Cover Picture



Yuki Tachibana, Garth L. Fletcher, Naoki Fujitani, Sakae Tsuda, Kenji Monde, and Shin-Ichiro Nishimura*

Antifreeze glycoproteins (AFGPs) found in the body fluids of polar fish are known to protect them from freezing by suppressing ice-crystal growth. The essential structural motifs of AFGPs were revealed by using a combination of chemical synthesis and spectroscopic analysis. The amphiphatic AFGPs form a threefold left-handed axis, which enables the sugar moieties to cluster on one side of the molecule. For further details see the Communication by S.-I. Nishimura and co-workers on page 856 ff.

Contents

Angewandte EarlyView

The following articles are available online (in Wiley InterScience). You can find them at www.angewandte.org, under Full Text, Early View.

F. F. Kneisel, M. Dochnahl, P. Knochel:*
Nucleophilic Catalysis of the Iodine–Zinc Exchange Reaction: Preparation of Highly Functionalized Diaryl Zinc Compounds
DOI: 10.1002/anie.200353316
Published online: January 27, 2004

C. L. M. Pereira, E. F. Pedroso, H. O. Stumpf, M. A. Novak, L. Ricard, R. Ruiz-García, E. Rivière, Y. Journaux*:*
A $Cu^{II}Co^{II}$ Metallacyclophane-Based Metamagnet with a Corrugated Brick Wall Sheet Architecture
DOI: 10.1002/anie.200352604
Published online: January 27, 2004

H. Chun, D. Kim, D. N. Dybtsev, K. Kim:*
Metal–Organic Replica of Fluorite Built with an Eight-Connecting Tetranuclear Cadmium Cluster and a Tetrahedral Four-Connecting Ligand
DOI: 10.1002/anie.200353139
Published online: January 27, 2004

D. Liu, S. Choi, B. Chen, R. J. Doerksen, D. J. Clements, J. D. Winkler, M. L. Klein, W. F. DeGrado:*
Nontoxic Membrane-Active Antimicrobial Arylamide Oligomers
DOI: 10.1002/anie.200352791
Published online: January 27, 2004

L. J. Gooßen, J. Paetzold:*
Decarbonylative Heck Olefination of Enol Esters: Salt-Free and Environmentally Friendly Access to Vinyl Arenes
DOI: 10.1002/anie.200352357
Published online: January 29, 2004

L. Hogg, D. A. Leigh, P. J. Lusby, A. Morelli, S. Parsons, J. K. Y. Wong:*
A Simple General Ligand System for Assembling Octahedral Metal–Rotaxane Complexes
DOI: 10.1002/anie.200353186
Published online: January 27, 2004

Articles judged by the referees or the editor as being either very important or very urgent are immediately edited, proof-read, and electronically published once the manuscript has arrived in the editorial office in final form. As long as there is no page number available these articles should be cited in the following manner:

Author(s) *Angew. Chem. Int. Ed.*, online publication date, DOI.

News

Organic Chemistry: Distinction to C. Djerassi — **776**

Organic Chemistry: T. Bach receives Novartis Award — **776**

Bioorganic Chemistry: D. Seebach and S. Kent recognized — **776**

Books

The Chemistry of Phenols — **778** — Zvi Rappoport — *reviewed by S. R. Waldvogel*

Modern Methods of Drug Discovery **779** — Alexander Hillisch, Rolf Hilgenfeld — *reviewed by N. Heinrich*

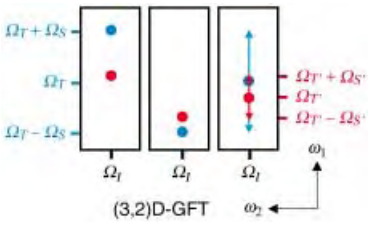
Organolithiums in Enantioselective Synthesis — **780** — David M. Hodgson — *reviewed by B. Goldfuss*

Highlights

Structure Determination

B. Simon, M. Sattler* — **782–786**

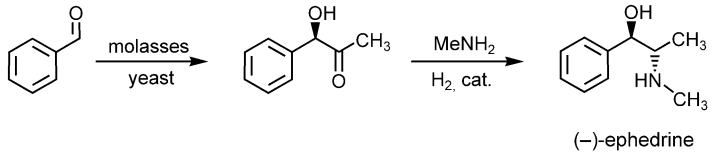
Speeding Up Biomolecular NMR Spectroscopy



A useful acquisition: Reducing the dimensionality of multidimensional NMR experiments dramatically decreases measurement times. Where signal-to-noise is not limiting, GFT NMR spectroscopy (see picture) provides a general scheme for fast data acquisition which can speed up NMR-based protein-structure determination.

© 2004 Wiley-VCH Verlag GmbH & Co. KGaA, Weinheim

Reviews



Of fundamental importance for the pharmaceutical industry is the large-scale availability of enantiomerically pure intermediates, such as amino acids, amino alcohols, amines, alcohols, and epoxides. In this Review industrially relevant syntheses of such intermediates are presented, based on chemical as well as enzymatic and fermentation processes (see scheme).

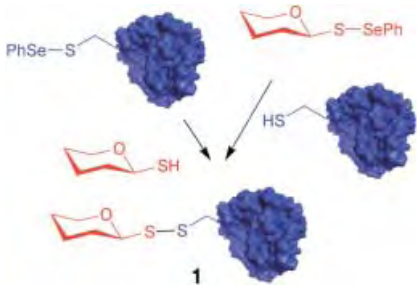
Industrial Chemistry

M. Breuer, K. Ditrich, T. Habicher, B. Hauer,* M. Keßeler, R. Stürmer, T. Zelinski ——— **788 – 824**

Industrial Methods for the Production of Optically Active Intermediates

Communications

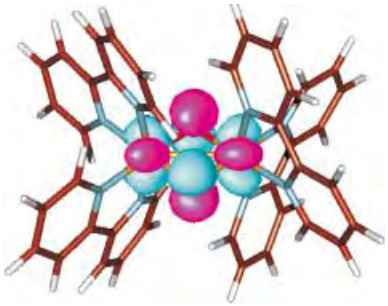
Site-selective glycosylation by Se–S-mediated ligation has led to the efficient formation of a wide variety of conjugates **1** without the need for a large excess of the carbohydrate reagent. By this convergent method it was possible to introduce a heptasaccharide glycan selectively, and to perform a multiple site-selective chemical glycosylation of protein. A chemically Cys-glycosylated glycoprotein was elaborated enzymatically.



Glycoproteins

D. P. Gamblin, P. Garnier, S. van Kasteren, N. J. Oldham, A. J. Fairbanks, B. G. Davis* ——— **828 – 833**

Glyco-SeS: Selenenylsulfide-Mediated Protein Glycoconjugation—A New Strategy in Post-Translational Modification



Insight into the electronic structures of high-valent intermediates with the $\{Fe^{IV}_2(\mu\text{-}O)_2\}$ "diamond core" is provided by density theory calculations. These electronic structures are contrasted with nitrido-bridged heme dimers that contain metal centers with the same oxidation state. Such diamond-core intermediates might actually occur in the catalytic cycles of diiron alkane monooxygenases such as AlkB.

Density Functional Calculations

A. Ghosh,* E. Tangen, E. Gonzalez, L. Que, Jr.* ——— **834 – 838**

Models of High-Valent Intermediates of Non-Heme Diiron Alkane Monooxygenases: Electronic Structure of a Bis(μ-oxo)diron(IV) Complex with Locally Low-Spin Metal Centers

For the USA and Canada:
ANGEWANDTE CHEMIE International Edition (ISSN 1433-7851) is published weekly by Wiley-VCH PO Box 191161, D 69451 Weinheim, Germany. Air freight and mailing in the USA by Publications Expediting Inc. 200 Meacham Ave., Elmont, NY 11003. Periodicals postage paid at Jamaica NY 11431. US POSTMASTER: send address changes to *Angewandte Chemie*, Wiley-VCH, 111 River Street, Hoboken, NJ 07030. Annual subscription price for institutions: Europe € 3430.00/3118.00; outside Europe US$ 4499.00/4090.00 (valid for print and electronic/print or electronic delivery); for individuals who are personal members of a national chemical society, or whose institution already subscribes, or who are retired or self-employed consultants, print only: Europe € 248.00/outside Europe US$ 378.00. Postage and handling charges included. All Wiley-VCH prices are exclusive VAT.

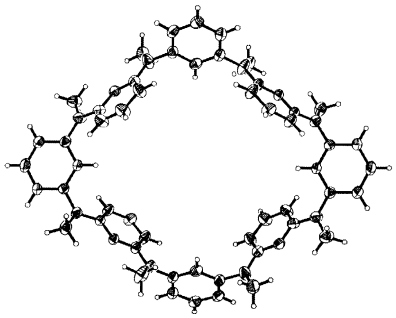
 © 2004 Wiley-VCH Verlag GmbH & Co. KGaA, Weinheim

Contents

Fullerene/Azacalixarene Complexes

M.-X. Wang,* X.-H. Zhang, Q.-Y. Zheng ——— **838 – 842**

Synthesis, Structure, and [60]Fullerene Complexation Properties of Azacalix[*m*]arene[*n*]pyridines



1

Remarkably stable C_{60} and C_{70} complexes with stability constants K_s of $70\,680 \pm 2060$ and $136\,620 \pm 3770\ M^{-1}$, respectively, are formed by azacalix[4]arene[4]pyridine **1**. The smaller-ring-homologue azacalix[2]arene[2]pyridine and compound **1** were readily synthesized, and they adopt a heavily twisted 1,3-*alternate* and a 1,2,3-*partial cone* conformation, respectively, in the solid state (see picture).

Protein–Ligand Interactions

S. Howorka,* J. Nam, H. Bayley, D. Kahne ——— **842 – 846**

Stochastic Detection of Monovalent and Bivalent Protein–Ligand Interactions

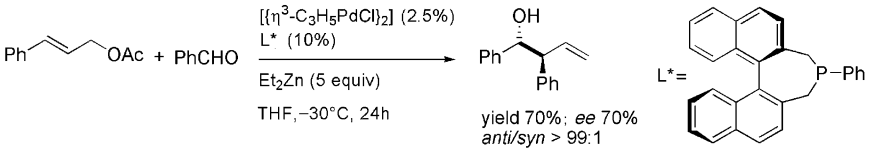


Single-molecule study on multivalency: The binding kinetics of a tetravalent lectin can be examined at the single-molecule level by using an engineered protein pore carrying up to seven carbohydrate ligands. The binding of the lectin to the pore (see molecular model) produces short and long reversible blockades in single-channel current recordings, which are interpreted as monovalent and bivalent binding events, respectively.

Enantioselective Allylation

G. Zanoni,* S. Gladiali, A. Marchetti, P. Piccinini, I. Tredici, G. Vidari ——— **846 – 849**

Enantioselective Catalytic Allylation of Carbonyl Groups by Umpolung of π-Allyl Palladium Complexes

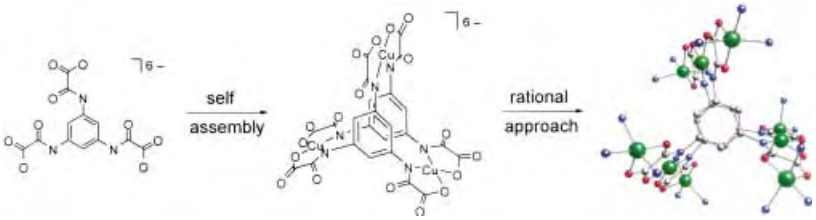


Diethylzinc mediates the asymmetric allylation of aldehydes through Umpolung of a π-allyl palladium complex. An investigation of the palladium source and the chiral monophosphane ligands have shown that the leaving group has a dramatic effect on the enantioselectivity of the reaction. The procedure furnished products in satisfactory yields and up to 70% *ee* (see scheme).

Metallacyclophanes

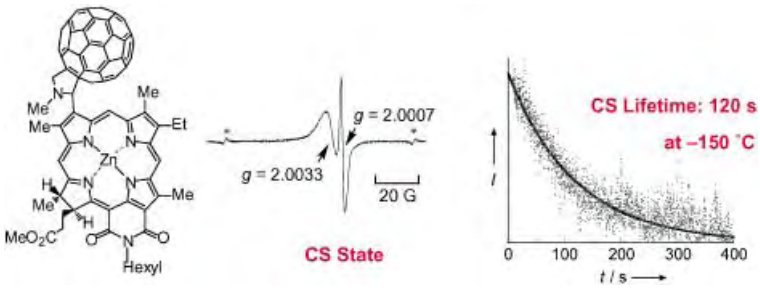
X. Ottenwaelder, J. Cano, Y. Journaux,* E. Rivière, C. Brennan, M. Nierlich, R. Ruiz-García ——— **850 – 852**

Rational Design of an Enneanuclear Copper(II) Complex with a Metallacyclophane Core



A hexakis-bidentate building block: Tricopper(II) and enneacopper(II) 1,3,5-metallacyclophanes were synthesized by a combination of self-assembly and a rational approach (see scheme). Both complexes exhibit ferromagnetic coupling in the core, through a spin-polarization mechanism.

© 2004 Wiley-VCH Verlag GmbH & Co. KGaA, Weinheim

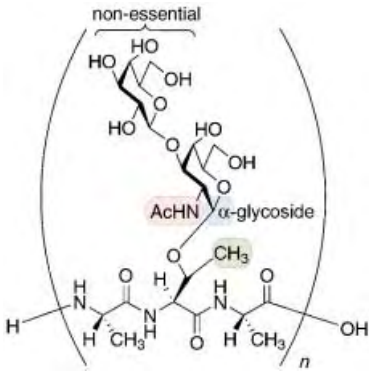


Long live the state! Photoexcitation of a zinc chlorin–fullerene dyad with a short linkage results in the formation of the ultra-long-lived charge-separated (CS) state by a one-step photoinduced electron transfer without loss of energy, which is inevitable for charge separation by multi-step electron-transfer processes. The lifetime of the charge-separated state was 120 s in frozen PhCN at −150 °C (see picture).

Intramolecular Electron Transfer

K. Ohkubo, H. Kotani, J. Shao, Z. Ou, K. M. Kadish,* G. Li, R. K. Pandey,* M. Fujitsuka, O. Ito,* H. Imahori,* S. Fukuzumi* _____ **853 – 856**

Production of an Ultra-Long-Lived Charge-Separated State in a Zinc Chlorin–C_{60} Dyad by One-Step Photoinduced Electron Transfer



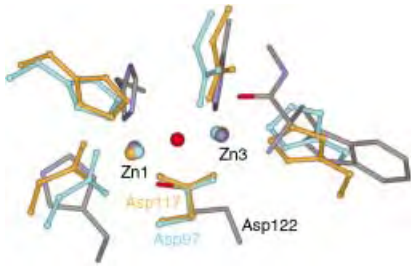
Good for winter: The structure–activity relationships of antifreeze glycoproteins (AFGPs) have been characterized by chemical synthesis and conformational analysis. The results revealed that the mode of glycosylation on the threonyl residue in the tripeptide unit is of primary importance in the formation of the specific structure for the antifreeze activity (see picture for the structural requirements of AFGPs).

Glycoproteins

Y. Tachibana, G. L. Fletcher, N. Fujitani, S. Tsuda, K. Monde, S.-I. Nishimura* _____ **856 – 862**

Antifreeze Glycoproteins: Elucidation of the Structural Motifs That Are Essential for Antifreeze Activity

Shaping up for inhibition: Identification of three-dimensional structural similarities (see picture) between the active sites of zinc dinuclear aminopeptidases and trinuclear phospholipase C hydrolytic enzymes that are not related by sequence or tertiary structure led to the discovery of phospholipase C inhibition by α-amino-hydroxamic acids, a typical family of aminopeptidase inhibitors.



Active-Site Inhibitors

A. González-Roura, I. Navarro, A. Delgado, A. Llebaria,* J. Casas _____ **862 – 865**

Disclosing New Inhibitors by Finding Similarities in Three-Dimensional Active-Site Architectures of Polynuclear Zinc Phospholipases and Aminopeptidases

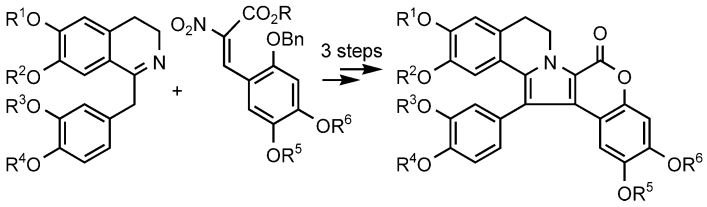
 © 2004 Wiley-VCH Verlag GmbH & Co. KGaA, Weinheim

Contents

Marine Alkaloid Synthesis

P. Ploypradith, C. Mahidol, P. Sahakitpichan, S. Wongbundit, S. Ruchirawat* ——— **866 – 868**

A Highly Efficient Synthesis of Lamellarins K and L by the Michael Addition/Ring-Closure Reaction of Benzyldihydroisoquinoline Derivatives with Ethoxycarbonyl-β-nitrostyrenes

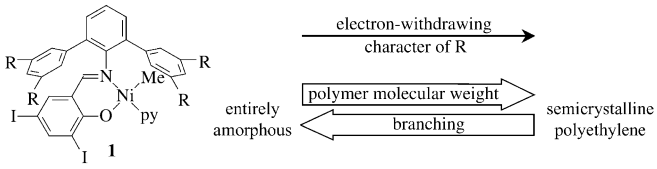


Alkaloid achievement: Lamellarins, a new class of potential nontoxic inhibitors of HIV-1 integrase that are also responsible for multidrug-resistance reversal in cancer cell lines, could be synthesized in three chemical steps and in 60% overall yields from two simple starting materials (see scheme). The key step in the convergent synthetic approach involved the novel Michael addition/ring-closure reaction to give the pyrrole core and the ester group required for subsequent lactonization in one step.

Polymerization Catalysis

M. A. Zuideveld, P. Wehrmann, C. Röhr, S. Mecking* ——— **869 – 873**

Remote Substituents Controlling Catalytic Polymerization by Very Active and Robust Neutral Nickel(II) Complexes



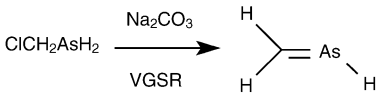
Remote control: Substituents strongly affect the catalytic properties of complexes **1** in ethylene polymerization, despite their remoteness from the active center. An appropriate substitution pattern provides very active and robust catalysts.

Organoarsenic Compounds

A. Chrostowska,* A. Dargelos, V. Lemierre, J.-M. Sotiropoulos, P. Guenot, J.-C. Guillemin* ——— **873 – 875**

First Synthesis and Characterization by Mass Spectrometry and UV-Photoelectron Spectroscopy of Methylenearsane

In a vacuum gas–solid reaction (VGSR; see scheme), the kinetically unstable methylenearsane was synthesized by dehydrohalogenation of gaseous chloromethylarsane on solid sodium carbonate and characterized in the gas phase by mass spectrometry and UV photoelectron spectroscopy. A new approach to theoretically evaluate ionization potentials is also demonstrated.

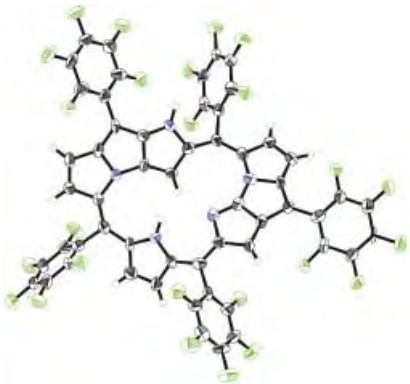


VIP

Confused Porphyrins

A. Srinivasan, T. Ishizuka, H. Furuta* ——— **876 – 879**

Doubly N-Fused Pentaphyrin



Inverted and fused: *Meso*-pentafluorophenyl-substituted N-confused, doubly N-fused pentaphyrin (see X-ray crystal structure; green: F, blue: N) was synthesized from [3+2] coupling of confused tripyrrane and dipyrromethane dicarbinol, followed by oxidation. Inverted pyrrole rings in pentaphyrin are easily transformed into N-fused tripentacyclic rings.

 © 2004 Wiley-VCH Verlag GmbH & Co. KGaA, Weinheim

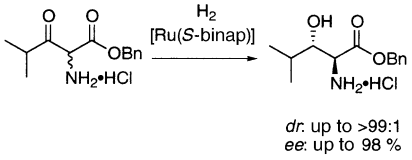


The stereoselective preparation and Pd-catalyzed cross-coupling reaction of boronates **2** provides a new general and convenient route to CF_3-substituted triaryl ethenes **3**, in which the CF_3 and Ar^3 groups are *cis* to each other. The synthetic potential was demonstrated by the total synthesis of panomifene ($Ar^1 = Ar^3 = Ph$, $Ar^2 = 4\text{-}(OHCH_2CH_2NHCH_2CH_2O)\text{-}C_6H_4$). Bpin = (pinacolato)boryl.

Organofluorine Compounds

X. Liu, M. Shimizu,*
T. Hiyama ——— 879 – 882

A Facile Stereocontrolled Approach to CF_3-Substituted Triarylethenes: Synthesis of Panomifene



Upping the *anti*: Asymmetric *anti*-selective hydrogenation of α-amino-β-keto esters through dynamic kinetic resolution has been achieved for the first time by using the Ru–binap catalyst. The reaction affords important *anti*-β-hydroxy-α-amino acids with 74–98% *ee* and high diastereomeric ratio in excellent yields (see scheme; binap = 2,2′-bis(diphenylphosphanyl)-1,1′-binaphthyl).

anti-Selective Hydrogenation

K. Makino, T. Goto, Y. Hiroki,
Y. Hamada* ——— 882 – 884

Stereoselective Synthesis of *anti*-β-Hydroxy-α-amino Acids through Dynamic Kinetic Resolution

The geological longevity of *Lingula*, depicted, suggests that the lightly mineralized carbonate-substituted fluorapatite (FAP) shell has remained well-adapted to evolutionary pressures. Contrary to earlier studies, soluble macromolecules isolated from *Lingula* shells are shown to specifically promote FAP crystallization by the destabilization of an amorphous calcium phosphate precursor.



Biomineralization

I. Lévêque, M. Cusack, S. A. Davis,
S. Mann* ——— 885 – 888

Promotion of Fluorapatite Crystallization by Soluble-Matrix Proteins from *Lingula Anatina* Shells

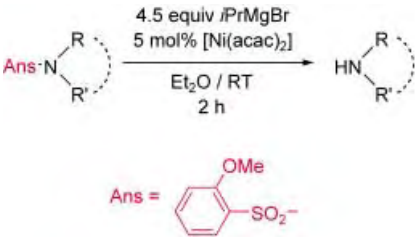
A mild method for the Ni^0-catalyzed hydrodesulfamoylation (see scheme, B) of aryl sulfonamides (**1**→**2**) with iPr_2Mg or *i*PrMgCl as β-hydride transfer sources can be linked with directed *ortho* metalation (A and C) to give *meta*-substituted aromatics **2**. Cross-coupling process with alkyl and aryl Grignard reagents furnish disubstituted benzenes and bi- and teraryl compounds.



Cross-Coupling Reactions

R. R. Milburn, V. Snieckus* ——— 888 – 891

The Tertiary Sulfonamide as a Latent Directed-Metalation Group: Ni^0-Catalyzed Reductive Cleavage and Cross-Coupling Reactions of Aryl Sulfonamides with Grignard Reagents



A potentially good alternative to the tosyl group (Ts) as a protecting group for amines is *N*-*ortho*-anisylsulfonyl (Ans), which is readily cleaved under mild, Ni^0-catalyzed reductive conditions (see scheme, acac = acetylacetonate). *N*-Anisylation of primary amines followed by alkylation and deprotection provides a route to a range of secondary amines.

Protecting Groups

R. R. Milburn, V. Snieckus* ——— 892 – 894

ortho-Anisylsulfonyl as a Protecting Group for Secondary Amines: Mild Ni^0-Catalyzed Hydrodesulfonylation

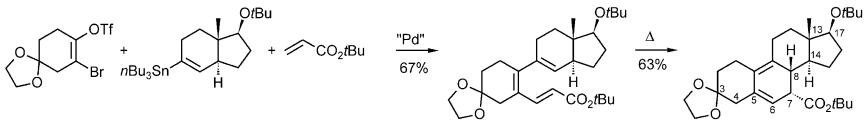
 © 2004 Wiley-VCH Verlag GmbH & Co. KGaA, Weinheim

Contents

Oligocyclic Dienes

H. W. Sünnemann, A. de Meijere* ____ 895 – 897

Steroids and Steroid Analogues from Stille–Heck Coupling Sequences

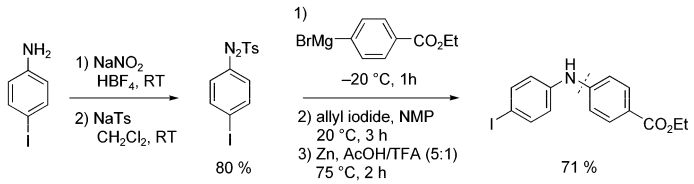


Tricyclic 1,3,5-hexatrienes were prepared from 4-substituted 2-bromocyclohexenyl triflate, enantiomerically pure hexahydroindenylstannanes, and *tert*-butyl acrylate in a sequence of Stille and Heck reactions. In the example shown, an enantiomerically pure steroid with protected functionalities in the 3-, 7-, and 17-positions is formed in a 6π-electrocyclization upon heating at 220 °C.

Amination

I. Sapountzis, P. Knochel* ____ 897 – 900

A General Amination Method Based on the Addition of Polyfunctional Arylmagnesium Reagents to Functionalized Arylazo Tosylates



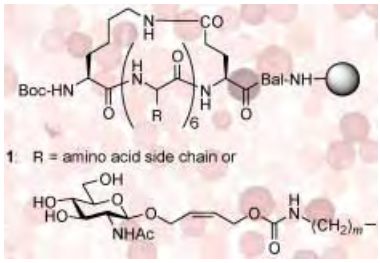
A one-pot reaction sequence consisting of a Grignard reaction, allylation, and reduction provides new functionalized diarylamines in good yields (see scheme, Ts = toluene-4-sulfonyl, NMP = *N*-methylpyrrolidine, TFA = trifluoroacetic acid). In the first step azoaryl tosylates, which are readily obtained from aromatic amines, are treated with a myriad of functionalized organomagnesium compounds.

Bioorganic Chemistry

V. Wittmann,* S. Seeberger ____ 900 – 903

Spatial Screening of Cyclic Neoglycopeptides: Identification of Polyvalent Wheat-Germ Agglutinin Ligands

Affinities enhanced by up to 619-fold were found for new ligands of the plant lectin wheat-germ agglutinin (compared to the binding of *N*-acetylglucosamine (GlcNAc)). These polyvalent neoglycopeptides were identified from screening of a spatially diverse library of type **1**. Binding affinity is determined not only by the number of GlcNAc residues but also by the ligand architecture.



VIP Communications labeled with this symbol have been judged by two referees as being "very important papers".

Looking for outstanding employees?

Do you need another expert for your excellent team?
... Chemists, PhD Students, Managers, Professors, Sales Representatives...

Place an advert in the printed version and have it made available online for 1 month, free of charge!

Angewandte Chemie International Edition
Advertising Sales Department: Marion Schulz
Phone: 0 62 01 - 60 65 65
Fax: 0 62 01 - 60 65 50
E-Mail: MSchulz@wiley-vch.de

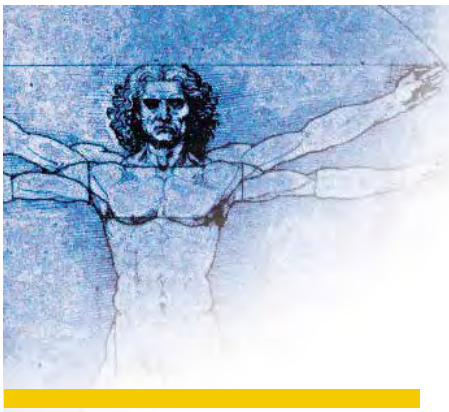
Service

Keywords ____ 906

Authors ____ 907

Angewandte's Sister Journals 904 – 905

Preview ____ 909



C. Djerassi Receives German Distinction

The Great Cross of Merit of the Federal Republic of Germany was awarded to Carj Djerassi for his many achievements in chemistry, as well as for the social impact of his research. In November 2003, he was keynote speaker and panel chairman at the Intergovernmental Forum on Chemical Safety in Bangkok. His Essay on "Chemical Safety in a Vulnerable World—A Manifesto" will be published in *Angewandte Chemie* soon.



C. Djerassi

Djerassi became known and widely honored as one of the originators of "the pill", for leading the small team at Syntex (Mexico) where the orally active ovulation inhibitor norethisterone was first synthesized in 1951. Further research in the same year led him and his colleagues to the synthesis of cortisone from a plant raw material and to many other important discoveries in steroid chemistry. As an author, he not only wrote over 1200 scientific publications, but since 1988 has also published five novels in the genre "science in fiction" and four plays as "science in theater". One of them, written jointly with Roald Hofmann, deals with the discovery of oxygen and the centenary of the Nobel prize.[1] Djerassi supports young artists through the Djerassi Resident Artists Program near Woodside, CA (USA) and owns one of the most important private collections of paintings by Paul Klee, which is exhibited in the Museum of Modern Art in San Francisco, CA (USA).

Djerassi was born in 1923 in Vienna, Austria, fled to the US in 1939, and received a PhD in chemistry from the University of Wisconsin (USA) in 1945. Subsequently, he worked as a research chemist for CIBA Pharmaceutical (Summit, NJ) and as a chemical research director for Syntex (Mexico City). In 1952, he accepted a position as a Professor of Chemistry at Wayne State University in Detroit. In 1959, he moved to Stanford University, where he became Professor Emeritus in 2002. The Austrian government presented him in 1999 with the Austrian Cross of Honor for Science and Art, and in 2003, on the occasion of his 80th birthday, with Austrian citizenship.

Novartis Award for T. Bach

Thorsten Bach, Professor of Organic Chemistry at the Technische Universität München (Germany) received the Novartis European Young Investigator Award in Chemistry. The award and prize money of SFr. 100000 is presented annually to an outstanding scientist under the age of 40 who is a European resident and is active in the areas of organic or bioorganic chemistry in the broadest sense.



T. Bach

Bach studied with G. Olah (University of Southern California), who received the Nobel Prize in Chemistry in 1994, and obtained a PhD under the guidance of M. Reetz from the University of Marburg, Germany. He carried out postdoctoral research with D. Evans (Harvard University) and obtained a habilitation from the University of Münster (Germany) in 1996. He became a Professor in Marburg (Germany) in 1997 and assumed his current position in Munich in 2000. His research is devoted to photochemistry, total synthesis of natural products, drug design, and organometallic chemistry. His latest Communication in *Angewandte Chemie* details the "[2+2] Photocycloaddition of Tetronates".[2]

Peptide Award for D. Seebach and S. Kent

The Vincent du Vigneau Award of the American Peptide Society is sponsored by Bachem Inc. and given for outstanding contributions to peptide science every two years. Du Vigneau (then Cornell University) received the Nobel Prize in Chemistry in 1955 for his work on biochemically important sulfur compounds, especially for the first synthesis of a polypeptide hormone. In 2004, the award will be presented to Professors Dieter Seebach (ETH Zurich, Switzerland) and Stephen B. H. Kent (University of Chicago, IL, USA). The award lectures will be presented during the Gordon Research Conference on the Chemistry and Biology of Peptides in February 2004.



D. Seebach

Seebach, a former member of *Angewandte*'s Editorial Board, received his PhD from the University of Karlsruhe, Germany, under the guidance of R. Criegee. He was a postdoctoral fellow with E. J. Corey (Harvard University), became a Professor in Giessen in 1971, and moved to the ETH in 1977. His research covers the development of new methods of organic synthesis in its broadest meaning. A Review of his research on β-peptides, which he is recognized for, will appear in *Angewandte Chemie* later this year. It is the twelfth Review he has contributed to the journal in almost 30 years on a variety of topics such as umpolung, the use of Ti- and Zr-nucleophiles, and asymmetric synthesis.



S. Kent

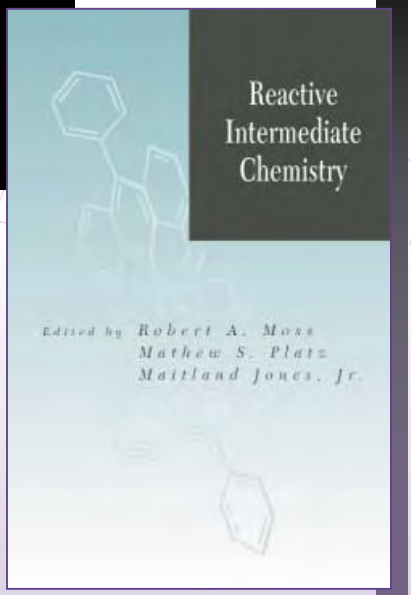
Kent earned his BSc and MSc degrees from Victoria and Massey University in New Zealand and a PhD from the University of California, Berkeley (1974). He carried out postdoctoral research with R. B. Merrifield (Rockefeller University, NY, Nobel

 © 2004 Wiley-VCH Verlag GmbH & Co. KGaA, Weinheim

Prize in Chemistry 1984) and subsequently took up a number of positions, which included appointments at the California Institute of Technology, Bond University (Queensland, Australia), and the Scripps Research Institute (USA) as well as in industry before he became a Professor (2001) and eventually Director of the Institute for Biophysical Dynamics (2003) at the University of Chicago. His research is devoted to the elucidation of the molecular basis of the biological functions of proteins through the application of the tools of chemistry. He is recognized for the development of general approaches to the total chemical synthesis of proteins and the application thereof to the study of structure–activity relationships of proteins of biomedical importance, notably the HIV-1 protease.[3]

[1] C. Djerassi, R. Hoffmann, *Oxygen*, Wiley-VCH, Weinheim, **2001**.
[2] M. Kemmler, T. Bach, *Angew. Chem.* **2003**, *115*, 4973; *Angew. Chem. Int. Ed.* **2003**, *42*, 4824.
[3] S. Kent, *J. Pept. Sci.* **2003**, *9*, 574.

Reactive Intermediate Chemistry



Robert A. Moss, *Rutgers University*
Matthew S. Platz, *Ohio State University*
Maitland Jones, *Princeton University*

ISBN 0-471-23324-2 • 1,080 pages • Cloth
$99.95 / £64.50 / €90.90
December 2003

Reactive Intermediate Chemistry presents a detailed and timely examination of key intermediates central to the mechanisms of numerous organic chemical transformations. Spectroscopy, kinetics, and computational studies are integrated in chapters dealing with the chemistry of carbocations, carbanions, radicals, radical ions, carbenes, nitrenes, arynes, nitrenium ions, diradicals, etc. Nanosecond, picosecond, and femtosecond kinetic realms are explored, and applications of current dynamics and electronic structure calculations are examined.

WILEY

Reactive Intermediate Chemistry provides a deeper understanding of contemporary physical organic chemistry, and will assist chemists in the design of new reactions for the efficient synthesis of pharmaceuticals, fine chemicals, and agricultural products. Among its features, this authoritative volume is:

- Edited and authored by world-renowned leaders in physical organic chemistry.
- Ideal for use as a primary or supplemental graduate textbook for courses in mechanistic organic
- Enhanced by supplemental reading lists and summary overviews in each chapter.

CONTENTS

Preface

PART 1: REACTIVE INTERMEDIATES

1. Carbocations (R.A. McClelland)
2. Crossing the Borderline Between SN1 and SN2 Nucleophilic Substitution at Aliphatic Carbon(T.L. Amyes, et al.)
3. Carbanions (S. Gronert)
4. Radicals (M. Newcomb)
5. Non-Kekul Molecules as Reactive Intermediates (J.A. Berson)
6. Organic Radical Ions (H.D. Roth)
7. Singlet Carbenes (M. Jones Jr. and R.A. Moss)
8. Stable Singlet Carbenes (G. Bertrand)
9. Triplet Carbenes (H. Tomioka)
10. Atomic Carbon (P.B. Shevlin)
11. Nitrenes (M.S. Platz)
12. Synthetic Carbene and Nitrene Chemistry (M.P. Doyle)
13. Nitrenium Ions (D.E. Falvey)
14. Silylenes (W. Ando and N. Tokitoh)
15. Strained Hydrocarbons: Structures, Stability, and Reactivity (K.B. Wiberg)
16. Arynes (M. Winkler, et al.)

PART 2: METHODS AND TEMPORAL REGIMES

17. Matrix Isolation (T. Bally)
18. Nanosecond Laser Flash Photolysis: A Tool for Physical Organic Chemistry (J.C. Scaiano)
19. The Picosecond Realm (E. Hilinski)
20. Reactions on the Femtosecond Time Scale (J.E. Baldwin)
21. Potential Energy Surfaces and Reaction Dynamics (B.K. Carpenter)
22. The Partnership Between Electronic Structure Calculations and Experiments in the Study of Reactive Intermediates (W.T. Borden)

 © 2004 Wiley-VCH Verlag GmbH & Co. KGaA, Weinheim

Structure Determination

Speeding Up Biomolecular NMR Spectroscopy**

*Bernd Simon and Michael Sattler**

Keywords:
GFT NMR spectroscopy · multidimensional NMR spectroscopy · proteins · structure determination

NMR spectroscopy is a well established method for the characterization of three-dimensional structures, dynamics, and molecular interactions of biomacromolecules. Today about 20% of the structures deposited in the Protein Data Bank (http://www.rcsb.org/pdb) are determined by NMR spectroscopy, and international structural genomics initiatives rely on both X-ray crystallography and NMR spectroscopy for large-scale protein structure determination.[1] A limitation for high-throughput NMR spectroscopy is the long time needed to record a set of multidimensional NMR experiments for the structure determination. In the past, long measurement times were required to improve the signal-to-noise ratio in NMR spectra, and to obtain sufficient spectral resolution in indirectly detected dimensions of multidimensional NMR data.

Continuous improvements in NMR hardware, for example, the introduction of highest magnetic-field strengths and cryogenic probes, have dramatically increased the sensitivity of NMR spectroscopy. Therefore, experimental times could be significantly shortened if sampling of indirect dimensions in multidimensional NMR experiments was optimized. Now, Kim and Szyperski report a general scheme for the acquisition of NMR spectra which involves reducing the dimensionality of multidimensional NMR experiments.[2] The method, called GFT NMR, greatly reduces measurement time without compromising spectral resolution and will be applicable where data acquisition is not limited by sensitivity but rather resolution.

[*] Dr. B. Simon, Dr. M. Sattler
European Molecular Biology Laboratory
Meyerhofstrasse 1, 69117 Heidelberg (Germany)
Fax: (+49) 6221-387-306
E-mail: sattler@embl.de

[**] We thank Christian Griesinger for stimulating discussions and critical reading of the manuscript.

Multidimensional NMR Spectroscopy

NMR structure determination involves two main parts: The first step comprises sequential assignment of all chemical shifts, while for the second step NMR spectra are recorded to derive structural information from nuclear Overhauser effects (NOEs), scalar couplings, and residual dipolar couplings.[3,4] Chemical shift and NOE assignments are hampered by spectral overlap owing to the growing number of NMR resonance signals associated with increasing molecular weight. About 15 years ago, the introduction of efficient isotope labeling schemes for the preparation of uniformly ^{13}C and ^{15}N labeled proteins allowed the use of heteronuclear correlation spectroscopy to resolve signal overlap in the ^{1}H NMR spectra.[5] Typically, magnetization of a proton spin I is transferred to a directly bound heteronucleus S (^{13}C or ^{15}N) through large one-bond J couplings. In the simplest case, this yields a two-dimensional (2D) NMR spectrum[6] which correlates proton (^{1}H) and heteronuclear (^{13}C, ^{15}N) chemical shifts. Since the introduction of multidimensional, that is, three-[7–9] or four-dimensional[10] experiments, a great variety of NMR pulse sequences has been developed.[11] These are used to obtain correlations between all ^{1}H, ^{13}C, and ^{15}N signals of a protein, based on one-bond J couplings.[12]

A 2D I,S correlation experiment uses a sequence of radio-frequency pulses and delays to transfer magnetization between spins S and I. Chemical shifts of the S spins are recorded in an indirect (digitized) time domain t_1 by stepwise incrementing a delay during which the chemical shift evolution of the S spins occurs. This approach leads to a modulation of the NMR signal with the S spin frequencies during t_1. After magnetization transfer, the chemical shifts of the I spins are directly observed during t_2. Fourier transformation of both time dimensions yields the chemical shifts of the S and I spins in a 2D NMR spectrum.

This concept is easily extended to more than two dimensions, by introducing additional indirect time domains.[7–9] For example, a three-dimensional (3D) I,S,T correlation experiment may involve magnetization transfer and chemical shift evolution for three spins I, S, and T (Figure 1a). For sensitivity reasons, excitation and detection is usually performed on proton spins.[6] With the introduction of additional indirect time domains, the total duration of an NMR experiment increases dramatically, since for the m time points in the indirect dimension of an N-dimensional (ND) experiment $m(N-1)$D spectra have to be acquired. The total experimental time is determined by the number of time points (m) sampled in the indirect dimensions, the number of scans (N_S) averaged in the directly detected dimension, and the duration of each scan, typically about one second. Thus, assuming $N_S = 1$ and 60 time points per indirect dimension the minimum experimental time is 1 min (60×1 s) for a 2D, 1 h ($60 \times 60 \times 1$ s) for a 3D, 2.5 days for a 4D, and almost 0.5 year for a 5D spectrum. Even with these estimates which reflect the absolute lower limit with respect to resolution, 5D experiments are not practical, and only spectra

 © 2004 Wiley-VCH Verlag GmbH & Co. KGaA, Weinheim DOI: 10.1002/anie.200301680

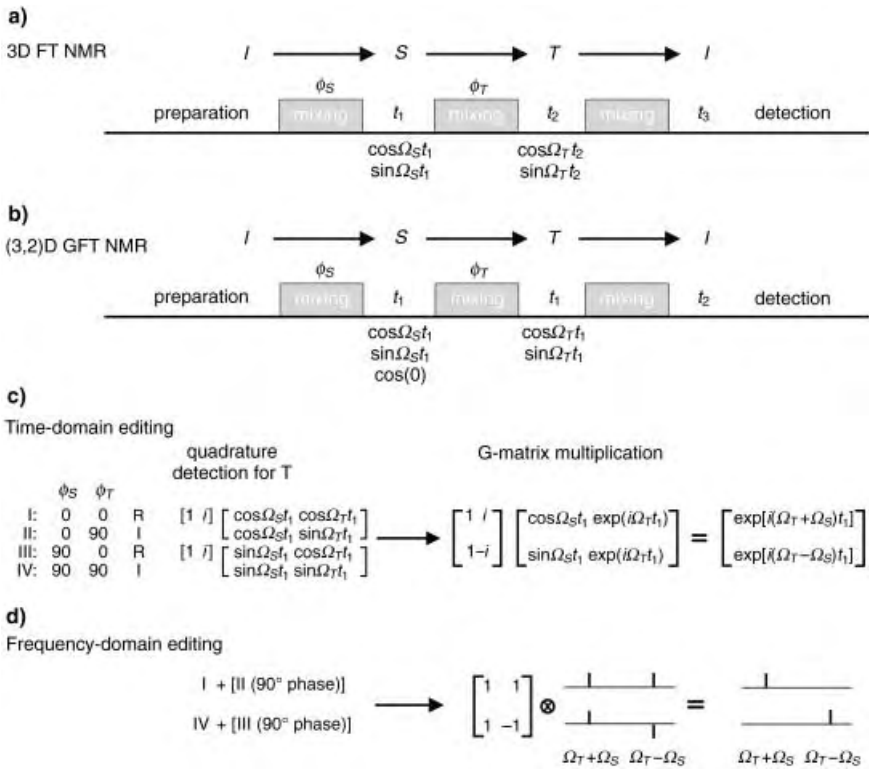


Figure 1. Schematic representation of a) a 3D NMR experiment and b) a corresponding (3,2)D reduced dimensionality (RD) experiment correlating three spins, *I*, *S* and *T*. During the preparation period, equilibrium magnetization is (re)established. Chemical shifts of *S* and *T* spins are recorded during indirect evolution periods, *I* spins are directly detected during acquisition. In the (3,2)D RD experiment, the chemical shift evolution period of the *S* spins is projected ($K=1$), and the chemical shifts of the *T* and *S* spins are recorded simultaneously during t_1. Quadrature detection for *S* and *T* spins is achieved by applying the mixing sequences with phases (θ_S, θ_T) 0° and 90°. This approach yields two pairs of signals with cosine and sine modulation, respectively (Figure 1c). For the (3,2)D GFT experiment, central-peak detection is achieved by performing an additional experiment with no chemical shift evolution of the *S* spins during t_1. This approach gives rise to a central-peak resonating at Ω_T during ω_1. c) Quadrature detection in the (3,2)D GFT experiment requires linear combinations of four different t_1 time-domain signals; R and I denote real and imaginary parts. Note, that there is a 90° phase shift between signals I,IV compared to II,III. In the first step, the cosine and sine modulated signals of the *T* spins are combined for quadrature detection of the *T* spin frequencies. Next, the two signals obtained are multiplied in the time domain with a G matrix (for $K=1$) to yield two phase-sensitive signals at frequencies $\Omega_T \pm \Omega_S$. d) Alternatively, the linear combinations required for quadrature detection of the *T* and *S* spin frequencies can also be performed in the frequency domain.

with up to four dimensions are routinely used.

Apart from the resolution requirements, sensitivity considerations also determine the minimum experimental time. Usually, a given NMR pulse sequence is averaged over N_S scans. The signals appear in all N_S repetitions at the same position, thus yielding N_S times the peak intensity of each scan, whereas the random noise only averages with square root of the number of scans. Therefore, the signal-to-noise ratio increases with $\sqrt{N_S}$.

Reduced Dimensionality NMR Spectroscopy

Until recently, poor signal-to-noise made it necessary to record a typical 3D experiment for 2–3 days. Therefore, experimental times were determined by the required signal-to-noise (sensitivity limited), which at the same time provided sufficient sampling of indirect time dimensions. Owing to dramatic improvements in NMR hardware in recent years, the intrinsic signal-to-noise ratio has increased by a factor 3–5, so that experimental times can be reduced 9–25-fold to achieve the same signal-to-noise ratio. Based on signal-to-noise considerations, 3D experiments could thus be recorded in less than a day, but the requirement to obtain sufficient resolution in indirect dimensions still necessitates longer measurement times, that is, these experiments are sampling limited. Amongst various strategies to optimize sampling of indirect time domains, such as nonlinear time domain sampling[13,14] or simultaneous acquisition,[15–17] reduced dimensionality NMR had already been proposed 10 years ago.[18,19]

Following the principle of accordion spectroscopy,[6] in reduced dimensionality (RD) experiments the evolution times of two or more[2,20,21] indirect dimensions are jointly sampled, in that the corresponding delays are increased simultaneously (Figure 1b). As a result, the dimensionality of the experiment is reduced, since K indirect dimensions of the ND experiment are projected onto $N-K$ dimensions in the RD experiment. Using quadrature detection (see next Section) by recording experiments I and II (Figure 1c), the frequency sign in the indirect time domain is determined only for one of the chemical shift modulations (Ω_T in Figure 1). The K projected dimensions lead to additional cosine modulations of the time-domain signal which give rise to cross peaks at $\Omega_1 \pm \Omega_2 \pm \Omega_{3\ldots} \pm \Omega_{K+1}$. Therefore, spectra are obtained with duplicated peaks at the sum and difference frequencies of the simultaneously incremented indirect dimensions. For example, a 3D experiment with a peak coordinate at $(\Omega_S,\Omega_T,\Omega_I)$ in the three frequency dimensions $(\omega_1, \omega_2, \omega_3$; Figure 2a) reduces to a 2D experiment with two peaks at $(\Omega_T+\Omega_S,\Omega_I)$ and $(\Omega_T-\Omega_S,\Omega_I)$ in (ω_1, ω_2) of the RD experiment (Figure 2c). For the equivalent of a 5D experiment eight peaks corresponding to $2\times2\times2$ sum/difference frequencies are obtained in the indirect dimension of a related 2D RD experiment, where three indirect dimensions are jointly sampled. In general, 2^K signals are obtained in the indirect dimension of a $(N,N-K)$D RD experiment with $K+1$ simultaneously sampled (K projected) dimensions, compared to one signal in the corresponding ND experiment.

 © 2004 Wiley-VCH Verlag GmbH & Co. KGaA, Weinheim

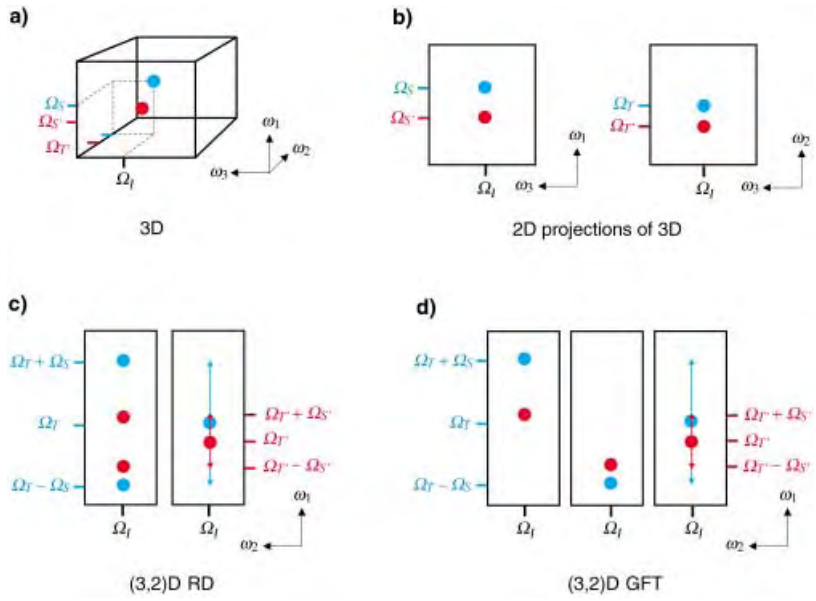


Figure 2. Schematic NMR spectra comparing conventional and RD implementations of a 3D experiment for two three-spin systems (blue and red) with degenerate chemical shifts of the *I* spin, which resonate at Ω_T,Ω_T,Ω_S, $\Omega_{S'}$ and Ω_I. a) Peak position in a conventional 3D FT NMR experiment. b) The chemical shift frequencies of the 3D experiment can be uniquely extracted from two 2D projections, if no signal overlap is present. Otherwise, the frequencies are not uniquely correlated and the partially overlapping spin systems cannot be assigned unambiguously. c) In a reduced dimensionality experiment, the frequencies of the *T* and *S* spins are measured as sum and difference chemical shifts (left). To unambiguously derive the underlying frequencies, also in the case of chemical shift degeneracy, a "central-peak" spectrum (right) is recorded, where no chemical shift modulation of the *S* spins has occurred during t_1. d) Spectra obtained in a (3,2)D GFT NMR spectrum. After linear combination (multiplication with a G matrix in the time domain, see Figure 1c), two signals are obtained at the sum or the difference frequencies of the *T* and *S* spins. To retrieve chemical shifts in case of degeneracies, the corresponding central-peak spectrum is required (right panel).

Reduced Dimensionality with Full Quadrature Detection: GFT NMR Spectroscopy

Serious drawbacks of this implementation of RD experiments are a reduction of signal-to-noise ratio by $v\sqrt{2^K}$ in the $(N,N-K)$D RD experiment compared to the corresponding *N*D experiment, and increased spectral overlap. This results from the cosine modulation obtained for each of the projected time domains which yields a duplication of peaks in the indirect frequency domain, thereby also reducing the signal intensity for each of the two peaks by or $1/(2^K)$ in a $(N,N-K)$D experiment (Figure 2c). However, if a second spectrum with sine modulation is recorded, one of the doublet components is inverted, and addition and subtraction of the two datasets yields two spectra with only a single peak (Figure 1c). Since the original doublet signals are added, the signal-to-noise ratio is improved by $\sqrt{2}$ compared to the RD experiment. This technique, called quadrature detection, is routinely used for frequency sign determination in all dimensions of a conventional multidimensional NMR experiment.[6] An improved implementation of RD experiments therefore employs quadrature detection for all jointly sampled time domains.[2,21–23] Cosine and sine modulation of the time-domain signals is achieved by independently shifting the phase of radio-frequency pulses preceding each indirect evolution time by 90° (Experiments I to IV in Figure 1c). In a (3,2)D RD experiment (Figure 1b, 2c), conventional quadrature detection is employed for the *T* spins. For full quadrature detection, two additional data sets with sine modulation for the chemical shift evolution of the *S* spins are recorded. After Fourier transformation the cosine- and sine-modulated *S* spin signals yield an in-phase and an anti-phase doublet at $\Omega_T \pm \Omega_S$, respectively. By linear combination, that is, addition and subtraction of these two datasets, two spectra are obtained with only one signal resonating at either $\Omega_T+\Omega_S$ or $\Omega_T-\Omega_S$ (Figure 1c,d and Figure 2d). For an $(N,N-K)$D RD experiment 2^K linear combinations have to be performed. The corresponding transformations can be summarized in a transformation matrix, which constitutes part of the "G matrix" as defined by Kim and Szyperski. This part of a 2×2 G matrix which achieves the appropriate linear combination of the time-domain signals in a (3,2)D RD experiment is shown in Figure 1c. Fourier transformation of the edited time-domain signals yields a set of basic spectra with a single peak at positions corresponding to all combinations of sum and difference frequencies in the indirect time domain (Figure 2d, left and middle). If full quadrature detection is applied, the signal-to-noise ratio of an $(N,N-K)$D RD experiment is equal to the corresponding *N*D experiment, since in an *N*D experiment quadrature detection is also employed for each time domain.

However, some information is lost in an RD experiment if resonance frequencies are degenerate in all of the conventionally sampled $(N-K-1)$ time domains, since only the sums and difference frequencies are measured—rather than the individual frequencies in separate time domains as in an *N*D experiment. While the RD experiment will still reveal that two signals with partial chemical shift degeneracy are present, the absolute resonance frequencies can not be retrieved from the sum and difference terms unless it is known which peaks in the basic spectra are correlated, that is, are derived from the same doublet. To overcome this problem, additional experiments have to be performed where for each projected dimension a peak centered between the cosine/sine modulated peak doublet is recorded ("central peak detection", for example, at Ω_T in Figure 2c,d right). If more than one dimension is projected, additional frequencies centered between the "first-order" central peaks need to be determined, and so on (Figure 2, 3 in ref. [2]). In a $(N,N-K)$ RD experiment 2^K basic and 2^{K-1} "central-peak" spectra have to be recorded. For example, a (3,2)D RD experiment

 © 2004 Wiley-VCH Verlag GmbH & Co. KGaA, Weinheim

requires only one additional central-peak spectrum, while a (5,2)D experiment ($K=3$) requires four first-order, two second-order, and one third-order central-peak spectra. By addition and subtraction of all $2^{K+1}-1$ time-domain signals (e.g. 15 signals for a (5,2)D RD experiment), $2^{K+1}-1$ spectra with a single peak at all combinations of the $K+1$ involved indirect frequencies ($\Omega_1,\Omega_2,\Omega_3,\Omega_4$) are obtained. The linear combination of these $2^{K+1}-1$ time-domain signals (2^K basic and 2^{K-1} central-peak spectra) can be combined and described by the complete G matrix. Since the data processing involves multiplication with the G matrix, followed by Fourier transformation, Kim and Szyperski propose the name GFT NMR for this implementation of RD experiments.

Assuming equivalent total measurement time, the signal-to-noise ratio in the basic spectra of GFT NMR is reduced by up to $1/\sqrt{2}$ compared to the equivalent *N*D experiment. This results, since $2^{K+1}-1$ rather than 2^K experiments have to be recorded for the indirect time domain, where signal contributions add up only in the 2^K basic spectra. Depending on K, up to almost half of the measurement time has to be used for central-peak acquisition which does not improve the signal-to-noise ratio in the basic peak spectra.

The measurement times of GFT NMR compared to *N*D FT can be estimated from Equation (1). This re-

$$\text{Minimal measurement time FT/GFT} = 2^K \prod_{j=0}^{K} (m_j)/(2^{K+1}\text{-}1) \sum_{j=0}^{K} (m_j) \quad (1)$$

flects the dramatic reduction in measurement time, especially for higher dimensionality experiments, that is, 1/20 for (3,2)D GFT compared to 3D and 1/30 000 for (5,2)D GFT compared to 5D assuming that 60 points are recorded for each time domain ($m=60$).

Another benefit of the GFT NMR approach results because individual chemical shifts are extracted from the various GFT spectra by a least-squares fitting routine. The accuracy for determination of the chemical shifts is improved and error analysis can be performed, since each frequency contributes to all $2^{K+1}-1$ spectra. This situation is in contrast to an *N*D experiment, where each frequency is measured only once, and with lower spectral resolution. However, the resolution in indirect dimensions of any multidimensional experiment can usually be improved by post-acquisition techniques, such as linear prediction or maximum entropy methods.[14]

Discussion and Perspectives

The generalized GFT NMR method introduced by Kim and Szyperski is an interesting approach to overcome the sampling problem in multidimensional NMR experiments—given that the sampling limit is fulfilled, that is, the total experimental time is not determined by sensitivity requirements. In that case, equivalents of 3D, 4D, and even 5D NMR experiments can be recorded in reasonable experimental time, and the chemical shifts can be determined with higher accuracy than those extracted from conventional experiments. Analysis of GFT NMR data is not as straightforward as that of *N*D experiments, since the chemical shifts are only recorded as sum and difference frequencies. Therefore, specialized software is required for data analysis, which has already been incorporated into automated assignment programs.[24]

An interesting simple alternative to GFT NMR is the acquisition of lower-dimensionality projections of an *N*D experiment. For example, chemical shifts recorded in a 3D experiment ($\Omega_1,\Omega_2,\Omega_3$) can also be extracted from two 2D spectra where only one of the indirect dimensions is recorded with peak positions at (Ω_2,Ω_3) and (Ω_1,Ω_3), respectively (Figure 2b). The signal-to-noise ratio of these experiments is equal to the corresponding 3D experiment, and high resolution can be achieved in the indirect time domain. The information obtainable corresponds to that in the basic spectra of GFT NMR. For a (5,2)D experiment, four 2D projections have to be recorded. Signal overlap can then be detected if chemical shifts are not degenerate in at least one dimension. An advantage of this alternative is that the chemical shifts can be directly extracted from the spectra. However, since the indirect dimensions are recorded separately in the projections, the frequencies are in fact uncorrelated. In unfavorable cases, chemical shift degeneracies between different spin systems can thus not be resolved. This situation is in contrast to the GFT NMR method, where all indirect dimensions contribute to the peak positions, and degeneracies can be resolved by central-peak detection (Figure 2).

GFT NMR still employs Fourier transformation to extract the frequencies from the time-domain signal. There are also interesting new alternatives for the fast recording of NMR spectra in the sampling limit, which include filter diagonalization[25] and maximum entropy methods[14] for which only a few (and not necessarily linearly sampled) time points are sufficient. Another exciting perspective is the combination of spatially and time encoded NMR detection within a single scan, as recently proposed by Frydman et al.[26]

A general problem when using FT or GFT NMR experiments with lower dimensionality is signal overlap, which is far better resolved in higher dimensionality experiments. Useful applications of reduced-dimensionality experiments will therefore be limited to relatively small protein domains, that is, of 10–15 kDa molecular weight.

It should also be noted, that the sensitivity of multidimensional NMR experiments still needs to be considered for both RD and *N*D implementations. Typically, these experiments involve at least $N-1$ magnetization transfer steps which involve numerous radio-frequency pulses and delays for magnetization transfers during which relaxation of the NMR resonance signal occurs. This effect reduces the overall sensitivity compared to, for example, a 2D experiment with just a single magnetization-transfer step.

In summary, GFT and other new strategies for optimized sampling of multidimensional spectra will significantly reduce measurement times for sampling-limited NMR experiments. Together with improved methods for automated chemical shift assignments and structure calculation this promises to reduce time requirements for NMR-based protein structure determination from months to few weeks in the future, which is likely to have a great impact

 © 2004 Wiley-VCH Verlag GmbH & Co. KGaA, Weinheim

and strengthen the application of NMR spectroscopy in structural biology and structural genomics.

[1] I. D. Campbell, *Nat. Rev. Mol. Cell Biol.* **2002**, *3*, 377.
[2] S. Kim, T. Szyperski, *J. Am. Chem. Soc.* **2003**, *125*, 1385.
[3] K. Wüthrich, *NMR of Proteins and Nucleic Acids*, Wiley-Interscience, New York, **1986**.
[4] G. M. Clore, A. M. Gronenborn, *Proc. Natl. Acad. Sci. USA Proc. Natl. Acad. Sci.* **1998**, *95*, 5891.
[5] S. W. Fesik, E. R. Zuiderweg, *Q. Rev. Biophys.* **1990**, *23*, 97.
[6] R. R. Ernst, G. Bodenhausen, A. Wokaun, *Principles of Nuclear Magnetic Resonance in One and Two Dimensions*, *Vol. 14*, Clarendon Press, Oxford, **1987**.
[7] C. Griesinger, O. W. Sørensen, R. R. Ernst, *J. Magn. Reson.* **1987**, *73*, 574.
[8] C. Griesinger, O. W. Sørensen, R. R. Ernst, *J. Magn. Reson.* **1989**, *84*, 14.
[9] H. Oschkinat, C. Griesinger, P. J. Kraulis, O. W. Sørensen, R. R. Ernst, A. M. Gronenborn, G. M. Clore, *Nature* **1988**, *332*, 374.
[10] L. E. Kay, G. M. Clore, A. Bax, A. M. Gronenborn, *Science* **1990**, *249*, 411.
[11] M. Ikura, L. E. Kay, A. Bax, *Biochemistry* **1990**, *29*, 4659.
[12] M. Sattler, J. Schleucher, C. Griesinger, *Prog. Nucl. Magn. Reson. Spectrosc.* **1999**, *34*, 93.
[13] C. Cieslar, A. Ross, T. Zink, T. A. Holak, *J. Magn. Reson. Ser. B* **1993**, *101*, 97.
[14] J. C. Hoch, A. S. Stern, *NMR data processing*, Wiley-Liss, New York, **1996**.
[15] S. M. Pascal, D. R. Muhandiram, T. Yamazaku, J. D. Forman-Kay, L. E. Kay, *J. Magn. Reson. Ser. B* **1994**, *103*, 197.
[16] R. Boelens, M. Burgering, R. H. Fogh, R. Kaptein, *J. Biomol. NMR* **1994**, *4*, 201.
[17] M. Sattler, M. Maurer, J. Schleucher, C. Griesinger, *J. Biomol. NMR* **1995**, *5*, 97.
[18] T. Szyperski, G. Wider, J. H. Bushweller, K. Wüthrich, *J. Am. Chem. Soc.* **1993**, *115*, 9307.
[19] B. Brutscher, J.-P. Simorre, M. S. Caffrey, D. Marion, *J. Magn. Reson. Ser. B* **1994**, *105*, 77.
[20] K. Ding, A. M. Gronenborn, *J. Magn. Reson.* **2002**, *156*, 262.
[21] W. Kozminski, I. Zhukov, *J. Biomol. NMR* **2003**, *26*, 157.
[22] Y. Xia, C. H. Arrowsmith, T. Szyperski, *J. Biomol. NMR* **2002**, *24*, 41.
[23] B. Brutscher, N. Morelle, F. Cordier, D. Marion, *J. Magn. Reson. Ser. B* **1995**, *109*, 238.
[24] T. Szyperski, D. C. Yeh, D. K. Sukumaran, H. N. Moseley, G. T. Montelione, *Proc. Natl. Acad. Sci. USA* **2002**, *99*, 8009.
[25] H. Hu, A. A. De Angelis, V. A. Mandelshtam, A. J. Shaka, *J. Magn. Reson.* **2000**, *144*, 357.
[26] L. Frydman, T. Scherf, A. Lupulescu, *Proc. Natl. Acad. Sci. USA* **2002**, *99*, 15858.

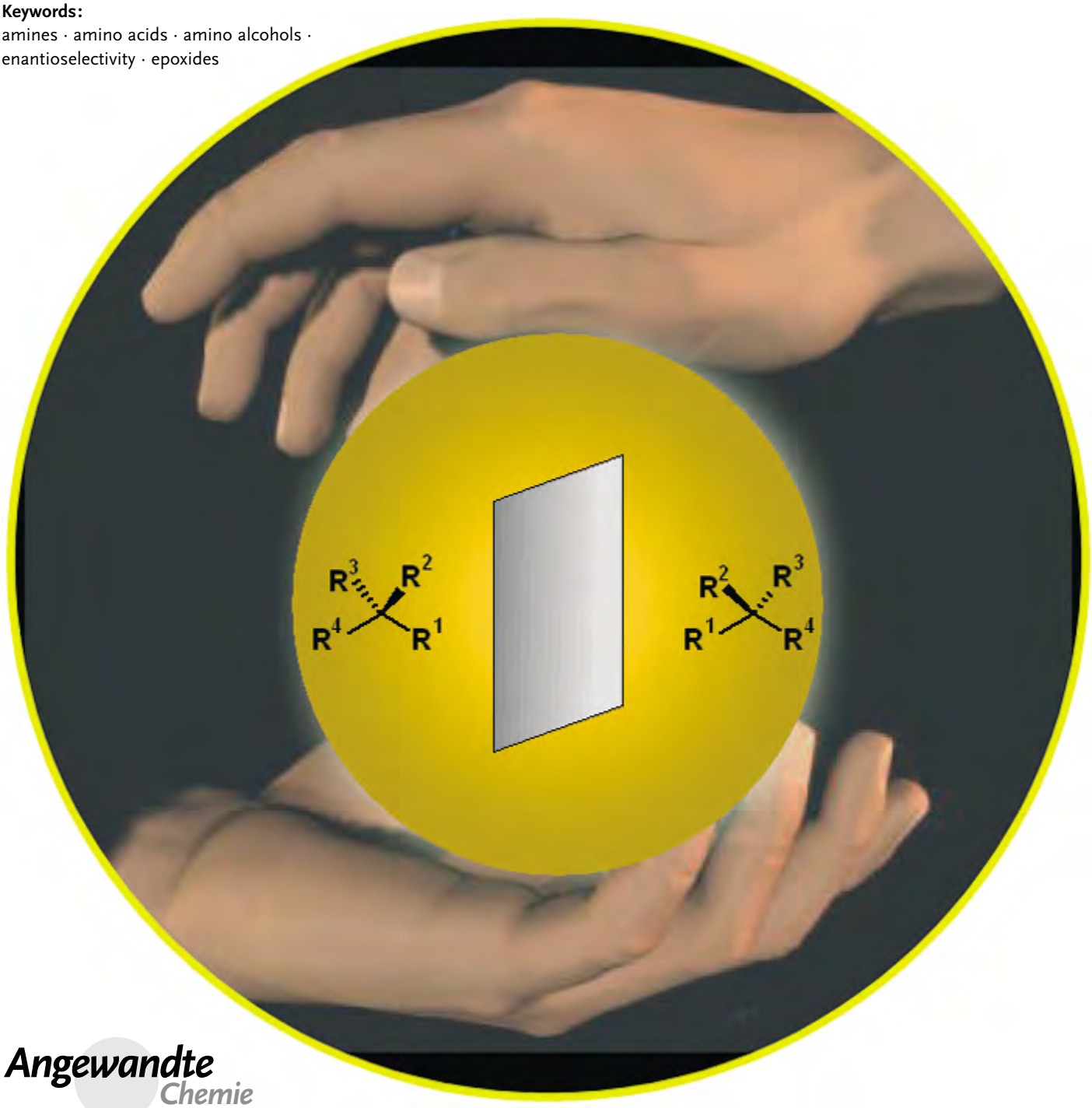
 © 2004 Wiley-VCH Verlag GmbH & Co. KGaA, Weinheim

Industrial Chemistry

Industrial Methods for the Production of Optically Active Intermediates

Michael Breuer, Klaus Ditrich, Tilo Habicher, Bernhard Hauer, Maria Keßeler, Rainer Stürmer, and Thomas Zelinski*

Keywords:
amines · amino acids · amino alcohols · enantioselectivity · epoxides



© 2004 Wiley-VCH Verlag GmbH & Co. KGaA, Weinheim

DOI: 10.1002/anie.200300599

Enantiomerically pure amino acids, amino alcohols, amines, alcohols, and epoxides play an increasingly important role as intermediates in the pharmaceutical industry and agrochemistry, where both a high degree of purity and large quantities of the compounds are required. The chemical industry has primarily relied upon established chemical methods for the synthesis of these intermediates, but is now turning more and more to enzymatic and biotechnological fermentation processes. For the industrial implementation of many transformations alternative methods are available. The advantages of the individual methods will be discussed herein and exemplified by syntheses of relevant compounds.

From the Contents

1. Introduction	789
2. Industrial Production of Amino Acids	789
3. Production of Carboxylic Acids	797
4. Production of Amines	803
5. Production of Alcohols	811
6. Production of Epoxides	814
7. Conclusions and Prospects	818

1. Introduction

The life-science industry is an important market for the chemical industry. The total revenue from sales in the pharmaceutical and agrochemical industries for the year 2000 is estimated to be in excess of €20 billion, of which the greatest share comes from the pharmaceutical industry. Optically active intermediates used as chemical building blocks, auxiliaries, or advanced intermediates have an estimated fraction of 15% of the market.

Sales of special intermediates are increasing at about 7–8% annually. Because of the increasing demand in the pharmaceutical industry for optically active intermediates, these compounds have a disproportionate share with 10% annually. About 80% of the active compounds that pharmaceutical companies have in the pipeline are chiral, and it is estimated that this fraction will increase, as the development of active compounds continues to be improved. The introduction of enantiopure active substances is also enforced through the ever stricter regulations of the US Food and Drug Administration (FDA). The authorities responsible for the registration of new active compounds increasingly demand the targeted synthesis of one stereoisomer. Since 1992 both the FDA and the European Committee for Proprietary Medicinal Products have stipulated that the physiological action of each enantiomer of a pharmaceutical product must be individually characterized, and since 1997 the fast-track, single-isomer program of the FDA has allowed pharmaceutical-product manufacturers shortened registration times with a so-called "chiral switch". In addition to lower dosages and improved efficacy the extension of patent term is also a driving force for pharmaceutical companies to convert a racemic active compound into the enantiomerically pure form.

Enantiomerically pure active compounds are also being used increasingly in the agrochemicals industry. The reasons for this trend are similar to those in the pharmaceutical sector. The targeted synthesis of the respective active enantiomer can improve the economics of the process and lead to reduced quantities applied and thus to reduced environmental impact.

Optically active amines, alcohols, and carboxylic acids are important classes of compounds for the synthesis of many active pharmaceutical and agricultural products. However, the availability of industrial quantities of many of these compounds with high optical purity was previously very limited. In recent years the development of new technologies and their implementation in large-scale industrial processes have opened up new perspectives and economically more attractive methods for the production of active compounds.

2. Industrial Production of Amino Acids

2.1. Introduction

In 1999 the total market for proteinogenic amino acids was about 1.5 million tons, with an estimated revenue of around €3.5 billion. Amino acids have this considerable economic importance because of their broad spectrum of industrial applications. Their use in human nutrition and health makes up about 40% of the market, and the animal-nutrition sector corresponds to about 55%. L-Glutamic acid, L-phenylalanine, L-aspartic acid, and glycine are produced as additives for foodstuffs. L-Lysine, methionine, L-threonine, and L-tryptophan are important additives in modern animal feed, as conventional feed sources are deficient in these amino acids.

In respect of market volume L-glutamic acid is the most important amino acid. More than 650000 tons are produced annually. Glutamic acid is mainly used in the form of its monosodium salt as a flavor enhancer in foodstuffs. The second-largest market volume is held by methionine with about 450000 tons per year ($t\,a^{-1}$). L-Phenylalanine and L-

[*] Dr. M. Breuer, Dr. K. Ditrich, Dr. T. Habicher, Dr. B. Hauer, Dr. M. Keßeler, Dr. R. Stürmer, Dr. T. Zelinski
BASF Aktiengesellschaft
Forschung Feinchemikalien & Biokatalyse
67056 Ludwigshafen (Germany)
Fax: (+49) 621-60-20914
E-mail: bernhard.hauer@basf-ag.de

 DOI: 10.1002/anie.200300599 © 2004 Wiley-VCH Verlag GmbH & Co. KGaA, Weinheim

aspartic acid are also important compounds, at about 12000 t a^{-1} each. They are required for the synthesis of the sweetener aspartame (α-L-aspartyl-L-phenylalanine methyl ester). In addition to the natural amino acids, nonnatural amino acids are also of industrial importance as building blocks for active compounds. Important examples are the D-amino acids used in the production of semisynthetic β-lactam antibiotics.

Three fundamentally different routes are used for the production of amino acids. In the extractive processes amino acids are isolated as components of natural protein-containing material. Alternative chemical and biological methods allow the targeted synthesis of amino acids.

2.2 Production of Amino Acids by Extraction

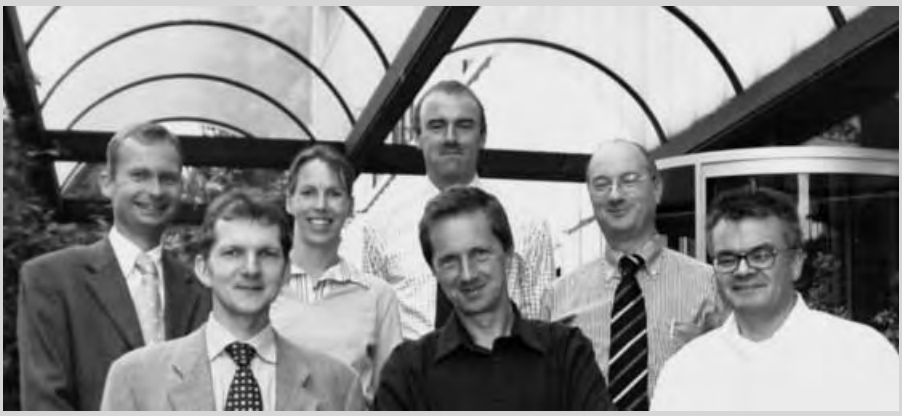
The oldest way of accessing amino acids is their extraction from protein-rich biological material, for which a wide variety of natural substances, such as hair, meat extracts, and plant hydrolysates, are used. These are mostly industrial by-products or waste, which are thus exploited for further utilization. An advantage of the extractive methods is the direct access to a series of different amino acids. Extractive isolation is particularly attractive for those amino acids for which demand is low. A feature of the extractive processes is the formation of salts as by-products, which can lead to considerable environmental impact. A number of more recent approaches attempt to avoid this disadvantage through biocatalytic processes. In particular, the use of extremophilic biocatalysts has already led to very promising results.[1,2] Extractive processes are currently used mainly for the production of L-cysteine. Keratin from hair and animal bristles is hydrolyzed by treatment with strong acids. The dimeric oxidation product cystine can be filtered from the hydrolysate because of its poor water solubility. Electrochemical reduction of the disulfide bridge in cystine yields cysteine.

A more recent method for the industrial production of cysteine has been developed by the Consortium für elektrochemische Industrie GmbH of Wacker Chemie.[3] This is a fermentation process in which the metabolic regulation of *Escherichia coli* is modified by genetic manipulation in such a way that the production strain produces far more cysteine than it needs itself. The excess cysteine enters the fermentation medium, where it is oxidized to the poorly soluble cystine by atmospheric oxygen. The workup is analogous to that of the conventional process. The product prepared biocatalytically is of higher quality than cysteine obtained from biological residues. Cysteine is marketed in the USA by Wacker Chemie in alliance with Kyowa Hakko.

2.3. Chemical Processes for the Manufacture of Amino Acids

Although asymmetric syntheses of amino acids are known,[4,5] no economical process has yet emerged. In the industrial manufacture of racemic amino acids, resort is usually made to the Bucherer–Bergs variant of the Strecker synthesis.[6] The respective α-aminonitrile is obtained from ammonia, hydrogen cyanide, and an aldehyde and is either hydrolyzed directly to the amino acid or converted into a hydantoin by reaction with CO_2. The hydantoin is then hydrolyzed to the racemic amino acid in a basic medium. An alternative route to racemic amino acids is amidocarbonylation catalyzed by a transition metal. In a three-component reaction *N*-acyl α-amino acids are formed from an aldehyde, an amide, and CO.[7]

Even though there is no commercially viable chemical process for the production of enantiomerically pure amino acids, the synthesis of racemic amino acids is still of considerable importance because racemates can be converted



From left to right: T. Habicher, M. Keßeler, M. Breuer, B. Hauer (top), T. Zelinski, K. Ditrich, R. Stürmer (bottom).

Tilo Habicher, born in 1969, studied chemistry at the Universität Leipzig and the Ecole Européenne des Hautes Etudes des Industries Chimiques in Strasbourg. After completing his PhD in 1998 in supramolecular chemistry in the research group of F. Diederich at the ETH Zürich, he took up a fellowship of the Studienstiftung des deutschen Volkes (BASF-research fellowship) at the UC, Berkeley and at The Scripps Research Institute in La Jolla with P. Schultz. There he studied the in vitro evolution of catalytic antibodies on phage surfaces. Since 2000 he has been at BASF AG in the biocatalysis division.

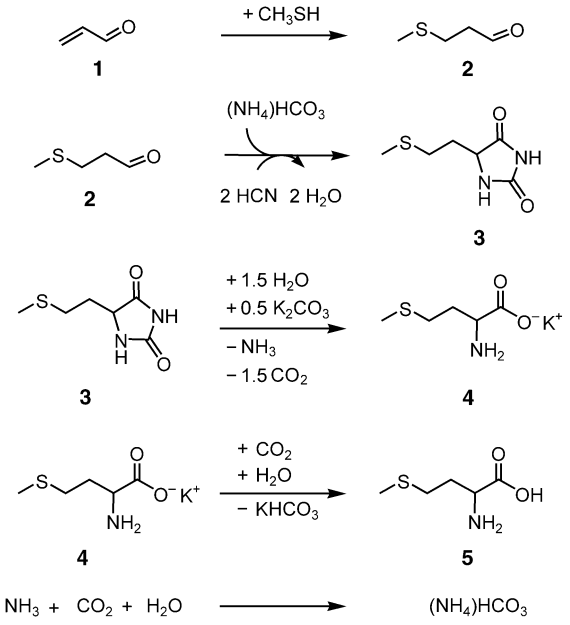
Maria Keßeler, born in 1969, received a biology degree at the Universität Marburg in 1993 and then took up a scholarship of the Studienstiftung des deutschen Volkes and of the Fonds der Chemischen Industrie for a research stay at the University of the Witwatersrand in Johannesburg. After completing her PhD at the Universität Göttingen (1996) she began at BASF AG in Ludwigshafen in 1997, where she is a laboratory group leader in the biotransformations group of the fine chemicals division.

 © 2004 Wiley-VCH Verlag GmbH & Co. KGaA, Weinheim

readily into enantiomerically pure compounds by a number of biocatalytic methods. Chemical procedures that do not provide enantiomerically pure amino acids are used for just two products on the amino acid market. Glycine is achiral and the nonnatural enantiomer D-methionine is converted in adults and animals into the biologically active L-enantiomer through a transamination reaction.

2.3.1. *Methionine Synthesis*

The chemical D,L-methionine synthesis developed by Degussa is especially elegant.[8] In this variant of the classical amino acid synthesis, in contrast to other processes, the formation of large quantities of salts is avoided (Scheme 1).



Scheme 1. Methionine synthesis by the Degussa process.

3-Methylmercaptopropionaldehyde (**2**) is prepared from acrolein (**1**) and methanethiol. Aldehyde **2** then reacts with hydrogen cyanide and ammonium hydrogen carbonate to form 5-(2-methylthioethyl)hydantoin (**3**), which is hydrolyzed at 170 °C in an alkaline solution with an excess of potassium carbonate. The product potassium D,L-methioninate (**4**) is formed along with carbon dioxide and ammonia, from which ammonium hydrogen carbonate is recovered for the second step. The potassium methioninate solution is then acidified under CO_2 pressure to produce D,L-methionine (D,L-**5**) and potassium hydrogen carbonate. The latter undergoes decomposition upon heating and concentration into CO_2 and potassium carbonate, which is recycled by use in the hydantoin hydrolysis.

2.4. *Production of Amino Acids by Biocatalysis*

In biocatalytic methods enzymes are employed as catalysts. Therefore biocatalysis is mostly carried out under moderate temperature and pressure, and frequently, if not exclusively, in aqueous media. Biocatalytic methods can be broken down into the categories biotransformations and fermentation methods.

2.4.1 *Fermentation Methods*

In fermentation methods the synthesis apparatus of living microorganisms is used to produce useful compounds from simple, cheap raw materials. In principle all proteinogenic amino acids are accessible by fermentation methods. In the production of the high-turnover, optically active products glutamic acid, lysine, and threonine fermentation processes have become established for economic reasons. In 1999 the world market for these amino acids was 650000 (glutamic acid), 40000 (lysine), and 6000 $t\,a^{-1}$ (threonine).

Michael Breuer, born in 1965, studied biology at the Universität Bonn. From 1992 to 1993 he held a scholarship of the Boehringer-Ingelheim-Fonds to carry out research in the research group of H. G. Floss at the University of Washington. He completed his PhD at the Universität Bonn under the guidance of E. Leistner on ansamacrolide bioynthesis in Actinomyceten (1995) and has been a laboratory group leader in the fine chemicals and biocatalysis research division at BASF AG since 1996.

Bernhard Hauer, born in 1955, studied biology at the Universität Hohenheim, where he completed his PhD in 1982 in the research group of F. Lingens on microbial alkaloid decomposition. During his postdoctoral research stay at the University of Chicago he investigated the transposon Tn7 under the guidance of J. A. Shapiro. In 1983 he joined BASF AG, where he is currently in charge of the research area biocatalysis as scientific director. He also completed his habilitation in 1996 at the Universität Heidelberg and is a professor of molecular biology there.

Thomas Zelinski, born in 1965, completed his PhD in chemistry in 1995 in the research group of Prof. M.-R. Kula at the Universität Düsseldorf. The topic of his thesis was enzymatic reductions. From 1996 to 1997 he undertook postdoctoral research with H. Waldmann at the Universität Karlsruhe, where he investigated a topic in phosphopeptide synthesis. He has been working in the research division fine chemicals and biocatalysis at BASF AG since 1997.

Klaus Ditrich, born in 1956, studied chemistry at the Universität Marburg and completed his PhD in 1986 on natural product synthesis in the research group of Prof. R. W. Hoffmann. He has been at BASF AG since 1987, first in the group active compound discovery (plant protection) and since 1992 in the division fine chemicals and biocatalysis. His main focus areas include asymmetric catalysis, enzymatic synthesis, and the development of production methods for optically active intermediates.

Rainer Stürmer, born in 1963, studied chemistry at the Universität Marburg. In 1992 he completed his PhD in the research group of Prof. R. W. Hoffmann with the synthesis of a natural product. During a postdoctoral stay at Harvard University (1992–1993), funded with a fellowship from the Studienstiftung des deutschen Volkes, he carried out research on lanthanoid catalysis under the guidance of Prof. D. A. Evans. He has been a laboratory group leader in the fine chemicals division of BASF AG since 1993. There he is primarily concerned with asymmetric catalysis, enzymatic synthesis, and optically active intermediates.

 © 2004 Wiley-VCH Verlag GmbH & Co. KGaA, Weinheim

In 1957 the bacterium *Corynebacterium glutamicum* was isolated. Organisms of this genus[9] were developed through a number of improvements to yield high-performance strains, which synthesize glutamic acid and lysine in remarkable space–time yields. With modern production strains amino acid concentrations of more than 160 g L^{-1} are reached.[10] Originally the explanation for this extraordinary synthetic efficiency relative to that of other microorganisms was that the cell membrane of the bacteria is permeable to amino acids, and that the compounds formed intracellularly can diffuse passively into the medium.[11] However, more recent work has shown that active transport across the cell membrane is responsible for the secretion of the amino acids.[12]

A detailed understanding of amino acid biosynthesis is required for improvement to be made in production strains. It was possible to take advantage of the results from the work on *Corynebacterium glutamicum* in this way. The first steps in the biosynthesis of glutamic acid, lysine, and threonine in *Corynebacterium* are catalyzed by the same enzymes. Thus, knowledge of regulatory mechanisms may be transferred to production strains for different amino acids. For example, by overproduction of the enzyme dihydropicolinate synthase the metabolism in *Corynebacterium* can be directed in favor of lysine production. In contrast, deletion of the appropriate gene leads to the biosynthesis of L-threonine.[13]

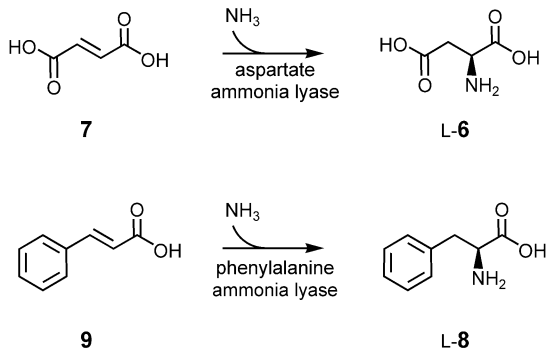
The economical fermentation production of L-threonine was first established in the 1980s when efficient *E. coli* mutants were developed. End concentrations of L-threonine of 100 g L^{-1} can be achieved with genetically modified *E. coli* or *Serratia marcescens*.[14,15] For the industrial production of L-threonine *E. coli* strains which contain an increased copy number of the threonine operon appear to be the most suitable.[16]

2.4.2 Biotransformations

Whereas living microorganisms are used as biocatalysts in the production of amino acids by fermentation, the catalysts in biotransformations are isolated enzymes or metabolically inactive cells. Depending on the specificity of the biocatalyst used, compounds that do not occur in natural metabolic pathways may also be transformed. Consequently biotransformations are the methods of choice for the production of enantiomerically pure D-amino acids and other nonnatural amino acids. In the production of natural amino acids biotransformations are used predominantly for those products whose market volume is less than 10000 t a^{-1}.[16,17]

2.4.3. Lyases as Biocatalysts in Amino Acid Synthesis

A well-established application of lyases is the production of L-aspartic acid (L-**6**) from fumaric acid (**7**) and ammonia with the enzyme L-aspartate ammonia lyase (Scheme 2). Variations of this biotransformation have been used since 1958. The synthesis of L-phenylalanine (L-**8**) from (*E*)-cinnamic acid (**9**) proceeds analogously with the enzyme phenylalanine ammonia lyase as the catalyst.[18] However, on an industrial scale this method has been replaced by a more

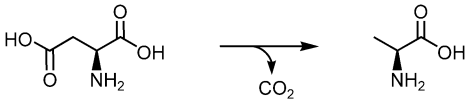


7 L-**6** 9 L-**8**

Scheme 2. Lyase reactions.

economical fermentation process with phenylalanine overproducers.[16]

L-Alanine (L-10) can also be produced through catalysis by a lyase. However, the lyase in question, L-aspartate β-decarboxylase, does not mediate the formation of a C–N bond as in the synthesis of L-phenylalanine or L-aspartic acid, but instead catalyzes the decarboxylation of L-aspartic acid (L-**6**) to L-**10** (Scheme 3). The catalysts used industrially are immobilized cells that contain L-aspartate β-decarboxylase.[19]



L-**6** L-**10**

Scheme 3. L-Alanine synthesis.

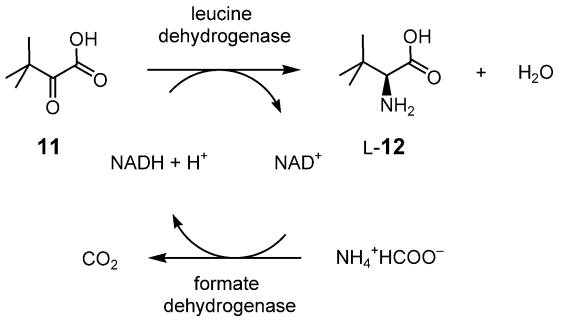
Based on the above, a direct synthesis of L-**10** from fumarate **7** and ammonia would appear feasible. However, as the optimal pH values for L-aspartate ammonia lyase and L-aspartate β-decarboxylase are very different, the procedure has to be carried out in two steps.[20] The synthesis of L-**10** from fumarate **7** and ammonia is the first two-step process based on biocatalysts. In the decarboxylation of L-**6** stoichiometric amounts of CO_2 are released. The formation of gas bubbles leads to inhomogeneity in the immobilization bed. To avoid this problem reactions are carried out in a special pressure reactor, in which a biotransformation can be carried out at 10 bar.[21] The increased pressure prevents the release of gaseous CO_2 and has no effect upon enzyme activity.

2.4.4 Amino Acid Dehydrogenases

Enantioselective biotransformations are also possible on an industrial scale with amino acid dehydrogenases (deaminating amino acid oxidoreductases). As a number of these enzymes are characterized by very low substrate specificity, nonnatural compounds can also be transformed. In addition to ammonia and the respective 2-oxocarboxylic acid, amino acid dehydrogenases need a cosubstrate, which supplies the hydride ions for the reduction of the intermediate Schiff bases.[22] For example, nicotinamide adenine dinucleotide

(NADH) is a suitable cosubstrate. The oxidized cosubstrates (e.g. NAD^+) must be regenerated in a further redox reaction because of their high cost.

One established regeneration system involves a formate dehydrogenase from *Candia boidinii*, which oxidizes formate irreversibly to CO_2 and thereby reduces the cosubstrate NAD^+ to NADH.[23] A combination of L-leucine dehydrogenase, formate dehydrogenase, and cosubstrate is used by Degussa to produce L-*tert*-leucine (L-**12**) on a ton scale from ammonium formate and trimethylpyruvic acid (**11**) (Scheme 4).[24]



Scheme 4. Production of L-*tert*-leucine (L-**12**) through reductive amination with leucine dehydrogenase.

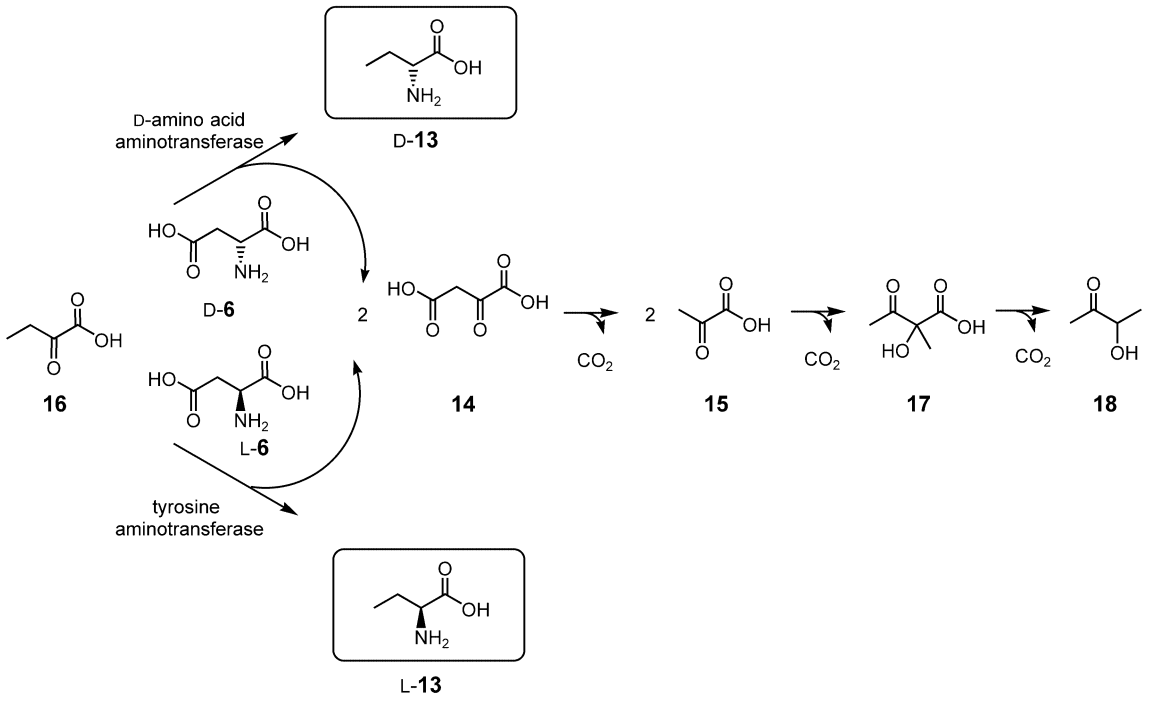
2.4.5 *Aminotransferases*

The use of aminotransferases allows the problem of cosubstrate regeneration to be circumvented. These enzymes transfer amino groups of amino acids to 2-oxocarboxylic acids. An illustrative example of their industrial application is the synthesis of L-2-aminobutyric acid (L-**13**) by Great Lakes Chemicals.[25] Genetically modified *E. coli* is used as the catalyst in this biotransformation (Scheme 5). L-Aspartic acid (L-**6**) functions as the amino-group donor. It is converted into 2-oxalylacetic acid (**14**) by aspartate aminotransferase. Intermediate **14** undergoes spontaneous decarboxylation to give pyruvate **15** and CO_2. The amino group of L-**6** is transferred to 2-oxobutyric acid (**16**). As **16** is not readily accessible, the gene for L-threonine deaminase is incorporated into the cells. In this way **16** can be prepared in situ from inexpensive L-threonine.

Because of an undesired side reaction of aminotransferases alanine (**10**) can be formed from **15**. To prevent this course two molecules of **15** are converted into acetolactate **17** by the enzyme acetolactate synthase. The acetolactate synthase gene from a *Bacillus* strain was transferred into *E. coli*. Compound **17** undergoes spontaneous decarboxylation to 2-hydroxybutane-3-one (acetoin, **18**), which can be removed from the reaction mixture by distillation. The removal of **18** displaces the reaction equilibrium in favor of the desired products and leads to a significant decrease in the formation of the by-product L-**10**. Thus, the ratio of the main product L-**13** to L-**10** is increased from 2.4:1 to 22.5:1, and end concentrations of L-**13** of 27 $g\,L^{-1}$ can be obtained.[25]

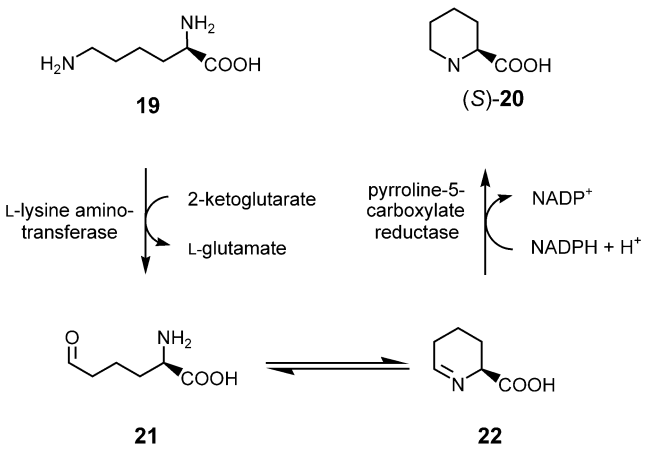
Depending on the choice of amino acid transferase, both enantiomers can be obtained. The L-tyrosine aminotransferase from *E. coli* is so indiscriminate that it can be used for the production of L-**13**. Strains that contain a D-amino acid transferase from *Bacillus sphaericus* accordingly form D-**13**.

The company Mercian (Japan) uses a combination of dehydrogenase and aminotransferase in an elegant whole-cell method for the production of L-piperidine-2-carboxylic acid



Scheme 5. Production of D- and L-aminobutyrate (D,L-**13**) from 2-oxobutyric acid (**16**) and L-aspartic acid (L-**6**) through enantioselective catalysis by aminotransferases.

 © 2004 Wiley-VCH Verlag GmbH & Co. KGaA, Weinheim



Scheme 6.

(*S*-**20**) from natural L-lysine (**19**; Scheme 6). The method is based on a biotransformation with recombinant *E. coli* bacteria. L-Lysine (**19**) enters the cells with the assistance of the overexpressed L-lysine permease transport system and is there deaminated to the aldehyde–amino acid **21** by the lysine aminotransferase from *Flavobacterium lutescens*. Amino acid **21** is in equilibrium with 2,3,4,5-tetrahydropyridine-2-carboxylic acid (**22**) and is reduced to (*S*)-**20** with the intrinsic pyrroline-5-carboxylate reductase of *E. coli* and NADPH.[26] The conversion observed is greater than 90% with respect to L-lysine, and (*S*)-**20** is obtained from the culture filtrate in 70% yield after purification. However, to reach high end concentrations of 50 $g L^{-1}$, long fermentation times (150 h) are necessary. (S)-20 serves as a building block for a number of pharmaceutical agents, for example, the local anesthetic bupivacaine (AstraZeneca). An alternative access to enantiomerically pure **20** is acylase-catalyzed racemate resolution (Section 2.4.8.3).

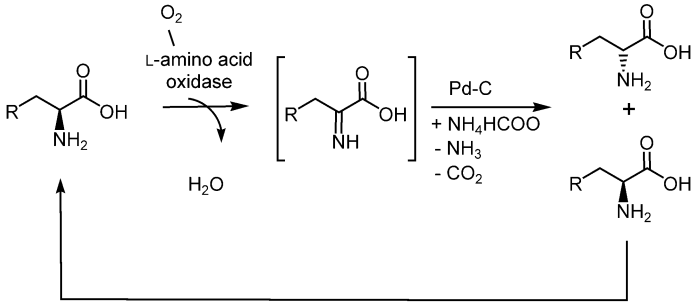
2.4.6. D-Amino Acids from Fermentation Processes

Monsanto has patented a fermentation process for the production of D-amino acids by genetically modified microorganisms.[2] For example, D-phenylalanine (D-**8**) can be synthesized with these biocatalysts (Scheme 7). The metabolism of the microorganisms is modified in such a way that no functional D-amino acid deaminases are produced. However, the strains contain additional genes for L-amino acid deaminases, D-amino acid aminotransferases, and a specific racemase. The growth medium of the cells is supplemented with an L-amino acid (L-**23**) as an amino-group donor, which may be L-alanine, L-glutamine, or L-aspartic acid.

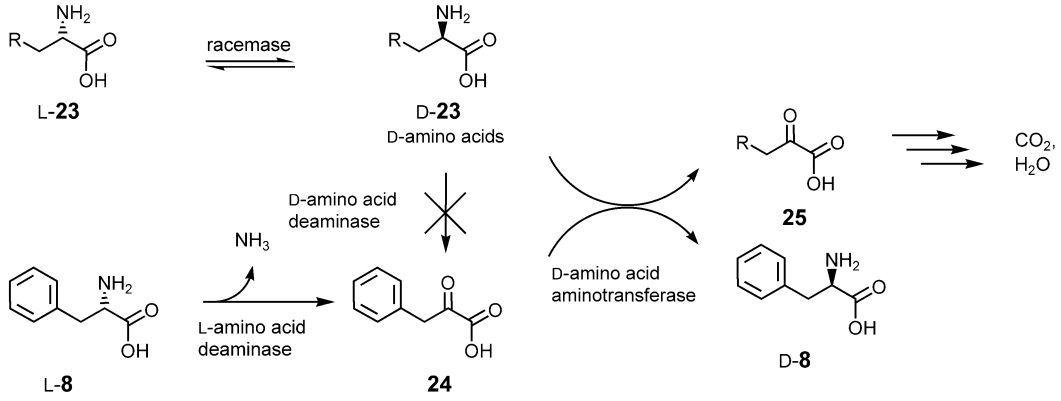
The carbon skeleton of D-**8** originates either from endogenously produced L-**8** or from L-**8** added to the medium, which is deaminated to phenylpyruvate **24** by L-amino acid deaminase. The amino-group donor L-**23** is racemized by the microorganisms to give D-**23**, a substrate for D-amino acid aminotranserases. The amino group of D-**23** is transferred to **24**, whereby D-**8** and the 2-oxocarboxylic acid **25** are formed. Carboxylic acid **25** is then degraded by the microbial metabolism with displacement of the equilibrium of the D-amino acid aminotransferase reaction toward D-**8** formation. As both L-amino acid deaminases and D-amino acid aminotransferases are highly nonspecific, this approach is applicable to the production of a wide variety of D-amino acids from the corresponding L-amino acids.[27]

2.4.7. Chemoenzymatic Synthesis of D-Amino Acids

There is also an elegant chemoenzymatic option for these amino acid syntheses.[28] In this case the L-amino acid is oxidized by an L-amino acid oxidase (Scheme 8). The intermediate imine is reduced by Pd-C in an ammonium



Scheme 8. Chemoenzymatic synthesis of D-amino acids.



Scheme 7. Production of D-phenylalanine (D-**8**) by fermentation with genetically modified microorganisms (according to reference [27]). Alanine, glutamine, or aspartic acid are added as the amino-group donor (L-**23**); L-**8** is formed by endogenous overproduction. The α-keto acid **25** is metabolized to CO_2 and H_2O.

 © 2004 Wiley-VCH Verlag GmbH & Co. KGaA, Weinheim

formate buffer. Only the L-enantiomer of the resulting racemic mixture is utilized by the oxidase, and the D-enantiomer accumulates. The enantiomeric form of the amino acid produced depends on the specificity of the oxidase. Yields of 90% and optical purities of 99% *ee* have been observed for this process.

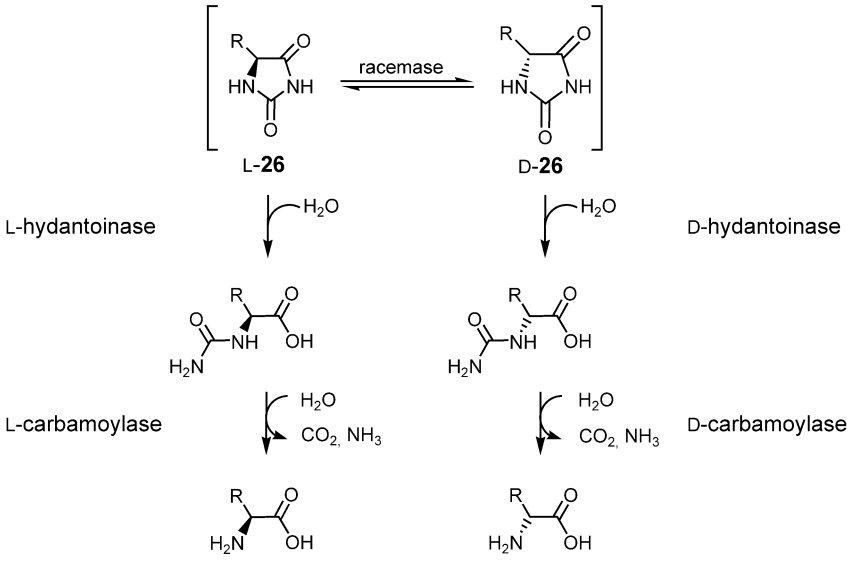
2.4.8. Preparation of Enantiomerically Pure Amino Acids by Racemate Resolution

2.4.8.1. Preparation of L- and D-Amino Acids with the Hydantoinase–Carbamoylase System

Racemic hydantoins **26** are readily accessible by chemical synthesis. A series of specific natural hydrolases have been isolated for their enantioselective hydrolysis to the corresponding carbamoyl derivatives. Specific hydrolases also exist for these compounds so that the preparation of optically active amino acids from the racemic hydantoins presents no difficulty.[29]

This method is particularly important for the preparation of D-amino acids. D-Phenylglycine and D-hydroxyphenylglycine, which are incorporated in the side chains of semisynthetic β-lactam antibiotics, are produced in this way.[30] As hydantoins racemize spontaneously at pH > 8, the complete conversion of the racemate into one enantiomer is possible. The rate of racemization is depends on side chain R. If the racemization of the hydantoin is the rate-determining step of the reaction, the reaction can be accelerated significantly by the addition of a racemase (Scheme 9).

Whereas the biocatalytic production of D-amino acids from D,L-hydantoins is a well-established process, the synthesis of L-amino acids with this system is not so well developed technically, mainly as a result of the poor stereoselectivity of the known L-hydantoinases. However, improvements in this field are ongoing. Thus, it was shown that the enantioselectivity of a D-hydantoinase from *Arthrobacter* sp. DSM 9771 could be reversed through evolutionary enzyme development ("directed evolution"), with a simultaneous increase in activity.[31] L-*tert*-Leucine can also be synthesized with the hydantoinase–carbamoylase system. Degussa currently produces this compound on a 100-kg scale through a novel biotransformation in a pilot process. In this process a recombinant microorganism that contains the aforementioned modified hydantoinase, a carboxylase, and the respective racemase is used.[32]



Scheme 9. Production of optically active amino acids with enantioselective hydantoinases and carbamoylases.

2.4.8.2. Preparation of L-Cysteine by Racemate Resolution

As early as the 1970s a biocatalytic procedure was developed as an alternative to the extraction of cysteine (**27**) from human hair, feathers, or animal bristles. The reaction starts from D,L-2-amino-Δ^2-thiazoline-4-carboxylic acid (D,L-**28**), which may be obtained by chemical synthesis from α-chloroacrylic acid (**29**) and thiourea (**30**; Scheme 10). The bacterium *Pseudomonas thiazolinophilum* transforms D,L-**28** into cysteine. Thus, L-**28** is cleaved to L-cysteine (L-**27**) by two specific hydrolases via (*S*)-carbamoyl-L-cysteine (L-**31**). A racemase converts D-**28** into the corresponding L-enantiomer, so that complete conversion of the racemate is possible. The process takes place in yields of 95% to give L-**27** in concentrations of 30 g L^{-1}.[33] It was implemented by Ajinomoto in 1982.

2.4.8.3. Racemate Resolution with Acylases and Amidases

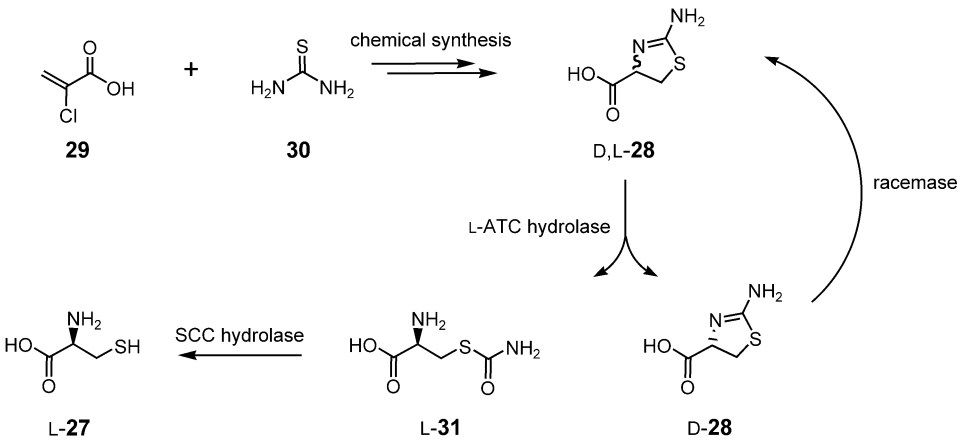
As well as hydantoinases, acylases and amidases are used for racemate resolution. L-Acylases catalyze the resolution of acyl D,L-amino acids to L-amino acids and *N*-acyl D-amino acids. After separation of the products, the *N*-acyl D-amino acid is racemized in a second step and returned to the enzyme reaction. One of the first industrial applications of an amino acid acylase was introduced by the Tanabe Seiyaku (Japan) in 1969.[34]

At Degussa L-methionine (**5**) is produced for use in foodstuffs through racemate resolution catalyzed by an acylase (Scheme 11). The process is carried out continuously in a stirred reactor. The acylase, which is not immobilized, is retained by ultrafiltration in a hollow fiber module.

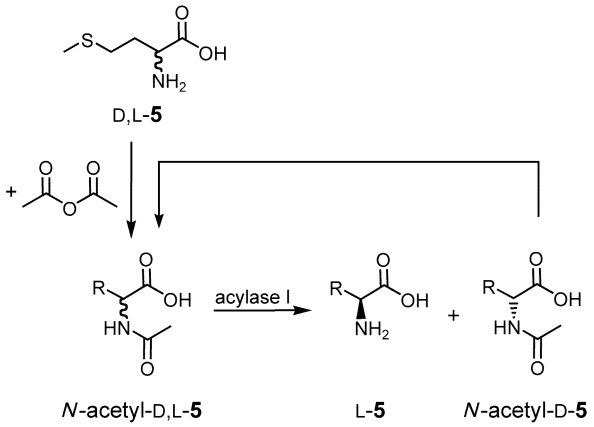
The amidase process developed by DSM operates by the same principle, but with a different biocatalyst. D,L-Amino acid amides are hydrolyzed enantioselectively with amidases. After separation of the L-amino acid and the D-amino acid amide, the latter can either be racemized or converted into the corresponding D-amino acid by chemical hydrolysis.[35]

Nonnatural cyclic amino acids, such as piperidine and proline derivatives, are also accessible through the use of enantioselective hydrolases. Often both enantiomers are of industrial interest. Exam-

 © 2004 Wiley-VCH Verlag GmbH & Co. KGaA, Weinheim



Scheme 10. Enantioselective synthesis of L-cysteine (L-**27**).



Scheme 11. Acylase-catalyzed racemate resolution of D,L-*N*-acetyl-**5** (Degussa).

ples are piperidine-2-carboxylic acids (**20**), which are incorporated into various active compounds, and *N*-CBZ-protected proline (*N*-CBZ-**32**). Researchers at Lonza have developed biocatalytic methods that allow access to this class of compounds through reactions with hydrolases.[36] Scheme 12 illustrates the synthesis of CBZ-protected proline derivatives.

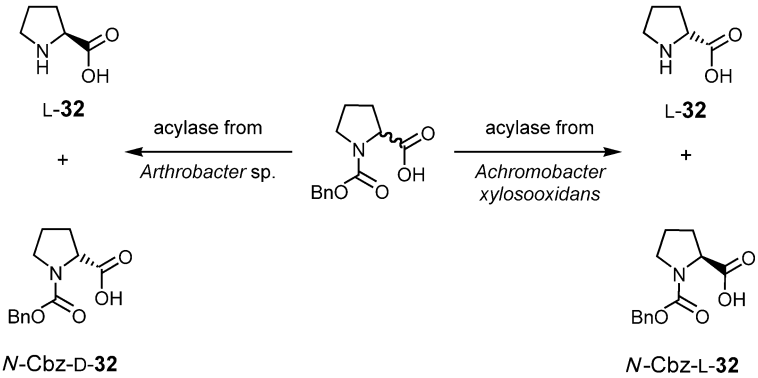
2.5. Improvements in Biocatalytic Amino Acid Synthesis

2.5.1 Improvements in Fermentation Processes

Classical improvement of production strains is based on undirected mutations. The genome of the production organisms is altered at random, and more efficient mutants are identified in a subsequent selection process. The mutants are characterized by, for example, increased membrane permeability,[37] regulation defects, or biosynthesis enzymes with altered kinetic characteristics.[38]

In the 1980s it was recognized that a fundamental understanding of the microbial amino acid metabolism would be necessary for further increases in productivity. Detailed analysis allows quantification of the flow of metabolites in a fermentation as a function of time (metabolic flux analysis). In this way the addition of nutrients can be optimized, and yields can be increased as a result. Metabolic flux analysis also makes it possible to model the metabolism of a given production strain (metabolic modeling). Moreover, conclusions drawn from metabolic flux analysis can then form the basis for targeted intervention in the metabolism by genetic methods.[39]

Another important requirement for the targeted improvement of amino acid production strains is knowledge about the genome of the microorganism concerned. The genome of *Corynebacterium glutamicum* has already been sequenced by at least three important amino acid producers.[8,40,41] It is merely a question of time before the results of genome sequencing and "metabolic modeling" lead to significantly improved amino acid production.



Scheme 12. Proline acylase process by Lonza for the production of enantiomerically pure *N*-Cbz-proline (*N*-Cbz-**32**).

2.5.2. Improvements in Biotransformations

Not only fermentation processes, but also biotransformations are undergoing continual improvement. As with chemical processes, in addition to selectivity, productivity (expressed in terms of the total turnover number) is the critical measure of the quality of the catalyst.

 © 2004 Wiley-VCH Verlag GmbH & Co. KGaA, Weinheim

A variety of strategies can be implemented to establish or improve a biocatalytic process. In the ideal situation a suitable biocatalyst is already available, and only the technical process itself must be elaborated. However, this situation rarely arises, and most frequently the development of a new catalyst is necessary. In wide-ranging screening programs, attempts are being made to identify novel enzymes. These are no longer targeted solely at isolating whole microorganisms from the biodiversity, as in classical screening, but instead at accessing genetic information directly. DNA is isolated from samples and transferred into suitable expression systems. The desired activity is then identified through high-throughput screening.[42] In this way direct access should be possible to the gene pool of nonculturable microorganisms, which by far outnumber culturable microorganisms.[43]

Of course, specific characteristics of known enzyme systems can also be improved.[44] In evolutionary enzyme optimization, also known as "directed evolution", natural evolution is mimicked in vitro. Mutations are incorporated randomly into the genes of the biocatalyst to generate an abundance of variants, which are then screened for those mutations with improved catalytic properties. The work of May et al. on the D-hydantoinase from *Arthrobacter* illustrates the potential of this methodology.[31] As well as untargeted modification, the recombination of genetic material plays a critical role in evolution. These mechanisms may also be copied and carried out in vitro.[45]

The development of biocatalysts for industrial applications is dominated by smaller companies, which offer their services to larger partners. Of course, fermentation processes for the production of amino acids can also be improved by means of evolutionary enzyme optimization. The optimized biocatalysts can also be transferred into production strains to avoid bottle necks in amino acid biosynthesis.

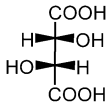
3. Production of Carboxylic Acids

As for amino acids, there are in principle three possible methods for the production optically active carboxylic acids. Naturally occurring carboxylic acids can be isolated from suitable raw materials. However, most carboxylic acids are produced in chemical and biocatalytic processes. In the case of natural carboxylic acids microbial fermentation processes are available, especially for quantities $>1000\,t\,a^{-1}$. Glucose or cheap industrial products, such as molasses, are used as the carbon source, which is metabolized by the microorganisms into biomass (growth), metabolic by-products, such as CO_2, and the desired carboxylic acid.

In this section examples of the different technologies are presented. The rapid development of enzyme-catalyzed syntheses has already been summarized in the form of reviews to which reference will be made where appropriate.

3.1. Isolation from Natural Sources (Chiral Pool)

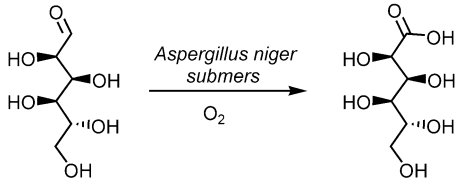
Natural chiral compounds (from the chiral pool) often offer an alternative to the synthesis of enantiomerically pure products.[46] One chiral carboxylic acid isolated from natural sources is L-(+)-tartaric acid (**33**). This isomeric form of tartaric acid separates out as tartar (potassium hydrogen tartrate) during the fermentation of grape must. Upon its reaction with calcium chloride or calcium hydroxide and sulfuric acid, **33** is released; yeast residues and gypsum occur as by-products. An alternative process has been established recently by Lurgi Life Science, whereby the tartar is transformed with potassium hydroxide into the water soluble dipotassium salt. After filtration and ion-exchange chromatography crystalline tartaric acid and feed yeast are obtained as by-products. Potassium sulfate and ammonium sulfate are formed as by-products during regeneration of the ion exchanger. In addition to numerous applications in the textile and food industries, 33 and derivatives, such as (−)-dibenzoyl-L-tartaric acid, are used as racemate resolving agents and for asymmetric synthesis, for example, of 2-aminotetralines[47] and methyl (*R*)-3-hydroxybutyrate.[48]



L-**33**

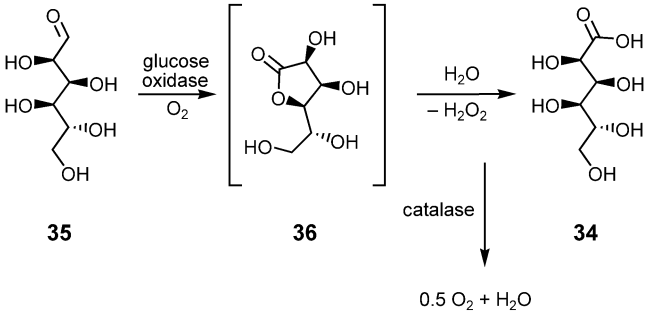
Natural carbohydrate building blocks have been used for decades for the preparation of enantiomerically pure sugar acids.[49] In industrial syntheses saccharides are oxidized selectively. During the middle of the last century oxidations with hypochlorite[50] and electrochemical oxidations[49] were developed for the preparation of D-gluconic acid (**34**) from D-glucose (**35**). These have been replaced by biotechnological processes in which the monosaccharide is selectively oxidized with microorganisms (mainly *Aspergillus niger* and *Gluconobacter sp.*) in a submersed aerobic process (Scheme 13).

A new method has been devised by DSM/Gist Brocades for use in the food industry. Glucose oxidase transforms **35** into the lactone **36**, which is then hydrolyzed to **34** and H_2O_2 Scheme 14). Catalase decomposes the H_2O_2 formed to



35 **34**

Scheme 13. Selective enzymatic oxidation of D-glucose (**35**) to D-gluconic acid (**34**).



35 **36** **34**

Scheme 14. Alternative synthesis of D-gluconic acid (**34**) of high enantiomeric purity through the oxidation of D-glucose (**35**) (DSM/Gist Brocades).

 © 2004 Wiley-VCH Verlag GmbH & Co. KGaA, Weinheim

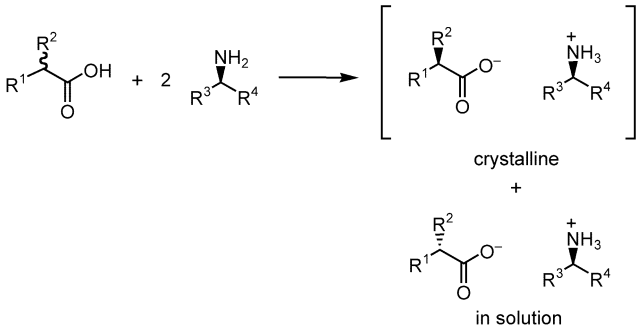
regenerate oxygen for the oxidation step and prevent deactivation of the enzyme by side reactions. The process is characterized by the high purity of the product **34** and the near-quantitative yield.[51]

D-Glyceric acid can be produced either by stepwise chemical oxidation of D-glucose with anthraquinone-2-sulfonate/H_2O_2 and hypochlorite or by enzymatic decarboxylation of L-tartrate.[52,53]

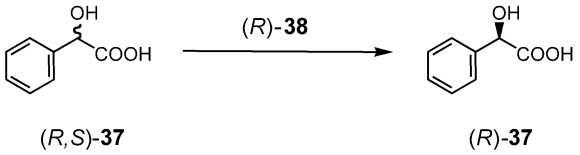
3.2. Classical Chemical Synthesis

3.2.1. Crystallization with Enantiomerically Pure Amines

The enantiomers of racemic carboxylic acids are separated by fractional crystallization of the diastereoisomeric salts that they form with enantiomerically pure amines (Scheme 15; see also Section 4.1.1). (*R*)-Mandelic acid ((*R*)-**37**) is produced by Yamakawa Chemical Industry Ltd (Japan) by classical racemate resolution from (*R*,*S*)-**37** with (*R*)-1-phenylethylamine ((*R*)-**38**; Scheme 16). The enantiomerically pure (*R*)-**38** can be recovered and reused several times as the resolving agent.[96]



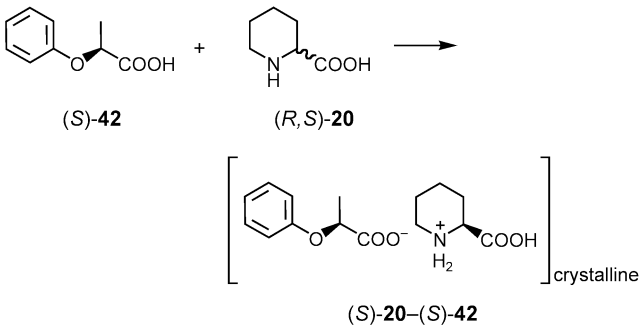
Scheme 15. Racemate resolution of optically active carboxylic acids through salt formation with enantiomerically pure amines and fractional crystallization.



Scheme 16.

The enantiomerically pure thiazolidinone carboxylic acid (*S*)-**39**, an intermediate in the synthesis of the new calcium antagonist CP-060-S ((*S*)-**40**), is isolated by resolution of the racemate with (*S*)-*N*-benzyl-1-phenylethylamine ((*S*)-**41**; Scheme 17). Although the salt-forming carboxy functionality is four bonds away from the stereogenic center, (*S*)-**39** was isolated with 99.8% *ee*.[54]

The chiral amino acid (*S*)-**20** can be synthesized in a similar way through fractional crystallization of diastereomeric salts with 2-phenoxypropionic acid (**42**). The less soluble salt (*S*)-**20**–(*S*)-**42** crystallizes with high diastereomeric purity from water/alcohol mixtures (Scheme 18).[55]

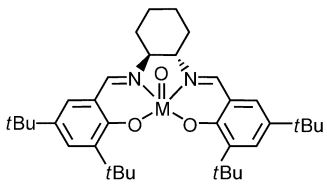


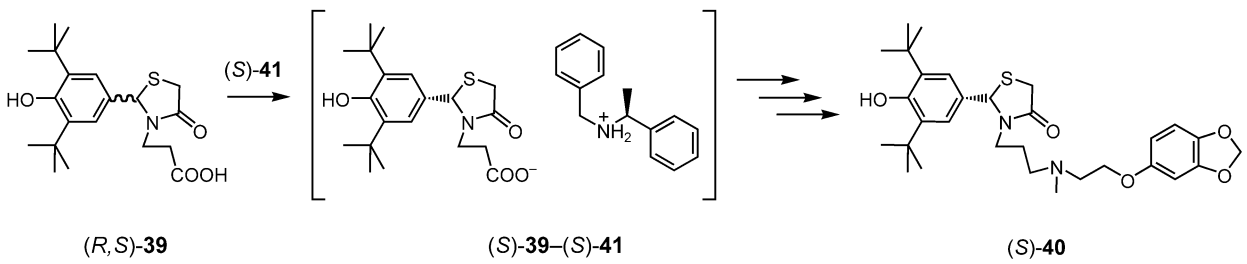
Scheme 18.

"Dutch resolution", a variant of diastereoisomeric crystallization in which carboxylic acid racemates are resolved through the use of amine mixtures, will be discussed in Section 4.1.1.

3.2.2. Asymmetric C–C Coupling

Recently new (salen)titanium and (salen)vanadium complexes **43** (CACHy-catalysts),[56] which mediate the asymmet-

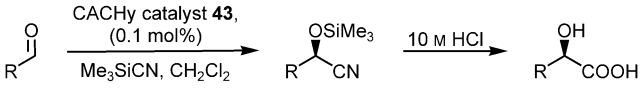




Scheme 17. Racemate resolution with (*S*)-*N*-benzyl-1-phenylethylamine ((*S*)-**41**) leads tp enantiomerically pure (*S*)-**39** for the synthesis of the calcium antagonist CP-060-S ((*S*)-**40**).

 © 2004 Wiley-VCH Verlag GmbH & Co. KGaA, Weinheim

ric addition of trimethylsilyl cyanide to aromatic and aliphatic aldehydes **44**[57] and ketones[58], have been described for the preparation of substituted α-hydroxycarboxylic acids (Scheme 19, Table 1). This method has been extended to the use of potassium cyanide as a cheaper nucleophile.[59] The α-hydroxycarboxylic acids **46** are available from the cyanohydrin trimethylsilyl ethers **45** by acid hydrolysis. As these reactions are in competition with the enzymatic processes described below, they can only be applied in a few special syntheses.



44 **45** **46**

Scheme 19. CACHy catalysts **43** mediate the enantioselective addition of trimethylsilyl cyanide to aromatic and aliphatic aldehydes **44**. The products **45** are hydrolyzed to enantiomerically pure α-hydroxycarboxylic acids **46**.

Table 1: Addition of trimethylsilyl cyanide to aldehydes with CACHy catalysts **43** (Scheme 19).[a]

R	Catalyst **43** (M = Ti)	Catalyst **43** (M = V)
	ee [%]	
Ph	82	94
p-OMe-Ph	84	90
o-Me-Ph	76	90
m-Me-Ph	90	95
p-Me-Ph	87	94
p-NO_2-Ph	50	73
Et	52	77
*t*Bu	66	68

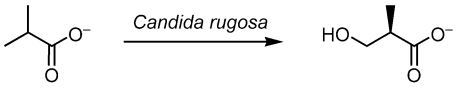
[a] Catalyst: 0.1 mol%; reaction time: M = Ti: < 5 min, M = V: 18 h; quantitative conversion; see reference [57].

3.3. Biotechnological Synthesis

3.3.1. Asymmetric Syntheses

3.3.1.1. Oxidations

In some hydroxylation processes bacterial mono- or dioxygenases are used to catalyze bond formation between one or both oxygen atoms of O_2, respectively, with non-activated carbon atoms. These hydroxylations are usually regio- but not stereoselective.[60,61] Many microbial hydroxylations to provide hydroxycarboxylic acids involve sequential α,β-dehydration and hydrolysis steps. The preparation of L-carnitine (L-**47**) from γ-butyrobetaine (**48**) by the Lonza process ($> 100\,t\,a^{-1}$) is an example of such a process. The biochemical transformation takes place via butyrobetainyl-CoA (**49**) and crotonobetainyl-CoA (**50**; Scheme 20).[62] The Kaneka process proceeds analogously through the β-hydroxylation of 2-methylpropionate (**51**) with *Candida rugosa* to give (*R*)-**52**, a building block for the synthesis of ACE inhibitors, such as captopril (Scheme 21).[63]



51 (*R*)-**52**

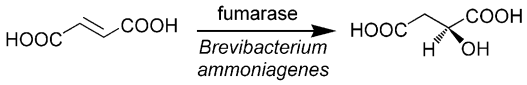
Scheme 21. β-Hydroxylation of 2-methylpropionate (**51**).

3.3.1.2. Reduction

In principle, the enantioselective biocatalytic reduction of keto acids is a possible route to enantiomerically pure hydroxycarboxylic acids. One current disadvantage is the dependence upon expensive cofactors such as NADH. A variety of approaches have been described for the regeneration or even the replacement of these reagents (see Section 2.4.4). Further examples are described in Section 5.

3.3.1.3. Hydrolysis

The enzyme-catalyzed enantioselective addition of water to the double bond of prochiral fumaric acid (**7**) is used in the preparation of L-malic acid (L-**53**) with immobilized brevibacteria or fungi (Tanabe process; Scheme 22).[64,65] L-Malic acid is used above all for the stabilization of fruit juices in food technology.

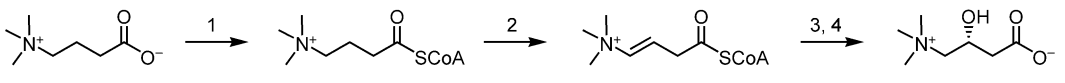


7 L-**53**

Scheme 22. Production of L-malic acid (L-**53**) through the enantioselective addition of water to **7** (Tanabe process).

3.3.1.4 C–C Coupling (Hydroxynitrile Lyase Process)

Hydroxynitrile lyases (HNL) catalyze the stereoselective addition of hydrogen cyanide to aldehydes and ketones or, depending on the reaction conditions, the cleavage of cyanhydrins.[66] The α-hydroxycarboxylic acids are obtained by hydrolysis of the chiral cyanhydrins with hydrochloric acid. In this efficient synthesis quantitative conversion of the aldehyde into the product is possible. HNL processes have recently been implemented in industrial syntheses of some chiral aromatic α-hydroxycarboxylic acids.

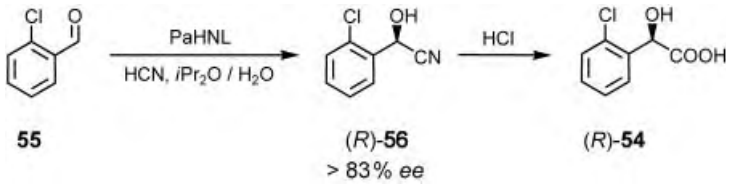


48 **49** **50** L-**47**

Scheme 20. Synthesis of L-Carnitin (L-**47**) according to the Lonza process. 1. Thioester synthetase, 2. dehydrogenase, 3. hydrolase, 4. thioesterase.

 © 2004 Wiley-VCH Verlag GmbH & Co. KGaA, Weinheim

Chiral mandelic acid derivatives are used as building blocks in diverse syntheses of active compounds and also as racemate resolving agents (Section 4.1.1). Chemical and biocatalytic synthetic routes have already been described on several occasions,[67] so we will restrict our discussion to a few more recent examples. HNL-based production processes have been developed for (*R*)-*o*-chloromandelic acid (**54**), an intermediate for the synthesis of the antidepressant and platelet-aggregation inhibitor clopidogrel,[68] by DSM Chemie Linz, Nippon Shokubai, and Clariant (Scheme 23).[69] Hydrocyanic acid adds enantioselectively to *o*-chlorobenzaldehyde (**55**) in microaqueous or biphasic[70] systems. Mandelonitrile lyase (PaHNL), for example, in the form of almond-flour extract or immobilized on Avicel microcrystalline cellulose, is used as the catalyst. Depending on the solvent employed, the enzyme can be used for several months. The (*R*)-*o*-chloromandelonitrile ((*R*)-**56**) thus formed is converted into the corresponding carboxylic acid by hydrolysis with concentrated HCl, without undergoing racemization. The advantage of this process over racemate resolution through the crystallization of diastereomeric ammonium salts or through enzymatic acylation/deacylation or transesterification, is that a 100% yield is theoretically possible.



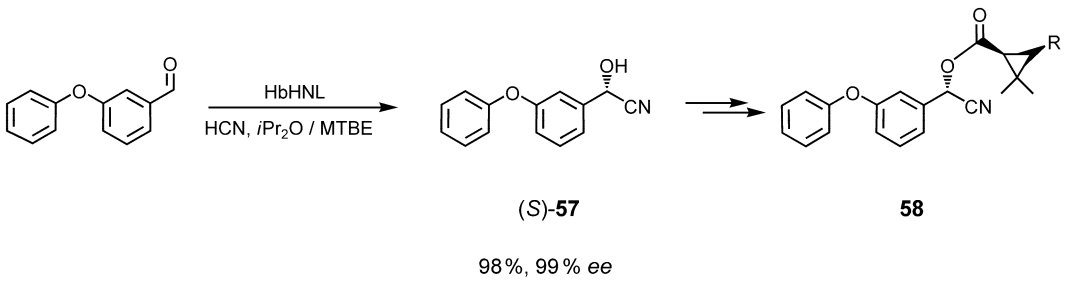
Scheme 23. HNL-catalyzed synthesis of (*R*)-*o*-chloromandelic acid ((*R*)-**54**).

In recent years processes for the production of *S* cyanohydrins and S hydroxycarboxylic acids catalyzed by HNLs from *Hevea brasiliensis* and *Manihot esculenta* have been made economically attractive by recombinant enzyme preparation in *E. coli*.[71] One recent example is the production of (*S*)-*m*-phenoxybenzaldehyde cyanohydrin ((*S*)-**57**) in a biphasic process by DSM Chemie Linz and Nippon Shokubai.[72] The cyanohydrin is an intermediate in the production of pyrethroids **58** (Scheme 24).

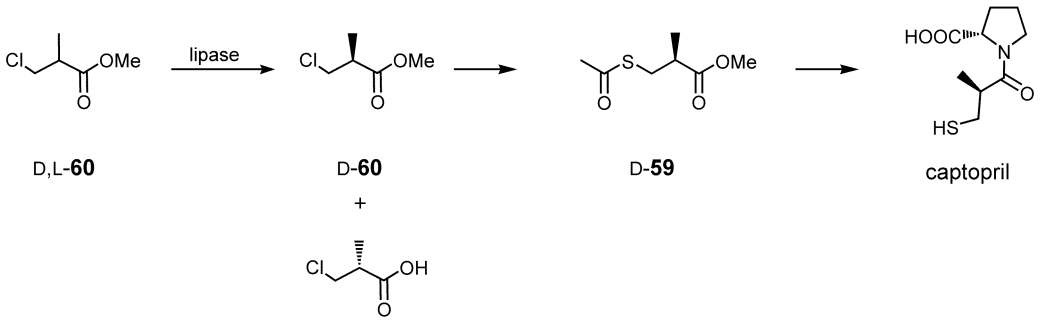
3.3.1.5 Ester Hydrolysis and Transacylation

Researchers at DSM have developed an enzymatic process for the production of the captopril intermediate D-**59**, whereby the enantiomers of methyl 3-chloro-2-methylpropionate (D,L-**60**) are separated with a lipase.[73] All lipases investigated hydrolyze L-**60**, and the unreacted D-**60** is converted into D-**59** (Scheme 25). Up to 98% *ee* at 64% conversion is observed with the lipase from *Candida cylindracea*.

The resolution of D,L-pantolactone (D,L-**61**) by enantioselective pantolactone hydrolases can be regarded as a special case of ester hydrolysis. D-Pantolactone (D-**61**) is a precursor of D-pantothenic acid (D-**62**, vitamin B5), which is required as a feed additive in pig and poultry breeding (Scheme 26). In the 1990s researchers at the Daiichi subsidiary Fuji Chemical Industries (now Daiichi Fine Chemical Co.) developed a process in cooperation with Yamada and co-workers[74] in which D,L-**61** is resolved into sodium D-pantoate (D-**63**) and L-**61** by a fungal aldonolactonase (capacity: 3500 t a^{-1}).[75] The

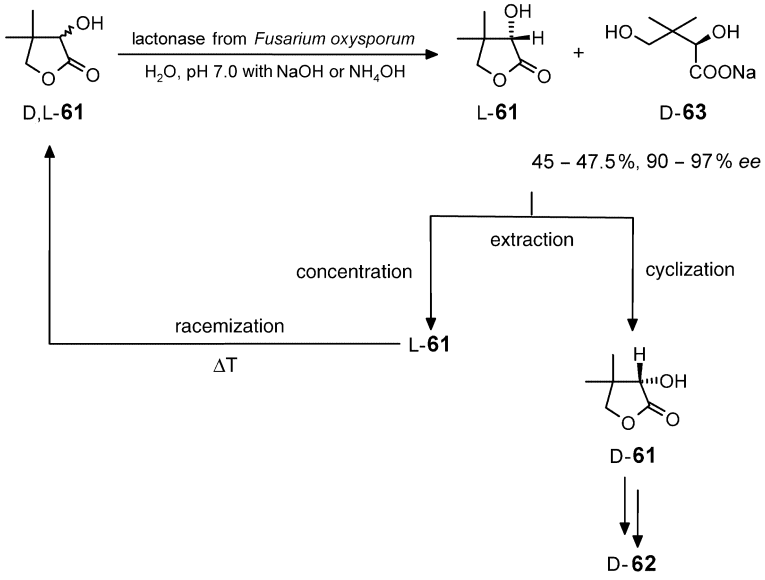


Scheme 24. (*S*)-*m*-Phenoxybenzaldehyde cyanohydrin ((*S*)-**57**) is an intermediate in the synthesis of pyrethroids, such as **58**.



Scheme 25. Synthesis of the ACE antagonist captopril.

 © 2004 Wiley-VCH Verlag GmbH & Co. KGaA, Weinheim

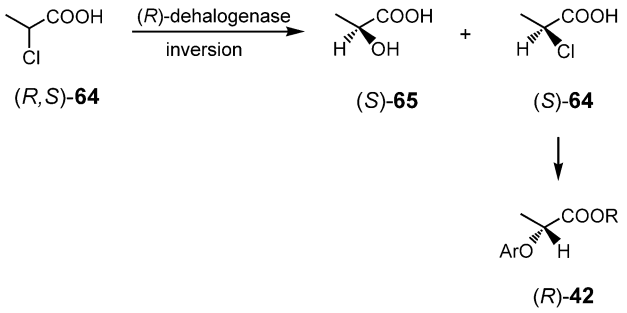


Scheme 26. Production of D-pantothenic acid (D-**62**) from D,L-pantolactone (D,L-**61**). Sodium D-pantoate (D-**63**) is formed in the enantioselective ester hydrolysis and is then converted into D-**61**. The enantiomer L-**61** is racemized to D,L-**61** and resubjected to the reaction sequence.

enzyme is highly selective and extremely stable in the form of immobilized fungal mycelia; >90% activity is observed after 180 runs (or 180 days).

3.3.1.6. *Dehalogenase Processes*

The enantioselective dehalogenation of (*R*)-2-chloropropionic acid ((*R*)-**64**) occurs with inversion of stereochemistry to give (*S*)-**64** and (*S*)-lactic acid ((*S*)-**65**; Scheme 27). This transformation is used in the industrial synthesis of (*R*)-α-phenoxypropionic acid ((*R*)-**42**).[76]

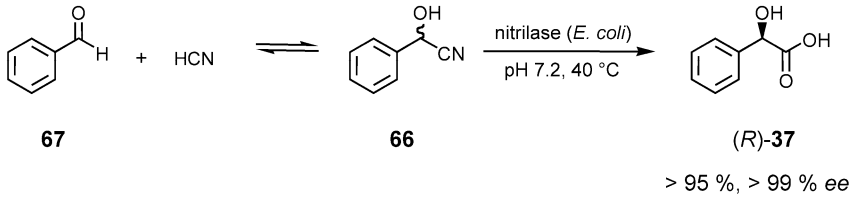


Scheme 27. Industrial synthesis of (*R*)-α-phenoxypropionic acid ((*R*)-**42**, R = H, Ar = Ph) starting from (*R*)-*o*-chloropropionic acid ((*R*)-**64**).

3.3.1.7. *Enzymatic Hydrolysis of Nitriles*

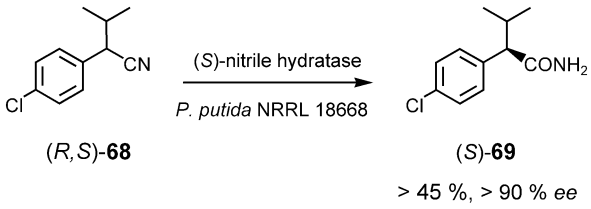
The hydrolysis of nitriles by nitrilases or nitrile hydratase/amidase systems in combination with hydrocyanic acid chemistry offers useful access to α-hydroxycarboxylic acids in a manner analogous to HNL processes.[77] In recent years a number of nitrilase processes have become established, for example, at Lonza (Section 3.3.1). BASF and Mitsubishi Rayon also use nitrilase processes for the production of (*R*)-mandelic acid ((*R*)-**37**) and its derivatives on a multiton scale.[78] (*R*)-Mandelic acid ((*R*)-**37**) is isolated by crystallization from the ammonium salt formed in the biocatalytic reaction. Because of the in situ racemization of the cyanohydrin **66**, this process represents a dynamic kinetic resolution (Scheme 28). If the rate of interconversion of the enantiomers of **66** is faster than the enzymatic hydrolysis, **67** can be converted completely into (*R*)-**37**. An advantage of the nitrilase process is that no organic solvents are required. Moreover, the synthesis of a nitrile is avoided, as the cyanohydrin **66** is formed from **67** and HCN under the reaction conditions.[79]

In principle nitrile hydratase/amidase systems, in which nitrile hydrolysis occurs via the free amide, also provide access to chiral carboxylic acids.[80] However, only a small number of enantioselective nitrile hydratases are known,[81,82] for example, the nitrile hydratase for the resolution of



Scheme 28. Industrial synthesis of (*R*)-mandelic acid ((*R*)-**37**) through the enantioselective hydrolysis of the cyanohydrin **66** (nitrilase process).

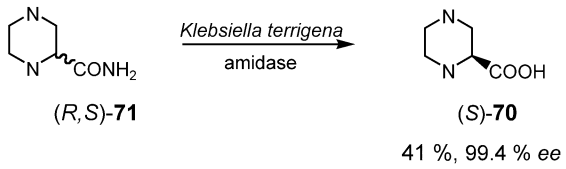
(*R*,*S*)-2-(*p*-chlorophenyl)-3-methylbutyronitrile (**68**) to (*S*)-**69** (Scheme 29).[83] The nonselective nitrile hydratase from *Rhodococcus rhodochrous J1* is used on an industrial scale



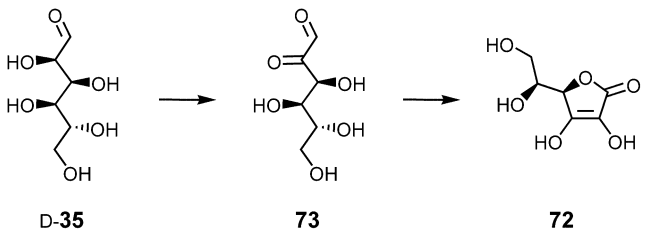
Scheme 29.

for acrylamide production (Nitto process, >20000 t a^{-1})[84] and nicotinamide synthesis (Lonza, 3000 t a^{-1}), and regioselective nitrile hydratase/amidase systems are used for the hydrolysis of dinitriles.[85] In most cases the racemic amides are resolved, so that a maximum yield of 50% is possible. An example of such a process is the production by Lonza of (*S*)-piperazinecarboxylic acid ((*S*)-**70**), an intermediate in the synthesis of the anti-HIV drug crixivan, whereby a *Klebsiella* amidase is used to resolve racemic (*R*,*S*)-piperazine-2-carboxamide ((*R*,*S*)-**71**; Scheme 30).[86]

 © 2004 Wiley-VCH Verlag GmbH & Co. KGaA, Weinheim



Scheme 30. Selective conversion of racemic (*R*,*S*)-piperazine-2-carboxamide ((*R*,*S*)-**71**) into (*S*)-piperazinecarboxylic acid ((*S*)-**70**).



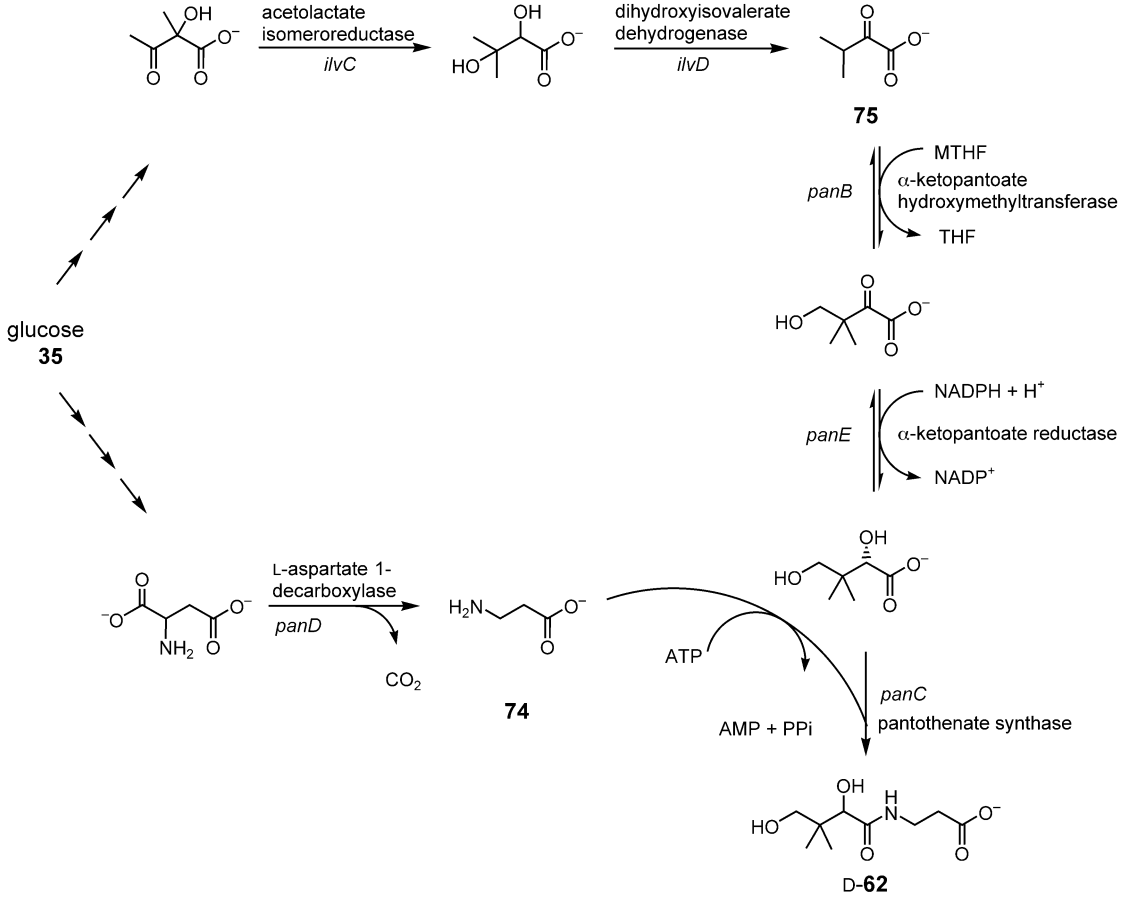
Scheme 31. Production of vitamin C (**72**) from D-glucose (D-**35**).

3.3.2. *Fermentation*

Owing to the advances made in the areas of strain development and metabolic engineering, microbial syntheses have become possible and economically attractive for many compounds produced on a large scale. These include amino acids, as well as lactic acid (*Lactobacilli* fermentation), ascorbic acid (**72**, vitamin C), and pantothenic acid (**62**, vitamin B5). In terms of the pharmaceutical market, penicillins must also be mentioned.

The world-wide production of vitamin C (**72**; 80000 t a^{-1}) still relies on the Reichstein process.[87] Biotechnological improvements are based in the first instance on the fermentation production of 2-keto-L-gulonic acid (**73**), an open-chain precursor of **72**, from D-glucose (D-**35**) (Scheme 31). These processes were compared recently by Hancock and Viola.[88]

In the 1990s researchers at Takeda Chemical Ind. developed a fermentation process in *E. coli* for the production of D-pantothenic acid (D-**62**), whereby high end concentrations were observed upon feeding with β-alanine (**74**; > 60 g L^{-1} of D-**62** after a fermentation time of 72 h).[89] Researchers at Degussa, in cooperation with the research groups of Pühler and Sahm, are currently working on a method based on this process for the synthesis of pantothenic acid by fermentation in *E. coli*[90] and *Corynebacterium glutamicum*,[91] respectively. The genes relevant for pantothenic acid biosynthesis were over-expressed, and the production of the precursor α-ketoisovalerate (**75**) was increased by *ilvBNCD* over-expression and *ilvA* deletion. For the workup of secreted D-**62**, the cells are separated from the fermentation broth. The pantothenic acid present as a mixed salt is converted into calcium D-pantothenate, for example, by addition of calcium hydroxide, concentration, and spray drying (Scheme 32).[92]



Scheme 32. Biosynthesis of deprotonated D-pantothenic acid (D-**62**). MTHF = 5-methyltetrahydrofolate, THF = tetrahydrofolate.

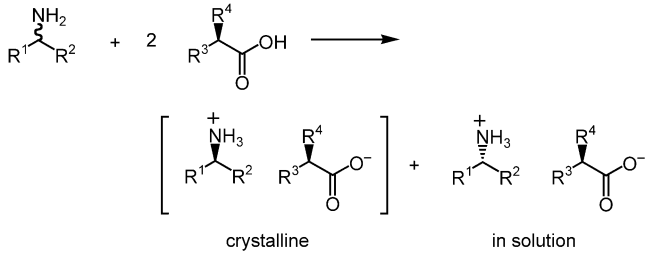
 © 2004 Wiley-VCH Verlag GmbH & Co. KGaA, Weinheim

4. Production of Amines

4.1. Classical Chemical Processes

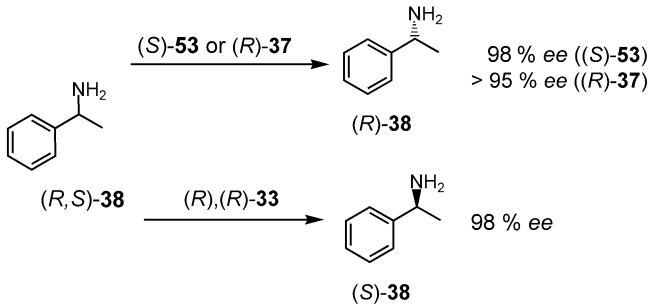
4.1.1. Crystallization with Chiral Carboxylic Acids

The crystallization of diastereomeric salts of chiral carboxylic acids with chiral amines is still of considerable importance today in the isolation of enantiomerically pure amines (Scheme 33).[93] Thus, (*R*)- or (*S*)-1-phenylethylamine



Scheme 33. Classical racemate resolution through fractional crystallization of salts of racemic amines and enantiomerically pure carboxylic acids.

((*R*)- or (*S*)-**38**) can be obtained on an industrial scale by crystallization either with (*S*)-malic acid ((*S*)-**53**)[94] or (*R*)-mandelic acid ((*R*)-**37**),[96] or with (*R*,*R*)-tartaric acid ((*R*,*R*)-**33**),[95] respectively (Scheme 34). Racemate resolution with

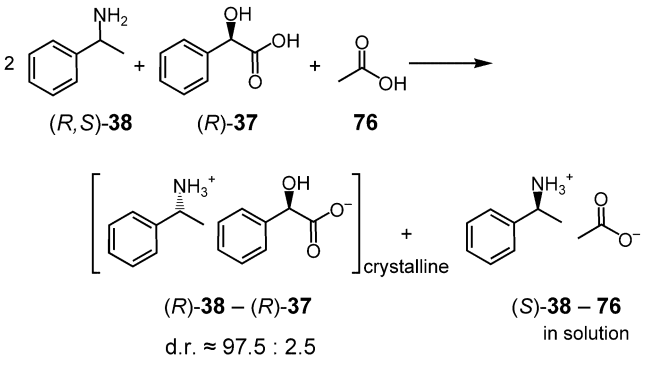


Scheme 34. Racemate resolution of (*R*,*S*)-1-phenylethylamine ((*R*,*S*)-**38**) through fractional crystallization.

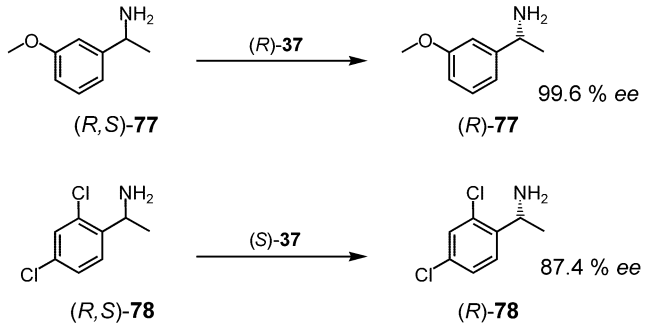
(*R*)-**37** is of particular commercial interest. During process optimization it was found that one equivalent of (*R*)-**37** could be replaced by acetic acid (**76**) (Scheme 35).[96a] During the process the *R*-**38**–*R*-**37** is formed with d.r. ≈ 97.5:2.5.

Mandelic acid (**37**) has proved to be a convenient resolving agent for a large number of amines. Racemates of substituted aryl alkyl amines, such as 1-(*m*-methoxyphenyl)-ethylamine (**77**)[97] and 1-(*o*,*p*-dichlorophenyl)ethylamine (**78**),[98] can also be resolved with **37** (Scheme 36).

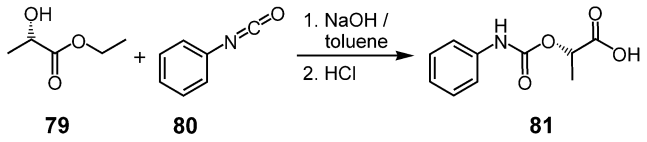
Another versatile resolving agent for the production of chiral amines is L-phenylcarbamoyllactic acid (L-**81**), which can be prepared readily and cheaply from the commercially available starting materials ethyl L-lactate (L-**79**) and phenylisocyanate (**80**; Scheme 37).[99] For example, (*R*)-1-phenylethylamine ((*R*)-**38**) is isolated with > 99 % *ee* upon treat-



Scheme 35.



Scheme 36. Racemate resolution with (*R*)- and (*S*)-mandelic acid ((*R*)- and (*S*)-**38**).



Scheme 37. Synthesis of L-phenylcarbamoyllactic acid (L-**81**), a reagent for the separation of the enantiomers of chiral amines.

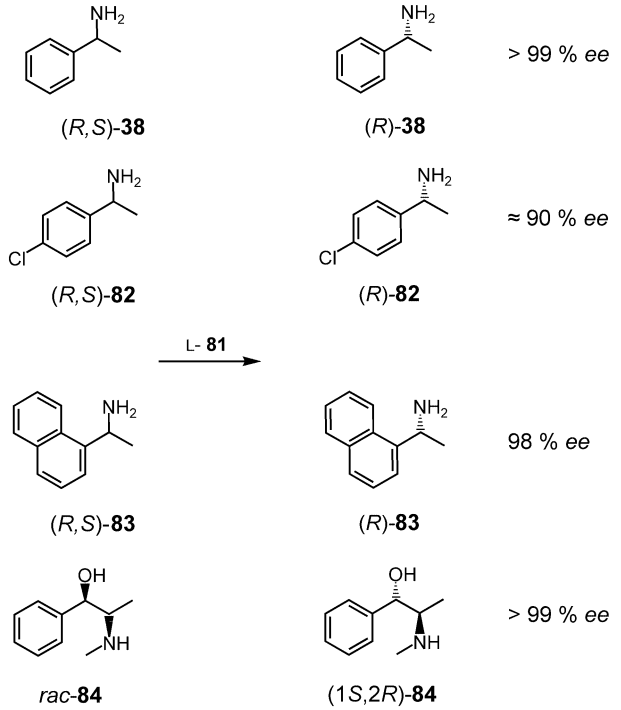
ment of (*R*,*S*)-**38** with L-**81**.[99b] Furthermore, L-**81** is suitable for the resolution of 1-(*p*-chlorophenyl)ethylamine (**82**), a key intermediate in the synthesis of a chiral fungicide,[100] as well as 1-(1-naphthyl)ethylamine (**83**)[99b] and ephedrine (*rac*-**84**; Scheme 38).[99b]

Derivatives of L-**81** are also accessible by treatment of L-lactic acid (L-**79**) with substituted aryl isocyanates (Scheme 37).[101] However, only L-**79** is available inexpensively, and therefore usually only one enantiomer of the amine can be obtained.

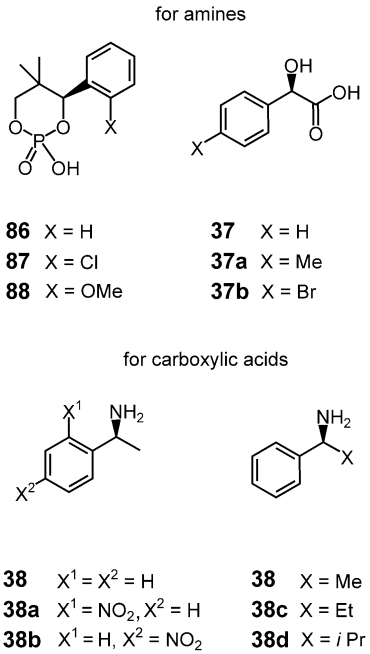
4.1.1.1. Dutch Resolution

A notable variant of classical racemate resolution is the so-called "Dutch resolution" developed by researchers at DSM and Syncom BV.[102] In an attempt to shorten the search for a suitable resolving agent for an amine through a combinatorial approach a mixture of several optically active acids was used, whereby salt precipitated that contained not *one*, but *several* acid anions.

 © 2004 Wiley-VCH Verlag GmbH & Co. KGaA, Weinheim

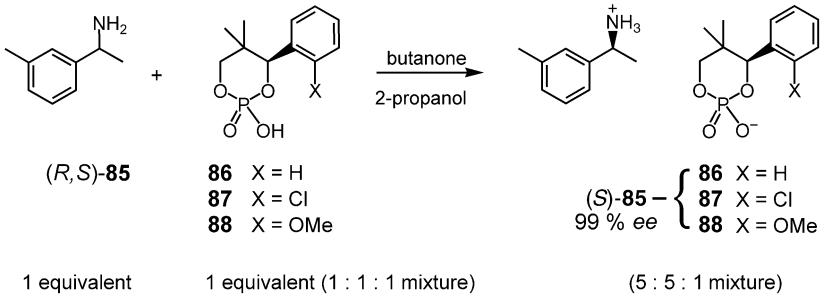


Scheme 38. Examples of racemate resolution with L-**81**.



Scheme 40. Dutch resolution: Frequently used reagents.

In a typical experiment racemic 1-(3-methylphenyl)ethylamine ((*R*,*S*)-**85**) is treated with one equivalent of an equimolar mixture of the chiral phosphoric acid esters **86**, **87**, and **88**. Upon mixing, an amine salt that contains the amine (*S*)-**85** in nearly enantiomerically pure form precipitates immediately (Scheme 39); the phosphates **86**, **87**, and **88** (5:5:1) act as counterions. Even after repeated recrystallization of the precipitated salt the counterion ratio does not change.



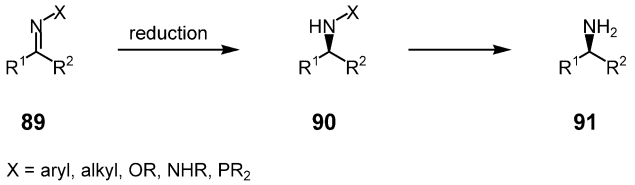
Scheme 39. Dutch resolution: The precipitation of salts of enantiomerically pure amines that contain a mixture of chiral acid anions.

The method is highly versatile, and various mixtures for the resolution of racemic amines and carboxylic acids have become since established (Scheme 40). However, as complex mixtures of the resolving agents are present in the mother liquor of the precipitated salt, the reuse of this auxiliary is problematic.

4.1.2. Reduction of C=N Bonds

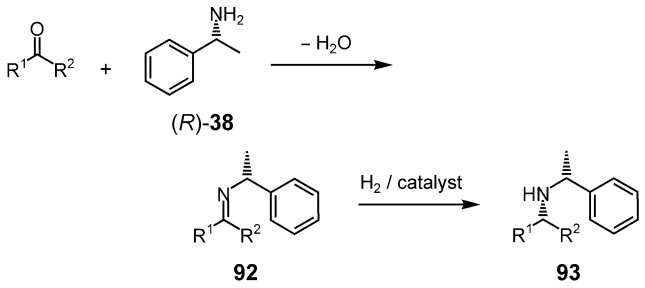
The production of optically active amines by reduction of a prochiral precursor **89** containing a C–N double bond has been treated in detail in several review articles (Scheme 41).[103] From an industrial viewpoint the problems generally lie in the synthesis of the precursor **89** and in the cleavage of the auxiliary group X from **90** to give the free amine **91** (for example, cleavage of the N–N bond in optically active hydrazines with SmI_2).[104] The diastereoselective hydrogenation of Schiff bases **92** derived from a ketone and (*R*)-**38**[105a,b] to secondary amines **93** can also be carried out on a large scale (Scheme 42).

The hydrogenation of the optically active Schiff base **95** from the electron-rich aryl ketone **94** gives a secondary amine **96** (Scheme 43). The two benzyl positions in **96** can be differentiated, so that selective cleavage of one benzylic C–N bond leads to (*R*)-**97**.[105c,d] The diastereoselectivity in the

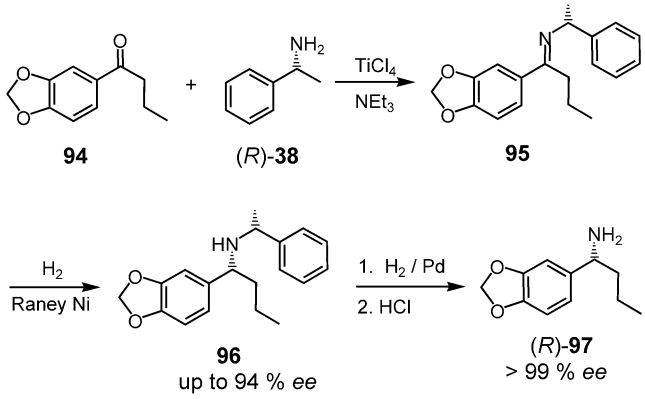


Scheme 41. Prochiral precursors **89** with a C–N double bond for the enantioselective synthesis of amines.

 © 2004 Wiley-VCH Verlag GmbH & Co. KGaA, Weinheim



Scheme 42.



Scheme 43.

hydrogenation of **95** is critically dependent upon the reaction conditions: At increased temperatures the selectivity observed is higher than at room temperature! The primary amine (*R*)-**97** can be obtained in greater than 99% *ee* through a single precipitation of the hydrochloride.[105c]

The three-step method developed by Burk and co-workers for the synthesis of optically active amides **98** by enantioselective catalytic hydrogenation of **99** with Rh^I/DuPHOS(**104**) is also interesting in terms of technical applications.[106] The enamides **99** are available in turn by reduction of the oximes **100** with iron (Scheme 44). The amide **103** is obtained from pinacolone oxime (**101**) via the enamine **102** in nearly enantiomerically pure form in the presence of just 0.1 mol% of the catalyst.

Researchers at Solvias [107] and Avecia Ltd.[108] take advantage of the facile cleavage of P–N bonds in their syntheses of optically active amines. The method of Solvias starts from the ketone oximes **105**, which are readily converted into diphenylphosphorylketimines **107** by treatment with chlorodiphenylphosphane (**106**; Scheme 45).[109] The asymmetric catalytic hydrogenation in the presence of a Rh^I/josiphos(**108**) catalyst system[110] results in the formation of optically active phosphonamides **109**, from which the corresponding chiral amines (*R*)-**110** are released readily by hydrolysis under acidic conditions. Under optimal conditions just 0.2 mol% of the Rh^I/**108** catalyst is sufficient for formation of the product **109** with >99% *ee* at complete conversion of **107**. When *para*-substituted acetophenones are used, the amines **110** are produced with significantly lower enantioselectivities (30–97% *ee*).

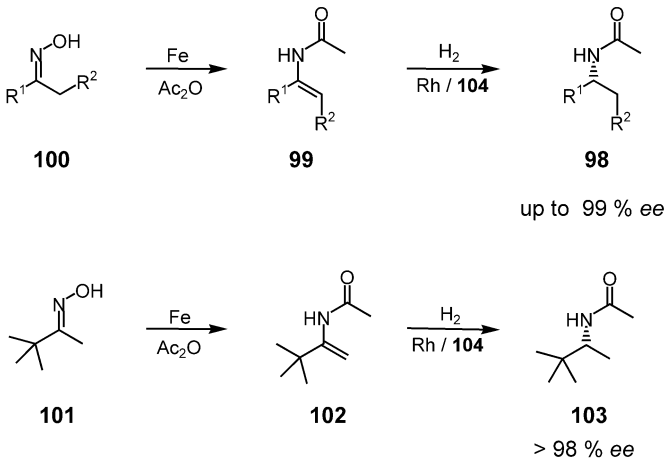
Avecia Ltd. uses a very similar approach in the synthesis of (*R*)-1-(1-naphthyl)ethylamine ((*R*)-**83**). Starting from ketone **111** a phosphorylated imine **113** is produced with diphenylphosphoramidate (**112**). Catalytic asymmetric transfer hydrogenation (CATHy; see Section 3.2.2) of **113** with the Rh complex **114** leads to the optically active phosphorylated amine **115**, from which the amine (*R*)-**83** is released by hydrolysis (Scheme 46). With 0.1 mol% of **114** and substrate concentrations of about 0.5 mol L^{-1} the products are obtained with >99% *ee* at satisfactory conversions.[108b]

4.2. Biotechnological Processes

4.2.1 Transaminations

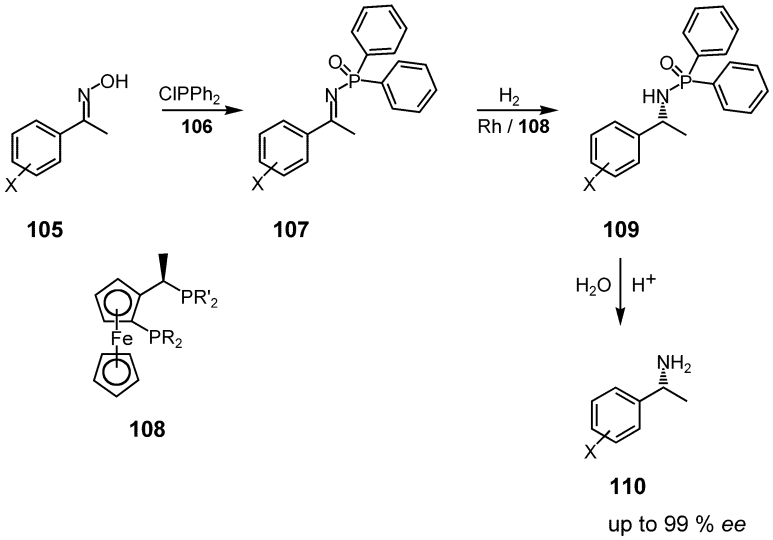
At the end of the 1980s a new biotechnology process for the production of optically active amines was devised at Celgene.[111] In this process transaminases are used, which are able to convert carbonyl compounds, such as ketones or α-keto acids **117** or **118**, into amines **119** and **116**, respectively. The enantioselective transfer of an amino group is dependent upon the cofactor pyridoxal phosphate (**120**; Scheme 47). To suppress the reverse reaction and shift the equilibrium in favor of the desired product, the reagents are normally used in different stoichiometries. The concentration of lipophilic substrates in the aqueous phase can also be kept low by using a two-phase system with an organic phase.

As researchers at Celgene have developed both *S*- and *R*-selective transaminases, both enantiomers of an amine **119** are accessible with this technology. Furthermore, the reaction can be carried out within the context of a synthesis or of a kinetic resolution (Scheme 48). In a synthesis the prochiral ketone **121** accepts an amino group from the amino-group donor isopropylamine (**122**). The amine (*S*)-**123** and acetone (**124**) are formed in more than 90% yield. It is possible to resolve the

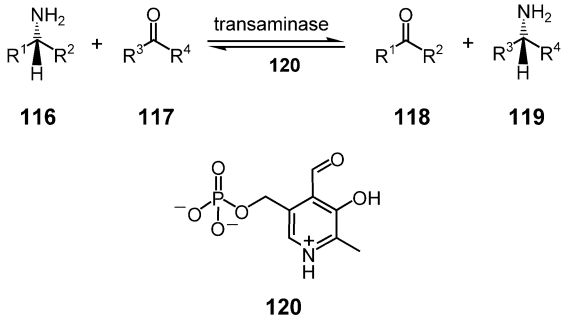


Scheme 44. Enantioselective catalytic hydrogenation with Rh^I/DuPHOS(**104**) to give optically active amides.

© 2004 Wiley-VCH Verlag GmbH & Co. KGaA, Weinheim



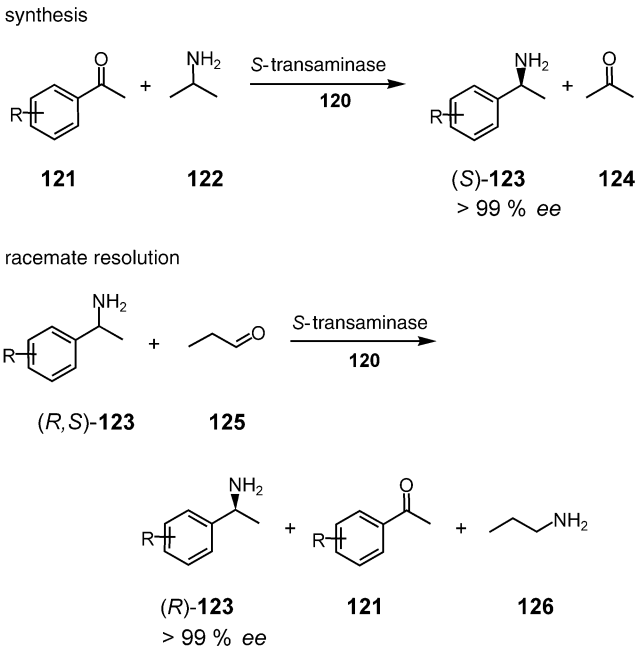
Scheme 45. The asymmetric hydrogenation of diphenylphosphorylketimines **107** with a Rh^{I}/josiphos(**108**) catalyst is the key step in the production of chiral amines (*R*)-**110**.



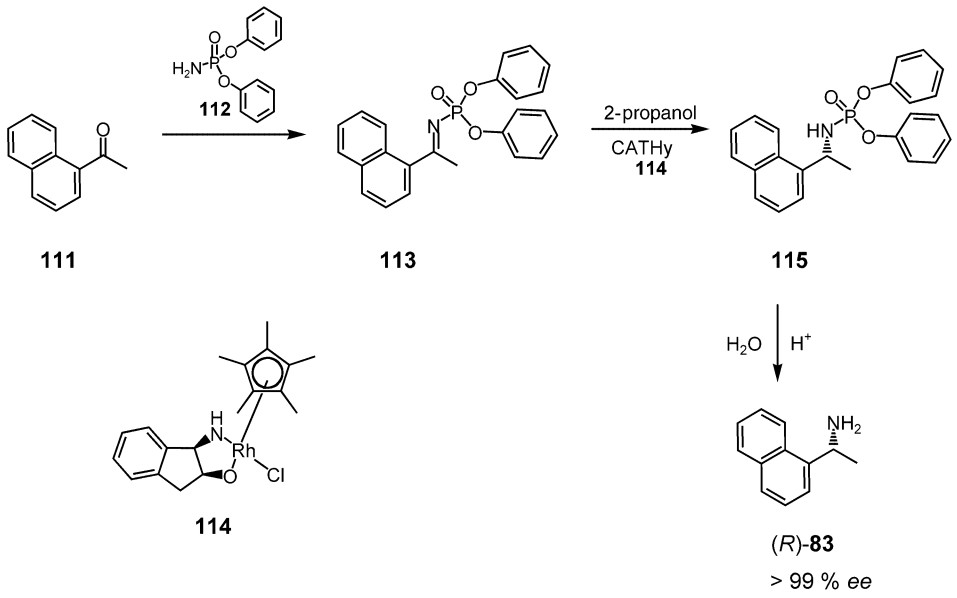
Scheme 47. Enantioselective transamination with pyridoxal phosphate (**120**) as the cofactor.

amine (*R*,*S*)-**123** with the same transamination. In this case (*S*)-**123** is converted into the ketone **121**. As amine-group acceptors low-molecular-weight aldehydes are used, such as propionaldehyde (**125**), from which propylamine (**126**) is obtained. When α-ketocarboxylic acids are used as the amino-group acceptor amino acids are formed.

The Celgene technology has already been used on a 2.5-m^3 scale. The transaminases accept many different aliphatic and aromatic ketones and amines as substrates.[111d]. However, one disadvantage is that in principle



Scheme 48. Examples of *S*-transaminase-catalyzed asymmetric amino-group transfer (Celgene).



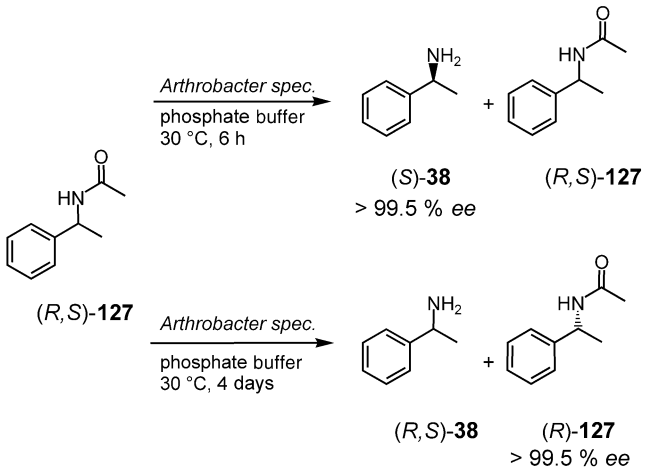
Scheme 46. Synthesis of enantiomerically pure (*R*)-1-(1-naphthyl)ethylamine ((*R*)-**83**; Avecia Ltd.).

 © 2004 Wiley-VCH Verlag GmbH & Co. KGaA, Weinheim

the reaction can only be carried out either in an aqueous solution or in mixtures of water and an organic solvent. For this reason only low product concentrations can usually be attained with hydrophobic substrates, and product mixtures from racemate resolution (Scheme 48) can only be separated by cumbersome methods.

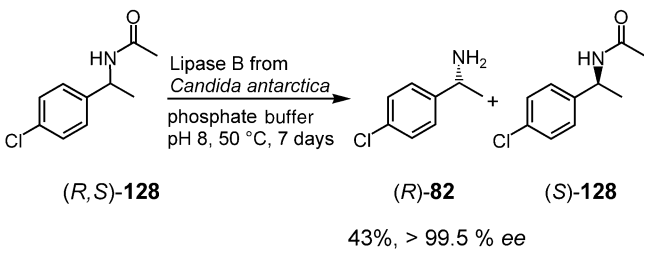
4.2.2 Kinetic Resolution

At the beginning of the 1990s initial work on the enantioselective hydrolysis of racemic amides was carried out at Shell.[112] Both enantiomerically pure (*S*)-1-phenylethylamine ((*S*)-**38**) and, after extended reaction times, enantiomerically pure (*R*)-**127** were thus produced through the selective, enzyme-mediated hydrolysis of racemic *N*-1-phenylethylacetamide ((*R*,*S*)-**127**; Scheme 49). The use of whole cells proved disadvantageous, as did the long reaction times required as a result of the low selectivity to provide the enantiomerically pure *R* amide.



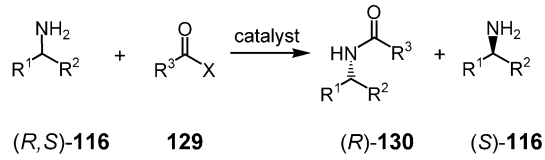
Scheme 49. Enantioselective hydrolysis of racemic *N*-(1-phenylethyl)-acetamide ((*R*,*S*)-**127**).

In the middle of the 1990s methods for the selective hydrolysis of the racemic acetamide (*R*,*S*)-**128** of 1-(*p*-chlorophenyl)ethylamine (**82**) were developed at Bayer.[113] It was found that lipase B from *Candida antarctica* was a suitable catalyst for the selective hydrolysis of (*R*)-**128** to the free amine (*R*)-**82** (Scheme 50). As high concentrations of the catalyst are apparently required for high space–time yields to be observed, this process is not yet exploited industrially.



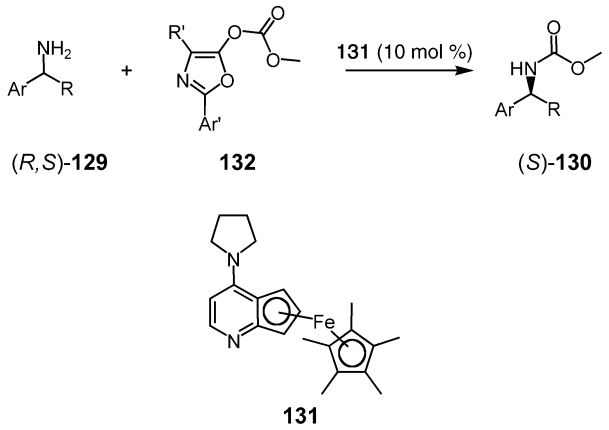
Scheme 50. Selective hydrolysis of (*R*,*S*)-**128** (Bayer).

Alternatively, the kinetic racemate resolution of amines can be carried out in a single synthetic step. In this case the racemic amine (*R*,*S*)-**116** is treated with an acylating agent **129** in the presence of a catalyst. The enantiomer (*R*)-**116** undergoes acylation to the amide (*R*)-**130**, whereas (*S*)-**116** remains unreacted as the free amine (Scheme 51). Fu and co-



Scheme 51.

workers recently described the successful use of planar-chiral DMAP derivatives, such as **131**, as acylation catalysts in combination with oxazoles of type **132** in the kinetic resolution of amines (Scheme 52).[114] Enantiomeric enrichment by a factor of 10–30 was observed in the formation of the amide.

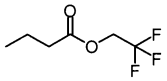
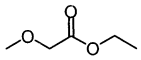
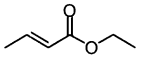
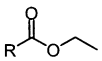
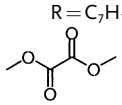
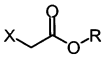
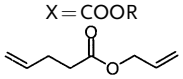
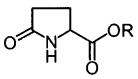
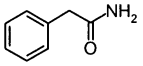


Scheme 52. Enantioselective amide formation in the presence of the ferrocene derivative **131** as the catalyst; selectivity: 10–30.

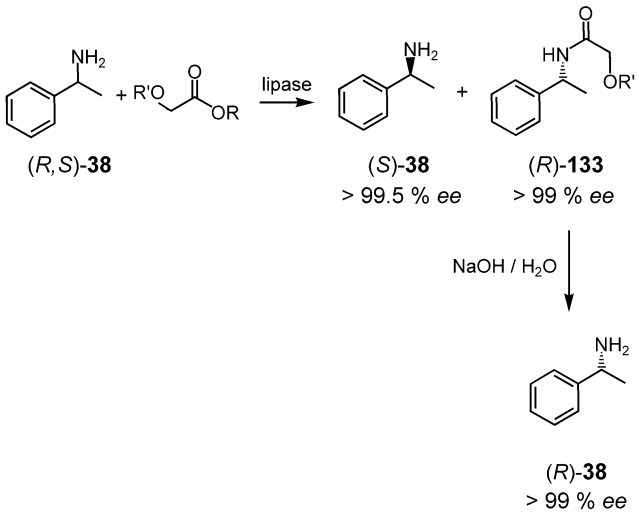
However, until now many results obtained through the use of biocatalysts in combination with acylating agents could not be surpassed (Table 2). An example is the selective acylation of (*R*)-1-phenylethylamine ((*R*)-**38**) in a process patented by BASF: In a single step (*S*)-**38** is produced in nearly enantiomerically pure form along with the amide (*R*)-**133** (Scheme 53).[116] After separation of (*S*)-**38** by distillation or extraction (*R*)-**38** is released through basic hydrolysis of the amide. In certain solvent mixtures the hydrolysis proceeds in nearly quantitative yield without racemization.[116d,125] A remarkable feature of this process is the broad substrate tolerance of the catalyst. Thus, a wide variety of amines have been resolved, in some cases on a multiton scale (Scheme 54). The versatility of the process with regard to possible substrates, the ability to recycle undesired enantiomers by racemization,[126] and the recovery of the acylating agent [127] are the main advantages of the process. At the beginning of

 © 2004 Wiley-VCH Verlag GmbH & Co. KGaA, Weinheim

Table 2: Biocatalysts and acylating agents used in the kinetic resolution of racemic amines.

Biocatalyst	Acylating agent	Reference
Subtillisin carlsberg		[115]
Burkolderia plantarii		[116a]
Candida antarctica lipase B		[117]
		[118]
		
	$R = C_3H_7$	[119a]
	$R = C_7H_{15}$	[119b]
		[120]
		
	$X = OCH_3$	[116c, 121a]
	$X = Cl$	[121a]
	$X = CN$	[121a]
	$X = COOR$	[121b]
		[122]
		[123]
Penicillin acylase		[124]

2002 a new tailor-made, cGMP-compliant (cGMP: current Good Manufacturing Practices) plant went on stream at BASF, which can produce more than 1000 t a^{-1} of optically active amines. In another BASF plant 2500 t a^{-1} of (*S*)-(1-methoxy)-2-propylamine ((*S*)-**164**) can be produced by this process (see Section 4.3.2).



Scheme 53. Lipase-catalyzed enantioselective amide formation from (*R*,*S*)-**38** to give (*S*)-**38** and (*R*)-**133**. The hydrolysis of (*R*)-**133** gives (*R*)-**38** (BASF).

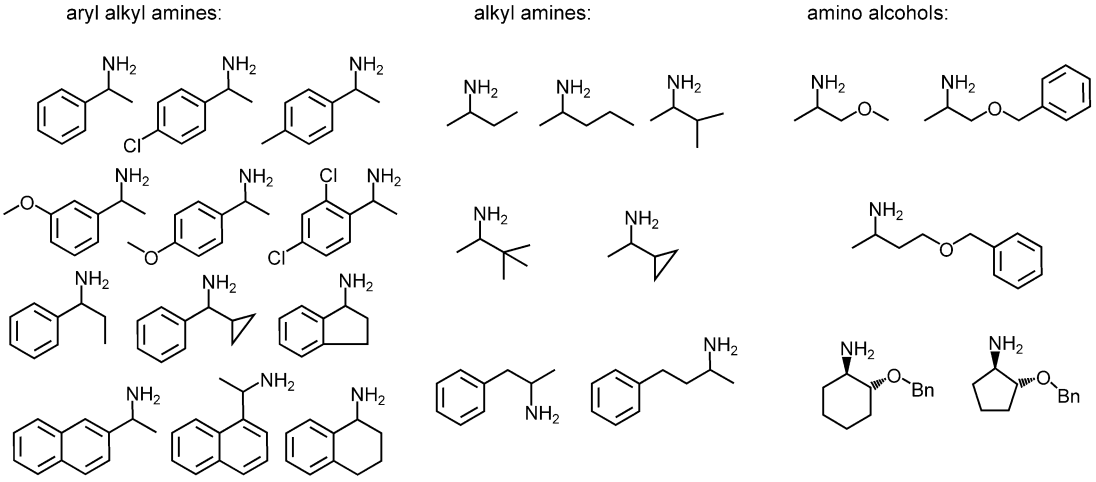
4.3. Production of Optically Active Amino Alcohols

4.3.1. Classical Chemical Processes

4.3.1.1. Crystallization with Chiral Carboxylic Acids

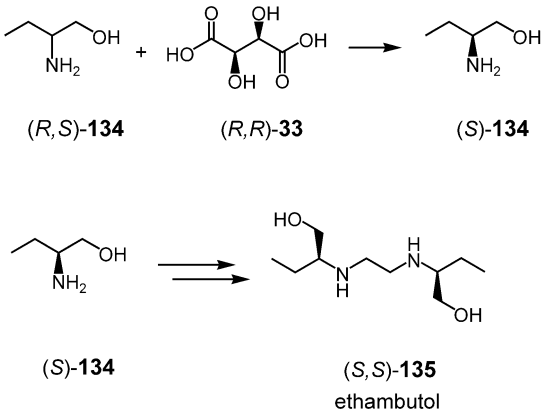
(*S*)-2-Aminobutanol (*S*-**134**) is one of the most important amino alcohol intermediates. It is required for the synthesis of the tuberculostatic ethambutol (*S*,*S*)-**135**; Scheme 55). This drug must be administered in its enantiomerically pure form, as the (*R*,*R*)-**135** causes blindness[128]. Enantiomerically pure (*S*)-**134** is obtained from the racemate by crystallization with L-tartaric acid (L-**33**).[129]

With the development of protease inhibitors for the treatment of AIDS[130] there has been intense demand for optically active intermediates since the beginning of the 1990s. Thus, during the course of the development of the drug indinavir (**136**) at Merck & Co considerable efforts were made world-wide toward the synthesis of (1*S*,2*R*)-1-amino-



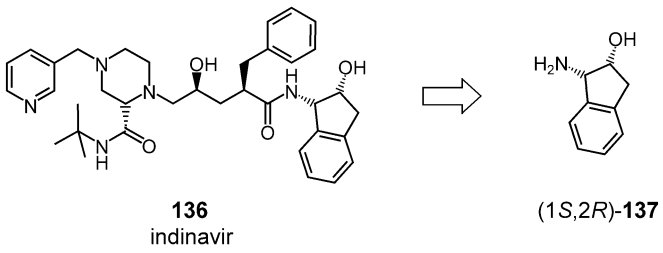
Scheme 54. The resolution of many chiral amines is possible by the BASF process (Scheme 53). Some compounds are resolved on a multiton scale.

 © 2004 Wiley-VCH Verlag GmbH & Co. KGaA, Weinheim



Scheme 55. The synthesis of the tuberculostatic ethambutol ((*S*,*S*)-**135**) proceeds via (*S*)-2-aminobutanol ((*S*)-**134**).

indan-2-ol ((1*S*,2*R*)-**137**; Scheme 56). However, no chemical[131] or biocatalytic[132] asymmetric syntheses can compare with the classical method, in which the racemate *rac*-**137** is



Scheme 56.

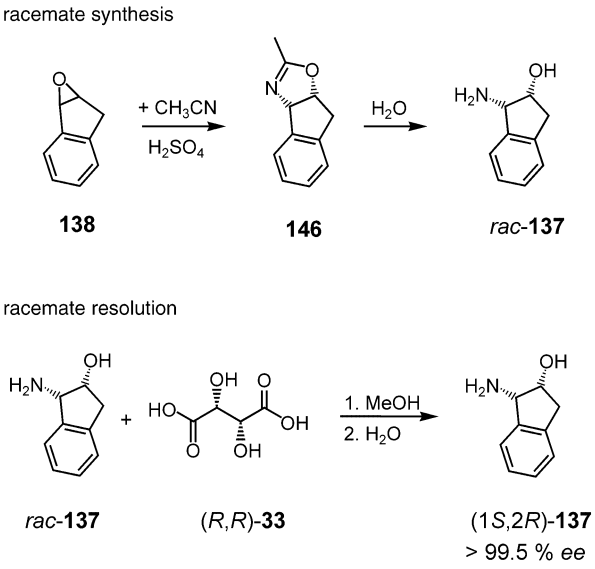
obtained through an elegant synthetic sequence from indene oxide (**138**) and in a second step resolved with (*R*,*R*)-**33** (Scheme 57). The crystallization of the tartrate as a hydrate is important:[133] The tartrate is first precipitated from methanol and then recrystallized from water to give enantiomerically pure (1*S*,2*R*)-**137**.

4.3.1.2 ***Reduction of Amino Acids***

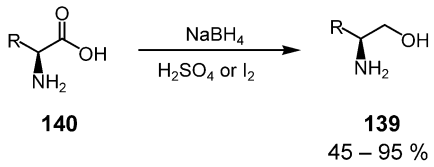
Researchers at Degussa have opened up an important route to amino alcohols **139** with a primary hydroxy functionality based on substrates from the chiral pool. Amino acids **140** are reduced with $NaBH_4$ in the presence of an activator (I_2[134a] or H_2SO_4[134b]), which transforms the $NaBH_4$ into B_2H_6 in situ (Scheme 58). The reduction takes place with retention of the configuration of the stereogenic center, and the products are isolated in good yields. L-Valinol (**141**), L-*tert*-leucinol (**142**), L-phenylglycinol (**143**), L-phenylalaninol (**144**), and L-neopentylglycinol (**145**) are prepared on a ton scale by this method (Scheme 59).[135]

4.3.1.3. ***Opening of Epoxides***

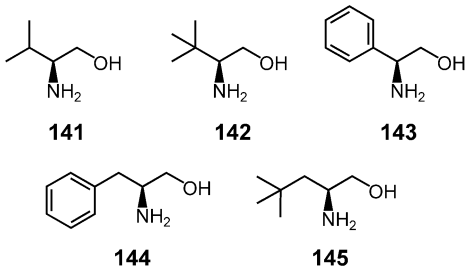
A very elegant method for the preparation of (1*S*,2*R*)-**137** is based on the enantioselective epoxidation of indene by



Scheme 57. Synthesis of enantiomerically pure (1*S*,2*R*)-1-aminoindan-2-ol ((1*S*,2*R*)-**137**), an intermediate in the synthesis of the anti-HIV agent indinavir (**136**, Scheme 56; Merck & Co.)



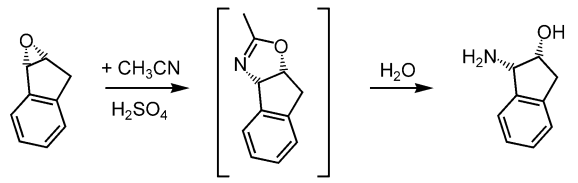
Scheme 58. Reduction of the natural amino acids L-**140** with $NaBH_4$ to the enantiomerically pure amino alcohols **139**.



Scheme 59. The amino alcohols L-valinol (**141**), L-*tert*-leucinol (**142**), L-phenylglycinol (**143**), L-phenylalaninol (**144**), and L-neopentylglycinol (**145**) are produced industrially through reduction of the corresponding amino acids.

Jacobsen and co-workers[131a] (Scheme 80, Section 6.1.3). The indene oxide (1*S*,2*R*)-**138** thus obtained with 84–86% *ee* is transformed into the oxazoline **146** by treatment with acetonitrile, and subsequent hydrolysis affords the desired amino alcohol (1*S*,2*R*)-**137**. Through this reaction sequence the enantiomeric excess of the epoxide (1*S*,2*R*)-**138** is transferred to the product (1*S*,2*R*)-**137** (Scheme 60). However, for the synthesis of indinavir (**136**) the optical purity of (1*S*,2*R*)-**137** must be improved by crystallization with (*R*,*R*)-tartaric acid ((*R*,*R*)-**33**) (Scheme 57).[131a,b]

 © 2004 Wiley-VCH Verlag GmbH & Co. KGaA, Weinheim

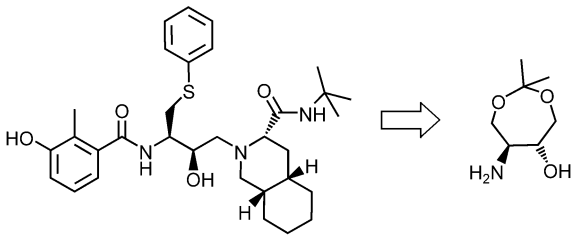


(1*S*,2*R*)-**138** **146** (1*S*,2*R*)-**137**

84 – 86 % *ee* 84 – 86 % *ee*

Scheme 60. The treatment of indene oxide ((1*S*,2*R*)-**138**) with acetonitrile, followed by hydrolysis, gives (1*S*,2*R*)-**137**. The enantiomeric excess of the starting epoxide, which is available through the Jacobsen epoxidation of indene, is transferred to the product in this process.

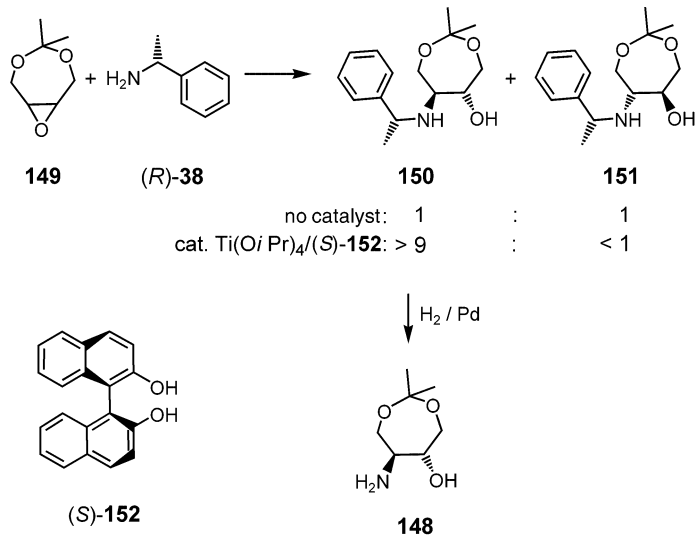
The optically active amino alcohol **148** is required for the synthesis of the HIV-protease inhibitor nelfinavir (**147**; Agouron, Roche; Scheme 61). This key intermediate is



147 nelfinavir **148**

Scheme 61.

produced on an industrial scale from the *meso* epoxide **149**. Upon treatment of **149** with (*R*)-1-phenylethylamine ((*R*)-**38**) in the absence of a catalyst the diastereomeric amino alcohols **150** and **151** are formed in equal amounts (Scheme 62). After separation of the desired diastereomer **150** by crystallization, the chiral auxiliary is removed by debenzylation to give **148** in an overall yield of 37–40 % (based upon **149**).[136] A significant advance was made with the addition of a catalytic amount of $Ti(OiPr)_4$ and (*S*)-1,1′-bis-2-naphthol ((*S*)-**152**). Under these conditions the ring opening of the *meso* epoxide **149** takes place with higher diastereoselectivity, and **148** can be isolated in 91 % yield.[137]



149 (*R*)-**38** **150** **151**

no catalyst: 1 : 1

cat. $Ti(O\,i\,Pr)_4$/(*S*)-**152**: > 9 : < 1

(*S*)-**152** **148**

Scheme 62. Selective ring opening of the epoxide in **149** with $Ti(OiPr)_4$ and (*S*)-1,1′-bi-2-naphthol ((*S*)-**152**) to give the diastereomeric amino alcohols **150** and **151** in a > 9:1 ratio.[137]

and **155** are isolated in nearly enantiomerically pure form (Scheme 63). Hydrazinolysis then affords the hydrazides **156** and **157**, respectively, which are transformed into the amino alcohols **158** and **159**, respectively, by the Curtius rearrangement.

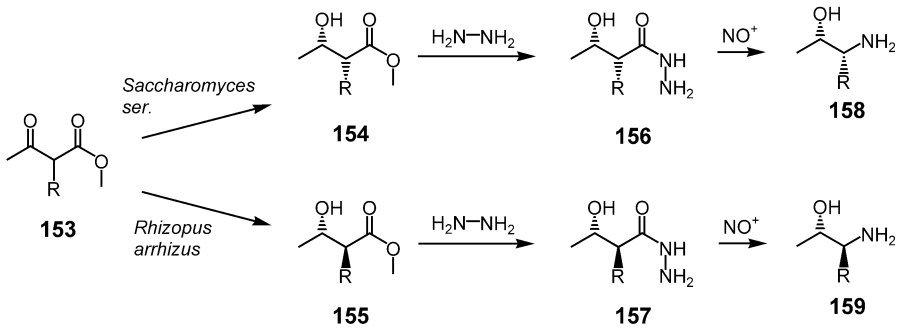
4.3.2. *Biotechnological Processes*

4.3.2.1. *Amino Acids from Hydroxy Acids*

The known high stereoselectivity of the enzyme-catalyzed reduction of 1,3-dicarbonyl compounds is exploited by Biocatalytics Inc. in the production of optically active amino alcohols.[138a,b] In the first step a β-ketoester **153** is reduced to a β-hydroxyester by enzyme catalysis. Depending on the enzyme used the diastereomeric β-hydroxyesters **154**

4.3.2.2. *Kinetic Resolution*

Effective access to optically active amino alcohols is provided by an enzyme-catalyzed kinetic resolution established at BASF. To suppress nonspecific side reactions the hydroxy functionality is protected as an ether. Thus, resolution of *trans*-2-aminocyclopentanol (*rac*-**160**) gives the amine (*S*,*S*)-**160** and the amide (*R*,*R*)-**161**, in each case with approximately 25 % *ee*. The reaction of the corresponding benzyl ether *rac*-**162**, however, proceeds with high enantioselectivity to give the amine (*S*,*S*)-**162** and the amide (*R*,*R*)-**163**) with > 99.5 % and 93 % *ee*, respectively (Scheme 64).[138c,d] This method can also be used with methyl ethers. For example, the enantiomers of racemic (1-methoxy)-2-propylamine ((*R*,*S*)-**164**) can be separated (Scheme 65).

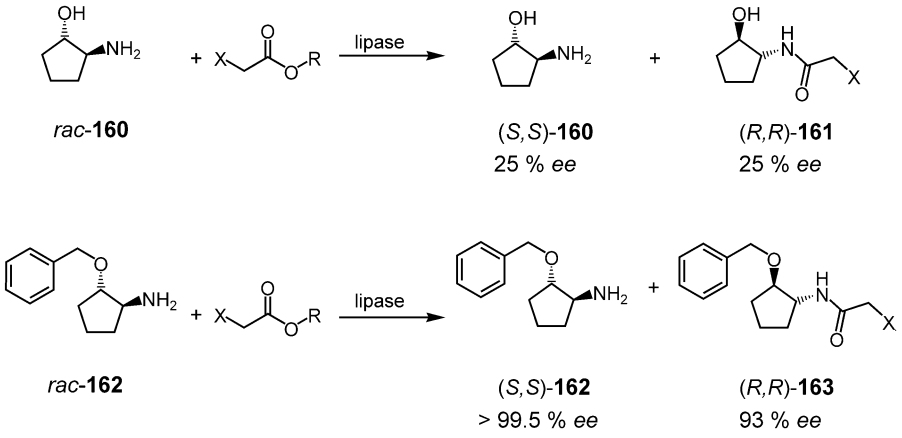


153 **154** **156** **158**

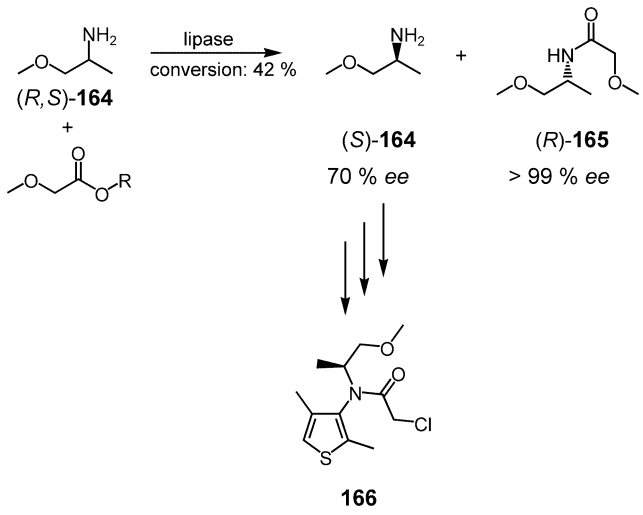
155 **157** **159**

Scheme 63. Enzyme-catalyzed stereoselective reduction of the 1,3-dicarbonyl compound **153** (Biocatalytics Inc.).

 © 2004 Wiley-VCH Verlag GmbH & Co. KGaA, Weinheim



Scheme 64. Enzyme-catalyzed kinetic resolution of racemic *trans*-2-aminocyclopentanol (*rac*-**160**) and its benzyl ether (*rac*-**162**; BASF).



Scheme 65. Resolution of racemic (1-methoxy)-2-propylamine ((*R*,*S*)-**164**) to give (*R*)-**165** und "S-MOIPA" ((*S*)-**164**), an intermediate in the synthesis of the chiral corn herbicide **166** ("Outlook", BASF).

The resulting (*S*)-**164** ("S-MOIPA"), formed along with the amide (*R*)-**165**, is required for the production of the chiral corn herbicide **166** ("*Outlook*", BASF). BASF currently produce up to 2500 t a^{-1} of (*S*)-**164** by enzyme-catalyzed kinetic resolution.

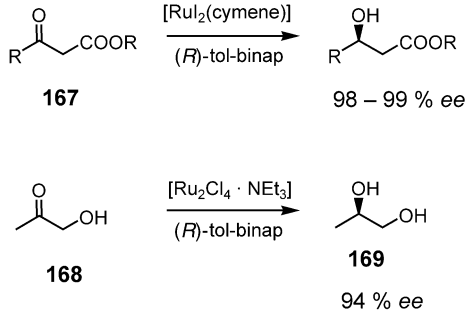
5. Production of Alcohols

5.1. Classical Chemical Processes

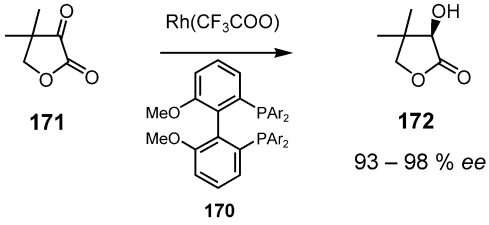
5.5.1. Asymmetric Hydrogenation of Ketones

The work of Noyori et al.[139] played a decisive role in the development of the asymmetric hydrogenation of ketoesters **167** and ketones **168**. Ruthenium complexes of binap[140] and derivatives, such as tol-binap[141] and segphos,[142] are used as catalysts. Industrial development of these reactions up to the ton scale was advanced by Takasago Inc. in Japan. (*R*)-Propanediol (**169**) can be obtained in this way with up to 94% *ee* (Scheme 66). Precursors of β-lactam antibiotics are also accessible by this route,[143] sometimes by exploiting dynamic kinetic resolution. Researchers at Roche developed the biphemp ligands **170**;[144] the conversion of ketopantolactone (**171**) into (*R*)-pantolactone (**172**) was carried out in a pilot plant (Scheme 67).

In more recent work Noyori et al. report efficient transfer hydrogenation catalysts[145] with which formic acid or 2-propanol serve as hydrogen donors, rather than H_2. An oxidative variant has also been described.[146] The heterogeneous asymmetric hydrogenation of Blaser and Studer,[147] which provides a precursor for ACE inhibitors, was operated on a ton scale at Ciba-Geigy. A cinchona-doped platinum catalyst was used for the hydrogenation of the ketoester **173** to the 4-phenylhydroxybutyrate **174** (Scheme 68).



Scheme 66. Ru^{II}/tol-binap-catalyzed asymmetric hydrogenation of carbonyl compounds.

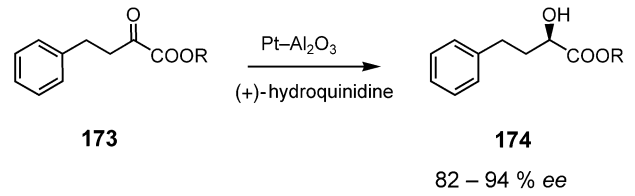


Scheme 67. Catalytic asymmetric hydrogenation of ketopantolactone (**171**) with Rh^{I}/(*R*)-**170** (Roche).

5.1.2 CBS Borane Reductions

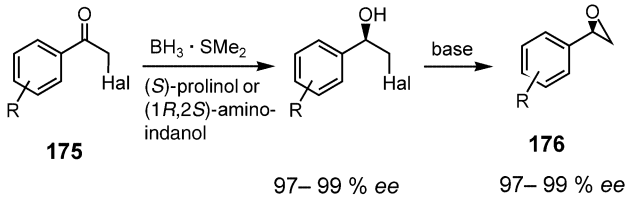
An efficient catalyst based on a chiral modified borane pioneered by Itsuno and co-workers[148] has undergone considerable further development by Corey et al.[149] Borane is used as an adduct with THF or dimethylsulfide as a stoichiometric reducing agent. The method has a broad scope and provides products with high *ee* values within short

 © 2004 Wiley-VCH Verlag GmbH & Co. KGaA, Weinheim



Scheme 68.

reaction times, not only with aryl alkyl ketones. Thus, substituted styrene oxides **176** can be prepared with high enantioselectivites in a two-step sequence from halogenated acetophenone derivatives **175** (Scheme 69).



Scheme 69. CBS borane reductions of halogenated acetophenone derivatives **175**.

Both enantiomers of the diphenylprolinol auxiliary are available and recoverable by extraction. The handling of relatively large quantities of the borane adduct is cumbersome and thus a disadvantage of this method. However, this disadvantage may be circumvented by generating borane in situ from sodium borohydride and trimethylchlorosilane[150] or a Lewis acid. Chemists at Merck, USA and Sipsy have described industrial applications of the process. [151,152] Commercially available borane adducts are frequently stabilized with sodium borohydride; this can strongly influence the enantioselectivity of the reaction.[153] A review by Deloux and Srebnik provides a comprehensive overview of borane-catalyzed reactions.[154]

5.1.3. Kinetic Resolution by Epoxide Hydrolysis

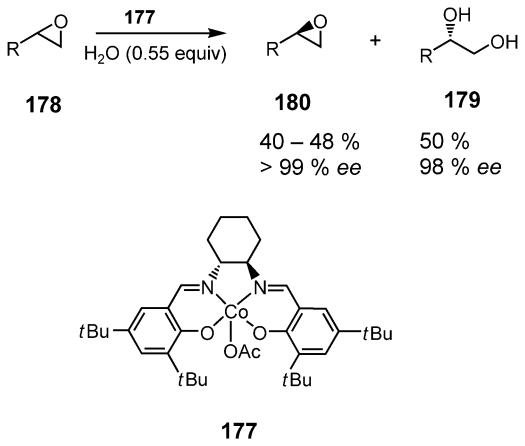
Jacobsen and co-workers developed the (salen)cobalt complex (*R*,*R*)-(salen)CoOAc (**177**) as a catalyst for the enantioselective hydrolysis of racemic epoxides **178**.[155] Through epoxide ring opening the *S* diols **179** are formed with excellent selectivities, and the remaining *R* epoxides **180** are also isolated with high enantiomeric purities (Scheme 70; see also Section 6.1.4).

Not only water but also phenols can be used as nucleophiles to open epoxide rings highly selectively.[156] The resulting 1-phenoxy-2-alkanols are intermediates for the synthesis of β-blockers.[157]

5.1.4. Further Methods

5.1.4.1. Kinetic Resolution of Alcohols with Organic Catalysts

This process has already been discussed in review articles by Dalko and Moisan[158] and by Jacobsen and co-workers,[196]



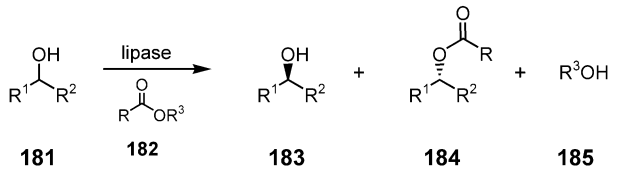
Scheme 70. Enantioselective hydrolysis of racemic epoxides **178** under the catalysis of the (salen)cobalt complex **177**.

which provide an excellent overview of more recent developments, for example, chiral ferrocene derivatives as catalysts for nucleophilic acylation, kinetic resolution, resolution with peptide enzyme mimetics, and kinetic acylation. No industrial applications of these reactions are yet known.

5.2. Biotechnological Processes

5.2.1. Enzyme-Catalyzed Resolution

Enzymatic acylations for the resolution of racemic alcohols were developed as early as the beginning of the 1980s (Scheme 71)[159] Racemic alcohols **181** are treated with



Scheme 71. Resolution of racemic alcohols through enzymatic acylation.

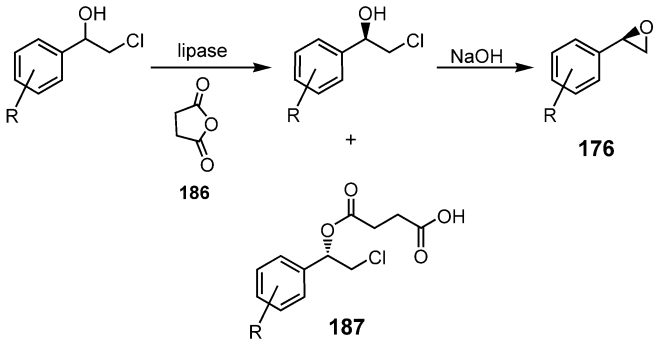
an acylating agent **182** under enzyme catalysis: One enantiomer **183** remains unconverted, whereas the second enantiomer is esterified to **184**. Bacterial and fungal lipases are normally used as biocatalysts.

Esterases also play a part. A number of research groups have made use of the astonishing stability of enzymes in organic solvents, which offer various advantages over aqueous media, such as higher substrate concentrations and simpler workup. Moreover, it is easier to separate the enzyme and to develop an industrially interesting continuous process.

Enzymatic resolutions are usually carried out irreversibly, for example, with a vinyl ester as an acylating agent.[160] The vinyl alcohol formed in the transesterifaction tautomerizes rapidly and irreversibly to acetaldehyde; the equilibrium is thus shifted in favor of the products. Many lipases are sensitive toward acetaldehyde, which forms Schiff bases with

 © 2004 Wiley-VCH Verlag GmbH & Co. KGaA, Weinheim

free amine groups. In a milder variant with propenyl esters, acetone is released.[161] Anhydrides, such as succinic anhydride (**186**), and diketenes are also suitable as acylating agents. The uncoverted enantiomer is separated from the acylated enantiomer **187** by distillation or, when succinic anhydride is used, by acid–base extraction Scheme 72). This process has been developed on an industrial scale at BASF for the synthesis of styrene oxides **176**.



Scheme 72. The enantioselective synthesis of styrene oxides **176** through the enzymatic acylation of α-chloroalcohols.

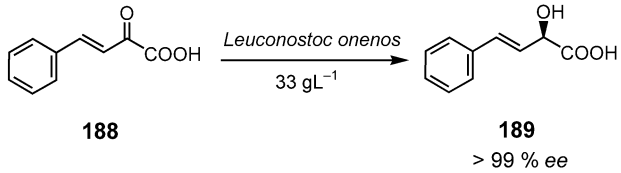
In general the selectivities observed are high, but enzymes, too, have their weaknesses with substrates that are difficult to differentiate sterically, such as 2-butanol. Not only high selectivity, but the highest possible activity is also important, so that good space–time yields can be attained in industrial applications. These and other properties, such as solvent tolerance, substrate versatility, and temperature spectrum, can now be improved remarkably in a targeted manner by enzyme engineering.[162] With modern genetic methods it is possible to produce several thousand mutants per day. To make it possible to screen such a large number of enzyme variants as quickly as possible, sophisticated screening systems must be developed.[163]

In most cases only one enantiomer of a specific intermediate in the synthesis of an active compound is required. For economic and ecological reasons the undesired enantiomer should be recycled, for example, by oxidation/reduction or by catalytic dehydrogenation/hydrogenation. More recent work by the research groups of Park,[164] Bäckvall,[165] Williams,[166] and others involves dynamic, kinetic resolution, whereby the nonacylated enantiomer is racemized in situ by a transition-metal-catalyzed Meerwein–Ponndorf–Verley reduction or Oppenauer oxidation. The resistance of many lipases toward these harsh conditions is astonishing. Up to 10 mol% of KO*t*Bu or KOH and temperatures of up to 70 °C are tolerated. As yet no industrial application of this process is known.

5.2.2 ***Fermentation Processes***

Microbial reactions with yeasts are amongst the oldest chemical processes used. As early as 1874 Dumas recognized the reductive effect of a *Saccharomyces* species.[167] Csuk and Glänzer provide a comprehensive overview;[168] industrially interesting biotransformations have been reviewed by Liese, Seelbach, and Wandrey.[169]

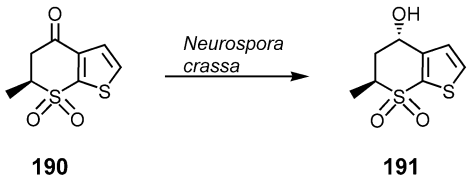
In fermentation processes for the production of optically active alcohols bacterial dehydrogenases in whole living cells are usually used. For example, a process at Daicel provides access to the hydroxycarboxylic acid **189**, an intermediate in the synthesis of ACE inhibitors, through reduction of the α-keto acid **188** (Scheme 73).



Scheme 73. Reduction of the α-ketocarboxylic acid **188** by a dehydrogenase (Daicel).

An interesting comparison of chemical and biocatalytic methods for the production of (*R*)-4-phenyl-2-hydroxybutyric acid, a key intermediate for ACE inhibitors, is presented by Blaser et al.[170] A more detailed comparison of chemical and biocatalytic reductions has been made by Hage et al.[171] It emerged that there is no sovereign route, but that depending on the nature of the substrate one route is more suitable than another. In practice economic and legal aspects play a critical role.

The reduction of the ketosulfone **190** to the corresponding alcohol **191** is the key step in the synthesis of Trusopt, a glaucoma remedy (Scheme 74). This reaction is carried out on a ton scale[172] and gives **191** with $>98\,\%$ *ee*.



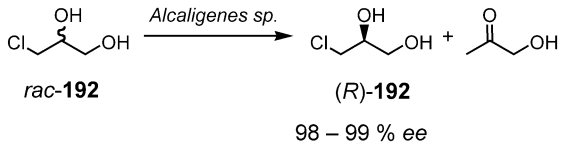
Scheme 74.

A fermentation method is only economical if high substrate concentrations ($>30\,g\,L^{-1}$) can be reached and if the product can be separated from the biomass in a straightforward manner. The advantages lie in the generally high selectivity of these reactions and the fact that they can be scaled up readily. Fermentations on a 100-m^3 scale can be carried out on an industrial scale without difficulty. Organic nutrients, such molasses or beet syrup, are available inexpensively in large amounts for the growth of the organisms.

Some examples of reductions with isolated dehydrogenases have also been described,[173] but these reactions usually require expensive cofactors, such as NAD or FAD. Such processes are only economical when the cofactor can be regenerated in situ in a second catalytic cycle.[174] Dehalogenating strains, such as *Alcaligenes* and *Pseudomonas*, are also

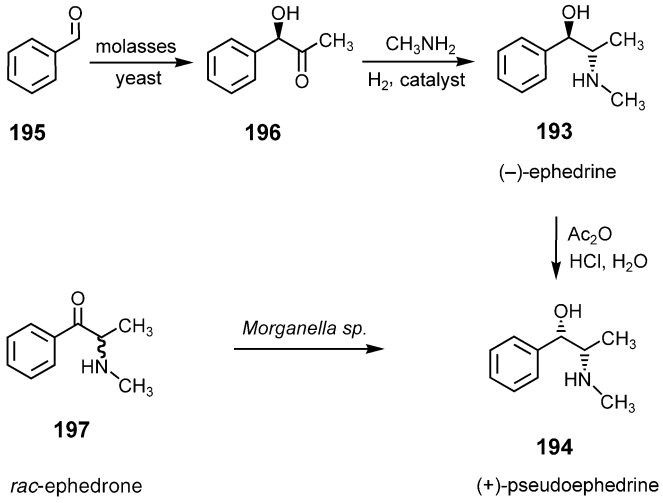
 © 2004 Wiley-VCH Verlag GmbH & Co. KGaA, Weinheim

used for the preparation of intermediates.[175] Daiso (Japan) used this technology for the synthesis of a portfolio of enantiomerically pure C_3 and C_4 building blocks, such as **192** (Scheme 75; see also Section 6.2.1). By means of modern gene technology many properties of the strains used can be improved in a targeted manner.



Scheme 75. Enantioselective dehalogenation of *rac*-**192** (Daiso).

The production of the sympathomimetics ephedrine (**193**) and pseudoephedrine (**194**) was one of the first processes to combine biotechnological and chemical synthetic steps (Scheme 76). As early as 1920 it was found that fermenting



Scheme 76. Synthesis of the sympathomimetics ephedrin (**193**) and pseudoephedrin (**194**), and an alternative biocatalytic synthesis of **194** through the dynamic kinetic resolution of ephedrone (**197**; Fuji).

yeast catalyzed the stereoselective acyloin condensation of benzaldehyde (**195**) and endogenous acetaldehyde to form (*R*)-1-hydroxy-1-phenylpropanone (**196**).[176]. A route to **193** and **194** by reductive methylamination of **196** was established at Knoll.[177] Even today most synthetic ephedrine derivatives are produced by this method (world market 1997: > €50 million).

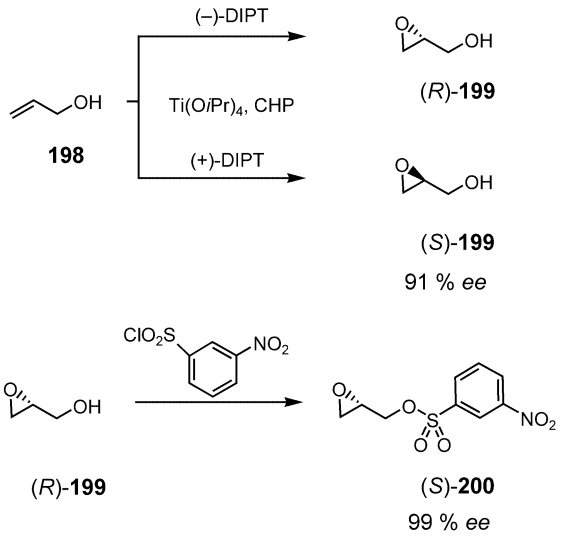
More recent work by researchers at Fuji Chemical Industries illustrates an alternative synthetic route based on biocatalysis (Scheme 76):[178] Chemically synthesized *rac*-2-methylamino-1-phenylpropanone (**197**, ephedrone) is reduced enantioselectively to pseudoephedrine (**194**) by a number of different microorganisms. The enantiomer that is not reduced racemizes in situ in this dynamic, kinetic resolution.

6. Production of Epoxides

6.1. Chemical Methods

6.1.1. Sharpless Asymmetric Epoxidation

One method for the direct epoxidation of primary allylic alcohols is the Sharpless epoxidation in which stoichiometric amounts of $Ti(OiPr)_4$ and an enantiomerically pure dialkyl tartrate are used in the presence of an oxygen-atom donor, for example, cumene hydroperoxide (CHP) or *tert*-butyl hydroperoxide (TBHP).[179] The breakthrough for industrial application came in 1986 with the discovery that upon addition of molecular sieves to the reaction mixture only catalytic amounts (5–10 mol%) of the titanium tartrate complex were required.[180] The oxidation of allyl alcohol (**198**) to (*R*)- and (*S*)-glycidol (**199**) were the first Sharpless epoxidations to be carried out on an industrial scale (Arco Chemical; Scheme 77).[181] With CHP as the oxygen-atom donor the



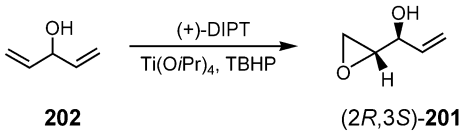
Scheme 77. Industrial application of the Sharpless epoxidation. CHP = cumene hydroperoxide, DIPT = diisopropyltartrate.

products were obtained with 91% *ee*.[182] The isolation of the product was greatly simplified by derivatization of the water-soluble and labile glycidol in situ, for example, as the *m*-nitrobenzene sulfonate **200**. After crystallization the sulfonate is obtained with > 99% *ee*.[183] PPG-Sipsy uses the Sharpless asymmetric epoxidation for the production of **199** under license from Arco Chemical.[184] Enantiomerically pure **199** and **200** are used as intermediates in the synthesis of cidofovir and indinavir (**136**).[185] (2*S*,3*R*)-1,2-Epoxy-4-penten-3-ol (**201**), an intermediate in the synthesis of the immunosuppressant FK-506 (tacrolimus), can be synthesized by the Sharpless epoxidation of divinylmethanol (**202**; Scheme 78).[186]

6.1.2. Sharpless Asymmetric Dihydroxylation

A further route to chiral epoxides is based on optically active diols, which can be converted into the corresponding

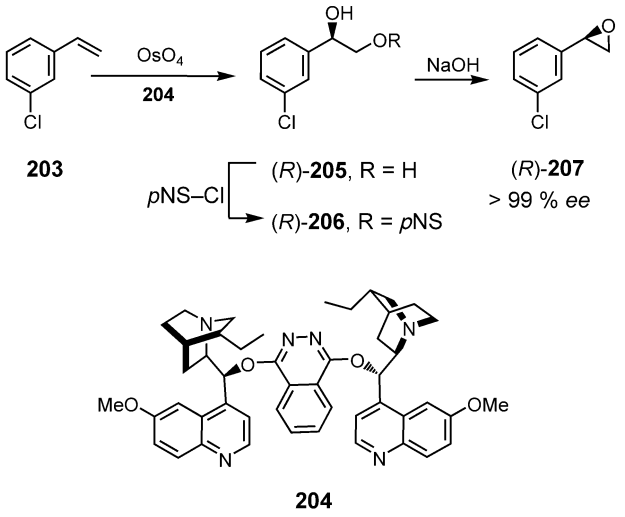
 © 2004 Wiley-VCH Verlag GmbH & Co. KGaA, Weinheim



Scheme 78.

oxiranes. In 1987 Sharpless and co-workers developed a catalytic procedure for the preparation of chiral vicinal diols. In this method a catalytic amount of a chiral tertiary-amine ligand (e.g. dihydroquinine) and OsO_4 are used for the oxidation of an alkene. A stoichiometric oxidizing agent (typically an amine *N*-oxide or $K_3[Fe(CN)_6]$) is used to reoxidize the osmium complex.[187]

In the production of (*R*)-*m*-chlorostyrene oxide (**207**) on a 100–4000-L scale (Rhodia ChiRex) *m*-chlorostyrene (**203**) is first converted into the diol **205** with OsO_4 in the presence of the phthalazine diquinine ligand **204** ($(DHQD)_2PHAL$). The diol **205** is then transformed into **207** (>99% *ee*) via the primary nitrobenzene sulphonate **206** (Scheme 79).[188] By



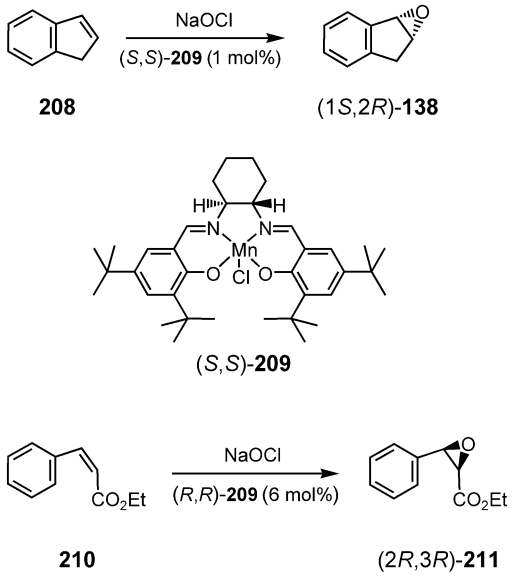
Scheme 79. (*R*)-*m*-Chlorostyrene oxide (**207**) is prepared on an industrial scale by the Sharpless dihydroxylation of **203**, followed by cyclization (Rhodia ChiRex). *p*NS = *p*-nitrophenylsulfonyl.

treatment with trimethoxyethane and acetyl bromide *cis* diols can also be converted into optically active epoxides with retention of configuration.[189]

To avoid effluent contamination, which occurs through the use of stoichiometric amounts of $K_3[Fe(CN)_6]$, an electrocatalytic variant of the asymmetric Sharpless dihydroxylation has been developed at Sepracor and ChiRex.[190] More recent work has shown that the osmium-catalyzed dihydroxylation can also be carried out at pH 10.4–12 with O_2 as the stoichiometric oxidizing agent.[191] This opens up new perspectives for the industrial synthesis of chiral diols and epoxides.

6.1.3. Jacobsen Asymmetric Epoxidation

The Jacobsen asymmetric epoxidation is based on a (salen)manganese(III) precatalyst; hypochlorite is used as the stoichiometric oxidizing agent.[192] Reactions of *cis* alkenes in the presence of 1 mol% of the catalyst afford epoxides with >98% *ee*. Jacobsen epoxidations of *trans*, tetra-substituted, and terminal alkenes give lower yields and lower *ee* values. ChiRex has exclusive rights to this technology, and applies it on a multiton scale. An example is the epoxidation of indene (**208**) to (1*S*,2*R*)-indene oxide ((1*S*,2*R*)-**138**) with catalytic amounts of the (*S*,*S*)-(salen)manganese(III) complex **209** (Scheme 80). Compound (1*S*,2*R*)-**138** is an intermediate in the synthesis of HIV-protease inhibitors, such as indinavir (**136**) by Merck (Section 4.3.1.1).[186,193]



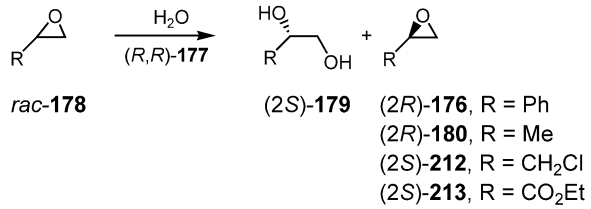
Scheme 80. Jacobsen epoxidations: The (*S*,*S*)-(salen)manganese(III) complex (*S*,*S*)-**209** and its *R*,*R* enantiomer (not shown) serve as catalysts.

A further example is the epoxidation of ethyl cinnamate (**210**) in 56% yield to *cis*-ethyl-3-phenylglycidate (**211**; 95–97% *ee*), an intermediate in the synthesis of paclitaxel (taxol) and docetaxel (Scheme 80).[194] The ligand for the chiral catalyst (*R*,*R*)-**209** is prepared from 1,2-diaminocyclohexane and 2,4-di-*tert*-butylphenol on a 100-kg scale.[195]

6.1.4. Jacobsen Hydrolytic Kinetic Resolution

In 1996 Jacobsen et al. developed a method for the resolution of racemic terminal epoxides by the enantioselective nucleophilic hydrolysis of one enantiomer (see Section 5.1.3, Scheme 70). With the (salen)cobalt(III) catalyst **177** enantioselectivities of >99% *ee* and yields of 40–48% are observed (Scheme 81), which corresponds to a selectivity of E = 500. The reaction is particularly suitable for terminal epoxides[196] and has been developed by Rhodia ChiRex,[197]

 © 2004 Wiley-VCH Verlag GmbH & Co. KGaA, Weinheim



Scheme 81. Selective hydrolysis of one enantiomer of the epoxide **178** with the (salen)cobalt(III) catalyst **177** (Scheme 70).

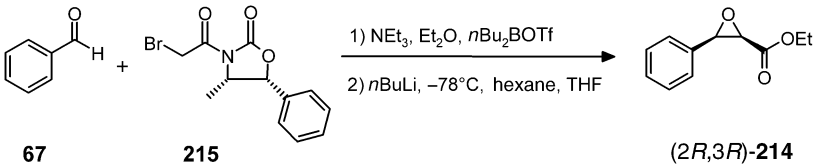
for example, for the resolution of styrene oxide (**176**), propylene oxide (**180**), epichlorohydrin (**212**), and ethyl 2,3-epoxyacrylate (**213**) on a ton scale.[198]

The epoxide opening proceeds by second-order kinetics with respect to the catalyst. Therefore it is assumed that a metal ion activates the epoxide as a Lewis acid, while a further metal center forms the counter ion of the nucleophile. As expected, oligomeric (salen)cobalt(III) complexes exhibit higher reactivities and selectivities than monomeric complexes, such as **177**.[199]

Researchers at Synetix are developing a Jacobsen catalyst in which the salen complex is immobilized on zeoliths, which should simplify separation and recycling of the catalyst and lead to less contamination of the product.[200] The company Daiso, which produces epichlorohydrin (**212**), glycidol (**199**), and chiral precursors by microbial resolution, recently announced the change to the Jacobsen technology in the production of **212**. The license was obtained from ChiRex, which also supplies the catalyst. Production capacity is to be extended to 50 t a^{-1} by 2004.[201]

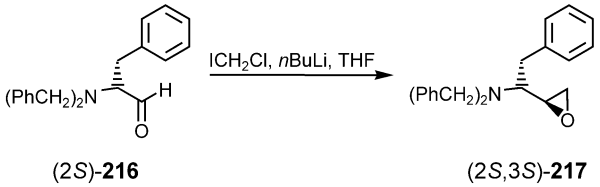
6.1.5. Other Methods

A further route to chiral epoxides is based on optically active α-halo alcohols, which are prepared through an enantioselective Darzens reaction.[202] In the production of the α,β-epoxycarboxylic acid ester **214**, an intermediate in the synthesis of docetaxel, the enolate of the *N*-α-bromoacyl oxazolidinone **215** reacts with benzaldehyde (**67**) in an aldol condensation.[203] The resulting bromohydrin was then cyclized to the epoxide **214** (Scheme 82).



Scheme 82.

A further example is the addition of chloromethyllithium generated in situ to the chiral α-aminoaldehyde **216** (Scheme 83). The epoxide (2*S*,3*S*)-**217** was isolated in 65% yield with 70% *de* after column chromatography.



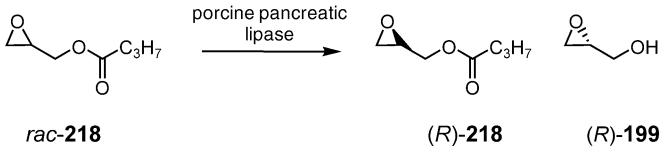
Scheme 83.

6.2. Biotechnological Processes

6.2.1. Racemate Resolution

6.2.1.1. Lipases

By the hydrolysis of racemic glycidylbutyrate (**218**) with porcine pancreatic lipase Ladner and Whitesides obtained (*R*)-**218** in 89% of the theoretical yield and with 92% *ee* (Scheme 84).[204] This process was developed further by

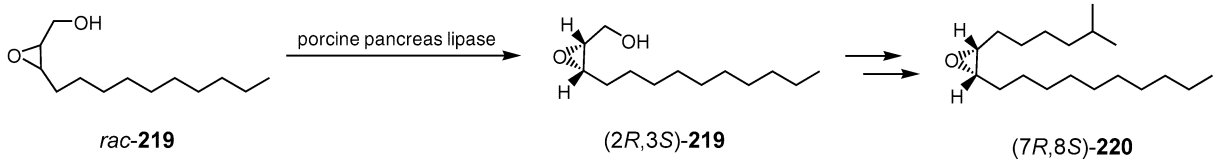


Scheme 84. Synthesis of (*R*)-**218** by porcine pancreatic lipase catalyzed hydrolysis (Andeno-DSM).

Andeno-DSM and implemented for the production of (*R*)-**218** and (*R*)-glycidol ((*R*)-**199**) on a multiton scale.[205]

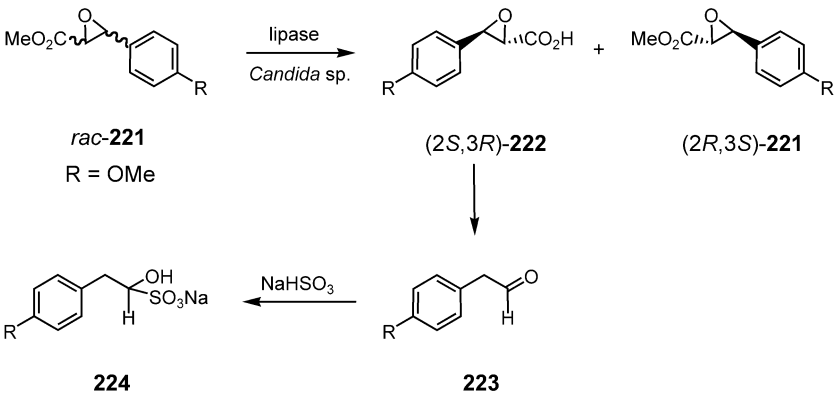
In the kinetic resolution of the epoxy alcohol **219** with porcine pancreatic lipase F and acetic anhydride the 2*S*,3*R* enantiomer is acylated preferentially. The unconverted (2*R*,3*S*)-**219** can be isolated in 27% yield and with 99% *ee* (Scheme 85).[206] This intermediate can be used in the synthesis of the moth pheromone disparlur ((7*R*,8*S*)-**220**). In the production of styrene oxides at BASF, the corresponding racemic styrene chlorohydrins are resolved with a lipase (Section 5.2.1, Scheme 70).

Hydrolysis of the undesired enantiomer of the epoxycarboxylic acid ester **221** with a lipase from *Candida sp.* affords (2*R*,3*S*)-**221** (Scheme 86). The carboxylic acid **222** formed decomposes spontaneously to CO_2



Scheme 85. The epoxide (2*R*,3*S*)-**219** is an intermediate in the synthesis of disparlur ((7*R*,8*S*)-**220**).

 © 2004 Wiley-VCH Verlag GmbH & Co. KGaA, Weinheim

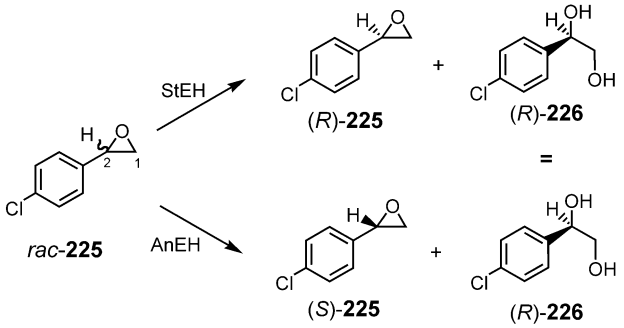


Scheme 86. The enantioselective hydrolysis of the epoxycarboxylic acid ester **221** affords (2*R*,3*S*)-**221**.

and the aldehyde **223**, which is a potent inhibitor of the lipase. Therefore, **223** is transformed into the bisulfite adduct **224** and separated.[207] In 1993 the company Tanabe started operation of a hollow-fiber reactor for the production of (2*R*,3*S*)-**221** with an immobilized lipase from *Serratina marescens*.[208] The glycidate (2*R*,3*S*)-**221** is used as an intermediate in the synthesis of the calcium antagonist diltiazem.[209]

6.2.1.2. Epoxide Hydrolases

Archelas and co-workers have been able to prepare both enantiomers of 4-chlorostyrene oxide (**225**) from the racemate with epoxide hydrolases from *Aspergillus niger* (AnEH) and *Solanum tuberosum* (StEH; Scheme 87). AnEH catalyzes

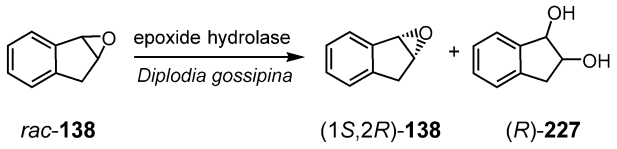


Scheme 87. Enantiomerically pure (*R*)- and (*S*)-*p*-chlorostyrene oxide ((*R*)- and (*S*)-**225**) are accessible through enzyme-catalyzed epoxide-ring opening. With both enzymes (*R*)-**226** is obtained as a by-product.

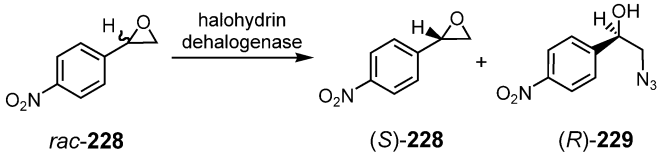
the epoxide-ring opening of (*R*)-**225** through the attack of a water molecule at the C-1 position to yield the diol (*R*)-**226** with retention of the stereochemistry. The *S* epoxide remains unconverted. In contrast, (*S*)-**225** is hydrolyzed with StEH to the same diol (*R*)-**226** through attack at the C-2 position and inversion of the stereochemistry, whereby (*R*)-**225** remains unconverted and can be isolated. Thus, Archelas and co-workers did not only develop a route to enantiomerically pure (*R*)- and (*S*)-*p*-chlorostyrene oxide, but also an enantioselective synthesis of (*R*)-**226**, a possible intermediate in the synthesis of the glutamate antagonist eliprodil, in 93% yield and with 94% *ee* starting from racemic **225**.[210]

At Merck an epoxide hydrolase from *Diplodia gossipina* has been used for the resolution of racemic indene oxide (**138**; Scheme 88). The enantiomer (1*S*,2*R*)-**138**, a precursor for HIV-protease inhibitors, is obtained in 14% yield and with 100% *ee*; indanediol (**227**) is also isolated (Scheme 88).[211]

Janssen and co-workers isolated (*S*)-*p*-nitrostyrene oxide ((*S*)-**228**; >99% *ee*) by selective azidolysis of (*R*)-**228** with a halohydrin dehalogenase from *Agrobacterium radiobacter* (Scheme 89). (*R*)-2-Azido-1-(*p*-nitrophenyl)ethanol ((*R*)-**229**) was obtained with 96% *ee*.[212]



Scheme 88.



Scheme 89. The selective azidolysis of *rac*-**228** leads to (*S*)-**228** and (*R*)-**229**.

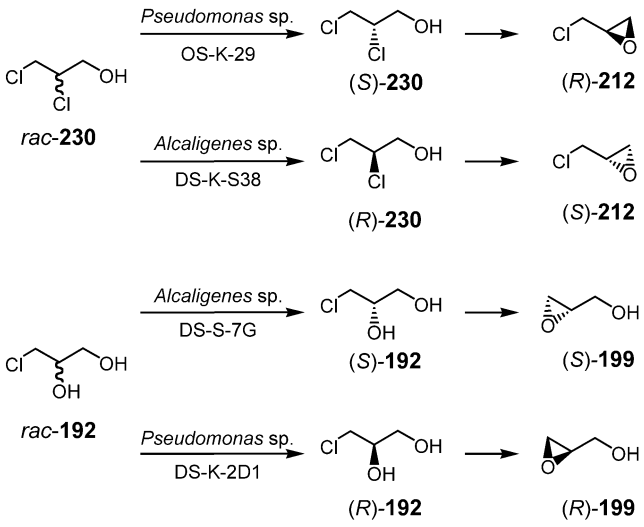
6.2.2. Microbial Methods for Racemate Resolution

In 1994 researchers at Daiso developed a process for the preparation of (*S*)-2,3-dichloro-1-propanol ((*S*)-**230**) by selective assimilation of (*R*)-**230** with *Pseudomonas* sp. (OS-K-29; Scheme 90).[213] The enantiomer (*R*)-**230** could be obtained by degradation of (*S*)-**230** with *Alcaligenes* sp. (DS-K-S38).[214] Under basic conditions (*R*)- and (*S*)-**230** are converted into optically active epichlorohydrin ((*S*)- and (*R*)-**212**, respectively). Under similar fermentation conditions 3-chloropropane-1,2-diol (**192**) can also be produced stereoselectively.[215] The enantiomers (*R*)- and (*S*)-**192** are converted into glycidol ((*R*)- and (*S*)-**199**, respectively).

6.2.3. Monooxygenases

Although monooxygenases of many microorganisms catalyze the stereoselective epoxidation of alkenes, their application is problematic for a number of reasons. First, the epoxides are frequently merely intermediates of a decomposition pathway and are not accumulated; second, the

 © 2004 Wiley-VCH Verlag GmbH & Co. KGaA, Weinheim



Scheme 90. Biotechnological preparation of enantiomerically pure epichlorohydrin ((*R*)- or (*S*)-**212**) and glycidol ((*S*)- or (*R*)-**199**) by fermentation (Daiso).

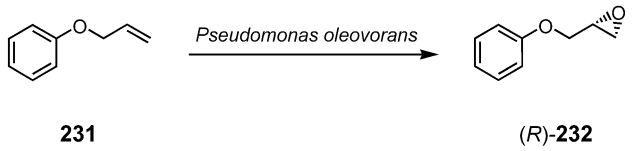
epoxides as alkylating agents act as toxins for the microorganisms, thus leading to product inhibition.

Nocardia corallina (Nippon Mining) can be used for the epoxidation of a broad spectrum of terminal and subterminal alkenes, such as styrenes (Table 3). Depending on the class of substrate three different procedures are used.[216] In the oxidation of short-chain, gaseous alkenes (C_3–C_5) the highly toxic epoxide is continuously expelled by using a fast gas flow. In this way propylene oxide can be obtained with 83% *ee* from propene in a space–time yield of 23 $g L^{-1} day^{-1}$. Epoxides of long-chain alkenes ($> C_{13}$) are less toxic and can be prepared with cells growing on glucose without product extraction. In the epoxidation of alkenes of medium chain length (C_6–C_{12}) and of styrenes the use of resting cells in the presence of a nontoxic organic phase (e.g. hexadecane) has proved effective.[217] The organic solvent lowers the concentration of the inhibitory epoxide in the aqueous phase and facilitates continuous product extraction.

Table 3: Epoxidations with *Nocardia* sp.

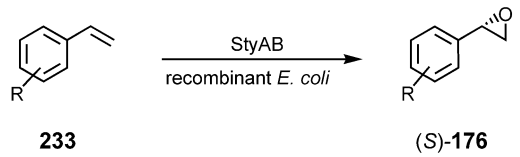
	Substrate	Configuration of the epoxide	*ee* [%]
C_3–C_5	1,2-propene	*R*	83
	3-chloropropene	*S*	81
C_6–C_{12}	1,2-heptene	*R*	94
	1,2-octene	*R*	91
	1,2-decene	*R*	86
	1,2-dodecene	*R*	87
	o-chlorostyrene	*R*	86
	m-chlorostyrene	*R*	82
	p-chlorostyrene	*R*	72
$> C_{13}$	1,2-tridecene	*R*	92
	1,2-pentadecene	*R*	81
	1,2-heptadecene	*R*	81

At Shell (*R*)-phenylglycidyl ether ((*R*)-**232**) was obtained by oxidation of 3-phenoxypropene (**231**) with suspended *Pseudomonas oleovorans* cells. This process provides (*R*)-**232**, an intermediate in the synthesis of β-adrenoreceptor blockers, with > 99.9% *ee* (Scheme 91).[218]



Scheme 91.

Styrene monooxygenases from styrene-degrading Pseudomonads were expressed in *E. coli* cells and used in the selective oxidation of styrene derivatives **233** to the corresponding *S* styrene oxides (*S*)-**176** (Scheme 92).[219] In the presence of an organic phase (dioctylphthalate) yields of 11 $g L^{-1}$ were observed.[220]

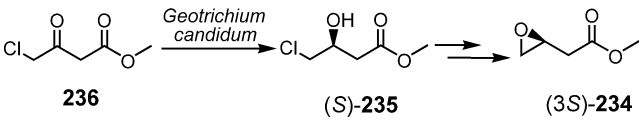


Scheme 92. Styrene monooxygenases oxidize **233** selectively to the *S* styrene oxides (*S*)-**176**.

6.2.4. Dehydrogenases

Access to chiral epoxides is also possible from enantiomerically pure α-halo alcohols (Scheme 70), which can be produced from the corresponding chloroketones by enantioselective reduction. The company Kaneka uses dehydrogenases in the form of whole cells for the production of *R* and *S* styrene oxides on a pilot-plant scale.

Bristol Meyers Squibb prepared methyl (3*S*)-3,4-epoxybutyrate (**234**) from the chlorohydrin (*S*)-**235**. The latter compound is available with 99% *ee* from the keto compound **236** on a multi-kg scale by enantioselective dehydrogenase reduction with whole cells from *Geotrichium candidum* (Scheme 93).[221]



Scheme 93.

7. Conclusions and Prospects

In comparing chemical processes with biotransformations no all-embracing judgment can be made with respect to

 © 2004 Wiley-VCH Verlag GmbH & Co. KGaA, Weinheim

economic efficiency and environmental impact. Advantages and disadvantages of individual methods must be assessed for specific cases. When the Sharpless epoxidation was compared with microbial epoxidation by life-cycle analysis (LCA), for example, neither process proved to be more environmentally friendly than the other.[222] The specific problems of chemical routes are often solvent emission or the toxicity of certain compounds, whereas with microbial procedures low yields relative to the biomass used or low product concentrations cause problems.

Chiral technologies are still developing very rapidly. For their successful implementation on an industrial scale a number of factors are important. Above all, highly versatile technologies are sought. Many chiral intermediates are produced in small quantities (10–100 t), and there are often competing manufacturers. Therefore, methods are desired that have a broad substrate spectrum, do not require specialist equipment, and enable cost-effective access to a comprehensive range of products.

In the case of biotechnological processes substrate concentration is often the deciding factor; in catalytic chemical methods the substrate/catalyst ratio is of critical importance. Today robot-assisted optimization helps us to meet these goals in the shortest possible time.

Catalytic technologies will be the way of the future. Auxiliary-based methods are loosing ground because the quantities of material required in each cycle are too large. Classical racemate resolution still has its place in the rapid provision of enantiomerically pure building blocks. Although dynamic kinetic resolution is still in an early phase of development, it clearly has considerable potential.

However, there will always be scope for a variety of technologies. Which technology is ultimately implemented in a production process often also depends on the general conditions, such as the availability of precursors and equipment, in the individual companies.

We thank Dr. Gisela Hieber for her support in procuring market information. Our special thanks go to Tanja Jenak, through whose enthusiastic involvement this Review first took shape.

Received: March 28, 2003 [A599]

[1] A. Friedrich, G. Antranikian, *Appl. Environ. Microbiol.* **1996**, *62*, 2875.
[2] S. Riessen, G. Antranikian, *Extremophiles* **2001**, *5*, 399.
[3] T. Maier, C. Winterhalter (Consortium für Electrochemische Industrie GmbH), WO 01/27307, **2001** [*Chem. Abstr.* **2000**, *133*, 361976].
[4] G. C. Barrett in *Chemistry and Biochemistry of the Amino Acids*, Chapman and Hall, New York, **1985**, p. 251, 261.
[5] L. Yet, *Angew. Chem.* **2001**, *113*, 900; *Angew. Chem. Int. Ed.* **2001**, *40*, 875.
[6] a) A. Strecker, *Justus Liebigs Ann. Chem.* **1850**, *75*, 27; b) H. T. Bucherer, H. T. Fischbeck, *J. Prakt. Chem.* **1934**, *140*, 69; c) H. T. Bucherer, W. Steiner, *J. Prakt. Chem.* **1934**, *140*, 291; d) H. Bergs, Deutsches Reichspatent No. 566094, **1929**.
[7] M. Beller, M. Eckert, *Angew. Chem.* **2000**, *112*, 1026; *Angew. Chem. Int. Ed.* **2000**, *39*, 1010.
[8] H. Wagner, H. Tanner, E. Liebetanz, S. P. Mannsfeld, A. Pfeiffer (Degussa AG), DE 1906405, **1969** [*Chem. Abstr.* **1971**, *74*, 64392].
[9] W. Liebl, M. Ehrmann, W. Ludwig, K. H. Schleifer, *Int. J. Syst. Bacteriol.* **1991**, *41*, 255.
[10] H. Sahm, L. Eggeling in *Encyclopedia of Microbiology* (Ed.: J. Lederberg), Academic Press, San Diego, CA, **2000**, p. 152.
[11] M. Kikuchi, Y. Nakao in *Biotechnology of Amino Acid Production* (Ed.: K. Aida, I. Chibata, K. Nakayama, K. Takinami, H. Yamada), Elsevier, Amsterdam, **1986**, p. 101.
[12] R. Krämer, *BioEngineering* **1993**, *9*, 51.
[13] S. Isamu, Y. Toride, A. Yokota, S. Sugimoto, K. Kawamura (Ajinomoto Co., Inc.), FR 2626286, **1990** [*Chem. Abstr.* **1989**, *113*, 38946].
[14] M. Masuda, S. Takamatu, N. Nishimura, S. Komatsubara, T. Tosa, *Appl. Biochem. Biotechnol.* **1992**, *37*, 255.
[15] K. Okamoto, K. Kino, M. Ikeda, *Biosci. Biotechnol. Biochem.* **1997**, *61*, 1877.
[16] W. Leuchtenberger in *Biotechnology* (Eds.: H.-J. Rehm, G. Reed), VCH, Weinheim, **1996**, p. 465.
[17] H. Kumagai, *Adv. Biochem. Eng./Biotechnol.* **2000**, *69*, 71.
[18] S. Yamada, K. Nabe, N. Izuo, *Appl. Environ. Microbiol.* **1981**, *42*, 773.
[19] I. Chibata, T. Tosa, S. Takamatsu, *Microbiol. Sci.* **1984**, *1*, 58.
[20] A. Liese, K. Seelbach, A. Buchholz, J. Haberland in *Industrial Biotransformations* (Eds.: A. Liese, K. Seelbach, C. Wandrey), Wiley-VCH, Weinheim, **2000**, p. 334.
[21] M. Furui, K. Yamashita, *J. Ferment. Technol.* **1983**, *61*, 587.
[22] E. L. Smith, B. M. Austen, K. M. Blumenthal, J. F. Nyc in *The Enzymes*, *Vol. XI* (Ed.: P. D. Boyer), Academic Press, **1975**, p. 293.
[23] R. Wichmann, C. Wandrey, A. F. Buckmann, M. R. Kula, *Biotechnol. Bioeng.* **2000**, *67*, 791.
[24] A. S. Bommarius, M. Schwarm, M. Stingl, K. Kotterhahn, K. Huthmacher, K. Drauz, *Tetrahedron: Asymmetry* **1995**, *6*, 2851.
[25] I. G. Fotheringham in *Biotechnology* (Ed.: D. Kelly), Wiley-VCH, Weinheim, **2000**, p. 313.
[26] a) H. Agematu, *ChiraSource Nov.* **2001**, Philadelphia; b) T. Fujii, T. Narita, H. Agematu, N. Agata, K. Isshiki, *J. Biochem.* **2000**, *128*, 975; c) T. Fujii, T. Narita, H. Agematu, N. Agata, K. Isshiki, *J. Biochem.* **2000**, *128*, 391.
[27] I. G. Fotheringham, P. P. Taylor, J. L. Ton (Monsanto Co.), US 5728555, **1998** [*Chem. Abstr.* **1999**, *128*, 216437].
[28] W. Liu, S. Laneman, D. J. Ager, P. P. Taylor (Great Lakes Chemical Corp.), WO 01/62948A2, **2001** [*Chem. Abstr.* **2001**, *135*, 209968].
[29] C. Syldatk, M. Pietzsch in *Enzyme Catalysis in Organic Synthesis* (Ed.: K. Drauz, H. Waldmann), VCH, Weinheim, **1995**, p. 409.
[30] M. A. Wegman, M. H. A. Janssen, F. van Rantwijk, R. A. Sheldon, *Adv. Synth. Catal.* **2001**, *343*, 559.
[31] O. May, P. T. Nguyen, F. H. Arnold, *Nat. Biotechnol.* **2000**, *18*, 317.
[32] O. May, personal communication.
[33] K. Sano, K. Mitsugi, *Agric. Biol. Chem.* **1978**, *42*, 2315.
[34] A. S. Bommarius, M. Schwarm, K. Drauz, *Chimia* **2001**, *55*, 50.
[35] H. E. Schoemaker, W. H. J. Boesten, Q. B. Broxterman, E. C. Roos, B. Kaptein, W. J. J. Van Den Tweel, J. Kamphuis, E. M. Meijer, F. P. J. T. Rutjes, *Chimia* **1997**, *51*, 308.
[36] M. Petersen, M. Sauter, *Chimia* **1999**, *53*, 608.
[37] H. Momose, T. Tagaki, *Agric. Biol. Chem.* **1978**, *42*, 1911.
[38] E. R. Börmann, B. J. Eikmanns, H. Sahm, *Mol. Microbiol.* **1992**, *6*, 317.
[39] H. Holms, *FEMS Microbiol. Rev.* **1996**, *19*, 85.
[40] M. Pompejus, B. Kröger, H. Schröder, O. Zelder, G. Haberhauer (BASF AG), WO 01/00844, **2001** [*Chem. Abstr.* **2001**, *134*, 67211].

 © 2004 Wiley-VCH Verlag GmbH & Co. KGaA, Weinheim

[41] S. Nakagawa, H. Mizoguchi, S. Ando, M. Hayashi, K. Ochiai, H. Yokoi, N. Tateishi, A. Senoh, M. Ikeda, A. Ozaki (Kyowa Hakko Kogyo Co. Ltd.), EP 1108790, **2001** [*Chem. Abstr.* **2001**, *135*, 283981].
[42] D. E. Robertson, E. J. Mathur, R. V. Swanson, B. L. Marrs, J. M. Short, *SIM news* **1996**, *46*, 3.
[43] R. I. Amann, W. Ludwig, K. H. Schleifer, *Microbiol. Rev.* **1995**, *59*, 143.
[44] a) I. P. Petrounia, F. H. Arnold, *Curr. Opin. Biotechnol.* **2000**, *11*, 325; b) K. A. Powell, S. W. Ramer, S. B. del Cardayre, W. P. C. Stemmer, M. B. Tobin, P. F. Longchamp, G. W. Huisman, *Angew. Chem.* **2001**, *113*, 4068; *Angew. Chem. Int. Ed.* **2001**, *40*, 3948; c) F. H. Arnold, *Nature* **2001**, *409*, 253.
[45] J. E. Ness, S. B. del Cardayre, J. Minshull, W. P. Stemmer, *Adv. Protein Chem.* **2000**, *55*, 261.
[46] a) C. Thomas, U. Ohnmacht, K. Zahn, K. Mohr, P, Gmeiner, *Pharmazie* **1999**, *54*, 248; b) F. Rahm, R. Stranne, U. Bremberg, K. Nordstrom, M. Cernerud, E. Macedo, C. Moberg, *J. Chem. Soc. Perkin Trans. 1* **2000**, 1983; c) A. Goti, S. Cicchi, F. M. Cordero, V. Fedi, A. Brandi, *Mol. Online* **1999**, *4*, 1; d) W. G. Liu in *Handbook of Chiral Chemicals* (Ed.: D. J. Ager), Marcel Dekker, New York, **1999**, p. 83; e) D. J. Ager, D. R. Allen, M. B. East I. G. Fotheringham, S. A. Laneman, W. G. Liu, D. P. Pantaleone, D. R. Schaad, P. P. Taylor in *Handbook of Chiral Chemicals* (Ed.: D. J. Ager), Marcel Dekker, New York, **1999**, p. 301.
[47] G. Amari, M. Del Canale, R. Razzetti, P. A. Monici Preti, I. Rondelli (Chiesi Farmaceutici S.p.A.), WO 01/085668, **2001** [*Chem. Abstr.* **2001**, *135*, 357780].
[48] H. Brunner, M. Muschiol, T. Wischert, J. Wiehl, *Tetrahedron: Asymmetry* **1990**, *1*, 159.
[49] H. G. J. De Wilt, *Ind. Eng. Chem. Prod. Res. Dev.* **1972**, *11*, 370.
[50] R. L. Whistler, R. Schweiger, *J. Am. Chem. Soc.* **1959**, *81*, 5190.
[51] A. J. Vroemen, M. Beverini (Gist Brocades B.V.), WO 96/35800, **1996** [*Chem. Abstr.* **1997**, *126*, 130654].
[52] C. H. H. Emons, B. F. M. Kuster, J. A. J. M. Vekemans, R. A. Sheldon, *Proc. Chiral 92 Symp.*, Spring Innovations, Stockport, UK, **1992**, p. 39.
[53] S. Furuyoshi, N. Kawabata, H. Tanaka, K. Soda, *Agric. Biol. Chem.* **1989**, *53*, 2101.
[54] T. Kato, T. Ozaki, K. Tsuzuki, N. Ohi, *Org. Process Res. Dev.* **2001**, *5*, 122.
[55] H. Hasegawa, T. Wataya, Y. Miura, N. Kou (Daito Kagaku KK), JP 2000-178253, **2000** [*Chem. Abstr.* **2000**, *133*, 43448].
[56] Y. N. Belokon, B. Green, N. S. Ikonnikov, V. S. Larichev, B. V. Lokshin, M. A. Moscalenko, M. North, C. Orizu, A. S. Peregudov, G. I. Timofeeva, *J. Org. Chem.* **2000**, *65*, 2655.
[57] a) Y. N. Belokon, S. Caveda-Cepas, B. Green, N. S. Ikonnikov, V. N. Krustalev, V. S. Larichev, M. A. Moscalenko, M. North, C. Orizu, V. I. Tararov, M. Tasinazzo, G. I. Timofeeva, L. V. Yashkina, *J. Am. Chem. Soc.* **1999**, *121* 3968; b) Y. N. Belokon, B. Green, N. S. Ikonnikov, M. North, T. Parsons, V. I. Tararov, *Tetrahedron* **2001** *57*, 771; c) Y. N. Belokon, M. North, T. Parsons, *Org. Lett.* **2000**, *2*, 1617.
[58] Y. N. Belokon, B. Green, N. S. Ikonnikov, M. North, V. I. Tararov, *Tetrahedron Lett.* **1999**, *40*, 8147.
[59] J. Blacker, *ChiraSource Nov.* **2001**, Philadelphia.
[60] A. Kiener (Lonza AG), EP 442430, **1991** [*Chem. Abstr.* **1992**, *116*, 57572].
[61] A. Kiener, *Angew. Chem.* **1992**, *104*, 748; *Angew. Chem. Int. Ed. Engl.* **1992**, *31*, 774.
[62] T. Zimmermann, J. Werlen (Lonza AG), WO 95/10613, **1995** [*Chem. Abstr.* **1995**, *123*, 135109].
[63] T. Ohashi, *Proc Chiral 90 Symp.*, Spring Innovations, Stockport, UK, **1990**, p. 65.
[64] I. Takata, K. Yamamoto, T. Tosa, I. Chibata, *Enzyme Microb. Technol.* **1980**, *2*, 30.
[65] F. Schindler (Hüls AG), EP 175007, **1983** [*Chem. Abstr.* **1985**, *102*, 4464].
[66] a) F. Effenberger, *Angew. Chem.* **1994**, *106*, 1609; *Angew. Chem. Int. Ed. Engl.* **1994**, *33*, 1555; b) F. Effenberger, *Enantiomer* **1996**, *1*, 359; c) F. Effenberger, *Chimia* **1999**, *53*, 3; d) F. Effenberger in *Stereoselective Biocatalysis* (Ed.: R. N. Patel), Marcel Dekker, New York, **2000**, p. 321; e) F. Effenberger, S. Forster, H. Wajant, *Curr. Opin. Biotechnol.* **2000**, *11*, 532; f) D. V. Johnson, H. Griengl, *Chim. Oggi* **1997**, *9/10*, 9; g) H. Griengl, A. Hickel, D. V. Johnson, C. Kratky, M. Schmidt, H. Schwab, *Chem. Commun.* **1997**, 1933; h) M. Schmidt, H. Griengl in *Biocatalysis—From Discovery to Application* (Ed.: W. D. Fessner) Springer, **1998**, p. 193; i) D. V. Johnson, A. A. Zabelinskaja-Mackova, H. Griengl, *Curr. Opin. Chem. Biol.* **2000**, *4*, 103; j) H. Griengl, H. Schwab, M. Fechter, *Opht. Gen.* **2000**, *18*, 252.
[67] H. Gröger, *Adv. Synth. Catal.* **2001**, *343*, 547.
[68] A. Bousquet, A. Musolino (Sanofi-Synthelabo), EP 1021449, **1998** [*Chem. Abstr.* **1999**, *130*, 296510].
[69] a) P. Pöchlauer, H. Mayrhofer (DSM Fine Chemicals Austria), EP 1148042, **2001** [*Chem. Abstr.* **2001**, *135*, 303603]; b) N. Okuda, H. Semba, Y. Dobashi (Nippon Shokubai), EP 1160235, **2001** [*Chem. Abstr.* **2002**, *136*, 5721]; c) H. Semba, Y. Dobashi (Nippon Shokubai), EP 1160329, **2001** [*Chem. Abstr.* **2002**, *136*, 4802]; d) H. Bühler, Dissertation, Universität Stuttgart, **2000**; e) Clartext 3/2001 (Clariant), C. Hanisch, *Von händigen Molekülen und ihren Spiegelbildern*, Clartext 3-2001 (Clariant), zu finden unter http://www.clariant.de/e2wportal/de/internet.nsf/directframe/CTX_Startpage, **2001**.
[70] See also: H. Griengl, N. Klempier, P. Pöchlauer, M. Schmidt, N. Y. Shi, A. A. Zabelinskaja-Mackova, *Tetrahedron* **1998**, *54*, 14477.
[71] a) Chemie Linz GmbH, DE 19529116, **1997** [*Chem. Abstr.* **1997**, *126*, 208953]; b) H. Semba (Nippon Shokubai), EP 1016712, **2000** [*Chem. Abstr.* **2000**, *133*, 85120]; c) F. Effenberger, H. Wajant, P. Lauble, S. Förster, H. Bühler, H. Schwab, C. Kratky, U. Wagner, E. Steiner (DSM Fine Chemicals Austria), EP 969095, **2000** [*Chem. Abstr.* **2000**, *132*, 191223].
[72] a) M. Hasslacher, M. Schall, H. Schwab, E. Hayn, S. Kohlwein, H. Griengl (DSM Chemie Linz), WO 97/03204, **1997** [*Chem. Abstr.* **2000**, *126*, 196118]; b) H. Semba (Nippon Shokubai), EP 1026256, **2000** [*Chem. Abstr.* **2000**, *133*, 134248]; c) P. Pöchlauer, M. Schmidt, I. Wirth, R. Neuhofer, A. A. Zabelinskaja-Mackova, H. Griengl, C. van den Broek, R. W. E. G. Reintjens, H. J. Wories (DSM Fine Chemicals Austria), EP 927766, **1999** [*Chem. Abstr.* **2000**, *131*, 72766].
[73] a) V. H. M. Elferink, J. G. T. Kierkels, M. Kloosterman, J. H. Roskam (Stamicarbon B.V.), EP 369553, **2000** [*Chem. Abstr.* **2000**, *114*, 41029]; b) J. Kamphuis, H. E. Schoemaker, W. H. J. Boesten, T. Sonke, H. Moody, B. Kaptein, W. J. J. Van den Tweel, *Meded. Fac. Landbouwwet. Univ. Gent* **1992**, *57*, 1731; c) J. Kamphuis, W. J. J. Van den Tweel, Q. B. Broxtermann, B. Kaptein, T. Sonke, W. H. J. Boesten, H. E. Schoemaker, 205th ACS National Meeting, Denver, **1993**.
[74] a) M. Kataoka, K. Shimizu, K. Sakamoto, H. Yamada, S. Shimizu, *Appl. Microbiol. Biotechnol.* **1995**, *43*, 974; b) S. Shimizu, M. Kataoka, K. Shimizu, M. Hirakata, K. Sakamoto, H. Yamada, *Eur. J. Biochem.* **1992**, *209*, 383; c) S. Shimizu, M. Kataoka, *Ann. N. Y. Acad. Sci.* **1996**, *799*, 650.
[75] a) K. Sakamoto, H. Yamada, S. Shimizu (Fuji Chemicals Industrial Co.), EP 436730, **1991** [*Chem. Abstr.* **1991**, *115*, 27689]; b) K. Sakamoto, H. Yamada, S. Shimizu (Fuji Yakuhin Kogyo K.K.), EP 504421, **1992** [*Chem. Abstr.* **1992**, *117*, 110119].
[76] S. C. Taylor in *Biocatalysis* (Ed.: D. A. Abramowicz), Van Nostrand Reinhold, New York, **1990**, p. 157, and references

therein; R. A. Sheldon, *Chirotechnology*, 1st ed., Marcel Dekker, New York, **1993**, p. 130.

[77] a) A. W. Bunch in *Biotransformations* (Ed.: D. R. Kelly), BLDSC, Shelfmark, **1998**, p. 277; b) T. Sugai, T. Yamazaki, M. Yokoyama, H. Ohta, *Biosci. Biotechnol. Biochem.* **1997**, *61*, 1419; c) D. Cowan, R. Cramp, R. Pereira, D. Graham, Q. Almatawah, *Extremophiles* **1998**, *2*, 207; d) M. Wieser, T. Nagasawa in *Stereoselective Biocatalysis* (Ed.: R. N. Patel), Marcel Dekker, New York, **2000**, p. 461.

[78] a) M. Ress-Löschke, T. Friedrich, B. Hauer, R. Mattes, D. Engels (BASF AG), DE 19848129, **2000** [*Chem. Abstr.* **2000**, *132*, 292813]; b) Y. Yamaguchi, M. Ushigome, T. Kato (Nitto Chem. Ind.), EP 773297, **1997** [*Chem. Abstr.* **1997**, *127*, 4190]; c) T. Endo, K. Tamura (Nitto Chem. Ind.), EP 449648, **1991** [*Chem. Abstr.* **1992**, *116*, 5338].

[79] T. Endo, K. Tamura (Nitto Chem. Ind.), EP 527553, **1993** [*Chem. Abstr.* **1993**, *118*, 167640].

[80] M. Kobayashi, S. Shimizu, *Curr. Opin. Chem. Biol.* **2000**, *4*, 95.

[81] L. Martíková, A. Stolz, H.-J. Knackmuss, *Biotechnol. Lett.* **1996**, *18*, 402.

[82] M. S. Payne, S. Wu, R. D. Fallon, G. Tudor, B. Stieglitz, I. M. Turner, M. J. Nelson, *Biochemistry* **1997**, *36*, 5447.

[83] R. D. Fallon, B. Stieglitz, I. Turner, *Appl. Microbiol. Biotechnol.* **1997**, *47*, 156.

[84] H. Yamada, M. Kobayashi, *Biosci. Biotechnol. Biochem.* **1996**, *60*, 1391.

[85] R. Di Cosimo, R. D. Fallon, J. E. Gavagan, F. E. Herkes (E. I. Du Pont), WO 97/44318, **1997** [*Chem. Abstr.* **1998**, *128*, 89231].

[86] a) A. Kiener, J.-P. Roduit, J. Kohr, N. Shaw (Lonza AG), EP 686698, **1995** [*Chem. Abstr.* **1996**, *124*, 115569]; b) M. Wieser, T. Nagasawa in *Stereoselective Biocatalysis* (Ed.: R. N. Patel), Marcel Dekker, New York, **2000**, p. 461.

[87] T. Reichstein, A. Grossner, *Helv. Chim. Acta* **1934**, *17*, 311.

[88] R. D. Hancock, R. Viola, *Appl. Microbiol. Biotechnol.* **2001**, *56*, 567.

[89] a) T. Moriya, Y. Hikichi, Y. Moriya, T. Yamaguchi (Takeda Chemical Ind.), WO 97/10340, **1997** [*Chem. Abstr.* **1997**, *126*, 263217]; b) Y. Hikichi, T. Moriya, I. Nogami, H. Miki, T. Yamaguchi (Takeda Chemical Ind.), EP 590857, **1994** [*Chem. Abstr.* **1994**, *121*, 55989].

[90] a) F. Elischewski, J. Kalinowski, A. Pühler, N. Dusch, J. Dohmen, M. Farwick, G. Thierbach (Degussa-Hüls AG), EP 1001027A2, **2000** [*Chem. Abstr.* **2000**, *132*, 278241]; b) N. Dusch, J. Kalinowski, A. Pühler (Degussa-Hüls AG), EP 1006192A2, **2000** [*Chem. Abstr.* **2000**, *133*, 29682]; c) M. Rieping, G. Thierbach, W. Pfefferle, N. Dusch, J. Kalinowski, A. Pühler (Degussa-Hüls AG), EP 1006193A2, **2000** [*Chem. Abstr.* **2000**, *133*, 29683]; d) N. Dusch, A. Pühler, J. Kalinowski, *Appl. Environ. Microbiol.* **1999**, *65*, 1530; e) F. Elischewski, A. Pühler, J. Kalinowski, *J. Biotechnol.* **1999**, *75*, 135.

[91] a) L. Eggeling, G. Thierbach, H. Sahm (Degussa-Hüls AG), EP 1006189A2, **2000** [*Chem. Abstr.* **2000**, *133*, 29681]; b) H. Sahm, L. Eggeling, *Appl. Environ. Microbiol.* **1999**, *65*, 1973.

[92] M. Binder, K.-E. Uffmann, I. Walger, U. Becker, W. Pfefferle, H. Friedrich (Degussa AG), DE 10016321, **2000** [*Chem. Abstr.* **2000**, *135*, 357110].

[93] J. Jacques, A. Collett, S. Wilen, *Enantiomers, Racemates, and Resolutions*, Wiley-Interscience, New York, **1980**.

[94] A. W. Ingersoll, *Org. Synth. Coll. Vol. II* **1950**, 506.

[95] A. Ault, *Org. Synth. Coll. Vol. V* **1973**, 932.

[96] a) W. Bryker, L. A. Avila (Hexcel Corp.), US 4983771, **1989** [*Chem. Abstr.* **1991**, *114*, 206739]; b) Yamakawa Yakuhin Ko, JP 56026848, **1979** [*Chem. Abstr.* **1981**, *95*, 115012].

[97] H. Hirotoshi (Sumitomo Chem. Co.), JP 11106368, **1997** [*Chem. Abstr.* **1999**, *130*, 311605]

[98] K. Hagiya, E. Harada, F. Goto (Sumitomo Chemical Co.), EP 0735018, **1994** [*Chem. Abstr.* **1996**, *125*, 167547].

[99] a) M. Littmann, A. Günther, U. Kraatz (Bayer AG), DE 19619445, **1996** [*Chem. Abstr.* **1997**, *127*, 293000]; b) E. Brown, F. Viot, *Tetrahedron Lett.* **1985**, *26*, 4451.

[100] W. Merz, M. Littmann, U. Kraatz, C. Mannheims (Bayer AG), DE 19624820, **1996** [*Chem. Abstr.* **1998**, *128*, 88664]; M. Littmann, A. Günther, U. Kraatz (Bayer AG), DE 19650081, **1996** [*Chem. Abstr.* **1998**, *128*, 22711]; U. Kraatz, M. Littmann, *Pflanzenschutz-Nachr. Bayer (Engl. Ed.)* **1998**, *51*, 203.

[101] E. Brown, M. Moudachirou, *Tetrahedron* **1994**, *50*, 10309.

[102] a) T. Vries, H. Wynberg, E. van Echten, J. Koek, W. ten Hoeve, R. M. Kellogg, Q. B. Broxterman, A. Minnaard, B. Kaptein, S. van der Sluis, L. Hulshof, J. Kooistra, *Angew. Chem.* **1998**, *110*, 2491; *Angew. Chem. Int. Ed.* **1998**, *37*, 2349; b) Q. B. Broxterman, E. van Echten, L. A. Hulshof, B. Kaptein, R. M. Kellog, A. J. Minaard, T. R. Vries, H. Wynberg, *Chim. Oggi* **1998**, *16*, 34.

[103] A. Johansson, *Contemp. Org. Synth.* **1995**, *2*, 393; H.-U. Blaser, F. Spindler, *Chim. Oggi* **1995**, *13*, 11.

[104] M. J. Burk, *J. Am. Chem. Soc.* **1991**, *113*, 8518; M. J. Burk, J. E. Feaster, *J. Am. Chem. Soc.* **1992**, *114*, 6266; M. J. Burk, J. P. Martinez, J. E. Feaster, N. Cosford, *Tetrahedron* **1994**, *50*, 4399.

[105] a) C. Lensink, J. G. de Vries, *Tetrahedron: Asymmetry* **1992**, *3*, 325; b) C. Lensink, J. G. de Vries, *Tetrahedron: Asymmetry* **1993**, *4*, 215; c) H.-Y. Li, L. Anzalone, R. E. Waltermire (DuPont Pharmaceutical Company), US 5932749, **1997** [*Chem. Abstr.* **1999**, *131*, 144591]; d) L. Storace, L. Anzalone, P. N. Confalone, W. P. Davis, J. M. Fortunak, M. Giangiordano, J. J. Haley, Jr., K. Kamholz, H.-Y. Li, P. Ma, W. A. Nugent, R. L. Parsons, Jr., P. J. Sheeran, C. E. Silverman, R. E. Waltermire, C. C. Wood, *Org. Process Res. Dev.* **2002**, *6*, 54; e) H.-Y. Li, L. Anzalone, R. E. Waltermire (DuPont Pharmaceutical Company), WO 9734887, **1996** [*Chem. Abstr.* **1997**, *127*, 318949].

[106] M. J. Burk, G. Casy, N. B. Johnson, *J. Org. Chem.* **1998**, *63*, 6084; N. B. Johnson, G. Casy, M. J. Burk (Chirotech Techn. Ltd.), WO 9918065, **1997** [*Chem. Abstr.* **1999**, *130*, 281579].

[107] F. Spindler, H.-U. Blaser, *Adv. Synth. Catal.* **2001**, *343*, 68.

[108] a) A. J. Blacker, L. Campbell (Avecia Ltd.), WO 00/18708, **2000** [*Chem. Abstr.* **2000**, *132*, 265099]; b) L. A. Campbell, Avecia Ltd., personal communication.

[109] B. Krzyzanowska, W. J. Stec, *Synthesis* **1982**, 270; B. Krzyzanowska, W. J. Stec, *Synthesis* **1978**, 521.

[110] A. Togni, C. Breutel, A. Schnyder, F. Spindler, H. Landert, A. Tijani, *J. Am. Chem. Soc.* **1994**, *116*, 4061.

[111] a) D. I. Sterling, A. L. Zeitlin, G. W. Matcham (Celgene Corp.), US 4950606, **1989** [*Chem. Abstr.* **1991**, *114*, 41055]; b) G. W. Matcham, J. D. Rozzell, D. I. Sterling, A. L. Zeitlin, (Celgene Corp.), US 5169780, **1990** [*Chem. Abstr.* **1993**, *118*, 190144]; c) G. W. Matcham, D. I. Sterling, A. L. Zeitlin, (Celgene Corp.), US 5300437, **1992** [*Chem. Abstr.* **1994**, *121*, 132394]; d) G. W. Matcham, A. R. S. Bowen, *Chim. Oggi* **1996**, *14*, 20; e) D. I. Sterling in *Chirality in Industry* (Eds.: A. N. Collins, G. N. Sheldrake, J. Crosby), Wiley, Chichester, **1992**, p. 209.

[112] G. T. Phillips, J. H. Shears (Shell Internationale Research Maatschappij B.V.), EP 399589, **1989** [*Chem. Abstr.* **1991**, *115*, 69951].

[113] H. Smidt, A. Fischer, P. Fischer, R. D. Schmidt, U. Stelzer (Bayer AG), EP 812363, **1995** [*Chem. Abstr.* **1996**, *125*, 219744].

[114] S. Arai, S. Bellemin-Laponnaz, G. C. Fu, *Angew. Chem.* **2001**, *113*, 240; *Angew. Chem. Int. Ed.* **2001**, *40*, 234.

[115] a) H. Kitaguchi, P. A. Fitzpatrick, J. E. Huber, A. M. Klibanov, *J. Am. Chem. Soc.* **1989**, *111*, 3094; b) A. L. Gutman, *Spec. Chem.* **1996**, *16*, 242; c) A. L. Gutman, E. Meyer, E. Kalerin, F. Polyak, J. Sterling, *Biotechnol. Bioeng.* **1992**, *40*, 760.

[116] a) F. Balkenhohl, K. Ditrich, B. Hauer, W. Ladner, *J. Prakt. Chem.* **1997**, *339*, 381; b) F. Balkenhohl, B. Hauer, W. Ladner,

 © 2004 Wiley-VCH Verlag GmbH & Co. KGaA, Weinheim

U. Pressler (BASF AG), DE 4332738, **1993** [*Chem. Abstr.* **1995**, *122*, 289035]; c) K. Ditrich, F. Balkenhohl, W. Ladner (BASF AG), DE 19534208, **1995** [*Chem. Abstr.* **1997**, 126, 277259].

[117] F. Rebolledo, V. Gotor, *Tetrahedron* **1993**, *49*, 4007.

[118] a) M. T. Reetz, C. Dreisbach, *Chimia* **1994**, *48*, 570; b) M. T. Reetz, K. Schimossek, *Chimia* **1996**, *50*, 668; c) C. Dreisbach, U. Stelzer (Bayer AG), WO 97/28271, **1996** [*Chem. Abstr.* **1997**, *127*, 160678]; d) C. D. Reeve (Zeneca Ltd.), WO 9931264, **1998** [*Chem. Abstr.* **1999**, *131*, 43668]; e) L. E. Iglesias, V. M. Sanchez, F. Rebolledo, V. Gotor, *Tetrahedron: Asymmetry* **1997**, *8*, 2675; f) F. Messina, M. Botta, F. Corelli, M. P. Schneider, *J. Org. Chem.* **1999**, *64*, 3767.

[119] a) M. Soledad de Castro, J. V. Sinisterra Gago, *Tetrahedron* **1998**, *54*, 2877; b) N. Öhrner, C. Orrenius, A. Mattson, T. Norin, K. Hult, *Enzyme Microb. Technol.* **1996**, *19*, 328.

[120] D. T. Chapman, D. H. G. Crout, M. Mahmoudian, D. I. C. Scopes, P. W. Smith, *Chem. Commun.* **1996**, 2415.

[121] a) U. Stelzer (Bayer AG), DE 19621686, **1996** [*Chem. Abstr.* **1998**, *128*, 60789]; b) A. Maestro, C. Astorga, V. Gotor, *Tetrahedron: Asymmetry* **1997**, *8*, 3153.

[122] S. Takayama, S. T. Lee, S.-C. Hung, C.-H. Wong, *Chem. Commun.* **1999**, 127.

[123] S. Conde, P. Lopez-Serrano, A. Martinez, *J. Mol. Catal. B* **1999**, *5*, 299.

[124] L. M. van Langen, N. H. P. Oosthoek, D. T. Guranda, F. van Rantwijk, V. K. Svedas, R. A. Sheldon, *Tetrahedron: Asymmetry* **2000**, *11*, 4593.

[125] K. Ditrich, W. Ladner, J.-P. Melder (BASF AG), DE 19913256, **1999** [*Chem. Abstr.* **2000**, *133*, 252151].

[126] a) H. Riechers, J. Simon, A. Höhn, A. Kramer, F. Funke, W. Siegel, C. Nübling (BASF AG), WO 2000047546, **1999** [*Chem. Abstr.* **2000**, *133*, 163769]; b) H. Riechers, J. Simon, A. Höhn, A. Kramer, F. Funke, W. Siegel, C. Nübling (BASF AG), US 6049007, **1999** [*Chem. Abstr.* **2000**, *132*, 236800]; c) H. Riechers, J. Simon, A. Höhn, A. Kramer, F. Funke, W. Siegel, C. Nübling (BASF AG), DE 19852282, **1998** [*Chem. Abstr.* **2000**, *132*, 308056]; d) K. Ditrich (BASF AG), DE 19606124, **1996** [*Chem. Abstr.* **1997**, *127*, 234169].

[127] K. Ditrich, U. Block (BASF AG), WO 2000046177, **1999** [*Chem. Abstr.* **2000**, *133*, 165414].

[128] J. Crosby in *Chirality in Industry* (Eds.: A. N. Collins, G. N. Sheldrake, J. Crosby), Wiley, Chichester, **1992**, p. 1.

[129] a) R. S. Samant, S. B. Chandalla, *Ind. Eng. Chem. Process Des. Dev.* **1985**, *24*, 426; b) R. A. Sheldon, *Chirotechnology: Industrial Synthesis of Optically Active Compounds*, Marcel Dekker, New York, **1993**, p. 173.

[130] I. S. Sigal, J. R. Huff, P. L. Darke, J. P. Vacca, S. D. Young, S. J. Desolms, W. J. Thompson, T. A. Lyle, S. L. Graham, A. K. Ghosh (Merck & Co., Inc., USA), EP 337714, **1988** [*Chem. Abstr.* **1990**, *112*, 199132].

[131] a) J. F. Larrow, E. Roberts, T. R. Verhoeven, K. M. Ryan, C. H. Sennayake, P. J. Reider, E. N. Jacobsen, *Org. Synth.* **1999**, *76*, 46; b) C. H. Sennayake, R. F. Edward, L. M. DiMichele, K. M. Ryan, J. Liu, L. E. Fredenburgh, B. S. Foster, A. W. Douglas, R. D. Larson, *Tetrahedron Lett.* **1995**, *36*, 3993; c) H. Kajiro, S. Mitamura, A. Mori, T. Hiyama, *Bull. Chem. Soc. Jpn.* **1999**, *72*, 1093.

[132] a) M. Takahashi, K. Ogasawara, *Synthesis* **1996**, 954; b) M. M. Chartrain, C. H. Sennayake, J. P. N. Rosazza, J. Zhang (Merck & Co., Inc., USA), WO 9612818, **1994** [*Chem. Abstr.* **1996**, *125*, 56385]; c) A. K. Ghosh, J. F. Kincaid, M. G. Haske, *Synthesis* **1997**, 541; d) K. Kuniro (Chisso Corp., Japan), JP 08332095, **1995** [*Chem. Abstr.* **1997**, *126*, 156476]; e) B. C. Buckland, M. M. Chartrain, N. C. Connors, F. P. Gailliot, R. L. Greasham, C. Lee, R. C. Olewinski, P. J. Reider, F. E. Roberts, C. H. Senanayake, T. R. Verhoeven (Merck & Co., Inc.; USA), WO 9700966, **1995** [*Chem. Abstr.* **1997**, *126*, 143388]; f) A. J. Blacker, D. R. Boyd, H. Dalton, N. Bowers (Zeneca Limited, UK), WO 9637628, **1995** [*Chem. Abstr.* **1997**, *126*, 88342]; g) A. T. Anilkumar, K. Goto, T. Takahashi, K. Ishizaki, H. Kaga, *Tetrahedron: Asymmetry* **1999**, *10*, 2501; h) A. S. Demir, H. Hamamci, F. Doganel, E. Ozgul, *J. Mol. Catal. B* **2000**, *9*, 157.

[133] a) T. R. Verhoeven, F. E. Roberts, C. H. Sennayake, K. M. Ryan (Merck & Co., Inc.; USA), US 5420353, **1994** [*Chem. Abstr.* **1995**, *123*, 314545]; b) P. R. Hof (DSM N.V., NL), EP 890571, **1997** [*Chem. Abstr.* **1999**, *130*, 110062].

[134] a) A. I. Meyers, K. Drauz, M. Schwarm, M. McKennon (Degussa AG), DE 4232505, **1992** [*Chem. Abstr.* **1994**, *121*, 10000]; b) A. Bommarius, K. Drauz, G. Krix, R.-M. Kula (Degussa AG), EP 692538, **1994** [*Chem. Abstr.* **1996**, *124*, 173602].

[135] M. Schwarm, *$NaBH_4$ Reductions of Amino Acids & Derivatives Using Electrophilic Assistance*, Rohm&Haas 6th European Metal Hydride Symposium, Schloss Reinach, Freiburg, **2001**.

[136] a) T. Inaba, A. G. Birchler, Y. Yamada, S. Sagawa, K. Yokota, K. Ando, I. Uchida, *J. Org. Chem.* **1998**, *63*, 7582; b) T. Inaba, Y. Yamada, H. Abe, S. Sagawa, H. Cho, *J. Org. Chem.* **2000**, *65*, 1623.

[137] T. Inaba, S. Sagawa, H. Abe (Japan Tobacco Inc.), EP 930312, **1998** [*Chem. Abstr.* **1999**, *131*, 116260].

[138] a) J. D. Rozzell (Biocatalytics Inc.), US 5834261, **1997** [*Chem. Abstr.* **1999**, *130*, 3114]; b) J. D. Rozzell (Biocatalytics Inc.), US 5942644, **1997** [*Chem. Abstr.* **1999**, *131*, 169389]; c) F. Balkenhohl, K. Ditrich, C. Nübling (BASF AG), WO 9623894, **1995** [*Chem. Abstr.* **1996**, *125*, 219729]; d) C. Nübling, K. Ditrich, C. Dully (BASF AG), DE 19837745, **1999** [*Chem. Abstr.* **1998**; *Chem. Abstr.* **2000**, *132*, 165214].

[139] R. Noyori, M. Tokunago, M. Kitamura, *Bull. Chem. Soc. Jpn.* **1995**, *68*, 36.

[140] S. Akutagawa, *Appl. Catal. A* **1995**, *128*, 171.

[141] H. Kumobayashi, *Recl. Trav. Chim. Pays-Bas* **1996**, *115*, 201.

[142] T. Saito, T. Yokozawa, T. Ishizaki, T. Moroi, N. Sayo, T. Miura, H. Kumobayashi, *Adv. Synth. Catal.* **2001**, *343*, 264.

[143] N. Sayo, T. Salto, Y. Okeda, N. Nagashima, H. Kumobayashi (Takasago Corp.), EP 369691, **1988** [*Chem. Abstr.* **1988**, 113, 190758].

[144] R. Schmid, E. A. Broger, *Proceedings of the Chiral Europe'94 Symposium*, Spring Innovations, Stockport, England, **1994**, p. 79.

[145] R. Noyori, T. Okhuma, *Angew. Chem.* **2001**, *113*, 41; *Angew. Chem. Int. Ed.* **2001**, *40*, 40; R. Noyori, T. Okhuma, *Pure Appl. Chem.* **1999**, *71*, 1493; R. Noyori, S. Hashigushi in *Applied Homogeneous Catalysis with Organometallic Compounds, Vol. 1* (Eds.: B. Cornils, W. A. Herrmann), VCH, Weinheim, **1996**, p. 559.

[146] a) S. Hashigushi, A. Fujii, J. Takehara, T. Ikariya, R. Noyori, *J. Am. Chem. Soc.* **1995**, *117*, 7562; b) S. Hashigushi, K.-J. Haack, K. Matsumura, T. Ikariya, R. Noyori, *Angew. Chem.* **1997**, *109*, 300; *Angew. Chem. Int. Ed. Engl.* **1997**, *36*, 288.

[147] H. U. Blaser, M. Studer, *Chirality* **1999**, *11*, 459.

[148] A. Hirao, S. Itsuno, S. Nakahama, N. Yamazaki, *J. Chem. Soc. Chem. Commun.* **1981**, 315.

[149] a) E. J. Corey, R. K. Bakshi, S. Shibata, C.-P. Chen, V. K. Singh, *J. Am. Chem. Soc.* **1987**, *109*, 7925; b) R. Hett, Q. K. Fang, Y. Gao, S. A. Wald, C. H. Senanayake, *Org. Process Res. Dev.* **1998**, *2*, 96.

[150] B. Jiang, Y. Feng, J. Zheng, *Tetrahedron Lett.* **2000**, *41*, 10281.

[151] E. J. Mathre, T. K. Jones, L. C. Xavier, T. J. Blacklock, R. A. Reamer, J. J. Mohan, E. T. Turner-Jones, K. Hoogsteen, M. W. Baum, E. J. J. Grabowski, *J. Org. Chem.* **1991**, *56*, 751; E. J. Mathre, T. K. Jones, L. C. Xavier, T. J. Blacklock, R. A. Reamer, J. J. Mohan, E. T. Turner-Jones, K. Hoogsteen, M. W. Baum, E. J. J. Grabowski, *J. Org. Chem.* **1991**, *56*, 763.

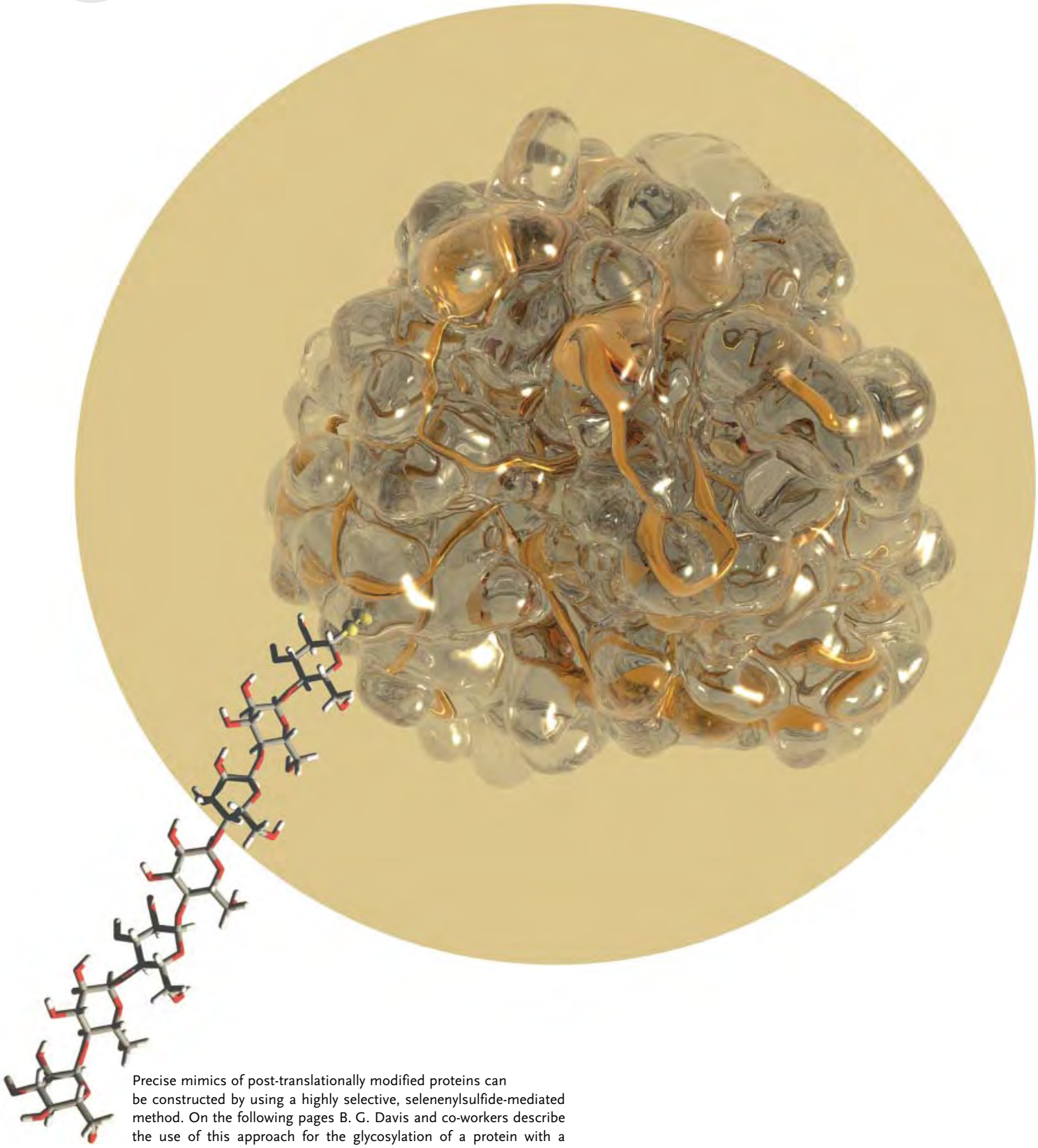
[152] a) J.-C. Caille, M. Bullaird, B. Laboue in *Chirality in Industry II*, Wiley, New York, **1997**, chap. 20; b) M. Bulliard, *Chiral Chemicals*, Marcel Dekker, New York, **1999**, chap. II.
[153] K. Matos, J. A. Corella, E. R. Burkhardt, S. M. Nettles (Mine Safety Appliances Company, USA), US 6218585 [*Chem. Abstr.* **2001**, *134*, 295546].
[154] L. Deloux, M. Srebnik, *Chem. Rev.* **1993**, *93*, 763.
[155] M. Tokunaga, J. F. Larrow, F. Kakiuchi, E. N. Jacobsen, *Science* **1997**, *277*, 937.
[156] J. M. Ready, E. N. Jacobsen, *J. Am. Chem. Soc.* **1999**, *121*, 6086.
[157] a) B. G. Main, H. Tucker in *Medicinal Chemistry*, 2nd ed. (Eds.: C. R. Genellin, S. M. Roberts), Academic Press, London, **1993**, p. 187; b) L. H. C. Lund in *Medicinal Chemistry*, 2nd ed. (Eds.: C. R. Genellin, S. M. Roberts), Academic Press, London, **1993**, p. 210; c) Y. Hong, Y. Gao, X. Nie, C. M. Zepp, *Tetrahedron Lett.* **1994**, *35*, 5551; d) C. Campo, E. F. Llama, J. L. Bermudez, J. V. Sinisterra, *Biocatal. Biotransform.* **2001**, *19*, 163.
[158] P. I. Dalko, L. Moisan, *Angew. Chem.* **2001**, *113*, 3840; *Angew. Chem. Int. Ed.* **2001**, *40*, 3726.
[159] a) B. Cambou, A. M. Klibanov, *Biotechnol. Bioeng.* **1984**, *26*, 1449; b) A. M. Klibanov, *Acc. Chem. Res.* **1990**, *23*, 114; c) *Enzymatic Reactions in Organic Media* (Eds.: A. M. P. Koskinen, A. M. Klibanov), Blackie Academic & Professional, Glasgow, UK, **1996**; d) G. M. Whitesides, C.-H. Wong, *Angew. Chem.* **1985**, *97*, 617; *Angew. Chem. Int. Ed. Engl.* **1985**, *24*, 617.
[160] Y.-F. Wang, J. L Lalonde, M. Momongan, D. E. Bergbreiter, C.-H. Wong, *J. Am. Chem. Soc.* **1988**, *110*, 7200.
[161] a) R. N. Patel, *Appl. Microbiol. Biotechnol.* **1992**, *38*, 56; R. N. Patel, *Adv. Appl. Microbiol.* **1997**, *43*, 91; b) R. Keller, W. Holla, G. Fülling, M. Schneider (Hoechst AG), EP 321918, **1988** [*Chem. Abstr.* **1988**, *112*, 137568].
[162] a) E. T. Farinas, T. Bulter, F. H. Arnold, *Curr. Opin. Biotechnol.* **2001**, *12*, 545; b) E. T. Farinas, U. Schwaneberg, A. Glieder, F. H. Arnold, *Adv. Synth. Catal.* **2001**, *343*, 601; c) F. H. Arnold, *Nature* **2001**, *409*, 253.
[163] a) M. T. Reetz, *Angew. Chem.* **2001**, *113*, 292; *Angew. Chem. Int. Ed.* **2001**, *40*, 284; b) K. A. Powell, S. W. Ramer, S. B. del Cardayré, W. P. C. Stemmer, M. B. Tobin, P. F. Longchamp, G. W. Huisman, *Angew. Chem.* **2001**, *113*, 4068; *Angew. Chem. Int. Ed.* **2001**, *40*, 3948.
[164] a) J. H. Park, J. H. Koh, J. Park, *Organometallics* **2001**, *20*, 1892; b) H. M. Jung, S. T. Shin, Y. H. Kim, M.-J. Kim, J. Park, *Organometallics* **2001**, *20*, 3370.
[165] a) O. Pamies, J. E. Bäckvall, *Adv. Synth. Catal.* **2001**, *343*, 726; b) F. F. Huerta, A. B. Minidis, J.-E. Bäckvall, *Chem. Soc. Rev.* **2001**, *30*, 321.
[166] a) P. M. Dinh, J. A. Howarth, A. R. Hudnott, J. M. J. Williams, W. Harris, *Tetrahedron Lett.* **1996**, *37*, 7623; b) J. V. Allen, J. M. J. Williams, *Tetrahedron Lett.* **1996**, *37*, 1859.
[167] J. B. Dumas, *Ann. Chim. Phys.* **1874**, *5*, 3.
[168] R. Csuk, B. I. Glänzer, *Chem. Rev.* **1991**, *91*, 49.
[169] A. Liese, K. Seelbach, C. Wandrey, *Industrial Biotransformations*, Wiley-VCH, Weinheim, **2000**.
[170] E. Schmidt, H. U. Blaser, P. F. Fauquez, G. Sedelmeier, F. Spindler in *Microbial Reagents in Organic Synthesis* (Ed.: S. Servi), Kluwer, Niederlande, **1992**, p. 377.
[171] A. Hage, D. G. I. Petra, J. A. Field, D. Schipper, J. B. P. A. Wijnberg, P. C. J. Kamer, J. N. H. Reek, P. W. N. M. van Leeuwen, R. Wever, H. E. Schoemaker, *Tetrahedron: Asymmetry* **2001**, *12*, 1025.
[172] R. A. Holt, S. R. Rigby (Zeneca Ltd.), WO 9405802, **1994** [*Chem. Abstr.* **1994**, *120*, 268348].
[173] U. Kragl, W. Kruse, W. Hummel, C. Wandrey, *Biotechnol. Bioeng.* **1996**, *52*, 309.
[174] W. Kruse, U. Kragl, C. Wandrey (Forschungszentrum Jülich GmbH), DE 4436149, **1996** [*Chem. Abstr.* **1996**, *124*, 315156].
[175] a) T. Suzuki, N. Kasai, R. Yamamoto, N. Minamiura, *Appl. Microbiol. Biotechnol.* **1994**, *42*, 270; b) T. Suzuki, H. Idogaki, N. Kasai, *Tetrahedron: Asymmetry* **1996**, *7*, 3109; c) for further information, see: http://www.daiso.co.jp.
[176] a) C. Neuberg, J. Hirsch, *Biochem. Z.* **1921**, *115*, 282; b) C. Neuberg, H. Ohle, *Biochem. Z.* **1922**, *127*, 327; c) for related C–C couplings, see: A. S. Demir, Ö. Sesenoglu, E. Eren, B. Hosrik, M. Pohl, E. Janzen, D. Kolter, R. Feldmann, P. Dünkelmann, M. Müller, *Adv. Synth. Catal.* **2002**, *344*, 96.
[177] G. Hildebrandt, W. Klavehn (Knoll A.-G. Chemische Fabriken in Ludwigshafen a.Rh.), DRP No.548 459, **1932**.
[178] K. Sakamoto, S. Kita, K. Tsuzaki, T. Morikawa (Fuji Chemical Industries Ltd), WO 0173100, **2001** [*Chem. Abstr.* **2001**, *135*, 256203].
[179] a) T. Katsuki, K. B. Sharpless, *J. Am. Chem. Soc.* **1980**, *102*, 5976; b) T. Katsuki, K. B. Sharpless (Stanford Junior University), US 4471130, **1984** [*Chem. Abstr.* **1985**, *102*, 24872].
[180] a) R. M. Hanson, K. B. Sharpless, *J. Org. Chem.* **1986**, *51*, 1922; b) Y. Gao, R. M. Hanson, J. M. Klunder, S. Y. Ko, H. Masamune, K. B. Sharpless, *J. Am Chem. Soc.* **1987**, *109*, 5765; c) R. M. Hanson, S. Y. Ko, K. B. Sharpless (Massachusetts Institute of Technology), US 4900847, **1986** [*Chem. Abstr.* **1987**, *106*, 66496].
[181] a) J. M. Klunder, S. Y. Ko, K. B. Sharpless, *J. Org. Chem.* **1986**, *51*, 3710; b) W. Dougherty, F. Liotta, D. Mondimore, W. Shum, *Tetrahedron Lett.* **1990**, *31*, 4389.
[182] N. Kasai, T. Suzuki, Y. Furukawa, *J. Mol. Catal. B* **1998**, *4*, 237.
[183] a) Y. Gao, R. M. Hanson, J. M. Klunder, S. Y. Ko, S. Masamune, K. B. Sharpless, *J. Am. Chem. Soc.* **1987**, *109*, 5765; b) J. M. Klunder, T. Onami, K. B. Sharpless, *J. Org. Chem.* **1989**, *54*, 1295.
[184] A. Richards, R. McCague, *Chem. Ind.* **1997**, *11*, 11422 – 11425.
[185] A. Kleemann, J. Engel, *Pharmaceutical Substances*, 4th ed., Thieme, Stuttgart, **2001**, p. 466 and 1067.
[186] A. Kleemann, J. Engel, *Pharmaceutical Substances*, 4th ed., Thieme, Stuttgart, **2001**, p. 1958.
[187] a) E. N. Jacobsen, I. Marko, W. S. Mungall, G. Schröder, K. B. Sharpless, *J. Am. Chem. Soc.* **1988**, *110*, 1968; b) I. E. Marko, K. B. Sharpless (Massachusetts Institute of Technology), US 4871855, **1989** [*Chem. Abstr.* **1990**, *112*, 75971]; c) D. Gilheany, B. M. Kim, H.-L. Kwong, K. B. Sharpless, T. Shibata (Massachusetts Institute of Technology), US 5126494, **1991** [*Chem. Abstr.* **1992**, *116*, 127820].
[188] http://www.rhodiachirex.com/default.htm; J. Hartung, K. B. Sharpless (Massachusetts Institute of Technology), US 5260461, **1993** [*Chem. Abstr.* **1993**, *119*, 139588].
[189] a) W. Harmann, H.-G. Heine, D. Wendisch, *Tetrahedron Lett.* **1977**, 2263; b) H. Kolb, K. B. Sharpless, *Tetrahedron* **1992**, *48*, 10515.
[190] a) R. A. Johnson, K. B. Sharpless in *Catalytic Asymmetric Synthesis*, 2nd ed. (Ed.: I. Ojima), Wiley-VCH, Weinheim, **2000**, p. 395; b) Y. Gao, C. Zepp (Sepracor), WO9317150, **1993** [*Chem. Abstr.* **1994**, *120*, 119437]; c) R. Pettman, *IBC International Symposium on New Synthetic Methods*, Sanibel Harbour, Fort Myers, Florida, **1998**; (http://www.albmolecular.com/features/tekreps/vol02/no20/)
[191] a) C. Döbler, G. Mehltretter, M. Beller, *Angew. Chem.* **1999**, *111*, 3211; *Angew. Chem. Int. Ed.* **1999**, *38*, 3026; b) M. Beller, C. Döbler, G. Mehltretter, U. Sundermeier (Bayer AG), WO 0064844, **2000** [*Chem. Abstr.* **2000**, *133*, 309573].
[192] a) W. Zhang, J. L. Loebach, S. R. Wilson, E. N. Jacobsen, *J. Am. Chem. Soc.* **1990**, *112*, 2801; b) E. N. Jacobsen, W. Zhang (Research Corporation Technologies Inc.), WO 9114694, **1991** [*Chem. Abstr.* **1992**, *116*, 106067]; c) E. N. Jacobsen, W. Zhang, L. Deng (Research Corporation Technologies Inc.), WO 9303838, **1993** [*Chem. Abstr.* **1994**, *120*, 7876].
[193] www.rhodiachirex.com.

 © 2004 Wiley-VCH Verlag GmbH & Co. KGaA, Weinheim

[194] a) A. Kleemann, J. Engel, *Pharmaceutical Substances*, 4th ed., Thieme, Stuttgart, **2001**, p. 1545; b) L. Deng, E. N. Jacobsen, *J. Org. Chem.* **1992**, *57*, 4320.
[195] J. F. Larrow, E. N. Jacobsen, Y. Gao, Y. Hong, X. Nie, C. M. Zepp, *J. Org. Chem.* **1994**, *59*, 1939.
[196] J. M. Keith, J. F. Larrow, E. N. Jacobsen, *Adv. Synth. Catal.* **2001**, *343*, 5.
[197] For information, see: http://www. chirex.com.
[198] http://www.rhodiachirex.com/default.htm; E. N. Jacobsen, M. Tokunaga, J. F. Larow (President and Fellows of Harvard College), WO 00/09463, **2000** [*Chem. Abstr.* **2000**, *132*, 180173].
[199] J. M. Ready, E. N. Jacobsen, *J. Am. Chem. Soc.* **2001**, *123*, 2687.
[200] S. C. Stinson, *Chem. Eng. News* **2001**, *79*, 65.
[201] http://www.daiso.co.jp/topics/e0072101.htm
[202] A. Abdel-Magid, L. N. Pridgen, D. S. Eggleston, I. Lantos, *J. Am. Chem. Soc.* **1986**, *108*, 4595.
[203] J.-D. Bourzat, A. Commercon (Rhone Poulenc Rorer), WO 9209589, **1991** [*Chem. Abstr.* **1992**, *117*, 251589].
[204] W. E. Ladner, G. M. Whitesides, *J. Am. Chem. Soc.* **1984**, *106*, 7250.
[205] R. A. Sheldon in *Speciality Chemicals*, Elsevier, London, **1991**.
[206] E.-I. Fukusaki, S. Satoda, S. Senda, T. Omata, *J. Biosci. Bioeng.* **1999**, *87*, 103.
[207] a) A. Gentil, C. Giordano, C. Fuganti, L. Ghirotto, S. Servi, *J. Org. Chem.* **1992**, *57*, 6635; b) D. R. Dodds, J. L. Lopez (Sepracor, Inc., USA), US 5274300, **1990** [*Chem. Abstr.* **1990**, *113*, 76620]; c) J. G. Kierkels (DSM N.V., Neth.), EP 0602740, **1994** [*Chem. Abstr.* **1994**, *121*, 177874].
[208] a) H. Matsumae, M. Furui, T. Shibatani, T. Tosa, *J. Ferment. Bioeng.* **1994**, *78*, 59; b) T. Tosa, T. Shibatani, *Ann. N. Y. Acad. Sci.* **1995**, *750*, 364; c) A. Liese, K. Seelbach, C. Wandrey, *Industrial Biotransformations*, Wiley-VCH, Weinheim, **2000**, p. 208; d) S. Matson (Sepracor, Inc., USA), WO 87/02381, **1986** [*Chem. Abstr.* **1988**, *108*, 127641].
[209] a) G. Rossy, L. Zard, A. E. Wick, *Manuf. Chem.* **1993**, *4*, 20; b) A. Kleemann, J. Engel, *Pharmaceutical Substances*, 4th ed., Thieme, Stuttgart, **2001**, p. 657.
[210] K. M. Manoj, A. Archelas, J. Baratti, R. Furstoss, *Tetrahedron* **2001**, *57*, 695.
[211] a) J. Zhang, J. Reddy, C. Roberge, C. Senanayake, R. Greasham, M. Chartrain, *J. Ferment. Bioeng.* **1995**, *80*, 244; b) M. Chartrain, C. H. Senanayake, J. P. Rosazza, J. Zhang (Merck & Co., Inc., USA), WO 9612818, **1996** [*Chem. Abstr.* **1996**, *125*, 56385].
[212] J. H. Spelberg, J. E. T. van Hylckama Vlieg, L. Tang, D. B. Janssen, R. M. Kellogg, *Org. Lett.* **2001**, *3*, 41.
[213] a) N. Kasai, K. Tsujimura, K. Unoura, T. Suzuki, *J. Ind. Microbiol.* **1992**, *9*, 97; b) N. Kasai, T. Suzuki, H. Idogaki (Daiso Co., Ltd., Japan), JP 2000287673, **1999** [*Chem. Abstr.* **2000**, *133*, 293205].
[214] N. Kasai, T. Suzuki, Y. Furukawa, *J. Mol. Catal. B* **1998**, *4*, 237 N. Kasai, T. Suzuki, Y. Furukawa (Daiso Co., Ltd., Japan), US 5177007, **1990** [*Chem. Abstr.* **1991**, *115*, 112848].
[215] a) T. Suzuki, N. Kasai, R. Yamamoto, N. Minamiura, *Appl. Microbiol. Biotechnol.* **1993**, *40*, 273; b) T. Suzuki, N. Kasai, R. Yamamoto, N. Minamiura, *Appl. Microbiol. Biotechnol.* **1994**, *42*, 270; c) T. Suzuki, N. Kasai (Daiso Co., Ltd., Japan), EP 0435551, **1990** [*Chem. Abstr.* **1991**, *115*, 278161]; d) N. Kasai, T. Suzuki (Daiso Co., Ltd., Japan), US 5246843 [*Chem. Abstr.* **1991**, *115*, 112850].
[216] a) K. Furuhashi, *CEER Chem. Econ. Eng. Rev.* **1986**, *18*, 21; b) K. Furuhashi (Nippon Mining Co., Ltd., Japan), JP 60214892, **1984** [*Chem. Abstr.* **1986**, *104*, 87153]; c) K. Furuhashi (Nippon Mining Co., Ltd., Japan), JP 62296888, **1986** [*Chem. Abstr.* **1986**, *109*, 5300].
[217] K. Furuhashi, M. Shintani, M. Takagi, *Appl. Microbiol. Biotechnol.* **1986**, *23*, 218.
[218] a) K. Kieslich, *Acta Biotechnol.* **1991**, *11*, 559; b) A. Liese, K. Seelbach, C. Wandrey, *Industrial Biotransformations*, Wiley-VCH, Weinheim, **2000**, p. 159; c) T. Gareth, M. A. Bertola, A. F. Marx, H. S. Koger (Gist Brocades N.V., Neth.; Shell Internationale Research Maatschappij B.V.), EP 0256586, **1987** [*Chem. Abstr.* **1989**, *110*, 7868].
[219] a) P. D. Gennaro, A. Colmegna, E. Galli, G. Sello, F. Pelizzoni, G. Bestetti, *Appl. Environ. Microbiol.* **1999**, *65*, 2794; b) S. Panke, V. de Lorenzo, A. Kaiser, B. Witholt, M. G. Wubbolts, *Appl. Environ. Microbiol.* **1999**, *65*, 5619; c) S. Bernasconi, F. Orsini, G. Sello, A. Colmegna, E. Galli, G. Bestetti, *Terahedron Lett.* **2000**, *41*, 9157.
[220] a) S. Panke, M. Wubbolts, A. Schmid, B. Witholt, *Biotechnol. Bioeng.* **2000**, *69*, 91; b) A. Schmid, K. Hofstetter, H.-J. Feiten, F. Hollmann, B. Witholt, *Adv. Synth. Catal.* **2001**, *343*, 732; c) A. Schmid, B. Witholt, H.-J. Feiten, S. Panke (ETH Zürich), EP 1106699, **2000** [*Chem. Abstr.* **2001**, *135*, 4579].
[221] R. N. Patel, C. G. McNamee, A. Banerjee, J. M. Howell, R. S. Robison, L. Szarka, *Enzyme Microb. Technol.* **1992**, *14*, 731.
[222] A. T. Boam, T. O. Carlsson, D. C. Stuckey, A. G. Livingston in *Proceedings of the Asia-Pacific Conference on Sustainable Energy and Environmental Technology*, World Scientific, Singapore, **1996**, p. 615.

 © 2004 Wiley-VCH Verlag GmbH & Co. KGaA, Weinheim

Communications



Precise mimics of post-translationally modified proteins can be constructed by using a highly selective, selenenylsulfide-mediated method. On the following pages B. G. Davis and co-workers describe the use of this approach for the glycosylation of a protein with a heptasaccharide glycan and for a multiple site-selective, chemical protein glycosylation.

DOI: 10.1002/anie.200352975
© 2004 Wiley-VCH Verlag GmbH & Co. KGaA, Weinheim

Glycoproteins

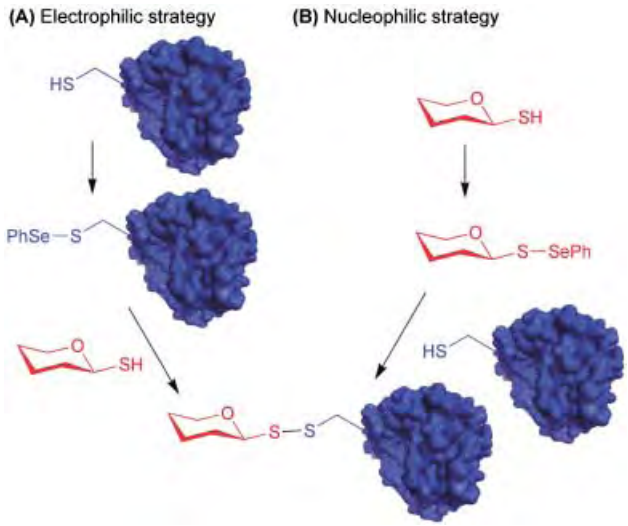
Glyco-SeS: Selenenylsulfide-Mediated Protein Glycoconjugation—A New Strategy in Post-Translational Modification**

*David P. Gamblin, Philippe Garnier, Sander van Kasteren, Neil J. Oldham, Antony J. Fairbanks, and Benjamin G. Davis**

The co- and post-translational glycosylation[1] of proteins[2,3] is a key factor in protein folding and stability,[4] and plays a major role in essential biological processes, such as cell signaling and regulation,[5,6] development,[7] and immunity.[8] The study of these events is made difficult by the fact that glycoproteins occur naturally as mixtures of so-called glycoforms,[9] which possess the same peptide backbone but differ in both the nature and the site of glycosylation. Furthermore, since protein glycosylation is not under direct genetic control, the expression of therapeutic glycoproteins in mammalian cell cultures leads to heterogeneous mixtures of glycoforms.[10] The ability to synthesize homogeneous glycoprotein glycoforms is therefore a prerequisite not only for purposes of accurate investigation, but is of increasing importance for the preparation of therapeutic glycoproteins, which are currently marketed as multiglycoform mixtures (e.g. erythropoietin[11,12] and interleukins[13]).

Several chemical synthetic strategies have been developed to this effect.[14–18] We showed previously that the combined use of site-directed mutagenesis and chemoselective glycoconjugation could be used for site-selective protein glycoconjugation.[19,20] In this approach, a cysteine residue is introduced through mutagenesis to generate a protein nucleophile with a single free thiol, which is subsequently modified chemoselectively with electrophilic thiol-specific carbohydrate reagents, such as glycosyl methanethiosulfonates[19,20] or glycosyl phenylthiosulfonates.[21] This method makes possible the introduction of spacer-linked free and protected glycans alike, but only allows the preparation of directly linked free glycosides after enzymatic deprotection on protein,[22] thus potentially limiting its utility. Several other methods have been developed for the synthesis of glycoproteins based on cysteine modification to create a linkage, for example, the use of a 5-nitropyridine-2-sulfenyl-activated *N*-acetylglucosamine (GlcNAc),[23] or glycosyl iodoacetamides.[16] However, these methods have so far been limited to the addition of a single GlcNAc monosaccharide[16,23] and can be plagued by a lack of selectivity (modification of histidine residues) and/or incomplete reactions.[16] Furthermore, no multiple site-selective glycoconjugation has been demonstrated, a weakness that was highlighted recently.[24]

Inspired by the occurrence, albeit rare, of selenenylsulfide proteins in Nature as selective electrophilic moieties,[25,26] we report herein a selenenylsulfide-mediated protein glycoconjugation,[27] which allows glycoconjugation with mono- and oligosaccharides of up to seven saccharide units in size at single and multiple sites in a variety of proteins. Two parallel strategies were investigated in which the protein cysteine residue plays potentially contrasting electrophilic and nucleophilic roles (Scheme 1). In the first approach **A**, a cysteine-containing protein is converted into the corresponding (phenylselenenyl)sulfide; the electrophilic character of the sulfur atom in the resulting S–Se bond[28] renders it susceptible to nucleophilic substitution by 1-thio mono- or oligosaccharides. In the opposite approach **B**, 1-thio mono- or oligosaccharides are first converted into their selenenylsulfide analogues, which can subsequently be coupled to a cysteine residue. Thus, the cysteine residue this time acts as a nucleophile. Importantly, the exquisite selectivity of S–Se chemistry would obviate all need for protecting groups during glycoconjugation.



Scheme 1. Two potential parallel glycoconjugation strategies. The protein cysteine plays either an electrophilic role (**A**) or a nucleophilic role (**B**).

The representative monosaccharides glucose (Glc), galactose (Gal), and *N*-acetylglucosamine (GlcNAc), and oligosaccharides (trisaccharides) Glcα(1,4)-Glcα(1,4)-Glc (**7**) and Glcα(1,4)-(Glcα(1,4))$_5$-Glc (**10**) were chosen for the glycoconjugation reactions. To evaluate the feasibility of approach **A**, the glycosyl halides **1a–c** were converted into the

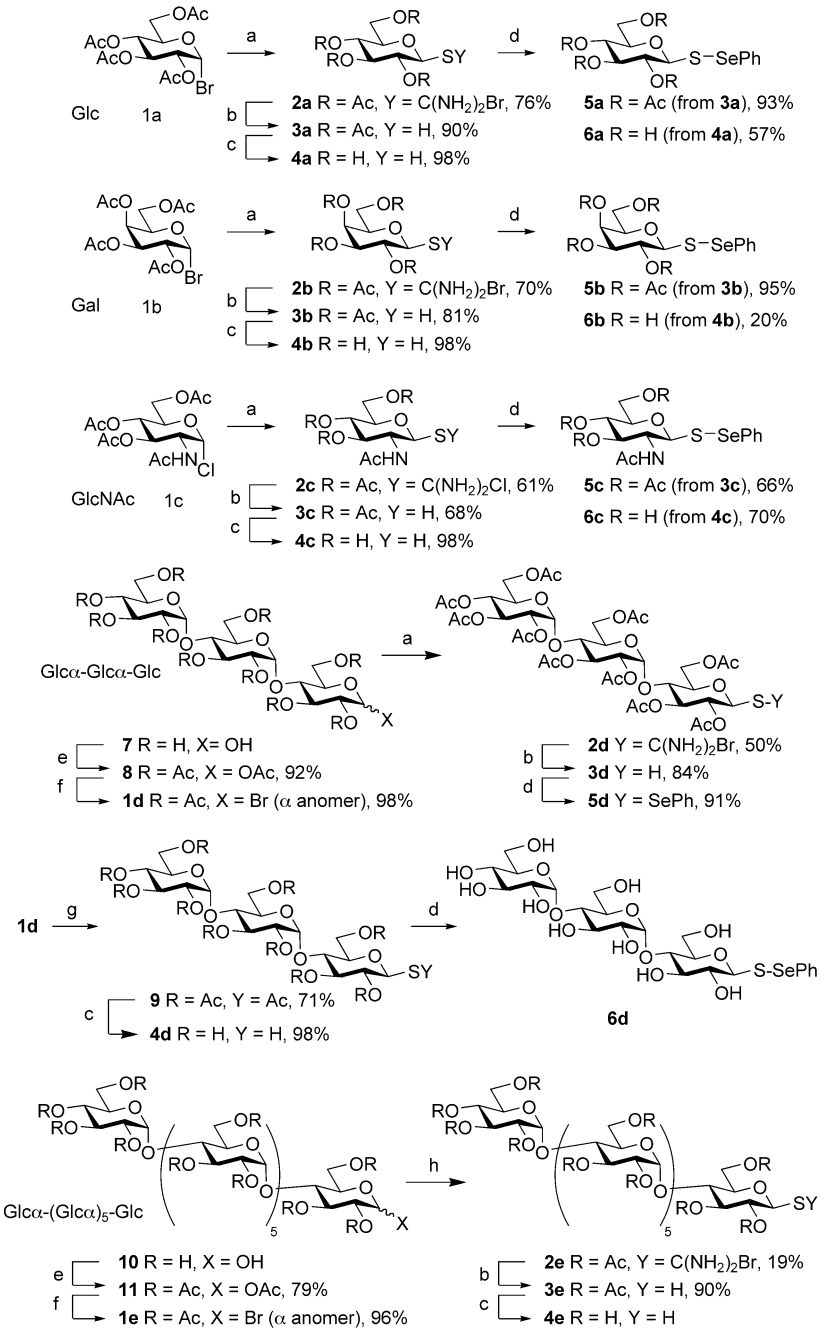
[*] D. P. Gamblin, Dr. P. Garnier, S. van Kasteren, Dr. N. J. Oldham, Dr. A. J. Fairbanks, Dr. B. G. Davis
Dyson Perrins Laboratory, University of Oxford
South Parks Road, Oxford, OX1 3QY (UK)
Fax: (+44) 1865-275674
E-mail: ben.davis@chem.ox.ac.uk

[**] This work was supported by the EPSRC (D.P.G.) and Glycoform (D.P.G., P.G., S.v.K.). We thank Dr. B. O'Neil, Dr. T. D. W. Claridge, and Dr. J. Kirkpatrick for invaluable technical support. We thank the EPSRC for access to the Mass Spectrometry Service at Swansea and the Chemical Database Service at Daresbury and for the award of a DTA studentship (D.P.G.). We also thank Dr. Mario Polywka for stimulating discussions and Susan M. Hancock for providing SSβG mutants.

Supporting information for this article is available on the WWW under http://www.angewandte.org or from the author.

 © 2004 Wiley-VCH Verlag GmbH & Co. KGaA, Weinheim DOI: 10.1002/anie.200352975

corresponding monosaccharide glycosyl-β-thiols **4a** (Glc), **4b** (Gal), and **4c** (GlcNAc) through treatment with thiourea to afford the corresponding isothiouronium salts,[29] followed by mild hydrolysis with sodium metabisulfite and Zémplen deacetylation (Scheme 2).[30] Following essentially similar procedures to those for the monosaccharides, the deprotected oligosaccharide thiols **4d** and **4e** were prepared from the maltotriose **7** and the maltoheptaose **10**, respectively (Scheme 2).



Scheme 2. Synthesis of protected and deprotected glycosylation reagents: a) thiourea, acetone, reflux; b) $Na_2S_2O_5$, CH_2Cl_2, water, 50 °C; c) NaOMe, MeOH; d) PhSeBr; e) NaOAc, Ac_2O, reflux; f) HBr (33%), AcOH, CH_2Cl_2; g) KSAc, acetone; h) thiourea, acetone, Bu_4NI (0.1 equiv), reflux.

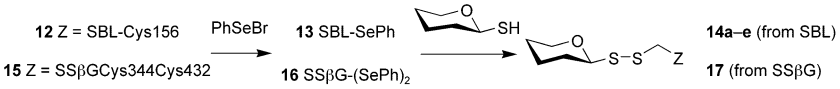
Single-site glycoconjugation was explored by using the model cysteine-containing protein serine protease subtilisin *Bacillus lentus* mutant S156C[19,31] (SBL-Cys156, **12**; Table 1). The protein **12** was treated with phenylselenenyl bromide (PhSeBr)[32,33] to give the corresponding selenenylsulfide **13**, which was subsequently treated with the deprotected 1-thio monosaccharides **4a–c** to afford the corresponding glycosylated proteins **14a** (SBL-Glc), **14b** (SBL-Gal), and **14c** (SBL-GlcNAc) in quantitative yields as confirmed by ESI-MS (Table 1).[34] The power of this method was such that we were also able to glycosylate **12** quantitatively with the bulky trisaccharide **4d** and even with the heptasaccharide **4e**. To our knowledge the latter carbohydrate is the largest to have been used in a convergent site-selective protein glycoconjugation to date (Figure 1). In all cases quantitative protein glycoconjugation occurred rapidly (within 60 min)[35] with a low ratio of reagent to protein (typically 10–20 equiv of thiol, and as little as 1 equiv in some cases).[36] Moreover, the compatibility of this procedure with deprotected thio sugars removes the need for a postmodification deprotection step.

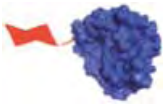
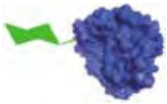
To demonstrate the applicability of this methodology to other proteins, and to carry out multiple-site glycoconjugations, we constructed a mutant of the thermophilic β-glycosidase from the archeon *Sulfolobus solfataricus*, which contains two cysteine residues (SSβG-Cys344Cys432, **15**). The doubly glycosylated protein **17** (SSβG-$[Glc]_2$) was obtained upon activation of **15** with PhSeBr, followed by treatment with the Glc thiol **4a**, as shown by ESI-MS (Table 1; m/z: calcd: 57775; found: 57760[37]). The three glycosylation sites in **12** (SBL-Cys156) and **15** (SSβG-Cys344Cys432) are found in a wide variety of protein structures and environments with different levels of exposure. This approach based on the modification of electrophilic cysteine residues can thus be used to prepare glycoproteins from very different proteins, and is not limited to single-site glycoconjugation, but is also amenable to multiple site-selective glycoconjugation. The site-selective modification of electrophilic protein residues is a rare but potentially powerful approach given the scarcity of other competing electrophiles.[15,38]

To probe approach **B** (Scheme 1) and the potential of a cysteine residue as a nucleophile, a series of protected glyco-SeS reagents were prepared readily from the thiols **3a–c** used above (Scheme 2). The protected glycosyl (phenylselenenyl)sulfides (glyco-SeS) **5a–c** were obtained from the

 © 2004 Wiley-VCH Verlag GmbH & Co. KGaA, Weinheim

Table 1: Glycoconjugation of **12** and **15** after activation with PhSeBr.[a]



Sugar thiol		Protein	Product		Conversion [%][b]	ESI-MS Found (calcd)
Glcβ-SH **4a**		SBL-SSePh	**14a**		>95	26908 (26909)
Galβ-SH **4b**		SBL-SSePh	**14b**		>95	26908 (26909)
GlcNAcβ-SH **4c**		SBL-SSePh	**14c**		>95	26944 (26950)
GlcαGlcαGlcβ-SH **4d**		SBL-SSePh	**14d**		>95	27228 (27233)
Glcα(Glcα)$_5$Glcβ-SH **4e**		SBL-SSePh	**14e**		>95	27878 (27881)
Glcβ-SH **4a**		SSβG-(SSePh)$_2$	**17**		>95	57760 (57775)

[a] Reagents: thiol (20 equiv), CHES (70 mM), MES (5 mM), $CaCl_2$ (2 mM), pH 9.5. [b] Conversion determined by ESI-MS.

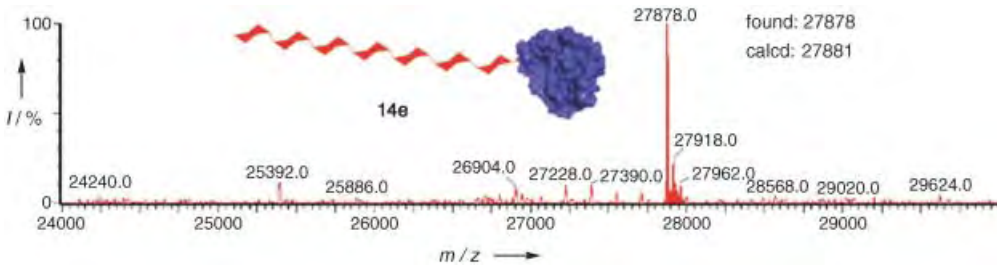


Figure 1. Deconvoluted ESI mass spectrum of **14e** (SBL-Glc(Glc)$_5$Glc).

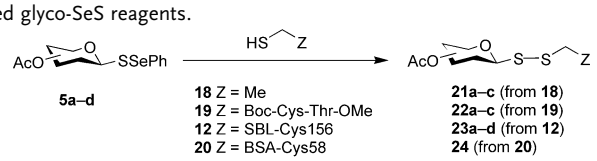
reaction of the acetylated thiols **3a–c** with PhSeBr. Their deprotected counterparts **6a–c** were obtained by using the same method following Zémplen deacetylation.[39] The protected and deprotected trisaccharides glyco-SeS **5d** and **6d**, respectively, were also prepared by this method (Scheme 2).

The protected and deprotected glyco-SeS reagents **5a–c** and **6a–c** were investigated in the glycoconjugation of the representative thiol EtSH (**18**) and dipeptide **19**. The corresponding protected glycoconjugate mixed disulfides **21a–c** and **22a–c** and their deprotected counterparts **25a**, **25c**, **26a**, and **26c** were all obtained in excellent yields, with complete retention of the anomeric β stereochemistry (Table 2 and Table 3). These novel glyco-SeS reagents were also investigated for their ability to glycosylate the model protein **12**. Again the glycoconjugation was quantitative, and the high purity of the eight glycoproteins **14a–d** and **23a–d** formed was confirmed by ESI-MS and Ellman titration.[40] The glycoprotein products **14a–d** were identical to those synthesized by using strategy **A**. To demonstrate the versatility of this methodology, we extended it to a larger cysteine-containing protein, bovine serum albumin (BSA-Cys58, **20**). The protein **20** was glycosylated successfully with both the protected and the deprotected Glc-SeS reagents **5a** and **6a** to afford **24** and **27**, respectively, and thus a third family of glycoproteins.

To further elucidate the mechanism of glycoconjugation with these glyco-SeS reagents, a time–course study of the reaction of **12** with the deprotected triose reagent **6d** was conducted, and the reaction conditions were explored (Figure 2). To our surprise, analysis by mass spectrometry

 © 2004 Wiley-VCH Verlag GmbH & Co. KGaA, Weinheim

Table 2: Glycoconjugation with protected glyco-SeS reagents.



5a–d

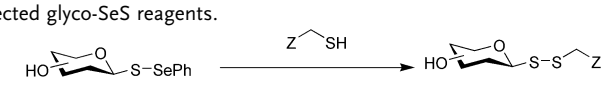
18 Z = Me
19 Z = Boc-Cys-Thr-OMe
12 Z = SBL-Cys156
20 Z = BSA-Cys58

21a–c (from **18**)
22a–c (from **19**)
23a–d (from **12**)
24 (from **20**)

	EtSH (**18**)[a]		Dipeptide **19**[b]		SBLCys156 (**12**)[c]		BSA-Cys58 (**20**)[c]	
	Product	Yield [%]	Product	Yield [%]	Product	Conv. [%][d]	Product	Conv. [%][d]
$Glc(Ac)_4$-SSePh **5a**	**21a**	82	**22a**	75	**23a**	>95	**24**	>95
$Gal(Ac)_4$-SSePh **5b**	**21b**	82	**22b**	93	**23b**	>95	[e]	–
$GlcNAc(Ac)_3$-SSePh **5c**	**21c**	93	**22c**	88	**23c**	>95	–	–
$Glc(Ac)_4Glc(Ac)_3Glc(Ac)_3$-SSePh **5d**	–	–	–	–	**23d**	90	–	–

[a] Et_3N, CH_2Cl_2, room temperature, glyco-SeS/**18** 1:1. [b] Et_3N, CH_2Cl_2/MeOH (20:1), room temperature, glyco-SeS/**19** 3:1. [c] CHES (70 mM), MES (5 mM), $CaCl_2$ (2 mM), pH 9.5, 10–75 equivalents of glyco-SeS. Different quantities of the reagent were used typically to increase rate and/or convenience. Although prolonged exposure of glyco-SeS reagents to aqueous conditions caused decomposition in some cases, the reactions described were fast enough to minimize decomposition. In all cases no side reactions with protein were observed. [d] Conversion (Conv.) was determined by ESI-MS. [e] Dash (–) indicates reaction was not studied.

Table 3: Glycoconjugation with deprotected glyco-SeS reagents.



6a Glcβ-SSePh
6b Galβ-SSePh
6c GlcNAcβ-SSePh
6d Glcα-Glcα-Glcβ-SSePh

18 Z = Me
19 Z = Boc-Cys-Thr-OMe
12 Z = SBL-Cys156
20 Z = BSA-Cys58

25a, 25c (from **18**)
26a, 26c(from **19**)
14a–d (from **12**)
27 (from **20**)

	EtSH (**18**)[a]		Peptide **19**[b]		SBLCys156 (**12**)[c]		BSA-Cys58 (**20**)[c]	
	Product	Yield [%]	Product	Yield [%]	Product	Conv. [%]	Product	Conv. [%]
Glc-SSePh **6a**	**25a**	90	**26a**	91	**14a**	>95	**27**	>95
Gal-SSePh **6b**	[d]	–	–	–	**14b**	>95	–	–
GlcNAc-SSePh **6c**	**25c**	77	**26c**	77	**14c**	>95	–	–
GlcGlcGlc-SSePh **6d**	–	–	–	–	**14d**	>95	–	–

[a] Et_3N, CH_2Cl_2, room temperature, glyco-SeS/**18** 1:1. [b] Et_3N, CH_2Cl_2/MeOH (20:1), room temperature, thioselenide/**19** 3:1. [c] 70 mM CHES, 5 mM MES, 2 mM $CaCl_2$, pH 9.5, 10–150 equivalents of glyco-SeS, conversion determined by ESI-MS. Different quantities of the reagent were used typically to increase rate and/or convenience. Although prolonged exposure of glyco-SeS reagents to aqueous conditions caused decomposition in some cases, the reactions described were fast enough to minimize decomposition. In all cases no side reactions with protein were observed. [d] Dash (–) indicates reaction was not studied.

showed the rapid formation of **13** (SBL-SePh; less than 1 min), followed by the subsequent formation of the glycosylated protein **14d** (Figure 2). This result suggests that an electrophilic glycoconjugation mechanism dominates regardless of the strategy (**A** or **B**) used. Thus, these two strategies may be used in a complementary manner, thereby increasing the flexibility of the glyco-SeS approach. We suggest that in strategy **B** an initial nucleophilic attack at the selenium center by the protein thiol generates **13** and liberates the sugar thiol **4d**, which is subsequently able to proceed exactly as in strategy **A** to displace SePh and form the glycosylated protein **14d** (SBL-GlcGlcGlc). Consistent with this mechanism, the use of a large excess of the glyco-SeS reagent was detrimental to the reaction, as the thiols released were then trapped by this reagent to give symmetrical disulfides. The reaction is pH-dependent: when carried out at pH 7.5 or pH 8.5 formation of the SBL-SePh intermediate **13** is observed, but just 10% conversion into the glycosylated protein **14d** occurs. Higher conversion is only observed at pH 9.5.[41] This observation is also consistent with the proposed mechanism of nucleophilic attack by the thiol **4d** (or the corresponding thiolate). These results show that glyco-SeS reagents in strategy **B** effectively act as the source of both the selenating reagent and the sugar thiol, thereby offering a convenient alternative to the two-step use of PhSeBr and a sugar thiol in strategy **A**.

Finally, to show the stability of the newly formed disulfide linkage towards enzymatic carbohydrate extension and to show that disulfide-linked glycoproteins may be processed by glycosyltransferases, this new glycoconjugation method was coupled with enzymatic carbohydrate extension (Figure 3). Inhibited GlcNAc-S-S-SBL was incubated with UDP-galactose (UDP-Gal) in the presence of β-1,4-galactosyltransferase,[42] which is known to catalyze the selective formation of the Galβ(1,4)-GlcNAc linkage.[43] The full conversion of the GlcNAc-S-S-SBL protein **14c** into the Galβ(1,4)-GlcNAc-S-S-SBL **28** was confirmed by ESI-MS (Figure 3), thereby further extending the utility of the glyco-SeS method.

In conclusion, we have described the synthesis of glycosyl selenenylsulfides (glyco-SeS), a novel class of glycosylating agents, and their use not only for the glycoconjugation of simple thiols and peptides (EtSH and dipeptides), but also of proteins. Whereas most site-specific glycoconjugation methods take advantage of the nucleophilic character of cysteine

 © 2004 Wiley-VCH Verlag GmbH & Co. KGaA, Weinheim

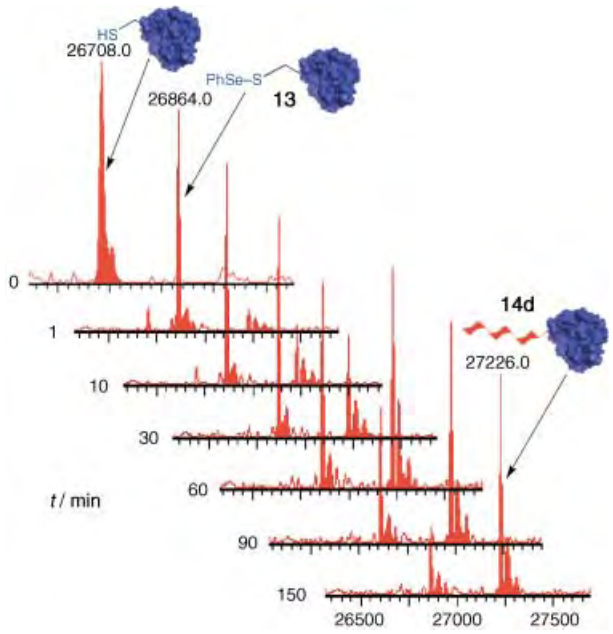


Figure 2. Deconvoluted ESI mass spectra showing glycoconjugation of **12** (SBLCys156; 26708 Da) with **6d** (GlcGlcGlc-SeS; 20 equiv) in a buffer solution (CHES (70 mM), MES (5 mM), $CaCl_2$ (2 mM); pH 9.5) after 1 min, 10 min, 30 min, 60 min, 90 min, 150 min. The selenenylated protein **13** (SBL-SePh; 26864 Da) is formed rapidly, followed by the glycoprotein **14d** (SBL-GlcGlcGlc; 27226 Da).

thiols (for example with glycosyl maleimides[44] or iodoacetamides[16,45]), our methodology is based upon a rarely exploited[15,38] but nonetheless powerful electrophilic glycoconjugation mechanism. In particular, this approach allows for the preparation of fully deprotected glycoconjugates and glycoproteins. We have demonstrated multiple site-selective glycoconjugation, which potentially provides access to polyvalent neoglycoproteins with control over valency,[24] the coupling of a heptasaccharide, and enzymatic elongation on a disulfide-linked glycoprotein after cysteine modification.[15] This methodology, combined with site-directed mutagenesis, allows the rapid, site-selective glycoconjugation of very different proteins with different fully deprotected carbohydrates, and the use of a low reagent-to-protein ratio. We are currently investigating the application of this novel selenenylsulfide methodology to other kinds of post-translational modification.

Received: September 29, 2003 [Z52975]
Published Online: January 21, 2004

Keywords: carbohydrates · glycoproteins · glycosylation · protein modifications · selenium

[1] The Gene Ontology Consortium has defined biological-process term-number GO:0006486 (protein amino acid glycosylation) as

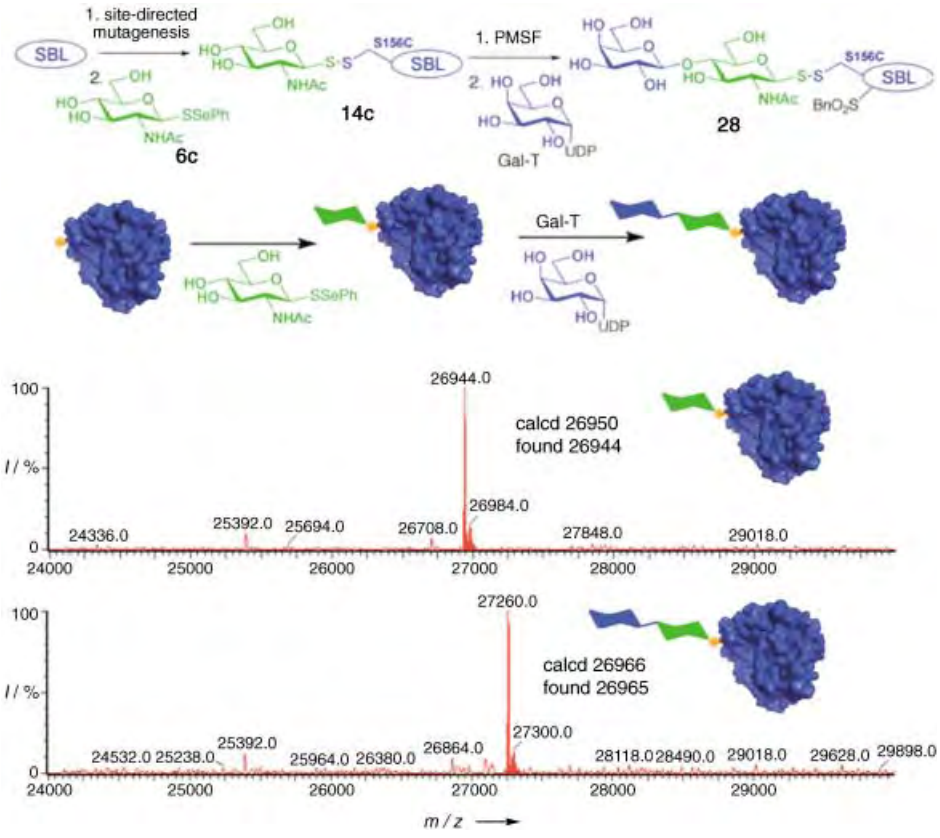


Figure 3. Chemical glycoconjugation of **12** (SBLCys156) with GlcNAc to form **14c** (GlcNAc-SBL; 2 mM), followed by the addition of a second monosaccharide unit (Gal) mediated by galactosyltransferase (Gal-T) to give **28** (Galβ(1,4)-GlcNAc-SBL): deconvoluted ESI mass spectra showing **14c** (GlcNAc-SBLCys156) before (top spectrum) and after (bottom spectrum) inactivation with phenylmethanesulfonyl fluoride (PMSF) and enzymatic galactosylation.

 © 2004 Wiley-VCH Verlag GmbH & Co. KGaA, Weinheim

"The addition of a sugar unit to a protein amino acid, for example, the addition of glycan chains to protein." (see *Genome Res.* **2001**, *11*, 1425). Herein we use the broader term glycoconjugation to refer to the general process of addition of a glycosyl-unit-containing moiety to another moiety through a covalent linkage.

[2] R. A. Dwek, *Chem. Rev.* **1996**, *96*, 683.
[3] J. B. Lowe, J. D. Marth, *Annu. Rev. Biochem.* **2003**, *72*, 643.
[4] A. J. Parodi, *Annu. Rev. Biochem.* **2000**, *69*, 69.
[5] A. Helenius, M. Aebi, *Science* **2001**, *291*, 2364.
[6] R. Kannagi, *Curr. Opin. Struct. Biol.* **2002**, *12*, 599.
[7] R. S. Haltiwanger, *Curr. Opin. Struct. Biol.* **2002**, *12*, 593.
[8] J. B. Lowe, *Cell* **2001**, *104*, 809.
[9] T. W. Rademacher, R. B. Parekh, R. A. Dwek, *Annu. Rev. Biochem.* **1988**, *57*, 785.
[10] The recent preparation of homogeneous *N*-glycosylated protein in yeast represents a remarkable achievement in this regard; see: S. R. Hamilton, P. Bobrowicz, B. Bobrowicz, R. C. Davidson, H. Li, T. Mitchell, J. H. Nett, S. Rausch, T. A. Stadheim, H. Wischnewski, S. Wildt, T. U. Gerngross, *Science* **2003**, *301*, 1244. Elegant in vitro misacylated tRNA systems may also facilitate powerful biological glycoprotein synthesis; see: R. R. Schmidt, J. C. Castro-Palomino, O. Retz, *Pure Appl. Chem.* **1999**, *71*, 729.
[11] R. S. Rush, P. L. Derby, D. M. Smith, C. Merry, G. Rogers, M. F. Rohde, V. Katta, *Anal. Chem.* **1995**, *67*, 1442.
[12] L. C. Wasley, G. Timony, P. Murtha, J. Stoudemire, A. J. Dorner, J. Caro, M. Krieger, R. J. Kaufman, *Blood* **1991**, *77*, 2624.
[13] C. King, R. Mueller Hoenger, M. Malo Cleary, K. Murali-Krishna, R. Ahmed, E. King, N. Sarvetnick, *Nat. Med.* **2001**, *7*, 206.
[14] B. G. Davis, *Chem. Rev.* **2002**, *102*, 579.
[15] H. Liu, L. Wang, A. Brock, C. H. Wong, P. G. Schultz, *J. Am. Chem. Soc.* **2003**, *125*, 1702.
[16] D. Macmillan, R. M. Bill, K. A. Sage, D. Fern, S. L. Flitsch, *Chem. Biol.* **2001**, *8*, 133.
[17] Y. Shin, K. A. Winans, B. J. Backes, S. B. H. Kent, J. A. Ellman, C. R. Bertozzi, *J. Am. Chem. Soc.* **1999**, *121*, 11684.
[18] K. Witte, P. Sears, R. Martin, C.-H. Wong, *J. Am. Chem. Soc.* **1997**, *119*, 2114.
[19] B. G. Davis, R. C. Lloyd, J. B. Jones, *J. Org. Chem.* **1998**, *63*, 9614.
[20] B. G. Davis, M. A. T. Maughan, M. P. Green, A. Ullman, J. B. Jones, *Tetrahedron: Asymmetry* **2000**, *11*, 245.
[21] D. P. Gamblin, P. Garnier, S. J. Ward, N. J. Oldham, A. J. Fairbanks, B. G. Davis, *Org. Biomol. Chem.* **2003**, *1*, 3642.
[22] B. G. Davis, R. C. Lloyd, J. B. Jones, *Bioorg. Med. Chem.* **2000**, *8*, 1527.
[23] W. M. Macindoe, A. H. van Oijen, G.-J. Boons, *Chem. Commun.* **1998**, 847.
[24] B. T. Houseman, M. Mrksich, *Top. Curr. Chem.* **2002**, *218*, 1.
[25] K. Anestål, E. S. J. Arnér, *J. Biol. Chem.* **2003**, *278*, 15966.
[26] L. Zhong, E. S. J. Arnér, A. Holmgren, *Proc. Natl. Acad. Sci. USA* **2000**, *97*, 5854.
[27] The reactions of thiols with unsymmetrical disulfides, in contrast to selenenylsulfides, are often slow and nonselective, typically require a large excess of the thiol, and lead to the release of thiol(ate), which may serve to cleave any disulfide formed. Reactions with selenenylsulfides are typically fast, favor S–S formation from S–Se through disproportionation, and release a selenate, which does not compete in the reaction.
[28] For examples of the behavior of S as an electrophile in S–Se-containing compounds, see: G. Bergson, G. Nordstrom, *Ark. Kemi* **1961**, *17*, 569; J. L. Kice, T. W. S. Lee, *J. Am. Chem. Soc.* **1978**, *100*, 5094; H. Fischer, N. Dereu, *Bull. Soc. Chim. Belg.* **1987**, *96*, 757. This reaction may compete with reaction at the electrophilic Se atom. However, reaction at the Se center would simply lead to in situ generation of glyco-SeS reagents, which would then feed into the same glycosylation sequence and ultimately lead to the required disproportionation of S–Se to S–S.
[29] W. A. Bonner, J. E. Kahn, *J. Am. Chem. Soc.* **1951**, *73*.
[30] B. D. Johnston, B. M. Pinto, *J. Org. Chem.* **2000**, *65*, 4607.
[31] G. DeSantis, P. Berglund, M. R. Stabile, M. Gold, J. B. Jones, *Biochemistry* **1998**, *37*, 5968.
[32] O. Behaghel, H. Seibert, *Justus Liebigs Ann. Chem.* **1932**, *65*, 812.
[33] H. Rheinboldt, E. Giesbrecht, *Justus Liebigs Ann. Chem.* **1950**, *568*, 198.
[34] Representative glycosylation procedure: The protein **12** (SBLCys156; 1 mg) was dissolved in a buffer solution (1 mL; CHES (70 mM), MES (5 mM), $CaCl_2$ (2 mM); pH 9.5). The thio sugar **4a** (Glc-SH; 20 equiv) was added as a solution in water to the solution of the protein, and the mixture was placed on an end-over-end rotator. After 1 h the reaction was analyzed by mass spectrometry.
[35] A comparable glycosylation with iodoacetamides may take as long as 24 h: see reference [16].
[36] Considerably smaller quantities of the reagent (1–20 equiv) are required than typically used in protein glycosylation or protein modification (often of the order of 1000 equiv); see: B. G. Davis, *Curr. Opin. Biotechnol.* **2003**, *14*, 379. For more information, see Supporting Information.
[37] For further details, see Supporting Information.
[38] K. L. Kiick, E. Saxon, D. A. Tirrell, C. R. Bertozzi, *Proc. Natl. Acad. Sci. USA* **2002**, *99*, 19.
[39] Attempted deprotection of the acetylated Glyco-SeS reagents only resulted in degradation.
[40] G. L. Ellman, K. D. Courtney, V. Andres, R. M. Featherstone, *Biochem. Pharmacol.* **1961**, *7*, 88.
[41] For further details, see Supporting Information.
[42] The glycoprotein **14c** (GlcNAc-S-S-SBL; 3 mg, as a solution in aqueous buffer (1 mg mL^{-1})) was deactivated with PMSF (500 equiv, as a solution in acetonitrile (100 mg mL^{-1})) at room temperature. The protein was purified (Sephadex G-25 PD-10 column), lyophilized, and redissolved in sodium cacodylate (0.1 M)/$MnCl_2$ buffer (0.05 M, 1.0 mL). The mixture was incubated for 40 min with UDP-Gal (1.6 mM) and recombinant bovine beta-1,4-galactosyltransferase (100 mU, Calbiochem) prior to analysis by mass spectrometry.
[43] F. L. Schanbacher, K. E. Ebner, *J. Biol. Chem.* **1970**, *245*, 5057.
[44] I. Shin, H.-j. Jung, M.-r. Lee, *Tetrahedron Lett.* **2001**, *42*, 1325.
[45] L. A. Marcaurelle, C. R. Bertozzi, *J. Am. Chem. Soc.* **2001**, *123*, 1587.

 © 2004 Wiley-VCH Verlag GmbH & Co. KGaA, Weinheim

Density Functional Calculations

Models of High-Valent Intermediates of Non-Heme Diiron Alkane Monooxygenases: Electronic Structure of a Bis(μ-oxo)diron(IV) Complex with Locally Low-Spin Metal Centers**

Abhik Ghosh, Espen Tangen, Emmanuel Gonzalez, and Lawrence Que, Jr.**

Long known as a common structural unit in inorganic chemistry, the bis(μ-chalcogeno)dimetal "diamond" core is increasingly recognized as important in a biological context.[1,2] Thus, a variety of clusters based on $\{Fe_2(\mu\text{-}S)_2\}$ rhombs occur in iron–sulfur proteins and are involved in redox reactions, while intermediates with $\{M_2(\mu\text{-}O)_2\}$ cores have been implicated more recently for non-heme metalloenzymes involved in oxygen metabolism.[1,2] For example, $\{Mn_2(\mu\text{-}O)_2\}$ units have been identified as components of the tetramanganese cluster involved in photosynthetic oxygen evolution,[3] while $\{Cu^{III}{}_2(\mu\text{-}O)_2\}$ intermediates have been recently synthesized and postulated as intermediates in the catalytic cycles of copper oxygenases such as particulate methane monooxygenase.[2,4] Strong evidence for a high-valent $\{Fe^{IV}{}_2(\mu\text{-}O)_2\}$ core has also been found for the key methane-hydroxylating intermediate **Q** of soluble methane monooxygenase (sMMO).[5,6] A related Fe^{III}–Fe^{IV} species called intermediate **X** produces the catalytically essential tyrosyl radical in the R2 protein of ribonucleotide reductase to initiate the process of ribonucleotide reduction in DNA biosynthesis.[7] By analogy, high-valent $\{Fe^{IV}{}_2(\mu\text{-}O)_2\}$ intermediates are also proposed for other non-heme diiron alkane-oxidizing enzymes such as fatty acid desaturases[8] and the membrane-bound ω-hydoxylase AlkB.[9]

In recent years, a number of synthetic complexes with $\{Fe_2(\mu\text{-}O)_2\}^{n+}$ ($n=3$ or 4) cores and tetradentate N_4 capping ligands have been isolated and characterized; these serve as models of the enzymatic intermediates **Q** and **X**. With the tpa ligand (tpa = tris(2-pyridylmethyl)amine) and its 5-alkyl derivatives, the complexes with an $\{Fe_2(\mu\text{-}O)_2\}^{3+}$ core exhibit an $S=3/2$ ground state (S is the total spin angular momentum).[10,11] Mössbauer spectroscopy indicated that the two iron centers in these species are electronically identical, thus suggesting a valence-delocalized diiron(III,IV) description for the dinuclear center.[10] Density-functional theory (DFT) calculations further indicated that the individual iron centers in these complexes could be described as locally low-spin.[12] More recently, the first synthetic $\{Fe^{IV}{}_2(\mu\text{-}O)_2\}$ intermediate has been reported,[13] which provides the closest synthetic model so far of **Q**. However, while **Q** has a carboxylate-rich ligand environment and antiferromagnetically coupled, locally high-spin Fe^{IV} centers,[14] the synthetic model is paramagnetic ($S=1$), features relatively strong-field *N*,*N*′-bis(2-pyridylmethyl)-*N*,*N*′-dimethyl-*trans*-1,2-diaminocyclohexane (bpmcn) terminal ligands and presumably low-spin Fe^{IV} centers.[13] Such an $\{Fe^{IV}{}_2(\mu\text{-}O)_2\}$ intermediate with locally low-spin iron centers may actually be involved in the catalytic cycle of the alkane ω-hydroxylase AlkB, which is thought to have a histidine-rich ligand environment.[15] Because of its importance, the catalytic cycle of sMMO has been the subject of several quantum-chemical studies.[16,17,18] To complement these efforts, we have undertaken a DFT study of an $\{Fe^{IV}{}_2(\mu\text{-}O)_2\}$ model complex with locally low-spin iron centers.

By using nonlocal DFT[19,20] as implemented in the ADF[21] program system, the VWN local exchange-correlation functional, PW91 gradient corrections for both exchange and correlation, triple-ζ plus polarization Slater-type basis sets, and a fine mesh for numerical integrations of matrix elements, we carried out full geometry optimizations of $[(bipy)_2Fe(\mu\text{-}O)_2Fe(bipy)_2]^{4+}$ (bipy = 2,2′-bipyridyl) for the lowest-energy $S=1$ and 2 electronic states and also of $[(bipy)_2Fe(\mu\text{-}O)_2Fe(bipy)_2]^{3+}$ for its $S=3/2$ ground state. Use of the bipy ligand instead of the bpmcn ligand used in the synthetic modeling studies permitted us to exploit D_2 symmetry in each of these calculations. We also carried out similar calculations with D_{4d} symmetry constraints on the high-valent nitrido-bridged heme dimer complexes $[(por)Fe]_2N$ ($S=1/2$)[22] and $[\{(por)Fe\}_2N]^+$ ($S=0$)[23] (por = porphyrinato) which feature the same formal metal oxidation states as $[(bipy)_2Fe(\mu\text{-}O)_2Fe(bipy)_2]^{3+}$ and $[(bipy)_2Fe(\mu\text{-}O)_2Fe(bipy)_2]^{4+}$, respectively. A spin-restricted formalism was used for $[\{(por)Fe\}_2N]^+$, a closed-shell species,[23] while spin-unrestricted calculations were used for all the other complexes.

Figure 1 presents the Kohn–Sham molecular orbital (MO) energy levels in the Fe 3d "band" of each of the three $\{Fe_2(\mu\text{-}O)_2\}$ species studied. Figure 2 provides pictorial representations of some of these MOs. Figure 1 reveals a substantial energy separation between the t_{2g} and e_g bands, with only the t_{2g} band populated, thus indicating the low-spin nature of the iron centers in the species studied. Note also that the t_{2g} band is fairly densely spaced, which provides a simple explanation for the $S=3/2$ ground state of $[(bipy)_2Fe(\mu\text{-}O)_2Fe(bipy)_2]^{3+}$ in terms of filling six MOs with nine 3d electrons according to Hund's rules.[12] Not surprisingly, the $S=1$ and $S=2$ states of

[*] Prof. Dr. A. Ghosh, E. Tangen, E. Gonzalez
Department of Chemistry
University of Tromsø
N-9037 Tromsø (Norway)
Fax: (+47) 77644765
E-mail: abhik@chem.uit.no
Prof. Dr. L. Que, Jr.
Department of Chemistry and the Center for Metals in Biocatalysis
University of Minnesota, Minnespolis
MN 55455 (USA)
Fax: (+1)612 6247029
E-mail: que@chem.umn.edu

[**] This work was supported by the Norwegian Research Council (AG), the VISTA program of Statoil (Norway) and of the Norwegian Academy of the Sciences and Letters (AG), a Senior Fellowship of the San Diego Supercomputer Center (AG), a Socrates/Erasmus scholarship (EM), and grant no. GM-38767 of the US National Institutes of Health (LQ).

Supporting information for this article is available on the WWW under http://www.angewandte.org or from the author. Optimized Cartesian coordinates of the molecules studied in this work are available.

 © 2004 Wiley-VCH Verlag GmbH & Co. KGaA, Weinheim DOI: 10.1002/anie.200351768

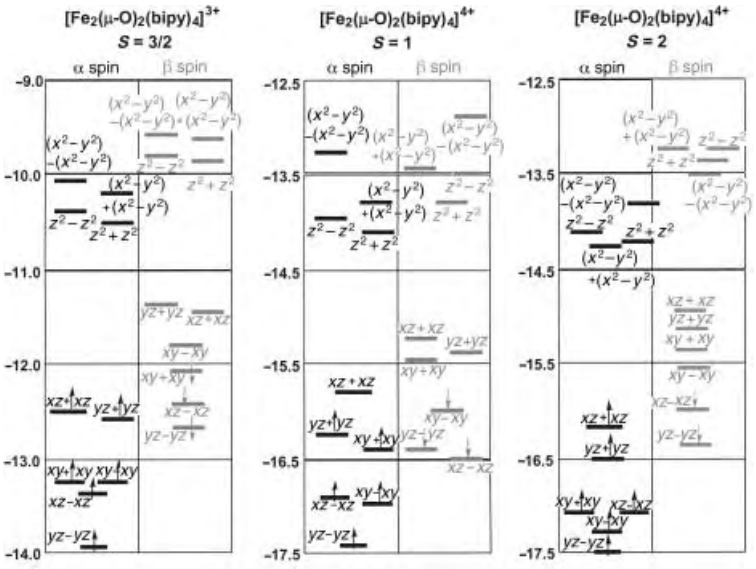


Figure 1. MO energy level diagrams for $\{Fe_2(\mu\text{-}O)_2\}$ model complexes studied. The energy scale is in eV. The orbital energies of these MOs are listed in the Supporting Information.

$[(bipy)_2Fe(\mu\text{-}O)_2Fe(bipy)_2]^{4+}$ are found to be comparable in energy, with the triplet state 0.18 eV above the quintet state. Although a triplet ground state has been found for the model complex studied experimentally,[13] the energy difference of 0.18 eV is at or below the threshold of the accuracy with which DFT can currently describe energy differences between spin states of transition-metal compounds.[24] By comparison, the $S=0$ state, which we also examined lies above the ground state by a substantial margin of 0.84 eV,[25] exhibits a distinctly non-aufbau orbital energy spectrum and is clearly excluded as a possible candidate as the ground state. Apparently, the dense spacing of the t_{2g} band discourages maximum spin pairing of the Fe 3d electrons, which is one of the key insights provided by these calculations.

Figure 3 presents MO energy-level diagrams for $[\{(por)Fe\}_2N]$ and $[\{(por)Fe\}_2N]^+$ and Figure 4 depicts some of these MOs pictorially. The linear Fe-N-Fe arrangement[22,23] in these compounds reflects strong Fe-N-Fe π-bonding resulting in much larger energy splittings within the t_{2g} bands in these compounds (Figure 4) compared with the $\{Fe_2(\mu\text{-}O)_2\}$ complexes described above. These band gaps result in maximum pairing of the Fe electron spins in the nitrido-bridged heme dimers. A similar scenario also holds for carbido-bridged Fe^{IV} porphyrin dimers[26,27] and oxo-bridged Fe^{IV} corrole dimers.[28,29] It thus appears that the paramagnetism of the $\{Fe_2(\mu\text{-}O)_2\}$ complexes studied and the maximal spin pairing in high-valent nitrido-bridged heme dimers reflect a difference in the coordination geometry in the two families of dinuclear complexes: an edge-sharing bioctahedral arrangement in the former versus a corner-sharing arrangement in the latter complexes.

Figure 5 presents key optimized geometry parameters for the complexes studied and these are in general in excellent agreement with those found from crystallographic analyses of closely related species. In the optimized structure of $[(bipy)_2Fe(\mu\text{-}O)_2Fe(bipy)_2]^{3+}$, the interatomic distances are Fe–O = 1.825 Å, $Fe–N_{pyridine}$ = 1.990 and 2.074 Å, Fe–Fe = 2.691 Å, and the Fe-O-Fe angle is 95°. These values can be compared with those obtained in a crystallographic analysis of $[Fe_2(\mu\text{-}O)_2(5\text{-}Et_3\text{-}TPA)_2](ClO_4)_3$ (5-Et_3-TPA = tris[(5-ethyl-2-pyridyl)methyl]amine), in which the interatomic distances are Fe–O = 1.827 (average of 1.805(3) and 1.860(3) Å), $Fe–N_{pyridine}$ = 2.003(3) and 2.025(3) Å, Fe–Fe = 2.683(1) Å, and the Fe-O-Fe angle is 94.1°.[11] For $[(bipy)_2Fe(\mu\text{-}O)_2Fe(bipy)_2]^{4+}$, the optimized interatomic distances for the $S=1$ state are Fe–O = 1.794 Å, Fe–N = 1.988 and 2.070 Å, and Fe–Fe = 2.834 Å; for the $S=2$ state Fe–O = 1.826 Å, Fe–N = 1.996 and 2.056 Å, and Fe–Fe = 2.805 Å, which may be compared with Fe K-edge EXAFS best-fit distances for $[Fe^{IV}_2(\mu\text{-}O)_2(bpmcn)_2](OTf)_4$ of 1 O at 1.79 Å, 3 N at 1.99 Å, and 1 Fe at 2.81 Å.[13] Note that while the iron–ligand distances are quite similar for all the $[(bipy)_2Fe(\mu\text{-}O)_2Fe(bipy)_2]^{3+,4+}$ species studied, there are significant variations in the Fe-O-Fe (and O-Fe-O angles). As a result, the Fe–Fe separation in $[(bipy)_2Fe(\mu\text{-}O)_2Fe(bipy)_2]^{4+}$ is slightly longer than that in $[(bipy)_2Fe(\mu\text{-}O)_2Fe(bipy)_2]^{3+}$, in agreement with a similar expansion observed for $[Fe^{IV}_2(\mu\text{-}O)_2(bpmcn)_2](OTf)_4$ compared with $[Fe_2(\mu\text{-}O)_2(5\text{-}Et_3\text{-}TPA)_2](ClO_4)_3$.[11,13] Without elaborating too much, we also note that the optimized geometry parameters for the nitrido-bridged heme dimers studied are also in excellent agreement with relevant crystallographic results. For example, the calculated $Fe–N_{nitrido}$ distances in $[(por)Fe]_2N$ of 1.645 Å and in $[\{(por)Fe\}_2N]^+$ of 1.619 Å agree closely with the corresponding distances of 1.662 and 1.628 Å in the crystal structures of $[(TPP)Fe]_2N$ and $[\{(TTP)Fe\}_2N]^+$ (TTP = *meso*-tetrakis(*p*-tolyl)porphyrin), respectively.[23] The overall excellent agreement between the calculated and observed geometry parameters constitutes powerful evidence that these calculations correctly describe the electronic structures of $\{Fe^{IV}_2(\mu\text{-}O)_2\}$ intermediates and, specifically, that the canonical MOs presented in Figure 1 and Figure 2 provide a correct description (although, of course, not a unique description) of the electron distributions in the relevant experimentally studied species.

Figure 5 also includes key gross atomic-spin populations for the various species studied. As in the case of heme peroxidase compound II models, the unpaired electronic-spin density is entirely concentrated on the Fe and O atoms for all the $\{Fe_2(\mu\text{-}O)_2\}$ model complexes studied, with small minority spin populations on the nitrogen atoms. The Fe/O spin partitioning ratio for $[(bipy)_2Fe(\mu\text{-}O)_2Fe(bipy)_2]^{3+}$ is approximately 3.04 (1.1653/0.3836); for $[(bipy)_2Fe(\mu\text{-}O)_2Fe(bipy)_2]^{4+}$ in the $S=1$ state, 3.29 (0.8122/0.2466) and in the $S=2$ state, 3.68 (1.5978/0.4345). These ratios are considerably higher than the approximately 1:1 ratio calculated for Fe^{IV}-(por)(O)[30,31,32] but similar to a ratio of about 3:1 calculated for $Fe^{IV}(por)(OCH_3)_2$,[33,34] thus indicating that a μ-oxo ligand, like the univalent methoxide ligand, is significantly less able than a terminal oxo ligand to delocalize electronic spin

 © 2004 Wiley-VCH Verlag GmbH & Co. KGaA, Weinheim

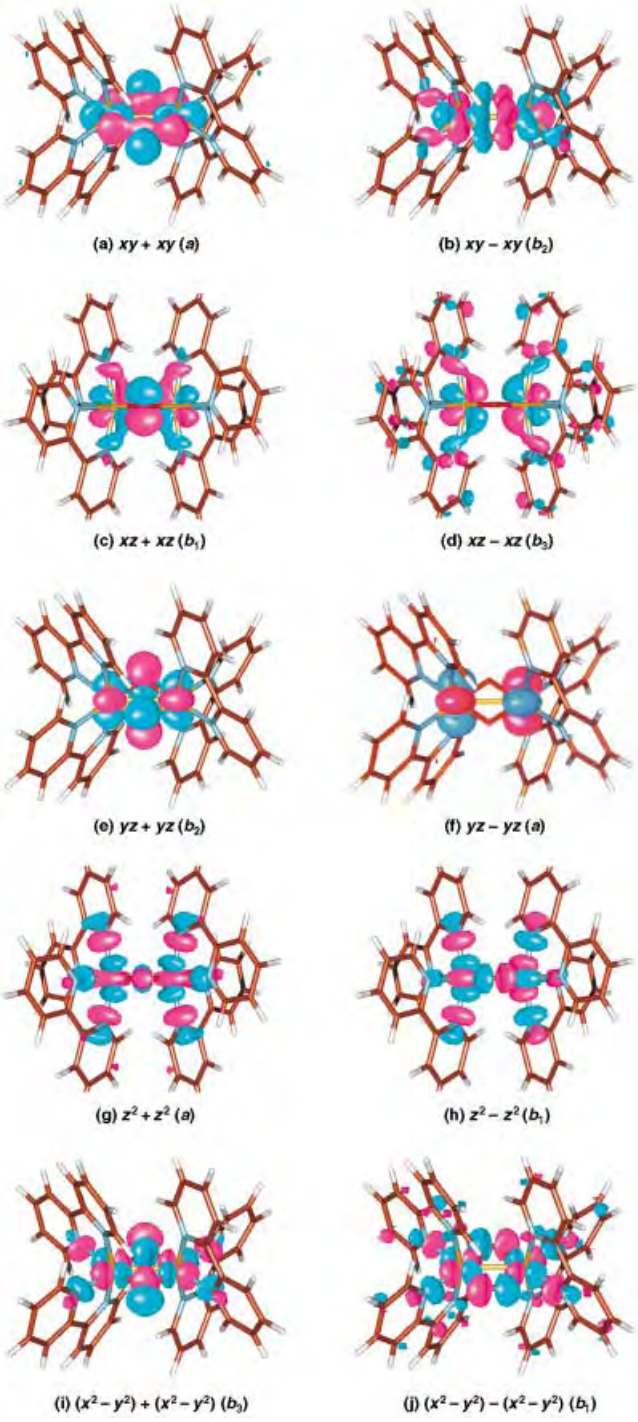


Figure 2. The primarily d-orbital-based α-spin MOs of $[(bipy)_2Fe(\mu\text{-}O)_2Fe(bipy)_2]^{3+}$. The corresponding β-spin MOs exhibit qualitatively similar shapes as the α-spin MOs. The primarily d-orbital-based MOs of the $S=1$ and $S=2$ states of $[(bipy)_2Fe(\mu\text{-}O)_2Fe(bipy)_2]^{4+}$ also exhibit the same qualitative shapes as the MOs depicted here.

density and presumably also positive charge away from high-valent iron centers.

An examination of the Mulliken charges of the three $\{Fe_2(\mu\text{-}O)_2\}$ species studied (Figure 5) provided further insights into this issue. The charges on the Fe, O, N_{axial}, and $N_{equatorial}$ atoms are +0.890, −0.632, −0.428 and −0.359 for

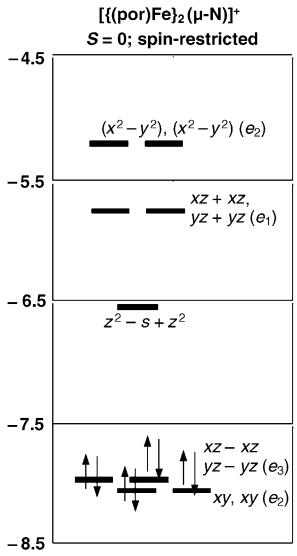


Figure 3. MO energy level diagrams for the nitrido-bridged heme dimers studied. The energy scale is in eV. The numerical values of the orbital energies are listed in the Supporting Information.

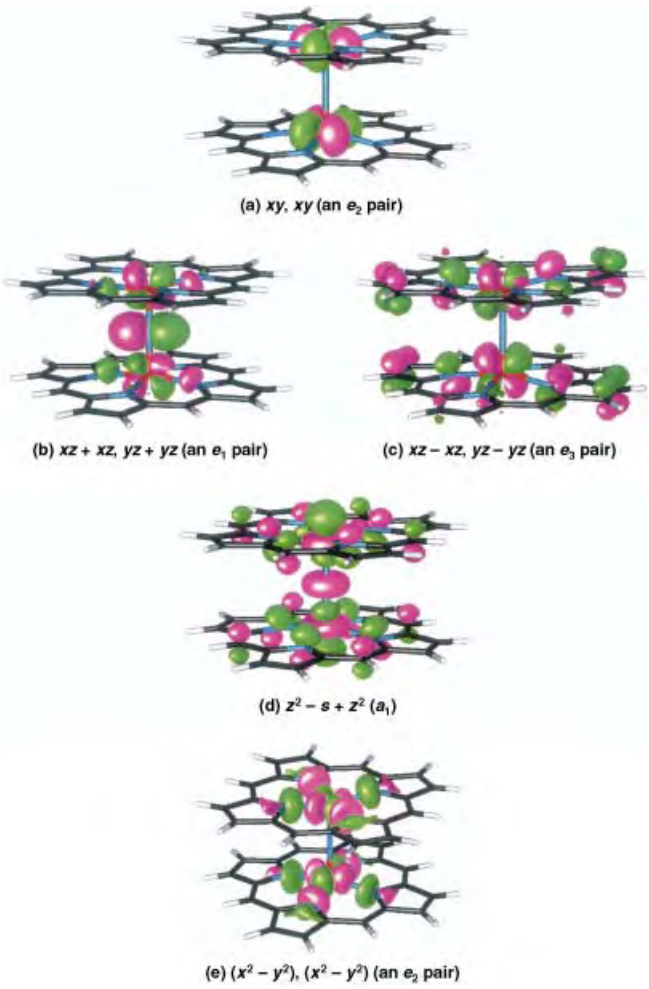


Figure 4. Some primarily d-orbital-based MOs of $[\{(por)Fe\}_2N]^+$ ($S=0$).

 © 2004 Wiley-VCH Verlag GmbH & Co. KGaA, Weinheim

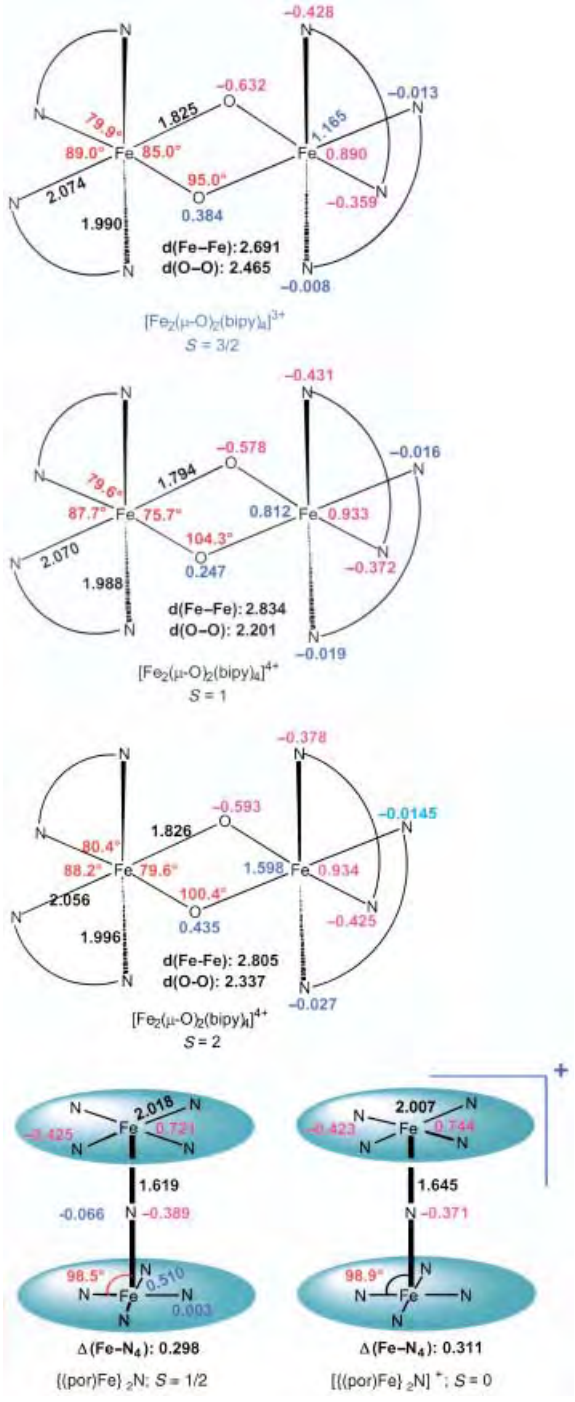


Figure 5. Selected optimized geometry parameters (bond lengths [Å] in black, angles [°] in red), Mulliken charges (magenta), and atomic spin populations (blue) for the molecules studied.

$[(bipy)_2Fe(\mu\text{-}O)_2Fe(bipy)_2]^{3+}$; 0.933, −0.578, −0.431 and −0.372 for the $S=1$ state of $[(bipy)_2Fe(\mu\text{-}O)_2Fe(bipy)_2]^{4+}$; and 0.934, −0.593, −0.425 and −0.378 for the $S=2$ state of $[(bipy)_2Fe(\mu\text{-}O)_2Fe(bipy)_2]^{4+}$, respectively, the equatorial plane being identified with the plane containing the $\{Fe_2(\mu\text{-}O)_2\}$unit. Some noteworthy aspects of these charge distributions are as follows: The equatorial nitrogen atoms carry smaller negative charges than the axial ones, as might be expected from the fact that $Fe-N_{equatorial}$ bonds are longer than the $Fe-N_{axial}$ bonds. The overall molecular charge density profiles of the +3 and +4 species are not radically different, which is consistent with the electroneutrality principle and reflects the ability of the bipy ligands to delocalize the high positive charges of these ionic species. That said, the total Mulliken electronic charge on the $\{Fe_2(\mu\text{-}O)_2\}$ unit is about 30–40% higher in the $[Fe_2(\mu\text{-}O)_2]^{4+}$ species, relative to the $[Fe_2(\mu\text{-}O)_2]^{3+}$ species, which is a significant difference. Accordingly, the oxygen atoms in the $[Fe_2(\mu\text{-}O)_2]^{4+}$ species may be expected to be much more electrophilic relative to the $[Fe_2(\mu\text{-}O)_2]^{3+}$ species. This has indeed been observed to be the case. Thus, in the context of C–H activation, while $[Fe_2(\mu\text{-}O)_2(tpa)_2]^{3+}$ only reacts with substrates with activated C–H bonds such as ethylbenzene and cumene, $[Fe^{IV}_2(\mu\text{-}O)_2(bpmcn)_2]^{4+}$ was found to react with adamantane at −40 °C under Ar, affording 1-adamantanol and 2-adamantanone in 56% and 20% yield, respectively.[13]

In summary, DFT calculations have provided a framework for understanding the electronic structures of $\{Fe^{IV}_2(\mu\text{-}O)_2\}$ intermediates with locally low-spin metal centers, species that may actually occur in Nature as reactive intermediates of non-heme diiron alkane monooxygenases such as AlkB. The calculations also explain why these intermediates exhibit different ground spin states relative to high-valent μ-nitrido/carbido heme dimers, despite the same formal metal oxidation states. The close agreement between theory and experiment with respect to key geometry parameters provides strong evidence that the calculations presented here faithfully describe the actual electronic structures of the relevant synthetic $\{Fe_2(\mu\text{-}O)_2\}$ intermediates.

Received: April 28, 2003 [Z51768]

Keywords: density functional calculations · iron · O ligands · porphyrinoids

[1] S. J. Lippard, J. M. Breg, *Principles of Bioinorganic Chemistry*, University Science Books, Mill Valley, CA, **1994**.
[2] L. Que, W. B. Tolman, *Angew. Chem.* **2002**, *114*, 1160; *Angew. Chem. Int. Ed.* **2002**, *41*, 1114–1137; Corrigendum: L. Que, W. B. Tolman, *Angew. Chem.* **2002**, *114*, 1900; *Angew. Chem. Int. Ed.* **2002**, *41*, 1821.
[3] V. K. Yachandra, K. Sauer, M. P. Klein, *Chem. Rev.* **1996**, *96*, 2927–2950.
[4] R. L. Lieberman, D. B. Shrestha, P. E. Doan, B. M. Hoffman, T. L. Stemmler, A. C. Rosenzweig, *Proc. Natl. Acad. Sci. USA* **2003**, *100*, 3820–3825, and references therein.
[5] L. Shu, J. C. Nesheim, K. Kauffman, E. Münck, J. D. Lipscomb, L. Que, Jr., *Science* **1997**, *275*, 515–518.
[6] M. Merkx, D. A. Kopp, M. H. Sazinsky, J. L. Blazyk, J. Müller, S. J. Lippard, *Angew. Chem.* **2001**, *113*, 2860–2888; *Angew. Chem. Int. Ed.* **2001**, *40*, 2782–2807.
[7] P. J. Riggs-Gelasco, L. Shu, S. Chen, D. Burdi, B. H. Huynh, L. Que, Jr., J. Stubbe, *J. Am. Chem. Soc.* **1998**, *120*, 849–860.
[8] J. A. Broadwater, J. Y. Ai, T. M. Loehr, J. Sanders-Loehr, B. G. Fox, *Biochemistry* **1998**, *37*, 14664–14671.
[9] R. N. Austin, H. K. Chang, G. J. Zylstra, J. T. Groves, *J. Am. Chem. Soc.* **2000**, *122*, 11747–11748.
[10] Y. Dong, H. Fujii, M. P. Hendrich, R. A. Leising, G. Pan, C. R. Randall, E. C. Wilkinson, Y. Zang, L. Que, Jr., B. G. Fox, K.

 © 2004 Wiley-VCH Verlag GmbH & Co. KGaA, Weinheim

Kauffmann, E. Münck, *J. Am. Chem. Soc.* **1997**, *119*, 12683–12684.
[11] H.-F. Hsu, Y. Dong, L. Shu, V. G. Young, Jr., L. Que, Jr., *J. Am. Chem. Soc.* **1999**, *121*, 5230–5237.
[12] A. Ghosh, J. Almlöf, L. Que, Jr., *Angew. Chem.* **1996**, *108*, 770–772; *Angew. Chem. Int. Ed. Engl.* **1996**, *35*, 770; A. J. Skulan, M. A. Hanson, H. -F. Hsu, L. Que, Jr, E. I. Solomon, *J. Am. Chem. Soc.* **2003**, *125*, 7344–7356.
[13] M. Costas, J.-U. Rohde, A. Stubna, R. Y. N. Ho, L. Quaroni, E. Münck, L. Que, Jr., *J. Am. Chem. Soc.* **2001**, *123*, 12931–12932.
[14] S.-K. Lee, B. G. Fox, W. A. Froland, J. D. Lipscomb, E. Münck, *J. Am. Chem. Soc.* **1993**, *115*, 6450–6451.
[15] J. Shanklin, E. B. Cahoon, *Annu. Rev. Plant Physiol. Plant Mol. Biol.* **1998**, *49*, 611–641.
[16] The reaction mechanism and intermediates of sMMO have been extensively studied by DFT. For a recent review, see: V. Guallar, B. F. Gherman, S. J. Lippard, R. A. Friesner, *Curr. Opin. Chem. Biol.* **2002**, *6*, 236–242.
[17] For a review on the mechanism of sMMO, see: D. A. Kopp, S. J. Lippard, *Curr. Opin. Chem. Biol.* **2002**, *6*, 568–576.
[18] For the latest major theoretical paper on the reaction mechanism of sMMO, see: M.-H. Baik, B. F. Gherman, R. A. Friesner, S. J. Lippard, *J. Am. Chem. Soc.* **2002**, *124*, 14608–14615.
[19] For a review of DFT calculations on transition metal-containing enzymes, see: P. E. M. Siegbahn, M. R. A. Blomberg, *Chem. Rev.* **2000**, *100*, 421–438.
[20] For a review of DFT calculations on high-valent transition metal porphyrins and related complexes, see: A. Ghosh, E. Steene, *J. Biol. Inorg. Chem.* **2001**, *6*, 739–752.
[21] For additional technical details, the reader is referred to the ADF program manual, available from: Scientific Computing and Modeling, Department of Theoretical Chemistry, Vrije Universiteit, 1081 HV Amsterdam, The Netherlands.
[22] For the first report of a nitrido-bridged heme dimer, $[(TPP)Fe]_2N$ (TPP = *meso*-tetraphenylporphyrinato), see: D. A. Summerville, I. A. Cohen, *J. Am. Chem. Soc.* **1976**, *98*, 1747–1752.
[23] For a recent study, see: M. Li, M. Shang, N. Ehlinger, C. E. Schulz, W. R. Scheidt, *Inorg. Chem.* **2000**. *39*, 580–583.
[24] A. Ghosh, P. R. Taylor, *Curr. Opin. Chem. Biol.* **2003**, *7*, 113–124.
[25] While an energy difference of 0.85 eV is substantial, we cannot be sure of the exact energy of the $S=0$ state relative to the lower-energy paramagnetic states. The present $S=0$ calculation was carried out in a simple-minded manner by a spin-unrestricted calculation with the assumption that there are no unpaired electrons. A broken-symmetry DFT or an MCSCF (CASSCF) calculation might be considered more meaningful, but as discussed elsewhere [24], even such calculations are unlikely to yield reliable energy differences. More advanced calculations such as CASPT2 or CCSD(T) are currently not feasible for the systems studied. Again, ref [24] provides a critical comparison of all these methods.
[26] D. Mansuy, J.-P. Lecompte, J.-C. Chottard, J.-F. Bartoli, *Inorg. Chem.* **1981**, *20*, 3119–3121.
[27] J. P. Battioni, D. Dupre, D. Mansuy, *J. Organomet. Chem.* **1981**, *214*, 303–309.
[28] E. Vogel, S. Will, A. Schulze Tilling, L. Neumann, J. Lex, E. Bill, A. X. Trautwein, K. Wieghardt, *Angew. Chem.* **1994**, *106*, 771; *Angew. Chem. Int. Ed. Engl.* **1994**, *33*, 731.
[29] E. Steene, T. Wondimagegn, A. Ghosh, *J. Phys. Chem. B* **2001**, *105*, 11406–11413; Erratum: E. Steene, T. Wondimagegn, A. Ghosh, *J. Phys. Chem. B* **2002**, *106*, 5312–5312.
[30] A. Ghosh, J. Almlöf, L. Que, Jr., *J. Phys. Chem.* **1994**, *98*, 5576–5579.
[31] H. Kuramochi, L. Noodleman, D. A. Case, *J. Am. Chem. Soc.* **1997**, *119*, 11442–11451.
[32] A. Dey, A. Ghosh, *J. Am. Chem. Soc.* **2002**, *124*, 3206–3207.
[33] DFT calculations on $Fe^{IV}(por)(OCH_3)_2$: J. Conradie, J. Swarts, A. Ghosh, *J. Phys. Chem. B*, **2004**, *108*, 452–456.
[34] Experimental characterization of $[Fe^{IV}(TMP)(OCH_3)_2]$ (TMP = *meso*-tetramesitylporphyrinato): J. T. Groves, R. Quinn, T. J. McMurry, M. Nakamura, G. Lang, B. Boso, *J. Am. Chem. Soc.* **1985**, *107*, 354–360.

 © 2004 Wiley-VCH Verlag GmbH & Co. KGaA, Weinheim

Fullerene/Azacalixarene Complexes

Synthesis, Structure, and [60]Fullerene Complexation Properties of Azacalix[*m*]arene[*n*]pyridines**

Mei-Xiang Wang, Xiao-Hang Zhang, and Qi-Yu Zheng*

Since Atwood et al.[1] and Shinkai et al.[2] independently discovered the selective formation of a sparingly soluble C_{60}/*p*-*t*Bu-calix[8]arene complex in toluene in 1994, there has been an increasing interest in supramolecular fullerene chemistry because of its potential applications in chemistry, biology, and materials sciences.[3] The design of host molecules capable of recognizing fullerenes, one of the most challenging and thrilling tasks in this field, is mainly based on the complementarity principle. The utilization of concave/convex interaction, for example, has resulted in the emergence of a few macrocyclic [60]fullerene receptors such as calix[*n*]arenes,[1,2,4] homooxacalix[3]arene,[4b,5] γ-cyclodextrin (γ-CD),[6] cyclotriveratrylene (CTV),[7] and crown ethers.[8] Intriguingly, however, porphyrins and metalloporphyrins with planar π surfaces have also been shown to interact with the curved π surface of fullerenes, predominantly through van der Waals dispersion forces.[9] To enhance the complexation power of receptors or to increase the stability of complexes, strategies for constructing molecular clefts such as bis(calix[*n*]arenes)[10] and "jaws porphyrins"[11] have been successfully followed.

The past decade has seen a tremendous development in calixarene chemistry, and it has now become an indispensable part of supramolecular chemistry.[12–15] While efforts are still being expended on derivatization of basic calixarene skeletons to improve their cavities and therefore their selective recognition properties towards various guest molecules, a

[*] Prof. Dr. M.-X. Wang, X.-H. Zhang, Dr. Q.-Y. Zheng
Laboratory of Chemical Biology, Center for Molecular Science
Institute of Chemistry, Chinese Academy of Sciences
Beijing 100080 (China)
Fax: (+86) 106-254-9563
E-mail: mxwang@iccas.ac.cn

[**] This research was supported by the National Science Foundation of China, the State Major Basic Research Development Program (No. G2000078100, G2000077502), MOST (Grant No. 2002CCA03100), and the Chinese Academy of Sciences.

Supporting information for this article is available on the WWW under http://www.angewandte.org or from the author.

 © 2004 Wiley-VCH Verlag GmbH & Co. KGaA, Weinheim DOI: 10.1002/anie.200351975

more recent development in this field is the construction of new calixarenes by replacing the methylene bridges with heteroatoms[16] such as nitrogen,[17] sulphur,[18] and other elements,[16,19] or their phenol units with pyrrole,[20] pyridine,[21] and other heteroarene species.[16,22] This has led to a number of intriguing macrocycles, such as thiacalixarenes[18] and calixpyrroles.[20] To develop novel and efficient host molecules, we envisaged that the incorporation of nitrogen atoms into calixarenes would generate intriguing azacalixarenes and azacalixpyridines or their hydrides. Because the bridging amino-nitrogen atoms can adopt sp^3- and/or sp^2-hybridized configurations with or without conjugation to the neighboring benzene or pyridine rings, the designed macrocycles would be subject to self-tuning by formation of various cavities corresponding to the presence or absence of a guest species. The conjugative effect of the bridging amino groups would also increase the electron density of the π surface of the resulting concave molecules and therefore enhance the binding affinity towards the electron-deficient curved π surfaces of fullerenes. Here we report a convenient fragment-coupling synthesis of novel azacalix[*m*]arene[*n*]pyridine host molecules, their molecular structures, and unique fullerene-complexation properties.

As illustrated in Scheme 1, *m*-phenylenediamine (**1**) condensed efficiently with 2,6-dibromopyridine (**2**) in the presence of an excess of KO*t*Bu to afford *N*,*N*′-bis(6′-bromopyrid-2′-yl)-*m*-phenylenediamine (**3**) in excellent yield. Treatment of **3** with methyl iodide and KO*t*Bu led efficiently to the formation of molecular fragment **4** in 90% yield. Palladium-catalyzed double aryl amination[23] of **4** with *N*,*N*′-dimethyl-*m*-phenylenediamine (**5**) in refluxing toluene furnished macrocyclic azacalix[2]arene[2]pyridine **6** ($n=1$) and azacalix[4]arene[4]pyridine **7** ($n=3$) in 26 and 22% yields, respectively (see Supporting Information). When the intermolecular cyclocondensation of **4** and **5** was performed at lower temperature (104 °C), the larger ring compound **7** was obtained as the major product in 26% yield.

Recrystallization of **6** from hexane/ethyl acetate gave crystals suitable for X-ray structure analysis.[27] As shown in Figure 1, **6** adopts a heavily twisted 1,3-alternate conformation. This is in sharp contrast to the solid-state structures of

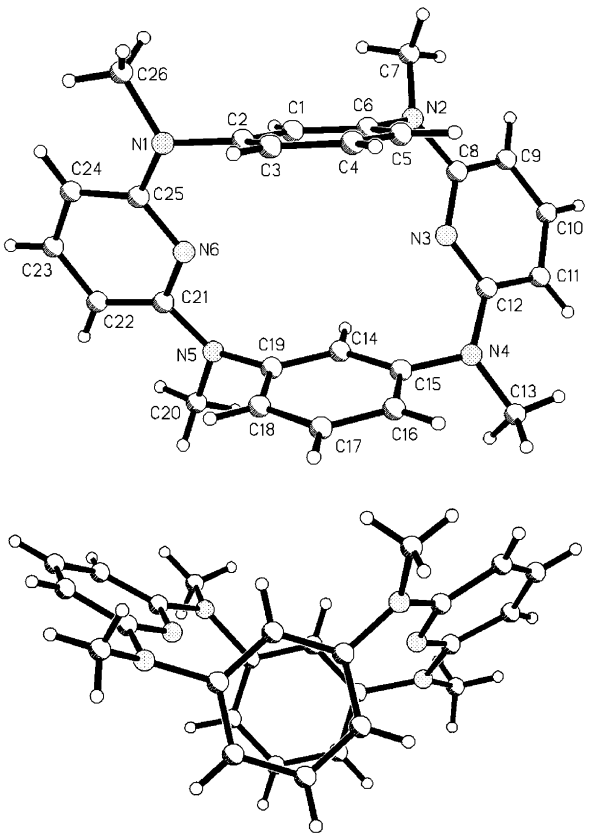
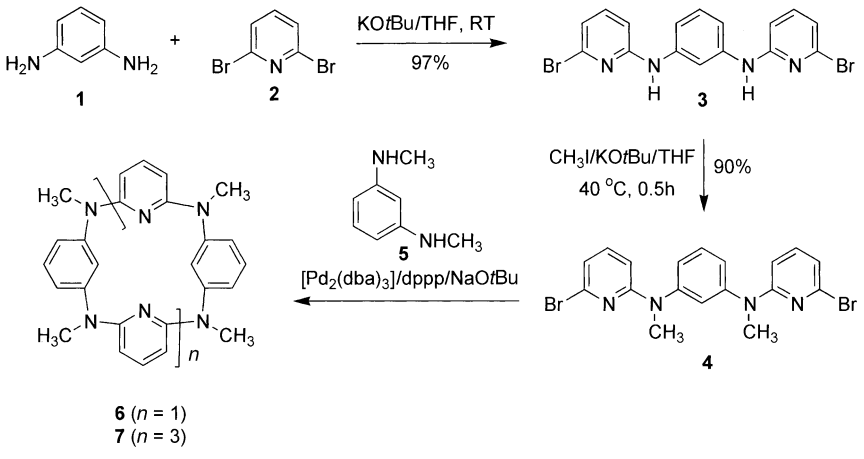


Figure 1. X-ray crystal structure of **6**.

azacalix[4]arene[17a] and of calix[4]pyridine,[21a] which have been determined as S_4 and a partial-cone conformation, respectively. Two of the benzene rings in the structure are almost face-to-face parallel but with a twist angel of 30°. The shortest C–C distance between these rings is 4.36 Å (C1–C14), while the C4–C17 distance is 5.09 Å. Interestingly, the crystal structure also reveals that all bridging amino groups conjugate with the neighboring pyridine rings rather than with benzene rings, with the two pairs of methyl groups located on the two pyridine planes. The four methyl groups are approximately *cis*-configured (rccc). The cavity of the azacalix[2]arene[2]pyridine **6** can be regarded as being constructed by two benzene and two conjugated 2,6-bis(methylamino)pyridine planar segments in a twisted 1,3-*alternate* fashion (Figure 1).

X-ray structure analysis of single crystals of azacalix[4]arene[4]pyridine **7**,[27] which were obtained directly from petroleum ether/ethyl acetate after column chromatography, showed an interesting molecular structure. First, as in **6**, all the bridging amino groups in **7** conjugate with the pyridine rings rather than with the benzene rings, and all methyl groups lie on the planes of the neighboring pyridine rings. Thus, all



Scheme 1. Fragment-coupling approach to azacalix[4]pyridine.

 © 2004 Wiley-VCH Verlag GmbH & Co. KGaA, Weinheim

nitrogen atoms of the bridging amino groups adopt sp^2 configurations, and the macrocycle is derived from four benzene rings and four conjugated 2,6-bis(methylamino)pyridine planar units. Second, the molecule forms a large, diamond-shaped cavity in which the longest distance between two opposite benzene rings is 12.2 Å (Figure 2, top view). In

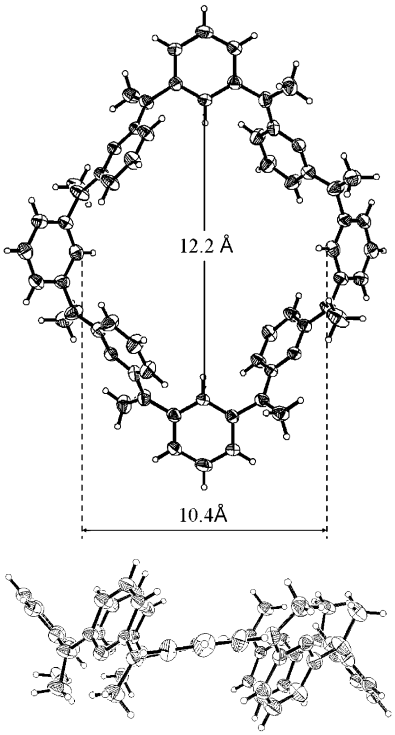


Figure 2. X-ray crystal structure of **7**.

addition, the whole cavity of the molecule is composed of two identical partial cone loops consisting of one benzene and two 2,6-bis(methylamino)pyridine planar segments. These two loops of opposite orientation are connected by two benzene moieties such that the molecule has S_2 symmetry. Accordingly, there are two sets of four *cis*-configured methyl groups (rccctttt) attached to the bottom rims of the two partial cone loops. The conformation of the molecule can thus be viewed as a 1,2,3-*partial cone*, resembling a double-ended spoon (Figure 2, side view). Furthermore, four pyridine nitrogen atoms lie on one plane, while eight bridging nitrogen atoms form another two rectangular planes.

Azacalix[*m*]arene[*n*]pyridines exhibit interesting [60]fullerene-complexation properties that depend on the size of the macrocyclic ring. By means of spectrophotometric measurements, for example, we found that **7** can strongly complex [60]fullerene, whereas its smaller homologue **6** has no affinity towards [60]fullerene. On addition of **7** to a solution of [60]fullerene in toluene, the absorption at 437.5 nm in the UV/Vis spectrum increases in intensity and shifts gradually to 452.5 nm (Supporting Information, Figure S1). The interaction of **7** with [60]fullerene was clearly evidenced by a color change of [60]fullerene in toluene from characteristic red-purple to light brown (Figure 3). A Job plot[10c,24] indicated 1:1



Figure 3. Color change from red-purple (left, $[C_{60}] = 1.084 \times 10^{-4}$ mol dm^{-3}) to light brown (right) on complexation with **6** (middle, colorless, 1.084×10^{-4} mol dm^{-3}).

complexation of **7** with [60]fullerene in toluene (Supporting Information, Figure S2). To further study the recognition of [60]fullerene by **7**, a fluorescence titration was conducted (Figure 4). The fluorescence intensity of **7** at about $\lambda_{em} =$ 402 nm decreased constantly with increasing concentration

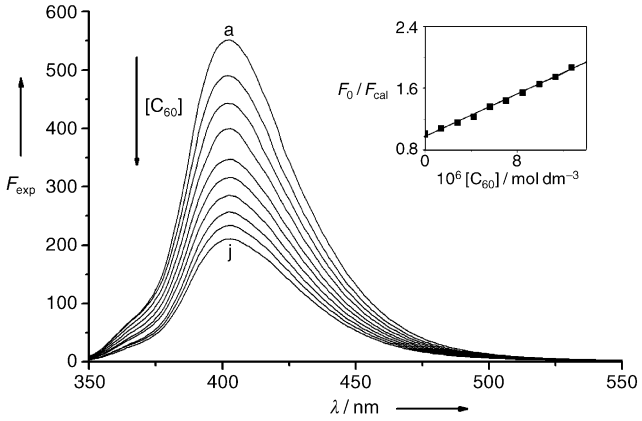


Figure 4. Emission spectra ($\lambda_{exc} = 336$ nm) of **7** (3.423×10^{-6} mol dm^{-3}) in the presence of C_{60} in toluene at 25 °C. The concentrations of C_{60} for curves a–j (from top to bottom) are 0.0, 1.419, 2.837, 4.256, 5.675, 7.093, 8.512, 9.931, 11.349, and 12.768×10^{-6} mol dm^{-3}. Inset: Variation of fluorescence intensity F_0/F_{cal} of **7** with increasing C_{60} concentration.

of [60]fullerene. To eliminate the competitive absorption of [60]fullerene at both the excitation and emission wavelengths, the fluorescence intensity F_{exp} of **7** was calibrated to F_{cal} according to a literature method.[25] The quenching was found to follow a Stern–Volmer equation, and the dependence of calibrated F_0/F_{cal} on the concentration of [60]fullerene is illustrated in the inset to Figure 4. The stability constant K_s calculated from the plot of F_0/F_{cal} versus [60]fullerene concentration is $70\,680 \pm 2060\ \text{M}^{-1}$.[26] To the best of our knowledge, this is the largest K_s value obtained up to date for complexation of [60]fullerene with a mono-macrocyclic receptor other than molecular clefts such as biscalix[*n*]arenes[10] and "jaws porphyrins".[11]

Azacalix[4]arene[4]pyridine **7** has even higher complexation capability towards [70]fullerene. As indicated by the

 © 2004 Wiley-VCH Verlag GmbH & Co. KGaA, Weinheim

UV/Vis spectrum (Supporting Information, Figure S3) and the Job plot[10c,24] (Supporting Information, Figure S4), **7** also forms a 1:1 complex with [70]fullerene. A fluorescence titration revealed a stability constant K_s of $136620 \pm 3770\,M^{-1}$, almost twice the stability constant for complexation of **7** and [60]fullerene (see Supporting Information, Figure S5). The stronger affinity of **7** towards [70]fullerene than towards [60]fullerene is most probably due to the giant cavity and the oval shape.[28]

We hoped to determine the solid-state structures of the **7**-[60]fullerene and **7**-[70]fullerene complexes, but no crystals could be obtained. No salient changes were observed in the ^1H and ^{13}C NMR spectra of the complexes in solution. The superior complexation of fullerenes by **7**, which contrasts with the noninteraction between **6** and fullerenes, suggests a steric requirement for fullerene recognition by the macrocyclic receptor. This is consistent with the results of [60]fullerene recognition with different calix[*n*]arenes.[4b] The much higher affinity of **7** ($K_s = 70680 \pm 2060\,M^{-1}$) relative to calix[5]- and [6]arene derivatives ($K_s = 87$–$2120\,M^{-1}$)[4b,d,e] and homooxacalix[3]arene ($K_s = 35 \pm 5\,M^{-1}$)[4b] indicates a clear advantage of introducing amino groups into the bridging positions of calixarenes. However, the strong interaction of **7** with fullerenes is not due to the formation of charge-transfer complexes, because neither new absorption nor emission peaks were observed in spectrophotometric titrations. The precise reason for efficient complexation of fullerenes by azacalix[4]arene[4]pyridine still remains unclear, although it is most probably rationalizble as the van der Waals force between sterically fitted concave and convex π surfaces. The introduction of electron-donating amino groups as the bridging units increases the electron density of the aromatic rings, and therefore might further contribute to enhancing the interaction of the curved surface of the macrocyclic receptor with electron-deficient fullerenes.

In summary, we have developed a fragment-coupling approach for the synthesis of azacalix[*m*]arene[*n*]pyridines. In the solid state, azacalix[2]arene[2]pyridine **6** and azacalix[4]-arene[4]pyridine **7** adopt a heavily twisted 1,3-*alternate* conformation and a double-ended spoon-shaped 1,2,3-*partial cone* conformation, respectively, in which the bridging nitrogen atoms conjugate with the neighboring pyridine rings. We have also shown that **7** is a novel and efficient macrocyclic host molecule that complexes [60]- and [70]fullerene in toluene with K_s values of $70680 \pm 2060\,M^{-1}$ and $136620 \pm 3770\,M^{-1}$, respectively. The color change of [60]fullerene on complexation and the linearity of the plot of F_0/F_{cal} of the receptor against [60]fullerene concentration make **7** a powerful spectrophotometric sensor for [60]fullerene.

Received: May 26, 2003
Revised: October 27, 2003 [Z51975]

Keywords: calixarenes · fullerenes · host–guest systems · supramolecular chemistry

[1] J. L. Atwood, G. A. Koutsantonis, C. L. Raston, *Nature* **1994**, *368*, 229.
[2] T. Suzuki, K. Nakashima, S. Shinkai, *Chem. Lett.* **1994**, 699.
[3] For reviews, see:a) F. Diederich, M. Gomez-Lopez, *Chem. Soc. Rev.* **1999**, *28*, 263; b) Z.-L. Zhong, A. Ikeda, S. Shinkai, Complexation of Fullerenes in *Calixarenes 2001* (Eds.: Z. Asfari, V. Bohmer, J. Vicens, M. Saadioui), Kluwer Academic Publishers, The Netherlands, **2001**, pp. 476–495.
[4] a) R. M. Williams, J. W. Verhoeven, *Recl. Trav. Chim. Pays-Bas* **1992**, *111*, 531; b) A. Ikeda, Y. Suzuki, M. Yoshimura, S. Shinkai, *Tetrahedron* **1998**, *54*, 2497; c) M. Makha, M. J. Hardie, C. L. Raston, *Chem. Commun.* **2002**, 1446; d) H. Haino, M. Yanase, Y. Fukazawa, *Angew. Chem.* **1997**, *109*, 288; *Angew. Chem. Int. Ed. Engl.* **1997**, *36*, 259; e) T. Haino, M. Yanase, Y. Fukazawa, *Angew. Chem.* **1998**, *110*, 1044; *Angew. Chem. Int. Ed.* **1998**, *37*, 997; f) J. L. Atwood, L. J. Barbour, C. L. Raston, I. B. N. Sudria, *Angew. Chem.* **1998**, *110*, 1029; *Angew. Chem. Int. Ed.* **1998**, *37*, 981.
[5] a) K. Tsubaki, K. Tanaka, T. Kinoshita, K. Fuji, *Chem. Commun.* **1998**, 895; b) A. Ikeda, T. Hatano, S. Shinkai, T. Akiyama, S. Yamada, *J. Am. Chem. Soc.* **2001**, *123*, 4855.
[6] Z.-I. Yoshida, H. Yakekuma, S.-I. Takekuma, Y. Matsubara, *Angew. Chem.* **1994**, *106*, 1658; *Angew. Chem. Int. Ed. Engl.* **1994**, *33*, 1597.
[7] J. L. Atwwod, M. J. Barnes, M. G. Gardiner, C. L. Raston, *Chem. Commun.* **1996**, 1449.
[8] S. Bhattacharya, A. Sharma, S. K. Nayak, S. Chattopadhyay, A. K. Mukherjee, *J. Phys. Chem. B* **2003**, *107*, 4213.
[9] a) Y. Sun, T. Drovetskaya, R. D. Bolskar, R. Bau, P. D. W. Boyd, C. A. Reed, *J. Org. Chem.* **1997**, *62*, 3642; M. M. Olmstead, D. A. Costa, K. Maitra, B. C. Noll, S. L. Phillips, P. M. Van Calcar, A. L. Balch, *J. Am. Chem. Soc.* **1999**, *121*, 7090; c) P. D. W. Boyd, M. C. Hodgson, C. E. F. Rickard, A. G. Oliver, L. Chaker, P. J. Brothers, R. D. Bolskar, F. S. Tham, C. A. Reed, *J. Am. Chem. Soc.* **1999**, *121*, 10487.
[10] a) T. Haino, M. Yanase, Y. Fukazawa, *Angew. Chem.* **1998**, *110*, 1044; *Angew. Chem. Int. Ed.* **1998**, *37*, 997; b) L. Wang, C. D. Gutsche, *J. Am. Chem. Soc.* **1998**, *120*, 12226; c) J. Wang, S. G. Bodige, W. H. Watson, C. D. Gutsche, *J. Org. Chem.* **2000**, *65*, 8260; d) T. Haino, H. Araki, Y. Fujiwara, Y. Tanimoto, Y. Fukazawa, *Chem. Commun.* **2002**, 2148; T. Haino, Y. Yamanaka, H. Araki, Y. Fukazawa, *Chem. Commun.* **2002**, 402.
[11] a) D. Sun, F. S. Tham, C. A. Reed, L. Chaker, M. Burgess, P. D. W. Boyd, *J. Am. Chem. Soc.* **2000**, *122*, 10704b) J.-Y. Zheng, K. Tashiro, Y. Hirabayashi, K. Kinbara, K. Saigo, T. Aida, S. Sakamoto, K. Yamaguchi, *Angew. Chem.* **2001**, *113*, 1909; *Angew. Chem. Int. Ed.* **2001**, *40*, 1857; c) Y. Kubo, A. Sugasaki, M. Ikeda, K. Sugiyasu, K. Sonoda, A. Ikeda, M. Takeuchi, S. Shinkai, *Org. Lett.* **2002**, *4*, 925; d) M. Ayabe, A. Ikeda, S. Shinkai, S. Sakamoto, K. Yamaguchi, *Chem. Commun.* **2002**, 1032; e) M. Ayabe, A. Ikeda, Y. Kubo, M. takeuchi, S. Shinkai, *Angew. Chem.* **2002**, *114*, 2914; *Angew. Chem. Int. Ed.* **2002**, *41*, 2790; f) D. Sun, F. S. Tham, C. A. Reed, L. Chaker, P. D. W. Boyd, *J. Am. Chem. Soc.* **2002**, *124*, 6604.
[12] *Calixarenes 2001* (Eds.: Z. Asfari, V. Böhmer, J. Harrowfield, J. Vicens, M. Saadioui), Kluwer Academic Publishers, Dordrecht, **2001**.
[13] C. D. Gutsche, *Calixarenes Revisited*, The Royal Society of Chemistry, Cambridge, **1998**.
[14] *Calixarenes in Action* (Eds.: L. Mandolini, R. Ungaro), Imperial College, London, **2000**.
[15] G. J. Lumetta, R. D. Rogers, A. S. Gopalan, *Calixarenes for Separation*, ACS, Washington, **2000**.
[16] For a useful overview of heteroatom-bridged calixarenes, see B. König, M. H. Fonseca, *Eur. J. Inorg. Chem.* **2000**, 2303.
[17] a) A. Ito, Y. Ono, K. Tanaka, *New J. Chem.* **1998**, 779; b) A. Ito, Y. Ono, K. Tanaka, *J. Org. Chem.* **1999**, *64*, 8236.
[18] a) H. Kumagai, M. Hasegawa, S. Miyanari, Y. Sugawa, Y. Sato, T. Hori, S. Ueda, H. Kamiyama, S. Miyano, *Tetrahedron Lett.* **1997**,

 © 2004 Wiley-VCH Verlag GmbH & Co. KGaA, Weinheim

38, 3971; b) H. Iki, C. Kabuto, T. Fukushima, H. Kumagai, H. Takeya, S. Miyanari, T. Miyashi, S. Miyano, *Tetrahedron* **2000**, *56*, 1437; c) H. Akdas, L. Bringel, E. Graf, M. W. Hosseini, G. Mislin, J. Pansanel, A. De Cian, J. Fischer, *Tetrahedron Lett.* **1998**, *39*, 2311.

[19] a) E. E. Boros, C. W. Andrews, A. O. Davis, *J. Org. Chem.* **1996**, *61*, 2553; b) B. König, M. Rödel, P. Bubenitschek, P. G. Jones, I. Thondorf, *J. Org. Chem.* **1995**, *60*, 7406; c) M. Yoshida, M. Goto, F. Nakanishi, *Organometallics* **1999**, *18*, 1465.

[20] a) P. A. Gale, J. L. Sessler, V. Král, *Chem. Commun.* **1998**, 1; b) S. Depraetere, M. Smet, W. Dehaen, *Angew. Chem.* **1999**, *111*, 3556; *Angew. Chem. Int. Ed.* **1999**, *38*, 3359; c) B. Turner, A. Shterenberg, M. Kapon, K. Suwinska, Y. Eichen, *Chem. Commun.* **2001**, 13; d) C. Bucher, R. S. Zimmerman, V. Lynch, V. Král, J. L. Sessler, *J. Am. Chem. Soc.* **2001**, *123*, 2099; e) G. Cafeo, F. H. Kohnke, G. L. La Torre, M. F. Parisi, R. P. Nascone, A. J. P. White, D. J. Williams, *Chem. Eur. J.* **2002**, *8*, 3148; f) C. Floriani, *Chem. Commun.* **1996**, 1257; g) P. A. Gale, P. Anzenbacher, J. L. Sessler, *Coord. Chem. Rev.* **2001**, *222*, 57.

[21] a) V. Král, P. A. Gale, P. Anzenbacher, K. Jursiková, V. Lynch, J. L. Sessler, *Chem. Commun.* **1998**, 9; b) J. L. Sessler, W.-S. Cho, V. Lynch, V. Král, *Chem. Eur. J.* **2002**, *8*, 1134; c) T. Gerkensmeier, J. Mattay, C. Näther, *Chem. Eur. J.* **2001**, *7*, 465.

[22] a) P. R. Dave, G. Doyle, *J. Org. Chem.* **1995**, *60*, 6946; b) N. Avarvari, N. Mezailles, L. Richard, P. Le Floch, F. Mathey, *Science* **1998**, *280*, 1587c) E. Vogel, M. Pohl, A. Herrmann, T. Wiss, C. König, J. Lex, M. Gross, J. P. Gisselbrecht, *Angew. Chem.* **1996**, *108*, 1677; *Angew. Chem. Int. Ed. Engl.* **1996**, *35*, 1520; d) J. Guillard, O. Meth-Cohn, C. W. Rees, A. J. P. White, D. J. Williams, *Chem. Commun.* **2002**, 232.

[23] S. Wagaw, S. L. Buchwald, *J. Org. Chem.* **1996**, *61*, 7240.

[24] J. Polster, H. Lachmann, *Spectrometric Titrations*, VCH, **1989**, pp. 256–259.

[25] M. Zheng, F. Bai, F. Li, D. Zhu, *J. Appl. Polym. Sci.* **1998**, *70*, 599.

[26] J. Wang, D. Wang, E. K. Miller, D. Moses, G. C. bazan, A. J. Heeger, *Macromolecules* **2000**, *33*, 5153. Both static and dynamic quenching processes can be quantitatively described by the Stern–Volmer equation: $F_0/F = 1 + K_{sv}[\text{quencher}]$, where the F_0 is the fluorescence intensity in the absence of the quencher, and F the fluorescence intensity in the presence of the quencher. The Stern–Volmer constant K_{sv} provides a quantitative measure of the quenching. In static quenching, the Stern–Volmer constant is the association constant for complex formation, that is, $K_{sv}^{S} = [FQ]/[F][Q]$, where [FQ], [F], and [Q] are the concentrations of complex, fluorophore, and quencher, respectively. From the above equation, it is straightforward to calculate the probability f that a fluorophore is not complexed: $f = [F]/([F] + [FQ]) = 1/(1 + K_{sv}^{S}[Q]) = F/F_0$ In our case, the stability constant K_s was calculated from the equation $F_0/F_{cal} = 1 + K_s[\text{fullerene}]$.

[27] Crystal data for **6** ($C_{26}H_{26}N_6$): $M_r = 422.53$, triclinic, space group $P\bar{1}$, $a = 9.6577(10)$, $b = 9.9349(11)$, $c = 12.3553(7)$ Å, $\alpha = 90.132(5)$, $\beta = 104.705(4)$, $\gamma = 109.768(3)°$, $V = 1074.0(17)$ Å^3, $T = 293(2)$ K, $Z = 2$, $\rho_{calcd} = 1.307$ g cm^{-3}, $\mu(Mo_{K\alpha}) = 0.081$ mm^{-1}; of a total of 7449 reflections, 4752 unique reflections ($R_{int} = 0.0523$) were used in the refinement by full-matrix least-squares methods on F^2, which converged to $R_F = 0.0649$ [$I > 2\sigma(I)$], 0.0935 (all data) and $Rw(F^2) = 0.1853$ [$I > 2\sigma(I)$], 0.2007 (all data). Crystal data for **7**·2 H_2O ($C_{52}H_{56}N_{12}O_2$): $M_r = 881.09$, triclinic, space group $P\bar{1}$, $a = 8.8164(18)$, $b = 11.5548(18)$, $c = 13.538(2)$ Å, $\alpha = 78.438(12)$, $\beta = 89.066(6)$, $\gamma = 75.572(3)°$, $V = 1307.8(4)$ Å^3, $T = 293(2)$ K, $Z = 1$, $\rho_{calcd} = 1.119$ g cm^{-3}, $\mu(Mo_{K\alpha}) = 0.071$ mm^{-1}; of a total of 9311 reflections, 5837 unique reflections ($R_{int} = 0.0471$) were used in the refinement by full-matrix least-squares methods on F^2, which converged to $R_F = 0.0642$ [$I > 2\sigma(I)$], 0.1944 (all data) and $Rw(F^2) = 0.1607$ [$I > 2\sigma(I)$], 0.1907 (all data). CCDC-211206 (**7**) and CCDC-211207 (**6**) contain the supplementary crystallographic data for this paper. These data can be obtained free of charge via www.ccdc.cam.ac.uk/conts/retrieving.html (or from the Cambridge Crystallographic Data Centre, 12, Union Road, Cambridge CB21EZ, UK; fax: (+44) 1223-336-033; or deposit@ccdc.cam.ac.uk).

[28] We thank one of the referees for suggesting an investigation on the complexation of **7** and [70]fullerene.

Protein–Ligand Interactions

Stochastic Detection of Monovalent and Bivalent Protein–Ligand Interactions**

Stefan Howorka, Joonwoo Nam, Hagan Bayley, and Daniel Kahne*

The term "multivalency" refers to the phenomenon in which a molecule that contains multiple binding sites binds simultaneously to multiple ligands.[1] Multivalency can lead to significant enhancements in binding strength for weakly binding ligands.[2] Prominent examples of multivalent systems include binding by antibodies and lectins, and the receptor-ligand interactions involved in cell adhesion or viral attachment. Both for fundamental reasons and so that the phenomenon can be exploited in the design of inhibitors,[3–6] there is great interest in understanding multivalent binding in detail.

[*] Dr. S. Howorka,[+] Prof. H. Bayley[++]
The Texas A&M University System Health Science Center
Department of Medical Biochemistry & Genetics
440 Reynolds Medical Building
College Station, TX 77843-1114 (USA)
E-mail: howorka@medicine.tamu.edu

J. Nam, Prof. D. Kahne
Department of Chemistry, Princeton University
Princeton, NJ 08544 (USA)

[+] Present address:
Upper Austrian Research GmbH
Scharitzerstrasse 6–8/4, A-4020 (Austria)
Fax: (+43) 732-6060-7930

[++] Present addresses:
Department of Chemistry, Texas A&M University
College Station, TX 77843-3255
and
Department of Chemistry, University of Oxford
Chemistry Research Laboratory, Mansfield Road
Oxford, OX1 3TA, England (UK)

[**] This work was supported by the U.S. Department of Energy, the DoD Tri-Service Technology Program, the National Institutes of Health, the Office of Naval Research (Multidisciplinary University Research Initiative 1999), and the Texas Advanced Technology Program. H.B. is the holder of a Royal Society-Wolfson Research Merit Award. S.H. held fellowships from the Austrian Science Foundation (Fonds zur Förderung der wissenschaftlichen Forschung) and the Max-Kade Foundation.

Supporting information for this article is available on the WWW under http://www.angewandte.org or from the author.

 © 2004 Wiley-VCH Verlag GmbH & Co. KGaA, Weinheim DOI: 10.1002/anie.200352614

Studying the physical chemistry of multivalency has been an enormous challenge, however. Although a wide variety of model systems and techniques have been employed to probe multivalent binding,[1,7–10] all of them have involved ensemble measurements in which specific characteristics of the multivalent systems are averaged and, thus, details of the interactions may be obscured. For example, monovalent and multivalent binding states cannot be observed independently within one experiment, and this complicates the kinetic analysis of multivalent binding. Herein, we describe a new approach to studying multivalent interactions. We show that the binding kinetics of a lectin to one or more ligands can be followed at the single-molecule level by monitoring the ionic current flow through a heptameric protein pore covalently modified with up to seven carbohydrates. This single-molecule approach permits the direct observation of individual monovalent and divalent binding events.

Chemically modified protein pores are powerful tools to study the binding kinetics of ligand receptor combinations at the single molecule level. An individual ligand is tethered to the protein pore and the reversible binding of the corresponding receptor produces transient current blockades in single-channel current recordings. In the past, this approach has been used to study the kinetics of monovalent binding of, for example, complementary DNA strands.[11–13] We wondered whether the single-molecule approach might also be applied to probe the multivalent interactions of carbohydrate binding proteins, with the aid of protein pores carrying

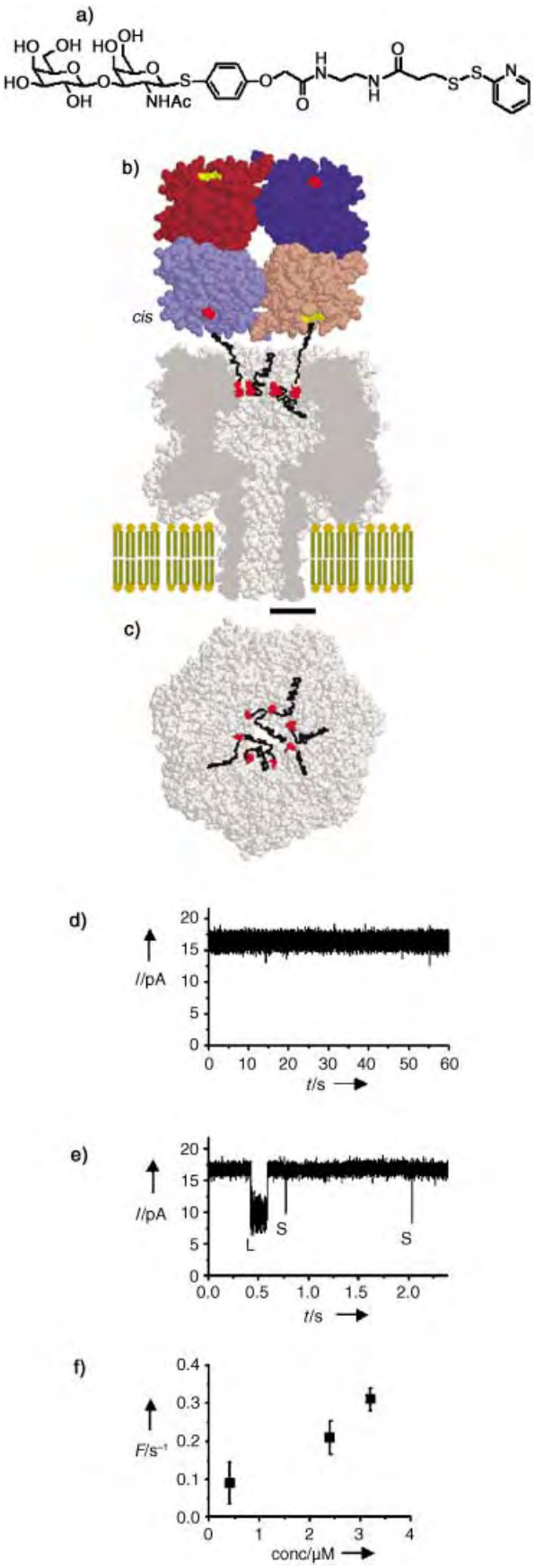


Figure 1. Protein pore 9C-NL_7, an engineered version of heptameric α-hemolysin (αHL) modified at seven sites with the disaccharide natural ligand, and its interaction with the tetrameric lectin from *Bauhinia purpurea*. a) Chemical structure of NL disaccharide D-gal-β-1,3-*N*-acetyl-galactosamine with a 16-atom linker terminated with an *S*-thiopyridyl group used for the coupling to αHL. b) A cross section of a model of 9C-NL_7 carrying the NL disaccharide covalently attached through the linker to each of the seven engineered cysteines residues at position C9 (red). The model of BP is based on the crystal structure of *Griffonia simplicifolia* lectin (PDP ID: 1HQL), which has a high extent of sequence similarity to the BP lectin. In the diagonally arranged pale red and dark red subunits the binding sites (yellow) are on the front side of the model, while those in the pale blue and dark blue subunits are on the back. Their projected positions on the front side are indicated in bright red. The distance between the two lectin binding sites in the pale red and pale blue subunits, which are close to αHL, is 4.6 nm. This value is the distance between the C4 carbon atoms of the galactose units of the two ligands in the crystal structure. The distance for the diagonally positioned subunits of the lectin (e.g. pale red and dark red) is 7.6 nm. This compares to a maximum distance of 5.5 nm between the C4 carbon atoms in galactose of two NL disaccharides attached to distal (i.e., the first and fourth) subunits of 9C-NL_7.The corresponding distance for the first and third subunit is 5.1 nm. Bar, 2 nm. c) Top view of 9C-NL_7. d) Representative single-channel current trace of 9C-NL_7 at a transmembrane potential of +50 mV relative to the *cis* side of the bilayer. e) Representative trace of 9C-NL_7 after the addition of 3.2 μM BP to the *cis* side of the bilayer. Negative current deflection with short (S) and long (L) lifetimes represent individual monovalent and bivalent binding events, respectively. The individual events were not clustered into groups as indicated by the single exponential decay of the distribution in the inter-event interval histogram (data not shown). f) The frequency of occurrence (*F*) of all binding events depends linearly on the concentration of BP.

 © 2004 Wiley-VCH Verlag GmbH & Co. KGaA, Weinheim

multiple copies of the ligand. To address this question, we prepared the thiopyridyl derivative (Figure 1a) of the disaccharide Gal-β-1,3-GalNAc (natural ligand, NL), which is a ligand for the carbohydrate binding protein *Bauhinia purpurea* (BP) lectin.[14,15] The NL disaccharide was then coupled to a cysteine residue engineered at position C9 of α-hemolysin (αHL), a bacterial polypeptide toxin, which forms heptameric pores of known structure .[16] Position C9 is located at the narrower part of the *cis* opening of the αHL pore (Figure 1b, c). By using a procedure based on published work[13] we were able to generate three different αHL heptamers, $H_6$9C-NL_1, $H_5$9C-NL_2, and 9C-NL_7, containing one, two, and seven NL-modified subunits, respectively, and unmodified subunits, H.

Single-channel current recordings of the homoheptamer 9C-NL_7 were performed in 0.6 M KCl, 0.6 mM $CaCl_2$, 0.3 mM $MnCl_2$, and 6 mM Tris-HCl, pH 7.2, at a potential of +50 mV with the *cis* side of the chamber connected to ground. In the absence of BP lectin, the current trace for the channel containing seven chemically modified subunits showed no fluctuations (Figure 1d) and the unitary conductance was 302 ± 50 pS ($n = 18$; *n*, number of independent recordings). This is lower than the conductance of the unmodified pore (Table 1) and suggests that the attached carbohydrates, which are tethered near a narrow part of the pore, can reduce the current flow through steric or electrostatic effects. Upon the addition of 3.2 μM BP lectin to the *cis* side of the homoheptamer, negative current deflections were observed with a mean amplitude of 110 ± 24 pS ($n = 5$) and a wide distribution of durations (Figure 1e). The frequency of occurrence of the events increased with the concentration of BP lectin (Figure 1f), but no events were observed in the presence of the lectin concanavalin A, which does not bind to Gal-β-1,3-GalNAc (data not shown). These results suggest that the current deflections are caused by specific binding of BP lectin to the carbohydrate ligands attached to the subunits. Consistent with this interpretation, the presence of the disulfide bond-breaking agent dithiothreitol led to a stepwise increase in mean conductance and the abolition of the binding events (data not shown). Furthermore, the presence of soluble *N*-acetyl-galactosamine (93 mM), which is known to compete with Gal-β-1,3-GalNAc for binding to BP lectin, led to a 2.4-fold decrease in the frequency of the events.

Two main types of binding events were discerned on further analysis of recordings of the carbohydrate-derivatized pore 9C-NL_7: short (Figure 1e, symbol S) with a mean lifetime, $\tau_{off\text{-}1}$, of 6.5 ± 1.2 ms (78 ± 5% of all events) and long (Figure 1e, symbol L) with a mean lifetime, $\tau_{off\text{-}2}$, of 110 ± 30 ms (22 ± 5% of all events; $n = 4$, Table 2). The two main types of events were separated based on the bi-exponential distribution of the lifetime histograms (see Supporting Information). The lifetime histogram also revealed a third component, and these rare events (less than 1% of all events) were longer ($\tau_{off} \approx 200$ ms) than the main type of long events. The analysis of the current traces yielded values for the frequencies of occurrence for the two main types of binding events, $8.4 \pm 3.1 \times 10^{-2}$ s^{-1} for short and $2.4 \pm 0.9 \times 10^{-2}$ s^{-1} for long events (values normalized to 1 μM BP). We speculated that the short events reflect monovalent binding of BP lectin to the channel while the long events reflect bivalent binding. Molecular modeling confirmed that two disaccharides can bind simultaneously to the tetravalent BP lectin (Figure 1b, see legend for the size of channel and approximate distances between disaccharide binding sites on the BP lectin).[17] The molecular models also indicate that trivalent binding is not possible.

To test the hypothesis that mono- and divalent binding events can be distinguished as short and long current blockades of derivatized channels, we evaluated the pattern of current flow through channels $H_6$9C-NL_1 and $H_5$9C-NL_2, which contain one and two chemically modified subunits, respectively. In the absence of BP lectin, no current fluctuations were observed and, as expected, the conductance values of $H_6$9C-NL_1 and $H_5$9C-NL_2 were higher than those of 9C-NL_7 (Table 1). In the presence of BP lectin, the pore containing a single carbohydrate gave rise to only short events ($\tau_{off\text{-}1} = 2.5 \pm 0.6$ ms, $n = 5$). The pore containing two

Table 2: The number of NL-disaccharides attached to αHL influences the type and the frequency of binding events.

Number of αHL subunits modified with NL	$\tau_{off\text{-}1}$ [ms][a]	$\tau_{off\text{-}2}$ [ms][a]	Frequency of occurrence for $\tau_{off\text{-}1}$ events [s^{-1}][a,b]	Frequency of occurrence for $\tau_{off\text{-}2}$ events [s^{-1}][a,b]	$\tau_{on\text{-}app}$ [s][a,b]
1	2.5 ± 0.6	not observed	$3.5 \pm 1.4 \times 10^{-3}$	not observed	180 ± 70
2	2.5 ± 0.7	80 ± 40	$9.1 \pm 3.2 \times 10^{-3}$	$9 \pm 3 \times 10^{-4}$	79 ± 17
7	6.5 ± 1.2	110 ± 30	$8.4 \pm 3.1 \times 10^{-2}$	$2.4 \pm 0.9 \times 10^{-2}$	10 ± 3.7

[a] Measured at +50 mV in 0.6 M KCl, 0.6 mM $CaCl_2$, 0.3 mM $MnCl_2$, and 6 mM Tris-HCl, pH 7.2. The concentration of BP ranged from 0.4 to 3.2 μM in the *cis* chamber. The values for $\tau_{off\text{-}1}$ and $\tau_{off\text{-}2}$, as well as τ_{on} were derived from the bi-exponential and mono-exponential fits, respectively, of lifetime histograms and represent the mean ± SD from five independent experiments for $H_6$9C-NL_1 and $H_5$9C-NL_2 and four experiments for 9C-NL_7. The frequencies of occurrence for $\tau_{off\text{-}1}$ and $\tau_{off\text{-}2}$ events were obtained by multiplying the frequency of occurrence for all events with fractions of the total events representing $\tau_{off\text{-}1}$ and $\tau_{off\text{-}2}$ events. The latter were obtained from the bi-exponential fits of the lifetime histograms. [b] Values are normalized to 1 μM BP.

Table 1: Conductance properties of αHL channels covalently modified with one, two and seven NL disaccharides at position 9C.

Number of αHL subunits modified with NL	Mean conductance of open channel [pS][a]	Mean amplitude of BP lectin binding event [pS][a,b]
1	550 ± 18 ($n = 9$)	194 ± 24 ($n = 5$)
2	536 ± 22 ($n = 7$)	164 ± 22 ($n = 5$)
7	302 ± 50 ($n = 18$)	110 ± 24 ($n = 5$)
0	578 ± 20 ($n = 4$)	not observed

[a] Measured at +50 mV in 0.6 M KCl, 0.6 mM $CaCl_2$, 0.3 mM $MnCl_2$, and 6 mM Tris-HCl, pH 7.2. [b] Comprises short and long binding events.

carbohydrate derivatives gave rise to both short ($\tau_{off\text{-}1} = 2.5 \pm 0.7$ ms) and long events ($\tau_{off\text{-}2} = 80 \pm 40$ ms, $n = 5$), and, in line with expectations, the frequencies of occurrence of both were lower than for the pores containing seven modified subunits (Table 2). These results are consistent with the hypothesis that single-channel current recordings can report on mono- and bivalent binding of receptors to ligands attached to the channel.

To evaluate the validity of our single-molecule data on lectin binding, we derived kinetic and equilibrium constants from single-channel current recordings of 9C-NL_7 and compared these values with the literature value of the equilibrium constant from ensemble measurements. The rate constants for lectin binding and dissociation, k_{on} and k_{off}, were obtained from the intervals between binding events, τ_{on}, the concentration of BP lectin, and the mean lifetimes of binding events, τ_{off}.[18] The apparent association rate constant, $k_{on\text{-}app}$, was dominated by the monovalent events and gave the value $1.0 \pm 0.4 \times 10^5\,\text{M}^{-1}\,\text{s}^{-1}$. The dissociation rate constants for the monovalent and bivalent events were $k_{off\text{-}1} = 160 \pm 20\ \text{s}^{-1}$ and $k_{off\text{-}2} = 9.6 \pm 2.4\ \text{s}^{-1}$.[19] The kinetic data were used to derive the overall dissociation constant, $K_{d\text{-}1\&2}$, by assuming a kinetic model with a monovalent step that preceded a bivalent binding step (see Supporting Information). By using $k_{off\text{-}1}$, $k_{off\text{-}2}$, and $k_{on\text{-}app}$, a value for $K_{d\text{-}1\&2}$ of 3.1×10^{-4} M was obtained. This compares well to the literature value[14] for macroscopic binding, $K_{d\text{-}lit}$, of 1.2×10^{-5} M, considering that $K_{d\text{-}lit}$ was obtained by affinity chromatography and includes trivalent binding and rebinding, which are excluded from $K_{d\text{-}1\&2}$. The kinetic analysis of the single-channel recordings also yielded $K_{d\text{-}1}$, the dissociation constant for monovalent binding, with a value of 1.7×10^{-3} M. Further comparison of $K_{d\text{-}1}$ and $K_{d\text{-}1\&2}$ with ensemble data affirmed the validity of the single-molecule data on lectin binding (see Supporting Information).

Our experiments show that ion channels derivatized with disaccharides are a valuable tool to study the binding kinetics of lectins. The single-molecule approach yields data in line with ensemble measurements but also reveals kinetic details, which would not have been discernible with conventional methods. For example, the dissociation rate constant for bivalent binding, $k_{off\text{-}2}$, with a value of $9.6 \pm 2.4\ \text{s}^{-1}$, is, by a factor of 17, smaller than the monovalent constant, $k_{off\text{-}1}$, with a value of $160 \pm 20\ \text{s}^{-1}$. The two dissociation rate constants $k_{off\text{-}1}$ and $k_{off\text{-}2}$ should not differ greatly given the similar molecular nature of the events. In further experiments, we will explore the reasons for the low value of $k_{off\text{-}2}$ at the molecular level. By using our single-molecule approach we will also be able to test the binding model used to derive $k_{off\text{-}2}$ from $\tau_{off\text{-}2}$. In this model, a bivalent event is thought to reflect the following molecular changes: A lectin tetramer binds a first and then a second ligand before it dissociates from the two ligands in sequential steps with a bivalent binding state preceding a monovalent state. In an extended model, the dissociating lectin molecule goes through a succession of several dissociation–rebinding steps that cycle between the monovalent and bivalent states before the molecule eventually dissociates from the derivatized pore. Presently, the current recordings do not show conductance substeps indicative of these different binding states. In future experiments, we will improve the temporal and conductance resolution of the bivalent binding events to detect potential substates within one bivalent binding event. The strategy to increase the conductance resolution will employ NL-conjugates with longer linkers to achieve different pore blockades for the monovalent and bivalent states. Currently, the monovalently bound lectin is likely to reside very close to the pore opening and subsequent bivalent binding does not alter the extent of pore blockade.

In summary, our approach to the kinetics of binding of a tetravalent lectin to a ligand-modified pore resulted in the detection of monovalent and bivalent binding events at the single molecule level, and yielded kinetic details, which would not have been available through conventional ensemble methods.

Experimental Section

The synthesis of the disaccharide ligand for *Bauhinia purpurea* lectin is described in detail in the Supporting Information. Briefly, an S-glycoside was synthesized in which the disaccharide D-galactose-β-1,3-*N*-acetyl-galactosamine (natural ligand, NL) was coupled through the C1 carbon of galactosamine to 4-hydroxy-thiophenol .[20] The phenolic hydroxyl was further modified to yield a 16-atom linker, which terminated with a thiol. The thiol was modified with 2,2′-dithiopyridine to yield the *S*-thiopyridyl NL conjugate (Figure 1a). The molecular weight of the conjugate is 678 Da, without the thiopyridyl group, and the effective length of the linker between the C1 atom of galactosamine and the thiol of the thiopyridyl group is 18 Å, assuming an extended conformation.

αHL heptamers modified with one, two, and seven NL-disaccharides were generated by using a published procedure[13] based on the formation of a disulfide linkage between an engineered cysteine residue of the protein and a compound containing a 2-pyridyl disulfide group. The heptamers with one and two NL-modified subunits were generated by combining modified and unmodified monomers and then isolating the heptameric assemblies containing the desired number of derivatized subunits. The heptamer containing seven modified subunits was prepared by using only modified monomers for the assembly. Details of the procedure are provided in the Supporting Information.

Single-channel current recordings of NL-modified heptamers were performed using a planar lipid bilayer apparatus[21,22] and details are available in the Supporting Information. The current recordings were analyzed as described.[11]

Received: August 11, 2003 [Z52614]

Keywords: carbohydrates · molecular recognition · polyvalency · protein engineering · single-molecule studies

[1] M. Mammen, S. K. Choi, G. M. Whitesides, *Angew. Chem.* **1998**, *110*, 2908; *Angew. Chem. Int. Ed.* **1998**, *37*, 2754.
[2] J. J. Lundquist, E. J. Toone, *Chem. Rev.* **2002**, *102*, 555.
[3] M. Mourez, R. S. Kane, J. Mogridge, S. Metallo, P. Deschatelets, B. R. Sellman, G. M. Whitesides, R. J. Collier, *Nat. Biotechnol.* **2001**, *19*, 958.
[4] P. I. Kitov, J. M. Sadowska, G. Mulvey, G. D. Armstrong, H. Ling, N. S. Pannu, R. J. Read, D. R. Bundle, *Nature* **2000**, *403*, 669.
[5] E. A. Merritt, Z. Zhang, J. C. Pickens, M. Ahn, W. G. Hol, E. Fan, *J. Am. Chem. Soc.* **2002**, *124*, 8818.

 © 2004 Wiley-VCH Verlag GmbH & Co. KGaA, Weinheim

[6] Z. Zhang, E. A. Merritt, M. Ahn, C. Roach, Z. Hou, C. L. Verlinde, W. G. Hol, E. Fan, *J. Am. Chem. Soc.* **2002**, *124*, 12991.
[7] B. C. Lagerholm, T. E. Starr, Z. N. Volovyk, N. L. Thompson, *Biochemistry* **2000**, *39*, 2042.
[8] C. W. Cairo, J. E. Gestwicki, M. Kanai, L. L. Kiessling, *J. Am. Chem. Soc.* **2002**, *124*, 1615.
[9] J. E. Gestwicki, C. W. Cairo, L. E. Strong, K. A. Oetjen, L. L. Kiessling, *J. Am. Chem. Soc.* **2002**, *124*, 14922.
[10] T. K. Dam, C. F. Brewer, *Chem. Rev.* **2002**, *102*, 387.
[11] L. Movileanu, S. Howorka, O. Braha, H. Bayley, *Nat. Biotechnol.* **2000**, *18*, 1091.
[12] S. Howorka, S. Cheley, H. Bayley, *Nat. Biotechnol.* **2001**, *19*, 636.
[13] S. Howorka, L. Movileanu, O. Braha, H. Bayley, *Proc. Natl. Acad. Sci. USA* **2001**, *98*, 12996.
[14] T. Osawa, T. Tsuji, *Annu. Rev. Biochem.* **1987**, *56*, 21.
[15] N. Horan, L. Yan, H. Isobe, G. M. Whitesides, D. Kahne, *Proc. Natl. Acad. Sci. USA* **1999**, *96*, 11782.
[16] L. Song, M. R. Hobaugh, C. Shustak, S. Cheley, H. Bayley, J. E. Gouaux, *Science* **1996**, *274*, 1859.
[17] According to the molecular modeling studies on the bivalent binding of BP lectin to homoheptamer 9C-NL_7, the lectin can bind two of the potential three NL carbohydrates combinations on the heptameric pore without sterical constraints. Conceivably, these two different bivalent binding states could have slightly different affinities and this could possibly account for the presence of a second type of longer events in addition to the $\tau_{off\text{-}2}$ events observed in the lifetime histograms. Future experiments will elucidate the molecular reason for these longer events.
[18] E. Moczydlowski in *Ion channel reconstitution* (Ed.: C. Miller), Plenum, New York, **1986**, p. 75.
[19] The dissociation rate constant for bivalent events, $k_{off\text{-}2}$, does not only include the dissociation from the bivalent to the monovalent state but also the dissociation to the unbound state. This is because $k_{off\text{-}2}$ was derived from $\tau_{off\text{-}2}$, which comprises both dissociation steps (see Supporting Information). The correction is, however, very small given that the second dissociation step is fast as indicated by the short duration of $\tau_{off\text{-}1}$.
[20] R. Liang, J. Loebach, N. Horan, M. Ge, C. Thompson, L. Yan, D. Kahne, *Proc. Natl. Acad. Sci. USA* **1997**, *94*, 10554.
[21] M. Montal, P. Mueller, *Proc. Natl. Acad. Sci. USA* **1972**, *69*, 3561.
[22] O. Braha, B. Walker, S. Cheley, J. J. Kasianowicz, L. Song, J. E. Gouaux, H. Bayley, *Chem. Biol.* **1997**, *4*, 497.

 © 2004 Wiley-VCH Verlag GmbH & Co. KGaA, Weinheim

Enantioselective Allylation

Enantioselective Catalytic Allylation of Carbonyl Groups by Umpolung of π-Allyl Palladium Complexes**

Giuseppe Zanoni, Serafino Gladiali, Alberto Marchetti, Paolo Piccinini, Ilenia Tredici, and Giovanni Vidari*

Dedicated to Luisa Beghi

The development of catalytic asymmetric C–C bond-forming reactions remains one of the main challenges in organic chemistry. Transformations mediated by transition-metal complexes with properly designed ligands have enabled this challenging synthetic goal to be achieved, often with remarkable results.[1] Among the transition-metal-catalyzed reactions known to form C–C bonds, the palladium-catalyzed allylic substitution developed by Trost and Tsuji stands out as one of the most valuable synthetic tools available.[2] In this reaction the key stage is the formation of a π-allyl palladium complex that can act both as an electrophilic and a nucleophilic species because of the ambiphilic nature of the metal-coordinated allylic ligand. Nucleophilic displacement across the π-allyl palladium complex has been extensively used in organic synthesis, particularly as its asymmetric variant—widely known as the asymmetric allylic alkylation (AAA), a strategically powerful option for the preparation of complex molecules such as natural products. On the other hand, nucleophilic metal-coordinated allylic moieties obtained from the so-called Umpolung of π-allyl palladium complexes have recently provided a versatile allylation method for aldehydes and ketones.[3] Of the various routes that utilize this Umpolung, the transmetalation of a π-allyl palladium complex with diethylzinc, according to the Tamaru protocol, has recently attracted attention. Here a putative allyl zinc species is delivered as an active allylating agent to a carbonyl electrophile.[3]

[*] Dr. G. Zanoni, A. Marchetti, P. Piccinini, I. Tredici, G. Vidari
Dipartimento di Chimica Organica
Università di Pavia
Viale Taramelli, 10–27100 Pavia (Italy)
Fax (+39) 038-250-7323
E-mail: gzanoni@unipv.it

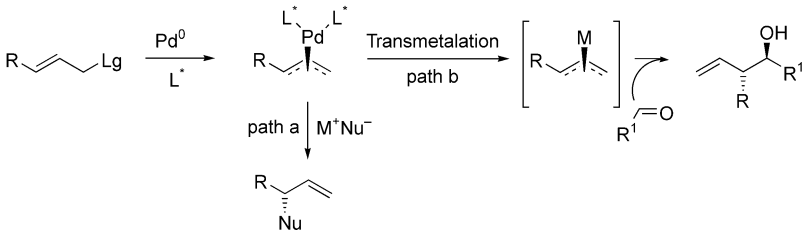
S. Gladiali
Dipartimento di Chimica
Università di Sassari
Via Vienna, 1-07100 Sassari (Italy)

[**] We would like to thank Prof. Stephen L. Buchwald (Massachusetts Institute of Technology, MA, USA) and Angela Marinetti (Laboratoire de Synthèse Sélective Organique et Produits Naturels, France) for their generous supply of ligands **24** and **10**, **14**, and **15**, respectively. We are indebted to Corrado Sangermani and Gloria Borin for their synthetic expertise and contributions. Special thanks go to Maurizio Franzini for his advice. This work was supported by the University of Pavia (Progetto Giovani Ricercatori).

Supporting information for this article is available on the WWW under http://www.angewandte.org or from the author.

 © 2004 Wiley-VCH Verlag GmbH & Co. KGaA, Weinheim DOI: 10.1002/anie.200352743

However, while impressive strides in asymmetric induction have been made in palladium-catalyzed AAA (Scheme 1, path a), to our knowledge the enantioselective allylation of carbonyl compounds by the Umpolung of π-allyl palladium complexes (Scheme 1, path b) has not been reported in the literature.



Scheme 1. Allylation of carbonyl compounds by Umpolung of π-allyl palladium complexes. Lg = leaving group.

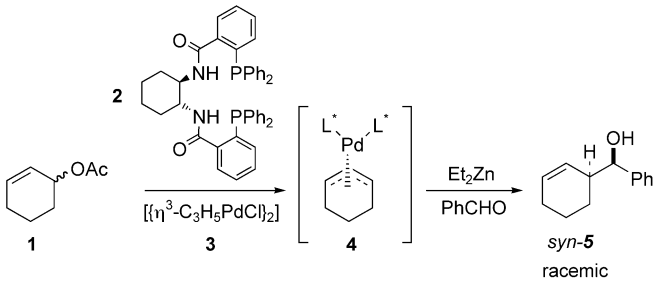
Here we report the first example of a catalytic asymmetric aldehyde addition of an allyl zinc reagent generated from an allyl ester and diethylzinc in the presence of a catalytic amount of a Pd complex and a chiral monophosphane.

Initial studies have dealt with the reaction of cyclohexenyl acetate **1** in the presence of 5 mol% of ligand (*R*,*R*)-**2**, 2.5 mol% of Pd complex **3** and 2.4 equivalents of diethylzinc (Scheme 2). According to Trost and Lee,[4] **2** emerges as the ligand of choice for the highly enantioselective allylic alkylation of cyclohexenyl acetate through intermediacy of π-allyl palladium complex **4**. In their work dealing with the palladium-catalyzed nucleophilic allylation of aldehydes, Tamaru et al. assumed that a reactive σ-allyl zinc species is stereospecifically generated with retention of configuration from the intermediate π-allyl palladium complex. Moreover, the Pd-catalyzed and Zn-mediated allylation of benzaldehyde with various cyclohexenyl moieties was shown to occur with high diastereoselectivity.[5]

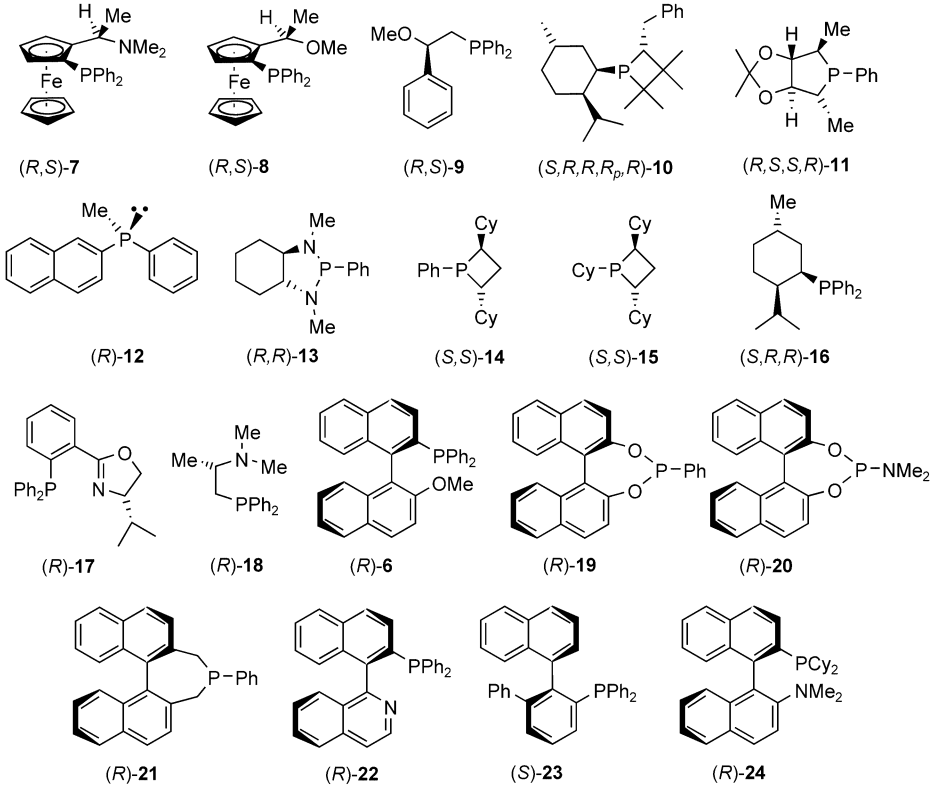
From these observations, we wondered whether the chiral information encoded in complex **4** could be transferred into the transmetalated Zn complex and then eventually into the final alcohol adduct. In a preliminary attempt, the expected homoallylic alcohol **5** was indeed obtained as a single *syn* diastereoisomer in a satisfying 70% yield, but as a racemic mixture.

The loss of the chiral information in complex **4** was assumed to happen at the transmetalation step, hence closer attention to the Pd–Zn exchange mechanism was demanded. While the diethylzinc-mediated Umpolung mechanism needs further elucidation, preliminary studies suggest transmetalation occurs after transfer of an ethyl group from the Zn to the Pd center, followed by elimination of diethylpalladium.[6]

The stereochemical discrimination that determines the enantioenrichment in the product may arise from the asymmetric induction exerted on the conjectural transient allyl zinc species by the chiral space where the ethyl transfer occurs. Whereas diphosphanyl ligand **2** was designed by Trost and Bunt for asymmetric induction on electrophilic π-allylic moieties reacting with soft nucleophiles through an outer-sphere mechanism,[7] chiral monophosphanes, such as Hayashi's (*R*)-2-(diphenylphosphanyl)-2′-methoxy-1,1′-binaphthyl ((*R*)-MOP **6**) or ferrocenylphosphane (*S*)-*N*,*N*-dimethyl-1-[(*R*)-2-diphenylphosphanylferroceneethylamine] (PPFA, **7**; Scheme 3), fared as the most efficient ligands when hard nucleophiles attacked the metal center of the π-allyl palladium complex to be and were subsequently relayed onto the electrophile (inner-sphere mechanism).[8] If the



Scheme 2. Allylation of benzaldehyde with cylohexenyl acetate **1** in the presence of chiral biphosphane ligand **2**.



Scheme 3. A list of chiral monodentate ligands. Cy = cyclohexyl.

 © 2004 Wiley-VCH Verlag GmbH & Co. KGaA, Weinheim

stereochemical discrimination occurs during the transfer of a "hard" ethyl group[7a] from the Zn to the Pd center in a inner-sphere fashion, asymmetric induction may be achieved by employing chiral monophosphanes. Our expectations were met by replacement of diphosphane **2** with monophosphane (*R*)-**6**. The *syn* addition product (3*S*,1′*R*)-**5** was obtained in 22% *ee* and 68% yield.

The absolute configuration of the adduct was assigned by comparson of the rotation with that of an identical compound from the literature,[9] the *ee* value was determined by chiral high-performance liquid chromatography (HPLC). Enhancement of the *ee* value was pursued using parallel synthesis—a particularly convenient technique when few mechanistic data are available.[10] A pool of chiral monophosphane ligands (Scheme 3) was screened against the reaction given in Scheme 2.[11] Nineteen ligands were selected because of their different electronic properties at the phosphorus center, and of the Tolman's cone angles (Scheme 3).[12] All reactions were carried out using acetate **1** and benzaldehyde in a 1.2:1 ratio, 2.4 equivalents of diethylzinc, 2.5 mol% of Pd complex **3**, and 10 mol% of the chiral ligand in THF (0.2 M with respect to benzaldehyde) at 4°C. The metal and ligand were premixed at room temperature in THF (1 mL) for 0.5 h, diluted with THF, and then cooled to 0°C.

Benzaldehyde, **1** and diethylzinc were sequentially added in a parallel synthesizer, and the mixture stirred under argon at 4°C (see Supporting Information). After quenching with NH_4Cl and simple work-up, the crude products were analyzed by high-resolution gas chromatography (HRGC) for chemical yields, and by chiral HPLC for their *ee* values (Figure 1).

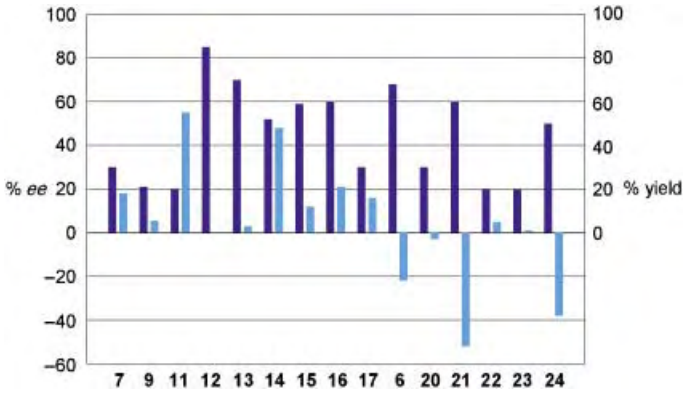
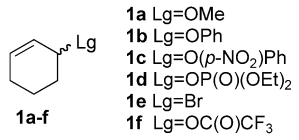


Figure 1. Results of allylation of cyclohexenyl acetate **1** with a selection of chiral ligands. Key: blue, yield as measured by high-resolution gas chromatography (HRGC); azure, percent enantiomeric excess as measured by chiral high-performance liquid chromatography (Kromasil CHI-DMB, heptane/*tert*-butylmethyl ether 98:2).

Employment of phosphanes **8**, **10**, and **18** as well as phosphonite **19** did not bring about any reaction, while the monophosphane **12** resulted in formation of **5** in 85% yield, albeit as a racemate. The best performing ligand was the phosphepine (*R*)-**21**, which provided the addition product (3*S*,1′*R*)-**5** in 60% yield and a promising 52% *ee*.

Ligand (*R*)-**21** was thenexamined further in a second screening so that the influence of the leaving group (Scheme 4), the palladium source and other reaction parameters on stereoselectivity could be determined (Figure 2).



Scheme 4. Cyclohexenyl derivatives employed in a second screening.[13]

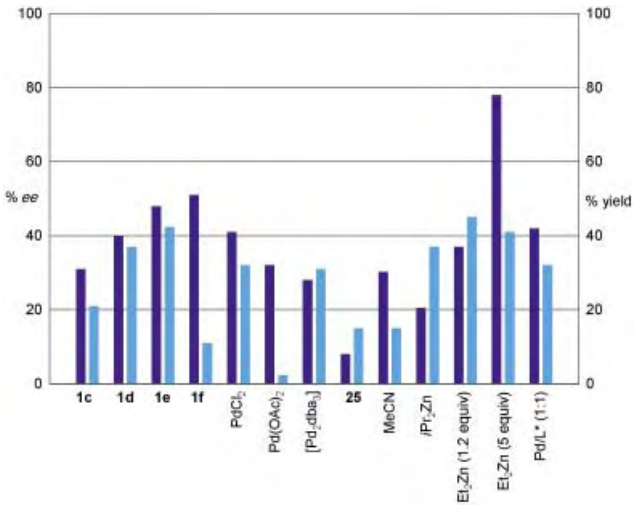


Figure 2. Results of allylation using phosphepine (*R*)-**21** with a selection of leaving groups on the cyclohexenyl moiety, Pd sources, Umpolung reagents (R_2Zn), Pd/ligand ratio and solvents. Key: blue, yield as measured by HRGC; azure, percent enantiomeric excess as measured by chiral high-performance liquid chromatography (Kromasil CHI-DMB, heptane/*tert*-butylmethyl ether 98:2).

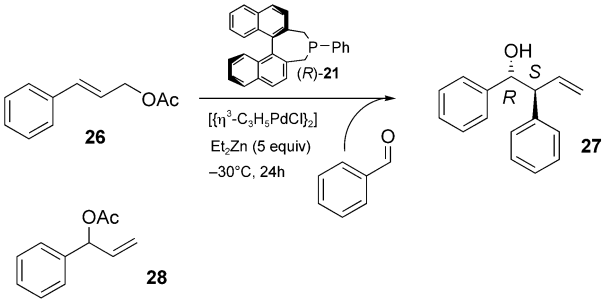
The results revealed that the leaving group had a dramatic effect on the enantioselectivity. The greater the ease with which the leaving group can ionize and depart from the allylic unit, the lower the *ee* value. Notably, trifluoroacetate **1f** afforded **5** in the highest yield, but only in 10% *ee*. To the best of our knowledge such a relationship between enantioselectivity in Pd-catalyzed AAAs and the nature of the leaving group has not been the subject of systematic studies published to date. In addition, we observed no addition products with ethers **1a** and **b**, despite them being reported to effect the allylation of benzaldehyde through Umpolung in good yields.[6a]

Variation of the solvent caused a detrimental effect both on the yield and enantioselectivity. A 1:1 mixture of DMF/THF, CH_2Cl_2, and MeCN all gave worse results than THF. $PdCl_2$, $Pd(OAc)_2$, $[Pd_2(dba)_3]$ (dba = *trans*,*trans*-dibenzylideneacteone), and the chloride-free allyl palladium complex $[Pd(\eta^3\text{-}C_3H_5)(MeCN)_2]OTf$ (**25**; Tf = trifluoromethanesulfonyl) were investigated as the palladium source,[14] but with unsatisfactory results (Figure 2).

 © 2004 Wiley-VCH Verlag GmbH & Co. KGaA, Weinheim

A change in the Pd/ligand ratio from 1:2 to 1:1 decreased the yield (42%) and *ee* value (32%), as did the reduction in the amount of diethylzinc to 1.2 equivalents (addition product **5** was obtained in 37% yield and 45% *ee*; Figure 2). Conversely, an increase in the amount of diethylzinc to 5 equivalents boosted the reaction rate and yield, with the allylation now being completed in 6 h at 4°C (instead of 24 h as required with 2.4 equivalents of diethylzinc at 4°C) in a 78% yield. Replacement of the ethyl group on the Zn center with the more sterically demanding isopropyl group did not affect the *ee* value (37%), but the yield was reduced to 21%. Finally, lowering the reaction temperature to −30°C and using 5 equivalents of Et_2Zn showed little effect on substrate **1**, whereas the trifluoroacetate **1f** product **5** was isolated with an *ee* value that was more than tripled (up to 38% from 11%).

Achiral cinnamyl acetate (**26**) performed even better as a substrate, with a faster and more stereoselective reaction being observed. Addition product (1*R*,2*S*)-*anti*-**27** was obtained in a 77% yield and 60% *ee* (Scheme 5) under our



Scheme 5. Allylation of benzaldehyde with cinnamyl acetate **26** as the substrate.

standard conditions with 5 equivalents of diethylzinc at 4°C.[15] The *ee* value gratifyingly climbed to 70% at −30°C (24 h, 70% yield). Isomeric racemic allyl acetate **28**, which is expected to originate the same intermediate π-allyl palladium complex as **26**, gave rise to (1*R*,2*S*)-*anti*-**27** in a 49% yield, while the *ee* value plummeted to 15%. This reduction in enantioselectivity is not unexpected in view of the possible intervention of memory effects, as amply investigated by Lloyd-Jones et al.[16]

In summary, we have documented the first catalytic asymmetric aldehyde allylation by Umpolung of a π-allyl palladium complex mediated by diethylzinc, which afforded products in satisfactory yields with *ee* values up to 70%.

Received: August 29, 2003 [Z52743]

Keywords: allylation · asymmetric synthesis · enantioselectivity · ligand design · Umpolung

[1] E. N. Jacobsen, A. Pfaltz, H. Yamamoto, *Comprehensive Asymmetric Catalysis*, *Vol. 2*, Springer, Berlin, **1999**.

[2] a) B. M. Trost, M. L. Crawley, *Chem. Rev.* **2003**, *103*, 2921–2944; b) T. Graening, H.-G. Schmalz, *Angew. Chem.* **2003**, *115*, 2684–2688; *Angew. Chem. Int. Ed.* **2003**, *42*, 2580–2584; c) B. M. Trost, C. Lee in *Catalytic Asymmetric Synthesis* (Ed.: I. Ojima), Wiley-VCH, **2000**, pp. 593–649; d) B. M. Trost, D. L. Van Vranken, *Chem. Rev.* **1996**, *96*, 395–422.

[3] a) M. Kimura, M. Shimizu, K. Shibata, M. Tazoe, Y. Tamaru, *Angew. Chem.* **2003**, *115*, 3514–3517; *Angew. Chem. Int. Ed.* **2003**, *42*, 3392–3395; b) Y. Tamaru in *Handbook of Organopalladium Chemistry for Organic Synthesis* (Ed.: E. Negishi), Wiley-Interscience, **2002**, pp. 1917–1943.

[4] B. M. Trost, C. Lee in *Catalytic Asymmetric Synthesis* (Ed.: I. Ojima), Wiley-VCH, **2000**, pp. 617–622.

[5] Y. Tamaru, A. Tanaka, K. Yasui, S. Goto, S. Tanaka, *Angew. Chem.* **1995**, *107*, 862–864; *Angew. Chem. Int. Ed. Engl.* **1995**, *34*, 787–789.

[6] a) Y. Tamaru, *J. Organomet. Chem.* **1999**, *576*, 215–231; b) Y. Tamaru, A. Tanaka, K. Yasui, S. Goto, Y. Takafumi, Y. Taniseki, K. Fugami, *Tetrahedron Lett.* **1993**, *34*, 7619–7622.

[7] a) G. Consiglio, R. M. Waymouth, *Chem. Rev.* **1989**, *89*, 257–276; b) B. M. Trost, R. C. Bunt, *J. Am. Chem. Soc.* **1994**, *116*, 4089–4090.

[8] a) T. Hayashi, *Acc. Chem. Res.* **2000**, *33*, 354–362; b) F. Lagasse, H. Kagan, *Chem. Pharm. Bull.* **2000**, *48*, 315–324.

[9] K. Kitayama, H. Tsuji, Y. Ouzumi, T. Hayashi, *Tetrahedron Lett.* **1996**, *37*, 4169–4172.

[10] M. T. Reetz, *Angew. Chem.* **2001**, *113*, 292–320; *Angew. Chem. Int. Ed.* **2001**, *40*, 284–310.

[11] With the exception of compounds **4**, **10**, **14**, and **15**, ligands of Scheme 3 were prepared according to literature procedures, as detailed in the Supporting Information.

[12] a) K. A. Bunten, L. Chen, A. L. Fernandez, A. J. Poë, *Coord. Chem. Rev.* **2002**, *233–234*, 41–51; b) a good supply of electronic parameters for trialkyl phosphane ligands can be found under web.bu.edu/quale, administered by W. P. Giering.

[13] All ligands were prepared according to published methods (see Supporting Information).

[14] B. Äkermark, B. Krakenberger, S. Hannson, A. Vitagliano, *Organometallics* **1987**, *6*, 620–628.

[15] Relative and absolute configuration have been assigned by comparison to the literature (A. Hafner, R. O. Duthaler, R. Marti, G. Rihs, P. Rothe-Streit, F. Schwarzenbach, *J. Am. Chem. Soc.* **1992**, *114*, 2321–2336) and by ^{1}H NMR spectroscopy, respectively.

[16] G. C. Lloyd-Jones, S. C. Stepen, M. Murray, C. P. Butts, Š. Vyskocil, P. Kočovsky, *Chem. Eur. J.* **2000**, *6*, 4348–4357.

 © 2004 Wiley-VCH Verlag GmbH & Co. KGaA, Weinheim

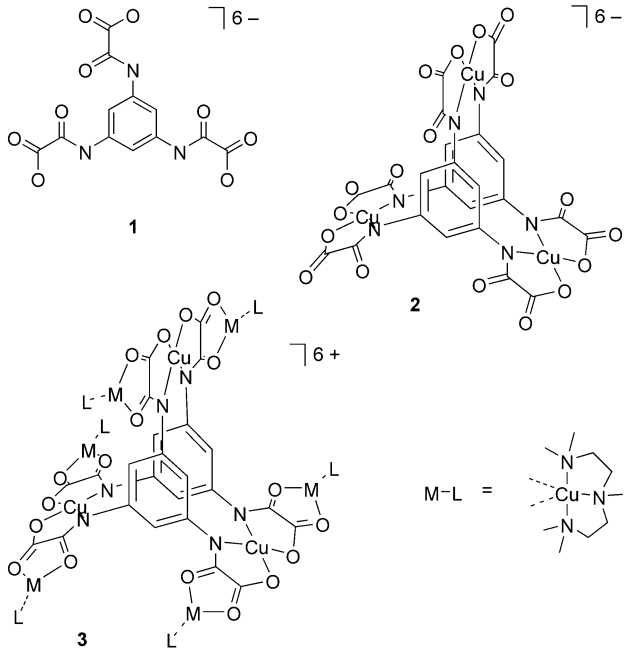
Metallacyclophanes

Rational Design of an Enneanuclear Copper(II) Complex with a Metallacyclophane Core**

Xavier Ottenwaelder, Joan Cano, Yves Journaux, Eric Rivière, Conor Brennan, Martine Nierlich, and Rafael Ruiz-García*

Design of complex molecular architectures starting from constituent subunits is a central theme in inorganic chemistry.[1] Among such species, those containing magnetic ions are of particular interest because their magnetic properties directly stem from the geometrical arrangement of the constituent subunits.[2] The main challenge in this field is the synthesis of single-molecule magnets whose ground states have high spin and considerable negative axial anisotropy.[3] Pathways to such complex molecular entities are based on two orthogonal synthetic schemes: self-assembly methods[4] and step-by-step strategies.[5] In the former, the nature of the final products cannot be determined a priori. In contrast, the latter provide an efficient means to control both nuclearity and dimensionality of the polymetallic edifice.

Following a step-by-step approach, we prepared the new ligand *N*,*N*′,*N*″-1,3,5-benzenetris(oxamate) (**1**). Being incapable of hexadentate ligation to a single metal center, this ligand rather self-assembles with Cu^{II} ions in a 2/3 ligand/metal ratio to give the trinuclear complex $Na_6[Cu^{II}_3(\mathbf{1})_2]\cdot 11.5\,H_2O$ (Na_6-**2**$\cdot 11.5\,H_2O$). In the $[Cu^{II}_3(\mathbf{1})_2]^{6-}$ core **2**, each ligand adopts a tris(N,O-bidentate) coordination mode (vide infra). Thus, the three bis(oxamate)copper(II) spin-bearing residues are bridged by two 1,3,5-benzenetriyl moieties, which have already proved to be efficient ferromagnetic spin-coupling units in π-conjugated organic polyradicals[6] and metal complexes.[7–10] Additionally, **2** is a potential hexakis-bidentate ligand that can coordinate six other metal ions through its external oxygen atoms. Using this "complex-as-ligand strategy" with ancillary ligands on the additional metal ions to avoid polymerization, we obtained the novel homometallic enneanuclear complex $[\{Cu^{II}_3(\mathbf{1})_2\}\{Cu^{II}(pmdien)\}_6](ClO_4)_6\cdot 12\,H_2O$ (**3**-$(ClO_4)_6\cdot 12\,H_2O$; pmdien = *N*,*N*,*N*′,*N*″,*N*″-pentamethyldiethylenetriamine).



Single-crystal X-ray characterization of **3** revealed the desired structure. The unit cell ($R\bar{3}$ space group) contains two types of hexacationic enneacopper molecules, one of which is disordered, as well as perchlorate ions and water molecules. The well-ordered enneanuclear molecules exhibit the anticipated pattern of six external $[Cu(pmdien)]^{2+}$ subunits ligated to a central $[Cu_3(\mathbf{1})_2]^{6-}$ unit (Figure 1). To the best of our knowledge, **3** is the second crystallographically characterized example of a 1,3,5-metallacyclophane.[11]

The central Cu^{II} ions have an elongated square-pyramidal (Cu2 and Cu4) or elongated octahedral (Cu5) geometry with distant axial ligands. These environments can be approximated as square-planar, created by one oxamate moiety of each ligand (maximum deviation from average N_2O_2 plane: 0.148 Å). The $[Cu_3(\mathbf{1})_2]^{6-}$ core is twisted to accomodate a noneclipsed disposition of the aromatic rings, with a distance of 3.237 Å between their average planes. In comparison to the binuclear 1,3-metallacyclophane analogue of **2**, [Cu_2-*m*],[10] coordination of the third Cu atom brings the aromatic rings closer, enhances electronic repulsions, and results in greater overall twisting of the molecule: the C-C-N-Cu torsion angles are farther from 90° in **3** (65.0–79.6°, av 73.8°) than in [Cu_2-*m*] (73.4–89.3°, av 78.9°). In the peripheral $[Cu(pmdien)]^{2+}$ subunit, the Cu^{II} ions are five-coordinate, close to square-pyramidal with τ values[12] ranging from 0.27 to 0.39, and with one Cu–O bond longer than the other (2.20 versus 1.97 Å on average).

The magnetic properties of **2** and **3** are depicted in Figure 2. Complex **2** exhibits ferromagnetic coupling between the three Cu^{II} ions: $\chi_M T$ continuously increases with decreasing temperature. A good fit to the experimental data was obtained with $g = 2.07$, $J = +11.6\ cm^{-1}$ and a Weiss constant $\theta = +0.41$ K (see Experimental Section). Despite the large separation between the Cu^{II} ions of about 6.9 Å, a strong ferromagnetic coupling J is present, as in [Cu_2-*m*]

[*] Dr. X. Ottenwaelder, Dr. J. Cano, Dr. Y. Journaux, Dr. E. Rivière, Dr. C. Brennan
Laboratoire de Chimie Inorganique, CNRS UMR 8613
Université Paris-Sud
91405 Orsay (France)
Fax: (+33) 169-154-754
E-mail: jour@icmo.u-psud.fr
Dr. M. Nierlich
CEA, Service de Chimie Moléculaire DSM/DRECAM
Centre d'Etudes de Saclay Bât. 125
91191 Gif sur Yvette Cedex (France)
Dr. R. Ruiz-García
Departament de Química Orgànica, Facultat de Química
Universitat de València
46100 Burjassot, València (Spain)

[**] This work was supported by the European Community (contract HPRN-CT-1999-00012/TMR network "MolNanoMag").

 © 2004 Wiley-VCH Verlag GmbH & Co. KGaA, Weinheim DOI: 10.1002/anie.200352851

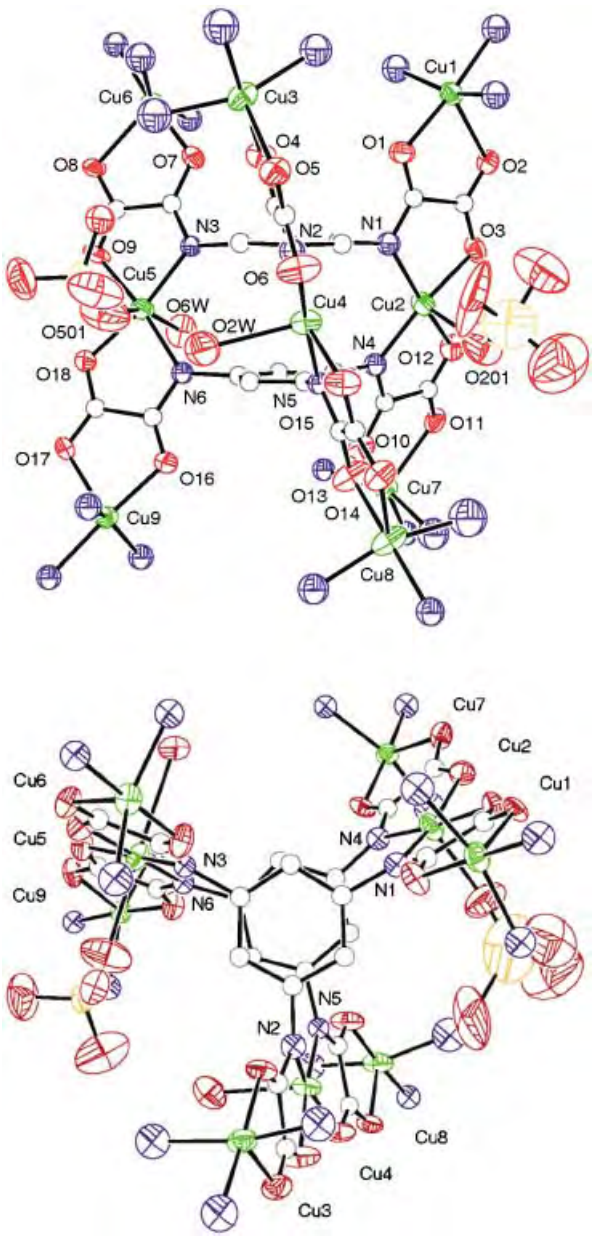


Figure 1. Side and top views of the well-ordered enneacopper unit **3**. Selected interatomic distances [Å] and angles [°]: Cu2-Cu4 6.899(7), Cu2-Cu5(7) 7.051, Cu4-Cu5(7) 6.836, Cu2-N1 1.980(6), Cu2-N4 1.957(6), Cu2-O201 2.417(7), Cu4-N2 1.961(5), Cu4-N5 1.980(5), Cu4-O2W 2.424(8), Cu5-N3 1.998(6), Cu5-N6 1.950(5), Cu5-O501 2.468(7), Cu5-O6W 2.835(8); N1-Cu2-N4 104.9(3), N2-Cu4-N5 105.1(2), N3-Cu5-N6 105.7(2).

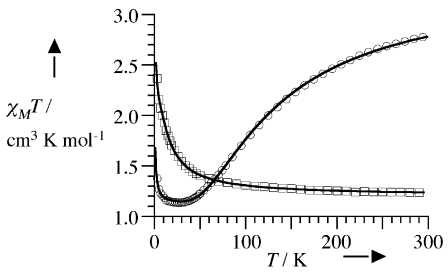


Figure 2. Magnetic behavior of **2** (squares) and **3** (circles); the solid lines are the calculated curves.

(+16.8 cm^{-1}),[10] due to spin-polarization effects through the aromatic *meta* linkage.[13] Aside from the organoiron complex reported by Lapinte et al.,[8] the couplings in **2** and [Cu_2-*m*] are larger than in other metal complexes.[9,14] This is due to the particular geometry of **2** in which the copper basal planes are nearly perpendicular to the benzene rings, which leads to a strong interaction between the Cu $d_{x^2-y^2}$ orbitals through the π system of the benzene rings.[10]

When the sample is cooled, $\chi_M T$ for **3** first decreases, then reaches a plateau between 20–30 K with a value of 1.17 cm^3 K mol^{-1} corresponding to three uncoupled 1/2 spins, and then increases below 20 K to reach 1.44 cm^3 K mol^{-1} at 2 K. This reproduces the expected behavior of **3**: antiferromagnetically coupled (J_{AF}) oxamato-bridged trinuclear Cu^{II} subunits, and, in the low-temperature region, ferromagnetic coupling (J_F) between the $S = 1/2$ ground states of the trinuclear subunits through the central $[Cu_3(\mathbf{1})_2]^{6-}$ core. A good fit of the experimental data was obtained with $J_{AF} = -106$ cm^{-1}, $J_F = +7.8$ cm^{-1}, and $g = 2.03$. The value of J_{AF} is in good agreement with that found for oxamate-bridged tricopper(II) complexes with pmdien as terminal ligand.[15,16] The magnitude of J_F was confirmed by the fit of the magnetization versus field at 2 K, which gave $J_F = +8.4$ cm^{-1}.[17] The smaller value of J_F in **3** (+7.8 cm^{-1}) compared to **2** (+11.6 cm^{-1}) and [Cu_2-*m*] (+16.8 cm^{-1}) likely originates from less efficient overlap between the aforementioned orbitals as a consequence of the greater helical twist in **3**.

In conclusion, ligand **1** allows the assembly of three Cu^{II} ions in a *meta* arrangement around bridging aromatic rings to give complex **2**. Being hexakis-bidentate, **2** is an efficient building block for larger assemblies with advantageous chelation of the peripheral metal ions, as observed in **3**. Through its rational construction, the enneanuclear complex **3** may be described as a first-generation metallodendrimer based on **2**. Importantly for magnetic assemblies, the ferromagnetic coupling by a spin-polarization mechanism in **2** is also operative in **3**. To extend these promising results, we aim at using this new class of ligands for the synthesis of 1) enneanuclear heterometallic complexes as potential single-molecule magnets, and 2) extended networks for molecule-based magnets.

Experimental Section

1,3,5-Triaminobenzene: A mixture of 3,5-dinitroaniline (1.46 g, 8.0 mmol) and 10% Pd/C (150 mg) in methanol (150 mL) was stirred overnight under hydrogen (40 bar). The suspension was filtered over Celite under inert atmosphere and washed with degassed methanol until the filtrate was colorless. Evaporation of the solvent gave 1,3,5-triaminobenzene as a light brown oil in quantitative yield. ^{1}H NMR (250 MHz, degassed [D_6]DMSO): $\delta = 4.34$ (br s, 6H; NH_2), 5.12 ppm (s, 3H; aromatic H).

1: The ligand was isolated as its triethyl ester. Under inert atmosphere, a solution of 1,3,5-triaminobenzene (972 mg, 7.9 mmol) in DMF (50 mL) was added to ethyloxalyl chloride (5.5 mL, 49 mmol). After the mixture had been stirred for 5 min, diisopropylethylamine (8.5 mL, 49 mmol) was added, and the solution was stirred at about 90 °C for 2 h, after which it was handled in air. After evaporation of the solvent, water (200 mL) was added to the resulting oil, to yield a white solid, which was collected by filtration, washed with water to neutrality of the filtrate, and dried under vacuum (2.7 g,

 © 2004 Wiley-VCH Verlag GmbH & Co. KGaA, Weinheim

80% yield). Elemental analysis (%) calcd for $C_{18}H_{21}N_3O_9$ (423): C 51.06, H 5.00, N 9.95; found: C 49.66, H 4.91, N 9.91; ^{1}H NMR ([D$_6$]DMSO): $\delta = 1.30$ (t, 9H; 3 CH_3), 4.29 (q, 6H; 3 CH_2O), 7.91 (s, 3H; aromatic H), 10.91 ppm (s, 3H; 3 NH); IR (KBr): $\tilde{\nu} = 3277$ (NH), 1739, 1695 cm^{-1} (C=O).

2: The trinuclear Cu^{II} complex was obtained by reaction of the proligand of **1** (2 equiv) with $Cu^{II}(NO_3)_2$ (3 equiv) in basic aqueous medium (6 equiv of NaOH), and isolated as its sodium salt (95%).[18] Elemental analysis (%) calcd for $C_{24}H_6Cu_3N_6Na_6O_{18}(H_2O)_{11.5}$ (1202): C 23.98, H 2.43, N 6.99; found: C 23.94, H 2.42, N 6.99; IR (KBr): $\tilde{\nu} =$ 1654, 1598 cm^{-1} (C=O).

3: Caution: Perchlorate-containing salts are potentially explosive and should be handled in very small quantities. The enneacopper(II) complex **3** was synthesized in a manner similar to that described in the literature,[16] with the appropriate 6:1 ratio of $[Cu(pmdien)](ClO_4)_2$ and **2** in water. After addition, the mixture was stirred for 10 min, then the precipitate was collected by filtration, washed with water and methanol, and dried under vacuum (75%). Crystallization of **3** as green rods occurred over a few days on slow evaporation of a saturated aqueous solution. Elemental analysis (%) calcd for $C_{78}H_{144}Cl_6Cu_9N_{24}O_{42}(H_2O)_{12}$ (3091): C 30.31, H 5.48, N 10.88, Cl 6.88, Cu 18.50; found: C 29.72, H 5.27, N 10.76, Cl 7.15, Cu 17.36; IR (KBr): $\tilde{\nu} = 1607$ br (C=O), 1088–1145 cm^{-1} (ClO).

Crystal data for **3**: $C_{91}H_{196}Cl_7Cu_{10.5}N_{28}O_{67}$, $M_r = 3270.08$, trigonal, space group $R\bar{3}$, $a = b = 65.137(9)$ Å, $c = 18.861(4)$ Å, $V =$ 69303(20) Å^3, $T = 123(2)$ K, $Z = 18$, $\rho_{calcd} = 1.410$ g cm^{-3}, $\mu(Mo_{K\alpha}) =$ 1.616 mm^{-1}. Data were corrected for Lorentzian and polarization effects and absorption. 23008 unique reflections, of which 9362 with $I > 2\sigma(I)$ were taken as as observed. The structure was solved by direct methods using SHELXS97 and refined by using the full-matrix least-squares method on F^2 using SHELXL97. The hydrogen atoms were neither found nor calculated. Refinement of 1296 variables with anisotropic thermal parameters gave $R = 0.1290$, $R_w = 0.3311$, and $S =$ 1.065. CCDC-208622 contains the supplementary crystallographic data for this paper. These data can be obtained free of charge via www.ccdc.cam.ac.uk/conts/retrieving.html (or from the Cambridge Crystallographic Data Centre, 12, Union Road, Cambridge CB2 1EZ, UK; fax: (+44) 1223-336-033; or deposit@ccdc.cam.ac.uk).

The moderate quality of the resolution likely arises from disorders. Two perchlorate ions (Cl3, Cl4) are disordered, as is a molecule of complex **3** (Cu10, Cu11, C88, C89, N28, O19, O21) lying on the $\bar{3}$ axis and disordered on two positions with occupancy factors of 0.5. The latter appear as dodecanuclear entities by superposition of the two enantiomers of a $[Cu_3[\mathbf{1}]_2[Cu(pmdien)]_6^{6+}$ complex. Even though a rigorous metrical analysis is precluded by the disorder, all Cu environments are very similar to those in well-ordered molecules.

Magnetic measurements were carried on a SQUID magnetometer on powdered samples in the range 2–300 K. The susceptibility curves were fitted with an analytical law with the $-J$ convention for **2**,[19] and by full Hamiltonian diagnalization for **3** with the Hamiltonian $\mathscr{H} = -J_F(S_2S_4 + S_2S_5 + S_4S_5) - J_{AF}(S_2S_1 + S_2S_7 + S_4S_3 + S_4S_8 + S_5S_6 + S_5S_9) + g\beta(S_1 + S_2 + S_3 + S_4 + S_5 + S_6 + S_7 + S_8 + S_9)$ B.

For **2**, at the lowest temperature attainable, $\chi_M T$ is 2.5 cm^3 K mol^{-1}, a value higher than expected for the $S = 3/2$ ground state. This is due to weak intermolecular ferromagnetic interactions, which were taken into account by a Weiss constant θ.[19]

Received: September 12, 2003 [Z52851]

Keywords: copper · cyclophanes · magnetic properties · metallacycles · N,O ligands · nonanuclear complex

[1] a) S. R. Seidel, P. J. Stang, *Acc. Chem. Res.* **2002**, *35*, 972; b) S. Leininger, B. Olenyuk, P. J. Stang, *Chem. Rev.* **2000**, *100*, 853; c) M. Fujita, *Chem. Soc. Rev.* **1998**, *27*, 417; d) D. L. Caulder, K. N. Raymond, *Acc. Chem. Res.* **1999**, *32*, 975.

[2] a) L. Zhao, Z. Q. Xu, L. K. Thompson, S. L. Heath, D. O. Miller, M. Ohba, *Angew. Chem.* **2000**, *112*, 3244; *Angew. Chem. Int. Ed.* **2000**, *39*, 3114; b) L. A. Zhao, C. J. Matthews, L. K. Thompson, S. L. Heath, *Chem. Commun.* **2000**, 265; c) J. J. Sokol, A. G. Hee, J. R. Long, *J. Am. Chem. Soc.* **2002**, *124*, 7656; d) J. J. Sokol, M. P. Shores, J. R. Long, *Inorg. Chem.* **2002**, *41*, 3052.

[3] a) J. Yoo, E. K. Brechin, A. Yamaguchi, M. Nakano, J. C. Huffman, A. L. Maniero, L. C. Brunel, K. Awaga, H. Ishimoto, G. Christou, D. N. Hendrickson, *Inorg. Chem.* **2000**, *39*, 3615; b) R. Sessoli, H.-L. Tsai, A. R. Schake, S. Wang, J. B. Vincent, K. Folting, D. Gatteschi, G. Christou, D. N. Hendrickson, *J. Am. Chem. Soc.* **1993**, *115*, 1804; c) A. L. Barra, P. Debrunner, D. Gatteschi, C. E. Schulz, R. Sessoli, *Europhys. Lett.* **1996**, *35*, 133.

[4] a) R. E. P. Winpenny, *Adv. Inorg. Chem.* **2001**, *52*, 1; b) R. E. P. Winpenny, *J. Chem. Soc. Dalton Trans.* **2002**, 1; c) G. L. Abbati, A. Cornia, A. C. Fabretti, A. Caneschi, D. Gatteschi, *Inorg. Chem.* **1998**, *37*, 3759; d) A. Caneschi, A. Cornia, S. J. Lippard, *Angew. Chem.* **1995**, *107*, 511; *Angew. Chem. Int. Ed. Engl.* **1995**, *34*, 467; e) G. Christou in *Magnetism a Supramolecular Function* (Ed.: O. Kahn), Kluwer Academic Publishers, Dordrecht, **1996**, p. 383; f) A. Caneschi, A. Cornia, A. C. Fabretti, S. Foner, D. Gatteschi, R. Grandi, L. Schenetti, *Chem. Eur. J.* **1996**, *2*, 1379; g) A. Caneschi, D. Gatteschi, J. Laugier, P. Rey, R. Sessoli, C. Zanchini, *J. Am. Chem. Soc.* **1988**, *110*, 2795.

[5] a) Y. Journaux, R. Ruiz, A. Aukauloo, Y. Pei, *Mol. Cryst. Liq. Cryst.* **1997**, *305*, 193; b) T. Mallah, C. Auberger, M. Verdaguer, P. Veillet, *J. Chem. Soc. Chem. Commun.* **1995**, 61; c) P. Yu, Y. Journaux, O. Kahn, *Inorg. Chem.* **1989**, *28*, 100; d) V. Marvaud, C. Decroix, A. Scuiller, F. Tuyeras, C. Guyard Duhayon, J. Vaissermann, M. Marrot, F. Gonnet, M. Verdaguer, *Chem. Eur. J.* **2003**, *9*, 1692.

[6] a) K. Itoh, *Pure Appl. Chem.* **1978**, *50*, 1251; b) N. Nakamura, K. Inoue, H. Iwamura, T. Fujioka, Y. Sawaki, *J. Am. Chem. Soc.* **1992**, *114*, 1484.

[7] T. Weyland, K. Costuas, A. Mari, J. F. Halet, C. Lapinte, *Organometallics* **1998**, *17*, 5569.

[8] T. Weyland, K. Costuas, L. Toupet, J. F. Halet, C. Lapinte, *Organometallics* **2000**, *19*, 4228.

[9] T. Glaser, M. Gerenkamp, R. Fröhlich, *Angew. Chem.* **2002**, *114*, 3984; *Angew. Chem. Int. Ed.* **2002**, *41*, 3823.

[10] I. Fernandez, R. Ruiz, J. Faus, M. Julve, F. Lloret, J. Cano, X. Ottenwaelder, Y. Journaux, M. C. Munoz, *Angew. Chem.* **2001**, *113*, 3129; *Angew. Chem. Int. Ed.* **2001**, *40*, 3039.

[11] P. M. VanCalcar, M. M. Olmstead, A. L. Balch, *Chem. Commun.* **1996**, 2597.

[12] A. W. Addison, T. N. Rao, J. Reedijk, J. van Rijn, G. C. Verschoor, *J. Chem. Soc. Dalton Trans.* **1984**, 1349.

[13] K. Itoh, M. Kinoshita, *Molecular Magnetism*, *New Magnetic Materials*, Kodansha Gordon and Breach Science, Tokyo, **2000**; A. S. Ovchinnikov, *Theor. Chim. Acta* **1978**, *47*, 259.

[14] a) J. A. McCleverty, M. D. Ward, *Acc. Chem. Res.* **1998**, *31*, 842; b) F. Lloret, G. De Munno, M. Julve, J. Cane, R. Ruiz, A. Caneschi, *Angew. Chem.* **1998**, *110*, 143; *Angew. Chem. Int. Ed.* **1998**, *37*, 135.

[15] R. Costa, A. Garcia, J. Ribas, T. Mallah, Y. Journaux, J. Sletten, X. Solans, *Inorg. Chem.* **1993**, *32*, 3733.

[16] A. Aukauloo, X. Ottenwaelder, R. Ruiz, Y. Journaux, Y. Pei, E. Riviere, M. C. Munoz, *Eur. J. Inorg. Chem.* **2000**, 951.

[17] The magnetization of **3** at low temperature can also be fitted in terms of an effective interaction between the doublet ground states of the trinuclear subunits. The best fit is obtained with a J_{eff} value of $+0.9$ cm^{-1}, which corresponds to a J_F value of $+8.4$ cm^{-1} ($J_F = 9J_{eff}$).

[18] H. O. Stumpf, Y. Pei, O. Kahn, J. Sletten, J.-P. Renard, *J. Am. Chem. Soc.* **1993**, *115*, 6738.

[19] O. Kahn, *Molecular Magnetism*, VCH, New York, **1993**.

 © 2004 Wiley-VCH Verlag GmbH & Co. KGaA, Weinheim

Intramolecular Electron Transfer

Production of an Ultra-Long-Lived Charge-Separated State in a Zinc Chlorin–C_{60} Dyad by One-Step Photoinduced Electron Transfer**

Kei Ohkubo, Hiroaki Kotani, Jianguo Shao, Zhongping Ou, Karl M. Kadish, Guolin Li, Ravindra K. Pandey,* Mamoru Fujitsuka, Osamu Ito,* Hiroshi Imahori,* and Shunichi Fukuzumi**

The natural photosynthetic reaction center utilizes sequential multistep electron transfer from the excited chromophore to the terminal electron acceptor via electron mediators, which are well-organized in a protein matrix, to attain a long lifetime (as long as seconds) of the final charge-separated (CS) state.[1] A number of linked electron-donor–acceptor dyads have been developed to mimic such multistep electron-transfer processes in natural photosynthesis. These systems have been extended to triads and more complex systems in which electron mediators are combined to achieve a longer lifetime of the final CS state.[2–7] A long lifetime of 380 ms, which is comparable to the lifetime of the natural system, has been achieved using a well-designed molecular tetrad (namely, ferrocene-zinc porphyrin-free base porphyrin-fullerene).[8] However, a significant amount of energy is lost during the multistep electron-transfer processes in both the natural and model systems. Thus, it is highly desired to develop donor–acceptor dyad systems in which the CS state has long lifetimes and does not lose energy by sequential electron transfer. The lifetime of the CS state has recently been reported to be elongated by decreasing the distance between the donor and acceptor in the dyads.[9–11]

We report herein that a zinc chlorin–fullerene dyad which has an extremely short donor–acceptor distance (ZnCh–C_{60}, Figure 1)[12–14] has a CS state with the longest lifetime reported for a linked donor–acceptor system. The large temperature dependence of the lifetime of the CS state has been examined over a wide temperature range (−150 to 65 °C).

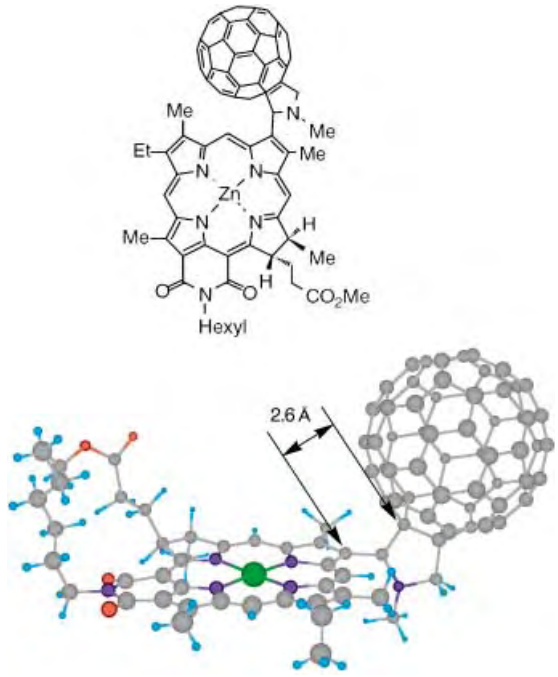


Figure 1. Structure of the ZnCh–C_{60} dyad, as well as the optimized structure determined by PM3 calculations.

The ZnCh–C_{60} dyad was synthesized by 1,3-dipolar cycloaddition of the 3-formylchlorin and sarcocine with fullerene.[13] The tetrapyrrolic compound contains a six-membered fused-imide ring system and presents an opportunity to design a fullerene conjugate containing a spacer with a defined

[*] Dr. K. Ohkubo, H. Kotani, Prof. Dr. S. Fukuzumi
Department of Material and Life Science
Graduate School of Engineering
Osaka University
CREST, Japan Science and Technology Agency
2-1 Yamada-oka Suita Osaka 565-0871 (Japan)
Fax: (+81) 6-6879-7370
E-mail: fukuzumi@chem.eng.osaka-u.ac.jp

Dr. J. Shao, Dr. Z. Ou, Prof. Dr. K. M. Kadish
Department of Chemistry, University of Houston
Houston, TX 77204-5003 (USA)
Fax: (+1) 713-743-2745
E-mail: kkadish@uh.edu

Dr. G. Li, Prof. Dr. R. K. Pandey
Chemistry Division, Photodynamic Therapy Center
and Department of Nuclear Medicine
Roswell Park Cancer Institute
Buffalo, NY, 14263 (USA)
Fax: (+1) 716-845-8920
E-mail: Ravindra.Pandey@RoswellPark.org

Dr. M. Fujitsuka,[+] Prof. Dr. O. Ito
Institute of Multidisciplinary Research for Advanced Materials
Tohoku University, CREST
Japan Science and Technology Agency (JST)
Sendai, Miyagi 980-8577 (Japan)
Fax: (+81) 22-217-5608
E-mail: ito@tagen.tohoku.ac.jp

Prof. Dr. H. Imahori
Graduate School of Engineering
Kyoto University, PRESTO (JST)
Kyoto 615-8510 (Japan)
Fax: (+81) 75-383-2571
E-mail: imahori@scl.kyoto-u.ac.jp

[+] Current address:
The Institute of Scientific and Industrial Research
Osaka University, Mihoga-oka, Ibaraki, Osaka 567-0047 (Japan)

[**] We wish to thank a grant in aid (13440216) from the Ministry of Education, Culture, Sports, Science, and Technology, Japan, and the Robert A. Welch Foundation (K.M.K., Grant E-680) for financial support, as well as the shared resources of the Roswell Park Cancer Center Support Grant (P30CA16056). Mass spectrometry analyses were performed at the Mass Spectrometry Facility, Michigan State University, East Lansing, Michigan (USA).

Supporting information for this article (the cyclic voltammogram of the dyad in PhCN, picosecond transient absorption spectra of ZnCh–C_{60}, and analytical data) is available on the WWW under http://www.angewandte.org or from the author.

 DOI: 10.1002/anie.200352870 © 2004 Wiley-VCH Verlag GmbH & Co. KGaA, Weinheim

length and geometry. The optimized structure of the dyad was obtained by PM3 calculations (Figure 1), and the edge-to-edge distance was determined to be 2.6 Å.

The absorption spectrum of ZnCh–C_{60} in benzonitrile (PhCN) is a reasonable superposition of the spectra of the component chromophores making up the dyads. Thus, there is no significant electronic interaction between the individual chromophores in the ground-state configuration despite the short linkage. The cyclic voltammogram of ZnCh–C_{60} in deaerated PhCN containing 0.1 M Bu_4NClO_4 consists of three one-electron reductions of the C_{60} molecule in the dyad (−0.53, −1.09, and −1.60 V versus the standard calomel electrode (SCE)), two one-electron reductions of ZnCh (−0.94 and −1.46 V), and a single one-electron oxidation of ZnCh (0.73 V; see the Supporting Information).

Photoexcitation of a deoxygenated solution of ZnCh–C_{60} in PhCN with 410-nm monochromatized light results in fluorescence with an emission maximum at 730 nm. The fluorescence decay was monitored at 730 nm, which corresponds to the emission of the zinc chlorin moiety.[9] The lifetime of the zinc chlorin fluorescence ($\tau = 2.7$ ns in an unlinked state)[9] was significantly reduced when it was in the dyad (τ(ZnCh–C_{60}) = 10 ps) as a result of electron transfer from the singlet excited state of ZnCh (^{1}ZnCh*) to the C_{60} molecule of the dyad. The rate constant of electron transfer (k_{ET}) from ^{1}ZnCh* to C_{60} was determined as 1.0×10^{11} s^{-1} from the difference between the reciprocal lifetimes of ZnCh–C_{60} and the unlinked zinc chlorin. The change in the free energy of the photoinduced electron transfer (ΔG^0_{ET}) from the ^{1}ZnCh* moiety to the C_{60} moiety in PhCN was determined as −0.44 eV from the one-electron oxidation potential and the excitation energy ($S_1 = 1.70$ eV) of the ZnCh moiety, as well as the one-electron reduction potential of the C_{60} moiety in ZnCh–C_{60}.

The k_{ET} value was also determined by picosecond transient absorption measurements. Application of a 388-nm laser pulse to a deoxygenated solution of ZnCh–C_{60} in PhCN gave rise to a transient absorption maximum at 460 nm, which corresponds to the singlet excited state of ZnCh (S2). The decay rate constant was determined as 1.0×10^{11} s^{-1}, which agrees with the value determined from measurements of the fluorescence lifetime. The decay of the absorbance at 460 nm, which corresponds to ^{1}ZnCh*, is accompanied by an increase in an absorbance at 590 nm, which results from the formation of ZnCh$^{\bullet+}$ (S2). This observation indicates that electron transfer from ^{1}ZnCh* to C_{60} occurs to form the CS state ZnCh$^{\bullet+}$–$C_{60}^{\bullet-}$.

The CS state can also be detected as a transient absorption spectrum upon excitation (355 nm) of a deoxygenated solution of ZnCh–C_{60} in PhCN with a nanosecond laser pulse (Figure 2a). The absorption band at 1000 nm is an attribute of the monofullerene radical anion.[8–11] The absorption band at 790 nm (Figure 2a) agrees with that of the π-radical cation of zinc chlorin. Thus, the transient absorption spectrum shown in Figure 2a indicates formation of the CS state (ZnCh$^{\bullet+}$–$C_{60}^{\bullet-}$). The quantum yield of the CS state was determined as 12%,[15,16] which is smaller than the efficiency of the fluorescence quenching (99.6%).[17] This result indicates that the singlet excited state is quenched to form a short-lived exciplex,[14] a part of which is converted into a long-lived CS state (Figure 2a). The CS state decays by back electron transfer (BET) to the ground state rather than to the triplet excited state since the CS state is lower in energy (1.26 eV) than both the triplet excited states of C_{60} (1.50 eV) and ZnCh (1.36–1.45 eV).[9] The rate of BET (k_{BET}) was determined from the disappearance of the absorption band at 790 nm, which is attributable to the ZnCh$^{\bullet+}$ species in the ZnCh$^{\bullet+}$–$C_{60}^{\bullet-}$ dyad. The decay of the absorption band at 790 nm was monitored using different laser power, and the decay was found to obey first-order kinetics with the same slope observed for all laser powers (Figure 2b). This observation indicates clearly that the decay of the CS state is ascribed to intramolecular BET and not to intermolecular BET. The k_{BET} value is determined as 4.2×10^3 s^{-1}, and thus the lifetime of the CS state is 230 μs at 25 °C.

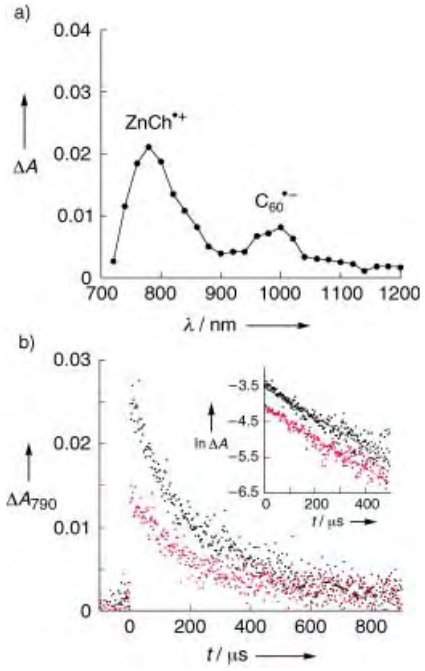


Figure 2. a) Transient absorption spectrum of ZnCh–C_{60} (1.0×10^{-4} M) in deaerated PhCN at 25 °C taken 1.0 μs after laser excitation at 355 nm; b) decay profiles at 790 nm with different laser power (30 mJ, black circles; 10 mJ, red circles). Inset: first-order plots.

The ESR spectra were measured by photoirradiation of ZnCh–C_{60} in frozen PhCN (Figure 3a). The resulting spectrum of the photoirradiated ZnCh–C_{60} in PhCN at −150 °C is shown in the inset of Figure 3a. The ESR spectrum consists of two characteristic signals, one of which is attributable to an organofullerene radical anion with a g value (2.0007) smaller than the free-spin value (2.0023), and the other to the zinc chlorin radical cation with a higher g value (2.0033).[9,10,18] The disappearance of the ESR signal intensity obeyed first-order kinetics (Figure 3a) under the experimental conditions, where a low concentration of ZnCh–C_{60} (1.0×10^{-5} M) was employed to avoid intermolecular decay of the CS state. The temperature dependence of the decay rate constant (k_{BET}) was examined in frozen PhCN by observing the decay of the ESR

 © 2004 Wiley-VCH Verlag GmbH & Co. KGaA, Weinheim

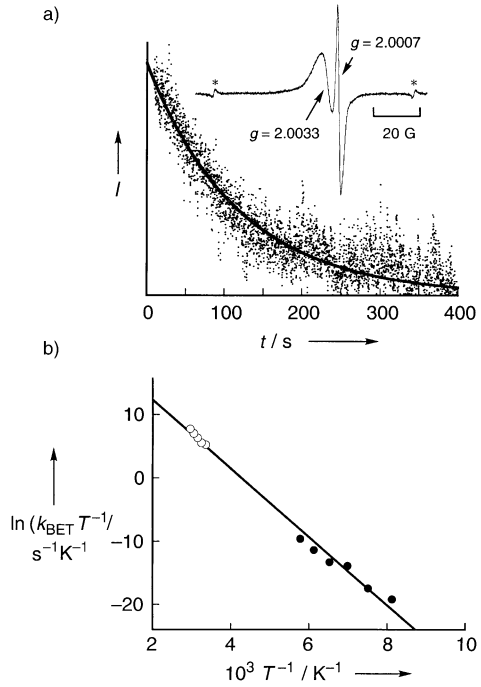


Figure 3. a) ESR spectrum and the decay time profile of the ESR signal intensity of $ZnCh^{\bullet+}$–$C_{60}^{\bullet-}$ in frozen PhCN at −150 °C. The asterisk denotes a Mn^{2+} marker; b) plot of $\ln(k_{BET}T^{-1})$ versus T^{-1} for BET in $ZnCh^{\bullet+}$–$C_{60}^{\bullet-}$ in PhCN as determined by laser flash photolysis (○) and ESR (●) measurements.

signal at −150 to −100 °C. The temperature dependence of the k_{BET} value in frozen PhCN (Figure 3b, filled circles) as well as in PhCN solution was observed by laser flash photolysis at 25–65 °C (Figure 3b, open circles). The activation enthalpy for the intramolecular BET was determined from the slope of the graph (Figure 3b) to be 5.4 kcal mol^{-1}. Such a large temperature dependence of the k_{BET} value indicates that the BET process is deeply in the Marcus inverted region because of the small amount of reorganization energy necessary for electron transfer in the ZnCh–C_{60} dyad with a short linkage and the rate of electron transfer decreases as the driving force increases.[19] This result is in sharp contrast with the case of the tetrad systems in which the BET is on the Marcus top region and the k_{BET} value exhibits no temperature dependence.[8,20] The lifetime of the CS state at −150 °C is as long as 120 s, which is the longest CS lifetime reported for linked donor–acceptor systems.

In summary, we have successfully shown that intramolecular electron transfer from the singlet excited state of zinc chlorin to fullerene occurs efficiently in a dyad with a short linkage. This process results in an ultra-long-lived CS state without the loss of energy that is inevitable in multistep electron-transfer processes.

Experimental Section

Ch–C_{60} dyad: A mixture of 3-formyl-3-devinylpurpurin-18-*N*-hexylimide methyl ester (104 mg, 1.0 equiv), C_{60} (127 mg, 1.1 equiv), and sarcosine (72 mg, 5.0 equiv) in dry toluene was refluxed under nitrogen for 17 h. The solution was cooled to room temperature and then passed through alumina (Brockmann Grade III) with dichloromethane as the eluent. The major fraction was collected, and the product obtained after evaporating the solvent was further purified by chromatography on alumina (Grade III) using hexanes/dichloromethane as the eluant (first 2/3 then 1/2 v/v) to give the title compound (67 mg) and recovered 3-formal-3-devinyl-purpurin-18-*N*-hexylimide methyl ester (25 mg). Analytical data are given in the Supporting Information.

ZnCh–C_{60}: A solution of zinc acetate dihydrate (500 mg) in methanol (15 mL) was added to a solution of the free-base dyad (42 mg) in chloroform (50 mL). The resultant solution was degassed by vacuum and stirred in a nitrogen atmosphere at room temperature for 19 h. The reaction mixture was then washed with water (6 × 50 mL), the organic layer collected, and then dried with sodium sulfate. After filtration, the solvent was removed and the title compound was obtained in quantitative yield. See the Supporting Information for analytical data.

The nanosecond and picosecond laser flash photolysis measurements were performed as reported previously.[9,21]

Received: September 15, 2003 [Z52870]
Published Online: January 22, 2004

Keywords: charge separation · chlorin · electron transfer · fullerenes · photosynthesis

[1] *The Photosynthetic Reaction Center* (Eds.: J. Deisenhofer, J. R. Norris), Academic, San Diego, **1993**.
[2] a) M. R. Wasielewski, *Chem. Rev.* **1992**, *92*, 435; b) K. D. Jordan, M. N. Paddon-Row, *Chem. Rev.* **1992**, *92*, 395; c) J. W. Verhoeven, *Adv. Chem. Phys.* **1999**, *106*, 603; d) A. Osuka, N. Mataga, T. Okada, *Pure Appl. Chem.* **1997**, *69*, 797.
[3] a) M.-J. Blanco, J. M. Consuelo, J.-C. Chambron, V. Heitz, M. Linke, J.-P. Sauvage, *Chem. Soc. Rev.* **1999**, *28*, 293; b) F. Diederich, M. Gómez-López, *Chem. Soc. Rev.*. **1999**, *28*, 263.
[4] F. D. Lewis, R. L. Letsinger, M. R. Wasielewski, *Acc. Chem. Res.* **2001**, *34*, 159.
[5] a) D. Gust, T. A. Moore, *The Porphyrin Handbook*, *Vol. 8* (Eds.: K. M. Kadish, K. M. Smith, R. Guilard), Academic Press, San Diego, CA, **2000**, p. 153.
[6] a) H. Imahori, Y. Sakata, *Adv. Mater.* **1997**, *9*, 537; b) H. Imahori, Y. Sakata, *Eur. J. Org. Chem.* **1999**, 2445; c) S. Fukuzumi, D. M. Guldi, *Electron Transfer in Chemistry*, *Vol. 2* (Ed.: V. Balzani), Wiley-VCH, Weinheim, **2001**, p. 270.
[7] D. Gust, T. A. Moore, A. L. Moore, A. N. Macpherson, A. Lopez, J. M. DeGraziano, I. Gouni, E. Bittersmann, G. R. Seely, F. Gao, R. A. Nieman, X. C. Ma, L. J. Demanche, S.-C. Hung, D. K. Luttrull, S.-J. Lee, P. K. Kerrigan, *J. Am. Chem. Soc.* **1993**, *115*, 11141.
[8] H. Imahori, D. M. Guldi, K. Tamaki, Y. Yoshida, C. Luo, Y. Sakata, S. Fukuzumi, *J. Am. Chem. Soc.* **2001**, *123*, 6617.
[9] S. Fukuzumi, K. Ohkubo, H. Imahori, J. Shao, Z. Ou, G. Zheng, Y. Chen, R. K. Pandey, M. Fujitsuka, O. Ito, K. M. Kadish, *J. Am. Chem. Soc.* **2001**, *123*, 10676.
[10] K. Ohkubo, H. Imahori, J. Shao, Z. Ou, K. M. Kadish, Y. Chen, G. Zheng, R. K. Pandey, M. Fujitsuka, O. Ito, *J. Phys. Chem. A* **2002**, *106*, 10911.
[11] Y. Kashiwagi, K. Ohkubo, J. A. MacDonald, I. M. Blake, M. J. Crossley, Y. Araki, O. Ito, H. Imahori, S. Fukuzumi, *Org. Lett.* **2003**, *5*, 2719.
[12] The atropisomerism arises from the short linkage between the C_{60} and the chlorin moieties, which restricts free rotation of the C_{60} moiety as reported for similar chlorin–C_{60} dyads.[13] The photophysical properties of atropisomers are reported to be the

 © 2004 Wiley-VCH Verlag GmbH & Co. KGaA, Weinheim

same.[14] Thus, the atropisomers of ZnCh–C_{60} are used for the photophysical and electrochemical characterizations.

[13] J. Helaja, A. Y. Tauber, Y. Abel, N. V. Tkachenko, H. Lemmetyinen, I. Klipeläinen, P. H. Hynninen, *J. Chem. Soc. Perkin Trans. 1* **1999**, 2403.

[14] N. V. Tkachenko, L. Rantala, A. Y. Tauber, J. Helaja, P. H. Hynninen, H. Lemmetyinen, *J. Am. Chem. Soc.* **1999**, *121*, 9378.

[15] The quantum yield of the CS state was determined using the comparative method.[16] In particular, the strong fullerene triplet–triplet absorption ($\varepsilon_{740\,nm} = 18\,800\,M^{-1}cm^{-1}$: $\Phi_{triplet} = 0.98$) served as a probe to obtain the quantum yield for the CS state, especially for ZnCh$^{\bullet+}$–C_{60} ($\varepsilon_{790\,nm} = 13\,000\,M^{-1}cm^{-1}$). The molar extinction coefficient of ZnCh$^{\bullet+}$–C_{60} was determined by thin-layer spectroelectrochemical measurements.

[16] C. Luo, M. Fujitsuka, A. Watanabe, O. Ito, L. Gan, Y. Huang, C.-H. Huang, *J. Chem. Soc. Faraday Trans.* **1998**, *94*, 527.

[17] The decay of the absorbance at 590 nm (see Supporting Information), which is much faster than the decay shown in Figure 2b, may be ascribed to the decay of the exciplex. The residual absorbance at 3 ns in the data shown in the Supporting Information may correspond to the absorbance arising from ZnCh$^{\bullet+}$ (Figure 2a), although the low signal-to-noise ratio has precluded the determination of the quantum yield from the picosecond laser measurements. It should be noted that the exciplex should have an absorption spectrum quite similar to the CS state.

[18] The observation of broad ESR signals arising from ZnCh$^{\bullet+}$ and $C_{60}^{\bullet-}$ moieties indicate that the spin–spin interaction is not strong enough to produce the singlet or triplet state.

[19] R. A. Marcus, N. Sutin, *Biochim. Biophys. Acta* **1985**, *811*, 265.

[20] A strong temperature dependence has rarely been observed. The absence of a temperature-dependent k_{BET} value has been ascribed to the occurrence of nuclear tunneling; see J. Kroon, H. Oevering, J. W. Verhoeven, J. M. Warman, A. M. Oliver, M. N. Paddon-Row, *J. Phys. Chem.* **1993**, *97*, 5065. In the case of ZnCh–C_{60}, the strong temperature dependence of the k_{BET} value shown in Figure 3b clearly indicates the absence of nuclear tunneling. At much lower temperatures, however, it may be possible to observe the tunneling effect.

[21] S. Fukuzumi, K. Okamoto, Y. Yoshida, H. Imahori, Y. Araki, O. Ito, *J. Am. Chem. Soc.* **2003**, *125*, 1007.

 © 2004 Wiley-VCH Verlag GmbH & Co. KGaA, Weinheim

Glycoproteins

Antifreeze Glycoproteins: Elucidation of the Structural Motifs That Are Essential for Antifreeze Activity**

*Yuki Tachibana, Garth L. Fletcher, Naoki Fujitani, Sakae Tsuda, Kenji Monde, and Shin-Ichiro Nishimura**

Antifreeze proteins (AFPs) and glycoproteins (AFGPs) collectively abbreviated as AF(G)Ps are essential to the survival of many marine teleost fishes that reside in polar and subpolar waters where temperatures decline below the colligative freezing points of their body fluids.[1] Although the AF(G)Ps are markedly diverse in structure, they all function by binding to the surface of embryonic ice crystals to inhibit their growth. This binding results in a freezing point depression without an appreciable change in the melting point. The difference between the melting and freezing temperatures, termed thermal hysteresis (TH), is used to detect and quantify the antifreeze activity. In addition to effecting a thermal hysteresis, concentrated fish AF(G)Ps alter the morphology of the ice crystal into a hexagonal bipyramid.[2]

The AFGPs isolated from fish blood plasma consist of repeating tripeptide units $(Ala\text{-}Thr\text{-}Ala)_n$ with a disaccharide moiety (Galβ1-3GalNAcα1-) attached to each threonyl residue.[3] They range in molecular mass from approximately 33 kDa (50 repeating units) to 2.6 kDa (four repeating units).

[*] Y. Tachibana, Dr. N. Fujitani, Dr. K. Monde, Prof. S.-I. Nishimura
Division of Biological Sciences
Graduate School of Science
Frontier Research Center for Post-Genomic Science and Technology
Hokkaido University
Sapporo 001-0021 (Japan)
Fax: (+81) 11-706-9042
E-mail: shin@glyco.sci.hokudai.ac.jp

Prof. G. L. Fletcher
Ocean Sciences Centre
Memorial University of Newfoundland
St. John's, Newfoundland A1c 5S7 (Canada)

Dr. S. Tsuda
Structural Biology Group
National Institute of Advanced Industrial Science and Technology (AIST)
Sapporo 062-8517 (Japan)

Prof. S.-I. Nishimura
Glycochemosynthesis Team
Research Center for Glycoscience
National Institute of Advanced Industrial Science and Technology (AIST)
Sapporo 062-8517 (Japan)

[**] This work was supported by the NEDO and the Ministry of Education, Science, and Culture. We also thank Ms. A. Maeda, Ms. H. Matsumoto, and Ms. S. Oka of the Center of Instrumental Analysis, Hokkaido University, for measuring elemental analyses and mass spectrometry studies.

Supporting information for this article is available on the WWW under http://www.angewandte.org or from the author.

 © 2004 Wiley-VCH Verlag GmbH & Co. KGaA, Weinheim DOI: 10.1002/anie.200353110

Although these AFGPs were the first antifreeze polypeptides to be described in detail, very little is known about their mechanism of action.[4] This contrasts with the considerable progress that has been made towards understanding the structure–function relationships of several of the AFPs.[5] This lack of progress is largely due to the structural complexity of the numerous isoforms of AFGP found in blood plasma and the ensuing difficulties in isolating sufficient quantities of pure material.[6] In addition, attempts to manufacture pure AFGP through the use of cell lines have not yet met with success. In light of these difficulties it would appear that chemical synthesis may be the only viable way to produce sufficient quantities of pure AFGP for detailed structure–function studies.

There have been a number of studies reporting the synthesis of AFGP-related compounds.[7] However, none of these compounds have been tested for antifreeze activity. This lack of success to date is largely because of the intrinsic difficulties involved in the construction of glycoproteins such as AFGPs that have relatively large molecular masses and contain a high density of sugar residues.

Recently, we have developed a strategy for the efficient chemical synthesis of sequential glycoproteins and have succeeded in synthesizing AFGPs (synthesized AFGPs are termed *sy*AFGPs) that are essentially identical to the naturally occurring AFGPs, and have the capacity to shape ice crystals into hexagonal bipyramids.[8] We now report on what we believe to be the structural motifs that are essential for the antifreeze activity of AFGPs, alter ice-crystal morphology and result in significant thermal hysteresis.

Antifreeze glycoproteins (*sy*AFGP$_{poly}$, **1**) were synthesized by directly polymerizing an unprotected glycopeptide macromonomer in the presence of diphenylphosphorylazide (DPPA) as a promoter.[8b] The weight-average molecular weight of **1** was estimated to be 6600 Da, which corresponded to 8–15 repeating units, and produced significant antifreeze activity (TH) (Figure 2C, b).

To determine the minimum number of tripeptide repeating units necessary for antifreeze activity, low-molecular-weight *sy*AFGPs were produced in a manner similar to that described for the *sy*AFGP$_{poly}$, **1**,[8b] but at a lower temperature and with a shorter reaction time. These *sy*AFGPs were then separated into homogeneous fractions of precise chain lengths by means of recycling preparative size-exclusion chromatography. As shown in Figure 1A, purification of up to seven repeating units was accomplished, and the calculated and observed mass for each glycopeptide was identical within experimental error (Figure 1C). The purity of each glycopeptide was demonstrated by using analytical reverse-phase (RP) HPLC (Figure 1B).

The relationship between thermal hysteresis activity, ice-crystal morphology, and synthetic AFGP chain length is presented in Figure 1D and E. Although high concentrations of the monomer *sy*AFGP$_1$, **1′**, exhibited no thermal hysteresis, it did produce hexagonal ice crystals (Figure 1E, a). This strongly suggests that the glycopeptide monomer is capable of some interaction with ice. All of the tripeptide *sy*AFGP polymers (**2**–**7**) displayed concentration-dependent thermal hysteresis and produced hexagonal bipyrimidal ice crystals. In addition there was a positive correlation between thermal hysteresis and chain length between two and five tripeptide repeating units (**2**–**5**). There was no increase in thermal hysteresis activity when the chain length increased from five–seven repeats (**5**–**7**), which suggests that the antifreeze activity of the *sy*AFGP was maximal at five repeats (Figure 1D). These results clearly demonstrate that a two-tripeptide *sy*AFGP is sufficiently large to control ice crystal growth.

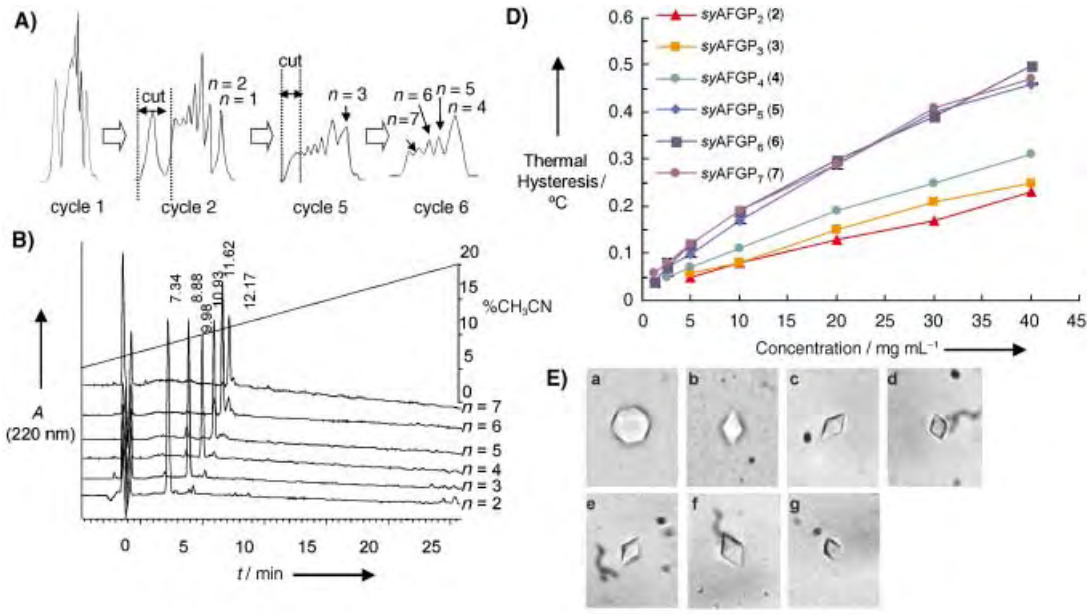
To identify the structural motifs that are essential for antifreeze activity, a number of AFGP analogues were synthesized (Figure 2A) by using established methods.[9] The antifreeze activity of each of the polypeptides and analogues was evaluated by using a Clifton nanoliter osmometer and by examining ice crystal morphology (Figure 2B and C). Synthetic **1** produced hexagonal bipyramidal ice crystals, and exhibited a thermal hysteresis that was somewhat greater than that of the naturally occurring AFGP-8 (2.6 kDa). A lack of carbohydrate moiety (nonglycosylated polypeptide, **8**) resulted in the complete loss of thermal hysteresis and structuring of the ice crystal (Figure 2C, c). This result confirms those of earlier studies that indicate that the carbohydrate is essential for AFGP activity.[10]

The β-*O*-linked type glycoprotein **9** was designed to probe the importance of α-glycosidic linkage between GalNAc residue and threonyl side chain. Although the formation of the hexagonal ice crystal (Figure 2C, d) suggests weak interactions between the glycopeptide and the ice, a complete lack of thermal-hysteresis activity attests to the essential nature of this linkage.

Sialylated glycoprotein **10** was prepared by the enzymatic introduction of sialic acid at the C3 position of the galactose residue of *sy*AFGP$_{poly}$ **1**, as previously described.[8b] The results of this modification confirm those reported for a similar study with naturally occurring AFGP: the complete loss of thermal hysteresis[2c] (data not shown).[8b] There are two possible reasons for this result: 1) The introduction of the sialic acid residue destroys the AFGP conformation; 2) The sialic acid residue interferes with the ability of the glycoprotein to prevent ice growth.

Glycoproteins **11**–**15** were synthesized to examine the importance of the NHAc group at the C2 position of the carbohydrate moiety attached to threonine residue and the hydroxyl groups. Interestingly, the AFGP analogue that only contained the GalNAc residue **11** was fully functional, and had a capacity to form bipyramidal crystals and a thermal hysteresis that was slightly lower than that of **1** (Figure 2B and C, e). This result indicates that the terminal galactose residue is not necessary for activity. However, the apparent lower thermal-hysteresis activity of GalNAc **11** polypeptide suggests that the galactose residue may enhance the binding of AFGP with the ice surface. The LacNAc **12** polypeptide also inhibited growth of ice crystals (Figure 2C, f). However the thermal hysteresis values were considerably lower than those of **1** (Figure 2B), thus implying that the configuration of the sugar hydroxyl groups is important for the activity. AFGP analogues carrying Galβ1-3Gal **13** (data not shown),[8b] Gal **14** or Lac **15** did not show any thermal hysteresis, although they were able to produce hexagonal-like crystals (Figure 2C, g and h), which indicates the presence of weak interactions with

 © 2004 Wiley-VCH Verlag GmbH & Co. KGaA, Weinheim



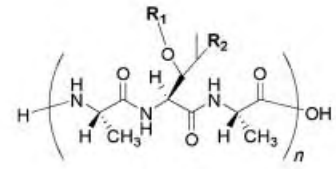
C)

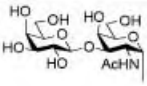
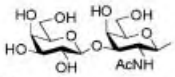
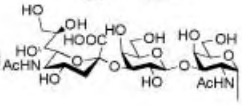
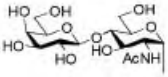
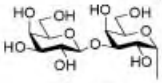
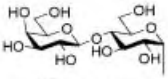
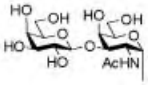
Codename	Structure	Calculated mass ([M + Na]+)	Observed mass
*syn*AFGP$_2$ (**2**)		1257.51	1257.29
*syn*AFGP$_3$ (**3**)		1865.76	1865.20
*syn*AFGP$_4$ (**4**)		2474.02	2473.82
*syn*AFGP$_5$ (**5**)		3082.27	3081.99
synAFGP$_6$ (**6**)		3690.53	3690.06
*syn*AFGP$_7$ (**7**)		4298.78	4298.00

Figure 1. Relationship between molecular weight and antifreeze activity. A) Recycling size-exclusion-chromatography profile of synthetic AFGP. Synthetic AFGP was separated into a homogeneous fraction of discrete length by means of RP-HPLC on Shodex size-exclusion columns (OHpak SB-2002.5×2-and OHpak SB-2003) with water as an eluent. B) RP-HPLC profiles of **2**–**7**. The right-hand axis gives the percentage of acetonitile in 0.1% aqueous trifluoroacetic acid (%CH_3CN). C) Structure and MALDI-TOF mass spectrometric analysis of *syn*AFGPs. D) Thermal hysteresis activity of **2**–**7**, measured by means of a Clifton nanolitre osmometer (Clifton Technical Physics, Hartford, NY).[15] E) The ice-crystal morphologies in the presence of a) **1′** (40 mg mL^{-1}), b) **2** (40 mg mL^{-1}), c) **3** (10 mg mL^{-1}), d) **4** (10 mg mL^{-1}), e) **5** (10 mg mL^{-1}), f) **6** (10 mg mL^{-1}), g) **7** (10 mg mL^{-1}) in water were observed as described previously.[16] Photos were taken at −0.1 °C (b–g) or 0.0 °C (a).

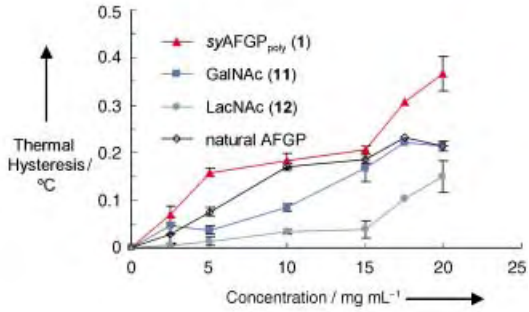
 © 2004 Wiley-VCH Verlag GmbH & Co. KGaA, Weinheim

A)



codename	R_1	R_2	Mn[a]	Mw[b]
*sy*AFGP$_{poly}$ (**1**)[8b]		CH_3	3 950	6 600
nonglycosylated polypeptide (**8**)	H	CH_3	1 690	2 400
β-*O*-linked glycoprotein (**9**)		CH_3	4 020	6 620
sialylated *sy*AFGP$_{poly}$(**10**)[8b]		CH_3	6 370	11 650
GalNAc (**11**)		CH_3	3 000	4 690
LacNAc (**12**)		CH_3	3 660	6 140
Galβ1-3Gal (**13**)[8b]		CH_3	4 100	5 480
Gal (**14**)		CH_3	3 180	4 230
Lac (**15**)		CH_3	4 700	7 000
ASA (**16**)		H	4 410	6 590

B)



C)

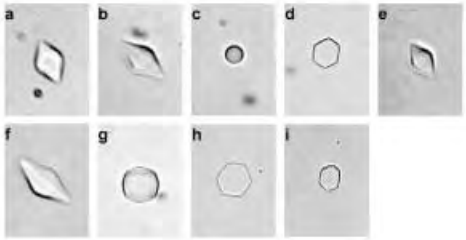


Figure 2. Structure–activity relationship of AFGP. A) AFGP analogues synthesized in this study. All compounds were used for the activity evaluation studies in polymeric form. B) Thermal hysteresis activity of synthetic AFGP. C) Ice-crystal morphology in the presence of a) natural AFGP, b) **1**, c) nonglycosylated polypeptide **8**, d) β-*O*-linked glycoprotein **9**, e) GalNAc **11**, f) LacNAc **12**, g) Gal **14**, h) Lac **15**, i) ASA **16**. Ice crystals were formed in the presence of 10 mg mL^{-1} glycoprotein in water. Photos were taken after 0.1 °C undercooling (a, b, e, f) or 0.0 °C (c,d, g–i).

ice. These results show that the acetamide (-NHCOCH$_3$) groups at the C2 position of the reducing end sugar residues are key functional groups required for the antifreeze activity. The Ala-Ser-Ala AFGP analogue **16**, was constructed to examine the importance of the γ-methyl groups on the Thr residue. This analogue exhibited no thermal hysteresis (Figure 2C, i), thus demonstrating that the γ-methyl groups of the Thr residues are also essential for activity.

From the evaluation of the activity discussed above, we conclude that the conformation of the glycoprotein is a key factor for antifreeze activity. Therefore, to study the relationship between the activity and the conformation, CD spectra of the synthetic (glyco)proteins in the far UV-absorption region were measured in aqueous solutions at neutral pH (Figure 3A–C). As reported previously, synthetic AFGP **1** gave a curve similar to that of natural AFGP[8b] thus providing evidence of the presence of polyproline type II (PPII) helix (Figure 3A, b).[4c,11] Similar spectra were also obtained in cases of active two-model glycoproteins **11** and **12** (Figure 3B, e and f), while Galβ1-3Gal **13** (data not shown),[8b] Gal **14**, Lac **15** (Figure 3B, g and h), β-Linked glycosides **9**, and nonglycosylated polypeptide **8** (Figure 3A, d and c) exhibited CD spectra typically found from the polypeptides of a disordered structure.[11c] It is reasonable to assume that acetamide group is a fundamental functional group for the construction of the specific structure of AFGPs. Interestingly, it was suggested that the Ser-replaced compound **16** seemed to contain a large α-helical structure (Figure 3B, i). In addition, sialylated glycoprotein **10**, which showed no antifreeze activity, still retains the similar secondary structure as AFGP (data not shown).[8b] Therefore, it seems that the terminal sialic acid residues introduced at the C3 position of the galactose residues might inhibit the successful adsorption of hydroxyl groups onto the surface of ice lattice. Alternatively, even small changes in the conformation might provide a drastic effect on the activity.

In the same manner, the chain-length dependency of the conformation of AFGP was also examined by use of **2**–**7** as

 © 2004 Wiley-VCH Verlag GmbH & Co. KGaA, Weinheim

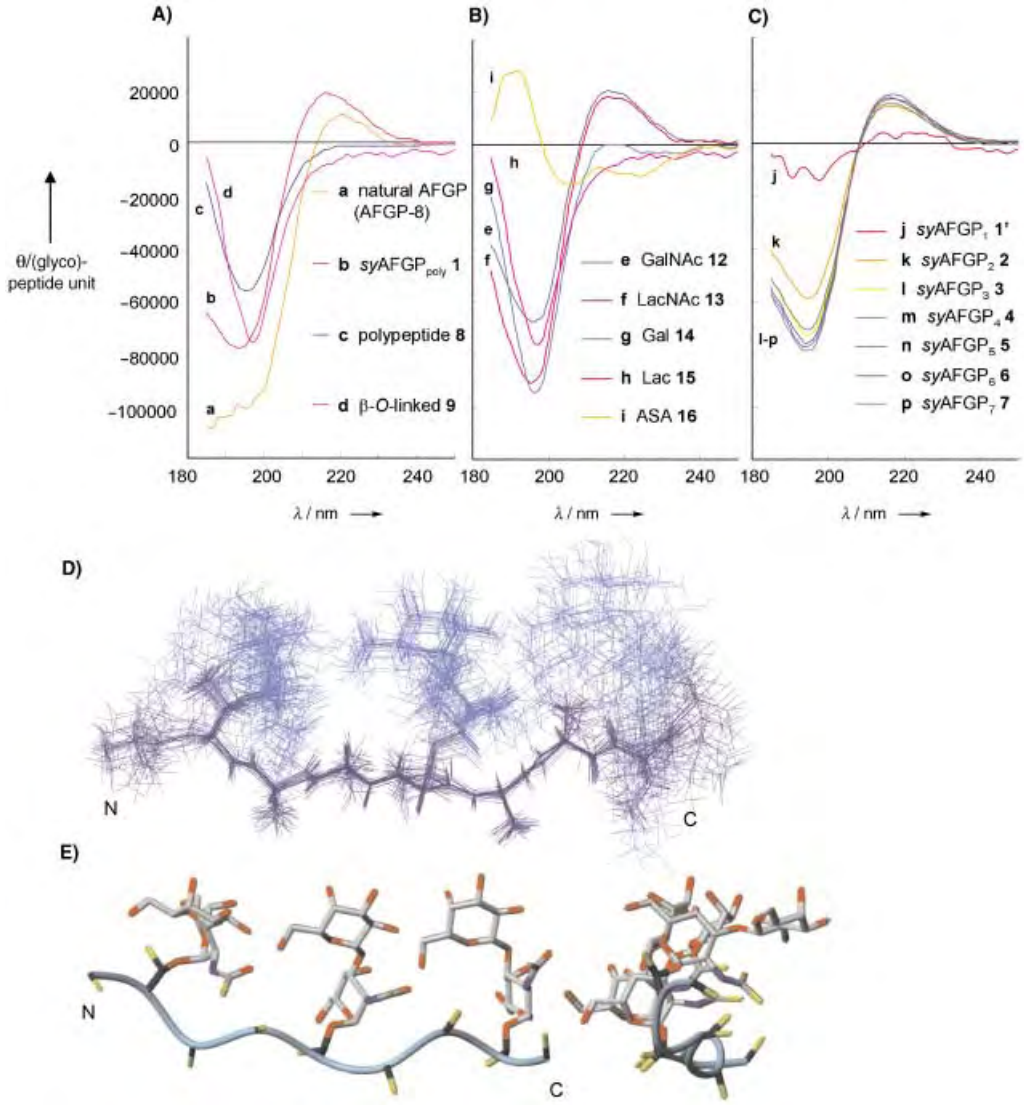


Figure 3. Structural analysis of synthetic compounds. A)–C) CD spectra of synthetic compounds. All curves were measured at 4 °C in water (0.1 mg mL^{-1}) in 1 mm path length quartz cells on a JASCO J-820 spectropolarimeter at 4 °C. D) Superposition of the 25 lowest energy structures of *sy*AFGP$_3$ calculated from NMR-based constraints. The peptide backbone is navy, and the carbohydrate moieties are royal blue. E) Structure closest to the average of the 25 best calculated models for **3**: yellow, methyl carbon; white, carbon in carbohydrate; gray, carbon in peptide side chains except for methyl carbon; blue, nitrogen; red, oxygen; the N- and C-terminal ends are identified. These images were generated by the program MOLMOL.[13]

shown in Figure 3 C. The CD spectral curves of active compounds, **2**–**7**, are almost the same, thus indicating that they form virtually the same secondary structure. In contrast, **1**′ showed no characteristic Cotton effect, which suggests that the chain length of *sy*AFGP$_1$ is not long enough for the formation of a specific conformation. These results are consistent with that obtained in the activity-evaluation study, and they concluded that two repeating units (M_w = 1.2 kDa) is the minimum required to form the specific conformation and induce the successful interaction with the diffuse ice/water interface.

From the above results, we conclude that the specific activity of AFGP is derived from its intrinsic conformation. A number of local structures have been proposed for AFGPs, such as three-hold left handed helix similar to PPII helix,[4c,11b] and γ-turn.[4f] However, the X-ray crystal structure for AFGP has not yet been obtained, presumably because of the difficulty in obtaining a good crystal of a molecule that contains a high density of carbohydrates. Similarly, NMR spectroscopic methods have not succeeded in giving a definite structure because of the difficulties in assigning the NOEs of the molecule due to the repeating structure in AFGPs, which leads to significant spectral overlap. Consequently, these studies concluded that AFGPs do not adopt a rigid, well-defined structure although maybe a part of the molecule adopts a preferred conformation in solution.[4g,h]

The smallest glycopeptide found in nature is a 14-residue glycopeptide that contains four disaccharides (AFGP-8, AAT*AAT*PAT*AAT*PA: *glycosylated residue), and this fact made the conformational analysis difficult. As discussed

 © 2004 Wiley-VCH Verlag GmbH & Co. KGaA, Weinheim

above, we have demonstrated that even *sy*$AFGP_2$ (AT*AAT*A: * glycosylated residue) has the antifreeze activity, and forms almost the same conformation as the larger *sy*AFGPs. These results encouraged us to examine the precise structure of AFGPs by use of *sy*AFGPs with short chain lengths, which should enable us to perform complete assignment of the spectrum. Thus, we choose *sy*$AFGP_3$ (AT*AAT*AAT*A: * = glycosylated residue) as a target for the structural analysis, which should make it easier to find the structural characteristics of AFGP compared with *sy*$AFGP_2$. Fortunately, we completed the sequence-specific assignments of *sy*$AFGP_3$ by using a combination of NOESY and COSY in both 9:1 H_2O/D_2O and D_2O, in which the spectral overlapping reduced significantly (see Supporting Information for details).

On the basis of the complete NMR assignment, we performed the structural calculations by using the program CNS with restraints[12] to determine the 3D solution structure of **3**. The statistical analysis of NMR restraints and a summary of structure statistics are given in Table 1 (see Supporting Information for NOE assignments, average glycosidic torsion angles for calculated models, and Ramachandran plots). An initial set of 50 structures was calculated by using the restraints, and a family of 25 accepted 3D structures was selected with the lowest potential energies. Figure 3D represents the superposition of the backbone coordinates for 25 converged structures, and the structure closest to the average of the 25 is shown in Figure 3E. Surprisingly, **3** appeared to form a well-defined structure, despite the absence of long- or medium-range constraints. As estimated from CD spectral analysis, the peptide backbone of **3** folds into a left handed helix in which three disaccharide moieties are on the same side of the molecule, thus constructing a hydrophilic face. In addition, it newly appeared that Ala–CH_3 groups and acetyl methyl groups in the GalNAc residues were clustered into one face of the molecule, forming a hydrophobic face. This amphiphatic structure of AFGP is similarly constructed in type I AFP, an amphiphatic single α-helix with consecutive alanines.[14] Taking into account of the results of CD experiments, one can imagine that a significant portion of larger AFGP also constructs a left handed helix. Again AFGP should have a more ordered structure than was previously estimated.[4g,h] Although detailed mechanism of action is unclear, the amphiphatic nature is presumed to be crucial for the AFGP specific activity.

Based on the structural results, we surmise that it is likely that antifreeze activity by AFGPs strongly depends on the presence of a specific-ordered helix similar to a PPII helix, and polymeric AFGP requires three key motifs such as *N*-acetyl group at C2 position of the reducing hexosamines, α-configuration of the *O*-glycosidic linkages between sugars and peptide chain, and γ-methyl group of the threonyl residue. We have also demonstrated that the antifreeze activity of AFPG was found even in the case of a dimer (**2**, $M_w = 1.2$ kDa). Further investigations that are aimed at elucidating the mechanism of action, and examining the potential use in clinical applications of AFGPs are under way and the results will be reported in due course.

Received: October 17, 2003 [Z53110]
Published Online: January 22, 2004

Table 1: Statistical analysis of NMR restraints and computed structure for **3**.

Summary of restraints and structural statistics	
Restraints	
Distance restraints[b]	
total	236
intraresidue	
peptide	26
glycan	97
sequential	
peptide	28
glycan	26
peptide to glycan	
within the same glycosylated residue	34
glycans on other peptide residues	25
dihedral restraints	
peptide backbone	5
peptide sidechain	3
glycans	3
Structural Statistics	
Average potential energies (kcal mol^{-1})[c]	
E_{total}	33.26 ± 0.30
E_{bonds}	1.15 ± 0.04
E_{angle}	16.28 ± 0.10
E_{impr}	3.87 ± 0.07
E_{VDW}[d]	0.54 ± 0.08
E_{NOE}[d]	5.99 ± 0.29
E_{cdih}[d]	0.00065 ± 0.00058
RMSD from idealized geometry	
bonds [Å]	0.0021 ± 0.00004
angles [°]	0.96 ± 0.0032
impropers [°]	0.63 ± 0.0056
Pairwise RMSD of 25 structures (Å)	
global region	
backbone atoms	0.69 ± 0.25
all heavy atoms	1.85 ± 0.81
(2–8) + T2GalNAc + T5GalNAc + T8GalNAc	
backbone atoms	0.39 ± 0.18
All heavy atoms	1.38 ± 0.62

[a] All energies and root mean square values were calculated by using the programs CNS1.1[12] and MOLMOL,[13] respectively. [b] See Supporting Information for details. [c] E_{impr}, E_{VDW}, E_{NOE}, and E_{cdih} are the energy of improper torsion angles, the van der Waals repulsion energy, the square-well NOE potential energy, and the dihedral potential energy, respectively. [d] The force constants for the calculations of E_{VDW}, E_{NOE}, and E_{cdih} were 4.0 kcal mol^{-1} Å^{-4}, 50 kcal mol^{-1} Å^{-1}, and 200 kcal mol^{-1} rad^{-2}, respectively.

Keywords: carbohydrates · computer chemistry · glycopeptides · glycoproteins

[1] a) Y. Yeh, R. E. Feeney, *Chem. Rev.* **1996**, *96*, 601; b) K. V. Ewart, Q. Lin, C. L. Hew, *Cell. Mol. Life Sci.* **1999**, *55*, 271; c) G. L. Fletcher, C. L. Hew, P. L. Davies, *Annu. Rev. Physiol.* **2001**, *63*, 359; d) M. M. Harding, P. I. Anderberg, A. D. J. Haymet, *Eur. J. Biochem.* **2003**, *270*, 1381.
[2] a) J. A. Raymond, A. L. DeVries, *Proc. Natl. Acad. Sci. USA* **1977**, *74*, 2589; b) C. L. Hew, D. S. Yang, *Eur. J. Biochem.* **1992**, *203*, 33; c) Z. Jia, P. L. Davies, *Trends Biochem. Sci.* **2002**, *27*, 101.
[3] A. L. DeVries, S. K. Komatsu, R. E. Feeney, *J. Biol. Chem.* **1970**, *245*, 2901.

 © 2004 Wiley-VCH Verlag GmbH & Co. KGaA, Weinheim

[4] a) R. E. Feeney, D. T. Osuga, Y. Yeh, *J. Carbohydr. Chem.* **1994**, *13*, 347; b) R. N. Ben, *ChemBioChem* **2001**, *2*, 161; c) C. A. Bush, S. Ralapati, G. M. Matson, R. B. Yamasaki, D. T. Osuga, Y. Yeh, R. E. Feeney, *Arch. Biochem. Biophys.* **1984**, *232*, 624; d) B. N. Rao, C. A. Bush, *Biopolymers* **1987**, *26*, 1227; e) C. A. Knight, E. Driggers, A. L. Devries, *Biophys. J.* **1993**, *64*, 252; f) J. A. Drewes, K. L. Rowlen, *Biophys. J.* **1993**, *65*, 985; g) A. N. Lane, L. M. Hays, R. E. Feeney, L. M. Crowe, J. H. Crowe, *Protein Sci.* **1998**, *7*, 1555; h) A. N. Lane, L. M. Hays, N. Tsvetkova, R. E. Feeney, L. M. Crowe, J. H. Crowe, *Biophys. J.* **2000**, *78*, 3195.
[5] M. M. Harding, L. G. Ward, A. D. J. Haymet, *Eur. J. Biochem.* **1999**, *264*, 653.
[6] Y. Wu, J. Banoub, S. V. Goddard, M. H. Kao, G. L. Fletcher, *Comp. Biochem. Physiol. Part B* **2001**, *128*, 265.
[7] a) F. Filira, L. Biondi, B. Scolaro, M. T. Foffani, S. Mammi, E. Peggion, R. Rocchi, *Int. J. Biol. Macromol.* **1990**, *12*, 41; b) W.-T. Jiaang, K.-F. Hsiao, S.-T. Chen, K.-T. Wang, *Synthesis* **1999**, 1687; c) R. N. Ben, A. A. Eniade, L. Hauer, *Org. Lett.* **1999**, *1*, 1759; d) P. H. Tseng, W. T. Jiaang, M. Y. Chang, S. T. Chen, *Chem. Eur. J.* **2001**, *7*, 585; e) A. Eniade, R. N. Ben, *Biomacromolecules* **2001**, *2*, 557.
[8] a) T. Tsuda, S.-I. Nishimura, *Chem. Commun.* **1996**, 2779; b) Y. Tachibana, N. Matsubara, F. Nakajima, S. Tsuda, K. Monde, S.-I. Nishimura, *Tetrahedron* **2002**, *58*, 10213.
[9] Details of the synthesis and analytical data of newly prepared AFGP analogues are available in the Supporting Information. For the synthesis of **10** and **13**, see reference [8b].
[10] S. T. Komatsu, A. L. DeVries, R. E. Feeney, *J. Biol. Chem.* **1970**, *245*, 2909.
[11] a) C. A. Bush, R. E. Feeney, *Int. J. Pept. Protein Res.* **1986**, *28*, 386; b) C. A. Bush, R. E. Feeney, D. T. Osuga, S. Ralapati, Y. Yeh, *Int. J. Pept. Protein Res.* **1981**, *17*, 125; c) R. W. Woody, *Adv. Biophys. Chem.* **1992**, *2*, 37.
[12] A. T. Brünger, P. D. Adams, G. M. Clore, W. L. DeLano, P. Gros, R. W. Grossekunstleve, J.-S. Jiang, J. Kuszewski, M. Nilges, N. S. Pannu, R. J. Read, L. M. Rice, T. Simonson, G. L. Warren, *Acta Crystallogr. Sect. D* **1998**, *54*, 905.
[13] R. Koradi, M. Billeter, K. Wüthrich, *J. Mol. Graphics* **1996**, *14*, 51.
[14] F. Sicheri, D. S. C. Yang, *Nature* **1995**, *375*, 427.
[15] M. H. Kao, G. L. Fletcher, N. C. Wang, C. L. Hew, *Can. J. Zool.* **1986**, *64*, 578.
[16] K. Miura, S. Ohgiya, T, Hoshino, N. Nemoto, T. Suetake, A. Miura, L. Spyracopoulos, H. Kondo, S. Tsuda, *J. Biol. Chem.* **2001**, *276*, 1304.

 © 2004 Wiley-VCH Verlag GmbH & Co. KGaA, Weinheim

Active-Site Inhibitors

Disclosing New Inhibitors by Finding Similarities in Three-Dimensional Active-Site Architectures of Polynuclear Zinc Phospholipases and Aminopeptidases**

Albert González-Roura, Isabel Navarro, Antonio Delgado, Amadeu Llebaria, and Josefina Casas*

Phosphatidylcholine-specific phospholipase C from *Bacillus cereus* (PC-PLC$_{Bc}$) is a bacterial enzyme that catalyzes the hydrolysis of choline phospholipids to form diacylglycerols and phosphorylcholine. This enzyme has been the subject of intense study as a model for the elusive mammalian PLC enzymes.[1,2] Several PC-PLC$_{Bc}$ inhibitors are known, including substrate analogues,[3] xanthate D609, and other related xanthate salts.[4] The interesting in vivo biological activities of D609[5] are counterbalanced by the fact that xanthates display limited chemical stability in water, especially at acidic pH values. Furthermore, D609 also inhibits other enzymes such as sphingomyelin synthase.[6] For these reasons, the development of more chemically stable and specific inhibitors for PC-PLC$_{Bc}$ was considered to be of interest.

Enzymatic catalysis is the result of a cooperative concatenation of several factors, which takes place in the enzyme active site under defined chemical and geometric constraints and specific conditions that have been evolutionarily optimized. The disruption of any of these essential elements for catalysis usually results in reduced or even abolished enzyme activity. Therefore, an enzyme inhibitor can be anticipated by finding a molecule that interferes with one (or several) of these cooperative factors. With this reasoning in mind, and since X-ray structural studies on PC-PLC$_{Bc}$ have led to a good knowledge of the three-dimensional structure of this enzyme,[7] we decided to look for structural similarities between PC-PLC$_{Bc}$ and other enzymes that may help us to define new PC-PLC$_{Bc}$ inhibitors. A prominent structural element in PC-PLC$_{Bc}$ is the presence of zinc ions, which are known to play a dominant role in catalysis,[8] as has been reported in related hydrolytic enzymes with zinc-containing active sites. We hypothesized that molecules interfering with

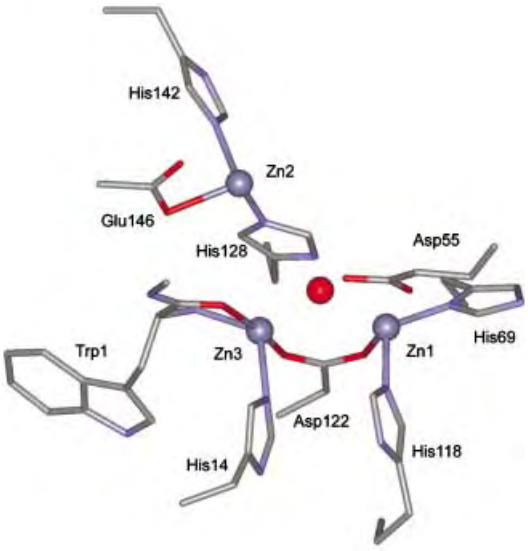
[*] A. González-Roura, Dr. I. Navarro, Dr. A. Llebaria, Dr. J. Casas
RUBAM, Department of Biological Organic Chemistry (IIQAB-CSIC)
Jordi Girona 18–26, 08034-Barcelona (Spain)
Fax: (+34) 93-2045904
E-mail: allebaria@iiqab.csic.es
Dr. A. Delgado
University of Barcelona, Faculty of Pharmacy
Unit of Medicinal Chemistry (CSIC Associated Unit)
Avgda. Joan XXIII, s/n, 08028 Barcelona (Spain)

[**] This work was supported by MCYT (BQU2002-03737), Fundación Ramón Areces, and DURSI, Generalitat de Catalunya (2001SGR00342 and 2001SGR00085). A.G.-R. thanks the MEC for a predoctoral fellowship. We thank Dr. M. Coll and Dr. F. X. Gomis-Rüth for their help with the X-ray protein structures and RUBAM members for their collaboration and interest.

 © 2004 Wiley-VCH Verlag GmbH & Co. KGaA, Weinheim DOI: 10.1002/anie.200352241

the essential binding of substrates to zinc ions in enzymes with active sites structurally similar to PC-PLC$_{Bc}$ might also behave as inhibitors of this phospholipase.[9]

The PC-PLC$_{Bc}$ active site contains three zinc ions (Figure 1). Zn1 and Zn3 appear to define a dinuclear center bridged by the carboxyl group of Asp122 and a water (or hydroxide) molecule, with an internuclear distance of 3.5 Å, whereas Zn2 is not bridged to either Zn1 or Zn3.[7] Dinuclear centers are common in different metallohydrolases[10] and (μ-carboxylato)dizinc(II) catalytic cores are found in several hydrolytic enzymes.[11] Several aminopeptidases, the enzymes involved in the hydrolysis of the N-terminal amino acid of polypeptides, contain a dizinc carboxylate-bridged center in the active site.[12] Although none of these proteins have sequence homology or tertiary-structure similarity with PC-PLC$_{Bc}$, comparison of the structures of *Streptomyces griseus* aminopeptidase (AP$_{Sg}$) and *Aeromonas proteolytica* aminopeptidase (AP$_{Ap}$)[13] with the available structure of PC-PLC$_{Bc}$ revealed a close structural relationship in the dizinc centers (Figure 2). Although the nature of the zinc ligands in the dinuclear centers of PC-PLC$_{Bc}$ and the aminopeptidases is not identical, the coordination geometries and distances are surprisingly similar.[14] This structural analogy does not appear to have been previously noted. The similarities between these enzymes were not only structural but also functional. An exceptionally high activity of AP$_{Sg}$ in phosphodiester hydrolysis was previously described.[15] Moreover, tris(hydroxymethyl)aminomethane, a common buffer solute, is a weak inhibitor for both dizinc aminopeptidases[16] and PC-PLC$_{Bc}$.[17] All this evidence led us to hypothesize that PC-PLC$_{Bc}$ inhibitors could be found among the reported inhibitors of these zinc-containing aminopeptidases.



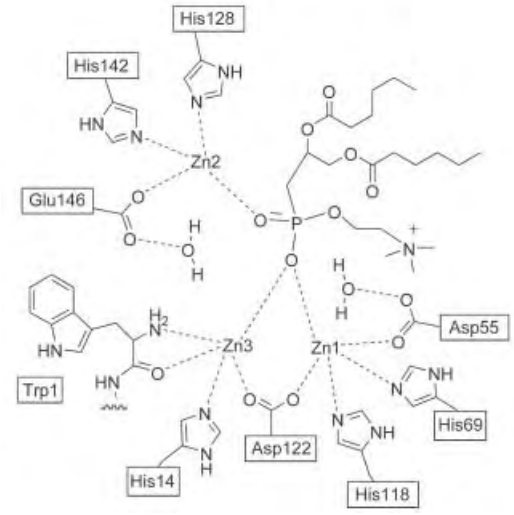


Figure 1. a) Native PC-PLC$_{Bc}$ active site (PDB file: 1AH7) showing amino acid side chains involved in zinc coordination, the bridging water molecule (red sphere), and the three zinc ions (blue spheres). Coordinative bonds of amino acid residues to zinc are displayed as covalent bonds. b) Schematic diagram of the binding mode of substrate analogue inhibitor (3*S*)-3,4-dihexanoylbutyl-1-phosphonylcholine to the active site of PC-PLC$_{Bc}$. (Adapted from Ref. [3].)

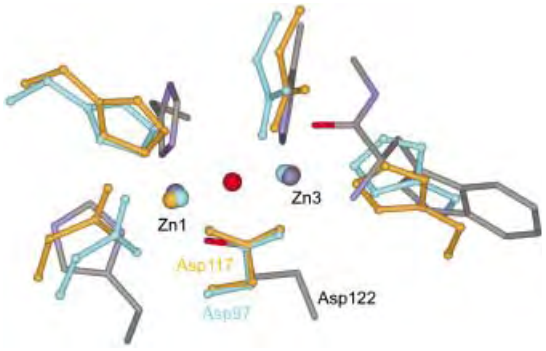
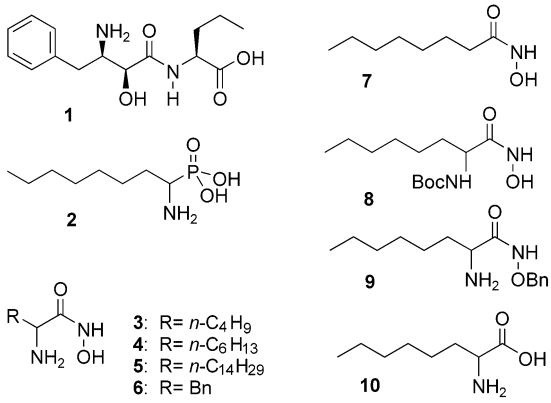


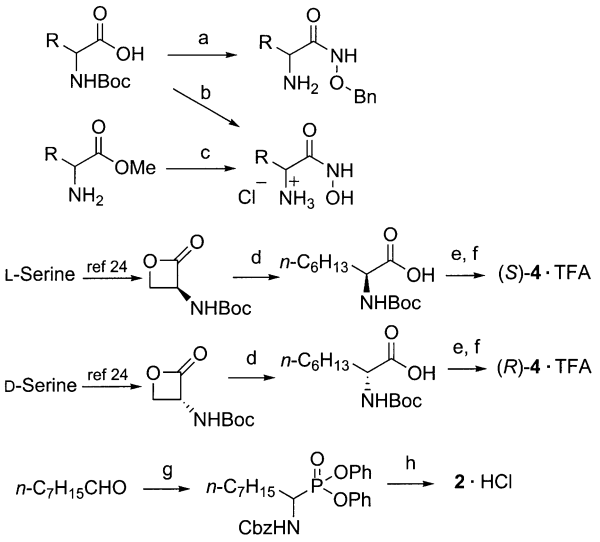
Figure 2. Superposition of dizinc catalytic centers of PC-PLC$_{Bc}$ (gray = carbon backbone, red = oxygen, dark blue = nitrogen, red sphere = μ-aqua ligand; PDB file: 1AH7), AP$_{Ap}$ (orange; 1AMP), and AP$_{Sg}$ (light blue; 1CP7). This arrangement results from overlay of the zinc atom and bridging carboxylate in the corresponding X-ray crystal structures.

Therefore, the effect of bestatin (**1**),[18] α-aminophosphonic acid[19] **2**, and α-aminohydroxamic acids[20] **3**–**6** (Scheme 1) on PC-PLC$_{Bc}$ was determined. Compounds **2**–**6** were obtained as depicted in Scheme 2. Gratifyingly, D,L-norleucine hydroxamic acid **3** showed a strong inhibition of



Scheme 1. Structures of the compounds used in this study. Bn = benzyl, Boc = *tert*-butoxycarbonyl.

 © 2004 Wiley-VCH Verlag GmbH & Co. KGaA, Weinheim



Scheme 2. Synthesis of compounds **2**–**6**. a) $NH_2OBn{\cdot}HCl$, EDC, THF/H_2O (1:2), 24 h; then HCl/MeOH, 25–32%; b) R = n-$C_{14}H_{29}$, $NH_2OH{\cdot}HCl$, *N*,*N*-carbonyldiimidazole, 48 h; then HCl/MeOH, 18%; c) $NH_2OH{\cdot}HCl$, NaOMe/MeOH, 25 °C, 72 h, 68%; d) n-$C_5H_{11}MgBr$, $CuBr{\cdot}Me_2S$, 5% Me_2S in THF, −23 °C, 2 h, 55–65%; e) $NH_2OtBu{\cdot}HCl$, DCC, HOBt, RT, 12 h, 95–98%; f) $B(OCOCF_3)_3$, TFA, 0 °C, 3 h, 90–94%; g) $BnOCONH_2$, $P(OPh)_3$, 2 h, 50 °C, 31%; h) HBr, AcOH; then conc. HCl, reflux, 60%. DCC = *N*,*N*′-dicyclohexylcarbodiimide, EDC = 3-(3-dimethylaminopropyl)-1-ethylcarbodiimide, HOBt = 1-hydroxy-1*H*-benzotriazole, TFA = trifluoroacetic acid, THF = tetrahydrofuran.

$PC\text{-}PLC_{Bc}$, although neither bestatin (**1**) nor (±)-α-aminooctylphosphonic acid (**2**) were inhibitors at 0.5 mM. The reasons for this different behavior are not clear at present. In any case, we have found that α-aminohydroxamates efficiently inhibit $PC\text{-}PLC_{Bc}$ with IC_{50} values in the low micromolar range at substrate/inhibitor ratios of 200 or higher (Table 1). A Lineweaver–Burk plot of inhibition for **4** established that it is a competitive inhibitor for $PC\text{-}PLC_{Bc}$, with an inhibition constant (K_i) of 3 μM (data not shown). This result is in agreement with our starting structural correlation, which would imply competition between the substrate and inhibitor for binding to the active-site zinc ions. Although only structural studies will fully confirm the binding mode of α-aminohydroxamic acids to $PC\text{-}PLC_{Bc}$, the present evidence would suggest a similar arrangement to that of the aminopeptidase–inhibitor complex. Further support for this was found by comparing the active-site structure of $PC\text{-}PLC_{Bc}$ with the dizinc center of AP_{Ap} complexed with *p*-iodophenylalanine hydroxamate[20a] (Figure 3). When the zinc ions and the bridging carboxylate carbon atom of the dizinc centers are overlapped, the bridging water molecule of the $PC\text{-}PLC_{Bc}$ dizinc center and the hydroxamate inhibitor oxygen atom on AP_{Ap} are placed in a close spatial arrangement (Figure 3). Interestingly, the α-amino group of the inhibitor is located near Zn2, which suggests a possible interaction.

Table 1: In vitro inhibitory concentration values on $PC\text{-}PLC_{Bc}$.

Compound	IC_{50} [μM][a]	Compound	IC_{50} [μM][a]	Compound	IC_{50} [μM][a]
1	>1000[b]	(*R*)-**4**	5	**7**	1200
2	>500[c]	(±)-**4**	5	**8**	250
3	7	**5**	45	**9**	750
(*S*)-**4**	5	**6**	4	**10**	>500[c]

[a] With 2 mM dihexanoylphosphatidylcholine as the substrate. [b] No inhibition at 1 mM. [c] No inhibition at 0.5 mM.

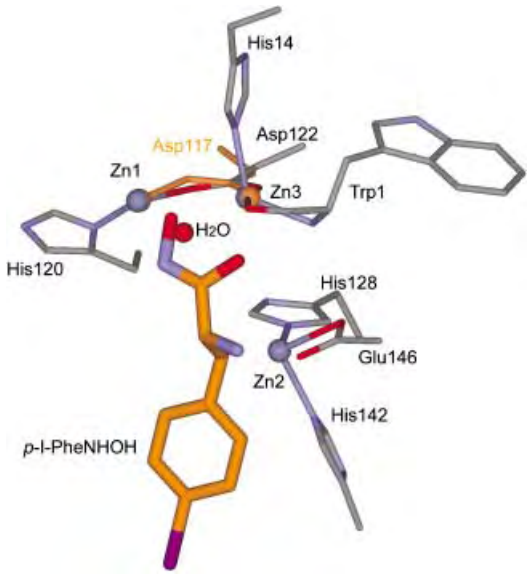


Figure 3. Superposition of $PC\text{-}PLC_{Bc}$ active site (gray = carbon, red = oxygen, dark blue = nitrogen, red sphere = μ-aqua ligand; PDB file: 1AH7) with the dizinc catalytic center of the AP_{Ap} (orange = Zn atoms and μ-carboxylato ligand; 1IGB) complexed with *p*-iodoPhe-NHOH (orange = carbon, red = oxygen, dark blue = nitrogen).

To find out about the influence of the different functional groups present in the active inhibitors we introduced some modifications on the α-aminohydroxamic acids (Scheme 1, **7**–**10**), which were obtained as depicted in Scheme 2 and assayed with $PC\text{-}PLC_{Bc}$ (Table 1). When the α-amino group was removed (**7**) or blocked as NHBoc (**8**), the inhibitory power of the compounds was considerably reduced. The importance of this group for strong inhibition is in agreement with the presumed interaction of the amino group with Zn2 (Figure 3). A similar result was found after *O*-benzylation (**9**) or removal of the *N*-hydroxyamino group (**10**). Finally, both (*R*)-**4** and (*S*)-**4** displayed very similar inhibitory potencies, a result indicating that $PC\text{-}PLC_{Bc}$ inhibition by α-aminohydroxamic acids is not enantioselective. This result is in sharp contrast with the inhibition of aminopeptidases, where the D-α-aminohydroxamic acids display higher potencies than their corresponding enantiomers.[20] In summary, the presence of both the *N*-hydroxyamino and α-amino groups is essential for strong inhibition of $PC\text{-}PLC_{Bc}$ by α-aminohydroxamic acids.[21] These results highlight the high degree of correlation between AP_{Sg}, AP_{Ap}, and $PC\text{-}PLC_{Bc}$.

The $PC\text{-}PLC_{Bc}$ activity was measured according to a described method[22] based on the quantification of phosphate ions arising from alkaline phosphatase (AlkP) catalyzed

 © 2004 Wiley-VCH Verlag GmbH & Co. KGaA, Weinheim

hydrolysis of the initially formed phosphorylcholine. AlkP is a zinc phosphoesterase that has been traditionally related to PC-PLC$_{Bc}$ because it also includes a trinuclear active site, although structural differences are evident. It is noteworthy that this enzyme was not inhibited by compounds **3**–**10** (data not shown) even at concentrations two orders of magnitude higher (0.5 mM) than those required for 50% inhibition of PC-PLC$_{Bc}$; this indicates that the presence of a dinuclear zinc active site is not the only element required for inhibition by α-aminohydroxamates. These results could be related to the different catalytic mechanism operating in AlkP, which involves a serine phosphate intermediate[23] that is subsequently hydrolyzed to the final phosphate product. In contrast, the accepted mechanism for PC-PLC$_{Bc}$ and related aminopeptidases involves a direct attack of water or a hydroxide ion on the phosphorus atom of phosphatidylcholine or on the carbonyl amide group. To stress the structural differences of AlkP and PC-PLC$_{Bc}$, the absence of a carboxylate group bridging the zinc ions in the AlkP active site and the presence of a magnesium ion in the place of the third zinc center is noteworthy.

In summary, a new family of PC-PLC$_{Bc}$ inhibitors has been disclosed by finding similarities among fold- and sequence-unrelated proteins, which, however, possess structurally and chemically related active sites. It is interesting to note the evolutionary convergence of the active-site architecture in dinuclear zinc aminopeptidases and lipid phosphohydrolases that leads to a similar solution for catalyzing the hydrolysis of amides and phosphodiesters. Appropriate modifications of the inhibitors to selectively address either phospholipase or aminopeptidase enzymes are to be found in future work. The results obtained show that when the structural determinants of the desired biological activity are available, alternative lead discovery procedures can be envisaged. With all necessary caution, we consider that the approach presented here may be useful not only for the identification of new inhibitors for a particular enzyme but also to unravel structurally related targets for known enzyme inhibitors.

Received: June 26, 2003
Revised: October 21, 2003 [Z52241]

Keywords: hydrolases · inhibitors · metalloenzymes · protein structures · zinc

[1] P. J. Hergenrother, S. F. Martin, *Top. Curr. Chem.* **2000**, *211*, 132–167.
[2] Although PC-PLC$_{Bc}$ is not toxic for mammals, it is structurally and functionally related to enzymatic pathogenic bacterial toxins such as the *Clostridium perfringens* gas gangrene α toxin: C. E. Naylor, J. T. Eaton, A. Howells, N. Justin, D. S. Moss, R. W. Titball, A. K. Basak, *Nat. Struct. Biol.* **1998**, *5*, 738–746.
[3] a) S. F. Martin, Y. Wong, A. S. Wagman, *J. Org. Chem.* **1994**, *59*, 4821–4831; b) C. L. Franklin, H. Li, S. F. Martin, *J. Org. Chem.* **2003**, *68*, 7298–7307.
[4] A. González-Roura, J. Casas, A. Llebaria, *Lipids* **2002**, *37*, 401–406.
[5] a) M. J. Wargovich, A. Jiménez, K. McKee, V. E. Steele, M. Velasco, J. Woods, R. Price, K. Gray, G. J. Kelloff, *Carcinogenesis* **2000**, *21*, 1149–1155; b) Y. Li, P. Maher, D. Schubert, *Proc. Natl. Acad. Sci. USA* **1998**, *95*, 7748–7753.
[6] C. Luberto, Y. A. Hannun, *J. Biol. Chem.* **1998**, *273*, 14550–14559.
[7] a) E. Hough, L. K. Hansen, B. Birkness, K. Jynge, S. Hansen, A. Hordvik, C. Little, E. Dodson, Z. Derewenda, *Nature* **1989**, *338*, 357–360; b) S. Hansen, L. K. Hansen, E. Hough, *J. Mol. Biol.* **1992**, *225*, 543–549; c) S. Hansen, L. K. Hansen, E. Hough, *J. Mol. Biol.* **1993**, *231*, 870–876; d) S. Hansen, E. Hough, L. A. Svensson, Y. L. Wong, S. F. Martin, *J. Mol. Biol.* **1993**, *234*, 179–187.
[8] D. S. Auld, *Biometals* **2001**, *14*, 271–313.
[9] For related reviews, see: a) R. Breinbauer, I. R. Vetter, H. Waldmann, *Angew. Chem.* **2002**, *114*, 3002–3015; *Angew. Chem. Int. Ed.* **2002**, *41*, 2878–2890; b) A. M. Davis, S. J. Teague, G. J. Kleywegt, *Angew. Chem.* **2003**, *115*, 2822–2841; *Angew. Chem. Int. Ed.* **2003**, *42*, 2718–2736.
[10] D. E. Wilcox, *Chem. Rev.* **1996**, *96*, 2435–2458.
[11] a) W. N. Lipscomb, N. Sträter, *Chem. Rev.* **1996**, *96*, 2375–2433; b) N. Sträter, W. N. Lipscomb, T. Klabunde, B. Krebs, *Angew. Chem.* **1996**, *108*, 2158–2191; *Angew. Chem. Int. Ed. Engl.* **1996**, *35*, 2024–2055.
[12] W. T. Lowther, B. W. Matthews, *Chem. Rev.* **2002**, *102*, 4581–4607.
[13] R. Gilboa, A. Spungin-Bialik, G. Wohlfahrt, D. Schomburg, S. Blumberg, G. Shoham, *Proteins Struct. Funct. Genet.* **2001**, *44*, 490–504, and references therein.
[14] For an example where the spatial position of catalytic residues is conserved, whereas their identity changes within a family of evolutionarily interrelated enzymes, see: M. S. Hasson, I. Schlichting, J. Moulai, K. Taylor, W. Barrett, G. L. Kenyon, P. C. Babbitt, J. A. Gerlt, G. A. Petsko, D. Ringe, *Proc. Natl. Acad. Sci. USA* **1998**, *95*, 10396–10401.
[15] L.-J. Ming, H. I. Park, *Angew. Chem.* **1999**, *111*, 3097–3100; *Angew. Chem. Int. Ed.* **1999**, *38*, 2914–2916.
[16] W. T. Desmarais, D. L. Bienvenue, K. P. Bzymek R. C. Holz, G. A. Petsko, D. Ringe, *Structure* **2002**, *10*, 1063–1072.
[17] S. E. Aakre, C. Little, *Biochem. J.* **1982**, *203*, 799–801.
[18] a) S. H. Wilkes, J. M. Prescott, *J. Biol. Chem.* **1985**, *260*, 13154–13162; b) S. K. Burley, P. R. David, R. M. Sweet, A. Taylor, W. N. Lipscomb, *J. Mol. Biol.* **1992**, *224*, 113–140.
[19] B. Bennett, R. C. Holz, *J. Am. Chem. Soc.* **1998**, *120*, 12139–12140, and references therein.
[20] a) B. Chevrier, H. D. Orchymont, C. Schalk, C. Tarnus, D. Moras, *Eur. J. Biochem.* **1996**, *237*, 393–398; b) S. H. Wilkes, J. M. Prescott, *J. Biol. Chem.* **1983**, *256*, 13517–13521.
[21] Related to our hydroxamic inhibitors, a series of cyclic *N,N′*-bishydroxyureas have been previously described as PC-PLC$_{Bc}$ inhibitors, although with substantially lower potency: S. F. Martin, B. C. Follows, P. J. Hergenrother, C. L. Franklin, *J. Org. Chem.* **2000**, *65*, 4509–4514.
[22] P. J. Hergenrother, S. F. Martin, *Anal. Biochem.* **1997**, *251*, 45–49.
[23] K. H. Holtz, B. Stec, E. R. Kantrowitz, *J. Biol. Chem.* **1999**, *274*, 8351–8354.

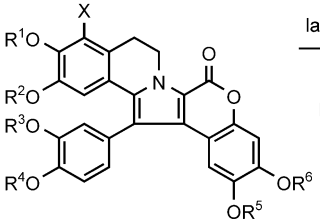
 © 2004 Wiley-VCH Verlag GmbH & Co. KGaA, Weinheim

Marine Alkaloid Synthesis

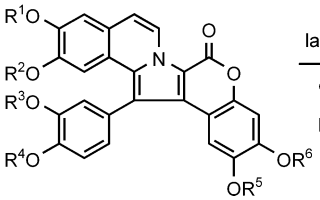
A Highly Efficient Synthesis of Lamellarins K and L by the Michael Addition/Ring-Closure Reaction of Benzyldihydroisoquinoline Derivatives with Ethoxycarbonyl-β-nitrostyrenes**

*Poonsakdi Ploypradith, Chulabhorn Mahidol, Poolsak Sahakitpichan, Siriporn Wongbundit, and Somsak Ruchirawat**

Among the recently discovered marine natural products isolated from the prosobranch mollusc *Lamellaria* sp. and also from the ascidians is a group of 3,4-diarylpyrroloisoquinoline lactone derivatives known as lamellarins, whose structures contain different patterns of polyoxygenated aromatics on their periphery (Scheme 1). Since the first four of these alkaloids were isolated by Faulkner and co-workers in 1985, a total of 35 lamellarins have been identified thus far.[1] Our research group has been particularly interested in lamellarins K (**1a**) and L (**1b**) for their reported biological activities which include cytotoxicity, HIV-1 integrase inhibition, and multidrug-resistance (MDR) reversal.[2,3] A recent biological evaluation by Faulkner and co-workers of lamellarin α (**2a**) and its 20-sulfate and 13,20-disulfate derivatives for inhibition of HIV-1 integrase showed that the presence of sulfate groups on the periphery could greatly influence selectivity in HIV-1 integrase inhibition.[4] It has also been found that lamellarins act as nontoxic inhibitors of acquired MDR. Lamellarin I (**1c**) showed sensitizing effects to doxorubicin in multidrug-resistant P388/Schabel cells at concentrations as low as 0.2 μM and showed full potentiation at a concentration 10-times lower than that of the prototype MDR inhibitor verapamil.[5] Fürstner and co-workers have recently shown that cytotoxicity and MDR reversal of lamellarins can be uncoupled.[6] The exact molecular mechanism of action of lamellarins and their related compounds is currently under extensive investigation.



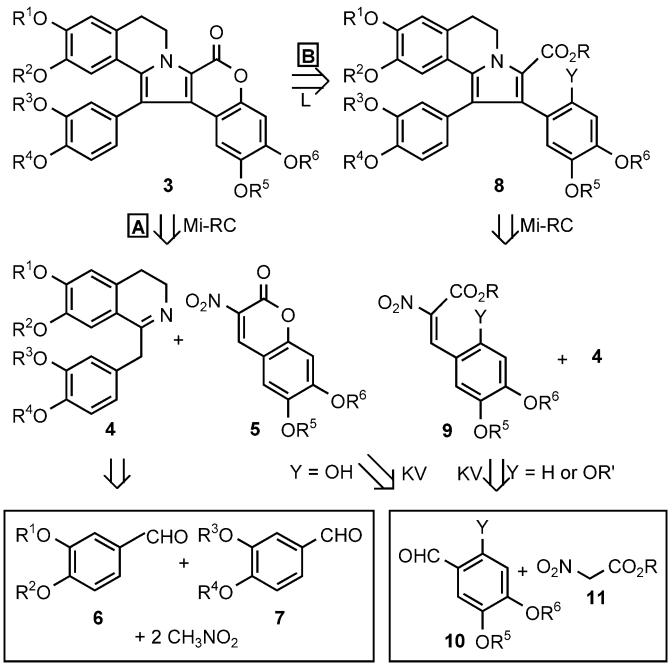
lamellarin	R^1	R^2	R^3	R^4	R^5	R^6	X
K (**1a**)	Me	Me	Me	H	Me	H	OH
L (**1b**)	H	Me	H	Me	Me	H	H
I (**1c**)	Me	Me	Me	Me	Me	H	OMe



lamellarin	R^1	R^2	R^3	R^4	R^5	R^6
α (**2a**)	Me	Me	H	Me	Me	H
N (**2b**)	H	Me	H	Me	Me	H

Scheme 1. Structures of lamellarins K (**1a**), L (**1b**), I (**1c**), α (**2a**), and N (**2b**).

There have been several studies[7] directed toward the total synthesis of lamellarins, notably by the research groups of Steglich,[8] Banwell,[9] Boger,[10] Ishibashi,[11] and ourselves.[12] Previously, we reported two synthetic approaches to the lamellarin skeleton, both of which involved the key condensation of the appropriately substituted benzyldihydroisoquinoline with phenacyl bromide derivatives to form the pyrrole core.[12] We now envisioned that the lamellarin skeleton **3** could arise from condensation of the benzyldihydroisoquinoline **4** with a Michael acceptor, such as **5** or **9**, which essentially would install the lactone or ester group on the 2-position (Scheme 2). This synthetic approach would prove highly convergent since, in a single step, it would form



Scheme 2. Retrosynthetic analysis and strategies for the synthesis of the lamellarin skeleton **3**. L = lactonization, Mi–RC = Michael addition/ring-closure reaction, KV = Knoevenagel reaction.

[*] Dr. P. Ploypradith, Prof. Dr. H.R.H. Princess C. Mahidol, Dr. P. Sahakitpichan, S. Wongbundit, Prof. Dr. S. Ruchirawat
Chulabhorn Research Institute
Vipavadee-Rangsit Highway, Bangkok 10210 (Thailand)
Fax: (+662) 574-2027
E-mail: somsak@tubtim.cri.or.th
Prof. Dr. H.R.H. Princess C. Mahidol, Prof. Dr. S. Ruchirawat
Chulabhorn Research Centre
Institute of Science and Technology for Research and Development
Mahidol University, Salaya Campus, Nakhon Pathom (Thailand)
Prof. Dr. S. Ruchirawat
Department of Chemistry
Mahidol University, Rama 6 Road, Bangkok 10400 (Thailand)

[**] We acknowledge financial contributions from the Thailand Research Fund to S.R. (RTA/07/2544 and Senior Research Scholar Award) and to P.P., and facilities provided by the Postgraduate Education and Research Program in Chemistry (PERCH), Department of Chemistry, Mahidol University.

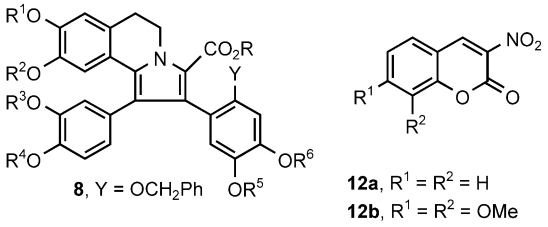
Supporting information for this article is available on the WWW under http://www.angewandte.org or from the author.

 © 2004 Wiley-VCH Verlag GmbH & Co. KGaA, Weinheim DOI: 10.1002/anie.200352043

the pyrrole as well as providing the lactone directly or the ester group for subsequent lactonization. Since imines, which exist in equilibrium with their enamines, have been shown to react with β-nitrostyrene to give the corresponding pyrroles,[13] it was expected that Michael addition of an enamine derived from benzyldihydroisoquinoline with a powerful Michael acceptor, such as **5** or **9**, followed by ring closure and aromatization could provide a more direct route to the lamellarin alkaloids than previous methods.

Modeling the Michael addition/ring-closure reaction between simple β-nitrostyrenes and 3,4-dihydropapavarine hydrochloride under basic conditions resulted in complete consumption of both starting materials but gave no desired product. We then examined the use of ester nitrostyrenes in place of the simple nitrostyrenes in a similar Michael addition/ring-closure reaction. The ester nitrostyrenes are more powerful Michael acceptors than the simple nitrostyrenes due to the additional electron-withdrawing effect provided by the ester group; this allows the ester nitrostyrenes to react under milder reaction conditions than those required for the simple nitrostyrenes.

We turned our attention to the coumarin derivatives **12a** and **12b** (Scheme 3) as the ester nitrostyrenes for the reaction under basic conditions (pathway A in Scheme 2). These

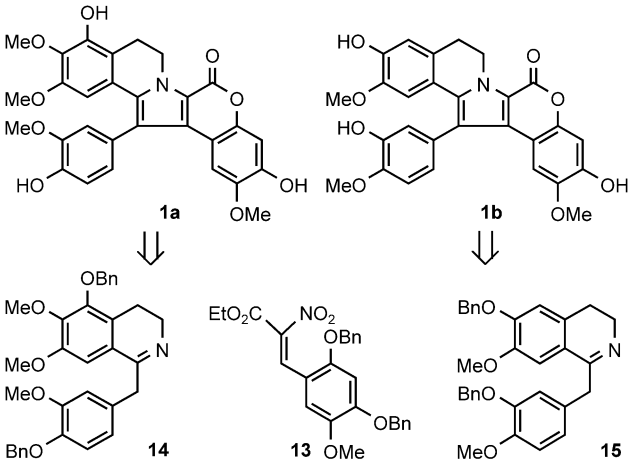


Scheme 3. Structures of intermediate pyrrole ester **8** and nitrocoumarins **12a** and **12b**.

coumarin derivatives offered a significant advantage in that their structures already contained the lactone moiety. We anticipated that, if the reaction occurred with these coumarins, all of the lamellarin skeleton, in particular the pyrrole and lactone moieties, would be successfully installed in one chemical operation. Unfortunately, such a reaction with these coumarins gave the desired lamellarins in only 5–6% yields.

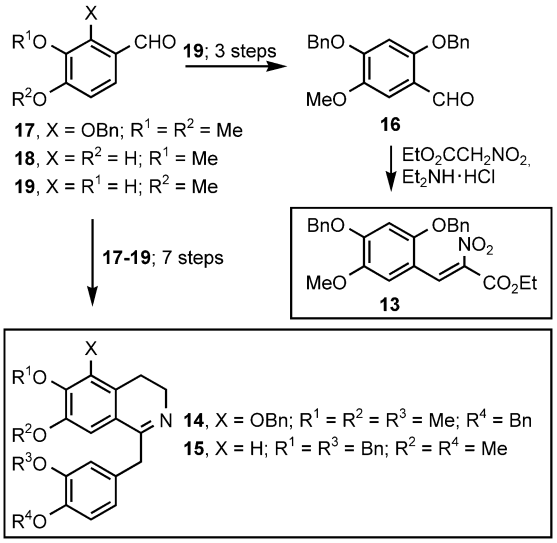
The poor yield resulting from the reaction with nitrocoumarins **12a** and **12b** prompted us to examine the use of acyclic ester nitrostyrenes like **9** (pathway B in Scheme 2). Despite adding one step of lactonization into the synthesis, this alternative synthetic route would probably allow for a more effective preparation of the lamellarin framework. Our required intermediate would then assume the structure of compound **8** (Scheme 3).

From the structure of compound **8**, it was apparent that the desired lactone moiety could be formed by unmasking the benzyloxy-protected phenol by hydrogenolysis and subsequently initiating base-mediated lactonization. Retrosynthetic analysis (Scheme 4) revealed that our target lamellarins K (**1a**) and L (**1b**) would require the same ester nitro-



Scheme 4. Retrosynthetic analysis for the synthesis of lamellarins K (**1a**) and L (**1b**). Bn = benzyl.

styrene, **13**, which could be prepared in 56% overall yield in four steps from **19** including the Knoevenagel condensation of aldehyde **16**[14] with ethyl nitroacetate (Scheme 5). As an alternative to the procedure depicted in Scheme 5, aldehyde



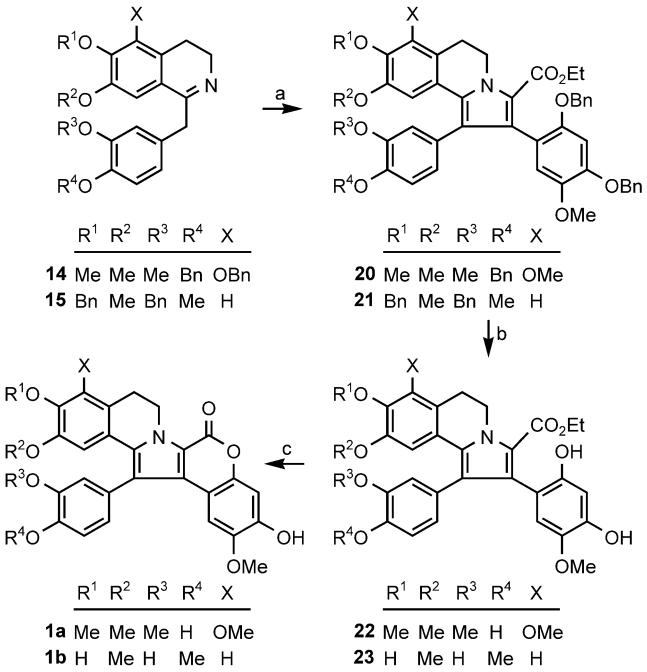
Scheme 5. Synthesis of ester nitrostyrene **13** and benzyldihydroisoquinoline derivatives **14** and **15**.

16 could be prepared in 79% overall yield by selective bisdemethylation of 2,4,5-trimethoxybenzaldehyde with $AlCl_3$[15] followed by benzylation. Synthesis of the substituted benzyldihydroisoquinolines **14** and **15** is well known in the literature[16–24] and both compounds were synthesized in seven steps by Bischler–Napieralski reactions of the appropriate aryl ethylamines and aryl acetic acids, which were readily prepared from three common starting materials, **17**–**19** (Scheme 5).

The Michael addition/ring-closure reaction of the imines **14** and **15** with the ester nitrostyrene **13** proceeded smoothly in refluxing anhydrous acetonitrile in the presence of

 © 2004 Wiley-VCH Verlag GmbH & Co. KGaA, Weinheim

$NaHCO_3$ to give the desired pyrroles **20** and **21**, both in 70% yield (Scheme 6). The syntheses were completed by subjecting pyrroles **20** and **21** to hydrogenolysis to give compounds **22** and **23** quantitatively, followed by base-mediated lactonization with sodium hydride in dry THF to produce lamellarin K (**1a**) in 93% yield and lamellarin L (**1b**) in 87% yield over two steps.



Scheme 6. Synthesis of lamellarins K (**1a**) and L (**1b**). a) $NaHCO_3$, **13**, CH_3CN, reflux, 70% (**20**), 70% (**21**); b) H_2, Pd/C, EtOAc; c) NaH, THF, 93% (**1a**, over two steps), 87% (**1b**, over two steps).

In summary, lamellarins K and L were successfully synthesized in three steps from benzyldihydroisoquinolines **14** and **15** with ester nitrostyrene **13** in 65% and 61% overall yields, respectively. The key step was the Michael addition/ring-closure reaction which proceeded in 70% yield for both lamellarins. The basic building blocks for the lamellarins are the simple and easily prepared substituted-benzaldehyde derivatives. Each lamellarin could be analyzed to consist of three such building blocks, two in the benzyldihydroisoquinoline derivative and the other in the ester nitrostyrene. Our convergent synthetic approach offers a significant improvement over others reported thus far in that it allows easy incorporation of all aryl groups on the lamellarin skeleton without the need for complex protecting-group strategies. The benzyl group was chosen as the only necessary hydroxy-protecting group since all of the benzyl groups could be removed in the same step by simple palladium-catalyzed hydrogenolysis. The syntheses of other lamellarins employing this similar approach will be reported in due course.

Received: June 3, 2003
Revised: November 14, 2003 [Z52043]

Keywords: alkaloids · cyclization · Michael addition · nitrostyrenes · total synthesis

[1] a) R. J. Andersen, D. J. Faulkner, C.-H. He, G. D. Van Duyne, J. Clardy, *J. Am. Chem. Soc.* **1985**, *107*, 5492; b) B. F. Bowden, *Stud. Nat. Prod. Chem. Part D* **2000**, *23*, 233; c) S. Urban, S. J. H. Hickford, J. W. Blunt, M. H. G. Munro, *Curr. Org. Chem.* **2000**, *4*, 765.
[2] a) J. Ham, H. Kang, *Bull. Korean Chem. Soc.* **2002**, *23*, 163; b) S. Urban, R. J. Capon, *Aust. J. Chem.* **1996**, *49*, 711.
[3] M. V. R. Reddy, M. R. Rao, D. Rhodes, M. S. T. Hansen, K. Rubins, F. D. Bushman, Y. Venkateswarlu, D. J. Faulkner, *J. Med. Chem.* **1999**, *42*, 1901.
[4] C. P. Ridley, M. Venkata Rami Reddy, G. Rocha, F. D. Bushman, D. J. Faulkner, *Bioorg. Med. Chem.* **2002**, *10*, 3285.
[5] A. R. Quesada, M. D. G. Gravalos, J. L. F. Puentes, *Br. J. Cancer* **1996**, *74*, 677.
[6] A. Fürstner, H. Krause, O. R. Thiel, *Tetrahedron* **2002**, *58*, 6373.
[7] a) M. Diaz, E. Guitian, L. Castedo, *Synlett* **2001**, *7*, 1164; b) O. Barun, S. Chakrabarti, I. H. H. Junjappa, *J. Org. Chem.* **2001**, *66*, 4457; c) S. Kim, S. Son, H. Kang, *Bull. Korean Chem. Soc.* **2001**, *22*, 1403.
[8] a) C. Peshko, C. Winklhofer, W. Steglich, *Chem. Eur. J.* **2000**, *6*, 1147; b) A. Heim, A. Terpin, W. Steglich, *Angew. Chem.* **1997**, *109*, 158; *Angew. Chem. Int. Ed. Engl.* **1997**, *36*, 155.
[9] a) M. G. Banwell, B. Flynn, D. Hockless, *Chem. Commun.* **1997**, 2259; b) M. G. Banwell, B. L. Flynn, E. Hamel, D. C. R. Hockless, *Chem. Commun.* **1997**, 207; c) M. G. Banwell, B. L. Flynn, D. C. R. Hockless, R. W. Longmore, A. D. Rae, *Aust. J. Chem.* **1999**, *52*, 755.
[10] D. L. Boger, C. W. Boyce, M. A. Labroli, C. A. Sehon, Q. Jin, *J. Am. Chem. Soc.* **1999**, *121*, 54.
[11] a) F. Ishibashi, Y. Miyazaki, M. Iwao, *Tetrahedron* **1997**, *53*, 5951; b) F. Ishibashi, S. Tanabe, O. Tatsuya, M. Iwao, *J. Nat. Prod.* **2002**, *65*, 500; c) M. Iwao, T. Takeuchi, N. Fujikawa, T. Fukuda, F. Ishibashi, *Tetrahedron Lett.* **2003**, *44*, 4443.
[12] a) S. Ruchirawat, T. Mutarapat, *Tetrahedron Lett.* **2001**, *42*, 1205; b) P. Ploypradith, W. Jinaglueng, C. Pavaro, S. Ruchirawat, *Tetrahedron Lett.* **2003**, *44*, 1363.
[13] a) S. Lim, I. Jabin, G. Revial, *Tetrahedron Lett.* **1999**, *40*, 4177; b) G. Revial, S. Lim, B. Viossat, P. Lemoine, A. Tomas, A. F. Duprat, M. Pfau, *J. Org. Chem.* **2000**, *65*, 4593.
[14] M. Tsukayama, A. Oda, Y. Kawamura, M. Nishiuchi, K. Yamashita, *Tetrahedron Lett.* **2001**, *42*, 6163.
[15] J. Demyttenaere, K. Van Syngel, A. P. Markusse, S. Vervisch, S. Debenedetti, N. De Kimpe, *Tetrahedron* **2002**, *58*, 2163.
[16] A. Bhattacharjya, R. Mukhopadhyay, S. C. Pakrashi, *Synthesis* **1985**, 886.
[17] T. Nakanishi, M. Suzuki, *Org. Lett.* **1999**, *1*, 985.
[18] a) L. Pouysegu, A.-V. Avellan, S. Quideau, *J. Org. Chem.* **2002**, *67*, 3425; b) Y.-C. Wang, P. E. Georghiou, *Synthesis* **2002**, 2187.
[19] A. Bermejo, I. Andreu, F. Suvire, S. Leonce, D. H. Caignard, P. Renard, A. Pierre, R. D. Enriz, D. Cortes, N. Cabedo, *J. Med. Chem.* **2002**, *61*, 709.
[20] L. F. Tietze, T. Eicher in *Reactions and Synthesis in the Organic Chemistry Laboratory*, University Science Books, Mill Valley, **1989**, pp. 177–178.
[21] C.-M. Chen, Y.-F. Fu, T.-H. Yang, *J. Nat. Prod.* **1995**, *58*, 1767.
[22] J. Z. Ginos, F. C. Brown, *J. Med. Chem.* **1978**, *21*, 155.
[23] C. Matt, A. Wagner, C. Mioskowski, *J. Org. Chem.* **1997**, *62*, 234.
[24] T. Kametani, K. Takahashi, K. Fukumoto, *J. Chem. Soc.* **1971**, 3617.

 © 2004 Wiley-VCH Verlag GmbH & Co. KGaA, Weinheim

Polymerization Catalysis

Remote Substituents Controlling Catalytic Polymerization by Very Active and Robust Neutral Nickel(II) Complexes**

*Martin A. Zuideveld, Peter Wehrmann, Caroline Röhr, and Stefan Mecking**

More than 70 million tons of polyethylene and polypropylene are produced annually. The majority is prepared by catalytic polymerization employing Ziegler or Phillips catalysts based on early transition metals. More recently, olefin polymerization by complexes of late transition metals has also received increasing attention.[1] A major motivation is their higher tolerance towards polar reagents due to a reduced oxophilicity by comparison to early transition-metal catalysts. Thus, ethylene and 1-olefins can be copolymerized with acrylates in a random fashion,[2] and ethylene homo- and copolymerizations can be carried out in aqueous emulsion to afford polymer latexes (i.e., aqueous dispersions of polymer particles of about 50–1000 nm size).[3]

The discovery by Brookhart and co-workers of the unique catalytic properties of cationic nickel and palladium diimine catalysts in olefin polymerization has given a strong impulse to the field.[4] As a result, polymerization with neutral Ni^{II} complexes has received renewed interest, as these catalysts are expected to be more functional-group tolerant than their cationic Ni^{II} counterparts. However, catalyst activity and stability over time and the capability to form polymers with higher molecular weights at the same time are critical issues, particularly if the effort for catalyst synthesis is also considered.[5–7] By analogy with the influence of bulky alkyl[4] or aryl[8] groups in cationic diimine complexes, in neutral Ni^{II} κ^2-*N,O* salicylaldiminato complexes bulky isopropyl groups on the *N*-aryl moiety retard chain transfer, which is supported by computational studies by Ziegler and co-workers.[9] Introduction of electron-withdrawing substituents in the *ortho* or *para* position of the *O* donor in neutral nickel(II) complexes has been reported to increase catalytic activities substantially, again in accordance with theoretical calculations.[6c,7a,9] Most specifically for this class of catalysts, Grubbs and co-workers have shown that bulky groups in the C3 position of the *O*-coordinating phenolate moiety of salicylaldimine ligands substantially increase polymerization activity. While these ligands afford highly active catalysts, their syntheses require multistep procedures with very low yields.[6c,d]

Our particular interest in the design of novel Ni^{II} salicylaldiminato complexes stems from the recent finding that the known isopropyl-substituted complexes enable the synthesis of latexes of high-molecular-weight polyethylene, which are, to date, inaccessible by other techniques.[3d] Such polyolefin latexes can provide environmentally friendly and economically attractive coatings, which, for example, can be stable towards UV light and hydrolysis at the same time in contrast to current commodity coatings.[10] In view of applications, a very active catalyst based on conveniently accessible ligands, and that is suited to polymerization in emulsion to higher-molecular-weight polyethylene is a prerequisite. Such a system is equally attractive for fundamental studies of catalytic polymerization in emulsion, in which well-defined catalyst precursors are also desirable. Our investigations subject to this report were initiated by the reasoning that an aryl substituent with strongly electron-withdrawing groups could provide steric bulk and electron withdrawing properties at the same time.

Suzuki coupling[11,8a] provided a convenient synthetic method for the introduction of electron-withdrawing substituted aryl groups in the C2 and C6 position of the aniline aryl ring (Scheme 1). A series of salicylaldimine ligands with systematically varied electronic properties, **1a–e**, resulted from the condensation of the corresponding substituted anilines with 3,5-diiodo-salicylaldehyde. The ^{13}C NMR resonances of the compounds were fully assigned by ^{1}H–^{1}H COSY, heteronuclear ^{1}H-^{13}C 2D NMR and ^{1}H–^{13}C 2D long-range-coupling NMR spectroscopy. The chemical shifts of the carbon atom *para* to the imine function in **1a–e** (atom labeled *p* in Scheme 1) are $\delta = 126.90$, 126.96, 126.55, 126.48, and 126.56 ppm, respectively, and for the imine carbon atom, C=N, $\delta = 168.42$, 168.05, 166.99, 166.23, and 166.26 ppm were observed. Although the differences in chemical shifts are moderate, this trend follows the electron withdrawing/donating character of the R group and indicates that the electronic character of the substituents R in **1** indeed affects the electronic properties of the neighboring aryl ring and the imine function.

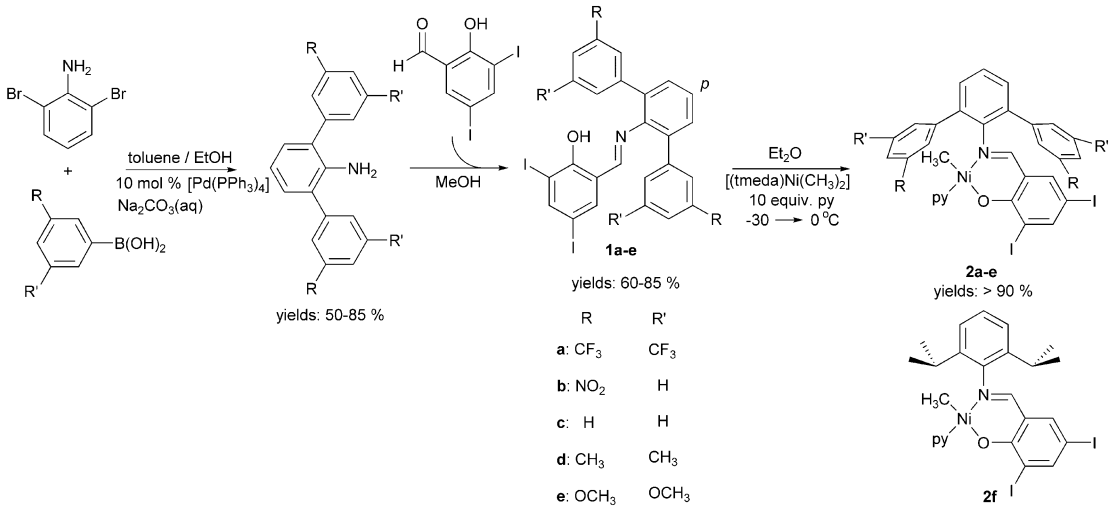
Reaction of **1a–e** in diethylether with [(tmeda)-$Ni(CH_3)_2$][12] (tmeda = *N,N,N′,N′*-tetramethylethylenediamine) in the presence of excess pyridine[3c,6b,6d,6g] afforded the neutral methylnickel(II) complexes **2a–e** in high yield (Scheme 1). The molecular structure of **2a** and **2c** was determined by single-crystal X-ray crystallography (Figure 1).[13,14] To our knowledge, these are the first examples of structurally characterized neutral methylnickel complexes, which are precursors to very active olefin polymerization catalysts. Such methyl complexes are of particular interest, in comparison to the more frequent phenyl complexes[5–7]

[*] Dr. M. A. Zuideveld, Dipl. Chem. P. Wehrmann, Priv.-Doz. Dr. S. Mecking
Institut für Makromolekulare Chemie und Freiburger Materialforschungszentrum der Albert-Ludwigs-Universität Freiburg
Stefan-Meier-Strasse 31, 79104 Freiburg (Germany)
Fax: (+49) 761-203-6319
E-mail: stefan.mecking@makro.uni-freiburg.de
Prof. Dr. C. Röhr
Institut für Anorganische Chemie der
Albert-Ludwigs-Universität Freiburg
Albertstrasse 20, 79104 Freiburg (Germany)

[**] We thank BASF AG and the Deutsche Forschungsgemeinschaft (Me1388/3 in the AM2Net) for financial support. M.A.Z. is grateful for a research stipend by the Alexander von Humboldt-Foundation. We thank G. Mörber for technical assistance and C. Stoz for participation in this research as part of her undergraduate studies. Catalyst deactivation studies by A. Warmbold, 2D NMR measurements by M. Keller and high-temperature GPC by D. Lilge (Basell GmbH) are gratefully acknowledged.

Supporting information for this article is available on the WWW under http://www.angewandte.org or from the author.

 DOI: 10.1002/anie.200352062 © 2004 Wiley-VCH Verlag GmbH & Co. KGaA, Weinheim



Scheme 1. Synthesis of ligands **1a–e** and of methylnickel(II) complexes **2a–e** (py = pyridine).

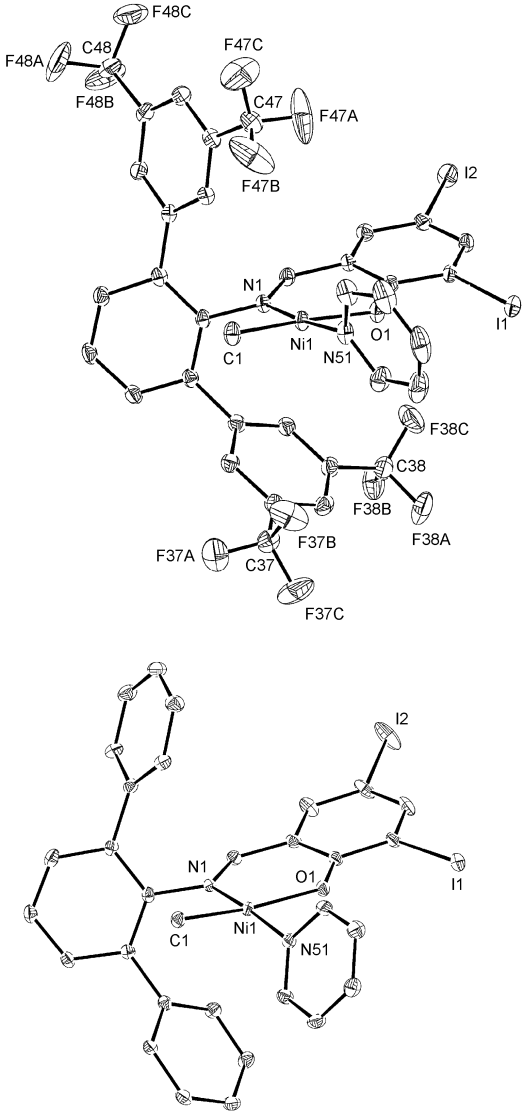


Figure 1. X-ray crystal structure of **2a** (top) and **2c** (bottom; ORTEP presentation with thermal ellipsoids drawn at the 50% probability level). Hydrogen atoms are omitted for clarity.

[(XO)NiPh(L)] (X = N or P), as the methyl group resembles the growing polymer chain much more closely than a phenyl group. For example, a hindered activation for polymerization due to slow insertion of ethylene in the Ni–C bond of the catalyst precursor need not be considered.[5e,15] The nickel-bound methyl group is located in the *trans* position to the O donor in both complexes **2a** and **2c**. A strong steric shielding of the apical positions of the metal center by the aryl groups bound to the C2,C6-position of the N-aryl moiety is evident for both compounds.

Complexes **2a–e**, and for comparison also the known complex **2f**,[3c] were employed as precursors for ethylene polymerization (Table 1). Alternatively, the mixing of ligands **1a–f** with one equivalent of $[(tmeda)Ni(CH_3)_2]$ in toluene solution under an ethylene atmosphere afforded an in situ catalyst (entry 3), which allowed a convenient rapid prescreening of these and other ligands in automated parallel pressure reactors.[16] The activity of all catalysts with 3,5-substituted aryl moieties (R,R′ = CF_3, Me and OMe; **2a, 2d**, and **2e**) is much higher by comparison to the well-known isopropyl substitution pattern represented by **2f** (entries 1, 7, 8 and 9). Catalysts formed from **2b** and **2c**, which do not bear substituents in the 3,5-position (R,R′ = H) or are only monosubstituted (R = NO_2, R′ = H), respectively, appear much less active. The catalyst stability over time was studied by monitoring the ethylene uptake by means of a mass flow meter. Whereas **2a**, **2d**, **2e**, and **2f** remain active for hours at 60 °C and 10 bar ethylene pressure, **2b** and **2c** are deactivated completely within 20 minutes (see Supporting Information). The initial activities are similar for all five catalysts **2a–e**, and thus the lower average activity of **2b** and **2c** in the 30 min experiments given in Table 1 is due to deactivation rather than to a strong difference in intrinsic activity between the five catalysts. Possibly, a deactivation of **2b** and **2c** by C–H activation of the hydrogen atom in *meta* position of the phenyl rings occurs.[17] Alternatively, the somewhat higher steric bulk in **2a**, **2d**, and **2e** may prevent possible bimolecular[6d] deactivation reactions. As for the known isopropyl-substituted catalysts,[3c] activities of the aryl-substituted catalysts

 © 2004 Wiley-VCH Verlag GmbH & Co. KGaA, Weinheim

Table 1: Results of ethylene polymerization reactions.[a]

Entry	Catalyst precursor (R/R′)	Amount of catalyst [μmol]	Pressure [bar]	Polymer yield [g]	TOF [mol(C_2H_4) mol(Ni)$^{-1}$ h^{-1}][b]	$\tilde{M}_n$ [g mol^{-1}][c]	$\tilde{M}_w/\tilde{M}_n$[c]	Branching (per 1000C)[d]	T_m [°C]
1	**2a** (CF_3)	40	40	23.4	41 800	1.9×10^4	5.1	10	123
2	**2a** (CF_3)	19	5	2.2	8270	1.6×10^4	6.7	10	124
3	**1a**[e] (CF_3)	56	5	7.3	9320	3.2×10^4	8.2	14	125
4	**2b** (NO_2)[i]	40	40	3.0	5360	1.1×10^4	2.6	26	106
5	**2c** (H)	40	40	9.0	16 080	2.9×10^3	2.3	52	78
6	**2c** (H)	56	5	2.5	3200	4.0×10^3	2.3	54	68
7	**2d** (Me)	40	40	24.0	42 800	1.1×10^3	2.1	76	–[f]
8	**2e** (OMe)	40	40	25.0	44 600	1.9×10^3	2.5	79	–[f]
9	**2f**	40	40	4.2	7500	1.2×10^4	2.5	5	127
10[g]	**2a** (CF_3)	19	40	3.0[h]	5640	1.8×10^4	3.1	14	122

[a] Reaction conditions: 100 mL of toluene, 50 °C, reaction time 0.5 h. [b] TOF = average turnover frequency. [c] Determined by GPC versus linear polyethylene standards. [d] Branches per 1000 carbon atoms (predominantly methyl branches). [e] In situ catalyst (**1** + [(tmeda)Ni(CH_3)$_2$]). [f] Completely amorphous polymer. [g] Reaction in aqueous emulsion; reaction time 1 h. [h] Formed as an aqueous polymer dispersion. [i] Monosubstituted, R = NO_2, R′ = H.

2a–e are strongly dependant on ethylene concentration (entries 1, 2, 5 and 6).

Surprisingly, despite their spatial remoteness from the metal center the nature of the substituents R,R′ has a dramatic effect on branching and thus crystallinity, and on polymer molecular weight (Table 1). With **2a** a semicrystalline, stiff polymer of 50% crystallinity (determined by differential scanning calorimetry, DSC) is obtained. Complexes **2b** and **2c** afford polyethylenes with a considerably higher degree of branching, and correspondingly low crystallinities (18% and <10%, respectively), and with **2d** and **2e** an entirely amorphous material is obtained. At the same time, the molecular weight of the polymer decreases by more than an order of magnitude going from **2a** to **2e**. The origin of the relatively broad molecular weight distributions obtained with **2a** is currently unclear. Given the similar intrinsic activities of all catalysts, the lower molecular weight obtained with **2d** and **2e** cannot result from a lower rate of chain growth, but must indeed result from a higher rate of chain transfer. This is also in reasonable accordance with the higher branching observed: methyl branching originates from a β-hydride transfer and a subsequent 2,1-reinsertion of the resulting metal-bound 1-olefin, and β-hydride transfer is also crucial in chain transfer.[18] Whereas the steric requirements of the substituents R,R′ are roughly similar in **2a** (R,R′ = CF_3), **2d** (R,R′ = CH_3) and **2e** (R,R′ = OCH_3) and higher than in **2c** (R,R′ = H),[19] their electron withdrawing character increases in the sequence **2e** ≈ **2d** < **2c** < **2b** ≈ **2a**.[20] Both the molecular weights and the branching of the polymers obtained with these different catalyst precursors vary systematically with the electronic nature of R rather than their steric requirements. This indicates that the effect of these remote substituents is related to their electronic properties. To our knowledge, there is no precedent for such a pronounced and systematic effect of such remote substituents on catalytic olefin polymerization by late transition-metal complexes, despite the enormous recent research efforts directed towards the latter field.[1] Future theoretical studies may provide insight on the correlation of the substitution pattern of the particular ligands and the reactivity of the metal center.

Ethylene polymerization with **2a** in aqueous emulsion was investigated. By comparison to polymerization with the isopropyl-substituted complex **2f**,[3d] activities are increased five-fold in preliminary experiments without further optimization. In experiments with reaction times from 1 to 5 h the polymer yield increased linearly with time, thus demonstrating the robustness of the catalyst system based on **2a** during polymerization in aqueous emulsion (Figure 2).

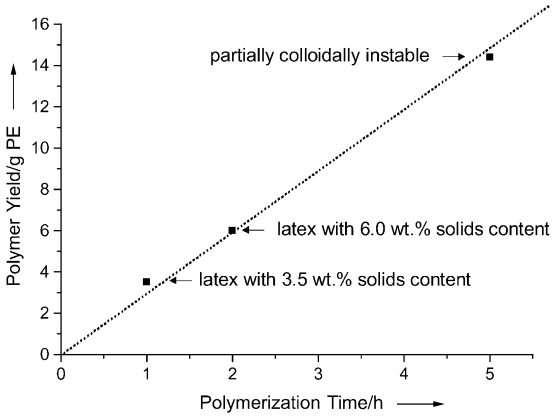


Figure 2. Polymer yield in polymerization in aqueous emulsion with catalyst precursor **2a** (ethylene pressure: 40 bar. Reaction temperature: 50 °C. Dotted line given only as a visual aid).

In summary, we present very active neutral methylnickel(II) complexes for ethylene polymerization based on a set of conveniently accessible ligands. A series of well-defined catalyst precursors with a systematically varied substitution pattern reveals a surprising and unprecedented effect of remote substituents on polymer branching and molecular weight, despite their spatial remoteness from the catalytically active center. An appropriate substitution pattern provides a catalyst that combines the capability to polymerize ethylene to higher-molecular-weight polymer with a high stability and activity in polymerization in aqueous emulsion.

 © 2004 Wiley-VCH Verlag GmbH & Co. KGaA, Weinheim

Experimental data is given in the Supporting Information: Synthesis and analytical data (^{1}H and ^{13}C NMR data and elemental analysis) of **1a–e** and **2a–e**; polymerization procedures; investigation on catalyst stability over time for **2a** and **2c** and ORTEP plots of **2a** and **2c** with full labeling schemes.

Received: June 5, 2003 [Z52062]

Keywords: alkenes · homogeneous catalysis · polymerization · polymers · substituent effects

[1] Reviews: a) G. J. P. Britovsek, V. C. Gibson, D. F. Wass, *Angew. Chem.* **1999**, *111*, 448–468; *Angew. Chem. Int. Ed.* **1999**, *38*, 428–447; b) V. C. Gibson, *Chem. Rev.* **2003**, *103*, 283–316; c) S. Mecking, *Coord. Chem. Rev.* **2000**, *203*, 325–351; d) S. D. Ittel, L. K. Johnson, M. Brookhart, *Chem. Rev.* **2000**, *100*, 1169–1204; e) S. Mecking, *Angew. Chem.* **2001**, *113*, 550–557; *Angew. Chem. Int. Ed.* **2001**, *40*, 534–540.

[2] a) S. Mecking, L. K. Johnson, L. Wang, M. Brookhart, *J. Am. Chem. Soc.* **1998**, *120*, 888–899; b) E. Drent, R. van Dijk, R. van Ginkel, B. van Oort, R. I. Pugh, *Chem. Commun.* **2002**, 744–745.

[3] a) A. Held, F. M. Bauers, S. Mecking, *Chem. Commun.* **2000**, 301–302; b) A. Held, S. Mecking, *Chem. Eur. J.* **2000**, *6*, 4623–4629; c) F. M. Bauers, S. Mecking, *Macromolecules* **2001**, *34*, 1165–1171; d) F. M. Bauers, S. Mecking, *Angew. Chem.* **2001**, *113*, 3112–3115; *Angew. Chem. Int. Ed.* **2001**, *40*, 3020–3022; e) F. M. Bauers, M. M. Chowdhry, S. Mecking, *Macromolecules* **2003**, *36*, 6711–6715; f) F. M. Bauers, R. Thomann, S. Mecking, *J. Am. Chem. Soc.* **2003**, *125*, 8838–8840; g) A. Tomov, J.-P. Broyer, R. Spitz, *Macromol. Symp.* **2000**, *150*, 53–58; h) R. Soula, C. Novat, A. Tomov, R. Spitz, J. Claverie, X. Drujon, J. Malinge, T. Saudemont, *Macromolecules* **2001**, *34*, 2022–2026; j) R. Soula, B. Saillard, R. Spitz, J. Claverie, M. F. Llaurro, C. Monnet, *Macromolecules* **2002**, *35*, 1513–123; Review: k) S. Mecking, A. Held, F. M. Bauers, *Angew. Chem.* **2002**, *114*, 564–582; *Angew. Chem. Int. Ed.* **2002**, *41*, 544–561; l) S. Mecking, J. Claverie in *Late Transition Metal Polymerization Catalysis* (Eds.: B. Rieger, L. S. Baugh, S. Kacker, S. Striegler), Wiley-VCH, Weinheim, **2003**, pp. 231–278.

[4] L. K. Johnson, C. M. Killian, M. Brookhart, *J. Am. Chem. Soc.* **1995**, *117*, 6414–6415.

[5] Earlier work on ethylene and 1-olefin polymerisation by neutral nickel(II) complexes: a) W. Keim, F. H. Kowaldt, R. Goddard, C. Krueger, *Angew. Chem.* **1978**, *90*, 493; *Angew. Chem. Int. Ed. Engl.* **1978**, *17*, 466–467; b) W. Keim, R. Appel, A. Storeck, C. Krueger, R. Goddard, *Angew. Chem.* **1981**, *93*, 91–92; *Angew. Chem. Int. Ed. Engl.* **1981**, *20*, 116–117; c) V. M. Moehring, G. Fink, *Angew. Chem.* **1985**, *97*, 982–984; *Angew. Chem. Int. Ed. Engl.* **1985**, *24*, 1001–1003; d) K. A. Ostoja-Starzewski, J. Witte, *Angew. Chem.* **1987**, *99*, 76–77; *Angew. Chem. Int. Ed. Engl.* **1987**, *26*, 63–64; e) U. Klabunde, S. D. Ittel, *J. Mol. Catal.* **1987**, *41*, 123–134; f) K. Kurtev, A. Tomov, *J. Mol. Catal.* **1994**, *88*, 141–150.

[6] recent work with κ^2-*N,O* complexes: a) S. Y. Desjardins, K. J. Cavell, J. L. Hoare, B. W. Skelton, A. N. Sobolev, A. H. White, W. Keim, *J. Organomet. Chem.* **1997**, *544*, 163–174; b) L. K. Johnson, A. M. A. Bennett, S. D. Ittel, L. Wang, A. Parthasarathy, E. Hauptman, R. D. Simpson, J. Feldman, E. B. Coughlin (DuPont), WO 98/30609, **1998**; c) C. Wang, S. Friedrich, T. R. Younkin, R. T. Li, R. H. Grubbs, D. A. Bansleben, M. W. Day, *Organometallics* **1998**, *17*, 3149–3151; d) T. R. Younkin, E. F. Connor, J. I. Henderson, S. K. Friedrich, R. H. Grubbs, D. A. Bansleben, *Science* **2000**, *287*, 460–462; e) D. A. Bansleben, S. Friedrich, T. R. Younkin, R. H. Grubbs, C. Wang, R. T. Li (W. R. Grace), WO 98/42664, **1998**; f) F. A. Hicks, M. Brookhart, *Organometallics* **2001**, *20*, 3217–3219; g) D. L. Schröder, W. Keim, M. A. Zuideveld, S. Mecking, *Macromolecules* **2002**, *35*, 6071–6073; h) E. F. Connor, T. R. Younkin, J. I. Henderson, S. J. Hwang, W. P. Roberts, J. J. Litzau, R. H. Grubbs, *J. Polym. Sci. Part A* **2002**, *40*, 2842–2854.

[7] recent work with κ^2-*P,O* phosphinoenolato complexes: a) R. Soula, J.-P. Broyer, M. F. Llauro, A. Tomov, R. Spitz, J. Claverie, X. Drujon, J. Malinge, T. Saudemont, *Macromolecules* **2001**, *34*, 2438–2442; b) V. C. Gibson, A. Tomov, A. J. P. White, D. J. Williams, *Chem. Commun.* **2001**, 719–720.

[8] a) M. Schmid, R. Eberhardt, M. Klinga, M. Leskelä, B. Rieger, *Organometallics* **2001**, *20*, 2321–2330; b) L. S. Moody, P. B. Mackenzie, C. M. Killian, G. G. Lavoie, J. A. Ponasik, Jr., A. G. M. Barret, T. W. Smith, J. C. Pearson (Eastman Chemical Company), WO 00/50470, **2000**.

[9] M. S. W. Chan, L. Deng, T. Ziegler, *Organometallics* **2000**, *19*, 2741–2750.

[10] a) *Wäßrige Polymerdispersionen* (Ed.: D. Distler), VCH, Weinheim, **1999**; b) *Polymer Dispersions and Their Industrial Applications* (Eds.: D. Urban, K. Takamura), Wiley-VCH, Weinheim, **2002.**

[11] N. Miyaura, T. Yanagi, A. Suzuki, *Synth. Commun.* **1981**, *11*, 513.

[12] W. Kaschube, K. R. Poerschke, G. Wilke, *J. Organomet. Chem.* **1988**, *355*, 525–532.

[13] Crystallographic data for **2a** and **2c**. **2a**: $C_{35}H_{20}F_{12}I_2N_2NiO$, $M_r = 1025.04$, monoclinic space group $P2_1/c$ (no. 14), $a = 12.840(2)$, $b = 14.681(2)$, $c = 20.919(3)$ Å, $\beta = 113.049(7)°$, $V = 3628.5(9)$ Å^3, $Z = 4$, $\rho_{calcd} = 1.8764(5)$ g cm^{-3}, $\mu = 23.30$ cm^{-1}, $R1$ (wR_2) = 0.035 (0.100), $T = 293(2)$ K, GOF = 1.031. **2c**: $C_{31}H_{24}I_2N_2NiO$, $M = 753.01$, triclinic space group $P\bar{1}$ (no. 2), $a = 8.460(3)$, $b = 12.243(4)$, $c = 14.917(5)$ Å, $\alpha = 113.380(5)$ $\beta = 90.876(5)°$, $\gamma = 95.868(6)$, $V = 1408.0(8)$ Å^3, $Z = 2$, $\rho_{calcd} = 1.7762(10)$ g cm^{-3}, $\mu = 29.08$ cm^{-1}, $R1$ ($wR2$) = 0.045 (0.101), $T = 223(2)$ K, GOF = 1.01. The intensity data were collected on a Bruker AXS CCD diffractometer with graphite-monochromated $Mo_{K\alpha}$ radiation ($\lambda = 0.71070$ Å). The structures were solved by direct methods with SHELXS-97. All hydrogen atoms were refined anisotropically. The final cycles of full-matrix least-squares refinement by using SHELXL-97 were based on 6396 (**2a**) and 6270 (**2c**) observed reflections (all data) and 485 (**2a**) and 340 (**2c**) variable parameters, respectively. CCDC-214669 (**2a**) and CCDC-214670 (**2c**) contain the supplementary crystallographic data for this paper. These data can be obtained free of charge via www.ccdc.cam.ac.uk/conts/retrieving.html (or from the Cambridge Crystallographic Data Centre, 12 Union Road, Cambridge CB2 1EZ, UK; fax: (+44) 1223-336-033; or deposit@ccdc.cam.ac.uk).

[14] Selected bond lengths (in Å) and angles for **2a**: Ni1-C1 1.931(4); Ni1-N1 1.896(3); Ni1-O 1.908(3); Ni1-N51 1.897(4); N1-Ni1-O1 92.6(1)°; C1-Ni1-N51 87.5(2)°; N1-Ni-C1 96.3(2); O1-Ni1-N51 83.7(1). **2c**: Ni1-C1 1.941(5) Å; Ni1-N1 1.903(4); Ni1-O1 1.920(3); Ni1-N51 1.908(4); N1-Ni1-O1 93.8(1); C1-Ni1-N51 87.3(2); N1-Ni1-C1 95.4(2); O1-Ni1-N51 84.7(2).

[15] a) R. M. Ceder, J. Cubillo, G. Muller, M. Rocamora, J. Sales, *J. Organomet. Chem.* **1992**, *429*, 391–401; b) R. Ceder, G. Muller, J. Sales, J. Vidal, D. Neibecker, I. Tkatchenko, *J. Mol. Catal.* **1991**, *68*, 23–31; c) W. Keim, A. Behr, B. Gruber, B. Hoffmann, F. H. Kowaldt, U. Kuerschner, B. Limbaecker, F. P. Sistig, *Organometallics* **1986**, *5*, 2356–2359; d) P. Braunstein, J. Pietsch, Y. Chauvin, S. Mercier, L. Saussine, A. DeCian, J. Fischer, *J. Chem. Soc. Dalton Trans.* **1996**, 3571–3574.

[16] A. Tuchbreiter, M. A. Zuideveld, S. Mecking, unpublished results.

[17] G. G. Hlatky, H. W. Turner, R. R. Eckman, *J. Am. Chem. Soc.* **1989**, *111*, 2728–2729.

 © 2004 Wiley-VCH Verlag GmbH & Co. KGaA, Weinheim

[18] Theoretical studies indicate, that instead of β-hydride elimination, transfer to monomer may also be a preferential mode of chain transfer.[9] However, the factors determining the energy barriers for both types of reactions appear to be similar.
[19] **2b** is omitted in this consideration, being the only monosubstituted compound ($R = NO_2$, $R' = H$) in the series.
[20] a) F. A. Carey, R. J. Sundberg, *Advanced Organic Chemistry. Part A: Structure and Mechanism*, Plenum, New York, 3rd ed. **1990**; b) L. P. Hammett, *Physical Organic Chemistry*, McGraw-Hill, New York, 2nd ed., **1970**; c) C. Hansch, A. Leo, R. W. Taft, *Chem. Rev.* **1991**, *91*, 165–195.

 © 2004 Wiley-VCH Verlag GmbH & Co. KGaA, Weinheim

Organoarsenic Compounds

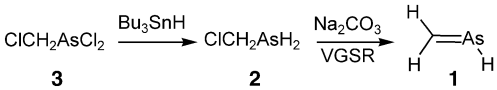
First Synthesis and Characterization by Mass Spectrometry and UV-Photoelectron Spectroscopy of Methylenearsane**

Anna Chrostowska, Alain Dargelos, Virginie Lemierre, Jean-Marc Sotiropoulos, Pierre Guenot, and Jean-Claude Guillemin**

The synthesis of the simplest unsaturated heterocompounds is a particular challenge since most of these compounds are kinetically unstable. Several of the simplest low-coordinated compounds bearing a nitrogen,[1] silicon, phosphorus, or sulfur atom have been prepared[2] but few of the corresponding derivatives with a heteroatom of the following rows of the periodic table have been characterized.[3] Due to a lack of any experimental data, the gas-phase proton affinity,[4] the π-bond strength,[5] or the reactivity trends[6] of the simplest arsaalkene, the methylenearsane **1**, have only been investigated from a theoretical point of view.

We report here the synthesis of the methylenearsane **1**, formed by dehydrohalogenation of gaseous chloromethylarsane on a solid support in a vacuum gas–solid reaction (VGSR).[7] The characterization was performed in the gaseous phase by mass spectrometry and UV photoelectron spectroscopy (UV-PES). Using methylenearsane **1** as an example, we also present the advantages of the very efficient and reliable time-dependent density functional theory (TDDFT) approach for the theoretical evaluation of ionization potentials (IPs).

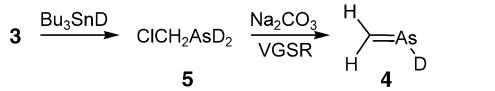
The synthesis of the chloromethylarsane **2** by chemoselective reduction of the chloromethyl arsonic acid has already been reported,[8] where the latter compound was formed by oxidation of the chloromethyldichloroarsane **3** with aqueous hydrogen peroxide. We reduced **3** directly to the arsane **2** in a 67% yield using tributyl tin hydride.[9] Compound **2** was then vaporized on solid sodium carbonate under VGSR conditions [Eq. (1)]. The gaseous flow was condensed with a co-solvent and then analyzed by ^{1}H NMR spectroscopy. With the temperature of the solid carbonate at 20°C, a small amount of arsane **2** was characterized along with some insoluble oligomeric products. The transformation was complete at a support temperature of 50°C, and at 80°C only the signals corresponding to methylarsane were observed. Attempts to characterize the very reactive species formed in the condensed phase under such conditions by low-temperature NMR (−100°C) or infrared (−196°C) spectroscopy were unsuccessful. Consequently we analyzed the gaseous flow by high-resolution mass spectrometry (HRMS).



(1)

To record the mass spectrum the reactor, which contained the solid support, was connected to the ionization chamber of a high-resolution mass spectrometer. Using sodium carbonate at 20°C as the solid base, the molecular ion of chloromethylarsane **2** was unambiguously observed (calcd for CH_4AsCl: 125.9217; found: 125.922). For a solid-base temperature of 50°C, this compound had completely disappeared from the mass spectrum and a base peak at m/z 90 attributed to the methylenearsane **1** was observed. The high-resolution mass spectrum confirms the composition of CH_3As for the product (calcd for CH_3As: 89.94507; found: 89.9449). Traces of methylarsane (calcd for CH_5As: 91.96072; found: 91.9608) and carbon dioxide were also observed. Experiments performed with a carbonate heated to 80°C showed the presence of methylarsane as the main product. All these results are consistent with the experiments analyzed by ^{1}H NMR spectroscopy.

On the other hand, reactions performed with a deuterated compound led to the expected results. Under similar experimental conditions, the chloromethylarsane-d_2 **5** gave a compound with a molecular ion at m/z 91, which we attributed to the methylenearsane-d **4** (calcd for CH_2DAs: 90.95134 ; found: 90.9504) [Eq. (2)]. [D_2]Methylarsane, carbon dioxide, and DCl were also observed as minor impurities.



(2)

[*] Prof. A. Chrostowska, Prof. A. Dargelos, V. Lemierre, J.-M. Sotiropoulos
Laboratoire de Chimie Théorique et Physico-Chimie Moléculaire
UMR CNRS 5624, Université de Pau et des Pays de L'Adour
Av. de L'Université, BP 1155, 64013 Pau Cedex (France)
Fax: (+33) 5-59-40-75-88
E-mail: anna.laporte-chrostowska@univ-pau.fr
Dr. J.-C. Guillemin
Laboratoire de Synthèse et Activation de Biomolécules
UMR CNRS 6052, ENSCR, Institut de Chimie de Rennes
35700 Rennes (France)
Fax: (+33) 2-23-23-81-08
E-mail: jean-claude.guillemin@ensc-rennes.fr
P. Guenot
Centre Régional de Mesures Physiques de L'Ouest
Université de Rennes 1, 35042 Rennes (France)

[**] J.-C.G. acknowledges the PNP (INSU-CNRS) for financial support. We thank P. Baylère for his efficient technical assistance.

Supporting information for this article is available on the WWW under http://www.angewandte.org or from the author.

 DOI: 10.1002/anie.200352445 © 2004 Wiley-VCH Verlag GmbH & Co. KGaA, Weinheim

To corroborate these results, we have chosen UV photoelectron spectroscopy experiments in conjunction with the theoretical evaluation of the ionization potentials, to understand the electronic structure of the methylenearsane **1**.

The UV photoelectron spectra of compounds **1** and **2** are displayed in Figure 1. In the spectrum of chloromethylarsane **2** (Figure 1a), three main ionizations are distinguished: two large peaks at around 9.85 and 12.5–13.1 eV, and a strong and intense band at 11.3 eV with a shoulder at 10.9 eV. In a further experiment, **2** was slowly vaporized over solid sodium carbonate (heated to 65 °C) and the gaseous flow was directly analyzed by UV photoelectron spectroscopy without further purification. The corresponding spectrum (Figure 1b) has a new intense ionization at 9.7 eV with a marked shoulder at 10.3 eV, as well as large peaks at 12.6 and 14.7 eV. The disappearance of the sharp band centered at 11.3 eV corresponding to the precursor **2** can be clearly observed. The ionizations at ≈8.8 and 11.8 eV, which varied in intensity, are attributed to other products (probably traces of methylarsane and oligomeric species). The detection of CO_2 is indicative of the effectiveness of the dehydrochlorination.

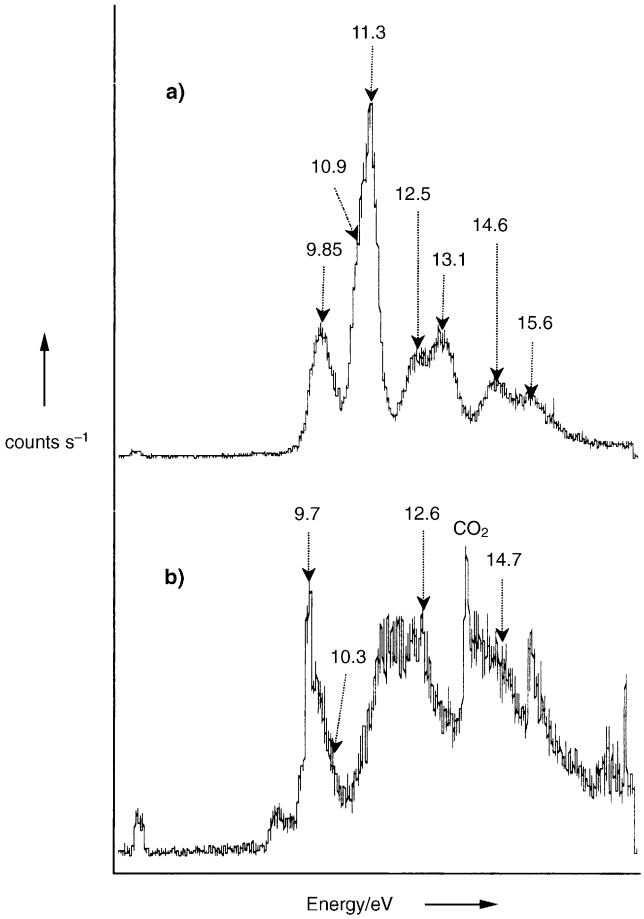


Figure 1. Photoelectron spectra of a) **2**, b) **2** vaporized on Na_2CO_3 (IP in eV).

The photoelectron spectrum of chloromethylarsane **2** was analyzed taking into account the ionization potentials of CH_3AsH_2 (9.50 eV n_{As}, 11.2–12.6 $\sigma_{As\text{-}C}$)[10] and CH_3Cl (11.29 n_{Cl}, 14.42 eV $\sigma_{C\text{-}Cl}$).[11] The first band is essentially assigned to the ejection of an electron from the arsenic lone pair, which is stabilized by 0.35 eV compared to the methylarsane because of the withdrawing effect of the chlorine atom. The next band is principally due to the ionization of the lone pairs of the chlorine atom, and the two large peaks correspond to the ejection of an electron from the σ orbitals.

For compound **1**, the disappearance of the signals corresponding to the chlorine atom lone pairs in the photoelectron spectrum confirms the formation of a nonchlorinated compound. For the methylenephosphane $CH_2{=}PH$,[2b] the vertical $\pi_{P=C}$ and n_P IPs were observed at 10.30 and 10.70 eV, respectively. Considering only these experimental results, we attribute the first band at 9.7 eV to the ejection of an electron from the $\pi_{C=As}$ orbital and the second band at 10.3 eV to the orbital corresponding to the n_{As} arsenic lone pair. The shift of the first band to lower energy relative to methylenephosphane clearly corresponds to a slightly more diffuse character of the carbon–arsenic double bond.

This qualitative interpretation of the PE spectra is not straightforward and comparison of theoretical and experimental IPs is necessary for a reliable identification. Considering that the scope of generally applicable methods for larger and more complicated systems is very limited, we tested the reliability of the TDDFT[12] approach in comparison with OVGF,[13] the more sophisticated CASPT2 calculations,[14] or by "shifting" the calculated Kohn–Sham energies[15] by taking compounds **1** and **2** as simple examples.

Table 1 displays the computed and estimated values of IPs for **1**. The first row of values correspond to the arsenic–carbon double bond, the second row is mainly localized on the arsenic lone pair, and the third and fourth row of figures are associated with simple carbon–arsenic and carbon–hydrogen bonds, respectively. It is worth mentioning that the three methods of calculation of the IPs are in excellent agreement with experimental data, since the deviations from experimental values are less than 0.2 eV. The performance of TDDFT is better than that of OVGF, but is much more favorable than the more expensive CASPT2 caluculations. On the other hand, considering Khon–Sham energies corrected by the uniform shift $x = 2.55$,[15] the estimated values of IPs agree surprisingly well with those calculated by TDDFT and CASPT2. This comparison of experimental IPs of methylenearsane **1** with high-level correlated ab initio calculations

Table 1: Comparison of calculated and experimental ionization potentials (IPs) for **1**; Kohn–Sham (K–S) energies and the nature of molecular orbitals ($x = 2.55$ for estimated IPs; all values in eV).

MOs nature	−K–S energies	IP TDDFT[12]	IP OVGF[13]	IP CASPT2[14]	IP estimated[15]	IP expt
$\pi_{C=As}$ (A″)	7.14	9.72[a]	9.52	9.69	9.7	9.7
n_{As} (A′)	7.76	10.37	10.22	10.13	10.3	10.3
$\sigma_{C\text{-}As}$ (A′)	9.93	12.63	12.64	12.53	12.5	12.6
$\sigma_{C\text{-}H}$ (A′)	12.13	14.74	14.85	14.62	14.7	14.7

[a] value of ΔSCF.

 © 2004 Wiley-VCH Verlag GmbH & Co. KGaA, Weinheim

proves the reliability of the TDDFT approach. However, OVGF-computed IPs are also satisfactory.

Table 2 lists the calculated and experimental values for the IPs of **2**. The first and third molecular orbitals correspond to the antibonding and bonding combinations of arsenic and chlorine lone pairs (in the same plane). The second orbital is associated with $n^{\pi}_{Cl,}$ while the fourth IP is mainly due to the ejection of an electron from σ^{-}_{As-H} bond. We note that the first ionic state is slightly underestimated ($\Delta SCF = 9.68$ eV), and as a direct consequence the following TDDFT ionization potentials are slightly too low. For IPs calculated by the OVGF method the first value is also underestimated (9.64 eV). However, values displayed in Table 2 correspond to the conformation in which the arsenic lone pair and the chlorine atom are antiperiplanar, thus allowing free rotation. A similar study performed on compound **3** also gave a very good correlation between TDDFT and the experimental data (see Supporting Information).

Table 2: Calculated and experimental ionization potentials (IPs) for **2** ($x = 2.5$ for estimated IPs; all values in eV).

MOs nature	−K–S energies	IP TDDFT	IP OVGF	IP estimated	IP expt
$n_{As}-n_{Cl}$ (A′)	7.34	9.68[a]	9.64	9.85	9.85
n_{Cl} (A″)	8.37	10.56	11.00	10.9	10.9
$n_{As} + n_{Cl}$ (A′)	8.59	11.28	11.09	11.1	11.3
σ^{-}_{As-H} (A″)	10.09	12.41	12.92	12.6	12.5
$n_{Cl}\ \sigma_{C\text{-}As}$ (A′)	10.50	12.91	13.04	13.0	13.1

[a] Value of ΔSCF.

In summary, the methylenearsane **1** has been prepared by dehydrohalogenation of a chloromethylarsane on solid sodium carbonate and characterized by mass spectrometry and UV photoelectron spectroscopy. The experimental and theoretical data for **1** emphasize an electronic similarity of arsenic and phosphorus double-bonded to the carbon atom, as well as a more diffuse character of the $\pi_{C=As}$ orbital originating from the 2pπ–4pπ overlap and weaker energy (0.6 eV) of this double bond relative to the phosphorus analogue (2pπ–3pπ). Moreover, the destabilization of the n_{As} orbital compared to the $\pi_{C=As}$ orbital is weaker than the one observed for the corresponding orbitals of the phosphorus analogue. This fact can be explained as the compromise between increasing s character of arsenic lone pair and its slightly smaller electronegativity. A significant separation (0.6 eV) of the two first ionic states (0.4 eV for the methylenephosphane) may also lead to the increased reactivity of this double-bond system. On the other hand, the performance of TDDFT method for evaluation of ionization potentials has been successfully demonstrated in the present case.

Experimental Section

All details of the synthesis of compounds **1**–**3**, mass spectrometry, UV-photoelectron spectroscopy, and the quantum chemical procedures employed in this study are given in the Supporting Information.

Received: July 22, 2003
Revised: October 6, 2003 [Z52445]

Keywords: arsenic · density functional calculations · ionization potentials · mass spectrometry · photoelectron spectroscopy

[1] a) H. Bock, R. Dammel, L. Horner, *Chem. Ber.* **1981**, *114*, 220–226; b) B. Braillon, M.-C. Lasne, J.-L. Ripoll, J.-M. Denis, *Nouv. J. Chim.* **1982**, *6*, 121–122.

[2] a) Methylenesilane: G. Maier, G. Mihm, H. P. Reisenauer, *Angew. Chem.* **1981**, *93*, 615–616; *Angew. Chem. Int. Ed. Engl.* **1981**, *20*, 597–598; b) Methylidynephosphane: T. E. Gier, *J. Am. Chem. Soc.* **1961**, *83*, 1769–1770. Methylenephosphane: S. Lacombe, D. Gonbeau, J.-L. Cabioch, B. Pellerin, J.-M. Denis, G. Pfister-Guillouzo, *J. Am. Chem. Soc.* **1988**, *110*, 6964–6967; c) Methanethial: B. Solouki, P. Rosmus, H. Bock, *J. Am. Chem. Soc.* **1976**, *98*, 6054–6055.

[3] a) Methaneselenal: H. Bock, S. Aygen, P. Rosmus, B. Solouki, E. Weissflog, *Chem. Ber.* **1984**, *117*, 187–202; b) R. D. Brown, P. D. Godfrey, D. McNaughton, P. R. Taylor, *J. Mol. Spectrosc.* **1986**, *120*, 292–297.

[4] L. L. Lohr, A. C. Scheiner, *J. Mol. Struct.* **1984**, *109*, 195–200.

[5] W. W. Schoeller, C. Begemann, U. Tubbesing, J. Strutwolf, *J. Chem. Soc. Faraday Trans.* **1997**, *93*, 2957–2962.

[6] a) A. Luna, M. Alcami, O. Mo, M. Yanez, *Int. J. Mass Spectrom.* **2000**, *201*, 215–231; b) J. A. Dobado, H. Martinez-Garcia, J. M. Molina, M. R. Sundberg, *J. Am. Chem. Soc.* **2000**, *122*, 1144–1149.

[7] a) J.-C. Guillemin, J.-M. Denis, *Angew. Chem.* **1982**, *94*, 715; *Angew. Chem. Int. Ed. Engl.* **1982**, *21*, 690–691; *Angew. Chem. Suppl.* **1982**, 1515–1524. For a review on the VGSR technique, see J.-M. Denis, A.-C. Gaumont, *Gas-Phase Reactions in Organic Synthesis*, Gordon & Breach Science, Amsterdam, **1997**, pp. 195–235.

[8] A. L. Rheingold, J. M. Bellama, *J. Organomet. Chem.* **1975**, *102*, 437–444.

[9] The synthesis of unstabilized low-boiling arsanes by this approach has already been reported: J.-C. Guillemin, L. Lassalle, *Organometallics* **1994**, *13*, 1525–1527.

[10] S. Elbel, H. T. Dieck, *J. Fluorine Chem.* **1982**, 349–362.

[11] K. Kimura, S. Katsumata, Y. Achiba, T. Yamazaki, S. Iwata, *Handbook of HeI Photoelectron Spectra of Fundamental Organic Molecules* Japan Scientific Societies Press, Tokyo, **1981**.

[12] a) R. E. Stratmann, G. E. Scuseria, M. J. Frisch, *J. Chem. Phys.* **1998**, *109*, 8218–8224; b) M. E. Casida, C. Jamorski, K. C. Casida, D. R. Salahub, *J. Chem. Phys.* **1998**, *108*, 4439–4449.

[13] a) W. von Niessen, J. Schirmer, L. S. Cederbaum, *Comput. Phys. Rep.* **1984**, *1*, 57–125; b) J. V. Ortiz, *J. Chem. Phys.* **1988**, *89*, 6348–6352.

[14] *MOLCAS* Version 5., Lund University, Sweden, **2000**.

[15] a) A. J. Arduengo, H. Bock, H. Chen, M. Denk, D. A. Dixon, J. C. Green, W. A. Hermann, N. L. Jones, M. Wagner, R. West, *J. Am. Chem. Soc.* **1994**, *116*, 6641–6649; b) H. Muchall, N. Werstiuk, J. Pitters, M. Workentin, *Tetrahedron* **1999**, *55*, 3767–3778; c) H. Muchall, N. Werstiuk, B. Choudury, J. Ma, J. Warkentin, J. Pezacki, *Can. J. Chem.* **1998**, *76*, 238–240; d) H. Muchall, N. Werstiuk, B. Choudury, *Can. J. Chem.* **1998**, *76*, 221–227; e) H. Muchall, P. Rademacher, *J. Mol. Struct.* **1998**, *471*, 189–194.

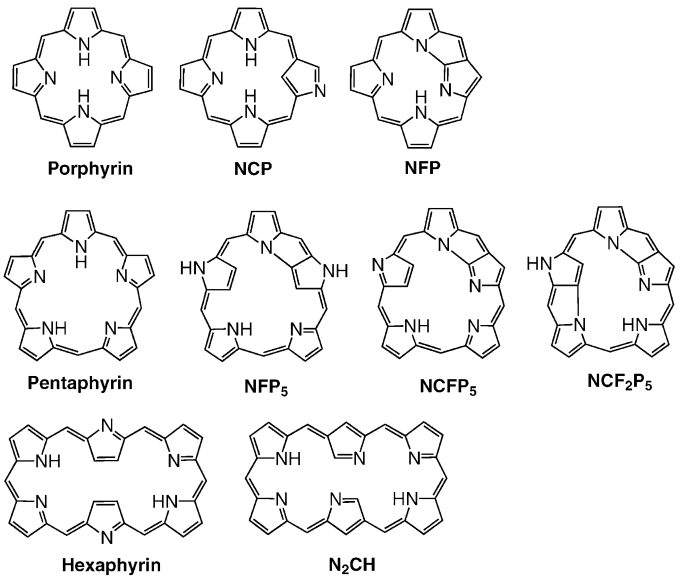
 © 2004 Wiley-VCH Verlag GmbH & Co. KGaA, Weinheim

Confused Porphyrins

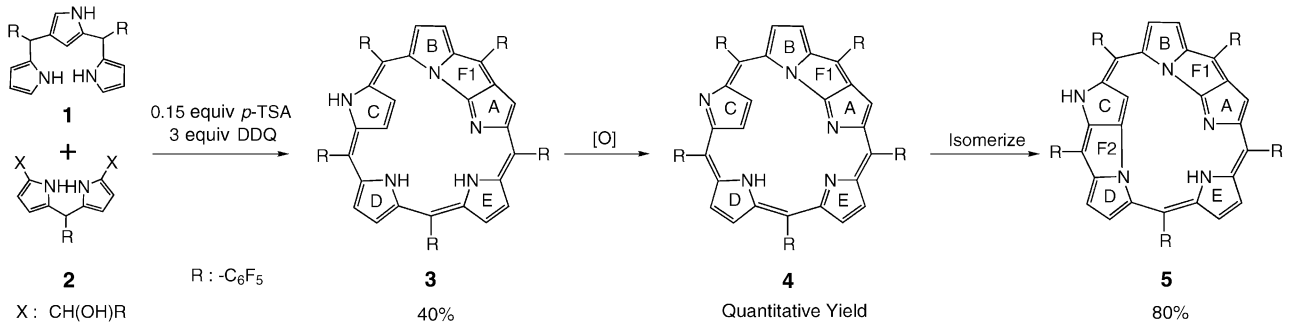
Doubly N-Fused Pentaphyrin

*Alagar Srinivasan, Tomoya Ishizuka, and Hiroyuki Furuta**

Increasing attention has recently been devoted to porphyrin analogues because of interest in their versatile electronic structures, rich coordination chemistry, and their possibilities for use in a variety of applications.[1] Among the various modifications of the porphyrin framework, changing the positions of the pyrrole linkage from α-α′ to α-β′ is of particular interest because so-called confused porphyrinoids could be synthesized easily by using one-pot pyrrole–aldehyde condensation or by replacing the oligopyrrole units with a confused ring in the standard porphyrin synthesis. Such analogues exhibit the peculiar chemistry already shown by N-confused porphyrin (NCP).[2] Previously, we reported the first example of hexapyrrolic confused porphyrinoids, the doubly N-confused hexaphyrins (N_2CH), that possess two N_3C compartments for the complexation of two metal ions in the cavity.[3] The successful results obtained with these hexaphyrins encouraged us to extend this approach to other expanded porphyrinoids. As a target, we chose a pentapyrrolic porphyrin, pentaphyrin,[4] because the *meso*-aryl pentaphyrin is shown to exist in the form of the N-fused pentaphyrin (NFP_5) and thus, the introduction of the confused pyrrole into its tripentacyclic ring may afford the isomer of NFP_5 which displays different chemical and physical properties.[5] Herein we report the first synthesis and structural characterization of the novel pentapyrrolic porphyrinoids: N-confused, N-fused pentaphyrin ($NCFP_5$) and N-confused, doubly N-fused pentaphyrin (NCF_2P_5). Amazingly, NCF_2P_5 has two different types of fused tripentacyclic rings (confused and normal) in the core. Such tripentacyclic rings were originally found in the N-fused porphyrin (NFP) derived from NCP and NFP_5.[5,6] Introduction of the confused pyrrole rings, at least in the tetra- and pentapyrrolic macrocycles, generally promotes the formation of a fused tripentacyclic ring.



The synthesis of the N-confused pentaphyrins is outlined in Scheme 1. Briefly, a [3+2] acid-catalyzed condensation of N-confused tripyrrane **1** and dipyrromethane dicarbinol **2** in the presence of *p*-toluenesulfonic acid (*p*-TSA), followed by oxidation with 2,3-dichloro-5,6-dicyano-1,4-benzoquinone (DDQ), resulted in the reduced form of N-confused, N-fused pentaphyrin ($NCFP_5$, **3**) as a brown solid in 40% yield. The FAB mass spectrum of **3** showed a signal for the molecular ion at *m*/*z* 1217, which suggests the presence of the pentapyrrolic macrocycle. Signals attributed to **3** appeared in the region from $\delta = 5$ to 13 ppm in the ^{1}H NMR spectrum recorded in $CDCl_3$ (Table 1). The pyrrolic β-CH and NH protons of inverted ring C resonated at $\delta = 7.38$, 7.02, and 8.82 ppm, while the singlet signal corresponding to the β-CH group of fused ring A was observed at $\delta = 5.67$ ppm, which



Scheme 1. Synthesis of N-confused, doubly N-fused pentaphyrin (**5**).

[*] Dr. A. Srinivasan, T. Ishizuka, Prof. Dr. H. Furuta[+]
Department of Chemistry and Biochemistry
Graduate School of Engineering
Kyushu University
Fukuoka 812-8581 (Japan)
Fax: (+81) 92-651-5606
E-mail: hfuruta@cstf.kyushu-u.ac.jp
[+] PRESTO, JST

Supporting Information for this article is available on the WWW under http://www.angewandte.org or from the author.

 © 2004 Wiley-VCH Verlag GmbH & Co. KGaA, Weinheim DOI: 10.1002/anie.200352946

Table 1: Selected physical data for **3**–**5**.

3: m.p. >300 °C (decomp); ^{1}H NMR ($CDCl_3$, 300 MHz): $\delta = 12.21$ (s, 1H, NH), 8.82 (s, 1H, NH), 7.38 (dd, $J = 3.6$, 2.4 Hz, 1H), 7.15 (br s, 1H, NH), 7.02 (dd, $J = 3.6$, 4.2 Hz, 1H), 6.39 (m, 1H), 6.21 (m, 3H), 5.91 (d, $J = 6.0$ Hz, 1H), 5.75 (d, $J = 6.0$ Hz, 1H), 5.67 (s, 1H, β-CH of ring A); UV/Vis (CH_2Cl_2): λ_{max} [nm] (ε [$mol^{-1}\,dm^3\,cm^{-1}$]): 448 (60000), 509 (41000), 718 (6600); HRMS (FAB): calcd for $C_{55}H_{13}F_{25}N_5$ $[M+H]^+$: 1218.0772; found: 1218.0789; elemental analysis calcd for $C_{55}H_{12}F_{25}N_5$: C 54.25, H 0.99, N 5.75; found: C 54.20, H 1.21, N 5.74.

4: m.p. >300 °C (decomp); ^{1}H NMR ($CDCl_3$, 300 MHz): $\delta = 8.68$ (m, 1H), 8.57 (d, $J = 6.0$ Hz, 1H), 8.26 (s, 1H, β-CH of ring A), 7.76 (m, 1H), 7.64 (d, $J = 6.0$ Hz, 1H), 7.57 (d, $J = 3.0$ Hz, 1H), 7.45 (d, $J = 6.0$ Hz, 1H), 4.04 (d, $J = 6.0$ Hz, 1H) 3.75 (d, $J = 6.0$ Hz, 1H), 3.65 (s, 1H, NH); UV/Vis (CH_2Cl_2): λ_{max} [nm] (ε [$mol^{-1}\,dm^3\,cm^{-1}$]): 351 (40000), 380 (43000), 517 (69000); HRMS (FAB): calcd for $C_{55}H_{11}F_{25}N_5$ $[M+H]^+$: 1216.0615; found: 1216.0601.

5: m.p. >300 °C (decomp); ^{1}H NMR ($CDCl_3$, 300 MHz): $\delta = 12.07$ (s, 1H, NH), 7.95 (s, 1H, β-CH of ring C), 7.38 (s, 1H, NH), 6.38 (m, 1H), 6.21 (m, 1H), 5.89 (m, 1H), 5.71 (d, $J = 6.0$ Hz, 1H), 5.66 (m, 1H), 5.61 (d, $J = 6.0$ Hz, 1H), 5.52 (s, 1H, β-CH of ring A); UV/Vis (CH_2Cl_2): λ_{max} [nm] (ε [$mol^{-1}\,dm^3\,cm^{-1}$]): 401 (57000), 503 (42000), 584 (13000), 630 (10000); HRMS (FAB): calcd for $C_{55}H_{11}F_{25}N_5$ $[M+H]^+$: 1216.0615; found: 1216.0672; elemental analysis calcd for $C_{55}H_{10}F_{25}N_5$: C 54.34, H 0.83, N 5.76; found: C 54.36, H 0.98, N 5.99.

proved that **3** was a 24π nonaromatic compound. Furthermore, the inner NH group of normal ring E appeared at $\delta =$ 12.21 ppm as a result of the strong hydrogen-bonding interaction with the neighboring nitrogen atom of ring A. Like NFP,[6] the absence of an α-CH (ring A) resonance suggested that it was directly fused with the adjacent pyrrole N atom, thus resulting in the formation of a tripentacyclic ring (A-F1-B). The electronic spectrum of **3** showed three broad bands between 445 and 720 nm, with the tail of the longest wavelength band reaching to around 1000 nm (Figure 1).

Further oxidation of **3** resulted in the quantitative formation of **4**. The FAB mass spctrum of **4** showed a molecular ion signal at m/z 1215, which is two mass units less than that of **3**. In contrast to **3**, the ^{1}H NMR spectrum of **4** (Table 1) was consistent with a 22π aromatic ring current effect, where the β-CH atoms on rings C and A resonated at $\delta = 4.04$, 3.75, and 8.26 ppm, and the inner NH proton was

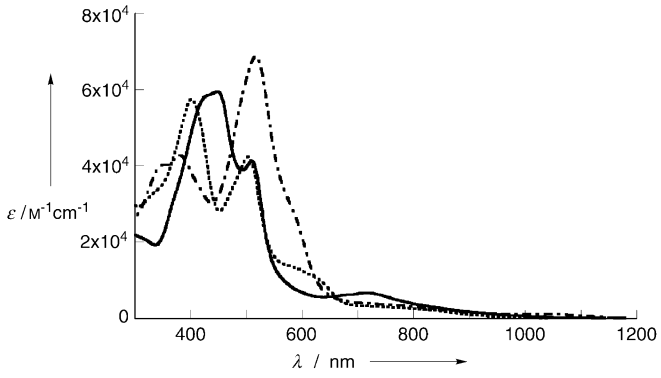


Figure 1. Absorption spectra of **3** (——), **4** (–•–•), and **5** (••••).

observed at $\delta = 3.65$ ppm. The aromatic nature of **4** was also suggested from a Soret-like band at 517 nm in the electronic spectrum. However, compound **4** was quite unstable and gradually isomerized in CH_2Cl_2 at room temperature over two days to form the doubly N-fused porphyrinoid **5** as a brown solid in 80% yield.[7]

The FAB mass spectrum of **5** showed a molecular ion signal at m/z 1215, which suggested that the compound was an isomer of **4**. Surprisingly, the ^{1}H NMR spectrum of **5** (Table 1) showed that one of the β-CH protons in ring C had disappeared. The newly formed NH group and the β-CH protons of ring C resonated at $\delta = 7.38$ and 7.95 ppm, respectively, while the β-CH group of ring A resonated at 5.52 ppm. In addition, the inner NH proton (ring D) of **4** shifted to the neighboring pyrrole (ring E) and resonated at $\delta = 12.07$ ppm. The NMR spectrum is thus consistent with the formation of a second tripentacyclic ring (C-F2-D) as well as the 24π anti-aromatic nature of the molecule. Thus, isomerization took place with loss of aromatic stabilization of the pentaphyrin core. The detailed mechanism for the isomerization of **4** is not clear yet, but it is likely that the release of steric repulsion between the inverted pyrrole rings C and D might be triggered by the formation of a shorter atomic distance between the pyrrolic N atom of ring D and the to-be-bonded carbon atom of ring C in **4**. This distance has been estimated to be 2.969 Å from the optimized structures calculated at the PM3 level (see the Supporting Information). The electronic absorption spectrum of **5** showed three broad bands between 300 and 800 nm, which further supports the anti-aromatic character of **5** (Figure 1).

The explicit structure of the N-confused, doubly N-fused pentaphyrin (NCF_2P_5, **5**) was revealed by X-ray single-crystal analysis (Figure 2).[8] As predicted from the above observations, there are two tripentacyclic rings (A-F1-B and C-F2-D) and a pyrrole ring in the macrocycle (**5**). Both the nitrogen atoms in one of the fused rings (A-F1-B) are inside the ring, while in the other tripentacyclic ring (C-F2-D), the outward and inward pointing nitrogen atoms were found in the macrocyclic core. The core plane consisting of 30 atoms is highly distorted from the least-squares plane, with a mean deviation of 0.413 Å. The dihedral angles between the core plane and the fused rings A-F1-B and C-F2-D, and the N5 pyrrole ring are 18.3(1), 162.2(2), and 130.1(3)°, respectively. Each asymmetric unit of the crystal data contains one pentaphyrin with a cocrystallized acetonitrile solvent molecule. The distance between N3 and the nitrogen atom of the acetonitrile molecule is 2.95(1) Å, which is within the range of a hydrogen-bonding interaction.

To confirm the positions of the nitrogen atoms unambiguously, the bond lengths and angles of the two fused rings were compared with those of NFP and NFP_5. The bond length (N1–C3) and angles (C1-N1-C3) of ring A-F1-B are 1.30(1) Å and 101.6(8)°, which are comparable to the values found in confused NFP (1.28 Å and 104°).[6] On the other hand, the corresponding bond length (C12–C13) and angle (C11-C12-C13) for ring C-F2-D are 1.37(1) Å and 107.1(9)°, which are similar to those of 1.39(1) Å and 107.3(9)° in normal NFP_5.[5] Thus, ring A-F1-B is considered to be a confused tripentacyclic ring, while ring C-F2-D is assigned as a normal

 © 2004 Wiley-VCH Verlag GmbH & Co. KGaA, Weinheim

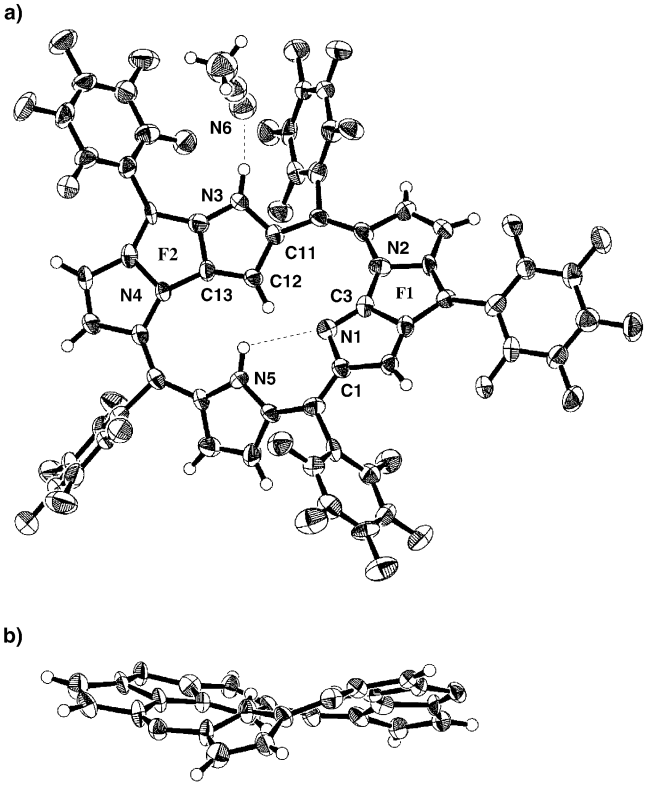


Figure 2. X-ray structure of N-confused, doubly N-fused pentaphyrin **5**: a) top view and b) side view. Hydrogen-bonding interactions are indicated by broken lines. The solvent molecule and the *meso*-pentafluorophenyl groups are omitted for clarity in (b).

tripentacyclic ring. Bond alternation (single, double) is very clearly observed in the structure, which reflects the non- or weak antiaromatic character of **5** (Figure 3). Similar to NFP and NFP_5, the proton on N5 shows an intramolecular hydrogen-bonding interaction with the adjacent pyrrolic nitrogen atom N1 that is at a distance of 2.95(1) Å.

In summary, we have successfully demonstrated the synthesis of N-confused, N-fused pentaphyrin and N-confused, doubly N-fused pentaphyrin. It has been clearly shown that the *meso*-aryl β-free derivatives display an interesting structural diversity,[9] which is unknown for the β-substituted pentaphyrins. The two different types of fused rings indicate that both the inverted conformation of normal and confused pyrrole rings can induce the formation of a tripentacyclic ring. The introduction of further confusion into the macrocyclic system would open the way to hitherto unexplored N-fused porphyrinoid chemistry. Efforts to prepare a series of confused expanded porphyrins are currently underway.

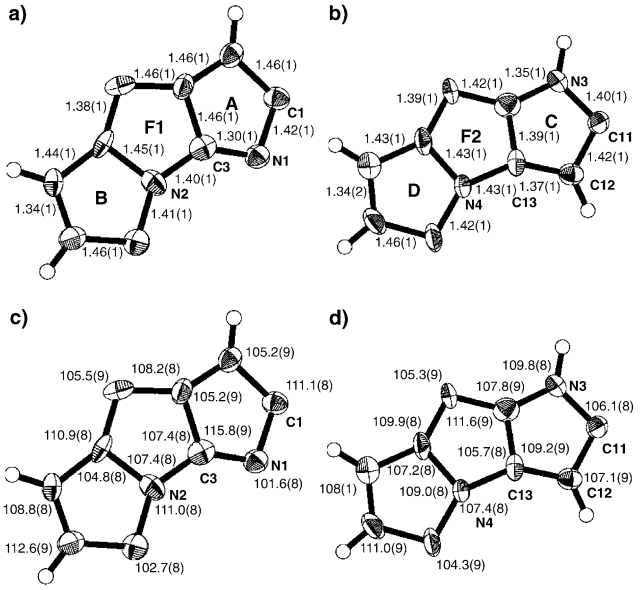


Figure 3. Bond lengths [Å] and angles [°] of the tripentacyclic rings: A-F1-B (a, c) and C-F2-D (b, d).

Experimental Section

3: A mixture of **1** (100 mg, 0.18 mmol) and **2** (126 mg, 0.18 mmol) in CH_2Cl_2 were stirred in a nitrogen atmosphere for 15 min at room temperature. *p*-Toluenesulfonic acid (*p*-TSA; 5.1 mg, 0.027 mmol) was then added to the above mixture and the solution stirred for a further 1 h in the dark. The reaction mixture was then passed through a column of silica gel using CH_2Cl_2 (200 mL) as the eluent. DDQ (122 mg, 0.54 mmol) was added to the combined solution and the mixture stirred for a further 1 h at room temperature. After removal of the solvent, the crude product was purified by column chromatography, first on basic alumina and then on silica gel. A brown fraction was eluted with CH_2Cl_2/hexane (40:60) which, on removal of the solvent, gave **3** (87 mg, 40%) as a brown solid.

4: DDQ (19 mg, 0.018 mmol) was added to a solution of **3** (20 mg, 0.016 mmol) in CH_2Cl_2 (10 mL), and the mixture was stirred at room temperature for 10 min. After removal of the solvent, the crude product was purified by column chromatography firstly on alumina and then on silica gel. A pink fraction eluted with CH_2Cl_2/hexane (90:10) which gave **4** (20 mg, 100%) as a green solid.

5: Compound **4** (15 mg, 0.012 mmol) was dissolved in CH_2Cl_2 (15 mL). The color of the solution gradually changed from pink to brown over 2 days at room temperature. The solvent was evaporated and the residue purified by column chromatography on silica gel. A brown fraction was eluted with CH_2Cl_2/hexane (20:80) which gave **5** (12 mg, 80%) as a brown solid. The remaining product was identified as starting material **4**.

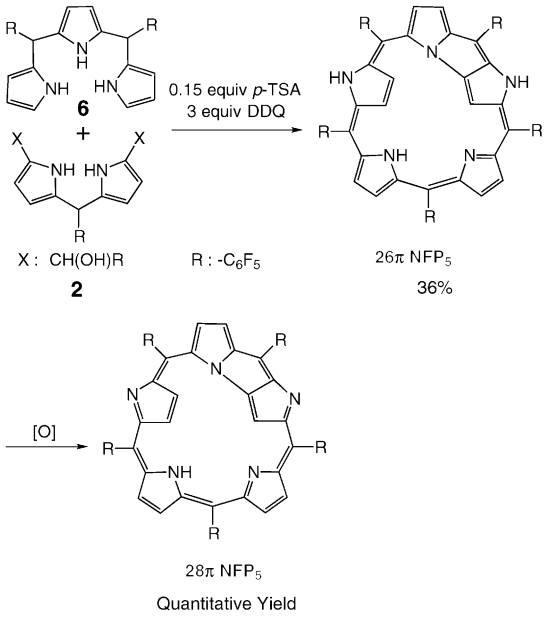
Received: September 24, 2003 [Z52946]
Published Online: January 22, 2004

Keywords: aromaticity · macrocyclic ligands · oxidation · porphyrinoids · structure elucidation

[1] *The Porphyrin Handbook*, *Vol. 2* (Eds.: K. M. Kadish, K. M. Smith, R. Guilard), Academic, San Diego, **2000**.
[2] a) H. Furuta, T. Asano, T. Ogawa, *J. Am. Chem. Soc.* **1994**, *116*, 767–768; b) P. J. Chmielewski, L. Latos-Grażyński, K. Rachlewicz, T. Głowiak, *Angew. Chem.* **1994**, *106*, 805–808; *Angew. Chem. Int. Ed. Engl.* **1994**, *33*, 779–781; c) H. Furuta, H. Maeda, A. Osuka, *Chem. Commun.* **2002**, 1795–1804; d) L. Latos-Grażyński in ref. [1], chapt. 14.
[3] A. Srinivasan, T. Ishizuka, A. Osuka, H. Furuta, *J. Am. Chem. Soc.* **2003**, *125*, 878–879.
[4] β-Alkyl *meso*-free pentaphyrins and their analogues are synthesized, see a) H. Rexhausen, A. Gossauer, *J. Chem. Soc. Chem. Commun.* **1983**, 275; b) A. Jasat, D. Dolphin, *Chem. Rev.* **1997**, *97*,

 © 2004 Wiley-VCH Verlag GmbH & Co. KGaA, Weinheim

2267 – 2340; c) J. L. Sessler, S. J. Weghorn, *Expanded, Contracted and Isomeric Porphyrins*, Pergamon, New York, **1997**.
[5] J.-Y. Shin, H. Furuta, A. Osuka, *Angew. Chem.* **2001**, *113*, 639 – 641; *Angew. Chem. Int. Ed.* **2001**, *40*, 619 – 621.
[6] a) H. Furuta, T. Ishizuka, A. Osuka, T. Ogawa, *J. Am. Chem. Soc.* **1999**, *121*, 2945 – 2946; b) H. Furuta, T. Ishizuka, A. Osuka, T. Ogawa, *J. Am. Chem. Soc.* **2000**, *122*, 5748 – 5757; c) B. Kiran, M. H. Nguyen, *J. Organomet. Chem.* **2002**, *643–644*, 265 – 271.
[7] It is noteworthy that the reported partially *meso*-aryl-substituted pentaphyrins were also quite unstable, even in the solid state, and decomposed when exposed to air with a half-live of several days: C. Brückner, E. D. Sternberg, R. W. Boyle, D. Dolphin, *Chem. Commun.* **1997**, 1689 – 1690.
[8] Crystal data for **6**: $C_{55}H_{10}N_5F_{25}\cdot CH_3CN$, $M_r = 1256.73$, triclinic, space group $P\bar{1}$ (no. 2), $a = 10.287(8)$, $b = 11.981(9)$, $c = 19.08(1)$ Å, $\alpha = 89.86(6)$, $\beta = 83.19(6)$, $\gamma = 87.38(6)°$, $V = 2332.8(3)$ Å^3, $T = -150.0\,°C$, $Z = 2$, 19939 measured reflections, 10250 unique reflections, 3169 with $I \geq 3\sigma(I)$ used in refinement, $R = 0.072$, $R_w = 0.057$, GOF = 0.756. CCDC-219943 contains the supplementary crystallographic data for this paper. These data can be obtained free of charge via www.ccdc.cam.ac.uk/conts/retrieving.html (or from the Cambridge Crystallographic Data Centre, 12 Union Road, Cambridge CB21EZ, UK; fax: (+44) 1223-336-033; or deposit@ccdc.cam.ac.uk).
[9] By applying the same synthetic procedure as used for **3**, the reduced form of normal N-fused pentaphyrin (NFP_5) was obtained from normal tripyrrane and dipyrromethane dicarbinol **6** in 36% yield, and further oxidation led to the quantitative formation of aromatic NFP_5, which was twofold higher than that of the reported Rothemund-type synthesis; see ref. [5].



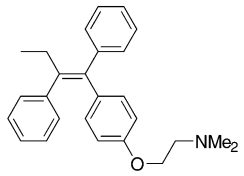
 © 2004 Wiley-VCH Verlag GmbH & Co. KGaA, Weinheim

Organofluorine Compounds

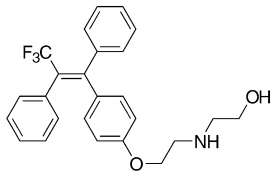
A Facile Stereocontrolled Approach to CF_3-Substituted Triarylethenes: Synthesis of Panomifene**

Xinyu Liu, Masaki Shimizu, and Tamejiro Hiyama*

Triaryl ethenes is a key structure in nonsteroidal antiestrogens.[1] In particular, tamoxifen (**1**) has been widely used for clinical treatment of breast cancer.[2] The antiestrogenic activity is known to depend on the olefin geometry of the triaryl ethene component.[3] On the other hand, selective replacement of C–H bonds with C–F bonds in biologically active compounds has been proved to be the most effective and powerful strategy in the optimization of parent compounds.[4] This strategy, when applied to the exploration of highly potent triaryl ethenes,[5,6] led to discovery of panomifene (**2**),[6] which exhibits antiestrogenic and tumor-inhibiting



Tamoxifen (**1**)



Panomifene (**2**)

activities superior to those of **1**. In view of this history, a general, convenient, and stereoselective synthetic method for the preparation of CF_3-substituted triaryl ethenes should definitely open a new entry to highly potent nonsteroidal antiestrogens.

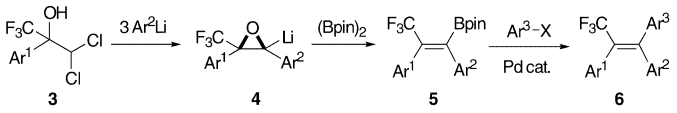
We recently found that treatment of CF_3-substituted dichlorohydrin **3** ($Ar^1 = PhC{\equiv}C$) with BuLi or PhLi (3 equiv) in THF at −98 °C generated the corresponding CF_3-substituted lithio-oxirane **4** ($Ar^1 = PhC{\equiv}C$, $Ar^2 = Bu$ or Ph), which reacted with bis(pinacolato)diboron, $(Bpin)_2$, to afford **5** ($Ar^1 = PhC{\equiv}C$, $Ar^2 = Bu$ or Ph) in high yields with excellent diastereoselectivity (Scheme 1).[7] We envisioned that the stereospecific cross-coupling reaction of β-CF_3-substituted alkenyl boronates **5** with Ar^3X, if feasible, would give rise to a series of compounds **6** conveniently and stereoselectively. Herein we describe the success of this

[*] X. Liu, Dr. M. Shimizu, Prof. Dr. T. Hiyama
Department of Material Chemistry
Graduate School of Engineering, Kyoto University
Katsura Campus, Nishikyo-ku, Kyoto 615-8510 (Japan)
Fax: (+81) 75-383-2445
E-mail: shimizu@npc05.kuic.kyoto-u.ac.jp

[**] This work was supported by a Grant-in-Aid for COE Research on Elements Science, no. 12CE2005, from the Ministry of Education, Culture, Sports, Science, and Technology, Japan. 1,1-Difluoro-3,3,3-trifluoropropan-2-one was kindly donated by Central Glass Co. Ltd. We are grateful to Dr. Yi-Chou Tsai for a helpful literature survey.

Supporting information for this article is available on the WWW under http://www.angewandte.org or from the author.

 DOI: 10.1002/anie.200353032 © 2004 Wiley-VCH Verlag GmbH & Co. KGaA, Weinheim



Scheme 1. Novel approach to CF_3-substituted triarylethenes **6**. Bpin = (pinacolato)boryl.

approach and demonstrate the versatility of the sequence through the total synthesis of panomifene (**2**).

Following our original protocol, we first treated a solution of **3**[8] in THF with Ar^2Li (3 equiv) at low temperatures and soon found that the corresponding lithio-oxiranes **4** could be generated at −78 °C. The 3-aryl derivatives **4** (Ar^2 = aryl) are stable at −78 °C, in sharp contrast to 3-alkyl-substituted lithio-oxiranes **4** (Ar^2 = alkyl) whose reactions had to be conducted at −98 °C. The enhanced stability of lithio-oxiranes **4** may be ascribed to the anion-stabilizing effect of an Ar^2 group in **4**,[9] which smoothly reacted with $(Bpin)_2$ at −78 °C to room temperature to give the corresponding compounds **5** in moderate to good yields with high *E* selectivity (Table 1). Fluorine, chlorine, methoxy, and methoxymethoxy (MOMO) substituents on Ar^1 and Ar^2 were tolerated under these conditions. The *E* configuration of **4** was confirmed by conversion of **5a** into a deborylated product (see below).

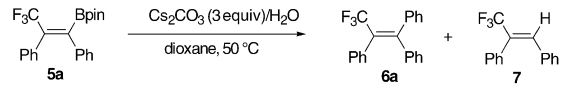
Table 1: Stereoselective preparation of **5** from **3** with Ar^2Li.[a]

Entry	3	Ar^1	Ar^2	5	Yield [%][b]	*E*/*Z*[c]
1	**a**	Ph	Ph	**a**	63	98:2
2	**a**	Ph	*p*-Cl-C_6H_4	**b**	73	97:3
3	**a**	Ph	*p*-MeO-C_6H_4	**c**	78	94:6
4	**a**	Ph	*p*-MOMO-C_6H_4[d]	**d**	75	92:8
5	**b**	*p*-F-C_6H_4	Ph	**e**	65	99:1
6	**c**	*p*-Cl-C_6H_4	Ph	**f**	80	99:1
7	**d**	*p*-MeO-C_6H_4	Ph	**g**	63	>99:<1

[a] A THF solution of **3** (5 mmol) was treated with Ar^2Li (15 mmol) at −78 °C for 0.5–2 h, and then with $(Bpin)_2$ (5.25 mmol) at −78 °C. The mixture was gradually warmed to room temperature before quenching with saturated aqueous NH_4Cl solution. [b] Yields of isolated products. [c] *E*/*Z* ratio was determined by ^{19}F NMR spectroscopic analysis. [d] MOM = methoxymethyl.

With **5** in hand, we next examined the Pd-catalyzed cross-coupling reaction with aryl iodide Ar^3I.[10] To the best of our knowledge, no examples of cross-coupling reactions of β-CF_3-substituted alkenyl boron reagents is available.[11,12] The reaction conditions were first optimized with iodobenzene as a typical coupling partner. The results are summarized in Table 2. When a dioxane solution of **5a** (*E*/*Z* = 98:2) and iodobenzene was heated in the presence of $[Pd(PPh_3)_4]$ (10 mol %) and Cs_2CO_3 (3 equiv) at 50 °C for 12 h, only protodeborylation took place to give (*E*)-1,2-diphenyl-3,3,3-trifluoropropene (**7**)[13] as the sole product (Table 2, entry 1).[14] The formation of **7** indicated that the Bpin group in **5a** was positioned *cis* to the CF_3 group. $[PdCl_2(PPh_3)_2]$ or $[Pd(tBu_3P)_2]$ catalyst produced **6a** as the major product though very slowly; fair amounts of **7** were still obtained (Table 2, entries 2 and 3). The use of TlOEt as base

Table 2: Coupling reaction of **5a** with iodobenzene.[a]



Entry	Catalyst	H_2O [equiv]	*t* [h]	Conv. [%][b]	**6a**/**7**[c]
1	$[Pd(PPh_3)_4]$	–	12	100	0:100
2	$[PdCl_2(PPh_3)_2]$	–	12	25	84:16
3	$[Pd(tBu_3P)_2]$	–	12	37	70:30
4[d]	$[Pd(tBu_3P)_2]$	–	2	100	22:78
5	$[PdCl_2(PPh_3)_2]$	3	4	100	77:23
6	$[Pd(tBu_3P)_2]$	3	1.5	100	82:18
7	$[Pd(tBu_3P)_2]$	6	2	100	91:9
8	$[Pd(tBu_3P)_2]$	15	5	100	93:7
9	$[Pd(tBu_3P)_2]$	[e]	6	100(94)[f]	98:2

[a] Reaction conditions: **5a** (0.5 mmol), iodobenzene (0.75 mmol), palladium catalyst (0.05 mmol), Cs_2CO_3 (1.5 mmol), H_2O (indicated amount), dioxane (0.1 mL), 50 °C. [b] For entries 1–3, reaction was terminated after 12 h. For entries 4–9, reaction was monitored by TLC and terminated when **5a** was completely consumed. [c] The ratio was determined by ^{19}F NMR analysis of crude product. [d] TlOEt was used instead of Cs_2CO_3. [e] A 5 M aqueous solution of Cs_2CO_3 was employed. [f] The value in parentheses is the yield of isolated **6a**.

accelerated the reaction remarkably, but led to preferential formation of **7** (Table 2, entry 4).[15] After several attempts, we found that the addition of water also accelerated the coupling reaction and was quite effective for the selective production of **6a** (Table 2, entries 5–9).[16] In particular, aqueous solution of Cs_2CO_3 (5 M) in combination with $[Pd(tBu_3P)_2]$ allowed the reaction to go to completion in 6 h, and **6a** was isolated as a single stereoisomer in 94 % yield (**6a**/**7** = 98:2; Table 2, entry 9). The minor stereoisomer of **5a** (*Z* isomer) did not undergo the coupling reaction under these conditions, although the reason is not clear at present.

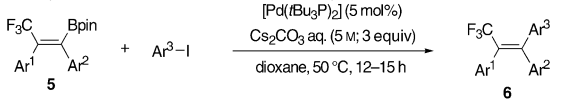
The optimized conditions were applied to the synthesis of several CF_3-substituted triaryl ethenes **6** (Table 3). The yields and selectivity of **6** were uniformly high. Both electron-withdrawing and -donating group at *para*-position of any of the aryl groups did not affect the performance of the coupling reaction. Notably, the coupling reaction cleanly discriminates Cl from I in **5** and Ar^3-I (Table 3, entries 3, 6, 7, 11, 12). The remaining Cl substituent can be elaborated for further transformation (see below). In all cases, the *Z* isomer of **5** did not undergo reaction, as determined by ^{19}F NMR spectroscopic and GC-MS analysis of the crude products, so that **6** was always obtained as a single diastereomer.

Synthetic transformations of chlorine-substituted **6** are illustrated in Scheme 2. The remaining Cl functionality in **6l** and **6g** was subjected to palladium-catalyzed C–N or C–O coupling reactions[17,18] to introduce nitrogen or oxygen functionality. Thus, aniline **8** and phenyl ether **9** were isolated in 83 % and 52 % yields, respectively.

Finally, we demonstrated the synthetic potential of the methodology described herein by conversion of **6i** into panomifene (**2**). Demethylation of **6i** with NaSEt proceeded without any isomerization of the double bond in **6i** to give **10**,[19] which was treated with $Cl(CH_2)_2OTs$ and then with ethanolamine to give rise to **2** as shown in Scheme 3.

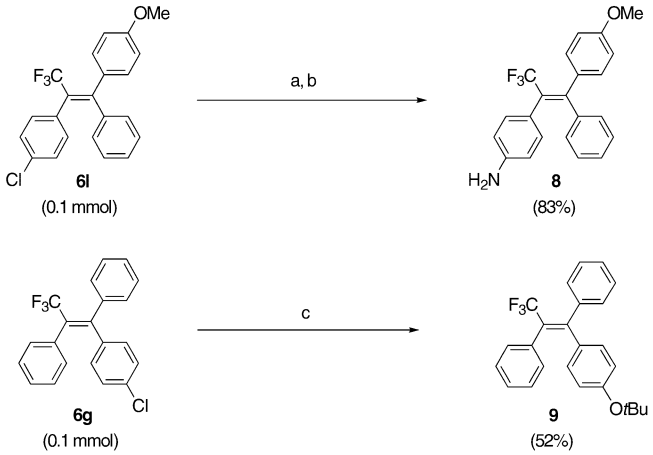
 © 2004 Wiley-VCH Verlag GmbH & Co. KGaA, Weinheim

Table 3: Synthesis of CF_3-substituted triarylethenes **6**.[a]



Entry	**5**	Ar^1	Ar^2	Ar^3	**6**	Yield [%][b]
1	**a**	Ph	Ph	*p*-EtO_2C-C_6H_4	**b**	92
2	**a**	Ph	Ph	*p*-F-C_6H_4	**c**	91
3	**a**	Ph	Ph	*p*-Cl-C_6H_4	**d**	96
4	**a**	Ph	Ph	*p*-MeO-C_6H_4	**e**	95
5	**a**	Ph	Ph	*p*-$Me_2N(CH_2)_2O$-C_6H_4	**f**	95
6	**b**	Ph	*p*-Cl-C_6H_4	Ph	**g**	92
7	**b**	Ph	*p*-Cl-C_6H_4	*p*-MeO-C_6H_4	**h**	89
8	**c**	Ph	*p*-MeO-C_6H_4	Ph	**i**	90
9	**d**	Ph	*p*-MOMO-C_6H_4	Ph	**j**	92
10	**e**	*p*-F-C_6H_4	Ph	*p*-F-C_6H_4	**k**	91
11	**f**	*p*-Cl-C_6H_4	Ph	*p*-MeO-C_6H_4	**l**	91
12	**f**	*p*-Cl-C_6H_4	Ph	*p*-F-C_6H_4	**m**	90
13	**g**	*p*-MeO-C_6H_4	Ph	*p*-F-C_6H_4	**n**	94

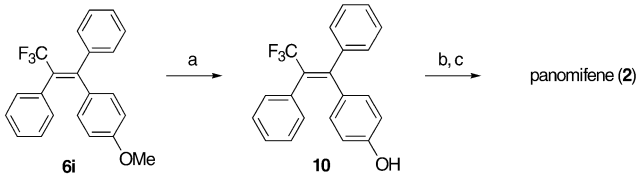
[a] Reaction conditions: **5** (0.2 mmol), Ar^3I (0.22 mmol), [Pd(tBu_3P)$_2$] (0.01 mmol), aqueous Cs_2CO_3 (5 M; 120 μL), dioxane (0.4 mL), 50 °C. [b] Yields of isolated products based on *E* isomer of **5**.



Scheme 2. Synthetic elaboration of chlorine-substituted **6**. Conditions: a) $LiN(SiMe_3)_2$, [$Pd_2(dba)_3$] (2.5 mol%), P(tBu)$_3$ (5 mol%), toluene, 100 °C, 12 h; b) HCl; c) NaO(tBu), [$Pd_2(dba)_3$] (5 mol%), 2-Cy_2P-2′-Me_2N-biphenyl (12 mol%), toluene, 100 °C, 18 h. dba = dibenzylideneacetone.

In summary, we have demonstrated a convenient and versatile synthetic strategy for CF_3-substituted triaryl ethenes through stereoselective preparation of **5** and its Pd-catalyzed cross-coupling. In particular, water was found to be effective in the acceleration of the Pd-catalyzed coupling reaction. This method can be applied to diverse CF_3-substituted triaryl ethenes, including panomifene, a potent nonsteroidal antiestrogen. Further studies on the preparation of organofluorine compounds, taking advantage of CF_3-substituted lithio-oxiranes and alkenyl–metal compounds are in progress.

Received: October 8, 2003 [Z53032]



Scheme 3. Application to the synthesis of panomifene (**2**). Conditions: a) NaSEt, DMF, 150 °C, 10 h, 78% yield; b) $Cl(CH_2)_2OTs$, K_2CO_3, MeCN, reflux, 12 h; c) $H_2N(CH_2)_2OH$, 2-methoxyethanol, reflux, 2 h, 66% (two steps from **10**). DMF = *N*,*N*-dimethylformamide, Ts = *p*-toluenesulfonyl.

Keywords: alkenes · boron · cross-coupling · fluorine · synthetic methods

[1] For a review on antiestrogens, see: a) R. A. Magarian, L. B. Overacre, S. Singh, K. L. Meyer, *Curr. Med. Chem.* **1994**, *1*, 61; b) V. C. Jordan, *J. Med. Chem.* **2003**, *46*, 883; c) V. C. Jordan, *J. Med. Chem.* **2003**, *46*, 1081.

[2] H. Wiseman, *Tamoxifen: Molecular Basis of Use in Cancer Treatment and Prevention*, Wiley, Chichester, **1994**.

[3] M. J. K. Harper, A. L. Walpole, *Nature* **1966**, *212*, 87.

[4] a) T. Hiyama, *Organofluorine Compounds. Chemistry and Applications*, Springer, Berlin, **2000**; b) M. Schlosser, *Angew. Chem.* **1998**, *110*, 1538–1556; *Angew. Chem. Int. Ed.* **1998**, *37*, 1496–1513; c) I. Ojima, J. R. McCarthy, J. T. Welch, *ACS Symp. Ser.* **1996**, *639*; d) M. Hudlicky, A. E. Pavlath in *Chemistry of Organic Fluorine Compounds II. A Critical Review*, American Chemical Society, Washington, DC, **1995**; e) J. T. Welch, *ACS Symp. Ser.* **1991**, *456*; f) J. T. Welch, *Tetrahedron* **1987**, *43*, 3123.

[5] W. J. Middleton, D. Metzger, J. A. Snyder, *J. Med. Chem.* **1971**, *14*, 1193.

[6] Monograph: a) *Drugs Future* **1985**, *10*, 395; b) *Drugs Future* **1990**, *15*, 532; Biological properties: c) J. Borvendeg, I. Hermann, O. Csuka, *Acta Physiol. Hung.* **1996**, *84*, 405 [*PubMed ID*, **1996**, 9328614]; d) V. Erdelyi-Toth, F. Gyergyay, I. Szamel, E. Pap, J. Kralovanszky, E. Bojti, M. Csorgo, S. Drabant, I. Klebovich, *Anti-Cancer Drugs* **1997**, *8*, 603 [*Chem. Abstr.* **1997**, *127*, 287616]; Synthesis: e) G. Nemeth, R. Kapiller-Dezsofi, G. Lax, G. Simig, *Tetrahedron* **1996**, *52*, 12821; Patents: f) G. Abraham, T. Horvath, L. Toldy, J. Borvendeg, E. Csanyi, E. Kiss, I. Hermann S, K. Tory (Gyogyszerkutato Intezet, Hung.), US 763078, **1989** [*Chem. Abstr.* **1989**, *111*, 77630].

[7] a) M. Shimizu, T. Fujimoto, H. Minezaki, T. Hata, T. Hiyama, *J. Am. Chem. Soc.* **2001**, *123*, 6947; b) M. Shimizu, T. Fujimoto, X. Liu, H. Minezaki, T. Hata, T. Hiyama, *Tetrahedron* **2003**, *59*, 9811.

[8] Dichlorohydrins **3** are readily available by carbonyl addition to 1,1-dichloro-3,3,3-trifluoropropan-2-one with Ar^1MgX (see Supporting Information).

[9] The lithio-oxirane generated from styrene oxide by deprotonation with *s*BuLi/TMEDA in THF at −98 °C was reportedly stable at −98 °C for only 30 min; the presence of a CF_3 group might contribute to the enhanced stability of **4**: V. Capriati, S. Florio, R. Luisi, A. Salomone, *Org. Lett.* **2002**, *4*, 2445.

[10] For reviews on the Suzuki–Miyaura coupling reaction, see: a) N. Miyaura, A. Suzuki, *Chem. Rev.* **1995**, *95*, 2457; b) A. Suzuki, *J. Organomet. Chem.* **1999**, *576*, 147; c) N. Miyaura, *Top. Curr. Chem.* **2002**, *219*, 11.

[11] For reviews on fluorinated organometallic compounds, see: a) D. J. Burton, Z.-Y. Yang, P. A. Morken, *Tetrahedron* **1994**, *50*, 2993; b) D. J. Burton, Z.-Y. Yang, *Tetrahedron* **1992**, *48*, 189.

[12] For the palladium-catalyzed coupling reaction of α-(trifluoromethyl)ethenyl boronic acid with aryl halides, see: a) B. Jiang,

 © 2004 Wiley-VCH Verlag GmbH & Co. KGaA, Weinheim

Q.-F. Wang, C.-G. Yang, M. Xu, *Tetrahedron Lett.* **2001**, *42*, 4083. β-CF_3-α,β-diphenylvinylstannane was prepared as a mixture of *E*/*Z* isomers (12:88) and coupled with aryl iodide using a catalyst system of [$Pd(PPh_3)_4$]/CuI to afford the corresponding CF_3-substituted triaryl ethenes as an *E*/*Z* mixture (12:88) in moderate yields: b) I. H. Jeong, Y. S. Park, M. S. Kim, Y. S. Song, *J. Fluorine Chem.* **2003**, *120*, 195.

[13] a) B. S. Nader, J. A. Cordova, K. E. Reese, C. L. Powell, *J. Org. Chem.* **1994**, *59*, 2898; b) J.-P. Begue, D. Bonnet-Delpon, D. Bouvet, M. H. Rock, *J. Org. Chem.* **1996**, *61*, 9111.

[14] Protodeborylation is often observed as a major side reaction; see: a) N. Miyaura, *Top. Curr. Chem.* **2002**, *219*, 20–23; N. Miyaura, *Top. Curr. Chem.* **2002**, *219*, 26–27; b) S. D. Brown, R. W. Armstrong, *J. Org. Chem.* **1997**, *62*, 7076.

[15] J.-i. Uenishi, J.-M. Beau, R. W. Armstrong, Y. Kishi, *J. Am. Chem. Soc.* **1987**, *109*, 4756.

[16] Some Pd-catalyzed coupling reactions of organoboron compounds were reported to be accelerated by the addition of water: a) reference [14a]; b) C. R. Johnson, M. P. Braun, *J. Am. Chem. Soc.* **1993**, *115*, 11014; c) C. Zhou, D. E. Emrich, R. C. Larock, *Org. Lett.* **2003**, *5*, 1579.

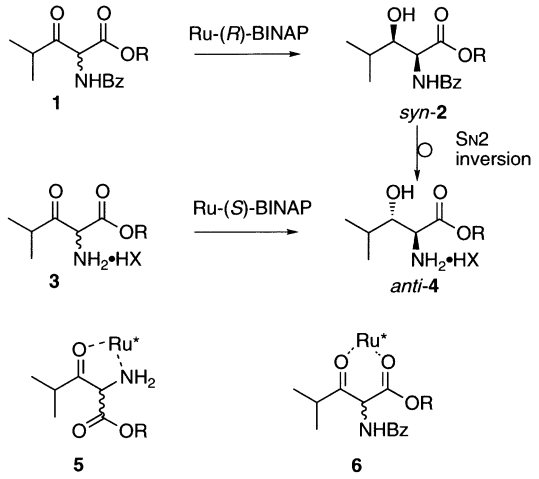
[17] S. Lee, M. Jorgensen, J. F. Hartwig, *Org. Lett.* **2001**, *3*, 2729.

[18] C. A. Parrish, S. L. Buchwald, *J. Org. Chem.* **2001**, *66*, 2498.

[19] In reference [6e], acidic demethylation was reported to result in the production of a 1:1 mixture of (*E*)- and (*Z*)-**10**.

 © 2004 Wiley-VCH Verlag GmbH & Co. KGaA, Weinheim

achieved stereoselective synthesis of all four stereoisomers of 3-hydroxyleucine.[3i] In this method, the *syn* isomer **2** of 3-hydroxyleucine was directly prepared by the asymmetric hydrogenation, but the *anti* isomer **4** needed to be constructed from **2** by two additional steps, oxazoline formation with internal SN2 inversion and acid hydrolysis (Scheme 1). To our knowledge, direct preparation of the *anti*-β-hydroxy-α-amino acids from the α-amino-β-keto esters by using an Ru–chiral-phosphane catalyst has not been reported. Herein, we describe the highly *anti*-selective hydrogenation of α-amino-β-keto esters through dynamic kinetic resolution with the Ru–BINAP catalyst. We envisioned hydrogenation through the five-membered transition state **5** (Scheme 1) with the 2-amino substituent of α-amino-β-keto ester **3** as a directing group; this reaction would directly produce *anti*-β-hydroxy-α-amino acid **4** in place of the *syn* product **2** that is produced through the six-membered transition state **6**.



Scheme 1. Synthesis of *syn*- and *anti*-β-hydroxy-α-amino acids through dynamic kinetic resolution with the Ru–BINAP catalyst. Bz = benzoyl.

anti-*Selective Hydrogenation*

Stereoselective Synthesis of *anti*-β-Hydroxy-α-amino Acids through Dynamic Kinetic Resolution

*Kazuishi Makino, Takayuki Goto, Yasuhiro Hiroki, and Yasumasa Hamada**

β-Hydroxy-α-amino acids are valuable constituents of a variety of biologically active natural products and medicinally important compounds, and many approaches for their enantioselective synthesis have been reported.[1–4] In connection with our ongoing research into the total synthesis of cyclodepsipeptides,[5] papuamides, and polyoxypeptins with biologically interesting activities, we needed a new method for the preparation of a large amount of (2*R*,3*R*)- and (2*S*,3*S*)-3-hydroxyleucine bearing the skeleton of an *anti*-β-hydroxy-α-amino acid, with control of both relative and absolute configuration. It is reported that *syn*-β-hydroxy-α-amino acid derivatives have been efficiently synthesized with high diastereo- and enantioselectivities from chirally labile α-amino-β-keto esters through dynamic kinetic resolution with the Ru–BINAP catalyst (BINAP = 2,2′-bis(diphenylphosphanyl)-1,1′-binaphthyl), which was originally developed by Noyori and co-workers.[3,4,6] Using this methodology, we have

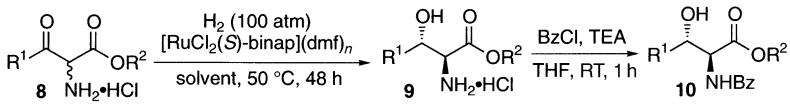
Hydrogenation of methyl 2-amino-4-methyl-3-oxo-pentanoate (**3**, where R = Me), the substrate producing 3-hydroxyleucine, was examined in detail, and the results are shown in Table 1. Reactions were carried out with the Ru–(*S*)-BINAP catalyst (4.2 mol%) at 50 °C under 100 atm of hydrogen. The absolute and relative configurations of the hydrogenated product were established, after transformation into benzoylamide derivative **7**, by comparison with authentic samples.[3i] In the preliminary experiment with the TsOH salt in methanol we were pleased to find that excellent *anti* selectivity (97:3) was observed by ^{1}H NMR analysis, although the enantioselectivity needed to be improved (Table 1, entry 1). With this encouraging result in hand, we extensively surveyed the conditions for the *anti*-selective hydrogenation with high enantioselectivity. First, the effect of counter anions in ammonium salts was investigated. The hydrochloric acid salt showed high *anti* diastereoselectivity with modest enantioselectivity (Table 1, entry 3). Interestingly, the tetrafluoroboric acid salt inhibited the hydrogenation, and the starting material was recovered (entry 2). Next, the effect of solvents was screened. The use of a polar solvent such as water,

[*] Dr. K. Makino, T. Goto, Y. Hiroki, Prof. Dr. Y. Hamada
Graduate School of Pharmaceutical Sciences
Chiba University, Yayoi-cho, Inage-ku, Chiba 263-8522 (Japan)
Fax: (+81) 43-290-2988
E-mail: hamada@p.chiba-u.ac.jp

 © 2004 Wiley-VCH Verlag GmbH & Co. KGaA, Weinheim DOI: 10.1002/anie.200353072

ethylene glycol, or *tert*-butyl alcohol was less or not effective for this hydrogenation. Methanol, *n*-propanol, 2-propanol, and dichloromethane were the solvents of choice for the diastereoselectivity. In particular, when the reaction was carried out in dichloromethane, the enantioselectivity of the desired *anti* product was increased to 95% *ee* but the yield was poor (entry 6). The decrease of the yield in dichloromethane may be due to very low solubility of the starting material. To improve the yield, the influences of the ester group and the solvent were next studied. Among the various ester derivatives examined in dichloromethane, the introduction of an isopropyl or a benzyl ester group led to the reaction being more effective in terms of yield (Table 1, entries 8 and 9). Especially in the case of a benzyl ester (Table 1, entry 9) the yield was increased to 87% with excellent diastereo- and enantioselectivity (>99% *de*, 96% *ee*). Although the reaction time was not optimized, the hydrogenation for 6 h under similar conditions was found to give almost the same result (Table 1, entry 11).

Table 2: The *anti*-selective asymmetric hydrogenation through dynamic kinetic resolution of other α-amino-β-keto esters.[a]

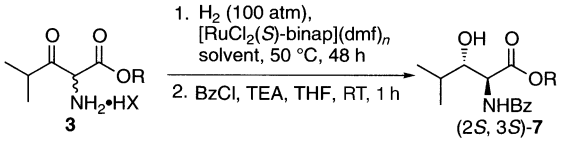


Entry	R^1	R^2	Solvent	Yield [%][b]	d.r.[c]	*ee* [%][d]
1	*i*Pr	Bn	CH_2Cl_2	87	>99:1	96
2	cyclobutyl	Bn	*n*PrOH	92	83:17	81
3	cyclopentyl	Bn	*n*PrOH	85	97.5:2.5	95
4	cyclohexyl	Bn	CH_2Cl_2	85	>99:1	97
5	cyclohexyl	Me	CH_2Cl_2	84	97.5:2.5	96
6	cycloheptyl	Bn	*n*PrOH	86	97:3	97
7	Et	Bn	CH_2Cl_2	89	89:11	76
8	*n*Pr	Bn	CH_2Cl_2	88	94:6	74
9	*n*Pr	Bn	*n*PrOH	53	91:1	58
10	*t*Bu	Bn	CH_2Cl_2	67	71:29	60
11	*t*Bu	Bn	*n*PrOH	89	96:4	79
12[e]	Ph	Bn	MeOH	93	>99:1	4
13[f]	cyclohexyl	Me	CH_2Cl_2	92	98:2	95

[a] Reaction conditions: Substrate (1 mmol), catalyst (3.8–4.6 mol%), and solvent (3 mL). [b] Yield over two steps. [c] *anti*:*syn* diastereomeric ratio. Determined by ^{1}H NMR analysis. [d] Value of the *anti*-3-hydroxyamino acid esters. Determined by HPLC analysis. [e] Reaction was carried out at 100°C. The product was analyzed after conversion into the corresponding acetamide. [f] The reaction was carried out by using 0.4 mol% of the catalyst under 30 atm of hydrogen for 6 h.

This method was then applied to various substrates to clarify the generality of the hydrogenation, and the results are shown in Table 2. The starting α-amino-β-keto ester hydrochlorides were easily prepared by the following three methods: 1) acid hydrolysis of 4-alkoxycarbonyloxazoles derived from carboxylic anhydrides and isocyanoacetic acid esters,[3i] 2) base-mediated N–C acyl migration of *N*-*tert*-butoxycarbonyl-*N*-acylglycine esters and then acid deprotection,[7] and 3) acylation of the benzophenone ketimine derived from a glycine ester in the presence of a strong base followed by acid hydrolysis.[8] Under our reaction conditions, the substrates with a secondary alkyl carbon, cyclobutyl, cyclopentyl, cyclohexyl, or cycloheptyl substituent at the α position of the ketone carbonyl group afforded the *anti* products with high diastereo- and enantioselectivities in excellent yields (Table 2, entries 2–6).[9] Furthermore, it was found that the hydrogenation of the cyclohexyl substrate was completed in 6 h even with a substrate/catalyst ratio of 250 under 30 atm of hydrogen (Table 2, entry 13). In the case of the *n*-alkyl substrate at the C4 position, the stereoselectivity was decreased to moderate (Table 2, entries 7–9). The hydrogenation of the α-amino-β-keto ester with the *tert*-butyl group was maximized in *n*-propanol to give the product in 89% yield and 79% *ee* with a diastereomeric ratio of 96:4 (Table 2, entry 11). In an aromatic substrate the hydrogenation in dichloromethane or *n*-propanol did not proceed under our reaction conditions. After some experiments we found that the hydrogenation of this substrate in MeOH at 100°C afforded exclusively the *anti* product in 93% yield. However, the enantioselectivity was poor. These results suggest that hydrogenation with the Ru–BINAP catalyst is affected by the structure at the C4 position of the α-amino-β-keto ester. Nonetheless, the results of the above asymmetric reaction with the Ru–BINAP catalyst are noteworthy not only because this represents the first example of *anti*-selective hydrogenation of α-amino-β-keto esters with high diastereo- and enantioselectivity through dynamic kinetic resolution but also because the amino group in the substrate is shown to serve as a stronger directing substituent than the ester function. Although the mechanism of the asymmetric induction with a high level of *anti* selectivity is not clear at present,

Table 1: The *anti*-selective asymmetric hydrogenation through dynamic kinetic resolution.[a]



Entry	R	HX	Solvent	Yield [%][b]	d.r.[c]	*ee* [%][d]
1	Me	TsOH	MeOH	72	97:3	22
2[e]	Me	HBF_4	MeOH	–	–	–
3	Me	HCl	MeOH	71	99:1	56
4	Me	HCl	*n*PrOH	69	99:1	69
5	Me	HCl	*i*PrOH	81	99:1	81
6	Me	HCl	CH_2Cl_2	38	99:1	95
7	Et	HCl	CH_2Cl_2	73	96:4	93
8	*i*Pr	HCl	CH_2Cl_2	96	98:2	92
9	Bn	HCl	CH_2Cl_2	87	>99:1	96
10	Bn	HCl	*i*PrOH	94	98:2	76
11[f]	Bn	HCl	CH_2Cl_2	82	>99:1	98

[a] Reaction conditions: Substrate (1 mmol), catalyst (3.8–4.6 mol%), and solvent (3.0 mL). Abbreviations: TsOH = toluene-4-sulfonic acid, Bn = benzyl. [b] Yield over two steps. [c] *anti*:*syn* diastereomeric ratio. Determined by ^{1}H NMR analysis. [d] Value of the *anti*-3-hydroxyamino acid ester. Determined by HPLC analysis. [e] No reaction. [f] Reaction time for hydrogenation: 6 h.

 © 2004 Wiley-VCH Verlag GmbH & Co. KGaA, Weinheim

we speculate that the reaction proceeds via a sterically constrained five-membered transition state.

In conclusion, we have succeeded in developing a new method for the preparation of *anti*-β-hydroxy-α-amino acids from α-amino-β-keto esters by using the Ru–BINAP catalyst in a dynamic kinetic resolution; this method provides the first example of the *anti*-selective hydrogenation and four-step access to the important (2*R*,3*R*)- and (2*S*,3*S*)-β-hydroxy-α-amino acids from readily available acid anhydrides or acid chlorides. Further studies to elucidate the reaction mechanism and extend the scope of the method's synthetic utility are in progress in our laboratory.

Experimental Section

Typical procedure: DMF (400 μL) was added to a mixture of $[\{RuCl_2(C_6H_6)\}_2]$ (9.8 mg, 19.6 μmol) and (*S*)-BINAP (26.4 mg, 42.4 μmol) in a Schlenk tube under an argon atmosphere. After being degassed, the mixture was stirred for 10 min at 100 °C. The resulting mixture was cooled and concentrated in vacuo at 50 °C for 2.5 h to give the reddish-brown catalyst. A degassed solution of α-amino-β-ketoester **8** ($R^1 = i$Pr, R^2 = Bn, 271.5 mg, 1.0 mmol) in CH_2Cl_2 (1 × 2.5 mL, 1 × 0.5 mL) was added dropwise to the catalyst through a canula under an argon atmosphere. The mixture was stirred at 50 °C under hydrogen (100 atm) for 6 h. The solvent was removed in vacuo to afford α-amino-β-hydroxy ester **9** which was used in the next step without further purification.

Benzoyl chloride (130 μL, 1.12 mmol) and triethylamine (440 μL, 0.316 mmol) were added dropwise to a solution of the crude **9** in THF (2.0 mL) at 0 °C. After stirring for 1 h at 23 °C, the reaction mixture was quenched with water and diluted with ethyl acetate/*n*-hexane (5:1). The mixture was washed with aqueous 1N HCl, water, saturated aqueous $NaHCO_3$, and brine, dried with Na_2SO_4, and filtered. The filtrate was then concentrated in vacuo. The residue was purified by silica gel column chromatography (ethyl acetate/*n*-hexane (1:2)) to give **10** (278.1 mg, 0.815 mmol, 82 % yield (2 steps), > 99 % *de*, 98 % *ee*): HPLC analysis with a Chiralcel OD-H chiral column (eluent = *n*-hexane/*i*PrOH (90:10, 0.5 mL min^{-1})): retention time for (2*R*,3*R*)-**10** = 21.6 min, for (2*S*,3*S*)-**10** = 30.3 min; $[\alpha]_D^{24} = +33.9$ (c = 1.00, $CHCl_3$); m.p. 95.5–96 °C; IR (KBr): $\tilde{\nu}$ = 3414, 2961, 2935, 2858, 1749, 1647, 1519, 1192, 1064 cm^{-1}; ^{1}H NMR (400 MHz, $CDCl_3$): δ = 0.95 (d, J = 6.6 Hz, 3H; $(CH_3)_2CH$), 1.13 (d, J = 6.6 Hz, 3H; $(CH_3)_2CH$), 1.71 (m, 1H; $(CH_3)_2CH$), 2.92 (d, J = 8.4 Hz, 1H; CHO*H*), 3.63 (dt, J = 3.1, 8.4 Hz, 1H; C*H*OH), 4.99 (dd, J = 3.3, 7.3 Hz, 1H; C*H*NH), 5.23 (d, J = 12 Hz, 1H; CH_2Ph), 5.29 (d, J = 12 Hz, 1H; CH_2Ph), 7.14 (d, J = 7.3 Hz, 1H; CHN*H*), 7.34–7.39 (m, 5H; Ar*H*), 7.43–7.47 (m, 2H; Ar*H*), 7.52–7.56 (m, 1H; Ar*H*), 7.81–7.83 ppm (m, 2H; Ar*H*); ^{13}C NMR (100 MHz, $CDCl_3$): δ = 18.9, 19.0, 31.5, 56.2, 67.6, 78.9, 127.2, 128.4, 128.6, 128.7, 132.0, 133.4, 134.9, 167.5, 170.8 ppm; HRMS (FAB, NBA): calcd for $C_{20}H_{24}NO_4$: 342.1705 [M^+ + 1]; found: 342.1682; elemental analysis: calcd for $C_{20}H_{23}NO_4$: C 70.36, H 6.79, N 4.10; found: C 70.26, H 6.82, N 4.06.

Received: October 13, 2003 [Z53072]

Keywords: amino acids · asymmetric synthesis · hydrogenation · kinetic resolution · ruthenium

[1] For representative reports on the synthesis of (2*S*, 3*S*)- and (2*R*, 3*R*)-3-hydroxyleucine, see: a) C. G. Caldwell, S. S. Bondy, *Synthesis* **1990**, 34–36; b) E. J. Corey, D.-H. Lee, S. Choi, *Tetrahedron Lett.* **1992**, *33*, 6735–6738; c) S. Kanemasa, T. Mori, A. Tatsukawa, *Tetrahedron Lett.* **1993**, *34*, 8293–8296; d) K. J. Hale, S. Manaviazar, V. M. Delisser, *Tetrahedron* **1994**, *50*, 9181–9188; e) L. Williams, Z. Zhang, F. Shao, P. J. Carroll, M. M. Joullié, *Tetrahedron* **1996**, *52*, 11673–11694; f) J. S. Panek, C. E. Masse, *J. Org. Chem.* **1998**, *63*, 2382–2384; g) M. Amador, X. Ariza, J. Garcia, S. Sevilla, *Org. Lett.* **2002**, *4*, 4511–4515; h) N. Yoshikawa, M. Shibasaki, *Tetrahedron* **2002**, *58*, 8289–8298.

[2] For recent reports on the stereoselective synthesis of *erythro*-β-hydroxy-α-amino acids, see: a) B. G. Jackson, S. W. Pedersen, J. W. Fisher, J. W. Misner, J. P. Gardner, M. A. Staszak, C. Doecke, J. Rizzo, J. Aikins, E. Farkas, K. L. Trinkle, J. Vicenzi, M. Reinhard, E. P. Kreoeff, C. A. Higginbotham, R. J. Gazak, T. Y. Zhang, *Tetrahedron*, **2000**, *56*, 5667–5677; b) A. Avenoza, C. Cativiela, F. Corzana, J. M. Peregrina, M. M. Zurbano, *Tetrahedron: Asymmetry* **2000**, *11*, 2195–2204; c) D. A. Evans, J. M. Janey, N. Magomedov, J. S. Tedrow, *Angew. Chem.* **2001**, *113*, 1936–1940; *Angew. Chem. Int. Ed.* **2001**, *40*, 1884–1888; d) J. B. MacMillan, T. F. Molinski, *Org. Lett.* **2002**, *4*, 1883–1886; e) T. Ooi, M. Taniguchi, M. Kameda, K. Maruoka, *Angew. Chem.* **2002**, *114*, 4724–4726; *Angew. Chem. Int. Ed.* **2002**, *41*, 4542–4544.

[3] For the synthesis of β-hydroxy-α-amino acids by dynamic kinetic resolution, see: a) R. Noyori, T. Ikeda, T. Ohkuma, M. Widhalm, M. Kitamura, H. Takaya, S. Akutagawa, N. Sayo, T. Saito, T. Taketomi, H. Kumobayashi, *J. Am. Chem. Soc.* **1989**, *111*, 9134–9135; b) J.-P. Genêt, S. Mallart, S. Jugé, French Patent 8911159, **1989**; c) K. Mashima, Y. Matsumura, K. Kusano, H. Kumobayashi, N. Sayo, Y. Hori, T. Ishizaki, S. Akutagawa, H. Takaya, *J. Chem. Soc. Chem. Commun.* **1991**, 609; d) J.-P. Genêt, C. Pinel, S. Mallart, S. Juge, S. Thorimbert, J. A. Laffitte, *Tetrahedron: Asymmetry* **1991**, *2*, 555–567; e) M. Kitamura, M. Tokunaga, R. Noyori, *J. Am. Chem. Soc.* **1993**, *115*, 144–152; f) K. Mashima, K. Kusano, N. Sato, Y. Matsumura, K. Nozaki, H. Kumobayashi, N. Sayo, Y. Hori, T. Ishizaki, S. Akutagawa, H. Takaya, *J. Org. Chem.* **1994**, *59*, 3064–3076; g) J.-P. Genêt, M. C. C. de Andrade, V. Ratovelomanana-Vidal, *Tetrahedron Lett.* **1995**, *36*, 2063–2066; h) E. Coulon, M. C. C. de Andrade, V. Ratovelomanana-Vidal, J.-P. Genêt, *Tetrahedron Lett.* **1998**, *39*, 6467–6470; i) K. Makino, N. Okamoto, O. Hara, Y. Hamada, *Tetrahedron: Asymmetry* **2001**, *12*, 1757–1762.

[4] For dynamic kinetic resolution under transfer hydrogenation, see: B. Mohar, A. Valleix, J.-R. Desmurs, M. Felemez, A. Wagner, C. Mioskowski, *Chem. Commun.* **2001**, 2572–2573.

[5] a) N. Okamoto, O. Hara, K. Makino, Y. Hamada, *Tetrahedron: Asymmetry* **2001**, *12*, 1353–1358; b) ref. [3i]; c) K. Makino, Y. Hennmi, Y. Hamada, *Synlett* **2002**, 613–615; d) K. Makino, A. Kondoh, Y. Hamada, *Tetrahedron Lett.* **2002**, *43*, 4695–4698; e) N. Okamoto, O. Hara, K. Makino, Y. Hamada, *J. Org. Chem.* **2002**, *67*, 9210–9215; f) K. Makino, T. Suzuki, S. Awane, O. Hara, Y. Hamada, *Tetrahedron Lett.* **2002**, *43*, 9391–9395.

[6] For reviews on dynamic kinetic resolution, see: a) R. Noyori, M. Tokunaga, M. Kitamura, *Bull. Chem. Soc. Jpn.* **1995**, *68*, 36–56; b) R. S. Ward, *Tetrahedron: Asymmetry* **1995**, *6*, 1475–1490; c) T. Ohkuma, M. Kitamura, R. Noyori in *Catalytic Asymmetric Synthesis*, 2nd ed. (Ed.: I. Ojima), Wiley-VCH, **2000**, pp. 1–110; d) H. Pellissier, *Tetrahedron* **2003**, *59*, 8291–8327.

[7] O. Hara, M. Ito, Y. Hamada, *Tetrahedron Lett.* **1998**, *39*, 5537–5540.

[8] J. Singh, T. D. Gordon, W. G. Earley, B. A. Morgan, *Tetrahedron Lett.* **1993**, *34*, 211–214.

[9] To optimize the cyclopentyl substrate, the catalyst derived from [(cod)Ru(methallyl)$_2$] (cod = cycloocta-1,5-diene) and (*S*)-BINAP was examined and was found to be less effective (34 % yield, 93:7 d.r., 92 % *ee*) than the one from $[\{RuCl_2(C_6H_6)\}_2]$ and (*S*)-BINAP.

Biomineralization

Promotion of Fluorapatite Crystallization by Soluble-Matrix Proteins from *Lingula Anatina* Shells**

*Ingrid Lévêque, Maggie Cusack, Sean A. Davis, and Stephen Mann**

One of the most persistent enigmas in the field of biomineralization is the evolutionary selection of calcium carbonate and calcium phosphate biominerals in invertebrate and vertebrate skeletal tissues, respectively. Whereas bones and teeth are constructed with carbonate-substituted hydroxyapatite ($Ca_{10}(PO_4)_6(OH)_2$), most mollusc shells consist of polymorphs of calcium carbonate such as calcite and aragonite.[1] One of the few modern exceptions to this carbonate–-phosphate dichotomy in skeletal biomineralization is the bivalved shell of extant Linguliform brachiopods such as *Lingula* and *Discinisca*, which consists of carbonate-substituted fluorapatite, ($Ca_{10}(PO_4)_6F_2$, francolite, FAP).[2] *Lingula* shells appeared along with phosphatic biominerals in the Problematica at the base of the Cambrian, about 545 million years ago (Mya),[3] possibly because of high concentrations of phosphorus in the seawater during the Precambrian and Cambrian eras (543 to 490 Mya).[4] The subsequent decrease in phosphate levels by the end of the Cambrian era may account for the extinction of the phosphatic Problematica due to arrested shell mineralization, although a switch to a carbonate regime may also have occurred in these invertebrates during this era.[3] The geological longevity of *Lingula*, in contrast, suggests that the lightly mineralized FAP shell has remained well adapted to evolutionary pressures even though by the middle of the Ordovician (ca. 470 Mya) phosphatic biomineralization was rare in invertebrates.

Previous studies have shown that the *Lingula* shell is produced by a rhythmic alternation of organic and mineralized layers.[2,5] The latter are constructed from FAP granules, 4–8 nm in diameter,[6] which are smaller at the anterior and periphery of the shell compared with those deposited in the central and posterior regions,[7] and become progressively aligned with the organic matrix during mineralization.[8] The matrix consists of a complex mixture of glycosaminoglycans, β-chitin, and proteins with molecular masses between 6 kDa to 46 kDa,[9] many of which are enriched in acidic amino-acid residues.[10,11] Because acidic macromolecules are considered in general to play a pivotal role in the nucleation and growth of calcium-containing biominerals,[12] we have investigated the potential role of *Lingula* shell proteins on the formation of carbonate-substituted FAP crystals in vitro. Herein we show for the first time that soluble macromolecules isolated from *Lingula* shells specifically promote FAP crystallization by the destabilization of an amorphous calcium phosphate precursor.

Proteins were sequentially extracted from powdered *L. anatina* whole valves or from four equally sized sections from the posterior to the anterior of the shell. Fractionation by sodium dodecyl sulfate/polyacrylamide gel electrophoresis (SDS PAGE) gave discrete bands that correspond to proteins with estimated molecular masses of 6, 8.5, 15.5, 21.5, 24, and 44 kDa for guanadine hydrochloride (GnHCl) and EDTA extracts (Figure 1 A). The EDTA extract contained significantly higher concentrations of the lower-molecular-weight proteins as well as additional proteins of molecular mass 4.5, 28, 35, 40, 50, 57.5, 60, and 69 kDa. The 21.5 and 24 kDa proteins in both extracts were glycosylated as determined by using concanavalin A binding (Figure 1 B,C).

The influence of *Lingula* shell proteins on the in vitro deposition of carbonate-substituted FAP was investigated by adding mixtures of the extracted macromolecules at various total concentrations to buffered calcium phosphate/fluoride metastable solutions at constant temperature. In each case, metastability was induced by raising the solution pH from 6.2 to 7.5, which resulted in relatively slow growth kinetics that were monitored by a progressive reduction in solution pH with time due to deprotonation of $[H_2PO_4]^-$ and $[HPO_4]^{2-}$ ions associated with the formation of mineral precipitates. Corresponding pH profiles (Figure 2) with (●) or without (■) added proteins showed a characteristic multistep process. This included an initial induction period of about 25 minutes during which the pH slowly decreased by approximately 0.05 units (Figure 2 stage I). This was followed by a faster reduction in pH to values of around 7.35, after which the pH remained constant for at least 7 mins (stage II). The pH then rapidly decreased to a value of about 6.9 within a further 15 mins (stage III), after which the pH remained approximately constant (stage IV). Analytical TEM and XRD investigations of samples removed at various time intervals indicated that the deposition of irregular particles of hydrated amorphous calcium phosphate (ACP) occurred during step I. The subsequent increase in the rate of proton release and onset of a steady state in stage II were associated with a progressive replacement of the ACP by irregularly shaped FAP nanorods. These increased in number, regularity, and size during the subsequent rapid pH reduction during step III, such that well-defined needle-shaped carbonate-substituted FAP crystals were predominant by the beginning of stage IV. In contrast, the addition of polyaspartate resulted in a slow reduction in pH of about 0.1 units and associated formation of ACP throughout the experimental period of 60 min (Figure 2, curve ▲), consistent with the known inhibitory properties of

[*] I. Lévêque, Dr. S. A. Davis, Prof. S. Mann
School of Chemistry
University of Bristol
Bristol BS8 1TS (UK)
Fax: (+44) 117-9290-509
E-mail: s.mann@bristol.ac.uk
Dr. M. Cusack
Division of Earth Sciences
Centre for Geosciences
University of Glasgow
Glasgow G12 8QQ (UK)

[**] We are grateful to William Chung for the generous provision of specimens of *L. anatina* for this research. We thank the Leverhulme Trust for financial support.

 DOI: 10.1002/anie.200353115 © 2004 Wiley-VCH Verlag GmbH & Co. KGaA, Weinheim

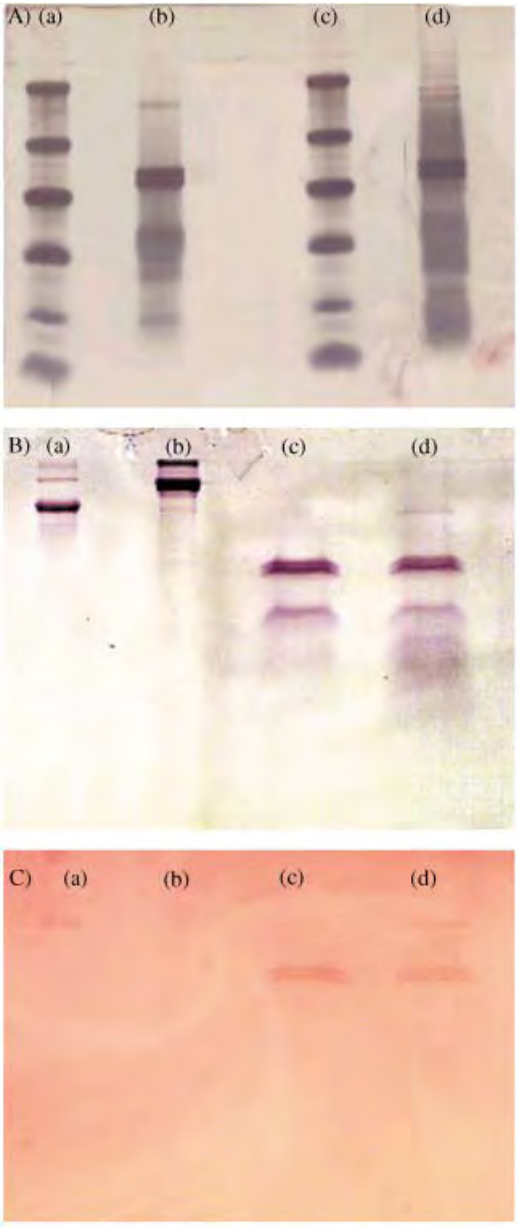


Figure 1. SDS PAGE gels and blot of protein extracts from *L. anatina* valves. A) SDS PAGE gels of (a and c) molecular weight markers corresponding to 44.7, 29.3, 20.2, 14.8, 5.7, and 2.9 kDa, (b) GnHCl-extracted proteins, and (d) EDTA-extracted proteins. Proteins were fractionated, fixed, then silver stained. B) SDS PAGE gels of (a) ovalbumin (1 mg, 43 kDa), (b) bovine serum albumin (1 mg, 66 kDa), (c) GnHCl extract (3.9 mg protein), and (d) EDTA extract (3.9 mg protein). Proteins were Coomassie stained. C) Electroblot of duplicate gel as in (B) probed for carbohydrate using Concanavalin A.

this macromolecule in calcium-phosphate crystal-growth studies.[13]

Significantly, no kinetic inhibition was observed in the presence of *Lingula* shell proteins; instead, the pH curves indicated a marked decrease in the time required for FAP crystallization (Figure 2, curve ●). For example, the induction period for FAP crystallization (t_{FAP} in Figure 2) was reduced by about 24 % for a protein concentration of 0.5 $\mu g\,mL^{-1}$, with the consequence that needlelike crystals, rather than ACP

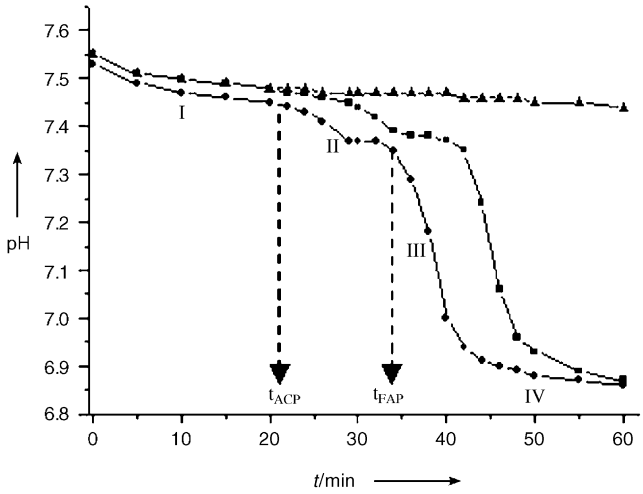


Figure 2. pH curves for FAP crystallization; control (■), +0.2 $\mu g\,mL^{-1}$ extracted *Lingula* shell proteins (●), +0.2 $\mu g\,mL^{-1}$ polyaspartate (▲). Typical stages of precipitation (I, II, III, IV) and induction times for ACP transformation (t_{ACP}) and FAP crystallization (t_{FAP}) are shown for curve ●. See text for details.

granules, were observed in samples removed after 30 min (Figure 3). The influence of protein-enhanced FAP nucleation was also evident in samples aged for 1 day, which in each case showed well-defined nanorods with a reduced mean length of 25 nm compared with the control crystals (35 nm). By 30 days, however, the FAP nanorods were not significantly different in size from the control sample, with mean lengths and widths of 33–35 and 7–8 nm, respectively. The absence of

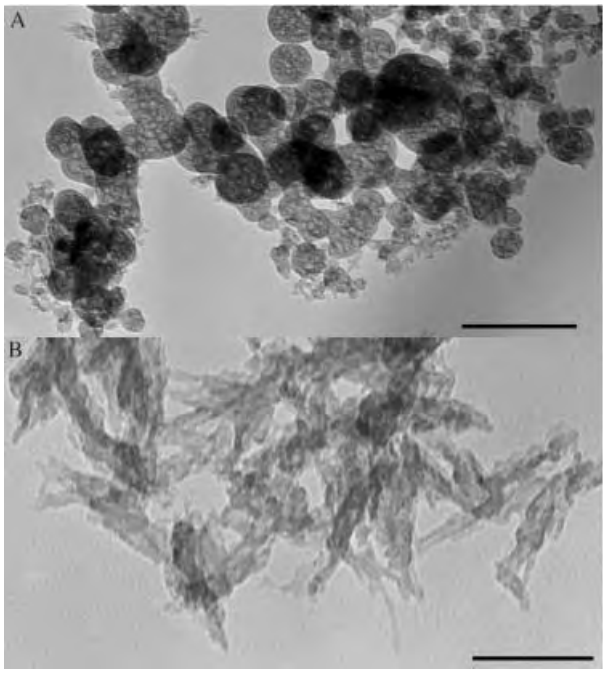


Figure 3. TEM images of samples extracted after 30 min; A) control experiment showing spherical particles of hydrated ACP, B) FAP crystals formed in the presence of *Lingula* shell proteins at 0.5 $\mu g\,mL^{-1}$. Scale bars, 100 nm.

 © 2004 Wiley-VCH Verlag GmbH & Co. KGaA, Weinheim

morphological changes in the protein-containing samples suggested that interactions between the macromolecules and growing FAP crystals were not generally surface-specific.

Interestingly, the ability of *Lingula* shell macromolecules to promote FAP crystallization showed a nonlinear bell-shaped dependence on protein concentration with a maximum effect at around 0.5 $\mu g\,mL^{-1}$ (Figure 4, curve ■). The main factor influencing this behavior was a reduction in the

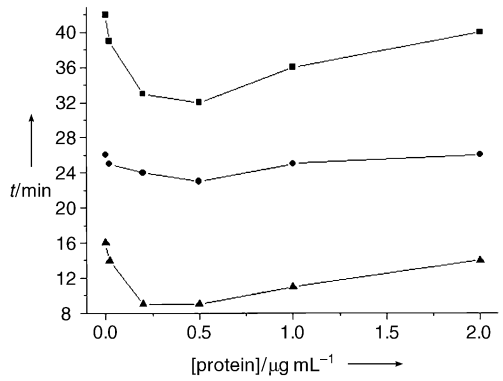


Figure 4. Influence of *Lingula* shell protein concentration on; FAP induction times (■), ACP induction times (●), and lifetime of ACP intermediate phase (▲).

time associated with the ACP to FAP transformation (Figure 2 stage II), which also showed a nonlinear dependence on protein concentration (Figure 4, curve ▲). Further analysis indicated that both the slope and plateau regions in stage II were similarly influenced by the bell-shaped relationship. In contrast, the induction period for ACP transformation (Figure 2, t_{ACP}), as well as the rate of FAP crystallization (defined by the tangent in stage III in Figure 2), were relatively unaffected by changes in protein concentration (Figure 4, curve ●).

Similar kinetic experiments were undertaken using *Lingula* shell proteins extracted from specific regions of the valve. Whereas, all extracts produced an enhancement in the rate of FAP crystallization by decreasing the ACP to FAP transformation time, macromolecules isolated from the heavily mineralized posterior and median regions of the shell showed the greatest activity with a 25% reduction in t_{FAP} in the presence of 1 $\mu g\,mL^{-1}$ protein. In contrast, protein extracts from the unmineralized anterior region produced a corresponding 16% reduction that was independent of the protein concentrations used.

The above results indicate that soluble macromolecules associated with the phosphatic shell of *L. anatina* can specifically promote the in vitro crystallization of FAP. This behavior is unusual and contrary to numerous previous studies in which a wide range of low- and high-molecular-weight additives have been shown to inhibit calcium-phosphate crystallization by stabilization of a hydrated ACP precursor.[14] Based on the above observations, we speculate on a possible mechanism for in vitro promotion. In general, transformation of ACP involves the formation of crystalline nuclei on the surface of the precursor in association with a solution-mediated process and dissolution of the amorphous phase.[15] Protons are released in the nucleation step but consumed during ACP dissolution, and this process gives rise to a transient steady state observed for example at around 30 minutes during stage II in the pH profiles (Figure 2). Strong adsorption of additives such as polyaspartate onto the surface of primary ACP nanoparticles reduces the surface charge on the primary ACP nanoparticles, with the consequence that the rate of dissolution of the amorphous phase is reduced due to colloidal aggregation. Moreover, the adsorbed macromolecules block the surface nucleation sites for FAP crystallization. In contrast, addition of the *Lingula* shell proteins at low concentration appears to destabilize the ACP particles. One possibility is that the surface charge on the primary nanoparticles is increased at low levels of protein adsorption such that the extent of secondary aggregation is reduced and rate of dissolution increased. Surface attachment of the *Lingula* proteins might also induce local ordering of FAP nuclei on the amorphous surface by facilitating structural relaxation through changes in surface dehydration and deprotonation. Finally, the adsorbed macromolecules could act as templates for FAP nucleation by inducing the clustering of aqueous ions at the ACP surface. This would occur for example if the proteins were anchored at low surface coverage such that appropriate functional groups remained exposed at the solution interface, rather than being buried by strong surface–macromolecule interactions associated with higher binding capacities. Indeed, it seems feasible that such conformational changes are responsible for the observed nonlinear dependence of FAP promotion on protein concentration.

Experimental Section

Specimens of *Lingula anatina* (Lamarck) were collected from intertidal silts of Starfish Bay, Hong Kong. Body tissue was stripped from the specimens and the periostracum and adherent body tissue removed from the shells by brushing with an aqueous solution of sodium hypochlorite (10 vol%). The valves (43 g) were placed in distilled water and repeatedly (x3) sonicated for periods of 3 minutes to remove loose organic material and air-dried. For protein extraction, shells were cut into small pieces and ground in a Teema agate grinder. The powdered valves were incubated with an aqueous solution of buffered guanidine HCl (GnHCl, 4 M, pH 7.4, Tris 50 mM) for 48 h at 4 °C with constant agitation. The biomineral powder was removed by centrifugation (3500 g for 30 min), and the supernatant concentrated followed by removal of guanidine by ultrafiltration with a Minitan tangential flow concentrator system. Protein extracts were concentrated further with Centriprep and Microcon concentrators, which resulted in a final volume of 285 μL and a protein concentration of 15.4 $\mu g\,\mu L^{-1}$. The GnHCl-treated shell fragments were resuspended in aqueous buffered EDTA (20 wt%, pH 8, Tris) and the mixture stirred at 4 °C for 11 days until the sample was demineralized completely. Samples were concentrated by centrifugation to give a final volume of 393 μL and a protein concentration of 3.6 $\mu g\,\mu L^{-1}$. All concentrators had a nominal cut-off value of 10 kDa.

Shell protein extracts were fractionated by SDS PAGE (15% polyacrylamide, gel size 9 cm × 7 cm × 0.75 mm) at 100 V for 3 hours. Samples were initially heated at 100 °C for 4 minutes in an equal volume of sample buffer (0.15 M Tris/HCl, pH 6.8) that contained 0.2 M βmercaptoethanol, 0.1% (*w*/*v*) SDS, 30% (*v*/*v*) glycerol and 0.0002% (w/v) of the tracking dye, Bromophenol Blue. Extracts loaded on the

 © 2004 Wiley-VCH Verlag GmbH & Co. KGaA, Weinheim

gel contained 3.1 μg protein for the guanidine extract and 4.5 μg protein for the EDTA extract. Prestained molecular-weight standards (ovalbumin/glycosylated ovalbumin, 44.7 kDa; carbonic anhydrase, 29.3 kDa; β-lactoglobulin, 20.2 kDa; lysozyme, 14.8 kDa; bovine trypsin inhibitor, 5.7 kDa; bovine serum albumin, 66 kDa) were included in the gels. Following electrophoresis, proteins were fixed and visualized by using Coomassie Brilliant Blue-R Silver staining.[16] In some experiments, the stained proteins were transferred onto ProBlott membranes by electroblotting and sugar groups detected by lectin binding by using Concanavalin A.[17]

Fluorapatite was prepared as described previously.[18] In brief, 6.25 mL of $NH_4H_2PO_4$ (60 mM) was added at 25 °C over a period of 1.5 min to a constantly stirring buffered Ca-containing solution prepared by mixing 12.5 mL of aqueous $Ca(CH_3CO_2)\cdot 2H_2O$ (100 mM) with 25 mL of $CH_3CO_2NH_4$ buffer (1.3 M). This was followed by the immediate addition of 6.25 mL of a solution containing $NH_4H_2PO_4$ (60 mM) and HF (20 mM) over a period of 1.5 min, followed by adjustment of the pH from around 6.2 to 7.5 with aqueous NH_4OH (1 M). The solution was left stirred and aliquots removed at various time intervals and air-dried onto TEM grids for analytical TEM. In general, the stirred solutions started to turn slightly cloudy within 2 to 5 minutes after raising the pH, and the reaction was complete within 60 min. Samples were also removed by centrifugation (0–30 days) or filtration (>1 month) and washed several times with ethanol. XRD patterns and FTIR spectroscopy confirmed the formation of carbonate-substituted fluorapatite. Calcium compositions were obtained by atomic absorption spectrophotometry ($\lambda = 423$ nm) of acid-dissolved precipitates.

For kinetic studies, changes in pH of the stirred reaction mixture were recorded at a constant temperature of 25 °C for up to 1 hr after mixing. Experiments were repeated five times with constant conditions. The influence of *Lingula* shell macromolecules on fluorapatite crystallization was studied by using the above procedures except that GnHCl-extracted proteins from entire valves, or from four sections of equal size from the posterior to anterior of the shell, were added to buffered calcium acetate prior to addition of aqueous $NH_4H_2PO_4$ and $NH_4H_2PO_4$/HF. Experiments were undertaken with final protein concentrations between 0.02 and 2 $\mu g\,mL^{-1}$. Dynamic light-scattering and small-angle X-ray scattering studies did not detect the presence of aggregates in the protein-containing solutions.

Received: October 20, 2003 [Z53115]
Published Online: January 22, 2004

Keywords: biomineralization · biosynthesis · crystal growth · natural products · proteins

[1] *Skeletal Biomineralization: Patterns, Processes and Evolutionary Trends.* (Eds.: J. G. Carter), Van Nostrand Reinhold, New York, **1990**.
[2] K. Iwata, *J. Fac. Sci. Hokkaido Univ. Ser. 1*, **1981**, *20*, 35.
[3] H. A. Lowenstam, S. Weiner, *On Biomineralization*, Oxford University Press, **1989**.
[4] P. J. Cook, J. H. Shergold, *Nature* **1984**, *308*, 231.
[5] A. Williams, M. Cusack, S. Mackay, *Philos. Trans. R. Soc. London Ser. B* **1994**, *346*, 223.
[6] A. Williams, M. Cusack, *J. Struct. Biol.* **1999**, *126*, 227.
[7] M. Iijima, Y. Moriwaki, T. Gyotoku, K. Hayashi , S. Imura, *Jpn. J. Oral Biol.* **1989**, *31*, 308.
[8] M. Iijima, Y. Moriwaki, *Calcif. Tissue Int.* **1990**, *47*, 237.
[9] M. Cusack, *Bull. Inst. Oceanogr.* **1996**, *14*, 271.
[10] M. Cusack, A. Williams, *Philos. Trans. R. Soc. London Ser. B* **1996**, *351*, 33.
[11] M. Iijima, H. Takita, Y. Moriwaki, Y. Kuboki, *Comp. Biochem. Physiol. Part A* **1996**, *98*, 379.
[12] S. Mann, *Biomineralization; Principles and Concepts in Bioinorganic Materials Chemistry*, Oxford University Press, **2001**.
[13] A. Bigi, E. Boanini, D. Walsh, S. Mann, *Angew. Chem.* **2002**, *114*, 2267; *Angew. Chem. Int. Ed.* **2002**, *41*, 2163.
[14] A. Bigi, G. Falini, E. Foresti, M. Gazzaro, A. Ripamonti, N. Roveri, *J. Inorg. Biochem.* **1993**, *49*, 69; J. Guerra-López, R. González, A. Gómez, R. Pomés, G. Punte, C. O. Della Védova, *J. Solid State Chem.* **2000**, *151*, 163A. Tsortos, G. H. Nancollas, *J. Colloid Interface Sci.* **2002**, *250*, 159; Z. Amjad, *Langmuir* **1987**, *3*, 1063.
[15] E. D. Eanes, J. D. Termine, M. U. Nylen, *Calcif. Tissue Res.* **1973**, *12*, 143; J. L. Meyer, E. D. Eanes, *Calcif. Tissue Res.* **1978**, *25*, 59; L. J. Brecevic, H. Furedi-Milhofer, *Calcif. Tissue Res.* **1972**, *10*, 82; R. Despotovic, N. Filipovic-Vincekovic, H. Furedi-Milhofer, *Calcif. Tissue Res.* **1975**, *11*, 13.
[16] J. H. Morrissey, *Anal. Biochem.* **1981**, *117*, 307.
[17] L. Faye, M. J. Chrispeels, *Anal. Biochem.* **1985**, *149*, 317.
[18] M. Okazaki, *Biomaterials* **2002**, *23*, 749.

 © 2004 Wiley-VCH Verlag GmbH & Co. KGaA, Weinheim

Cross-Coupling Reactions

The Tertiary Sulfonamide as a Latent Directed-Metalation Group: Ni^0-Catalyzed Reductive Cleavage and Cross-Coupling Reactions of Aryl Sulfonamides with Grignard Reagents

*Robert R. Milburn and Victor Snieckus**

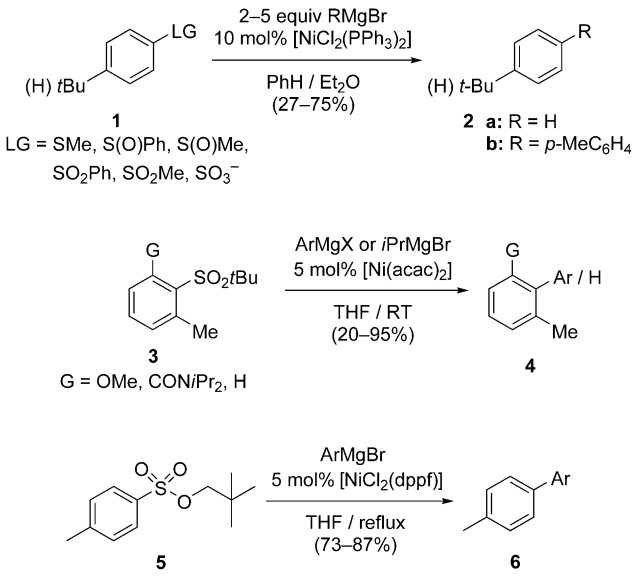
In the rich portfolio of transition-metal-catalyzed cross-coupling reactions that have been added to the synthetic chemist's repertoire during the last thirty years,[1] sulfur-based leaving groups of the organometallic coupling partners have been underdeveloped. Thus application of sulfur groups in modern cross-coupling chemistry has been largely neglected in favor of the highly successful and readily available halo,[2] triflate,[3] and, to some extent, *O*-carbamate[4] leaving groups in combination with various aryl metal partners. Exceptionally, Wenkert et al.[5] demonstrated coupling of sulfur derivatives in several oxidation states with RMgX reagents (**1**→**2**), our group[6,7] and Julia and co-workers[8] married the directed *ortho* metalation strategy with the Corriu–Kumada–Tamao reaction to allow access to 1,3-di- and 1,2,3-trisubstituted benzenes, (e.g., **3**→**4**), and Takei and co-workers[9] explored the cross-coupling of vinyl sulfones, and the coupling of aryl sulfonates (**5**→**6**) was recently reported (Scheme 1).[10]

Herein we report that tertiary aryl sulfonamides undergo Ni^0-catalyzed reductive cleavage with β-hydride donors (iPr$_2$Mg or iPrMgCl)[11] under especially mild conditions,

[*] R. R. Milburn, Prof. V. Snieckus
Department of Chemistry, Queens University
Kingston, Ontario, K7L 3N6 (Canada)
Fax: (+1) 613-533-6089
E-mail: snieckus@chem.queensu.ca

Supporting information for this article is available on the WWW under http://www.angewandte.org or from the author.

 © 2004 Wiley-VCH Verlag GmbH & Co. KGaA, Weinheim DOI: 10.1002/anie.200352633



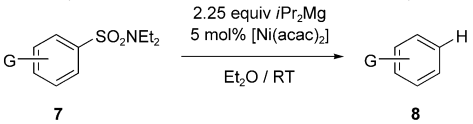
Scheme 1. Application of sulfur leaving groups in modern cross-coupling chemistry. acac = acetylacetonate; dppf = 1,1′-bis(diphenylphosphanyl)ferrocene.

(Tables 1 and 2) and cross-coupling with Grignard reagents (Table 3), thus presenting a new directed *ortho* metalation—connected methodology for the construction of polysubstituted aromatic and biaryl compounds. The hydrodesulfamoylation reaction establishes a latent quality to the powerful sulfonamide directed-metalation group[12] and thereby allows the construction of 1,3-disubstituted aromatic compounds (Table 2), which are unavailable by traditional electrophilic aromatic substitution protocols. The increasing prominence of aryl sulfonamides as commercial entities or lead-drug candidates[13] constitutes an appropriate backdrop in which this new chemistry may find application and extension.

Table 1 summarizes the initial results of the Ni-catalyzed hydrodesulfamoylation reaction of substituted tertiary aryl sulfonamides, **7**→**8**.[14] Several qualitative trends in the screened aryl sulfonamides deserve attention. The reaction is very sensitive to both steric and electronic effects. Large *ortho* substituents (Table 1, entries 7, 11, 14) and *para*-substituted electron-donating groups (Table 1, entries 8, 13) promote lower yields. Groups *ortho* to the sulfonamide that are capable of metal coordination[15] (Table 1, entry 9) appear to enhance the yield significantly, which may also be used to overcome inhibitory effects of electron-donating substituents (compare Table 1, entries 8 and 13 with Table 2, entries 4 and 2, respectively).

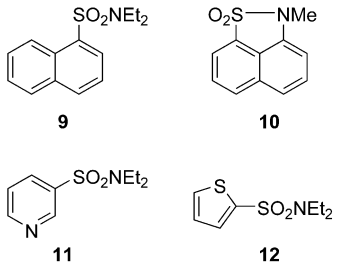
As a further test of scope, cyclic and other aryl and heteroaryl sulfonamides were subjected to the representative hydrodesulfamoylation conditions (Scheme 2). Thus *N*,*N*-diethyl-1-naphthalenesulfonamide (**9**) furnished naphthalene in moderate yield (59%) while the *N*-methyl-1,8-naphthalene sultam (**10**) afforded the reductive SO_2 extrusion product, *N*-methyl-1-naphthylamine in 43% yield.[16] *N*,*N*-Diethylpyridinesulfonamide (**11**) gave pyridine in 29% yield (complete consumption of starting material) while the corresponding 2-thiophenesulfonamide (**12**) was quantitatively recovered.

Table 1: Ni^0-catalyzed reduction of monosubstituted aryl sulfonamides.



Entry	7	G	8	Yield [%][a]
1	**a**	H	**a**	(74)
2	**b**	2-Me	**b**	(74)
3	**c**	3-Me	**b**	(94)
4	**d**	4-Me	**b**	(56)
5	**e**	2-$CONEt_2$	**c**	60(64)
6	**f**	4-$CONEt_2$	**c**	58(67
7	**g**	2-N(Me)Ph	**d**	53
8	**h**	4-N(Me)Ph	**d**	18
9	**i**	2-OMe	**e**	(97)
10	**j**	2-OCH_2Ph	**f**	68
11	**k**	2-O*i*-Pr	**g**	59
12	**l**	3-OMe	**e**	(91)
13	**m**	4-OMe	**e**	(18)
14	**n**	2-TMS	**h**	(48)
15	**o**	4-TMS	**h**	(76)
16	**p**	2-(*p*-MeO-C_6H_4)	**i**	90
17	**q**	4-(*p*-MeO-C_6H_4)	**i**	85

[a] Values in parenthesis indicate yields determined by GC analysis. TMS = trimethylsilyl.



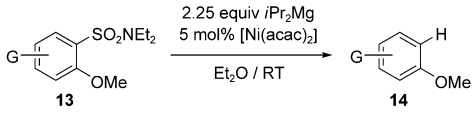
Scheme 2. Heteroaryl sulfonamides and sultams for the hydrodesulfamoylation reaction.

To develop a new combined directed *ortho* metalation–hydrodesulfamoylation route to *meta*-substituted aromatic compounds that overrides the standard electrophilic substitution approach, a selected group of aryl sulfonamides, readily available from inexpensive commercial entities, was tested (**13**→**14**, Table 2). Thus, prototypes of 1,3-dioxygenated (Table 2, entries 2, 8, 9) and 3-aminoanisole (Table 2, entry 4) were obtained in modest to good yields. Additional synthetic advantage is gained by the availability of products that originate from Negishi cross-coupling[17] (Table 2, entry 7) and Buchwald–Hartwig C–N coupling[18] (Table 2, entry 4) regimens.

To take advantage of the mechanistic implications of the above results, the cross-coupling of aryl sulfonamides with Grignard reagents was studied (**7**→**15**, Table 3). Screening of catalysts led to optimization using the [Ni(acac)$_2$]–bidentate phosphane ligand (dppp) combination, although higher temperatures were required to achieve efficient coupling.[19] Electronic effects appear to have little influence on the yields of products (Table 3, entries 3, 7, and 9) while comparison of *ortho* and *para* substituents shows consistently lower yields

 © 2004 Wiley-VCH Verlag GmbH & Co. KGaA, Weinheim

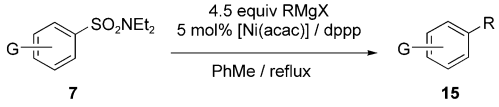
Table 2: Ni^0-catalyzed reduction of di- and trisubstituted aryl sulfonamides.



Entry	13	G	14	Yield [%][a]
1	**a**	4-TMS	**a**	91
2	**b**	4-OMe	**b**	(87)
3	**c**	4-Me	**c**	(80)
4	**d**	4-N(Me)Ph	**d**	77
5	**e**	4-NBn_2	**e**	10
6	**f**	4-Cl	**f**	63
7	**g**	6-(*p*-MeO-C_6H_4)	**g**	89
8	**h**	6-OMe	**h**	(54)
9	**i**	6-OMe, 4-TMS	**i**	53(60)

[a] Values in parenthesis indicate yields determined by GC analysis.

Table 3: Ni^0-catalyzed cross-coupling of aryl sulfonamides.

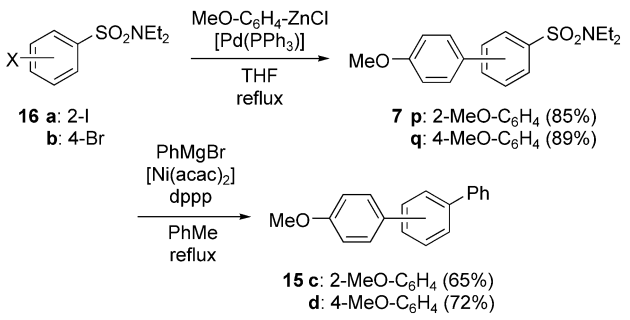


Entry	7	G	R	15	Yield [%][a]
1	**i**	2-OMe	Me	**a**	(60)
2	**i**	2-OMe	Ph	**b**	52
3	**m**	4-OMe	Ph	**i**	79
4	**p**	2-(*p*-MeO-C_6H_4)	Ph	**c**	65
5	**q**	4-(*p*-MeO-C_6H_4)	Ph	**d**	72
6	**b**	2-Me	Ph	**e**	(69)
7	**d**	4-Me	Ph	**f**	(80)
8	**n**	2-TMS	Ph	**g**	(73)
9	**o**	4-TMS	Ph	**h**	(84)

[a] Values in parenthesis indicate yields determined by GC analysis.

for the former with the exception of the OMe group (Table 3, entries 2 vs. 3, 6 vs. 7, 8 vs. 9).

To demonstrate the iterative cross-coupling potential, haloaryl sulfonamides (Scheme 3, **16a**,**b**) were subjected to Negishi cross-coupling to afford biaryl compounds **7p**,**q** which, upon sulfonamide–PhMgBr coupling, furnished teraryls **15c**,**d** in good overall yields. Further regioselective polyaryl construction by taking advantage of the directed *ortho* metalation potential of **7p**,**q** followed by the above modular coupling approach may be envisaged.



Scheme 3. Iterative Negishi/Kumada cross-coupling of haloaryl sulfonamides to furnish teraryls. dppp = propane-l,3-diylbis(diphenylphosphane).

The established oxidative addition into the C–S bond[20] for most oxidation states of sulfur, including sulfonates[5,8,9] suggest a similar mechanistic path for the aryl sulfonamide–Grignard desulfamoylation and cross-coupling reactions. Reduction of *N*,*N*-diethyl-2,6-dimethoxy-4-trimethylsilylbenzenesulfonamide (Table 2, entry 9) with [D_7]*i*PrMgBr afforded 1,3-dimethoxy-5-trimethylsilylbenzene (85% [D] by GC–MS, ^{1}H- and ^{2}H NMR) supports the proposed mechanism. These results, in combination with regiospecific cross-coupling of aryl sulfonamides with aryl Grignard reagents (Table 3), suggest that the aryl sulfonamide cross-coupling reaction proceeds predominantly through the catalytic cycle proposed for the Corriu–Kumada–Tamao reaction.[11]

In conclusion, a new Ni^0-catalyzed aryl sulfonamide–Grignard reagent reaction has been developed, which provides reductive desulfamoylation (Et_2O, room temperature) and cross-coupling (toluene/reflux)[21] processes of synthetic interest. The former reaction, paralleling the work of Julia and co-workers[8] on aryl-*tert*-butyl sulfones, allows the powerful sulfonamide directed-metalation group to act in a latent capacity, thus providing a route to aromatic compounds with 1,3-substitution patterns (Table 2) which are in opposition to those available, usually as mixtures, by classical electrophilic aromatic substitution chemistry. The cross-coupling process represents a new variant of the Corriu–Kumada–Tamao protocol but enjoys the advantage of the directed *ortho* metalation connection (Table 3).[22] Although the sensitivity of the reaction to both electronic and steric effects somewhat constrains functional-group flexibility, the enhancing, unprecedented *ortho* coordination group effect bodes well for further synthetic utility.[23]

Experimental Section

Representative Procedure for Desulfamoylation: iPr_2Mg (5.4 mL, 0.65 M in *t*BuOMe, 3.6 mmol) was added to a solution of **7q** (510 mg, 1.6 mmol) and [Ni(acac)$_2$] (20.0 mg, 0.08 mmol) in a mixture of Et_2O (20 mL) and *t*BuOMe (15 mL) at room temperature, and the reaction mixture was stirred for 8 h. The reaction mixture was cooled in an ice bath and quenched with saturated aqueous NH_4Cl solution, partitioned between Et_2O and H_2O, and the organic layer was extracted twice with Et_2O. The combined organic layer was washed twice with saturated aqueous NH_4Cl solution, and then once with H_2O, and once with brine. The solution was dried (Na_2SO_4), and the solvent was removed in vacuo to give **8i**[24] (249 mg, 85%) as a colorless solid after column chromatography (20:1 hexane/EtOAc). M.p. 82–83 °C (hexane); ^{1}H NMR (200 MHz): $\delta = 7.58$–7.22 (m, 6H), 6.97 (d, 2H, $J = 8.9$ Hz), 3.84 ppm (s, 3H); ^{13}C NMR (50.3 MHz): $\delta = 159.2$, 140.8, 133.8, 128.7, 128.1, 126.7, 126.6, 114.2, 55.3 ppm; LRMS (EI): *m*/*z* (%): 184 [M^+] (100), 169 [$M-15$] (60), 141 (61), 115 (37).

Representative Procedure for Cross-Coupling: PhMgBr (1.33 mL, 3.0 M in Et_2O, 4.0 mmol) was added to a solution of **7p** (319 mg, 1.0 mmol), [Ni(acac)$_2$] (13.0 mg, 0.05 mmol), and dppp (13.0 mg, 0.10 mmol) in toluene (10 mL), and the reaction mixture was heated at reflux for 6 h. The reaction mixture was cooled in an ice bath, quenched with saturated aqueous NH_4Cl solution, partitioned between EtOAc and H_2O, and the organic components were extracted twice with EtOAc. The combined organic layer was washed twice with saturated aqueous NH_4Cl solution, once with H_2O, and once with brine. The solution was dried (Na_2SO_4), and the

 © 2004 Wiley-VCH Verlag GmbH & Co. KGaA, Weinheim

solvent was removed in vacuo to give **15c**[25] (168 mg, 65%) as a colorless oil after chromatography (50:1 hexane/Et_2O). ^{1}H NMR (200 MHz): $\delta = 7.62$–7.50 (m, 4H), 7.45–7.30 (m, 4H), 7.21 (d, 2H, $J =$ 8.9 Hz), 6.90 (d, 2H, $J = 8.9$ Hz), 3.89 ppm (s, 3H); ^{13}C NMR (50.3 MHz): $\delta = 159.0$, 142.4, 141.1, 140.8, 134.6, 131.6, 131.3, 131.2, 130.5, 129.4, 128.5, 128.1, 127.7, 127.4, 127.0, 114.0, 55.7 ppm.

Received: August 12, 2003 [Z52633]

Keywords: arenes · cross-coupling · magnesium · nickel · sulfonamides

[1] For a summary, see the special issue dedicated to the field: Eds.: K. Tamao, T. Hiyama, E.-i. Negishi, *J. Organomet. Chem.* **2002**, *653*; Stille coupling**:** I. P. Beletskaya, *J. Organomet. Chem.* **1983**, *250*, 551; Negishi coupling: A. O. King, E.-i. Negishi, F. J. Villani, A. Silveira, *J. Org. Chem.* **1978**, *43*, 358; I. Klement, M. Rottlander, C. E. Tucker, T. N. Majid, P. Knochel, P. Venegas, G. Cahiez, *Tetrahedron* **1996**, *52*, 7201; Hiyama coupling: Y. Hatanaka, T. Hiyama, *Synlett* **1991**, 845; S. E. Denmark, T. F. Sweis, *Acc. Chem. Res.* **2002**, *35*, 835; Suzuki–Miyaura coupling: N. Miyaura, A. Suzuki, *J. Chem. Soc. Chem. Commun.* **1979**, 867; S. Kotha, K. Lahiri, S. Kashinath, *Tetrahedron* **2002**, *58*, 9633; Corriu–Kumada–Tamao reaction: K. Tamao, K. Sumitani, M. Kumada, *J. Am. Chem. Soc.* **1972**, *94*, 4374; R. J. P. Corriu, J. P. Masse, *J. Chem. Soc. Chem. Commun.* **1972**, 144; for a recent copper-catalyzed coupling of siloxanes, see**:** P. Y. S. Lam, S. Deudon, K. M. Averill, R. Li, M. Y. He, P. DeShong, C. G. Clark, *J. Am. Chem. Soc.* **2000**, *122*, 7600; for the copper-catalyzed coupling of boronic acids, see: P. Y. S. Lam, C. G. Clark, S. Saubern, J. Adams, M. P. Winters, D. M. T. Chan, A. Combs, *Tetrahedron Lett.* **1998**, *39*, 2941; P. Y. S. Lam, D. Bonne, G. Vincent, C. G. Clark, A. P. Combs, *Tetrahedron Lett.* **2003**, *44*, 1691; for iron-catalyzed coupling, see**:** A. Fürstner, A. Leitner, M. M. Menendez, H. Krause, *J. Am. Chem. Soc.* **2002**, *124*, 13856, and references therein.

[2] N. Kataoka, Q. Shelby, J. P. Stambuli, J. F. Hartwig, *J. Org. Chem.* **2002**, *67*, 5553; A. F. Littke, G. C. Fu, *Angew. Chem.* **2002**, *114*, 4350; *Angew. Chem. Int. Ed.* **2002**, *41*, 4176.

[3] J. E. McMurry, S. Mohanraj, *Tetrahedron Lett.* **1983**, *24*, 2723.

[4] S. Sengupta, M. Leite, D. S. Raslan, C. Quesnelle, V. Snieckus, *J. Org. Chem.* **1992**, *57*, 4066.

[5] E. Wenkert, T. W. Ferreira, Michelotti, E. L. *J. Chem. Soc. Chem. Commun.* **1979**, 637; E. Wenkert, T. W. Ferreira, *J. Chem. Soc. Chem. Commun.* **1982**, 840.

[6] C. Quesnelle, T. Iihama, T. Aubert, H. Perrier, V. Snieckus, *Tetrahedron Lett.* **1992**, *33*, 2625.

[7] M. Iwao, T. Iihama, K. K. Mahalanabis, H. Perrier, C. Snieckus, *J. Org. Chem.* **1989**, *54*, 24.

[8] J. Clayden, M. Julia, *J. Chem. Soc. Chem. Commun.* **1993**, 1682; J. Clayden, J. A. Cooneym, M. Julia, *J. Chem. Soc. Perkin Trans. 1* **1995**, 7.

[9] H. Okamura, M. Miura, H. Takei, *Tetrahedron Lett.* **1979**, *20*, 43.

[10] C.-H. Cho, H.-S. Yun, K. Park, *J. Org. Chem.*.**2003**, *69*, 3017.

[11] K. Tamao, K. Sumitani, Y. Kiso, S. F. Zembayashi, S. Kodama, I. Nakajima, A. Minato, M. Kumada, *Bull. Chem. Soc. Jpn.* **1976**, *49*, 1958; M. Kumada, *Pure Appl. Chem.* **1980**, *52*, 669.

[12] V. Snieckus, *Chem. Rev.* **1990**, *90*, 879.

[13] See also: *Annu. Rep. Med. Chem.* **2002**, *37*, pp. 3, 4, 17, 46–48, 54–57, 66, 70, 72, 81, 87, 88, 91, 131, 135, 136, 139, 142, 242, 252; G. Bouchain, S. Leit, S. Frechette, E. A. Khalil, R. Lavoie, O. Moradei, S. H. Woo, M. Fournel, P. T. Yan, A. Lakita, M.-C. Trachy-Bourget, C. Beaulieu, Z. Li, M.-F. Robert, R. MacLeod, J. M. Besterman, D. Delorme, *J. Med. Chem.* **2003**, *46*, 820; E. Pomarnzcka, M. Gdaniec, *Bioorg. Med. Chem.* **2003**, *11*, 1259; M. Nakamura, M. Yamaguchi, O. Sakai, J. Inoue, *Bioorg. Med. Chem.* **2003**, *11*, 1371; N. Murugesan, Z. Gu, S. Spergel, M. Young, P. Chen, A. Mathur, L. Leith, M. Hermsmeier, E. C.-K. Liu, R. Zhang, E. Bird, T. Waldron, A. Marino, B. Koplowitz, W. G. Humphreys, S. Chong, R. A. Morrison, M. L. Webb, S. Moreland, N. Trippodo, J. C. Barrish, *J. Med. Chem.* **2003**, *46*, 125; Y. M. Choi-Sledeski, R. Kearney, G. Poli, H. Pauls, C. Gardner, Y. Gong, M. Becker, R. Davis, A. Spada, G. Liang, V. Chu, K. Brown, D. Collussi, R. Leadley, S. Rebello, P. Moxey, S. Morgan, R. Bentley, S. Lasiewshi, S. Maignan, J.-P. Guilloteau, V. Mikol, *J. Med. Chem.* **2003**, *46*, 681.

[14] Excess Grignard reagent was necessary. [Ni(cod)] (cod = cyclo-octa-1,5-diene), $NiCl_2$, and $Ni(OAc)_2$ gave negligible reduction. [$NiCp_2$] was found to be an effective catalyst. The control experiment without catalyst gave no reaction. Catalyst loadings of 1 mol% gave slightly lower yields. Use of THF and hexanes as solvents and the addition of phosphane ligands gave poor yields. The nature of the amine portion of the sulfonamide (e.g. sterically demanding or aromatic) had a negligible influence on the yield. Secondary amines were inert to the reaction conditions, possibly due to the insolubility of their magnesium salts.

[15] M. Alami, C. Amatore, S. Bensalem, A. Choukchou-Brahim, A. Jutand, *Eur. J. Inorg. Chem.* **2001**, 2675.

[16] Other cyclic sulfonamides gave synthetically unproductive results: 2-methyl-3,3-diphenyl-2,3-dihydro-benzo[d]isothiazole 1,1-dioxide was inert while 2-methyl-1,1-dioxo-1,2-dihydro-Δ^6-benzo[d]isothiazol-3-one (*N*-methyl saccharin) gave *N*-methyl-benzamide in 15% yield.

[17] For Suzuki cross-coupling chemistry of aryl sulfonamides, see: S. L. MacNeil, O. B. Familoni, V. Snieckus, *J. Org. Chem.* **2001**, *66*, 3662.

[18] H Tomori, J. M. Fox, S. L. Buchwald, *J. Org. Chem.* **2000**, *65*, 1158; B. H. Yang, S. L. Buchwald, *J. Organomet. Chem.* **1999**, *576*, 125.

[19] Use of $Pd(OAc)_2$, [$Pd(PPh_3)_4$] and [Pd(dppp)]Cl_2 resulted in complex mixtures. The [$NiCl_2$]–dppp combination was an ineffective catalyst, while under [$Ni(acac)_2$] alone, cross-coupling products were obtained in low yields.

[20] E. Wenkert, M. E. Shepard, A. T. McPhail, *J. Chem. Soc. Chem. Commun.* **1986**, 1390.

[21] Recently, the conversion of **7i**→**15b** (Table 3) was effected at room temperature in 54% yield in the presence of catalytic [CpNi(IMes)Cl]: C. D. Abernethy, A. H. Cowley, R. A. Jones, *J. Organomet. Chem.* **2000**, *596*, 3; R. R. Milburn, A. Pla, V. Snieckus, unpublished results (Mes = mesityl = 2,4,6-trimethylphenyl).

[22] For other directed *ortho* metalation–cross-coupling links, see: J.-G. Anctil, V. Snieckus, *J. Organomet. Chem.* **2002**, *653*, 150.

[23] For the use of reductive chemistry in the development of a new amine-protecting group, see subsequent communication in this issue: R. R. Milburn, V. Snieckus, *Angew. Chem.* **2004**, *116*, 910; *Angew. Chem. Int. Ed.* **2004**, *43*, 892.

[24] S. Saito, S. Oh-tani, N. Miyaura, *J. Org. Chem.* **1997**, *62*, 8024.

[25] B. M. Trost, H. C. Arndt, *J. Am. Chem. Soc.* **1973**, *95*, 5288.

 © 2004 Wiley-VCH Verlag GmbH & Co. KGaA, Weinheim

Protecting Groups

ortho-Anisylsulfonyl as a Protecting Group for Secondary Amines: Mild Ni^0-Catalyzed Hydrodesulfonylation

*Robert R. Milburn and Victor Snieckus**

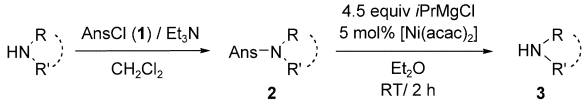
In the current armamentarium of amine-protecting groups,[1] aryl sulfonamides occupy an ambivalent position of facile formation and ease of handling but extreme robust character, undergoing cleavage only under harsh reductive (e.g. sodium naphthalenide)[1a,2] or acidic (e.g. 48% HBr/cat. phenol)[3] conditions.[4] The *p*-toluenesulfonyl (Ts) and, to a lesser extent, the benzenesulfonyl groups are central in synthetic practice, not only as protecting groups for amines, but also as part of reagents and in derivatization procedures.[5] The Achilles heel position of the Ts group can be seen in the difficult deprotection measures in multifunctional organic molecules[6] and/or lack of further manipulation of the obtained NTs derivatives.[7] A second long-standing feature of the NTs function is its enabling use as a method for the synthesis of pure secondary amines,[8] which, although advanced by the development of Mitsunobu alkylation conditions,[9] suffers from the harsh cleavage conditions. Thus, the Fukuyama method[10] has been a welcome addition to the arsenal of amine-deprotection protocols.

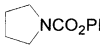
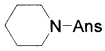
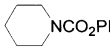
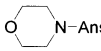
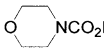
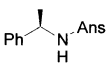
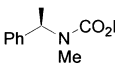
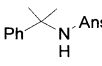
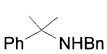
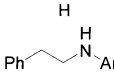
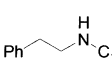
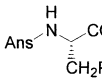
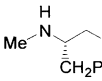
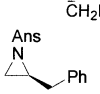
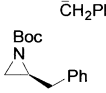
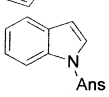
As a logical sequel to the finding of hydrodesulfamoylation and cross-coupling reaction of aromatic sulfonamides,[11] we report herein that the readily appended *ortho*-anisylsulfonyl (Ans = 2-MeO-$C_6H_4SO_2$-) group is cleanly detached from secondary amines by using the β-hydride transfer conditions of the standard Corriu–Kumada–Tamao cross-coupling procedure (Ni^0, *i*PrMgCl, Et_2O, room temperature).[12]

Thus, use of the Ni^0-catalyzed reductive cross-coupling protocol[11] results in the smooth and rapid deprotection of *N*-Ans acyclic and cyclic amines, chiral amines and amino alcohols, anilines, pyrrole, indole, and aziridines (Table 1). Furthermore, stepwise alkylation of *N*-Ans primary amines followed by cleavage allows the synthesis of unsymmetrical secondary amines. Taken together, this new methodology promises generality and provides a significant alternative to the established *N*-Ts and *N*-benzenesulfonamide protection tactics.

An array of diverse amines were derivatized with the readily prepared *ortho*-anisylsulfonyl chloride (AnsCl; **1**) and subjected to deprotection in the presence of excess *i*PrMgCl (commercially available as a solution in Et_2O), [Ni(acac)$_2$] (5 mol%), in diethyl ether at room temperature (Table 1).[13]

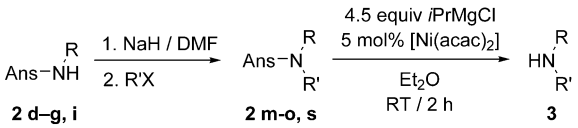
Table 1: Protection and deprotection of *N*-Ans amines



Entry	Protection		Yield [%][a]	Deprotection		Yield [%]
1		**2a**	72		**3a**	68[e]
2		**2b**	82		**3b**	73[e]
3		**2c**	76		**3c**	69[e]
4		**2d**	81		**3d**	92[e,f]
5		**2e**	66		**3e**	78
6		**2f**	87		**3f**	88[e]
7		**2g**	74		**3g**	74[e]
8		**2h**	81[b]		**3h**	89[f]
9		**2i**	97[c]		**3i**	95
10		**2j**	85[c]		**3j**	82
11		**2k**	65[d]		**3k**	82[g]
12		**2l**	77[d]		**3l**	77

[a] Conditions: Et_3N/CH_2Cl_2 unless otherwise indicated. [b] Conditions: **2g**/DIBAL/CH_2Cl_2; TsCl, aq KOH/THF/reflux. [c] Conditions: DMAP/Pyridine. [d] Conditions: 1. *n*BuLi/ −78 °C; 2. AnsCl. [e] Compound isolated as carbamate for ease of purification or due to volatile nature of amine. [f] Amines were converted into their *N*-acetyl derivatives for HPLC analysis (Chiracel OD column (hexane/*i*PrOH). [g] Yield by GC analysis. DIBAL = diisobutylaluminum hydride, DMAP = 4-dimethylaminopyridine.

Aliphatic and aromatic primary *N*-Ans amines **2d–g,i** were readily alkylated to form **2m–o,qs** (Scheme 1) and cleaved to provide unsymmetrical secondary amines **3d–g,i** (Table 1, entries 4–10). The application of the *N*-cumylsulfonamide[14] allows, after decumylation, the synthesis of primary amines (Table 1, entry 5). No decrease in optical activity was observed for chiral substrates (Table 1, entries 4 and 7). Although α-amino esters, as expected, do not tolerate the reaction conditions, a corresponding reduced and *O*-benzylated amino alcohol is readily deanisylated in high yield (Table 1, entry 7). The cleavage of the *N*-Ans aziridine



Scheme 1. Alkylation and hydrodesulfonylation of *N*-Ans amines. DMF = *N*,*N*-dimethylformamide, acac = acetoacetonate.

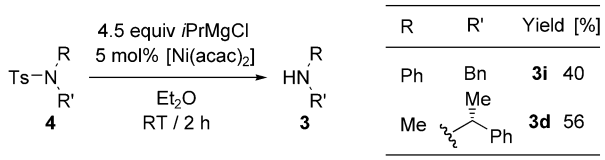
[*] R. R. Milburn, Prof. V. Snieckus
Department of Chemistry, Queens University
Kingston, Ontario K7L 6 (Canada)
Fax: (+1) 613-533-6089
E-mail: snieckus@chem.queensu.ca

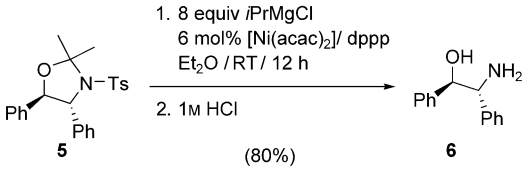
Supporting information for this article is available on the WWW under http://www.angewandte.org or from the author.

 © 2004 Wiley-VCH Verlag GmbH & Co. KGaA, Weinheim DOI: 10.1002/anie.200352634

(Table 1, entry 8) also proved unexceptional. *N*-Ans-pyrrole and indole[15] are smoothly deprotected. However, *N*-Ans-allyl amines are not compatible with the hydrodesulfonylation conditions and give products of deallylation.[16]

The poor reaction of *N*-Ts amines **4** has thus far precluded its deprotection under Ni^0-catalyzed conditions (Scheme 2).[17] However, the widespread use of the Ts protecting group makes the development of a Ni^0-catayzed deprotection protocol a priority. To this end, preliminary experiments with oxazolidine **5** indicate that Ni–phosphane catalysts, extended reaction times (12–18 h), and the use of a large excess of the Grignard reagent result in increased yields of the product of *N*-Ts cleavage.[18]





Scheme 2. Ni^0-catalyzed hydrodesulfonylation of *N*-Ts amines. dppp = propane-l,3-diylbis(diphenylphosphane)

To conclude, the *N*-Ans group constitutes a new amine-protecting group that overcomes the necessity for harsh cleavage conditions normally demanded by the *N*-Ts and related sulfonamides.[1] Furthermore, its value for the synthesis of unsymmetrical secondary amines and primary amines has been demonstrated. Although the scope and limitations of the new methodology, and hence its potential complementarity to the Fukuyama[4a,b,10] and Gabriel[19] syntheses of primary amines, remains to be established, it allows a significant departure from the classical *N*-Ts deprotection modes.[20] The combined advantages of convenient derivatization with mild and rapid deprotection bodes well for its broader application in organic synthesis.

Experimental Section

2-Methoxybenzenesulfonyl chloride (**1**):[20] *n*BuLi (35.4 mL, 2.85 M, 101 mmol) was added to a solution of TMEDA (15.2 mL, 101 mmol) in Et_2O (200 mL) at 0 °C, and the reaction mixture was stirred for 5 min. Anisole (10 mL, 92 mmol) was added and the mixture was stirred for 1 h, cooled to −78 °C, treated with SO_2 (g) passed through a syringe for 30 min, and allowed to warm to room temperature over 1 h. SO_2Cl_2 (8.8 mL 110 mmol) was added, and the mixture was stirred at room temperature for 6 h. The mixture was partitioned between Et_2O and H_2O, the organic layer was separated, washed with brine, and dried (Na_2SO_4), and the solvent was removed in vacuo to give AnsCl (10.1 g, 81 %). M.p. 53–54 °C (hexanes) [Lit.[21] m.p. 56 °C]; ^{1}H NMR (300 MHz): $\delta = 7.95$ (dd, 1 H, $J = 8.0$, 1.7 Hz), 7.70(ddd, 1 H, $J = 8.5$, 7.5, 1.7 Hz), 7.13 (t, 1 H, $J = 8.3$ Hz), 7.09 (d, 1 H, $J = 7.5$ Hz), 4.06 ppm (s, 3 H); ^{13}C NMR (75.5 MHz): $\delta = 157.3$, 137.3, 131.7, 129.7, 120.2, 113.2, 56.6 ppm; LRMS (EI): *m*/*z* (%): 205 [M^+] (1), 163 (10), 83 (58), 81 (39), 67 (16), 55 (100).

N-Benzylphenylamine (**3i**): A solution of *i*PrMgCl (6.34 mL, 2.13 M in Et_2O, 13.5 mmol) was added to a solution of **2s** (1.06 g, 3.0 mmol) and [Ni(acac)$_2$] (39.0 mg, 0.15 mmol) in Et_2O (80 mL), and the reaction mixture stirred at room temperature for 2 h. The reaction was quenched with saturated NH_4Cl solution, and the aqueous layer was extracted twice with EtOAc. The organic layer was washed three times with saturated NH_4Cl solution, once with H_2O, and once with brine. The solution was dried (Na_2SO_4), and the solvent was removed in vacuo to give **3i** (395 mg, 95 %) as a colorless solid after chromatography (20:1 hexane/EtOAc). M.p. 35.5–37.8 °C (Lit.[21]); ^{1}H NMR (300 MHz): $\delta = 7.38$–7.13 (m, 7 H), 6.78–6.50 (m, 3 H), 4.87 ppm (br s, 1 H), 4.26 (s, 2 H); ^{13}C NMR (50.3 MHz): $\delta = 148.1$, 139.4, 129.2, 128.5, 127.4, 127.1, 117.5, 112.8, 48.2.

Received: August 12, 2003 [Z52634]

Keywords: amines · magnesium · nickel · protecting groups · sulfonamides

[1] a) *Protective Groups in Organic Synthesis*, 3rd ed. (Eds.: T. W. Green, P. G. Wuts), Wiley, New York, **1999**, pp. 600–613; b) P. J. Kocienski, *Protecting Groups*, 2nd ed., Theime, Stuttgart, **2000**.

[2] B. J. Paul, E. Hobbs, P. Buccino, Hudlicky, T. *Tetrahedron Lett.* **2001**, *42*, 6433.

[3] C. J. Opalka, T. E. D'Ambra, J. J. Faccone, G. Bodson, E. Cossement, *Synthesis* **1995**, *7*, 766.

[4] For recent developments, see 2-nitrophenylsulfonyl (cleavage PhSH/K_2CO_3/DMF): a) T. Fukuyama, C.-k. Jow, M. Cheung, *Tetrahedron Lett.* **1995**, *36*, 6373; b) W. Kurosawa, T. Kan, T. Fukuyama, *Org. Synth.* **2002**, *79*, 186; c) T. Messeri, D. D. Sternbach, N. C. O. Tomkinson, *Tetrahedron Lett.* **1998**, *39*, 1669; *p*-toluenesulfonyl cleavage (SmI_2): d) E. Vedejs, S. Lin, *J. Org. Chem.* **1994**, *59*, 1602; e) D. C. Hill, L. A. Flugge, P. A. Petillo, *J. Org. Chem.* **1997**, *62*, 4864; Ti^0: f) S. K. Nayak, *Synthesis* **2000**, *11*, 1575.

[5] Sharpless asymmetric aminohydroxylation**:** a) V. V. Fokin, K. B. Sharpless, *Angew. Chem.* **2001**, *113*, 3463; *Angew. Chem. Int. Ed.* **2001**, *40*, 3455; b) P. O'Brien, *Angew. Chem.* **1999**, *111*, 339; *Angew. Chem. Int. Ed.* **1999**, *38*, 326; for a short review on the scope and limitations, see: c) D. Nilov, O. Reiser, *Adv. Synth. Catal.* **2002**, *344*, 1169, for recent work, see: d) T. J. Donohoe, P. D. Johnson, A. Cowley, M. Keenan, *J. Am. Chem. Soc.* **2002**, *124*, 12934; e) V. Nesterenko, J. T. Byers, P. J. Hergenrother, *Org. Lett.* **2003**, *5*, 281; asymmetric addition to imines: f) R. Hori, T. Aoya ma, T. Shioiri, *Tetrahedron Lett.* **2000**, *41*, 9455; g) G. K. S. Prakash, M. Mandal, Olah, G. A. M. Ueda, A. Saito, N. Miyaura, *Synlett* **2000**, *11*, 1637; h) W. Lu, T. H. Chan, *J. Org. Chem.* **2001**, *66*, 3467; aziridination: i) L. Simkhovich, Z. Gross, *Tetrahedron Lett.* **2001**, *42*, 8089; j) P. Dauban, R. H. Dodd, *Tetrahedron Lett.* **2001**, *42*, 1037; k) B. M. Chana, R. Vyas, A. V. Bedekar, *J. Org. Chem.* **2001**, *66*, 30; l) S. Handy, M. Czopp, *Org. Lett.* **2001**, *3*, 1423; m) M. T. Baros, C. D. Maycock, M. R. Ventura, *Tetrahedron Lett.* **2002**, *43*, 4329; n) J. J. Caldwell, D. Craig, S. P. East, *Synlett* **2001**, 1602; o) V. K. Aggarwal, E. Alonso, M. Ferrara, S. E. Spey, *J. Org. Chem.* **2002**, *67*, 2335; p) D. Caine, P. O'Brien, C. M. Rosser, *Org. Lett.* **2002**, *4*, 1923; q) K. M. Gillespie, C. J. Sanders, P. O'Shaughnessy, I. Westmoreland, C. P. Thickitt, P. Scott, *J. Org. Chem.* **2002**, *67*, 3450; r) L. Simkhovich, Z. Gross, *Tetrahedron Lett.* **2001**, *42*, 8089; α-amino acid synthesis: (cleavage: Na/NH_3) s) E. Fischer, *Ber. Dtsch. Chem. Ges.* **1915**, *48*, 93; t) V. du Vigneaud, O. K. Behrens, *J. Biol. Chem.* **1937**, *212*, 27; (cleavage HBr/HOAc) u) B. E. Haskell, S. B. Bowlus, *J. Org. chem.* **1976**, *41*, 159; β-

 © 2004 Wiley-VCH Verlag GmbH & Co. KGaA, Weinheim

amino acid synthesis: v) A. E. Taggu, A. M. Hafez, T. Lectka, *Acc. Chem. Res.* **2003**, *36*, 10; w) N. Jiang, J. Wang, *Synlett* **2002**, 149; Baylis–Hillman reaction: x) M. Shi, Y.-m. Xu, *Angew. Chem.* **2002**, *114*, 4689; *Angew. Chem. Int. Ed.* **2002**, *41*, 4507; β-lactam synthesis: y) A. E. Taggi, A. M. Hafez, H. Wack, B. Young, D. Ferraris, T. Lectka, *J. Am. Chem. Soc.* **2002**, *124*, 6626; Ugi multicomponent synthesis: z) E. Campian, B. Lou, H. Saneii, *Tetrahedron Lett.* **2002**, *43*, 8467; sulfonamide library derivation: aa) H. Ohno, K. Kawamura, A. Otake, H. Nagase, H. Tanaka, T. Takabashi, *Synlett* **2002**, 93; azamacrocycle construction: ab) G. J. Briger, E. M. Boehringe, Z. Wang, D. Schols, R. I. Skerlj, D. E. Bogucki, PCT Patent Appl. WO 0144229A1, **2001**; ac) R. T. Skerlj, S. Nan, Y. Zhou, G. J. Bridger, *Tetrahedron Lett.* **2002**, *43*, 7569; ad) J. P. Hill, C. E. Anson, A. K. Dovell, *Tetrahedron Lett.* **2002**, *43*, 7301; ae) C. Bazzicalupi, A. Bencini, E. Berni, A. Bianchi, S. Ciattini, C. Giorgi, S. Maoggi, P. Paoletti, B. Valtancoli, *J. Org. Chem.* **2002**, *67*, 9107; af) B. M. Kim, S. M. So, H. Choi, *J. Org. Lett.* **2002**, *4*, 949.

[6] For selected references, see: a) D. F. Taber, T. D. Neubert, A. L. Rheingold, *J. Am. Chem. Soc.* **2002**, *124*, 12416; b) S. Minakata, D. Kano, Y. Oderaotoshi, M. Komatsu, *Org. Lett.* **2002**, *4*, 2097; c) T. Hudlicky, U. Rinner, D. Gonzalez, H. Akgun, S. Schilling, P. Siengewicz, T. A. Martinot, G. R. Pettit, *J. Org. Chem.* **2002**, *67*, 8726; K. A. Parker, S. Fokas, *J. Am. Chem. Soc.* **1992**, *114*, 9688; d) S. R. Fix, J. L. Brice, S. S. Stahl, *Angew. Chem.* **2002**, *114*, 172; *Angew. Chem. Int. Ed.* **2002**, *41*, 164; e) W. Lu, T. H. Chan, *J. Org. Chem.* **2001**, *66*, 3467; f) O. Kitagawa, Y. Yamada, H. Fujiwara, T. Taguchi, *Angew. Chem.* **2001**, *113*, 3983; *Angew. Chem. Int. Ed.* **2001**, *40*, 3865; R. Mukhopadhyay, N. G. Kundu, *Synlett* **2001**, 1143; g) M. Ueda, A. Saito, N. Miyaura, *Synlett* **2000**, 1637.

[7] P. A. Evans, J. E. Robinson, K. K. Moffett, *Org. Lett.* **2001**, *3*, 3269.

[8] Stems from the outdated Hinsberg qualitative organic test for amines, see: R. L. Shriner, R. C. Fuson, D. Y. Curtin, *The Systematic Identification of Organic Compounds*, 4th ed., Wiley, New York, **1956**, p. 103; J. March, *Advanced Organic Chemistry*, 4th ed., Wiley, New York, **1992**, p. 499.

[9] J. R. Henry, L. R. Marcin, M. C. McIntosh, P. M. Scola, F. D. Harris, Jr., S. M. Weinreb, *Tetrahedron Lett.* **1989**, *30*, 5709.

[10] See reference [4b]; for limitations of the Ns protection, see: P. G. M. see Wuts, J. M. Northuis, *Tetrahedron Lett.* **1998**, *39*, 3889.

[11] See previous Communication in this issue: R. R. Milburn, V. Snieckus, *Angew. Chem.* **2004**, *116*, 906; *Angew. Chem. Int. Ed.* **2004**, *43*, 888.

[12] a) K. Tamao, *J. Organomet. Chem.* **2002**, *653*, 23; b) K. Tamao, Y. Kiso, K. Sumitani, M. Kumada, *J. Am. Chem. Soc.* **1972**, *94*, 9268; c) Y. Kiso, K. Tamao, M. Kumada, *J. Organomet. Chem.* **1973**, *50*, C12.

[13] Volatile amines were isolated as the phenyl carbamates formed by addition of phenyl chloroformate to the cooled reaction mixture prior to addition of saturated aqueous NH_4Cl. Use of less than 4.5 equivalents of *i*PrMgBr gave significantly lower yields.

[14] C. Metallinos, S. Nerdinger, V. Snieckus, *Org. Lett.* **1999**, *1*, 1183.

[15] Standard conditions for cleavage of *N*-Ts pyrrole and indole: 2% aqueous KOH.[1a]

[16] J. Pawlas, Y. Nakao, M. Kawatsura, J. F. Hartwig, *J. Am. Chem. Soc.* **2002**, *124*, 3669.

[17] Considerable effort was expended to use the benzenesulfonyl, Ts and *meta*-toluenesulfonyl derivatives in order to present the most cost-effective new *N*-protecting group. Thus, in a comparison of deprotection ease with the *N*-Ans group, the selected *N*-Ts amines **4** underwent Ni^0-catalyzed hydrodesulfonylation to give **3** only in modest yield. Similarly, although *meta*-toluenesulfonyl amides are conveniently prepared from the commercial *meta*-toluenesulfonyl chloride, their deprotection, while proceeding in high yields, occurs much more slowly (8–12 h) than that of the Ans group (2 h).[11]

[18] J. C. Espuga, V. Snieckus, unpublished results.

[19] For general synthesis of amines, see S. R. Sandler, W. Karo, *Organic Functional Group Preparations*, 2nd ed., Academic, New York, **1983**, chap. 13.

[20] The sluggish reaction of *N*-Ts amines under the Ni^0-catalyzed conditions has, to date, stifled the development of this widely used Ts protective group. However, preliminary experiments on oxazoline **5** with Ni–phosphane catalysts, extended reaction times (12–18 h), and excess Grignard reagent have shown promise in the improved yields of the *N*-detosylation reaction.[18]

[21] S. N. Bhattacharga, C. Earborn, D. R. M. Walton, *J. Chem. Soc. C* **1968**, 1265..

[22] T. Kawakami, T. Sugimoto, A. Baba, H. Matsuda, N. Sonoda, *J. Org. Chem.* **1995**, *60*, 2677.

 © 2004 Wiley-VCH Verlag GmbH & Co. KGaA, Weinheim

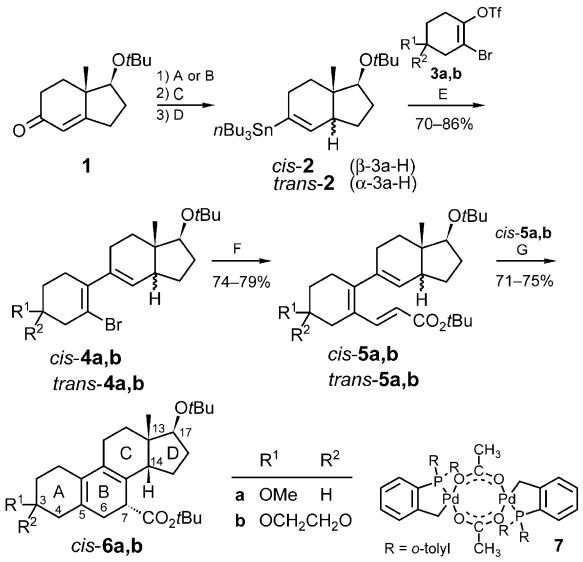
Oligocyclic Dienes

Steroids and Steroid Analogues from Stille–Heck Coupling Sequences**

*Hans Wolf Sünnemann and Armin de Meijere**

Steroids have been synthesized in many different ways,[1] and to a certain extent they have become one of the preferred testing grounds for the development of more efficient methods for organic synthesis. A maximum increase of structural complexity in a minimum number of operational steps in synthesis can be achieved either by completely new transformations or by new sequential combinations of previously established reactions. A striking example is the total synthesis of estrone by Vollhardt et al., in which a cobalt-mediated intramolecular cocyclization of two alkynes and an alkene is applied followed by an intramolecular Diels–Alder reaction.[2] Our previously reported selective Stille–Heck coupling sequences of 1-bromo-2-trifluoromethanesulfonyloxycyclohexenes with alkenylstannanes and alkyl acrylates to yield unsymmetrically 1,6-disubstituted 1,3,5-hexatrienes, which can be transformed by 6π-electrocyclizations into oligocyclic dienes,[3] appeared to be suitable to access steroids and steroid analogues efficiently by a convergent A + CD → ACD → ABCD strategy.

The sequence (Scheme 1) starts with a Stille coupling[4] of the enantiomerically pure hexahydroindenylstannanes *cis*-**2** and *trans*-**2** onto the 4-substituted 2-bromocyclohexenol triflates **3a**,**b** to yield the tricyclic bromobutadienes *cis*-**4a**,**b** and *trans*-**4a**,**b**, respectively. The bicycloalkenylstannanes *cis*-**2** and *trans*-**2** were prepared in high yields (82–97%) with a tributylstannyl cuprate[5] from the corresponding *cis*-[6] and *trans*-configurated[7] enol triflates, which were obtained in 55–79% yield[8] by reductive enolate formation from the α,β-unsaturated bicyclic ketone **1**.[9] The bromocyclohexenol triflate **3a** was assembled from *p*-methoxyphenol by Birch reduction,[10] and bromination,[11] (74% yield) regioselective formation of the lithium enolate, and trapping with *N*,*N*-bis(trifluoromethanesulfonyl)aniline (69% yield).[3] The starting compound for the synthesis of **3b** was 1,4-cyclohexanedione monoethyleneacetal, which was converted into the trimethylsilyl enol ether.[12] Since the bromination product 2-bromo-1,4-cyclohexanedione monoethyleneacetal is not stable, it was transformed directly into the bromocyclohexenol triflate **3b** (53% yield over two steps from the trimethylsilyl enol ether).[13] Of the reaction conditions tried, the protocol for Stille couplings developed by Farina et al.[14] with triphenylarsane[15] as a ligand and a copper(I) cocatalyst proved to be best and gave yields in the range of 70–86% (Table 1). From the racemic 4-methoxy derivative **3a** the products *cis*-**4a** and *trans*-**4a** were obtained as 1:1 mixtures of diastereomers. The tricyclic bromodienes *cis*-**4a**,**b** and *trans*-**4a**,**b** were immediately subjected to subsequent Heck reactions with *tert*-butyl acrylate[16] to form the



Scheme 1. A) NH_3, Li (2.30 equiv), $PhNH_2$ (0.75 equiv), THF, −33 °C, 2 h; B) CuBr·SMe_2 (1.00 equiv), *t*BuLi (1.10 equiv), DIBAH (1.50 equiv), HMPA (8.00 equiv), TMSCl (2.00 equiv), THF, −100 → −40 °C, 6 h; MeLi (1.50 equiv), THF, 0 °C, 45 min; C) $PhN(Tf)_2$ (1.10–2.40 equiv), THF, −78 → 25 °C, 22–24 h; D) LDA (2.60 equiv), Bu_3SnH (2.20 equiv), CuCN (1.10 equiv), THF, −30 °C, 2.5 h; AgOAc (3.00 equiv), EtOAc, 25 °C, 1 h; E) $[Pd_2(dba)_3·CHCl_3]$ (10 mol%), $AsPh_3$ (8 mol%), CuI (5 mol%), LiCl (3.00 equiv), NMP, 65 °C, 5 h; F) **7** (8 mol%), nBu_4NOAc (2.00 equiv), *tert*-butyl acrylate (5.00 equiv), DMF, MeCN, H_2O (5:5:1), 105 °C, 4 h; G) decalin, 215 °C, 45 min. DIBAH = diisobutylaluminum hydride, HMPA = hexamethylphosphoramide, TMS = trimethylsilyl, Tf = trifluoromethanesulfonyl, LDA = lithium diisopropylamide, NMP = *N*-methylpyrrolidone.

Table 1: Chemoselective Stille and Heck coupling reactions of 4-substituted 2-bromocyclohexenol triflates leading to tricyclic 1,3,5-hexatrienes (see Scheme 1).

Starting cmpd.	Alkene	Product	Yield [%][a]	d.r.[b]
3a	*cis*-**2**	*cis*-**4a**	80	1:1
3b	*cis*-**2**	*cis*-**4b**	83	–
3a	*trans*-**2**	*trans*-**4a**	70	1:1
3b	*trans*-**2**	*trans*-**4b**	86	–
cis-**4b**	CO_2tBu	*cis*-**5a**	74	1:1
cis-**4b**	CO_2tBu	*cis*-**5b**	76	–
trans-**4b**	CO_2tBu	*trans*-**5a**	79	1:1
trans-**4b**	CO_2tBu	*trans*-**5b**	78	–

[a] Yield of isolated product. [b] The diastereomeric ratio was determined by ^1H NMR spectroscopy.

[*] Dipl.-Chem. H. W. Sünnemann, Prof. Dr. A. de Meijere
Institut für Organische Chemie der
Georg-August-Universität Göttingen
Tammannstrasse 2, 37077 Göttingen (Germany)
Fax: (+49) 551-399475
E-mail: Armin.deMeijere@chemie.uni-goettingen.de

[**] This work was supported by the Fonds der Chemischen Industrie as well as by the companies BASF AG and Chemetall GmbH (chemicals). The authors are indebted to Dr. E. Ottow, Schering AG, Berlin, for a generous gift of the Hajos-Wiechert ketone **1**, and to Dr. Burkhard Knieriem, Göttingen, for his careful proofreading of the final manuscript.

Supporting information for this article is available on the WWW under http://www.angewandte.org or from the author.

 DOI: 10.1002/anie.200352162 © 2004 Wiley-VCH Verlag GmbH & Co. KGaA, Weinheim

unsymmetrically substituted tricyclic 1,3,5-hexatrienes *cis*-**5a**,**b** and *trans*-**5a**,**b**, respectively.

The best catalyst for this step turned out to be the palladacycle **7**[17] in the presence of tetrabutylammonium acetate as a base. For higher yields (74–79%), a solvent mixture consisting of DMF, MeCN, and water[18] was required (Table 1). The methoxy-substituted hexatrienes *trans*-**5a** and *cis*-**5a** were also isolated as 1:1 mixtures of diastereomers.

The tricyclic 1,3,4,5,6-pentasubstituted hexatrienes *cis*-**5a**,**b** and *trans*-**5a**,**b** are reasonably well set up for an additional ring closure by thermal 6π-electrocyclization (Scheme 1).[19,20] The best conditions for this turned out to be by heating in decalin solution at temperatures in the range 215–220 °C.[21] After 30 min at 215 °C, the hexatriene *cis*-**5b** had been completely converted into a mixture of the expected product of the 6π-electrocyclization and that arising from a subsequent 1,5-hydrogen shift, the apparently thermodynamically more stable isomer *cis*-**6b**. Upon extended heating, *cis*-**6b** was the sole product. Heating the hexatrienes *cis*-**5a,b** in decalin at 215–220 °C for 45 min provided the steroid analogues *cis*-**6a,b** cleanly with yields in the range of 71–75% (Table 2). Thus, the new sequence provides interesting new 7-substituted 19-*nor*-steroid analogues with an unnatural *cis* CD-ring fusion.

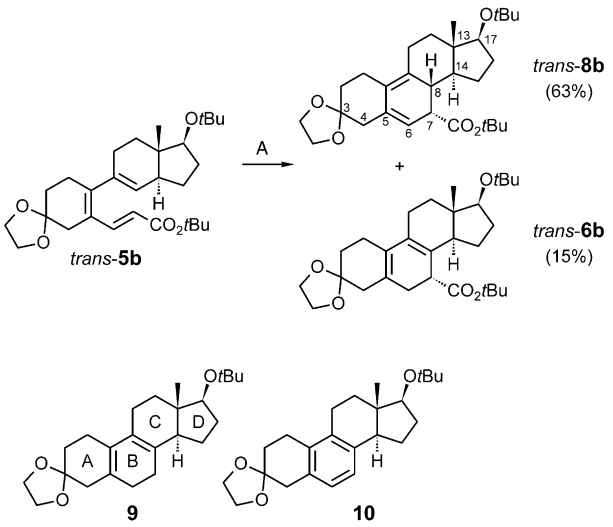
Table 2: Thermal 6π-electrocyclizations of tricyclic 1,3,4,5,6-pentasubstituted 1,3,5-hexatrienes.

Starting cmpd.	Product	Yield [%][a]	d.r.[b]	$[\alpha]_D^{20}$ [c]
cis-**5a**	*cis*-**6a**	75	1:1	+54.5 (10.0)
cis-**5b**	*cis*-**6b**	71	–	+49.7 (6.00)
trans-**5b**	*trans*-**8b**	63[d]	–	+27.0[d] (10.0)

[a] Yield of isolated product. [b] The diastereomeric ratio was determined by ^{1}H NMR spectroscopy. [c] Concentration *c* [mg mL^{-1}] in parentheses. [d] Plus 15% of *trans*-**6b**, which has an optical rotation of $[\alpha]_D^{20} = +24.4$ (12.4 mg mL^{-1}, C_6H_6).

Heating the isomer *trans*-**5b** with *trans* CD-ring fusion at 220 °C for 30 min led to a separable mixture of the primary 6π-electrocyclization product *trans*-**8b** and the product of a subsequent 1,5-hydrogen shift, *trans*-**6b**, in a ratio of 4:1 (Scheme 2). The overall yield is 78%, and the 63% yield of the main product *trans*-**8b** is preparatively satisfying. When a sample of *trans*-**6b** was heated in decalin at 215 °C for 45 min, *trans*-**8b** was again the main product, which proves reversibility for the 1,5-hydrogen shift. In view of this, complete transformation of *trans*-**6b** into *trans*-**8b** may be possible. Because of the *trans* relationship of the hydrogens on C8 and C14 and the *trans* CD-ring fusion, this product is more closely related to the natural steroids than *cis*-**6a,b**.

Variation of the temperature (190–260 °C) and extended heating (up to 90 min) of *trans*-**5b** (Table 2) did not significantly affect the ratio of two regioisomers *trans*-**8b** and *trans*-**6b**, unlike the observation for the hexatrienes *cis*-**5a**,**b.** However, at 260 °C, the hexatriene *trans*-**5b** furnished not only a mixture of the regioisomeric cyclohexadienes *trans*-**8b** *and trans*-**6b** but also significant amounts (10–15%) of the products **9** and **10**, which are formed by de-*tert*-butoxycarbonylation without and with subsequent aromatization, respectively, of the B ring (Scheme 2).



Scheme 2. A) Decalin, 215 °C, 30 min.

It is noteworthy that all the 6π-electrocyclizations occur with a high degree of outward disrotational selectivity,[22] as the tetracycles *cis*-**6b**, *trans*-**6b**, and *trans*-**8b** were all isolated as single diastereomers.[23] These steroidal products ought to be enantiomerically pure as well, since the bicycloalkenylstannanes *cis*-**2** and *trans*-**2** were enantiomerically pure starting materials and any racemization along the route would not be probable.

Received: June 18, 2003 [Z52162]

Keywords: cross-coupling · homogeneous catalysis · pericyclic reactions · steroids · total synthesis

[1] a) S. N. Ananchenko, I. V. Torgov, *Tetrahedron Lett.* **1963**, 1553–1558; b) N. Cohen, B. L. Banner, W. F. Eichel, D. R. Parrish, G. Saucy, J.-M. Cassal, W. Meier, A. Fürst, *J. Org. Chem.* **1975**, *40*, 681–685; c) Y. Zhang, E.-i. Negishi, *J. Am. Chem. Soc.* **1989**, *111*, 3454–3456; d) H. Nemoto, N. Matsuhashi, M. Imaizumi, M. Nagai, K. Fukumoto, *J. Org. Chem.* **1990**, *55*, 5625–5631; e) C. D. Dzierba, K. S. Zandi, T. Möllers, K. J. Shea, *J. Am. Chem. Soc.* **1996**, *118*, 4711–4712; f) K. C. Nicolaou, D. Vourloumis, N. Winssinger, P. S. Baran, *Angew. Chem.* **2000**, *112*, 47–126; *Angew. Chem. Int. Ed.* **2000**, *39*, 44–122.

[2] a) R. L. Funk, K. P. C. Vollhardt, *J. Am. Chem. Soc.* **1980**, *102*, 5253–5261; b) R. L. Funk, K. P. C. Vollhardt, *J. Am. Chem. Soc.* **1979**, *101*, 215–217.

[3] P. v. Zezschwitz, F. Petry, A. de Meijere, *Chem. Eur. J.* **2001**, *7*, 4035–4046.

[4] For reviews on the Stille reaction see: a) T. N. Mitchell in *Metal-Catalyzed Cross-Coupling Reactions* (Eds.: F. Diederich, P. J. Stang), Wiley-VCH, Weinheim, **1998**, pp. 167–202; b) V. Farina, V. Krishnamurthy, W. J. Scott, *Org. React.* **1997**, *50*, 1–652; c) T. N. Mitchell, *Synthesis* **1992**, 803–815; d) M. Kosugi, K. Fugami in *Handbook of Organopalladium Chemistry for Organic Synthesis* (Eds.: E.-i. Negishi, A. de Meijere), Wiley, New York, **2002**, pp. 263–284.

[5] S. R. Gilbertson, C. A. Challener, M. E. Bos, W. D. Wulff, *Tetrahedron Lett.* **1988**, *29*, 4795–4798.

 © 2004 Wiley-VCH Verlag GmbH & Co. KGaA, Weinheim

[6] J. E. McMurry, W. J. Scott, *Tetrahedron Lett.* **1983**, *24*, 979 – 982.
[7] U. Groth, T. Köhler, T. Taapken, *Tetrahedron* **1991**, *47*, 7583 – 7592.
[8] For the *trans*-configurated enol triflate the yield was determined over two steps since the diisobutylaluminum enolate was first trapped as the trimethylsilyl enol ether, which was cleaved with MeLi to form the more reactive lithium enolate.
[9] a) Z. G. Hajos, D. R. Parrish, *J. Org. Chem.* **1974**, *39*, 1612 – 1614; b) Z. G. Hajos, D. R. Parrish, *J. Org. Chem.* **1974**, *39*, 1615 – 1621; c) R. A. Micheli, Z. G. Hajos, N. Cohen, D. R. Parrish, L. A. Portland, W. Sciamanna, M. A. Scott, P. A. Wehrli, *J. Org. Chem.* **1975**, *40*, 675 – 681.
[10] J. A. Marshall, G. A. Flynn, *Synth. Commun.* **1979**, *9*, 123 – 127.
[11] K. A. Parker, H.-J. Kim, *J. Org. Chem.* **1992**, *57*, 752 – 755.
[12] W. J. Kerr, M. McLaughlin, A. J. Morrison, P. L. Pauson, *Org. Lett.* **2001**, *3*, 2945 – 2948.
[13] P. L. Stotter, K. A. Hill, *J. Org. Chem.* **1973**, *38*, 2576 – 2578.
[14] V. Farina, B. Krishnan, D. R. Marshall, G. P. Roth, *J. Org. Chem.* **1993**, *58*, 5434 – 5444.
[15] More recent experiments showed that triphenylarsane does not play any significant role in the Stille coupling of **3b** with *trans*-**2**. Even without the presence of $AsPh_3$ the product *trans*-**4b** was obtained in a comparable yield of 84%.
[16] Reactions with *tert*-butyl acrylate proved to give consistently better yields those with methyl acrylate, from which early precipitation of palladium black was observed. This may be attributed to a better stabilization of the palladium(0) catalyst by the less electron-deficient *tert*-butyl acrylate. Cf. a) M. Buback, T. Perkovic, S. Redlich, A. de Meijere, *Eur. J. Org. Chem.* **2003**, 2375 – 2382; b) T. Perkovic, Dissertation, Universität Göttingen, **1999**.
[17] The palladacycle was prepared from $Pd(OAc)_2$ and $(o\text{Tol})_3P$: a) W. A. Herrmann, C. Brossmer, K. Öfele, C.-P. Reisinger, T. Priermeier, M. Beller, H. Fischer, *Angew. Chem.* **1995**, *107*, 1989 – 1992; *Angew. Chem. Int. Ed. Engl.* **1995**, *34*, 1844 – 1848; b) W. A. Herrmann, C. Brossmer, C.-P. Reisinger, T. Riermeier, K. Öfele, M. Beller, *Chem. Eur. J.* **1997**, *3*, 1357 – 1364.
[18] Cf. a) F. Ozawa, A. Kubo, T. Hayashi, *Chem. Lett.* **1992**, 2177 – 2180; b) S. Lemaire-Audoire, M. Savignac, C. Dupuis, J.-P. Genêt *Tetrahedron Lett.* **1996**, *37*, 2003 – 2006; c) F. Y. Zhao, M. Shirai, M. Arai, *J. Mol. Catal. A* **2000**, *154*, 39 – 44; d) L. F. Tietze, T. Nöbel, M. Spescha, *Angew. Chem.* **1996**, *108*, 2385 – 2386; *Angew. Chem. Int. Ed. Engl.* **1996**, *35*, 2259 – 2261.
[19] Cf. a) T. L. Gilchrist, R. J. Summersell, *J. Chem. Soc. Perkin Trans. 1* **1988**, 2595 – 2601; b) A. Lansky, Dissertation, Universität Göttingen, **1992**.
[20] K. Voigt, P. von Zezschwitz, K. Rosauer, A. Lansky, A. Adams, O. Reiser, A. de Meijere, *Eur. J. Org. Chem.* **1998**, 1521 – 1534.
[21] When the hexatrienes were heated at lower temperatures (150–160 °C), the reaction required significantly longer times. For example, even after 12 h traces of the starting materials could be detected and, besides the desired products, several side products were formed.
[22] a) B. M. Trost, P. G. McDougal, *J. Org. Chem.* **1984**, *49*, 458 – 468. This rotational selectivity has also been termed torquoselectivity. Cf. b) E. A. Kallel, Y. Wang, D. C. Spellmeyer, K. N. Houk, *J. Am. Chem. Soc.* **1990**, *112*, 6759 – 6763; c) J. D. Evanseck, B. E. Thomas IV, D. C. Spellmeyer, K. N. Houk, *J. Org. Chem.* **1995**, *60*, 7134 – 7141.
[23] The structures were confirmed by ^1H–^1H NOESY NMR experiments in which interactions within the steroid analogue *cis*-**6b** between the protons of the methyl group at C13 and the proton at C14 as well as between the proton at C14 and the proton at C7 were detected. For the steroid *trans*-**8b** interactions between the methyl group at C13 and the proton at C8 could be observed, and also interactions between the proton at C7 and the proton at C8 as well as the proton at C14 and one proton at C15 were found.

 © 2004 Wiley-VCH Verlag GmbH & Co. KGaA, Weinheim

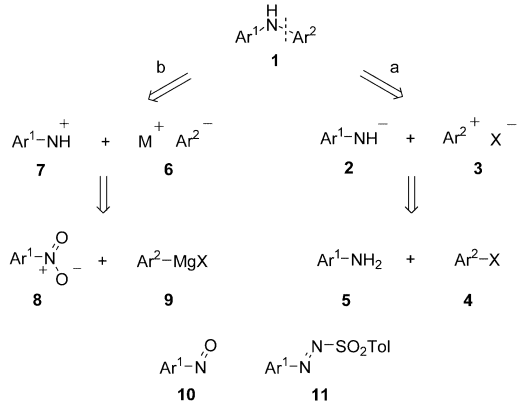
Amination

A General Amination Method Based on the Addition of Polyfunctional Arylmagnesium Reagents to Functionalized Arylazo Tosylates**

*Ioannis Sapountzis and Paul Knochel**

Dedicated to Professor Gernot Boche

The preparation of polyfunctional diarylamines of type **1** is an important goal in synthesis since these building blocks are present in many pharmaceuticals and various fine chemicals. There are two approaches to such target molecules[1] involving either the generation of a nucleophilic amino synthon **2** which will react with an electrophilic aromatic reagent (Ar^+X^- **3**, path a in Scheme 1). This retrosynthetic analysis has been successfully demonstrated recently with palladium-[2] and copper-catalyzed[3] reactions between aryl halides **4** and various amines **5**.



Scheme 1. Retrosynthetic analysis for the preparation of diarylamines.

Alternatively, one may envision adding an organometallic reagent **6** to a positively charged arylamine synthon **7** (path b in Scheme 1).[4] We reported recently that nitroarenes of type **8** are excellent equivalents for electrophilic nitrogen synthons. They react with arylmagnesium halides **9** and provide after

[*] Dipl.-Chem. I. Sapountzis, Prof. Dr. P. Knochel
Department Chemie
Ludwig-Maximilians-Universität München
Butenandtstrasse 5–13, Haus F, 81377 München (Germany)
Fax: (+49) 089-21-80-776-80
E-mail: paul.knochel@cup.uni-muenchen.de

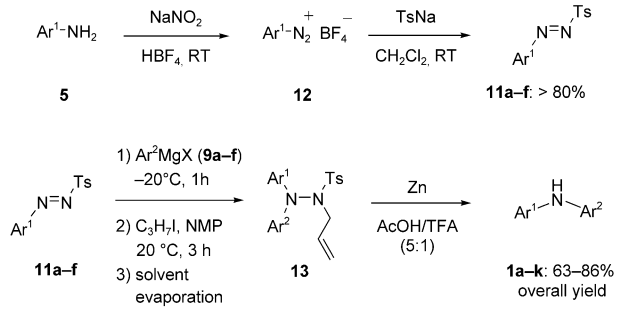
[**] We thank Aventis Pharma (Frankfurt a.M.) for a fellowship (I.S.) and the Fonds der Chemischen Industrie for financial support. We also thank K. Becker for the preparation of starting materials as well as Chemetall GmbH (Frankfurt a.M.), Wacker Chemie GmbH (München), and BASF AG (Ludwigshafen) for generous gifts of chemicals.

Supporting information for this article is available on the WWW under http://www.angewandte.org or from the author.

 DOI: 10.1002/anie.200353241 © 2004 Wiley-VCH Verlag GmbH & Co. KGaA, Weinheim

reductive workup diarylamines of type **1** in excellent overall yields.[5] A drawback of this method is requirement of two equivalents of the Grignard reagent **9**, since one equivalent of Ar^2MgX is consumed in the reduction of the nitroarene to an intermediate arylnitroso species **10**.[5d] We have examined the direct use of the arylnitroso derivatives **10** as starting materials for the amination procedure[6] since this would preclude the use of an excess of the arylmagnesium reagent. Although the reaction of nitrosoarenes of type **10** with arylmagnesium species proceeds well, their stability is limited and their synthesis is complicated by dimerization reactions which reduce the scope of this approach.[6]

We report herein that arylazo tosylates[7] of type **11** are powerful synthetic equivalents of the electrophilic arylamino synthon **7** (Schemes 1 and 2). They are readily prepared from



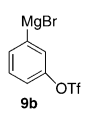
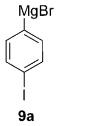
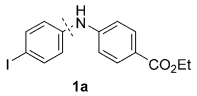
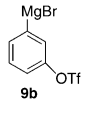
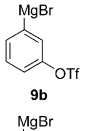
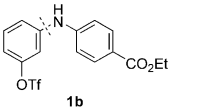
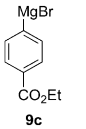
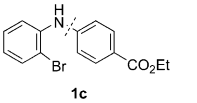
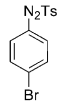
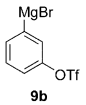
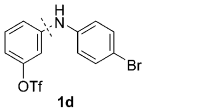
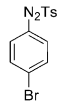
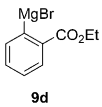
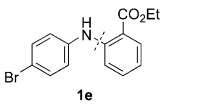
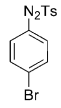
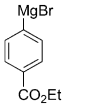
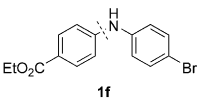
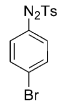
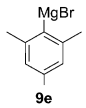
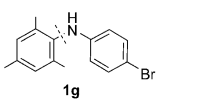
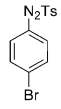
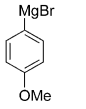
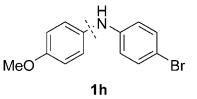
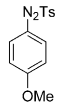
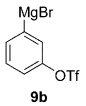
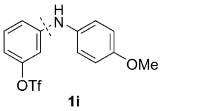
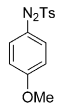
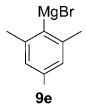
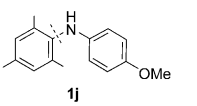
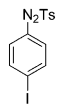
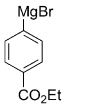
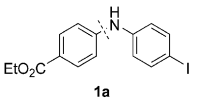
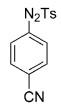
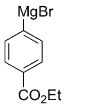
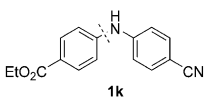
Scheme 2. Preparation of arylazo tosylates and diarylamines.

aromatic amines of type **5** in a two step-sequence consisting of a diazotation ($NaNO_2$, 50% HBF_4 in water, 25 °C, 1 h)[8] and subsequent reaction of the resulting diazonium tetrafluoroborates **12** with sodium *p*-toluenesulfinate (NaTs) in dichloromethane (CH_2Cl_2, 25 °C, overnight). Various functionalized arylazo tosylates of type **11** result in overall yields of over 80%.[7]

We have now found that these highly electrophilic diazo derivatives react under mild conditions (−20 °C, 1 h) with a broad range of polyfunctional arylmagnesium halides prepared by an iodine–magnesium exchange reaction.[9] The intermediate addition products were allylated in situ by addition of first *N*-methylpyrrolidinone (NMP) and then allyl iodide. The resulting hydrazine derivatives **13** were treated, after evaporation of the solvents, with zinc in a 5:1 mixture of acetic acid and trifluoroacetic acid (TFA; 75 °C, 1–8 h). This one-pot procedure furnishes polyfunctionalized diarylamines **1a**–**k** in overall yields of 63–86% (Scheme 2 and Table 1).

Various functionalized arylazo tosylates **11a**–**f** undergo addition reactions with magnesium compounds. Thus, the presence of electron-withdrawing groups such as an ester (entries 1 and 2), a halogen substituent (entries 3–8 and 11), and a nitrile function (entry 12) or an electron-donating group like a methoxy substituent (entries 9 and 10) is compatible with the reaction of a range of functionalized Grignard reagents. Remarkably, both the Grignard reagent as well as the arylazo tosylates of type **11** can bear a bromine (entries 3–8) or an iodine substituent (entries 1 and 11). A highly electrophilic functionality like a triflate (entries 2, 4, and 9) is

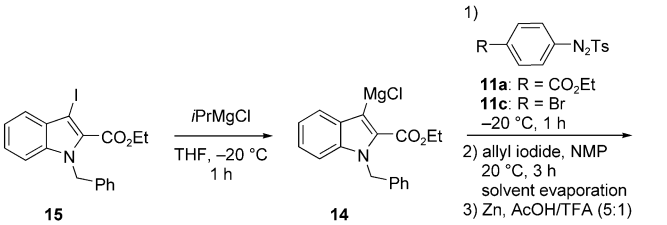
Table 1: Polyfunctional diarylamines **1a**–**l** obtained by the addition of functionalized Grignard reagents **9a**–**f** to functionalized arylazo tosylates **11a**–**f** followed by in situ allylation and reductive workup.

Entry	Diazo reagent	Ar^2MgBr	Product[a]	Yield [%][b]
1	 **9b**	 **9a**	 **1a**	63
2	 **9b**	 **9b**	 **1b**	76
3	 **11b**	 **9c**	 **1c**	65
4	 **11c**	 **9b**	 **1d**	70
5	 **11c**	 **9d**	 **1e**	80
6	 **11c**	 **9c**	 **1f**	83
7	 **11c**	 **9e**	 **1g**	69
8	 **11c**	 **9f**	 **1h**	86
9	 **11d**	 **9b**	 **1i**	81
10	 **11d**	 **9e**	 **1j**	83
11	 **11e**	 **9c**	 **1a**	71
12	 **11f**	 **9c**	 **1k**	64

[a] The dotted lines indicate the new carbon–nitrogen bond. [b] Overall yields of analytically pure product from the one-pot procedure including the allylation with allyl iodide and subsequent zinc reduction in AcOH/TFA (5:1).

 © 2004 Wiley-VCH Verlag GmbH & Co. KGaA, Weinheim

also tolerated under the mild reaction conditions. In this respect our amination method differs from the Pd-, Cu-, and Ni-catalyzed amination reactions of aromatic halides,[2,3] and our method is thus complementary to the Buchwald–Hartwig amination procedure. Steric hindrance is also not problematic, since in both the arylazo tosylate as well as in the Grignard reagent the presence of an *ortho* substituent does not reduce the amination yields (entries 3, 7, and 10). Our procedure can also be applied successfully to heterocyclic systems. Thus, the functionalized 3-indolylmagnesium reagent **14** prepared from the corresponding heterocyclic iodide **15** by iodine–magnesium exchange reacts with the arylazo tosylates **11a** and **11c** under the usual reaction conditions, providing the new 3-arylaminated indole derivatives **16a–b** in 58–71% yield (Scheme 3).

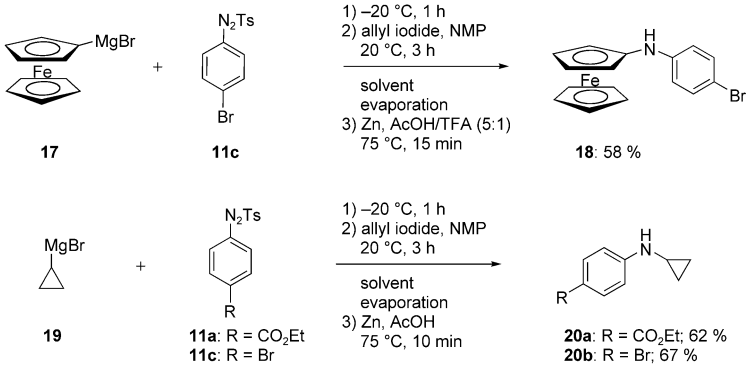


Scheme 3. Preparation of (3-arylamino)indole derivatives.

Finally, the new amination reaction has a broad scope and can be extended to other classes of organomagnesium reagents. Thus, the preparation of elusive ferrocenyl aryl amines[10] can be readily achieved by treating ferrocenylmagnesium bromide (**17**), which is prepared from tributylstannylferrocene,[11] with the arylazo tosylate **11c** followed by the usual reductive workup. Under these conditions, the new aminated ferrocenyl derivative **18** is obtained in 58% yield (Scheme 4).

Aliphatic magnesium compounds undergo the amination reaction as well. Thus cyclopropylmagnesium bromide **19** reacts with the arylazo tosylates **11a** and **11c** to afford the expected *N*-arylcyclopropylamines **20a** and **20b**, respectively,[12] in 62–67% yields (Scheme 4).

In summary, we have shown that arylazo tosylates of type **11**, which are easily prepared from arylamines, are excellent amination reagents. They react with various aromatic and heterocyclic magnesium compounds providing a range of new polyfunctional amines, some of which are difficult to prepare by standard methods. The extension of this method to other organometallic reagents is currently being investigated in our laboratories.



Scheme 4. Preparation of ferrocenyl aryl amine **18** and *N*-arylcyclopropylamines **20a** and **20b**.

Experimental Section

General procedure for the synthesis of arylazo tosylates: **11c**: 4-Bromoaniline (1.72 g, 10 mmol) was dissolved in 15 mL aq HBF_4 solution (50% in water) and cooled to 0°C before a solution of $NaNO_2$ (760 mg, 11 mmol) in water (5 mL) was added dropwise. After 30 min of stirring, the reaction mixture was allowed to warm to room temperature and was stirred for an additional hour. The white precipitate was filtered off and washed subsequently with aq HBF_4 solution (10 mL), ethanol (10 mL), and diethyl ether (20 mL). The white crystalline powder was dissolved in dichloromethane without further purification or drying. NaTs (2.14 g, 12 mmol) was added, and the reaction mixture was stirred overnight. The salts were removed by filtration, and the crude reaction mixture was concentrated in vacuo. Recrystallization from ethanol yielded **11c** (2.71 g, 80%) as an orange solid.

General procedure for the amination: **1f**: A dry and argon-flushed 25-mL round-bottom flask equipped with a magnetic stirrer and a septum was charged with ethyl 4-iodobenzoate (306 mg, 1.1 mmol) dissolved in dry THF (5 mL) and cooled to −20°C. *i*PrMgCl (1.15 mL, 1.1 mmol, 0.95 M in THF) was added dropwise and the I/Mg exchange was monitored by GC analysis until completion (30 min). 4-Bromophenylazo tosylate (**11c**) (339 mg, 1 mmol) was dissolved in THF (3 mL) and added dropwise to the Grignard reagent. After 1 h of stirring at −20°C, the reaction mixture was treated with allyl iodide (510 mg, 3 mmol) and NMP (2 mL), and stirred for additional 2 h at room temperature. The solvents were removed in vacuo and the residue taken up in glacial acetic acid (10 mL). Zinc powder (10 mmol) and TFA (2 mL) were added, and the reaction mixture was heated to 75°C until no starting material was evident by TLC analysis (2 h). The reaction mixture was allowed to cool to room temperature and was poured on crushed ice (ca. 30 g) and 20 mL of 2 M NaOH. The aqueous phase was extracted with diethyl ether (3 × 30 mL), and the combined organic phases were washed successively with sat. $NaHCO_3$ solution and brine. The organic phases were dried over Na_2SO_4, filtered, and concentrated in vacuo. Flash chromatography on silica gel (pentane/diethyl ether 9:1) furnished **1f** (265 mg, 83%) as a colorless solid.

Received: November 3, 2003 [Z53241]

Keywords: amination · Grignard reaction · halogen–magnesium exchange · heterocycle synthesis · synthetic methods

[1] a) A. Ricci, *Modern Amination Methods*, Wiley-VCH, Weinheim, **2000**; b) P. Dembech, G. Seconi, A. Ricci, *Chem. Eur. J.* **2000**, *6*, 1281; c) E. Erdik, M. Ay, *Chem. Rev.* **1989**, *89*, 1947; d) G. Boche, *Houben-Weyl*, *Methods of Organic Chemistry* (Eds.: G. Helmchen, R. W. Hoffmann, J. Mulzer, E. Schaumann), Thieme, Stuttgart, **1995**.

 © 2004 Wiley-VCH Verlag GmbH & Co. KGaA, Weinheim

[2] a) J. P. Wolfe, S. Wagaw, J.-F. Marcoux, S. L. Buchwald, *Acc. Chem. Res.* **1998**, *31*, 805; b) J. F. Hartwig, *Angew. Chem.* **1998**, *110*, 2155; *Angew. Chem. Int. Ed.* **1998**, *37*, 2046; c) L. M. Alcazar-Roman, J. F. Hartwig, A. L. Rheingold, L. M. Liable-Sands, I. A. Guzei, *J. Am. Chem. Soc.* **2000**, *122*, 4618; d) U. K. Singh, E. R. Strieter, D. G. Blackmond, S. L. Buchwald, *J. Am. Chem. Soc.* **2002**, *124*, 14104; d) T. E. Mueller, M. Beller, *Chem. Rev.* **1998**, *98*, 675; e) For a nickel-catalyzed amination, see: B. H. Lipshutz, H. Ueda, *Angew. Chem.* **2000**, *112*, 4666; *Angew. Chem. Int. Ed.* **2000**, *39*, 4492.

[3] a) J. C. Antilla, S. L. Buchwald, *Org. Lett.* **2001**, *3*, 2077; b) J. P. Collman, M. Zhong, *Org. Lett.* **2000**, *2*, 1233; c) P. Y. S. Lam, G. Vincent, D. Bonne, C. G. Clark, *Tetrahedron Lett.* **2003**, *44*, 4927; d) P. Y. S. Lam, S. Deudon, K. M. Averill, R. Li, M. Y. He, P. DeShong, C. G. Clark, *J. Am. Chem. Soc.* **2000**, *122*, 7600; e) J. Zanon, A. Klapars, S. L. Buchwald, *J. Am. Chem. Soc.* **2003**, *125*, 2890; f) F. Y. Kwong, S. L. Buchwald, *Org. Lett.* **2003**, *5*, 793; g) D. Zim, S. L. Buchwald, *Org. Lett.* **2003**, *5*, 2413.

[4] a) G. Boche, H. U. Wagner, *J. Chem. Soc. Chem. Commun.* **1984**, 1591; b) G. Boche, C. Boie, F. Bosold, K. Harms, M. Marsch, *Angew. Chem.* **1994**, *106*, 90; *Angew. Chem. Int. Ed. Engl.* **1994**, *33*, 115; c) A. Casarini, P. Dembech, D. Lazzari, E. Marini, G. Reginato, A. Ricci, G. Seconi, *J. Org. Chem.* **1993**, *58*, 5620; d) J. P. Genêt, S. Mallart, C. Greck, E. Piveteau, *Tetrahedron Lett.* **1991**, *32*, 2359; e) C. Greck, J. P. Genêt, *Synlett* **1997**, 741; f) P. Beak, A. Basha, B. Kokko, *J. Am. Chem. Soc.* **1984**, *106*, 1511; g) B. M. Trost, W. H. Pearson, *J. Am. Chem. Soc.* **1981**, *103*, 2483; h) H. Tsutsui, T. Ichikawa, K. Narasaka, *Bull. Chem. Soc. Jpn.* **1999**, *72*, 1869.

[5] a) I. Sapountzis, P. Knochel, *J. Am. Chem. Soc.* **2002**, *124*, 9390; b) H. Wieland, *Ber. Dtsch. Chem. Ges.* **1903**, *36*, 2315; c) H. Gilman, R. McCracken, *J. Am. Chem. Soc.* **1927**, *49*, 1052; d) G. Koebrich, P. Buck, *Chem. Ber.* **1970**, *103*, 1412.

[6] a) F. Kopp, I. Sapountzis, P. Knochel, *Synlett* **2003**, 885; b) N. Momoyama, H. Yamamoto, *Angew. Chem.* **2002**, *114*, 3112; *Angew. Chem. Int. Ed.* **2002**, *41*, 2986; c) N. Momoyama, H. Yamamoto, *Org. Lett.* **2002**, *4*, 3579.

[7] a) M. J. Evers, L. E. Christiaens, M. R. Guillaume, M. J. Renson, *J. Org. Chem.* **1985**, *50*, 1779; b) M. J. Evers, L. E. Christiaens, M. J. Renson, *J. Org. Chem.* **1986**, *51*, 5196; c) N. Kimigata, A. Satoh, T. Kondoh, M. Mameyama, *Bull. Chem. Soc. Jpn.* **1988**, *61*, 3575; d) C. Dell'Erba, M. Novi, G. Petrillo, C. Tafani, *Tetrahedron* **1995**, *51*, 3905; e) C. Dell'Erba, M. Novi, G. Petrillo, C. Tafani, *Tetrahedron* **1997**, *53*, 2125.

[8] S. H. Karzeniowski, G. W. Gokel, *Tetrahedron Lett.* **1977**, 3519.

[9] a) P. Knochel, W. Dohle, N. Gommermann, F. Kneisel, F. Kopp, T. Korn, I. Sapountzis, V. A. Vu, *Angew. Chem.* **2003**, *115*, 4438; *Angew. Chem. Int. Ed.* **2003**, *42*, 4302; b) A. Staubitz, W. Dohle, P. Knochel, *Synthesis* **2003**, 233; c) F. F. Kneisel, P. Knochel, *Synlett* **2002**, 1799; d) N. Gommermann, C. Koradin, P. Knochel, *Synthesis* **2002**, 2143; e) A. E. Jensen, W. Dohle, I. Sapountzis, D. M. Lindsay, V. A. Vu, P. Knochel, *Synthesis* **2002**, 565.

[10] a) G. R. Knox, P. L. Pauson, D. Willison, E. Solcaniova, S. Toma, *Organometallics* **1990**, *9*, 301; b) F. S. Arimoto, A. C. Haven, *J. Am. Chem. Soc.* **1955**, *77*, 6295; c) D. W. Hall, J. H. Richards, *J. Org. Chem.* **1963**, *28*, 1549; d) E. M. Acton, R. M. Silverstein, *J. Org. Chem.* **1959**, *24*, 1487.

[11] D. Giullaneux, H. B. Kagan, *J. Org. Chem.* **1995**, *60*, 2502.

[12] a) A. de Meijere, S. I. Kozhushkov, A. I. Savchenko in *Titanium and Zirconium in Organic Synthesis* (Ed.: I. Marek), Wiley-VCH, Weinheim, **2002;** b) W. Cui, R. N. Loeppky, *Tetrahedron* **2001**, *57*, 2953.

 © 2004 Wiley-VCH Verlag GmbH & Co. KGaA, Weinheim

Bioorganic Chemistry

Spatial Screening of Cyclic Neoglycopeptides: Identification of Polyvalent Wheat-Germ Agglutinin Ligands**

Valentin Wittmann and Sonja Seeberger*

Natural and synthetic polyvalent ligands can act as inhibitors of biological processes or as effectors of signal-transduction pathways.[1,2] In the case of carbohydrate–lectin interactions, polyvalency is of particular importance because individual carbohydrate epitopes are usually bound with only weak affinity and often broad specificity.[3,4] The potency of a polyvalent inhibitor depends on the spatial presentation of the carbohydrates and the associated possibility of occupying several binding sites simultaneously. If the 3D structure of the protein is known, suitable polyvalent ligands may be obtained by rational design. This has been impressively demonstrated for the bacterial AB_5 toxins[5] as well as for non-carbohydrate systems[6] ("directed" polyvalency). However, if the three-dimensional orientation of the binding sites of a polyvalent lectin is not known, many potential ligands have to be synthesized and screened to determine the required orientation of the carbohydrate units.[4,7] This holds true particularly for conformationally restricted glycoclusters which may lead in such cases to ligands with especially strong affinities.[1,6,8] Screening of a library of spatially diverse glycoclusters could accelerate this process significantly. St. Hilaire, Meldal, et al. reported on split-and-mix libraries of linear glycopeptides.[9] First studies on the behavior of dynamic combinatorial carbohydrate libraries of four[10] and 21[11] compounds in the presence of lectins have been published as well.

Here we report the first example of a split-and-mix library of conformationally restricted, spatially diverse glycoclusters, and their screening for binding to the *N*-acetylglucosamine-(GlcNAc)-binding plant lectin wheat-germ agglutinin (WGA). As scaffold molecules (templates) for the presentation of the carbohydrate residues we chose side-chain-cyclized pep-

[*] Dr. V. Wittmann,[+] Dipl.-Chem. S. Seeberger
Institut für Organische Chemie und Chemische Biologie
Johann Wolfgang Goethe-Universität
Marie-Curie-Strasse 11, 60439 Frankfurt (Germany)
E-mail: mail@valentin-wittmann.de

[+] New address:
Universität Konstanz, Fachbereich Chemie
Fach M 709, 78457 Konstanz (Germany)
Fax: (+49) 7531-88-4573

[**] This work was supported by the Deutsche Forschungsgemeinschaft and by the Adolf-Messer-Stiftung (Adolf Messer Prize 2000 for interdisciplinary basic research to V.W.). We thank Prof. Joachim W. Engels for his support, Prof. Hermann Schägger for performing microsequence analyses, Degussa AG for a donation of amino acids, and Aventis AG for providing an HPLC system.

Supporting information for this article (syntheses of **1**, **3**, **5**, and **9**, and the procedure for the solid-phase enzyme-immuno lectin-binding assay) is available on the WWW under http://www.angewandte.org or from the author.

 © 2004 Wiley-VCH Verlag GmbH & Co. KGaA, Weinheim DOI: 10.1002/anie.200352055

tides.[12] Figure 1 shows the composition of library **1**, which was obtained by convergent solid-phase synthesis on TentaGel without employing a linker according to a synthetic strategy[13] described by us. At the combinatorially varied positions marked in gray, L- and D-amino acids without further side-chain functionality as well as L- and D-diamino acids, such as L-2,3-diaminopropionic acid (Dpr), D-2,4-diaminobutyric acid (D-Dab), and D-lysine, were used. The latter served as attachment points for GlcNAc residues by means of urethane formation with a linker especially developed for this purpose based on the allyloxycarbonyl (Aloc) protecting group. With this library design, spatial diversity may be generated in two "dimensions". Positional diversity leads to different carbohydrate patterns on the peptide scaffolds. Variation of the stereochemistry of the amino acids (stereodiversity) increases spatial diversity by modulating the folding of the peptide backbones.[14] In addition, this library design allows for the analysis of the neoglycopeptides bound to single beads.[15] The carbohydrate contents of all 19440 library members ranges from 0 (2.6% of all compounds) through 1 (14.5%), 2 (30.3%), 3 (30.9%), 4 (16.6%), 5 (4.5%), and 6 (0.5%).

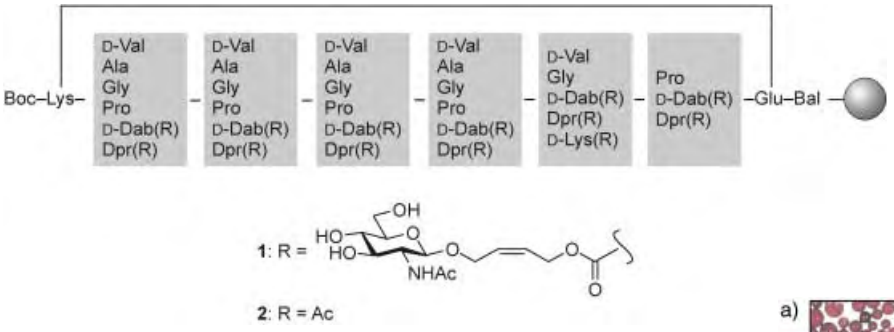


Figure 1. Neoglycopeptide library **1** consisting of 19440 compounds and control library **2** for the spatial screening of WGA ligands.

WGA is a 36-kDa lectin composed of two identical glycine- and cysteine-rich subunits. The WGA dimer contains a total of eight binding sites for GlcNAc and oligomers thereof.[16] Therefore, WGA was a promising candidate for a polyvalent interaction. To screen for binding properties to WGA, we developed the on-bead enzyme-immuno lectin-binding assay shown in Figure 2. Approximately 100 mg of library **1** (corresponding almost 100000 resin beads or five copies of every library member) were incubated with biotinylated WGA, and after washing, a conjugate of a monoclonal anti-biotin antibody and alkaline phosphatase (AP) was added. After further washing the resin beads bearing WGA ligands were visualized by an alkaline phosphatase (AP)-catalyzed reaction delivering a water-insoluble dye.

As shown in Figure 3a, initially approximately 97–98% of all the beads were colored. This result was not unexpected, since this corresponds to the proportion of compounds within **1** with at least one GlcNAc residue. To select for the best WGA ligands in **1**, we added competing monomeric GlcNAc in varying concentrations during incubation with WGA and all subsequent washing steps (Figure 3b and c).[17] Thus it was possible to reduce the number of colored beads to approximately 0.1% (Figure 3c) or in the extreme case even completely. Screening of the non-glycosylated library **2** and a control experiment omitting the addition of

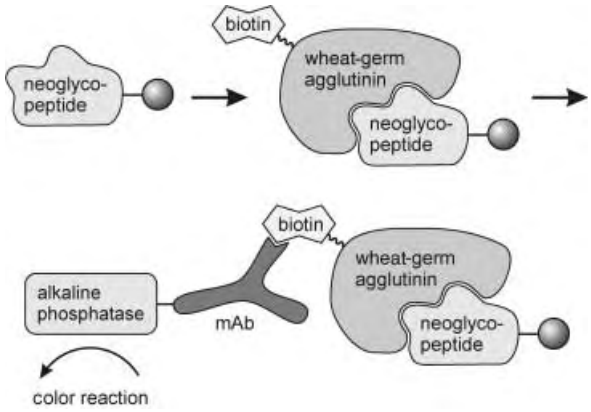


Figure 2. Solid-phase enzyme-immuno lectin-binding assay for screening of **1** for WGA ligands. mAb = monoclonal antibody.

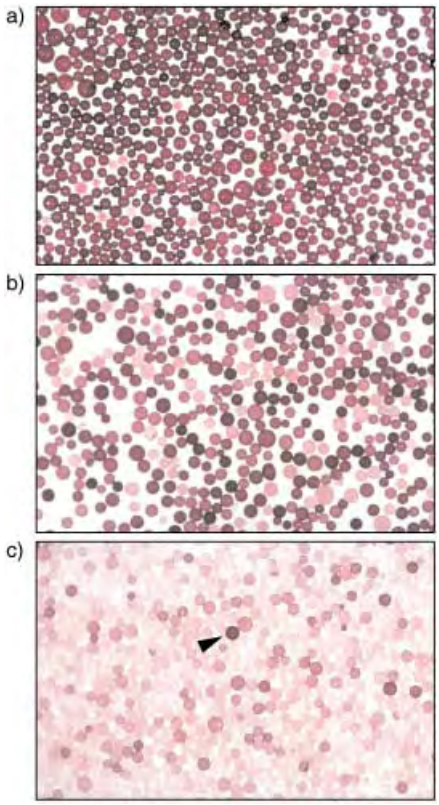
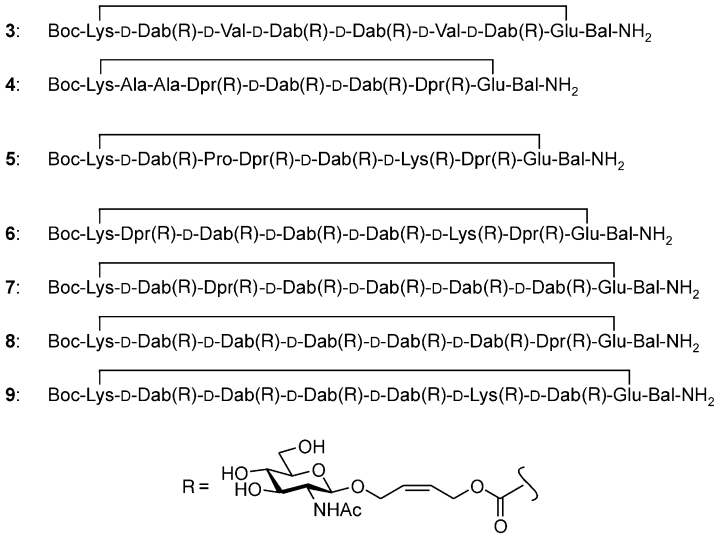


Figure 3. Resin beads of library **1** stained by the WGA binding assay shown in Figure 2. a) Assay carried out without addition of GlcNAc; b) WGA incubation with 225 mM GlcNAc, all further steps with 16 mM GlcNAc; c) WGA incubation with 680 mM GlcNAc, all further steps with 167 mM GlcNAc. The marked bead was identified as a hit. Average diameter of the beads is 130 μm.

 © 2004 Wiley-VCH Verlag GmbH & Co. KGaA, Weinheim

biotinylated WGA led to colorless beads as well. From this we conclude that the result of the binding assay is indeed evoked by a carbohydrate–lectin interaction. In contrast, the initially used binding assay developed by Kahne et al.[18] to screen an oligosaccharide library, in which an AP–streptavidin conjugate is used instead of the AP–antibody conjugate, was not suitable since library **1** apparently contains a small proportion of streptavidin ligands.

The most darkly stained beads were manually selected under a low-power stereo microscope and analyzed by microsequencing (Edman degradation) after palladium-catalyzed detachment of the sugars according to a strategy described by us.[15] Two tetravalent (**3**, **4**), one pentavalent (**5**), and four hexavalent (**6–9**) neoglycopeptides could be identified. If the performed binding assay responds to polyvalency, we expected to find many compounds with a high GlcNAc content. For **3–9** this is clearly the case. Interestingly, however, not all hexavalent neoglycopeptides in library **1** (0.5 %) lead to comparable staining. Instead, one



pentavalent and two tetravalent compounds are among the ligands on the most intensively stained resin beads.

To verify that the result of the binding assay is reproducible in solution, neoglycopeptides **3**, **5**, and **9** were resynthesized as single compounds. IC_{50} values for inhibition of the binding of porcine stomach mucin to peroxidase-labeled WGA (Figure 4, Table 1) were determined by an enzyme-linked lectin assay (ELLA) as described by Zanini and Roy.[19] According to this assay the affinities of the tetra- (**3**), penta- (**5**), and hexavalent (**9**) neoglycopeptides are 218-, 619-, and 568-fold higher, respectively, than that of the monomeric GlcNAc reference (β values[1]). This shows that the result of the solid-phase lectin-binding assay correlates with the binding properties of **3**, **5**, and **9** in solution and is not dominated by a surface effect on the resin beads. This is remarkable in light of observations made by Kahne et al. upon screening a library of immobilized monovalent oligosaccharides against the lectin from *Bauhinia purpurea*. They did not find a

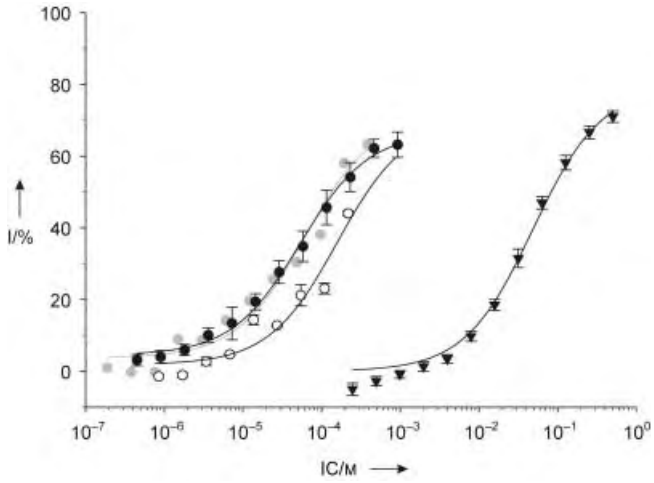


Figure 4. Dose–response curves for inhibition of the binding of porcine stomach mucin to peroxidase-labeled WGA obtained from an enzyme-linked lectin-binding assay (ELLA). Triangles: GlcNAc, white circles: **3**, gray circles: **5**, black circles: **9**. I = inhibition, IC = inhibitor concentration.

Table 1: IC_{50} values for inhibition of the binding of porcine stomach mucin to peroxidase-labeled WGA by **3**, **5**, and **9** obtained from the dose–response curves shown in Figure 4.

Compound	IC_{50} [mM]	β
GlcNAc	83	1
3	0.381	218
5	0.134	619
9	0.146	568

correlation between the solution affinities of monovalent ligands and the corresponding avidities on the surface of resin beads.[18] The fact that **5** and **9** have similar IC_{50} values illustrates that the binding affinity is not only determined by the number of GlcNAc residues but that ligand architecture is important as well. This coincides with observations on other systems.[20]

In summary, we have presented the first example of a split-and-mix library of conformationally restricted, spatially diverse glycoclusters and their screening by a novel solid-phase lectin-binding assay which does not produce false-positive results due to an interaction with streptavidin. The binding enhancement of the identified polyvalent ligands **3**, **5**, and **9** compared to monovalent GlcNAc is the highest ever found for GlcNAc clusters of that size binding to WGA.[19,21] Since the non-glycosylated cyclopeptide library **2** does not contain any WGA ligands, we assume the spatial presentation of the GlcNAc residues on the cyclopeptide templates to be responsible for the high affinity to WGA. The presented procedure of a spatial screening[22] of polyvalent lectin ligands can easily be applied to other lectins because the carbohydrates are coupled to the neoglycopeptide library in the last synthetic step and, therefore, can be replaced easily.

Received: June 4, 2003 [Z52055]

 © 2004 Wiley-VCH Verlag GmbH & Co. KGaA, Weinheim

Keywords: bioorganic chemistry · carbohydrates · glycopeptides · lectins · polyvalency

[1] M. Mammen, S.-K. Choi, G. M. Whitesides, *Angew. Chem.* **1998**, *110*, 2908 – 2953; *Angew. Chem. Int. Ed.* **1998**, *37*, 2754 – 2794.

[2] L. L. Kiessling, J. E. Gestwicki, L. E. Strong, *Curr. Opin. Chem. Biol.* **2000**, *4*, 696 – 703.

[3] a) T. K. Dam, C. F. Brewer, *Chem. Rev.* **2002**, *102*, 387 – 429; b) J. J. Lundquist, E. J. Toone, *Chem. Rev.* **2002**, *102*, 555 – 578; c) B. T. Houseman, M. Mrksich, *Top. Curr. Chem.* **2002**, *218*, 1 – 44; d) T. K. Lindhorst, *Top. Curr. Chem.* **2002**, *218*, 201 – 235; e) L. L. Kiessling, T. Young, K. H. Mortell in *Glycoscience: Chemistry and Chemical Biology, Vol. II* (Eds.: B. Fraser-Reid, K. Tatsuta, J. Thiem), Springer, Heidelberg, **2001**, pp. 1817 – 1861; f) R. Roy, *Top. Curr. Chem.* **1997**, *187*, 241 – 274.

[4] R. T. Lee, Y. C. Lee, *Glycoconjugate J.* **2000**, *17*, 543 – 551.

[5] a) P. I. Kitov, J. M. Sadowska, G. Mulvery, G. D. Armstrong, H. Ling, N. S. Pannu, R. J. Read, D. R. Bundle, *Nature* **2000**, *403*, 669 – 672; b) E. Fan, Z. Zhang, W. E. Minke, Z. Hou, C. L. M. J. Verlinde, W. G. J. Hol, *J. Am. Chem. Soc.* **2000**, *122*, 2663 – 2664.

[6] N. Schaschke, G. Matschiner, F. Zettl, U. Marquardt, A. Bergner, W. Bode, C. P. Sommerhoff, L. Moroder, *Chem. Biol.* **2001**, *8*, 313 – 327.

[7] a) Y. C. Lee, R. T. Lee, *Acc. Chem. Res.* **1995**, *28*, 321 – 327; b) *Neoglycoconjugates. Preparation and Applications* (Eds.: Y. C. Lee, R. T. Lee), Academic Press, San Diego, **1994**.

[8] J. Rao, J. Lahiri, R. M. Weis, G. M. Whitesides, *J. Am. Chem. Soc.* **2000**, *122*, 2698 – 2710.

[9] a) P. M. St. Hilaire, T. L. Lowary, M. Meldal, K. Bock, *J. Am. Chem. Soc.* **1998**, *120*, 13312 – 13320; b) K. M. Halkes, P. M. St. Hilaire, P. R. Crocker, M. Meldal, *J. Comb. Chem.* **2003**, *5*, 18 – 27.

[10] S. Sakai, Y. Shigemasa, T. Sasaki, *Tetrahedron Lett.* **1997**, *38*, 8145 – 8148.

[11] O. Ramström, J.-M. Lehn, *ChemBioChem* **2000**, *1*, 41 – 48.

[12] For the use of cyclic peptides as templates see: a) U. Sprengard, M. Schudok, W. Schmidt, G. Kretzschmar, H. Kunz, *Angew. Chem.* **1996**, *108*, 359 – 362; *Angew. Chem. Int. Ed. Engl.* **1996**, *35*, 321 – 324; b) H. Franzyk, M. K. Christensen, R. M. Jørgensen, M. Meldal, H. Cordes, S. Mouritsen, K. Bock, *Bioorg. Med. Chem.* **1997**, *5*, 21 – 40; c) G. Tuchscherer, M. Mutter, *Pure Appl. Chem.* **1996**, *68*, 2153 – 2162; d) J. Eichler, A. W. Lucka, R. A. Houghten, *Peptides* **1994**, *7*, 300 – 307.

[13] V. Wittmann, S. Seeberger, *Angew. Chem.* **2000**, *112*, 4508 – 4512; *Angew. Chem. Int. Ed.* **2000**, *39*, 4348 – 4352.

[14] R. Haubner, D. Finsinger, H. Kessler, *Angew. Chem.* **1997**, *109*, 1440 – 1456; *Angew. Chem. Int. Ed. Engl.* **1997**, *36*, 1374 – 1389.

[15] V. Wittmann, S. Seeberger, H. Schägger, *Tetrahedron Lett.* **2003**, *44*, 8243 – 9246.

[16] C. S. Wright, G. E. Kellogg, *Protein Sci.* **1996**, *5*, 1466 – 1476.

[17] Other attempts to increase the selectivity of the assay, such as lowering the lectin concentration, were not successful.

[18] a) R. Liang, L. Yan, J. Loebach, M. Ge, Y. Uozumi, K. Sekanina, N. Horan, J. Gildersleeve, C. Thompson, A. Smith, K. Biswas, W. C. Still, D. Kahne, *Science* **1996**, *274*, 1520 – 1522; b) R. Liang, J. Loebach, N. Horan, M. Ge, C. Thompson, L. Yan, D. Kahne, *Proc. Natl. Acad. Sci. USA* **1997**, *94*, 10554 – 10559.

[19] D. Zanini, R. Roy, *Bioconjugate Chem.* **1997**, *8*, 187 – 192.

[20] a) J. E. Gestwicki, C. W. Cairo, L. E. Strong, K. A. Oetjen, L. L. Kiessling, *J. Am. Chem. Soc.* **2002**, *124*, 14922 – 14933; b) S. André, R. J. Pieters, I. Vrasidas, H. Kaltner, I. Kuwabara, F.-T. Liu, R. M. J. Liskamp, H.-J. Gabius, *ChemBioChem* **2001**, *2*, 822 – 830.

[21] T. Furuike, S. Aiba, S.-I. Nishimura, *Tetrahedron* **2000**, *56*, 9909 – 9915.

[22] The term "spatial screening" was first used by Kessler et al. in connection with the screening of libraries of stereoisomeric peptides: H. Kessler, B. Diefenbach, D. Finsinger, A. Geyer, M. Gurrath, S. L. Goodman, G. Hoelzemann, R. Haubner, A. Jonczyk, G. Müller, E. Graf von Roedern, J. Wermuth, *Lett. Pept. Sci.* **1995**, *2*, 155 – 160.

 © 2004 Wiley-VCH Verlag GmbH & Co. KGaA, Weinheim

Cover Picture

Rainer A. Böckmann and Helmut Grubmüller*



Membrane–cation interactions can greatly affect the properties of biological membranes. In their Communication on page 1021 ff. H. Grubmüller and R. A. Böckmann describe the simulation of the binding of sodium and calcium ions to neutral, zwitterionic lipid membranes. The cover picture shows a snapshot from the molecular dynamics simulation of a membrane with Ca^{2+} ions.

Contents

Angewandte EarlyView

The following articles are available online (in Wiley InterScience). You can find them at www.angewandte.org, under Full Text, Early View.

M. Somer, A. Yarasik, L. Akselrud, S. Leoni, H. Rosner, W. Schnelle, R. Kniep:*
$Ae[Be_2N_2]$: Nitridoberyllates of the Heavier Alkaline-Earth Metals
DOI: 10.1002/anie.200352796
Published online: February 2, 2004

M. A. Sanchez-Castillo, C. Couto, W. B. Kim, J. A. Dumesic:*
Gold-Nanotube Membranes for the Oxidation of CO at Gas–Water Interfaces
DOI: 10.1002/anie.200353238
Published online: February 3, 2004

M. J. Rauterkus, B. Krebs:*
Pentanuclear Platinum(II) Macrocycles with Nucleobases
DOI: 10.1002/anie.200352950
Published online: February 2, 2004

H. Imai, Y. Oaki:*
Emergence of Morphological Chirality from Twinned Crystals
DOI: 10.1002/anie.200352891
Published online: January 27, 2004

D. A. Colby, G. M. Ferrence, T. D. Lash:*
Oxidative Metalation of Azuliporphyrins with Copper(II) Salts: Formation of a Porphyrin Analogue System with a Unique Fully Conjugated Nonaromatic Azulene Subunit
DOI: 10.1002/anie.200353189
Published online: January 27, 2004

G. Sonmez, C. K. F. Shen, Y. Rubin, F. Wudl:*
A Red, Green, and Blue (RGB) Polymeric Electrochromic Device (PECD): The Dawning of the PECD Era
DOI: 10.1002/anie.200352910
Published online: January 27, 2004

Articles judged by the referees or the editor as being either very important or very urgent are immediately edited, proof-read, and electronically published once the manuscript has arrived in the editorial office in final form. As long as there is no page number available these articles should be cited in the following manner:

Author(s) *Angew. Chem. Int. Ed.*, online publication date, DOI.

Obituary

Saturo Masamune (1928–2003): Natural Products and Small Rings ——— **922** — Koji Nakanishi and Rick L. Danheiser

Books

An Introduction to Theoretical Chemistry ——— **923** — Jack Simons — *reviewed by B. C. Rinderspacher*

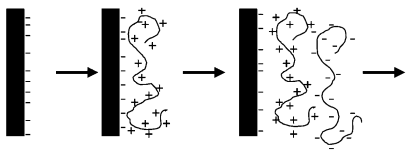
Magnetic Resonance in Chemistry and Medicine ——— **924** — Ray Freeman — *reviewed by G. Gemmecker*

Highlights

Medicinal Chemistry

T. Groth,* A. Lendlein ——— **926–928**

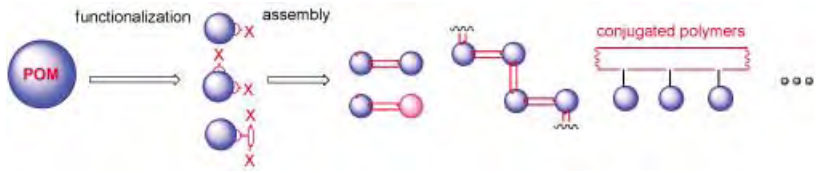
Layer-by-Layer Deposition of Polyelectrolytes—A Versatile Tool for the In Vivo Repair of Blood Vessels



Layer-by-layer adsorption of polygenic polyelectrolytes is a promising method of treatment in which multilayers are formed on the inner arterial wall (see scheme). An advantage of this technique, which has already proved successful in animal models, is that it is very simple to apply, in contrast to in situ polymerization, which requires irradiation with UV light. Furthermore, it is rapid and allows the incorporation of active drugs in the layer.

© 2004 Wiley-VCH Verlag GmbH & Co. KGaA, Weinheim

Minireviews



A modular building-block strategy is used to rationally synthesize conjugated molecules and polymers containing polyoxometalate (POM) clusters that are covalently linked in a variety of architectures (see picture). The most recent advances in organic–inorganic hybrids that are connected by an imido linkage are highlighted.

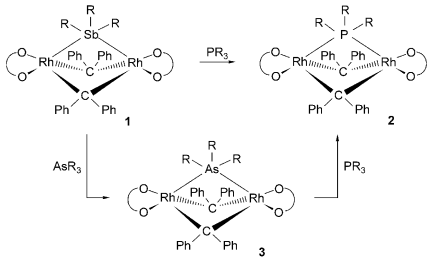
Organic–Inorganic Hybrids

Z. Peng* ——— **930 – 935**

Rational Synthesis of Covalently Bonded Organic–Inorganic Hybrids

Reviews

Until recently, phosphanes, arsanes, and stibanes were considered to bind to transition-metal centers only in a terminal coordination mode. Replacement of the bridging stibane in complex **1** with tertiary phosphanes leads to the formation of compounds **2** and **3** (see scheme). Other dinuclear analogues, even with bulky phosphanes such as P*i*Pr$_3$ and PPh$_3$, are accessible by an unexpected route.

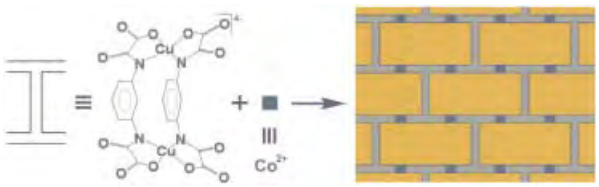


Bridging Ligands

H. Werner* ——— **938 – 954**

The Way into the Bridge: A New Bonding Mode of Tertiary Phosphanes, Arsanes, and Stibanes

Communications



Magnet brickwork: A two-dimensional molecule-based metamagnet is obtained by the reaction of Co^{II} ions and the *tetra*-bidentate {Cu$_2$(mpba)$_2$}$^{4-}$ moiety. The Co^{II} ions act as cement between {Cu$_2$(mpba)$_2$} units to form a brick-wall assembly (see picture). The strong Co^{II} anisotropy and weak interplanar interactions lead to a metamagnetic transition and glassy behavior.

Molecular Magnets

C. L. M. Pereira, E. F. Pedroso, H. O. Stumpf,* M. A. Novak, L. Ricard, R. Ruiz-García, E. Rivière, Y. Journaux* ——— **956 – 958**

A Cu^{II}Co^{II} Metallacyclophane-Based Metamagnet with a Corrugated Brick-Wall Sheet Architecture

For the USA and Canada:
ANGEWANDTE CHEMIE International Edition (ISSN 1433-7851) is published weekly by Wiley-VCH PO Box 191161, D 69451 Weinheim, Germany. Air freight and mailing in the USA by Publications Expediting Inc. 200 Meacham Ave., Elmont, NY 11003. Periodicals postage paid at Jamaica NY 11431. US POSTMASTER: send address changes to *Angewandte Chemie*, Wiley-VCH, 111 River Street, Hoboken, NJ 07030. Annual subscription price for institutions: Europe € 3430.00/3118.00; outside Europe US$ 4499.00/4090.00 (valid for print and electronic/print or electronic delivery); for individuals who are personal members of a national chemical society, or whose institution already subscribes, or who are retired or self-employed consultants, print only: Europe € 248.00/outside Europe US$ 378.00. Postage and handling charges included. All Wiley-VCH prices are exclusive VAT.

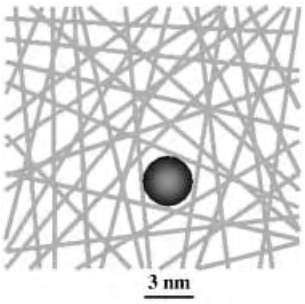
 © 2004 Wiley-VCH Verlag GmbH & Co. KGaA, Weinheim

Contents

Cluster Compounds

B. Corain,* K. Jerabek,* P. Centomo, P. Canton* ——— **959 – 962**

Generation of Size-Controlled Pd^0 Nanoclusters inside Nanoporous Domains of Gel-Type Resins: Diverse and Convergent Evidence That Supports a Strategy of Template-Controlled Synthesis

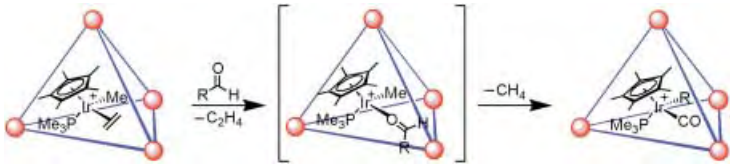


Resin molds for clusters: The nanoporous domains of a gel-type microporous functional resin are used as templates for the production of size-controlled Pd^0 nanoclusters, the size of which is governed by the largest mesh available (see picture). Inverse steric exclusion chromatography provides the quantitative estimate of resin nanoporosity in its swollen state.

Supramolecular Chemistry

D. H. Leung, D. Fiedler, R. G. Bergman,* K. N. Raymond* ——— **963 – 966**

Selective C–H Bond Activation by a Supramolecular Host–Guest Assembly

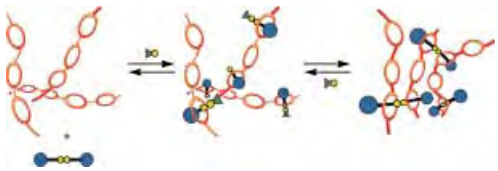


Interior design: A chiral supramolecular tetrahedral $[Ga_4L_6]^{12-}$ host (L = bis(bidentate) ligand) is shown to encapsulate a half-sandwich iridium complex. This host–guest assembly reacts with aldehydes through C–H bond activation, which occurs within the host interior. This activation occurs with high size and shape specificity as well as modest diastereoselectivity (d.r. 55:45–70:30) owing to the well-defined shape of the host cavity.

Supramolecular Polymers

T. Oku, Y. Furusho, T. Takata* **966 – 969**

A Concept for Recyclable Cross-Linked Polymers: Topologically Networked Polyrotaxane Capable of Undergoing Reversible Assembly and Disassembly

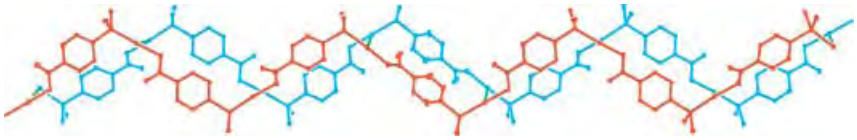


It's physical: A novel concept for recyclable cross-linked polymers is presented by utilizing mechanical linkages in a polyrotaxane network capable of undergoing reversible assembly and disassembly (see schematic representation).

Au–Au Interactions

F. Mohr, M. C. Jennings, R. J. Puddephatt* ——— **969 – 971**

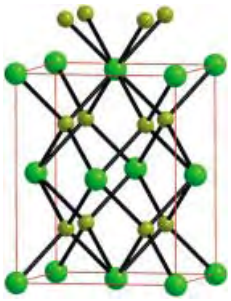
Self-Assembly in Gold(I) Chemistry: A Double-Stranded Polymer with Interstrand Aurophilic Interactions



Raising the gold standard: Hybrid organic–inorganic side-by-side double-chain polymers have been prepared in which individual polymer chains are connected through the aurophilic interactions of gold(I) centers (see picture). The use of alternative isomers of the monomeric building blocks leads to the formation of dimeric or trimeric complexes.

© 2004 Wiley-VCH Verlag GmbH & Co. KGaA, Weinheim

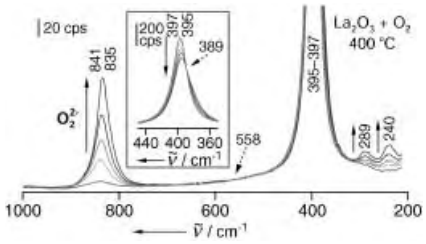
A non-interpenetrating 3D metal–organic framework, synthesized by a solvothermal reaction of cadmium nitrate and a tetracarboxylate ligand, is the first metal–organic analogue of fluorite (CaF_2). In the structure of the title compound, depicted, an eight-connecting tetranuclear cadmium cluster (green sphere) and a tetracarboxylate ligand (brown sphere) play the role of Ca^{2+} and F^- ions, respectively, in fluorite.



Metal–Organic Frameworks

H. Chun, D. Kim, D. N. Dybtsev, K. Kim* ——— 971 – 974

Metal–Organic Replica of Fluorite Built with an Eight-Connecting Tetranuclear Cadmium Cluster and a Tetrahedral Four-Connecting Ligand



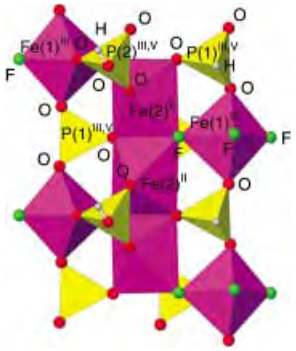
Laser irradiation of La_2O_3 under oxygen at 300–500 °C with the beam of a microprobe Raman spectrometer ($\lambda = 325$, 514.5, or 632.8 nm) caused the emergence of a peroxide band at $\approx 840\ cm^{-1}$ at the expense of the $\nu_{La-O''}$ band at $\approx 400\ cm^{-1}$ with clear isosbestic points at 389 and 558 cm^{-1} (see picture). This photoexcitation process has implications for laser Raman spectroscopic studies on lanthanide oxide catalysts under working conditions.

Photooxidation

W. Z. Weng,* H. L. Wan,* J. M. Li, Z. X. Cao ——— 975 – 977

Laser-Induced Formation of Metal–Peroxide Linkages on the Surface of Lanthanum Sesquioxide under Oxygen

Site insights: The title compound has been synthesized by mild hydrothermal conditions. The iron(II) and iron(III) cations are trapped in two different crystallographic positions, whereas the phosphite and hydrogenphosphate–phosphate oxoanions are disordered in two phosphorus sites (see structure). The compound has antiferromagnetic interactions and the nature of the iron centers is investigated by Mössbauer spectroscopy.

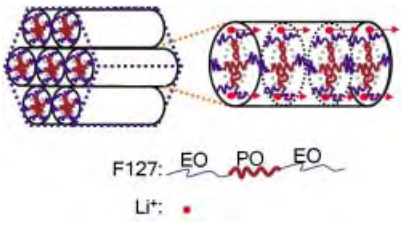


Open-Framework Materials

S. Fernández-Armas, J. L. Mesa,* J. L. Pizarro, J. S. Garitaonandia, M. I. Arriortua, T. Rojo* ——— 977 – 980

$(C_4N_2H_{12})[Fe^{II}_{0.86}Fe^{III}_{1.14}(HPO_3)_{1.39}(HPO_4)_{0.47}(PO_4)_{0.14}F_3]$: A Fluoro–Phosphite–Hydrogenphosphate–Phosphate Iron(II,III) Mixed-Valence Organically Templated Compound

High lithium ionic conductivity is exhibited by an organic–inorganic hybrid electrolyte prepared by self-assembly of a PEO-PPO-PEO triblock copolymer (Pluronic F127; PEO = poly(ethylene oxide), PPO = poly(propylene oxide)), complexed with $LiClO_4$, on a silica framework. The good performance of the hybrid material with an [O]:[Li] ratio of 16:1 is due to its well-ordered mesophase consisting of a hexagonal arrangement of cylinders (see diagram).



Conducting Materials

H.-M. Kao,* C.-L. Chen ——— 980 – 984

An Organic–Inorganic Hybrid Electrolyte Derived from Self-Assembly of a Poly(Ethylene Oxide)–Poly(Propylene Oxide)–Poly(Ethylene Oxide) Triblock Copolymer

 © 2004 Wiley-VCH Verlag GmbH & Co. KGaA, Weinheim

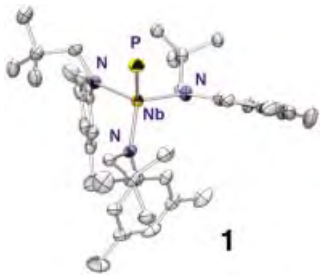
Contents

P Ligands

J. S. Figueroa, C. C. Cummins* ——— 984 – 988

Diorganophosphanylphosphinidenes as Complexed Ligands: Synthesis via an Anionic Terminal Phosphide of Niobium

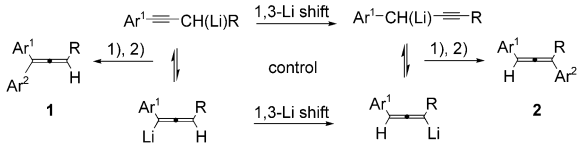
Reductive cleavage of a bridging diphosphide complex with sodium amalgam affords the sodium salt of the terminal niobium phosphide anion $[PNb(N[Np]Ar)_3]^-$ (**1**; Np = neopentyl, Ar = 3,5-$Me_2C_6H_3$), which is best formulated as containing an Nb–P triple bond. The phosphorus atom of **1** is nucleophilic. Treatment of **1** with $ClP(tBu)_2$ or $ClP(Ph)_2$ provides η^2-phosphanylphosphinidene complexes, which are the first examples of such complexed ligands bound to an early-transition-metal fragment.



Li Reactions in Organic Synthesis

S. Ma,* Q. He ——— 988 – 990

A 1,3-Lithium Shift of Propargylic/Allenylic Lithium and the Subsequent Transmetalation Coupling Reaction with Aryl Halides

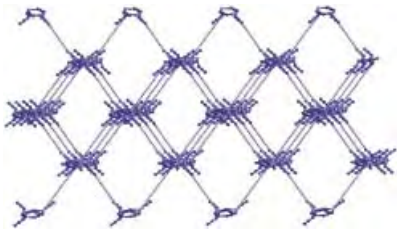


The lithiation reagent and temperature may be the key factors controlling the 1,3-lithium shift of propargylic/allenylic lithium (see scheme). Under the right conditions, 1,1-diarylallenes and 1,3-diarylallenes can be easily and highly selectively synthesized by the lithiation of 1-aryl-1-alkynes and the subsequent transmetalation (1), and Pd-catalyzed coupling with aryl halides (2).

Coordination Polymers

C.-M. Liu,* S. Gao, D.-Q. Zhang,* Y.-H. Huang, R.-G. Xiong, Z.-L. Liu, F.-C. Jiang, D.-B. Zhu* ——— 990 – 994

A Unique 3D Alternating Ferro- and Antiferromagnetic Manganese Azido System with Threefold Interpenetrating (10,3) Nets

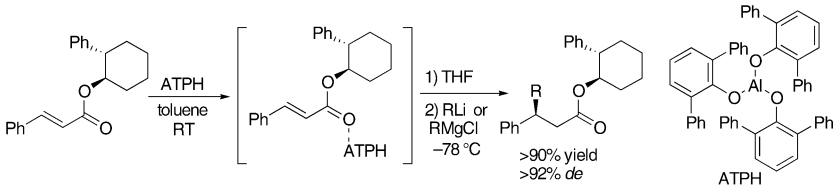


Alternative bridging: Alternating ferro- and antiferromagnetic interactions are mediated by alternating end-on and end-to-end azido bridges, respectively, in a novel manganese azido complex. The compound has an interesting framework of threefold interpenetrating (10,3) nets, one of which is shown in the picture.

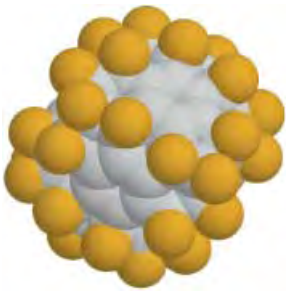
Michael Addition

H. Ito, T. Nagahara, K. Ishihara, S. Saito,* H. Yamamoto* ——— 994 – 997

Chiral Molecular Recognition by Aluminum Tris(2,6-diphenylphenoxide) in an Asymmetric 1,4-Addition



A precomplex of a chiral α,β-unsaturated ester and a bulky aluminum oxide is crucial to setting the diastereoselectivity in the 1,4-addition of a Grignard or organolithium reagent. This approach based on chiral recognition broadens the potential of the strategies relying on stoichiometric reagents.



Experimental support for the IPR-D_{3h} structure of the empty-cage C_{74} fullerene (IPR = isolated pentagon rule) has been obtained from an exohedral derivative of the small-bandgap fullerene D_3-$C_{74}F_{38}$ (see picture). Selective fluorination is proposed as a general procedure for protecting nonextractable fullerenes and their endohedral derivatives.

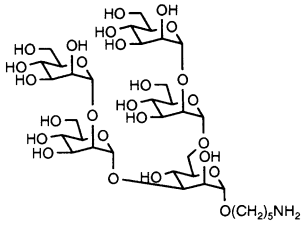
Fullerene Derivatives

A. A. Goryunkov, V. Y. Markov, I. N. Ioffe, R. D. Bolskar, M. D. Diener, I. V. Kuvychko, S. H. Strauss,* O. V. Boltalina* _____ **997 – 1000**

$C_{74}F_{38}$: An Exohedral Derivative of a Small-Bandgap Fullerene with D_3 Symmetry

---

An HIV-1 vaccine may eventually be developed from oligomannoses synthesized by a reactivity-based one-pot self-condensation strategy. The compounds were tested for their ability to inhibit the binding of gp120 to the broadly neutralizing HIV-1 antibody 2G12. New epitope mimics (see structure for example) were identified that inhibit this binding as well as, or better than the natural epitope $Man_9GlcNAc_2$ (Man = mannose, Glc = glucose).



Drug Development

H.-K. Lee, C. N. Scanlan, C.-Y. Huang, A. Y. Chang, D. A. Calarese, R. A. Dwek, P. M. Rudd, D. R. Burton, I. A. Wilson, C.-H. Wong* _____ **1000 – 1003**

Reactivity-Based One-Pot Synthesis of Oligomannoses: Defining Antigens Recognized by 2G12, a Broadly Neutralizing anti-HIV-1 Antibody

---



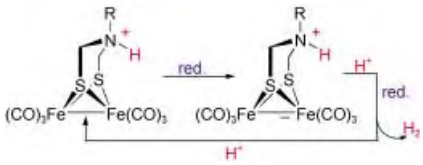
Cleaner fuels: Preferential adsorption of organonitrogen compounds from commercial diesel can be achieved by using a Faujasite zeolite in which Cu ions occupy the 6-ring windows sites. The key to this denitrogenation process is π complexation with the Cu^{I} ion, as illustrated for pyrrole.

Denitrogenation of Fuels

A. J. Hernández-Maldonado, R. T. Yang* _____ **1004 – 1006**

Denitrogenation of Transportation Fuels by Zeolites at Ambient Temperature and Pressure

---



Good potential: A biomimetic model of the iron hydrogenase active site functions as a catalyst for electrochemical proton reduction at relatively moderate negative potentials. The catalytic cycle (see scheme) involves the protonation of the azadithiolate nitrogen atom as its initial step. This system may eventually be used to achieve light-activated hydrogen evolution.

Biomimetic Electrochemistry

S. Ott,* M. Kritikos, B. Åkermark, L. Sun, R. Lomoth* _____ **1006 – 1009**

A Biomimetic Pathway for Hydrogen Evolution from a Model of the Iron Hydrogenase Active Site

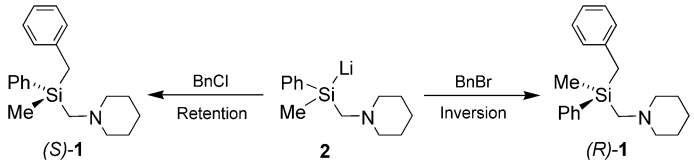
 © 2004 Wiley-VCH Verlag GmbH & Co. KGaA, Weinheim

Contents

Stereochemistry

C. Strohmann,* M. Bindl, V. C. Fraaß, J. Hörnig ——— 1011 – 1014

Enantiodivergence in the Reactions of a Highly Enantiomerically Enriched Silyllithium Compound with Benzyl Halides: Control of Inversion and Retention by Selection of Halide

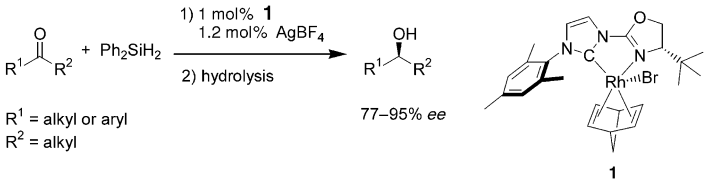


Inversion of the configuration at the silicon center is observed for the reaction of benzyl bromide with the highly enantiomerically enriched silyllithium compound **2**. In contrast, retention of configuration occurs at the silicon center with benzyl chloride, which suggests two different reaction mechanisms.

Hydrosilylation Catalysts

L. H. Gade,* V. César, S. Bellemin-Laponnaz* ——— 1014 – 1017

A Modular Assembly of Chiral Oxazolinylcarbene–Rhodium Complexes: Efficient Phosphane-Free Catalysts for the Asymmetric Hydrosilylation of Dialkyl Ketones

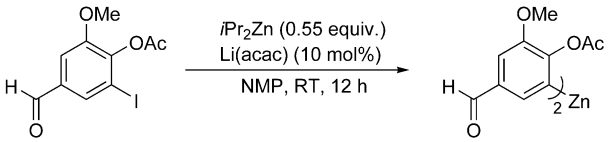


A novel class of chiral bidentate ligands with a carbene and an oxazoline moiety is obtained by the coupling of *N*-arylimidazoles and a 2-bromooxazoline derivative. The rhodium complex **1** catalyzes the hydrosilylation of aryl alkyl ketones and otherwise problematic dialkyl ketones in high yields and good enantioselectivities (up to 95% *ee*).

Organometallic Reagents

F. F. Kneisel, M. Dochnahl, P. Knochel* ——— 1017 – 1021

Nucleophilic Catalysis of the Iodine–Zinc Exchange Reaction: Preparation of Highly Functionalized Diaryl Zinc Compounds

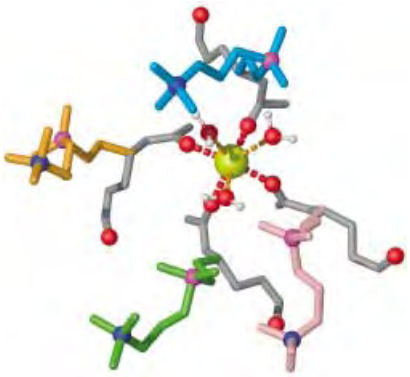


Sensitive functional groups are tolerated in an iodine–zinc exchange reaction catalyzed by Li(acac). Aryl and heteroaryl diorganozinc compounds with keto, aldehyde, or isothiocyanate substituents can be prepared by this method (see example in scheme; acac = acetylacetone, NMP = 1-methyl-2-pyrrolidinone). Such zinc reagents serve as substrates for a wide variety of coupling reactions.

Ion–Membrane Interactions

R. A. Böckmann, H. Grubmüller* ——— 1021 – 1024

Multistep Binding of Divalent Cations to Phospholipid Bilayers: A Molecular Dynamics Study



Step by step: The sequential coordination of calcium ions (yellow) to four lipid carbonyl oxygen atoms in neutral zwitterionic phospholipid bilayers has been studied by molecular dynamics simulations.

VIP Communications labeled with this symbol have been judged by two referees as being "very important papers".

The publication of Communications labeled with this symbol has been accelerated because of their topical or highly competitive nature.

 © 2004 Wiley-VCH Verlag GmbH & Co. KGaA, Weinheim

Looking for outstanding employees?

Do you need another expert for your excellent team?
... Chemists, PhD Students, Managers, Professors, Sales Representatives...

Place an advert in the printed version and have it made available online for 1 month, free of charge!

Angewandte Chemie International Edition
Advertising Sales Department: Marion Schulz
Phone: 0 62 01 - 60 65 65
Fax: 0 62 01 - 60 65 50
E-Mail: MSchulz@wiley-vch.de

Service

Keywords ____ *1028*

Authors ____ *1029*

Angewandte's Sister Journals ____ *1026 – 1027*

Preview ____ *1031*

Speakers

Steve Adams (UCSD, San Diego)
Philippe Bastiaens (EMBL Heidelberg)
Annette Beck-Sickinger (Leipzig University)
Craig Crews (Yale University, New Haven)
Michael Famulok (Bonn University)
Theodorus Gadella (Amsterdam University)
A. Ganesan (University of Southampton)
Carine Giovannangeli (MNHN, Paris)
Kai Johnson (EPFL Lausanne)
Thomas Mayer (MPI Martinsried)
Tim Mitchison (Harvard Univ., Cambridge)
Peter Nielsen (PI Copenhagen)
Jan-Michael Peters (IMP Vienna)
Greg Petsko (Brandeis University, Waltham)
Orlando Schärer (Zürich University)
Ilme Schlichting (MPI Heidelberg)
Carsten Schultz (EMBL Heidelberg)
Peter Seeberger (ETH Zürich)
Oliver Seitz (Humboldt University, Berlin)
Herbert Waldmann (MPI Dortmund)

Speakers

2nd **EMBO Young Investigator Programme** Symposium

EMBO

Chemistry meets Biology

Chemical Approaches to the Study of Biology

5–6 June 2004

EMBL Heidelberg | Germany

For further information and online registration please visit **www.embo.org/projects/yip/chemicalbiologyindex.html** or send an e-mail **yip@embo.org**

 © 2004 Wiley-VCH Verlag GmbH & Co. KGaA, Weinheim

Saturo Masamune (1928–2003): Natural Products and Small Rings

Satoru Masamune died on November 9, 2003 at the age of 75 from complications following a cardiac arrest. Born in Fukuoka (Japan), he completed his science degree in 1952 at Tohoku University under the guidance of Tetsuo Nozoe. He completed his PhD in 1957 at the University of California, Berkeley (USA), under the supervision of Henry Rapoport, as one of the first Fulbright Fellows. He went as a postdoctoral fellow to Eugene van Tamelen at the University of Wisconsin (1956–1959), and then took up positions first at the Mellon Institute (1960–1964), and then at the University of Alberta (1964–78), before moving to the Massachusetts Institute of Technology (MIT) in 1978, where he became the Arthur C. Cope Professor in 1991. Masamune received the Award for Creative Work in Synthetic Organic Chemistry of the American Chemical Society in 1978 and the A. C. Cope Scholar Award in 1987. He was a Fellow of the Royal Society of Canada, a Fellow of the American Academy of Arts and Sciences, and a Centenary Scholar of the Chemical Society in London (1980), and he received the Fujiwara Award in 1997. He retired in 2000 but continued to visit his MIT office nearly every day until his death.



The breadth of Masamune's interests and accomplishments is extraordinary. His selection of research projects was always guided by what he identified as the most important problems of the day, even if that might require him to abandon his current comfortable and familiar sphere of research in which he had perhaps already established his preeminence. He made significant contributions to two broad fields, the synthesis of natural products and the chemistry of small ring systems. Masamune's research interests spanned topics ranging from the synthesis of organic and organometallic compounds to the chemistry of theoretically interesting molecules, and later included catalytic antibodies, enzyme-catalyzed reactions, and polymer gels. When he visited Columbia University in the late 1970s, his interests overlapped with those of Ron Breslow, Tom Katz, Gilbert Stork, and Nick Turro; Koji Nakanishi was the only one whose research interests did not overlap with those of Masamune.

Masamune is best known for his work on methods for the synthesis of naturally occurring substances, particularly compounds with biological activity. He attracted the attention of the chemical community early in his career when he published three consecutive single-author communications in *JACS* in 1964 on the synthesis of the complex polycyclic diterpene alkaloids kaurene, garryine, and atisine. [1] He reported these results as an invited speaker at the 3rd IUPAC Symposium on Natural Products Chemistry in Kyoto in 1964, which was attended by 1500 scientists. This probably triggered his invitation by Ray Lemieux to join the faculty of the University of Alberta.

Masamune pioneered the development of a general strategy known as "double asymmetric synthesis",[2] which in the 1980s and 1990s revolutionized the ability of chemists to prepare certain classes of molecules with complex three-dimensional structures. He and his students demonstrated the power of this strategy in syntheses of a number of organic compounds with high structural complexity. Particularly significant were his landmark syntheses of several important macrolide antibiotics and carbohydrates, including the L-hexoses as mirror-image isomers of the naturally occuring sugars.[3] His contributions to chemistry also include the first syntheses of a number of unusual and theoretically important nonnatural compounds, whose high degree of strain and instability had defeated previous synthetic efforts. Especially significant was his work on the synthesis of cyclobutadiene,[4] [10]-annulenes, and small ring compounds of Si, Ge, and Sn.

Masamune was a constant source of off-beat humor, which came from his uniquely honest and candid nature. On the other hand, he often could not comprehend common humor, reflecting his purist personality. According to his wife Takako he was not known for, or was incapable of helping with chores around the house. However, he was a truly warm, loving, devoted husband, and an emotional pillar. He was extremely bright, always did his best, and had an unusually unspoiled personality. He had a great passion for classical music, especially for Beethoven, and had been an excellent pianist since his youth. He regularly attended concerts of the Boston Symphony Orchestra and was a close friend of the conductor Seiji Ozawa. He also avidly followed baseball and sumo wrestling. We will all miss this smiling person, who was always willing to help. He is survived by his wife and two children.

Koji Nakanishi
Columbia University, New York

Rick L. Danheiser
Massachusetts Institute of Technology

[1] a) S. Masamune, *J. Am. Chem. Soc.* **1964**, *86*, 289; b) S. Masamune, *J. Am. Chem. Soc.* **1964**, *86*, 290; c) S. Masamune, *J. Am. Chem. Soc.* **1964**, *86*, 291.
[2] S. Masamune, W. Choy, J. S. Petersen, L. R. Sita, *Angew. Chem.* **1985**, *97*, 1; *Angew. Chem. Int. Ed. Engl.* **1985**, *24*, 1.
[3] S. Y. Ko, A. W. M. Lee, S. Masamune, L. A. Reed, K. B. Sharpless, F. J. Walker, *Tetrahedron* **1990**, *46*, 245.
[4] S. Masamune, M. Suda, H. Ona, L. M. Leichter, *J. Chem. Soc. Chem. Commun.* **1972**, 1268.

 © 2004 Wiley-VCH Verlag GmbH & Co. KGaA, Weinheim

Medicinal Chemistry

Layer-by-Layer Deposition of Polyelectrolytes—A Versatile Tool for the In Vivo Repair of Blood Vessels

Thomas Groth and Andreas Lendlein*

Keywords:
layer-by-layer techniques · medicinal chemistry · nanolayers · polyelectrolytes

Background

Polyelectrolytes are macromolecules that have a large number of charged or chargeable groups when dissolved in polar solvents, primarily water.[1] Polyelectrolytes are typically weak polyacids or polybases. Upon dissolution of polyelectrolytes in water, they dissociate into a macromolecular ion and counterions. The effective charge of each segment is controlled by the pH value of the solution.[2] For polyelectrolytes, electrostatic interactions provide the driving force for their behavior in solution and at interfaces. A characteristic aspect of polyelectrolytes is the high expansion or stretching of the polyion chain owing to the strong electrostatic repulsion between equally charged segments of the chain.[3]

The layer-by-layer technique, which was introduced by Decher,[4] is based on the attractive electrostatic force between a charged surface and an oppositely charged polyelectrolyte.[5] The charge of the polyelectrolyte must alternate from layer to layer to build up multilayer systems (see Figure 1). The polyelectrolyte to be adsorbed must have a critical number of binding sites to the previously adsorbed layer. On the other hand, it must also retain an adequate number of bonds for the adsorption of the subsequent layer.[5]

Electrostatic interaction is definitely the most important force for the adsorption process. In addition to these Coulombic interactions, van der Waals and entropic effects are also important for the stability of the system.[2] The layer-by-layer technology was developed as a versatile surface-coating, -modification, and -engineering tool. The technique was recently applied to functionalize surfaces with proteins or nucleic acids for use in sensor technology, gene transfer, and other biotechnological applications.[4]

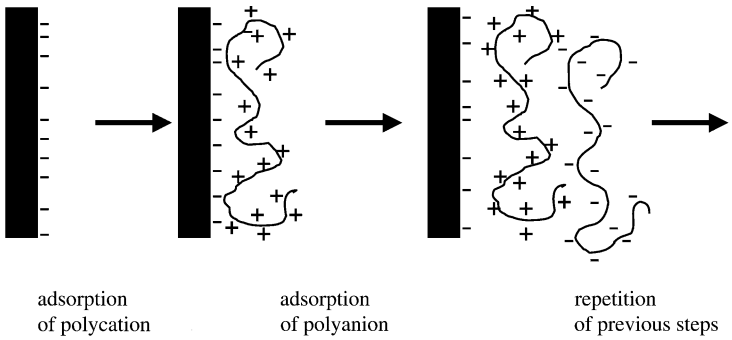


Figure 1. Alternating adsorption of polyelectrolytes in the layer-by-layer deposition technique.

Current Clinical Problems

Arteriosclerosis is a major cause of death in western countries. Balloon dilatation (e.g., percutaneous transluminal coronary angioplasty—PTCA) is applied to open obstructed blood vessels and to improve the blood flow. PTCA is an alternative method to bypass surgery and may have considerable advantages as a minimum-invasive therapy, which should lead to less pain, lower risk, shorter durations of hospitalization, and reduced costs.[6]

However, restenosis of blood vessels is still a major complication in the maintenance of vessel patency after treatment. Restenosis results from a number of factors, such as the collapse of the dilated vessel, negative vascular remodeling, and neointimal hyperplasia.[7] Collapse of blood vessels can be prevented by stents,[8] which are tubular placeholders made of metal that are introduced during the balloon-dilation process to support the vessels. Vascular remodeling and neointimal hyperplasia are believed to be caused by injuries induced during the intervention. These injuries comprise the removal of the protective endothelial cell lining from the luminal vessel surface and a partial destruction of the arterial wall. As a consequence, activation of blood clotting and blood cells occurs, which may result in thrombus formation on the vessel surface. Reocclusion of the blood vessel and embolus formation may be a consequence. A long-term consequence is neointimal hyperplasia due to extensive growth of smooth-muscle cells, which may lead to narrowing and reocclusion of the vessel.[9]

Figure 2 shows the principal structure and components of an arterial wall. Figure 3 illustrates the process of reste-

[*] Prof. Dr. T. Groth, Prof. Dr. A. Lendlein
GKSS Forschungszentrum
Institut für Chemie
Kantstrasse 55, 14513 Teltow (Germany)
Fax: (+49) 3328-352-452
E-mail: Thomas.Groth@gkss.de

 © 2004 Wiley-VCH Verlag GmbH & Co. KGaA, Weinheim DOI: 10.1002/anie.200301708

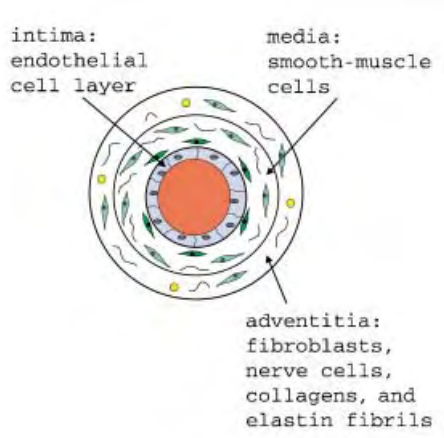


Figure 2. Cross-section through an artery.

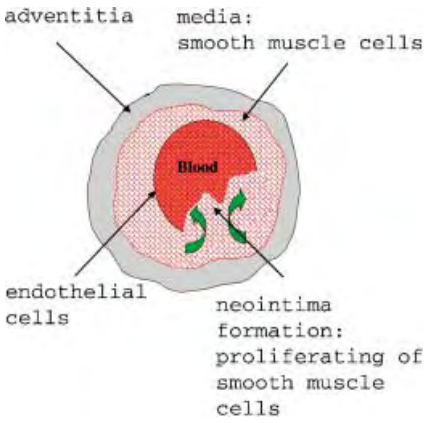


Figure 3. Restenosis of the arterial wall caused by the formation of a neointima owing to smooth-muscle cell proliferation.

nosis after balloon dilatation owing to excessive neointimal hyperplasia. Systemic and local delivery of drugs such as heparin has been used to prevent immediate onset of blood clotting on stents and the vessel wall, but also to reduce the growth of smooth-muscle cells.[10] Whereas blood clotting can be prevented successfully, restenosis occurs in about 15–30% of cases as a result of neointimal hyperplasia.[11]

Approaches to Repair Arteries

Prevention of blood clotting and excessive smooth-muscle cell growth together with an enhanced re-endothelization of the luminal surface of the vessel is highly desirable for the above-mentioned reasons. Different strategies, such as drug-eluting stents, have been developed to reduce proliferation of smooth-muscle cells.[12] On the other hand a number of techniques have been developed that aim at the reconstitution of the architecture of the vessel wall. Such approaches are based on the in situ polymerization of degradable hydrogels from macromers to cover the inner vessel surface. These hydrogels can prevent blood clotting and platelet adhesion, and reduce the proliferation of smooth-muscle cells.[13,14]

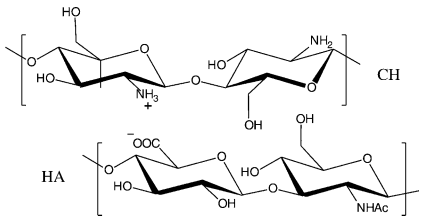
To allow photopolymerization, macromers based on poly(ethylene glycol) and lactic acid were capped with diacrylates.[13] Experiments on animals have shown that a thin layer of hydrogel on the arterial wall obtained by in situ photopolymerization reduces thrombosis and neointimal thickening of damaged blood vessels. These hydrogels can also be used as a depot for local drug delivery.

Other photopolymerized hydrogels are based on acrylate esters of hyaluronic acid (HA).[15] HA is not only biodegradable but also non-adhesive to blood cells and hence nonthrombogenic. It also inhibits the proliferation of vascular smooth-muscle cells. Hence, polymerized HA has been used to coat intravascular stents and showed an inhibitory effect on the neointimal formation in a porcine coronary model.[11]

In situ photopolymerization is practically possible but requires intraluminal application of UV light and a photoinitiator, which might be toxic to vascular cells. It is also possible that incomplete conversion of the acrylates and the formation of degradation products (such as oligoacrylates) may be toxic to the vascular environment. It would therefore be advantageous to simplify the procedures for the in situ repair of blood vessels even further and to avoid a polymerization process altogether.

Recent Developments

Thierry et al.[16] presented a promising technique to prepare nanocoatings on arteries through layer-by-layer deposition of two naturally occurring polyelectrolytes: the cationic polysaccharide chitosan (CH) and anionic HA. As the denuded arterial wall is composed of



polyanionic collagen, alternating coatings with CH and HA resulted in the deposition of a multilayer. The adsorption of the polyelectrolytes occurred rapidly within a few seconds. These multilayers were built on collagen-coated glass slides and denuded porcine arteries. It is remarkable that these multilayers were stable in buffer solutions, which indicates a sufficient stability under physiological conditions when salt ions and blood proteins are present. The coating significantly reduced the adhesion of blood platelets, thus demonstrating a restored blood compatibility of the denuded arteries. It was shown that these multilayers can be used for the incorporation and release of drugs that prevent platelet adhesion and smooth-muscle cell proliferation. Other biocompatible polyelectrolytes that are of interest are alginate, collagen, different glycosaminoglycans (e.g., heparin), fucoidans, poly(L-lysine), but also synthetic polyelectrolytes, such as poly(ethylene imine).

The layer-by-layer technique has several clear advantages: 1) the ease of the procedure without the need for initiators or an energy supply (e.g. light), 2) the use of water-soluble biocompatible polymers, and 3) the high rate of adsorption. Furthermore, it is possible to incorporate a multitude of molecules such as bioactive drugs, proteins (i.e., adhesion and growth factors), or nucleic acids. These molecules regulate the blood response and vascular repair in the desired manner. For example, heparin reduces blood clotting, enhances the re-endothelization of the luminal vessel surface, and diminishes the growth of smooth-muscle cells.

The layer-by-layer deposition of polyelectrolytes may therefore become an interesting alternative to current minimum-invasive cardiovascular interventions. However, before this technique can be applied clinically, certain limitations must still be overcome. For

 © 2004 Wiley-VCH Verlag GmbH & Co. KGaA, Weinheim

example, all blood (which contains a mixture of ions and polyelectrolytes (proteins)) must be drained from the vessel to be repaired so that the vessel lumen can be rinsed and treated with the desired polyelectrolytes. This demands a temporary blockage of blood flow, which can only be tolerated in peripheral regions of the body that do not suffer too much from a temporary lack of oxygen supply. In other regions, an anastomosis has to be created to circumvent the hypooxygenation of tissue.

Besides this limitation, the layer-by-layer technique holds great potential in clinical applications for the in situ repair of damaged blood vessels. Nanocoatings obtained from layer-by-layer deposition are also versatile tools to prepare biocompatible coatings on implant materials. For example, the technique was shown to improve the biocompatibility of silicon, on which the growth of neuronal cells could be enhanced.[17] The technique was also used to prepare thromboresistant surfaces on biomedical stainless-steel surfaces.[18]

Outlook

Layer-by-layer assembly is a promising, robust, and simple technique for the modification of the surfaces of objects with different shapes and sizes.[4] It can be anticipated that the layer-by-layer technique will attain an increasing application in the biomedical field, particularly in cardiovascular interventions but also in wound healing and the processing of implant materials.

[1] H. Dautzenberg, W. Jäger, J. Kötz, B. Phillip, C. Seidel, D. Stscherbina, *Polyelectrolytes*, Carl Hanser, Munich, **1994**.

[2] R. R. Netz, D. Andelman, *Phys. Rep.* **2003**, *380*, 1 – 95.

[3] P.-G. DeGennes, P. Pincus, R. M. Velasco, F. Brochard, *J. Phys.* **1976**, *37*, 1461 – 1473.

[4] *Multilayer Thin Films: Sequential assembly of Nanocomposite Materials* (Eds.: G. Decher, J. B. Schlenoff), Wiley-VCH, Weinheim, **2002**.

[5] S. Schwarz, K.-J. Eichhorn, E. Wischerhoff, A. Laschewsky, *Colloids Surf. A* **1999**, *159*, 491 – 501.

[6] A. Gruntzig, R. Myler, S. Stertzer, *Circulation* **1979**, *60*, 264 – 265.

[7] G. Pasterkamp, D. P. de Kleijn, C. Borst, *Cardiovasc. Res.* **2000**, *45*, 843 – 852.

[8] E. Noldge, G. M. Richter, J. C. Palmaz, *Radiology* **1987**, *27*, 431 – 432.

[9] H. C. Lowe, S. N. Oesterle, L. M. Khachigian, *J. Am. Coll. Cardiol.* **2002**, *39*, 183 – 193.

[10] C. W. Hwang, E. R. Edelman, *Circ. Res.* **2002**, *90*, 826.

[11] B. Heublein, E. G. Evagorou, R. Rohde, S. Ohse, R. R. Meliss, S. Barlach, A. Haverich, *Int. J. Artif. Organs* **2002**, *25*, 1166 – 1173.

[12] a) J. E. Sousa, P. W. Serruys, M. A. Costa, *Circulation* **2003**, *107*, 2274 – 2279; b) Y. Huang, L. Wang, X. Liu, S. Li, E. K. Verbeken, I. de Scheerder, *Business Briefing: European Pharmacotherapy* **2003**, 1 – 6.

[13] J. L. Hill-West, S. M. Chowdhury, M. J. Slepan, J. A. Hubbell, *Proc. Natl. Acad. Sci. USA* **1994**, *91*, 5967 – 5971.

[14] Y. An, J. A. Hubbell, *J. Controlled Release* **2000**, *64*, 205 – 215.

[15] Y. D. Park, N. Tirelli, J. A. Hubbell, *Biomaterials* **2003**, *24*, 893 – 900.

[16] B. Thierry, F. M. Winnik, Y. Merhi, M. Tabrician, *J. Am. Chem. Soc.* **2003**, *125*, 7494 – 7495.

[17] H. Ai, H. Meng, I. Ichinose, S. A. Jones, D. K. Mills, Y. M. Lvov, X. Qioa, *J. Neurosci. Methods* **2003**, *128*, 1 – 8.

[18] Q. Tan, J. Ji, M. A. Barbosa, C. Forensa, J. Shen, *Biomaterials* **2003**, *24*, 4699 – 4705.

 © 2004 Wiley-VCH Verlag GmbH & Co. KGaA, Weinheim

Organic–Inorganic Hybrids

Rational Synthesis of Covalently Bonded Organic–Inorganic Hybrids

*Zhonghua Peng**

Keywords:
molybdenum · organic–inorganic hybrid composites · polymers · polyoxometalates

Hybrid materials based on covalently linked inorganic polyoxometalates (POMs) and organic species containing a delocalized π system have drawn increasing attention. These hybrids, traditionally prepared by cluster assembly approaches that lack predictability and controllability, can now be synthesized through common organic reactions by using organically functionalized POM clusters as building blocks. This minireview highlights some of the most recent advances on a particular type of hybrids where the organic and inorganic components are connected by an imido linkage.

1. Introduction

Polyoxometalates (POMs) are a unique class of metal–oxygen clusters, whose molecular identity is maintained both in the solid state and in solutions.[1–4] Coupled with interesting electrical and optical properties such as electrochromism, photochromism, conductivity, and redox activitities,[5–6] POMs are considered electrically active molecular materials. On the other hand, conjugated molecules and polymers are electrically active organic materials.[7] Such materials have drawn tremendous attention in the last decade and have found numerous exciting applications in, for example, light emitting diodes,[8] field-effect transistors,[9] and solid-state lasers.[10] The molecular nature of these two types of materials offers the opportunity to generate covalently bonded molecular hybrids where the interplay between cluster d electrons and organic delocalized π-electrons can be explored at the molecular level.

Organically derived POMs have been extensively studied.[11] Among the many organic derivatives of POMs, organoimido derivatives have attracted particular interest because the organic π electrons may extend their conjugation to the inorganic framework, thus resulting in strong d–π interactions. Moreover, organoimido derivatives of POMs with a remote organic functional group can be utilized as building blocks to construct more complicated POM–organic hybrids. This modular building block approach brings rational design and structure control into the synthesis of organic–inorganic hybrids. In this review, various approaches to organoimido derivatives of POMs are surveyed and the ability of the functionalized POMs to undergo further organic reactions is discussed. Different hybrid molecules and polymers rationally assembled will then be highlighted.

[*] Prof. Z. Peng
Department of Chemistry
University of Missouri-Kansas City
Kansas City, MO 64110 (USA)
Fax: (+1) 816-235-5502
E-mail: pengz@umkc.edu

2. Preparation of Organoimido Derivatives of POM Clusters

2.1. Monofunctionalization

The organoimido derivatives of POM clusters have been extensively studied in recent years and the majority of the work has been focused on the hexamolybdate ion, $[Mo_6O_{19}]^{2-}$ (the cation is the tetrabutylammonium ion, unless otherwise stated). The hexamolybdate ion has the so-called Lindquist structure,[12] which features six terminal oxygen atoms aligned along the Cartesian axes. These terminal oxygen atoms are reactive enough to be replaced by various organic species, including the nitrosyl,[13] diazenido, hydrazido,[14] organometallic,[15] diazoalkyl,[16] and imido ligands.[17–25] For imido derivatives of hexmolybdates, so far, three types of reactions have been discovered; namely, reactions with phosphinimines [Eq. (1)],[17–18] isocyanates [Eq. (2)],[19–22] and aromatic amines [Eq. (3)].[23–25]

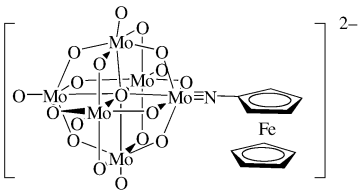
$$[Mo_6O_{19}]^{2-} + Ph_3P{=}NAr \xrightarrow[85\,^{o}C,\ 48\,h]{\text{pyridine}} [Mo_6O_{18}(NAr)]^{2-} + Ph_3P{=}O \quad (1)$$

$$[Mo_6O_{19}]^{2-} + ArNCO \xrightarrow[110\,^{o}C,\ 2-13\,days]{\text{pyridine}} [Mo_6O_{19-x}(NAr)_x]^{2-} + CO_2 \quad (2)$$

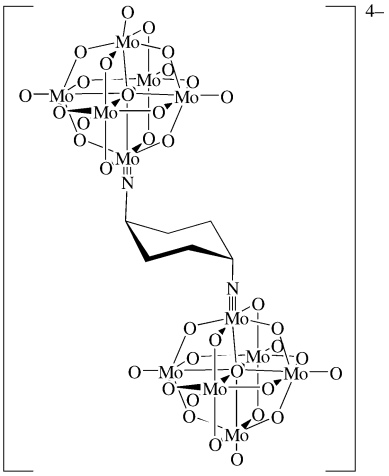
$$[Mo_6O_{19}]^{2-} + ArNH_2 \xrightarrow[150\,^{o}C]{PhCN,\ Et_3N} [Mo_6O_{18}(NAr)]^{2-} + H_2O \quad (3)$$

© 2004 Wiley-VCH Verlag GmbH & Co. KGaA, Weinheim
DOI: 10.1002/anie.200301682

The first reaction [Eq. (1)] was discovered by Maatta et al. a little over a decade ago.[17] Although the reaction involves a not-easily accessible phosphinimine reactant, it nonetheless demonstrates that direct functionalization can be carried out on parent clusters in a straightforward manner. The second reaction [Eq. (2)] was first reported by Errington et al.,[19] who have shown that both alkyl and aryl imido derivatives of hexamolybdates could be prepared by using organoisocyanates. Maatta and co-workers have modified the reaction conditions (anhydrous pyridine was used as the solvent instead of acetonitrile or benzonitrile, which was initially used by Errington) and have applied this approach to prepare a number of organoimido derivatives,[20–22,26] including the ferrocenylimido complex **1**[21] and the diimido-bridged hexamolybdates **2**.[22] It is noted that the reaction needs to be carried out in strictly anhydrous conditions at high temperature for a prolonged time.



1



2



Zhonghua Peng received his PhD in chemistry from the University of Chicago in 1997. After one-year postdoctoral studies at Bell laboratories, Lucent Technologies, he joined the University of Missouri-Kansas City (UMKC) as an Assistant Professor in 1998 and became full Professor in 2003. He received the US National Science Foundation CAREER award in 2001, the UKC Trustees' Faculty Scholar award from UMKC in 2000, and the Research Innovative Award from Research Corporation in 1999. His research interests include organic/inorganic hybrids, conducting polymers, conjugated dendrimers, and polymer assemblies.

The third reaction [Eq. (3)] was reported by Errington and co-workers, who found that the reaction of 1,4-diaminobenzene with $[Mo_6O_{19}]^{2-}$ could proceed, albeit under rather harsh conditions.[23] A mixture that includes various oligomers is obtained, from which pure imidoderivatives are difficult to isolate.

We recently discovered that carbodiimides, such as dicyclohexylcarbodiimide (DCC) can dramatically facilitate the reaction of $[Mo_6O_{19}]^{2-}$ with aromatic amines [Eq. (4)].[24] In the presence of one equivalent of DCC, $[Mo_6O_{19}]^{2-}$ reacts smoothly with a variety of aromatic amines under refluxing acetonitrile. It also tolerates additional functional groups such as iodo, ethynyl, and diethylamino groups. Figure 1 shows the X-ray crystal structures of the resulting three imidoderivatives. It should be pointed out that the reactivity of aryl amines with hexamolybdates appears to correlate with their basicity; 4-aminopyridine, for example, was found to be unreactive under refluxing acetonitrile.

$$[Mo_6O_{19}]^{2-} + ArNH_2 \xrightarrow{DCC,\ CH_3CN} [Mo_6O_{18}(NAr)]^{2-} \quad (4)$$

All arylimido derivatives have some characteristic structural features, such as a short Mo–N bond length (~1.74 Å), a near-linear Mo-N-C bond angle (>170°), a closer distance of the central oxygen to the imido-bearing Mo atom than to the *para* Mo atom, and a long–short bond length alteration pattern in the Mo_4O_4 belt perpendicular to the Mo–N imido-bond axis.

2.2. Multiple Functionalization

The six terminal oxygen ligands in the hexamolybdate anion can be partially or completely replaced with organoimido ligands. Maatta and co-workers have shown that by carefully controlling the molar ratios of the isocyanate over the cluster, multiple-functionalized $[Mo_6O_{(19-x)}(NAr)_x]^{2-}$ (x = 2–6) systems could be prepared.[20,26] While all five multiply substituted derivatives have been isolated and characterized, the nonselective nature of the reaction, which results in a mixture of various multiple functionalized products, makes the isolation process difficult. It was recently discovered that instead of using $[Mo_6O_{19}]^{2-}$ as the parent cluster, the reaction of $[\alpha\text{-}Mo_8O_{26}]^{4-}$ with aromatic amines give the bisimido derivative selectively [Eq. (5)].[27] This approach has allowed the facile synthesis of a number of difunctionalized hexamolybdates, including compounds **4a** and **4b**, one with two iodo and the other with two ethynyl groups (Figure 2).

$$[\alpha\text{-}Mo_8O_{26}]^{4-} + ArNH_2 \xrightarrow[\text{reflux, 6–12 h}]{DCC,\ CH_3CN} [Mo_6O_{17}(NAr)_2]^{2-} \quad (5)$$

2.3. Functionalization of other POMs

Attempts to extend the various above-mentioned reactions to other POM clusters have so far found only limited success. Hexatungstate, $[W_6O_{19}]^{2-}$, another Linquist cluster, does not react with aromatic amines or isocyanates,[28–29]

 © 2004 Wiley-VCH Verlag GmbH & Co. KGaA, Weinheim

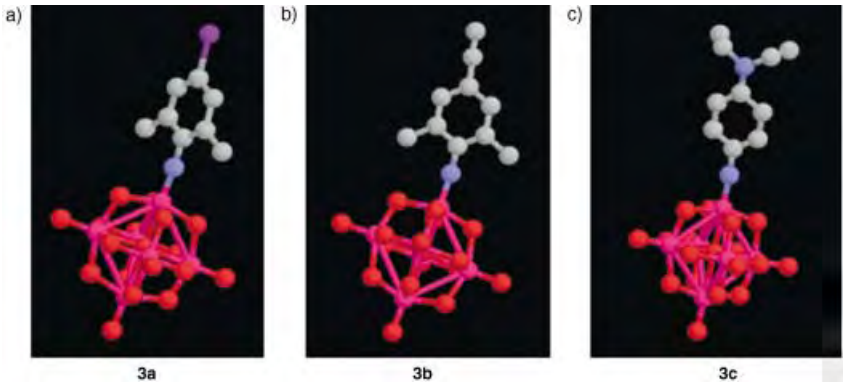


Figure 1. X-ray crystal structures (Rasmol drawing) of three $[Mo_5O_{18}(MoNAr)]^{2-}$ anions. a) **3a**, Ar = 2,6-dimethyl-4-iodophenyl; b) **3b**, Ar = 2,6-dimethyl-4-ethynylphenyl; c) **3c**, Ar = 4-(*N*,*N*-diethyl)aminophenyl.

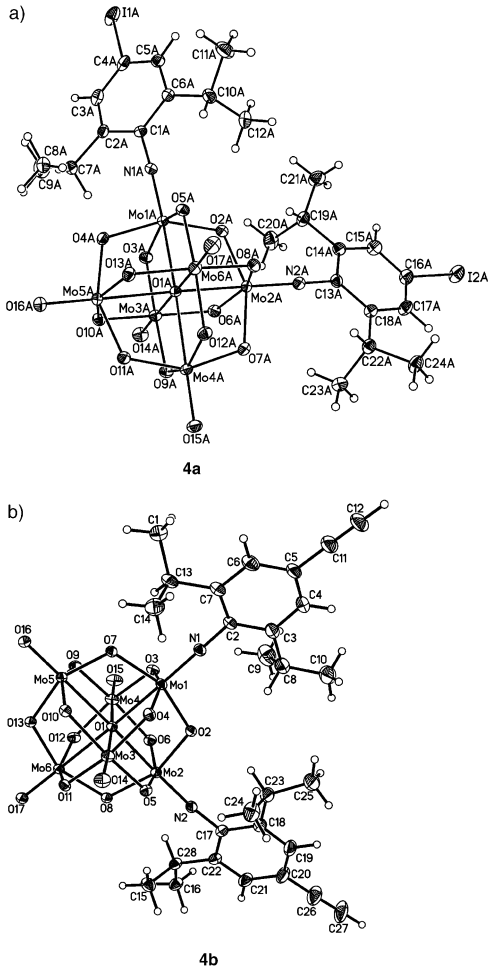


Figure 2. The structures of two bisimido derivatives of hexamolybdate $[Mo_6O_{17}(NAr)_2]^{2-}$. a) **4a**, Ar = 2,6-diisopropyl-4-iodophenyl; b) **4b**, Ar = 2,6-diisopropyl-4-ethynylphenyl.

although an example of organoimido hexatungstate has been prepared by an assembly approach.[29] However, the reaction of $[MoW_5O_{19}]^{2-}$ with aromatic amines does proceed and aryl imido derivatives of the mixed metal $[MoW_5O_{19}]^{2-}$ cluster can be synthesized.[30] Two examples are shown in Figure 3.

The reaction of aryl amines with $[Mo_2O_7]^{2-}$ or $[Mo_7O_{24}]^{6-}$ in the presence of DCC yielded imido derivatives of hexamolybdate.[27] Clearly, cluster rearrangement occurs. It is not clear at this moment whether rearrangement occurs first followed by functionalization, or vice versa. For the majority of the Keggin structures, their redox activities result in oxidation of aromatic amines, thus preventing the functionalization reaction from occurring. By using isocyanates, the reaction yields a mixture of products involving cluster rearrangements.[31]

3. Synthesis of Organic–Inorganic Molecular Hybrids

A characteristic feature of those imido-formation reactions is their tolerance of various organic functional groups. Many of the organoimido derivatives of POMS, such as compounds **3a**,**3b**,**4a**,**4b** and **5b** have remote functional groups, namely, iodo or ethynyl groups. It is well

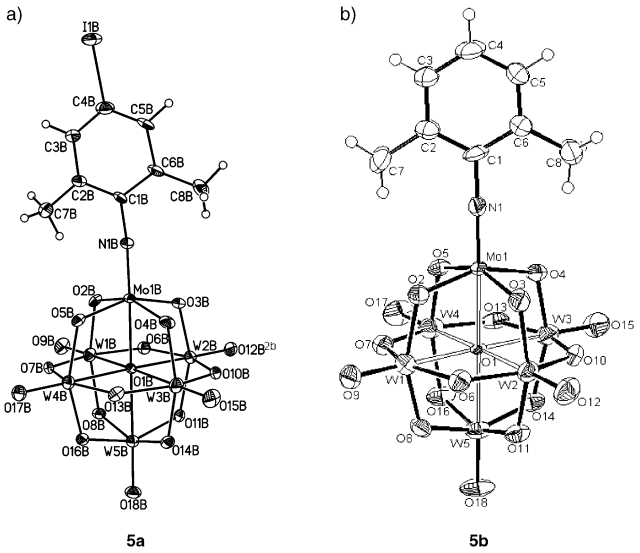
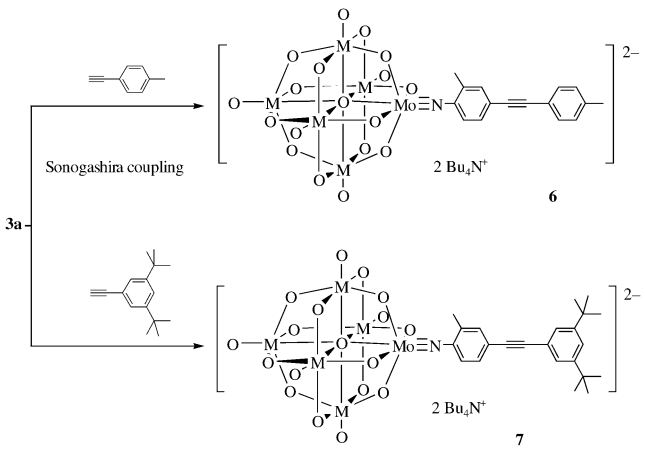


Figure 3. X-ray crystal structures of $[W_5O_{18}(MoNAr)]^{2-}$. a) **5a**, Ar = 2,6-dimethyl-4-iodophenyl; b) **5b**, Ar = 2,6-dimethylphenyl.

known that aryl halides and ethynyl arenes can undergo Pd-catalyzed coupling reactions.[32] If the iodo or ethynyl groups on functionalized POM clusters can undergo Pd-catalyzed coupling reactions, and if the imido linkage is stable under the coupling reaction conditions, such functionalized clusters would be ideal building blocks for the rational synthesis of novel molecular POM–organic hybrids.

The Pd-catalyzed coupling reaction of **3a** with 3,5-di-*tert*-butyl-1-ethynylbenzene or 4-methyl-1-ethynylbenzene (Scheme 1) has been carried out.[33] It is shown that compounds **6** and **7** can be synthesized in over 80% yield although the reaction has proceeded for merely 15 min. The hexamolybdate cluster not only survives under the reaction conditions, it actually activates the coupling reaction.

 © 2004 Wiley-VCH Verlag GmbH & Co. KGaA, Weinheim



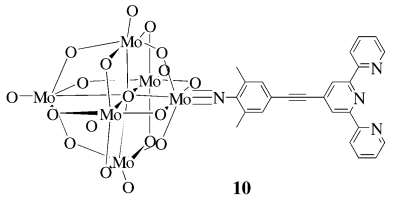
Scheme 1. Pd-catalyzed coupling reactions of iodo-functionalized hexamolybdate **3a** with ethynylarenes.

With the demonstration that iodo- or ethynyl-functionalized POM clusters can undergo Pd-catalyzed coupling reactions, an essentially unlimited number of hybrids with various linking geometries can be rationally designed and synthesized. For example, hybrid molecular dumbbells with two POM clusters, either identical or different, linked by a rigid conjugated organic rod with controllable lengths can be prepared. Indeed, two hybrid dumbbells, shown in Scheme 2, with different bridge lengths have been prepared.[34] The X-ray crystal structure of dumbbell **8** has been determined. UV/Vis absorption spectroscopy studies show that the lowest-energy electronic transition is significantly bathochromically shifted from compounds **3a** (362 nm) and **3b** (368 nm), to hybrid dumbbells **8** (426 nm) and **9** (438 nm), which indicates that the Mo–N π bond is delocalized with the organic conjugated π system. Static fluorescence studies show that hybrids **8** and **9** show no fluorescence under excitation from 200 nm to 500 nm, thus indicating efficient fluorescence quenching by the covalently bonded clusters. Cyclic-voltammetry studies reveal a reversible one-electron reduction wave at −891 mV (vs Ag/Ag^+) for both **8** and **9**, which is very close to the reduction potential of other monoaryl imido derivatives such as **3a** (−909 mV), **3b** (−893 mV), **6** (−893 mV), and **7** (−895 mV).[35] These results indicate that strong electronic interactions exist between the two clusters.

It should be pointed out that hybrid dumbbells linking two different clusters together can be synthesized in the same approach. For example, the coupling reaction between **3b** and **5b** yields a dumbbell with one $\{Mo_6\}$ cluster on one end and one $\{W_5Mo\}$ cluster on the other.[36] It remains to be seen how the two clusters, with different redox potentials, interact electronically through the organic conducting bridge.

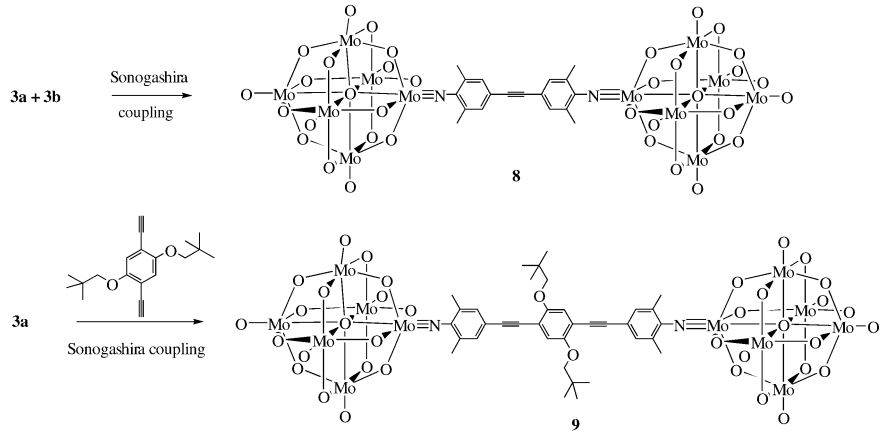
One of the most important features of POMs is their electron-accepting properties. Efforts have thus been made to develop molecular charge transfer hybrids.[5,37–38] Compound **1** is one example, in which a ferrocenyl donor is bound covalently to a hexamolybdate acceptor.[21] A charge-transfer transition from the Fe^{2+} center to the cluster is observed.

Charge-transfer hybrids that use transition metal complexes as electron donors have also been pursued. An imido derivative with a terpyridine ligand, shown as compound **10**, has been prepared.[39] The structure of compound **10** was



characterized by X-ray single-crystal diffraction. The aromatic frame in **10** shows a near-planar conformation with a small dihedral angle of only 5.7° between the phenyl ring and the central pyridine ring. Within the lattice, the hybrid ions are organized into dimers. As shown in Figure 4, the "dimerization" is clearly driven by the π–π stacking of the two parallel aromatic systems where the vertical separation distance is only 3.60 Å. They also appear to have some C–H···O hydrogen bonds, as evidenced by the short separation distances observed for O2–H19A at 2.49 Å, O2–H24A at 2.61 Å, O14-H18A at 2.88 Å and O15-H23A at 2.72 Å, which further stabilizes the dimers.

Preliminary studies on the coordination of hybrid ligand **10** with transition-metal ions such as Zn^{2+} and Ru^{2+} have shown that the complex formation process is facile.[39] The structural and physical property characterizations of the resulting POM–transition-metal complex hybrids are in progress.



Scheme 2. Synthesis of hybrid molecular dumbbells.

4. Covalently Bonded POM–Polymer Hybrids

Hybrid materials combining POMs with organic conducting polymers have been actively pursued.[40–44] Most of the research, however, has focused on

 © 2004 Wiley-VCH Verlag GmbH & Co. KGaA, Weinheim

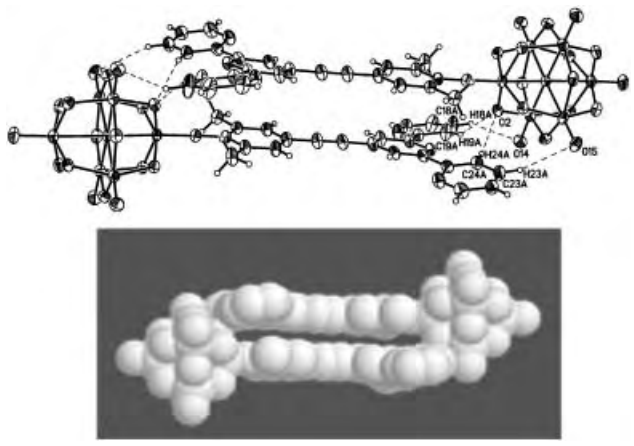
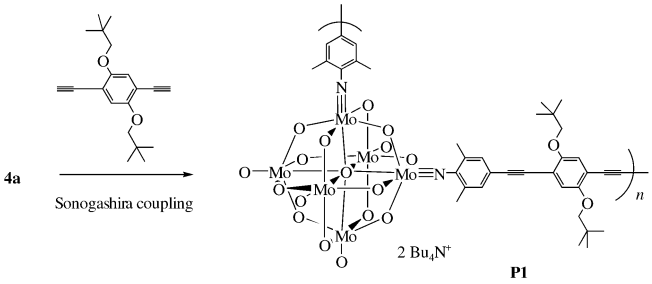


Figure 4. Dimer formation of the anion in the lattice of **10**. The inset shows the space-filling model of the dimer.

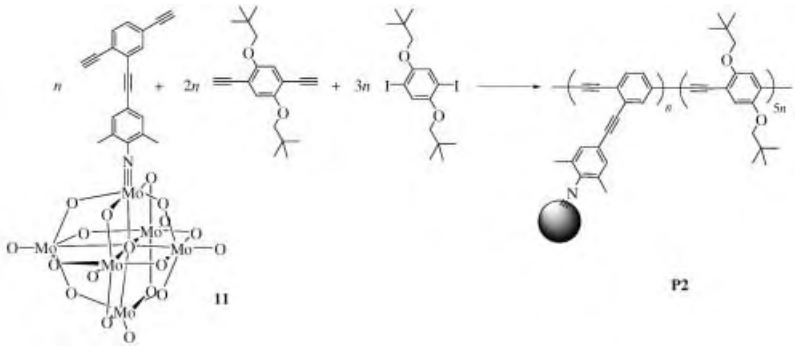
composite materials where POMs are embedded in the conducting polymer matrix. With the demonstration that functionalized hexamolybdates can undergo Pd-catalyzed coupling reactions, conjugated polymers containing covalently linked POM clusters, either in the main chain or in the side chains, can be synthesized. Main-chain POM-containing polymers have been synthesized by using difunctionalized cluster **4a** or **4b** as the monomer, as shown in Scheme 3.[27] The polymer (**P1**) contains about 18 repeating units. Its electronic spectrum is nearly identical to that of hybrid dumbbell **9**, which indicates that the organic π delocalization extends only to the two imido-bearing Mo atoms and the electronic interaction between the two orthogonally jointed organic π systems is limited. Cyclicvoltammetry studies reveal a reversible one-electron reduction wave at −1.2 V (vs Ag/Ag^+) which is consistent with bis(arylimido)-substituted hexamolybdates.



Scheme 3. Synthesis of main chain POM-containing hybrid polymers.

POM clusters as side-chain pendants have been grafted to a number of polymers.[45–48] Judeinstein reported the first POM–polymer hybrid ten years ago where a lacunary Keggin POM cluster was covalently linked to a polystyrene or polymethacrylate backbone through Si–O bonds.[45] This approach has been expanded recently by Lalot and co-workers to prepare polymer–POM cross-linked networks[46] and by Johnson and Stein to generate macroporous silica materials functionalized with POM clusters.[47] A polymer–POM hybrid has also been reported recently by Maatta and co-workers.[48] All these polymeric hybrids, however, involve insulating nonconjugated polymers. We have recently synthesized the first conjugated polymer–POM hybrid. The structure of the polymer and its synthesis is shown in Scheme 4.[49]

Monomer **11** has been characterized by, in addition to other spectroscopy methods, single-crystal diffraction.[50] Polymer **P2** has a maximum absorption at 424 nm. Cyclicvoltammetry studies show a reversible one-electron reduction at −930 mV, which is consistent with monoarylimido-substituted hexamolybdates. Preliminary fluorescence studies show that polymer **P2** exhibits only very weak fluorescence, thus indicating significant fluorescence quenching of the POMs on the conjugated backbone.



Scheme 4. Synthesis of conjugated polymers with POMs as side-chain pendants.

5. Summary and Outlook

The field of covalently bonded POM–organic hybrids, particularly those involving organic π-conjugated systems, is still in its infancy. Only a very few molecular hybrids and polymeric hybrids have been prepared, and studies of the physical property studies of these systems have yet to be systematically carried out. Nonetheless, with the rational synthetic strategies developed, a large number of hybrids including molecular, dendritic, and polymeric systems are sure to be prepared in the near future. Efforts on exploring the electrical, optical, and photophysical properties of this new class of hybrids are expected.

The author gratefully acknowledges the contributions of undergraduate and graduate students, and postdoctoral associates: Ms Calida Fung-chi Cheung, Ms Meng Lu, Dr Yongge Wei, Mr Bubin, Xu, and Dr. Lin Xu. Financial support by the National Science Foundation, Office of Naval Research, and Research Corporation is gratefully acknowledged. Acknowledgement is also made to the Donors of Petroleum Research Fund, administered by the American Chemical Society for the support of this work.

Received: July 14, 2003 [M1682]

 © 2004 Wiley-VCH Verlag GmbH & Co. KGaA, Weinheim

[1] M. T. Pope, *Heteropoly and Isopoly Oxometalates*, Springer, New York, **1983**.
[2] M. T. Pope, A. Müller, *Angew. Chem.* **1991**, *103*, 56; *Angew. Chem. Int. Ed. Engl.* **1991**, *30*, 34.
[3] *Polyoxometalates: From Platonic Solids to Anti-Retroviral Activity* (Eds.: M. T. Pope, A. Müller), Kluwer Academic Publishers, Dordrecht, The Netherlands, **1994**.
[4] *Chem. Rev.* **1998**, *98*, 1–390 (guest editor: C. L. Hill).
[5] E. Coronado, C. J. Gómez-García, *Chem. Rev.* **1998**, *98*, 273.
[6] T. Yamase, *Chem. Rev.* **1998**, *98*, 307.
[7] *Handbook of Organic Conductive Molecules and Polymers I–IV* (Ed.: H. S. Nalwa), Wiley, Chichester, England, **1997**.
[8] For recent reviews, see: a) A. Kraft, A. C. Grimsdale, A. B. Holmes, *Angew. Chem.* **1998**, *110*, 416; *Angew. Chem. Int. Ed.* **1998**, *37*, 40; b) S. M. Kelly, *Flat Panel Displays: Advanced Organic Materials*, Royal Society of Chemistry, Cambridge, **2002**.
[9] For a recent review, see: a) H. E. Katz, Z. Bao, S. L. Gilat, *Acc. Chem. Res.* **2001**, *34*, 359; b) H. E. Katz, Z. Bao, *J. Phys. Chem. B* **2000**, *104*, 671–678.
[10] a) F. Hide, M. A. Diaz-Garcia, B. J. Schwartz, A. J. Heeger, *Acc. Chem. Res.* **1997**, *30*, 450; b) M. D. McGehee, A. J. Heeger, *Adv. Mater.* **2000**, *12*, 1655.
[11] P. Gouzerh, A. Proust, *Chem. Rev.* **1998**, *98*, 77.
[12] H. R. Allcock, E. C. Bissell, E. T. Shawl, *Inorg. Chem.* **1973**, *12*, 2963.
[13] a) P. Gouzerh, Y. Jeannin, A. Proust, F. Robert, *Angew. Chem.* **1989**, *101*, 1377; *Angew. Chem. Int. Ed. Engl.* **1989**, *28*, 1363; b) A. Proust, R. Thouvenot, F. Robert, P. Gouzerh, *Inorg. Chem.* **1993**, *32*, 5299.
[14] S. Bank, S. Liu, S. N. Shaikh, X. Sun, J. Zubieta, P. D. Ellis, *Inorg. Chem.* **1988**, *27*, 3535.
[15] A. Proust, R. Thouvenot, P. Herson, *J. Chem. Soc. Dalton Trans.* **1999**, 51.
[16] H. Kwen, V. G. Young, Jr., E. A. Maatta, *Angew. Chem.* **1999**, *111*, 1215; *Angew. Chem. Int. Ed.* **1999**, *38*, 1145.
[17] Y. Du, A. L. Rheingold, E. A. Maatta, *J. Am. Chem. Soc.* **1992**, *114*, 346.
[18] A. Proust, R. Thouvenot, M. Chaussade, F. Robert, P. Gouzerh, *Inorg. Chim. Acta* **1994**, *224*, 81.
[19] W. Clegg, R. J. Errington, K. A. Fraser, C. Lax, D. G. Richards, *Polyoxometalates: From Platonic Solids to Anti-Retroviral Activity* (Eds.: M. T. Pope, A. Müller), Kluwer Academic Publishers, Dordrecht, The Netherlands, **1994**, p. 113.
[20] J. B. Strong, G. P. A. Yap, R. Ostrander, L. M. Liable-Sands, A. L. Rheingold, R. Thouvenot, P. Gouzerh, E. A. Maatta, *J. Am. Chem. Soc.* **2000**, *122*, 639–649.
[21] J. L. Stark, V. G. Young, Jr., E. A. Maatta, *Angew. Chem.* **1995**, *107*, 2751; *Angew. Chem. Int. Ed. Engl.* **1995**, *34*, 2547.
[22] J. L. Stark, A. L. Rheingold, E. A. Maatta, *J. Chem. Soc. Chem. Commun.* **1995**, 1165–1166.
[23] W. Clegg, R. J. Errington, K. Fraser, S. A. Holmes, A. Schäfer, *J. Chem. Soc. Chem. Commun.* **1995**, 455–456.
[24] Y. Wei, B. Xu, C. L. Barnes, Z. Peng, *J. Am. Chem. Soc.* **2001**, *123*, 4083.
[25] R. A. Roesner, S. C. McGrath, J. T. Brockman, J. D. Moll, D. X. West, J. K. Swearingen, A. Castineiras, *Inorg. Chim. Acta* **2003**, *342*, 37.
[26] J. B. Strong, B. S. Haggerty, A. L. Rheingold, E. A. Maatta, *Chem. Commun.* **1997**, 1137.
[27] L. Xu, M. Lu, B. Xu, Y. Wei, Z. Peng, D. R. Powell, *Angew. Chem.* **2002**, *114*, 4303; *Angew. Chem. Int. Ed.* **2002**, *41*, 4129.
[28] R. J. Errington, C. Lax, D. G. Richards, W. Clegg, K. A. Fraser, *Polyoxometalates: From Platonic Solids to Anti-Retroviral Activity* (Eds.: M. T. Pope, A. Müller), Kluwer Academic Publishers, Dordrecht, The Netherlands, **1994**, p. 105.
[29] T. R. Mohs, G. P. A. Yap, A. L. Rheingold, E. A. Maatta, *Inorg. Chem.* **1995**, *34*, 9.
[30] Y. Wei, M. Lu, C. F.-C. Cheung, C. L. Barnes, Z. Peng, *Inorg. Chem.* **2001**, *40*, 5489–5490.
[31] A. Proust, S. Taunier, V. Artero, F. Robert, R. Thouvenot, P. Gouzerh, *Chem. Commun.* **1996**, 2195.
[32] K. Sonogashira, Y. Tohda, N. Hagihara, *Tetrahedron Lett.* **1975**, 4467.
[33] B. Xu, Y. Wei, C. L. Barnes, Z. Peng, *Angew. Chem.* **2001**, *113*, 2353–2356; *Angew. Chem. Int. Ed.* **2001**, *40*, 2290.
[34] M. Lu, Y. Wei, B. Xu, C. F.-C. Cheung, Z. Peng, D. Powell, *Angew. Chem.* **2002**, *114*, 1636; *Angew. Chem. Int. Ed.* **2002**, *41*, 1566.
[35] Cyclic voltammetry was carried out in DMSO at room temperature by using a 1 mm^2 platinum disc as the working electrode, an Ag/Ag^+ electrode (0.01 M $AgNO_3$) as the reference electrode, and a platinum wire as the counter electrode. (Bu_4N)(PF_6) (0.1 M) was the electrolyte. The scan rate was 50 $mV\,s^{-1}$.
[36] M. Lu, B. Xu, Z. Peng, unpublished results.
[37] M. Clemente-Leon, E. Coronado, C. Gimenez-Saiz, C. J. Gomez-Garcia, E. Martinez-Ferrero, M. Almeida, E. B. Lopes, *J. Mater. Chem.* **2001**, *11*, 2176.
[38] P. Le Magueres, S. M. Hubig, S. V. Lindeman, P. Veya, J. K. Kochi, *J. Am. Chem. Soc.* **2000**, *122*, 10073.
[39] B. Xu, Z. Peng, Y. Wei, D. R. Powell, *Chem. Commun.* **2003**, 2562.
[40] T. Shimidzu, A. Ohtani, M. Aiba, K. Honda, *J. Chem. Soc. Faraday Trans. 1* **1988**, *84*, 3941.
[41] G. Bidan, E. M. Geniès, M. Lapkowski, *J. Chem. Soc. Chem. Commun.* **1988**, 533.
[42] G. Fabre, G. Bidan, M. Laplowski, *J. Chem. Soc. Chem. Commun.* **1994**, 1509.
[43] P. Gómez-Romero, M. Lira-Cantu, *Adv. Mater.* **1997**, *9*, 144.
[44] T. F. Otero, S. A. Cheng, E. Coronado, E. M. Ferrero, C. J. Gomez-Garcia, *ChemPhysChem* **2002**, *3*, 808.
[45] P. Judeinstein, *Chem. Mater.* **1992**, *4*, 4.
[46] a) C. R. Mayer, V. Cabuil, T. Lalot, R. Thouvenot, *Angew. Chem.* **1999**, *111*, 3878; *Angew. Chem. Int. Ed.* **1999**, *38*, 3672; b) C. R. Mayer, R. Thouvenot, T. Lalot, *Chem. Mater.* **2000**, *12*, 257.
[47] a) R. C. Schroden, C. F. Blanford, B. J. Melde, B. J. S. Johnson, A. Stein, *Chem. Mater.* **2001**, *13*, 1074; b) B. J. S. Johnson, A. Stein, *Inorg. Chem.* **2001**, *40*, 801.
[48] A. R. Moore, H. Kwen, A. B. Beatty, E. A. Maatta, *Chem. Commun.* **2000**, 1793.
[49] B. Xu, Z. Peng, D. R. Powell, unpublished results.
[50] CCDC-205080 (**11**) contains the supplementary crystallographic data for this paper. These data can be obtained free of charge via www.ccdc.cam.ac.uk/conts/retrieving.html (or from the Cambridge Crystallographic Data Centre, 12 Union Road, Cambridge CB2 1EZ, UK; fax: (+44) 1223-336-033; or deposit@ccdc.cam.ac.uk).

 © 2004 Wiley-VCH Verlag GmbH & Co. KGaA, Weinheim

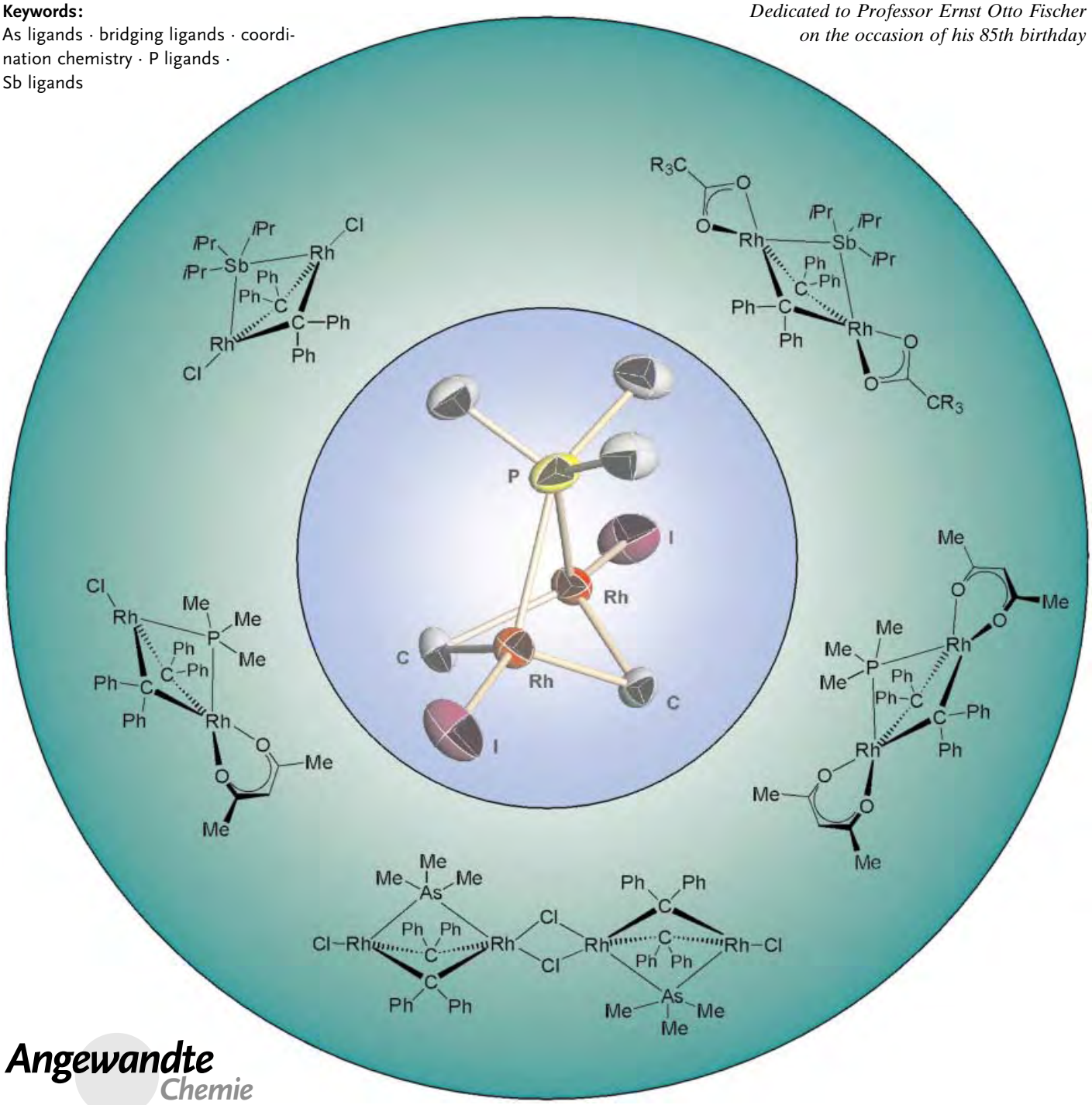
Bridging Ligands

The Way into the Bridge: A New Bonding Mode of Tertiary Phosphanes, Arsanes, and Stibanes

*Helmut Werner**

Keywords:
As ligands · bridging ligands · coordination chemistry · P ligands · Sb ligands

Dedicated to Professor Ernst Otto Fischer on the occasion of his 85th birthday



© 2004 Wiley-VCH Verlag GmbH & Co. KGaA, Weinheim
DOI: 10.1002/anie.200300627

Until recently, tertiary phosphanes, arsanes, and stibanes were considered to bind to transition-metal centers only in a terminal coordination mode. Investigations on the reactivity of square-planar trans-*[RhCl(=CRR′)(L)$_2$] compounds revealed that compounds in which L = SbiPr$_3$ can be converted upon heating into dinuclear complexes [Rh$_2$Cl$_2$(μ-CRR′)$_2$(μ-SbiPr$_3$)] with the carbene and stibane ligands in bridging positions. Although attempts to replace the stibane in these complexes with a tertiary arsane or phosphane failed, substitution of the chloro ligands for acetylacetonates followed by bridge–ligand exchange allowed the preparation of the phosphane- and arsane-bridged compounds [Rh$_2$(acac)$_2$(μ-CRR′)$_2$(μ-PR$_3$)] and [Rh$_2$(acac)$_2$(μ-CRR′)$_2$(μ-AsMe$_3$)]. The acac ligands can be replaced by anionic Lewis bases to give either monomeric [Rh$_2$X$_2$(μ-CRR′)$_2$(μ-ER$_3$)] or dimeric chain-like [XRh(μ-CRR′)$_2$(μ-ER$_3$)Rh(μ-X)$_2$Rh(μ-CRR′)$_2$(μ-ER$_3$)RhX] molecules.*

From the Contents

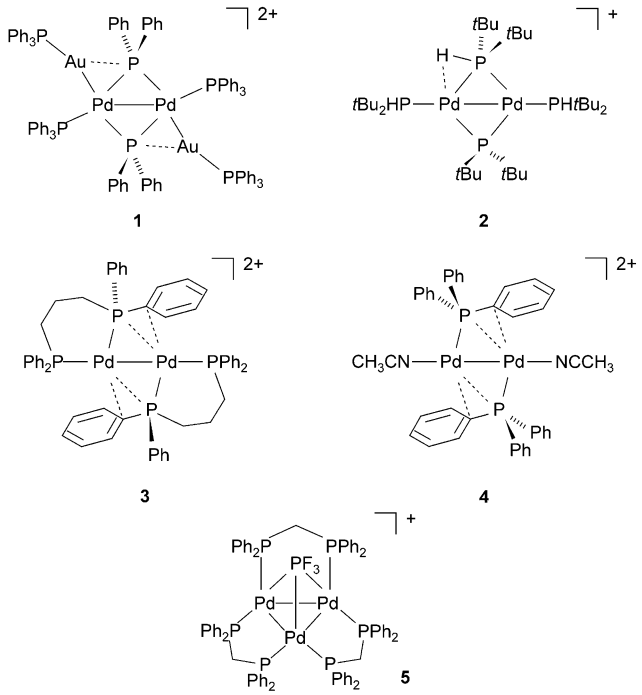
1. Introduction 939
2. The First Steps into a New Field 940
3. The Rich Chemistry of the Stibane-Bridged Complexes 942
4. The Unexpected Entry into a Family of Mixed-Valence Rhodium Complexes 944
5. The Breakthrough: Tertiary Phosphanes in Semibridging and Doubly Bridging Positions 945
6. The Youngest Members of the {Rh(μ-PR$_3$)Rh} Family 948
7. The Final Goal: Trimethylarsane as a Semibridging and a Doubly Bridging Ligand 950
8. Theoretical Studies 951
9. Concluding Remarks 952

1. Introduction

Tertiary phosphanes PR$_3$ with R = alkyl or aryl groups belong, together with CO, to the most well-known ligands in the chemistry of low-valent transition-metal complexes. With regard to CO, not only numerous metal compounds with terminal but also with doubly bridging carbonyl ligands have been reported, in contrast it is generally accepted that tertiary phosphanes (as well as tertiary arsanes and stibanes) behave exclusively as terminal coordinated ligands.[1,2]

In spite of this clear statement, there were some hints in the literature that a doubly bridging bonding mode for phosphane ligands could be achieved. By investigating the chemistry, including the molecular structure, of platinum–gold clusters, Braunstein and co-workers observed that in compound **1** the Au–PPh$_2$ distances are relatively short (see Scheme 1).[3] Owing to this structural feature, and by virtue of the isolobal analogy between Au(PPh$_3$) and H, the authors predicted "that polynuclear systems containing a *bridging phosphane ligand* might exist".[3]

Shortly after this paper appeared, Pasquali, Pregosin et al. described the molecular structure of the dinuclear palladium complex **2**, in which the *t*Bu$_2$P–H···Pd unit has an agostic-like interaction.[4] Although the P–H···Pd hydrogen atom was not found in the X-ray crystal structure analysis, one- and two-dimensional NMR spectroscopy revealed different electronic environments for the two phosphido ligands. Preliminary calculations based on heteronuclear Overhauser experiments suggested a P–H distance of about 1.9 Å, which places the P–H proton between the palladium and the bridging phosphide unit.[4,5] Thus, **2** has a similar structural feature to that



Scheme 1.

[*] Prof. Dr. H. Werner
Institut für Anorganische Chemie der Universität Würzburg
Am Hubland, 97074 Würzburg (Germany)
Fax: (+49) 931-888-4623
E-mail: helmut.werner@mail.uni-wuerzburg.de

DOI: 10.1002/anie.200300627
© 2004 Wiley-VCH Verlag GmbH & Co. KGaA, Weinheim

found in compound **1**, which underlies the prediction made by Braunstein and co-workers.

One year after the publication of the work by Pasquali, Pregosin and co-workers, the group of van Leeuwen reported the preparation and molecular structure of the palladium(I) dimer **3**, in which one phosphorus atom of each 1,3-bis(diphenylphosphino)propane (dppp) ligand occupies an asymmetrically bridging position.[6] The X-ray crystal-structure analysis also suggests an interaction between the *ipso*-carbon atom of a phenyl group at a bridging PPh_2 moiety and a palladium atom which, according to the ^{13}C NMR spectrum, persists in solution. As not only this agostic-like interaction but also the bridging or side-on Pd–P bond is rather weak, the dimer is easily split by donor groups such as CO or CH_3CN to give monomeric species.[6]

A compound somewhat related to **3** was described recently by Kurosawa and co-workers.[7] During investigations aimed to create at least two vacant coordination sites on a Pd^I–Pd^I framework, these authors observed that the dication $[Pd_2(CH_3CN)_4(PPh_3)_2]^{2+}$ easily loses two acetonitrile ligands to give the stable dipalladium complex **4**, in which each of the two vacant sites is occupied by an *ipso*-carbon atom of a η^1-bound phenyl ring. Since according to the X-ray crystal-structure analysis there is a strong Pd–P bond to one metal center and a weak Pd–P bond to the second, the triphenylphosphane can be formally considered as a four-electron donor similar to the $HPtBu_2$ unit in compound **2**. For this reason, the bonding scheme of the bridging phosphane neither in **2** nor in **4** is comparable to that of a bridging CO group in a {M(μ-CO)M} moiety.

The nearest analogy between the two-electron donor capabilities of CO and a molecule of the general composition PR_3 was found by Balch et al.[8] In attempting to obtain a dinuclear palladium compound with {Pd(μ-PF_3)Pd} as the core unit, these authors reported in 1990 the preparation and structural characterization of a cationic Pd_3 complex, **5**, which consists of a nearly equilateral triangle of palladium atoms bridged at the edges by bis(diphenylphosphino)methane ligands and capped by the triply bridging phosphorus atom of PF_3. This situation is reminiscent of that of various carbonylmetal clusters, in which molecular building blocks of the general type {M_3(μ-CO)} exist.[9] However, from a comparison of complex **5** with the other compounds shown in Scheme 1, because of its strong π-acceptor character, PF_3 can be considered as an atypical phosphane as it is closer to CO than to trialkyl- or triarylphosphanes.



Helmut Werner was born in 1934 at Mühlhausen (Thüringen) and studied chemistry in Jena and Munich. He did his PhD with E. O. Fischer and was a postdoctoral fellow with J. H. Richards at Caltech in Pasadena. After his Habilitation at the Technical University in Munich (1966), he joined the University of Zürich (1968). In 1975 he was appointed Professor and Head of the Institute of Inorganic Chemistry at the University of Würzburg where he became Professor Emeritus (2002). He has gained numerous international awards and in 2001 received an honorary doctorate from the University of Zaragoza (Spain).

2. The First Steps into a New Field

The detective story entitled "How to find a route to generate a phosphane-bridge {M(μ-PR_3)M} as an analogue to a {M(μ-CO)M} bridge" began far away from the real topic. After we had investigated in detail the chemistry of square-planar vinylidene- and allenylidene-rhodium(I) complexes of type B and C,[10] we also became interested in the preparation of the corresponding rhodium carbenes A, which represent the missing link in the series of Rh=C double-bond systems A-B-C (see Figure 1). However, the reaction of the dimer

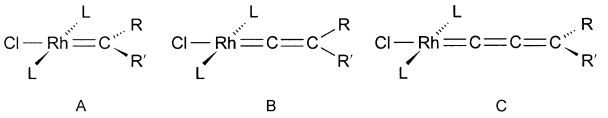


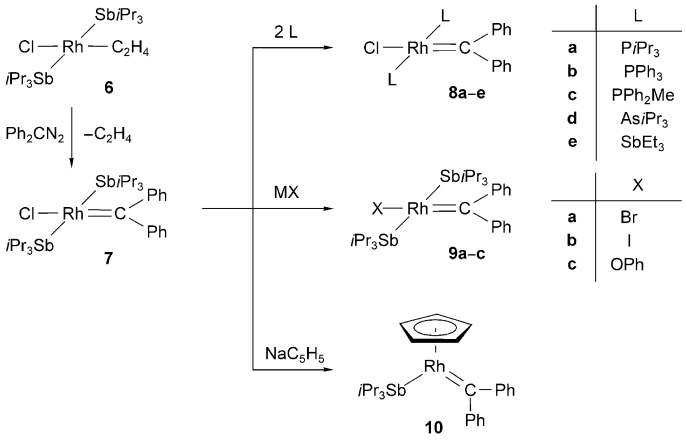
Figure 1. A series of square-planar rhodium(I) complexes containing rhodium-carbon double bonds (L = $PiPr_3$).

[{Rh(μ-Cl)($PiPr_3$)$_2$}$_2$], used as the starting material for the synthesis of compounds B and C, with either CH_2N_2, $PhCHN_2$, or Ph_2CN_2 did not lead to the formation of the required carbene complexes of type A but gave instead olefin- or diazoalkane-rhodium(I) derivatives.[11] Since we were convinced, owing to the composition of the products and their reactivity towards diazoalkanes, that rhodium carbenes were involved in these reactions, we attempted to achieve the original goal by varying the coordination sphere around the rhodium(I) center.

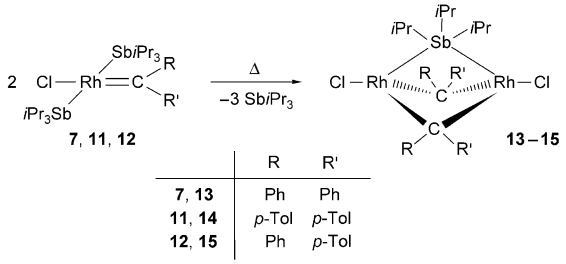
The key to success was the use of triisopropylstibane, instead of triisopropylphosphane, as the supporting (formally innocent) ligand. Treatment of *trans*-[RhCl(C_2H_4)($SbiPr_3$)$_2$] (**6**) with Ph_2CN_2, other diaryldiazoalkanes, or with $PhC(CF_3)N_2$ afforded complexes of type A (L = $SbiPr_3$) in good to excellent yields.[12] Although these compounds are quite stable and can even be handled in air for short periods of time, they are highly reactive and undergo a variety of ligand substitution reactions with either neutral or anionic Lewis bases. As illustrated in Scheme 2, which uses compound **7** as an example, it is possible to exchange the chloride, the stibane, or both for other donor ligands without breaking the metal–carbene bond.[12,13]

However, the most interesting reaction of **7** was discovered when we investigated the thermal behavior of the compound. We observed that slightly below the decomposition point of 61 °C, the compound changed from dark green to red. A repetition of the process in benzene at 60 °C led to the formation of the dinuclear complex **13** (Scheme 3) which, after chromatographic workup, was isolated in 81 % yield. While the square-planar precursors **11** and **12** behaved similarly and afforded in nearly quantitative yields compounds **14** and **15**, respectively, under the same conditions the

 © 2004 Wiley-VCH Verlag GmbH & Co. KGaA, Weinheim



Scheme 2.



Scheme 3.

bis(phosphane) derivatives **8a–c** were inert and after a solution of these complexes had been stirred in benzene for two days, the starting material was recovered unchanged. Since during the thermal reactions of **7**, **11**, and **12** the formation of free triisopropylstibane was observed, we originally thought that one Sb*i*Pr$_3$ ligand from the precursors had been eliminated and two of the resulting 14-electron species [RhCl(=CRR′)(Sb*i*Pr$_3$)] had formed a dimer with either chloro or diarylcarbene bridges. Although this does not occur, it is nevertheless conceivable that the supposed dimer [RhCl(=CRR′)(Sb*i*Pr$_3$)]$_2$ with two bridging carbene ligands is generated as an intermediate from which subsequent loss of one stibane affords the final product.[14]

The dinuclear compounds **13–15** are red, slightly air-sensitive solids that, remarkably, decompose only above 180 °C. With regard to the spectroscopic data, a characteristic feature is that, in contrast to those of **7**, the phenyl groups of complex **13** are spectroscopically nonequivalent. Moreover, the ^{13}C NMR spectrum of the less symmetrical complex **15** reveals that all three possible isomers *syn-syn*, *syn-anti*, and *anti-anti* (see Figure 2) with different orientations of the aryl groups are present. Since the intensity of the resonances for the carbene carbon atoms of the three isomers remain unchanged upon stirring a solution of **15** in C_6D_6 for 12 h at 25 °C, the conclusion is that under these conditions the isomeric mixture is already at equilibrium.[14]

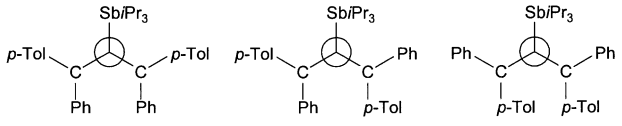


Figure 2. Newman projections of the configurational isomers of compound **15** viewed along the Cl-Rh-Rh-Cl axis.

The X-ray crystal-structure analysis of **13** (Figure 3) established the hitherto unknown capability of trialkylstibanes to behave as bridging ligands and to form two metal–antimony bonds. Quite surprisingly, there is almost no influence of the bridging function of the stibane on the Sb–C bond lengths and, despite the increase in the coordination number of antimony from three to five, on the C-Sb-C bond angles. The relatively short Rh–Rh distance in **13** (2.5349(5) Å) is indicative of a direct metal–metal interaction. Noteworthy are the larger Rh–Sb distances in **13** (2.6868(5) and 2.6695(5) Å) compared with those in **7** (2.5843(5) and 2.5633(5) Å), which is in agreement with the bridging function of the stibane ligand. The arrangement of the Cl-Rh-Rh-Cl moiety is nearly linear, the somewhat slight bending away from the antimony atom being possibly due to the steric repulsion between the chloro ligands and the bulky isopropyl groups.[14]

Studies that concerned the ability of compound **7** to undergo C–C coupling reactions with various substrates offered an alternative route to dinuclear rhodium complexes with a bridging stibane ligand. While attempts to connect the CPh_2 unit of **7** with CH_2 or $CH(CO_2Et)$ by using CH_2N_2 or $CH(CO_2Et)N_2$ as a carbene source did not generate the corresponding olefin but gave a mixture of products, treatment of **7** with $(p\text{-Tol})_2CN_2$ or $PhC(p\text{-Tol})N_2$ under the same conditions led to the formation of the more unsymmetrical dirhodium complexes **16** and **17** in about 75% yield (Scheme 4). Compounds **16** and **17** are also accessible by conproportionation of equimolar amounts of **13** and **14,** or of **13** and **15**, respectively. It is remarkable that although complexes **13–15** are probably very similar in structure and bonding, after a solution of **13** and **14** had been stirred in diethyl ether for 5 h at room temperature, instead of an equilibrium mixture of **13**, **14**, and **16** in the ratio of 1:1:2, the less symmetrical product **16** was obtained nearly quantita-

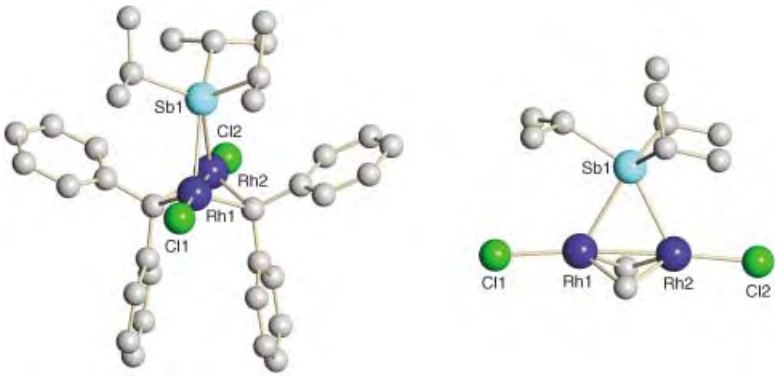
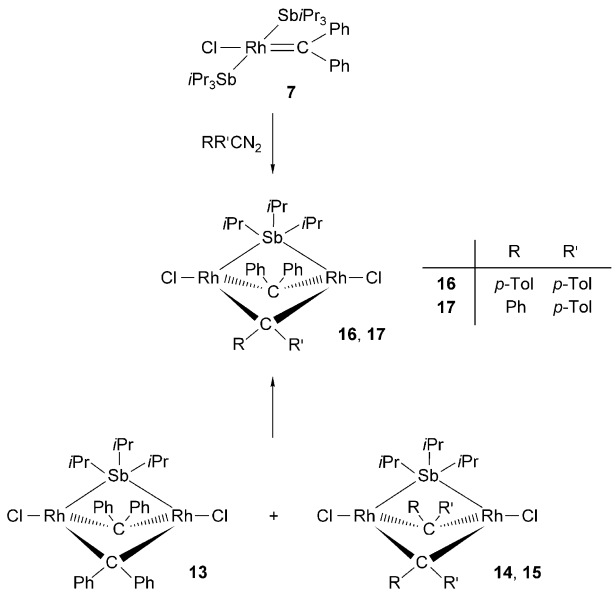
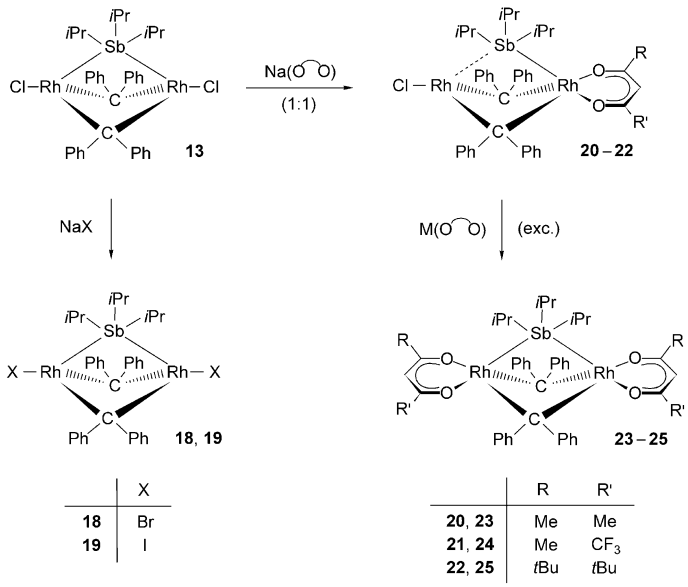


Figure 3. Molecular structure (SCHAKAL representation) of compound **13** (hydrogen atoms omitted for clarity).

 © 2004 Wiley-VCH Verlag GmbH & Co. KGaA, Weinheim



Scheme 4.



Scheme 5.

tively. Moreover, in contrast to **7** the dinuclear complex **13** is inert toward $(p\text{-Tol})_2CN_2$ and does not generate either **14** or one of the olefins $R_2C{=}CR'_2$ (R, R′ = Ph, *p*-Tol).[14]

3. The Rich Chemistry of the Stibane-Bridged Complexes

Since **13** is a 26-electron compound and appears not only electronically but also coordinatively unsaturated, it is not surprising that it is highly reactive toward Lewis bases. While attempts to convert the mononuclear precursors *trans*-$[RhX(=CPh_2)(Sb\textit{i}Pr_3)_2]$ (X = Br, I) to the corresponding dinuclear complexes **18** and **19** remained unsuccessful, the reactions of **13** with an excess of NaBr or NaI in acetone affords the required dibromo and diiodo derivatives **18** and **19** in virtually quantitative yield (Scheme 5).[15] The ^{1}H and ^{13}C NMR spectra of **18** and **19** are quite similar to those of the dichloro counterpart **13** and thus there is no doubt that the proposed structure is correct. Attempts to replace the chloro ligands in **13** with fluoride, by using either NaF or CsF as fluoride source, failed.

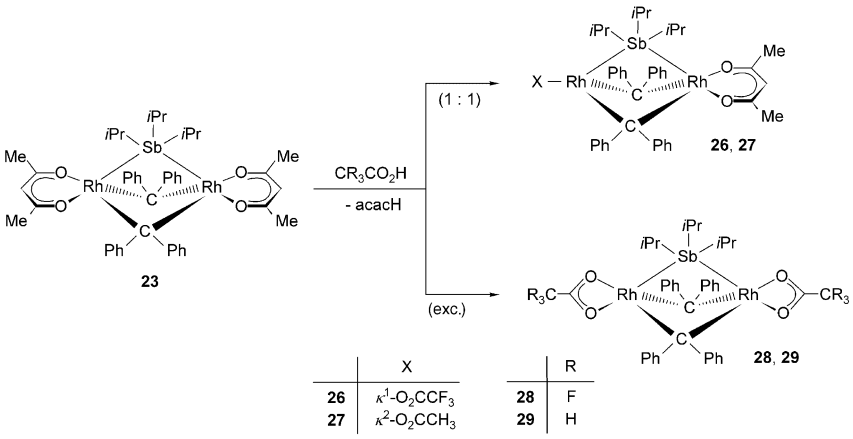
The reactions of **13** with equimolar amounts of the sodium salts of acetylacetone (acacH), trifluoroacetylacetone (acac-f_3-H), and dipivaloylmethane (dpmH) led to the formation of the unsymmetrical dinuclear rhodium(I) compounds **20**–**22** in 92–95 % yield of the isolated products.[15] Although in our initial studies we used Tl(acac) as the acac source, [16] for the preparation of **20**, Na(acac) is the preferred substrate. The bis(di-*p*-tolylcarbene) complex $[Rh_2(acac)_2\{\mu\text{-}C(p\text{-Tol})_2\}_2(\mu\text{-}Sb\textit{i}Pr_3)]$ is also accessible by using the same route. With respect to the spectroscopic data of **20**–**22**, the remarkable feature is that the resonance for the ^{13}C nuclei of the bridging carbene atoms appears in the ^{13}C NMR spectra of **20** and **21** as a multiplet but in the spectrum of **22** as a doublet of doublets owing to the coupling of this carbon atom to two different rhodium atoms. In the case of the symmetrical complexes **13**, **18**, and **19** the corresponding signal is a triplet.

The X-ray crystal structure analysis of **20** revealed that owing to the asymmetry of the dinuclear molecule, the stibane and one of the diphenylcarbene ligands are linked to the two rhodium centers in an unsymmetrical fashion.[16] The bond lengths Sb–Rh1 and Sb–Rh2 differ by about 0.35 Å and those between one of the carbene carbon atoms and Rh1, and between C2 and Rh2 differ by approximately the same value. In **20** the Sb–Rh1 bond is about 0.19 Å shorter and the Sb–Rh2 about 0.18 Å longer than the corresponding bonds found in the starting material **13**; the longer Sb–Rh bond being directed to the lower-coordinated metal center. It is also noteworthy that the acetylacetonate is coordinated in an unsymmetrical mode, such that the shorter Rh–O bond is opposite to the shorter Rh–C(carbene) bond. The Rh–Rh distance in **20** is about 0.15 Å longer than that in **13**, but the value still lies within the range of distances of other dinuclear rhodium(I) complexes with a metal–metal bond.[17]

From the reaction of **13** with an excess of either M(acac) or M(acac-f_3) (M = Na, Tl) the bis(acetylacetonato) compounds **23** or **24** were obtained in excellent yields.[15,16] If under the same conditions the reaction of **13** or **22** was carried out with Na(dpm), a mixture of products was isolated with **25** as the dominating species. While it was possible to separate **25** from **22** and other by-products by column chromatography, attempts to remove small amounts of Na(dpm), used in excess, failed. Therefore, compound **25** was characterized spectroscopically. Quite remarkably, the symmetrical complexes **23** and **24** are thermally significantly less stable than the unsymmetrical counterparts **20** and **21**, which might be because of the steric requirements imposed by the chelating ligands (see Section 5). In this context it is worth mentioning that all attempts to obtain dirhodium compounds with a $\{Rh(\mu\text{-}CR_2)_2(\mu\text{-}Sb\textit{i}Pr_3)\}$ framework and one or two hexafluorinated acetylacetonates remained unsuccessful.

 © 2004 Wiley-VCH Verlag GmbH & Co. KGaA, Weinheim

Not only **13** but also the bis(acac) complex **23** has been used as a starting material for the preparation of new dinuclear rhodium(I) derivatives with a bridging Sb*i*Pr$_3$ ligand. Treatment of **23** with CF_3CO_2H in the molar ratio of 1:1.1 gave the compound **26** in almost quantitative yield (Scheme 6). In contrast, the reaction of **23** with an equimolar amount of acetic acid led to a mixture of **27** (ca. 80%), **29** (ca. 10%), and the starting material **23** (ca. 10%), which could not be separated. However, compound **23** reacted unequivocally with an excess of CH_3CO_2H to give the bis(acetato) complex **29** in 85% yield. The $\{Rh_2(O_2CCF_3)_2\}$ analogue, **28**, which had also been prepared from **13** and TlO_2CCF_3,[16] was obtained in the same way. From the IR data, it can be seen that the trifluoroacetate behaves as a monodentate ligand in compound **26**, whereas it is coordinated in a chelating fashion in **28**.



Scheme 6.

The bidentate coordination mode of the acetate units in complex **29** was confirmed crystallographically (Figure 4).[15] The coordination geometry around each of the rhodium centers can be best described as distorted square-pyramidal with the antimony atom in the apical position. The respective metal atom lies above the plane formed by the oxygen atoms and the carbene carbon atoms of the bridging CPh_2 ligands. Whereas the Rh1–Rh2 distance (2.5429(3) Å) in **29** is practically identical to that of the dichloro analogue **13**, the Rh–Sb bond lengths in **29** (2.6902(2) and 2.7126(2) Å) are slightly longer than in **13**. The fact that most of the structural data for the core units $\{Rh_2(\mu\text{-}CPh_2)_2(\mu\text{-}Sb\textit{i}Pr_3)\}$ of **13** and **29** are quite similar is noteworthy insofar as the coordination number of the rhodium atoms in the two molecules is different. It should also be emphasized that while in the bis(acac) complexes $[Rh_2(\kappa^2\text{-acac})_2(\mu\text{-}CPh_2)_2(\mu\text{-}CO)]$ and $[Rh_2(\kappa^2\text{-acac})_2(\mu\text{-}CPh_2)_2(\mu\text{-}PMe_3)]$ (Section 5) the two planes containing the chelating systems are twisted (like a propeller), the two rhodium atoms and the four oxygen atoms of **29** lie in the same plane.

However, even more remarkable than the smooth exchange of the anionic units in **13** and **23** is the fact that the bridging stibane ligand of these compounds can be substituted by a variety of Lewis bases without breaking the $\{Rh(\mu\text{-}CPh_2)Rh\}$ bridges. Whereas the dichloro derivative **13** is inert towards ethene and terminal alkynes, it reacts with CO in benzene at room temperature to afford a brick-red solid that is practically insoluble in all common organic solvents. Since the elemental analysis of the solid is consistent with the composition $[RhCl(CPh_2)(CO)]$, we assume that the (presumably polymeric) product is identical to a compound obtained by Sonogashira and co-workers from $[\{Rh(\mu\text{-}Cl)(CO)_2\}_2]$ and diphenylketene.[18] Although it is conceivable, as suggested by the Sonogashira group, that two CO groups bridges two adjacent rhodium centers, we think that the structure **31** shown in Scheme 7 is more likely. An argument in favor of this proposal is that **31** reacts with NaC_5H_5 to give $[(\eta^5\text{-}C_5H_5)_2Rh_2(\mu\text{-}CPh_2)_2(\mu\text{-}CO)]$ and with pyridine to afford $[Rh_2Cl_2(py)_2(\mu\text{-}CPh_2)_2(\mu\text{-}CO)]$, respectively.[17a]

In contrast to **31**, the product **32** obtained from the bis(acac) complex **23** and CO is monomeric and this has been substantiated by an X-ray crystal-structure analysis.[16b] In a similar way to **29**, the coordination geometry around the rhodium centers is best described as square-pyramidal with the carbene carbon atom in the apical position. The molecule is highly symmetric and in contrast to **20** also the two acetylacetonato ligands are symmetrically linked to the metal centers. The bond length Rh–CO in **32** is slightly shorter than the bond lengths between rhodium and the carbene carbon atoms which is in agreement with the data for the above-mentioned compounds $[(\eta^5\text{-}C_5H_5)_2Rh_2(\mu\text{-}CPh_2)_2(\mu\text{-}CO)]$ and $[Rh_2Cl_2(py)_2(\mu\text{-}CPh_2)_2(\mu\text{-}CO)]$.

With *t*BuNC, compounds **13** and **23** react in an analogous fashion and afford the two isocyanide-bridged complexes **34** and **35** in

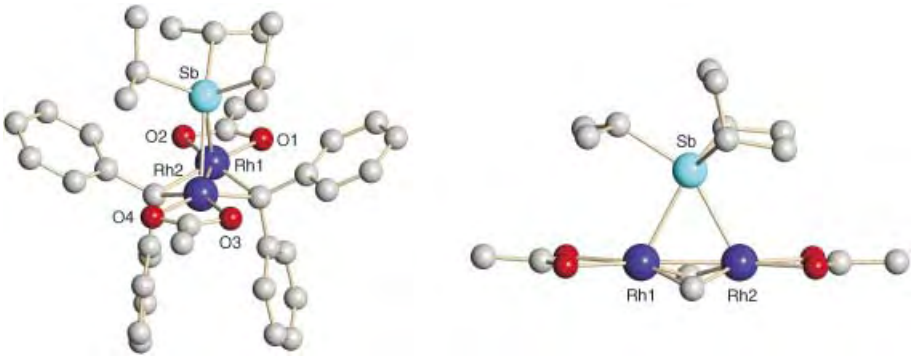
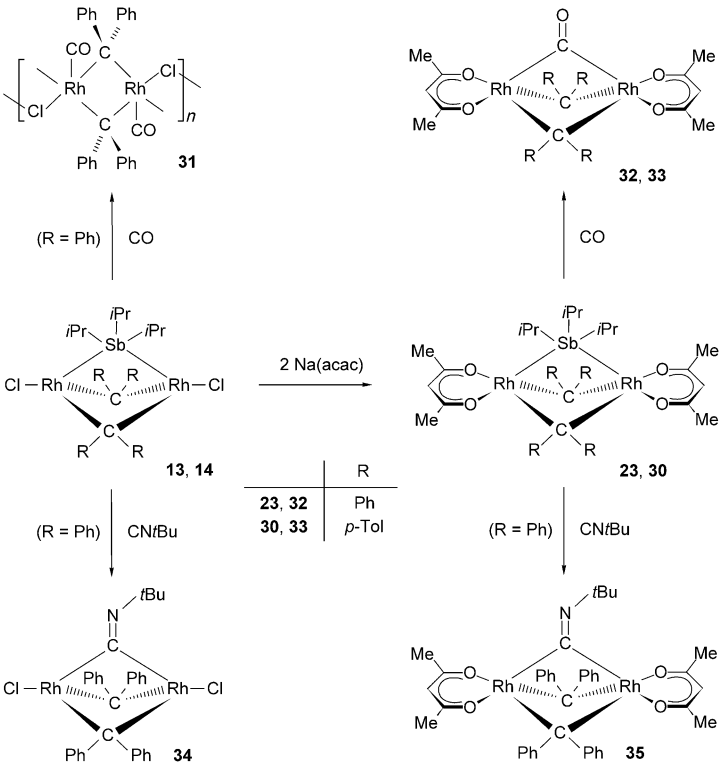


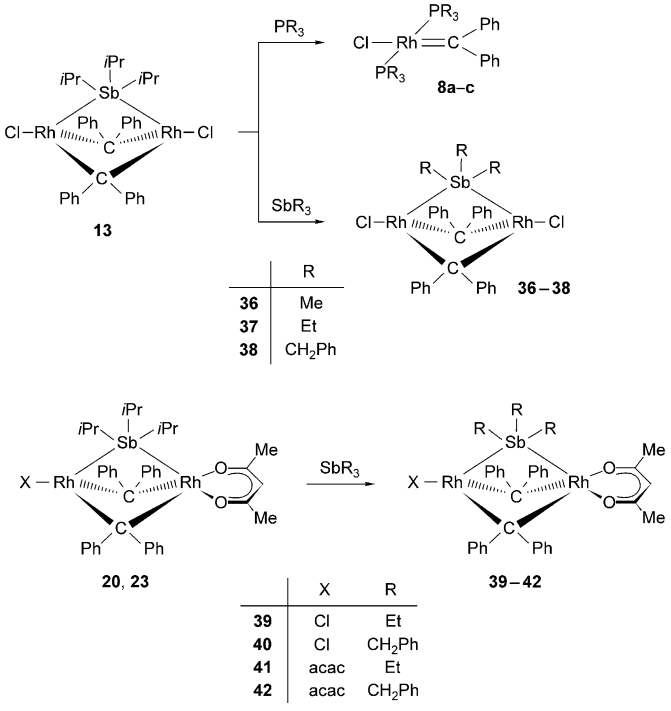
Figure 4. Molecular structure (SCHAKAL representation), including a side-view, of compound **29** (hydrogen atoms omitted for clarity).

 © 2004 Wiley-VCH Verlag GmbH & Co. KGaA, Weinheim



Scheme 7.

nearly quantitative yields. A clean and quick bridge–ligand exchange also occurs between **13** and $SbMe_3$, $SbEt_3$, and $Sb(CH_2Ph)_3$ to give the dirhodium counterparts **36–38** (Scheme 8).[14,15] Quite remarkably, the $SbMe_3$-bridged compound is even more stable than the precursor **13** and decomposes at 242 °C! The mono(acac) and bis(acac) derivatives **20** and **23** behave in a similar way as **13** and upon treatment with $SbEt_3$ or $Sb(CH_2Ph)_3$ form the products **39–42** in excellent yields.[15,16] We note, however, that while it is easy to substitute the bridging Sb*i*Pr$_3$ ligand in **13**, **20**, and **23** for trialkylstibanes, all attempts to prepare a dinuclear rhodium complex with $SbPh_3$ in the bridging position failed.



Scheme 8.

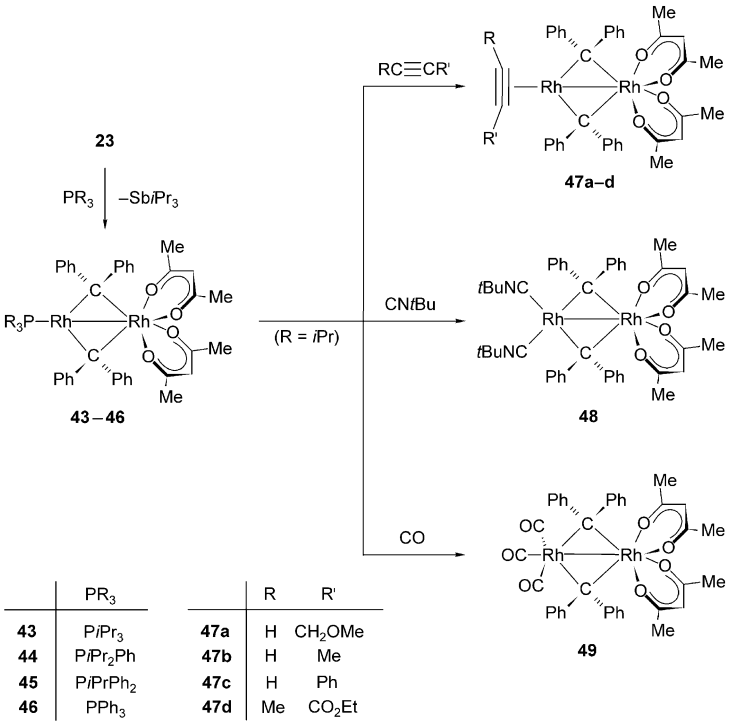
4. The Unexpected Entry into a Family of Mixed-Valence Rhodium Complexes

Although we were convinced, from the time when we had isolated the first stibane-bridged compound **13**, that it could be possible to prepare an analogue of **13** with $\{Rh(\mu\text{-}CPh_2)_2(\mu\text{-}PR_3)Rh\}$ as the central core, the way to achieve this goal was paved not only with several set-backs but also with a big surprise. Since we speculated that, owing to the stability and the ease of formation of **13**, P*i*Pr$_3$ could be similar in its coordination capabilities to Sb*i*Pr$_3$, we first considered triisopropylphosphane as an appropriate candidate for the formation of a $\{Rh(\mu\text{-}PR_3)Rh\}$ bridge. However, the reaction of **13** with one equivalent of P*i*Pr$_3$ gave the square-planar carbene complex **8a** in about 25% yield. With four equivalents of the phosphane, the mononuclear product was obtained nearly quantitatively. Other tertiary phosphanes such as PPh_3 or $PMePh_2$ behaved similarly (see Scheme 8).[14] In contrast to **13**, the bis(acac) compound **23** reacts with an excess of P*i*Pr$_3$ much more slowly and affords, after four hours at 60 °C in benzene, the novel dinuclear complex **43** in 68% yield of the isolated product (Scheme 9).[16] The reactions of **23** with P*i*Pr$_2$Ph, P*i*PrPh$_2$, and PPh_3 proceed analogously and gave, after reaction times of 8, 24 and 48 h, respectively, the related compounds **44–46** in equally good yields. By using the same methodology, the bis(di-*p*-tolylcarbene) complex $[(PiPr_3)Rh\{\mu\text{-}C(p\text{-}Tol)_2\}_2Rh(acac)_2]$ is obtained from **30** and excess triisopropylphosphane. Since the ^1H and ^{13}C NMR spectra of **43–46** displayed two sets of signals for the protons and carbon atoms of the $OC(CH_3)$ moieties of the acac ligands, it was apparent that an unsymmetrical environment around the central $[Rh(\mu\text{-}CPh_2)_2Rh]$ core should exist.

This proposal was confirmed by the X-ray crystal-structure analysis of **43**. Evidently, one of the chelating ligands has migrated from one metal center to the other and its former position is occupied by the phosphane. The stibane ligand has been replaced, while the bridging diphenylcarbene units are maintained. Not unexpectedly, the distances between the less coordinated rhodium atom and the carbene carbon atoms are shorter than the others. Moreover, in analogy to the mixed $\{Rh_2Cl(acac)\}$ complex **20**, the acetylacetonato ligands are not coordinated in a symmetrical fashion and, therefore, in both six-membered chelate rings the Rh–O bond lengths differ by 0.08 to 0.10 Å. The unsymmetrical structure is, without any doubt, also maintained in solution since the ^{31}P NMR spectrum of **43** displays a sharp doublet of doublets with a large $^1J(^{103}Rh,^{31}P)$ and a small $^2J(^{103}Rh,^{31}P)$ coupling constant.[16]

However, the novel mixed-valence compounds are not only interesting from a structural point of view but also with

 © 2004 Wiley-VCH Verlag GmbH & Co. KGaA, Weinheim



	PR_3
43	P*i*Pr$_3$
44	P*i*Pr$_2$Ph
45	P*i*PrPh$_2$
46	PPh$_3$

	R	R'
47a	H	CH_2OMe
47b	H	Me
47c	H	Ph
47d	Me	CO_2Et

Scheme 9.

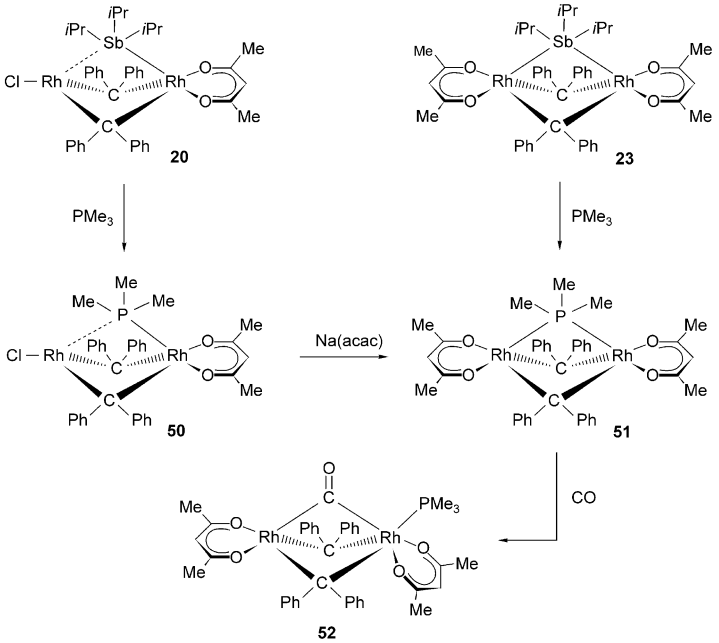
respect to their reactivity toward Lewis bases. With the P*i*Pr$_3$ derivative as the starting material the corresponding dinuclear monoalkyne, bis(isocyanide) and tricarbonyl complexes **47a–d**, **48** and **49** can be obtained in good to excellent yields (Scheme 9). As the X-ray crystal structure analysis of **47a** revealed, the Rh–Rh distance in **47a** is about 0.03 Å shorter than in **43**, while the Rh–C(carbene) and Rh–O bond lengths differ only slightly to those of the P*i*Pr$_3$ counterpart. The axis of the alkyne carbon atoms lies perpendicular to the Rh-C-C-Rh plane with the CH_2OMe fragment bent away from the nearby rhodium center. Notably, all attempts to rearrange the coordinated alkyne to an isomeric vinylidene ligand either by heating or photolyzing solutions of **47a** or **47b** failed.[16]

The reactions of **43** with CN*t*Bu and CO did not only lead to a displacement of the phosphane but also to an increase of the coordination number at the low-valent rhodium center. It is thus evident that the coordination sphere around Rh^0 can change and, depending on the size of the ligands, is quite flexible. As confirmed crystallographically, in the bis(isocyanide) complex **48** the low-valent metal center is coordinated in a considerably distorted square-planar fashion with C-Rh-C bond angles that deviate significantly from the ideal 90° value.[16] The coordination geometry around the higher-valent metal center is distorted octahedral and quite similar to that found in **43** and **47a**. A further increase in the coordination number at Rh^0 occurs if P*i*Pr$_3$ is replaced by CO as is substantiated by the appearance of three CO stretching modes in the IR spectrum of **49**. This increase in coordination number is accompanied by lability, as indicated by the observation that compound **49** loses smoothly in solution one carbonyl ligand and thus it can be stored unchanged only under a CO atmosphere.

5. The Breakthrough: Tertiary Phosphanes in Semibridging and Doubly Bridging Positions

All attempts undertaken between 1994 and 1999 to replace the bridging stibane in compounds such as **13** or **23** by a tertiary phosphane remained unsuccessful. The breakthrough occurred when we used the unsymmetrical complex **20** as the starting material and the smaller trimethylphosphane as the substrate, instead of the more bulky phosphanes that were essential in our work on metallacumulenes.[10,19] The treatment of a solution of **20** in either pentane/diethyl ether or in dichloromethane at −78 °C with an equimolar amount of PMe_3 gave the substitution product **50** as a red-brown, slightly air-sensitive solid in about 85% yield of the isolated product (Scheme 10). The ^{31}P NMR spectrum of **50** displayed a doublet of doublets with two relatively large $^1J(^{103}Rh,^{31}P)$ coupling constants, thus indicating that the phosphane is not linked to one of the metal centers in a terminal mode.[20]

The X-ray crystal structure analysis of **50** established that the position of the PMe_3 ligand can be best described as semibridging (see Figure 5).[21] Apart from the different bond lengths (Rh1–P (2.2406(15) Å) and Rh2–P (2.8410(14) Å), characteristic features are in particular the Rh-Rh-P bond angles, which are significantly smaller than 90°. Because of the higher coordination number of Rh1 compared with Rh2, not only the phosphane but also the two diphenylcarbene ligands are linked to the metal centers in an unsymmetrical fashion. The bond lengths Rh2–C1 and Rh2–C2 are about 0.11 Å shorter than those from Rh1–C1 and Rh1–C2, quite similar to the situation found for the stibane-bridged compound **20**. How-



Scheme 10.

 © 2004 Wiley-VCH Verlag GmbH & Co. KGaA, Weinheim

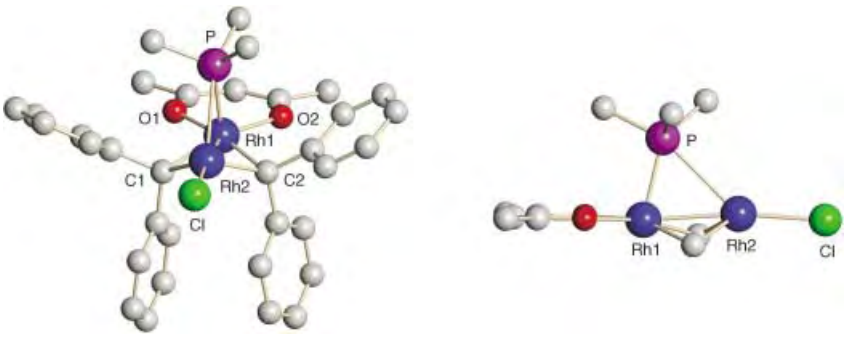


Figure 5. Molecular structure (SCHAKAL representation), including a side-view, of compound **50** (hydrogen atoms omitted for clarity).

ever, in contrast to **20** the acetylacetonate unit in **50** is coordinated in a symmetrical mode. The three P–C distances are nearly the same and lie in the range of rhodium(I) compounds with a terminal PMe_3 ligand. While the Rh1–Rh2 bond length of 2.5318(8) Å is practically identical to that in **13**, it is significantly shorter than in the Sb*i*Pr_3 counterpart **20**.

Compound **50** reacts not only with Tl(acac)[20] but also with Na(acac) in the molar ratio of 1:4 at room temperature by replacement of the chloro for the acetylacetonato ligand to give the dinuclear complex **51** (see Scheme 10). An alternative procedure to obtain **51** involves the substitution of Sb*i*Pr_3 in compound **23** for PMe_3; in both cases the yields are excellent.[22] As has already been observed for **20** and **23**, the symmetrical complex **51** is thermally considerably less stable than the unsymmetrical counterpart **50**. Regarding the spectroscopic data of **51**, it is important to note that, in contrast to **50**, the ^{31}P NMR spectrum does not display a doublet of doublets but a sharp triplet, thus illustrating that in solution the phosphane ligand is coordinated to both rhodium centers in an identical mode.

The result of the X-ray crystal structure analysis of **51** is shown in Figure 6. Although the two Rh–P bond lengths are not exactly the same, the difference of about 0.3 Å is only half of that in **50**. Since both the ^{31}P and the ^{13}C NMR spectra suggest that the core unit $\{Rh_2(\mu\text{-}CPh_2)_2(\mu\text{-}PMe_3)\}$ in **51** is symmetrical, it is conceivable that the deviation from the ideal symmetry for the sterically hindered molecule found in the crystal is due to steric reasons or simply packing effects.

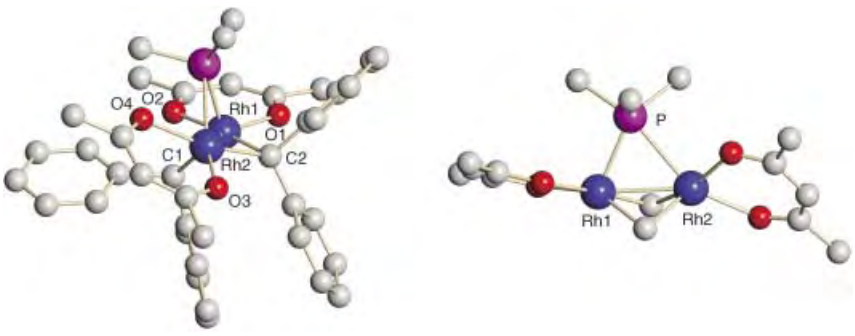
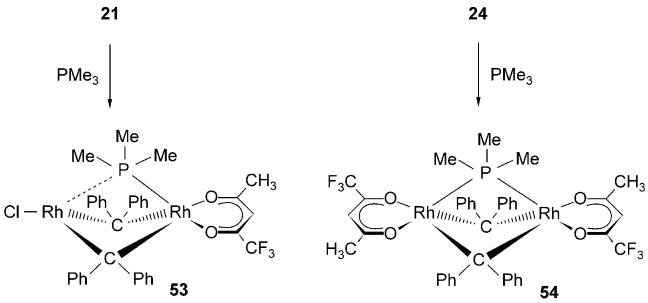


Figure 6. Molecular structure (SCHAKAL representation), including a side-view, of compound **51** (hydrogen atoms omitted for clarity).

The coordination geometry of both rhodium centers corresponds to a distorted square pyramid, the difference being that for the polyhedron around Rh1 the phosphorus atom and for the polyhedron around Rh2 the carbene carbon atom C1 is in the apical position. The two planar six-membered rings formed by the metals and the acac ligands lie not in the same plane but are twisted; the dihedral angle between the two planes is 30.2°. In contrast with Rh1–O1 and Rh1–O2, the bond lengths Rh2–O3 and Rh2–O4 are not the same, a fact which reflects the loss of symmetry in the crystal.

Compound **51** is highly reactive toward carbon monoxide and upon treatment in benzene affords the dinuclear complex **52** in nearly quantitative yield.[22] The shift of the PMe_3 ligand from a bridging to a terminal position is indicated by the splitting of the ^{31}P NMR resonance, which is a doublet of doublets with one large and one small $J(^{103}Rh,^{31}P)$ coupling constant. The appearance of a ν(CO) stretching mode at $\tilde{\nu} = 1829\ cm^{-1}$ in the IR spectrum of **52** leaves no doubt that the carbonyl ligand occupies a doubly bridging position.

Compounds **21** and **24** that have one or two acac-f_3 ligands coordinated to the rhodium centers (instead of one or two acac ligands), behave similarly to **20** and **23**, and react with an equimolar amount of PMe_3 to give the dinuclear complexes **53** and **54** (Scheme 11). Also in this case, the unsymmetrical compound **53** is considerably more stable than the symmetrical counterpart. In agreement with the different bonding mode (semibridging versus doubly bridging), the ^{31}P NMR



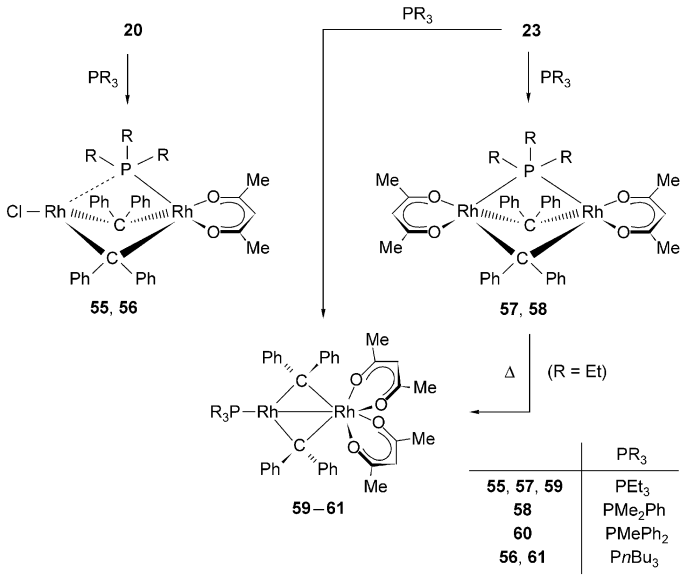
Scheme 11.

spectrum of **53** displays a doublet of doublets while that of **54** shows a sharp triplet with a $^1J(^{103}Rh,^{31}P)$ coupling constant that is virtually identical to that of **51**.

In contrast to PMe_3, the more bulky triisopropylphosphane reacts with **20** to give a mixture of products, among which a species with a bridging P*i*Pr_3 unit could not be detected. Thus, we decided to study the reactivity of those phosphanes toward **20** that, owing to Tolman's cone angles,[23] are of a size between PMe_3 and P*i*Pr_3. Treatment of **20** with PEt_3 under the same conditions as used for the preparation of **50**

 © 2004 Wiley-VCH Verlag GmbH & Co. KGaA, Weinheim

affords the analogous dinuclear compound **55** as a dark brown solid in 81 % yield of the isolated product (Scheme 12).[20] The somewhat larger P*n*Bu$_3$ behaves similarly, although in this case besides the required complex **56**, some by-products were also obtained. Both the ^{31}P NMR spectra of **55** and **56** display



Scheme 12.

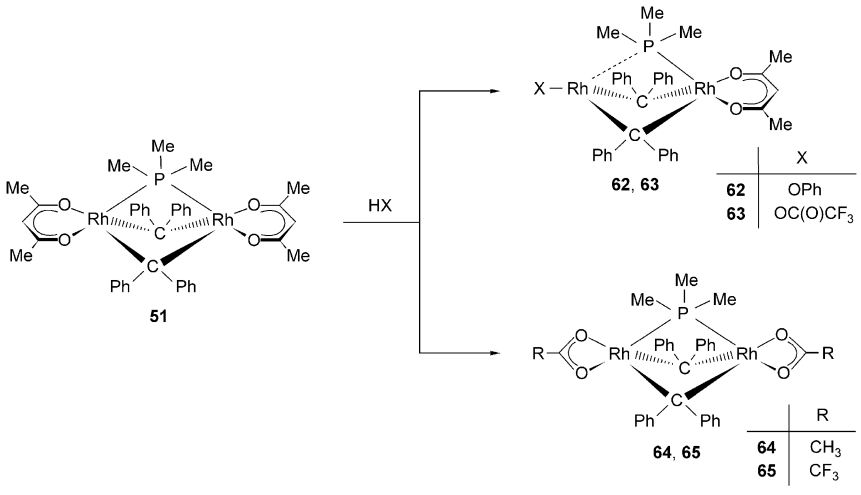
the expected doublet of doublets and thus there is no doubt that the PEt$_3$ as well as the P*n*Bu$_3$ ligand occupies a semibridging position.

An interesting situation arises if the symmetrical complex **23** is treated with PEt$_3$ or P*n*Bu$_3$. If the reaction of **23** with PEt$_3$ is carried out in diethyl ether at −30 °C to 0 °C, after low-temperature crystallization from Et$_2$O the symmetrical phosphane-bridged complex **57** is isolated in 61 % yield (see Scheme 12). The reaction of **23** with P*n*Bu$_3$, under exactly the same conditions, affords a mixture of products, among which the analogue of **57** is the dominating species. If the reaction of **23** with P*n*Bu$_3$ in C$_6$D$_6$ in an NMR tube is monitored by NMR spectroscopy and not stopped after [Rh$_2$(acac)$_2$(μ-CPh$_2$)$_2$(μ-P*n*Bu$_3$)] has been generated, a subsequent slow rearrangement to isomer **61** can be observed. On a preparative scale, this complex is obtained from **23** with a twofold excess of P*n*Bu$_3$ in benzene at room temperature in nearly quantitative yield. The PEt$_3$ analogue, **59**, is accessible either by using the same route or by stirring a solution of **57** in benzene for 15 h at 25 °C. The ^{31}P NMR spectra of the mixed-valence compounds **59** and **61** display the typical doublet of doublet resonance, with one resonance being very large (265–270 Hz) and one very small (5 Hz) J(^{103}Rh,^{31}P) coupling constant.

The dominating role, played by the size of the reacting phosphane, is also evident in the reactions of **23** with PMe$_2$Ph and PMePh$_2$. While the smaller ligand PMe$_2$Ph generates exclusively the phosphane-bridged complex **58**, the more bulky ligand PMePh$_2$ produces the unsymmetrical compound **60** in high yield. In contrast to the rearrangement of **57** to **59**, attempts to convert **58** to the corresponding Rh^0–Rh^{II} isomer failed.

To get an insight into the mechanism of the isomerization of the PR$_3$-bridged complexes to the mixed-valence counterparts, the kinetics of the conversion of **57** to **59** were investigated. In C$_6$D$_6$ at 293.5 K the reaction is strictly first order with a Gibbs free energy of activation $\Delta G^{*} = 94.5(5)$ kJ mol^{-1}. Thus one can assume that an intramolecular rearrangement occurs and that the migration of the phosphane from the bridging into a terminal position is accompanied by the migration of an acac ligand from one metal center to the next.

The reactivity of the phosphane-bridged {Rh$_2$(acac)$_2$} compound **51** towards Brønsted acids HX, such as CH$_3$CO$_2$H, CF$_3$CO$_2$H, and phenol, is quite similar to that of the stibane-bridged analogue **13** (see Scheme 6). Independent of whether only one acac ligand or both are replaced by the anion of the acid, the core unit {Rh$_2$(μ-CPh$_2$)$_2$(μ-PMe$_3$)} remains unchanged. While even with an excess of phenol the substitution of the remaining acac unit in **62** could not be achieved, the starting material **51** reacts cleanly with excess acetic or trifluoroacetic acid to give the symmetrical complexes **64** and **65** in excellent yields (Scheme 13). In agreement with the proposed structure, the ^{31}P NMR spectra of **64**



Scheme 13.

and **65** show in each case a sharp triplet with coupling constants that are very similar to those of **51**. The fact, that the ^{1}J(^{103}Rh,^{31}P) values for the ^{31}P NMR resonances (doublets of doublets) for **62** and **63** differ only slightly, supports the proposal that in **63** the trifluoroacetate is coordinated as a monodentate ligand.

 © 2004 Wiley-VCH Verlag GmbH & Co. KGaA, Weinheim

6. The Youngest Members of the {Rh(μ-PR_3)Rh} Family

After the X-ray structure analysis of **51** revealed that in the crystal the two acetylacetonates are not symmetrically arranged to each other, thus leading to the conclusion that this asymmetry could be the reason for the difference in the bond lengths between the two rhodium atoms and the phosphorus atom of the bridging trimethylphosphane, attempts were made to reconvert the {Rh(acac)} to {RhX} units (X = Cl, Br, I). This change of the terminal ligands should not only reduce the coordination number but also the steric crowding around the metal centers.

Treatment of **51** with an excess of Me_3SiCl in benzene at room temperature led indeed to a smooth replacement of the acac ligands with chloride and gave a red solid, **66**, correctly analyzed as $[Rh_2Cl_2(CPh_2)_2(PMe_3)]$, in 91% yield.[24] If the reaction of **51** with Me_3SiCl was carried out in the molar ratio of 1:1, the unsymmetrical complex **50**, originally prepared from **20** by bridge-ligand exchange (see Scheme 10), was obtained. While we anticipated, owing to the ^1H and ^{13}C NMR spectra, that compound **66** has a structure analogous to the stibane-bridged complex **13**, the X-ray crystal structure analysis showed that in the lattice two dinuclear moieties are connected by two bridging chlorides to give a Rh_4 species with a chain-like $\{ClRh_2(\mu Cl)_2Rh_2Cl\}$ core (Figure 7). Moreover, the midpoint of the planar $\{Rh(\mu\text{-}Cl)_2Rh\}$ unit is a center of symmetry. The coordination geometry around Rh1 is distorted tetrahedral, whereas that around Rh2 is best described as square-pyramidal with the phosphorus atom in the apical position. The structure of the fragment $\{ClRh(\mu\text{-}CPh_2)_2(\mu\text{-}PMe_3)RhCl_2\}$ is thus similar to that of the unsymmetrical molecule **50**. Besides the Rh–Rh bond length of about 2.50 Å (there are two independent molecules in the unit cell), which differs only slightly to that of the stibane-bridged compound **13**, the most important structural features of **66** are the Rh–P bond lengths; they are 2.3625(6) and 2.4826(6) Å in the first molecule (Figure 7) and 2.3890(6) and 2.4173(6) Å in the second molecule. Most noteworthy, the difference between the two Rh–P bond lenghts in each case is much less than for the bis(acac) complex **51**, thus indicating that—at least in the crystal lattice—the type of anionic ligands bonded to rhodium influences significantly the position of the bridging phosphane unit. Because of the similarity of the Rh–Rh and Rh–P interatomic distances, the bond angles of the Rh_2P triangle are nearly the same and deviate only marginally from the 60° value.

Although cryoscopic measurements with a saturated solution of **66** in benzene confirm that under these conditions the tetranuclear compound is present, the ^{31}P NMR spectrum of **66** in C_6D_6 at room temperature is concentration-dependent. The spectrum of a nearly saturated solution (4 mmol L^{-1}) exhibits a somewhat broadened triplet at $\delta = -24.6$ ppm, which, after lowering the concentration to 0.1 mmol L^{-1}, transforms into a sharp triplet with a chemical shift of $\delta = -20.4$ ppm. Since the data in CD_2Cl_2 are quite similar, it is to assume that both in benzene and dichloromethane a rapid equilibrium between the Rh_4 and the Rh_2 species exists (see Scheme 14) and that at low concentrations the Rh_2 species **66′** dominates. At −80 °C in $[D_8]$toluene, the ^{31}P NMR spectrum of **66** displays a doublet of doublets at $\delta = -30.4$ ppm with $J(^{103}Rh,^{31}P)$ coupling constants of 128.4 and 95.4 Hz, thus indicating that under these conditions the conversion of **66** to **66′** is inhibited on the NMR time scale.[24]

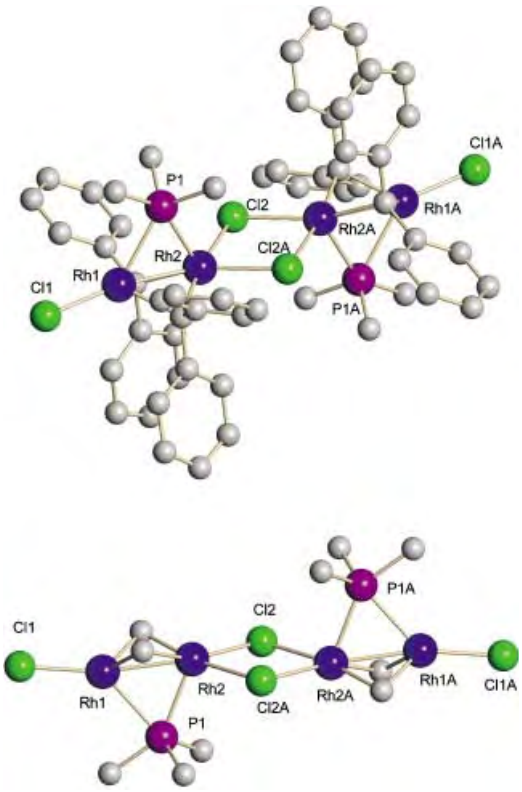
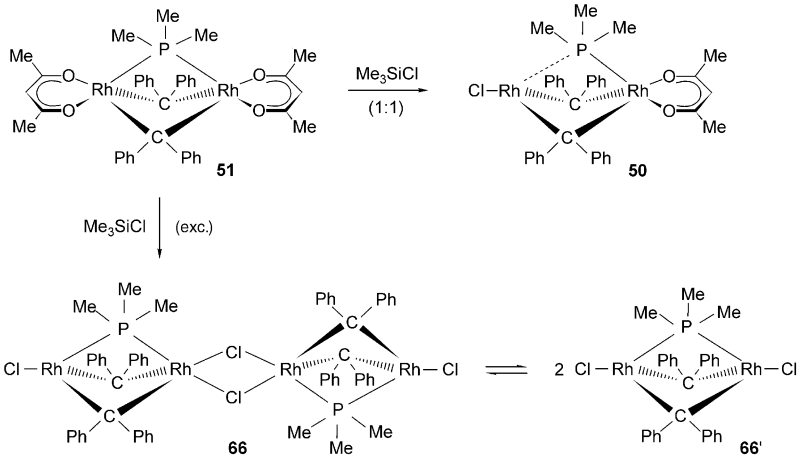


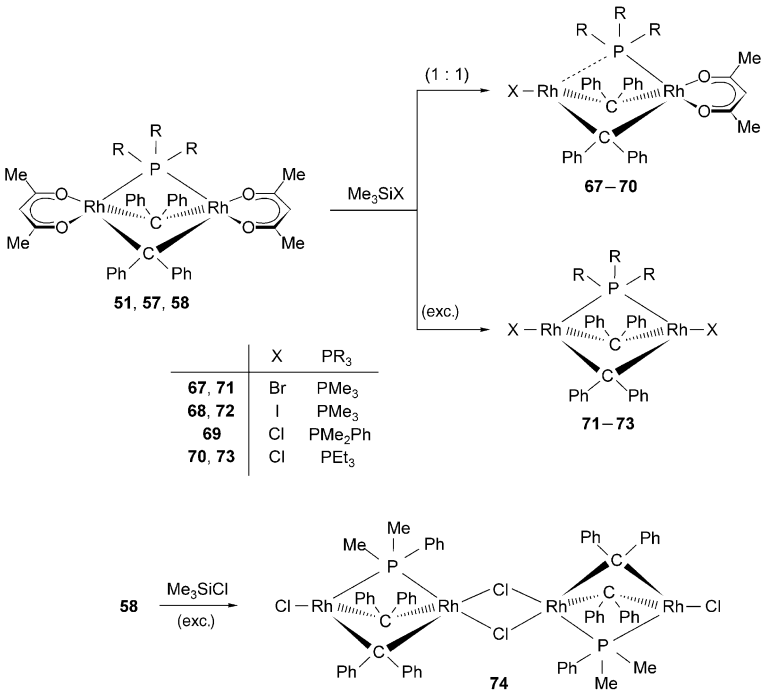
Figure 7. Molecular structure (SCHAKAL representation), including a side-view, of compound **66** (hydrogen atoms omitted for clarity).



Scheme 14.

 © 2004 Wiley-VCH Verlag GmbH & Co. KGaA, Weinheim

The reactivity of the bis(acac) compound **51** with Me_3SiBr and Me_3SiI is similar to that of **51** with Me_3SiCl. With equimolar amounts of the substrates, the unsymmetrical complexes **67** and **68** are formed and isolated as deeply colored, moderately air-stable solids in nearly quantitative yields (Scheme 15). An alternative procedure consists of the reaction of **50** with NaBr or NaI, which equally affords **67** and **68** in good to excellent yields.[25] Both **67** and **68** are thermally less stable than **50** but can be stored at room temperature under argon for weeks. The same is true for the $\{Rh_2Cl(acac)\}$ compounds **69** and **70**, which were obtained from **57** or **58** and Me_3SiCl in the molar ratio of 1:1. The ^{31}P NMR spectra of **67** and **68** display, similarly to the spectrum of **50**, one doublet of doublets with $J(^{103}Rh,^{31}P)$ coupling constants that differ for **67** by 93.3 Hz and for **68** by 111.7 Hz (for a comparison see **50**: $\Delta J = 84.3$ Hz). As for transition-metal complexes that contain terminal phosphane ligands, the size of the coupling constant $^1J(^{103}Rh,^{31}P)$ is, to a first approximation, inversely proportional to the Rh–P bond length,[26] it is conceivable that the difference in the distances between the phosphorus atom of the semibridging trimethylphosphane and the two rhodium centers is larger in **67,** and particularly in **68**, than in **50**.



Scheme 15.

The reactions of **51** with a twofold excess of Me_3SiBr or Me_3SiI proceed quite slowly and afford in toluene at room temperature the dibromo and diiodo complexes **71** and **72** in about 90% yield of the isolated product. In contrast to that of **66**, the ^{31}P NMR spectra of **71** and **72** are independent of the concentration of the solution and display in each case a sharp triplet at $\delta = -18.3$ (**71**) and -20.8 ppm (**72**). However, while the ^{31}P NMR spectrum of **72** remains unchanged by lowering the temperature to 193 K, the corresponding spectrum of **71** changes and at 193 K shows together with the triplet at $\delta = -17.5$ ppm a doublet of doublets at $\delta = -31.8$ ppm. If we take the data reported for **66** and **66′** into consideration, the appearance of these two signals indicate that in the case of **71** at low temperature, in addition to the presence of dinuclear compound **71**, the tetranuclear species $[BrRh(\mu\text{-}CPh_2)_2(\mu\text{-}PMe_3)Rh(\mu\text{-}Br)_2Rh(\mu\text{-}CPh_2)_2(\mu\text{-}PMe_3)RhBr]$ is present. At 193 K, the equilibrium between the monomer and the dimer is evidently very slow on the NMR time scale, thus both the Rh_2 and the Rh_4 complexes can be observed.

The assumption that the PMe_3 ligand in **72** indeed occupies a truly symmetrical doubly bridging position was confirmed by an X-ray crystal-structure analysis.[27] As shown in Figure 8, the molecule contains a C_2 axis passing through the phosphorus atom and the midpoint of the Rh–Rh bond. Therefore, the structure is quite similar to that of the stibane-bridged compound **13**. The I-Rh-Rh-I axis in **72** is nearly linear with bond angles Rh1-Rh1A-I1A = Rh1A-Rh1-I1 = 174.37(2)°. The Rh–P bond lengths are 2.412(3) Å and thus lie exactly between those of the bis(acac) derivative **51** (2.2707(7) and 2.5700(8) Å).

The reactions of **57** and **58** with an excess of Me_3SiCl also led to the displacement of the acac ligands by chloride to afford the compounds **73** and **74** in excellent yields. Surprisingly, the ^{31}P NMR spectrum of **73** displays a sharp triplet, which does not change either at higher concentrations of the solution or at lowering the temperature to 193 K. Therefore, it is assumed that in contrast to the PMe_3-counterpart **66**, under the experimental conditions, only the dinuclear complex **73** exists. The ^{31}P NMR spectrum of **74** shows at room temperature a broadened triplet at $\delta = -17.0$ ppm with $^1J(^{103}Rh,^{31}P) = 101.7$ Hz, which at 193 K becomes a doublet of doublets with $J(^{103}Rh,^{31}P)$ coupling constants of 139.8 and 68.6 Hz.[25] These data clearly indicate that in the case of the PMe_2Ph-bridged compound the dimer **74** dominates at low temperature, whereas at room temperature the dimer is in

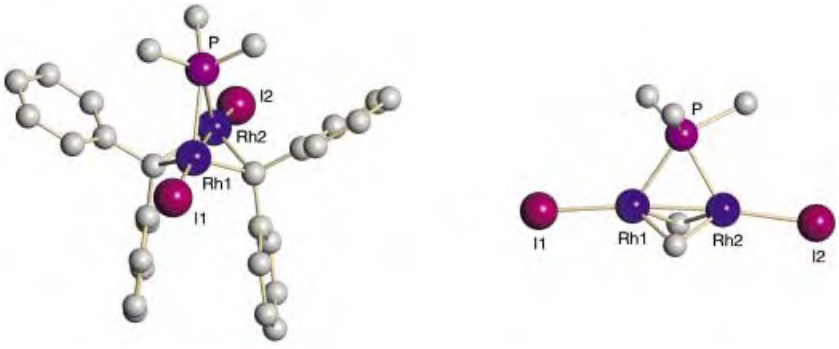
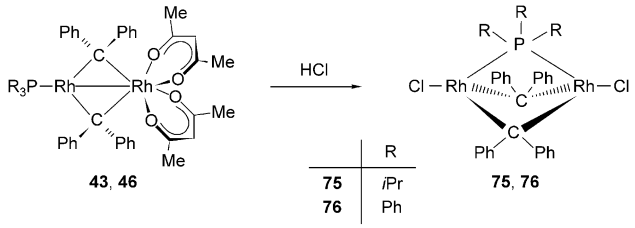


Figure 8. Molecular structure (SCHAKAL representation), including a side-view, of compound **72** (hydrogen atoms omitted for clarity).

 © 2004 Wiley-VCH Verlag GmbH & Co. KGaA, Weinheim

equilibrium with the corresponding monomeric Rh_2 species. It should be mentioned that attempts to prepare **73** and **74** from **13** and PEt_3 or PMe_2Ph by ligand exchange failed.

After it had been confirmed that PMe_3, PMe_2Ph, and PEt_3 can behave as doubly bridging ligands, we finally also succeeded with transferring the more bulky triisopropylphosphane from a terminal into a bridging position. It was already mentioned that while the dichloro compound **13** reacts with P*i*Pr$_3$ to give *trans*-[RhCl(=CPh$_2$)(P*i*Pr$_3$)$_2$], the bis(acac) counterpart **23** affords upon treatment with P*i*Pr$_3$ the mixed-valence complex **43** exclusively (see Scheme 9). Since we considered it as conceivable that the latter reaction proceeds via the phosphane-bridged isomer **75**, we attempted to trap this species by replacing the acac ligands with chloride. The mixed-valence compound **43** was thus treated with an excess of Me_3SiCl resulting in a mixture of products. A clean reaction occurred, however, when a solution of HCl in benzene was dropped into a vigorously stirred solution of **43** in the same solvent; after workup, the required complex was isolated as a red solid in 91% yield. In the same way, the PPh_3 analogue, **76**, could be generated from **46** (see Scheme 16).[27] Since the ^{31}P NMR



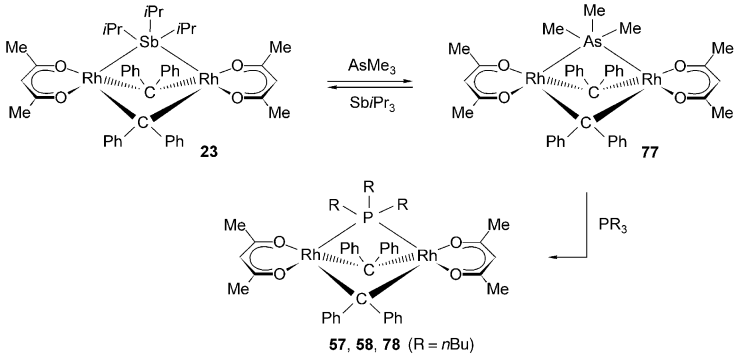
Scheme 16.

spectra of both **75** and **76** display a sharp triplet at room temperature and below, there is no doubt that the proposed structure with P*i*Pr$_3$ and PPh_3 in a doubly bridging position between the two rhodium centers is correct.

7. The Final Goal: Trimethylarsane as a Semibridging and a Doubly Bridging Ligand

While the stibane-bridged compound **13** reacts with P*i*Pr$_3$ and PPh_3 by bridge cleavage, it is inert toward As*i*Pr$_3$ and $AsPh_3$. A slow reaction takes place when **13** is treated with $AsMe_3$, but in this case a mixture of products results, which could not be separated by fractional crystallization or column chromatography.

The successful route to bind trimethylarsane in a bridging position was similar to that found for PMe_3. Treatment of the bis(acac) complex **23** with $AsMe_3$ in benzene leads to an equilibrium between **23** and the $AsMe_3$ analogue, which, even in the presence of a large excess of the arsane, could not be completely shifted to the side of the required product. However, in hexane as the solvent, in which **77** is only sparingly soluble, the arsane-bridged compound **77** precipitates and is isolated in excellent yield (Scheme 17).[24] The light-brown solid is thermally more stable than the PMe_3



Scheme 17.

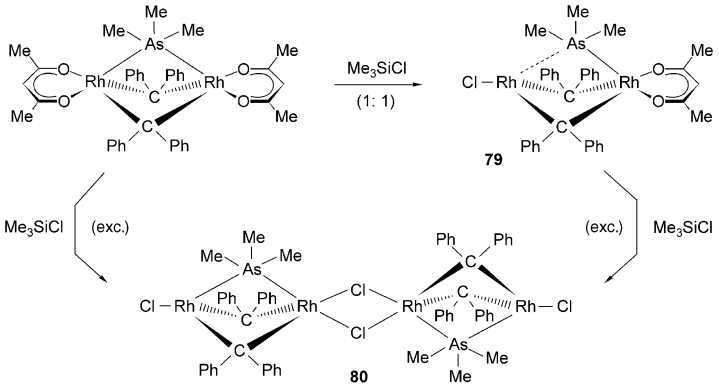
analogue **51** and can be stored under argon at low temperatures for weeks. The ^1H and ^{13}C NMR spectra of **77** suggest that the two acac as well as the two CPh_2 ligands are equivalent and thus it can be assumed that the trimethylarsane is symmetrically bound to the two rhodium centers.

In contrast to **51**, the related $AsMe_3$ complex **77** is rather labile and reacts not only with Sb*i*Pr$_3$ but also with tertiary phosphanes such as PMe_2Ph, PEt_3, and P*n*Bu$_3$ by bridge-ligand exchange. While compounds **57** and **58** had originally been prepared from **23** and PMe_2Ph or PEt_3 (see Scheme 12), it was already mentioned that attempts to obtain **78** in an analogous way resulted in the formation of the mixed-valence isomer **61** (see Section 5). The successful procedure to isolate the phosphane-bridged complex **78** consists of the treatment of a solution of **77** in toluene at −50 °C with one equivalent of P*n*Bu$_3$, followed by warming of the solution to 0 °C and stirring of the reaction mixture at this temperature under reduced pressure for 20 min. Under these conditions, the volatile trimethylarsane is removed and the product **78** isolated in 89% yield.[25] The ^{31}P NMR spectrum of **78** displays a sharp triplet at $\delta = -9.6$ ppm with a $J(^{103}Rh,^{31}P)$ coupling constant that is identical to that of **58**. Notably, both **57** and **58** are obtained from **77** in much better yields than when **23** is used as the precursor.

In a similar way to the PMe_3 analogue **51**, compound **77** reacts with Me_3SiCl in the molar ratio of 1:1.1 to give the dinuclear complex **79**, which probably contains the arsane in a semibridging coordination mode (Scheme 18). As already observed for the {Rh$_2$Cl(acac)(μ-Sb*i*Pr$_3$)} and {Rh$_2$Cl(acac)(μ-PR$_3$)} derivatives, the unsymmetrical species **79** is significantly more stable than the symmetrical precursor **77** and does not decompose in benzene even after it had been stored for 3 days.[24]

Replacement of the remaining acac ligand of **79** by chloride is more difficult and, even with a large excess of Me_3SiCl, the formation of **80** takes place slowly at room temperature. Nevertheless, after removal of the volatiles, the dichloro compound could be isolated as a red-brown solid in 91% yield. As shown by the X-ray crystal-structure analy-

 © 2004 Wiley-VCH Verlag GmbH & Co. KGaA, Weinheim



Scheme 18.

sis,[24] the $AsMe_3$-bridged complex **80** is isomorphous to **66** and also has the midpoint of the Rh(μ-Cl)$_2$Rh unit as a center of symmetry (see Figure 9). The Rh–Rh distance in each dinuclear subunit is slightly larger than in **66**, probably

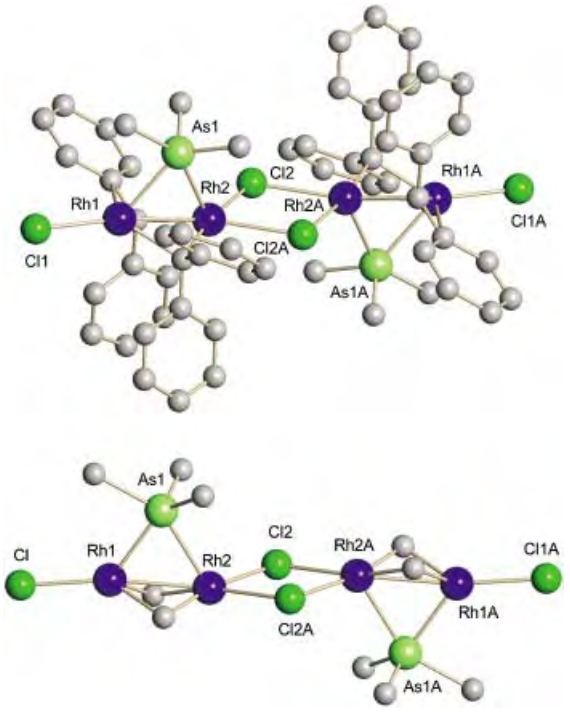


Figure 9. Molecular structure (SCHAKAL representation), including a side-view, of compound **80** (hydrogen atoms omitted for clarity).

because of the increase in the covalent radius of arsenic compared with phosphorus. The two Rh–As bond lengths in each subunit differ somewhat, which reflects the nonequivalence of the "outer" and "inner" metal centers of the {ClRh$_2$(μ-Cl)$_2$Rh$_2$Cl} chain. Since not only the arsane but also the two diphenylcarbene ligands are linked to the two rhodium atoms of each dinuclear subunit in an unsymmetrical fashion, no mirror plane exists along the Cl-Rh-Rh axis. As expected, the terminal Rh1–Cl1 distance is shorter than the Rh2–Cl2 and Rh2–Cl2A distances of the bridging unit in the center of the molecule. In this respect it should be mentioned that in the unit cell of **80** there are no contacts either between the terminal chloro ligands and the corresponding Rh–Cl fragment of a neighboring Rh_2 subunit or between these chloro ligands and the benzene molecules incorporated in the crystal. The ^{1}H and ^{13}C NMR spectra of **80** remain unchanged in the temperature range between 193 and 333 K, which indicates that under these conditions no dissociation of the dimeric Rh_4 to the monomeric Rh_2 species, analogous to the dissociation of **66** to **66′**, takes place.

8. Theoretical Studies

DFT calculations for dinuclear compounds of the general composition [A^{1}M^1(μ-CH$_2$)$_2$(μ-EX$_3$)M^{2}A^2] (M^1, M^2 = Co, Rh, Ir; A^1, A^2 = monoanionic ligands) have been carried out by Kaupp, Schinzel, and Straka by using the B3LYP functional with the Gaussian 98 program.[28] The present results can be summarized as follows:

a) For phosphanes PX_3 as the bridging unit, a more symmetrical position between two rhodium centers is expected along the series X = CH$_3$ < H < F. With the increase of the electronegativity of X, the π-acceptor strength of PX_3 increases and thus the bonding capability becomes more similar to that of CO.

b) For the parent phosphane, arsane, and stibane EH_3, the formation of a symmetrical bridge is favored along the series E = P < As < Sb. In a similar way to a), the polarity of the E–H bond increases from phosphorus to antimony and thus also the π-acceptor strength increases in the same order. Taking both points a) and b) into consideration, it follows that SbF_3 should be the preferred candidate for building a doubly bridging {M(μ-EX$_3$)M} framework. This has to be proven by experiment.

c) For halides as anionic ligands A^1 and A^2, the most symmetrical {Rh(μ-PH$_3$)Rh} bridge in the model compound [A^{1}Rh^1(μ-CH$_2$)$_2$(μ-PH$_3$)Rh^{2}A^2] should be formed in the case of A^1 = A^2 = I and the less symmetrical bridge in the case of A^1 = A^2 = F. For A^1 = Cl and A^2 = F, Cl, Br, I, the smallest difference in the two Rh–P distances should result for A^2 = Cl and the largest for A^2 = F. It appears that an increase in the difference of the electronegativity of two halogens also leads to an increase in the difference of the Rh–P bond lengths.

d) For A^1 = Cl and A^2 = κ^2-acac, the distance Rh^2–P in the model compound [ClRh^1(μ-CH$_2$)$_2$(μ-PH$_3$)Rh^2(κ^2-acac)] should be smaller than the distance Rh^1–P, despite the increase in the coordination number at Rh^2. This is in agreement with the results found for the isolated complex **50**. Since Rh^1 is linked to one chloride and Rh^2 to two oxygen atoms, the positive charge at Rh^2 should be higher than at Rh^1 and this should strengthen the Rh^2–P bond.

e) By changing the metal in Group 9, the asymmetry of the {Ir(μ-EH$_3$)Ir} bridge should decrease along the series E = P > As > Sb following the trend observed for rhodium as the metal center. In contrast, for M = Co the highest

 © 2004 Wiley-VCH Verlag GmbH & Co. KGaA, Weinheim

asymmetry is found for E = As and the smallest for M = Sb. For PF_3 as the bridging ligand, the difference in the two M–P distances (M = Co, Rh, Ir) is significantly smaller than for PH_3 while the ratio $d(M^1–P)/d(M^2–P)$ is about the same for all three elements of Group 9. The calculations leave no doubt that rhodium is the preferred candidate for forming a {M(μ-EX_3)M} bridge.

f) The bonding analyses for the model compound [ClRh(μ-CH_2)$_2$(μ-PH_3)RhCl)], based on the electron localization functions (ELF), reveals an asymmetric attractor from the phosphorus to the rhodium atoms being in agreement with a delocalized three-center bond. The coordination geometry around the phosphorus atom in the {Rh(μ-PH_3)Rh} fragment corresponds to a distorted trigonal bipyramid with one hydrogen atom in axial and two hydrogen atoms in equatorial positions. The calculated distance P–H_{ax} is slightly larger than the distances P–H_{eq}, which could be explained by the more efficient π back bonding from a metal d orbital into the in-plane σ* orbital of the phosphane. However, by comparing the values of the positive charge at the phosphorus atom in free PH_3 with the doubly bridging PH_3 in the respective model compound, it is nevertheless apparent that σ bonding is much more dominant than π bonding, which is also found for complexes that have terminal PH_3 ligands.

9. Concluding Remarks

The studies described in this Review opens the gate to a new field in coordination chemistry. After it had been supposed for decades that tertiary phosphanes, arsanes, and stibanes behave exclusively as terminal ligands, it was only recently that this postulate became weakened. The work by the groups of Braunstein, Pasquali, van Leeuwen, and Balch provided the hint that it might be possible to bind tertiary phosphanes in a bridging position, whereby the d^8 and d^9 metal centers presumably play a crucial role. However, for the preparation of compound **13**—the first "outsider" according to Caulton[29]—it was important to have not tertiary phosphanes but tertiary stibanes, in particular Sb*i*Pr_3, as supporting ligands. This facet has to be emphasized insofar as trialkylstibanes complexes of the late transition-metals are quite rare,[2,30] probably because the M–SbR_3 bond is weaker than the M–AsR_3 and M–PR_3 bonds. Because of the reduced bond energy, trialkylstibanes can thus be considered as good leaving groups, which is not only in agreement with the smooth bridge–ligand exchange of Sb*i*Pr_3 to PR_3 but also with the fact that compound **13** is generated from *trans*-[RhCl(=CPh_2)(Sb*i*Pr_3)$_2$] by partial elimination of Sb*i*Pr_3 in high yield. In contrast, *trans*-[RhCl(=CPh_2)(P*i*Pr_3)$_2$] is quite inert and neither heating nor UV irradiation transforms this complex into [Rh_2Cl_2(μ-CPh_2)$_2$(μ-P*i*Pr_3)] (**75**).

However, the stibane-bridged compounds (of which 25 have been prepared to date) are not only interesting in themselves, but are even more interesting as starting materials for the preparation of the phosphane- and arsane-bridged analogues. Moreover, the bis(acac) compound **23** with bridging triisopropylstibane is the precursor for a series of mixed-valence Rh^0–Rh^{II} complexes in which the coordination number of the low-valent metal center can vary between three and five. At present, the chemistry of these complexes is mainly unexplored and it would be particularly interesting to find out whether they can be oxidized, possibly electrochemically, to Rh^{II}–Rh^{II} or Rh^{I}–Rh^{III} species.

Despite these challenging perspectives, the present work is, without any doubt, highlighted by the preparation and characterization of a variety of di- and tetranuclear phosphane-bridged rhodium compounds. These compounds are really exceptional not only from a structural point of view but equally with respect to their reactivity. Various substitution reactions with both hard and soft Lewis bases had been carried out in the periphery of the molecules without destroying the bridging framework. While the increase in the coordination number from four to five at the metal centers has, besides an increase in the steric crowd, no significant effect, the decrease in the coordination number from five to four favors in some cases a dimerization of the Rh_2 species and leads to the formation of chainlike {$XRh_2X_2Rh_2X$} complexes. Another interesting facet is that in contrast to the initial observations, not only small phosphanes such as PMe_3, PMe_2Ph, or PEt_3 but also more bulky analogues such as P*n*Bu_3, P*i*Pr_3, or PPh_3 can be forced to bind to two metal centers in a doubly bridging mode.

The question, of how large the bond energy of a tertiary phosphane in a doubly bridging position is, cannot be answered at present. From thermochemical studies it is known that the bond energy of doubly bridged carbonyls is about half of the bond energy of terminal CO ligands.[31] Moreover, since the bond energy for M–PPh_3 (as shown for M = Mo) is significantly smaller (ca. 120 kJ mol^{-1}) than the bond energy for M–CO,[32] one can assume that a similar relation holds for the bond energy of an {M(μ-PR_3)M} and an {M(μ-CO)M} bridge. From a kinetic point of view, the formation of an {M(μ-CO)M} bond appears to be considerably more favored compared with an {M(μ-PR_3)M} bond, as indicated by the course of the reaction of compound **51** with CO. In this case (see Scheme 10) instead of the complex [(κ^2-acac)Rh(μ-CPh_2)$_2$(μ-PMe_3)Rh(CO)(κ^2-acac)], formed by the addition of CO to one of the rhodium centers of the starting material, the isomer **52** with bridging CO and terminal coordinated trimethylphosphane ligands is formed. Since this compound does not rearrange, neither by heating nor by photolysis, into the {Rh(μ-PMe_3)Rh(CO)} isomer, we assume that it is not only kinetically but also thermodynamically preferred.

With regard to future studies, it would be interesting to find out whether dinuclear compounds with {M(μ-ER_3)M} (E = P, As, Sb) as the core fragment are also accessible with other transition metals, in particular with the neighboring elements of rhodium in the periodic table, that is, cobalt, ruthenium, palladium, and iridium. From the previous investigations mentioned in the Introduction, palladium seems to be the preferred candidate. The recent discovery by Reau and co-workers[33] that the phosphorus atom of substituted phospholes is able to bridge two palladium atoms in a symmetrical fashion supports this prediction. In a Microreview published

in 2001, Braunstein and Boag argued that compounds with an {M(μ-ER_3)M} molecular building block should in general not be considered as thermodynamically disfavored.[34] These authors took the isolobal analogy between PR_3 and SiR_3^-, as well as the existence of various silyl-bridged transition-metal complexes, into consideration.[35] Independent of whether this expectation will be fulfilled or not, the successful steps discussed in this article should encourage additional work in this field.

Our own research described in this Review was mainly carried out by three exceptionally able Ph.D. students: Peter Schwab opened up this field by discovering the unique role that $SbiPr_3$ played as a ligand in carbenerhodium chemistry, Ulrich Herber discovered the ability of the $Rh(\mu\text{-}SbiPr_3)Rh$ compounds to generate the new family of mixed-valence Rh^0–Rh^{II} complexes, and Thomas Pechmann made the breakthrough in preparing the whole series of phosphane- and arsane-bridged Rh_2 and Rh_4 species. I would also like to acknowledge the indispensible contributions of other members of our group (Norbert Mahr, Paul Steinert, Birgit Weberndörfer, Kerstin Ilg and in particular Carsten D. Brandt), who elucidated the crystal and molecular structures of the dinuclear and tetranuclear complexes reported. Moreover, I am very grateful to Justin Wolf who not only contributed with numerous fruitful discussions but also encouraged the younger students in continuing their efforts to achieve the final goal. It was a great pleasure to collaborate with Professor Martin Kaupp and his group on the bonding capabilities of bridging EX_3 ligands. The constant and unbureaucratic financial support by the Deutsche Forschungsgemeinschaft, the Fonds der Chemischen Industrie and the University of Würzburg is also gratefully acknowledged. Finally, I thank Professor Luis A. Oro for his generous hospitality during my time as a visiting professor at the University of Zaragoza when this Review was written.

Received: August 21, 2003 [A627]

[1] a) L. H. Gade, *Koordinationschemie*, Wiley-VCH, Weinheim, **1998**; b) F. A. Cotton, G. Wilkinson, C. A. Murillo, M. Bochmann, *Advanced Inorganic Chemistry*, 6nd ed., Wiley, New York, **1999**, chap. 16.4; c) E. Riedel, *Moderne Anorganische Chemie*, de Gruyter, Berlin, **1999**, chap. 4.3.

[2] a) G. Booth in *Organic Phosphorus Compounds*, *Vol. 1* (Eds.: G. M. Kosolapoff, L. Maier), Wiley, New York, **1972**, chap. 3A; b) O. Stelzer, *Top. Phosphorus Chem.* **1977**, *9*, 1–229; c) W. Levason, C. A. McAuliffe, *Phosphine, Arsine and Stibine Complexes of the Transition Elements*, Elsevier, Amsterdam, **1979**; d) W. Levason, C. A. McAuliffe, *Acc. Chem. Res.* **1978**, *11*, 363–368; e) C. A. McAuliffe in *Comprehensive Coordination Chemistry*, *Vol. 2* (Eds.: G. Wilkinson, R. D. Gillard, J. A. McCleverty), Pergamon, Oxford, **1987**, pp. 989–1066.

[3] R. Bender, P. Braunstein, A. Dedieu, Y. Dusausoy, *Angew. Chem.* **1989**, *101*, 931–934; *Angew. Chem. Int. Ed. Engl.* **1989**, *28*, 923–925.

[4] A. Albinati, F. Lianza, M. Pasquali, M. Sommovigo, P. Leoni, P. S. Pregosin, H. Rüegger, *Inorg. Chem.* **1991**, *30*, 4690–4692.

[5] P. Leoni, M. Pasquali, M. Sommovigo, F. Laschi, P. Zanello, A. Albinati, F. Lianza, P. S. Pregosin, H. Rüegger, *Organometallics* **1993**, *12*, 1702–1713.

[6] P. H. M. Budzelaar, P. W. N. M. van Leeuwen, C. F. Roobeek, A. G. Orpen, *Organometallics* **1992**, *11*, 23–25.

[7] T. Murahashi, T. Otani, T. Okuno, H. Kurosawa, *Angew. Chem.* **2000**, *112*, 547–550; *Angew. Chem. Int. Ed.* **2000**, *39*, 537–540.

[8] a) A. L. Balch, B. J. Davis, M. M. Olmstead, *J. Am. Chem. Soc.* **1990**, *112*, 8592–8593; b) A. L. Balch, B. J. Davis, M. M. Olmstead, *Inorg. Chem.* **1993**, *32*, 3937–3942.

[9] P. R. Raithby in *Transition Metal Clusters* (Ed.: B. F. G. Johnson), Wiley, Chichester, **1980**, pp. 5–192.

[10] Short reviews: a) H. Werner, *Nachr. Chem. Tech. Lab.* **1992**, *40*, 435–444; b) H. Werner, *J. Organomet. Chem.* **1994**, *475*, 45–55; H. Werner, *Chem. Commun.* **1997**, 903–910.

[11] J. Wolf, L. Brandt, A. Fries, H. Werner, *Angew. Chem.* **1990**, *102*, 584–586; *Angew. Chem. Int. Ed. Engl.* **1990**, *29*, 510–512.

[12] a) P. Schwab, N. Mahr, J. Wolf, H. Werner, *Angew. Chem.* **1993**, *105*, 1498–1500; *Angew. Chem. Int. Ed. Engl.* **1993**, *32*, 1480–1482; b) H. Werner, P. Schwab, E. Bleuel, N. Mahr, P. Steinert, J. Wolf, *Chem. Eur. J.* **1997**, *3*, 1375–1384.

[13] a) H. Werner, P. Schwab, E. Bleuel, N. Mahr, B. Windmüller, J. Wolf, *Chem. Eur. J.* **2000**, *6*, 4461–4470; b) E. Bleuel, P. Schwab, M. Laubender, H. Werner, *J. Chem. Soc. Dalton Trans.* **2001**, 266–273.

[14] a) P. Schwab, N. Mahr, J. Wolf, H. Werner, *Angew. Chem.* **1994**, *106*, 82–84; *Angew. Chem. Int. Ed. Engl.* **1994**, *33*, 97–99; b) H. Werner, *J. Organomet. Chem.* **1995**, *500*, 331–336; c) P. Schwab, J. Wolf, N. Mahr, P. Steinert, U. Herber, H. Werner, *Chem. Eur. J.* **2000**, *6*, 4471–4478.

[15] T. Pechmann, C. D. Brandt, H. Werner, *J. Chem. Soc. Dalton Trans.* **2003**, 1495–1499.

[16] a) U. Herber, B. Weberndörfer, H. Werner, *Angew. Chem.* **1999**, *111*, 1707–1710; *Angew. Chem. Int. Ed.* **1999**, *38*, 1609–1613; b) U. Herber, T. Pechmann, B. Weberndörfer, K. Ilg, H. Werner, *Chem. Eur. J.* **2002**, *8*, 309–319.

[17] a) T. Yamamoto, A. R. Garber, J. R. Wilkinson, C. B. Boss, W. E. Streib, L. J. Todd, *J. Chem. Soc. Chem. Commun.* **1974**, 354–356; b) H. Ueda, Y. Kai, N. Yasuoka, N. Kasai, *Bull. Chem. Soc. Jpn.* **1977**, *50*, 2250–2254; c) W. A. Herrmann, *Adv. Organomet. Chem.* **1982**, *20*, 159–263; d) M. J. Krause, R. G. Bergman, *Organometallics* **1986**, *5*, 2097–2108.

[18] P. Hong, N. Nishii, K. Sonogashira, N. Hagihara, *J. Chem. Soc. Chem. Commun.* **1972**, 993.

[19] H. Werner, K. Ilg, R. Lass, J. Wolf, *J. Organomet. Chem.* **2002**, *661*, 137–147.

[20] T. Pechmann, C. D. Brandt, H. Werner, *Angew. Chem.* **2000**, *112*, 4069–4072; *Angew. Chem. Int. Ed.* **2000**, *39*, 3909–3911.

[21] For definition of "semibridging" see: C. Elschenbroich, A. Salzer, *Organometallics*, 2nd Ed., VCH, Weinheim, **1992**, p. 225.

[22] T. Pechmann, C. D. Brandt, H. Werner, *Chem. Eur. J.*, **2004**, *10*, 729–737.

[23] C. A. Tolman, *Chem. Rev.* **1977**, *77*, 313–348.

[24] T. Pechmann, C. D. Brandt, C. Röger, H. Werner, *Angew. Chem.* **2002**, *114*, 2398–2401; *Angew. Chem. Int. Ed.* **2002**, *41*, 2301–2303.

[25] T. Pechmann, Dissertation, Universität Würzburg, **2003**.

[26] a) P. S. Pregosin, R. W. Kunz, *^{31}P and ^{13}C NMR of Transition Metal Phosphine Complexes*, Springer, New York, **1979**, p. 25; b) D. W. Meek, T. J. Mazanek, *Acc. Chem. Res.* **1981**, *14*, 266–274.

[27] T. Pechmann, C. D. Brandt, H. Werner, *Chem. Commun.* **2003**, 1136–1137.

[28] M. Kaupp, S. Schinzel, M. Straka, unpublished results.

[29] K. G. Caulton, *Chemtracts: Inorg. Chem.* **1999**, 592–595.

[30] N. R. Champness, W. Levason, *Coord. Chem. Rev.* **1994**, *133*, 115–217.

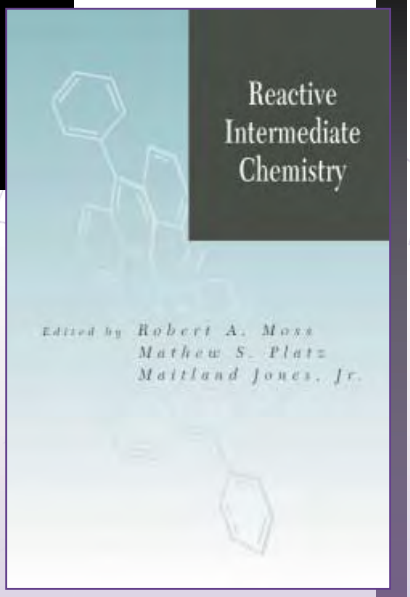
[31] J. A. Connor in *Transition Metal Clusters* (Ed.: B. F. G. Johnson), Wiley, New York, **1980**, chap. 5.

[32] H. A. Skinner, J. A. Connor, *Pure Appl. Chem.* **1985**, *57*, 79–88.

 © 2004 Wiley-VCH Verlag GmbH & Co. KGaA, Weinheim

[33] a) M. Sauthier, B. Le Guennic, V. Deborde, L. Toupet, J.-F. Halet, R. Reau, *Angew. Chem.* **2001**, *113*, 234–237; *Angew. Chem. Int. Ed.* **2001**, *40*, 228–231; b) F. Leca, M. Sauthier, V. Deborde, L. Toupet, R. Reau, *Chem. Eur. J.* **2003**, *9*, 3785–3795.
[34] P. Braunstein, N. M. Boag, *Angew. Chem.* **2001**, *113*, 2493–2499; *Angew. Chem. Int. Ed.* **2001**, *40*, 2427–2433.
[35] For a recent example of a complex with [Rh(μ-SiR_3)Rh] as a molecular building block see: K. Osakada, T. Koizumi, T. Yamamoto, *Angew. Chem.* **1998**, *110*, 364–366; *Angew. Chem. Int. Ed.* **1998**, *37*, 349–351.

Reactive Intermediate Chemistry



Robert A. Moss, *Rutgers University*
Matthew S. Platz, *Ohio State University*
Maitland Jones, *Princeton University*

ISBN 0-471-23324-2 • 1,080 pages • Cloth
$99.95 / £64.50 / €90.90
December 2003

Reactive Intermediate Chemistry presents a detailed and timely examination of key intermediates central to the mechanisms of numerous organic chemical transformations. Spectroscopy, kinetics, and computational studies are integrated in chapters dealing with the chemistry of carbocations, carbanions, radicals, radical ions, carbenes, nitrenes, arynes, nitrenium ions, diradicals, etc. Nanosecond, picosecond, and femtosecond kinetic realms are explored, and applications of current dynamics and electronic structure calculations are examined.

WILEY

Reactive Intermediate Chemistry provides a deeper understanding of contemporary physical organic chemistry, and will assist chemists in the design of new reactions for the efficient synthesis of pharmaceuticals, fine chemicals, and agricultural products. Among its features, this authoritative volume is:

- Edited and authored by world-renowned leaders in physical organic chemistry.
- Ideal for use as a primary or supplemental graduate textbook for courses in mechanistic organic
- Enhanced by supplemental reading lists and summary overviews in each chapter.

CONTENTS

Preface

PART 1: REACTIVE INTERMEDIATES

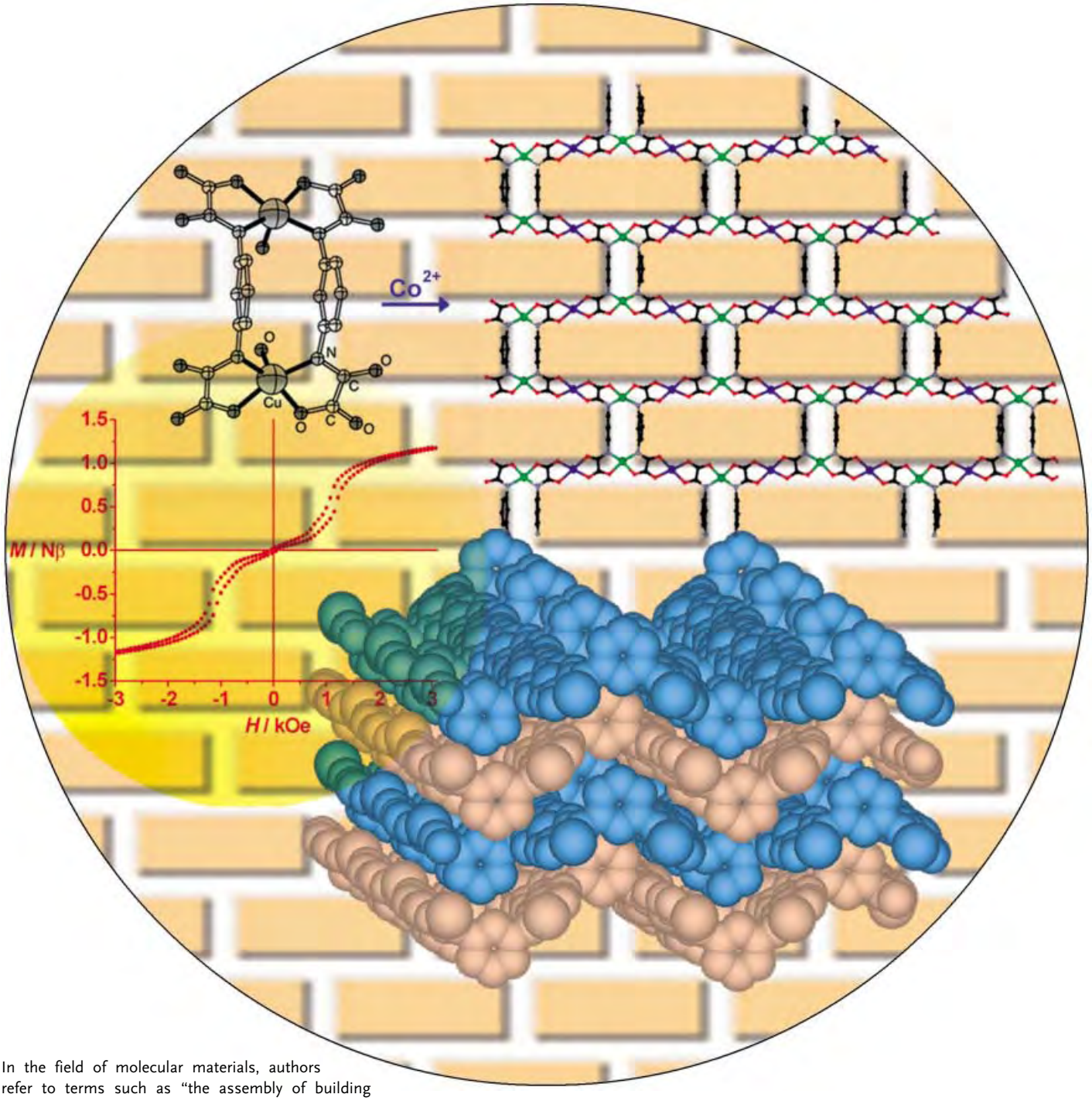
1. Carbocations (R.A. McClelland)
2. Crossing the Borderline Between SN1 and SN2 Nucleophilic Substitution at Aliphatic Carbon(T.L. Amyes, et al.)
3. Carbanions (S. Gronert)
4. Radicals (M. Newcomb)
5. Non-Kekul Molecules as Reactive Intermediates (J.A. Berson)
6. Organic Radical Ions (H.D. Roth)
7. Singlet Carbenes (M. Jones Jr. and R.A. Moss)
8. Stable Singlet Carbenes (G. Bertrand)
9. Triplet Carbenes (H. Tomioka)
10. Atomic Carbon (P.B. Shevlin)
11. Nitrenes (M.S. Platz)
12. Synthetic Carbene and Nitrene Chemistry (M.P. Doyle)
13. Nitrenium Ions (D.E. Falvey)
14. Silylenes (W. Ando and N. Tokitoh)
15. Strained Hydrocarbons: Structures, Stability, and Reactivity (K.B. Wiberg)
16. Arynes (M. Winkler, et al.)

PART 2: METHODS AND TEMPORAL REGIMES

17. Matrix Isolation (T. Bally)
18. Nanosecond Laser Flash Photolysis: A Tool for Physical Organic Chemistry (J.C. Scaiano)
19. The Picosecond Realm (E. Hilinski)
20. Reactions on the Femtosecond Time Scale (J.E. Baldwin)
21. Potential Energy Surfaces and Reaction Dynamics (B.K. Carpenter)
22. The Partnership Between Electronic Structure Calculations and Experiments in the Study of Reactive Intermediates (W.T. Borden)

 © 2004 Wiley-VCH Verlag GmbH & Co. KGaA, Weinheim

Communications



In the field of molecular materials, authors refer to terms such as "the assembly of building blocks", molecular "architecture", or "engineering", terms normally associated with the building trade. H. O. Stumpf, Y. Journaux, and co-workers report in the following Communication a Cu^{II}/Co^{II} complex that really resembles a brick wall! The complex was prepared by using a "design-and-synthesize" strategy and has interesting magnetic properties.

DOI: 10.1002/anie.200352604
© 2004 Wiley-VCH Verlag GmbH & Co. KGaA, Weinheim

Molecular Magnets

A $Cu^{II}Co^{II}$ Metallacyclophane-Based Metamagnet with a Corrugated Brick-Wall Sheet Architecture**

Cynthia L. M. Pereira, Emerson F. Pedroso, Humberto O. Stumpf, Miguel A. Novak, Louis Ricard, Rafael Ruiz-García, Eric Rivière, and Yves Journaux**

The design and synthesis of polynuclear metal complexes and extended networks with predictable magnetic properties have been an intellectual challenge for inorganic chemists interested in the field of molecular magnetism over the last two decades.[1] In particular, the design of molecule-based magnets[2] have focused the interest of many research groups around the world. Along this line the synthetic approach we exploit consists of designing heterobimetallic coordination polymers of varying dimensionality (1D–3D) that show ferrimagnetic behavior and of assembling these polymers within the crystal lattice in a ferromagnetic fashion.[3] It is well known that a pure 1D system cannot present magnetic ordering at $T \neq 0$.[4] Only interchain interactions can lead to ordering with spontaneous magnetization. In two dimensions long-range ordering occurs only in the Ising limit.[5] This thermodynamic behavior is the major drawback of our approach due to the weak control of the interchain interaction.

Recently, we designed a new building block, namely the ferromagnetically-coupled binuclear $[Cu_2(mpba)_2]^{4-}$ entity (mpb*a* = *m*-phenylenebis(oxamato)).[6] The $\{Cu_2(mpba)_2\}^{4-}$ unit is a metallamacrocycle of the [3,3]*meta*cyclophane type, with a π-stacked arrangement of the aromatic rings connected by two N–Cu–N linkages. When coordinated to divalent metal ions through the oxamato groups, this building block is able to link the ferrimagnetic chains, thus ensuring a ferromagnetic interaction between them.

In the work presented herein, we have used $\{Cu_2(mpba)_2\}^{4-}$ units and Co^{II} centers to obtain the first extended network with this building block, a bimetallic complex whose formula is $[Co_2Cu_2(mpba)_2(H_2O)_6]\cdot 6H_2O$ (**1**). Single crystals of **1** were obtained by slow diffusion in aqueous solution by using an H tube. Its structure consists of brick wall 2D networks assembled by chains linked with cyclophane moieties (Figure 1).[7] The end result is a corrugated structure.

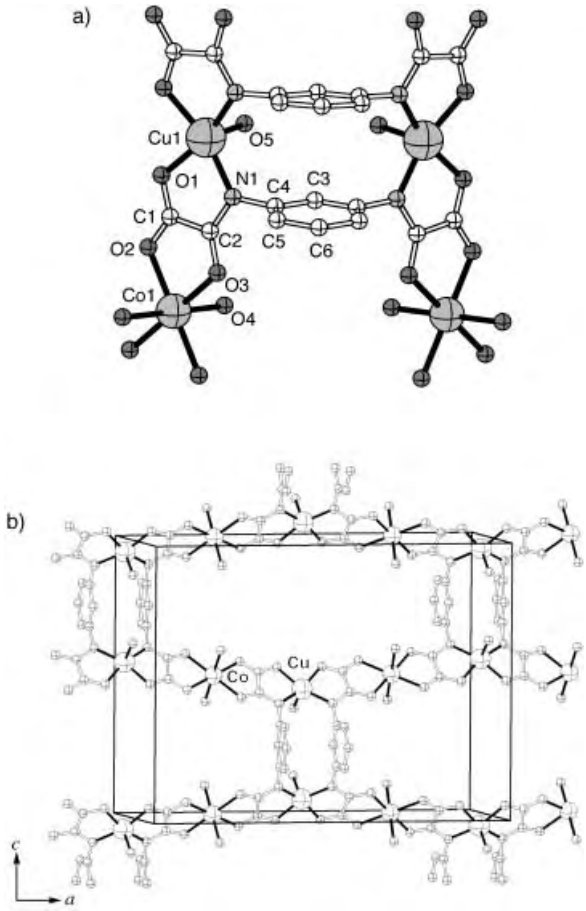


Figure 1. View of the structure of **1**. a) Detail of a Cu_2Co_2 unit emphasizing the atom labels and b) a simplified view of the content of the unit cell showing a layer.

Each brick is formed by four Co^{II} ions and six Cu^{II} ions (see Figure 1b). The Cu–Cu distance across the cyclophane moiety is 6.398 Å while the distance Cu–Cu in the middle of the brick is longer (10.683 Å). The length of each brick is equal to the *a* axis of the unit cell, namely 21.108 Å. The copper atoms are in a square pyramidal environment and the Co^{II} ions form a bis-chelate in a distorted octahedral geometry with two water molecules in *trans* positions. The aromatic rings almost face each other (dihedral mean angle of 8.1°; mean separation of 3.5 Å).

[*] Dr. C. L. M. Pereira, E. F. Pedroso, Prof. H. O. Stumpf
Departamento de Química, ICEX
Universidade Federal de Minas Gerais
Av. Antônio Carlos 6627, Belo Horizonte-MG, 31270-901 (Brazil)
Fax: (+55) 313-499-5700
E-mail: stumpf@dedalus.lcc.ufmg.br
Dr. E. Rivière, Dr. Y. Journaux
Laboratoire de Chimie Inorganique, UMR 8613
Université de Paris-Sud, 91405, Orsay (France)
Fax: (+33) 169-154-754
E-mail: jour@icmo.u-pud.fr
Prof. M. A. Novak
Instituto de Física, Universidade Federal do Rio de Janeiro
21945-970, Rio de Janeiro- RJ (Brazil)
L. Ricard
Ecole Polytechnique- UMR 7653, Lozère (France)
Dr. R. Ruiz-García
Departament de Química Orgànica
Facultat de Química, Universitat de València
46100 Burjassot, València (Spain)

[**] This work was partially supported by Instituto do Milênio de Nanociências/CNPq, Procad/CAPES, FAPEMIG, FAPERJ, and CNRS. We thank also Dr. L. Ghivelder for the use of the PPMS System and A. M. Moreira for the X-pattern.

Supporting information for this article is available on the WWW under http://www.angewandte.org or from the author.

 © 2004 Wiley-VCH Verlag GmbH & Co. KGaA, Weinheim DOI: 10.1002/anie.200352604

Figure 2 shows the corrugated layers stacking along the crystallographic *b* axis. Each sheet packs above each other, corner to corner, in a perfect stack. The aromatic rings change the catenation direction in a zigzag fashion with an angle of

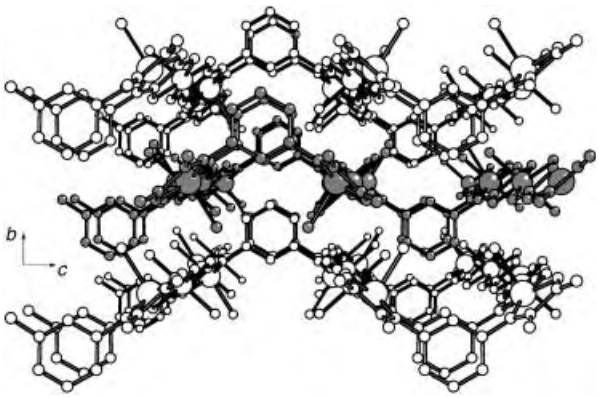


Figure 2. Perspective view of the stacking of corrugated sheets. The solvent molecules have been omitted for the sake of clarity.

121.5°, nearly the expected for the *meta* substitution pattern of the benzene rings. The shortest metal–metal interlayer separations involve ions of the same nature: Cu–Cu = 5.111 and 5.133 Å; Co–Co = 4.848 Å. The distances between Cu–Co of different layers are 7.210 and 7.217 Å. Hydrogen bondings are also present between the layers. The shortest intermolecular contacts are between an oxygen atom (O4) of water molecule coordinated to the Co^{II} ion and an oxygen atom (O3) belonging to the oxamato group of an adjacent layer with a distance of 2.795 Å.

The magnetic properties of **1** have been investigated in the 2–300 K temperature range by using a polycrystalline powder. The temperature dependence of the dc magnetic susceptibility is shown in Figure 3a in the form of the $\chi_M T$ versus T plot, χ_M being the molar magnetic susceptibility. At room temperature $\chi_M T$ is equal to 5.4 emu K mol^{-1}. This value is slightly below those expected for isolated Co^{II} and Cu^{II} ions in similar compounds which falls in the 5.5–7.5 emu K mol^{-1} range.[8] This indicates that strong AF (antiferromagnetic) coupling between Cu^{II} and Co^{II} ions, as found for similar oxamato ligands ($J_{Cu-Co} \approx -30$ cm^{-1}),[2] are operative at room temperature. $\chi_M T$ decreases further owing to this AF interaction passing through a minimum at 76 K ($\chi_M T$ = 4.0 emu K mol^{-1}) and then increases owing to ferrimagnetic correlation within the chain. In addition, the presence of ferromagnetic coupling between the Cu^{II} ions ($J_{Cu-Cu} \approx +17$ cm^{-1})[6] enhances further the value of $\chi_M T$. Short-range 2D ferrimagnetic order is thus expected to be established.

The temperature dependence of the magnetization at various fields is shown in the inset of Figure 3a. For applied fields below 1.2 kOe, the field-cooled (FC) curves present a maximum at 8.5 K indicating that some interlayer antiferromagnetic interactions are operative. However, a magnetic field of 1.2 kOe is sufficient to overcome these weak interactions and the compound presents a field-induced

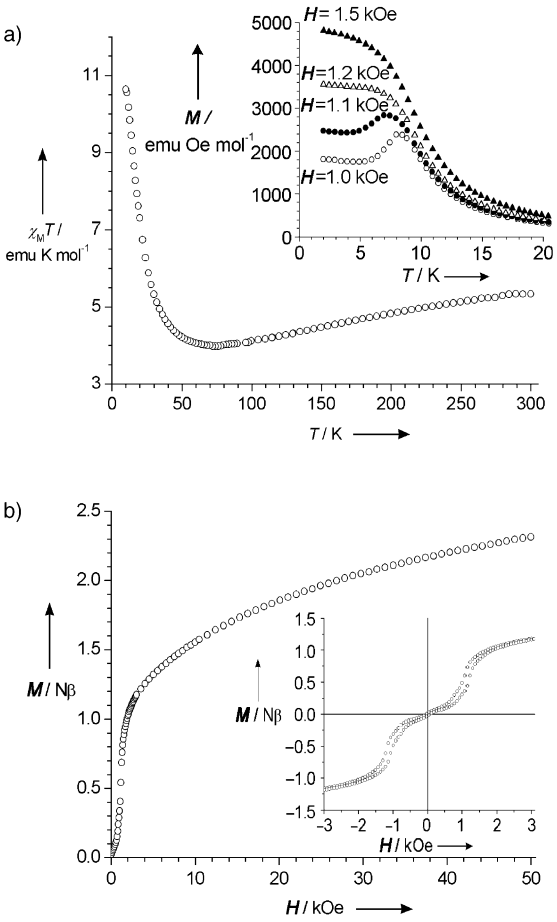


Figure 3. a) $\chi_M T$ versus T for the field strength $H = 5$ kOe. Inset: Magnetization (M) versus T at 1.0, 1.1, 1.2 and 1.5 kOe ; b) First Magnetization at 2 K. Inset: Hysteresis loop at 2 K.

transition from an antiferromagnetic to a ferromagnetic-like state.

The field dependence of the magnetization was also measured in the 2–10 K temperature range. In Figure 3b we show the 2 K isotherm in which it is clear that even with 50 kOe the saturation is not reached ($M = 2.3\,N\beta$). At this temperature, only the doublet ground state of Co^{II} ions in the octahedral geometry is populated. An effective spin $S = 1/2$ and $g_{\|}$values between 6 and 8 is normally used (g is the g factor).[9] In this limit the expected saturation magnetization (per $\{Cu_2Co_2\}$ unit) is $2(g_{Co}S_{Co} - g_{Cu}S_{Cu}) = 4\,N\beta$. High-field measurements and single-crystal measurements should be carried out to explain this point.

The low-field magnetization presents a small butterfly-shaped hysteresis (inset of Figure 3b) with a metamagnetic-like transition around 1200 Oe, in agreement with the FC results (inset of Figure 3a). This value may be accounted by considering the weak interactions between neighboring planes (dipolar and through hydrogen bonds). We attribute this behavior to the reversal of ferrimagnetic sheets from antiparallel to parallel configuration. This reversal involves an increase of approximately 1 Bohr magneton/$\{Cu_2Co_2\}$ units.

 © 2004 Wiley-VCH Verlag GmbH & Co. KGaA, Weinheim

The ac magnetic susceptibility presented in Figure 4 shows a frequency-independent peak of the real component at 9.5 K due to AF interactions discussed above and a frequency-dependent shoulder around 5 K. The imaginary component presents a maximum with a frequency dependence characterized by $\Delta\log(f)/\Delta T = 4.3$, which is reminiscent of spin-glass dynamics.[10]

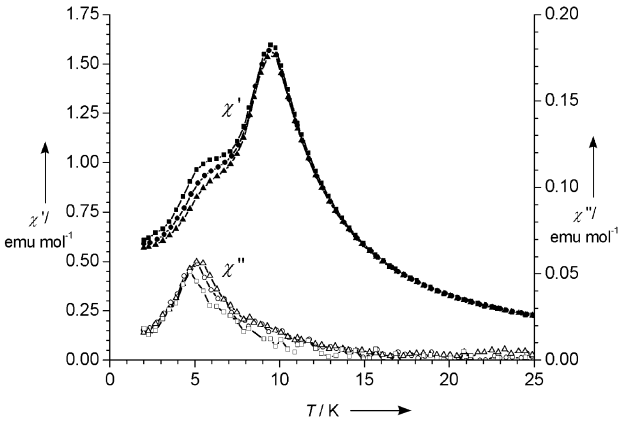


Figure 4. Temperature dependence of the in-phase, χ', and out-of-phase, χ'', ac magnetic susceptibilities for **1**, measured at 100 Hz (■), 1 kHz (●) and 5 kHz (▲) for χ', and 100 Hz (□), 1 kHz(○) and 5 kHz (△) for χ''. The solid lines joining the experimental points are to guide the eyes.

The origin of the observed small hysteresis, related to this slow relaxation is an interesting open problem observed in several molecule-based magnets[11] and should be further investigated. In our case the glassy behavior may be attributed to interacting magnetically correlated planar regions, which become progressively blocked as the temperature is lowered.

In conclusion, we have synthesized and characterized a new compound with a planar corrugated structure. Among the oxamato-ligand compounds, it is rare to obtain good single crystals with 2D architectures. In addition, this system presents a beautiful low-field metamagnetic-like transition and magnetic glassy behavior and finally to the best of our knowledge, **1** is the first example of brick-wall sheet structure to be reported on this field.

Experimental Section

Synthesis: The precursor $Na_4[Cu_2(mpba)_2]\cdot 10H_2O$ was synthesized as already described.[6] Green crystals of **1** were obtained by slow diffusion in an H tube: $Na_4[Cu_2(mpba)_2]\cdot 10H_2O$ (48.1 mg, 0.056 mmol) and $Co(NO_3)_2\cdot 6H_2O$ (16.2 mg, 0.056 mmol) are placed in each side of the tube, then water was added slowly; after two months, at room temperature, the product was separated by filtration. Yield: 13 mg (25%). Elemental analyses calcd (%) for $C_{20}H_{32}Co_2Cu_2N_4O_{24}$ (957): C 25.09, H 3.34, N 5.85, Cu 13.27; Co 12.31; found C 24.30, H 3.25, N 5.59, Cu 12.70, Co 11.77. The presence of 12 molecules of H_2O was confirmed by thermogravimetric analysis.

Crystal data for $[Co_2Cu_2(mpba)_2(H_2O)_6]\cdot 6H_2O$ (**1**): $C_{20}H_{32}Co_2Cu_2N_4O_{24}$, $M_r = 957.44$, orthorhombic, space group *Cmcm*, $a = 21.108(5)$, $b = 9.697(5)$, $c = 16.102(5)$ Å, $\alpha = 90$, $\beta = 90$, $\gamma = 90°$, $V = 3296.2$ Å^3, $T = 150.0$ K, $Z = 8$, $\rho_{calcd} = 1.930$ g cm^{-3}, μ ($Mo_{K\alpha}$) = 0.71069 nm, 6181 unique reflections, and 1441 observed with $I > 2\sigma(I)$. Crystal size: $0.22 \times 0.10 \times 0.03$ mm^3. The structure was solved by direct methods by using SHELXS 97, and refined by the full-matrix least squares method on F^2 by using SHELXL 97.[12] The hydrogen atoms from the organic ligand were located from a difference synthesis and refined with an overall isotropic thermal parameter, while those from the water molecules were not found or calculated. Refinement of 127 variables with anisotropic thermal parameters for all non-hydrogen atoms gave $R = 0.0414$ and $R_w = 0.0807$, with $S = 0.892$. CCDC-216906 contains the supplementary crystallographic data for this paper. These data can be obtained free of charge via www.ccdc.cam.ac.uk/conts/retrieving.html (or from the Cambridge Crystallographic Data Centre, 12, Union Road, Cambridge CB21EZ, UK; fax: (+44) 1223-336-033; or deposit@ccdc.cam.ac.uk).

Magnetic measurements: The magnetic measurements have been studied in commercial Quantum Design PPMS system and Quantum Design SQUID MPMS instruments. The diamagnetism of the sample and sample holder were taken into account.

Received: August 8, 2003
Revised: November 27, 2003 [Z52604]
Published Online: January 27, 2004

Keywords: cobalt · copper · magnetic properties · metallacyclophanes · molecule-based magnets

[1] a) O. Kahn, *Angew. Chem.* **1985**, *97*, 837; *Angew. Chem. Int. Ed. Engl.* **1985**, *24*, 834; b) Y. Journaux, J. Sletten, O. Kahn, *Inorg. Chem.* **1985**, *24*, 4063.
[2] O. Kahn, *Adv. Inorg. Chem.* **1995**, *43*, 179.
[3] a) H. O. Stumpf, Y. Pei, O. Kahn, J. Sletten, J. P. Renard, *J. Am. Chem. Soc.* **1993**, *115*, 6738; b) H. O. Stumpf, L. Ouahab, Y. Pei, D. Grandjean, O. Kahn, *Science* **1993**, *261*, 447; c) R. Ruiz, C. Surville-Barland, A. Aukauloo, Y. Journaux, I. Castro, B. Cervera, M. Julve, L. Lloret, F. Sapiñã, *Chem. Mater.* **1997**, *9*, 201; d) M. G. F. Vaz, L. M. M. Pinheiro, H. O. Stumpf, A. F. C. Alcântara, L. Ouahab, O. Cador, C. Mathonière, O. Kahn, *Chem. Eur. J.* **1999**, *5*, 1486.
[4] O. Kahn, *Molecular Magnetism*, VCH, New York, **1993**.
[5] J.-P. Renard in *Organic and Inorganic Low Dimensional Crystalline Materials* (Eds.: M. Drillon, P. Delhaes), Plenum, New York, **1987**, p. 125.
[6] I. Fernandez, R. Ruiz, J. Faus, M. Julve, F. Lloret, J. Cano, X. Ottenwaelder, Y. Journaux, M. C. Munoz, *Angew. Chem.* **2001**, *113*, 3129; *Angew. Chem. Int. Ed.* **2001**, *40*, 3039.
[7] B. Moulton, M. J. Zaworotko, *Chem. Rev.* **2001**, *101*, 1629, and references therein.
[8] A. Earnshaw, *Introduction to Magnetochemistry*, Academic Press, London, **1968**.
[9] R. L. Carlin, *Magnetochemistry*, Springer, Berlin, **1986**.
[10] J. A. Mydosh, *Spin Glasses: An Experimental Introduction*, Taylor & Francis Ltd., London, **1993**.
[11] M. A. Novak, *J. Magn. Magn. Mater.*, in press.
[12] G. M. Sheldrick, SHELXS-97, Program for Crystal Structure Resolution, University of Göttingen, Göttingen (Germany), **1997**.

 © 2004 Wiley-VCH Verlag GmbH & Co. KGaA, Weinheim

Cluster Compounds

Generation of Size-Controlled Pd^0 Nanoclusters inside Nanoporous Domains of Gel-Type Resins: Diverse and Convergent Evidence That Supports a Strategy of Template-Controlled Synthesis**

Benedetto Corain, Karel Jerabek,* Paolo Centomo, and Patrizia Canton**

In the realm of supported metal catalysis, the metal component is usually present as nanoparticles dispersed on the surface of suitable metal oxides[1] or on active carbon.[2] Synthetic procedures are normally directed to the generation of size-controlled metal nanoclusters, whose circumstances become mandatory when reactions to be catalyzed are "structure sensitive".[3] A paramount example of the necessity of size control is given in the area of Au^0 catalytic chemistry, specifically, the low-temperature oxidation of carbon monoxide in the presence of excess dihydrogen and the case of water gas shift reaction.[4]

In general, size control has been achieved by: directly manufacturing metal-oxide-supported catalysts;[5] by the generation of kinetically stabilized metal nanoclusters in the liquid phase[6] and subsequent transfer of the protected nanoclusters on to suitable supports;[7] by generating metal nanoclusters inside isoporous inorganic materials such as mesoporous silicas. [8]

In addition to the still-common practice of employing inorganic supports (and active carbon), a few examples of metal catalysts supported on functional resins are cited in the realm of chemical processing (such as industrial synthesis of methylisobutylketone, chemoselective hydrogenation of diolefins, acetylenes, carbonyl compounds in the presence of isobutene) and very efficient removal of dioxygen (down to the ppb levels) from industrial waters upon hydrogenation.[9] A considerable advantage of these catalysts is that they are multifunctional,[9] and may allow size control in the generation of metal nanoclusters inside polymer frameworks after the metallation–reduction steps (Figure 1).[10]

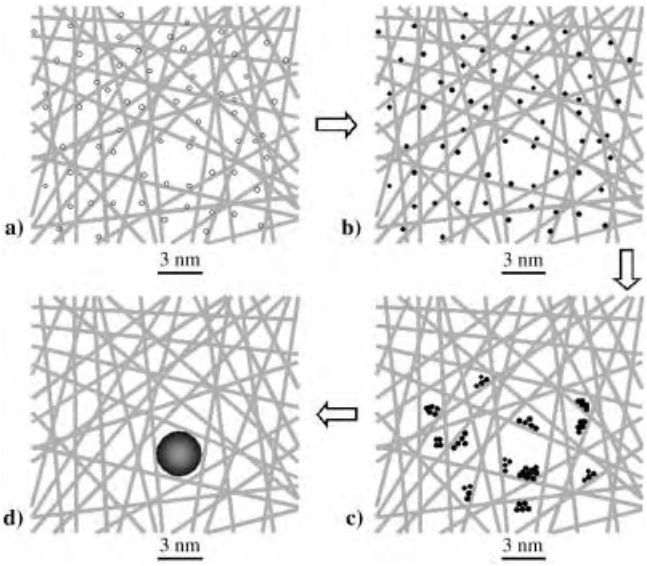


Figure 1. Model for the generation of size-controlled metal nanoparticles inside metallated resins. a) Pd^{II} is homogeneously dispersed inside the polymer framework; b) Pd^{II} is reduced to Pd^0; c) Pd^0 atoms start to aggregate in subnanoclusters; d) a single 3 nm nanocluster is formed and "blocked" inside of the largest mesh present in that "slice" of polymer framework, see text. The polymer network is drawn according to Ogston's model, reference[16].

Herein, we report on three independent, convergent pieces of structural evidence of this template-controlled synthesis strategy to obtain size-controlled metal nanoclusters suitable for synthesizing resin-supported metal catalysts. In fact, in the course of our long-standing interest in the generation and catalytic exploitation of resin-supported Pd^0 nanoclusters[9] we discovered in 1998[11] and subsequently confirmed in 2001[12] that gel-type, lightly cross-linked resins (2–8 % mol, in the absence of any porogenic agent[9]) are suitable templates for the generation of 2–4 nm Pd^0 nanoclusters. The strategy for this achievement is the dispersion of individual "Pd^{2+}" centers in the interior of the organic functional frameworks followed by their chemical reduction to Pd^0 atoms that rapidly evolve into metal nanoclusters, the size of which was tentatively expected to be controlled by the matrix nanoporosity (Figure 1). Details of the concepts outlined in Figure 1 are given in reference [12]. In this context, our previous results were encouraging,[11,12] but a quantitative confirmation of both findings and relevant rationale was lacking. We report herein on a detailed unambiguous quantitative support of the tentative conclusions of our previous papers.

[*] Prof. Dr. B. Corain
Dipartimento di Chimica Inorganica Metallorganica Analitica
Via Marzolo 1, 35131 Padova (Italy)
Fax: (+39) 049-827-5223
E-mail: benedetto.corain@unipd.it
and
Istituto di Scienze e Tecnologie Molecolari, C. N. R.
Sezione di Padova
c/o Dipartimento di Chimica Inorganica Metallorganica Analitica
Via Marzolo 1, 35131 Padova (Italy)
Fax: (+39) 049 827 5233
Dr. K. Jerabek
Institute of Chemical Process Fundamentals
Rozvojova 135, CR-16502 Suchdol, Praha 6 (Czech Republic)
E-mail: KJER@icpf.cas.cz.
Dr. P. Canton
Dipartimento di Chimica Fisica
Via Torino, 155/B, 30172 Venezia-Mestre (Italy)
Fax: (+39) 041 2346747
E-mail: cantonpa@unive.it
Dr. P. Centomo
Dipartimento di Chimica Inorganica Metallorganica Analitica
Via Marzolo 1, 35131 Padova (Italy)

[**] We are grateful to Mr. Finotto for skilled technical assistance. This work was partially supported by P.R.I.N. funding 2001–2003, Ministero dell'Università e della Ricerca Scientifica, Italy (project number 2001038991).

Supporting information for this article is available on the WWW under http://www.angewandte.org or from the author.

 DOI: 10.1002/anie.200352640 © 2004 Wiley-VCH Verlag GmbH & Co. KGaA, Weinheim

The object of our investigation is a Pd^0/resin material that we described as a chemoselective catalyst for the hydrogenation of 2-ethylanthraquinone to 2-ethylanthrahydroquinone,[13] slightly superior to the long-established commercial catalyst (Pd^0 on inorganic supports) industrially employed in a key step of the Ausimont process in the production of hydrogen peroxide. The support is a gel-type very lipophilic resin, that is polydodecylmethacrylate (92% mol)–4-vinylpyridine (4% mol)–ethylene glycol dimethacrylate (4% mol), hereafter coded as DOMA-VP.

The synthesis of Pd^0/DOMA-VP is carried out upon introducing Pd^{II} ions onto the support by using $Pd(OAc)_2$ in THF at room temperature, followed by reduction of Pd^{II} to Pd^0 in THF. The final Pd content is 1% w/w. The black material is analyzed with TEM and contains size-controlled nanoclusters (see Figure 2 and Experimental Section).

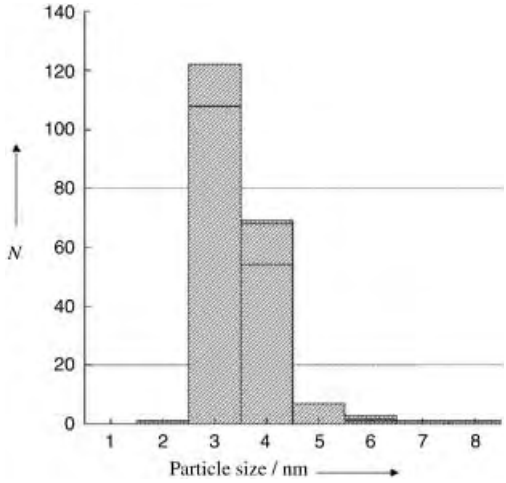


Figure 2. Size dispersion of Pd^0 nanoclusters in Pd^0/DOMA-VP. Several relevant TEM pictures are available as Supplementary Material. N = number of particles.

The surface-weighted average size [Eq.(1)]:

$$\frac{\sum_i n_i d_i^3}{\sum_i n_i d_i^2} \qquad (1)$$

obtained by TEM histogram is 3.6, in which n is the number of particles, and d is particle size.

Resin DOMA-VP was structurally investigated by ISEC (inverse steric exclusion chromatography)[14] in THF.[13] This technique provides detailed information on the nanometer-scale morphology of a given resin, after it has been swelled in a convenient liquid medium. It is based on measurements of elution behavior of standard solutes with known effective molecular sizes on a column filled with the investigated material at conditions such that the elution is influenced exclusively by the (nano)morphology of the stationary phase. As in the case of the other porosimetric methods, mathematical treatment of the elution data allows one to obtain information on the morphology of the investigated material by using a simple geometrical model. It is now established[15] that for the description of the morphology of swollen polymer gels the best tool is the so called Ogston's model,[16] which depicts pores as spaces between randomly oriented solid rods. This geometry, albeit a substantially simplified description of the morphology of swollen polymer networks, provides a fair description of both the intensive parameters (polymer chain densities) and extensive properties (specific volumes of variously dense polymer fractions). On the other hand, the conventional cylindrical-pore model commonly employed for the characterization of solid porous materials[15] relies on a geometry that is not directly related to the physical reality of the polymer framework but, from the purely mathematical point of view, it can be used to correlate the chromatographic data to the morphology of the polymer framework at the nanometer scale with essentially the same accuracy provided by Ogston's model. As a matter of fact, the porosity of a swollen gel described by using cylindrical pore geometry gives easily understandable information about the effective size of the cavities among the polymer chains, although the actual data for the specific-volume of the pores might be somewhat erroneous. However, for an investigation of the factors affecting the formation of metal nanoclusters inside the swollen polymer matrix, the effective size of the cavities used in the templating molds is much more important than their specific volume. Results of ISEC characterization of the swollen state morphology in THF of the polymer DOMA-VP are given in Table 1 and illustrated in Figure 3.

DOMA-VP has only "pores" with diameters between 2.5 and 4 nm with a clear maximum at 3.5 nm. The choice of THF

Table 1: ISEC characterization of resin DOMA-VP in THF.[a]

Pore diameter [nm]		Volume fraction [$cm^3 g^{-1}$]		Specific surface [$m^2 g^{-1}$]
	2.5	0.185	0.158	253.2
	3.0	0.927	0.791	1054.7
	3.5	1.217	1.038	1185.3
	4.0	0.637	0.544	543.7
average diameter [nm]		3.4[b]		
cumulative pore volume [$cm^3 g^{-1}$]		2.531		
cumulative surface [$m^2 g^{-1}$]		3037.9		
sum of squared errors		0.340		
number of iteration		15212		

[a] Pores from 1.0 to 2.0 nm and from 5 to 10 nm are not detected. [b] Datum calculated from Equation (1).

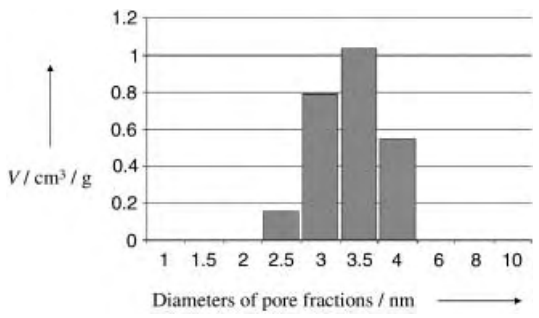


Figure 3. Nanoporosity of DOMA-VP as determined with ISEC; V = volume of the pore fractions.

 © 2004 Wiley-VCH Verlag GmbH & Co. KGaA, Weinheim

as the swelling medium was dictated by the fact that the catalyst, Pd^0/DOMA-VP, could only be obtained in this solvent. From these results, one can see that the agreement between TEM evaluation of Pd^0 nanoclusters diameter and dominant pores size is almost perfect. However, we do consider this finding to be very encouraging but not conclusive.

TEM information on nanoparticle size, albeit practical and perceivable by human senses (see below), rests on the evaluation of a few hundred metal nanoclusters (if they are 3 nm in diameter, each of cluster has about 1000 Pd atoms) that is a mass of about 10^{-17} g. As we are searching for unambiguous evidence to support a general strategy of metal nanoclusters size control (TCS), it was necessary to exploit a procedure that was able to give the average nanocluster size representative of the whole specimen. In the study of supported metal catalyst the nano- and microstructural characteristics of the metal component could be determined by using X-ray-diffraction methods, which in fact are more sensitive to dimensions greater than 4–5 nm.

The determination of average particle size dimension uses Fourier coefficient analysis, which exploits the information contained in the shape and width of the XRD peak profile, corrected for the instrument contribution, to extract the average particle size and particle-size distribution.[17–19] In the case of a very dispersed catalyst, the determination of the particle size is not an easy task, as it is very difficult to establish the true background because of the large breadth of the peaks, peak overlap, and the scattering of the support. In the case in which there are very small particle sizes (less than 3 nm) the peak width is so wide that it almost disappears from the XRD pattern. This phenomenon is more striking in the case of a supported catalyst in which the scattering of the support could effectively mask the signal coming from the active phase. To take into account the signal coming from the whole active phase, that is, from particles greater than 3 nm and from particles less than 3 nm, an accurate description of the support and catalyst is mandatory. For this purpose a modified Rietveld analysis[20,21] with a physically based background, is employed in this investigation.

This method calculates the diffracted intensity of the metal phase and the background contribution due to the crystalline phase (the metal) and allows the proper scaling of the high scattering coming from the support without using any arbitrary assumption in the background description. This approach separates the scattering of the metal phase from the background, and allows the determination of the particle dimension taking into account also the contribution of sizes smaller than 2 nm. To obtain reliable results the scattering coming from the support must superimpose exactly in the region where there is no scattering contribution coming from the metal; for this reason the support and the catalyst underwent the same drying treatment by using H_2 and N_2 flux (see Experimental Section).

The sample here analyzed is a particularly difficult one as the scattering of the support peaks at a Bragg angle near to the (111) Pd reflection (see Figure 4). The Rietveld refinement is reported in Figure 4, and shows the experimental pattern, the calculated pattern, and the contribution coming

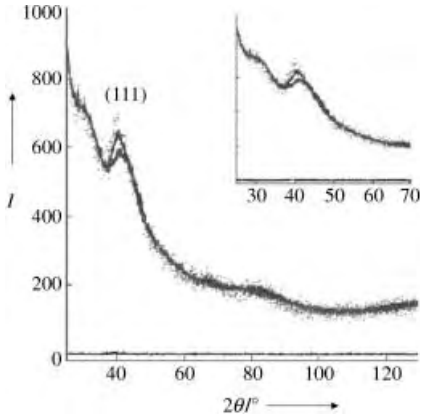


Figure 4. Rietveld refinement. In the inset the magnification of the 2θ range from 25 to 70 is reported evidencing the (111) Pd Bragg reflection. Dots are the experimental data the lower straight line is the total background the upper straight line is the calculated pattern. I = intensity (counts).

from the background. The profile parameters, obtained with Rietveld analysis, of the (111) Pd reflection, the only reflection visible in the XRD pattern, were used in the Fourier analysis; for this reason it was not possible to study the presence of strain in the sample. The procedure used to calculate the metal particle size is discussed in reference.[22]

As indicated by Guinier and other authors,[17,23] the surface weighted average sizes (defined as columns or chords in case of spherical crystallites) perpendicular to (*hkl*) planes, ⟨Ds⟩ can be obtained from the intercepts on the L axis (L being a distance in the real space) of the tangent of the size-dependent Fourier coefficients $A^S(L)$ at $L=0$ (Figure 5). By multiplying this size ⟨Ds⟩ by a factor of 3/2 the diameter of the corresponding spherical particle could be obtained, which, for this sample, is equal to 3.3(3) nm. The assumption that the particle is spherical is shown to be well justified by TEM micrographs.

Due to the importance of the determination of particle size, another independent approach was used that provides

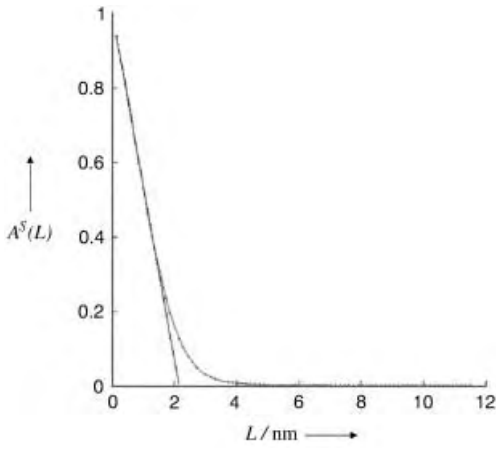


Figure 5. $A^S(L)$ Fourier transforms due to crystallite size broadening only. The intercept, with the L axis at the origin gives the surface-weighted average crystallite size.

 © 2004 Wiley-VCH Verlag GmbH & Co. KGaA, Weinheim

also the number distribution function $\prod(L)$, [24] in the case of spherically shaped crystallites:

$$\prod(L) = -C\frac{\mathrm{d}}{\mathrm{d}L}\frac{\frac{\mathrm{d}^2 A^S(L)}{\mathrm{d}L^2}}{L} \quad (2)$$

in which C is a normalization constant, and the surface-averaged diameter is:

$$\langle d\rangle_S^{\mathrm{diam}} = \frac{\int_0^\infty \prod(L)\, L^3\, \mathrm{d}L)}{\int_0^\infty \prod(L)\, L^2\, \mathrm{d}L)} \quad (3)$$

the thus obtained $\langle \mathrm{d}\rangle_s$ diameter is equal to 2.6(3) nm.

In conclusion, the set of ISEC, TEM, and XRD data (Table 2) are in agreement, and provide robust evidence to support the rationale depicted in Figure 1. Intense work aimed at supporting this template-controlled-synthesis strategy for other metal centers, particularly for gold (0) is in progress.[25]

Table 2: Consistency among nanostructural features of Pd^0/DOMA-VP.

Feature	Technique	Datum	Remarks
cavities size [nm]	ISEC	3.4	–
nanocluster diameter [nm]	TEM	3.6	–
nanocluster diameter [nm]	XRD	3.3	Rietveld
nanocluster diameter [nm]	XRD	2.6	from number distribution function

Experimental Section

Catalysts Pd^0/DOMA-VP was available in the lab.[13] Solvents were of reagent grade and were used as received.

TEM analyses: JEOL 2010 with GIF, samples for TEM analysis were prepared by extensive grinding of the as-prepared material to be examined, which was subsequently ultrasonically dispersed in methanol and then transferred as a suspension to a copper grid covered with a lacey carbon film. TEM images are available in the Supporting Information.

ISEC analysis: ISEC measurements were carried out by using an established procedure and a standard chromatographic setup described elsewhere.[14,15]

XRD measurements: Philips X'Pert vertical goniometer connected to a highly stabilized generator, $Cu_{K\alpha}$ Ni-filtered radiation, a graphite monochromator, and a proportional counter with a pulse-height discriminator were used. Measurements were performed by using a sample holder that allows a gas flow[26] to avoid any contamination from air humidity, in fact both the sample and the support were extremely hygroscopic such that the water content was able to change the XRD pattern. For this reason, they were dried with a N_2 flux for 72 h. The drying process was monitored by XRD measurements by comparing the XRD patterns of each run. The corresponding diffractograms are available in the Supporting Information. The contribution due to the adsorbed water clearly affects the shape of the XRD pattern.

The sample, contained in the XRD sample holder, was subjected to a second in situ treatment with H_2 (20 mL min^{-1} 4 h) thus producing a β-PdH phase. Finally, the sample was washed with N_2 flux and monitored by XRD until β-PdH disappears and metallic Pd appears. Patterns of the sample and of the support were recorded at 295 K on a 10–140° range with a step size of 0.05° (10 s/step). For each sample seven runs were performed to have a final time of 70 s for each point. This longer period of time was used to drop the noise of data as much as possible.

Received: August 13, 2003 [Z52640]

Keywords: cluster compounds · micorporous materials · nanostructures · palladium · template synthesis

[1] For two technology-related reviews see a) E. Gallei, E. Schwab, *Catal. Today* **1999**, *51*, 535–546; b) F. Schmidt, *Appl. Catal. A* **2001**, *221*, 15–21.
[2] See for example: S. Biella, M. Rossi, *Chem. Commun.* **2003**, *3*, 378–379).
[3] a) For a classic reference see: M. Che, C. O. Bennet, *Adv. Catal.* **1989**, *36*, 54–171; b) for a recent reference see: S. Naito, M. Iwahashi, I. Kawakami, T. Miyao, *Catal. Today* **2002**, *73*, 355–361.
[4] G. Schmid, B. Corain, *Eur. J. Inorg. Chem.* **2003**, *17*, 3081–3098.
[5] S. Schimpf, M. Lucas, C. Mohr, U. Rodemerk, A. Brückner, J. Radnik, H. Hofmeister, P. Claus, *Catal. Today* **2002**, *72*, 63–78,and references therein.
[6] For an extensive review see H. Bönnemann, R. M. Richards, *Eur. J. Inorg. Chem.* **2001**, *10*, 2455–2480.
[7] C. L. Bianchi, S. Biella, A. Gervasini, L. Prati, M. Rossi *Catal. Lett.* **2003**, *85*, 91, and references therein.
[8] For two recent papers see a) Z. Konya, V. F. Puntes, I. Kiricsi, J. Zhu, J. W. Ager III, M. K. Ko, H. Frei, P. Alivisatos, G. A. Somorjai, *Chem. Mater.* **2003**, *15*, 1242–1248; b) I. Yuranov, P. Moeckli, E. Suvorova, P. Buffat, L. Kiwi-Minsker, A. Renken, *J. Mol. Catal. A* **2003**, *192*, 239–251).
[9] B. Corain, P. Centomo, S. Lora, M. Kralik, *J. Mol. Catal. A* **2003**, *204–205*, 755–762, and references therein.
[10] a) N. Toshima, Y. Shiraishi, T. Teranishi, *J. Mol. Catal. A* **2001**, *177*, 139–147b) Y. Uozumi, R. Nakao, *Angew. Chem.* **2003**, *115*, 204–207; *Angew. Chem. Int. Ed.* **2003**, *42*, 194–197.
[11] A. Biffis, A. A. D'Archivio, K. Jerabek, G. Schmid, B. Corain, *Adv. Mater.* **2000**, *12*, 1909.
[12] F. Artuso, A. A. D'Archivio, S. Lora, K. Jerabek, M. Kralik, B. Corain, *Chem. Eur. J.* **2003**, *9*, 5292–5296.
[13] A. Biffis, R. Ricoveri, S. Campestrini, M. Kralik, K. Jerabek, B. Corain, *Chem. Eur. J.* **2002**, *8*, 2962–2967.
[14] a) K. Jerábek, *Anal. Chem.* **1985**, *57*, 1595; b) K. Jerábek, *Anal. Chem.* **1985**, *57*, 1598; c) K. Jerabek, K. Setinek, *J. Polym. Sci. Part A* **1990**, *28*, 1387.
[15] "Cross Evaluation of Strategies in Size-Exclusion Chromatography": K. Jeràbek, *ACS Symp. Ser.* **1996**, *635*, 211.
[16] A. G. Ogston, *Trans. Faraday Soc.* **1958**, *54*, 1754.
[17] A. Guinier, *X-Ray Diffraction*, Freeman & Company San Francisco, **1963**, pp. 131–148.
[18] B. E. Warren, *X-Ray Diffraction*, Addison-Wesley, Reading, MA, **1969**, pp. 251–275.
[19] S. Enzo, G. Fagherazzi, A. Benedetti, S. Polizzi, *J. Appl. Crystallogr.* **1988**, *21*, 536–542.
[20] P. Riello, G. Fagherazzi, D. Clemente, P. Canton, *J. Appl. Crystallogr.* **1995**, *28*, 115- 120.
[21] G. Fagherazzi, P. Canton, P. Riello, N. Pernicone, F. Pinna, M. Battagliarin, *Langmuir* **2000**, *16*, 4539–4546.
[22] P. Canton, G. Fagherazzi, M. Battagliarin, F. Menegazzo, F. Pinna, N. Pernicone. *Langmuir* **2002**, *18*, 6530–6535.
[23] R. J. Matyi, L. H. Schwartz, J. B. Butt, *Catal. Rev. Sci. Eng.* **1987**, *29*, 41–99.
[24] S. Ciccariello, G. Fagherazzi, A. Benedetti, *Acta Crystallogr. Sect. A* **1990**, *46*, 187–194.
[25] B. Corain, C. Burato, P. Centomo, S. Lora, W. Meyer-Zaika, G. Schmid, contribution to GOLD2003, Vancouver, **2003**; submitted to *Gold Bull.*
[26] P. Canton, P. Riello, A. Furlan, A. Minesso, L. Bertoldo, F. Pinna, A. Benedetti, *Catal. Lett.* **2000**, *69*, 17–20.

 © 2004 Wiley-VCH Verlag GmbH & Co. KGaA, Weinheim

Supramolecular Chemistry

Selective C–H Bond Activation by a Supramolecular Host–Guest Assembly**

Dennis H. Leung, Dorothea Fiedler, Robert G. Bergman, and Kenneth N. Raymond**

The development of synthetic supramolecular compounds that mimic enzyme catalysts with well-defined internal environments represents a novel approach to improving the ability to control the rate and selectivity of organometallic reactions. Rather than using many different inner-sphere ligands to effect changes in reactivity, the outer-sphere environment of a self-assembled host cavity may be used to introduce new types of size and shape selectivity. A number of such synthetic "nanovessels" have been reported and their ability to encapsulate organic guests has been investigated.[1–5] While a number of thermal and photochemical organic transformations have been performed inside some of these nanovessel cavities,[6–9] there are very few reports on the encapsulation of reactive metal complexes in such host assemblies and their resultant reactivity.[10–13] We have recently shown that a synthetic supramolecular nanovessel can induce high diastereoselectivies in the encapsulation reactions of chiral guests.[14] We report herein the first supramolecular encapsulations and reactivity studies of organometallic complexes, in the specific context of carbon–hydrogen bond activation, in a self-assembled nanovessel host cavity.

Raymond and co-workers have reported the formation and host–guest properties of supramolecular tetrahedral assemblies of $[M_4L_6]^{12-}$ stoichiometry (M = Ga^{3+}, Al^{3+}, Fe^{3+}; L = bis(bidentate) catecholamide).[15] These structures are formed through the self-assembly of achiral components to yield exclusively a racemic mixture of homochiral Δ,Δ,Δ,Δ- or Λ,Λ,Λ,Λ-clusters with Δ or Λ configuration at each metal center. One such $[Ga_4L_6]^{12-}$ assembly utilizes a naphthalene-based catecholamide ligand backbone (Figure 1). This highly negatively charged capsule is soluble in polar solvents, such as water, but the naphthalene-based ligand scaffold generates a hydrophobic cavity of approximately 0.5 nm^3. This hydrophobic cavity allows the assembly to encapsulate a variety of hydrophobic monocationic species,[16] for example, organic cations, such as $[NMe_4]^+$ and $[NEt_4]^+$, as well as organometallic sandwich complexes, such as $[Cp_2Fe]^+$, $[Cp_2Co]^+$, and $[CpRu(C_6H_6)]^+$ (Cp = η^5-C_5H_5).[11,17,18] This supramolecular host was initially prepared in the presence of NMe_4Cl to form $[Na_4(NMe_4)_7][NMe_4{\subset}Ga_4L_6]$ (⊂ denotes guest encapsulation within host), which helps to stabilize the tetrahedral assembly during its formation. The $[NMe_4]^+$ cation binds weakly to the host interior and can be easily displaced by more strongly binding guests. Since sandwich complexes were observed to be suitable guests, the encapsulation of more chemically reactive organometallic half-sandwich compounds was attempted.

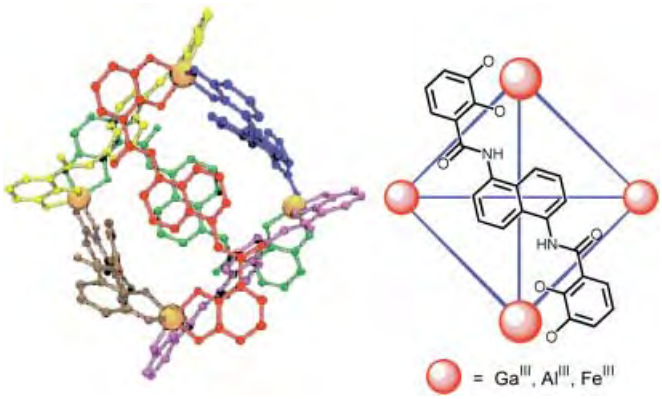


Figure 1. Left: view down the twofold axis of the crystal structure of the tetrahedral supramolecular $[M_4L_6]^{12-}$ host which can encapsulate monocationic guest molecules. Ligands are colored for differentiation. Right: schematic representation showing the structure of one of the six identical ligands that span the edges of the tetrahedral host.

In organic solvents, the half-sandwich complex [Cp*(PMe_3)Ir(Me)OTf] (**1**; Cp* = η^5-C_5Me_5, OTf = OSO_2CF_3 = triflate) thermally activates the C–H bonds of a wide range of organic molecules, including methane, at low temperatures. This process is believed to occur by dissociation of the anionic triflate ligand to form a reactive monocationic iridium intermediate $[Cp^*(PMe_3)Ir(Me)]^+$.[19–21] Therefore, we chose to explore the encapsulation of **1** with the intention that encapsulation of this species would allow for the observation of similar C–H bond-activation reactions with selectivity preferences controlled by the well-defined cavity of the host assembly.

However, upon addition of $[Na_4(NMe_4)_7][NMe_4{\subset}Ga_4L_6]$ to **1** in aqueous solution, no encapsulation was observed, presumably a result of the relatively high desolvation enthalpy of the hydrated species [Cp*(PMe_3)Ir(Me)(OH_2)][OTf]. The iridium methyl ethene adduct [Cp*(PMe_3)Ir(Me)(C_2H_4)][OTf][22] (**2**) was then targeted as a better guest candidate, since it was anticipated that the additional ethene

[*] D. H. Leung, D. Fiedler, Prof. R. G. Bergman
Department of Chemistry
University of California
Berkeley, CA 94720-1460 (USA)
Fax: (+1) 510-642-7714
E-mail: bergman@cchem.berkeley.edu
Prof. K. N. Raymond
Department of Chemistry
University of California
Berkeley, CA 94720-1460 (USA)
Fax: (+1) 510-486-5283
E-mail: raymond@socrates.berkeley.edu

[**] Supported by the Director, Office of Energy Research, Office of Basic Energy Sciences, Chemical Sciences Division, of the U.S. Department of Energy under contract DE-AC03-7600098. We gratefully acknowledge Ms. Cathleen M. Yung for insightful commentary on iridium chemistry, Ms. Anna V. Davis for helpful discussions on host–guest chemistry, and Mr. Robert M. Yeh for assistance with mass spectrometry.

Supporting information (experimental and spectroscopic details) for this article is available on the WWW under http://www.angewandte.org or from the author.

 DOI: 10.1002/anie.200352772 © 2004 Wiley-VCH Verlag GmbH & Co. KGaA, Weinheim

ligand would increase π–π interactions with the host interior as well as increase the hydrophobicity of **2** owing to the absence of a coordinated solvent molecule.

In contrast to the lack of encapsulation of **1**, a mixture of racemic **2** and racemic $[Na_4(NMe_4)_7][NMe_4{\subset}Ga_4L_6]$ in aqueous solution led to displacement of the internal $[NMe_4]^+$ ion and immediate formation of the host–guest assembly $[Na_3(NMe_4)_8][Cp^*(PMe_3)Ir(Me)(C_2H_4){\subset}Ga_4L_6]$ (**3a**), as established by ^1H and ^{31}P NMR spectroscopy. Owing to the ring-current effect of the naphthalene backbone surrounding the host cavity, the NMR resonance signals for an encapsulated guest are shifted upfield, a useful diagnostic feature. The host–guest assembly is a mixture of two diastereomers owing to encapsulation of the chiral iridium guest within the chiral host assembly with only modest diastereoselectivity. Evidence for these diastereomers is seen in two sets of upfield-shifted resonance signals in ^1H and ^{31}P NMR spectra (Figure 2a).

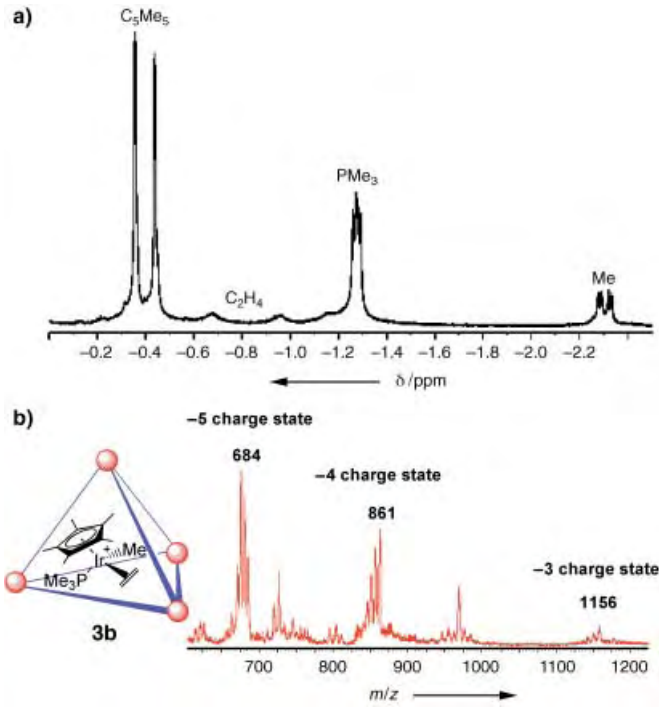


Figure 2. a) ^1H NMR spectrum of **3a** showing upfield resonances corresponding to the diastereomeric encapsulated guest molecule. b) Electrospray mass spectrum of **3b** displaying peaks corresponding to the intact host–guest complex with varying numbers of sodium counterions. Minor peaks correspond to the intact host–guest complex with a second equivalent of the iridium species associated with it, presumably coordinated to the exterior of the host assembly.

Notably, the peaks corresponding to the Cp* protons of the iridium complex are now shifted upfield from a single peak at $\delta = 1.96$ ppm for the unbound species to two signals at $\delta = -0.35$ and -0.44 ppm corresponding to the two diastereomeric host–guest assemblies. In the ^{31}P NMR spectrum, the resonance corresponding to the encapsulated iridium species has been shifted upfield from a single peak at $\delta = -29.1$ ppm to two diastereomeric signals at $\delta = -37.1$ and -37.9 ppm.

To reduce the number of counterions in solution and to remove the possible complications of $[NMe_4]^+$ guest competition, **2** was added to the formally "empty" $Na_{12}[Ga_4L_6]$ assembly (prepared in the absence of NMe_4Cl) to form $Na_{11}[Cp^*(PMe_3)Ir(Me)(C_2H_4){\subset}Ga_4L_6]$ (**3b**). Electrospray mass spectrometry data afforded signals of the intact host–guest assembly corresponding to the $\{Na_8[Cp^*(PMe_3)Ir(Me)(C_2H_4){\subset}Ga_4L_6]\}^{3-}$, $\{Na_7[Cp^*(PMe_3)Ir(Me)(C_2H_4){\subset}Ga_4L_6]\}^{4-}$, and $\{Na_6[Cp^*(PMe_3)Ir(Me)(C_2H_4){\subset}Ga_4L_6]\}^{5-}$ charge states at 1156 *m/z*, 861 *m/z*, and 684 *m/z*, respectively (Figure 2b). An MM2 molecular mechanics optimized structure of **3b** predicts that the iridium species will fit within the cavity of the host assembly with ample room for small substrates (Figure 3).[23]

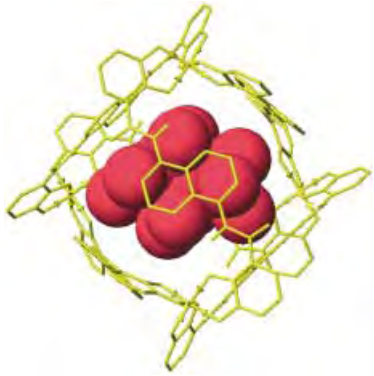
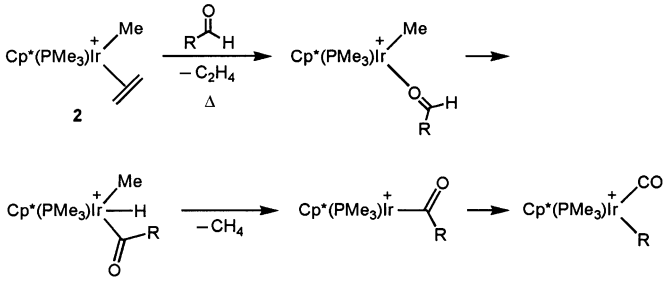


Figure 3. Molecular mechanics optimized structure of host–guest assembly **3b** containing encapsulated iridium species (red).

Despite ethene coordination, complex **2** (unencapsulated) remains reactive and undergoes C–H bond activation reactions with aldehydes (RCHO) in aqueous solution at 75 °C. Presumably, the ethene ligand is able to dissociate at this temperature, which allows the metal center to activate the aldehyde C–H bond and form an iridium acyl intermediate. This step is followed by migratory deinsertion of the carbonyl group to give a cationic iridium alkyl carbonyl product $[Cp^*(PMe_3)Ir(R)(CO)][OTf]$, analogous to the mechanism of activation of aldehydes by **1** (Scheme 1).[24]

When acetaldehyde (**4**) was added to an aqueous solution of iridium host–guest assembly **3b** and heated to 75 °C, a new encapsulated product was detected in moderate yield after



Scheme 1. Mechanism of C–H bond activation with aldehydes.

 © 2004 Wiley-VCH Verlag GmbH & Co. KGaA, Weinheim

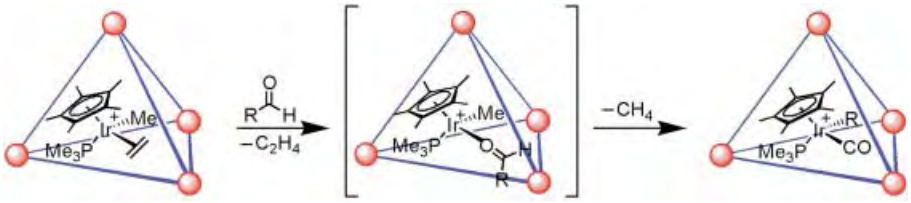
several days.[25] This guest species was identified as $[Cp^*(PMe_3)Ir(Me)(CO)]^+$, which results from the C–H bond activation of acetaldehyde by the supramolecular host–guest assembly (reaction illustrated at the top of Table 1). In addition to ^1H and ^{31}P NMR spectroscopy, and electrospray mass spectrometry data consistent with the formation of this product host–guest assembly, infrared spectroscopy revealed a sharp absorbance for a new metal carbonyl stretch $\tilde{\nu}_{CO}$ at 2022 cm^{-1}, which confirms the formation of an iridium carbonyl species. Furthermore, addition of independently prepared product iridium methyl carbonyl species to $Na_{12}[Ga_4L_6]$ at 75 °C yielded the spectroscopically identical host–guest assembly. Since the product iridium alkyl carbonyl guest is also chiral, the host assembly induces product formation with a diastereomeric ratio (d.r.) that can easily be detected by NMR spectroscopy. In this case, the diastereoselectivity is relatively small, 60:40.

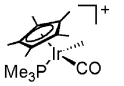
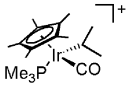
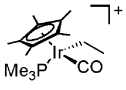
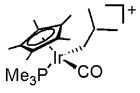
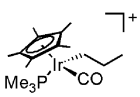
The selectivity in the encapsulated C–H bond-activation reactions was explored by examining a variety of aldehyde substrates (Table 1). The products were all characterized as above. These results display significant dependence on the size and shape of the aldehyde during diastereoselective product formation. As the size of straight-chain alkyl aldehyde substrates increased progressively from acetaldehyde (**4**) to propionaldehyde (**5**) and then to butyraldehyde (**6**), the d.r. also increased from 60:40 to 65:35 and then to 70:30. Presumably, the larger guests come into closer contact with the interior of the host assembly and the chirality of the host cavity is expressed more effectively. However, while substrates with sizes from acetaldehyde to butyraldehyde react with the host–guest assembly **3b**, *no reaction* occurred with larger aldehydes, such as valeraldehyde (**7**) and benzaldehyde (**8**). These aldehydes are apparently too large to enter the cavity of the host assembly and, as such, cannot interact with the encapsulated iridium complex. This result emphasizes the ability of the well-defined cavity of the host assembly to control the access of substrates to the reactive, but encapsulated, metal center. This selectivity is remarkably effective: even after weeks at elevated temperatures, the iridium methyl ethene guest does not "leak out" of the host and react with the substrate.

In addition to size selectivity, shape selectivity plays a key role in the encapsulated C–H bond-activation reactions. The host–guest assembly **3b** reacts with isobutyraldehyde (**9**) with a lower diastereomeric ratio than with butyraldehyde (d.r. of 55:45 vs. 70:30). We hypothesize that the iridium isobutyraldehyde intermediate has a more spherical shape than the butyraldehyde complexes, which results in decreased diastereoselective recognition by the host nanovessel. Valeraldehyde (**7**), isovaleraldehyde (**10**), 2-methylbutanal (**11**), and pivalaldehyde (**12**) are all five-carbon-skeleton structural isomers. However, only **10** reacts with the encapsulated iridium complex **3b**, with a d.r. of 58:42. Even after extended periods at elevated temperatures, the structural isomers **7**, **11**, and **12** do not react with the encapsulated metal center. It appears that, of this group of isomeric compounds, only **10** has the right shape to fit inside the host interior containing the reactive metal center.[26,27]

The above selectivity results require that the C–H bond activation of aldehydes must occur within the cavity of the host assembly rather than by dissociation from the capsule, reaction with aldehyde, and then re-entry into the nanovessel. This selectivity is markedly illustrated in two competition experiments. When 0.5 equivalents each of **4** and **8** were added at 75 °C to one equivalent of the unencapsulated iridium complex **2** in aqueous solution, two products corresponding to the methyl carbonyl and the phenyl carbonyl iridium complexes are formed in a 1:1 ratio. Thus, there is no selectivity in the reaction of the unbound complex with regard to the activation of these two aldehydes. However, when the same competition experiment was performed with the encapsulated iridium complex **3b**, only the methyl carbonyl guest product was detected upon heating to 75 °C. Compound **4** reacts quantitatively to form the 0.5 equivalents of encapsulated methyl carbonyl product, leaving 0.5 equivalents of host–guest assembly **3b** and 0.5 equivalents of **8**, thus demonstrating the ability of the host–guest complex

Table 1: Observed steric and diastereoselectivities in the C–H bond activation of aldehydes by the encapsulated iridium host–guest complex.



	Substrate	Guest product[a]	d.r.		Substrate	Guest product[a]	d.r.
4			60:40	**9**			55:45
5			65:35	**10**			58:42
6			70:30	**11**		n. r.	n/a
7		n. r.	n/a	**12**		n. r.	n/a
8		n. r.	n/a				

[a] n. r. = no reaction.

 © 2004 Wiley-VCH Verlag GmbH & Co. KGaA, Weinheim

to selectively activate one substrate from a mixture of chemically very similar substrates in situ.

In conclusion, we have described the supramolecular encapsulation of reactive transition-metal complexes in a host nanovessel and the first case of C–H bond activation under such reaction conditions. The C–H bond activation of aldehydes proceeds with highly specific size and shape selectivity, as well as modest diastereoselectivity, in this new iridium host–guest assembly.

Received: September 2, 2003 [Z52772]

Keywords: C–H activation · diastereoselectivity · gallium · host–guest systems · iridium · supramolecular chemistry

[1] J.-M. Lehn, *Supramolecular Chemistry*, Weinheim, **1995**.
[2] J. Rebek, *Acc. Chem. Res.* **1999**, *32*, 278.
[3] J. P. Sauvage, *Acc. Chem. Res.* **1998**, *31*, 611.
[4] D. L. Caulder, K. N. Raymond, *J. Chem. Soc. Dalton Trans.* **1999**, 1185.
[5] M. Fujita, N. Fujita, K. Ogura, K. Yamaguchi, *Nature* **1999**, *400*, 52.
[6] J. M. Kang, J. J. Rebek, *Nature* **1997**, *385*, 50.
[7] M. Ziegler, J. L. Brumaghim, K. N. Raymond, *Angew. Chem.* **2000**, *112*, 4285; *Angew. Chem. Int. Ed.* **2000**, *39*, 4119.
[8] M. Yoshizawa, Y. Takeyama, T. Okano, M. Fujita, *J. Am. Chem. Soc.* **2003**, *125*, 3243.
[9] M. Fujita, K. Umemoto, M. Yoshizawa, N. Fujita, T. Kusukawa, *Chem. Commun.* **2001**, 509.
[10] V. F. Slagt, J. N. H. Reek, P. C. J. Kamer, P. W. N. M. van Leeuwen, *Angew. Chem.* **2001**, *113*, 4401; *Angew. Chem. Int. Ed.* **2001**, *40*, 4271.
[11] D. Fiedler, D. Pagliero, J. L. Brumaghim, R. G. Bergman, K. N. Raymond, *Inorg. Chem.* **2004**; in press.
[12] M. L. Merlau, M. d. P. Mejia, S. T. Nguyen, J. T. Hupp, *Angew. Chem.* **2001**, *113*, 4369; *Angew. Chem. Int. Ed.* **2001**, *40*, 4239.
[13] W. Sun, T. Kusukawa, M. Fujita, *J. Am. Chem. Soc.* **2002**, *124*, 11570.
[14] D. Fiedler, D. H. Leung, R. G. Bergman, K. N. Raymond, J. Am. Chem. Soc., **2004**; in press .
[15] D. L. Caulder, R. E. Powers, T. N. Parac, K. N. Raymond, *Angew. Chem.* **1998**, *110*, 1940; *Angew. Chem. Int. Ed.* **1998**, *37*, 1840.
[16] Current efforts are underway to understand the mechanism and the thermodynamics of encapsulation. Hydrophobic monocations are efficiently encapsulated within the host, while strongly solvated monocations (e.g., alkali cations) and dicationic species remain unencapsulated. Neutral molecules do not strongly interact with the host. Encapsulation of guests appears to rely upon electrostatic as well as hydrophobic interactions.
[17] T. N. Parac, M. Scherer, K. N. Raymond, *Angew. Chem.* **2000**, *112*, 1288; *Angew. Chem. Int. Ed.* **2000**, *39*, 1239.
[18] T. N. Parac, D. L. Caulder, K. N. Raymond, *J. Am. Chem. Soc.* **1998**, *120*, 8003.
[19] P. Burger, R. G. Bergman, *J. Am. Chem. Soc.* **1993**, *115*, 10462.
[20] B. A. Arndtsen, R. G. Bergman, *Science* **1995**, *270*, 1970.
[21] H. F. Luecke, R. G. Bergman, *J. Am. Chem. Soc.* **1997**, *119*, 11538.
[22] C. M. Yung, R. G. Bergman, unpublished results.
[23] *CAChe Workstation Pro*, Fujitsu Limited, 5.04, **2002**.
[24] P. J. Alaimo, B. A. Arndtsen, R. G. Bergman, *Organometallics* **2000**, *19*, 2130.
[25] Yields ranging from 40–60% were obtained in these aldehyde activation reactions. At this temperature, some decomposition of the iridium metal complex to intractable products is observed for both the free and encapsulated species. Specific experimental yields are presented in the Supporting Information.
[26] This selectivity is due to differences in shape and size rather than hydrophobicity of the substrate. Both **10** and **12** have the same hydrophobicity value as determined by an octanol/water partition experiment, but only **10** is activated by the encapsulated iridium host–guest complex.
[27] CAChe MM2 force field molecular mechanics calculations could not detect a substantial difference in substrate binding selectivity. More sophisticated calculations have not yet been undertaken.

 © 2004 Wiley-VCH Verlag GmbH & Co. KGaA, Weinheim

Supramolecular Polymers

A Concept for Recyclable Cross-Linked Polymers: Topologically Networked Polyrotaxane Capable of Undergoing Reversible Assembly and Disassembly**

*Tomoya Oku, Yoshio Furusho, and Toshikazu Takata**

The development of methodologies for material recycling and/or chemical recycling of cross-linked polymers such as thermosetting resins and rubbers is one of the most important issues in polymer and material science.[1] Because of the difficulty in developing suitable recycling methodologies due to the network structure of polymers, a new recycling concept has long been sought after. Reversible cross-linking–decross-linking may constitute an effective recycling protocol. We have previously shown a concept for the "recycling of cross-linked polymers" by the application of reversible acid-catalyzed ring-opening polymerization of spiroorthoester.[2] The formation and decomposition of cross-linked polymers was reversible enough to recover the original monomers in high yields.[3] Although a number of approaches to the recycling of cross-linked polymers have been reported to date,[1,4] much work remains to be done to develop new concepts and materials based on this protocol.

We have recently unveiled a new synthetic method for [2] and [3]rotaxanes based on the concept of "dynamic covalent chemistry",[5] which involves the thermodynamic control of

[*] T. Oku, Prof. T. Takata
Department of Organic and Polymeric Materials
Tokyo Institute of Technology
Ookayama, Meguro-ku, Tokyo 152-8550 (Japan)
Fax: (+81) 03-5734-2888
E-mail: ttakata@polymer.titech.ac.jp
Y. Furusho
JST, ERATO, Yashima super-structured helix project

[**] The authors are grateful to the Ministry of Education, Science, Sports, Culture, and Technology for a Grant-in-Aid for Scientific Research on Priority Areas (A; 413/14045262).

Supporting information for this article is available on the WWW under http://www.angewandte.org or from the author.

 © 2004 Wiley-VCH Verlag GmbH & Co. KGaA, Weinheim DOI: 10.1002/anie.200353046

the thiol-catalyzed reversible cleavage of a disulfide linkage.[6] Furthermore, the first poly[3]rotaxane in which the monomer unit is linked through topological linkages has been synthesized by using this protocol.[7]

We now report a reversible cross-linking–decross-linking system directed towards a new concept for the recycling of cross-linked polymers by utilizing a polyrotaxane network.[8] In this system, no apparent chemical bond formation or breaking takes place because the reversible disulfide bond cleavage occurring in the axle component is the only reaction during the cross-linking and decross-linking in which a polyrotaxane network is formed and disassembled.[8] Therefore, this protocol provides a novel concept for effective recycling: that is, the trunk polymer undergoes both cross-linking and decross-linking without receiving any injury because it does not participate directly in either of the two reactions.

The cross-linking reaction was carried out by treating 0.25 M of poly(crown ether) (**1**; $\bar{M}_n = 5100$, $\bar{M}_w/\bar{M}_n = 7.1$, $\bar{M}_n$ and $\bar{M}_w$ are the weight-average and number-average molar mass, respectively; 10% weight loss temperature (T_{d10}) = 256 °C and glass transition temperature (T_g) = 81 °C) based on the cyclic unit with bisammonium salt (**2**, 0.063 M), and benzenethiol (0.013 M) in a mixed solvent of acetonitrile and chloroform (1:3) at 50 °C (Scheme 1). After 20 h, a gelled product was formed quantitatively. The swelled gel, which was originally elastic and transparent, was dried under reduced pressure to form a hard solid with plasticity. Without **2** or benzenethiol, no gelation took place. The above result suggests that the gelation arises from cross-linking, especially from the formation of the [3]rotaxane-like structure composed of the dumbbell-shaped disulfide (**2**) and the crown ether units of **1**, as shown in Scheme 1.

To confirm the formation of the mechanical linkage as the cross-linking structure, the gelation process was examined by ^{1}H NMR spectra (Figure 1). The reaction was carried out in an NMR tube that contained **1** (0.10 M based on the cyclic unit), of **2** (0.040 M), and benzenethiol (0.0080 M) in CD_3CN/$CDCl_3$ (1:4) at 50 °C. Before the addition of benzenethiol, the

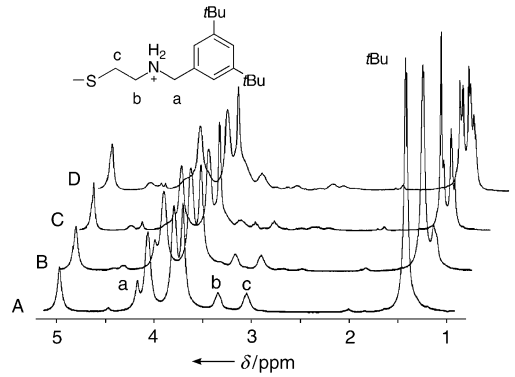
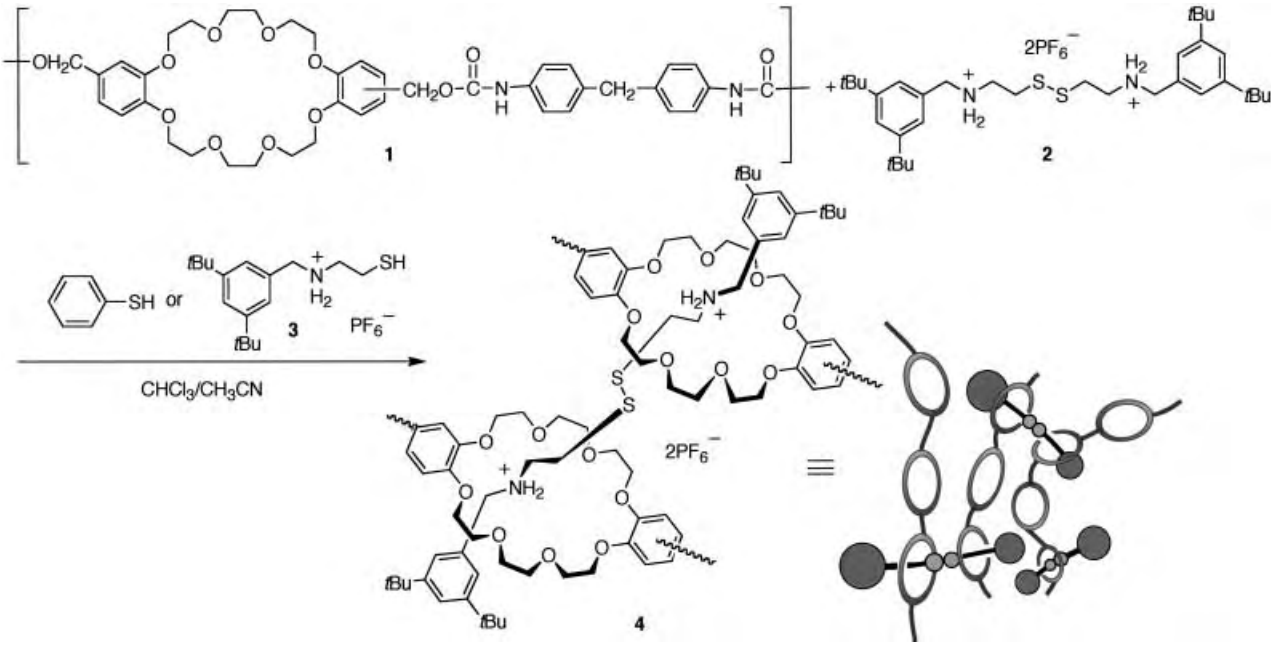


Figure 1. ^{1}H NMR spectral changes during the gelation (270 MHz, $CDCl_3/CD_3CN$ 4:1, 60 °C). A) Before adding benzenethiol, B) soon after adding benzenethiol, C) after 10 h, and D) after 24 h.

spectrum of the mixture was almost equal to that of the simple mixture of **1** and **2**. Just after the addition of benzenethiol, a splitting of the *tert*-butyl signal and a downfield shift of the signal from the benzylic proton (a) to about 4.5 ppm were observed. Similar spectral changes were also observed with the model crown ether: that is, **2** and dibenzo-[24]crown-8 ether (see Supporting Information).[6] After 24 h, the tube was filled with the formed gelled material, which had no fluidity. The remaining small signals of the methylene protons of **2** (b, c) observed at this time imply that most of **2** had been used in the formation of the rotaxane. In fact, the association ratio between the ammonium salt moiety of **2** and the cyclic unit of **1** was calculated to be 74% by ^{1}H NMR spectrum,[6] which



Scheme 1. Polyrotaxane network **4** was synthesized from **1** and **2** by the catalysis of thiol.

 © 2004 Wiley-VCH Verlag GmbH & Co. KGaA, Weinheim

suggests that the [3]rotaxane structure had been incorporated leading to cross-linking (at least 48%). Thus, the obtained results clearly indicate that the mechanical linkage between the two caused the cross-linking of **1** with **2**.

Gel **4** swelled well in *N*,*N*-dimethylformamide (DMF; percentage swelling = 1400% = [weight of swelled gel]−[weight of dried gel]/[weight of dried gel] × 100) and dimethylsulfoxide (DMSO; percentage swelling = 840%). In methanol, gel **4** hardly swelled (percentage swelling = 27%). Figure 2 depicts two pictures of gel **4** before and after swelling

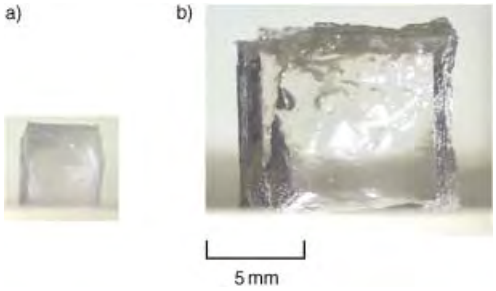


Figure 2. The pictures of gel **4** obtained, a) before swelling and b) after swelling in DMF.

in DMF, revealing a colorless transparent gel. The percentage swelling and glass transition temperature of **4** were controlled by the feed ratio of [**2**] to [**1**] or by the concentration (see Supporting Information). The most characteristic feature of the cross-linking mentioned above is that both the trunk polymer (**1**) and the cross-linker (**2**) seem not to participate in any apparent chemical reaction, because their structures do not change at all besides the topological linkage produced through space between them, as shown in Scheme 1. Since the cross-linking is a reversible process, the starting materials can be perfectly recovered, if the cross-linked polymer is treated under appropriate conditions.

To confirm this proposition, the cross-linked polymer **4** was treated with an equimolar amount of benzenethiol in DMF at 60 °C.[9] The initial heterogeneous mixture turned to a colorless clear solution within a few minutes, yielding 100% of the original poly(crown ether) (**1**) by precipitation in methanol. Given the above effective decross-linking results, we examined the chemical recycling of cross-linked polymer **4**.

Thiol **3**[10] which is a reduced derivative of the disulfidic axle (**2**), was used instead of benzenethiol in the decross-linking. Thiol **3** (50 mol%) was added to **4**, which had been previously immersed in DMF. The mixture became a colorless homogeneous solution after 70 min at 60 °C. Precipitation in methanol gave **1** quantitatively by filtration, while a mixture of **2** and **3** was recovered in 92% yield by the precipitation of the filtrate in water. As mentioned above, the starting materials recovered by these procedures underwent no change in chemical structure and composition before or after cross-linking and decross-linking. Therefore, the recycling of the recovered materials was accomplished.

We have succeeded in synthesizing novel polyrotaxane networks by using the reversible thiol–disulfide interchange reaction based on dynamic covalent chemistry.[5] The polyrotaxane network was readily removed by treatment with DMF that contained thiols, and the starting materials were almost quantitatively recovered when thiol **3** was used. We have thus demonstrated a new concept for recyclable cross-linked polymer based on the reversible mechanical bonding characteristic of the rotaxane system.

Supporting Information (^{1}H NMR spectra of the model rotaxanes, the effect of the cross-linking ratio on the glass transition temperature and swelling behavior of **4**, and the experimental procedures of the cross-linking and decross-linking) is available.

Received: October 9, 2003 [Z53046]

Keywords: gels · green chemistry · rotaxanes · sulfur · supramolecular chemistry

[1] a) F. Sanda, T. Endo, *Eco Ind.* **2001**, *6*, 18–26; b) M. Mori, N. Sato, *Sokeizai* **2000**, *4*, 17–21; c) F. Sanda, T. Endo, *Polym. Recycl.* **1998**, *3*, 159–163.

[2] a) S. Chikaoka, T. Takata, T. Endo, *Macromolecules* **1991**, *24*, 331–332; b) S. Chikaoka, T. Takata, T. Endo, *Macromolecules* **1991**, *24*, 6557–6562; c) S. Chikaoka, T. Takata, T. Endo, *Macromolecules* **1991**, *24*, 6563–6565; d) S. Chikaoka, T. Takata, T. Endo, *Macromolecules* **1992**, *25*, 625–628.

[3] a) T. Endo, F. Sanda, *React. Funct. Polym.* **1997**, *33*, 241–245; b) T. Endo, T. Suzuki, F. Sanda, T. Takata, *Bull. Chem. Soc. Jpn.* **1997**, *70*, 1205–1210; c) T. Endo, F. Sanda, *Macromol. Symp.* **1998**, *132*, 371–376; c) S. Chikaoka, T. Takata, T. Endo, *Macromolecules* **1994**, *27*, 2380–2382; d) T. Endo, T. Suzuki, F. Sanda, T. Takata, *Macromolecules* **1996**, *29*, 3315–3316; e) For a similar system, see K. Yoshida, F. Sanda, T. Endo, *J. Polym. Sci. Part A* **1999**, *37*, 2551–2558; f) T. Endo, T. Suzuki, F. Sanda, T. Takata, *Macromolecules* **1996**, *29*, 4819–4819.

[4] a) H. J. Sawada, *J. Macromol. Sci. Part C* **1972**, *8*, 235–288; b) I. C. McNeill in *Comprehensive Polymer Science*, *Vol. 6*, Pergamon, New York, **1989**, pp. 451–500; c) W. Egan, R. Schneerson, K. E. Werner, G. Zon, *J. Am. Chem. Soc.* **1982**, *104*, 2898–2910; d) B. E. Christensen, O. Smidsroed, A. Elgsaeter, B. T. Stokke, *Macromolecules* **1993**, *26*, 6111–6120; e) J. C. W. Chien, P. H. Lu, *Macromolecules* **1989**, *22*, 1042–1048; f) L. E. Manring, R. C. Blume, G. T. Dee, *Macromolecules* **1990**, *23*, 1902–1907; g) P. Dubois, I. Baraket, R. Jerome, P. Teyssie, *Macromolecules* **1993**, *26*, 4407–4412.

[5] Reviews on the "Dynamic Covalent Chemistry"; a) Y. Furusho, T. Takata, *Kagaku* **2002**, *57*, 72; b) S. J. Rowan, S. J. Cantrill, G. R. L. Cousins, J. K. M. Sanders, J. F. Stoddart, *Angew. Chem.* **2002**, *114*, 1528; *Angew. Chem. Int. Ed.* **2002**, *41*, 898–952.

[6] a) Y. Furusho, T. Hasegawa, A. Tsuboi, N. Kihara, T. Takata, *Chem. Lett.* **2000**, 18–19; b) Y. Furusho, T. Oku, T. Hasegawa, A. Tsuboi, N. Kihara, T. Takata, *Chem. Eur. J.* **2003**, *9*, 2895–2903.

[7] T. Oku, Y. Furusho, T. Takata, *J. Polym. Sci. Part A* **2003**, *41*, 119–123.

[8] Several polyrotaxane networks have been reported: a) C. Gong, H. W. Gibson, *J. Am. Chem. Soc.* **1997**, *119*, 5862–5866; b) C. Gong, H. W. Gibson, *J. Am. Chem. Soc.* **1997**, *119*, 8585–8591; c) C. Gong, H. W. Gibson, *Macromol. Chem. Phys.* **1998**, *199*, 1801–1806; d) A. Zada, Y. Avny, A. Zilkha, *Eur. Polym. J.* **1999**, *35*, 1159–1164; e) A. Zada, Y. Avny, A. Zilkha, *Eur. Polym. J.* **2000**, *36*, 351–357; f) A. Zada, Y. Avny, A. Zilkha, *Eur. Polym. J.* **2000**, *36*, 359–364; g) T. Ichi, J. Watanabe, T. Ooya, N. Yui, *Biomacromolecules* **2001**, *2*, 204–210; h) J. Watanabe, T. Ooya,

 © 2004 Wiley-VCH Verlag GmbH & Co. KGaA, Weinheim

K. D. Park, Y. H. Kim, N. Yui, *J. Biomater. Sci. Polym. Ed.* **2000**, *11*, 1333 – 1345; i) H. Oike, T. Mouri, Y. Tezuka, *Macromolecules* **2001**, *34*, 6229 – 6234; j) M. Kubo, T. Hibino, M. Tamura, T. Uno, T. Itoh, *Macromolecules* **2002**, *35*, 5816 – 5820; k) Y. Okumura, K. Ito, *Adv. Mater.* **2001**, *13*, 485 – 487.

[9] Here, the association between dibenzo-24-crown-8 and *sec*-ammonium salt is reported to be largely prevented in a solvent with a high donor number such as DMF. P. R. Ashton, E. J. T. Chrystal, P. T. Glink, S. Menzer, C. Schiavo. N. Spencer, J. F. Stoddart, P. A. Tasker, A. J. P. White, D. J. Williams, *Chem. Eur. J.* **1996**, *2*, 709.

[10] Y. Furusho, G. A. Rajkumar, T. Oku, T. Takata, *Tetrahedron* **2002**, *58*, 6609 – 6613.

 © 2004 Wiley-VCH Verlag GmbH & Co. KGaA, Weinheim

Au–Au Interactions

Self-Assembly in Gold(I) Chemistry: A Double-Stranded Polymer with Interstrand Aurophilic Interactions**

*Fabian Mohr, Michael C. Jennings, and Richard J. Puddephatt**

There has been remarkable progress and interest in the design and synthesis of hybrid organic–inorganic molecular materials, and a key strategy is to design simple building blocks that can be induced to form complex molecular structures by self-assembly.[1] Gold(I) centers are particularly versatile as components of such building blocks based on their tendency for linear coordination,[2,3] their high reactivity towards ligand substitution,[2] and their ability to form secondary aurophilic bonds that can be used to direct the self-assembly.[2–9] These properties have made it possible to design macrocycles, molecular triangles, catenanes, and polymers with gold(I) centers coordinated to a phosphane and a nitrogen or carbon donor ligand.[2–10] The gold–carboxylate linkage is important in self-assembled monolayers on gold colloids[11] and is well known in simple complexes,[2,12] but it has not yet been exploited in molecular materials. Here we show that a simple condensation procedure can lead to the self-assembly of a cyclic dimer or trimer, or of a linear polymer for gold(I) complexes of the three isomers of diphenylphosphanylbenzoic acid, and that the polymer forms a remarkable double-stranded structure through aurophilic attractions. The ligands themselves are already known to give interesting gold compounds[13,14] and bimetallic compounds,[15] and this work further highlights their potential in the field of hybrid organic–inorganic molecular materials.

The synthetic strategy was to eliminate HCl from the *ortho* (**1**), *meta* (**2**), and *para* (**3**) isomers of $[AuCl(Ph_2PC_6H_4CO_2H)]$,[13,14] to yield the corresponding oligomers or polymers $[\{Au(Ph_2PC_6H_4CO_2)\}_n]$, with the expectation that the degree of aggregation would be different for the different isomers. Preliminary experiments with $[AuCl(4\text{-}Ph_2PC_6H_4CO_2H)]$ (**3**), which forms a hydrogen-bonded dimer in the solid state (Figure 1), were unsuccessful since the complex

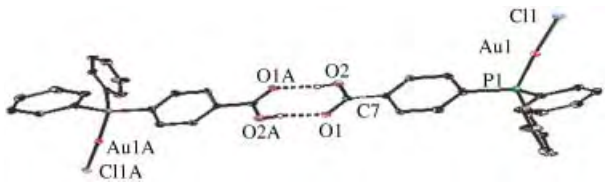


Figure 1. A view of the hydrogen-bonded dimeric structure of **3**.

was resistant to dehydrochlorination with mild bases and was decomposed by stronger ones. However, success was achieved by a two-step reaction involving abstraction of the chloride ligand from each complex **1**–**3** using silver(I) trifluoroacetate to form the corresponding gold(I) trifluoroacetate complex, which was not isolated but was treated in situ with a base to eliminate trifluoroacetic acid and give the product, as outlined in Scheme 1. Complex **1** gave a mixture of dimer **4** and trimer **5**, while complex **2** gave only a molecular triangle **6**, and complex **3** gave an insoluble polymer **7**.

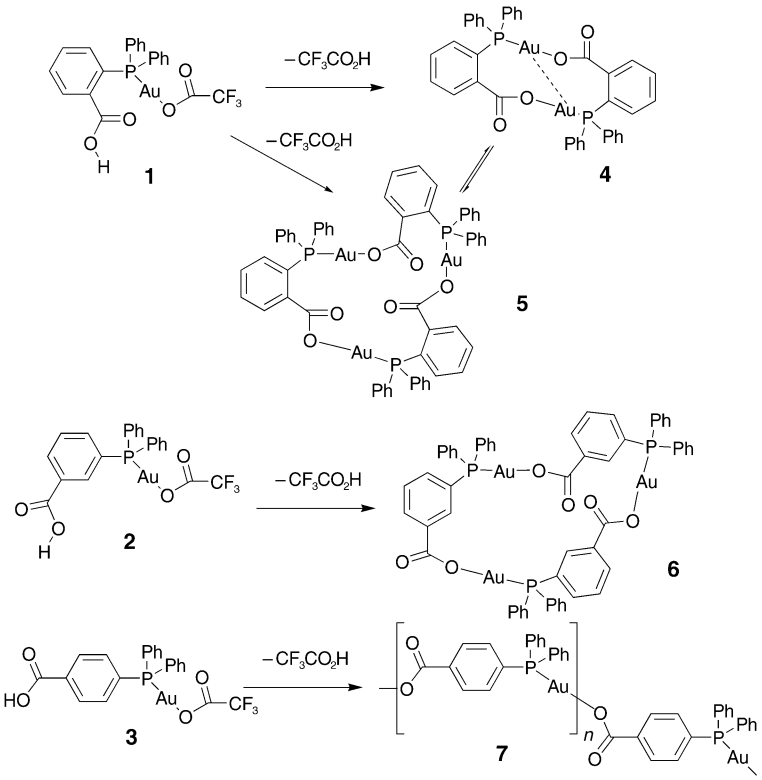
The soluble complexes **4**–**6** were characterized in solution by NMR spectroscopy and ESI mass spectrometry. Complex **6** gave a singlet in the ^{31}P NMR spectrum (in $CDCl_3$) at $\delta = 28.8$ ppm and a peak at $m/z = 1639$ in the ESI-MS (in CH_2Cl_2/CH_3CN, with CsI present to enhance ionization), which corresponds to the $[\{Au(Ph_2PC_6H_4CO_2)\}_3]\cdot Cs^+$ ion, and indicates the presence of the molecular triangle structure only. Complexes **4** and **5** formed an equilibrium mixture in solution. Thus, the ^{31}P NMR spectrum gave two resonances at $\delta = 33.0$ (trimer) and 27.9 ppm (dimer) while the ESI-MS contained two major ions at $m/z = 1639$ and 1137 corresponding to $[\{Au(Ph_2PC_6H_4CO_2)\}_n]\cdot Cs^+$, with $n = 3$ or 2, respectively. Crystallization of the mixture gave the molecular triangle complex **5**, whose structure is shown in Figure 2. The 18-membered macrocycle contains three linear gold(I) units with gold atoms separated by 3.56–4.31 Å, which is too long to be indicative of aurophilic bonding. Molecular modeling indicates that the dimer **4** has more ring strain than **5** but that this is compensated by the presence of a shorter Au···Au contact of approximately 2.9 Å. In solution, **4** will also be favored with respect to **5** through entropic effects.

Complex **7** was insufficiently soluble for characterization in solution, but the remarkable structure shown in Figure 3 was determined using crystals that were grown by the diffusion of 2,2′-bipyridyl into a solution of $[Au(O_2CCF_3)(4\text{-}Ph_2PC_6H_4CO_2H)]$ in $CHCl_3$. The structure (Figure 3) contains infinite polymer chains $[\{Au(4\text{-}Ph_2PC_6H_4CO_2)\}_n]$; there is a degree of helicity in these chains arising from the usual

[*] Dr. F. Mohr, Dr. M. C. Jennings, Prof. R. J. Puddephatt
Department of Chemistry
University of Western Ontario
London, Ontario N6A 5B7 (Canada)
Fax: (+1) 519-661-3022
E-mail: pudd@uwo.ca

[**] We thank NSERC (Canada) for financial support. R.J.P. holds a Canada Research Chair.

 DOI: 10.1002/anie.200353127 © 2004 Wiley-VCH Verlag GmbH & Co. KGaA, Weinheim



Scheme 1. Self-assembly processes from monomers **1**–**3**.

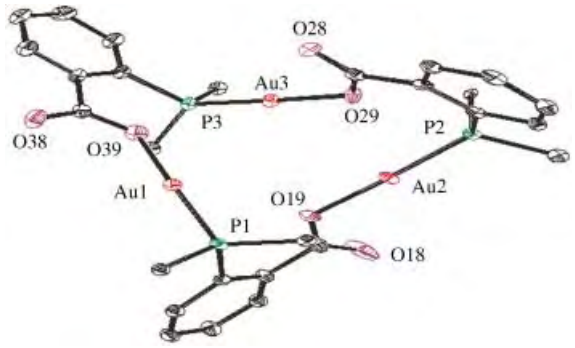


Figure 2. A view of the molecular triangle structure of **5**.

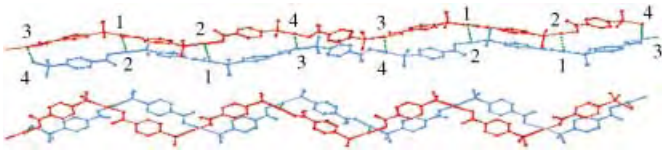


Figure 3. Two views of the double-stranded polymeric structure of **7**. Only the gold atoms are labeled with the labels 1–4 representing Au(1)–Au(4), respectively, and only the *ipso* carbon atoms of the phenyl groups are shown for clarity.

propeller-like arrangement of phenyl groups at the phosphorus centers, and all units within the same polymer chain have the same helicity *P* or *M*. The polymer chains associate in pairs primarily through gold–gold aurophilic contacts (Au(1)···Au(2) = 3.1643(9) Å) to give a racemic *P*,*M* double-helical structure. Complex **7** appears to be the first example of a hybrid organic–inorganic double-chain polymer of this type. However, there is a related inorganic double-chain polymer containing $[AuSe_5]_n^{n-}$ ions, in which chains are connected through aurophilic interactions (Au···Au = 2.950(3) Å).[16] In addition, the antiarthritic drug gold thiomalate contains a classic chiral double-helical structure with chains connected through interchain aurophilic bonds (Au···Au = 3.227(5) Å).[17] Together, these structures demonstrate the remarkable ability of gold(I) centers to form several classes of double-stranded polymeric structures through aurophilic bonding.

Experimental Section

4, **5**: A solution of [AuCl(2-$Ph_2PC_6H_4CO_2H$)] (0.050 g, 0.093 mmol) in CH_2Cl_2 (10 mL) was treated with AgO_2CCF_3 (0.021 g, 0.095 mmol) for 0.5 h. The solution was filtered through celite. Et_3N (0.010 g, 0.099 mmol) was then added to the filtrate, the volume was reduced to 5 mL, and pentane (20 mL) was added to precipitate the product as a pale-yellow solid. Yield: 54 %. ^{31}P NMR ($CDCl_3$): $\delta = 33.0$ (**5**); 27.9 ppm (**4**). IR (KBr disk): $\tilde{\nu} = 1635$ (s, C=O), 1336 cm^{-1} (s, C–O); ESI-MS (*m*/*z*): 1639 [**5**+Cs]$^+$, 1137 [**4**+Cs]$^+$; elemental analysis (%) calcd for $C_{19}H_{14}AuO_2P$: C 45.4, H 2.8, found: C 45.2, H 2.9.

6: This complex was prepared similarly from [AuCl(3-$Ph_2PC_6H_4CO_2H$)]. Yield: 40 %. ^{31}P NMR ($CDCl_3$): $\delta =$ 28.8 ppm; IR (KBr disk): $\tilde{\nu} = 1627$ (s, C=O), 1334 cm^{-1} (s, C–O); ES-MS (*m*/*z*): 1639 [**6**+Cs]$^+$; elemental analysis (%) calcd for $C_{19}H_{14}AuO_2P$: C 45.4, H 2.8, found: C 45.1, H 2.5.

7: This was prepared similarly from [AuCl(4-$Ph_2PC_6H_4CO_2H$)], but precipitated on addition of Et_3N, and was isolated at that stage by filtration. Yield: 65 %. IR (KBr disk): $\tilde{\nu} = 1625$ (s, C=O), 1334 cm^{-1} (s, C–O); elemental analysis (%) calcd for [$C_{19}H_{14}AuO_2P \cdot 0.25\,CH_2Cl_2$]: C 44.8, H 2.8, found: C 44.6, H 2.8.

X-ray structure analysis:[18] Nonius Kappa-CCD diffractometer ($Mo_{K\alpha}$ radiation), data collection and refinement SHELXTL-NT V6.1, empirical absorption correction. CCDC-221124–6 contain the supplementary crystallographic data for this paper. These data can be obtained free of charge via www.ccdc.cam.ac.uk/conts/retrieving.html (or from the Cambridge Crystallographic Data Centre, 12, Union Road, Cambridge CB21EZ, UK; fax: (+44) 1223-336-033; or deposit@ccdc.cam.ac.uk).

Received: October 21, 2003 [Z53127]

Keywords: gold · macrocycles · polymers · self-assembly · supramolecular chemistry

[1] S. Leininger, B. Olenyuk, P. J. Stang, *Chem. Rev.* **2000**, *100*, 853–908.
[2] H. Schmidbaur, *Gold: Progress in Chemistry, Biochemistry and Technology*, Wiley, Chichester, **1999**.
[3] G. A. Bowmaker, C. L. Brown, R. D. Hart, P. C. Healy, C. E. F. Rickard, A. H. White, *J. Chem. Soc. Dalton Trans.* **1999**, 881–889.
[4] H. Ehlich, A. Schier, H. Schmidbaur, *Inorg. Chem.* **2002**, *41*, 3721–3727.
[5] J. P. Fackler, Jr., *Inorg. Chem.* **2002**, *41*, 6959–6972.

 © 2004 Wiley-VCH Verlag GmbH & Co. KGaA, Weinheim

[6] a) R. J. Puddephatt, *Coord. Chem. Rev.* **2001**, *216–217*, 313 – 332; b) F. Mendizabal, P. Pyykkö, N. Runeberg, *Chem. Phys. Lett.* **2003**, *370*, 733 – 740.
[7] P. Schwerdtfeger, H. L. Hermann, H. Schmidbaur, *Inorg. Chem.* **2003**, *42*, 1334 – 1342.
[8] A. Codina, E. J. Fernandez, P. G. Jones, A. Laguna, J. M. Lopez de Luzuriaga, M. Monge, M. E. Olmos, J. Perez, M. A. Rodriguez, *J. Am. Chem. Soc.* **2002**, *124*, 6781.
[9] L. J. Hao, M. A. Mansour, R. J. Lachicotte, H. J. Gysling, R. Eisenberg, *Inorg. Chem.* **2000**, *39*, 5520 – 5529.
[10] V. W. W. Yam, K. K. W. Lo, *Chem. Soc. Rev.* **1999**, *28*, 323 – 334. V. W. W. Yam, *Pure Appl. Chem.* **2001**, *73*, 543 – 548.
[11] S. Y. Lin, T. K. Tsai, C. M. Lin, C. H. Chen, Y. C. Chan, H. W. Chen, *Langmuir* **2002**, *18*, 5473 – 5478.
[12] P. Rombke, A. Schier, H. Schmidbaur, *Z. Naturforsch. B* **2002**, *57*, 605 – 609.
[13] B. P. Howe, R. V. Parish, R. G. Pritchard, *Quim. Nova* **1998**, *21*, 564 – 568.
[14] H. Schmidbaur, B. Brachthaeuser, S. Gamper, A. Schier, O. Steigelmann, *Z. Naturforsch. B* **1992**, *47*, 1725 – 1735.
[15] S.-M. Kuang, P. E. Fanwick, R. A. Walton, *Inorg. Chem.* **2002**, *41*, 1036 – 1038; S.-M. Kuang, P. E. Fanwick, R. A. Walton, *Inorg. Chim. Acta* **2002**, *338*, 219 – 227.
[16] Y. Park, M. G. Kanatzidis, *Angew. Chem.* **1990**, *102*, 945 – 946; *Angew. Chem. Int. Ed. Engl.* **1990**, *29*, 914 – 915.
[17] R. Bau, *J. Am. Chem. Soc.* **1998**, *120*, 9380 – 9381.
[18] **3**: $C_{19}H_{15}AuClO_2P$, $M_r = 538.70$, triclinic, space group $P\bar{1}$, $Z = 4$, $a = 12.0996(3)$, $b = 12.4632(3)$, $c = 13.7806(3)$ Å, $\alpha = 112.200(1)$, $\beta = 91.268(1)$, $\gamma = 108.774(1)°$, $V = 1797.04(7)$ Å^3, $T = 148(2)$ K, $\mu(Mo_{K\alpha}) = 8.432$ mm^{-1}, 18665 reflections, 8195 independent reflections, R_1 $[I > 2\sigma(I)] = 0.069$, $wR_2 = 0.160$. **5**·3.25 acetone: $C_{66.75}H_{61.5}Au_3O_{9.25}P_3$, $M_r = 1695.47$, monoclinic, space group $P2_1/c$, $Z = 4$, $a = 13.6996(2)$, $b = 19.7912(3)$, $c = 23.1202(3)$ Å, $\beta = 97.756(1)$, $V = 6211.3(1)$ Å^3, $T = 150(2)$ K, $\mu(Mo_{K\alpha}) = 7.202$ mm^{-1}, 62032 reflections, 10958 independent reflections, R_1 $[I > 2\sigma(I)] = 0.044$, $wR_2 = 0.110$. **7**·6.5 $CHCl_3$: $C_{82.5}H_{62.5}Au_4Cl_{19.5}O_8P_4$, $M_r = 2784.85$, monoclinic, space group $P2_1/c$, $Z = 4$, $a = 34.8469(3)$, $b = 12.6874(1)$, $c = 23.3187(2)$ Å, $\beta = 108.645(1)°$, $V = 9768.5(1)$ Å^3, $T = 150(2)$ K, $\mu(Mo_{K\alpha}) = 6.638$ mm^{-1}, 86413 reflections, 16218 independent reflections, R_1 $[I > 2\sigma(I)] = 0.074$, $wR_2 = 0.151$.

 © 2004 Wiley-VCH Verlag GmbH & Co. KGaA, Weinheim

Metal–Organic Frameworks

Metal–Organic Replica of Fluorite Built with an Eight-Connecting Tetranuclear Cadmium Cluster and a Tetrahedral Four-Connecting Ligand**

*Hyungphil Chun, Dongwoo Kim, Danil N. Dybtsev, and Kimoon Kim**

The last decade has seen remarkable progress in the development of new materials based on transition-metal ions and organic ligands, often termed as coordination polymers (networks) or metal–organic frameworks. Although this relatively new field of chemistry aims at the discovery and synthesis of new materials for practical applications emphasizing their functional aspects, it would be difficult to achieve a true advance without understanding the structural aspects of such materials at a molecular or an atomic resolution. Recent reviews on the framework topologies and other geometrical characteristics of network solids reflect this importance.[1]

As the number of infinite network structures based on molecular building blocks increases, it becomes easier to analyze and categorize their framework topologies. It appears that for the majority of 3D metal–organic framework structures, there are well-known prototypes in metallic or binary inorganic solids. For example, diamond-related nets composed of one or two kinds of tetrahedral nodes and linear linkers are the most common,[2] and a primitive cubic net (α-Po) based on octahedral nodes with linear linkers is also frequently observed.[3] Other 3D structures have recently been reported to have the following topologies: boracite,[4] $CdSO_4$,[5] CaB_6,[6] feldspar,[7] NbO,[8] perovskite,[9] Pt_3O_4,[10] PtS,[7,11] pyrite,[12] quartz,[13] rutile,[14] sodalite,[15] $SrSi_2$,[16] and tungsten bronze.[17] Note that the connectivity of the building blocks in any of these frameworks does not exceed six and, in general, coordination networks with a local connectivity higher than six is very rare.[18] One of the most important and frequently encountered structure types in minerals that have not been reported in metal–organic frameworks is fluorite (CaF_2), in which the cation is eight coordinated in a cubic geometry and the anion is in tetrahedral environment. The

[*] Dr. H. Chun, D. Kim, Dr. D. N. Dybtsev,[+] Prof. Dr. K. Kim
National Creative Research Initiative Center for Smart Supramolecules, and Department of Chemistry
Division of Molecular and Life Sciences
Pohang University of Science and Technology
San 31 Hyojadong, Pohang 790-784 (Republic of Korea)
Fax: (+82) 54-279-8129
E-mail: kkim@postech.ac.kr

[+] Permanent address:
Institute of Inorganic Chemistry
3, Lavrenteva st., Novosibirsk, 630090 (Russia)

[**] We gratefully acknowledge the Creative Research Initiative Program of the Korean Ministry of Science and Technology for support of this work, and the Brain Korea 21 Program of the Korean Ministry of Education for graduate studentship to D. Kim.

Supporting information for this article is available on the WWW under http://www.angewandte.org or from the author.

 DOI: 10.1002/anie.200353139 © 2004 Wiley-VCH Verlag GmbH & Co. KGaA, Weinheim

design of a metal–organic framework with such a topology, based on deduction, would require an eight-coordinated metal center or an eight-connecting polynuclear metal cluster unit; however, none of the two can easily be envisioned since stereochemically unconstrained eight coordination almost always results in a square antiprism geometry, as exemplified by a 3D framework based on octacyanomolybdate building units,[18a] and an eight-connecting polynuclear metal cluster in a cubic geometry is hitherto unprecedented. Herein, we report a non-interpenetrating cadmium-carboxylate framework built upon a new type of tetranuclear clusters that act as eight-connecting vertices. Together with a tetrahedral four-connecting ligand, tetrakis(4-carboxyphenyl)methane (TCPM),[19] the resulting 3D framework is defined as the first metal–organic replica of fluorite.

A solvothermal reaction of $Cd(NO_3)_2{\cdot}4H_2O$ and H_4TCPM in DMF gives light brown cube-shaped crystals, which maintain single-crystallinity after washing with DMF and drying under vacuum at room temperature. A single-crystal X-ray diffraction study established the formula as $[Cd_4(TCPM)_2(DMF)_4]{\cdot}4DMF{\cdot}4H_2O$ (**1**), and the bulk purity of the product was independently confirmed by elemental analysis and X-ray powder diffraction measurements in which a number of sharp signals closely match those of a simulated diffractogram based on the single-crystal X-ray data (see Supporting Information).

In the structure, a tetranuclear cluster with a general formula $[M_4(O_2CR)_8]$ is observed in which four Cd^{II} ions lie on the same plane, and a total of eight carboxylate groups bridge the Cd ions from above and below the plane of the Cd ions (Figure 1). Along with a solvent DMF molecule bonded to each metal center, the coordination environment around the Cd ion is best described as a monocapped trigonal prism, in which the oxygen atom of the solvent molecule is capping a tetragonal face of the trigonal prism formed by six oxygen atoms from three carboxylate moieties. The Cd–O bond lengths are uniform in the range 2.263(7)–2.299(3) Å except for the bridging oxygen atoms that form asymmetrical bonds with two adjacent Cd ions (2.285(3) and 2.553(4) Å). Each Cd ion in the tetranuclear cluster is related to its neighbor by crystallographic fourfold symmetry, and the two sets of four carboxylate groups above and below the plane of Cd ions are related to each other by mirror plane symmetry. Therefore, the $[Cd_4(O_2CR)_8(DMF)_4]$ cluster mimics the geometry of a twisted square prism or tetragonally compressed cube (see below). The extension of the structure into a 3D network is accomplished by connecting eight tetrahedral shape TCPM ligands to the building block with 4/*m* symmetry. The arrangement of eight TCPM ligands around a $[Cd_4(O_2CR)_8(DMF)_4]$ cluster is shown in Figure 2.

To understand the framework topology, it is necessary to simplify the building blocks from which the 3D net of **1** is built. The $[Cd_4(O_2CR)_8(DMF)_4]$ cluster unit and TCPM ligand can be represented by cubic and tetrahedral units, respectively. The former building block is achieved by connecting the carboxylate carbon (C1) atoms to its nearest neighbors and the latter by drawing a tetrahedron around the central sp^3 carbon atom of the TCPM ligand (Figure 3a and b). This process, when repeated over the extended network, results in the simplified view of the framework of **1** as shown in Figure 3c. The (4,8)-connected net has a strong resemblance to fluorite (CaF_2), one of the most important and

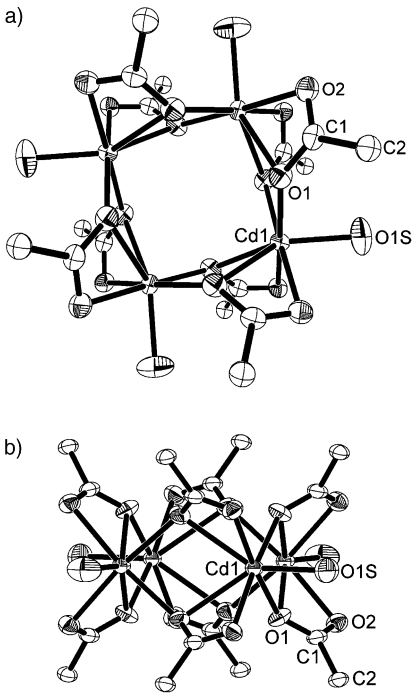


Figure 1. a) Top and b) side view of the $[Cd_4(O_2CR)_8(DMF)_4]$ building unit in the structure of **1** (ORTEP, 40% probability ellipsoids). Only oxygen atoms (O1S) of the coordinated DMF molecules are shown for clarity.

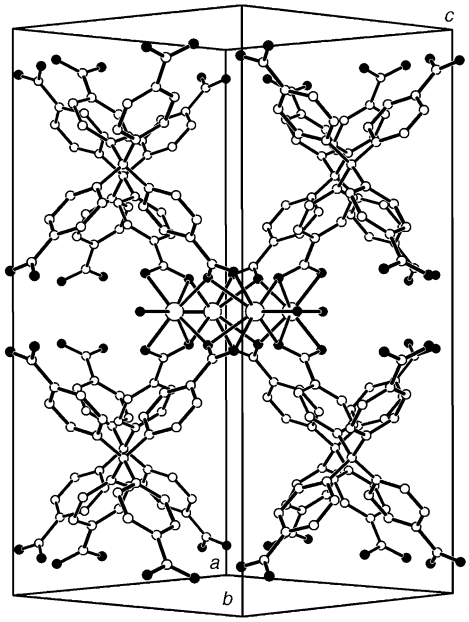


Figure 2. Perspective view showing the arrangement of eight TCPM ligands around one Cd_4 cluster in the unit cell of **1**. Solvent molecules and hydrogen atoms are omitted for clarity. Large and small open circles represent cadmium and carbon atoms, respectively, and oxygen atoms are shown as filled circles.

 © 2004 Wiley-VCH Verlag GmbH & Co. KGaA, Weinheim

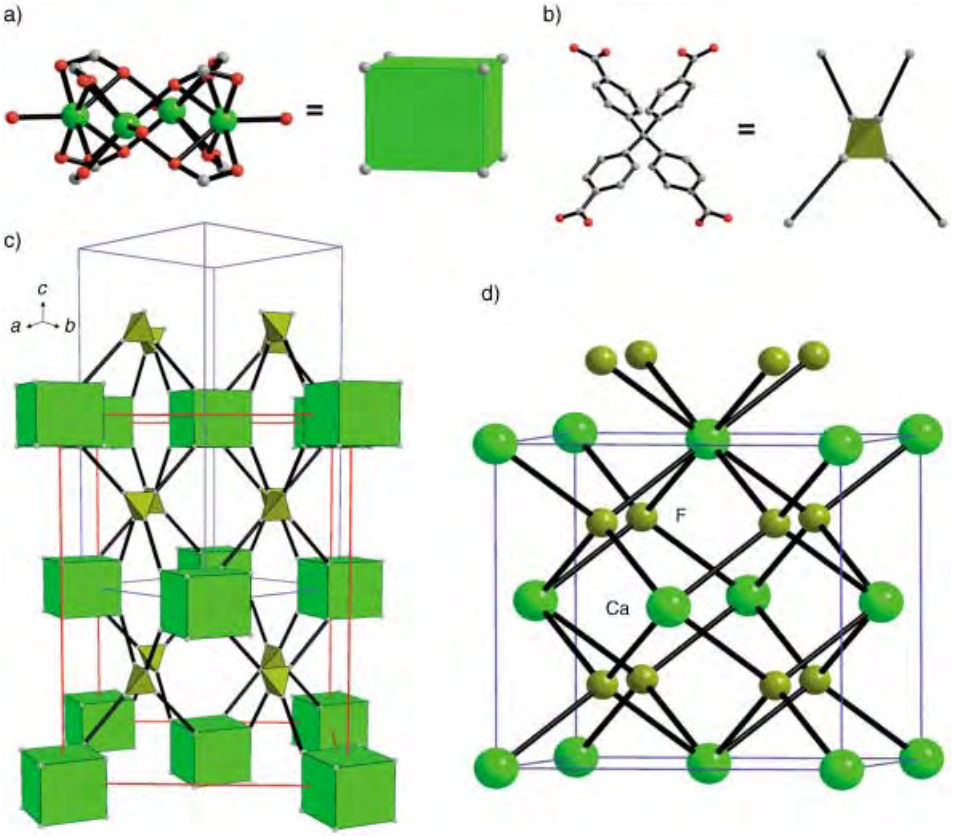


Figure 3. Simplified views of a) cubic and b) tetrahedral building blocks in **1**. c) Perspective view of the framework **1** stylized according to (a) and (b). The red lines represent an imaginary unit cell having the face-centered symmetry (not allowed in tetragonal system). d) Crystal structure of fluorite (CaF_2) in a face-centered cubic unit cell ($Fm\bar{3}m$).

preferred structure for AB_2 type compounds, and is a unique topology for connecting regular cubic and tetrahedral building blocks.[1b] In the structure of fluorite, which has a face-centered cubic symmetry, Ca^{2+} ions are coordinated by eight F^- ions in a cubic geometry, and F^- ions occupy all the tetrahedral sites in the face-centered cubic unit cell (Figure 3d). In the simplified structure of **1**, the cubic and tetrahedral building blocks replace Ca^{2+} and F^- ions in fluorite, respectively, and as one can easily see from the comparison in Figure 3, the similarity in the structures of the genuine fluorite and its metal–organic analogue is striking, except for the slight tetragonal distortion in the structure of **1**. The decorated fluorite net of **1** does not allow interpenetration owing to the size of the Cd_4 cluster, the organic linker, and the void space. The inside the cagelike substructure of **1** comprising six cubes and eight tetrahedra is divided into two compartments by coordinated DMF molecules, which lie approximately at the same height as Cd ions along the *c* axis, and the void space is occupied by solvent DMF and water molecules. A thermogravimetric analysis reveals that the free guest molecules and a coordinated DMF molecule are released from the framework upon heating to about 270 °C (see Supporting Information). Further heating results in the loss of the remaining coordinated DMF molecule before a sharp weight loss corresponding to the decomposition of the TCPM ligand is observed shortly after 370 °C.[20]

In summary, we have synthesized a metal–organic framework that contains eight-connecting tetranuclear cadmium–carboxylate clusters and tetrahedral organic building blocks. The non-interpenetrating, 3D framework is best described as a decorated fluorite net, a topology that has been expected but never been observed in metal–organic or organometallic compounds prior to this work. The new tetranuclear metal-carboxylate cluster may also prove to be a useful building motif in designing a metal–organic framework with a specific topology.

Experimental Section

1: H_4TCPM (103 mg, 0.21 mmol) and $Cd(NO_3)_2{\cdot}4H_2O$ (112 mg, 0.36 mmol) were dissolved in DMF (2.4 mL), and the solution was heated in a screw-capped vial at 95 °C for 2 days. The light brown crystals formed were collected, washed with DMF, and dried under a reduced pressure at room temperature (104 mg, 61 % based on $Cd(NO_3)_2{\cdot}4H_2O$). Elemental analysis calcd (%) for $[Cd_4(TCPM)_2(DMF)_4]{\cdot}4DMF{\cdot}4H_2O$: C 47.09, H 4.63, N 5.36; found: C 46.99, H 4.66, N 5.62. Single-crystal X-ray crystallography: The full hemisphere data were collected on a Siemens SMART CCD diffractometer with $Mo_{K\alpha}$ radiation ($\lambda = 0.71073$ Å) at −60 °C. After the data integration (SAINT) and semiempirical absorption correction based on equivalent reflections (SADABS), the structure was solved by direct methods and subsequent difference Fourier techniques (SHEXLTL). Crystal data for $[Cd_4(TCPM)_2(DMF)_4]{\cdot}$

 © 2004 Wiley-VCH Verlag GmbH & Co. KGaA, Weinheim

4 DMF·4 H_2O (**1**): crystal size 0.19 × 0.17 × 0.17 mm, tetragonal, space group *I*4/*m* (No. 87), $a = 13.480(1)$, $c = 24.582(5)$ Å, $V = 4467(1)$ Å^3, $Z = 2$, $\rho_{calcd} = 1.555$ g cm^{-3}, $\mu = 1.02$ mm^{-1}, $2\theta_{max} = 52°$, $T_{max} = 0.85$ $T_{min} = 0.83$. Total number of reflections 2254 ($R_{int} = 0.0507$). All the non-hydrogen atoms except for those of disordered solvent molecules were refined anisotropically, and hydrogen atoms were added to their geometrically ideal positions. The disordered solvent molecules could not be fully modeled, and were left without hydrogen atoms. The refinements were carried out with full-matrix least-squares on F^2. $R_1 = 0.0522$, w$R_2 = 0.1298$ and GOF = 1.058 for 1824 reflections ($I > 2\sigma(I)$) and 155 parameters. CCDC-221907 contains the supplementary crystallographic data for this paper. These data can be obtained free of charge via www.ccdc.cam.ac.uk/conts/retrieving.html (or from the Cambridge Crystallographic Data Centre, 12 Union Road, Cambridge CB2 1EZ, UK; fax: (+44) 1223-336-033; or deposit@ccdc.cam.ac.uk).

Received: October 22, 2003 [Z53139]
Published Online: January 27, 2004

Keywords: cadmium · carboxylate ligands · coordination polymers · metal–organic frameworks · topochemistry

[1] a) S. R. Batten, R. Robson, *Angew. Chem.* **1998**, *110*, 1558–1595; *Angew. Chem. Int. Ed.* **1998**, *37*, 1460–1494; b) M. O'Keeffe, M. Eddaoudi, H. Li, T. Reineke, O. M. Yaghi, *J. Solid State Chem.* **2000**, *152*, 3–20; c) R. Robson, *J. Chem. Soc. Dalton Trans.* **2000**, 3735–3744; d) M. Eddaoudi, D. B. Moler, H. Li, B. Chen, T. M. Reineke, M. O'Keeffe, O. M. Yaghi, *Acc. Chem. Res.* **2001**, *34*, 319–330; e) B. Moulton, M. Zaworotko, *Chem. Rev.* **2001**, *101*, 1629–1658; f) O. R. Evans, W. Lin, *Acc. Chem. Res.* **2002**, *35*, 511–522; g) O. M. Yaghi, M. O'Keeffe, N. W. Ockwig, H. K. Chae, M. Eddaoudi, J. Kim, *Nature* **2003**, *423*, 705–714; h) S. L. James, *Chem. Soc. Rev.* **2003**, *32*, 276–288.

[2] See refs. [1a–c,e–h, 12] and references therein.

[3] Most recent and representative examples: a) B. F. Hoskins, R. Robson, D. A. Slizys, *Angew. Chem.* **1997**, *109*, 2861–2863; *Angew. Chem. Int. Ed. Engl.* **1997**, *36*, 2752–2755; b) H. Li, M. Eddaoudi, M. O'Keefe, O. M. Yaghi, *Nature* **1999**, *402*, 276–279; c) S. Noro, S. Kitagawa, M. Kondo, K. Seki, *Angew. Chem.* **2000**, *112*, 2161–2164; *Angew. Chem. Int. Ed.* **2000**, *39*, 2081–2084; d) E. Lee, J. Heo, K. Kim, *Angew. Chem.* **2000**, *112*, 2811–2813; *Angew. Chem. Int. Ed.* **2000**, *39*, 2699–2701; e) M. Eddaoudi, J. Kim, N. Rosi, D. Vodak, J. Wachter, M. O'Keeffe, O. M. Yaghi, *Science* **2002**, *295*, 469–472.

[4] a) B. F. Abrahams, S. R. Batten, H. Hamit, B. F. Hoskins, R. Robson, *Angew. Chem.* **1996**, *108*, 1794–1796; *Angew. Chem. Int. Ed. Engl.* **1996**, *35*, 1690–1692; (later reported as α-Po-related net,[1a] but a close examination reveals that the structure is better described as a boracite topology) b) For a twisted boracite net, see S. S.-Y. Chu, S. M.-F. Lo, J. P. H. Charmant, A. G. Orpen, I. D. Williams, *Science* **1999**, *283*, 1148–1150.

[5] a) M. Eddaoudi, J. Kim, D. Vodak, A. Sudik, J. Wachter, M. O'Keeffe, O. M. Yaghi, *Proc. Natl. Acad. Sci. USA* **2002**, *99*, 4900–4904; b) B. Moulton, H. Abourahma, M. W. Bradner, J. Lu, G. J. McManus, M. J. Zaworotko, *Chem. Commun.* **2003**, 1342–1343; c) V. Niel, A. L. Thompson, M. C. Muñoz, A. Galet, A. E. Goeta, J. A. Real, *Angew. Chem.* **2003**, *115*, 3890–3893; *Angew. Chem. Int. Ed.* **2003**, *42*, 3760–3763.

[6] J. Kim, B. Chen, T. M. Reineke, H. Li, M. Eddaoudi, D. B. Moler, M. O'Keeffe, O. M. Yaghi, *J. Am. Chem. Soc.* **2001**, *123*, 8239–8247.

[7] S. W. Keller, *Angew. Chem.* **1997**, *109*, 295–297; *Angew. Chem. Int. Ed. Engl.* **1997**, *36*, 247–248.

[8] a) M. Eddaoudi, J. Kim, M. O'Keeffe, O. M. Yaghi, *J. Am. Chem. Soc.* **2002**, *124*, 376–377; b) B. Chen, F. R. Fronczek, A. W. Maverick, *Chem. Commun.* **2003**, 2166–2167.

[9] a) ref. [3d]; b) for organic perovskite, see C. A. Bremner, M. Simpson, W. T. A. Harrison, *J. Am. Chem. Soc.* **2002**, *124*, 10960–10961.

[10] a) R. P. Farrell, T. W. Hambley, P. A. Lay, *Inorg. Chem.* **1995**, *34*, 757–758; b) B. Chen, M. Eddaoudi, S. T. Hyde, M. O'Keeffe, O. M. Yaghi, *Science* **2001**, *291*, 1021–1023

[11] a) R. W. Gable, B. F. Hoskins, R. Robson, *J. Chem. Soc. Chem. Commun.* **1990**, 762–763; b) B. F. Abrahams, B. F. Hoskins, D. M. Michael, R. Robson, *Nature* **1994**, *369*, 727–729; c) B. Chen, M. Eddaoudi, T. M. Reineke, J. W. Kampf, M. O'Keeffe, O. M. Yaghi, *J. Am. Chem. Soc.* **2000**, *122*, 11559–11560.

[12] H. K. Chae, J. Kim, O. D. Friedrichs, M. O'Keeffe, O. M. Yaghi, *Angew. Chem.* **2003**, *115*, 4037–4039; *Angew. Chem. Int. Ed.* **2003**, *42*, 3907–3909.

[13] a) B. F. Hoskins, R. Robson, N. V. Y. Scarlett, *Angew. Chem.* **1995**, *107*, 1317–1318; *Angew. Chem. Int. Ed. Engl.* **1995**, *34*, 1203–1204; b) J. Sun, L. Weng, Y. Zhou, J. Chen, Z. Chen, Z. Liu, D. Zhao, *Angew. Chem.* **2002**, *114*, 4651–4653; *Angew. Chem. Int. Ed.* **2002**, *41*, 4471–4473.

[14] a) S. R. Batten, B. F. Hoskins, R. Robson, *J. Chem. Soc. Chem. Commun.* **1991**, 445–447; b) S. R. Batten, B. F. Hoskins, B. Moubaraki, K. S. Murray, R. Robson, *J. Chem. Soc. Dalton Trans.* **1999**, 2977–2986.

[15] B. F. Abrahams, M. G. Haywood, R. Robson, D. A. Slizys, *Angew. Chem.* **2003**, *115*, 1144–1147; *Angew. Chem. Int. Ed.* **2003**, *42*, 1111–1115.

[16] Also known as (10, 3)-a net. a) O. M. Yaghi, C. E. Davis, G. Li, H. Li, *J. Am. Chem. Soc.* **1997**, *119*, 2861–2868; b) C. J. Kepert, T. J. Prior, M. J. Rosseinsky, *J. Am. Chem. Soc.* **2000**, *122*, 5158–5168. For (10,3)-b net or $ThSi_2$, see K. Biradha, M. Fujita, *Angew. Chem.* **2002**, *114*, 3542–3545; *Angew. Chem. Int. Ed.* **2002**, *41*, 3392–3395.

[17] E. B. Rusanov, V. V. Ponomarova, V. V. Komarchuk, H. Stoeckli-Evans, E. Fernandez-Ibañez, F. Stoeckli, J. Sieler, K. V. Domasevitch, *Angew. Chem.* **2003**, *115*, 2603–2605; *Angew. Chem. Int. Ed.* **2003**, *42*, 2499–2501.

[18] a) A. K. Sra, G. Rombaut, F. Lahitête, S. Golhen, L. Ouahab, C. Mathonière, J. V. Yakhmi, O. Kahn, *New J. Chem.* **2000**, *24*, 871–876; b) D.-L. Long, A. J. Blake, N. R. Champness, C. Wilson, M. Schröder, *Angew. Chem.* **2001**, *113*, 2509–2513; *Angew. Chem. Int. Ed.* **2001**, *40*, 2443–2447.

[19] M. Grimm, B. Kirste, H. Kurreck, *Angew. Chem.* **1986**, *98*, 1095–1099; *Angew. Chem. Int. Ed. Engl.* **1986**, *25*, 1097–1098.

[20] To study the gas-sorption property, we heated as-synthesized **1** at 120 °C under a high vacuum (10^{-5} Torr) for 24 h, upon which the sample lost its weight by 26 %; however, no significant amount of sorption was observed for N_2, or H_2, and the evacuated sample showed severe line broadening in its powder XRD pattern. This may be attributed to the instability of the framework caused by the loss of coordinated DMF molecules.

 © 2004 Wiley-VCH Verlag GmbH & Co. KGaA, Weinheim

Photooxidation

Laser-Induced Formation of Metal–Peroxide Linkages on the Surface of Lanthanum Sesquioxide under Oxygen**

Wei Zheng Weng, Hui Lin Wan,* Jian Mei Li, and Ze Xing Cao*

Dedicated to Professor Khi Rui Tsai on the occasion of his 90th birthday

Laser Raman spectroscopy (LRS) is extensively used for analyzing molecular vibrational spectra, generally as a complimentary technique to IR spectroscopy, and specifically for in situ applications owing to its simplicity and maneuverability. In particular, LRS has been widely used for in situ examination of surface structures and reaction intermediates in metal oxide catalysts under working conditions.[1] When studying lanthanide oxide based catalysts for selective oxidation of methane or ethane by in situ LRS, measurements must be carried out at an elevated temperature in the presence of oxygen to simulate the catalytic conditions and provide information on, amongst others, active oxygen species.[2] Recently, during a study on La_2O_3-based catalysts by microprobe LRS, we discovered that the laser not only acted as an excitation source for Raman scattering but also induced the formation of a metal peroxide on the La_2O_3 surface. The implications of the observation are far reaching, since they indicate that LRS results may be complicated by an artifact arising from laser excitation. This also raises questions about the photophysics and photochemistry of La_2O_3 surfaces and their relation to catalytic activity. We took advantage of the ready-made configuration and energy-delivery and detection systems of microprobe LRS to study surface photooxygenation of some lanthanide sesquioxides and thier subsequent reaction with ethane. We demonstrate that a lanthanum peroxide linkage is formed by irradiating La_2O_3 with a laser under oxygen and reacts with ethane in a catalytic fashion. The results reported below were obtained in an in situ Raman cell designed for microprobe LRS under standard conditions (under flowing oxygen, 514.5 nm excitation laser at 5 mW, 400 °C) unless otherwise specified. Further experimental details are given in the Supporting Information.

La_2O_3 is characterized by three Raman bands in the regions 406–397, 190–184, and 104–101 cm^{-1} arising from the stretching and bending of La–O^{II} bonds;[3] elevated temperatures (e.g., 400 °C) may cause shifts to lower frequencies. On irradiation of La_2O_3 in the in situ Raman cell with a continuous-wave excitation laser (514.5 nm) at 400 °C under oxygen, a new set of bands at 835–841, 289, and 240 cm^{-1} start to emerge at the expense of the $\nu_{La-O^{II}}$ stretching band at 397 cm^{-1} (Figure 1). These concurrent changes induced by

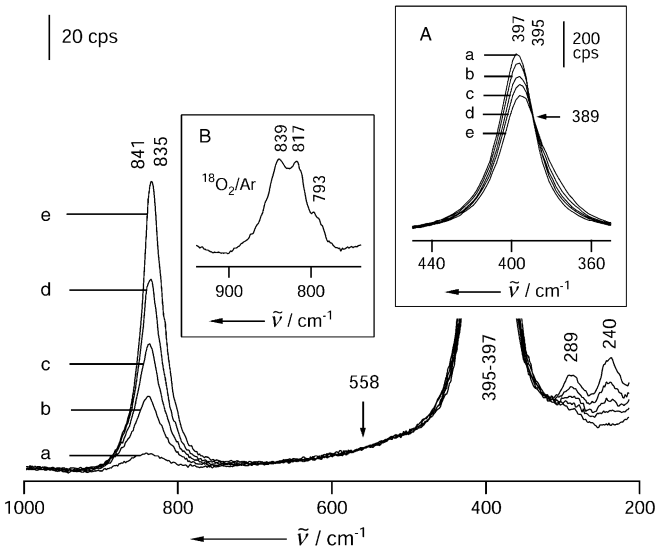


Figure 1. In situ Raman spectra of La_2O_3 continuously irradiated with a focused laser beam (514.5 nm, 5 mW) under $^{16}O_2$ in a microprobe Raman spectrometer at 400 °C for 1, 4, 9, 18, and 60 min (a–e). Inset A: the $\nu_{La-O^{II}}$ peak recorded under $^{16}O_2$ atmosphere. Inset B: the pattern of ν_{O-O} isotopic peaks recorded for the ^{18}O-labeled sample at room temperature.

laser irradiation became noticeable after several minutes and displayed well-defined isosbestic points at 558 and 389 cm^{-1}. Comparable changes in LRS bands were also recorded for other Ln_2O_3 samples under O_2 at elevated temperatures; for example, the stretching band of Nd_2O_3 at 434 cm^{-1} was replaced by a band at 849 cm^{-1}, and that of Sm_2O_3 at 331 cm^{-1} by one at 836 cm^{-1}, on laser irradiation (Supporting Information). As such changes did not occur under nitrogen, the new Raman bands must arise from photooxygenation of the La_2O_3 surface to a lanthanum peroxide. The major band at $\approx$840 cm^{-1} can be assigned to the O_2^{2-} stretching mode, and the other two minor bands to the La^{3+}–O_2^{2-} bending mode, by comparison with the assignment for neodymium(III) oxide peroxide $[Nd_2O_2(O_2)]$.[4] The spectrum of photooxygenated La_2O_3 (Supporting Information) is comparable to, but shifted from, that of $[Nd_2O_2(O_2)]$ prepared from Nd_2O_3 and KO_2 at 1500 °C and 40 kbar.[4] In contrast to such extreme conditions, the present peroxide is formed by mild photooxidation, where laser excitation provides the necessary energy to power the unique surface reaction transforming La–O^{II} into La^{3+}–O_2^{2-} under oxygen, as cogently demonstrated by the exact

[*] Prof. Dr. W. Z. Weng, Prof. Dr. H. L. Wan, J. M. Li, Prof. Dr. Z. X. Cao
State Key Laboratory for Physical Chemistry of Solid Surfaces
Department of Chemistry, Institute of Physical Chemistry
Xiamen University, Xiamen, 361005 (China)
Fax: (+86) 592-218-1395
E-mail: wzweng@xmu.edu.cn
hlwan@xum.edu.cn

[**] Supported by the Ministry of Science and Technology of China (G1999022408) and the National Natural Science Foundation of China (20021002 and 20233020). We thank Prof. Yuan L. Chow for stimulating discussions and revision of the manuscript, Prof. Yuan Yan Liao for designing and manufacturing the in situ Raman cell, and Prof. Chuan Jing Huang and Guo Kun Liu for their help in the experiments.

Supporting information for this article is available on the WWW under http://www.angewandte.org or from the author.

 DOI: 10.1002/anie.200351706 © 2004 Wiley-VCH Verlag GmbH & Co. KGaA, Weinheim

isosbestic points in Figure 1. Formation of a peroxide linkage with a band at $\approx 840\ cm^{-1}$ was further confirmed by using 3% $^{18}O_2$ in Ar to perform the laser-induced photooxygenation. Figure 1B shows side peaks at 817 and 793 cm^{-1} corresponding to isotopic peroxide linkages $[^{16}O^{18}O]^{2-}$ and $^{18}O_2^{2-}$, respectively, perched on the slope of the main peak at 839 cm^{-1} (for $^{16}O_2^{2-}$).

The requirement for laser excitation was further demonstrated by three experiments. On irradiating La_2O_3 under oxygen at 400 °C with a 514.5 nm laser, the 837 cm^{-1} band increased in intensity in proportion to the irradiation time, remained static when the laser was switched off, and increased again when the laser was switched back on (Figure 2a).

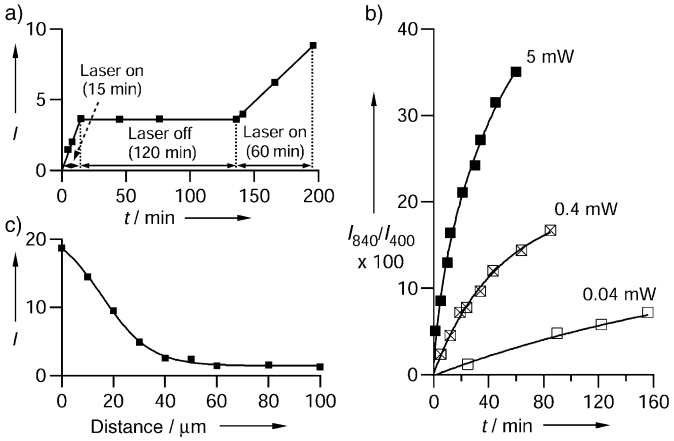


Figure 2. Effects of 514.5 nm laser irradiation (at 5 mW and 400 °C unless otherwise specified) on the formation of peroxide species over La_2O_3 under O_2. a) Response of 837 cm^{-1} peak intensity to the duration of laser action. b) Intensity ratio of the peaks at ≈ 840 and $\approx 400\ cm^{-1}$ (I_{840}/I_{400}) as a function of time with laser powers of 5, 0.4, and 0.04 mW. c) Plot of 837 cm^{-1} peak intensity against the distance from the center of the laser beam (≈ 4 μm in diameter) after irradiation at 400 °C for 130 min followed by at 300 °C for a further 85 min.

Figure 2b shows the response of the same band as a function of the applied laser power under similar conditions. Finally, Figure 2c plots the intensity of the same 837 cm^{-1} band against the distance from the center of the laser beam (≈ 4 μm in diameter); the intensity attenuated with increasing distance from the center, and became almost zero at 40–50 μm. The pattern indicated that laser irradiation but not thermal heating causes the formation of La–peroxide linkages, although so far the latter interpretation has been generally considered to be correct.[2a,5]

Whereas extended heating of La_2O_3 at high temperature (> 650 °C) resulted in insignificant intensity at 840 cm^{-1}, the formation and decay of this peroxide band was closely related to laser energy output in conjunction with operating temperatures. In microprobe LRS measurements under oxygen with laser excitation at 514.5 nm (55.6 kcal mol^{-1}) for a fixed time, the 840 cm^{-1} band intensity was insignificant at 100 °C, but increased slowly from 200 °C and peaked at about 450 °C, above which the intensity started to decrease and became weak at about 600 °C (see Figure 3a). Under comparable conditions, laser excitation at 632.8 nm (45.2 kcal mol^{-1})

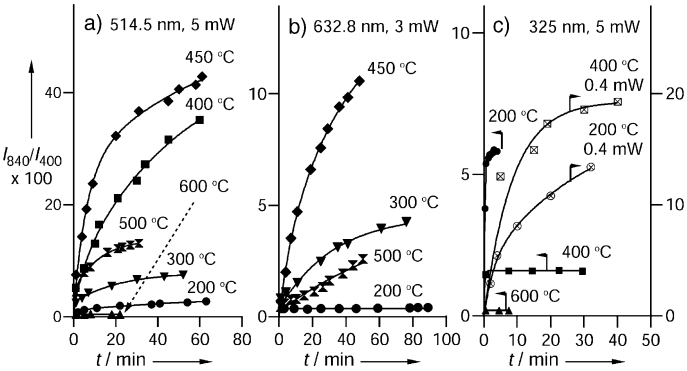


Figure 3. Plots of I_{840}/I_{400} as a function of time for continuous irradiation of La_2O_3 under O_2 with lasers at the indicated temperatures: a) 514.5 nm, 5 mW; b) 632.8 nm, 3 mW; c) 325 nm, 5 mW (unless where otherwise indicated: the measurements at 0.4 mW correspond to values of I_{840}/I_{400} shown on the axis on the right-hand side).

resulted in a weaker buildup of the peroxide-band intensity (see Figure 3b), but the higher energy 325 nm (88 kcal mol^{-1}) excitation led to weak signals even at lower temperatures, clearly owing to peroxide decomposition (see Figure 3c). In contrast, laser excitation at 785 nm (36.4 kcal mol^{-1}) did not cause formation of peroxide species up to 500 °C. The pattern of formation of the 840 cm^{-1} band is typical for the requirement of photoexcitation, whereby the intensity is proportional to irradiation time and power, and a certain minimum laser energy (energy threshold) is required to cause the transition.

Such transformations are intimately related to the photophysics and photochemistry of molecular oxygen, as well as to the interaction of O_2 with lanthanum oxide. Preliminary theoretical calculations with a simplified surface cluster model show that the triplet ground state of O_2 is only loosely associated with the La_2O_3 surface structure, while singlet O_2 can be dissociatively adsorbed on the La_2O_3 surface to generate peroxide species with an activation energy of about 20 kcal mol^{-1}. O_2 has two low-lying singlet excited states: $a^1\Delta_g$ (at 22.5 kcal mol^{-1}) and $b^1\Sigma_g^+$ (at 37.5 kcal mol^{-1}). Owing to the prevailing heavy-atom effects of lanthanides arising from spin–orbit coupling, as is observed in solution,[6] on excitation at the metal oxide center the loose complexes can undergo facile intersystem crossing to reach singlet oxygen in the bound state. Considering the available irradiation energy (> 36.4 kcal mol^{-1}, corresponding to a 785 nm laser) and the transition probabilities from the ground state of oxygen ($^3\Sigma_g^-$) to $^1\Sigma_g^+$ and $^1\Delta_g$, singlet oxygen in the $^1\Sigma_g^+$ state (at 37.5 kcal mol^{-1}) should be more accessible than that in the $^1\Delta_g$ state, and its surface-adsorbed state can be regarded as a precursor for the formation of oxidizing species.

The requirement for photoexcitation led us to study the reactivity of the peroxide. As shown in the Supporting Information, the peroxide species generated on the La_2O_3 surface by laser excitation under oxygen and the usual conditions decomposed slowly under N_2 (spectra b, c), but was immediately consumed by ethane (spectrum d). When the gas flow was changed to a mixture of C_2H_6/O_2 (2/1), as used in the actual oxidative dehydrogenation (for 6 min),

 © 2004 Wiley-VCH Verlag GmbH & Co. KGaA, Weinheim

peroxide-band intensity was regained (spectrum e) and became stronger on switching to pure oxygen again (spectrum f). Both changes in the peroxide band in spectra d and e were accompanied by growth of the band at 1071 cm^{-1} for carbonate formed by adsorption of CO_2 (a by-product of the reaction between C_2H_6 and O_2^{2-}) on La_2O_3. The pattern clearly demonstrates that the surface peroxide not only reacts with ethane but also does so in catalytic fashion in the presence of oxygen. Similar sequential spectral progressions can be recorded for Sm_2O_3 under comparable conditions (Supporting Information). However, since the total amount of peroxide generated by the laser is very limited (the focused laser spot on the sample is only a few micrometers in diameter), we are unable to analyze the other products of the reaction (e.g., C_2H_4) in the gas phase.

A peroxide has been proposed as active oxygen species in catalytic oxidation of methane and ethane to ethylene over metal (including lanthanides) oxide catalysts in thermal processes.[7] The spectral comparison described here suggests that the present peroxide should have the same type of linkage but may be located in a different environment than that generated in thermal catalytic processes. The possibility of using photoinduced surface activation of oxygen in related catalytic processes remains to be studied.

We have shown that laser excitation causes photoinduced formation of lanthanide peroxide linkages on the Ln_2O_3 surface under oxygen, and demonstrated the reactivity of the peroxide with ethane at elevated temperature. Thus, we have defined a limiting condition for LRS measurements, and established a prototype instrument for investigating photoreactions of a solid surface by LRS.

Received: April 22, 2003
Revised: November 19, 2003 [Z51706]

Keywords: lanthanides · laser chemistry · oxides · peroxides · Raman spectroscopy

[1] a) G. Mestl, H. Knözinger in *Handbook of Heterogeneous Catalysis*, *Vol. 2* (Eds.: G. Ertl, H. Knözinger, J. Weitkamp), VCH, Weinheim, **1997**, p. 539; b) H. Knözinger, *Catal. Today* **1996**, *32*, 71; c) G. Mestl, T. K. K. Srinivasan, *Catal. Rev. Sci. Eng.* **1998**, *40*, 451; d) H. Knözinger, G. Mestl, *Top. Catal.* **1999**, *8*, 45; e) I. E. Wachs, *Top. Catal.* **1999**, *8*, 57; f) G. Mestl, *J. Mol. Catal. A* **2000**, *158*, 45; g) A. Bruckner, *Catal. Rev.* **2003**, *45*, 97.

[2] a) G. Mestl, H. Knözinger, J. H. Lunsford, *Ber. Bunsen-Ges. Phys. Chem.* **1993**, *97*, 319; b) Y. D. Liu, H. B. Zhang, G. D. Lin, Y. Y. Liao, K. R. Tsai, *J. Chem. Soc. Chem. Commun.* **1994**, 1871; c) H. B. Zhang, G. D. Lin, H. L. Wan, Y. D. Liu, W. Z. Weng, J. X. Cai, Y. F. Shen, K. R. Tsai, *Catal. Lett.* **2001**, *73*, 141.

[3] a) C. R. Gopinath, I. D. Brown, *J. Raman Spectrosc.* **1982**, *12*, 278; b) J. Gouteron, D. Michel, A. M. Lejus, J. Zarembowitch, *J. Solid State Chem.* **1981**, *38*, 288.

[4] a) A. M. Heyns, K. J. Range, *J. Raman Spectrosc.* **1994**, *25*, 855; b) K. J. Range, M. Stadler, F. Rau, U. Klement, *Angew. Chem.* **1987**, *99*, 1176; *Angew. Chem. Int. Ed. Engl.* **1987**, *26*, 1174.

[5] M. S. Palmer, M. Neurock, M. M. Olken, *J. Am. Chem. Soc.* **2002**, *124*, 8452.

[6] J. H. Zhou, S. Q. Xia, J. R. Chen, X. S. Wang, B. W. Zhang, *Chem. Commun.* **2003**, 1372.

[7] a) K. Otsuka, K. Jinno, *Inorg. Chim. Acta* **1986**, *121*, 237; b) K. Otsuka, A. A. Said, K. Jinno, T. Komatsu, *Chem. Lett.* **1987**, 77; c) K. C. C. Kharas, J. H. Lunsford, *J. Am. Chem. Soc.* **1989**, *111*, 2336; d) J. H. Lunsford, X. Yang, K. Haller, J. Laane, G. Mestl, H. Knözinger, *J. Phys. Chem.* **1993**, *97*, 13810; e) H. Yamashita, Y. Machida, A. Tomita, *Appl. Catal.* **1991**, *79*, 203; f) D. Dissanayake, J. H. Lunsford, M. P. Rosynek, *J. Catal.* **1993**, *143*, 286; g) H. X. Dai, C. F. Ng, C. T. Au, *Appl. Catal. A* **2000**, *202*, 1.

 © 2004 Wiley-VCH Verlag GmbH & Co. KGaA, Weinheim

Open-Framework Materials

$(C_4N_2H_{12})[Fe^{II}_{0.86}Fe^{III}_{1.14}(HPO_3)_{1.39}(HPO_4)_{0.47}(PO_4)_{0.14}F_3]$: A Fluoro–Phosphite–Hydrogenphosphate–Phosphate Iron(II,III) Mixed-Valence Organically Templated Compound**

Sergio Fernández-Armas, José L. Mesa, José L. Pizarro, José S. Garitaonandia, María I. Arriortua, and Teófilo Rojo**

The search for new open-framework materials has developed with a great interest owing to their potential applications in catalysis, sorption, and ion-exchange processes.[1] Zeolites are one of the best known and widely used open-framework materials, many efforts have been made to introduce transition-metal cations into these compounds, or substitute the silicate anions by other tetrahedral groups, such as the phosphate.[2] In this way, the introduction of organic molecules to the reaction medium as structure-directing agents has led to the hydrothermal synthesis of a great variety of inorganic–organic hybrid phosphates.[3] In particular, iron phosphates, some of them mixed-valent, have shown interesting magnetic behaviors.[4] Recently, the pyramidal hydrogenphosphite $[HPO_3]^{2-}$ oxoanion, has also been incorporated

[*] Dr. S. Fernández-Armas, Dr. J. L. Mesa, Prof. T. Rojo
Departamento de Química Inorgánica
Facultad de Ciencias
Universidad del País Vasco
Apdo. 644, 48080 Bilbao (Spain)
Fax: (+34) 94-464-8500
E-mail: qipmeruj@lg.ehu.es
qiproapt@lg.ehu.es

Dr. J. L. Pizarro, Prof. M. I. Arriortua
Departamento de Mineralogía-Petrología
Universidad del País Vasco
Apdo. 644, 48080 Bilbao (Spain)

Dr. J. S. Garitaonandia
Departamento de Física Aplicada II
Universidad del País Vasco
Apdo. 644, 48080 Bilbao (Spain)

[**] This work was financially supported by the Ministerio de Educación y Ciencia (PB97-0640; BQU2001-0678) and Universidad del País Vasco/EHU (9/UPV00169.310-13494/2001; 9/UPV00130.310-13700/2001), which we gratefully acknowledge.

 DOI: 10.1002/anie.200352219 © 2004 Wiley-VCH Verlag GmbH & Co. KGaA, Weinheim

into the structural framework of these kinds of compounds, giving rise to new purely inorganic[5] or organically templated[6] phases.

To date, many organically templated mixed valence $Fe^{II,III}$ phosphates are known.[4] However, less exploratory work has been carried out on incorporating a mixed-valent anionic part into the inorganic framework of these organically templated compounds. As far as we are aware, this is the first time in which both the pyramidal phosphite, $[HPO_3]^{2-}$, and the tetrahedral hydrogenphosphate, $[HPO_4]^{2-}$, as well as the phosphate, $[PO_4]^{3-}$, oxoanions form part of the inorganic skeleton of a mixed-valent iron(II,III) phase. This phase has the formula $(C_4N_2H_{12})[Fe^{II}_{0.86}Fe^{III}_{1.14}(HPO_3)_{1.39}(HPO_4)_{0.47}(PO_4)_{0.14}F_3]$ (**1**). Herein we describe the synthesis, crystal structure, Mössbauer and magnetic behavior of this fluoro–phosphite–hydrogenphosphate–phosphate iron(II,III) mixed-valence organically templated compound.

Compound **1** has been prepared under mild hydrothermal conditions from a mixture of phosphorous, phosphoric, and hydrofluoric acids, Fe^{II} and Fe^{III} sulfates, piperazine, ethanol, and water. Dark brown prismatic single-crystals were obtained. Pattern matching analysis of the X-Ray powder diffraction data of the bulk sample provided a good agreement with single-crystal structure data.

The structure consists of $[Fe^{II}_{0.86}Fe^{III}_{1.14}(HPO_3)_{1.39}(HPO_4)_{0.47}(PO_4)_{0.14}F_3]^{2-}$ chains running along the [010] direction (Figure 1 a). The piperazinium cations are in the cavities of the structure delimited by three different chains. These organic cations establish both ionic interactions and hydrogen bonds with the anionic chains, which are surrounded by six piperazinium cations, and hydrogen bonded to four neighboring chains.

The $[Fe^{II}_{0.86}Fe^{III}_{1.14}(HPO_3)_{1.39}(HPO_4)_{0.47}(PO_4)_{0.14}F_3]^{2-}$ chains are formed by a central chain built of $[Fe(2)^{II}O_4F_2]$ edge-sharing octahedra, and two side chains formed by alternating $[Fe(1)^{III}O_3F_3]$ octahedra and $[HP(1)O_{3.11}]$ tetrahedra. The O(3) and F(3) atoms form the common edge of the $[Fe(2)^{II}O_4F_2]$ polyhedra, and are also shared with the $[HP(1)O_{3.11}]$ and $[Fe(1)^{III}O_3F_3]$ polyhedra, respectively. The $[HP(2)O_{3.50}]$ tetrahedra link two edge-sharing $[Fe(2)^{II}O_4F_2]$ octahedra and one $[Fe(1)^{III}O_3F_3]$ octahedron along the chains (Figure 1 b).

Direct methods[7] were employed to solve the structure, and refined by the full-matrix least-squares method based on F^2, by using the SHELXL 97[8] computer program belonging to the WINGX software package.[9] Throughout solution and refinement processes only three oxygen atoms near P(1) and four near P(2) were found. Finally, a 2 e Å^3 peak near P(1) appeared in the difference electron-density map that was assigned to the phosphite hydrogen atom. At the end of the refinement, the P(1)–H separation (1.54 Å) was much greater than the theoretical value (1.30 Å) and the isotropic thermal factor was extremely low. Instead, the isotropic thermal factor of the O(8) oxygen atom, which is not coordinated to any metal atom and belongs to the $(HP(2)O_4)$ group, was very high.

The presence of both phosphite and hydrogenphosphate groups in the two P(1) and P(2) phosphorus sites was considered. The P(1)–H separation was fixed to the theoretical value, 1.30 Å, and the site occupation factor of the O(8) atom was considered as a variable. After some refinement cycles the peak near P(1) was assigned to the fourth oxygen atom O(7) from the hydrogenphosphate unit. Finally, the protons corresponding to the hydrogenphosphate groups were geometrically placed and the H- and HO- groups were treated as disordered groups with complementary occupation factors.

After convergence was achieved, we found that all thermal factors shown reasonable values, and the phosphorus–oxygen separations were in excellent agreement with those expected for the hydrogenphosphate groups. The final occupation factors were 0.11 for the hydrogenphosphate in

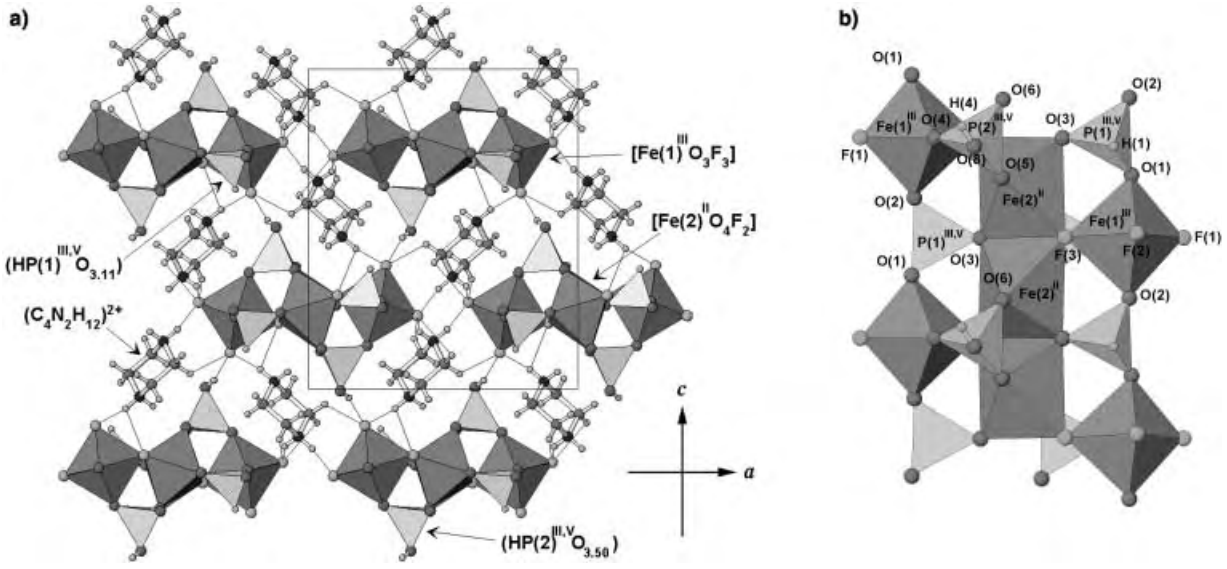


Figure 1. a) Polyhedral view of **1** along the [010] direction. b) Detailed polyhedral view of the anionic triple chain. Both phosphite and hydrogenphosphate–phosphate groups are present in two phosphorus crystallographic sites, only those with site occupation factors equal or greater than 0.50 have been represented.

 © 2004 Wiley-VCH Verlag GmbH & Co. KGaA, Weinheim

P(1) and 0.50 for the phosphite in P(2). Bond-valence calculations[10] for the P(1) and P(2) phosphorus atoms treated as a part of the hydrogenphosphate groups provided values of 4.86 and 4.77, respectively. However, when these calculations were made by treating both phosphorus atoms as belonging to phosphite[11] groups we obtained 4.08 for the $HP(1)^{4+}$ and 4.00 for $HP(2)^{4+}$ groups. Bond-valence sum calculations were also carried out for the iron atoms, which gave values of 3.06 and 2.04 for Fe(1) and Fe(2), respectively. Finally, the electroneutrality of the formula of this compound also requires the existence in the chemical composition of the $[PO_4]^{3-}$ oxoanion in an amount of 0.14 ions per formula. The presence of this anion was confirmed by IR spectroscopy where a band at approximately 1010 cm^{-1} appears. Bands corresponding to the $[HPO_4]^{3-}$ and $[HPO_3]^{2-}$ oxoanions were also observed.

The Mössbauer spectrum shows the presence of pure electric hyperfine interactions, and seems to be formed by two doublets corresponding to the Fe^{III} and Fe^{II} ions in the Fe(1) and Fe(2) sites, respectively (Figure 2). The simulation for Fe^{II}

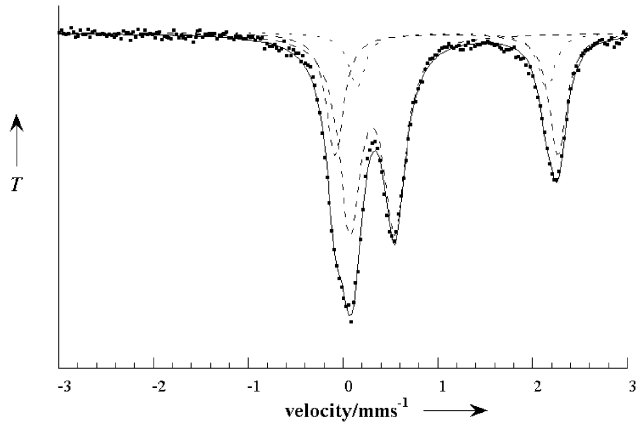


Figure 2. Simulation (-----) of the Mössbauer spectrum employing three doublets. (● data points, —— fit.)

in the Fe(2) site was performed by using a convolution of doublets with the same line-width, isomer shift, and intensity distribution over a quadrupole splitting interval. A distribution with two maxima was obtained. This result was attributed to the presence of slightly different chemical environments for Fe(2) related to the substitution of phosphite (P^{III}) by hydrogen-phosphate (P^{V}) in the P(2) neighboring position. In this way, the best simulation was made considering two doublets for the Fe^{II} ions in Fe(2)a and Fe(2)b positions (see Table 1) taking into account the two chemical environments, and one doublet for the Fe^{III} ions in Fe(1), allowing us to obtain a reasonably good fit (Figure 2). Attempts to simulate the spectrum by employing only two doublets corresponding to the Fe^{II} and Fe^{III} cations gave unsatisfactory results.

The isomer-shift and quadropole-spliting values are in good agreement with those expected for Fe^{III} and Fe^{II} ions in octahedral coordination environments (Table 1). Oxidation states are trapped in their positions and evidence of Fe^{III}/Fe^{II} substitution is not observed, which is in good agreement with

Table 1: Values of isomer shift (IS), quadrupolar splitting (QS), area percentage, and assignation of each doublet in the final simulation of the Mössbauer spectrum.

Site	IS [mm s^{-1}]	QS [mm s^{-1}]	Ox. State	Area percentage	
Fe(1)	0.419	0.474	+3	57.1	
Fe(2)a	1.202	2.352	+2	29.9	42.9
Fe(2)b	1.255	2.003	+2	13.0	

the bond-valence calculations. The ratio between Fe(1) and Fe(2) is close to 1, which is in accord with their multiplicities.

Magnetic measurements on powdered samples have been performed from room temperature to 5.0 K. The thermal evolution of $1/\chi_m$ follows the Curie–Weiss law for temperatures higher than 130 K, with $C_m = 8.00\ cm^3\,K\,mol^{-1}$ and $\theta = -65.2$ K. Considering, $g = 2$ and $S = 5/2$ for Fe^{III} and the Fe^{III}/Fe^{II} ratio obtained from the Mössbauer spectrum, an effective magnetic moment of 5.30 μ_B per Fe^{II} ion was calculated, in good agreement with those usually found for octahedral high-spin Fe^{II} ions. The molar susceptibility increases from room temperature with decreasing temperature and reaches a maximum at approximately 22 K, which indicates the existence of antiferromagnetic interactions, with a magnetic ordering at temperatures below 22 K. The complexity of this system prevented us from modeling the magnetic behavior.

In conclusion, the new organically templated phase synthesized by using mild hydrothermal conditions exhibits a mixed-valence nature and the phosphite and hydrogenphosphate–phosphate oxoanions are both present together.

Experimental Section

Hydrothermal synthesis (443 K, 5 days) was carried out in a PTFE-lined stainless steel pressure vessel in which a previously stirred mixture of H_3PO_3 (15 mmol), H_3PO_4 (85%; 5.2 mmol), HF (48%), $Fe(SO_4)\cdot 7H_2O$ (1.5 mmol), $Fe_2(SO_4)_3\cdot 5H_2O$ (0.75 mmol), $C_4N_2H_{10}$ (37 mmol) ethanol, and water was placed. The percentage of the elements in the product was calculated by inductively coupled plasma atomic emission spectroscopy (ICP-AES) and elemental analysis. Fluoride content was measured with an ion-selective electrode. A chemical analysis confirmed the existence of two oxidation states for iron (Fe^{II}:Fe^{III} close to 1). Calcd (%) for $(C_4N_2H_{12})[Fe^{II}_{0.86}Fe^{III}_{1.14}(HPO_3)_{1.39}(HPO_4)_{0.47}(PO_4)_{0.14}F_3]$: C 11.1, H 3.3, N 6.5, F 13.1, Fe 25.7, P 14.8; found: C 10.7, H 3.0, N 6.4, F 13.0, Fe 25.5,P 14.5.

Mössbauer measurements were recorded at room temperature in the transmission geometry using a conventional constant-acceleration spectrometer with a $^{57}CoRh$ source. The fit of the Mössbauer spectrum has been performed using the NORMOS program.[12] Magnetic measurements on powdered sample were performed at temperatures between 5.0–300 K, using a Quantum Design MPMS-7 SQUID magnetometer. The magnetic field was 0.1, 0.05, and 0.01 T, values in the range of linear dependence of magnetization versus magnetic field, even at 5.0 K.

Crystal data of $C_4H_{13.86}F_3Fe_2N_2O_{6.61}P_2$: $M = 426.57$, orthorhombic, $P2_12_12_1$, $a = 12.790(2)$, $b = 6.440(1)$, $c = 15.167(1)$ Å, $V = 1249.3(3)$ Å^3, $Z = 4$, $\rho_{calcd} = 2.268\ g\,cm^{-3}$, $D_M = 2.25(1)\ g\,cm^{-3}$, $\mu(Mo_{K\alpha}) = 2.646\ mm^{-1}$, 2049 total (2049 independent) reflections, $2.08 < \theta < 29.94$, $R = 0.045$ and $R_w = 0.113$ for 1822 reflections with $I > 2\sigma(I)$, absolute structure parameter 0.05(3). Further details on the crystal structure investigations may be obtained from the Fachinformationszentrum Karlsruhe, 76344 Eggenstein-Leopoldshafen, Germany (fax:

 © 2004 Wiley-VCH Verlag GmbH & Co. KGaA, Weinheim

(+49) 7247-808-666; e-mail: crysdata@fiz-karlsruhe.de), on quoting the depository number CSD-413223.

Received: June 25, 2003 [Z52219]

Keywords: iron · magnetic behavior · mixed-valent compounds · mössbauer spectroscopy · phosphates · phosphites

[1] P. B. Venuto, *Microporous Mater.* **1994**, *2*, 297 – 411.
[2] S. T. Wilson, B. M. Lok, C. A. Messian, T. R. Cannan, E. M. Flanigen, *J. Am. Chem. Soc.* **1982**, *104*, 1146 – 1147.
[3] a) T. Loisseau, G. Ferey, *J. Solid State Chem.* **1994**, *111*, 416 – 421; b) G. Bonavia, R. C. Haushalter, C. J. O'Connor, J. Zubieta, *Inorg. Chem.* **1996**, *35*, 5603 – 5612; c) S. Natarajan, M. Eswaramoorthy, A. K. Cheetham, C. N. R. Rao, *Chem. Commun.* **1998**, 1561 – 1562; d) A. K. Cheetham, G. Ferey, T. Loiseau, *Angew. Chem.* **1999**, *111*, 3466 – 34920; *Angew. Chem. Int. Ed.* **1999**, *38*, 3268 – 3292; e) S. Neeraj, M. L. Noy, C. N. R. Rao, A. K. Cheetham, *J. Solid State Chem.* **2002**, *167*, 344 – 353; f) C. Serre, F. Tauelle, G. Ferey, *Chem. Mater.* **2002**, *14*, 998 – 1003.
[4] a) M. Cavellec, G. Ferey, J. M. Greneche, *J. Magn. Magn. Mater.* **1997**, *174*, 109 – 116; b) J. R. D. DeBord, W. H. Reiff, C. J. Warren, R. C. Haushalter, J. Zubieta, *Chem. Mater.* **1997**, *9*, 1994 – 1998; c) V. Zima, K.-H. Lii, N. Nguyen, A. Ducouret, *Chem. Mater.* **1998**, *10*, 1914 – 1920; d) C.-Y. Huang, S.-L. Wang, K.-H. Lii, *J. Porous Mater.* **1998**, *5*, 147 – 152; e) M. Riou-Cavellec, D. Riou, G. Ferey, *Inorg. Chim. Acta* **1999**, *291*, 317 – 325; f) S. Mandal, S. Natarajan, J. M. Greneche, M. Riou-Cavellec, G. Ferey, *Chem. Mater.* **2002**, *14*, 3751 – 3757.
[5] a) M. Shieh, K. J. Martin, P. J. Squattrito, A. Clearfield, *Inorg. Chem.* **1990**, *29*, 958 – 963; b) F. Sapiña, P. Gomez, M. D. Marcos, P. Amoros, R. Ibañez, D. Beltran, *Eur. J. Solid State Inorg. Chem.* **1989**, *26*, 603 – 617; c) M. D. Marcos, P. Amoros, A. Beltran, R. Martinez, J. P. Attfield, *Chem. Mater.* **1993**, *5*, 121 – 128; e) M. P. Attfield, R. E. Morris, A. K. Cheetham, *Acta Crystallogr. Sect. C* **1994**, *50*, 981 – 984; f) M. D. Marcos, P. Amoros, A. Le Bail, *J. Solid State Chem.* **1993**, *107*, 250 – 257.
[6] a) G. Bonavia, J. DeBord, R. C. Haushalter, D. Rose, J. Zubieta, *Chem. Mater.* **1995**, *7*, 1995 – 1998; b) M. L. F. Phillips, T. M. Nenoff, C. T. Thompson, W. T. A. Harrison, *J. Solid State Chem.* **2002**, *167*, 337 – 343; c) S. Fernandez, J. L. Pizarro, J. L. Mesa, L. Lezama, M. I. Arriortua, R. Olazcuaga, T. Rojo, *Inorg. Chem.* **2001**, *40*, 3476 – 3483; d) S. Fernandez, J. L. Pizarro, J. L. Mesa, L. Lezama, M. I. Arriortua, T. Rojo, *Int. J. Inorg. Mater.* **2001**, *3*, 331 – 336; e) S. Fernandez, J. L. Mesa, J. L. Pizarro, L. Lezama, M. I. Arriortua, T. Rojo, *Chem. Mater.* **2002**, *14*, 2300 – 2307; f) S. Fernandez, J. L. Mesa, J. L. Pizarro, L. Lezama, M. I. Arriortua, T. Rojo, *Angew. Chem.* **2002**, *114*, 3835 – 3837; *Angew. Chem. Int. Ed.* **2002**, *41*, 3683 – 3685; g) S. Fernandez, J. L. Mesa, J. L. Pizarro, L. Lezama, M. I. Arriortua, T. Rojo, *Chem. Mater.* **2003**, *15*, 1204 – 1209; Y. Wang, J. Yu, Y. Du, Z. Shi, Y. Zou. R. Xu, *J. Chem. Soc. Dalton Trans.* **2002**, 4060 – 4063.
[7] G. M. Sheldrick, SHELXS97 Program for the Solution of Crystal Structures, University of Göttingen, Germany, **1997**.
[8] G. M. Sheldrick, SHELXL97 Program for the Refinement of Crystal Structures, University of Göttingen, Germany, **1997**.
[9] J. Farrugia, WINGX Version 1.63.02 An Integrated System of Windows Programs for the Solution, Refinement and Analysis of Single Crystal X-Ray Diffraction Data J. Farrugia, *J. Appl. Crystallogr.* **1999**, *32*, 837 – 838.
[10] a) N. E. Brese, M. O'Keeffe, *Acta Crystallogr. Sect. B* **1991**, *47*, 192 – 197; b) I. D. Brown , D. Altermatt, *Acta Crystallogr. Sect. B* **1985**, *41*, 244 – 247.
[11] J. Loub, *Acta Crystallogr. Sect. B* **1991**, *47*, 468 – 473.
[12] R. A. Brand, J. Lauerm D. M. Herlach, *J. Phys. F* **1983**, *13*, 675 – 683.

 © 2004 Wiley-VCH Verlag GmbH & Co. KGaA, Weinheim

Conducting Materials

An Organic–Inorganic Hybrid Electrolyte Derived from Self-Assembly of a Poly(Ethylene Oxide)–Poly(Propylene Oxide)–Poly(Ethylene Oxide) Triblock Copolymer**

Hsien-Ming Kao and Chien-Liang Chen*

Intensive studies have focused on the development of new types of solid polymer electrolytes (SPEs) which combine high mechanical strength with high ionic conductivity, as needed for applications in, for example, solid-state lithium polymer batteries.[1,2] While poly(ethylene oxide) (PEO), chains act as solvents for lithium salts, practical use of PEO-based electrolytes is often hindered by their low conductivity at room temperature (ca. 10^{-7}–10^{-8} S cm^{-1}) and poor mechanical properties. Moreover, PEO-based electrolytes are prone to crystallization. To alleviate these drawbacks of polyether-based electrolytes, considerable effort is being devoted to synthesizing new organic–inorganic hybrid materials by sol–gel routes, which usually involve hydrolysis and condensation of alkoxysilanes. A variety of organic–inorganic hybrids with covalent bonds or only weak physical bonds between the inorganic and organic phases have been proposed.[3–7] These solid polymer electrolytes, so-called ormolytes (organically modified electrolytes), combine the solvating power of the ether units with an inorganic network, which provides simultaneously an amorphous structure and good thermal, mechanical, and chemical stability. However, miscibility between the organic and inorganic entities is a major concern, but this can be overcome by the use of functionalized alkoxysilanes.

Block copolymers can be regarded as macromolecular analogues of low-molecular-weight surfactants, and they can self-assemble under certain conditions to give a variety of nanoscale morphologies.[8] In particular, PEO-PPO-PEO triblock copolymers (PPO = poly(propylene oxide)) consisting of two dissimilar moieties, that is, hydrophilic EO blocks and hydrophobic PO blocks, were recently used as structure-directing agents to prepare ordered mesoporous silica by self-assembly in acidic medium.[9] Herein we report the design and synthesis of a new organic–inorganic hybrid electrolyte derived from the self-assembly of a PEO-PPO-PEO triblock copolymer by co-condensation of (3-glydicyloxypropyl)trimethoxysilane (GLYMO) and tetraethoxysilane (TEOS). We

[*] Prof. H.-M. Kao, C.-L. Chen
Department of Chemistry, National Central University
Chung-Li, Taiwan 32054 (Republic of China)
Fax: (+886) 342-27664
E-mail: hmkao@cc.ncu.edu.tw

[**] Financial support of this work by the National Science Council of Taiwan is gratefully acknowledged. The authors thank Dr. U-Ser Jeng, Prof. H. P. Lin, Mr. C. Y. Tang, and Ms. R. R. Wu for their contributions to SAXS, TEM, and NMR experiments.

Supporting information for this article is available on the WWW under http://www.angewandte.org or from the author.

 © 2004 Wiley-VCH Verlag GmbH & Co. KGaA, Weinheim DOI: 10.1002/anie.200352243

used commercially available Pluronic F127 triblock copolymer ($EO_{106}PO_{70}EO_{106}$, $M_w = 12\,600$, BASF) both as the structure-directing amphiphilic surfactant and as the polymer matrix. Since the EO and PO units of F127 are relatively short, the mechanical properties of F127-based solid polymer electrolyte are a major concern for its practical applications. These properties can be greatly improved if the silica domain is incorporated within the polymer matrix. The F127 triblock copolymer was recently used for the self-assembly of ordered cubic mesoporous silica SBA-16 in acidic medium.[9] We therefore expected that F127 triblock copolymer would self-assemble on a functionalized silica network to generate a nanocomposite film. Moreover, the epoxide functionality of GLYMO can provide a cross-linking center for blending the triblock copolymer and thus improving the compatibility between organic and inorganic phases.

Figure 1a shows the powder X-ray diffraction (XRD) patterns of the hybrids with various [O]/[Li] ratios. The appearance of peaks at $2\theta = 0.5°$ indicates that the hybrids exhibit mesoscopically ordered structures. The degree of ordering depends on the lithium content. The much sharper and more intense peak for the hybrid with [O]/[Li] = 16 indicates a higher degree of order than in the other two samples. The small-angle X-ray scattering (SAXS) profile of this hybrid (Figure 1b) exhibits more and sharper peaks and thus also indicates superior ordering in this sample. For [O]/[Li] = 16, five scattering peaks with a spacing ratio of $1:\sqrt{3}:2:\sqrt{7}:3$ are observed. This spacing sequence is indicative of a hexagonal array of cylinders, with a cylinder spacing of 180 Å.[10a] The TEM images in Figure 2 also show a well-organized hexagonal mesophase with cylindrical assemblies in the hybrid with [O]/[Li] = 16. Unlike mesoporous silica materials, N_2 adsorption–desorption isotherms (Supporting Information) show that no significant adsorption is observed for the sample after calcination at 560 °C for 8 h, because the mesostructure collapses on removal of the copolymer. This effect is due to the relatively low inorganic fraction (silica) in these materials. Above its critical micellar concentration, F127 forms micelles in water, in which a hydrophobic core consisting of the PPO blocks is surrounded by an outer shell,

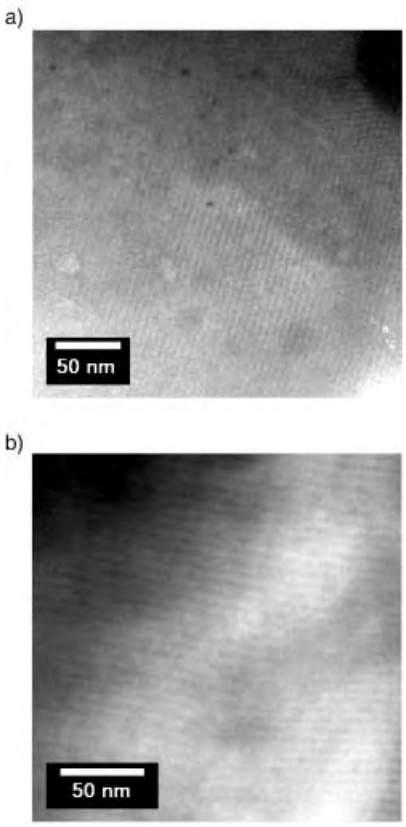


Figure 2. TEM images of the hybrid material with [O]/[Li] = 16 revealing a well-ordered hexagonal array of cylinders, viewed a) from above and b) from the side.

or corona, of hydrated PEO blocks.[10b] Consequently, the silica species adopt the mesoscopic organization imposed by the block copolymer and are preferentially partitioned into the hydrophilic regions of the sample, where they form a rigid cross-linked network. A schematic representation of the mesophase formed by self-assembly of F127 is shown in Scheme 1.

The glass transition temperature T_g and melting temperature T_m of the hybrid samples were measured by differential scanning calorimetry (DSC; Table 1). The T_g of pure F127 copolymer is about −64 °C. The T_g value increases (becomes less negative) with increasing lithium content, and this suggests that the presence of lithium salts leads to the formation of transient cross-links between ether oxygen atoms and lithium cations. This cross-linking decreases segmental motion of the polymer chains and thus increases T_g. Except for the hybrid with [O]/[Li] = 32, no clear melting transitions were observable, that is, F127 crystallization is successfully suppressed by high levels of salt doping. Thermogravimetric analysis shows that the present hybrid electrolytes are thermally stable up to at least 200 °C.

Figure 3 shows the ionic conductivity σ as a function of temperature for hybrids with various [O]/[Li] ratios. The hybrid with [O]/[Li] = 16 has well-ordered mesophases and exhibits the highest ionic conductivity,

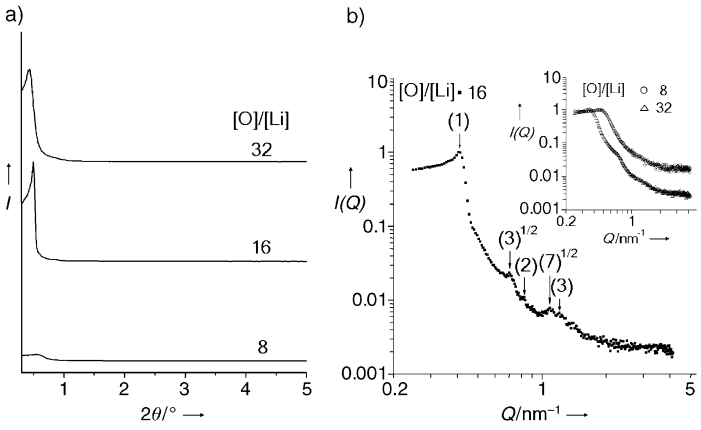
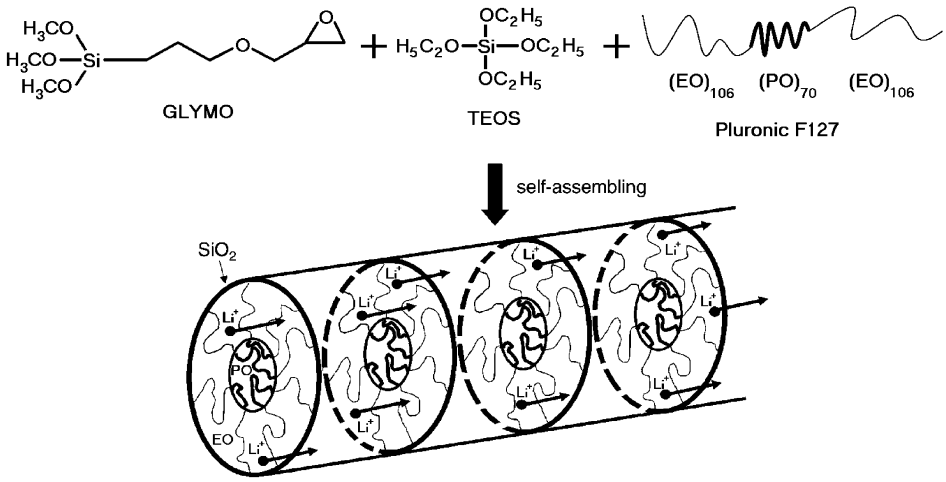


Figure 1. a) XRD and b) SAXS profiles of hybrids with various [O]/[Li] ratios. The scattering wave vector Q is given in terms of $Q = (4\pi/\lambda)\sin\theta$, where 2θ is the scattering angle and λ is the X-ray wavelength.

 © 2004 Wiley-VCH Verlag GmbH & Co. KGaA, Weinheim



Scheme 1. Schematic illustration of the formation of a mesophase by self-assembly of Pluronic F127 triblock copolymer. For the sake of clarity, only the copolymer molecules and lithium cations at the cross-section of the cylinder assemblies are depicted, and the dissociated anions are not shown. TEOS = tetraethoxysilane.

Table 1: DSC and ionic conductivity of hybrids with various [O]/[Li] ratios.

[O]/[Li]	T_g [°C]	T_m [°C]	Conductivity [S cm^{-1}]	
			at 30 °C	at 80 °C
32	−44.1	45.7	1.20×10^{-6}	1.58×10^{-3}
16[a]	−38.2	–	3.17×10^{-5}	1.71×10^{-3}
8	−32.9	–	7.83×10^{-6}	7.24×10^{-4}

[a] The silica-free F127-based electrolyte at the same salt concentration exhibits a conductivity of only 2.30×10^{-7} S cm^{-1} at 30 °C.

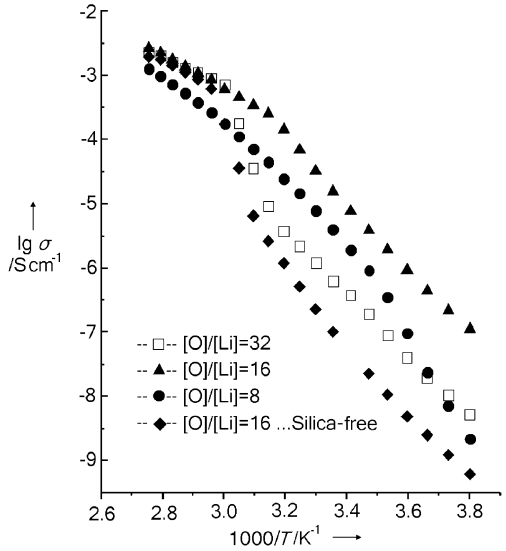


Figure 3. Temperature dependence of ionic conductivity of hybrids with various [O]/[Li] ratios. For comparison, the conductivity of silica-free F127-based electrolyte with [O]/[Li] = 16 is also shown.

especially in the temperature range from −10 to 45 °C. An optimal value of approximately 3×10^{-5} S cm^{-1} at 30 °C is obtained at [O]/[Li] = 16, which is comparable with the conductivity of PEO-based electrolytes containing nanoscale TiO_2 and Al_2O_3.[11] This conductivity is much better than those of composite polymer electrolytes containing other nanoscale ceramics, and it is at least two orders of magnitude higher than the conductivity of conventional PEO electrolytes. Interestingly, the conductivity of a silica-free F127-based electrolyte of the same [O]/[Li] ratio, which does not have a mesoscopically ordered structure, is only 2.30×10^{-7} S cm^{-1} at 30 °C. The conductivity of the silica-containing electrolytes increases with increasing temperature and reaches around 10^{-3} S cm^{-1}, the level needed for many practical applications, at about 80 °C. The hybrid electrolyte with [O]/[Li] = 8 shows Vogel–Tamman–Fulcher (VTF) behavior over the studied temperature range, that is, the ion mobility is coupled with the segmental motion of the polymer chain, while the other two hybrid electrolytes exhibit Arrhenius behavior between −10 and 40 °C. The hybrid with [O]/[Li] = 32 shows a conductivity jump at the temperature associated with its melting point and exhibits similar conductivity to the hybrid with [O]/[Li] = 16 at high temperatures. The hybrid with the largest amount of lithium salt (i.e., [O]/[Li] = 8), which has less ordered mesophases, exhibits the lowest ionic conductivity among the studied hybrid electrolytes.

Solid-state ^{29}Si and ^{13}C NMR spectroscopy measurements were performed in order to determine the structure of the inorganic and organic parts of the hybrid, respectively. Three major ^{29}Si NMR signals at $\delta = -58$, −67, and −110 ppm are observed, and can be assigned to silicon sites of T^2 (R*Si*(O-Si)$_2$OH), T^3 (R*Si*(OSi)$_3$), and Q^4 (*Si*(OSi)$_4$) groups, respectively, where R represents an alkyl group belonging to GLYMO. The ^{13}C cross-polarization/magic-angle spinning (CP/MAS) spectrum shows six major resonances, assigned to −C−O− linkages (δ = 71, 74, and 76 ppm), −CH_2− groups (δ = 24 ppm), −CH_3 (δ = 18 ppm, PPO), and −C−Si− (δ = 10 ppm, GLYMO). The relative intensities of T and Q and ^{13}C signals are all as expected on the basis of the synthesis. The absence of the ^{13}C peaks at δ = 44 and 51 ppm for the epoxide ring of GLYMO is indicative of complete epoxide ring opening. Variable-temperature ^{7}Li{^{1}H} MAS NMR measurements were performed to probe the local environments of the Li^+

 © 2004 Wiley-VCH Verlag GmbH & Co. KGaA, Weinheim

cations. At 213 K, the ^{7}Li resonance at $\delta = -0.9$ ppm (site I) with a shoulder at about $\delta = -0.4$ ppm (site II) indicates that two distinct ^{7}Li local environments exist in the hybrid (Figure 4). On raising the temperature of the sample to

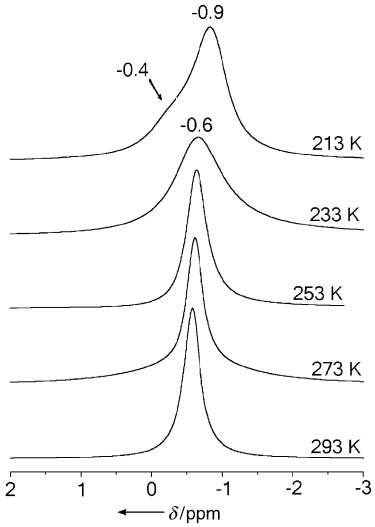


Figure 4. Variable-temperature ^{7}Li{^{1}H} MAS NMR spectra, acquired at a spinning speed of 3.4 kHz, of the hybrid with a [O]/[Li] ratio of 16.

233 K, which is close to T_g, these two sites merge together into a signal at $\delta = -0.6$ ppm. Site I with the higher intensity peak is assigned to lithium cations in the polyether domain, whereas the site II possibly corresponds to the lithium cations in the polymer/silica interface or silica-rich domain. Thus variable-temperature ^{7}Li{^{1}H} MAS NMR spectroscopy is able to resolve the different lithium local environments in the hybrid system.

Previous NMR spectroscopic investigations on similar hybrid materials showed that the hydrophilic PEO blocks are firmly anchored in the inorganic silica phase, which substantially restricts the molecular mobility, while the hydrophobic PPO blocks show a flexibility comparable to that observed for the bulk copolymer.[12] Therefore, the hybrid electrolyte is expected to exhibit low ionic conductivity, as the mobility of the lithium cations is associated with the segmental motion of the polymer chains. In contrast, the present hybrid electrolytes exhibit conductivity two orders-of-magnitude higher than that of silica-free F127-based polymer electrolyte. The resistive dynamics of polymer–salt electrolytes can be mediated by introducing nanoscale ceramics that function as solid plasticizers.[11] In the present system the surface interaction of the copolymer, cations, and anions with the nanoscale silica network is believed to play a key role in stabilizing the hybrid structure and facilitating motion of the Li^+ ions while retarding that of the anions. A possible explanation for the lower conductivity of the hybrid with [O]/[Li] = 8 relative to that with [O]/[Li] = 16 is increased ion-pair formation with increasing salt concentration. However, FTIR spectroscopy shows that the hybrids with [O]/[Li] = 16 and 8 exhibit similar degrees of salt dissociation. The conductivity data in combination with the structural characterization suggests that the drastically enhanced conductivity for the hybrid with [O]/[Li] = 16 is closely related to its well-ordered mesophase, which might improve the arrangement of Li^+-ion conducting pathways, as illustrated in Scheme 1. Both effects (i.e., surface interaction and formation of a well-ordered mesophase) are manifested as a substantial enhancement of the Li^+ ionic conductivity at room temperature. The ordered region of the mesophase and the amorphous region of the polyether moieties are possibly active simultaneously and work synergistically to yield favorable lithium-ion transport and thus contribute to the high ionic conductivity of the materials.

In summary, we have demonstrated that the complexation of Pluronic F127 triblock copolymer with $LiClO_4$ by a sol–gel route involving the co-condensation of alkoxysilanes can give rise to a well-ordered mesophase that is dependent on the salt concentration. The SAXS and TEM results confirm the formation of stabilized and well-ordered hexagonal mesophase by self-assembly of F127 and lithium salts, especially at a [O]/[Li] ratio of 16. The present self-organized nanocomposite network provides a novel architecture for ionically conductive materials with a combination of several advantageous properties, for example, simple preparation from commercially available components, substantial suppression of polymer crystallization, reasonably high ionic conductivity with copolymers of relatively low molecular weight, excellent mechanical strength, and potential for nanostructurablility. The present work can be extended to other similar triblock copolymers which are capable of self-assembling on a silica network, to make electrolytes with high ionic conductivity for use in the field of lithium-battery technology.

Experimental Section

The organic–inorganic hybrid electrolyte based on F127 was synthesized by a sol–gel route. In a typical synthesis (3-glydicyloxypropyl)-trimethoxysilane (1.5 g; GLYMO, Fluka) and tetraethoxysilane (0.3 g; TEOS) were mixed and hydrolyzed with 0.01N HCl (30 mL) at room temperature for 5–6 h. A solution of F127 (5.0 g) in acetonitrile (30 mL) was mixed with $LiClO_4$ to give the desired [O]/[Li] ratio, and the mixture was stirred for 5–6 h. Then the two solutions were mixed and stirred at room temperature for 2 days. The resulting gels were dried at room temperature for 2 days and then heated at 95 °C under vacuum for 2–5 days to give a piece of transparent and crack-free material. Samples prepared with other ratios of GLYMO/TEOS tended to be structurally unstable after drying. They exhibited nonuniform shrinkage or had a constantly wet surface. The salt concentrations were expressed as the ratio of the total concentration of EO and PO ether oxygen atoms to the lithium-ion concentration (i.e., [O]/[Li] ratio).

Powder XRD and SAXS data were collected on BL17A Wiggler-A beamline ($\lambda = 0.1326$ nm) at National Synchrotron Radiation Research Center of Taiwan. TEM images were taken with a Hitachi H-7100 instrument operated at 75 keV. The samples were embedded in Spur resin and cured at 60 °C overnight. Ultrathin sections (ca. 60–90 nm) were cut from the embedded specimen with a diamond knife. DSC studies were performed in the range of −60 to 125 °C by using a Mettler Toledo DSC system at a heating rate of 5 °C min^{-1}. Alternating-current impedance measurements on the polymer electrolytes were performed with a CH Instrument Model 604A Electrochemical Analyzer over a frequency range of 10 Hz to 100 kHz with an amplitude of 10 mV. All solid-state NMR experiments were performed on a Bruker AVANCE-400 spectrometer, equipped with a

 © 2004 Wiley-VCH Verlag GmbH & Co. KGaA, Weinheim

Bruker double-tuned 7 mm probe. The Larmor frequencies for ^{7}Li, ^{13}C, and ^{29}Si nuclei were 155.45, 100.58, and 79.46 MHz, respectively. A repetition time of 5 s was used for ^{13}C CP/MAS NMR experiments. A pulse length of 2 μs (π/6 pulse) and a repetition time of 50 s were used to obtain ^{29}Si MAS NMR spectra. Both ^{13}C and ^{29}Si chemical shifts were referenced to external TMS at 0 ppm. To remove the heteronuclear ^{7}Li–^{1}H dipolar interactions from the ^{7}Li resonance, high-power proton decoupling (^{7}Li{^{1}H} NMR) was used. ^{7}Li chemical shifts were referenced to external 1M aqueous LiCl at 0 ppm.

Received: June 30, 2003
Revised: September 9, 2003 [Z52243]

Keywords: block copolymers · conducting materials · lithium · organic–inorganic hybrid composites

[1] C. A. Vincent, B. Scrosati, *Modern Batteries: An Introduction to Electrochemical Power Sources*, Butterworth-Heinemann, London, **1997**.
[2] F. M. Gary, *Solid Polymer Electrolytes: Fundamentals and Technological Applications*, VCH, New York, **1991**.
[3] P. Judeinstein, J. Titman, M. Stamm, H. Schmidt, *Chem. Mater.* **1994**, *6*, 127 – 134.
[4] N. C. Mello, T. J. Bonagamba, H. Panepucci, K. Dahmouche, P. Judeinstein, M. A. Aegerter, *Macromolecules* **2000**, *33*, 1280 – 1288.
[5] M. Popall, M. Andrei, J. Kappel, J. Kron, K. Olma, B. Olsowski, *Electrochim. Acta* **1998**, *10–11*, 1155 – 1161.
[6] L. M. Bronstein, C. Joo, R. Karlinsey, A. Ryder, J. W. Zwanziger, *Chem. Mater.* **2001**, *13*, 3678 – 3684.
[7] Ö. Dag, A. Verma, G. A. Ozin, C. T. Kresge, *J. Mater. Chem.* **1999**, *9*, 1475 – 1482.
[8] P. F. W. Simon, R. Ulrich, H. W. Spiess, U. Wiesner, *Chem. Mater.* **2001**, *13*, 3464 – 3486.
[9] D. Zhao, Q. Huo, J. Feng, B. F. Chmelka, G. D. Stucky, *J. Am. Chem. Soc.* **1998**, *120*, 6024 – 6036.
[10] a) B. Chu, B. Hsiao, *Chem. Rev.* **2001**, *101*, 1727 – 1761; b) C. Booth, D. Attwood, *Macromol. Rapid Commun.* **2000**, *21*, 501 – 527.
[11] a) G. B. Appetecchi, F. Crose, L. Persi, B. Scrosati, *Electrochim. Acta* **2000**, *45*, 1481 – 1490; b) F. Crose, G. B. Appetecchi, L. Persi, B. Scrosati, *Nature* **1998**, *394*, 456.
[12] N. A. Melosh, P. Lipic, F. S. Bates, F. Wudl, G. D. Stucky, G. H. Fredrickson, B. F. Chmelka, *Macromolecules* **1999**, *32*, 4332 – 4342.

 © 2004 Wiley-VCH Verlag GmbH & Co. KGaA, Weinheim

P Ligands

Diorganophosphanylphosphinidenes as Complexed Ligands: Synthesis via an Anionic Terminal Phosphide of Niobium**

*Joshua S. Figueroa and Christopher C. Cummins**

Compounds with multiple bonding between adjacent phosphorus atoms are of interest both as free molecules and as complexed ligands.[1] As one proceeds formally from triply bonded P_2, via intermediate states of reduction, all the way to two equivalents of PH_3, several interesting P–P bonded systems (and isomers thereof) may be considered. Phosphanylphosphinidene, PPH_2, a neutral isomer of HP=PH (diphosphene) is an intriguing parent species in this regard and its geometric and electronic structure have been the subject of several theoretical investigations.[2–5]

Organic derivatives of phosphanylphosphinidene have generated interest as complex ligands capable of η^2-binding to transition-metal centers.[2] A prototypical example is the structurally characterized complex $[(\eta^2\text{-}t\text{Bu}_2\text{PP})\text{Pt}(\text{PPh}_3)_2]$.[6] That organic phosphanylphosphinidenes, exemplified by $t\text{Bu}_2\text{PP}$, are novel π-electron ligands in a manner reminiscent of alkenes or alkynes is recognized and was the subject of a recent review article.[7] Fritz and co-workers have pioneered the synthesis of such derivatives by utilization of the "phosphanylphosphinidene transfer" reagent, $t\text{Bu}_2\text{PP}{=}\text{PX}(t\text{Bu}_2)$ (X = Me or Br),[6,7] which represented, until now, the only synthetic entry to complexes of phosphanylphosphinidenes.

Herein we report an alternative synthetic entry to complexed organic derivatives of phosphanylphosphinidene. Our method takes advantage of our ability to synthesize an unprecedented anionic, niobium, terminal phosphide complex, $Na^+[\text{PNb}(\text{N}[\text{Np}]\text{Ar})_3]^-$ (Np = neopentyl, Ar = 3,5-$\text{Me}_2\text{C}_6\text{H}_3$) that permits assembly[8] of R_2PP ligands directly within the metal's protective coordination sphere. Furthermore, the complexes $[(\eta^2\text{-}\text{R}_2\text{PP})\text{Nb}(\text{N}[\text{Np}]\text{Ar})_3]$, are the first examples of η^2-phosphanylphosphinidene complexation by an early-transition-metal fragment.

Our recent discovery that the niobaziridine-hydride complex $[\text{Nb}(\text{H})(\eta^2\text{-}t\text{Bu}(\text{H})\text{C}{=}\text{NAr})(\text{N}[\text{Np}]\text{Ar})_2]$ reacts with white phosphorus (P_4) to afford the dinuclear, bridging diphosphide complex $[(\mu_2{:}\eta^2,\eta^2\text{-}\text{P}_2)\{\text{Nb}(\text{N}[\text{Np}]\text{Ar})_3\}_2]$ (**1**)[9] presented us with a unique entry into low-coordinate

[*] J. S. Figueroa, Prof. Dr. C. C. Cummins
Department of Chemistry, Room 2-227
Massachusetts Institute of Technology
77 Massachusetts Ave., Cambridge, MA 02139-4307 (USA)
Fax: (+1) 617-258-5700
E-mail: ccummins@mit.edu

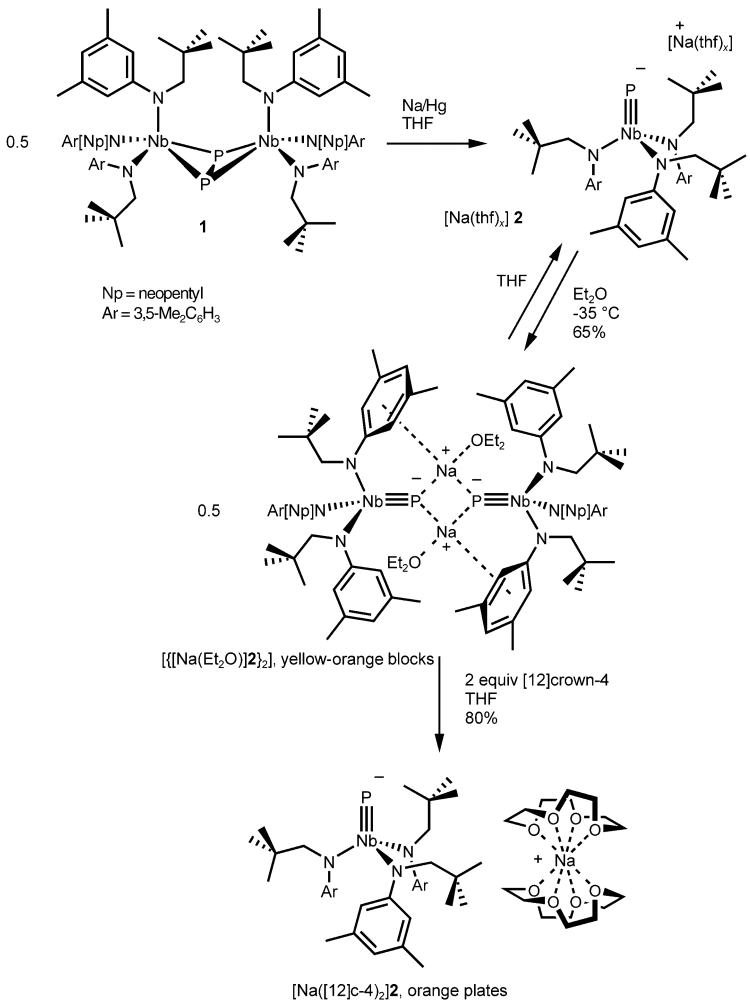
[**] We gratefully acknowledge the U.S. National Science Foundation (CHE-9988806) for financial support. Diorganophosphanylphosphinidenes (1,1-R_2PP; R = *t*Bu, Ph).

Supporting information for this article (experimental details, spectroscopic data, computational details) is available on the WWW under http://www.angewandte.org or from the author.

 © 2004 Wiley-VCH Verlag GmbH & Co. KGaA, Weinheim DOI: 10.1002/anie.200352779

phosphorus chemistry. It was recognized that the P_2 unit in complex **1** could be further reduced by two electrons to afford a species featuring a terminal, uninegative phosphorus atom bound to a single niobium center. Accordingly, treatment of a green THF solution of **1** with an excess of 1.0% sodium amalgam gradually produced a dark orange mixture over 2.5 h. Analysis of the crude reaction mixture by $^{31}P\{^1H\}$ NMR spectroscopy indicated the presence of a new signal centered near $\delta =$ 1010 ppm, characteristic of early-transition-metal phosphido species containing one-coordinate phosphorus.[10]. Solvent removal followed by diethyl ether extraction and crystallization produced the hydrocarbon-soluble, sodium etherate dimer $[\{[Na(Et_2O)]\mathbf{2}\}_2]$ (Scheme 1), as yellow orange blocks in 65% yield.[11]

The $^{31}P\{^1H\}$ NMR spectrum of pure $[\{[Na(Et_2O)]\mathbf{2}\}_2]$ in C_6D_6 solution gives rise to a single signal located at $\delta = 949.2$ ppm ($\nu_{1/2} =$ 495 Hz), which shifts to 1019.8 ppm ($\nu_{1/2} = 166$ Hz) when the spectrum is obtained in THF solution. Whereas the broad nature of the signals is caused by relaxation effects owing to the quadrupolar niobium nucleus,[12] the chemical shift difference presumably arises from formation of a monomeric $[Na(thf)_x]\mathbf{2}$ species in THF solution. Such downfield movement in ^{31}P chemical shift in polar solvents may be attributed to diminished Na–P contact ion pairing, with concomitant strengthening of $P_{(p\pi)} \rightarrow Nb_{(d\pi)}$ bonding interactions as the electropositive niobium center compensates for the buildup of negative charge.[13] Complete sequestration of the sodium counterion from the phosphorus nuclei can be achieved by treatment of a THF solution of $[\{[Na(Et_2O)]\mathbf{2}\}_2]$ (i.e. $[Na(thf)_x]\mathbf{2}$) with 2.0 equivalents of the crown ether [12]crown-4 ([12]c-4). The resulting hydrocarbon insoluble salt, $[Na([12]c\text{-}4)_2]\mathbf{2}$, gives rise to a single ^{31}P NMR signal at 1110.2 ppm ($\nu_{1/2} = 170$ Hz, $[D_8]$THF), further emphasizing the downfield progression of chemical shift as the $[PNb(N[Np]Ar)_3]^-$ unit becomes discrete and separated from its counterion.



Scheme 1.

Crystallization from a THF/*n*-pentane mixture produced red-orange plates of $[Na([12]c\text{-}4)_2]\mathbf{2}$ in 80% yield. The single-crystal X-ray structure of $[Na([12]c\text{-}4)_2]\mathbf{2}$ (Figure 1) clearly shows the anion–cation separation imposed by 2.0 equivalents of [12]c-4 and confirms the terminal nature of the phosphido substituent. The Nb–P bond length of 2.186(2) Å in $[Na([12]c\text{-}4)_2]\mathbf{2}$ is short when compared to the related four-coordinate, tantalum phosphinidene complex, [PhP=Ta(OSi-tBu$_3$)$_3$] (Ta–P 2.317(4) Å), which can be viewed as containing a short Ta–P double bond.[14] However, the Nb–P bond length in $[Na([12]c\text{-}4)_2]\mathbf{2}$ agrees well with the Mo–P triple bonds in [P≡Mo(N[tBu]Ar)$_3$] (2.119(4) Å)[15] and [P≡Mo(N[iPr]Ar)$_3$] (2.116(3) Å),[16] when the 0.07 Å difference in covalent radii between Nb and Mo is considered.[17] Thus, we suggest $[Na([12]c\text{-}4)_2]\mathbf{2}$ is accurately described as containing a Nb–P triple bond, the notion of which has also been substantiated by DFT calculations on the model complex $[PNb(NH_2)_3]^-$.[18]

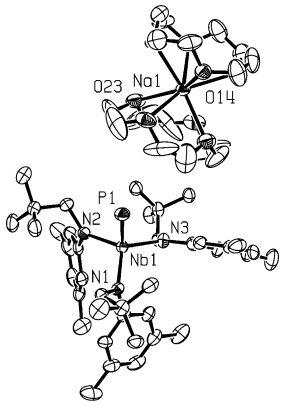


Figure 1. ORTEP diagram of $[Na([12]c\text{-}4)_2]\mathbf{2}$ (ellipsoids set at 35% probability). Selected bond lengths [Å] and angles [°]: Nb1-P1 2.186(2), Nb-N 2.073 av; P-Nb-N 103.43 av.

It is also noteworthy that $[Na([12]c\text{-}4)_2]\mathbf{2}$ is the first definitive example of a terminal phosphide complex of a transition metal outside of group 6.[19]

The terminal phosphorus atom in $[Na(thf)_x]\mathbf{2}$ has proven to be nucleophilic and readily provides terminal phosphini-

 © 2004 Wiley-VCH Verlag GmbH & Co. KGaA, Weinheim

denes upon treatment with electrophiles. For example, treatment of thawing THF solutions of $[Na(thf)_x]$**2** with 0.95 equivalents[20] of trimethylsilyl or trimethylstannyl chloride produced the trimethysilyl, $[Me_3SiP{=}Nb(N[Np]Ar)_3]$ (**3**), and trimethylstannyl, $[Me_3SnP{=}Nb(N[Np]Ar)_3]$ (**4**), phosphinidene complexes in 75% and 85% yield, respectively (see Scheme 2). The $^{31}P\{^1H\}$ NMR spectral resonances for **3** ($\delta =$ 528.6 ppm) and **4** ($\delta = 607.0$ ppm) indicate bent[14,21] phosphinidene moieties typical for four-coordinate early-transition-metal phosphinidene complexes supported by hard, π-donating, ancillary ligands.[22] A solid-state structural determination of **4**[23] confirmed this spectroscopic assignment and revealed an elongated Nb–P bond (2.2731(8) Å) relative to that in $[Na([12]c\text{-}4)_2]$**2**, consistent with formulation of this product as a doubly bonded Nb=P phosphinidene. Furthermore, the P–Sn bond length of 2.4778(8) Å matches the sum of covalent radii for these atoms,[17] attesting to a single bond between tin and phosphorus in **4**.[24]

Our attention then turned to the construction of η^2-bound phosphanylphosphinidenes, species known to contain multiple bonding between adjacent phosphorus atoms.[7] Accordingly, treatment of a thawing THF solution of $[Na(thf)_x]$**2** with 0.95 equivalents[20] of di-*tert*-butylchlorophosphane (tBu$_2$PCl) readily provided the orange phosphanylphosphinidene complex, $[(\eta^2\text{-}t\text{Bu}_2\text{PP})\text{Nb}(\text{N[Np]Ar})_3]$ (**5**) in 65% yield (Scheme 2). Formation of phosphanylphosphinidene **5** from **2** and tBu$_2$PCl represents a synthetic method complementary to Fritz and co-workers' use of a transfer reagent[6,7] in which the P–P bond is already intact. However, our method is applicable to the synthesis of novel, Nb-complexed R_2PP derivatives. Thus, treatment of $[Na(thf)_x]$**2** with diphenylchlorophosphane (Ph_2PCl) afforded the red diphenylphosphanylphosphinidene complex, $[(\eta^2\text{-}Ph_2PP)\text{Nb}(\text{N[Np]Ar})_3]$ (**6**) in 60% isolated yield.

The solid-state structures of **5** and **6** (Figure 2 and Figure 3, respectively) show the η^2-interaction of the R_2PP unit with the niobium center. The Nb1–P1 bond for both **5** and **6** (2.4149(12) and 2.429(3) Å, respectively) are much longer than typically found in early-transition-metal phosphinidene complexes[22] and more closely approximate an Nb–P single bond. Contrastingly, the P1–P2 separations of 2.0888(15) and 2.073(4) Å in **5** and **6**, respectively are approximately 0.13 Å shorter than expected for a P–P single bond,[25] lending credence to the notion of multiple-bond character in R_2PP unit, itself complexed according to the standard Dewar–Chatt–Duncanson model. Resonance structures including those shown in Scheme 2 may

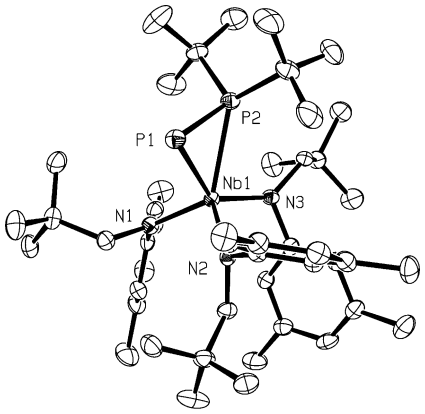


Figure 2. ORTEP diagram of **5** (ellipsoids set at 35% probability). Selected bond lengths [Å] and angles [°]: Nb1-P1 2.4149(12), Nb1-P2 2.6126(11), P1-P2 2.0888(15), Nb1-N 2.027 av; Nb1-P1-P2 70.49(4), P1-P2-Nb1 60.61(4), P1-Nb1-P2 48.90(4).

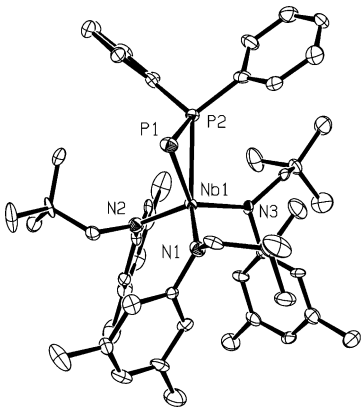
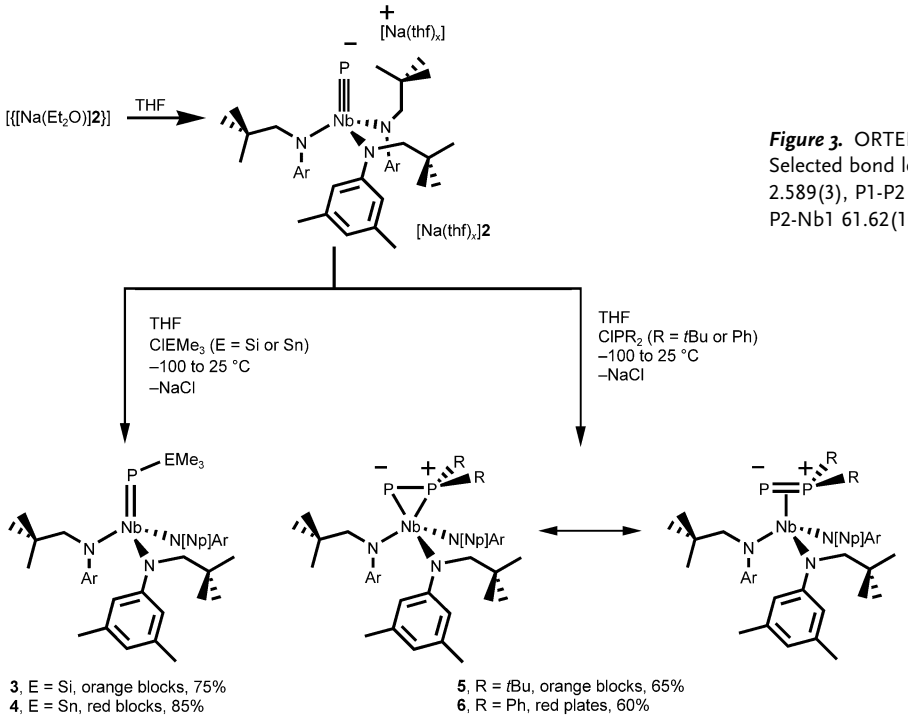


Figure 3. ORTEP diagram of **6** (ellipsoids set at 35% probability). Selected bond lengths [Å] and angles [°]: Nb1-P1 2.429(3), Nb1-P2 2.589(3), P1-P2 2.073(4), Nb1-N 2.016 av; Nb1-P1-P2 69.71(11), P1-P2-Nb1 61.62(10), P1-Nb1-P2 48.66(9).



Scheme 2.

 © 2004 Wiley-VCH Verlag GmbH & Co. KGaA, Weinheim

reasonably approximate the bonding attendant with R_2PP complexation in this system.[26]

The $^{31}P\{^1H\}$ NMR spectrum of **5** (C_6D_6) exhibits two sets of doublets located at $\delta = 405.5$ and 80.6 ppm for the phosphinidene (P_α) and phosphanyl (P_β) atoms, respectively, with a large $^1J_{PP}$ coupling constant of 425 Hz also reflective of multiple-bonding interactions[27] ($P_\alpha = 401.3$ ppm, $P_\beta = 19.0$ ppm, $^1J_{PP} = 439$ Hz for **6**). NMR calculations carried out on the hypothetical construct, $[(\eta^2\text{-}Me_2PP)Nb(NH_2)_3]$, support the assignment of a downfield shift for P_α relative to P_β in this system.[26] However, the highly downfield signals for P_α in **5** and **6** are in stark contrast to the mononuclear $[(\eta^2\text{-}t\text{Bu}_2PP)PtL_2]$ (L = phosphane) complexes of Fritz and coworkers,[6] in which P_α resonates upfield of P_β, which indicates a small contribution from P_α in the frontier-orbital region[28] for the latter and nicely highlighting a major spectroscopic differentiation between these early- and late-transition-metal systems.

In conclusion, nucleophilic, terminal, triply-bonded functional groups are of interest for building novel complexed moieties "from the ground up", as demonstrated previously for niobium nitride[8,29] and molybdenum carbide[13,30] anions. Now to this category we add the niobium phosphide anion, the versatility of which is demonstrated by the present synthesis of novel stannyl and phosphanyl phosphinidene complexes. Furthermore, incorporation of phosphorus atoms derived directly from the element into complexed ligands represents a potentially powerful method for the generation of synthetically useful phosphorus-containing molecules.

Experimental Section

General: Unless otherwise stated, all manipulations were preformed at room temperature in a glovebox (N_2) using dried and deoxygenated solvents and reagents. Full spectroscopic details for all new compounds can be found in the Electronic Supporting Information.

$[\{[Na(Et_2O)]\mathbf{2}\}_2]$: 1.0% sodium amalgam (Na: 0.115 g, 3.3 equiv/Nb) was added to a green THF solution of **1**[9] (1.00 g, 1.50 mmol, 10 mL). The mixture was stirred vigorously for 2.5 h, it gradually changed in color to dark orange. The supernatant solution was decanted from the amalgam, filtered through Celite, and evaporated to dryness. The resulting dark orange residue was then dissolved in Et_2O (5 mL), filtered through Celite again, and cooled at −35 °C for 3 days whereupon large yellow-orange crystals were obtained. Yield: 0.759 g, 65% in two crops.

$[Na([12]c\text{-}4)_2]\mathbf{2}$: A THF solution of [12]crown-4 (0.040 g, 0.231 mmol, 2 mL) was added to a solution of $[\{[Na(Et_2O)]\mathbf{2}\}_2]$ (0.100 g, 0.115 mmol) dissolved in THF (5 mL) over the course of 5 min. The reaction mixture was stirred for 30 min, after which it was concentrated to a volume of 2 mL and filtered through a small plug of Celite. *n*-Pentane (2 mL) was added and the resulting solution was stored at −35 °C overnight whereupon small red-orange crystals were obtained. Yield: 0.099 g, 80%.

3–**6**: Separately, a solution of $[\{[Na(Et_2O)]\mathbf{2}\}_2]$ (0.250 g, 0.316 mmol) dissolved THF (5 mL) and a THF solution (2 mL) containing 0.95 equiv of the corresponding electrophile ($ClSiMe_3$ for **3**, $ClSnMe_3$ for **4**, $ClPtBu_2$ for **5**, and $ClPPh_2$ for **6**) were frozen in a glove box cold well (liquid N_2). Upon removal from the cold well, approximately 0.6 mL of the thawing solution containing the electrophile was added dropwise over 1 min to the thawing solution of $[\{[Na(Et_2O)]\mathbf{2}\}_2]$, eliciting a color change from dark yellow to red-orange. The reaction mixture stirred for an additional 3 min whereupon both solutions were placed back into the cold well. This procedure was repeated two more times until complete addition of the electrophile was achieved. The reaction mixture was then allowed to warm to room temperature and stirred for an additional 30 min before being evaporated to dryness in vacuo. The residue was extracted with *n*-pentane (3 mL), filtered through Celite, and the filtrate evaporated to dryness again in vacuo. Crystallizations were effected by storing Et_2O (**3**, **4**, **6**) or *n*-pentane (**5**) solutions at −35 °C for 1–2 days. Color, yield: **3**: Orange, 75%; **4**: Red, 85%; **5**: Orange, 65%; **6**: Red, 60%.

Crystallographic Data: Crystal data can be found in the Supporting Information. CCDC-218230 ($[\{[Na(Et_2O)]\mathbf{2}\}_2]$), CCDC-218231 ($[Na([12]c\text{-}4)_2]\mathbf{2}\cdot(THF)$), CCDC-218229 (**4**), CCDC-218232 (**5**), CCDC-218228 (**6**) contain the supplementary crystallographic data for this paper. These data can be obtained free of charge via www.ccdc.cam.ac.uk/conts/retrieving.html (or from the Cambridge Crystallographic Data Centre, 12, Union Road, Cambridge CB21EZ, UK; fax: (+44) 1223-336-033; or deposit@ccdc.cam.ac.uk).

Received: September 3, 2003 [Z52779]

Keywords: anions · multiple bonds · niobium · P ligands · phosphorus

[1] *Multiple bonds and low coordination in Phosphorus chemistry* (Eds.: M. Regitz, O. J. Scherer), Thieme, New York, **1990**.
[2] G. Trinquier, G. Bertrand, *Inorg. Chem.* **1985**, *24*, 3842–3856.
[3] S. Jin, B. T. Colegrove, H. F. Schaefer III, *Inorg. Chem.* **1991**, *30*, 2969–2977.
[4] S. Creve, K. Pierloot, M. T. Nguyen, L. G. Vanquickborne, *Eur. J. Inorg. Chem.* **1999**, 107–115.
[5] S. Grigoleit, A. Alijah, A. B. Rozhenko, R. Streubel, W. W. Schoeller, *J. Organomet. Chem.* **2002**, *643–644*, 223–230.
[6] H. Krautscheid, E. Matern, I. Kovacs, G. Fritz, J. Pikies, *Z. Anorg. Allg. Chem.* **1997**, *623*, 1917; E. Matern, J. Pikies, G. Fritz, *Z. Anorg. Allg. Chem.* **2000**, *626*, 2136–2142.
[7] J. Olkowska-Oetzel, J. Pikies, *Appl. Organomet. Chem.* **2003**, *17*, 28–35.
[8] J. K. Brask, M. G. Fickes, P. Sangtrirutnugul, V. Dura-Villa, A. L. Odom, C. C. Cummins, *Chem. Commun.* **2001**, 1676–1677.
[9] J. S. Figueroa, C. C. Cummins, *J. Am. Chem. Soc.* **2003**, *125*, 4020–4021.
[10] G. Wu, D. Rovnyak, M. J. A. Johnson, N. C. Zanetti, D. G. Musaev, K. Morokuma, R. R. Schrock, R. G. Griffin, C. C. Cummins, *J. Am. Chem. Soc.* **1996**, *118*, 10654–10655.
[11] Full structural details for $[\{[Na(Et_2O)]\mathbf{2}\}_2]$ can be found in CCDC-218230, see Experimental Section.
[12] *NMR and the Periodic Table* (Eds.: R. K. Harris, B. E. Mann), Academic Press, London, **1978**.
[13] J. B. Greco, J. C. Peters, T. A. Baker, W. M. Davis, C. C. Cummins, G. Wu, *J. Am. Chem. Soc.* **2001**, *123*, 5003.
[14] J. B. Bonanno, P. T. Wolczanski, E. B. Lobkovsky, *J. Am. Chem. Soc.* **1994**, *116*, 11159–11160.
[15] C. E. Lalplaza, W. M. Davis, C. C. Cummins, *Angew. Chem.* **1995**, *107*, 2181–2183; *Angew. Chem. Int. Ed. Engl.* **1995**, *34*, 2042–2044.
[16] J. P. F. Cherry, F. H. Stephens, M. J. A. Johnson, P. L. Diaconescu, C. C. Cummins, *Inorg. Chem.* **2001**, *40*, 6820–6862.
[17] L. Pauling, *The Nature of the Chemical Bond*, 3rd ed., Cornell University Press, Cornell, **1960**, chap. 11, p. 405.
[18] Input and results for this calculation can be found in the Supporting Information, ADF Program Package (release 2000.02).
[19] J. S. Freundlich, R. R. Schrock, W. M. Davis, *J. Am. Chem. Soc.* **1996**, *118*, 3643–3655.

 © 2004 Wiley-VCH Verlag GmbH & Co. KGaA, Weinheim

[20] Sub-stoichiometric quantities of halo-electrophiles, cold temperatures, and slow addition rates are necessary to prevent over halogenation of the $\{PNbL_3\}^-$ fragment.
[21] A. H. Cowley, B. Pellerin, J. L. Atwood, G. S. Bott, *J. Am. Chem. Soc.* **1990**, *112*, 6734 – 6735.
[22] A. H. Cowley, *Acc. Chem. Res.* **1997**, *30*, 445 – 451.
[23] Full structural details for complex **4** can be found in CCDC-218229, see Experimental Section.
[24] $^1J_{(Sn,P)}$ coupling is not fully resolved in the $^{31}P\{^1H\}$ NMR spectrum of **4**, but rather observed as shoulders to the main peak.
[25] The experimentally determined P–P interatomic distance in $P_4(g)$ is 2.21 Å, N. N. Greenwood, A. Earnshaw, *Chemistry of the Elements*, 2nd ed., Butterworth–Heinemann, Oxford, **1997**, chap. 12, p. 479.
[26] Two of many possible resonance structures are presented here. Detailed DFT calculations to elucidate the bonding in this system are currently in progress and will be presented in due course.
[27] S. Shah, J. D. Protasiewicz, *Coord. Chem. Rev.* **2000**, *210*, 181 – 201.
[28] See for example: G. Schreckenbach, T. Ziegler, *J. Phys. Chem.* **1995**, *99*, 606 – 611.
[29] M. G. Fickes, A. L. Odom, C. C. Cummins, *Chem. Commun.* **1997**, 1993 – 1994.
[30] T. Agapie, P. L. Diaconescu, C. C. Cummins, *J. Am. Chem. Soc.* **2002**, *124*, 2412 – 2413.

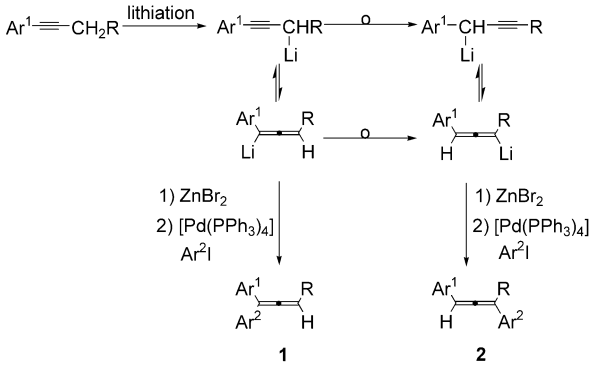
 © 2004 Wiley-VCH Verlag GmbH & Co. KGaA, Weinheim

Li Reactions in Organic Synthesis

A 1,3-Lithium Shift of Propargylic/Allenylic Lithium and the Subsequent Transmetalation Coupling Reaction with Aryl Halides**

Shengming Ma and Qiwen He*

Selective synthesis has been a formidable challenge in organic synthesis, especially controlled highly selective synthesis beginning from the same starting materials.[1] Herein, we report a novel clean 1,3-lithium shift reaction of propargylic/allenylic lithium (Scheme 1). Based on this observation, the corresponding sequential transmetalation and Pd-catalyzed coupling with aryl halides leading to 1,1-diarylallenes (**1**) or 1,3-diarylallenes (**2**) highly selectively from the same 1-aryl-1-alkynes has been developed (Scheme 1).

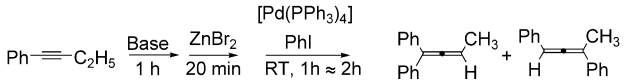


Scheme 1. Protocol for the selective synthesis of 1,1-diarylallenes or 1,3-diarylallenes by monolithiation of 1-aryl-1-alkynes, transmetalation, and Pd-catalyzed coupling with aryl halides.

Recently, we developed a monolithiation reaction of 1-aryl-1-alkynes with or without the mediation of $HgCl_2$.[2,3] The propargylic/allenylic lithium formed in this reaction undergoes sequential transmetalation and Pd-catalyzed coupling with organic halides leading to alkynes or allenes depending on the structures of the starting materials.[4] Quite recently, however, we observed that the sequential monolithiation of 1-aryl-1-alkynes beyond 1-aryl-1-propyne, (1-phenyl-1-butyne), the transmetalation, Pd-catalyzed coupling reaction with aryl halides when conducted by different chemists, or even the same chemist at different times, surprisingly gave two products. These products were identified as allenes **1a** and **2a** and formed in very different ratios ranging from 0:100 to 100:0; in other words, in terms of the ratio of **1a** to **2a**, the results were difficult to reproduce (entries 1 and 2, Table 1).

Further investigations showed that with different lithiation reagents, the ratios of **1a** and **2a** are also different, some of the representative results are summarized in Table 1 with the following noteworthy points: (1) No lithiation was observed with *n*BuLi or *t*BuLi at −78 °C (entry 7, Table 1);

Table 1: The effect of base on the lithiation of 1-aryl-1-butyne, transmetalation, and the Pd-catalyzed coupling with phenyl iodide.



1a **2a**

Entry	*T*[a]	Yield[b] (**1a**/**2a**) *n*BuLi	*t*BuLi	LDA
1	8 °C	100:0–0:100	100:0–0:100	84%[c] (0:100)
2	−10 °C	100:0–0:100	54% (89:11)	–
3	−20 °C	70% (100:0)	28% (93:7)	98% (0:100)
4	−40 °C	54% (100:0)	54% (100:0)	96% (19:81)
5	−55 °C	–	–	94% (45:55)
6	−65 °C	–	–	88% (77:23)
7	−78 °C	no lithiation	no lithiation	50% (91:9)

[a] Lithiation temperature. [b] NMR yield determined with CH_2Br_2 as the internal standard. [c] Yield of the isolated product.

[*] Prof. S. Ma, Ms. Q. He
State Key Laboratory of Organometallic Chemistry
Shanghai Institute of Organic Chemistry
Chinese Academy of Sciences
354 Fenglin Lu, Shanghai 200032 (P. R. China)
Fax: (+86) 21-6416-7510
E-mail: masm@mail.sioc.ac.cn

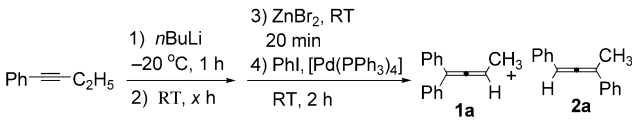
[**] Financial supports from the Major State Basic Research Development Program (Grant No. G2000077500), National Natural Science Foundation of China, and Shanghai Municipal Committee of Science and Technology are greatly appreciated. Shengming Ma is the recipient of 1999 Qiu Shi Award for Young Scientific Workers issued by Hong Kong Qiu Shi Foundation of Science and Technology (1999–2003).

Supporting information for this article is available on the WWW under http://www.angewandte.org or from the author.

 © 2004 Wiley-VCH Verlag GmbH & Co. KGaA, Weinheim DOI: 10.1002/anie.200352924

(2) Lithiation with LDA at −78 °C followed by transmetalation and coupling afforded **1a** and **2a** in 50% yield with a ratio of 91:9 (entry 7, Table 1). Lithiation with LDA at a higher temperature favors the formation of **2a**; (3) lithiation with *n*BuLi or *t*BuLi at −20 °C or −40 °C led to the highly selective or exclusive formation of the nonisomerized product **1a** (entries 3 and 4, Table 1). These facts indicate that the temperature and amine may be the factors that control the isomerization of 1-aryl-1-alkyn-3-yl or 1-aryl-1,2-alkadien-1-yl lithium to 1-aryl-2-alkyn-1-yl or 1-aryl-1,2-alkadien-3-yl lithium, respectively (Scheme 1).

In fact, it was observed that when the lithiation of 1-phenyl-1-butyne was conducted at −20 °C for 1 h then at room temperature for 2 h, instead of 1,1-diphenyl-1,2-butadiene (**1a**), the sequential reaction afforded 1,3-diphenyl-1,2-butadiene (**2a**) in 74% yield (Scheme 2). With a longer

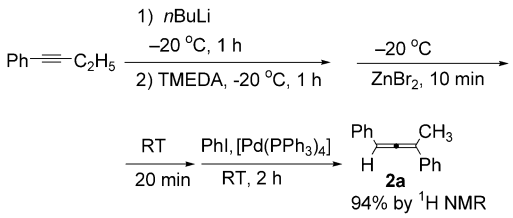


x (h)	yield by ^{1}H-NMR (%) (**1a**/**2a**)
1	90 (29:71)
2	74 (<1:99)
5	10 (0:100)
> 11	unidentified mixture

Scheme 2. Different lithiation conditions gave different ratios of **1a**/**2a**.

reaction time for the lithiation at room temperature, the yields of **1a** and **2a** decreased dramatically. When the lithiation was performed at −20 °C for 1 h followed by the addition of *N*,*N*,*N*′,*N*′-tetramethyl ethylene diamine (TMEDA) at −20 °C, the same sequential reaction also afforded the isomerized product 1,3-diphenyl-1,2-butadiene (**2a**) in 94% yield, thus indicating an interesting effect of amine on the 1,3-lithium shift (Scheme 3).

Through trial and error, we were happy to identify two suitable sets of reaction conditions: A) lithiation at −20 °C with *n*BuLi for 1 h followed by transmetalation ($ZnBr_2$ was added at −20 °C followed by stirring at room temperature) and coupling at room temperature for the selective formation of 1,1-diarylallenes; B) lithiation at room temperature with LDA for 1 h followed by transmetalation and coupling at room temperature for the selective formation of 1,3-diarylallenes. Under conditions A and B, the results can be easily reproduced. Some typical results are presented in Table 2, which indicates that: 1) the reaction is general for differently substituted 1-aryl-1-alkynes/aryl halides; 2) the regioselectivity for the formation of 1,1-diarylallenes and 1,3-diarylallenes is excellent.



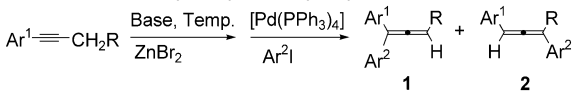
Scheme 3. The effect of TMEDA on the 1,3-lithium shift.

In conclusion, we have observed a clean and complete 1,3-lithium shift reaction of 1-aryl-1-alkyn-3-yl or 1-aryl-1,2-alkadien-1-yl lithium leading to 1-aryl-1,2-alkadien-3-yl or 1-aryl-2-alkyn-1-yl lithium, respectively. Although this kind of 1,3-metal shift has been observed,[5–7] the present protocol provides a clear-cut control of the lithiation as well as the isomerization. Under conditions A and B, 1,1-diarylallenes and 1,3-diarylallenes, respectively, can be prepared starting from the same alkynes. Although the mechanism of 1,3-lithium shift is not clear, this work may open up a new area for the study and control of 1,3-metal shifts in propargyl/allenylic species. Further investigations in this area are continuing in our laboratory.

Experimental Section

Typical procedure (conditions A): *n*BuLi (0.45 mL, 1.6 M in hexanes, 0.72 mmol) was added to a solution of 1-phenyl-1-butyne (78 mg, 0.6 mmol) in THF (3 mL) in a dry Schlenk tube at −20 °C under N_2. The reaction mixture was stirred at −20 °C for 1 h, then a solution of dry $ZnBr_2$ (275 mg, 1.2 mmol) in THF (4 mL) was added. After a further 10 min at this temperature the reaction mixture was warmed up to room temperature and kept there for 20 min. $[Pd(PPh_3)_4]$ (35 mg, 5 mol%) and iodobenzene (83 μL, 0.72 mmol) were subsequently added, and the resulting mixture was stirred at room

Table 2: Reaction under conditions A (*n*BuLi) and B (LDA)



Entry (**1**/**2**)	Ar^1	CH_2R	Ar^2I	Base	*T* [°C]	Yield [%][a]
1	Ph	C_2H_5	C_6H_5I	*n*BuLi	−20	55 (**1a**:**2a** = 100:0)
2	Ph	C_2H_5	C_6H_5I	LDA	8	84 (**1a**:**2a** = 0:100)
3	Ph	C_4H_9	C_6H_5I	*n*BuLi	−20	71 (**1b**:**2b** = 99:1)
4	Ph	C_4H_9	C_6H_5I	LDA	10	89 (**1b**:**2b** = 0:100)
5	Ph	C_4H_9	*p*-MeC_6H_4I	*n*BuLi	−20	79 (**1c**:**2c** = 99:1)
6	Ph	C_4H_9	*p*-MeC_6H_4I	LDA	20	99 (**1c**:**2c** = 0:100)
7	Ph	C_4H_9	α-$C_{10}H_8I$	*n*BuLi	−20	63 (**1d**:**2d** = 100:0)
8	Ph	C_4H_9	α-$C_{10}H_8I$	LDA	20	56 (**1d**:**2d** = 0:100)
9	Ph	C_4H_9	*p*-$MeOC_6H_4I$	*n*BuLi	−20	74 (**1e**:**2e** = 98:2)
10	Ph	C_4H_9	*p*-$MeOC_6H_4I$	LDA	30	83 (**1e**:**2e** = 0:100)
11	Ph	C_4H_9	*p*-$MeO_2CC_6H_4I$	*n*BuLi	−20	93 (**1f**:**2f** = 100:0)
12	Ph	C_4H_9	*p*-$MeO_2CC_6H_4I$	LDA	19	71 (**1f**:**2f** = 0:100)
13	Ph	C_3H_7	C_6H_5I	*n*BuLi	−20	76 (**1g**:**2g** = 100:0)
14	Ph	C_3H_7	C_6H_5I	LDA	11	96[b] (**1g**:**2g** = 0:100)
15	*p*-PhC_6H_4	C_3H_7	C_6H_5I	*n*BuLi	−20	77 (**1h**:**2h** = 100:0)
16	*p*-PhC_6H_4	C_3H_7	C_6H_5I	LDA	18	72 (**1h**:**2h** = 0:100)

[a] Yield of isolated products with the ratios determined by 300 MHz ^{1}H NMR analysis. [b] NMR yield determined with CH_2Br_2 as the internal standard.

 © 2004 Wiley-VCH Verlag GmbH & Co. KGaA, Weinheim

temperature. After the reaction was complete, as monitored by TLC (eluent: petroleum ether, 60–90 °C), it was quenched with saturated NH_4Cl and extracted with ether. The product solution was dried over $MgSO_4$, the solvent was removed by rotary evaporation, and the crude product was purified by flash chromatography on silica gel (petroleum ether) to afford **1a**[8] (68 mg, 55 %) as a liquid. ^{1}H NMR ($CDCl_3$, 300 MHz): $\delta = 7.43$–7.25 (m, 10 H), 5.72 (q, $J = 7.1$ Hz, 1 H), 1.89 ppm (d, $J = 7.1$ Hz, 3 H); ^{13}C NMR ($CDCl_3$, 75.4 MHz): $\delta =$ 206.32, 137.24, 128.42, 128.28, 126.98, 109.18, 88.85, 14.33 ppm; MS (70 eV): *m*/*z* (%): 206 (84.30) [M^+], 191 (100) [$M^+ - CH_3$]; IR (neat): $\tilde{\nu} = 1943\ cm^{-1}$; HRMS calcd for $C_{16}H_{14}$ [M^+]: 206.10955, found: 206.10914.

Typical procedure (conditions B)**:** LDA (0.4 mL, 2.0 M in THF/ethylbenzene/pentane, 0.8 mmol) was added to a solution of 1-phenyl-1-butyne (58 mg, 0.45 mmol) in THF (3 mL) in a dry Schlenk tube at room temperature under N_2. After the solution had been stirred for 1 h at room temperature, a solution of dry $ZnBr_2$ (499 mg, 2.22 mmol) in THF (4 mL) was added. After a further 25 min at this temperature, [$Pd(PPh_3)_4$] (22 mg, 5 mol %) and iodobenzene (42 μL, 0.38 mmol) were added. After the reaction was complete as monitored by TLC (eluent: petroleum ether, 60–90 °C), it was quenched with saturated NH_4Cl and extracted with ether. The resulting solution was dried over $MgSO_4$, the solvent was removed by rotary evaporation, and the crude product was purified by flash chromatography on silica gel (petroleum ether) to afford **1b**[9] (65 mg, 84 %) as a liquid. ^{1}H NMR ($CDCl_3$, 300 MHz): $\delta = 7.53$–7.47 (m, 2 H), 7.40–7.20 (m, 8 H), 6.50 (q, $J = 2.7$ Hz, 1 H), 2.25 ppm (d, $J = 2.7$ Hz, 3 H); ^{13}C NMR ($CDCl_3$, 75.4 MHz): $\delta = 206.77$, 136.23, 134.44, 128.67, 128.43, 127.01, 126.99, 126.85, 125.78, 104.48, 96.56, 16.75 ppm; MS (70 eV): *m*/*z* (%): 206 (79.98) [M^+], 191 (100) [$M^+ - CH_3$]; IR (neat): $\tilde{\nu} = 1936\ cm^{-1}$.

Received: September 22, 2003 [Z52924]

Keywords: allenes · cross-coupling · isomerization · lithiation · palladium

[1] For some of the most recent excellent results in this area, see: a) P. Wipf, C. Kendall, C. R. Stephenson, *J. Am. Chem. Soc.* **2003**, *125*, 4020; b) J. Barluenga, J. Alonso, F. J. Fananas, *J. Am. Chem. Soc.* **2003**, *125*, 2610; c) M. P. Doyle, M. Yan, W. Hu, L. S. Gronenberg, *J. Am. Chem. Soc.* **2003**, *125*, 4692; d) S. E. Denmark, W. Pan, *Org. Lett.* **2003**, *5*, 1119; e) Y. Zhang, A. J. Raines, R. A. Flowers II, *Org. Lett.* **2003**, *5*, 2363; For our own results, see: f) S. Ma, J. Zhang, *Angew. Chem.* **2003**, *115*, 194; *Angew. Chem. Int. Ed.* **2003**, *42*, 184; g) S. Ma, G. Wang, *Angew. Chem.* **2003**, *115*, 4347; *Angew. Chem. Int. Ed.* **2003**, *42*, 4215.

[2] a) S. Ma, L. Wang, *J. Org. Chem.* **1998**, *63*, 3497; b) S. Ma, L. Wang, *Chin. J. Chem.* **1999**, *17*, 531.

[3] a) R. L. P. De Jong, L. Brandsma, *J. Organomet. Chem.* **1982**, *238*, C17; b) R. L. P. De Jong, L. Brandsma, *J. Organomet. Chem.* **1986**, *312*, 277; c) J. Y. Becker, J. Klein, *J. Organomet. Chem.* **1978**, *157*, 1; d) J. Y. Becker, *J. Organomet. Chem.* **1976**, *118*, 247.

[4] a) S. Ma, A. Zhang, *J. Org. Chem.* **1998**, *63*, 9601; b) S. Ma, A. Zhang, Y. Yu, W. Xia, *J. Org. Chem.* **2000**, *65*, 2287; c) S. Ma, A. Zhang, *J. Org. Chem.* **2002**, *67*, 2287.

[5] For an incomplete 1,3-lithium shift in 2-alkynyl lithium, see: C. Huynh, G. Linstrumelle, *J. Chem. Soc. Chem. Commun.* **1983**, 1133.

[6] For a NMR observation, see: A. Maercker, J. Fischenich, *Tetrahedron* **1995**, *51*, 10209.

[7] For a 1,3-potassium shift in 1-alkoxy-2-alkynyl potassium, see: R. D. Verkruijsse, W. Verboom, P. E. Vanrijn, L. Brandsma, *J. Organomet. Chem.* **1982**, *232*, C1.

[8] M. Kazuhiro, I. Hiroshi, *J. Org. Chem.* **1989**, *54*, 2701.

[9] K. Ehud, B. Eric, *J. Org. Chem.* **1986**, *51*, 4013.

 © 2004 Wiley-VCH Verlag GmbH & Co. KGaA, Weinheim

Coordination Polymers

A Unique 3D Alternating Ferro- and Antiferromagnetic Manganese Azide System with Threefold Interpenetrating (10,3) Nets**

Cai-Ming Liu, Song Gao, De-Qing Zhang,* Yong-Hong Huang, Ren-Gen Xiong, Zhi-Liang Liu, Feng-Chi Jiang, and Dao-Ben Zhu**

Azide-containing coordination polymers have received considerable attention for the construction of new molecule-based magnets.[1–4] The versatility of the azido ligand lies not only in its diverse bridging modes but also in it being an efficient magnetic coupler. The azido ligand generally mediates antiferromagnetic interactions when it bridges in an end-to-end (EE) mode, and ferromagnetic interactions in an end-on (EO) mode.[2] The many coordination polymers with azido bridges which have been reported include one-dimensional (1D) chains,[3] two-dimensional (2D) layers,[4] and three-dimensional (3D) networks,[5] and antiferromagnetic, ferromagnetic, alternating, and canted systems have been observed. Because it is believed that increasing dimensionality can enhance bulk magnetic properties,[6] the design of high-dimensionality (especially 3D) transition-metal–azido coordination polymers is attractive, but it still remains a great challenge. One approach to high-dimensionality magnetic coordination polymers is the designed self-assembly of azido bridging ligands with bis(monodentate) or bis(bidentate) ligands by. Several bis(monodentate) ligands such as 4,4-bipyridine, pyrazine, and pyrazine dioxide and the bis(bidentate) ligand bipyrimidine have successfully been utilized to construct 3D azide-containing coordination polymers.[5]

To date most azide-containing magnetic coordination polymers were synthesized by methods of conventional

[*] Dr. C.-M. Liu, D.-Q. Zhang, Z.-L. Liu, Prof. D.-B. Zhu
Center for Molecular Science
Institute of Chemistry, Organic Solids Laboratory
Chinese Academy of Sciences, Beijing 100080 (P.R. China)
Fax: (+86) 106-255-9373
E-mail: cmliu@iccas.ac.cn

Prof. S. Gao
State Key Laboratory of Rare Earth Materials and Applications
College of Chemistry and Molecular Engineering
Peking University, Beijing 100871 (P.R. China)

Y.-H. Huang, Prof. F.-C. Jiang
Department of Chemistry
Jiangxi Normal University, Nanchang, 330027 (P.R. China)

Prof. R.-G. Xiong
State Key Laboratory of Coordination Chemistry
Institute of Coordination Chemistry
Nanjing University, Nanjing, 210093 (P.R. China)

[**] This work was supported by National Natural Science Foundation of China (No. 20201012, 90101025), the Major State Basic Research Development Program of P.R. China (G2000077500 and 2001CB610507), and Chinese Academy of Sciences.

Supporting information (structural and magnetic details) for this article is available on the WWW under http://www.angewandte.org or from the author.

 © 2004 Wiley-VCH Verlag GmbH & Co. KGaA, Weinheim DOI: 10.1002/anie.200352780

coordination chemistry, and there are still few reports on solvothermal synthesis of this type of complexes, although the solvothermal technique, which can not only overcome difficulties arising from differing solubilities of organic and inorganic precursors but can also produce metastable phases, has proved to be a powerful tool for crystallizing many novel transition-metal coordination polymers.[7] The only reported example of a metal coordination polymer with azido bridges prepared by solvothermal reaction is $[CdN_3(3\text{-ptz})]$ (3-ptz = 5-(3-pyridyl)tetrazolate),[7e] in which the metal centers are diamagnetic $3d^{10}$ cadmium ions. We are now exploring the solvothermal chemistry of azide-containing manganese coordination polymers and report herein the isolation of the novel 3D azide-containing magnetic complex $[(Mn\text{-}\mu_{1,3}\text{-}N_3\text{-}\mu_{1,1}\text{-}N_3)_2L]$ (**1**) by using the bis(bidentate) Schiff base ligand 4,5-diazafluoren-9-one azine (L) as the long link and the infinite $Mn\text{-}\mu_{1,3}\text{-}N_3\text{-}\mu_{1,1}\text{-}N_3$ chain as the secondary building unit (SBU). This complex exhibits an interesting forbidden catenation framework with triple interpenetrating 3D (10,3) nets.

The 3D coordination polymer **1** was synthesized solvothermally from a mixture of L, $Mn(ClO_4)_2\cdot 6H_2O$, NaN_3, H_2O, and methanol in a thick Pyrex glass tube. The brown block crystals obtained are insoluble in common solvents. The IR spectrum of **1** shows two sharp bands at 2099 and 2077 cm^{-1}, which suggest the presence of both EO and EE azide bridges.

The crystal structure of **1** shows a 3D network that is composed of the 4,5-diazafluoren-9-one azine links and chains of Mn^{II} ions alternately connected by two EO and two EE azido bridges (Figure 1).[8] Each manganese atom is octahedrally coordinated to one ligand L (Mn–N1, N2, 2.248(6), 2.376(5) Å), two *cis*-EO (Mn–N6, N6#1, 1.952(6), 2.473(8) Å;#1 $1-x$, y, $-z+1/2$), and two *cis*-EE [Mn–N3, N5#2, 2.522(7), 2.150(5) Å; #2 $-x+1/2$, $-y+1/2$, $-z$) azido ligands. The nearest two Mn^{II} centers are bonded to each other by two EO azide bridges to generate an asymmetrical planar entity formed by two neighboring manganese ions and two terminal nitrogen atoms from two EO azido ligands (plane 1, defined by Mn1-N6-Mn1A-N6A). These dinuclear entities are further connected to each other through double EE azide bridges to form a manganese–azido chain running along the [101] direction. The double EE azide bridges and the two manganese atoms to which they connected are almost in a plane. The plane formed by Mn1-N3-N4-N5-Mn1B-N3B-N4B-N5B (plane 2) and the plane defined by Mn1A-N3A-N4A-N5A-Mn1D-N3D-N4D-N5D (plane 3) have a dihedral angle of 2.3°. The dihedral angles between planes 1 and 2 and planes 1 and 3 are 88.8 and 91.2°, respectively, that is, the three planes are almost perpendicular to one another.

Unusually, the double EE azide bridges connect the dinuclear entities in a *cis* arrangement (Figure 1 a), and this unique structural feature is quite different from other

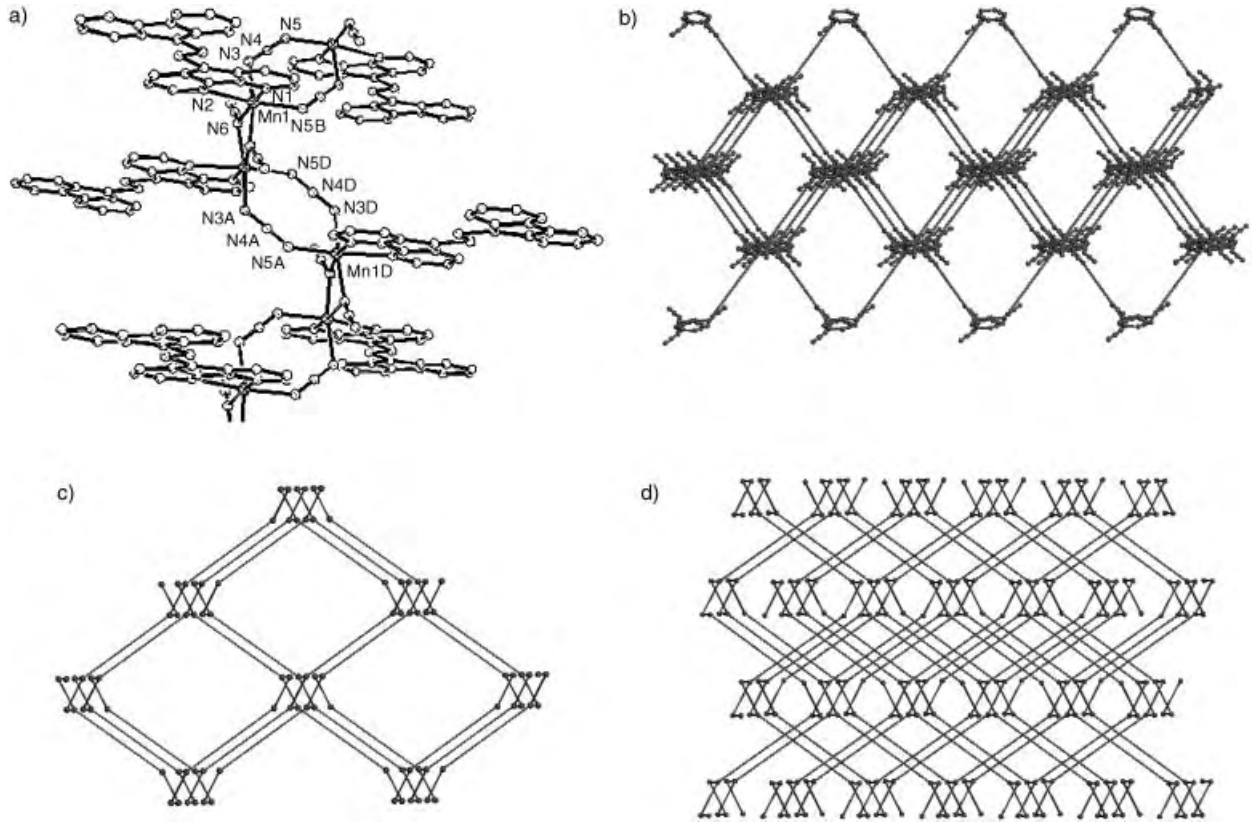


Figure 1. a) Infinite Mn–azido SBU linked by bis(bidentate) ligands L (4,5-diazafluoren-9-one azine). b) A 3D network in **1** along the [101] direction. For clarity, the long link represents the Schiff base ligand L. c) Projection of **1** along the [101] direction showing a 3D (10,3) network based on the topology of Mn–Mn connections. The short, medium, and long links represent the double EO azido, double EE azido, and bis(bidentate) Schiff base ligand L, respectively. d) Three parallel interpenetrating (10,3) nets in the structure of **1**.

 © 2004 Wiley-VCH Verlag GmbH & Co. KGaA, Weinheim

reported chains of metal atoms and alternating EO/EE azido ligands, in which only *trans* arrangements of double EE azide bridges are present.[3a,h,e,i,m,q,p] The intrachain Mn···Mn distance through the EO azide bridges is 2.790 Å, much smaller than typical for this type of bridging,[2–5] and that through the EE bridges of 5.794 Å is longer than typical values.[2–5] The Mn-N-Mn bond angle in the EO azide bridges is 77.2(3)°, which is smaller than normal values.[2–5] For the EE azide bridges, the Mn1-N3-N4 and Mn1-N5-N4#2 angles are 134.5(5) and 131.8(5)°, respectively. The Mn-azido-Mn torsion angle τ, defined by the dihedral angle between the mean planes of Mn1-N3-N4-N5 and Mn1B-N5-N4-N3, is 5.5°, and the dihedral angle δ between the $(EE\text{-}N_3)_2$ plane and the N3-Mn1-N5B plane is only 2.9°. Both τ and δ values are significantly smaller than those for previously reported Mn^{2+} chains with alternating EE and EO azido bridges (τ = 19–64°, δ = 10–35°).[3p,r,4]

The structure of **1** consists of three identical interpenetrating nets, one of which is shown in Figure 1 b. The infinite Mn^{II}/alternating EO-EE azido chains are stacked parallel to one another and connected by bis(bidentate) ligands L to generate a 3D framework. The ligands L between the EE azido bridges are mutually parallel, while those between the EO azido bridges form an angle of 106°. 1D rhombic channels would be formed if no interpenetration happened. The threefold interpenetration in **1** increases the calculated filled space to 77.7 %, and the unit cell therefore contains no area accessible to residual solvent. To better illustrate this structure, the topology of Mn–Mn connections is presented in Figure 1 c and Figure 1 d. It exhibits interpenetrating three-connected 3D (10,3) nets, which are reminiscent of nets of the (10,3)-a type.[9] A characteristic feature of the (10,3)-a nets is the presence of parallel fourfold helices, all of the same handedness, and the net as a whole is thus chiral.[9] However, the manganese/alternating EO-EE azido chains in **1** run in a quite different way, similar to a shoelace, running around and crossing two parallel axes in a figure-of-eight fashion. Consequently, such a chain will have no handedness, because it is counteracted automatically by the opposite handedness owing to the double axes. To our knowledge, this type of (10,3) nets had not been reported before.[9]

The variation of the molar magnetic susceptibility χ_M for **1** was investigated in the temperature range 2–300 K (Figure 2). The χ_M value increases on cooling, reaches a rounded maximum at about 60 K, and then tends to zero at low temperature. The $\chi_M T$ value at room temperature is 8.0 $cm^3 K mol^{-1}$, somewhat smaller than the value expected for two uncoupled spin-only Mn^{II} ions (8.76 $cm^3 K mol^{-1}$). The $\chi_M T$ value decreases continuously upon cooling. These features indicate a dominant antiferromagnetic interaction. According to the structure, this complex should have alternating ferro (F)- and antiferromagnetic (AF) interactions mediated by double EO and double EE azido bridges, respectively. To evaluate the superexchange coupling constants, we tried to simplify this 3D magnetic system by treating it with the theoretical model for alternating F/AF S = 5/2 chains proposed by Cortés et al.[3i] Equation (1). This

$$\chi = [N g^2 \beta^2 S(S+1)/(3kT)][(1+u_1+u_2+u_1u_2)/(1-u_1u_2)] \qquad (1)$$

expression is based on the spin Hamiltonian $\mathcal{H} = -J_1 \Sigma S_{2i} S_{2i+1} - J_1 \Sigma S_{2i} S_{2i+1}$, where J_1 and J_2 are the alternating exchange constants for the EE and EO superexchange pathways, respectively, and the S operators are treated as classical spins where $u_i = \coth[J_i S(S+1)/kT] - kT/[J_i S(S+1)]$ (i = 1, 2).

A Weiss constant θ was then introduced by replacing T with $T-\theta$ in Equation (1) because of the possible presence of interchain antiferromagnetic interactions,[3p] mediated by the bis(bidentate) ligand L. By varying all the parameters, the best agreement between theory and experiment was obtained with $J_1 = -8.09$ cm^{-1}, $J_2 = 3.82$ cm^{-1}, $\theta = -2.0$ K, $g = 2.094$, and $R = 5.80 \times 10^{-4}$, which confirms alternating AF and F interactions with domination by the former, and the small negative θ value suggests a weak AF interchain interaction mediated by the bis(bidentate) ligand L. The J_{AF} (J_1) value is smaller than, but the J_F (J_2) and the θ values are comparable to, the corresponding values ($J_{AF} = -11.8$–-15.4 cm^{-1}, J_F = 3.8–8.0 cm^{-1}, and $\theta = -1.1$–-2.6 K) for reported Mn^{2+} chains with alternating EE and EO azido bridges and Schiff base ligands.[3p]

Interestingly, weak ferromagnetism, probably arising from spin canting, was observed at temperatures below 2 K. The divergence of the zero-field cooled (ZFC) and the field cooled (FC) magnetization $M(T)$ below 2 K indicates irreversible long-range magnetic order. Alternating-current susceptibility measurements show that both $\chi'_{acac}(T)$ and $\chi''_{ac}(T)$ are frequency-independent, and this excludes any glassy behavior. The $\chi'_{ac}(T)$ curve exhibits a transition temperature at about 2 K, and a nonzero $\chi''_{ac}(T)$ component suggests hysteresis effects and an uncompensated moment. The small magnetization value at 1.8 K suggests the existence of a weakly spin canted moment. Isothermal magnetization experiments performed at 1.8 K showed hysteresis with a coercive field around 20 Oe and a remnant magnetization of 2.95 emu Oe mol^{-1} (Figure 3). The field dependence of the magnetization at 1.9 K shows a pronounced sigmoid shape corresponding to a spin-flop transition[5b,d,f] when the field is large enough (ca. 30 kOe), which happens if the Ising-like anisotropy is small with respect to the weakest antiferromagnetic interaction.[5b] This anisotropy interaction is probably produced by the strong intrachain interaction in the [101] direction through azido bridges in comparison with the weak

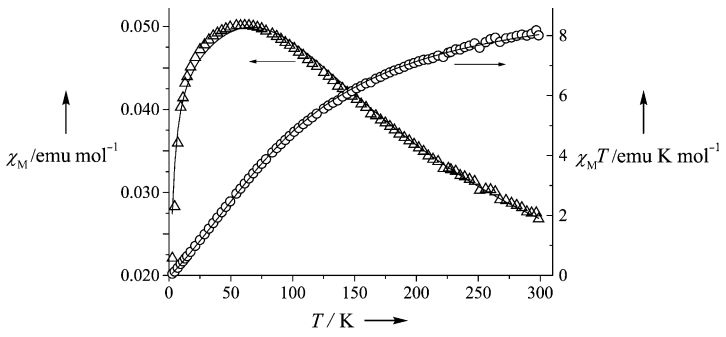


Figure 2. χ_M (△and $\chi_M T$ (●) versus T plots for **1**; the solid lines represent the best fit of the experimental data to Equation (1).

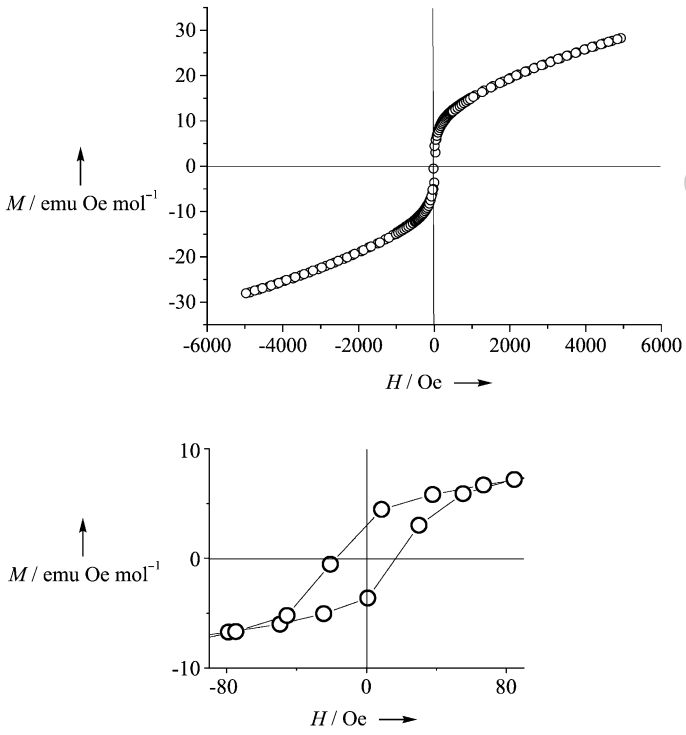


Figure 3. Top: hysteresis loop of **1** recorded at 1.8 K. Bottom: expansion of hysteresis region.

interchain interaction through 4,5-diazafluoren-9-one azine ligands. The magnetization is only 0.11 $N\beta$ at 70 kOe, far from the saturation value of 5 $N\beta$ expected for an $S = 5/2$ system, which is consistent with weak ferromagnetism owing to spin canting.[5f]

Recently, spin-canted ferromagnetism was found in a 1D Ni^{II} complex with single EE azido bridges[3l] and two 3D Mn^{II} complexes with double EE azido bridges.[5d,f] We have now found a 3D manganese coordination polymer with alternating EE azido and EO azido ligands that exhibits spin-canted long-range ferromagnetic ordering, which probably arises from a Dzyaloshinski–Moriya interaction.[11] Furthermore, this work also demonstrates that the solvothermal technique allows the crystallization of novel high-dimensionality azide-containing coordination polymers with magnetic properties.

Experimental Section

The ligand 4,5-diazafluoren-9-one azine was synthesized as described earlier.[10] A mixture of 4,5-diazafluoren-9-one azine (0.4 mmol), $Mn(ClO_4)_2{\cdot}6H_2O$ (0.4 mmol), NaN_3 (0.4 mmol), H_2O (0.2 mL), and methanol (1 mL) was placed in a thick Pyrex tube (ca. 15 cm long), the tube was frozen with liquid N_2, evacuated under vacuum and sealed with a torch. The tube was then heated at 110 °C under autogenous pressure for 2 days to give brown block crystals of **1** in 60 % yield. The elemental analysis of the bulk material was consistent with the formula proposed. IR (KBr pellet): $\tilde{\nu} = 2099$ (vs, $\nu_{as}(\mu_{1,1}\text{-}N_3^-)$), 2077 (vs, $\nu_{as}(\mu_{1,3}\text{-}N_3^-)$), 1330 (w, $\nu_s(\mu_{1,1}\text{-}N_3^-)$), 1631(w, ν_s(C=N)), 1577(m, ν_s(C=C)), 1476(w), 1404(m), 1280(w), 1165(w), 1091(w), 830(w), 753 cm^{-1} (m).

Caution: $Mn(ClO_4)_2{\cdot}6H_2O$ and NaN_3 are potentially explosive and should be handled with care.

Received: September 3, 2003
Revised: October 8, 2003 [Z52780]

Keywords: azides · interpenetrating nets · magnetic properties · manganese · solvothermal reactions

[1] a) O. Kahn, *Molecular Magnetism*, VCH, Weinheim, **1993**; b) D. Gatteschi, O. Kahn, J. S. Miller, F. Palacio, *Magnetic Molecular Materials*, NATO ASI, Kluwer, Dordrecht, **1991**.

[2] J. Ribas, A. Escuer, M. Monfort, R. Vicente, R. Cortés, L. Lezama, T. Rojo, *Coord. Chem. Rev.* **1999**, *193–195*, 1027.

[3] a) R. Cortés, L. Lezama, J. L. Pizarro, M. I. Arriortua, X. Solans, T. Rojo, *Angew. Chem.* **1994**, *106*, 2520; *Angew. Chem. Int. Ed. Engl.* **1994**, *33*, 2488; b) A. Escuer, R. Vicente, M. S. EI Fallah, J. Ribas, X. Solans, M. Font-Bardia, *J. Chem. Soc. Dalton Trans.* **1993**, 2975; c) A. Escuer, R. Vicente, M. S. El Fallah, J. Ribas, X. Solans, M. Font-Bardia, *Inorg. Chem.* **1993**, *32*, 3727; d) R. Cortés, M. K. Urtiaga, L. Lezama, J. L. Pizzarro, A. Goòi, M. I. Arriortua, T. Rojo, *Inorg. Chem.* **1994**, *33*, 4009; e) J. Ribas, M. Monfort, B. Kumar-Gosh, X. Solans, *Angew. Chem.* **1994**, *106*, 2177; *Angew. Chem. Int. Ed. Engl.* **1994**, *33*, 2087; f) J. Ribas, M. Monfort, C. Diaz, X. Solans, *Inorg. Chem.* **1994**, *33*, 484; g) J. Ribas, M. Monfort, B. Kumar-Gosh, X. Solans, M. Font-Bardia, *J. Chem. Soc. Chem. Commun.* **1995**, 2375; h) J. Ribas, M. Monfort, I. Resino, X. Solans, P. Rabu, F. Maingot, M. Drillon, *Angew. Chem.* **1996**, *108*, 2671; *Angew. Chem. Int. Ed. Engl.* **1996**, *35*, 2520; i) R. Cortés, M. Drillon, X. Solans, L. Lezama, T. Rojo, *Inorg. Chem.* **1997**, *36*, 677; j) G. Viau, M. G. Lombardi, G. De Munno, M. Julve, F. Lloret, J. Faus, A. Caneschi, J. M. Clemente-Juan, *Chem. Commun.* **1997**, 1195; k) K. R. Reddy, M. V. Rajasekharan, J.-P. Tuchagues, *Inorg. Chem.* **1998**, *37*, 5978; l) C. S. Hong, Y. Do, *Angew. Chem.* **1999**, *111*, 153; *Angew. Chem. Int. Ed.* **1999**, *38*, 193; m) H.-Y. Shen, W.-M. Bu, E.-Q. Gao, D.-Z. Liao, Z.-H. Jiang, S.-P. Yan, G.-L. Wang, *Inorg. Chem.* **2000**, *39*, 396; n) T. K. Maji, P. S. Mukherjee, G. Mostafa, T. Mallah, J. Cano-Boquera, N. R. Chaudhuri, *Chem. Commun.* **2001**, 1012; o) L. Li, D. Liao, Z. Jiang, S. Yan, *Inorg. Chem.* **2002**, *41*, 1019; p) E.-Q. Gao, S.-Q. Bai, Y.-F. Yue, Z.-M. Wang, C.-H. Yan, *Inorg. Chem.* **2003**, *42*, 3642; q) A. Escuer, R. Vicente, M. S. El Fallah, S. B. Kumar, F. A. Mautner, D. Gatteschi, *J. Chem. Soc. Dalton Trans.* **1998**, 3905; r) M. A. M. Abu-Youssef, M. Drillon, A. Escuer, M. A. S. Goher, F. A. Mautner, R. Vicente, *Inorg. Chem.* **2000**, *39*, 5022; s) T.-F. Liu, D. Fu, S. Gao, Y.-Z. Zhang, H.-L. Sun, G. Su, Y.-J. Liu, *J. Am. Chem. Soc.* **2003**, *125*, 13976.

[4] a) M. Monfort, J. Ribas, X. Solans, *J. Chem. Soc. Chem. Commun.* **1993**, 350; b) J. Ribas, M. Monfort, X. Solans, M. Drillon, *Inorg. Chem.* **1994**, *33*, 742; c) A. Escuer, R. Vicente, M. A. S. Goher, F. A. Mautner, *Inorg. Chem.* **1995**, *34*, 5707; d) M. Monfort, M. Resino, J. Ribas, H. Stoeckli-Evans, *Angew. Chem.* **2000**, *112*, 197; *Angew. Chem. Int. Ed.* **2000**, *39*, 191; e) Z. Shen, J. L. Zuo, S. Gao, Y. Song, C. M. Che, H. K. Fun, X.-Z. You, *Angew. Chem.* **2000**, *112*, 3779; *Angew. Chem. Int. Ed.* **2000**, *39*, 3633; f) E.-Q. Gao, S.-Q. Bai, Z.-M. Wang, C.-H. Yan, *J. Am. Chem. Soc.* **2003**, *125*, 4984. g) R. Cortés, L. Lezama, J. L. Pizarro, M. I. Arriortua, T. Rojo, *Angew. Chem.* **1996**, *108*, 1934; *Angew. Chem. Int. Ed. Engl.* **1996**, *35*, 1810.

[5] a) F. A. Mautner, R. Cortes, L. Lezama, T. Rojo, *Angew. Chem.* **1996**, *108*, 96; *Angew. Chem. Int. Ed. Engl.* **1996**, *35*, 78; b) B. Q. Ma, H. L. Sun, S. Gao, G. Su, *Chem. Mater.* **2001**, *13*, 1946; c) C.-M. Liu, Z. Yu, R.-G. Xiong, K. Liu, X.-Z. You, *Inorg. Chem. Commun.* **1999**, *2*, 31; d) S. Han, J. L. Manson, J. Kim, J. S. Miller, *Inorg. Chem.* **2000**, *39*, 4182; e) A. Fu, X. Huang, J. Li, T. Yuen,

 © 2004 Wiley-VCH Verlag GmbH & Co. KGaA, Weinheim

C. L. Lin, *Chem. Eur. J.* **2002**, *8*, 2239; f) E.-Q. Gao, Z.-M. Wang, C.-H. Yan, *Chem. Commun.* **2003**, 1748; h) G. De Munno, M. Julve, G. Viau, F. Lloret, J. Faus, D. Viterbo, *Angew. Chem.* **1996**, *108*, 1931; *Angew. Chem. Int. Ed. Engl.* **1996**, *35*, 1807.

[6] Z.-N. Chen, J. Qiu, Z.-K. Wu, D.-G. Fu, K.-B. Yu, W.-X. Tang, *J. Chem. Soc. Dalton Trans* **1994**, 1923.

[7] For examples: a) H. K. Chae, J. Kim, O. D. Friedrichs, M. O'Keeffe, O. Yaghi, *Angew. Chem.* **2003**, *115*, 4037; *Angew. Chem. Int. Ed.* **2003**, *42*, 3907; b) W. Lin, O. R. Evans, R.-G. Xiong, Z. Wang, *J. Am. Chem. Soc.* **1998**, *120*, 13272; c) O. R. Evans, R.-G. Xiong, Z. Wang, G. K. Wong, W. Lin, *Angew. Chem.* **1999**, *111*, 557; *Angew. Chem. Int. Ed.* **1999**, *38*, 536; d) R.-G. Xiong, X.-Z. You, B. F. Abrahams, Z. Xue, C.-M. Che, *Angew. Chem.* **2001**, *113*, 4554; *Angew. Chem. Int. Ed.* **2001**, *40*, 4422; e) X. Xue, X.-S. Wang, R.-G. Xiong, X.-Z. You, B. F. Abrahams, Z. Xue, C.-M. Che, H.-X. Ju, *Angew. Chem.* **2002**, *114*, 3068; *Angew. Chem. Int. Ed.* **2002**, *41*, 2944; f) R.-G. Xiong, X. Xue, H. Zhao, X.-Z. You, B. F. Abrahams, Z. Xue, *Angew. Chem.* **2002**, *114*, 3954; *Angew. Chem. Int. Ed.* **2002**, *41*, 3800; g) C.-M. Liu, D.-Q. Zhang, J.-L. Luo, N.-L. Wang, H.-M. Hu, D.-B. Zhu, *Eur. J. Inorg. Chem.* **2003**, 3618.

[8] Crystal data ($C_{22}H_{12}Mn_2N_{18}$): monoclinic, space group $C2/c$; $a = 9.2645(19)$, $b = 23.269(5)$, $c = 11.678(2)$ Å, $\beta = 103.04(3)°$, $V = 2452.5(9)$ Å^3, $Z = 4$, $\rho_{calc} = 1.729$ g cm^{-3}, $\mu = 1.085$ mm^{-1}, $R_1 = 0.0700$, $wR_2 = 0.1415$; Rigaku RAXIS RAPID IP imaging plate system with $Mo_{K\alpha}$ radiation ($\lambda = 0.71073$ Å), $T = 293(2)$ K; 3822 measured reflections ($5.00 \le 2\theta \le 71.54°$; $-15 \le h \le 15$, $-29 \le k \le 29$, $-11 \le l \le 11$), of which 2538 were unique ($R_{int} = 0.0955$) and 828 with $I > 2\sigma(I)$ were used in the refinement. The data were corrected for Lorentzian and polarization effects, and absorption corrections were applied. The structure was solved by direct methods and refined by a full-matrix least-squares technique based on F^2 using the SHELXL97 program. All non-hydrogen atoms were refined anisotropically. The end-on azido ligand was found to be disordered, and the refinement was carried out by considering two positions for each of the two uncoordinated nitrogen atoms with occupation factors fixed at 10.5. All hydrogen atoms were introduced at calculated positions as riding on a bonded atom. CCDC-218191 contains the supplementary crystallographic data for this paper. These data can be obtained free of charge via www.ccdc.cam.ac.uk/conts/retrieving.html (or from the Cambridge Crystallographic Data Centre, 12 Union Road, Cambridge CB21EZ, UK; fax: (+44) 1223-336-033; or deposit@ccdc.cam.ac.uk).

[9] a) S. R. Batten, R. Robson, *Angew. Chem.* **1998**, *110*, 1558; *Angew. Chem. Int. Ed.* **1998**, *37*, 1460; b) A. F. Wells, *Three-dimensional Nets and Polyhedra*, Wiley-Interscience, New York, **1977**; c) *Further Studies of Three-dimensional Nets*, ACA Monograph No. 8, American Crystallographic Association, **1979**.

[10] J. Mlochowski, Z. Szulc, *Pol. J. Chem.* **1983**, *57*, 33.

[11] a) J. Dzyaloshinski, *J. Phys. Chem. Solids* **1958**, *4*, 241; b) T. Moriya, *Phys. Rev.* **1960**, *120*, 91.

 © 2004 Wiley-VCH Verlag GmbH & Co. KGaA, Weinheim

Michael Addition

Chiral Molecular Recognition by Aluminum Tris(2,6-diphenylphenoxide) in an Asymmetric 1,4-Addition**

Hirotsugu Ito, Takashi Nagahara, Kazuaki Ishihara, Susumu Saito, and Hisashi Yamamoto**

Asymmetric conjugate addition, the most popular reaction in organocopper chemistry, can be used to generate stereogenic centers, both stoichiometrically[1] and catalytically.[2] Recently there have been important advances in the strategies based on catalytic reagents. Earlier work focused on the stoichiometric approach, which required chiral conjugated esters, amides, and their variants, each bearing a chiral auxiliary.[1c,3] We report here an approach relying on molecular recognition, which broadens the potential of strategies based on stoichiometric reagents. This method involves the use of organolithium reagent, chiral ester, and aluminum tris(2,6-diphenylphenoxide) (ATPH) (Figure 1).[4] A wide range of the most reactive nucleophiles could be used with high selectivity and generality.

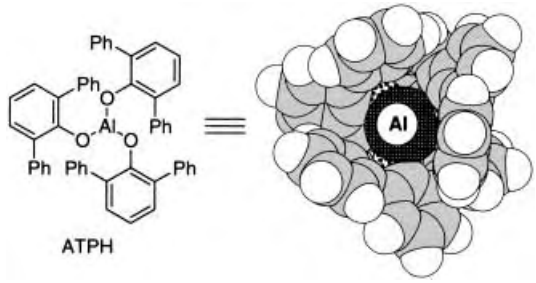


Figure 1. Molecular structure of aluminum tris(2,6-diphenylphenoxide) (ATPH).

[*] Prof. Dr. S. Saito
Institute for Advanced Research & Graduate School of Science
Nagoya University
Chikusa, Nagoya 464-8602 (Japan)
Fax: (+81) 52-789-5945
E-mail: susumu@chem.nagoya-u.ac.jp

Prof. Dr. H. Yamamoto
Department of Chemistry
University of Chicago
5735 South Ellis Aveue, Chicago, IL 60637 (USA)
Fax: (+1) 773-702-0805
E-mail: yamamoto@uchicago.edu

H. Ito, T. Nagahara, Prof. Dr. K. Ishihara
Graduate School of Engineering
Nagoya University
Chikusa, Nagoya 464-8603 (Japan)

[**] This work was supported by SORST and by the Japan Science and Technology Corporation (JST). We are grateful to Professor A. Yamamoto and N. Tamura (JST) for their support and valuable advice.

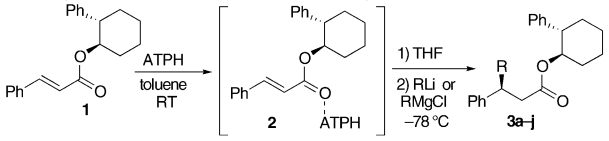
Supporting information for this article is available on the WWW under http://www.angewandte.org or from the author.

 © 2004 Wiley-VCH Verlag GmbH & Co. KGaA, Weinheim DOI: 10.1002/anie.200352809

Precomplexation of the chiral ester **1** (1.0 equiv) with ATPH (1.1 equiv) in toluene at room temperature was followed by treatment with THF at −78 °C for 1 h and then subsequent addition of a solution of BuLi (1.5 equiv) in hexane. After 1 h the reaction was quenched, and subsequent purification by silica gel column chromatography gave the 1,4-adduct **3a** quantitatively in 97 % *de* (*S*). If precomplexation was performed at −78 °C, a somewhat lower diastereomeric excess was observed (88 % *de* (*S*)). If the equilibration period with THF is eliminated from the procedure and the reaction mixture is treated directly with a solution of BuLi in THF, the diastereoselectivity decreases slightly (94 % *de*). The use of 1.0 equiv BuLi slightly decreased the product yield (ca. 90 %). In each case the 1,2-adduct could not be detected by ^{1}H NMR analysis. The ester of the opposite chirality to **1** gave comparable results but with complete reversal of the diastereofacial selectivity (97 % *de* (*R*)). Other nucleophiles were also tested, and results are listed in Table 1. These results can be summarized by three points.

1) Optimal conditions resulted in clean reactions, affording **3a–f** in nearly quantitative yields and more than 91 % *de*. Several reagents favored the attack from the *si* face of **1**, which is consistent with the behavior of BuLi.
2) Surprisingly, unusual α-selectivity was observed from screening allylic reagents. With prenyllithium, the addition proceeded preferentially at its α-carbon to give good selectivity (91 % *de*; α:γ = 1.8:1), while the γ-addition was gave even better selectivity (99 % *de*). In contrast, prenylmagnesium chloride reacted exclusively by γ-addition[5] with 92 % *de* (entry 6).
3) A positive effect of lithium halide[6] was observed when **2** was formed at −78 °C (92 % *de* for BuLi–LiBr), in contrast to the negative halide effect when **2** was formed at room temperature (87 % *de*). Thus chiral recognition events by ATPH are strongly temperature-dependent. With the exception of the acetate enolate, the best results were obtained when the complexation was carried out at room temperature and the ATPH–ester complex **2** was "aged" with THF[7] at −78 °C for approximately 1 h in the absence of LiBr.

Table 1: Asymmetric 1,4-addition of **1** in the presence of ATPH.[a]



Entry	Nucleophile	Prod.	R	Yield [%][b]	*de* [%][c]	Abs. config.[d]
1	BuLi	**3a**	Bu	99	97	*S*
2	prenyl-Li	**3b**		98[g]	α:91	–
		3c			γ:99	–
3	2-propenyl-Li	**3d**		99	99	–
4	vinyl-Li	**3e**		94	98	*R*
5[e]		**3f**		90	93	–
6[f]	prenyl-MgCl	**3c**		98[h]	92	–

[a] Unless otherwise specified, the reaction was performed with ATPH (1.1 equiv), the chiral ester (1.0 equiv), THF (100 vol %), and RM (1.5 or 2.0 equiv) in toluene. Precomplexation was performed at room temperature. [b] Yield of the isolated, purified alcohols obtained by reduction of crude **3a–f**. [c] The *de* values were determined by chiral HPLC analysis of the corresponding alcohols. [d] The absolute configurations were determined by comparison to literature values. See the Supporting Information. [e] Precomplexation was performed at −78 °C, and a solution of the enolate with TMEDA (1.5 equiv) in THF was used. [f] A solution of the Grignard reagent with TMEDA (1.5 equiv) in THF was used. [g] α-Adduct **3b**:γ-adduct **3c** 1.8:1. [h] **3b**:**3c** < 5:> 95.

To better understand these unprecedented observations, we determined the X-ray single-crystal structure of the ATPH–**1** complex **2** (Figure 2).[8] In addition to resolving arguments concerning the conformational of **1** in the complex,[9,10] the X-ray data may also help explain the role of ATPH in the chiral recognition. A large portion of the chiral ester **1** is under the considerable steric influence of ATPH. Fortunately, however, from the X-ray crystal structure, the difference in steric bulk around both sides of the diastereoface involving the β-carbon is discernible. The *re* face is more shielded by ATPH, allowing a favorable attack from the *si* face, which is totally consistent with the configurations that have been assigned so far (Table 1, entries 1 and 4; Table 2, entries 1–3). In addition, the X-ray structure shows that the chiral auxiliary is relatively exposed, at least to the region distal from the β-carbon, and thus likely to have little influence on the diastereofacial events. Rather, the effective chiral environment that seems to induce the high diastereoselectivity is created by the conformational chirality of ATPH, which is induced by the chirality of the ester. Although ATPH possesses C_3 symmetry[11,12] and thus has conformational enantiomers rapidly interconverting in an equilibrium, these enantiomers are optically resolved. In other words, the conformational enantiomers are rendered homochiral by the chiral recognition of the optically pure ester (Figure 2).

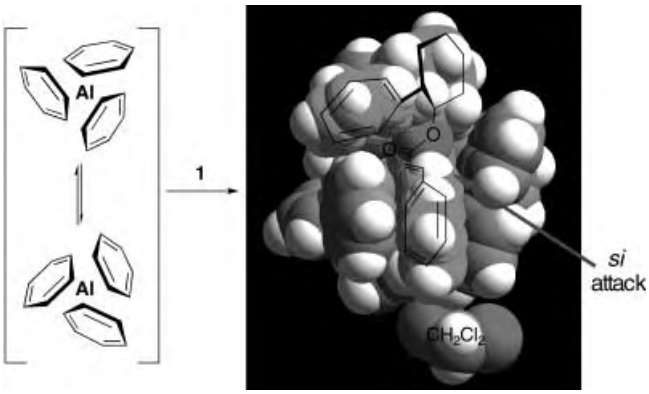


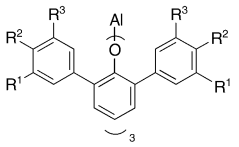
Figure 2. Possible inversion of the C_3 enantiomers of ATPH and the X-ray single-crystal structure of **2**.

 © 2004 Wiley-VCH Verlag GmbH & Co. KGaA, Weinheim

Table 2: Asymmetric 1,4-addition of **1** in the presence of ATPH analogues.[a]

Entry	Organolithium	Al reagent	Product	R	Yield [%][b]	*de* [%][c]	Abs. config.[d]
1	MeLi	**5**	**3g**	Me	99	94	*S*
2	allyl-Li	**4**	**3h**		97	93	*S*
3	allyl-Li	**5**	**3h**		99	95	*S*
4	methallyl-Li	**5**	**3i**		92	97	–
5	prenyl-Li	**4**	**3b**		99	α: 98;	–
			3c		(6.0:1)[e]	γ: 97	
6	prenyl-Li	**5**	**3b**		99	α: 99;	–
			3c		(5.5:1)[e]	γ: 99	
7	prenyl-Li	**6**	**3b**		99	α: 99;	–
			3c		(8.5:1)[e]	γ: 98	
8		**5**	**3j**		99	99	–

[a] Unless otherwise specified, the reaction was performed with ATPH (1.1 equiv), the chiral ester (1.0 equiv), THF (100 vol%), and RM (1.5 or 2.0 equiv) in toluene.[b] Yield of isolated, purified alcohols derived by reduction of crude **3**. [c] Diastereomeric excess was determined by chiral HPLC analysis of the corresponding alcohols. [d] Absolute configurations were determined by comparison to literature values. See the Supporting Information. [e] α-Adduct **3b**:γ-adduct **3c**.



4: $R^1 = R^3 = H$, $R^2 = Me$
5: $R^1 = R^3 = H$, $R^2 = Et$
6: $R^1 = R^2 = Me$, $R^3 = H$

Although the reactions gave virtually complete yields and diastereoselectivities for several organolithium reagents, we found that MeLi and allylic reagents were less suitable. For example, attempts to use MeLi and allyllithium resulted in lower diastereoselectivities (86% and 78% *de*, respectively). The present strategy facilitates the rational molecular design of ATPH. Several ATPH analogues were synthesized based on the X-ray structure and used for the asymmetric 1,4-addition (Table 2). We observed considerable increase not only in diastereoselectivities for **3b**, **g–j** (entries 1–8) but also in the α-selectivity in the reaction with prenyllithium (entries 5–7). The effectiveness of these ATPH analogues in remote stereocontrol, such as asymmetric 1,6-addition, is now being investigated in our laboratory.

Experimental Section

The following procedure for the reaction of (1*R*,2*S*)-2-phenylcyclohexyl cinnamate and *n*-butyllithium is representative. To a solution of ATPH (0.33 mmol) in toluene (3.0 mL) was added (1*R*,2*S*)-2-phenylcyclohexyl cinnamate (**1**) (91.9 mg, 0.30 mmol) in toluene (0.5 mL) at room temperature under Ar. After the mixture had been stirred for 5 min, it was cooled to −78°C. THF (3.0 mL) was added dropwise, and the reaction mixture was stirred for 1 h. To the mixture was added *n*BuLi (1.55 M, 290 μL, 0.45 mmol) dropwise at the same temperature. The reaction mixture was stirred for 1 h and quenched with aqueous hydrogen chloride (1.0 M, 5 mL). The organic layer was extracted with ether, dried over Na_2SO_4, and concentrated. The residue was dissolved in THF (9.0 mL) and reduced with $LiAlH_4$ (92%, 63 mg, 1.5 mmol) under Ar at 0°C, and stirred for 1 h at room temperature. The reaction mixture was quenched by a dropwise addition of MeOH and neutralized with a 1.0 M aqueous HCl. The organic layer was extracted with ether, dried over Na_2SO_4, and concentrated. The residue was purified by column chromatography on silica gel (ether/hexane 1:3 to 1:2 as the eluent) to give 3-phenylheptanol (99% yield, 97% *de*) as the reduced 1,4-adduct. (*S*)-**3**-Phenylheptan-1-ol, known compound:[13] $[\alpha]_D^{20} = -1.28$ ($c = 1.02$, $CHCl_3$, for 94% *ee*); ^1H NMR (300 MHz, $CDCl_3$): $\delta = 7.50$ (m, 5H), 3.50 (m, 2H), 2.67 (m, 1H,), 1.83 (m, 2H), 1.61 (m, 2H), 1.22 (m, 4H), 0.83 ppm (t, 3H, $J = 6.9$ Hz). HPLC analysis (OD-H, 1.0 mL min^{-1} flow rate, hexane/2-propanol 40:1 as eluent): $t_R = 12.8$ (minor) and $t_R = 15.4$ min (major; *S*, determined by comparing the value in ref. [13b]). After converting to the corresponding acid: $[\alpha]_D^{20} = +6.42$ ($c = 1.04$, $CHCl_3$).

Experimental procedures, spectroscopic, and analytical data for all new compounds, and the X-ray data for the ATPH complex **2** (PDF) are included in the Supporting Information.

Received: September 8, 2003 [Z52809]

Keywords: aluminum · asymmetric synthesis · chiral auxiliaries · Michael addition · molecular recognition

[1] a) J. Leonard, E. Díez-Barra, S. Merino, *Eur. J. Org. Chem.* **1998**, 2051; b) M. Kanai, Y. Nakagawa, K. Tomioka, *Synth. Org. Chem. Jpn.* **1996**, *54*, 474; c) B. E. Rossiter, N. M. Swingle, *Chem. Rev.* **1992**, *92*, 771.

[2] a) B. L. Feringa, *Acc. Chem. Res.* **2000**, *33*, 346; b) K. Tomioka, Y. Nagaoka in *Comprehensive Asymmetric Catalysts, Vol. III* (Eds.: E. N. Jacobsen, A. Pfaltz, H. Yamamoto), Springer, Berlin, **1999**, p. 1105; c) D. A. Evans, T. Rovis, J. S. Johnson, *Pure Appl. Chem.* **1999**, *71*, 1407; d) Y. Takaya, M. Ogasawara, T. Hayashi, M. Sakai, N. Miyaura, *J. Am. Chem. Soc.* **1998**, *120*, 5579; e) T. Hayashi, T. Senda, Y. Takaya, M. Ogasawara, *J. Am. Chem. Soc.* **1999**, *121*, 11591; f) T. Hayashi, T. Senda, M. Ogasawara, *J. Am. Chem. Soc.* **2000**, *122*, 10726; g) S. J. Degrado, H. Mizutani, A. H. Hoveyda, *J. Am. Chem. Soc.* **2002**, *124*, 13362; h) A. W. Hird, A. H. Hoveyda, *Angew. Chem.* **2003**, *115*, 1314; *Angew. Chem. Int. Ed.* **2003**, *42*, 1276.

[3] G. Roos, *Compendium of Chiral Auxiliary Applications*, Academic Press, San Diego, **2002**.

[4] For preliminary communication and related work for the present article, see: a) S. Saito, M. Shiozawa, T. Nagahara, M. Nakadai, H. Yamamoto, *J. Am. Chem. Soc.* **2000**, *122*, 7847; b) S. Saito, M.

 © 2004 Wiley-VCH Verlag GmbH & Co. KGaA, Weinheim

Shiozawa, H. Yamamoto, *Angew. Chem.* **1999**, *111*, 1884; *Angew. Chem. Int. Ed.* **1999**, *38*, 1769; c) S. Saito, M. Ito, M. Shiozawa, H. Yamamoto, *J. Am. Chem. Soc.* **1998**, *120*, 813; d) S. Saito, H. Yamamoto, *Chem. Eur. J.* **1999**, *5*, 1959. For very recent applications of ATPH, see: e) S. Saito, T. Sone, M. Murase, H. Yamamoto, *J. Am. Chem. Soc.* **2000**, *122*, 10216; f) S. Saito, S. Yamazaki, H. Yamamoto, *Angew. Chem.* **2001**, *113*, 3725; *Angew. Chem. Int. Ed.* **2001**, *40*, 3613; g) S. Saito, T. Nagahara, M. Shiozawa, M. Nakadai, H. Yamamoto, *J. Am. Chem. Soc.* **2003**, *125*, 6200. For a review on ATPH, see: h) S. Saito, H. Yamamoto, *Chem. Commun.* **1997**, 1585; i) H. Yamamoto, S. Saito, *Pure Appl. Chem.* **1999**, *71*, 239.

[5] a) A. Yanagisawa, S. Habaue, K. Yasue, H. Yamamoto, *J. Am. Chem. Soc.***1994**, *116*, 6130; b) A. Yanagisawa, H. Hibino, N. Nomura, H. Yamamoto, *J. Am. Chem. Soc.* **1993**, *115*, 5879; c) A. Yanagisawa, S. Habaue, H. Yamamoto, *J. Am. Chem. Soc.* **1991**, *113*, 8955, and references therein.

[6] For effects of the halide salts of alkali metals, see: S. Saito in *Handbook on Lewis Acids* (Ed.: H. Yamamoto), Wiley-VCH, Weinheim, **2000**, pp. 1–67, and references therein.

[7] We have no good explanation for the THF effect, which is now under investigation. However, one reasonable explanation might be that THF coordinates to the aluminum atom of ATPH to make a higher coordination complex. This was also invoked to explain the effect of Et_2O, which also enhanced asymmetric induction, see: M. Murakata, T. Jono, Y. Mizuno, O. Hoshino, *J. Am. Chem. Soc.* **1997**, *119*, 11713.

[8] CCDC-217071 (**2**) contains the supplementary crystallographic data for this paper. These data can be obtained free of charge via www.ccdc.cam.ac.uk/conts/retrieving.html (or from the Cambridge Crystallographic Data Centre, 12, Union Road, Cambridge CB21EZ, UK; fax: (+44) 1223-336-033; or deposit@ccdc.cam.ac.uk). The ^{1}H NMR (300 MHz, [D_8]toluene) data showed a solution structure of the complex **2** adopting a single, presumably the most favorable conformation. ^{1}H NMR data: $\delta = 7.80$–6.40 (m, 50H), 5.16 (d, 1H, $J = 15.9$ Hz), 3.57 (td, 1H, $J = 10.0$, 4.0 Hz), 2.21 (td, 1H, $J = 11.1$, 3.9 Hz), 1.50–0.60 (m, 7H), 0.22 ppm (m, 1H).

[9] The complex **2** adopts the s-*trans* conformation with respect to the carbonyl compound and the *syn* coordination by ATPH. The alkoxy group of the ester prefers *Z* (or *trans*) orientation with respect to the carbonyl group and is arranged around the single-bond axis of (O=C)–(OR*). For the definition of conformations of conjugated carbonyl compounds, see: S. Saito, H. Yamamoto in *Modern Carbonyl Chemistry* (Ed.: J. Otera), Wiley-VCH, Weinheim, **2000**, pp. 33–65.

[10] For NMR analyses of Lewis acid/carbonyl complexes, see: a) R. F. Childs, D. L. Mulholland, A. Nixon, *Can. J. Chem.* **1982**, *60*, 801; b) S. Saito in *Main Group Metals in Organic Synthesis* (Eds.: H. Yamamoto, K. Oshima), Wiley-VCH, Weinheim, in press.

[11] For C_3 symmetry of ATPH, see: K. Maruoka, H. Imoto, S. Saito, H. Yamamoto, *J. Am. Chem. Soc.* **1994**, *116*, 6153. See also ref. [4h].

[12] For C_3 symmetry in chiral recognition, see: C. Moberg, *Angew. Chem.* **1998**, *110*, 260; *Angew. Chem. Int. Ed.* **1998**, *37*, 248.

[13] a) H. Ahlbrecht, G. Bonnet, D. Enders, G. Zimmermann, *Tetrahedron Lett.* **1980**, *21*, 3175; b) B. Mikael, I. Tommy, N. Martin, O. Thomas, *Tetrahedron Lett.* **1995**, *36*, 3227.

 © 2004 Wiley-VCH Verlag GmbH & Co. KGaA, Weinheim

Fullerene Derivatives

$C_{74}F_{38}$: An Exohedral Derivative of a Small-Bandgap Fullerene with D_3 Symmetry**

Alexey A. Goryunkov, Vitaliy Y. Markov, Ilya N. Ioffe, Robert D. Bolskar, Michael D. Diener, Igor V. Kuvychko, Steven H. Strauss, and Olga V. Boltalina**

Toluene-soluble fullerenes with large HOMO–LUMO energy gaps (e.g., C_{60}, C_{70}) have been intensely studied.[1] In contrast, toluene-insoluble fullerenes with HOMO–LUMO gaps less than 0.5 eV have not been extensively studied due to their low solubility and air sensitivity. An important example of the latter is C_{74}, which may have a HOMO–LUMO gap as small as 0.05 eV.[2–4] We present here the isolation and characterization of a single regioisomer (pair of enantiomers) of the $C_{74}F_{38}$ fullerene derivative with D_3 symmetry (denoted D_3-$C_{74}F_{38}$), the first exohedral derivative of C_{74}.

Pure samples of the small-bandgap (SBG) fullerene C_{74} were reported for the first time in 1998.[2] Diener and Alford at TDA processed solutions containing the stable C_{74}^{2-} ion by anaerobic HPLC, then reoxidized the C_{74}^{2-}-enriched fraction to yield solid C_{74}.[2] Up until that point, the insolubility of empty (i.e., metal-free) C_{74}, which may be a consequence of the small HOMO–LUMO gap,[2] had prevented the exploration of its exohedral derivative chemistry. However, there were indications that some fluoro[74]fullerenes might be prepared. The gas-phase difluoro monoanion $C_{74}F_2^-$ was observed in 1994 by Knudsen-cell mass spectrometry.[5] Significantly, the C–F bonds in $C_{74}F_2^-$ appeared to be stronger than the C–F bonds in $C_{60}F_2^-$ and $C_{70}F_2^-$.[6] In addition, it was recently shown that a specific set of Knudsen-cell conditions led to the generation of $C_{74}F_{38}^+$ as the dominant gas-phase [74]fullerene species.[7] Highly fluorinated [60]fullerenes are well known to be stable and to have higher volatilities and solubilities than the parent fullerene C_{60}.[8,9] With this in mind,

[*] I. V. Kuvychko, Prof. S. H. Strauss
Department of Chemistry
Colorado State University
Fort Collins, CO 80523 (USA)
Fax: (+1) 970-491-1801
E-mail: strauss@lamar.colostate.edu

A. A. Goryunkov, Dr. V. Y. Markov, Dr. I. N. Ioffe, Prof. O. V. Boltalina
Chemistry Department
Moscow State University
Moscow 119992 (Russia)
Fax: (+7) 095-939-1240
E-mail: ovbolt@lamar.colostate.edu

Dr. R. D. Bolskar, Dr. M. D. Diener
TDA Research Inc., 12345 W. 52nd Avenue
Wheat Ridge, CO 80033 (USA)

[**] This work was supported by the Volkswagen Stiftung (I-77/855), the Russian Foundation for Basic Research (03-03-32756), the council on Grants of the President of the Russian Federation (MK-832.2003.03), and the U.S. National Science Foundation (CHE-9905482). We thank Prof. D. W. Grainger for the use of his HPLC equipment.

 DOI: 10.1002/anie.200352960 © 2004 Wiley-VCH Verlag GmbH & Co. KGaA, Weinheim

we began to investigate the selective fluorination of enriched samples of C_{74} and herein report our initial results.

The high-temperature solid-state reaction of C_{74} and K_2PtF_6 followed by sublimation and HPLC purification resulted in the isolation of milligram amounts of $C_{74}F_{38}$ with $>90\%$ compositional purity. This compound, the first isolable exohedral derivative of any SBG fullerene, is stable in air even when dissolved in common organic solvents and has been characterized by electron-ionization (EI) mass spectrometry, FTIR, and ^{19}F NMR spectroscopy.

The 20 eV EI mass spectrum of purified $C_{74}F_{38}$ is shown in Figure 1 along with an FTIR spectrum of a KBr pellet of $C_{74}F_{38}$. The relatively simple $\tilde{\nu}$(CF) region, dominated by one

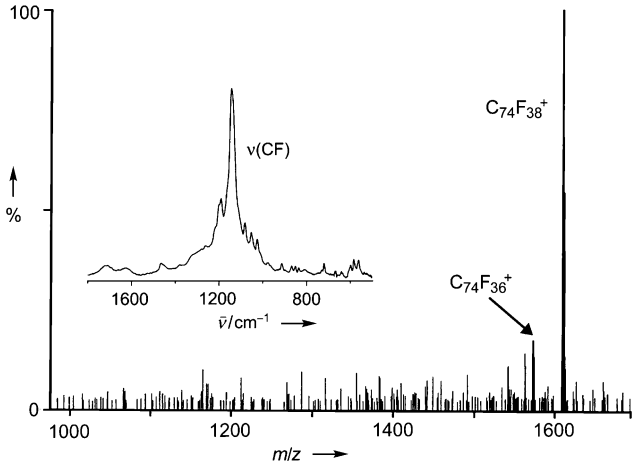


Figure 1. Electron-ionization mass spectrum of HPLC-purified $C_{74}F_{38}$ ($U_e = 20$ eV) showing very little fragmentation of the parent ion $C_{74}F_{38}^+$. Inset: FTIR spectrum of a KBr pellet of the same batch of $C_{74}F_{38}$.

intense band (1142 cm^{-1}), and the absence of intense bands in the 500–800 cm^{-1} region are reminiscent of the IR spectrum of $C_{60}F_{36}$[10] but not of the spectra of $C_{60}F_{18}$[11] and $C_{60}F_{48}$,[12] both of which exhibit many intense bands in the $\tilde{\nu}$(CF) and 500–800 cm^{-1} regions.

The 1D and 2D ^{19}F NMR spectra of $C_{74}F_{38}$ are shown in Figures 2 and 3. The 2:6:6:6:6:6:6 intensity pattern (signals a–g, respectively) for the 38 F atoms requires D_3, C_{3h}, or D_{3h} point symmetry, with two F atoms situated on the C_3 axis. The ^{19}F signal for these F atoms (a) is split by three equivalent F atoms into a 1:3:3:1 quartet with $J_{FF} = 32.4$ Hz. The other signals are complex multiplets, some of which exhibit unresolved ^{19}F–^{19}F couplings. The range of δ values (−129 to −164 ppm) is the same as observed for C_{3v}-$C_{60}F_{18}$,[11] T- and C_3-$C_{60}F_{36}$,[10] and D_3- and S_6-$C_{60}F_{48}$.[13] The network of correlations in the 2D COSY spectrum of $C_{74}F_{38}$ confirms that all seven signals belong to the same molecular species and suggests that each sp^3 C atom is adjacent to at least one other sp^3 C atom, as in $C_{60}F_{18}$, $C_{60}F_{36}$, and $C_{60}F_{48}$.

To propose a structure for what appears to be a single isomer of $C_{74}F_{38}$, it was first necessary to consider the structure of the C_{74} cage. There is only one isomer of C_{74} that obeys the isolated-pentagon rule (IPR), and it has long been assumed (but never experimentally verified) that empty

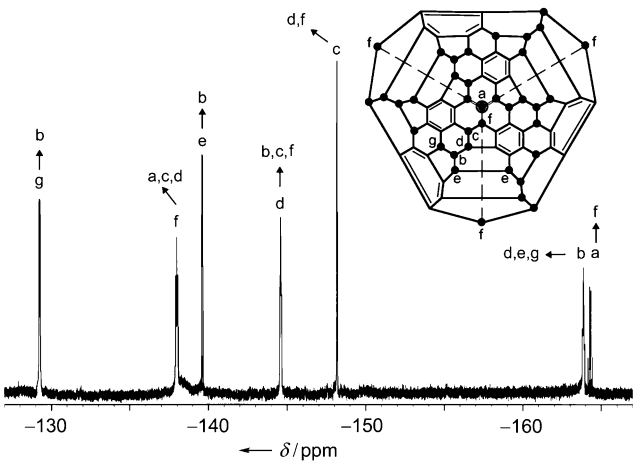


Figure 2. ^{19}F NMR spectrum of HPLC-purified $C_{74}F_{38}$ (376.5 MHz, CD_2Cl_2, 25 °C). The solid isolated from an aliquot of this sample was used to collect the FTIR and mass spectra shown in Figure 1. The relative integrated intensities of the signals labeled a–g are, respectively, 2:6:6:6:6:6:6. The arrows indicate the correlations observed in the 2D spectrum shown in Figure 3. The Schlegel-like diagram is a view down the C_3 axis of the proposed D_3 structure of $C_{74}F_{38}$. The spectral assignments are based on chemical shifts, integrated intensities, ^{19}F–^{19}F coupling constants, and the 2D spectrum. The solid black circles represent fluorine-bearing carbon atoms. The two fluorine-bearing carbon atoms on the C_3 axis (a) are superimposed, and one is depicted as an open circle connected by dashed lines to the three f carbon atoms at the periphery.

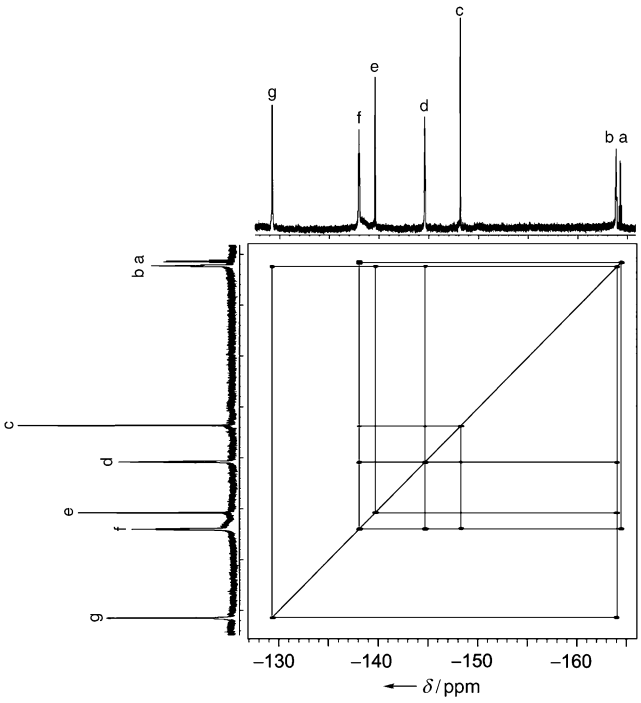


Figure 3. 2D COSY ^{19}F NMR spectrum of HPLC-purified $C_{74}F_{38}$ (376.5 MHz, CD_2Cl_2, 25 °C). The signals labeled a–g are assigned to the corresponding fluorine atoms in the Schlegel-like diagram in Figure 2. The assignments of resonances e and g, which cannot be distinguished by the COSY correlations, are based on chemical shift similarities with structurally characterized fluoro-[60]fullerenes.

 © 2004 Wiley-VCH Verlag GmbH & Co. KGaA, Weinheim

(i.e., metal-free) C_{74} has the IPR-D_{3h} structure.[14–16] This assumption is consistent with the nearly isoenergetic singlet and triplet ground states (i.e., small bandgap) predicted for IPR-D_{3h}-C_{74}.[2–4,14–17] We have calculated, for the first time, the relative energies of IPR-D_{3h}-C_{74} and the nine other isomers of C_{74} that have C_{3h}, D_3, or D_{3h} symmetry. The most stable of these, a D_3 isomer with three pentalene fragments, was found to be nearly 400 kJ mol^{-1} less stable than IPR-D_{3h}-C_{74}. We conclude that the carbon core of $C_{74}F_{38}$ is, as previously assumed, IPR-D_{3h}-C_{74}.

Our proposed structure of $C_{74}F_{38}$ is depicted in the Schlegel-like diagram in Figure 2 and will be referred to as **1**. This D_3 isomer was proposed when $C_{74}F_{38}^+$ was observed by Knudsen-cell mass spectrometry[7] by analogy with *T*-$C_{60}F_{36}$, which is believed to be especially stable because it contains four stabilizing isolated benzenoid (SIB) rings.[10] Structure **1** contains six SIB rings, the maximum number possible for any derivative of IPR-D_{3h}-C_{74}. It is the only possible isomer of $C_{74}F_{38}$ that is consistent with the NMR data and that has six SIB rings. The proposed contiguous pattern of adjacent fluorine-bearing C atoms in **1** is a structural feature common to $C_{60}F_{18}$, $C_{60}F_{36}$, and $C_{60}F_{48}$, and therefore may be a feature common to many fluorofullerenes prepared at high temperatures, regardless of cage size. There is an additional similarity between **1** and *T*-$C_{60}F_{36}$: each pentagon in both structures has three F atoms.[10] The similarities suggest that fluorinated derivatives of higher fullerenes with compositions and structures that lead to the maximum possible number of SIB rings, a contiguous pattern of sp^3 C atoms, and three F atoms per pentagon should be considered as worthwhile synthetic targets.

Structure **1** is supported by DFT calculations. In addition to **1**, other possible isomers of $C_{74}F_{38}$ were considered that were consistent with the NMR data. All were found to be less stable than **1** by $\geq$ 200 kJ mol^{-1}. To explore the possibility that **1** might represent a kinetic product and not the most stable isomer, we also investigated isomers that are not consistent with the ^{19}F NMR pattern. Given the enormous number of possible isomers, some restrictions were necessary. All possible C_{3v} and C_3 isomers were considered, some of which contain three SIB rings. We also considered a number of lower-symmetry four- or five-SIB-ring isomers that were formed by moving one or both of the F atoms, labelled (a) in Figure 2, which are attached to the two unique triple-hexagon junctions (THJs) of IPR-D_{3h}-C_{74}. These lower-symmetry isomers were chosen taking into account the theoretical results on C_{76} hydrogenation, which demonstrated that addition to THJs was energetically unfavorable relative to the usual junction of two hexagons and one pentagon.[18] However, in that work the two isomers of $C_{76}H_{18}$ considered both had one SIB ring. Therefore, it may be that an isomerization involving loss of an SIB is more destabilizing than one involving attachment of an atom to a THJ. All of the alternative isomers we considered were less stable than **1** by $\geq$ 120 kJ mol^{-1}.

In summary, the high-temperature fluorination of purified C_{74} by K_2PtF_6 afforded milligram quantities IPR-D_3-$C_{74}F_{38}$, the first isolable exohedral derivative of any small-bandgap fullerene and the first structurally characterized fluorinated higher fullerene. The excellent isomeric purity and high compositional purity are especially noteworthy. In addition, the IPR-D_{3h} structure of C_{74} now has direct experimental support as well as additional theoretical support from the first DFT study of alternative cage structures. Finally, our results suggest that selective fluorination should be explored as a general procedure for solubilizing and stabilizing other nonextractable and/or reactive carbon clusters, including endohedral molecules, that represent the bulk of fullerene soots.

Experimental Section

Arc-generated fullerenes were sublimed out of the soot at 750 °C and 10^{-3} Torr. Under an argon atmosphere, the sublimate was collected and washed with *o*-dichlorobenzene at 100 °C and 40 Torr using a Soxhlet extractor until the washings were colorless. The remaining C_{74}-enriched solid residue was washed with hexane and dried under vacuum.

In a typical preparation, the C_{74}-enriched solid (32 mg, 0.036 mmol based on C_{74}) was ground with K_2PtF_6 (459 mg, 1.19 mmol) in a nitrogen-filled glove box. The mixture was heated under dynamic vacuum at 500 °C for 8 h in the sealed end of a long glass reactor, as previously described for other solid-state fullerene fluorinations.[19] The volatile products, which had condensed in a broad zone near the 25 °C end of the reactor, were collected as two approximately equal-length fractions. EI mass spectrometry (EI-MS) revealed that the fraction that was closer to the reactor hot zone consisted mainly of $C_{74}F_{38}$. This fraction was processed by HPLC (10 × 250 mm Cosmosil Buckyprep column; 5 mL toluene min^{-1}, UV detector, 300 nm). A typical chromatogram (Figure 4) clearly illustrates that selective fluorination is possible when many sets of reaction conditions are pre-screened with only a few Knudsen-cell experiments.[7] The most intense HPLC peak, with a retention time of 2.92 min, was shown by EI-MS to contain $C_{74}F_{38}$ with >90% compositional purity ($\leq$10% may be due to the presence of $C_{74}F_{36}$).The yield of $C_{74}F_{38}$ was as high as 3 mg in some batches.

Geometry optimizations for a large set of possible isomers were carried out at the AM1 level of theory. The most stable structures were reoptimized by DFT using the program PRIRODA, the TZ2P basis set[20] and the PBE exchange-correlation functional.[21] Since

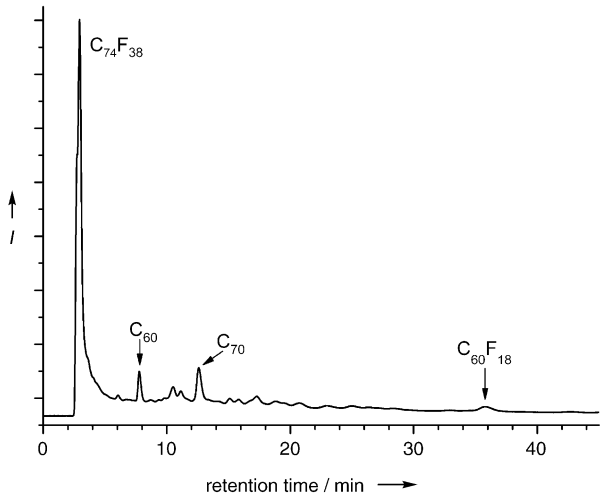


Figure 4. HPLC trace of the hot-zone crude sublimate from a reaction of C_{74} and K_2PtF_6 (10 × 250 mm Cosmosil Buckyprep, 5 mL toluene/min, UV detector, 310 nm). The intense peak at 2.92 min is due to $C_{74}F_{38}$. *I* = relative intensity.

 © 2004 Wiley-VCH Verlag GmbH & Co. KGaA, Weinheim

AM1 calculations are known to underestimate the stabilizing effects of SIB rings in fullerene derivatives,[22] only DFT-derived relative energies have been considered in this paper.

Received: September 26, 2003 [Z52960]

Keywords: carbon · density functional calculations · fluorination · fullerenes · NMR spectroscopy

[1] K. M. Kadish, R. S. Ruoff, *Fullerenes: Chemistry, Physics, and Technology*, Wiley-Interscience, New York, **2000**.
[2] M. D. Diener, J. M. Alford, *Nature* **1998**, *393*, 668.
[3] C. Hong, F. Ji-Kang, Z. Xin, R. Ai-Min, W. Q. Tian, J. D. Goddard, *J. Mol. Struct.* **2003**, *620*, 271.
[4] V. I. Kovalenko, A. R. Khamatgalimov, *Chem. Phys. Lett.* **2003**, *377*, 263.
[5] O. V. Boltalina, L. N. Sidorov, E. V. Sukhanova, I. D. Sorokin, *Chem. Phys. Lett.* **1994**, *230*, 567.
[6] O. V. Boltalina, D. B. Ponomarev, A. Y. Borchshevskii, L. N. Sidorov, *J. Phys. Chem. A* **1997**, *101*, 2574.
[7] O. V. Boltalina, A. A. Goryunkov, V. Y. Markov, I. N. Ioffe, L. N. Sidorov, *Int. J. Mass Spectrom.* **2003**, *228*, 807.
[8] Y. A. Makeev, Ph.D. thesis, Moscow State University, **2001**.
[9] O. V. Boltalina, V. Y. Markov, A. Y. Borschevskii, N. A. Galeva, L. N. Sidorov, G. Gigli, G. Balducci, *J. Phys. Chem. B* **1999**, *103*, 3828.
[10] O. V. Boltalina, J. M. Street, R. Taylor, *J. Chem. Soc. Perkin Trans. 2* **1998**, 649.
[11] O. V. Boltalina, V. Y. Markov, R. Taylor, M. P. Waugh, *Chem. Commun.* **1996**, 2549.
[12] V. F. Bagryantsev, A. S. Zapolskii, O. V. Boltalina, N. A. Galeva, L. N. Sidorov, *Dokl. Akad. Nauk* **1997**, *357*, 487.
[13] A. A. Gakh, A. A. Tuinman, J. L. Adcock, R. A. Sachleben, R. N. Compton, *J. Am. Chem. Soc.* **1994**, *116*, 819.
[14] X. Liu, T. G. Schmaltz, D. J. Klein, *Chem. Phys. Lett.* **1992**, *188*, 550.
[15] B. L. Zhang, C. Z. Wang, K. Ho, C. T. Chan, *J. Chem. Phys.* **1993**, *98*, 3095.
[16] P. W. Fowler, D. E. Manolopoulous, *An Atlas of Fullerenes*, Clarendon, Oxford, **1995**.
[17] S. Saito, S. Okada, S. A. N. Hamada, *Phys. Rev. Lett.* **1995**, *75*, 685.
[18] B. W. Clare, D. L. Kepert, *J. Mol. Struct. (THEOCHEM)* **2001**, *536*, 99.
[19] A. Y. Lukonin, V. Y. Markov, O. V. Boltalina, *Moscow Univ. Chem. Bull. (Engl. Transl.)* **2001**, *42*, 3.
[20] D. N. Laikov, *Chem. Phys. Lett.* **1997**, *281*, 151.
[21] J. P. Perdew, K. Burke, M. Ernzerhof, *Phys. Rev. Lett.* **1996**, *77*, 3865.
[22] B. W. Clare, D. L. Kepert, *J. Mol. Struct. (THEOCHEM)* **2002**, *589–590*, 195.

 © 2004 Wiley-VCH Verlag GmbH & Co. KGaA, Weinheim

Drug Development

Reactivity-Based One-Pot Synthesis of Oligomannoses: Defining Antigens Recognized by 2G12, a Broadly Neutralizing Anti-HIV-1 Antibody**

*Hing-Ken Lee, Christopher N. Scanlan, Cheng-Yuan Huang, Aileen Y. Chang, Daniel A. Calarese, Raymond A. Dwek, Pauline M. Rudd, Dennis R. Burton, Ian. A. Wilson, and Chi-Huey Wong**

The design of immunogens capable of eliciting broadly neutralizing antibodies is a major, but elusive, goal of HIV vaccine research.[1] However, a small panel of broadly neutralizing human monoclonal antibodies (mAbs)[2] isolated from seropositive donors may be very valuable in guiding the design of such immunogens.[3] One antibody from this panel is mAb 2G12, which recognizes a conserved and unusually dense cluster of oligomannose residues on the "silent face" of gp120, the envelope protein of HIV-1.[4]

The crystal structure of the Fab fragment of 2G12 shows that the antibody adopts a highly unusual domain-exchanged dimeric structure.[5] The structure produces an array of antibody combining sites in proximity to one another (Figure 1). Two conventional combining sites composed of heavy (V_H) and light (V_L) variable domains sandwich an unconventional site composed of residues from the two neighboring V_H domains.

The structure of Fab 2G12 complexed with $Man_9GlcNAc_2$ (**1**) shows that the conventional binding sites are occupied by the D1 arms of the $Man_9GlcNAc_2$ moieties, and that the terminal Manα1-2Man residues make 85% of the protein

[*] Dr. H.-K. Lee, C.-Y. Huang, Dr. A. Y. Chang, Prof. Dr. C.-H. Wong
Department of Chemistry and
The Skaggs Institute for Chemical Biology
The Scripps Research Institute
10550 North Torrey Pines Road, La Jolla, CA 92037 (USA)
Fax: (+1) 858-784-2409
E-mail: wong@scripps.edu

C. N. Scanlan, Prof. Dr. D. R. Burton
Departments of Immunology and Molecular Biology
The Scripps Research Institute
10550 North Torrey Pines Road, La Jolla, CA 92037 (USA)

D. A. Calarese, Prof. Dr. I. A. Wilson
Department of Molecular Biology and
The Skaggs Institute for Chemical Biology
The Scripps Research Institute
10550 North Torrey Pines Road, La Jolla, CA 92037 (USA)

Prof. Dr. R. A. Dwek, Dr. P. M. Rudd
Glycobiology Institute
Department of Biochemistry
University of Oxford
Oxford, OX1 3QU (UK)

[**] This work was supported by Optimer Pharmaceuticals, San Diego (C.H.W.) and the National Institutes of Health (Grant no. AI33292 to D.R.B. and GM 46192 to I.A.W.).

Supporting information for this article is available on the WWW under http://www.angewandte.org or from the author.

 © 2004 Wiley-VCH Verlag GmbH & Co. KGaA, Weinheim DOI: 10.1002/anie.200353105

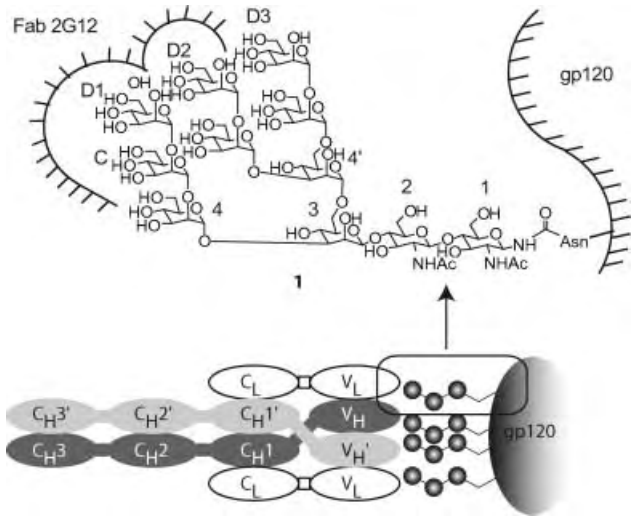


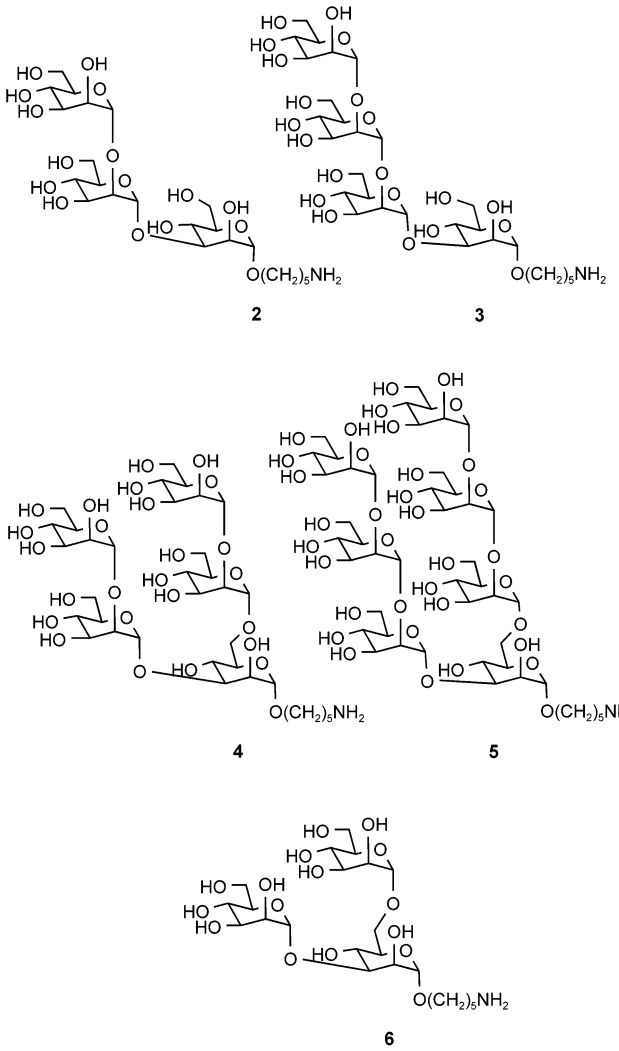
Figure 1. The structure of $Man_9GlcNAc_2$ (**1**; Man = mannose; Glc = glucose; Ac, acetyl) on gp120 interacting with the Fab fragment of the broadly neutralizing 2G12 antibody.

contacts. In the crystal, the D2 arms from two neighboring $Man_9GlcNAc_2$ moieties occupy the nonconventional site.

We are attempting to use the structural information obtained from the complexes of 2G12 with oligomannose chains to design novel immunogens that will elicit a 2G12-like antibody response. As part of these efforts toward development of an HIV vaccine, we have designed and synthesized the Manα1-2Man-containing oligomannoses **2**–**6** (Scheme 1) by using a reactivity-based, modular one-pot synthesis method that requires a minimal number of building blocks.

The programmable reactivity-based one-pot method for oligosaccharide synthesis[6] has since been successfully applied to the synthesis of several biologically significant oligosaccharides, which include Globo H,[7] Lewis Y,[8] *N*-acetyllactosamine oligomers,[9] and fucosyl-GM_1.[10] Before the one-pot synthesis could be applied to oligomannosides the relative reactivity value (RRV) of each monomer had first to be determined by a competitive HPLC assay. The RRV of each mannoside is then used as a guide for the selection of thioglycoside building blocks (Figure 2a).

An analysis of the RRVs of mannose building blocks for the one-pot synthesis of trimannose Manα1-2Manα1-2Man, the D1 arm of $Man_9GlcNAc_2$, suggests that D-mannose thioglycosides are less reactive than other thioglycosides, such as fucose and galactose.[6] In addition, 2-hydroxymannose thioglycosides are in general much more reactive than the corresponding 2-protected derivatives (Scheme 2), which makes a one-pot synthesis with a universal leaving group (used to simplify the protocol and conditions) difficult to carry out. This problem was overcome by Ley and co-workers, who synthesized trimannose with a one-pot strategy by



Scheme 1. The structures of oligomannoses **2**–**6**.

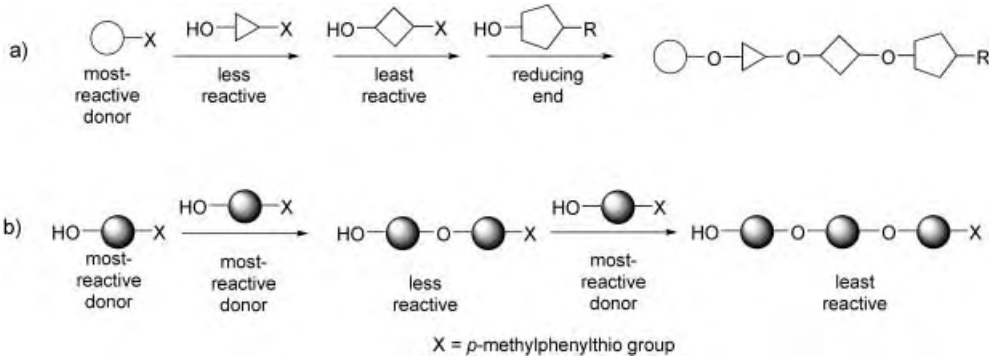
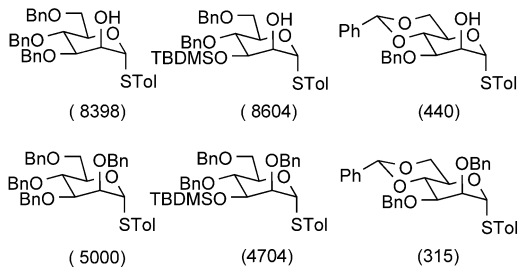


Figure 2. Strategy for a) sequential one-pot synthesis and b) one-pot self-condensation synthesis.

 © 2004 Wiley-VCH Verlag GmbH & Co. KGaA, Weinheim



Scheme 2. RRV values of 2-hydroxymannose thioglycosides. Bn = benzyl, Tol = tolyl, TBDMS = *tert*-butyldimethylsilyl.

Table 1: The reaction conditions used for reactivity-based one-pot self-condensation of **7**.

Entry	*T* [°C]	NIS [molar equiv][a]	*t* [h]	Yield of **8** [%]	Yield of **9** [%]
1	−60	0.7	24	0	0
2[b]	−50	0.7	24	70	5
3	−45	0.7	2	40	20
4	−40	0.7	1	35	25
5	−40	0.6	1	38	30
6	−40	0.5	1	50	15
7	−30	0.7	0.5	25	15
8[c]	−20	0.7	0.5	0	10

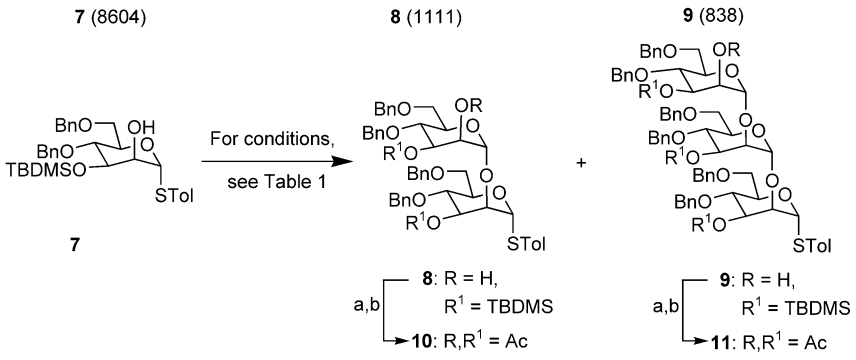
[a] NIS = *N*-iodosuccinimide. [b] The yield was calculated based on the amount of **7** recovered. [c] Polymerization was observed.

changing the anomeric leaving group on mannose from F to SePh to SEt, and thus changing the reactivity of this group.[11]

While we continue to find new protecting groups to tune the reactivity of mannose thioglycosides for the one-pot synthesis of oligomannoses, we report herein a new one-pot strategy for the synthesis of both mannose dimer **8** and trimer **9**. In our strategy, the most reactive monomer undergoes self-condensation to give a less-reactive dimer. The dimer then serves as an acceptor for another monomer molecule, which leads to formation of the trimer (Figure 2b). Several 2-hydroxymannose thioglycosides were designed and tested for self-condensation but their reactions were not clean and separation of the monomer, dimer, and trimer by column chromatography was required. This problem was overcome by introducing the nonpolar protecting group *tert*-butyldimethylsilyl to form **7**, which undergoes self-condensation to give dimer **8** and trimer **9** (Scheme 3).

Entry 5 in Table 1 lists the optimal conditions for the one-pot self-condensation of **7** to produce **8** and **9**. The reaction temperature is key to the degree of self-condensation. No self-condensation occurred at −60 °C (Entry 1) and mainly dimer **8** and monomer **7** were found at −50 °C (Entry 2). Uncontrollable self-condensation was observed at temperatures over −20 °C (Entry 8). The overall yield was reduced when more than 0.6 molar equivalents NIS were added (Entry 4), probably as a result of decomposition of the thioglycosides, dimer **8**, and trimer **9**.

The RRVs of **7**–**9** were determined and, as expected, monomer **7** (RRV = 8604) is the most reactive and undergoes self-condensation to give the less-reactive dimer **8** (RRV = 1111), which is then glycosylated by monomer **7** again to give the least reactive molecule in the series, trimer **9** (RRV = 838). Subsequent removal of the TBDMS group and acetylation of **8** and **9** gave **10** and **11**, respectively (Scheme 3).



Scheme 3. One-pot self-condensation synthesis of building blocks **10** and **11**. a) Tetrabutylammonium fluoride, tetrahydrofuran, RT, 24 h; b) Ac_2O, Et_3N, 4-dimethylaminopyridine, CH_2Cl_2, RT, 2 h.

Donors **10**–**12**[12] were coupled to acceptor **13** or **14** (Bz, benzoyl)[13] to give trimannose **15**, tetramannose **16**, pentamannose **17**, heptamannose **18**, or trimannose **19**. Details of these syntheses are shown in Table 2. Donors **10**–**12** exhibited excellent Manα1-6Man or Manα1-3Man selectivity as a result of steric bulk at the 2-position of **10** and **11** and participation of the acetyl group of **12**. As shown in Table 2, deprotection of oligomannoses **15**–**19** gave the corresponding deprotected oligomannoses **2**–**6**, respectively, in good yields.[9]

$Man_9GlcNAc_2$ (**1**)[5] and deprotected oligosaccharides **2**–**6** were evaluated for their ability to inhibit the interaction between 2G12 and gp120 in an enzyme-linked immunosorbent assay (see Figure 3).[4a] We will ultimately take the best synthetic inhibitors found in this assay forward into experiments to develop multivalent constructs as potential HIV vaccine candidates for eliciting 2G12-like antibodies. The results for trimannose **2** (15% inhibition at 2 mM) and tetramannose **3** (79%) indicate that an extra α1-2 linked mannose unit significantly enhances the inhibitory effect to a level comparable with that achieved by $Man_9GlcNAc_2$ (71%). This result is consistent with crystallographic studies that identified the D1 arm of $Man_9GlcNAc_2$ as the primary carbohydrate recognition motif for 2G12; compound **3** contains the same arrangement of mannose units as the D1 arm. The Manβ1-4GlcNAcβ1-4GlcNAc core of $Man_9GlcNAc_2$ appears not to be critical for binding as it is absent from compound **3**. Pentamannose **4** (79% inhibition at 2 mM), though lacking two sequential Manα1-2Man units, is divalent which may explain its more efficient inhibition of 2G12–gp120 binding compared to that of compound **2** (15%). Surprisingly, heptamannose **5** (65% inhibition at 2 mM), which contains both residues mimicking the D1 arm of $Man_9GlcNAc_2$ and an additional Manα1-2Manα1-2Manα1-6Man-linked branch, does not offer a further increased affinity over that of compound **3**. The second branch, not found in mammalian glycans, may force compound **5** to adopt an unusual conformation that is not optimal for 2G12 recognition.

 © 2004 Wiley-VCH Verlag GmbH & Co. KGaA, Weinheim

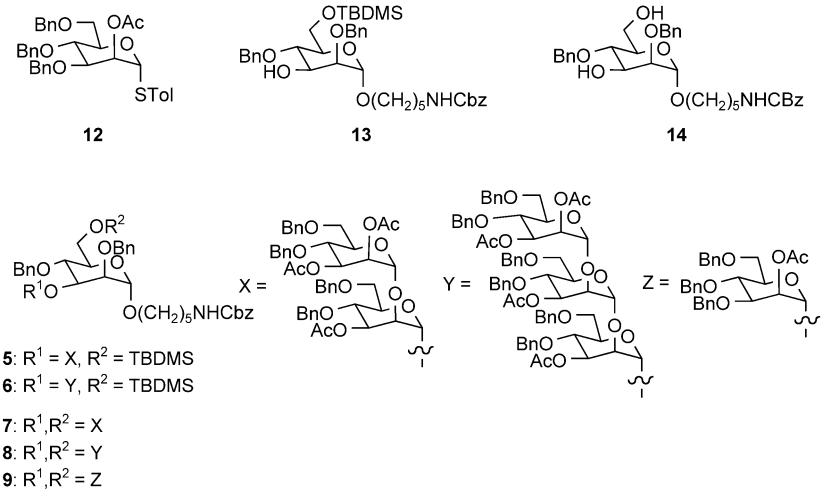


Table 2: The reaction conditions for the synthesis of oligosaccharides **15**–**18** and **2**–**6**.

Donor	Acceptor	NIS [equiv]	TfOH[a] [equiv]	T [°C]	t [h]	Protected oligosaccharide (yield [%])	Deprotected oligosaccharide (yield [%])
10	**13**	1.3	0.13	−20	2	**15** (85)	**2** (75)[b]
11	**13**	1.3	0.13	−10	4	**16** (83)	**3** (72)[b]
10	**14**	2.6	0.26	−20	2	**17** (65)	**4** (68)[c]
11	**14**	2.6	0.26	−10	4	**18** (63)	**5** (65)[c]
12	**14**	2.6	0.26	0	24	**19** (50)	**6** (60)[c]

[a] TfOH, trifluoroacetic acid. [b] a) 80% acetic acid, RT, 4 h; b) NaOMe, RT, 2 h; c) Pd black, 5% formic acid/MeOH, H_2, RT, 24 h. [c] a) NaOMe, RT, 2 h; b) Pd black, 5% formic acid/MeOH, H_2, RT, 24 h.

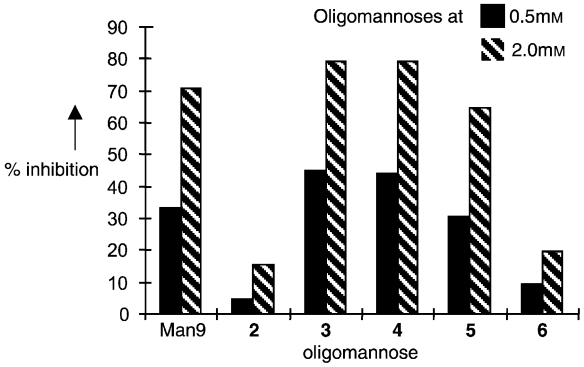


Figure 3. Inhibition (%) of 2G12 binding to gp120. Man9 = $Man_9GlcNAc_2$ (**1**).

In conclusion, we have developed a novel and efficient route to high-mannose oligosaccharides through a reactivity-based one-pot self-condensation reaction. By using this method we have prepared several Manα1-2Man-containing oligosaccharides and found they effectively inhibit the binding of 2G12 to gp120. We have identified new synthetic epitope mimics that are as effective as, or better than, $Man_9GlcNAc_2$ at inhibiting this interaction. Work is in progress to develop multivalent constructs as candidates for the development of an HIV vaccine.

Received: October 16, 2003 [Z53105]

Keywords: antibodies · drug design · oligosaccharides · self-condensation · synthetic methods

[1] a) N. L. Letvin, B. D. Walker, *Nat. Med.* **2003**, *9*, 861–866; b) A. J. McMichael, T. Hanke, *Nat. Med.* **2003**, *9*, 874–880.

[2] a) D. R. Burton, *Proc. Natl. Acad. Sci. USA* **1997**, *94*, 10018–10023; b) R. M. Ruprecht, R. Hofmann-Lehmann, B. A. Smith-Franklin, R. A. Rasmussen, V. Liska, J. Vlasak, W. Xu, T. W. Baba, A. L. Chenine, L. A. Cavacini, M. R. Posner, H. Katinger, G. Stiegler, B. J. Bernacky, T. A. Rizvi, R. Schmidt, L. R. Hill, M. E. Keeling, D. C. Montefiori, H. M. McClure, *Transfus. Clin. Biol.* **2001**, *8*, 350–358; c) J. R. Mascola, *Vaccine* **2002**, *20*, 1922–1925.

[3] D. R. Burton, *Nat. Rev. Immunol.* **2002**, *2*, 706–713.

[4] a) C. N. Scanlan, R. Pantophlet, M. R. Wormald, E. O. Saphire, R. Stanfield, I. A. Wilson, H. Katinger, R. A. Dwek, P. M. Rudd, D. R. Burton, *J. Virol.* **2002**, *76*, 7306–7321; b) R. W. Sanders, M. Venturi, L. Schiffner, R. Kalyanaraman, H. Katinger, K. O. Lloyd, P. D. Kwong, J. P. Moore, *J. Virol.* **2002**, *76*, 7293–7305.

[5] D. A. Calarese, C. N. Scanlan, M. B. Zwick, S. Deechongkit, Y. Mimura, R. Kunert, P. Zhu, M. R. Wormald, R. L. Stanfield, K. H. Roux, J. W. Kelly, P. M. Rudd, R. A. Dwek, H. Katinger, D. R. Burton, I. A. Wilson, *Science* **2003**, *300*, 2065–2071.

[6] Z. Y. Zhang, I. R. Ollmann, X.-S. Ye, R. Wischnat, T. Baasov, C.-H. Wong, *J. Am. Chem. Soc.* **1999**, *121*, 734–753.

[7] F. Burkhart, Z. Y. Zhang, S. Wacowich-Sgarbi, C.-H. Wong, *Angew. Chem.* **2001**, *113*, 1314–1317; *Angew. Chem. Int. Ed.* **2001**, *40*, 1274–1277.

[8] K.-K. T. Mong, C.-H. Wong, *Angew. Chem.* **2002**, *114*, 4261–4264; *Angew. Chem. Int. Ed.* **2002**, *41*, 4087–4090.

[9] T. K.-K. Mong, C.-Y. Huang, C.-H. Wong, *J. Org. Chem.* **2003**, *68*, 2135–2142.

[10] T. K.-K. Mong, H.-K. Lee, S. G. Durón, C.-H. Wong, *Proc. Natl. Acad. Sci. USA* **2003**, *100*, 797–802.

[11] a) P. Grice, S. V. Ley, J. Pietruszka, H. W. M. Priepke, *Angew. Chem.* **1996**, *108*, 206–208; *Angew. Chem. Int. Ed. Engl.* **1996**, *35*, 197–200; b) P. Grice, S. V. Ley, J. Pietruszka, H. M. I. Osborn, H. W. M. Priepke, S. L. Warriner, *Chem. Eur. J.* **1997**, *3*, 431–440; c) D. K. Baeschlin, L. G. Green, M. G. Hahn, B. Hinzen, S. J. Ince, S. V. Ley, *Tetrahedron: Asymmetry* **2000**, *11*, 173–197; for other syntheses of oligomannoses, see: d) D. M. Ratner, O. J. Plante, P. H. Seeberger, *Eur. J. Org. Chem.* **2002**, *5*, 826–833; e) I. Matsuo, M. Wada, S. Manabe, Y. Yamaguchi, K. Otake, K. Kato, Y. Ito, *J. Am. Chem. Soc.* **2003**, *125*, 3402–3403.

[12] a) N. E. Franks, R. Montgomery, *Carbohydr. Res.* **1968**, *6*, 286–298; b) C. S. Callam, T. L. Lowary, *J. Org. Chem.* **2001**, *66*, 8961–8972.

[13] T. Ogawa, K. Katano, K. Sasajima, M. Matsui, *Tetrahedron* **1981**, *37*, 2779–2786.

 © 2004 Wiley-VCH Verlag GmbH & Co. KGaA, Weinheim

Denitrogenation of Fuels

Denitrogenation of Transportation Fuels by Zeolites at Ambient Temperature and Pressure**

*Arturo J. Hernández-Maldonado and Ralph T. Yang**

The oil industry is facing increasing pressure to remove organic nitrogen compounds from transportation fuels (gasoline, diesel, and jet fuels).[1–5] Denitrogenation and desulfurization are accomplished commercially by hydrotreating using catalysts in reactors under high temperature and pressure. Denitrogenation is considerably more difficult than desulfurization because the organonitrogen compounds are much less reactive than the organosulfur compounds.[1–5] In this work, we show that denitrogenation can be achieved effectively by using a zeolite sorbent that removes the nitrogen-containing molecules by selective adsorption at ambient temperature and pressure. The sorbent can remove nitrogen from a commercial diesel fuel that contains 83 parts per million by weight (ppmw) nitrogen to well below 0.1 ppmw nitrogen at a sorbent capacity of 43 cm^3 diesel per gram of sorbent. The sorbent can be regenerated for re-use.

There is an increasing need to remove organonitrogen compounds from liquid fuels for two reasons: 1) denitrogenation is essential to many different refinery processes, and 2) to lower emission of nitrogen oxides from combustion processes.[1–3] In addition, it becomes increasingly important to process heavy, low-quality stocks and the anticipated syncrudes, both are rich in highly refractory nitrogen compounds. Denitrogenation and desulfurization are coupled and are performed simultaneously in catalytic hydrotreating, which is an integral part of oil refining. Thus, hydrodenitrogenation (HDN) is accomplished by reacting with hydrogen at 20–100 atm pressure and 300–380 °C using $CoMo/Al_2O_3$ or $NiMo/Al_2O_3$ as the catalyst. Two types of organic nitrogen compounds are found in petroleum and syncrudes: heterocycles and non-heterocycles. The latter consist of anilines and aliphatic amines that are relatively easy to remove by HDN. The heterocycles include compounds containing the six-membered pyridine ring and those containing the five-membered pyrrole ring. The derivatives of pyridine and pyrrole include those with one or two benzene rings as well as alkyl-substituted benzene rings. The kinetics of HDN are not well understood; however, some basic facts are known. The reactivities of the organonitrogen compounds are significantly lower than that of the corresponding organosulfur compounds.[1–5] For example, the alkyl-substituted carbazoles (i.e., pyrrole sandwiched between two benzene rings, the most abundant nitrogen compounds) appear to react at rates about 1/10 as fast as those of alkyl-dibenzothiophenes of comparable structures.[2] Thus, it is considerably more difficult to remove organonitrogen compounds than organosulfur compounds.

The new challenge is to use adsorption to selectively remove these nitrogen compounds from transportation fuels. Because adsorption would be accomplished at ambient temperature and pressure, success in this development would lead to major advances in petroleum refining. However, the commercially available sorbents[6] cannot selectively adsorb the nitrogen compounds.

A class of highly nitrogen-selective and high-nitrogen-capacity sorbents have been discovered and are reported here. This class of sorbents bind the organonitrogen compounds selectively by π complexation. This class of sorbents has been reported recently for desulfurization of transportation fuels, also by π complexation.[7]

The new sorbent for denitrogenation is a zeolite containing cuprous cations and was prepared by ion exchange of zeolites using known ion-exchange procedures.[8] First, this candidate was identified in a screening study that used molecular orbital (MO) theory to search for sorbents that would bond the organonitrogen molecules more strongly than benzene. Here benzene was used as a model compound for aromatic compoundss in transportation fuel that would compete for adsorption sites (by π complexation) against the nitrogen compounds. The calculations were performed at the Hartree–Fock (HF) and density functional theory (DFT) level using effective core potentials (ECPs).[9] The restricted Hartree–Fock (RHF) theory at the LanL2DZ level basis set[10] was used to determine the geometries and the adsorption bonding energies.[11] Moreover, natural bond orbital (NBO) analysis at the B3LYP/LanL2DZ level was used for studying the electron density distribution of the adsorption system.[11] A cluster model was used to represent the zeolite framework structure to which Cu^+ ions were bonded. The results for the adsorption bond energies are shown in Figure 1. Thiophene, the basic molecule for organosulfur compounds in transportation fuels, was also included for comparison. These results indicate that the Cu^+–zeolite could adsorb organonitrogen compounds preferentially over benzene. Thiophene is also preferentially adsorbed by CuY, but the adsorption of the organonitrogen compounds is significantly stronger. The natural bond orbital analysis showed that the bonding followed the classical picture of π complexation, with some donation of electron charges from the π orbital of the pyrrole ring to the vacant s orbital of metals known as σ donation and, simultaneously, back donation of electron charges from the d orbitals of metals to the π* orbital (i.e., antibonding π orbital) of pyrrole, or π back donation. Since many of the d-block metals and their cations are capable of π complexation,[6–8] zeolites with other d-block cations are expected to preferentially adsorb the organonitrogen compounds as well. It should be mentioned that for molecules containing amine or other functional

[*] A. J. Hernández-Maldonado, Dr. R. T. Yang
Chemical Engineering Department, University of Michigan
Ann Arbor, MI, 48109 (USA)
Fax: (+1) 734-764-7453
E-mail: yang@umich.edu

[**] We thank Dr. Alice He and Dr. William Cannella of Chevron-Texaco Research & Technology Company for the nitrogen analysis and discussion. This work was partially funded by Chevron Texaco and NSF. U.S. and foreign patents are pending.

Supporting information for this article is available on the WWW under http://www.angewandte.org or from the author.

 © 2004 Wiley-VCH Verlag GmbH & Co. KGaA, Weinheim DOI: 10.1002/anie.200353162

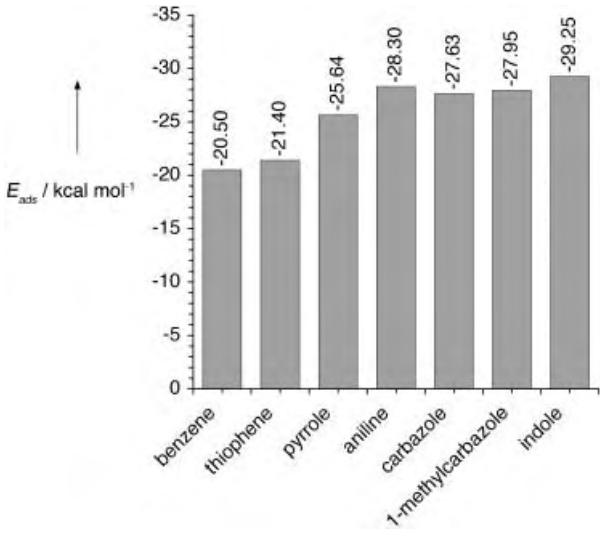


Figure 1. Energy of adsorption for different molecules on CuY zeolite.

groups, the adsorption energy is higher because of the electron-donating effect of the methyl group to the aromatic ring (Figure 1). A schematic representation of an aniline molecule interacting with a cuprous zeolite cluster is shown in Figure 2. Because of π complexation, all organonitrogen molecules adsorb on CuY in a flatwise, face-down manner, and hence are devoid of steric hindrance which inhibits their reaction in HDN.

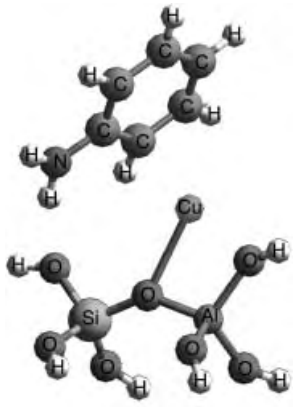


Figure 2. Optimized structure of aniline on Cu–Zeolite.

Then we proceeded to perform adsorption experiments for denitrogenation of a commercial diesel in a fixed-bed adsorber that contained particles of CuY zeolite, at ambient temperature and pressure. The zeolite was prepared by ion exchange of NaY zeolite (Si/Al = 2.43) with Cu^{2+}. The Cu^{2+} exchanged form was subsequently subjected to auto-reduction[12] to form $Cu^{I}Y$. The adsorber bed contained 1–2 g zeolite, while the feed flow rate was maintained at 0.5 $cm^3 min^{-1}$. Effluent (or eluent) samples were collected at regular intervals until saturation was reached, and the samples were subsequently analyzed for nitrogen-containing compounds with a gas chromatograph (GC) equipped with a chemiluminescent nitrogen detector (CLND, by Antek Instruments, Inc.). The CLND was operated at a sensitivity (or detection limit) of approximately 0.015 ppbw N.[2]

The results with the commercial diesel (containing 83 ppmw nitrogen) are summarized in Figure 3 for CuY as the sorbent in the main bed. A thin layer of activated carbon

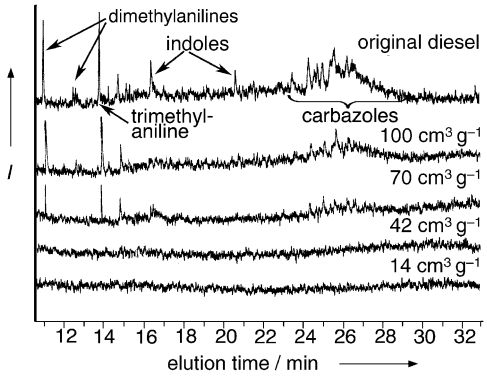


Figure 3. GC-CLND chromatograms of a commercial diesel for nitrogen analysis and progression of nitrogen breakthrough during diesel adsorption in the bed. The sampling time is expressed by cumulative effluent volume normalized by the sorbent weight ($cm^3 g^{-1}$). I = intensity in arbitrary units.

(15 % of the bed) was used as the guard bed that extended the sorbent capacity of the main bed by adsorbing the largest molecules from the fuels. For desulfurization, the sulfur capacity was increased by about 20 % by the guard bed.[7] However, the concentration of nitrogen in the effluent (before nitrogen breakthrough) remained the same without the guard bed. The nitrogen contents in the effluent product before the breakthrough point were below 0.1 ppmw nitrogen. The detailed nitrogen breakthrough behavior is shown in Figure 4. The detailed nitrogen analysis showed that the earliest nitrogen breakthrough appeared at a cumulative effluent volume of 43 $cm^3 g^{-1}$. This corresponds to a very high and practical sorbent capacity of 3 mg nitrogen per gram

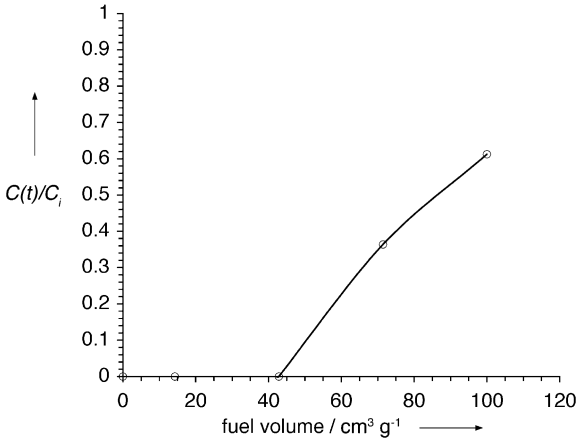


Figure 4. Breakthrough of total nitrogen heterocyclic compounds in a fixed-bed adsorber with AC/Cu^{I}-Y adsorbent, for diesel feed at room temperature. C_i is the total nitrogen concentration of the feed (83 ppmw).

 © 2004 Wiley-VCH Verlag GmbH & Co. KGaA, Weinheim

sorbent.[6] It should be mentioned that the zeolite sorbent selectively and effectively remove all alkylcarbazoles (see Figure 3). It is well known that substituted carbazoles poison the hydrodesulfurization (HDS) of the refractory sulfur species in diesel.[13,14]

Experiments on sorbent regeneration were also performed, which showed that CuY can be effectively regenerated either thermally or with solvents. CuY was regenerated by first treating with air at 350 °C (to burn off sulfur) followed by auto-reduction (of Cu^{2+} to Cu^{+}). Afterwards, the original adsorption capacity was completely recovered. For thermal regeneration, activated carbon would not be suitable for the guard bed; activated alumina would be effective.[8]

Received: October 27, 2003 [Z53162]

Keywords: adsorption · denitrogenation · desulfurization · pi-complexation · zeolites

[1] P. Zeuthen, K. G. Knudsen, D. D. Whitehurst, *Catal. Today* **2001**, *65*, 307 – 314.
[2] P. Wiwel, K. Knudsen, P. Zeuthen, D. D Whitehurst, *Ind. Eng. Chem. Res.* **2000**, *39*, 533 – 540.
[3] T. C. Ho, *Catal. Rev. Sci. Eng.* **1988**, *30*, 117 – 160.
[4] B. C. Gates, H. Topsoe, *Polyhedron* **1997**, *16*, 3213 – 3217.
[5] D. D. Whitehurst, T. Isoda, I. Mochida, *Adv. Catal.* **1998**, *42*, 345 – 471.
[6] R. T. Yang, *Adsorbents: Fundamentals and Applications*, Wiley, New York, **2003**.
[7] R. T. Yang, A. J. Hernández-Maldonado, F. H. Yang, *Science* **2003**, *301*, 79 – 81.
[8] A. J. Hernández-Maldonado, R. T. Yang, *Ind. Eng. Chem. Res.* **2003**, *42*, 123 – 129.
[9] P. J. Hay, W. R. Wadt, *J. Chem. Phys.* **1985**, *82*, 299 – 310.
[10] T. V. Russo, R. L. Martin, P. J. Hay, *J. Phys. Chem.* **1995**, *99*, 17085 – 17087.
[11] A. Takahashi, F. H. Yang, R. T. Yang, *Ind. Eng. Chem. Res.* **2002**, *41*, 2487 – 2496.
[12] S. C. Larsen, A. Aylor, A. T. Bell, J. A. Reimer, *J. Phys. Chem.* **1994**, *98*, 11533 – 11540.
[13] T. C. Ho, *J. Catal.* **2003**, *219*, 442 – 451.
[14] S. D. S. Murti, H. Yang, K. H. Choi, Y. Korai, I. Mochida, *Appl. Catal. A* **2003**, *252*, 331 – 346.

 © 2004 Wiley-VCH Verlag GmbH & Co. KGaA, Weinheim

Biomimetic Electrochemistry

A Biomimetic Pathway for Hydrogen Evolution from a Model of the Iron Hydrogenase Active Site**

Sascha Ott, Mikael Kritikos, Björn Åkermark, Licheng Sun, and Reiner Lomoth**

The recent elucidation of the structures of two iron hydrogenases isolated from different organisms[1,2] has provided a unique insight into the active site of these hydrogen-producing enzymes. This knowledge has fueled intense research aimed at the synthesis of close mimics of the active site that can achieve catalytic activities comparable to that found in the natural system.[3] The particular interest in this system arises from the fact that the enzyme relies exclusively on readily available iron cations in the active site.[4] Apart from a thiolate-linked $[Fe_4S_4]$ cluster, cyanide and carbonyl ligands populate the whole coordination sphere of the two iron nuclei in the site, which are within bonding distance of one another and are additionally connected by a nonproteic dithiolate bridge.[5–7] Although a subject of some controversy in the past, recent spectroscopic, crystallographic, and theoretical studies suggest the structure of this tether is S-CH_2-NH-CH_2-S (azadithiolate, ADT).[8,9] The importance of the nitrogen heteroatom in the disulfide bridge arises from its potential for protonation in its position close to the active site, which offers a thermodynamically and kinetically favorable pathway for hydrogen evolution in the natural system. Model complexes that exhibit catalytic features related to those of the iron hydrogenases have so far relied solely on propyldithiolate (PDT) bridges. For example, Rauchfuss and co-workers demonstrated that $[(\mu\text{-PDT})Fe_2(CO)_4PMe_3(CN)]^-$ serves as a catalyst for electrochemical hydrogen evolution,[10,11] and Darensbourg and co-workers have reported that $[(\mu\text{-H})(\mu\text{-PDT})Fe_2(CO)_4(PMe_3)_2]^+$ is a catalyst for H_2/D_2 scrambling.[12] In these models, the electron-donating cyanide

[*] Dr. S. Ott, Prof. Dr. B. Åkermark, Dr. L. Sun
Department of Organic Chemistry
Arrhenius Laboratory, Stockholm University
10691 Stockholm (Sweden)
Fax: (+46) 8-154-908
E-mail: sascha.ott@organ.su.se

Dr. R. Lomoth
Department of Physical Chemistry
BMC, Uppsala University
BOX 579, 75123 Uppsala (Sweden)
Fax: (+46) 18-471-3654
E-mail: reiner.lomoth@fki.uu.se

Dr. M. Kritikos
Department of Structural Chemistry
Arrhenius Laboratory, Stockholm University
10691 Stockholm (Sweden)

[**] We thank Fernando Lopes Pinto (Uppsala University) for his help with the hydrogen GC analysis. Financial support for this work was provided by the Swedish Energy Agency, the Knut and Alice Wallenberg Foundation, and the Swedish Research Council (VR).

 © 2004 Wiley-VCH Verlag GmbH & Co. KGaA, Weinheim DOI: 10.1002/anie.200353190

and phosphane ligands are crucial because they increase the electron density of the Fe^{I}–Fe^{I} bond and thereby facilitate protonation at this position.[13] In our approach, which involves light-driven proton reduction by utilizing a suitable photosensitizer,[14] such electronegative ligands are counterproductive as they shift the reduction potential of the respective diiron complex to more negative values and render electron transfer to this site unfavorable.[15] Once the first examples of mimics containing the azadithiolate (ADT) tether had been made available by us[14] and others,[16–18] we anticipated that an alternative, more biomimetic pathway for catalytic evolution of hydrogen may be accessible that involves the nitrogen heteroatom of the bridge acting as a basic site and allows electronically unfavorable ligands to be omitted.

To investigate this possibility, [(μ-ADT)$Fe_2(CO)_6$] (**1**; ADT = S-CH_2-NR-CH_2-S, R = *p*-bromobenzyl) was synthesized by a procedure similar to that previously used for the synthesis of analogous complexes.[14,17] The bromide functionality on the aromatic ring in complex **1** acts as a synthetic handle for the attachment of further redox-active components. Single-crystal x-ray diffraction analysis of **1** (Figure 1)[19] reveals the usual distorted square-pyramidal geometry around the iron centers.[14,16–18] In contrast to the crystal structures of phenyl-substituted ADT-bridged diiron complexes,[14] the benzyl moiety in that of **1** resides in a pseudo-equatorial position relative to the metalloheterocycle, with the nitrogen lone-pair pointing towards an iron nucleus. In the solid state, the nonbonding C···N distance between the ADT nitrogen atom and the nearest carbonyl carbon atom is significantly shorter in **1** than in the phenyl-substituted analogues (3.02 and 3.5 Å, respectively). After protonation of **1**, the proton is anticipated to be in proximity to the diiron active site. Protonation of **1** to form $\mathbf{1H^+}$ occurs in an acetonitrile solution upon addition of a strong acid such as triflic, hydrochloric, or perchloric acid.[20] The resonances in the ^{1}H NMR spectrum (CD_3CN) of $\mathbf{1H^+}$ are generally shifted to lower magnetic field strengths than those in **1**; the protons in proximity to the nitrogen atom are displaced by 0.64 and 0.31 ppm, respectively. The carbonyl frequencies in the IR spectrum of $\mathbf{1H^+}$ are shifted 15 cm^{-1} higher in energy relative to those of **1**, which is consistent with observations made during the protonation of a related complex.[18] Protonation of **1** is accompanied by a color change from orange to yellow. The UV absorption maximum is shifted from 328 to 332 nm, and during titration with acid an isosbestic point is preserved at 320 nm, which indicates the formation of a single protonation product at all acid concentrations (Figure 2).[21]

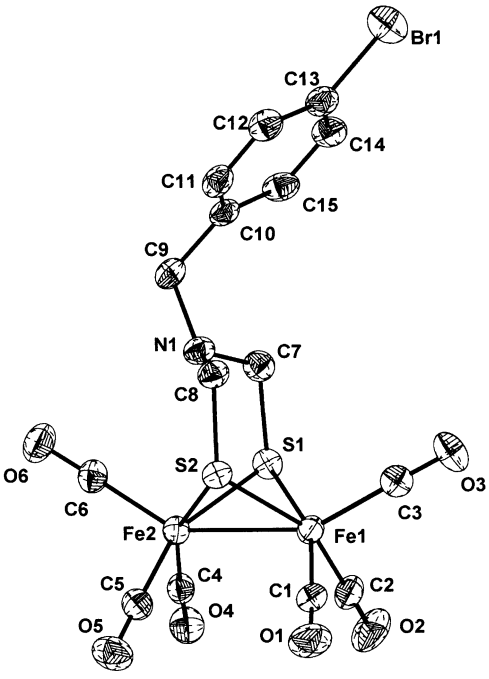


Figure 1. ORTEP view (ellipsoids at 30% probability level) of $C_{15}H_{10}BrFe_2NO_6S_2$ (**1**). Selected bond lengths [Å]: Fe1–Fe2 2.5083(7), Fe1–S1 2.2460(12), Fe1–S2 2.2526(10), Fe2–S1 2.2573(10), Fe2–S2 2.2682(10), Fe1–C1 1.785(5), Fe1–C2 1.791(4), Fe1–C3 1.803(4), Fe2–C4 1.790(4), Fe2–C5, 1.778(4), Fe2–C6 1.804(4), N1–C7 1.433(5).

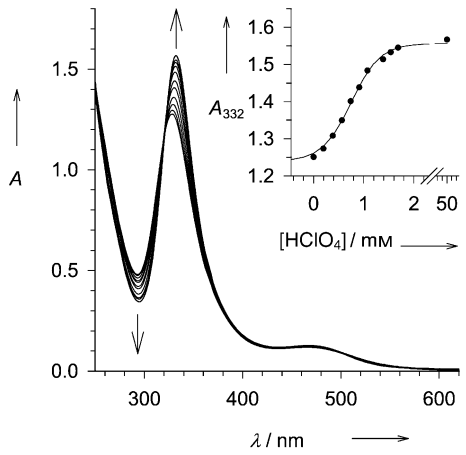


Figure 2. UV/Vis spectra (l = 1 mm) of **1** (1 mM) in acetonitrile. Arrows indicate spectral changes upon addition of increasing amounts of acid (concentrations as shown in the inset). Inset: absorbance at λ = 332 nm as a function of acid concentration.

The reduction behavior of **1** and $\mathbf{1H^+}$ was investigated by cyclic and differential pulse voltammetry. In dry acetonitrile, electrochemically irreversible one-electron reduction of **1** occurs at −1.56 V versus the ferrocene/ferrocenium couple (Fc/Fc^+; Figure 3a and inset).[22] Addition of excess perchloric acid to a 1 mM solution of **1** in acetonitrile resulted in the cyclic voltammogram of $\mathbf{1H^+}$ being observed. The first reduction peak is shifted by around 400 mV towards more positive potential, which is consistent with the introduced positive charge.[23] The position of this peak is independent of the acid concentration[21] and corresponds to a one-electron reduction of the protonated complex to **1H**. Following this reduction, a second reduction peak occurs around −1.4 V, the height of which increases and which shifts to more negative potential with increasing acid concentration (Figure 3a, inset). Both of these features are indicative of catalytic proton reduction,[24] which is also supported by the observation of gas evolution at this potential. Analysis of the reaction

 © 2004 Wiley-VCH Verlag GmbH & Co. KGaA, Weinheim

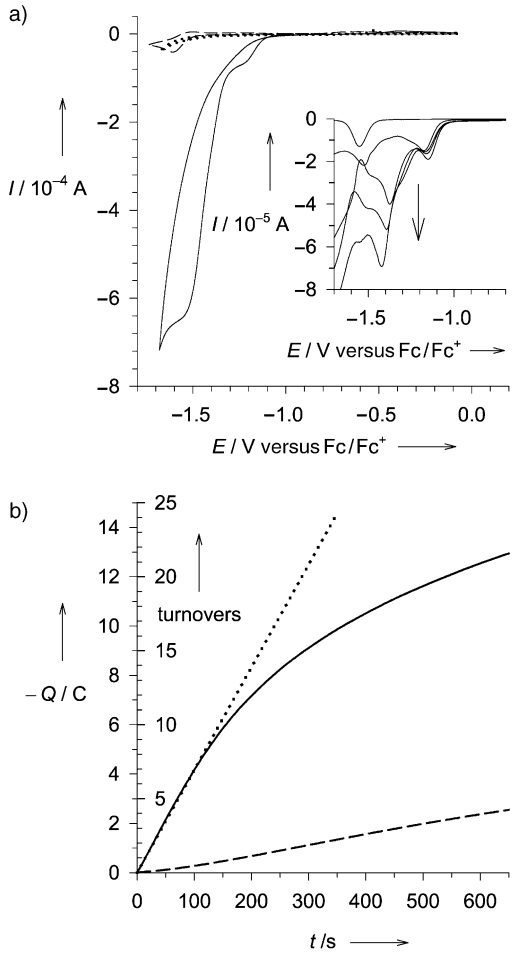
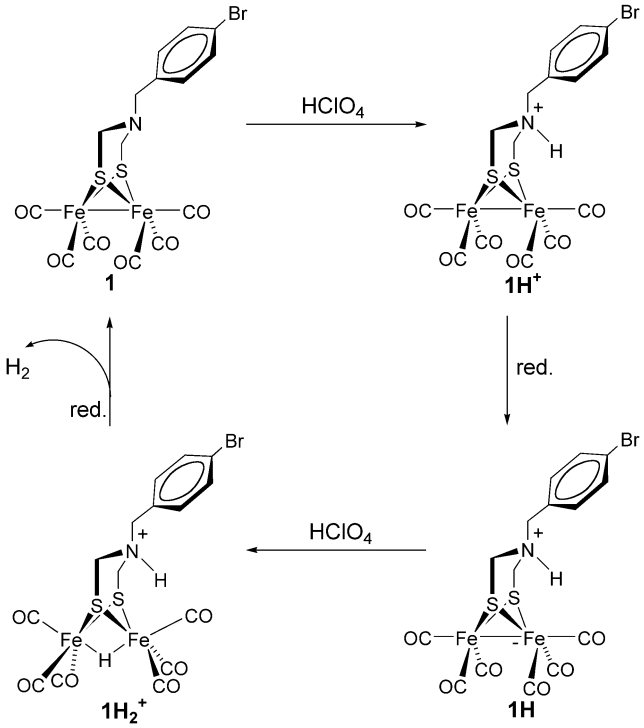


Figure 3. a) Cyclic voltammograms ($\nu = 0.100\ V s^{-1}$) of **1** (-----), $HClO_4$ (50 mM; •••••), and **1** in the presence of $HClO_4$ (50 mM; ——); inset: differential pulse voltammograms of **1** in the presence of increasing acid concentrations (0, 10, 30, 50, 70 mM) as indicated by the arrow; working electrode: glassy carbon; surface area: 0.07 cm^2. b) Coulometry for bulk electrolysis of $HClO_4$ (50 mM) at a graphite electrode in the presence of **1** (——) and without **1** (-----); extrapolation of the catalytic reduction at the initial electrolysis rate (•••••); electrolysis potential: −1.48 V; volume: 3 mL; electrode surface area: 1.4 cm^2. All measurements were made on 1 mM solutions of **1** in CH_3CN, with $(Bu)_4NPF_6$ (0.1 M) as the supporting electrolyte. All potentials given are versus Fc/Fc^+.

by gas chromatography showed hydrogen to be the sole gaseous product. Without the diiron complex, reduction of protons at the carbon electrode is slow at the potential of the second reduction peak.

Further evidence for the catalytic activity of **1** was obtained when solutions of **1** with excess perchloric acid were electrolyzed at −1.48 V, a potential slightly beyond the second reduction peak (Figure 3b). When the cell is loaded with a 1 mM solution of **1** containing 50 mM perchloric acid, the initial rate of electrolysis is more than 10 times higher than that in the absence of the catalyst, and 9 F (based on the amount of **1**) pass through the cell in 1 minute, which corresponds to 4.5 turnovers. The rate of electrolysis slows down as the proton concentration decreases and after approximately 10 minutes the total charge passed through the cell approaches its maximum of 50 F, which is equivalent to 25 turnovers. Once the current has dropped during electrolysis, the initial value can be recovered by replacing the consumed protons.

Based on the structural, spectroscopic, and electrochemical data described above, we propose the catalytic cycle shown in Scheme 1. After protonation, $\mathbf{1H^+}$ is electrochemically reduced to **1H** at −1.18 V. We anticipate that the reduction increases the electron density of the Fe^I–Fe^I bond and creates a situation similar to that achieved by the presence of electron-donating cyanide and phosphane ligands in other model complexes.[11,12] The electron-rich Fe–Fe bond is then available for protonation, which leads to $\mathbf{1H_2^+}$. This protonation enables the complex to undergo a second reduction at around −1.4 V, molecular hydrogen is then released, and the catalyst is liberated and made available for another cycle.



Scheme 1. Proposed catalytic cycle for the electrochemical reduction of protons in the presence of **1**.

Electrochemical production of hydrogen catalyzed by a mimic of the iron hydrogenase active site has been reported once before, with a potential of −1.2 V versus Ag/AgCl (corresponding to −1.71 V versus Fc/Fc^+)[25] required to drive the reduction of protons.[10] Omission of electron-withdrawing ligands at the diiron site and utilization of the basicity of the ADT nitrogen atom enabled us to shift this potential by 230 mV to a more positive value and thus make this reduction significantly easier. The shift in potential can be rationalized by considering the altered catalytic mechanism, which in our system commences with the protonation of the ADT nitrogen atom. In this way, the catalytic cycle proposed for **1** resembles the natural system more closely than other reported models.

 © 2004 Wiley-VCH Verlag GmbH & Co. KGaA, Weinheim

With a mimic of the iron hydrogenase active site that operates at a moderately negative potential, we are currently pursuing the incorporation of **1** into a device capable of using the action of light to drive the evolution of hydrogen.

Experimental Section

1: Reaction of *p*-bromobenzylamine,[26] *p*-CH_2O, thionylchloride, and the lithium salt of diironhexacarbonyldisulfide[27] on a 0.5-mmol scale gave 151 mg (0.27 mmol, 54%) of **1** as a red solid. Elemental analysis (%): calcd for $C_{15}H_{10}BrFe_2NO_6S_2$: C 32.40, H 1.81, N 2.52; found: C 32.44, H 1.99, N 2.52; ^{1}H NMR (300 MHz, CD_3CN): $\delta = 7.48$ (d, $J =$ 8.4 Hz, 2H), 7.12 (d, $J = 8.4$ Hz, 2H), 3.72 (s, 2H), 3.40 ppm (s, 4H); ^{13}C NMR (75 MHz, $CDCl_3$): $\delta = 207.7$, 134.9, 131.8, 130.3, 121.8, 61.2, 52.3 ppm; IR (CH_3CN): $\tilde{\nu} = 2074$, 2036, 1997 cm^{-1} (C=O); UV/Vis (CH_3CN): 328 (12800), 465 nm ($1200\,M^{-1}cm^{-1}$).

1H$^+$: ^{1}H NMR (300 MHz, CD_3CN): $\delta = 7.65$ (d, $J = 8.4$ Hz, 2H), 7.36 (d, $J = 8.4$ Hz, 2H), 4.36 (s, 2H), 3.71 ppm (very broad, 4H); ^{13}C NMR (75 MHz, CD_3CN): $\delta = 206.9$, 134.7, 133.6, 126.9, 125.9, 64.2, 49.4 ppm; IR (CH_3CN): $\tilde{\nu} = 2089$, 2052, 2016 cm^{-1} (C=O); UV/Vis (CH_3CN): 332 (15700), 465 nm ($1200\,M^{-1}cm^{-1}$).

Received: October 30, 2003 [Z53190]

Keywords: bioinorganic chemistry · biomimetic catalysis · electrochemistry · hydrogen · iron hydrogenase

[1] J. W. Peters, W. N. Lanzilotta, B. J. Lemon, L. C. Seefeldt, *Science* **1998**, *282*, 1853 – 1858.
[2] Y. Nicolet, C. Piras, P. Legrand, E. C. Hatchikian, J. C. Fontecilla-Camps, *Structure* **1999**, *7*, 13 – 23.
[3] J. Alper, *Science* **2003**, *299*, 1686 – 1687.
[4] M. Y. Darensbourg, E. J. Lyon, J. J. Smee, *Coord. Chem. Rev.* **2000**, *206–207*, 533 – 561.
[5] M. Frey, *ChemBioChem* **2002**, *3*, 152 – 160.
[6] J. W. Peters, *Curr. Opin. Struct. Biol.* **1999**, *9*, 670 – 676.
[7] Y. Nicolet, B. J. Lemon, J. C. Fontecilla-Camps, J. W. Peters, *Trends Biochem. Sci.* **2000**, *25*, 138 – 143.
[8] H.-J. Fan, M. B. Hall, *J. Am. Chem. Soc.* **2001**, *123*, 3828 – 3829.
[9] Y. Nicolet, A. L. de Lacey, X. Vernede, V. M. Fernandez, E. C. Hatchikian, J. C. Fontecilla-Camps, *J. Am. Chem. Soc.* **2001**, *123*, 1596 – 1602.
[10] F. Gloaguen, J. D. Lawrence, T. B. Rauchfuss, M. Benard, M.-M. Rohmer, *Inorg. Chem.* **2002**, *41*, 6573 – 6582.
[11] F. Gloaguen, J. D. Lawrence, T. B. Rauchfuss, *J. Am. Chem. Soc.* **2001**, *123*, 9476 – 9477.
[12] X. Zhao, I. P. Georgakaki, M. L. Miller, R. Mejia-Rodriguez, C.-Y. Chiang, M. Y. Darensbourg, *Inorg. Chem.* **2002**, *41*, 3917 – 3928.
[13] M. S. Arabi, R. Mathieu, R. Poilblanc, *J. Organomet. Chem.* **1979**, *177*, 199 – 209.
[14] S. Ott, M. Kritikos, B. Åkermark, L. Sun, *Angew. Chem.* **2003**, *115*, 3407 – 3410; *Angew. Chem. Int. Ed.* **2003**, *42*, 3285 – 3288.
[15] R. Mathieu, R. Poilblanc, P. Lemoine, M. Gross, *J. Organomet. Chem.* **1979**, *165*, 243 – 252.
[16] H. Li, T. B. Rauchfuss, *J. Am. Chem. Soc.* **2002**, *124*, 726 – 727.
[17] J. D. Lawrence, H. Li, T. B. Rauchfuss, *Chem. Commun.* **2001**, 1482 – 1483.
[18] J. D. Lawrence, H. Li, T. B. Rauchfuss, M. Benard, M.-M. Rohmer, *Angew. Chem.* **2001**, *113*, 1818 – 1821; *Angew. Chem. Int. Ed.* **2001**, *40*, 1768 – 1771.
[19] CCDC-222734 (**1**) contains the supplementary crystallographic data for this paper. These data can be obtained free of charge via www.ccdc.cam.ac.uk/conts/retrieving.html (or from the Cambridge Crystallographic Data Centre, 12 Union Road, Cambridge CB2 1EZ, UK; fax: (+44) 1223-336-033; or deposit@ccdc.cam.ac.uk).
[20] Unexpectedly, addition of acid to solutions of the related phenyl-substituted comlex [(μ-ADT)$Fe_2(CO)_6$] (where R = phenyl) did not result in protonation of the bridge nitrogen atom, as evidenced by unchanged UV/Vis, IR, and NMR spectra.
[21] Acid titrations, monitored by electrochemical, UV/Vis, and IR techniques indicate that a slight excess of acid is required for exhaustive protonation of **1** (see the inset in Figure 2).
[22] All potentials are given versus Fc/Fc$^+$ and as differential pulse voltammetry peak potentials E_{pk}.
[23] A similar effect can be observed for the irreversible oxidation potential of **1**, which is shifted anodically by about 400 mV upon protonation and formation of **1H$^+$**.
[24] I. Bhugun, D. Lexa, J.-M. Savéant, *J. Am. Chem. Soc.* **1996**, *118*, 3982 – 3983.
[25] The different reference systems were compared by using [(μ-$S(CH_2)_3S)Fe_2(CO)_6$] as a calibrating agent, which is reduced at −1.16 V versus Ag/AgCl (F. Gloaguen, J. D. Lawrence, M. Schmidt, S. R. Wilson, T. B. Rauchfuss, *J. Am. Chem. Soc.* **2001**, *123*, 12518 – 12527). With our reference system and under otherwise identical conditions, this complex is reduced at −1.67 V, which gives rise to a ΔE value of 0.51 V.
[26] R. P. Bonar-Law, A. P. Davis, B. J. Dorgan, *Tetrahedron* **1993**, *49*, 9855 – 9866.
[27] P. F. Brandt, D. A. Lesch, P. R. Stafford, T. B. Rauchfuss, *Inorg. Synth.* **1997**, *31*, 112 – 116.

 © 2004 Wiley-VCH Verlag GmbH & Co. KGaA, Weinheim

Stereochemistry

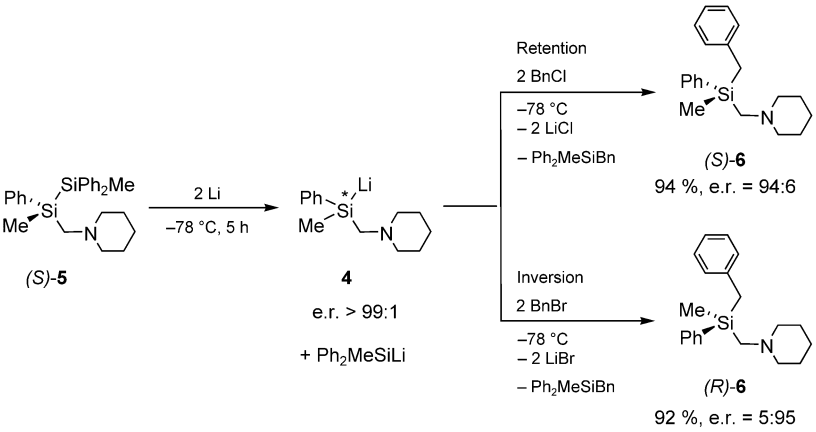
Enantiodivergence in the Reactions of a Highly Enantiomerically Enriched Silyllithium Compound with Benzyl Halides: Control of Inversion and Retention by Selection of Halide**

Carsten Strohmann, Martin Bindl, Verena C. Fraaß, and Jan Hörnig*

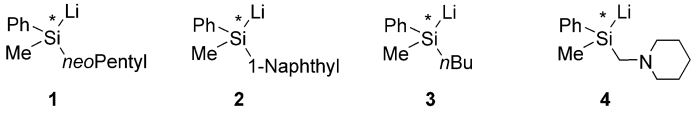
The reaction behavior of optically active silyllithium compounds was first described and investigated in detail by Sommer et al.[1] and later by Corriu et al.[2] and Kawakami et al.[3] The absolute configurations of the investigated compounds **1** and **2** were stable at room temperature. Their reactions with H_2O and H_2O/HCl gave the respective hydridosilanes with retention at the silicon center. It was deduced from these results that "silyl anions" react with electrophiles under retention.[4]

An alternative synthetic route by means of tin–lithium exchange has been described for **2** as has the racemization of **2** and **3** in solution.[3] The only reactions of enantiomerically enriched silyllithium compounds with chlorosilanes have been carried out by Kawakami et al. and our group.[3,5] Kawakami et al. described retention of configuration but in this work it was not made clear by the authors how the absolute configurations were unambiguously assigned and how these conclusions were reached. By our route the highly enantiomerically enriched silyllithium compound **4** (Scheme 1) is accessible which racemizes within a few hours at room temperature in THF. However, at low temperatures the resulting **4** reacts further with chlorosilanes selectively with retention starting from (*R*)-**5** and (*S*)-**5**, respectively.[5] The aminomethyl substituent allows resolution of the disilane (*S*)-**5** and simplifies analysis of the silanes investigated. The unexpected stereochemical reaction courses of the highly enantiomerically enriched silyllithium compound **4** with benzyl halides—the first reactions of an optically active silyllithium compound with organic electrophiles—is reported in the following.

Racemic silyllithium compounds react with chlorosilanes in good yields with the formation of disilanes. In contrast, reactions with alkyl halides give only modest yields, which probably accounts for why these reactions have aroused only little interest.[6] This is partly attributable to the observable coupling products (disilanes and products of C–C couplings) which can be the consequence of halogen–lithium exchange reactions.[7] These side reactions may be partially suppressed by lithium–copper exchange, but the respective silyl cuprates usually show an altered regioselectivity.[8] We therefore asked ourselves how the highly enantiomerically enriched silyllithium compound **4** reacts with benzyl halides and whether the stereochemical probe at the silicon center can provide information on the course of the reaction.



Scheme 1. Products of the reactions of the highly enantiomerically enriched compound **4** with benzyl chloride (retention) and benzyl bromide (inversion). The assignment of the stereochemical pathways relates to the disilane(*S*)-**5** used.



A solution of **4** was freshly prepared by cleavage of the unsymmetrical disilane (*S*)-**5** with lithium at −78 °C (it contains a molar equivalent $Ph_2MeSiLi$; see Scheme 1). A solution of **4** in THF[5] was added to the respective benzyl halide in THF (2.6 equivalents relative to (*S*)-**5**) at different temperatures. After warming to room temperature the product composition of the respective reaction mixture was determined before and after workup by GC-MS and NMR spectroscopy, and the enantiomeric ratios were determined by ^{1}H NMR spectroscopy in the presence of (*S*)-mandelic acid. Assuming that the Si–Si bond of (*S*)-**5** is cleaved with retention (see reference [5]) the reaction of **4** with benzyl chloride leads to benzylsilane (*S*)-**6** with retention. The analogous reaction with benzyl bromide yields in contrast the benzylsilane (*R*)-**6** with inversion.

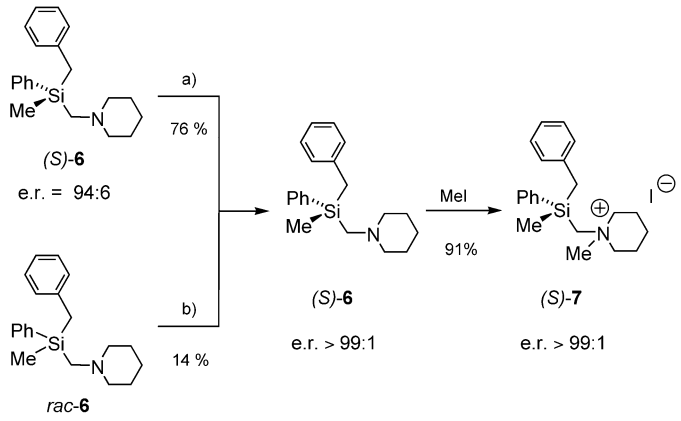
The assignment of the absolute configurations of (*S*)-**6** and (*R*)-**6** was carried out by single-crystal X-ray structure analysis of the methiodide (*S*)-**7** (Scheme 2).[9] Compound (*S*)-**7** was synthesized on the one hand from an enantiomerically pure sample of (*S*)-**6** obtained by repeated recrystallization as hydrochloride (Scheme 2, path (a)), and on the other

[*] Priv.-Doz. Dr. C. Strohmann, M. Bindl, V. C. Fraaß, J. Hörnig
Institut für Anorganische Chemie
Universität Würzburg
Am Hubland, 97074 Würzburg (Germany)
Fax: (+49) 931-888-4605
E-mail: mail@carsten-strohmann.de

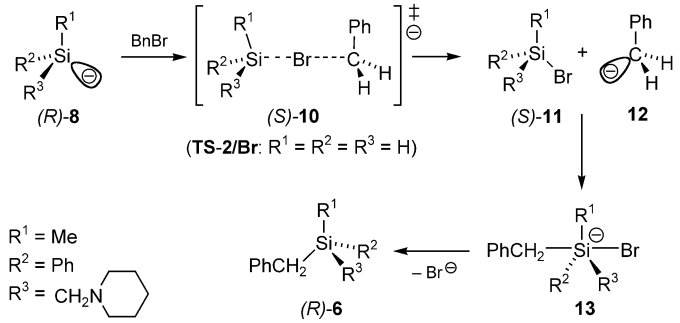
[**] We thank the Deutsche Forschungsgemeinschaft, the Graduiertenkolleg 690, and the Fonds der Chemischen Industrie for financial support of this work and Wacker-Chemie GmbH for providing us with special chemicals.

Supporting information for this article is available on the WWW under http://www.angewandte.com or from the author.

 DOI: 10.1002/anie.200352700 © 2004 Wiley-VCH Verlag GmbH & Co. KGaA, Weinheim



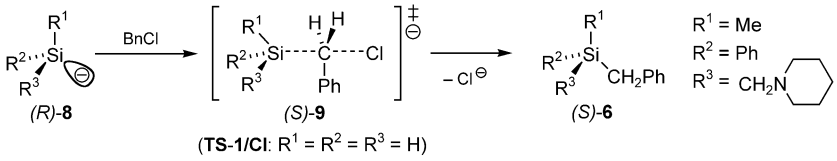
Scheme 2. Synthesis of enantiomerically pure (*S*)-**6** and methylation to (*S*)-**7**: a) recrystallization as hydrochloride, release with NaOH; b) resolution with di-*O*-4-toluoyl-D-tartaric acid, recrystallization as hydrochloride, release with NaOH.



Scheme 4. Proposed mechanism for the observed stereochemical reaction pathway of inversion with benzyl bromide.

from an enantiomerically pure sample of (*S*)-**6** prepared by resolution (Scheme 2, path (b)). Solutions prepared from single crystals of (*S*)-**7** measured by X-ray structure analysis exhibited the same rotation for linearly polarized light as the solutions of the respective enantiomerically pure total material.

With the assumption that the cleavage of the disilane (*S*)-**5** to **4** takes place with retention and formation of the anion (*R*)-**8**, two different reaction mechanisms can be proposed as explanation for the unusual stereochemical courses: the formation of the Si–C bond in the reaction of **4** or (*R*)-**8** with benzyl chloride follows an S_N2 mechanism under substitution of chloride at the benzylic carbon center with retention of configuration at the silicon center (Scheme 3). In



Scheme 3. Proposed mechanism for the observed stereochemical reaction pathway of retention with benzyl chloride. (Due to the change of substituents the priorities of CIP nomenclature and thus the absolute configurations are inverted here and in Scheme 4.)

the reaction of **4** or (*R*)-**8** with benzyl bromide, however, a bromine-lithium exchange occurs first with retention of the configuration at the silicon center (Scheme 4). The enantiomerically pure bromosilane (*S*)-**11** then reacts with benzyllithium under inversion of configuration at the silicon center so that the whole reaction sequence occurs with inversion.[10] If the first reaction step is sufficiently rapid few or no further coupling products of the halosilanes, silylithium and alkyllithium compounds should be formed—as observed in the experiment.[11]

Whereas in reactions with other nucleophiles the S_N2 mechanism has already been established,[12] the mechanism of halogen–lithium exchange reactions is still controversial.[13] The two extreme cases for the latter reaction are a radical mechanism with SET steps, and a mechanism with intermediate ate complexes. Experimental evidence has been described for both mechanisms. Several reports suggest that the courses of the reactions are highly associated with the type of electrophile, which greatly impairs a study of this mechanism.[13] Quantum-chemical studies of Boche et al. on methyl-ate complexes suggest that ate complexes are pivotal intermediates in halogen–lithium exchange reactions with alkyllithium compounds.[13e] Experimental and theoretical studies of Hoffmann et al. as part of the synthesis of optically active alkylmagnesium compounds show that ate complexes are also involved in iodine–magnesium exchange reactions with alkylmagnesium compounds.[13a–c]

In order to support the proposed mechanisms for our experimental observations (S_N2 mechanism and halogen–lithium exchange via an ate complex) DFT calculations (B3LYP/6-31 + G(d)) were carried out on the model system $H_3Si^-/ClCH_2Ph$ and $H_3Si^-/BrCH_2Ph$ (Figure 1).[14] The methods for the description of the relevant stationary points have been discussed comprehensively in a quantum-chemical study on the S_N2 mechanism published recently.[12] Since S_N2 reactions in the gas phase and in solution differ because of solvent effects, calculations with solvent models are necessary. The stationary points were energy optimized in THF solution by means of the self-consistent reaction field (SCRF) method based on the On-

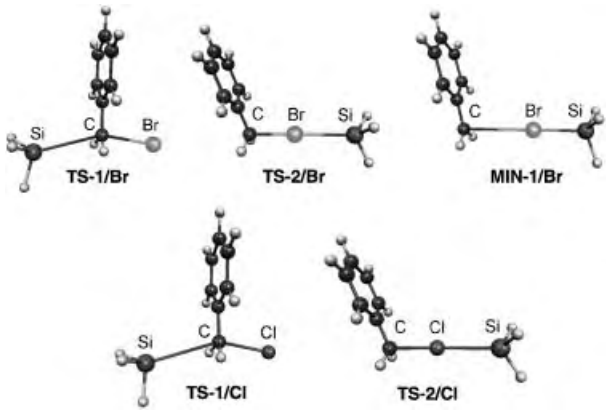


Figure 1. Molekel plots[16] of the calculated stationary points for the studied model systems $H_3Si^-/ClCH_2Ph$ und $H_3Si^-/BrCH_2Ph$.

 © 2004 Wiley-VCH Verlag GmbH & Co. KGaA, Weinheim

sager model, and the energies for the structures obtained were also calculated with the polarizable conductor calculation model (CPCM).[12,15] From the calculations with the CPC solvent model we obtained the following trends for the model systems studied (Table 1): in the case of benzyl chloride the transition state **TS-2/Cl** for a chlorine–lithium exchange lies about 12.9 kJ mol^{-1} higher than the alternative path through direct substitution of the halogen (**TS-1/Cl**). However, for benzyl bromide these energy relationships are reversed, and the bromine–lithium exchange (**TS-2/Br**) is favored by 9.5 kJ mol^{-1} over the substitution (**TS-1/Br**). Likewise, the ate complex **MIN-1/Br** can be characterized as a minimum. We were unable to localize an analogous ate complex for benzyl chloride. The DFT calculations on the model systems thus showed the trends observed in the experiment (Table 1).

Table 1: Relative energies E_{rel} of the calculated stationary points from Figure 1.

Relative energies E_{rel} [+zero point correction (ZPVE)] [kJ mol^{-1}]					
Method	**TS-1/Br**	**TS-2/Br**	**MIN-1/Br**	**TS-1/Cl**	**TS-2/Cl**
Onsager	19.3	0	−27.2	0	1.0
CPCM[a]	9.5	0	−38.4	0	12.9

[a] The energy values for zero-point correction (ZPVE) are derived from the frequency calculations with the Onsager model.

The small energy difference between the respective stationary points suggests a significant temperature dependency for the reaction of **4** with benzyl chloride and benzyl bromide. It emerged in the investigation that indeed in these reactions the resulting enantiomeric ratios were critically dependent upon the reaction temperature (Table 2), whereby the temperature dependency was less pronounced for benzyl bromide. However, no reduction in yield through formation of coupling products of the participating lithium and halogen compounds was observed on increasing the trapping reaction temperature.[11]

Table 2: Relationship between the enantiomeric ratios for the reaction of **4** with benzyl chloride and benzyl bromide and the reaction temperature.

Trapping reagent	*T* [°C]	(*S*):(*R*)
benzyl chloride	0	>55:45
	−40	83:17
	−78	94:6
benzyl bromide	0	18:82
	−40	8:92
	−78	5:95

It is unusual that two competing reaction mechanisms, which are associated with an opposing stereochemical course, supply such high yields. In initial experiments it emerged that other alkyl halides such as butyl halides or cyclopentyl halides exhibit an analogous trend in their reaction behavior. The nature of the halogen here too has a pivotal influence on the stereochemical outcome of reactions with the silyllithium compound **4**. It is thus not always necessary to convert a silyllithium compound into the corresponding cuprate to increase the respective selectivities.[8] Leaving group and temperature are furthermore critical for selective reactions with the silyllithium compound **4**. Only the stereochemical probe at the silicon center permitted us to obtain an insight into the described processes since the products of both reaction pathways differ merely in their absolute configuration at the silicon center. Currently we are investigating the question of how further specific influences can be exerted on the course of the reaction, for example, through choice of solvent.

Methods

The calculations were carried out with Gaussian 98,[14] energy minimizations and calculations were carried at the B3LYP/6-31+G(d) level with C_s symmetry. The SCRF method based on the Onsager model ($\varepsilon = 7.58$ for THF) was used for structure optimization and energy calculation. Single point energy calculations were carried out by means of CPCM for the stationary points minimized with the Onsager model. Zero-point corrections were obtained from the frequency calculations with the Onsager model. The transition states exhibited in each case exactly one imaginary frequency in the direction of the expected reaction coordinate. Because of the low rotational barriers of the SiH_3 groups a further weak imaginary frequency was found in each case for **TS-1/Cl**, **TS-1/Br**, and **TS-2/Cl** which are attributed to this process (see also lit. [13e] for related systems). Absolute electronic energies are collated in Table 3.

Table 3: Absolute electronic energies of the quantum-chemical calculations in atomic units.

Structure	*E* according to Onsager[a]	*E* according to CPCM
TS-1/Br	−3134.00838976 (0.138686)	−3134.06740722
TS-2/Br	−3134.01539512 (0.138354)	−3134.07068775
MIN-1/Br	−3134.02585360 (0.138438)	−3134.08538291
TS-1/Cl	−1022.47347412 (0.138720)	−1022.53251263
TS-2/Cl	−1022.47250767 (0.138126)	−1022.52701893

[a] The ZPVE values (in parentheses) for the zero-point correction are derived from the frequency calculations with the Onsager model.

Received: August 22, 2003 [Z52700]

Keywords: benzyl halides · density functional calculations · organosilanes · silyllithium compounds · stereochemistry

[1] L. H. Sommer, R. Mason, *J. Am. Chem. Soc.* **1965**, *87*, 1619–1620.
[2] a) E. Colomer, R. Corriu, *J. Chem. Soc. Chem. Commun.* **1976**, 176–177; b) E. Colomer, R. J. P. Corriu, *J. Organomet. Chem.* **1977**, *133*, 159–168.
[3] a) M. Omote, T. Tokita, Y. Shimizu, I. Imae, E. Shirakawa, Y. Kawakami, *J. Organomet. Chem.* **2000**, *611*, 20–25; b) H. Oh, M. Omote, K. Suzuki, I. Imae, Y. Kawakami, *Polym. Prepr. Am. Chem. Soc., Div. Polym. Chem.* **2001**, *42*, 194–195.
[4] a) J. L. Brefort, R. Corriu, C. Guerin, B. Henner, *J. Organomet. Chem.* **1989**, *370*, 9–15; b) L. H. Sommer, *Intra-Sci. Chem. Rep.* **1973**, *7*, 1–44; c) R. J. P. Corriu, C. Guerin, J. J. E. Moreau in *The Chemistry of Organic Silicon Compounds, Vol. 1* (Eds.: S. Patai, Z. Rappoport), Wiley, Chichester, **1989**, p. 305–370; d) E. Colomer, R. J. P. Corriu, *Top. Curr. Chem.* **1981**, 96, 79–107.
[5] C. Strohmann, J. Hörnig, D. Auer, *Chem. Commun.* **2002**, 766–767.

 © 2004 Wiley-VCH Verlag GmbH & Co. KGaA, Weinheim

[6] I. Fleming, R. S. Robert, S. C. Smith, *J. Chem. Soc. Perkin Trans. 1* **1998**, 1209 – 1214.
[7] A. Sekiguchi, M. Nanjo, C. Kabuto, H. Sakurai, *Organometallics* **1995**, *14*, 2630 – 2632.
[8] I. Fleming in *Organocopper Reagents* (Ed.: R. J. K. Taylor), Oxford University Press, Oxford (England), **1994**, p. 257 – 292.
[9] Crystal structure data for (*S*)-**7** ($C_{21}H_{30}INSi$): $M_r = 451.45$, orthorhombic, space group $P2_12_12_1$, $a = 9.877(5)$, $b = 9.917(3)$, $c = 22.001(8)$ Å, $V = 2154.8(15)$ Å^3, $Z = 4$, $\rho_{calcd} = 1.392$ Mg m^{-3}, $Mo_{K\alpha}$ radiation ($\lambda = 0.71073$ Å), $T = 173$ K; a single colorless platelet ($0.2 \times 0.2 \times 0.1$ mm^3) was mounted on a Stoe-IPDS diffractometer in an inert oil at −60 °C in a nitrogen stream (X-TEMP 2).[17] The intensities were collected in the 2θ range 5 – 52°. Of a total of 17272 reflections 4233 were independent ($R_{int} = 0.0586$). The structure was refined anisotropically on F^2 (G. M. Sheldrick, SHELXS-97, Universität Göttingen, Göttingen, **1997**): $R_1 = 0.0459$, $wR_2 = 0.1231$ (all data). The absolute configuration was determined by refinement of the Flack parameter to −0.03(3). CCDC-217658 contain the supplementary crystallographic data for this paper. These data can be obtained free of charge via www.ccdc.can.ac.uk/conts/retrieving.html (or from the Cambridge Crystallographic Centre, 12 Union Road, Cambridge CB2 1EZ, UK; Fax: (+44) 1223-336033; or deposit@ccdc.cam.ac.uk).
[10] The previously investigated optically active halosilanes reacted with organolithium compounds with inversion; especially for the benzyl anion as nucleophile inversion at the silicon center was always observed independent of the leaving group (see ref [4b] und [4c]).
[11] Coupling products of the compounds $MePh_2SiX$, $PhCH_2X$, and $PhMeSi(CH_2NC_5H_{10})X$ with X = Li, Cl, Br present in the reaction solutions were observed in only small amounts (< 1%) at reaction temperatures between −78 and 0 °C. The fraction of these coupling products rises significantly, however, if care is not taken during the reaction procedure to ensure that the reaction solution is immediately and thoroughly mixed (particularly pronounced in the reaction with benzyl chloride at 0 °C).
[12] Y. Fang, Y. Gao, P. Ryberg, J. Eriksson, M. Kolodziejska-Huben, A. Dybala-Defratyka, S. Madhavan, R. Danielsson, P. Paneth, O. Matsson, K. C. Westaway, *Chem. Eur. J.* **2003**, *9*, 2696 – 2709, and references therein.
[13] a) R. W. Hoffmann, M. Brönstrup, M. Müller, *Org. Lett.* **2003**, *5*, 313 – 316; b) M. Müller, M. Brönstrup, O. Knopff, V. Schulze, R. W. Hoffmann, *Organometallics* **2003**, *22*, 2931 – 2937; c) V. P. W. Böhm, V. Schulze, M. Brönstrup, M. Müller, R. W. Hoffmann, *Organometallics* **2003**, *22*, 2925 – 2930; d) K. B. Wiberg, S. Sklenak, W. F. Bailey, *J. Org. Chem.* **2000**, *65*, 2014 – 2021; e) G. Boche, M. Schimeczek, J. Cioslowski, P. Piskorz, *Eur. J. Org. Chem.* **1998**, 1851 – 1860; f) P. Beak, D. J. Allen, *J. Am. Chem. Soc.* **1992**, *114*, 3420 – 3425; g) W. F. Bailey, J. J. Patricia, *J. Organomet. Chem.* **1988**, *352*, 1 – 46, and refrences therein; h) H. Gilman, G. D. Lichtenwalter, *J. Am. Chem. Soc.* **1958**, *80*, 608 – 611; i) K.-W. Lee, J. S. Filippo, Jr., *Organometallics* **1983**, *2*, 906 – 908; j) J. S. Filippo, Jr., J. Silbermann, *J. Am. Chem. Soc.* **1982**, *104*, 2831 – 2836, and references therein.
[14] Gaussian 98 (Revision A.7), M. J. Frisch, G. W. Trucks, H. B. Schlegel, G. E. Scuseria, M. A. Robb, J. R. Cheeseman, V. G. Zakrzewski, J. A. Montgomery, R. E. Stratmann, J. C. Burant, S. Dapprich, J. M. Millam, A. D. Daniels, K. N. Kudin, M. C. Strain, O. Farkas, J. Tomasi, V. Barone, M. Cossi, R. Cammi, B. Mennucci, C. Pomelli, C. Adamo, S. Clifford, J. Ochterski, G. A. Petersson, P. Y. Ayala, Q. Cui, K. Morokuma, D. K. Malick, A. D. Rabuck, K. Raghavachari, J. B. Foresman, J. Cioslowski, J. V. Ortiz, B. B. Stefanov, G. Liu, A. Liashenko, P. Piskorz, I. Komaromi, R. Gomperts, R. L. Martin, D. J. Fox, T. Keith, M. A. Al-Laham, C. Y. Peng, A. Nanayakkara, C. Gonzalez, M. Challacombe, P. M. W. Gill, B. G. Johnson, W. Chen, M. W. Wong, J. L. Andres, M. Head-Gordon, E. S. Replogle, J. A. Pople, Gaussian, Inc., Pittsburgh, PA, **1998**.
[15] T. Mineva, N. Russo, E. Sicilia, *J. Comput. Chem.* **1998**, *19*, 290 – 299.
[16] P. Flükiger, H. P. Lüthi, S. Portmann, J. Weber, Swiss Center for Scientific Computing, MOLEKEL 4.0, Manno (Schweiz), **2000**.
[17] a) D. Stalke, *Chem. Soc. Rev.* **1998**, *27*, 171 – 178; b) T. Kottke, R. J. Lagow, D. Stalke, *J. Appl. Crystallogr.* **1996**, *29*, 465 – 468; c) T. Kottke, D. Stalke, *J. Appl. Crystallogr.* **1993**, *26*, 615 – 619.

 © 2004 Wiley-VCH Verlag GmbH & Co. KGaA, Weinheim

Hydrosilylation Catalysts

A Modular Assembly of Chiral Oxazolinylcarbene–Rhodium Complexes: Efficient Phosphane-Free Catalysts for the Asymmetric Hydrosilylation of Dialkyl Ketones**

Lutz H. Gade, Vincent César, and Stéphane Bellemin-Laponnaz**

The modular combination of a strongly bonded "anchor" unit with a chiral stereodirecting structural element is an underlying principle in the development of many phosphane-heteroatom-based chiral catalysts.[1] In the optimization of their catalytic performance, the assembly of such systems in essentially one step represents the ideal practical strategy. Given their facile chemical accessibility and stability, the replacement of phosphanes by N-heterocyclic carbenes and their combination with chiral donor units such as oxazolines provides an attractive alternative to the established catalytic systems.

N-heterocyclic carbenes have emerged as a new family of ligands for homogeneous catalysis.[2–4] However, despite the numerous efforts to prepare chiral carbene complexes,[5] there have been relatively few reports on highly enantioselective

[*] Prof. Dr. L. H. Gade,[+] V. César, Dr. S. Bellemin-Laponnaz
Laboratoire de Chimie Organométallique et de Catalyse (UMR 7513)
Institut Le Bel, Université Louis Pasteur
4, rue Blaise Pascal, 67070 Strasbourg (France)
Fax: (+33) 390-241-531
E-mail: gade@chimie.u-strasbg.fr
bellemin@chimie.u-strasbg.fr

[+] New address:
Anorganisch-Chemisches Institut
Universität Heidelberg
Im Neuenheimer Feld 270, 69120 Heidelberg (Germany)

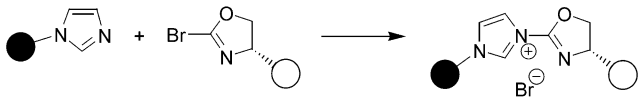
[**] We thank the CNRS (France) and the Institut Universitaire de France for support of this work and the Ministère de L'Education Nationale de la Recherche et de la Technologie for a Ph.D. grant to V.C. Support by BASF (Ludwigshafen) and Degussa (Hanau) is gratefully acknowledged. We thank Dr. A. De Cian and N. Gruber for the X-ray diffraction study.

Supporting information for this article is available on the WWW under http://www.angewandte.org or from the author.

 © 2004 Wiley-VCH Verlag GmbH & Co. KGaA, Weinheim DOI: 10.1002/anie.200353133

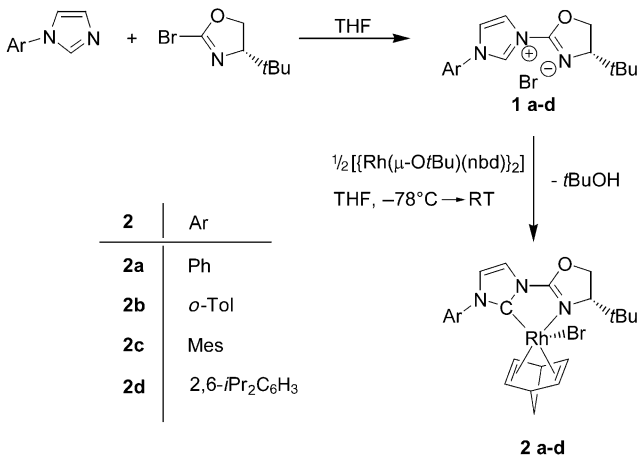
catalytic transformations using these systems. Notable examples include a chiral olefin metathesis catalyst reported by Hoveyda and co-workers[6] as well as the development of highly efficient asymmetric hydrogenation catalysts based on carbene–oxazoline iridium complexes reported by Burgess et al.[7] However, most examples of asymmetric catalysis using chiral carbenes, such as the hydrosilylation of ketones, have provided much lower enantioselection.[8–10]

We recently reported the synthesis of an achiral oxazolinyl-carbene ligand (A-B), which is easily obtained by a direct linkage between the two heterocycles A and B.[11] This



modular approach, which assembles both the "anchor" and the chiral directing unit(s) in a single coupling step, was thought to be an efficient strategy for the development of novel (chiral) catalysts. Based on this general consideration, we report a chiral N-heterocyclic carbene derivative that is highly efficient as a ligand for the Rh-catalyzed asymmetric hydrosilylation of, in particular, dialkyl ketones.

The chiral oxazoline–carbene ligands were prepared by reacting 2-bromo-4(*S*)-*tert*-butyl oxazoline with several imidazole derivatives in THF at room temperature to generate the corresponding aryl imidazolium salts **1a–d** in good yields (Scheme 1).[12,13] The steric demand at the *ortho* position of



2	Ar
2a	Ph
2b	*o*-Tol
2c	Mes
2d	2,6-*i*Pr$_2$C$_6$H$_3$

Scheme 1. Synthesis of the catalysts **2a–d**.

the *N*-phenyl substituent increases in the series from **1a** to **1d**. The reaction of **1a–d** with [{Rh(μ-O*t*Bu)(nbd)}$_2$] generated in situ leads to the corresponding N-heterocyclic complexes **2a–d** in 80–89% yield.[14]

Crystals suitable for X-ray structure analysis were obtained for complex **2c**, and its molecular structure is represented in Figure 1. The complex possesses a slightly distorted square-pyramidal coordination geometry with the

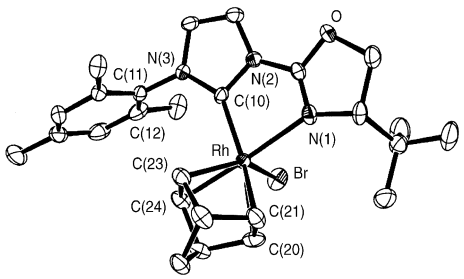


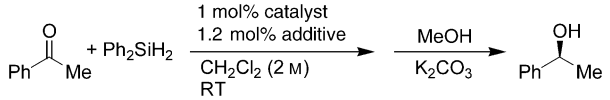
Figure 1. Molecular structure of the rhodium complex **2c**. Selected bond lengths [Å] and angles [°]: Rh-N(1) 2.285(3), Rh-C(10) 2.001(4), Rh-Br 2.6775(5), Rh-C(20) 2.231(4), Rh-C(21) 2.231(4), Rh-C(23) 2.084(4), Rh-C(24) 2.070(4); Br-Rh-N(1) 91.72(9), Br-Rh-C(10) 96.5(1), N(1)-Rh-C(10) 77.0(1).

bromo ligand in the apical position.[15] The mesityl ring plane is twisted almost orthogonally out of the plane of the central molecular unit (C(10)-N(3)-C(11)-C(12) 81.6°). The Rh–C bond lengths of 2.231(4) Å for the norbornadiene carbon atoms in *trans* disposition to the carbene ligand are significantly longer than those *trans* to the oxazoline-N donor atom (Rh–C(23) 2.084(4), Rh–C(24) 2.070(4) Å). This is consistent with the previously observed strong *trans* influence of the N-heterocyclic carbene ligands.[16]

Recently, a number of very efficient phosphane-hetero-donor-based catalysts for the stereoselective hydrosilylation of ketones have been reported, notably by Fu and Tao[17] and Evans et al.[18] Whereas aryl-alkyl-substituted ketones are transformed with very high enantioselectivity, the application of this catalytic reaction to unsymmetrical dialkyl ketones remains a challenge. One goal of our work therefore was the asymmetric hydrosilylation of such ketones with the new class of rhodium complexes **2a–d**. These complexes would represent the first carbene complexes to display high enantioselectivity for this reaction.

We chose the hydrosilylation of acetophenone with diphenylsilane as the reference reaction to test the potential of the catalysts. Complexes **2a–d**, which differ in the pattern of the *ortho*-substituents at the aryl group and which were used with a catalyst loading of 1.0 mol% in the presence of a slight excess of $AgBF_4$, gave the results displayed in Table 1. The *N*-mesityl-substituted catalyst **2c** (Table 1, entry 3) gave the highest selectivity at 20 °C with 65% *ee*.[19] The formation of the square-planar cationic rhodium species as active

Table 1: Asymmetric hydrosilylation of acetophenone with catalysts **2a–d** at room temperature.

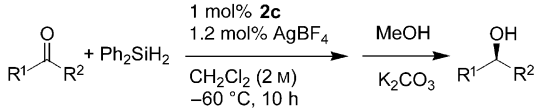


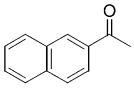
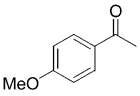
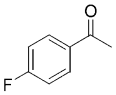
Entry	Catalyst	Additive	*ee* [%]	Yield [%]
1	**2a**	$AgBF_4$	0	90
2	**2b**	$AgBF_4$	31	82
3	**2c**	$AgBF_4$	65	90
4	**2c**	none	13	53
5	**2d**	$AgBF_4$	20	89

 © 2004 Wiley-VCH Verlag GmbH & Co. KGaA, Weinheim

catalyst appears to be crucial since the use of compound **2c** without the silver salt gave both poor yield and enantioselectivity (Table 1, entry 4). Lowering the reaction temperature led to a significant increase in stereoselectivity, while, remarkably, barely altering the activity of the catalysts. The catalytic runs performed at −60 °C gave the best results, with acetophenone being hydrosilylated cleanly giving the product with an enantiomeric excess of 90 % after a reaction time of 10 h. Similarly high enantioselectivities were obtained in the reduction of a variety of aryl alkyl ketones under these optimized reaction conditions (Table 2).

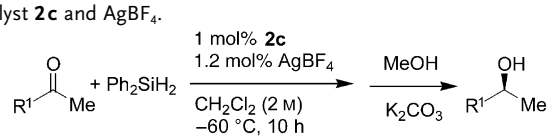
Table 2: Asymmetric hydrosilylation of aryl alkyl ketones with catalyst **2c** and $AgBF_4$.

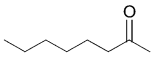
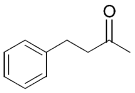
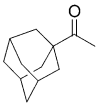


Entry	Ketone	*ee* [%]	Yield [%]
1		90	92
2		91	99
3		89	93
4		88	92
5		91	90

Whereas the selectivity in the hydrosilylation of aryl alkyl ketones is much higher than for previously reported chiral carbene catalysts, it is nevertheless somewhat below that of the most efficient phosphane-based systems with which values of over 95 % *ee* were obtained.[10,17,18,20] This may be related to the absence of an aryl-directing group in complex **2c**, the principal stereodirecting function most probably being the *tert*-butyl group in the oxazoline ring. We therefore probed the efficiency of precatalyst **2c** in the hydrosilylation of unsymmetrical *dialkyl* ketones which have proved to be difficult substrates for the known chiral catalysts, although recent progress has been reported by Fu and co-workers.[17] Carrying out the Rh-catalyzed transformation under conditions identical to those described above gave the corresponding secondary alcohols in high enantiopurity (Table 3). In particular, the relatively high *ee* values obtained for the ketones that do not contain an α-branching point is remarkable (Table 3, entries 1 and 2) and makes this novel class of chiral catalysts promising candidates for the further development of this field aimed at the general application of this methodology in stereoselective organic synthesis.

Table 3: Asymmetric hydrosilylation of a series of dialkyl ketones with catalyst **2c** and $AgBF_4$.



Entry	Ketone	*ee* [%]	Yield [%]
1		79	95
2		77	97
3		81	63[a]
4		88	53[b]
5		95	70[a]
6		89	96

[a] A conversion of > 98 % was observed by ^{1}H NMR spectroscopy. The moderate yield was due to the volatility of the products. [b] A conversion of 85 % was observed by ^{1}H NMR spectroscopy.

In summary, we have reported a readily accessible, efficient chiral *N*-heterocyclic carbene ligand for asymmetric hydrosilylation of ketones. Moreover, the modular synthesis of the oxazolinylcarbene ligands allows the facile access to a large ligand library. Future work will explore the potential of this class of C,N-heterodonor ligands in other stereoselective catalytic reactions.[21]

Experimental Section

General procedure for the hydrosilylation reaction (Table 2, entry 1): A solution of **2c** (5.9 mg, 0.01 mmol) in CH_2Cl_2 (0.3 mL) was added to $AgBF_4$ (2.3 mg, 1.2 equiv) under a nitrogen atmosphere. After the mixture had been stirred for 5 min, the red solution was filtered over a bed of celite and rinsed with additional CH_2Cl_2 (0.2 mL). Acetophenone (117 μL, 1.0 mmol) was added to this solution, the reaction mixture was cooled to −60 °C, and diphenylsilane (210 μL, 1.1 mmol) was subsequently added dropwise over a period of 2 min. The bright yellow reaction mixture was stirred at −60 °C for 10 h. A solution of K_2CO_3 (2.0 mL) in methanol (0.1 %) was then added and the resulting mixture was stirred for 4 h at room temperature. After evaporation of the solvents, the product (*S*)-*sec*-phenethyl alcohol (112 mg, 92 %) was purified by silica gel chromatography. GC analysis showed 90 % *ee*.

Crystal data for **2c**: $C_{26}H_{33}BrN_3ORh$, $M_r = 586.39$, orange crystals, dimensions $0.25 \times 0.20 \times 0.20$ mm, orthorhombic, space group $P2_12_12_1$, $a = 9.7117(1)$, $b = 13.7354(2)$, $c = 18.3991(2)$ Å, $U = 2454.33(5)$ Å^3, $Z = 4$, $\rho_{calcd} = 1.59$ g cm^{-3}, $\mu = 2.347$ mm^{-1}, $F(000) = 1192$, number of data measured: 7139 ($2.5 < \theta < 30.03°$) at 173 K, number of data with $I > 3\sigma(I)$: 3461, number of variables: 289, $R = 0.030$, $Rw = 0.048$, GOF = 1.020, largest peak in final difference: 0.532 e Å^{-3}. CCDC-221154 contains the supplementary crystallo-

 © 2004 Wiley-VCH Verlag GmbH & Co. KGaA, Weinheim

graphic data for this paper. These data can be obtained free of charge via www.ccdc.cam.ac.uk/conts/retrieving.html (or from the Cambridge Crystallographic Data Centre, 12, Union Road, Cambridge CB2 1EZ, UK; fax: (+44) 1223-336-033; or deposit@ccdc.cam.ac.uk).

Received: October 22, 2003 [Z53133]

Keywords: asymmetric catalysis · carbene ligands · hydrosilylation · ketones · rhodium

[1] a) G. Helmchem, A. Pfaltz, *Acc. Chem. Res.* **2000**, *33*, 326; b) for a general review, covering phosphane-oxazoline ligands in catalysis, see: P. Braunstein, F. Naud, *Angew. Chem.* **2001**, *113*, 702; *Angew. Chem. Int. Ed.* **2001**, *40*, 681.

[2] Reviews: a) W. A. Herrmann, *Angew. Chem.* **2002**, *114*, 1342; *Angew. Chem. Int. Ed.* **2002**, *41*, 1290; b) D. Bourissou, O. Guerret, F. Gabbaï, G. Bertrand, *Chem. Rev.* **2000**, *100*, 39; c) W. A. Herrmann, C. Köcher, *Angew. Chem.* **1997**, *109*, 2257; *Angew. Chem. Int. Ed. Engl.* **1997**, *36*, 2162.

[3] Selected examples for palladium-catalyzed coupling reactions: a) G. Altenhoff, R. Goddard, C. W. Lehmann, F. Glorius, *Angew. Chem.* **2003**, *115*, 3818; *Angew. Chem. Int. Ed.* **2003**, *42*, 3690; b) C. W. K. Gstöttmayr, V. P. W. Böhm, E. Herdtweck, M. Grosche, W. A. Herrmann, *Angew. Chem.* **2002**, *114*, 1421; *Angew. Chem. Int. Ed.* **2002**, *41*, 1363; c) G. A. Grasa, M. S. Viciu, J. Huang, C. Zhang, M. L. Trudell, S. P. Nolan, *Organometallics* **2002**, *21*, 2866; d) D. S. McGuinness, K. J. Cavell, *Organometallics* **2000**, *19*, 741.

[4] Selected examples of ruthenium-catalyzed olefin ring-closing metathesis: a) T. Weskamp, F. J. Kohl, W. Hieringer, D. Gleich, W. A. Herrmann, *Angew. Chem.* **1999**, *111*, 2573; *Angew. Chem. Int. Ed.* **1999**, *38*, 2416; b) M. Scholl, T. M. Trnka, J. P. Morgan, R. H. Grubbs, *Tetrahedron Lett.* **1999**, *40*, 2247; c) J. Huang, H. Z. Schanz, E. D. Stevens, S. P. Nolan, *Organometallics* **1999**, *18*, 5375; d) L. Ackermann, A. Fürstner, T. Weskamp, F. J. Kohl, W. A. Herrmann, *Tetrahedron Lett.* **1999**, *40*, 4787.

[5] Review on N-heterocyclic carbene ligands in asymmetric catalysis: M. C. Perry, K. Burgess, *Tetrahedron: Asymmetry* **2003**, *14*, 951.

[6] J. J. Van Veldhuizen, S. B. Garber, J. S. Kingsbury, A. H. Hoveyda, *J. Am. Chem. Soc.* **2002**, *124*, 4954.

[7] M. C. Perry, X. Cui, M. T. Powell, D. R. Hou, J. H. Reibenspies, K. Burgess, *J. Am. Chem. Soc.* **2003**, *125*, 113.

[8] Herrmann et al. obtained enantiomeric excesses of up to 32% *ee*: W. A. Herrmann, L. J. Goossen, C. Kocher, G. R. J. Artus, *Angew. Chem.* **1996**, *108*, 2580; *Angew. Chem. Int. Ed. Engl.* **1996**, *35*, 2805.

[9] Enders et al. reported maximum enantiomeric excesses of 44% *ee* in hydrosilylation catalysis with chiral N-heterocyclic carbenes: a) D. Enders, H. Gielen, J. Runsink, K. Breuer, S. Brode, K. Boehn, *Eur. J. Inorg. Chem.* **1998**, 913; b) D. Enders, H. Gielen, J . *Organomet. Chem.* **2001**, *617–618*, 70.

[10] a) For a review on asymmetric hydrosilylation, see: H. Nishiyama, K. Itoh, *Catalytic Asymmetric Synthesis* (Ed.: I. Ojima), Wiley-VCH, New York, **2000**, chap. 2.

[11] V. César, S. Bellemin-Laponnaz, L. H. Gade, *Organometallics* **2002**, *21*, 5204.

[12] For the synthesis of the 2-bromo-oxazoline, see: A. I. Meyers, K. A. Novachek, *Tetrahedron Lett.* **1996**, *37*, 1747.

[13] We also recently reported a very efficient way to synthesize trisoxazolines using 2-bromooxazoline, see: a) S. Bellemin-Laponnaz, L. H. Gade, *Chem. Commun.* **2002**, 1286; b) S. Bellemin-Laponnaz, L. H. Gade, *Angew. Chem.* **2002**, *114*, 3623; *Angew. Chem. Int. Ed.* **2002**, *41*, 3473.

[14] C. Köcher, W. A. Herrmann, *J. Organomet. Chem.* **1997**, *532*, 261.

[15] Due to the arrangement of the ligands, a stereogenic center at the metal atom is created leading to the existence of a possible second diastereoisomer. However, we were not able to detect any trace of the second diastereomer by classical spectroscopic methods.

[16] Similar examples for the *trans* influence of carbene ligands, see: a) A. R. Chianese, X. Li, M. C. Janzen, J. W. Faller, R. H. Crabtree, *Organometallics* **2003**, *22*, 1663; b) J. A. Loch, M. Albrecht, E. Peris, J. Mata, J. W. Faller, R. H. Crabtree, *Organometallics* **2002**, *21*, 700; c) A. C. Hillier, H. M. Lee, E. D. Stevens, S. P. Nolan, *Organometallics* **2001**, *20*, 4246.

[17] Fu and Tao reported a new P,N ligand family giving high enantioselectivities: B. Tao, G. C. Fu, *Angew. Chem.* **2002**, *114*, 4048; *Angew. Chem. Int. Ed.* **2002**, *41*, 3892.

[18] Evans et al. reported a new P,S ligand family giving very high activity and selectivity in Rh-catalyzed hydrosilylation: D. A. Evans, F. E. Michael, J. S. Tedrow, K. R. Campos, *J. Am. Chem. Soc.* **2003**, *125*, 3534.

[19] The influence of the silane structure on the enantioselectivity of the reaction was investigated and we found that the standard reducing agent diphenylsilane gave the best results.

[20] a) R. Kuwano, M. Sawamura, J. Shirai, M. Takahashi, Y. Ito, *Bull. Chem. Soc. Jpn.* **2000**, *73*, 485, and references therein; b) Y. Yamanoi, T. Imamoto, *J. Org. Chem.* **1999**, *64*, 2988.

[21] Note added in proof (14.1.2004): While this work was in press an efficient chiral biscarbene–rhodium hydrosilylation catalyst was reported: W.-L. Duan, M. Shi, G. B. Rong, *Chem. Commun.* **2003**, 2916.

 © 2004 Wiley-VCH Verlag GmbH & Co. KGaA, Weinheim

Organometallic Reagents

Nucleophilic Catalysis of the Iodine–Zinc Exchange Reaction: Preparation of Highly Functionalized Diaryl Zinc Compounds**

*Florian F. Kneisel, Maximilian Dochnahl, and Paul Knochel**

Halogen–metal exchange reactions are among the most powerful methods for preparing organometallic reagents. Pioneered by Wittig et al.[1] and Gilman et al.,[2] the halogen–lithium exchange has become an important method for the preparation of functionalized aryl and heteroaryl lithium compounds.[3] The halogen–magnesium[4] and the halogen–

[*] Dipl.-Chem. F. F. Kneisel, M. Dochnahl, Prof. Dr. P. Knochel
Ludwig-Maximilians-Universität München
Department Chemie
Butenandtstrasse 5–13, Haus F, 81377 München (Germany)
Fax: (+49) 89-218-077-680
E-mail: knoch@cup.uni-muenchen.de

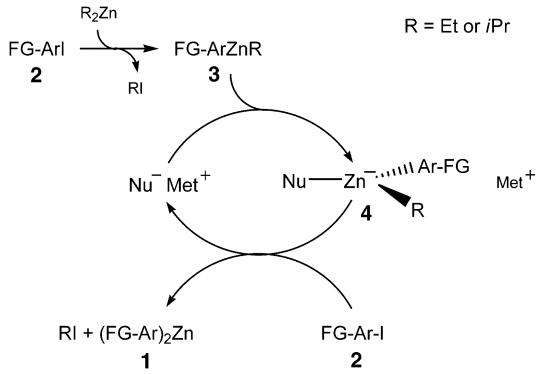
[**] We thank the Deutsche Forschungsgemeinschaft for a fellowship to F.F.K. (KN 347/6-1) and the Fonds der Chemischen Industrie for generous financial support. We thank BASF AG (Ludwigshafen) and Chemetall GmbH (Frankfurt) for generous gifts of chemicals and Florence Darbour for preliminary experiments.

Supporting information for this article is available on the WWW under http://www.angewandte.org or from the author.

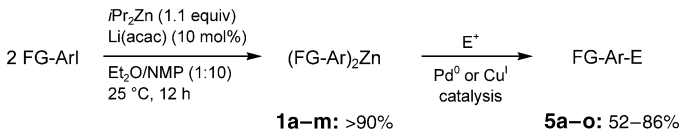
 DOI: 10.1002/anie.200353316 © 2004 Wiley-VCH Verlag GmbH & Co. KGaA, Weinheim

copper[5] exchange reactions were recently investigated extensively, as they allow convenient access to polyfunctional organometallic compounds.[6] However, the exchange rate of these reactions is considerably slower than that of the halogen–lithium exchange. Similary, the halogen–zinc exchange reaction can only be used for the preparation of primary and secondary dialkyl zinc compounds[7] and fails in the case of aromatic iodides.[8,9] During the course of our investigations into iodine–zinc exchange reactions of alkyl iodides, we found that magnesium salts accelerate the reaction by a factor of ≈ 200.[7a] However, this effect was not sufficient for the preparation of diaryl zinc compounds. We therefore studied the reaction parameters (solvent, additives) of this exchange reaction in detail and report herein the first catalyzed iodine–zinc exchange reaction.

The iodine–zinc exchange provides access to functionalized diaryl zinc compounds of type **1** from the corresponding aryl iodides of type **2** (Schemes 1 and 2). Preliminary experiments showed that no exchange reaction occurs when an aryl iodide is treated with Et_2Zn or iPr_2Zn in Et_2O or THF. However, when mixtures of Et_2O and *N*-methylpyrrolidinone (1:10) are used at 25 °C, an exchange reaction occurs to furnish the mixed diorganozinc reagent FG-ArZnR (**3**, R = Et or *i*Pr, FG = functional group).[10] To promote the transfer of the second alkyl group R we envisaged that it might be necessary to activate the intermediate zinc species **3** through the formation of an ate complex of type **4**, in analogy with the Suzuki reaction in which the boronic acid is converted into a boronate through the addition of a base.[11]



Scheme 1. Catalytic cycle of the iodine–zinc exchange reaction.



Scheme 2. Nucleophilic catalysis of the iodine–zinc exchange with Li(acac) as the catalyst (acac = acetylacetone, NMP = 1-methyl-2-pyrrolidinone).

After transfer of the first R group, with formation of RI and FG-ArZnR, the nucleophilic catalyst Nu^-Met^+ is regenerated, thus, in principle, making it possible to use this activator in catalytic amounts. We therefore treated methyl 4-iodobenzoate (**2a**) with iPr_2Zn[12] in Et_2O/NMP (1:10) at 25 °C in the presence of various salts (Table 1). $Mg(acac)_2$ and $MgCl_2$ were found to be the most active magnesium additives (Table 1, entries 1–3 and 9), and Li(acac) to be by far the most active lithium additive (Table 1, entries 5–8). Interestingly, Cs(acac) was as active as Li(acac), but $Zn(acac)_2$ did not display any catalytic activity (Table 1, entries 10 and 11).

Table 1: The influence of metallic salts on the rate of the iodine–zinc exchange of **2a** with iPr_2Zn in Et_2O/NMP (1:10) at 25 °C.

Entry	Additive[a]	Conversion [%][b]
1	$MgCl_2$	30
2	$MgBr_2$	15
3	MgI_2	2
4	Bu_4NI	10
5	LiCl	0
6	$LiBF_4$	2
7	$LiClO_4$	2
8	Li(acac)	87
9	$Mg(acac)_2$	33
10	Cs(acac)	84
11	$Zn(acac)_2$	2

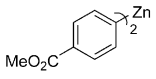
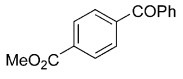
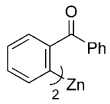
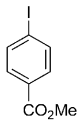
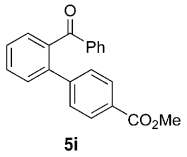
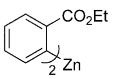
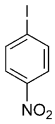
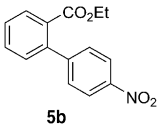
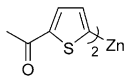
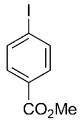
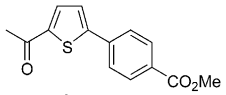
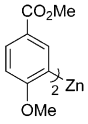
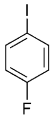
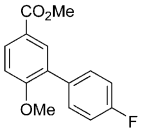
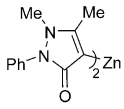
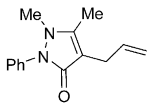
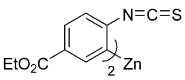
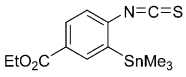
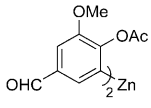
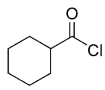
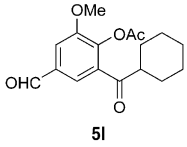
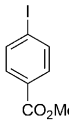
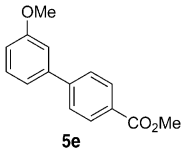
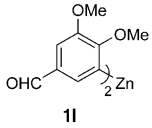
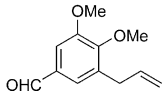
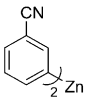
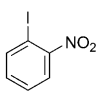
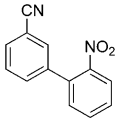
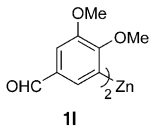
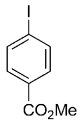
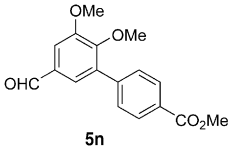
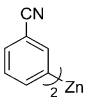
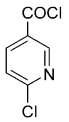
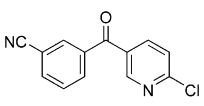
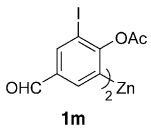
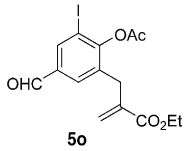
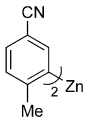
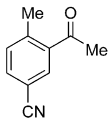
[a] Metal salt: 10 mol%. [b] The conversion was determined after a reaction time of 15 min by analysis of reaction aliquots by GC with tetradecane as an internal standard; accuracy: ±2%.

These results support the nucleophilic catalysis proposed above (Scheme 1). iPr_2Zn[12] proved to be a better organozinc reagent than Et_2Zn or Me_2Zn for the exchange reaction. As iPr_2Zn is highly inflammable, we developed an alternative procedure in which sBu_2Zn is prepared in situ by the reaction of *s*BuLi with $ZnCl_2$ (0.5 equiv, −78 °C→RT, Et_2O, reaction overnight), followed by filtration (see experimental section). Thus, the treatment of **2a** (1 equiv) with iPr_2Zn (0.55 equiv) in the presence of Li(acac) (10 mol%) in Et_2O/NMP (1:10) furnished the desired diaryl zinc **1a** in 12 h at 25 °C (Scheme 2). Acylation of **1a** with benzoyl chloride (1.5 equiv) in the presence of CuCN·2 LiCl[13] (10 mol%) at 50 °C for 5 h provided 4-carbomethoxybenzophenone (**5a**) in 82% yield when the reaction was performed on a 2-mmol scale and in 75% yield when the reaction was performed on a 25-mmol scale (Table 2, entry 1). Palladium-catalyzed Negishi cross-coupling reactions[14] of the zinc reagents prepared by this method proceeded very well. The reaction of di(2-carboethoxyphenyl)zinc (**1b**) with 1-iodo-4-nitrobenzene in the presence of a catalytic amount of $[Pd(dba)_2]$ (2.5 mol%) and tri(2-furyl)phosphane (tfp, 5.0 mol%) for 10 h at room temperature provided the functionalized biphenyl **5b** in 71% yield (Table 2, entry 2).[15] The presence of an additional methoxy group on the aryl ring of the zinc substrate enhances its reactivity. Thus, the diaryl zinc compound **1c** reacted to give the biphenyl **5c** in 83% yield (Table 2, entry 3).

Organozinc reagents with a wide range of functional groups can be prepared by this method. Thus, it was possible to prepare the isothiocyanate-substituted zinc compound **1d**. The treatment of **1d** with Me_3SnCl (4 h, 25 °C) provided the aryl tin derivative **5d** in 66% yield. Both electron-donor substituents (e.g. methoxy groups) and electron-acceptor substituents (e.g. cyano groups) can be present in the diaryl

 © 2004 Wiley-VCH Verlag GmbH & Co. KGaA, Weinheim

Table 2: The reaction of the polyfunctional diaryl zinc compounds **1** with electrophiles in the presence of a copper or palladium catalyst.

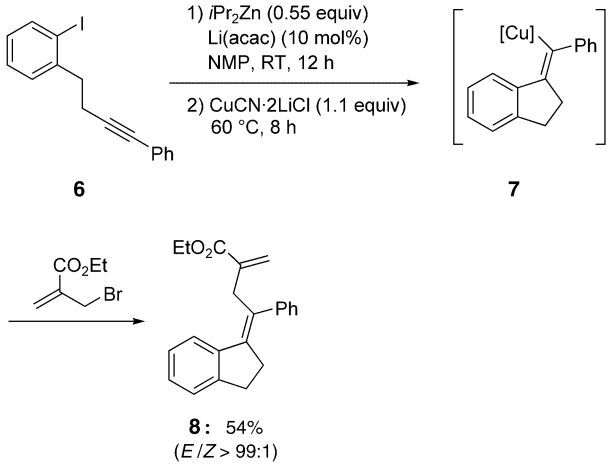
Entry	1	Electrophile	Product 5	Yield [%][a]	Entry	1	Electrophile	Product 5	Yield [%][a]
1	 **1a**	PhCOCl	 **5a**	82[c,f] 75[b,c,f]	9	 **1h**		 **5i**	81[d,e]
2	 **1b**		 **5b**	71[d,e]	10	 **1i**		 **5j**	52[d,e]
3	 **1c**		 **5c**	83[d,e]	11	 **1j**		 **5k**	84[c,e]
4	 **1d**	Me_3SnCl	 **5d**	66[f]	12	 **1k**		 **5l**	75[d,e]
5	 **1e**		 **5e**	86[d,e]	13	 **1l**		 **5m**	77[c,f]
6	 **1f**		 **5f**	84[d,e]	14	 **1l**		 **5n**	60[d,e]
7	 **1f**		 **5g**	77[d,e]	15	 **1m**		 **5o**	60[c,e] 54[c,f]
8	 **1g**	MeCOCl	 **5h**	87[d,e]					

[a] Yields of analytically pure products. [b] Yield of the reaction on a 25-mmol scale. [c] In the presence of CuCN·2 LiCl (20 mol%). [d] In the presence of $[Pd(dba)_2]$ (2.5 mol%) and tfp (5.0 mol%). [e] With iPr_2Zn as the reagent for the exchange. [f] With sBu_2Zn, generated in situ by transmetalation of *s*BuLi, as the reagent for the exchange.

zinc compounds (**1e**–**g**; Table 2, entries 5–8). Interestingly, a keto group is also compatible with the mild reaction conditions for the I–Zn exchange. The diaryl zinc compounds **1h** and **1i** underwent Negishi cross-coupling with methyl 4-iodobenzoate (**2a**) under palladium catalysis. The reaction proceeded in good yield for **1h** (81%, Table 2, entry 9) and in moderate yield for the dithienylzinc derivative **1i** (52%, Table 2, entry 10), which suggests that competitive deprotonation of the acetyl group may occur in the latter case. We also prepared the heterocyclic zinc species **1j**, which underwent copper(I)-catalyzed allylation to give the expected product **5k** in 84% yield (Table 2, entry 11). To our surprise, it was even possible to prepare diaryl zinc compounds with an aldehyde functional group under our standard conditions (**1k**–**m**, Table 2, entries 12–15).[16] Subsequent acylation or allylation led to the polyfunctional products **5l**, **5m**, and **5o** in yields of 75, 77, and 60%, respectively (Table 2, entries 12, 13, and 15). Negishi cross-coupling of **1l** with **2a** provided the expected biphenyl **5n** in 60% yield (Table 2, entry 14).

Finally, we examined an intramolecular carbometalation reaction[17] starting from the readily available alkynyl iodide **6** (Scheme 3).[18] The treatment of **6** with iPr_2Zn (0.55 equiv) in the presence of Li(acac) (10 mol%) in NMP at 25°C for 12 h provided the desired diaryl zinc reagent, which underwent a

 © 2004 Wiley-VCH Verlag GmbH & Co. KGaA, Weinheim



Scheme 3. Carbocupration preceded by an iodine–zinc exchange.

smooth carbocupration in the presence of CuCN·2 LiCl[13] (1.1 equiv) to give the copper reagent **7** stereoselectively. This intermediate was trapped with ethyl (2-bromomethyl)-acrylate[19] to provide the tetrasubstituted *E* alkene **8** (*E*/*Z* > 99:1) in 54% overall yield (THF/NMP, 25 °C, 12 h).

In summary, we have reported the first example of nucleophilic catalysis of the iodine–zinc exchange reaction. Under the mild reaction conditions a range of sensitive functionalities (ketones, isothiocyanates, aldehydes) are tolerated, thus facilitating the synthesis of a wide range of polyfunctional diaryl zinc reagents. We are currently studying the scope of this reaction as well as the extension of this catalytic approach to other systems.

Experimental Section

In situ preparation of sBu$_2$Zn: A solution of *sec*-butyllithium in cyclohexane (ca. 1.4 M) was filtered through celite. The concentration of the alkyl lithium reagent was determined according to a literature procedure.[20] The solution was cooled to 0 °C, then concentrated in vacuo to about 10% of its initial volume to give an orange, highly viscous mixture, which was then cooled to −78 °C. A solution of zinc chloride in Et_2O (1.0 M, 0.5 equiv) was added slowly. The resulting solution was allowed to warm up slowly to room temperature and was stirred overnight under light exclusion. The lithium chloride that precipitated was removed from the solution by decantation, filtration, or centrifugation. The resulting light-sensitive solution of sBu$_2$Zn in Et_2O had a concentration of 0.6–0.8 M (determined by iodolytic titration, see also Supporting Information).

Typical procedure for the I–Zn exchange reaction and subsequent copper-catalyzed allylation: A dried 10-mL round-bottomed flask was charged with 3-iodo-4,5-dimethoxybenzaldehyde (584 mg, 2.0 mmol, 1.0 equiv) and Li(acac) (21 mg, 0.2 mmol, 0.1 equiv) in dry NMP (1.5 mL) under an argon atmosphere and cooled to 0 °C. The previously prepared sBu$_2$Zn solution (1.4 mL of a 0.8 M solution, 1.1 mmol, 0.55 equiv) was added and the reaction mixture was stirred at room temperature for 3 h. The formation of the zinc reagent **11** was monitored by gas chromatography with tetradecane as an internal standard. The zinc reagent **11** was treated with allyl bromide (363 mg, 3.0 mmol, 1.5 equiv) in the presence of CuCN·2 LiCl (0.2 mL, 0.2 mmol, 0.1 equiv). The reaction was complete after 5 h. (The consumption of the zinc reagent was monitored by gas chromatography). A saturated solution of NH_4Cl was added to the mixture, the aqueous phase was extracted with Et_2O (3 × 30 mL), the solvent was evaporated, and the product was then purified by column chromatography (SiO_2, pentane/Et_2O 80:20). The aldehyde **5m** (317 mg, 77%) was obtained as a colorless oil).

Received: November 13, 2003 [Z53316]
Published Online: January 27, 2004

Keywords: copper · cross-coupling · iodine–zinc exchange · nucleophilic catalysis · palladium

[1] a) G. Wittig, U. Pockels, H. Dröge, *Ber. Dtsch. Chem. Ges. A* **1938**, *71*, 1903; b) G. Wittig, U. Schöllkopf, *Tetrahedron* **1958**, 91; c) W. F. Bailey, J. J. Patricia, *J. Organomet. Chem.* **1988**, *352*, 1.
[2] a) H. Gilman, W. Langham, A. L. Jacoby, *J. Am. Chem. Soc.* **1939**, *61*, 106; b) R. G. Jones, H. Gilman, *Org. React.* **1951**, *6*, 339.
[3] a) W. F. Bailey, J. J. Patricia, *J. Organomet. Chem.* **1988**, *352*, 1; b) W. F. Bailey, E. R. Punzalan, *J. Org. Chem.* **1990**, *55*, 5404; c) W. F. Bailey, J. D. Brubaker, K. P. Jordan, *J. Organomet. Chem.* **2003**, *681*, 210; d) E. Negishi, D. R. Swanson, C. J. Rousset, *J. Org. Chem.* **1990**, *55*, 5406; e) G. Boche, M. Schimeczek, J. Cioslowski, P. Piskorz, *Eur. J. Org. Chem.* **1998**, 1851; f) H. J. Reich, M. J. Bevan, B. O. Gudmundsson, C. L. Puckett, *Angew. Chem.* **2002**, *114*, 3586; *Angew. Chem. Int. Ed.* **2002**, *41*, 3436; g) C. E. Tucker, T. N. Majid, P. Knochel, *J. Am. Chem. Soc.* **1992**, *114*, 3983.
[4] a) L. Boymond, M. Rottländer, G. Cahiez, P. Knochel, *Angew. Chem.* **1998**, *110*, 1801; *Angew. Chem. Int. Ed.* **1998**, *37*, 1701; b) A. E. Jensen, W. Dohle, I. Sapountzis, D. M. Lindsay, V. A. Vu, P. Knochel, *Synthesis* **2002**, 565; c) P. Knochel, W. Dohle, N. Gommermann, F. F. Kneisel, F. Kopp, T. Korn, I. Sapountzis, V. A. Vu, *Angew. Chem.* **2003**, *115*, 4438; *Angew. Chem. Int. Ed.* **2003**, *42*, 4302.
[5] a) C. Piazza, P. Knochel, *Angew. Chem.* **2002**, *114*, 3397; *Angew. Chem. Int. Ed.* **2002**, *41*, 3263; b) X. Yang, T. Rotter, C. Piazza, P. Knochel, *Org. Lett.* **2003**, *5*, 1229.
[6] A. Boudier, L. O. Bromm, M. Lotz, P. Knochel, *Angew. Chem.* **2000**, *112*, 4584; *Angew. Chem. Int. Ed.* **2000**, *39*, 4415.
[7] a) L. Micouin, P. Knochel, *Synlett* **1997**, 327; b) for an iodine–magnesium exchange catalyzed by $Mg(OTf)_2$, see: R. W. Hoffmann, M. Brönstrup, M. Müller, *Org. Lett.* **2003**, *5*, 313.
[8] For a cobalt-catalyzed synthesis of organozinc reagents with zinc metal, see: a) H. Fillon, C. Gosmini, J. Perichon, *J. Am. Chem. Soc.* **2003**, *125*, 3867; for the use of activated zinc, see: b) R. D. Rieke, *Science* **1989**, *246*, 1260; c) L. Zhu, R. M. Wehmeyer, R. D. Rieke, *J. Org. Chem.* **1991**, *56*, 1445.
[9] For the use of lithium zincates as transmetalation agents, see: M. Uchiyama, M. Koike, M. Kameda, Y. Kondo, T. Sakamoto, *J. Am. Chem. Soc.* **1996**, *118*, 8733.
[10] For the enantioselective addition of mixed ArZn(alkyl) compounds, see: C. Bolm, J. P. Hildebrand, K. Muniz, N. Hermanns, *Angew. Chem.* **2001**, *113*, 3382; *Angew. Chem. Int. Ed.* **2001**, *40*, 3284.
[11] N. Miyaura, A. Suzuki, *Chem. Rev.* **1995**, *95*, 2457.
[12] A. Boudier, C. Darcel, F. Flachsmann, L. Micouin, M. Oestreich, P. Knochel, *Chem. Eur. J.* **2000**, *6*, 2748.
[13] P. Knochel, M. C. P. Yeh, S. C. Berk, J. Talbert, *J. Org. Chem.* **1988**, *53*, 2390.
[14] a) E. Negishi, L. F. Valente, M. Kobayashi, *J. Am. Chem. Soc.* **1980**, *102*, 3298; b) M. Kobayashi, E. Negishi, *J. Org. Chem.* **1980**, *45*, 5223; c) E. Negishi, *Acc. Chem. Res.* **1982**, *15*, 340.
[15] a) I. Klement, M. Rottländer, C. E. Tucker, T. N. Majid, P. Knochel, P. Venegas, G. Cahiez, *Tetrahedron* **1996**, *52*, 7201; b) A. Staubitz, W. Dohle, P. Knochel, *Synthesis* **2003**, 233.
[16] No clear results were obtained with 2-iodobenzaldehyde. Dimeric products could be detected by gas chromatography

 © 2004 Wiley-VCH Verlag GmbH & Co. KGaA, Weinheim

during the preparation of the corresponding diaryl zinc reagent, which suggests that this species has moderate stability.
[17] The alkynyl iodide **6** was prepared in two steps from 1-bromomethyl-2-iodobenzene according to a literature procedure: D. Bouyssi, G. Balme, *Synlett* **2001**, 1191.
[18] S. A. Rao, P. Knochel, *J. Am. Chem. Soc.* **1991**, *113*, 5735.
[19] J. Viliéras, M. Rambaud, *Synthesis* **1982**, 924.
[20] H.-S. Lin, L. Paquette, *Synth. Commun.* **1994**, *24*, 2503.

 © 2004 Wiley-VCH Verlag GmbH & Co. KGaA, Weinheim

Ion–Membrane Interactions

Multistep Binding of Divalent Cations to Phospholipid Bilayers: A Molecular Dynamics Study**

*Rainer A. Böckmann and Helmut Grubmüller**

The specific interaction of cations—particularly divalent cations—with biological membranes is essential not only for the structure, dynamics, and stability of membranes, but also for the binding or insertion of proteins to or into membranes, for membrane fusion, and for the transport of small molecules across membranes. Membrane fusion, for example, has been shown to be triggered by calcium ions.[1,2] Moreover, calcium ions are an integral part of neural signal transduction, and so is their interaction with the neural membrane.[3]

Various experimental methods have been applied in the past to shed light on the interaction of cations with membranes. NMR experiments[4,5] suggested a conformational change in the polar region of dipalmitoylphosphatidylcholine (DPPC) bilayers[4] and a calcium ion/phospholipid stoichiometry of 1:2 at 5 M $CaCl_2$.[5] Additional rearrangements or conformational changes in the carbonyl region of palmitoyloleoylphosphatidylcholine (POPC) lipids were revealed by IR spectroscopy.[6] From neutron diffraction experiments, the distribution of calcium in the lipid headgroup of DPPC bilayers in the liquid-crystalline state could be determined.[7]

Taken together, these experiments suggest a picture in which the calcium ion is predominantly bound to the phosphate moieties of two lipids. However, up to now, there has been no direct evidence for this model and, accordingly, there is no proposal for the structure of the ion–lipid complex. The main experimental obstacle here is the low signal-to-noise ratio, typically resulting from the fact that the two-dimensional lipid–solvent interface comprises only a small fraction of the sample volume. Therefore, the current consensus leaves considerable room for diverging interpretations as, for example, evidenced by a fluorescence study on the influence of anions and cations on the dipole potential of phosphatidylcholine vesicles.[8] In this study—in accord with the available experimental data, but quite in contrast to the above picture—a measured reduction of the overall dipole potential was interpreted in terms of anion binding to the headgroup. More detailed structural information can be expected from recent X-ray diffraction studies on oligolamellar bilayers,[9] which do not suffer from this drawback.

These difficulties on the experimental side give considerable weight to theoretical studies. Indeed, molecular dynamics (MD) simulations of solvated lipid bilayers have yielded information on the conformation and arrangement of the lipids in membranes. In many cases the results were in quantitative agreement with experimental data.[10–13,15]

However, up to now, MD studies of ion binding to lipid bilayers have not been possible because of the apparently slow kinetics of ion binding to and dissociation from lipid membranes. Typically the simulation systems do not reach sufficient equilibration within the nanosecond simulation time spans.[14] Only very recently, we were able to carry out a simulation sufficiently long to observe the binding of sodium ions to the carbonyl oxygens of phospholipids.[15] This study confirmed that even the binding of monovalent ions is unexpectedly slow, and it predicted a reduced self-diffusion coefficient for the lipids under the influence of sodium chloride, which was subsequently confirmed by fluorescence correlation spectroscopy.[15]

The above-mentioned simulation, however, would have been too short to yield sufficiently converged results for calcium binding, which called for a further increase of simulation lengths. Here we present 200-ns MD simulations of calcium binding, which are sufficiently converged for the analysis of calcium binding. These simulations were also suitable for elucidating the differences between the binding of monovalent and divalent cations to phospholipid bilayers. Finally, our simulations enabled us to characterize the different binding kinetics.

Two simulation systems (A and B) were studied, each comprising ca. 20000 atoms (Figure 1). Both systems contained 128 POPC lipids arranged in a bilayer and approximately 5000 water molecules. To system A we added 10 sodium and 10 chloride ions, and to system B, 8 calcium and 16 chloride ions. All ions were randomly placed within the water phase. The sodium chloride simulation system has been described.[15] In the present study the simulation was extended to 200 ns. The simulation time for system B was also 200 ns.

We note that the system had to be relatively small in order to attain sufficiently long simulation times. However, for the chosen concentration of calcium ions (0.089 M), the Debye–Hückel length of $\lambda_D = 5.9$ Å is much smaller than the size of the periodic box ($62 \times 62 \times 80$ Å^3). Therefore, the interactions

[*] Dr. R. A. Böckmann,[+] Priv.-Doz. Dr. H. Grubmüller
Theoretical and Computational Biophysics Department
Max Planck Institute for Biophysical Chemistry
Am Fassberg 11, 37077 Göttingen (Germany)
Fax: (+49) 551-201-2302
E-mail: hgrubmu@gwdg.de

[+] Current address: Department of Biochemistry, University Zürich
Winterthurerstrasse 190, CH-8057 Zürich (Switzerland)

[**] This work was supported by the BIOTECH programs of the EU, grants QLRT-2000/00778 and QLRT-2000/00504. We thank B. de Groot, T. Heimburg, G. Schröder, C. Schütte, and P. Vöhringer for stimulating discussions and for carefully reading the manuscript, and B. de Groot also for help with the GROMACS program package. Computer time was provided by the Göttingen computer center, GWDG.

 DOI: 10.1002/anie.200352784 © 2004 Wiley-VCH Verlag GmbH & Co. KGaA, Weinheim

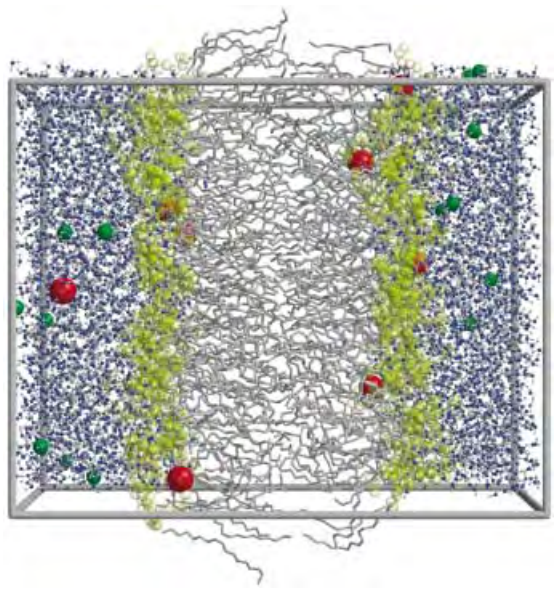


Figure 1. Snapshot of simulation system B after 100 ns (128 POPC lipids; carbon chains = gray, water = light blue, Ca^{2+} = red, Cl^- = green, hydrophilic headgroups = yellow).

between ions in adjacent periodic units should be small, even at the very end of the simulation when all the calcium ions are bound to the membrane ($\lambda_D = 10.2$ Å). This nearly equilibrated end state thus corresponds to a state with a rather low concentration of calcium ions in solution, close to physiological conditions.

Figure 2 shows snapshots from our simulations of the binding of monovalent (top row) and divalent cations (bottom row) to lipid carbonyl oxygens. The progression of the equilibration of the cations is monitored by the averaged number of coordinating water oxygens (black lines) and lipid carbonyl oxygens (red) as a function of simulation time (Figure 3). Monoexponential fits (blue lines) to these curves yield binding times of 23 ns and 86 ns for sodium and calcium

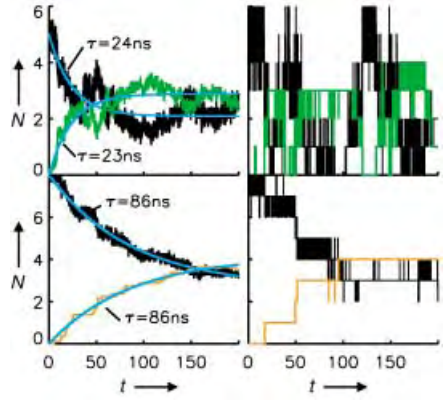


Figure 3. Total number N of water oxygens (black) and lipid carbonyl oxygen atoms (green, orange) within 2.8 Å of the sodium ions (upper panel) and within 3 Å of the calcium ions (lower panel) as a function of simulation time t. The relaxation times τ from the exponential fits (blue) to the data are also given. The right row shows the quantities for representative single cations.

ions, respectively. The fits yield also equilibrium coordination numbers for the binding of lipid carbonyl oxygens of 2.9 for Na^+ and 4.2 for Ca^{2+}.

In the simulations a sequential binding of the lipid carbonyl oxygens to the calcium ions is observed (see Figure 4). Binding of the first carbonyl oxygen requires penetration of the Ca^{2+} ions through the hydrophilic headgroups of the lipids and occurs, for the concentration chosen, within 30–40 ns (red line). After 200 ns of simulation time,

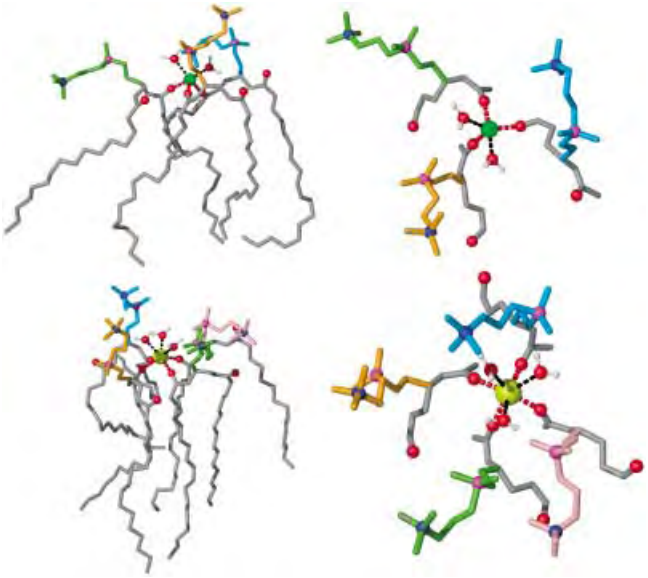


Figure 2. Typical snapshots of the coordination of Na^+ (top row) and Ca^{2+} ions (bottom row) by lipid carbonyl oxygens (dotted lines in red) and by water oxygens (dotted lines in black). Left: side view; right: top view.

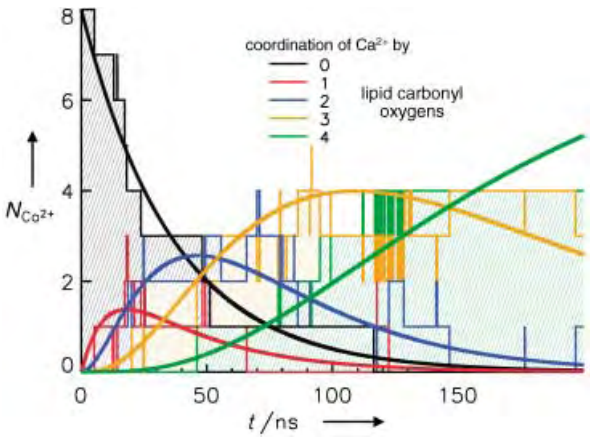


Figure 4. Coordination of Ca^{2+} by lipid carbonyl oxygens as a function of simulation time t ($N_{Ca^{2+}}$ is the number of Ca^{2+} ions with a given coordination number). The colors differentiate between coordination by only water oxygens (black) and by one (red), two (blue), three (orange), and four lipid carbonyl oxygens (green). Also shown is a fit of the simulation data (thick lines) assuming a multilevel process for the sequential binding of the calcium ions to finally four lipid carbonyl oxygens (see text).

 © 2004 Wiley-VCH Verlag GmbH & Co. KGaA, Weinheim

about half of the ions reached the preferred coordination by at least four phosphatidylcholines (green line). The red, blue, and orange traces show the population of intermediates of one-, two-, and threefold lipid coordination, respectively.

The observed sequence of intermediates suggests that the binding of the lipid carbonyl oxygens to the Ca^{2+} ions can be described by a sequential rate equation [Eq. (1)]. Since in our

$$Ca^{2+} \xrightarrow{k_0} Ca^{2+}\cdot L \xrightarrow{k_1} Ca^{2+}\cdot 2L \xrightarrow{k_2} Ca^{2+}\cdot 3L \xrightarrow{k_3} Ca^{2+}\cdot 4L \qquad (1)$$

simulations the flux of binding ions is significantly larger than the flux of dissociating ions, we simplify the treatment by neglecting the back reactions. The bold lines in Figure 4 show fits of the solution of these rate equations to the coordination numbers obtained from the simulations, which yield the corresponding rate coefficients k_i and binding times $\tau_i = 1/k_i$. The agreement is well within the statistical error of the finite number of observed events.

After the calcium ion binds to the first lipid carbonyl oxygen ($\tau_0 = 36^{+16}_{-11}$ ns[*]), the second coordination is faster ($\tau_1 = 10^{+5}_{-4}$ ns). In contrast, coordination by the third and fourth lipid carbonyl oxygen is much slower again, as can be seen from the significantly increased decay times ($\tau_2 = 31^{+14}_{-10}$ ns, $\tau_3 = 107^{+90}_{-50}$ ns). Closer inspection of the structure of the complexes (cf. Figure 2) shows that binding of the third and fourth lipid requires major reorientation and fine-tuning of the lipid–ion packing. Accordingly, the slow kinetics can be explained in terms of entropic barriers, which is also the main determinant of the slow kinetics of the whole binding process. Due to saturation effects we expect a deviation from the above binding times for higher salt concentration.

Like our previous findings for sodium ions,[15] complex formation for calcium ions here is also found to reduce lipid self-diffusion. In addition we predict a decreased rotational diffusion coefficient for the lipid headgroups, as evidenced by the increase of the half-life $t_{1/2} \propto 1/D_R$ of the rotational correlation function [Eq. (2)]. For the vector $\boldsymbol{p}$ connecting

$$C_2(t) = \frac{1}{2}\langle 3[\boldsymbol{p}(t)\,\boldsymbol{p}(0)]^2 - 1\rangle \qquad (2)$$

the phosphate and the nitrogen atom in the headgroup, the half-life increases from 0.96 ns for the case without ions to approximately 1.83 ns in the presence of 330 mM $CaCl_2$ (1.11 ns at 110 mM NaCl, 1.58 ns at 330 mM NaCl).

The different binding of monovalent and divalent cations to the lipid bilayer entails differences in the lipid headgroup conformation (see Figure 2). In particular, the tight packing of lipids around the Ca^{2+} ions leads to a smaller angle ($\approx 60°$) between the dipole moment of the lipid headgroup and the membrane normal (63.5° on average vs. 69.8° for the case without ions[15]). Additionally, a significant increase of the order of the lipid acyl chain is observed.

In conclusion, our simulations provide an atomistic model for the binding of potassium and calcium ions to neutral, zwitterionic POPC lipid bilayers. Key features of these models are a sequential multistep binding and coordination of the cations by three and four lipid carbonyl oxygens, respectively. These predictions will likely be tested in the near future by X-ray diffraction studies on oligolamellar bilayers and by solid-state NMR experiments. Our results should enable construction and/or refinement of quantitative models for biological processes involving calcium binding such as neural signal transduction and membrane fusion.[16]

[*] The exponents and indices on these numbers correspond to the values of the error bars.

Experimental Section

Both simulations were carried out with the GROMACS suite[17] using the force field devised by Berger et al.;[18] parameters for the unsaturated carbons were taken from the GROMOS87 force field. Application of the Lincs[19] and Settle[20] methods allowed for an integration step size of 2 fs. We note that the force field used is not a polarizable one and may provide an inaccurate description of the ion–carbonyl interactions. Therefore, the actual binding rates may differ from those reported here, most likely roughly by a common scaling factor. The Particle-Mesh Ewald (PME) method[21] was used, and an NPT ensemble was applied in the simulations, with separate coupling of the membrane and the solvent to a 300 K heat bath, and a semiisotropic pressure coupling in the lateral direction and perpendicular to the membrane surface, as described.[15] Coordination numbers for the ions were calculated from the cumulative radial distribution function at distances of 2.8 Å (Na^+) and 3.0 Å (Ca^{2+}) as a function of simulation time.

Error bars (1σ) for the rate coefficients k_i were determined from multiple Monte Carlo simulations of Equation (1) using the values for k_i given above and eight calcium ions, as in the MD simulation. Many, statistically independent replica of the data shown in Figure 4 were obtained. From each of these replica, four rate coefficients k_i were computed using the same fitting procedure as was used for the MD data. The statistical scatter of these sets of k_i provided the statistical error expected in the rate coefficients derived from the MD simulation. Note that the scatter was computed on a logarithmic scale, which is more appropriate for rates; for this reason the error bars are asymmetric.

The simulations were performed on a dual-processor PC with two Athlon MP 2200+ processors; each ns of simulation time required about 26 h of computation time.

Received: September 8, 2003 [Z52784]
Published Online: December 4, 2003

Keywords: calcium · cations · membranes · molecular dynamics · phospholipids

[1] D. Papahadjopoulos, S. Nir, N. Düzgünes, *J. Bioenerg. Biomembr.* **1990**, *22*, 157.
[2] J. A. Szule, S. E. Jarvis, J. E. Hibbert, J. D. Spafford, J. E. A. Braun, G. W. Zamponi, G. M. Wessel, J. R. Coorssen, *J. Biol. Chem.* **2003**, *278*, 24251.
[3] B. Alberts, A. Johnson, J. Lewis, M. Raff, K. Roberts, P. Walter, *Molecular Biology of the Cell*, Garland Science, New York, **2002**.
[4] H. Akutsu, J. Seelig, *Biochemistry* **1981**, *20*, 7366.
[5] C. Altenbach, J. Seelig, *Biochemistry* **1984**, *23*, 3913.
[6] H. Binder, O. Tschörnig, *Chem. Phys. Lipids* **2002**, *115*, 39.
[7] C. A. N. L. Herbette, R. V. McDaniel, *Biophys. J.* **1984**, *46*, 677.
[8] R. J. Clarke, C. Lüpfert, *Biophys. J.* **1999**, *76*, 2614.
[9] T. Salditt, M. Vogel, W. Fenzl, *Phys. Rev. Lett.* **2003**, *90*, 178101.
[10] P. van der Ploeg, H. J. C. Berendsen, *J. Chem. Phys.* **1982**, *76*, 3271.

 © 2004 Wiley-VCH Verlag GmbH & Co. KGaA, Weinheim

[11] H. Heller, M. Schaefer, K. Schulten, *J. Phys. Chem.* **1993**, *97*, 8343.
[12] R. M. Venable, Y. Zhang, B. J. Hardy, R. W. Pastor, *Science* **1993**, *262*, 223.
[13] D. P. Tieleman, S. J. Marrink, H. J. C. Berendsen, *Biochim. Biophys. Acta* **1997**, *1331*, 235.
[14] S. A. Pandit, D. Bostick, M. L. Berkowitz, *Biophys. J.* **2003**, *84*, 3743.
[15] R. A. Böckmann, A. Hac, T. Heimburg, H. Grubmüller, *Biophys. J.* **2003**, *85*, 1647.
[16] R. Jahn, H. Grubmüller, *Curr. Opin. Cell Biol.* **2002**, *14*, 488.
[17] E. Lindahl, B. Hess, D. van der Spoel, *J. Mol. Model.* **2001**, *7*, 306.
[18] O. Berger, O. Edholm, F. Jähnig, *Biophys. J.* **1997**, *72*, 2002.
[19] B. Hess, H. Bekker, H. J. C. Berendsen, J. G. E. M. Fraaije, *J. Comput. Chem.* **1997**, *18*, 1463.
[20] S. Miyamoto, P. A. Kollman, *J. Comput. Chem.* **1992**, *13*, 952.
[21] T. Darden, D. York, L. Pedersen, *J. Chem. Phys.* **1993**, *98*, 10089.

 © 2004 Wiley-VCH Verlag GmbH & Co. KGaA, Weinheim

Cover Picture



Dahui Liu, Sungwook Choi, Bin Chen, Robert J. Doerksen, Dylan J. Clements, Jeffrey D. Winkler, Michael L. Klein, and William F. DeGrado*

The amphiphilic nature of a highly selective antimicrobial arylamide oligomer is shown by the simulation of its conformation at a water/octane interface. Arginine end groups make this oligomer the most amphiphilic in the series studied and increase its overall hydrophobic moment. While the former property correlates with its low toxicity, the latter correlates with a high antimicrobial activity. More details are described in the Communication by DeGrado and co-workers on page 1158 ff.

Contents

Angewandte EarlyView

The following articles are available online (in Wiley InterScience). You can find them at www.angewandte.org, under Full Text, Early View.

N. D. Clement, K. J. Cavell, C. Jones, C. J. Elsevier:*
Oxidative Addition of Imidazolium Salts to Ni^0 and Pd^0: Synthesis and Structural Characterization of Unusually Stable Metal–Hydride Complexes
DOI: 10.1002/anie.200353409
Published online: February 11, 2004

N. Halland, P. S. Aburel, K. A. Jørgensen:*
Highly Enantio- and Diastereoselective Organocatalytic Asymmetric Domino Michael–Aldol Reaction of β-Ketoesters and α,β-Unsaturated Ketones
DOI: 10.1002/anie.200353364
Published online: February 11, 2004

J. K. Cammack, H. Amouri, P. W. Leonard, R. L. Myrabo, K. P. C. Vollhardt:*
Electron Exchange Along the Tercyclopentadienyltrimetallic Scaffold: Kinetics, Equilibria, and Bond Strengths
DOI: 10.1002/anie.200352479
Published online: February 9, 2004

S. E. McLain, C. J. Benmore, J. E. Siewenie, J. Urquidi, J. F. C. Turner:*
On the Structure of Liquid Hydrogen Fluoride
DOI: 10.1002/anie.200353289
Published online: February 11, 2004

J. M. Ready, S. E. Reisman, M. Hirata, M. M. Weiss, K. Tamaki, T. V. Ovaska, J. L. Wood:*
A Mild and Efficient Synthesis of Oxindoles: Progress Towards the Synthesis of Welwitindolinone A Isonitrile.
DOI: 10.1002/anie.200353282
Published online: February 11, 2004

E. Hittinger, A. Kokil, C. Weder:*
Synthesis and Characterization of Cross-Linked Conjugated Polymer Milli-, Micro-, and Nanoparticles
DOI: 10.1002/anie.200352863
Published online: February 29, 2004

Articles judged by the referees or the editor as being either very important or very urgent are immediately edited, proof-read, and electronically published once the manuscript has arrived in the editorial office in final form. As long as there is no page number available these articles should be cited in the following manner:

Author(s) *Angew. Chem. Int. Ed.*, online publication date, DOI.

News

Cotton Award to J. Ellis ——— **1044**

Research Prizes to P. Schwille and P. Fromherz ——— **1044**

F. Diederich: New Editorial Board Chairman ——— **1044**

Books

Biochemistry ——— **1045** David E. Metzler *reviewed by B. Schwenzer, K.-H. van Pée*

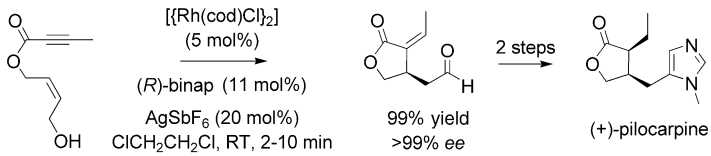
In Situ Spectroscopy of Monomer and Polymer Synthesis ——— **1045** Judit E. Puskas, Timothy E. Long, Robson F. Storey *reviewed by B. Abel*

Highlights

Synthetic Methods

I. J. S. Fairlamb* ——— **1048 – 1052**

Asymmetric Cycloisomerization of 1,6- and 1,7-Enynes by Transition-Metal Catalysts



Highly functionalized carbo- and heterocycles can be prepared enantioselectively from simple enynes in transition-metal-catalyzed reactions. This versatile, atom-economic, and environmentally friendly approach has become a mainstay in natural product synthesis. The concise synthesis of (+)-pilocarpine is one example (see scheme). binap = 2,2′-bis-(diphenylphosphanyl)-1,1′-binaphthyl), cod = cyclooctadiene, RT = room temperature.

© 2004 Wiley-VCH Verlag GmbH & Co. KGaA, Weinheim

Essays

History of Science

R. Mülhaupt* ——— 1054 – 1063

Hermann Staudinger and the Origin of Macromolecular Chemistry

Staudinger's visions paved the way for the development of modern polymeric materials with very versatile properties and new opportunities at the interface of materials and life sciences. This is confirmed in this Essay, written to mark the 50th anniversary of the award of the Nobel Prize for Chemistry to Hermann Staudinger. His revolutionary concept, which initially attracted heavy opposition, marked the beginning of the new era of rational molecular design of structural and functional polymeric materials, whose property profiles are tailored by varying their molecular architectures.

History of Science

H. Ringsdorf* ——— 1064 – 1076

Hermann Staudinger and the Future of Polymer Research: Jubilees—Beloved Occasions for Cultural Piety

Chemistry was his life, but Hermann Staudinger's dreams belonged to biology and to the unity of chemistry and biology. That is the central theme of this Essay, which, on the occasion of the fiftieth anniversary of the award of the Nobel Prize to Hermann Staudinger, discusses the significance of Staudinger's discoveries for the biosciences, not only retrospectively, but deliberately also prospectively. General questions of science ethics and the interplay of research, politics, and responsibility are also considered.

Minireviews

Plastics

S. Mecking* ——— 1078 – 1085

Nature or Petrochemistry?—Biologically Degradable Materials

Biodegradable plastics based on renewable raw materials are interesting alternatives considering the limited availability of fossil fuel feedstocks and the emission of greenhouse gases. Biological degradability has been defined in Germany since 1998 by an industrial standard, the logo of which is depicted.

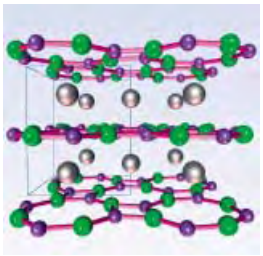


Communications

Layered Compounds

M. Somer, A. Yarasik, L. Akselrud, S. Leoni, H. Rosner, W. Schnelle, R. Kniep* ——— 1088 – 1092

Ae[Be_2N_2]: Nitridoberyllates of the Heavier Alkaline-Earth Metals



Complex anionic partial structures of the general formula [BeN^-] occur in nitridoberyllates *Ae*[Be_2N_2] (*Ae* = Mg, Ca, Sr, Ba). Planar 4.8^2 nets are present in Ca[Be_2N_2] and Sr[Be_2N_2] (see structure; Ca, Sr: gray; Be: purple; N: green), whereas Mg[Be_2N_2] displays puckered 6^3 nets connected to form double layers and a peculiar bonding situation for nitrogen.

For the USA and Canada:
ANGEWANDTE CHEMIE International Edition (ISSN 1433-7851) is published weekly by Wiley-VCH PO Box 191161, D 69451 Weinheim, Germany. Air freight and mailing in the USA by Publications Expediting Inc. 200 Meacham Ave., Elmont, NY 11003. Periodicals postage paid at Jamaica NY 11431. US POSTMASTER: send address changes to *Angewandte Chemie*, Wiley-VCH, 111 River Street, Hoboken, NJ 07030. Annual subscription price for institutions: Europe € 3430.00/3118.00; outside Europe US$ 4499.00/4090.00 (valid for print and electronic/print or electronic delivery); for individuals who are personal members of a national chemical society, or whose institution already subscribes, or who are retired or self-employed consultants, print only: Europe € 248.00/outside Europe US$ 378.00. Postage and handling charges included. All Wiley-VCH prices are exclusive VAT.

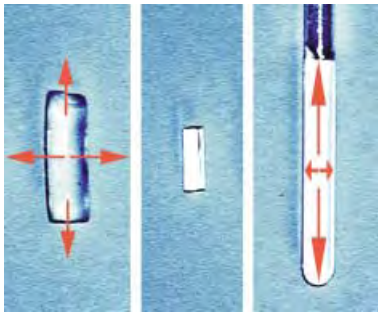
 © 2004 Wiley-VCH Verlag GmbH & Co. KGaA, Weinheim

Contents

NMR Spectroscopic Methods

B. Luy, K. Kobzar, H. Kessler* ——— **1092 – 1094**

An Easy and Scalable Method for the Partial Alignment of Organic Molecules for Measuring Residual Dipolar Couplings



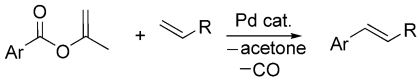
Stretched polystyrene gel (see picture) induces partial alignment of small molecules in an organic solvent for the measurement of residual dipolar couplings in high-resolution NMR spectroscopy. The degree of orientation can be varied over a wide range by the amount of cross-linking of the polymer. An important NMR parameter can thus be measured routinely.

Pd-Catalyzed Couplings

L. J. Gooßen,* J. Paetzold — **1095 – 1098**

Decarbonylative Heck Olefination of Enol Esters: Salt-Free and Environmentally Friendly Access to Vinyl Arenes

Thank you, no salt on the side. In this variant of the Heck olefination, enol esters serve as environmentally friendly synthetic equivalents of aryl halides. These reactants, in turn, are available from a waste-free synthesis from carboxylic acids and propyne. Thus, a salt-free overall process



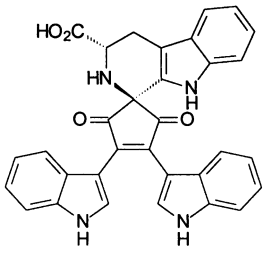
has been devised for preparing vinyl arenes from a variety of aromatic carboxylic acids.

Biosynthesis

B. Irlinger, H.-J. Krämer, P. Mayser,* W. Steglich* ——— **1098 – 1100**

Pityriarubins, Biologically Active Bis(indolyl)spirans from Cultures of the Lipophilic Yeast *Malassezia furfur*

Indole alkaloids, such as pityriarubin A (**1**), may be of importance for the pathogenesis of the common skin disease pityriasis versicolor. The metabolite **1** is produced in cultures of the lipophilic yeast *Malassezia furfur* with tryptophan present as the sole source of nitrogen. The structures of the pityriarubins were derived from spectroscopic investigations, and insight into their biosynthesis was gained by feeding experiments with [1′-^{13}C]tryptophan.

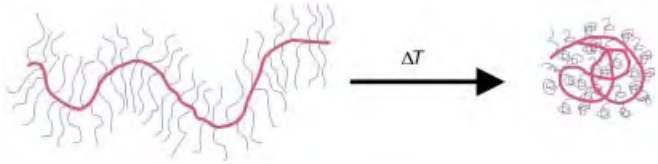


1

Structures of Macromolecules

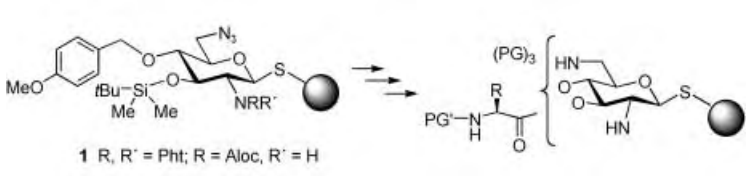
C. Li, N. Gunari, K. Fischer, A. Janshoff, M. Schmidt* ——— **1101 – 1104**

New Perspectives for the Design of Molecular Actuators: Thermally Induced Collapse of Single Macromolecules from Cylindrical Brushes to Spheres



Polymethacrylates with densely grafted poly-*N*-isopropylacrylamide side chains change their shape at the lower critical solution temperature from cylindrical brushes (left) to spherical structures (right). This is an interesting example of a temperature-induced cylinder-to-sphere transition observed for single macromolecules.

 © 2004 Wiley-VCH Verlag GmbH & Co. KGaA, Weinheim



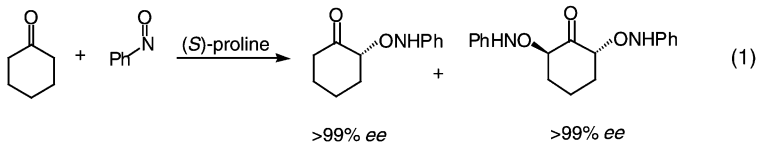
1 R, R' = Pht; R = Aloc, R' = H

Irrespective of the sequence, the carbohydrate scaffold **1** as a molecular platform for combinatorial diversification can be selectively deprotected and equipped with side chains, for example amino acids or peptides, in every position (see picture). This allows the flexible arrangement of functional groups and structural elements. PG = protective group.

Solid-Phase Synthesis

U. Hünger, J. Ohnsmann, H. Kunz* ——— **1104 – 1107**

Carbohydrate Scaffolds for Combinatorial Syntheses That Allow Selective Deprotection of All Four Positions Independent of the Sequence



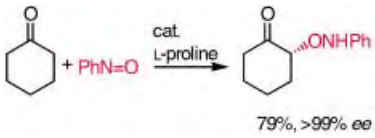
Proline-catalyzed reactions between unmodified ketones and nitrosobenzene proceed with excellent diastereo- and enantioselectivities to provide protected α-hydroxy and α,α′-dihydroxy ketones [Eq. (1)]. Such compounds with chiral α-hydroxy carbonyl units are crucial in natural product synthesis.

Asymmetric Catalysis

A. Bøgevig, H. Sundén, A. Córdova* ——— **1109 – 1112**

Direct Catalytic Enantioselective α-Aminoxylation of Ketones: A Stereoselective Synthesis of α-Hydroxy and α,α′-Dihydroxy Ketones

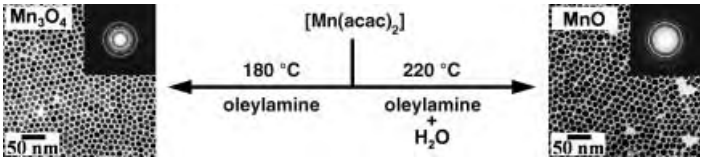
Nitrosobenzene is the oxygen source in the direct catalytic enantioselective α-aminoxylation of ketones catalyzed by L-proline [Eq. (1)]. Versatile α-aminoxylated ketones are obtained in high yield and with excellent enantioselectivities.



Asymmetric Catalysis

Y. Hayashi,* J. Yamaguchi, T. Sumiya, M. Shoji ——— **1112 – 1115**

Direct Proline-Catalyzed Asymmetric α-Aminoxylation of Ketones

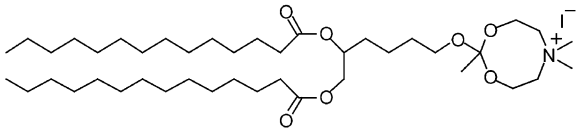


Highly crystalline and monodisperse MnO and Mn_3O_4 nanoparticles are prepared by thermal decomposition of $[Mn(acac)_2]$ in oleylamine under an inert atmosphere in the presence and absence of a small amount of water, respectively (see picture). The particle size of both manganese oxide systems can be easily manipulated by changing the employed reaction temperature, and it has been demonstrated that the magnetic behavior depends on the size of the particles.

Magnetic Nanoparticles

W. S. Seo, H. H. Jo, K. Lee, B. Kim, S. J. Oh, J. T. Park* ——— **1115 – 1117**

Size-Dependent Magnetic Properties of Colloidal Mn_3O_4 and MnO Nanoparticles



Making and breaking lipids: A general synthesis of a new class of ortho ester lipids from a dioxazocinium ketene acetal is disclosed. Both single- and dual-chain analogues were prepared, and the most sensitive of these (see structure) was shown to disassemble at 38 °C within 6 h at pH 5.0.

Lipid Amphiphiles

K. By, M. H. Nantz* ——— **1117 – 1120**

Dioxazocinium Ortho Esters: A Class of Highly pH-Vulnerable Amphiphiles

 © 2004 Wiley-VCH Verlag GmbH & Co. KGaA, Weinheim

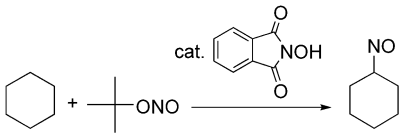
Contents

Synthesis Techniques

T. Hirabayashi, S. Sakaguchi, Y. Ishii* ——— 1120 – 1123

A New Route to Lactam Precursors from Cycloalkanes: Direct Production of Nitrosocycloalkanes or Cycloalkanone Oximes by Using *tert*-Butyl Nitrite and *N*-Hydroxyphthalimide

Clean and selective: Nitrosation and oximation of cycloalkanes was achieved by treating them with *t*BuONO under Ar in the presence of a catalytic amount of *N*-hydroxyphthalimide (see scheme). The novel, clean nitrosation procedure uses halogen-free, relatively mild reaction conditions and results in good product

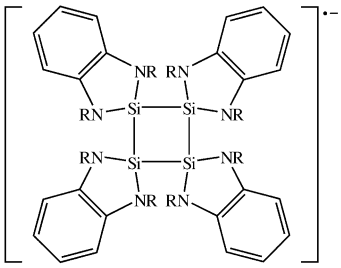


selectivity (almost no organic byproducts) and high recovery of the catalyst.

Silanes

B. Gehrhus,* P. B. Hitchcock, L. Zhang ——— 1124 – 1126

An Isolable Radical Anion and Dianion of a Cyclotetrasilane: Synthesis and Structure of $[Si\{1,2\text{-}(NEt)_2C_6H_4\}]_4^{-\bullet}$ and $[Si\{1,2\text{-}(NEt)_2C_6H_4\}]_4^{2-}$

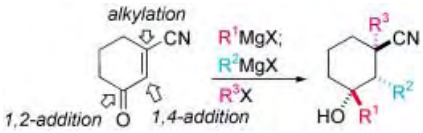


Silicon squares up: The silylene Si[1,2-$(NR)_2C_6H_4$] (R = CH_2tBu) is thermally stable owing to its bulky substituent. What effect will a reduction of the size of R have on the stability of a two-coordinate Si^{II} species? Results show that a silylene with R = Et cannot be isolated but will yield a stable radical anion (see picture) and dianion of a cyclotetrasilane.

Conjugate Addition–Alkylations

F. F. Fleming,* Z. Zhang, Q. Wang, O. W. Steward ——— 1126 – 1129

Oxonitriles: Multicomponent Grignard Addition–Alkylations



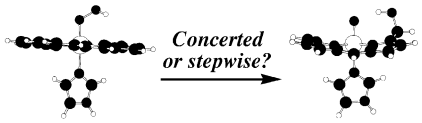
Three at a time: Sequential carbonyl addition, chelation-controlled conjugate addition, and alkylation triggers the multicomponent assembly of diverse nitriles. The chelation-controlled conjugate addition–alkylation installs three new stereocenters (see scheme), thereby generating substituted nitriles that are ideal terpenoid precursors as illustrated in the synthesis of *epi*-dehydroabietic acid.

Heme Degradation

P. K. Sharma, R. Kevorkiants, S. P. de Visser, D. Kumar, S. Shaik* ——— 1129 – 1132

Porphyrin Traps Its Terminator! Concerted and Stepwise Porphyrin Degradation Mechanisms Induced by Heme-Oxygenase and Cytochrome P450

Concerted or stepwise? A homolytic stepwise pathway is taken by the enzyme heme-oxygenase (HO) to degrade the porphyrin ring in heme species. The porphyrin ring assists the enzyme by trapping the hydroxyl radical during the degradation (see scheme). HO is compared to cytochrome P450.

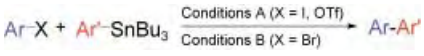


Stille Coupling

S. P. H. Mee, V. Lee, J. E. Baldwin* ——— 1132 – 1136

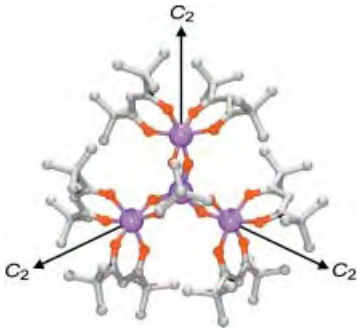
Stille Coupling Made Easier—The Synergic Effect of Copper(I) Salts and the Fluoride Ion

CsF and CuI do the trick: Stille coupling reactions of aryl/vinyl iodides, triflates, and bromides with aryl/vinyl stannanes are greatly enhanced by the inclusion of CsF and CuI in the reaction mixture (see scheme; Conditions A: $[Pd(PPh_3)_4]$/CsF/CuI/DMF/45 °C; Conditions B: $PdCl_2$/$Pt Bu_3$/CsF/CuI/DMF/45 °C).



 © 2004 Wiley-VCH Verlag GmbH & Co. KGaA, Weinheim

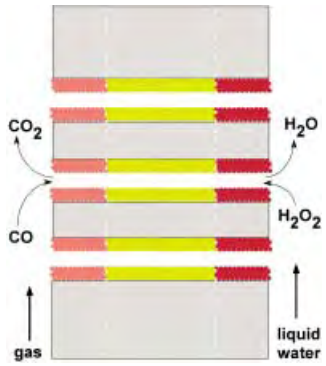
A relaxing time: A dramatic increase of the energy barrier (U_{eff}) in tetrairon(III) single-molecule magnets can be achieved by simple chemical modification. Site-specific replacement of the six methoxide bridges in $[Fe_4(OMe)_6(dpm)_6]$ (Hdpm = dipivaloylmethane; $U_{eff}/k_B = 3.5$ K) with two tripodal 1,1,1-tris-(hydroxymethyl)ethane (H_3thme) ligands affords the compound $[Fe_4(thme)_2(dpm)_6]$ (see figure) with $U_{eff}/k_B = 15.6(2)$ K and a magnetic relaxation time exceeding 1000 s below 0.2 K.



Magnetic Properties

A. Cornia,* A. C. Fabretti, P. Garrisi, C. Mortalò, D. Bonacchi, D. Gatteschi, R. Sessoli, L. Sorace, W. Wernsdorfer, A.-L. Barra ——— **1136 – 1139**

Energy-Barrier Enhancement by Ligand Substitution in Tetrairon(III) Single-Molecule Magnets

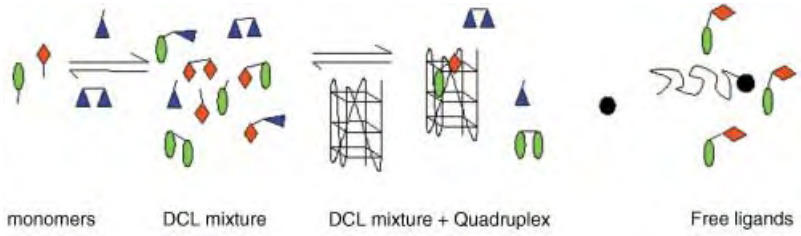


Membranes of gold nanotubes in polycarbonate films are used to study catalytic reactions at gas–liquid interfaces. The catalytic properties of gold for CO oxidation with O_2 can be enhanced by liquid water and promoted by increasing the pH value of the solution. The membrane is sandwiched between other membranes that contain thiol-functionalized gold nanotubes, which control mass transport to the central reaction zone (see picture).

Nanotubes as Catalysts

M. A. Sanchez-Castillo, C. Couto, W. B. Kim, J. A. Dumesic* ——— **1140 – 1142**

Gold-Nanotube Membranes for the Oxidation of CO at Gas–Water Interfaces



Reversible disulfide chemistry is used to identify ligands that bind G-quadruplex DNA from a small dynamic combinatorial library (DCL) (see scheme). The biological macromolecular target is shown to induce an equilibrium shift. Surface plasmon resonance demonstrates that the two amplified species bind the quadruplex DNA.

DNA Recognition

A. M. Whitney, S. Ladame, S. Balasubramanian* ——— **1143 – 1146**

Templated Ligand Assembly by Using G-Quadruplex DNA and Dynamic Covalent Chemistry



Long-range forces (capillary force) are used in the self-assembly of three-dimensional (3D) micropatterns of aligned carbon nanotubes films. This method involves the spreading of a droplet of water after the growth of the carbon nanotube film. Controlling the density of the carbon nanotube film is crucial to the formation of 3D patterned structures (see picture).

Carbon Nanotubes

H. Liu, S. Li, J. Zhai, H. Li, Q. Zheng, L. Jiang,* D. Zhu ——— **1146 – 1149**

Self-Assembly of Large-Scale Micropatterns on Aligned Carbon Nanotube Films

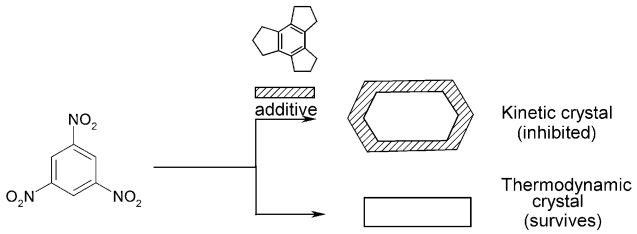
 © 2004 Wiley-VCH Verlag GmbH & Co. KGaA, Weinheim

Contents

Crystal Growth

P. K. Thallapally, R. K. R. Jetti, A. K. Katz, H. L. Carrell, K. Singh, K. Lahiri, S. Kotha, R. Boese,* G. R. Desiraju* _ **1149 – 1155**

Polymorphism of 1,3,5-Trinitrobenzene Induced by a Trisindane Additive

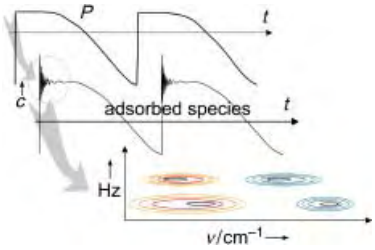


The most stable is not necessarily the most easy to obtain! Two new stable crystal forms of the 120 year old compound *sym*-trinitrobenzene are reported. These elusive forms have been obtained by the use of an additive, trisindane, that can act as a mimic in the crystallization experiment (see scheme).

Analyzing Zeolites

S. Chenevarin, F. Thibault-Starzyk* _____ **1155 – 1158**

Two-Dimensional IR Pressure-Jump Spectroscopy of Adsorbed Species for Zeolites



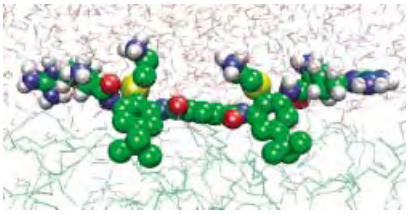
Probing pores: Adsorbed species on a zeolite are perturbed by pressure jumps (see picture; top), relaxation by means of diffusion and adsorption follows and is monitored by fast IR (middle). 2D maps are obtained by a second Fourier transform (bottom): the spectrum of each adsorbate/site pair is distinguished.

Antimicrobial Agents

D. Liu, S. Choi, B. Chen, R. J. Doerksen, D. J. Clements, J. D. Winkler, M. L. Klein, W. F. DeGrado* _____ **1158 – 1162**

Nontoxic Membrane-Active Antimicrobial Arylamide Oligomers

Cracking the case: Aryl amide oligomers with amphiphilic secondary structure were designed that attack bacteria by lysing their membranes. A variety of groups were appended to the lead compound to adjust its overall charge, hydrophobicity, and hydrophobic moment. An Arg-containing oligomer (see figure) was found to have good antimicrobial activity and low toxicity towards human erythrocytes.



VIP Communications labeled with this symbol have been judged by two referees as being "very important papers".

The issues for February 2004 appeared online on the following dates
Issue 5: January 21 · Issue 6: January 27 · Issue 7: February 2 · Issue 8: February 11

 © 2004 Wiley-VCH Verlag GmbH & Co. KGaA, Weinheim

Sources

Product and Company Directory

You can start the entry for your company in "Sources" in any issue of *Angewandte Chemie*.

If you would like more information, please do not hesitate to contact us.

Wiley-VCH Verlag – Advertising Department
Tel.: 0 62 01 - 60 65 65
Fax: 0 62 01 - 60 65 50
E-Mail: MSchulz@wiley-vch.de

Service

Keywords ____ *1164*

Authors ____ *1165*

Sources ____ *A17*

Vacancies ____ *A19*

Preview ____ *1167*

Corrigendum

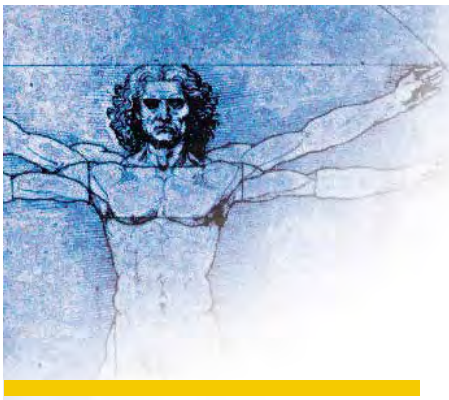
In the Review "Modern Synthetic Methods for Copper-Mediated C(aryl)—O, C(aryl)—N, and C(aryl)—S Bond Formation" by S. V. Ley and A. W. Thomas (*Angew. Chem. Int. Ed.* **2003**, *42*, 5400–5449), the "Avendano-Modified Ullmann Condensation Reaction" (Section 1.1, Equation 11) should be correctly termed the "Barton Plumbane-Modified Ullmann Condensation Reaction".

Furthermore, the following important references are missing: D. H. R. Barton, N. Yadav-Bhatnagar, J.-P. Finet, J. Khamsi, *Tetrahedron Lett.* **1987**, *28*, 3111–3114; D. H. R. Barton, D. M. X. Donnely, J.-P. Finet, P. J. Guiry, *Tetrahedron Lett.* **1989**, *30*, 1377–1380; D. H. R. Barton, D. M. X. Donnely, J.-P. Finet, P. J. Guiry, *J. Chem. Soc. Perkin Trans. 1* **1991**, 2095–2102.

Apology

In the Communication "Chiral, Porous, Hybrid Solids for Highly Enantioselective Heterogeneous Asymmetric Hydrogenation of β-Keto Esters" by A. Hu, H. L. Ngo, and W. Lin (*Angew. Chem. Int. Ed.* **2003**, *42*, 6000–6003), the authors neglected to cross-reference their thematically related communication in *J. Am. Chem. Soc.* **2003**, *125*, 11 490–11 491. The latter publication reported the hydrogenation of aromatic ketones with up to 99.2% *ee* by a different mechanism in the presence of a different [Ru(4,4'-binap)(diamine)Cl_2]–derived solid catalyst. The authors apologize for this accidental oversight.

 © 2004 Wiley-VCH Verlag GmbH & Co. KGaA, Weinheim



Cotton Award to J. Ellis

The first F. Albert Cotton Award in Synthetic Inorganic Chemistry of the American Chemical Society has been awarded to John E. Ellis. Ellis studied chemistry at the University of Southern California (USA), completed his PhD in 1971 in the research group of Alan Davison at the Massachusetts Institute of Technology (MIT, USA), and then went to the University of Minnesota in Minneapolis (USA), where he has been full professor since 1984. He is known for the synthesis and characterization of unusual transition-metal complexes and carbonylmetalates,[1a] some of which have found their way into text books, including one co-written by Cotton himself.[1b] In his most recent Communication[1c] in *Angewandte Chemie* Ellis describes the synthesis of bis(1,2,3,4-η^4-anthracene)cobaltate(1−).



J. Ellis

Research Prizes to P. Schwille and P. Fromherz

The Philip Morris Foundation awards research prizes worth a total of €100000 annually. This year Petra Schwille and Peter Fromherz are among the four recipients.

Schwille has been recognized for the development of two-photon cross-correlation spectroscopy, with which the interaction of individual biomolecules can be observed.[2] Schwille studied physics in Stuttgart and Göttingen (Germany) and completed her PhD in 1996 at the Max-Planck-Institut (MPI) für Biophysikalische Chemie in Göttingen under the guidance of Manfred Eigen (Nobel Prize 1967) on the topic "Fluorescence Correlation Spectroscopy: Analysis of Biophysical Systems on a Single-Molecule Level". She undertook postdoctoral research with W. Webb at Cornell University from 1997 to 1999, and then became a junior group leader in experimental biophysics at the MPI in Göttingen. In 2002 she took up a position as Professor of Biophysics at the Technische Universität (TU) Dresden (Germany).



P. Schwille

Fromherz has been recognized for his work at the interface between nerve cells and semiconductor chips: How can these two systems be coupled with one another for the transfer of information?[3] Fromherz studied chemistry at the Universität Karlsruhe (Germany), completed his PhD in 1969 in the research group of Hans Kuhn at the MPI für biophysikalische Chemie in Göttingen on lipid–protein films, and completed his habilitation there in 1978 with work on an enzyme–lipid–dye assembly between an electrolyte and a semiconductor. In 1981 he took up a position at the Universität Ulm (Germany) and in 1994 was made director of the MPI für Biochemie in Martinsried (Germany).



P. Fromherz

F. Diederich: New Editorial Board Chairman

At the beginning of 2004 François Diederich replaced Horst Kessler as Chairman of the Editorial Board of *Angewandte Chemie*. The members of this board advise the editorial staff on all matters regarding the content and presentation of the journal. Kessler (TU München, Germany) has been a member of the Editorial Board since 1996 and was chairman for two terms (2000–2003). For more information about him, see the news item on the award of the Philip Morris Research Prize in issue 08/2003 of *Angewandte Chemie*.

Diederich studied chemistry at the Universität Heidelberg (Germany) and completed his PhD in 1977 under the supervision of Heinz Staab at the MPI für medizinische Forschung in Heidelberg. After a postdoctoral period with Donald Cram (Nobel Prize in Chemistry 1987) at the University of California, Los Angeles (UCLA, USA) from 1979 to 1981, he returned to the MPI für medizinische Forschung in Heidelberg. Following his habilitation in 1985, he took up a position at the Department of Chemistry and Biochemistry, UCLA and was made full professor there in 1989. Since April 1992 he has been Professor of Organic Chemistry at the ETH Zürich (Switzerland). His research interests include synthetic fullerenes, supramolecular chemistry, molecular recognition, and medicinal chemistry. Diederich recently discussed "Interactions with Aromatic Rings in Chemical and Biological Recognition" in a comprehensive Review.[4] He has been a member of the Editorial Board since 1995.



F. Diederich

[1] a) W. Beck, *Angew. Chem.* **1991**, *103*, 173; *Angew. Chem. Int. Ed. Engl.* **1991**, *30*, 168; b) F. A. Cotton, G. Wilkinson, C. A. Murillo, M. Bochmann, *Advanced Inorganic Chemistry*, Wiley, New York, **1999**; c) W. W. Brennessel, V. G. Young, Jr., J. E. Ellis, *Angew. Chem.* **2002**, *114*, 1259; *Angew. Chem. Int. Ed.* **2002**, *41*, 1211.

[2] P. Schwille, K. G. Heinze, *ChemPhysChem* **2001**, *2*, 269.

[3] P. Fromherz, *ChemPhysChem* **2002**, *2*, 276.

[4] E. A. Meyer, R. K. Castellano, F. Diederich, *Angew. Chem.* **2003**, *115*, 1244; *Angew. Chem. Int. Ed.* **2003**, *42*, 1210.

 © 2004 Wiley-VCH Verlag GmbH & Co. KGaA, Weinheim DOI: 10.1002/anie.200481027

Dateiname: G81027E
Seite: 1 te von 1
Status Neusatz
Sprache

Pagina: 1044
Umfang (Seiten): 1
Datum: 8 KW., 17. Februar 2004 (Dienstag)
Zeit: 6:26:12 Uhr

Synthetic Methods

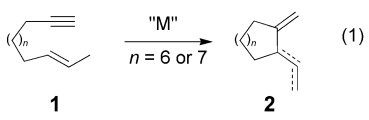
Asymmetric Cycloisomerization of 1,6- and 1,7-Enynes by Transition-Metal Catalysts

*Ian J. S. Fairlamb**

Keywords:
atom economy · cyclization · enantioselectivity · palladium · rhodium · ruthenium

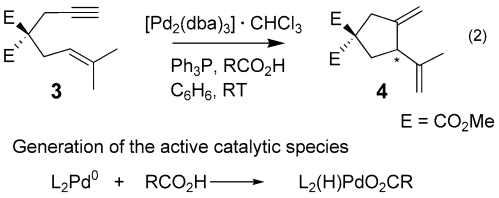
Introduction

An abundance of optically active molecules found in nature contain highly functionalized carbo- and heterocycles. These important structural features, which are often absolutely essential for biological activity and function, provide an impetus for synthetic chemists to design and develop new and more efficient methods for the synthesis of such compounds. Transition-metal-catalyzed cyclizations are arguably some of the most useful methods, and high selectivity and efficiency are often realized. It is somewhat surprising to find that asymmetric transition-metal-catalyzed cyclization reactions are generally quite limited, particularly when compared to other asymmetric reactions, such as hydrogenation or allylic alkylation, often referred to as the benchmark asymmetric reactions for testing new chiral transition-metal catalysts. Clearly, asymmetric cyclization reactions have great potential to facilitate access to both simple and structurally complex cyclic compounds in an efficient, but enantioselective fashion. Over the past twenty years, the transition-metal-catalyzed (Ti, Ru, Co, Rh, Ni–Cr, Pd, and Pt) "Alder-ene" cycloisomerization reaction of 1,*n*-enynes ($n = 6,7$)[1] has emerged as an extremely powerful, atom-economic, and environmentally friendly method for the rapid assembly of complex carbo- and heterocyclic frameworks in a highly regio-, diastereo-, and chemoselective way [Eq. (1), **1**→**2**].[2]



(1)

Trost is without doubt a pioneer in this area, particularly in the development of catalysts and their employment in the total syntheses of natural products, where the scope and limitations of the methodology have been studied extensively. Over the past few years there has been a resurgence of interest in the development of the asymmetric variant of the cycloisomerization reaction, particularly of 1,6-enynes. Here, these developments, as well as the initial investigations on the asymmetric reaction, are highlighted.



(2)

Asymmetric Pd-Catalyzed Cycloisomerization

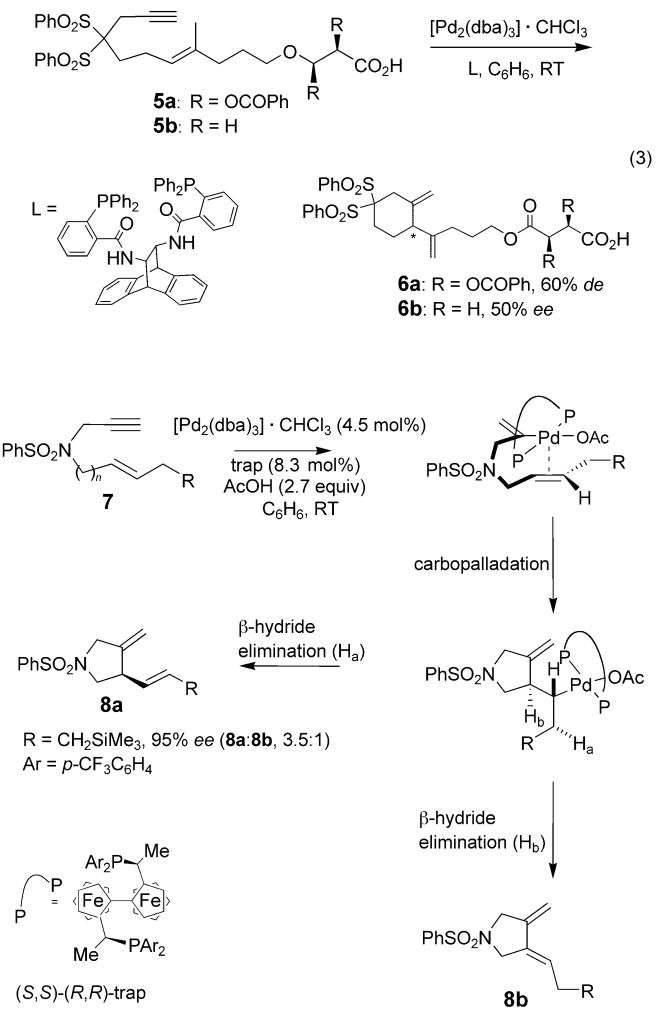
Trost was first to report an asymmetric protocol. It was found that a combination of $[Pd_2(dba)_3]{\cdot}CHCl_3$ (dba = *trans,trans*-dibenzylideneacetone) plus a carboxylic acid, such as acetic acid, effectively catalyzed the cycloisomerization of 1,6-enynes [Eq. (2), **3**→**4**].[3] The catalytic intermediate was proposed to be a palladium(II) hydride species "H–Pd–OAc", which is the oxidative-addition product of acetic acid and Pd^0. This was extended to the use of enantiomerically pure carboxylic acids, such as Mosher's acid, ((*S*)-(−)-2-methoxy-2-trifluoromethylphenyl acetic acid) and (*S*)-(−)-binaphthoic acid, which facilitated the asymmetric cycloisomerization reaction, although with modest, but encouraging enantioselectivity (33% *ee* was the highest).

Asymmetric induction was improved by the employment of amidodiphosphane ligands (Trost modular ligands) in combination with a tartrate chiral auxiliary contained within the 1,6- or 1,7-enyne, allowing a double stereodifferentiation to occur [Eq. (3), **5a**→**6a**].[4] It was found that the chiral ligand operates independently of the chirality of the tartrate auxiliary. The distant carboxylic acid unit in the substrate is essential for asymmetric induction, but the presence of the chiral tartrate is not. This was proven by comparison with reactions with the ethyl and methyl esters, which gave poor selectivity. A model was proposed where the carboxylic acid rigidifies the substrate by coordination to Pd in the chiral discriminating step (carbopalladation).

More efficient bidentate ligands for palladium were introduced by Ito and co-workers, namely the *trans*-coordinating bisferrocenyldiphosphanes based on (*S*,*S*)-(*R*,*R*)-trap [Eq. (4)].[5] Phosphane ligands reduce the rate of cyclization, although they are crucial for smooth conversion, minimizing side reactions,

[*] Dr. I. J. S. Fairlamb
Department of Chemistry
University of York
Heslington, York, YO10 5DD
(United Kingdom)
Fax: (+44) 1904-432-516
E-mail: ijsf1@york.ac.uk

 © 2004 Wiley-VCH Verlag GmbH & Co. KGaA, Weinheim DOI: 10.1002/anie.200301699



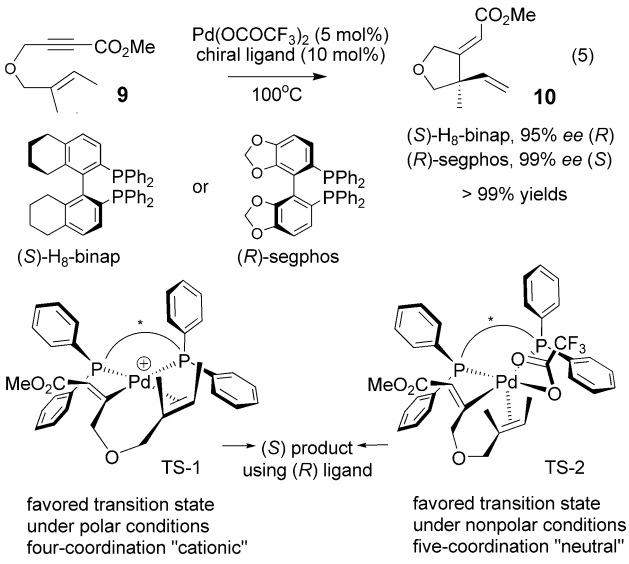
and prolonging the lifetime of the catalytic species. In this reaction, H_a elimination is the favored process to give 1,4-diene **8a** as the major product (H_b elimination gives the 1,3-diene **8b**). Increasing the electron-withdrawing ability on the P–aryl substituents results in higher enantioselectivities and reactivities (up to 95% *ee*), but this appears to be substrate sensitive (nine examples, 34–76% *ee*). Alteration of the alkene configuration from *Z* to *E* resulted in a reversal of the observed configuration of the newly formed stereogenic center in the product (*E*→*R*) to (*Z*→*S*).

In addition to these results, it was shown that other optically active *cis*-chelating phosphanes, such as chiraphos and diop, amongst others, gave poor selectivities (6–15% *ee*), whereas for binap and the electron-donating ettrap no conversion occurred even at 80°C.

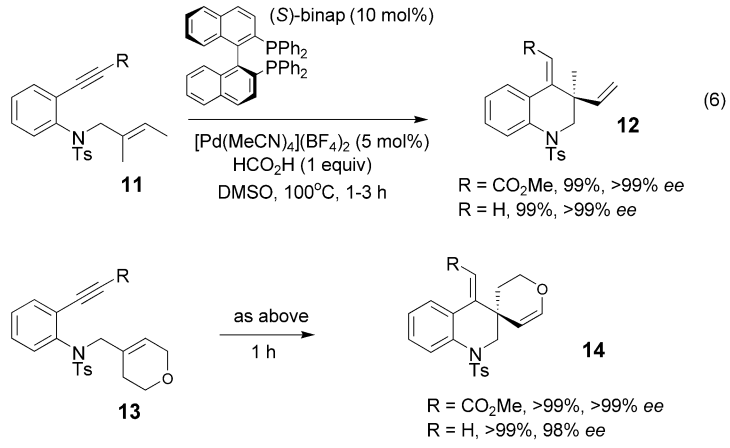
Mikami et al. found that the cycloisomerization of 1,6-enyne **9**→**10**, in benzene at 100°C, with typical palladium catalysts ($Pd(OAc)_2$, $[Pd_2(dba)_3]\cdot CHCl_3$/AcOH, and $[Pd_2(dba)_3]\cdot CHCl_3$/$F_3CCO_2H$) and (*R*)-binap gave higher enantioselectivity (up to 84% *ee*), although with insufficient catalytic activity (<25% yield) [Eq. (5)].[6]

On switching to $Pd(OCOCF_3)_2$ an improvement in yield (>99%) and enantioselectivity (93% *ee*) was seen. Use of the related binap ligands (*S*)-H_8-binap and (*R*)-segphos increased enantioselectivity to >99% *ee*. For these ligands, changing the solvent to dimethyl sulfoxide (DMSO) resulted in improved reaction rates but with a slight reduction in enantioselectivity (ca. 90–96% *ee*). It is proposed that the CF_3COO^- ion is released associatively in DMSO and gives up one coordination site on a square-planar cationic complex [TS-1 in Eq. (5)]. In the nonpolar solvent, the counterion remains coordinated to the Pd^{II} species, where the olefin is forced to coordinate the fully square-planar Pd^{II}, producing a relatively unfavorable five-coordinate intermediate, which is proposed to slow down the reaction [TS-2 in Eq. (5)].

Mikami and Hatano extended this work to the asymmetric cycloisomerization of 1,7-enynes to provide six-membered rings, which are more difficult to form than the five-membered-ring systems.[7] In particular, a highly efficient asymmetric synthesis of quinoline derivatives bearing a quaternary carbon center (**11**→**12**) or a spiro ring (**13**→**14**) was achieved using the catalyst combination (*S*)-binap/$[Pd(MeCN)_4](BF_4)_2$ in the presence of formic acid in DMSO at



 © 2004 Wiley-VCH Verlag GmbH & Co. KGaA, Weinheim



(6)

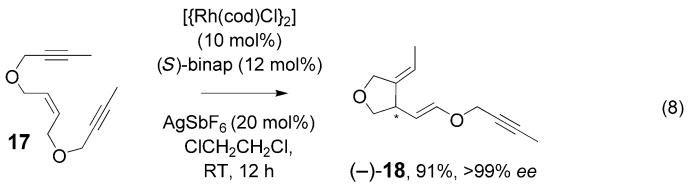
100 °C [Eq. (6)]. Interestingly, these reactions can be monitored by following changes in the color of the solution. The reaction solution is light yellow initially and becomes a deep green clear solution after only 2 min at 100 °C. The color lightens as the reaction proceeds, finally turning to a yellow-orange color when the reaction is complete.

Asymmetric Rh-Catalyzed Cycloisomerization

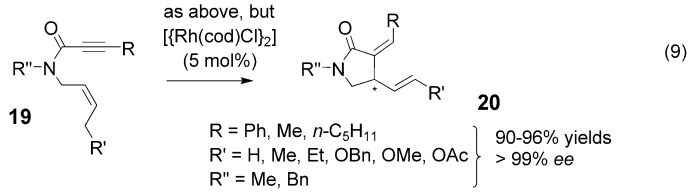
Zhang and co-workers reported the first asymmetric Rh-catalyzed 1,6-enyne cyclosiomerization reactions employing precursor catalysts containing chiral bidendate phosphanes and phosphinites [Eq. (7), **15**→**16**].[8] Surprisingly no reactivity was observed with the Rh/binap system, whereas Me-duphos, bicp, and bicpo were very useful. Generally, the catalyst system proved quite responsive to subtle changes in the electronic nature of the substrate and ligand—a limiting feature with respect to broader substrate scope.

It was subsequently found that simply preparing the catalysts in situ led to a significant improvement in reactivity and enantioselectivity for several prototypical substrates containing heteroatom tether linkages. The catalyst prepared from binap, in particular, gave excellent asymmetric induction and demonstrated good reactivity [Eq. (8), **17**→**18**].[9]

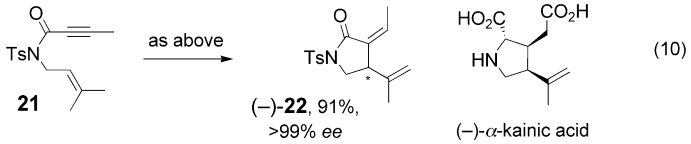
Substrate scope has been broadened by application of the new protocol to the highly enantioselective cyclosiomerization of enyne amides to give functionalized lactams in extraordinarily high enantioselectivities [Eq. (9), **19**→**20**].[10] These reactions demonstrate broad functional-group tolerance, but notably, functionalized vinyl derivatives such as vinyl ether, vinyl acetate, vinyl allylic ether, and enamides containing lactams are accessible. This further offers a new asymmetric approach to kainic acid analogues [Eq. (10), **21**→**22**]. A limitation is in the use of (*E*)-olefins, where poor conversion and low enantioselectivities are observed. This is possibly



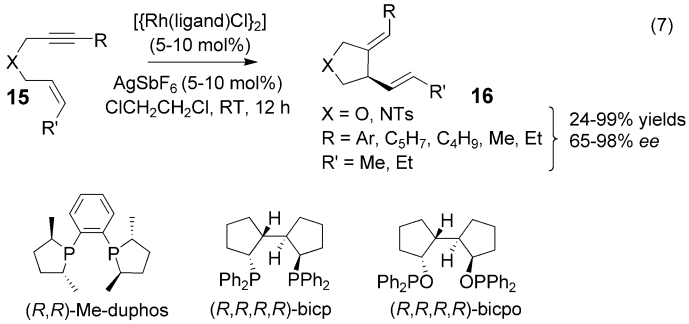
(8)



(9)



(10)

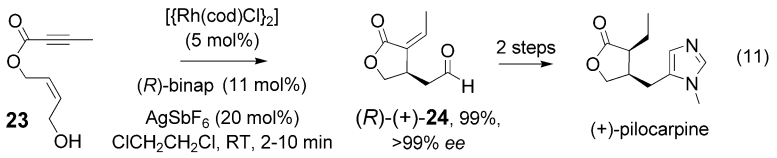


(7)

attributable to weaker coordination of *E* substrates to Rh^I. A highly stereoselective kinetic resolution of 1,6-enynes and a Rh^I-catalyzed intramolecular cycloisomerization reaction have also been developed, allowing access to polyfunctional tetrahydrofurans and 1,6-enynes with two stereogenic centers with high enantioselectivity.[11]

Zhang and his team have employed this catalyst system in an asymmetric "formal" synthesis of (+)-pilocarpine

 © 2004 Wiley-VCH Verlag GmbH & Co. KGaA, Weinheim

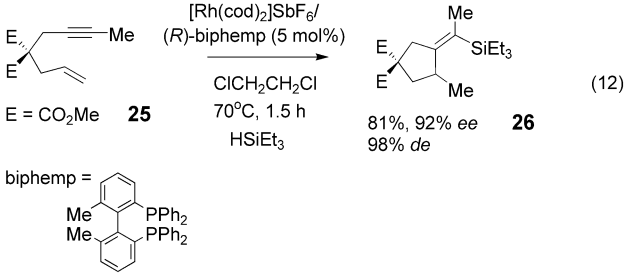


[Eq. (11), **23**→**24**].[12] Functionalized α-methylene-γ-butyrolactones are accessible in high yields (90–98%) and enantioselectivities (all examples given are >99% *ee*!). A number of these reactions were complete in <5 min! Clearly this catalyst system is extremely powerful.

A catalytic cycle for the Rh-catalyzed cycloisomerization reaction has been proposed (Scheme 1).[10] This consists of bidentate coordination of the enyne with a Rh^I species to form a coordinated intermediate **II**. Depending on the substituent R^2, either oxidative cyclization of the enyne or oxidative addition could be expected. Here, only oxidative cyclization occurs, affording metallacyclopentenes **III**. A regiospecific β-H elimination of metallacyclopentene **III-A** provides the Rh–H species **IV**, which then undergoes reductive elimination to provide the expected 1,4-diene product. The *E* geometry of the double bond is expected, as β-H elimination is favored from the less sterically hindered metallacyclopentene **III-A**, as opposed to the more sterically congested metallacyclopentene **III-B**, which provides the *Z* isomer. Under Rh catalysis, the cycloisomerization reaction tolerates the presence of allylic acetate and carbonate groups, which generally show a high reactivity towards oxidative addition with low-valent transition metals. It is clear that in this system that oxidative cyclization is strongly favored over oxidative addition.

In a variation of the cycloisomerization reaction, Widenhoefer et al. have developed the first asymmetric 1,6-enyne cyclization/hydrosilylation reaction using rhodium catalysts containing (*R*)-biphemp [Eq. (12), **25**→**26**].[13]

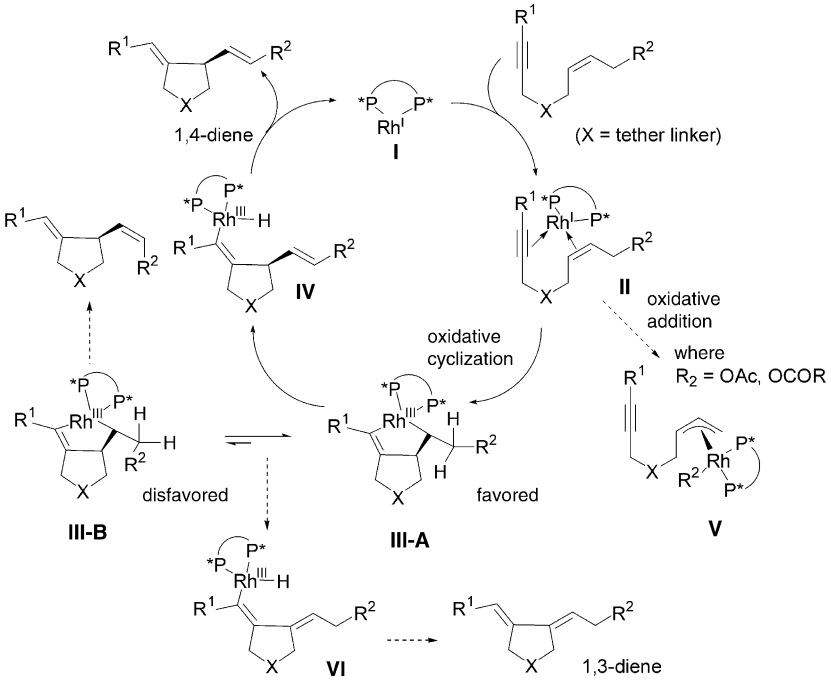
Various 1,6-enynes gave functionalized silylated alkylidenecyclopentanes in generally good yields and enantioselectivities of up to 92% *ee*. These results are very encouraging, given that they present the first highly enantioselective transformations of malonate-type enyne substrates.



Summary and Outlook

The future perspectives for asymmetric cycloisomerization reactions, catalyzed by transition metals, are very positive and encouraging. The rhodium-catalyzed reaction is without doubt the current leader in terms of substrate scope (including (*Z*)-olefins), enantioselectivity, and catalyst reactivity. The ruthenium-catalyzed asymmetric variant represents a new challenge. Trost has reported that $[CpRu(CH_3CN)_3]PF_6$ is an excellent catalyst for enyne cycloisomerization, which is proposed to proceed via a ruthenacyclopentene intermediate (Ru^{IV}), formed by oxidative cyclometalation, in the catalytic cycle.[14] This catalyst possibly precludes the use of chiral phosphanes,[15] and alternative strategies may be required if this versatile metal is to enjoy similar success as rhodium and palladium in catalyzed asymmetric reactions. It should be noted that the cycloisomerization reactions catalyzed by Pt^{II}, similar to those with Ru^{II}, also proceed by an oxidative cyclometalation process.[16] Asymmetric variants of the Pt-catalyzed reaction remain to be developed.

The emergence of efficient protocols for the asymmetric cycloisomerization



Scheme 1. The proposed mechanism for the Rh-catalyzed cycloisomerization of enynes.

 © 2004 Wiley-VCH Verlag GmbH & Co. KGaA, Weinheim

of enynes to provide nonracemic carbo- and heterocyclic compounds has been demonstrated. Further application of these protocols to the synthesis of other natural products and molecules of biological importance and interest is expected over the coming years.

[1] For comprehensive reviews, see: a) C. Aubert, O. Buisine, M. Malacria, *Chem. Rev.* **2002**, *102*, 813; b) B. M. Trost, M. J. Krische, *Synlett* **1998**, 1; c) B. M. Trost, *Acc. Chem. Res.* **1990**, *23*, 34; d) For a mechanistic overview, see: G. C. Lloyd-Jones, *Org. Biomol. Chem.* **2003**, *1*, 215.

[2] The thermal Alder reaction, in the absence of a transition metal, has had few applications in organic synthesis, due to limitations in scope, particularly as extremely high temperatures are required.

[3] B. M. Trost, D. C. Lee, F. Rise, *Tetrahedron Lett.* **1989**, *30*, 651.

[4] B. M. Trost, B. A. Czeskis, *Tetrahedron Lett.* **1994**, *35*, 211.

[5] A. Goeke, M. Sawamura, R. Kuwano, Y. Ito, *Angew. Chem.* **1996**, *108*, 686; *Angew. Chem. Int. Ed. Engl.* **1996**, *35*, 662 [trap = 2,2″-bis[1-(diarylphosphanyl)-ethyl]-1,1″-biferrocene].

[6] M. Hatano, M. Terada, K. Mikami, *Angew. Chem.* **2001**, *113*, 255; *Angew. Chem. Int. Ed.* **2001**, *40*, 249 [binap = 2,2′-bis(diphenylphosphanyl)-1,1′-binaphthyl), chiraphos = 2,3-bis(diphenylphosphanyl)butane, diop = 2,3-*O*-isopropylidene-2,3-dihydroxy-1,4-bis(diphenylphosphanyl)butane].

[7] M. Hatano, K. Mikami, *J. Am. Chem. Soc.* **2003**, *125*, 4704.

[8] P. Cao, X. Zhang, *Angew. Chem.* **2000**, *112*, 4270; *Angew. Chem. Int. Ed.* **2000**, *39*, 4104 [duphos = 1,2-bis(phospholano)benzene, bicp = 2,2′-bis(diphenylphosphanyl)-1,1′-dicyclopentane, bicpo = 2,2′-bis(diphenylphosphinite)-1,1′-dicyclopentane].

[9] A. Lei, M. He, S. Wu, X. Zhang, *Angew. Chem.* **2002**, *114*, 3607; *Angew. Chem. Int. Ed.* **2002**, *41*, 4104.

[10] A. Lei, J. P. Waldkirch, M. He, X. Zhang, *Angew. Chem.* **2002**, *114*, 4708; *Angew. Chem. Int. Ed.* **2002**, *41*, 4526. Pd-catalyzed asymmetric cyclization of similar enynes initiated by acetoxypalladation results in β-deacetoxypalladation (elimination). This protocol is very useful for the asymmetric synthesis of substituted γ-butyrolactones, see: a) Q. Zhang, X. Lu, X. Han, *J. Org. Chem.* **2001**, *66*, 7676; b) Q. Zhang, X. Lu, *J. Am. Chem. Soc.* **2000**, *122*, 7604.

[11] A. Lei, M. He, X. Zhang, *J. Am. Chem. Soc.* **2003**, *125*, 11472.

[12] A. Lei, M. He, X. Zhang, *J. Am. Chem. Soc.* **2002**, *124*, 8198.

[13] H. Chakrapani, C. Liu, R. A. Widenhoefer, *Org. Lett.* **2003**, *5*, 157. It was found that Rh/binap complexes were not effective catalysts for cyclization/hydrosilylation. [biphemp = 6,6′-bis-(diphenylphosphanyl)-2,2′-dimethyl-biphenyl].

[14] a) B. M. Trost, F. D. Toste, *J. Am. Chem. Soc.* **1999**, *121*, 9728; b) B. M. Trost, F. D. Toste, *J. Am. Chem. Soc.* **2000**, *122*, 714; c) B. M. Trost, F. D. Toste, *J. Am. Chem. Soc.* **2002**, *124*, 5025; for a related article, see: d) M. Mori, N. Saito, D. Tanaka, M. Takimoto, Y. Sato, *J. Am. Chem. Soc.* **2003**, *125*, 5606 and references therein.

[15] The presence of phosphane ligands with this catalyst might slow down the rate of cycloisomerization.

[16] M. Méndez, M. P. Muñuz, C. Nevado, D. J. Cárdenas, A. M. Echavarren, *J. Am. Chem. Soc.* **2001**, *123*, 10511.

 © 2004 Wiley-VCH Verlag GmbH & Co. KGaA, Weinheim

History of Science

Hermann Staudinger and the Origin of Macromolecular Chemistry

*Rolf Mülhaupt**

Keywords:
history of science · ketenes · macromolecular chemistry · polymers · Staudinger, Hermann

1. Introduction

On December 10th, 1953 Hermann Staudinger's pioneering research on macromolecules was acknowledged by the award of the Nobel Prize for Chemistry.[1] The headline "High Polymers bring High Honors" went all around the world.[2] Staudinger had discovered the molecular blueprints of high molecular weight natural and man-made polymeric materials. His revolutionary concept, involving linking of a large number of small monomer molecules by means of covalent bond formation to form macromolecules, marked the beginning of the new era of molecular design of high molecular weight structural and functional polymeric materials. At the beginning of the 20th century the trial-and-error-type polymer development was aimed primarily at imitating natural polymeric materials such as silk, natural rubber, and ivory. Most early imitations exhibited rather poor product qualities with respect to those of the corresponding natural products. It was Staudinger's molecular blueprint that was applied successfully to design modern high-value-in-use polymers with property profiles unparalleled in nature. Polymeric materials are exceptional with respect to their unique combination of attractive cost/performance ratio, low-energy demand during preparation and processing, flexible supply of feedstocks, attractive ecobalances and ecoefficiency, easy processing with short cycle times typical for the modern industrial mass production, and their extraordinary versatility with respect to their property profiles, application ranges, and recycling of wastes.

No other class of materials is capable of matching similarly diversified property profiles. As a function of their molecular and supermolecular architectures it is possible to render polymers rigid like steel, soft, or rubbery, permeable or impermeable, conducting or insulating, optically transparent or opaque, durable or biodegradable. Typical polymer applications include food packaging, light-weight construction and engineering materials, functional textiles, corrosion-resistant coatings, durable adhesives, agricultural films used to enhance food production, and biomedical applications ranging from artificial teeth and dental fillings to advanced drug-release systems and biocompatible materials for bone, cartilage, and tissue replacement. Since the mid 1970s industrial polymer production increased tenfold and is now rapidly approaching 200 million metric tons per year.[3] In nature the annual production of biopolymers such as carbohydrates is much larger, exceeding 200 billion metric tons per year, and exploits photosynthesis based upon carbon dioxide, water, and solar energy. Today high molecular weight polymer products are integral parts of our daily life and secure high quality of life. Staudinger's visions remain important key issues in modern macromolecular chemistry, materials science, and biotechnology. His concepts continue to provide the solid and still expanding base on which we build new structural and functional polymers in the fields of our modern key technologies.

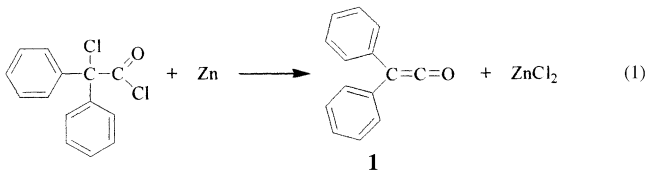
[*] Prof. Dr. R. Mülhaupt
Institut für Makromolekulare Chemie
Albert-Ludiwig-Universität Freiburg
Stefan-Meier-Strasse 31
79104 Freiburg (Germany)
Fax: (+49) 761-203-6319
E-mail: rolf.muelhaupt@makro.uni-freiburg.de

2. Staudinger's Route to Macromolecular Chemistry

Hermann Staudinger's academic career is exceptional, especially with respect to the outstanding scientific achievements of young Staudinger and his very rapid academic career development. Important stages of his life and his research were highlighted by Hermann Staudinger himself in his "*Arbeitserinnerungen*" (work memoirs).[4] Several authors have published Hermann Staudinger's bibliography and acknowledged his scientific contributions.[5] Hermann Staudinger, born in Worms, Germany on March 23, 1881, started to study botany with Klebs at the University of Halle in 1899. Soon he was attracted by the field of chemistry in the laboratory of Volhard and decided to shift his academic focus to chemical research. After studying chemistry in Darmstadt and Munich, he got his PhD degree in 1903 in Halle, only four years after his enrolment at the university. His PhD thesis with Vorländer in Halle was concerned with the addition of malonates to unsaturated compounds.[6] In the same year he accepeted an assistant position with J. Thiele at the University of Strasbourg. During his research in Thiele's laboratory, which was aimed at exploring the conversion reactions of carboxylic acids into the corresponding aldehydes, Staudinger discovered the ketenes as a new class of chemical substances in 1905. When he treated diphenylchloroacetyl chloride with zinc,

 © 2004 Wiley-VCH Verlag GmbH & Co. KGaA, Weinheim DOI: 10.1002/anie.200330070

he succeeded in isolating and identifying diphenylketene (**1**) [Eq. (1)].[7]

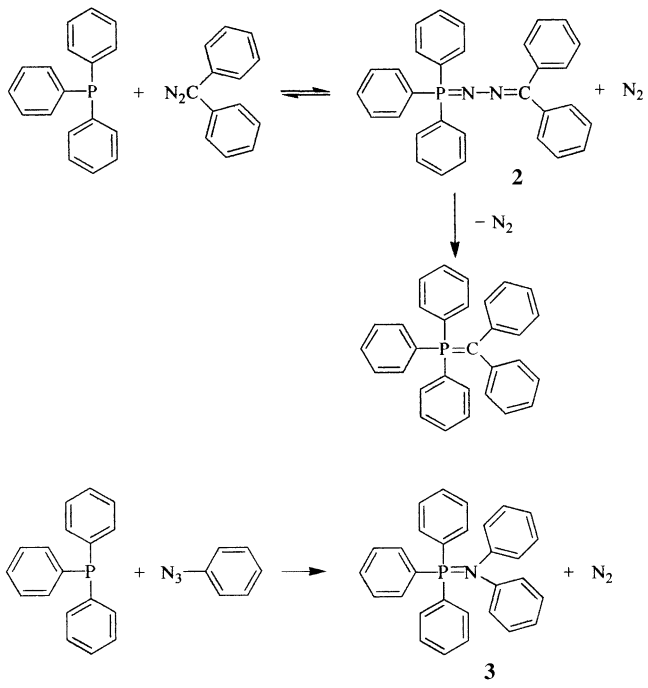


1

During the spring of 1907 he received his "habilitation" degree at the University of Strasbourg after submitting his "habilitation" thesis on ketene chemistry. Already in October 1907 young Staudinger, then 26 years old, was appointed the "*planmässige Extraordinariat*" (Assistant Professor) for organic chemistry at the Technical University of Karlsruhe, Germany (successor of R. Scholl) in C. Engler's laboratory. Within a very short time Hermann Staudinger acquired his outstanding international reputation as a chemist doing research on the organic chemistry of small molecules. In the summer of 1912, at the age of only 31 years old, Hermann Staudinger was appointed successor to Richard Willstätter at the Swiss Federal Institute ETH Zürich in Switzerland. During his research in Karlsruhe and afterwards in Zürich Staudinger continued his investigations of ketene chemistry and started his research on oxalyl chloride, aliphatic diazo compounds, carbene reactions, new organophosphorus compounds, autoxidation of organic compounds, drugs, preparation and polymerization of isoprene and butadiene. Important discoveries at this time included Staudinger's new route to novel phosphazenes such as **2** and **3** by reacting tertiary phosphanes with diazo compounds[8] and especially with azides (Scheme 1).[9,10] His azide route to produce phosphazenes became soon known as the "Staudinger reaction".[11,12]

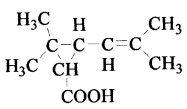
Staudinger's pyrolysis of six-membered rings represented one of the first industrial routes to 1,3-dienes, for example, isoprene was obtained from terpenes such as limonene.[13] This process was patented by Staudinger[14] and applied by the BASF AG, where butadiene was prepared in an analoguous manner by pyrolysis of cyclohexadiene. At that time large amounts of isoprene and butadiene were needed at the BASF AG in Ludwigshafen for the evaluation of the diene polymerization and the preparation of synthetic rubbers.[15] Staudinger's basic research on explosions encountered when mixing together alkali metals and halogen compounds can be found cited in most modern handbooks and safety instructions of organic chemistry. It was Staudinger who recognized that the mixture of alkali metals together with inorganic or organic halogen compounds formed systems that are extremely shock-sensitive. Minute agitations of such mixtures are sufficient to trigger heavy detonations. This is why it is strictly prohibited to dry halogen compounds by refluxing them over alkali metals. According to Staudinger the simple mixture of tetrachloromethane with sodium/potassium alloy is 200-fold more shock-sensitive than mercury fulminate.[16–18] Five patent applications of Staudinger claimed the use of such mixtures as primers for explosives. However, industrial applications failed because in contrast to mercury fulminate his mixtures did not manage to initiate effectively the detonations of picric acid and dynamite.

In 1910 Staudinger started his successful research on biofunctional small molecules. Jointly with his student L. Ruzicka (Nobel Prize for Chemistry in 1939) he identified the active ingredient of the Dalmatian insect-powder (pyrethrum). Pyrethrum was a powder made from finely ground blossom of the chrysanthemum flower (*Chrysanthemum cinerariifolium Bocc.*), which was extracted with petroleum ether. The ester of the cyclopropanecaboxylic acid chrysanthemic acid (**4**) and pyrethrin acid (**5**) with the cyclopentenyl alcohol pyrethrolone (**6**) and cinerolone proved to be very active insecticides, as successfully tested on the common German cockroach (*Blatta germanica*). The natural pyrethrins pyrethrin I and II are esters of the (+)-*trans* acids with (+)-**6**. The structures of the chrysanthemic acids[19] were identified by Staudinger's group beyond a shadow of doubt, whereas they failed to pin-point the actual position of the OH group and the double bond in the side chain.[20]

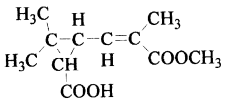


Scheme 1. Examples of the Staudinger reaction.

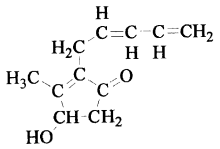
 © 2004 Wiley-VCH Verlag GmbH & Co. KGaA, Weinheim



4



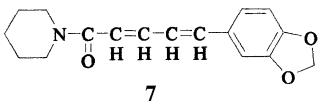
5



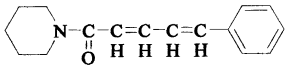
6

This problem was solved later by other groups. Pyrethrins are very effective insecticides which continue to attract a lot of attention today. At Staudinger's time, cheap competing insecticides were based on hexachloroethane, dichlorobenzene, and later also DDT, all of which are banned today. All of Staudinger's attempts to make syntheic pyrethrins had failed because, although he synthesized **4** and **5**, he did not succeed in synthesizing pyrethrolone (**6**). However, his research achievements provided the solid base for the modern pyrethrin development and our state-of-the-art insecticide protection.

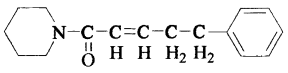
During World War I the shortage of raw materials stimulated the quest for research on surrogates. Staudinger's surrogate research was very successful! His discovery of synthetic pepper and his synthetic coffee flavor attracted considerable attention. In fact, the allied naval blockage caused a natural pepper shortage in Germany. Therefore, attempts were made to explore surrogates for the piperidine derivative **7**, which is a component of natural pepper (7–10%). Schneider and Staudinger recog-



7



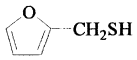
8



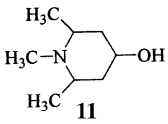
9

nized that the dioxomethylene ring substitution did not affect the pepper flavor. They prepared and patented the piperidine **8** and the partially hydrogenated derivative **9**, both of which exhibited the typical pepper flavor.[21] They clarified the basic correlations between molecular architectures and pepper flavor.[22] In 1917 the hydrogenated derivative **9** was introduced commercially as synthetic pepper and thereby helped the Germans to improve the taste of their beetroot-based surrogate food during the dramatic food shortage in Germany at the end of World War I. During World War II Farbweke Hoechst AG produced **8** as synthetic pepper. Although Staudinger claimed that his synthetic pepper was a very satisfactory pepper surrogate, natural pepper was much cheaper during peace time.

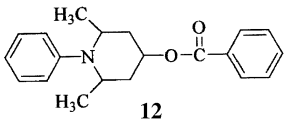
During World War I Staudinger also approached the problem of the natural coffee shortage in Germany. Jointly with Reichstein he succeed in distilling and isolating more than 70 coffee-flavored compounds from roasted coffee in high vacuum. Among this fairly large number of compounds they were very surprised to find furfurylthiol (**10**) as a very effective coffee flavor although this compound in high concentrations is well known for its very unpleasant odor. Finally, a typical coffee flavor was achieved from a synthetic mixture of more than 40 compounds, at an appropriate dilution. Jointly with the Swiss company International Genussmittel AG in Schaffhausen, Switzerland, Staudinger filed patents on the extraction of coffee flavor and his synthetic coffee flavor.[23] The company Haarmann & Reimer in Holzminden, Germany introduced Staudinger's synthetic coffee as "Caffarom" on a commercial scale shortly before the outbreak of World War II and the renewed German interest in coffee surrogates. Staudinger and Reichstein published their research on synthetic coffee flavor when World War II was over.[24] The atropin shortage during World War I prompted Staudinger and Reichstein to prepare and to patent 1,2,6-dimethyl-4-oxypiperdine (**11**) as "open-chain tropin" together with a large number of its derivatives.[25] These patents were transferred to the "Gesellschaft für Chemische Industrie" (Society of The Chemical Industry) in Basel, Switzerland. The benzoates, especially the *N*-phenyl derivative **12** proved to be effective as a local anaesthetic. Staudinger's research in the field of small molecule chemistry was published in 215 publications.



10



11



12

Around 1920 Staudinger started his investigations on macromolecular compounds with special emphasis being placed upon polyoxymethylene, rubber, and polystyrene. In 1926 Staudinger moved to the Albert-Ludwigs University in Freiburg and became the successor of Heinrich Wieland. He was Director of the "Chemisches Laboratorium" (chemical laboratory) at the University of Freiburg till 1951 and Director of his Institute of Macromolecular Chemistry till 1956. His change of location was paralleled by a complete change of his research topics: In Freiburg Staudinger focused his research exclusively on macromolecular compounds. Why did Staudinger leave the safe harbor of organic chemistry and embark on the stormy seas of the new high-risk research field named macromolecular chemistry, especially in view of the heavy opposition and even sarcasm of his colleagues?

3. Polymerization and Staudinger's Macromolecules

At the beginning of the 20th century the successful research for surrogates of natural fibers, ivory, and natural rubber—an important raw material decisive for the war effort—was accompanied by substantial progress in the development of novel structural and functional polymeric materials. A comprehensive view on the history of polymer sciences was presented by Herbert Morawetz in *Angewandte Chemie*[26] and in his excellent

 © 2004 Wiley-VCH Verlag GmbH & Co. KGaA, Weinheim

book entitled "*Polymers - The Origins and Growth of a Science*". At the end of the 19th century only chemically modified natural polymeric materials were available. In 1839 Charles Goodyear's discovery that sulfur-based vulcanization converted tacky natural rubber into elastomers gave birth to the rubber industry.[27] In 1833 it was Braconnot[28] who first described the nitration of cellulose and the explosive decomposition of the corresponding nitrocellulose. The nitration process was improved significantly by Schönbein, Professor of Chemistry in Basel, Switzerland, in 1847. His process was the basis for the production of nitrocellulose explosives that became well known as smokeless gunpowder. In contrast to the insoluble and infusible cellulose, the corresponding nitrocellulose derivative was found to be soluble and was successfully applied as a component of coatings.[29] Graf de Chardonnet first reported the extrusion of nitrocellulose solution followed by precipitation in water to spin the first man-made fibers which resembled those of silk.[30] Since nitrocellulose was highly flammable, de Chardonnet developed various processes for cleaving the nitro groups after spinning. This led to the development of the first man-made silk fibers based upon cellulose.[31]

The breakthrough in the development of thermoplastics occurred in 1870 when Hyatt discovered the plasticizing effect of camphor.[32] The camphor plasticizer rendered nitrocellulose melt processable and moldable. Placticized camphor (celluloid) became known as man-made ivory and saved the lives of many thousand elephants. It was applied to manufacture combs, toys, toothbrushes and even artificial teeth, billiard balls, and films. In sharp contrast to billiard balls made from natural ivory, however, the nitrocellulose billiard balls were reported to explode immediately upon contact with burning cigars.[33] Soon the plasticized nitrocellulose films proved to be excellent carriers for photographic layers. The explosive nature of nitrocellulose and its high flammability caused many fires in cinemas when celluloid films were introduced commercially at the beginning of the 20th century. The lifetime of celluloid films was very limited due to embrittlement resulting from plasticizer migration.[34]

At the beginning of the 20th century the true breakthrough in industrial polymer chemistry is attributed to Baekeland who in 1907 managed to control the polycondensation of phenol and formaldehyde in the presence of acid catalysts, forming melt processable novolacs which he cured with formaldehyde or urotropin, respectively.[35] Baekeland's phenolic thermoset resins were introduced into the market under the tradename of Baekelite. These first fully synthetic polymeric materials proved to be excellent electrical insulators and came just in time to enable the victorious advances of the electrification and electrical engineering. At the beginning of the 20th century the molecular design and the molecular architectures of natural and man-made polymeric materials was unknown although the first polymer products, developed by trial-and-error optimizations, had reached the market place.

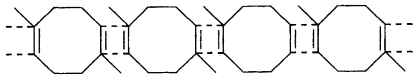
The terms polymer and polymerization were introduced a long time before Staudinger started his pioneering research. However, during the early days they had a very different meaning with respect to our modern understanding. The word "polymer" appeared in the literature in 1833. According to Berzelius "polymeric states" and "polymers" were compounds of the same chemical composition that exhibited very different properties.[36] Berzelius' polymers had nothing in common with our modern idea of polymers and high molecular weight long polymer chains! At that time polymer was ill-defined and included isomers, homologues, and polymorphisms without taking into account any molecular weight limits. For example, Berthelot reported in 1866 that heating acetylene afforded the "polymers" benzene and styrene.[37] During those days "polymers" included compounds with different molecular weights and the same chemical composition without paying attention to their molecular architectures, high molecular weights, and chemicals bonds.

The term "polymerization" was introduced by Berthelot in 1863.[38] He concluded that all molecules (today we would call them unsaturated compounds), which are able to add hydrogen, chlorine, or water can also add to themselves. In 1853 Berthelot reported the thermal and catalytic polymerization of pinene[39] and in 1869 published his research on the polymerization of ethene, propene, pentene, and pinene.[40] In the presence of alkali metals ethene was "polymerized" to produce high boiling olefins such as hexadecane, which he named polyethylene. Propene was "polymerized" in the presence of sulfuric acids, thus producing olefin fractions boiling at 200–220 and 260–280 °C. The term oligomer was introduced in the literature much later during the first half of the 20th century.[41] Solid polyethylene or polymethylene, which was identical with Ziegler's linear high density polyethylene produced in catalytic low-pressure polymerization, was successfully prepared by decomposition of diazomethane, as reported by von Pechmann[42] in 1899 and by Bamberger and Tschirner[43] in 1900. At that time nobody identified the enormous industrial impact of high-density polyethylene. Also the presence of long polymer chains was not recognized. In Berthelot's meaning of "polymerization" the actual nature of the chemical bonds and the role of the molecular weight was not an issue.

At the beginning of the 20th century the properties of polymers were explained by using concepts of colloid chemistry, which Graham had introduced in 1861.[44] It was believed that micellar self-assembly of small molecules in the absence of covalent bond formation between them accounted for the polymer properties. During the 1920s the leading scientists of the emerging field of crystallography ardently opposed the existence of high molecular weight polymers formed by covalent linking of small monomer molecules. At that time it was believed that the entire polymer molecule would have to fit into the crystallographic unit cell which was much too small to accommodate such giant molecules. For example, in 1923 Brill calculated from his crystallographic study on silk fibroin that only protein molecules with molecular weights varying between 500 and 600 $g\,mol^{-1}$ would fit into the dimensions of the unit cell.[45] Later it was recognized that only segments of the long polymer chains are present in the unit cell.

 © 2004 Wiley-VCH Verlag GmbH & Co. KGaA, Weinheim

One should not forget that the concepts of molecules and molecular structures are well established today but this was not the case a hundred years ago when thinking in terms of molecules was new. Therefore it is not surprising that the early proposals for polymer architectures were based upon self-assembly of small monomer molecules without covalent bond formation between them. A prominent example is the polymer structure that Harries proposed in 1905 for natural rubber.[46] Since the ozonolysis produced exclusively levulinic aldehyde, Harries concluded that natural rubber was composed of dimethylcyclooctadiene which polymerizes by self-assembly involving noncovalent interactions between the two double bonds to give **13**. This concept was in accord with



13

Thiele's partial valence hypothesis, which claimed that the C atoms of the double bond possess an affinity or partial valence because their potential binding affinity is not fully used.[47] In 1914 it was Pickles who questioned the self-assembly as claimed by colloid chemistry because his bromination of natural rubber was not accompanied by degradation.[48] He proposed for the first time the covalent bond formation between isoprene monomer molecules. However, he completely underestimated the actual molecular weights of natural rubber and favored the formation of cyclic polymers without end groups.

In protein chemistry the modern structural concepts for the existence of high molecular weight biopolymers were established during the first years of the 20th century. In 1906 Emil Fischer examined the hydrolysis of proteins and concluded that proteins are polypeptides formed by covalent bond formation between amino acid units.[49] In his tedious multistep synthesis Fischer built a polypeptide chain containing 18 amino acid units linked together by covalent bond formation: $LeuGly_3LeuGly_3$-$LeuGly_9$.[50] Fischer concluded that synthetic polypeptides exhibited properties that were very similar to those of natural proteins. Interestingly, in 1913 even Fischer[51] himself expressed his sincere doubts with respect to the existence of high molecular weight polymers exceeding 4000 $g\,mol^{-1}$. In spite of his own experiments, he fully agreed with the established opinion opposing Staudinger's new idea of high molecular weight polymers consisting of covalently linked monomer units.

During his research in Karlsruhe and Zürich Staudinger had acquired first experimental experiences relating to the polymerization of isoprene, the synthesis of polyoxymethylene, and rubber chemistry. In 1920 he drew his conclusions and postulated in his famous essay in *"Berichte der Deutschen Chemischen Gesellschaft"* his revolutionary concept that high molecular weight polymerization products such as polyoxymethylene, polystyrene, polyvinyl chloride, polymalonic aldehyde, polyglycolide as well as natural rubber (**14**) and other similar compounds were composed of long polymer chains consisting of a very large number of molecular base units (today we would call them monomeric units) linked together by covalent bond formation.[52] At this early time Staudinger did not present convincing experimental evidence for his hypothesis. Many of his colleagues did not share either his opinion or his enthusiasm. In his research memoirs Staudinger referred to friendly advice he had received from H. Wieland: "*Dear colleague, abandon your idea of large molecules, organic molecules with molecular weights exceeding 5000 do not exist. Purify your products such as rubber, they will crystallize and turn out to out to be low molecular weight compounds.*"[53] Staudinger also wrote in his memoirs: "*Those colleagues who were aware of my early publications in the field of low molecular weight chemistry asked me why I decided to quit these beautiful fields of research and why I devoted myself to such disgusting and ill-defined compounds such as rubber and synthetic polymers which at that time in view of their properties were referred to as grease chemistry ("Schmierenchemie").*"[54]

Staudinger recognized the outstanding potential of this "grease chemistry" and accepted this new scientific challenge. He was courageous enough to completely abandon his traditional fields of research and to focus exclusively on polymer research when he moved to the University of Freiburg in 1926. His remarkable decision to shift his major research thrust to polymers also indicated the beginning of an intense struggle which raged for many decades and exposed Staudinger to heavy attacks of his colleagues from many disciplines and the self-proclaimed guards of the old concepts. Figure 1 displays Hermann Staudinger together with a molecular model of a macromolecule which he was convinced would be highly ordered with rigid-rod-like shape.

The first experimental evidence for the existence of long polymer chains was provided by Staudinger and Fritschi who performed the polymer-analogous hydrogenation of natural rubber.[55] The hydrogenation of the double bonds was not accompanied by the formation of volatile cyclic hydrocarbons, as expected for the polymer with molecular architecture **13**. Since the hydrogenated rubber did not contain double bonds, Staudinger concluded that also this polymer-analogous derivative exhibited high molecular weight. In 1922 in his paper on rubber hydrogenation he coined the term "macromolecules" for his giant polymer chains containing covalent bonds between the monomeric units in the backbone. In 1924 he stated a precise definition of macromolecules: "*For such colloid particles, in which the molecule is identical with the primary particle, and in which the individual atoms of this colloid molecule are linked together by covalent bonds, we propose for better differentiation the name macromolecule.*"[56] By the end of the 1920s additional experimental evidence for this concept of macromolecules was available from extensive viscosity measurements. Staudinger's viscosity law[57]

$$-CH_2\text{-}C(CH_3)=CH\text{-}CH_2\text{-}CH_2\text{-}C(CH_3)=CH\text{-}CH_2\text{-}CH_2\text{-}C(CH_3)=CH\text{-}CH_2\text{-}CH_2\text{-}C(CH_3)=CH\text{-}CH_2\text{-}$$

14

 © 2004 Wiley-VCH Verlag GmbH & Co. KGaA, Weinheim

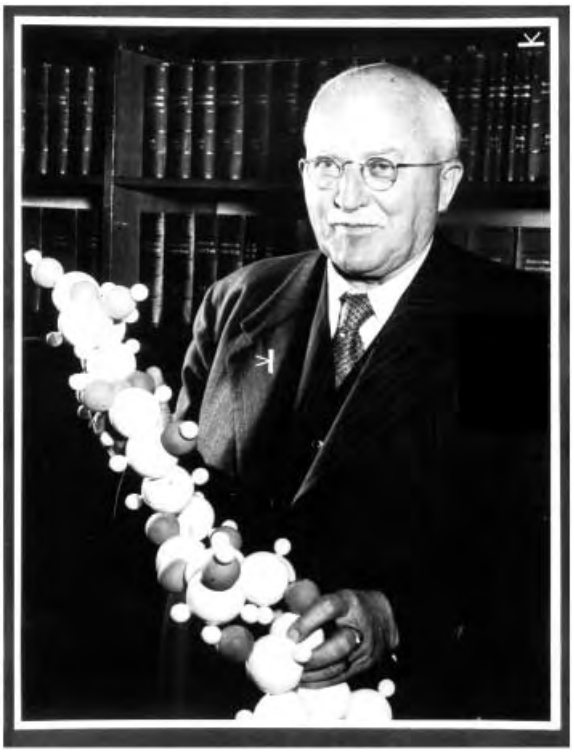


Figure 1. Hermann Staudinger (1881–1965).

and later the Staudinger index, which correlates with molecular weight, attracted attention. Later Mark and Houwink established viscosity correlations with both the molecular weights and the shapes of the polymer chains. Progress in polymer analytics, for example, molecular weight determination by means of ultracentrifuge, membrane osmometry, and light scattering played a key role in supporting Staudinger's idea of macromolecules. Staudinger's study on crystalline polyoxymethylene and his polyoxymethylene single crystals by means of X-ray crystallography clearly proved that polyoxymethylene consists of long-chain macromolecules although only four CH_2O groups occupy the crystallographic unit cell.[58]

In his study on the physical properties of polystyrene Staudinger recognized the influence of the degree of polymerization as well as the influence of diastereoisomerism (today we would call it stereoregularity). This happened quite a long time before G. Natta discovered the stereospecific polymerization and distinguished between atactic and isotactic polymers.[59] Staudinger considered polyoxymethylene to be a model for cellulose and polystyrene a model for rubber. Finally during the 1930s Staudinger's concept of macromolecules was accepted in science and technology. Molecular design of polymeric materials stimulated the rational development of materials, which was purely empirical during the earlier days. Within a short period of time new polymers were produced on an industrial scale. Prominent examples of such polymers introduced commercially during the 1920s and 1930s are polystyrene, polyvinyl chloride, high-pressure polyethylene, polyesters, and polyamides ("Nylon"). Staudinger performed extensive research projects on polymer synthesis, structure analysis, polymerization mechanisms, analytical polymer chemistry, and control of polymer properties. His research on macromolecules led to 644 publications.

After countless disputes at conferences, red-hot debates, and his very passionate promotion of his macromolecules, Staudinger was acknowledged in 1953 when he was awarded the Nobel Prize for Chemistry. Professor A. Fredga, a member of the Nobel committee, summarized Staudinger's achievements and the turbulent pioneering days of polymer sciences when he stated in his laudation: "*It is no secret that for a long time many colleagues rejected your views which some of them even regarded as abderitic. This was understandable perhaps. In the world of high polymers almost everything was new and untried. Long standing, established concepts had to be revised or new ones created. The development of macromolecular sciences does not present a picture of peaceful idyll.*"[1]

4. Hermann Staudinger, Technology and Society

Hermann Staudinger had very clear visions on how to establish and to promote the new field of macromolecular chemistry and polymer sciences. In 1940 he founded his research institute for macromolecular chemistry in Freiburg as the first European research institute which was devoted exclusively to polymer research. A new communication platform for the research results generated in this field was established when Staudinger founded the first polymer journal, the "*Journal für makromolekulare Chemie*" (journal of macromolecular chemistry)[60] in 1943 as a new branch of the "*Journal für praktische Chemie*" (journal for practical chemistry), for which he had served as the Editor-in-chief since 1939 with the Barth publishers in Leipzig, Germany. After World War II was over Staudinger's journal was published under the new title of "*Die makromolekulare Chemie*" (the macromolecular chemistry) by the publishers Wepf & Co. in Basel, Switzerland. Today this journal, renamed *Macromolecular Chemistry and Physics*, together with a family of other macromolecular journals is published by Wiley-VCH.[61] In several textbooks Staudinger taught the basic principles of polymer sciences for experienced readers as well as young students.[62] In the "*Förderverein*" (support association) of his institute Staudinger rallied prominent representatives from industry in an early version of a public–private partnership. This support was essential in difficult political times and continues to serve as the Advisory Board today. In 1950 Staudinger opened his internal colloquium for external participants from academia and industry. Today Staudinger's "*Makromolekulares Kolloquium*" (Macromolecular Colloquium) represents the largest annual polymer conference in Germany attracting around 600 to 700 participants every year.

Staudinger was very well aware that technological breakthroughs are closely associated with significant changes of the society, especially in view the major impact which epoch-making progress in chemistry had on human life. He felt obliged to address these consequences

 © 2004 Wiley-VCH Verlag GmbH & Co. KGaA, Weinheim

of technological advances. In his lectures he included economic and cultural changes fueled by progress in technology. He developed a model to quantify the power of technology. His approach was rather simple and straightforward: Without technology support in the early days of human history a human being had to rely exclusively on his own manpower and the additional manpower supplied by his human slaves. With emerging technologies each human disposes of a vast invisible technical support, which Staudinger referred to as "technical slaves". He calculated the number of technical slaves from power production, taking into account coal mining, oil production, hydroelectric power, and steel production. This technical power, measured as "horsepower years", he divided by the population and the average horsepower years contributed by an individual human being to obtain the number of "technical slaves" available for each person per year. The order of magnitude of the "technical slaves" enabled Staudinger to compare the economic and also the military powers of different countries. In 1917 he published this concept in the journal "*Friedens-Warte*"[63] (peace watch) and in 1947 in his booklet entitled "*Vom Aufstand der technischen Sklaven*"[64] (rebellion of the technical slaves).

From his calculations Staudinger concluded that when the USA entered World War I in 1917 the war was lost for Germany because of the obvious imbalance of power caused by adding the very large US power resources to the existing power of their allied countries. At that time, shortly after Russia signed a separate peace treaty, the Germans were still confident of winning World War I because they did not see this imbalance when counting only the number of soldiers, artillery pieces, and airplanes of both sides. Staudinger informed the German High Command in Berlin about his power assessment and proposed emphatically to stop the war and to start the peace negotiations immediately. Although the Germans checked on Staudinger's scheme, his view was not shared. Later in World War II Staudinger's calculations also predicted the failure of the German war effort around 1943 after the allied power superiority was achieved when both the industrialized Soviet Union and the USA had entered the war. However, during World War II the Nazis kept Staudinger under very tight surveillance and he did not dare anymore to go public. Shortly after World War II was over he published his booklet and modified his scheme by taking into account the emerging nuclear power. Staudingers's conclusion relating to the social consequences of technology and the nuclear power are quite remarkable. According to Staudinger without technology support humans were forced to fight wars for survival. With increasing power from technology there is no reason to fight wars because this power can be applied peacefully to secure life. Therefore, Staudinger demanded that the highest priority must be placed upon securing peace by keeping technology support under control, that is, to prevent the "rebellion of the technical slaves" and to promote the exploitation of technology exclusively for the well-being of humans. It is easy to understand that Staudinger's pacifism was not very well received in public during the time of the two World Wars and also afterwards during the time of the Cold War. Staudinger's views on the impact of technology on peace were lost in history.

During World War I Staudinger proved his remarkable courage. He published a paper written in French in a Red Cross journal and openly expressed his ideas concerning the role of modern technology in war.[65] Staudinger strictly opposed the development of chemical weapons for mass destruction and pointed out the unbearable suffering of humans exposed to chemical warfare. In public he opposed Fritz Haber, who was Staudinger's friend during the early days in Karlsruhe. Jointly with the German military Haber promoted chemical warfare and guided the research on chemical weapons, which he continued after the end of World War I under the cover of research on pest control chemicals.

During the time of German patriotism and German war enthusiasm in World War I Staudinger was completely isolated with respect to his pacifism and anti-war attitude. Since then his political correctness was questioned by many Germans. Before he was offered the Full Professorship at the University of Freiburg in 1926, he was asked by the Faculty Committee to clearly state his attitude towards Germany. Shortly after the Nazi party took over the German government, the Dean of the Freiburg University and famous philosopher Martin Heidegger questioned again Staudinger's loyality to Germany and to the Nazi movement. In 1934 Heidegger proposed to the state government to fire Staudinger. Staudinger was interrogated by the Gestapo (German secret police) and had to sign a formal written request demanding his discharge without listing the date. This was the Nazi's dead pledge to blackmail Staudinger and to prevent him from opposing their regime. During the Nazi rule Staudinger was exposed to many repressions and humiliations. He was not permitted to travel abroad and experienced a very difficult time with respect to the poor support of his research activities. Staudinger's life during the Third Reich and the history of his institute is described comprehensively by Priesner.[5g] On November 27, 1944 the city of Freiburg and Staudinger's Macromolecular Institute were destroyed completely by the allied bombing. When the Nazi regime collapsed, Staudinger's Institute was left as a pile of rubble and required tremendous effort to rebuild it during the very difficult post-war time.

Staudinger was supported by his second wife Magda (Figure 2). After Staudinger died on September 8, 1965 she continued his battles and pushed his



Figure 2. Hermann Staudinger and his wife Magda (from reference [4]).

 © 2004 Wiley-VCH Verlag GmbH & Co. KGaA, Weinheim

ideas for another three decades. In 1961 she became a member of the German UNESCO committee. A long time before the Green Party appeared in Germany she placed her major emphasis on environmental issues. For example, she devoted herself to create and establish the UNESCO program entitled "Man and Biosphere".

5. Conclusions

Staudinger's research on small and macromolecular compounds is published in his 859 publications, including 51 patents. Some of his patents on small molecules led to commercial products such as artificial pepper and artificial coffee flavor. Commercial applications of Staudinger's polymer patents and polymer products named after Staudinger do not exist. However, without any doubt Staudinger and his basic research have had a major impact on industrial polymer development. In Germany some of Staudinger's students and coworkers became leading directors of industrial polymer research and promoted technology transfer and industrial applications of polymers, for example, A. Steinhofer at the BASF AG in Ludwigshafen, G. Bier at the Hoechst AG in Frankfurt-Hoechst, Hans Batzer at the Ciba-Geigy AG in Basel, Switzerland, and H. Schnell at the Bayer AG in Leverkusen. All over the world scientists in academia and industry, among them Wallace Carothers at Du Pont, were stimulated by Staudinger's concept of macromolecules and his new approach to molecular design of structural and functional polymeric materials. His rational polymer design expanded the frontiers of polymer technology, which was dominated by purely empirical optimization during the pioneering days. On April 19, 1999 the American Chemical Society jointly with the German Chemical Society (GDCh) honored the Staudinger laboratory in Freiburg as an "International Historic Landmark of Chemistry". At the entrance of the Institute for Macromolecular Chemistry in a building named "Hermann Staudinger Haus" the bronze plaque (Figure 3) reads: "*International Historic Landmark of Chemistry. Foundation of Polymer Science. This building is named after Hermann Staudinger, who between 1926 and 1956 carried out his poineering research on macromolecular chemistry in Freiburg. His theories on the polymer structures of fibers and plastics and his later research on biological macromolecules formed the basis for countless modern developments in the fields of materials science and bioscience and supported the rapid growth of the plastics industry. For his work in the field of polymers, Staudinger was awarded the Nobel Prize for Chemistry in 1953.*"

Hermann Staudinger's visions continue to stimulate the progress of modern science and technology. His molecular blueprint idea for preparing polymeric materials with tailor-made property profiles still represents the important key to the development of functional and structural high-tech materials meeting the highly diversified demands of modern technologies. Innovative polymerization processes and modern programmed biosyntheses are offering new opportunities for this molecular polymer design. Moreover, Staudinger's concept is highly attractive in nanotechnology for building complex three-dimensional architectures through the covalent linking of nanometer-scaled molecules and nanoparticles. In fact, many of Staudingers giant macromolecules represent dwarfs when taking into account their actual dimensions of just a few nanometers. So it was Staudinger who also discovered the new class of nanomolecules which are a prime focus of modern research. Today we urgently need strong individuals like Hermann Staudinger who go out of their way to create new ideas, to explore courageously new unexplored fields, to challenge the established communities, and to push the frontiers of science and technology with special emphasis being placed upon effective public–private partnerships and sustainable development.



Figure 3. The plaque mounted on Hermann Staudinger's laboratory in Freiburg to mark it as an International Historic Landmark of Chemistry. The idea behind this program is explained, for example, on the website http://nasw.org/users/randywedin/Millennium2/IChCAnnualreport.pdf.

[1] The web page of the Nobel Foundation contains Prof. A. Fredgas "Presentation Speech" (http://www.nobel.se/chemistry/laureates/1953/press.html), the Staudinger Biography (http://www.nobel.se/chemistry/laureates/1953/staudinger-bio.html), as well as Staudinger's Nobel Lecture (http://www.nobel.se/chemistry/laureates/1953/staudinger-lecture.html) and his "Banquet Speech" (http://www.nobel.se/chemistry/laureates/1953/staudinger-speech.html).

[2] *Chem. Eng. News*, January 11, **1954**.

[3] Economic data, recycling aspects, and special applications are presented on the homepage of the "Verbandes der kunststofferzeugenden Industrie" (vke, German plastic manufacturer's association, www.vke.de)

[4] H. Staudinger, *Arbeitserinnerungen*, Hüthig, Heidelberg, **1961**.

 © 2004 Wiley-VCH Verlag GmbH & Co. KGaA, Weinheim

[5] a) "Hermann Staudinger, His Life and Work": V. E. Yarsely, *Chem. Ind.* **1967**, *18*, 250–271; b) "Hermann Staudinger zum Gedenken": H. F. Mark, *Naturwissenschaften* **1966**, *53*, 93; "Hermann Staudinger zu Technik und Politik": H. Sachsse, *Nachr. Chem. Tech. Lab.* **1984**, *32*, 974–976; c) "Hermann Staudinger": A. Steinhofer, *Chem. Unserer Zeit* **1967**, *1*, 123–125; d) "Hermann Staudinger": V. E. Yarsley in *Pioneers of Polymers*, The Plastics and Rubber Institute, London, **1981**; e) "Hermann Staudinger – zu seinem 80. Geburtstag": E. Trommsdorff, *Chem.-Ztg.* **1961**, *85*, 173–20; f) "Makromolekulare Gerontographie": D. G. Hummel, *Nachr. Chem. Tech. Lab.* **1981**, *29*, 169–171; g) "Hermann Staudinger und die makromolekulare Chemie in Freiburg": C. Priesner, *Chem. Unserer Zeit* **1987**, *21*, 151–160; h) "Hermann Staudinger und die Entwicklung der Makromolekularen Chemie": R. Mülhaupt, *Nachr. Chem. Tech. Lab.* **1999**, *47*, 413–418; i) "The Foundation of Polymer Science by Hermann Staudinger": R. Mülhaupt, *Macromol. Chem. Phys.* **1999**, *200*, NIL5-NIL8; i) "Hermann Staudinger (1881–1965, Nobelpreis für Chemie:1953) – Makromoleküle oder Polymere? Ein Professorenleben im Oerstedschen Gesetz des Umfelds, Jubiläumsfeiern – selbstbestimmter Anlass kultureller Frömmigkeit": L. Jaenicke, *BIOspektrum* **2003**, *5*, 601.

[6] H. Staudinger, *Anlagerung des Malonesters an ungesättigte Verbindungen (addition of malonic acid esters to unsaturated compounds)*, Dissertation, Universität Halle **1903**.

[7] H. Staudinger, *Ber. Dtsch. Chem. Ges.* **1905**, *38*, 1735–1739.

[8] H. Staudinger, J. Meyer, *Helv. Chim. Acta* **1919**, *2*, 619–635.

[9] H. Staudinger, J. Meyer, *Helv. Chim. Acta* **1919**, *2*, 635–646.

[10] H. Staudinger, E. Hauser, *Helv. Chim. Acta* **1921**, *4*, 861–886.

[11] Y. G. Gololobov, I. N. Zhmurova, L. F. Kasukhin, *Tetrahedron* **1981**, *37*, 437–472.

[12] In the literature (Scifinder, accessed on 22.08.2003) 412 citations are concerned with the Staudinger reaction. In addition to Staudinger's phosphane synthesis from azides, also Staudinger's synthesis of β-lactams by the [2+2] cycloaddition of imines and ketenes is referred to as the Staudinger reaction, for example a) B. C. Borer, D. W. Balogh, *Tetrahedron Lett.* **1991**, *32*, 1039–1040; b) G. I. Georg, P. M. Mashava, E. Akgun, M. W. Milstead, *Tetrahedron Lett.* **1991**, *32*, 3151–3154; c) I. Banik, L. Hackfeld, B. K. Banik, *Heterocycles* **2003**, *59*, 505–508; d) E. Hevia, J. Perez, V. Riera, D. Miguel, P. Campomanes, M. I. Menendez, T. L. Sordo, S. Garcia-Granda, *J. Am. Chem. Soc.* **2003**, *125*, 3706–3707.

[13] H. Staudinger, H. W. Klever, *Ber. Dtsch. Chem. Ges.* **1911**, *44*, 2212–2215.

[14] a) H. Staudinger, DRP 257 640, **1910**; b) H. Staudinger, DRP 264 923, **1911**.

[15] A. Holt, *Z. Angew. Chem.* **1914**, *27*, 153.

[16] H. Staudinger, *Z. Angew. Chem.* **1922**, *35*, 657–659.

[17] H. Staudinger, *Z. Elektrochem.* **1925**, *31*, 549–552.

[18] H. Staudinger in ref. [4], chapter VII, p. 46.

[19] H. Staudinger, L. Ruzicka, *Helv. Chim. Acta* **1922**, *7*, 201–211.

[20] H. Staudinger, L. Ruzicka, *Helv. Chim. Acta* **1922**, *7*, 212–235.

[21] a) H. Staudinger, Schweizer Patent P.94436, **1919**, priority March 30, 1916; b) H. Staudinger, DRP 384295, **1920**; Hungarian priority October 10, 1916.

[22] a) H. Staudinger, H. Schneider, *Ber. Dtsch. Chem. Ges.* **1923**, *56*, 699–711; b) H. Staudinger, F. Müller, *Ber. Dtsch. Chem. Ges.* **1923**, *56*, 711–715.

[23] a) H. Staudinger (Internationale Nahrungs- und Genussmittel AG), EP 246454, **1926**; b) H. Staudinger (Internationale Nahrungs- und Genussmittel AG), EP 286152, **1927**; c) H. Staudinger, DRP 457 266, **1925**; d) H. Staudinger, T. Reichstein (Internationale Nahrungs- und Genussmittel AG), AP 4448/1926, **1926**; e) H. Staudinger, T. Reichstein, AP 1715795, **1927.**

[24] a) T. Reichstein, H. Staudinger, *Angew. Chem.* **1950**, *62*, 292; b) T. Reichstein, H. Staudinger, *Experientia* **1950**, *6*, 280; c) T. Reichstein, H. Staudinger, *Ciba Z.* **1951**, *127*(11), 4692–4694.

[25] a) H. Staudinger, DRP 436 442, **1924**; b) H. Staudinger, DRP 451 731, **1924**.

[26] "Difficulties with the concept of a polymer—an essay: H. Morawetz, *Angew. Chem.* **1987**, *99*, 95–100; *Angew. Chem. Int. Ed. Engl.* **1987**, *26*, 93–97

[27] a) C. Goodyear, *Gum-Elastic and Its Varieties with a Detailed Account of its Applications and Uses*, New Haven, **1855**; b) R. F. Wolf, *India Rubber Mnan—the Story of Charles Goodyear*, Caxton Printers, Caldwell, ID, **1939.**

[28] H. Braconnot, *Justus Liebigs Ann. Chem.* **1833**, *7*, 242–245.

[29] D. R. Wiggam, W. E. Gloor, *Ind. Eng. Chem.* **1934**, *26*, 551.

[30] H. deChardonnet, *C. R. Hebd. Seances Acad. Sci.* **1887**, *105*, 899

[31] a) H. deChardonnet, Fr. Pat. 203 202, **1890**; b) V. Hottenroth, *Die Kunstseide*, Hirzel, Leipzig, **1926**, english translation *Artificial Silk*, Pitman, London, **1928**; b) *Technologie der Textilfasern*, *Vol. 7* (Ed.: R. O. Herzog), Springer, Berlin, **1927.**

[32] J. W. Hyatt, I. J. Hyatt, US Pat. 105 338, **1870**.

[33] M. Kaufman, *The First Century of Plastics, Celluloid and ist Sequel*, The Plastics and Rubber Institute, London, **1963**.

[34] W. E. Gloor in *Cellulose and Cellulose* Derivatives (Ed.: E. Ott), Interscience, New York, **1943**, chap. 10.

[35] a) L. H. Baekeland, US Pat. 942 699, **1907**; b) L. H. Baekeland, *Ind. Eng. Chem.* **1909**, *1*, 202; c) L. H. Baekeland, *Ind. Eng. Chem.* **1909**, *1*, 545.

[36] J. Berzelius, *Jahresber. Fortsch. Phys. Wissensch.* **1833**, *12*, 63.

[37] a) P. E. M. Berthelot, *C. R. Hebd. Seances Acad. Sci.* **1866**, *63*, 479; P. E. M. Berthelot, *C. R. Hebd. Seances Acad. Sci.* **1866**, *63*, 515; b) P. E. M. Berthelot, *Bull. Soc. Chim. Fr.* **1866**, 6, 268; c) P. E. M. Berthelot, *Justus Liebigs Ann. Chem.* **1867**, 141, 173

[38] M. Berthelot, *Lecons de chimie professees en 1864 et 1865*, Societe chimique de Paris, Paris, **1866**, S. 18–65; M. Berthelot, *Lecons de chimie professees en 1864 et 1865*, Societe chimique de Paris, Paris, **1866**, S. 148–167.

[39] a) M. Berthelot, *C. R. Hebd. Seances Acad. Sci.* **1853**, *36*, 425; b) M. Berthelot, *Ann. Chim. Phys.* **1853**, *38*, 38; c) M. Berthelot, *Ann. Chim. Phys.* **1853**, *39*, 5.

[40] M. Berthelot, *Bull. Soc. Chim. Fr.* **1869**, *11*, 4.

[41] B. Helferich, *Ber. Dtsch. Chem. Ges.* **1930**, *63*, 989, here the prefix "oligo" was used for the first time, for example, in "oligosaccharide" and "oligopeptide", to distinguish these compounds from the corresponding high molecular weight polymers.

[42] H. Von Pechmann, *Ber. Dtsch. Chem. Ges.* **1899**, *31*, 2640.

[43] E. Bamberger, F. Tschirner, *Ber. Dtsch. Chem. Ges.* **1900**, *33*, 955.

[44] T. Graham, *Philos. Trans. R. Soc. London* **1861**, *151*, 183.

[45] R. Brill, *Justus Liebigs Ann. Chem.* **1923**, *434*, 204.

[46] a) C. Harries, *Ber. Dtsch. Chem. Ges.* **1902**, *35*, 3256; b) C. Harries, *Ber. Dtsch. Chem. Ges.* **1903**, *36*, 1937; c) C. Harries, *Ber. Dtsch. Chem. Ges.* **1904**, *37*, 2708; d) C. Harries, *Ber. Dtsch. Chem. Ges.* **1903**, *36*, 1937; e) C. Harries, *Angew. Chem.* **1907**, *20*, 1265.

[47] J. Thiele, *Justus Liebigs Ann. Chem.* **1899**, *306*, 87.

[48] S. S. Pickles, *J. Chem. Soc.* **1910**, *97*, 1085

[49] E. Fischer, *Ber. Dtsch. Chem. Ges.* **1906**, *39*, 530.

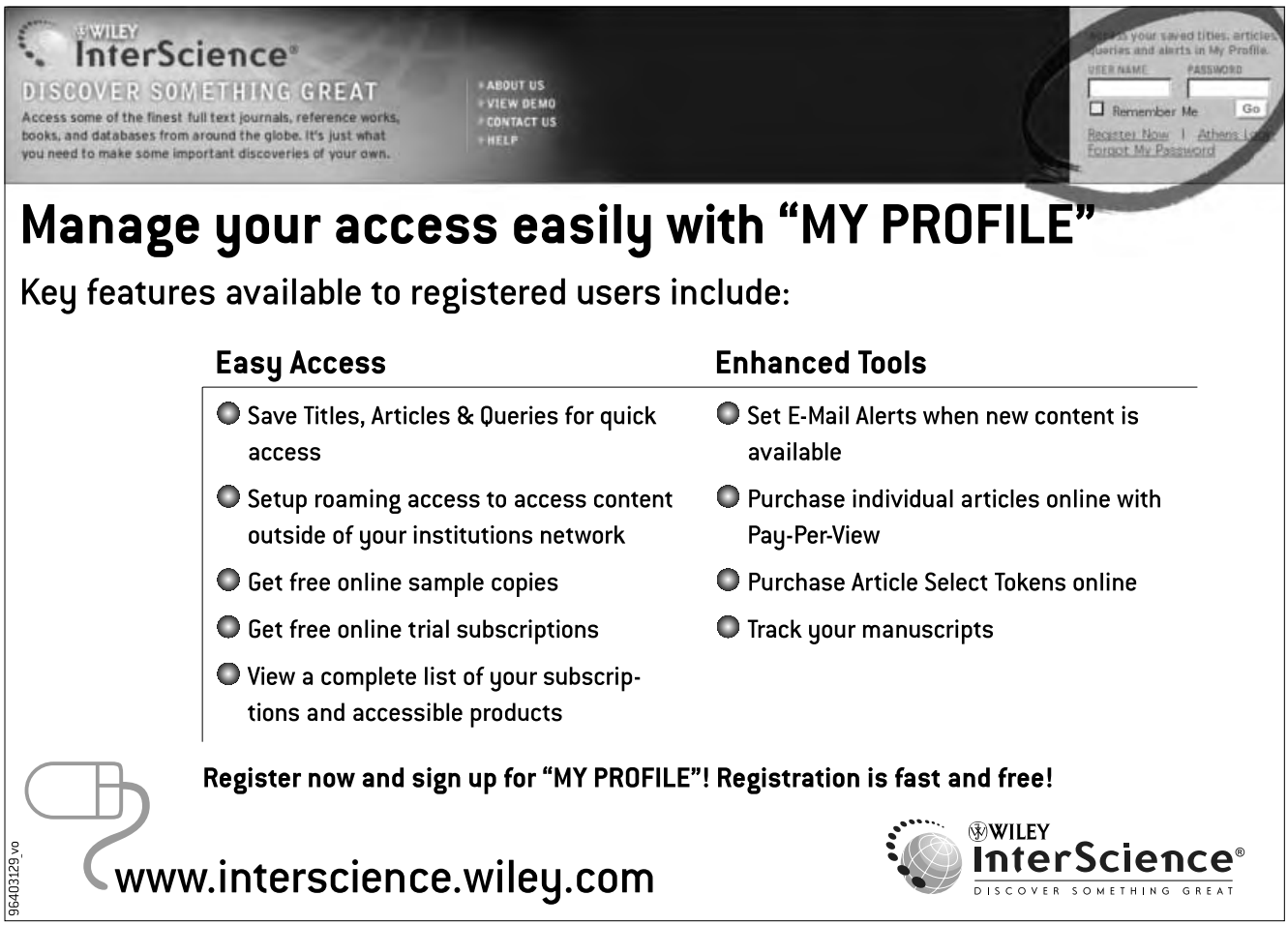
[50] E. Fischer, *Ber. Dtsch. Chem. Ges.* **1907**, *40*, 1754.

[51] E. Fischer, *Ber. Dtsch. Chem. Ges.* **1913**, *46*, 3288.

[52] H. Staudinger, *Ber. Dtsch. Chem. Ges.* **1920**, *53*, 1073–1085.

 © 2004 Wiley-VCH Verlag GmbH & Co. KGaA, Weinheim

[53] H. Staudinger in ref. [4], p. 79.
[54] H. Staudinger in ref. [4], p. 77.
[55] H. Staudinger, J. Fritschi, *Helv. Chim. Acta* **1922**, *5*, 785 – 806.
[56] H. Staudinger, *Ber. Dtsch. Chem. Ges.* **1924**, *57*, 1203 – 1208.
[57] H. Staudinger, W. Heuer, *Ber. Dtsch. Chem. Ges.* **1930**, *63*, 222 – 234.
[58] H. Staudinger, H. Johner, H. Signer, G. Mie, J. Hengstenberg, *Z. Phys. Chem.* **1927**, *126*, 425 – 448.
[59] H. Staudinger, *Die hochmolekularen organischen Verbindungen – Kautschuk und Cellulose*, Springer, Berlin, **1932**, S. 164.
[60] The first paper was authored by Staudinger himself and was entitled *"Makromolekulare Naturstoffe und makromolekulare synthetische Produkte (Macromelecular natural materials and macromolecular synthetic products)"*, H. Staudinger, *Makromol. Chem.* **1947**, *1*, 7 – 21.
[61] "The 60th anniversary of the first polymer journal – ("Die Makromolekulare Chemie"—Moving to New Horizons": I. Meisel, R. Mülhaupt, *Macromol. Chem. Phys.* **2003**, *204*, 195 – 206.
[62] a) H. Staudinger, *Die hochmolekularen organischen Verbindungen – Kautschuk und Cellulose*, Springer, Berlin, **1932**; b) W. Röhres, H. Staudinger, R. Vieweg, *Fortschritte der Chemie, Physik und Technik der makromolekularen Stoffe*, Bd. I, J. F. Lehmann, München, **1939**; W. Röhres, H. Staudinger, R. Vieweg, *Fortschritte der Chemie, Physik und Technik der makromolekularen Stoffe*, Bd. II, J. F. Lehmann, München, **1942**; c) H. Staudinger, *Über die makromolekulare Chemie*, Hans Ferdinand Schulz, Freiburg i.Br., **1939**; H. Staudinger, *Über die makromolekulare Chemie*, 2nd expanded edition, Hans Ferdinand Schulz, Freiburg i.Br., **1954**; d) H. Staudinger, *Makromolekulare Chemie und Biologie*, Wepf & Co., Basel, **1947**.
[63] H. Staudinger, *Friedens-Warte*, **1917**, *19*, 196.
[64] H. Staudinger, *Vom Aufstand der technischen Sklaven*, Chamier, Essen, **1947.**
[65] "La technique moderen et la guerre": H. Staudinger, *Rev. Int. Croix-Rouge Geneve* **1919**, *1*, 508 – 515.



 © 2004 Wiley-VCH Verlag GmbH & Co. KGaA, Weinheim

History of Science

Hermann Staudinger and the Future of Polymer Research

Jubilees—Beloved Occasions for Cultural Piety[1]

*Helmut Ringsdorf**

Keywords:
history of chemistry · macromolecular chemistry · polymers · Staudinger, Hermann

Without any apprehension and without concern for the question still on occasion discussed today of who thought, knew, or wrote something about polymers when, where, and how in the initial phase of macromolecular chemistry, the Nobel Foundation awarded Hermann Staudinger (1881–1965, Figure 1) the Nobel Prize in 1953 "for his discoveries in the field of macromolecular chemistry"—that is, not for the discovery of macromolecules, and not for the establishment of macromolecular chemistry. Hermann Staudinger never claimed to have discovered macromolecules. He was aware that much was known about polymers, but he had to prove their existence as chain molecules within the context of Kekulé valence theory with all his farsightedness, his brilliance, and his doggedness against the dominance of those who maintained that polymers were colloidal systems or aggregates of smaller molecules.



Figure 1. Hermann Staudinger in 1964 in his Freiburg study—a year before his death.

[*] Prof. Dr. H. Ringsdorf
Institut für Organische Chemie
Universität Mainz
Duesbergweg 10–14
55099 Mainz (Germany)
Fax: (+49) 6131-39-23145
E-mail: ringsdor@mail.uni-mainz.de

Chemistry was his life, but Hermann Staudinger's dreams belonged to biology and to the unity of chemistry and biology. The timing of the award of the Nobel Prize was indeed late, but it could not have been better chosen to honor the already blossoming sciences surrounding synthetic as well as biological macromolecules: In that year Paul Flory published his textbook which became the "bible for polymer researchers", Ziegler–Natta catalysts were discovered, H. A. Krebs and F. A Lipmann reported on enzymes and coenzymes as important biological macromolecules at the same Nobel Prize celebration, and J. D. Watson and F. H. Crick rang in molecular biology definitively with the *Nature* article on their DNA model.

If tribute is paid to Herman Staudinger, his genius, and his contribution to the development of the natural sciences, then one must also be reminded fifty years after the award of the Nobel Prize of the tense backdrop against which everyone carried out research and taught in the 1920s and 1930s between two world wars: science as an alliance of objectivity, responsibility, and human behavior. Although this problem is "painted" differently today, it is no less topical.

1. The Kaiser's Carriage Ran on Tires of Synthetic Rubber before H. Staudinger Had Even Begun His Battle for Macromolecules

It is today something of a curiosity to show a picture of Wilhelm II, the last German Kaiser. However, this picture (Figure 2) appears for scientific reasons, as it is more about the automobile than "His Divine Majesty".[2a] Herbert Morawetz published it in his book *Polymers: The Origins and Growth of a Science.*[2b] This book should still be required reading today for all who wish to be informed first hand and from personal experience[2c] about the origin of the science of macromolecules, about polymer science.

In the picture Wilhelm II (in a white coat) is watching with his generals the mounting of the first wheels of synthetic rubber onto his automobile: Dawn of the First World War, independence from natural rubber from the British and Dutch tropics. Even then, in 1912, the natural and synthetic rubber industry was blossoming in Europe and in the USA. Although they were not yet "his" macromolecules, Hermann Staudinger was also involved. As an organic chemist he was interested in the synthesis of isoprene by the pyrolysis of terpenoid hydrocarbons. In praise of the purity of the isoprene thus prepared, he wrote in 1911:[3] "*…it contains only small amounts of trimethylethylene, as was determined through its conversion into rubber.*" How this was determined he failed to mention in his article, but nevertheless: polymerization as proof of purity. The intense phase of his interest in macromolecules first began with an article "Über Polymerisation"

 © 2004 Wiley-VCH Verlag GmbH & Co. KGaA, Weinheim DOI: 10.1002/anie.200330071



Figure 2. Not the "Emperor's new clothes", but new synthetic tires on the Emperor's old carriage.

(On Polymerization) published in 1920,[4] and especially in 1922 with the definition of macromolecules[5] as primary-valence chain systems. With this article he began his almost ten-year feud with classical organic chemists, particularly with colloid chemists, who continued to define large molecules, polymers (multiples), as colloids and aggregates of small molecules.[6] The story of this academic dispute—industry bothered little about it—was frequently and controversially described and is mentioned in the book by H. Morawetz,[2b] as well as in a number of other publications on polymer history.[7–11] The mood of this relatively short and stormy interlude of polymer history was described in 1980 by Hermann F. Mark, one of the players involved intimately and creatively from the beginning of this sequence of scientific events. In his essay "Aus den frühen Tagen der Makromolekularen Chemie" (From the Early Days of Macromolecular Chemistry)[12] he commented in very general, but directly and demonstrably accurate terms such as rarely used to comment on a scientific development: "*Most branches of science pass through a 'pioneering period' where different concepts and approaches create, for a while, a turbulent atmosphere until, on the basis of new experimental evidence, clear and durable principles emerge, which lead to a broad and continuous growth of basic understanding and practical application. The author of this article recalls how, temporarily, conflicting ideas created confusion in the chemistry and technology of giant molecules before these disciplines developed into what they are now: indispensable contributors to the comfort, safety and expansion of our society from medicine to astronautica.*"

2. Nobel Prizes: Momentary Successes and Key Events of the Century

All work distinguished with the Nobel Prize is important and valuable in its time. It can be differentiated by its timeless significance to science, and by the areas and levels of its effectiveness.[13] There are Nobel Prizes for outstanding specialized individual performances, for example, in 1912 to V. Grignard for the discovery of the reaction which carries his name. This reaction is still fundamental in synthetic organic chemistry today—and still the terror of chemistry students in laboratory courses, when "the Grignard does not get going". A fantastic building block for chemical cottages, houses, and cathedrals—the trend-setting impulse lies, however, in the respective building plan. The same applies to the recognition of a series of technically or medically important procedures and also for a few analytical methods. Then there are those Nobel Prizes awarded for work that extends beyond the currently accepted scientific horizons, which opens up borders and creates new sciences. These prizes sometimes prove to be "chain reactions", as the Nobel Prizes in chemistry and physics for nuclear science illustrate: 1903: discovery of radioactivity (H. Becquerel, P. and M. Curie), 1908: chemistry of radioactive substances (E. Rutherford), 1911: isolation of radium (M. Curie), 1935: synthesis of new radioactive substances (F. Joliot and I. Juliot-Curie), and 1944: discovery of nuclear fission (O. Hahn)—a consequential development process, with war-resolving explosions, for a long time the force to maintain peace, and now—hopefully!—only with more peaceful applications.

Equally autocatalytic, perhaps still more "explosive" (in terms of the rate at which significance and recognition grew) was the development of a new science initiated by Hermann Staudinger. He left the safe haven of organic chemistry in which he was already famous to fight with vision, at faced with condescension, for the recognition of macromolecules. The time was ripe! There was much prior knowledge at hand and, as mentioned at the beginning, polymeric materials were already in use. However, at the start of the 1920s the front of the classical organic chemists of the Liebig school, the colloid chemists about Wolfgang Ostwald, and a few crystallographers was too united to accept the existence of macromolecules without a struggle: They swore by submicroscopic particles and aggregates. That is now all water under the bridge, but it required the expert ability of Hermann Staudinger, his astounding, usually underestimated steadfastness, and his almost missionary zeal to wrench the investigation of polymers from the grips of colloidal chemists and their devotees. When this stronghold was broken research and technology could connect, and a new science that had long been at the starting blocks could develop: the polymer science of today. What happened to colloid science as a consequence is a further interesting chapter in the history of science. It disappeared for quite a while—at least from the laboratories of universities—and is today justifiably celebrating a remarkable rebirth in academia, partly in nanoscience.

3. Genius Is Not a Permanent Condition—Creativity Is Necessary, Intelligence Helpful, Composure Sensible: Staudinger's Dreams and the Nobel Prize

Is there such a thing as systematic development in basic research? Of

 © 2004 Wiley-VCH Verlag GmbH & Co. KGaA, Weinheim

course, but it rarely, if ever, leads linearly to the next step. Instead it must go through a "confusion period" of perplexity until the next paradigm shift occurs.[14] Light bulbs were not discovered by the systematic modification of oil lamps, and we do not thank the systematic development of the steam engine for the modern electric locomotive.

Hermann Staudinger's move from his previous and considerable successes in "low-molecular-weight" organic chemistry (e.g. ketenes, ozonolysis, aliphatic diazo compounds, explosives, aromas, the Staudinger reaction[7,15]) to macromolecules was a step that needed vision and courage—surely a paradigm shift.[14] It was thanks to his convincing obstinacy that large molecules entered the conceptions of chemists in the 1920s. And when, at the beginning of the 1930s, the existence of macromolecules was inescapable, all were in agreement. Only insignificant rearguard actions remained, the usual "scientific" deployment actions—yet Hermann Staudinger allowed himself to be obstructed by them. The wounds were too deep,[16] and the impending "1000-Year Reich" (Nazi rule in Germany 1933–1945) was already tainting the clear skies of research brown. The times derailed Hermann Staudinger's train of creativity, and his great intelligence did not help him to continue to follow his visions and dreams with composure.

In the 1930s polymer science exploded in many laboratories around the world, the age of plastics had arrived; Hermann Staudinger looked upon it with joy and pride. However, he personally could not give up the fight for his macromolecules supported rigorously with Baltic patriotism by his second wife Magda (neé Woit). Moreover, he loved his macromolecules as long, rigid rods. Their rigidity suited his perseverance and his empirical relationship between the specific viscosity of a dissolved polymer and its molecular weight, that he at times intentionally shut out the work he knew well of Werner and Hans Kuhn, Paul Flory, and others on the "tangled behavior" of polymers. He devoted much of his Nobel lecture, too, to his love of viscosity (see reference [7]). Of course, Kuhn and Flory were cited, but I would be amazed if Staudinger, on his one and only visit to the USA (in 1958 to Herman Mark's then world-renowned Institute of Polymer Research in Brooklyn), had not packed in his luggage his beloved wooden rods as models of his macromolecules![17]

In an appraisal of this inspired scientist fifty years after he was awarded the Nobel Prize, his charismatic dreams should not be forgotten against the backdrop of his campaigning in the 1920s: All his life Hermann Staudinger's visions and hopes belonged to biology and biological macromolecules—and here, too, his wife Magda, herself a scientist with a PhD in biology, supported him with passion and considerable energy. It has to be mentioned that alongside the chemistry of synthetic macromolecules of Staudinger, the science of biopolymers had already started to develop at the start of the 20th century with the emergence of protein chemistry.[10,11,18,19] In 2002 Lother Jaenicke wrote:[18] "*It is not futile to go back to the origins of how Emil Fischer built up oligopeptides of up to 18 residues. The deliberations of Hofmeister and the experiments of Fischer laid the foundation for the conviction that proteins are built up in large numbers and different sequences by the linear coupling of* L-α-*amino acids through peptide bonds.*"

Staudinger's view of biomacromolecules was at that time shaped by his knowledge of natural rubber and cellulose, structural and framework polymers: in principle "simply knitted" polymerisates or polycondensates of like monomers. The complexity of functional biological polymers can not have been present to him in the clarity with which we can see it today. Only with this in mind can one understand that he was able to look upon polystyrene as a chemically model for natural rubber, polyformaldehyde as a model for cellulose, and even polyacrylic acid as a model for proteins. In the same way it is perhaps also understandable that his dream regarding the biological importance of macromolecules ended with the following beautiful and correct, if also very general concept: "*Macromolecules exist, and in the future they will have considerable significance for biology, for only with such large molecules can living cells be built up. Because of their size they have different shapes; thus, different structures are possible, as needed for living cells. Again because of their size they can accommodate different reactive groups.*"

That was his vision, characteristically related only to structure and not to function, but it does not detract from Staudinger's genius that the foundation of his dreams were his synthetic macromolecules, which, apart from their high molecular weight, have almost nothing in common with functional biological polymers. If, at the beginning of polymer science, Hermann Staudinger had not eroded his energy and tenacity in defending the existence of synthetic macromolecules against the lack of understanding and perseverance of a number of colleagues, and if the brutality of world events brought about by the Third Reich had not subsequently seamlessly closed in on him, perhaps he, who had started out as a biologist, would have succeeded in crossing the bridge to his beloved biology with its molecular children. That is particularly evident when one considers what former colleagues of Hermann Staudinger had already achieved in biochemistry and even molecular biology by then.[20a] For most peptide chemists of that time the "mystery of macromolecules" was almost already a matter of course; they did not involve themselves in the energy-absorbing tussle with colloid chemists, were perhaps not even much aware of it.

Protein chemistry[19] and R. Signer's knowledge of DNA[20a] would have been an immensely important bridge to the biosciences and molecular biology, a bridge which Herman Staudinger never had the good fortune to cross. Thus his vision and desire for the union of his chemistry and his biology remained for him a dream.[20b] Towards the end he was so trapped in the Don Quixotic battle for his synthetic macromolecules that he could no longer recognize the extent to which the biosciences and the blossoming field of molecular biology had long taken on board his macromolecules and used his analytical methods almost routinely as a working basis. This is an example of the "human" nature of science, an example whereby it is difficult to know what one should admire more: the creativity of the scientist or the constancy of his adherence to his original idea.

 © 2004 Wiley-VCH Verlag GmbH & Co. KGaA, Weinheim

Polymer science and bioscience had developed in parallel and were both already in full bloom when Hermann Staudinger received the Nobel Prize in 1953, justified recognition of outstanding achievements and earlier successes. There is no better example of the parallelism of two scientific developments—and no director could have set the scene more perfectly—than the fact that Staudinger received the Nobel Prize in Chemistry in Stockholm at the same time as Hans Adolf Krebs[21] and Fritz Albert Lipmann[22] were able to accept the Nobel Prize for Medicine.

It is delightful to be able to see such a great moment in the history of science portrayed so openly (Figure 3).[23] Seen in the picture beside those named is the Dutch physicist Fritz Zernike, who had developed the phase-contrast microscope, also fundamental for the then-emerging membrane and cell biology.[24] In their Nobel Lectures the two biochemists H. A. Krebs and F. A Lipmann reported much that was concrete and still more that was trend-setting about the numerous structures and the biological function of biological macromolecules—biochemists on the path to molecular biology.[25] And almost as if to further emphasize this, J. D. Watson and F. H. Crick published their initial work on the double-helix structure of DNA in the same year,[26] based in part on Erwin Chargaff's observation[27,28] that the same number of thymine and adenine, and of cytosine and guanine molecules were always present in deoxyribonucleic acids (see also reference [20a]). The initial work of the two ended with the now classic "understatement": "*It has not escaped our notice that the specific pairing we have postulated immediately suggests a possible copying mechanism for the genetic material.*"



Figure 3. Time check: the moment before the award of the Nobel Prizes of 1953—a historic moment for science. From left to right: F. Lipmann, H. Krebs, H. Staudinger, and F. Zernike.

What a span of genius and development from the achievements of Hermann Staudinger and his dreams on the biology of life up to this great moment of science in 1953! I do not believe that Hermann Staudinger was aware of the work published in the April volume of *Nature* as he traveled to Stockholm in December 1953. Would he have been pleased? In any case, he ended his Nobel Lecture with precisely what he could have read in that publication and what he had dreamt of all his life with farsightedness and hope: "*In light of this new knowledge of macromolecular chemistry the wonder of life reveals itself from its chemical side in the unending diversity and masterful molecular architectonics of living material*" (see reference [7]).

4. Rifts in Science That Are Not Bridged Immediately Are Later Difficult to Close: Also a Generation Problem!

The heading says it all! How can the rift between polymer science and bioscience be bridged? This question has often been raised over the last thirty years, and yet must still be discussed today, of how polymer science, bioscience, and biomedicine, can be considered with a common denominator. They are certainly closer than in Staudinger's time, but separated siblings they are still, in spite of all assertions to the contrary. Although many collaborations are in existence today, they are divided too swiftly into areas of the practical and the calculable—and if such areas are not available, the epiphets missing, then they are invented: nano, bionano, supranano, nanotec, bionanotec, etc., etc.

According to Wolfgang Frühwald, President of the Alexander von Humboldt Foundation in Germany, the flood of ignorance also increases simultaneously with the flood of knowledge. That no longer applies only to the broad fields of natural science, the humanities, and philosophy, but has for some time also been the case within more specialized scientific disciplines.[29] Thus, as knowledge is gained in one field the lack of insight into other areas grows and hinders effective collaboration. Is it therefore to be feared that after the great success of their science in technology and everyday life polymer chemists will once more withdraw quietly to Staudinger's classical polymers? One could sometimes think so, especially when one comes across such symposium topics as "Classical Polymer Science Revisited".

Of the biopolymers only the structural polymers, biomaterials, such as rubber and cellulose, and perhaps also the degradable carbohydrates of the food chain, actually belong to polymer science today, as in Staudinger's time. Biochemistry and molecular biology consider themselves responsible for all important functional biological polymers from DNA to proteins and glycoproteins, which is historically not at all incorrect and therefore understandable. If the term biopolymer had not existed for some time it would have to be invented today. However, it would then not apply exclusively to natural macromolecules, but would also be used for many synthetic polymers which have aroused interest in biology as functional macromolecules, composite and hybrid materials, or co- and terpolymers, or which are important as biomembrane model systems. The current generation of polymer chemists can and will be much more cooperative, although even they only learn the vocabulary of molecular and membrane biology slowly.

And again, only fifty years after the Nobel Prize for Hermann Staudinger and the DNA helix of Watson and Crick, only a few years after the elucidation of the human genome, *Science* published the "Derivation of Oocytes from Mouse Embryonic Stem Cells" in 2003.[30] Until then embryonic stem cells grown in culture were regarded only as pluripotent—now they are recognized as totipotent. What a jump! Here, too, it appears that polymer science has some leeway to make up if it still loves its biological sister and wishes not only to keep up with her leaps in knowledge but also wishes to be involved.

 © 2004 Wiley-VCH Verlag GmbH & Co. KGaA, Weinheim

Where does polymer science stand today? Do you expect an answer? It will certainly not have escaped the reader that I, infected by Staudinger's dream, am drawn towards the biological sister of polymer science. Nor can this attachment be renounced in the next section. It may be regarded as an excuse that in the attempt to answer the question posed bias will come into play, in spite of all attempts at objectivity. However, it is also possible that insufficient breadth of knowledge further restricts the view.[31]

5. Macromolecules to Garnish: Classical Polymer Science as a Welcome Ingredient in Materials Science and Other Scientific Disciplines

A paradigm shift occurred to mark the beginning of macromolecular chemistry,[14] which then developed into polymer science almost as soon as it was born. At that time it welded together chemistry and physics, was the midwife of materials science, and therefore fundamental to the development of our modern world. The term "plastics age" is nowadays already antiquated. It is no longer possible to imagine technology and biotechnology, daily life, and even art and culture, without polymers as basic materials. In addition and as a result of the enormous breadth of materials properties offered by macromolecules, polymer science has long since become an essential part of many modern areas of science, such as the chemistry and physics of supramolecular systems[32] and supramolecular materials,[33,34] the whole of nanotechnology, surface chemistry,[35] and the rejuvenated colloid chemistry.[36] Many important functional, structure-forming macromolecules are no longer prepared in the kitchens of classical polymer science: macromolecules to garnish! It is clear that polymer science has become a sister or even a part of materials science,[37] and for some time has no longer been a stranger to the biosciences: polymeric biomaterials[38a] and tissue engineering.[38b]

If this were merely a "jubilee" for a great scientist and his Nobel Prize, a laudation for Hermann Staudinger and all those other midwives of polymer science fifty years ago and more, then in the face of so much success in this "new" science there would be nothing more to add. But it will continue!

Just two points are singled out. Two new thoughts? Not by a long way, but as aphoristically formulated by André Gide in his self-deprecating way: "*It has all been said before, but as no-one listens it all has to be said again*". [39] At present the discipline of biomedicine[38] is also still discreetly coupled to materials science: polymers as medical materials and biomaterials, for example, as heart valves, veins, and arteries, as eye lenses, as surgical threads, as skin and organ substitutes. The next step—synthetic polymers as pharmacologically active compounds—is apparent and has already begun: synthetic polymers as cell components and synthetic polymers as therapeutics.

5.1. From Synthetic Macromolecules to Biological Structures

The factor that is still lacking in terms of understanding and wide application has just begun: the detailed study of the interaction of cells with synthetic "biopolymers" and the biologization of synthetic macromolecules. Without wishing to evaluate and review, I would like to cite a number of topics from this interface: polymers and biomimicry,[40] the targeted preparation of biopolymers,[41] bioactive polymers,[42] polyvalent ligands,[43a] topologically linked catalysts,[43b] the inhibition of the cell adhesion of fibrinoectin by polynorbornene,[44a] and nanocontainers which deliver to defined cytoplasmatic organelles.[44b] Along these lines of thought and on the basis of modern knowledge about water-soluble, structure-forming homo-, co-, and terpolymers,[45] old—and at that time really only light-hearted—work on polymeric monolayers and lipid assemblies[46] is increasing in importance as biomembrane and cell models.

Broadly based consideration is today being given to self-replicating systems within the context of molecular biology. However, the polymer chemist still has much to learn from biology to progress from "simple" synthetic systems to complex cell-analogue systems. Molecular biologists also need modern polymer science to translate their knowledge into synthetic "molecular machines" and cell-like systems. Examples could be viral vectors, stable, ATP-producing Bacteriorhodopsin, and F_0F_1–ATP-ase-containing polymeric cell models, systems for transmembrane impulse transmission (under-membrane fishing). I believe that cell, membrane, and molecular biologists still have little to no idea of what role polymer science can and will play in their disciplines. Here, too, clarification and interaction is necessary.

"From Macromolecules to Biological Assemblies"—a beautiful title! What a topic! It was the title of the Nobel Lecture by Aaron Klug in 1982.[47] In describing the decisive role of macromolecules in all biological processes of living cells, he said, "*These macromolecules do not of course function in isolation but often interact to form ordered aggregates or macromolecular complexes, sometimes so distinctive in form and function as to deserve the name of organelles.*" Of course he was referring to nucleic acid–protein complexes—no mention of synthetic macromolecules. Naturally—it was 1982. But today? In the times of proteomics, hybrid structures, self-organization and self-association, supramolecular systems, modern colloid chemistry, and enormous synthetic possibilities all the prerequisites are actually in place. The missing link, as said again and again—is the absence of any matter-of-course proximity of polymer chemists to cell and molecular biologists and their already thrillingly perfect insight into molecular processes. We polymer chemists must learn to speak their language and teach it in lectures and practical courses. We must reach out to the cell and molecular biologists, who also do not yet know how much they will need us for "artificial cells" and self-replicating systems.

5.2. Polymers as Pharmacologically Active Compounds: The Pharmaceuticals of the Future?

There is another dream of Staudinger mintage closely associated with the idea of "synthetic biological" structures,

 © 2004 Wiley-VCH Verlag GmbH & Co. KGaA, Weinheim

and for which a close, long-term collaboration of polymer science with membrane and cell biology, with pharmacy, pharmacology, and medicine is an absolute necessity: polymers as pharmacologically active compounds—polymeric therapeutics.[48] It is certainly only a matter of time before pharmaceuticals are required not only affect cells and tissues specifically, but must also exhibit specific behavior in the cytoplasm of the cell: a defined interaction with the plethora of membranes and cell organelles. First thoughts regarding this interface between pharmacy and polymer science may be almost a half a century old, but their acceptance in pharmacy and pharmacology, and above all in the often short-term and merely profit-driven pharmaceutical industry, is not yet sufficient. Ruth Duncan summarized the foundations, the results, the possibilities, and the future of this interface in a publication that appeared in 2003.[48] In the preface to this work the term "Polymer Therapeutics" she coined is defined and the potential outlined: "*As we enter the twenty-first century, research at the interface of polymer chemistry and the biomedical sciences has given rise to the first nano-sized (5–100 nm) polymer-based pharmaceuticals, the Polymer Therapeutics. Polymer Therapeutics include rationally designed macromolecular drugs, polymer–drug and polymer–protein conjugates, polymeric micelles containing covalently bound drug, and polyplexes for DNA delivery. The successful clinical application of polymer–protein conjugates, and promising clinical results arising from trials with polymer–anticancer-drug conjugates, bode well for the future design and development of the even more sophisticated bionanotechnologies that are needed to realize the full potential of the post-genomics age.*"

To insiders the subject is familiar, the results are known,[49–52] but only the first steps have been taken. What could be achieved in tumor research and has already shown to be possible in tumor therapy is currently being applied to other clinical pictures.[48] The necessary knowledge is there on both sides: in biomedicine and pharmacology the insight into molecular details and the course of most diseases, and in polymer science the ability to produce degradable, narrow-range homo- and block copolymers with a breadth of functional and structure-forming groups which can even surpass the possibilities available in nature. The meeting point of these two fields is again molecular and membrane biology: knowledge about cell membranes, as well as transmembrane and intracellular transport (which ties in well with the Nobel Prize in Chemistry for 2003).[53] One might predict that the interactions of "tailor-made" synthetic macromolecules with cells, cell membranes, and intracellular systems will also give rise to new effects. These effects could lead to fundamental questions, the answers to which may not be found in the catalogue of knowledge of the molecular biologists, who have until now only been biologically orientated.

The more we know about the interaction of natural and synthetic macromolecules with cell membranes and cell organelles, and the better we understand endosomal and lyspsomal systems and the processes of intracellular transport of novel polymers, the closer we will come to an understanding that will allow the development of disease-specific polymers. Here, too, the close and mutually planned collaboration between polymer science, membrane and molecular biology, and pharmacy and pharmacology is required. It is a question of the synthesis of macromolecules based on biological rationale. That should not put an end to the pure joy of synthesizing novel macromolecules for the sake of synthesis, but this approach belongs—and this is said without deprecation—to classical polymer science. It is foreseeable that only polymeric therapeutics will be able to fulfill the plethora of ever more stringent demands on the pharmaceuticals of the future. Not without reason has Mother Nature always made use of macromolecules when it was a matter of viability, regulation, self-replication, and stability.

Polymer science has found its place as a fundamental science. We, the old polymer scientists, will die out, and with us the old days of classical macromolecules. The creative minds of the young generation will then be free to make their dreams and those of Hermann Staudinger become reality. They will find ways in close cooperation with biomedicine, with membrane and molecular biology, to use the diversity of possible polymer systems for the construction of new cell- and tissue-specific pharmaceuticals and of functioning artificial cells—and that while once again on the road to new goals.

6. Science Directed and Disturbed by Two World Wars

What do we actually know, we who are able to teach and research in a liberal democracy and in relative freedom today, of the constraints of the sciences?[54] Hermann Staudinger's research largely took place against the backdrop of two world wars (1914–1918 and 1939–1945). He taught and did research (1907–1912) during the last German empire (Kaiserreich), in liberal, neutral Switzerland (1912–1926), and during the Nazi dictatorship, (1933–1945) which immediately aryanized the universities in 1933 and then "generously" supported each branch of science that accepted its obsessive racism and its war plans.[55] In between there was a short period of the democratic Weimar Republic (1926–1933) for Hermann Staudinger, but this was also highly charged with patriotic empathies. No, the history and the—mostly shameful and often tragic—entanglement of science and politics of that time will not be rolled out here. Much has been written about it.[55–60] However, to understand this great scientist one must point out, even fifty years after the award of the Nobel Prize, how very bound up in those tragic times he was, as a researcher, a teacher, and a person.

Hermann Staudinger loved the liberal, politically tolerant climate of the ETH Zürich (Switzerland), where he worked from 1912. From there he followed the politics and development of the First World War with great skepticism and concern.[61] He did not consider engaging in direct political activities, and he was reluctant to comment on questions that lay outside his sphere of competence. However, he considered it his duty to discuss politics and science, and he was supported in this by his first wife, Mina Mathilde (neé Förster), the mother of his four children and a dedicated socialist.

 © 2004 Wiley-VCH Verlag GmbH & Co. KGaA, Weinheim

At that time he went into great detail in his lectures about the economic and cultural consequences of the immense processes of change ensuing from modern technology. We find an expression of this concern in 1917, in his courageous appeal directly to the German imperial general staff for an end to the bloodshed of the war. In his article "Technik und Krieg" (Technology and War) he described the considerable superiority of the allies and inferred from this the defeat of Germany.[61] The appeal and this publication led to the well-known serious dispute with Fritz Haber, his friend from Karlsruhe days, whom he had attacked because of his active involvement in gas warfare. How important the association of scientist, technology, and society was to Hermann Staudinger is also demonstrated by his renewed publication of these thoughts in 1946 as a book—with a somewhat antiquated title and content (Figure 4).[62]



Figure 4. The inside cover of the 1946 book of Herrmann Staudinger [62] with his corrections and his signature.

After the First World War, in the admittedly democratic but still very patriotic Weimar Republic, the reaction to such little national pride—and that from neutral Switzerland—was not long in the coming. When he wanted to move from the ETH Zürich to the Universität Freiburg (Germany) in 1926, Staudinger was ordered by the dean in Freiburg to comment officially on his appeal of 1917 to remove suspicions of his patriotic stance[63]—and he did.

Science as "neuronal network": a sensitive temporal coupling of human, scientific, and political events, the simultaneousness of events, and the parallelism or conflict of developments. Everything is connected, but we, imprisoned in our specialized fields,[29] are usually not aware of it, often do not want to admit it for professional zeal, factual blindness, and lack of objectivity, and often see it first in the light of history. The Nobel Prizes in Chemistry and Medicine of fifty years ago are themselves a good example of the network of scientific hope and political reality. The lives and research paths of the polymer scientist Hermann Staudinger and the medical doctor Hans Krebs could have crossed long before their joint honor in 1953—perhaps they even did. The future biochemist worked from 1931 as a ward physician in the university clinic in Freiburg. That did not last long; he had just enough time to carry out his research into the orthinine cycle and for his habilitation. Then came the "turning point", which Lothar Jaenicke described so bitterly yet truthfully:[64] "*In 1932 H. A. Krebs—Freiburg—received the Venia docendi and a considerable number of estimable offers for his advancement. Eight weeks later he was ordered to stay away: The Nazis had come to power and with them Germanity had broken out virulently. The highly praised lecturer became a Jew and persona non grata overnight. His old, mildly resistant teacher von Möllendorf was replaced as Rector magnificus by the mystical opportunist Heidegger as Führerrektor, who existentialistically provided the philosophical arguments for what came to pass: The students drifted brainlessly but dangerously.*"

Thus seen in a historical perspective political attitude naturally played a role, not for the Nobel Prize, but for the Nobel Laureate. Hermann Staudinger's path during the Third Reich did not run in a straight line. It was a difficult time, and strongly influenced by his love for his macromolecules. For him, too, it looked tragic at first: The above-mentioned Nazi, status-seeking philosopher Martin Heidegger pursued his ostracism and planned his dismissal on the grounds of his unpatriotic behavior during the First World War. The Second World War saved Hermann Staudinger, as plastics were now important war materials for the Nazis. Hermann Staudinger was no friend of the NS regime, but he was not an opponent either. His attitude in the Third Reich was for the sake of his research and retaining his research group. Thus, to be able to travel to conferences abroad, he made offers to the university management to represent German science abroad, to defend his "German" macromolecules against those that had meanwhile become "Jewish" polymers.[63,65] If Hermann Staudinger had held to his pacifist stance of the First World War to only the slightest extent he could not have become editor of the renowned German *Journal für praktische Chemie* in 1939, he would not have been allowed to found the first European institute for macromolecular chemistry in Freiburg in 1940, and he would not have been able to rename his journal the *Journal für Mackromolekulare Chemie* in 1943.[66] If none of this had happened it would not have lessened the recognition of the scientific achievements of Hermann Staudinger, nor delayed polymer science,[67] and not at all would it have prejudiced the Nobel Prize in Chemistry in 1953.

One has to read the profound and reflective Essay[68] of Roald Hoffmann and Pierre Laszlo on Fritz Haber and that period to be able to comprehend the profound tragedy and entanglement of science and humanity in the conflicting field of politics and society. What do we really know today of such pressures of lack of freedom and political tendencies in science? What can we do to also understand something of this today, for today? None other than Roald Hoffmann[68] both raises and answers this question from his own experience—not then, but now, in 2001! I would like to reproduce his answer at this point—and I ask the author for understanding and forgiveness—in a somewhat altered form as a concluding comment on this scientific–political part of our jubilee celebration of the Nobel Prize of 1953: "*Most of us are also university teachers and responsible. We have to do better than the usual, traditional presentation of technical successes. We have to talk about the scientist, the historical figure and the person. And we must get involved where our competence is required!*"[69,70]

[1] Admitted: copied! This most appropriate subtitle comes from L. Jaenicke, Universität Köln, and he uses it to mark the same occasion. As his article appeared in a biochemical journal and the rifts to polymer science are still not completely closed over, I cite it here and

 © 2004 Wiley-VCH Verlag GmbH & Co. KGaA, Weinheim

in this way try not only to justify my title plagiarism, but also to direct interest toward a fantastic, technically critical, and philosophically human contribution on H. Staudinger: L. Jaenicke, *BIOspektrum* **2003**, *9*, 601 – 604.

[2] a) Does the following document show the PhD certificate of His Majesty the last German Emperor? Of course not!



AVGVSTISSIMI ET POTENTISSIMI PRINCIPIS AC DOMINI
DOMINI
WILHELMI II
GERMANORVM IMPERATORIS
BORVSSIAE REGIS
PATRIS PATRIAE
REGIS ET DOMINI NOSTRI LONGE CLEMENTISSIMI
ACADEMIAE FRIDERICIANAE HALENSIS CVM VITEBERGENSI CONSOCIATAE
RECTORE MAGNIFICO
VIRO CLARISSIMO
RVDOLFO STAMMLER
EX DECRETO AMPLISSIMI PHILOSOPHORVM ORDINIS
HERMANNVS SUCHIER
VIRO PRAENOBILISSIMO ET DOCTISSIMO
HERMANNO STAUDINGER
DOCTORIS PHILOSOPHIAE ET AA. LL. MAGISTRI
RITE CONFERRI

But because everything that happened in those days happened by the grace of His Majesty, his name crowns Hermann Staudinger's PhD certificate (1903)—Historical traditions have their own value. (This is a copy of the original PhD certificate (M. AUGUSTI A. MDCCCCIII), which is in the archives of the Martin-Luther-Universität Halle-Wittenberg. The topic of the PhD thesis was "The Addition of Malonic Esters to Unsaturated Compounds".)

b) H. Morawetz, *Polymers: The Origins and the Growth of a Science*, Wiley-Interscience, New York, **1985**. A book, scientifically accurate, in which the footnotes are as worth reading as the text. In the introduction Herbert Morawetz says he read each of his 1042 literature citations himself in the original language wherever he was able—and Herbert Morawetz, a highly educated former citizen of Prague and central European who emigrated to the USA under duress, is multilingual. I would not buy this statement from many scientists, but in his case I do it blind. The book, long out of print, has at last been republished by Dover Publications.

c) Herbert Morawetz is Professor of Polymer Science and one of the early comrades-in-arms of Herman Mark at the Institute of Polymer Research founded in 1946 at the Polytechnic Institute of Brooklyn (nowadays: of New York).

[3] "Über die Darstellung von Isopren aus Terpenkohlenwasserstoffen" (On the Synthesis of Isoprene from Terpenoid Hydrocarbons): H. Staudinger, H. W. Klever, *Ber. Dtsch. Chem. Ges.* **1911**, *44*, 2212.

[4] "Über Polymerisation" (On Polymerization): H. Staudinger, *Ber. Dtsch. Chem. Ges.* **1920**, *53*, 1073.

[5] a) "Über die Hydrierung des Kautschuks und über seine Konstitution" (On the Hydrogenation of Rubber and on Its Constitution): H. Staudinger, J. Fritschi, *Helv. Chim. Acta* **1922**, *5*, 785 – 806; b) "Difficulties in the Emergence of the Polymer Concept—an Essay": H. Morawetz, *Angew. Chem.* **1987**, *99*, 95 – 100; *Angew. Chem. Int. Ed. Engl.* **1987**, *26*, 93 – 97.

[6] Just a reminder: the terms polymers and colloids had already been coined in the 19th century, "polymeric" by J. J. Berzelius and "colloids" by T. Graham (J. J. Berzelius, *Jahresber. Fortschr. Phys. Wissensch.* **1833**, *12*, 63; T. Graham, *Philos. Trans. R. Soc. London* **1861**, *151*, 183). If the definitions and the relevant examples are looked at side-by-side, the conflict of that time, first resolved by Hermann Staudinger, can be understood. "High polymers" such as rubber, cellulose, starch, and synthetic resins were already classified in the century before last as "colloidal substances"; see H. Morawetz in reference [2a] (p. 5, p. 47). How very attached Hermann Staudinger also remained to colloids is confirmed by his book, republished in 1941: H. Staudinger, *Organische Kolloidchemie*, Vieweg, Braunschweig, **1941.**

[7] H. Staudinger, *From Organic Chemistry to Macromolecules: A Scientific Autobiography Based on My Original Papers*, Wiley-Interscience, New York, **1970** (translated by J. Fock and M. Fried). The book, the German edition of which had already appeared in 1961 (H. Staudinger, *Arbeitserinnerungen*, A. Hüthig Verlag, Heidelberg, **1961**), so during Staudinger's lifetime, contains as the conclusion his Nobel Lecture of December 11, 1953 in Stockholm. The English edition is introduced with a preface by Herman F. Mark, which is written so affectionately, circumspectly, and farsightedly that it could have been printed confidently as a jubilee article in celebration of the fifty years since Staudinger's Nobel Prize.

[8] C. Priesner, *H. Staudinger, H. Mark und K. H. Meyer: Thesen zur Größe und Struktur der Makromoleküle*, Verlag Chemie, Weinheim, **1980.**

[9] Y. Furukawa, *Staudinger, Carothers and the Emerge of Macromolecular Chemistry*, University of Pennsylvania Press, Pennsylvania, **1998.**

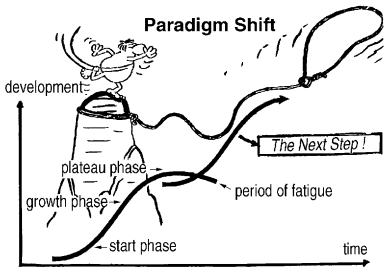
[10] C. Tanford, J. Reynolds, *Proteins versus Polymers: History needs Revising*, The Chemical Intelligencer, July **1999**, p. 24–27.

[11] "Protein Chemists Bypass the Colloid/Macromolecule Debate": C. Tanford, J. Reynolds, *Ambix* **1999**, *46*, 33 – 51.

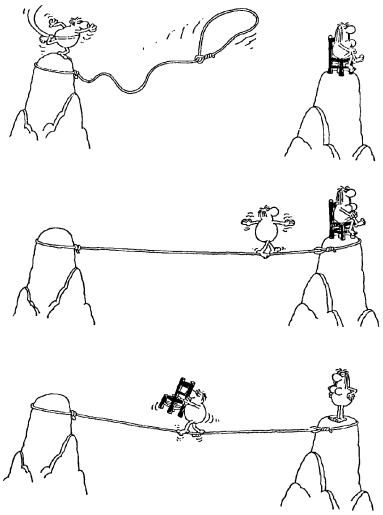
[12] H. F. Mark, *Naturwissenschaften* **1980**, *67*, 477.

[13] Far from wishing to give a critically comparative review on Nobel Prizes, I would still like to mention two examples of Nobel Prizes for medicine, physics, and chemistry, each—in my opinion—with a different breadth of influence and different scientific significance. In medicine: 1908 to Paul Ehrlich and Ilya Mechnikov "in recognition of their work on immunity", the foundation of modern chemotherapy, 1911 to Allvar Gullstrand "for his work on the dioptrics of the eye"; in physics: 1903 to Henri Becquerel for "his discovery of spontaneous radioactivity" and to Pierre Curie and Marie Curie for "their joint researches on the radiation phenomena discovered by H. Becquerel", 1906 to Joseph J. Thomson for "his theoretical and experimental investigations of the conduction of electricity by gases"; in chemistry: 1953 to Hermann Staudinger "for his discoveries in the field of macromolecular chemistry", 1912 to Victor Grignard "for the discovery of the so-called Grignard reagent".

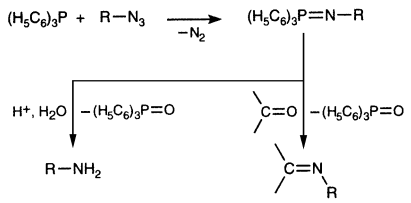
[14] T. S. Kuhn, *The Structure of Scientific Revolutions*, 2nd ed., University of Chicago, Chicago, **1970**: Progress in science does not happen through the continuous collection of facts, but by revolutionary processes, which induce the replacement of existing explanation models (paradigms) by new concepts: A paradigm shift. Two pictures may illustrate paradigm shift in science. Picture 1: beginning the next step; picture 2: scientist on the march to new objectives: materials science or bioscience, that is the question. It is amazing how well G. Modillo, the Argentinian caricaturist, knows polymer chemists…



 © 2004 Wiley-VCH Verlag GmbH & Co. KGaA, Weinheim



[15] The Staudinger reaction: The reaction of organic azides with phosphanes leads to phosphanimides (iminophosphoranes) with the release of nitrogen. In a reaction analogous to the Wittig reaction these compounds can be converted upon reaction with carbonyl compounds into imines (azomethines, Schiff bases), which can be hydrolyzed in turn to amines. Thus, by means of this reaction amines can be prepared from azides under relatively mild conditions.



[16] The intensity of the verbal and written disputes of that time are hard to imagine today. A particularly extreme example was the great mutual aversion of H. Staudinger and K. H. Meyer. Staudinger did not attempt to conceal his antipathy. However, one also has to search long and hard in Meyer's textbook[16a] to find the first reference to Staudinger's work on page 34, and much of his work is only mentioned in passing. a) K. H. Meyer, *Natural and Synthetic High Polymers*, 2nd revised and expanded edition, Interscience, New York, **1950**; b) Herbert Morawetz also mentions this book in reference [2] (p. 97), but the first edition, which was vehemently criticized by H. Staudinger.

[17] a) Pure fantasy? Not really: In 1958, as a PhD student of Elfriede Husemann, H. Staudinger's successor—after completing my diploma with Hermann Staudinger at the Institut für Macromolekulare Chemie in Freiburg, and when I was still relatively unburdened by a knowledge of polymers—I had the real pleasure of working three mornings a week as a "personal assistant" with Hermann Staudinger, to help him to perfect his "Arbeitserinnerungen" and with the writing of his four USA lectures. The original slides of these lectures are still in Mainz.
b) Temporally it was directly against the backdrop of the Nobel Prize awards of 1953 that rodlike polymers were detected in the helix–coil transition of polypeptides: L. Pauling, R. B. Corey, H. R. Branson, *Proc. Natl. Acad. Sci. USA* **1951**, *37*, 205; P. Doty, A. M. Holtzer, J. H. Bradbury, E. Blout, *J. Am. Chem. Soc.* **1954**, *76*, 493, to read about in detail in reference [2a] (p. 231–234). It took somewhat longer before Hermann Staudinger's rigid synthetic macromolecules could be prepared, for example, "Dendronized Polymers: Recent Progress in Synthesis": D. Schlüter, *Macromol. Chem. Phys.* **2003**, *204*, 328.

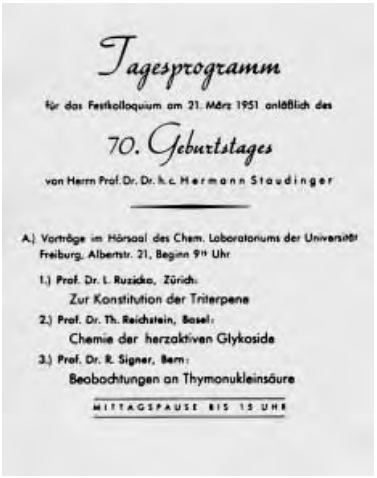
[18] "Ein Jahrhundertdatum—1902. Das Geburtsjahr der Peptidchemie" (An Key Date of the Century—1902. The Year of the Birth of Peptide Chemistry): L. Jaenicke, *Chem. Unserer Zeit* **2002**, *36*, 338.

[19] "The Physical Chemistry of the Proteins": E. J. Cohn, *Physiol. Rev.* **1925**, *5*, 349.

[20] a) Two of H. Staudinger's students, who originally worked with him on terpenes, received the Nobel Prize before him: L. Ruzicka obtained the Nobel Prize in Chemistry in 1939 together with A. Butenandt "for his work on polymethylenes and higher terpenes"; Tadeus Reichstein, who had obtained his PhD with Staudinger in 1922 and was later an assistant of L. Ruzicka, received the Nobel Prize in Medicine in 1950 together with Edward C. Kendall and Philip S. Hench "for their discoveries relating to the hormones of the adrenal cortex, their structure and biological effects".
Much more directly associated with Staudinger's Nobel Prize in 1953 and even more so with the solving of the structure of DNA by Watson and Crick 50 years ago was Rudolf Signer (Universität Bern, Switzerland), one of Staudinger's co-workers in the 1920s: He would have been 100 years of age in 2003! His contribution to the elucidation of the structure of DNA has almost been forgotten and does not appear in the literature on the critical phase. It can be said unequivocally that without his input the elucidation of the structure of DNA would not have been possible so early, certainly not in 1953. During the time with Staudinger the work by Singer together with J. Hengstenberg on the X-ray crystallographic investigation of polyoxymethylene fractions was crucial for the proof that the unit cell of a macromolecule can be much smaller than the molecule itself. This achievement would actually have been the perfect basis for the discovery and significance of the double helix. For it was Rudolf Signer's highly purified DNA samples that led to the DNA diffraction patterns in the laboratories of Maurice H. Wilkins and Raymond Gosling, which made the interpretation of Watson and Crick possible.
The official scientific world has almost entirely forgotten this essential contribution by R. Signer. He is not cited, although Maurice Wilkins formulated the facts of the case with rare clarity and with the highest recognition for R. Signer in his Nobel Lecture of December 1962. He describes how impressed he was to be able to draw threads like a spider's web from the DNA gel of the Signer DNA samples. He passed the samples on to Raymond Gosling and emphasized in his Nobel Lecture: "We obtained good diffraction patterns with DNA made by Signer and Schwander which Signer brought to London to a Faraday Society Meeting on nucleic acids and which he generously distributed so that all workers, using their various techniques, could study it." ("The molecular configuration of nucleic acids", M. H. F. Wilkins in *Nobel Lectures*, *Medicine*, published for the Nobel Foundation in **1964**, Elsevier, New York, p. 754–782.) In the same Nobel Lecture Maurice Wilkins also cited the following work by Signer and co-workers: "109. Isolierung hochmolekularer Nucleinsäure aus Kalbsthymus" (Isolation of High-Molecular-Weight Nucleic Acids from the Thymus of a Calf): R. Signer, H. Schwander, *Helv. Chim. Acta* **1949**, *32*, 853; "Molecular Shape and Size of Thymonucleic Acid": R. Signer, T. Caspersson, E. Hammarsten, *Nature* **1938**, *141*, 122. In the *Nature* article, one of the conclusions drawn by R. Signer and co-workers based on viscosity and optical investigations was that in solution DNA had the form of long, thin rods, and that the purine and pyrimidine rings occupied planes at right angles to the axis of the molecule: at that time, 15 years before Watson and Crick, a revolutionary insight. It will probably always remain an open question as to why, with his X-ray crystallographic experience from his time with Staudinger, his interest in biopolymers, and his lucid recognition of the importance of his DNA samples, he did not himself try

 © 2004 Wiley-VCH Verlag GmbH & Co. KGaA, Weinheim

to elucidate the structure of DNA by X-ray crystallography; see also: "Signer's Gift—Rudolf Signer and DNA": M. Meili, *Chimia* **2003**, *57*, 735 – 740.
b) H. Staudinger, *Makromolekulare Chemie und Biologie*, Wepf, Basel, **1947**: In this book, which was perhaps written as a type of "textbook" for biologists, Hermann Staudinger presented his thoughts on the unity of chemistry and biology enthusiastically. Therein he also speaks of viruses, genes, polynucleotides, enzymes, and crystalline proteins, but only from the viewpoint of his experience with synthetic polymers (see p. 49, p. 60), and expounds his ideas of long, threadlike molecules (see, for example, p. 61, p. 103, p. 107). In this connection it is historically interesting that in a one-day colloquium for Hermann Staudinger's 70th birthday (March 21, 1951), his former co-workers L. Ruzicka (Zürich), T. Reichstein (Basel), and R. Signer (Bern) gave the first three talks (see picture). It has to be emphasized especially that on this occasion Rudolf Signer also discussed the properties of his highly purified nucleic acids mentioned above (in reference [20]).


Tagesprogramm

für das Festkolloquium am 21. März 1951 anläßlich des

70. Geburtstages

von Herrn Prof. Dr. Dr. h. c. Hermann Staudinger

A.) Vorträge im Hörsaal des Chem. Laboratoriums der Universität Freiburg, Albertstr. 21, Beginn 9¹⁵ Uhr

1.) Prof. Dr. L. Ruzicka, Zürich:
Zur Konstitution der Triterpene

2.) Prof. Dr. Th. Reichstein, Basel:
Chemie der herzaktiven Glykoside

3.) Prof. Dr. R. Signer, Bern:
Beobachtungen an Thymonukleinsäure

MITTAGSPAUSE BIS 15 UHR

[21] Sir Hans Adolf Krebs (1900–1981), Professor of Biochemistry at Oxford University; areas of research: biochemistry, metabolic energetics, elucidation of the urea cycle and the citric acid cycle, which was named after him (Krebs cycle).

[22] Fritz Albert Lipmann (1899–1986), Professor of Biochemistry at Harvard University; areas of research: coenzyme A and its central role in energy transfer in cells, energetics of metabolic processes, cellular synthesis of peptides.

[23] In the issue of *Chemical and Engineering News* of January 11, 1954 the award of the Nobel Prize of 1953 is described under "The Cover: Nobel Ceremony Honors Chemists": *Chem. Eng. News* **1954**, *32,* No. 2, 162 – 163.

[24] Fritz Zernike (1888–1966), Professor of Physics at Groningen University.

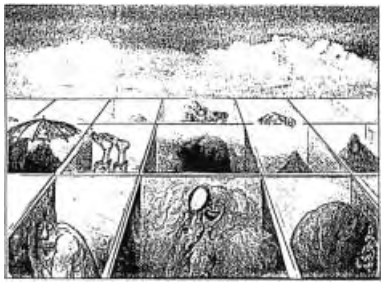
[25] In view of the parallel development of polymer science and the biosciences it is worth mentioning that the polymer book of Herbert Morawetz also contains a chapter on "The Rise of Molecular Biology" (see reference [2a], p. 197–213).

[26] J. D. Watson, F. H. Crick, *Nature* **1953**, *171*, 737; J. D. Watson, F. H. Crick, *Nature* **1953**, *171*, 964.

[27] E. Chargaff, *Experientia* **1950**, *6*, 201 – 204; also well worth reading is what Lothar Jaenicke wrote upon the death of this all-round genius in 2002.[28]

[28] "The Torch of Erwin Chargaff and the Fire of Heraklitus Devour Their Children": L. Jaenicke, *Angew. Chem.* **2002**, *114*, 4387; *Angew. Chem. Int. Ed.* **2002**, *41*, 4213.

[29] Ronald Searle, the British cartoonist, called this caricature "Human Beings". In analogy, we scientists usually sit in the boxes of our specialty areas: naturally, we are interested in what is going on next door! But beyond there?



[30] "Derivation of Oocytes from Mouse Embryonic Stem Cells": K. Hübner, G. Fuhrmann, L. K. Christenson, J. Kehler, R. Reinbold, R. LaFuente, J. Wood, J. F. Strauss, M. Boiani, H. R. Schöler, *Science* **2003**, *300*, 1251.

[31] An old Mongolian adage: The frog who sits at the bottom of a deep well, for him is the expanse of the heavens and horizon narrow and small.

[32] Supramolecular chemistry and polymer science actually fraternized quite early in the chemistry and physics of supramolecular systems: In 1987 Donald J. Cram, Jean-Marie Lehn, and Charles J Pedersen received the Nobel Prize in Chemistry "for their development and use of molecules with structure-specific interactions of high selectivity", and in 1988, in addition to the Nobel Lecture by Jean-Marie Lehn,[32a] *Angewandte Chemie*—-an issue commemorating its 100-year existence—contained a contribution on the molecular architecture of polymer-orientated systems.[32b]
a) "Supramolecular Chemistry—Scope and Perspectives: Molecules, Supermolecules, and Molecular Devices": J. M. Lehn, *Angew. Chem.* **1988**, *100*, 91 – 116; *Angew. Chem. Int. Ed. Engl.* **1988**, *27*, 89 – 112; b) "Molecular Architecture and Function of Polymeric Oriented Systems: Models for the Study of Organization, Surface Recognition, and Dynamics of Biomembranes": H. Ringsdorf, B. Schlarb, J. Venzmer, *Angew. Chem.* **1988**, *100*, 117 – 162; *Angew. Chem. Int. Ed. Engl.* **1988**, *27*, 113 – 158.

[33] a) *Supramolecular Polymers* (Ed.: A. Ciferri), Marcel Dekker, New York, **2000**; b) "Supramolecular Polymer Chemistry—Scope and Perspectives": J.-M. Lehn in reference [33a] (chap. 14, p. 615).

[34] *Supramolecular Materials and Technologies* (Ed.: D. N. Reinhoudt), Wiley-Interscience, New York, **1999.**

[35] a) "Supramolecular Structures with Macromolecules": U. Beginn, M. Möller in reference [34] (chap. 3, p. 89); b) "Layer-by-Layer Adsorption: The Solid Liquid Interface as a Template for the Controlled Growth of Well Defined Nano Structures of Polyelectrolytes, Proteins, DNA and Polynucleotides, Self-Production of Supramolecular Structures": G. Decher, J. D. Hong, K. Lowaki, *NATO ASI Ser. Ser. C* **1999**, *446*, 267; c) "Smart Inorganic/Organic Nanocomposite Hollow Microcapsules": D. G. Shchukin, G. B. Sukhorukov, H. Möhwald, *Angew. Chem.* **2003**, *115*, 4610 – 4613; *Angew. Chem. Int. Ed.* **2003**, *42*, 4472 – 4475; d) "Nanocomposites of Hairy Rod Macromolecules: Concepts, Constructs, and Materials": G. Wegner, *Macromol. Chem. Phys.* **2003**, *204*, 347 – 357.

[36] Colloid chemistry has long since found the place it deserves, is once again a fundamental part of polymer science, as it was at the outset, and is now more vigorous than ever. a) Two historical sources, the second of which also confirms Hermann Staudinger's enduring interest in colloids: W. Ostwald, *Die Welt der vernachlässigten Dimensionen*, 10th ed., Steinkopf, Leipzig, **1927**; H. Staudinger, *Organische Kolloidchemie*, 3rd ed., Vieweg, Braunschweig, **1950**; b) "90 Years of Polymer Latexes and Heterophase Polymerization: More Vital Than Ever": M. Antonietti, *Macromol. Chem. Phys.* **2003**, *204*, 207; c) "Polymerization in Inverse Microemulsions": F. Candau in *Comprehensive Polymer Science*, *Vol. 4* (Eds.: J. C. Eastmond, A. Ledwith, S. Russo) Pergamon, Oxford, **1989**, chap. 13, p. 225.

[37] The presence and future of modern polymer science could be formulated somewhat more ironically: The classical

 © 2004 Wiley-VCH Verlag GmbH & Co. KGaA, Weinheim

part is basic science, such as organic and inorganic chemistry, significant parts have long since become materials science, and the most recent developments are disappearing into the abyss of nanotechnology, which, before it is also swallowed up by materials science, is being given the life-saving prefix "bio".

[38] a) *Polymeric Biomaterials* (Ed.: S. Dumitrin), 2nd revised and extended ed., Marcel Dekker, New York, **2002**, 1168 pages (!); b) *Synthetic Biodegradable Polymer Scaffolds* (Eds.: A. Atala, D. J. Mooney, J. Vacanti, R. S. Langer), Birkhäuser, Boston, **1997**; c) "The History of Tissue Engineering Using Biodegradable Synthetic Polymer Scaffolds and Cells": B. E. Chaignand, R. S. Langer, J. Vacanti in reference [38b] (p. 1).

[39] It was no-one less than Herman Mark who, on the occasion of the 100th anniversary of the birth of Hermann Staudinger in 1981, reflected upon the future of polymer science. In his Essay "Macromolecular Chemistry Today—Aging Roots, Sprouting Branches" he speaks amongst other things of "stabilized cells" and the "synthesis of a cell" as long-term objectives. Discussing a possible cooperation of polymer science and cell biology, Hermann Mark wrote: "… there is a 'multilingual' borderland, beyond which only a well established interdisciplinary team can expect to progress. This cooperation may give rise to an entirely new discipline which survives the old ones. 'Material science' thus originated from metallurgy, ceramics and plastics technology. What about 'Life Science'? Can polymer chemistry, cell biology and medicine overlap and strive together for new goals?": H. F. Mark, *Angew. Chem.* **1981**, *93*, 309 – 310; *Angew. Chem. Int. Ed. Engl.* **1981**, *20*, 303 – 304.

And even much earlier, in 1959, J. Lederberg almost wrote a contribution to this Essay on the 50th anniversary of the award of the Nobel Prize to Hermann Staudinger: "If the ingenuity and craftsman-ship so successfully directed at the fabrication of organic polymers for the practical needs of mankind were to be concentrated on the problem of constructing a self-replicating assembly along these lines I predict that the construction of an artificial molecule having the essential function of primitive life would fall within the grasp of our current knowledge of organic chemistry." ("A View of Genetics": J. Lederberg, *Science* **1960**, *131*, 275). What a compliment for us polymer chemists, and what trust in us. This publication is based on Lederberg's lecture on the occasion of his receiving the Nobel Prize in Medicine in 1958. H. Morawetz also cites J. Lederberg's mental leap in his book on the history of polymer science (reference [2], p. 213).

[40] "Polymers and Biomimicry": V. Percec, C. H. Ahn, W. D. Cho, A. M. Jamiesson, J. Kim, M. Schmidt, M. Gerte, M. Möller, *J. Am. Chem. Soc.* **1998**, *120*, 8619 – 8631.

[41] "Engineered Biopolymers": K. Dizio, D. A. Tirell, *Macromolecules* **2003**, *36*, 1553 – 1558.

[42] "Bioactive Polymers": J. L. West, J. A. Hubbel in reference [38b] (p. 83–96).

[43] a) "Influencing Receptor–Ligand Binding Mechanisms with Multivalent Ligand Architecture": J. E. Gestwicki, C. W. Cairo, L. E. Strong, K. A. Oetjen, L. L. Kiessling, *J. Am. Chem. Soc.* **2002**, *124*, 14922 – 14933; b) "Epoxidation of Polybutadiene by a Topologically Linked Catalyst": P. Thordarson, E. Bijsterveld, A. Rowan, R. Nolde, Nature **2003**, *424*, 915 – 918.

[44] a) "Inhibition of Cell Adhesion to Fibronectin by Oligopeptide Substituted Polynorbornes": H. D. Maynard, S. Y. Okada, R. H. Grubbs, *J. Am. Chem. Soc.* **2001**, *123*, 1275 – 1279; b) "Nanocontainers Distribute to Defined Cytoplasmic Organelles": R. Savic, L. Luo, A. Eisenberg, D. Maysinger, *Science* **2003**, *300*, 615 – 616.

[45] "Polymerosomes: Tough Vescicles Made from Diblock Copolymers": B. M. Discher, Y. Y. Won, D. S. Ege, J. Lee, F. S. Bates, D. E. Discher, D. Hammer, *Science* **1999**, *284*, 1143.

[46] a) "Polymerization and Domain Formation in Lipid Assemblies": B. Armitage, D. E. Bernett, H. G. Lamparski, D. F. O'Brien, *Adv. Polym. Sci.* **1996**, *126*, 53; b) "Attempts to Mimic Docking Processes of the Immune System: Recognition Induced Formation of Protein Multilayers": W. Müller, H. Ringsdorf, E. Rump, G. Wildburg, X. Zhang, L. Angermaier, W. Knoll, M. Liley, J. Spinke, *Science* **1993**, *262*, 1706 – 1708; c) "Ultrathin Organic Films: Molecular Architecture for Advanced Optical, Electronic and Bio-Related Systems": H. Fuchs, H. Ohst, W. Prass, *Adv. Mater.* **1991**, *3*, 10 – 18; d) "Preformed Polymers for Langmuir–Blodgett Films—Molecular Concepts": F. Embs, D. Funhoff, A. Laschewsky, U. Licht, H. Ohst, W. Praß, H. Ringsdorf, G. Wegner, R. Wehrmann, *Adv. Mater.* **1991**, *3*, 25 – 31; e) "Specific Interaction of Proteins with Functional Lipid Monolayers—Ways of Simulating Biomembrane Processes": M. Ahlers, W. Müller, A. Reichert, H. Ringsdorf, J. Venzmer, *Angew. Chem.* **1990**, *102*, 1310 – 1327; *Angew. Chem. Int. Ed. Engl.* **1990**, *29*, 1269 – 1285.

[47] "From Macromolecules to Biological Assemblies": A. Klug, *Nobel Lectures, Chemistry 1981–1990* (Eds.: A. G. Frängsmye, B. G. Malström), World Scientific, London, **1992**, p. 77; A. Klug, *Angew. Chem.* **1983**, *95*, 579 – 596; *Angew. Chem. Int. Ed. Engl.* **1983**, *22*, 565 – 582; see also reference [39].

[48] "The Dawning Era of Polymer Therapeutics": R. Duncan, *Nat. Rev. Drug Discovery* **2003**, *2*, 347 – 360.

[49] a) "Macromolecular Therapeutics. Advantages and Prospects with Special Emphasis on Solid Tumour Targeting": K. Greish, J. Fang, T. Inutsuka, A. Nagamitsu, H. Maeda, *Clin. Pharmacokinetic* **2003**, *42*, 1089 – 1105.

If one compares the titles of references [48] and [49a], one notices that "polymers" and "macromolecules" stand alongside "polymer therapeutics" and "macromolecular therapeutics"—like in the old Staudinger days in the 1920s, but with less political significance. For the sake of accuracy the term polymeric therapeutics must be accepted, as it sensibly includes polymeric micelles and polymer-modified liposomes alongside classical polymer systems. Magda Staudinger would be pleased, because for her only main-chain-coupled giant molecules came under the term macromolecules—scientifically exact (see reference [63, 65]), but for her personally very politically colored. The term polymer therapeutics was coined in 1996 by Ruth Duncan in a review ("The Role of Polymer Conjugates in the Diagnosis and Treatment of Cancer": R. Duncan, S. Dimitrijevic, E. G. Evagoron, *S.T.P. Pharma Sciences* **1996**, 6, 237 – 263). Since then it has also been adopted for the symposia "International Symposia on Polymer Therapeutics" in Great Britain and Japan, which were also begun in 1966. It is also clearly defined and used in the contribution "Challenges in Polymer Therapeutics" by A. Kabanov and T. Okano on p. 1 of the following book: b) *Polymer Drugs in the Clinical Stage. Advantages and Prospects* (Eds.: H. Maeda, A. Kabanov, K. Kataoka, T. Okano), Kluwer Academic/Plenum, New York, **2003**; c) *Self-Assembling Complexes for Gene Delivery. From Laboratory to Clinical Trial* (Eds.: A. V. Kabanov, P. L. Felgner, L. W. Seymour), Wiley-VCH, Weinheim, **1998**.

[50] a) "HPMA Copolymer–Anticancer Agents: Design, Activity, and Mechanism of Action": J. Kopacek, P. Kopeckova, T. Minko, Z. Lu, *Eur. J. Pharm. Biopharm.* **2000**, *50*, 61 – 81; b) "Doxorubicin–Polymer Conjugates: Further Demonstration of the Concept of Enhanced Permeability and Retention": F. M. Muggin, *Clin. Cancer Res.* **1999**, *5*, 7 – 8.

[51] a) "Phase I Clinical and Pharmacokinetic Study of PK1 (HPMA Copolymer Doxorubicin): First Member of a New Class of Chemotherapeutic Agents—Drug–Polymer Conjugates": P. Vasey, S. Kaye, R. Morrison, C. Twelves, P. Wilson, R. Duncan, R. Thomson, J. Cassidy, *Clin. Cancer Res.* **1999**, *5*, 83–94; b) "Polymer Conjugates for Tumour Targeting and Intracytoplasmic Delivery. The EPR Effect as a Common Gateway": R. Duncan, *Pharm. Sci. Technol. Today* **1999**, *2*, 441 – 449.

[52] A number of studies on polymer therapeutics are already cited in reference [38a]: "Systematic Cancer Therapy using Polymer-Based Prodrugs and Progenes" by L. W. Seymour, p. 843; "Anticancer Drug Conjugates with Macromolecular Carriers" by F. Kratz, A. Warnecke, K. Riebesee, P. Rodriguez, p. 851; "Enzyme-Prodrug Therapy of Cancer" by R. J. Knox, R. G. Melton, R. Satchi, p. 895; "Recent Developments in Drug Delivery to the Nervous System" by D. Maysinger, R. Savic, A. Eisenberg, p. 1083.

[53] It is a pleasure to be able to include the Nobel Prize in Chemistry for 2003 in this Essay. It was almost as if the Nobel Committee wanted to join in the celebration of Hermann Staudinger's scientific achievements and his dreams of the importance of polymer science to biology on the occasion of the 50th anniversary of his receiving the Nobel Prize in Chemistry. Peter Agre and Roderick MacKinnon received the Nobel Prize in 2003 for work on the membrane function of polymers—admittedly, still natural proteins. P. Agre was recognized for the discovery of water channels in cells, and R. MacKinnon for structural and mechanistic studies of ion channels. The justification states that the discoveries "have contributed to fundamental chemical knowledge on how cells function." Not many chemists and certainly still fewer polymer scientists had expected this topic as the basis for the 2003 Nobel Prize in Chemistry. But it will certainly—or hopefully!—rekindle and intensify our interest as chemists in cell-membrane processes!

[54] Admittedly, teaching and research are still today not entirely free. Wars are still waged, biological and chemical weapons are stored "as a precaution", as are atom bombs, land mines may be detected scientifically with sensors, but are still manufactured zealously in some countries—independent of the children still becoming crippled by the old land mines. However, unlike previously, it is often no longer a political dictatorship, but sometimes an economic one that enforces the development. New problems grow out of a—so-called—free market economy and unrestricted laissez-faire capitalism. Research is bound up in this network of industrial development with its short-term outlook—in spite of the immanent necessity for intuitive and long-term work in research. This does not fit in very well with the often shareholder-value-driven globalization tendencies. The stock market mercilessly demands the rapid attainment of imposed—often only formal—targets and thereby restricts broad fields of research and development in industry and at universities to a short-term amusement of our pleasure-driven society.

[55] U. Deichmann, *Flüchten, Mitmachen, Vergessen. Chemiker und Biochemiker in der NS-Zeit*, Wiley-VCH, Weinheim, **2001**. Those who find the book too thick, the subject too foreign, the material too old, are directed to the publication of U. Deichmann in *Angewandte Chemie*: U. Deichmann, *Angew. Chem.* **2002**, *114*, 1364 – 1383; *Angew. Chem. Int. Ed.* **2002**, *41*, 1310 – 1328. In the summary of this article the author writes: "…after the war the common stance to forget the 12 years of National Socialist rule … delayed affiliation of the weakened fields of research to the level of international research." This applies especially to biochemistry and molecular biology, as documented extensively in her article. As the Essay of Roald Hoffmann [68] this publication of U. Deichmann should—in my opinion—be part of one of the curriculum courses in chemistry. This is not an "anti-German" remark, but an attempt to point out again that we scientists have to learn from our mistakes! We all know: "Those who don't learn from history are condemned to repeat it " (see reference [54, 56]).

[56] *Science in the Twentieth Century* (Eds.: J. Krige, D. Pestre), Harwood Academic, **1997.** The book not only describes the development of scientific disciplines during the 20th century in various countries, but also examines the interplay of science and cultural aspects, industrial and state interests. Thereby it shows how time after time financial backing from military sources drives scientific development forward during wars and political conflicts. Differences in this trend from country to country are virtually nonexistent. Have we still not learnt enough from history? "War is the father of all things." The old, famous and infamous saying of Heraclitus (550–450 B.C.), a sentence I already hated as a boy.

[57] H. Kahlert, *Chemiker unter Hitler*, Bernhardus, Grevenbroich, **2001.**

[58] I would like to point out to those who do not wish to read further because it is all news from yesterday, because everything has already been said, that the same applies to the science we are extolling. Is it more important? The all-too-frequent denial of the past[55] at German universities during precisely those fifty years of which we speak has resulted, for example, in the fact that the Max-Planck-Gesellschaft (MPG) only published in 2001 two volumes on the history of its predecessor, the Kaiser-Wilhelm-Gesellschaft, under National Socialism.[59] One major reason why these volumes were published so late was that with Adolf Butenandt (1903–1995) as president of the MPG (1960–1971) a critical and reflective discussion on the Third Reich was not possible, and that not only because his bequeathed works (letters, etc) are locked away in the archives of the MPG until 2025![60] Together with L. Ruzicka, one of Staudinger's colleagues from his time in Zurich, Butenandt received the Nobel Prize in Chemistry in 1937.

[59] *Geschichte der Kaiser-Wilhelm-Gesellschaft im Nationalsozialismus. Bestandsaufnahme und Perspektive der Forschung* (Eds.: R. Rürup, W. Schieder), Wallstein, Hubert and Co., Göttingen, **2000** (commissioned by the presidential committee of the MPG)**.**

[60] In reference [59] (*Vol. 1*, p. 210)**.**

[61] "Ein Chemiker zur Friedensdiskussion. Hermann Staudinger zu Technik und Politik" (A Chemist's Position in the Peace Movement. Hermann Staudinger and his Opinions on Technology and Politics): H. Sachsse, *Nachr. Chem. Tech. Lab.* **1984**, *32*, 974.

[62] Hermann Staudinger, *Vom Aufstand der technischen Sklaven*, Hans V. Cahmir, Essen, **1947.**

[63] "Hermann Staudinger und die makromolekulare Chemie in Freiburg. Dokumente zur Hochschulpolitik 1925–1955" (Hermann Staudinger and Macromolecular Chemistry in Freiburg. Documents on University Politics 1925–1955): C. Priesner, *Chem. Unserer Zeit* **1987**, *21*, 151.

[64] L. Jaenicke, *BIOspektrum* **2001**, *7*, 45.

[65] Until the end of her life, out of love for her husband and his primary-valence-coupled macromolecules, Magda Staudinger fought against the term "polymer". Formally she was correct in so far as this term taken from ancient Greek (poly = many, meros = parts) can naturally also be applied to colloids, liposomes, and crystals. However, she was a woman of such pride and conviction that in my opinion in this case her stand had less to do with technically formal

 © 2004 Wiley-VCH Verlag GmbH & Co. KGaA, Weinheim

aspects and more to do with human emotion.

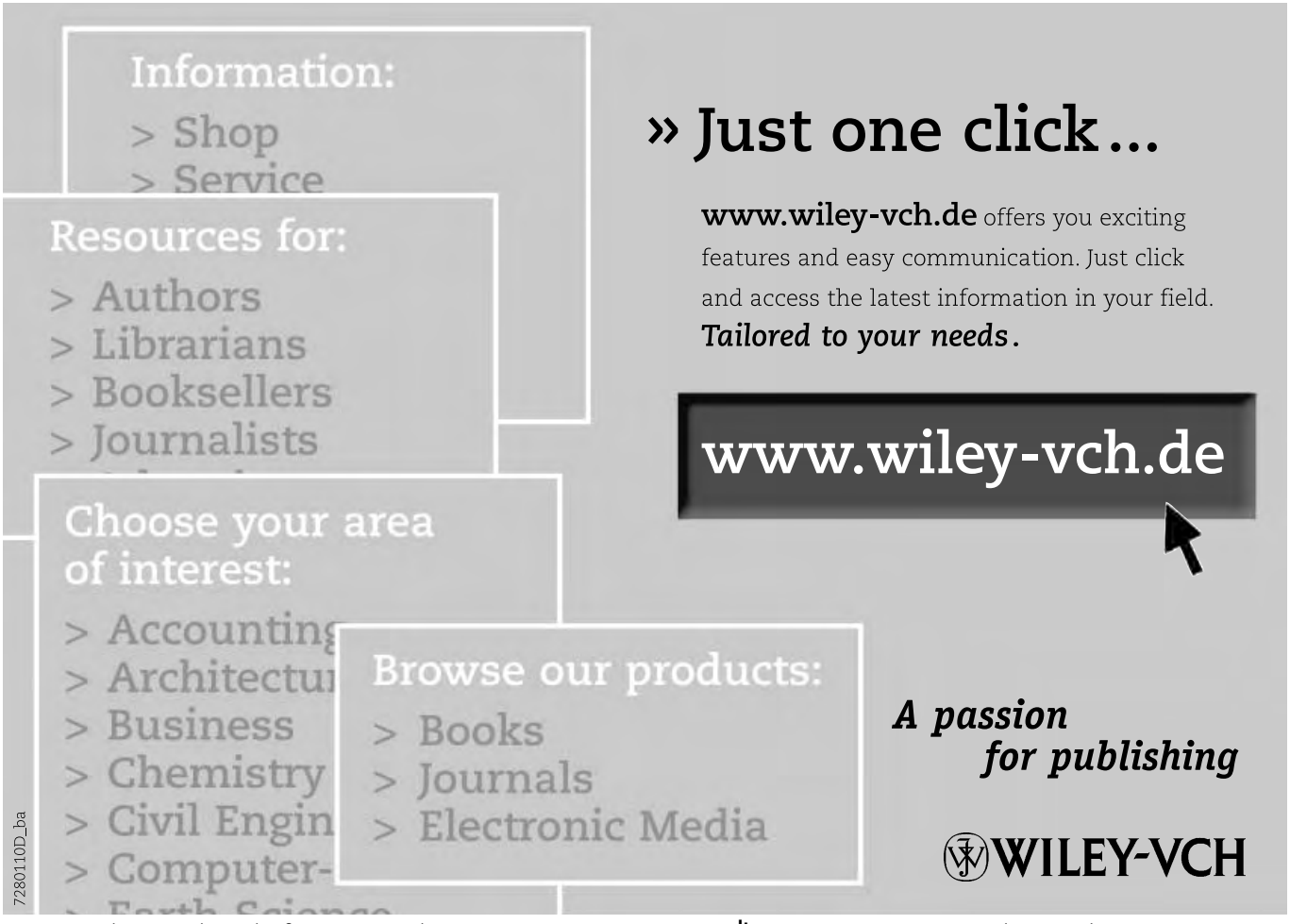
[66] A detailed history of the journal *Macromolecular Chemistry and Physics*, woven into the development of polymer science, was published on the occasion of the 60th birthday of the journal: "The 60th Anniversary of the First Polymer Journal ('Die Makromolekulare Chemie'): Moving to New Horizons": I. Meisel, R. Mühlhaupt, *Macromol. Chem. Phys.* **2003**, 199–206.

[67] Already in 1945 in the USA Herman Mark published the journal *Polymer Bulletin*, which in 1946 was renamed *Journal for Polymer Science*. In the same year he founded the Institute of Polymer Research at the Polytechnic Institute of Brooklyn. From 1947 *Die Makromolekulare Chemie* appeared in Europe under the leadership of Hermann Staudinger, and in the same year Charles Sadron started the Centre de Recherches sur les Macromolecules in Strasbourg (France).

[68] "Coping with Fritz Haber's Somber Literary Shadow": R. Hoffmann, P. Laszlo, *Angew. Chem.* **2001**, *113*, 4733–4739; *Angew. Chem. Int. Ed.* **2001**, *40*, 4599–4604.

[69] Today it is certainly no longer a matter of fighting Hitler. Our current willingness to do so comes too late! The young generation today will ask us, the then young and now old, whether we have learnt anything from that dark period of German science, and whether we today as scientists take our responsibility for society seriously. Or have we, too, smothered it again in the zeal of professionalism and busyness, or allowed it to be smothered by politics and commercialism? At times I fear that we natural scientists are still too unwilling to become involved. In peaceful and neutral times we continue to meet at conferences in many countries and to pat each other benevolently and appreciatively on the back. If it gets serious, or even just a little more serious, we withdraw into our laboratories and work on "pure" science, even when outside the chimneys of human injustice, social or political, are smoking! And yet: "Optimism is our duty. We are all jointly responsible for what is to come!"[70] And what is to come? Almost as if in explanation under "News of the Week" *Science* published two short items in September and October 2003: "IEEE, Under Fire for Withdrawing Iranian Members' Benefits" (*Science* **2003**, *301*, 1646) and "U.S. License Needed to Edit Iranian Papers" (*Science* **2003**, *302*, 210). Can what Y. Bhattacharjee wrote in the October issue of *Science* **2003** really be true?: "The U.S. Department of Treasury has ruled that scientific journals based in the United States cannot edit papers submitted by authors from Iran unless they have the government's permission. The policy, described in a letter sent last week to the Institute of Electrical and Electronics Engineers (IEEE), stems from rules prohibiting U.S. organizations from engaging in trade with Iran. Although the trade embargo has been in place since 1997, the 1 October letter is the first time Treasury has spelled out how it would affect publishers." I simply can not imagine that the American chemical societies and the respective publishing houses in the USA would collaborate in this matter! However, it seems no less strange to see that "on the other side of the battlefield" each issue of the *Iranian Polymer Journal* bears the caption "In the Name of Allah".

[70] K. Popper, *Alles Leben ist Problemlösen. Über Erkennen, Geschichte und Politik*, Piper, München, **1996**.



 © 2004 Wiley-VCH Verlag GmbH & Co. KGaA, Weinheim

Plastics

Nature or Petrochemistry?—Biologically Degradable Materials

*Stefan Mecking**

Keywords:
environmental chemistry · green chemistry · petrochemistry · plastics · polymers

Naturally occurring polymers have been utilized for a long time as materials, however, their application as plastics has been restricted because of their limited thermoplastic processability. Recently, the microbial synthesis of polyesters directly from carbohydrate sources has attracted considerable attention. The industrial-scale production of poly(lactic acid) from lactic acid generated by fermentation now provides a renewable resources-based polyester as a commodity plastic for the first time. The biodegradability of a given material is independent of its origin, and biodegradable plastics can equally well be prepared from fossil fuel feedstocks. A consideration of the overall carbon dioxide emissions and consumption of non-renewable resources over the entire life-cycle of a product is not necessarily favorable for plastics based on renewable resources with current technology—in addition to the feedstocks for the synthesis of the polymer materials, the feedstock for generation of the overall energy required for production and processing is decisive.

Introduction

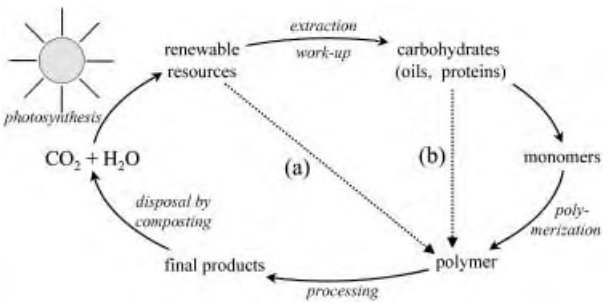
The evolution and the success of the chemical industry in the second half of the 19th century was intimately related to the introduction of fossil feedstocks as a basis for synthesis. With synthetic dyes made from coal replacing scarce naturally occurring dyes, light-stable colorants became accessible to larger portions of the population for the first time. Today fossil feedstocks in the form of oil and gas are by far the most important raw materials for the chemical industry, accounting for more than 90%. After energy generation (54% in the OECD countries) and transportation (35%), the chemical industry follows in third position as user of fossil feedstocks (12%, of which approximately equal shares are used as raw materials for syntheses and for energy generation).[1] In the chemical industry, the larger part of the raw materials is converted to polymers. The success of commodity plastics over the past 50 years can be attributed not only to the reliable raw materials basis and to their versatile applications properties, but also to their thermoplastic processability. Processing from the melt enables a cost effective and environmentally benign fabrication of mass products such as films and molded articles.

As a result of the oil crisis in 1973, alternative energy and raw materials sources such as biomass were propagated and investigated intensely. With decreasing crude oil prices public interest diminished again. Contemporary geopolitical and economical developments have brought back to mind the disadvantages of a dependence on crude oil and also its limited availability. The range of proven oil reserves accessible with conventional recovery techniques is currently estimated to be 40 years.[2] Albeit past estimates of this type have always proven to be to pessimistic in hindsight, on the other hand without doubt the dependence on the oil reserves in the Middle East will increase substantially. The ultimate formation of the greenhouse gas CO_2 from fossil feedstocks has unpredictable and irreversible consequences on the global climate. A disposal of traditional plastics in landfills will occupy the latter for indefinite amounts of time due to the very slow degradation. A cycle according to Scheme 1 based on renewable resources therefore appears attractive, and would also satisfy the general desire for "natural" products.

[*] Priv.-Doz. Dr. S. Mecking[+]
Institut für Makromolekulare Chemie
und Freiburger Materialforschungszentrum
der Albert Ludwigs-Universität Freiburg
Stefan-Meier-Strasse 31, 79104 Freiburg (Germany)
Fax: (+49) 761-203-6319
E-mail: stefan.mecking@uni-konstanz.de

[+] New address: Universität Konstanz
Fachbereich Chemie
78457 Konstanz (Germany)

 © 2004 Wiley-VCH Verlag GmbH & Co. KGaA, Weinheim DOI: 10.1002/anie.200301655



Scheme 1. Simplified schematic materials cycle for biologically degradable materials based on renewable resources.



Figure 1. Symbol for the certification of biodegradability of plastics according to the German standard test method DIN V 54900.

In the following discussion the term of biodegradablility will be defined. Subsequently the synthesis and properties of biologically degradable materials based on naturally occurring polymers, polyesters from microbial synthesis, lactic acid as a monomer prepared from renewable resources, and petrochemical monomers will be presented. Finally, materials based on renewable resources and petrochemistry-based materials are compared with respect to their ecological potential.

Biological Degradability

Biologically degradable materials are currently receiving considerable attention. In this context, biodegradability and the preparation from renewable resources should be differentiated from one another. While it is true that naturally occurring polymers, such as cellulose or natural rubber, are also biodegradable, the degradability of a given chemical structure will be independent of whether it was generated from renewable resources or from fossil resources.

As a definition of the term biodegradability, a German standard test method exists since 1998, which is entitled "test of the compostability of plastics" (Figure 1).[3,4] In addition to an analysis of the chemical composition (e.g. of any heavy metals present) this standard test includes probing the complete degradability in laboratory experiments, probing the degradability under real-life conditions and the quality of the resulting compost, and probing the ecotoxicity of the compost for barley, rain worms, and daphnia. To be classified as biodegradable, in laboratory experiments more than 60 % of the organic carbon must be converted within a maximum of six months; moreover under real-life conditions of composting more than 90 % of the plastic is required to be degraded to fragments not more than 2 mm in size.

Besides naturally occurring polymers, the use of microbially or chemically prepared polyesters as biodegradable materials is currently the center of attention. Degradation occurs in two steps: An initial extracellular enzymatic or chemical hydrolysis results in low molecular weight fragments, in some cases this can proceed to the original monomers. These fragments can be resorbed by cells, and are ultimately mineralized to carbon dioxide and water. As erosion usually occurs much faster in the amorphous regions of the polymer than in the crystalline regions, crystallinity and crystallite sizes can have a strong impact on the degradation rate.[5] The predominance of structures with a high crystallinity amongst traditional polyesters and polyamides is certainly related to the corresponding desirable mechanical properties, which, for example, enable their use as molded parts and in fibers. In addition it can be speculated that the non-degradability and the resulting stability towards undesired environmental influences during the useful lifetime of the products contributed to establishing them in the early days of the polymer industry.

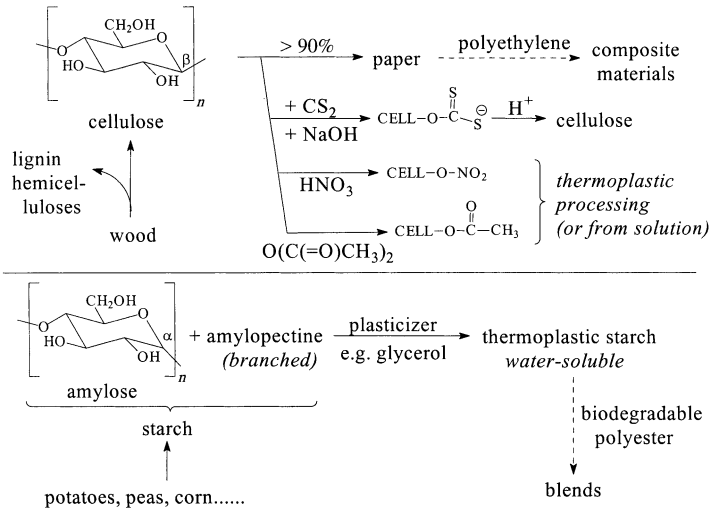


Dr. Stefan Mecking, born October 1966, studied chemistry at RWTH Aachen. In 1994 he received his Ph.D. degree there in the group of W. Keim. After a postdoctoral stay in the group of M. Brookhart as a Feodor-Lynen-Fellow, he joined the corporate research of Hoechst AG in Frankfurt in 1996 as a research chemist heading a laboratory in the polymers group. In 1998 he moved on to the Institut für Makromolekulare Chemie and Freiburger Materialforschungszentrum of the Albert Ludwigs-Universität Freiburg, where he habilitated in 2002. His research interests include catalytic polymerizations in aqueous systems, catalytically or biologically active colloidal polymer/nanoparticle hybrids, and the recycling of soluble catalysts. Mostly recently, he was awarded the BASF Catalysis Award 2003, a DECHEMA young lecturer prize, a Hermann-Schnell-Stipend, the Otto-Roelen-Medal, and a Chemiedozenten-Stipend by the Fonds der Chemischen Industrie.

Naturally Occurring Polymers

More than 10^{11} t of biomass is formed by photosynthesis annually, consisting for the most part of cellulose, starch, other polysaccharides, and lignin. Paper has been known for more than 2000 years. The current annual worldwide production of paper and cardboard amounts to 320×10^6 t, clearly exceeding that of petrochemical plastics (200×10^6 t).[6] However, the hydrophilicity and the resulting sensitivity of the mechanical properties towards water limits the utility as a material—a soaked paper bag is of little use. Moreover, unlike commodity plastics such as polyolefins, cellulose cannot be processed thermoplastically. Thus, celluose fibers (viscose) or sheets (cellophane) are manufactured from solution by decomposition of cellulose xanthogenate

 © 2004 Wiley-VCH Verlag GmbH & Co. KGaA, Weinheim



Scheme 2. Materials based on cellulose and starch.

(Scheme 2).[7,8] Derivatization can yield materials suited for thermoplastic processing, for example, cellulose acetate or celluloid (that is cellulose nitrate with camphor as a plasticizer).[8,9] However, this requires additional synthetic steps which today consume fossil resources, and the degradability of these derivatives is less than that of unmodified cellulose.

Pulp (which consists primarily of cellulose) for paper production or serving as a raw material for the chemical industry is made from wood by separating the hemicelluloses and lignin. The processes currently applied for pulp production consume significant amounts of energy and water, and pollutants such as sulfur compounds are released into the environment.[10] Accordingly, for example, paper bags offer no advantage over polyethylene bags with regard to the overall environmental impact from the raw materials to their disposal.[11]

Composite materials can combine the low cost of pulp with the water stability of polyethylene. In beverage containers, marketed under the tradename Tetrapak in Europe on a very large scale, a thin polyethylene film protects both sides of the cardboard container. Upon "recycling" after use, the pulp is dissolved and employed for other applications less demanding with regard to fiber quality, and the polyethylene is burnt to generate energy.[12]

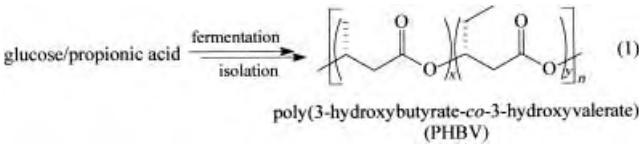
In contrast to cellulose, starch can be processed thermoplastically without the need for modification if it has a suitable water content. In addition to its water sensitivity, the overall mechanical properties of starch pose a strong limitation, however. Both issues can be improved upon by blending with thermoplastics, such as polyethylene or polyesters. Blends with biologically degradable polyesters are completely compostable. Such blends are produced by Novamont under the tradename Mater-Bi on a scale of 20000 t per year.[13]

Naturally occurring polymers perform versatile vital functions in living organisms, and they represent highly attractive materials. Employing naturally occurring polymers as materials is a beneficial "shortcut" (route a) in terms of Scheme 1. The necessity for their isolation from biomass and their limited processability impose significant limitations. Therefore other thermoplastic biodegradable materials, mostly polyesters—prepared microbially or chemically—have become the focus of attention in recent years.[14–16]

Microbially Synthesized Polyester

Poly(3-hydroxybutyrate) (PHB) is produced by various bacteria by fermentation of carbohydrates under controlled nutrition conditions. Similar to the function of starch or glycogen in other organisms, it serves as an energy-storage reservoir. It is located in the cytoplasm in the form of granules of approximately 0.5 μm size. Under suitable conditions, up to 90% polymer can be accumulated with respect to bacteria dry mass. Isolation of the PHB requires breaking of the cell walls by means of mechanical shear or by enzymatic digestion, followed by extraction of the polymer. This extraction can be performed by means of washing in centrifuges, or with organic solvents such as dichloromethane.[17]

As early as the 1960s, PHB was produced on a kilogram scale temporarily, motivated by potential commercial applications as a biodegradable plastic based on renewable resources.[18] During the oil crisis in 1973 interest in PHB reintensified, and poly(3-hydroxybutyrate-*co*-3-hydroxyvalerate) (PHBV) was successfully prepared by a fermentative route [Eq. (1)].[19] By comparison to (stereoregular) PHB,



which melts at 180 °C, the melting point of PHBV can be lowered to 137 °C by introduction of 25 mol% of hydroxyvaleriate units. This strongly improves thermoplastic processability. In addition, mechanical stability (impact strength) is improved by an order of magnitude. Overall properties are comparable to those of polypropylene. With the stabilization of oil prices, interest in commercial uses of PHBs decreased again for some time. However, in the late 1980s PHBV was commercialized by ICI under the tradename Biopol. In Germany a blowmolded shampoo bottle was marketed. An example of another potential application is commercial fishing nets, which upon loss sink to the bottom of the ocean where they degrade. In 1996 the Biopol technology was acquired by Monsanto, which investigated the direct synthesis of polyhydroxyalkanoates in transgenic plants intensively. The production was stopped by Monsanto in 1998.[20,17c] The company Biomer in Munich has been producing PHB with their own proprietary bacteria strains since 1994. Current annual production amounts to several tons per year, with prices around € 15 to 20 per kg. The material is applied for instance in fireworks rockets, which degrade in the environment.[21]

A direct synthesis of carbohydrates again represents a favorable "shortcut" (route b) in terms of Scheme 1. A

 © 2004 Wiley-VCH Verlag GmbH & Co. KGaA, Weinheim

disadvantage of the current syntheses of polyhydroxyalkanoates is the necessity to use glucose as a relatively costly substrate, which is converted to PHBV with limited yield (ca. 40%), as well as the effort required to isolate the polymer. Designed bacteria with a lower demand with regard to the substrate, or a direct production of polyhydroxyalkanoates in genetically modified plants could provide potential future alternatives.[22]

Poly(lactic acid)

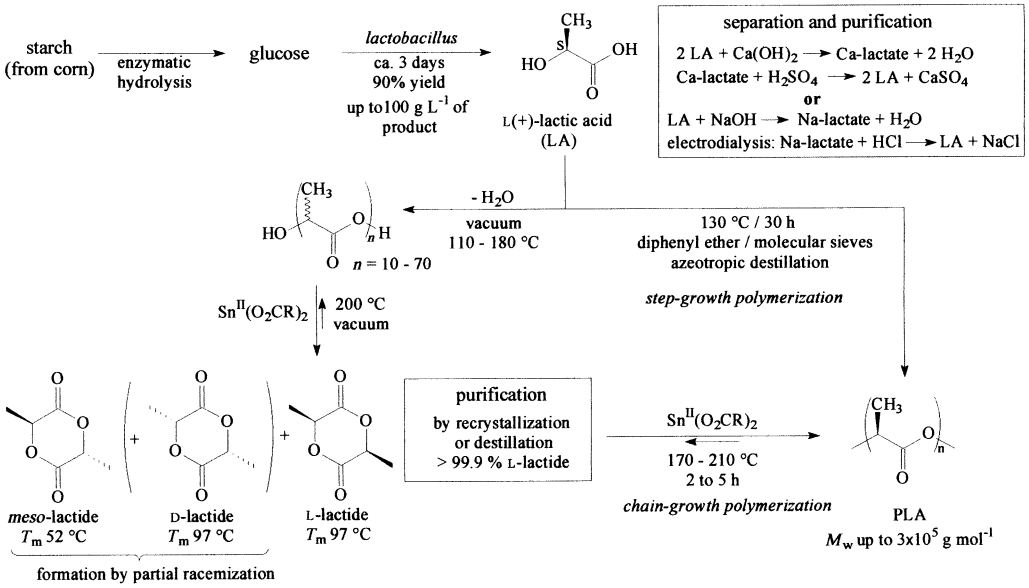
The synthesis of higher molecular weight poly(lactic acid) (PLA) was reported by Carothers et al. already in 1932.[23] Since the 1970s copolymers based on lactic acid and glycolic acid have been utilized for medical applications, for example, as a degradable matrix for the slow release of dugs.[24] A broader larger scale application as a biodegradable material has only become reality very recently.

The biotechnological production of lactic acid by fermentation of carbohydrates, which can provide either enantiomer in high purity, dominates over chemical routes. In conventional processes, lactic acid is isolated by precipitation of the calcium salt with $Ca(OH)_2$, followed by redissolution with H_2SO_4. For each kilogram of lactic acid produced, about one kilogram of gypsum is formed as a coproduct. Membrane-separation processes, such as electrodialysis, provide a more environmentally friendly alternative.[25]

The direct synthesis of PLA by polycondensation of lactic acid features the typical drawbacks of step-growth polymerizations:[26] owing to the correlation $DP_n = 1/(1-p)$ between the degree of polymerization (DP_n) and the conversion (p) high molecular weights are only achieved at very high conversions (>99% conversion for a degree of polymerization of 100), and monofunctional impurities such as ethanol or acetic acid from fermentation limit the molecular weights attainable.[27] Nonetheless, high molecular weight PLA (M_w 3×10^5 g mol^{-1}) can be obtained by employing highly pure lactic acid and removing the water formed azeotropically during the polycondensation. The presence of solvents such as diphenyl ether is disadvantageous by comparison to solvent-free processes. Mitsui has developed this process to an industrial scale.[28]

By contrast, CargillDow, which was founded in 1997 by Dow Chemical and the agricultural company Cargill, produces PLA by ring-opening polymerization of the dimeric lactide. The latter is prepared from lactic acid via linear oligomers as intermediates in the presence of Sn^{II}–carboxylates or –alkoxides (Scheme 3). Small impurities of, for example, the *meso*-lactide, formed by racemization during the oligomerization and cyclization, can be removed from the L-lactide by distillation or crystallization. This is of importance, as the polymer properties are strongly dependent upon the stereostructure. By continuous distillation 99.9% pure L-lactide can be produced on a large scale. As a chain-growth polymerization, ring-opening polymerization affords high molecular weight polymer rapidly. For this equilibrium reaction the suitable temperature range is limited, as on the one hand the polymerization rate should be reasonably high and on the other hand the position of the equilibrium is required to be largely in favor of polymer formation. Therefore, small residues of lactide usually remain in the polymer. Polymerization can be performed anionically, cationically, or by a coordination mechanism. Coordination polymerization in the presence of Sn^{II}–octanoate occurs rapidly and with a low degree of racemization.[29] Toxicologically, traces of Sn^{II}–octanoate are regarded as uncritical for most plastics applications. Industrially, the polymerization is carried out in the melt or as a solid-state reaction.

PLA is a transparent stiff thermoplast with a glass transition temperature (T_g) around 60 °C and a melt temperature (T_m) of 170 to 180 °C. Its high modulus compares to that of PET or cellophane. Controlled incorporation of *meso*-lactide can reduce the stereoregularity, yielding a softer



Scheme 3. Synthesis of poly(lactic acid) (PLA).

 © 2004 Wiley-VCH Verlag GmbH & Co. KGaA, Weinheim

material. Melt viscosity can be varied across a broad range, enabling processing by, for example, injection molding, melt spinning of fibers, film casting, and thermoforming. Amongst numerous potential applications stiff containers and fibers are pursued in particular (Figure 2). Clothing made from PLA is claimed to provide the same wearing comfort as PET or cotton at a better dimensional stability.[30,32]

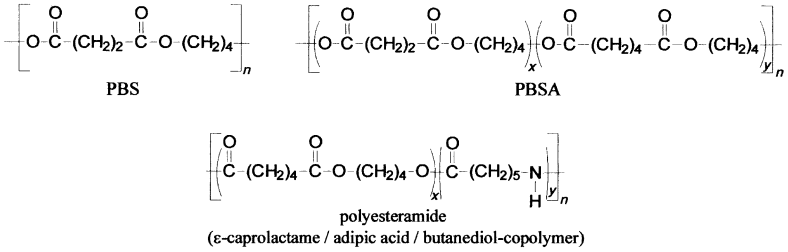




Figure 2. Examples for applications of poly(lactic acid). Left: food containers; right: pillow liners. Photographs: CargillDow.

In April 2002 CargillDow started operation of a PLA plant with a capacity of 140000 t per year in Blair, Nebraska (tradename "NatureWorks") with .[31] Starch isolated from corn serves as a raw material, which is hydrolyzed to glucose.[32] In Japan PLA is marketed by Mitsui under the tradename LACEA.[28,33]

Aliphatic Polyesters and Polyesteramides

Polyesters prepared from petroleum-based terephthalic acid and ethylene glycol (PET) or 1,4-butanediol (PBT) are commodity polymers used for a broad range of applications.[34] They are not biologically degradable. By contrast, aliphatic polyesters have been known since the 1960s to be biodegradable.[35]

Regarding the choice of dicarboxylic acids and diols (or lactones) suited for the synthesis of such entirely aliphatic polyesters, in addition to their availability the melting temperature of the polyesters which is required to be significantly above room temperature for most applications ($>$ ca. 80 °C), as well as the crystallization temperature impose restrictions. Poly(butylene succinate) (PBS) has a melting temperature of 114 °C and crystallizes at about 75 °C. Blown films have mechanical properties similar to the ubiquitous low density polyethylene (LDPE) films. Incorporation of adipic acid in poly(butylenesuccinate-*co*-butylene adipate) (PBSA) increases the degradation rate by lowering the crystallinity; however, the lower crystallization temperatures can be disadvantageous. PBS and PBSA are marketed by Showa Denko under the tradename Bionolle.

Polyamides such as Nylon-6 or Nylon-6,6 are produced on a large scale. Like PET these semicrystalline polyamides are biodegraded only extremely slowly. By contrast, aliphatic polyesteramides with a sufficient ester content and a random distribution of amide and ester moieties are biologically degradable. Copolymers of ε-caprolactam (ca. 60 wt %), adipic acid, and butanediol possess mechanical properties and a melting temperature similar to those of LDPE, and they are suited for film applications. Copolymers of hexamethylenediamine, adipic acid, butanediol, and diethylene glycol (amide content ca. 40 wt %) are more rigid, making them suited for injection molded parts such as flower pots and disposable cutlery as well as for fibers. Like PBS and PBSA, the synthesis of aliphatic polyesters is based on petrochemicals. The polymers are biodegradable, fulfilling the requirements of the aforementioned standard test method DIN V 54900.

Polyesteramides were sold commercially by Bayer from 1997 to 2001 under the tradename BAK.[36] A combination of the high costs associated with establishing any new plastic in the market with the disadvantages imposed on biodegradable polymers based on petroleum versus materials based on renewable resources by current legislation in Germany (vide infra) was given as a reason for abandoning this business.[37]

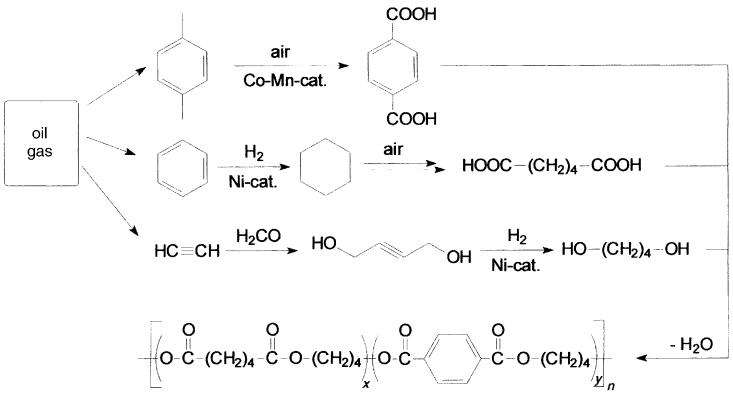
Aliphatic–Aromatic Polyesters

Various companies are currently marketing copolyesters of adipic acid and terephthalic acid with butanediol (BASF: trade name Ecoflex; DuPont: Biomax; Eastman Chemical: Eastar Bio).[38] By contrast to traditional terephthalic acid copolymers (PET and PBT) such aliphatic–aromatic copolyesters are biologically degradable, however the chain stiffness is increased compared to that of the entirely aliphatic polyesters discussed in the previous section.[39] The monomers are made petrochemically (Scheme 4).[40]

Ecoflex is a random copolymer containing approximately equal amounts of adipic acid and of terephthalic acid. The glass transition occurs at −30 °C, the melting temperature is 110–115 °C. The physical and mechanical properties of this soft thermoplastic are similar to those of LDPE, and it can be processed on conventional equipment for LDPE (Figure 3).

The material is marketed as a compostable packaging film, for agricultural films, as a hydrophobic protective coating for food containers made from foamed starch of from paper, and as a blend component (Figure 4).[41] Copolyesters with a higher terephthalic acid content have been reported to be suited for fiber applications.[38c] Ecoflex is currently produced by BASF in a pilot plant with an annual capacity of 8000 t. This aliphatic–aromatic polyester also fulfills the requirements of the standard test method DIN V 54900 for

 © 2004 Wiley-VCH Verlag GmbH & Co. KGaA, Weinheim



Scheme 4. Synthesis of aliphatic–aromatic polyesters from fossil resources.



Figure 3. Film blowing with an aliphatic–aromatic copolyester (Ecoflex). Photograph: BASF AG.



Figure 4. Examples of applications of aliphatic–aromatic copolyesters. a) Packaging film made from Ecoflex. b) Coated paper cup. c) Shopping bag suited for subsequent use as a compost bag made from Mater-Bi (a blend with starch). Photographs: BASF AG (a,b) and Novamont (c).

biological degradability. Complete hydrolysis to the monomers is observed, which are metabolized further to carbon dioxide and water.[42]

In 2002 Rieger et al. reported on the synthesis of the biodegradable poly(hydroxybutyrate) (PHB) by cobalt-catalyzed alternating copolymerization of carbon monoxide with propylene oxide.[43a] The currently attainable molecular weights of 5×10^4 g mol^{-1} [43b] are still limited, and by comparison to the other polymer syntheses reviewed, the reaction remains to be transferred to an industrial scale. Nonetheless this new reaction certainly represents an attractive alternative based on classical petrochemicals to the aforementioned microbial synthesis of PHB.

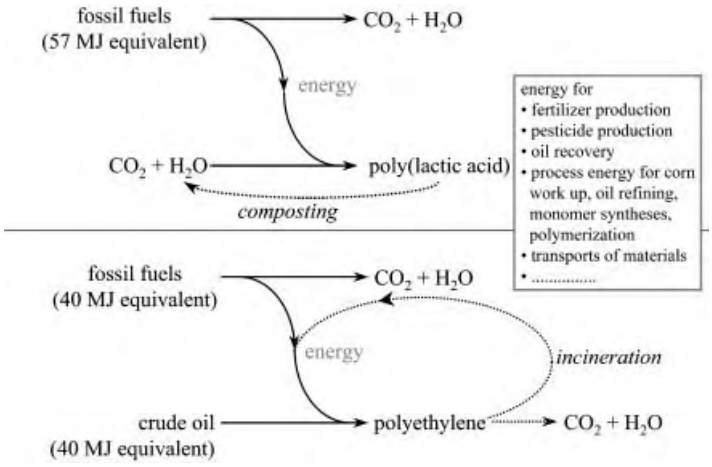
Nature or Petrochemistry?

Regarding the source of raw materials, biologically degradable polymers can be produced based on renewable resources, as well as on a petrochemical basis. For the commercial success the price is decisive primarily. While consumers may be willing to pay a slightly higher price for, for example, a biodegradable package, this willingness has its limits. Today an indefinite variety of consumer goods claims to be ecologically beneficial—whether justified or not—reducing willingness to pay an obvious premium in an individual case. Although the price of a polymer resin is always a snapshot due to variable raw materials cost, economy of production scale, and marketing strategy etc., the contemporary pricing is nonetheless instructive. Ecoflex, produced by BASF in a pilot plant with 8000 t annual capacity, is currently sold for € 3.10 per kg, placing it in the price range of engineering plastics.[44] PLA, produced by CargillDow on a large scale, is currently available for less than € 2.20 per kg.[45] For comparison, the price of PET has been fluctuating between € 1 and 1.50 per kg in the past few years, and polyethylene is priced at about € 0.80 per kg currently.[52] Thus, a biologically degradable polyester based on renewable resources is approaching prices of commodity plastics for the first time. As an example of the impact of legislation, in Germany lower mandatory costs for a disposal by means of biodegradable compostable waste (which is collected separately in many German cities) could represent an advantage for biodegradable materials over conventional plastics.[46] A field test in the city of Kassel, Germany, conducted from May 2001 to the end of 2002 probed the reliability of separation of biodegradable plastics from conventional plastics by consumers.[47] It is also worth mentioning that currently in Germany one is only allowed to dispose of biodegradable plastics by the compostable waste collection if these were produced from renewable resources—although the ecological merits of the latter are debatable as the following paragraph reveals.

The production of poly(lactic acid) as an example can be roughly considered as a complete closed cycle with regard to the raw materials (Scheme 1). However, this picture neglects the energy required for the production of fertilizers, pesticides, transport of raw materials and of intermediates, and

 © 2004 Wiley-VCH Verlag GmbH & Co. KGaA, Weinheim

process energy for polymer production, which is generated from fossil fuels primarily today. According to Cargill-Dow[32,48] production of 1 kg of PLA resin (Scheme 5; steps



Scheme 5. Current raw materials and CO_2 balance for poly(lactic acid) and polyethylene for disposal of poly(lactic acid) by composting and of polyethylene by incineration with energy generation.

from CO_2 to polymer in Scheme 1) currently consumes 57 MJ energy equivalents of fossil fuels. For comparison, production of 1 kg of PET or of 1 kg of LDPE requires 80 MJ energy equivalents.[49] The latter corresponds to 2 kg of crude oil, half of which is not burnt for energy generation but serves as a raw material for the polymer. The *higher* amount of CO_2 formed from fossil fuels during PLA synthesis than during PET or LDPE synthesis is approximately matched by the amount of CO_2 consumed during photosynthesis of the biomass used as a raw material.[48,49] The overall balance for PHB as an example of a polymer produced microbially is no better with the currently available technology.[50]

Considering the further life cycle of the polymer, composting as a frequently propagated solution is not necessarily the most useful scenario: incineration provides additional energy at a similar CO_2-balance, and even upon disposal in landfills at least no CO_2 is released (fermentation of organic waste to methane, which can be used as an energy sources, has a better energy balance by comparison to composting, however it is performed only sporadically today). The provocative suggestion to improve the global CO_2-balance by depositing materials based on renewable resources in landfills, where they will degrade very slowly despite their principle degradability, is worth mentioning.[51]

Biologically degradable materials based on renewable resources are certainly not per se as "green" as they might appear at first sight. Notwithstanding, they can certainly offer ecological advantages. However, the fuel source employed for energy generation is more decisive than the raw materials source for polymer synthesis. If the overall energy demand were satisfied for the largest part from non-fossil sources such as wind energy, solar power, or water power (or also nuclear power, which is however obviously subject to debate for other reasons), polymers based on renewable resources could possess a significantly better balance by comparison to petrochemical polymers. CargillDow has announced that it intends to use wind energy for PLA production in the future, and to improve the ecological and economical balance by using waste plant parts such as stems and leaves instead of corn. The contained cellulose and hemicelluloses will serve as a raw material, and the lignin will be incinerated for energy generation.[48]

Ultimately, society must balance such different factors as the emission of greenhouse gases, environmental pollution by pesticides and also by oil production, leakage of pollutants from compost or landfills, land consumption for farming, and the willingness to pay slightly higher prices against one another in a rational discussion. It should be noted that in some countries a complex system of regulations already provides a strict framework, for example, in the EU.

Independent of these considerations the biodegradable materials developed over the past decade enable new niche applications, which strictly require biodegradability. Examples previously outlined comprise compost bags or agricultural films. In addition, beyond the issue of degradability and the raw materials source, newly available polymers such as poly(lactic acid) and aliphatic–aromatic copolyesters are also attractive materials due to their property profile.

Received: April 9, 2003 [M1655]

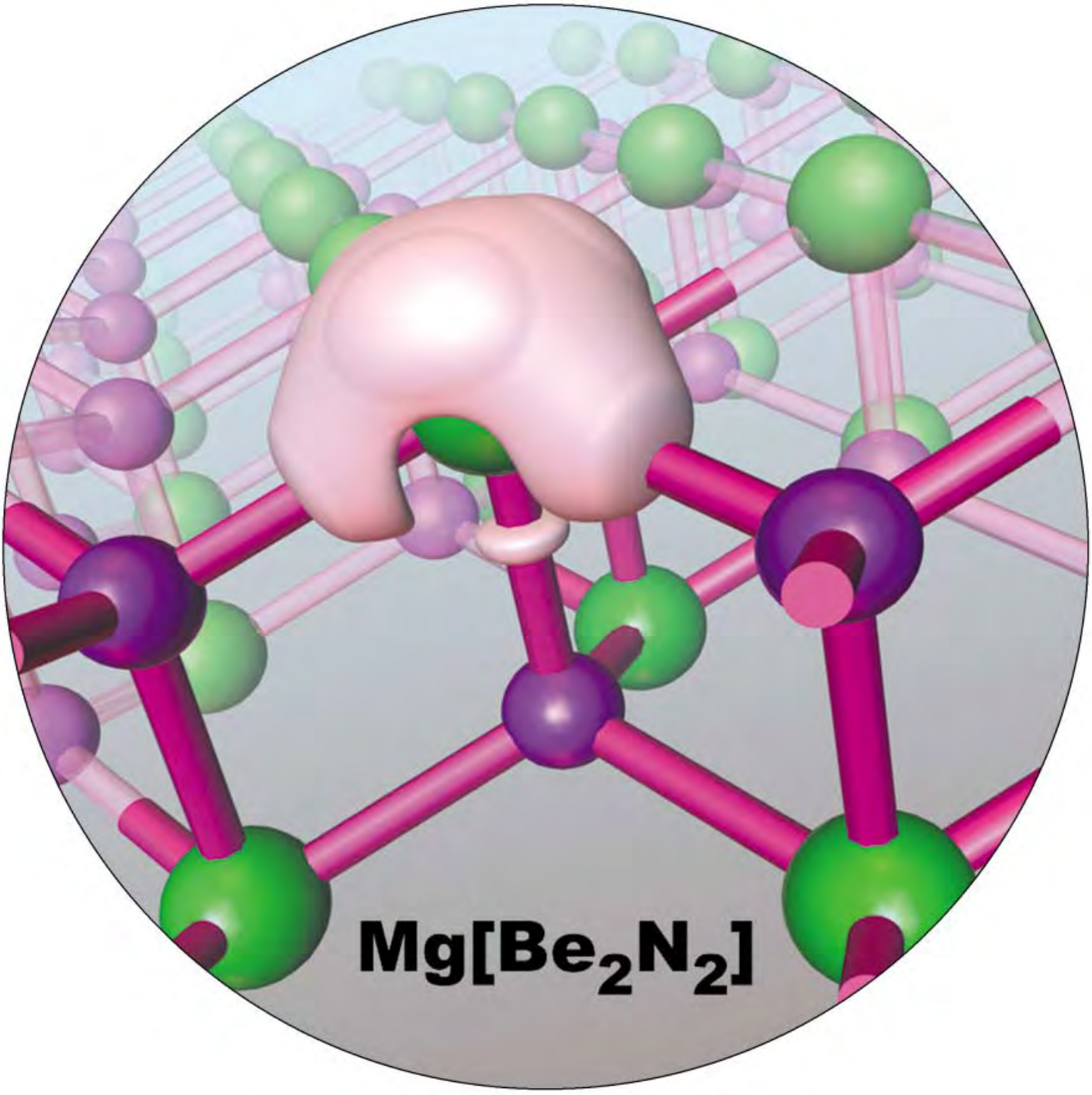
[1] International Energy Agency: *Energy Balances of OECD Countries 1999–2000*, **2002**.
[2] *BP Statistical Review of World Energy*, 51st ed., **2002**.
[3] DIN V 54900 "Prüfung der Kompostierbarkeit von Kunststoffen" (German standard test method "Probing the compostability of plastics").
[4] For a discussion of the term "biodegradable" exemplified by packaging films: a) H. Haschke, I. Tomka, A. Keilbach, *Monatsh. Chem.* **1998**, *129*, 253–279; overview of test methods: b) A. Calmon-Decriaud, V. Bellon-Maurel, F. Silvestre, *Adv. Polym. Sci.* **1998**, *135*, 207–226; educational experiments: c) J. Storrer, S. Rohrmann, *Biol. Unserer Zeit* **2001**, *31*, 116–122.
[5] a) Y. Doi, S. Kitamura, H. Abe, *Macromolecules* **1995**, *28*, 4822–4828; b) H. Abe, Y. Doi, H. Aoki, T. Akehata, *Macromolecules* **1998**, *31*, 1791–1797.
[6] Verband deutscher Papierfabriken e.V.: *Papier 2002 - Ein Leistungsbericht*, **2002**.
[7] H. Krässig, J. Schurz, R. G. Steadman, K. Schliefer, W. Albrecht in *Ullmann's Encyclopedia of Industrial Chemistry*, *Vol. A5* (Eds.: W. Gerhartz, B. Elvers), Wiley-VCH, Weinheim, **1992**, pp. 375–418.
[8] D. Klemm, B. Philipp, T. Heinze, U. Heinze, W. Wagenknecht, *Comprehensive Cellulose Chemistry* (two volumes), Wiley-VCH, **1998**.
[9] a) K. Balser, L. Hoppe, T. Eicher, M. Wandel, H.-J. Astheimer, *Ullmann's Encyclopedia of Industrial Chemistry*, *Vol. A5* (Eds.: W. Gerhartz, B. Elvers), Wiley-VCH, Weinheim, **1992**, pp. 419–459; b) L. Brandt, *Ullmann's Encyclopedia of Industrial Chemistry*, *Vol. A5* (Eds.: W. Gerhartz, B. Elvers), Wiley-VCH, Weinheim, **1992**, pp. 461–488.
[10] R. Patt, O. Kordsachia, R. Süttinger, Y. Ohtani, J. F. Hoesch, P. Ehrler, R. Eichinger, H. Holik, U. Hamm, M. E. Rohmann, P. Mummenhoff, E. Petermann, R. F. Miller, D. Frank, R. Wilken, H. L. Baumgarten, G.-H. Rentrop in *Ullmann's Encyclopedia of*

 © 2004 Wiley-VCH Verlag GmbH & Co. KGaA, Weinheim

Industrial Chemistry, *Vol. A18* (Eds.: W. Gerhartz, B. Elvers), Wiley-VCH, Weinheim, **1995**, pp. 545 – 691.
[11] Umweltbundesamt: Vergleich der Umweltauswirkungen von Polyethylen- und Papiertragetaschen, **1988** (German Federal Environmental Agency: comparison of the environmental impact of polyethylene and paper bags)
[12] Information brochure TetraPak GmbH.
[13] a) R. F. T. Stepto, I. Tomka, *Chimia* **1987**, *41*, 76 – 81; b) information provided by Novamont (cf. www.novamont.com).
[14] a) *Biopolymers from Renewable Resources* (Eds.: D. L. Kaplan), Springer, Berlin, **1998**; b) W. Tänzer, *Biologisch abbaubare Polymere*, Deutscher Verlag für Grundstoffindustrie/Wiley-VCH, Stuttgart, **2000**; c) Renewable resources in general: R. Mülhaupt, *Chimia* **1996**, *50*, 191 – 198.
[15] *Biopolymers* (Eds.: A. Steinbüchel, Y. Doi), Wiley-VCH, Weinheim, **2002**; a) "Polyesters I: Biological Systems and Biotechnological Production": *Biopolymers*, *Vol. 3a* (Eds.: A. Steinbüchel, Y. Doi), Wiley-VCH, Weinheim, **2002**; b) "Polyesters II: Properties and Chemical Synthesis": *Biopolymers*, *Vol. 3b* (Eds.: A. Steinbüchel, Y. Doi), Wiley-VCH, Weinheim, **2002**; c) "Polyesters III: Applications and Commercial Products": *Biopolymers*, *Vol. 4* (Eds.: A. Steinbüchel, Y. Doi), Wiley-VCH, Weinheim, **2002**.
[16] J. Schroeter, *Kunststoffe* **2000**, *90*, 64 – 70.
[17] a) Y. Doi, *Microbial Polyesters*, VCH, Weinheim, **1990**; b) P. J. Hocking, R. H. Marchessault in *Biopolymers from Renewable Resources* (Ed.: D. L. Kaplan), Springer, Berlin, **1998**, pp. 220 – 248; c) J. Asrar, K. J. Gruys in *Biopolymers*, *Vol. 4* (Eds.: A. Steinbüchel, Y. Doi), Wiley-VCH, Weinheim, **2002**, pp. 53 – 90.
[18] J. N. Baptist, F. X. Werber, *SPE Trans* **1964**, *4*, 245 – 250.
[19] P. P. King, *J. Chem. Technol. Biotechnol.* **1982**, *32*, 2 – 8.
[20] W. Tänzer, *Biologisch abbaubare Polymere*, Deutscher Verlag für Grundstoffindustrie/Wiley-VCH, Stuttgart, **2000**, p. 88.
[21] Information by Biomer (Munich; www.biomer.de).
[22] a) A. Steinbüchel, *Kautschuk*, *Gummi*, *Kunststoffe* **1996**, *49*, 120 – 124; b) Y. Poirier, *Curr. Opin. Biotechnol.* **1999**, *10*, 181 – 185; c) C. Jung, A. Steinbüchel, *Biol. Unserer Zeit* **2001**, *31*, 250 – 258.
[23] W. H. Carothers, G. L. Dorough, F. J. van Natta, *J. Am. Chem. Soc.* **1932**, *54*, 761 – 772.
[24] M. Vert in *Biopolymers*, *Vol. 4* (Eds.: A. Steinbüchel, Y. Doi), Wiley-VCH, Weinheim, **2002**, pp. 179 – 202.
[25] a) M. Hongo, Y. Nomura, M. Iwahara, *Appl. Environ. Microbiol.* **1986**, *52*, 314 – 319; b) C. J. Wang, R. K. Bajpai, E. L. Iannotti, *Appl. Biochem. Biotechnol.* **1991**, *28/29*, 589 – 603; c) N. Boniardi, R. Rota, G. Nano, B. Mazza, *J. Appl. Electrochem.* **1997**, *27*, 125 – 133; d) K. Hofvendahl, B. Hahn-Hägerdal, *Enzyme Microb. Technol.* **2000**, *26*, 87 – 107.
[26] a) W. H. Carothers, *Trans. Faraday Soc.* **1936**, *32*, 39 – 52; b) P. J. Flory, *Principles of Polymer Chemistry*, Cornell University Press, Ithaca, **1953**.
[27] M. H. Hartmann in *Biopolymers from Renewable Resources* (Ed.: D. L. Kaplan), Springer, Berlin, **1998**, pp. 367 – 411.
[28] N. Kawashima, S. Ogawa, S. Obuchi, M. Matsuo, T. Yagi in *Biopolymers*, *Vol. 4* (Eds.: A. Steinbüchel, Y. Doi), Wiley-VCH, Weinheim, **2002**, pp. 251 – 274.
[29] H. R. Kricheldorf, I. Kreiser-Saunders, C. Boettcher, *Polymer* **1995**, *36*, 1253 – 1259.
[30] *Chem. Eng. News* **2003**, *81*(13), 11.
[31] a) *Chem. Eng. News* **2002**, *80*(14), 13; b) S. K. Ritter, *Chem. Eng. News* **2002**, *80*(47), 19 – 23.
[32] P. Gruber, M. O'Brien in *Biopolymers*, *Vol. 4* (Eds.: A. Steinbüchel, Y. Doi), Wiley-VCH, Weinheim, **2002**, pp. 235 – 250. Also cf. www.cargilldow.com
[33] Mitsui has developed PLA independently and produced it in a pilot plant. According to an agreement signed in 2001 Mitsui is supplied by CargillDow with PLA for the Japanese market: press release by CargillDow of September 26, 2001.
[34] Worldwide capacity for PET production in 2001 was 8×10^6 t. Information provided by the Association of Plastics Manufacturers Europe.
[35] R. T. Darby, A. M. Kaplan, *Appl. Microbiol.* **1968**, *16*, 900 – 905.
[36] R. Timmermann in *Biopolymers*, *Vol. 4* (Eds.: A. Steinbüchel, Y. Doi), Wiley-VCH, Weinheim, **2002**, pp. 315 – 327.
[37] Press release by Bayer AG of February 9, 2001.
[38] a) BASF AG: product brochure Ecoflex (also cf. www.basf.de/ecoflex); b) DuPont: technical data sheet Biomax; c) Eastman Chemical: technical data sheet Eastar Bio.
[39] K. Kuwabara, Z. Gan, T. Nakamura, H. Abe, Y. Doi, *Biomacromolecules* **2002**, *3*, 390 – 396.
[40] a) R. J. Sheehan, *Ullmann's Encyclopedia of Industrial Chemistry*, *Vol. A26* (Eds.: W. Gerhartz, B. Elvers), Wiley-VCH, Weinheim, **1995**, pp. 193 – 203; b) D. D. Davis, *Ullmann's Encyclopedia of Industrial Chemistry*, *Vol. A1* (Eds.: W. Gerhartz, B. Elvers), Wiley-VCH, Weinheim, **1992**, pp. 269 – 278; c) H. Gräfje, W. Körnig, H.-M. Weitz, W. Reiß, G. Steffan, H. Diehl, H. Bosche, K. Schneider, H. Kieczka, *Ullmann's Encyclopedia of Industrial Chemistry*, *Vol. A4* (Eds.: W. Gerhartz, B. Elvers), Wiley-VCH, Weinheim, **1992**, pp. 455 – 462.
[41] a) D. Stärke, G. Skupin, *Kunststoffe* **2001**, *91*, 100 – 104; b) M. Yamamoto, U. Witt, G. Skupin, D. Beimborn, R.-J. Müller in *Biopolymers*, *Vol. 4* (Eds.: A. Steinbüchel, Y. Doi), Wiley-VCH, Weinheim, **2002**, pp. 299 – 311; c) see also: *Chem. Eng. News* **2002**, *80*(31), 13.
[42] a) U. Witt, M. Yamamoto, U. Seeliger, R.-J. Müller, V. Warzelhan, *Angew. Chem.* **1999**, *111*, 1540 – 1544; *Angew. Chem. Int. Ed.* **1999**, *38*, 1438 – 1442; b) U. Witt, T. Einig, M. Yamamoto, I. Kleeberg, W.-D. Deckwer, R.-J. Müller, *Chemosphere* **2001**, *44*, 289 – 299.
[43] a) M. Allmendinger, R. Eberhardt, G. Luinstra, B. Rieger, *J. Am. Chem. Soc.* **2002**, *124*, 5646 – 5647; b) B. Rieger, personal communication.
[44] Information provided by BASF AG (price for an order of 20 t).
[45] Information provided by CargillDow Europe (price for an order of 20 t).
[46] Disposal fees of conventional plastics in the German DSD disposal system € $1.50\,kg^{-1}$; upon composting about € $0.35\,kg^{-1}$.
[47] a) Information provided by the Interessengemeinschaft biologisch abbaubare Werkstoffe (association for the promotion of biologically degradable materials; see also: www.ibaw.org); b) information brochure on the model project on consumer recycling of biodegradable plastics in Kassel (see also: www.modellprojekt-kassel.de).
[48] E. T. H. Vink, K. R. Rabago, D. A. Glassner, P. R. Gruber, *Polym. Degrad. Stab.* **2003**, *80*, 403 – 419.
[49] Information for PET and LDPE by the Association of Plastics Manufacturers Europe (www.apme.org) based on detailed ecoprofiles. This data is recommended for example, by the German federal environmental agency.
[50] T. Gerngross, *Nat. Biotechnol.* **1999**, *17*, 541 – 544.
[51] T. U. Gerngross, S. C. Slater, *Sci. Am.* **2000**, 20. August, 36 – 41; *Spektrum der Wissenschaft* **2000**, December, 58 – 63.
[52] Price information provided by Kunstoff Information.

 © 2004 Wiley-VCH Verlag GmbH & Co. KGaA, Weinheim

Communications



The nitridoberyllates of the heavier alkaline-earth metals contain anion layers with covalent Be—N bonds. $Mg[Be_2N_2]$ occupies a special position among this class of compounds, since, unlike the Ca, Sr, and Ba compounds, it contains puckered [BeN] layers. For more information on these structures see the Communication by R. Kniep et al. on the following pages.

DOI: 10.1002/anie.200352796
© 2004 Wiley-VCH Verlag GmbH & Co. KGaA, Weinheim

Layered Compounds

$Ae[Be_2N_2]$: Nitridoberyllates of the Heavier Alkaline-Earth Metals**

*Mehmet Somer, Alper Yarasik, Lev Akselrud, Stefano Leoni, Helge Rosner, Walter Schnelle, and Rüdiger Kniep**

Dedicated to Professor Bernt Krebs on the occasion of his 65th birthday

The first and only known nitridoberyllate up to now, Li[BeN],[1] was reported in 1996. The crystal structure contains puckered 4.8^2 nets in which Be and N alternate. Neighboring $^2_\infty[(Be_{3/3}N_{3/3})^-]$ nets are connected through Li cations, which are tetrahedrally coordinated by nitrogen. Attempts to replace Li by the heavier and larger alkali metals Na or K, have not been successful. However, success could be achieved with the heavier homologues of beryllium. Compounds of the composition $Ae[Be_2N_2]$ (Ae = Mg, Ca, Sr, Ba) were synthesized as microcrystalline powders.[2] On the basis of the chemical formula alone, the compounds could be expected to crystallize as a substitutional variant of the polymorphic modifications of beryllium nitride: Be_3N_2 exists in a cubic low-temperature modification[3,4] with the α-Mn_2O_3-type structure and beryllium tetrahedrally coordinated by nitrogen, as well as in a hexagonal high-temperature modification[5,6] in which beryllium is coordinated in a tetrahedral and trigonal-planar fashion by nitrogen. Another likely structure could be the (anti-)La_2O_3-type structure,[7] which is often found in ternary phases. The mixed alkaline-earth metal nitride $CaMg_2N_2$[8] and the ternary nitrides Li_2ZrN_2[9] and Li_2CeN_2[10] also crystallize in this latter type.

The crystal structures[11] of the novel compounds $Ae[Be_2N_2]$ contain complex anion layers with covalent bonds between beryllium and nitrogen and are therefore characterized as nitridoberyllates. $Mg[Be_2N_2]$ crystallizes in the above-mentioned La_2O_3-type structure,[7] whereas the Ca, Sr, and Ba compounds are isostructural to the boride–carbide $Ca[B_2C_2]$.[12] The latter contains planar 4.8^2 layers of alternating boron and carbon atoms. The anionic partial structure $[B_2C_2^{2-}]$ is isoelectronic with $[Be_2N_2^{2-}]$ (16 e^- systems).

$Mg[Be_2N_2]$ contains puckered Be–N six-membered rings in chair conformation, which are condensed to single layers parallel (001) and which are pairwise connected to form double layers along [001] (Figure 1). The stacking of the puckered double nets is such that Be and N alternate, as they do within a single net. Nitrogen occupies the positions at the outer boundaries of the double layers. Beryllium and nitrogen are surrounded by four nitrogen and four beryllium atoms, respectively, with distances d(Be–N) = 178.4(4) pm (3×) and 176.0(1) pm. Beryllium is tetrahedrally coordinated by nitrogen, while nitrogen occupies the apex of a trigonal pyramid whose base is made of three Be positions (Be′). The fourth Be position (Be″) belongs to the adjacent net of the double layer and is placed therefore below the base of the trigonal pyramid. The resulting nitrogen coordination can be described as an inverse tetrahedron. The angle Be′-N-Be″ is 73.1(4)°, and the angle Be′-N-Be′ is 111.9(3)° and thus close to the value for a tetrahedral arrangement. Magnesium is placed between the complex double-layer anions $^2_\infty[(Be_2N_2)^{2-}]$ and is octahedrally surrounded by nitrogen (d(Mg–N) = 220.9(2) pm).

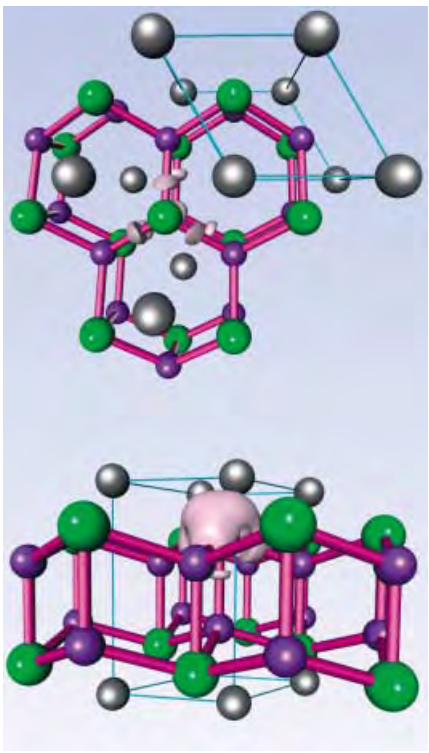


Figure 1. Crystal structure of $Mg[Be_2N_2]$. Mg: gray; Be: purple; N: green. Top: View along [001]. The electron localization function (ELF) (η = 0.84) shows localization domains between Be and N in the puckered 6^3 nets. Bottom: Skew view along [110]. The ELF (η = 0.80) shows a localization domain as a large maximum around N as well as a smaller axial localization domain.

$Ca[Be_2N_2]$ and $Sr[Be_2N_2]$ are isotypic. Analogously to Li[BeN],[1] the crystal structure contains 4.8^2 nets $^2_\infty[(Be_{3/3}N_{3/3})^{2-}]$ that are stacked along [001]. Unlike Li[BeN], the nets are not puckered but strictly planar. The (···AB···) stacking of the planar nets, which are slightly rotated with respect to each other, causes Be and N to alternate also along [001] (Figure 2). The octagonal prismatic voids between the

[*] Dr. S. Leoni, Dr. H. Rosner, Dr. W. Schnelle, Prof. Dr. R. Kniep
Max-Planck-Institut für Chemische Physik fester Stoffe
Nöthnitzer Strasse 40, 01187 Dresden (Germany)
Fax: (+49) 351-4646-3002
E-mail: Kniep@cpfs.mpg.de
Prof. Dr. M. Somer, A. Yarasik
Koç University, Istanbul (Turkey)
Dr. L. Akselrud
University Lviv (Ukraine)

[**] Ae = Mg, Ca, Sr, Ba. We gratefully aknowlegde Dr. Wilder Carrillo-Cabrera for his support with the analysis of the X-ray powder data, and Prof. Dr. Matthias Driess for stimulating discussions.

 © 2004 Wiley-VCH Verlag GmbH & Co. KGaA, Weinheim DOI: 10.1002/anie.200352796

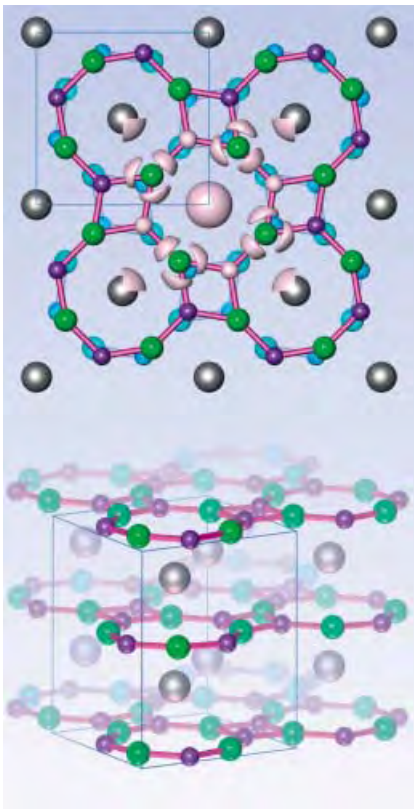


Figure 2. Crystal structure of $Ca[Be_2N_2]$. Ca: gray; Be: purple; N: green. Top: View along [001]. ELF localization domains ($\eta = 0.81$) show up in the planar 4.8^2 net between Be and N. See text for details. The next lower lying layer is displayed in slightly different colors while preserving the atom sizes. Bottom: stacking of the layers along [001] and cations in between in the centers of the octagonal prisms.

nitridoberyllate layers are centered by charge-balancing Ca^{2+} or Sr^{2+} ions. The Be–N distances within the layers, of 163.2(6) pm ($2\times$) and 165.7(6) pm for the Ca compound, 163.0(2) pm ($2\times$) and 167.0(2) pm for the Sr compound, are clearly shorter than the ones in $Mg[Be_2N_2]$.

Planar 4.8^2 nets are also present in the anionic partial structure of the isotypic boride-carbide $Ca[B_2C_2]$.[12] Here also the stacking sequence of the layers causes the nonmetal atoms in neighboring layers to alternate. The structurally closely related compound $Ce[B_2C_2]$[13] shows the same stacking sequence, whereby the arrangement of the two kinds of atoms in neighboring anionic layers is congruent: boron is placed over boron, and carbon over carbon. The same congruent motif is also adopted by the lithium–nitrogen anionic partial structure in $Ca\{Li_2[Mn^{I}N]_2\}$.[14] Here the 4.8^2 nets are additionally connected to each other by (N-Mn^{I}-N) groups, such that the Ca^{2+} ions abandon the octagonal prismatic voids to occupy the centers of the net octagons. The succession of Be and N along [001] in the crystal structure of $Ca[Be_2N_2]$ was checked with a full-potential calculation[15] with the FPLO method (full potential minimum basis local orbital scheme).[16] For this two ordering schemes (congruent and alternating sequence of the atom sorts along [001]) were defined in space group *P*4/*mbm*. The alternation of Be and N within the layers was preserved. With an energy gain of 0.6 eV per Be–N bond the alternating sequence along [001] is clearly favored and confirms thereby the experimental finding. Unlike the significantly high gain in energy for the Be–N bond, the gain for the C–B bond in the isotypic compound $Ca[B_2C_2]$[12] is more than one order of magnitude smaller. The still controversial discussion on the layer stacking in the boride–carbide compound can therefore be only partially clarified with ab initio calculations.[17]

The magnetic susceptibilities $\chi(T) = M(T)/H$ of samples of the $Ae[Be_2N_2]$ compounds consist of a constant and a field- and temperature-dependent contribution. The latter can be explained by minor paramagentic and ferromagnetic impurities. The corrected values for the susceptbility $\chi_{corr}(300\ K)$ amount to -28.5 ($Mg[Be_2N_2]$), -35.3 ($Ca[Be_2N_2]$), and -60.3×10^{-6} emu mol^{-1} ($Ba[Be_2N_2]$). Using the diamagnetic increments χ_{dia}[18] for the alkaline-earth ions Ae^{2+} a value of $\chi_A(300\ K) = (-27\pm2)\times10^{-6}$ emu mol^{-1} can be calculated for the $[Be_2N_2]$ anion. The nitridoberyllates are therefore diamagnetic. In agreement with the electronic density of state no Pauli paramagnetism was detected. Phase transitions were also not observed.

The bonding situation in the compounds $Mg[Be_2N_2]$, $Ca[Be_2N_2]$, and $Sr[Be_2N_2]$ was analyzed by means of electron localization function (ELF) calculations.[19–21] For $Mg[Be_2N_2]$ the ELF ($\eta = 0.80$) shows a large valence basin around nitrogen and a smaller basin between Be and N along the geometric line parallel to the *c* axis (Figure 1 and 3). At $\eta =$

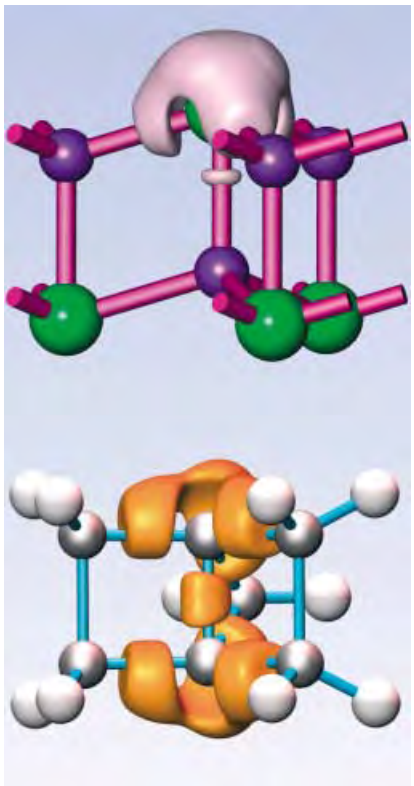


Figure 3. Comparison of ELF topologies. Top: Around nitrogen in $Mg[Be_2N_2]$ ($\eta = 0.80$). Bottom: At a bridgehead carbon atom in [2.2.1]propellane ($\eta = 0.73$). The ELF characteristics of such an inverse geometry consist of a large basin, which decays into three localization domains as well as a smaller axial basin. See text for details.

 © 2004 Wiley-VCH Verlag GmbH & Co. KGaA, Weinheim

0.84 the valence basin around nitrogen decays into three equivalent localization domains between Be and N, corresponding to the bonds of the puckered 6^3 nets, while the small axial basin has disappeared (Figure 1). Upon integration of the electronic density in the ELF basins[22] a value of 2.4 electrons per Be–N bond in the 6^3 nets is found. The smaller basin contains 0.8 electrons. The bonding situation of nitrogen is thus the one of an inverse tetrahedron and is reminiscent of the bridgehead carbon atoms in propellanes.[23] ELF calculations of different propellanes with varying ring sizes ([*l.m.n*]propellanes; $l,m,n = 1,2$) show in each case a small basin between the bridgehead carbon atoms, and a large valence basin that decays into three localization domains.[24] This situation is illustrated in Figure 3 for the example of the bridgehead carbon atoms in [2.2.1]propellane. For the whole $[Be_2N_2]$ net in the crystal structure of $Mg[Be_2N_2]$ the integration over all bonding basins amounts to 1.93 electrons, which is in agreement with the description of the compound as a nitridoberyllate.

The ELFs of the isotypic compounds $Ca[Be_2N_2]$ and $Sr[Be_2N_2]$ are topologically identical. For reasons of symmetry, within the planar 4.8^2 nets there are two different bonds. Accordingly, for $\eta = 0.82$ the ELF shows two different localization domains (Figure 2). The eccentric position of one of the domains with respect to the geometric line between Be and N reflects the local strain caused by the four-membered ring. The bond that belongs to the eight-membered ring only is represented by a localization domain, which is found on the geometric bonding line. Both bonds correspond to 2.7 and 2.5 electrons, respectively (by integration of the electronic density in the ELF basins[22]). For the whole $[Be_2N_2]$ net an excess of 1.65 electrons (Ca compound) and 1.6 electrons (Sr compound), respectively, is found. This value, which clearly deviates from two electrons, together with the structuring of the Ca- and Sr-core basins at higher ELF values,[25] is indicative of a participation of Ca and Sr d orbitals in the covalent chemical bonding. Accordingly, a Bader analysis[26] of the electronic density yields values of $Ca^{1.4+}$ and $Sr^{1.4+}$.

Figure 4 shows the electronic structures (band structures and DOS)[20] of $Mg[Be_2N_2]$ and $Ca[Be_2N_2]$ ($Sr[Be_2N_2]$). For $Mg[Be_2N_2]$ the region from −7 eV up to the Fermi level is dominated by nitrogen states. The quasi-two-dimensional character of the (Be–N)-2p-σ bands is reflected in a small dispersion orthogonal to the hexagonal plane, and generates a large density of states below the Fermi level. No band crosses the Fermi level. At the Γ point a large band gap of about 4.5 eV is opened. This gap is caused by the heteropolar Be–N bonds within the Be–N layers (in analogy to the band gap in Li[BC] with covalent bonds in the anionic partial structure).[27] The bands above 4.5 eV are mainly characterized by Mg states. The DOS shows the large contribution of N p states close to the Fermi level. For $Ca[Be_2N_2]$ ($Sr[Be_2N_2]$) the region from −5.0 eV up to the Fermi level is also dominated by N states. Like in $Mg[Be_2N_2]$, the quasi-two-dimensional character of some bands brings a considerable density of states just below the Fermi level, which is again not crossed by any band. At the Γ point a direct band gap of approximately 1.8 eV (1.4 eV) is opened. The bands above 1.8 eV (1.4 eV) show Ca and Sr character, respectively.

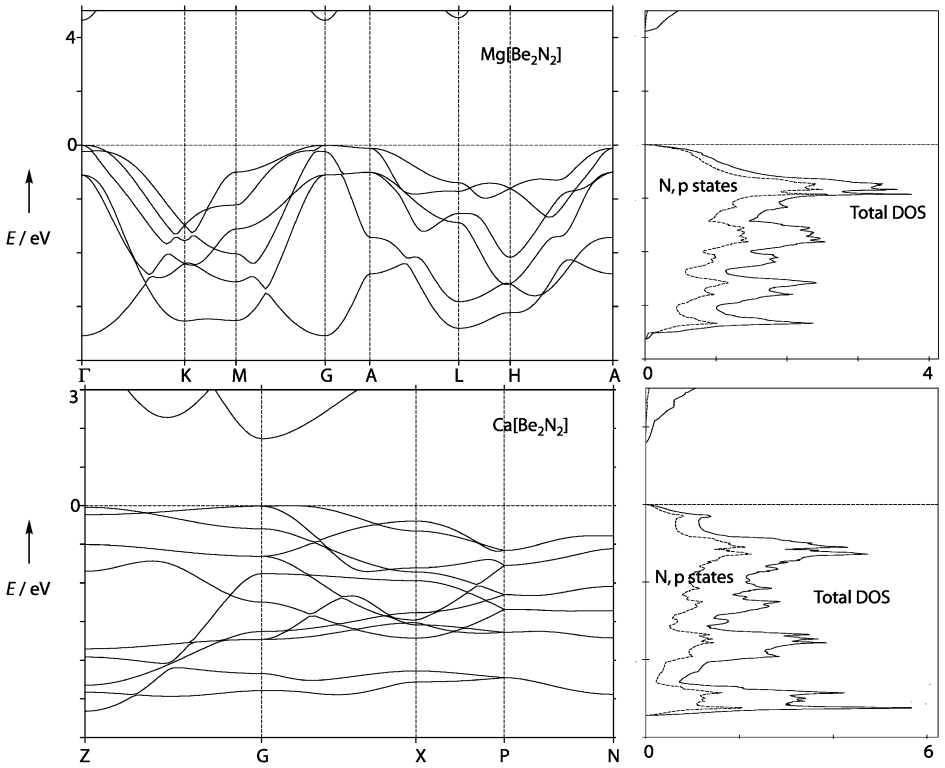


Figure 4. Electronic band structures along selected directions of the Brillouin zone (left) and DOS (right) of $Mg[Be_2N_2]$ (top) and $Ca[Be_2N_2]$ (bottom). See text for details.

 © 2004 Wiley-VCH Verlag GmbH & Co. KGaA, Weinheim

Form a crystal-chemical point of view the nitridoberyllates can be assigned to a large class of compounds, which comprises complex anionic partial structures of lighter nonmetallic elements, like borides and boride–carbides with eight valence electrons per pair of atoms ($[B_2^{2-}]$, $[BC^-]$). The nitridoberyllates extend this concept by the inclusion of a light metallic element (Be) in combination with nitrogen and by the formation of complex anionic partial structures of general formula $[BeN^-]$. A large number of such compounds with alkali or alkaline-earth metals contain planar anionic units like $Mg[B_2]$,[28,29] $Mg[B_2C_2]$,[30] or $Li[BC]$[27] with 6^3 nets; planar 4.8^2 nets are present for example in $Ca[B_2C_2]$[12] and in the nitridoberyllates of calcium and strontium presented in this work. Puckered 4.8^2 nets are present in the crystal structure of Li[BeN].[1] Having puckered nets connected into double layers and a peculiar nitrogen bonding situation, $Mg[Be_2N_2]$ occupies a special position in this class of compounds. It is expected that interesting physical properties will appear after appropriate chemical modifications.

Received: September 4, 2003 [Z52796]
Published Online: February 2, 2004

Keywords: ab initio calculations · electron localization function · layered compounds · nitridoberyllates · propellanes

[1] M. Somer, W. Carrillo-Cabrera, E.-M. Peters, K. Peters, H. G. von Schnering, *Z. Kristallogr.* **1996**, *211*, 635.

[2] Synthesis: The compounds $Ae[Be_2N_2]$ (Ae = Mg, Ca, Sr, Ba) were synthesized from mixtures of the binary nitrides Be_3N_2 (obtained from Be powder and ammonia at 1373 K[2a]) and Ae_3N_2 (Ae = Mg, Ca) or Ae_2N (Ae = Sr, Ba) in molar ratios of 2:1 and 3:4, respectively, in closed Nb ampoules at 1473 and 1373 K (Ba). The small nitrogen deficiency ($AeBe_2N_{1.84}$) arising from Sr_2N as a starting material does not affect the synthesis of the Sr compound, probably due to the easy formation of diazenides.[2b] On the contrary, the synthesis with Ba_2N in closed ampoules produces a multiphasic product. For the preparation of $Ba[Be_2N_2]$ it is thus necessary to pre-process the starting materials (pellets, Ta crucible) under N_2 flow (1273 K, 24 h). The resulting microcrystalline product, which is uniformly yellow-green, is held at 1323 K for 36 h in closed Nb ampoules for the reaction to complete. The alkaline-earth nitridoberyllates are obtained as microcrystalline powders, which are air- and moisture-sensitive. $Mg[Be_2N_2]$ is transparent, while the Ca and Sr compounds are transparent to bright-yellow. $Ba[Be_2N_2]$ is yellow-green. a) G. Brauer, *Handbuch der Präparativen Anorganischen Chemie*, Ferdinand Enke, Stuttgart, **1954**, p. 678; b) Yu. Prots, G. Auffermann, M. Tovar, R. Kniep, *Angew. Chem.* **2002**, *114*, 2392; *Angew. Chem. Int. Ed.* **2002**, *41*, 2288.

[3] M. von Stackelberg, R. Paulus, *Z. Phys. Chem. Abt. B* **1933**, *22*, 305.

[4] O. Reckeweg, C. Lind, A. Simon, F. J. DiSalvo, *Z. Naturforsch. B* **2003**, *58*, 159.

[5] P. Eckerlin, A. Rabenau, *Z. Anorg. Allg. Chem.* **1960**, *304*, 218.

[6] D. Hall, G. E. Gurr, G. A. Jeffrey, *Z. Anorg. Allg. Chem.* **1969**, *369*, 108.

[7] P. Aldebert, J. P. Traverse, *Mater. Res. Bull.* **1979**, *14*, 303.

[8] V. Schultz-Coulon, W. Schnick, *Z. Naturforsch. B* **1995**, *50*, 619.

[9] R. Juza, A.-P. Palisaar, *Z. Anorg. Allg. Chem.* **1971**, *384*, 1.

[10] D. Halot, J. Flahout, *C. R. Seances Acad. Sci. Ser. C* **1971**, *272*, 465.

[11] X-ray powder diffraction diagrams of the nitridoberyllates were measured on a Huber 644 diffractometer with $Cu_{K\alpha1}$ radiation (Ge monochromator, NaI(Tl) scintillation counter). Data analyses and subsequent Rietveld refinements were performed with the programs WinXPOW[11a] and WinCSD.[11b] Weak reflections belonging to other phases were identified in the powder diagrams of $Mg[Be_2N_2]$ (α-Be_3N_2) and $Sr[Be_2N_2]$ (α-Be_3N_2 plus another unknown phase) and were subtracted from the patterns before Rietveld refinements. $Mg[Be_2N_2]$ at 298 K: hexagonal, space group $P\bar{3}m1$, $a = 295.53(2)$ pm, $c = 508.80(5)$ pm; $V = 38.48 \times 10^6$ pm^3, $Z = 1$; Mg on (1*b*); Be on (2*d*) $z = 0.622(2)$; N on (2*d*) $z = 0.2759(13)$, $R_{prof} = 0.0433$, $R_{int} = 0.0274$; measurement range $10° < 2\Theta < 100°$: measured reflections: 18. $Ca[Be_2N_2]$ at 298 K: tetragonal, space group *I*4/*mcm*, $a = 556.15(2)$ pm, $c = 687.96(3)$ pm; $V = 212.79 \times 10^6$ pm^3, $Z = 4$; Ca on (4*a*); Be on (8*h*) $x = 0.3794(9)$; N on (8*h*) $x = 0.8312(5)$; $R_{prof} = 0.0924$, $R_{int} = 0.0684$; measurement range $10° < 2\Theta < 90°$: measured reflections: 30. $Sr[Be_2N_2]$ at 298 K: tetragonal, space group *I*4/*mcm*, $a = 562.13(1)$ pm, $c = 755.12(2)$ pm; $V = 238.61 \times 10^6$ pm^3, $Z = 4$; Sr on (4*a*); Be on (8*h*) $x = 0.372(3)$; N on (8*h*) $x = 0.833(2)$; $R_{prof} = 0.0778$, $R_{int} = 0.0697$; measurement range $10° < 2\Theta < 100°$: measured reflections: 35. $Ba[Be_2N_2]$ at 298 K: tetragonal, space group: *I*4/*mcm*, $a = 5.66.46(5)$ pm, $c = 839.42(9)$ pm. Further details on the crystal structure investigation may be obtained from the Fachinformationszentrum Karlsruhe, 76344 Eggenstein-Leopoldshafen, Germany (fax: (+49) 7247-808-666; e-mail: crysdata@fiz-karlsruhe.de), on quoting the depository numbers CSD-413356, CSD-413357, and CSD-413358). a) STOE WinXPOW, *Version 1.2, STOE & Cie GmbH*, Darmstadt; b) L. G. Akselrud, P. Yu. Zavalii, Yu. N. Grin, V. K. Pecharski, B. Baumgartner, E. Wölfel, *Mater. Sci. Forum* **1993**, *335*, 133–136.

[12] B. Albert, K. Schmitt, *Inorg. Chem.* **1999**, *38*, 6159.

[13] J. Van Dujin, K. Suzuki, J. P. Attfield, *Angew. Chem.* **2000**, *112*, 373; *Angew. Chem. Int. Ed.* **2000**, *39*, 365.

[14] J. Klatyk, R. Niewa, R. Kniep, *Z. Naturforsch. B* **2000**, *55*, 988.

[15] A full potential method is necessary for a meaningful energetic comparison of different structures. In the scalar relativistic calculations we used the exchange and correlation potential of Perdew and Wang.[15a] Ca(3s, 3p, 4s, 4p, 4d), Be and N (2s, 2p, 3d) states were chosen as the basis sets. Lower lying states were treated as core states. The 3d states of Ca, Be, and N were taken into account to increase the completeness of the basis set. The inclusion of the Ca 3s and 3p states in the valence states was necessary to account for non-negligible core–core overlaps. The spatial extension of the basis orbitals, controlled by a confining potential,[15b] was optimized to minimize the total energy. A *k*-mesh of 196 points in the irreducible part of the Brillouin zone was used. Convergency with respect to *k*-points and basis sets were carefully checked. a) J. P. Perdew, Y. Wang, *Phys. Rev. B* **1992**, *45*, 13244; b) H. Eschrig, *Optimized LCAO Method and the Electronic Structure of Extended Systems*, Springer, Berlin, **1989**.

[16] K. Koepernik, H. Eschrig, *Phys. Rev. B* **1999**, *59*, 1743.

[17] J. Akimitsu, K. Takenawa, K. Suzuki, H. Harima, Y. Kuramoto, *Science* **2001**, *293*, 1125–1127.

[18] P. W. Selwood, *Magnetochemistry*, 2nd ed., Interscience, New York, **1956**.

[19] A. D. Becke, K. E. Edgecombe, *J. Chem. Phys.* **1990**, *92*, 5397–5403; A. Savin, O. Jepsen, J. Flad, O. K. Andersen, H. Preuss, H. G. von Schnering, *Angew. Chem.* **1992**, *104*, 186–188; *Angew. Chem. Int. Ed. Engl.* **1992**, *31*, 187–188.

[20] O. Jepsen, O. K. Andersen, The Stuttgart TB-LMTO-ASA Program, Version 4.7, Max-Planck-Institut für Festkörperforschung, Stuttgart, **2000**.

[21] The one-electron scalar relativistic Schrödinger equation was solved self-consistently within the LMTO–ASA scheme. Inter-

 © 2004 Wiley-VCH Verlag GmbH & Co. KGaA, Weinheim

stitial empty spheres had to be added to correct for large sphere overlaps and to fill the interstitial space. The basis set consisted of 3s, 3p and 3d (downfolded) for Mg, 4s, 4p and 3d for Ca, 5s, 5p (downfolded), 4d, 4f (downfolded) for Sr, 2s, 2p (downfolded), 3d (downfolded) for Be, 2s, 2p and 3d (downfolded) for N. Radii of the atoms and of the interstitial spheres (in Å): $Mg(BeN)_2$: $r(Mg) = 1.544$, $r(Be) = 1.024$, $r(N) = 1.016$, $r(E) = 1.080$; $Ca(BeN)_2$: $r(Ca) = 1.970$, $r(Be) = 0.925$, $r(N) = 0.943$, $r(E) = 1.215$; $Sr(BeN)_2$: $r(Sr) = 2.143$, $r(Be) = 0.926$, $r(N) = 0.941$, $r(E) = 1.046$.

[22] M. Kohout, Program Basin, Version 2.4, Max-Planck-Institut für Chemische Physik fester Stoffe, Dresden, **2003**.

[23] K. B. Wiberg, *Chem. Rev.* **1989**, *89*, 975 – 983.

[24] The geometry of [1.1.1]-, [2.1.1]-, [2.2.1]-, and [2.2.2]propellanes was optimized in internal coordinates (z-matrix) with the 6-311G basis set at the HF level (program GAUSSIAN98).[24a] The ELF was calculated from the resulting electron density with the program dgrid.[24b] The η value, at which the small basin becomes visible, depends on the size of the rings. As soon as the bridgehead carbon atoms have reached tetrahedral geometry (as in [3.3.3]propellane), the ELF shows four localization domains around C. a) Gaussian 98 (Revision A.7), M. J. Frisch, G. W. Trucks, H. B. Schlegel, G. E. Scuseria, M. A. Robb, J. R. Cheeseman, V. G. Zakrzewski, J. A. Montgomery, R. E. Stratmann, J. C. Burant, S. Dapprich, J. M. Millam, A. D. Daniels, K. N. Kudin, M. C. Strain, O. Farkas, J. Tomasi, V. Barone, M. Cossi, R. Cammi, B. Mennucci, C. Pomelli, C. Adamo, S. Clifford, J. Ochterski, G. A. Petersson, P. Y. Ayala, Q. Cui, K. Morokuma, D. K. Malick, A. D. Rabuck, K. Raghavachari, J. B. Foresman, J. Cioslowski, J. V. Ortiz, B. B. Stefanov, G. Liu, A. Liashenko, P. Piskorz, I. Komaromi, R. Gomperts, R. L. Martin, D. J. Fox, T. Keith, M. A. Al-Laham, C. Y. Peng, A. Nanayakkara, C. Gonzalez, M. Challacombe, P. M. W. Gill, B. G. Johnson, W. Chen, M. W. Wong, J. L. Andres, M. Head-Gordon, E. S. Replogle, J. A. Pople, Gaussian, Inc., Pittsburgh, PA, **1998**. b) M. Kohout, Program dgrid, Max-Planck-Institut für Chemische Physik fester Stoffe, Dresden, **2003**.

[25] M. Kohout, F. R. Wagner, Yu. Grin, *Theor. Chem. Acc.* **2002**, *108*, 150 – 156.

[26] R. F. W. Bader, *Atoms in Molecules: A Quantum Theory*, Oxford University Press, Oxford, **1990**.

[27] H. Rosner, A. Kitaigorodsky, W. E. Pickett, *Phys. Rev. Lett.* **2002**, *88*, 127001.

[28] M. E. Jones, R. E. Marsh, *J. Am. Chem. Soc.* **1954**, *76*, 1434.

[29] J. Nagamatsu, N. Nakagawa, T. Muranaka, Y. Zenitani, J. Akimitsu, *Nature* **2001**, *410*, 63.

[30] M. Wörle, R. Nesper, *J. Alloys Compd.* **1994**, *216*, 75.

 © 2004 Wiley-VCH Verlag GmbH & Co. KGaA, Weinheim

NMR Spectroscopic Methods

An Easy and Scalable Method for the Partial Alignment of Organic Molecules for Measuring Residual Dipolar Couplings**

*Burkhard Luy, Kyryl Kobzar, and Horst Kessler**

Residual dipolar couplings contain important structural information about the distance between two atoms and the angle between a pair of atoms and a static magnetic field. Their measurement in high-resolution NMR spectroscopy requires the partial alignment of the molecules in the sample.[1–5] A number of standard methods are known for biological molecules in aqueous solution, for example, phospholipid bicelles,[6] filamentous phages,[7] or other liquid-crystalline phases,[8] which orient themselves in the magnetic field and partially orient the molecules by steric or electrostatic interactions.

In organic solvents, so far only liquid-crystalline poly-γ-benzyl-L-glutamate (PBLG) in $CDCl_3$ has been used successfully for the orientation of molecules in the magnetic field.[9–13] Liquid-crystalline phases, however, have the disadvantage that a minimal concentration is necessary and therefore a minimal alignment of the molecules in a sample is introduced, which strongly limits the applicability of standard methods for the measurement of coupling constants.[12] An alternative is given by strain induced alignment in a gel (SAG), which is independent of the magnetic field and scalable over a wide range. In aqueous solutions, mechanically stretched polyacrylamide[14–17] and an acrylamide/acrylate copolymer[18] were applied. But polymeric gels are also generally suited for partial alignment in organic solvents, as was shown by the pioneering work of Deloche and Samulski[19] and many follow-up applications in polymer NMR spectroscopy (e.g. see refs. [20–23]). Herein we present an easy to apply and scalable method for the alignment of organic molecules and measurement of residual dipolar couplings in cross-linked polystyrene in $CDCl_3$ which, in principle, can be extended to a large number of polymer/solvent combinations.

Cross-linked polystyrene (PS) can easily be obtained by the polymerization of styrene with divinylbenzene (DVB) for branching and dibenzoylperoxide (DBP) as the radical initiator.[24] If a cylindrical PS stick(≈ 1 cm length, ≈ 3 mm diameter) is introduced into an NMR tube together with

[*] Dr. B. Luy, Dipl.-Chem. K. Kobzar, Prof. Dr. H. Kessler
Institut für Organische Chemie und Biochemie
Technische Universität München
Lichtenbergstrasse 4, 85 747 Garching (Germany)
Fax: (+49) 89-289-13210
E-mail: horst.kessler@ch.tum.de

[**] B.L. and H.K. acknowledge the Fonds der Chemischen Industrie and the DFG (Emmy-Noether-fellowships LU 835/1-1, KC 147/35) for financial support. We thank Prof. Dr.-Ing O. Nuyken, Dr. R. Jordan, Dr. M. Zweckstetter, Dr. R. Marx, O. Hiltner, and W. Günther for their help.

Supporting information for this article is available on the WWW under http://www.angewandte.org or from the author.

 © 2004 Wiley-VCH Verlag GmbH & Co. KGaA, Weinheim DOI: 10.1002/anie.200352860

$CDCl_3$, the polymer starts to swell and stretches owing to the constraints of the glass wall of the tube (Figure 1). Since the friction of PS against the glass wall is low, no additional tools such as a teflon funnel[17] are necessary. After a few hours a

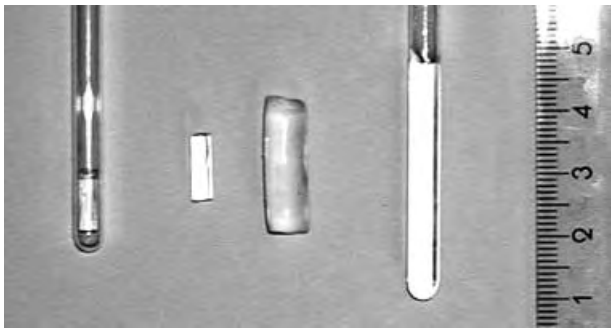


Figure 1. Photograph of the cross-linked PS stick in different states of swelling. From left to right: unswollen polymer stick in a standard 5-mm NMR tube, polymer stick directly after polymerization, free polymer stick completely swollen, polymer stick swollen in the NMR tube.

splitting in the deuterium spectrum of $CDCl_3$ can already be measured; the full splitting with narrow lineshapes can be seen after a few days after full equilibration of the gel. We could not determine any correlation between the linewidth of signals and the appearance of the sample or the degree of cross-linking, but after an equilibration time of about 5 days, no significant changes in the lineshape could be measured for the tested samples. The actual sample molecule can be added to the polymer together with the solvent or after the polymer is already swollen. In the case of strychnine and menthol, diffusion at room temperature overnight was enough to measure residual dipolar couplings.

The degree of alignment can be influenced by the consistency of the polymer stick. First, the stretching of the gel depends on the diameter of the unswollen stick. With a diameter of 3 mm, we achieved good results with an orientation range useful for high-resolution NMR spectroscopy. The degree of cross-linking and therefore also the NMR properties can be tuned by the amount of DVB and DBP added and the polymerization conditions used (e.g. temperature). The deuterium splitting of $CDCl_3$ as a measure of the anisotropy of the gel is shown in Figure 2 with respect to DVB and DBP concentration and a constant polymerization temperature of 80 °C. An increase in the orientation of the solvent with higher DVB and lower DBP concentrations is clear. The quadrupolar couplings of samples produced under identical conditions varied in the order of $\pm 10\,\%$, which can already be explained by variations in the wall thickness of the NMR tubes and the variations in the diameter of the cylinders used for polymerization. Furthermore, the polymer itself is probably quite heterogeneous and a certain bandwidth under the polymerization conditions used cannot be avoided. In a few cases, the top of the gel was broken for yet unknown reasons. In these cases, it was more difficult to shim the samples, but residual dipolar couplings could still be determined.

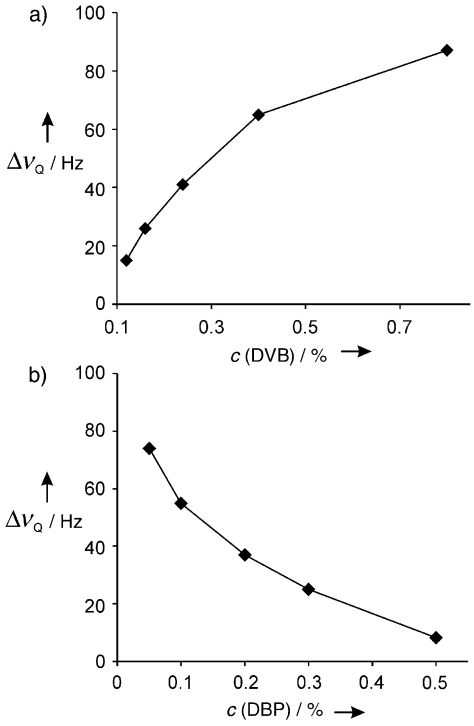


Figure 2. Quadrupolar splitting $\Delta\nu_Q$ in the deuterium signal of $CDCl_3$ with respect to a) DVB concentration at 0.25 % (w/v) DBP and b) DBP concentration at 0.16 % (v/v) DVB (b). Technical-grade DVB and DBP were used, and therefore absolute concentrations are only approximations.

For the orientation of strychnine, a standard sample in NMR spectroscopy,[25] a polymer stick with DVB (0.16 % v/v) and DBP (0.3 % w/v) was used, which resulted in a quadrupolar splitting of 25 Hz in the deuterium spectrum. Two HSQC spectra were recorded without heteronuclear decoupling during acquisition: 1) strychnine in $CDCl_3$ alone as reference and 2) dissolved in the aligned polymer gel. All ^1J(H,C) couplings from the reference sample and ^1J(H,C)+D(H,C) couplings from the oriented sample were measured by using the program Sparky.[26,27] The PS signals could easily be distinguished from strychnine signals because of their broad lines, and practically no overlap between the resonances was observed (Figure 3). The difference between the two coupling constants directly results in the residual dipolar couplings D(H,C). All dipolar couplings are in the range of -11 to 13 Hz, so that the sign of the couplings is unambiguously given by the larger ^1J(H,C) coupling (>120 Hz).

The program PALES[28] was used to fit 18 measured dipolar couplings to an unoptimized crystal structure of strychnine with a correlation factor of $R = 0.978$ (see Supporting Information for more details). A comparison to the fit of the residual dipolar couplings obtained in PBLG[12] shows an alignment tensor with axial and rhombic components of $D_a = -2.23 \times 10^{-3}$ and $D_r = -8.63 \times 10^{-4}$, respectively, which are about 12 times stronger than those for strychnine in the PS gel with $D_a = -1.77 \times 10^{-4}$ and $D_r = -8.82 \times 10^{-5}$, respectively. The ratio D_a/D_r and the orientations of the alignment tensors in space are different in the two cases, so that studies

 © 2004 Wiley-VCH Verlag GmbH & Co. KGaA, Weinheim

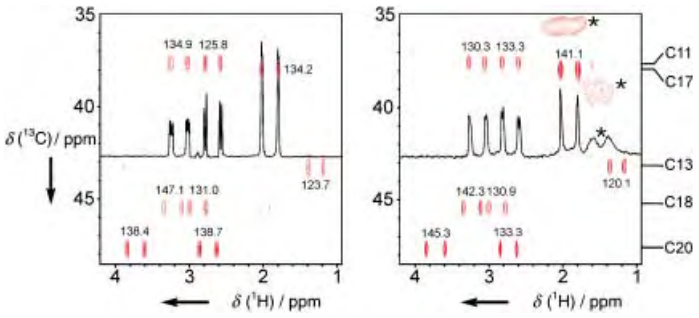


Figure 3. The region of the $^{1}H,^{13}C$-correlation spectra (HSQC) acquired on ~50 mg strychnine in $CDCl_3$ (left) and in a PS gel swollen in $CDCl_3$ (right) at 300° K. $^{1}J(H,C)$ and $^{1}J(H,C)+D(H,C)$ couplings, respectively, are given next to the corresponding cross peaks. As can be seen from the 1D slice at 37.8 ppm the couplings are easily measured. The broad signals of the PS polymer are indicated with an asterisk (*).

of the dynamic behavior of molecules (for example, see references[29–31] seem to be possible. Whether the difference in alignment is large enough has yet to be shown.

As a second model system, residual dipolar couplings for menthol were measured, for which dipolar couplings aligned in PBLG are also reported.[13] Menthol is a far more globular molecule than strychnine, and we decided to use a PS stick with DVB (0.8% v/v) and DBP (0.25% w/v), which resulted in a quadrupolar splitting of 87 Hz of the $CDCl_3$ signal. The measured D(H,C) couplings are in the range of −6.2 to 7.2 Hz and a comparison with the residual dipolar couplings measured in PBLG[13] shows a fourfold stronger alignment tensor for PBLG with a different orientation in space. The D_a/D_r ratio is 2.1 in both cases, but the axes of the rhombic component are oriented differently in space and relative to each other, so that also here additional structurally relevant information can be obtained in principle (see Supporting Information).

We can only speculate on the origin of the variation in the alignment tensors induced by PBLG and the PS gel. Certainly, the relatively small organic molecules can interact efficiently with the polar groups of the orienting media and small apolar cavities might lead to strong steric effects. The properties of the helical and somewhat polar PBLG differ significantly from those of the PS gel.

In summary, the usefulness of cross-linked polymer gels for the partial alignment of molecules in organic solvents could be demonstrated. With PS in $CDCl_3$ as a model system the simple handling and the scalability through the degree of cross-linking of the polymer could be shown. A disadvantage of the method is the long time that is sometimes required for equilibration of the stretched polymer gel and for diffusion of the sample into the gel. This problem can be partially overcome by storage of a number of already swollen and characterized gels in an NMR tube. Many solvent/polymer combinations are possible and will be the subject of future studies to ensure a broad applicability and a variation in orientation tensors for a wide range of samples for NMR spectroscopy. With the corresponding methods adapted to small molecules, the structure determination of natural products will be significantly simplified and many ambiguities in NMR spectroscopy will be clarified.

Received: September 12, 2003 [Z52860]

Keywords: gels · NMR spectroscopy · partial alignment · polystyrene · residual dipolar coupling

[1] C. R. Sanders, B. J. Hare, K. P. Howard, J. H. Prestegard, *Prog. Nucl. Magn. Reson. Spectrosc.* **1994**, *26*, 421 – 444.
[2] J. R. Tolman, J. M. Flanagan, M. A. Kennedy, J. H. Prestegard, *Proc. Natl. Acad. Sci. USA* **1995**, *92*, 9279 – 9283.
[3] N. Tjandra, A. Bax, *Science* **1997**, *278*, 1111 – 1114.
[4] B. Simon, M. Sattler, *Angew. Chem.* **2002**, *114*, 453 – 456; *Angew. Chem. Int. Ed.* **2002**, *41*, 437 – 440.
[5] A. Bax, *Protein Sci.* **2003**, *12*, 1 – 16.
[6] J. H. Prestegard, *Nat. Struct. Biol.* **1998**, *5*, 517 – 522.
[7] M. R. Hansen, L. Mueller, A. Pardi, *Nat. Struct. Biol.* **1998**, *5*, 1065 – 1074.
[8] M. Rückert, G. Otting, *J. Am. Chem. Soc.* **2000**, *122*, 7793 – 7797.
[9] A. Meddour, I. Canet, A. Loewenstein, J. M. Pechine, J. Courtieu, *J. Am. Chem. Soc.* **1994**, *116*, 9652 – 9656.
[10] P. Lesot, D. Merlet, A. Loewenstein, J. Courtieu, *Tetrahedron: Asymmetry* **1998**, *9*, 1871 – 1881.
[11] C. Canlet, D. Merlet, P. Lesot, A. Meddour, A. Loewenstein, J. Courtieu, *Tetrahedron: Asymmetry* **2000**, *11*, 1911 – 1918.
[12] C. M. Thiele, S. Berger, *Org. Lett.* **2003**, *5*, 705 – 708.
[13] L. Verdier, P. Sakhaii, M. Zweckstetter, C. Griesinger, *J. Magn. Reson.* **2003**, *163*, 353 – 359.
[14] R. Tycko, F. J. Blanco, Y. Ishii, *J. Am. Chem. Soc.* **2000**, *122*, 9340 – 9341.
[15] H. J. Sass, G. Musco, S. J. Stahl, P. T. Wingfield, S. Grzesiek, *J. Biomol. NMR* **2000**, *18*, 303 – 309.
[16] Y. Ishii, M. A. Markus, R. Tycko, *J. Biomol. NMR* **2001**, *21*, 141 – 151.
[17] J. J. Chou, S. Gaemers, B. Howder, J. M. Louis, A. Bax, *J. Biomol. NMR* **2001**, *21*, 377 – 382.
[18] S. Meier, D. Haussinger, S. Grzesiek, *J. Biomol. NMR* **2002**, *24*, 351 – 356.
[19] B. Deloche, E. T. Samulski, *Macromolecules* **1981**, *14*, 575 – 581.
[20] P. Sentosa, F. Fujara, H. Sillescu, *Makromol. Chem.* **1992**, *193*, 2421 – 2431.
[21] L. C. ter Beek, F. M. Linseisen, *Macromolecules* **1998**, *31*, 4986 – 4989.
[22] R. J. Cormier, M. L. Kilfoil, P. T. Callaghan, *Phys. Rev. E* **2001**, *64*, 051809.
[23] P. Medick, M. Vogel, E. Rossler, *J. Magn. Reson.* **2002**, *159*, 126 – 136.
[24] H. G. Elias, *Makromoleküle*, 6th ed., Wiley-VCH, Weinheim, **2001**.
[25] S. Braun, H.-O. Kalinowski, S. Berger, *150 and More Basic NMR Experiments*, 2nd ed., Wiley-VCH, Weinheim, **1998**.
[26] D. G. Kneller, I. D. Kuntz, *J. Cell Biochem.* **1993**, *17C Suppl*, 254.
[27] T. D. Goddard, D. G. Kneller, University of California, San Francisco.
[28] M. Zweckstetter, A. Bax, *J. Am. Chem. Soc.* **2000**, *122*, 3791 – 3792.
[29] J. Meiler, W. Peti, C. Griesinger, *J. Am. Chem. Soc.* **2003**, *125*, 8072 – 8073.
[30] J. Meiler, J. J. Prompers, W. Peti, C. Griesinger, R. Bruschweiler, *J. Am. Chem. Soc.* **2001**, *123*, 6098 – 6107.
[31] W. Peti, J. Meiler, R. Bruschweiler, C. Griesinger, *J. Am. Chem. Soc.* **2002**, *124*, 5822 – 5833.

 © 2004 Wiley-VCH Verlag GmbH & Co. KGaA, Weinheim

Pd-Catalyzed Couplings

Decarbonylative Heck Olefination of Enol Esters: Salt-Free and Environmentally Friendly Access to Vinyl Arenes**

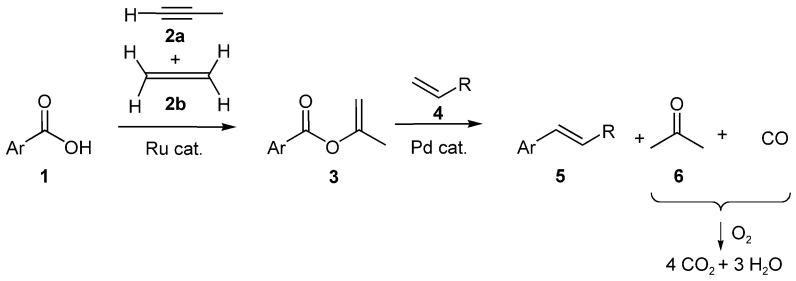
Lukas J. Gooßen and Jens Paetzold*

Dedicated to Prof. Dr. Manfred Reetz on the occasion of his 60th birthday

The Mizoroki–Heck reaction, one of the most elegant methods for the attachment of carbon chains onto aromatic rings, has found many applications in both academic and industrial laboratories.[1] The standard process starting from aryl halides,[2] triflates,[3] diazonium salts,[4] aroyl-[5] and arylsulfonyl halides[6] suffers from the requirement of stoichiometric amounts of base to neutralize the acid released in the reaction. The large quantities of salts inevitably formed must then be separated and disposed of in an environmentally acceptable way—a complex procedure, particularly on an industrial scale.

The reduction of the salt load of Heck reactions has previously been approached in two ways: In the first, nonfunctionalized arenes are used for the oxidative coupling with olefins.[7] In analogy to the Friedel–Crafts reaction, this reaction is regioselective for very few substrates; usually product mixtures are obtained that can be hard to separate. The second, more generally applicable approach makes use of carboxylic acids as the source of the aryl residue.[8–10] These are first converted into the corresponding anhydrides or *p*-nitrophenyl esters, which are then used in a palladium-catalyzed decarbonylative olefination step. The substitution pattern on the aromatic ring is determined by the position of the carboxylate group. Along with the desired vinyl arenes, the corresponding carboxylic acid or *p*-nitrophenol is produced as the by-product, which can be converted back into the starting material with fresh carboxylic acid. In the overall process, the only by-products eliminated are hence CO and water. However, the technical realization of such a cyclic process would be rather difficult, and the ecological advantage of a salt-free reaction might not balance the energy required for the separation and recycling of the by-products. Based on both economical and ecological considerations, there is still a high demand for alternative processes that start from environmentally benign compounds, produce no waste salts, and require no energetically demanding material streams.

Herein, we report on a novel strategy for the introduction of carbon chains to arenes that fulfills these requirements in an excellent way (Scheme 1). Aromatic carboxylic acids **1** are initially converted into the isopropenyl esters **3** in a waste-free

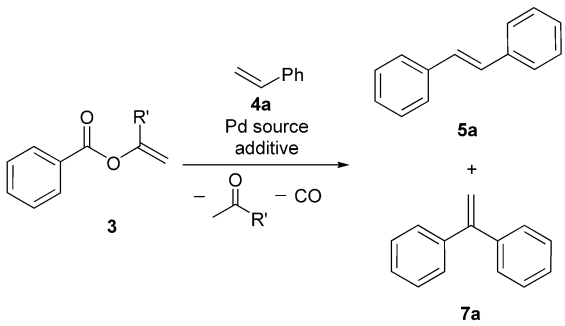


Scheme 1. Salt-free synthesis of vinyl arenes from carboxylic acids.

and atom-economical fashion by coupling to propyne (**2a**) or allene (**2b**), which are available from the C_3 fraction from the steam cracker.[11a] These intermediates **3** then react further to give the vinyl arenes **5** in a newly developed decarbonylative Heck olefination. The only by-products, CO and acetone (**6**), can be burned in an environmentally neutral way, potentially providing some of the energy required for the reaction.

While a number of active catalyst systems are available for the first reaction step,[11] metal-catalyzed coupling reactions of enol esters are still unknown. This second step in the process would require metal complexes with enough activity to insert into the C–O bond of the poorly reactive enol esters. Such catalysts could undergo a cycle consisting of the oxidative addition of the enol ester to give an acyl–metal enolate, decarbonylation to give the aryl complex, insertion of the olefin into the metal–aryl bond, β-hydride elimination, and protonation of the enolate with formation of the corresponding ketone.[12]

Using the model reaction depicted in Scheme 2, a conversion of isopropenyl benzoate (**3a**, R′ = Me) with styrene (**4a**) to yield *trans*-stilbene (**5a**), we investigated the catalytic activity of various combinations of palladium precursors, additives, and ligands (Table 1). While barely any conversion was observed for palladium acetate or $[Pd_2(dba)_3]$ (dba = dibenzylideneacetone) modest catalytic activity for the desired reaction was displayed by palladium(II)



Scheme 2. Decarbonylative Heck olefination of vinyl benzoates.

[*] Dr. L. J. Gooßen, J. Paetzold
Max-Planck-Institut für Kohlenforschung
Kaiser-Wilhelm-Platz 1, 45470 Mülheim an der Ruhr (Germany)
Fax. (+49) 208-306-2985
E-mail: goossen@mpi-muelheim.mpg.de

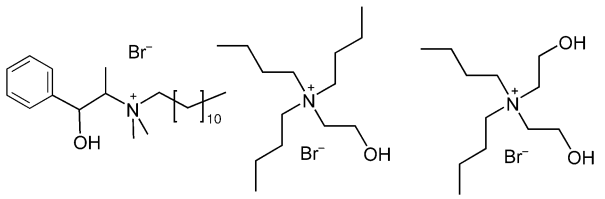
[**] We thank Prof. Dr. M. T. Reetz for generous support and constant encouragement, D. Neis for technical assistance, and the DFG, the FCI, and the BMBF for financial support.

 DOI: 10.1002/anie.200352357 © 2004 Wiley-VCH Verlag GmbH & Co. KGaA, Weinheim

Table 1: Optimization of the catalyst system for the reaction in Scheme 2.[a]

No.	Pd source	Additive	R′	Solvent	Conv.	Sel.[b]
1	$Pd(OAc)_2$	–	Me	NMP	0	n.d.[c]
2	$(dba)_3Pd_2$	–	Me	NMP	0	n.d.[c]
3	$PdCl_2$	–	Me	NMP	45	80
4	$PdBr_2$	–	Me	NMP	50	90
5	$PdCl_2$	LiCl	Me	NMP	60	>95
6[d]	$PdCl_2$	LiCl	Me	NMP	38	95
7[e]	$PdCl_2$	LiCl	Me	NMP	10	n.d.[c]
8	$PdCl_2$	LiBr	Me	NMP	70	>95
9	$PdBr_2$	NaBr	Me	NMP	75	70
10	$PdBr_2$	KBr	Me	NMP	80	>95
11	$PdBr_2$	LiBr	Me	NMP	70	>95
12	$PdBr_2$	$(n\text{Bu})_4N^+Br^-$	Me	NMP	100	90
13	$PdBr_2$	$(n\text{Oct})_4P^+Br^-$	Me	NMP	95	90
14	$PdBr_2$	**8a**	Me	NMP	100	>95
15	$PdBr_2$	**8b**	Me	NMP	100	>95
16	$PdBr_2$	**8c**	Me	NMP	100	75
17[f]	$PdBr_2$	**8b**	Me	NMP	100	95
18	$PdBr_2$/celite	**8b**	Me	NMP	100	95
19[g]	$PdBr_2$/celite	**8b**	Me	NMP	100	95
20	$PdBr_2$	**8b**	Me	DMF	35	50[h]
21	$PdBr_2$	**8b**	Me	*o*-$C_6H_4Cl_2$	40	55
22	$PdBr_2$	**8b**	Me	sulfolane	90	50
23	$PdBr_2$	**8b**	Me	–	90	80
24	$PdBr_2$	**8b**	H	NMP	40	80
25	$PdBr_2$	**8b**	*t*Bu	NMP	80	90
26	$PdBr_2$	**8b**	Ph	NMP	90	90
27	$PdBr_2$	**8b**	*n*Bu	NMP	100	<10[i]

[a] Reaction conditions: 1.00 mmol vinyl benzoate (**3**), 2.00 mmol styrene (**4a**), 0.03 mmol Pd source, 0.03 mmol additive, 0.03 mmol ligand, 4 mL solvent, 16 h, 160 °C. Conversions and selectivities (both in %) were determined by GC analysis with *n*-tetradecane as the internal standard. The ratio **5a**/**7a** was around 10:1 in all conversions. [b] Main side products: benzoic acid and benzoic anhydride. [c] n.d.: not determined. [d] With isoquinoline as a ligand. [e] With PPh_3 as a ligand. [f] 0.5 mL solvent, 0.005 mmol $PdBr_2$, and additive. [g] Experiment conducted with regenerated catalyst. [h] Side product: *N*,*N*-dimethylbenzamide. [i] Isomerization to the product with the internal C=C bond.



8a **8b** **8c**

halides (entries 1–4). In analogy to decarbonylative olefinations of anhydrides and *p*-nitrophenyl esters, the conversion could be improved by adding metal halides (entries 5, 8–11); however, early precipitation of metallic palladium could not totally be prevented by these additives. Coordinating ligands, such as amines or phosphanes, succeeded in stabilizing the palladium in solution, but at the same time decreased its catalytic activity (entries 6, 7). Hence, only unsatisfactory yields could be obtained when the catalytic systems optimal for anhydrides[8d] or *p*-nitrophenyl esters[8b] were applied to isopropenyl esters (entries 5, 6).

A combination of palladium bromide and tetraalkylammonium or tetraalkylphosphonium bromides proved to be active and selective catalysts for these substrates (entries 12, 13). Finally, the hydroxy-substituted ammonium salts *N*-dodecyl-*N*-methylephedrinium bromide (**8a**) and tri-*n*-butyl(2-hydroxyethyl)ammonium bromide (**8b**) were found to stabilize the palladium in solution for sufficient time to give quantitative conversion along with high selectivity (entries 14–16).[13] With this additive, the catalyst load could be reduced to 0.5 mol% without losses in the yield (entry 17).

The catalyst was recycled successfully following the method of de Vries (entries 18, 19).[14] Thus, celite was added to the reaction mixture, and palladium in reduced form precipitated on it over the course of the reaction. After complete conversion, the solid was removed by centrifugation and treated with the corresponding amount of Br_2 and **8b** as solutions in *N*-methylpyrrolidone (NMP). The resulting mixture displayed the same catalytic activity as the original catalyst.

N-Methylpyrrolidone proved to be a particularly suitable solvent (entries 15, 20–22). In contrast to traditional Heck reactions, the dilution can be significantly reduced since there is no longer a necessity to dissolve stoichiometric amounts of inorganic salts (entry 17). Notable product yields are obtained even in the absence of a solvent—a major advantage of the new protocol from an ecological perspective (entry 23).

Besides isopropenyl esters, other enol esters with terminal double bonds, for example, vinyl benzoate (**3b**, R′ = H), 1-(*tert*-butyl)vinylbenzoate (**3c**, R′ = *t*Bu), and 1-phenylvinyl benzoate (**3d**, R′ = Ph) were successfully olefinated (entries 24–26). In the reaction of 2-hex-1-enyl benzoate (**3e**, R′ = *n*Bu), however, mainly isomerization to a mixture of (*E*)- and (*Z*)-2-hex-2-enyl benzoate was observed (entry 27).

In the model reaction of the relatively unreactive styrene, the principal product was *trans*-stilbene (**5a**); under optimized conditions, 1,1-diphenylethylene (**7a**) was formed in less than 10% yield. The only side-product observed was triphenylethylene, at levels of around 2%. In analogy to the traditional Heck olefination, yet higher selectivities were obtained with activated olefins such as acrylates (Table 2, **5p**).

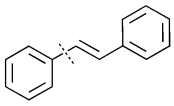
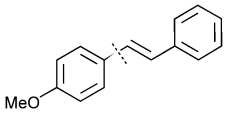
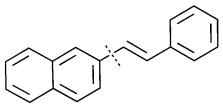
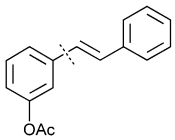
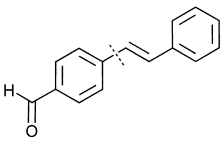
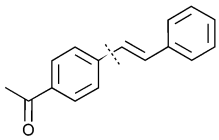
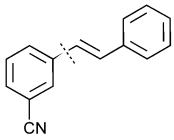
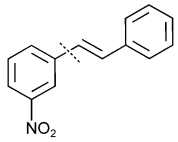
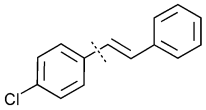
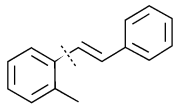
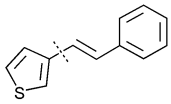
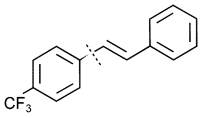
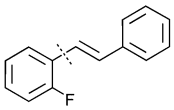
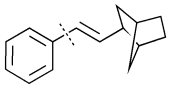
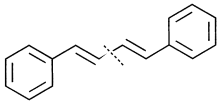
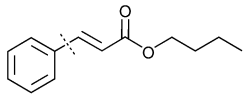
The general applicability of the new reaction was investigated with a series of isopropenyl carboxylates **3a**,**f**–**r**, previously prepared from the corresponding carboxylic acids and propyne gas,[11c] and with the olefins **4a**–**c** following Scheme 3. Table 2 shows the broad applicability of the new Heck reaction variant. Electron-rich and electron-deficient aryl, heteroaryl, and vinyl carboxylic acid esters were coupled to various olefins in good yields. The reaction tolerates many functionalities, including esters, ethers, nitro, keto, trifluoromethyl, and even formyl groups.

The workup is particularly easy since only volatile side products are formed: the celite is removed by filtration or centrifugation together with the precipitated palladium(0), the solvent is evaporated under high vacuum along with excess olefin, then the vinyl arene is purified by distillation.

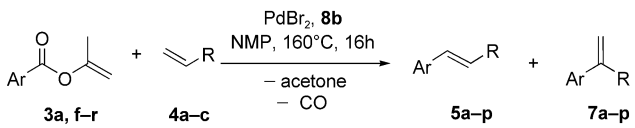
Overall, for the first time an efficient and selective catalyst system for the decarbonylative Heck olefination of enol esters

 © 2004 Wiley-VCH Verlag GmbH & Co. KGaA, Weinheim

Table 2: Conversion of various isopropenyl carboxylates with olefins (Scheme 3).[a]

Cmpd.	Structure	Yield [%][b]	**5**:**7**[c]	Cmpd.	Structure	Yield [%][b]	**5**:**7**[c]
5a		95	10:1	**5i**		92	8:1
5b		85	9:1	**5j**		75	9:1
5c		78	13:1	**5k**		98	9:1
5d		92	13:1	**5l**		77	9:1
5e		96	10:1	**5m**		95	15:1
5f		75	10:1	**5n**		87	15:1
5g		99	15:1	**5o**		67	5:1[d]
5h		63	9:1	**5p**		98	>50:1

[a] Reaction conditions: 1.00 mmol isopropenyl benzoate, 2.00 mmol olefin, 0.03 mmol $PdBr_2$, 0.03 mmol **8b**, 4 mL NMP, 16 h, 160 °C. [b] Overall yield [%] of vinyl arenas as isolated products. [c] The relative amounts of 1,2- and 1,1-substituted vinyl arenes were determined by gas chromatography. [d] Mixture of double-bond isomers.



Scheme 3. Decarbonylative Heck olefination of isopropenyl carboxylates.

has been developed. In contrast to traditional Heck reactions, the addition of both base and solvent can be avoided, and instead of waste salts, only volatile, flammable by-products are formed. This reaction combined with a waste-free synthesis of the isopropenyl ester substrates by addition of a carboxylic acid onto propyne results in a salt-free, environmentally benign overall process. This is the first example of a palladium-catalyzed coupling reaction of the poorly reactive enol esters and could open up new perspectives for related reactions, such as ketone syntheses or reductions.[15]

Experimental Section

5p: A 20-mL flask was charged with $PdBr_2$ (8.00 mg, 0.03 mmol), **8b** (9.30 mg, 0.03 mmol), and celite (200 mg). The flask was then heated to 140 °C under vacuum for 15 min and flushed with argon. Subsequently, **3a** (162 mg, 1.00 mmol), **4c** (175 μL, 1.20 mmol), and NMP (4.00 mL) were added by syringe. The resulting mixture was then stirred for 16 h at 160 °C. After filtration of Pd^0/celite and removal of the volatiles under high vacuum, the residue was fractionally distilled to give **5p** (195 mg, 95%) as a colorless liquid. The spectroscopic data of the product correspond to those of (*E*)-3-phenyl-2-propenoic acid 1-butylester, CAS registry number [538-65-8]. The Pd^0/celite mixture was dried under vacuum then treated with Br_2 (2.00 μL, 0.037 mmol) in NMP (1 mL) and stirred for 15 min. Following addition of **8b** (9.30 mg, 0.03 mmol), the mixture can be reused as the catalyst.

The experiments in Table 2 were carried out analogously. The products were purified by column chromatography and characterized by NMR, MS, and HRMS.

Received: July 11, 2003
Revised: October 27, 2003 [Z52357]
Published Online: January 29, 2004

 © 2004 Wiley-VCH Verlag GmbH & Co. KGaA, Weinheim

Keywords: alkenes · enol esters · Heck reaction · homogeneous catalysis · palladium

[1] a) R. F. Heck, *Org. React.* **1982**, 27 – 390; b) A. de Meijere, F. E. Meyer, *Angew. Chem.* **1994**, *106*, 2473 – 2506; *Angew. Chem. Int. Ed. Engl.* **1994**, *33*, 2379 – 2411; c) C. E. Tucker, J. G. de Vries, *Top. Catal.* **2002**, *19*, 111 – 118.

[2] For examples of particularly active catalysts, see: a) W. A. Herrmann, C. Broßmer, K. Öfele, M. Beller, H. Fischer, *J. Mol. Catal. A* **1995**, *103*, 133 – 146; b) K. H. Shaughnessy, P. Kim, J. F. Hartwig, *J. Am. Chem. Soc.* **1999**, *121*, 2123 – 2132; c) A. F. Littke, G. C. Fu, *Angew. Chem.* **2002**, *114*, 4350 – 4386; *Angew. Chem. Int. Ed.* **2002**, *41*, 4176 – 4211; d) A. Ehrentraut, A. Zapf, M. Beller, *Synlett* **2000**, *11*, 1589 – 1592; e) M. T. Reetz, E. Westermann, *Angew. Chem.* **2000**, *112*, 170 – 173; *Angew. Chem. Int. Ed.* **2000**, *39*, 165 – 168.

[3] a) S. Cacchi, E. Moreau, G. Ortar, *Tetrahedron Lett.* **1984**, *25*, 2271 – 2274; b) W. J. Scott, G. T. Crisp, J. K. Stille, *J. Am. Chem. Soc.* **1984**, *106*, 4630 – 4632.

[4] a) K. Kikukawa, T. Matsuda, *Chem. Lett.* **1977**, 159 – 162; b) K. Kikakuwa, K. Ikenaga, K. Kono, K. Toritani, F. Wada, T. Matsuda, *J. Organomet. Chem.* **1984**, *270*, 277 – 282.

[5] M. Miura, H. Hashimoto, K. Itoh, M. Nomura, *J. Chem. Soc. Perkin Trans. 1* **1990**, *8*, 2207 – 2211.

[6] H. U. Blaser, A. Spencer, *J. Organomet. Chem.* **1982**, *233*, 267 – 274.

[7] a) T. Yokota, M. Tani, S. Sakaguchi, Y. Ishii, *J. Am. Chem. Soc.* **2003**, *125*, 1476 – 1477; b) M. Dams, D. E. De Vos, S. Celen, P. A. Jacobs, *Angew. Chem.* **2003**, *115*, 3636 – 3639; *Angew. Chem. Int. Ed.* **2003**, *42*, 3512 – 3515.

[8] a) M. S. Stephan, A. J. J. M. Teunissen, G. K. M. Verzijl, J. G. de Vries, *Angew. Chem.* **1998**, *110*, 688 – 690; *Angew. Chem. Int. Ed.* **1998**, *37*, 662 – 664; b) L. J. Gooßen, J. Paetzold, *Angew. Chem.* **2002**, *114*, 1285 – 1289; *Angew. Chem. Int. Ed.* **2002**, *41*, 1237 – 1241; c) L. J. Gooßen, J. Paetzold, L. Winkel, *Synlett* **2002**, 1721 – 1723; d) A. F. Shmidt, V. V. Smirnov, *Kinet. Catal.* **2000**, *41*, 743 – 744.

[9] For a direct, but not salt-free olefination of carboxylic acids, see: A. G. Myers, D. Tanaka, M. R. Mannion, *J. Am. Chem. Soc.* **2002**, *124*, 11 250 – 11 251.

[10] For an alternative concept, see: T. Sugihara, T. Satoh, M. Miura, M. Nomura, *Angew. Chem.* **2003**, *115*, 4820 – 4822; *Angew. Chem. Int. Ed.* **2003**, *42*, 4672 – 4674.

[11] a) C. Bruneau, M. Neveux-Duflos, P. H. Dixneuf, *Green Chem.* **1999**, *1*, 183 – 185, and references therein; b) T. Mitsudo, Y. Hori, Y. Yamakawa, Y. Watanabe, *J. Org. Chem.* **1987**, *52*, 2230 – 2239; c) L. J. Gooßen, J. Paetzold, D. Koley, *Chem. Commun.* **2003**, 706 – 707.

[12] For mechanistic investigation of Pd-catalyzed reactions, see: C. Amatore, A. Jutand, *Acc. Chem. Res.* **2000**, *33*, 314 – 321.

[13] Compound **8a** is commercially available; **8b**,**c** were prepared by alkylation of the corresponding amines with 2-bromoethanol.

[14] A. H. M. de Vries, F. J. Parlevliet, L. Schmieder-van de Vondervoort, J. H. M. Mommers, H. J. W. Henderickx, M. A. M. Walet, J. G. de Vries, *Adv. Synth. Catal.* **2002**, *344*, 996 – 1002.

[15] a) L. J. Gooßen, K. Ghosh, *Angew. Chem.* **2001**, *113*, 3566 – 3568; *Angew. Chem. Int. Ed.* **2001**, *40*, 3458 – 3460; b) K. Nagayama, F. Kawataka, M. Sakamoto, I. Shimizu, A. Yamamoto, *Chem. Lett.* **1995**, 367 – 368; c) L. J. Gooßen, K. Ghosh, *Chem. Commun.* **2002**, 836 – 837.

 © 2004 Wiley-VCH Verlag GmbH & Co. KGaA, Weinheim

Biosynthesis

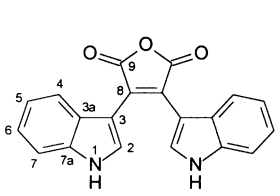
Pityriarubins, Biologically Active Bis(indolyl)spirans from Cultures of the Lipophilic Yeast *Malassezia furfur***

Bernhard Irlinger, Hans-Joachim Krämer, Peter Mayser, and Wolfgang Steglich**

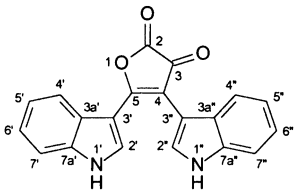
In memory of Ernst Habermann

Lipophilic yeasts of the genus *Malassezia* (earlier: *Pityrosporum*) belong to the resident flora of the human skin and that of many mammals.[1] One of seven species of such yeasts currently defined, *M. furfur* exhibits certain biochemical peculiarities. When L-tryptophan is added as the only nitrogen source to cultures of this yeast, it induces the production of numerous indole alkaloids, including colored and fluorescent compounds.[2–4] This may be of importance for the pathogenesis of pityriasis versicolor, a skin disease associated with *Malassezia* and characterized by flaky lesions with a hitherto unexplained variation in color and fluorescence.[5]

We now report on the isolation of three biologically active bis(indolyl)spirans from cultures of *M. furfur*. Extraction of the culture medium with ethyl acetate was followed by separation of the extract into several fractions on a Sephadex LH-20 chromatographic column. Each of these fractions was subjected to thin-layer chromatography (TLC) on silica gel, and the individual TLC zones were purified by two consecutive HPLC steps to afford the three orange-red pityriarubins A–C (**3**, **6**, and **7**), as well as the red pityrianhydride (**1**) and pityrialactone (**2**). The last compound is readily recognizable by its yellow-green fluorescence under UV light.



1



2

[*] Dr. H.-J. Krämer, Priv.-Doz. P. Mayser
Zentrum für Dermatologie und Andrologie
Justus-Liebig-Universität
Gaffkystrasse 14, 35385 Gießen (Germany)
Fax: (+49) 641-9943349
E-mail: Peter.Mayser@derma.med.uni-giessen.de
Dr. B. Irlinger, Prof. Dr. W. Steglich
Department Chemie
Ludwig-Maximilians-Universität
Butenandtstrasse 5–13, Haus F, 81377 München (Germany)
Fax: (+49) 89-2180-77756
E-mail: wos@cup.uni-muenchen.de

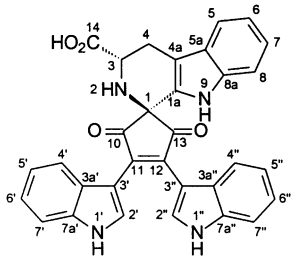
[**] We thank the Deutsche Forschungsgemeinschaft for generous support.

Supporting information for this article is available on the WWW under http://www.angewandte.org or from the author.

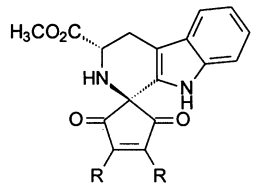
 © 2004 Wiley-VCH Verlag GmbH & Co. KGaA, Weinheim DOI: 10.1002/anie.200352549

Based on its spectroscopic data and direct comparison with an authentic sample, **1** was identified as 3,4-bis(indol-3-yl)maleic anhydride, an intermediate in the synthesis of arcyriarubin A,[6] but previously unknown as a natural product. The unusual bis(indolyl)oxobutenolide structure of **2** was described by us recently.[7]

The optically active pityriarubin A (**3**) showed a molecular ion at *m*/*z* 525 in the negative-ion FAB mass spectrum, which corresponds to the molecular formula $C_{32}H_{22}N_4O_4$. In addition to aromatic signals, the ^{1}H NMR spectrum revealed three signals in the aliphatic region, which result from an ABC spin system. Signals at $\delta = 2.92$ and 3.26 ppm were assigned to the diastereotopic protons of a CH_2 group, and characteristic singlets at $\delta = 9.16$ (1H) and 9.99 ppm (2H) could be attributed to three protons bonded to indole N atoms. In the ^{13}C NMR spectrum two signals at $\delta = 200.2$ and 200.7 ppm were ascribed to the carbonyl C atoms of two α,β-unsaturated ketone functionalities. Signals corresponding to a carboxy C atom and a quaternary C atom were observed at $\delta = 174.3$ and 62.7 ppm, respectively. From this evidence the spiro structure **3** was deduced for pityriarubin A, which is in accord with all the other spectroscopic data.

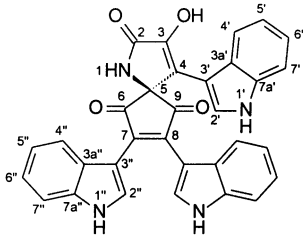


3

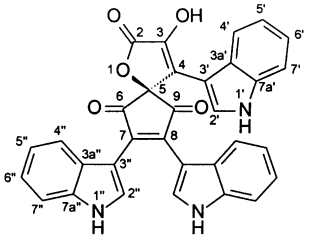


4: R R = CH=CH-CH=CH
5: R = Ph

To confirm the *S* configuration of **3**, the spiro-fused model compounds **4** and **5** were synthesized from L-tryptophan and the corresponding triketones. Like compound **3**, both **4** and **5** have a negative optical-rotation value, and their CD curves and ^{13}C NMR spectra agree well with those of **3**.[8]



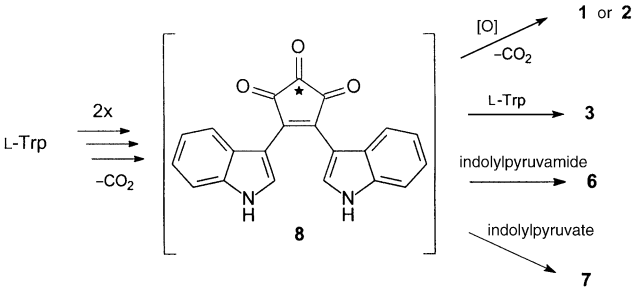
6



7

The ^{1}H NMR spectra of the achiral pityriarubins B (**6**) and C (**7**) differ from that of **3** by virtue of their lack of aliphatic signals. In the aromatic region, signals for two of the three indole units overlap, as a result of structural symmetry. The ^{13}C NMR spectra are also simplified with respect to that of **3**. Based on the chemical shifts and HMBC correlations observed the symmetrical structures **6** and **7** were assigned to pityriarubins B and C, respectively.

Biosynthetically speaking, the structures of these *Malassezia* metabolites can be derived in a straightforward manner from the triketone **8** (or its hydrate) as a hypothetical precursor (Scheme 1). Pictet–Spengler condensation of **8** with



Scheme 1. Proposal for the biosynthesis of bisindolyl metabolites in cultures of *Malassezia furfur* (*: ^{13}C labeling after treatment with DL-[1′-^{13}C]tryptophan).

L-tryptophan would lead to pityriarubin A (**3**), whereas the reaction of **8** with (indol-3-yl)pyruvamide or the corresponding carboxylic acid would lead to pityriarubins B (**6**) and C (**7**), respectively. Similar reactions are known for ninhydrin.[9] Pityrianhydride (**1**) and pityrialactone (**2**) could also be formed from **8** through selective oxidative cleavage, followed by oxidative decarboxylation of the resulting α-keto acid and lactonization.

To test this proposal, a culture of *M. furfur* was treated with DL-[1′-^{13}C]tryptophan. After 14 days, the bisindolyl metabolites were isolated and the degree of incorporation of ^{13}C was determined by ^{13}C NMR spectroscopy. As shown in Table 1, the spiro carbon atoms of the pityriarubins originate

Table 1: Labeling of the *Malassezia furfur* metabolites after treatment with DL-[1′-^{13}C]tryptophan.

	Position of labeling (incorporation rate [%])
pityrialactone (**2**)	C2 (62.6)
pityriarubin A[a] (**3**)	C1 (32.1); C14 (44.4)
pityriarubin B (**6**)	C2 (16.1); C5 (8.5)
pityriarubin C (**7**)	C2;[b] C5 (3.8)

[a] Optically inactive. [b] Because of contamination with a labeled co-metabolite, the extent of ^{13}C enrichment could not be determined.

from the carboxy group of tryptophan, whereas the carboxy group of the second tryptophan unit is lost. This supports the intermediacy of the triketone **8** and its formation from two molecules of indolylpyruvic acid. We are as yet unable to explain the significant differences observed in the ^{13}C-incorporation rates for the different compounds and the differences in their individual labeling positions.

The interesting biological activity exhibited by the pityriarubins reflects their close structural relationship with bis(indolyl)maleimides, which have recently attracted attention as protein kinase inhibitors.[10] Both types of compound suppress the "oxidative burst" of human granulocytes at μM

 © 2004 Wiley-VCH Verlag GmbH & Co. KGaA, Weinheim

levels in a concentration-dependent manner.[11] The activity of the pityriarubins is comparable to that of arcyriarubin A. However, in the case of the former compounds a more pronounced selectivity is observed with regard to the applied stimulus. The target site has yet to be determined. If in vivo formation of the metabolites is postulated, the inflammation-inhibition properties of the pityriarubins are consistent with the remarkably weak granulocytic reaction observed clinically in lesions of pityriasis versicolor.[11] The isolation and structural elucidation of additional indole metabolites from *M. furfur* will be reported in a separate publication.

Experimental Section

Cultivation and isolation: *Malassezia furfur* (CBS 1878) was cultivated for 14 days at 30 °C on an agar medium treated with L-tryptophan, as reported in reference [2]. Details of the cultivation and the exact procedure for the isolation of the metabolites are provided in the Supporting Information.

1: Orange-colored solid; m.p. 227–230 °C. Spectroscopic data identical with those of the synthetic compound.[6]

2: Pale-yellow powder; m.p. > 250 °C; UV/Vis (MeOH): λ_{max} ($\lg\varepsilon$) = 224 (4.07), 292 (sh, 3.55), 356 nm (3.55); IR (KBr): $\tilde{\nu}$ = 3400 (s, br), 1736 (s), 1639 (s), 1536 (m), 1458 (m), 1424 (m), 744 cm^{-1} (m); ^{1}H NMR (600 MHz, [D$_6$]acetone): δ = 6.48 (dd, J = 7.4, 7.4 Hz, 1H, 5′-H), 6.65 (m, 2H, 4′/5″-H), 6.88 (dd, J = 7.4, 7.4 Hz, 1H, 6′-H), 6.94 (dd, J = 8.2, 8.2 Hz, 1H, 6″-H), 7.00 (d, J = 8.2 Hz, 1H, 4″-H), 7.27 (d, J = 7.4 Hz, 1H, 7′-H), 7.32 (d, J = 8.2 Hz, 1H, 7″-H), 7.41 (d, J = 2.3 Hz, 1H, 2″-H), 7.57 (br s, 1H, 2′-H), 11.24 (s, 1H, 1″-H), 11.48 ppm (br s, 1H, 1′-H); ^{13}C NMR (151 MHz, CD_3CN): δ = 107.0 (C3″), 108.4 (C3′), 111.5 (C7′), 111.6 (C7″), 117.3 (C4), 118.7 (C5″), 119.1 (C5′), 120.8 (C4″), 121.1 (C6″), 121.3 (C6′), 121.4 (C4′), 125.4 (C3a′), 126.4 (C2″,C3a″), 128.1 (C2′), 135.8 (C7a″), 136.2 (C7a′), 151.9 (C5), 168.1 (C2), 172.8 ppm (C3); MS (EI): m/z (%): 329 (15), 328 (92) $[M]^+$, 315 (15), 314 (64), 270 (16), 269 (22), 257 (38), 256 (100), 255 (38), 207 (59), 128 (20); HRMS (EI): m/z calcd for $C_{20}H_{12}N_2O_3$ $[M]^+$: 328.0866; found: 328.0848.

3: Orange-red powder; m.p. > 200 °C (decomp); $[\alpha]_D^{25} = -80$ (c = 0.05, CH_3CN); UV/Vis (CH_3CN): λ_{max} ($\lg\varepsilon$) = 198 (4.46), 219 (4.43), 277 (4.04), 385 (3.63), 436 nm (3.68); CD (CH_3CN): λ_{max} ($\Delta\varepsilon$) = 207 (−1.77), 211 (0), 222 (+2.07), 231 (0), 241 (−1.72), 255 (0), 265 (+0.82), 278 (0), 298 (−2.23), 350 (0), 374 (+0.44), 391 (0), 434 (−0.94), 503 nm (0); IR (KBr): $\tilde{\nu}$3400 (s, br), 2927 (w), 1683 (s), 1516 (m), 1458 (w), 1422 (s), 1336 (w), 1243 (m), 1202 (s), 1135 (s), 1012 (w), 744 (m), 723 cm^{-1} (w); ^{1}H NMR (600 MHz, CD_3CN): δ = 2.92 (dd, J = 15.5, 10.7 Hz, 1H, 4-H$_a$), 3.26 (dd, J = 15.5, 4.3 Hz, 1H, 4-H$_b$), 4.52 (dd, J = 10.7, 4.3 Hz, 1H, 3-H), 6.66 (m, 2H, 5′/5″-H), 6.86 ("d", J = 8.2 Hz, 2H, 4′/4″-H), 7.02 (m, 2H, 6′/6″-H), 7.08 (dd, J = 8.0, 8.0 Hz, 1H, 6-H), 7.12 (dd, J = 8.0, 8.0 Hz, 1H, 7-H), 7.25 (d, J = 8.0 Hz, 1H, 8-H), 7.42 (m, 2H, 7′/7″-H), 7.55 (d, J = 8.0 Hz, 1H, 5-H), 8.03 ("d", J = 3.0 Hz, 2H, 2′/2″-H), 9.16 (br s, 1H, 9-H), 9.99 ppm (br s, 2H, 1′/1″-H); ^{13}C NMR (151 MHz, CD_3CN): δ = 25.8 (C4), 54.1 (C3), 62.7 (C1), 107.9 (C3′/3″), 112.3 (C8), 112.7 (C7′/7″), 112.8 (C4a), 119.1 (C5), 120.5 (C6), 120.9 (C5′/5″), 122.7 (C4′), 122.8 (C4″), 123.2 (C6′), 123.3 (C6″), 123.4 (C7), 126.6 (C3a′), 126.7 (C3a″), 127.6 (C5a), 129.9 (C1a), 131.8 (C2′), 131.9 (C2″), 137.1 (C7a′/7a″), 137.8 (C8a), 144.7 (C11), 144.9 (C12), 174.3 (C14), 200.2 (C10), 200.7 ppm (C13); HRMS (FAB)$^-$: m/z calcd for $C_{32}H_{21}N_4O_4$ $[M-H]^-$: 525.1548; found: 525.1563.

6: Orange-colored powder; m.p. 180–183 °C (decomp); UV/Vis (CH_3CN): λ_{max} ($\lg\varepsilon$) = 196 (4.38), 218 (4.34), 277 (4.05), 382 (3.55), 446 nm (3.61); IR (KBr): $\tilde{\nu}$ = 3401 (s, br), 2927 (w), 2228 (w), 1732 (m), 1689 (s), 1618 (w), 1518 (m), 1423 (m), 1275 (w), 1244 (m), 1198 (m), 1133 (m), 1014 (w), 816 (w), 744 (m), 720 cm^{-1} (w); ^{1}H NMR (600 MHz, [D$_6$]acetone): δ = 6.52 (ddd, J = 7.8, 7.8, 1.1 Hz, 2H, 5″-H), 6.65 (d, J = 7.8 Hz, 2H, 4″-H), 6.91 (ddd, J = 7.8, 7.8, 1.1 Hz, 2H, 6″-H), 6.98 (ddd, J = 7.8, 7.8, 1.1 Hz, 1H, 5′-H), 7.00 (d, J = 2.6 Hz, 1H, 2′-H), 7.02 (ddd, J = 7.8, 7.8, 1.1 Hz, 1H, 6′-H), 7.21 (d, J = 7.8 Hz, 1H, 7′-H), 7.34 (d, J = 7.8 Hz, 2H, 7″-H), 7.88 (d, J = 7.8 Hz, 1H, 4′-H), 7.92 (s, 1H, 1-H), 7.98 (d, J = 2.6 Hz, 2H, 2″-H), 10.26 (br s, 1H, 1′-H), 10.95 ppm (br s, 2H, 1″-H); ^{13}C NMR (151 MHz, [D$_6$]acetone): δ = 68.5 (C5), 107.1 (C3′), 107.8 (C3″), 112.0 (C7′), 112.5 (C3a′), 117.9 (C4), 120.1 (C5′), 120.7 (C5″), 122.2 (C4″), 122.7 (C4′), 122.8 (C6′), 122.9 (C6″), 124.2 (C2′), 126.5 (C3a″), 127.5 (3-a′), 131.5 (C2″), 137.1 (C7a′), 137.2 (C7a″), 144.2 (C3), 145.1 (C7/8), 170.5 (C2), 199.0 ppm (C6/9); MS (EI): m/z (%): 524 (52) $[M]^+$, 496 (4), 340 (4), 256 (22), 255 (13), 207 (10), 157 (4), 144 (8), 130 (10), 117 (24), 90 (8), 89 (6), 44 (100), 43 (25); HRMS (EI): m/z calcd for $C_{32}H_{20}N_4O_4$ $[M]^+$: 524.1525; found: 524.1509.

7: Red solid; m.p. 125–130 °C (decomp); UV/Vis (CH_3CN): λ_{max} ($\log\varepsilon$) = 195 (4.66), 218 (4.60), 277 (4.37), 323 (sh, 4.08), 394 (3.74), 4.62 nm (3.83). IR (KBr): $\tilde{\nu}$ = 3415 (s, br), 2924 (w), 1765 (s), 1686 (s), 1619 (w), 1571 (w), 1514 (m), 1459 (m), 1422 (s), 1337 (w), 1241 (m), 1199 (w), 1128 (m), 1095 (m), 1014 (m), 744 cm^{-1} (m); ^{1}H NMR (600 MHz, [D$_6$]acetone): δ = 6.60 (dd, J = 8.2, 8.2 Hz, 2H, 5″-H), 6.77 (d, J = 8.2 Hz, 2H, 4″-H), 6.98 (dd, J = 8.2, 8.2 Hz, 2H, 6″-H), 7.06 (dd, J = 8.2, 8.2 Hz, 1H, 5′-H), 7.11 (dd, J = 8.2, 8.2 Hz, 1H, 6′-H), 7.22 (s, 1H, 2′-H), 7.31 (d, J = 8.2 Hz, 1H, 7′-H), 7.42 (d, J = 8.2 Hz, 2H, 7″-H), 8.06 (d, J = 8.2 Hz, 1H, 4′-H), 8.16 (s, 2H, 2″-H), 10.59 (br s, 1H, 1′-H), 11.14 ppm (br s, 2H, 1″-H); ^{13}C NMR (151 MHz, [D$_6$]acetone): δ = 82.2 (C5), 105.9 (C3′), 107.5 (C3″), 112.4 (C7′), 112.6 (C7″), 120.8 (C5′), 121.0 (C5″), 122.3 (C4″), 122.9 (C4′), 123.2 (C6″), 123.4 (C6′), 124.6 (C4), 125.2 (C2′), 126.3 (C3a″), 126.7 (C3a′), 132.3 (C2″), 137.1 (C7a″), 137.2 (C7a′), 138.0 (C3), 145.6 (C7/8), 169.4 (C2), 195.4 ppm (C6/9); MS (FAB)$^+$ (glycerin): m/z (%): 526 (13) $[M+H]^+$, 256 (25); HRMS (FAB)$^+$: m/z calcd for $C_{32}H_{20}N_3O_5$ $[M+H]^+$: 526.1403; found: 526.1382.

Received: August 4, 2003 [Z52549]

Keywords: alkaloids · biosynthesis · skin diseases · yeasts

[1] G. Midgley, *Med. Mycol.* **2000**, *38*(Suppl. 1), 9–16.
[2] P. Mayser, G. Wille, A. Imkampe, W. Thoma, N. Arnold, T. Monsees, *Mycoses* **1998**, *41*, 265–271.
[3] G. Wille, P. Mayser, W. Thoma, T. Monsees, A. Baumgart, H.-J. Schmitz, D. Schrenk, K. Polborn, W. Steglich, *Bioorg. Med. Chem.* **2001**, *9*, 955–960.
[4] P. Mayser, U. Schäfer, H.-J. Krämer, B. Irlinger, W. Steglich, *Arch. Dermatol. Res.* **2002**, *294*, 131–134.
[5] A. K. Gupta, R. Bluhm, R. Summerbell, *J. Eur. Acad. Dermatol. Venereol.* **2002**, *16*, 19–33.
[6] M. Brenner, H. Rexhausen, B. Steffan, W. Steglich, *Tetrahedron* **1988**, *44*, 2887–2892.
[7] P. Mayser, H. Stapelkamp, H.-J. Krämer, M. Podobinska, W. Wallbott, B. Irlinger, W. Steglich, *Antonie van Leeuwenhoek* **2003**, *84*, 185–191.
[8] For details, see Supporting Information.
[9] a) A. Heesing, R. Müller-Matthesius, H. Rose, *Justus Liebigs Ann. Chem.* **1970**, *735*, 72–76; b) H. N. Song, J. S. Son, M. R. Seong, J. N. Kim, *Synth. Commun.* **1998**, *28*, 687–692.
[10] Reviews: a) W. Steglich, *Pure Appl. Chem.* **1989**, *61*, 281–288; b) M. Gill, W. Steglich, *Prog. Chem. Org. Nat. Prod.* **1987**, *51*, 1–317; c) G. W. Gribble, S. J. Berthel, *Stud. Nat. Prod. Chem.* **1993**, *12*, 365–409 (stereoselective synthesis); d) J. Bergman, T. Janosik, N. Wahlstrom, *Adv. Heterocycl. Chem.* **2001**, *80*, 1–71.
[11] H.-J. Krämer, D. Kessler, W. Steglich, P. Mayser, *Arch. Dermatol. Res.* **2003**, *294*, 492.

 © 2004 Wiley-VCH Verlag GmbH & Co. KGaA, Weinheim

Structures of Macromolecules

New Perspectives for the Design of Molecular Actuators: Thermally Induced Collapse of Single Macromolecules from Cylindrical Brushes to Spheres**

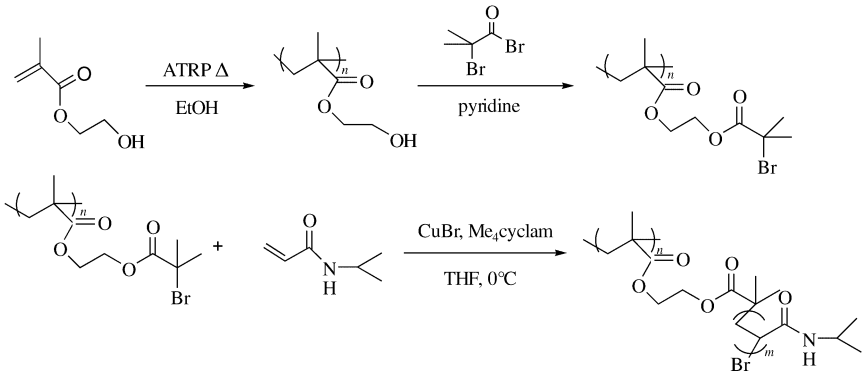
*Chengming Li, Nikhil Gunari, Karl Fischer, Andreas Janshoff, and Manfred Schmidt**

Linear flexible chains with densely grafted long side chains exhibit the shape of cylindrical brushes provided that the main chain is much longer than the side chains. Such structures may be prepared by polymerization of macromonomers,[1] by grafting from a linear macro initiator,[2] and by grafting onto a multifunctional linear chain.[3] Each of the methods has its particular advantages and disadvantages.[4]

The conformation of the main chain in cylindrical-brush polymers is not fully stretched, as revealed by light-scattering measurements and atomic force microscopy (AFM). The length of the cylinder per main chain monomer decreases with decreasing side-chain length and with decreasing solvent quality for the side chain.[5] This behavior is understood in terms of the simple picture that with increasing repulsion of the side chains the main chain is stretched until the entropic restoring force of the main chain balances the repulsive forces originating from the interactions between the side chains.

Nanomanipulation of single macromolecular objects and responsive polymers or particles is an exciting challenge in contemporary research on polymers and supramolecular systems. Recently, dendronized polymers consisting of a long main chain and regularly branched side chains (dendrons of up to the fourth generation) were successfully moved and manipulated on a graphite surface by an AFM tip.[6] Statistical copolymers of two different macromonomers were observed to exhibit a transition from cylindrical brushes to regularly curved structures, such as horseshoe- or meanderlike shapes, when the side chains were made incompatible by chemical transformations.[7] Homopolymer cylindrical brushes spread on the air–water interface were found to adopt a spherical shape upon lateral compression of the monolayer.[8] This cylinder–sphere transition was shown to be reversible upon expanding the film.

Here we report on the synthesis, characterization, and properties of cylindrical-brush polymers comprising poly-*N*-isopropyl-acrylamide (PNIPAM) side chains, in which the side-chain repulsion can be controlled easily by variation of the temperature due to the well-known lower critical solution temperature in aqueous solution.[9] In the present approach the macro initiator poly-2-bromoisobutyryloxyethyl methacrylate (PBIEM) was prepared by atom-transfer radical polymerization (ATRP) of hydroxyethylmethacrylate and subsequent reaction with α-bromoisobutyric acid bromide (Scheme 1, for details see the Supporting Information).



Scheme 1. Synthesis of the macro initiator and of the cylindrical PNIPAM brush polymers.

The characterization of the macro initiator PBIEM is summarized in Table 1. The observed values for the square root of the *z*-average mean squared radius of gyration, which describes the squared distance of all monomers from the center of gravity of a macromolecule, $R_g \equiv \langle s^2 \rangle_z^{1/2}$, and the hydrodynamic radius $R_h \equiv \langle R_h^{-1} \rangle_z^{-1}$, which represents an inverse *z*-average, are typical for an expanded flexible coil. ATRP grafting from macro initiator chains are well known for a variety of monomers like *tert*- and *n*-butyl-acrylate, methylacrylate, and styrene.[2] Although ATRP of acrylamides is known to proceed uncontrolled,[10] grafting of NIPAM from planar substrates was reported to yield planar brushes with a high grafting density.[11] However, polymerization of NIPAM in THF at room temperature utilizing the macro initiator always resulted in gel formation. Eventually, a soluble polymer could be obtained by polymerization at 0 °C. Gel-permeation chromatography (GPC) showed a high and a low molar mass peak, the latter of which obviously originates from the linear homopolymer which, however, could be

Table 1: Characterization of the macro initiator PBIEM in THF.

M_w [g^{-1} mol^{-1}]	R_g [nm]	R_h [nm]	M_w/M_n[a]	f [%][b]	N_w^{Br}[c]	L_w^{LS} [nm][d]
213 000	20.8	10.5	1.37	94.7	744	196

[a] Determined by GPC (polystyrene calibration). [b] Conversion of HEMA into bromoisobutyrate macro initiator. [c] Number of bromoisobutyrate groups per chain. [d] Contour length $L_w = P_w 0.25$ nm.

[*] Dr. C. Li, N. Gunari, Dr. K. Fischer, Prof. Dr. A. Janshoff, Prof. Dr. M. Schmidt
Institut für Physikalische Chemie, Johannes Gutenberg Universität
Jakob-Welder-Weg 11, 55128 Mainz (Germany)
Fax: (+49) 6131-3922970
E-mail: mschmidt@mail.uni-mainz.de

[**] Financial support by the Fond der Chemischen Industrie, the BMBF (FKZ: 03N6500) and the Deutsche Forschungsgemeinschaft is gratefully acknowledged.

Supporting information for this article is available on the WWW under http://www.angewandte.org or from the author.

 DOI: 10.1002/anie.200352845 © 2004 Wiley-VCH Verlag GmbH & Co. KGaA, Weinheim

completely removed by repeated precipitation and ultrafiltration.

The purified cylindrical-brush polymers were investigated by light scattering and by AFM (Table 2). The contour length of the macro initiator is calculated to $L_w^{AFM} = 193$ nm from the

Table 2: Characterization of the PNIPAM brushes in water at 20 °C.

M_w [$\times 10^{-6}$ g mol^{-1}]	R_g [nm]	R_h [nm]	L_w^{AFM} [nm]
10 ± 1	61.0	51.8	110

measured weight average molar mass M_w according to $L_w = l M_w M_0^{-1}$ (with M_0 the molar mass of one repeat unit) assuming $l = 0.25$ nm per repeat unit. This value ought to be compared to the length L_w^{AFM} derived from AFM pictures. Figure 1 a displays an image obtained from the cylindrical-

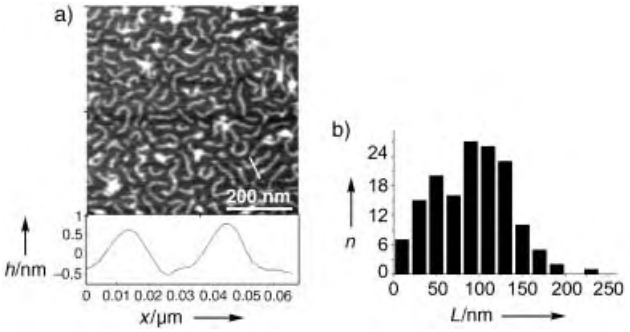


Figure 1. a) AFM picture of the cylindrical PNIPAM brush polymers spin cast at 20 °C from aqueous solution. b) Histogram of the contour length yielding $L_w^{AFM} = 110$ nm, $L_w L_n^{-1} = 1.23$ (average of 152 molecules).

brush polymers in the dry state (spin cast from aqueous solution), and Figure 2 a shows the cylindrical-brush polymers in water at room temperature, respectively. Remarkably, the values measured in the dry state and under water do not differ significantly, that is, the conformation of the cylindrical-brush polymers does not change during the drying process. The cylinder length per monomer, l, is calculated to $l = 0.25\, L_w^{AFM} (L_w^{LS})^{-1} = 0.14$ nm. This small value for l means

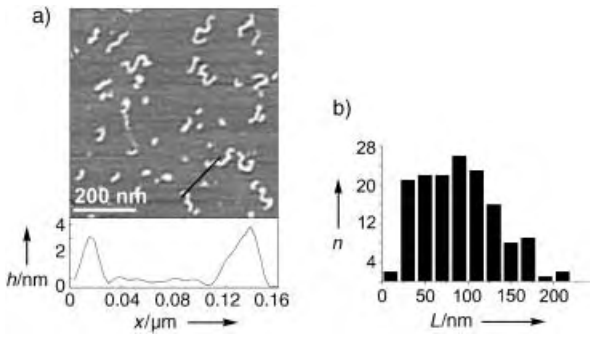


Figure 2. a) AFM picture of the cylindrical PNIPAM brush polymers in water at $T = 20$ °C. b) Histogram of the contour length yielding $L_w^{AFM} = 109$ nm, $L_w L_n^{-1} = 1.22$ (average of 152 molecules).

that the main chain is not completely stretched out but locally coiled. The number of grafted side chains per macro initiator chain as well as the side-chain molar mass and molar mass distribution cannot be determined unless the side chains are cleaved off the main chain and are investigated separately. This is beyond the scope of the present communication. However, usually the molar mass of the grafted side chains is similar to that of the free homopolymer formed by chain transfer in solution, which was determined to the number average molar mass $M_n = 15\,000$ g mol^{-1}, $M_w M_n^{-1} = 1.48$ (GPC in DMF, PMMA calibration). So far, there is no rigorous proof in the literature that each bromoisobutyrate group indeed has started a side chain nor any proof for intramolecular loop formation due to recombination. In view of the fact that for many systems at high monomer conversion chemically cross-linked gels are obtained, intramolecular loop formation is quite likely. From the molar mass of the PNIPAM brushes and the number of initiating groups per chain, N_w^{Br}, a lower limit of the side-chain molar mass is estimated to $M_n(\text{PNIPAM}) = M_w^{LS} (N_w^{Br})^{-1} = 13\,000$ g mol^{-1}. This represents a lower limit because possibly not all initiation sites had started a side chain.

On the first sight the stiff wormlike cylinders observed by AFM do not seem to be compatible with the light-scattering results since for high aspect ratios in the order of 10 the ratio $\rho \equiv R_g R_h^{-1}$ should have values of roughly 2,[12] which are significantly larger than $\rho = 1.1$–1.2 observed experimentally. Also, for a given contour length $L_w = 110$ nm the radius of gyration should not exceed $R_g = 44$ nm, the maximum value calculated for a polydisperse rod with $M_w M_n^{-1} = 1.33$ (assuming a Schulz–Zimm distribution with a convolution parameter $m = 3$). This discrepancy is resolved by inspection of the AFM picture shown in Figure 3, which was measured on a sample in the dry state spin cast from an acetone solution. Here the side-chain corona is clearly resolved, and we anticipate that this picture better resembles the situation of the swollen PNIPAM side chains in solution.

The discussion above has two important consequences: 1) The aspect ratio is much lower than estimated from the AFM pictures taken in water, where most probably the PNIPAM side chains could not be resolved or are collapsed onto the main chain. 2) The contour length has to be

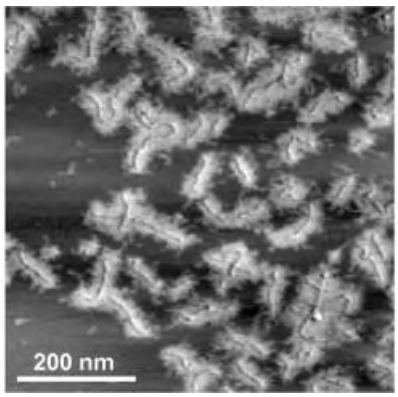


Figure 3. AFM picture of the cylindrical PNIPAM brush polymers spin cast from a dilute solution in acetone. The extended side-chain corona is clearly resolved.

 © 2004 Wiley-VCH Verlag GmbH & Co. KGaA, Weinheim

increased by twice the thickness of the side-chain corona because the side chains at both ends of the main chain do contribute to the cylinder length. From Figure 3 the extension of the side chains is estimated to 20 nm thus increasing the contour length to $L_w \cong 150$ nm and decreasing the aspect ratio to $L_w d^{-1} \cong 3$. With these numbers the calculations yield a maximum value of $R_g = 60$ nm and $\rho \approx 1.26$, which now are compatible with the experimental data.

In Figure 4 the variation of R_g, R_h, and M_w with temperature are summarized. Between 20 °C and 38 °C the molar

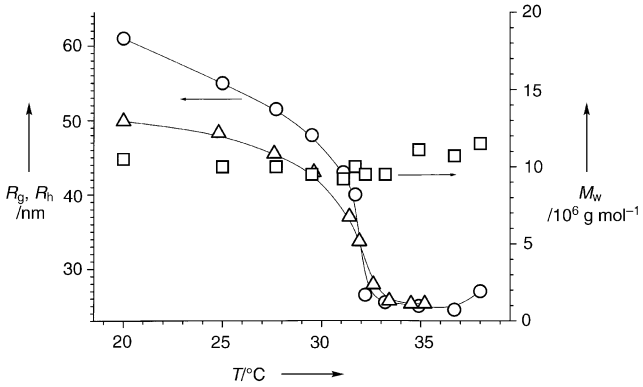


Figure 4. Molar mass M_w (□, right axis), radius of gyration R_g (○, left axis), and hydrodynamic radius R_h (△, left axis) as function of the temperature T.

mass of the polymer remains constant at about $(10 \pm 1) \times 10^6$ g mol^{-1}. This proves that the collapse of the cylindrical-brush polymer is a single macromolecule phenomenon. The radius of gyration R_g is observed to gradually decrease from 61 nm at 20 °C to about 40 nm at 31 °C, followed by a strong decrease from 40 nm to 25 nm within a small temperature interval of only 0.5 °C. The first slow decrease of R_g from 60 to 40 nm reflects the shrinkage of the brush polymer caused by the decreasing solvent quality, similar to that reported earlier for a different system.[5] AFM on spin-cast samples at 30 °C also revealed a reduced cylinder length $L_w^{AFM}(30°) = 94$ nm, which is in good agreement with the observed decrease of R_g if the reduced contribution of the collapsed side chains to L_w is reduced to only 10 nm; in other words, the side chains should be at least partly collapsed.

When the known lower critical solution temperature of the PNIPAM side chains is reached, the transition from a cylindrical-brush polymer to a collapsed structure takes place. It should be noted that the solution remains stable up to 38 °C, above which aggregation and eventually precipitation occurs. This shape transition is completely reversible. However, we have not yet investigated if a hysteresis is possible. The value of $\rho \approx 0.9$ in the collapsed regime indicates the formation of very compact objects, probably spheres that have collapsed to a solution density of ≈ 0.25 g cm^{-3}. The AFM picture from a sample spin cast at 38 °C from aqueous solution (Figure 5) corroborates this interpretation because oblate ellipsoids are observed. This is typically found for soft spheres which deform at the surface either due to tip–sample interaction or adhesion on the substrate.

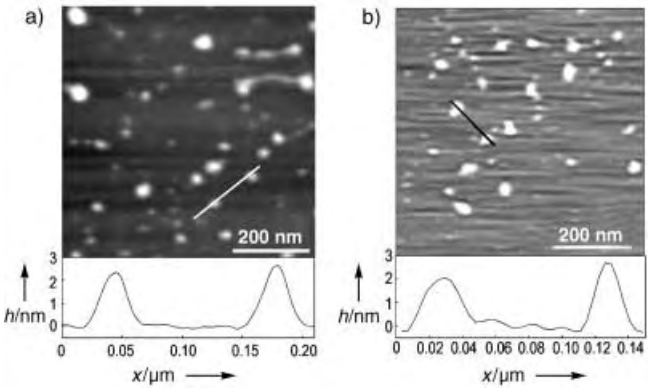


Figure 5. a) AFM picture of the collapsed PNIPAM brush polymers spin cast from aqueous solution at $T = 38$ °C and b) measured in water at $T = 38$ °C.

Whereas the temperature-induced coil collapse of linear PNIPAM chains is known,[9b,c] to the best of our knowledge the present communication reports the first observation of a transition of a single macromolecule cylinder to a sphere for a synthetic system within an extremely small temperature range. Possibly this could be the basis for future experiments towards the realization of soft nanomachines, in which mechanical action is triggered by variation of the temperature.

Received: September 11, 2003 [Z52845]

Keywords: molecular actuators · nanostructures · polymers · scanning force microscopy

[1] a) Y. Tsukahara, K. Mizuno, A. Segawa, Y. Yamashita, *Macromolecules* **1989**, *22*, 1546; b) Y. Tsukahara, K. Tsusumi, Y. Yamashita, S. Shimada, *Macromolecules* **1990**, *23*, 5201; c) K. Ishizu, K. Tsubaki, *Polymer* **1998**, *39*, 2935; d) M. Wintermantel, M. Schmidt, Y. Tsukahara, K. Kajiwara, S. Kohjiya, *Macromol. Rapid Commun.* **1994**, *15*, 279; e) M. Wintermantel, M. Gerle, K. Fischer, M. Schmidt, I. Wataoka, H. Urakawa, K. Kajiwara, Y. Tsukahara, *Macromolecules* **1996**, *29*, 978; f) P. Dziezok, S. S. Sheiko, K. Fischer, M. Schmidt, M. Möller, *Angew. Chem.* **1997**, *109*, 2894; *Angew. Chem. Int. Ed.* **1997**, *36*, 2812; g) S. S. Sheiko, M. Gerle, K. Fischer, M. Schmidt, M. Möller, *Langmuir* **1997**, *13*, 5368; h) M. Gerle, M. Schmidt, K. Fischer, S. Roos, A. H. E. Müller, S. S. Sheiko, S. Prokhorova, M. Möller, *Macromolecules* **1999**, *32*, 2629; i) R. Djalali, N. Hugenberg, K. Fischer, M. Schmidt, *Macromol. Rapid Commun.* **1999**, *20*, 444; j) K. Ito, H. Tanaka, G. Imai, S. Kawaguchi, S. Isuno, *Macromolecules* **1991**, *24*, 2348; k) K. Tsubaki, K. Ishizu, *Polymer* **2001**, *42*, 8387; l) S. Kawaguchi, K. Akaike, Z.-M. Zhang, H. Matsumoto, K. Ito, *Polym. J.* **1998**, *30*, 1004; m) S. Kawaguchi, M. Maniruzzaman, K. Katsuragi, H. Matsumoto, Iriany, K. Ito, N. Hugenberg, M. Schmidt, *Polym. J.* **2002**, *34*, 253; n) V. Heroguez, S. Breunig, Y. Gnanou, M. Fontanille, *Macromolecules* **1996**, *29*, 4459.

[2] a) K. L. Beers, S. G. Gaynor, K. Matyjaszewski, S. S. Sheiko, M. Möller, *Macromolecules* **1998**, *31*, 9413; b) H. G. Börner, K. L. Beers, K. Matyjaszewski, S. S. Sheiko, M. Möller, *Macromolecules* **2001**, *34*, 4375; c) G. Cheng, A. Böker, M. Zhang, G. Krausch, A. H. E. Müller, *Macromolecules* **2001**, *34*, 6883; d) M. Zhang, T. Breiner, H. Mori, A. H. E. Müller, *Polymer* **2003**, *44*, 1449.

 © 2004 Wiley-VCH Verlag GmbH & Co. KGaA, Weinheim

[3] a) A. Deffieux, M. Schappacher, *Macromolecules* **1999**, *32*, 1797; b) A. Deffieux, M. Schappacher, *Macromolecules* **2000**, *33*, 7371.
[4] M. W. Neiser, J. Okuda, M. Schmidt, *Macromolecules* **2003**, *36*, 5437.
[5] a) K. Fischer, M. Schmidt, *Macromol. Rapid Commun.* **2001**, *22*, 787; b) K. Fischer, M. Gerle, M. Schmidt, *Polym. Mater. Sci. Eng.* **1999**, *80*, 133.
[6] a) L. Shu, A. D. Schlüter, C. Ecker, N. Severin, J. P. Rabe, *Angew. Chem.* **2001**, *113*, 4802; *Angew. Chem. Int. Ed.* **2001**, *40*, 4666; b) J. Barner, F. Mallwitz, L. Shu, A. D. Schlüter, J. P. Rabe, *Angew. Chem.* **2003**, *115*, 1976; *Angew. Chem. Int. Ed.* **2003**, *42*, 1932.
[7] T. Stephan, S. Muth, M. Schmidt, *Macromolecules* **2002**, *35*, 9857.
[8] a) S. S. Sheiko, S. A. Prokhorova, K. L. Beers, K. Matyjaszewski, I. I. Potemkin, A. R. Khokhlov, M. Möller, *Macromolecules* **2001**, *34*, 8354; b) S. S. Sheiko, M. Möller, *Chem. Rev.* **2001**, *101*, 4099.
[9] a) H. G. Schild, Prog. *Polym. Sci.* **1992**, *17*, 163; b) K. Kubota, S. Fujishige, I. Ando, *J. Phys. Chem.* **1990**, *94*, 5154; c) C. Wu; S. Zhou, *Phys. Rev. Lett.* **1996**, *77*, 3053.
[10] a) J. T. Rademacher, M. Baum, M. E. Pallack, W. J. Brittain, W. J. Simonsick, *Macromolecules* **2000**, *33*, 284; b) M. Teodorescu, K. Matyjaszewski, *Macromolecules* **1999**, *32*, 4826.
[11] a) L. K. Ista, S. Mendez, V. H. Pérez-Luna, G. P. López, *Langmuir* **2001**, *17*, 2552; b) S. Mendez, L. K. Ista, G. P. López, *Langmuir* **2003**, *19*, 8115; c) D. M. Jones, W. T. S. Huck, *Adv. Mater.* **2001**, *13*, 1256; d) D. M. Jones, A. A. Brown, W. T. S. Huck, *Langmuir* **2002**, *18*, 1265.
[12] M. Schmidt, *Macromolecules* **1984**, *17*, 553.

 © 2004 Wiley-VCH Verlag GmbH & Co. KGaA, Weinheim

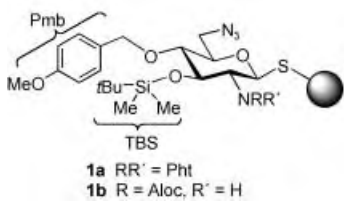
Solid-Phase Synthesis

Carbohydrate Scaffolds for Combinatorial Syntheses That Allow Selective Deprotection of All Four Positions Independent of the Sequence**

*Udo Hünger, Janina Ohnsmann, and Horst Kunz**

Combinatorial chemistry[1] has accelerated the syntheses of novel active compounds in both pharmaceutical and agrochemical industries. To carry out solution-phase parallel combinatorial syntheses, sophisticated robots have been developed, but the applied procedures are limited by the total number of synthetic operations achievable. Thus, combinatorial syntheses on solid support remain particularly important for the generation of libraries of active compounds with highly diverse structures. Besides linear sequential syntheses of peptides and peptidomimetic compounds[1] as the origin of combinatorial chemistry,[2] and multicomponent reactions,[3] selective transformations on multifunctional scaffolds are increasingly attractive for combinatorial applications. In this sense cyclopeptides with various side chains,[4] bile acid derivatives,[5] aryl-[6] and squaric acid building blocks[7] have been combinatorially applied as scaffolds for the introduction of side chains.

Carbohydrates, more specifically monosaccharides, hold an extraordinary density of functional groups and chiral information per molecular unit. This feature has previously been used in synthesizing peptido-[8] and aminoglycoside mimics.[9] In the form of immobilized scaffolds on solid support, monosaccharides have proved suitable for combinatorial diversification as aminouronic acid derivatives[10] at three positions, in the case of selectively deprotectable glucose and galactose scaffolds at four,[11] and even at all five positions.[13] Nevertheless these systems require a certain sequence of deprotection and introduction of the desired side chains. So far it has not been feasible to selectively remove an individual protective group from any arbitrary position, whilst leaving the protective groups on the other positions untouched. Herein we report the first successful application of such a strategy for 2,6-diaminoglucose scaffolds. The strategy is based on the protective group concept **1** shown in Scheme 1.



Scheme 1. Protective group concept for a selectively deprotectable carbohydrate scaffold. Aloc = allyloxycarbonyl.

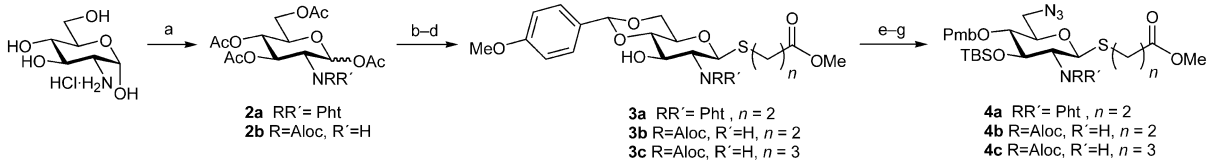
Preserving the thioglycosidic anchoring group[11,12,14] and all other protected functionalities, the tBuMe$_2$Si (TBS) group is removable with fluoride and at the same time stable towards all deprotection conditions for the other functionalities. Corresponding demands have to be applied to the reduction of the 6-azido group and the oxidative cleavage of the *p*-methoxy benzyl (Pmb) group in position 4. For the protection of the 2-amino group the phthaloyl (Pht) as well as the allyloxycarbonyl (Aloc) group have been utilized. The thioglycosidic linker of the scaffold, which can be activated for glycosylations with bromine as has been shown previously,[11,12] was attached to tentagel[14] resin through the acid-labile Rink benzhydryl amide linker.[15] The Rink linker facilitates cleavage of the products from the solid phase without affecting any other functional group incorporated in the scaffold. In this way, removal from the solid support can be achieved after every synthetic step and the products can be analyzed.

To synthesize the completely protected diaminoglucose scaffold, glucosamine hydrochloride was N-acylated with either phthalic anhydride or allyl chloroformate and directly per-O-acetylated to form the products **2a** or **2b**, respectively (Scheme 2). BF$_3$·Et$_2$O-Induced stereoselective glycosylation

[*] Dr. U. Hünger, Dipl.-Chem. J. Ohnsmann, Prof. Dr. H. Kunz
Institut für Organische Chemie der Universität Mainz
Duesbergweg 10–14, 55128 Mainz (Germany)
Fax: (+49) 6131-392-4786
E-mail: hokunz@uni-mainz.de

[**] This work was supported by the Deutschen Forschungsgemeinschaft and the Fonds der Chemischen Industrie. U.H. is grateful to the Fonds der Chemischen Industrie for a Kekulé Fellowship.

 © 2004 Wiley-VCH Verlag GmbH & Co. KGaA, Weinheim DOI: 10.1002/anie.200352919



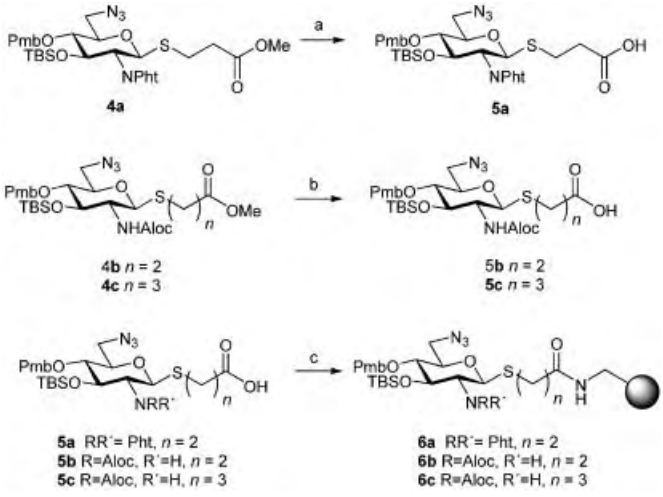
Scheme 2. a) **2a**: 1. Phthalic anhydride, $NaHCO_3$ aq., dioxane, 20 °C, 6 h; 2. Ac_2O, pyridine, 20 °C, 12 h, 72 %; **2b**: 1. AlocCl, $NaHCO_3$ aq., dioxane, 20 °C, 10 h; 2. Ac_2O, pyridine, 20 °C, 12 h, 73 %; b) methyl mercaptoalkylcarboxylate, $BF_3{\cdot}OEt_2$, CH_2Cl_2, 20 °C, 12 h, 46 %–82 %; c) NaOMe, MeOH, 20 °C, 4 h, quant.; d) anisaldehyde dimethyl acetal, TsOH, DMF, 50 °C, 20 mbar, 6 h, 68–70 %; e) TBSOTf, pyridine, CH_2Cl_2, 0–20 °C, 4 h, 78–97 %; f) $NaBH_3CN$, TMSCl, acetonitrile, 0–20 °C, 12 h, 56–85 %; g) 1. MsCl, pyridine, CH_2Cl_2, 0 −20 °C, 6 h; 2. NaN_3, DMF, 75 °C, 50–84 %. Ts = *p*-tolylsulfonyl; Ms = methanesulfonyl.

of methyl mercaptopropionate (to form **3a** or **3b**) and methyl 4-mercaptobutyrate (to form **3c**) introduced the respective thioglycosidic anchor. After the O-acetyl groups were removed upon treatment with catalytic amounts of sodium methoxide in methanol, the 4,6-*p*-methoxybenzylidene acetal was installed to furnish carbohydrates **3a–c**. *tert*-Butyldimethylsilyltriflate (TBSOTf) was used to silylate the 3-OH group in the presence of pyridine. Subsequently, 6-OH deprotection was achieved regioselectively by reductive ring opening of the benzylidene acetal with sodium cyanoborohydride and trimethylsilyl chloride.[16] The resulting free hydroxy group was converted to the corresponding methanesulfonate. The latter was then displaced using sodium azide in DMF to give access to the scaffolds **4a–c**.

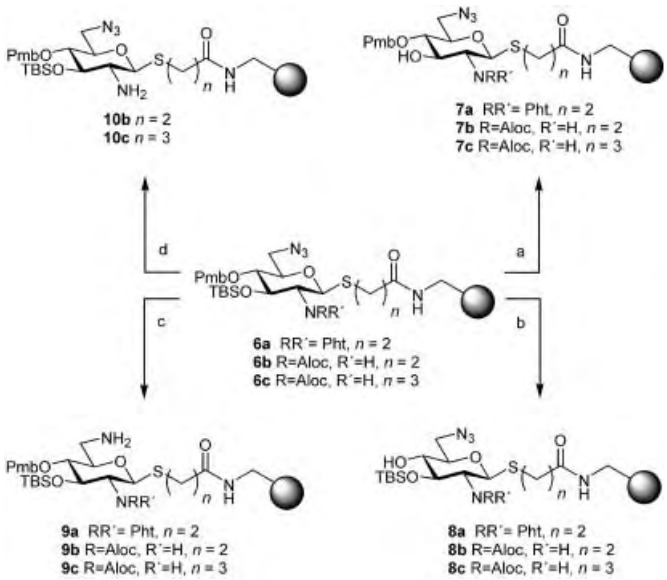
To attach the scaffold to the Rink amide tentagel resin it was necessary to convert the methyl ester of the anchor to the carboxylic acid without affecting any base-labile protective groups incorporated in scaffolds **4a–c**. In case of **4a** the ester was cleaved with lithium chloride and thiophenol[17] in DMF at 75 °C under S_N2 conditions (Scheme 3a). The base-stable Aloc group of **4b** and **4c** remains after saponification with lithium hydroxide in a mixture of water/THF (Scheme 3b).

The resulting carboxylic acids **5a–c** were coupled to the Rink benzylhydrylamine resin in high yields by using *O*-(1*H*-benzotriazolyl)-*N*,*N*,*N*′,*N*′-tetramethyluronium hexafluorophosphate (HTBU)[18] and 1-hydroxy-benzotriazole (HOBt) in the presence of Hünigs base (Scheme 3c). The coupling reactions were monitored by both FTIR and high-resolution magic angle spinning (HRMAS) NMR spectroscopy.[19] Following the coupling reaction unreacted benzhydryl functionalities were end-capped with methanesulfonyl chloride in the presence of pyridine.

Selective deprotections of the polymer-bound scaffolds **6a–c** were conducted to prove the concept of the orthogonal stability for the chosen set of protective groups. By using tetrabutylammonium fluoride (TBAF) trihydrate in THF or its HF adduct, the TBS groups were, according to HRMAS-NMR spectroscopy, quantitatively removed[20] yielding the 3-OH-deprotected scaffolds **7a–c** (Scheme 4, route a).



Scheme 3. a) PhSH, LiCl, DMF, 75 °C, 12 h, 52 %; b) LiOH, H_2O/THF, 20 °C, 5 h, 86 %; c) HBTU, HOBt, DMF, NEt*i*Pr_2, Rink amide tentagel, 90 %.



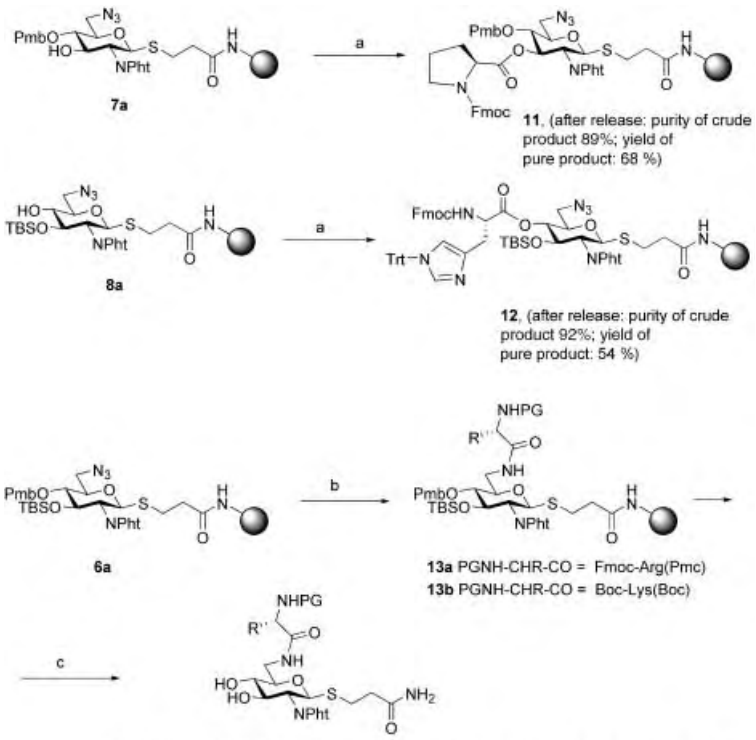
Scheme 4. a) TBAF, THF; b) DDQ, CH_2Cl_2/H_2O; c) 1. Bu_3P, DMF; 2. Et_3N, DMF/H_2O; d) **6b** and **6c**: [$Pd_2(dba)_3$], *p*-toluenesulfinic acid, DMF. dba = *trans*,*trans*-dibenzylideneacetone.

Treatment of **6a–c** with 2,3-dichloro-5,6-dicyano-1,4-quinone (DDQ)[21] in CH_2Cl_2 and 10 vol % water led to the selective removal of the methoxybenzyl ether portective groups and thus to the resin-bound compounds **8a–c** (Scheme 4, route b). The 6-azido groups were reduced under Staudinger conditions with tri-*n*-butylphosphane, followed by hydrolysis of the resulting phosphine imines with triethylamine in DMF in the presence of water to give **9a–c** (Scheme 4, route c). Only the cleavage of the phthaloyl group

 © 2004 Wiley-VCH Verlag GmbH & Co. KGaA, Weinheim

from **6a** with hydrazine hydrate, which can be achieved readily in solution for an analogous compound, gave unsatisfactory results on the resin. In DMF at 30 °C the Rink linker was obviously cleaved and the structure of the polymer was affected in a way, which the intended reaction could not proceed. In contrast, the Aloc groups in **6b** and **6c** were cleaved selectively by palladium(0)-catalyzed allyl transfer reactions in *p*-toluenesulfinic acid[22] to form carbohydrates **10b** and **10c** without any problems (Scheme 4, route d). The 2-*N*-Aloc-protected frameworks **6b** and **6c** satisfy all requirements for a multifunctional chiral scaffold selectively deprotectable in any position independently of the sequence. In the case of the phthaloyl-protected analogue **6a**, diversity at the 2-amino group can be applied after cleavage from the solid phase.

Position-selective introduction of side chains as demonstrated herein for the esterification and amidation with Fmoc-protected amino acids, was conducted without affecting any of the protecting groups. To esterify position 3 in **7a** or position 4 in **8a** the Fmoc-amino acids were activated with *N*,*N*′-diisopropylcarbodiimide (DIC) and 4-dimethylaminopyridine (DMAP; Scheme 5).[23] All reactions gave quantitative conversion of the starting materials at ambient temperature, as has been shown by UV-control of the Fmoc-cleavage[24] from analytical resin samples. Neither the phthaloyl group nor the Pmb (**11**) or the TBS groups (**12**) showed instability in the presence of DMAP.

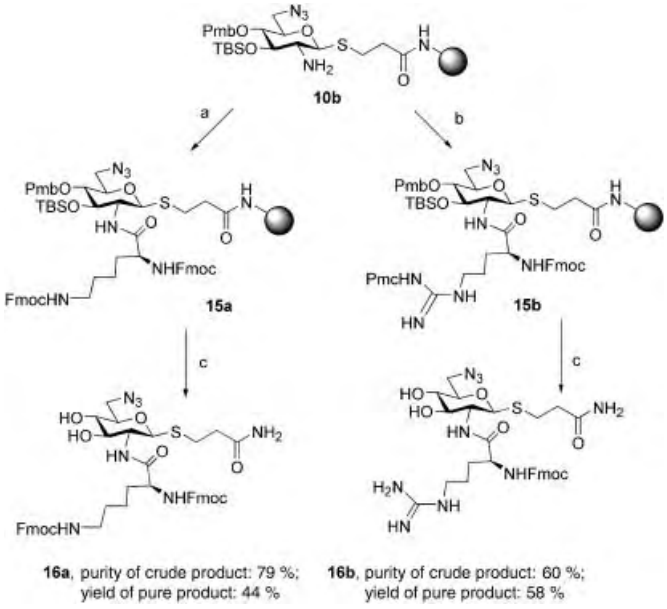


Scheme 5. a) PG-AA-OH, DIC, DMAP, DMF, 20 °C; b) PG-AA-OH, DIC, HOBt, Bu_3P, THF, 20 °C; c) TFA/CH_2Cl_2 1:1, mercaptomethyl polystyrene, 30 min, 20 °C. PG = protective group. Yields given refer to products purified by HPLC (purity > 95 %); purities of crude products determined by HPLC-MS directly after detachment from the resin are also quoted.

To prevent side reactions at the base-labile phthaloyl group during modification of the 6-position, model compound **6a** was converted directly to the amide in one step without isolating intermediate **9a** by combining the Staudinger reaction[25] with the subsequent amide coupling (Scheme 5). To this end, **6a** was treated with a solution of N- and side-chain-protected amino acids, DIC, HOBt,[26] and tri-*n*-butylphosphane in THF at ambient temperature. According to the UV spectroscopic determination of *N*-(9-fluorenylmethyl)piperidine after Fmoc cleavage from analytical samples of **13a** and **13b**, the reactions proceed quantitatively.

Finally the products **13a** and **13b**, like **11** and **12**, were detached from the Rink linker with trifluoroacetic acid (50 % in dichloromethane). Simultaneously all acid-labile protective groups, such as the Pmc group[27] of **13a** and the Boc group of **13b** or the trityl group of **12** as well as the Pmb and TBS groups were cleaved. mercaptomethyl polystyrene was used as scavenger nucleophile. The yields given for products **14a** and **14b** as well as those from **11** and **12** are based on **6a** as the starting material and involve at least three steps.

To introduce substituents in position 2, Aloc-protected scaffold **6b** was converted to 2-amino compound **10b**, which was subjected to peptide condensation with different amino acids. To monitor the reaction, analytical samples of **15a** and **15b** were treated with piperidine and the resulting Fmoc-adduct was examined by UV spectroscopy (Scheme 6).



Scheme 6. a) Fmoc-Lys(Fmoc)-OH, DIC, DMAP, DMF, 20 °C; b) Fmoc-Arg(Pmc)-OH, DIC, DMAP, DMF, 20 °C; c) TFA/CH_2Cl_2 1:1, mercaptomethyl polystyrene, 30 min, 20 °C. Pmc: 2,2,5,7,8-pentamethylchromane-6-sulfonyl. All yields (based on **6b**) refer to products purified by HPLC (purity > 95 %); purities of crude products determined by HPLC-MS are also quoted.

 © 2004 Wiley-VCH Verlag GmbH & Co. KGaA, Weinheim

Cleavage from the solid support and simultaneous deprotection of the acid-labile products gave the amino acid–carbohydrate conjugates **16a** and **16b**. The analysis of the remarkably clean cleavage products (78–95%; **16b** contains some TBS-protected compound) from **11**, **12**, **13**, and **15** was performed by HPLC using LD-detection combined with ESI mass spectrometry.

The described results show that 2,6-diaminoglucose **6** can be selectively deprotected and functionalized in every position of the polyfunctional chiral scaffold. The potential of this methodology lies in the ability to generate high diversity especially if the diversifications would be performed not only with Fmoc-protected amino acids, as demonstrated herein, but with an array of different compounds. This applies especially to compounds bearing a function corresponding to that of the replaced protective group. This would be the case for coupling a TBS or 2-trimethylsilylethoxycarbonyl-protected compound to the 3 position or a *p*-methoxybenzyl or *p*-methoxybenzyloxycarbonyl(MOZ)-protected compound to the 4 position. In this way, the initial orthogonal set of protective groups would be reproduced to form another building block of the type of **6** and thus offer enormous potential for the construction of ligand and receptor structures.

Received: September 19, 2003 [Z52919]

Keywords: carbohydrates · combinatorial chemistry · orthogonal protecting groups · protecting groups · solid-phase synthesis

[1] Reviews: a) L. A. Thomson, J. A. Ellman, *Chem. Rev.* **1996**, *96*, 555; b) J. S. Früchtel, G. Jung, *Angew. Chem.* **1996**, *108*, 19; *Angew. Chem. Int. Ed. Engl.* **1996**, *35*, 17; c) F. Balkenhohl, C. von dem Bussche-Hünnefeld, A. Lansky, C. Zechel, *Angew. Chem.* **1996**, *108*, 2436; *Angew. Chem. Int. Ed. Engl.* **1996**, *35*, 2288; d) A. Netzi, J. M. Ostresh, R. A. Houghten, *Chem. Rev.* **1997**, *97*, 449.

[2] a) H. M. Geysen, S. J. Bartling, R. H. Meloen, *Proc. Natl. Acad. Sci. USA* **1985**, *82*, 178; b) R. A. Houghten, *Proc. Natl. Acad. Sci. USA* **1985**, *82*, 5131; A. Furka, F. Sebestyen, M. Asgedom, G. Dibo, *Int. J. Pept. Protein Res.* **1991**, *37*, 487.

[3] a) I. Ugi, *J. Prakt. Chem.* **1997**, *339*, 499; b) P. A. Tempest, S. D. Brown, R. W. Armstrong, *Angew. Chem.* **1996**, *108*, 689; *Angew. Chem. Int. Ed. Engl.* **1996**, *35*, 640.

[4] a) D. Leipert, D. Nopper, M. Bauser, G. Gauglitz, G. Jung, *Angew. Chem.* **1998**, *110*, 3506; *Angew. Chem. Int. Ed.* **1998**, *37*, 3308.

[5] G. Wess, K. Bock, H. Kleine, M. Kurz, W. Guba, H. Hemmerle, E. Lopez-Calle, K.-H. Baringhaus, H. Glombik, A. Ehnsen, W. Kramer, *Angew. Chem.* **1996**, *108*, 2363; *Angew. Chem. Int. Ed. Engl.* **1996**, *35*, 2222.

[6] M. J. Plunkett, J. A. Ellman, *J. Org. Chem.* **1997**, *62*, 2885.

[7] P. A. Tempest, R. W. Armstrong, *J. Am. Chem. Soc.* **1997**, *119*, 7607.

[8] a) R. Hirschmann, K. C. Nicolaou, S. Pietramico, J. Salvino, E. M. Lealy, W. C. Shakespeare, P. S. Spengler, P. Hamley, A. B. Smith, T. Reisine, K. Raynor, C. Donaldson, W. Vale, L. Maechler, R. M. Freidinger, C. D. Strader, *J. Am. Chem. Soc.* **1993**, *115*, 12550; b) E. Graf von Roedern, E. Lohof, G. Hessler, M. Hoffmann, H. Kessler, *J. Am. Chem. Soc.* **1996**, *118*, 10156; c) T. Q. Dinh, C. D. Smith, X. Du, R. W. Armstrong, *J. Med. Chem.* **1998**, *41*, 981.

[9] C.-H. Wong, M. Hendrix, D. D. Manning, C. Rosenbohm, W. A. Greenberg, *J. Am. Chem. Soc.* **1998**, *120*, 8319.

[10] M. J. Sofia, R. Hunter, T. Y. Chan, A. Vaughan, R. Dulina, H. Wang, D. Gange, *J. Org. Chem.* **1998**, *63*, 2802.

[11] a) T. Wunberg, C. Kallus, T. Opatz, S. Henke, W. Schmidt, H. Kunz, *Angew. Chem.* **1998**, *110*, 2620; *Angew. Chem. Int. Ed.* **1998**, *37*, 2503; b) T. Opatz, C. Kallus, T. Wunberg, W. Schmidt, S. Henke, H. Kunz, *Carbohydr. Res.* **2002**, *337*, 2089.

[12] C. Kallus, T. Opatz, T. Wunberg, W. Schmidt, S. Henke, H. Kunz, *Tetrahedron Lett.* **1999**, *40*, 7783.

[13] T. Opatz, C. Kallus, T. Wunberg, W. Schmidt, S. Henke, H. Kunz, *Eur. J. Org. Chem.* **2003**, 1527.

[14] E. Bayer, W. Rapp, *Chem. Pept. Proteins* **1986**, *3*, 3.

[15] H. Rink, *Tetrahedron Lett.* **1987**, *28*, 3787.

[16] To prevent hydrolysis of the methyl ester, reported conditions (R. Johansson, B. Samuelsson, *J. Chem. Soc. Chem. Commun.* **1984**, 201) had to be changed, we used $NaCNBH_3$/Me_3SiCl in the ratio 15:1 and subsequent treatment of the reaction mixture with K_2CO_3 instead of Na_2CO_3 solution.

[17] With lithium iodide/thiophenol at 100°C (F. Elsing, J. Schreiber, A. Eschenmoser, *Helv. Chim. Acta* **1960**, *43*, 113) in DMF/pyridine no reaction was observed. Only after the addition of [12]crown-4 did the cleavage of the methyl ester begin (yield: 47%)

[18] R. Knorr, A. Trzeciak, W. Bannwarth, D. Gillessen, *Tetrahedron Lett.* **1989**, *30*, 1927.

[19] K. Thieme, G. Zech, H. Kunz, H. W. Spiess, I. Schnell, *Org. Lett.* **2002**, *4*, 1559. Rink tentagel resin (Rapp Polymere, Tübingen, Germany) loaded with 0.24 mmol g^{-1} benzhydryl amine was shaken in dimethyl formamide with 1.2 equivalents of the S-glycosylmercaptocarboxylic acid **5** for 12 h. After extensive washing with dimethyl formamide, dichloromethane, methanol, dichloromethane, and diethyl ether and drying, the remaining amino groups were treated with methanesulfonyl chloride. The loading with the carbohydrate scaffolds was determined by integration of the TBS and methanesulfonamide signals in the HRMAS NMR spectra, by elemental analysis, and by UV analysis of subsequent products (**11**–**13**) and amounted correspondingly to 0.19 mmol g^{-1} (yield of 80%).

[20] E. J. Corey, A. Venkateswarlu, *J. Am. Chem. Soc.* **1972**, *94*, 6190.

[21] Y. Oikawa, T. Nishi, O. Yonemitsu, *Tetrahedron Lett.* **1983**, *24*, 4037.

[22] a) M. Honda, H. Morita, I. Nakagura, *J. Org. Chem.* **1997**, *62*, 8932; b) T. Opatz, H. Kunz, *Tetrahedron Lett.* **2000**, *41*, 10185.

[23] B. Neises, W. Steglich, *Angew. Chem.* **1978**, *90*, 556; *Angew. Chem. Int. Ed.* **1978**, *17*, 522.

[24] L. A. Carpino, G. Y. Han, *J. Am. Chem. Soc.* **1970**, *92*, 5748.

[25] H. Staudinger, J. Meyer, *Helv. Chim. Acta* **1919**, *2*, 635.

[26] W. König, R. Geiger. *Chem. Ber.* **1970**, *103*, 788.

[27] R. Ramage, J. Green, *Tetrahedron Lett.* **1987**, *28*, 2287.

 © 2004 Wiley-VCH Verlag GmbH & Co. KGaA, Weinheim

Asymmetric Catalysis

Direct Catalytic Enantioselective α-Aminoxylation of Ketones: A Stereoselective Synthesis of α-Hydroxy and α,α′-Dihydroxy Ketones**

*Anders Bøgevig, Henrik Sundén, and Armando Córdova**

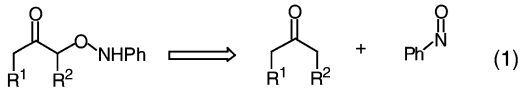
One of the ultimate goals and challenges in chemistry is to develop catalytic stereoselective transformations for the creation of optically active molecules from simple and easily available starting materials.[1] Optically active α-hydroxy carbonyl moieties are commonly found in numerous important natural products. This has led to extensive research to find new diastereoselective and enantioselective routes for their syntheses.[2] One way of preparing these compounds is the asymmetric α-hydroxylation of enolates.[3] Despite extensive research in this area it was not until recently that Yamomoto et al. reported a more efficient catalytic system based on AgX/binap complexes (binap = 2,2′-bis(diphenylphosphanyl)-1,1′-binaphthyl), which mediate indirect α-oxidation of activated tin enolates.[4]



1a

Asymmetric reactions catalyzed by metal-free organic catalysts have received increased attention in recent years.[5] Interestingly, following the discovery of amino acid catalyzed stereoselective Robinson annulations in the early 1970s,[6] there was no intensive research on this concept for other C–C bond-forming reactions for several decades even though the reaction is frequently used to prepare building blocks in natural products synthesis.[7] It was not until recently that researchers demonstrated that amino acid derivatives function as catalysts for direct asymmetric intermolecular reactions.[8–16]

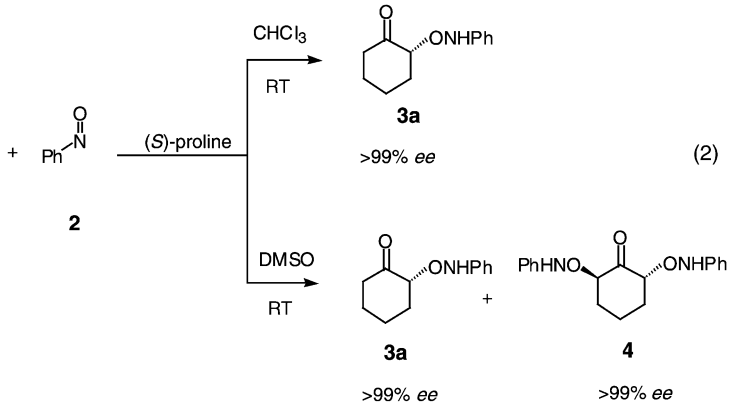
Based on the elegant work of Yamomoto et al. and our previous research on amine-catalyzed asymmetric synthesis, we envisioned that an amino acid could catalyze the α-oxyamination of unmodified ketones [Eq. (1)].[4,8d,f,g,i,9b–9g,10a,10c] We believed that the enhanced Brønstedt basicity of the nitrogen atom would favor O-addition over N-addition. Hence, we embarked on the quest to develop a novel enamine-catalyzed asymmetric route for the synthesis of α-hydroxy-containing molecules.[17]



(1)

Herein, we present a method for the direct catalytic α-oxidation of ketones. This new transformation yields protected α-hydroxy ketones with excellent regioselectivity and >99% *ee*. In addition, unsubstituted cyclic ketones were α,α′-dioxylated with remarkable high selectivity affording the corresponding C_2-symmetric ketodiols in >99% *ee*.

In an initial experiment, we treated cyclohexanone (**1a**) (10 mmol) with nitrosobenzene (**2**) (1 mmol) in the presence



(2)

of a catalytic amount of (*S*)-proline (20 mol%) in $CHCl_3$ (4 mL) at room temperature [Eq. (2)]. The initial light blue solution changed first to light green, then to dark green, and finally to orange within 30 min. The reaction was quenched after 2 h, and NMR analysis of the crude product revealed that no starting material remained and only α-aminooxylated ketone **3a** had formed. Most satisfying we could not observe the N-addition product, and ketone **3a** was isolated in 91% yield and >99% *ee* as determined by chiral HPLC analysis. The reactions also proceed with only two equivalents of cyclohexanone and 10 mol% of the catalyst.

Next, we tested a number of solvents (THF, $CHCl_3$, dimethylformamide (DMF), Et_2O, *N*-methylpyrrolidinone (NMP), toluene, dimethyl sulfoxide (DMSO), CH_3CN, and neat) for the proline-catalyzed α-aminoxylation with **1a** as the donor and found that the best solvents with regard to the reactivity of proline were $CHCl_3$ and DMSO. In all cases tested, the corresponding product **3a** was isolated with >95% *ee*. For example, the reaction in DMSO was complete within 30 min providing not only ketone **3a** in 70% yield and >99% *ee* but also the corresponding C_2-symmetric α,α′-diaminoxy ketone **4** in 22% yield and >99% *ee*. The formation of **4** could be circumvented by slow addition of **3a** (1M solution in DMSO) with a syringe pump to the reaction mixture. The second O-addition exhibited remarkable selectivity, since no *meso*-diol adduct was detected either by NMR or HPLC analyses during the course of the reaction. This is the first time that this type of double stereoselective nucleophilic attack to an electrophile has been reported in a

[*] Dr. A. Bøgevig, H. Sundén, Prof. Dr. A. Córdova
Department of Organic Chemistry
The Arrhenius Laboratory, Stockholm University
10691 Stockholm (Sweden)
Fax: (+46) 8-154-908
E-mail: acordova@organ.su.se
acordova1a@netscape.net

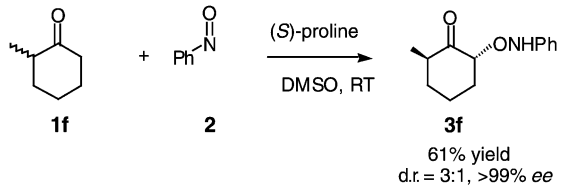
[**] We thank Prof. J.-E. Bäckvall and Prof. H. Adolfsson for valuable discussions and the Swedish National Research council and Wenner-Gren-Foundation for financial support. We also thank Prof. Hayashi and the referees for helpful discussions concerning the absolute configuration.

 DOI: 10.1002/anie.200353018 © 2004 Wiley-VCH Verlag GmbH & Co. KGaA, Weinheim

proline-catalyzed reaction, which indicates that nitrosobenzene is more reactive and/or provides less steric hindrance than other electrophiles such as diazocarboxylates or α-imino glyoxylates.[9,10]

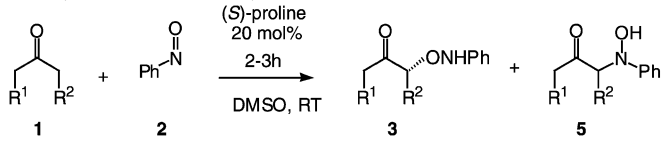
Next, we performed the corresponding reaction with a set of different aliphatic ketones (Table 1). The reactions were effective, and the corresponding α-aminoxy ketones **3a**–**3e** were isolated in good yield with >99% *ee*.[18] In addition, excellent regioselectivities were observed for α-aminoxylation of acyclic ketones and no α,α′-diaminoxylated ketones were observed. The oxidation occurred exclusively on the methylene carbon of the ketones. For example, protected hydroxy ketone **3b** was isolated as a single regioisomer in 70% yield with >99% *ee*. With regards to the O- or N-selectivity of the reaction, we found that the reaction was chemoselective, furnishing no N-addition products for transformations with cyclic ketones as donors. However, α-aminoxylation of acyclic ketones afforded small amounts (<25%) of the corresponding 2-aminated ketones **5** with the same regioselectivity as the O-addition adducts with a minor chiral induction.

Furthermore, the sterically hindered, racemic 2-methylcyclohexanone **1f** was also efficiently α- aminoxylated oxyaminated, providing the corresponding keto adduct **3f** as a 3:1 mixture of diastereomers (*trans/cis*) in >99% *ee* (Scheme 1). In this case, excellent O-selectivity was observed since no N-addition product was observed. The reactions were readily performed on gram scale in not strictly anhydrous solvents and in the presence of air. In addition, the progress of the reaction can be monitored simply by the human eye since the reaction mixture changes colors from light blue to green and finally to orange when the reaction is complete.



Scheme 1. Direct catalytic asymmetric synthesis of **3f**.

Table 1: Proline-catalyzed direct α-aminoxylation of different ketones.[a]

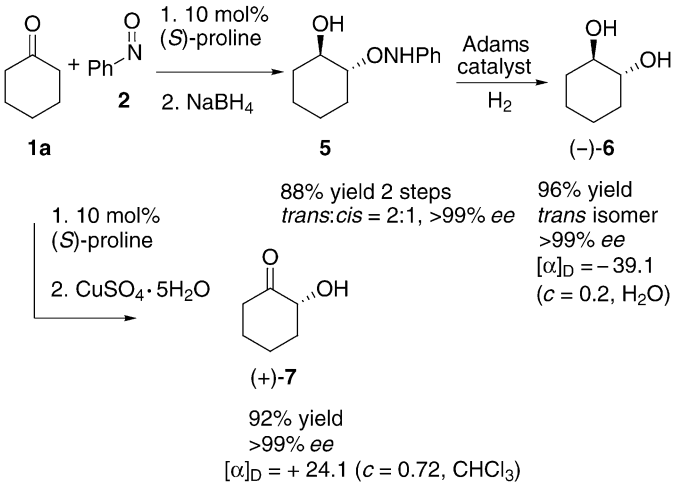


Entry	Ketone	R^1	R^2	Yield [%][b]	**3**:**5**	*ee* [%] of **3**[c]	*ee* [%] of **5**[c]
1	**1a**		$-(CH_2)_3-$	70	>100/1	>99	–
				(91)[d]	(>100/1)[d]	(>99)[d]	–
2	**1b**	H	Me	93	81:19	>99	11
3	**1c**	Et	Me	66	98:2	99	7
4	**1d**	H	$CH_2CH{=}CH_2$	87	8:22	>99	n.d.[e]
5	**1e**	H	*i*Pr	64	90:10	>99	n.d.[e]

[a] Experimental conditions: A mixture of **1** (10 mmol, 10 equiv), **2** (1 mmol), and (*S*)-proline was stirred at room temperature for 2–3 h. The crude product obtained after aqueous workup was purified by column chromatography. [b] Combined yield of isolated products after silica gel column chromatography. [c] Determined by chiral-phase HPLC analyses. [d] The reaction was performed in $CHCl_3$. [e] Not determined.

As selective reduction of α-hydroxy ketones to both *syn*- and *anti*-1,2-diols is known, the present procedure is one practical route for the preparation of all the possible stereoisomers of chiral 1,2-diols. In addition, the ketones **3a** and **4** were readily deprotected with $CuSO_4$ to afford the corresponding α-hydroxy ketone **7** and α,α′-dihydroxy ketone adducts in >90% yield without loss of enantioselectivity.[4]

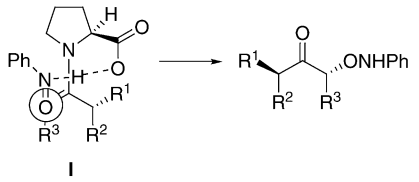
On the basis of the absolute configuration, which is opposite to adducts **3** derived from Yamamoto's reaction,[19] we propose



Scheme 2. Asymmetric synthesis of (1*R*,2*R*)-*trans*-1,2-cyclohexanediol (**6**) and (2*R*)-hydroxycyclohexanone (**7**).

 © 2004 Wiley-VCH Verlag GmbH & Co. KGaA, Weinheim

transition-state model **I** to account for the regio- and enantioselectivity of the α-oxidation reaction of unmodified substituted ketones (Scheme 3). Hence, (*S*)-proline forms an enamine with the ketone, which is attacked by the nitro-



I

Scheme 3. Transition-state models evoked to account for the regio- and enantioselectivity of the (*S*)-proline-catalyzed reaction.

sobenzene from its *se* face providing (2*R*)-α-aminoxylated ketones. This is in accordance with the transition states of previously reported proline-catalyzed Mannich and α-amination reactions, in which a *si*-facial attack occurs.[9,10,20] The proposed transition state **I** also explains how the unprecedented second attack of the electrophile could occur for the monoaminoxylated intermediate ($R^1 = ONHPh$).

In conclusion, we have developed the first direct enantioselective method that provides protected α-hydroxy ketones in $>99\%$ *ee*. The reactions were performed without tedious elaboration in wet solvents in the presence of air and are readily scaled up. In addition, reactions with α-unsubstituted cyclic ketones as donors in DMSO were remarkably selective, affording the corresponding C_2-symmetric α,α′-dihydroxy ketones with $>99\%$ *ee*. Further elaboration of this transformation and its synthetic application is being studied in our laboratory.[21]

Experimental Section

Typical experimental procedure (Table 1, entry 1): To a vial containing **2** (1 mmol) and a catalytic amount of (*S*)-proline (20 mol%) in $CHCl_3$ (4 mL) was added the ketone **1a** (1 mL, 10 equiv). After 2 h of vigorous stirring the reaction was quenched by the addition of aqueous NH_4Cl, and the aqueous phase was extracted three times with EtOAc. The combined organic layers were dried over $MgSO_4$, the solvent was removed under reduced pressure, and the crude product mixture was purified by silica gel column chromatography (EtOAc/pentane 1:8) to afford α-aminooxy ketone **3a** in 91% yield as slightly yellow solid. The enantiomeric excess of **3a** was $>99\%$ as determined by chiral-phase HPLC analysis. **3a**: ^{1}H NMR ($CDCl_3$): $\delta = 1.71$–1.79 (m, 4H), 2.00–2.02 (m, 2H), 2.34–2.48 (m, 2H), 4.35 (q, 1H, $J = 6.0$ Hz), 6.94 (t, 3H, $J = 8.1$ Hz), 7.25 (t, 2H, $J = 8.4$ Hz), 7.82 ppm (brs, 1H); ^{13}C NMR: $\delta = 23.7$, 27.2, 32.5, 40.8, 86.2, 114.3, 122.0, 128.8, 148.0, 209.9 ppm; HPLC (Daicel Chiralpak AD, hexanes/*i*PrOH 90:10, flow rate 0.5 mL min^{-1}, $\lambda = 242$ nm): major isomer: $t_R = 30.31$ min; minor isomer: $t_R = 25.79$ min; $[\alpha]_D = +111.3$ ($c = 0.15$, $CHCl_3$); MALDI-TOF MS: 228.101; $C_{12}H_{15}NO_2$ (M+Na$^+$: calcd 228.100).

Received: October 6, 2003 [Z53018]
Published Online: February 9, 2004

Keywords: asymmetric catalysis · ketones · oxidation · proline

[1] a) *Comprehensive Asymmetric Catalysis* (Eds.: E. N. Jacobsen, A. Pfaltz, H. Yamamoto), Springer, Heidelberg, **1999**; b) R. Noyori, *Asymmetric Catalysis in Organic Synthesis*, Wiley, New York, **1994**; c) *Catalytic Asymmetric Synthesis*, 2nd ed (Ed.: I. Ojima, Wiley-VCH, New York, **2000**.

[2] F. A. Davis, B. C. Chen in *Houben-Weyl: Methods of Organic Chemistry*, *Vol. E21* (Eds.: G. Helmchen, R. W. Hoffmann, J. Mulzer, E. Schaumann), Georg Thieme, Stuttgart, **1995**, p. 4497.

[3] F. A. Davis, B. C. Chen, *Chem. Rev.* **1992**, *92*, 919, and references therein.

[4] N. Momiyama, H. Yamamoto, *J. Am. Chem. Soc.* **2003**, *125*, 6038.

[5] a) P. I. Dalko, L. Moisan, *Angew. Chem.* **2001**, *113*, 3840; *Angew. Chem. Int. Ed.* **2001**, *40*, 3726; b) B. List, *Tetrahedron* **2002**, *58*, 5573; c) J. Gröger, J. Wilken, *Angew. Chem.* **2001**, *113*, 545; *Angew. Chem. Int. Ed.* **2001**, *40*, 529; d) E. R. Jarvo, S. J. Miller, *Tetrahedron* **2002**, *58*, 2481; e) R. O. Duthaler, *Angew. Chem.* **2003**, *115*, 1005; *Angew. Chem. Int. Ed.* **2003**, *42*, 975.

[6] a) "Asymmetric Synthesis of Optically Active Polycyclic Organic Compounds": Z. G. Hajos, D. R. Parrish, German patent DE 2102623, July 29, **1971**; b) Z. G. Hajos, D. R. Parrish, *J. Org. Chem.* **1974**, *39*, 1615; c) "Optically Active 1,5-Indanone and 1,6-Naphthalenedionene": U. Eder, G. Sauer, R. Wiechert, German patent DE 2014757, October 7, **1971**; d) U. Eder, G. Sauer, R. Wiechert, *Angew. Chem.* **1971**, *83*, 492; *Angew. Chem. Int. Ed. Engl.* **1971**, *10*, 496; e) C. Agami, *Bull. Soc. Chim. Fr.* **1988**, 499.

[7] For example, the total synthesis of taxol: S. J. Danishefsky, *J. Am. Chem. Soc.* **1996**, *118*, 2843.

[8] For aldol reactions, see: a) B. List, R. A. Lerner, C. F. Barbas III, *J. Am. Chem. Soc.* **2000**, *122*, 2395; b) W. Notz, B. List, *J. Am. Chem. Soc.* **2000**, *122*, 7386; c) K. Saktihvel, W. Notz, T. Bui, C. F. Barbas III, *J. Am. Chem. Soc.* **2001**, *123*, 5260; d) A. Córdova, W. Notz, C. F. Barbas III, *J. Org. Chem.* **2002**, *67*, 301; e) B. List, P. Pojarliev, C. Castello, *Org. Lett.* **2001**, *3*, 573; f) A. Córdova, W. Notz, C. F. Barbas III, *Chem. Commun.* **2002**, *67*, 3034; g) A. Bøgevig, K. Juhl, N. Kumaragurubaran, K. A. Jørgensen, *Chem. Commun.* **2002**, 620; h) A. B. Northrup, D. W. C. MacMillan, *J. Am. Chem. Soc.* **2002**, *124*, 6798; i) N. S. Chowdari, D. B. Ramachary, A. Córdova, C. F. Barbas III, *Tetrahedron Lett.* **2002**, *43*, 9591; j) C. Pidathala, L. Hoang, N. Vignola, B. List, *Angew. Chem.* **2003**, *115*, 2891; *Angew. Chem. Int. Ed.* **2003**, *42*, 2785; k) Z. Tang, F. Jiang, L.-T. Yu, X. Cui, L.-Z. Gong, A.-Q. Mi, Y.-Z. Jiang, Y.-D. Wu, *J. Am. Chem. Soc.* **2003**, *125*, 5262.

[9] For Mannich reaction, see: a) B. List, *J. Am. Chem. Soc.* **2000**, *122*, 9336; b) A. Córdova, W. Notz, G. Zhong, J. M. Betancort, C. F. Barbas III, *J. Am. Chem. Soc.* **2002**, *124*, 1844; c) A. Córdova, S. Watanabe, F. Tanaka, W. Notz, C. F. Barbas III, *J. Am. Chem. Soc.* **2002**, *124*, 1866; d) A. Córdova, *Synlett* **2003**, 1651; e) A. Córdova, C. F. Barbas III, *Tetrahedron Lett.* **2002**, *43*, 7749; f) S.-i. Watanabe, A. Córdova, F. Tanaka, C. F. Barbas III, *Org. lett.* **2002**, *4*, 4519; g) A. Córdova, C. F. Barbas III, *Tetrahedron Lett.* **2003**, *44*, 1923; h) B. List, P. Porjalev, W. T. Biller, H. J. Martin, *J. Am. Chem. Soc.* **2002**, *124*, 827; i) W. Notz, K. Sakthivel, T. Bui, G. Zhong, C. F. Barbas III, *Tetrahedron Lett.* **2001**, *42*, 199; j) Y. Hayashi, W. Tsuboi, I. Ashimine, T. Urushima, M. Shoji, K. Sakai, *Angew. Chem.* **2003**, *115*, 3805; *Angew. Chem. Int. Ed.* **2003**, *42*, 3677; k) E. N. Wenzel, E. N. Jacobsen, *J. Am. Chem. Soc.* **2002**, *124*, 12964.

[10] For α-aminations, see: a) A. Bøgevig, K. Juhl, N. Kumaragurubaran, W. Zhuang, K. A. Jørgensen, *Angew. Chem.* **2002**, *114*, 1868; *Angew. Chem. Int. Ed.* **2002**, *41*, 1790; b) B. List, *J. Am. Chem. Soc.* **2002**, *124*, 5656; c) N. Kumaragurubaran, K. Juhl, W. Zhuang, A. Bøgevig, K. A. Jørgensen, *J. Am. Chem. Soc.* **2002**, *124*, 6254.

[11] For Michael reactions, see: a) B. List, H. Pojarliev, H. J. Martin, *Org. Lett.* **2001**, *3*, 2423; b) M. Yamaguchi, T. Shiraishi, M.

 © 2004 Wiley-VCH Verlag GmbH & Co. KGaA, Weinheim

Hirama, *J. Org. Chem.* **1996**, *61*, 3520; b) M. Yamaguchi, Y. Igarashi, R. S. Reddy, T. Shiraishi, M. Hirama, *Tetrahedron* **1997**, *53*, 11223; c) M. Yamaguchi, Y. Igarashi, T. Shiraishi, M. Hirama, *Tetrahedron Lett.* **1994**, *35*, 8233; d) S. Hanessian, V. Pham, *Org. Lett.* **2000**, *2*, 2975; e) J. M. Betancort, K. Sakthivel, R. Thayumanavan, C. F. Barbas III, *Tetrahedron Lett.* **2001**, *42*, 4441; f) J. M. Betancort, C. F. Barbas III, *Org. Lett.* **2001**, *3*, 3737; g) D. J. Hortsmann, D. J. Guerin, S. J. Miller, *Angew. Chem.* **2000**, *112*, 3781; *Angew. Chem. Int. Ed.* **2000**, *39*, 3635; h) A. Alexakis, O. Andrey, *Org. Lett.* **2002**, *4*, 3611; i) D. J. Guerin, S. J. Miller, *J. Am. Chem. Soc.* **2002**, *124*, 2134; j) N. Halland, P. S. Aburel, K. A. Jørgensen, *Angew. Chem.* **2003**, *115*, 685; *Angew. Chem. Int. Ed.* **2003**, *42*, 661; j) N. Halland, R. G. Hazell, K. A. Jørgensen, *J. Org. Chem.* **2002**, *67*, 8331; k) O. Andrey, A. Alexakis, G. Bernardinelli, *Org. Lett.* **2003**, *5*, *2559*; l) N. Halland, T. Hansen, K. A. Jørgensen, *Angew. Chem.* **2003**, *115*, 5105; *Angew. Chem. Int. Ed.* **2003**, *42*, 4955; m) D. Enders, A. Seki, *Synlett* **2002**, 26.

[12] For Diels–Alder reactions, see: a) A. B. Northrup, D. W. C. MacMillan, *J. Am. Chem. Soc.* **2002**, *124*, 2458; b) K. A. Ahrendt, C. J. Borths, D. W. C. MacMillan, *J. Am. Chem. Soc.* **2000**, *122*, 4243; for hetero-Diels–Alder reactions, see: d) K. Juhl, K. A. Jørgensen, *Angew. Chem.* **2003**, *115*, 1536; *Angew. Chem. Int. Ed.* **2003**, *42*, 1498; e) Y. Huang, K. Unni, A. N. Thadani, V. H. Rawal, *Nature* **2003**, *424*, 146.

[13] For alkylation of electron-rich benzene systems, see: a) N. A. Paras, D. W. C. MacMillan, *J. Am. Chem. Soc.* **2001**, *123*, 4370; b) J. F. Austin, D. W. C. MacMillan, *J. Am. Chem. Soc.* **2002**, *124*, 1172; c) N. A. Paras, D. W. C. MacMillan, *J. Am. Chem. Soc.* **2002**, *124*, 7894.

[14] For 1,3-dipolar cycloadditions, see: a) W. S. Jen, J. J. M. Wiener, D. W. C. MacMillan, *J. Am. Chem. Soc.* **2000**, *122*, 9874; b) S. Karlsson, H. Högberg, *Tetrahedron: Asymmetry* **2002**, *13*, 923.

[15] For an example of a Strecker reaction, see: P. Vachal, E. N. Jacobsen, *J. Am. Chem. Soc.* **2002**, *124*, 10012.

[16] For other reactions, see: a) A. E. Taggi, A. M. Hafez, H. Wack, B. Young, W. J. Drury III, T. Lectka, *J. Am. Chem. Soc.* **2000**, *122*, 7831; b) B. R. Sculimbrene, A. J. Morgan, S. J. Miller, *J. Am. Chem. Soc.* **2002**, *124*, 11653; c) M. Harmata, S. K. Ghosh, X. Hong, S. Wacharasindhu, P. Kirchhoefer, *J. Am. Chem. Soc.* **2003**, *125*, 2058.

[17] During the preparation of this manuscript two excellent independent reports of proline-catalyzed α-oxidations of aldehydes were reported, see: a) G. Zhong, *Angew. Chem.* **2003**, *115*, 4379; *Angew. Chem. Int. Ed.* **2003**, *42*, 4247; b) S. P. Brown, M. P. Brochu, C. J. Sinz, D. W. C. MacMillan, *J. Am. Chem. Soc.* **2003**, *125*, 10808.

[18] The α-oxy aniline adducts racemize and decompose upon storage in solution and at room temperature and should therefore be stored as solids at 4 °C or reduced to the more stable corresponding monoprotected diols.

[19] The optical rotation of **3a** obtained from the (*S*)-proline-catalyzed reaction was $[\alpha]_D = +111.3$ ($c = 0.15$, $CHCl_3$); reported rotation for (−)-**3a** is $[\alpha]_D = -53.0$ ($c = 0.62$, $CHCl_3$).[4] The optical rotation of **3c** was $[\alpha]_D = +57.7$ ($c = 2.1$, $CHCl_3$); the reported rotation for (−)-**3c** is $[\alpha]_D = -12.8$ ($c = 0.3$, $CHCl_3$).[4]

[20] S. Bahmanyar, K. N. Houk, *Org. Lett.* **2003**, *5*, 1249, and references therein.

[21] Note added in proof (19.1.2004): Please see the following communication by Hayashi et al., which describes related chemistry: Y. Hayashi, J. Yamaguchi, T. Suniya, M. Shoji, *Angew. Chem.* **2004**, *116*, 1132; *Angew. Chem. Int. Ed.* **2004**, *43*, 1112.

 © 2004 Wiley-VCH Verlag GmbH & Co. KGaA, Weinheim

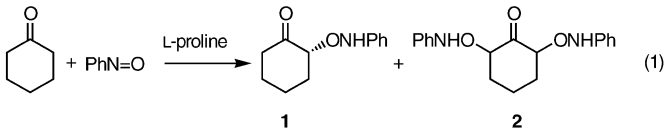
Asymmetric Catalysis

Direct Proline-Catalyzed Asymmetric α-Aminoxylation of Ketones**

Yujiro Hayashi, Junichiro Yamaguchi, Tatsunobu Sumiya, and Mitsuru Shoji*

Optically active α-hydroxy carbonyl compounds, important building blocks in organic synthesis, can be prepared by several methods such as the electrophilic α-hydroxylation of enolates using chiral oxaziridines as the oxidizing agent.[1] As for methods based on asymmetric catalytic reactions, there are several, including the asymmetric dihydroxylation of enol ethers developed by Sharpless et al.,[2] the asymmetric epoxidation of silyl enol ethers with a chiral dioxirane,[3] and the asymmetric epoxidation of enol ether with a chiral Mn–salen catalyst.[4] Recently Yamamoto et al. have developed an excellent asymmetric, catalytic nitroso-aldol reaction:[5] a catalytic amount of a binap–AgOTf complex promotes the reaction of tin enolate and nitrosobenzene, affording an α-aminoxy ketone, which is easily converted into the α-hydroxy ketone. In most of these reactions, however, the ketones must be converted into isolable enolate or enol derivatives, and there is as yet no direct catalytic method for the synthesis of chiral α-hydroxy ketones from the corresponding ketones. In this communication, we disclose the direct catalytic enantioselective α-aminoxylation of ketones, which is complementary to the recent asymmetric α-aminoxylation of aldehydes.[6]

Proline[7] has been found to be an excellent catalyst of asymmetric aldol[8] and Mannich reactions[9] and of the asymmetric α-amination of carbonyl compounds.[10] In our continuing research on asymmetric reactions catalyzed by proline,[6c,9c,11] we have found the asymmetric α-aminoxylation of a ketone: The reaction of cyclohexanone and nitrosobenzene was conducted in dimethyl sulfoxide (DMSO) at room temperature in the presence of a catalytic amount of L-proline. The desired α-aminoxylated cyclohexanone **1** was obtained in 31% yield, along with the α,α′-diaminoxylated product **2** in 11% yield [Eq. (1)]. Dimerized nitrosobenzene



1 **2** (1)

[*] Prof. Dr. Y. Hayashi, J. Yamaguchi, T. Sumiya, Dr. M. Shoji
Department of Industrial Chemistry, Faculty of Engineering
Tokyo University of Science, Kagurazaka, Shinjuku-ku
Tokyo 162-8601 (Japan)
Fax: (+81) 3-5261-4631
E-mail: hayashi@ci.kagu.tus.ac.jp

[**] This work was supported by a Grant-in-Aid for Scientific Research on Priority Areas (A) "Exploitation of Multi-Element Cyclic Molecules" from the Ministry of Education, Culture, Sports, Science and Technology, Japan. We thank Prof. K. Tachibana and Dr. S. Fukuzawa, The University of Tokyo, for measurement of CD spectra and T. HASEGAWA Co., LTD. for chiral GC analysis.

 © 2004 Wiley-VCH Verlag GmbH & Co. KGaA, Weinheim DOI: 10.1002/anie.200353085

was also generated. This α-aminoxylation is readily accomplished in highly polarized solvents such as DMSO, dimethylformamide (DMF), CH_3NO_2, *N*-methylpyrrolidinone (NMP), and CH_3CN, affording the α-aminoxylated product in 26–37% yield with excellent enantioselectivity (>99% *ee*, Table 1). As the best yield was obtained for the reaction in DMF, further investigations were performed with this solvent.

Slow addition of nitrosobenzene was found to be crucial for obtaining a high yield without affecting the enantioselectivity. That is, addition of nitrosobenzene by syringe pump to a solution of cyclohexanone and 10 mol% proline effectively suppresses both homodimerization of nitrosobenzene and α,α′-diaminoxylation, affording **1** in 77% yield with >99% *ee* (Table 2, entry 2). No α-hydroxyamino ketone, a major product in the reaction of nitrosobenzene with a variety of alkali metals or tin enolates,[12] is formed at all.

As the best reaction conditions had been established, the generality of the reaction was examined (Table 2). 1,4-Cyclohexanedione monoethylene ketal and 4,4-dimethylcyclohexanone were transformed into the α-aminoxylated cyclohexanones in good yield with very high enantioselectivity (entries 4–6).[13] Not only cyclohexanones, but also tetrahydro-4*H*-pyran-4-one and 1-methyl-4-piperidinone were successfully employed in this reaction, affording α-aminoxylated compounds with moderate yield and excellent enantioselectivity (entries 7 and 8). In the reaction of 1-methyl-4-piperidinone, CH_3NO_2 was used as solvent instead of DMF, owing to the difficulty of separating the product from the solvent. It is noteworthy that the basic tertiary amine moiety has no detrimental effect on the proline catalyst. Though the reactivity of acyclic ketones is different from that of cyclic ketones under our conditions, the aminoxylated product is generated in moderate yield: 2-Butanone reacts with nitrosobenzene in DMSO at room temperature, affording 2-aminoxy-3-butanone in 40% yield with >99% *ee*, together with the hydroxyaminated product in 33% yield with 4% *ee* (entry 9). It is noteworthy that hydroxyaminated product is racemic and that the possible regioisomer, 1-aminoxy-2-butanone, was not formed at all.

Though the optimum addition time for nitrosobenzene varies according to the ketone, in the case of cyclic ketones a good yield is generally obtained using addition over 24 h when 10 mol% of proline is employed, while addition over 2 h affords a moderate yield in the reaction of 2-butanone. The catalyst loading can be reduced to 5 mol% without significant loss in yield and enantioselectivity, but a longer reaction time is required (entry 5).

The conversion of **1** into α-hydroxycyclohexanone was successfully carried out in 87% yield with only partial racemization (>99% *ee*→96% *ee*[14]) by treatment with $CuSO_4$,[5] and the stereochemistry of the product was determined to be *R* by comparison with the literature.[15] This was also confirmed after conversion to (−)-1,2-cyclohexanediol[16] by the reduction with $NaBH_4$. The transition state model shown in Figure 1,

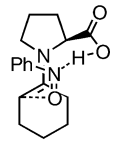
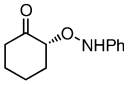
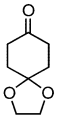
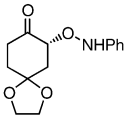
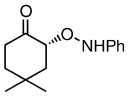
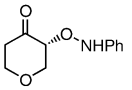
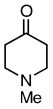
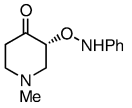
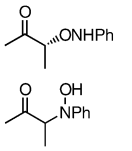


Figure 1. The transition-state model for the L-proline-catalyzed α-aminoxylation of cyclohexanone.

Table 2: Aminoxylation of various ketones.[a]

Entry	Ketone	Product	Cat. [mol%]	Add. time [h]	Yield [%][b]	*ee* [%]
1			30	5.5	79	>99[c]
2			10	5.5	77	>99[c]
3			30	12	96	>99[d]
4			10	24	93	>99[d]
5			5	60	86	>99[d]
6			10	24	84	>99[d]
7			10	24	53	96[c]
8[e]			10	24	44	99[c]
9[f]			10	2[g]	40, 33	>99[d], 4[d]

[a] Unless otherwise shown, reactions were conducted with 10 mol% catalyst, 1.0 equiv nitrosobenzene, and 2.0 equiv ketone in DMF at 0°C with slow addition of nitrosobenzene. [b] Yield of isolated product. [c] Determined by HPLC using a Chiralpak AD-H column. [d] Determined by HPLC using a Chiralpak OD-H column. [e] CH_3NO_2 was used as solvent. [f] The reaction was conducted with 10 mol% catalyst, 1.0 equiv nitrosobenzene, and 10.0 equiv ketone in DMSO at room temperature. [g] After addition of nitrosobenzene, the reaction mixture was stirred for a further 4 h at room temperature.

Table 1: Solvent effect on the α-aminoxylation of cyclohexanone.[a]

Entry	Solvent	Yield [%][b]		*ee* [%] of **1**[c]
		1	**2**	
1	DMSO	31	11	>99
2	DMF	37	7	>99
3	CH_3NO_2	34	2	>99
4	NMP	29	6	>99
5	CH_3CN	26	2	>99
6	CH_2Cl_2	11	0	>99
7	THF	0	0	–

[a] Reactions were conducted with 30 mol% catalyst, 1.0 equiv nitrosobenzene, and 2.0 equiv cyclohexanone at room temperature, and nitrosobenzene was added in one portion. The reaction time was 1 h. [b] Yield of isolated product. [c] Determined by chiral HPLC with a Chiralpak AD-H column.

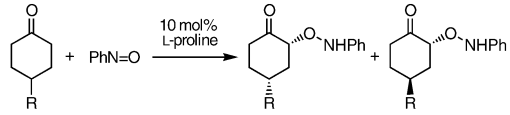
 © 2004 Wiley-VCH Verlag GmbH & Co. KGaA, Weinheim

which is similar to that proposed for the α-aminoxylation of aldehydes,[6] explains the absolute stereochemistry of the α-aminoxylated products.

Next this asymmetric α-aminoxylation was applied to the asymmetric desymmetrization of a 4-substituted cyclohexanone (Table 3). When 4-*tert*-butylcyclohexanone was treated with nitrosobenzene in the presence of L-proline, (2*R*,4*R*)-2-anilinoxy-4-*tert*-butylcyclohexanone and the (2*R*,4*S*) isomer were obtained in 31% yield and >99% *ee* and 31% yield and 94% *ee*, respectively. The absolute stereochemistry of the (2*R*,4*R*) isomer was deduced based on that of the corresponding hydroxycyclohexanone,[17] while that of the (2*R*,4*S*) isomer was determined by the CD-chirality method after conversion into (1*S*,2*R*,4*S*)-4-*tert*-butyl-1,2-dibenzoyloxycyclohexane. 4-*tert*-Butyldiphenylsilyloxycyclohexanone gave almost the same results, affording (2*R*,4*R*)-2-anilinooxy-4-*tert*-butyldiphenylsilyloxycyclohexanone and the (2*R*,4*S*) isomer in 46% yield and >99% *ee*, and 23% yield and 96% *ee*, respectively. These reactions are composed of two successive steps, an asymmetric desymmetrization for the enamine formation, and diastereoselective α-aminoxylation of the generated enamine. These results indicate that the asymmetric induction in the initial enamine formation is not high, while the diastereoselectivity of the second α-aminoxylation is excellent.

In summary, we have developed the direct catalytic enantioselective α-aminoxylation of ketones by using nitrosobenzene as the oxygen source and L-proline as the catalyst. This reaction has several noteworthy features: The reaction proceeds with high yield and excellent enantioselectivity. This α-aminoxylation can be successfully applied not only to cyclohexanone derivatives but also to 4-monosubstituted cyclohexanones with asymmetric desymmetrization, affording both α-aminoxylated products with very high enantioselectivities. Because of the easy conversion of α-aminoxylated ketones into α-hydroxy ketones, operational simplicity, and the availability and low cost of the catalyst, the present method is one practical approach to the preparation of optically active α-hydroxy ketones.

Table 3: Asymmetric desymmetrization of 4-substituted cyclohexanones.[a]



3 **4**

R	Yield [%]		*ee* [%][b]	
	3	**4**	**3**	**4**
*t*Bu	31	31	>99	94
OSi-*t*BuPh$_2$	46	23	>99	96

[a] Reactions were conducted with 10 mol% catalyst, 1.0 equiv nitrosobenzene, and 2.0 equiv ketone in DMF at 0°C with slow addition of nitrosobenzene. [b] Determined by chiral HPLC.

Experimental Section

Typical experimental procedure (Table 2, entry 6): To a solution of 4,4-dimethylcyclohexanone (151.4 mg, 1.2 mmol) and L-proline (6.9 mg, 0.06 mmol) in DMF (2.7 mL) was added a solution of nitrosobenzene (64.2 mg, 0.6 mmol) in DMF (0.9 mL) over 24 h at 0°C by syringe pump, and the mixture was stirred for 30 min at that temperature. The reaction was quenched with phosphate buffer solution (pH 7.0), and the organic materials were extracted with ethyl acetate three times. The combined organic extracts were washed with brine, dried over anhydrous Na_2SO_4, and concentrated in vacuo. Purification by silica gel column chromatography (ethyl acetate/hexane 1:10–1:5) gave α-aminoxy ketone (116.7 mg, 0.50 mmol) in 84% yield and >99% *ee*, as determined by chiral HPLC analysis.[18]

Received: October 14, 2003 [Z53085]
Published Online: February 11, 2004

Keywords: asymmetric catalysis · ketones · oxidation · proline

[1] a) Review: F. A. Davis, B. C. Chen, *Chem. Rev.* **1992**, *92*, 919, and references therein; b) D. Enders, V. Bhushan, *Tetrahedron Lett.* **1988**, *29*, 2437; c) B. B. Lohray, D. Enders, *Helv. Chim. Acta* **1989**, *72*, 980; d) D. Enders, U. Reinhold, *Synlett* **1994**, 792; e) D. Enders, U. Reinhold, *Liebigs Ann.* **1996**, 11; f) D. Enders, B. Bockstiegel, *Synthesis* **1989**, 493.

[2] a) K. Morikawa, J. Park, P. G. Andersson, T. Hashiyama, K. B. Sharpless, *J. Am. Chem. Soc.* **1993**, *115*, 8463; b) T. Hashiyama, K. Morikawa, K. B. Sharpless, *J. Org. Chem.* **1992**, *57*, 5067.

[3] a) Y. Zhu, Y. Yu, H. Yu, Y. Shi, *Tetrahedron Lett.* **1998**, *39*, 7819; b) W. Adam, R. T. Fell, C. R. Saha-Moller, C.-G. Zhao, *Tetrahedron: Asymmetry* **1998**, *9*, 397.

[4] a) T. Fukuda, T. Katsuki, *Tetrahedron Lett.* **1996**, *37*, 4389; b) W. Adam, R. T. Fell, V. R. Stegmann, C. R. Saha-Moller, *J. Am. Chem. Soc.* **1998**, *120*, 708.

[5] N. Momiyama, H. Yamamoto, *J. Am. Chem. Soc.* **2003**, *125*, 6038.

[6] a) S. P. Brown, M. P. Brochu, C. J. Sinz, D. W. C. MacMillan, *J. Am. Chem. Soc.* **2003**, *125*, 10808; b) G. Zhong, *Angew. Chem.* **2003**, *115*, 4379; *Angew. Chem. Int. Ed.* **2003**, *42*, 4247; c) Y. Hayashi, J. Yamaguchi, K. Hibino, M. Shoji, *Tetrahedron Lett.* **2003**, *44*, 8293.

[7] Reviews, see a) B. List, *Synlett* **2001**, 1675; b) B. List, *Tetrahedron* **2002**, *58*, 5573.

[8] a) A. B. Northrup, D. W. C. MacMillan, *J. Am. Chem. Soc.* **2002**, *124*, 6798; b) C. Pidathala, L. Hoang, N. Vignola, B. List, *Angew. Chem.* **2003**, *115*, 2797; *Angew. Chem. Int. Ed.* **2003**, *42*, 2785, and references therein.

[9] a) B. List, P. Pojarliev, W. T. Biller, H. J. Martin, *J. Am. Chem. Soc.* **2002**, *124*, 827; b) A. Córdova, S. Watanabe, F. Tanaka, W. Notz, C. F. Barbas III, *J. Am. Chem. Soc.* **2002**, *124*, 1866; c) Y. Hayashi, W. Tsuboi, I. Ashimine, T. Urushima, M. Shoji, K. Sakai, *Angew. Chem.* **2003**, *115*, 3805; *Angew. Chem. Int. Ed.* **2003**, *42*, 3677; d) A. Córdova, *Synlett* **2003**, 1651, and referenes therein.

[10] a) B. List, *J. Am. Chem. Soc.* **2002**, *124*, 5656; b) N. Kumaragurubaran, K. Juhl, W. Zhuang, A. Bøgevig, K. A. Jørgensen, *J. Am. Chem. Soc.* **2002**, *124*, 6254; c) A. Bøgevig, K. Juhl, N. Kumaragurubaran, W. Zhuang, K. A. Jørgensen, *Angew. Chem.* **2002**, *114*, 1868; *Angew. Chem. Int. Ed.* **2002**, *41*, 1790; d) Review, see R. O. Duthaler, *Angew. Chem.* **2003**, *115*, 1005; *Angew. Chem. Int. Ed.* **2003**, *42*, 975.

[11] Y. Hayashi, W. Tsuboi, M. Shoji, N. Suzuki, *J. Am. Chem. Soc.* **2003**, *125*, 11208.

[12] a) N. Momiyama, H. Yamamoto, *Angew. Chem.* **2002**, *114*, 3112; *Angew. Chem. Int. Ed.* **2002**, *41*, 2986; b) N. Momiyama, H. Yamamoto, *Org. Lett.* **2002**, *4*, 3579.

 © 2004 Wiley-VCH Verlag GmbH & Co. KGaA, Weinheim

[13] Cyclopentanone and cycloheptanone do not react under the present reaction conditions.
[14] The enantiomeric excess of 2-hydroxycyclohexanone (96% *ee*) was determined by chiral GC analysis using CHIRAMIX column (0.25 mm I.D./df = 0.25 mm). Column temp.: 60–160 °C (0.7 °C min^{-1}); flow rate: 1.2 mL min^{-1}. *S* isomer: $t_R = 70.81$ min; *R* isomer: $t_R = 71.68$ min. CHIRAMIX is licensed by T. HASEGAWA Co., LTD.
[15] L. G. Lee, G. M. Whitesides, *J. Org. Chem.* **1986**, *51*, 25.
[16] $[\alpha]_D^{20} = -38.4$ ($c = 0.17$, H_2O). Lit. $[\alpha]_D^{20} = +39.0$ ($c = 1.6$, H_2O) for (*S*,*S*)-1,2-cyclohexanediol (O. Bortolini, G. Fantin, M. Fogagnolo, P. P. Giovannini, A. Guerrini, A. Medici, *J. Org. Chem.* **1997**, *62*, 1854).
[17] C. M. Cain, R. P. C. Cousins, G. Coumbarides, N. S. Simpkins, *Tetrahedron* **1990**, *46*, 523.
[18] HPLC conditions: Chiralcel OD-H column (hexane/2-propanol 40:1), 1.0 mL min^{-1}; $t_R = 9.1$ min (major) and 12.2 min (minor). $[\alpha]_D^{19} = +85.7$ ($c = 0.33$, $CHCl_3$).
[19] Note added in proof (19.1.2004): Please see the preceding communication by Córdova and co-workers, which describes related chemistry: A. Bøgevig, H. Sundén, A. Córdova, *Angew. Chem.* **2004**, *116*, 1129; *Angew. Chem. Int. Ed.* **2004**, *43*, 1109.

 © 2004 Wiley-VCH Verlag GmbH & Co. KGaA, Weinheim

Magnetic Nanoparticles

Size-Dependent Magnetic Properties of Colloidal Mn_3O_4 and MnO Nanoparticles**

*Won Seok Seo, Hyong Hoon Jo, Kwangyeol Lee, Bongsoo Kim, Sang Jun Oh, and Joon T. Park**

Metal-oxide nanocrystals are expected to find useful applications in catalysis, energy storage, magnetic data storage, sensors, and ferrofluids.[1] In particular, colloidal metal-oxide nanocrystals are of great interest for technological applications owing to their unique size-dependent properties and excellent processability. Recent advances in the colloidal synthesis of metal oxides reveal that thermal decomposition of metal acetylacetonates,[2] metal cupferronates,[3] metal alkoxides,[4] and metal carbonyls[5] in complex organic solvent systems can lead to monodisperse metal oxide nanoparticles in certain cases.

Manganese oxides are widely used as electrode materials,[6] catalysts,[7] and soft magnetic materials.[8] In spite of their important applications, there has been only one report on synthesis of monodisperse colloidal manganese-oxide nanoparticles.[3] Furthermore, a systematic study on the relationship between particle size and physical properties has never been conducted. Herein we report a simple, reliable synthesis of size-focused colloidal nanocrystals of two different manganese oxides, Mn_3O_4 and MnO, from thermal decomposition of a single precursor $[Mn(acac)_2]$ (acac = acetylacetonate) in oleylamine, as well as their unique size-dependent magnetic properties.

A slurry of $[Mn(acac)_2]$ (0.3 g) in oleylamine (7.6 g; 1:24 molar ratio) was heated at 180 °C for 9 h under an atmosphere of argon, and the resulting reaction mixture was cooled to room temperature to form a brown suspension. After centrifugation at 3000 rpm for 10 min, the supernatant was removed to afford a brown precipitate. Dichloromethane (10 mL) was added to the resulting brown precipitate to give a brown suspension, which was sonicated for 10 min to form a clear solution. Removal of the insoluble material, if any, by centrifugation and precipitation by adding ethanol (40 mL) produced a brown powder, which could be easily redispersed in various organic solvents such as hexane, toluene, and dichloromethane. The low-resolution transmission-electron-microscope (TEM) image of the powder shows nearly monodisperse spherical nanoparticles of 10 nm in diameter as shown in Figure 1a, and its high resolution TEM image in Figure 1b reveals the highly crystalline nature of Mn_3O_4

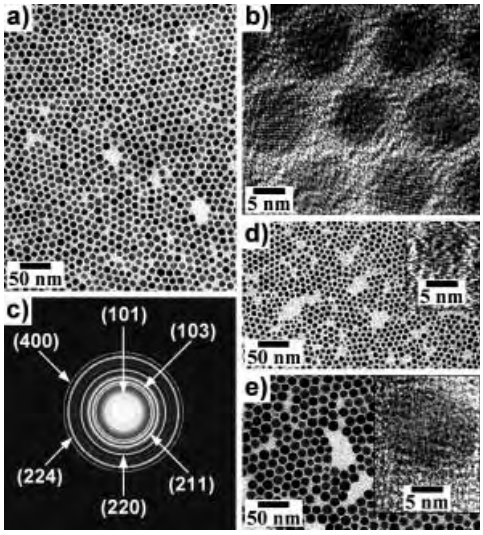


Figure 1. TEM micrographs of Mn_3O_4 nanoparticles: a) TEM image, b) high resolution TEM image, and c) an SAED pattern of 10 nm ($\sigma = 1.0$) nanoparticles. TEM images of d) 6 nm ($\sigma = 0.9$) and e) 15 nm ($\sigma = 1.2$) nanoparticles. High resolution TEM images are shown in the insets.

[*] W. S. Seo, H. H. Jo, Prof. B. Kim, Prof. J. T. Park
National Research Laboratory
Department of Chemistry and School of Molecular Science (BK 21)
Korea Advanced Institute of Science and Technology
Daejeon, 305-701 (Korea)
Fax: (+82) 42-869-5826
E-mail: joontpark@kaist.ac.kr
Prof. K. Lee
Department of Chemistry
Korea University
Seoul, 136-701 (Korea)
Dr. S. J. Oh
Korea Basic Science Institute
Daejeon, 305-333 (Korea)

[**] This research was financially supported by National Research Laboratory (NRL) Program of the Korean Ministry of Science & Technology (MOST), the Korea Science & Engineering Foundation (Project No. 1999-1-122-001-5) for J.T.P, and a Korea University Grant for K.L. We thank staffs of KBSI and KAIST for TEM analyses. We also thank Prof. S. A. Majetich at Carnegie Mellon Univ. for helpful comments.

Supporting information for this article is available on the WWW under http://www.angewandte.org or from the author.

 DOI: 10.1002/anie.200352400 © 2004 Wiley-VCH Verlag GmbH & Co. KGaA, Weinheim

nanoparticles. The selected-area electron-diffraction pattern (SAED) of the nanoparticles is consistent with tetragonal Mn_3O_4 (JCPDS card No.: 24-0734) with strong ring patterns due to (101), (103), (211), (220), (224), and (400) planes (Figure 1c; see Supporting Information for the X-ray diffraction pattern (XRD)). The particle size can be varied easily by a simple change in the reaction temperatures (see Supporting Information for experimental details); smaller nanoparticles of 6 nm in diameter were obtained at 150 °C (Figure 1d) and larger nanoparticles of 15 nm in diameter were prepared at 250 °C (Figure 1e). Although the mechanism leading to Mn_3O_4 and the accompanied oxidation of Mn^{II} to Mn^{III} ions under the employed reaction conditions is not clear at the moment, the oxygen in nanoparticles should originate from the decomposition of acetylacetonate ligand in the $[Mn(acac)_2]$ precursor because the reaction has been conducted with rigorous exclusion of other oxygen sources. Several metal oxides have been prepared by thermal decomposition of metal acetylacetonates under an inert atmosphere,[2a,9] and it has been proposed that carbon dioxide acts as the main oxidant among the various products from ligand decomposition.[9b]

A dramatic change in the decomposition behavior of the precursor $[Mn(acac)_2]$ was observed when 10 equiv of water was introduced to the reaction slurry of $[Mn(acac)_2]$ in oleylamine (1:24 molar ratio). Only pure cubic MnO (JCPDS card No.: 07–0230) was obtained without contamination by Mn_3O_4 (see Supporting Information for the XRD pattern). The presence of water prohibits further oxidation of the formed MnO, presumably because the water is involved in the decomposition of the acetylacetonate ligand, which acts as the oxygen source. Again a simple change in the reaction temperatures results in variation of the MnO nanoparticle size as shown in Figure 2 (see Supporting Information for experimental details): 11 nm particles (220 °C, 9 h), 17 nm particles (220 °C, 3 h and then 250 °C, 6 h), and 22 nm particles (250 °C, 9 h).

Size-dependent magnetic properties of the Mn_3O_4 nanoparticles of varying sizes were studied by using a superconducting quantum interference device (SQUID). As expected, the three Mn_3O_4 nanoparticle samples showed ferromagnetic behaviors at low temperatures, whereas they were paramagnetic at room temperature.[10] Under zero-field-cooling (ZFC) measurements at 100 Oe, the observed blocking temperatures T_B were 36 K, 40 K, and 41 K for 6 nm, 10 nm, and 15 nm Mn_3O_4 nanoparticles, respectively, as shown in Figure 3. This result is consistent with the linear relationship between crystal volume V and blocking temperature T_B as predicted from the equation $KV = 25 k_B T_B$ (K is the anisotropy constant and k_B is Boltzmann's constant;[11] a similar trend was also observed for other ferromagnetic materials such as Co[12] and Fe_2O_3 nanoparticles.[5]

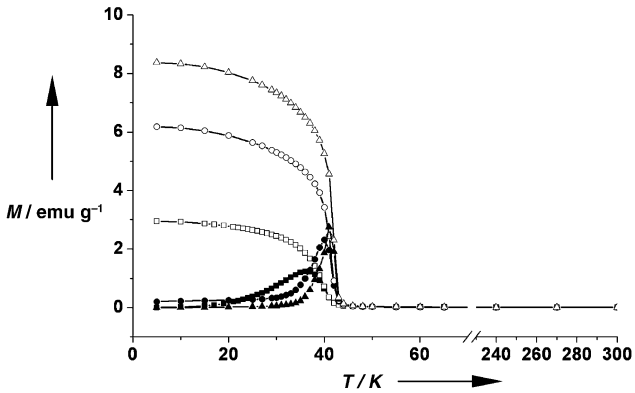


Figure 3. ZFC (filled symbols) and FC (open symbols) magnetization curves of 6 nm (squares), 10 nm (circles), and 15 nm (triangles) Mn_3O_4 nanoparticles under an applied field of 100 Oe.

It has been recently reported that very small MnO nanoparticles (5–10 nm in diameter) show weak ferromagnetic behavior at low temperatures,[13] although bulk MnO shows antiferromagnetic behavior with $T_N \approx 125$ K. The observed weak ferromagnetism has been ascribed to the presence of noncompensated surface spins on the antiferromagnetic core of the MnO nanoparticle.[13] Measurements of size-dependent magnetism, however, have never been reported for MnO nanoparticles. The three MnO samples showed the expected weak ferromagnetic behavior at low temperatures, but unusual size-dependency of magnetic properties was observed for MnO nanoparticles. Under ZFC measurements at 100 Oe, the observed blocking temperatures T_B were 25 K, 18 K, and 10 K for 11 nm, 17 nm, and 22 nm MnO nanoparticles, respectively (Figure 4). This result is, to the best of our knowledge, the first demonstration of an inverse proportionality of the blocking temperature to the particle size. It is likely that smaller MnO nanoparticles with higher surface-to-volume ratio exhibit much larger proportion of noncompensated surface spins on the antiferromagnetic core and thus reveal higher T_B and magnetization values than those of larger nanoparticles.

In summary, we have prepared soluble, highly crystalline, monodisperse, and size-controlled Mn_3O_4 and MnO nanoparticles by thermal decomposition of a single precursor $[Mn(acac)_2]$ in oleylamine under an inert atmosphere, and have demonstrated their unique size-dependent magnetic properties. The particle size can be easily manipulated by

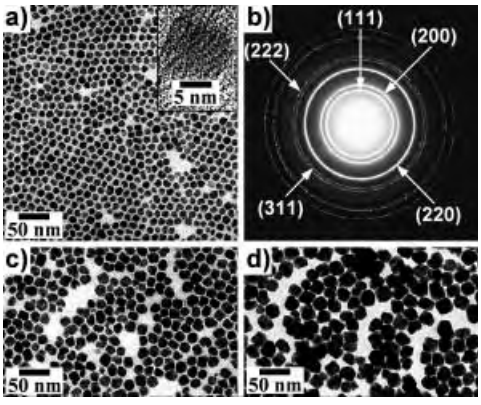


Figure 2. TEM micrographs of MnO nanoparticles: a) TEM image and b) a SAED pattern of 11 nm ($\sigma = 1.1$) nanoparticles. High resolution TEM image is in the inset. TEM images of c) 17 nm ($\sigma = 1.6$) and d) 22 nm ($\sigma = 2.3$) nanoparticles.

 © 2004 Wiley-VCH Verlag GmbH & Co. KGaA, Weinheim

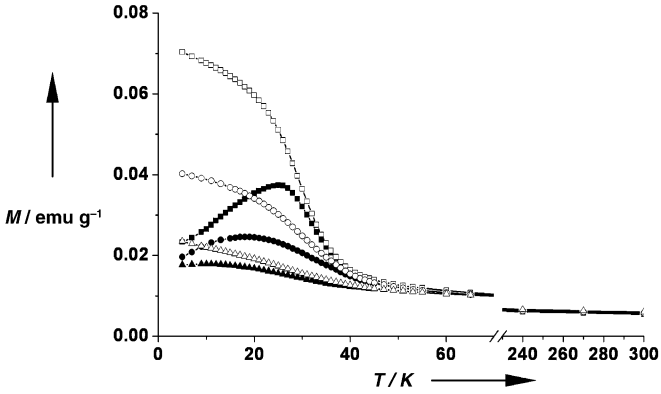


Figure 4. ZFC (filled symbols) and FC (open symbols) magnetization curves of 11 nm (squares), 17 nm (circles), and 22 nm (triangles) MnO nanoparticles under an applied field of 100 Oe.

simply changing the employed reaction temperature, and moreover the metal-oxide phase was effectively controlled by the presence or absence of a small amount of water. Detailed magnetic property measurements and theoretical calculations for the observed unusual magnetic behavior are underway for the prepared manganese oxide nanoparticles.

Experimental Section

Syntheses of MnO and Mn_3O_4 nanoparticles: See Supporting Information.

Characterization: The prepared nanoparticles were characterized by XRD (Rigaku D/MAX-RB (12 kW) diffractometer with a graphite-monochromatized $Cu_{K\alpha}$ radiation source at 40 kV and 120 mA), TEM (low resolution: Omega EM912 operated at 120 kV; high resolution: Philips F20Tecnai operated at 200 kV), selected area electron diffraction (SAED) patterns attached to EM912, and energy dispersive analyses of X-ray emission (EDAX) attached to EM912. Samples for TEM investigations were prepared by putting an aliquot of dichloromethane solution of nanoparticles onto an amorphous carbon substrate supported on a copper grid. The excess liquid was then removed with tissue, and the grid was allowed to dry at room temperature. Magnetic measurements were performed on a SQUID magnetometer (Quantum Design MPMS-7). DC susceptibility and hysteresis measurements were recorded for powdered samples of nanoparticles in a gelatin capsule. The temperature was varied between 5 and 300 K according to a zero-field-cooling/field-cooling (ZFC/FC) procedure at 100 Oe, and the hysteretic loops were obtained in a magnetic field that varied from +7 to −7 T.

Received: July 17, 2003
Revised: November 11, 2003 [Z52400]

Keywords: colloids · magnetic properties · manganese · nanoparticles

[1] a) A. J. Zarur, J. Y. Ying, *Nature* **2000**, *403*, 65–67; b) S. A. Majetich, Y. Jin, *Science* **1999**, *284*, 470–473; c) C. Nayral, E. Viala, P. Fau, F. Senocq, J.-C. Jumas, A. Maisonnat, B. Chaudret, *Chem. Eur. J.* **2000**, *6*, 4082–4090; d) K. Raj, R. Moskowitz, *J. Magn. Magn. Mater.* **1990**, *85*, 233–245.

[2] a) W. S. Seo, H. H. Jo, K. Lee, J. T. Park, *Adv. Mater.* **2003**, *15*, 795–797; b) S. Sun, H. Zeng, *J. Am. Chem. Soc.* **2002**, *124*, 8204–8205.

[3] J. Rockenburger, H. C. Scher, A. P. Alivisatos, *J. Am. Chem. Soc.* **1999**, *121*, 11595–11596.

[4] S. O'Brien, L. Brus, C. B. Murray, *J. Am. Chem. Soc.* **2001**, *123*, 12085–12086.

[5] T. Hyeon, S. S. Lee, J. Park, Y. Chung, H. B. Na, *J. Am. Chem. Soc.* **2001**, *123*, 12798–12801.

[6] a) J. C. Nardi, *J. Electrochem. Soc.* **1985**, *132*, 1787–1790; b) A. R. Armstrong, P. G. Bruce, *Nature* **1996**, *381*, 499–500.

[7] a) L. Hegedus, J. W. Beckman, W. H. Pan, J. P. Solor, Eur. Pat. Appl. 345,695, **1989**; b) M. Baldi, E. Finocchio, F. Milella, G. Busca, *Appl. Catal. B* **1998**, *16*, 43–51.

[8] Chugai Electric Industrial Co. Ltd., Japan Pat. Appl. 82,209,833, **1982**.

[9] a) L. A. Ryabova, V. S. Salun, L. A. Serbinov, *Thin Solid Films* **1982**, *92*, 327–332; b) A. G. Nasibulin, P. P. Ahonen, O. Richard, E. I. Kauppinen, I. S. Altman, *J. Nanopart. Res.* **2001**, *3*, 385–400.

[10] K. Dwight, N. Menyuk, *Phys. Rev.* **1960**, *119*, 1470–1479.

[11] C. P. Bean, J. D. Livingston, *J. Appl. Phys.* **1959**, *30*, 120S-129S.

[12] J.-I. Park, N.-J. Kang, Y.-W. Jun, S. J. Oh, H.-C. Ri, J. Cheon, *ChemPhysChem* **2002**, *3*, 543–547.

[13] G. H. Lee, S. H. Huh, J. W. Jeong, B. J. Choi, S. H. Kim, H.-C. Ri, *J. Am. Chem. Soc.* **2002**, *124*, 12094–12095.

 © 2004 Wiley-VCH Verlag GmbH & Co. KGaA, Weinheim

Lipid Amphiphiles

Dioxazocinium Ortho Esters: A Class of Highly pH-Vulnerable Amphiphiles**

*Kolbot By and Michael H. Nantz**

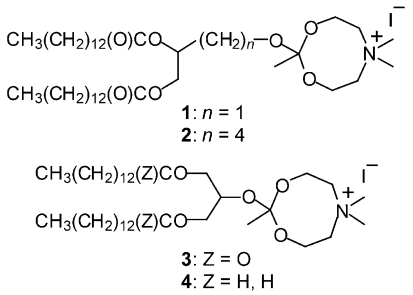
Micelles and vesicles derived from pH-sensitive amphiphiles continue to attract attention for a variety of applications.[1,2] Of particular recent interest is the use of cationic, pH-sensitive liposomes as delivery vehicles for DNA therapeutics.[3] Our interest in lipids that disassemble on exposure to mild acid conditions, such as the pH 5–6 environment within endosomes,[4] led us to engineer lipids that feature the highly pH-vulnerable ortho ester moiety.[5] We disclose herein the synthesis of an even more sensitive class of pH-vulnerable lipids from a novel dioxazocinium ketene acetal reagent. The results of formulation and hydrolysis studies with representative lipids **1**–**4** (Scheme 1) and a single-chain analogue are presented to illustrate the versatility of the synthesis and pH sensitivity.

[*] K. By, Prof. M. H. Nantz
Department of Chemistry
University of California, Davis, CA 95616 (USA)
Fax: (+1) 530-752-8995
E-mail: mhnantz@ucdavis.edu

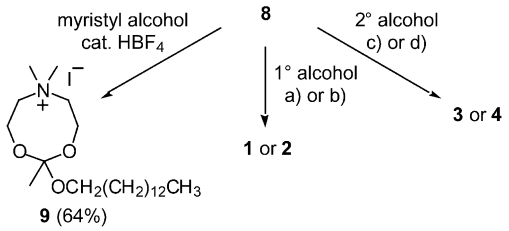
[**] This work was partly supported by the Cystic Fibrosis Foundation. We thank Grete N. Adamson for the transmission electron micrographs and Dara E. Gilbert for technical assistance.

Supporting information for this article is available on the WWW under http://www.angewandte.org or from the author.

 DOI: 10.1002/anie.200352589 © 2004 Wiley-VCH Verlag GmbH & Co. KGaA, Weinheim

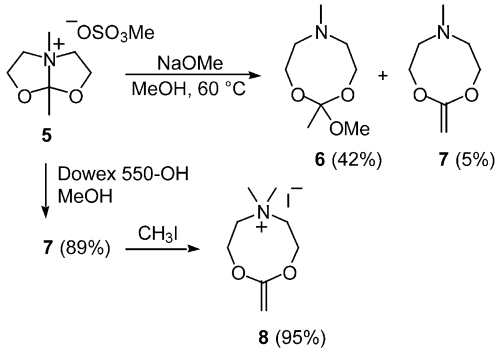


Scheme 1. Dioxazocinium ortho ester lipids.



Scheme 3. Ortho ester synthesis: a) 1,2-ditetradecanoyl-*rac*-glycerol, DMF, 69% (**1**); b) 1,2-dimyristoyloxy-6-hexanol, CH_2Cl_2:DMF (3:1), 86% (**2**); c) 1,3-ditetradecanoyl-*rac*-glycerol, DMF, 61% (**3**); d) 1,3-dimyristyloxy-2-propanol, CH_2Cl_2:DMF (3:1), 43% (**4**). DMF = *N*,*N*-dimethylformamide.

Lipid synthesis: Exposure of ammonium salt **5**[6] (Scheme 2) to NaOMe gives rise to methyl ortho ester **6** and to ketene acetal **7** as the consequence of a competing Hofmann-type elimination.[7] We reasoned that the ketene acetal moiety in **7** could serve as a progenitor of amphiphilic ortho esters. Hence, we aimed to optimize the yield of **7** from **5**. Our initial efforts resulted in a protocol in which sodium



Scheme 2. Synthesis of the ketene acetal reagent **8**.

triphenylmethoxide and **5** were heated under vacuum in tetrahydrothiophene 1,1-dioxide (sulfolane). Ketene acetal **7** was collected by direct distillation. Final purification afforded a 36% yield of pure **7** on a 20-gram scale. Ultimately, we discovered that simple elution of **5** as a methanol solution through an anion-exchange resin gave ketene acetal **7** in 89% yield. Although hydroxide ion exchange resins are often used to prepare ammonium hydroxide salts, temperatures in excess of 100 °C are typically required to effect subsequent Hofmann eliminations.[8] Thus the formation of **7** under these mild conditions represents a convenient but unusual ketene acetal synthesis.[9]

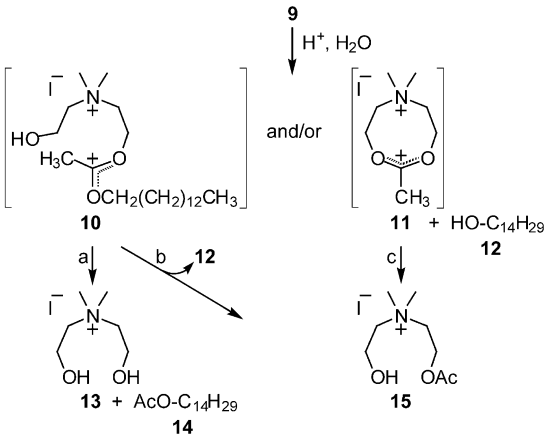
Ortho ester formation with **7** proved to be sluggish without the assistance of an acid catalyst and low yielding when only catalytic amounts of acid were employed. However, quaternization of **7** cleanly afforded **8** (Scheme 2). In contrast to **7**, ammonium salt **8** can be stored without decomposition[10] and readily converted into ortho esters (Scheme 3). The synthesis is general. For example, under HBF_4 catalysis, reaction of **8** with myristyl alcohol provided ortho ester **9**. Other catalysts were examined (trifluoromethanesulfonic acid, methanesulfonic acid, anhydrous HCl in diethyl ether), but none were as effective as HBF_4. Reaction of **8** with dual-chain substituted primary and secondary alcohols gave the ortho esters **1**–**4** in good to moderate yields depending on the degree of substitution of the alcohol.

Lipid properties: With the dioxazocinium lipids prepared, we turned our attention toward liposome formulation and pH-vulnerability issues. Incorporation of dioloeylphosphatidylethanolamine (DOPE) during the hydration and sonication of the dual-chain analogues **1**–**4** greatly improved the ability of these lipids to assemble in water.[11] In separate D_2O experiments, ^1H NMR analysis showed that sonication and heating of **1**–**4** at 50 °C for 1 h did not hydrolyze the ortho ester. Transmission electron microscopy (TEM) analyses of representative preparations derived from **1** and **3** revealed multilamellar lipid aggregates with sizes of 95–220 nm.[12] Light-scattering-particle size measurements also indicated aggregates with mean diameters of 165 and 159 nm for the DOPE preparations of **1** and **3**, respectively.

To examine the susceptibility of the dioxazocinium ortho ester linkage toward acid-induced cleavage under different conditions, we considered the case of the single-chain derivative **9**. Ortho ester hydrolysis is believed to proceed through a three-stage reaction mechanism that involves, as the first stage, the generation of a dioxocarbenium ion intermediate.[13] Though many variables are involved in the hydrolysis,[14] cyclic ortho esters form dioxocarbenium ions either by endocyclic C–O or exocyclic C–O bond cleavage, with the latter being the preferred mode in small to medium-size rings.[15] In the case of **9**, endocyclic C–O bond cleavage would give rise to dioxocarbenium species **10** (Scheme 4), while heterolysis of an exocyclic C–O bond would give **11** with concomitant formation of myristyl alcohol (**12**). Subsequent interception of these dioxocarbenium species by water results in products from paths a–c. While **10** may serve as a precursor to diol **13** (path a), the monoacetate **15** (path b), and the accompanying myristyl hydrolysates **14** and **12**, respectively, the cyclic species **11** can form only monoacetate **15**. This mechanistic interpretation suggests that the appearance of the myristyl hydrolysis products could be used as a convenient probe for monitoring the progress of the hydrolysis.

Incubation of **9** in HOAc/NaOAc buffer solutions at pH 5.0, 5.5, and 6.0 with monitoring by GC/MS to quantify the appearance of **12** and **14** revealed that myristyl acetate was the predominant by-product, thereby implicating path a as the principal mode of hydrolysis.[12] Only trace amounts of

 © 2004 Wiley-VCH Verlag GmbH & Co. KGaA, Weinheim



Scheme 4. Hydrolysis of the ortho esters.

myristyl alcohol (**12**, $<5\%$) were detected in these experiments. The data (Figure 1) suggest an apparent zero-order rate law consistent with the acid-catalyzed dissociative mechanism reported for ortho ester hydrolysis.[13] The rate of hydrolysis of **9** is faster than that of other cationic lipids—**9** was completely hydrolyzed at pH 5.0 within six hours ($t_{1/2} = 120 \pm 1$ min). Extrapolation of the linear plot data for the pH 5.5 and 6.0 conditions gave $t_{1/2}$ values of 250 ± 17 and 407 ± 15 min, respectively.

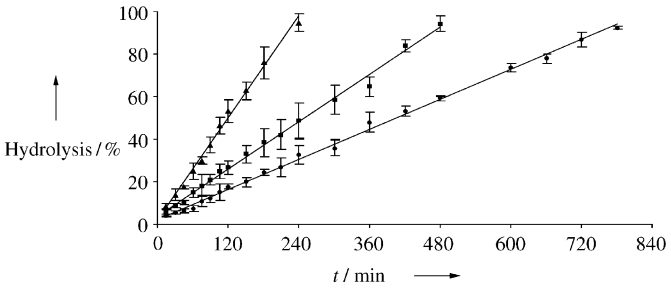


Figure 1. Linear plots for the hydrolysis of **9** in HOAc/NaOAc buffer solutions at pH 5.0 (▲), pH 5.5 (■), and pH 6.0 (●). Hydrolyses were performed at 38 °C in the presence of 1-methoxydodecane as an internal standard. Each data point represents the average of three experiments; the bars for each point represent the standard deviation.

The high sensitivity of **9** toward acid-catalyzed cleavage can be attributed to a combination of structural features. The flexibility imparted by the eight-membered ring of **9** increases the possibility for either *anti*- or *syn*-periplanar dissociation[15] to the dioxocarbenium species **10**. The proximal ammonium group may also facilitate formation of the dioxocarbenium ion by improving the leaving-group ability of the endocyclic oxygen atoms. While this hypothesis is consistent with the interpretation of the rate study, the details of the factors that govern the hydrolysis of dioxazocinium ortho esters have yet to be confirmed.

Substitution of the ortho ester influences the rate of hydrolysis. Exposure of the liposome suspensions derived from lipids **1**–**4** to pH 5.0 for 6 h at 38 °C revealed that the ortho ester moieties in **1**, **3**, and **4** had undergone only partial (approximately 10–50 %) hydrolysis. While the hydrolysis rate certainly is influenced by differences in the aggregation state (that is, micellar with **9**, lamellar with **1**–**4**), substituent effects also contribute. Lipid **3** is the slowest to hydrolyze, a fact which is consistent with the expected electron-withdrawing influences of the β-acyloxy and β-alkoxy groups. Lipid **2**, which closely approximates the alkyl side-chain structure of **9**, is the most sensitive of the dual-chain amphiphiles. In competition hydrolysis experiments of **9** mixed with each dual-chain lipid we found that **9** was clearly more vulnerable except when mixed with **2**, where we observed essentially no difference in the rate of hydrolysis between **2** and **9**. The ortho ester moiety in **2** undergoes complete hydrolysis at pH 5.0 within 6 h. These results show that subtle structural differences can be used to adjust the pH sensitivity of a dioxazocinium ortho ester. This facet may be useful in tailoring amphiphiles of this type to cleave at a targeted, mild pH value.

In summary, we have reported an efficient synthesis of a dioxazocinium ketene acetal that can serve as a reagent for the transformation of hydrophobic primary or secondary alcohols into pH-vulnerable ortho ester amphiphiles. Hydrolysis studies revealed unprecedented pH-sensitivity among the cationic lipids and provided preliminary indications that hydrolysis of dioxazocinium ortho esters occurs through the endocyclic C–O bond cleavage mode.

Received: August 7, 2003 [Z52589]

Keywords: amphiphiles · cleavage reactions · hydrolysis · lipids · ortho esters

[1] a) C. Wang, Q. Gao, J. Huang, *Langmuir* **2003**, *19*, 3757; b) Y. Rui, S. Wang, P. S. Low, D. H. Thompson, *J. Am. Chem. Soc.* **1998**, *120*, 11213; c) D. A. Jaeger, B. Li, T. Clark, Jr., *Langmuir* **1996**, *12*, 4314; d) D. Ono, S. Yamamura, M. Nakamura, T. Takeda, A. Masuyama, Y. Nakatsuji, *J. Am. Oil Chem. Soc.* **1995**, *72*, 853; e) D. A. Jaeger, J. Jamrozik, T. G. Golich, M. W. Clennan, J. Mohebalian, *J. Am. Chem. Soc.* **1989**, *111*, 3001.

[2] For a recent review on liposome delivery, see: T. Lian, R. J. Y. Ho, *J. Pharm. Sci.* **2001**, *90*, 667.

[3] a) J. S. Choi, J. A. MacKay, F. C. Szoka, Jr., *Bioconjugate Chem.* **2003**, *14*, 420; b) J. A. Boomer, D. H. Thompson, S. M. Sullivan, *Pharm. Res.* **2002**, *19*, 1289; c) E. Liang, M. N. Rosenblatt, P. S. Ajmani, J. A. Hughes, *Eur. J. Pharm. Sci.* **2000**, *11*, 199.

[4] J. A. Reddy, P. S. Low, *J. Controlled Release* **2000**, *64*, 27.

[5] J. Zhu, R. J. Munn, M. H. Nantz, *J. Am. Chem. Soc.* **2000**, *122*, 2645.

[6] a) K. Burzin, R. Feinauer, *Angew. Chem.* **1973**, *85*, 1055; *Angew. Chem. Int. Ed. Engl.* **1973**, *12*, 996; b) R. Feinauer, *Angew. Chem.* **1968**, *80*, 703; *Angew. Chem. Int. Ed. Engl.* **1968**, *7*, 731.

[7] R. Feinauer, *Synthesis* **1971**, 16.

[8] For example, see: C. Kaiser, J. Weinstock, *Org. Synth.* **1976**, *55*, 3.

[9] a) S. M. McElvain, L. R. Morris, *J. Am. Chem. Soc.* **1951**, *73*, 206; b) W. J. Bailey, L.-L. Zhou, *Tetrahedron Lett.* **1991**, *32*, 1539; c) L. H. Trogen, *Acta Chem. Scand.* **1993**, *47*, 841.

[10] Analysis of a sample of **8** that had been stored for six months at room temperature revealed no decomposition.

[11] As expected, single-chain analogue **9** did not form lamellate structures.

[12] See Supporting Information for TEM images and representative GC chromatographs.

 © 2004 Wiley-VCH Verlag GmbH & Co. KGaA, Weinheim

[13] a) M. Ahmad, R. G. Bergstrom, M. J. Cashen, Y. Chiang, A. J. Kresge, R. A. McClelland, M. F. Powell, *J. Am. Chem. Soc.* **1979**, *101*, 2669; b) C. A. Bunton, R. H. De Wolfe, *J. Org. Chem.* **1965**, *30*, 1371.
[14] a) P. Deslongchamps, Y. L. Dory, L. Shigui, *Tetrahedron* **2000**, *56*, 3533; b) S. Li, A. J. Kirby, P. Deslongchamps, *Tetrahedron Lett.* **1993**, *34*, 7757.
[15] S. Li, Y. L. Dory, P. Deslongchamps, *Tetrahedron* **1996**, *52*, 14841.

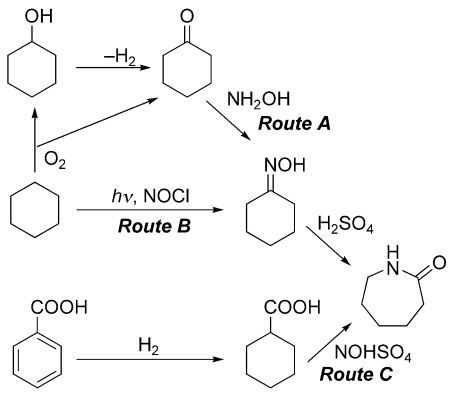
 © 2004 Wiley-VCH Verlag GmbH & Co. KGaA, Weinheim

Synthesis Techniques

A New Route to Lactam Precursors from Cycloalkanes: Direct Production of Nitrosocycloalkanes or Cycloalkanone Oximes by Using *tert*-Butyl Nitrite and *N*-Hydroxyphthalimide**

*Tomotaka Hirabayashi, Satoshi Sakaguchi, and Yasutaka Ishii**

The development of an innovative methodology for the production of bulk and commodity chemicals, in particular one that takes account of effects on the environment, becomes more and more important in industrial chemistry worldwide.[1,2] ε-Caprolactam is one of the monomers most widely used for the production of nylon 6; the world production capacity of ε-caprolactam in 1998 was about 4.2 million tons.[3] Currently, ε-caprolactam is produced by the following methods (Scheme 1): 1) Beckmann rearrangement of cyclohexanone oxime derived from cyclohexanone and hydroxylamine (Route A) or from cyclohexane and NOCl by the photonitrosation of cyclohexane (PNC) process (Route B), or 2) nitrosation of cyclohexane carboxylic acid with $NOHSO_4$ (Route C). Of these approaches, Route A is most often employed and accounts for about 70% of the total production of ε-caprolactam worldwide. However, this method has several drawbacks. Cyclohexanone is supplied by the aerobic oxidation of cyclohexane, which leads to a mixture of cyclohexanone and cyclohexanol (K/A oil), but the conversion of cyclohexane must be kept at only 3–6% to avoid the formation of further oxidation products such as adipic acid and glutaric acid.[4] Another serious drawback of this method is the coproduction of a large amount of ammonium sulfate waste in both the hydroxylamine production and the Beckmann rearrangement processes.[3]



Scheme 1. The routes currently used for the manufacture of ε-caprolactam.

Several new approaches to the synthesis of ε-caprolactam and its precursors have recently been developed. Researchers at EniChem Co. have synthesized the oxime by ammoximation of cyclohexanone with hydrogen peroxide and ammonia catalyzed by titanium silicate-1 (TS-1), followed by Beckmann rearrangement in the presence of a high-content silicate catalyst developed by Sumitomo Chemical Co.[3,5] Thomas and co-workers have reported that a bifunctional transition-metal-ion-substituted aluminophosphate molecular sieve promotes the reaction of cyclohexanone with ammonia and hydrogen peroxide or molecular oxygen to give cyclohexanone oxime along with a small amount of ε-caprolactam.[6] These methods, however, require cyclohexanone as the starting material. If direct conversion of cyclohexane into ε-caprolactam precursor could be achieved, the reaction would represent an innovative method. Although the PNC process fits this purpose, very corrosive NOCl must be used as a key compound together with HCl.[1] In addition, cyclohexanone oxime is obtained as its hydrochloric acid salt and the formation of NOCl is very troublesome. Therefore, the development of a new system for the nitrosation or oximation of cyclohexane that overcomes these disadvantages is desirable.

We have shown previously that the phthalimide *N*-oxyl radical (PINO; generated in situ by reaction of *N*-hydroxyphthalimide (NHPI) with dioxygen in the presence or absence of a transition-metal salt or nitrogen dioxide) serves as a carbon-radical-producing catalyst (CRPC) and abstracts hydrogen atoms from C–H bonds in hydrocarbons under relatively mild conditions.[7] For example, cyclohexane was oxidized in the presence of a catalytic amount of NHPI combined with $[Mn(acac)_2]$ (acac = acetylacetonate) under dioxygen to give a cyclohexyl radical, which was eventually converted into adipic acid in high yield.[8] Cyclohexane was also efficiently nitrated by treatment with nitrogen dioxide and NHPI to form nitrocyclohexane.[9] In the course of our studies on the NHPI-catalyzed functionalization of cyclohexane, we have now found that the nitrosation of cyclohexane

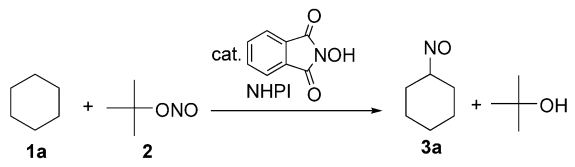
[*] T. Hirabayashi, S. Sakaguchi, Prof. Y. Ishii
Department of Applied Chemistry
Faculty of Engineering & High Technology Research Center
Kansai University, Suita, Osaka 564-8680 (Japan)
Fax: (+81) 06-6339-4026
E-mail: ishii@ipcku.kansai-u.ac.jp

[**] This work was supported by the 2003 Industrial Technology Research Grant Program of the New Energy and Industrial Technology Development Organization of Japan, and a Grant-Aid for Scientific Research (KAKENHI; Grant no. 13853008 to Y.I.) from the Japan Society for the Promotion of Science.

Supporting information for this article is available on the WWW under http://www.angewandte.org or from the author.

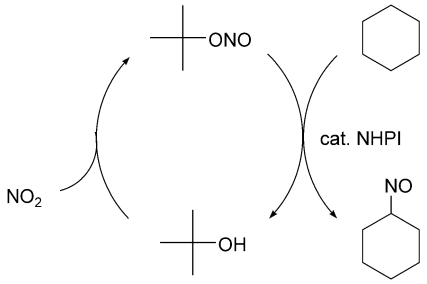
 © 2004 Wiley-VCH Verlag GmbH & Co. KGaA, Weinheim DOI: 10.1002/anie.200352741

by *tert*-butyl nitrite can be successfully achieved without photoirradiation and under halogen-free conditions by using NHPI as a catalyst (Scheme 2).



Scheme 2. Nitrosation of cyclohexane under halogen-free conditions, catalyzed by NHPI in AcOH at 80 °C under argon.

Cyclohexane (**1a**; 8 mmol, 1 mL) was allowed to react with *tert*-butyl nitrite (**2**; 1 mmol) in the presence of NHPI (0.1 mmol) in AcOH (1 mL) at 80 °C for 2 h under argon (standard conditions). Evaporation of the solvent and remaining starting materials followed by short column chromatography on acidic alumina (hexane/ethyl acetate, 5:1) gave nitrosocyclohexane (**3a**; 0.51 mmol) as a dimer. The yield of isolated **3a** was 51 % based on the amount of **2** used. This process is the first catalytic transformation of **1a** into **3a** under relatively mild conditions (at 80 °C for 2 h). The majority of **2** was found to be converted into *tert*-butyl alcohol (see below). Since *tert*-butyl alcohol is known to react with NO_2 or sodium nitrite to produce **2**,[10] reagent **2** may be regenerated from the *tert*-butyl alcohol formed. This fact suggests that this nitrosation of **1a** with **2** provides a "green" route to **3a** (Scheme 3). LC-MS analysis of the reactant showed that most of the NHPI catalyst remains in the reaction mixture after the reaction and is not decomposed. In fact, 80 % of the NHPI catalyst used could be recovered from the reaction mixture.



Scheme 3. A new route to ε-caprolactam precursors.

Figure 1 shows the ^1H and ^{13}C NMR spectra of the reactant after reaction in CD_3COOD under standard conditions. Signals at $\delta = 5.06$ ppm and $\delta = 66.0$ ppm in the ^1H and ^{13}C NMR spectrum, respectively, were assigned to protons and carbon atoms in **3a**. The signals at $\delta = 7.79$–7.67 ppm in the ^1H spectrum and $\delta = 163.9$, 133.6, 129.1, and 122.7 ppm in the ^{13}C spectrum were attributed to NHPI and small amounts of phthalimide and phthalic anhydride, which were detected by LC-MS analysis. The ^{13}C signal at $\delta = 69.5$ ppm corresponds to the tertiary carbon atom of the *tert*-butyl alcohol derived from **2**. The signals around $\delta = 4.40$ ppm in

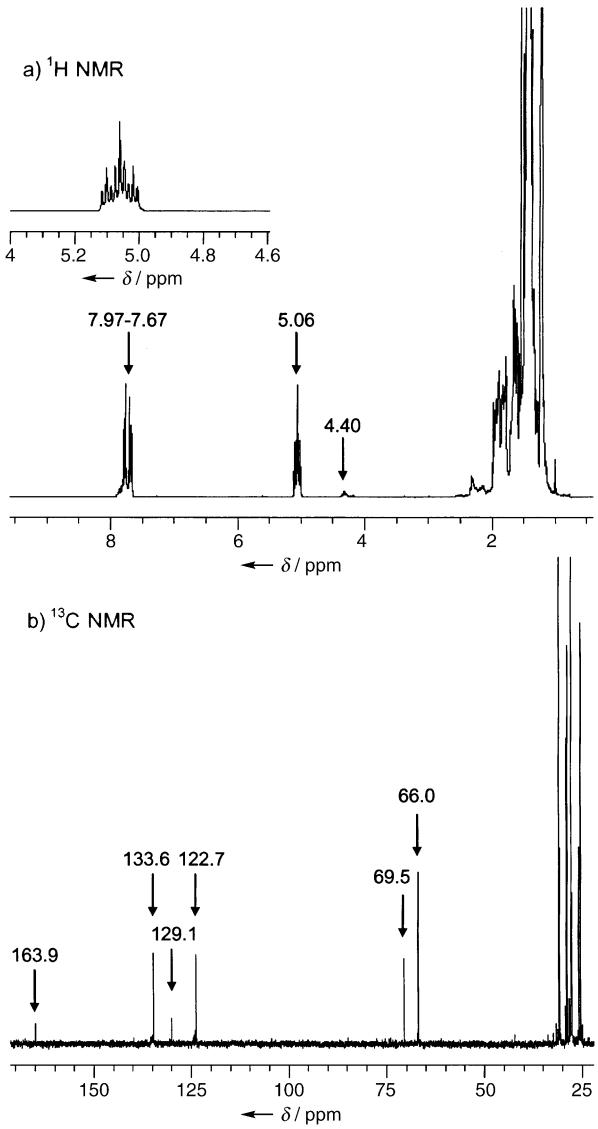


Figure 1. The NMR spectra of the reaction mixture after reaction of cyclohexane (**1a**) with *tert*-butyl nitrite (**2**) catalyzed by NHPI in CD_3COOD under standard conditions.

the ^1H spectrum were ascribed to a trace amount of nitrocyclohexane (**4a**), which was confirmed by GC-MS analysis. Compound **2** was not detected at all after the reaction. Part of **2** seems to cleave to form NO_2, which was observed as a brown gas during the reaction. HNO_2 and HNO_3 generated from NO_2 made the reaction solution very acidic.

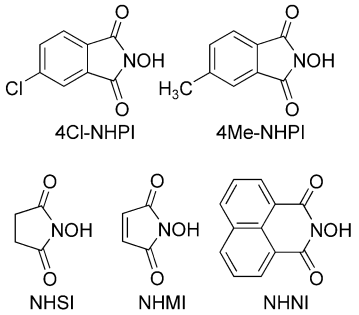
Table 1 summarizes representative results for the nitrosation of **1a** by treatment with **2** to form **3a** under various reaction conditions. The yield of **3a** was determined by ^1H NMR spectroscopy by using a known amount of nitromethane as an internal standard. Among the *N*-hydroxyimide analogues shown in Scheme 4, NHPI and *N*-hydroxy-4-chlorophthalimide (4Cl-NHPI) were found to be effective catalysts (entries 1–6). Compound **3a** was obtained in 51 % yield within only 1 h when 4Cl-NHPI was used as a catalyst (entry 3). The reaction proceeded even at 70 °C (entry 7). Recovered NHPI was also efficient when reused for a further

 © 2004 Wiley-VCH Verlag GmbH & Co. KGaA, Weinheim

Table 1: Nitrosation of cyclohexane (**1a**) by treatment with *tert*-butyl nitrite (**2**), catalyzed by NHPI.[a]

Entry	Catalyst[b]	*t* [h]	Yield of **3a** [%]
1	NHPI	2	58
2	NHPI	1	33
3	4Cl-NHPI	1	51
4	4Me-NHPI	2	19
5	NHSI	2	32
6	NHNI	2	20
7[c]	NHPI	2	63
8[d]	NHPI	2	56
9[e]	NHPI	2	40
10[f]	NHPI	2	52
11[g]	NHPI	2	0
12[h]	NHPI	2	<1
13[i]	NHPI	2	28
14[j]	NHPI	2	64
15[k]	NHPI	2	1
16[l]	NHPI	6	18

[a] **1a** (4 mmol, 0.5 mL) was allowed to react with *tert*-butyl nitrite (**2**; 0.5 mmol) in the presence of NHPI (0.05 mmol) in CD_3COOD (0.5 mL) at 80 °C under argon for 2 h. The yield of **3a** based on the amount of **2** was determined by ^1H NMR spectroscopy with a known amount of nitromethane as an internal standard and is given as the average of two runs. [b] The abbreviations refer to the structures in Scheme 4. [c] The reaction was carried out at 70 °C. [d] The catalyst recovered from the reaction described in entry 1 was used. [e] 2 mmol (0.25 mL) of **1** was used. [f] 0.25 mL of CD_3COOD was used. [g] In the absence of CD_3COOD. [h] CD_3CN (0.5 mL) was used instead of CD_3COOD. [i] The reaction was carried out in an O_2 atmosphere. [j] The reaction was carried out in the dark. [k] *n*-Butyl nitrite (**5**, 0.5 mmol) was used instead of **2**. [l] See the text for details.

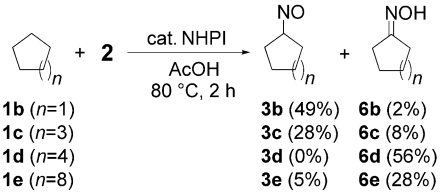


Scheme 4. The catalysts involved in the reactions listed in Table 1. 4Cl-NHPI = *N*-hydroxy-4-chlorophthalimide, 4Me-NHPI = *N*-hydroxy-4-methylphthalimide, NHSI = *N*-hydroxysuccinimide, NHMI = *N*-hydroxymaleimide, NHNI = *N*-hydroxynaphthalimide.

nitrosation (entry 8). When the amount of **1a** or CD_3COOD was halved, **3a** was formed in slightly lower yield (entries 9 and 10). The reaction did not take place at all in the absence of CD_3COOD (entry 11). Almost no reaction occurred when CD_3CN was employed in place of acetic acid (entry 12). No reaction was observed in other solvents such as PhCl, AcOEt, and α,α′,α″-trifluorotoluene.

The reaction carried out in an O_2 atmosphere was accompanied by the formation of **3a** (28%) and considerable amounts of **4a** (19%), as well as oxygenated products (<5%) such as cyclohexanol and cyclohexanone (entry 13). This result may be caused by trapping of the generated cyclohexyl radical by NO_2 derived from NO and O_2, or by O_2 itself to form **4a** and the oxygenated products, respectively. The reaction carried out in the dark gave the same results as that in the light, which indicates that the nitrosation is not initiated by photoirradiation (entry 14). When **1a** was allowed to react with *n*-butyl nitrite (**5**) instead of **2**, only a trace amount of **3a** was produced because of the formation of *n*-butyl acetate by the ready reaction of **5** with acetic acid (entry 15). A prolonged reaction time (6 h) led to a complex mixture of products other than **3a** (18%) and cyclohexanone oxime **6a** (8%; entry 16).

On the basis of these results, the reactions of several cycloalkanes with **2** catalyzed by NHPI under standard conditions were examined (Scheme 5). Cyclopentane (**1b**)

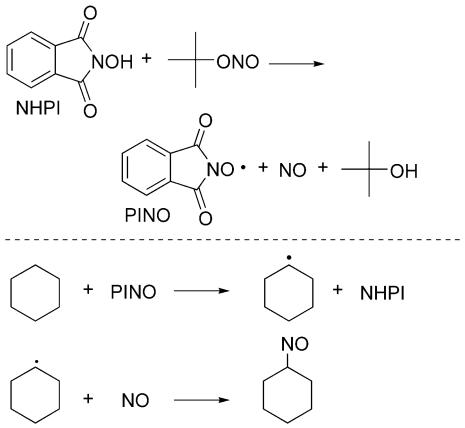


Scheme 5. The reactions of cycloalkanes with **2**, catalyzed by NHPI under standard conditions.

was nitrosated in a similar manner to **1a** to afford nitrosocyclopentane (**3b**) in 49% yield. A small amount (2%) of cyclopentanone oxime (**6b**) was also obtained. Interestingly, the reaction of cyclooctane (**1d**) produced cyclooctanone oxime (**6d**) as a major product (56%). A longer reaction time (4 h) led to **6d** in 65% yield. Direct transformation of cycloalkanes to cycloalkanone oximes, which has so far been very difficult to carry out by conventional methods, was thus achieved. It seems likely that the nitrosocyclooctane (**3d**) formed is rapidly isomerized into **6d** under these reaction conditions, probably as a result of the lower stability of nitroso dimer **3d** compared to **6d**.

ESR measurements were made to obtain information on the reaction pathway. After reaction of **2** with NHPI for 15 minutes under standard conditions, ESR measurement of the reaction mixture showed a triple signal at $g = 2.0073$ with $A_N = 4.23$ G, which we attributed to the phthalimide *N*-oxyl radical. The nitrosation process is complex and the reaction pathway is difficult to explain clearly at this stage, but a plausible reaction pathway is outlined in Scheme 6. In this suggested pathway, the reaction is initiated by the formation of PINO and NO through the reaction of NHPI with **2**. Since NHPI is easily oxidized by a weak oxidizing agent, *tert*-butyl nitrite (**2**) may serve as an oxidizing agent for NHPI and allow the formation of PINO and NO. A brown gas (nitrogen dioxide) was observed upon heating **2** with NHPI in acetic acid in the presence or absence of **1a**, which suggests that **2** decomposed to form NO and reaction with a small amount of the dissolved dioxygen gave NO_2. The PINO thus generated abstracts a hydrogen atom from **1a** to form a cyclohexyl radical and NHPI. Subsequently, the cyclohexyl radical is trapped by NO to produce nitrosocyclohexane (**3a**).

 © 2004 Wiley-VCH Verlag GmbH & Co. KGaA, Weinheim



Scheme 6. A plausible reaction pathway for the reaction of **1a** with **2**, catalyzed by NHPI.

According to this reaction pathway, nitrosation of **1a** under an NO atmosphere instead of under Ar should improve the yield of **3a**. However, it was found to be difficult to obtain **3a** selectively by NHPI-catalyzed reaction of **1a** with **2** under NO. When **1a** was allowed to react with **2** in the presence of NHPI at 80 °C for 2 h under an NO atmosphere, the reaction resulted in a complex mixture of several products. We have previously shown that the reaction of an alkane in the presence of the catalyst NHPI under an NO atmosphere proceeds by the formation of an alkyl cation intermediate that is produced when the alkyl radical generated from the alkane is oxidized by excess amounts of NO.[11] We therefore suggest that transformation of the cyclohexyl radical into the cyclohexyl cation may occur as a side reaction in the nitrosation of **1a** with **2** in the presence of excess amounts of NO. The cyclohexyl cation generated could be converted into cyclohexyl acetate by trapping with AcOH, into cyclohexene by β-proton elimination, and into several reaction products of the resulting cyclohexene. As a consequence, the reaction of **1a** with **2** in an NO atmosphere would lead to a complex mixture of products. We think that NO may be generated slowly from **2** during nitrosation of **1a** by treatment with **2** under an Ar atmosphere and that this explains why **3a** was obtained in only moderate yield. Further investigations aiming to optimize the reaction conditions are now in progress.

In conclusion, we have developed a novel, clean procedure for the nitrosation of **1a** by treatment with **2** in the presence of NHPI as a catalyst. This method has some advantages over conventional methods, such as the halogen-free, relatively mild reaction conditions, good product selectivity (almost no organic byproducts), and high recovery of the catalyst.

Experimental Section

Representative procedure: NHPI (0.1 mmol) was added to a solution of **1a** (1 mL, 8 mmol) and **2** (1 mmol) in AcOH (1 mL) in a Schlenk tube. The tube was cooled to −78 °C to freeze the solvent, degassed in vacuo, then filled with Ar gas. The frozen solvent was melted at room temperature and refrozen to repeat the evacuation/Ar purge procedure. The series of operations was repeated three times. The reaction mixture was allowed to react under an atmospheric pressure of argon at 80 °C for 2 h. After the reaction, GC and GC-MS analyses were performed. The yields of products were estimated from the areas under the peaks in the spectra by incorporating an internal standard.

Received: August 29, 2003
Revised: November 28, 2003 [Z52741]

Keywords: alkanes · lactams · nitrosation · oximation · synthesis design

[1] V. D. Luedeke in *Encyclopedia of Chemical Processing and Design* (Ed.: J. J. Mcketta), Marcel Dekker, New York, **1978**, pp. 73–95; W. N. Fisher, L. Crescentini in *Kirk-Othmer Encyclopedia of Chemical Technology, 4th ed., Vol. 4* (Ed.: J. I. Kroschwitz), Wiley, New York, **1990**, pp. 827–839; J. Ritz, H. Fuchs, H. Kiecza, W. C. Moran in *Ullmann's Encyclopedia of Industrial Organic Chemicals, Vol. 2* (Eds.: B. Elvers, S. Hawkins), Wiley-VCH, Weinheim, **1999**, pp. 1013–1043.

[2] Selected recent papers: R. Neumann, M. Dahan, *Nature* **1997**, *388*, 353–355; K. Sato, M. Aoki, R. Noyori, *Science* **1998**, *281*, 1646–1647; M. Thomas, R. Raja, G. Sankar, R. G. Bell, *Nature* **1999**, *398*, 227–230; G.-J. Brink, I. W. C. E. Arends, R. A. Sheldon, *Science* **2000**, *287*, 1636–1639; K. Ishihara, S. Ohara, H. Yamamoto, *Science* **2000**, *290*, 1140–1142; X. Zuwei, Z. Ning, S. Yu, L. Kunlan, *Science* **2001**, *292*, 1139–1141.

[3] About 2.8 kg of ammonium sulfate is generated per kilogram of cyclohexanone oxime produced: G. Bellussi, C. Perego, *Cattech* **2000**, *4*, 4–16.

[4] D. D. Davis in *Ullmann's Encyclopedia of Industrial Chemistry, 5th ed., Vol. A1* (Ed.: W. Gerhartz), Wiley, New York, **1985**, pp. 270–272; D. D. Davis, D. R. Kemp in *Kirk-Othmer Encyclopedia of Industrial Chemistry, 4th ed., Vol. 1* (Ed.: J. I. Kroschwitz), Wiley, New York, **1990**, pp. 71–480, and references cited therein.

[5] A. Cesana, M. A. Mantegazza, M. Pastori, *J. Mol. Catal. A* **1997**, *117*, 367–373; M. A. Mantegazza, G. Petrini, A. Cesana (Enichem Anic S.r.L.), EP 00564040, **1993** [*Chem. Abstr.* **1994**, *120*, 76939].

[6] R. Raja, G. Sankar, J. M. Thomas, *J. Am. Chem. Soc.* **2001**, *123*, 8153–8154.

[7] For a review, see: Y. Ishii, S. Sakaguchi, T. Iwahama, *Adv. Synth. Catal.* **2001**, *343*, 393–427.

[8] T. Iwahama, S. Sakaguchi, Y. Ishii, *Org. Process Res. Dev.* **1998**, *2*, 255–260.

[9] S. Sakaguchi, Y. Nishiwaki, T. Kitamura, Y. Ishii, *Angew. Chem.* **2001**, *113*, 228–230; *Angew. Chem. Int. Ed.* **2001**, *40*, 222–224.

[10] *The Merck Index*, *13th ed.* (Eds.: M. J. O'Neil, A. Smith, P. E. Heckelman), MERCK & CO., Whitehouse Station, **2001**, p. 266; J. C. Treacy (Notre Dame, Ind.), US 2739166, **1956** [*Chem. Abstr.* **1956**, *50*, 82174]; F. S. Olan (USA), US 4980496, **1990** [*Chem. Abstr.* **1991**, *114*, 121474].

[11] S. Sakaguchi, M. Eikawa, Y. Ishii, *Tetrahedron Lett.* **1997**, *38*, 7075–7078; M. Eikawa, S. Sakaguchi, Y. Ishii, *J. Org. Chem.* **1999**, *64*, 4676–4679.

 © 2004 Wiley-VCH Verlag GmbH & Co. KGaA, Weinheim

Silanes

An Isolable Radical Anion and Dianion of a Cyclotetrasilane: Synthesis and Structure of $[Si\{1,2\text{-}(NEt)_2C_6H_4\}]_4^{-\cdot}$ and $[Si\{1,2\text{-}(NEt)_2C_6H_4\}]_4^{2-}$**

Barbara Gehrhus, Peter B. Hitchcock, and Lihong Zhang*

The stability of isolable N-heterocyclic silylenes[1,2] has its origin in a significant π delocalization in the five-membered ring of Si[N(*t*Bu)CHCHN*t*Bu] (**A**)[3] or the benzo-annulated Si[1,2-$(NCH_2tBu)_2C_6H_4$] (**B**)[4] with incorporation of the formally empty silicon out-of-plane p orbital.[5,6] In contrast, the silylene Si[N(*t*Bu)-CH_2CH_2N*t*Bu] (**C**),[7] which lacks π delocalization is only marginally stable and converts into its stable tetramer.[8] But how important is the steric protection provided by the bulky *t*Bu or CH_2*t*Bu groups in the stable silylenes **A** and **B**, respectively, and what effect will a reduction of the size of the substituent at the nitrogen atom have on the stability of a two-coordinate silicon species? Herein we report 1) the reduction of the $Cl_2Si[1,2\text{-}(NR)_2C_6H_4]$ (R = Et; **3**) analogue of the silylene precursor of **B** (R = CH_2*t*Bu) with potassium, 2) the synthesis of the first isolable and structurally characterized radical anion of a cyclotetrasilane, $[Si\{1,2\text{-}(NEt)_2C_6H_4\}]_4^{-\cdot}$, and 3) its dianion $[Si\{1,2\text{-}(NEt)_2C_6H_4\}]_4^{2-}$.

Reduction of $Cl_2Si[1,2\text{-}(NEt)_2C_6H_4]$ (**3**)[9] with potassium in THF at ambient temperature afforded a product mixture of the potassium salt of the radical anion $\mathbf{1}^{-\cdot}$ and the dianion $\mathbf{2}^{2-}$ (Scheme 1). Complex **1** could be isolated from the mixture as green crystals at −25 °C whereas the orange complex **2** was crystallized from DME.

The structure of **1**[10] shows the potassium cation solvent-separated from the cyclotetrasilane radical anion (Figure 1) whilst for the structure of **2**[11] the solvated potassium cations have η^2-coordination to the 3,3′-C atoms (C14, C15) of the *o*-phenylene ring (Figure 2). In both, **1** and **2**, the cyclotetrasilane ring lies on an inversion centre and the $\{Si_4\}$ core is planar. The Si1–Si2 bond length in **1** of 2.347(2) Å (see Table 1) is slightly shorter compared to Si–Si bond lengths

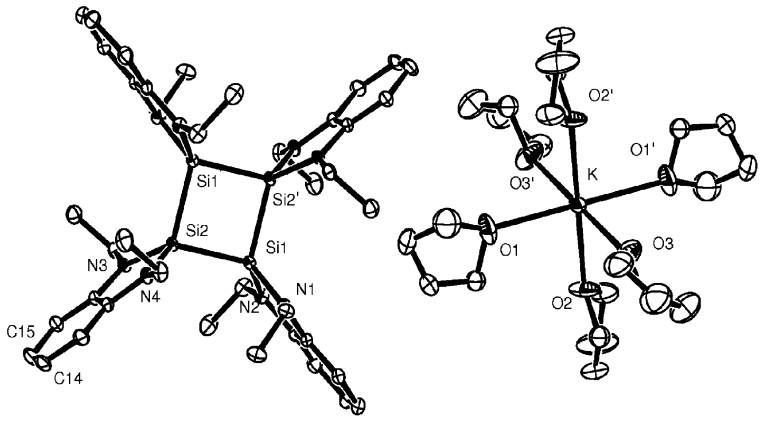
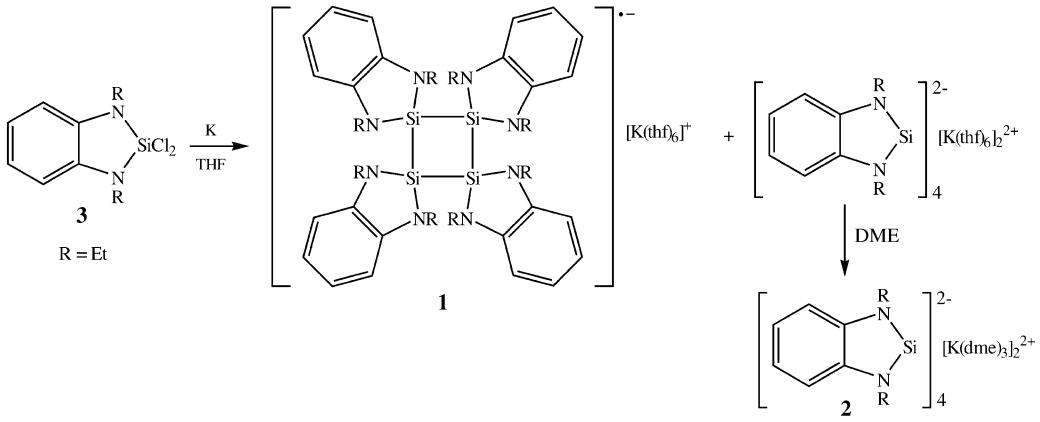


Figure 1. Molecular structure of **1** (thermal ellipsoids set at 20 % probability).



Scheme 1.

[*] Dr. B. Gehrhus, Dr. P. B. Hitchcock, L. Zhang
Department of Chemistry
School of Life Science
University of Sussex
Brighton, BN1 9QJ (UK)
Fax: (+44) 1273-677-196
E-mail: b.gehrhus@sussex.ac.uk

[**] We thank the EPSRC for the award of an Advanced Fellowship for B.G.

which are found in cyclopolysilanes (av. 2.372 Å)[12] or for tetrasilacyclobutanes (2.363–2.445 Å).[13] Even further reduction of the Si1–Si2 bond length is found for complex **2** (2.284(2) Å), which is close to the range of Si–Si double bonds (2.138–2.261 Å)[12] and may also be compared to the Si=Si bonds in a *Z*-diaminodisilyldisilene (the tetramer of **C**; 2.289 Å)[8] or cyclotetrasilenes (2.174, 2.257 Å).[14,15] The substantial shortening of the Si–Si bond in **1** and **2** can be

 © 2004 Wiley-VCH Verlag GmbH & Co. KGaA, Weinheim DOI: 10.1002/anie.200352882

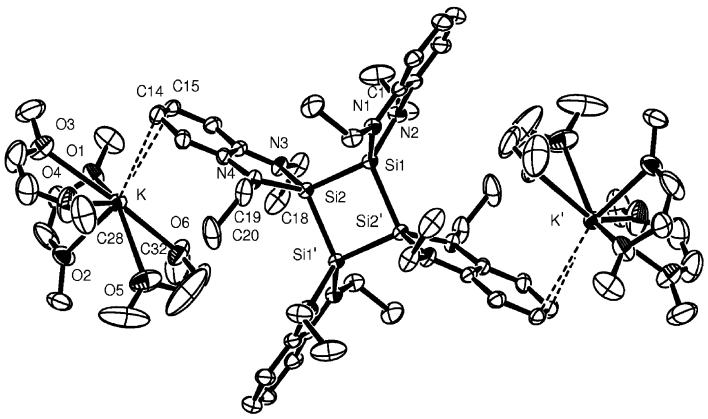


Figure 2. Molecular structure of **2** (thermal ellipsoids set at 20 % probability).

Table 1: Selected bond lengths [Å] and angles [°] of compounds **1** and **2**.

Bond	1	2	Angle	1	2
Si1-Si2′	2.346(2)	2.284(2)	Si2′-Si1-Si2	90.27(6)	89.87(5)
Si1-Si2	2.347(2)	2.284(2)	Si1′-Si2-Si1	89.73(6)	90.13(5)
Si1-N1	1.768(4)	1.814(3)	N1-Si1-N2	88.6(2)	85.2(2)
Si1-N2	1.775(4)	1.799(4)	N3-Si2-N4	88.6(2)	84.7(2)
Si2-N3	1.770(4)	1.807(3)			
Si2-N4	1.765(4)	1.812(3)			
K···C14		3.137(5)			
K···C15		3.266(5)			

attributed to the additional one or two electrons, respectively, which are delocalized in the Si_4 ring.

ESR-spectroscopic analysis[16] (Figure 3a) of **1** ($g_{iso}=2.0025$, $a=3.5$ G) shows 15 of the 17 expected lines ($2nI+1$, $I=1$, $n=8$) consistent with the electron being delocalized over the Si_4 ring and is in good agreement with the simulated spectrum (Figure 3b).

Alkali-metal reduction of a cyclosilane to obtain a radical anion is a long established method. A wide range of ESR spectroscopic analysis shows that the unpaired electron is delocalized over the resulting cyclopolysilane ring.[17–19] All of these radical anions of cyclosilanes are labile and are only detected at low temperature. Persistent radical anions of ladder oligosilanes were reported recently.[20] The radical anion $\mathbf{1}^{-\cdot}$ of complex **1** is the first thermally robust, crystalline and structurally characterized radical anion of a cyclopolysilane.

The proposed mechanism leading to **1** and **2** may involve pathways (a), (b) and/or (c) (Scheme 2). Precedence for pathway (a) is found in the reported formation of **6** and **7** (where (NN)Si = **C**)[21] by reduction of **C** with Na/K or the formation of **7** (where (NN)Si = **B**) by reduction of **B** with potassium.[22] Precedence for pathway (b) is the report that the transient silylene (tBu$_3$Si)SiCl inserts into the Si–Na bond of its precursor (tBuSi)SiCl$_2$Na; in the present context this corresponds to the insertion of **5** into the Si–K bond of **4** to form **8**. This insertion was found to proceed more readily than insertion into the Si–H bond of the common silylene trap Et_3SiH and was accompanied by one or two further insertions of (tBuSi)SiCl into the Si–Na bond of the successive intermediates, which led, after elimination of NaCl, to the corresponding cyclosilanes (tBuSiSiCl)$_3$ and (tBuSiSiCl)$_4$.[23] A third pathway (c) is possible, which is commonly suggested for the synthesis of cyclooligosilanes by reductive dehalogenation of halosilanes, which in this case would proceed by reaction of **4** with the dichlorosilane **3** to yield a 1,2-dichlorodisilane **10**. Successive metallation and reaction with **3** followed by elimination of NaCl would also lead to intermediate **9**.

Complex **2** can readily be converted into **1** by, for example, treatment with **3**. Attempts to isolate the neutral cyclotetrasilane [Si{1,2-(NEt)$_2$C$_6$H$_4$}]$_4$ (cf., **9** in Scheme 2) have so far been unsuccessful, presumably owing

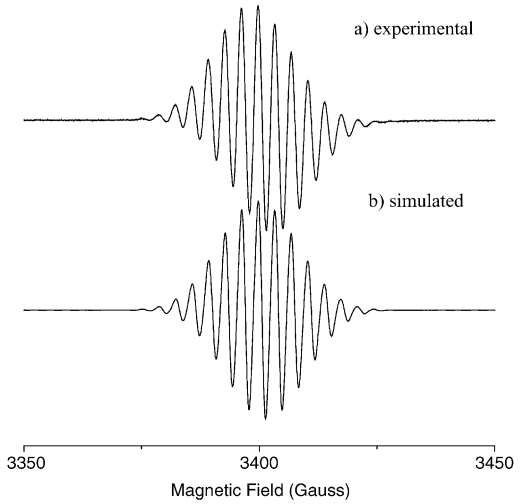
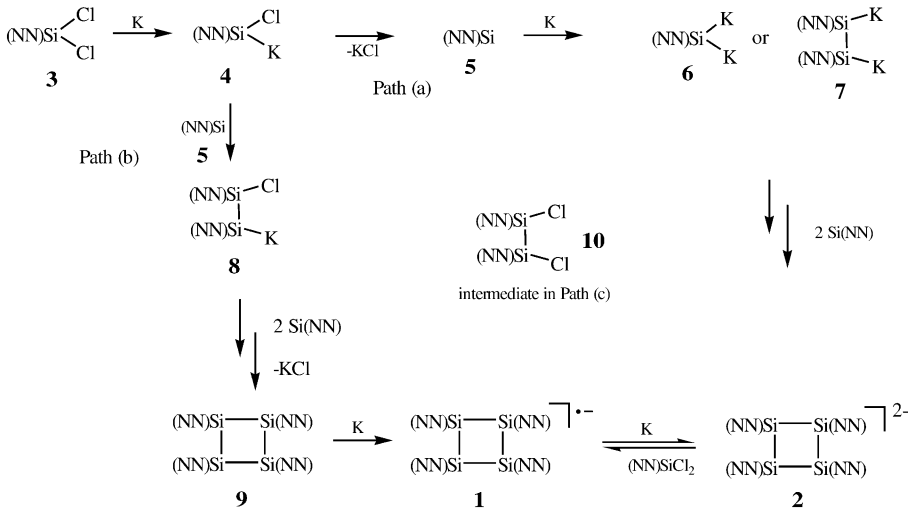


Figure 3. ESR spectrum of **1**.



Scheme 2.

 © 2004 Wiley-VCH Verlag GmbH & Co. KGaA, Weinheim

to the readiness of $[Si\{1,2\text{-}(NEt)_2C_6H_4\}]_4$ to take up a single electron. Surprisingly, the reduction of $Cl_2Si[1,2\text{-}(NR)_2C_6H_4]$ upon changing the substituent at N from R = Et to the bulkier *i*Bu led to a similar formation of a cyclotetrasilane radical anion and dianion, which will be reported in the full paper. The neopentyl substituent ($R = CH_2tBu$) therefore seems ideally suited to provide steric protection for the silylene **B**.

Experimental Section

1: Potassium (1.45 g, 0.037 mol) was added to a solution of **3** (4.85 g, 0.019 mol) in THF (150 mL) at ambient temperature. The mixture initially turned green and after stirring for 2 days to green brown. The mixture was filtered and the green residue was extracted with hot THF. The extract was concentrated and green crystals of compound **1** were obtained at −25 °C.

2: Potassium (3.5 g, 0.89 mol) was added to a solution of **3** (5.85 g, 0.022 mol) in THF (150 mL) at ambient temperature. The mixture initially turned green. The mixture was stirred for 5 days then filtered and the solvent was removed from the red-brown filtrate. The residue was crystallized from DME yielding orange crystals of compound **2** (4.9 g, 64 %). ^{1}H NMR (300 MHz, $[D]_8$THF): $\delta = 1.05$ (br,s, 6H, CH_3), 3.26 (dme), 3.42 (dme), 3.78 (br,d, 4H, CH_2), 5.95 (m, 2H, phenyl), 6.09 ppm (m, 2H, phenyl). ^{29}Si{^{1}H} NMR (99.3 MHz, $[D]_8$THF): $\delta = -45.2$ ppm.

Received: September 16, 2003 [Z52882]

Keywords: radical anions · silanes · silicon · silylene · small ring systems

[1] M. Haaf, T. A. Schmedake, R. West, *Acc. Chem. Res.* **2000**, *33*, 704.
[2] B. Gehrhus, M. F. Lappert, *J. Organomet. Chem.* **2001**, *617*, 209.
[3] M. Denk, R. Lennon, R. Hayashi, R. West, A. V. Belyakov, H. P. Verne, A. Haaland, M. Wagner, N. Metzler, *J. Am. Chem. Soc.* **1994**, *116*, 2691.
[4] B. Gehrhus, P. B. Hitchcock, M. F. Lappert, J. Heinicke, R. Boese, D. Bläser, *J. Organomet. Chem.* **1996**, *521*, 211.
[5] M. Denk, J. C. Green, N. Metzler, M. Wagner, *J. Chem. Soc. Dalton Trans.* **1994**, 2405.
[6] P. Blakeman, B. Gehrhus, J. C. Green, J. Heinicke, M. F. Lappert, M. Kindermann, T. Veszprémi, *J. Chem. Soc. Dalton Trans.* **1996**, 1475.
[7] R. West, M. Denk, *Pure Appl. Chem.* **1996**, *68*, 785.
[8] T. A. Schmedake, M. Haaf, Y. Apeloig, T. Müller, S. Bukalov, R. West, *J. Am. Chem. Soc.* **1999**, *121*, 9479.
[9] Synthesis of **3** is similar to the synthesis of $Cl_2Si[1,2\text{-}(NCH_2tBu)_2C_6H_4]$ in ref. [4].
[10] Crystal data for **1**: $C_{64}H_{104}KN_8O_6Si_4$, $M_r = 1233.01$, specimen $0.20 \times 0.05 \times 0.05$ mm^3, monoclinic, space group $P2_1/n$ (No. 14), $a = 18.2955(7)$, $b = 9.4645(4)$, $c = 20.0260(8)$ Å, $\beta = 91.757(2)°$, $U = 3466.0(2)$ Å^3, $Z = 2$, $\mu = 0.20$ mm^{-1}, $T = 173(2)$ K, 4775 unique reflections collected, $R_1 = 0.069$ for 3212 reflections with $I > 2\sigma(I)$, $wR_2 = 0.174$ for all reflections, Data collection KappaCCD, full-matrix least-squares refinement on F^2, SHELX-97. CCDC-218118 (**1**) and CCDC-218119 (**2**) contains the supplementary crystallographic data for this paper. These data can be obtained free of charge via www.ccdc.cam.ac.uk/conts/retrieving.html (or from the Cambridge Crystallographic Data Centre, 12 Union Road, Cambridge CB21EZ, UK; fax: (+44) 1223-336-033; or deposit@ccdc.cam.ac.uk).
[11] Crystal data for **2**: $C_{64}H_{116}K_2N_8O_{12}Si_4$, $M_r = 1380.21$, specimen $0.20 \times 0.20 \times 0.05$ mm^3, monoclinic, space group $P2_1/n$ (No. 14), $a = 12.7165(2)$, $b = 19.0891(4)$, $c = 17.2205(4)$ Å, $\beta = 109.724(1)°$, $U = 3934.96(14)$ Å^3, $Z = 2$, $\mu = 0.24$ mm^{-1}, $T = 173(2)$ K, 5295 unique reflections collected, $R_1 = 0.0631$ for 3774 reflections with $I > 2\sigma(I)$, $wR_2 = 0.178$ for all reflections, Data collection KappaCCD, full-matrix least-squares refinement on F^2, SHELX-97. (CCDC reference number 218119.)
[12] M. Kaftory, M. Kapon, M. Botoshansky, *The Chemistry of Organosilicon Compounds*, *Vol. 2*, Wiley, New York, **1998**.
[13] H. Suzuki, K. Okabe, R. Kato, N. Sato, Y. Fukuda, H. Watanabe, M. Goto, *Organometallics* **1993**, *12*, 4833.
[14] M. Kira, T. Iwamoto, C. Kabuto, *J. Am. Chem. Soc.* **1996**, *118*, 10303.
[15] N. Wiberg, H. Auer, H. Nöth, J. Knizek, K. Polborn, *Angew. Chem.* **1998**, *110*, 3030; *Angew. Chem. Int. Ed.* **1998**, *37*, 2869.
[16] ESR measurement and simulation: D. M. Murphy at the EPSRC National ENDOR Service, Cardiff University, UK.
[17] R. West, *Pure Appl. Chem.* **1982**, *54*, 1041.
[18] C. L. Wadsworth, R. West, *Organometallics* **1985**, *4*, 1659.
[19] E. Hengge, R. Janoschek, *Chem. Rev.* **1995**, *95*, 1495.
[20] S. Kyushin, Y. Miyajima, H. Matsumoto, *Chem. Lett.* **2000**, 1420.
[21] R. West, T. A. Schmedake, M. Haaf, J. Becker, T. Mueller, *Chem. Lett.* **2001**, 68.
[22] B. Gehrhus, P. B. Hitchcock, R. Pongtavornpinyo, unpublished results.
[23] N. Wiberg, W. Niedermayer, *J. Organomet. Chem.* **2001**, *628*, 57.

 © 2004 Wiley-VCH Verlag GmbH & Co. KGaA, Weinheim

Conjugate Addition–Alkylations

Oxonitriles: Multicomponent Grignard Addition–Alkylations**

Fraser F. Fleming, Zhiyu Zhang, Qunzhao Wang, and Omar W. Steward*

Dedicated to Professor Edward Piers on the occasion of his retirement

Efficiently installing high molecular complexity is a fundamental pursuit in organic synthesis.[1] Several excellent strategies have emerged for installing multiple bonds in a single synthetic operation; bidirectional synthesis,[2] domino reactions,[3] biomimetic cascades,[4] and multicomponent reactions.[5] Each strategy exhibits complementary advantages, with multicomponent reactions benefiting from an inherent convergence that fulfills the synthetic criteria of assembling complex targets from fragments of similar size.[6]

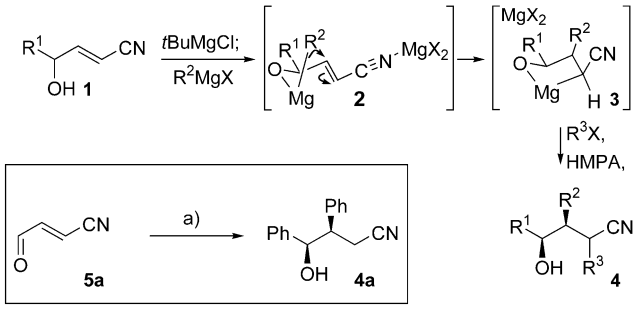
[*] Prof. Dr. F. F. Fleming, Z. Zhang, Q. Wang, Prof. Dr. O. W. Steward
Department of Chemistry and Biochemistry
Duquesne University
Pittsburgh, PA 15282-1530 (USA)
Fax: (+1) 412-396-5683
E-mail: flemingf@duq.edu

[**] Financial support from the National Institutes of Health (USA) is gratefully acknowledged.

Supporting information for this article is available on the WWW under http://www.angewandte.org or from the author.

 © 2004 Wiley-VCH Verlag GmbH & Co. KGaA, Weinheim DOI: 10.1002/anie.200352920

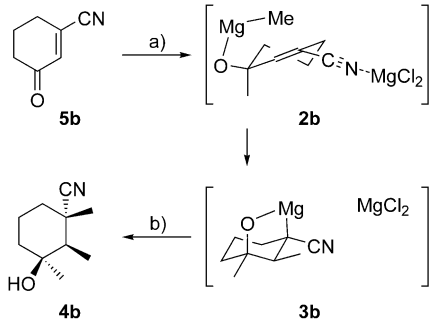
As a subclass of multicomponent reactions, conjugate addition–alkylation reactions install two new bonds and up to three stereocenters in a single synthetic operation.[7] Chelation-controlled conjugate addition–alkylations exhibit the additional advantage of promoting conjugate additions with less reactive Michael acceptors. The strategy is particularly effective for γ-hydroxyalkenenitriles (Scheme 1, **1**→**4**)[8] where chelation permits a facile conjugate addition–alkylation with a recalcitrant class of Michael acceptors that are unreactive toward many conventional nucleophiles.[9]



Scheme 1. Chelation-controlled conjugate additions to alkenenitriles. a) PhMgBr (3 equiv), THF, RT, 1.5 h, (58%).

The highly efficient chelation-controlled conjugate additions to γ-hydroxyalkenenitriles **1** stimulated a multicomponent variation with Grignard reagents and oxonitriles for potentially installing three new stereocenters in one operation (inset, Scheme 1). Conceptually, the addition of a Grignard reagent to the γ-oxonitrile **5a** was envisaged to directly generate an alkylmagnesium alkoxide intermediate **2**, which triggered conjugate addition and generated the dimagnesiated nitrile **3** for potential alkylation (Scheme 1). Addition of excess PhMgBr to oxonitrile **5a**[10] triggers sequential carbonyl and conjugate additions, generating **4a** as the sole stereoisomer.

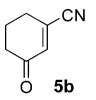
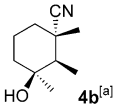
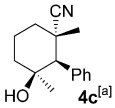
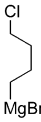
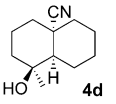
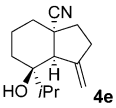
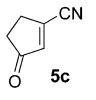
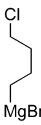
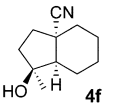
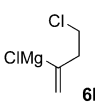
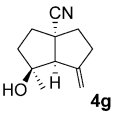
Although the formation of **4a** validates the multicomponent concept, optimizing the reaction was frustrated by the volatility and instability of **5a**.[10a] Attention was therefore redirected toward the more stable six-membered oxonitrile **5b**[11] (Scheme 2). Addition of excess methylmagnesium chloride to **5b** triggers the sequential carbonyl addition–conjugate addition affording the cyclic magnesiated nitrile **3b**.[8] Intercepting this formal dianion with methyl iodide installs a third stereocenter,[12] generating **4b** as a single stereoisomer.[13]



Scheme 2. Multicomponent addition–alkylation with oxonitrile **5b**. a) MeMgCl, THF, −78°C, 1 h; b) −78°C→RT, 2 h, MeI, 86%.

The efficient three-component addition–alkylation of **5b** is typical of the reactivity exhibited in a range of multicomponent reactions (Table 1). Grignard reagents react significantly faster with the carbonyl group than in the subsequent chelation-controlled conjugate addition, permitting the sequential addition of two different Grignard reagents, first to the ketone and second in the conjugate addition (Table 1, entry 2). Employing ω-haloalkyl Grignard

Table 1: Multicomponent oxonitrile conjugate addition–alkylations.

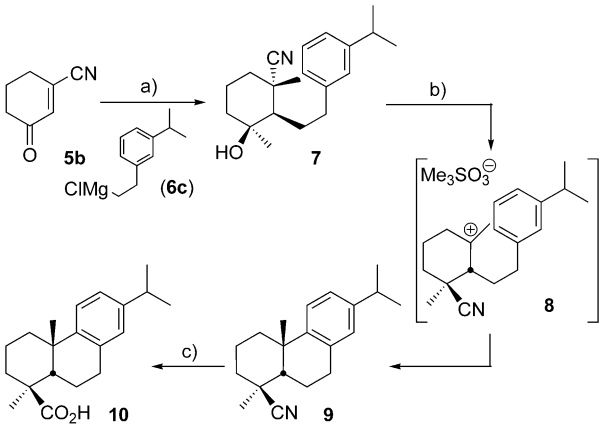
Entry	Oxonitrile	Reagents	Alkanenitrile	Yield [%]
1	 **5b**	MeMgCl, MeI	 **4b**[a]	86
2	 **5b**	MeMgCl, PhMgCl, MeI	 **4c**[a]	71
3	 **5b**	MeMgCl,  **6a**	 **4d**	53
4	 **5b**	*i*PrMgBr,  **6b**[b]	 **4e**	58
5	 **5c**	MeMgCl,  **6a**	 **4f**	53
6	 **5c**	MeMgCl,  **6b**[c]	 **4g**	50[b]

[a] Stereochemistry assigned by X-ray crystallography.[14] [b] Prepared by *i*PrMgCl exchange.[15] [c] An equivalent of *t*BuLi is added after addition of **6b** to promote conjugate addition through the ate complex.[16]

 © 2004 Wiley-VCH Verlag GmbH & Co. KGaA, Weinheim

reagents, such as chlorobutylmagnesium bromide (**6a**) or the related Grignard reagent **6b**, for the conjugate addition allows a smooth annulation route to the *cis*-fused decalin **4d** and hydrindane **4e**, respectively (Table 1, entries 3 and 4, respectively). Similarly, carbonyl additions to the corresponding five-membered oxonitrile **5c**,[11] followed by addition of the ω-haloalkyl Grignard reagents **6a** and **6b**, generates nitrile-substituted hydrindane and octalin rings in one synthetic operation (Table 1, entries 5 and 6).

The rapid installation of three new stereocenters makes the multicomponent Grignard addition to oxonitriles ideally suited to terpenoid synthesis. Combining the multicomponent addition with cationic cyclization provides a particularly efficient entry to the dehydroabietic acid skeleton, several congeners of which exhibit antitumor, antibiotic, and cytotoxic actitvity.[17] Sequential addition of MeMgCl and Grignard **6c**[18] to **5b** followed by methylation with MeI installs the entire abietane carbon skeleton (Scheme 3).



Scheme 3. Multicomponent *epi*-dehydroabietic acid synthesis. a) MeMgCl, THF, 1 h; **6c**, −78 °C→RT; MeI, 2 h, 54%; b) Me_3SO_3H, $MeNO_2$, 0 °C, 1.5 h, 75%; c) NaOH, H_2O, diethylene glycol, 16 h, 170 °C; 6 h, 246 °C; HCl 90%.

Intramolecular Friedel–Crafts alkylation affords predominantly[19] the *cis*-abietane **9**, illustrating the advantage of the small, non-nucleophilic nitrile that permits arylation without prior interception of the carbocation intermediate **8** that occurs with the corresponding ester.[20] Nitrile hydrolysis completes the synthesis of *epi*-dehydroabietic acid **10**.[21]

Multicomponent Grignard addition–alkylations of oxonitriles rapidly assembles highly substituted mono- and bicyclic nitriles. Employing ω-haloalkyl Grignard reagents permits an efficient route to octalins, hydrindanes, and decalins with aryl-substituted Grignards being ideally suited for annulation by Friedel–Crafts alkylations. Collectively the strategy rapidly assembles a diverse array of cyclic nitriles, with complete control over the three stereogenic centers.

Received: September 19, 2003 [Z52920]

Keywords: alkylation · Grignard reagents · Michael addition · multicomponent reactions · oxonitriles

[1] T. Hudlicky, *Chem. Rev.* **1996**, *96*, 3.
[2] a) S. R. Magnuson, *Tetrahedron* **1995**, *51*, 2167; b) C. S. Poss, S. L. Schreiber, *Acc. Chem. Res.* **1994**, *27*, 9.
[3] a) L. F. Tietze, *Chem. Rev.* **1996**, *96*, 115; b) T.-L. Ho, *Tandem Organic Reagents*, Wiley, New York, **1992**.
[4] U. Scholz, E. Winterfeldt, *Nat. Prod. Rep.* **2000**, *17*, 349.
[5] a) L. F. Tietze, A. Modi, *Med. Res. Rev.* **2000**, *20*, 304; b) A. Dömling, I. Ugi, *Angew. Chem.* **2000**, *112*, 3300; *Angew. Chem. Int. Ed.* **2000**, *39*, 3168; c) R. W. Armstrong, A. P. Combs, P. A. Tempest, S. D. Brown, T. A. Keating, *Acc. Chem. Res.* **1996**, *29*, 123.
[6] E. J. Corey, X.-C. Cheng, *The Logic of Chemical Synthesis*, Wiley, New York, **1989**, chap. 1.
[7] M. Hulce, M. J. Chapdelaine in *Comprehensive Organic Synthesis*, *Vol. 4* (Eds.: B. M. Trost, I. Fleming), Pergamon, Oxford, **1991**, pp. 237–268.
[8] F. F. Fleming, Q. Wang, O. W. Steward, *J. Org. Chem.* **2003**, *68*, 4235.
[9] F. F. Fleming, Q. Wang, *Chem. Rev.* **2003**, *103*, 2035.
[10] Prepared by oxidation[10a] of **1**, $R^1 = H$.[10b] a) A. Nudelman, E. Keinan, *Synthesis* **1982**, 687; b) F. F. Fleming, Q. Wang, O. W. Steward, *J. Org. Chem.* **2001**, *66*, 2171.
[11] Oxidation of cyclohexenecarbonitrile and cyclopentenecarbonitrile with CrO_3-3,5-dimethylpyrazole,[11a] rather than pyridine,[11b] afforded oxonitriles **5b** and **5c** in 65% and 25% yield, respectively. a) J. N. Johnson, *Encyclopedia of Reagents for Organic Synthesis*, *Vol. 2* (Ed.: L. A. Paquette), Wiley, Chichester, **1995**, pp. 1275–1277. a) H. E. Zimmerman, R. J. Pasteris, *J. Org. Chem.* **1980**, *45*, 4864.
[12] ^{1}H NMR analysis of the crude reaction mixture failed to identify any of the independently prepared diastereomeric nitrile.
[13] Methylation of **3b** corresponds to a retentive alkylation of the chiral C-magnesiated nitrile, as consistently observed in the inter- and intramolecular alkylations (Table 1). The retentive alkylations of **3b** contrast with invertive acylations of a closely related magnesiated nitrile[8] implying an unusual electrophile-dependent stereoselectivity analogous to that observed with selected chiral organolithium reagents.[a] Interception of **3b** with a range of electrophiles is being pursued to determine if the alkylation stereoselectivity of this magnesiated nitrile is indeed electrophile dependent. a) A. Basu, S. Thayumanavan *Angew. Chem.* **2002**, *114*, 740; *Angew. Chem. Int. Ed.* **2002**, *41*, 717.
[14] X-ray crystallography of **4b** and **4c** confirmed the stereochemical assignment. CCDC-218678 (**4b**) and CCDC-218679 (**4c**) contain the supplementary crystallographic data for this paper. These data can be obtained free of charge via www.ccdc.cam.ac.uk/conts/retrieving.html (or from the Cambridge Crystallographic Data Centre, 12, Union Road, Cambridge CB21EZ, UK; fax: (+44) 1223-336-033; or deposit@ccdc.cam.ac.uk).
[15] M. Abarbri, J. Thibonnet, L. Bérillon, F. Dehmel, M. Rottländer, P. Knochel, *J. Org. Chem.* **2000**, *65*, 4618.
[16] F. F. Fleming, Z. Zhang, Q. Wang, O. W. Steward, *Org. Lett.* **2002**, *4*, 2493.
[17] a) Y. Kinouchi, H. Ohtsu, H. Tokuda, H. Nishino, S. Matsunaga, R. Tanaka, *J. Nat. Prod.* **2000**, *63*, 817; b) A. M. El-Sayed, *Zagazig J. Pharm. Sci.* **1998**, *7*, 80; c) I. Rogers, H. Mahood, J. Servizi, R. Gordon, *Pulp Pap. Can.* **1979**, *80*, 94.
[18] The Grignard reagent **6c**[18a] is synthesized from 1-bromo-3-isopropylbenzene:[18b] 1. Mg; ethylene oxide. 2. Ph_3P, CCl_4. a) R. D. Haworth, R. L. Barker, *J. Chem. Soc.* **1939**, 1299. b) Commercially available from Lancaster.
[19] Cyclization affords a 9:1 ratio of *cis*:*trans* abietanes in favor of **9**.
[20] a) K. Fuji, S.-Z. Zheng, M. Node, X.-J. Hao, *Chem. Pharm. Bull.* **1991**, *39*, 202. b) A 13% yield of the carbocyclic ester is formed from a carbocationic cyclization from the corresponding alkene.[18a]

 © 2004 Wiley-VCH Verlag GmbH & Co. KGaA, Weinheim

[21] *epi*-Abietic acid **10** is used as a biological marker for diterpenoids[21a] in geochemical sediments and has been previously synthesized.[21b,c] a) B. R. T. Simoneit, *Geochim. Cosmochim. Acta* **1977**, *41*, 463; b) R. E. Ireland, R. C. Kierstead, *J. Org. Chem.* **1966**, *31*, 2543; c) M. Sharma, U. R. Ghatak, P. C. Dutta, *Tetrahedron* **1963**, *19*, 985.

 © 2004 Wiley-VCH Verlag GmbH & Co. KGaA, Weinheim

Heme Degradation

Porphyrin Traps Its Terminator! Concerted and Stepwise Porphyrin Degradation Mechanisms Induced by Heme-Oxygenase and Cytochrome P450**

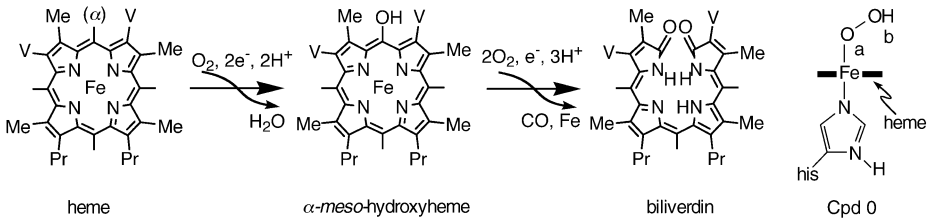
*Pankaz K. Sharma, Rouslan Kevorkiants, Sam P. de Visser, Devesh Kumar, and Sason Shaik**

Dedicated to Don Truhlar on the occasion of his 60th birthday

The enzyme heme-oxygenase (HO) traps heme species and induces their degradation.[1] The degradation process (Scheme 1) is thought to serve three key functions: a) maintenance of iron homeostasis, b) creation of CO in the brain that acts as a neurotransmitter akin to NO, and c) generation of products (e.g., biliverdin) that play a role in the defense mechanism against oxidative stress. Structural studies by Poulos and co-workers[2] of the human form (hHO-1) of the enzyme-heme complex show that the trapped heme undergoes ligation by an imidazole ring of a histidine side chain and a water molecule. Upon dioxygen uptake, followed by two-electron reduction and protonation, which activate the O=O bond, the heme unit undergoes hydroxylation at the α-*meso* position and subsequently opens up, releasing iron and carbon monoxide.

Decisive mechanistic studies by Wilks et al.[3] and Davydov et al.,[4] showed that the active species of the enzyme is the ferric hydroperoxide, Compound 0 (Cpd 0 in Scheme 1), which is the competent reaction intermediate that leads to biliverdin is the α-*meso* hydroxyheme species (Scheme 1). Furthermore, Wilks et al.[3] and Ortiz de Montellano,[1a] considered two viable mechanisms for the hydroxylation of the *meso* carbon atom. The first one involves homolytic O–O bond dissociation of Cpd 0, followed by OH· attack at the *meso* carbon atom, while the second one is an acid-catalyzed concerted electrophilic attack of the OOH moiety on the *meso* carbon atom, that is, a formal "OH^+" transfer. Ortiz de Montellano[1a] and Wilks et al.[3] preferred the electrophilic mechanism over the homolytic alternative primarily because a free OH· radical would be expected to attack the heme in a nonselective manner, unlike the regioselective reaction of Cpd 0 in HO. However, as pointed out by Poulos and co-workers,[2] there are no specific acid or basic residues close enough to the FeOOH moiety to take part directly in the reaction. One wonders, therefore, how an electrophilic mechanism can be acid catalyzed. Could there, alternatively, be a homolytic scenario with a regioselective OH· attack on the *meso* position?

Another intriguing issue is the reactivity of Cpd 0 in HO, which is unusual for a heme enzyme. In most other heme enzymes the primary active form is the high-valent iron–oxo species, Cpd I,[2,5] whereas Cpd 0 is either inactive or reacts by default in the absence of Cpd I.[6] Indeed, theoretical calculations show that Cpd 0 in the enzyme P450 is a poor electrophilic species.[7] Could the change of the proximal ligand from thiolate (in P450) to imidazole (in HO) be really so dramatic to endow Cpd 0 with appreciable reactivity? Eventual resolution of these mechanistic questions may require the assistance of theory. To this end, and with an eye on promoting interplay between experiment and theory, it was deemed necessary to study computationally the mechanism of the initial step of heme activation by Cpd 0 of HO, by comparison to the putative process in P450.



Scheme 1. Degradation of heme catalyzed by heme-oxygenase. V = vinyl.

Following established procedures,[7a] we used hybrid density functional B3LYP calculations; the double zeta LACVP(Fe)/6-31G(H,C,N,O,S) basis set (hereafter, LACVP) was employed for geometry optimization, followed by single-point calculations with the LACVP** (Fe)/6-31G**(H,C,N,O,S) basis set (hereafter, LACVP**).[8] The two model systems involve an imidazole (ImH) ligand for HO and an HS^- ligand for P450; in both cases iron porphine represented the heme. For the reactions of Cpd 0(HO), we

[*] Dr. P. K. Sharma, Dr. R. Kevorkiants, Dr. S. P. de Visser, Dr. D. Kumar, Prof. S. Shaik
Department of Organic Chemistry and
the Lise Meitner-Minerva Center for Computational Quantum Chemistry
The Hebrew University of Jerusalem
91904 Jerusalem (Israel)
Fax: (+972) 2-658-4680
E-mail: sason@yfaat.ch.huji.ac.il

[**] This research is supported by an Israel Science Foundation (ISF) grant. Discussions with P. R. Ortiz de Montellano, T. L. Poulos, S. Sligar, J. D. Dawson, and W.-D. Woggon are acknowledged.

Supporting information for this article (16 Tables and 28 Figures) is available on the WWW under http://www.angewandte.org or from the author.

 DOI: 10.1002/anie.200352943 © 2004 Wiley-VCH Verlag GmbH & Co. KGaA, Weinheim

also explored the effects of the environment on the reaction. Following the findings of La Mar and co-workers[9] for buried water molecules, we calculated the reaction in the presence of two water molecules hydrogen bonded to the proximal oxygen atom of Cpd 0 (O_a, Scheme 1). As a limiting situation, we studied the reaction in the presence of a proton source, $H_2O{\cdot}H_3O^+$, hydrogen bonded to the proximal oxygen atom. The effect of pocket polarity was mimicked by a dielectric constant, ε, of 5.7.[7a] Finally, the structure of the heme complex in HO,[2] reveals a significant steric crowding above the would-be site of the FeOOH moiety. Indeed, the electron paramagnetic resonance (EPR) spectrum of Cpd 0 of HO[4] suggests that the FeOOH moiety possesses an acute Fe-O-O angle, unlike analogous species in other systems. The most likely candidate for this steric pressure is the methylene group of the residue Gly143, which points toward the FeOO moiety, and was found by NMR spectroscopy to move 0.5 Å towards the iron center and cause bending of the Fe-CN unit in the corresponding Fe^{III} cyanide complex.[9a] We mimicked the effect of this methylene group by placing a CH_4 molecule initially at the position coresponding to Gly143 in the crystal structure, and subsequently letting it slide 0.5 Å closer to the heme. The data generated by the calculations are summarized in the Supporting Information, while herein we present the key data.

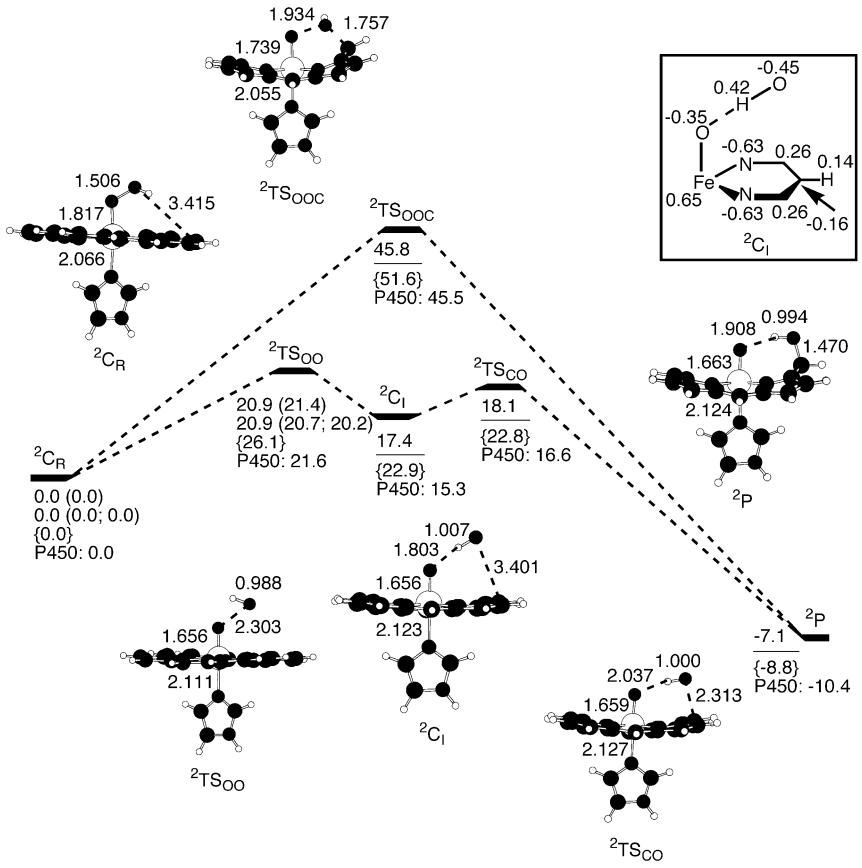


Figure 1. Energy profiles for a concerted and a stepwise reaction mechanism for the hydroxylation of the *meso* carbon atom of porphine by Cpd 0 of heme-oxygenase model (^2C_R) versus a P450 model. The energies are reported, relative to ^2C_R, as follows: the first line gives the LACVP energies in the gas-phase (with hydrogen bond to the proximal oxygen atom by two H_2O molecules in $\varepsilon = 5.7$). The second line relists the LACVP energies in the gas phase (with CH_4 at the distance of Gly143 in the crystal structure; with CH_4 translated 0.5 Å closer to the heme iron atom). The third line shows the LACVP** energies in braces. The fourth line shows the corresponding relative energies (relative to ^2C_R of P450) for the reaction with Cpd 0(P450). ε is a dielectric constant. The hydrogen-bond distance with two H_2O molecules is 2.0 Å. The C···O distance of the CH_4 molecule from the hydroperoxo oxygen atom is 3.85 Å.

Figure 1 displays the two located mechanisms of *meso* hydroxylation by Cpd 0(HO). In the first mechanism the hydroxy group is transferred to the *meso* position in a concerted reaction, akin to the proposed electrophilic mechanism.[1a,b,3] However, the computed spin densities and charge distribution of $^2TS_{OOC}$, show that there are virtually no charge and no spin on the migrating OH group, in line with its synchronous bonding situation. The second mechanism is a stepwise one, initiated by O–O homolysis followed by OH· attack on the *meso* position of porphine. Note that the barrier for the second step is extremely small (< 1 kcal mol^{-1}), as would be expected for an OH· attack on a double bond. The O–OH bond energy was also calculated and found to be 28.8 kcal mol^{-1} (32.3 kcal mol^{-1} with LACVP**), significantly higher than the energy of the intermediate, ^2C_I. As such, the ^2C_I intermediate is bound by approximately 11 kcal mol^{-1} (10 kcal mol^{-1} with LACVP**), and the energy cost of OH· escape would be much higher than the barrier for OH· attack. Thus, although formally part of a stepwise mechanism, once formed, the OH· radical will immediately attack the *meso* position.

To understand the origins of the binding of the OH· radical in the ^2C_I intermediate, we verified that a gradual increase of the O···O separation indeed takes this intermediate to the dissociation limit (Cpd II + OH·). The inset in Figure 1 shows that the OH· radical in ^2C_I is bound by hydrogen bonding and electrostatic stabilization to the Fe^{IV}-oxo group and to the porphyrin nitrogen atoms; it is fixed in space above the *meso* position. Thus, the OH· radical is trapped by the heme-oxo moiety by noncovalent interactions that lower the homolytic-cleavage barrier, the energy of the intermediate, and the barrier for the subsequent regioselective addition to the *meso* position. Comparison of the two mechanisms (Figure 1) shows that the truly concerted mechanism is highly unfavorable compared with the homolytic mechanism, most likely because of the poor bonding of the migrating hydroxyl radical (note the long O···O and O···C separations in Figure 1) and the severe heme deformation.

The homolytic mechanism involves a doublet triradicaloid species, since it results in a Fe^{IV} (FeO) unit that has two

 © 2004 Wiley-VCH Verlag GmbH & Co. KGaA, Weinheim

triplet-coupled electrons, and a radical in the porphine moiety, in an orbital of a_{2u} origin. To rule out lower barriers in other spin states, we also calculated the corresponding quartet and sextet surfaces. The resulting $^{6,4}TS_{OO}$ species were found to be higher in energy than the corresponding $^{2}TS_{OO}$ species (see Supporting Information). Thus, the first step of the heme activation is dominated by a single spin state.

The data in Figure 1 (see more details in the Supporting Information) shows that the hydrogen bonding of two water molecules to the proximal oxygen atom (O_a) raises the barrier. The resulting hydrogen bonding effect is in line with experimental evidence, which indicates that the chain of water molecules, which was found buried in the enzyme, serves to stabilize Cpd 0(HO).[9] Apparently, this stabilization is greater than the corresponding one in the transition state (TS).

Applying a steric pressure to the FeOOH moiety, by using the CH_4 unit pointing towards the proximal oxygen atom (as a mimic of the effect of the Gly143 methylene group), did not change the barriers significantly. However, the actual steric pressure in the enzyme may be more severe than our simplified modeling suggests.[2] A series of calculations showed that the energy of Cpd 0 is raised by approximately 4–8 kcal mol^{-1} when the Fe-O-O angle is reduced from 115 to 100–95°. If such a pressure[2,4,9] indeed exists in the pocket, it will lower the barriers for both concerted and homolytic mechanisms. Thus, in any event the homolytic mechanism would prevail.

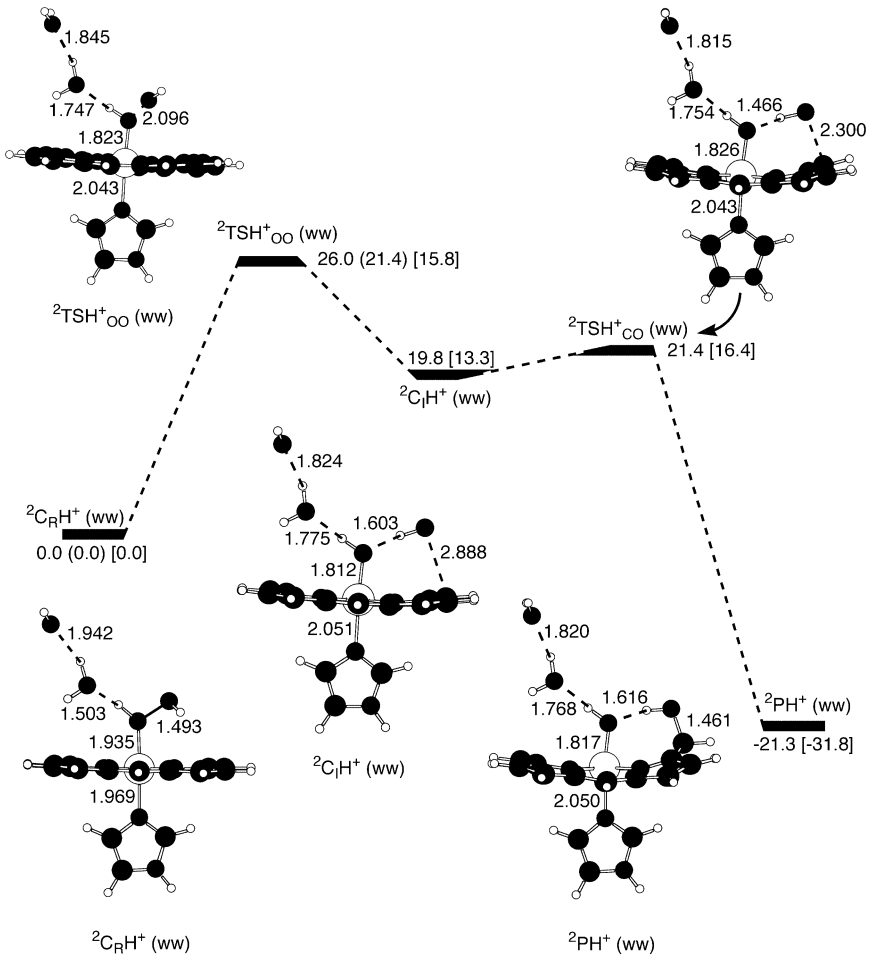


Figure 2. The mechanism of *meso* carbon atom hydroxylation initiated from the protonated Cpd 0 species ($[Fe^{III}(H_2O_2)]^+$) which is coordinated by two water molecules, ($^{2}C_RH^+$ (ww)). Energy values correspond to LACVP. The energy values in parentheses include the effect of a dielectric constant ($\varepsilon = 5.7$), while the values in square brackets correspond to the reaction of the bare $[Fe^{III}(H_2O_2)]^+$ complex ($^{2}C_RH^+$).

To explore an acid–base assisted mechanism, we used an $H_2O{\cdot}H_3O^+$ cluster coordinated to the proximal oxygen atom (O_a) by a hydrogen bond donated by the water molecule (see Supporting Information). Optimizing the structure of Cpd 0 in the presence of this cluster resulted in a spontaneous proton transfer, in a Grotthuss-type mechanism,[10] to give the iron hydrogen peroxide complex, $[Fe^{III}(H_2O_2)]^+$, coordinated by two water molecules and indicated in Figure 2 as $^{2}C_RH^+$(ww). The mechanism remains, however, stepwise with O–O homolysis leading to the intermediate $^{2}C_IH^+$(ww) in which the OH$^{\cdot}$ radical (spin density 0.91) is trapped by the heme hydroxo complex. Subsequently, the radical collapses by attacking the *meso* carbon atom. The barrier for the acid-catalyzed process, in the presence of a dielectric medium ($\varepsilon = 5.7$) is comparable to that of the pristine Cpd 0 in Figure 1 ($\Delta E^{\neq} = 21.4$ and 21.4 kcal mol^{-1}; $\Delta G^{\neq}(298\ K) = 20.8$ (16.2 with $\varepsilon = 5.7$) for the proton-assisted mechanism versus 18.5 kcal mol^{-1} for the pristine). Removal of the two water molecules and repeating the process, starting with the $[Fe^{III}(H_2O_2)]^+$ complex, lead to the same homolytic mechanism, and a significantly lower barrier (Figure 2). The lower barrier in the absence of the water molecules may not be physically significant since it is not apparent that the water molecules would detach from the $^{2}C_RH^+$(ww) complex after protonation. However, the homolytic mechanism prevails, and the remaining question is whether the reaction is proton assisted or not. This question may be settled by experimental means (such as equilibrium or kinetic solvent isotope effect) or by QM/MM calculations within the native protein. Should the proton-assisted mechanism prove to be the path taken by HO, the QM/MM calculations would be expected to reveal the reason why Cpd 0 is protonated only on the proximal oxygen atom, rather than forming Cpd I by distal protonation.

The homolytic mechanism can account for some key experimental findings.[1a,b,3] Firstly, since the OH$^{\cdot}$ radical is locked by the heme moiety, the OH$^{\cdot}$ species will not behave as a nonselective free radical, but on the contrary, its subsequent reaction will be regioselective. Secondly, since the OH$^{\cdot}$ radical is held by polar interactions, there will be a competition between the heme and the amino acid residues on the OH$^{\cdot}$ species. Thus, in some cases, a small fraction of the OH$^{\cdot}$ radicals will be trapped by the surrounding protein and will oxidize one of these residues or abstract a hydrogen atom from it, which generates a protein radical along with a Cpd II

 © 2004 Wiley-VCH Verlag GmbH & Co. KGaA, Weinheim

heme species (for example, ImH-PorFeO). These are indeed the experimental observations.[1a,b,3]

Finally, comparison of the data in Figure 1 to that of Cpd 0 of P450 shows very small quantitative differences; the LACVP barrier for the concerted reaction (45.5 kcal mol^{-1}) is virtually identical to that of HO (see Figure 1) while the barrier for homolytic cleavage (21.6 kcal mol^{-1}) is marginally higher than that for Cpd 0 of HO. Clearly, there does not seem to be anything unique about Cpd 0(HO) as such. Indeed, as a rule, heme enzymes have a protonation machinery that protonates the distal oxygen atom and converts Cpd 0 rapidly[5,10] into Cpd I, thereby avoiding HO-type activity. HO appears to lack such protonation machinery.[2] Thus, if our calculations are correct, it might be expected that upon mutation of the amino acid residues that convert Cpd 0(P450) into Cpd I(P450), the enzyme should exhibit some HO activity. In such a case, if some OH$^{\bullet}$ radical escapes the porphyrin cage, either the radical or Cpd II,[11a] may be responsible for the observation of residual epoxidation reactivity in some of the P450 mutants (for example, the T252A mutant in $P450_{cam}$).[6,11]

Note added in proof: A recent mechanistic study[12] shows solvent kinetic isotope effect (KIE) and C_{meso}–D KIE which point to a proton-catalyzed concerted mechanism. KIE calculations carried out by us will be reported elsewhere.

Received: September 24, 2003 [Z52943]

Keywords: density functional calculations · enzyme catalysis · enzyme models · heme proteins · oxygenation

[1] a) P. R. Ortiz de Montellano, *Acc. Chem. Res.* **1998**, *31*, 543; b) P. R. Ortiz de Montellano, *Curr. Opin. Chem. Biol.* **2000**, *4*, 221; c) T. Yoshida, C. T. Migita, *J. Inorg. Biochem.* **2000**, *82*, 33.

[2] D. J. Schuller, A. Wilks, P. R. Ortiz de Montellano, T. L. Poulos, *Nat. Struct. Biol.* **1999**, *6*, 860.

[3] A. Wilks, J. Torpey, P. R. Ortiz de Montellano, *J. Biol. Chem.* **1994**, *269*, 29553.

[4] R. Davydov, V. Kofman, H. Fujii, T. Yoshida, M. Ikeda-Saito, B. M. Hoffman, *J. Am. Chem. Soc.* **2002**, *124*, 1798.

[5] a) M. Sono, M. P. Roach, E. D. Coulter, J. H. Dawson, *Chem. Rev.* **1996**, *96*, 2841; b) T. L. Poulos in *The Porphyrin Handbook*, *Vol. 4* (Eds.: K. M. Kadish, K. M. Smith, R. Guillard), Academic Press, New York, **2000**, chap. 32, pp. 189–218.

[6] S. Jin, T. M. Makris, T. A. Bryson, S. G. Sligar, J. H. Dawson, *J. Am. Chem. Soc.* **2003**, *125*, 3406.

[7] a) F. Ogliaro, S. P. de Visser, S. Cohen, P. K. Sharma, S. Shaik, *J. Am. Chem. Soc.* **2002**, *124*, 2806; b) T. Kamachi, Y. Shiota, T. Ohta, K. Yoshizawa, *Bull. Chem. Soc. Jpn.* **2003**, *76*, 721.

[8] a) Geometry optimization was done with JAGUAR 4.2 package, Schrödinger, Portland OR, **2000**; b) Frequencies were calculated with Gaussian 98, M. J. Frisch, G. W. Trucks, H. B. Schlegel, G. E. Scuseria, M. A. Robb, J. R. Cheeseman, V. G. Zakrzewski, J. A. Montgomery, Jr., R. E. Stratmann, J. C. Burant, S. Dapprich, J. M. Millam, A. D. Daniels, K. N. Kudin, M. C. Strain, O. Farkas, J. Tomasi, V. Barone, M. Cossi, R. Cammi, B. Mennucci, C. Pomelli, C. Adamo, S. Clifford, J. Ochterski, G. A. Petersson, P. Y. Ayala, Q. Cui, K. Morokuma, D. K. Malick, A. D. Rabuck, K. Raghavachari, J. B. Foresman, J. Cioslowski, J. V. Ortiz, B. B. Stefanov, G. Liu, A. Liashenko, P. Piskorz, I. Komaromi, R. Gomperts, R. L. Martin, D. J. Fox, T. Keith, M. A. Al-Laham, C. Y. Peng, A. Nanayakkara, C. Gonzalez, M. Challacombe, P. M. W. Gill, B. G. Johnson, W. Chen, M. W. Wong, J. L. Andres, M. Head-Gordon, E. S. Replogle, J. A. Pople, Gaussian, Inc., Pittsburgh, PA, **1998**.

[9] a) Y. Li, R. T. Syvitski, K. Auclair, A. Wilks, P. R. Ortiz de Montellano, G. N. La Mar, *J. Biol. Chem.* **2002**, *277*, 33018; b) R. T. Syvitski, Y. Li, K. Auclair, P. R. Ortiz de Montellano, G. N. La Mar, *J. Am. Chem. Soc.* **2002**, *124*, 14296.

[10] D. L. Harris, *J. Inorg. Biochem.* **2002**, *91*, 568.

[11] a) Cpd II-epoxidized olefins: J. T. Groves, Z. Gross, M. K. Stern, *Inorg. Chem.* **1994**, *33*, 5065; b) O–O homolysis of Cpd 0(P450) into Cpd II + OH$^{\bullet}$ is preferred over heterolysis to Cpd I + OH^{-}, because the electron affinity of OH is much smaller than that of Cpd II (see, F. Ogliaro, S. P. de Visser, S. Shaik, *J. Inorg. Biochem.* **2002**, *91*, 554). TD-DFT calculation (see Supporting Information) shows that the heterolytic state is 38.5 kcal mol^{-1} higher than the homolytic state at the geometry of the ^2C_I intermediate in Figure 1. Hydrogen-bonding and polarity effects will reduce the energy difference between the dissociation modes, but may not reverse it, at least not at the intermediate geometry. The heterolytic species will be more stable at the dissociation limit.

[12] R. Davydov, T. Matsui, H. Fujii, M. Ikeda-Satio, B. M. Hoffman, *J. Am. Chem. Soc.* **2003**, *125*, 16208.

 © 2004 Wiley-VCH Verlag GmbH & Co. KGaA, Weinheim

Stille Coupling

Stille Coupling Made Easier—The Synergic Effect of Copper(I) Salts and the Fluoride Ion**

*Simon P. H. Mee, Victor Lee, and Jack E. Baldwin**

The union of two trigonal carbon centers through the Stille coupling[1] is a versatile process which has found numerous applications in organic synthesis. However the reaction between an aryl or vinyl halide/triflate and an organostannane under palladium catalysis sometimes presents difficulties.[2] The choice of catalyst, ligands, additives, solvent, and temperature can substantially affect the outcome and yield of the reaction.

We encountered a difficult Stille reaction in the course of a recent natural product synthesis,[3] a reaction which was very low yielding under typical conditions. After extensive optimization studies we discovered a combination of co-reagents that has proven to be remarkably effective in promoting the Stille reaction, that is, a copper(I) salt in conjunction with fluoride ions.

The beneficial effect of Cu^{I} salts in the Stille coupling is well documented[4–7] and it is believed that the function

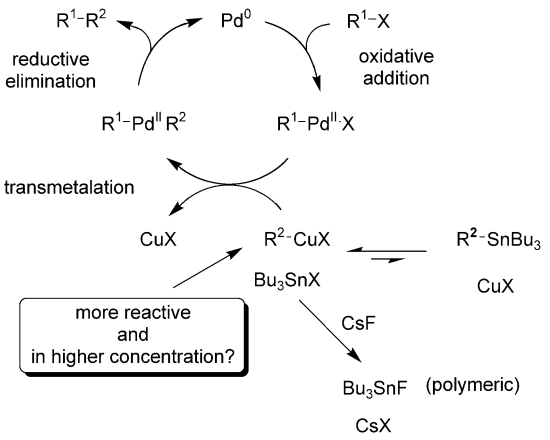
[*] S. P. H. Mee, Dr. V. Lee, Prof. J. E. Baldwin
The Dyson Perrins Laboratory
University of Oxford
South Parks Road, Oxford OX1 3QY (UK)
Fax: (+44) 1865-275-632
E-mail: jack.baldwin@chem.ox.ac.uk

[**] We thank the Overseas Research Student awards scheme for a scholarship (to S.P.H.M.).

 © 2004 Wiley-VCH Verlag GmbH & Co. KGaA, Weinheim DOI: 10.1002/anie.200352979

performed by the Cu^I salt in the catalytic cycle is solvent dependent.[5] In ethereal solvents such as THF and dioxane, the proposed role of Cu^I is as a scavenger for free neutral ligand that otherwise causes autoretardation of the rate-determining associative transmetalation.[5,6] However in highly polar solvents such as *N*-methylpyrrolidone (NMP) and DMF, the rate-accelerating effect of Cu^I has been attributed to a preliminary transmetalation reaction from the organostannane to generate a more reactive organocopper intermediate, which then takes part in the catalytic cycle.[6,7] Stille and Scott have observed previously that the fluoride ion increases the rate of the palladium-catalyzed coupling reaction between vinyl triflates and organostannanes.[8] It was also noted that the Bu_3SnCl by-product could be efficiently transformed into insoluble Bu_3SnF, which could be removed from the reaction mixture by filtration. More recently others have also employed the fluoride ion to enhance the Stille reaction.[9–11,16]

On this basis we hypothesized that if the preliminary transmetalation between the organostannane and CuI did exist and it was in equilibrium, then removal of the Bu_3SnI by-product as insoluble Bu_3SnF should favor the formation of the more reactive organocopper species, resulting in enhancement of the reaction (Scheme 1). To our knowledge, the tandem use of CuI and CsF to promote the Stille reaction has not been reported.

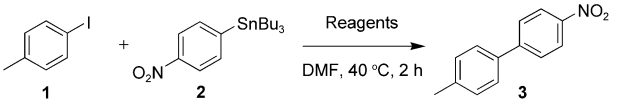


Scheme 1. Hypothesis leading to the investigation of the simultaneous use of copper(I) and fluoride in the Stille reaction.

We emphasize here that Scheme 1 presents an outline of our hypothesis. Detailed mechanistic studies will be required to determine the precise role of copper(I) and fluoride in the Stille reaction. This is beyond the scope of our current investigation; nonetheless the improvement they afford is significant however it comes about.

To investigate the effect of CuI and CsF on the Stille reaction we chose to couple 4-iodotoluene (**1**) and a deactivated electron-deficient aryl stannane, 4-(tri-*n*-butylstannyl)nitrobenzene (**2**), as a model reaction. Since **1** would be expected to undergo facile oxidative addition,[12] any variation in the rate and yield of this reaction should reflect the relative ease of the transmetalation step involving organostannane **2**. A series of reactions were carried out to determine the individual effects of CuI and CsF and then the combined effect of these two additives on this coupling reaction (Table 1).

Table 1: The individual and combined effects of CuI and CsF on the coupling of **1** and **2**.



Entry	Reagents[a]	Yield [%][b]
1	$[Pd(PPh_3)_4]$	2
2	$[Pd(PPh_3)_4]$, CsF	8
3	$[Pd(PPh_3)_4]$, CuI	46
4	$[Pd(PPh_3)_4]$, CsF and CuI	98
5	CsF and CuI	0

[a] $[Pd(PPh_3)_4]$ (10%), CuI (20%), CsF (2.0 equiv). [b] Yields are isolated yields of **3** and are the average of two repeat experiments. Remaining mass balance is recovered starting materials.

When the reaction between **1** and **2** was conducted at 40 °C for two hours using $[Pd(PPh_3)_4]$ as catalyst, only a trace of product **3** was isolated and most of the starting materials were recovered (Table 1, entry 1). The addition of CsF had a very minor positive effect on the yield of this reaction (Table 1, entry 2). A significant improvement in the yield of **3** was observed when CuI was included as an additive; the recovered starting materials again accounted for the remaining mass balance (Table 1, entry 3). When both CuI and CsF were present, the coupling reaction proceeded to completion with a near-quantitative yield of **3** (Table 1, entry 4). However no product formation was observed when the coupling between **1** and **2** was attempted with only CuI and CsF (Table 1, entry 5). This eliminated the possibility of CuI directly catalyzing the coupling of **1** and **2**.[13–15] It is clear that in the presence of palladium(0), CuI and CsF exert a synergic effect that promotes this reaction considerably.

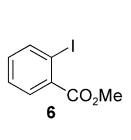
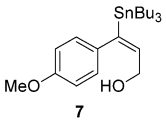
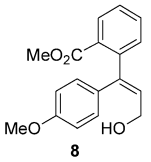
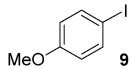
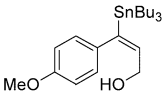
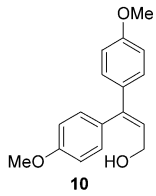
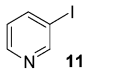
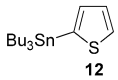
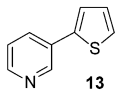
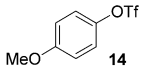
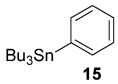
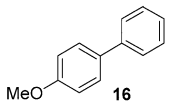
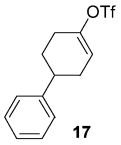
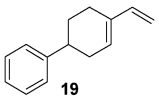
Before exploring the scope of this combined effect, we evaluated the optimal conditions for the reaction. Variables investigated were: solvent, palladium source, ligands, fluoride source, and copper(I) source. We observed that aryl iodides and triflates undergo facile coupling with organostannanes using a mixture of $[Pd(PPh_3)_4]$/CuI/CsF in DMF (Conditions A). For the less reactive aryl bromides, the most effective reagent combination has proven to be $PdCl_2/PtBu_3$/CuI/CsF in DMF (Conditions B). However, in both cases these were not necessarily the only conditions that gave high yields. Highly polar solvents such as DMSO and NMP were also effective and tetrabutylammonium fluoride (TBAF) seemed comparable to CsF in enhancing the reaction, whereas other fluoride sources (LiF, NaF, KF) were less effective.

Recently Fu et al. reported a procedure for the Stille coupling that also makes use of $PtBu_3$.[16] To investigate whether our Conditions B provide an improvement over the procedure described by Fu et al. for the coupling of bromides, a series of reactions were carried out on the challenging coupling of electron-rich 4-bromoanisole (**4**) and electron-deficient 4-(tri-*n*-butylstannyl)nitrobenzene (**2**; Table 2).

 © 2004 Wiley-VCH Verlag GmbH & Co. KGaA, Weinheim

The coupling of **4** and **2** under Conditions B afforded 92% of the desired product **5** after 4 h at 45°C (Table 2, entry 1). To demonstrate that CuI is necessary when using P*t*Bu$_3$ under Conditions B the coupling of **4** and **2** was repeated in the absence of CuI. After the same reaction time only 29% of the coupled product **5** was isolated, with the remaining starting material being recovered (Table 2, entry 2). This indicates that even though Conditions B generate a coordinatively unsaturated catalytic system, CuI is still necessary to provide the highest yields. When the coupling of **4** and **2** was carried out using the reagent combination described by Fu et al.,[16] a 16% yield of the coupled product **5** was isolated along with recovered starting materials (Table 2, entry 3). Interestingly when CuI was included in the same reaction there was a slight decrease in yield (Table 2, entry 4). This observation is supported by our optimization studies in which it was discovered that highly polar solvents are necessary to ensure the synergic effect of CuI and CsF. We also observed that $PdCl_2$ was a superior palladium source to [Pd$_2$(dba)$_3$] (dba = *trans*,*trans*-dibenzylideneacetone) when using DMF as the solvent.

Table 3: Scope of the combined copper(I)/fluoride effect on a variety of cross coupling reactions of iodides and triflates.

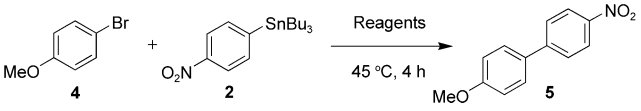
Entry	Iodide/Triflate	Stannane	Product	Conditions	Time [h]	Yield [%][a]
1	 **6**	 **7**	 **8**	A	8	92
2	 **9**	 **7**	 **10**	A	8	94
3	 **11**	 **12**	 **13**	A	1	99
4	 **14**	 **15**	 **16**	A	2	92
5	 **17**	 **18**	 **19**	A	1	98

Conditions A: [Pd(PPh$_3$)$_4$] (5%), CuI (10%), CsF (2 equiv), DMF, 45°C. [a] Yields are isolated yields and are the average of two repeat experiments.

To investigate the efficiency of our new conditions we studied a number of different coupling reactions which are summarized in Table 3 and Table 4. Some of these examples were selected from the literature.

The coupling of hindered iodide **6** and hindered stannane **7** to give **8** has previously been achieved in an optimized yield of only 27%, following reaction for 15 h at 80°C.[17] When conducted under the new conditions, this same reaction delivered **8** in an excellent yield of 92% (Table 3, entry 1). It is noteworthy that with Cu^{I} and CsF present, the reaction between **6** and **7** was complete after 6 h at just 45°C. Similarly, reaction of iodide **9** and stannane **7** afforded **10** in 94% yield (Table 3, entry 2), whereas the previously reported best yield of this reaction was a moderate 42%.[17] Heterocycles are well tolerated under our coupling conditions, as demonstrated by the near-quantitative coupling of 3-iodopyridine (**11**) and 2-(tributylstannyl)thiophene (**12**; Table 3, entry 3). Organotriflates were also shown to be excellent substrates under the new conditions: reaction of deactivated triflate **14** with stannane **15** gave the coupled product **16** in 92% yield (Table 3, entry 4), and diene **19** was obtained in 98% yield from coupling of vinyl triflate **17** and stannane **18** (Table 3, entry 5).

Table 2: Evaluating alternative conditions on the coupling of **4** and **2**.



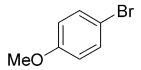
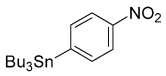
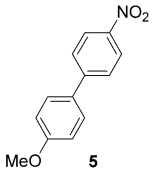
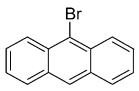
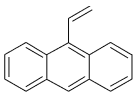
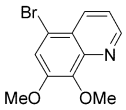
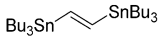
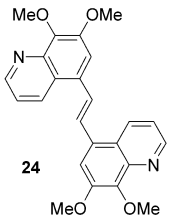
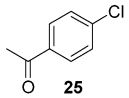
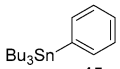
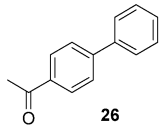
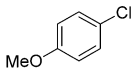
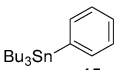
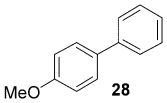
Entry	Reagents[a]	Yield [%][d]
1	$PdCl_2$, P*t*Bu$_3$, CuI, CsF, DMF[b]	92
2	$PdCl_2$, P*t*Bu$_3$, CsF, DMF	29
3	[Pd$_2$(dba)$_3$], P*t*Bu$_3$, CsF, dioxane[c]	16
4	[Pd$_2$(dba)$_3$], P*t*Bu$_3$, CuI, CsF, dioxane	10

[a] $PdCl_2$ (2%) *or* [Pd$_2$(dba)$_3$] (1%), P*t*Bu$_3$ (4%), CuI (4%), CsF (2.0 equiv). [b] Conditions B. [c] Reagent combination reported by Fu et al.[16]. [d] Yields are isolated yields and are the average of two repeat experiments. Remaining mass balance is recovered starting materials.

Coupling reactions with aryl bromides or chlorides warranted the use of $PdCl_2$/P*t*Bu$_3$/CuI/CsF (Conditions B) (Table 4). These reactions were carried out overnight for convenience, but did not necessarily require this extended reaction time. For example the electronically disfavored coupling of electron-rich bromide **4** and electron-deficient stannane **2** afforded the product **5** in 97% yield overnight (Table 4, entry 1), however it was essentially complete after 4 h (92%) as demonstrated above in Table 2 (entry 1). The sterically unfavorable coupling of di-*ortho*-substituted bromide **20** and stannane **18** gratifyingly provided the coupled product **21** in 96% yield (Table 4, entry 2). This is substantially higher than the previous reported yield of 66%,[16] although our reaction was carried out at higher temperature and for a longer time. In our hands the coupling of **20** and **18**

 © 2004 Wiley-VCH Verlag GmbH & Co. KGaA, Weinheim

Table 4: Scope of the combined copper(I)/fluoride effect on a variety of cross coupling reactions of bromides and chlorides.

Entry	Bromide/Chloride	Stannane	Product	Conditions	Time [h]	Yield [%][c]
1	 **4**	 **2**	 **5**	B	15	97
2[a]	 **20**	 **18**	 **21**	B	15	96
3	 **22**	 **23**	 **24**	B	15	93
4[b]	 **25**	 **15**	 **26**	B	15	81
5[b]	 **27**	 **15**	 **28**	B	15	40–60

Conditions B: $PdCl_2$ (2%), $PtBu_3$ (4%), CuI (4%), CsF (2 equiv), DMF, 45°C. [a] 1.3 equivalents of organostannane. [b] Reaction temperature: 100°C. [c] Yields are isolated yields and are the average of two repeat experiments (entry 5 shows the range).

under the conditions applied by Fu and co-workers ($[Pd_2(dba)_3]$, $PtBu_3$, toluene, RT, 3 h) gave 54% of the product **21**, whereas when the reaction was repeated using our catalytic system under identical conditions (RT, 3 h) a 68% yield of the product **21** was isolated. In both cases the remaining mass balance was largely recovered starting materials. As an example of a double Stille coupling, the quinoline derivative **22** and stannane **23** were subjected to our conditions, and delivered the desired product **24** in 93% yield (Table 4, entry 3).

We have also investigated the coupling of aryl chlorides under the Cu^I/CsF conditions. With these substrates we observed that the electronic effect of the substituents on the aromatic ring of the aryl chloride has a considerable influence on the reactivity of the substrate. Reaction of electron-deficient aryl chloride **25** with stannane **15** using Conditions B at 100°C provided **26** in a respectable 81% yield (Table 4, entry 4). However the coupling of the electron-rich chloride **27** to stannane **15**, proceeded in lower yields of 40–60% (Table 4, entry 5). In both cases, coupling of the aryl chlorides did not proceed to completion even with extended reaction times, suggesting that the catalytic system may be decomposing under the more forcing conditions. Thus our new conditions appear effective for the coupling of electron-deficient aryl chlorides, but less effective when it comes to electron-rich aryl chlorides.[18]

In summary, we have demonstrated that the combination of copper(I) iodide and cesium fluoride can significantly enhance the Stille reaction. We found that the $PdCl_2/PtBu_3$ catalytic system with copper(I) iodide and cesium fluoride in DMF is most effective for coupling aryl bromides, while $[Pd(PPh_3)_4]$ in combination with copper(I) iodide and cesium fluoride is optimal when coupling iodides and triflates. Furthermore, our conditions are mild and compatible with a variety of functional groups. This combination of copper(I) iodide and cesium fluoride should widen the scope of the Stille reaction, allowing synthesis of sterically hindered systems and promote electronically disfavored coupling reactions.[19]

Received: September 30, 2003
Revised: December 4, 2003 [Z52979]

Keywords: copper · cross-coupling · fluorides · Stille reaction

[1] a) J. K. Stille, *Angew. Chem.* **1986**, *98*, 504–519; *Angew. Chem. Int. Ed. Engl.* **1986**, *25*, 508–524; b) J. K. Stille, *Pure Appl. Chem.* **1985**, *57*, 1771–1780.
[2] For a review of the Stille reaction see: V. Farina, V. Krishnamurthy, W. J. Scott, *Org. React.* **1997**, *50*, 1–652.
[3] S. P. H. Mee, V. Lee, J. E. Baldwin, unpublished results.
[4] a) L. S. Liebeskind, R. W. Fengi, *J. Org. Chem.* **1990**, *55*, 5359–5364.
[5] V. Farina, S. Kapadia, B. Krishnan, C. Wang, L. S. Liebeskind, *J. Org. Chem.* **1994**, *59*, 5905–5911.
[6] A. L. Casado, P. Espinet, *Organometallics* **2003**, *22*, 1305–1309.
[7] X. Han, B. M. Stolz, E. J. Corey, *J. Am. Chem. Soc.* **1999**, *121*, 7600–7605.
[8] W. J. Scott, J. K. Stille, *J. Am. Chem. Soc.* **1986**, *108*, 3033–3040.
[9] A. García Martínez, J. Osío Barcina, A. de Fresno Cerezo, L. R. Subramanian, *Synlett* **1994**, *12*, 1047–1048.
[10] E. Fouquet, M. Pereyre, A. L. Rodriguez, *J. Org. Chem.* **1997**, *62*, 5242–5243.
[11] E. Ābele, K. Rubina, M. Fleicher, J. Popelis, P. Arsenyan, L. Edmunds, *Appl. Organometal. Chem.* **2002**, *16*, 141–147.
[12] V. Farina, B. Krishnan, *J. Am. Chem. Soc.* **1991**, *113*, 9585–9595.
[13] S. Zhang, D. Zhang, L. S. Liebeskind, *J. Org. Chem.* **1997**, *62*, 2312–2313.
[14] G. D. Allred, L. S. Liebeskind, *J. Am. Chem. Soc.* **1996**, *118*, 2748–2749.
[15] E. Piers, T. Wong, *J. Org. Chem.* **1993**, *58*, 3609–3610.
[16] A. F. Littke, L. Schwarz, G. C. Fu, *J. Am. Chem. Soc.* **2002**, *124*, 6343–6348.
[17] F. Liron, M. Gervais, J.-F. Peyrat, M. Alami, J.-D. Brion, *Tetrahedron Lett.* **2003**, *44*, 2789–2794.
[18] For an effective method of Stille coupling using aryl chlorides, see reference [16].

 © 2004 Wiley-VCH Verlag GmbH & Co. KGaA, Weinheim

[19] General experimental: A mixture of the organohalide (or triflate) (0.840 mmol) and the organotin reagent (0.930 mmol) was dissolved in DMF (2 mL), then cesium fluoride (256 mg, 1.685 mmol) was added. The palladium catalyst and copper(I) iodide [Conditions A: $[Pd(PPh_3)_4]$ (5%), CuI (10%); Conditions B: $PdCl_2$ (2%), P*t*Bu_3 (4%), CuI (4%)] were added and the flask was evacuated and refilled with argon five times. The mixture was stirred at 45°C for the specified duration, then diluted with CH_2Cl_2 (50 mL) and water (20 mL). After vigorous shaking the mixture was filtered through celite with CH_2Cl_2/EtOAc (200 mL, 1:1). The organic layer was separated, dried over $Na_2SO_4/MgSO_4$ and the solvent was removed under reduced pressure. The residue was purified by column chromatography.

 © 2004 Wiley-VCH Verlag GmbH & Co. KGaA, Weinheim

Magnetic Properties

Energy-Barrier Enhancement by Ligand Substitution in Tetrairon(III) Single-Molecule Magnets**

Andrea Cornia, Antonio C. Fabretti, Pierfrancesco Garrisi, Cecilia Mortalò, Daniele Bonacchi, Dante Gatteschi, Roberta Sessoli, Lorenzo Sorace, Wolfgang Wernsdorfer, and Anne-Laure Barra*

The tailoring of the structure and properties of single-molecule magnets (SMMs) is a very active branch of modern coordination chemistry. Investigations on classes of structurally related SMMs, such as those of the Mn_{12} family, have helped unravel the mechanisms underlying slow magnetic relaxation in high-spin molecules, a key step in both fundamental and application-oriented research.[1] At the same time, the search for new SMMs with higher blocking temperatures has fueled synthetic efforts aimed, on one side, at increasing structural control on cluster architectures[2] and, on the other side, at developing the so-called serendipitous-assembly approach.[3] An elegant strategy for structural design is based on site-specific modification of preformed clusters.[4] Carboxylate abstraction from Mn_{12} clusters, for instance, has been carried out site specifically using a variety of incoming ligands, such as nitrates,[4a] phosphanates,[4b] phosphates,[4c] or different carboxylates.[4d] However, these substitutions are accompanied by only small perturbation of the magnetic properties.

The SMM behavior is associated with the magnetic anisotropy of clusters, which in turn depends on local anisotropies and on the way they vectorially add to give a resulting total anisotropy.[5a] Herein we show that site-specific ligand replacement provides a means to raise the symmetry of Fe_4 clusters from C_2 to D_3, which results in a dramatic increase of magnetic anisotropy and energy barrier. Fe_4 clusters are among the simplest inorganic systems showing SMM behavior.[5,6] The archetypal member of this class is the tetrairon(III) compound $[Fe_4(OMe)_6(dpm)_6]$ (**1**) (Hdpm = dipivaloylmethane). The six μ-methoxide ligands bridge a central iron(III) ion to three peripheral iron centers arranged at the vertices of an isosceles triangle[5a] with a crystallographic C_2 symmetry, and some disorder which yields three different isomers in the lattice. At low temperature, the cluster has a high-spin state ($S = 5$) and an easy-axis magnetic anisotropy, two requisites for the observation of slow magnetic relaxation. For the major component, the second-order zero-field splitting (ZFS) parameters are $D = -0.206(1)\ cm^{-1}$ and $E = 0.010(3)\ cm^{-1}$. In addition, the presence of sizeable fourth-order contributions has been demonstrated.[5b]

To eliminate the lattice disorder, we attempted to replace the methoxide bridges in **1** with a tripodal ligand, 1,1,1-tris(hydroxymethyl)ethane (H_3thme), which affords facial coordination in octahedral iron(III) complexes [Eq. (1)].[7]

$$\underset{\mathbf{1}}{[Fe_4(OMe)_6(dpm)_6]} + 2\,H_3thme \rightarrow \underset{\mathbf{2}}{[Fe_4(thme)_2(dpm)_6]} + 6\,MeOH \quad (1)$$

The new tetrairon(III) cluster **2** (see Experimental Section) crystallizes in a highly ordered trigonal lattice and exhibits an enhanced SMM behavior compared with **1**.

The molecular structure of **2**, as revealed by a single-crystal X-ray study at 100(2) K, has crystallographic D_3 symmetry (Figure 1). The C_3 axis passes through Fe1, C2, and C3, whereas the three C_2 axes are directed along Fe1···Fe2, Fe1···Fe2′ and Fe1···Fe2″. As a consequence, the Fe_4 moiety is perfectly planar and the six alkoxide bridges are crystallographically equivalent to each other. The main structural differences between **1** and **2** directly reflect the geometric constraints imposed by the thme^{3-} ligand. In particular, the ligand "bite" reduces the O1-Fe1-O1′ angle

[*] Dr. A. Cornia, Prof. Dr. A. C. Fabretti, P. Garrisi, C. Mortalò
Dipartimento di Chimica—Centro SCS
Università di Modena e Reggio Emilia, UdR INSTM
Via G. Campi 183, 41100 Modena (Italy)
Fax: (+39) 059-373543
E-mail: acornia@unimore.it

D. Bonacchi, Prof. Dr. D. Gatteschi, Prof. Dr. R. Sessoli
Dipartimento di Chimica
Università di Firenze, UdR INSTM
Polo scientifico universitario, via della Lastruccia 3
50019 Sesto Fiorentino (Italy)

Dr. W. Wernsdorfer
Laboratoire Louis Néel-CNRS
BP166, 25 Avenue des Martyrs
38042 Grenoble Cedex 9 (France)

Dr. L. Sorace, Dr. A.-L. Barra
Laboratoire des Champs Magnetiques Intenses-CNRS
BP166, 25 Avenue des Martyrs
38042 Grenoble Cedex 9 (France)

[**] Work in part financed by the networks MOLNANOMAG, SENTINEL, and High Field ICN (under contract Nos. HPRN-CT-1999-00012, HPRI-CT-2000-40022 and HPRI-CT-1999-40013, respectively), and by italian MIUR and CNR and by the German DFG (SPP 1137). Mass spectral data were kindly provided by Dr. Adriano Benedetti (Università di Modena e Reggio Emilia). We gratefully acknowledge Ina Dix and the staff of the Bruker AXS company in Karlsruhe (Germany) for their helpful collaboration in collecting X-ray data, and Dr. Patrick Rosa for assistance in the magnetic measurements.

 © 2004 Wiley-VCH Verlag GmbH & Co. KGaA, Weinheim DOI: 10.1002/anie.200352989

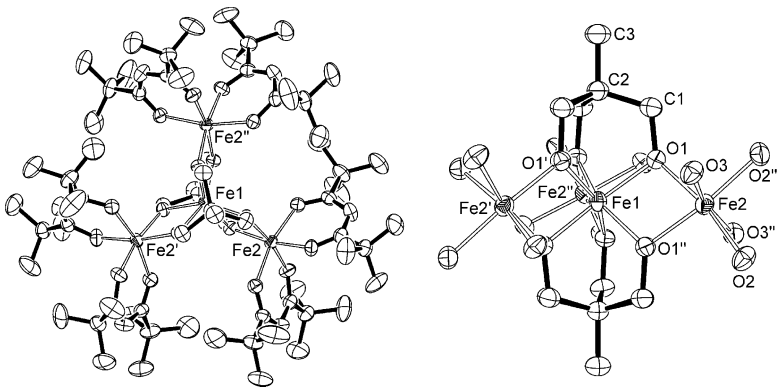


Figure 1. ORTEP[17c] representation of the molecular structure of **2** viewed slightly off the trigonal axis (left) and perpendicular to it (right; only the Fe/O framework and the thme^{3-} ligands are shown). Thermal ellipsoids are set at 50% probability and hydrogen atoms have been omitted for clarity. Selected interatomic distances [Å] and angles [°]: Fe1···Fe2 3.0858(4), Fe2···Fe2′ 5.3448(7), Fe1-O1 1.9810(12), Fe2-O1 1.9639(12); Fe1-O1-Fe2 102.92(5), O1-Fe1-O1′ 89.16(5), O1-Fe1-O1″ 76.68(7), O1-Fe2-O1″ 77.47(7).

(89.16(5) versus 93.6°), which leads to a shorter Fe1···Fe2 separation (3.0857(3) versus 3.137 Å).

The temperature dependence of the molar magnetic susceptibility (Figure 2) is characteristic of antiferromagnetic

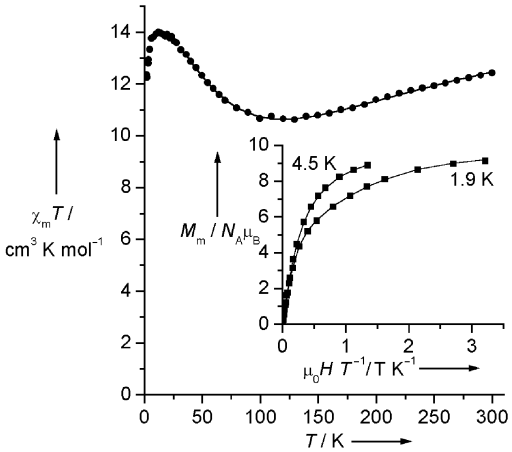


Figure 2. $\chi_m T$ versus T and M_m versus $\mu_0 H/T$ plots for a powder sample of **2**, along with best-fit calculated data (solid lines).

clusters with incomplete spin cancellation. The fitting of susceptibility data gives $J_1 = 16.51(8)\ cm^{-1}$ (antiferromagnetic) and $J_2 = -0.62(8)\ cm^{-1}$ (ferromagnetic) for the nearest-neighbor and next-nearest-neighbor Heisenberg constants, respectively. J_1 is significantly smaller in **2** than in **1** ($J_1 = 21.1\ cm^{-1}$), consistent with the smaller Fe-O-Fe angle subtended by the alkoxide bridges (102.92(5) versus 104.3°).[5a]

The occurrence of an $S = 5$ ground spin state, expected to afford a $\chi_m T$ value close to 15 cm^3 K mol^{-1} at low temperature, is confirmed by molar magnetization versus field data at 4.5 and 1.9 K (Figure 2 inset), which approach the appropriate saturation value $M_m = 10 N_A \mu_B$ in high fields. The detailed field dependence at both temperatures can be accurately fitted using an axial ZFS Hamiltonian with $D = -0.42(1)\ cm^{-1}$ and $S = 5$. To further support these conclusions, variable-temperature high-frequency EPR (HF-EPR) spectra have been recorded at 190 and 230 GHz. In the 190 GHz spectrum at 10 K (Figure 3) two sets of EPR signals arising from the transitions with magnetic field parallel and perpendicular to the symmetry axis are clearly visible in the low- and high-field regions, respectively. The largest extension of the spectrum is observed at low field and the lines in the parallel set gain intensity with decreasing field, a clear indication of a large spin ground state and a negative D parameter. In fact, when the energy quantum of the microwave radiation (≈ 9 K at 190 GHz) is comparable with the thermal energy, the $M_S = -4 \leftarrow -5$ signal has the strongest intensity owing to the enhanced population of the $M_S = -5$ state. The spectra can be accurately reproduced with $S = 5$, $g = 2.00$, and $D = -0.445\ cm^{-1}$, in good agreement with the magnetization data. To our knowledge, compound **2** has the largest D value so far reported for an iron(III)-based SMM.

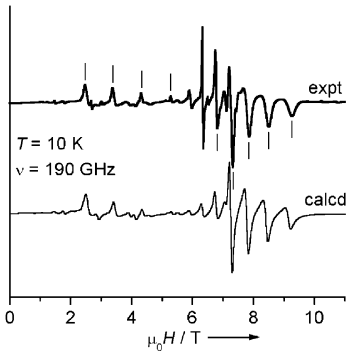


Figure 3. Experimental and simulated HF-EPR powder spectra of **2** at 10 K and 190 GHz. The pattern of signals discussed in the text is marked with vertical lines.

The twofold increase of the $|D|$ parameter following site-specific ligand substitution demonstrates the subtle structural dependence of magnetic anisotropy in iron(III) clusters. Two main terms associated with dipole–dipole interactions and single-ion anisotropies need to be considered.[8] Dipolar interactions contribute -0.034 and $-0.036\ cm^{-1}$ to the ground state D parameter of **1** and **2**, respectively, the difference being due to the slightly shorter Fe···Fe separation in the latter.[5a,9] Arguably, the large D variation in the two compounds has to be ascribed to different single-ion terms, which are known to be very sensitive to structural distortions. Angular-overlap model (AOM) calculations have previously been used to analyze the effect of trigonal compression and rotation on the magnetic anisotropy of a FeO_6 chromophore (the two types of distortions are measured by the angles θ and ϕ, whose values are 54.74° and 60°, respectively, in a regular octahedron[10,11]). The results show that trigonal compression

 © 2004 Wiley-VCH Verlag GmbH & Co. KGaA, Weinheim

leads to a positive single-ion D value (elongation to a negative value), while rotation of an octahedral face along the threefold axis favors a negative D value.[5a,10] The central iron(III) ion Fe1 shows a larger extent of trigonal rotation in **2** ($\phi = 29.2°$) than in **1** ($\phi = 41.8°$). Moreover, trigonal compression occurs in **1** ($\theta = 57.3°$), whereas slight elongation is observed in **2** ($\theta = 54.1°$). Hence, the AOM predicts a greater tendency of the Fe1 spin in **2** to lie along the unique molecular axis, which leads to an enhanced easy-axis anisotropy in the $S = 5$ ground state of the cluster.

AC and DC susceptibility measurements with the polarizing magnetic field directed along the c axis have been used to study the temperature dependence of the magnetic relaxation time τ in zero field (Figure 4). In the high-temperature limit, $\ln(\tau)$ varies linearly with $1/T$ as predicted by the Arrhenius law.[1] A linear fit of the data at $T \geq 1.9$ K gives thermal activation parameters $U_{eff}/k_B = 15.6(2)$ K and $\tau_0 = 3.4(2) \times 10^{-8}$ s. In contrast, τ approaches a temperature-independent value of approximately 1500 s below 0.2 K, a clear signature of quantum tunneling (QT) within the ground $M_S = \pm 5$ doublet. U_{eff} represents the actual barrier to be overcome for the reversal of the magnetization and its value is found to be very close to the energy gap between the $M_S = 0$ and $M_S = \pm 5$ states, $U/k_B = (|D|/k_B)S^2 = 16.0$ K (11.1 cm^{-1}). This result indicates that barrier short-cuts by QT are rather ineffective. By contrast, U_{eff} in compound **1** was found to be significantly smaller than U (3.5 versus 7.4 K).[5a] The difference can be qualitatively explained recalling that barrier short-cuts are activated by transverse anisotropies.[1,12] A dominant role is played by second-order terms, which are present in **1** but are forbidden in **2** because of its strictly axial symmetry. Fourth-order terms are also expected to be rather ineffective in **2** because for trigonal symmetry they can promote tunneling only between states whose M_S values differ by multiples of ± 3,[1] that is, only within the excited $M_S = \pm 3$ doublet in absence of external field.

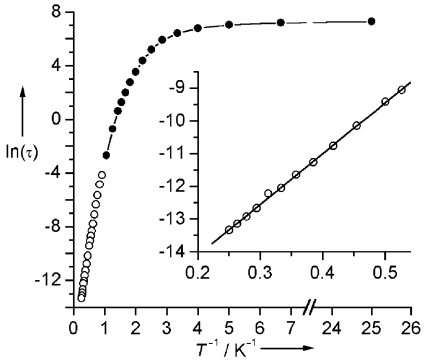


Figure 4. Magnetic relaxation time measured on a single crystal of **2** by DC (●) and AC (○) techniques (the solid line is a guide to the eye). The inset shows the high-temperature region along with the best-fit line.

Hysteresis loops on single crystals of **2** have also been recorded (Figure 5). Abrupt variations of the magnetization occur at regular field intervals $\Delta(\mu_0 H) = D/g\,\mu_B \cong 0.5$ T, that is, whenever the applied fields brings energy levels of the zero-field split multiplet into coincidence.[1] Spin–spin cross relaxation may contribute to the fine structure of the $M_S = 4 \leftarrow\!-5$ and $M_S = 3 \leftarrow\!-5$ transitions around 0.5 and 1.0 T.[13] Below around 0.2 K the relaxation becomes temperature independent, which shows that it occurs purely by a QT mechanism.

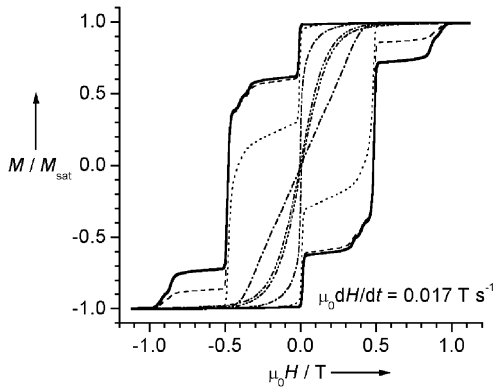


Figure 5. Hysteresis loops recorded on a single crystal of **2** with a field sweep rate of 0.017 T s^{-1} and at different temperatures: 0.04 to 0.2 K (——), 0.4 K (- - - -), 0.6 K (••••), 0.8 K (–•–•), and 1.15 K (····). The magnetic field has been applied along the crystallographic c axis.

In conclusion, site-specific ligand replacement heavily affects the ground-state anisotropy of Fe_4 SMMs and, in addition, provides a simple way to control molecular symmetry and tunneling mechanisms. We are now applying the same technique for the functionalization of Fe_4 clusters with surface-binding groups that may promote the formation of ordered molecular adsorbates on solid supports.[14]

Experimental Section

All chemicals were used as received, except for methanol which was dried by distillation over $Mg(OMe)_2$ before use. NaOMe was used as a 2.96 M solution in methanol, freshly prepared by careful addition of sodium metal to anhydrous methanol under inert atmosphere.

1: The compound was obtained by a variation on the reported synthesis.[5a,15] The dimer $[Fe_2(OMe)_2(dpm)_4]$ (**3**) was prepared as described by Rossman and co-workers by reaction of resublimed $FeCl_3$ with Hdpm in anhydrous methanol, but replacing piperidine with sodium methoxide.[16] Resublimed $FeCl_3$ (0.119 g, 0.735 mmol) was added to a stirred suspension of **3** (1.00 g, 1.10 mmol) in MeOH/Et_2O 1:2 v/v (93 mL) to give a deep red solution, and then NaOMe (0.75 mL, 2.22 mmol) was added. The yellow mixture was stirred for 40 min and diluted with MeOH/Et_2O 1:4 v/v (312 mL). After additional 15 min stirring, NaCl was removed by gooch filtration (G4) and the resulting yellow solution was divided into five 80-mL portions. Slow diffusion of methanol vapors (100 mL) into each portion over 2 weeks gave yellow rod-like crystals of **1** in 60–65% yield. Elemental analysis calcd (%) for $C_{72}H_{132}O_{18}Fe_4$: C 57.30, H 8.82; found: C 57.75, H 9.13.

2: Compound **1** (0.180 g, 0.12 mmol) was dissolved in dry Et_2O (75 mL) and treated with H_3thme (0.035 g, 0.29 mmol). Slow diffusion of methanol vapors (75 mL) into the filtered solution over 4–5 days gave yellow prisms of **2** in 70–75% yield. Elemental analysis calcd (%) for $C_{76}H_{132}O_{18}Fe_4$: C 58.62, H 8.54; found: C 58.49, H 8.55. MS (D.I.P., 70 eV): m/z (%): 1557 (<1) [M^+], 1374 (7) [M^+–dpm], 850 (50), 768 (5), 651 (6), 595 (12), 545 (10), 535 (5), 422 (100) [$Fe(dpm)_2^+$], 365 (59), 239 (29) [$Fe(dpm)^+$], 127 (7).

 © 2004 Wiley-VCH Verlag GmbH & Co. KGaA, Weinheim

Crystal structure data for **2**: $C_{76}H_{132}O_{18}Fe_4$, $M_r = 1557.22$, crystal dimensions $0.28 \times 0.23 \times 0.21$ mm, trigonal, space group $R\bar{3}c$, $a = 16.1893(12)$, $c = 56.712(10)$ Å, $V = 12873(3)$ Å^3, $Z = 6$, $\rho_{calcd} = 1.205$ g cm^{-3}, $2\theta_{max} = 56.56°$, $Mo_{K\alpha}$ radiation, $\lambda = 0.71073$ Å, $T = 100(2)$ K. Of the 33070 reflections collected on a BRUKER X8APEX system, 3564 were independent and were used in the structure refinement (Lorentz, polarization and absorption corrections applied, $\mu = 0.723$ mm^{-1}, min./max. transmission = 0.8233/0.8631). The structure was solved by direct methods using BRUKER-SHELXTL-V6.12 package and refined on F_o^2 using SHELXL-97 program[17a] implemented in the WINGX suite.[17b] One *tert*-butyl group was found to be disordered over two positions with 0.849(5) and 0.151(5) occupancies, respectively. All non-hydrogen atoms were refined anisotropically, except for the methyl carbon atoms of the disordered *t*Bu group in the lower-occupancy position. Hydrogen atoms were added in idealized positions, with torsion angle refinement for Me groups. The values of $R1$ and w$R2$ are 0.0370 [$I > 2\sigma(I)$] and 0.1089 (all data) for 172 parameters and 7 restraints. The maximum and minimum residual electron density are 0.454 and -0.285 e Å^{-3}, respectively. CCDC-220804 (**2**) contains the supplementary crystallographic data for this paper. These data can be obtained free of charge via www.ccdc.cam.ac.uk/conts/retrieving.html (or from the Cambridge Crystallographic Data Centre, 12 Union Road, Cambridge CB21EZ, UK; fax: (+44) 1223-336-033; or deposit@ccdc.cam.ac.uk).

HF-EPR spectra of **2** were recorded on a home-build spectrometer equipped with two Gunn oscillators working at fundamental frequencies of 95 and 115 GHz respectively, with double and triple harmonic generator at the Grenoble High Magnetic Field Laboratory. The sample was pressed in a pellet to prevent preferential orientation of the crystallites. Simulations of HF-EPR spectra were obtained by full diagonalization of the spin Hamiltonian matrix, using an already described calculation procedure.[18] Magnetic data on microcrystalline powder samples have been recorded using a Cryogenic S600 SQUID magnetometer, with applied fields of 0.1 T (for $T \leq 50$ K) and 1 T (for $T > 50$ K) in susceptibility versus T measurements. The diamagnetic contribution of the sample was estimated from Pascal's constants and subtracted from the data. Low-temperature magnetic measurements on single crystals were performed using an array of micro-SQUIDS.[19] Measurements were performed on this magnetometer in the temperature range 0.035–7.0 K, with fields up to 1.4 T. The field can be applied in any direction by separately driving three orthogonal coils. AC susceptibility measurements on single crystals of the order of 0.1 mm were performed with a home-built Hall probe magnetometer. It works in the temperature range between 30 mK and 30 K, for frequencies between 1 Hz and 1 MHz, and for applied fields up to 1.4 T. The field can be applied in any direction with a precision better than 0.1°.

Received: October 1, 2003 [Z52989]

Keywords: cluster compounds · iron · magnetic properties · single-molecule magnets · tripodal ligands

[1] D. Gatteschi, R. Sessoli, *Angew. Chem.* **2003**, *115*, 278; *Angew. Chem. Int. Ed.* **2003**, *42*, 268, and references therein.
[2] G. L. Abbati, A. Caneschi, A. Cornia, A. C. Fabretti, Y. A. Pozdniakova, O. I. Shchegolikhina, *Angew. Chem.* **2002**, *114*, 4699; *Angew. Chem. Int. Ed.* **2002**, *41*, 4517.
[3] R. E. P. Winpenny, *J. Chem. Soc. Dalton Trans.* **2002**, 1.
[4] a) P. Artus, C. Boskovic, J. Yoo, W. E. Streib, L.-C. Brunel, D. N. Hendrickson, G. Christou, *Inorg. Chem.* **2001**, *40*, 4199; b) C. Boskovic, M. Pink, J. C. Huffman, D. N. Hendrickson, G. Christou, *J. Am. Chem. Soc.* **2001**, *123*, 9914; c) T. Kuroda-Sowa, S. Fukuda, S. Miyoshi, M. Maekawa, M. Munakata, H. Miyasaka, M. Yamashita, *Chem. Lett.* **2002**, 682; d) M. Soler, P. Artus, K. Folting, J. C. Huffman, D. N. Hendrickson, G. Christou, *Inorg. Chem.* **2001**, *40*, 4902.
[5] a) A. L. Barra, A. Caneschi, A. Cornia, F. Fabrizi de Biani, D. Gatteschi, C. Sangregorio, R. Sessoli, L. Sorace, *J. Am. Chem. Soc.* **1999**, *121*, 5302; b) A. Bouwen, A. Caneschi, D. Gatteschi, E. Goovaerts, D. Schoemaker, L. Sorace, M. Stefan, *J. Phys. Chem. B* **2001**, *105*, 2658.
[6] R. W. Saalfrank, I. Bernt, M. M. Chowdhry, F. Hampel, G. B. M. Vaughan, *Chem. Eur. J.* **2001**, *7*, 2765.
[7] A. Cornia, D. Gatteschi, K. Hegetschweiler, L. Hausherr-Primo, V. Gramlich, *Inorg. Chem.* **1996**, *35*, 4414, and references therein.
[8] G. L. Abbati, L.-C. Brunel, H. Casalta, A. Cornia, A. C. Fabretti, D. Gatteschi, A. K. Hassan, A. G. M. Jansen, A. L. Maniero, L. Pardi, C. Paulsen, U. Segre, *Chem. Eur. J.* **2001**, *7*, 1796.
[9] D. Gatteschi, R. Sessoli, A. Cornia, *Chem. Commun.* **2000**, 725.
[10] D. Gatteschi, L. Sorace, *J. Solid State Chem.* **2001**, *159*, 253.
[11] E. L. Muetterties, L. J. Guggenberger, *J. Am. Chem. Soc.* **1974**, *96*, 1748.
[12] A. L. Barra, D. Gatteschi, R. Sessoli, *Chem. Eur. J.* **2000**, *6*, 1608.
[13] W. Wernsdorfer, S. Bhaduri, R. Tiron, D. N. Hendrickson, G. Christou, *Phys. Rev. Lett.* **2002**, *89*, 197201.
[14] A. Cornia, A. C. Fabretti, M. Pacchioni, L. Zobbi, D. Bonacchi, A. Caneschi, D. Gatteschi, R. Biagi, U. Del Pennino, V. De Renzi, L. Gurevich, H. S. J. Van der Zant, *Angew. Chem.* **2003**, *115*, 1683; *Angew. Chem. Int. Ed.* **2003**, *42*, 1645.
[15] G. Amoretti, S. Carretta, R. Caciuffo, H. Casalta, A. Cornia, M. Affronte, D. Gatteschi, *Phys. Rev. B* **2001**, *64*, 104403.
[16] C.-H. S. Wu, G. R. Rossman, H. B. Gray, G. S. Hammond, H. J. Schugar, *Inorg. Chem.* **1972**, *11*, 990.
[17] a) G. M. Sheldrick, SHELXL-97, Program for Crystal Structure Refinement (Release 97–2), Institüt für Anorganische Chemie der Universität, Göttingen, Germany, **1998**; b) L. J. Farrugia, *J. Appl. Crystallogr.* **1999**, *32*, 837; c) L. J. Farrugia, *J. Appl. Crystallogr.* **1997**, *30*, 565.
[18] C. J. H. Jacobsen, E. Pedersen, J. Villadsen, H. Weihe, *Inorg. Chem.* **1993**, *32*, 1216.
[19] W. Wernsdorfer, *Adv. Chem. Phys.* **2001**, *118*, 99.

 © 2004 Wiley-VCH Verlag GmbH & Co. KGaA, Weinheim

Nanotubes as Catalysts

Gold-Nanotube Membranes for the Oxidation of CO at Gas–Water Interfaces**

*Marco A. Sanchez-Castillo, Claudia Couto, Won Bae Kim, and James A. Dumesic**

An exciting discovery in the area of heterogeneous catalysis is the observation that nanoparticles of gold on high-surface-area supports exhibit high activity for oxidation of CO with O_2 ($CO + 1/2\,O_2 \rightarrow CO_2$) at room temperature.[1,2] This discovery is of particular relevance for the production of fuel-cell-grade hydrogen, since carbon monoxide must be removed from hydrogen streams generated by catalytic reforming of hydrocarbons.[3] The origins for the unique catalytic properties of supported gold catalysts are still unresolved. These properties have been related to changes in the electronic properties, the presence of defect sites, and the existence of strain for metallic gold nanoparticles.[4–8] Unique catalytic properties have also been related to the presence of sites associated with the catalyst support, such as cationic gold species, and sites at gold–support interfaces.[9,10]

Here we show that it is possible to study the catalytic properties of metallic gold, without interference from a catalyst support, by using nanotubes of gold in polycarbonate membranes. These nanotubes exhibit catalytic activity for the oxidation of carbon monoxide by O_2 at room temperature, and this activity is enhanced by liquid water, promoted by increasing the pH of the solution, and increased using H_2O_2 as the oxidizing agent. The rate can also be increased by depositing KOH within these nanotubes. These rates are comparable with those found in heterogeneous catalysis studies with gold nanoparticles on oxide supports, which suggests that the high activity of these latter catalysts may be related to the promotional effect of hydroxyl groups.

Gold nanotubes of uniform size were prepared via a template-synthesis method by electroless deposition of gold[11] within the pores of a 10-μm-thick, track-etched polycarbonate membrane containing 220-nm-diameter pores.[12] All surfaces of the template membrane were first sensitized with a Sn^{II} salt, activated by formation of a metallic Ag layer, followed by electroless deposition of gold for a period of 2 h. The gold nanotubes were cleaned with a 25% HNO_3 solution for 15 h.[13] Hydrophobic or hydrophilic self-assembled monolayers were formed on gold nanotubes by rinsing the samples in ethanol for 20 min, followed by immersion for 17 h in solutions of ethanol containing $HS(CH_2)_{15}CH_3$ or $HS(CH_2)_{15}COOH$, respectively.[14]

Gold nanotubes embedded within the pores of the polycarbonate template membranes were exposed by reactive ion etching (RIE) using an oxygen plasma to selectively etch approximately 2.3 μm of polycarbonate, leaving the gold nanotubes intact.[15] Figure 1 shows images from field-emission scanning electron microscopy (SEM) of the top surface of a template membrane after electroless deposition of gold followed by RIE. The images in Figure 1 reveal a high level of surface roughness; the length scale is ≈53 nm.

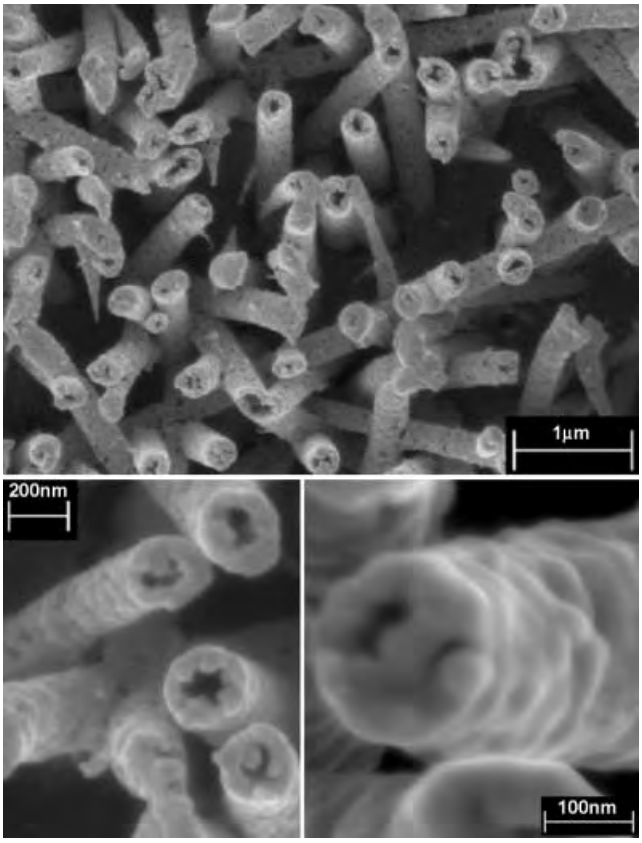


Figure 1. Field-emission SEM images of gold nanotubes at different magnifications. Micrographs were taken on the etched side of the membrane.

The membrane reactor used to study CO oxidation over gold nanotubes is shown schematically in Figure 2.[12] Table 1 shows results for the rate of CO oxidation by O_2 at 300 K and 1 bar total pressure for a $CO:O_2$ ratio of 1:1. The rate of CO_2 production is low in the absence of water, but it is increased by about 50% in the presence of water vapor at a pressure of 30 mbar (the vapor pressure of water at 298 K). The rate is significantly higher (by a factor of 10) when the $CO:O_2$ gas stream saturated with water-vapor at 298 K is passed over a gold membrane that had been previously in contact with

[*] M. A. Sanchez-Castillo, C. Couto, W. B. Kim, Prof. J. A. Dumesic
Chemical and Biological Engineering Department
University of Wisconsin
Madison, WI 53706 (USA)
Fax: (+1) 608-262-5434
E-mail: dumesic@engr.wisc.edu

[**] This work was supported by the National Science Foundation and Daimler-Chrysler. Fellowships were provided by the Ford Foundation, Graduate Engineering Scholars program, Camille and Henry Dreyfus Foundation, and Korea Science and Engineering Foundation. We thank the Wisconsin Center for Applied Microelectronics for providing facilities, and we thank P. F. Nealey, T. F. Kuech, and M. Mavrikakis for invaluable assistance.

Supporting information for this article is available on the WWW under http://www.angewandte.org or from the author.

 © 2004 Wiley-VCH Verlag GmbH & Co. KGaA, Weinheim DOI: 10.1002/anie.200353238

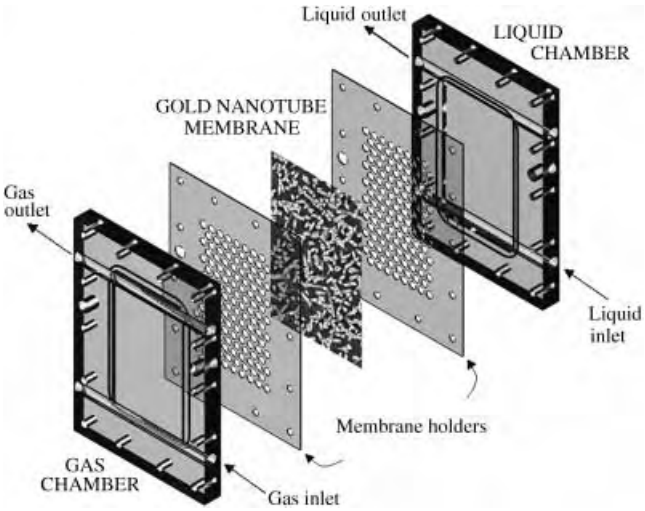


Figure 2. Diagram of the membrane reactor used to study CO oxidation on gold nanotubes positioned at the interface between two reaction chambers.

Table 1: Rate of CO_2 production for combinations of gas and liquid streams. Data collected using a gold membrane treated by RIE, with the etched side of the membrane facing the gas chamber.

Gas chamber[a]	Membrane	Liquid chamber[b]	CO_2 rate[c]
$CO:O_2$	Au	None	3
$CO:O_2$ H_2O (30 mbar)	Au[d]	None	30
$CO:O_2$ H_2O (30 mbar)	Au/KOH[d]	None	77
$CO:O_2$	Au	H_2O	47
$CO:O_2$	Au	H_2O (pH 13)	230
CO[e]	Au	H_2O (0.5% H_2O_2)	590

[a] Total gas flow rate = 100 $cm^3 min^{-1}$ (STP); $CO:O_2$ ratio = 1:1. [b] Liquid flow rate = 2 $cm^3 min^{-1}$. [c] In units of μmol of CO_2 per gram of Au per minute. [d] Liquid water or KOH solution filled inside gold nanotubes. [e] Total gas flow rate = 100 $cm^3 min^{-1}$ (STP); CO:He ratio = 1:1.

liquid water,[12] which suggests that liquid water within the gold nanotubes is responsible for the observed enhancement in the rate of CO oxidation. Indeed, a high rate of CO oxidation is achieved when the membrane containing the gold nanotubes is positioned at the interface between a $CO:O_2$ gas stream and a stream of flowing liquid water. Furthermore, the rate of CO oxidation by O_2 in the presence of liquid water is increased further (by a factor of 5) when the pH value of the solution is increased to 13. High rates of CO oxidation over the gold nanotubes were also achieved by bringing a gas stream containing CO (balanced with He to CO/He = 1) on one side of the membrane into contact with an aqueous solution containing 0.5 wt% H_2O_2 on the other side ($CO + H_2O_2 \rightarrow CO_2 + H_2O$).

The promotional effect of liquid water at high pH values on the rate of CO oxidation by O_2 can also be achieved by depositing KOH within the gold nanotubes, by first bringing gold nanotubes into contact with an aqueous solution containing KOH (0.1M). As seen in Table 1, when the membrane containing the gold nanotubes is subsequently exposed to a gas stream containing CO and O_2 saturated with water vapor at 298 K, the rate of CO oxidation is about three times higher than for the original gold membrane. Thus by using gold nanotubes that have been filled with an aqueous KOH solution and using a gas stream saturated with water vapor, high rates of CO oxidation over a long reaction time (> 40 h) were observed, with a slow decline of the rate due to a possible loss of the liquid water from the nanotubes. In this way, by taking advantage of water within gold nanotubes, it is possible to achieve high rates of CO oxidation on metallic gold without the need for a continuous flow of liquid water over the sample at high pH values.

It has recently been shown that the energetics for water dissociation and the activation energy barrier for this process are more favorable on Pt surfaces in liquid versus gas phases, and negatively charged hydroxyl groups formed by the heterolytic dissociation of liquid water may be reactive intermediates for the oxidation of CO to CO_2.[16] This behavior is apparently operative on gold surfaces as well, since we detect the formation of small amounts (0.5 μmol min^{-1} per g of gold) of H_2 when gold nanotubes are brought into contact with gaseous CO on one side of the membrane and liquid water on the other side, which leads to water-gas shift at room temperature ($CO + H_2O \rightleftarrows CO_2 + H_2$). Negatively charged hydroxyl groups may also be supplied to the metal surface by increasing the pH value of the solution. While the details of the mechanism for CO oxidation by O_2 over gold are still not fully understood, it appears that one of the key steps is the activation of O_2.[8,17–19] We suggest that the presence of hydroxyl groups facilitates the interaction of CO with O_2, thus leading to the formation of CO_2 and peroxyl species, since we have observed the formation of small amounts (1.5 μmol min^{-1} per g of gold) of hydrogen peroxide in the liquid phase during oxidation of CO by O_2 on gold nanotubes in the presence of liquid water. In addition, gold is an effective metal for the catalytic synthesis of hydrogen peroxide from hydrogen and oxygen.[20] Finally, we note that the higher catalytic activity for the oxidation of CO by H_2O_2 compared to oxidation by O_2 in liquid water may be related to the weaker O–O bond in the former oxidizing agent.

The participation of hydroxyl groups in the oxidation of CO by O_2 is in accordance with results from studies of catalysts consisting of gold supported on high-surface-area oxide supports. Previous studies have found that the rate of CO oxidation by O_2 is strongly influenced by the nature of the catalyst support, which suggests the importance of catalytic sites at the gold–support interface.[21,22] Furthermore, the rate of CO oxidation by O_2 is enhanced by the presence of water vapor[23–26] and by treatment of the catalyst in water-containing atmospheres.[27,28] Findings such as these have led researchers to suggest that CO oxidation is promoted by hydroxyl groups associated with cationic gold species on the support or associated with the support itself. Our results provide strong evidence for the role of hydroxyl groups in promoting the rate of CO oxidation by O_2 on gold, and these hydroxyl groups need not only be associated with the support but may be supplied by liquid water, especially at high pH values.

 © 2004 Wiley-VCH Verlag GmbH & Co. KGaA, Weinheim

It is noteworthy that the rates of CO oxidation by O_2 measured for gold nanotubes in the presence of liquid water at high pH values are comparable to those rates measured in heterogeneous catalysis reactions using gold nanoparticles on oxide supports. The BET surface area of the gold-nanotube membrane used in our reaction studies is 5.2 $m^2 g^{-1}$ of gold (8×12 cm sheet containing 0.19 g of gold). Assuming a site density of 10^{15} sites cm^{-2} for a gold surface, we thus estimate that the turnover frequency for CO oxidation by O_2 in liquid water at high pH values is about 0.04 s^{-1}. Indeed, the turnover frequency for CO oxidation on supported gold catalysts typically ranges from 0.01 to 0.5 s^{-1}.[21,23]

Finally, we note that placing nanotubes in a membrane reactor offers a unique opportunity to study reactions at gas–liquid interfaces, since the gas and liquid reactants may access the active sites by counterdiffusion from opposite ends of the nanotubes. Transport can be controlled by placing the catalytic membrane between additional membranes containing gold nanotubes that have been functionalized with self-assembled monolayers of hydrophobic and hydrophilic thiols, as demonstrated previously for molecular filtrations.[11] Table 2 presents results for the oxidation of CO by H_2O_2 for cases where the gold nanotubes were placed between such hydrophilic and/or hydrophobic membranes, which were themselves inactive for CO oxidation under all experimental conditions of this study. It can be seen that only small effects are caused by placing a hydrophilic membrane between the gold nanotubes and the liquid water (entries 2 and 3), and by placing a hydrophobic membrane between the gold nanotubes and the gas phase (entries 2 and 6). However, a strong inhibiting effect on the rate of CO oxidation is caused by placing a hydrophobic membrane between the gold nanotubes and the liquid water (entries 1 and 5), which hinders the transport of liquid water to the reactive interface. Also, the rate of CO oxidation is inhibited by placing a hydrophilic membrane between the gold nanotubes and the gas phase (entries 1 and 4), which hinders the transport of gaseous species through liquid-filled nanotubes that are positioned between the gas phase and the reactive interface. It should be noted by comparing the rates in Tables 1 and 2 that higher rates of CO oxidation are achieved by the RIE treatment, which exposes the gold nanotubes from the polycarbonate membrane at the gold–gas interface.

Table 2: Rate of CO_2 production for combinations of hydrophobic and/or hydrophilic membranes surrounding a gold nanotube membrane. Data collected using a gold membrane without RIE.

Entry	Gas–Au membrane	Au–liquid membrane	CO_2 rate[a,b]
1	Hydrophilic	Hydrophobic	9
2	Hydrophobic	Hydrophilic	84
3	None	Hydrophilic	130
4	Hydrophilic	None	10
5	None	Hydrophobic	7
6	Hydrophobic	None	79
7	None	None	150

[a] Total gas flow rate = 100 $cm^3 min^{-1}$ (STP); CO:He ratio = 1:1. Liquid flow rate = 2 $cm^3 min^{-1}$; 0.5 wt% H_2O_2. [b] Rate is given in units of μmol of CO_2 per gram of Au per minute.

Received: November 3, 2003 [Z53238]
Published Online: February 3, 2004

Keywords: carbon monoxide · gold · heterogeneous catalysis · membranes · nanotubes

[1] M. Haruta, T. Kobayashi, H. Sano, N. Yamada, *Chem. Lett.* **1987**, *2*, 405.
[2] G. C. Bond, D. T. Thompson, *Gold Bull.* **2000**, *33*, 41.
[3] R. R. Davda, J. A. Dumesic, *Angew. Chem.* **2003**, *115*, 4202; *Angew. Chem. Int. Ed.* **2003**, *42*, 4068.
[4] M. Valden, X. Lai, D. W. Goodman, *Science* **1998**, *281*, 1647.
[5] M. Mavrikakis, P. Stoltze, J. K. Norskov, *Catal. Lett.* **2000**, *64*, 101.
[6] H. G. Boyen, G. Kastle, F. Weigl, B. Koslowski, C. Dietrich, P. Ziemann, J. P. Spatz, S. Riethmuller, C. Hartmann, M. Moller, G. Schmid, M. G. Garnier, P. Oelhafen, *Science* **2002**, *297*, 1533.
[7] S. K. Shaikhutdinov, R. Meyer, M. Naschitzki, M. Bäumer, H.-J. Freund, *Catal. Lett.* **2003**, *86*, 211.
[8] Y. Xu, M. Mavrikakis, *J. Phys. Chem. B* **2003**, *107*, 9298.
[9] R. J. Davis, *Science* **2003**, *301*, 926.
[10] Q. Fu, H. Saltsburg, M. Flytzani-Stephanopoulos, *Science* **2003**, *301*, 935.
[11] C. R. Martin, M. Nishizawa, K. Jirage, M. Kang, *J. Phys. Chem. B* **2001**, *105*, 1925.
[12] Details of materials, methods, and diagrams of experimental apparatus are available as Supporting Information.
[13] Z. Hou, N. L. Abbott, P. Stroeve, *Langmuir* **1998**, *14*, 3287.
[14] K. B. Jirage, J. C. Hulteen, C. R. Martin, *Science* **1997**, *278*, 655.
[15] S. Yu, N. Li, J. Wharton, C. R. Martin, *Nano Lett.* **2003**, *3*, 815.
[16] S. K. Desai, M. Neurock, *Phys. Rev. B* **2003**, *68*, 075420.
[17] T. V. Choudhary, D. W. Goodman, *Top. Catal.* **2002**, *21*, 25.
[18] Z. P. Liu, P. Hu, A. Alavi, *J. Am. Chem. Soc.* **2002**, *124*, 14770.
[19] T. S. Kim, J. D. Stiehl, C. T. Reeves, R. J. Meyer, C. B. Mullins, *J. Am. Chem. Soc.* **2003**, *125*, 2018.
[20] M. Okamura, Y. Kitagawa, K. Yamaguchi, T. Akita, S. Tsubota, M. Haruta, *Chem. Lett.* **2003**, *32*, 822.
[21] H. H. Kung, M. C. Kung, C. K. Costello, *J. Catal.* **2003**, *216*, 425.
[22] M. Haruta, *Stud. Surf. Sci. Catal.* **2003**, *145*, 31.
[23] M. Daté, M. Haruta, *J. Catal.* **2001**, *201*, 221.
[24] R. J. H. Grisel, B. E. Nieuwenhuys, *J. Catal.* **2001**, *199*, 48.
[25] W. T. Wallace, R. B. Wyrwas, R. L. Whetten, R. Mitric, V. Bonacic-Koutecky, *J. Am. Chem. Soc.* **2003**, *125*, 8408.
[26] C. K. Costello, J. H. Yang, H. Y. Law, Y. Wang, J. N. Lin, L. D. Marks, M. C. Kung, H. H. Kung, *Appl. Catal. A* **2003**, *243*, 15.
[27] D. A. Bulushev, L. Kiwi-Minsker, I. Yuranov, E. I. Suvorova, *J. Catal.* **2002**, *210*, 149.
[28] C. K. Costello, M. C. Kung, H. S. Oh, Y. Wang, H. H. Kung, *Appl. Catal. A* **2002**, *232*, 159.

 © 2004 Wiley-VCH Verlag GmbH & Co. KGaA, Weinheim

DNA Recognition

Templated Ligand Assembly by Using G-Quadruplex DNA and Dynamic Covalent Chemistry**

*Andrew M. Whitney, Sylvain Ladame, and Shankar Balasubramanian**

Dynamic covalent chemistry (DCC) is a reversible exchange process which allows noncovalent interactions to template covalent-bond formation.[1] A dynamic combinatorial library (DCL) is an equilibrating mixture, under thermodynamic control, in which each of the species is represented in proportion to its free energy.[2] The introduction of a molecular template to a DCL will shift the equilibrium to favor individual library members that bind the template and are thus stabilized. Since its conception, DCC has been applied to both small-molecule[2] and macromolecular targets.[3] Examples of DCC that involve biomolecules include the work of Ramström and Lehn[3b] who generated a small disulphide-based carbohydrate library and screened in situ against the common jack bean-lectin Concanavalin A, and of Miller and co-workers[4] who targeted oligonucleotides with non-nucleotide building blocks and selected metal–ligand complexes that bind nucleic acid hairpins with high affinity and selectivity. An experimentally challenging aspect of employing biomolecules as templates in DCLs is the analysis of the reversibility of the dynamic chemistry and quantitation of ligand amplification. This analysis requires detailed investigations on a relatively simple DCL, and has been a key objective of the work we report in this paper.

The molecular target for our study is a four-stranded G-quadruplex formed by DNA sequences with stretches of G-nucleotides under near physiological salt conditions in vitro.[5] Quadruplex structures may be involved in cellular functions that include chromosomal alignment[6] and telomere length regulation.[7] In particular, the latter has been implicated in the control of cellular aging and mechanisms of cancer proliferation.[7] Furthermore, recent studies reported for the oncogene *c-myc*[8] suggest that quadruplex stabilization might have the potential to control gene expression. Therefore, there is considerable interest in developing quadruplex-stabilizing ligands for novel therapeutic approaches and a desire to understand the molecular basis of quadruplex recognition.[9] The G-quadruplex structural motif has features that distinguish it from double-stranded B-DNA and that can be exploited in the design of quadruplex specific ligands. A number of promising small-molecule ligands have been reported based on recognition of the terminal G-tetrad through hydrophobic and π–π interactions.[9] There is potential for specific ligands that make contacts with loop and groove regions of quadruplex DNA.[10] The philosophy of combining distinct binding elements to generate improved ligands has been effective for nucleic acids.[11] Herein, we investigate the potential of DCC to generate quadruplex ligands through a reversible, covalent combination of two distinct recognition elements: a hydrophobic acridone unit, designed to interact with the terminal G tetrad of a parallel quadruplex,[12] and a tetrapeptide sequence (FRHR), which was recently shown by us to have quadruplex-recognition properties.[13]

Disulphide chemistry was chosen because it is water compatible, relatively fast, and thiol exchange operates at mild pH. It allows the mixture of DCL components to interconvert and reach equilibrium, and can be switched off by lowering the pH value to ≤ 5.[14] The peptide fragment, FRHR, was derivatized with sulfanylacetic acid at the N terminus to give monomer **P**, which has an N-terminal thiol group. **P** was synthesized by using standard solid-phase Fmoc-peptide chemistry (Fmoc = 9-fluorenylmethoxycarbonyl) on Rink amide resin. Acridone **A** was prepared by coupling of 3,6-bis[(2-carbamoylethyl)methylamino]acetic acid-substituted acridone[15] onto cysteine-loaded Wang resin. Based on preliminary modeling studies, the sarcosine linker was shown to position the cysteine residue at the top of a quadruplex groove (data not shown). In our DCC experiments we employed a human telomeric quadruplex, formed from the deoxyoligonucleotide 5′-biotin$(GTTAGG)_5$.[16]

The experimental design principles are detailed in Scheme 1. An exchange buffer containing an excess of both oxidized (**G-G**) and reduced glutathione (**G**) mediates exchange between the components of the DCL, which enables the use of relatively low concentrations of **A** and **P**. Furthermore, both, **G** and **G-G**, have the potential to interact with the quadruplex and thus act as competitive library members. When equilibrium is reached, the exchange reaction is stopped by lowering the pH from 7.4 to 2 and the biotinylated quadruplex target, with bound ligands, can be isolated from the solution by immobilization onto streptavidin beads. The quadruplex is heat-denatured at 85 °C to release any bound ligand and HPLC is used to identify and quantify all members of the DCL. A parallel control experiment, without quadruplex target, enabled us to make a comparison that identified species amplified by the quadruplex-DNA template.

Critical features of any DCC experiment are the need to prove thermodynamic control and demonstrate an equilibrium shift induced by a template. To investigate disulfide-exchange reactions of **A** and **P** under thermodynamic control, a glutathione-containing buffer was used. The glutathione was utilized in a large excess to mediate fast exchange at relatively low levels of **A** and **P**.[14,17]

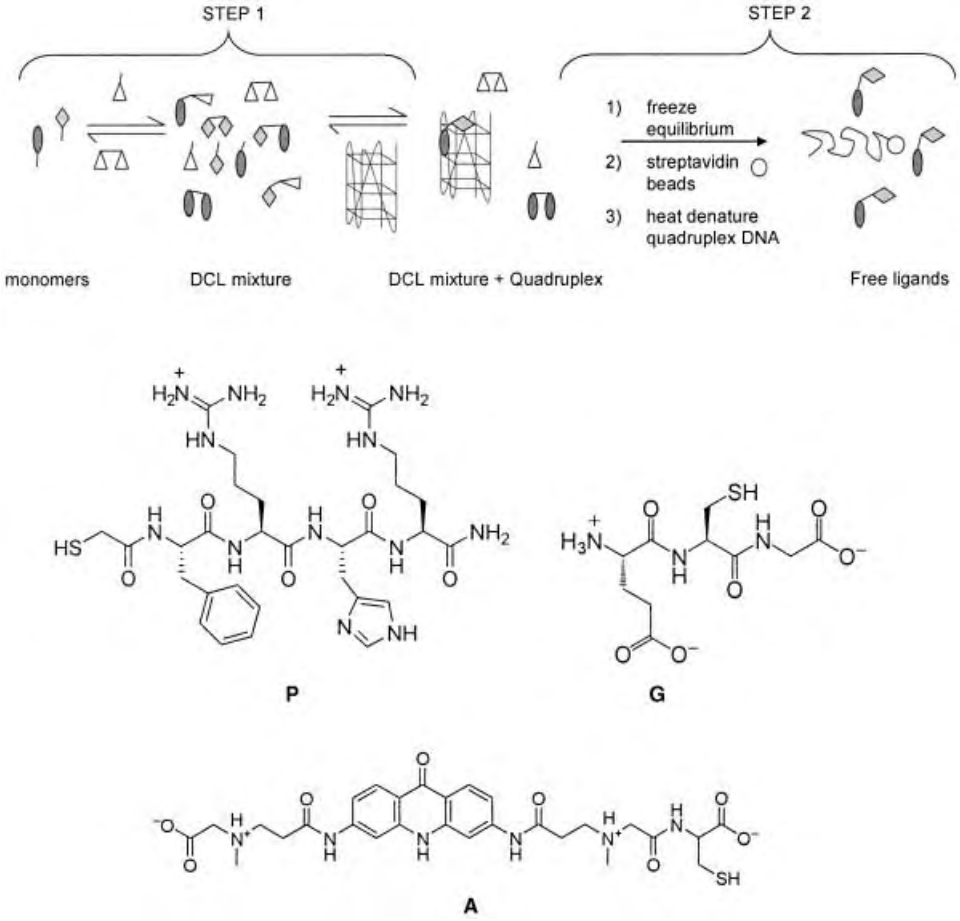
In the absence of target quadruplex DNA, the system equilibrated within 22 hours and remained unchanged over

[*] A. M. Whitney, Dr. S. Ladame, Dr. S. Balasubramanian
University Chemical Laboratories
University of Cambridge
Lensfield Road, Cambridge CB2 1EW (UK)
Fax: (+44) 1223-336-913
E-mail: sb10031@cam.ac.uk

[**] This work was funded by the BBSRC. We thank Drs. Y. Krishnan-Ghosh and S. Otto for critically reading the manuscript and helpful comments.

Supporting information for this article is available on the WWW under http://www.angewandte.org or from the author.

 DOI: 10.1002/anie.200353069 © 2004 Wiley-VCH Verlag GmbH & Co. KGaA, Weinheim



Scheme 1. Schematic experimental method. Step 1: Monomers **P** and **A** are used in the presence of glutathione (oxidized: **G-G** (375 μM), reduced: **G** (1.5 mM)) in redox exchange buffer to equilibrate in either the presence or absence of the target quadruplex DNA. Step 2: The exchange is frozen by reducing the pH to 2 with 0.1% TFA in water, the quadruplex (+ ligand) is removed from solution by streptavidin immobilization and heat denatured to dissociate bound ligands. All ligands are analyzed by HPLC. TFA = trifluoroacetic acid.

the next 26 hours (Figure 1a). The same distribution of species was reached in 48 hours but starting from homodisulfides **A-A** and **P-P** (data not shown), which showed that the system is truly reversible and under thermodynamic control. At equilibrium, building block **P** was predominantly found in the form of a heterodisulfide with glutathione, **P-G**. In contrast, building block **A** was predominantly found as the homodisulfide **A-A**, despite the excess of competing **G** present. This observation is in accordance with air oxidation experiments (see Supporting Information) and suggests self-recognition of the acridone.[14]

Parallel experiments were carried out in the presence of 200 μM 5′-biotinylated, folded[16] human telomeric quadruplex, under otherwise identical conditions. Equilibrium was achieved within 48 hours (Figure 1b) and the same distribution of species was reached starting with **A** and **P** as either free thiols or as homodisulfides **A-A** and **P-P**, which confirmed a true equilibration of the system in the presence of quadruplex DNA. Analysis of the reaction stopped at 12, 24, 48, and 100 hours revealed an increase in the proportion of both, acridone–peptide heterodisulfide (**A-P**) and peptide homodisulfide (**P-P**), until equilibrium was reached within 48 hours with a constant **A-P**/**P-P** ratio of 1.4:1. The formation of **A-P** and **P-P** was at the expense of disulfides **P-G** and **A-A** and thiols **A** and **P**. At equilibrium the acridone–peptide heterodisulfide **A-P** and peptide homodisulfide **P-P** are 19 and 12%, respectively, of the library's mole composition (Figure 1c). This is a four and fivefold amplification of **A-P** and **P-P**, respectively, induced by the presence of the quadruplex DNA (Figure 1d).

The amplification of **P-P** was particularly surprising since there are no reports of short peptide ligands that bind quadruplex DNA with high affinity. To confirm this result, exchange experiments were carried out by using **P** alone in the **G**/**G-G**-containing buffer. In the absence of quadruplex DNA the major species observed was **P-G**, as expected. Upon introduction of the quadruplex DNA, the proportion of **P-P** in the exchange mixture rose from 2 to 12%, a sixfold increase at the expense of **P-G** (see Supporting Information).

Quantitative-binding studies of species **A-P**, **P-P**, and **A-A** were carried out by using surface plasmon resonance (SPR) with the same quadruplex-DNA target. SPR is a valuable and extensively used method for the study of DNA small molecule interactions.[13,18] Figure 2 shows the binding curves derived from the SPR data. **A-P** and **P-P** bind the human telomeric quadruplex DNA with dissociation constants of 30 ± 1.5 and

 © 2004 Wiley-VCH Verlag GmbH & Co. KGaA, Weinheim

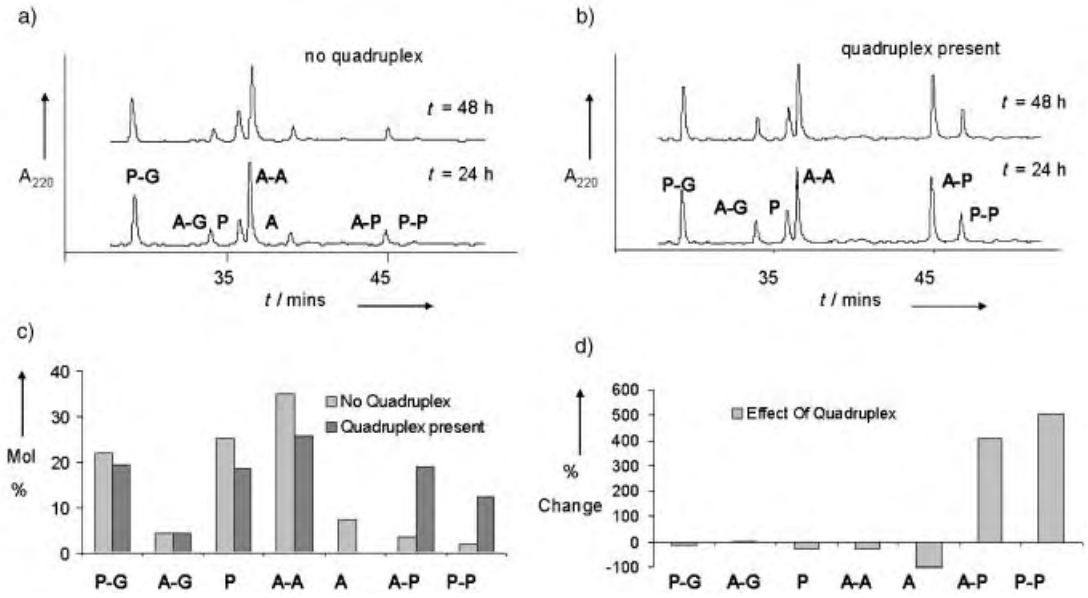


Figure 1. a) HPLC traces showing the component composition for exchange experiments in glutathione-containing buffer with use of **A** and **P** (200 μM each) in the absence of quadruplex DNA, at times denoted. b) HPLC traces showing the component composition for exchange experiments in glutathione-containing buffer with use of **A** and **P** (200 μM each) in the presence of quadruplex DNA, at times denoted. c) Histogram showing the change in equilibrium mixture composition on introduction of quadruplex DNA. Values were measured by HPLC-peak area, taking into account differences in extinction coefficients. d) Histogram showing the percentage changes in each species of the equilibrium mixture upon introduction of quadruplex DNA.

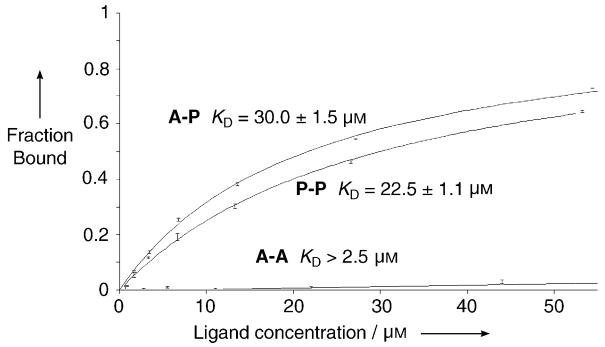


Figure 2. Binding curves obtained from SPR measurements for the determination of K_D values for **A-P**, **P-P**, and **A-A** with quadruplex DNA.

22.5 ± 1.1 μM, respectively, consistent with their selection in the DCC experiments. No binding of **A-A** was detected at 88 μM indicative of a lower limit for the K_D of 2.5 mM (see Supporting Information).

This study shows that dynamic covalent chemistry can be used to evolve molecules that bind to quadruplex DNA from a DCL. The critical requirements of thermodynamic control and target-mediated shifting of the position of equilibrium, have been satisfied. The heterodisulfide **A-P** and, more surprisingly, homodisulfide **P-P** have been selected from a library of nine species and shown to have good quadruplex affinity. Based on the design principles, we propose that binding of **A-P** is mediated by acridone–π–π interactions with the top tetrad of the quadruplex and quadruplex-loop/groove interactions with the appended peptide. This result is also suggested by modeling studies of amide-linked acridone–peptide conjugates with human telomeric quadruplexes (data not shown). The mode by which **P-P** binds quadruplex DNA is presently unknown and will be the subject of future high-resolution NMR spectroscopic studies. Thus, the DCC approach has generated two novel quadruplex-binding ligands and will be exploited to select aromatic cores and peptide/nonpeptide side chains against G-quadruplex targets in future studies.

Received: October 13, 2003 [Z53069]

Keywords: combinatorial chemistry · DNA recognition · quadruplex ligands · surface plasmon resonance · template synthesis

[1] For selected reviews see a) A. Ganesan, *Angew. Chem.* **1998**, *110*, 2989; *Angew. Chem. Int. Ed.* **1998**, *37*, 2828; b) J.-M. Lehn, *Chem. Eur. J.* **1999**, *5*, 2455; c) O. Ramstrom, T. Bunyapaiboonsri, S. Lohmann, J.-M. Lehn, *Biochim. Biophys. Acta* **2002**, *1572*, 178; d) S. J. Rowan, S. J. Cantrill, G. R. L. Cousins, J. K. M. Sanders, J. F. Stoddart, *Angew. Chem.* **2002**, *114*, 1528; *Angew. Chem. Int. Ed.* **2002**, *41*, 898.

[2] a) H. Hioki, W. C. Still, *J. Org. Chem.* **1998**, *63*, 904; b) V. Berl, I. Huc, J.-M. Lehn, A. DeCian, J. Fischer, *Eur. J. Org. Chem.* **1999**, 3089; c) S. Otto, R. L. E. Furlan, J. K. M. Sanders, *J. Am. Chem. Soc.* **2000**, *122*, 12063; d) R. L. E. Furlan, Y.-F. Ng, S. Otto, J. K. M. Sanders, *J. Am. Chem. Soc.* **2001**, *123*, 8876; e) R. L. E. Furlan, Y.-F. Ng, G. R. L. Cousins, J. E. Redman, J. K. M. Sanders, *Tetrahedron* **2002**, *58*, 771; f) S. L. Roberts, R. L. E. Furlan, G. R. L. Cousins, J. K. M. Sanders, *Chem. Commun.* **2002**, 938; g) E. Stulz, Y.-F. Ng, S. M. Scott, J. K. M. Sanders, *Chem. Commun.* **2002**, 524; h) S. Otto, R. L. E. Furlan, J. K. M. Sanders, *Science* **2002**, *297*, 590; i) B. Brisig, J. K. M. Sanders, S.

 © 2004 Wiley-VCH Verlag GmbH & Co. KGaA, Weinheim

Otto, *Angew. Chem.* **2003**, *115*, 1308; *Angew. Chem. Int. Ed.* **2003**, *42*, 1270; j) S. Otto, S. Kubik, *J. Am. Chem. Soc.* **2003**, *125*, 7804.
[3] a) I. Huc, J.-M. Lehn, *Proc. Natl. Acad. Sci. USA* **1997**, *94*, 2106; b) O. Ramström, J.-M. Lehn, *ChemBioChem* **2000**, *1*, 41; c) M. Hochgürtel, H. Kroth, D. Piecha, M. W. Hofmann, C. Nicolau, S. Krause, O. Schaaf, G. Sonnenmoser, A. V. Eliseev, *Proc. Natl. Acad. Sci. USA* **2002**, *99*, 3382.
[4] a) B. Klekota, B. L. Miller, *Tetrahedron* **1999**, *55*, 11687; b) C. Karan, B. L. Miller, *J. Am. Chem. Soc.* **2001**, *123*, 7455.
[5] For selected reviews see a) S. Neidle, G. N. Parkinson, *Curr. Opin. Struct. Biol.* **2003**, *13*, 275; b) T. Simonsson, *Biol. Chem.* **2001**, *382*, 621.
[6] D. Sen, W. Gilbert, *Nature* **1988**, *334*, 364.
[7] a) E. Blackburn, *Nature* **2000**, *408*, 53; b) T. R. Cech, *Angew. Chem.* **2000**, *112*, 34; *Angew. Chem. Int. Ed.* **2000**, *39*, 34.
[8] A. Siddiqui-Jain, C. L. Grand, D. J. Bearss, L. H. Hurley, *Proc. Natl. Acad. Sci. USA* **2002**, *99*, 11593.
[9] D. Sun, B. Thompson, B. E. Cathers, M. Salazar, S. Kerwin, J. O. Trent, T. C. Jenkins, S. Neidle, L. H. Hurley, *J. Med. Chem.* **1997**, *40*, 2113.
[10] G. N. Parkinson, M. P. Lee, S. Neidle, *Nature* **2002**, *417*, 876.
[11] For selected examples, see: a) T. Bentin, P. E. Nielsen, *J. Am. Chem. Soc.* **2003**, *125*, 6378; b) C. Carrasaco, P. Helissey, M. Haroun, B. Baldeyrou, A. Lansiaux, P. Colson, C. Houssier, S. Giorgi-Renault, C. Bailly, *ChemBioChem* **2003**, *4*, 50; c) C. B. Carlson, O. M. Stephens, P. A. Beal, *Biopolymers* **2003**, *70*, 86.
[12] a) S. M. Gowan, J. R. Harrison, L. Patterson, M. Valenti, M. A. Read, S. Neidle, L. R. Kelland, *Mol. Pharmacol.* **2002**, *61*, 1154; b) G. R. Clark, P. D. Pytel, C. J. Squire, S. Neidle, *J. Am. Chem. Soc.* **2003**, *125*, 4066; c) S. M. Haider, G. N. Parkinson, S. J. Neidle, *J. Mol. Biol.* **2003**, *326*, 117.
[13] J. A. Schouten, S. Ladame, S. J. Mason, M. A. Cooper, S. Balasubramanian, *J. Am. Chem. Soc.* **2003**, *125*, 5594.
[14] Y. Krishnan-Ghosh, S. Balasubramanian, *Angew. Chem.* **2003**, *115*, 2221; *Angew. Chem. Int. Ed.* **2003**, *42*, 2171.
[15] S. Ladame, R. J. Harrison, S. Neidle, S. Balasubramanian, *Org. Lett.* **2002**, *4*, 2509.
[16] The G-quadruplex was folded under standard conditions. The single-stranded oligonucleotide, 5′-biotinylated $(GTTAGG)_5$, was heated in buffer to 90 °C and slowly cooled to room temperature overnight. Its fully folded structure was confirmed by circular dichroism spectroscopy and UV melting experiments.
[17] A. Saghatelian, Y. Yokobayashi, K. Soltani, M. R. Ghadiri, *Nature* **2001**, *409*, 797.
[18] a) E. R. Lacy, N. M. Le, C. A. Price, M. Lee, W. D. Wilson, *J. Am. Chem. Soc.* **2002**, *124*, 2153; b) C. Carrasco, M. Facompre, J. D. Chisholm, D. L. Van Vranken, W. D. Wilson, C. Bailly, *Nucleic Acids Res.* **2002**, *30*, 1774; c) C. Carrasco, F. Rosu, V. Gabelica, C. Houssier, E. De Pauw, C. Garbay-Jaureguiberry, B. Roques, W. D. Wilson, J. B. Chaires, M. J. Waring, C. Bailly, *ChemBioChem* **2002**, *3*, 1235.

 © 2004 Wiley-VCH Verlag GmbH & Co. KGaA, Weinheim

Carbon Nanotubes

Self-Assembly of Large-Scale Micropatterns on Aligned Carbon Nanotube Films**

Huan Liu, Shuhong Li, Jin Zhai, Huanjun Li, Quanshui Zheng, Lei Jiang, and Daoben Zhu*

The fabrication of well-defined structures with nanoscale materials is a key technology,[1] and self-assembly is an efficient and often preferred process to build micro- and nanoparticles into ordered macroscopic structures.[2] As carbon nanotubes are attractive materials for nanotechnology because of their interesting physicochemical properties and molecular symmetries,[3–6] it is necessary to control the architecture of carbon nanotubes on the substrates. Most patterned carbon nanotubes are formed on prepatterned substrates or prepatterned catalysts during the fabrication process.[7–9] Herein we report the first use of a long-range force (capillary force) in the self-assembly of three-dimensional (3D) micropatterns on aligned carbon nanotube films through a water-spreading method after the growth of the carbon nanotube. It is considered that low-density regions or vacancies of carbon nanotube films play an important role in the formation of the pattern. Therefore different kinds of highly ordered micropatterned structures have been built in a controlled fashion by introducing vacancies artificially.

Hydrophobic aligned carbon nanotube films were grown on quartz substrates by pyrolysis of iron(II) phthalocyanine (FePc) by methods described in the literature.[10–12]

Interestingly, when a water droplet was placed on the fresh carbon nanotube film, the color of the water region changed from black to grey. Water permeates slowly into the film, accompanied by a change in the height and shape of the droplet, but its contact area with the film is almost unchanged (See Supporting Information Figure S1). Detailed scanning electron microscopic (SEM) observations show that the structures in the grey color region are micropatterns composed of honeycomb-like polygons with sizes ranging from 30 to 60 μm (Figure 1 a). An oblique view shows that these

[*] Dr. H. Liu,[+] Dr. S. Li,[+] Dr. J. Zhai, Dr. H. Li, L. Jiang, D. Zhu
Center of Molecular Sciences, Institute of Chemistry,
Chinese Academy of Sciences
Beijing 100080 (P. R. China)
Fax: (+86) 10-8262-7566
E-mail: jianglei@infoc3.icas.ac.cn
Prof. Q. Zheng
Tsinghua University
Beijing 100084 (P. R. China)
[+] PhD students of the Graduate School of the Chinese Academy of Sciences. They contributed equally to this work.

[**] The authors thank the State Key Project Fundamental Research (G1999064504) and the Special Research Foundation of the National Nature Science Foundation of China (29992530) for continuing financial support. The Chinese Academy of Sciences is gratefully acknowledged.

Supporting information for this article is available on the WWW under http://www.angewandte.org or from the author.

 © 2004 Wiley-VCH Verlag GmbH & Co. KGaA, Weinheim DOI: 10.1002/anie.200351988

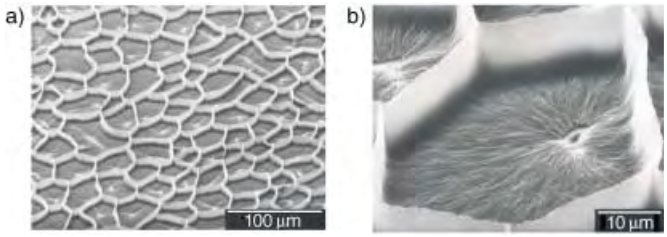


Figure 1. a) The SEM image of patterned carbon nanotubes induced by water spreading. These patterns are mostly honeycomb-like structures with the sizes ranged from 30 to 60 μm. b) Enlarged oblique view of an individual honeycomb structure with the honeycomb "wall" vertical to the substrate.

honeycomb-like patterns have 3D structures in which the "walls" are vertical to the substrate. Figure 1b is a high-resolution SEM image of an individual polygon. All carbon nanotubes inside this polygon are bent radially toward the "walls" from the center. In particular, all carbon nanotubes originally on the substrate of the "cave" region were flattened, bundled, and eventually formed the cave (See Supporting Information Figure S2). The height and thickness of the "walls" are 6–10 μm and ca. 0.5 μm, respectively, in this image.

All these phenomena can be explained as the self-assembly of carbon nanotubes as a result of the capillary action of water. A variety of strategies for self-assembly have been proposed and employed to fabricate two- and three-dimensional structures,[13–18] and the driving forces are usually van der Waals forces,[19] hydrogen bonding,[20] and Coulombic forces.[21,22] However, these short-range forces can only act on a molecular level, whereas longer-range forces, such as surface tension, capillary force, convection, etc., can be used for constructing microstructures with nanostructured materials. Although carbon is hydrophobic, it is known that flat graphite surfaces are hydrophilic, with a water contact angle ϕ_g of $\approx 86°$.[22] Transmission electron microscopy images (See Supporting Information Figure S3) of carbon nanotubes dispersed from the film show their bamboolike structure, with diameters ranging from 40 to 60 nm. We have not found measurement water contact angle values of carbon nanotubes. However, it is believed that the water contact angle of perfect carbon nanotubes of large diameters (40–60 nm) would be almost the same as that of the graphite plane. The bamboo structures should lead to better hydrophilicity than that of perfect nanotubes, as generally observed for that of rough surfaces. This means that the water contact angles ϕ_{nt} of the bamboolike carbon nanotubes are generally smaller than 86°. The SEM image of the film surface (See Supporting Information Figure S4) shows that thinner tubes extend from thicker aligned tubes and grovel on the film surface. These hydrophilic flattened tubes guide the water droplet along the corresponding aligned carbon nanotubes into the film.

Once the water is guided into the spaces between the aligned tubes, the resulting capillary action forces the water down to the quartz substrate. The water then spreads over the substrate because the quartz is hydrophilic. All interspaces among aligned tubes over the water-spread region become to be soaked due to the capillary force. The capillary force supplied by a single nanotube of radius r can be estimated to be $2\pi r\gamma_w \cos\phi_{nt}$ through the water surface tension or surface energy[23] $\gamma_w = 72.8\ mN\,m^{-1}$ and the water contact angle ϕ_{nt}. The capillary force thus generates a hydrostatic dilation stress p to the water. To have an estimate of p, we modeled an aligned carbon nanotube cluster by a hexagonal distribution of their cross-section (Figure 2a,b), with diameter $2r$ and distance $2R$ of tubes, which gives rise to Equation (1), in which $c = (rR^{-1})^2$ is the density of carbon nanotubes.

$$p = \frac{2r\gamma_w \cos\phi_{nt}}{R^2 - r^2} = p_{0.5}\frac{c}{1-c},\ p_{0.5}\frac{2\gamma_w \cos\phi_{nt}}{r}, \qquad (1)$$

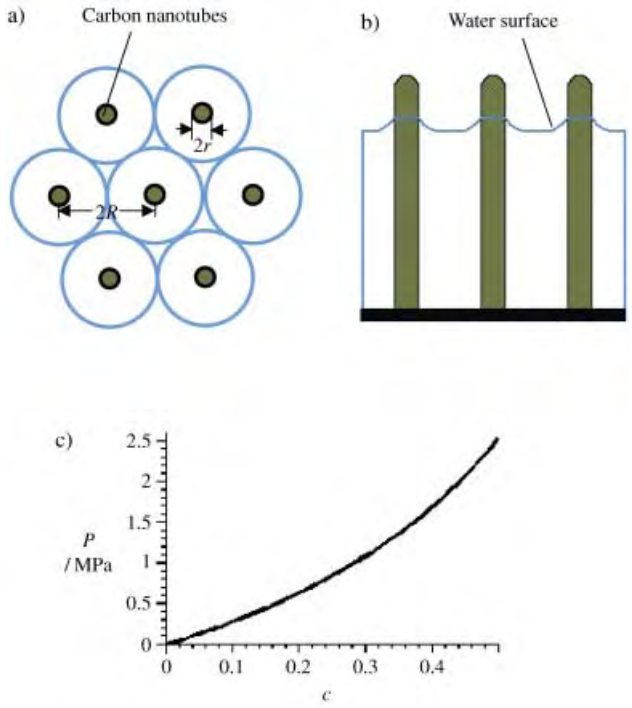


Figure 2. a) Top view and b) side view of the model of the aligned carbon nanotube cluster with tubes of diameter $2r$ at a distance $2R$. The blue lines represent the water surface, the dark green dots and pillars are the carbon nanotubes. c) The relationship between hydrostatic dilation stress p and the volume fraction of nanotubes.

Using the values $\gamma_w = 72.8\ mN\,m^{-1}$, $r = 40$ nm, $\phi_{nt} < \phi_g = 86°$ yields $p > (0.25c)(1-c)^{-1}$ in MPa. The relationship between the dilation stress p and the volume fraction of nanotubes c is shown in Figure 2c, indicating the nonlinear increase in p as the carbon nanotube density increases. This hydrostatic dilation stress alone causes the nanotubes to flatten.

SEM images of the grown carbon nanotube films show that the carbon nanotube densities are not homogeneous. There are both low-density and high-density regions in all carbon nanotube films. With the above estimate of hydrostatic dilation stress p, the nanotubes along the boundary between a lower-density $-c_l$ and higher-density $-c_h$ regions are subjected to a load q per unit tube length toward the higher-density region (Equation (2)).

 © 2004 Wiley-VCH Verlag GmbH & Co. KGaA, Weinheim

$$q = p_{0.5}\, r\left(\frac{\sqrt{c_h}}{1-c_h} - \frac{\sqrt{c_l}}{1-c_l}\right) \qquad (2)$$

From Equation (2) it can be concluded that aligned nanotubes may be bent, flattened, or even burst through from lower- toward higher-density regions. For example, with the observed typical values $R_h r^{-1} = 2$ and $R_l r^{-1} = 3$, we have $q = 3.7 \times 10^{-3}\ \mathrm{N\,m^{-1}}$. The bundling force and bending moment experienced by a single nanotube of length $L = 19\ \mu\mathrm{m}$ near the substrate are $qL = 70.3$ nN and $(qL^2)/2 = 6.7 \times 10^{-4}$ nN m, respectively. If the axial Young modulus of the carbon nanotubes is assumed to be 1 TPa, then the maximum bending strain is 11 %, that is, much larger than the critical rippling strain of $\approx 0.6\,\%$.[24,25] It means that the estimated load q experienced by a single carbon nanotube can even force a dozen carbon nanotubes to be severely bent. During the above bending and bundling procedures, $-c_l$ decreases and $-c_h$ increases further. This leads to a stronger and stronger q, until micropatterns are formed in which nanotubes are very closely aligned so that the van der Waals repulsive forces between the nanotubes become effective and balance q. That is, the hydrostatic dilation stress at higher densities is larger than that at lower densities, so this difference leads to the flattening of the nanotubes, while the "wall" is formed when the collapsing nanotubes from opposite directions meet between two regions of lower density. The lower-density region is the center of the micropatterns.

Therefore, it is possible to control the patterns artificially, for example, to etch the regular vacancies by pulse laser. The vacancy etched by laser is 2–3 μm in diameter and various patterns with different vacancy distances were prepared when a water droplet was placed on the surface. Figure 3 shows that the morphologies after the water has spread are dependent on the etching distance. There are two kinds of areas in the same film. One is the controlled assembling region in which the etching vacancy is the center; the other is the freely assembling region, which is determined by the density of the carbon nanotube film. The freely assembling region is decreased as the etching vacancy distance decreases (the etching distance is 150 μm and 100 μm in Figures 3a and 3b, respectively). When the etching distance approaches ≈ 40 μm, highly ordered aligned micropatterns are obtained without the freely assembling region because of the interference of the etching vacancies (Figure 3c), suggesting that if vacancies are arranged artificially, then various desired highly ordered polygon micropatterns may be fabricated.

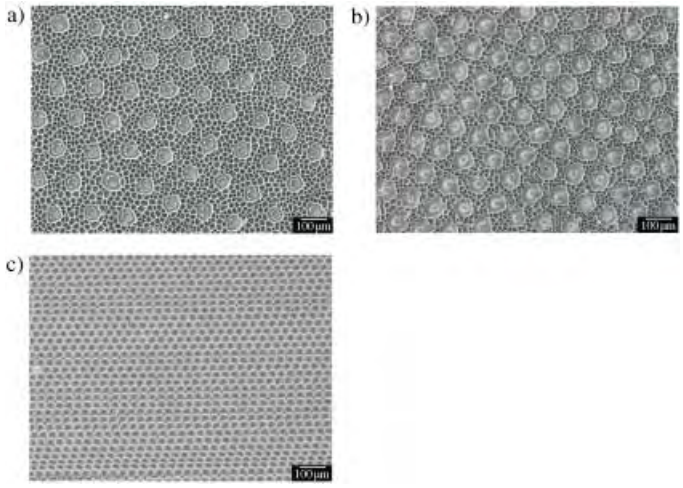


Figure 3. SEM images of micropatterned carbon nanotubes induced by water spreading on the laser-etched films with different etching distances: a) 150, b) 100, and c) 30 μm.

According to the above idea, ordered micropatterns were designed and obtained successfully by designing the position of the etching vacancies. The "wall" of the polygon is supposed to stand up approximately at the vertical bisector of two adjacent vacancies. Some designs of the etching positions are given in the inserts of Figure 4a–d, in which the blue dots represent vacancies and the lines represent "walls". In terms of these designs, the cubic, pentagonal, and hexagonal aligned micropatterns were fabricated (Figure 4a–c) by water spreading on the etched carbon nanotube film, and parallel lines were also formed in Figure 4d. All these demonstrate that large-scale aligned micropatterned structures can be obtained in a controlled fashion by water spreading and capillary force.

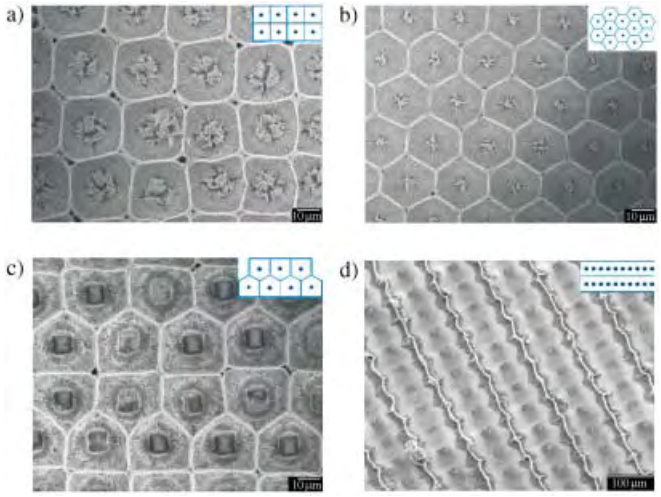


Figure 4. Highly ordered aligned patterns (a) cubic, b) hexagon, c) pentagon and d) parallel lines) are prepared by adjusting the arrangement of the vacancies. The inserts are the designs, the blue dots represent the laser etched vacancies and the blue lines the "walls" of carbon nanotubes.

In summary, the present results provide evidence for self-assembly of carbon nanotubes to form large-scale 3D micropatterns through the water-spreading effect, and highly ordered patterned structures can be built controllably by adjusting the density of carbon nanotubes films artificially. Two-dimensional carbon nanotube films can be easily transformed into three-dimensional architectures after the growth of the film. This method might not only be extended to both inorganic nanotube/wire arrays[26,27] and organic nanotubes/fibers[28–30] to realize the transformation of 1D and 2D to 3D architectures, but also useful in fabricating microelectrical devices as well.

 © 2004 Wiley-VCH Verlag GmbH & Co. KGaA, Weinheim

Experimental Section

Aligned carbon nanotubes films were prepared on cleaned quartz glass plates by pyrolysis of iron(II) phthalocyanine (FePc), which contains both the carbon source and the iron catalyst required. FePc (0.23 g) in a quartz boat was decomposed at approximately 550 °C, and the carbon nanotube film was prepared at approximately 900 °C in a flow reactor consisting of a quartz tube and a tube furnace fitted with a temperature controller under Ar/H_2. The growth time of the carbon nanotube films in this case was 5 min. After that, a water drop was carefully placed on the films. The artificial vacancies were induced by the Pulse Laser Etching System with 355 nm (New Wave Research Inc. in California), the size of the facula was 35×35 (2–3 μm) and the energy was 1.8–2.9 μW.

Optical microscope images were obtained on Olympus TH3 optical microscopy equipped with a CCD camera. SEM images were obtained on a JEOL JSM-6700F scanning electron microscope at 3.0 kV. Transmission electron microscopy images were obtained with an Hitachi JEM 200-CX instrument at 120 kV.

Received: May 27, 2003
Revised: November 17, 2003 [Z51988]

Keywords: carbon · electron microscopy · nanotubes · self-assembly · water

[1] T. Nishikawa, J. Nishida, R. Ookura, S. Nishimura, S. Wada, T. Karino, M. Shimomura, *Mater. Sci. Eng. C* **1999**, *10*, 141 – 146.
[2] H. Shimoda, S. J. Oh, H. Z. Geng, R. J. Walker, X. B. Zhang, L. E. McNeil, O. Zhou, *Adv. Mater.* **2002**, *14*, 899 – 901.
[3] N. Bowden, A. Terfort, J. Carbeck, G. M. Whitesides, *Science* **1997**, *276*, 233 – 235.
[4] Z. F. Ren, Z. P. Huang, J. W. Xu, J. H. Wang, P. Bush, M. P. Siegal, P. N. Provencio, *Science* **1998**, *282*, 1105 – 1107.
[5] L. Dai, A. W. H. Mau, *Adv. Mater.* **2001**, *13*, 899 – 913.
[6] S. Fan, M. G. Chapline, N. R. Franklin, T. W. Tombler, A. M. Cassell, H. Dai, *Science* **1999**, *283*, 512 – 514.
[7] S. Sun, C. B. Murray, D. Weller, L. Folks, A. Moser, *Science* **2000**, *287*, 1989 – 1992.
[8] S. Huang, A. W. H. Mau, T. W. Turney, P. A. White, L. Dai, *J. Phys. Chem. B* **2000**, *104*, 2193 – 2196.
[9] Y. Yang, S. Huang, H. He, A. W. H. Mau, L. Dai, *J. Am. Chem. Soc.* **1999**, *121*, 10832 – 10833.
[10] X. Wang, Y. Liu, D. Zhu, *Appl. Phys. A* **2000**, *71*, 347 – 348.
[11] H. Li, X. Wang, Y. Song, Y. Liu, Q. Li, L. Jiang, D. Zhu, *Angew. Chem.* **2001**, *113*, 1793 – 1796; *Angew. Chem. Int. Ed.* **2001**, *40*, 1743 – 1746.
[12] S. Li, H. Li, X. Wang, Y. Song, Y. Liu, L. Jiang, D. Zhu, *J. Phys. Chem. B* **2002**, *106*, 9274 – 9276.
[13] S. H. Park, D. Qin, Y. Xia, *Adv. Mater.* **1998**, *10*, 1028 – 1032.
[14] Y. Xia, J. A. Rogers, K. E. Paul, G. M. Whitesides, *Chem. Rev.* **1999**, *99*, 1823 – 1848.
[15] A. Ulman, *Chem. Rev.* **1996**, *96*, 1533 – 1554.
[16] S. A. Jenekhe, X. L. Chen, *Science* **1999**, *283*, 372 – 375.
[17] N. Maruyama, T. Koito, J. Nishida, T. Sawadaishi, X. Cieren, K. Ijiro, O. Karthaus, M. Shimomura, *Thin Solid Films* **1998**, *327–329*, 854 – 856.
[18] B. Q. Wei, R. Vajtai, Y. Jung, J. Ward, R. Zhang, G. Ramanath, P. M. Ajayam, *Nature* **2002**, *416*, 495 – 496.
[19] J. Jin, T. Iyoda, C. Cao, Y. Song, L. Jiang, T. Li, D. Zhu, *Angew. Chem.* **2001**, *113*, 2193 – 2196; *Angew. Chem. Int. Ed.* **2001**, *40*, 2135 – 2138.
[20] G. Decher, *Science* **1997**, *277*, 1232 – 1237.
[21] M. P. Pileni, *Langmuir* **1997**, *13*, 3266 – 3276.
[22] A. W. Adamson, A. P. Gast, *Physical Chemistry of Surfaces*, New York, Wiley, **1997**, pp. 358 – 359.
[23] E. W. Weisstein, *Handbook of Chemistry and Physics*, 61st ed., CRC Press, Boca Raton, FL, **1981**, p. F-45
[24] J. Z. Liu, Q. S. Zheng, Q. Jiang, *Phys. Rev. B.* **2003**, *67*, o75414-1–o75414-8.
[25] J. Z. Liu, Q. S. Zheng, Q. Jiang, *Phys. Rev. Lett.* **2001**, *86*, 4843 – 4846.
[26] J. Wu, S. Liu, *Adv. Mater.* **2002**, *14*, 215 – 218.
[27] Z. Zhang, G. Ramanath, P. M. Ajayan, D. Goldberg, Y. Bando, *Adv. Mater.* **2001**, *13*, 197 – 200.
[28] G. Shi, S. Jin, G. Xue, C. Li, *Science* **1995**, *267*, 994 – 996
[29] M. Fu, Y. Zhu, R. Tan, G. Shi, *Adv. Mater.* **2001**, *13*, 1874 – 1877.
[30] H. Qiu, M. Wan, B. Matthews, L. Dai, *Macromolecules* **2001**, *34*, 675 – 677.

 © 2004 Wiley-VCH Verlag GmbH & Co. KGaA, Weinheim

Crystal Growth

Polymorphism of 1,3,5-Trinitrobenzene Induced by a Trisindane Additive**

Praveen K. Thallapally, Ram K. R. Jetti, Amy K. Katz, H. L. Carrell, Kuldeep Singh, Kakali Lahiri, Sambasivarao Kotha, Roland Boese, and Gautam R. Desiraju**

Additive-induced polymorphism has always interested the solid-state chemist for fundamental and practical reasons.[1] Polymorphism is, in itself, an enigmatic phenomenon and the reasons for its occurrence are only now beginning to be unraveled.[2] The role of tailor-made additives (auxiliaries) in the control of various aspects of crystallization (nucleation,

[*] Dr. R. K. R. Jetti, Prof. Dr. R. Boese
Institut für Anorganische Chemie
Universität Duisburg-Essen, Standort Essen
Universitätstrasse 5–7, 45177 Essen (Germany)
Fax: (+49) 201-183-2535
E-mail: roland.boese@uni-essen.de

Dr. P. K. Thallapally, Prof. G. R. Desiraju
School of Chemistry
University of Hyderabad
Hyderabad 500 046 (India)
Fax: (+91) 40-2301-0567
E-mail: desiraju@uohyd.ernet.in

A. K. Katz, Dr. H. L. Carrell
The Institute for Cancer Research, Fox Chase Cancer Center, 7701 Burholme Avenue, Philadelphia, PA 19111 (USA)

K. Singh, Dr. K. Lahiri, Prof. S. Kotha
Department of Chemistry, Indian Institute of Technology
Powai, Mumbai, 400 076 (India)

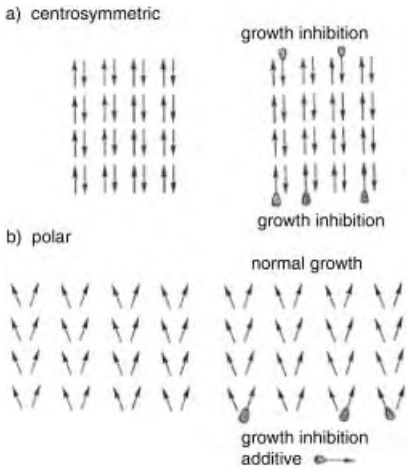
[**] P.K.T thanks the CSIR for a fellowship. G.R.D. is a recipient of the Alexander von Humboldt research award. R.K.R.J. and R.B. are grateful to the DFG for financial assistance. H.L.C. and A.K.K. acknowledge financial support from grant CA-10925 of the NIH. K.S., K.L., and S.R.K. thank RSIC IIT-Mumbai for spectral data.

Supporting information for this article (experimental details, spectroscopic data, computational details) is available on the WWW under http://www.angewandte.org or from the author.

 DOI: 10.1002/anie.200352253 © 2004 Wiley-VCH Verlag GmbH & Co. KGaA, Weinheim

growth, morphology, dissolution, structure) has been described.[3] Polymorphism is one of the least controllable aspects of crystallization. Therefore it would be extremely useful if there were a reliable and general way of engineering additive-induced polymorphism. These ideas are also relevant in crystal-structure prediction.[4] Three questions are pertinent: 1) Does the presence of an additive change the polymorph that is obtained? 2) If so, can the structure of the polymorph so obtained be correlated with the structure of the additive? 3) What is the mechanism of enhancement/inhibition of a polymorph? Despite the importance of these questions, the number of well-documented examples of additive-induced polymorphism is very limited.

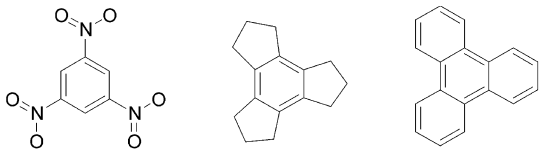
Leiserowitz, Lahav, and co-workers[1f,g] have provided a basic model for additive-induced polymorphism (Scheme 1). The additive is structurally similar to the molecule of interest



Scheme 1. Basic model for additive-induced polymorphism, see text for details.

(host) and it may be selectively adsorbed on its crystal faces. Depending on the degree of similarity between the host and the additive, the latter may selectively inhibit the growth of a few faces of the embryonic crystal of the host. These ideas find a practical application in the preferred crystallization of a noncentrosymmetric polymorph (Scheme 1b, left) at the expense of a centrosymmetric one (Scheme 1a, left). An appropriate tailor-made additive will inhibit growth of the centrosymmetric form at two opposite ends thereby precluding it (Scheme 1a, right), but it will inhibit growth of the polar form at only one end of the crystal (Scheme 1b, right) so that it survives. This concept was demonstrated for *N*-(2-acetamido-4-nitrophenyl)pyrrolidine (PAN) with the 2-nitro and 2-amino derivatives as additives, and for the γ-form of glycine in aqueous solution with racemic hexafluorovaline as an additive. [1f,g] Another clear example is provided by Davey and co-workers[5] who selected trimesic acid and *trans*-glutaconic acid as inhibitors of the stable β-polymorph of L-glutamic acid leading to the metastable α-polymorph. He, Stowell, and co-workers[6] designed isomorphous additives that induced crystallization of a metastable form of 4-methyl-2-nitroacetanilide. The phenomenon has been reviewed.[7,8]

Herein we report on the polymorphism of 1,3,5-trinitrobenzene (TNB) induced by the additive trisindane (TI). TNB has been known for 120 years as an explosive and in the formation of crystalline π–π donor–acceptor complexes.[9] However, and in contrast to the related molecule 2,4,6-trinitrotoluene (TNT),[2a,10] there has been no report of its polymorphism.[11] The only known crystal structure of TNB is that of the centrosymmetric orthorhombic form (space group *Pbca*, $Z' = 2$), which we shall call Form **I**.[12] More recently, TNB has been used as a component of C–H···O hydrogen-bonded molecular complexes for applications in nonlinear optics (NLO). For example, we co-crystallized an equimolar mixture of TNB and triphenylene (TP) to obtain a 1:1



molecular complex, which we studied in detail.[13] Continuing this strategy, we attempted to co-crystallize 1:1 and 2:1 mixtures of TNB and the closely related TI from CCl_4.[14] There was distinct evidence of complex formation in solution in that the solution changed from pale yellow to dark red. However, instead of obtaining the desired 1:1 or 2:1 molecular complexes, we obtained (from a 2:1 experiment in CCl_4) a new polymorph of TNB, henceforth, Form **II**.

Figure 1 shows the crystal structure of the new and unexpected noncentrosymmetric polymorph, in the orthorhombic space group $Pca2_1$, also with $Z' = 2$.[15] Close inspection of this intricate structure shows two patterns generated, respectively, from the two independent molecules in the asymmetric unit. These patterns are shown in green and yellow in Figure 1. The green colored molecules form a V-shaped trough while the yellow colored molecules form a zigzag arrangement. The V-shaped trough and the zigzag chains are linked with weak C–H···O, C–H···N, and $NO_2 \cdots NO_2$ contacts.[16]

We next redetermined the structure of Form **I** because we wished to verify the Lahav–Leiserowitz model for additive induced polymorphism.[15] Figure 2 shows that the *Pbca* structure of Form **I** is closely related to the $Pca2_1$ structure of Form **II**. In both forms, there are V-shaped troughs made up of one of the two symmetry independent molecules in the crystal (green). The major distinction is that the V-shaped troughs point in opposite directions in the centrosymmetric Form **I** crystal and only in one direction in the polar Form **II** crystal. The *Pbca* structure is in effect a doubled version of the $Pca2_1$ structure across an inversion center[18] so that the mechanism in Scheme 1 broadly applies leading to Form **II** crystals. The unit cell parameters (Form **I**, $a = 12.587$, $b = 9.684$, $c = 26.86$; Form **II**, $a = 9.297$, $b = 18.730$, $c = 9.633$) show some relationship in that $b_{\mathbf{I}} \cong c_{\mathbf{II}}$ and that $(a_{\mathbf{I}} c_{\mathbf{I}}) \cong 2\,(a_{\mathbf{II}} b_{\mathbf{II}})$. While the V-shaped troughs point along [010] and [0−10] in Form **I** they point only along [001] in Form **II**.

 © 2004 Wiley-VCH Verlag GmbH & Co. KGaA, Weinheim

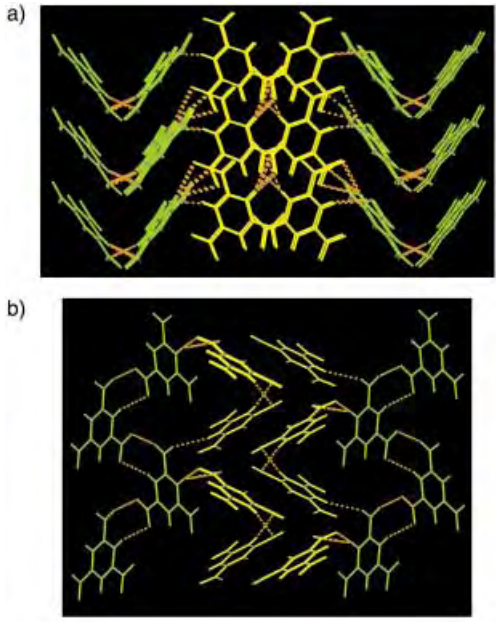


Figure 1. Noncentrosymmetric Form **II** crystal of TNB. The two symmetry-independent molecules are shown in green and yellow. a) View down the *a* axis showing alternate V-shaped troughs and zigzag chains. b) View down the *c* axis showing TNB tape based on C–H···O and NO_2···NO_2 interactions along the *a* axis (green), and zigzag chains (yellow). For clarity C–H···N and ON–O···NO_2 interactions are removed between the green TNB molecules. Molecular graphics were generated using X-seed and POV-Ray.[17]

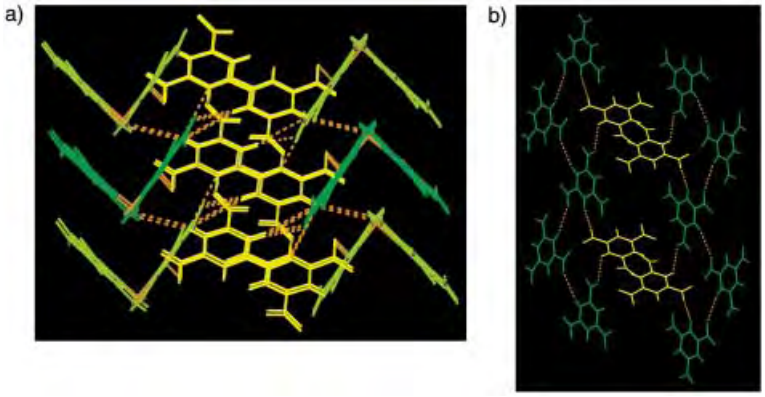


Figure 2. Centrosymmetric Form **I** crystal structure of TNB (*Pbca*). a) View down the *a* axis. b) View down the *b* axis.

The experimental morphology of the Form **I** crystals was determined. Figure 3 shows the crystal faces in a well-grown specimen. The main faces are (010) and (001) and their centrosymmetrically related equivalents. From the direction of the V-shaped troughs in the two forms, it may be assumed that binding of TI on the (010) faces is likely. If the binding is slightly different on (010) and (0–10) there will be a symmetry reduction from *Pbca* to $Pb2_1a$. A permutation of the *b* and *c* axes ($b_{\mathbf{I}} \cong c_{\mathbf{II}}$) leads to space group $Pca2_1$ for Form **II**. According to this model it is not mandatory that $a_{\mathbf{I}} \cong a_{\mathbf{II}}$ with $c_{\mathbf{I}} \cong 2\,(b_{\mathbf{II}})$. It is sufficient if $(a_{\mathbf{I}}\, c_{\mathbf{I}}) \cong 2\,(a_{\mathbf{II}}\, b_{\mathbf{II}})$ and this condition is achieved by a slight shearing of molecules in the

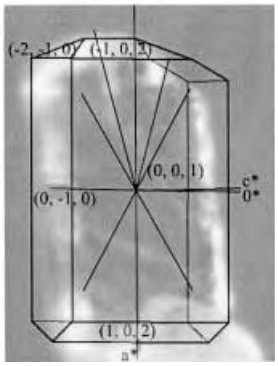


Figure 3. Experimental morphology of Form **I** crystal of TNB. Note the (010) and (0–10) faces.

(010) planes of the Form **I** crystal. Indeed such shearing is unsurprising. It would have been more exceptional if the preferential growth along +b or –b were accompanied by no change whatsoever in the (010) planes, in effect along the *a* and *c* directions. These results also demonstrate that it is the adsorption of TI additive on (010) and (0–10) that is critical to the formation of the new polymorph because it is the *b* axis of Form **I** that is unchanged in length in going to Form **II** (where it is termed the *c* axis), while the *a* and *c* axes of Form **I** (renamed as the *a* and *b* axes in Form **II**) change in length. The experimental morphology shows that (010) and (001) are major faces, with (001) being more prominent. Yet, only adsorption of TI on (010) is critical to the growth of Form **II** with any possible adsorption on (001) being innocuous.

In considering the growth of Form **II** crystals from a CCl_4 solution of TNB that contains TI additive, an important assumption that is implicit in the Lahav–Leiserowitz model needs to be mentioned,[3a] namely that any solution contains a variety of molecular aggregates, some of which have structures akin to those of the macroscopic crystalline forms. This assumption is a triviality when polymorphs appear concomitantly. However, if say solution *A* normally results in polymorph *A* and one wishes to design an additive that will yield polymorph *B* from this solution, then this assumption must be taken into account. This is pertinent in the present case because both Forms **I** and **II** were obtained from CCl_4 solution. Another consideration that has been utilized in certain layered structures wherein layer stabilities and bulk stabilities are inverted in two polymorphs is to induce nucleation layer by layer so as to obtain the less stable polymorph.[3a] But this is not applicable in the present case because the structures of Forms **I** and **II** are not layered and Form **II** is more stable than Form **I** (see below).

In attempting to reproduce these results we set up a series of crystallization experiments from various solvents (in Essen) with varying mole proportions of TNB and TI.[19] However, we never again were able to obtain the noncentrosymmetric Form **II** (which had appeared originally in Hyderabad), even after nearly 100 crystallization attempts

 © 2004 Wiley-VCH Verlag GmbH & Co. KGaA, Weinheim

spread over a six-month period. However, during these experiments, we isolated another polymorph, Form **III**, when TNB (80%) and TI (20%) were taken in EtOAc. This form of TNB crystallizes in the centrosymmetric space group $P2_1/c$ with $Z' = 1$ (Figure 4). Unlike Form **II**, we were

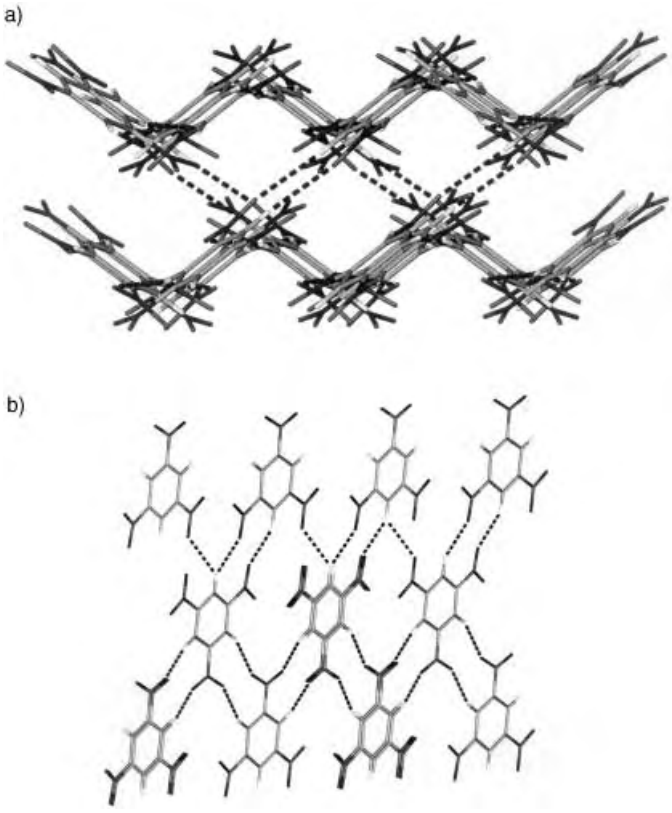


Figure 4. Centrosymmetric Form **III** crystal of TNB. a) View down the *a* axis. b) View down the *b* axis showing the TNB tape.

able to obtain crystals of Form **III** a second time but only after several attempts. Close inspection of this new(est) structure of TNB shows that it is not obviously related to Form **I** and Form **II**. There are no V-shaped troughs or zigzag chains. The structure is "normal" and emphasizes Kitaigorodskii-type close packing.[20] The TNB tape building block shown in Figure 4b is common in TNB molecular complexes[21] but is not seen in Forms **I** and **II** (see Supporting Information).

These results, unanticipated as they were, open up several lines of discussion. What is the role of TI in inducing the appearance of Form **III** crystals? First, although many crystallization experiments were carried out,[22] Forms **II** and **III** were only obtained when TI was present. An additional indication that TI is indispensable for the production of polymorphic structures is that there is no evidence of any phase transformation of Form **I** crystals, at least as evidenced from differential scanning calorimetry (DSC), thermogravimetric analysis (TGA), and variable-temperature powder diffraction traces. Second, we note that TNB gives stoichiometric molecular complexes with a very large number of planar π donors.[23,24] Thus, TNB readily gives a 1:1 molecular complex with the planar TP. It is possible that the difficulty of formation of a molecular complex between TNB and TI arises from the nonplanarity of the TI molecule. In any event, we observed the formation of small amounts of red microcrystalline material coating the crystals of TNB (shown in a photograph in the Supporting Information) in most of the cocrystallization experiments (regardless of the crystalline form of TNB obtained). We made several attempts to isolate a single crystal from this microcrystalline mass but were unsuccessful. We infer that this material corresponds largely to a TNB–TI molecular complex of unknown structure. Whilst formation of a stoichiometric molecular complex between TNB and TI may be difficult as explained above, there is a close degree of molecular similarity as is revealed in the overlap diagram in Figure 5. This situation leads to the



Figure 5. Overlay of TNB and TI molecules.

possibility of nonstoichiometric solid–solution formation at the surface. As very little of this red material was obtained (we estimate less than 5% according to powder X-ray diffractometry) we conclude that the degree of molecular similarity is not high enough.[25,26] In summary, it is this serendipitous duality of events that appears to favor the formation of Form **III**. The nonplanar TI cannot form a stoichiometric molecular complex readily with TNB, for if this were so there would be no other result in the cocrystallization experiments,[9a] and the degree of molecular similarity between TI and TNB is not so high as to lead to the formation of nonstoichiometric solid–solutions. Yet the interaction between TNB and TI is sufficiently good to promote some sort of association. What appears plausible, is an ill-defined outcome with an indiscriminate adsorption of TI molecules over all the faces of the growing TNB crystals.

Such nonselective adsorption of TI on the TNB faces may be rationalized by considerations of molecular and crystal symmetry. It is not straightforward to establish at which faces of the centrosymmetric Form **I** crystal the additive is adsorbed, since TI has molecular threefold symmetry, as does TNB. This issue is resolved for adsorption leading to Form **II**, because it is noncentrosymmetric, but Form **III** is centrosymmetric. How does the additive work in this case? The clue lies in the actual point groups of Forms **I** and **III** which are *2/m 2/m 2/m* and *2/m*, respectively. The idea here is that the higher the crystal point symmetry, the more different orientations in the lattice the constituent molecules may occupy, making the inhibition process less selective, or in other words, more indiscriminate. This principle was enunciated by Weissbuch et al.[3b] but no examples have been found to support this

 © 2004 Wiley-VCH Verlag GmbH & Co. KGaA, Weinheim

conjecture until the present case. Here, we may suggest that the threefold symmetric additive molecule may substitute for the threefold symmetric host molecule, of roughly the same size and shape, at several locations because many of the orientations that the host molecule presents in the growing crystal are equivalent.

Finally, let us consider the energetics of the three polymorphs of TNB. To compare the relative stability of the three polymorphs one should consider their lattice energies,[27] melting points, densities, and packing coefficients (see Supporting Information). The crystallographic and physical details are given in Table 1. The data in Table 2 shows that

Table 1: Crystallographic data for the compounds studied

Parameter	I	II	III
crystal system	orthorhombic	orthorhombic	monoclinic
space group	*Pbca*	$Pca2_1$	$P2_1/c$
Z	16	8	4
Z'	2	2	1
ρ_{calcd} [g cm^{-3}]	1.729	1.688	1.717
C_{k*}	72.5	71.0	72.5
m.p. [°C]	121.8	119.2	122.7

Table 2: Lattice energy calculations on the polymorphs of TNB

Energy	Form I [Kcal mol^{-1}]	per molecule	Form II [Kcal mol^{-1}]	per molecule	Form III [Kcal mol^{-1}]	per molecule
Van der Waals	−267.830	−16.739	−124.327	−15.541	−65.817	−16.454
electrostatic	−261.686	−16.355	−176.639	−22.079	−82.907	−20.727
hydrogen bond	−43.158	−2.697	−29.152	−3.644	−17.655	−4.414
total energy	−572.67	−35.792	−330.118	−41.265	−166.38	−41.595

Form **III** is the most stable polymorph being more stable than Form **II** by 0.33 kcal mol^{-1} and more stable than Form **I** by as much as 5.80 kcal mol^{-1}.[28] The observed melting points of Forms **I** and **III** support these calculations. Surprisingly, the least stable polymorph (Form **I**) is also the densest. This is not unprecedented but it is uncommon.[29] That a crystal form that is of such high relative energy has been reported after more than a century of experimental work on TNB is noteworthy, and suggests that Form **I** is distinctly favored kinetically.[30] The adsorption of TI on the faces of the kinetic Form **I** crystal leads (in an orderly fashion according to Scheme 1) to Form **II** and the adsorption is selective. If the adsorption is indiscriminate, the growth of all faces of all possible kinetic forms may be affected,[31] and what crystallizes out might be the most stable (thermodynamically favored) Form **III**. The fact that the highest melting Form **III** has a "normal"[20] packing ($P2_1/c$, $Z'=1$) also corroborates that it is the thermodynamic form, or at any rate close to the thermodynamic form, which may still remain to be isolated. Whether Form **II** is a disappearing form[32] or not is an open question, and we reserve comment at present.[33]

In conclusion, it may be said that the isolation and detection of new polymorphs is still unpredictable. A combination of serendipity and subsequent rigorous observation could well lead to novel and unanticipated polymorphs. For instance, in this work, crystal forms have been found that were hitherto unreported. In general, it would appear that McCrone's dictum[34] is correct but again, perhaps only for some categories of molecules.[35] In the present instance, the fact that molecules of TI can interact with those of TNB, but not too well, seems to be the critical factor that determines the appearance of new polymorphs. But why is so much of additive required? And why is it that while additives change crystal morphology easily,[3] they do not seem to be able to change the polymorph that is obtained so readily? It appears that if the additive completely surrounds the embryonic crystal of the kinetic forms (through an indiscriminate adsorption on all the crystal faces), then only the most stable crystal form is able to survive.[31] Normally, thermodynamic forms are obtained under conditions when nucleation is inhibited (dilute solutions, annealing, supercritical fluids, hydrothermal methods, gel crystallization, high pressure). The present study shows that there may be another way of inhibiting nucleation, namely through the use of additives that bind nonselectively to all crystal faces of all kinetic forms.[36] However, this does not mean that such an additive may be designed, in advance, with our present understanding of the crystallization event although the appearance of Form **II** may be rationalized on the basis of an accepted model. Could one have computed the structure of the stable Form **III**? What would happen if TNB was given as a candidate molecule in a blind test for crystal structure prediction (CSP)?[4] Why is it that the presence of TI in the crystallization vessel does not invariably lead to the formation of Forms **II** or **III**? In other words, why is the formation of these more stable forms much less frequent? We are not particularly disappointed that we obtained Form **II** only once and Form **III** only twice. It is possible that if the crystallization is carried out with TI and also employing some other condition that inhibits nucleation (such as those listed above), the appearance of more stable crystal forms might become much more frequent. We are pursuing these and other related experiments currently. On a more speculative note, is the occurrence of multiple molecules in the crystallographic asymmetric unit for nonpseudosymmetric structures correlated with the appearance of kinetic forms? Perhaps some of the questions posed in this paragraph might appear to be rhetorical, or even fanciful. However, they do show that the phenomenon of polymorphism is one of the most difficult frontiers in the chemistry of the molecular solid state today.

Received: June 27, 2003
Revised: September 22, 2003 [Z52253]

Keywords: additives · crystal growth · inhibition · polymorphism

[1] a) M. Kuhnert-Brandstätter, M. Aepkers, *Mikroskopie* **1961**, *16*, 189–197; b) M. Kuhnert-Brandstätter, M. Aepkers, *Mitt. Mik-*

 © 2004 Wiley-VCH Verlag GmbH & Co. KGaA, Weinheim

rochim. Acta **1963**, 360–375; c) A. R. Ebian, M. A. Moustafa, S. A. Khalil, M. M. Motawi, *J. Pharm. Sci.* **1973**, *25*, 13–20; d) A. R. Ebian, M. A Moustafa, S. A. Khalil, M. M. Motawi, *J. Pharm. Sci.* **1975**, *64*, 1481–1484; e) S. N. Black, R. J. Davey, M. Halcrow, *J. Cryst. Growth* **1986**, *79*, 765–774; f) E. Staab, L. Addadi, L. Leiserowitz, M. Lahav, *Adv. Mater.* **1990**, *2*, 40–43; g) I. Weissbuch, L. Leiserowitz, M. Lahav, *Adv. Mater.* **1994**, *6*, 952–956; h) B. D. Chen, J. Garside, R. J. Davey, S. J. Maginn, M. Matsuoka, *J. Phys. Chem.* **1994**, *98*, 3215–3221; i) B. D. Chen, G. D. Potts, R. J. Davey, J. Garside, D. Bergmann, S. Niehoerster, S. Ulrich, *J. Cryst. Growth* **1994**, *144*, 297–303; j) D. Lechuga-ballesteros, N. Rodriguezhornedo, *Int. J. Pharm.* **1995**, *115*, 139–149; k) B. A. Hendriksen, D. J. W. Grant, P. Meenan, D. A. Green, *J. Cryst. Growth* **1998**, *183*, 629–640; l) C.-H. Gu, K. Chatterjee, V. Young, D. J. W. Grant, *J. Cryst. Growth* **2002**, *235*, 471–481.

[2] Selected books and reviews: a) J. Bernstein, *Polymorphism in Molecular Crystals*, *Clarendon*, Oxford, **2002**; b) T. L. Threlfall, *Analyst* **1995**, *120*, 2435–2460; c) "Polymorphism and Pseudo-polymorphism in Organic Crystals: A Cambridge Structural Database Study": by J. A. R. P. Sarma, G. R. Desiraju in *Crystal Engineering* (Eds.: K. R. Seddon, M. Zaworotko), Kluwer, Norwell, MA, **1999**, pp. 325–356; d) G. R. Desiraju, *Science*, **1996**, *278*, 404–405; d) R. J. Davey, *Chem. Commun.* **2003**, 1463–1467; recent papers include: e) R. K. R. Jetti, R. Boese, J. A. R. P. Sarma, L. S. R. Reddy, P. Vishweshwar, G. R. Desiraju, *Angew. Chem.* **2003**, *115*, 2008–2012; *Angew. Chem. Int. Ed.* **2003**, *42*, 1963–1967; f) L. Yu, *J. Am. Chem. Soc.* **2003**, *125*, 6380–6381; g) A. Kálmán, L. Fábián, G. Argay, G. Bernáth, Z. Gyarmati, *J. Am. Chem. Soc.* **2003**, *125*, 34–35.

[3] a) I. Weissbuch, M. Lahav, L. Leiserowitz, *Cryst. Growth Des.* **2003**, *3*, 125–150; b) I, Weissbuch, R. Popovitz-Biro, M. Lahav, L. Leiserowitz, *Acta Crystallogr. Sect. B* **1995**, *51*, 115–148.

[4] a) G. R. Desiraju, *Nat. Mater.* **2002**, *1*, 77–79; b) J. D. Dunitz, *Chem. Commun.* **2003**, 545–548.

[5] R. J. Davey, N. Blagden, G. D. Potts, R. Docherty, *J. Am. Chem. Soc.* **1997**, *119*, 1767–1972.

[6] X. He, J. G. Stowell, K. R. Morris, R. R. Pfeiffer, H. Li, G. P. Stahly, S. R. Byrn, *Cryst. Growth Des.* **2001**, *1*, 305–312.

[7] a) M. R. Caira, *Top. Curr. Chem.* **1998**, *198*, 163–208; b) M. R. Caira, *J. Chem. Crystallogr.* **1994**, *24*, 695–701.

[8] It is possible that additive-induced polymorphism is far more widespread than has been actually documented. In industrial crystallization, it is known, for example, that the crystal form of a substance obtained from the reaction mixture is sometimes different from the forms obtained upon subsequent crystallization of purified material. Considering that the synthetic precursor of a particular molecule of interest is likely to have a related chemical structure, it may well be able to behave as an unintended crystallization auxiliary. For a general reference on industrial crystallization, see *Crystal Growth of Organic Materials* (Eds.: A. S. Myerson, D. A. Green, P. Meenan), ACS Conference Proceedings Series, American Chemical Society, Washington DC, **1996**.

[9] a) R. Foster, *Organic Charge-Transfer Complexes*. Academic, New York, **1969**; b) P. Pfeiffer, *Organische Molekülverbindungen*, 2nd ed., Ferdinand Enke, Stuttgart, **1927**; c) C. Becker, *Ber. Dtsch. Chem. Ges.* **1883**, *16*, 1597.

[10] a) R. M. Vrcelj, H. G. Gallagher, J. N. Sherwood, *J. Am. Chem. Soc.* **2001**, *123*, 2291–2295; b) R. M. Vrcelj, J. N. Sherwood, A. R. Kennedy, H. G. Gallagher, T. Gelbrich, *Cryst. Growth Des.* **2003**, *3*, 1027–1032.

[11] There is solitary report in the patent literature, [G. B. Ravich, O. F. Bogush, *Dokl. Akad. Nauk. SSSR* **1962**, *142*, 831–834] but the forms reported there do not bear a resemblance to the new crystal forms in the present work.

[12] The crystal structure of TNB has been determined by C. S. Choi, J. E. Abel, *Acta Crystallogr. Sect. B* **1972**, *23*, 198–201 using neutron radiation at room temperature. We redetermined the structure using X-ray radiation at 183 K (see ref. [15]), and our analysis is based on this data.

[13] J. Zyss, I, Ledoux, H.-C. Weiss, R. Boese, P. K. Thallapally, V. R. Thalladi, G. R. Desiraju, *Chem. Mater.* **2003**, *15*, 3063–3073.

[14] TI was synthesized by using a literature procedure (S. Kotha, K. Chakraborty, E. Brahmachary, *Synlett* **1999**, 1621–1623). TNB was either synthesized by using a literature procedure (P. Segura, J. F. Bunnett, L. Villanova, *J. Org. Chem.* **1985**, *50*, 1041–1049) or obtained from Dynamit Nobel AG. We attempted to cocrystallize TNB and TI in 1:1 and 2:1 proportions from chloroform, dichloromethane, ethyl acetate, acetonitrile, acetone, dioxane, nitromethane, and from solvent combinations but in none of these cases could we isolate any diffraction-quality crystals of any molecular complexes.

[15] Crystal data for TNB Form **I**: orthorhombic, *Pbca*, $a = 12.587(11)$, $b = 9.684(9)$, $c = 26.86(2)$ Å, $V = 3274(5)$ Å^3, $Z = 16$, $\rho_{calcd} = 1.729$ g cm^{-3}, $T = 183$ K, $\mu = 0.159$ mm^{-1}, $2\theta_{max} = 57.5°$, 36564 measured, 4188 independent, 1396 observed ($I > 2\sigma_1$) reflections, 271 parameters, $R1 = 0.0450$, $wR2 = 0.0985$ (for $I > 2\sigma_1$), residual electron density $+0.188/-0.191$ e Å^{-3} (CCDC-213310); Crystal data for TNB Form **II**: orthorhombic, $Pca2_1$, $a = 9.2970(19)$, $b = 18.730(4)$, $c = 9.6330(19)$ Å, $V = 1677.4(6)$ Å^3, $Z = 8$, $\rho_{calcd} = 1.688$ g cm^{-3}, $T = 120$ K, $\mu = 0.155$ mm^{-1}, $2\theta_{max} = 55.8°$, 2117 measured, 2117 independent, 1924 observed ($I > 2\sigma_1$) reflections, 271 parameters, $R1 = 0.0397$, $wR2 = 0.0985$ (for $I > 2\sigma_1$), residual electron density $+0.240/-0.317$ e Å^{-3} (CCDC-213311); Crystal data for TNB Form **III**: monoclinic, $P2_1/c$, $a = 12.896(5)$, $b = 5.723(2)$, $c = 11.287(5)$ Å, $\beta = 98.190(8)°$, $V = 824.5(6)$ Å^3, $Z = 4$, $\rho_{calcd} = 1.717$ g cm^{-3}, $T = 183$ K, $\mu = 0.158$ mm^{-1}, $2\theta_{max} = 56.60°$, 4936 measured, 2008 independent, 1221 observed ($I > 2\sigma_1$) reflections, 136 parameters, $R1 = 0.0609$, $wR2 = 0.1462$ (for $I > 2\sigma_1$), residual electron density $+0.419/-0.231$ e Å^{-3} (CCDC-213312); Crystal data for TI: monoclinic, $P2_1/c$, $a = 11.920(3)$, $b = 6.0733(13)$, $c = 16.584(4)$ Å, $\beta = 110.670(4)°$, $V = 1123.4(4)$ Å^3, $Z = 4$, $\rho_{calcd} = 1.172$ g cm^{-3}, $T = 203$ K, $\mu = 0.065$ mm^{-1}, $2\theta_{max} = 54°$, 12490 measured, 2443 independent, 1428 observed ($I > 2\sigma_1$) reflections, 136 parameters, $R1 = 0.0559$, $wR2 = 0.1260$ (for $I > 2\sigma_1$), residual electron density $+0.208/-0.139$ e Å^{-3} (CCDC-213313). The data for Form **I**, **III**, and TI were collected on a SMART diffractometer using $Mo_{K\alpha}$ radiation. For Form **II** the instrument used was Nonius FAST area detector. Structure solution by direct methods and refinements on F^2 with SHELXTL (Version 6.10 and 6.12). Non-hydrogen atoms were refined anisotropically and the H atoms of the phenyl groups were generated at idealized geometries and refined isotropically using a riding model. CCDC 213310–213312 contain the supplementary crystallographic data for this paper. These data can be obtained free of charge via www.ccdc.cam.ac.uk/conts/retrieving.html (or from the Cambridge Crystallographic Data Centre, 12 Union Road, Cambridge CB2 1EZ, UK; fax: (+44) 1223-336-033; or deposit@ccdc.cam.ac.uk).

[16] a) G. R. Desiraju, T. Steiner, *The Weak Hydrogen Bond in Structural Chemistry and Biology*, Oxford University Press, Oxford, **1999**; b) M. Mascal, *Chem. Commun.* **1998**, 303–304; c) K. Wozniak, H. He, J. Klinowski, W. Jones, E. Grech, *J. Phys. Chem.* **1994**, *98*, 13755–13765; d) R. K. R. Jetti, P. K. Thallapally, A. Nangia, C.-K. Lam, T. C. W. Mak, *Chem. Commun.* **2002**, 952–953.

[17] a) L. J. Barbour, *J. Supramol. Chem.* **2001**, *1*, 189–191; b) J. L. Atwood, L. J. Barbour, *Cryst. Growth Des.* **2003**, *3*, 3–8.

[18] See Supporting Information for details of the calculated crystal morphology.

 © 2004 Wiley-VCH Verlag GmbH & Co. KGaA, Weinheim

[19] Cocrystallization of TNB with TI in these exhaustive trials was attempted with mole percentages of TI from 10% to 50%. Recrystallization was carried out separately for both TNB and TI and as well as for mixtures from a variety of solvents, such as EtOAc, MeOH, EtOH, CH_2Cl_2, $CHCl_3$, CCl_4, benzene, toluene, *m*-xylene, *p*-xylene, mesitylene, acetone, MeCN, *n*BuOH, *n*PrOH, *i*PrOH, $MeNO_2$, THF, dioxane, Et_2O, DMF, and DMSO. Solvent combinations, such as MeOH–MeCN, benzene–CCl_4, benzene–hexane, EtOAc–hexane, and benzene–MeCN, were also tried. Invariably, we obtained crystals of Form **I** or TI. In all, approximately 100 single crystals from different crystallization experiments were selected for cell measurements. While the crystals very often had different morphologies, all of them turned out to be those of either Form **I** or TI.

[20] A. I. Kitaigorodskii, *Molecular Crystals and Molecules*, Academic Press, New York, **1973**. By "normal" is meant a three-dimensionally close-packed structure without any easily identifiable substructural motifs, such as V-shaped troughs, molecular tapes.

[21] a) P. K. Thallapally, A. K. Katz, H. L. Carrell, G. R. Desiraju, *CrystEngComm* **2003**, *5*, 87–92; b) P. K. Thallapally, K. Chakraborty, H. L. Carrell, S. Kotha, G. R. Desiraju, *Tetrahedron* **2000**, *56*, 6721–6728.

[22] We carried out around 150 crystallization experiments with TNB. In roughly 50 of these trials, we did not use any TI. In these cases, there were two outcomes. For non-aromatic solvents, only Form **I** was obtained. With some aromatic solvents (benzene, toluene, chlorobenzene, *m*-xylene, *p*-xylene, mesitylene) we obtained solvates with a greater or lesser degree of difficulty.[23] With other aromatic solvents (nitrobenzene, bromobenzene, triflurotoluene, pyridine, collidine, picolines), only Form **I** was obtained.

[23] R. K. R. Jetti, P. K. Thallapally, R. Boese, G. R. Desiraju, *Cryst. Growth Des.* **2003**, *3*, 1033–1040.

[24] The current version of the CSD contains 61 (CSD version 5.23, April **2002**) of these molecular complexes; F. H. Allen, O. Kennard, *Chem. Des. Autom. News* **1993**, 8, 1–57.

[25] A. I. Kitaigorodskii, *Mixed Crystals*, Springer, Berlin, **1984** (Springer Series in Solid-State Science 33).

[26] We redetermined the crystal structure of pure TI (the earlier CSD known crystal structure is of limited precision with no hydrogen-atom positions reported; E. R. Boyko, P. O. Vaughan, *Acta Crystallogr.* **1964**, *17*, 152–154; see ref. [15]) but this is quite different from any of the forms of TNB. If the structures were isomorphous, solid–solution formation would be more likely.

[27] The lattice energies were carried out using "Smart Minimizer" option of the Cerius2 package. All molecules in the crystal were treated as rigid entries. Atom–atom potentials were estimated using Dreiding 2.21 force field and atomic charges were estimated using the charge equilibration method. Cerius2, Accelrys, Cambridge (UK). See www.accelrys.com.

[28] These energy values include the small variations in energy owing to the conformational differences between the nitro groups in the three forms.

[29] a) J. M. Robertson, *Proc. R. Soc. London Ser. A* **1936**, *157*, 79–83; b) J. M. Robertson, A. R. Ubbelohde, *Proc. R. Soc. London Ser. A* **1938**, *167*, 122–125.

[30] The relationship between the kinetic accessibility, higher relative energy, and high density of the most common Form **I** and the explosive character of TNB is an aspect that might need to be investigated in the future.

[31] We estimate that at a 20% loading of the additive, the embryonic TNB crystal contains 24580 molecules (crystal radius 107 Å) if the additive coats the crystal at monomolecular thickness, this is reasonable for a crystal in the very early stages of growth. Both TNB and TI are assumed to be spherical and the embryonic crystal is also assumed to be spherical. We thank Mr. T. Omlor for these calculations.

[32] J. D. Dunitz, J. Bernstein, *Acc. Chem. Res.* **1995**, *28*, 193–200.

[33] We do not rule out the possibility that Form **II** may be isolated in another laboratory at a future date, see for example the work on tetraacetyl ribofuransose by P. Bombicz, M. Czugler, R. Tellgren, A. Kálmán, *Angew. Chem.* **2003**, *115*, 2001–2004; *Angew. Chem. Int. Ed.* **2003**, *42*, 1957–1960.

[34] W. C. McCrone, *Polymorphism in Physics and Chemistry of the Organic Solid-State* (Eds.: D. Fox, M. M. Labes, A. Weissberger), Interscience, New York, **1965**.

[35] One of us (GRD) has pointed out on several occasions that despite rigorous experimentation, compounds such as benzoic acid, anthracene, and D-glucose do not yield normal pressure polymorphs.

[36] Leiserowitz et al. made a similar observation with PAN (see refs. [1f, 1g]).

 © 2004 Wiley-VCH Verlag GmbH & Co. KGaA, Weinheim

Analyzing Zeolites

Two-Dimensional IR Pressure-Jump Spectroscopy of Adsorbed Species for Zeolites**

*Stéphane Chenevarin and Frédéric Thibault-Starzyk**

Infrared spectroscopy of adsorbed probe molecules is a well established technique for the characterization of surface sites on zeolites and other solid catalysts. Time resolution in modern spectrometers increases the power of the technique for use with complex adsorption systems, with multiple adsorption sites and a microporous structure, by allowing the study of transient systems and of adsorption dynamics out of equilibrium. Step-scan Fourier transform interferometers can easily reach the microsecond timescale if the observation can be repeated with sufficient reproducibility. At this timescale, adsorbed molecules in a zeolite each have their eigen-response frequency to a pressure perturbation or modulation. Using pressure and temperature measurements, Rees and co-workers[1] and Grenier and co-workers[2] have explored the pressure modulation frequencies, indicated the frequencies for given adsorbates on given zeolites, and extracted diffusion kinetic parameters from their results. We

[*] Dr. F. Thibault-Starzyk
Laboratoire Catalyse et Spectrochimie
CNRS-ENSICAEN
14050 Caen CEDEX (France)
Fax: (+33) 2-3145-2822
E-mail: fts@ismra.fr
and
Department of Chemistry
University of Cambridge (UK)
S. Chenevarin
Laboratoire Catalyse et Spectrochimie
Caen (France)

[**] This work was supported by Bruker Optique. The authors acknowledge fruitful discussions with G. Zachmann (Bruker Optiks GmbH, Ettlingen (Germany)), J. C. Boulou (Bruker Optique, Wissembourg, France), and Prof. C. Fernandez (LCS, Caen).

 DOI: 10.1002/anie.200352754 © 2004 Wiley-VCH Verlag GmbH & Co. KGaA, Weinheim

thought we could use these eigen frequencies to extract spectral information for complex mixtures on surfaces. Thus, several adsorption sites, or several adsorbed molecules in a mixture, would each lead to a specific eigen-response frequency to a pressure modulation, and we could obtain the spectral signature for each individual species on each individual adsorption site. Instead of having to vary the modulation frequency progressively to explore the whole frequency domain, we decided to generate a square pressure wave on the surface (or more exactly a pressure jump), which would be equivalent to the generation of an infinite number of pressure oscillations with different frequencies (Figure 1).

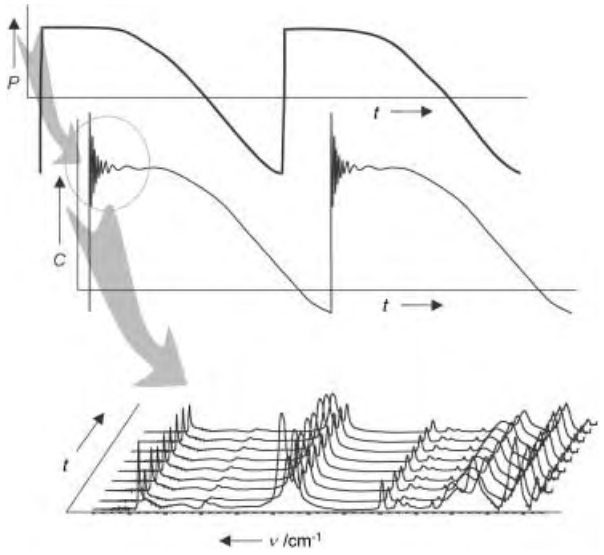


Figure 1. principle of the PJAS-IR method. A pressure jump is generated (top), which leads to a relaxation process by adsorption and diffusion on the surface (middle). The middle graph shows how the concentration *C* of adsorbed species varies following pressure jumps. IR spectra can be recorded for each pressure jump in step or rapid-scan modes (bottom: spectra shown here do not correspond to a specific experiment).

Such a pressure jump can be described as a shift of the adsorption in an excited state, with a relaxation by diffusion and adsorption equilibria. The relaxation process can be followed by fast time-resolved IR spectroscopy. The infrared spectra collected can be analysed by Fourier transform to extract the relaxation processes eigen frequencies, with correlations with the infrared frequencies. The technique is named IR pressure-jump spectroscopy of adsorbed species (PJAS-IR).

Mordenite is an important zeolite as a result of its many industrial applications and its specific pore structure: large 12-membered rings channels (ca. 6.7 × 7.0 Å) which run along the *c* crystallographic axis, with 8-membered-ring side pockets (ca. 3.9 Å free diameter) in the *b* direction. Owing to such different possible locations for catalytic sites, confinement effects are important in mordenites,[3,4] and have been used to tune catalytic activity.[5,6] The location and strength of Brønsted acid sites have long been studied by IR spectroscopy: these sites are due to H^+ ions compensating the charge defects of aluminium atoms in the framework, which leads to very clear ν(OH) vibration bands in the IR spectrum. The ν(OH) band in H-mordenite (H-Mor) has fine structure (Figure 2), in which two main ν(OH) vibration bands are

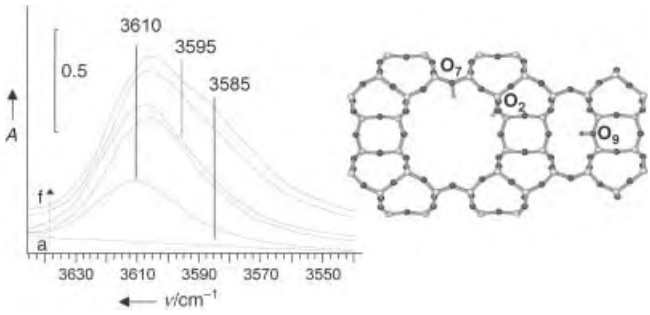


Figure 2. Left: IR room-temperature spectra of Na,H-Mor samples with various sodium contents (a–f, adapted from ref. [9]) showing the fine structure in the ν(OH) vibration region, and right: view of the mordenite framework along the *c* axis, showing the three possible OH groups in H-Mor that were assigned to the three corresponding ν(OH) vibration bands (in ref [10]).

usually identified, for OH groups in the main channels (MC; $\nu(OH_{MC})$ at 3610 cm^{-1}), and in the side pockets (SP) of the structure ($\nu(OH_{SP})$ at 3585 cm^{-1}).[7] Using mainly crystallographic data, Alberti proposed three different OH groups in the structure, at positions O7 in the main channels (OH_{MC}), O2 at the 8-R opening between large channels and side pockets (denoted here as OH_{8R}), and O9 at the end of the side pockets (OH_{SP}).[8] The ν(OH) vibration band for OH_{8R} groups has been identified recently,[9] but remains unclear and can not be seen directly on the spectrum of the fully acidic sample.

Deuterated acetonitrile is an important probe molecule for acid sites in mordenites,[3,4,6,7,10,11] its properties are strongly influenced by temperature, pressure, and confinement. At room temperature and low coverage, a hydrogen bond is formed between acetonitrile and OH groups. At high coverage, a very strong hydrogen bond is formed between probe molecules (probably dimers) and OH groups in the side pockets.[4] If the pressure is reduced, or if the temperature is risen, this particular hydrogen bond disappears. At very high temperature, acetonitrile is protonated and a nitrilium is formed.[10] The formation of this nitrilium ion seems very much influenced by confinement,[11] and probably takes place in the side pockets, but this has so far not been established.

We studied the acetonitrile adsorption on H-Mor by 2D-PJAS IR, which allowed the measurement of spectroscopic and dynamic features of adsorption in the micropores. The time trace (shown for a given wavenumber at 523 K, Figure 3, top) was obtained for the whole of the mid-infrared (by the first set of Fourier transforms). The pressure jump was detected between 0 and 1 s. The relaxation process on the surface was clearly visible after the pressure pulse: some oscillations and envelopes were visible on the time trace, with intensities rapidly decreasing. The decrease of the baseline from 5 to 8 s was due to the modification of the volume of the cell to prepare for the next jump, at 9 s. The frequencies of the

 © 2004 Wiley-VCH Verlag GmbH & Co. KGaA, Weinheim

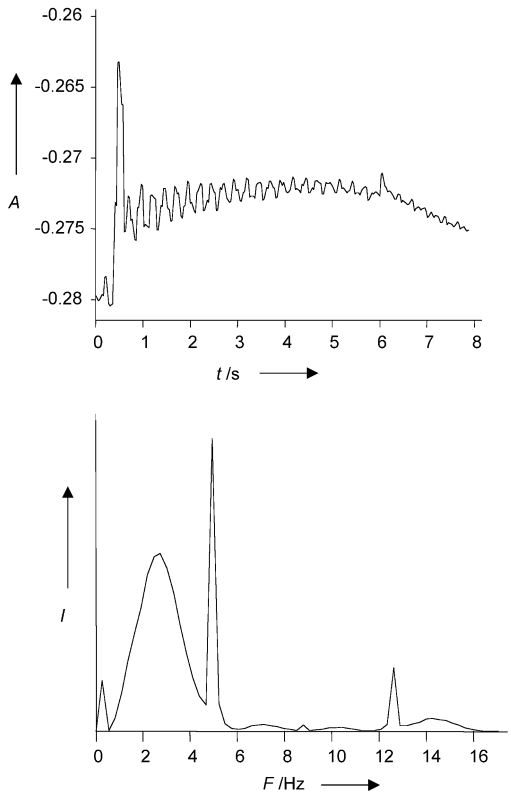


Figure 3. PJAS-IR experiment on H-Mor at 525 K under 78 Pa of acetonitrile (8 cm^{-1} and 28 ms resolution). The data were averaged on 100 pressure jumps. Top: time trace of the IR intensity *A* at 2295 cm^{-1}; Bottom: corresponding Fourier transform on the first 128 points (3.58 s) after the maximum pressure. *F* = Fourier frequency, and *I* = intensity of the Fourier transform.

oscillations were obtained by the second Fourier transforms in the time domain (Figure 3, bottom). Figure 4 shows the whole 2D map.

The Fourier transform in the time domain leads to four main peaks, indicating four oscillation frequencies as a result of the pressure pulse. The two very intense and narrow peaks at 5 and 12.5 Hz (Figure 3, bottom) were also observed in the absence of a sample. They were not damped quickly, and were not affected by surface dynamics on the sample. They were eigen vibration frequencies of the cell itself. The two broad bands at 2.5 and 14 Hz could be observed only in the presence of a solid sample in the cell. Their broadness indicates a rapid relaxation and damping, owing to diffusion and adsorption kinetics on the surface.

The experiment was performed at various temperatures: 300, 423, and 523 K. The four peaks in the pressure-response frequency scale were observed in all three experiments. They were at higher frequencies at higher temperatures, because of diffusion and adsorption activation at higher temperature. The two narrow and intense peaks at 5 and 12.5 Hz at 523 K affected all wavenumbers the same way, but the two surface responses at 2.5 and 14 Hz presented a more complex correlation with wavenumber values. The low-frequency response was particularly interesting since it presented a fine structure in the ν(OH) and in the ν(CN) vibration regions (Figure 5). In the ν(OH) vibration region, the three ν(OH)

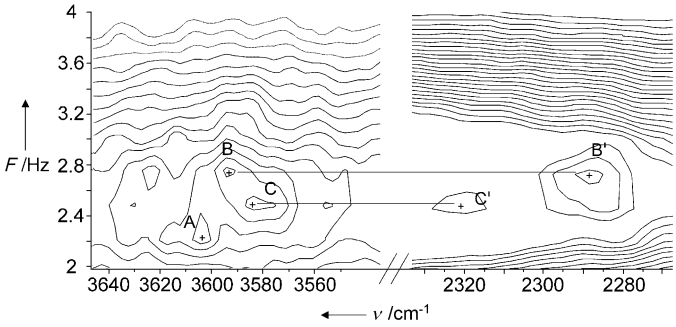


Figure 5. Enlargement of the ν(OH) and ν(CN) regions around 2.5 Hz from Figure 4. The same eigen frequencies for points C and C′ and for points B and B′ indicate correlations between hydrogen-bonded acetonitrile and OH_{8R} (B–B′) and between protonated acetonitrile and OH_{SP} (C–C′).

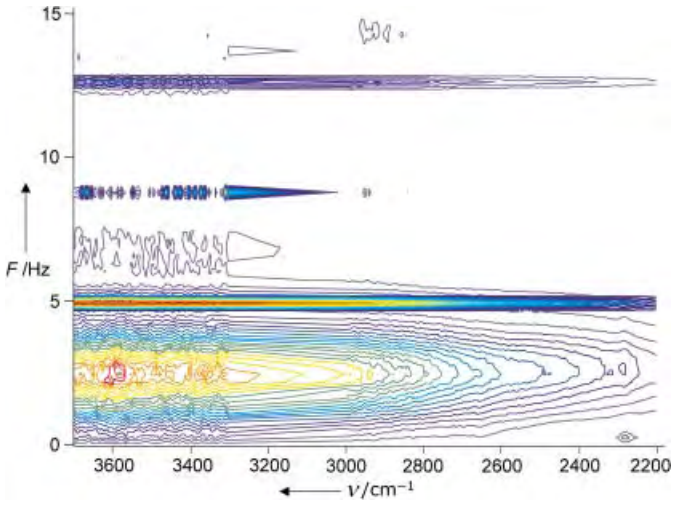


Figure 4. 2D-PJAS-IR spectrum of acetonitrile on H-Mor at 525 K (Fourier intensity contours: blue (minimum), red (maximum), versus pressure response frequency *F* and infrared wavenumbers).

vibration bands of the OH groups in the three possible locations (OH_{MC} 3605 cm^{-1}, OH_{8R} at 3595 cm^{-1} and OH_{SP} at 3585 cm^{-1}) were identified (at points A, B, and C in Figure 5: 2.25 Hz, 2.73, and 2.5 Hz, respectively). This is the first direct IR detection of the three OH groups in H-Mor.

In the ν(CN) vibration region, at 523 K, two ν(CN) vibration bands were expected: one around 2290 cm^{-1} for the hydrogen bond, and a second one above 2315 cm^{-1} for protonated acetonitrile. They could indeed be observed, at points C′ (2.73 Hz) and B′ (2.5 Hz), respectively. This was a clear indication that protonation of acetonitrile was linked to the OH group in the side pockets, OH_{SP}, and was favored by confinement in this constrained environment.[4] Interestingly, the perturbation of the hydrogen bond by the pressure jump was only detected at the opening of the side pockets (OH_{8R}), and the OH groups in the main channels (ν3605 cm^{-1}) were not involved in the change in the hydrogen bond. This situation is probably due to the number of perturbed sites remaining mostly constant in the main channels during the

 © 2004 Wiley-VCH Verlag GmbH & Co. KGaA, Weinheim

pressure jump. It had been shown by molecular dynamics simulations[3] that a pressure increase in the main channels allowed a higher proportion of acetonitrile to enter the side pockets: the main channels act as a pipe leading acetonitrile to the side pockets, in which the loading variation becomes important.

When the experiment is performed at room temperature, no difference can be detected between the three OH groups, which give a broad signal in the ν(OH) vibration region. At intermediate temperature, 423 K, the pressure jump leads to the formation of the acetonitrile dimer and the particularly strong hydrogen bond reported in ref.[4] This bond formation also leads to a correlation with the OH_{SP} on the 2D map, which confirms the formation of this specific hydrogen bond in the side pockets only.

In conclusion we have presented a new spectroscopic 2D IR technique for the study of adsorption in micro and mesoporous systems. It is based on µs time-resolved spectroscopy and sudden pressure changes in the infrared cell containing the solid sample and the gas probe molecule. The pressure jump leads to a relaxation process by diffusion and adsorption, which is monitored by IR spectroscopy. The 2D spectrum is obtained by two Fourier transforms in the IR wavelength domain and in the time domain. The potential of the technique was shown by studying probe molecule (acetonitrile) adsorption on mordenite, and confirmed previous studies performed in classical adsorption cells. 2D-PJAS-IR allowed the first direct detection of three distinct OH vibration bands in the IR spectrum of mordenite, and revealed three different interactions with acetonitrile, which depend on the adsorption site. Protonation of acetonitrile at high temperature was shown to take place only in the side pockets.

Experimental Section

A Bruker IFS66s spectrometer was used in the step scan or rapid scan mode. The IR cell allowed in situ heating of the sample in the IR beam, it was connected to a vacuum/gas line. In a typical experiment, the catalyst was activated by in situ heating to 400 °C under vacuum (10^{-4} Pa), and the probe molecule (perdeuterated acetonitrile 99.9 % pure; Aldrich) was introduced in the cell ($\approx$100 Pa) at room temperature. A 30 % pressure jump was applied every 9 s in the cell, and the IR spectrum was recorded at 0.2–30 ms time resolution and 64–8 cm^{-1} spectral resolution, at temperature between 300 and 525 K.

Received: September 1, 2003 [Z52754]

Keywords: acetonitrile · adsorption · IR spectroscopy · pressure-jump spectroscopy · zeolites

[1] G. Onyestyák, J. Valyon, L. V. C. Rees, *Phys. Chem. Chem. Phys.* **2000**, *2*, 3077.
[2] V. Bourdin, Ph. Grenier, F. Meunier, L. M. Sun, *AIChE J.* **1996**, *42*, 700.
[3] K. S. Smirnov, F. Thibault-Starzyk, *J. Phys. Chem. B* **1999**, *103*, 8595.
[4] O. Marie, F. Thibault-Starzyk, J. C. Lavalley, *Phys. Chem. Chem. Phys.* **2000**, *2*, 5341.
[5] T. Terlouw, J. P. Gilson (Shell Int. Res. Mij. B.V.), EP 458378, **1991**.
[6] O. Marie, F. Thibault-Starzyk, P. Massiani, J. C. Lavalley, *Stud. Surf. Sci. Catal.* **2001**, *135*, 220 (ref on the CD: 12-P-14).
[7] M. Maache, A. Janin, J. C. Lavalley, E. Benazzi, *Zeolites* **1995**, *15*, 507.
[8] A. Alberti, *Zeolites* **1997**, *19*, 411.
[9] O. Marie, F. Thibault-Starzyk, P. Massiani, *J. Phys. Chem. B*, in press.
[10] J. Czyzniewska, S. Chenevarin, F. Thibault-Starzyk, *Stud. Surf. Sci. Catal.* **2002**, *142*, 342.
[11] F. Thibault-Starzyk, A. Travert, J. Saussey, J.-C. Lavalley, *Top. Catal.* **1998**, *6*, 111.

 © 2004 Wiley-VCH Verlag GmbH & Co. KGaA, Weinheim

Antimicrobial Agents

Nontoxic Membrane-Active Antimicrobial Arylamide Oligomers**

*Dahui Liu, Sungwook Choi, Bin Chen, Robert J. Doerksen, Dylan J. Clements, Jeffrey D. Winkler, Michael L. Klein, and William F. DeGrado**

Non-natural polymers can adopt specific secondary and tertiary structures that resemble those of naturally occurring biopolymers.[1–4] As a result of their stability towards enzymatic degradation and their virtually unlimited diversity, non-natural polymers and oligomers are excellent candidates for therapeutic biomimetics. We previously designed a series of easily synthesized aryl amide oligomers[5] that mimic the properties of membrane-interactive antimicrobial peptides such as the magainins and cecropins. Although these oligomers are highly active, they have significant toxicities toward human cells, as assessed from the hemolytic activities of the compounds. Herein, we describe the fine-tuning of the

[*] Dr. D. Liu, D. J. Clements, Prof. Dr. W. F. DeGrado
Department of Biochemistry and Biophysics
University of Pennsylvania
Philadelphia, PA 19104-6059 (USA)
Fax: (+1) 215-573-7229
E-mail: wdegrado@mail.med.upenn.edu

S. Choi, Prof. Dr. B. Chen,[+] Dr. R. J. Doerksen, Prof. Dr. J. D. Winkler, Prof. Dr. M. L. Klein, Prof. Dr. W. F. DeGrado
Department of Chemistry
University of Pennsylvania
Philadelphia, PA 19104-6323 (USA)

[+] Current address:
Department of Chemistry
Louisiana State University
232 Choppin Hall, Baton Rouge, LA 70803-1804

[**] We thank the NIH BECON program and PolyMedix. Inc. for financial support.

Supporting information for this article is available on the WWW under http://www.angewandte.org or from the author.

 © 2004 Wiley-VCH Verlag GmbH & Co. KGaA, Weinheim DOI: 10.1002/anie.200352791

physicochemical properties of these oligomers to enhance their potency while eliminating their toxicity.

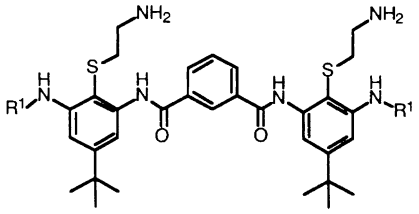
Antimicrobial peptides act on the membranes of their targets,[6–9] and bacteria appear to develop resistance to these surface-active peptides less easily than to antibiotics that act on more-specific enzymatic targets. The peptides appear to differentiate bacterial from mammalian membranes by virtue of the fact that bacterial membranes present a greater density of negatively charged phospholipids and lack cholesterol. Although these peptides differ in sequence and in their detailed secondary structure, they all adopt amphiphilic conformations with spatially segregated hydrophobic and positively charged surfaces. Upon binding to a membrane, these peptides cause the formation of pores and disruption of the integrity of the bilayer.[9–11]

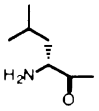
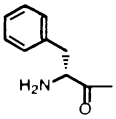
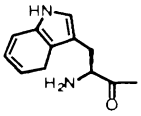
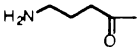
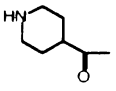
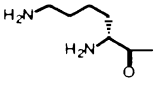
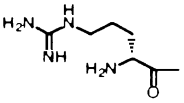
Several research groups have recently reported antimicrobial oligomers that act by this mechanism, such as β-peptides,[12–14] cyclic D,L-peptides,[15] diastereomeric peptides,[9] peptoids,[16] and cyclic peptides related to gramicidin S.[17] However, these peptides are rather closely related to traditionally studied peptides and have relatively high molecular weights (for example, the antimicrobial β-peptides are 1379–1719 Da), and hence can be expected to suffer from many of the limitations inherent to this class of compounds. We therefore recently designed a new class of facially amphiphilic aryl amide oligomers[5] related to compound **1** (see Table 1). However, although these oligomers have potencies comparable to those of host defense peptides, they are toxic towards human red blood cells at comparable concentrations.

The selectivity of natural antimicrobial peptides for lysing bacterial rather than mammalian cells depends on the appropriate balance of conformational rigidity, hydrophobicity, and the distribution of charged side chains in the peptide.[14,17,18] If the compounds are too polar they have little affinity for bacterial membranes; if they are too hydrophobic they fail to discriminate between mammalian and bacterial targets.

The short triaryl amide **1** served as the starting point for optimization of the selectivity of the aryl amide series of antimicrobial oligomers, whose amphiphilic structure is stabilized by weak hydrogen bonds between the sulfur

Table 1: Antibacterial activity and selectivity.



Compound	R^1	MIC [μg mL^{-1}]		HC50 [μg mL^{-1}]	Selectivity (HC50/MIC)		Relative hydrophobicity (log K_{OW})[a]
		E. coli	*S. aureus*		*E. coli*	*S. aureus*	
1	H	12.5	50	12	0.96	0.24	3.51
2		6.25	12	40	6.4	3.3	3.12
3		6.25	6.25	9	1.4	1.4	3.74
4		6.25	6.25	7	1.1	1.1	3.86
5		25	50	790	32	16	1.45
6		25	100	1230[b]	49	12	2.99
7		50		370	7.4		0.33
8		6.25	12.5	715	110	57	−1.71
MSI-78		12.5		120	9.6		

[a] K_{OW} = *n*-octanol/water partition coefficient. [b] The HC50 value (concentration required for 50% cell lysis) was obtained by extrapolating the fitted curve to 50% lysis.

 © 2004 Wiley-VCH Verlag GmbH & Co. KGaA, Weinheim

atoms and neighboring amide groups.[5,19] Amino acids appeared to be good candidates for appendage to this template; their amino groups introduce an additional positively charged center, while their side chains provide a ready source of diversity. Examination of a small collection of amino acids revealed two means of increasing the activity of the peptide: Compounds **2**–**4**, which have increasingly hydrophobic substituents, show good activity against both Gram-negative and Gram-positive bacteria (minimal inhibitory concentration (MIC) 6–12 $\mu g\,mL^{-1}$ against both *Escherichia coli* and *Staphylococcus aureus*; Table 1). However, these compounds are also toxic towards human red blood cells, and the toxicity increases as a function of the hydrophobicity of the side chain. By contrast, the introduction of more polar substituents to give **5**–**8** led to oligomers with significantly lower toxicity towards erythrocytes. Compound **8**, which contains the dibasic Arg substituent, was the most active of this series. This compound displays antibacterial activity similar to that of the potent magainin analogue MSI-78,[8] and has significantly greater selectivity. Encouraged by these results, we introduced an additional polar, positively charged aminoalkyl substituent onto the central isophthaloyl group. This substitution enhanced the selectivity of the compounds without greatly altering their potency, irrespective of the amino acid component present (Table 2). The Arg-containing analogue **12** did not lyse red blood cells at concentrations as high as 800 μM.

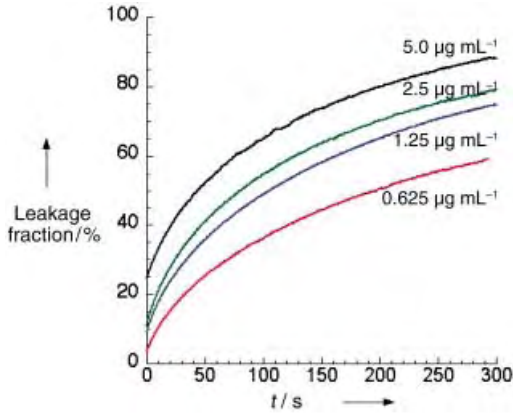
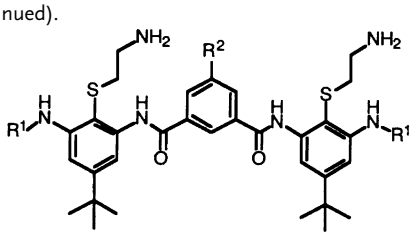
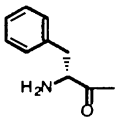
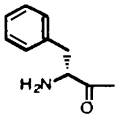
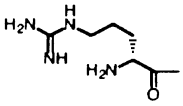
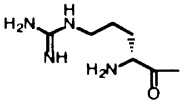
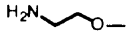


Figure 1. Amphiphilic oligomer **8** induces vesicle leakage at the oligomer concentrations indicated.

To confirm the mechanism of action of this series of compounds, we examined the ability of **8** to induce leakage of the fluorescent dye calcein from large unilamellar vesicles composed of 90% stearolyloleoyl-phosphatidylcholine and 10% stearolyloleoyl-phosphatidylserine.[14] Lysis occurred in a concentration-dependent manner and began at oligomer

Table 2: Antibacterial activity and selectivity (continued).



Compound	R^1	R^2	MIC [$\mu g\,mL^{-1}$]		HC50 [$\mu g\,mL^{-1}$]	Selectivity (HC50/MIC)		Relative hydrophobicity (log K_{OW})
			E. coli	*S. aureus*		*E. coli*	*S. aureus*	
1	H	H	12.5	50	12	0.96	0.24	3.51
9	H		25	25	110[a]	4.4	4.4	2.61
10			50	200	400	8.0	2.0	1.53
3		H	6.25	6.25	9	1.4	1.4	3.74
11			12.5	12.5	61	4.9	4.9	2.84
8		H	6.25	12.5	715	110	57	−1.71
12			12.5	12.5	>800	>64	>64	−2.61
MSI-78			12.5		120	9.6		

[a] The HC50 value was obtained by extrapolating the fitted curve to 50% lysis.

 © 2004 Wiley-VCH Verlag GmbH & Co. KGaA, Weinheim

concentrations as low as 0.625 μg mL^{-1}. At oligomer concentrations near the MIC value for inhibition of bacterial growth, the vesicle leakage is close to 90% after 300 s (Figure 1).

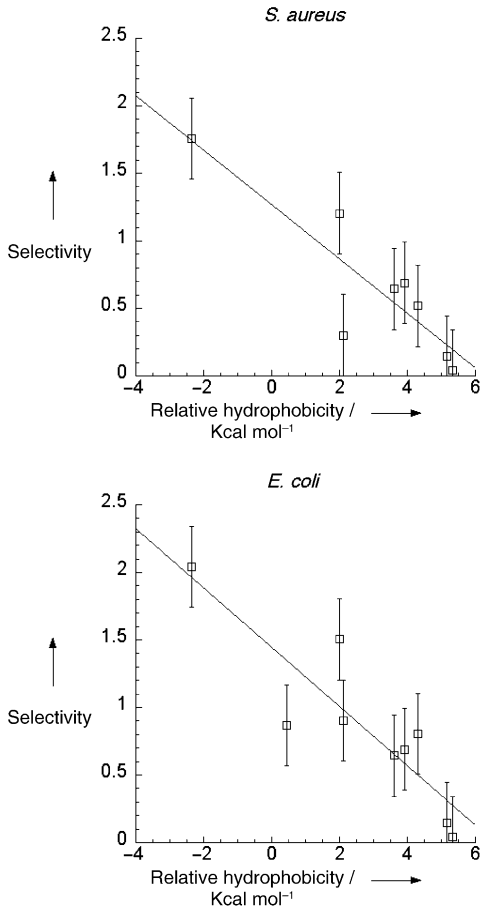


Figure 2. Relative hydrophobicity (measured as $\log K_{OW}$) and selectivity (HC50/MIC) of the aryl amides.

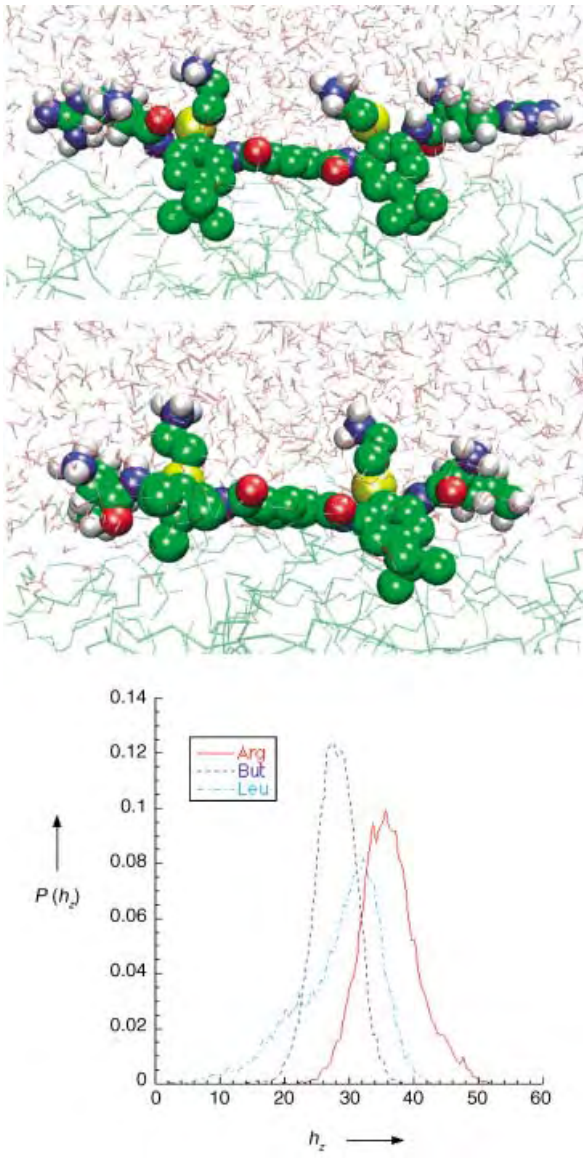


Figure 3. Snapshots showing aryl amide with D-Arg (**8**, top) and D-Leu (**2**, middle) end groups at the *n*-octane/water interface; hydrophobic moment distributions for **2**, **5**, and **8** (bottom).

The finding that the amino acid side chain influences the selectivity of the compounds prompted us to examine the relationship between their selectivity ratios (the ratio of the MIC value for a given bacteria to the HC50 value (concentration required for 50% cell lysis) of the compound) and their hydrophobicities. The *n*-octanol/water partition coefficient K_{OW} is a common measure of the hydrophobicity of a molecule and has been successfully used in quantitative structure–activity relationship studies to correlate and predict a plethora of solute properties, including toxicity.[20,21] We chose to use the atom/fragment approach[22] to estimate the value of K_{OW} since the members of this group of oligo(aryl amide)s are structurally similar and all share a rigid and open backbone. Figure 2 shows that the logarithm of the selectivity ratio varies linearly with $\log K_{OW}$. This simple measure thus provides a rapid method to screen for safe compounds. However, although this parameter correlates well with selectivity, it does not explain the antimicrobial potency: the least hydrophobic Arg-containing compound has an antimicrobial activity comparable to that of the most hydrophobic compound.

Calculations of the hydrophobic moment, however, provide an explanation. The atom/fragment approach[22] allows a straightforward definition of the hydrophobic moment.[23] The hydrophobic moment distributions of a few selected aryl amides at an *n*-octane/water interface at 300 K obtained from extensive molecular dynamics simulations of these aryl amides (5–10 ns in each case) are plotted in Figure 3. From the conformational ensembles it is clear that the Arg-containing compound has the largest hydrophobic moment and therefore has the most amphiphilic conformations. Visual inspection of the configurations reveals that the benzene rings on the two sides to which the Arg groups are attached appear to be roughly perpendicular to the interface, with the *tert*-butyl groups sliding into the *n*-octane phase and

 © 2004 Wiley-VCH Verlag GmbH & Co. KGaA, Weinheim

the polar side chains exposed in the water phase, a conformation that maximizes both polar and nonpolar interactions. We expect that such a conformation would also enable the molecule to bind favorably to the lipid bilayer/water interface. Thus, hydrophobic moment calculations provide an additional useful measure for predicting potency.

In summary, we have designed a series of oligo(aryl amide)s that have amphiphilic secondary structure. By varying the appending group so as to adjust the overall charge, hydrophobicity, and hydrophobic moment, we obtained molecules with both good activity and selectivity. The oligomers are significantly smaller than comparable antimicrobial oligomers, which might provide significant advantages in terms of tissue distribution, as well as cost of production.

Experimental Section

The synthesis of representative oligomers is described in the Supporting Information. Antibacterial assays, hemolysis assays, and vesicle leakage experiments were carried out as previously described.[5] In the atom/fragment approach,[22] the K_{OW} value is estimated by using the equation: $\log K_{OW} = \Sigma(f_i n_i) + 0.229$, where f_i is the coefficient for fragment I, and n_i is the number of times that fragment i occurs. The molecular dynamics calculations were conducted as previously described.[5] After equilibration, which consisted of short NPT (constant pressure and temperature) and NVT (constant volume and temperature) runs (ca. 100 ps each) and a longer NVE (constant energy) run (ca. 500 ps), snapshots were taken every 0.5 ps, and the hydrophobic moments of the resulting configurations were calculated by using the atom-based method of Eisenberg.[23] The hydrophobic moment is defined as $\boldsymbol{\mu}_H = \Sigma(f_i n_i \mathbf{r}_i)$, where $\mathbf{r}$ is a vector from an origin, which must be specified, to the center of fragment i. We considered only the component of $\boldsymbol{\mu}_H$ normal to the interface, and chose the origin to be in the plane (parallel to the interface) in which the *n*-octane carbon density and water oxygen density profiles cross.

Received: September 4, 2003 [Z52791]
Published Online: January 27, 2004

Keywords: amphiphiles · antimicrobial agents · aryl amides · oligomers · peptides

[1] A. E. Barron, R. N. Zuckermann, *Curr. Opin. Chem. Biol.* **1999**, *3*, 681.
[2] R. P. Cheng, S. H. Gellman, W. F. DeGrado, *Chem. Rev.* **2001**, *101*, 3219.
[3] S. H. Gellman, *Acc. Chem. Res.* **1998**, *31*, 173.
[4] D. J. Hill, M. J. Mio, R. B. Prince, T. S. Hughes, J. S. Moore, *Chem. Rev.* **2001**, *101*, 3893.
[5] G. N. Tew, D. Liu, B. Chen, R. J. Doerksen, J. Kaplan, P. J. Carroll, M. L. Klein, W. F. DeGrado, *Proc. Natl. Acad. Sci. USA* **2002**, *99*, 5110.
[6] M. Zasloff, *Nature* **2002**, *415*, 389.
[7] M. Zasloff, *Curr. Opin. Immunol.* **1992**, *4*, 3.
[8] W. L. Maloy, U. P. Kari, *Biopolymers* **1995**, *37*, 105.
[9] Y. Shai, *Biopolymers* **2002**, *66*, 236.
[10] L. Yang, T. M. Weiss, R. I. Lehrer, H. W. Huang, *Biophys. J.* **2000**, *79*, 2002.
[11] K. B. B. A. Matsuzaki, *Biochim. Biophys. Acta* **1999**, *1462*, 1.
[12] Y. Hamuro, J. P. Schneider, W. F. DeGrado, *J. Am. Chem. Soc.* **1999**, *121*, 12200.
[13] E. A. Porter, X. Wang, H.-S. Lee, B. Weisblum, S. H. Gellman, *Nature* **2000**, *404*, 565.
[14] D. Liu, W. F. DeGrado, *J. Am. Chem. Soc.* **2001**, *123*, 7553.
[15] S. Fernandez-Lopez, H. S. Kim, E. C. Choi, M. Delgado, J. R. Granja, A. Khasanov, K. Kraehenbuehl, G. Long, D. A. Weinberger, K. M. Wilcoxen, M. R. Ghadiri, *Nature* **2001**, *412*, 452.
[16] J. A. Patch, A. E. Barron, *J. Am. Chem. Soc.* **2003**, *125*, 12092.
[17] D. L. Lee, R. S. Hodges, *Biopolymers* **2003**, *71*, 28.
[18] Z. Oren, Y. Shai, *Biopolymers* **1998**, *47*, 451.
[19] R. J. Doerksen, B. Chen, M. L. Klein, *Chem. Phys. Lett.* **2003**, *380*, 150.
[20] J. Sangster, *Octanol–Water Partitioning Coefficients: Fundamentals and Physical Chemistry*, Wiley, Chichester, **1997**.
[21] C. Hansch, A. Leo, *Exploring QSAR: Fundamentals and Applications in Chemistry and Biology*, American Chemical Society, Washington, **1995**.
[22] W. M. Meylan, P. H. Howard, *Perspect. Drug Discovery Des.* **2000**, *19*, 67.
[23] D. Eisenberg, R. M. Weiss, T. C. Terwilliger, W. Wilcox, *Faraday Symp. Chem. Soc.* **1982**, *17*, 109.

 © 2004 Wiley-VCH Verlag GmbH & Co. KGaA, Weinheim

Cover Picture

Michael J. Rauterkus and Bernt Krebs*



Metallocalixarenes such as the pentanuclear platinum(II) macrocycle shown in the cover picture, are prepared from a cisplatin analogue with tertiary amine ligands and the nucleobase uracil or thymine. The platinum(II) complex used in the synthesis of the macrocycle has a significant cytostatic activity as a result of its ability to bind to DNA. The background shows a crystal of calf thymus DNA. More details can be found in the Communication by M. J. Rauterkus and B. Krebs on page 1300 ff.

Contents

Angewandte EarlyView

The following articles are available online (in Wiley InterScience). You can find them at www.angewandte.org, under Full Text, Early View.

L. Quebatte, R. Scopelliti, K. Severin:*
Combinatorial Catalysis with Bimetallic Complexes: Robust and Efficient Catalysts for Atom-Transfer Radical Additions
DOI: 10.1002/anie.200353084
Published online: February 16, 2004

B. H. Lipshutz, H. Shimizu:*
Copper(I)-Catalyzed Asymmetric Hydrosilylations of Imines at Ambient Temperatures
DOI: 10.1002/anie.200353294
Published online: February 16, 2004

C. Nieto-Oberhuber, M. P. Muñoz, E. Buñuel, C. Nevado, D. J. Cárdenas, A. M. Echavarren:*
Cationic Gold(I) Complexes: Highly Alkynophilic Catalysts for the *Exo*- and *Endo*-Cyclization of Enynes
DOI: 10.1002/anie.200353207
Published online: February 16, 2004

R. K. Haynes, W.-Y. Ho, H.-W. Chan, B. Fugmann, J. Stetter, S. L. Croft, L. Vivas, W. Peters, B. L. Robinson:*
Highly Antimalaria-Active Artemisinin Derivatives: Biological Activity Does Not Correlate with Chemical Reactivity
DOI: 10.1002/anie.200352343
Published online: February 16, 2004

T. Müller, M. Juhasz, C. A. Reed*:*
The X-ray Structure of a Vinyl Cation
DOI: 10.1002/anie.200352986
Published online: February 16, 2004

Articles judged by the referees or the editor as being either very important or very urgent are immediately edited, proof-read, and electronically published once the manuscript has arrived in the editorial office in final form. As long as there is no page number available these articles should be cited in the following manner:

Author(s) *Angew. Chem. Int. Ed.*, online publication date, DOI.

News

H. tom Dieck Made Honorary Member of the GDCh — **1182**

H. Schnöckel Receives Alfred Stock Memorial Prize — **1182**

Carl Duisberg Memorial Award to A. Terfort — **1182**

Books

Esterification — **1183** — Junzo Otera — *reviewed by P. J. Kocienski*

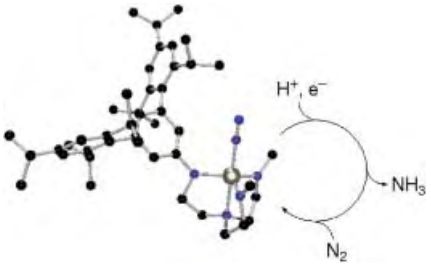
Hydrocarbon Chemistry — **1184** — George A. Olah, Árpád Molnár — *reviewed by P. R. Schreiner*

Highlights

Nitrogen Fixation

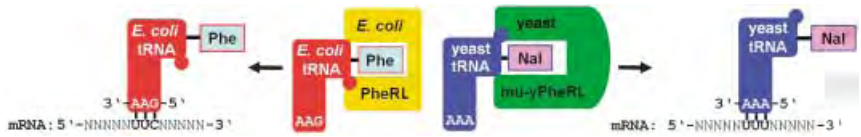
C. M. Kozak,*
P. Mountford* — **1186 – 1189**

Revelations in Dinitrogen Activation and Functionalization by Metal Complexes



A monumental achievement for coordination chemistry that also re-addresses the role of molybdenum in the nitrogenase FeMo cofactor is the discovery of the catalytic reduction of dinitrogen at a well-defined molybdenum complex by protons and electrons (see picture).

© 2004 Wiley-VCH Verlag GmbH & Co. KGaA, Weinheim



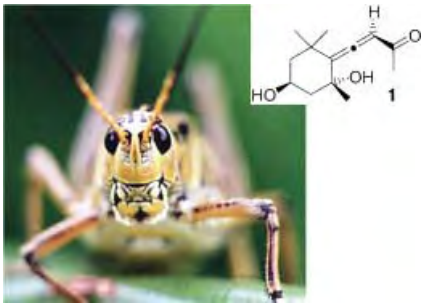
The degeneracy of the genetic code—the fact that 61 codons in mRNA direct only 20 different amino acid monomers in ribosomal polypeptide synthesis—provides the necessary ambiguity for reassigning codons for the sequence-specific incorporation of artificial amino acids. Genetic engineering of specific tRNA and aminoacyl-tRNA ligase is a tool for the insertion of nonstandard amino acids in ribosomal polypeptide elongation.

Alloproteins

U. Hahn, G. J. Palm, W. Hinrichs* ——— **1190 – 1193**

Old Codons, New Amino Acids

Reviews



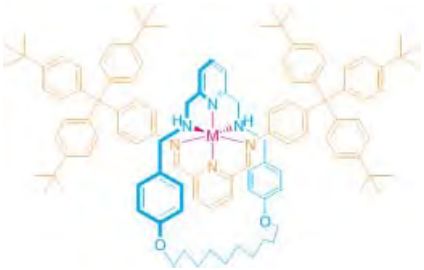
Fascinating structures are displayed by many allenic natural products. Among these stimulating synthetic targets is the grasshopper ketone **1**, which was isolated from the defense secretion of the large flightless grasshopper *Romalea microptera* (see picture). Allenes are being applied more and more frequently as enzyme inhibitors, cytotoxic, or antiviral agents.

Allenes

A. Hoffmann-Röder,* N. Krause* ——— **1196 – 1216**

Synthesis and Properties of Allenic Natural Products and Pharmaceuticals

Communications



Full Metal Jacket: Simple stirring of a five component mixture at room temperature is sufficient to assemble a wide range of octahedrally coordinated [2]metallorotaxanes under thermodynamic control (see picture).

Rotaxanes VIP

L. Hogg, D. A. Leigh,* P. J. Lusby, A. Morelli, S. Parsons, J. K. Y. Wong ——— **1218 – 1221**

A Simple General Ligand System for Assembling Octahedral Metal–Rotaxane Complexes

For the USA and Canada:
ANGEWANDTE CHEMIE International Edition (ISSN 1433-7851) is published weekly by Wiley-VCH PO Box 191161, D 69451 Weinheim, Germany. Air freight and mailing in the USA by Publications Expediting Inc. 200 Meacham Ave., Elmont, NY 11003. Periodicals postage paid at Jamaica NY 11431. US POSTMASTER: send address changes to *Angewandte Chemie*, Wiley-VCH, 111 River Street, Hoboken, NJ 07030. Annual subscription price for institutions: Europe € 3430.00/3118.00; outside Europe US$ 4499.00/4090.00 (valid for print and electronic/print or electronic delivery); for individuals who are personal members of a national chemical society, or whose institution already subscribes, or who are retired or self-employed consultants, print only: Europe € 248.00/outside Europe US$ 378.00. Postage and handling charges included. All Wiley-VCH prices are exclusive VAT.

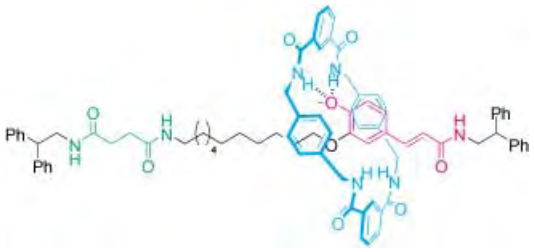
 © 2004 Wiley-VCH Verlag GmbH & Co. KGaA, Weinheim

Contents

Molecular Shuttles

C. M. Keaveney,
D. A. Leigh* ——— 1222 – 1224

Shuttling through Anion Recognition

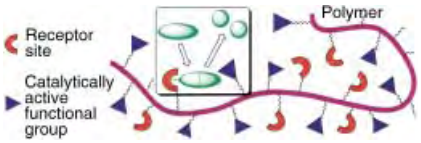


A negative response: Anion formation induces translocation of the macrocycle in a molecular shuttle (see picture). Shuttling only occurs in polar solvents and is unaffected by the nature of the counter-cation or the presence of other anions.

Artificial Enzymes

W. B. Motherwell,* C. E. Atkinson,
A. E. Aliev, S. Y. F. Wong,
B. H. Warrington ——— 1225 – 1228

A Simple Protocol for the Modular Assembly of "Millipede" Artificial Enzymes

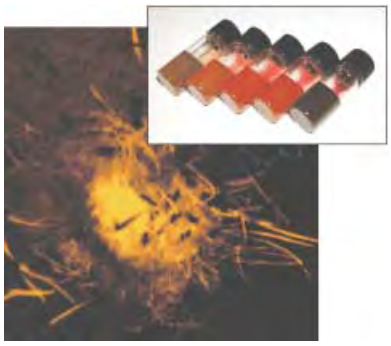


A step-by-step strategy for the assembly of "millipede" artificial enzymes involves attachment of two separate molecular strands to a flexible polymeric backbone. One strand contains a substrate receptor site designed around a transition state mimic, whilst the other carries a catalytically active group (see picture).

Photochemical Processes

K. Sugiyasu, N. Fujita,
S. Shinkai* ——— 1229 – 1233

Visible-Light-Harvesting Organogel Composed of Cholesterol-Based Perylene Derivatives



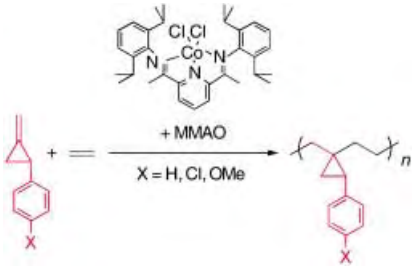
A rich harvest: A visible-light-harvesting system has been created utilizing an organogel medium (see picture; the inset shows different gel mixtures). Mixing four different perylene derivatives in the gel phase sets up an energy gradient in the gel fibrils. The well-defined nanofibers harvest a wide range of light energy in the visible region (i.e., sunlight) to the energy sink in a stepwise manner.

Alternating Copolymerization

D. Takeuchi, K. Anada,
K. Osakada* ——— 1233 – 1235

Cobalt-Complex-Catalyzed Copolymerization of Ethylene with 2-Aryl-1-methylenecyclopropanes

The importance of tolerance: A Cobalt complex with bis(imino)pyridine ligand promotes the alternating copolymerization of ethylene with 2-aryl-1-methylenecyclopropanes to give polymers with regulated C_4 repeating units that have a three-membered ring (see scheme). The polymerization is tolerant of functional groups on the three-membered ring such as methoxy and chloro groups.



 © 2004 Wiley-VCH Verlag GmbH & Co. KGaA, Weinheim

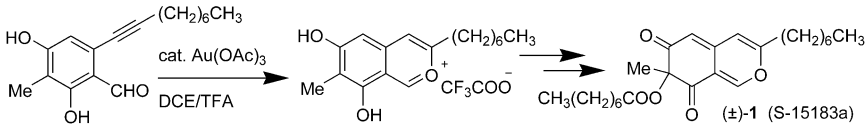


A radical step: The addition of radicals to amino acrylates and subsequent H-atom transfer in the presence of chiral Lewis acid activators provides β²-amino acids in high yields and enantiomeric purity (see scheme; Ln* = chiral ligands, Fmoc = 9-fluorenylmethoxycarbonyl).

Amino Acid Synthesis

M. P. Sibi,* K. Patil ——— 1235 – 1238

Enantioselective H-Atom Transfer Reactions: A New Methodology for the Synthesis of β²-Amino Acids

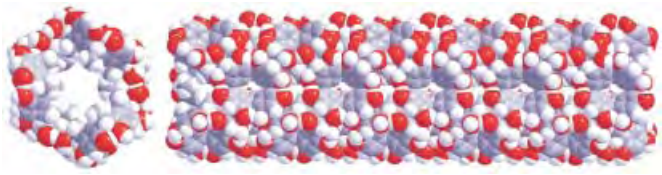


Right to the core: Gold(III)-catalyzed cycloisomerization of *o*-alkynylbenzaldehydes to 2-benzopyrylium salts and subsequent in situ oxidation have been employed to prepare the core structure of azaphilone natural products, such as the sphingosine kinase inhibitor S-15183 (see scheme, DCE = 1,2-dichloroethane, TFA = trifluoroacetic acid)), and several unnatural azaphilones.

Natural Product Synthesis

J. Zhu, A. R. Germain, J. A. Porco, Jr.* ——— 1239 – 1243

Synthesis of Azaphilones and Related Molecules by Employing Cycloisomerization of *o*-Alkynylbenzaldehydes



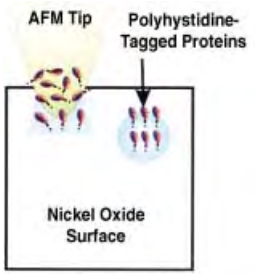
By manipulating the crystallization conditions of *C*-methyl recorcinarene, a motif of self-assembled helical nanotubes held together by extensive π···π interactions is obtained. The tube, depicted (red = O, white = H, gray = C), has an exo-functionalized hydrophilic outer surface capable of complex formation with cationic or neutral guests and a hydrophobic interior potentially suitable for the transportation of small hydrophobic molecules.

Nanostructures

H. Mansikkamäki, M. Nissinen, K. Rissanen* ——— 1243 – 1246

Noncovalent π···π-Stacked Exo-Functional Nanotubes: Subtle Control of Resorcinarene Self-Assembly

Ink flowing from a pen: Direct-write dip-pen nanolithography of His-tagged proteins (ubiquitin and thioredoxin) has been used to generate biologically active protein nanoarrays with feature sizes as small as 80 nm on nickel oxide surfaces without the need for an applied electric field. The protein molecules in this system seem to diffuse from the Ni-coated atomic force microscopy (AFM) tips to the Ni-coated substrate (see diagram).



Bioactive Protein Nanoarrays

J.-M. Nam, S. W. Han, K.-B. Lee, X. Liu, M. A. Ratner, C. A. Mirkin* ——— 1246 – 1249

Bioactive Protein Nanoarrays on Nickel Oxide Surfaces Formed by Dip-Pen Nanolithography

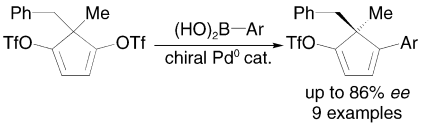
 © 2004 Wiley-VCH Verlag GmbH & Co. KGaA, Weinheim

Contents

Asymmetric Catalysis

M. C. Willis,* L. H. W. Powell, C. K. Claverie, S. J. Watson — **1249 – 1251**

Enantioselective Suzuki Reactions: Catalytic Asymmetric Synthesis of Compounds Containing Quaternary Carbon Centers

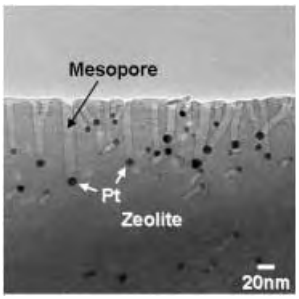


Prochiral ditriflates can act as substrates in asymmetric Suzuki couplings by using an enantioselective desymmetrization strategy. The products are obtained with selectivities up to 86% *ee* and contain a quaternary carbon center and a synthetically useful vinyl triflate functionality (see scheme).

Making Materials Mesoporous

H. Kato,* T. Minami, T. Kanazawa, Y. Sasaki — **1251 – 1254**

Mesopores Created by Platinum Nanoparticles in Zeolite Crystals

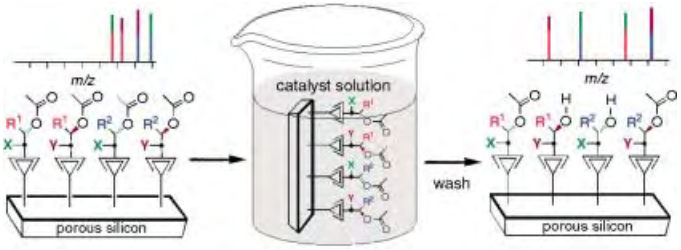


Platinum drops in and eats out: Platinum nanoparticles penetrate from the surface of the zeolite into its bulk, creating hexagonal mesopores of about the same width as the platinum particles (see micrograph). It is as if the platinum particles tunnel into the crystal. The mesopores are formed along particular directions in the zeolite crystal, and their walls consisted of specific zeolite crystal faces.

Mass Spectrometry

J.-C. Meng, C. Averbuj, W. G. Lewis, G. Siuzdak, M. G. Finn* — **1255 – 1260**

Cleavable Linkers for Porous Silicon-Based Mass Spectrometry



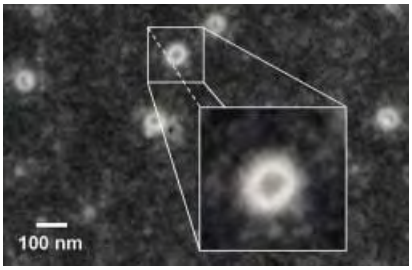
Dip, wash, and analyze: Molecules can be attached to tailored porous silicon wafers by using Diels–Alder reactions and efficiently detached and detected in the laser pulse of a MALDI mass spectrometer in a positionally encoded manner (see scheme).

Polymer Self-Assembly

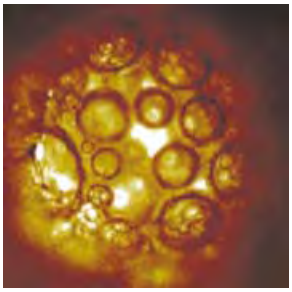
K. N. Power-Billard, R. J. Spontak,* I. Manners* — **1260 – 1264**

Redox-Active Organometallic Vesicles: Aqueous Self-Assembly of a Diblock Copolymer with a Hydrophilic Polyferrocenylsilane Polyelectrolyte Block

A water-soluble poly(dimethylsiloxane-*b*-ferrocenylsilane) diblock copolymer containing a hydrophilic cationic polyferrocene block, which is formed in a self-assembly process, yields redox-active vesicles with a diameter of approximately 85 nm (see figure) in which the organometallic block is located on both the outside and the inside of the formed aggregates.



© 2004 Wiley-VCH Verlag GmbH & Co. KGaA, Weinheim

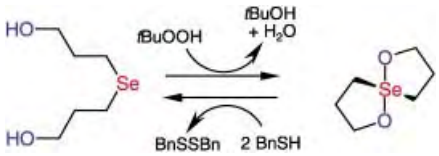


Not a creature from the ocean depths, but the product of synthetic chemistry aided by self-assembly is shown in the photomicrograph. The densely packed, hollow spheres with highly blistered surfaces offer the possibility of a useful encapsulation system which is simple, cheap, and endowed with a particularly high capture volume.

Soft Materials

F. M. Menger,* J. Bian, V. A. Seredyuk ——— 1265 – 1267

Vesicular Latex

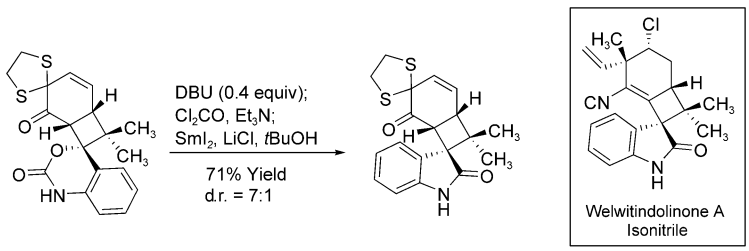


A new mechanism for reducing oxidative stress: Di(3-hydroxypropyl) selenide has exceptionally high glutathione peroxidase-like catalytic activity in the reduction of *tert*-butyl hydroperoxide with benzyl thiol. The catalytic cycle proceeds via a novel spirodioxaselenanonane, which was isolated and characterized spectroscopically, as well as by X-ray crystallography.

Enzyme Mimetics

T. G. Back,* Z. Moussa, M. Parvez ——— 1268 – 1270

The Exceptional Glutathione Peroxidase-Like Activity of Di(3-hydroxypropyl) Selenide and the Unexpected Role of a Novel Spirodioxaselenanonane Intermediate in the Catalytic Cycle

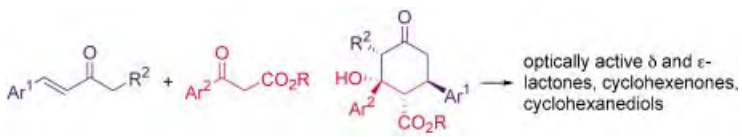


The complete carbon skeleton of welwitindolinone A isonitrile has been prepared by using a [2+2] cycloaddition to establish the bicyclo[4.2.0]octane core and a SmI_2-mediated intramolecular reductive cyclization between an enone and an aryl isocyanate to stereoselectively install the spiro-oxindole (see scheme; DBU = 1,8-diazabicyclo[5.4.0]undec-7-ene).

Natural Product Synthesis

J. M. Ready, S. E. Reisman, M. Hirata, M. M. Weiss, K. Tamaki, T. V. Ovaska, J. L. Wood* ——— 1270 – 1272

A Mild and Efficient Synthesis of Oxindoles: Progress Towards the Synthesis of Welwitindolinone A Isonitrile.



Three to four contiguous stereogenic centers are formed in the title reaction (see scheme). The optically active cyclohexanones are formed as single diastereomers with excellent enantioselectivities (up to 99% *ee*) and can be transformed into synthetically useful building blocks.

Addition Reactions

N. Halland, P. S. Aburel, K. A. Jørgensen* ——— 1272 – 1277

Highly Enantio- and Diastereoselective Organocatalytic Asymmetric Domino Michael–Aldol Reaction of β-Ketoesters and α,β-Unsaturated Ketones

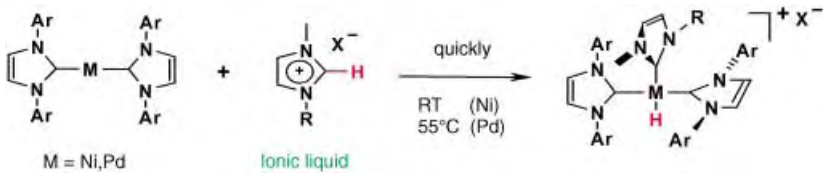
 © 2004 Wiley-VCH Verlag GmbH & Co. KGaA, Weinheim

Contents

Metal–Hydride Complexes

N. D. Clement, K. J. Cavell,* C. Jones, C. J. Elsevier ——— **1277 – 1279**

Oxidative Addition of Imidazolium Salts to Ni^0 and Pd^0: Synthesis and Structural Characterization of Unusually Stable Metal–Hydride Complexes

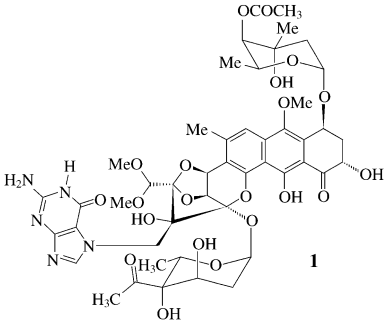


C–H activation of imidazolium salts by coordinatively unsaturated low-valent Ni and Pd complexes occurs under mild conditions. Surprisingly stable hydrido–metal–N-heterocyclic carbene complexes were isolated (see scheme), which demonstrates the ease with which imidazolium-based ionic liquids may react with transition-metal complexes during catalysis.

Marine Natural Products

R. P. Maskey, M. Sevvana, I. Usón, E. Helmke, H. Laatsch* ——— **1281 – 1283**

Gutingimycin: A Highly Complex Metabolite from a Marine Streptomycete



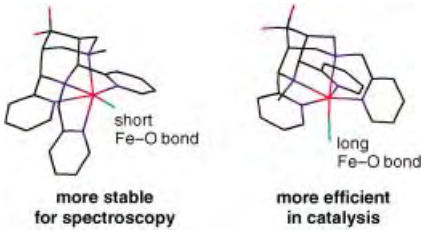
An intriguing catch: Gutingimycin (**1**) from the marine streptomycete isolate B8652 is a conjugate of guanine and trioxacarcin A, as extensive NMR measurements and a crystal structure analysis show. The natural product is formed most likely by the selective attack of trioxacarcin A on the bacterial DNA, which results in strand breakage and may explain the high cytotoxicity of the latter.

Coordination Chemistry

M. R. Bukowski, P. Comba,* C. Limberg, M. Merz, L. Que, Jr., T. Wistuba* ——— **1283 – 1287**

Bispidine Ligand Effects on Iron/Hydrogen Peroxide Chemistry

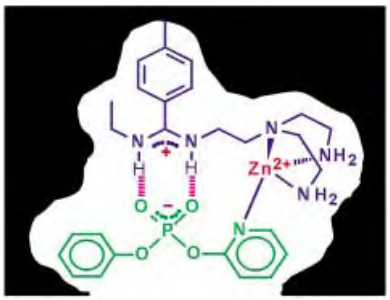
...and yet so different. Non-heme iron complexes catalyze the stereoselective oxidation of C–H and C=C bonds. Isomeric Fe^{III}-η^1-hydroperoxo and Fe^{III}-η^2-peroxo complexes (see picture), important intermediates in these reactions, were studied by EPR, resonance Raman, and UV/Vis spectroscopies.



Enzyme Models

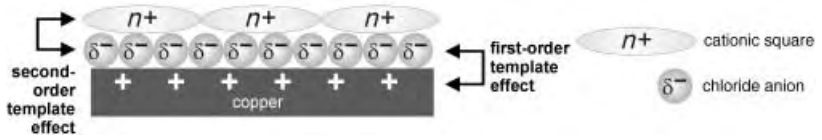
J.-q. Liu, G. Wulff* ——— **1287 – 1290**

Molecularly Imprinted Polymers with Strong Carboxypeptidase A-Like Activity: Combination of an Amidinium Function with a Zinc-Ion Binding Site in Transition-State Imprinted Cavities



Impressing models: A novel polymer catalyst shows even higher catalytic activity for the hydrolysis of carbonates than catalytic antibodies prepared for the same purpose. The catalyst was prepared by molecular imprinting with a stable transition state analogue and the introduction of an amidinium function and a Zn^{2+} ion in the active site in a defined orientation (see picture).

 © 2004 Wiley-VCH Verlag GmbH & Co. KGaA, Weinheim



Beneath the surface lies the answer: Metallosupramolecular cations are deposited in an ordered manner on a copper surface, which had previously been covered with chloride ions. The anion layer acts as a second-order template, whose interactions with the cation determine the adsorption process (see scheme).

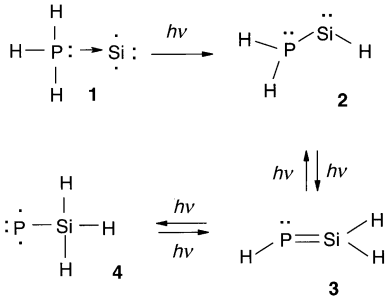
Adsorption

C. Safarowsky, L. Merz, A. Rang, P. Broekmann,* B. A. Hermann,* C. A. Schalley* ——— **1291 – 1294**

Second-Order Templation: Ordered Deposition of Supramolecular Squares on a Chloride-Covered Cu(100) Surface

---

Four isomers with the formula H_3PSi (**1**–**4**) were detected directly by matrix isolation spectroscopy. The n-adduct **1** is formed upon cocondensation of silicon atoms and phosphane. Subsequent irradiation leads to **2**, **3**, and **4**. The structures were elucidated by comparing experimental and calculated IR spectra.



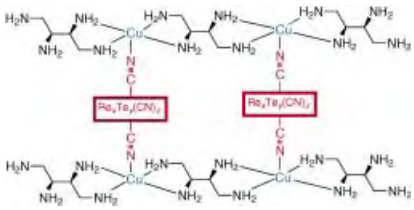
P–Si Compounds

J. Glatthaar, G. Maier* ——— **1294 – 1296**

Reaction of Atomic Silicon with Phosphane: A Matrix-Spectroscopic Study

---

Tuned to the right network: Chiral, heterometallic coordination polymers can be prepared readily by using the chiral (2S,3S)-1,2,3,4-butanetetramine, a labile, divalent transition-metal cation such as Cu^{2+}, and an oligonuclear, rhenium–chalcogenide–cyano cluster as starting materials (see picture).

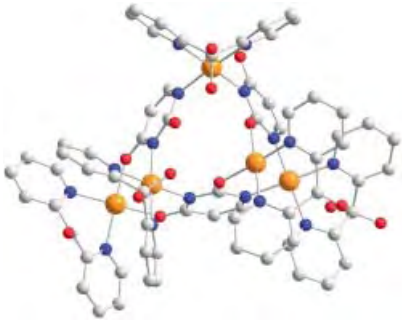


Chiral Solid-State Structures

Y. V. Mironov, N. G. Naumov, K. A. Brylev, O. A. Efremova, V. E. Fedorov,* K. Hegetschweiler* ——— **1297 – 1300**

Rhenium–Chalcogenide–Cyano Clusters, Cu^{2+} Ions, and 1,2,3,4-Tetraaminobutane as Molecular Building Blocks for Chiral Coordination Polymers

---



Pent-up potential: A novel type of metallocalixarenes for molecular recognition processes is synthesized. The self-assembling platinum(II) macrocycles are built from cisplatin analogues with tertiary amine ligands and the nucleobases uracil or thymine (see picture red O, blue N, orange Pt). The pentanuclear complex cations exhibit an asymmetric structure and bind anions by supramolecular interactions.

Metallocalixarenes

M. J. Rauterkus, B. Krebs* ——— **1300 – 1303**

Pentanuclear Platinum(II) Macrocycles with Nucleobases

 © 2004 Wiley-VCH Verlag GmbH & Co. KGaA, Weinheim

Contents

Communications labeled with this symbol have been judged by two referees as being "very important papers".

Deadline for recruitment adverts

14/2004	March 11	Publication date:	March 26
15/2004	March 18	Publication date:	April 2

Angewandte Chemie International Edition
Advertising Sales Department:
Marion Schulz
Phone: 0 62 01 – 60 65 65
Fax: 0 62 01 – 60 65 50
E-Mail: MSchulz@wiley-vch.de

Place an advert in the printed version
and have it made available online for 1 month, free of charge!

Service

Keywords ____ *1304*

Authors ____ *1305*

Preview ____ *1307*



Green, M.M. / Wittcoff, H.A.

Organic Chemistry Principles and Industrial Practice

3527-30289-1 2003
341pp with 166 figs and 5 tabs Pbk
€ 39.90 /£ 29.95 /US$ 39.00

"This very interesting book is going to find a unique place in the repertoire of organic textbooks."
James Canary, New York University

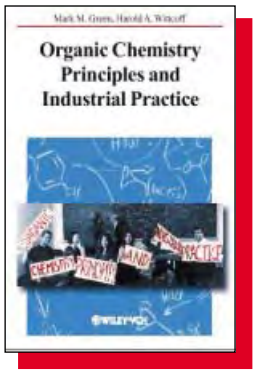
"This book is a joy to read (and re-read)."
James A. Moore, Rensselaer Polytechnic Institute

"Simply put, this book is a gem. The chemistry described is rigorous but the warm, humorous, and conversational writing style makes the book a joy to read."
Dasan M. Thamattoor, Colby College

"I have never come across such an enticing mix of stories of discovery with basic chemistry!"
Roald Hoffmann, Cornell University

"This is a highly original book filling an obvious need."
Herbert Morawetz, Polytechnic University

"This book is a delightful contribution to the field of organic chemistry that offers a useful pedagogical approach."
Pedro Cintas, Facultad de Ciencias-UEX Badajoz, Spain



08622083_gu

Wiley-VCH · P.O. Box 10 11 61 · D-69451 Weinheim · Germany · Tel: +49 (0) 62 01- 60 64 00
Fax: +49 (0) 62 01- 60 61 84 · E-mail: service@wiley-vch.de · Internet: www.wiley-vch.de
WILEY-VCH



H. tom Dieck Made Honorary Member of the GDCh

The former long-standing director of the Gesellschaft Deutscher Chemiker (GDCh, German Chemical Society) Heindirk tom Dieck is to receive honorary membership of this society. During his more than 11 years in office he made outstanding contributions toward the reorganization of chemical journals in Europe, for example, in the launching of *Chemistry—A European Journal* and conversion of a series of traditional national journals into the *European Journals of Inorganic* and *Organic Chemistry*. He was also instrumental in setting up numerous foundations for the sponsorship of young scientists and various bilateral named lectures.



H. tom Dieck

H. tom Dieck completed his PhD in 1966 at the Ludwig-Maximilians-Universität München (Germany) under the supervision of H. Bock and moved with him in 1969 to the Universität Frankfurt am Main (Germany), where he completed his habilitation in 1971. In 1972 he was made Professor of Organometallic Chemistry there; in 1977 he took up a position as Professor of Inorganic and Applied Chemistry at the Universität Hamburg (Germany). His research includes organometallic chemistry, catalysis, and low-dimensional materials. From 1991 to 2002 he had a large impact on the development of the GDCh. Since 1986 he has been working on committees to support German–French contacts in education and technology. In 1993 tom Dieck received an honorary doctorate from the University of Rennes (France).

H. Schnöckel Receives Alfred Stock Memorial Prize

Every two years the Alfred Stock Memorial Prize is awarded by the GDCh for outstanding scientific experimental work in inorganic chemistry and presented at the Congress of Chemistry Lecturers. The recipient for 2004 is Hansgeorg Schnöckel of the Universität Karlsruhe (Germany).

Schnöckel completed his PhD in 1970 in the research group of H. J. Becher at the Universität Münster (Germany) and completed his habilitation there in 1981. In 1989 he took up a position at the Universität München, and from there went on to the Universität Karlsruhe in 1993. His research is focused on matrix investigations of reactive molecules, such as molecular SiO_2, the spectroscopy and quantum chemistry of such molecules, the synthetic chemistry of gallium(I) and aluminum(I) compounds, including the first low-valent organometallic compounds of these main-group elements: $[Al_4Cp_4^*]$ (Cp^*: C_5Me_5) and [GaCp],[1a,b] and also on Ga and Al clusters. He recently published a Review in *Angewandte Chemie* on "Metalloid Aluminum and Gallium Clusters: Element Modifications on the Molecular Scale?"[1c]. A Communication on the stability and structure of $GaAs_5$ and $InAs_5$ will appear soon.



H. Schnöckel

Carl Duisberg Memorial Award to A. Terfort

The Carl Duisberg Memorial Award is presented annually at the Congress of Chemistry Lecturers to a young scientist who has completed his or her habilitation, and who has excelled with original work. The Award for 2004 goes to Andreas Terfort of the Universität Hamburg.



A. Terfort

Terfort studied chemistry at the Universität Göttingen (Germany) and completed an undergraduate research project and dissertation under the supervision of G. von Kiedrowski. He completed his PhD in 1994 on ligands in enantioselective catalysis under the guidance of H. Brunner at the Universität Regensburg (Germany) and then went to Harvard University (USA) to undertake postdoctoral work with G. Whitesides on two- and three-dimensional self-assembly.[2] In 2003 Terfort completed his habilitation at the Universität Hamburg. His research interests include the synthesis, characterization, and application of self-assembled monolayers of functionalized molecules on substrate surfaces. Through the use of aromatic compounds he has been able to prepare robust films, which could be of interest for applications in molecular electronics and bioanalytics.

[1] a) C. Dohmeier, C. Robl, M. Tacke, H. Schnöckel, *Angew. Chem.* **1991**, *103*, 594; *Angew. Chem. Int. Ed. Engl.* **1991**, *310*, 564; b) D. Loos, H. Schnöckel, J. Gauss, U. Schneider, *Angew. Chem.* **1992**, *104*, 1376; *Angew. Chem. Int. Ed. Engl.* **1992**, *31*, 1362; c) A. Schnepf, H. Schnöckel, *Angew. Chem.* **2002**, *114*, 3682; *Angew. Chem. Int. Ed.* **2002**, *41*, 3532; *Angew. Chem.* **2002**, *114*, 4344; *Angew. Chem. Int. Ed.* **2002**, *41*, 4170.

[2] A. Terfort, G. M. Whitesides, *Adv. Mater.* **1998**, *10*, 470.

 © 2004 Wiley-VCH Verlag GmbH & Co. KGaA, Weinheim DOI: 10.1002/anie.200481028

Nitrogen Fixation

Revelations in Dinitrogen Activation and Functionalization by Metal Complexes**

Christopher M. Kozak and Philip Mountford**

Keywords:
coordination modes · enzyme catalysis · molybdenum · nitrogen fixation · nitrogenases

The fixation of atmospheric nitrogen is fundamentally important for the synthesis of nitrogen-containing molecules essential to all life. Nature converts nitrogen from the atmosphere into a form readily exploitable by organisms using a class of enzymes called nitrogenases;[1–3] the most well-studied of these enzymes possesses an Fe- and Mo-containing cofactor (FeMoco) at its active site, where dinitrogen binds and is converted into ammonia. Despite considerable effort by many researchers over the years, uncertainty still persists with regard to the mechanism and even the metal center at which N_2 is bound and reduced.

Early attempts to obtain synthetic models of nitrogenase focused on the assumption that dinitrogen binds to the molybdenum center of the cofactor, as even in the absence of crystallographic data, it was known that it contained both Fe and Mo ions. The pioneering work by Chatt et al.[4] utilized low oxidation state Group 6 metal centers supported by ancillary phosphane ligands to create monometallic dinitrogen complexes. These systems were shown to react with reducing agents and protons to yield reduced nitrogen compounds, including hydrazine and ammonia. The drawback to this model is the presence of molybdenum in the zero oxidation state, which is not easily accommodated by biological systems.[5]

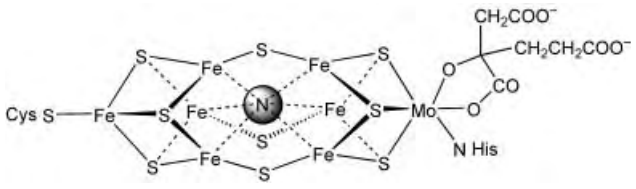
In recent years the proposed mechanisms by which nitrogenase reduces dinitrogen to ammonia have been guided largely by the crystallographic data[6] obtained for the active site of the enzyme, although structural characterization of a FeMoco cluster possessing a coordinated dinitrogen molecule is still elusive. These data describe the cofactor as a cagelike arrangement of one molybdenum and seven iron centers linked by sulfide ions. Six three-coordinate iron atoms appeared to occupy the periphery of the central cavity of the cluster, while the unique molybdenum atom was coordinatively saturated. This led to theories that suggested the three-coordinate iron centers constituted the coordination site of dinitrogen while the molybdenum center, which is surrounded by three sulfide ligands, a histidine imidazole group, and a bidentate homocitrate ligand, was considered by some to be a less likely binding site.

Higher resolution crystallographic data have recently revealed a new ligand bound within the iron cage.[7] An additional atom, possibly N, C, or O, occupies the central cavity of the cluster which results in four-coordinate iron centers (Scheme 1). Theoretical studies[8] support the identity of the interstitial ligand as nitrogen and, taking this implication into account, various bonding motifs have been suggested where the dinitrogen ligand coordinates externally to an Fe_4S_4 face of the cofactor. Furthermore, labeling studies combining ENDOR and ESEEM experiments have shown that the central nitrogen atom does not exchange with N_2 during catalysis.[9] Whether or not it resides there as a "resting state" of nitrogen reduction, or is merely structural is arguable. It has been proposed that the homocitrate ligand, which occupies two coordination sites of the molybdenum ion, may disconnect itself from one or both sites to create a vacancy for dinitrogen bonding.[5] A re-evaluation of current theories regarding the interaction of nitrogenase with dinitrogen, particularly the role of molybdenum, will be required as new observations are presented.[10]

Intimately connected to biological nitrogen fixation are efforts to discover new chemical processes that are capable of utilizing molecular nitrogen as a feedstock. Practically, this entails the synthesis of complexes that not only coordinate dinitrogen, but also allow it to undergo the stepwise addition of electrons and/or protons or other reagents. Hundreds of N_2 complexes are now known,[11] but only a small number of homogeneous systems have shown the ability to reduce N_2 to NH_3, at least

[*] Dr. C. M. Kozak, Dr. P. Mountford
Inorganic Chemistry Laboratory
University of Oxford
South Parks Road, Oxford OX1 3QR (UK)
Fax: (+44) 1865-272690
E-mail:
Christopher.Kozak@chemistry.oxford.ac.uk
Philip.Mountford@chemistry.oxford.ac.uk

[**] C.M.K. thanks the NSERC (Canada) for a postdoctoral fellowship.



Scheme 1. Representation of the FeMo cofactor showing the central ligand (assigned as N).

 © 2004 Wiley-VCH Verlag GmbH & Co. KGaA, Weinheim DOI: 10.1002/anie.200301712

stoichiometrically.[4,12–15] It is believed that dinitrogen cleavage is fundamental to the fixation process, and although there are now a number of reports of species that induce N–N bond cleavage,[11,16–21] they often form stable, unreactive metal nitrides.

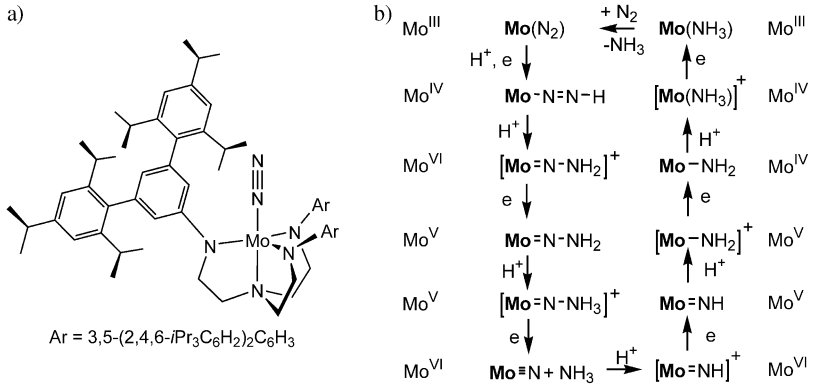
The very recent discovery of a molybdenum species (Scheme 2)[22,23] that allows the catalytic stepwise reduction and protonation of a coordinated dinitrogen ligand to form ammonia is the realization of a goal that has challenged chemists since the discovery of the first dinitrogen complex.[24] This seminal work demonstrates the utility of the triamidoamine ligand that has borne a rich cache of dinitrogen-activation chemistry. The use of extremely bulky hexaisopropylterphenyl (hipt) groups on the amide substituents prevents the formation of dinuclear, end-on-bridged molybdenum dinitrogen complexes[25] (which arise when smaller substituents are used) and results in the formation of a cavity where only small moieties (such as dinitrogen, protons, and electrons) may access the molybdenum center.[26,27] Reduction of the molybdenum chloride precursor under N_2 generates a terminal end-on-bound dinitrogen complex (Scheme 2a). The use of carefully selected and tuned reducing [Cp^*_2Cr] and protonating [(2,6-lutidinium)$B(Ar'_F)_4$], ($Cp^* = C_5Me_5$, $Ar'_F = 3,5\text{-}(CF_3)_2C_6H_3$) agents, and by carefully controlling the reaction conditions enables the catalytic reduction of dinitrogen to ammonia to progress for at least four turnovers (Scheme 2b).

In contrast to the Chatt cycle, these results provide a more viable model system for the reduction of dinitrogen to ammonia catalyzed by a molybdenum center in nitrogenase. The proposed intermediates in the reduction process cycle between Mo^{III} and Mo^{VI} species, oxidation states which are biologically relevant. These results certainly lend themselves to the implication of the molybdenum center in nitrogenase as being more than merely a spectator.

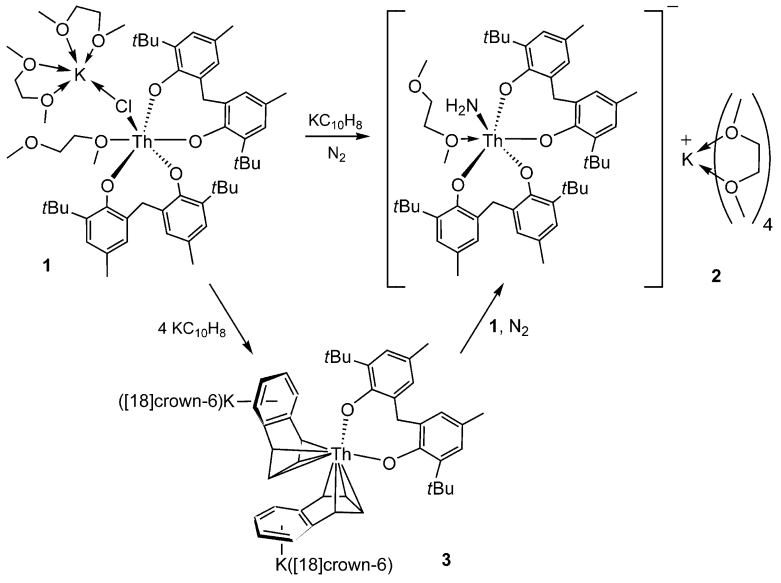
Another remarkable dinitrogen cleavage and hydrogenation transformation has very recently been reported, this time using an actinide complex. Potassium naphthalenide reduction of the potassium salt of a thorium chloride complex supported by bis(aryloxide) ligands, namely [{(2-*t*Bu-4-$MeC_6H_2O)_2CH_2$}$_2$Th(dme)(μ-Cl)K(dme)$_2$] (**1**; dme = dimethoxyethane), generates the thorium amide complex [{{(2-*t*Bu-4-$MeC_6H_2O)_2CH_2$}$_2$Th(dme)(NH_2)}-{K(dme)$_4$}] (**2**) in nearly 50% yield (Scheme 3).[28] This remarkable reaction is proposed to result from the cleavage of dinitrogen and subsequent hydrogen-atom abstraction from the DME solvent. In addition to the crystallographic evidence, this structure is supported by NMR data from $^{15}N_2$ labeling experiments.

An intermediate color change is observed for this reaction, and the nature of this bright-red species has been examined to shed some light on the process. Indeed, this intensely colored intermediate species can be isolated if the reaction is conducted with two to four equivalents of K(naphthalenide); preliminary structural data suggests that this product is [{{[2-(*t*Bu),4-$MeC_6H_2O]_2CH_2$}Th($C_{10}H_8$)$_2$}{K([18]-crown-6)}$_2$] (**3**). The oxidation state of the thorium center is not altogether clear, as the distortion of the coordinated naphthalene fragments suggests a non-zero-valent metal center. It is suggested that this colored intermediate undergoes reaction with the colorless thorium(IV) starting complex **1** to trigger a cascade of transformations resulting in dinitrogen cleavage and partial hydrogenation.

While the discovery of a catalytic homogeneous process that converts di-



Scheme 2. a) [Mo(hiptN$_3$N)N$_2$] ([**Mo**N$_2$]) and b) proposed intermediates in the reduction of N_2 at **Mo** by stepwise addition of protons and electrons.



Scheme 3. Reduction of a thorium complex under dinitrogen generates an amido-thorium species.

 © 2004 Wiley-VCH Verlag GmbH & Co. KGaA, Weinheim

nitrogen into ammonia (in the presence of protons and electrons) represents a coveted "trophy" of coordination chemistry, related goals are no less highly desirable. Organonitrogen materials such as amines, amino acids, and nitrogen heterocycles, for example, are all worthy targets. To develop advancement in this area, dinitrogen complexes capable of undergoing novel nitrogen bond-forming reactions at the coordinated N_2 molecule are particularly significant.

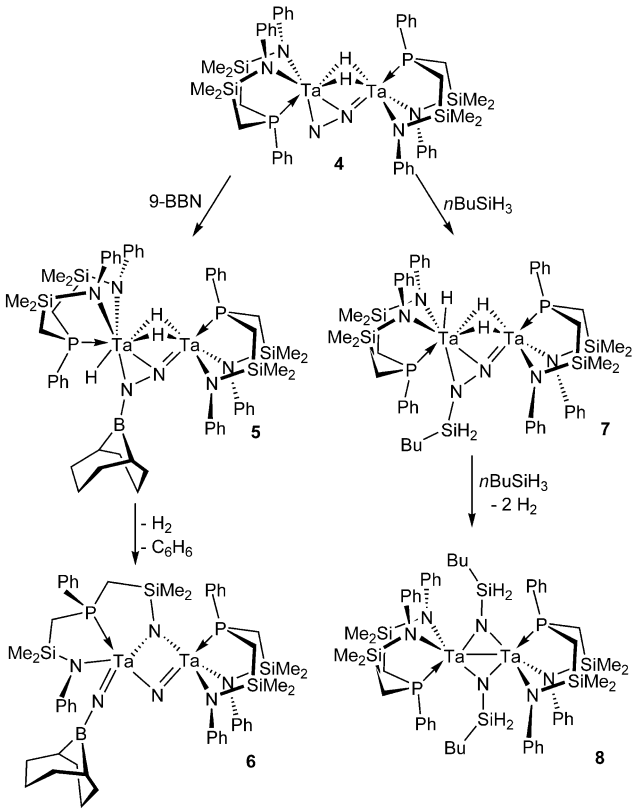
The bonding mode of the dinitrogen ligand appears to be of utmost importance. In addition to N–N bond elongation, the employment of coordinated dinitrogen as a nucleophile capable of reacting not only with protons, but alkylating agents, silanes, boranes, etc., may lead to new realms of stoichiometric and even catalytic reactivity. The asymmetric side-on, end-on bonding mode present in the tantalum–dinitrogen complex $[\{(NPN)Ta\}_2(\mu\text{-}H)_2(\mu\text{-}\eta^1{:}\eta^2\text{-}N_2)]$ (**4**) (where NPN = $(PhNSiMe_2CH_2)_2PPh$) undergoes N–N bond cleavage and functionalization as a result of reaction with boranes[29] and silanes[30] (Scheme 4).

Reaction of the dinitrogen complex with 9-borabicyclo[3.3.1]nonane (9-BBN) generates the hydroboration product $[\{(NPN)Ta(H)(\mu\text{-}H)_2(\mu\text{-}N_2\text{-}BC_8H_{14})\}\{Ta(NPN)\}]$ (**5**). This product, however, is thermally unstable and over a period of several weeks in solution is transformed into the imide–nitride complex **6**. A multistep mechanism is proposed which includes N–N bond scission accompanied by the loss of H_2 and benzene.

The reaction of **4** with *n*-butylsilane gives stepwise functionalization of the dinitrogen fragment to yield **7** with a new Si–N bond and a new terminal hydride at one Ta center. This product, however, is thermally unstable and readily loses H_2 concurrently with N–N bond cleavage. The addition of a second equivalent of nBuSiH$_3$ across the {Ta-N=Ta} unit of this species causes the loss of one more equivalent of H_2 to give the bridging diimide complex **8**. This reaction is more intriguing in terms of leading to a potentially catalytic cycle as, unlike the borane-induced dinitrogen bond cleavage, the ancillary NPN ligand remains intact.

This manifold of reactivity may be an important step towards generating dinitrogen-derived products. The fact that these reactions possess "built-in" reduction capability through the reductive elimination of H_2, and that the dinitrogen complex itself originates from the reductive elimination of H_2 from a tantalum(IV) tetrahydride bridged dimer, imply that a catalytic cycle of N_2 activation, functionalization, and elimination may be possible. Clearly, the challenge for this system is whether the nitrogen-containing fragment can be removed from the {Ta(NPN)} units, ideally by a process leading to the regeneration of the side-on, end-on dinitrogen complex **4**.

The recent outpouring of papers in the field of dinitrogen activation clearly suggests that this area is not only undergoing a renaissance, but that the reactivity exhibited by dinitrogen complexes is reaching ever more exciting levels of sophistication. The development of a mild homogeneous process for the synthesis of ammonia from dinitrogen is the realization of a long-standing challenge faced by chemists. What then, will be the new directions taken? Can, for example, dinitrogen be used in insertion chemistry, one of the fundamental processes at the heart of organometallic chemistry and many catalytic cycles? Can transformations exhibited by isoelectronic carbon monoxide and acetylene be found for N_2? Developing catalytic cycles that employ dinitrogen as a feedstock for the synthesis of high-value organonitrogen compounds is a lofty goal,[31] but as is evident from recent discoveries, the chemistry of dinitrogen is providing ingenious researchers ever more opportunities to achieve this objective.



Scheme 4. N–N bond cleavage in a tantalum dinitrogen complex results from reaction with 9-BBN or nBuSiH$_3$.

[1] B. K. Burgess, *Chem. Rev.* **1990**, *90*, 1377.
[2] B. K. Burgess, D. J. Lowe, *Chem. Rev.* **1996**, *96*, 2983.
[3] R. L. Richards in *Biology and Biochemistry of Nitrogen Fixation* (Eds.: M. J. Dilworth, A. R. Glenn), Elsevier, Amsterdam, **1991**, p. 58.
[4] J. Chatt, J. R. Dilworth, R. L. Richards, *Chem. Rev.* **1978**, *78*, 589.

 © 2004 Wiley-VCH Verlag GmbH & Co. KGaA, Weinheim

[5] G. J. Leigh, *Science* **2003**, *301*, 55.
[6] J. Kim, D. C. Rees, *Nature* **1992**, *360*, 563.
[7] O. Einsle, F. A. Texcan, S. L. A. Andrade, B. Schmid, M. Yoshida, J. B. Howard, D. C. Rees, *Science* **2002**, *297*, 1696.
[8] I. Dance, *Chem. Commun.* **2003**, 324.
[9] H.-I. Lee, P. M. C. Benton, M. Laryukhin, R. Y. Igarashi, D. R. Dean, L. C. Seefeldt, B. M. Hoffman, *J. Am. Chem. Soc.* **2003**, *125*, 5604.
[10] F. Barriere, *Coord. Chem. Rev.* **2003**, *236*, 71.
[11] M. D. Fryzuk, S. A. Johnson, *Coord. Chem. Rev.* **2000**, *200–202*, 379.
[12] C. J. Pickett, J. Talarmin, *Nature* **1985**, *317*, 652.
[13] M. Hidai, Y. Mizobe, *Chem. Rev.* **1995**, *95*, 1115.
[14] M. Hidai, *Coord. Chem. Rev.* **1999**, *185–186*, 99.
[15] R. L. Richards, *Coord. Chem. Rev.* **1996**, *154*, 83.
[16] A. Caselli, E. Solari, R. Scopelliti, C. Floriani, N. Re, C. Rizzoli, A. Chiesi-Villa, *J. Am. Chem. Soc.* **2000**, *122*, 3652.
[17] G. K. B. Clentsmith, V. M. E. Bates, P. B. Hitchcock, F. G. N. Cloke, *J. Am. Chem. Soc.* **1999**, *121*, 10444.
[18] J. C. Peters, J. F. Cherry, J. C. Thomas, L. Baraldo, D. J. Mindiola, W. M. Davis, C. C. Cummins, *J. Am. Chem. Soc.* **1999**, *121*, 10053.
[19] C. E. Laplaza, C. C. Cummins, *Science* **1995**, *268*, 861.
[20] M. D. Fryzuk, C. M. Kozak, M. R. Bowdridge, B. O. Patrick, S. J. Rettig, *J. Am. Chem. Soc.* **2002**, *124*, 8389.
[21] E. Solari, C. Da Silva, B. Iacono, J. Hesschenbrouck, C. Rizzoli, R. Scopelliti, C. Floriani, *Angew. Chem.* **2001**, *113*, 4025; *Angew. Chem. Int. Ed.* **2001**, *40*, 3907.
[22] D. V. Yandulov, R. R. Schrock, *Science* **2003**, *301*, 76.
[23] R. R. Schrock, *Chem. Commun.* **2003**, 2389.
[24] A. D. Allen, C. V. Senoff, *J. Chem. Soc. Chem. Commun.* **1965**, 621.
[25] M. Kol, R. R. Schrock, R. Kempe, W. M. Davis, *J. Am. Chem. Soc.* **1994**, *116*, 4382.
[26] D. V. Yandulov, R. R. Schrock, *J. Am. Chem. Soc.* **2002**, *124*, 6252.
[27] D. V. Yandulov, R. R. Schrock, A. L. Rheingold, C. Ceccarelli, W. M. Davis, *Inorg. Chem.* **2003**, *42*, 796.
[28] I. Korobkov, S. Gambarotta, G. P. A. Yap, *Angew. Chem.* **2003**, *115*, 5108–5111; *Angew. Chem. Int. Ed.* **2003**, *42*, 4598–4961.
[29] M. D. Fryzuk, B. A. MacKay, S. A. Johnson, B. O. Patrick, *Angew. Chem.* **2002**, *114*, 3861; *Angew. Chem. Int. Ed.* **2002**, *41*, 3709.
[30] M. D. Fryzuk, B. A. MacKay, B. O. Patrick, *J. Am. Chem. Soc.* **2003**, *125*, 3234.
[31] M. D. Fryzuk, *Chem. Rec.* **2003**, *3*, 2.

 © 2004 Wiley-VCH Verlag GmbH & Co. KGaA, Weinheim

Alloproteins

Old Codons, New Amino Acids**

*Ulrich Hahn, Gottfried J. Palm, and Winfried Hinrichs**

Keywords:
gene expression · ligases · mRNA · protein modifications · tRNA

Dedicated to Professor Wolfram Saenger on the occasion of his 65th birthday

Introduction

Today it is possible to incorporate non-proteinogenic amino acids into proteins by genetic engineering. This is a promising way to expand the structural, chemical, and functional diversity of proteins. The resulting alloproteins[1] can have unusual biophysical and biochemical properties, and may have potential in protein analysis in biochemistry and cell biology. Further applications in biotechnology and medicine are also feasible.

Numerous nonstandard amino acid residues in proteins are known,[2] but these are all enzymatically modified after ribosomal polypeptide syntheses or introduced by nonribosomal peptide syntheses. Direct chemical modifications seldom fulfill the prerequisites of site-specificity and -selectivity and often alter the three-dimensional structure or even denature the treated protein. Both solid-phase peptide syntheses and successful chemical ligation on native proteins in reasonable yields and in large amounts require extensive efforts.[3]

A common strategy to force site-specific incorporation of a desired unnatural amino acid in vivo requires specific additional tools for the biosynthetic protein factory. A new pair of tRNA and an appropriate aminoacyl-tRNA ligase (aaRL, formerly called aminoacyl-tRNA ligase) must work efficiently in the translation step. The new tRNA must be esterified exclusively with the novel amino acid and must read a unique codon not used by any other standard aminoacyl-tRNA. Up to now, this codon has been a stop codon or an artificial four-base codon of the mRNA.

What Was Possible So Far

The first case refers to an exception, where in addition to the 20 standard amino acids, a selenocysteine (often referred as the 21st amino acid) had been incorporated into the growing polypeptide chain by overwriting a stop codon.[4] This was discovered in naturally occurring enzymes, which exhibit a selenocysteine in the active site. Recently a similar case has been reported for pyrrolysine as the 22nd naturally occurring amino acid.[5] These redefined stop codons are "in the frame" of the other codons on the mRNA, but not at the end of the coding region and will not terminate polypeptide elongation, if the appropriate aminoacyl-tRNA is present.

A more general approach was developed to upgrade the translational machinery of the cell by introduction of an additional novel tRNA/stop-codon pair.[6] A specific tRNA is not sufficient for the site-specific insertion of a synthetic amino acid into a growing polypeptide chain; an aminoacyl-tRNA ligase must also be designed that charges the tRNA with the requested amino acid. The new set of tRNA/aminoacyl-tRNA ligase must function orthogonal to the common 20 amino acids. This means that only the new amino acid is a substrate for the designed ligase/tRNA pair, and the tRNA exclusively responds to the unique codon.[7] This was the basis for the selective incorporation of L-3-(2-naphthyl)alanine, functionalized phenylalanine, and tyrosine derivatives.[6,8]

The method works perfectly for the incorporation of noncanonical amino acids at single sites, but the suppression efficiencies for multisite substitutions are moderate. This can be circumvented by using auxotrophic *Escherichia coli* strains with reduced substrate specificity of the modified aminoacyl-tRNA ligases. These ligases are designed to aminoacylate their cognate tRNA with a synthetic amino acid which replaces the native counterpart in ribosomal polypeptide elongation. In this case the novel amino acid shares a codon with the replaced natural one.[9]

Applications

Hendrickson et al. were the first to introduce the selenium-homologue of methionine into proteins for crystallographic protein structure analyses.[10] This approach has become standard for direct three-dimensional structure determination by multiwavelength anomalous diffraction (MAD). Selenomethionine can be incorporated easily into any protein simply by overproducing the desired protein with the aid of an *E. coli* methionine auxotroph, which is grown in selenomethionine-containing medium.

[*] Dr. G. J. Palm, Prof. Dr. W. Hinrichs
Institut für Chemie und Biochemie
Mathematisch-Naturwissenschaftliche Fakultät
Universität Greifswald
Soldmannstrasse 16, 17489 Greifswald (Germany)
Fax: (+49) 3834-86-4373
E-mail: hinrichs@uni-greifswald.de
Prof. Dr. U. Hahn
Abteilung Biochemie und Molekularbiologie
Institut für Biochemie und Lebensmittelchemie
Fachbereich Chemie, Universität Hamburg
Martin-Luther-King-Platz 6
20146 Hamburg (Germany)

[**] Financial support to both groups by Fonds der Chemischen Industrie is gratefully acknowledged.

 © 2004 Wiley-VCH Verlag GmbH & Co. KGaA, Weinheim DOI: 10.1002/anie.200301720

Other examples are fluorotryptophans incorporated into annexin V, 3-fluoro- and 3-chlorotyrosine into azurin and annexin V, respectively, and 4-aminotryptophan into green fluorescent protein (GFP) to study the structure, stability, activity, and spectroscopic properties of these alloproteins.[11] A recent example is the exchange of all 13 methionine residues against the methionine analogue norleucine in the heme domain (463 amino acids) of cytochrome P450 BM-3. The resulting alloprotein showed doubled peroxygenase activity and significantly reduced thermostability.[12]

The Genetic Code Is Degenerate

Another way to edit the genetic code is based on the fact that 64 nucleotide triplets (codons) define three stop codons, but the remaining 61 combinations define only 20 proteinogenic amino acids. This situation is usually refered to as the degeneracy of the genetic code.[13] Methionine and tryptophan are single-codon-based, but the remaining 18 amino acids are defined by two to six different triplets. Interestingly, in most cases the first two nucleotides of redundant codons are identical and already unambiguously define the amino acid selected during polypeptide synthesis. This situation might also be discussed as a (2+1) letter code. On the other hand, we can think about an ancestral two-letter code during evolution. However, this degeneracy of the genetic code is the provides the necessary ambiguity for forcing the ribosome to accept nonstandard amino acids in defined positions during polypeptide-chain elongation. Recently, the possibility of reassigning degenerate sense codons was demonstrated by Tirell et al.,[14] and we will focus on this in the following discussion.

The New Aproach

In *E. coli* the two codons UUC and UUU of the mRNA encode sequence-specific incorporation of phenylalanine (Phe) during protein biosynthesis. The organism provides only one tRNA to transfer Phe to the mRNA at the ribosome. It carries the anticodon GAA and interacts well with the codon UUC in a standard Watson–Crick manner, but slightly more weakly with UUU, creating a "wobble" base pair G-U.[13] Remember that the polynucleotide sequences are written from the 5′ to the 3′ terminus, and the codon and anticodon nucleotide chains are complementary in antiparallel orientation. The interaction of UUC (codon) with GAA (anticodon) is approximately $10\,kJ\,mol^{-1}$ stronger than that of UUU with GAA.[15] Nevertheless, *E. coli* will incorporate Phe into the growing polypeptide in both cases.

To discriminate between the two codons, an exogenous Phe-transfering but modified pair of tRNA/aminoacyl-tRNA ligase from yeast was incorporated into *E. coli*. The new tRNA comprises the anticodon AAA ($ytRNA^{Phe}_{AAA}$) leading to the optimal recognition of the target codon UUU in *E. coli* by Watson–Crick base-pairing. This tRNA can be charged with a nonstandard amino acid by its corresponding but genetically modified aminoacyl-tRNA ligase. In the work discussed here L-3-(2-naphthyl)alanine (Nal) was chosen as an example.[14] Mutational screening of the yeast ligase was restrained to some amino acid residues of the active site pocket, and a variant form with relaxed substrate specificity was prepared to accommodate Nal.[16] In vitro the designed yeast ligase showed eightfold larger activation by the artificial amino acid than Phe,[14] and it has to be pointed out that the aminoacylation rate of yeast $tRNA^{Phe}$ by endogenous *E. coli* enzymes can be ignored.[17] Additionally, the aminoacyl-tRNA ligase variant from yeast does not accept any tRNA from the *E. coli* host as substrate. The latter two properties ensure orthogonality of the yeast $tRNA^{Phe}$/phenylalanyl-tRNA ligase pair to the *E. coli* system (Figure 1).

In a further attempt, a Phe auxotroph *E. coli* strain was established which carries the gene for the exogenous $ytRNA^{Phe}_{AAA}$, the gene for a mutated aaRL variant from yeast (mu-yPheRL), and the gene of murine dihydrofolate reductase (mDHFR) as test protein, which is also foreign to *E. coli*. This set of these genes in the presence of Nal in the culture medium made possible the expression of mDHFR, which had specifically incorporated the new amino acid in defined positions.

Proteolytic digests of mDHFR were analyzed by MALDI mass spectrometry and liquid chromatography/tandem mass spectrometry (LC/MS/MS) to prove complete replacement of Phe by Nal in response to the five UUU codons but Phe incorporation at the four UUC codons. The translation of the two codons is now distinct and Phe and Nal are incorporated into the polypeptide. Thus, the genetic code of this *E. coli* construct is enriched by a nonstandard but specific amino acid codon for ribosomal polypeptide synthesis, as the artificial amino acid has its own codon in addition to the 20 canonical ones.

Orthogonality Is a Prerequisite for tRNA/aminoaycl-tRNA Ligase Pairs

The structural basis for the specificity of the orthogonality of corresponding tRNA/aminoacyl-tRNA ligases for engineered expansion of the genetic code was highlighted by the crystal structure analysis of the complex of the tyrosyl-tRNA/tyrosyl-tRNA ligase of the archaeal organism *Methanococcus jannaschii*.[18] The structural information allowed improved application by site-directed mutagenesis of the ligase and by modification of the tRNA, which suppresses a stop codon. The groups of Cusack and Yokoyama pointed out that orthogonality arises from the difference in the recognition of the tRNA structure by tyrosyl-tRNA ligase in bacterial and archaeal/eukaryotic systems. The primary and tertiary structures the tyrRL of bacteria are highly homologous, but they differ from their functional equivalents in archaea and eukaryotes.

Conclusion

The new approach for redefining redundant codons, which are recognized with divergent specificity in the translation step, became possible with the use of the orthogonal pairs of tRNA and the cognate aminoacyl-tRNA ligase. As previously pointed out, it is not sufficient to consider simply the genetic information as a sequence variation of

 © 2004 Wiley-VCH Verlag GmbH & Co. KGaA, Weinheim

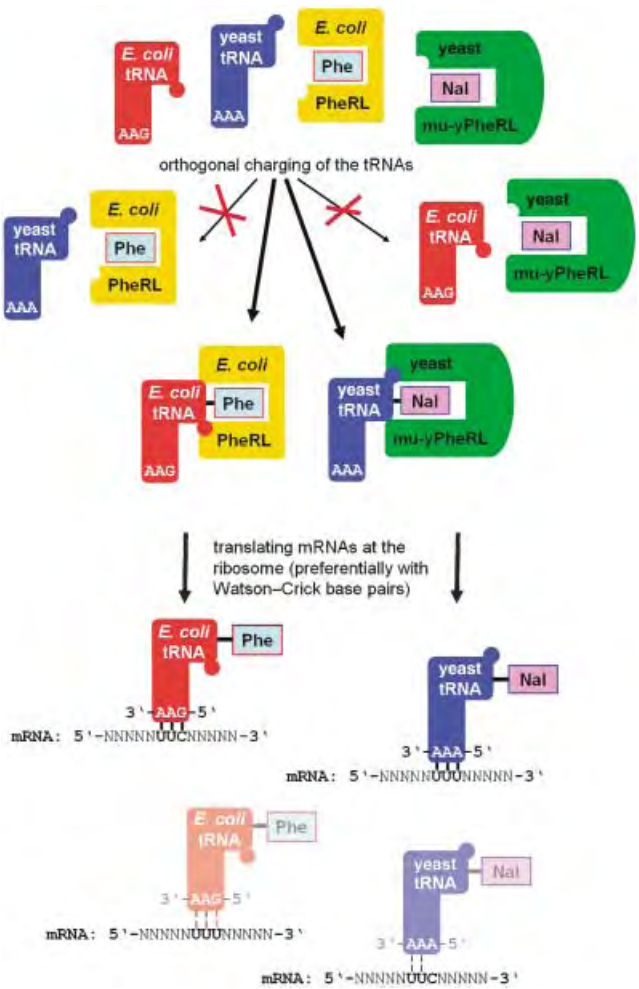


Figure 1. Use of orthogonal pairs of tRNA/aminoacyl-tRNA ligase for incorporation of Phe and Nal during ribosomal protein synthesis. Owing to the orthogonality of the *E. coli* $tRNA^{Phe}$/PheRL and yeast $tRNA^{Nal}$/mutated PheRL pairs, the $tRNA^{Phe}$ is only aminoacylated with Phe and $tRNA^{Nal}$ only with Nal. The *E. coli* genome comprises 21 aaRL and 84 tRNAs. Therefore, it is a formidable task to prevent over 1600 wrong aminoacylations, but enable only the 84 correct ones. The charged tRNAs are utilized at the ribosome with different preferences for the canonical Phe codons UUC and UUU: $tRNA^{Phe}$ binds better to UUC and $tRNA^{Nal}$ only to UUU triplets on the mRNA due to optimized hydrogen-bond pattern (Watson–Crick) of the codon/anticodon recognition. Suppressed tRNA/codon recognition is shown at the bottom with pale colors. Thus, 5′-NNN **UUC UUU** NNN-3′ on the mRNA will be translated specifically to NH_2-Xaa **Phe Nal** Xaa-COOH.

the four nucleotide bases, but it is also the biochemistry of the reading system that determines the biological function.[19]

Unfortunately, it is still not straightforward to predict exactly the structural and functional changes of alloproteins (polypeptide folding and stability, ligand recognition). In this light, structural analyses at atomic resolution, such as NMR spectroscopy and X-ray crystallography, supported by molecular dynamics simulations, further spectroscopic studies, and computing methods will have further targets.

Additional amino acids can function as probes for these new challenges in structural biochemistry, biology, and biotechnology. To this end the group of Tirell has added a method to the protein chemist's repertoire, but the restless biochemist asks for more: Each new nonstandard amino acid still needs selection of an adapted aminoacyl-tRNA ligase. Mutants exist that lack the adenylylation activity but still bind amino acids and ATP.[20] Changing the specificity of the purine binding pocket of phosphoribosyltransferase has also been demonstrated.[21] Could we create a modified aminoacyl-tRNA ligase that accepts an activated derivative (e.g. replacing adenylyl by the analogue guanylyl) of any amino acid and charges a tRNA? We are looking forward to exciting protein chemistry.

[1] H. Koide, S. Yokoyama, G. Kawai, J. M. Ha, T. Oka, S. Kawai, T. Miyake, T. Fuwa, T. Miyazawa, *Proc. Natl. Acad. Sci. USA* **1988**, *85*, 6237–6241.

[2] G. C. Barrett in *Amino Acid Derivatives: A Practical Approach* (Ed.: G. C. Barrett), Oxford University Press, New York, **1999**, pp. 15–30.

[3] P. E. Dawson, S. B. H. Kent, *Annu. Rev. Biochem.* **2000**, *69*, 923–960.

[4] a) F. Zinoni, J. Heider, A. Böck, *Proc. Natl. Acad. Sci. USA* **1990**, *87*, 4660–4664; b) A. Böck, K. Forchhammer, J. Heider, W. Leinfelder, G. Sawers, B. Veprek, F. Zinoni, *Mol. Microbiol.* **1991**, *5*, 515–520; c) M. Rother, R. Wilting, S. Commans, A. Böck, *J. Mol. Biol.* **2000**, *299*, 351–358.

[5] a) G. Srinivasan, C. M. James, J. A. Krzycki, *Science* **2002**, *296*, 1459–1462; b) B. Hao, W. Gong, T. K. Ferguson, C. M. James, J. A. Krzycki, M. K. Chan, *Science* **2002**, *296*, 1462–1466.

[6] a) L. Wang, A. Brock, B. Herberich, P. G. Schultz, *Science* **2001**, *292*, 498–500; b) Z. Zhang, L. Wang, A. Brock, P. G. Schultz, *Angew. Chem.* **2002**, *114*, 2964–2966; *Angew. Chem. Int. Ed.* **2002**, *41*, 2840–2842; c) L. Wang, A. Brock, P. G. Schultz, *J. Am. Chem. Soc.* **2002**, *124*, 1836–1837; d) L. Wang, Z. Zhang, A. Brock, P. G. Schultz, *Proc. Natl. Acad. Sci. USA* **2003**, *100*, 56–61.

[7] R. Furter, *Protein Sci.* **1998**, *7*, 419–426.

[8] S. Ohno, T. Yokogawa, I. Fujii, H. Asahara, H. Inokuchi, K. Nishikawa, *J. Biochem.* **1998**, *124*, 1065–1068.

[9] V. Döring, H. D. Mootz, L. A. Nangle, T. L. Hendrickson, V. de Crécy-Lagard, P. Schimmel, P. Marlière, *Science* **2001**, *292*, 501–504.

[10] W. A. Hendrickson, J. R. Horton, D. M. LeMaster, *EMBO J.* **1990**, *9*, 1665–1672.

[11] a) C. Minks, R. Huber, L. Moroder, N. Budisa, *Biochemistry* **1999**, *38*, 10649–10659; b) C. Minks, S. Alefelder, L. Moroder, R. Huber, N. Budisa, *Tetrahedron* **2000**, *56*, 9431–9442; c) J. H. Bae, M. Rubini, G. Jung, G. Wiegand, M. H. Seifert, M. K. Azim, J.-S. Kim, A. Zumbusch, T. A. Holak, L. Moroder, R. Huber, N. Budisa, *J. Mol. Biol.* **2003**, *328*, 1071–1081.

[12] P. C. Cirino, Y. Tang, K. Takahashi, D. A. Tirrell, F. H. Arnold, *Biotechnol. Bioeng.* **2003**, *83*, 729–734.

 © 2004 Wiley-VCH Verlag GmbH & Co. KGaA, Weinheim

[13] F. H. C. Crick, *J. Mol. Biol.* **1966**, *19*, 548 – 555.
[14] I. Kwon, K. Kirshenbaum, D. A. Tirrell, *J. Am. Chem. Soc.* **2003**, *125*, 7512 – 7513.
[15] M. Meroueh, C. S. Chow, *Nucleic Acids Res.* **1999**, *27*, 1118 – 1125.
[16] P. Wang, N. Vaidehi, D. A. Tirrell, W. A. Goddard III, *J. Am. Chem. Soc.* **2002**, *124*, 14442 – 14449.
[17] E. C. T. Peterson, O. C. Uhlenbeck, *Biochemistry* **1992**, *31*, 10380 – 10389.
[18] T. Kobayashi, O. Nureki, R. Ishitani, A. Yaremchuk, M. Tukalo, S. Cusack, K. Sakamoto, S. Yokoyama, *Nat. Struct. Biol.* **2003**, *10*, 425 – 432.
[19] C. Fenske, G. Palm, W. Hinrichs, *Angew. Chem.* **2003**, *115*, 626 – 630; *Angew. Chem. Int. Ed.* **2003**, *42*, 606 – 610.
[20] R. J. Leatherbarrow, A. R. Fersht, G. Winter, *Proc. Natl. Acad. Sci. USA* **1985**, *82*, 7840 – 7844.
[21] N. R. Munagala, C. C. Wang, *Biochemistry* **1998**, *37*, 16612 – 16619.

Why Wait to Make Great Discoveries

When you can make them in an instant with

Wiley InterScience® Pay-Per-View and ArticleSelect™

Now you can have instant, full-text access to an extensive collection of journal articles or book chapters available on Wiley InterScience. With Pay-Per-View and ArticleSelect™, there's no limit to what you can discover...

ArticleSelect™ is a token-based service, providing access to full-text content from non-subscribed journals to existing institutional customers (EAL and BAL)

Pay-Per-View is available to any user, regardless of whether they hold a subscription with Wiley InterScience.

Benefits:

- Access online full-text content from journals and books that are outside your current library holdings
- Use it at home, on the road, from anywhere at any time
- Build an archive of articles and chapters targeted for your unique research needs
- Take advantage of our free profiled alerting service, the perfect companion to help you find specific articles in your field as soon as they're published
- Get what you need instantly, no waiting for document delivery
- Fast, easy, and secure online credit-card processing for Pay-Per-View downloads
- Special, cost-savings for EAL customers: whenever a customer spends tokens on a title equaling 115% of its subscription price, the customer is auto-subscribed for the year
- Access is instant and available for 24 hours

96203129_vo

www.interscience.wiley.com

WILEY InterScience® DISCOVER SOMETHING GREAT

 © 2004 Wiley-VCH Verlag GmbH & Co. KGaA, Weinheim

Allenes

Synthesis and Properties of Allenic Natural Products and Pharmaceuticals

Anja Hoffmann-Röder and Norbert Krause**

Keywords:
allenes · cumulenes · natural products · pharmaceuticals · stereoselective synthesis



Angewandte Chemie

 © 2004 Wiley-VCH Verlag GmbH & Co. KGaA, Weinheim DOI: 10.1002/anie.200300628

Nowadays, about 150 natural products comprising an allenic or cumulenic structure are known. The chemistry of these compounds has turned out to be a very attractive and prolific area of interest: advances in the isolation and characterization of new allenic natural products have led to the establishment of efficient synthetic procedures which in many cases also open up an access to enantiomerically pure target molecules. Inspired by the intriguing biological activities of many allenic natural products, allene moieties are now systematically introduced in pharmacologically active classes of compounds (steroids, prostaglandins, amino acids, nucleosides). The functionalized allenes thus obtained often exhibit impressive activities as mechanism-based enzyme inhibitors, cytotoxic, or antiviral agents. A prerequisite for further developments in this field is the efficient stereoselective synthesis of allene derivatives.

From the Contents

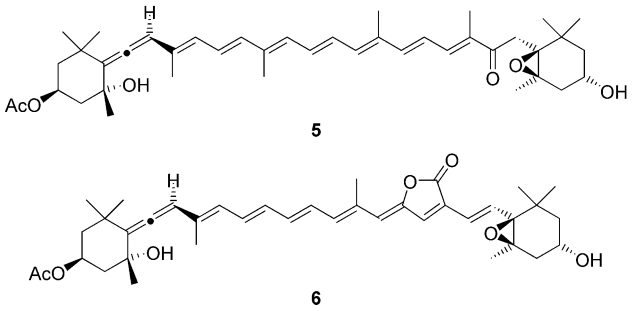
1. Introduction	1197
2. Allenic Natural Products	1198
3. Pharmacologically Active Allenes	1206
4. Conclusion	1212

1. Introduction

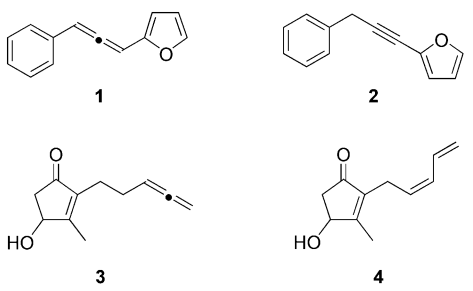
For a long period allenes[1] have been regarded mostly as chemical curiosities. Already in 1874–1875 Van't Hoff[2] had predicted in one of the most relevant publications for the development of organic chemistry the correct structures of allenes and higher cumulenes in line with the tetrahedral geometry of alkanes. But even though first experimental investigations in this area followed closely, most chemists had their doubts about Van't Hoff's predictions, and considered such systems to be highly unstable—a common prejudice that can be even encountered nowadays. Not surprisingly, the first documented synthesis of an allene carried out by Burton and von Pechmann[3] in 1887 was initially an attempt to prove the non-existence of this class of compounds. At that time, however, with all the analytical tools available (mostly synthesis of derivatives) it was almost impossible to distinguish between allenes and the corresponding alkynes. Only when IR and Raman spectroscopy were introduced as tools for structural investigations, was it possible to prove, by its characteristic allenic C–C vibration at about 1950 cm^{-1}, that Burton and von Pechmann had indeed synthesized an allenic molecule.[4]

Similar problems were encountered in the characterization of certain allenic natural products[5] (Scheme 1). For example, Semmler[6] had proposed an allenic structure **1** for a furan derivative extracted from the roots of *Carlina acaulis*, which was corrected later with the aid of Raman spectroscopy in favor of the isomeric alkyne **2**.[7] Much wider known, however, is the case of the pyrothrolone from *Chrysanthemum cinerariaefolium* for which Staudinger and Ruzicka[8] had published the structure **3** in 1924. Also this assignment, which relied on the cleavage of the natural product by ozonolysis, turned out to be incorrect, and spectroscopic investigations finally revealed the conjugated diene moiety of compound **4**.[9,10]

In addition, for quite a large number of well-known natural products the (correct) assignment of their allenic structure took place long after their isolation (Scheme 2). For example, the most abundant of all carotinoids, fucoxanthin (**5**) which occurs in brown algae and diatomees, was isolated by Willstätter and Page[11] in 1914, whereas its structural assignment was afforded almost 50 years later.[12] Even more strikingly, the closely related carotinoid peridinin (**6**) which



Scheme 2. Structure of the allenic carotinoids fucoxanthin (**5**) and peridinin (**6**).



Scheme 1. Proposed (left) and correct (right) structures of unsaturated natural products.

[*] Dr. A. Hoffmann-Röder
ETH Zürich
Laboratorium für Organische Chemie
ETH-Hönggerberg
8093 Zürich (Switzerland)
Fax: (+41) 1-632-1109
E-mail: anja.hoffmann-roeder@carb.org.chem.ethz.ch
Prof. Dr. N. Krause
Organic Chemistry II
University of Dortmund
44221 Dortmund (Germany)
Fax: (+49) 231-755-3884
E-mail: norbert.krause@uni-dortmund.de

 DOI: 10.1002/anie.200300628 © 2004 Wiley-VCH Verlag GmbH & Co. KGaA, Weinheim

plays an important role in the photosystem of dinoflagellates was already isolated in 1890, but fully characterized in 1971.[13]

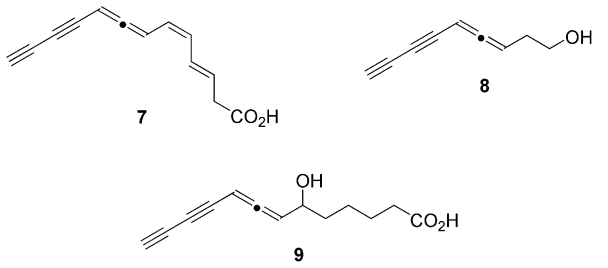
Nowadays, about 150 natural products comprising an allenic or cumulenic structure are known.[14] This number clearly proves that allenes cannot simply be considered as curiosities, but instead they represent important structural elements for a wide variety of different classes of compounds. The majority of these naturally occurring allenes can be divided into three classes (linear allenes, allenic carotinoids and terpenoids, and bromoallenes). Moreover, almost all allenic natural products reported to date are chiral and were isolated in non-racemic form, albeit not necessarily as enantiomerically pure compounds (vide infra). A substantial number of these allenes show interesting biological activities, and in recent years, many attempts have been made to further "tune" the biological and pharmacological properties of certain pharamacologically active compounds simply by introducing an allenic moiety into the existing backbone of the molecule.

In this review we will report on recent developments in the field of allenic natural products and pharmaceuticals, emphasizing their (normally stereoselective) synthesis[1,15] as well as investigations of their biological properties.

2. Allenic Natural Products

2.1. Linear Allenes

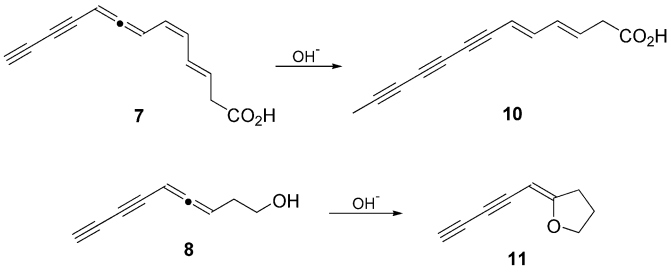
Linear allenes form the structurally simplest group of allenic natural products and comprise more than 30 compounds[5,14] isolated from such diverse sources as microorganisms, fungi, higher plants, and insects. Moreover, to this class belongs the first "authentic" allenic natural product, the fungal metabolite mycomycin (**7**)[16] which shows (as the related marasin (**8**)[17]) high antibiotic activity (Scheme 3). Interestingly, both enantiomers of marasin can be found in nature: (*R*)-(−)-marasin is isolated from *Marasmium rameallis*, while its (*S*)-(+)-enantiomer was found in *Aleurodiscus roseus*. To date quite an impressive number of naturally occurring linear allenes possessing a diyneallene structure[18,19] have been characterized, such as the antibiotic



Scheme 3. Mycomycin (**7**), marasin (**8**), and 07F275 (**9**).

diynoic allenol 07F275 (**9**)[18i] which was isolated in 1995 from a fungus originating from Panama.

The low stability of these unbranched polyenynes, however, prevented any exploitation of their biological activity. While mycomycin (**7**) readily rearranges into the dienetriyne isomycomycin (**10;** Scheme 4),[16b] the corresponding marasin (**8**) is cycloisomerized into the tetrahydrofuran analogue isomarasin (**11**).[17a]



Scheme 4. Rearrangement of linear allenes into alkynes.

With respect to crop protection, the insect pheromone methyl (*R*,*E*)-(−)-tetradeca-2,4,5-trienoate (**12**) represents also an interesting allenic target molecule. This compound was isolated in 1970 by Horler[20] from male "dried bean beetles" *Acanthoscelides obtectus* (Scheme 5). Interestingly, the beetle contains rather large amounts (ca. 0.5%) of the chiral allene which does not occur in enantiomerically pure form but with an enantiomeric excess of about 80%.



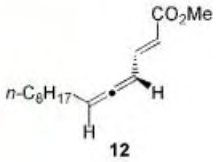
Norbert Krause, born 1959 in Wolfsburg, Germany, obtained his Ph.D. degree in chemistry in 1986 with H. Hopf at the Technical University of Braunschweig. After one-year postdoctoral appointments with D. Seebach (ETH Zürich) and M. Saunders (Yale University), he obtained his habilitation in the group of K. Hafner at the Technical University of Darmstadt in 1993. He was appointed to the University of Bonn in 1994 and subsequently moved to become a Professor of Organic Chemistry at the University of Dortmund in 1998. His research interests include the development and mechanistic understanding of metal-promoted and -catalyzed reactions, for which he has received several awards such as the Heinz–Maier–Leibnitz Preize (1991), a Heisenberg scholarship (1994), and a JSPS Fellowship (2003).



Anja Hoffmann-Röder, born 1972 in Bonn, Germany, became laboratory technician at the Degussa AG and then studied chemistry at the University of Bonn, where she obtained her Diploma for work on chiral allenophanes. Parts of her Ph.D thesis (completed in 2003 with N. Krause) on stereoselective syntheses with copper, silver, and gold were carried out with A. Alexakis (Geneva), Y. Yamamoto (Sendai), and P. Knochel (Munich). She is currently an Emmy-Noether fellow in the group of F. Diederich (ETH Zürich). For her research activities she has received the Heinrich-Hörlein-Gedächtnispreis and a DSM Award for Chemistry and Technology 2003.

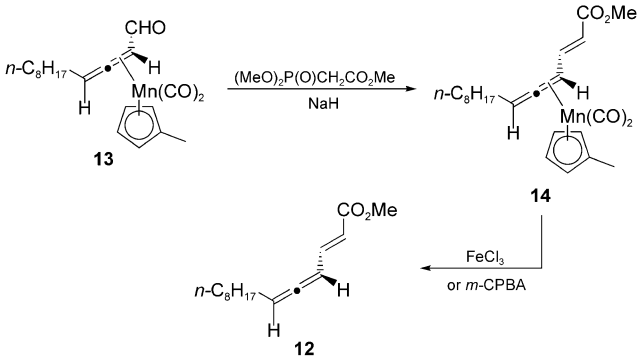
 © 2004 Wiley-VCH Verlag GmbH & Co. KGaA, Weinheim





Scheme 5. Dried bean beetle *Acanthoscelides obtectus* (left) and insect pheromone **12** (right).

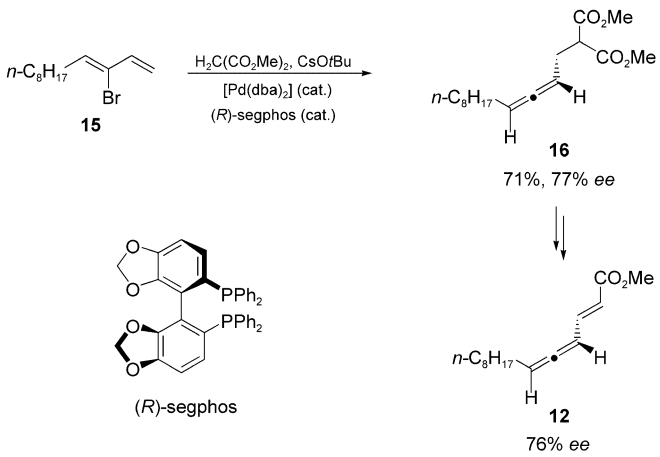
Although several syntheses of the racemic[21] as well as of the enantiomerically pure[22] allene are already known, the pheromone **12** was recently targeted again by different groups to probe newly developed stereoselective methods for the synthesis of such chiral allenes. Whereas Satoh et al.[23] benefited from the stereoselective replacement of a chiral sulfinyl group using a magnesium organometallic followed by subsequent elimination for the generation of both enantiomers of **12** with about 80% *ee*, Franck-Neumann and co-workers[24] utilized the manganese complex **13** (formed by deracemization) to obtain the enantiomerically pure target molecule **12** by Horner–Wadsworth–Emmons olefination and oxidative decomplexation of the intermediate vinylallene complex **14** (Scheme 6).



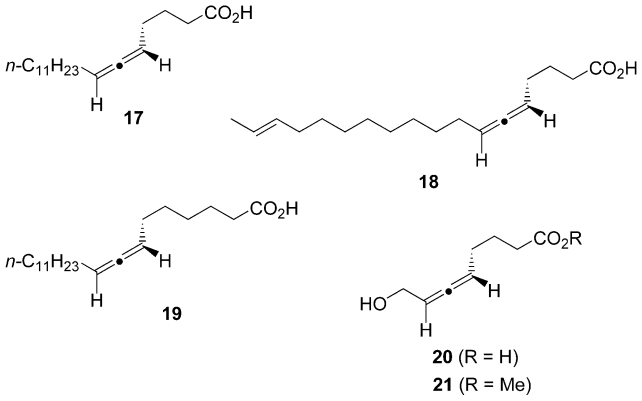
Scheme 6. Synthesis of the insect pheromone **12** from the manganese complex **13** (*m*CPBA = *m*-chloroperbenzoic acid).

Furthermore, the first *catalytic* synthesis of allenes with high enantiomeric purity[15c,25] was applied recently to the pheromone **12** by Ogasawara and Hayashi[26] (Scheme 7). The palladium-catalyzed S_N2'-substitution of the bromodiene **15** with dimethyl malonate in the presence of cesium *tert*-butanolate and catalytic amounts of the chiral ligand (*R*)-segphos furnished allene **16** with 77% *ee*. Subsequent transformation into the desired target molecule **12** by decarboxylation and selenoxide-mediated dehydrogenation proceeded without appreciable loss of stereochemical purity and led to the formation of the allenic pheromone in practically the same enantiomeric ratio as in the natural sample.

A number of closely related linear allenes has also been isolated from seed oils (Scheme 8). Examples are laballenic



Scheme 7. Synthesis of the insect pheromone **12** by palladium-catalyzed S_N2'-substitution (dba = dibenzylideneacetone).

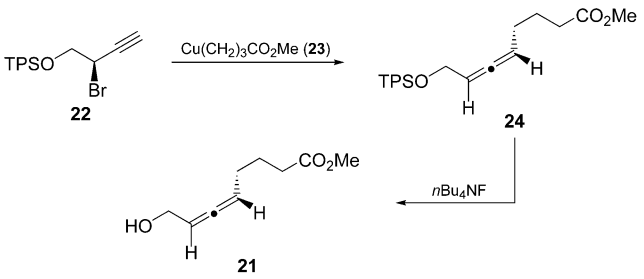


Scheme 8. Linear allenes isolated from seed oils.

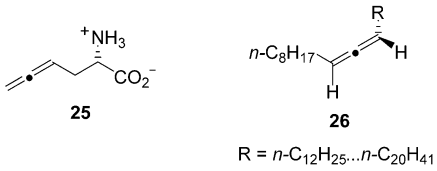
acid (**17**),[27] lamenallenic acid (**18**),[28] and phlomic acid (**19**).[29] The hydroxyacid **20** was isolated as part of a triglyceride from the chinese tallow tree *Sapium sebiferum*[30] and as its methyl ester **21** from the related species *Sapium japonicum*[31] which is found in Japan. As a consequence of its antifungal activity that efficiently prevents infections of the leaves, the allenic ester **21** had been the target of several non-stereoselective[32] and enantioselective syntheses. While Huguet and del Carmen Reyes[33] in their synthesis of **21** relied on the S_N2'-reduction of a chiral propargylic ether with lithium aluminum hydride, Gooding, Cooper, and co-workers[34] took advantage of an *anti*-stereoselective S_N2'-substitution of the propargylic bromide **22** with the functionalized organocopper compound **23** (Scheme 9).

The amino acid **25**, which has been isolated from various *Amanita* fungi,[35] is one of the few examples of a natural product with an achiral allene moiety (Scheme 10) and was prepared inter alia by Strecker synthesis as well as by substitution reactions of allenic bromides and phosphates.[36] Recently, even *unfunctionalized* allenes have been found in nature: seven allenic hydrocarbons **26** with chain lengths ranging from C_{23} to C_{31} were isolated from the skin of the Australian scarab beetle *Antitrogus consanguineus* and

 © 2004 Wiley-VCH Verlag GmbH & Co. KGaA, Weinheim



Scheme 9. Synthesis of methyl (*R*)-8-hydroxyocta-5,6-dienoate (**21**; TPS = *tert*-butyldiphenylsilyl).



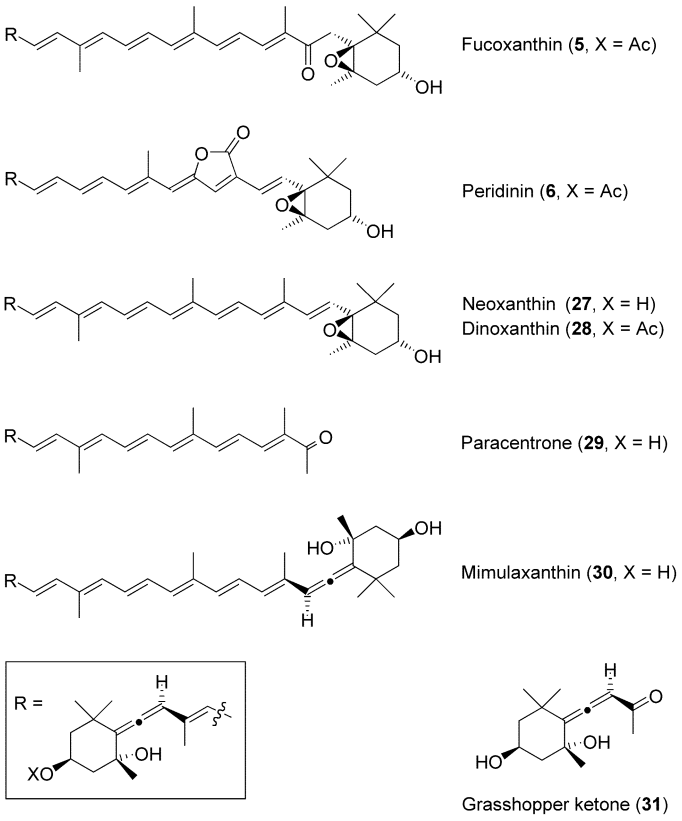
Scheme 10. Naturally occurring allenic amino acid (**25**) und allenic hydrocarbons (**26**).

related species (Scheme 10).[37] Also these allenes do not occur in enantiomerically pure form, but with enantiomeric excesses of 86–89 % *ee*. A stereoselective synthesis of the enantiomerically enriched allenic hydrocarbons was achieved by hydrostannylation and elimination (or by Mitsunobu reaction and [3,3]-sigmatropic rearrangement).[37]

2.2. Carotinoids and Terpenoids

Carotinoids and terpenoids form the largest group of allenic natural products with nowadays more than 40 isolated compounds.[5,14] As has been mentioned in the introduction, the majority of these compounds has been known for a long time, whereas the structural assignments often were accomplished after the introduction of spectroscopic methods. As a common structural feature most carotinoids bear a cyclohexylidene ring but differ in the structure of the second ring and its periphery (Scheme 11). Typical examples are (besides the already mentioned compounds fucoxanthin (**5**)[11,12] and peridinin (**6**)[13]) neoxanthin (**27**),[38] dinoxanthin (**28**),[39] and paracentrone (**29**),[40] whereas mimulaxanthin (**30**)[41] finally represents a carotinoid comprising even two allenic groups. One of the best-known allenic natural products, the so-called "grasshopper ketone" (**31**),[42] is probably a dietary metabolite of one or several of these allenic carotinoids.

Many allenic carotinoids are readily available in large amounts from natural sources and consequently, early preparative work was concentrated mainly on their interconversions. Until now, total syntheses have been documented only for fucoxanthin (**5**), peridinin (**6**), neoxanthin (**27**), paracentrone (**29**), mimulaxanthin (**30**), and the grasshopper ketone (**31**).[43] The allenic terpenoid **31** was isolated in 1968 from the defense secretion of the large flightless grasshopper *Romalea microptera* which occurs in southern USA



Scheme 11. Structures of allenic carotinoids und terpenoids.

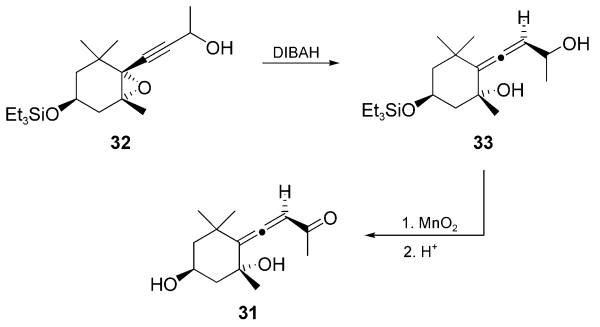
(Scheme 12).[42] The strong similarity of **31** to the carotinoids fucoxanthin (**5**) and neoxanthin (**27**) present in many plants suggests that those are oxidatively metabolized in vivo to **31**, which could also be demonstrated by in vitro experiments.[44]

The first synthesis of the racemic natural product **31** was already described in 1969,[45] and numerous (also enantioselective[46]) syntheses have followed. The introduction of the allenic moiety was achieved either by photochemical oxidation of a β-ionol-type molecule with singlet oxygen or by reduction of appropiate propargylic electrophiles with complex hydrides. Thus, the key step in the synthesis of enantiomerically pure **31** by Eugster et al.[46d] comprises a S_N2'-reduction of the propargylic oxirane **32** with diisobutylaluminum hydride (Scheme 13). The high *syn*-diastereoselec-



Scheme 12. Large flightless grasshopper *Romalea microptera* (right) and grasshopper ketone (**31**, left).

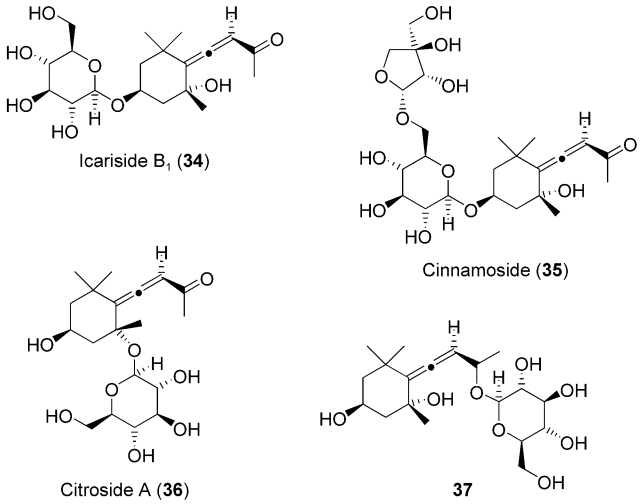
 © 2004 Wiley-VCH Verlag GmbH & Co. KGaA, Weinheim



Scheme 13. Synthesis of the grasshopper ketone (**31**) according to Eugster et al.[46d] (DIBAH = diisobutylaluminum hydride).

tivity observed in this transformation is most presumably due to a precoordination of the aluminum hydride to the epoxide oxygen atom. Since allenyl ketones of type **31** are prone to undergo a facile light-induced epimerization, this reaction sequence also provides an efficient access to stereoisomers of the grasshopper ketone.[46d]

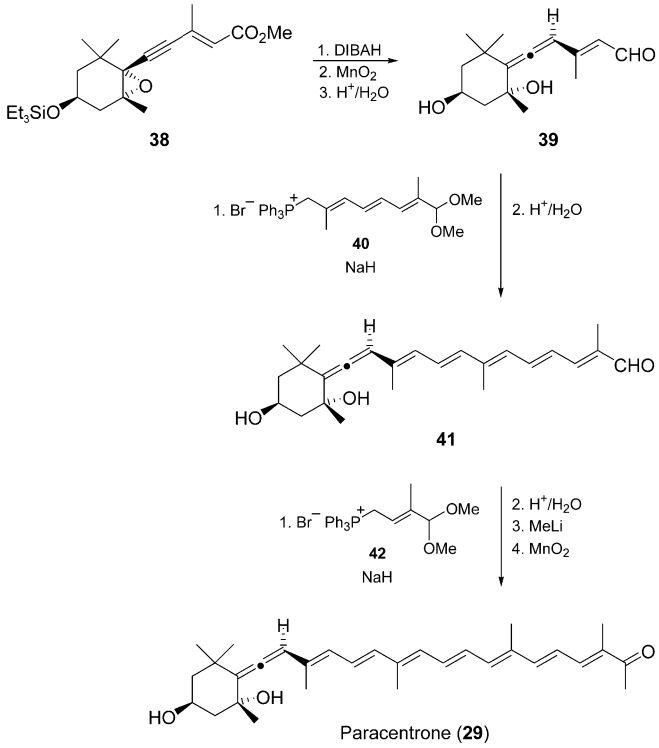
In addition to the free grasshopper ketone (**31**), the 3-*O*-acetyl derivative (apo-9′-fucoxanthinone),[47] as well as various glycosides also occur in nature (Scheme 14). Thus, the



Scheme 14. Naturally occurring glycosides of the grasshopper ketone.

terpenoid icariside B_1 (**34**) bearing a pyranose ring in 3-position was found in a variety of different plants,[49] whereas the related disaccharide cinnamoside (**35**) has only been isolated from cinnamon (*Cinnamomum cassia*).[50] This spice is used in the Asian folk medicine as "Goreisan" (China) or "Kannan Keihi" (Japan) for the treatment of fever, pain, and stomach trouble. Two further terpenoids, citroside A (**36**) and citroside B (the epimer with regard to the allenic chirality axis), bear a pyranose ring in the 5-position and are contained in the leaves of the tangerine tree *Citrus unshiu*,[51] while the terpenoid **37** (formally derived from the reduced grasshopper ketone by glycosylation in 9-position) was isolated from the leaves of the solanaceous herb *Lycium halimifolium*.[52] The first syntheses of **37**, and of derivatives of icariside B_1 (**34**), were reported recently. Here, once more the allenic entity was formed by diastereoselective reduction of propargylic oxiranes by using DIBAH.[53]

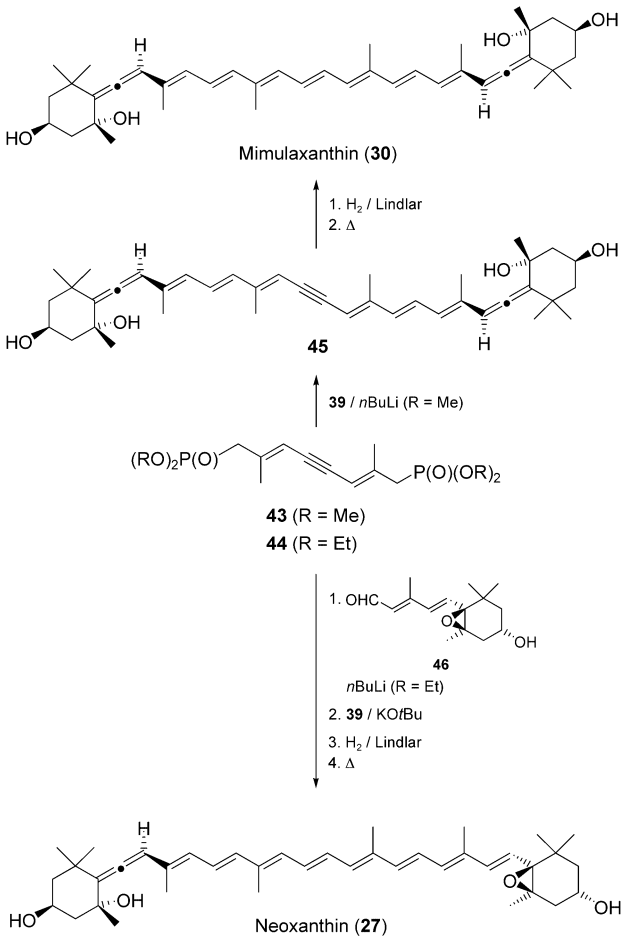
The synthesis of higher allenic carotinoids could apparently benefit from the use of the grasshopper ketone (**31**) or related allenic carbonyl compounds as substrates for olefination reactions. Thorough investigations by Eugster et al.,[54] however, have shown that derivatives of **31** are not only very unreactive in Wittig olefinations, but that the allene system may epimerize easily. Consequently, these reaction conditions are usually not suitable for the stereoselective synthesis of allenic carotinoids, although aldehyde **39** (available through *syn*-selective S_N2'-substitution reaction of the corresponding propargylic oxirane **38** with DIBAH and subsequent oxidation[54,55]) was employed successfully in the preparation of various carotinoids. In the sole reported synthesis of the C_{31}-apocarotinoid paracentrone (**29**; isolated from the sea urchin *Paracentrotus lividus*[40]), olefination of **39** with the phosphonium salt **40** furnished aldehyde **41**, which after two further chain elongation steps (by another Wittig reaction with the C_5 building block **42** followed by MeLi addition) finally provided the desired target molecule **29** (Scheme 15).[56]



Scheme 15. Synthesis of the C_{31}-apocarotinoide paracentrone (**29**).[56]

Analogous olefination reactions were used by Eugster and co-workers during their syntheses of neoxanthin (**27**)[38,57] and mimulaxanthin (**30**)[41,54] (Scheme 16). Thus, Horner–Wadsworth–Emmons reaction of two equivalents of **39** with the bisphosphonate **43** according to the building block scheme $C_{15}+C_{10}+C_{15}$ furnished the symmetrical product **45**, which was transformed into mimulaxanthin (**30**) by Lindlar hydrogenation and thermal isomerization of the central double

 © 2004 Wiley-VCH Verlag GmbH & Co. KGaA, Weinheim

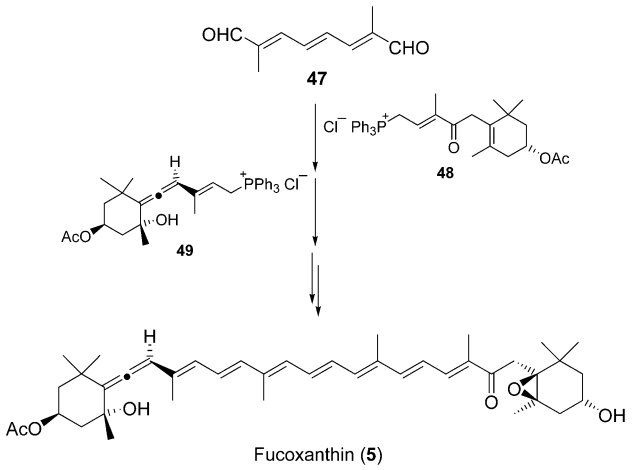


Scheme 16. Synthesis of neoxanthin (**27**) and mimulaxanthin (**30**) from the bisphosphonates **43**/**44** according to Eugster et al.[38,54,57]

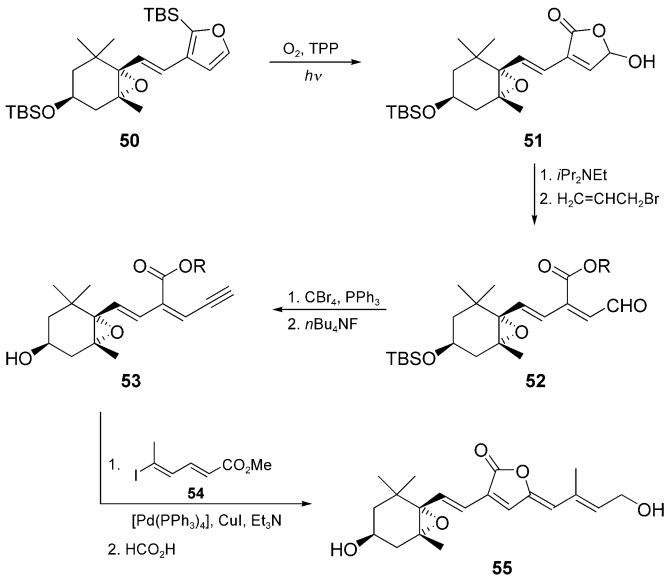
bond.[54] In contrast, stepwise olefinations of the bisphosphonate **44** with the violaxanthin building block **46** and the allenic C_{15} aldehyde **39** led to the formation of neoxanthin (**27**).[38,57]

The sole synthesis of fucoxanthin (**5**) known to to date by M. Ito et al. relied upon the opposite building block scheme, that is, the C_{10}-dialdehyde **47** was linked with the two C_{15}-phosphorane termini **48** and **49** (Scheme 17).[58] However, several steps of this synthetic approach are hardly efficient; for example, the introduction of the epoxide ring carried out in the last step furnishes mainly the non-natural diastereomer.

In contrast to this, the recently described first stereoselective[59] synthesis[43,60] of peridinin (**6**)[13] can be regarded without exaggeration as a highlight in the chemistry of allenic natural products (Scheme 18, 19). Several challenges had to be met in this synthesis, namely, the stereoselective construction of the all-*trans*-polyene chain and of the chiral allene moiety, as well as the generation of the (*Z*)-γ-alkylidenebutenolide ring. To generate the key building block **55**, the authors started with the silylfurane **50** which was oxidized chemoselectively with singlet oxygen to the corresponding butenolide **51** (Scheme 18). Subsequent ring-opening and esterification provided the aldehyde **52** which was converted into the terminal alkyne **53** by the Corey–Fuchs reaction. The



Scheme 17. Synthesis of fucoxanthin (**5**) according to Ito et al.[58]

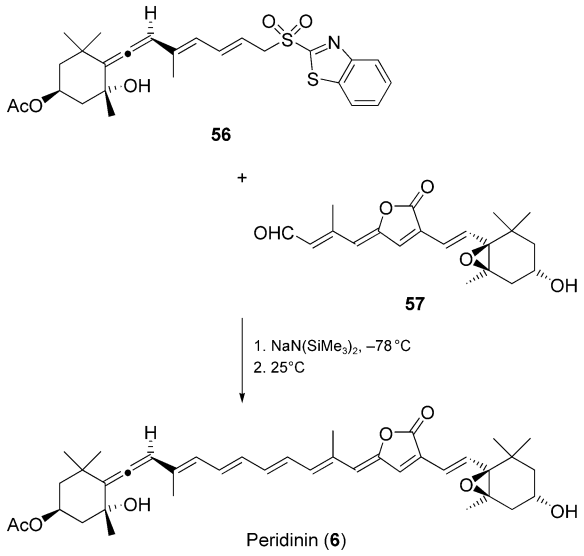


Scheme 18. Synthesis of peridinin (**5**):[59] formation of the key building block **55** (TBS = *tert*-butyldimethylsilyl, TPP = 5,10,15,20-tetraphenyl-21*H*,23*H*-porphin, R = allyl).

resulting alkyne **53** was then submitted to a Sonogashira coupling with the iododiene **54** and furnished after reductive deallylation and stereoselective lactonization the desired building block **55**. Remarkably, three of these subsequent steps were realized in an elegant one-pot procedure using different Pd^0 and Pd^{II} compounds as catalysts.

To link the two half moieties of the molecule, a Julia–Kocienski olefination was carried out between the C_{19} building block **56** (again prepared by *syn*-S_N2'-substitution of a propargylic oxirane with DIBAH) and the C_{20} building block **57**, formed by oxidation of **55** with MnO_2 (Scheme 19). Although this reaction initially led to the formation of the *Z* isomer as the major product, the latter was readily isomerized at room temperature to the desired all-*trans*-polyene peridinin (**6**).

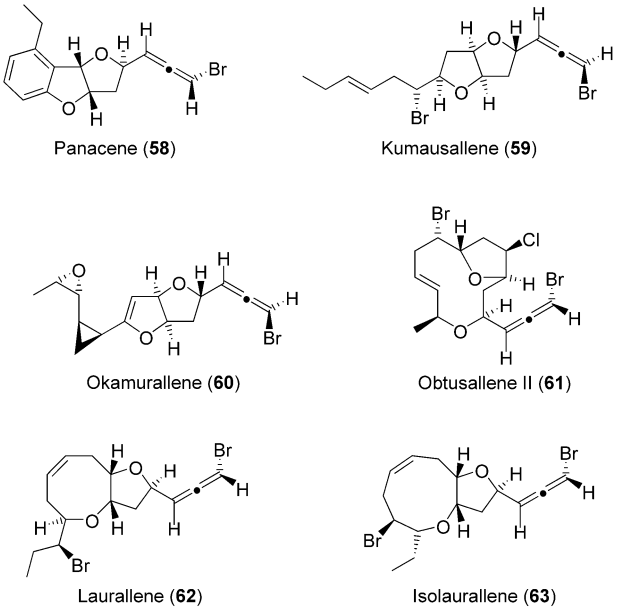
 © 2004 Wiley-VCH Verlag GmbH & Co. KGaA, Weinheim



Scheme 19. Synthesis of peridinin (**6**):[59] linking of the building blocks **56** and **57**.

2.3. Bromoallenes

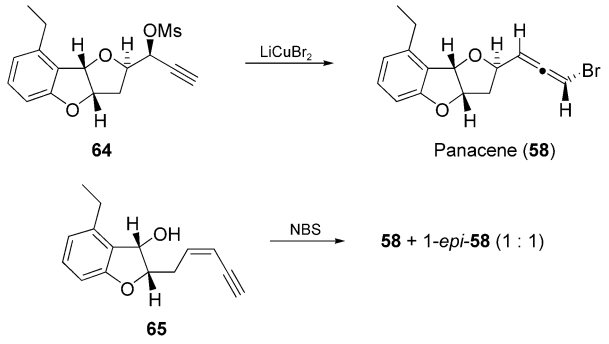
Among allenic natural products, bromoallenes form the most recently discovered group (the first example, panacene (**58**), was isolated in 1977[61]) but comprises already more than 30 members.[5,14] These are mainly C_{15}-dioxabicyclic compounds with an exocyclic bromoallene moiety[62] which were isolated from red algae or molluscs (Scheme 20).



Scheme 20. Naturally occurring bromoallenes.

The structural complexity of this class of natural products is highly impressive. The most abundant bicyclics are 2,6-dioxabicyclo[3.3.0]octanes[63] (panacene (**58**),[61] kumausallene (**59**),[64] okamurallene (**60**),[65] aplysiallene[66]) and 4,13-dioxabicyclo[8.2.1]-tridecanes (dactylallene,[67] obtusallene II (**61**),[68] obtusallenes III/IV and VII–IX[68,69]). In addition to these bicyclo[6.3.0]undecanes (laurallene (**62**),[70] pannosallene,[71] aplyparvunin[72]), bicyclo[6.4.0]dodecanes (microcladallene A–C[73]), as well as bicyclo[7.3.0]dodecanes (isolaurallene (**63**),[74] neolaurallene[75]), bicyclo[7.3.1]tridecanes (obtusallene I,[68,69] kasallene[76]), and even tricyclo[8.2.1.1^{1,4}]-tetradecanes (obtusallenes V/VI[69d]) have been observed. Of this large number of potential target molecules, so far only panacene (**58**), kumausallene (**59**), laurallene (**62**), and isolaurallene (**63**) have been the target of total syntheses.

Panacene (**58**) is a metabolite of the sea hare *Aplysia brasiliana* and acts as a fish antifeedent.[61] The synthesis of the racemic natural product published by Feldman et al.[77] in 1982 takes advantage of the *anti*-selective S_N2'-substitution of the propargylic mesylate **64** with $LiCuBr_2$ (Scheme 21). In



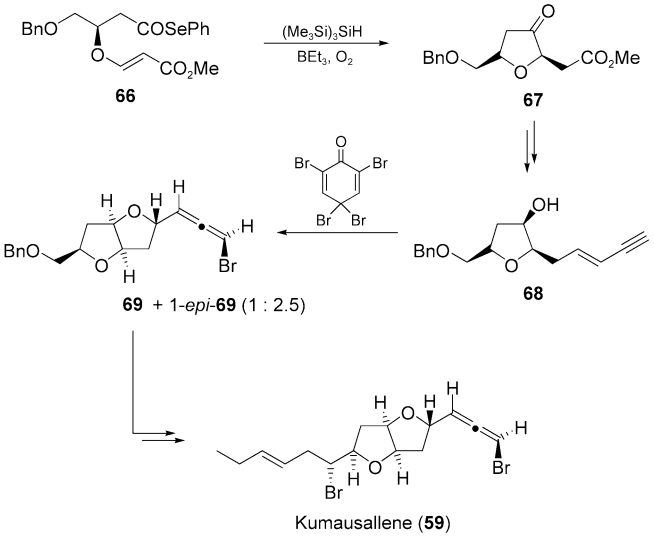
Scheme 21. Synthesis of (±)-panacene (**58**)[77,78] (Ms = methanesulfonyl, NBS = *N*-bromosuccinimide).

contrast, the later attempted biomimetic synthesis by treatment of the enyne **65** with NBS or 2,4,4,6-tetrabromocyclohexadienone did not proceed stereoselectively and led to a 1:1 mixture of the target molecule **58** together with its allenic epimer.[78]

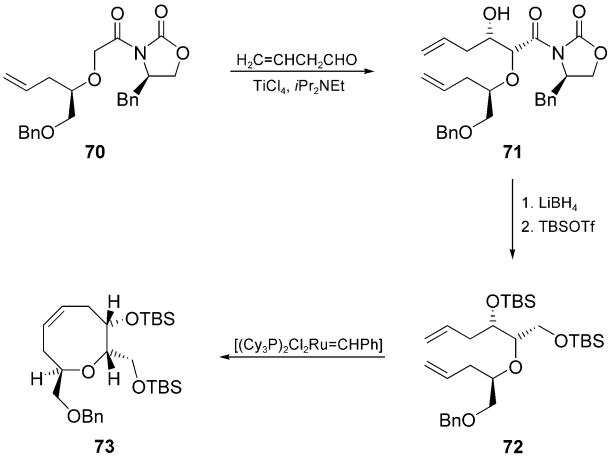
The bromoallene (−)-kumausallene (**59**) was isolated in 1983 from the red alga *Laurencia nipponica* Yamada.[64a] The synthesis of the racemic natural product by Overman et al. once more employed the S_N2'-substitution of a propargyl mesylate with lithium dibromocuprate.[79] Two formal syntheses of (−)-[80] and (+)-kumausallene[81] followed this route and relied on the enantioselective preparation of the 2,6-dioxabicyclo[3.3.0]octane system starting from diethyl tartrate or an appropriate chiral sulfoxide.

In contrast, Evans and co-workers[82] used a distinct biomimetic approach in their synthesis of the natural product (−)-**59** (Scheme 22). In this approach the *cis*-disubstituted tetrahydrofuranone **67** (accessible with high diastereoselectivity by radical cyclization of the acylselenide **66** with tris(trimethylsilyl)silane and triethylborane) was transformed into the corresponding enyne **68** by reduction and Wittig olefination. The subsequent electrophilic cyclization was carried out in analogy to the biomimetic synthesis of panacene (Scheme 21) and led to the desired bicyclic bromoallene **69**, albeit with the non-natural epimer as the major product. However, the latter can be transformed into

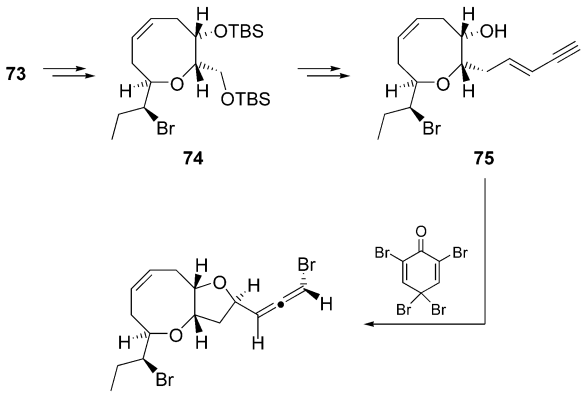
 © 2004 Wiley-VCH Verlag GmbH & Co. KGaA, Weinheim



Scheme 22. Synthesis of (−)-kumausallene (**59**)[82] (Bn = benzyl).



Scheme 23. Synthesis of laurallene (**62**):[84] aldol reaction and ring-closing metathesis (Bn = benzyl, TBS = *tert*-butyldimethylsilyl).



Scheme 24. Synthesis of laurallene (**62**):[84] formation of the side chains and electrophilic cyclization.

the desired intermediate **69** upon treatment with samarium(II) iodide and 2,4,4,6-tetrabromocyclohexadienone. The final steps in the synthesis of (−)-kumausallene (**59**) comprise deprotection of the benzyl ether, oxidation of the resulting alcohol, followed by Sakurai reaction with 3-triethylsilylpent-1-ene, as well as an Appel bromination (CBr_4/PPh_3).

The closely related bromoallenes laurallene (**62**),[70] isolaurallene (**63**),[74] and neolaurallene[75] (which is a stereoisomer of **63**) are likewise metabolites of *Laurencia nipponica* Yamada and other red algae. From a preparative point of view, interest in these natural products is mainly due to their challenging eight- and nine-membered cyclic ether structure. Moreover, in analogy to panacene and kumausallene, biomimetic studies suggest the enyne prelaureatin as the presumable precursor for laurallene (**62**).[83] However, the total syntheses of laurallene (**62**)[84] and isolaurallene (**63**)[85] published recently by Crimmins et al. do not follow this biomimetic pathway but use a ring-closing metathesis reaction for the formation of the eight- and nine-membered rings.

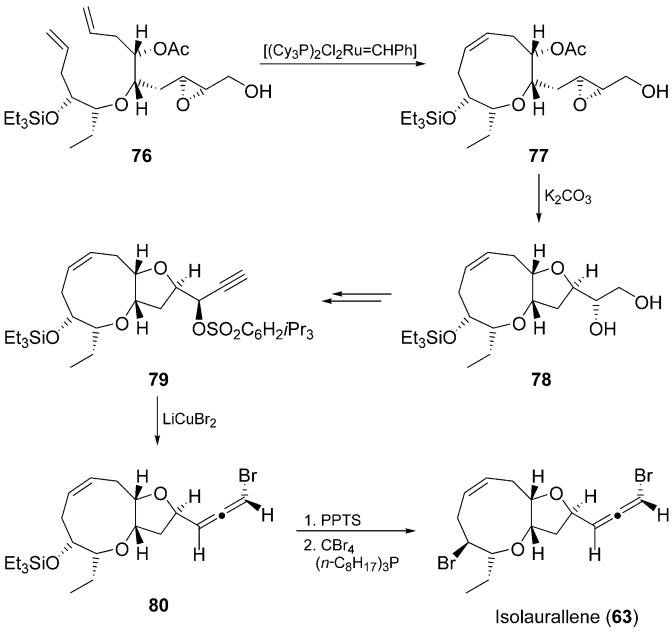
To generate the two stereogenic centers of the bicyclic system, the synthesis of laurallene (**62**) takes in one of its key steps advantage of an aldol reaction between the titanium enolate formed from the chiral oxazolidinone **70** and but-3-enal (Scheme 23). Subsequent reduction and protection of the aldol adduct **71** led to the diene **72**, which was converted with an excellent chemical yield of 95% into oxocine **73** by ring-closing metathesis using the Grubbs-I catalyst. Subsequently, the construction of the bromopropane side chain and the formation of the enyne moiety was tackled with the aid of two Wittig reactions employing a C_1 and a C_3 building block (Scheme 24). Finally, another electrophilic cyclization (cf. Scheme 21, 22) with 2,4,4,6-tetrabromcoyclohexadienone converted enyne **75** into a 1:1 mixture of the target molecule laurallene (**62**) and its allenic epimer.

In their total synthesis of isolaurallene (**63**), Crimmins et al.[85] relied upon the *anti*-selective S_N2'-substitution of a propargylic sulfonate with $LiCuBr_2$ (cf. the synthesis of panacene) instead of the enyne cyclization sequence which had turned out to be unsatisfactory in terms of stereocontrol (Scheme 25). Again, the formation of the nine-membered cyclic ether was accomplished by ring-closing metathesis of the diene **76** (formed by enantioselective alkylation and Sharpless epoxidation) with the Grubbs-I catalyst proceeding with high efficiency (94% yield). Treatment of the cyclic product **77** with potassium carbonate led to the formation of the bicyclo[7.3.0]dodecane system, and the resulting diol **78** was converted over several steps into the required propargylic sulfonate **79**. As expected, the formation of the bromoallene **80** by S_N2'-substitution took place with high *anti*-stereoselectivity, allowing the synthesis of the natural product **63** to be concluded by using the already outlined sequence of deprotection and incorporation of the secondary bromide by Appel bromination.

2.4. Other Naturally Occurring Allenes and Cumulenes

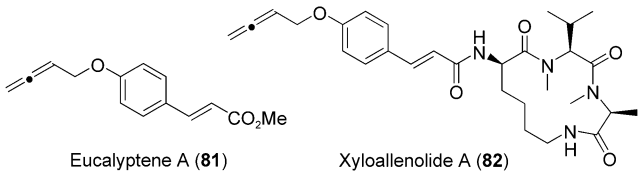
About 30 allenic natural products cannot be assigned to the three classes covered so far.[5,14] These comprise com-

 © 2004 Wiley-VCH Verlag GmbH & Co. KGaA, Weinheim



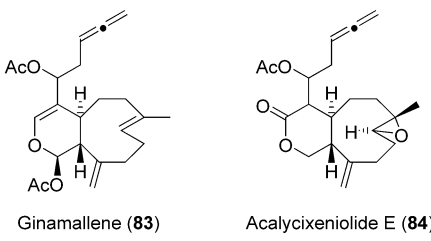
Scheme 25. Synthesis of isolaurallene (**63**)[85] (PPTS = pyridinium *p*-toluenesulfonate).

pounds with an acyclic, often achiral allene group[86] such as the cinnamate eucalyptene A (**81**) which was isolated together with the *Z* isomer eucalyptene B from the fungus *Citocybe eucalyptorum* (Scheme 26).[87] Interestingly, a fungus of the *Xylaria* species does not only contain **81** and the corresponding allenic carboxylic acid but also the cyclic peptide **82** which was labeled xyloallenolide A.[88]



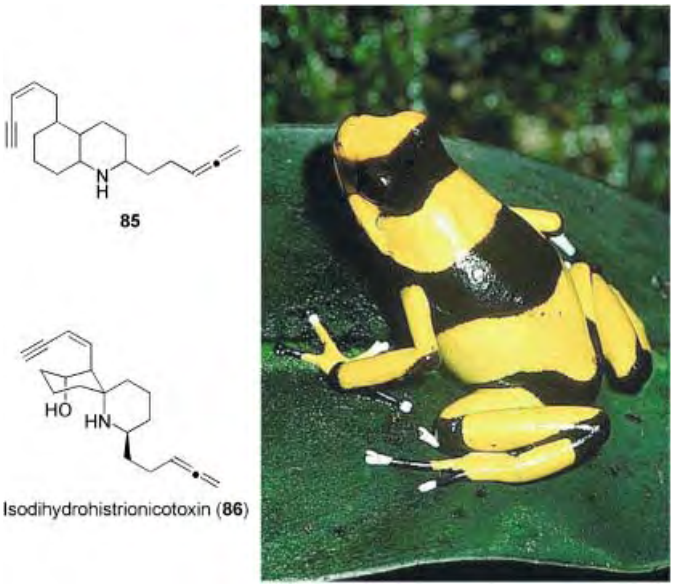
Scheme 26. Naturally occurring allenic cinnamate derivatives.

A further group of bicyclic natural products bearing a terminal allene moiety has been found in corals of the *Acalycigorgia* species.[89] Examples of these are ginamallene (**83**) and the acalycixeniolides B–F (Scheme 27). A common structural feature of these compounds is a *trans*-bicyclo[7.4.0]-tridecane system comprising an *E*-configured double bond in the larger ring that (as in acalycixeniolide E) can also be epoxidized. Several acalycixeniolides inhibit the growth of sea urchin eggs and are found to be cytotoxic against certain leukemia cell lines.[89] Furthermore, acalycixeniolide E (**84**) has been shown to possess strong anti-angiogenetic properties.[90] To date, however, no syntheses of these interesting allenic natural products have been described.



Scheme 27. Allenic natural products from *Acalycigorgia* corals.

The skin of several *Dendrobates* "poison-dart frogs" from Columbia contains some allenic alkaloids with either a decahydroquinoline[91] or an azaspiro[5.5]undecane structure[92] (Scheme 28). The decahydroquinolines of type **85**

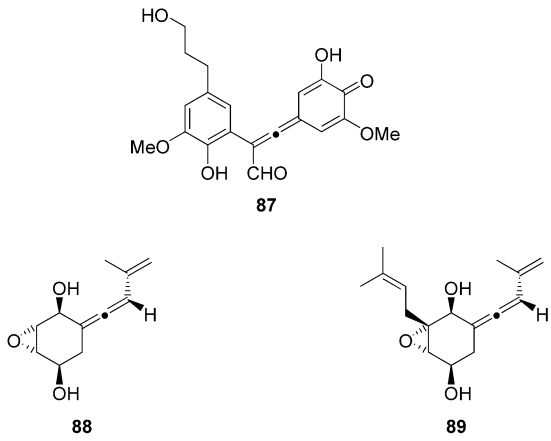


Scheme 28. "Poison-dart frog" *Dendrobates leucomelas* (right) and allenic alkaloids (left) isolated from its skin.

exist as *cis* and *trans* isomers with regard to the decalin system as well as to the attached side chains. Since frogs raised in captivity do not form these toxins, they are probably part of their diet; indeed, related compounds were also found in the ant *Solenopsis azte*ca.[91b] The allenic azaspiro[5.5]undecanes comprise isodihydrohistrionicotoxin (**86**) and isotetrahydrohistrionicotoxin which bears a 1,3-butadiene side chain instead of the enyne side chain.[92] Investigations of the interaction with ion channels of the nicotin acetylcholin receptor revealed strong similarities between the histrionicotoxins with different side chains; the strongly unsaturated allenic natural products isodihydro- (**86**) and isotetrahydrohistrionicotoxin, however, usually displayed the highest activities.[92b] Also for these allenic alkaloids no total syntheses have been reported so far.

The following natural products **87**–**89** provide examples of exocyclic allenes that do not belong to the class of carotinoids and terpenoids (Scheme 29). For example, the quinone derivative **87** has been isolated recently from the bark of the tree *Brosimum acutifolium* which occurs in the Amazon region.[93] This bark ("Murure") is used in the Brazilian folk medicine because of its anti-inflammatory and anti-rheumatic properties. In contrast, the vinylallenes **88**[94] and **89**[95]

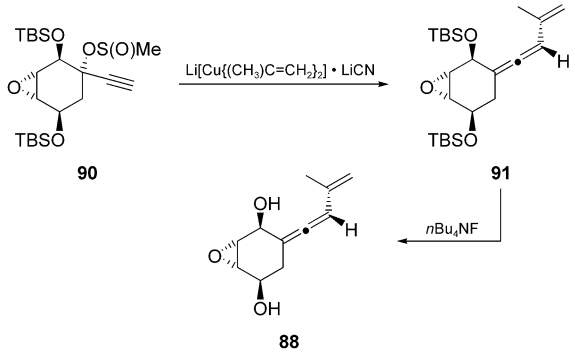
 © 2004 Wiley-VCH Verlag GmbH & Co. KGaA, Weinheim



Scheme 29. Naturally occurring exocyclic allenes.

represent once more fungal metabolites. Hence, compound **88** has been isolated from the fungus *Eutypa lata* that infects fruit trees and grapevine and causes the eutypiosis disease that finally leads to the death of the plants.

A diastereoselective synthesis of the racemic vinylallene **88** was described by Gordon and Tabacchi[96] in 1992 (Scheme 30). Here, the exocyclic allene was formed by *anti*-

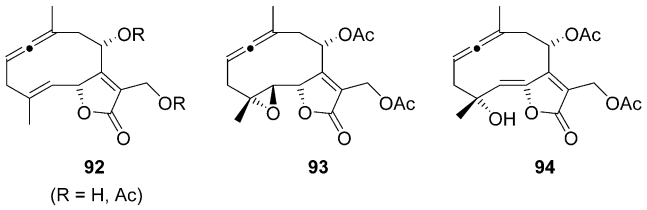


Scheme 30. Synthesis of the exocyclic vinylallene **88**.[96]

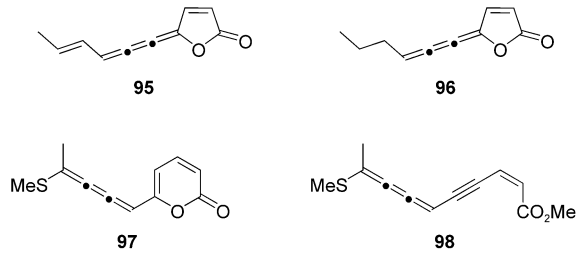
S_N2'-substitution of the propargylic sulfinate **90** with lithium diisopropenylcyanocuprate which, however, was also found to undergo side reactions such as reduction and direct attack of the nucleophile at the sulfinate. Deprotection of the substitution product **91** (which was obtained with only 35% yield) finally provided the desired target molecule **88**.

About 20 years ago, Bohlmann and co-workers examined South American plants of the widespread *Vernonia* species and found the first and (until now) only naturally occurring endocyclic allenes (Scheme 31).[97] These are the bicyclic sesquiterpene lactones **92**–**94** bearing a 10-membered ring,[98] in which the *E*-configured double bond of the larger ring can also be present in its oxidized form (**93**, **94**). As in other cases, these fascinating natural products have not been synthesized until now.

Bohlmann et al. furthermore described the sole natural products with a cumulene structure (Scheme 32).[99] These



Scheme 31. Cyclic allenes isolated from *Vernonia sp.*[97]



Scheme 32. Naturally occurring cumulenes.[99]

compounds **95**–**98** (which were isolated between 1965–1971 from the roots of camomile and other plants) are highly unstable, a fact that made their structural assignment rather difficult.

3. Pharmacologically Active Allenes

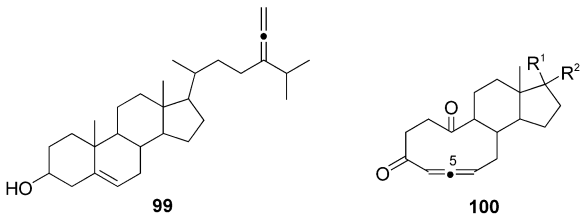
The manifold biological activities of the allenic natural products described in the previous sections might lead to the notion that it could be auspicious to include an allenic moiety also in (non-natural) pharmacologically active compounds. To estimate the potential benefit of such a cumulated double bond systems in pharmaceuticals, information about structure–activity relationships and the biogenesis of allenes should be helpful. Unfortunately, mostly (plausible) speculations but only very few experimental investigations are to be found in this field.[5] For example, it seems reasonable to ascribe the activity of the insect pheromone **12** to the allene topology (rigid C_3 unit with axial chirality), although the existence of a specific receptor for this structural element has not been proven so far. Similarly, experimental evidence is lacking for the biosynthesis of allenes which are usually thought to be formed by oxidative or reductive rearrangements of the corresponding alkynes[5,100,101] (cf. biomimetic syntheses of the bromoallenes panacene (**58**),[78] kumausallene (**59**),[82] and laurallene (**62**)[83] in Section 2.3). In spite of the lack of information about structure–activity relationships, quite a number of different allenic pharmaceuticals has been synthesized and examined in terms of their activity so far, with the results up to 1980 being reviewed already.[5] Recent advances in this field focus mainly on the inhibition of enzymes by allenic steroids, prostaglandins, amino acid, and nucleoside analogues. In this respect, a "mechanism-based inhibition" is observed frequently in which a "suicide substrate" is unmasked at the active site by the natural catalytic activity of the enzyme leading to the formation of a

 © 2004 Wiley-VCH Verlag GmbH & Co. KGaA, Weinheim

highly reactive acceptor-substituted allene which then undergoes an irreversible Michael addition with a suitable nucleophilic group of the enzyme.[5,102]

3.1. Steroids

Pharmacologically active allenic steroids have been examined intensively for about 30 years.[5] Thus, the only naturally occurring allenic steroid **99** had been synthesized three years *before* its isolation from *Callyspongia diffusa*, and it had been identified as an inhibitor of the sterol biosynthesis of the silkworm *Bombyx mori* (Scheme 33).[86d] In this early

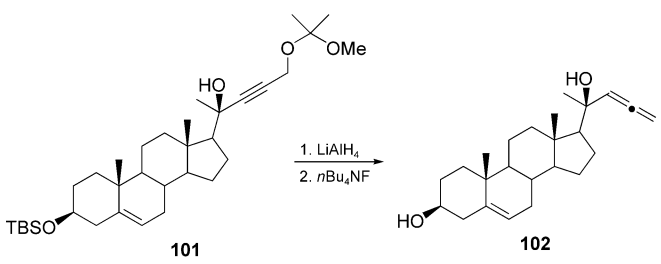


Scheme 33. Allenic steroids as inhibitors of sterol biosynthesis.

stage, allenic 3-oxo-5,10-secosteroids of type **100** have also been used for the irreversible inhibition of ketosteroid isomerases in bacteria, assuming that their activity is probably caused by Michael addition of a nucleophilic amino acid side chain of the enzyme at the 5-position of the steroid.[103,104] Since this activity is also observed in the corresponding β,γ-acetylenic ketones, it can be rationalized that the latter are converted in vivo into the allenic steroids **100** by enzymatic isomerization.[104,105]

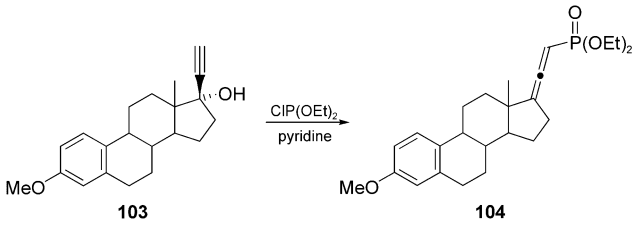
Most of the more recently described allenic steroids bear an allene group in the 17-position, which was usually formed by a S_N2'-substitution[106] or S_N2'-reduction[86d] process of a suitable propargylic electrophile. Thus, reduction of the propargylic ether **101** with lithium aluminum hydride followed by deprotection of the silyl ether resulted in the formation of the allenic steroid **102**, which irreversibly inhibits the biosynthesis of the insect-moulting hormone ecdysone (Scheme 34).[107]

Alternative, also stereoselective routes to allenic steroids take advantage of cationic cyclization reactions[108] or [2,3]-sigmatropic rearrangements.[109] For example, the allenic Michael acceptor **104** was prepared with 57% yield by



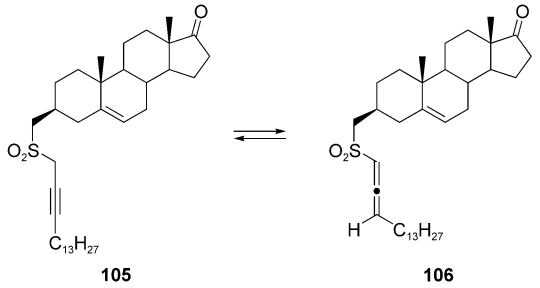
Scheme 34. Synthesis of the allenic steroid **102** by S_N2'-reduction.[107]

reaction of mestranol (**103**) with chlorodiethylphosphite and was found to inhibit the sterol biosynthesis of the pathogen responsible for *Pneumocystis-carinii* pneumonia (PCP), the most abundant AIDS-related disease (Scheme 35).[110]



Scheme 35. Synthesis of the allenic phosphonate **104** by [2,3]-sigmatropic rearrangement.[110]

Further variations of allenic steroids comprise the introduction of an allene moiety in the 10-,[111] 11-,[112] or 3-position. Williams and Boehm[113] investigated a number of steroids with propargylic sulfone side chains as inhibitors for the glucose-6-phosphate dehydrogenase (G6PDH) and observed the highest activity for substrates bearing lipophilic alkyl chains in the 3β-position (e.g., **105**; Scheme 36). Again, it is



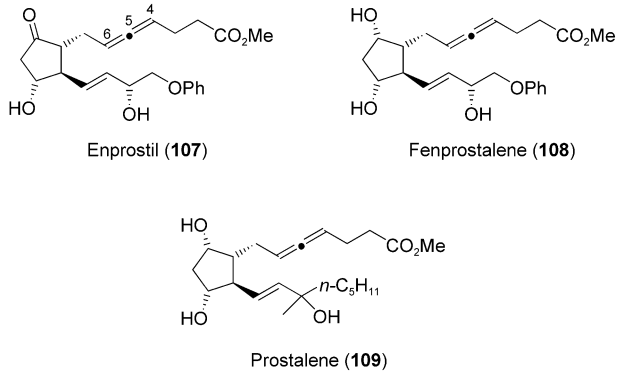
Scheme 36. Steroids substituted in the 3β-position as inhibitors of glucose-6-phosphate dehydrogenase.

assumed that an isomerization to the allenic sulfone **106** occurs in the enzymatic active site, with the latter undergoing an irreversible Michael addition with nucleophilic amino acid side chains.

3.2. Prostaglandins and Carbacyclins

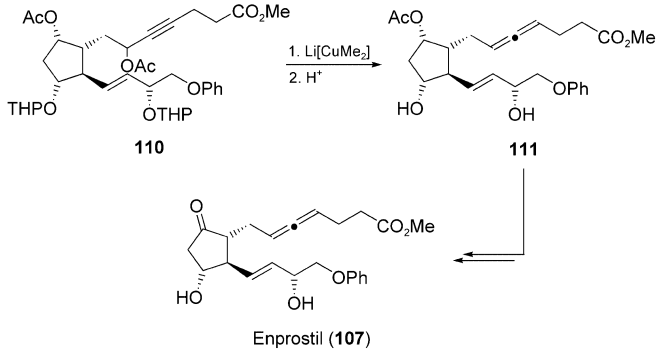
Variations of the prostaglandin and prostacyclin structures by introduction of an allenic group in the α- or ω-side chain have been the subject of many research activities in the last 30 years. Here, the major goals were not only a modulation of the pharmacological activity but also an improvement of the metabolic stability and bioavailibility of the molecules.[114] Although only few examples (with minor biological activities) have been reported for prostaglandins with allenic ω-side chains so far,[115] several compounds with an allenic entity in the 4-5-6-position have been developed and marketed (Scheme 37),[114] with the most noted example being enprostil (**107**),[114] a PGE_2-analogue that strongly

 © 2004 Wiley-VCH Verlag GmbH & Co. KGaA, Weinheim



Scheme 37. Allenic prostaglandins introduced into the market.

inhibits gastric acid secretion.[116,117] The compound is (or was) marketed in several countries under the trade names Gardrin, Camleed, or Syngard for the prevention and treatment of gastric and duodenal ulcers. The allene and phenoxy groups were introduced to decrease the metabolic susceptibility of the oral drug. Interestingly, the effect of either modification alone is rather modest, whereas enprostil is over 600 times as potent as PGE_2 in inhibiting gastric acid secretion.[118] Enprostil is usually administered as a racemic mixture of diastereomers with regard to the allenic axis of chirality. In the first synthesis of this isomeric mixture (Scheme 38),[119] the

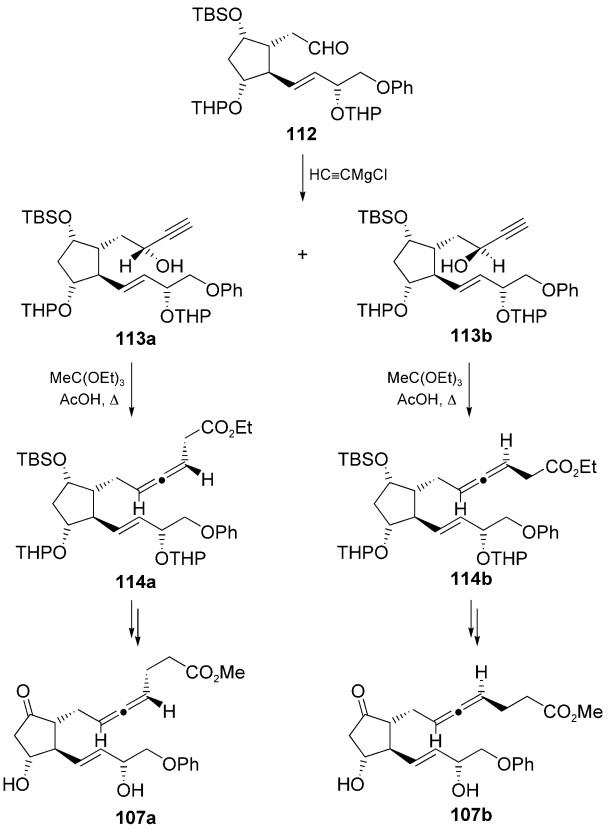


Scheme 38. Synthesis of racemic enprostil (**107**)[119,120] (THP = tetrahydropyranyl).

allenic moiety was installed by an S_N2'-reduction of the propargylic acetate **110** with lithium dimethylcuprate.[115,120] Subsequent manipulation of the protective groups and oxidation of the 9-OH group finally provided the target molecule **107**.

During the last decade, a substantial number of novel (sometimes even stereoselective) strategies for the preparation of allenic prostaglandins have been devised. The most convergent approach used by Patterson and co-workers involves the three-component coupling by a 1,4-addition of an organocopper compound to an enone, followed by alkylation of the enolate formed.[121] However, unsatisfactory yields are often obtained in this sequence which are due to the notoriously low reactivity in the alkylation of the mixed copper/lithium enolates formed during the Michael addition.[122] Hence, a detour by trapping the enolate as a silyl enol ether, subsequent transmetalation to the corresponding lithium enolate, and alkylation turned out to be more efficient.[123] In contrast to this, Sato et al.[124] employed two consecutive 1,4-addition reactions of organocopper compounds to a suitable substrate for the assembly of the enprostil framework.

Additionally, a selective synthesis of all four stereoisomers of enprostil was accomplished by Cooper and coworkers[125a] using an orthoester-Claisen rearrangement (Scheme 39). Acetylide addition to the aldehyde **112** thus



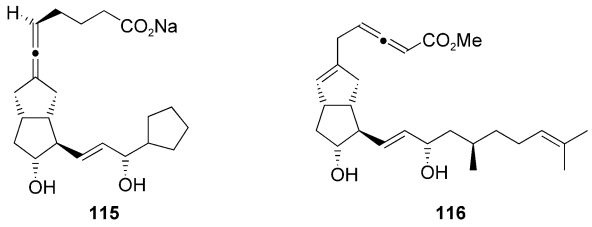
Scheme 39. Stereoselective synthesis of enprostil by orthoester–Claisen rearrangement.[125a]

furnished a 3:2 mixture of the epimeric propargylic alcohols **113a** and **113b**, which were separated chromatographically and subjected to the *syn*-stereoselective Claisen rearrangement to furnish **114a** and **114b**, respectively. The pure enprostil isomers **107a** and **107b** were finally obtained through a sequence of homologization, oxidation, and deprotection (their enantiomers were prepared accordingly). Interestingly, of these four stereoisomeric prostaglandin analogues, compound **107a** exhibits by far the highest antisecretoric activity[116b] and strongest binding to PG receptors.[117a]

The allenic $PGF_{2\alpha}$-analogues fenprostalene (**108**) and prostalene (**109**) are closely related to enprostil and are used in veterinary medicine for the synchronization of estrus. As in the synthesis of enprostil (Scheme 38), the allenic α-side chain

 © 2004 Wiley-VCH Verlag GmbH & Co. KGaA, Weinheim

is formed by a copper-mediated S_N2'-reduction.[114] Besides these prostaglandin analogues, some examples for the hydrolytically stable allenic prostacyclin analogues, namely the carbacyclin **115** and the isocarbacyclin **116** (Scheme 40) have been reported. Allene **115** is a promising antithrombotic

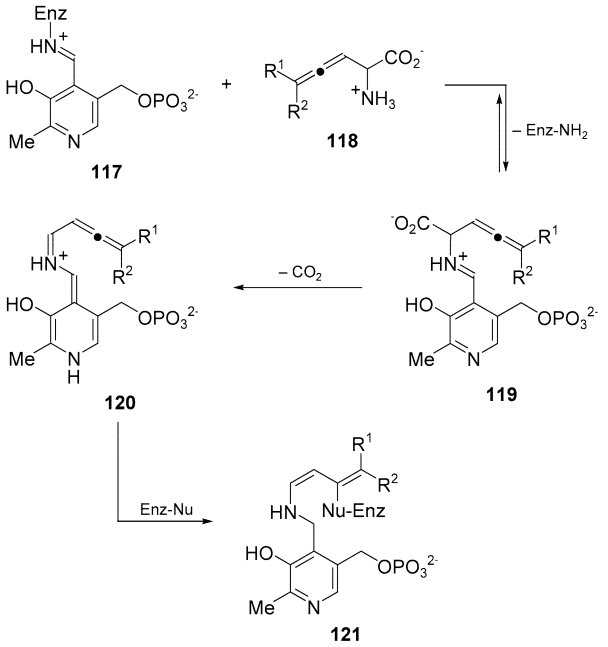


Scheme 40. Allenic carbacyclins.

agent[114] that was prepared through a [2,3]-sigmatropic rearrangement of a propargylic sulfenate and reaction of the resulting allenic sulfoxide with methyllithium.[126] In contrast to this, Mikami et al.[127] generated the allenic side chain of isocarbacyclin **116** by a palladium-catalyzed and samarium-mediated reduction of a secondary propargylic phosphate.

3.3. Amino Acids

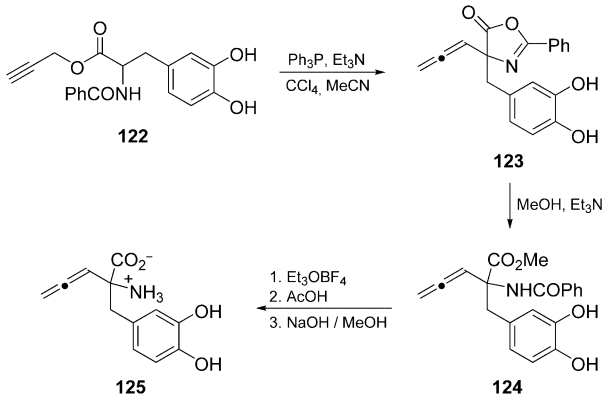
Allenic amino acids belong to the classical "suicide substrates" for the irreversible "mechanism-based inhibition" of enzymes.[5] Among the different types of allenic substrates used for enzyme inhibition,[128,129] the deactivation of vitamin-B_6-(pyridoxalphosphate)-dependent decarboxylases by α-allenic α-amino acids plays an important role (Scheme 41).



Scheme 41. Postulated inhibition mechanism of pyridoxal phosphate-dependent decarboxylases by α-allenic α-amino acids.

In analogy to the corresponding activity of other β,γ-unsaturated amino acids[102,130] it is assumed that the allenic amino acid **118** reacts with the decarboxylase **117** to furnish the imine **119**, which is transformed into a Michael acceptor of type **120** by decarboxylation. Subsequent attack of a suitable nucleophilic group of the active site then leads to inhibition of the decarboxylase by irreversible formation of the adduct **121**.[131,132]

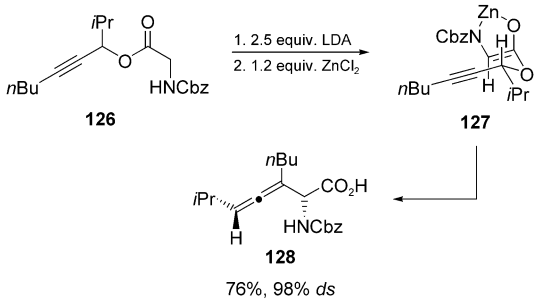
The first syntheses of α-allenic α-amino acids[131,133] took advantage of the protocol developed by Steglich and coworkers[134] for the oxazole–Claisen rearrangement of unsaturated *N*-benzoyl amino acid esters (Scheme 42). Thus,



Scheme 42. Synthesis of α-allenyl-DOPA (**125**).[133]

treatment of the propargylic ester **122** with PPh_3 and CCl_4 furnished the allenic oxazolone **123** which was converted into the amino acid derivative **124** by methanolysis. Stepwise deprotection finally led to the allenic DOPA analogue **125**, which shows a much higher decarboxylase-inhibiting activity than α-vinyl- and α-ethynyl-DOPA.[133]

Further variations of the Claisen rearrangement protocol were also utilized for the synthesis of allenic amino acid derivatives. Whereas the Ireland–Claisen rearrangement only led to unsatisfactory results,[133b] a number of variously substituted α-allenic α-amino acids were prepared by Kazmeier and Görbitz[135] by using the chelate-controlled Claisen rearrangement of ester enolates. (Scheme 43). For example, deprotonation of the propargylic ester **126** with two equiv-

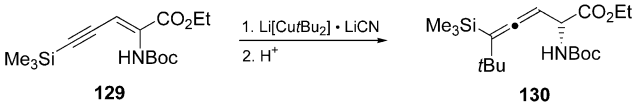


Scheme 43. Synthesis of the allenic amino acid derivative **128** by chelate-controlled Claisen rearrangement[135] (LDA = lithium diisopropylamide, Cbz = benzyloxycarbonyl).

 © 2004 Wiley-VCH Verlag GmbH & Co. KGaA, Weinheim

alents of lithium diisopropylamide and transmetalation with zinc chloride furnished the chelate complex **127**, which underwent a highly *syn*-stereoselective rearrangement to the amino acid derivative **128**.

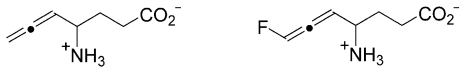
Alternative routes to α-allenic α-amino acids were described more recently and utilize radical[136] or transition-metal-catalyzed[137] allenylations, as well as copper-promoted Michael additions.[15b] Thus, sterically demanding amino acid derivatives (e.g., **130**) are accessible by the 1,6-addition reaction of lithium di-(*tert*-butyl)cyanocuprate to acceptor-substituted enynes of type **129** (Scheme 44).



129 **130**

Scheme 44. Synthesis of the allenic amino acid derivative **130** by 1,6-cuprate addition[15b] (Boc = *tert*-butoxycarbonyl).

Besides α-allenic α-amino acids, the corresponding allenic derivatives of γ-aminobutyric acid (GABA) have also been synthesized as potential inhibitors of the pyridoxalphosphate-dependent enzyme GABA-aminotransferase (Scheme 45).[131,138–142] The synthesis of γ-allenyl-GABA



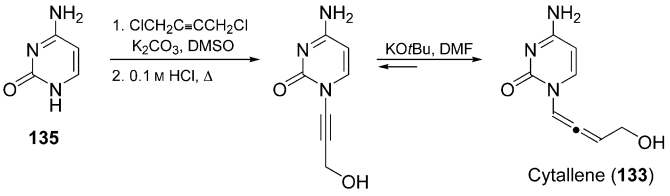
131 **132**

Scheme 45. Allenic derivatives of γ-aminobutyric acid (GABA).

(**131**) and its methylated derivatives was accomplished through Crabbé-reaction,[131] aza-Cope rearrangement,[138] and lactam allenylation,[139] while the fluoroallene **132** was prepared by S_N2'-reduction of a propargylic chloride.[141]

3.4. Nucleoside Analogues

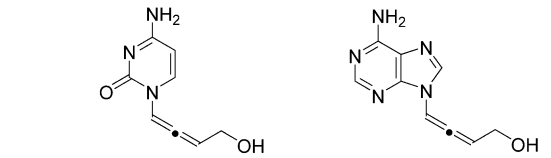
Allenic nucleoside analogues are currently of high interest as cytotoxic and antiviral agents. Prototypes of this class of compounds (Scheme 46) are the nucleoside analogues cytallene (**133**) and adenallene (**134**) that were developed by Zemlicka.[143] After the first reports of cytallene and adenallene in 1988, the array of allenic nucleoside analogues of this type has expanded considerably (e.g., guanallene, hypoxallene).[143] Cytallene (**133**) and adenallene (**134**) were selected as target molecules because of their close similarity to cytosin and adenosin (with the hydroxyallene side chain mimicking the topology of the ribose ring) and their ability to undergo in vivo phosphorylation of the hydroxy group. Both nucleoside analogues were synthesized by alkylation of the free nucleobase (e.g., cytosin **135**) with 1,4-dichlorbut-2-yne, hydrolysis to the propargylic alcohols **136**, and basic equilibration, followed by chromatographic separation of the allene **133** from the equilibrium mixture (Scheme 47).[144]



135 **136** Cytallene (**133**)

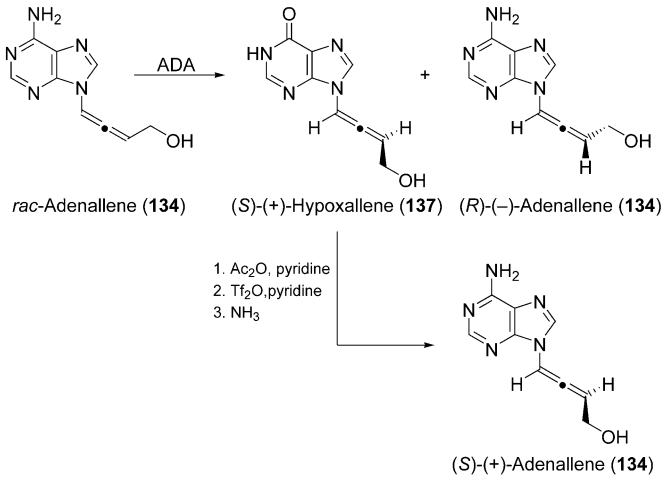
Scheme 47. Synthesis of racemic cytallene (**133**).[144]

Quickly, a number of impressive biological activities was determined for cytallene and adenallene, such as cytotoxicity and inhibition of the replication of HIV and other retroviruses.[144] In contrast to this, no antiviral activity could be detected for an adenallene analogue bearing two terminal CH_2OH groups.[145] To investigate the dependence of the antiviral activity upon the absolute configuration of the allenic side chain, the pure enantiomers of the allenic nucleoside analogues were prepared by kinetic deracemization. Whereas in the case of cytallene, this could be accomplished through a simple lipase-catalyzed acylation reaction,[146] a deamination catalyzed by adenosin deaminase had to be used for adenallene (Scheme 48).[147] Hence, the deamination reaction led to the formation of (*R*)-(−)-**134** and (*S*)-(+)-hypoxallene (**137**), with the latter being converted



Cytallene (**133**) Adenallene (**134**)

Scheme 46. Allenic nucleoside analogues.



rac-Adenallene (**134**) (*S*)-(+)-Hypoxallene (**137**) (*R*)-(−)-Adenallene (**134**)

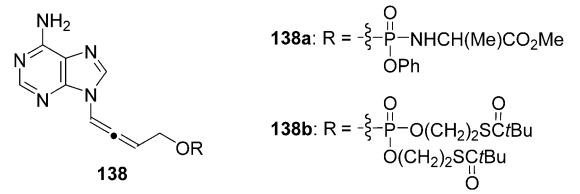
(*S*)-(+)-Adenallene (**134**)

Scheme 48. Kinetic deracemization of adenallene (**134**) by enzyme-catalyzed deamination[147] (ADA = adenosin deaminase, Tf = trifluoromethanesulfonyl).

 © 2004 Wiley-VCH Verlag GmbH & Co. KGaA, Weinheim

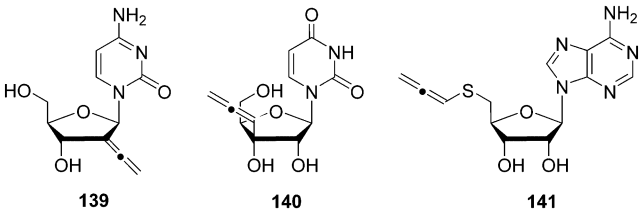
into (*S*)-(+)-adenallene by esterification, ammonolysis, and ester hydrolysis.

Attempts to inhibit HIV-1 with either enantiomer of cytallene and adenallene revealed that only the *R* enantiomer is active.[146,147] Moreover, (*R*)-(−)-cytallene is capable of inhibiting the replication of the hepatitis-B virus.[148] The activation of these nucleoside analogues (which act as "prodrugs") takes place via an enzymatic phosphorylation. Since cells resistant against antiviral agents like AZT often lack the kinases necessary for the formation of the monophosphate,[143c] a number of lipohilic phosphodiester derivatives of these allenic nucleoside analogues was designed for the inhibition of retroviruses. As expected, an increased anti-HIV activity was observed for the phosphorylated adenallene derivatives **138** (Scheme 49). Thus, the phosphodiester amidate **138a** is found to be 16 times (racemate) and 28 times (*R* enantiomer) more active than adenallene itself.[149] Interestingly, this enhanced activity, albeit less pronounced, was also found determined for the S-acylthioethylphosphate **138b**.[150] However, this increase in activity is accompanied by an enhanced cytotoxicity and a lower selectivity.



Scheme 49. Phosphodiester derivatives of adenallene.

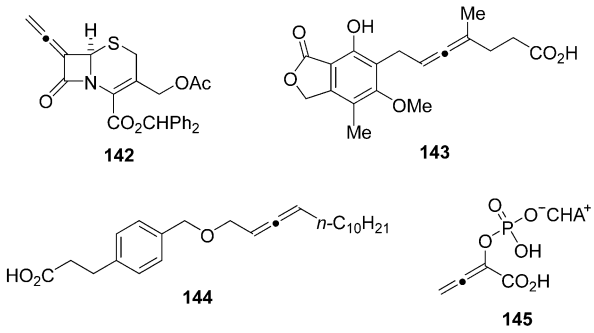
Besides these nucleoside analogues bearing an allenic chain instead of the ribofuranose ring, a few derivatives with an intact sugar ring modified by introduction of an allenic moiety have been described recently (Scheme 50). Thus, Jarvi und McCarthy[151] prepared 2′-desoxy-2′-ethenylidenecytidine (**139**) and the corresponding adenosin analogue (which are of interest as possible inhibitors for the ribonucleotide reductase or *S*-adenosyl-L-homocysteine hydrolase) by palladium-catalyzed S_N2'-reduction of the corresponding propargylic carbonates. In contrast, 3′-allenyluridine (**140**) was synthesized by Crabbé homologization of the corresponding 3′-ethynyl derivative, but did not show any antitumor activity.[152] However, similarly to cytallene and adenallene, the allenic thioether **141** is active against the vaccinia virus and was prepared by basic isomerization of the corresponding propargylic thioether.[153]



Scheme 50. Allenic nucleoside analogues with a modified ribofuranose ring.

3.5. Other Pharmacologically Active Allenes

In addition to the aforementioned allenic steroids, prostaglandins, amino acids, and nucleoside analogues, a number of other functionalized allenes has been employed (albeit with limited success) in enzyme inhibition (Scheme 51).[154–159]



Scheme 51. Functionalized allenes used for enzyme inhibition (CHA^+ = cyclohexylammonium).

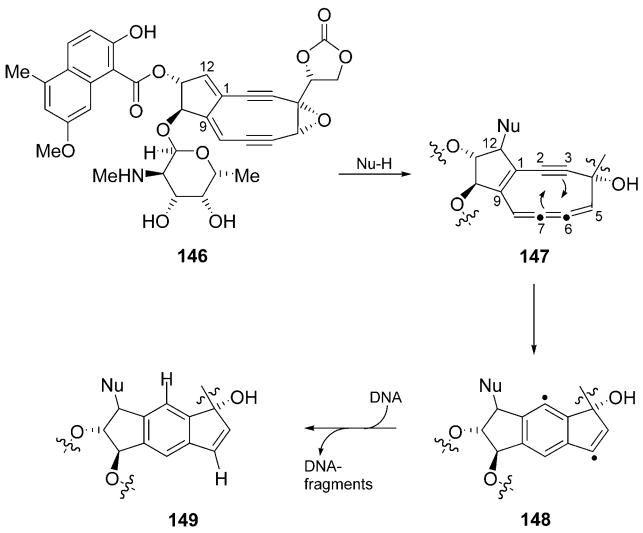
Thus, the 7-vinylidenecephalosporin **142** and related allenes did not show the expected activity as inhibitors of human leukocyte elastase, but a weak inhibition of porcine pancreas elastase.[156] Similarly disappointing were the immunosuppressive activity of the allenic mycophenolic acid derivative **143**,[157] as well as the inhibition of 12-lipoxygenase by the carboxylic acid **144**.[158] In contrast to this, the carboxyallenyl phosphate **145** turned out to be a potent inhibitor of phosphoenolpyruvate carboxylase and pyruvate kinase.[159] Hydrolysis of this allenic phosphate probably leads to 2-oxobut-3-enoate, which then undergoes an irreversible Michael addition with suitable nucleophilic side chains of the enzyme.

For a number of other pharmacologically active unsaturated compounds it is assumed that a reactive allene is formed in situ by an alkyne isomerization[160] or an elimination reaction.[161] The prime example of the formation of such a highly reactive allene through chemical activation of an unsaturated precursor is the enediyne antibiotic neocarzinostatin (Scheme 52).[162]

The strong cytotoxicity of neocarzinostatin is ascribed to an activation of the neocarzinostatin chromophore (**146**) by attack of a nucleophile (usually a thiol) in the 12-position of the bicyclo[7.3.0]dodecane core. This induces a ring-opening of the epoxide and the formation of the enynecumulene **147**, which under physiological conditions subsequently undergoes a Myers–Saito cyclization between C-3 and C-7 to give the aromatic biradical **148**. This radical is stabilized by abstraction of hydrogen atoms from the carbohydrate backbone of DNA, which causes fragmentation of the latter.[162]

Since the double bond between C-5 and C-6 of the enynecumulene **147** is not required for the Myers–Saito cyclization, a large number of enyneallenes has been synthe-

 © 2004 Wiley-VCH Verlag GmbH & Co. KGaA, Weinheim



Scheme 52. Postulated mechanism of the DNA cleavage by the neocarzinostatin chromophore **146**.[162]

sized as model compounds for the neocarzinostatin chromophore and tested for DNA-cleaving activity in recent years, with the results being already summarized extensively.[162]

4. Conclusion

From its beginnings 50 years ago, the chemistry of allenic natural products and pharmaceuticals has developed into a very attractive and prolific area of interest. Advances in the isolation and characterization of new allenic natural products were accompanied by the establishment of efficient synthetic procedures that also opened up an access to enantiomerically pure target molecules in many cases. Highlights of these developments are the enantioselective total syntheses of the allenic carotinoid peridinin (**6**) and of the bromoallenes laurallene (**62**) and isolaurallene (**63**).

Inspired by the intriguing biological activities of many allenic natural products, the systematic introduction of allenic moieties in pharmacologically active classes of compounds (steroids, prostaglandins, amino acids, nucleosides) began about 30 years ago. The functionalized allenes thus obtained often exhibit interesting activities as mechanism-based enzyme inhibitors, cytotoxic, or antiviral agents. The development of efficient methods for the stereoselective synthesis of allenes has been important in establishing allenes as a pharmacological important class of compounds, and future exciting developments in this field can be expected.

Received: August 25, 2003 [A628]

[1] a) *The Chemistry of Ketenes, Allenes and Related Compounds* (Ed.: S. Patai), Wiley, New York, **1980**; b) *The Chemistry of the Allenes* (Ed.: S. R. Landor), Academic Press, London, **1982**; c) H. F. Schuster, G. M. Coppola, *Allenes in Organic Synthesis*, Wiley, New York, **1984**; d) C. J. Elsevier in *Methods of Organic Chemistry (Houben-Weyl)*, *Vol. E21a* (Eds.: G. Helmchen, R. W. Hoffmann, J. Mulzer, E. Schaumann), Thieme, Stuttgart, **1995**, pp. 537–566; e) *Modern Allene Chemistry* (Eds.: N. Krause, A. S. K. Hashmi), Wiley-VCH, Weinheim, **2004**.

[2] J. H. Van't Hoff, *La Chimie dans L'Espace*, Bazendijk, Rotterdam, **1875**.

[3] B. S. Burton, H. v. Pechmann, *Ber. Dtsch. Chem. Ges.* **1887**, *20*, 145–149.

[4] E. R. H. Jones, G. H. Mansfield, M. L. H. Whiting, *J. Chem. Soc.* **1954**, 3208–3212.

[5] a) "Naturally Occurring Allenes": S. R. Landor in *The Chemistry of the Allenes* (Ed.: S. R. Landor), Academic Press, London, **1982**, pp. 679–707; b) A. Claesson, Biologically Active Allenes in *The Chemistry of the Allenes* (Ed.: S. R. Landor), Academic Press, London, **1982**, pp. 709–733; c) "*Biological Formation and Reactions*": C. H. Robinson, D. F. Covey in *The Chemistry of Ketenes, Allenes and Related Compounds* (Ed.: S. Patai), Wiley, Chichester, **1980**, pp. 451–485.

[6] F. W. Semmler, *Ber. Dtsch. Chem. Ges.* **1906**, *39*, 726–731.

[7] a) H. Gilman, P. R. van Ess, R. R. Burtner, *J. Am. Chem. Soc.* **1933**, *55*, 3461–3463; b) A. St. Pfau, J. Pictet, P. Plattner, B. Susz, *Helv. Chim. Acta* **1935**, *18*, 935–951.

[8] H. Staudinger, L. Ruzicka, *Helv. Chim. Acta* **1924**, *7*, 212–235.

[9] L. Crombie, S. H. Harper, D. Thompson, *J. Chem. Soc.* **1951**, 2906–2915.

[10] Interestingly, this correction has not been included in the well-known monograph by Schuster and Coppola;[1c] here, pyrothrolone is mentioned on p. 1 as the first naturally occurring allene!

[11] R. Willstätter, H. J. Page, *Justus Liebigs Ann. Chem.* **1914**, *404*, 237–271.

[12] R. Bonnett, A. A. Spark, J. L. Tee, B. C. L. Weedon, *Proc. Chem. Soc. London* **1964**, 419.

[13] a) F. Schütt, *Ber. Dtsch. Bot. Ges.* **1890**, *8*, 9–32; b) H. H. Strain, W. A. Svec, K. Aitzetmüller, M. C. Grandolfo, J. J. Katz, H. Kjøsen, S. Norgard, S. Liaaen-Jensen, F. T. Haxo, P. Wegfahrt, H. Rapoport, *J. Am. Chem. Soc.* **1971**, *93*, 1823–1825.

[14] A literature survey carried out in August 2003 in the Beilstein database BS0302PR (allene with maximum degrees of freedom in the structure editor, inp = * in the fact editor) gave 194 hits. After taking into account redundant or wrong entries and several compounds not included in this database, 146 allenic natural products (38 linear allenes, 46 allenic carotinoids and terpenoids, 33 bromoallenes, 29 other allenes) and 4 natural products with cumulene structure remained.

[15] a) "Copper-Mediated Addition and Substitution Reactions of Extended Multiple Bond Systems": N. Krause, A. Hoffmann-Röder in *Modern Organocopper Chemistry* (Ed.: N. Krause), Wiley-VCH, Weinheim, **2002**, pp. 145–166; b) N. Krause, A. Hoffmann-Röder, J. Canisius, *Synthesis* **2002**, 1759–1774; c) A. Hoffmann-Röder, N. Krause, *Angew. Chem.* **2002**, *114*, 3057–3059; *Angew. Chem. Int. Ed.* **2002**, *41*, 2933–2935.

[16] a) E. A. Johnson, K. L. Burdon, *J. Bacteriol.* **1947**, *54*, 281; b) W. D. Celmer, I. A. Solomons, *J. Am. Chem. Soc.* **1952**, *74*, 1870–1871; W. D. Celmer, I. A. Solomons, *J. Am. Chem. Soc.* **1952**, *74*, 2245–2248; W. D. Celmer, I. A. Solomons, *J. Am. Chem. Soc.* **1952**, *74*, 3838–3842.

[17] a) G. Bendz, *Arkiv. Kemi* **1959**, *14*, 305–321; G. Bendz, *Arkiv. Kemi* **1959**, *14*, 475–481; b) R. C. Cambie, A. Hirschberg, E. R. H. Jones, G. Lowe, *J. Chem. Soc.* **1963**, 4120–4130; Synthesen: c) F. Bohlmann, P. Herbst, H. Gleinig, *Chem. Ber.* **1961**, *94*, 948–957; c) R. J. D. Evans, S. R. Landor, J. P. Regan, *J. Chem. Soc. Perkin Trans. 1* **1974**, 552–556; d) S. R. Landor, B. J. Miller, J. P. Regan, A. R. Tatchell, *J. Chem. Soc. Perkin Trans. 1* **1974**, 557–561; e) W. de Graaf, A. Smits, J. Boersma, G. van Koten, W. P. Hoekstra, *Tetrahedron* **1988**, *44*, 6699–6704.

[18] a) R. E. Bew, J. R. Chapman, E. R. H. Jones, B. E. Lowe, G. Lowe, *J. Chem. Soc. C* **1966**, 129 – 135; b) R. E. Bew, R. C. Cambie, E. R. H. Jones, G. Lowe, *J. Chem. Soc. C* **1966**, 135 – 138; c) P. D. Landor, S. R. Landor, P. Leighton, *J. Chem. Soc. Perkin Trans. 1* **1975**, 1628 – 1632; d) F. Bohlmann, W. Sucrow, I. Queck, *Chem. Ber.* **1964**, *97*, 2586 – 2597; e) J. D. Bu'Lock, E. R. H. Jones, P. R. Leeming, *J. Chem. Soc.* **1955**, 4270 – 4276; f) J. D. Bu'Lock, E. R. H. Jones, P. R. Leeming, *J. Chem. Soc.* **1957**, 1097 – 1101; g) J. D. Bu'Lock, H. Gregory, *J. Chem. Soc.* **1960**, 2280 – 2285; h) E. R. H. Jones, P. R. Leeming, W. A. Remers, *J. Chem. Soc.* **1960**, 2257 – 2263; i) G. Schlingmann, L. Milne, C. J. Pearce, D. B. Borders, M. Greenstein, W. M. Maise, G. T. Carter, *J. Antibiot.* **1995**, *48*, 375 – 379.

[19] Isolation of 9-oxadeca-2,4,5,7-tetraenoic acid from *Streptomyces kitasatoensis*: S. Omura, H. Imai, H. Takeshima, A. Nakagawa, *Chem. Pharm. Bull.* **1976**, *24*, 3139 – 3143.

[20] D. F. Horler, *J. Chem. Soc. C* **1970**, 859 – 862.

[21] a) P. J. Kocienski, G. Cernigliaro, G. Feldstein, *J. Org. Chem.* **1977**, *42*, 353 – 355; b) R. W. Lang, E. Kohl-Mines, H.-H. Hansen, *Helv. Chim. Acta* **1985**, *68*, 2249 – 2253c) N. Krause, A. Gerold, *Angew. Chem.* **1997**, *109*, 194 – 213; *Angew. Chem. Int. Ed. Engl.* **1997**, *36*, 186 – 204.

[22] a) W. H. Pirkle, C. W. Boeder, *J. Org. Chem.* **1978**, *43*, 2091 – 2093; b) K. Mori, T. Nukada, T. Ebata, *Tetrahedron* **1981**, *37*, 1343 – 1347.

[23] T. Satoh, N. Hanaki, Y. Kuramochi, Y. Inoue, K. Hosoya, K. Sakai, *Tetrahedron* **2002**, *58*, 2533 – 2549.

[24] M. Franck-Neumann, D. Martina, D. Neff, *Tetrahedron: Asymmetry* **1998**, *9*, 697 – 708.

[25] a) M. Ogasawara, H. Ikeda, T. Nagano, T. Hayashi, *J. Am. Chem. Soc.* **2001**, *123*, 2089 – 2090; b) M. Ogasawara, K. Ueyama, T. Nagano, T. Mizuhata, T. Hayashi, *Org. Lett.* **2003**, *5*, 217 – 219.

[26] M. Ogasawara, T. Nagano, T. Hayashi, unpublished results.

[27] a) M. O. Bagby, C. R. Smith, Jr., I. A. Wolff, *J. Org. Chem.* **1965**, *30*, 4227 – 4229; b) F. Bohlmann, K.-M. Rode, M. Grenz, *Chem. Ber.* **1967**, *100*, 3201 – 3203; c) S. R. Landor, N. Punja, *Tetrahedron Lett.* **1966**, 4905 – 4907.

[28] a) K. L. Mikalaijczak, M. F. Rogers, C. R. Smith, I. A. Wolff, *Biochem. J.* **1967**, *105*, 1245 – 1249; b) J. S. Cowie, P. D. Landor, S. R. Landor, N. Punja, *J. Chem. Soc. Perkin Trans. 1* **1972**, 2197 – 2201.

[29] K. Aitzetmüller, N. Tsevegsüren, K. Vosmann, *Fett/Lipid* **1997**, *99*, 74 – 78.

[30] H. W. Sprecher, R. Maier, M. Barber, R. T. Holman, *Biochemistry* **1965**, *4*, 1856 – 1863.

[31] H. Ohigashi, K. Kawazu, H. Egawa, T. Mitsui, *Agric. Biol. Chem.* **1972**, *36*, 1399 – 1403.

[32] a) D. J. Rodini, B. B. Snider, *Tetrahedron Lett.* **1980**, *21*, 3857 – 3860; b) T. G. Back, B. P. Dyck, *Tetrahedron Lett.* **1992**, *33*, 4725 – 4726.

[33] J. Huguet, M. del Carmen Reyes, *Tetrahedron Lett.* **1990**, *31*, 4279 – 4280.

[34] O. W. Gooding, C. C. Beard, D. Y. Jackson, D. L. Wren, G. F. Cooper, *J. Org. Chem.* **1991**, *56*, 1083 – 1088.

[35] a) W. S. Chilton, G. Tsou, L. Kirk, R. G. Benedict, *Tetrahedron Lett.* **1968**, 6283 – 6284; b) S.-I. Hatanaka, Y. Niimura, K. Takishima, J. Sugiyama, *Phytochemistry* **1998**, *49*, 573 – 578.

[36] a) D. K. Black, S. R. Landor, *J. Chem. Soc. C* **1968**, 281 – 283; D. K. Black, S. R. Landor, *J. Chem. Soc. C* **1968**, 283 – 287; b) J. E. Baldwin, R. M. Adlington, A. Basak, *J. Chem. Soc. Chem. Commun.* **1984**, 1284 – 1285; c) B. Cazes, D. Djahanbini, J. Goré, J.-P. Genet, J.-M. Gaudin, *Synthesis* **1988**, 983 – 985; d) M. J. Dunn, R. F. W. Jackson, J. Pietruszka, D. Turner, *J. Org. Chem.* **1995**, *60*, 2210 – 2215, and references therein.

[37] a) M. T. Fletcher, M. J. McGrath, W. A. König, C. J. Moore, B. W. Cribb, P. G. Allsopp, W. Kitching, *Chem. Commun.* **2001**, 885 – 886; b) M. J. McGrath, M. T. Fletcher, W. A. König, C. J. Moore, B. W. Cribb, P. G. Allsopp, W. Kitching, *J. Org. Chem.* **2003**, *68*, 3739 – 3748.

[38] Isolation and structure:A. Baumeler, C. H. Eugster, *Helv. Chim. Acta* **1992**, *75*, 773 – 790, and references therein.

[39] a) Isolation: H. H. Strain, W. M. Manning, G. Hardin, *Biol. Bull.* **1944**, *86*, 169 – 191; structure: b) J. E. Johansen, W. A. Svec, S. Liaaen-Jensen, F. T. Haxo, *Phytochemistry* **1974**, *13*, 2261 – 2271; c) J. E. Johansen, G. Borch, S. Liaaen-Jensen, *Phytochemistry* **1980**, *19*, 441 – 444.

[40] Isolation and structure: G. Galasko, J. Hora, T. P. Toube, B. C. L. Weedon, D. Andre, M. Barbier, E. Lederer, V. R. Villanueva, *J. Chem. Soc. C* **1969**, 1264 – 1265.

[41] a) Isolation: T. W. Goodwin, D. M. Thomas, *Phytochemistry* **1964**, *3*, 47 – 50; b) structure: H. Nitsche, *Z. Naturforsch. C* **1973**, *28*, 481 – 487.

[42] a) Isolation and structure: J. Meinwald, K. Erickson, M. Hartshorn, Y. C. Meinwald, T. Eisner, *Tetrahedron Lett.* **1968**, 2959 – 2962; b) configuration: T. E. DeVille, M. B. Hursthouse, S. W. Russell, B. C. L. Weedon, *J. Chem. Soc. Chem. Commun.* **1969**, 754 – 755.

[43] Review: M. Ito, Y. Yamano, S. Sumiya, A. Wada, *Pure Appl. Chem.* **1994**, *66*, 939 – 946.

[44] a) A. Jensen, *Acta Chem. Scand.* **1964**, *18*, 2005 – 2007; b) R. Bonnett, A. K. Mallams, J. L. Tee, B. C. L. Weedon, A. McCormick, *J. Chem. Soc. Chem. Commun.* **1966**, 515 – 516; c) R. Bonnett, A. K. Mallams, A. A. Spark, J. L. Tee, B. C. L. Weedon, A. McCormick, *J. Chem. Soc. C* **1969**, 429 – 454; d) T. E. DeVille, M. B. Hursthouse, S. W. Russell, B. C. L. Weedon, *J. Chem. Soc. Chem. Commun.* **1969**, 1311 – 1312.

[45] a) S. W. Russell, B. C. L. Weedon, *J. Chem. Soc. Chem. Commun.* **1969**, 85 – 86; b) J. Meinwald, L. Hendry, *Tetrahedron Lett.* **1969**, 1657 – 1660; c) S. Isoe, S. Katsumura, S. B. Hyeon, T. Sakan, *Tetrahedron Lett.* **1971**, 1089 – 1092; d) J. R. Hlubucek, J. Hora, S. W. Russell, T. P. Toube, B. C. L. Weedon, *J. Chem. Soc. Perkin Trans. 1* **1974**, 848 – 852.

[46] a) K. Mori, *Tetrahedron Lett.* **1973**, 723 – 726; b) K. Mori, *Tetrahedron* **1974**, 1065 – 1072; c) M. Ito, Y. Hirata, K. Tsukida, N. Tanaka, K. Hamada, R. Hino, T. Fujiwara, *Chem. Pharm. Bull.* **1988**, *36*, 3328 – 3340; d) A. Baumeler, W. Brade, A. Haag, C. H. Eugster, *Helv. Chim. Acta* **1990**, *73*, 700 – 715.

[47] Y. Doi, M. Ishibashi, N. Yamaguchi, J. Kobayashi, *J. Nat. Prod.* **1995**, *58*, 1097 – 1099.

[48] In grapes (*Vitis vinifera*): M. A. Sefton, G. A. Skouroumounis, R. A. Massy-Westropp, P. J. Williams, *Aust. J. Chem.* **1989**, *42*, 2071 – 2084.

[49] a) T. Miyase, A. Ueno, N. Takizawa, H. Kobayashi, H. Karasawa, *Chem. Pharm. Bull.* **1987**, *35*, 1109 – 1117; b) S. Shimiyu, T. Miyase, A. Ueno, K. Usmanghani, *Phytochemistry* **1989**, *28*, 3399 – 3402; c) T. Miyase, A. Ueno, N. Takizawa, H. Kobayashi, H. Oguchi, *Phytochemistry* **1989**, *28*, 3483 – 3485; d) F. Abe, T. Yamauchi, *Phytochemistry* **1993**, *33*, 1499 – 1501.

[50] Y. Shiraga, K. Okano, T. Akira, C. Fukaya, K. Yokoyama, S. Tanaka, H. Fukui, M. Tabata, *Tetrahedron* **1988**, *44*, 4703 – 4711.

[51] K. Umehara, I. Hattori, T. Miyase, A. Ueno, S. Hara, C. Kageyama, *Chem. Pharm. Bull.* **1988**, *36*, 5004 – 5008.

[52] a) R. Näf, A. Velluz, W. Thommen, *Tetrahedron Lett.* **1990**, *31*, 6521 – 6522; b) H. Sudo, T. Ide, H. Otsuka, E. Hirata, A. Takushi, T. Shinzato, Y. Takeda, *Chem. Pharm. Bull.* **2000**, *48*, 542 – 546.

[53] Y. Yamano, Y. Watanabe, N. Watanabe, M. Ito, *J. Chem. Soc. Perkin Trans. 1* **2002**, 2833 – 2844.

[54] A. Baumeler, C. H. Eugster, *Helv. Chim. Acta* **1991**, *74*, 469 – 486.

[55] Biomimetic synthesis of the aldehyde **39**: M. Nakano, N. Furuichi, H. Mori, S. Katsumura, *Tetrahedron Lett.* **2001**, *42*, 7307 – 7310.

 © 2004 Wiley-VCH Verlag GmbH & Co. KGaA, Weinheim

[56] a) J. A. Haugan, *Tetrahedron Lett.* **1996**, *37*, 3887 – 3890; b) J. A. Haugan, *J. Chem. Soc. Perkin Trans. 1* **1997**, 2731 – 2737.
[57] A. Baumeler, O. Zerbe, R. Kunz, C. H. Eugster, *Helv. Chim. Acta* **1994**, *77*, 909 – 930.
[58] a) Y. Yamano, M. Ito, *Chem. Pharm. Bull.* **1994**, *42*, 410 – 412; b) Y. Yamano, C. Tode, M. Ito, *J. Chem. Soc. Perkin Trans. 1* **1995**, 1895 – 1904.
[59] N. Furuichi, H. Hara, T. Osaki, H. Mori, S. Katsumura, *Angew. Chem.* **2002**, *114*, 1065 – 1068; *Angew. Chem. Int. Ed.* **2002**, *41*, 1023 – 1026.
[60] Synthesis of racemic peridinin: a) M. Ito, Y. Hirata, Y. Shibata, K. Tsukida, *J. Chem. Soc. Perkin Trans. 1* **1990**, 197 – 199; b) M. Ito, *Pure Appl. Chem.* **1991**, *63*, 13 – 22; c) M. Ito, Y. Yamano, Y. Shibata, *Methods Enzymol.* **1992**, *213*, 13 – 22; d) Y. Yamano, M. Ito, *J. Chem. Soc. Perkin Trans. 1* **1993**, 1599 – 1610.
[61] R. Kinnel, A. J. Duggan, T. Eisner, J. Meinwald, *Tetrahedron Lett.* **1977**, 3913 – 3916.
[62] Isolation of bromoallene fatty acids from Asian lichens: T. Rezanka, V. M. Dembitsky, *Phytochemistry* **2001**, *56*, 869 – 874.
[63] Graciosallene (isolated from the red alga *Laurencia obtusa*) can be considered to be an opened 2,6-dioxabicyclo[3.3.0]octane: a) M. Norte, J. J. Fernandez, J. Z. Ruano, M. L. Rodriguez, P. Perez, *Phytochemistry* **1988**, *27*, 3537 – 3539; b) M. Norte, J. J. Fernandez, J. Z. Ruano, *Tetrahedron* **1989**, *45*, 5987 – 5994.
[64] a) T. Suzuki, K. Koizumi, M. Suzuki, E. Kurosawa, *Chem. Lett.* **1983**, 1639 – 1642; cf.: b) M. Suzuki, E. Kurosawa, *Phytochemistry* **1985**, *24*, 1999 – 2002.
[65] Isolation: a) M. Suzuki, E. Kurosawa, *Tetrahedron Lett.* **1981**, *22*, 3853 – 3856; b) M. Suzuki, E. Kurosawa, *Chem. Lett.* **1982**, 289 – 292; structure: c) M. Suzuki, Y. Sasage, M. Ikura, K. Hikichi, E. Kurosawa, *Phytochemistry* **1989**, *28*, 2145 – 2148; d) M. Suzuki, H. Kondo, I. Tanaka, *Chem. Lett.* **1991**, 33 – 34.
[66] Y. Okamoto, N. Nitanda, M. Ojika, Y. Sakagami, *Biosci. Biotechnol. Biochem.* **2001**, *65*, 474 – 476.
[67] M. L. Ciavatta, M. Gavagnin, R. Puliti, G. Cimino, E. Martinez, J. Ortea, C. A. Mattia, *Tetrahedron* **1997**, *53*, 17343 – 17350.
[68] a) P. J. Cox, S. Imre, S. Islimyeli, R. H. Thomson, *Tetrahedron Lett.* **1982**, *23*, 579 – 580; b) G. Guella, G. Chiasera, I. Mancini, A. Öztunc, F. Pietra, *Chem. Eur. J.* **1997**, *3*, 1223 – 1231.
[69] a) A. Öztunc, S. Imre, H. Wagner, M. Norte, J. J. Fernandez, R. Gonzalez, *Tetrahedron* **1991**, *47*, 2273 – 2276; b) G. Guella, I. Mancini, A. Öztunc, F. Pietra, *Helv. Chim. Acta* **2000**, *83*, 336 – 348.
[70] a) A. Fukuzawa, E. Kurosawa, *Tetrahedron Lett.* **1979**, 2797 – 2800; b) M. Suzuki, K. Koizumi, H. Kikuchi, T. Suzuki, E. Kurosawa, *Bull. Chem. Soc. Jpn.* **1983**, *56*, 715 – 718; compare: c) A. D. Wright, G. M. Koenig, O. Sticher, *J. Nat. Prod.* **1991**, *54*, 1025 – 1033; d) ref. [65c].
[71] M. Suzuki, Y. Takahashi, Y. Matsuo, M. Masuda, *Phytochemistry* **1996**, *41*, 1101 – 1103.
[72] T. Miyamoto, Y. Ebisawa, R. Higuchi, *Tetrahedron Lett.* **1995**, *36*, 6073 – 6074.
[73] a) D. J. Kennedy, I. A. Selby, H. J. Cowe, P. J. Cox, R. H. Thomson, *J. Chem. Soc. Chem. Commun.* **1984**, 153 – 155; b) M. Suzuki, S. Nakano, Y. Takahashi, T. Abe, M. Masuda, H. Takahashi, K. Kobayashi, *J. Nat. Prod.* **2002**, *65*, 801 – 804.
[74] K. Kurata, A. Furusaki, K. Suehiro, C. Katayama, T. Suzuki, *Chem. Lett.* **1982**, 1031 – 1034.
[75] a) M. Suzuki, E. Kurosawa, A. Furusaki, S.-I. Katsuragi, T. Matsumoto, *Chem. Lett.* **1984**, 1033 – 1034; b) J. C. Coll, A. D. Wright, *Aust. J. Chem.* **1989**, *42*, 1685 – 1694.
[76] A. Öztunc, S. Imre, H. Wagner, M. Norte, J. J. Fernandez, R. Gonzalez, *Tetrahedron Lett.* **1991**, *32*, 4377 – 4380.
[77] K. S. Feldman, C. C. Mechem, L. Nader, *J. Am. Chem. Soc.* **1982**, *104*, 4011 – 4012.
[78] a) K. S. Feldman, *Tetrahedron Lett.* **1982**, *23*, 3031 – 3034; b) J. G. Stuart, K. M. Nicholas, *Heterocycles* **1991**, *32*, 949 – 963.
[79] T. A. Grese, K. D. Hutchinson, L. E. Overman, *J. Org. Chem.* **1993**, *58*, 2468 – 2477.
[80] E. Lee, S.-K. Yoo, H. Choo, H. Y. Song, *Tetrahedron Lett.* **1998**, *39*, 317 – 318.
[81] a) R. Fernández de la Pradilla, C. Montero, J. Priego, L. A. Martínez-Cruz, *J. Org. Chem.* **1998**, *63*, 9612 – 9613; b) R. Fernández de la Pradilla, A. Viso, *Recent Res. Dev. Org. Bioorg. Chem.* **2001**, *4*, 123 – 132.
[82] P. A. Evans, V. S. Murthy, J. D. Roseman, A. L. Rheingold, *Angew. Chem.* **1999**, *111*, 3370 – 3372; *Angew. Chem. Int. Ed.* **1999**, *38*, 3175 – 3177.
[83] J. Ishihara, Y. Shimada, N. Kanoh, Y. Takasugi, A. Fukuzawa, A. Murai, *Tetrahedron* **1997**, *53*, 8371 – 8382.
[84] M. T. Crimmins, E. A. Tabot, *J. Am. Chem. Soc.* **2000**, *122*, 5473 – 5476.
[85] a) M. T. Crimmins, K. A. Emmitte, *J. Am. Chem. Soc.* **2001**, *123*, 1533 – 1534; b) M. T. Crimmins, K. A. Emmitte, A. L. Choy, *Tetrahedron* **2002**, *58*, 1817 – 1834.
[86] a) Sistopyrone: A. K. Amegadzie, W. A. Ayer, L. Sigler, *Can. J. Chem.* **1995**, *73*, 2119 – 2125; b) chestersiene: R. L. Edwards, J. R. Anderson, A. J. S. Whalley, *Phytochemistry* **1982**, *21*, 1721 – 1724; c) dicraenone B_1: T. Ichikawa, M. Namikawa, K. Yamada, K. Sakai, K. Kondo, *Tetrahedron Lett.* **1983**, *24*, 3337 – 3340; d) allenic steroid: N. Theobald, J. N. Shoolery, C. Djerassi, T. R. Erdman, P. J. Scheuer, *J. Am. Chem. Soc.* **1978**, *100*, 5574 – 5575 (isolation); M. Morisaki, N. Awata, Y. Fujimoto, N. Ikekawa, *J. Chem. Soc. Perkin Trans. 1* **1975**, 362 – 363 (synthesis); Y. Fujimoto, M. Morisaki, N. Ikekawa, *J. Chem. Soc. Perkin Trans. 1* **1975**, 2302 – 2307 (synthesis).
[87] A. Arnone, R. Cardilla, G. Nasini, O. V. De Pava, *Phytochemistry* **1993**, *32*, 1279 – 1281.
[88] Y. Lin, X. Wu, S. Feng, G. Jiang, S. Zhou, L. L. P. Vrijmoed, E. B. G. Jones, *Tetrahedron Lett.* **2001**, *42*, 449 – 451.
[89] a) N. Fusetani, M. Asano, S. Matsunaga, K. Hashimoto, *Tetrahedron Lett.* **1987**, *28*, 5837 – 5840; b) S. Hokama, J. Tanaka, T. Higa, N. Fusetani, M. Asano, S. Matsunaga, K. Hashimoto, *Chem. Lett.* **1988**, 855 – 856; c) N. Fusetani, M. Asano, S. Matsunaga, K. Hashimoto, *Tetrahedron* **1989**, *45*, 1647 – 1652; d) M. Ochi, K. Kataoka, A. Tatsukawa, H. Kotsuki, K. Shibata, *Heterocycles* **1994**, *38*, 151 – 158; e) J.-R. Rho, H.-S. Lee, Y. Seo, K. W. Cho, J. Shin, *J. Nat. Prod.* **2000**, *63*, 254 – 257.
[90] H. J. Kwon, J. H. Kim, H. J. Jung, Y.-G. Kwon, M. Y. Kim, J.-R. Rho, J. Shin, J. *Microbiol. Biotechnol.* **2001**, *11*, 656 – 662.
[91] a) J. W. Daly, B. Witkop, T. Tokuyama, T. Nishikawa, I. L. Karle, *Helv. Chim. Acta* **1977**, *60*, 1128 – 1140; b) T. F. Spande, P. Jain, H. M. Garaffo, L. K. Pannell, H. J. C. Yeh, J. W. Daly, S. Fukumoto, K. Imamura, T. Tokuyama, J. A. Torres, R. R. Snelling, T. H. Jones, *J. Nat. Prod.* **1999**, *62*, 5 – 21.
[92] a) T. Tokuyama, K. Uenoyama, G. Brown, J. W. Daly, B. Witkop, *Helv. Chim. Acta* **1974**, *57*, 2597 – 2604; b) C. E. Spivak, M. A. Maleque, A. C. Oliveira, L. M. Masukawa, T. Tokuyama, J. W. Daly, E. X. Albuquerque, *Mol. Pharmacol.* **1982**, *21*, 351 – 361; c) T. Tokuyama, J. Yamamoto, J. W. Daly, R. J. Highet, *Tetrahedron* **1983**, *39*, 49 – 53; d) T. Tokuyama, N. Nishimori, I. L. Karle, M. W. Edwards, J. W. Daly, *Tetrahedron* **1986**, *42*, 3453 – 3460.
[93] J. Takashima, S. Asano, A. Ohsaki, *Tennen Yuki Kagobutsu Toronkai Koen Yoshishu* **2000**, 487 – 492 [*Chem. Abstr.* **2001**, *135*, 104986].
[94] J.-M. Renaud, G. Tsoupras, H. Stoeckli-Evans, R. Tabacchi, *Helv. Chim. Acta* **1989**, *72*, 1262 – 1267.
[95] D. R. Sanson, H. Gracz, M. S. Tempesta, D. S. Fukuda, W. M. Nakatsukasa, T. H. Sands, P. J. Baker, J. S. Mynderse, *Tetrahedron* **1991**, *47*, 3633 – 3644.
[96] J. Gordon, R. Tabacchi, *J. Org. Chem.* **1992**, *57*, 4728 – 4731.

 © 2004 Wiley-VCH Verlag GmbH & Co. KGaA, Weinheim

[97] a) F. Bohlmann, R. K. Gupta, J. Jakupovic, R. M. King, H. Robinson, *Liebigs Ann. Chem.* **1980**, 1904 – 1906; b) F. Bohlmann, J. Jakupovic, R. K. Gupta, R. M. King, H. Robinson, *Phytochemistry* **1981**, *20*, 473 – 480; c) F. Bohlmann, C. Zdero, R. M. King, H. Robinson, *Phytochemistry* **1982**, *21*, 695 – 699; d) J. Jakupovic, G. Schmeda-Hirschmann, A. Schuster, C. Zdero, F. Bohlmann, R. M. King, H. Robinson, J. Pickardt, *Phytochemistry* **1986**, *25*, 145 – 158; e) U. Warning, J. Jakupovic, F. Bohlmann, S. B. Jones, *Liebigs Ann. Chem.* **1987**, 467 – 468.

[98] The structures of five additional endocyclic allenes found in the Beilstein database (e.g., an 11-membered ring system[97e]) are probably incorrect.

[99] a) F. Bohlmann, H. Bornowski, C. Arndt, *Chem. Ber.* **1965**, *98*, 2236 – 2242; b) F. Bohlmann, K.-M. Kleine, C. Arndt, *Justus Liebigs Ann. Chem.* **1966**, *694*, 149 – 156; c) F. Bohlmann, C. Zdero, *Tetrahedron Lett.* **1970**, 2465 – 2466; F. Bohlmann, C. Zdero, *Chem. Ber.* **1971**, *104*, 1329 – 1331.

[100] H. Kikuchi, T. Suzuki, E. Kurosawa, M. Suzuki, *Bull. Chem. Soc. Jpn.* **1991**, *64*, 1763 – 1775.

[101] Results of investigations on the biosynthesis of neoxanthin (**27**) and peridinin (**6**) from ^{3}H- and ^{14}C-marked mevanolate by the alga *Amphidinium carterae* are not in accordance with the formation of the exocyclic allene from an alkyne: I. E. Swift, B. V. Milborrow, *Biochem. J.* **1981**, *199*, 69 – 74.

[102] C. Walsh, *Tetrahedron* **1982**, *38*, 871 – 909.

[103] D. F. Covey, C. H. Robinson, *J. Am. Chem. Soc.* **1976**, *98*, 5038 – 5040.

[104] F. H. Batzold, D. F. Covey, C. H. Robinson, *Cancer Treat. Rep.* **1977**, *61*, 255 – 257.

[105] a) F. H. Batzold, C. H. Robinson, *J. Am. Chem. Soc.* **1975**, *97*, 2576 – 2578; b) F. H. Batzold, C. H. Robinson, *J. Org. Chem.* **1976**, *41*, 313 – 317.

[106] a) H. Westmijze, I. Nap, J. Meijer, H. Kleijn, P. Vermeer, *Recl. Trav. Chim. Pays-Bas* **1983**, *102*, 154 – 157; b) C. J. Elsevier, P. M. Stehouwer, H. Westmijze, P. Vermeer, *J. Org. Chem.* **1983**, *48*, 1103 – 1105.

[107] a) A. Burger, J.-P. Roussel, C. Hetru, J. A. Hoffmann, B. Luu, *Tetrahedron* **1989**, *45*, 155 – 165; b) J.-P. Roussell, A. Burger, C. Hetru, *Arch. Int. Physiol. Biochim.* **1990**, *98*, 253 – 259.

[108] D. Guay, W. S. Johnson, U. Schubert, *J. Org. Chem.* **1989**, *54*, 4731 – 4732.

[109] A. S. Craig, A. W. Norman, W. H. Okamura, *J. Org. Chem.* **1992**, *57*, 4374 – 4380.

[110] D. H. Beach, F. Chen, M. T. Cushion, R. S. Macomber, G. A. Krudy, M. A. Wyder, E. S. Kaneshiro, *Antimicrob. Agents Chemother.* **1997**, *41*, 162 – 168.

[111] B. W. Metcalf, C. L. Wright, J. P. Burkhart, J. O. Johnston, *J. Am. Chem. Soc.* **1981**, *103*, 3221 – 3222.

[112] H. Faraj, A. Aumelas, M. Claire, A. Rondot, G. Auzou, *Steroids* **1991**, *56*, 558 – 561.

[113] a) J. R. Williams, J. C. Boehm, *Bioorg. Med. Chem. Lett.* **1992**, *2*, 933 – 936; b) J. R. Williams, J. C. Boehm, *Steroids* **1995**, *60*, 699 – 708.

[114] Review: P. W. Collins, S. W. Djuric, *Chem. Rev.* **1993**, *93*, 1533 – 1564.

[115] a) J. H. Fried, J. M. Muchowski, H. Carpio, *Prostaglandins* **1977**, *14*, 807 – 811; b) P. Baret, E. Barreiro, A. E. Greene, J.-L. Luché, M.-A. Teixeira, P. Crabbé, *Tetrahedron* **1979**, *35*, 2931 – 2938.

[116] a) A. P. Roszkowski, G. L. Garay, S. Baker, M. Schuler, H. Carter, *J. Pharmacol. Exp. Ther.* **1986**, *239*, 382 – 389; b) R. P. Rosenkranz, P. E. Fischer, M. L. Turke, M. R. Perry, A. G. Wong, D. L. Wren, G. F. Cooper, W. L. Smith, *Arzneim.-Forsch.* **1989**, *39*, 1568 – 1571; c) W. Schepp, C. B. Chan, A. S. Giraud, D. Avedian, M. C. Y. Chen, P. Chew, J. H. Walsh, A. H. Soll, *Am. J. Physiol.* **1994**, *266*, G194-G200; d) C. K. Ching, S. K. Lam, *J. Gastroenterol.* **1995**, *30*, 607 – 614; e) N. Omura, H. Kashiwagi, T. Aoki, K. Omura, Y. Fukuchi, *J. Gastroenterol.* **1997**, *32*, 740 – 746.

[117] Additional pharmacological activities of enprostil: a) R. M. Eglen, R. L. Whiting, *Br. J. Pharmacol.* **1989**, *98*, 1335 – 1343; b) B. Donatini, C. Bognel, J.-N. Munck, L. Ramirez, P. Ardouin, P. Rougier, *J. Cancer Res. Clin. Oncol.* **1994**, *120*, 529 – 532; c) H. Vanhanen, T. A. Miettinen, *Scand. J. Gastroenterol.* **1995**, *30*, 33 – 37; d) A. Murai, A. E. Murakami, J. Okamura, M. Furuse, *Biochem. Mol. Biol. Int.* **1996**, *39*, 329 – 334; e) K. Toshina, I. Hirata, K. Maemura, S. Sasaki, M. Murano, M. Nitta, H. Yamauchi, T. Nishikawa, N. Hamamoto, K. Katsu, *Scand. J. Immunol.* **2000**, *52*, 570 – 575.

[118] H. Carpio, G. F. Cooper, J. A. Edwards, J. H. Fried, G. L. Garay, A. Guzman, J. A. Mendez, J. M. Muchowski, A. P. Roszkowski, A. R. Van Horn, *Prostaglandins* **1987**, *33*, 169 – 180.

[119] A. R. Van Horn, G. Garay, J. A. Edwards, US-Patent 4178457, **1980** [*Chem. Abstr.* **1980**, *92*, 146339p].

[120] P. Crabbé, H. Carpio, *J. Chem. Soc. Chem. Commun.* **1972**, 904 – 905.

[121] J. W. Patterson, *J. Org. Chem.* **1990**, *55*, 5528 – 5531.

[122] B. H. Lipshutz, M. R. Wood, *J. Am. Chem. Soc.* **1994**, *116*, 11 689 – 11 702, and references therein.

[123] a) O. W. Gooding, *J. Org. Chem.* **1990**, *55*, 4209 – 4211; b) O. W. Gooding, C. C. Beard, G. F. Cooper, D. Y. Jackson, *J. Org. Chem.* **1993**, *58*, 3681 – 3686.

[124] N. Ono, Y. Kawanaka, Y. Yoshida, F. Sato, *J. Chem. Soc. Chem. Commun.* **1994**, 1251 – 1252.

[125] a) G. F. Cooper, D. L. Wren, D. Y. Jackson, C. C. Beard, E. Galeazzi, A. R. Van Horn, T. T. Li, *J. Org. Chem.* **1993**, *58*, 4280 – 4286; compare: b) Y. S. Lee, K. H. Nam, S. H. Jung, H. Park, *Synthesis* **1994**, 792 – 794.

[126] S. W. Djuric, M. Miyano, M. Clare, R. M. Rydzewski, *Tetrahedron Lett.* **1987**, *28*, 299 – 302.

[127] K. Mikami, A. Yoshida, Y. Matsumoto, *Tetrahedron Lett.* **1996**, *37*, 8515 – 8518.

[128] Allenic tripetides as substrates for isopenicillin-N synthetase: J. E. Baldwin, R. M. Adlington, A. Basak, H.-H. Ting, *J. Chem. Soc. Chem. Commun.* **1986**, 1280 – 1281.

[129] Inhibition of monoamine oxidase B by allenic amines: R. A. Smith, R. L. White, A. Krantz, *J. Med. Chem.* **1988**, *31*, 1558 – 1566.

[130] a) R. R. Rando, *Acc. Chem. Res.* **1975**, *8*, 281 – 288; b) C. Angst, *Pure Appl. Chem.* **1987**, *59*, 373 – 380.

[131] P. Casara, K. Jund, P. Bey, *Tetrahedron Lett.* **1984**, *25*, 1891 – 1894.

[132] The activity as enzyme inhibitors of halogenated amino acids (which can be transformed into allenic amino acids by enzymatic dehydrohalogenation) may be caused by the same mechanism: a) N. Esaki, H. Takada, M. Moriguchi, S. Hatanaka, H. Tanaka, K. Soda, *Biochemistry* **1989**, *28*, 2111 – 2116; b) Y. Xu, R. H. Abeles, *Biochemistry* **1993**, *32*, 806 – 811.

[133] a) A. Castelhano, P. H. Pliura, G. J. Taylor, K. C. Hsieh, A. Krantz, *J. Am. Chem. Soc.* **1984**, *106*, 2734 – 2735; b) A. Castelhano, S. Horne, G. J. Taylor, R. Billedeau, A. Krantz, *Tetrahedron* **1988**, *44*, 5451 – 5466.

[134] a) B. Kübel, G. Höfle, W. Steglich, *Angew. Chem.* **1975**, *87*, 64 – 66; *Angew. Chem. Int. Ed. Engl.* **1975**, *14*, 58 – 60; b) N. Engel, B. Kübel, W. Steglich, *Angew. Chem.* **1977**, *89*, 408 – 410; *Angew. Chem. Int. Ed. Engl.* **1977**, *16*, 394 – 396; c) J. Fischer, C. Kilpert, U. Klein, W. Steglich, *Tetrahedron* **1986**, *42*, 2063 – 2074.

[135] a) U. Kazmaier, C. H. Görbitz, *Synthesis* **1996**, 1489 – 1493; b) U. Kazmaier, *Liebigs Ann. Chem.* **1997**, 285 – 295.

[136] D. P. G. Hamon, R. A. Massy-Westropp, P. Razzino, *Tetrahedron* **1995**, *51*, 4183 – 4194.

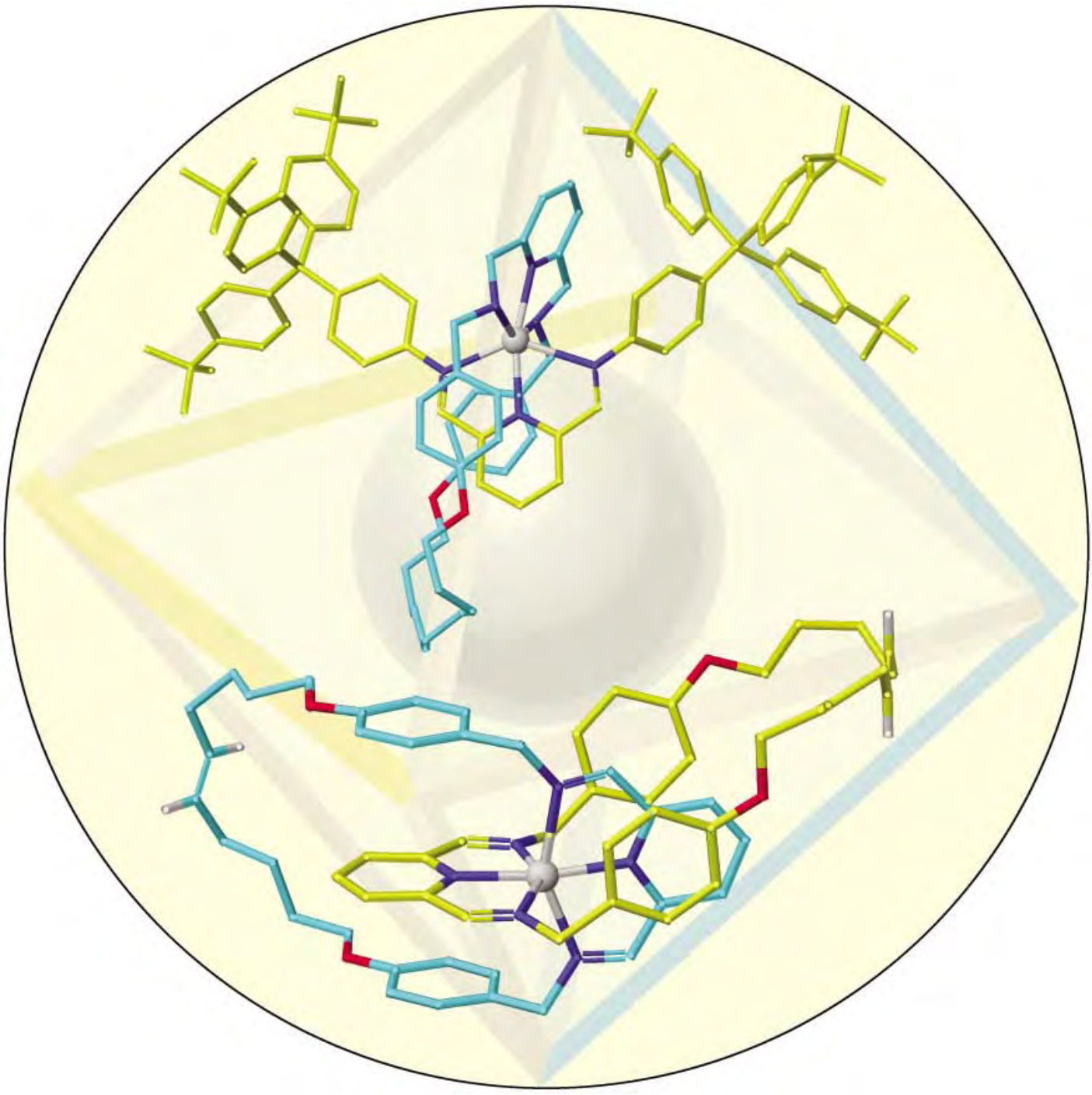
[137] H. Kagoshima, T. Uzawa, T. Akiyama, *Chem. Lett.* **2002**, 298 – 299.

 © 2004 Wiley-VCH Verlag GmbH & Co. KGaA, Weinheim

[138] A. Castelhano, A. Krantz, *J. Am. Chem. Soc.* **1984**, *106*, 1877 – 1879.
[139] H. Hiemstra, H. P. Fortgens, W. N. Speckamp, *Tetrahedron Lett.* **1984**, *25*, 3115 – 3118.
[140] Enzyme-catalyzed kinetic deracemization of unsaturated GABA derivatives: A. L. Margolin, *Tetrahedron Lett.* **1993**, *34*, 1239 – 1242.
[141] A. Castelhano, A. Krantz, *J. Am. Chem. Soc.* **1987**, *109*, 3491 – 3493.
[142] Compare: a) formation of γ-allenyl-GABA from 4-amino-5-fluorohex-5-enoic acid by enzymatic dehydrohalogenation: R. B. Silverman, K. A. Bichler, A. J. Leon, *J. Am. Chem. Soc.* **1996**, *118*, 1241 – 1252; b) methyl α-allenylpipecolinate: C. Agami, D. Bihan, L. Hamon, C. Kadouri-Puchot, M. Lusinchi, *Eur. J. Org. Chem.* **1998**, 2461 – 2465.
[143] Reviews: a) J. Zemlicka, *Nucleosides Nucleotides* **1997**, *16*, 1003 – 1012; b) J. Zemlicka, *Pharmacol. Ther.* **2000**, *85*, 251 – 266; c) J. Zemlicka, *Biochim. Biophys. Acta* **2002**, *1587*, 276 – 286.
[144] a) S. Hayashi, S. Phadtare, J. Zemlicka, M. Matsukura, H. Mitsuya, S. Broder, *Proc. Natl. Acad. Sci. USA* **1988**, *85*, 6127 – 6131; b) S. Phadtare, J. Zemlicka, *J. Am. Chem. Soc.* **1989**, *111*, 5925 – 5931; c) S. Phadtare, D. Kessel, T. H. Corbett, H. E. Renis, B. A. Court, J. Zemlicka, *J. Med. Chem.* **1991**, *34*, 421 – 429.
[145] Z.-Q. Xu, R. V. Joshi, J. Zemlicka, *Tetrahedron* **1995**, *51*, 67 – 76.
[146] B. C. N. M. Jones, J. V. Silverton, C. Simons, S. Megati, H. Nishimura, Y. Maeda, H. Mitsuya, J. Zemlicka, *J. Med. Chem.* **1995**, *38*, 1397 – 1405.
[147] S. Megati, Z. Goren, J. V. Silverton, J. Orlina, H. Nishimura, T. Shirasaki, H. Mitsuya, J. Zemlicka, *J. Med. Chem.* **1992**, *35*, 4098 – 4104 (correction: S. Megati, Z. Goren, J. V. Silverton, J. Orlina, H. Nishimura, T. Shirasaki, H. Mitsuya, J. Zemlicka, *J. Med. Chem.* **1993**, *36*, 634).
[148] Y.-L. Zhu, S. B. Pai, S.-H. Liu, K. L. Grove, B. C. N. M. Jones, C. Simons, J. Zemlicka, Y.-C. Cheng, *Antimicrob. Agents Chemother.* **1997**, *41*, 1755 – 1760.
[149] H. Winter, Y. Maeda, H. Mitsuya, J. Zemlicka, *J. Med. Chem.* **1996**, *39*, 3300 – 3306.
[150] D. Egron, C. Perigaud, G. Gosselin, A.-M. Aubertin, H. Gatanaga, H. Mitsuya, J. Zemlicka, J.-L. Imbach, *Bioorg. Med. Chem. Lett.* **2002**, *12*, 265 – 266.
[151] E. T. Jarvi, J. R. McCarthy, *Nucleosides Nucleotides* **1994**, *13*, 585 – 598.
[152] J. Dauvergne, A. Burger, J.-F. Biellmann, *Nucleosides Nucleotides Nucleic Acids* **2001**, *20*, 1775 – 1781.
[153] G. Guillerm, D. Guillerm, C. Vandenplas-Witkowski, H. Rogniaux, N. Carte, E. Leize, A. Van Dorsselaer, E. De Clerq, C. Lambert, *J. Med. Chem.* **2001**, *44*, 2743 – 2752.
[154] F. Diaz, A. Ortega, C. Guerrero, A. Guzman, B. E. Lizama, A. F. Benitez, C. F. Jankowski, *Nat. Prod. Lett.* **1998**, *12*, 241 – 254.
[155] V. Tumiatti, J. Wehrle, C. Hildebrandt, U. Moser, G. Dannhardt, E. Mutschler, G. Lambrecht, *Arzneim.-Forsch.* **2000**, *50*, 11 – 15.
[156] J. D. Buynak, A. S. Rao, G. P. Ford, C. Carver, G. Adam, B. Geng, B. Bachmann, S. Shobassy, S. Lackey, *J. Med. Chem.* **1997**, *40*, 3423 – 3433.
[157] P. H. Nelson, E. Eugui, C. C. Wang, A. C. Allison, *J. Med. Chem.* **1990**, *33*, 833 – 838.
[158] G. Gorins, L. Kuhnert, C. R. Johnson, L. J. Marnett, *J. Med. Chem.* **1996**, *39*, 4871 – 4878.
[159] P. Wirsching, M. H. O'Leary, *Biochemistry* **1988**, *27*, 1355 – 1360.
[160] a) R. Wood, T. Lee, *J. Biol. Chem.* **1981**, *256*, 12379 – 12386; b) W. H. Johnson, Jr., R. M. Czerwinski, M. C. Fitzgerald, C. P. Whitman, *Biochemistry* **1997**, *36*, 15724 – 15732.
[161] a) P. C. Ruenitz, R. F. Arrendale, G. D. George, C. B. Thompson, C. M. Mokler, N. T. Nanavati, *Cancer Res.* **1987**, *47*, 4015 – 4019; b) P. C. Ruenitz, R. F. Arrendale, W. F. Schmidt, C. B. Thompson, N. T. Nanavati, *J. Med. Chem.* **1989**, *32*, 192 – 197.
[162] Reviews: a) K. C. Nicolaou, W.-M. Dai, *Angew. Chem.* **1991**, *103*, 1453 – 1481; *Angew. Chem. Int. Ed. Engl.* **1991**, *30*, 1387 – 1416; b) M. E. Maier, *Synlett* **1995**, 13 – 26; c) J. W. Grissom, G. U. Gunawardena, D. Klingberg, D. Huang, *Tetrahedron* **1996**, *52*, 6453 – 6518; d) K. K. Wang, *Chem. Rev.* **1996**, *96*, 207 – 222; e) R. Brückner, J. Suffert, *Synlett* **1999**, 657 – 679.

 © 2004 Wiley-VCH Verlag GmbH & Co. KGaA, Weinheim

Communications



In their Communication on the following pages, D. A. Leigh and co-workers describe a general ligand system for rotaxane complexes of transition-metal ions that prefer octahedral coordination—a rare coordination mode for rotaxanes. Simple mixing of the components at room temperature is sufficient to assemble a broad range of octahedrally coordinated [2]metallorotaxanes in high yields.

DOI: 10.1002/anie.200353186
© 2004 Wiley-VCH Verlag GmbH & Co. KGaA, Weinheim

Rotaxanes

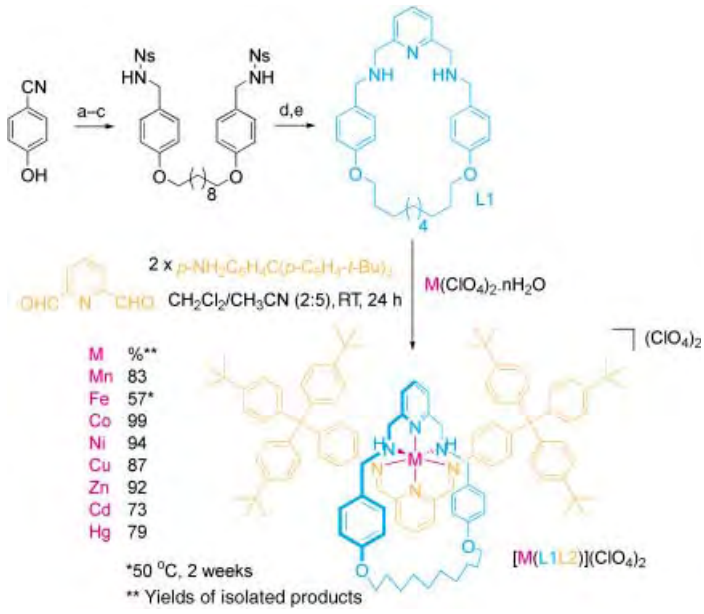
A Simple General Ligand System for Assembling Octahedral Metal–Rotaxane Complexes**

Louise Hogg, David A. Leigh, Paul J. Lusby, Alessandra Morelli, Simon Parsons, and Jenny K. Y. Wong*

Coordination complexes in which rotaxanes act as ligands for transition-metal atoms are amongst the most celebrated examples of mechanically interlocked molecular level architectures.[1] This is not only because coordination chemistry makes possible a rich diversity of structures, but also because the metal atom can be locked in unusual environments for subsequent electrochemical,[2] photochemical[3] and catalysis[4] studies. Efficient synthetic methods have been developed for rotaxanes based on tetrahedral and trigonal-bipyrimidal metal complexes by using the metal-bis-phenanthroline synthon pioneered in Strasbourg.[1a,b,5] Herein we describe a general ligand system for rotaxane complexes of ions that prefer octahedral coordination—the commonest ligand geometry amongst transition metals, but up to now a rare[6] coordination mode for rotaxanes. Simple mixing of the components at room temperature is sufficient to assemble a broad range of octahedrally coordinated [2]metallorotaxanes in excellent yields. The reactions have few, if any, by-products and proceed under thermodynamic control in the absence of a catalyst or any other external reagents.

Catenanes have previously been synthesized around octahedral metal templates by employing macrocycles containing tridentate 2,6-diiminopyridine chelating units.[7] This system is not well-suited to forming rotaxanes, however, because thread–thread–metal and macrocycle–macrocycle–metal (catenate) complexes can form in competition with the desired thread–macrocycle–metal assembly. Replacement of the macrocycle imine ligand set by nonlabile amine groups removes the possibility of forming catenates and introduces a structural asymmetry that can potentially be tailored to favor rotaxane formation under dynamic exchange conditions.[8]

After exploring several unsuccessful designs, we investigated the chemistry of macrocycle **L1**, which is conveniently prepared on a multigram scale in five steps from readily available materials (Scheme 1). The key step to **L1** is the macrocyclization of a bis-2-nitrobenzenesulfonamide (NsNH) derivative with 2,6-dibromomethylpyridine to give the protected macrocycle in 67% yield. Cyclization of the analogous Boc-protected diamine proceeded with a low yield



Scheme 1. Five-component self-assembly of octahedral metal(II)[2]rotaxanes, [M(**L1L2**)]$(ClO_4)_2$. Reagents and conditions: a) 1,10-dibromodecane, K_2CO_3, NaI, butanone, reflux, 18 h, 83%, b) $LiAlH_4$, THF, 0–60°C, 3 h, 92%, c) 2-nitrobenzenesulfonyl chloride (NsCl), NEt_3, CH_2Cl_2, 18 h, 93%, d) 2,6-dibromomethylpyridine, K_2CO_3, butanone, reflux, 18 h, 67%, e) mercaptoacetic acid, LiOH, DMF, 24 h, 80%.

(< 20%) and routes based on ring-closing olefin metathesis to form the C_{10} chain also proved uncompetitive. The use of aniline, rather than benzylamine, in the thread was designed to destabilize the dithread–metal complex with respect to the desired interlocked structure (see below).

Octahedral metal–rotaxane formation was achieved by sequential treatment of **L1** with $Zn(ClO_4)_2 \cdot 6H_2O$ (0.8 equiv), 2,6-diformylpyridine (1 equiv) and (*p*-aminophenyl)tris(*p*-*tert*-butylphenyl)methane (2 equiv), Scheme 1. Remarkably, after 24 h at room temperature no metal-containing species other than the zinc(II)[2]rotaxane was evident by either ^{1}H NMR or electrospray mass spectrometry and the analytically pure [Zn(**L1L2**)]$(ClO_4)_2$ rotaxane was isolated in 92% yield by simply washing the crude product with diethyl ether. The generality of the reaction was explored by using divalent metal ions both across and down the periodic table with respect to zinc (i.e., Mn←Zn and Zn→Hg). Pleasingly, each of [M(**L1L2**)]$(ClO_4)_2$ ($M = Mn^{II}$, Co^{II}, Ni^{II}, Cu^{II}, Cd^{II}, Hg^{II}) could be efficiently prepared by using the procedure in isolated yields ranging from 73 to 99% (Scheme 1). In all cases no other metal-containing species could be detected[9] after 24 h, which suggests near-quantitative formation of the interlocked metal-rotaxane complex. Formation of [Fe(**L1L2**)]$(ClO_4)_2$ required a longer reaction time and gentle heating (CH_2Cl_2/CH_3CN, N_2, 40°C, 2 weeks) and

[*] L. Hogg, Prof. D. A. Leigh, Dr. P. J. Lusby, A. Morelli, Dr. S. Parsons, Dr. J. K. Y. Wong
School of Chemistry
University of Edinburgh
The King's Buildings, West Mains Road
Edinburgh EH9 3JJ (United Kingdom)
Fax: (+44) 131-667-9085
E-mail: david.leigh@ed.ac.uk

[**] This work was supported by the European Union Future and Emerging Technology Program *MechMol* and the EPSRC.

Supporting information for this article is available on the WWW under http://www.angewandte.org or from the author.

 © 2004 Wiley-VCH Verlag GmbH & Co. KGaA, Weinheim DOI: 10.1002/anie.200353186

resulted in a lower yield of rotaxane (57%). The sluggish rate of reaction is characteristic of the slow rate of ligand exchange of low spin d^6 metal complexes, but a potentially useful feature of the slower dynamics is that Fe^{II} therefore locks the rotaxane architecture in a particularly kinetically stable form.

The nonparamagnetic metal–rotaxane complexes all have similar ^{1}H NMR spectra; those of the zinc(II)[2]rotaxane [Zn(**L1L2**)]$(ClO_4)_2$ and macrocycle **L1** are shown in Figure 1.[10] The shielding of the H_C and H_D protons of the benzyl rings of the macrocycle and several protons of the thread indicate that extensive intercomponent π stacking occurs in solution. Single crystals of [Cd(**L1L2**)]$(ClO_4)_2$ suitable for investigation by X-ray crystallography were obtained by slow vapor diffusion of diethyl ether into a solution of the rotaxane in acetonitrile.[11] The crystal structure (Figure 2) confirms the interlocked molecular architecture, the pseudooctahedral geometry of the cadmium(II) ion, and shows π stacking of both the macrocycle benzylic rings with the pyridyl unit and an imine group of the thread.

The mechanism of the rotaxane-forming reaction provides insight into the reasons for the effectiveness of the ligand assembly. When **L1** is treated with $Zn(ClO_4)_2 \cdot 6H_2O$ (CH_2Cl_2/CH_3CN, room temperature) followed by the preformed thread, **L2**, electrospray mass spectrometry shows that within 10 minutes the thread has extracted the zinc(II) ion from the macrocycle to form the dithread complex,

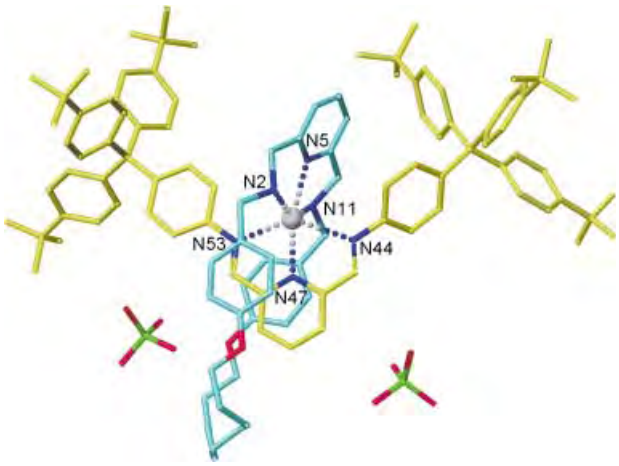


Figure 2. X-ray crystal structure of [Cd(**L1L2**)]$(ClO_4)_2$.[11] Carbon atoms of the macrocycle, **L1**, are shown in light blue and those of the thread, **L2**, in yellow; oxygen atoms are red; nitrogen dark blue; chlorine green; cadmium grey. Hydrogen atoms and a molecule of acetonitrile are omitted for clarity. Selected bond lengths [Å]: Cd-N2 2.40, Cd-N5 2.30, Cd-N11 2.40, Cd-N44 2.52, Cd-N47 2.26, Cd-N53 2.38; other selected interatomic distances [Å]: N2-N11 4.52, N5-N47 4.52, N44-N53 4.59; ligand bite angles [°]: N2-Cd-N11 141.5, N44-Cd-N53 139.2.

$[Zn(\mathbf{L2})_2](ClO_4)_2$ in >95% yield (Scheme 2). The $[Zn(\mathbf{L2})_2](ClO_4)_2$ species is then quantitatively converted to the rotaxane [Zn(**L1L2**)]$(ClO_4)_2$ over 24 h.[12] Whilst the

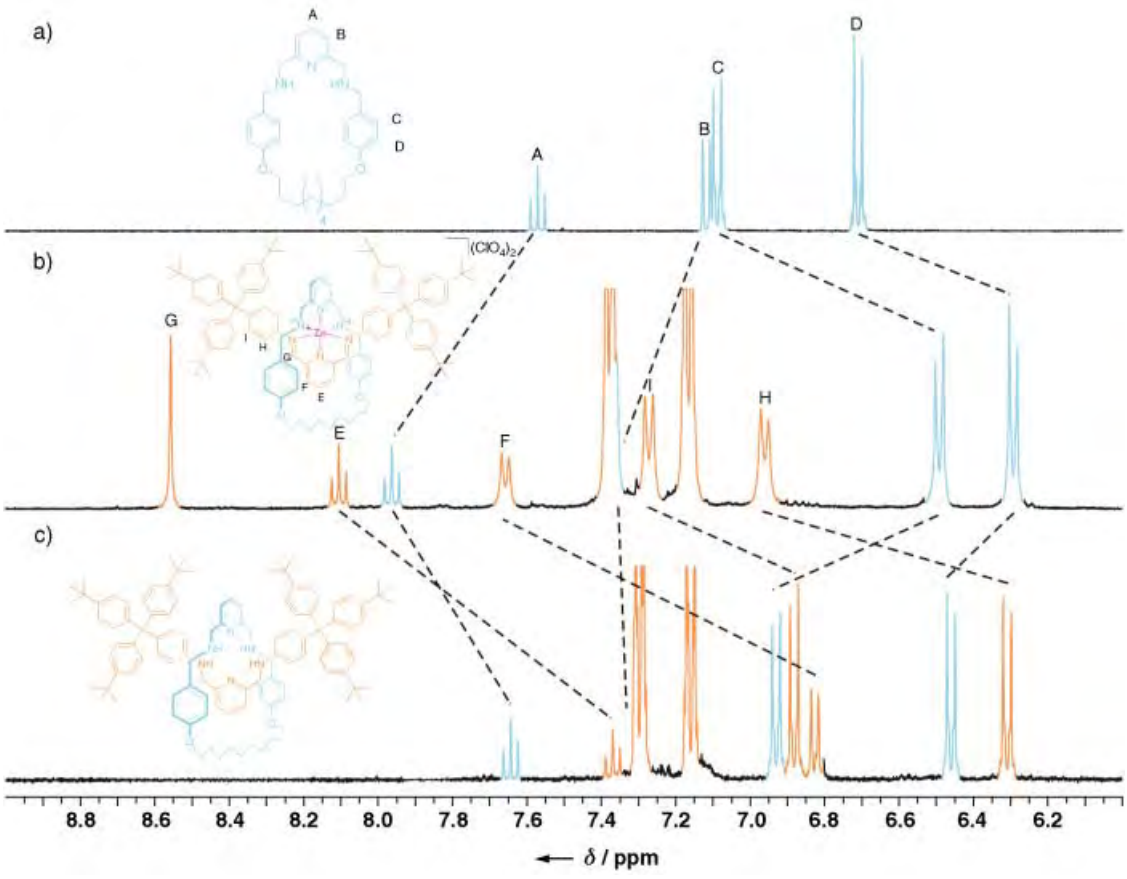
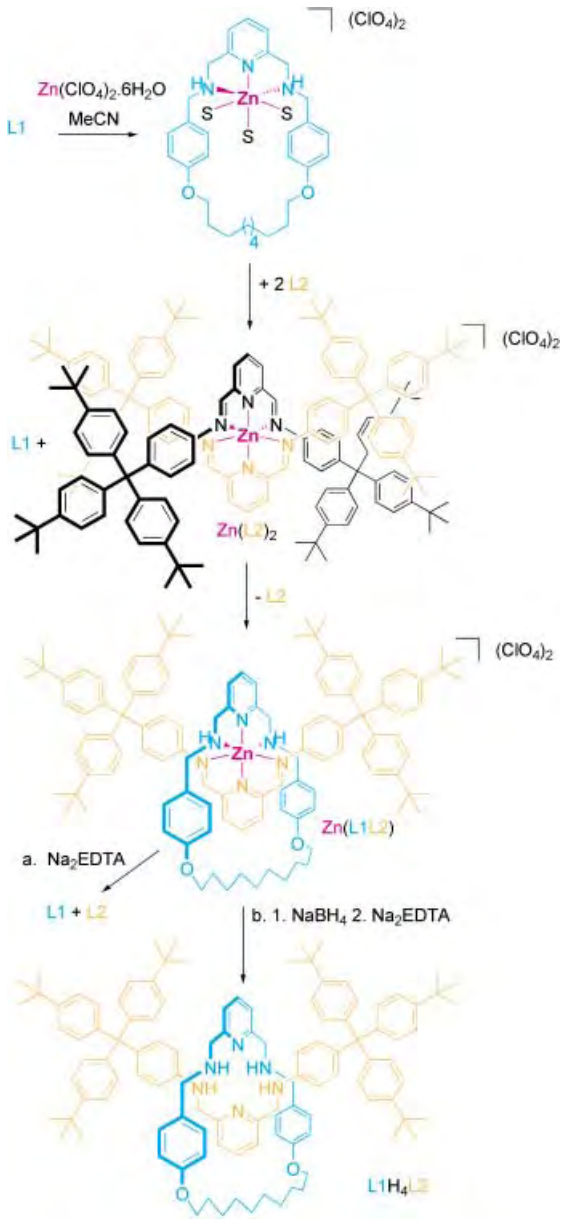


Figure 1. Partial ^{1}H NMR spectra (400 MHz, CD_3CN, 298 K) of a) macrocycle **L1** b) zinc(II)[2]rotaxane [Zn(**L1L2**)]$(ClO_4)_2$ c) demetallated, reduced, rotaxane **L1**H_4**L2**.

 © 2004 Wiley-VCH Verlag GmbH & Co. KGaA, Weinheim



Scheme 2. Mechanism of formation and reactivity of [Zn(**L1L2**)](ClO$_4$)$_2$. Rapid formation of Zn(**L2**)$_2$ is followed by quantitative conversion to Zn(**L1L2**) under thermodynamic control. Demetallation of the rotaxane by using Na$_2$EDTA occurs both with (b) and without (a) prior reduction of the imine groups.

reversible nature of imine bond formation accounts for the dynamics of the system, the reasons for the metal–rotaxane complex being the thermodynamic product rather than the dithread–metal complex are rather more subtle. In fact, imine N donors often form stronger coordination bonds than the corresponding amines,[13] which leads to dithread–metal complexes being thermodynamically favored in other ligand systems we investigated. However, the use of aniline rather than, for example, benzylamine groups in the thread does not allow geometries in which the dithread–metal complex can form attractive intercomponent π-stacking interactions, such as those observed in the rotaxane between the benzyl groups of the macrocycle and the extended π system of the thread in both solution (NMR spectroscopy) and the solid state (X-ray crystal studies). We believe these favorable secondary interactions are important for the thermodynamic stability of the rotaxane over the other possible products of the reaction.

The 2,6-diminopyridyl motif imparts high kinetic stability in metal-coordinated interlocked structures. Tetraimine metal(II) catenates are not demetallated by Na$_2$EDTA (EDTA = ethylenediaminetetracetate), which required reduction to the more labile tetraamine catenates for the metal atom to be extracted.[7] The [M(**L1L2**)](ClO$_4$)$_2$ rotaxanes, which contain a combination of imine and amine N donors, do react with excess Na$_2$EDTA when heated (10 equiv, CH$_3$CN/MeOH, 60 °C, 0.5 h) to remove the metal. However, without the stabilization provided by metal coordination the rotaxane decomposes through imine bond exchange and only free macrocycle and thread are observed experimentally (Scheme 2, path a). If the rotaxane imine bonds are reduced beforehand ([Zn(**L1L2**)](ClO$_4$)$_2$, 10 equiv NaBH$_4$, CH$_3$CN/MeOH, Δ, 1.5 h), however, treatment with Na$_2$EDTA (10 equiv, CH$_3$CN/MeOH, 60 °C, 0.5 h) gives the demetallated, reduced, rotaxane **L1**H$_4$**L2** (88 % yield) with no evidence of dethreading (Scheme 2, path b). The ^{1}H NMR of **L1**H$_4$**L2** is shown in Figure 1c. The downfield shift in the resonances of the benzyl groups with respect to [Zn(**L1L2**)](ClO$_4$)$_2$ indicates that π stacking with the thread is less pronounced in the demetallated rotaxane in which there are no coordination bonds to organize the geometry of the components.

In conclusion, we have developed a general ligand system for the efficient assembly of [2]rotaxanes around octahedral metal ions. The five component self-assembly reaction produces rotaxanes under true thermodynamic control in excellent yields without the need for large excesses of reagents, subsequent derivatization to stabilize the rotaxane architecture, chromatography or any other complicated purification processes. The system is remarkable in terms of its simplicity and expands both the range and geometry of metal ions that can be readily encapsulated within rotaxane structures.

Experimental Section

Typical example of octahedral metal(II)[2]rotaxane formation, [Zn(**L1L2**)](ClO$_4$)$_2$: Zinc(II) perchlorate hexahydrate (0.127 g, 0.342 mmol) in acetonitrile (5 mL), 2,6-pyridinedicarboxaldehyde (0.055 g, 0.410 mmol) in acetonitrile (10 mL), and *p*-aminophenyltris(*p*-*tert*-butylphenyl)methane (0.413 g, 0.820 mmol) in dichloromethane (10 mL) were added sequentially over five-minute periods to a solution of **L1** (0.200 g, 0.410 mmol) in acetonitrile (10 mL). The resulting solution was stirred at room temperature for 24 h, after which the solvent was removed under reduced pressure, the crude residue dissolved in acetonitrile (30 mL), filtered, and finally the solvent removed under reduced pressure. The crude residue was washed with diethyl ether (30 mL) for 10 min, isolated by filtration and dried in air to give [Zn(**L1L2**)](ClO$_4$)$_2$ as a bright yellow solid (0.582 g, yield = 92 %). Mp 266 °C (decomp). ^{1}H NMR (400 MHz, CD$_3$CN, 298 K): δ = 1.32 (s, 54 H, C(CH$_3$)$_3$), 1.48–1.68 (bm, 12 H, alkyl), 1.79 (m, 4 H, OCH$_2$C*H*$_2$), 3.84 (br, 4 H, OCH$_2$), 4.06–4.55 (br, 8 H, pyC*H*$_2$NHC*H*$_2$Ar; py = pyridyl), 6.29 (d, J = 8.6 Hz, 4 H, macrocycle ArH), 6.49 (d, J = 8.6 Hz, 4 H, macrocycle ArH), 6.96 (d, J = 8.6 Hz, 4 H, thread ArH), 7.16 (d, J = 8.6 Hz, 12 H, thread ArH), 7.27

 © 2004 Wiley-VCH Verlag GmbH & Co. KGaA, Weinheim

(d, $J = 8.6$ Hz, 4H, thread ArH), 7.37 (m, 14H, thread ArH plus macrocycle pyridyl H), 7.65 (d, $J = 7.8$ Hz, 2H, thread pyridyl H), 7.96 (t, $J = 7.8$ Hz, 1H, macrocycle pyridyl H), 8.11 (t, $J = 7.8$ Hz, 1H, thread pyridyl H), 8.57 ppm (s, 2H, thread HC=N); ^{13}C NMR (100 MHz, $CDCl_3$, 298 K): $\delta = 25.6$, 28.4, 28.5, 29.4, 31.5, 34.5, 52.2, 55.3, 63.9, 67.4, 114.1, 120.8, 123.0, 124.1, 124.3, 124.6, 127.0, 128.5, 130.6, 141.5, 141.9, 143.3, 143.4, 145.9, 148.9, 149.0, 155.0, 158.2, 158.7 ppm; IR (KBr pressed pellet): $\tilde{\nu} = 3465$, 2960, 2865, 1611, 1582, 1513, 1464, 1395, 1363, 1251, 1180, 1109, 1089, 1017, 840, 823, 637, 625, 582 cm^{-1}; LRESI-MS: $m/z = 830$ $[Zn(\mathbf{L1L2})]^{2+}$, 1759 $[Zn(\mathbf{L1L2})](ClO_4)^+$; HRFAB-MS (3-NOBA matrix): $m/z =$ 1657.97065 (calcd for $^{12}C_{111}{}^{13}CH_{132}N_6O_2{}^{64}Zn$ $[(\mathbf{L1L2})Zn]$, 1657.97363).

Received: October 29, 2003 [Z53186]
Published Online: January 27, 2004

Keywords: coordination modes · rotaxanes · self-assembly · template synthesis · thermodynamic control

[1] a) J.-P. Sauvage, C. Dietrich-Buchecker, G. Rapenne in *Molecular Catenanes, Rotaxanes and Knots* (Eds.: J.-P. Sauvage, C. Dietrich-Buchecker), Wiley-VCH, **1999**; b) J.-P. Collin, C. Dietrich-Buchecker, P. Gaviña, M. C. Jimenez-Molero, J.-P. Sauvage, *Acc. Chem. Res.* **2001**, *34*, 477–487; For complexes in which metal coordination forms part of the macrocycle in a rotaxane see: c) K.-S. Jeong, J. S. Choi, S.-Y. Chang, H.-Y. Chang, *Angew. Chem.* **2000**, *112*, 1758–1761; *Angew. Chem. Int. Ed.* **2000**, *39*, 1692–1695; d) S.-Y. Chang, J. S. Choi, K.-S. Jeong, *Chem. Eur. J.* **2001**, *7*, 2687–2697; e) S.-Y. Chang, K.-S. Jeong, *J. Org. Chem.* **2003**, *68*, 4014–4019; f) S.-Y. Chang, H.-Y. Jang, K.-S. Jeong, *Chem. Eur. J.* **2003**, *9*, 1535–1541; For complexes in which metal coordination forms part of the thread in a rotaxane see: g) K.-M. Park, D. Whang, E. Lee, J. Heo, K. Kim, *Chem. Eur. J.* **2002**, *8*, 498–508; For complexes in which metal coordination forms the stoppers in a rotaxane see: h) R. B. Hannak, G. Färber, R. Konrat, B. Kräutler, *J. Am. Chem. Soc.* **1997**, *119*, 2313–2314; i) J.-C. Chambron, J.-P. Collin, J.-O. Dalbavie, C. O. Dietrich-Buchecker, V. Heitz, F. Odobel, N. Solladié, J.-P. Sauvage, *Coord. Chem. Rev.* **1998**, *178–180*, 1299–1312; j) A. J. Baer, D. H. Macartney, *Inorg. Chem.* **2000**, *39*, 1410–1417; k) S. J. Loeb, J. A. Wisner, *Chem. Commun.* **1998**, 2757–2758; l) G. J. E. Davidson, S. J. Loeb, N. A. Parekh, J. A. Wisner, *J. Chem. Soc. Dalton Trans.* **2001**, 3135–3136; For polyrotaxanes based on metal coordination polymers see: m) S. R. Batten, R. Robson, *Angew. Chem.* **1998**, *110*, 1558–1595; *Angew. Chem. Int. Ed.* **1998**, *37*, 1460–1494; n) A. J. Blake, N. R. Champness, P. Hubberstey, W.-S. Li, M. A. Withersby, M. Schröder, *Coord. Chem. Rev.* **1999**, *183*, 117–138; o) K. Kim, *Chem. Soc. Rev.* **2002**, *31*, 96–107.

[2] a) N. Armaroli, V. Balzani, J.-P. Collin, P. Gaviña, J.-P. Sauvage, B. Ventura, *J. Am. Chem. Soc.* **1999**, *121*, 4397–4408; b) L. Raehm, J.-M. Kern, J.-P. Sauvage, *Chem. Eur. J.* **1999**, *5*, 3310–3317.

[3] a) J.-C. Chambron, A. Harriman, V. Heitz, J.-P. Sauvage, *J. Am. Chem. Soc.* **1993**, *115*, 6109–6114; b) M. Andersson, M. Linke, J.-C. Chambron, J. Davidsson, V. Heitz, L. Hammarström, J.-P. Sauvage, *J. Am. Chem. Soc.* **2002**, *124*, 4347–4362; c) N. Watanabe, N. Kihara, Y. Furusho, T. Takata, Y. Araki, O. Ito, *Angew. Chem.* **2003**, *115*, 705–707; *Angew. Chem. Int. Ed.* **2003**, *42*, 681–683.

[4] P. Thordarson, E. J. A. Bijsterveld, A. E. Rowan, R. J. M. Nolte, *Nature* **2003**, *424*, 915–918.

[5] a) C. Wu, P. R. Lecavalier, Y. X. Shen, H. W. Gibson, *Chem. Mater.* **1991**, *3*, 569–572; b) J.-C. Chambron, V. Heitz, J.-P. Sauvage, *J. Chem. Soc. Chem. Commun.* **1992**, 1131–1133.

[6] D. Pomeranc, D. Jouvenot, J.-C. Chambron, J.-P. Collin, V. Heitz, J.-P. Sauvage, *Chem. Eur. J.* **2003**, *9*, 4247–4254.

[7] D. A. Leigh, P. J. Lusby, S. J. Teat, A. J. Wilson, J. K. Y. Wong, *Angew. Chem.* **2001**, *113*, 1586–1591; *Angew. Chem. Int. Ed.* **2001**, *40*, 1538–1543.

[8] a) S. J. Cantrill, S. J. Rowan, J. F. Stoddart, *Org. Lett.* **1999**, *1*, 1363–1366; b) S. J. Rowan, J. F. Stoddart, *Org. Lett.* **1999**, *1*, 1913–1916; c) P. T. Glink, A. I. Oliva, J. F. Stoddart, A. J. P. White, D. J. Williams, *Angew. Chem.* **2001**, *113*, 1922–1927; *Angew. Chem. Int. Ed.* **2001**, *40*, 1870–1875; d) M. J. Gunter, N. Bampos, K. D. Johnstone, J. K. M. Sanders, *New J. Chem.* **2001**, *25*, 166–173; e) S. J. Rowan, S. J. Cantrill, G. R. L Cousins, J. K. M. Sanders, J. F. Stoddart, *Angew. Chem.* **2002**, *114*, 938–993; *Angew. Chem. Int. Ed.* **2002**, *41*, 898–952; f) K. D. Johnstone, N. Bampos, J. K. M. Sanders, M. J. Gunter, *Chem. Commun.* **2003**, 1396–1397; g) R. G. E. Coumans, J. A. A. W. Elemans, P. Thordarson, R. J. M. Nolte, A. E. Rowan, *Angew. Chem.* **2003**, *115*, 674–678; *Angew. Chem. Int. Ed.* **2003**, *42*, 650–654; h) A. F. M. Kilbinger, S. J. Cantrill, A. W. Waltman, M. W. Day, R. H. Grubbs, *Angew. Chem.* **2003**, *115*, 3403–3407; *Angew. Chem. Int. Ed.* **2003**, *42*, 3281–3285; i) J. S. Hannam, T. J. Kidd, D. A. Leigh, A. J. Wilson, *Org. Lett.* **2003**, *5*, 1907–1910; j) Y. Furusho, T. Oku, T. Hasegawa, A. Tsuboi, N. Kihara, T. Takata, *Chem. Eur. J.* **2003**, *9*, 2895–2903; k) M. Horn, J. Ihringer, P. T. Glink, J. F. Stoddart, *Chem. Eur. J.* **2003**, *9*, 4046–4054.

[9] Reactions were monitored by electrospray mass spectrometry in all cases and by ^{1}H NMR spectroscopy for systems not containing paramagnetic metals.

[10] The **L1** and **L2** resonances in $[Zn(\mathbf{L1L2})](ClO_4)_2]$ were distinguished by a combination of COSY and ROESY experiments.

[11] $[Cd(\mathbf{L1L2})](ClO_4)_2 \cdot 2\,MeCN \cdot 1.5\,Et_2O$: $C_{124}H_{153}CdCl_2N_8O_{11.5}$, $M_r = 2098.82$, yellow block, crystal size $0.15 \times 0.12 \times 0.10$ mm, monoclinic Cc, $a = 31.636(2)$, $b = 22.4269(14)$, $c = 22.2668(15)$ Å, $\beta = 133.7570(10)°$, $V = 11410.8(13)$ Å^3, $Z = 4$, $\rho_{calcd} = 1.222$ Mg m^{-3}; $Mo_{K\alpha}$ radiation (graphite monochromator, $\lambda = 0.71073$ Å), $\mu = 0.300$ mm^{-1}, $T = 150(2)$ K. 36017 data (22989 unique, $R_{int} = 0.03170$, $1.27 < \theta < 28.96°$), were collected on a Bruker SMARTApex CCD diffractometer by using narrow frames (0.3° in ω), and were corrected semiempirically for absorption and incident beam decay. The structure was solved by direct methods and refined by full-matrix least-squares on F^2 values of all data (G. M. Sheldrick, SHELXTL manual, Siemens Analytical *X*-ray Instruments, Madison WI, USA, **1994**, version 5) to give $wR = \{\Sigma[w(F_o^2 - F_c^2)^2]/\Sigma[w(F_o^2)^2]\}^{1/2} = 0.1536$, conventional $R = 0.0627$ for F values of 22989 reflections with $F_o^2 > 2\sigma F_o^2$), $S = 1.048$ for 1371 parameters. Residual electron density extremes were 1.12 and -0.89 e Å^{-3}. Hydrogens were added in calculated positions and constrained to a Riding model. CCDC-224059 contains the supplementary crystallographic data for this paper. These data can be obtained free of charge via www.ccdc.cam.ac.uk/conts/retrieving.html (or from the Cambridge Crystallographic Data Centre, 12 Union Road, Cambridge CB21EZ, UK; fax: (+44) 1223-336-033; or deposit@ccdc.cam.ac.uk).

[12] Under identical experimental conditions the reduced thread, $H_4\mathbf{L2}$, does not afford $[Zn(\mathbf{L1}H_4\mathbf{L2})](ClO_4)_2$, thus precluding the possibility of a "slippage" mechanism.

[13] G. J. P. Britovesk, V. C. Gibson, S. Mastroianni, D. C. H. Oakes, C. Redshaw, G. A. Solan, A. J. P. White, D. J. Williams, *Eur. J. Inorg. Chem.* **2001**, 431–437. The greater stability of octahedral metal–imine complexes, compared with metal–amine complexes, is also illustrated by the facile demetallation of amine—but not imine—octahedral metal catenates.[7]

 © 2004 Wiley-VCH Verlag GmbH & Co. KGaA, Weinheim

Molecular Shuttles

Shuttling through Anion Recognition**

*Claire M. Keaveney and David A Leigh**

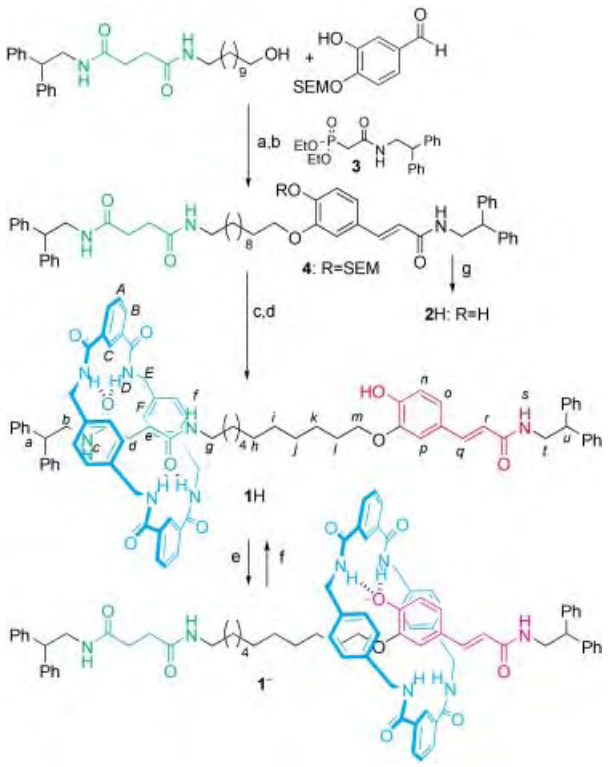
The reversible hydrogen bonding of anions is a key feature of many biological processes, including the remarkable trigger of molecular (and, ultimately, macroscopic) motion in photoactive yellow proteins (PYPs).[1,2] The photoisomerization-induced protonation of a hydrogen-bonded cinnamate anion in PYPs coincides with a large conformational change in the protein, which acts as the signal for *E. halophilia* and other bacteria to swim away from harmful blue light. Despite considerable advances[3–5] in the understanding of noncovalent anion binding in recent years, its application in synthetic systems beyond sensors[4] and templating[5] is still rare. Here we describe the use of anion hydrogen bonding to induce translocation of a macrocycle in a bistable molecular shuttle.[6]

The polarity of the N–H bond, combined with its relatively high pK_a value, makes secondary amides excellent hydrogen-bond donors for neutral[7] functional groups (particularly amides, sulfoxides, nitrones, and phosphane oxides) and anions[8] which are insufficiently basic to deprotonate the amide. Isophthalamide groups, in particular, bind strongly to halides[9] and oxyanions[10] in a variety of solvents and such observations have been exploited to template the synthesis of rotaxanes through isophthalamide-anion hydrogen bonding where the anion is either consumed (phenolate as the template[10]) or retained (chloride as the template[11]) during the synthesis. Although there is limited data or theory with which to reliably compare the hydrogen-bonding ability of anions with neutral functional groups,[12] it seemed plausible that such strong anion binding might be able to translocate an isophthalamide-based macrocycle from a neutral hydrogen-bonding station in a molecular shuttle.

Rotaxane **1**H contains a thread which features two potential hydrogen-bonding stations for a benzylic amide macrocycle. The succinamide group (Scheme 1, green) has previously been shown[13] to be an excellent geometrical and electronic fit for benzylic amide macrocycles. The second station is related to the cinnamate group found in PYPs and is weakly hydrogen bonding as either a donor or acceptor in the phenol form (red) but a powerful hydrogen-bond acceptor as the phenolate anion (purple).

The shuttle was prepared according to Scheme 1. The rotaxane-forming reaction was unusually low yielding (19%) as a result of a difficult chromatographic separation of the rotaxane from the unconsumed thread. Deprotonation of the rotaxane and thread phenol groups to form **1**$^-$ and **2**$^-$, respectively, could be accomplished with a variety of bases (for example, HO^-, $tBuO^-$, DBU, and Schwesinger's P_1 base[14]). Since the xylylene units of the macrocycle shield the encapsulated regions of the thread, the position of the ring in rotaxanes **1**H and **1**$^-$ could be readily determined from the chemical-shift differences of the protons in the corresponding threads, **2**H and **2**$^-$ (Figure 1). In the neutral form, the succinic methylene protons are shielded by >1.2 ppm in the rotaxane in a range of solvents ($CDCl_3$, CD_2Cl_2, [D_3]MeCN, [D_7]DMF),[15] which indicates that the macrocycle resides preferentially on the succinamide station. Remarkably, this is true even in DMF (>95% succinamide-bound translational isomer, 298 K, [D_7]DMF, Figure 1a and b) where the solvent is comparable, and probably slightly superior, in terms of hydrogen-bond basicity to the succinamide amide groups.[16]

^{1}H NMR confirms that deprotonation of the phenol provides an excellent alternative hydrogen-bonding station for the macrocycle. The shielding of the protons of **1**$^-$ (Figure 1d) and **2**$^-$ (Figure 1c) in [D_7]DMF (298 K, P_1H^+ counterion) show the ring is now located overwhelmingly over the phenolate anion (H_p shifted by $\delta = -0.6$ ppm in the rotaxane anion compared to the thread anion) and the adjacent parts of the alkyl chain (relative shifts of H_m $\delta =$



Scheme 1. Synthesis of the bistable molecular shuttle **1**H/**1**$^-$ (SEM = $Me_3SiCH_2CH_2OCH_2$-): a) Diisopropylazodicarboxylate (DIAD), PPh_3, 70%; b) **3**, NaH, THF, 85%; c) isophthaloyl dichloride, *p*-xylylene diamine, Et_3N, $CHCl_3$, 19%; d) tetrabutylammonium fluoride (TBAF), 1,3-dimethyl-3,4,5,6-tetrahydro-2(1H)-pyrimidinone (DMPU), 4Å molecular sieves, 75%; e) various bases, DMF; f) CF_3CO_2H (1 equiv), DMF; g) TBAF, DMPU, 4Å molecular sieves, 61%. Full experimental procedures can be found in the Supporting Information.

[*] Dr. C. M. Keaveney, Prof. D. A. Leigh
School of Chemistry, University of Edinburgh, The King's Buildings, West Mains Road, Edinburgh EH9 3JJ (UK)
Fax: (+44) 131-667-9085
E-mail: David.Leigh@ed.ac.uk

[**] This work was supported by the European Union Future and Emerging Technology Program *MechMol* and the EPSRC.

Supporting information for this article is available on the WWW under http://www.angewandte.org or from the author.

 © 2004 Wiley-VCH Verlag GmbH & Co. KGaA, Weinheim DOI: 10.1002/anie.200353248

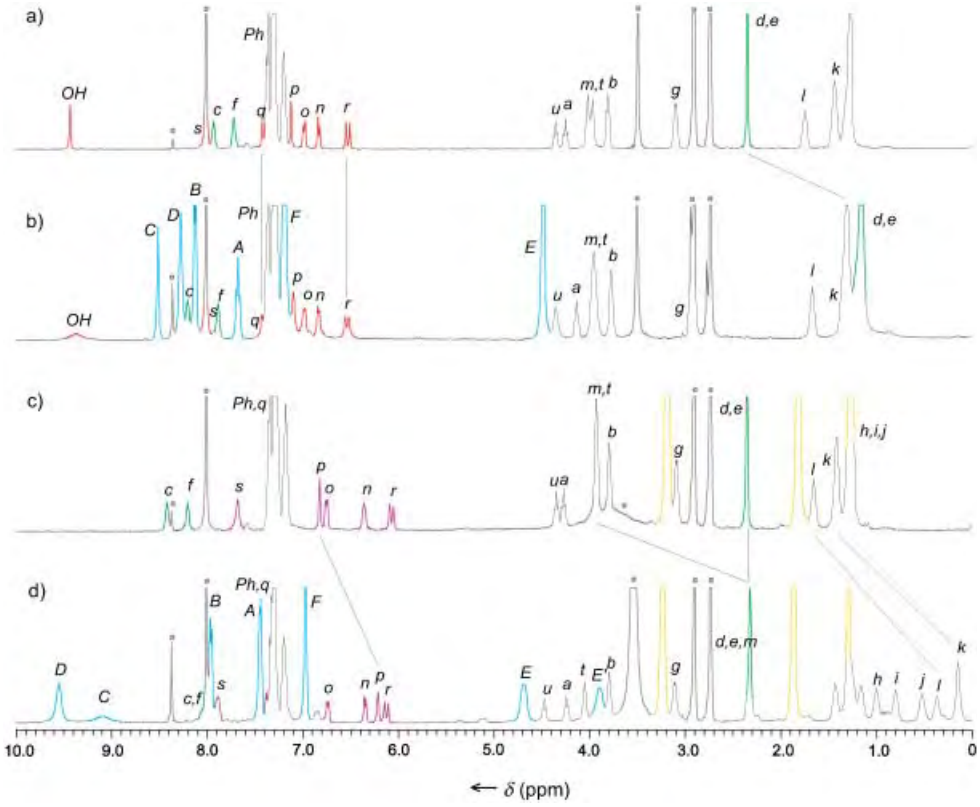


Figure 1. 400 MHz ^{1}H NMR spectra ([D$_7$]DMF, 298 K) of a) thread **2**H; b) rotaxane **1**H; c) thread **2**$^-$ with the P$_1$H$^+$ counterion; d) rotaxane **1**$^-$ with the P$_1$H$^+$ counterion. The color coding and assignments correspond to those indicated in Scheme 1. The resonances of P$_1$H$^+$ ions are shown in orange and those of the residual solvent and H$_2$O in grey (°).

−1.7 ppm, H_l $\delta = -1.3$ ppm, H_k $\delta = -0.8$ ppm, H_j $\delta = -0.7$ ppm, H_i $\delta = -0.4$ ppm). Note also the virtually unchanged chemical-shift values of the succinic methylene protons $H_{d,e}$ in **1**$^-$ and **2**$^-$. The shuttling is reversible and protonation of **1**$^-$ with CF_3CO_2H smoothly regenerates **1**H, which returns the macrocycle to the original succinamide station.

The anion-induced shuttling is highly solvent dependent. Normally hydrogen-bonded molecular shuttles work best in nonpolar solvents where the designed intercomponent hydrogen bonding is strongest.[13] For **1**$^-$, however, the opposite is true. The degree of discrimination of the macrocycle for the phenolate station over succinamide is excellent in [D$_7$]DMF, [D$_3$]MeCN, and [D$_4$]MeOH but not in $CDCl_3$ or CD_2Cl_2, where the ^{1}H NMR spectra shows that intramolecular folding occurs but the macrocycle remains located over the succinamide station.[17] This is presumably because the phenolate anion only provides a hydrogen-bonding site for one of the two isophthalamide units of the macrocycle. Good hydrogen-bond-accepting solvents are able to adequately solvate the second isophthalamide site (and, equally important, the succinamide groups of the thread) and induce shuttling, but $CDCl_3$ and CD_2Cl_2 cannot. It is indicative of the strength of the anion hydrogen bonding in **1**$^-$ that the isophthalamide–phenolate interaction can displace the macrocycle from the succinamide binding site in [D$_3$]MeCN, a solvent of modest hydrogen-bond basicity ($\beta_2^H = 0.45$[12b]) compared to an amide ($\beta_2^H \sim 0.66$[12b]).

The proton-mediated translocation of the macrocycle in **1**H/**1**$^-$ was investigated in the presence of other ions.[18] First, shuttling was found to be independent of the base used. The same ^{1}H NMR chemical shifts were observed using various bases capable of deprotonating the phenol (LiOH, NaOH, KOH, CsOH, Bu$_4$NOH, *t*BuOK, DBU, phosphazine P$_1$) but not bases that do not generate the rotaxane anion (Et$_3$N, pyridine). Although the strength of anion hydrogen bonding can be strongly influenced by the nature of the accompanying cation,[19] the co-conformation adopted by rotaxane anion **1**$^-$ is unaffected by the counterion.

Second, not only is the macrocycle observed to switch with excellent positional integrity between the different stations in **1**H and **1**$^-$ in the presence of strong alternative neutral hydrogen-bond acceptors (e.g. [D$_7$]DMF), the shuttling also proved unaffected by competition from anionic hydrogen-bond acceptors. The addition of up to 10 equivalents of Bu$_4$NX (X = F$^-$, Cl$^-$, Br$^-$, I$^-$, HO$^-$, NO$_3^-$, AcO$^-$) had no effect on the degree of translational isomerism exhibited by either rotaxane.[18] The shuttling in **1**$^-$ can therefore be considered to result from a precise recognition event rather than an unselective anion interaction with the amide groups in the macrocycle or thread.

In conclusion, we have demonstrated the reversible control of translation motion in a rotaxane through hydrogen bonding to an anion. The shuttle has several remarkable features, including that translocation of the macrocycle only occurs in solvent systems where the designed hydrogen-

 © 2004 Wiley-VCH Verlag GmbH & Co. KGaA, Weinheim

bonding interactions are relatively weak (and competing hydrogen-bonding interactions weaker still), and that under these conditions shuttling is unaffected by the nature of the countercation or the presence of alternative anionic hydrogen-bond acceptors. This adds to the range of methods already developed for switching the position of macrocycles in bistable molecular shuttles and provides a new type of model system for probing anion hydrogen-bonding interactions.

Received: November 4, 2003 [Z53248]

Keywords: anions · hydrogen bonds · molecular recognition · molecular shuttles · rotaxanes

[1] T. E. Meyer, *Biochim. Biophys. Acta* **1985**, *806*, 175 – 183.
[2] For a recent review see K. J. Hellingwerf, J. Hendriks, T. Gensch, *J. Phys. Chem. A* **2003**, *107*, 1082 – 1094.
[3] a) F. P. Schmidtchen, M. Berger, *Chem. Rev.* **1997**, *97*, 1609 – 1646; b) *The Supramolecular Chemistry of Anions* (Eds.: A. Bianchi, K. Bowman-James, E. García-España), Wiley, Chichester, **1997**; c) *Special issue on Anion Recognition* (Ed.: P. A. Gale), *Coord. Chem. Rev.* **2003**, *240*, 1 – 221.
[4] P. D. Beer, P. A. Gale, *Angew. Chem.* **2001**, *113*, 502 – 532; *Angew. Chem. Int. Ed.* **2001**, *40*, 487 – 516.
[5] R. Vilar, *Angew. Chem.* **2003**, *115*, 1498 – 1516; *Angew. Chem. Int. Ed.* **2003**, *42*, 1460 – 1477.
[6] For examples of control over translational isomerism through the protonation/deprotonation of cationic binding sites in molecular shuttles see a) R. A. Bissell, E. Córdova, A. E. Kaifer, J. F. Stoddart, *Nature*, **1994**, *369*, 133 – 137; b) P. R. Ashton, R. Ballardini, V. Balzani, I. Baxter, A. Credi, M. C. T. Fyfe, M. T. Gandolfi, M. Gómez-López, M.-V. Martínez-Díaz, A. Piersanti, N. Spencer, J. F. Stoddart, M. Venturi, A. J. P. White, D. J. Williams, *J. Am. Chem. Soc.* **1998**, *120*, 11932 – 11942; c) J. W. Lee, K. Kim, K. Kim, *Chem. Commun.* **2001**, 1042 – 1043; d) A. M. Elizarov, S.-H. Chiu, J. F. Stoddart, *J. Org. Chem.* **2002**, *67*, 9175 – 9181.
[7] G. A. Jeffrey, *An Introduction to Hydrogen Bonding*, Oxford University Press, New York, **1997**.
[8] C. R. Bondy, S. J. Loeb, *Coord. Chem. Rev.* **2003**, *240*, 77 – 99.
[9] a) K. Kavallieratos, S. R. De Gala, D. J. Austin, R. H. Crabtree, *J. Am. Chem. Soc.* **1997**, *119*, 2325 – 2326; b) K. Kavallieratos, C. M. Bertao, R. H. Crabtree, *J. Org. Chem.* **1999**, *64*, 1675 – 1683; c) J. A. Wisner, P. D. Beer, M. G. B. Drew, *Angew. Chem.* **2001**, *113*, 3718 – 3721; *Angew. Chem. Int. Ed.* **2001**, *40*, 3606 – 3609; d) J. M. Mahoney, A. M. Beatty, B. D. Smith, *J. Am. Chem. Soc.* **2001**, *123*, 5847 – 5848.
[10] a) G. M. Hübner, J. Gläser, C. Seel, F. Vögtle, *Angew. Chem.* **1999**, *111*, 395 – 398; *Angew. Chem. Int. Ed.* **1999**, *38*, 383 – 386; b) C. Seel, F. Vögtle, *Chem. Eur. J.* **2000**, *6*, 21 – 24; c) R. Shukla, M. J. Deetz, B. D. Smith, *Chem. Commun.* **2000**, 2397 – 2398; d) C. A. Schalley, G. Silva, C. F. Nising, P. Linnartz, *Helv. Chim. Acta* **2002**, *85*, 1578 – 1596; e) P. Ghosh, O. Mermagen, C. A. Schalley, *Chem. Commun.* **2002**, 2628 – 2629; f) J. M. Mahoney, R. Shukla, R. A. Marshall, A. M. Beatty, J. Zajicek, B. D. Smith *J. Org. Chem.* **2002**, *67*, 1436 – 1440; g) M. J. Deetz, R. Shukla, B. D. Smith, *Tetrahedron* **2002**, *58*, 799 – 805.
[11] J. A. Wisner, P. D. Beer, M. G. B. Drew, M. R. Sambrook, *J. Am. Chem. Soc.* **2002**, *124*, 12469 – 12476.
[12] The relative efficacy of neutral functional groups as hydrogen-bond acceptors can be accurately estimated using hydrogen-bond basicity tables (a) R. W. Taft, F. G. Bordwell, *Acc. Chem. Res.* **1988**, *21*, 463 – 469; b) M. H. Abraham, *Chem. Soc. Rev.* **1993**, *22*, 73 – 83). However, the large effects of solvation and ion pairing make it far harder to assess the inherent hydrogen-bond accepting ability of anions beyond their pK_a value or position in a Hofmeister series.
[13] a) A. M. Brouwer, C. Frochot, F. G. Gatti, D. A. Leigh, L. Mottier, F. Paolucci, S. Roffia, G. W. H. Wurpel, *Science* **2001**, *291*, 2124 – 2128; b) A. Altieri, F. G. Gatti, E. R. Kay, D. A. Leigh, F. Paolucci, A. M. Z. Slawin, J. K. Y. Wong, *J. Am. Chem. Soc.* **2003**, *125*, 8644 – 8654; c) A. Altieri, G. Bottari, F. Dehez, D. A. Leigh, J. K. Y. Wong, F. Zerbetto, *Angew. Chem.* **2003**, *115*, 2398 – 2402; *Angew. Chem. Int. Ed.* **2003**, *42*, 2296 – 2300.
[14] R. Schwesinger, C. Hasenfratz, H. Schlemper, L. Walz, E.-M. Peters, K. Peters, H. G. von Schnering, *Angew. Chem.* **1993**, *105*, 1420 – 1422; *Angew. Chem. Int. Ed. Engl.* **1993**, *32*, 1361 – 1363.
[15] The chemical shift difference for the succinic methylene protons of **1**H/**2**H is 0.5 ppm in [D_6]DMSO and 0.4 ppm in [D_4]MeOH, which indicates a lower occupancy of the succinamide station in these solvents.
[16] J. Y. Le Questel, C. Laurence, A. Lachkar, M. Helbert, M. Berthelot, *J. Chem. Soc. Perkin Trans. 2* **1992**, 2091 – 2094.
[17] The chemical shifts of $H_{d,e}$ are virtually unchanged between rotaxanes **1**H and $\mathbf{1}^-$ in $CDCl_3$ or CD_2Cl_2 (see Supporting Information), which shows that the macrocycle of $\mathbf{1}^-$ is preferentially located over the succinamide station in these solvents. Similarly, with the exception of H_m, the alkyl chain protons are shielded by < 0.2 ppm in $\mathbf{1}^-$ compared with $\mathbf{2}^-$, which confirms that the alkyl chain near the phenolate unit is not encapsulated by the macrocycle. However, there are significant shifts in the amide protons of the macrocycle (≈ 1.2 ppm, which indicates their involvement in stronger hydrogen bonding in the deprotonated rotaxane), H_c, H_m, and some of the phenolate resonances in $\mathbf{1}^-$ compared to **1**H, all consistent with a folded, hydrogen-bonded structure for $\mathbf{1}^-$ where the macrocycle is situated over the succinamide station while simultaneously hydrogen bonding to the phenolate anion.
[18] The standard experimental set up for all our experiments, from which one variable was changed or another component added, was: rotaxane or thread (0.009 mmol), P_1 base (0.010 mmol), and [D_7]DMF (0.6 mL) as solvent at 298 K. The base-induced shuttling in the rotaxane is rapid on the NMR timescale (the spectrum shown in Figure 1d is immediately apparent and not time dependent). Shuttling away from a succinamide binding site in a similar rotaxane has been shown to occur on the microsecond timescale.[13a,b]
[19] R. Shukla, T. Kida, B. D. Smith, *Org. Lett.* **2000**, *2*, 3099 – 3102.

 © 2004 Wiley-VCH Verlag GmbH & Co. KGaA, Weinheim

Artificial Enzymes

A Simple Protocol for the Modular Assembly of "Millipede" Artificial Enzymes**

William B. Motherwell, Catherine E. Atkinson, Abil E. Aliev, Stephanie Y. F. Wong, and Brian H. Warrington*

Successful strategies for the creation of effective artificial enzymes can be broadly classified into two contrasting approaches.[1] The first involves rational design of macromolecules that present a perfectly engineered array of catalytic functional groups.[2] The smallest miscalculation in orchestrating a tailored active site can however lead to disastrous results. The second approach,[3] which requires selection of a few catalytically active biomolecules from a large pool of randomly generated molecules can be seen in such areas as catalytic antibodies,[4,5] catalytic RNA molecules,[6] and the successful screening developments pioneered by Reetz and co-workers for in vitro evolution.[7] Whilst such selection processes often lead to active catalysts, retrospective structural analysis is then required to obtain a detailed understanding of a possible mode of action. Within this framework, the highly creative and original contribution of Menger and co-workers[8] in recognizing that automated combinatorial derivatization of polymers would produce large libraries of randomly functionalized polymers which could then be screened for catalytic activity is especially significant. Thus, for example, by attaching various combinations of carboxylic acids (some of which contained the well known catalytically active groups of enzymes) to a polyallylamine backbone it was possible to demonstrate significant phosphatase catalytic activity in the presence of a metal ion within the resultant mixture. As emphasized by Menger and co-workers, the goal of this approach, as in many selection systems, is directed towards a polymeric system that serves a useful function, even though any given "combinatorial polymer" is composed of an inseparable mixture of polymeric variations whose structure is impossible to determine.

In light of the above situation, we have therefore sought to develop a simple protocol for the modular assembly of artificial enzymes which combines the positive elements of both rational design and selection, and hence, through programmed variation, provides an exploratory mechanism-based framework for catalyst discovery. The essence of our approach was to concentrate on the most simple but dynamic view of an enzyme as a molecule which can both "hold" and "bite" and also possesses the flexibility to achieve the operation of bringing the "hands" (substrate binding) to the "mouth" (catalytically active group). The idea of attaching nucleophilic groups for solvolysis to a polymeric backbone and thereby creating an artificial enzyme is of course a well-established approach[9] and is also implicit in the aforementioned combinatorial polymers prepared by Menger and co-workers.[8] We reasoned however that the installation of an additional designed and selected unit, whose primary function is to act as a binding region with the role of transition-state stabilization, should considerably enhance the catalytic activity in such polymeric systems. The resultant design in Figure 1

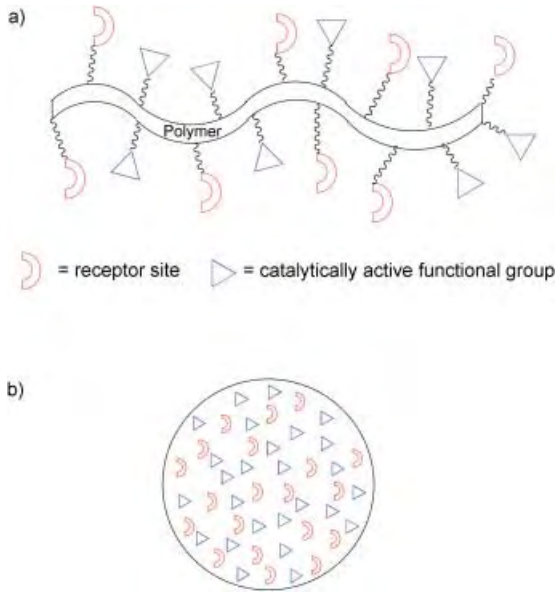


Figure 1. A schematic view of the modular approach to the synthesis of flexible artificial enzymes. a) Linear view: receptor sites and potential catalytic groups are grafted onto a polymer backbone at random intervals. b) Aerial view: each receptor site is surrounded by several catalytic groups, and once a substrate is bound, any one of these may be in the correct position to attack the substrate.

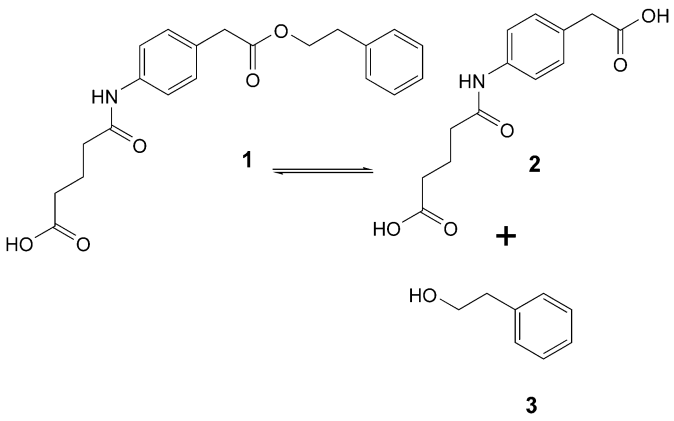
therefore features a polymeric backbone to which separate strands possessing either a designed receptor site based on a transition-state analogue or a catalytically active group are randomly attached. Although this distribution of binding sites and catalytically active groups means that the precise tertiary structure which will evolve is unknown, we considered that the resultant polymer, for which we have coined the name "millipede", would confer a statistical advantage in terms of developing effective regions for catalysis. Thus, any given receptor site could be surrounded by several proximal catalytic groups potentially capable of adopting the necessary stereoelectronic trajectory for attack on the bound substrate (Figure 1).

To illustrate this concept, we chose to study the hydrolysis of ester **1** (Scheme 1), with the classical phosphonate ester **4**

[*] Prof. W. B. Motherwell, Dr. C. E. Atkinson, Dr. A. E. Aliev
Department of Chemistry, Christopher Ingold Laboratories
University College London
20 Gordon Street, London, WC1H 0AJ (UK)
Fax: (+44) 207-679-7524
E-mail: w.b.motherwell@ucl.ac.uk
S. Y. F. Wong, Dr. B. H. Warrington
GlaxoSmithKline, New Frontiers Science Park
Harlow, Essex, CM19 5AW (UK)

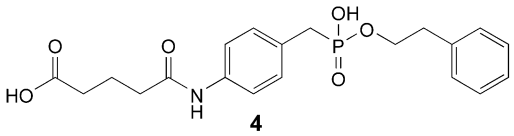
[**] We are grateful to GlaxoSmithKline for the provision of a CASE studentship (C.E.A.). We also acknowledge the provision of a Leverhulme Trust grant which initiated our studies in this area. We also thank Dr. Grant Wishart (Wolfson Institute of Biomedical Research) for his help with molecular modeling studies.

 DOI: 10.1002/anie.200352370 © 2004 Wiley-VCH Verlag GmbH & Co. KGaA, Weinheim



Scheme 1. The hydrolysis reaction chosen for study.

selected as a suitable transition-state analogue (TSA). These compounds were prepared by standard synthetic sequences.



The most important objective in this approach was to select and prepare a complementary binding unit for phosphonate **4**. Initially, to facilitate this process, **4** was chosen to contain two acidic residues, the carboxylic acid, and the phosphonic acid, together with an additional amide bond all on the acid side of the ester bond in the substrate. Consequently, a suitable binding unit would be bidentate and contain either basic or hydroxy groups at each end capable of binding to the two acidic groups. Dipeptides with hydrogen bonding potential were of course the natural choice. With these thoughts in mind, nine commercially available dipeptides were selected for use in binding studies with phosphonate **4**.

The affinity of the dipeptides for the TSA **4** was then studied by measuring the change in diffusion coefficient (D) upon complexation by using the pulsed field gradient NMR BPPLED technique.[10] The translational diffusion coefficient of a molecule in solution is molecular mass dependent, and on complexation with a host molecule a decrease in diffusion coefficient is observed.[11]

The translational diffusion coefficients of the nine dipeptides and the TSA **4** were measured in D_2O at pD7.[12] The value of D was measured both in free solution, and in mixtures containing one peptide and the TSA in a ratio of 3 mM:30 mM. The diffusion coefficient of free TSA was measured to be $3.38 \times 10^{-10}\ m^2 s^{-1}$. In the presence of the peptides, this value was not expected to change significantly, since even if a stable complex formed, only 10% of the TSA molecules could be involved in binding at any one time. Hence it was the observed change in D for the dipeptides that was of interest.

As revealed in Table 1, the basic dipeptide, Arg–Arg clearly displayed the most significant change in D as might be anticipated from the well-established interaction between guanidine groups and carboxylic acids.[13] The binding constant (K_a) for the interaction between Arg–Arg and the TSA was calculated to be $86\ L M^{-1}$ by measuring D at varying concentrations, and using a curve-fitting procedure.[11a,14] This value was more than acceptable to us since hydrogen bonding between two small molecules in water would be interrupted by solvent molecules. Molecular modeling was then undertaken to verify whether the geometries of preferred conformations for both the TSA and Arg–Arg were suitable for a bidentate interaction. As envisaged, the lowest energy complexes showed each guanidine unit of the dipeptide interacting, one with the phosphonate and the other with the carboxylic acid moieties of the TSA. There was no evidence for amide hydrogen bond association. Even though it does not necessarily follow that the dipeptide with the strongest binding interaction with the TSA **4** will provide the most effective unit for catalysis, the ability to rank this affinity using the above NMR protocol[12] provides a valuable method for ordered selection.

Table 1: Observed diffusion coefficients of dipeptides in D_2O at 298 K: D for 3 mM solutions of dipeptide and D' for mixtures containing dipeptide (3 mM) and TSA (30 mM).

Entry	Dipeptide	D [$\times 10^{-10}\ m^2 s^{-1}$]	D' [$\times 10^{-10}\ m^2 s^{-1}$]	R_d [%][a]
1	H-Arg-Arg-OH	4.10	3.40	17
2	H-Ala-Arg-OH	4.76	4.18	12
3	H-βAla-Lys-OH	4.91	4.39	11
4	H-βAla-His-OH	5.18	4.71	9
5	H-Ser-His-OH	4.89	4.46	9
6	H-Gly-Tyr-OH	4.97	4.64	7
7	H-βAla-Leu-OH	4.97	4.62	7
8	H-Gly-Thr-OH	5.54	5.19	6
9	H-Ala-Gly-OH	6.08	5.72	6

[a] R_d reflects the relative change in diffusion coefficient ($100\,(D-D')/D$).

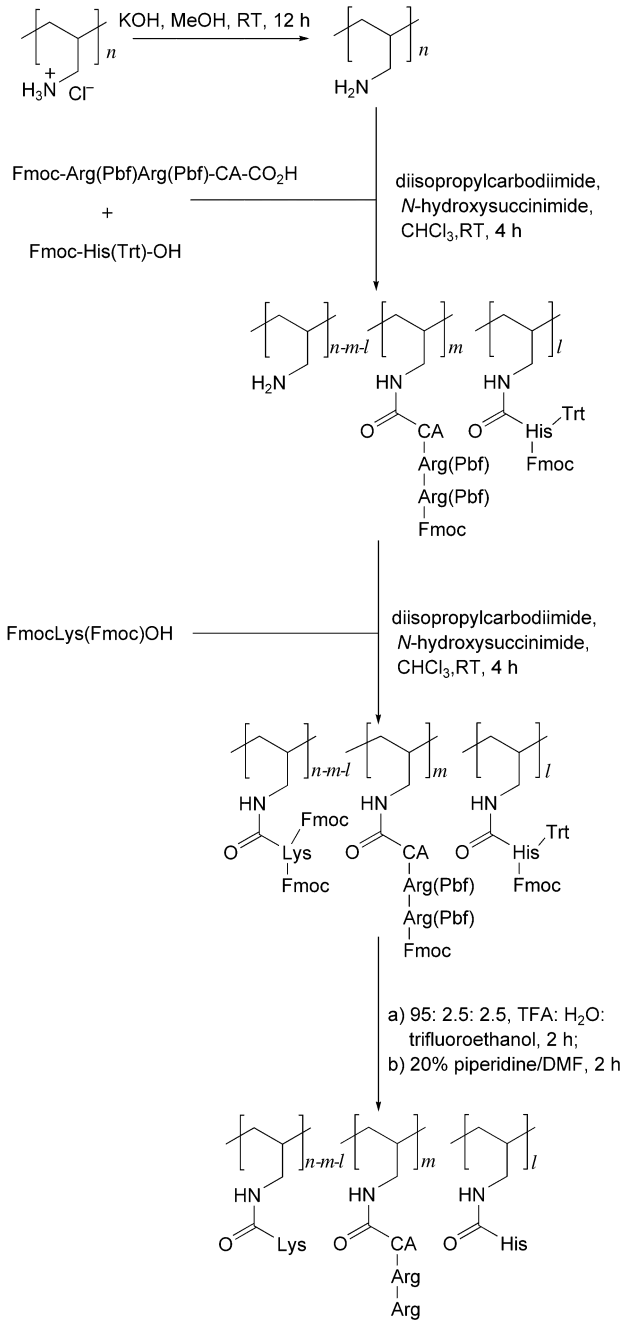
With a suitable "receptor unit" in hand, we then had to consider how to incorporate this fragment into a polymer backbone, and also to select a catalytically active group for concomitant incorporation. Based on nature's principles, the obvious choice was to use an amino acid, such as histidine, cysteine, lysine, tyrosine, or serine, which have such a role in the natural proteases.[15]

Preliminary studies reported here focus on the use of histidine. As in the combinatorial polymers described by Menger and co-workers,[8] a polyallylamine thread was chosen for the polymer backbone since it was flexible, soluble, and the free amino groups provided an easy method for incorporation of the binding and catalytic moieties into the polymer by standard peptide coupling procedures. It was also decided at this point to lengthen the leg of the millipede by using 6-amino caproic acid as a linker between the polymer and the dipeptides such that the conformational freedom of the binding unit would not be restricted by being placed too close to the polymer backbone. The required protected tripeptide

 © 2004 Wiley-VCH Verlag GmbH & Co. KGaA, Weinheim

6-(Fmoc-Arg(Pbf)-Arg(Pbf)-)amido caproic acid was prepared by solid-phase synthesis.

Polymer **5** was then assembled in sequential fashion as shown in Scheme 2. Polyallylamine hydrochloride was converted to the free base by stirring with KOH in methanol.[16] One third of the amino sites were functionalized with 6-(Fmoc-Arg(Pbf)-Arg(Pbf)-)amido caproic acids, and one third with Fmoc-His(Trt)-OH by coupling with diisopropylcarbodiimide and *N*-hydroxysuccinimide. Both of these units were introduced to the polymer at the same time to encourage the desired statistically random distribution. All of the unfunctionalized amino groups on the polymer were then capped with lysine residues. In principle, this third type of leg in the millipede can be chosen to create a more hydrophilic or hydrophobic environment as desired. In addition to the fully armed polymer, three further polymers were also prepared, one containing lysine and the "binding unit" (2:1) **6**, another lysine and the catalytic group (2:1) **7**, with the third being the blank polymer **8** with only lysine residues. In this way the significance of each component can be identified and hence cooperativity in catalysis can be examined. Deprotection of acid-labile groups with 95% trifluoroacetic acid (TFA), followed by base deprotection of the Fmoc groups afforded the fully deprotected polymers in free base form.



Scheme 2. Synthesis of catalytic polymers (CA = $-(CH_2)_5NH-$).

Hydrolysis reactions were then performed by adding 15 mg of the appropriate polymer to a 0.5 mM solution of ester **1** in aqueous phosphate buffer at pH 7.[*] The changes in the concentration of both the ester substrate and the acid product **2** were monitored by HPLC.

In blank reactions containing either no polymer, or the blank lysine polymer **8**, no hydrolysis whatsoever was observed. The preliminary kinetic data for formation of the free acid **2** from ester **1** in the presence of polymers **5**–**7** are displayed in Figure 2. The initial relative rates for product formation were calculated to be 1:90:890 for polymers **7**:**6**:**5**, respectively. The fact that polymer **7** embodying the imida-

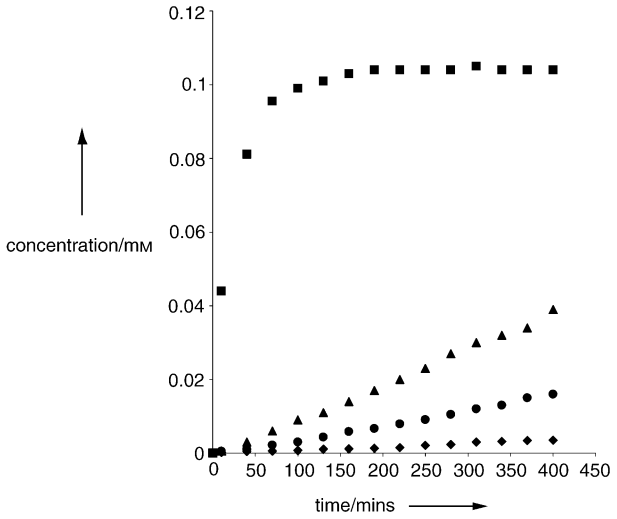


Figure 2. Graph showing rate of formation of product **2** using polymers **5** (■), **6** (▲), and **7** (◆). Also shown (●) is a competition experiment for polymer **6**, when the hydrolysis was performed in the presence of an equimolar quantity of TSA **4**.

[*] As shown by our diffusion NMR measurements,[12] significant self-association effects are observed for the ester analogue **4** on increasing its concentration. Similar concentration-dependent self-association is also expected for ester **1**, hence a dilute 0.5 mM solution of **3** was used in all our measurements and no variation of substrate concentration was attempted when comparing catalytic properties of polymers **5**–**8** in this study.

 © 2004 Wiley-VCH Verlag GmbH & Co. KGaA, Weinheim

zole group alone can function as a catalyst is not surprising since, as we have emphasized, polymer-supported nucleophilic catalysts of this type are known.[9] At first sight, polymer **6** containing the receptor site should function only by binding of the tetrahedral intermediate for ester hydrolysis. However, within the environs of the polymer, positively charged guanidine groups may induce a higher local concentration of hydroxide anions, and this may contribute to the observed rate enhancement and help to explain why the "hands" are more effective than the "teeth". The behavior of polymer **5** clearly indicates that the whole is greater than the sum of the parts, and that, irrespective of mechanistic detail, the initial premise of designing a flexible polymer with separately selected binding regions and catalytic groups offers a valuable strategic approach.

Interestingly polymer **5** appears to demonstrate the often-encountered phenomenon of product inhibition, as implied by the saturation kinetics curve displayed in Figure 2. Such a result can be anticipated since the product diacid is produced in close proximity to the bidentate and highly basic Arg–Arg site. The fact that even with such a challenging substrate, a 25% conversion to product was achieved in two hours using only 5 mol% of the polymer was a very encouraging observation. We have also verified the binding role of the Arg–Arg unit in polymer **6** using the phosphonate TSA **4**. The change in the diffusion coefficient of the TSA upon binding to the polymer was found to be significantly reduced by 80% relative to the value of D found in free solution. Using these values K_a was estimated to be $\geq 1500\ \mathrm{L\,M^{-1}}$, indicating the strong affinity of **4** for polymer **6**. This measurement encouraged us to demonstrate the phenomenon of competitive inhibition of enzyme action. Thus, when the hydrolysis of ester **1** by polymer **6** was attempted in the presence of an equimolar amount of the TSA **4**, the rate of hydrolysis decreased by a factor of 2. A further feature of interest is that, in contrast to combinatorial polymers[8] which can display an induction period of up to 24 h while the polymer "learns to recognize the substrate", polymer **5** did not exhibit this phenomenon. This observation therefore provides additional circumstantial evidence for the effectiveness of binding site incorporation.

In summary, the foregoing study has indicated that this modular "step-by-step" strategy, which combines both design and selection elements for the attachment of separately considered receptor sites and catalytically active groups to a flexible polymer backbone, can be used to construct an artificial enzyme. The method outlined is clearly amenable to a parallel synthesis approach for optimization and can also provide, at every step along the way, detailed information about the relative importance and cooperativity of the groups contributing to the molecular environment of active sites within enzymes.

Received: July 14, 2003 [Z52370]

Keywords: catalysis · enzyme mimics · esters · hydrolysis · polymers

[1] a) J. D. Stevenson, N. R. Thomas, *Nat. Prod. Rep.* **2000**, *17*, 535; b) W. B. Motherwell, M. J. Bingham, Y. Six, *Tetrahedron* **2001**, *57*, 4663.

[2] a) R. Breslow, S. D. Dong, *Chem. Rev.* **1998**, *98*, 1997; b) L. J. Twyman, A. S. H. King, I. K. Martin, *Chem. Soc. Rev.* **2002**, *31*, 69; c) G. Wulff, *Chem. Rev.* **2002**, *102*, 1; d) J. H. Suh, *Synlett* **2001**, *9*, 1343.

[3] P. A. Brady, J. K. M. Sanders, *Chem. Soc. Rev.* **1997**, *26*, 327.

[4] a) A. Tramontano, K. D. Janda, R. A. Lerner, *Science* **1986**, *234*, 1566; b) S. J. Pollack, J. W. Jacobs, P. G. Schultz, *Science* **1986**, *234*, 1570.

[5] a) F. Tanaka, *Chem. Rev.* **2002**, *102*, 4885; b) J. L. Raymond, *Top. Curr. Chem.* **1999**, *200*, 59.

[6] a) V. J. DeRose, *Chem. Biol.* **2002**, *9*, 961; b) C. Frauendorf, A. Jäschke, *Angew. Chem.* **1998**, *110*, 1449; *Angew. Chem. Int. Ed.* **1998**, *37*, 1378.

[7] a) K.-E. Jaeger, T. Eggert, A. Eipper, M. T. Reetz, *Appl. Microbiol. Biotechnol.* **2001**, *55*, 519; b) M. T. Reetz, M. Hermes, M. H. Becker, *Appl. Microbiol. Biotechnol.* **2001**, *55*, 531; c) H. Y. Tao, V. W. Cornish, *Curr. Opin. Chem. Biol.* **2002**, *6*, 858.

[8] a) F. M. Menger, A. V. Eliseev, V. A. Migulin, *J. Org. Chem.* **1995**, *60*, 6666; b) F. M. Menger, C. A. West, J. Ding, *Chem. Commun.* **1997**, 633; c) F. M. Menger, J. Ding, V. Barragan, *J. Org. Chem.* **1998**, *63*, 7578.

[9] I. M. Klotz in *Enzyme Mechanisms* (Eds.: M. I. Page, A. Williams), Royal Society of Chemistry, London, **1987**, pp. 14–34.

[10] D. H. Wu, A. D. Chen, C. S. Johnson, *J. Magn. Reson. Ser. A* **1995**, *115*, 260.

[11] a) L. Fielding, *Tetrahedron* **2000**, *56*, 6151; b) M. F. Lin, D. A. Jayawickrama, R. A. Rose, J. A. Delviscio, C. K. Larive, *Anal. Chim. Acta* **1995**, *307*, 449; c) A. Gafni, Y. Cohen, *J. Org. Chem.* **1997**, *62*, 120.

[12] C. E. Atkinson, A. E. Aliev, W. B. Motherwell, *Chem. Eur. J.* **2003**, *9*, 1714.

[13] C. G. Suresh, J. Ramaswamy, M. Vilayan, *Acta Crystallogr. Sect. B* **1986**, *42*, 473.

[14] a) D. R. Carcanague, F. Diederich, *Angew. Chem.*, **1990**, *102*, 836; *Angew. Chem. Int. Ed. Engl.* **1990**, *29*, 769; b) B. R. Peterson, P. Wallimann, D. R. Carcanague, F. Diederich, *Tetrahedron* **1995**, *51*, 401.

[15] A. R. Ferscht, *Structure and mechanism in protein science. A guide to enzyme catalysis and protein folding*, W. H. Freeman, New York, **1999**.

[16] N. Tanaka, K. Nakagawa, H. Iwasaki, K. Hosoya, K. Kimata, T. Araki, D. G. Patterson, Jr., *J. Chromatogr. A* **1997**, *781*, 139.

 © 2004 Wiley-VCH Verlag GmbH & Co. KGaA, Weinheim

Photochemical Processes

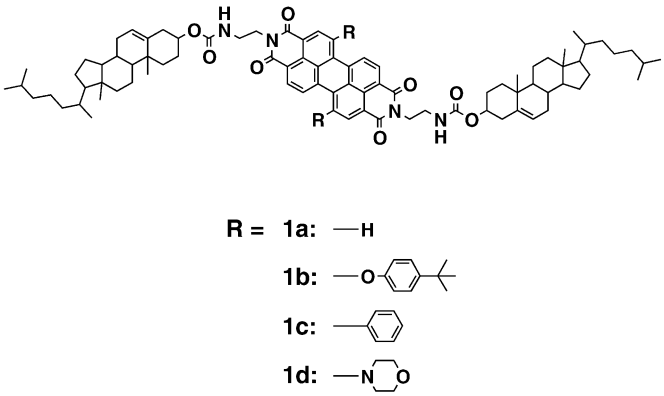
Visible-Light-Harvesting Organogel Composed of Cholesterol-Based Perylene Derivatives**

*Kazunori Sugiyasu, Norifumi Fujita, and Seiji Shinkai**

In nature, photosynthesis commences with the absorption of sunlight, and continuous unidirectional energy or electron transfer between chromophores plays a key role in efficient light harvesting.[1] The chromophores (i.e., chlorophyll molecules) are arranged by noncovalent interactions at suitable distances and in an appropriate orientations within the peptide matrix. To mimic a natural photosynthetic system with artificial molecular systems, numerous attempts have been made to arrange chromophores in a one-dimensional (1D) manner utilizing the methodologies developed in self-assembly and supramolecular chemistry. The supramolecular architectures used so far to design light harvesting systems are molecular arrays,[2] supramolecular complexes,[3] dendrimers,[4] monolayer systems,[5] etc. In particular, photochemical studies conscious of the reaction medium (matrix) are very important not only to create efficient energy and electron transfer systems but also to consider what kind of reaction is taking place in green plants.

Recently, novel supramolecular architectures constructed in organogels have attracted the widespread attention of supramolecular chemists. The origin of organogel formation is considered to be through 1D alignment of gelator molecules supported by dipole–dipole, van der Waals, and hydrogen-bonding interactions.[6,7] Such 1D alignment of functional molecules constructed through the gelation process can provide a novel chromophore assembly. Thus, gelators based on porphyrins,[8] phthalocyanines,[9] and conjugate oligomers[10] have been developed. In addition, the gel phase, which is different from either the solid phase or the liquid phase, is so unique as a medium that it is expected to provide a novel environment to arrange functional molecules indispensable to a natural photosynthetic system. Herein, we report on the design of a novel "visible"-light-harvesting system utilizing the 1D alignment nature of perylene-containing cholesterol-based gelators. Perylene and its derivatives are known to be the photofunctional dyes with unique optical and electrochemical properties. They have excellent light fastness, high chemical stability, high photoluminescence yield, and a wide range of colors that are tunable by various substituents at the bay position.[11] The gel-forming ability of cholesterol derivatives is useful to arrange them into a 1D alignment.[12] As a result, it is expected that perylene-containing organogels[13] will provide well-defined nanomaterials that feature a "visible"-light-harvesting function.[14]

The gelation ability of **1a–d** (Scheme 1) was evaluated in various solvents. In most of these solvents gels were not



Scheme 1. Structure of cholesterol-based perylene derivatives.

formed, however, aromatic solvents (such as benzene, toluene, and *p*-xylene) are partially gelated by **1a,** whereas it is virtually insoluble in most alcoholic solvents (such as methanol, ethanol, 1-propanol, and 1-butanol). Thus, we modified the solubility of **1a** in *p*-xylene by adding alcoholic solvents; as expected, most mixed solvents were finely gelated by **1a** (Figure 1a). We could also use toluene, *o*-xylene, and

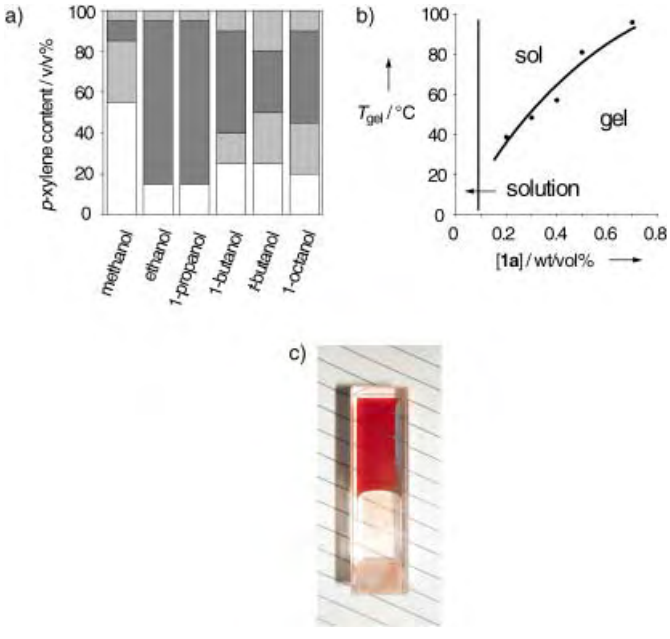


Figure 1. a) Gelation test for **1a** in *p*-xylene and alcoholic solvent mixtures: dark gray = gel, light gray = precipitate, white = insoluble material; b) plot of T_{gel} versus **1a** concentration in *p*-xylene/1-propanol (3:1 v/v); c) photo of **1a** gel prepared from *p*-xylene/1-propanol (3:1 v/v), [**1a**] = 0.5 wt/vol% (3.8 mM).

[*] K. Sugiyasu, Dr. N. Fujita, Prof. Dr. S. Shinkai
Department of Chemistry & Biochemisry
Graduate School of Engineering, Kyushu University
6-10-1 Hakozaki, Higashi-ku, Fukuoka 812–8581 (Japan)
Fax: (+81) 92-642-3611
E-mail: seijitcm@mbox.nc.kyushu-u.ac.jp

[**] We thank Hongyue Li and Yumiko Kitada at Kyushu University for ^{1}H NMR and AFM measurements. This work is financially supported by the 21st Century COE Project, "Functional Innovation of Molecular Informatics".

Supporting information for this article is available on the WWW under http://www.angewandte.org or from the author.

 DOI: 10.1002/anie.200352458 © 2004 Wiley-VCH Verlag GmbH & Co. KGaA, Weinheim

nitrobenzene for gelation instead of *p*-xylene. The **1a** gel was formed very stably above 0.5 wt/vol% (3.8 mM) and showed a high sol–gel phase-transition temperature (T_{gel}; Figure 1b) as well as high transparency even in the high gelator concentration region (Figure 1c), which is a condition that is indispensable for applying this system to photochemical purposes. In contrast, **1b–d** could not gelate these mixed solvents. However, mixtures containing more than 50 mol% of **1a** formed stable, transparent organogels from the mixed solvents. Hereafter, we used a mixed solvent of *p*-xylene and 1-propanol (3:1 v/v) as a standard medium.

First, to obtain visual images of the **1a** gel we took pictures with confocal laser scanning microscope (CLSM), SEM, and AFM (Figure 2). Although the scale of the pictures is

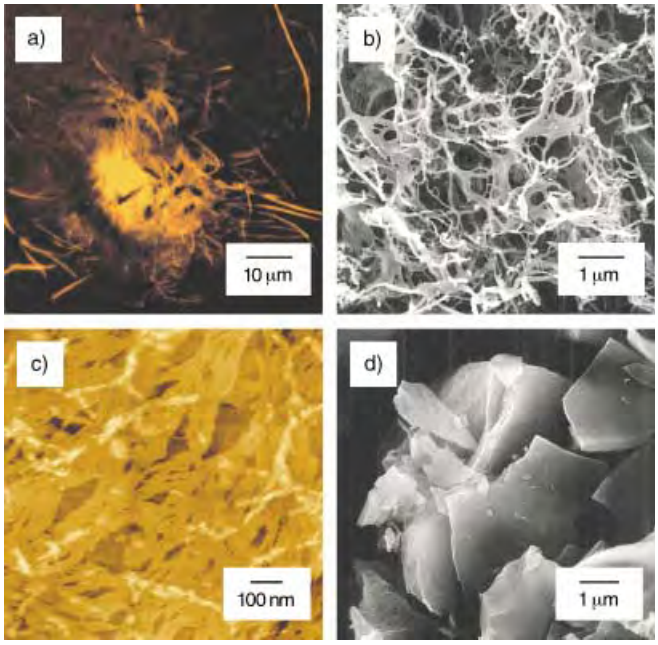


Figure 2. a–c) CLSM (λ_{ex} = 488 nm, prepared from *p*-xylene/1-propanol (3:1 v/v)), SEM (*p*-xylene/*tert*-butanol (4:1 v/v)), and AFM images (*p*-xylene/1-propanol (3:1 v/v)) of a **1a** gel; d) SEM image of **1a** crystals precipitated from *p*-xylene.

increased 10 times from Figure 2c (AFM) to Figure 2b (SEM) and from Figure 2b to Figure 2a (CLSM), one can consistently observe a network structure composed of fibrous aggregates. This means that the gel fibers present consist of hierarchical structures. The smallest fiber diameter observed with AFM is ≈3 nm, which is almost comparable with the length of the molecular long axis of **1a**.[15] On the other hand, an SEM picture of the precipitate formed from *p*-xylene showed a cubic structure (Figure 2d). The difference indicates that added 1-propanol plays a role in changing the aggregation mode of **1a** from the 3D aggregate to the 1D aggregate.

Second, we measured the absorption and fluorescence spectra of **1a–d** (2.0×10^{-5} M) in homogeneous solutions to obtain an insight into their photochemical properties. As shown in Figure 3, **1a**, **b**, **c**, and **d** have their absorption maxima at 527 (and weaker maxima 490 and 457), 550 (and 513), 557, and 660 nm, respectively, and their emission

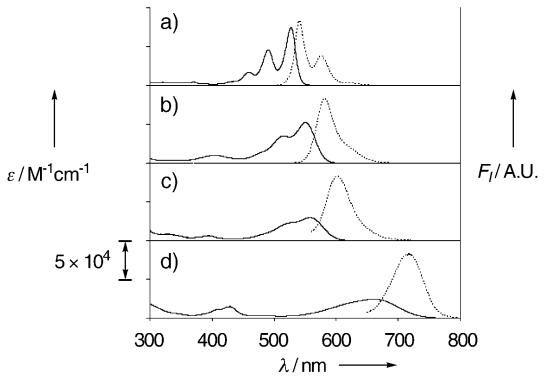


Figure 3. Absorption (——) and fluorescence (•••••) spectra of a) **1a**, b) **1b**, c) **1c**, and d) **1d** in diluted homogeneous solutions; [**1a–d**] = 2.0×10^{-5} M in $CHCl_3$. λ_{ex} = 477 for **1a**, 494 for **1b**, 507 for **1c**, and 622 nm for **1d**, respectively.

maxima at 540 (and 575), 580, 602, and 718 nm, respectively. We estimated the fluorescence quantum yields of **1a–d** in the solution phase using a reported compound *N*,*N*′-di(1-hexylheptyl)-3,4,9,10-perylenetetracarboxylic diimide as a standard: the fluorescence quantum yield is 0.93.[16] We could thus determine the quantum yields of **1a**, **b**, **c**, and **d** to be 0.93, 0.49, 0.28, and ≈0.001, respectively. Comparison of Figure 4a

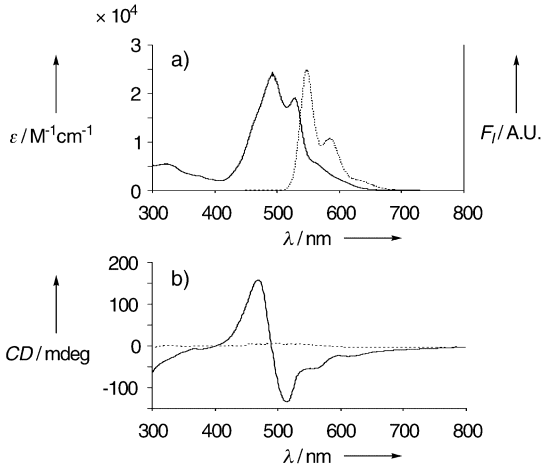


Figure 4. a) Absorption (——) and fluorescence (•••••) spectra of a **1a** gel; b) CD spectra of a **1a** gel (——) and a **1a** sol (•••••, 70°C): *p*-xylene/1-propanol (3:1 v/v), [**1a**] = 0.2 wt/vol% (1.5 mM), λ_{ex} used for fluorescence measurements was 457 nm.

with Figure 3a reveals that the relative absorbance of the 0→0 transition (527 nm) against the 0→1 transition (490 nm) is decreased in the gel phase. This change indicates that the gel formation intensifies the π–π stacking interaction among perylene moieties.[17] It was found that the fluorescence intensity of **1a** in the gel phase is decreased by about two orders of magnitude from that in the solution phase, but the relative intensity of a fluorescence peak at 630 nm is rather intensified. Interestingly, only the gel phase (but not the sol phase) showed CD activity, which features a negative exciton coupling consisting of a negative first Cotton effect and a

 © 2004 Wiley-VCH Verlag GmbH & Co. KGaA, Weinheim

positive second Cotton effect (Figure 4b). The contribution of linear dichroism (LD) observed under the same measurement conditions was negligibly small. This CD sign implies that the dipole moments in the perylene moiety of **1a** are oriented into an anticlockwise direction (that is, *S* chirality). The π–π stacking interaction among the perylene moieties is so strong that one can imagine an aggregation mode in which a 1D-aligned perylene column is twisted by the chirality of the tethered cholesterol groups. Addition of **1b** to the **1a** gel weakened the CD intensity (Figure 1 in Supporting Information). This is probably because the perylene moiety of **1b** is intercalated into the **1a** gel fibrils and the helical sense of **1a** is reduced by the bulky *p-tert*-butylphenoxy substituents of **1b**.[18]

Third, we evaluated whether efficient energy transfer can take place from **1a** to others or in a stepwise manner from **1a** to **1d** using **1b** and **1c** as stepping stones (Figure 5). In diluted

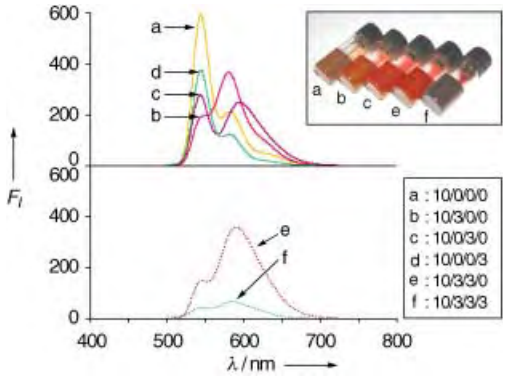


Figure 5. Fluorescence spectra of **1a/1b/1c/1d** mixed gels: [**1a**] = 0.5 wt/vol% (3.8 mM), [**1b–d**] = 0 or 1.3 mM, *p*-xylene/1-propanol (3:1 v/v), λ_{ex} = 457 nm. the numbers in inset denote the molar ratios for **1a/1b/1c/1d**. Inset: a photograph displaying the **1a/1b/1c/1d** mixed gels.

homogeneous solutions ([**1a**] = 2.0×10^{-5} M), perceptible energy transfer from **1a** to other forms was not detected, although the mixtures (**1a/1b/1c/1d** = 10:3:0:0, 10:0:3:0, 10:3:3:0, and 10:3:3:3 molar ratios) were excited at various wavelengths: that is, the presence of **1b**, **1c**, and/or **1d** scarcely affects the fluorescence intensity of **1a** (Figure 2 in the Supporting Information). In contrast, when the **1a/1b/1c/1d** (10:3:3:3 molar ratio) mixed gel was excited at 457 nm where **1a** mainly absorbs light (Figure 3 in the Supporting Information), it was confirmed that efficient energy transfer from **1a** takes place. Figure 5 illustrates the fluorescence spectra of **1a/1b**, **1a/1c**, and **1a/1d** (all 10:3 molar ratio) binary systems, which clearly show that energy is transferred from excited **1a** to **1b**, **1c**, and **1d**, respectively. Energy-transfer efficiency was estimated by the quenching efficiency for **1a** at the emission maximum of 544 nm, which appeared in the order of **1b** (68%), **1c** (53%), and **1d** (34%). This order is consistent with the order of the overlap between the fluorescence of **1a** and the absorbance of **1b**, **1c**, and **1d**, respectively. We have found that $FI_{acceptor}/FI_{donor}$ values in the gel phase are increased 10-fold for the **1a/1b** system and 19-fold for **1a/1c** system when compared to the solution phase.[19]

It should be noted that fluorescence of **1b** and **1c** becomes stronger in the mixed-gel systems in spite of their low fluorescence quantum yields relative to **1a**. As shown by spectrum e in Figure 5, the emission band of a **1a/1b/1c** (10:3:3 molar ratio) ternary system is decreased in the shorter wavelength region whereas it is increased in the longer wavelength region. This change supports the view that energy transfer from **1b** to **1c** is also taking place. Overall, the emission spectrum of the **1a/1b/1c** ternary system is similar to that of **1c**. This means that even though the ternary system has a broad absorption wavelength region that is photo-irradiated by visible light, the excited energy is collected by **1c** and thus it is mainly the emission from **1c** is observable. In a quaternary system including **1d**, 1D alignment of four different perylene groups constitutes an energy gradient, and consequently, the excited energy of **1a** was given to **1b** and **1c**, and finally collected by **1d**. Because of the low emissive nature of **1d** arising from the twisted intramolecular charge-transfer (TICT) band,[20] it acts rather as an energy sink (note the weak fluorescence intensity of spectrum f in Figure 5). These trends are visually shown in the inset in Figure 5.[21]

In conclusion, we have demonstrated that a new visible-light-harvesting system can be designed utilizing a superstructure created in an organogel medium. As is common to organogel systems, gelator molecules tend to assemble into 1D aggregates and thus energy transfer among such 1D aligned chromophores can take place.[22] Since perylene derivatives can absorb a wide range of light energy by subtle modification of the substituents, one can harvest sunlight to the energy sink through perylene-stacked assemblies in the gel system. Well-defined nanoscale 1D alignment of photofunctional molecules, ease of fabrication,[23] and thermo-reversible properties of organogels will lead to the development of novel photofunctional materials from the organogel system. We believe that these soft materials based on molecular assemblies can be applied as model systems for light-emitting diodes, signal amplifiers, fluorescence sensors, energy filters, and other photonic devices.

Experimental Section

Cholesterol-based perylene derivatives (**1a**, **b**, **c**, and **d**) were synthesized from 3,4,9,10-perylene tetracarboxylic dianhydride. The synthetic procedures are explained in the Supporting Information.[24]

^{1}H NMR spectra were measured on a Bruker DMX 600 spectrometer. IR spectra were obtained using a Perkin Elmer ATR FTIR spectrometer. Mass spectral data were obtained using a Perseptive Voyager RP MALDI TOF mass spectrometer. UV/Vis and CD spectra were measured on a Shimadzu UV-2500PC spectrophotometer and a Jasco J-720WI spectrometer, respectively. Fluorescence spectral measurements were performed using a Hitachi F-4500 spectrometer. The gels were photoexcited with an incidence angle of 45° to the quartz-cell surface and the fluorescence was detected along the normal angle. Comparison of each absorption coefficient reveals that even in the **1a/1b/1c/1d** quaternary gel system, **1a** is mainly photoexcited at an excitation wavelength of 457 nm (Figure 3S).

Gelation test: The gelator and the solvent were put in a septum-capped test tube and heated until the solid was dissolved. The sample vial was cooled in air to 25 °C, then left for 1 h at this temperature. The

 © 2004 Wiley-VCH Verlag GmbH & Co. KGaA, Weinheim

state of the materials were evaluated by the "stable-to-inversion of a test tube" method.

CLSM measurements: **1a** gel (prepared from *p*-xylene/1-propanol (3:1)) was placed on a glass plate and observed with a BIO-RAD Radiance 2000 AGR3 microscope. The excitation wavelength was 488 nm (argon laser with reflector turret).

SEM measurements: The specimens were obtained by freezing and pumping the sample of **1a** for 12 h (the gel was prepared from *p*-xylene/*tert*-butanol (4:1); the precipitate was prepared from *p*-xylene). The xerogel and precipitate of **1a** thus obtained were shielded by Pt and examined with a Hitachi S-5500 scanning electron microscope. The accelerating voltage of SEM was 15 kV.

AFM measurements: **1a** gel (prepared from *p*-xylene/1-propanol (3:1)) was collapsed by strong vibration and the supernatant was cast on to freshly cleaved highly oriented pyrolytic graphite (HOPG) by spin-coating. The surface was examined by a Topometrix TMX-2100 microscope (non-contact mode).

Received: July 23, 2003
Revised: December 8, 2003 [Z52458]

Keywords: absorption · chromophores · nanostructures · self-assembly · sol–gel processes

[1] a) W. Kühlbrandt, D. N. Wang, Y. Fujiyoshi, *Nature* **1994**, *367*, 614 – 621; b) G. McDermott, S. M. Prince, A. A. Freer, A. M. Hawthornthwaite-Lawless, M. Z. Papiz, R. J. Cogdell, N. W. Isaacs, *Nature* **1995**, *374*, 517 – 521; c) X. Hu, A. Damjanovic, T. Ritz, K. Schulten, *Proc. Natl. Acad. Sci. USA* **1998**, *95*, 5935 – 5941.

[2] a) S. Prathapan, T. N. Johnson, J. S. Lindsey, *J. Am. Chem. Soc.* **1993**, *115*, 7519 – 7520; b) K.-y. Tomizaki, R. S. Loewe, C. Kirmaier, J. K. Schwartz, J. L. Retsek, D. F. Bocian, D. Holten, J. S. Lindsey, *J. Org. Chem.* **2002**, *67*, 6519 – 6534; c) A. Nakano, A. Osuka, I. Yamazaki, T. Yamazaki, Y. Nishimura, *Angew. Chem.* **1998**, *110*, 3172; *Angew. Chem. Int. Ed.* **1998**, *37*, 3023; d) H. S. Cho, H. Rhee, J. K. Song, C. K. Min, M. Takase, N. Aratani, S. Cho, A. Osuka, T. Joo, D. Kim, *J. Am. Chem. Soc.* **2003**, *125*, 5849 – 5860; e) C. V. K. Sharma, G. A. Broker, J. G. Huddleston, J. W. Baldwin, R. M. Metzger, R. D. Rogers, *J. Am. Chem. Soc.* **1999**, *121*, 1137 – 1144.

[3] a) C. A. Hunter, R. K. Hyde, *Angew. Chem.* **1996**, *108*, 2064 – 2067; *Angew. Chem. Int. Ed. Engl.* **1996**, *35*, 1936 – 1939; b) R. Takahashi, Y. Kobuke, *J. Am. Chem. Soc.* **2003**, *125*, 2372 – 2373; c) T. S. Balaban, R. Goddard, M. Linke-Schaetzel, J.-M. Lehn, *J. Am. Chem. Soc.* **2003**, *125*, 4233 – 4239; d) M. D. Ward, *Chem. Soc. Rev.* **1997**, *26*, 365 – 375.

[4] a) C. Devadoss, P. Bharathi, J. S. Moore, *J. Am. Chem. Soc.* **1996**, *118*, 9635 – 9644; b) D.-L. Jiang, T. Aida, *Nature* **1997**, *388*, 454 – 456; c) M.-S. Choi, T. Aida, T. Yamazaki, I. Yamazaki, *Angew. Chem.* **2001**, *113*, 3294 – 3297; *Angew. Chem. Int. Ed.* **2001**, *40*, 3194 – 3198; d) A. Adronov, J. M. Fréchet, *Chem. Commun.* **2000**, 1701 – 1710; e) J. M. Serin, D. W. Brousmiche, J. M. Fréchet, *J. Am. Chem. Soc.* **2002**, *124*, 11848 – 11849; f) V. Vicinelli, P. Ceroni, M. Maestri, V. Balzani, M. Gorka, F. Vögtle, *J. Am. Chem. Soc.* **2002**, *124*, 6461 – 6468.

[5] a) N. Kimizuka, T. Kunitake, *J. Am. Chem. Soc.* **1989**, *111*, 3758 – 3759; b) L. A. J. Chrisstoffels, A. Adronov, J. M. Fréchet, *Angew. Chem.* **2000**, *112*, 2247 – 2251; *Angew. Chem. Int. Ed.* **2000**, *39*, 2163 – 2167.

[6] For recent comprehensive reviews see a) P. Terech, R. G. Weiss, *Chem. Rev.* **1997**, *97*, 3133 – 3160; b) D. J. Abdallah, R. G. Weiss, *Adv. Mater.* **2000**, *12*, 1237 – 1247; c) J. H. van Esch, B. L. Feringa, *Angew. Chem.* **2000**, *112*, 2351 – 2354; *Angew. Chem. Int. Ed.* **2000**, *39*, 2263 – 2266; d) S. Shinkai, K. Murata, *J. Mater. Chem.* **1998**, *8*, 485 – 495; e) O. Gronwald, S. Shinkai, *Chem. Eur. J.* **2001**, *7*, 4328 – 4334.

[7] a) K. Hanabusa, M. Yamada, M. Kimura, H. Shirai, *Angew. Chem.* **1996**, *108*, 2086 – 2088; *Angew. Chem. Int. Ed. Engl.* **1996**, *35*, 1949 – 1951; b) J. van Esch, S. De Feyter, R. M. Kellogg, F. De Schryver, B. L. Feringa, *Chem. Eur. J.* **1997**, *3*, 1238 – 1243; c) R. Oda, I. Huc, S. J. Candau, *Angew. Chem.* **1998**, *110*, 2835 – 2838; *Angew. Chem. Int. Ed.* **1998**, *37*, 2689 – 2691; d) K. Yoza, N. Amanokura, Y. Ono, T. Akao, H. Shinmori, M. Takeuchi, S. Shinkai, D. N. Reinhoudt, *Chem. Eur. J.* **1999**, *5*, 2722 – 2729; e) G. Wang, A. D. Hamilton, *Chem. Eur. J.* **2002**, *8*, 1954 – 1961; f) S. Kiyonaka, S. Shinkai, I. Hamachi, *Chem. Eur. J.* **2003**, *9*, 976 – 983.

[8] a) S.-i. Tamaru, M. Nakamura, M. Takeuchi, S. Shinkai, *Org. Lett.* **2001**, *3*, 3631 – 3634; b) M. Shirakawa, S.-i. Kawano, N. Fujita, K. Sada, S. Shinkai, *J. Org. Chem.* **2003**, *68*, 5037 – 5044.

[9] H. Engelkamp, S. Middelbeek, R. J. M. Nolte, *Science* **1999**, *284*, 785 – 788.

[10] a) F. S. Schoonbeek, J. H. van Esch, B. Wegewijs, D. B. A. Rep, M. P. de Haas, T. M. Klapwijk, R. M. Kellogg, B. L. Feringa, *Angew. Chem.* **1999**, *111*, 1486 – 1490; *Angew. Chem. Int. Ed.* **1999**, *38*, 1393 – 1397; b) A. Ajayaghosh, S. J. George, *J. Am. Chem. Soc.* **2001**, *123*, 5148 – 5149.

[11] a) Y. Zhao, M. R. Wasielewski, *Tetrahedron Lett.* **1999**, *40*, 7047 – 7050; b) C. Ego, D. Marsitzky, S. Becker, J. Zhang, A. C. Grimsdale, K. Müllen, J. D. MacKenzie, C. Silva, R. H. Friend, *J. Am. Chem. Soc.* **2003**, *125*, 437 – 443; c) F. Würthner, S. Ahmed, C. Thalacker, T. Debaerdemaeker, *Chem. Eur. J.* **2002**, *8*, 4742 – 4750.

[12] a) Y.-c. Lin, B. Kachar, R. G. Weiss, *J. Am. Chem. Soc.* **1989**, *111*, 5542 – 5551; b) K. Murata, M. Aoki, T. Suzuki, T. Harada, H. Kawabata, T. Komori, F. Ohseto, K. Ueda, S. Shinkai, *J. Am. Chem. Soc.* **1994**, *116*, 6664 – 6676; c) D. C. Duncan, D. G. Whitten, *Langmuir* **2000**, *16*, 6445 – 6452; d) S.-i. Kawano, N. Fujita, K. J. C. van Bommel, S. Shinkai, *Chem. Lett.* **2003**, *32*, 12 – 13.

[13] The perylene-containing organogel has never been reported. For perylene-based supramolecular systems, see a) F. Würthner, C. Thalacker, A. Sautter, W. Schärtl, W. Ibach, O. Hollricher, *Chem. Eur. J.* **2000**, *6*, 3871 – 3886; b) F. Würthner, C. Thalacker, S. Diele, C. Tschierske, *Chem. Eur. J.* **2001**, *7*, 2245 – 2253; c) T. van der Boom, R. T. Hayes, Y. Zhao, P. J. Bushard, E. A. Weiss, M. R. Wasielewski, *J. Am. Chem. Soc.* **2002**, *124*, 9582 – 9590; d) A. P. H. J. Schenning, J. van Herrikhuyzen, P. Jonkheijm, Z. Chen, F. Würthner, E. W. Meijer, *J. Am. Chem. Soc.* **2002**, *124*, 10252 – 10253; e) E. Peeters, P. A. van Hal, C. J. Meskers, R. A. J. Janssen, E. W. Meijer, *Chem. Eur. J.* **2002**, *8*, 4470 – 4474; f) F. Würthner, A. Sautter, *Org. Biomol. Chem.* **2003**, *1*, 240 – 243.

[14] For similar reports on gelation-assisted light-harvesting systems, see a) T. Nakashima, N. Kimizuka, *Adv. Mater.* **2002**, *14*, 1113 – 1116; b) A. Ajayaghosh, S. J. George, V. K. Praveen, *Angew. Chem.* **2003**, *115*, 346 – 349; *Angew. Chem. Int. Ed.* **2003**, *42*, 332 – 335; c) K. Sugiyasu, N. Fujita, M. Takeuchi, S. Yamada, S. Shinkai, *Org. Biomol. Chem.* **2003**, *1*, 895 – 899.

[15] The molecular parameters of **1a**, as estimated by CPK molecular modeling, is $\approx 5 \times 1$ nm.

[16] H. Langhals, J. Karolin, L. B.-A. Johansson, *J. Chem. Soc. Faraday Trans.* **1998**, *94*, 2919; $[\mathbf{1a}\text{–}\mathbf{d}] = 1.0 \times 10^{-5}$ M: Excitation wavelengths used for **1a**, **b**, **c**, and **d** were 477, 494, 507, and 622 nm, respectively, where these molecules have molar absorptivities of 20000.

[17] a) F. F. So, S. R. Forrest, *Phys. Rev. Lett.* **1991**, *66*, 2649; b) M. H. Hennessy, Z. G. Soos, R. A. Pascal, A. Girlando, *Chem. Phys.* **1999**, *245*, 199; c) W. Wang, L.-S. Li, G. Helms, H.-H. Zhou, A. D. Q. Li, *J. Am. Chem. Soc.* **2003**, *125*, 1120 – 1121.

 © 2004 Wiley-VCH Verlag GmbH & Co. KGaA, Weinheim

[18] **1b–d** are not soluble in the mixed solvent of *p*-xylene and 1-propanol but form precipitates. From this fact, it is reasonable to deduce that **1a–d** coassemble to form gels.
[19] To determine how many times the fluorescence of the acceptor was intensified, total fluorescence spectra of mixed systems (spectra b and c in Figure 5 and b and c in Figure 2 of the Supporting Information) were divided into those of donor and acceptors. Thus, we could calculate the values for $FI_{acceptor}/FI_{donor}$.
[20] E. U. Akkaya, H. T. Baytekin, *27th Annual Symposium of International Symposium of Macrocyclic Chemistry (ISMC)*, **2002**, PA1.
[21] As one of the referees pointed out, the suggested coassembly of **1a–d** should lead to assemblies with a random distribution of the four units, and consequently many different decay pathways are likely to exist, instead of a "clean" decay channel to the lowest energy state of **1d**.
[22] We have found that when *N*,*N*′-di-*n*-butyl-1,7-bis(4-*tert*-butylphenoxy)-3,4,9,10-perylenetetracarboxylic diimide (compound **4** without the cholesterol group shown in the Supporting Information) was added as an energy acceptor, emission from **4** was not intensified as for **1b**. This result further supports the view that the structural similarity of the perylene–cholesterol conjugates **1a–d** plays an important role in coassembling acceptors and mediating efficient energy transfer.[18]
[23] K. J. C. van Bommel, A. Friggeri, S. Shinkai, *Angew. Chem.* **2003**, *115*, 1010 – 1030; *Angew. Chem. Int. Ed.* **2003**, *42*, 980 – 999.
[24] Cholesterol-based perylene derivatives were synthesized according to the following references: a) H. Quante, P. Schlichting, U. Rohr, Y. Geerts, K. Müllen, *Macromol. Chem. Phys.* **1996**, *197*, 4029 – 4044; b) T. Ishii, R. Iguchi, E. Snip, M. Ikeda, S. Shinkai, *Langmuir* **2001**, *17*, 5825 – 5833; c) A. Böhm, H. Arms, G. Henning, P. Blaschka, US Pat. 6,184,378, **2001**; d) T. Watanabe, N. Miyaura, A. Suzuki, *Synlett* **1992**, 207 – 210.

 © 2004 Wiley-VCH Verlag GmbH & Co. KGaA, Weinheim

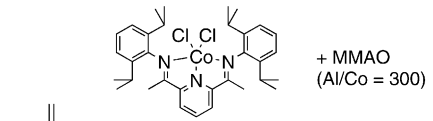
Alternating Copolymerization

Cobalt-Complex-Catalyzed Copolymerization of Ethylene with 2-Aryl-1-methylenecyclopropanes

*Daisuke Takeuchi, Kouhei Anada, and Kohtaro Osakada**

Copolymers of ethylene and monomers having polar functional groups, such as COOR and OR, have attracted attention because polymers with polar substituents exhibit properties that are not available to hydrocarbon polyolefins. Ni and Pd complexes with chelating N-ligands were reported to catalyze the random copolymerization of ethylene with acrylic esters[1] and with norbornene containing a COOR group,[2] while samarocenes initiate the block copolymerization of ethylene with acrylic esters to form AB type block copolymers.[3] Although the alternating copolymerization of ethylene with an α-olefin[4] and with norbornene[5] was promoted by Ti, Zr, Ni, and Pd complexes, there have been no reports on alternating copolymers of ethylene and vinyl monomers that have polar functional groups. Herein, we report the copolymerization of ethylene with 2-aryl-1-methylenecyclopropanes[6,7] that have OR or Cl groups promoted by a Co complex to afford new polymers comprising functionalized C_4 repeating units.

2-Aryl-1-methylenecyclopropanes (**1**–**3**) were smoothly polymerized in the presence of [$CoCl_2L$] (L = bis(imino)pyridine)[8,9] and MMAO (MMAO = modified methylaluminoxane) at room temperature to produce the polymer with a three-membered ring in each structural unit [Eq. (1)]. 2-



(1)

1: Ar = C_6H_5
2: Ar = C_6H_4OMe-4
3: Ar = C_6H_5Cl-4

Phenyl-1-methylenecyclopropane (**1**) underwent living polymerization and gave the polymer with molecular weights of $\bar{M}_n = 8500$ to 200000 ($\bar{M}_w/\bar{M}_n = 1.12$–$1.19$; $\bar{M}_n$ is the number-average molar mass, $\bar{M}_w$ is the weight-average molar mass) as shown in Figure 1.[10] Monomers **2** and **3**, with OMe and Cl groups on their respective phenyl rings, were also polymerized smoothly to form polymers with molecular weights of $\bar{M}_n = 3000$–43000, which varied depending on the initial monomer-to-catalyst ratio.

Copolymerization was conducted by adding MMAO to a toluene solution of the Co complex and 2-aryl-1-methylene-

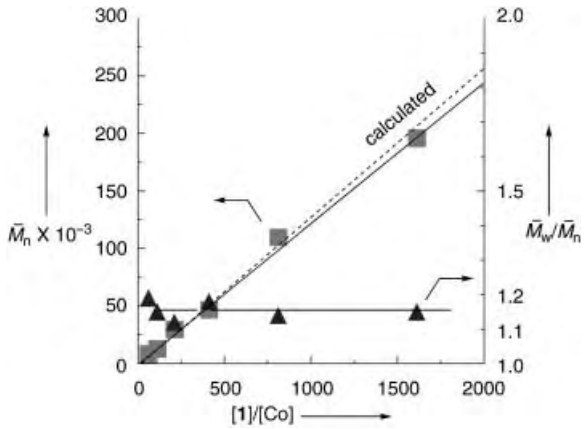


Figure 1. $\bar{M}_n$ and $\bar{M}_w/\bar{M}_n$ of the polymer of **1** plotted against initial monomer-to-Co molar ratio. Conditions: [Al]/[Co] = 300 in toluene at −40 °C. Dashed line shows the molecular weights calculated from $[\mathbf{1}]_0/[Co]$.

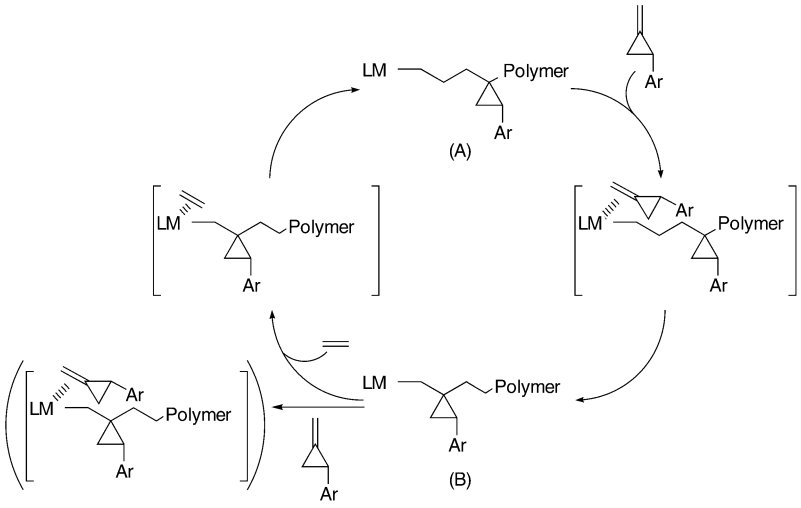
[*] Dr. D. Takeuchi, K. Anada, Prof. Dr. K. Osakada
Chemical Resources Laboratory
Tokyo Institute of Technology
4259 Nagatsuta, Midori-ku, Yokohama 226-8503 (Japan)
Fax: (+81) 45-924-5224
E-mail: kosakada@res.titech.ac.jp

Supporting information for this article is available on the WWW under http://www.angewandte.org or from the author.

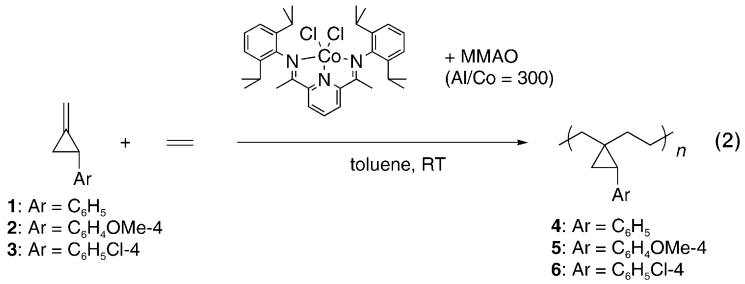
 DOI: 10.1002/anie.200352837 © 2004 Wiley-VCH Verlag GmbH & Co. KGaA, Weinheim

cyclopropane under ethylene (1 atm). The ^1H and $^{13}C\{^1H\}$ NMR spectra and GPC elution pattern of the copolymer from ethylene and **2** indicate a structure composed of two alternating monomer units as shown in Equation (2). Figure 2 shows the $^{13}C\{^1H\}$ NMR spectrum of the copolymer, which exhibits six sharp signals due to the aliphatic carbons at $\delta = 18$–40 ppm. The spectrum does not contain signals that arise from a homopolymer of the monomers or random copolymer units. A comparison of the spectrum with that of a model compound (1,1-dibutyl-2-phenylcyclopropane) and results from DEPT NMR spectroscopy also support the proposed structure.

Scheme 1 depicts the mechanism proposed for the alternating copolymerization. The growing polymer with the Co–CH_2–CH_2 chain (A) undergoes coordination of **2** and



Scheme 1. Mechanism of alternating copolymerization of ethylene with monomers **1**–**3**. ML denotes Co bonded to the bis(imino)pyridine ligand. See reference [8c,d] for the active species of the catalyst proposed for ethylene polymerization.



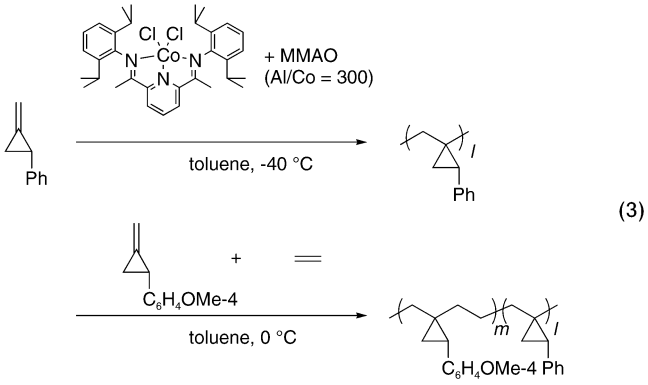
(2)

1: Ar = C_6H_5
2: Ar = C_6H_4OMe-4
3: Ar = C_6H_5Cl-4

4: Ar = C_6H_5
5: Ar = C_6H_4OMe-4
6: Ar = C_6H_5Cl-4

1,2-insertion of its C=C bond into the Co–C bond.[11,12] The formed intermediate (B) undergoes preferential ethylene insertion to regenerate A. The monomer reactivity ratios r_2 and $r_{ethylene}$[13] are determined to be 1.1 and 0.05, respectively, from the Fineman–Ross plots. The strong coordination of **2** to A suppresses the double insertion of ethylene to make the $r_{ethylene}$ value small because the addition of 2-methyl-2-phenyl-1-methylenecyclopropane, which does not polymerize under these conditions, inhibits the ethylene polymerization catalyzed by the Co complex. All these results are in contrast with the alternating copolymerization of ethylene with norbornene catalyzed by Zr and Ti complexes, in which the double insertion of ethylene is much easier than that of the cyclic monomer ($r_{ethylene} > 1$, $r_{norbornene} = 0.36$–0.03).

The alternating copolymerization, which is initiated by the living polymer of 2-phenyl-1-methylenecyclopropane ($\bar{M}_n = 9300$, $\bar{M}_w/\bar{M}_n = 1.14$), affords an AB block copolymer, -(CH_2-$\overline{C}CH_2\overline{C}HPh$)$_l$-($CH_2$-$CH_2$-$CH_2$-$\overline{C}CH_2\overline{C}H$($C_6H_4OMe$-4))$_m$- ($l$:$m = 29$:71, $\bar{M}_n = 28000$, $\bar{M}_w/\bar{M}_n = 1.77$) [Eq. (3)]. The



(3)

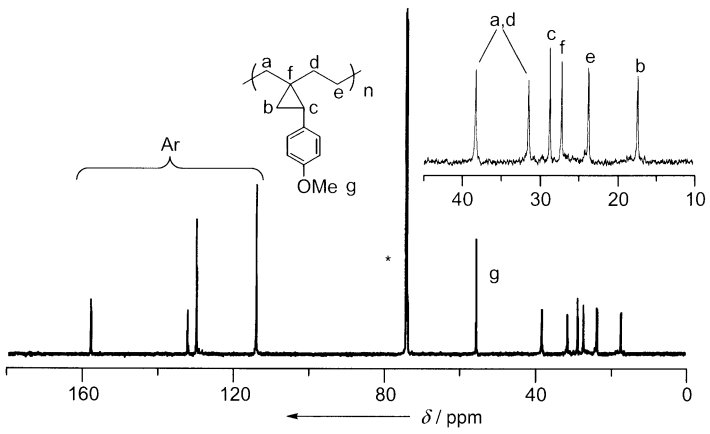


Figure 2. $^{13}C\{^1H\}$ NMR spectrum of poly(2-(4-methoxyphenyl)-1-methylenecyclopropane-*alt*-ethyene). Conditions: 1 atm of ethylene in toluene −40 °C ([**2**]$_0$ = 28 mM, [ethylene]$_0$ = 135 mM). The signal with the asterisk is due to the solvent ($C_2D_2Cl_4$).

produced polymer molecules contain the segment composed of C_4 units that have an OMe group, which is probably softer than the other segment composed of C_2 units with phenylcyclopropylidene group.[6c]

In summary, we have found that the Co complex promotes the living addition polymerization of 2-phenyl-1-methylenecyclopropane and the alternating copolymerization of ethylene with 2-aryl-1-methylenecyclopropanes. The resulting copolymers have a regulated structure composed of C_4

 © 2004 Wiley-VCH Verlag GmbH & Co. KGaA, Weinheim

repeating units with a three-membered ring. The polymerization is tolerant of functional groups such as methoxy and chloro groups. We are continuing to investigate the copolymerization of ethylene with other functionalized monomers.

Received: September 10, 2003
Revised: November 10, 2003 [Z52837]

Keywords: cobalt · copolymerization · ethylene · N-ligand · reaction mechanisms

[1] a) S. Mecking, L. K. Johnson, L. Wang, M. Brookhart, *J. Am. Chem. Soc.* **1998**, *120*, 888–899; b) E. Drent, R. van Dijk, R. van Ginkel, B. van Oort, R. I. Pugh, *Chem. Commun.* **2002**, 744–745.

[2] a) T. R. Younkin, E. F. Connor, J. I. Henderson, S. K. Friedrich, R. H. Grubbs, D. A. Bansleben, *Science* **2000**, *287*, 460–462; b) G. M. Benedikt, E. Elce, B. L. Goodall, H. A. Kalamarides, L. H. McIntosh III, L. F. Rhodes, K. T. Selvy, C. Andes, K. Oyler, A. Sen, *Macromolecules* **2002**, *35*, 8978–8988.

[3] a) H. Yasuda, M. Furo, H. Yamamoto, A. Nakamura, S. Miyake, N. Kibino, *Macromolecules* **1992**, *25*, 5115–5116; b) H. Frauenrath, S. Balk, H. Keul, H. Höcker, *Macromol. Rapid Commun.* **2001**, *22*, 1147–1151.

[4] a) T. Miyatake, K. Mizunuma, M. Kakugo, *Makromol. Chem. Macromol. Symp.* **1993**, *66*, 203–214; b) T. Uozumi, K. Miyazawa, T. Sano, K. Soga, *Macromol. Rapid Commun.* **1997**, *18*, 883–889; c) M. K. Leclerc, R. M. Waymouth, *Angew. Chem.* **1998**, *110*, 964–967; *Angew. Chem. Int. Ed.* **1998**, *37*, 922–925.

[5] a) W. Kaminsky, I. Beulich, M. Arndt-Rosenau, *Macromol. Symp.* **2001**, *173*, 211–225; b) J. Kiesewetter, W. Kaminsky, *Chem. Eur. J.* **2003**, *9*, 1750–1758; c) A. L. McKnight, R. M. Waymouth, *Macromolecules* **1999**, *32*, 2816–2825.

[6] Polymerization of methylenecyclopropanes by Pd and Ni complexes. a) D. Takeuchi, S. Kim, K. Osakada, *Angew. Chem.* **2001**, *113*, 2757–2760; *Angew. Chem. Int. Ed.* **2001**, *40*, 2685–2688; b) D. Takeuchi, K. Osakada, *Chem. Commun.* **2002**, 646–647; c) D. Takeuchi, K. Anada, K. Osakada, *Macromolecules* **2002**, *35*, 9628–9633.

[7] Copolymerization of methylenecyclopropanes with ethylene by early transition metal complexes. a) L. Jia, X. Yang, A. M. Seyam, I. D. L. Albert, P.-F. Fu, S. Yang, T. J. Marks, *J. Am. Chem. Soc.* **1996**, *118*, 7900–7913; b) T. R. Jensen, T. J. Marks, *Macromolecules* **2003**, *36*, 1775–1778.

[8] a) B. L. Small, M. Brookhart, A. M. A. Bennett, *J. Am. Chem. Soc.* **1998**, *120*, 4049–4050; b) G. J. P. Britovsek, V. C. Gibson, B. S. Kimberley, P. J. Maddox, S. J. McTavish, G. A. Solan, A. J. P. White, D. J. Williams, *Chem. Commun.* **1998**, 849–850; c) V. C. Gibson, M. J. Humphries, K. P. Tellmann, D. F. Wass, A. J. P. White, D. J. Williams, *Chem. Commun.* **2001**, 2252–2253; d) T. M. Kooistra, Q. Knijnenburg, J. M. M. Smits, A. D. Horton, P. H. M. Budzelaar, A. W. Gal, *Angew. Chem.* **2001**, *113*, 4855–4858; *Angew. Chem. Int. Ed.* **2001**, *40*, 4719–4722.

[9] a) B. L. Small, *Organometallics* **2003**, *22*, 3178–3183; b) F. Pelascini, F. Peruch, P. J. Lutz, M. Wesolek, J. Kress, *Macromol. Rapid Commun.* **2003**, *24*, 768–771.

[10] Re-addition of **1** to the reaction mixture after consumption of the initially charged monomer ($\bar{M}_n = 8300$, $\bar{M}_w/\bar{M}_n = 1.16$) induces the polymerization to afford a product with an increased molecular weight and a narrow molecular weight distribution ($\bar{M}_n = 26000$, $\bar{M}_w/\bar{M}_n = 1.14$); this result also indicates that the living polymerization is efficient. A slightly lower efficiency of the initiation than the ideal living polymerization is ascribed to slow or insufficient activation of the Co complex by MMAO. See also: P. Mehrkhodavandi, R. R. Schrock, L. L. Pryor, *Organometallics* **2003**, *22*, 4569–4583.

[11] Polymerization of methylenecyclopropane catalyzed by Zr and Ni complexes is proposed to involve the 1,2-insertion of the monomer into the M–C σ bond (See refs [6b] and [7]). The 1,2-insertion of monomer is also supported by an end functionalization experiment.

[12] Recent papers on ethylene polymerization by Co catalyst (Ref [8c,d]) suggested that the Co^{III} complex is most likely the active species in the reaction.

[13] $r_{\mathbf{2}} = k_{\mathbf{2},\mathbf{2}}/k_{\mathbf{2},\text{ethylene}}$ and $r_{\text{ethylene}} = k_{\text{ethylene,ethylene}}/k_{\text{ethylene},\mathbf{2}}$, in which $k_{\mathbf{2},\mathbf{2}}$ and $k_{\mathbf{2},\text{ethylene}}$ denote the rate constants for the insertion reactions of **2** and ethylene into the Co–C bond of $Co{-}CH_2{-}\overline{C\underline{CH_2}CH(C_6H_4OMe\text{-}4)}$, respectively.

 © 2004 Wiley-VCH Verlag GmbH & Co. KGaA, Weinheim

Amino Acid Synthesis

Enantioselective H-Atom Transfer Reactions: A New Methodology for the Synthesis of β^2-Amino Acids**

Mukund P. Sibi and Kalyani Patil*

The development of new methods for the synthesis of β-amino acids and their derivatives is important.[1] Several enantioselective catalytic methods have been developed recently for the synthesis of β-substituted β-amino acids (β^3-amino acids).[2] In contrast, there are very few reports on enantioselective methods for the synthesis of α-substituted β-amino acids (β^2-amino acids).[3] This substitution pattern is of interest since it is present in naturally occurring amino acids as well as in compounds with potential therapeutic value.[4]

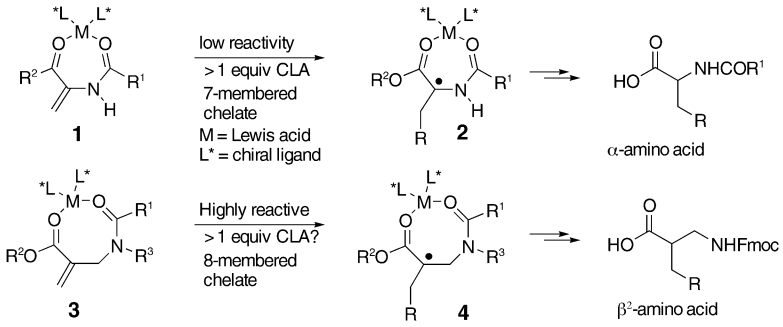
Enantioselective H-atom transfer,[5] an underdeveloped complementary strategy to enolate protonation,[6] is well suited to the preparation of β-amino acids. We showed recently that α-amino acrylates undergo radical addition followed by an enantioselective H-atom transfer in the presence of a chiral Lewis acid (**1**→**2**, Scheme 1).[5d] In this transformation, a stoichiometric amount of the Lewis acid is required to achieve good selectivity because of the low reactivity of the substrate. Development of a similar protocol starting with β-amino acrylate would provide access to α-substituted β-amino acids. At the outset, we were not certain if substrate **3** would be suitable for the catalytic process

[*] Prof. M. P. Sibi, K. Patil
Department of Chemistry
North Dakota State University
Fargo, ND 58105-5516 (USA)
Fax: (+1) 701-231-1057
E-mail: mukund.sibi@ndsu.nodak.edu

[**] This work was supported by the National Institutes of Health (Grant no. NIH-GM-54656). We thank Dr. Kennosuke Ito and Dr. Craig Jasperse for helpful discussions.

Supporting information for this article is available on the WWW under http://www.angewandte.org or from the author.

 DOI: 10.1002/anie.200353000 © 2004 Wiley-VCH Verlag GmbH & Co. KGaA, Weinheim

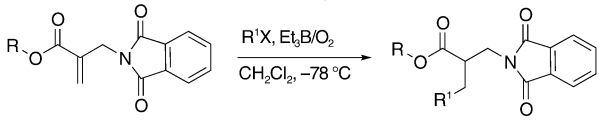


Scheme 1. Synthesis of amino acid derivatives from amino acrylates by radical addition and subsequent enantioselective H-atom transfer.

because of its high reactivity towards conjugate addition. The requirement of a very flexible eight-membered chelate[7] to control the face selectivity posed an additional concern. Herein, we report the successful development of catalytic methods for the synthesis of β^2-amino acids in high chemical yield and with high enantioselectivity by radical addition[8] followed by H-atom transfer.

We began our work by examining conjugate radical additions to acrylates **5** and **6**. These substrates were readily prepared in good overall yields in three steps.[9] The addition of various radicals was examined by using triethylborane/O_2 as an initiator in the absence of any Lewis acid activation (Table 1). As can be discerned from the results (entries 1–6),

Table 1: Radical addition to amino acrylates.[a]



5 R = Me
6 R = *t*Bu

7a–c R = Me
8a–c R = *t*Bu

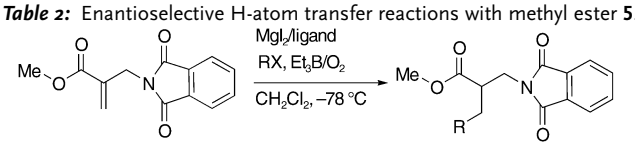
Entry	R	R^1	Compd	Yield [%],[b] No Lewis acid	MgI_2 (1 equiv)
1	Me	isopropyl-I	**7a**	99	78
2	Me	cyclohexyl-I	**7b**	95	80
3	Me	cycloheptyl-Br	**7c**	94	85
4	*t*Bu	isopropyl-I	**8a**	99	86
5	*t*Bu	cyclohexyl-I	**8b**	99	77
6	*t*Bu	cycloheptyl-I	**8c**	91	80

[a] For detailed reaction conditions see the Supporting Information. [b] Yields are for column-purified, isolated materials.

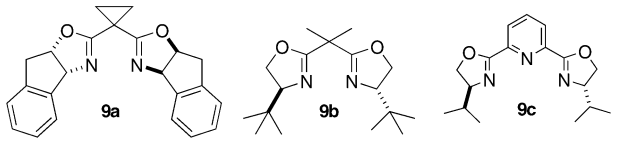
both substrates are very reactive and undergo very efficient uncatalyzed radical addition even at −78 °C. Reactions were also carried out with a stoichiometric amount of MgI_2 which was present as a representative Lewis acid (Table 1, entries 1–6).[10] The results show that the uncatalyzed reactions are slightly more efficient than reactions mediated by a Lewis acid. The results also suggest that the reactions catalyzed by chiral Lewis acids have to be substantially faster than the background reaction to achieve enantioselective H-atom transfer.

Enantioselective H-atom transfer reactions catalyzed by chiral Lewis acids derived from bisoxazolines and magnesium salts were evaluated.[11] Addition of an isopropyl radical to **5** in the presence of **9a** and MgI_2 (100 mol%) gave the product in good yield and with modest enantioselectivity (Table 2, entry 1). A change of ligand to either **9b** or **9c** did not lead to improvements in selectivity (entries 2 and 3). The effect of the H-atom donor on the level of selectivity was also examined and was found to have very little impact.[12] This trend is similar to that observed in our previous work on α-amino acids.[5d] The addition of a series of acyclic and cyclic radicals to **5** was investigated with **9a** as the ligand.

Table 2: Enantioselective H-atom transfer reactions with methyl ester **5**.



5 **7a–i**



9a **9b** **9c**

Entry	RX	Ligand	Compd	Yield [%][a]	*ee* [%][b]
1	isopropyl-I	**9a**	**7a**	91	40
2	isopropyl-I	**9b**	**7a**	98	6
3	isopropyl-I	**9c**	**7a**	76	−6
4	CH_3OCH_2-Br	**9a**	**7d**	85	30
5	CH_3CH_2-I	**9a**	**7e**	91	40
6	MeC(O)Br	**9a**	**7f**	80	55
7	*tert*-butyl-I	**9a**	**7g**	81	20
8	cyclopentyl-Br	**9a**	**7h**	68	60
9	cyclohexyl-I	**9a**	**7b**	71	79
10	cycloheptyl-Br	**9a**	**7c**	70	75
11	1-adamantyl-I	**9a**	**7i**	64	27
12[c]	isopropyl-I	**9a**	**7a**	95	20
13[c]	cyclohexyl-I	**9a**	**7b**	76	40

[a] Yields of isolated products. 100 mol% catalyst was used. [b] Enantiomeric excess determined by chiral HPLC analysis. A negative value indicates that the enantiomer opposite to that of the starting material is favored. [c] Reaction with 30 mol% chiral Lewis acid.

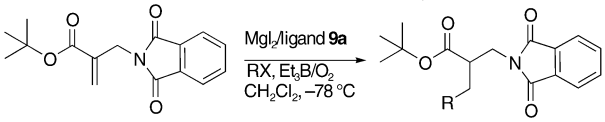
Reactions with the primary radicals methoxymethyl and ethyl were chemically efficient but selectivities were low (entries 4 and 5). Addition of the acetyl radical was not highly selective either (entry 6). The yield from the addition of the bulky *tert*-butyl radical was high, but the reaction gave the product in only 20% *ee* (entry 7). The observed trend of lower selectivity with bulkier radicals is the same as that found in our previous work on the synthesis of α-amino acids. Reactions with cyclic radicals were more rewarding: the addition products were formed in good yield and high *ee* values (entries 8–10). Addition of the bulky adamantyl radical occurred with a low enantioselectivity similar to that observed for the *tert*-butyl radical (entry 11). Reactions in the presence of 30 mol% of the chiral Lewis acid gave lower *ee* values for the products than when 100 mol% of the Lewis acid was used

 © 2004 Wiley-VCH Verlag GmbH & Co. KGaA, Weinheim

(compare entries 1 and 9 with entries 12 and 13, respectively). These results clearly suggest that background reactions compete with the catalyzed reactions.

In our next set of experiments we used the *tert*-butyl ester **6** as the substrate and investigated the addition of various radicals of different size in the presence MgI_2/**9a** as the chiral Lewis acid catalyst. The results of these experiments are presented in Table 3. The reactions with primary radicals

Table 3: Enantioselective H-atom transfer reactions with *tert*-butyl ester **6**.[a]



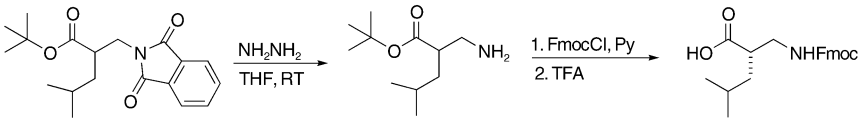
6 **8a–j**

Entry	RX	Compd	100 mol% LA[b] Yield [%][c]	100 mol% LA[b] *ee* [%][d]	30 mol% LA[b] Yield [%][c]	30 mol% LA[b] *ee* [%][d]
1	CH_3OCH_2-Br	**8d**	85	68	78	36
2	$ClCH_2$-I	**8e**	84	36	84	34
3	CH_3CH_2-I	**8f**	82	36	83	62
4	isopropyl-I	**8a**	91	62	95	84
5	*tert*-butyl-I	**8g**	85	92	88	71
6	$ClCH_2CH_2CH_2(CH_3)_2C$-Br	**8h**	72	98	70	50
7	cyclopentyl-I	**8i**	86	94	74	47
8	cyclohexyl-I	**8b**	95	88	86	90
9	1-adamantyl-I	**8j**	71	97	72	61

[a] For detailed reaction conditions see the Supporting Information. [b] LA = Lewis acid. [c] Yields are for column-purified, isolated materials. [d] *ee* values were determined by chiral HPLC.

were efficient but their enantioselectivity was modest (entries 1–3). Interestingly, addition of the ethyl radical occurred more selectively with substoichiometric amounts of the Lewis acid (*ee* = 62%, entry 3) than with 100 mol% of the Lewis acid. The isopropyl radical behaved similarly and led to a higher *ee* value of 84% when 30 mol% of the catalyst was used (entry 4).[13] Substrate **6**, a *tert*-butyl ester, reacted with higher selectivity than the corresponding methyl ester (compare entry 5 in Table 3 with entry 7 in Table 2). Reactions with tertiary and cyclic radicals gave excellent yields and proceeded with high enantioselectivity (entries 5–9). The functionalized tertiary radical gave the highest selectivity (98%, entry 6). These results demonstrate that a variety of β^2-amino acids can be prepared with high levels of selectivity by employing a novel enantioselective H-atom transfer reaction. Disappointingly, there was no clear correlation between the catalytic loading and level of selectivity.[14]

The absolute stereochemistry of **8a** was assigned by converting it into a known β^2-amino acid[15] by using standard reactions (Scheme 2). This sequence also establishes that the



8a

Scheme 2. Conversion of **8a** into a β^2-amino acid. Fmoc = 9-fluorenylmethoxycarbonyl, Py = pyridine, TFA = trifluoroacetic acid.

products of the radical reaction can be converted into compounds that can be employed in solid-phase peptide synthesis.

A stereochemical model for the H-atom transfer reactions must be consistent with four key observations: 1) the effect of the ester substituent (*tert*-butyl versus methyl) on selectivity, 2) the increased enantioselectivity observed with bulky radicals and with **6** as the substrate, 3) the absolute stereochemistry of the addition product, and 4) the effect of catalytic loading on selectivity. We propose an eight-membered chelate model with a tetrahedrally coordinated magnesium ion to account for most of these observations (Figure 1).[16] In this model, the conformation of the ester substituent (*S-cis* or *S-trans*) is dependent on its size and is controlled by the ligand.[17] Substrate **6**, which has a bulky *tert*-butyl ester substituent, is predominantly in an *S-trans* arrangement.[18] The conformation of **5**, which has a smaller methyl ester substituent, is not fixed but is predominantly *S-trans*. After radical addition from the top face (see structure **B**), the face selectivity of the H-atom transfer is dependent

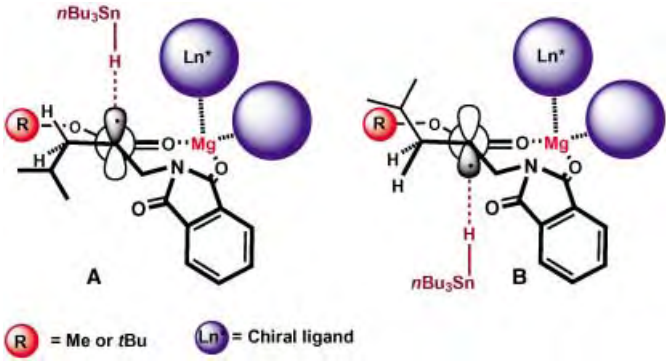


Figure 1. Stereochemical model.

upon the size of the ester substituent as well as that of the radical fragment. The high enantioselectivities observed in reactions between bulky radicals and **6** suggests that the local conformation of the substituent at the carbon atom β to the radical center[19] has a large impact on the selectivity. Metzger and co-workers.[7a] also noted unusual relationships between selectivity and the size of the radical fragment. Steric interactions between the *tert*-butyl ester and the radical fragment in the complex force the radical to adopt the orientation shown in Figure 1A. H-atom transfer

 © 2004 Wiley-VCH Verlag GmbH & Co. KGaA, Weinheim

then occurs *anti* to the radical fragment. This analysis is consistent with the dependence of the level of enantioselectivity on the steric bulk of the radical fragment. In reactions with **5**, steric interactions between the methyl group of the ester and the radical fragment are less demanding (both models **A** and **B** are feasible) but reactions occur predominantly through model **A**.

The absolute stereochemistries of **8a** and **7a** were determined to be *S* (see above). The proposed model predicts the correct face selectivity (*S*) for H-atom transfer in reactions with both **5** and **6**. In the methyl ester (**5**) series, the lower selectivity of reactions with 30 mol% of the catalyst suggests that background reactions compete effectively with the catalyzed process. In contrast, there is no discernable relationship between catalytic loading and selectivity in the reactions with **6**. The broad range of results observed with these reactions is more difficult to explain and further work is required.

In conclusion, we have developed a novel and efficient enantioselective H-atom transfer process to prepare α-substituted β-amino acids (β^2-amino acids) in high enantiomeric purity. Work is underway to develop more efficient catalytic reactions and to extend the methodology to more complex substrates.

Received: October 2, 2003 [Z53000]

Keywords: amino acids · asymmetric catalysis · enantioselective H-atom transfer · Lewis acids · radical reactions

[1] For a recent review, see: M. Liu, M. P. Sibi, *Tetrahedron* **2002**, *58*, 7991; see also: E. Juaristi, H. Lopez-Ruiz, *Curr. Med. Chem.* **1999**, *6*, 983.

[2] For selected recent examples, see: a) W. Tang, W. Wang, Y. Chi, X. Zhang, *Angew. Chem.* **2003**, *115*, 973; *Angew. Chem. Int. Ed.* **2003**, *42*, 3509; b) W. Tang, S. Wu, X. Zhang, *J. Am. Chem. Soc.* **2003**, *125*, 9570; c) H. Ishitani, M. Ueno, S. Kobayashi, *J. Am. Chem. Soc.* **2000**, *122*, 8280; d) M. P. Sibi, M. Liu, *Org. Lett.* **2000**, *2*, 3393; e) J. K. Myers, E. N. Jacobsen, *J. Am. Chem. Soc.* **1999**, *121*, 8959; f) M. P. Sibi, J. J. Shay, M. Liu, C. P. Jasperse, *J. Am. Chem. Soc.* **1998**, *120*, 6615; g) M. P. Sibi, N. Prabagaran, S. G. Ghorpade, C. P. Jasperse, *J. Am. Chem. Soc.* **2003**, *125*, 11796.

[3] a) H. M. L. Davies, C. Venkataramani, *Angew. Chem.* **2002**, *114*, 2301; *Angew. Chem. Int. Ed.* **2002**, *41*, 2197; b) U. Eilitz, F. Leßmann, O. Seidelmann, V. Wendisch, *Tetrahedron: Asymmetry* **2003**, *14*, 189; c) A. Duursma, A. J. Minnaard, B. L. Feringa, *J. Am. Chem. Soc.* **2003**, *125*, 3700; d) O. Muñoz-Muñiz, E. Juaristi, *Tetrahedron* **2003**, *59*, 4223; e) H.-S. Lee, J.-S. Park, B. M. Kim, S. H. Gellman, *J. Org. Chem.* **2003**, *68*, 1575; f) D. Seebach, L. Schaeffer, F. Gessier, P. Bindschädler, C. Jäger, D. Josien, S. Kopp, G. Lelais, Y. R. Mahajan, P. Micuch, R. Sebesta, B. W. Schweizer, *Helv. Chim. Acta* **2003**, *86*, 1852.

[4] Cryptophycins: a) G. V. Subbaraju, T. Golakoti, G. M. L. Patterson, R. E. Moore, *J. Nat. Prod.* **1997**, *60*, 302; biologically active β-peptides: b) M. Werder, H. Hausre, S. Abele, D. Seebach, *Helv. Chim. Acta* **1999**, *82*, 1774.

[5] For recent reviews on enantioselective radical processes, see: a) M. P. Sibi, S. Manyem, J. Zimmerman, *Chem. Rev.* **2003**, *103*, 3263; M. P. Sibi, N. A. Porter, *Acc. Chem. Res.* **1999**, *32*, 163; for examples of H-atom transfer mediated by chiral Lewis acids, see: b) M. Murakata, H. Tsutsui, N. Takeuchi, O. Hoshino, *Tetrahedron* **1999**, *55*, 10295; c) H. Urabe, K. Yamashita, K. Suzuki, K. Kobayashi, F. Sato, *J. Org. Chem.* **1995**, *60*, 3576; d) M. P. Sibi, Y. Asano, J. B. Sausker, *Angew. Chem.* **2001**, *113*, 1333; *Angew. Chem. Int. Ed.* **2001**, *40*, 1293; e) M. P. Sibi, J. B. Sausker, *J. Am. Chem. Soc.* **2002**, *124*, 984; for selected examples of enantioselective reductions with chiral H-atom transfer reagents, see: f) M. Blumenstein, K. Schwarzkopf, J. O. Metzger, *Angew. Chem.* **1997**, *109*, 245; *Angew. Chem. Int. Ed. Engl.* **1997**, *36*, 235; g) C. H. Schiesser, M. A. Skidmore, J. M. White, *Aust. J. Chem.* **2001**, *54*, 199; h) D. Nanni, D. P. Curran, *Tetrahedron: Asymmetry* **1996**, *7*, 2417; i) D. Dakternieks, K. Dunn, V. T. Perchyonok, C. H. Schiesser, *Chem. Commun.* **1999**, 1665; j) for general information on radical reactions, see: *Radicals in Organic Synthesis* (Eds.: P. Renaud, M. P. Sibi), Wiley-VCH, Weinheim, **2001**.

[6] a) O. Muñoz-Muñiz, E. Juaristi, *Tetrahedron Lett.* **2003**, *44*, 2023, and references cited therein; b) for a recent review, see: J. Eames, N. Weerasooriya, *Tetrahedron: Asymmetry* **2001**, *12*, 1.

[7] For reports on seven- and eight-membered metal chelates in stereoselective radical reactions, see: a) A. Hayen, R. Koch, W. Saak, D. Haase, J. Metzger, *J. Am. Chem. Soc.* **2000**, *122*, 12458; b) A. Hayen, R. Koch, J. O. Metzger, *Angew. Chem.* **2000**, *112*, 2898; *Angew. Chem. Int. Ed.* **2000**, *39*, 2758; c) H. Nagano, H. Ohkouchi, T, Yajima, *Tetrahedron* **2003**, *59*, 3649; d) H. Nagano, T. Hirasawa, T. Yajima, *Synlett* **2000**, 1073.

[8] For a report on radical additions to acrylates leading to racemic products, see: J. Huck, J.-M. Receveur, M.-L. Roumestant, J. Martinez, *Synlett* **2001**, 1467.

[9] For the synthesis of substrates and details on experimental conditions, see the Supporting Information and D. Basavaiah, M. Krishnamacharyulu, J. Rao, *Synth. Commun.* **2000**, *30*, 2061.

[10] Several other Lewis acids were evaluated. They gave similar results to those obtained with MgI_2. The details of these experiments will be reported in a separate full account.

[11] Several ligand–Lewis acid combinations were also evaluated. Of these, magnesium salts with ligand **9a** gave the best results.

[12] Of the three H-atom donors tested (Bu_3SnH, Ph_3SnH, and $(TMS)_3SiH$; TMS = trimethylsilyl), tributyltin hydride gave the addition products most efficiently (clean with very few byproducts) and with the highest enantioselectivity.

[13] The catalytic loading was varied from 10 to 100 mol%. The enantioselectivity remained nearly constant (ca. 80% *ee*) for loadings between 20 and 75 mol%.

[14] The higher enantioselectivities observed for **8a** and **8f** at 30 mol% catalytic loading are not an experimental artifact. Further experimentation is required to identify the origin(s) of this anomaly.

[15] P. E. Coffey, K. Drauz, S. M. Roberts, J. Skidmore, J. A. Smith, *Chem. Commun.* **2001**, 2330. See also ref. [3e]. Product **7a** also has the *S* configuration (see the Supporting Information). By analogy, we assume that the face selectivity is the same for the other substrates.

[16] This model is similar to that proposed by Metzger and coworkers in their work on diastereoselective H-atom transfer reactions with methylene glutarates (see ref. [7a]).

[17] At the present time we do not have a clear picture of the influence of the chiral ligand on the rotamer geometry of the ester substituent and its impact on the observed enantioselectivity.

[18] For the conformations of the ester substituents, see: A. G. Pinkus, E. Y. Lin, *J. Mol. Struct.* **1975**, *24*, 9.

[19] The size of the exocyclic substituent has been shown to have an impact on H-atom transfer reactions: B. Giese, W. Damm, T. Witzel, H.-G. Zeitz, *Tetrahedron Lett.* **1993**, *34*, 7053.

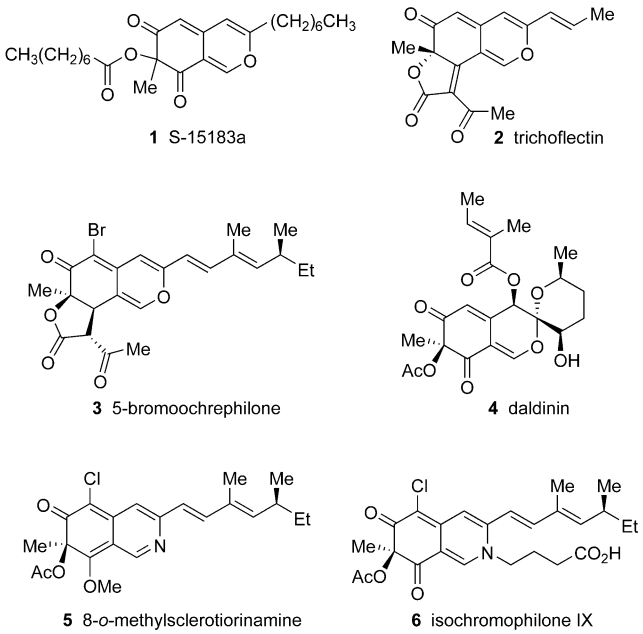
 © 2004 Wiley-VCH Verlag GmbH & Co. KGaA, Weinheim

Natural Product Synthesis

Synthesis of Azaphilones and Related Molecules by Employing Cycloisomerization of *o*-Alkynylbenzaldehydes**

*Jianglong Zhu, Andrew R. Germain, and John A. Porco, Jr.**

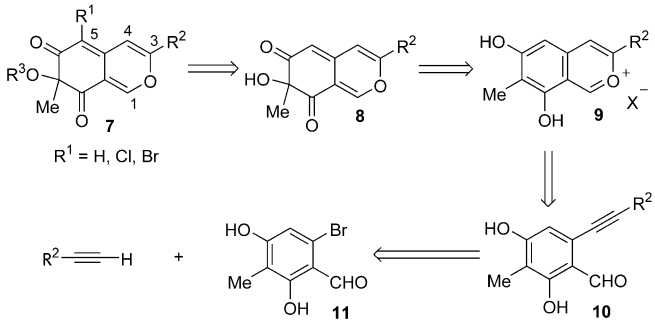
The azaphilones are a structurally diverse family of natural products containing a highly oxygenated bicyclic core and a quaternary center (see **1**–**6**, Scheme 1).[1] These molecules



Scheme 1. Representative azaphilone natural products.

exhibit a wide range of biological activities, including gp120-CD4,[1c] Grb2-SH2,[1d] and sphingosine kinase inhibition.[1e] The potent biological activities of this class of compounds may be related to reaction of the 4*H*-pyran nucleus with amines to produce the corresponding vinylogous 4-pyridones (see **6**).[2] A number of synthetic efforts concerning azaphilones have been reported.[3] In general, pyronoquinones[3a] and pyrylium salts[3b,c] have been employed as precursors. Herein we report an approach to the synthesis of the azaphilones involving cycloisomerization of *o*-alkynylbenzaldehydes to 2-benzopyrylium salts and subsequent oxidation to the 6*H*-isochromene ring system.

Our retrosynthetic analysis for the azaphilones is shown in Scheme 2. Core structure **7** may be prepared by acylation of



Scheme 2. Retrosynthetic analysis for the azaphilone core structure.

tertiary carbinol **8**, which may be derived from oxidation of 2-benzopyrylium salt **9**.[3c,4] We planned to prepare **9** by transition-metal-catalyzed cycloisomerization[5,6] of *o*-alkynylbenzaldehyde **10**. This approach takes advantage of readily available alkynes to construct azaphilones with diverse side chains at C3. Alkynylbenzaldehyde **10** may be obtained by Sonogashira coupling of 2-bromobenzaldehyde **11**.

S-15183a (**1**), a sphingosine kinase inhibitor isolated from *Zopfiella inermis* SANK 15183,[1e] was chosen as our initial target and the basis for model experiments. Nitration of commercially available 2,4-dimethoxy-3-methylbenzaldehyde (**12**) with $Cu(NO_3)_2$ in acetic anhydride afforded **13** in which the aldehyde was protected in situ as the geminal diacetate (85%).[7] Compound **13** was then reduced (Pd/C, H_2) and brominated to afford *o*-bromoaniline **14** (92%). Deamination of **14** and in situ deprotection of the geminal diacetate produced 6-bromo-2,4-dimethoxy-3-methylbenzaldehyde (**15**; 87%). Demethylation of **15** proceeded smoothly with BBr_3 to afford 2-bromobenzaldehyde **11** (95%). Sonogashira coupling of **11** with 1-nonyne afforded the desired *o*-alkynylbenzaldehyde **16** (92%, Scheme 3).[8]

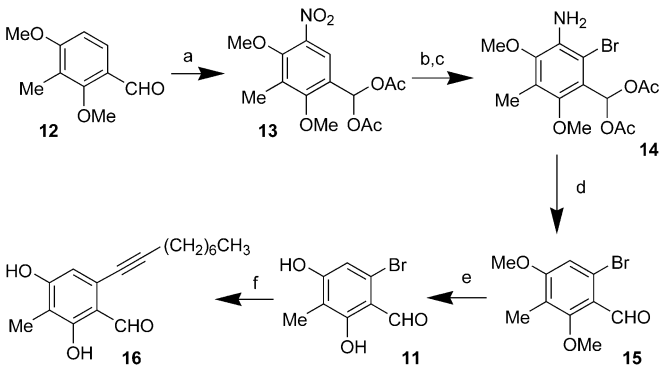
We next investigated cycloisomerization reactions of *o*-alkynylbenzaldehyde **16**. Recent reports have highlighted the utility of Lewis acids for alkyne activation,[5,6,9,10] including formal [4+2] benzannulations of *o*-alkynylbenzaldehydes and alkynes/alkenes by employing gold(III) catalysis.[5e–g,6] It was envisaged that substrates such as **16** could be converted directly into 2-benzopyrylium salts in the presence of a catalytic amount of a carbophilic Lewis acid and stoichiometric amounts of a proton source. A number of Lewis acid catalysts were investigated for the cycloisomerization (Table 1). Among these Lewis acids, gold(III) acetate ($Au(OAc)_3$)[11] was found to be optimal and led to formation of 2-benzopyrylium salt **17** in 1 min at room temperature with 1,2-dichloroethane/trifluoroacetic acid (10:1) as the solvent

[*] J. Zhu, A. R. Germain, Prof. Dr. J. A. Porco, Jr.
Department of Chemistry
Center for Chemical Methodology and Library Development
Boston University, 590 Commonwealth Avenue
Boston, MA 02215 (USA)
Fax: (+1) 617-353-6466
E-mail: porco@chem.bu.edu

[**] We thank Dr. Takafumi Kohama (Sankyo Co. LTD.) for providing ^1H and ^{13}C NMR spectra of S-15183a and Dr. Emil Lobkovsky (Cornell University) for X-ray crystal structure analysis. We thank CEM Corporation (Matthews, NC) for providing the Explorer microwave system, Bristol-Myers Squibb for an unrestricted Grant in Synthetic Organic Chemistry (J.A.P, Jr.), and Novartis Pharma AG for research support.

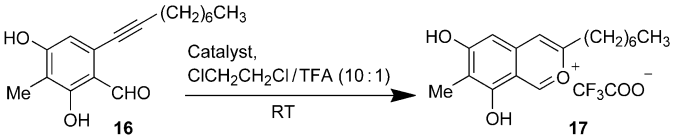
Supporting information for this article is available on the WWW under http://www.angewandte.org or from the author.

 DOI: 10.1002/anie.200353037 © 2004 Wiley-VCH Verlag GmbH & Co. KGaA, Weinheim



Scheme 3. a) $Cu(NO_3)_2 \cdot 3H_2O$, Ac_2O, RT, 85%; b) Pd/C, H_2, THF, RT; c) Br_2, HOAc, RT, 92% for two steps; d) $NaNO_2$, conc. HCl, THF/H_2O, −5 °C; H_3PO_2, 0 °C→40 °C, 87%; e) BBr_3, CH_2Cl_2, −78 °C→RT, 95%; f) $[PdCl_2(PPh_3)_2]$, 1-nonyne, CuI, Et_3N, DMF, 60 °C, 92%. THF = tetrahydrofuran, DMF = *N*,*N*-dimethylformamide.

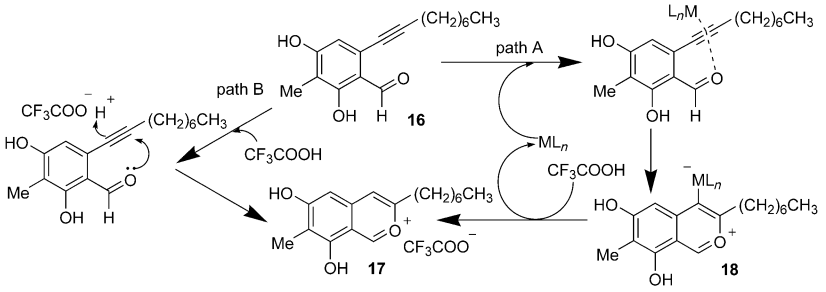
Table 1: Lewis acid catalyzed formation of 2-benzopyrylium salt **17**.[a]



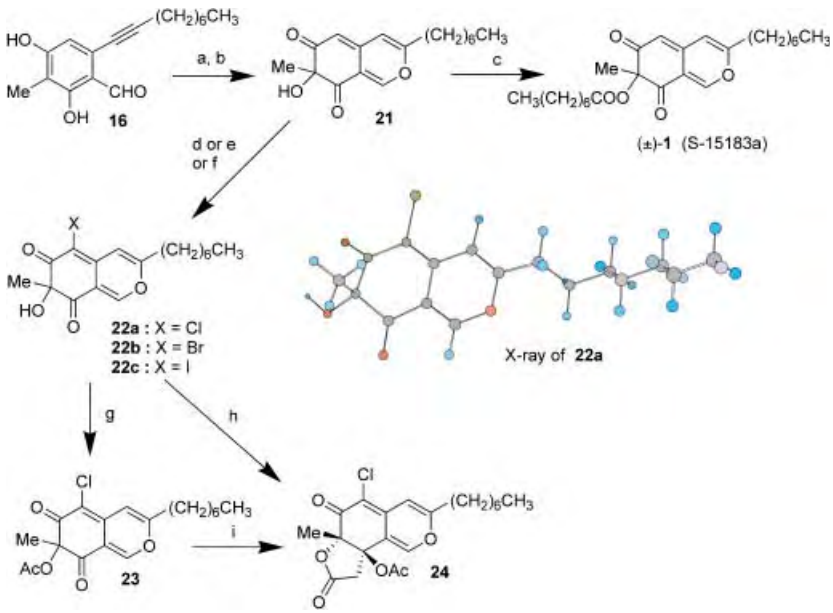
Entry	Catalyst (equiv)	*t* [min]	Conversion [%][b]
1[c]	None	20	< 1
2	$AuCl_3$ (0.05)	20	75
3	$AuBr_3$ (0.05)	20	48
4	$Au(OAc)_3$ (0.05)	1	100
5	$Cu(OTf)_2$ (0.05)	20	41
6	$[CuOTf]_2$·toluene (0.025)	20	74
7	$AgNO_3$ (0.05)	20	94

[a] Reactions were conducted on a 0.1-mmol scale in $ClCH_2CH_2Cl$ (1.0 mL) and CF_3COOH (0.1 mL). [b] Reactions were quenched with CH_3CN/H_2O and conversion was determined by reversed-phase HPLC analysis of the recovered starting material with benzophenone used as an internal standard. See the Supporting Information for a detailed procedure. [c] Less than 1% conversion was observed after 20 min at 40 °C.

(entry 4).[12,13] In comparison, $AuCl_3$ (entry 2) led to 75% conversion in 20 minutes (entry 2). In the absence of Lewis acid catalyst, less than 1% conversion was observed at 40 °C (entry 1). However, 2-benzopyrylium salt **17** was formed completely in 2 h at 60 °C by using trifluoroacetic acid (TFA) as the solvent. The 2-benzopyrylium salt **17** may thus be formed by two possible pathways (Scheme 4). Lewis acid activation of the triple bond of *o*-alkynylbenzaldehyde **16** should provide metal ate complex **18**[5e] which may be protonated to afford **17** (path A). In the absence of a Lewis acid catalyst, the protic acid may also activate the alkyne for attack by the aldehyde carbonyl group to afford **17** directly (path B).[5b] Although Lewis acid catalysis was not necessary for cycloisomerization of **16** into **17**, subsequent experiments revealed that Lewis acid catalysis is advantageous for cycloisomerization of certain *o*-alkynylbenzaldehyde substrates (see below). This methodology may be a general approach for the preparation of 2-benzopyrylium salts.[14]



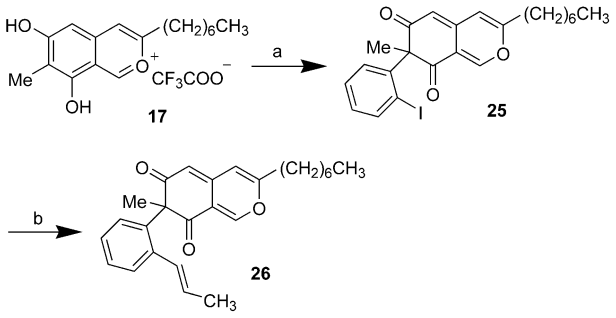
Scheme 4. Proposed mechanism for cycloisomerization. M = metal, L = ligand.



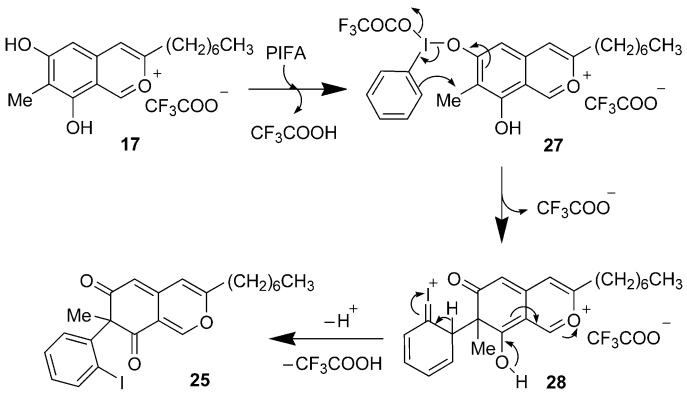
Scheme 5. a) $Au(OAc)_3$ (5 mol%), $ClCH_2CH_2Cl/CF_3COOH$ (10:1), RT; b) IBX, tetrabutylammonium iodide (5 mol%), RT, then sat. $Na_2S_2O_3$, 84% (two steps); c) $CH_3(CH_2)_6COCl$, iPr_2NEt, DMAP, CH_2Cl_2, RT, 61%; d) NCS, CH_3CN, RT, 83%;[24] e) NBS, CH_3CN, RT, 88%; f) NIS, CH_3CN, RT, 66%; g) Ac_2O (4.0 equiv), Et_3N (2.0 equiv), DMAP, CH_2Cl_2, RT, 73%; h) Ac_2O (4.0 equiv), Et_3N (5.0 equiv), DMAP, RT, CH_2Cl_2, 42%; i) Ac_2O (4.0 equiv), Et_3N (5.0 equiv), DMAP, CH_2Cl_2, RT, 47%. DMAP = 4-dimethylaminopyridine, NCS = *N*-chlorosuccinimide, NBS = *N*-bromosuccinimide, NIS = *N*-iodosuccinimide.

Previous studies on the oxidation of 2-benzopyrylium salts related to **17** to form the azaphilone nucleus have typically involved the use of lead tetraacetate.[3a–c] However, after screening alternative oxidants we found that *o*-iodoxybenzoic acid (IBX)[15] in 1,2-dichloroethane/TFA cleanly afforded the desired azaphilone **21** in 84% yield after reductive workup (Scheme 5). A key to this transformation was the use of tetrabutylammonium iodide as a phase-transfer catalyst and apparent IBX activator.[16,17] Acylation of **21** afforded (±)-S-15183a (**1**; 61%) whose

^{1}H NMR, ^{13}C NMR, and mass spectra were found to be identical to those of an authentic sample. Since a number of azaphilone natural products contain chlorine or bromine at the C5 position, we next investigated halogenation of **21**. It was found that chloroazaphilone **22a** could be obtained in 83% yield when azaphilone **21** was treated with *N*-chlorosuccinimide in CH_3CN. The structure of **22a** was confirmed by single-crystal X-ray structure analysis. Similarly, bromination



Scheme 6. a) PIFA, RT, then sat. $Na_2S_2O_3$, 46%; b) $Pd(OAc)_2$, (*o*-tolyl)$_3$P, (*E*)-tributyl-1-propenylstannane, DMF, 80°C, 81%.



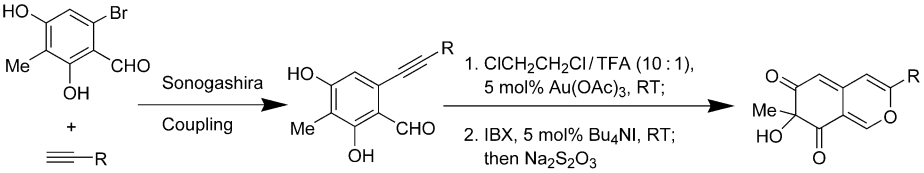
Scheme 7. Proposed mechanism for the formation of **25**.

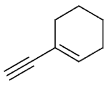
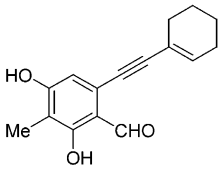
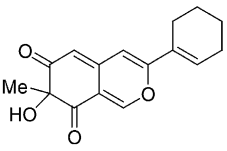
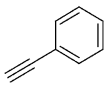
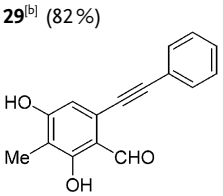
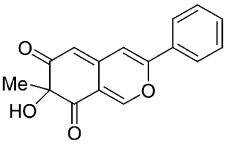
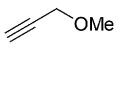
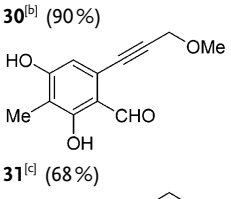
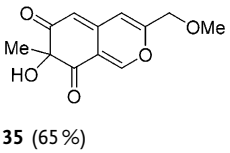
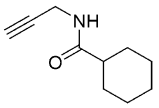
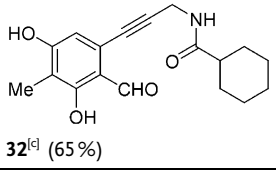
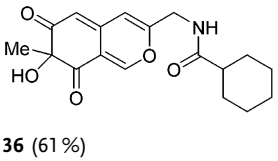
or iodination of alcohol **21** with *N*-bromosuccinimide or *N*-iodosuccinimide, respectively, afforded bromoazaphilone **22b**[1c] (88%) and iodoazaphilone **22c** (66%). These results reaffirm that halogenation of the azaphilone nucleus may be performed at a late stage.[18] Attempted acylation of **22a** led to acetate **23** or angular azaphilone **24**, which is related to trichoflectin (**2**)[1b] and 5-bromoochrephilone (**3**),[1c] depending on the reaction conditions employed.

Interestingly, treatment of 2-benzopyrylium salt **17** with the hypervalent iodine reagent (bis(trifluoroacetoxy)-iodo)benzene (PIFA) did not afford the desired azaphilone but provided C-arylated azaphilone **25** (46%; Scheme 6). A proposed mechanism for this transformation is shown in Scheme 7. Reaction of 2-benzopyrylium salt **17** with PIFA affords intermediate **27**, which may undergo [3,3] sigmatropic rearrangement to dearomatized intermediate **28**.[19] Rearomatization and elimination of trifluoroacetic acid affords C-arylated azaphilone **25**. Preliminary experiments showed that **25** may undergo further functionalization by Pd-catalyzed cross-coupling to afford novel styrenyl azaphilone **26** (81%; Scheme 6).

The cycloisomerization–oxidation sequence was next applied to the synthesis of several unnatural azaphilones (Table 2). Sonogashira coupling of 2-bromobenzaldehyde **11** with 1-ethynylcyclohexene and phenylacetylene with P*t*Bu$_3$ employed as the ligand[20] cleanly afforded the desired *o*-alkynylbenzaldehydes **29** and **30**, respectively (entries 1 and 2). In contrast, microwave conditions[21] were required for efficient coupling with methyl propargyl ether and propargyl cyclohexyl amide to prepare substrates **31** and **32**, respectively (entries 3 and 4). $Au(OAc)_3$-catalyzed cyclo-

Table 2: Synthesis of several unnatural azaphilones.



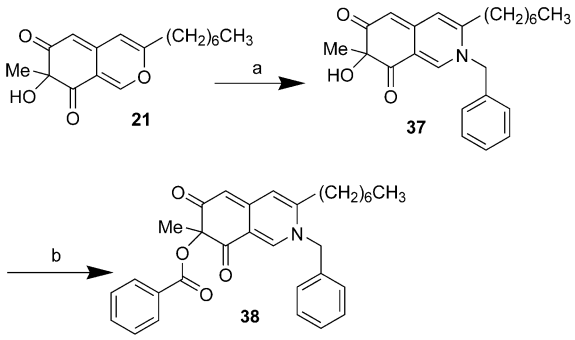
Entry	Alkyne	*o*-Alkynylbenzaldehyde (yield[a])	Azaphilone (yield[a])
1		 **29**[b] (82%)	 **33** (65%)
2		 **30**[b] (90%)	 **34** (82%)
3		 **31**[c] (68%)	 **35** (65%)
4		 **32**[c] (65%)	 **36** (61%)

[a] Yield of isolated product. [b] Method A: $[PdCl_2(PhCN)_2]$, CuI, P*t*Bu$_3$·HBF$_4$, *i*Pr$_2$NH, 1,4-dioxane, RT. [c] Method B: $[PdCl_2(PPh_3)_2]$, CuI, Et$_3$N, 1,2-dimethoxyethane, microwave (300 W, 120°C, 25 min).

 © 2004 Wiley-VCH Verlag GmbH & Co. KGaA, Weinheim

isomerization of the resulting *o*-alkynylbenzaldehydes in 1,2-dichloroethane/TFA (10:1) at room temperature produced the corresponding 2-benzopyrylium salts.[22] Oxidation of the 2-benzopyrylium salts with IBX in the presence of tetrabutylammonium iodide afforded the corresponding C3-functionalized azaphilones **33**–**36** (61–82%).

As a prelude to the anticipated use of the azaphilones as scaffolds in a chemical library synthesis, we conducted the functionalization sequence shown in Scheme 8. Reaction of



Scheme 8. a) Benzylamine (1.2 equiv), CH_3COOH (3.6 equiv), THF, RT, 90%; b) benzoyl chloride (1.5 equiv), Et_3N (1.0 equiv), DMAP (0.5 equiv), CH_2Cl_2, RT, 86%.

azaphilone **21** with benzylamine in THF in the presence of acetic acid[23] proceeded smoothly to afford the corresponding vinylogous 4-pyridone **37**, which underwent acylation with benzoyl chloride to produce vinylogous 4-pyridone ester **38**. These experiments demonstrate access to three orthogonal diversification points on the azaphilone core structure.

In conclusion, an approach to the synthesis of diverse azaphilones has been developed by employing gold(III)-catalyzed cycloisomerization of *o*-alkynylbenzaldehydes into 2-benzopyrylium salts and subsequent oxidation to form the azaphilone ring system by using IBX in conjunction with a phase-transfer catalyst. Preliminary results suggest that the azaphilones may be functionalized to afford highly functionalized vinylogous 4-pyridones. Further studies including asymmetric synthesis of select azaphilone targets and preparation of azaphilone-based chemical libraries are in progress and will be reported in due course.

Received: October 8, 2003 [Z53037]

Keywords: alkynes · azaphilones · cycloisomerization · gold · Lewis acid catalysis

[1] Daldinin: a) T. Hashimoto, S. Tahara, S. Takaoka, M. Tori, Y. Asakawa, *Chem. Pharm. Bull.* **1994**, *42*, 2397–2399; trichoflectin: b) E. Thines, H. Anke, O. Sterner, *J. Nat. Prod.* **1998**, *61*, 306–308; 5-bromoochrephilone: c) K. Natsuzaki, H. Tahara, J. Inokoshi, H. Tanaka, *J. Antibiot.* **1998**, *51*, 1004–1011; 8-*o*-methylsclerotiorinamine: d) J.-Y. Nam, H.-K. Kim, J.-Y. Kwon, M. Y. Han, K.-H. Son, U. C. Lee, J.-D. Choi, B.-M. Kwon, *J. Nat. Prod.* **2000**, *63*, 1303–1305; S-15183a: e) K. Kono, M. Tanaka, Y. Ono, T. Hosoya, T. Ogita, T. Kohama, *J. Antibiot.* **2001**, *54*, 415–420; isochromophilone IX: f) A. P. Michael, E. J. Grace, M. Kotiw, R. A. Barrow, *Aust. J. Chem.* **2003**, *56*, 13–15.

[2] M. Natsume, Y. Takahashi, S. Marumo, *Agric. Biol. Chem.* **1988**, *52*, 307–312.

[3] For representative synthetic efforts on azaphilones, see: a) R. Chong, R. R. King, W. B. Whalley, *J. Chem. Soc. C* **1971**, 3566–3571; b) R. Chong, R. R. King, W. B. Whalley, *J. Chem. Soc. C* **1971**, 3571–3575; c) T. Suzuki, C. Okada, K. Arai, A. Awall, T. Shimizu, K. Tanemura, T. Horaguchi, *J. Heterocycl. Chem.* **2001**, *38*, 1409–1418; d) T. Kamino, Y. Murata, N. Kawai, S. Hosokawa, S. Kobayashi, *Tetrahedron Lett.* **2001**, *42*, 5249–5252.

[4] For reviews on the chemistry of 2-benzopyrylium salts, see: E. Kuznetsov, I. V. Shcherbakova, A. T. Balaban, *Adv. Heterocycl. Chem.* **1990**, *50*, 157–254.

[5] For recent examples of cycloisomerization of alkynyl substrates, see: a) K. R. Roesch, R. C. Larock, *Org. Lett.* **1999**, *1*, 553–556; b) J. D. Tovar, T. M. Swager, *J. Org. Chem.* **1999**, *64*, 6499–6504; c) A. V. Kel'in, A. W. Sromek, V. Gevorgyan, *J. Am. Chem. Soc.* **2001**, *123*, 2074–2075; d) A. V. Kel'in, V. Gevorgyan, *J. Org. Chem.* **2002**, *67*, 95–98; e) N. Asao, K. Takahashi, S. Lee, T. Kasahara, Y. Yamamoto, *J. Am. Chem. Soc.* **2002**, *124*, 12650–12651; f) N. Asao, T. Kasahara, Y. Yamamoto, *Angew. Chem.* **2003**, *115*, 3628–3630; *Angew. Chem. Int. Ed.* **2003**, *42*, 3504–3506; g) N. Asao, T. Nogami, S. Lee, Y. Yamamoto, *J. Am. Chem. Soc.* **2003**, *125*, 10921–10925; h) N. Asao, K. Sato, Y. Yamamoto, *Tetrahedron Lett.* **2003**, *44*, 5675–5677.

[6] During the preparation of this manuscript, a publication appeared reporting the gold(III)-catalyzed formation of isobenzopyrylium (2-benzopyrylium) cations and their cycloaddition with olefins and electron-rich heteroarenes: G. Dyker, D. Hildebrandt, J. Liu, K. Merz, *Angew. Chem.* **2003**, *115*, 4536–4538; *Angew. Chem. Int. Ed.* **2003**, *42*, 4399–4402.

[7] For use of a geminal diacetate (acylal) as a protecting group for aldehydes, see: a) K. S. Kochhar, B. S. Bal, R. P. Deshpande, S. N. Radadhyaksha, H. W. Pinnick, *J. Org. Chem.* **1983**, *48*, 1765–1767; b) A. Kawada, S. Takeda, K. Yamashita, H. Abe, T. Harayama, *Chem. Pharm. Bull.* **2002**, *50*, 1060–1065.

[8] For Sonogashira coupling with 2,3-dibromobenzaldehyde as a substrate, see: A. Fkyerat, G. Dubin, R. Tabacchi, *Helv. Chim. Acta* **1999**, *82*, 1418–1422.

[9] For catalysis by gold species, see: a) G. Dyker, *Angew. Chem.* **2000**, *112*, 4407–4409; *Angew. Chem. Int. Ed.* **2000**, *39*, 4237–4239; b) two special issues on gold catalysis have appeared: *Catal. Today* **2002**, *72*, 1–169.

[10] For gold(III)-mediated activation of alkynes, see: a) R. O. C. Norman, W. J. E. Parr, C. B. Thomas, *J. Chem. Soc. Perkin Trans. 1* **1976**, 1983–1987; b) Y. Fukuda, K. Utimoto, *J. Org. Chem.* **1991**, *56*, 3729–3731; c) Y. Fukuda, K. Utimoto, *Bull. Chem. Soc. Jpn.* **1991**, *64*, 2013–2015; d) Y. Fukuda, K. Utimoto, *Synthesis* **1991**, 975–978; e) F. Gasparrini, M. Giovannoli, D. Misiti, G. Natile, G. Palmieri, L. Maresca, *J. Am. Chem. Soc.* **1993**, *115*, 4401–4402; f) J. H. Teles, S. Brode, M. Chabanas, *Angew. Chem.* **1998**, *110*, 1475–1478; *Angew. Chem. Int. Ed.* **1998**, *37*, 1415–1418; g) E. Mizushima, K. Sato, T. Hayashi, M. Tanaka, *Angew. Chem.* **2002**, *114*, 4745–4747; *Angew. Chem. Int. Ed.* **2002**, *41*, 4563–4565.

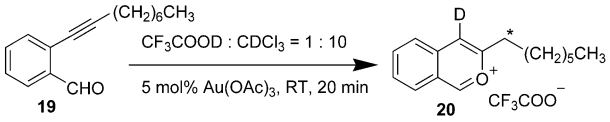
[11] Synthetic applications of $Au(OAc)_3$ appear to be limited thus far to sol–gel preparations for the reduction of NO_x; see: E. Seker, E. Gulari, *Appl. Catal. A* **2002**, *232*, 203–217.

[12] Formation of 2-benzopyrylium salt **17** was verified by ^1H and ^{13}C NMR spectroscopy (see the Supporting Information). For previous NMR studies of 2-benzopyrylium salts, see ref. [3c].

[13] It is possible that gold(III) acetate may undergo ligand exchange with trifluoroacetic acid to form gold(III) trifluoroacetate. For preparation of gold(III) triflate by exchange of $AuBr_3$ with triflic acid, see: N. E. Drysdale, R. E. Bockrath, WO 9409055, **1994**.

 © 2004 Wiley-VCH Verlag GmbH & Co. KGaA, Weinheim

[14] ^{1}H NMR analysis showed that cycloisomerization of *o*-alkynylbenzaldehyde **19** cleanly afforded 2-benzopyrylium salt **20**. In contrast to salt **17**, deuterium incorporation at the C* position of **20** was approximately 87% as determined by ^{1}H NMR analysis.



[15] For IBX oxidation of phenols to *o*-quinones, see: D. Magdziak, A. A. Rodriguez, R. W. Van De Water, T. R. R. Pettus, *Org. Lett.* **2002**, *4*, 285–288.

[16] For the use of phase-transfer catalysis for the oxidation of sulfides with IBX, see: V. G. Shukla, P. D. Salgaonkar, K. G. Akamanchi, *J. Org. Chem.* **2003**, *68*, 5422–5425.

[17] For further examples of ligand complexation/activation of IBX, see: a) K. C. Nicolaou, T. Montagnon, P. S. Baran, *Angew. Chem.* **2002**, *114*, 1035–1038; *Angew. Chem. Int. Ed.* **2002**, *41*, 993–996; b) K. C. Nicolaou, D. L. F. Gray, T. Montagnon, S. T. Harrison, *Angew. Chem.* **2002**, *114*, 1038–1042; *Angew. Chem. Int. Ed.* **2002**, *41*, 996–1000.

[18] For previous work on chlorination at the C5 position of azaphilones (rotiorin), see: R. W. Gray, W. B. Whalley, *J. Chem. Soc. C* **1971**, 3575–3577.

[19] For [3,3] sigmatropic rearrangement of an allenyl (aryl) iodine(III) intermediate ("iodonio Claisen" rearrangement), see: a) M. Ochiai, T. Ito, Y. Takaoka, Y. Masaki, *J. Am. Chem. Soc.* **1991**, *113*, 1319–1323; b) M. Ochiai, M. Kida, T. Okuyama, *Tetrahedron Lett.* **1998**, *39*, 6207–6210.

[20] For the use of P*t*Bu$_3$ in low-temperature Sonogashira couplings, see: a) T. Hundertmark, A. F. Littke, S. L. Buchwald, G. C. Fu, *Org. Lett.* **2000**, *2*, 1729–1731; b) M. R. Netherton, G. C. Fu, *Org. Lett.* **2001**, *3*, 4295–4298.

[21] For microwave-promoted Sonogashira couplings, see: a) M. Erdélyi, A. Gogoll, *J. Org. Chem.* **2001**, *66*, 4165–4169; b) M. Erdélyi, A. Gogoll, *J. Org. Chem.* **2003**, *68*, 6431–6434.

[22] In contrast, formation of the 2-benzopyrylium salts from *o*-alkynylbenzaldehydes **31** or **32** in CF_3CO_2D (60 °C) was extremely slow and was accompanied by severe side reactions, as observed by ^{1}H NMR analysis.

[23] Control experiments revealed that acetic acid was required to buffer the benzylamine and prevent decomposition of azaphilone **21**.

[24] CCDC 219685 (**22a**) contains the supplementary crystallographic data for this paper. These data can be obtained free of charge via www.ccdc.cam.ac.uk/conts/retrieving.html (or from the Cambridge Crystallographic Data Centre, 12, Union Road, Cambridge CB2 1EZ, UK; fax: (+44) 1223-336-033; or deposit@ccdc.cam.ac.uk).

 © 2004 Wiley-VCH Verlag GmbH & Co. KGaA, Weinheim

Nanostructures

Noncovalent π···π-Stacked Exo-Functional Nanotubes: Subtle Control of Resorcinarene Self-Assembly**

*Heidi Mansikkamäki, Maija Nissinen, and Kari Rissanen**

An exciting research challenge in supramolecular chemistry is to design, synthesize, and characterize nanosized tubular architectures with applications in biology, chemistry, and materials science.[1] Predicting and designing noncovalently bound supramolecular structures is difficult because of the weakness of the interactions involved, and the resulting superstructure is often a compromise between the geometrical constraints of the building blocks and the competing weak intermolecular interactions.[2]

Hollow tubular architectures can be constructed from radial disk-shaped or nondisk-shaped building blocks.[1] Several cyclopeptides create flat, disk-shaped supramolecular synthons that self-assemble, by stacking, into stable nanotubes.[3] Examples of nondisk-shaped building blocks include the calixarene derivatives *p*-sulfonatocalixarene[4] and calix[4]hydroquinone.[5] In the self-assembly process of calix[4]-hydroquinone nanotubes, stable ultrathin silver wires are formed in an electro-/photochemical redox reaction.[5a]

Resorcinarenes, which are structurally closely related to calixarenes, are attractive building blocks for a variety of supramolecular architectures owing to their ability to bind neutral and cationic molecules inside their electron-rich cavity and simultaneously to form multiple hydrogen bonds with the eight hydroxy groups of the upper rim of the molecule (Scheme 1).[6] Resorcinarenes are known to form dimeric and hexameric hydrogen-bonded spherical assemblies and to act as supramolecular hosts for smaller molecules.[6,7]

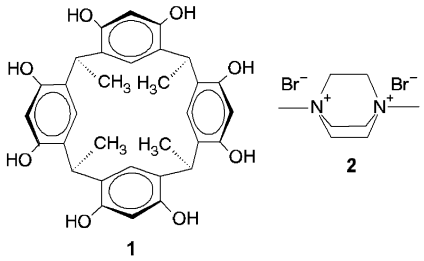
Our earlier work on the complexation of small molecules and self-assembly of various resorcinarenes has mostly resulted in spherical dimeric capsule-type assemblies[7b,c] or 1:1 inclusion complexes, that is, open complexes.[8] To our surprise, instead of a spherical assembly, the cocrystallization of *C*-methyl resorcinarene (**1**; Scheme 1) with a rigid diquaternary alkyl ammonium salt (**2**; 1,4-dimethyl-1,4-diazoniabicyclo[2.2.2]octane dibromide) resulted in an intriguing nano-

[*] H. Mansikkamäki, Dr. M. Nissinen, Prof. Dr. K. Rissanen
University of Jyväskylä
NanoScience Center
Department of Chemistry
PO Box 35, 40014 Jyväskylä (Finland)
Fax: (+358) 14-2602-501
E-mail: kari.rissanen@cc.jyu.fi

[**] Dr. M. Luostarinen and Dr. C. A. Schalley are thanked for providing compounds **1** and **2**, respectively. H.M. wishes to thank the Graduate School of Bioorganic Chemistry and K.R. and M.N. the Academy of Finland for financial support.

Supporting information for this article is available on the WWW under http://www.angewandte.org or from the author.

 DOI: 10.1002/anie.200353112 © 2004 Wiley-VCH Verlag GmbH & Co. KGaA, Weinheim



Scheme 1. Molecular structure of *C*-methyl resorcin[4]arene, **1**, and diquaternary alkyl ammonium salt **2**.

tubular structure held together by well-ordered intratubular π···π interactions.

Single crystals suitable for X-ray analysis of the nanotube structure were grown by slow evaporation of a 2:1 mixture of **1** and **2**, in aqueous *n*-propanol.[9] The asymmetric unit of the nanotube structure comprises three resorcinarene hosts, four alkyl ammonium guests, eight bromide anions, and six water molecules (Figure 1a). All resorcinarene molecules are in crown conformation, each stabilized by four intramolecular hydrogen bonds of length 2.7–2.8 Å. Three of the four $\mathbf{2}^{+}$ guests are present in the upright position in the resorcinarene host cavities allowing close C–H···π and cation···π interactions with the host (2.8–3.0 Å from methyl groups and 3.3–3.5 Å from methylene carbons of $\mathbf{2}^{+}$ to the closest aromatic ring of the host). Five of the eight bromides in the asymmetric unit are disordered over two or three locations, making detailed investigation of hydrogen bonding pattern extremely difficult. Anions interact with the cations by electrostatic forces, being at a distance of 3.3–4.7 Å from the closest cationic nitrogen; at the same time they are hydrogen bonded to water molecules or free hydroxy groups of resorcinarenes (≈2.7 Å for O–H···OH_2 and 3.1–3.4 Å for O–H···Br^{-}).

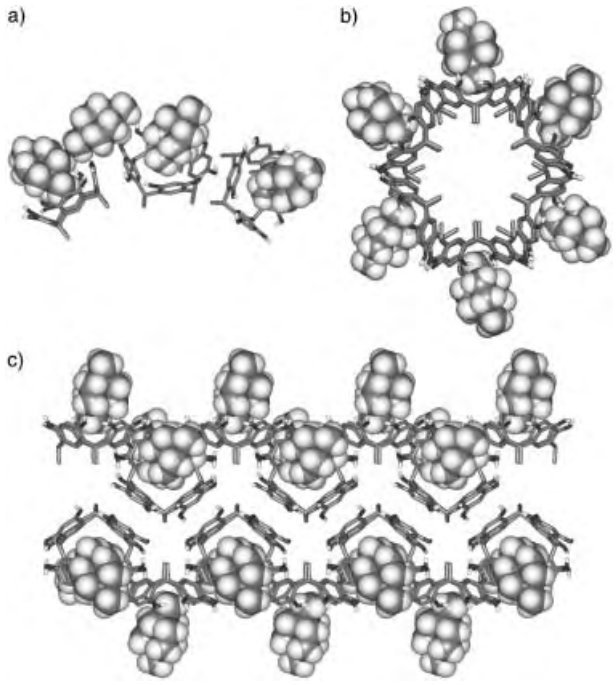


Figure 1. The structure of the nanotube showing resorcinarenes, **1**, in stick representation and diquaternary cations $\mathbf{2}^{+}$, shown with Van der Waals radii. Anions, water molecules, non-hydrogen bonding hydrogens of resorcinarenes, and disorder of the cations are omitted for clarity. a) The asymmetric unit. b) A view of the tube along the crystallographic *a* axis. c) A perpendicular view of the tube showing the regular π···π interaction pattern.

The crystal lattice reveals a novel tubular superstructure, in which neighboring resorcinarenes are connected to each other though multiple π···π interactions (Figure 1b and c). The nature of the interactions is offset face-to-face π···π stacking with facing aromatic rings bent by 22–28° and turned by 41–47° with respect to each other. The shortest distances between the centroids of the facing rings are 3.8–3.9 Å, while the closest individual carbon-adjacent aromatic ring distances are about 3.2 Å. The cavities and upper-rim hydroxy groups of the resorcinarenes create a hydrophilic exo-functional outer surface to the tube, which is capable of binding small guest molecules (in this case 1,4-dimethyl-1,4-diazoniabicyclo[2.2.2]octane, $\mathbf{2}^{+}$) and of forming hydrogen bonds to surrounding hydrophilic solvent molecules and anions.

For both 1:1 inclusion complexes and spherical assemblies, the usual governing intermolecular force between the resorcinarenes is multiple hydrogen bonding, either directly or through solvent molecules or anions[7,8] In the present case, however, the distance between the hydroxy groups of adjacent resorcinarenes varies from 3.4 to 4.1 Å, thus indicating that there is no direct hydrogen bonding between them. Neither is there any obvious bridging through anions or water molecules. This means that hydrogen bonding does not govern the self-assembly. Rather, the driving force in the crystal packing is the slightly weaker and yet significant π···π interactions, supplemented by cation···π interactions and weak hydrogen bonding between the adjacent tubes through the diquaternary cation $\mathbf{2}^{+}$.

The asymmetric unit is a curved building block which, repeated in the crystal packing, forms a chiral helical tube (Figure 2a and b). The crystal itself, however, is a racemic mixture of antiparallel tubes. The top view (Figure 3a), down the channel of the nanotube, shows the hexagonal outer shape of the tube, which is also repeated in the packing of the tubes. The adjacent nanotubes are linked through the $\mathbf{2}^{+}$ ions (Figure 3b): one methyl group of the cation is lodged in the π-basic resorcinarene cavity, while the other forms a C–H···O hydrogen bond to a hydroxy group of the resorcinarene of the adjacent tube. Interstices between the adjacent nanotubes are filled with cations, as well as bromide ions and water molecules, so that each tube is surrounded by a layer of **2** and water molecules that glues the tubes together.

Some electron density is present inside the hydrophobic tube interior, but the contents could not be reliably defined. It is nevertheless reasonable to assume from the location of the highest electron density near the lower-rim methyl groups of the resorcinarene molecules (3.8–4.4 Å) and from the X-ray structure determination of the 1:1 complex of *C*-methyl resorcinarene with 1,4-dibenzyl-1,4-diazoniabicyclo[2.2.2]octane dibromide crystallized from *n*-propanol[10] that the residual electron density inside the tube is indeed *n*-propanol. In this position the propanol hydroxy groups would point

 © 2004 Wiley-VCH Verlag GmbH & Co. KGaA, Weinheim

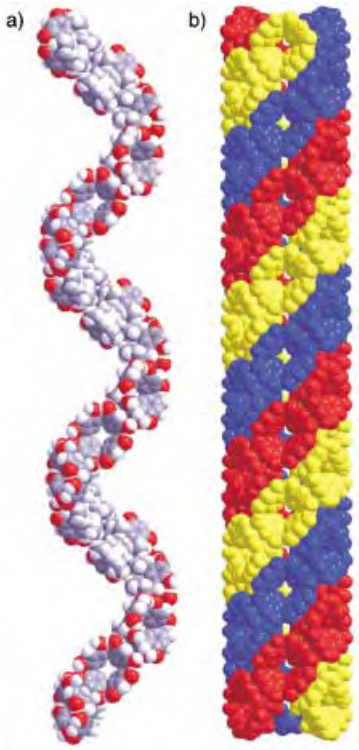


Figure 2. Tubular resorcinarene assembly shown with Van der Waals radii: a) adjacent resorcinarenes connected and rotated with respect to each other forming a single helix, b) the resorcinarene triple helix tube.

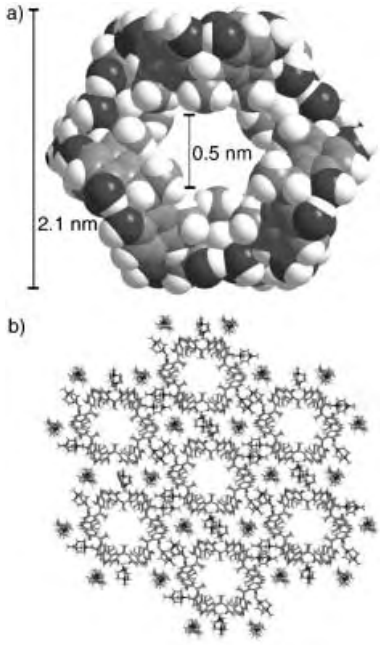


Figure 3. a) Resorcinarene nanotube shown with Van der Waals radii. b) Packing picture along the crystallographic *a* axis. Anions and water molecules are omitted for clarity.

inwards in the tube, thus allowing hydrogen bonding at the center of the tube.

The outside diameter of the nanotube is about 2.1 nm and the inner diameter about 0.5 nm, when measured as the longest Van der Waals distance between opposite resorcinarene hydroxy groups and the shortest Van der Waals distance between the centroids of opposite resorcinarene methyl groups (Figure 3 a). Overall the interior of the tube is shaped like a series of stacked hourglasses, in which the narrowest point is between the resorcinarene methyl groups. The internal diameter of the nanotube, at its narrowest, is about the same as that of the widely studied and well-known α-cyclodextrin cavity (0.5 nm), which is capable of incorporating organic guests such as benzene and phenol.[11] It is reasonable to assume that similar guests may be stored and transported by the *C*-methyl resorcinarene nanotube.

Our attempts to crystallize similar tubular architectures from **1** and a corresponding diquaternary alkyl ammonium dichloride and diiodide (1,4-dimethyl-1,4-diazoniabicyclo[2.2.2]octane dichloride and diiodide) by using aqueous *n*-propanol as solvent and host-guest ratios of 2:1, 1:1, 3:4, and 1:2 have so far been unsuccessful. Only an open 1:1 complex with dichloride has been obtained[10] In this 1:1 complex the cation, as in the nanotube, is complexed inside the resorcinarene cavity, but the chloride ions are hydrogen-bonded to the resorcinarene hydroxy groups in a highly organized manner, thus mediating the facing resorcinarenes with relatively strong -O–H···Cl^- ···H–O- bonds (O···Cl^- separations 3.0–3.4 Å).

The role of the solvent in the formation of supramolecular structures should not be ignored or underestimated, especially if some solvent molecules are cocrystallized in the crystal lattice, as is usual in resorcinarene complexes. Earlier attempts to cocrystallize resorcin[4]arenes with **2** and tetramethyl ammonium salts from methanol or ethanol resulted in spherical complexes or open complexes in which the solvent alcohol was hydrogen-bonded to resorcin[4]arene hydroxy groups. Propanol, which is less hydrophilic and is able to interact with the resorcinarene alkyl groups through lipophilic interactions, is propably able to assist the self-assembly of *C*-methyl resorcin[4]arene towards π-stacked nanotubular structure.

We have shown that with use of a less electronegative and larger anion, that is, a weaker hydrogen bond acceptor (bromide instead of chloride) and appropriate conditions, the self-assembly process of *C*-methyl resorcinarene can be driven to favor weaker interactions such as π···π and cation···π interactions instead of hydrogen bonding. The *C*-methyl resorcinarene-based nanotube represents a new motif for nanotubular structures and opens up a wide range of possibilities for crystal engineering and nanochemical and biological research and applications. Appealing possibilities are offered by a hydrophilic and functional outer surface capable of both complexing small guest molecules and binding to hydrogen-bonding surfaces or other media. The hydrophobic interior could act as a transport channel or as storage for small lipophilic molecules. Challenges for the future include optimization of the conditions of tube formation and studies on the transport properties of the tube structure.

Received: October 20, 2003 [Z53112]

 © 2004 Wiley-VCH Verlag GmbH & Co. KGaA, Weinheim

Keywords: crystal engineering · host–guest systems · nanotubes · self-assembly · supramolecular chemistry

[1] D. T. Bong, T. D. Clark, J. R. Granja, M. R. Ghadiri, *Angew. Chem.* **2001**, *113*, 1016; A *ngew. Chem. Int. Ed.* **2001**, *40*, 988.

[2] a) G. R. Desiraju, *Nature* **2001**, *412*, 397; b) T. Steiner, *Angew. Chem.* **2002**, *114*, 50; *Angew. Chem. Int. Ed.* **2002**, *41*, 48; d) E. A. Meyer, R. K. Castellano, F. Diederich, *Angew. Chem.* **2003**, *115*, 1244; *Angew. Chem. Int. Ed.* **2003**, *42*, 1210; e) J. C. Ma, D. A. Dougherty, *Chem. Rev.* **1997**, *97*, 1303.

[3] a) M. R. Ghadiri, J. R. Granja, R. A. Milligan, D. E. McRee N. Khazanovich, *Nature* **1993**, *366*, 324; b) J. Sánchez-Quesada, M. P. Isler, M. R. Ghadiri, *J. Am. Chem. Soc.* **2002**, *124*, 10004; c) D. Gauthier, P. Baillargeon, M. Drouin, Y. L. Dory, *Angew. Chem.* **2001**, *113*, 4771; *Angew. Chem. Int. Ed.* **2001**, *40*, 4635; d) S. Ferdinander-Lopez, H.-S. Kim, E. C. Choi, M. , Delgado, J. R. Granja, A. Khasanov, K. Kraehenbuehl, G. Long, D. A. Weinberger, K. M. Wilcoxen, M. R. Ghadiri, *Nature* **2001**, *412*, 452.

[4] G. W. Orr, L. J. Barbour, J. L. Atwood, *Science* **1999**, *285*, 1049.

[5] a) B. H. Hong, S. C. Bae, C.-W. Lee, S. Jeong, K. S. Kim, *Science* **2001**, *294*, 348; b) B. H. Hong, J. Y. Lee, C.-W. , Lee, J. C. , Kim, S. C. Bae, K. S. Kim, *J. Am. Chem. Soc.* **2001**, *123*, 10748.

[6] L. R. MacGillivray, J. L. Atwood, *J. Solid State Chem.* **1999**, *152*, 199.

[7] a) K. Murayama, K. Aoki, *Chem. Commun.* **1998**, 607; b) H. Mansikkamäki, M. Nissinen, K. Rissanen, *Chem. Commun.* **2002**, 1902; c) H. Mansikkamäki, M. Nissinen, C. A. Schalley, K. Rissanen, *New J. Chem.* **2003**, *27*, 88; d) L. R. MacGillivray, J. L. Atwood, *Nature* **1997**, *389*, 469; e) A. Shivanyuk, J. Rebek, *J. Am. Chem. Soc.* **2003**, *125*, 3432.

[8] M. Nissinen, K. Rissanen, *Supramol. Chem.* **2003**, *15*, 581.

[9] Crystal data for nanotube: formula $3C_{32}H_{32}O_8{\cdot}4C_8H_{18}N_2Br_2{\cdot}6H_2O$, crystal size $0.1\times0.1\times0.3$ mm, triclinic, space group $P\bar{1}$ (No.2), $a=13.9358(2)$ Å, $b=23.6272(2)$ Å, $c=23.9065(3)$ Å, $\alpha=64.617(1)°$, $\beta=85.811(1)°$, $\gamma=87.348(1)°$, $V=7091.7$ Å^3, $Z=2$, $\rho_{calcd}=1.38$ cm^{-3}, $Mo_{K\alpha}$ radiation, $\lambda=0.71073$ Å, $\mu=2.33$ mm^{-1}, $T=173$ K, Nonius Kappa CCD diffractometer, 85764 reflections measured, 24119 independent, 10857 used ($5.86<2\theta<49.50°$), number of parameters 1680, $R_{int}=0.121$, $R1=0.090$ ($I>2\sigma I$), $wR2=0.227$, GOF = 1.034. Minimum and maximum peaks in the difference map -0.891 and 2.735 e Å^{-3}. CCDC-220735 contains the supplementary crystallographic data for this paper. These data can be obtained free of charge via www.ccdc.cam.ac.uk/conts/retrieving.html (or from the Cambridge Crystallographic Data Centre, 12 Union Road, Cambridge CB2 1EZ, UK; fax: (+44) 1223-336-033; or deposit@ccdc.cam.ac.uk).

[10] Supporting information for this article is available on the WWW under http://www.angewandte.com or from the authors.

[11] F. Vögtle, *Supramolecular Chemistry*, Wiley, Chichester, **1991**, p. 135.

 © 2004 Wiley-VCH Verlag GmbH & Co. KGaA, Weinheim

Bioactive Protein Nanoarrays

Bioactive Protein Nanoarrays on Nickel Oxide Surfaces Formed by Dip-Pen Nanolithography**

*Jwa-Min Nam, Sang Woo Han, Ki-Bum Lee, Xiaogang Liu, Mark A. Ratner, and Chad A. Mirkin**

Biologically functional protein arrays are important for chip-based protein detection assays and proteomic profiling experiments.[1–3] Nanoscale arrays allow for smaller chips with more reaction sites, smaller test sample volumes, potentially higher sensitivity and speed, and direct feature analysis with a scanning probe instrument.[4–11] Several promising routes to protein nanoarrays with submicrometer and even sub-100-nm features have been reported.[9–11] The activity of the immobilized proteins in some of the arrays generated by dip-pen nanolithography (DPN)[4] has been confirmed by fluorescence labeling studies and direct imaging by atomic force microscopy (AFM).[9–11]

Nickel is a commonly used substrate for biological arrays because the oxidized Ni surface has a high affinity for polyhistidine residues, and this specific interaction, in principle, can provide control over the uniformity of protein binding and presentation to the analyte solution. The histidine tag allows for protein adsorption without direct contact between the active area of the protein and the substrate surface.[2,12–14]

The deposition of histidine-tagged peptides and proteins on Ni substrates by using electrochemical DPN[7] was recently reported; however, it was concluded that peptide and protein transport could not be effected without an applied field, and the biological activities of the generated nanofeatures were not studied.[15,16] The requirement of an applied field is limiting with respect to chemical compatibility of the protein inks and protein denaturation under such conditions (−2 to −3 V) and the complexity of the hardware used to effect such a process. Herein, we report a methodology based upon DPN and conditions that allow one to generate biologically active protein nanoarrays with feature sizes as small as approximately 80 nm on Ni surfaces without the need for an applied field (Figure 1).

To facilitate ink wetting and transport, AFM tips were coated with a thin layer of Ni (ca. 5 nm) by thermal

[*] J.-M. Nam,[+] Dr. S. W. Han,[+] K.-B. Lee, X. Liu, M. A. Ratner, Prof. C. A. Mirkin
Department of Chemistry and Institute for Nanotechnology
Northwestern University
2145 Sheridan Road, Evanston, Illinois 60208-3113 (USA)
Fax: (+1) 847-467-5123
E-mail: camirkin@chem.northwestern.edu

[+] These authors contributally equally to this work.

[**] C.A.M. and M.A.R. acknowledge the National Sciences Foundation NSEC program and the Department of Defence MURI/DURINT program for support of this research. S.W.H. acknowledges KOSEF for support of a postdoctoral fellowship.

Supporting information for this article is available on the WWW under http://www.angewandte.org or from the author.

 © 2004 Wiley-VCH Verlag GmbH & Co. KGaA, Weinheim DOI: 10.1002/anie.200353203

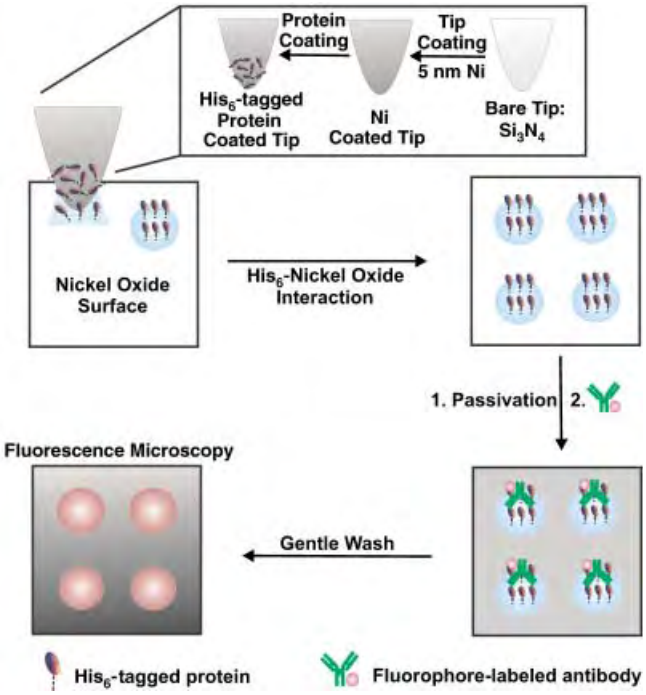


Figure 1. Tip-coating and direct-write DPN protocols.

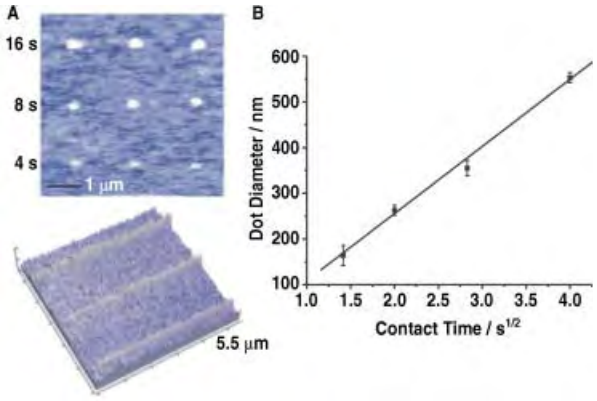


Figure 2. A) Dot and line patterns of ubiquitin generated by direct-write DPN and B) ubiquitin dot size as a function of contact time at pH 7.4.

evaporation prior to DPN deposition experiments. The Ni-coated tips were immersed in solutions of His-tagged (His_6) proteins (ubiquitin ($300\,\mu g\,mL^{-1}$) or thioredoxin ($250\,\mu g\,mL^{-1}$) in 0.1 M phosphate-buffered saline (PBS) at pH 7.4) for 1–2 min. Ubiquitin and thioredoxin were chosen as initial ink candidates because they are biologically important. (The attachment of ubiquitin to a lysine residue of a protein tags the protein for intracellular proteolytic destruction by a proteasome, and thioredoxin mediates the reduction of disulfide bonds in proteins.[21,22]) The Ni-coated tip presumably adsorbs His-tagged protein molecules as a result of the interaction between the nickel oxide surface and the polyhistidine tag. Bare Si_3Ni_4 AFM tips could not be homogeneously coated with proteins under the conditions employed, and this resulted in inconsistent transport and non-uniform protein patterns on the nickel oxide surfaces, an outcome consistent with previous observations by Stone and co-workers.[19,20]

Ni substrates were prepared by thermal evaporation of Ni (30 nm) on Si(100) wafers. The Ni substrates were oxidized by exposing them to air (ambient conditions) for 24 h prior to use. All DPN experiments were done with a ThermoMicroscopes CP AFM apparatus interfaced with customized software (DPNWrite, Nanoink, Inc., Chicago, IL). Protein patterning was performed in a closed environment with 80% humidity at 24 °C. High humidity was used to effect uniform and rapid protein diffusion from the tip to the surface and to prevent the denaturation of the protein structures on the Ni substrate. Patterning could be effected down to 50% relative humidity, but in general, lower quality results were obtained with humidity values below 80%. N-terminal His-tagged ubiquitin nanoarrays were constructed in direct-write fashion in the form of dots and lines (Figure 2A). The height profile of the nanofeatures shows that each ubiquitin structure is approximately 5 nm tall, which is consistent with a monolayer of ubiquitin proteins being attached to the underlying nickel oxide surface (the size of ubiquitin = $5.1 \times 4.3 \times 2.9\ nm^3$).[21] Patterns could not be generated under comparable conditions when ubiquitin proteins without histidine tags were used as inks. This suggests that the interaction between the oxidized nickel substrate and the polyhistidine residues is critical for the patterning process.

An important attribute of DPN is the ability to pattern various molecules (small organic molecules, polymers, DNA, and proteins) with control over feature size (micrometer to sub-100-nm length scale) and shapes. One of the major obstacles of direct-write DPN of proteins has been the diffusion of protein molecules on a surface. Proteins on both modified Si and Au surfaces diffuse very slowly.[10,11] On nickel oxide surfaces, however, His-tagged proteins show tip to substrate diffusion behavior similar to that observed for small alkanethiol molecules diffusing from the tip to an Au substrate (Figure 2B), but different from the stamping behavior observed for protein transport to other substrates.[5–7,10,11] The transport process is facilitated on Ni because of the high hydrophilicity of the oxidized substrate and its ability to support a meniscus, in addition to the strong binding interaction between the histidine-tagged ink and the nickel oxide substrate (see the Supporting Information).

Nanoarrays of ubiquitin and thioredoxin (Sigma–Aldich) were patterned with DPN (Figure 3). Ubiquitin and thioredoxin ($6.8 \times 2.7 \times 5.2\ nm^3$) have similar dimensions.[21,22] Regularly spaced arrays with feature sizes as large as 500 nm and as small as approximately 80 nm could be easily constructed (Figure 3). To address the biological activity of the nanopatterned proteins the nanoarrays were treated with fluorophore-labeled antibodies (Figures 1 and 4). The area surrounding the ubiquitin pattern was passivated with His-tagged polypeptides (ASASHH, $10\,\mu g\,mL^{-1}$ in PBS, pH 7.4; Sigma–Genosys) for 30 min, and this was followed by copious gentle rinsing with buffer solution (0.1 M PBS solution, pH 7.4) and NANOpure water (18 megohm, Barnstead International, Dubuque, IA). The ubiquitin nanoarray was then incubated in a solution containing fluorophore-labeled (Alexa Fluor 594)

 © 2004 Wiley-VCH Verlag GmbH & Co. KGaA, Weinheim

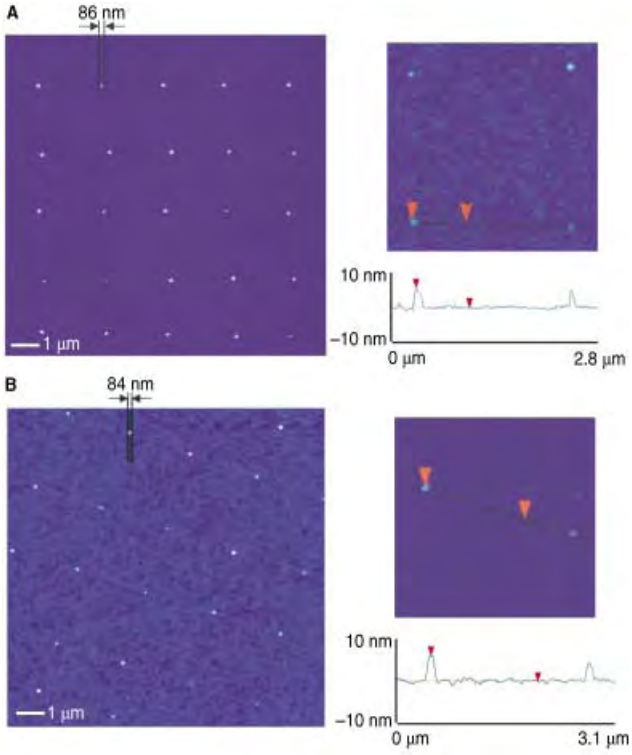


Figure 3. Protein nanoarrays of: A) ubiquitin and B) thioredoxin. Images were taken at 0.5 Hz in tapping mode (Nanoscope IIIa and multimode microscope from Digital Instruments). The contact time was 3 s for the ubiquitin array and 5 s for the thioredoxin array.

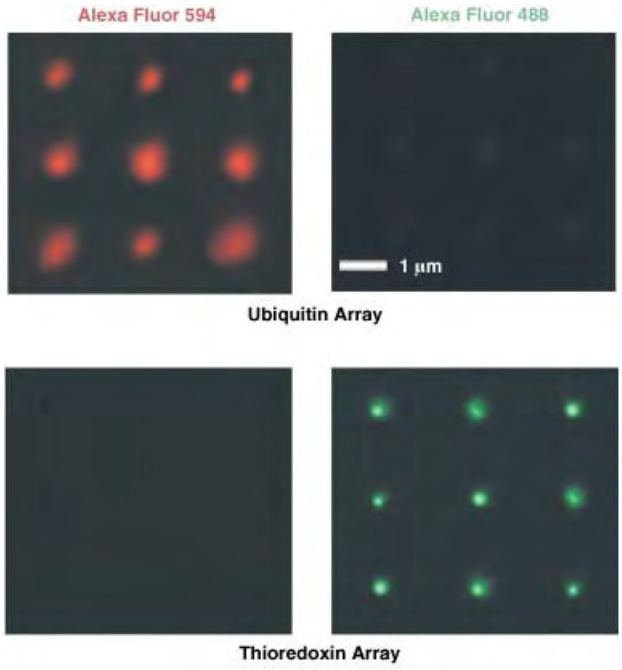


Figure 4. Probing the biorecognition properties of the ubiquitin and thioredoxin nanoarrays with dye-labeled anti-ubiquitin (red) and anti-thioredoxin (green).

anti-ubiquitin (50 $\mu g\,mL^{-1}$) mixed with anti-thioredoxin labeled with Alexa Fluor 488 (50 $\mu g\,mL^{-1}$) in PBS buffer for 2 h. After gentle rinsing of the substrate with PBS buffer solution and NANOpure water, labeled anti-ubiquitin molecules were bound to the ubiquitin-immobilized nanofeatures (red in Figure 4), while no detectable nonspecific binding of anti-thioredoxin (green) was found within the ubiquitin pattern region (Zeiss Axiovert 100 microscope). A similar result was obtained with the comparable labeling studies involving the thioredoxin arrays (that is, fluorophore-labeled anti-thioredoxin only attaches to the thioredoxin features, Figure 4).

In summary, a straightforward method for the preparation of biologically active protein nanoarrays on nickel oxide surfaces is reported. Importantly, with this new method, an applied potential is not necessary to generate active biological structures with excellent control over the feature size. Unlike previous studies involving the transport of proteins,[10,11] the protein molecules in this system seem to diffuse from the Ni-coated tips to the Ni-coated substrate, behavior similar to that observed for the alkanethiol on gold system.[5] This technique could be combined with multiple-pen AFM techniques[23,24] to generate protein arrays with extraordinary complexity in massively parallel fashion.

Received: October 30, 2003 [Z53203]

Keywords: atomic force microscopy · nanolithography · nickel · protein arrays · proteins

[1] G. MacBeath, S. L. Schreiber, *Science* **2000**, *289*, 1760.
[2] H. Zhu, M. Bilgin, R. Bangham, D. Hall, A. Casamayor, P. Bertone, N. Lan, R. Jansen, S. Bidlingmaier, T. Houfek, T. Mitchell, P. Miller, R. A. Dean, M. Gerstein, M. Snyder, *Science* **2001**, *293*, 2101.
[3] B. B. Haab, M. J. Dunham, P. O. Brown, *Genome Biol.* **2001**, *2*(2), research 0004.1.
[4] R. D. Piner, J. Zhu, F. Xu, S. Hong, C. A. Mirkin, *Science* **1999**, *283*, 661.
[5] A. Ivanisevic, C. A. Mirkin, *J. Am. Chem. Soc.* **2001**, *123*, 7887.
[6] P. E. Sheehan, L. J. Whitman, *Phys. Rev. Lett.* **2002**, *88*, 156104.
[7] Y. Li, B. W. Maynor, J. J. Liu, *J. Am. Chem. Soc.* **2001**, *123*, 2105.
[8] D. L. Wilson, R. Martin, S. Hong, M. Cronin-Golomb, C. A. Mirkin, D. L. Kaplan, *Proc. Natl. Acad. Sci. USA* **2001**, *98*, 13660.
[9] K.-B. Lee, S.-J. Park, C. A. Mirkin, J. C. Smith, M. Mrksich, *Science* **2002**, *295*, 1702.
[10] K.-B. Lee, J.-H. Lim, C. A. Mirkin, *J. Am. Chem. Soc.* **2003**, *125*, 5588.
[11] J.-H. Lim, D. S. Ginger, K.-B. Lee, J. Heo, J.-M. Nam, C. A. Mirkin, *Angew. Chem.* **2003**, *115*, 2411; *Angew. Chem. Int. Ed.* **2003**, *42*, 2309.
[12] G.-Y. Liu, S. Xu, Y. Qian, *Acc. Chem. Res.* **2000**, *33*, 457.
[13] J. R. Kenseth, J. A. Harnisch, V. W. Jones, M. D. Porter, *Langmuir* **2001**, *17*, 4105.
[14] M. A. Case, G. L. McLendon, Y. Hu, T. K. Vanderlick, G. Scoles, *Nano. Lett.* **2003**, *3*, 425.
[15] D. J. Zhou, X. Wang, L. Birch, T. Rayment, C. Abell, *Langmuir*, **2003**, *19*, 10557.
[16] R. Gentz, C.-H. Chen, C. A. Rosen, *Proc. Natl. Acad. Sci. USA* **1989**, *86*, 821.
[17] G. B. Sigal, C. Bamdad, A. Barberis, J. Strominger, G. M. Whitesides, *Anal. Chem.* **1996**, *68*, 490.
[18] R. Yasuda, H. Noji, K. Kinosita, M. Yoshida, *Cell* **1998**, *93*, 1117.

 © 2004 Wiley-VCH Verlag GmbH & Co. KGaA, Weinheim

[19] G. Agarwal, L. A. Sowards, R. R. Naik, M. O. Stone, *J. Am. Chem. Soc.* **2003**, *125*, 580.
[20] G. Agarwal, R. R. Naik, M. O. Stone, *J. Am. Chem. Soc.* **2003**, *125*, 7408.
[21] S. Vijay-Kumar, C. E. Bugg, W. J. Cook, *J. Mol. Biol.* **1987**, *194*, 531.
[22] J. F. Anderson, D. A. R. Sanders, J. R. Gasdaska, A. Weichsel, G. Powis, W. R. Montfort, *Biochemistry* **1997**, *36*, 13979.
[23] M. Zhang, D. Bullen, S.-W. Chung, S. Hong, K. S. Ryu, Z. Fan, C. A. Mirkin, C. Liu, *Nanotechnology* **2002**, *13*(2), 212.
[24] J. Zou, D. Bullen, X. Wang, C. Liu, C. A. Mirkin, *Appl. Phys. Lett.* **2003**, *83*, 581.

 © 2004 Wiley-VCH Verlag GmbH & Co. KGaA, Weinheim

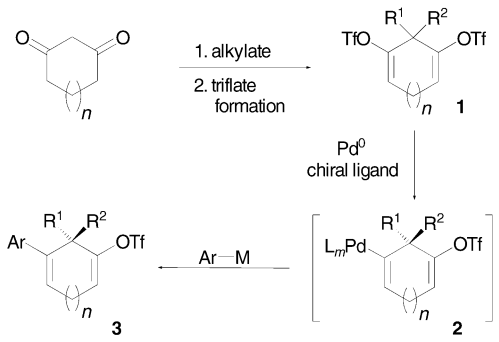
Asymmetric Catalysis

Enantioselective Suzuki Reactions: Catalytic Asymmetric Synthesis of Compounds Containing Quaternary Carbon Centers**

Michael C. Willis, Luke H. W. Powell, Christelle K. Claverie, and Simon J. Watson*

Palladium-catalyzed coupling reactions are some of the most widely used and reliable transformations available to organic chemists, and it is therefore not surprising that the efforts taken to adapt these key transformations to asymmetric processes are ongoing.[1] The use of enantiomerically pure palladium catalysts in inter- and intramolecular Heck reactions is well established and has been applied to a number of successful total syntheses.[2] The systems studied in Heck reactions generally involve carbon–carbon double bond transposition, thus resulting in the stereoselective formation of a new sp^3 center. The development of enantioselective cross-coupling reactions, such as Suzuki and Stille couplings, is more complex, in that generally the reactions result in the union of two sp^2 centers with no stereogenic sp^3 centers being produced. An elegant solution, reported recently by the research groups of both Buchwald and Cammidge, is to use Suzuki coupling reactions to produce axially chiral systems.[3–5] Hayashi et al. have developed a metal-catalyzed asymmetric biaryl synthesis; a desymmetrization approach was employed to allow palladium- and nickel-catalyzed enantioselective Kumada couplings to generate axially chiral systems with high selectivities.[6] A similar approach has also been employed to prepare systems containing planar chirality.[7] Herein, we utilize a desymmetrization strategy to detail the first report on the intermolecular enantioselective Suzuki couplings that produce compounds containing stereodefined sp^3 carbon centers.[8]

An important consideration with desymmetrization strategies is that the *meso*- or the achiral substrates are readily available and do not require laborious synthetic sequences.[9] For this reason we were drawn to the use of ditriflates **1**, derived from the corresponding cyclic 1,3-diketones, as attractive and readily available desymmetrization substrates (Scheme 1). We reasoned that the reaction of the triflates



Scheme 1. Desymmetrization-based enantioselective palladium couplings. Tf = trifluoromethanesulfonyl.

such as **1** with a chiral palladium catalyst should allow selective oxidative addition to produce enantiomerically enriched vinyl–palladium species **2**. Coupling of intermediate **2** with a nucleophilic partner should deliver the enantiomerically enriched desymmetrized products **3** containing a defined quaternary stereocenter. Intermediates similar to **2** are common in many cross-coupling processes and variation in the coupling partner should allow a range of enantioselective palladium-catalyzed coupling reactions to be developed. The wide availability, low toxicity, and good tolerance towards oxygen and water of boronic acids and esters prompted us to focus our initial study on the development of an enantioselective Suzuki reaction.[10]

We focused on the coupling of a five-membered ditriflate **1a** and boronic acid **4** as a platform to evaluate conditions for the proposed Suzuki couplings.[11,12] Experiments revealed that the optimal catalyst for this coupling was generated from MeO–MOP (MOP = (diphenylphosphanyl)-2′-methoxy-1,1′-binaphthyl) and $Pd(OAc)_2$ using dioxane as the reaction solvent (Scheme 2).[13] Under these conditions, the coupled product could be obtained with 77% *ee*.

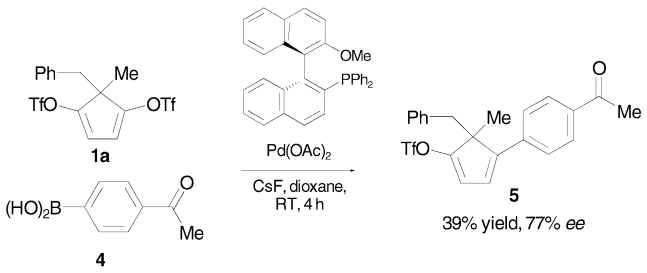
With optimized conditions for the selective union of **1a** and **4** in hand, we further explored the tolerance of the process towards a range of boronic acids (Table 1).[15] Both the *para*- and the *meta*-substituted acetylbenzene boronic

[*] Dr. M. C. Willis, L. H. W. Powell, C. K. Claverie
Department of Chemistry
University of Bath
Bath, BA2 7AY (UK)
Fax: (+44) 1225-386231
E-mail: m.c.willis@bath.ac.uk
S. J. Watson
Novartis Horsham Research Centre
Wimblehurst Road
Horsham, RH12 4AB (UK)

[**] This work was supported by the EPSRC, the University of Bath, and Novartis Pharmaceuticals. The EPSRC Mass Spectrometry service at the University of Wales Swansea is also thanked for their assistance. Dr. Alastair Denholm is thanked for his helpful discussions.

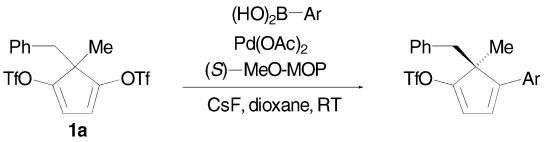
Supporting information for this article is available on the WWW under http://www.angewandte.org or from the author.

 DOI: 10.1002/anie.200352648 © 2004 Wiley-VCH Verlag GmbH & Co. KGaA, Weinheim



Scheme 2. Desymmetrization of the ditriflate **1a**.

Table 1: Enantioselective Suzuki coupling of the ditriflate **1a** with representative boronic acids.[a]

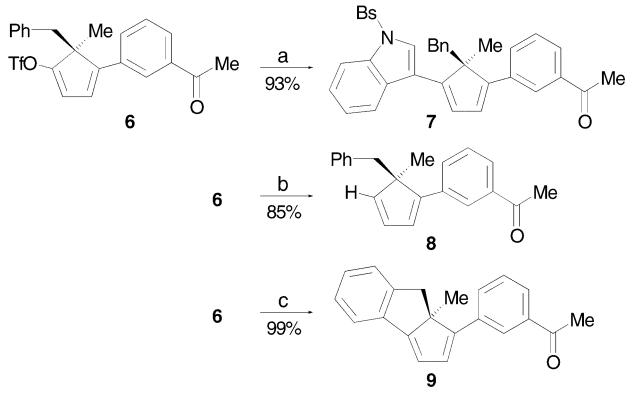


entry	Ar	Yield [%][b]	*ee* [%][c]
1	4-$C_6H_5C(O)Me$	46	77
2	3-$C_6H_5C(O)Me$	51	86
3	2-$C_6H_5C(O)Me$	< 5	–
4	4-C_6H_5CHO	47	73[d]
5	3-C_6H_5CHO	57	80[d]
6	2-C_6H_5CHO	41	82
7	4-C_6H_5-OH	43	74
8	3-furyl	53	72
9	3-*N*-Bs-indolyl[e]	66	85

[a] For all the reactions: 10 mol% Pd, 11 mol% ligand, 2.0 equiv base, 2.0 equiv boronic acid. [b] Yield of the isolated pure material. [c] Determined by chiral HPLC analysis using a Chiracel OD, OA, or OJ column. [d] *ee* values were determined (chiral HPLC) on a derivative, see Supporting Information for details. [e] Bs = benzenesulfonyl.

acids performed well, and provided the coupled products in 77 and 86% *ee*, respectively (entries 1 and 2). However, the corresponding *ortho*-substituted boronic acid displayed poor reactivity, presumably because of steric factors (entry 3). All the three positional isomers of formylbenzene boronic acid performed well (entries 4–6). The hydroxy functionality is compatible with the reaction conditions, thus allowing 4-hydroxybenzene boronic acid to deliver the product with 74% *ee* (entry 7). Finally, heterocyclic boronic acids are also tolerated well, with 3-furyl- and *N*-phenylsulfonyl-3-indole boronic acids providing the coupled products with enantioselectivities of 72 and 85%, respectively (entries 8 and 9). The enantiopurity of the products can be improved by simple recrystallization. For example, the enantioselectivity of the material obtained in entry 1 can be increased from 77 to 97% *ee* by a single recrystallization from a dichloromethane/hexane mixture (31% yield). The relatively close enantioselectivities obtained over a range of boronic acids are consistent with the oxidative addition being the enantiodetermining step; the variations observed are most likely as a consequence of differing reactivities between the boronic acids. The moderate to good yields obtained are a reflection on the catalyst's lifetime, with starting material (15%–25%) being recovered in all cases.

The enantioselective synthesis of quaternary carbon centers remains a considerable challenge;[16] the presence of such centers in the monocoupled products, obtained above, together with the remaining triflate group results in these compounds being useful synthetic intermediates. To demonstrate their utility we elaborated the remaining triflate functionality by a series of palladium-catalyzed reactions (Scheme 3). Monotriflate **6** was initially subjected to a second



Scheme 3. Functionalization of the monotriflate **6**. Reagents: a) KOH, *N*-phenylsulfonyl-3-indoleboronic acid, $Pd(OAc)_2$ (10 mol%), PPh_3 (22 mol%), THF, room temperature, 1 h; b) $Pd(OAc)_2$ (10 mol%), PPh_3 (22 mol%), NBu_3, HCO_2H, DMF, 60°C, 1 h; c) $Pd(OAc)_2$ (15 mol%), PPh_3 (30 mol%), NBu_3, DMF, 60°C, 1 h. Bs = benzenesulfonyl. Bn = benzyl

Suzuki coupling to provide bisaryl **7** in 93% yield. The triflate functionality present in **6** could also undergo palladium-catalyzed reduction (HCO_2H, NBu_3) to yield alkene **8** in 85% yield. Finally, the triflate functionality of **6** could be exploited in an intramolecular C–H coupling procedure to deliver tricylic **9** in quantitative yields.[17]

In conclusion, we have demonstrated that the use of a desymmetrization strategy allows highly enantioselective Suzuki coupling reactions that can deliver compounds containing stereodefined quaternary carbon centers. The process can tolerate a variety of functionalized boronic acids and also delivers products containing vinyl triflate units that can be functionalized by a range of palladium-catalyzed reactions. The enantioselectivities obtained are good and represent the highest that have been achieved for a Suzuki coupling in which stereogenic carbon centers are created.

Experimental Section

Dry degassed 1,4-dioxane (2 mL) was added to a mixture of ditriflate **1a** (93.20 mg, 0.20 mmol), the relevant boronic acid (0.40 mmol), $Pd(OAc)_2$ (4.50 mg, 0.02 mmol, 10 mol%), (*S*)-MeO–MOP (10.30 mg, 0.022 mmol, 10 mol%), and cesium fluoride (91.40 mg, 0.60 mmol). The reaction mixture was stirred for 6–10 h at room temperature. EtOAc (10 mL) and water (8 mL) were added and the aqueous layer was extracted using EtOAc (2 × 10 mL). The combined organic phases were dried ($MgSO_4$), filtered, and concentrated under reduced pressure. The residue was purified by flash chromatography (gradient elution 1–40% diethyl ether:hexane) to give the monotri-

 © 2004 Wiley-VCH Verlag GmbH & Co. KGaA, Weinheim

flate products. See the Supporting Information for complete data for all novel compounds.

Received: August 13, 2003
Revised: October 23, 2003 [Z52648]

Keywords: asymmetric catalysis · cross-coupling · enantioselectivity · palladium

[1] For reviews of enantioselective palladium-catalyzed coupling reactions, see: a) T. Hayashi in *Comprehensive Asymmetric Catalysis*, *Vol. 2* (Eds.: E. N. Jacobsen, A. Pfaltz, H. Yamamoto), Springer, Berlin, **1999**, pp. 887–907; b) M. Ogasawara, T. Hayashi in *Catalytic Asymmetric Synthesis*, 2nd ed. (Ed.: I. Ojima), Wiley, New York, **2000**, pp. 651–674; c) C. G. Frost in *Rodd's Chemistry of Carbon Compounds*, *Vol. 5*, 2nd ed. (Ed.: M. Sainsbury), Elsevier, Amsterdam, **2001**, pp. 315–350.

[2] For recent reviews of enantioselective Heck reactions, see: a) M. Shibasaki, E. M. Vogl in *Comprehensive Asymmetric Catalysis*, *Vol. 1* (Eds.: E. N. Jacobsen, A. Pfaltz, H. Yamamoto), Springer, Berlin, **1999**, pp. 457–487; b) M. Shibasaki, E. M. Vogl, *J. Organomet. Chem.* **1999**, *576*, 1–15; c) O. Loiseleur, M. Hayashi, M. Keenan, N. Schmees, A. Pfaltz, *J. Organomet. Chem.* **1999**, *576*, 16–22; d) Y. Donde, L. E. Overman in *Catalytic Asymmetric Synthesis*, 2nd ed. (Ed.: I. Ojima), Wiley, New York, **2000**, pp. 675–697.

[3] J. Yin, S. L. Buchwald, *J. Am. Chem. Soc.* **2000**, *122*, 12051–12052.

[4] A. N. Cammidge, K. V. L. Crépy, *Chem. Commun.* **2000**, 1723–1724.

[5] For the application of an antropo-enantioselective Suzuki reaction to the synthesis of the analogues of rhazinilam, see: A. Herrbach, A. Marinetti, O. Baudoin, D. Guénard, F. Guéritte, *J. Org. Chem.* **2003**, *68*, 4897–4905.

[6] a) T. Hayashi, K. Hayashizaki, T. Kiyoi, Y. Ito, *J. Am. Chem. Soc.* **1988**, *110*, 8153–8156; b) T. Hayashi, S. Niizuma, T. Kamikawa, N. Suzuki, Y. Uozumi, *J. Am. Chem. Soc.* **1995**, *117*, 9101–9102; c) T. Kamikawa, T. Hayashi, *Tetrahedron* **1999**, *55*, 3455–3466.

[7] a) M. Uemura, H. Nishimura, T. Hayashi, *J. Organomet. Chem.* **1994**, *473*, 129–137. For a palladium-catalyzed carbonylation route to planar chiral systems, see: b) B. Gotov, H.-G. Schmalz, *Org. Lett.* **2001**, *3*, 1753–1756.

[8] For a desymmetrization-based enantioselective intramolecular Suzuki coupling that delivers products with selectivities up to 31% *ee*, see: S. Y. Cho, M. Shibasaki, *Tetrahedron: Asymmetry* **1998**, *9*, 3751–3754.

[9] For a review of enantioselective desymmetrization, see: M. C. Willis, *J. Chem. Soc. Perkin Trans. 1* **1999**, 1765–1784.

[10] For reviews of Suzuki reactions, see: a) N. Miyaura, A. Suzuki, *Chem. Rev.* **1995**, *95*, 2457–2483; b) A. Suzuki, *J. Organomet. Chem.* **1999**, *576*, 147–168.

[11] For the synthesis of **1a** and its use in achiral Suzuki couplings, see: M. C. Willis, C. K. Claverie, *Tetrahedron Lett.* **2001**, *42*, 5105–5107.

[12] For the use of substrates related to **1a** in enantioselective intramolecular Heck reactions, see: S. Bräse, *Synlett* **1999**, 1654–1656.

[13] Initial catalyst evaluation was conducted using a KOH–THF combination at room temperature; bidentate ligands such as 2,2′-bis(diphenylphosphanyl)-1,1′-binaphthyl (BINAP), *O*-isopropylidene-2,3-dihydroxy-1,4-bis(diphenylphosphanyl)butane (DIOP), and 2,3-bis(diphenylphosphanyl)butane (CHIRAPHOS) produced inactive catalysts. 4,12-Bis(diphenylphosphanyl)-[2,2]paracyclophane (PHANEPHOS; 36, 12% *ee*), neomenthyldiphenylphosphane (29, 6% *ee*), and 1-(2-methoxyphenyl)-2-phenylhexahydropyrrolo[1,2-c][1,3,2]diazaphosphole[14] (SEMI-ESPHOS; 36, 16% *ee*) were more encouraging although MeO–MOP (33, 55% *ee*) performed best. The use of $[Pd_2(dba)_3]$/MeO–MOP (dba = *trans,trans*-dibenzylideneacetone) and CsF, dioxane conditions resulted in 30% yield and 51% *ee*.

[14] S. Breeden, D. J. Cole-Hamilton, D. F. Foster, G. J. Schwarz, M. Wills, *Angew. Chem.* **2000**, *112*, 4272–4274; *Angew. Chem. Int. Ed.* **2000**, *39*, 4106–4108.

[15] The absolute configuration of compound **5** was established by X-ray diffraction analysis of the recrystallized material (97% *ee*). The absolute configurations of the remaining adducts are assigned by analogy.

[16] For reviews detailing the enantioselective construction of quaternary centers, see: a) J. Christoffers, A. Mann, *Angew. Chem.* **2001**, *113*, 4725–4732; *Angew. Chem. Int. Ed.* **2001**, *40*, 4587–4591; b) E. J. Corey, A. Guzman-Perez, *Angew. Chem.* **1998**, *110*, 402–415; *Angew. Chem. Int. Ed.* **1998**, *37*, 388–401; c) K. Fuji, *Chem. Rev.* **1993**, *93*, 2037–2066.

[17] M. C. Willis, C. K. Claverie, M. F. Mahon, *Chem. Commun.* **2002**, 832–833.

 © 2004 Wiley-VCH Verlag GmbH & Co. KGaA, Weinheim

Making Materials Mesoporous

Mesopores Created by Platinum Nanoparticles in Zeolite Crystals

Hitoshi Kato, Takashi Minami, Takaaki Kanazawa, and Yukichi Sasaki*

Zeolites are important catalytic materials because they have large surface areas, good heat-resistance, solid-state acidity, and molecular-shape selectivity owing to their framework structures.[1,2] Many types of zeolites and related materials have been synthesized and utilized.[3] For example, zeolite Y and zeolite ZSM-5 are used industrially to refine oil and convert methanol into gasoline, respectively. NOx reduction over metal-exchanged zeolite Cu-ZSM-5 has also been examined.[4] In each case, the shape of the channels and pores in the zeolite framework contributes to the catalytic reactions. Synthesis methods and applications for ordered mesoporous materials have also been researched in recent years.[2] These materials are potential catalysts and adsorbents

[*] H. Kato, Dr. Y. Sasaki
Materials Research and Development Laboratory
Japan Fine Ceramics Center
2-4-1 Mutsuno, Atsuta-ku, Nagoya 456-8587 (Japan)
Fax: (+81) 52-871-3599
E-mail: hkato@jfcc.or.jp
T. Minami, T. Kanazawa
Materials Engineering Division
Toyota Motor Corporation
1 Toyota-cho, Toyota 471-8572 (Japan)

Supporting information (gas absorption–desorption measurements) for this article is available on the WWW under http://www.angewandte.org or from the author.

 DOI: 10.1002/anie.200352706 © 2004 Wiley-VCH Verlag GmbH & Co. KGaA, Weinheim

because their mesopores are of the same order as the size of many industrially important molecules. Researchers have also attempted to make the amorphous wall surfaces crystalline or add a zeolite-like function to them.[5] Judicious use of micropores (< 2 nm diameter) and mesopores (2–50 nm diameter) should enable the reaction field to be accurately controlled so that a wide range of applications can be expected.

The constituents of catalysts undergo various structural changes under actual operating conditions. In the case of automobile catalysts, sintering of the noble metal particles and chemical reactions between the support, particles, and atmosphere occur at high temperature.[6] Understanding such changes on a nanostructural level will provide information for developing high-performance catalyst materials.

Herein, we report the structural changes of a platinum/zeolite catalyst under actual operating conditions. We found that platinum particles penetrated from the surface of the zeolite into its crystalline bulk, with mesopores of about the same size as the platinum particles being formed as if the platinum had tunneled into the structure. This surprising phenomenon has never been observed before in Pt/zeolite catalysts, and might be useful as a technique for controlling the structure of the catalyst. We therefore examined the mesopores in detail to understand their properties better.

Zeolite ZSM-5 ($SiO_2/Al_2O_3 = 1900$) was used as the support in this study. Platinum particles were prepared on the ZSM-5 with a $[Pt(NH_3)_4](OH)_2$ solution. The solution was evaporated to dryness and annealed at 673 K for 2 h in air. The platinum density on the catalyst was 8.4×10^{-5} mol g^{-1}. The prepared catalyst powder was pressed into a pellet, and was exposed to an atmosphere containing gases similar to the actual exhaust gases of an automotive engine (0.11–1.75 % CO, 0.03–0.11 % C_3H_6, 0.19–0.23 % NO, 0.03–2.52 % O_2, 15 % CO_2, 3.0 % H_2O in N_2, total flow-rate = 0.01 m^3 min^{-1}.) at 1073 K for 100 h. We examined the nanostructure of the catalyst particles before and after the aging process with a field-emission scanning electron microscope (FE-SEM, Hitachi S-5200) and transmission electron microscopes (TEM, JEOL JEM-2010 and Hitachi HF-2000). The sample for TEM observation was dispersed on a carbon-covered copper mesh. Composition analysis was carried out by energy dispersive X-ray spectroscopy (EDS). Pore volumes were measured by N_2 gas adsorption and desorption experiments using a Shimadzu ASAP-2010 analyzer.

SEM and TEM images of the surface of catalyst particles in the initial state are shown in Figure 1 a and b. EDS confirmed that the small bright particles in Figure 1 a and dark particles in Figure 1 b were platinum. Most of the platinum particles were widely dispersed on the surface of the zeolite crystal, and their size was under 10 nm.

After aging the platinum particles were no longer visible on the surfaces of the zeolite particle, on which many dark spots appeared which looked like holes penetrating the surface (Figure 1 c). Platinum particles about 10 nm in size associated with channels were observed near the surface of the zeolite crystal (Figure 1 d). These characteristic channels seem to be tracks caused by the platinum particles penetrating from the surface of the zeolite crystal into its bulk. The width

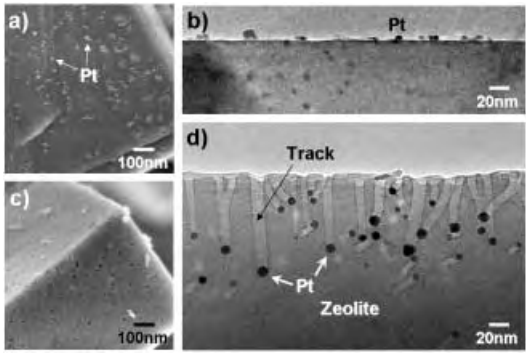


Figure 1. Micrographs of the Pt/ZSM-5 catalyst. a) SEM image of the catalyst particle before aging. b) TEM image near the surface of a catalyst particle before aging. Platinum particles several nanometers in size are distributed over the surface of the zeolite. c) SEM image of the aged catalyst. Many pores are visible on the surfaces. d) The surface of the aged catalyst. All the platinum particles have penetrated into the zeolite. The tracks in the lower part of the image at odd angles to the surface are those formed by particles which have penetrated from other sides of the zeolite crystal.

of the channels is almost equal to that of the platinum particles and the platinum particles are located at the end of the tracks. We assume that the platinum clusters sintered and grew to sizes of about 10 nm on the surface of the zeolite and then penetrated into the zeolite during the aging process.

The length of the tracks caused by platinum-particle penetration sometimes reached several hundreds of nanometers. Most platinum particles appear to have moved in a straight line in directions usually parallel to the crystal faces of the zeolite ZSM-5. Powder X-ray diffraction of the zeolite before and after aging produced the diffraction patterns of zeolite ZSM-5 in both cases, with no significant differences between them.

A thin sample including a section of the track along which a platinum particle migrated was prepared for TEM observation by Ar^+ ion polishing. The cross section of the track in the thin sample was observed to produce a very bright contrast about 10 nm in diameter. No contrast corresponding to an amorphous region was observed around it. From the EDS analysis, we confirmed that apart from the platinum particle the channel was vacant. In other words, the channel corresponds to a mesopore in the zeolite. The gas absorption–desorption experiments also showed that mesopores had been formed (see Supporting Information). The total volume of the measured mesopores agrees well with the volume estimated from the amount of loaded Pt, particle size, and the length of the mesopores.

TEM observation under a very low-intensity electron beam is one of the most effective techniques for studying the fine structure of materials, such as zeolites, which are easily damaged by electron-beam irradiation.[7] We applied this technique to determine the crystal condition of the zeolite around the "mesopore" formed by the platinum particle.

Figure 2 a is a TEM image of a mesopore observed from the [100] direction of the zeolite ZSM-5. This image indicates that the region of the zeolite around the mesopore is in the crystalline state. Figure 2 b is a micrograph of a mesopore

 © 2004 Wiley-VCH Verlag GmbH & Co. KGaA, Weinheim

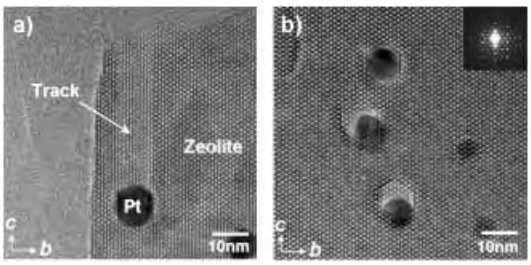


Figure 2. TEM images of mesopores formed by platinum particles in the aged catalyst. Both images were taken along the [100] zone axis. a) The region around the mesopore remains crystalline. b) The width of the mesopore is almost equal to that of a platinum particle. The walls of the mesopore are formed from zeolite crystal facets.

viewed normal to its long axis. This micrograph shows that the width of the mesopore is almost equal to that of the platinum particle. A characteristic feature of all mesopores is their internal walls are constructed from facets of the zeolite crystal.

The high-resolution TEM image in Figure 3 shows a typical cross section of a mesopore observed along the [010] zone axis. This micrograph reveals that the crystal structure of the zeolite ZSM-5 is maintained right up to the edges of the

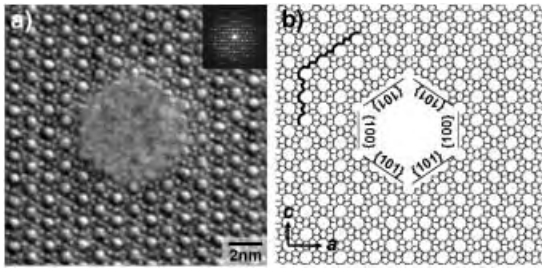


Figure 3. a) HR-TEM image of the cross section of a mesopore observed along the [010] zone axis compared with a structural model (b) see main text for details.

mesopore. By comparison with the structural model in Figure 3b viewed along the same direction, we can see that the apexes of the hexagonal mesopore correspond to the main channels of the zeolite's 10-ring. The sides of the hexagonal mesopore correspond to {100} planes and {101} planes of the zeolite ZSM-5. The surfaces of the mesopores were found to be terminated by rows of atoms from the split main channels and the neighboring 5- and 6-rings as shown in Figure 3b. This configuration corresponds to planes of high atomic density, so that the stability of the observed facets can be explained in terms of the greater number of chemical bonds that must be broken compared to in less dense planes of the same orientation.

When observed along the [010] axis of the ZSM-5, the mesopore cross-sections tended to be hexagonal (Figure 3). Cross sections observed along the [100] axis were also hexagonal with the mesopores bounded by {010} and {011} planes (see Figure 2b). When viewed along these two axes, large channels 0.51–0.56 nm in diameter which are arranged regularly can be seen.[3] We consider these to be easy directions for making hexagonal tunnels. When observed along the [001] axis, the cross section was an irregular polygon, with {100} and {010} planes forming the long sides. Such irregular polygons were rarely observed, however, and most mesopores grew perpendicular to the [001] direction. When projected along the [001] axis, material density varies periodically along the x and y axes. Such a configuration can result in mesopores whose cross sections are polygons containing {100} and {010} planes. The cross-sectional shapes of mesopores formed by platinum particles therefore seem to strongly reflect the framework structure of the zeolite.

In the micrograph of Figure 4a, lattice fringes from the {101} planes of the ZSM-5 and mesopores along the planes were observed. While still observing this region, we tilted the

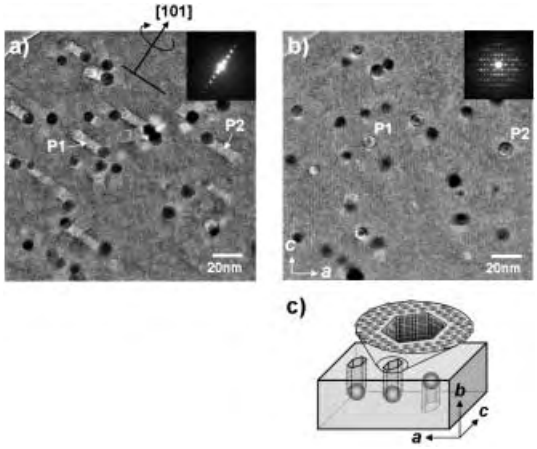


Figure 4. TEM images of mesopores and platinum particles. a) Most of the mesopores formed along the {101} plane of the ZSM-5, the diffraction pattern of which is also shown. b) The crystal tilted by 0.29 radians, observed along the [010] zone axis of ZSM-5. The mesopores mainly formed along the [010] direction. c) Schematic diagram of the zeolite surface.

sample about the [101] direction. The apparent length of the mesopores decreased with increasing tilt angle, until the cross sections of the mesopores and their Pt particles perfectly coincided in most cases at an angle of 0.29 radians (Figure 4b). In this position, the incident electron beam was aligned with the [010] direction of the zeolite. This result indicates that hexagonal mesopores about 80 nm in length formed selectively along the [010] axis of the ZSM-5 crystal. It can be seen that the mesopores in Figure 4 marked P1 and P2 both formed in the [010] direction of the ZSM-5, while the platinum particles moved in the reverse direction. Hence, they appear to have penetrated into the zeolite crystal along the [010] axis but from opposite surfaces of the particle. By examining several other particles, we confirmed that mesopores formed mainly along the [100] and [010] axes.

The mechanism of the phenomenon reported here is considered to be as follows: The width of the mesopores is equivalent to the diameter of the platinum particles, and the framework structure of the zeolite is not perturbed by the

 © 2004 Wiley-VCH Verlag GmbH & Co. KGaA, Weinheim

presence of a mesopore. This feature suggests that the mesopores formed by selective reaction with atoms in the zeolite structure at the interface between the platinum and zeolite. Under hydrothermal conditions siloxane bonds in zeolites are broken and recombined.[8] When silica is heated in contact with silicon, carbon, hydrogen, or a hydrocarbon at high temperatures, SiO is given off as a gaseous product.[9] The surfaces of the platinum particles act as catalytic reaction sites, so that water forms on them by reaction between the molecules in the atmosphere during aging according to Equation (1):

$$C_mH_n + (m + n/4)O_2 \rightarrow m\,CO_2 + (n/2)\,H_2O \quad (1)$$

Heat is also generated by this reaction. Water and hydrogen can also be formed by other catalytic reactions. Around a single platinum particle there are a greater number of active agents, such as radicals produced by catalytic reactions, water and hydrogen reaction products, and active H^+ and OH^- ions (from the dissociation of these products as well as from Si–OH terminating species of the zeolite) than in other regions. It is likely that these active agents at high temperature cause the decomposition of siloxane bonds at the interface between the platinum particle and zeolite. It is conceivable that broken zeolite components diffuse out of the system in forms of SiO or $Si(OH)_4$ because no amorphous phases were observed around the mesopores by electron microscopy, and because the mesopores increased in volume according to gas absorption–desorption measurements. While the decomposition of the siloxane bonds gradually progresses at the interface between platinum and the zeolite, the platinum particle itself tends to remain in contact with the zeolite because this is the most energetically stable position. As a result, the platinum particle gradually penetrates into the zeolite.

The mesopores formed along particular directions in the zeolite ZSM-5 crystal, and their walls were formed from specific ZSM-5 crystal faces. Such shape selectivity during the mesopore formation process can be explained as follows: There is a spatial distribution in the densities and directions of siloxane bonds in the framework of zeolite. Vacancies are most easily formed by the decomposition and removal of siloxane bonds in directions where the bond density is lower. The platinum particle continues to "eat" its way into the zeolite, but the final shape of the mesopore is strongly influenced by the framework structure of the zeolite. In addition, the structure of the zeolite may also affect the diffusion rates of reactants to the reactive interface.

Formation of mesopores using carbon during synthesis of zeolites or by generation of noble-metal particles has been reported.[10,11] However, the shapes of the mesopores and their arrangement could not be controlled. With a technique based on the phenomenon reported here, it might be possible to control the shape and size of the mesopores by altering the size of the platinum particles, the processing time, the type of zeolite, and the crystal orientation of the support material. Such a technique would produce materials for applications in which both structure-controlled mesopores and micropores based in a zeolite framework are needed, such as fine catalysts, adsorbents, and nano-ordered devices, with high precision and efficiency.

Received: August 25, 2003
Revised: November 11, 2003 [Z52706]

Keywords: mesoporous materials · nanostructures · platinum · surface chemistry · zeolites

[1] D. W. Breck, *Zeolite Molecular Sieves*, Wiley, New York, **1974**.
[2] M. E. Davis, *Nature* **2002**, *417*, 813 – 821.
[3] C. Baerlocher, W. M. Meier, D. H. Olson, *Atlas of Zeolite Structure Types*, 5th revised ed., Elsevier, London, **2001**.
[4] a) M. Iwamoto, H. Hamada, *Catal. Today* **1991**, *10*, 57 – 71; b) W. Held, A. Konning, T. Richter, L. Puppe, *SAE Prepr.* **1990**, 900496.
[5] a) Y. Liu, W. Zhang, T. J. Pinnavaia, *Angew. Chem.* **2001**, *113*, 1295 – 1298; *Angew. Chem. Int. Ed.* **2001**, *40*, 1255 – 1258b) Z. Zhang, Y. Han, L. Zhu, R. Wang, Y. Yu, S. Qiu, D. Zhao, F. S. Xiao, *Angew. Chem.* **2001**, *113*, 1288 – 1302; *Angew. Chem. Int. Ed.* **2001**, *40*, 1258 – 1262.
[6] a) P. J. F. Harris, E. D. Boyes, J. A. Cairns, *J. Catal.* **1983**, *82*, 127 – 146; b) H. C. Yao, H. K. Stepien, H. S. Gandhi, *J. Catal.* **1980**, *61*, 547 – 550; c) N. Miyoshi, S. Matsumoto, M. Ozawa, M. Kimura, *SAE Tech. Pap. Ser.* **1989**, 891970; d) S. J. Tauster, S. C. Fung, *J. Catal.* **1978**, *55*, 29 – 35.
[7] a) L. A. Bursill, E. A. Lodge, J. M. Thomas, *Nature* **1980**, *286*, 111 – 113; b) Y. Sasaki, T. Suzuki, Y. Ikuhara, *J. Am. Ceram. Soc.* **1995**, *78*, 1411 – 1413.
[8] H. Stach, U. Lohse, H. Thamm, W. Schirmer, *Zeolites* **1986**, *6*, 74 – 90.
[9] R. B. Sosman, *The Phases of Silica*, Rutgers University Press, New Brunswick, **1965**, pp. 9 – 10.
[10] a) C. J. H. Jacobsen, C. Madsen, J. Houzvicka, I. Schmidt, A. Carlsson, *J. Am. Chem. Soc.* **2000**, *122*, 7116 – 7117; b) I. Schmidt, A. Boisen, E. Gustavsson, K. Stahl, S. Pehrson, S. Dahl, A, Carlsson, C. H. Jacobsen, *Chem. Mater.* **2001**, *13*, 4416 – 4418.
[11] N. I. Jaeger, J. Rathousky, G. Schulz-Ekloff, A. Svensson, A. Zukal, *Zeolites: Facts*, *Figures*, *Future B*, Elsevier, Amsterdam, **1989**, pp. 1005 – 1013.

 © 2004 Wiley-VCH Verlag GmbH & Co. KGaA, Weinheim

Mass Spectrometry

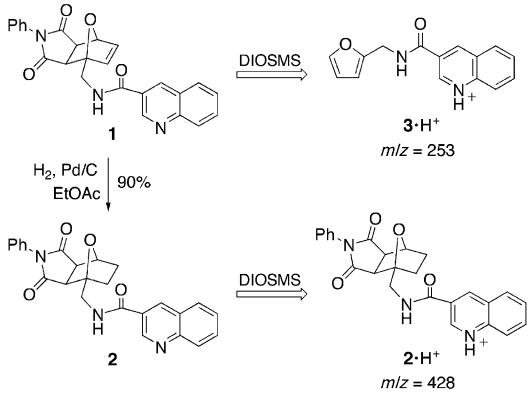
Cleavable Linkers for Porous Silicon-Based Mass Spectrometry**

*Jun-Cai Meng, Claudia Averbuj, Warren G. Lewis, Gary Siuzdak, and M. G. Finn**

Desorption/ionization on silicon mass spectrometry (DIOSMS) uses porous silicon (pSi) to generate gas-phase ions of small (< 3000 Da) molecules without a matrix by using standard MALDI (matrix-assisted laser desorption/ionization) instrumentation.[1] The unique laser desorption/ionization surface properties of DIOSMS allow for the simultaneous detection of a broad range of small molecules as their molecular ions, and the chemical properties of DIOSMS facilitate the attachment of a variety of organic fragments through surface Si–H[2] and Si–OH groups.[3] We aim to combine these advantages with the proven ability of covalent immobilization to facilitate combinatorial chemistry and the extraction of molecular information from complex mixtures.[4] Previous reports in this vein include the use of self-assembled monolayers of functionalized alkanethiols to purify mixtures (usually of proteins) by specific molecular interactions or properties such as hydrophobicity or charge complementarity prior to MALDI analysis.[5] DIOS has been similarly employed to detect small molecules bound to pSi-immobilized proteins.[6] We report herein that Diels–Alder adducts undergo retro-[4+2] fragmentation in DIOSMS analysis, thus providing a convenient way to covalently attach and detach probe structures for chip-based mass analysis.

The most useful covalent linkers for our purposes should be stable under organic synthetic conditions, yet cleavable during desorption/ionization. While photocleavable groups are commonly used in solid-phase organic synthesis,[7] most (but not all[8]) of these systems require a workup step after irradiation to complete the cleavage, and are therefore poorly suited to detachment in the MALDI laser pulse. The retro-Diels–Alder (rDA) reaction was one of the first dissociation pathways to be investigated in mass spectrometry,[9] and has since been characterized with a variety of ionization methods.[10] Some studies showed that the fragmentation is highly stereospecific for *cis*-annelated systems, which suggests a concerted mechanism.[11]

We have found that Diels–Alder adducts undergo [4+2] cycloreversion readily upon desorption/ionization by the laser pulse in DIOS analyses. Thus, the maleimide–furan adduct **1** bearing a 3-quinoline carboxamide moiety showed only a single intense peak in the DIOSMS spectrum, which corresponds to the protonated diene $[\mathbf{3}\cdot H]^+$ (Scheme 1). The



Scheme 1. Retero Diels–Alder cleavage of a furan–maleimide adduct.

maleimide was not detected because it is poorly ionized, as verified by control experiments. Hydrogenation of **1** into **2** eliminated fragmentation in the DIOS mass spectrum, thus supporting the notion that cycloreversion is the cleavage mechanism. A survey of a set of Diels–Alder adducts suggested that the ease of thermal cycloreversion in solution may be correlated with retro-Diels–Alder fragmentation in DIOSMS (see Supporting Information). Furan–maleimide adducts were found to be conveniently accessible, of sufficient chemical stability,[12] and to undergo uniformly clean rDA cleavage, and were therefore used in subsequent studies.

The use of a Diels–Alder moiety as a connector allows small molecules to be both covalently attached to the porous silicon surface and detected by mass spectrometry when desired. This was illustrated by the derivatization of freshly-etched pSi by hydrosilylative attachment of *N*-(4-vinylphenyl)maleimide to give **4** (Scheme 2 and Supporting Information). It should be noted that many of the hydrosilylation reactions described here were performed at room temperature in the absence of air, which is in contrast to the higher temperatures (ca. 100 °C) that appear to be standard in previous cases.[1d,13] Under our mild conditions, it is assumed that only the most reactive surface silicon-hydride sites are derivatized giving rise to incomplete surface coverage, but a sufficient density for DIOSMS detection was invariably achieved. 1,3-Diphenylisobenzofuran was then introduced in a CH_2Cl_2 solution, followed by extensive washing with organic solvent. DIOSMS analysis showed a strong signal for the expected rDA peak at *m*/*z* 270. Control samples, involving noncovalently deposited diene and dienophile, as well as the diene alone, showed no signal after they had been washed (Scheme 2).

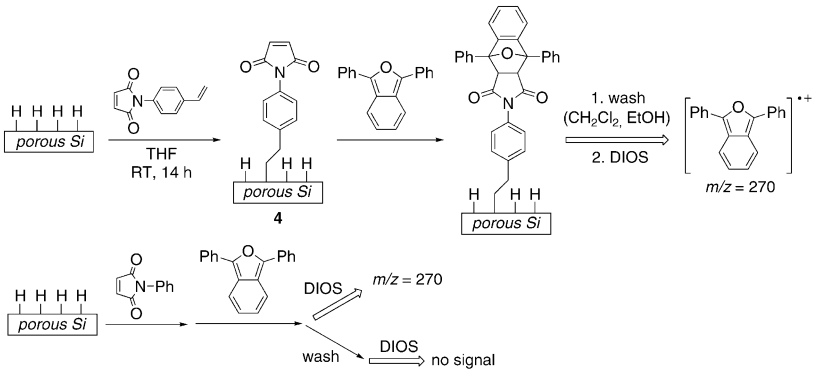
As in all mass-spectrometry techniques, the strength of the DIOS signal is affected by many factors, especially the

[*] Prof. G. Siuzdak
Department of Molecular Biology
The Scripps Research Institute
10550 N. Torrey Pines Rd., La Jolla, CA 92037 (USA)
Dr. J.-C. Meng, Dr. C. Averbuj, W. G. Lewis, Prof. M. G. Finn
Department of Chemistry
The Scripps Research Institute
10550 N. Torrey Pines Rd., La Jolla, CA 92037 (USA)
Fax: (+1) 858-784-8850
E-mail: mgfinn@scripps.edu

[**] We thank the National Institutes of Health (RR-15066) and The Skaggs Institute for Chemical Biology for support of this work; WGL is a Skaggs Predoctoral Fellow. We are grateful to Dr. Zhouxin Shen for helpful discussions.

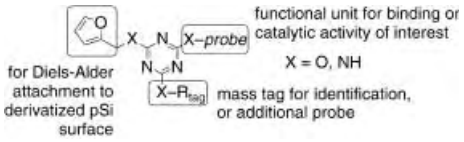
Supporting information for this article is available on the WWW under http://www.angewandte.org or from the author.

 DOI: 10.1002/anie.200352803 © 2004 Wiley-VCH Verlag GmbH & Co. KGaA, Weinheim



Scheme 2. Attachment and detachment of isobenzofuran by using a maleimide-derivatized porous-silicon surface.

ionization efficiency of the analyte. The combination of a retro-Diels–Alder linkage with an easily ionizable spacer should provide a useful platform for the analysis of a number of chip-based phenomena. The 1,3,5-triazine unit proved to be an effective scaffold, since it provides a strong DIOSMS signal regardless of the attached species and can be addressed sequentially in three positions from trihalide (cyanuric) derivatives.[14] The general design of such a system is shown in Scheme 3, and Figure 1 depicts an example of the synthetic manipulations performed.



Scheme 3. Trifunctional 1,3,5-triazine core.

Furfurylamine addition to cyanuric chloride at low temperature afforded **5**, which was subsequently converted into the fully substituted triazine–diene **6**. Compounds **7** and **8** were prepared analogously. Diels–Alder attachment to *N*-phenethylmaleimide (giving **9a**) and to the maleimide-decorated porous silicon surface **4** (giving **9b**) occurred under mild conditions. Both **9a**, deposited on a DIOS chip, and modified pSi **9b** gave a single dominant MS peak at *m*/*z* 387, indicative of clean cycloreversion to **6** upon laser desorption/ionization. Furthermore, immersion of a *p*Si-maleimide chip in a toluene solution of equimolar amounts of **6**, **7**, and **8** (10 μmol each in 2 mL), or deposition of a drop of this solution on the chip, showed all three species in approximately equal intensity. When the immersed chip was subsequently rinsed thoroughly with toluene and ethanol, only **6** appeared, presumably held by covalent attachment to the surface, whereas the other species were washed away. A nonfunctionalized pSi wafer retained none of these species after identical analyte deposition and washing procedures.

The sequence shown in Figure 2 illustrates the application of an alternative pSi-attachment strategy that incorporates a preformed oxanorbornene structure. Hydrosilyation of 1,6-heptadiyne with freshly prepared pSi afforded the terminal alkyne surface **10**. In spite of the presence of unconverted surface Si–H sites, at least some terminal alkyne residues remained available, as established by IR spectroscopy and subsequent reactivity; samples prepared by thermal or photochemical[15] hydrosilylation methods behaved very similarly. Attachment of **10** to azide **11** was then performed by using the Cu^{I}-catalyzed procedure recently reported by Fokin and Sharpless,[16] in a mixture of acetonitrile and pH 8 buffer at room temperature. The capture of azide at 10 μM concen-

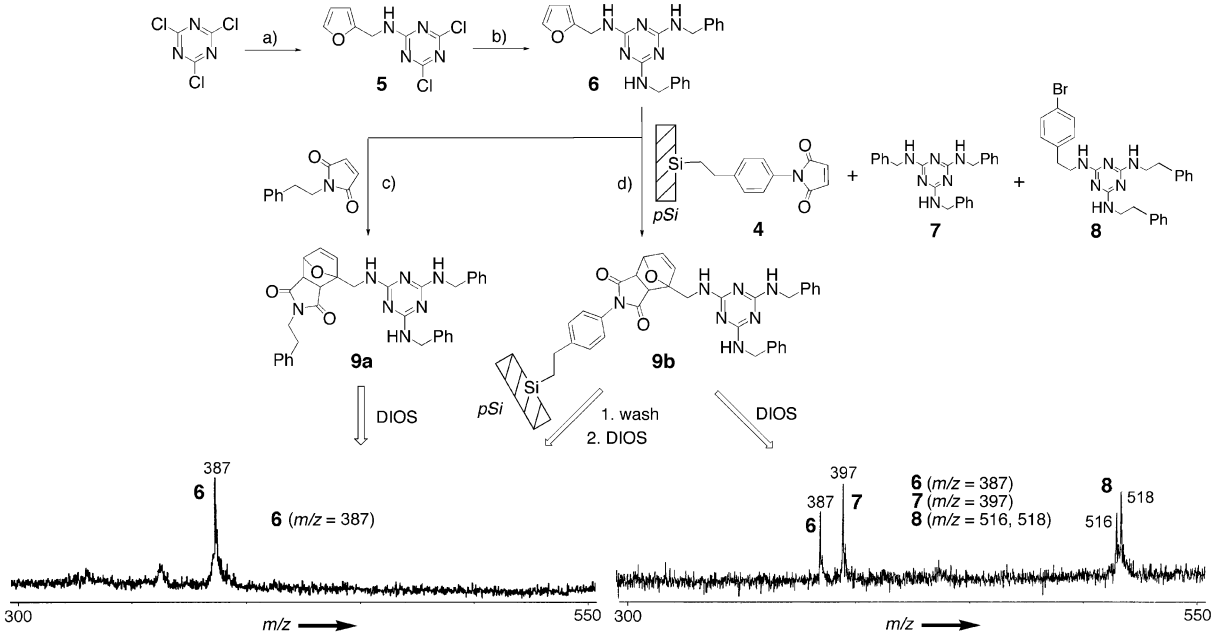


Figure 1. Detection of deposited and covalently attached compounds by DIOSMS. a) Furfurylamine (1 equiv), $NaHCO_3$, 2:3 acetone/H_2O, 93%. b) Benzylamine (10 equiv), THF, reflux, 90%. c) Toluene (25 °C) or benzene (reflux), 75–80%. d) Toluene, 25 °C, 12 h.

 © 2004 Wiley-VCH Verlag GmbH & Co. KGaA, Weinheim

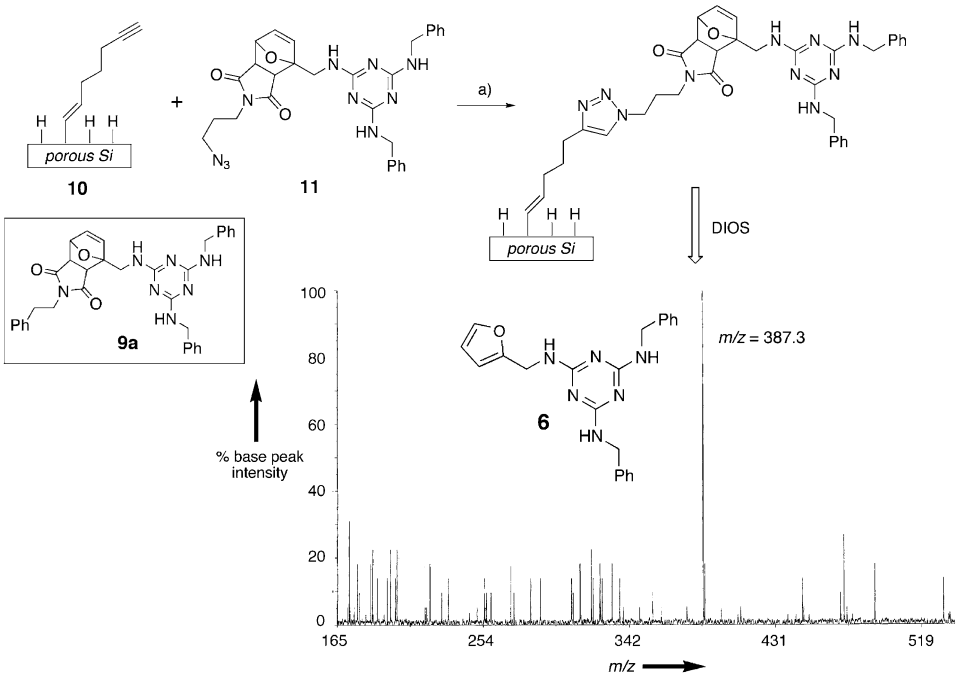


Figure 2. a) (I) 10 μM **11**, 1.0 μM $CuSO_4$, 2.0 μM L-ascorbic acid; 1:1 (v:v) MeCN:Tris buffer (pH 8.0), room temperature, 8 h. (II) Wash with THF and ethanol.

tration by the surface-attached alkyne by using 1 μM copper catalyst is among the most impressive examples of this "click reaction"[17] so far reported,[18] thus illustrating the extraordinary ability of the process to join appropriate pieces at low concentration.[19] After the product had been washed, DIOS analysis showed the expected rDA product **6** as the dominant signal. The corresponding control compound **9a** gave no MS signal after incubation with **10** and washing of the product under identical conditions.

The capture of a set of azides by an immobilized alkyne was demonstrated as shown in Figure 3. In this case, the alkyne was brought to the pSi surface as part of the triazenyl

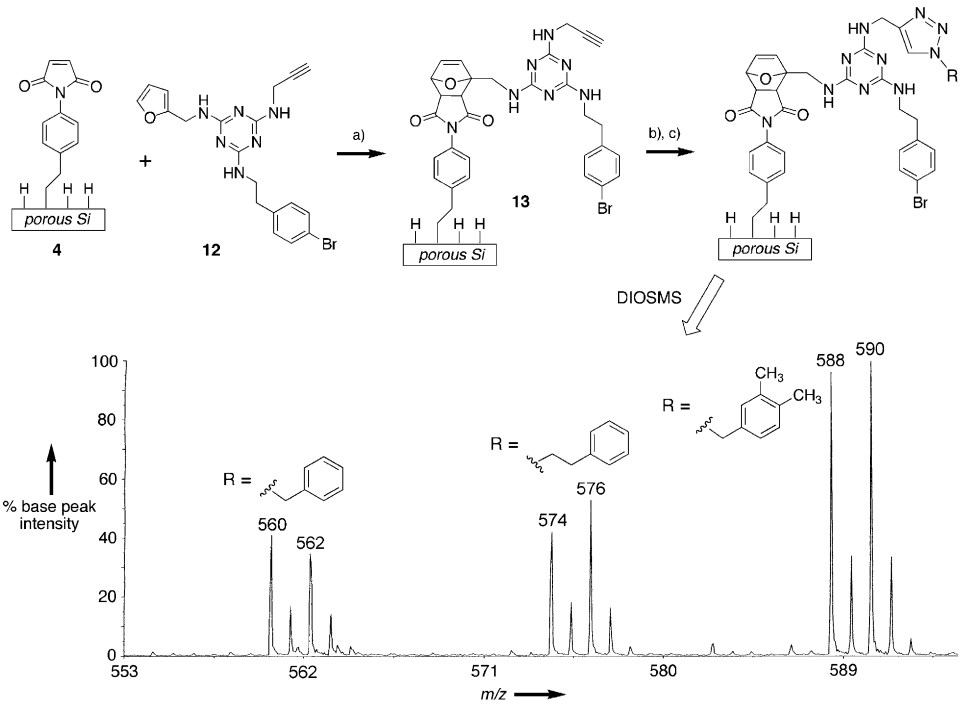
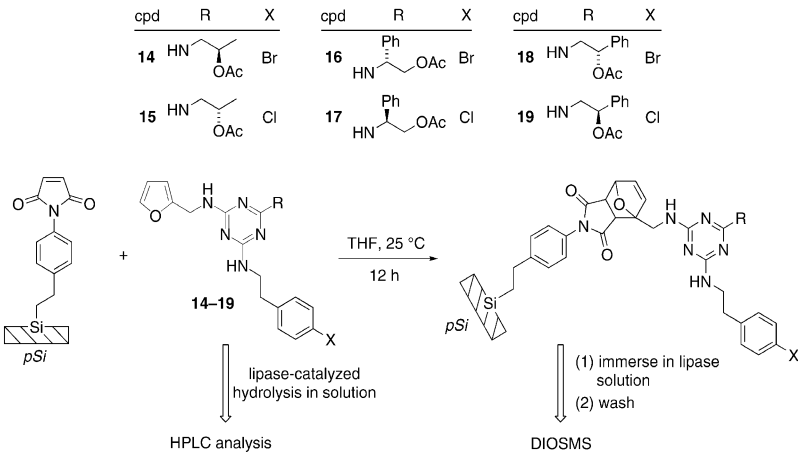


Figure 3. Capture and detection of solution-phase azides by DIOSMS. a) Toluene, 25 °C, 12 h. b) Mixture of indicated R–N_3 (10 μM each), 3.0 μM $CuSO_4$, 6.0 μM L-ascorbic acid, 1:1 (v/v) MeCN:Tris buffer (pH 8.0), RT, 8 h. c) Wash with THF, then ethanol.

 © 2004 Wiley-VCH Verlag GmbH & Co. KGaA, Weinheim

furan dienophile **12**. The resulting wafer, **13**, was then exposed to an equimolar mixture of three azides, chosen to differ in mass by successive methylene units. Washing of the product followed by DIOSMS analysis gave a clean set of signals for the three $[M+H]^+$ species, each showing the expected bromine isotope pattern arising from the Br label introduced to the triazine core. As before, the negative controls (allyl in place of propargyl in **12**, nonderivatized pSi in place of **4**) gave no MS signals, thus demonstrating that both the covalent connections (Diels–Alder and [3+2] cycloaddition) were made.



Scheme 4. Lipase-mediated hydrolysis of soluble and pSi-bound acetate esters.

To show that the covalent attachment and detachment events enabled by the Diels–Alder reaction can be useful in catalyst screening, we explored the enantioselective hydrolysis of acetate esters by two lipase enzymes.[20] Triazines **14**–**19** comprise three pairs of pseudoenantiomers (Scheme 4). Each member of a pair has the opposite absolute configuration of the chiral component and was tagged with a bromide or chloride substituent to encode this information into the MS signal.[21]

Pseudoracemic mixtures of triazine–acetates (equimolar amounts of **14**+**15**, **16**+**17**, and **18**+**19**) were subjected to hydrolysis by lipases from *Pseudomonas cepacia* (PCL) and *Candida rugosa* (CRL) in aqueous buffer and the results were analyzed by reversed-phase HPLC (Figure 4). A range of outcomes was observed. In two cases, the enzymes differed dramatically in their reactivity: for the **14**/**15** pair, PCL gave excellent resolution ($k_{rel} > 50$) and CRL was nonselective ($k_{rel} = 1$), whereas for **18**/**19**, CRL catalyzed a moderately successful resolution ($k_{rel} = 16$) and PCL was inactive. In the case of **16**/**17**, the lipases were more similar in their activity, with PCL being somewhat more selective ($k_{rel} = 5.1$ versus 1.1). The good performance of PCL with **14**/**15** and the absolute configuration of the faster-reacting compound are consistent with previous results involving structures that are related to the substrates used here.[22] All the other cases are sufficiently far removed from prior reports as to constitute new results, although it was expected that the primary acetates **16**/**17** would undergo less efficient kinetic resolution than secondary acetates, which have the chiral center of interest closer to the reactive bond.[23] Few lipase-catalyzed transformations of alcohols and esters bearing nitrogen substituents in the α position have been reported.[24]

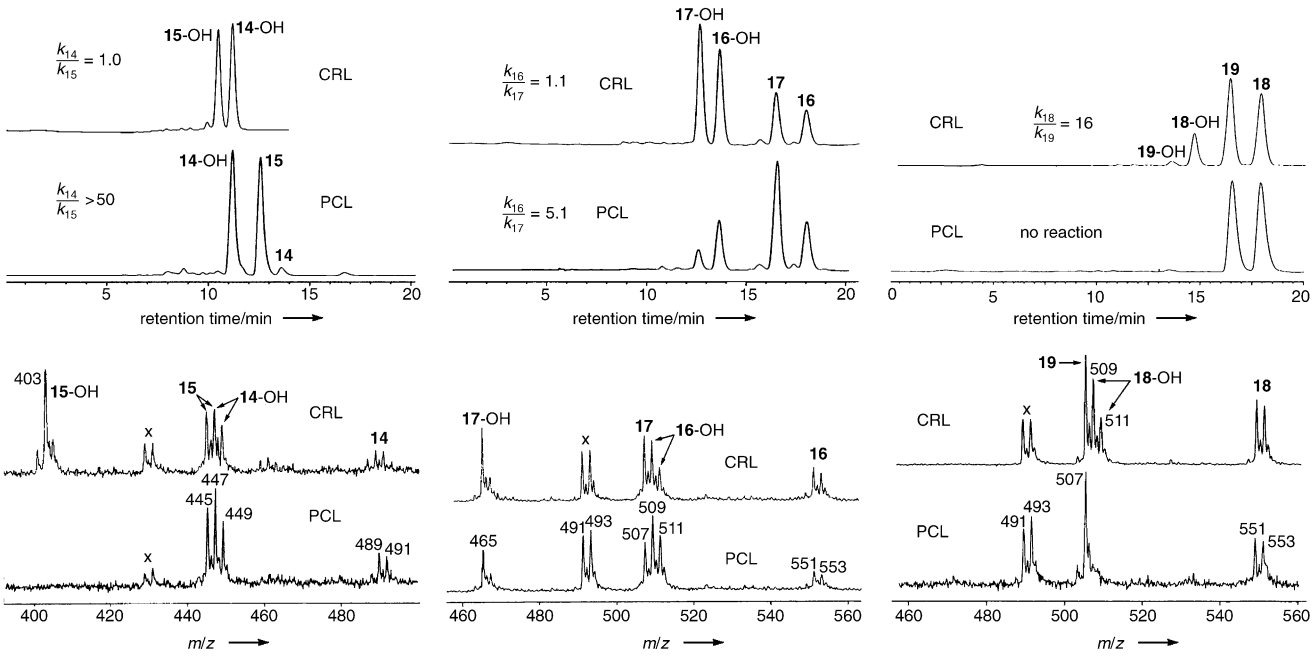


Figure 4. HPLC (top; I = relative intensity arbitrary units) and DIOSMS (bottom; %I = percentage base peak intensity) analyses of hydrolysis reactions using CRL and PCL on acetates **14**–**19**.

 © 2004 Wiley-VCH Verlag GmbH & Co. KGaA, Weinheim

The pseudoenantiomeric mixtures of acetates were also separately incubated with maleimide-functionalized porous silicon as described above and the chips were then thoroughly rinsed with toluene and ethanol. Alternatively, each pair of acetates was attached to a different spot of the same pSi chip. The resulting wafers were swirled together in an aqueous buffer solution containing either CRL or PCL (12 h at room temperature), washed with water and ethanol, and then analyzed directly by DIOSMS. The resulting spectra, shown in Figure 4, reproduced the solution-phase/HPLC findings quite well. For example, with PCL, only the alcohol derived from **14** was observed, and no hydrolysis product from **15** was evident, whereas both alcohols were detected in comparable amounts with CRL. Similarly, in all other cases the relative reactivity observed by HPLC were clearly reproduced in the chip-based format. As a control, undecorated porous silicon was incubated with the same mixtures of substrates **14**–**19** and lipase in phosphate buffer under identical conditions. The substrates and the hydrolyzed products were poorly detected by DIOS, and washing of the products removed the signals entirely.

Analytical methods based on mass spectrometry have the general advantage over optical and radiolabel assays in that the installation of chromophoric or radioactive tags is not required and that detection of mass provides a general means to monitor chemical changes in the analytes of interest. The combination of the ability to detect analytes of different mass in a single spectrum with the rapid data acquisition provided by the chip-based format makes both DIOSMS and MALDI well suited to high-throughput screening. Covalent attachment of analytes further enhances these approaches by enabling spatially addressable and multistep synthesis on the chip. Most importantly, the making of a cleavable covalent link between the analyte/probe and the surface allows the user to wash the chips vigorously and thus overcome problems of nonspecific adsorption and signal suppression. Mrksich and Su have described the use of MALDI in this fashion to analyze the conversion of surface-bound substrates by a galactosyltransferase enzyme by using functionalized alkanethiols, which relies on the ability of the MALDI laser pulse to dissociate the Au–thiol bond.[5a]

Here we have shown Diels–Alder adducts to be cleavable covalent linkers compatible with the DIOSMS technique, useful in probing the reactivity of species attached to the porous silicon surface. The triazine unit is a well-ionized tripodal spacer, which allows for the attachment of tagging residues or other components. Enzyme-catalyzed transformations on pSi-immobilized substrates were found to proceed with similar relative activity and selectivity as those observed in solution. Our methodology allows covalent attachment and detachment to be implemented in the mass spectrometer without added matrix material, and should be applicable to a wide variety of analytes, chemical transformations, and washing conditions.

Received: September 5, 2003 [Z52803]

Keywords: cleavage reactions · combinatorial chemistry · lipases · mass spectrometry · porous silicon

[1] a) J. Wei, J. Buriak, G. Siuzdak, *Nature* **1999**, *399*, 243 – 246; b) Z. Shen, J. J. Thomas, C. Averbuj, K. M. Broo, M. Engelhard, J. E. Crowell, M. G. Finn, G. Siuzdak, *Anal. Chem.* **2001**, *73*, 612 – 619; c) J. J. Thomas, Z. Shen, J. E. Crowell, M. G. Finn, G. Siuzdak, *Proc. Natl. Acad. Sci. USA* **2001**, *98*, 4932 – 4937; d) S. Tuomikowki, K. Huikko, K. Grigoras, P. Östman, R. Kostiainen, M. Baumann, J. Abian, T. Kotiaho, S. Franssila, *Lab Chip* **2002**, *2*, 247 – 253.

[2] a) M. P. Stewart, J. M. Buriak, *Comments Inorg. Chem.* **2002**, *23*, 179 – 203; b) J. M. Schmeltzer, L. A. Porter, Jr., M. P. Stewart, C. M. Lopez, J. M. Buriak, *Mater. Res. Soc. Symp. Proc.* **2003**, *737*, 561 – 566; c) J. M. Buriak, M. J. Allen, *J. Am. Chem. Soc.* **1998**, *120*, 1339 – 1340; d) B. R. Hart, S. E. Létant, S. R. Kane, M. Z. Hadi, S. J. Shields, J. G. Reynolds, *Chem. Commun.* **2003**, 322 – 323; e) F. Effenberger, G. Götz, B. Bidlingmaier, M. Wezstein, *Angew. Chem.* **1998**, *110*, 2651 – 2654; *Angew. Chem. Int. Ed.* **1998**, *37*, 2462 – 2464; f) A. R. Pike, L. H. Lie, R. A. Eagling, L. C. Ryder, S. N. Patole, B. A. Connolly, B. R. Horrocks, A. Houlton, *Angew. Chem.* **2002**, *114*, 637 – 639; *Angew. Chem. Int. Ed.* **2002**, *41*, 615 – 617; g) A. Janshoff, K.-P. S. Dancil, C. Steinem, D. P. Greiner, V. S.-Y. Lin, C. Gurtner, K. Motesharei, M. J. Sailor, M. R. Ghadiri, *J. Am. Chem. Soc.* **1998**, *120*, 12108 – 12116; h) C. Gurtner, A. W. Wun, M. J. Sailor, *Angew. Chem.* **1999**, *111*, 2132 – 2135; *Angew. Chem. Int. Ed.* **1999**, *38*, 1966 – 1968; i) N. Y. Kim, P. E. Laibinis, *J. Am. Chem. Soc.* **1997**, *119*, 2297 – 2298; j) N. Y. Kim, P. E. Laibinis, *J. Am. Chem. Soc.* **1998**, *120*, 4516 – 4517; k) L. H. Lie, S. N. Patole, E. R. Hart, A. Houlton, B. R. Horrocks, *J. Phys. Chem. B* **2002**, *106*, 113 – 120.

[3] K.-P. S. Dancil, D. P. Greiner, M. J. Sailor, *J. Am. Chem. Soc.* **1999**, *121*, 7925 – 7930.

[4] a) M. C. Pirrung, *Chem. Rev.* **1997**, *97*, 473 – 488; b) R. W. Nelson, D. Nedelkov, K. A. Tubbs, *Electrophoresis* **2000**, *21*, 1155 – 1163; c) G. MacBeath, S. L. Schreiber, *Science* **2000**, *289*, 1760 – 1763.

[5] a) J. Su, M. Mrksich, *Angew. Chem.* **2002**, *114*, 4909 – 4912; *Angew. Chem. Int. Ed.* **2002**, *41*, 4715 – 4718; b) M. Merchant, S. R. Weinberger, *Electrophoresis* **2000**, *21*, 1164 – 1167; c) R. W. Nelson, J. R. Krone, O. Jansson, *Anal. Chem.* **1997**, *69*, 4363 – 4368; d) J. L. Bundy, C. Fenselau, *Anal. Chem.* **2001**, *73*, 751 – 757.

[6] H. Zou, Q. Zhang, Z. Guo, B. Guo, Q. Zhang, X. Chen, *Angew. Chem.* **2002**, *114*, 668 – 670; *Angew. Chem. Int. Ed.* **2002**, *41*, 646 – 648.

[7] a) V. N. R. Pillai, *Synthesis* **1980**, 1 – 26; b) V. N. R. Pillai in *Organic Photochemistry*, *Vol. 9* (Ed.: A. Padwa), Marcel Dekker, New York, **1987**, pp. 225 – 323; c) F. Guiller, D. Orain, M. Bradley, *Chem Rev.* **2000**, *100*, 2091 – 2157; d) R. Glatthar, B. Giese, *Org. Lett.* **2000**, *2*, 2315 – 2317.

[8] a) M. C. Fitzgerald, K. Harris, C. G. Shevlin, G. Siuzdak, *Bioorg. Med. Chem. Lett.* **1996**, *6*, 979 – 982; b) J. M. Gerdes, H. Waldmann, *J. Comb. Chem.* **2003**, *5*, 814 – 820.

[9] a) H. Budzikiewicz, J. I. Brauman, C. Djerassi, *Tetrahedron* **1965**, *21*, 1855 – 1879; b) H. Kwart, K. King, *Chem. Rev.* **1968**, *68*, 415 – 447.

[10] a) J. H. Bowie, A. H. Ho, *J. Chem. Soc. Perkin Trans. 2* **1975**, 724 – 728; b) D. J. Burinsky, R. Dunphy, J. D. Alves-Santana, M. L. Cotter, *Org. Mass Spectrom.* **1991**, *26*, 669 – 670; c) A. Etinger, A. Mandelbaum, *Org. Mass Spectrom.* **1992**, *27*, 761 – 762; d) K. P. Madhusudanan, T. S. Dhami, A. Rani, S. N. Suryawanshi, *Rapid Commun. Mass Spectrom.* **1993**, *7*, 92 – 94; e) A. Lucas, J. Fernández-Gadea, N. Martin, R. Martínez, C. Seoane, *Rapid Commun. Mass Spectrom.* **2000**, *14*, 1783 – 1786; f) N. Martin, R. Martínez-Alvarez, C. Seoane, M. Suárez, E. Salfran, Y. Verdecia, N. K. Sayadi, *Rapid Commun. Mass Spectrom.* **2001**, *15*, 20 – 24.

 © 2004 Wiley-VCH Verlag GmbH & Co. KGaA, Weinheim

[11] A. Mandelbaum in *Applications of Mass Spectrometry to Stereochemical Problems* (Eds.: J. Splitter, F. Turecek), VCH Publishers, New York, **1992**, and references therein.
[12] D. Tobia, R. Harrison, B. Phillips, T. L. White, M. DiMare, B. Rickborn, *J. Org. Chem.* **1993**, *58*, 6701 – 6706.
[13] J. T. C. Wojtyk, K. A. Morin, R. Boukherroub, D. D. M. Wayner, *Langmuir* **2002**, *18*, 6081 – 6087.
[14] Our use of triazines was inspired by their elegant adaptation to dendrimer synthesis described by Simanek and co-workers: W. Zhang, E. E. Simanek, *Org. Lett.* **2000**, *2*, 843 – 845; W. Zhang, D. T. Nowlan III, L. M. Thomson, W. M. Lackowski, E. E. Simanek, *J. Am. Chem. Soc.* **2001**, *123*, 8914 – 8922.
[15] M. P. Stewart, J. Buriak, *J. Am. Chem. Soc.* **2001**, *123*, 7821 – 7830.
[16] V. V. Rostovtsev, L. G. Green, V. V. Fokin, K. B. Sharpless, *Angew. Chem.* **2002**, *114*, 2708 – 2711; *Angew. Chem. Int. Ed.* **2002**, *41*, 2596 – 2599.
[17] H. C. Kolb, M. G. Finn, K. B. Sharpless, *Angew. Chem.* **2001**, *113*, 2056 – 2075; *Angew. Chem. Int. Ed.* **2001**, *40*, 2004 – 2021.
[18] a) Q. Wang, T. R. Chan, R. Hilgraf, V. V. Fokin, K. B. Sharpless, M. G. Finn, *J. Am. Chem. Soc.* **2003**, *125*, 3192 – 3193; b) A. E. Speers, G. C. Adam, B. F. Cravatt, *J. Am. Chem. Soc.* **2003**, *125*, 4686 – 4687; c) A. J. Link, D. A. Tirrell, *J. Am. Chem. Soc.* **2003**, *125*, 11164 – 11165d) A. Deiters, T. A. Cropp, M. Mukherji, J. W. Chin, J. C. Anderson, P. G. Schultz, *J. Am. Chem. Soc.* **2003**, *125*, 11782 – 11783.
[19] The azide–alkyne cycloaddition reactions described in this paper were performed in the absence of the tris(triazolyl)amine ligand previously shown to be helpful to the solution-phase process.[18a–c] While the rate of the ligand-free process may be great enough to effect the necessary degree of coupling to surface-tethered alkynes, we suspect that the pSi surface can play an important role in the reaction mechanism,[16] perhaps by providing active hydride to preserve the Cu^{I} oxidation state or assist in Cu–C bond cleavage.
[20] S. Servi, *Top. Curr. Chem.* **1999**, *200*, 127 – 158.
[21] M. T. Reetz, M. H. Becker, H.-W. Klein, D. Stöckigt, *Angew. Chem.* **1999**, *111*, 1872 – 1875; *Angew. Chem. Int. Ed.* **1999**, *38*, 1758 – 1761.
[22] R. J. Kazlauskas, A. N. E. Weissfloch, A. T. Rappaport, L. A. Cuccia, *J. Org. Chem.* **1991**, *56*, 2656 – 2665.
[23] a) A. N. E. Weissfloch, R. J. Kazlauskas, *J. Org. Chem.* **1995**, *60*, 6959 – 6969; b) B.-V. Nguyen, O. Nordin, C. Voerde, E. Hedenstroem, H.-E. Hoegberg, *Tetrahedron: Asymmetry* **1997**, *8*, 983 – 986.
[24] a) T. Izumi, K. Fukaya, *Bull. Chem. Soc. Jpn.* **1993**, *66*, 1216 – 1221; b) K. Kundell, L. T. Kanerva, *Tetrahedron: Asymmetry* **1995**, *6*, 2281 – 2286.

 © 2004 Wiley-VCH Verlag GmbH & Co. KGaA, Weinheim

Polymer Self-Assembly

Redox-Active Organometallic Vesicles: Aqueous Self-Assembly of a Diblock Copolymer with a Hydrophilic Polyferrocenylsilane Polyelectrolyte Block**

K. Nicole Power-Billard, Richard J. Spontak, and Ian Manners**

The formation of nanoscopic aggregates via the self-assembly of block copolymers in a selective solvent for one of the blocks is currently a flourishing area of polymer and materials science.[1] While early studies of such systems reported mainly spherical micelles, more recent efforts have yielded an interesting variety of other morphologies such as cylinders, vesicles, and lamellae, as well as more complex structures particularly in systems containing a short, corona-forming polyelectrolyte block.[2] Diblock copolymers capable of self-assembling in water are of intense interest due to their potential applications as nanocontainers for drug delivery technologies and as emulsifiers for heterogeneous catalysis.[3,4] Although the aqueous self-assembly of organic diblock copolymers has been well studied and copolymers with polyelectrolyte blocks have received particular attention in this vein,[4] analogous investigations of metal-containing block copolymers are extremely rare.[5] Micelles derived from a metal-containing block copolymer offer potentially interesting redox tunability, in addition to conductive and preceramic characteristics.[5,6] In this communication, we report on the molecular self-assembly of a water-soluble block copolymer possessing a hydrophilic organometallic polyferrocene polyelectrolyte block. This chemical constitution results in the formation of novel redox-active vesicles with a metal-containing block on both the outside and inside of the nanoscale aggregates. In addition, our studies demonstrate how sample preparation can influence the complex morphologies of such aqueous colloidal systems as discerned by transmission electron microscopy (TEM).

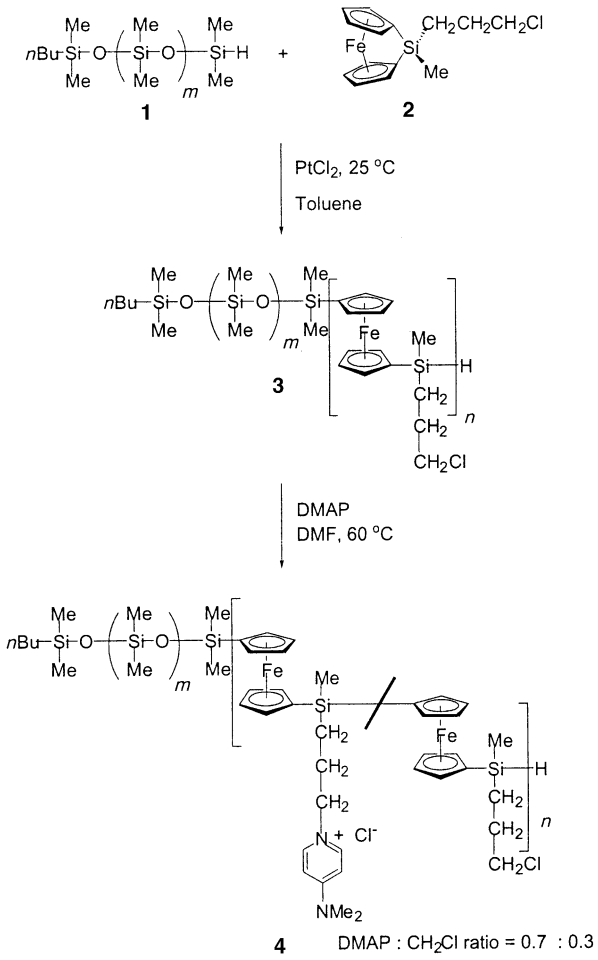
[*] K. N. Power-Billard, Prof. I. Manners
Department of Chemistry, University of Toronto, 80 St. George Street, Toronto, Ontario, M5S 3H6 (Canada)
Fax: (+1) 416-978-6157
E-mail: imanners@alchemy.chem.utoronto.ca
Prof. R. J. Spontak
Departments of Chemical Engineering and Materials Science & Engineering, North Carolina State University, Raleigh, NC 27695 (USA)
Fax: (+1) 919-515-3465
E-mail: rich_spontak@ncsu.edu

[**] I.M. thanks the Canadian Government for a Canada Research Chair and would like to thank the Natural Sciences and Engineering Research Council (NSERC) for support. R.J.S. thanks the STC Program of the National Science Foundation under Agreement No. CHE-9876674 for support. Special thanks to Mr. Fred Pearson at McMaster University for the TEM analysis of LN2-quenched solutions of polymer **4**. We thank Alex Bartole-Scott and John Halfyard for performing the electrochemistry experiments.

 © 2004 Wiley-VCH Verlag GmbH & Co. KGaA, Weinheim DOI: 10.1002/anie.200352819

Previous work has demonstrated that polyferrocenylsilane (PFS) block copolymers[7] form a variety of micellar morphologies.[8] To generate vesicles via aqueous self-assembly, we targeted a block copolymer with a hydrophilic PFS block and a hydrophobic polydimethylsiloxane (PDMS) coblock. We also utilized the synthetic design strategy suggested by the recent work of Eisenberg and co-workers,[9] who elucidated a mechanism for the thermodynamic stabilization of block copolymer vesicles. In their studies, they demonstrated that the curvature of poly(styrene-*b*-acrylic acid) (PS-*b*-PAA) vesicles was stabilized by preferential segregation of long hydrophilic PAA chains towards the outside of the vesicle and short PAA chains towards the inside of the vesicle. This chain arrangement generated greater interchain repulsion between PAA chains outside than inside the vesicle. The polydispersity of the hydrophilic PAA block was believed to be of crucial importance in the formation of such structures (even though the molecular-weight distribution was narrow). In this work, a hydrophobic PDMS block was synthesized by anionic polymerization so that it was nearly monodisperse. However, we chose to prepare the hydrophilic PFS block by Pt-catalyzed ring-opening polymerization (ROP), which is known[10] to yield polymers with polydispersity indices (PDIs) in the range of 1.3 to 1.5. Thus, we anticipated that the resultant polydispersity of the hydrophilic PFS block would help promote the formation of the desired vesicular morphology.

Specifically, the PDMS-*b*-PFS diblock copolymer **4** (block ratio 2.9:1, $\bar{M}_n \approx 8600$, PDI ≈ 1.5) employed in this work was synthesized according to Scheme 1.[11] First, the chloropropyl-substituted ferrocenophane **2** was induced to undergo transition-metal-catalyzed ROP in the presence of Si–H-terminated polydimethylsiloxane **1** ($\bar{M}_n = 3110$, PDI = 1.19), which was prepared by anionic polymerization. The PDMS telechelic functioned as a capping group for the growing PFS chain to yield the diblock copolymer **3** ($\bar{M}_n = 7490$, PDI = 1.49). Second, the latter material was then treated with dimethylaminopyridine (DMAP) to yield the final PDMS-*b*-PFS diblock copolymer **4** containing a hydrophilic PFS polyelectrolyte block with 70% substitution by DMAP.[11]



Scheme 1. Synthesis of **4**.

Self-assembly of **4** was initiated via direct dissolution in water. Solutions of block copolymer **4** were initially investigated by dynamic light scattering (DLS), which revealed an average hydrodynamic diameter of 84 nm for a 0.5 mg mL^{-1} solution of **4**. The morphology of **4** in a 0.5 mg mL^{-1} aqueous solution was also investigated by TEM. Specimens were prepared either by an "as-dropped" method or by freeze-drying. In the former, a drop of solution was placed on a carbon-coated copper grid and excess liquid was blotted away with filter paper. In the sample prepared by this method, spherical and compound aggregates with diameters ranging from 12 to 50 nm were observed (Figure 1a). These diameters most likely correspond to aggregates that collapsed during drying. Since contrast in phase-contrast TEM is attributed to differences in electron density, the dark regions in the TEM images are assigned to the water-soluble PFS block. A small population of cylindrical aggregates with widths of ≈ 30 nm and lengths that varied from 140 to 230 nm were also observed. Freeze-drying was performed by first placing a drop of solution on a carbon-coated copper grid resting on a metal block cooled by liquid nitrogen (LN2). Once the drop was solidified, it was immediately placed in a Schlenk tube under vacuum (≈ 0.003 mm Hg) until the solvent was completely removed. Surprisingly, the samples prepared in this fashion using LN2 as the cryogen displayed a variety of structural elements, which include ribbons, vesicles, strands of hollow hoops, and pearl necklaces (Figure 1b). The strands of hollow hoops and ribbon morphologies extended for several tens of microns, while vesicular structures ranged from several hundreds of nanometers to several microns in diameter. It must be recognized, however, that the observed sizes of the aggregates are substantially greater than those expected on the basis of the companion DLS data. In light of this result, we postulated that the methods of sample preparation used may dramatically influence the observed morphologies, which constitutes the first time that this effect has been observed in our studies regarding the self-assembly of polyferrocene-based diblock copolymers. We therefore undertook more detailed studies to address this issue.

Samples of **4** identical to those used in the DLS studies were used to explore the influence of TEM sample preparation on the observed aggregate morphology. First, solutions of **4** were freeze-dried in liquid ethane (LE) as a quenching medium. Plunging into LE (bp = −88 °C) supercooled to

 © 2004 Wiley-VCH Verlag GmbH & Co. KGaA, Weinheim

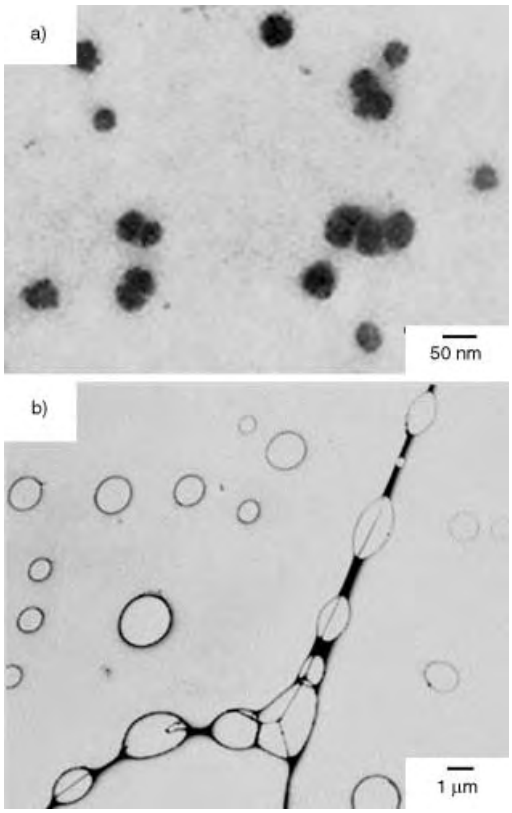


Figure 1. TEM images of block copolymer **4** (0.5 mg mL^{-1} in water) wherein the sample was prepared by a) the "as-dropped" method, and b) freeze-drying using liquid nitrogen as the quenching agent.

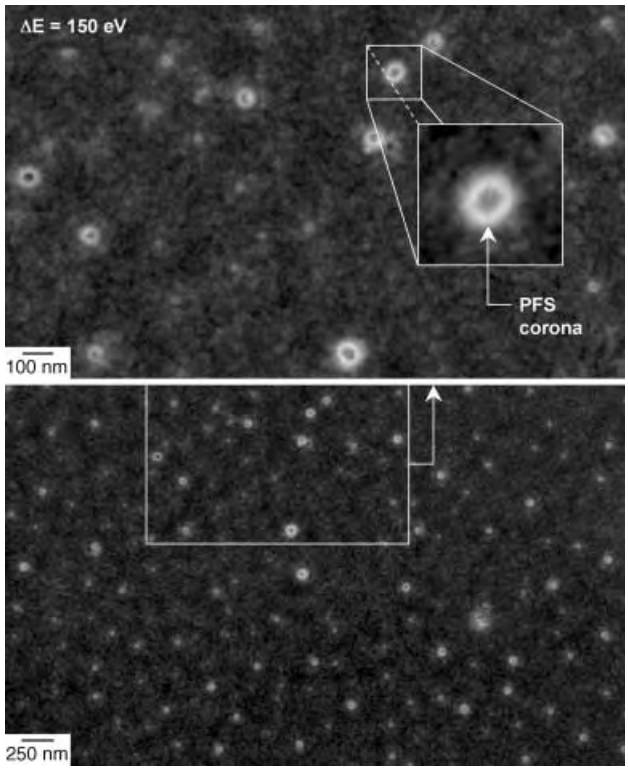


Figure 2. Energy-filtered TEM image of block copolymer **4** (0.5 mg mL^{-1} in water). The sample was prepared by quenching in liquid ethane.

−196 °C provides a cooling rate in excess of 15000 K s^{-1}, in marked contrast to LN2 (bp = −196 °C), which cools at a much slower rate of ≈1000 K s^{-1}.[12] The difference in cooling rate is attributed to the insulating liquid nitrogen vapor layer that forms and surrounds the sample during immersion into the liquid reservoir, since LN2 is at its normal boiling point. This vapor layer slows the rate of heat exchange between the sample and cryogen (thereby permitting water crystallization and probable morphological alteration), but does not occur in the case of LN2-cooled LE since the ethane is at a temperature below its normal freezing point (−183 °C). By using LE instead of LN2 as a quenching medium, water crystallization in ultrathin aqueous films should be altogether avoided, in which case the intrinsic polymer morphology is expected to remain intact. This is essentially the same methodology used to investigate the complex morphological characteristics of aqueous polymer solutions in situ (at cryogenic temperatures) by cryo-TEM.[13] Care was exercised to ensure that the sample temperature did not rise during freeze-drying so that neither water crystallization (at a transition temperature[14] of −125 °C) nor aggregate reorganization could occur as the water was removed by sublimation.

Transmission electron microscopy of polymer **4** after rapid quenching in LE and subsequent freeze-drying revealed the presence of vesicular-like aggregates with diameters measuring 85 nm on average (Figure 2). This structure-sensitive image was obtained using energy-filtered TEM.[15] In this imaging mode, electrons inelastically scattered due to carbon at an energy loss (ΔE) of ≈150 eV are effectively removed from image formation so that contrast is generally enhanced and non-carbonaceous elements appear highlighted. Thus, the light circular features in Figure 2 clearly identify the water-soluble PFS block. The relatively low-magnification image provides evidence that this morphology is representative, whereas the enlargements permit more detailed analysis of the aggregates. Recall, for instance, that the PDMS block is relatively short and that it is likewise composed of a non-carbonaceous element. Taken together, these two attributes explain why the PDMS-rich core of the copolymer bilayer comprising each vesicular aggregate is undetectable in Figure 3. The bilayer measures on the order of 15–20 nm in thickness, which compares well with four times the copolymer gyration radius, estimated to be ≈4 nm. It is further satisfying that the size of the vesicular aggregates gleaned from this TEM analysis is in favorable quantitative agreement with the corresponding measurement obtained by DLS.

This comparison clearly demonstrates that the method of sample preparation dramatically affects the solution aggregate morphology observed by TEM. Relative to our previous studies of the solution self-assembly of polyferrocene-based block copolymers, this is the first detailed study in which the solvent is water instead of a volatile organic solvent. Therefore, factors such as solvent crystallization, surface tension, and the rate of solvent evaporation during sample preparation become increasingly important, as rearrangement of the aggregate structure can occur if the matrix crystallizes during quenching or freeze-drying, or a receding solvent front forms

 © 2004 Wiley-VCH Verlag GmbH & Co. KGaA, Weinheim

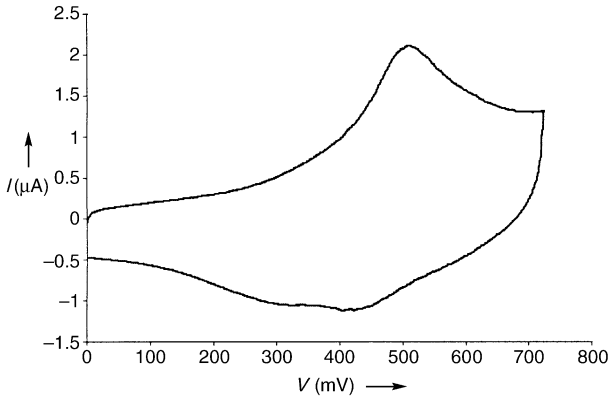


Figure 3. Cyclic voltammogram of **4** in 0.01 M aqueous NaCl. The scan rate was 100 $mV s^{-1}$.

during solvent removal. Solvent surface-tension effects constitute an especially important consideration when aqueous polymer solutions are prepared by placing a small sample volume onto a carbon-coated grid and allowing the (liquid) water to evaporate at ambient temperature. To preclude artifacts arising from such preparation, aqueous polymer solutions have been quenched and freeze-dried at LN2 temperature. Due to the low heat-transfer efficacy of LN2 relative to LE, water crystallization during quenching becomes a critical factor that could potentially promote gross alteration of the solution morphology. For this reason, LE is a far more suitable cryogen for preparing aqueous TEM samples than LN2. During solvent sublimation, the solution structure ideally should not be able to rearrange. It is, however, important to prevent the sample from warming up during freeze-drying so as to avoid morphological deformation due to solvent crystallization. Special care may further be required to ensure that sample temperature remains not only low, but also consistent. Finally, it is important to note that, due to the chemical nature of the diblock copolymer **4** (e.g., the glass-transition temperature of PDMS is −123 °C), our material is relatively fluid, which would not be expected to help preserve the structural integrity of complex morphologies during TEM sample preparation.

On the basis of previous work,[16] which established that low-molecular-weight ferrocene-based surfactants can be reversibly opened and reformed by sequential oxidation and reduction of the ferrocene units, the PDMS-*b*-PFS vesicles described herein may provide access to aggregate structures with redox-tunable encapsulation properties. To examine the redox chemistry of the vesicles, cyclic voltammetric studies have been performed on a 10^{-4} M solution of the vesicles in 0.1 M aqueous NaCl. Reversible oxidation of the ferrocene units in the PFS block is apparent from the detection of a single reversible oxidation wave (Figure 3).[17] This result underscores the interesting potential of these novel supramolecular vesicular assemblies as switching materials.

In summary, a water-soluble PDMS-*b*-PFS diblock copolymer prepared by combining both anionic and transition-metal-catalyzed ring-opening polymerization techniques has been found to form nanoscale vesicular aggregates upon direct dissolution in water. The mean diameter of these aggregates (≈85 nm) is in favorable agreement with that derived from dynamic light scattering. The method of TEM sample preparation has been shown to drastically affect the observed aggregate morphology. Contrary to the water-soluble PFS-containing block copolymers investigated thus far, self-assembly of materials such as **4** is of considerable interest since the electroactive PFS block, rather than the organic block, is hydrophilic and in aqueous media constitutes the aggregate corona. The potentially redox-tunable encapsulation properties of these structures are currently under study.

Experimental Section

4:[11] The chloropropyl-substituted ferrocenophane **2**[18] was subject to ROP in toluene over 24 h using a catalytic amount of $PtCl_2$ in the presence of Si–H-terminated polysiloxane **1**. The solution was then precipitated into an excess of MeOH and dried in vacuo to yield diblock copolymer **3** as a viscous amber fluid (GPC in THF versus polystyrene standards: $M_n = 7490$, PDI = 1.49). The diblock copolymer **3** was heated at 60 °C over 5 days in DMF with excess 4-dimethylaminopyridine (DMAP). The DMF was removed by vacuum distillation and the crude product was dissolved in distilled water and dialyzed against distilled water for 3 days to eliminate small-molecule impurities. The product was then dried at 100 °C to afford **4** as an amber viscous fluid (yield ≈20 %). ^{1}H NMR analysis showed that 70 % of the Cl substituents of the CH_2Cl groups of **4** had been replaced by DMAP under these reaction conditions. The approximate molecular weight and polydispersity of **4** ($M_n = 8600$, PDI = 1.5) was calculated from that for **3** assuming negligable chain cleavage during the substitution step.[19]

3: ^{1}H NMR (C_6D_6, 400 MHz): $\delta = 0.03$–0.31 (br, $SiMe_2O$), 0.41 (s, SiMe), 0.55 (t, CH_2 (*n*Bu)), 0.87–0.89 (m, CH_2 + CH_2 (*n*Bu)), 1.32 (m, CH_2CH_3 (*n*Bu)), 1.70 (br, CH_2), 3.18 (br, CH_2Cl), 3.95–4.19 ppm (m, Cp). ^{13}C NMR (C_6D_6, 100 MHz): $\delta = -3.0$ (SiMe), −1.3 to −1.7 ($SiMe_2O$), 14.0 (*n*Bu), 14.2 ($SiCH_2$), 18.3 (*n*Bu), 25.9 (*n*Bu), 26.8 (*n*Bu), 28.2 (CH_2), 48.2 (CH_2Cl), 70.5 (ipso-Cp), 71.9–74.0 ppm (Cp). ^{29}Si NMR (C_6D_6, 79.3 MHz): $\delta = 7.6$ (*n*BuSiMe_2O), 0.1 ($SiMe_2$fc), −5.4 (fcSi(Me)$CH_2CH_2CH_2Cl$), −17.7 (fcSi(Me)($CH_2CH_2CH_2Cl$)H), −21.5 to −22.2 ppm ($SiMe_2O$). GPC: $M_n = 7490$, $M_w = 11200$, PDI = 1.49.

4: ^{1}H NMR ([D_7]DMF, 400 MHz): $\delta = -$ 0.20–0.37 (br, $SiMe_2O$), 0.54–0.64 (s, SiMe + $SiCH_2$ (*n*Bu)), 0.82–1.18 (br, $SiCH_2$ + CH_2 (*n*Bu)), 1.41 (br, CH_2CH_3 (*n*Bu)), 1.80–2.05 (br, CH_2CH_2N + CH_2CH_2Cl), 3.28 (s, $N(CH_3)_2$)), 3.50 (H_2O), 3.71 (br, CH_2Cl), 4.09–4.55 (br, Cp + CH_2N), 7.24 (br, aromatic DMAP), 8.62–8.90 ppm (br, aromatic DMAP). ^{13}C NMR ([D_7]DMF, 100 MHz): $\delta = -$ 2.4 ($SiCH_3$), 1.1–1.9 ($SiMe_2O$), 13.3 (*n*Bu), 14.7 ($SiCH_2$), 18.9 (*n*Bu), 26.5 (*n*Bu), 27.4 (*n*Bu), 29.2 (CH_2), 40.7 ($N(CH_3)_2$), 49.5 (CH_2Cl), 60.8 (CH_2N), 71.5 (*ipso*-Cp), 72.6 (Cp), 74.6 (Cp), 108.9 (aromatic DMAP), 143.8 (aromatic DMAP), 157.4 ppm (aromatic DMAP). ^{29}Si NMR ([D_7]DMF, 79.3 MHz): $\delta = -5.4$ and −5.0 (fcSi(Me)-$CH_2CH_2CH_2Cl$ + fcSi(Me)$CH_2CH_2CH_2N$), −23.0 to −21.5 ppm ($SiMe_2O$).

The copolymer gyration diameter was estimated to be 7–10 nm based on light-scattering studies of PFS materials.[20]

Microscopy and Light Scattering: Solutions of polymer **4** were prepared by dissolving the sample in water at a concentration of 0.5 $mg mL^{-1}$ and filtering the solution with a 0.2 μm filter. Scattering intensity was recorded at a scattering angle of 90°. TEM was performed with comparably prepared solutions at the same concentration. Samples were prepared by three methods. In the first, a drop of solution was placed on a carbon-coated copper grid and excess solution was removed by blotting with filter paper. In the second method, a drop of solution was placed on a carbon-coated copper grid

 © 2004 Wiley-VCH Verlag GmbH & Co. KGaA, Weinheim

lying on a metal block cooled by LN2. Once the drop was solidified, it was immediately placed in vacuo until the solvent was completely removed. The third method involved placing a 2 μL drop of sample onto a carbon-coated copper grid that was then rapidly plunged into LE at −196 °C. The sample was then freeze-dried by placing the resultant vitrified sample on a metal block kept in equilibrium with LN2 and placed under vacuum until the solvent was fully sublimed. TEM images were obtained on a Phillips CM12 electron microscope operated at an accelerating voltage of 120 kV (for samples of **4** quenched in LN2 or prepared by the "as-dropped" method) or a Zeiss EM902 electron spectroscopic microscope operated at an accelerating voltage of 80 kV and $\Delta E = 150$ eV (for samples of **4** quenched in LE).

Electrochemistry: Cyclic voltammetry was performed on a BAS 1000 B/W instrument with a Ag/AgCl electrode as a reference. The solution was $\approx 10^{-4}$ M of **4** in 0.01M aqueous NaCl. The peak potentials were 0.51 V (ox) and 0.42 V (red).

Received: September 8, 2003 [Z52819]

Keywords: block copolymers · liposomes · nanostructures · ring-opening polymerization · self-assembly

[1] a) M. Antonietti, C. Göltner, *Angew. Chem.* **1997**, *109*, 944; *Angew. Chem. Int. Ed. Engl.* **1997**, *36*, 910; b) P. Alexandridis, R. J. Spontak, *Curr. Opin. Colloid Interface Sci.* **1999**, *4*, 130; c) P. Alexandridis, B. Lindman, *Amphiphilic Block Copolymers: Self-Assembly and Applications*, Elsevier, Amsterdam, **2000**. d) S. Förster, B. Berton, H. P. Hentze, E. Krämer, M. Antonietti, P. Lindner, *Macromolecules* **2001**, *34*, 4610.

[2] For examples of recent work on nonspherical morphologies of block copolymers in solution, see a) L. Zhang, A. Eisenberg, *J. Am. Chem. Soc.* **1996**, *118*, 3168; b) K. Yu, C. Bartels, A. Eisenberg, *Langmuir* **1999**, *15*, 7157; c) X. H. Yan, G. J. Liu, F. T. Liu, B. Z. Tang, H. Peng, A. B. Pakhomov, C. Y. Wong, *Angew. Chem.* **2001**, *113*, 3705; *Angew. Chem. Int. Ed.* **2001**, *40*, 3593; d) Y. Y. Won, H. D. Davis, F. S. Bates, *Science* **1999**, *283*, 960; e) S. Stewart, G. Liu, *Angew. Chem.* **2000**, *112*, 348; *Angew. Chem. Int. Ed.* **2000**, *39*, 340; f) L. Zhang, A. Eisenberg, *Science* **1995**, *268*, 1728; g) J. P. Spatz, S. Mössmer, M. Möller, *Angew. Chem.* **1996**, *108*, 1673; *Angew. Chem. Int. Ed. Engl.* **1996**, *35*, 1510.

[3] a) A.-Y. A. I. Lebdeh, P. M. Budd, V. M. Nace, *J. Mater. Chem.* **1998**, *8*, 1839; b) R. Gref, Y. Minamitake, M. T. Peracchia, V. Trubetskoy, V. Torchilin, R. Langer, *Science* **1994**, *263*, 1600.

[4] a) S. Y. Liu, S. P. Armes, *Angew. Chem.* **2002**, *114*, 1471; *Angew. Chem. Int. Ed.* **2002**, *41*, 1413.b) S. Y. Liu, N. C. Billingham, S. P. Armes, *Angew. Chem.* **2001**, *113*, 2390; *Angew. Chem. Int. Ed.* **2001**, *40*, 2328; c) V. Bütün, S. P. Armes, N. C. Billingham, Z. Tuzar, A. Rankin, J. Eastoe, R. K. Heenan, *J. Am. Chem. Soc.* **2001**, *123*, 9910; d) A. V. Kabanov, T. K. Bornich, V. A. Kabanov, K. Yu, A. Eisenberg, *J. Am. Chem. Soc.* **1998**, *120*, 9941; e) J. Zhu, A. Eisenberg, R. B. Lennox, *J. Am. Chem. Soc.* **1991**, *113*, 5583; f) F. Henselwood, G. Liu, *Macromolecules* **1997**, *30*, 488; g) J. F. Gohy, N. Willet, S. Varshney, J. X. Zhang, R. Jerome, *Angew. Chem.* **2001**, *113*, 3314; *Angew. Chem. Int. Ed.* **2001**, *40*, 3214; h) K. L. Wooley, *Chem. Eur. J.* **1997**, *3*, 1397.

[5] Recent works on the self-assembly of metal-containing block copolymers include a) S. J. Hou, W. K. Chan, *Macromol. Rapid Commun.* **1999**, *20*, 440; b) S. J. Hou, K. Y. K. Man, W. K. Chan, *Langmuir* **2003**, *19*, 2485; c) C. M. Park, J. E. McAlvin, C. L. Fraser, E. L. Thomas, *Chem. Mater.* **2002**, *14*, 1225; d) J. F. Gohy, B. G. G. Lohmeijer, S. K. Varshney, U. S. Schubert, *Macromolecules* **2002**, *35*, 7427; e) J. F. Gohy, H. Hofmeier, A. Alexeev, U. S. Schubert, *Macromol. Chem. Phys.* **2003**, *204*, 1524.

[6] I. Manners, *Science* **2001**, *294*, 1664.

[7] a) R. Rulkens, Y. Z. Ni, I. Manners, *J. Am. Chem. Soc.* **1994**, *116*, 12121; b) Y. Ni, R. Rulkens, I. Manners, *J. Am. Chem. Soc.* **1996**, *118*, 4102.

[8] a) J. A. Massey, K. N. Power, M. A. Winnik, I. Manners, *Adv. Mater.* **1998**, *10*, 1559; b) J. A. Massey, M. A. Winnik, I. Manners, V. Z.-H. Chan, J. M. Ostermann, R. Enchelmaier, J. P. Spatz, M. Möller, *J. Am. Chem. Soc.* **2001**, *123*, 3147; c) J. Raez, I. Manners, M. A. Winnik, *J. Am. Chem. Soc.* **2002**, *124*, 10381.

[9] a) L. Luo, A. Eisenberg, *J. Am. Chem. Soc.* **2001**, *123*, 1012; b) D. E. Discher, A. Eisenberg, *Science* **2002**, *297*, 967.

[10] a) P. Gómez-Elipe, P. M. Macdonald, I. Manners, *Angew. Chem.* **1997**, *109*, 780; *Angew. Chem. Int. Ed. Engl.* **1997**, *36*, 762; b) P. Gómez-Elipe, R. Resendes, P. M. Macdonald, I. Manners, *J. Am. Chem. Soc.* **1998**, *120*, 8348.

[11] K. N. Power-Billard, I. Manners, *Macromol. Rapid Commun.* **2002**, *23*, 607.

[12] P. Echlin, *Low-Temperature Microscopy and Analysis*, Plenum, New York, **1992**.

[13] P. Terech, A. de Geyer, B. Struth, Y. Talmon, *Adv. Mater.* **2002**, *14*, 495.

[14] J. R. Harris, *Negative Staining and Cryoelectron Microscopy: The Thin Film Techniques*, Bios Scientific, Oxford, **1997**.

[15] a) A. Du Chesne, *Macromol. Chem. Phys.* **1999**, *200*, 1813; b) R. Thomann, R. J. Spontak in *Science, Technology and Education of Microscopy: An Overview* (Ed.: A. Mendez-Vilas), Formatex, Badajoz, Spain, **2003**, pp. 249–254.

[16] a) Y. Kakizawa, H. Sakai, A. Yamaguchi, Y. Kondo, N. Yoshino, M. Abe, *Langmuir* **2001**, *17*, 8044; b) T. Saji, K. Hoshino, S. Aoyagui, *J. Am. Chem. Soc.* **1985**, *107*, 6865.

[17] The presence of a single wave is anticipated based on the formation of ion pairs between ferrocenium units and the chloride anions in the supporting electrolyte, which reduces any metal–metal interactions present: see a) R. Rulkens, A. J. Lough, I. Manners, S. R. Lovelace, C. Grant, W. E. Geiger, *J. Am. Chem. Soc.* **1996**, *118*, 12683; b) F. Barriere, N. Camire, W. E. Geiger, U. T. Mueller-Westerhoff, R. Sanders, *J. Am. Chem. Soc.* **2002**, *124*, 7262.

[18] K. N. Power-Billard, T. J. Peckham, A. Butt, F. Jäkle, I. Manners, *J. Inorg. Organomet. Polym.* **2000**, *10*, 157.

[19] Halide substitution reactions on PFS materials have previously been shown to take place without any significant molecular-weight decline. See, for example, a) K. N. Power-Billard, I. Manners, *Macromolecules* **2000**, *33*, 26; b) D. L. Zechel, K. C. Hultszch, R. Rulkens, B. Balaishis, Y. Ni, J. K. Pudelski, A. J. Lough, I. Manners, *Organometallics* **1996**, *15*, 1972.

[20] J. A. Massey, K. Kulbaba, M. A. Winnik, I. Manners, *J. Polym. Sci. Polym. Phys. Part B* **2000**, *28*, 3032.

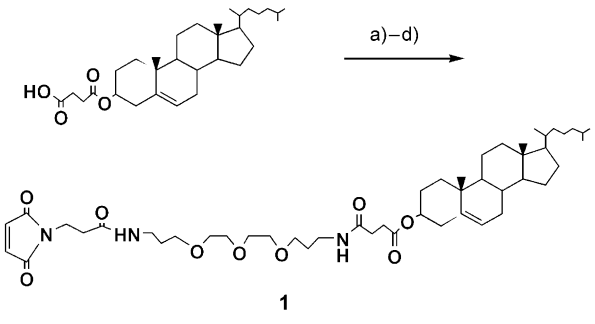
 © 2004 Wiley-VCH Verlag GmbH & Co. KGaA, Weinheim

Soft Materials

Vesicular Latex**

Fredric M. Menger, Jianwei Bian, and Victor A. Seredyuk*

Hydrophobic attraction among projecting lipid chains assembles vesicles into long "strings" capable of gelating water.[1] Exposure to shear stress reversibly disrupts the hydrophobic association, thus breaking the strings and fluidizing the gel. The question arose as to whether vesicles can be joined covalently to render the gels more robust.[2–5] Toward this end we synthesized compound **1** (Scheme 1) in which a vesicle-



Scheme 1. Synthesis of compound **1**. a) $(COCl)_2$; b) $BocNH(CH_2)_3O(CH_2)_2O(CH_2)_3NH_2$; c) TFA, CH_2Cl_2; d) succinimido-3-maleimidopropanoate. Boc = *tert*-butoxycarbonyl, TFA = trifluoroacetic acid.

binding unit (a cholesterol derivative) is attached by a spacer to a maleimide group to which thiols are known to readily undergo Michael addition.[6,7]

When lipid dispersions containing **1** were exposed to dithiothreitol (Cleland's reagent), a room-temperature reaction ensued that interconnected the vesicles [Eq. (1)] to give a material resembling shaving cream in consistency. Its characterization constitutes the basis of this communication.

A more detailed preparation of the new soft material follows. Solutions of DPPC[8] (1.46 mL, 10 mg mL^{-1}), DOPG[8] (88.4 μL, 10 mg mL^{-1}), and **1** (464 μL, 2 mg mL^{-1}) in $CHCl_3$ were added to a 10-mL flask. The solvent was removed by evaporation and vacuum drying, after which degassed phosphate buffer (pH 7; 1 mL) was added and the mixture was either stirred for 10 min (400 rpm) or bath-sonicated for 15 min, to form polydisperse vesicular structures. According to dynamic light-scattering analysis, the vesicles averaged 200 nm in diameter. Finally, dithiothreitol (146 μL, 0.58 mg mL^{-1} in buffer) was added, and the mixture was stirred magnetically under N_2 at high speed (1100 rpm) for 24 h at room temperature to give a thick cream. Only a fluid opalescent suspension of particulate lipid was obtained when dithiothreitol was omitted from the preparation.

The lipid/**1** ratio was such that, prior to cross-linking, a component vesicle with 10000 lipid molecules would contain 550 cross-linking sites. Sufficient dithiothreitol was added to react with all the maleimide units. If, after the addition of dithiothreitol, stirring was set at slow speeds (250 and 550 rpm), then only fluid suspensions were observed. On the other hand, cross-linking with rapid stirring produced a thick, white, slow-flowing cream, as seen in the inverted vial in Figure 1.

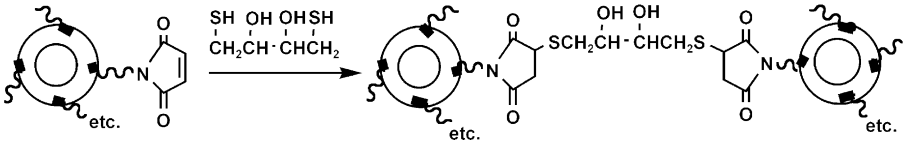


Figure 1. An inverted vial containing cross-linked product.

Examination by phase-contrast microscopy (Nikon Diaphot-TMD inverted microscope) showed that the material is composed of round, densely packed particles ranging from 5–150 μm in diameter (Figure 2). For brevity we call this material a "latex" as a result of its superficial resemblance to colloidal dispersions of polymer particles given that name.

Detailed photos taken by phase-contrast microscopy (Figure 3 A) revealed an unusual "blistered" texture of the particle surface. Confocal microscopy (Figure 3 B, Zeiss 510 Meta laser scanning confocal microscope, $\lambda = 488$ nm) showed more clearly that the blisters (nonremovable by suction with a micropipette) are indeed integrated with the particle surface.

When the sample preparation was carried out at 55 °C (exceeding by 14 °C the gel-to-liquid-crystal transition temperature T_m of DPPC), then only a translucent liquid containing no microscopically visible particles was produced. Absence of latex formation high above the T_m value was also seen with POPC[8] ($T_m = -2.5$ °C) when the synthesis was performed at room temperature with this lipid instead of DPPC.



(1)

Three possibilities presented themselves. The particles could be solid lipid or they could be lipid shells filled either with water or with air (as in a conventional foam). All the evidence points to hollow, water-filled structures: a) No volume increase was observed. Such an increase would be expected if the material was a conventional foam with air-filled "bubbles". b) Since the preparation was carried out in water, the water must logically reside within the particles making up the dense material. c) Dilution with water

[*] Prof. F. M. Menger, J. Bian, Dr. V. A. Seredyuk
Department of Chemistry
Emory University
Atlanta, GA 30322 (USA)
Fax: (+1) 404-727-6586
E-mail: menger@emory.edu

[**] This research was supported by the National Institutes of Health. We thank Dr. Robert P. Apkarian and Ashley L. Galloway for the high-resolution scanning-electron-microscopy picture.

 DOI: 10.1002/anie.200352936 © 2004 Wiley-VCH Verlag GmbH & Co. KGaA, Weinheim

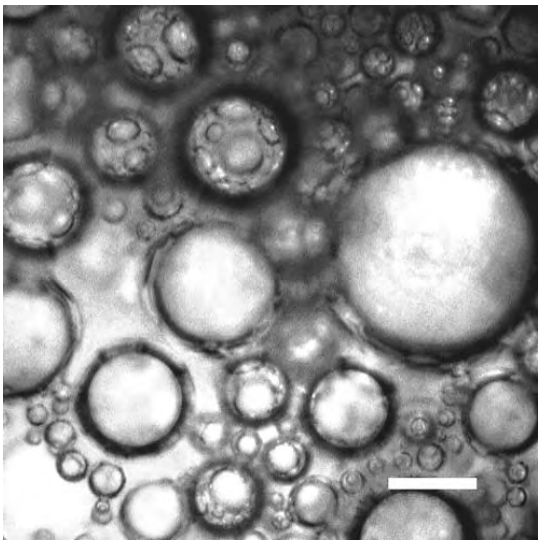


Figure 2. Phase-contrast photomicrograph of a latex smear showing a high particle density. The tops of the larger particles are out of focus. The bar represents 40 μm.

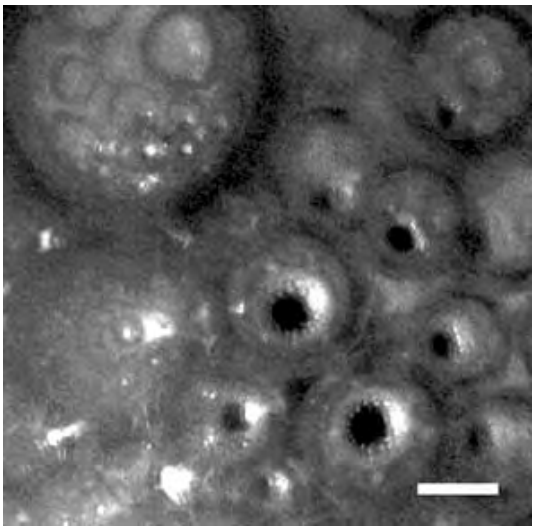
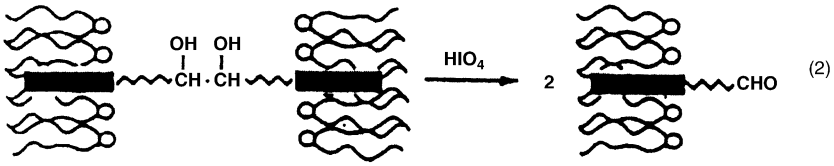


Figure 4. Latex particles showing open pores, as seen by phase-contrast microscopy. The bar represents 30 μm.

produced individual particles that sank rather than floated, a result suggesting the absence of air. d) The particles are tough and, rather than bursting when dragged through water or compressed by a cover slip, merely deform from their spherical shape. e) On occasion, particles are seen with an apparent opening to a hollow sphere (Figure 4). Being hollow, the particle morphology offers the possibility of a useful encapsulation system[9] which is simple, cheap, and endowed with a particularly high capture volume.



(2)

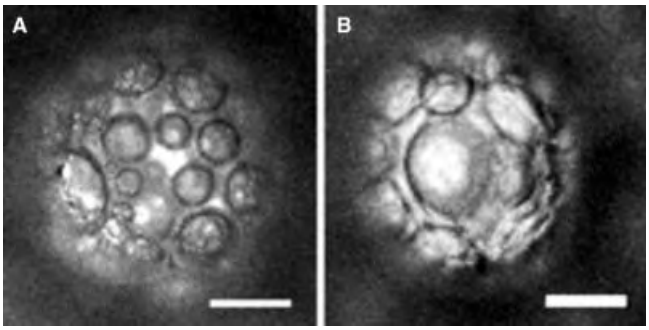


Figure 3. Organic synthesis and self-assembly combine to form the exotic structures seen by A) phase-contrast microscopy and B) confocal microscopy. The bars represent 50 μm.

No change in the material was observed after bath-sonication for 45 min. On the other hand, the vesicular latex particles disintegrate into tiny ill-defined fragments (not shown) upon exposure to periodate (50 μL, 0.1M added to microscope slide). Periodate rapidly cleaves the central C–C bond of the spacer's glycol unit,[10] and this allows the particle constituents to disconnect. The interconnected bilayers are thereby "depolymerized" [Eq. (2)].

The response of the latex particle morphology to drying and freezing was examined next. Slow evaporative drying of a latex cream led to compression and distortion of the spheres (Figure 5A) and ultimately to a dry film (Figure 5B) where small vesicular substructures are visible at the hexagonal peripheries. Freezing of the latex samples causes the particles to divide into small particles that have lost their blistered texture (Figure 5C). As the sample warms up, the particles fuse (Figure 5D) but remain smooth until the original size and mottled appearance are reestablished above the T_m value of 14 °C (DPPC). The blisters are apparently associated with the liquid-crystalline state above the T_m value requiring more space per lipid than the gel state does below the T_m value.

Finally, we carried out high-resolution scanning electron microscopy studies (HRSEM; Figure 6). The photomicrographs showed that the water-filled vesicular latex particles had burst under the high-vacuum conditions. The thickness of the particle shells is < 100 nm. We surmise that the film consists of < 25 lipid bilayers (formed from the shearing of vesicles under the high-speed stirring) in which small vesicles (< 100 nm; visible in Figures 4–6) are embedded. The lamellar/vesicular composite is bonded together by the cross-linking agent.

Experimental Section

1: Oxalyl chloride (3 g, 23.6 mol) was added to cholesteryl hemisuccinate (0.56 g, 1.15 mmol) in CH_2Cl_2 (30 mL), and the mixture was stirred at room temperature for 12 h to give the acid chloride in 98%

 © 2004 Wiley-VCH Verlag GmbH & Co. KGaA, Weinheim

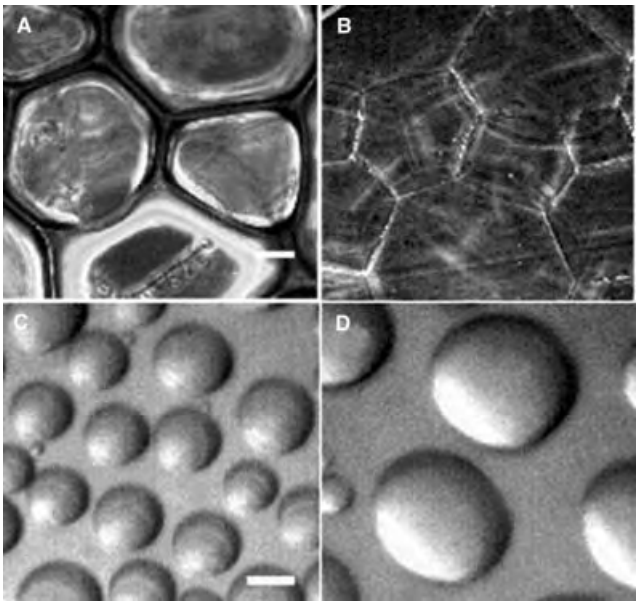


Figure 5. Phase-contrast micrographs of: A) Partial and B) total drying of a vesicular latex; C) a frozen sample of a vesicular latex; D) fused particles of the sample shown in (C) during partial thawing. The bar represents 25 μm. At room temperature the blistered structures of Figure 3 reappear.

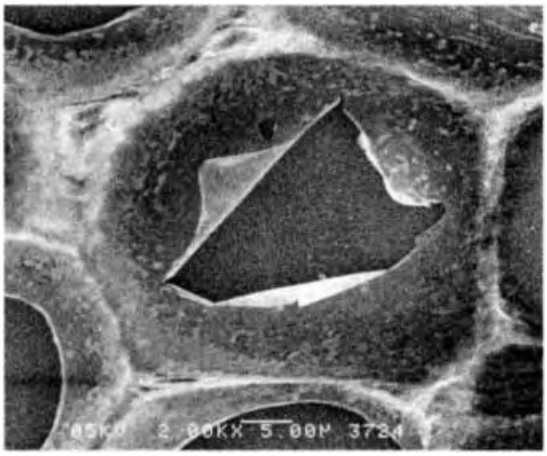


Figure 6. HRSEM photomicrograph of a ruptured latex particle at 2000× enlargement. The bar (7 mm) represents 5 μm. As in Figure 5A, the particles have been forced into proximity by drying.

yield. $(Boc)_2O$ (1.98 g, 9.08 mmol) in $CHCl_3$ (60 mL) was added to 4,7,10-trioxa-1,13-tridecanediamine (10 g, 45.4 mmol) in $CHCl_3$ (100 mL), and the mixture was heated to reflux for 24 h. Purification by chromatography ($MeOH/CH_2Cl_2/NH_4OH$ (5:5:1) over silica) gave 70% of the monoprotected diamine. The acid chloride product of the first reaction (0.4 g, 0.79 mmol) in $CHCl_3$ (20 mL) was added to a mixture of this diamine compound (0.25 g, 0.78 mmol) and Et_3N (0.26 g, 2.34 mmol) in $CHCl_3$ (30 mL). This resulting mixture was then stirred at room temperature for 20 h. Chromatographic purification (CH_2Cl_2/MeOH (10:1)) gave the monoprotected diamine–cholesterol conjugate in 85% yield. Trifluoroacetic acid (1 g, 8.77 mmol) was added to the conjugate (0.2 g, 0.25 mmol) in CH_2Cl_2 (20 mL), and the mixture was stirred for 6 h, washed with 5 N $NaHCO_3$, dried over $MgSO_4$, and stripped of solvent to quantitatively remove the Boc group on the terminal amine. The deprotected product (0.63 g, 0.92 mmol) in *N*,*N*-dimethylformamide (DMF; 30 mL) was added to succinimido-3-maleimidopropanoate (0.32 g, 1.2 mmol) plus Et_3N (0.35 g, 3 mmol) in DMF (12 mL), and the resulting mixture was stirred for 12 h. Purification of the final product **1** (following removal of the solvent) was effected by gradient elution chromatography ($MeOH/CHCl_3$, 10→33%). The structures of the protected cholesterol conjugate, the deprotected conjugate, and compound **1** were all affirmed by ^1H NMR spectroscopy, HRMS, and elemental analysis. For example, for **1**: HRMS: calcd for $C_{48}H_{77}O_9N_3$ [M+Li^+]: 846.5820; found 846.5790; elemental analysis: calcd for $C_{48}H_{77}O_9N_3$: C 68.62, H 9.24, N 5.00; found: C 68.47, H 9.36, N 4.81.

Received: September 23, 2003 [Z52936]

Keywords: cross-linking · nanoparticles · self-assembly · soft materials · vesicles

[1] F. M. Menger, A. V. Peresypkin, *J. Am. Chem. Soc.* **2003**, *125*, 5340.
[2] H. Hayashi, K. Kono, T. Takagishi, *Bioconjugate Chem.* **1998**, *9*, 382.
[3] H. Bader, K. Dorn, B. Hupfer, H. Ringsdorf, *Adv. Polym. Sci.* **1985**, 64.
[4] A. A. Yaroslavov, O. Yu. Udalykh, N. S. Melik-Nubarov, V. A. Kabanov, Y. A. Ermakov, V. A. Azov, F. M. Menger, *Chem. Eur. J.* **2001**, *7*, 4835.
[5] S. A. Walker, J. A. Zasadzinski, *Langmuir* **1997**, *13*, 5076.
[6] J. T. Elliott, G. D. Prestwich, *Bioconjugate Chem.* **2000**, *11*, 832.
[7] M. D. Partis, D. G. Griffiths, G. C. Roberts, R. B. Beechey, *J. Protein Chem.* **1983**, *2*, 263.
[8] DPPC = 1,2-dipalmitoyl-*sn*-glycero-3-phosphocholine, DOPG = 1,2-dioleoyl-*sn*-glycero-3-phosphoglycerol, POPC = 1-palmitoyl-2-oleoyl-*sn*-glycero-3-phosphocholine (from Avanti).
[9] D. D. Lasic, *Liposomes: From Physics to Applications*, *Part III*, Elsevier, Amsterdam, **1993**.
[10] Z. Skrzypczynski, S. Wayland, *Bioconjugate Chem.* **2003**, *14*, 642.

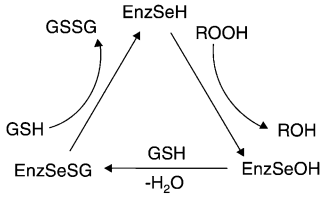
 © 2004 Wiley-VCH Verlag GmbH & Co. KGaA, Weinheim

Enzyme Mimetics

The Exceptional Glutathione Peroxidase-Like Activity of Di(3-hydroxypropyl) Selenide and the Unexpected Role of a Novel Spirodioxaselenanonane Intermediate in the Catalytic Cycle**

Thomas G. Back, Ziad Moussa, and Masood Parvez*

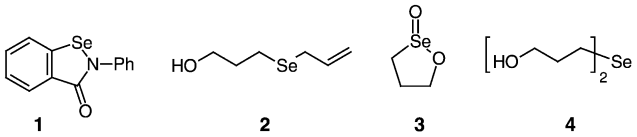
Oxidative stress results from the formation of peroxides and other reactive oxygen species during the course of normal aerobic metabolism.[1] These reactive intermediates and the free radicals they produce cause damage to various biologically important molecules present in cells. Peroxides have been implicated in a number of degenerative processes and disease states, including inflammation, mutagenesis, and cancer, atherosclerosis, Alzheimer's disease, and the aging process.[2] Glutathione peroxidase (GPx) is a selenoenzyme that protects cells by catalyzing the reduction of peroxides with the stoichiometric reductant glutathione.[3] The catalytic cycle of the enzyme is shown in Scheme 1 and involves the



Scheme 1. Catalytic cycle of glutathione peroxidase (EnzSeH). GSH = glutathione.

reduction of a peroxide molecule by the selenol moiety of a selenocysteine residue of the enzyme, followed by reduction of the corresponding selenenic acid with glutathione. The resulting selenenyl sulfide then reacts with a second mole equivalent of glutathione to regenerate the original selenol and the disulfide of glutathione.

In view of the biological importance of GPx as a natural protective agent against oxidative stress, considerable effort has been expended to discover small-molecule selenium compounds that emulate GPx.[4] One such compound, ebselen (**1**),[5] has undergone clinical trials as an antiinflammatory agent. Ebselen and many other GPx mimetics that have been studied contain a covalent Se–N bond or an amino substituent capable of coordinating with the selenium atom at various stages of its redox cycle.[6,7] Aryl selenides generally display poor catalytic activity in the thiol-mediated reduction of peroxides,[7] while alkyl selenides are prone to decomposition by *syn* elimination of their corresponding selenoxides. However, we recently reported that allyl 3-hydroxypropyl selenide (**2**) possesses remarkably high GPx-like activity (ca. one order of magnitude greater than that of ebselen) by producing the corresponding cyclic seleninate **3** in situ by a series of oxidation and [2,3] sigmatropic rearrangement steps.[8] Seleninate **3** then serves as the true catalyst and is recovered at the end of the catalytic cycle. These experiments revealed that O–Se compounds can be even more effective catalysts than the more widely studied N–Se analogues. We now report that di(3-hydroxypropyl) selenide (**4**)[9] serves as a highly effective GPx mimetic and functions by a remarkable mechanism that involves a novel spirodioxaselenanonane as an intermediate.



1 **2** **3** **4**

In the course of our studies on GPx mimetics, we have employed a model system in which excess *tert*-butyl hydroperoxide (*t*BuOOH) is treated with benzyl thiol (BnSH), which serves as the sacrificial reductant, in the presence of 10 mol% of the selenium-containing catalyst at 18 °C.[6g,8] The reaction is easily followed by HPLC with naphthalene as an internal standard, and the time ($t_{1/2}$) required for the oxidation of 50% of the thiol to its disulfide (BnSSBn) provides a convenient means for comparing the effectiveness of various catalysts. Thus, under identical conditions, **4** gave $t_{1/2} = 2.9$ h, compared with 4.8 h for **2**, 2.5 h for **3**, 42 h for **1,** and >300 h for a control reaction conducted in the absence of a catalyst (see Figure 1).[10]

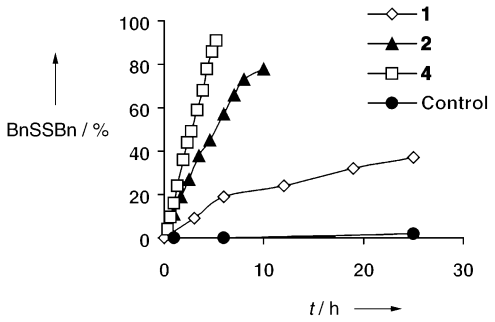


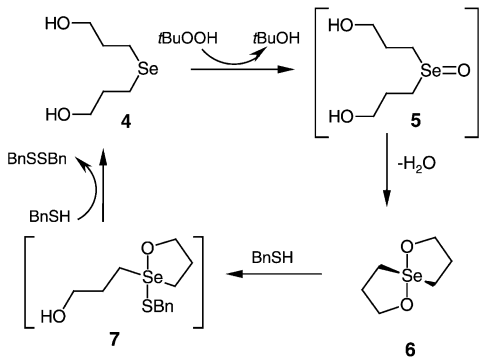
Figure 1. Rates of formation of BnSSBn from oxidation of BnSH (0.031 M) with 90% aqueous *t*BuOOH (0.043 M) in the presence of catalysts **1**, **2**, and **4** (0.0031 M) in dichloromethane/methanol (95:5) at 18 °C.

Further investigation revealed that selenide **4** was, as expected, inert toward BnSH but reacted rapidly (complete reaction in less than 5 min) with excess *t*BuOOH in the absence of the thiol to afford the novel spirodioxaselenanonane **6** quantitatively (see Scheme 2). The latter product could be readily isolated and stored at −5 °C. When **6** was subjected to our assay with excess *t*BuOOH and BnSH, it displayed the same $t_{1/2}$ as the original selenide **4** and was the

[*] Prof. Dr. T. G. Back, Z. Moussa, Dr. M. Parvez
Department of Chemistry
University of Calgary
Calgary, AB T2N1N4 (Canada)
Fax: (+1) 403-289-9488
E-mail: tgback@ucalgary.ca

[**] We thank the Natural Sciences and Engineering Research Council of Canada for financial support.

 © 2004 Wiley-VCH Verlag GmbH & Co. KGaA, Weinheim DOI: 10.1002/anie.200353128



Scheme 2. Catalytic cycle of selenide **4** and spirodioxaselenanonane **6**.

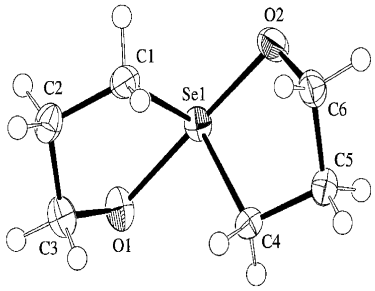
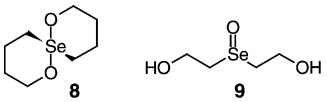


Figure 2. X-ray crystal structure of **6** (ORTEP diagram).

sole selenium-containing product that remained in the mixture upon completion of the reaction. This confirms its catalytic role in the process. Moreover, when **6** was treated with 2 mol BnSH in the absence of *t*BuOOH, it rapidly afforded the disulfide BnSSBn and regenerated selenide **4** quantitatively. Based on these observations, we propose that the catalytic activity of selenide **4** is the result of the mechanism shown in Scheme 2. Evidently, oxidation of **4** with *t*BuOOH produces the transient selenoxide **5**, which spontaneously cyclizes to give the dioxaselenanonane **6**, as confirmed by the control experiment conducted in the absence of the thiol. In the presence of BnSH, however, we propose that **6** undergoes substitution of one alkoxy group to produce intermediate **7**, followed by reductive elimination with a second equivalent of thiol to regenerate selenide **4** along with BnSSBn.[11] In the presence of excess *t*BuOOH, **4** is recycled to **6** and the catalytic process continues.

The homologous di(2-hydroxyethyl) and di(4-hydroxybutyl) selenides were also investigated under similar conditions. The latter afforded the corresponding dioxaselenaundecane **8**, which showed lower catalytic activity ($t_{1/2} = 5.1$ h) than **6**. On the other hand, the 2-hydroxyethyl derivative produced only the corresponding selenoxide **9** when oxidized with *t*BuOOH. Failure of **9** to cyclize under the usual conditions is attributed to the increased strain in the corresponding spiro compound.



The novel dioxaselenanonane **6**[12] was fully characterized by spectroscopic methods and by X-ray crystallography.[13] The X-ray structure revealed that the O-Se-O moiety is roughly linear with a bond angle of 172.99°, while the C-Se-C bond angle is only 102.95° (Figure 2). Thus, the oxygen atoms occupy the apical positions of a distorted trigonal bipyramid centered around the selenium atom, while the carbon substituents and the selenium lone pair occupy the equatorial positions.

These experiments reveal that selenide **4** is a remarkably potent catalyst for the reduction of *t*BuOOH with BnSH, displaying a half-life that is 14.5 times shorter than that of the widely studied compound ebselen (**1**) under the same conditions. This is especially noteworthy because the mechanism for the present process proceeds via the unusual spirodioxaselenanonane **6** and is thus distinct from that employed by GPx itself and by many of its small-molecule mimetics.

Experimental Section

6: *tert*-Butyl hydroperoxide (0.47 mL, 3.4 mmol, 70 %) was added to a solution of di(3-hydroxypropyl) selenide (300 mg, 1.52 mmol) in 10 mL dichloromethane, and the mixture was stirred at room temperature for 17 h. The solvent was removed in vacuo, and the residue was purified by chromatography (elution with 30 % methanol/ethyl acetate) to afford 260 mg (87 %) of the product as a colorless oil, which solidified upon standing. IR (neat): $\tilde{\nu} = 1052$, 785 cm^{-1}; ^1H NMR (200 MHz, $CDCl_3$): $\delta = 4.08$–3.90 (m, 2H), 3.88–3.70 (m, 2H), 3.39–2.98 (m, 4H), 2.17–1.78 ppm (m, 4H); ^{13}C NMR (50 MHz, $CDCl_3$): $\delta = 65.4$, 42.2, 27.3 ppm; ^{77}Se NMR ($CDCl_3$): $\delta = 769.0$ ppm (relative to Me_2Se at $\delta = 0.0$ ppm); MS: *m*/*z* (%): 196 (3, M^+), 195 (6), 138 (62), 107 (100), 58 (65); Exact mass calcd for $C_6H_{12}O_2{}^{80}Se$: 196.0003; found: 196.0007; Anal. calcd for $C_6H_{12}O_2Se$: C 36.93, H 6.20; found: C 36.80, H 6.40.

Received: October 21, 2003 [Z53128]

Keywords: oxidative stress · peroxidases · selenium · spiro compounds · thiols

[1] a) *Oxidative Stress* (Ed.: H. Sies), Academic Press, London, **1985**; b) *Free Radicals and Oxidative Stress: Environment, Drugs and Food Additives* (Eds.: C. Rice-Evans, B. Halliwell, G. G. Lunt), Portland Press, London, **1995**; c) *Oxidative Processes and Antioxidants*, (Eds.: R. Paoletti, B. Samuelsson, A. L. Catapano, A. Poli, M. Rinetti), Raven Press, New York, **1994**; d) H. Sies, *Exp. Physiol.* **1997**, *82*, 291; e) H. Sies, *Eur. J. Biochem.* **1993**, *215*, 213; f) L.-O. Klotz, K.-D. Kroncke, D. P. Buchczyk, H. Sies, *J. Nutr.* **2003**, *133*, 1448.

[2] a) *Free Radicals in Biology, Vol. 1–5* (Ed.: W. A. Pryor), Academic Press, New York, **1976–1982**; b) *Free Radicals in Molecular Biology, Aging and Disease* (Eds.: D. Armstrong, R. S. Sohal, R. G. Cutler, T. F. Slater), Raven Press, New York, **1984**; c) B. Halliwell in *Oxygen Radicals and the Disease Process* (Eds.: C. E. Thomas, B. Kalyanaraman), Harwood, Amsterdam, **1997**, pp. 1–14; d) B. Halliwell, *Free Radical Res.* **1999**, *31*, 261; e) J. M. C. Gutteridge, B. Halliwell, *Ann. N. Y. Acad. Sci.* **2000**, *899*, 136.

[3] a) *Selenium in Biology and Human Health* (Ed.: R. F. Burk), Springer, New York, **1994**; b) H. E. Ganther, *Chem. Scr.* **1975**, *8*,

 © 2004 Wiley-VCH Verlag GmbH & Co. KGaA, Weinheim

79; c) H. E. Ganther, R. J. Kraus in *Methods in Enzymology, Vol. 107* (Eds.: S. P. Colowick, N. O. Kaplan), Academic Press, New York, **1984**, pp. 593–602; d) T. C. Stadtman, *J. Biol. Chem.* **1991**, *266*, 16257; e) A. L. Tappel, *Curr. Top. Cell. Regul.* **1984**, *24*, 87; f) L. Flohé, *Curr. Top. Cell. Regul.* **1985**, *27*, 473; g) O. Epp, R. Ladenstein, A. Wendel, *Eur. J. Biochem.* **1983**, *133*, 51.

[4] For recent reviews, see: a) G. Mugesh, W.-W. du Mont, H. Sies, *Chem. Rev.* **2001**, *101*, 2125; b) G. Mugesh, H. B. Singh, *Chem. Soc. Rev.* **2000**, *29*, 347; c) G. Mugesh, W.-W. du Mont, *Chem. Eur. J.* **2001**, *7*, 1365.

[5] a) A. Müller, E. Cadenas, P. Graf, H. Sies, *Biochem. Pharmacol.* **1984**, *33*, 3235; b) A. Wendel, M. Fausel, H. Safayhi, G. Tiegs, R. Otter, *Biochem. Pharmacol.* **1984**, *33*, 3241; c) M. J. Parnham, S. Kindt, *Biochem. Pharmacol.* **1984**, *33*, 3247; d) A. Müller, H. Gabriel, H. Sies, *Biochem. Pharmacol.* **1985**, *34*, 1185; e) H. Safayhi, G. Tiegs, A. Wendel, *Biochem. Pharmacol.* **1985**, *34*, 2691; f) A. Wendel, G. Tiegs, *Biochem. Pharmacol.* **1986**, *35*, 2115; g) H. Fischer, N. Dereu, *Bull. Soc. Chim. Belg.* **1987**, *96*, 757; h) G. R. M. M. Haenen, B. M. De Rooij, N. P. E. Vermeulen, A. Bast, *Mol. Pharmacol.* **1990**, *37*, 412; i) R. S. Glass, F. Farooqui, M. Sabahi, K. W. Ehler, *J. Org. Chem.* **1989**, *54*, 1092.

[6] For examples of Se–N compounds as GPx mimetics, see: a) Y. Liu, B. Li, L. Li, H.-Y. Zhang, *Helv. Chim. Acta* **2002**, *85*, 9; b) H. J. Reich, C. P. Jasperse, *J. Am. Chem. Soc.* **1987**, *109*, 5549; c) P. V. Jacquemin, L. E. Christiaens, M. J. Renson, M. J. Evers, N. Dereu, *Tetrahedron Lett.* **1992**, *33*, 3863; d) I. Erdelmeier, C. Tailhan-Lomont, J.-C. Yadan, *J. Org. Chem.* **2000**, *65*, 8152; e) V. Galet, J.-L. Bernier, J.-P. Hénichart, D. Lesieur, C. Abadie, L. Rochette, A. Lindenbaum, J. Chalas, J.-F. Renaud de la Faverie, B. Pfeiffer, P. Renard, *J. Med. Chem.* **1994**, *37*, 2903; f) M. Iwaoka, S. Tomoda, *J. Am. Chem. Soc.* **1994**, *116*, 2557; g) T. G. Back, B. P. Dyck, *J. Am. Chem. Soc.* **1997**, *119*, 2079.

[7] S. R. Wilson, P. A. Zucker, R.-R. C. Huang, A. Spector, *J. Am. Chem. Soc.* **1989**, *111*, 5936.

[8] a) T. G. Back, Z. Moussa, *J. Am. Chem. Soc.* **2002**, *124*, 12104; b) T. G. Back, Z. Moussa, *J. Am. Chem. Soc.* **2003**, *125*, 13455.

[9] I. Cordova-Reyes, E. VandenHoven, M. Ali, B. M. Pinto, *Can. J. Chem.* **1995**, *73*, 113.

[10] The assay of the catalytic activity and the measurement of the half-life ($t_{1/2}$) of **2**–**4**, **6**, and **8** were performed by the method described in reference [8].

[11] We cannot unequivocally rule out the possibility that both oxygen moieties of **6** are first displaced by BnSH in successive reactions, followed by a reductive elimination of the corresponding dithioselena compound.

[12] Although a few aryl dioxaselena compounds have been reported, they contain aromatic moieties attached to the Se atom or acyloxy instead of alkyloxy Se substituents. The parent compounds **6** and **8** are novel. For examples of aryl and acyldioxy derivatives, see: a) H. J. Reich, *J. Am. Chem. Soc.* **1973**, *95*, 964; b) B. Dahlén, B. Lindgren, *Acta Chem. Scand.* **1973**, *27*, 2218; c) S. Claeson, V. Langer, S. Allenmark, *Chirality* **2000**, *12*, 71; d) J. Drabowicz, J. Luczak, M. Mikolajczyk, Y. Yamamoto, S. Matsukawa, K. Akiba, *Tetrahedron: Asymmetry* **2002**, *13*, 2079; e) J. Zhang, S. Takahashi, S. Saito, T. Koizumi, *Tetrahedron: Asymmetry* **1998**, *9*, 3303; f) F. Ohno, T. Kawashima, R. Okazaki, *Chem. Commun.* **1997**, 1671; g) T. Kawashima, F. Ohno, R. Okazaki, *J. Am. Chem. Soc.* **1993**, *115*, 10434.

[13] X-ray crystallographic data for **6**: $C_6H_{12}O_2Se$, $M_w = 195.12$, monoclinic, space group $P2_1/c$, $a = 9.767(5)$, $b = 8.414(5)$, $c = 8.855(7)$ Å, $\beta = 91.928(3)°$, $V = 727.3(8)$ Å^3, $T = 173(2)$ K, 2573 reflections collected. CCDC-222210 (**6**) contains the supplementary crystallographic data for this paper. These data can be obtained free of charge via www.ccdc.cam.ac.uk/conts/retrieving.html (or from the Cambridge Crystallographic Data Centre, 12, Union Road, Cambridge CB21EZ, UK; fax: (+44) 1223-336-033; or deposit@ccdc.cam.ac.uk).

 © 2004 Wiley-VCH Verlag GmbH & Co. KGaA, Weinheim

Natural Product Synthesis

A Mild and Efficient Synthesis of Oxindoles: Progress Towards the Synthesis of Welwitindolinone A Isonitrile**

*Joseph M. Ready, Sarah E. Reisman, Makoto Hirata, Matthew M. Weiss, Kazuhiko Tamaki, Timo V. Ovaska, and John L. Wood**

Recently, Moore and co-workers reported the isolation and structural elucidation of several oxindole-containing natural products from blue-green algae. Termed the welwitindolinones, this structurally intriguing class of alkaloids displays diverse and valuable biological properties, including multiple drug resistance (MDR) reversing, insecticidal, and antifungal activities.[1] To date, ten congeners have been identified, nine of which contain a 3,4-bridged oxindole core as exemplified by *N*-methyl welwitindolinone C isothiocyanate (**1**). Welwitindolinone A isonitrile (**2**) accounts for the antifungal activity associated with the extracts and is the proposed biosynthetic precursor to welwitindolinones B–D.[1a] Motivated by its antifungal activity, topological complexity, and the possibility of accessing other welwitindolinones (e.g. **1**), we targeted **2** for total synthesis. Herein we report a novel method for the preparation of spiro-oxindoles and its application in a synthesis of an advanced intermediate that contains the complete welwitindolinone A carbon framework.[2]

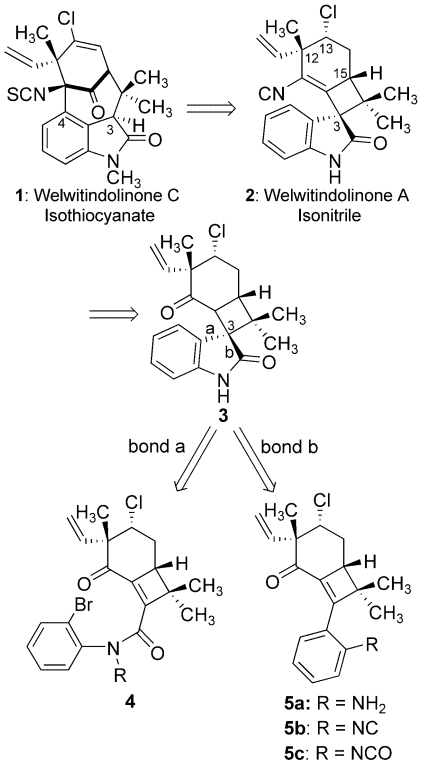
Recognizing that the sensitive vinyl isonitrile region found in **2** could potentially derive from a ketone, we began devising a synthetic approach that targeted **3** as a key intermediate (Scheme 1). For the construction of **3** we envisioned routes that, in a retrosynthetic sense, involved disconnection of either the C3–C_{aryl} bond (Scheme 1, bond a), or the C3–$C_{carbonyl}$ bond (bond b). Although ring formation by closure of bond a (i.e., **4** → **3**) was well precedented in either radical[3] or metal catalyzed modes,[4] concern over the thermal stability of the proposed cyclobutene intermediate and the likelihood that bond formation would occur on the convex face (thus delivering the incorrect stereochemistry at C3) led us to focus on strategies involving formation of bond b (i.e., **5**→**3**). To this end, Pd-catalyzed carbonylative cyclization of aniline **5a** ($R = NH_2$)[5] or radical cyclization of isonitrile **5b** ($R = NC$)[6] held potential; however, remaining

[*] Dr. J. M. Ready, S. E. Reisman, Dr. M. Hirata, Dr. M. M. Weiss, Dr. K. Tamaki, Dr. T. V. Ovaska, Prof. Dr. J. L. Wood
Department of Chemistry, Yale University
Sterling Chemistry Laboratory
PO Box 208107, New Haven, CT 06520–8107 (USA)
Fax: (+1) 203-432-6144
E-mail: john.wood@yale.edu

[**] We gratefully acknowledge financial support from Yamanouchi, Merck, Pfizer, and Amgen. J.M.R. is the recipient of an NIH postdoctoral fellowship. K.R. thanks Sankyo Co., LTD.; M.H. thanks Daiso Co., LTD., M.M.W. thanks Bristol Myers Squibb for a graduate fellowship.

Supporting information for this article is available on the WWW under http://www.angewandte.org or from the author.

 © 2004 Wiley-VCH Verlag GmbH & Co. KGaA, Weinheim DOI: 10.1002/anie.200353282

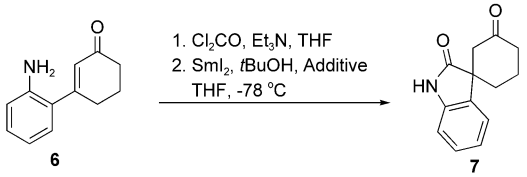


Scheme 1. Brief retrosynthetic analysis of welwitindolinone A isonitrile.

concerns regarding the stability of cyclobutenes to the prolonged heating required by these approaches led us to seek alternatives. Of particular interest in this regard was a recent report describing the SmI_2-mediated reductive coupling of acrylates with isocyanates to furnish amides.[7] In the context of a welwitindolinone synthesis, we anticipated that a similar reaction involving isocyanate **5c** would deliver spiro-oxindole **3** under reaction conditions that would be compatible with the sensitive cyclobutene.

To test the viability of the proposed SmI_2-mediated oxindole synthesis, aniline **6** was converted to its corresponding isocyanate and treated with SmI_2; unfortunately, only trace amounts of oxindole **7** were obtained (Table 1, entry 1).

Table 1: SmI_2-mediated synthesis of spiro-oxindoles.[a]



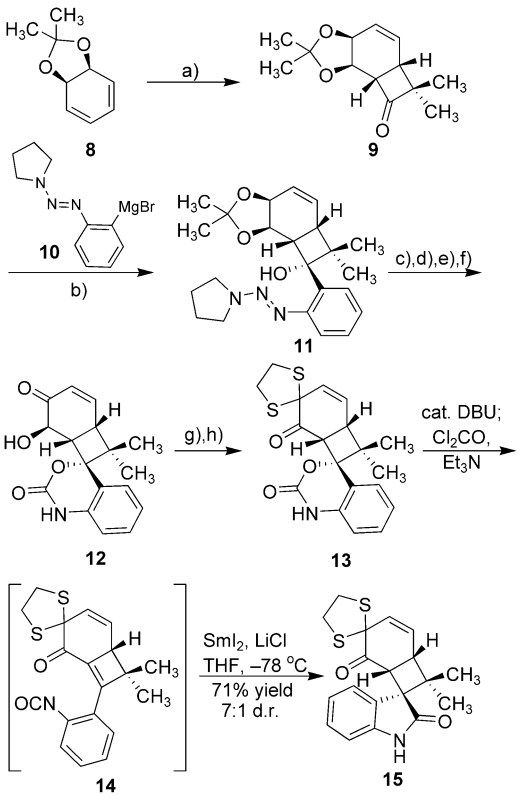
Entry	Additive	Yield [%][b]
1	None	5
2	NiI_2[c]	15
3	HMPA[d]	32
4	LiBr[e]	47
5	LiCl[e]	88

[a] Reactions carried out with 1 equiv **6**, 1 equiv *t*BuOH and 2.1 equiv SmI_2. [b] Yield of isolated product. [c] 0.05 equiv. [d] 6.2 equiv. [e] 8.4 equiv.

In an effort to improve the chemical yield, the effects of additives known to modulate the activity of SmI_2 were examined.[8] In contrast to conventional additives such as NiI_2 and HMPA (hexamethyl phosphoramide; entries 2,3), simple, nontoxic lithium salts provided substantially improved yields (entries 4,5). Thus, brief exposure (2 min) of the isocyanate derived from **6** to a mixture of SmI_2, LiCl, and *t*BuOH at −78 °C furnished the corresponding oxindole in 88% isolated yield (entry 5).[8c,9–11]

Having developed a new method for the synthesis of spiro-oxindoles, we turned towards preparing a fully elaborated cyclobutene-containing substrate that would be poised for conversion to **2**. As the point of departure, the readily available cyclohexadiene acetonide **8** was found to participate in an exquisitely stereo- and regioselective [2+2] cycloaddition that furnished **9** in excellent yield (Scheme 2).[12] Diastereoselective introduction of the requisite aryl amine was achieved through the aegis of ortho-metallated aniline **10**,[13] which proved uniquely effective for this transformation as attempts with numerous other aryl metal species led to enolization or decomposition.[14]

In ongoing studies, Grignard addition product **11** was routinely converted to α,β-unsaturated ketone **12** on multigram scale by an efficient four step sequence involving chemoselective reduction of the triazene, protection of the



Scheme 2. a) Isobutyryl chloride, Et_3N, THF (85% yield). b) **10**, THF, −78%°C (88% yield). c) Raney Ni, MeOH. d) 4-Nitrophenyl chloroformate, $NaHCO_3$, MTBE; 1 M NaOH. e) 60% AcOH/H_2O, reflux. f) Bu_2SnO, MeOH, reflux; NBS, $CHCl_3$ (73% yield, 4 steps). g) $HSCH_2CH_2SH$, $BF_3{\cdot}Et_2O$, 0 °C. h) $(COCl)_2$, DMSO, Et_3N, CH_2Cl_2, −78 °C to −20 °C (46% yield, 2 steps). MBTE = methyl *tert*-butyl ether, NBS = *N*-bromosuccinimide, Cat. = catalyst.

 © 2004 Wiley-VCH Verlag GmbH & Co. KGaA, Weinheim

resultant amino alcohol, acetonide removal, and selective oxidation of the allylic alcohol.[15] Although the derived ketone **12** provides a potential branch point for several synthetic end-games, our initial efforts have focused on applying our recently developed oxindole synthesis to this fully elaborated system.

To this end, protection of **12** as the corresponding dithiolane followed by oxidation of the secondary alcohol provided the masked cyclization substrate **13**.[16] Addition of 1,8-diazabicyclo[4.3.0]undec-7-ene (DBU, 0.4 equiv) to a solution of **13** in THF effected the smooth elimination of CO_2 and provided an unstable β-(2-aminophenyl)-α,β-unsaturated ketone, which was converted to isocyanate **14** in the same reaction vessel (Cl_2CO, Et_3N). After removal of HCl salts by filtration, the isocyanate was exposed to a mixture of SmI_2 and LiCl at −78 °C. Chromatographic purification on silica gel furnished a 71 % yield of **15** as an inseparable 7:1 mixture of diastereomers. The major diastereomer was determined by NOE analysis to be appropriately configured for conversion to **2** (Scheme 1) and is consistent with bond formation on the less hindered, convex face of **14**.

Inspired by the unique and challenging structural features presented by the welwitindolinone alkaloids, we have discovered and developed a new SmI_2-mediated synthesis of spiro-oxindoles. This stereoselective reaction, in conjunction with a highly regio- and diastereoselective [2+2] cycloaddition provides efficient access to the carbon skeleton of welwitindolinone A isonitrile. These reactions serve as key steps in our ongoing total synthesis of this important natural product. The new reductive cyclization constitutes a significant expansion of the scope of SmI_2-mediated reactions, and suggests that other intramolecular cyclizations of α,β-unsaturated ketones may by possible. Results related to both areas of inquiry will be reported in due course.

Received: November 10, 2003 [Z53282]
Published Online: February 11, 2004

Keywords: alkaloids · natural products · samarium · total synthesis

[1] a) K. Stratmann, R. E. Moore, R. Bonjouklian, J. B. Deeter, G. M. L. Patterson, S. Shaffer, C. D. Smith, T. A. Smitka, *J. Am. Chem. Soc.* **1994**, *116*, 9935 – 9942; b) J. I. Jimenez, U. Huber, R. E. Moore, G. M. L. Patterson, *J. Nat. Prod.* **1999**, *62*, 569 – 572.

[2] Synthetic efforts directed toward welwitindolinone alkaloids: a) J. L. Wood, A. A. Holubec, B. M. Stoltz, M. M. Weiss, J. A. Dixon, B. D. Doan, M. F. Shamji, J. M. Chen, T. P. Heffron, *J. Am. Chem. Soc.* **1999**, *121*, 6326 – 6327; b) H. B. Deng, J. P. Konopelski, *Org. Lett.* **2001**, *3*, 3001 – 3004; c) M. E. Jung, F. Slowinski, *Tetrahedron Lett.* **2001**, *42*, 6835 – 6838; d) P. Lopez-Alvarado, S. Garcia-Granda, C. Alvarez-Rua, C. Avendano, *Eur. J. Org. Chem.* **2002**, 1702 – 1707.

[3] a) S. Atarashi, J. K. Choi, D. C. Ha, D. J. Hart, D. Kuzmich, C. S. Lee, S. Ramesh, S. C. Wu, *J. Am. Chem. Soc.* **1997**, *119*, 6226 – 6241; b) S. T. Hilton, T. C. T. Ho, G. Pljevaljcic, K. Jones, *Org. Lett.* **2000**, *2*, 2639 – 2641.

[4] A. Madin, L. E. Overman, *Tetrahedron Lett.* **1992**, *33*, 4859 – 4862.

[5] B. ElAli, K. Okuro, G. Vasapollo, H. Alper, *J. Am. Chem. Soc.* **1996**, *118*, 4264 – 4270.

[6] T. Fukuyama, X. Q. Chen, G. Peng, *J. Am. Chem. Soc.* **1994**, *116*, 3127 – 3128.

[7] Y. H. Kim, H. S. Park, D. W. Kwon, *Synth. Commun.* **1998**, *28*, 4517 – 4524.

[8] For the use of a) NiI_2: F. Machrouhi, B. Hamann, J. L. Namy, H. B. Kagan, *Synlett* **1996**, 633 – 634; b) HMPA: J. Inanaga, M. Ishikawa, M. Yamaguchi, *Chem. Lett.* **1987**, 1485 – 1486; c) LiBr and LiCl: R. S. Miller, J. M. Sealy, M. Shabangi, M. L. Kuhlman, J. R. Fuchs, R. A. Flowers, *J. Am. Chem. Soc.* **2000**, *122*, 7718 – 7722. It has been suggested that addition of LiCl to SmI_2 generates $SmCl_2$ in situ, which is a stronger reductant toward ketones.

[9] For complete experimental details, see Supporting Information.

[10] Reactions of α,β-unsaturated ketones with SmI_2: a) Y. Fujita, S. Fukuzumi, J. Otera, *Tetrahedron Lett.* **1997**, *38*, 2121 – 2124; b) A. Cabrera, R. Le Lagadec, P. Sharma, J. L. Arias, R. A. Toscano, L. Velasco, R. Gavino, C. Alvarez, M. Salmon, *J. Chem. Soc. Perkin Trans. 1* **1998**, 3609 – 3617.

[11] Y. S. Liu, M. Z. Bei, Z. H. Zhou, K. Takaki, Y. Fujiwara, *Chem. Lett.* **1992**, 1143 – 1144.

[12] L. Ghosez, M. J. O'Donnell, *Pericyclic Reactions*, *Vol. II*, Academic, New York, **1997**.

[13] M. L. Gross, D. H. Blank, W. M. Welch, *J. Org. Chem.* **1993**, *58*, 2104 – 2109.

[14] For a discussion of the acidity of cyclobutanones, see: R. J. Cantlin, J. Drake, R. W. Nagorski, *Org. Lett.* **2002**, *4*, 2433 – 2436.

[15] P. Soderman, G. Widmalm, *Carbohydr. Res.* **1999**, *316*, 184 – 186.

[16] A. J. Mancuso, S. L. Huang, D. Swern, *J. Org. Chem.* **1978**, *43*, 2480 – 2482.

 © 2004 Wiley-VCH Verlag GmbH & Co. KGaA, Weinheim

Addition Reactions

Highly Enantio- and Diastereoselective Organocatalytic Asymmetric Domino Michael–Aldol Reaction of β-Ketoesters and α,β-Unsaturated Ketones**

*Nis Halland, Pompiliu S. Aburel, and Karl Anker Jørgensen**

The catalytic asymmetric formation of chiral building blocks represents an increasingly important field in organic chemistry owing to the usefulness of these products in further synthetic transformations. The catalytic enantioselective for-

[*] Dr. N. Halland, Dr. P. S. Aburel, Prof. Dr. K. A. Jørgensen
The Danish National Research Foundation: Center for Catalysis
Department of Chemistry, Aarhus University
8000 Aarhus C (Denmark)
Fax: (+45) 8919-6199
E-mail: kaj@chem.au.dk

[**] We are grateful to Dr. R. G. Hazell for X-ray crystallographic analysis of compounds **6a**, **c**, **e**. This work was made possible by a grant from The Danish National Research Foundation.

Supporting information for this article is available on the WWW under http://www.angewandte.org or from the author.

 © 2004 Wiley-VCH Verlag GmbH & Co. KGaA, Weinheim DOI: 10.1002/anie.200353364

mation of C–C bonds is a widely developed method for achieving this goal and a number of reactions and methodologies have been developed.[1] Among the various asymmetric C–C bond-forming reactions, the direct catalytic domino[2] and cycloaddition[3] reactions are of particular interest as multiple stereogenic centers can be formed in a single reaction.

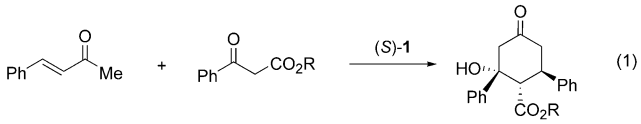
Recently we reported the environmentally benign imidazolidine-catalyzed Michael reaction of malonates,[4] cyclic β-ketoesters,[5] and nitroalkanes.[6] Herein we present the first organocatalytic asymmetric domino Michael–aldol reaction of acyclic β-ketoesters and unsaturated ketones to afford optically active cyclohexanones with up to four stereogenic centers with excellent enantio- and diastereoselectivity. The domino Michael–aldol reaction reported herein is related to the proline-catalyzed Robinson annulation pioneered by Wiechert and co-workers and by Hajos and Parrish 30 years ago,[7] but was originally discovered by Fischer and Dieckmann almost a century ago and more recently reinvestigated by Christoffers.[8] The potential of this novel catalytic enantioselective domino Michael–aldol reaction is demonstrated by the easy formation of optically active cyclohexanone and cyclohexanediol, as well as γ- and ε-lactone building blocks in high yields and enantioselectivities.

The phenylalanine-derived imidazolidine catalyst **1** has proved to be a powerful catalyst for the catalytic asymmetric Michael reaction of unsaturated ketones **2** with various Michael donors. Herein we present its application to the catalytic asymmetric domino Michael–aldol reaction with acyclic β-ketoesters **3** (Scheme 1).

An initial screening of reaction conditions was carried out to optimize the reaction of benzylideneacetone (**2a**) with several β-ketoesters **3** [Eq. (1)] and some representative results obtained during the screening are presented in Table 1.[9] The results of the initial screening experiments revealed that catalyst **1** is an excellent catalyst for the domino Michael–aldol reaction and that higher enantioselectivities were obtained when using benzyl benzoylacetate (**3b**) than when using ethyl benzoylacetate (**3a**). Furthermore, it was observed that the reaction proceeded readily in various solvents, as well as under solvent-free conditions; excellent enantioselectivities were obtained in all solvents, although yields varied somewhat. Protic solvents such as MeOH and EtOH gave the highest reaction rates and up to 80% yield with 95% *ee* could be obtained (Table 1, entries 9–11) and therefore EtOH was chosen for further reactions. We also tested other chiral amines as catalysts: for example, L-proline gave a fast reaction, but the product was formed as a racemate. Notably, to obtain analytically pure domino Michael–aldol adducts no chromatography was required as the optically active cyclohexanones precipitated from the reaction mixture and were recovered by simple filtration, washing with Et_2O (to remove unconverted starting materials), and drying under vacuum. This very simple work-up procedure suggests that a continuous recrystallization takes place during the reaction, but reactions purified by flash chromatography afforded domino Michael–aldol adducts with the same optical purity as those recovered by filtration.

After optimization of the reaction conditions, various α,β-unsaturated ketones were treated with benzyl benzoylacetate (**3b**) to determine the scope of the reaction ([Eq. (2)], Table 2). The various α,β-unsaturated ketones **2** carrying aromatic and heteroaromatic β-substituents (Ar^1) all reacted well with β-ketoester **3b**, affording cyclohexanones in moderate to good yields and with excellent enantioselectivities (Table 2, entries 1–10). Furthermore, several other aromatic β-ketoesters **3c**,**d** could be employed in the reaction and led

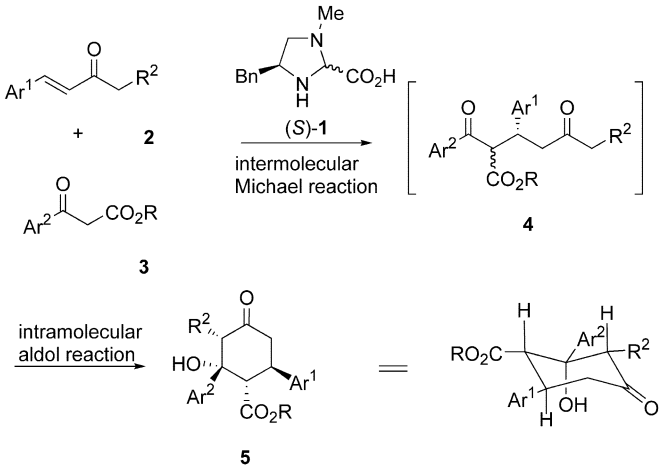
Table 1: Optimization of the diastereo- and enantioselective domino Michael–aldol reaction catalyzed by (*S*)-**1**.



2a **3** **5**

Entry	R	**3**	**1** [mol%]	Solvent	**5**	*t* [h]	Yield [%][a]	d.r.[b]	*ee* [%][c]
1	Et	**a**	20	neat	**a**	110	89	>97:3	70
2	Et	**a**	10	CH_2Cl_2	**a**	144	60	>97:3	88
3	Et	**a**	10	H_2O	**a**	93	<5	–	–
4	Et	**a**	10	$EtOH/H_2O$[d]	**a**	93	57	>97:3	87
5	Bn	**b**	10	neat	**b**	96	20	>97:3	94
6	Bn	**b**	10	neat	**b**	120	60	>97:3	95
7	Bn	**b**	10	THF	**b**	96	10	>97:3	99
8	Bn	**b**	10	CH_2Cl_2	**b**	80	42	>97:3	94
9	Bn	**b**	10	EtOH	**b**	44	89	>97:3	89
10	Bn	**b**	10	EtOH	**b**	190	80	>97:3	95[e]
11	Bn	**b**	10	MeOH	**b**	44	52	>97:3	90
12	Bn	**b**	10	CH_3CN	**b**	68	70	>97:3	90
13	Bn	**b**	10	CH_3CN	**b**	42	30	>97:3	91[e]

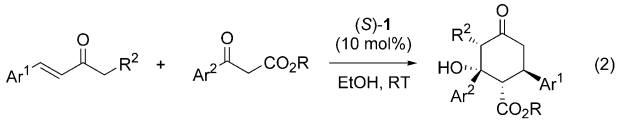
Experimental conditions: β-Ketoester **3** (1.0 mmol, 2 equiv) and catalyst (*S*)-**1** were added to a solution of benzylideneacetone **2a** (0.5 mmol) in solvent (1.0 mL), and the reaction mixture was stirred at ambient temperature for the time indicated in the table. [a] Yields of isolated products. [b] Determined by ^1H NMR spectroscopic analysis. [c] Determined by CSP-HPLC. [d] Performed in $EtOH/H_2O$ 4:1. [e] Reaction performed at 10°C.



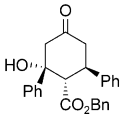
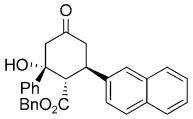
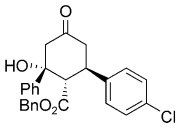
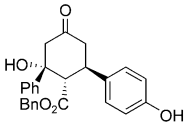
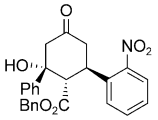
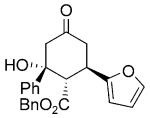
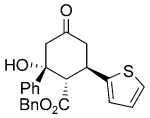
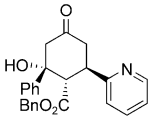
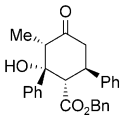
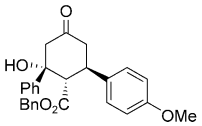
Scheme 1. Domino Michael–aldol reaction of acyclic β-ketoesters **2** with α,β-unsaturated ketones **3** catalyzed by (*S*)-**1**.

 © 2004 Wiley-VCH Verlag GmbH & Co. KGaA, Weinheim

Table 2: Domino Michael–aldol reaction of α,β-unsaturated ketones **2** with β-ketoesters **3** catalyzed by (*S*)-**1**.

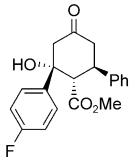
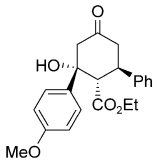


2 **3** **5**

Entry	**2**	Ar^1	R^2	**3**	Ar^2	R	*t* [h]	Product	**5**	Yield [%][a]	d.r.[b]	*ee* [%][c]
1	**a**	Ph	H	**b**	Ph	Bn	192		**b**	80	>97:3	95[d]
2	**b**	2-Np	H	**b**	Ph	Bn	95		**c**	85	>97:3	91
3	**c**	4-Cl-Ph	H	**b**	Ph	Bn	95		**d**	60	>97:3	97
	c	4-Cl-Ph	H	**b**	Ph	Bn	240		**d**	80	>97:3	93[c]
4	**d**	4-HO-Ph	H	**b**	Ph	Bn	95		**e**	20	>97:3	99
5	**e**	2-NO_2-Ph	H	**b**	Ph	Bn	125		**f**	56	>97:3	96
6	**f**	2-furyl	H	**b**	Ph	Bn	140		**g**	40	>97:3	85
7	**g**	2-thienyl	H	**b**	Ph	Bn	165		**h**	52	>97:3	83
8	**h**	2-pyrimidyl	H	**b**	Ph	Bn	240		**i**	84	>97:3	89[d]
9	**i**	Ph	Me	**b**	Ph	Bn	95		**j**	50	>97:3	95
	i	Ph	Me	**b**	Ph	Bn	165		**j**	61	>97:3	96
10	**j**	Ph	H	**b**	Ph	Bn	140		**k**	70	>97:3	86

 © 2004 Wiley-VCH Verlag GmbH & Co. KGaA, Weinheim

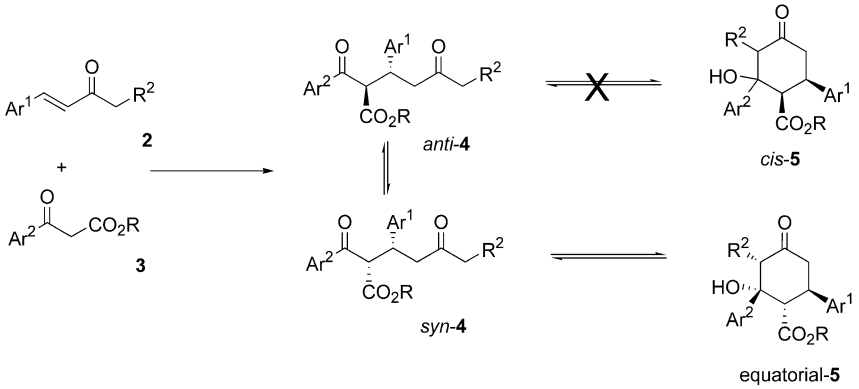
Table 2: (Continued)

Entry	2	Ar^1	R^2	3	Ar^2	R	*t* [h]	Product	5	Yield [%][a]	d.r.[b]	*ee* [%][c]
11	**a**	Ph	H	**c**	4-F-Ph	Me	160		**l**	44	>97:3	92
12	**a**	Ph	H	**d**	4-MeO-Ph	Et	165		**m**	22	>97:3	90

Experimental conditions: β-Ketoester **3** (1.0 mmol, 2.0 equiv) and catalyst (*S*)-**1** (10 mol%) were added to α,β-unsaturated ketone **2** (0.5 mmol) in EtOH[14] (1.0 mL), and the reaction mixture was stirred for the time indicated in the table. [a] Yields of isolated products. [b] Determined by ^{1}H NMR spectroscopic analysis. [c] Determined by CSP-HPLC. [d] Reaction performed at 10°C.

to the formation of cyclohexanones with excellent enantioselectivities, although the yields were moderate (Table 2, entries 11 and 12). The low yield of **5e** (Table 2, entry 4) is due to low conversion because of the electron-donating substituent at the *para* position of Ar^1 in **2d**.

In all cases only a single diastereomer of the domino Michael–aldol adduct was formed, something that is easily rationalized. The reaction proceeds through initial formation of the Michael adduct **4**, which bears two stereogenic centers, but only the Ar^1-substituted stereogenic carbon center is stable, whereas the stereogenic carbon center with both the ketone and ester substituents epimerizes in the reaction mixture as the proton is highly acidic and therefore the Michael adduct **4** exists as a mixture of *syn* and *anti* isomers (Scheme 2).

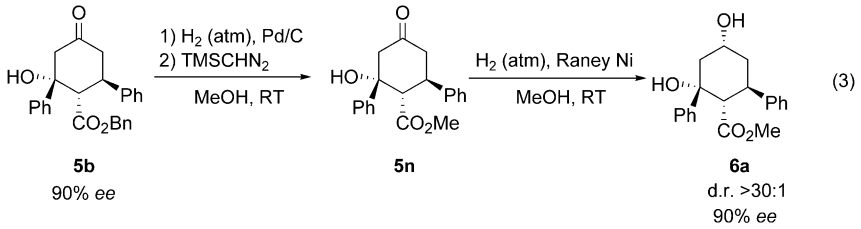


Scheme 2. Diastereoselectivity in the domino Michael–aldol reaction.

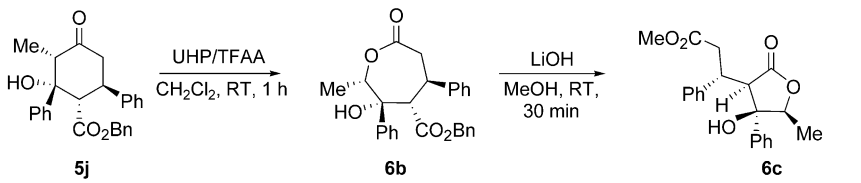
Fortunately, the intramolecular aldol reaction proceeds in a highly diastereoselective fashion to form the six-membered ring so that all large substituents are equatorial and thus are controlled by the stable stereogenic center formed in the initial Michael reaction. It should be noted that the high-energy diastereomers *cis*-**5** are not observed in the course of the reaction. Furthermore, in contrast to the intermolecular Michael reaction, which is catalyzed by the chiral imidazolidine catalyst, the intramolecular aldol reaction is believed to be base-catalyzed, as shown by Dieckmann and Fischer and by Christoffers,[8] with the imidazolidine catalyst acting as the base. The catalyst plays three roles in the reaction: a) it activates the Michael acceptor by iminium-ion formation, b) it generates the active Michael donor by deprotonation of the β-ketoester, and c) it acts as a base in the intramolecular aldol reaction. However, it cannot be completely excluded that the intramolecular aldol reaction is catalyzed by the imidazolidine compound and proceeds through an enamine mechanism.

The assignment of the relative stereochemistry of the cyclohexanones is based on X-ray crystallographic studies (see Supporting Information) of cyclohexanol **6a** formed by a diastereoselective reduction of cyclohexanone **5n** as outlined below [Eq. (3)].[10]

As we were unable to obtain X-ray-quality crystals of the domino Michael–aldol adduct **5j** with four stereogenic centers, we subjected **5j** to Baeyer–Villiger oxidation followed by a translactonization as outlined below [Eq. (4)].[11]



(3)

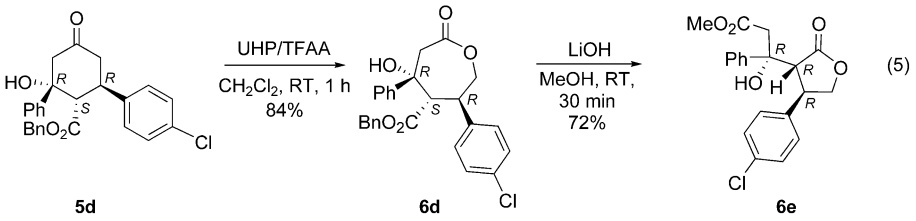


(4)

 © 2004 Wiley-VCH Verlag GmbH & Co. KGaA, Weinheim

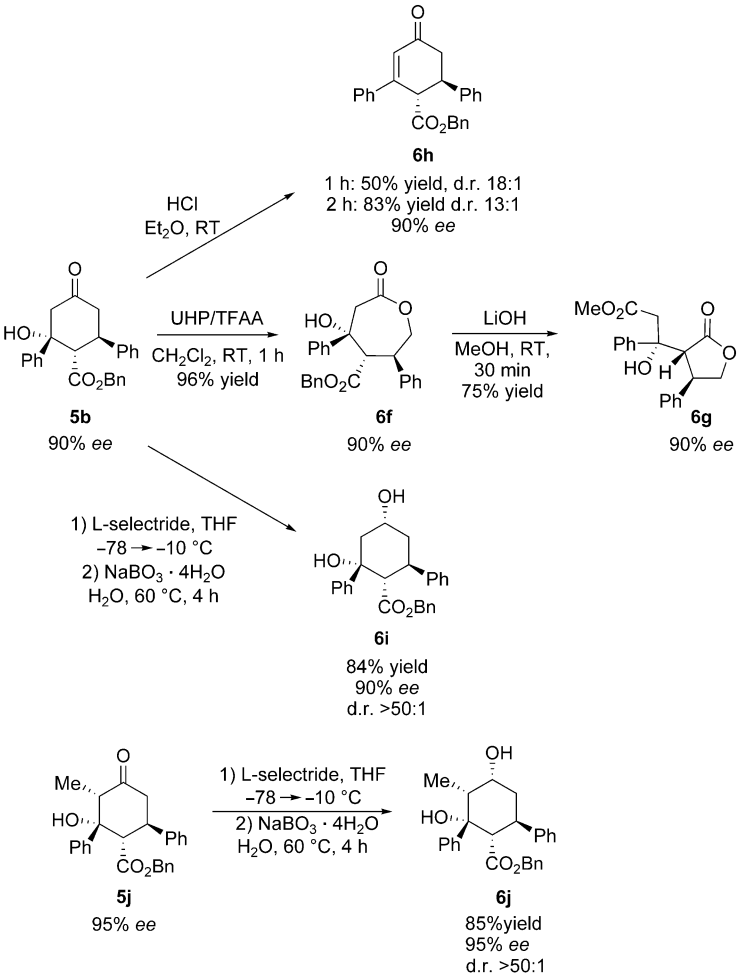
This afforded the γ-lactone **6c**, which readily afforded X-ray-quality crystals upon recrystallization from MeOH, and the relative stereochemistry of **6c** was determined by X-ray crystallography, thus providing information on the relative stereochemistry of the α-keto compound (see Supporting Information).[12]

The absolute stereochemistry of the domino Michael–aldol adducts was similarly determined from the γ-lactone **6e** derived from domino Michael–aldol adduct **5d** [Eq. (5)].



(5)

The absolute stereochemistry of γ-lactone **6e** was determined to be *R*,*R*,*R* by X-ray crystallography, and the absolute configuration of the domino Michael–aldol adduct **5d** was therefore determined to be 3*R*,4*S*,5*R*, as indicated in Equation (5).[12]



Scheme 3. Transformations of cyclohexanones **5**.

To demonstrate the potential of the domino Michael–aldol reaction, several product modifications were performed on the domino Michael–aldol adducts to determine the versatility of the cyclohexanone derivatives **5** (Scheme 3). Baeyer–Villiger oxidation of **5b** proceeded smoothly, with complete regioselectivity, in the presence of urea–hydrogen peroxide (UHP) and trifluoroacetic anhydride (TFAA) as a very convenient way of generating trifluoro peroxyacetic acid, giving the optically active ε-lactone **6f** in 96% yield.[13] The ε-lactone **6f** was easily translactonized to γ-lactone **6g** in good yield by brief exposure to LiOH/MeOH, maintaining the high enantiopurity. Furthermore, the cyclohexenone **6h** could be formed by acid-catalyzed dehydration of **5b**, although some epimerization occurred at C4 under the reaction conditions. However, diastereoselectivities of up to 18:1 were obtained. Lastly, the cyclohexanediols **6i**,**j** were prepared in good yields as single diastereomers by reduction of the corresponding cyclohexanones **5b**,**j** with L-selectride.

These optically active building blocks with up to five contiguous stereogenic centers are all formed in one or two simple high-yielding transformations, without racemization, from the domino Michael–aldol adducts.

In summary, we have developed the first highly enantio- and diastereoselective organocatalytic domino Michael–aldol reaction of acyclic β-ketoesters and α,β-unsaturated ketones in the presence of an imidazolidine catalyst, which is easily prepared from phenylalanine. The reaction proceeds for a number aromatic and heteroaromatic β-ketoesters and α,β-unsaturated ketones, forming adducts with 3–4 contiguous stereogenic centers. Furthermore, the synthetic scope of the reaction was demonstrated by the easy formation of various optically active building blocks.

Received: November 19, 2003 [Z53364]
Published Online: February 11, 2004

Keywords: aldol reaction · domino reaction · esters · ketones · Michael addition

[1] *Comprehensive Asymmetric Catalysis* (Eds.: E. N. Jacobsen, A. Pfaltz, H. Yamamoto), Springer, Berlin, **1999**.

[2] For recent examples of catalytic enantioselective domino reactions in which multiple stereogenic centers are formed, see: a) M. P. Sibi, J. Chen, *J. Am. Chem. Soc.* **2001**, *123*, 9472; b) L. A. Arnold, R. Naasz, A. J. Minnaard, B. L. Feringa, *J. Org. Chem.* **2002**, *67*, 7244; c) H. M. L. Davies, B. D. Doan, *J. Org. Chem.* **1999**, *64*, 8501; d) D. F. Cauble, J. D. Gipson, M. J. Krische, *J. Am. Chem. Soc.* **2003**, *125*, 1110; e) J. Tian, N. Yamagiwa, S. Matsunaga, M. Shibasaki, *Angew. Chem.* **2002**, *114*, 3788; *Angew. Chem. Int. Ed.* **2002**, *41*, 3636; f) A. Alexakis, S. March, *J. Org. Chem.* **2002**, *67*, 8753; g) O. Knopff, A. Alexakis, *Org. Lett.* **2002**, *4*, 3835; h) S.-I. Watanabe, A. Córdova, F. Tanaka, C. F. Barbas III, *Org. Lett.* **2000**, *2*, 4519; i) A. Córdova, C. F. Barbas III, *Tetrahedron Lett.* **2003**, *44*, 1923; j) N. Halland, T. Velgaard, K. A. Jørgensen, *J. Org. Chem.* **2003**, *68*, 5067.

 © 2004 Wiley-VCH Verlag GmbH & Co. KGaA, Weinheim

[3] For some recent examples of direct catalytic asymmetric cycloaddition reactions, see: a) W. S. Jen, J. J. M. Wiener, D. W. C. MacMillan, *J. Am. Chem. Soc.* **2000**, *122*, 9874; b) A. B. Northrup, D. W. C. MacMillan, *J. Am. Chem. Soc.* **2002**, *124*, 2458; c) K. A. Ahrendt, C. J. Borths, D. W. C. MacMillan, *J. Am. Chem. Soc.* **2000**, *122*, 4243; d) K. Juhl, K. A. Jørgensen, *Angew. Chem.* **2003**, *115*, 1536; *Angew. Chem. Int. Ed.* **2003**, *42*, 1498; e) A. S. Gothelf, K. V. Gothelf, R. G. Hazell, K. A. Jørgensen, *Angew. Chem.* **2002**, *114*, 4410; *Angew. Chem. Int. Ed.* **2002**, *41*, 4236; f) K. A. Jørgensen, *Angew. Chem.* **2000**, *112*, 3702; *Angew. Chem. Int. Ed.* **2000**, *39*, 3558, and references therein; g) J. S. Johnson, D. A. Evans, *Acc. Chem. Res.* **2000**, *33*, 325, and references therein; h) K. Gademann, D. E. Chavez, E. N. Jacobsen, *Angew. Chem.* **2002**, *114*, 3185; *Angew. Chem. Int. Ed.* **2002**, *41*, 3059; i) E. J. Corey, *Angew. Chem.* **2002**, *114*, 1724; *Angew. Chem. Int. Ed.* **2002**, *41*, 1650; j) D. A. Evans, J. Wu, *J. Am. Chem. Soc.* **2003**, *125*, 10162; k) D. B. Ramachary, N. S. Chowdari, C. F. Barbas III, *Angew. Chem.* **2003**, *115*, 4365; *Angew. Chem. Int. Ed.* **2003**, *42*, 4233; l) *Cycloaddition Reactions in Organic Synthesis* (Eds.: S. Kobayashi, K. A. Jørgensen), Wiley-VCH, **2000**.

[4] N. Halland, P. S. Aburel, K. A. Jørgensen, *Angew. Chem.* **2003**, *115*, 685; *Angew. Chem. Int. Ed.* **2003**, *42*, 661.

[5] N. Halland, T. Hansen, K. A. Jørgensen, *Angew. Chem.* **2003**, *115*, 4955; *Angew. Chem. Int. Ed.* **2003**, *42*, 5105.

[6] N. Halland, R. G. Hazell, K. A. Jørgensen, *J. Org. Chem.* **2002**, *67*, 8331.

[7] a) U. Eder, G. Sauer, R. Wiechert, *Angew. Chem.* **1971**, *83*, 492; *Angew. Chem. Int. Ed. Engl.* **1971**, *10*, 496; b) Z. G. Hajos, D. R. Parrish, *J. Org. Chem.* **1974**, *39*, 1615; see also; c) T. Arai, H. Sasai, K.-I. Aoe, K. Okamura, T. Date, M. Shibasaki, *Angew. Chem.* **1996**, *108*, 103; *Angew. Chem. Int. Ed. Engl.* **1996**, *35*, 104; d) T. Bui, C. F. Barbas III, *Tetrahedron Lett.* **2000**, *41*, 6951.

[8] a) W. Dieckmann, K. Fischer, *Ber. Dtsch. Chem. Ges.* **1911**, *44*, 966; b) J. Christoffers, *J. Chem. Soc. Perkin Trans. 1*, **1997**, 3141, see also: F. Tanaka, R. Thayumanavan, C. F. Barbas III, *J. Am. Chem. Soc.* **2002**, *124*, 8523.

[9] The 4,5-diphenyl-imidazolidine-2-carboxylic acid catalyst recently reported for the catalytic enantioselective formation of warfarin,[5] also promoted the domino Michael–aldol reaction in up to 90% *ee* in moderate yield.

[10] CCDC-224447 (**6a**), CCDC-224448 (**6c**), and CCDC-224449 (**6e**) contain the supplementary crystallographic data for this paper. These data can be obtained free of charge via www.ccdc.cam.ac.uk/conts/retrieving.html (or from the Cambridge Crystallographic Data Centre, 12, Union Road, Cambridge CB21EZ, UK; fax: (+44) 1223-336-033; or deposit@ccdc.cam.ac.uk).

[11] Baeyer-Villiger oxidations generally occur with retention of stereochemistry at the migrating center; see, for example: *Comprehensive Organic Synthesis* (Ed.: B. M. Trost), Pergamon, Berlin, **1991**.

[12] Inversion of the α-carbonyl stereogenic center was observed during the translactonization procedure.

[13] M. S. Cooper, H. Heaney, A. J. Newbold, W. R. Sanderson, *Synlett* **1990**, 533.

[14] The reaction rate is strongly concentration-dependent (see Supporting Information).

 © 2004 Wiley-VCH Verlag GmbH & Co. KGaA, Weinheim

Metal–Hydride Complexes

Oxidative Addition of Imidazolium Salts to Ni^0 and Pd^0: Synthesis and Structural Characterization of Unusually Stable Metal–Hydride Complexes**

Nicolas D. Clement, Kingsley J. Cavell, Cameron Jones, and Cornelis J. Elsevier*

Ionic liquids (ILs) and especially imidazolium-based ionic liquids have found important applications in catalysis over the last decade or so as non-aqueous solvents for biphasic catalysis.[1] Interestingly, improved catalyst stability and, in some examples, improved overall catalytic performance were observed for reactions conducted in ILs. Although ILs have been considered to be nonparticipative or "innocent" solvents, a number of reports have suggested possible formation of metal–carbene complexes in situ during the course of catalysis.[2] Deprotonation of C2 of imidazolium salts to generate N-heterocyclic carbene ligands (NHC) is well-documented.[3] A weak base is often all that is necessary to deprotonate such salts under the reaction conditions and therefore it seems likely that carbene formation may occur if a basic entity is present during catalytic reactions. This has effectively been demonstrated through isolation of carbene–-metal complexes from the ionic liquid solvents used for Heck and Suzuki–Miyaura coupling reactions.[2b,c]

We have also shown, using theoretical and experimental methods, that in the absence of base, imidazolium cations can oxidatively add to a low-valent metal center of Group 10 to form carbene complexes via C2–X (X = halogen) or –H activation.[4] Stone and co-workers,[5a] and more recently Fürstner et al.[5b] utilized the oxidative addition of C2–X species in the synthesis of metal–carbene complexes. Nolan and co-workers[6a] and Crabtree and co-workers[6b] provided evidence for the oxidative addition of imidazolium salts to Pd^0, although no Pd–hydride complex was isolated. Experimentally, C2–H activation and M–H formation had only been unambiguously observed with Pt^0 complexes.[4b,c] We

[*] N. D. Clement, Prof. K. J. Cavell, Prof. C. Jones
Department of Chemistry, Cardiff University
PO Box 912, Cardiff CF10 3TB, Wales (UK)
Fax: (+44) 29-2087-5899
E-mail: cavellkj@cf.ac.uk
Prof. C. J. Elsevier
Institute of Molecular Chemistry,
Organometallic and Coordination Chemistry
University of Amsterdam
Nieuwe Achtergracht 166, 1018 WV Amsterdam (The Netherlands)

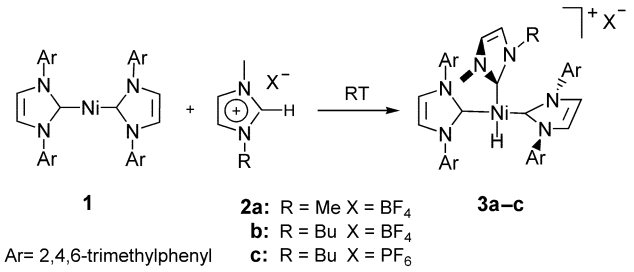
[**] We are grateful to the Engineering and Physical Sciences Research Council (EPSRC) for financial support and for a stipend for N.D.C. We also thank Solvent Innovation GmbH for the generous gift of ionic liquids, Johnson-Matthey for the loan of palladium chloride, and R. Jenkins for help with NMR spectroscopic measurements.

Supporting information for this article is available on the WWW under http://www.angewandte.org or from the author (preparation procedures and spectroscopic data for complexes **3a–c** and **5**).

 DOI: 10.1002/anie.200353409 © 2004 Wiley-VCH Verlag GmbH & Co. KGaA, Weinheim

now report the synthesis of stable (carbene)M–hydride complexes of Ni and Pd formed by "insertion" of the metal center into the C2–H bond of imidazolium salts.

We employed electron-rich, coordinatively unsaturated L_2M^0 complexes (L = 1,3-aryl-NHC) to facilitate low-temperature oxidative addition of imidazolium salts. When equimolar quantities of various imidazolium salts **2a–c** were stirred with the Ni^0 complex **1** generated in situ,[7] the deep purple color of **1** quickly disappeared at room temperature to give a light yellow solution (Scheme 1). Concentration of the



Scheme 1. C–H oxidative addition of imidazolium salts to Ni^0 complex **1**: a) THF, 5 min; b) toluene, 1 h; c) toluene, 5 min.

solution and addition of *n*-hexane led to the isolation of triscarbene–nickel–hydrido complexes **3a–c** as light-yellow crystalline solids in 70–76% yield. The Ni–H signals appear at $\delta = -14.96$, -15.02, and -15.02 ppm, respectively in the ^{1}H NMR spectra (CD_2Cl_2). These represent the first examples of (carbene)nickel–hydride complexes. All three complexes are surprisingly stable both in solution and in the solid state. They can be heated at reflux in THF for 16 hours without evidence of major decomposition and they can be stored under an inert atmosphere for an extended period of time. They also may be manipulated in air without any sign of degradation.

The full molecular geometry of complex **3b** was elucidated by single-crystal X-ray diffraction, and the ORTEP diagram is given in Figure 1 together with selected bond distances and angles.[8]

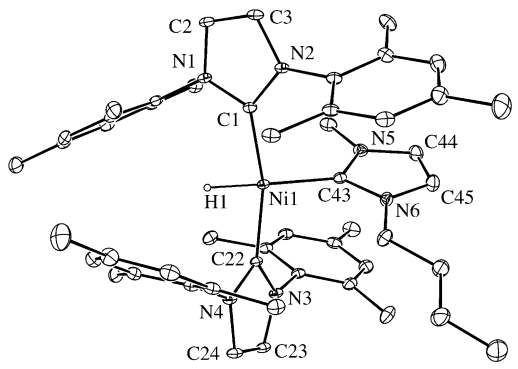
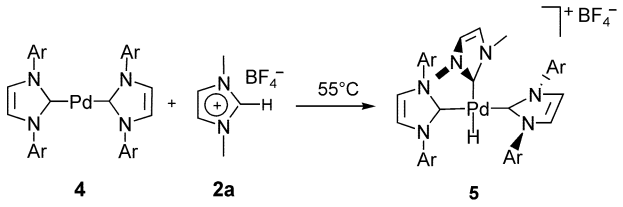


Figure 1. Molecular structure of **3b** (ORTEP diagram drawn at the 25% probability level). Selected bond lengths [Å] and bond angles [°]: Ni1-C22 1.891(3), Ni1-C1 1.895(4), Ni1-C43 1.936(4), Ni1-H1 1.38(5), C22-Ni1-C1 164.22(16), C22-Ni1-C43 98.40(15), C1-Ni1-C43 97.30(15), C22-Ni1-H1 83(2), C1-Ni1-H1 81(2), C43-Ni1-H1 179(2).

Complex **3b** exhibits a distorted square-planar geometry in which the two mesityl-substituted carbenes have a *trans* disposition. Steric crowding between the two mesityl-substituted carbenes and the 1-butyl-3-methyl-substituted carbene causes the bulky mesityl-substituted carbenes to be pushed towards the small hydride group with an angle C22-Ni-C1 of 164.22(16)°. The surprising stability of such complexes could be rationalized in terms of both steric and electronic effects imparted by the three carbene ligands. Steric bulk around the metal center hinders orbital overlap between the hydride and the carbene carbon that would favor reductive elimination of imidazolium salt.[9] As well as protecting the mesityl-substituted carbenes against reductive elimination, the bulk of these two carbenes forces the hydride to be *trans* to the 1-butyl-3-methyl-substituted carbene.

We employed a similar approach to synthesize a stable Pd–H complex from coordinatively unsaturated L_2Pd^0 complexes[10] (L = NHC). For example, when equimolar quantities of imidazolium salt **2a** and complex **4** were stirred together at 55 °C in an acetone/THF mixture, the yellow color of **4** quickly disappeared to give a colorless solution (Scheme 2).



Scheme 2. C–H oxidative addition of imidazolium salt to Pd^0 complex **4**: acetone/THF, 15 min.

The triscarbene–palladium–hydrido complex **5**, which was isolated as colorless crystals in 62% yield, gives rise to a Pd–H signal at $\delta = -10.17$ ppm in the ^{1}H NMR spectrum (C_6D_6). As observed for its nickel counterpart, this complex is surprisingly stable both in solution and in the solid state. The full molecular geometry of **5** was elucidated by single-crystal X-ray crystallography (Figure 2).[8] This complex represents the first fully characterized palladium hydride complex with carbene ligands. During the synthesis of complex **5**, small amounts of several other palladium–hydride complexes were noted in solution in the nonrecrystallized product. A Pd–hydride complex with a ^{1}H NMR resonance at $\delta = -15.84$ ppm was frequently observed (a Pd–H resonance at $\delta = -14.85$ ppm was reported by Nolan and co-workers for an unidentified complex formed during the reaction of an imidazolium salt with Pd^0[6a]). We were unable to isolate or identify the complex with the resonance observed at $\delta = -15.84$ ppm.

It is interesting to note in complex **5** a possible $H^{\delta+}\cdots H^{\delta-}$ intramolecular interaction in view of the short H42b–H1 distance of 2.07 Å (significantly less than twice the van der Waals radius for H of 2.4 Å expected in the absence of an attractive interaction) together with angles Pd-H···H and

 © 2004 Wiley-VCH Verlag GmbH & Co. KGaA, Weinheim

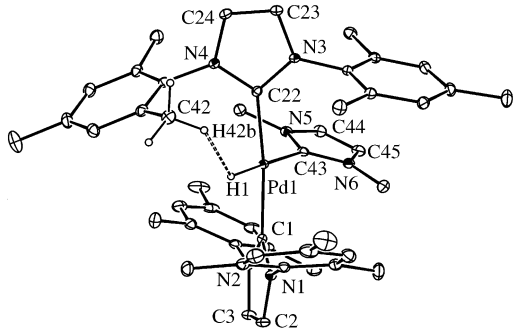


Figure 2. Molecular structure of **5** (ORTEP diagram drawn at the 25% probability level). Selected bond lengths [Å] and bond angles [°]: Pd1-C1 2.030 (2), Pd1-C22 2.031(2), Pd1-C43 2.111(2), Pd1-H1 1.57(3), C1-Pd1-C22 168.02(8), C1-Pd1-C43 95.78(9), C22-Pd1-C43 96.20(8), C1-Pd1-H1 82.0(10), C22-Pd1-H1 86.0(10), C43-Pd1-H1 177.0(10).

H···H-C of 132.0° and 129.8°, respectively. This is an unusual example of such an H···H interaction; it involves a Group 10 metal hydride (other examples involve Group 8 and 9 metals) with a hydrogen atom coordinated to a carbon atom rather than to an electronegative heteroatom, as is commonly the case.[11] Further characterization of this hydridic-to-protonic interaction will be reported elsewhere. The nickel–hydride complex also shows a similar, but less significant H–H close-approach (shortest H(Me)–H1 distance of 2.41 Å].

These observations have a number of important ramifications for NHC chemistry: a) The results show irrevocably that carbene or carbene–metal–hydride species readily form under mild conditions in the presence of imidazolium salts, especially with Group 10 metals. This is likely to occur in situ when a coordinatively unsaturated, low-valent metal species (particularly when bearing strong σ-donor ligands) are present or are formed during a reaction, for example, under catalytic conditions in an ionic liquid solvent. b) The direct generation of a carbene–M–H species in situ may provide an important atom-efficient route to active catalytic species under mild conditions. Metal–carbene complexes are being applied more and more widely in catalysis, and metal hydrides are implicated in many catalytic processes. c) The almost directional distribution of steric bulk, encapsulating sites on the metal center, and the unusual electronic features of carbene ligands allow the stabilization of normally highly reactive species.[12]

The ease of formation of complexes **3** and **5** together with their remarkable stability is an example of how NHC ligands may allow the isolation of new and normally reactive species. In summary, we have demonstrated that direct C2–H activation of imidazolium salts by coordinatively unsaturated low valent Ni and Pd complexes such as **1** and **4** can be a facile process.

Received: November 26, 2003 [Z53409]
Published Online: February 11, 2004

Keywords: C–H activation · carbene ligands · hydride ligands · hydrogen bonding · ionic liquids

[1] T. Welton, *Chem. Rev.* **1999**, *99*, 2071; P. Wasserscheid, W. Keim, *Angew. Chem.* **2000**, *112*, 3926; *Angew. Chem. Int. Ed.* **2000**, *39*, 3772; R. Sheldon, *Chem. Commun.* **2001**, 2399; J. Dupont, R. F. de Souza, P. A. Z. Suarez, *Chem. Rev.* **2002**, *102*, 3667.

[2] a) A. J. Carmichael, M. J. Earle, J. D. Holbrey, P. B. McCormac, K. R. Seddon, *Org. Lett.* **1999**, *1*, 997; b) L. Xu, W. Chen, J. Xiao, *Organometallics* **2000**, *19*, 1123; c) C. J. Mathews, P. J. Smith, T. Welton, A. J. P. White, D. J. Williams, *Organometallics* **2001**, *20*, 3848; d) other reactions involving imidazolium type ionic liquids and transition-metal complexes have also been described, for example, dealkylation of the imidazolium ring: J. E. L. Dullius, P. A. Z. Suarez, S. Einloft, R. F. de Souza, J. Dupont, J. Fischer, A. De Cian, *Organometallics* **1998**, *17*, 815; the hydrolysis of the anion, such as PF_6^-: G. S. Fonseca, A. P. Umpierre, P. F. P. Fichtner, S. R. Teixeira, J. Dupont, *Chem. Eur. J.* **2003**, *9*, 3263.

[3] A. J. Arduengo III, R. L. Harlow, M. Kline, *J. Am. Chem. Soc.* **1991**, *113*, 361; A. J. Arduengo III, *Acc. Chem. Res.* **1999**, *32*, 913; W. A. Herrmann, C. Köcher, *Angew. Chem.* **1997**, *109*, 2256; *Angew. Chem. Int. Ed. Engl.* **1997**, *36*, 2162, and references therein.

[4] a) D. S. McGuinness, K. J. Cavell, B. F. Yates, *Chem. Commun.* **2001**, 355; b) D. S. McGuinness, K. J. Cavell, B. F. Yates, B. W. Skelton, A. H. White, *J. Am. Chem. Soc.* **2001**, *123*, 8317; c) M. A. Duin, N. D. Clement , K. J. Cavell, C. J. Elsevier, *Chem. Commun.* **2003**, 400.

[5] a) P. J. Fraser, W. R. Roper, F. G. A. Stone, *J. Chem. Soc. Dalton Trans.* **1974**, 102; P. J. Fraser, W. R. Roper, F. G. A. Stone, *J. Chem. Soc. Dalton Trans.* **1974**, 760; b) A. Fürstner, G. Seidel, D. Kremzow, C. W. Lehmann, *Organometallics* **2003**, *22*, 907.

[6] a) M. S. Viciu, G. A. Grasa, S. P. Nolan, *Organometallics* **2001**, *20*, 3607; b) S. Gründemann, M. Albrecht, A. Kovacevic, J. W. Faller, R. H. Crabtree, *J. Chem. Soc. Dalton Trans.* **2002**, *10*, 2163.

[7] A. J. Arduengo III, S. F. Gamper, J. C. Calabrese, F. Davidson, *J. Am. Chem. Soc.* **1994**, *116*, 4391.

[8] Crystal data for **3b**·$(CH_2Cl_2)_2$: $C_{52}H_{67}BCl_4F_4N_6Ni$, $M = 1063.44$, monoclinic, space group $P2_1/n$, $a = 14.121(3)$, $b = 15.464(3)$, $c = 25.045(5)$ Å, $\beta = 93.12(3)°$, $V = 5460.9(19)$ Å^3, $Z = 4$, $\rho_{calcd} = 1.293$ g cm^{-3}, $F(000) = 2232$, $\mu(Mo_{K\alpha}) = 0.604$ mm^{-1}, 150(2) K, 9970 unique reflections ($R_{int} = 0.0669$), R (on F) 0.0679, wR (on F^2) 0.1771 ($I > 2\sigma(I)$). Crystal data for **5**·$(C_6H_6)_{0.5}$: $C_{50}H_{60}BF_4N_6Pd$, $M = 938.25$, triclinic, space group $P\bar{1}$, $a = 10.697(2)$, $b = 12.118(2)$, $c = 20.101(4)$ Å, $\alpha = 102.78(3)$, $\beta = 90.78(3)$, $\gamma = 108.65(3)°$, $V = 2397.6(8)$ Å^3, $Z = 2$, $\rho_{calcd} = 1.300$ g cm^{-3}, $F(000) = 978$, $\mu(Mo_{K\alpha}) = 0.442$ mm^{-1}, 150(2) K, 9770 unique reflections ($R_{int} = 0.0684$), R (on F) 0.0352, wR (on F^2) 0.0834 ($I > 2\sigma(I)$). CCDC-223761 (**3b**) and CCDC-223762 (**5**) contain the supplementary crystallographic data for this paper. These data can be obtained free of charge via www.ccdc.cam.ac.uk/conts/retrieving.html (or from the Cambridge Crystallographic Data Centre, 12, Union Road, Cambridge CB21EZ, UK; fax: (+44) 1223-336-033; or deposit@ccdc.cam.ac.uk).

[9] D. S. McGuinness, N. Saendig, B. F. Yates, K. J. Cavell, *J. Am. Chem. Soc.* **2001**,*123*, 4029.

[10] V. P. W. Böhm, C. W. K. Gstöttmayr, T. Weskamp, W. A. Herrmann, *J. Organomet. Chem.* **2000**, *595*, 186.

[11] T. B. Richardson, T. F. Koetzle, R. H. Crabtree, *Inorg. Chim. Acta* **1996**, *250*, 69; W. Xu, A. J. Lough, R. H. Morris, *Can. J. Chem.* **1997**, *75*, 475; Y. A. Abramov, L. Brammer, W. T. Klooster, R. M. Bullock, *Inorg. Chem.* **1998**, *37*, 6317; R. Custelcean, J. E. Jackson, *Chem. Rev.* **2001**, *101*, 1963.

[12] R. Dorta, E. D. Stevens, C. D. Hoff, S. P. Nolan, *J. Am. Chem. Soc.* **2003**, *125*, 10490.

 © 2004 Wiley-VCH Verlag GmbH & Co. KGaA, Weinheim

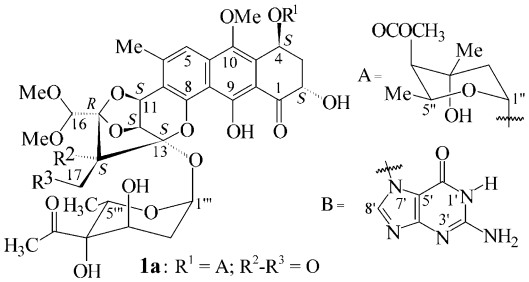
Marine Natural Products

Gutingimycin: A Highly Complex Metabolite from a Marine Streptomycete**

*Rajendra P. Maskey, Madhumati Sevvana, Isabel Usón, Elisabeth Helmke, and Hartmut Laatsch**

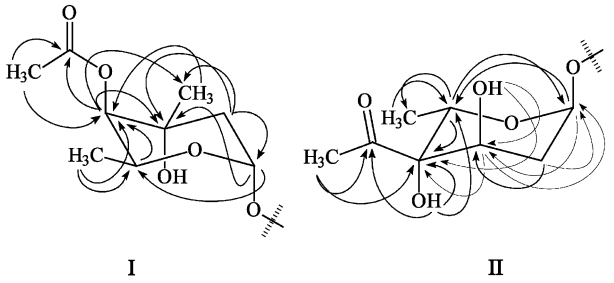
In our search for novel bioactive secondary metabolites of marine streptomycetes, the ethyl acetate extract of the isolate B8652 drew our attention by its high antibiotic activity against *Staphylococcus aureus*, *Escherichia coli*, *Bacillus subtilis*, and *Streptomyces viridochromogenes* (Tü57). The new 2,3-dihydro-1,4-anthraquinone parimycin[1] and the yellow trioxacarcines A–F,[2] which exhibit intensive green fluorescence in solution, were mainly responsible for this activity.

For the isolation of a further, highly polar trioxacarcin derivative, the culture filtrate had to be concentrated and lyophilized, and the residue was further extracted with methanol. In this way, a 50-L fermentation yielded 120 mg of a novel natural product with the trioxacarcin skeleton, however, with higher complexity, which we have named gutingimycin (**1c**), after Gutingi, the old name of Göttingen.



1a: R^1 = A; R^2-R^3 = O
1b: R^1 = A; R^2 = R^3 = OH
1c: R^1 = A; R^2 = OH; R^3 = B
1d: R^1 = H; R^2 = OH; R^3 = B

Like the other trioxacarcines, gutingimycin (**1c**) is yellow in substance, fluoresces green in solution upon irradiation with 366-nm light, and delivers an ^{1}H NMR spectrum typical for this group of compounds. The (+)- and (−)-ESI mass spectra exhibit signals at $m/z = 1050$ ($[M+Na]^+$) and 1028 ($[M+H]^+$), and at $m/z = 1063$ ($[M+Cl]^-$) and 1026 ($[M-H]^-$), respectively, which indicate a molecular weight of 1027. High-resolution mass spectrometry suggest the molecular formula to be either $C_{49}H_{57}NO_{23}$ or $C_{47}H_{57}N_5O_{21}$. The ^{13}C NMR, H,H COSY, HMQC, and HMBC spectra as well as the coupling constants in the ^{1}H NMR spectrum confirm that the sugar residues **I** and **II** are the same those as in trioxacarcin B (**1b**) (Figure 1). The aglycon (Figure 2) is identical to that of **1b** as



I II

Figure 1. HMBC couplings (H→C) of the sugar residues in gutingimycin (**1c**).

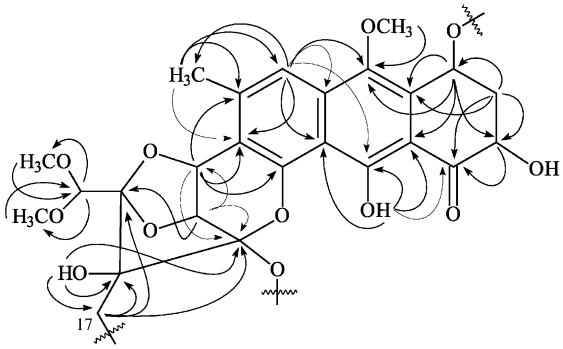


Figure 2. HMBC couplings (H→C) in the aglycon of gutingimycin (**1c**).

well, except for the residue at C17. The HMBC couplings of the anomeric protons at $\delta = 5.74$ (1‴H), 5.52 (1″H), and 5.36 ppm (4H) with the carbon signals at $\delta = 103.3$ (C13), 72.2 (C4), and 100.8 ppm (C1″), respectively, allow the connection of the sugars with the aglycon, yielding the partial structure **1c** with the mass 877 ($C_{42}H_{53}O_{20}$) and a still-unknown residue R^3. This initial assignment was further confirmed by comparison of the ^{13}C NMR data with those of trioxacarcin B (**1b**).

In the 1D and 2D NMR spectra of gutingimycin, altogether nine acidic protons were detected. Three of them can be assigned unambiguously to the aglycon and two to the sugars. The third OH group of the sugar **I** showed couplings neither in the H,H COSY nor in the HMBC spectrum. From the remaining signals at $\delta = 8.86$, 7.55, 6.64, and 6.10 ppm, three must belong therefore to the residue R^3 in **1c**.

In the ^{1}H NMR spectrum a CH singlet at $\delta = 8.23$ ppm is observed, which is not present in the spectrum of **1b**. According to the ^{13}C NMR spectrum, the heteroatom-con-

[*] Dr. R. P. Maskey, Prof. Dr. H. Laatsch
Institut für Organische und Biomolekulare Chemie
Georg-August-Universität Göttingen
Tammannstrasse 2, 37077 Göttingen (Germany)
Fax: (+49) 551-399-660
E-mail: hlaatsc@gwdg.de
M. Sevvana, Dr. I. Usón
Institut für Anorganische Chemie
Georg-August-Universität Göttingen (Germany)
Dr. E. Helmke
Alfred-Wegener-Institut für Polar- und Meeresforschung
Bremerhaven (Germany)

[**] Marine Bacteria, Part 26. This work was supported by the Bundesministerium für Bildung und Forschung (BMBF 03F0346A). R.P.M. thanks the Deutschen Akademischen Austauschdienst (DAAD) for a Ph.D. scholarship. Part 25: R. P. Maskey, E. Helmke, H. Laatsch, *J. Antibiot.* **2003**, *56*, 942–949.

 DOI: 10.1002/anie.200352312 © 2004 Wiley-VCH Verlag GmbH & Co. KGaA, Weinheim

nected C atoms with signals at $\delta = 157.7$, 153.4, and 151.7 ppm, a CH group at $\delta = 140.4$ ppm, and a C atom at $\delta = 108.3$ ppm must be attributed to the partial structure R^3. In the HMBC spectrum, the aromatic proton signal at $\delta =$ 8.23 ppm couples to the carbon signals of the residue R^3 at $\delta =$ 157.7, 153.4, and 108.3 ppm.

Formally, gutingimycin (**1c**) is formed from trioxacarcin A (**1a**) by the attack of a nucleophile, which the mass difference indicates to have a molecular weight of 151. Among the compounds isolated from microorganisms with this mass and the same number of C atoms and acidic protons, only guanine, isoguanine, and akalone are plausible candidates.[3] As HMBC correlations connecting the residue R^3 with the trioxacarcin skeleton or determining its connectivity were missing, further confirmation of the structure was not possible.

The remaining questions were finally solved by a crystal structure analysis: Gutingimycin (**1c**) crystallizes in the monoclinic space group $P2_1$ with one molecule of the metabolite and four molecules of water in the asymmetric unit[4] (Figure 3). It consists of the trioxacarcin A substructure

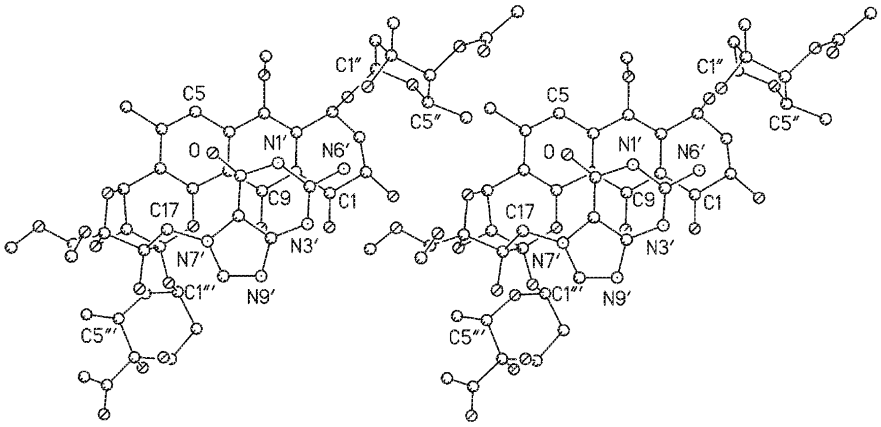
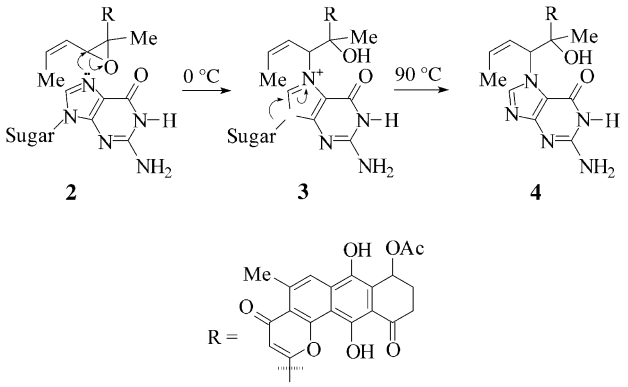


Figure 3. X-ray crystal structure of gutingimycin (**1c**) as a stereoplot.

(**1a**), whose epoxide ring has been opened, however, through the nucleophilic attack of N7 of the guanine base at atom C17. The guanine substructure is oriented nearly parallel to the planar condensed ring system of **1c** with a distance of approximately 3.2 Å between the two planes. This conformation is stabilized by an intramolecular hydrogen bond between 2″-OH and the hydrogen atom at N6′. Based on the previously reported absolute configuration of the sugars L-trioxacarcinose A and B,[5] we assigned the absolute configuration of the trioxacarcines as well as that of **1c**.

A compound structurally related to gutingimycin (**1c**) was obtained by Saito et al.[6] from the reaction of kapurimycin A3 (**2**) with DNA as well as with synthetic oligonucleotides (Scheme 1). At 0 °C the ionic intermediate **3** was produced, which on heating at 90 °C decomposed to form **4**. The latter had not been obtained previously as a natural product. Trioxacarcin A (**1a**) forms a highly polar, stable complex with DNA in the same manner, from which at 100 °C **1c** is easily liberated. It seems plausible, therefore, that gutingimycin (**1c**) is not formed from smaller precursors, but by the attack of **1a**



Scheme 1. In the reaction of kapurimycin A3 (**2**) with DNA as well as with synthetic oligonucleotides the ionic intermediate **3** is produced, which on heating at 90 °C decomposes to form **4**, a compound related to gutingimycin.

on the cellular DNA in analogy to the attack of **2**. In this way alkylation at N7 occurs, the aminal bond of the nucleotide breaks, and with strand cleavage, the extremely water-soluble **1c** is formed.

According to the structure, gutingimycin (**1c**) should not exhibit alkylating properties, which coincides with the fact that **1c** ($IC_{70} =$ 3.4 $\mu g\,mL^{-1}$) is much less cytotoxic than **1a** ($IC_{70} = < 0.3\ \mu g\,mL^{-1}$). The MIC values of trioxacarcin A (**1a**) for *Bacillus subtilis*, *Streptomyces viridochromogenes* (Tü 57), *Staphylococcus aureus*, and *Escherichia coli* are in the range of 0.15–2.5 $\mu g\,mL^{-1}$ in comparison to gutingimycin (**1c**) which has $> 20\ \mu g\,mL^{-1}$.

The highly cytotoxic actinomycin D intercalates in a similar way into the DNA at neighboring guanine–cytosine base pairs,[7] however, does not lead to strand breakage. The numerous alkylating agents used in the cancer therapy, like the N- or S-lost derivatives, also attack the guanine residues preferably, although without intercalating. It is now of great interest to determine which intermediates in this reaction may occur and if structurally related antibiotics, for example, the indomycinones, react in a similar manner. Details of the interaction of **1a** and **1c** with DNA are currently under investigation.

Experimental Section

Materials, methods, and test procedures have been described previously.[8] The marine streptomycete isolate B8652 was incubated in a 50-L fermenter under our standard conditions[1] with malt extract/yeast extract/glucose for 3 d at 28 °C and extracted with ethyl acetate (extract A). The aqueous phase was concentrated under vacuum (40 °C water-bath temperature) to approximately 3 L and lyophilized. Extraction of the residue with methanol gave extract B.

Preseparation of extract A on silica gel gave a polar, yellow, gutingimycin-containing fraction with green fluorescence under UV light. Further separation of the fraction by preparative thin-layer chromatography (4 plates 20×20 cm, $CHCl_3$/15 % MeOH/0.1 % AcOH) delivered a crude product with $R_f = 0.21$ ($CHCl_3$/10 % MeOH) and intensive green fluorescence at 366 nm, which yielded

 © 2004 Wiley-VCH Verlag GmbH & Co. KGaA, Weinheim

60 mg yellow gutingimycin (**1c**) after twofold chromatography on Sephadex LH-20 (4 × 100 cm, $CHCl_3$/40% MeOH). Purification of extract B in the similar way delivered an additional 60 mg of **1c**.

^{1}H NMR ($CDCl_3$, 500 MHz): $\delta = 13.88$ (s, H/D exchangeable, 1H, 9-OH), 8.86 (br s, H/D exchangeable, 1H, NH), 8.23 (s, 1H, 8′H), 7.55 (br s, H/D exchangeable, 1H, NH), 7.51 (s, 1H, 5H), 6.64 (br s, H/D exchangeable, 1H, NH), 6.52 (br s, H/D exchangeable, 1H, 2OH), 6.10 (br s, H/D exchangeable, 1H, OH), 5.74 (d, $^3J = 3.2$ Hz, 1H, 1‴H), 5.52 (d, $^3J = 4.2$ Hz, 1H, 1″H), 5.42 (s, H/D exchangeable, 1H, 16OH), 5.36 (t, $^3J = 2.4$ Hz, 1H, 4H), 5.28 (d, $^3J = 4.0$ Hz, 1H, 12H), 5.13 (1H, 4″H), 5.12 (1H, 11H), 5.11 (s, 1H, 16H), 5.05 (d, $^2J = 15.1$ Hz, 1H, $17H_A$), 5.02 (q, $^3J = 6.3$ Hz, 1H, 5‴H), 4.93 (q, $^3J = 6.6$ Hz, 1H, 5′H), 4.77 (t, $^3J = 3.2$ Hz, 1H, 2H), 4.73 (d, $^3J = 4.1$ Hz, H/D exchangeable, 1H, 3″OH), 4.37 (d, $^2J = 15.9$ Hz, 1H, $17H_B$), 4.01 (s, H/D exchangeable, 1H, 4″OH), 3.97 (s, 3H, $10OCH_3$), 3.75 (m, 1H, 3‴H), 3.67 (s, 3H, $16OCH_3$), 3.55 (s, 3H, $16OCH_3$), 2.99 (td, $^3J = 3.9$ Hz, $^2J = 13.3$ Hz, 1H, $3H_A$), 2.64 (s, 3H, $6CH_3$), 2.51 (s, 3H, 4‴$COCH_3$), 2.30 (td, $^3J = 3.4$ Hz, $^2J = 14.2$ Hz, 1H, $2'''H_A$), 2.24 (s, 3H, 4″$OCOCH_3$), 2.23 (m, 1H, $2''H_A$), 2.00 (td, $^2J = 13.2$ Hz, $^3J = 13.2$, 2.7 Hz, 1H, $3H_B$), 1.85 (d, $^2J = 14.8$ Hz, 1H, $2''H_B$), 1.78 (d, $^2J = 13.6$ Hz, 1H, $2'''H_B$), 1.25 (d, $^3J = 6.7$ Hz, 3H, $5''CH_3$), 1.18 (s, 3H, $3''CH_3$), 1.08 ppm (d, $^3J = 6.6$ Hz, 3H, $5'''CH_3$); ^{13}C NMR ($CDCl_3$, 125.7 MHz): $\delta = 210.9$ (4‴*C*OCH_3), 207.6 (C1), 173.2 (4″*O*COCH_3), 162.9 (C9), 157.7 (C6′), 153.0 (C4′), 152.7 (C8), 151.7 (C2′), 144.6 (C10), 142.4 (C6), 140.4 (C8′), 135.7 (C10a), 128.4 (C4a), 116.8 (C5), 114.5 (C8a), 113.1 (C7), 108.8 (C9a), 108.3 (C5′), 108.2 (C15), 103.3 (C13), 100.8 (C1″), 99.5 (C16), 92.9 (C1‴), 84.4 (C14), 78.5 (C4‴), 75.8 (C4″), 72.2 (C4), 71.6 (C12), 69.5 (C3‴), 69.0 (C11), 68.2 (C2), 67.2 (C3″), 63.7 (C5‴), 62.7 (10*O*CH_3), 62.2 (C5″), 55.4 (16*O*CH_3), 56.2 (16*O*CH_3), 46.2 (C17), 37.8 (C2″), 37.0 (C3), 32.9 (C2‴), 27.8 (4‴CO*C*H_3), 27.2 (3″*C*H_3), 21.2 (4″OCO*C*H_3), 20.2 (6*C*H_3), 16.8 (5″*C*H_3), 14.6 ppm (5‴*C*H_3); (+)-ESI-MS: $m/z = 1050$ [M+Na], 1028 [M+H]; (−)-ESI-MS: $m/z = 1063$ [M+Cl], 1027 [M−H]; HRMS calcd for $C_{47}H_{57}N_5O_{21}$: 1027.354604, found: 1027.3257; UV/Vis (MeOH): λ_{max} (lg ε) = 269 (5.53), 399 (4.96) nm; IR (KBr): $\tilde{\nu} = 3438$, 2938, 2362, 1695, 1626, 1445, 1385, 1225, 1089, 1000, 871, 822, 755, 672, 554 cm^{-1}; $[\alpha]_D^{20} = -56.5$ ($c = 584$ μg mL^{-1}, $CHCl_3$).

Received: July 4, 2003 [Z52312]

Keywords: antibiotics · glycosides · gutingimycin · natural products · structure determination

[1] R. P. Maskey, E. Helmke, H. H. Fiebig, H. Laatsch, *J. Antibiot.* **2002**, *55*, 1031 – 1035.

[2] a) R. P. Maskey, E. Helmke, O. Kayser, H. H. Fiebig, H. Laatsch, *J. Antibiot.*, submitted; b) F. Tomita, T. Tamaoki, M. Morimoto, K. Fujimoto, *J. Antibiot.* **1981**, *34*, 1519 – 1524; c) T. Tamaoki, K. Shirahata, T. Iida, F. Tomita, *J. Antibiot.* **1981**, *34*, 1525 – 1530.

[3] H. Izumida, K. Adachi, M. Nishijima, M. Endo, W. Miki, *J. Mar. Biotechnol.* **1995**, *2*, 115 – 118.

[4] Crystallographic data for **1c**: $C_{47}H_{57}O_{21}N_5 + 4H_2O$, $M_r = 1100.04$, monoclinic, space group $P2_1$, $a = 17.736(3)$, $b = 7.091(2)$, $c = 19.816(3)$ Å, $\gamma = 90.00°$, $V = 2510.3(9)$ Å^3, $Z = 2$, $\rho_{calc} = 1.379$, $F(000) = 1164$, $\lambda = 1.54178$ Å, $T = 133$ K, crystal dimensions 0.3 × 0.1 × 0.05 mm^3, $2 \le 2\theta \le 118$, of 18834 measured data, 3897 were independant ($R_{int} = 0.015$ Friedel mates merged). Refinement: 737 parameters, 729 restraints, $R_1(\%) = \Sigma F_o - F_c / \Sigma F_o = 4.41$ for 3357 $F_o > 4\sigma(F_o)$ and 5.67 for 3897 (all data), $wR_2 = [\Sigma w(F_o^2 - F_c^2 / \Sigma w(F_o^2)^2]^{1/2} = 0.1100$ (all data), min/max residual electron density −0.24/0.23 e Å^3. Data for **2c** were collected on a three-circle diffractometer with a CCD detector and φ scans on a flash-frozen crystal in an oil drop in a loop. The data was integrated with the program SAINT. All data were corrected semiempirically for systemic errors such as absorption. The structure was solved by using the dual-space recycling method (SHELXD[9]) and refined against F^2 by least squares. All non-hydrogen atoms were refined anisotropically. The hydrogen atoms were placed in geometrically ideal positions and refined with a riding model, in which the methyl groups can rotate on their local axes. CCDC-213711 contains the supplementary crystallographic data for this paper. These data can be obtained free of charge via www.ccdc.cam.ac.uk/conts/retrieving.html (or from the Cambridge Crystallographic Data Centre, 12, Union Road, Cambridge CB2 1EZ, UK; fax: (+44) 1223-336-033; or deposit@ccdc.cam.ac.uk).

[5] K. Shirahata, T. Iida, N. Hirayama, *Tennen Yuki Kagobutsu Toronkai Koen Yoshishu* **1981**, *24*, 199 – 206.

[6] a) K. L. Chan, H. Sugiyama, I. Saito, M. Hara, *Phytochemistry* **1995**, *40*, 1373 – 1374; b) K. L. Chan, H. Sugiyama, I. Saito, *Tetrahedron Lett.* **1991**, *32*, 7719 – 7722.

[7] U. Hollstein, *Chem. Rev.* **1974**, *74*, 625 – 652.

[8] R. P. Maskey, R. N. Asolkar, E. Kapaun, I. Wagner-Döbler, H. Laatsch, *J. Antibiot.* **2002**, *55*, 643 – 649.

[9] I. Usón, G. M. Sheldrik, *Curr. Opin. Struct. Biol.* **1999**, *9*, 643 – 648.

 © 2004 Wiley-VCH Verlag GmbH & Co. KGaA, Weinheim

Coordination Chemistry

Bispidine Ligand Effects on Iron/Hydrogen Peroxide Chemistry**

Michael R. Bukowski, Peter Comba, Christian Limberg, Michael Merz, Lawrence Que, Jr.,* and Tobias Wistuba*

The long-term interest in dioxygen activation by heme centers has recently been extended to non-heme iron systems,[1–3] both of which can catalyze the stereoselective oxidation of C–H and C=C bonds. Key intermediates include Fe^{III} η^1-hydroperoxo and Fe^{III} η^2-peroxo species, which have been identified for cytochrome P450,[4] bleomycin,[5] and naphthalene dioxygenase.[6] A range of synthetic non-heme iron complexes with amine/pyridine ligand combinations has been

[*] Prof Dr. P. Comba, Dr. M. Merz, Dr. T. Wistuba
Universität Heidelberg, Anorganisch-Chemisches Institut
Im Neuenheimer Feld 270, 69120 Heidelberg (Germany)
Fax: (+49) 6226-546617
E-mail: peter.comba@aci.uni-heidelberg.de

M. R. Bukowski, Prof. Dr. L. Que, Jr.
Department of Chemistry and Center for Metals in Biocatalysis
University of Minnesota
207 Pleasant Street SE, Minneapolis MN 55455 (USA)
Fax: (+1) 612-624-7029
E-mail: que@chem.umn.edu

Prof. Dr. C. Limberg
Humboldt-Universität zu Berlin
Institut für Chemie
Brook-Taylor-Strasse 2, 12489 Berlin (Germany)
Fax: (+49) 30-2093-6966

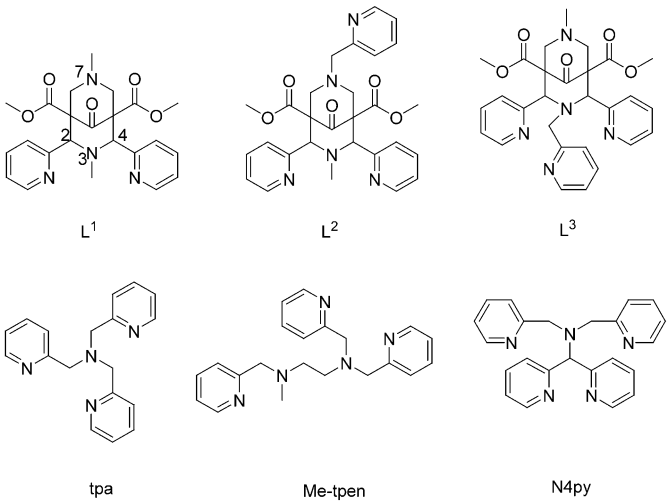
[**] Financial support by the German Science Foundation (DFG to P.C. and C.L.) and the U.S. National Institutes of Health (GM-33162 to L.Q.) are gratefully acknowledged.

 DOI: 10.1002/anie.200352523 © 2004 Wiley-VCH Verlag GmbH & Co. KGaA, Weinheim

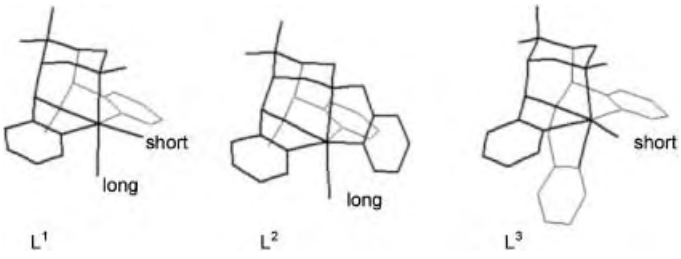
found to catalyze hydrocarbon oxidations with H_2O_2 as oxidant.[3] Extensive spectroscopic and labeling studies have led to a thorough understanding of the properties of the Fe^{III} intermediates,[3] and support for a mechanistic proposal involving high-valent iron-oxo species for the catalytic alkane hydroxylation, olefin epoxidation, and olefin *cis*-dihydroxylation has been obtained.

A set of iron complexes with pentadentate N_5 ligands that react with H_2O_2 to afford metastable low-spin Fe^{III} η^1-OOH intermediates with hydroperoxo-to-Fe^{III} charge-transfer bands in the 500-nm region has been extensively studied.[7–9] Deprotonation of these species affords their respective conjugate bases with lower energy charge-transfer bands; spectroscopic studies support their assignment as the corresponding high-spin Fe^{III} side-on peroxo derivatives. To date, no crystal structures are available for any of these Fe^{III} intermediates, so their precise structures remain to a large extent a matter of speculation.

The rigid tetra- and pentadentate bispidine derivatives L^1–L^3 have donor sets similar to tpa and N4py, the iron complexes of which represent the most active oxidation catalysts in non-heme iron chemistry (for ligand structures see Scheme 1, for complex structures see Scheme 2).[7,10,11] L^1–L^3 provide a rigid ligand backbone and enforce *cis*-octahedral (or square-pyramidal) coordination geometries for a range of metal ions.[12,13] The most relevant structural feature is that for the two coligands (substrates) in $[Fe^{II}(L^1)(X)(Y)]^{n+}$ the metal–ligand distances are significantly different, with that



Scheme 1. Molecular formula of the ligands discussed.



Scheme 2. Representations of the metal–ligand complexes.

trans to N3 being shorter than that *trans* to N7 (see Scheme 2). With the two isomeric ligands L^2 and L^3, the coordination sites *trans* to N3 and *trans* to N7, respectively, are blocked by an additional pendant pyridine arm. This leaves one coordination site for H_2O_2 binding and thus provides us with the opportunity to explore the effects of steric and electronic constraints on the properties of the Fe–OOH and Fe–OO units. Based on extensive structural, spectroscopic, electrochemical, and computational studies of $Cu^{II/I}$ bispidine complexes,[13–16] the iron complexes with L^2 and L^3 are expected to have strikingly different structural[12] and electronic properties. Here we report the spectroscopic properties of the Fe^{III} hydroperoxo and peroxo complexes; the reactivities of these oxidation catalysts will be reported separately.[17]

Following the precedent for the observation of the $[Fe(OOH)(N4py)]^{2+}$ intermediate,[18] we have investigated the reactions of the high-spin Fe^{II} complexes of L^2 and L^3 with excess H_2O_2 in MeOH at −40 °C. Purple chromophores are observed that can be assigned to the formation of low-spin Fe^{III} complexes with end-on hydroperoxo ligands. Thus, addition of ten equivalents of H_2O_2[19] to $[Fe(L^3)(solvent)]^{2+}$[21] leads to a new species with a charge-transfer transition at 561 nm (Figure 1), similar to those observed for a

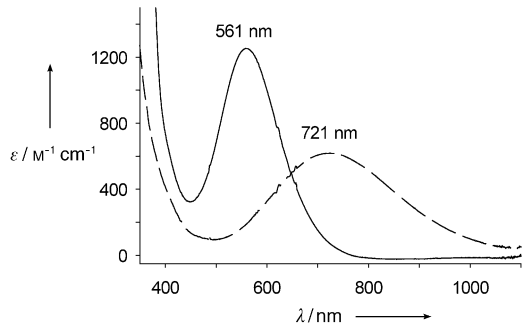


Figure 1. Absorption spectra of $[Fe^{III}(OOH)(L^3)]^{2+}$ (——; from the reaction of $[Fe^{II}(L^3)](BF_4)_2$ with 100 equiv H_2O_2 in methanol at −40 °C) and of $[Fe^{III}(O_2)(L^3)]^{+}$ (-----; after addition of 14 equiv base).

number of low-spin Fe^{III} hydroperoxo complexes (see Table 1 for data of the iron bispidine and similar compounds).[22] The low-spin character of $[Fe(OOH)(L^3)]^{2+}$ is confirmed by its EPR signals at $g = 2.18, 2.12, 1.95$ (Table 1). Similar results are obtained for the complex with L^2 (Table 1, Figure 2).

Resonance Raman studies show that $[Fe(OOH)(L^2)]^{2+}$ and $[Fe(OOH)(L^3)]^{2+}$ give rise to the two expected features that can be assigned to $\nu_{Fe\text{-}OOH}$ and $\nu_{O\text{-}O}$ (Table 1). Isotopic labeling studies (shown in Figure 3 for $[Fe(OOH)(L^3)]^{2+}$) establish these assignments. The ^{18}O and ^{2}H isotope shifts for the $\nu_{Fe\text{-}OOH}$ vibration for the L^2 and L^3 complexes, unlike those observed for $[Fe(OOH)(N4py)]^{2+}$,[9,18] are almost precisely as predicted by a simple calculation based on Hooke's law, assuming the hydroperoxo moiety to be a single mass unit. Interestingly, while the $\nu_{O\text{-}O}$ vibrations of the two intermediates are identical, the $\nu_{Fe\text{-}OOH}$ vibration for the L^2 complex is shifted to lower energy by 12 cm^{-1} relative to that of the L^3 isomer, consistent with the expectation of a weaker bond (see Scheme 2).

 © 2004 Wiley-VCH Verlag GmbH & Co. KGaA, Weinheim

Table 1: Spectroscopic properties of $[Fe^{III}(\eta^1\text{-OOH})(L)]^{2+}$ and $[Fe^{III}(\eta^2\text{-OO})(L)]^{+}$ intermediates.

Ligand	$[Fe(L)OOH]^{2+}$, $S=1/2$				$[Fe(L)OO]^{+}$, $S=5/2$			
	λ_{max} [nm] (ε [$M^{-1}cm^{-1}$])	EPR *g*-values	ν(Fe-O) [cm^{-1}] ($\Delta^{18}O$) [$\Delta^{2}H$]	ν(O-O) [cm^{-1}] ($\Delta^{18}O$)	λ_{max} [nm] (ε [$M^{-1}cm^{-1}$])	EPR E/D	ν(Fe-O) [cm^{-1}]	ν(O-O) [cm^{-1}]
L^2	561 (1260)	2.19, 2.13, 1.96	608 (−24) [−5]	804 (−44)	780 ($\geq$350)	0.24	not observed	not observed
L^3	561 (1300)	2.18, 2.12, 1.95	620 (−22) [−6]	804 (−43)	721 (540)	0/0.33	493	827
N4py[9,18]	548 (1100)	2.17, 2.12, 1.98	627 (−16) [−5]	790 (−44)	685 (520)	0.11	495	827
Me-tpen[25,31]	537 (1000)	2.19, 2.12, 1.95	617	796	740 (500)	0.08	470	819
tpa[32,33]	538 (1000)	2.19, 2.15, 1.97	626	789	not observed			

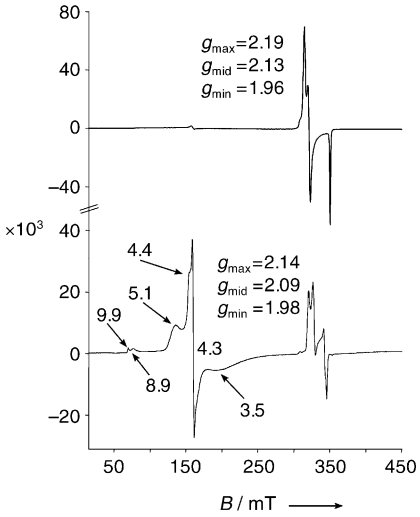


Figure 2. X-band EPR spectra of $[Fe^{III}(OOH)(L^2)]^{2+}$ at 25 K (top) and $[Fe^{III}(OO)(L^2)]^{+}$ at 2 K (bottom) in methanol. Conditions: 10 GHz modulation frequency, 0.3181 mW power.

The distinction between $[Fe(OOH)(L^2)]^{2+}$ and $[Fe(OOH)(L^3)]^{2+}$ is emphasized by the properties of their conjugate bases. Deprotonation of $[Fe(OOH)(L^3)]^{2+}$ in methanol at −40 °C (2 equiv NaOMe) leads to a blue solution with an absorption maximum at $\lambda = 721$ nm (Figure 1); this conversion is easily reversed by back titration with acid (2 equiv $HClO_4$).[23] All spectra go through an isosbestic point at $\lambda =$ 650 nm, indicating the presence of a fully reversible acid–base equilibrium. This set of data allows the determination of the extinction coefficients of the pure complexes ($\varepsilon_{560} =$ 1300 $L\,mol^{-1}cm^{-1}$ for $[Fe(OOH)(L^3)]^{2+}$ and $\varepsilon_{721} =$ 540 $L\,mol^{-1}cm^{-1}$ for $[Fe(O_2)(L^3)]^{+}$), and an estimate of its pK value (−40 °C, MeOH, $4.5 < pK < 5.0$).[24] When this interconversion is monitored by EPR, the low-spin EPR spectrum of $[Fe(OOH)(L^3)]^{2+}$ is replaced by a new signal at $g = 5.9$ that corresponds to an axial high-spin Fe^{III} species. We attribute these changes to the conversion of the low-spin Fe^{III} η^1-OOH complex to a high-spin η^2-peroxo species, as previously observed for corresponding complexes of N4Py and R-tpen (see Scheme 1). This notion is confirmed by its resonance Raman spectrum showing features at 493 and 827 cm^{-1} (see Table 1 and Figure 3). These peaks can be assigned, respectively, to the $\nu_{Fe\text{-}O2}$ and $\nu_{O\text{-}O}$ modes of $[Fe(\eta^2\text{-}O_2)(L^3)]^{+}$, by analogy to the very similar features observed for the corresponding N4py and Me-tpen complexes (Table 1).

The conjugate base of $[Fe(OOH)(L^2)]^{2+}$ appears to be less stable. Unlike its L^3 analogue, $[Fe(OOH)(L^2)]^{2+}$ could not be converted to its conjugate base at −40 °C; addition of base affords only an Fe^{III} decomposition product. However, deprotonation could be effected at −80 °C, and a new chromophore can be observed with a broad absorption band centered near $\lambda =$ 760 nm ($\varepsilon \geq 350\,L\,mol^{-1}cm^{-1}$), which presumably is the corresponding side-on peroxo complex for L^2. This species is associated with an EPR spectrum with $g = 9.9$, 8.9, 5.1, 4.3, and 3.5, corresponding to an $S = 5/2$ species with $E/D = 0.24$ (Figure 2). As for the L^3 complex, there is also a new but minor $S = 1/2$ signal that appears when a significant amount of $[Fe(\eta^2\text{-}OO)(L^2)]^{+}$ has formed.[23] Unfortunately, attempts to obtain a Raman spectrum of $[Fe(\eta^2\text{-}OO)(L^2)]^{+}$ have not been successful thus far. Although $[Fe(OO)(L^2)]^{+}$ cannot be characterized as well as its L^3 counterpart, it is clear that

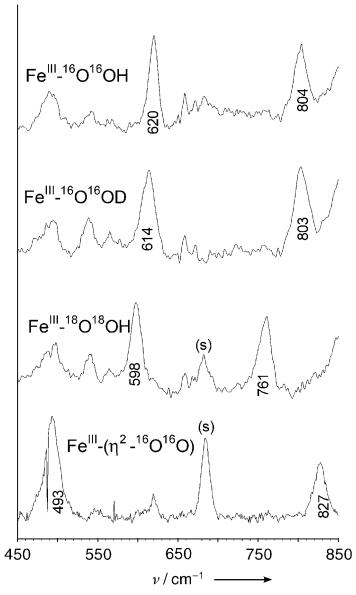


Figure 3. Resonance Raman spectra of $Fe^{III}(L^3)$-peroxo complexes in methanol. $\lambda_{ex} = 568.2$ nm for the Fe^{III}-OOH samples, $\lambda_{ex} = 647.1$ nm for the Fe^{III}-O_2 sample; 100 mW power.

 © 2004 Wiley-VCH Verlag GmbH & Co. KGaA, Weinheim

the two complexes have quite different temperature-dependent stabilities and optical properties.

These differences give novel insights into the nature of side-on peroxo complexes with $Fe^{III}N_5$ chromophores, for which there is as yet no crystal structure. For the related $[Fe(\eta^2\text{-}OO)(Me\text{-}tpen)]^+$ species it has been suggested that its formation from the Fe^{III} η^1-OOH precursor may involve the dissociation of one of the pendant pyridine ligands to generate a six-coordinate FeN_4O_2 complex;[25,26] this structure was postulated by analogy to that proposed for $[Fe^{III}(edta)(O_2)]^{3-}$ (edta = ethylenediamine tetraacetate) on the basis of a comprehensive spectroscopic investigation.[11] On the other hand, DFT calculations for $[Fe(\eta^2\text{-}OO)(N4py)]^+$ suggest that the N4py ligand remains pentadentate and that the $Fe\text{–}N_{amine}$ bond lengthens from 2.1 to 2.4 Å to accommodate the side-on peroxo binding; the calculated structure affords iron–ligand bond lengths fully consistent with those derived from EXAFS analysis.[9] The significant difference in properties of the side-on peroxo complexes of L^2 and L^3 argues against the dissociation of the third, additional pyridine donor and leads us to consider seven-coordinate η^2-O_2 structures.

Seven-coordination for transition-metal complexes with bispidine ligands has been observed before[13] and is supported for the high-spin Fe^{III} η^2-O_2 complexes by DFT calculations (UB3LYP functional at the 6-31G(d) level; this method reproduces the crystal structure of $[FeCl(L^2)]^+$ reasonably well).[28] The results of the structure optimization[29] of the two peroxo complexes are shown in Figure 4. The $Fe(\eta^2\text{-}O_2)(L^3)$ unit is quite symmetrical in the L^3 complex; the peroxo group is coplanar with N3, the Fe^{III} center, and the two pyridine N donors (Figure 4). The two Fe–O bonds are close to identical and comparably short, and the O–O bond is relatively long. In $[Fe(\eta^2\text{-}O_2)(L^2)]^+$ the peroxo group is coplanar with the Fe^{III} center, N3, and N7. The two Fe–O bonds are relatively long and significantly different from each other, and the O–O bond is shorter than in the complex with L^3 (Figure 4b). The structures of the corresponding hydroperoxo complexes were also optimized, and the Fe–O bond length in $[Fe(OOH)(L^2)]^{2+}$ is 1.88 Å while that in $[Fe(OOH)(L^3)]^{2+}$ is 1.78 Å. Hence, the low-spin hydroperoxo (six-coordinate) and the high-spin peroxo complexes (seven-coordinate) have relatively weak Fe–O bonds in the case of L^2 and stronger bonds in the case of L^3. This is as expected from structural studies with iron(II)[12] and other transition-metal bispidine complexes (Scheme 2).[13,14,31] The strong interaction of the peroxo ligand with the Fe^{III} center coordinated to L^3 leads to a weakening of the O–O bond, while the weaker interaction in the complexes with L^2 gives rise to an O–O bond that is stronger and less activated.

Based on extensive studies of bispidine coordination compounds, also including structural studies of Fe^{II} bispidines, the isomeric pair of Fe complexes with L^2 and L^3 was predicted to have significantly different hydrogen peroxide chemistry. This expectation is largely fulfilled. Raman spectra and computed structures indicate that the Fe–O bonds are, as expected, consistently weaker *trans* to N7 (L^2), specifically for the seven-coordinate high-spin peroxo complex. This also indicates that the two complexes might differ considerably in terms of their activity as oxidation catalysts.[17]

Received: July 31, 2003 [Z52523]

Keywords: coordination modes · iron · ligands · stereochemistry

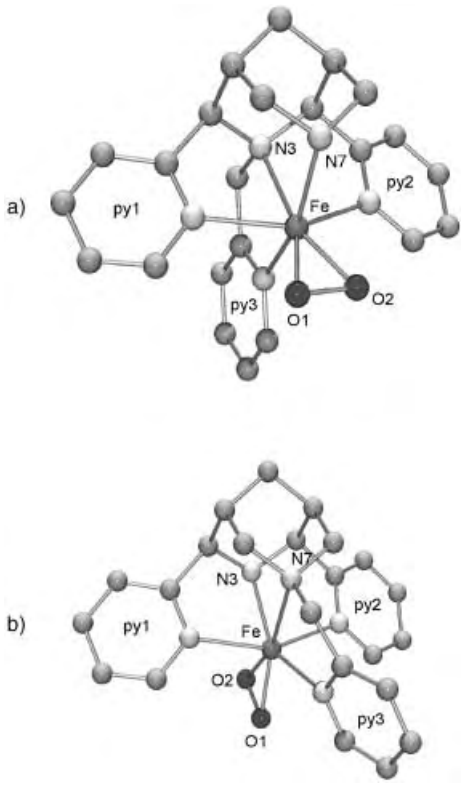


Figure 4. Computed structures (UB3LYP/6-31G(d)) of the two high-spin peroxo complexes. a) $[Fe^{III}(\eta^2\text{-}O_2)(L^3)]^+$: Fe-N3 2.33, Fe-N7 2.24, Fe-py1 2.29, Fe-py2 2.29, Fe-py3 2.16, Fe-O1 1.91, Fe-O2 1.91, O1-O2 1.41 Å. b) $[Fe^{III}(\eta^2\text{-}O_2)(L^2)]^+$: Fe-N3 2.21, Fe-N7 2.53, Fe-py1 2.23, Fe-py2 2.27, Fe-py3 2.21, Fe-O1 1.97, Fe-O2 1.99, O1-O2 1.36 Å.

[1] B. Meunier, *Struct. Bonding (Berlin)* **2000**, *97*.
[2] *Biomimetic Oxidations Catalyzed by Transition Metal Complexes* (Ed.: B. Meunier), Imperial College, London, **2000**.
[3] K. Chen, M. Costas, L. Que, Jr., *J. Chem. Soc. Dalton Trans.* **2002**, 672.
[4] R. Davydov, T. M. Makris, V. Kofman, D. E. Werst, S. G. Sligar, B. M. Hoffman, *J. Am. Chem. Soc.* **2001**, *123*, 1403.
[5] R. M. Burger, *Struct. Bonding (Berlin)* **2000**, *97*, 287.
[6] A. Karlsson, J. V. Parales, R. E. Parales, D. T. Gibson, H. Eklund, S. Ramaswamy, *Science* **2003**, *299*, 1039.
[7] "Metal-Oxo and Metal-Peroxo Species in Catalytic Oxidations": J.-J. Girerd, F. Banse, A. J. Simaan, *Struct. Bonding (Berlin)* **2000**, *97*, 145.
[8] K. B. Jensen, C. J. McKenzie, L. P. Nielsen, J. Z. Pedersen, H. M. Svendsen, *J. Chem. Soc. Chem. Commun.* **1999**, 1313.
[9] G. Roelfes, V. Vrajmasu, K. Chen, R. Y. N. Ho, J.-U. Rohde, C. Zondervan, R. M. la Crois, E. P. Schudde, M. Lutz, A. L. Spek, R. Hage, B. Feringa, E. Münck, L. Que, Jr., *Inorg. Chem.* **2003**, *42*, 2639.
[10] L. Que, Jr., R. Y. N. Ho, *Chem. Rev.* **1996**, *96*, 2607.
[11] E. I. Solomon, T. C. Brunold, M. I. Davis, J. N. Kensley, S.-K. Lee, N. Lehnert, F. Neese, A. J. Skulan, Y.-S. Yang, J. Zhou, *Chem. Rev.* **2000**, *100*, 235.

 © 2004 Wiley-VCH Verlag GmbH & Co. KGaA, Weinheim

[12] H. Börzel, P. Comba, K. S. Hagen, M. Merz, Y. D. Lampeka, A. Lienke, G. Linti, H. Pritzkow, L. V. Tsymbal, *Inorg. Chim. Acta* **2002**, *337*, 407.
[13] P. Comba, M. Kerscher, M. Merz, V. Müller, H. Pritzkow, R. Remenyi, W. Schiek, Y. Xiong, *Chem. Eur. J.* **2002**, *8*, 5750.
[14] P. Comba, A. Lienke, *Inorg. Chem.* **2001**, *40*, 5206.
[15] P. Comba, A. Hauser, M. Kerscher, H. Pritzkow, *Angew. Chem.* **2003**, *115*, 4675 – 4679; *Angew. Chem. Int. Ed.* **2003**, *42*, 4536 – 4540.
[16] P. Comba, M. Kerscher, A. Roodt, *Inorg. Chem.*, submitted.
[17] The tetra- and pentadentate ligand complexes (L^1 vs. L^2 and L^3) follow mechanistically different pathways (product distribution, ^{18}O-labeling experiments, aerobic vs anaerobic conditions). Under standard conditions[3] the reactivity of the L^1-based catalyst is comparable to that with tpa. The catalyst based on L^2 has, under aerobic conditions, a similar reactivity, that of L^3 is less reactive by a factor of 5–10.
[18] G. Roelfes, M. Lubben, K. Chen, R. Y. N. Ho, A. Meetsma, S. Genseberger, R. M. Hermant, R. Hage, S. K. Mandal, V. G. Young, Jr., Y. Zang, H. Kooijman, A. L. Spek, L. Que, Jr., B. L. Feringa, *Inorg. Chem.* **1999**, *38*, 1929.
[19] 35% aqueous solution, quantitative analysis by iodometric titration.[20]
[20] D. H. R. Barton, V. N. L. Gloahec, H. Patin, F. Launay, *New J. Chem.* **1998**, *22*, 559.
[21] BF_4 salts, crystallized from CH_3CN and fully characterized.
[22] These transitions are attributed to ligand-to-metal charge transfer from the hydroperoxo group.
[23] At high base concentrations there is formation of a new but minor species not yet fully characterized, with a low-spin electronic configuration (L^3: $g_1 = 2.13$, $g_2 = 2.08$, $g_3 = 1.98$; L^2: $g_1 = 2.14$, $g_2 = 2.09$, $g_3 = 1.98$) and a low-energy ligand field. We propose that this may arise from the end-on isomers $[Fe(\eta^1\text{-}O_2)(L^3)]^+$ and $[Fe(\eta^1\text{-}O_2)(L^2)]^+$, respectively.
[24] The ε-values of the hydroperoxo and peroxo Fe^{III} complexes as well as the corresponding acid–base equilibrium constant are based on the assumption of 100% conversion to the Fe^{III} peroxo–hydroperoxo system and full reversibility. Admittedly, this is an oversimplification.[23] The pK value was calculated from the intensities of the bands at $\lambda = 561$ nm and $\lambda = 721$ nm (and the known ε-values) at different amounts of acid ($HClO_4$) added to the fully deprotonated form.
[25] A. J. Simaan, S. Döpner, F. Banse, S. Bourcier, G. Bouchoux, A. Boussac, P. Hildebrandt, J.-J. Girerd, *Eur. J. Inorg. Chem.* **2000**, 1627.
[26] For a related tpen derivative a seven-coordinate peroxo complex was proposed.[27]
[27] A. Hazell, C. J. McKenzie, L. Preuss Nielsen, S. Schindler, M. Weitzer, *J. Chem. Soc. Dalton Trans.* **2002**, 310.
[28] The comparison of the results of a structure optimization at that level with those of a single-crystal X-ray diffraction study[12] showed that all Fe–N bond lengths are only slightly overestimated with a mean deviation of 2.5%, while the Fe–Cl bond length is underestimated by 4.6%; that is, the agreement between experiment and theory is acceptable at that level.
[29] All structures were characterized as minima by frequency analysis.
[30] However, the expected structural differences, which correlate well with the different stabilities and reactivities, might have been expected to also lead to significantly different spectroscopic properties. Reasons why this is not so are currently under investigation.
[31] A. J. Simaan, F. Banse, P. Mialane, A. Boussac, S. Un, T. Kargar-Grisel, G. Bouchoux, J.-J. Girerd, *Eur. J. Inorg. Chem.* **1999**, 993.
[32] Y. Zang, J. Kim, Y. Dong, E. C. Wilkinson, E. H. Appelman, L. Que, Jr., *J. Am. Chem. Soc.* **1997**, *119*, 4197.
[33] R. Y. N. Ho, G. Roelfes, B. L. Feringa, L. Que, Jr., *J. Am. Chem. Soc.* **1999**, *121*, 264.

 © 2004 Wiley-VCH Verlag GmbH & Co. KGaA, Weinheim

Enzyme Models

Molecularly Imprinted Polymers with Strong Carboxypeptidase A-Like Activity: Combination of an Amidinium Function with a Zinc-Ion Binding Site in Transition-State Imprinted Cavities**

*Jun-qiu Liu and Günter Wulff**

Mimicking of natural enzyme systems with catalytically active arrangements in designed receptors is a challenging topic for chemists. Notable achievements to date have been obtained with several model systems, such as synthetic macrocyclic compounds, molecular assemblies, catalytic antibodies, and molecularly imprinted polymers.[1] Among these models, molecular imprinting has been demonstrated to be an attractive strategy for creating catalytically active binding sites for enzyme mimetics.[2] This method should give the opportunity to generate more complicated active sites with a high similarity to natural systems. For this purpose, to mimic enzyme behavior, especially esterase activity, numerous experiments have been undertaken by imprinting with transition-state analogues (TSAs).[3,4] Although the earlier attempts to mimic enzyme behavior using imprinted polymers showed only limited catalytic efficiency, significant rate enhancement by catalysis with imprinted polymers has been obtained in recent years.[4] Evidently, increasing the transition-state binding, as well as correctly incorporating and positioning the functional groups is essential for the construction of an effective enzyme model.[1–4] In our previous work on preparing polymer catalysts by molecular imprinting,[4] amidinium functional groups were oriented in imprinted cavities. These groups acted as anchors for binding the tetrahedral transition states of basic ester or carbonate hydrolysis in a similar manner to the catalytic role of guanidinium moieties in certain catalytic antibodies[1c] and in carboxypeptidase A.[5] The catalytic action of carboxypeptidase A involves two guanidinium groups and a Zn^{2+} ion. The guanidinium moiety of Arg 127 binds the oxyanion generated in the rate-limiting formation of the tetrahedral transition

[*] Prof. Dr. G. Wulff
Institute of Organic Chemistry and Macromolecular Chemistry
Heinrich-Heine-University Düsseldorf
Universitaetsstrasse 1, 40225 Düsseldorf (Germany)
Fax: (+49) 211-811-5840
E-mail: wulffg@uni-duesseldorf.de

Prof. Dr. J.-q. Liu
Key Laboratory of Supramolecular Structure and Materials
Jilin University, Changchun, 130023 (P.R. China)

[**] This research was supported by Deutsche Forschungsgemeinschaft and Fonds der Chemischen Industrie. J.-q. Liu acknowledges a fellowship from the Alexander von Humboldt Foundation. Helpful discussions with Prof. Dr. W. Kläui, Institute of Inorganic Chemistry of our university are greatly acknowledged.

Supporting information (synthetic and kinetic details) for this article is available on the WWW under http://www.angewandte.org or from the author.

 DOI: 10.1002/anie.200352770 © 2004 Wiley-VCH Verlag GmbH & Co. KGaA, Weinheim

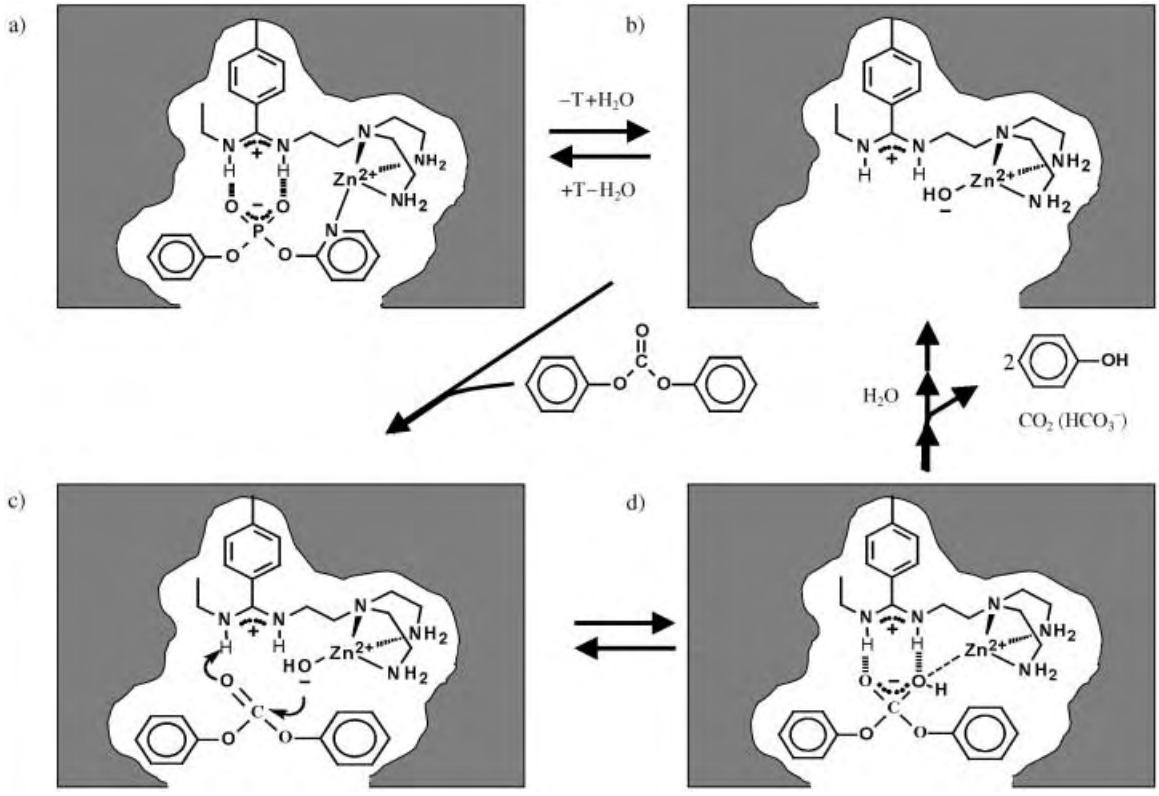
state.[6] The zinc ion coordinated to the amino acid residues of His 69, Glu 72, and His 196 plays a decisive role in the catalysis of the enzyme. Substrate specificity is brought about by a hydrophobic pocket and another guanidinium moiety of Arg 145.[5]

Herein we report on a novel molecularly imprinted polymer, in which an amidinium group and a Zn^{2+} center are oriented in a TSA imprinted cavity, in a similar way to the active site in carboxypeptidase A.[5] These imprinted polymers exhibited strong rate enhancements for carbonate hydrolysis.

Our recent studies have clearly shown that the amidinium group of the functional monomer *N*,*N*′-diethyl-4-vinylbenzamidine **1**,[4] which is responsible for binding and catalysis, can be positioned in imprinted cavities by complexation with carboxyl groups or with a TSA, such as a phosphate or a phosphonate through stoichiometric noncovalent interaction.[7] A similar amidinium group was incorporated in our new monomer **2**. In this functional monomer an additional triamine group was introduced with a defined proximity to the amidinium group. This group gives rise to a strong threefold coordination of the Zn^{2+} ion leaving the fourth coordination site free for other ligands.[8] Coordination of the Zn^{2+} ion to the amidinium group is much weaker.[9]

As with previous templates for carbonate hydrolysis (see for example, **3**)[1c,4b] the new template **4** acts as a stable TSA for the tetrahedral transition state of the basic carbonate hydrolysis. One phenyl ring in **3** is replaced by a pyridine ring in **4**. This change gives the possibility of incorporating the pyridine nitrogen atom as the fourth ligand in the Zn^{2+} coordination sphere (Scheme 1 a). This additional coordination permits the formation of more stable complexes between the functional monomer and the template.[10] Furthermore, the amidinium group and the Zn^{2+} ion are brought into defined proximity to each other and to the template molecule in the cross-linking polymerization during the imprinting process.

Imprinted polymers were prepared in bulk by radical initiation at 60 °C from polymerization mixtures consisting of cross-linker, ethylene dimethacrylate (EDMA), methylme-



Scheme 1. Schematic representation of a) the molecular imprinting with template (T) **4** and monomer **2** in the presence of Zn^{2+}, b) removal of the template, and c,d) catalysis.

 © 2004 Wiley-VCH Verlag GmbH & Co. KGaA, Weinheim

thacrylate (MMA), the functional monomer **2**, and either diphenylphosphate (**3**) or phenyl-2-pyridyl-phosphate (**4**) as template molecules in the presence of $ZnCl_2$ in acetonitrile (MeCN). This procedure corresponds to earlier preparations (in absence of Zn^{2+}) of imprinted polymers from **1** and **3**.[4b] The templates were removed from the crushed polymer (particles 45–125 μm) with a solution of 0.1M NaOH and MeCN (1:1, v/v), to give 73–86% of free cavities. The zinc ions bound at the triamine moiety during imprinting were not removed in the process of template removal.[11] In addition, a control polymer of identical composition to that of the imprinted polymer but without the template was prepared.

The catalytic activity of the imprinted polymers and of the controls was investigated in the hydrolysis of the substrate diphenylcarbonate (**5**) in a 1:1 solution of 2-[4-(2-hydroxyethyl)-1-piperazine] ethanesulfonic acid (HEPES) buffer (pH 7.3; 1 mM **5** in buffer/acetonitrile) and MeCN. To follow the reaction kinetics, aliquots were taken at regular intervals and checked by HPLC; phenol as one of the products of hydrolysis was determined quantitatively. The kinetics were measured at low conversion and were calculated as pseudo first-order rate constants.

Table 1 shows the results obtained with different catalysts prepared by molecular imprinting. Table 2 gives control data for the kinetics of the hydrolysis either in the same solution without any added polymer, or with added control polymer, or with added monomer **2** and Zn^{2+}. As in earlier investigations[4] the efficiency of the catalyst was expressed by the ratio of reaction in presence of polymer catalyst to that in neat HEPES–MeCN solution (k_{impr}/k_{soln}). Effects that are only connected to the imprinting in the polymer (the imprinting effect)[2a] can be elucidated from the ratio k_{impr}/k_{contr}. In our earlier investigations with a polymer of monomer **1** and template **3** (**P1**,**3**) a rate enhancement of 455-fold compared to solution and an imprinting effect of 10.7 was obtained.[4b] Our new polymers with template **3** but with monomer **2** and Zn^{2+} (**PZn2**,**3**) showed a much stronger rate enhancement of 1800-fold and an improved imprinting factor of 34.0. By using the template **4** and the monomer **2** under Zn^{2+} complexation (**PZn2**,**4**) a much better orientation in the cavity during imprinting is possible (Scheme 1a). This polymer gives rise to a further improved catalytic activity of more than 3200-fold and an imprinting factor of 61.5 (Table 1). This strong rate enhancement is in accord with the postulated cooperativity between the amidinium group and the Zn^{2+} ion. The high activity can best be explained by the complexation of the pyridine group of template **4** that stabilizes a favorable conformation during imprinting. To establish the influence of the functional groups in the polymer on the catalysis, the soluble monomer **2** with Zn^{2+} was investigated in HEPES–MeCN solution. Their impact on catalysis is only small, a rate enhancement of 18-fold is observed in comparison to reaction in neat solution (Table 2).

Table 1: Kinetic parameters for the hydrolysis of diphenylcarbonate (**5**) in presence of imprinted polymers in buffer (pH 7.3)/MeCN 1:1.[a]

Imprinted polymer[b]	Monomer	Template	k_{impr} [min^{-1}]	k_{impr}/k_{soln}	k_{impr}/k_{contr}
P1,**3**[c]	–	**1** **3**	2.80×10^{-4}	455	10.7
PZn2,**3**	Zn^{2+}	**2** **3**	1.30×10^{-3}	1806	34.0
PZn2,**4**	Zn^{2+}	**2** **4**	2.35×10^{-3}	3264	61.5

[a] Hydrolysis of diphenylcarbonate (**5**) in a solution of 50 mM HEPES buffer (pH 7.3)/MeCN 1:1 at 20°C. There are 2 mM of available cavities in the polymer in relation to 1 mM substrate. All *k* values are the average of at least three measurements and standard deviations were less than 5%. k_{impr} is the pseudo first-order rate constant in presence of the imprinted polymer at this catalyst to substrate ratio; k_{contr} the rate constant in presence of the control polymer; k_{soln} is the rate constant for hydrolysis in HEPES buffer (pH 7.3)/MeCN 1:1 solution. [b] The composition of the monomer mixture for the preparation of the imprinted polymers consisted of 83.3 wt% of EDMA, 10.4 wt% of MMA, 6.3 wt% of the monomer-template 1:1 complex, and 1 wt% of azobis(isobutyronitrile), diluted by the same weight of the porogen MeCN. The control polymer was prepared accordingly but without template. For details see Supplemental Material. [c] This data is taken from ref. [4b] and is measured at 15°C.

Table 2: Kinetic parameters for control experiments of the hydrolysis of **5** in buffer (pH 7.3)/MeCN 1:1 of and with addition of control substances.

Control	*k* [min^{-1}]	k/k_{soln}
no addition	7.20×10^{-7}	≡1.00
monomer **2** and Zn^{2+}[a]	1.29×10^{-5}	17.9
control polymer and Zn^{2+}	3.82×10^{-5}	53.1

[a] The concentration of the monomer and Zn^{2+} corresponded to that of the available binding sites in the polymer.

As with natural enzymes the catalysis of carbonate hydrolysis by **PZn2**,**4** shows typical Michaelis–Menten kinetics. A plot of initial velocities of the reaction versus the substrate concentration shows at first an increase in the rate of reaction with increasing substrate, the rate then levels off. At higher substrate concentration, when all the active sites are occupied, the rate remains constant which means it is zero-order with respect to carbonate concentration (saturation kinetics). From this data the Michaelis constant $K_m = 2.01$ mM and the turnover number $k_{cat} = 0.035\ min^{-1}$ can be calculated (Table 3). k_{cat} is higher than k_{impr} which is determined for only one ratio of catalyst to substrate. The ratio k_{cat}/k_{uncat} is used to express the catalytic activity of antibodies and natural enzymes. In our case, by using k_{soln} as k_{uncat} for **PZn2**,**4** a k_{cat}/k_{soln} value of 6900 is obtained. These are the highest values that have been obtained for imprinted polymers of this type. These values are considerably higher than those for catalytic antibodies for which $k_{cat}/k_{uncat} = 810$[12] has been reported for carbonate hydrolysis.

Table 3: Data for Michaelis–Menten kinetics of hydrolysis of **5** in presence of **PZn2**,**4**.

K_m	k_{cat}	k_{cat}/K_m	k_{cat}/k_{soln}
2.01 mM	0.035 min^{-1}	17.0 $min^{-1}\,M^{-1}$	6900

With regard to the mechanism it can be assumed that the Zn^{2+} ion is tetrahedrally coordinated by three amine groups and one water molecule.[13] This Zn^{2+}-bound water molecule is ionized through base catalysis that is facilitated by the amidinium group. The Zn^{2+} bound water is more acidic than usual water (Scheme 1b).[13] The pH–rate profile for the

 © 2004 Wiley-VCH Verlag GmbH & Co. KGaA, Weinheim

carbonate hydrolysis by **PZn2**,**4** is shown in Figure 1. The reaction is strongly dependent on the pH value, it has an inversion point at pH 7.5 which is in agreement with data for Zn^{2+}-bound water[14] and is also in reasonable accord with the pK_s value of 7.4 obtained by potentiometric titration of the catalyst **PZn2**,**4**.

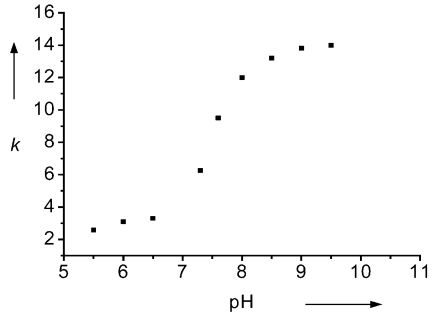


Figure 1. pH profile of the rate of the hydrolysis of **5** in the presence of 1 mM **PZn**2,4 active sites. Buffer solution/MeCN 1:1. Buffer used were MES (pH 5.5–6.5), HEPES (pH 7.3–8.1), CHES (pH 8.4–9.5). $k = 10^{-4}$ min^{-1}. MES = 2-(4-morpholinyl) ethanesulfonic acid, CHES = 2-(cyclohexylamino) ethanesulfonic acid.

The catalysis occurs as follows: After binding the substrate (Scheme 1 c) and polarization of the carbonyl group by the amidinium ion a nucleophilic attack of the Zn^{2+}-bound OH^- ion results, via the transition state, in the tetrahedral intermediate (Scheme 1 d). The reaction is accelerated by the preferred binding of the transition state (compared to the substrate) in the active site of the catalyst (transition-state stabilization). In this way the activation energy of the reaction is reduced. After this rate-determining step one molecule of CO_2 (as HCO_3^-) and two molecules of phenol are formed in a number of further faster reaction steps regenerating the catalyst (Scheme 1 b).

In summary, this novel catalytic system shows a remarkable rate enhancement of $k_{cat}/k_{soln} = 6900$. This is the first example in which molecularly imprinted catalysts are clearly more efficient than catalytic antibodies. In earlier work[4b] the efficiency of antibody catalysis[15] could be reached in the case of carbamate hydrolysis. These new catalysts are very promising for broad application since in contrast to antibodies molecularly imprinted polymers show a much higher chemical, mechanical, and thermal stability, can easily be prepared, and have the potential of simple variation of structure.[16]

Received: September 2, 2003 [Z52770]

Keywords: enzyme models · heterogeneous catalysis · molecular imprinting · polymers · reaction kinetics

[1] For reviews see: a) A. Kirby, *Angew. Chem.* **1996**, *108*, 770–790; *Angew. Chem. Int. Ed. Engl.* **1996**, *35*, 707–724; b) R. Breslow, S. D. Dong, *Chem. Rev.* **1998**, *98*, 1997–2011; c) R. A. Lerner, S. J. Benkovic, P. G. Schultz, *Science* **1991**, *252*, 659–667; d) G. Wulff, *Angew. Chem.* **1995**, *107*, 1958–1979; *Angew. Chem. Int. Ed. Engl.* **1995**, *34*, 1812–1832; e) K. Mosbach, *Trends Biochem. Sci.* **1994**, *19*, 9–14; f) K. J. Shea, *Trends Polym. Sci.* **1994**, *5*, 166–173.

[2] For reviews see: a) G. Wulff, *Chem. Rev.* **2002**, *102*, 1–27; b) O. Ramstrom, K. Mosbach, *Curr. Opin. Chem. Biol.* **1999**, *3*, 759–764.

[3] For examples see: a) D. K. Robinson, K. Mosbach, *J. Chem. Soc. Chem. Commun.* **1989**, 969–970; b) B. Sellergren, R. N. Karmalkar, K. J. Shea, *J. Org. Chem.* **2000**, *65*, 4009–4027; c) K. Ohkubo, Y. Urata, Y. Honda, Y. Nakashima, K. Yoshinaga, *Polymer* **1994**, *35*, 5372–5374.

[4] a) G. Wulff, T. Gross, R. Schoenfeld, *Angew. Chem.* **1997**, *109*, 2049–2052; *Angew. Chem. Int. Ed. Engl.* **1997**, *36*, 1961–1964; b) A. G. Strikovsky, D. Kasper, M. Gruen, B. S. Green, J. Hradil, G. Wulff, *J. Am. Chem. Soc.* **2000**, *122*, 6295–6296; c) M. Emgenbroich, G. Wulff, *Chem. Eur. J.* **2003**, *9*, 4106–4117.

[5] D. W. Christianson, W. N. Lipscomb, *Acc. Chem. Res.* **1989**, *22*, 62–69.

[6] M. A. Phillips, R. Fletterick, W. J. Rutter, *J. Biol. Chem.* **1990**, *265*, 20692–20698.

[7] G. Wulff, K. Knorr, *Bioseparation* **2002**, *10*, 257–276.

[8] For the cooperativity of guanidinium and metal ions in recent enzyme model studies for small molecule enzyme models, see: H. Haddou, J. Sumaoka, S. L. Wiskur, J. F. Anderson, E. V. Anslyn, *Angew. Chem.* **2002**, *114*, 4186–4188; *Angew. Chem. Int. Ed.* **2002**, *41*, 4014–4016. For a macromolecular enzyme model, see: B.-B. Jang, K.-P. Lee, D.-H. Min, J. Suh, *J. Am. Chem. Soc.* **1998**, *120*, 12008–12016

[9] In case of guanidinium functionalities: S. Aoki, K. Iwaida, N. Hanamoto, M. Shiro, E. Kimura, *J. Am. Chem. Soc.* **2002**, *124*, 5256–5257.

[10] The association constant for a 1:1 complex of monomer **2** and template **3** was determined to be 5.6×10^3 M^{-1} in $CDCl_3$ by ^1H NMR spectroscopic titration. Zn^{2+} complexes with the triamine part of the monomer **2** showed a binding constant of $\log K$ 9.3 determined by potentiometric titration in aqueous solution. Although we could not directly measure the complexation constant of **2** with **4** in the presence of Zn^{2+}ions, it should be expected that the complexation of **2** with **4** is stronger than that of **1** and **3** ($K = 4.6 \times 10^3$ in MeCN at 25 °C)[7b] owing to the multiple binding of amidinium ion with phosphate as well as of the Zn^{2+} ion with the pyridine ring in template **4**.

[11] The amount of zinc ions in the imprinted polymers was determined by elemental analysis. Only a slight loss of Zn^{2+} ions was detected during spitting off the template from the imprinted polymer, for example, in **PZn2**,**4** the zinc-ion content was 0.84 wt% prior to, and 0.82 wt% after template removal.

[12] J. W. Jacobs, P. G. Schultz, R. Sugasawara, M. Powell, *J. Am. Chem. Soc.* **1987**, *109*, 2174–2176.

[13] R. P. Sheridan, L. C. Allen, *J. Am. Chem. Soc.* **1981**, *103*, 1544–1550.

[14] E. Kimura, T. Shiota, T. Koike, M. Shiro, M. Kodama, *J. Am. Chem. Soc.* **1990**, *112*, 5805–5811.

[15] P. Wentworth, A. Datta, S. Smith, A. Marshall, L. J. Partridge, G. M. Blackburn, *J. Am. Chem. Soc.* **1997**, *119*, 2315–2316.

[16] In antibodies functional groups can not be easily varied, for example, it is difficult to introduce a Zn^{2+} center in defined orientation by using site-directed mutagenesis.

 © 2004 Wiley-VCH Verlag GmbH & Co. KGaA, Weinheim

Adsorption

Second-Order Templation: Ordered Deposition of Supramolecular Squares on a Chloride-Covered Cu(100) Surface**

Caroline Safarowsky, Leo Merz, Alexander Rang, Peter Broekmann, B. A. Hermann,* and Christoph A. Schalley**

Scanning tunneling microscopy (STM) has become a valuable tool for the characterization[1] and manipulation[2] of surface-deposited macrocycles[3] and supramolecular species such as gridlike and other metal complexes[4] and mechanically interlocked species.[5] Self-assembly within the deposited monolayer often causes long-range order, which can also be influenced or even be controlled by the surface. For example, Stoddart et al.[6] reported a cationic cyclophane to stand upright on a highly ordered pyrolytic graphite (HOPG) surface and—in marked contrast to the crystal structure of the cyclophane—to self-assemble into nanotubes. For a direct observation of guest molecules[7] incorporated into supramolecular hosts such as the cyclophane-analogous square **1** (Figure 1), cavities are however required with an orientation of the macrocyclic host parallel to the surface.

A strategy to achieve this particular orientation of the host could be the enhancement of the interaction between the substrate and the host molecules by templating the arrangement of charged substrates on ionic adsorbates (Figure 2a).[8]

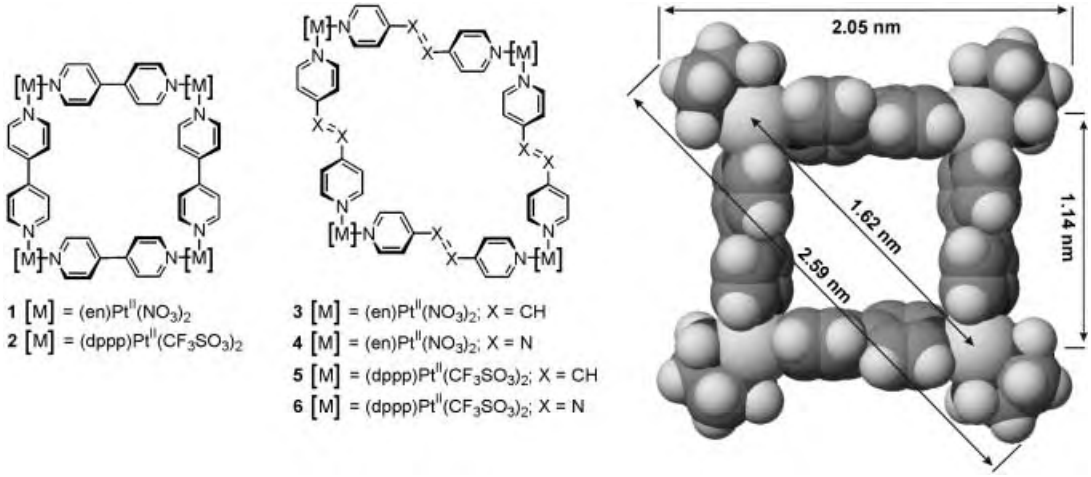


Figure 1. Structural formulas of the metallo-supramolecular squares **1**–**6** (left) and a MM2 minimized[15] space-filling model of square **1** (right). The dimensions along the edge and along the diagonal are given as metal–metal distances and as the total width inclusive of van der Waals radii.

[*] Dipl.-Chem. C. Safarowsky, Dr. P. Broekmann
Institut für Physikalische und Theoretische Chemie der Universität
Wegelerstrasse 12, 53115 Bonn (Germany)
Fax: (+49) 228-732-551
E-mail: broekman@thch.uni-bonn.de
Dipl.-Chem. L. Merz, Prof. Dr. B. A. Hermann[+]
Institut für Physik der Universität
Klingelbergstrasse 82, 4056 Basel (Switzerland)
E-mail: b.hermann@cens.de
Dipl.-Chem. A. Rang, Dr. C. A. Schalley
Kekulé-Institut für Organische Chemie und Biochemie der Universität
Gerhard-Domagk-Strasse 1, 53121 Bonn (Germany)
Fax: (+49) 228-735-662
E-mail: c.schalley@uni-bonn.de
[+] Present address: Walther-Meissner-Institut für Tieftemperaturforschung der Bayerischen Akademie der Wissenschaften und Fakultät für Physik/Center for Nano Science (CeNS) der LMU München
Walther-Meissner-Strasse 8, 85748 Garching (Germany)
Fax: (+49) 89-289-14206

[**] This work was supported by the SFB 624 of the Deutsche Forschungsgemeinschaft and the NRP 47 of the Swiss National Science Foundation. C.A.S. and B.A.H. gratefully acknowledge the Fonds der Chemischen Industrie and the BMBF for financial support.

A substrate-induced templating effect is often overruled, when self-organization from intermolecular interactions is the structure-determining factor rather than molecule–substrate interactions, in particular when ions such as the cations in the square **1** are deposited on uncharged substrates (e.g. HOPG, see below). Hence, the molecule–substrate interaction must be fine-tuned and enlarged to overcome the domination of self-organization due to intermolecular interactions.

To prepare such a charged substrate, we utilize the fact that chloride anions specifically adsorb on a positively polarized Cu(100) electrode from chloride-containing electrolytes (e.g. 10 mM HCl).[9] The fourfold symmetry of the resulting c(2×2)-Cl adsorbate structure (coverage $\Theta = 0.5$ ML)[10] with chloride particles residing in fourfold hollow sites is clearly indicative for a strong impact of the copper substrate on the structural properties of the adsorbate layer (Figure 2b, c). In contrast to a fourfold-symmetric Au(100) substrate with a chloride absorbate layer of almost hexagonal symmetry,[11] the chloride layer on Cu(100) adopts the symmetry of the copper substrate (the first-order template effect in Figure 2a). Not only the atomic structure of the copper electrode is altered by the presence of the chloride

 DOI: 10.1002/anie.200352968 © 2004 Wiley-VCH Verlag GmbH & Co. KGaA, Weinheim

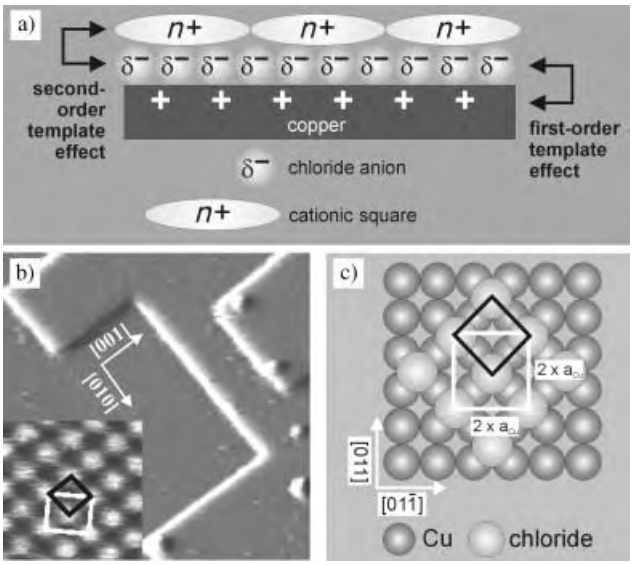


Figure 2. a) The principle of second-order templation: First, chloride ions are deposited on a Cu(100) surface. Electrostatic interactions between the chloride layer and the cationic squares lead to an ordered structure. b) STM image of the chloride-covered Cu(100) surface with the direction of the steps visible, 45 nm × 45 nm, $U_b = 45$ mV, $I_t = 1$ nA, $E = -400$ mV (Ag/AgCl). The inset shows the same surface at atomic resolution as well as the square unit cell. The steps are oriented parallel to the main symmetry axis of the chloride layer, 1.7 nm × 1.7 nm. c) Schematic representation of the chloride layer on the Cu substrate.

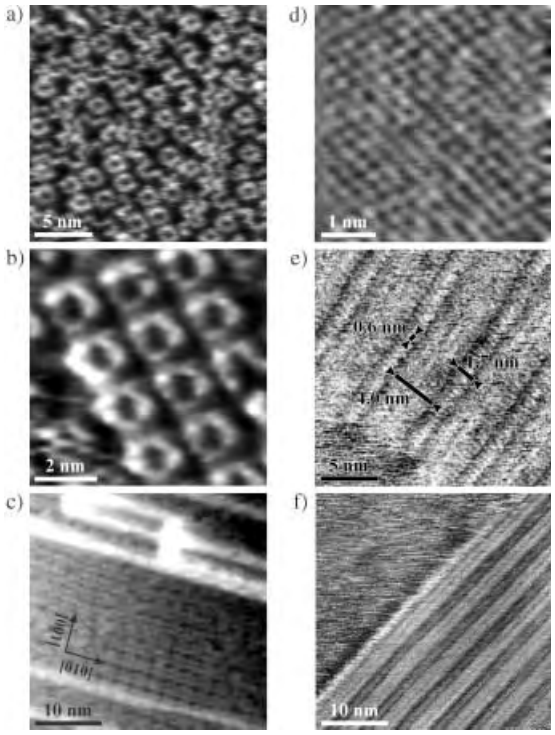


Figure 3. a) Squares **1** deposited onto the anion-covered surface. Several oligomer chains can be seen due to the acidic conditions used for the sample preparation, 20.5 nm × 20.5 nm, $U_b = 280$ mV, $I_t = 0.7$ nA, $E = -550$ mV (Ag/AgCl). b) Lateral ordering of **1**, 7.6 nm × 7.6 nm, $U_b = 280$ mV, $I_t = 0.7$ nA, $E = -550$ mV (Ag/AgCl). c) Long-range order of **1** yields large perfect domains under optimized sample preparation conditions (see text), 35.6 nm × 35.6 nm, $U_b = -110$ mV, $I_t = 0.7$ nA, $E = -480$ mV (Ag/AgCl). d) Image of the underlying chloride adlayer. e) Compound **5** deposited on graphite from a solution in CH_2Cl_2. After evaporation of the solvent a striped pattern can be observed. Arrows indicate a fine pattern reflecting observed periodicities (20.5 nm × 20.5 nm, $U_b = -700$ mV, $I_t = -0.001$ nA). f) Stripes shown in e) on a larger scale (35.6 nm × 35.6 nm, $U_b = -700$ mV, $I_t = -0.001$ nA). For comparability, images e) and f) are depicted on the same scale as a) and c), respectively.

layer, but also the surface morphology on a mesoscopic length scale. Copper steps are preferentially oriented parallel to the close-packed chloride rows which are rotated by 45° with respect to the main symmetry axis of the copper.[9] In particular, chloride layers are ideal substrates and templates for the adsorption of cationic species such as **1**, since the chloride retains practically its full charge upon adsorption,[12] while the heavier homologues bromide and iodide exhibit an increased partial charge transfer to the metal.

After preparation and characterization of the negatively charged chloride layer on top of the positively charged copper electrode, the pure supporting electrolyte (10 mM HCl, 5 mM KCl) was exchanged *under potential control* by a solution containing 10 mM HCl, 5 mM KCl, and 0.1 mM of the water-soluble metallosupramolecular square **1**.[13] The attractive Coulomb interactions force the cationic square to adsorb on the negatively charged chloride layer (the second-order template effect indicated in Figure 2a).[14] Clearly visible in Figure 3a is a local ordering of molecular assemblies revealing a pronounced cavity in the center. This feature points to supramolecular squares lying flat on the electrode surface. The distance of 1.9 nm to the nearest neighbor (Figure 3b) agrees well with the calculated[15] size of the square (Figure 1).[16] Most likely, the adsorbate–substrate interactions are mainly governed by attractive electrostatic interactions between the negatively charged chloride layer and the positively charged Pt^{2+} ions, while the lateral ordering is apparently dominated by van der Waals interactions.

The lateral ordering is strongly hindered by the presence of chainlike oligomers coadsorbed with the fourfold symmetric supramolecular squares (Figure 3a). Indeed, ^{1}H NMR experiments for **1** in 0.1M DCl/D_2O solution confirmed that some of the squares opened and new signals for oligomers were found. The degradation does not take place instantaneously, but proceeds on a time scale of about 30 min. Consequently, sample preparation could be modified to reduce the formation of oligomers by injecting some droplets of a freshly prepared aqueous solution of square **1** into the electrochemical cell to the pure supporting electrolyte to keep the presence of **1** in the acidic medium in the STM cell as short as possible. With this optimized sample preparation procedure, large perfectly ordered domains of the squares are observed for which the amount of oligomers is reduced to a minimum (Figure 3c). Characteristically, the squares are oriented parallel to the chloride-stabilized step edges and thus parallel to the main symmetry axes of the c(2 × 2) chloride adlayer. This observation also points to a strong second-order template effect of the chloride layer on the metallo-organic film. Please note that the copper step edges in Figure 3c appear as bright stripes parallel to the substrate ⟨001⟩ directions (Figure 2b).

 © 2004 Wiley-VCH Verlag GmbH & Co. KGaA, Weinheim

To prove the presence of the chloride ion layer underneath the metallo-organic layer, the STM tunneling parameters were systematically varied. Higher tunneling currents and lower bias voltages lead to a local removal of the metallo-organic layer from the surface through an increased tip–sample interaction.[17] Using these more drastic tunneling conditions, the chloride c(2 × 2) adsorbate layer becomes visible in the STM experiment (Figure 3d). After retracting the tip from the surface the metallo-organic layer is fully restored again.

To evaluate how important the anion-covered surface is for the arrangement of the squares, preliminary experiments were performed on HOPG: A series of molecular squares in different solvents (**1** and **4** in H_2O; **2**, **5**, and **6** in CH_2Cl_2) have been deposited by solution casting on HOPG. All measurements show a striped pattern, which could result from a self-organization that is probably unstable under the scanning tip (even with soft tunneling parameters) or from stacking of the molecules dominated by intermolecular interactions. The best high-resolution images were obtained with square **5** (Figure 3e,f).[18] A careful comparison of Figure 3e with Figure 3a strongly suggests that a complex molecular stacking—potentially in analogy to the structures observed with the adsorbed cyclophanes by Stoddart et al.[6]—rather than a formation of chainlike oligomers cause the observed pattern. On a graphite surface in a dry[19] environment, the intermolecular interactions clearly dominate over the molecule–substrate interactions and thus prohibit the molecular species to lie flat.

In conclusion, the two-dimensional structure formed by the weakly bound metallosupramolecular square **1** is dependent on the nature of the surface. If designed suitably, the surface can act as a template that forces the squares into a horizontal orientation through strong attractive interactions between squares and substrate. The orientation is dictated by the arrangement of chloride ions which again is controlled by the Cu(100) surface itself. We have clearly demonstrated the use of a second-order template effect to connect a metal electrode surface to a supramolecular assembly through an intermediate layer of anions. The stage is now set to attempt the insertion of guest molecules into the cavities of the squares and directly observe the guests within the host at electrified solid/liquid interfaces by means of high-resolution scanning probe techniques.

Received: September 29, 2003 [Z52968]

Keywords: adsorption · monolayers · scanning tunnel microscopy · self-organization

[1] For recent reviews, see: a) S. De Feyter, A. Gesquière, M. M. Abdel-Mottaleb, P. C. M. Grim, F. C. De Schryver, C. Meiners, M. Sieffert, S. Valiyaveetil, K. Müllen, *Acc. Chem. Res.* **2000**, *33*, 520–531; b) J. Michl, T. F. Magnery, *Proc. Natl. Acad. Sci. USA* **2002**, *99*, 4788–4792; c) E. Mena-Osteritz, *Adv. Mater.* **2002**, *14*, 609–616; d) S. De Feyter, F. C. De Schryver, *Chem. Soc. Rev.* **2003**, *32*, 139–150.

[2] Selected examples: a) H. Shigekawa, K. Miyake, J. Sumaoka, A. Harada, M. Komiyama, *J. Am. Chem. Soc.* **2000**, *122*, 5411–5412; b) L. Shu, A. D. Schlüter, C. Ecker, N. Severin, J. P. Rabe, *Angew. Chem.* **2001**, *113*, 4802–4805; *Angew. Chem. Int. Ed.* **2001**, *40*, 4666–4669.

[3] a) J. Kroner, I. Rios-Carreras, G. Fuhrmann, C. Musch, M. Wunderlin, T. Debaerdemaeker, E. Mena-Osteritz, P. Bäuerle, *Angew. Chem.* **2000**, *112*, 3628–3632; *Angew. Chem. Int. Ed.* **2000**, *39*, 3481–3486; b) E. Mena-Osteritz, P. Bäuerle, *Adv. Mater.* **2001**, *13*, 243–246; c) G. B. Pan, J. M. Liu, H. M. Zhang, L. J. Wan, Q. Y. Zheng, C. L. Bai, *Angew. Chem.* **2003**, *115*, 2853–2857; *Angew. Chem. Int. Ed.* **2003**, *42*, 2747–2751; d) G. B. Pan, L. J. Wan, Q. Y. Zheng, C. L. Bai, *Chem. Phys. Lett.* **2003**, *367*, 711–716.

[4] a) A. Semenov, J. P. Spatz, M. Möller, J.-M. Lehn, B. Sell, D. Schubert, C. H. Weidl, U. S. Schubert, *Angew. Chem.* **1999**, *111*, 2701–2705; *Angew. Chem. Int. Ed.* **1999**, *38*, 2547–2550; b) M. E. Williams, J. T. Hupp, *J. Phys. Chem. B* **2001**, *105*, 8944–8950; c) U. Ziener, J.-M. Lehn, A. Mourran, M. Möller, *Chem. Eur. J.* **2002**, *8*, 951–957; d) D. G. Kurth, N. Severin, J. P. Rabe, *Angew. Chem.* **2002**, *114*, 3833–3835; *Angew. Chem. Int. Ed.* **2002**, *41*, 3681–3683; e) A. Dmitriev, H. Spillmann, N. Lin, J. V. Barth, K. Kern, *Angew. Chem.* **2003**, *115*, 2774–2777; *Angew. Chem. Int. Ed.* **2003**, *42*, 2670–2673; f) D. Wouters, S. Höppener, R. Lunkwitz, L. Chi, H. Fuchs, U. S. Schubert, *Adv. Funct. Mater.* **2003**, *13*, 277–280.

[5] a) P. Samori, F. Jäckel, Ö. Ünsal, A. Godt, J. P. Rabe, *ChemPhysChem* **2001**, *2*, 461–464; b) Y. Liu, L. Li, H.-Y. Zhang, Y.-L. Zhao, X. Wu, *Macromolecules* **2002**, *35*, 9934–9938; c) Y. Liu, Y.-L. Zhao, H.-Y. Zhang, H.-B. Song, *Angew. Chem.* **2003**, *115*, 3382–3385; *Angew. Chem. Int. Ed.* **2003**, *42*, 3260–3263.

[6] P. Laitenberger, C. G. Claessens, L. Kuipers, F. M. Raymo, R. E. Palmer, J. F. Stoddart, *Chem. Phys. Lett.* **1997**, *279*, 209–214.

[7] a) S. Yoshimoto, K. Suto, K. Itaya, N. Kobayashi, *Chem. Commun.* **2003**, 2174–2175; b) S. Griessl, M. Lackinger, M. Edelwirth, M. Hietschold, W. M. Heckl, *Single Mol.* **2002**, *3*, 25–31.

[8] M. Kunitake, N. Batina, K. Itaya, *Langmuir* **1995**, *11*, 2337–2340; b) G. B. Pan, L. J. Wan, Q. Y. Zheng, C. L. Bai, K. Haya, *Chem. Phys. Lett.* **2002**, *359*, 83–88.

[9] a) D. W. Suggs, A. J. Bard, *J. Phys. Chem.* **1995**, *99*, 8349–8355; b) M. R. Vogt, A. Lachenwitzer, O. M. Magnussen, R. J. Behm, *Surf. Sci.* **1998**, *399*, 49–69.

[10] The Θ value is defined as the chloride to copper ratio. At $\Theta = 0.5$ the maximum coverage of the surface with chloride is reached.

[11] a) A. Cuesta, D. M. Kolb, *Surf. Sci.* **2000**, *465*, 310–316. Also, see: b) G.-Z. Yang, Q.-D. Zeng, L.-J. Wan, C.-L. Bai, *Surf. Sci.* **2002**, *511*, L298-L302; c) G. Janssens, F. Touhari, J. W. Gerritsen, H. van Kempen, P. Callant, G. Deroover, D. Vandenbroucke, *Chem. Phys. Lett.* **2001**, *344*, 1–6.

[12] M. T. M. Koper, *J. Electroanal. Chem.* **1998**, *450*, 189–201.

[13] Synthesis and characterization of squares: a) M. Fujita, J. Yazaki, K. Ogura, *J. Am. Chem. Soc.* **1990**, *112*, 5645–5647; b) M. Fujita, J. Yazaki, K. Ogura, *Chem. Lett.* **1991**, 1031; c) P. J. Stang, D. H. Cao, S. Saito, A. M. Arif, *J. Am. Chem. Soc.* **1995**, *117*, 6273–6283; d) C. A. Schalley, T. Müller, P. Linnartz, M. Witt, M. Schäfer, A. Lützen, *Chem. Eur. J.* **2002**, *8*, 3538–3551; for recent reviews, see: e) D. L. Caulder, K. N. Raymond, *Acc. Chem. Res.* **1999**, *32*, 975–982; f) S. Leininger, B. Olenyuk, P. J. Stang, *Chem. Rev.* **2000**, *100*, 853–908; g) B. J. Holliday, C. A. Mirkin, *Angew. Chem.* **2001**, *113*, 2076–2098; *Angew. Chem. Int. Ed.* **2001**, *40*, 2022–2042; h) M. Fujita, K. Umemoto, M. Yoshizawa, N. Fujita, T. Kusukawa, K. Biradha, *Chem. Commun.* **2001**, 509–518.

[14] The nitrate counterions remain in the aqueous solution above the surface.

[15] The augmented MM2 force field as implemented in the CACHE 5.0 program package for Windows was used for the calculation (Fujitsu Ltd., Krakow, Poland, **2001**).

 © 2004 Wiley-VCH Verlag GmbH & Co. KGaA, Weinheim

[16] The value of 2.05 nm given in Figure 1 is inclusive of the Van der Waals radius of the peripheral hydrogen atoms. The lower observed value of 1.9 nm seems reasonable, when one takes into account that the peripheries of two adjacent squares may well interdigitate thus maximizing the Van der Waals contacts. The Pt–Pt distance of 1.14 nm determined by molecular modeling agrees well with the values of 1.109 and 1.112 nm reported in a recent X-ray crystal structure analysis of **1**. See: M. Aoyagi, K. Biradha, M. Fujita, *Bull. Chem. Soc. Jpn.* **1999**, *72*, 2603 – 2606.
[17] C. Safarowsky, K. Wandelt, P. Broekmann, unpublished results.
[18] L. Merz, P. Linnartz, H. Mansikkamäki, C. A. Schalley, B. A. Hermann, unpublished results.
[19] STM measurements in dry environment were carried out with a standard commercial microscope with a low current converter employing PtIr tips. For linear unbranched molecules the contrast is often enhanced by studying these molecules with the STM tip submerged in the liquid. In contrast, a reduced resolution was observed for large, flexible three-dimensional molecules when measured in solution. This was attributed to the half-room being open for arrangement in solution (leading to a more natural three-dimensional arrangement) and the increased interaction with the solvent molecules. These observations support the fact that the results presented in this paper are attributed to a template effect. See: I. Widmer, U. Hubler, M. Stöhr, L. Merz, H.-J. Güntherodt, B. A. Hermann, P. Samorí, J. P. Rabe, P. B. Rheiner, G. Greiveldinger, P. Murer, *Helv. Chim. Acta* **2002**, *85*, 4255 – 4263.

 © 2004 Wiley-VCH Verlag GmbH & Co. KGaA, Weinheim

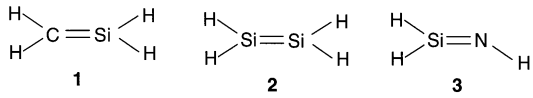
P–Si Compounds

Reaction of Atomic Silicon with Phosphane: A Matrix-Spectroscopic Study**

*Jörg Glatthaar and Günther Maier**

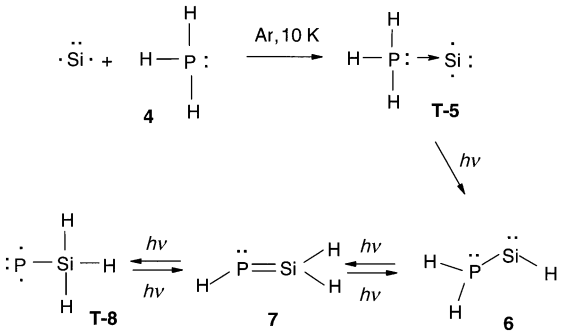
Dedicated to Professor Peter Jutzi on the occasion of his 65th birthday

Matrix isolation spectroscopy is the ideal method for the generation and identification of unsubstituted heteroolefins. Examples are silene **1**,[1a–e] disilene **2**,[1e] and silanimine **3**.[1f,g] The easiest access to these species is the cocondensation of thermally produced Si atoms with CH_4 (this reaction needs additional photochemical activation[1e]), SiH_4,[1e] or NH_3[1h,i] in an argon matrix at 10 K.



1 **2** **3**

As shown herein the reaction of atomic silicon with phosphane (**4**) opens in an analogous manner the door to the H_3PSi isomers **5**–**8** (Scheme 1). These parent compounds bearing only hydrogen atoms have the advantage that their properties can especially well be compared with the results of quantum-chemical calculations. Theoretical studies of the H_3PSi energy hypersurface have already been carried out several times.[2] Additional calculations of our own (B3LYP/6-311+G**) were performed above all to identify the new species by comparing the frequencies and intensities of the experimental and theoretical IR spectra (Table 1).



4 **T-5** **T-8** **7** **6**

Scheme 1. Generation and transformations of the H_3PSi isomers **5**–**8**.

In contrast to phosphanylcarbenes[3] so far phosphanylsilylenes are not known at all, phosphasilenes only in the form of highly substituted derivatives.[4] Phosphanidenes play an important role as synthetic intermediates. They have been identified trapped mainly by trapping addition reactions with olefines or dienes[5] and are well known as ligands in transition-metal complexes.[5]

Upon cocondensation of a gas mixture of phosphane (**4**) and argon (ratio 1:200) together with thermally generated silicon atoms[6] on a spectroscopic window at 10 K one observes in the matrix IR spectrum beside the bands of phosphane (**4**) a new, intense absorption at 1003.5 cm^{-1}. This band belongs to the *n*-adduct **5** (phosphane–silicon). Additional, weak absorptions of **5** can be registered at 1075.0/1078.3 (splitting by matrix effects), 2312.3/2314.5, and 2320.3/2326.1 cm^{-1} (Figure 1). The assignment of the bands of **5** is supported by the study of the reaction of Si atoms with a mixture of PH_3, PH_2D ([D_1]**5**: 910.6 cm^{-1}), PHD_2 ([D_2]**5**: 902.2 cm^{-1}), and PD_3 ([D_3]**5**: 741.5 cm^{-1}). There is accordance between the experimental and calculated isotopic shifts. The small differences in the band positions of the *n*-adducts compared with those of the free phosphanes show that the original geometry of the phosphane is only slightly changed upon formation of the corresponding n-adduct. Beside the bands of **5** an additional weak absorption at 2001.5 cm^{-1} can be detected in the spectrum of the cocondensation product.

[*] Dr. J. Glatthaar, Prof. Dr. G. Maier
Institut für Organische Chemie
Justus-Liebig-Universität
Heinrich-Buff-Ring 58, 35392 Giessen (Germany)
Fax: (+49) 641-99-34309
E-mail: guenther.maier@org.chemie.uni-giessen.de

[**] Hetero π Systems, Part 37. This work was supported by Wacker-Chemie GmbH, Burghausen, the Fonds der Chemischen Industrie, and the Deutsche Forschungsgemeinschaft. We thank Dr. H. P. Reisenauer for many helpful discussions. Part 36: G. Maier, J. Glatthaar, H. P. Reisenauer, *J. Organomet. Chem.* **2003**, *686*, 341–362.

Supporting information for this article is available on the WWW under http://www.angewandte.org or from the author.

 © 2004 Wiley-VCH Verlag GmbH & Co. KGaA, Weinheim DOI: 10.1002/anie.200353111

Table 1: Calculated (B3LYP/6-311+G**) and experimental (Ar, 10 K) wavenumbers [cm^{-1}] of the H_3PSi isomers **5**–**8**.[a]

T-5, calcd	**T-5**, exptl	**6**, calcd	**6**, exptl	**7**, calcd	**7**, exptl	**T-8**, calcd	**T-8**, exptl
301.6(0.1)	–	235.0(27.8)	–	478.8(23.1)	482.1(w)	432.0(0.2)	–
416.1(1.4)	–	480.1(0.4)	–	503.7(0.2)	–	505.6(29.7)	506.5(w)
1044.5(250.2)	1003.5(vs)	501.7(11.1)	–	598.4(1.9)	597.2(vw)	901.3(299.0)	884.9(vs)
1091.3(9.3)	1075.0(w) 1078.3(w)	520.8(9.7)	–	614.4(0.0)	–	938.3(44.0)	925.2(m)
2367.3(33.8)	2312.3(m)2314.5(m)	813.9(53.7)	801.0(m)	773.1(12.4)	748.0(w)	2203.8(60.3)	2172.1(m)
2383.2(201.7)	2320.3(m)2326.1(m)	1105.4(35.6)	1080.6(w)	967.0(85.1)	938.2(w)	2212.5(100.9)	2177.9(m)
		2043.7(215.5)	2001.5(s)	2231.0(61.4)	2184.1(m)		
		2433.0(30.3)	2360.6(w)	2263.4(72.3)	2207.2(m)		
		2462.6(28.8)	2379.8(w)	2354.9(61.2)	2293.4(w)		

[a] Calculated absolute intensities [km mol^{-1}] and relative experimental intensities (vs = very strong, s = strong, m = medium, w = weak) in parentheses.

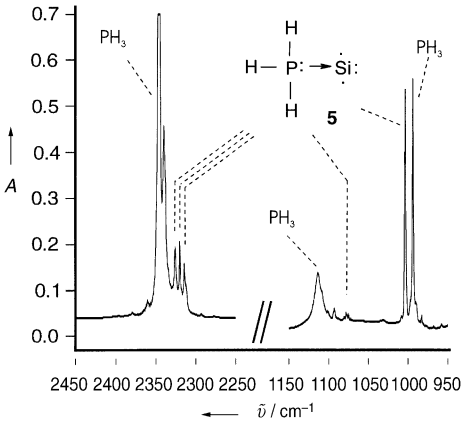


Figure 1. Sections of the IR spectrum of the products of the cocondensation of silicon atoms with a PH_3–Ar gas mixture (1:200) at 10 K.

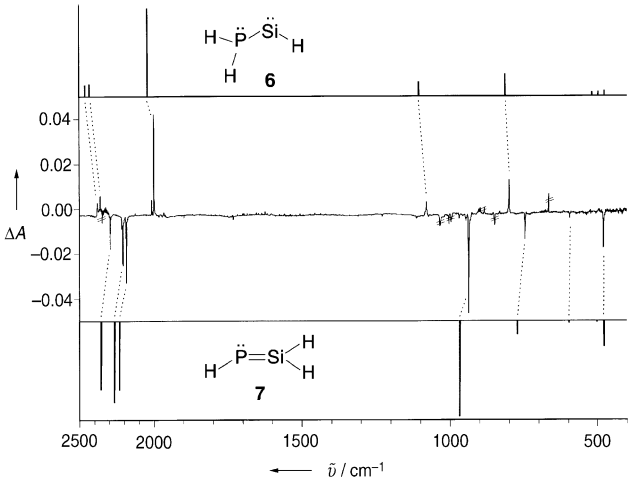


Figure 2. IR spectrum of the photochemically induced isomerization of phosphasilene **7** into phosphanylsilylene **6**. Top: Calculated (B3LYP/6-311+G**) IR spectrum of **6**. Middle: Difference IR spectrum after irradiation at 290 nm; the positive bands of **6** increase during irradiation, the negative ones of **7** decrease. Bottom: Calculated (B3LYP/6-311+G**) IR spectrum of **7**.

This band corresponds with the expected SiH stretching vibration of phosphanylsilylene **6**.

The observed transformation **5**→**6** can in principle be initiated thermally or photochemically. But independent experiments showed that the *n*-adduct **5** is thermally stable up to about 30 K, when the matrix begins to soften. On the other hand a fast photochemical isomerization **5**→**6** occurs if the matrix formed directly upon cocondensation is irradiated with light of the wavelength 366 nm. The bands of **5** disappear, those of **6** (migration of the first hydrogen atom) and **7** (successive 1,2 shift of the second hydrogen atom) increase. During longer irradiation (3.5 h) with 366-nm light the absorptions of **6** (2001.5 cm^{-1}) and **7** (2184.1, 2207.2, and 2293.4 cm^{-1}) decrease again. Now even the third hydrogen atom migrates from the phosphorus to the silicon atom and silylphosphanidene **8** is formed, which is characterized by a strong band at 884.9 cm^{-1}. The back reaction **8**→**7** can be induced with light of the wavelength 534 nm. By suitable selection of the wavelength of the irradiating light it is possible to establish photoequilibria between varying concentrations of the isomers **6**, **7**, and **8**. With 290-nm light the main component is silylene **6**, with 366-nm light phosphanidene **8**, with 534 nm silene **7**. The difference spectra (Figure 2 and 3) derived from theses mutual transformations are of particular value in extracting the spectroscopic data of the isomers concerned, which are the basis for their structural elucidation.

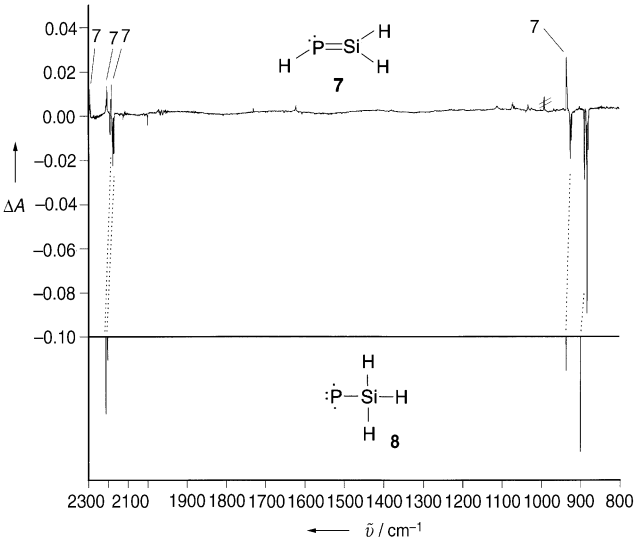
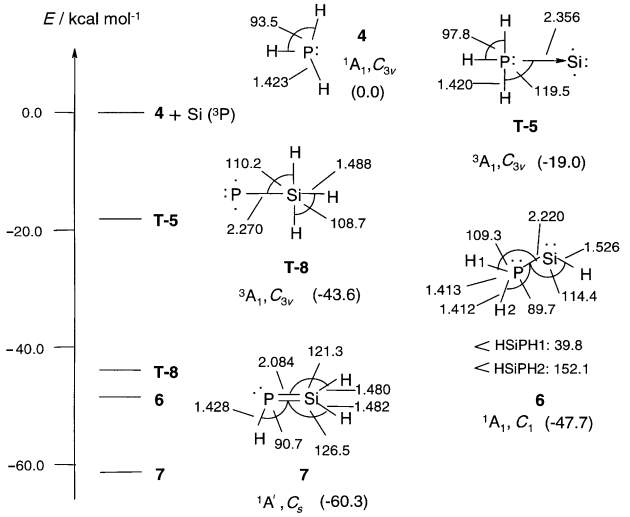


Figure 3. IR spectrum of the photochemically induced isomerization of silylphosphanidene **8** into phosphasilene **7**. Top: Difference IR spectrum after irradiation at 534 nm; the positive bands of **7** increase during irradiation, the negative ones of **8** decrease. Bottom: Calculated (B3LYP/6-311+G**) IR spectrum of **8**.

 © 2004 Wiley-VCH Verlag GmbH & Co. KGaA, Weinheim

The relative energies and geometries of H_3PSi isomers **5**–**8** determined by density functional calculations (B3LYP/6-311+G**) are shown in Scheme 2. Phosphane–silicon (*n*-adduct) **5**, which has not been discussed in the earlier



Scheme 2. Calculated (B3LYP/6-311+G**) relative energies and geometries of H_3PSi isomers **5**–**8**; zero-point vibrational energies included. Distances are given in Å, angles in degrees.

theoretical treatments,[2] possesses according to calculations and experiment a triplet ground state. The measured IR spectrum is in very good accordance with the expectation for the triplet molecule **T-5** (C_{3v} symmetry), the energetically higher-lying singlet **S-5** (C_s symmetry; calculated T/S-energy difference: 34.0 kcal mol^{-1}) should show another spectrum. The formation of **T-5** starting from a Si atom and phosphane (**4**) is predicted to be exothermic (calculated reaction enthalpy $\Delta H_r = -19.0$ kcal mol^{-1}). The calculated relative energies (related to Si(^{3}P) + **4**; zero-point energies included) of the other three H_3PSi isomers are much lower (**T-8**: −43.6; **6**: −47.7; **7**: −60.3 kcal mol^{-1}, global minimum). In this context it is astonishing that in the series of the corresponding derivatives of ammonia the same theoretical method indicates the silylene isomer to be the most stable species. Silylene **6** is a singlet molecule (nonplanar; C_1 symmetry) and is similar in its properties to aminosilylene.[1h] The photoisomerization of phosphanylsilylene **6** into phosphasilene **7** (planar; C_s symmetry) has its parallel in analogous observations in the π systems **1**–**3**, which can also be generated by irradiation of the corresponding silylenes.[1] Silylphosphophanidene **8** is, the same is true for the parent compound HP,[7] characterized by a triplet ground state. It should also be mentioned, that mesitylphosphanidene has been identified by ESR spectroscopy as a triplet molecule.[8] So it is no surprise, that the calculated IR spectrum of **T-8** (C_{3v} symmetry) agrees well with the experimental one (Table 1). In this peculiar case a comparison with the corresponding singlet molecule **S-8** is not possible since this species does not represent an energy minimum.

Matrix isolation is the method of choice for the identification of the H_3PSi isomers **5**–**8**. It remains to be seen whether these compounds undergo—in analogy to the reaction **3**→HSiN + HNSi + SiN[1g]—upon irradiation with short wavelength light also a dehydrogenation, resulting in the formation of HSiP, HPSi, and SiP with a formal Si–P triple bond.

Received: October 17, 2003 [Z53111]

Keywords: matrix isolation · phosphorus · photochemistry · reactive intermediates · silicon

[1] a) G. Maier, G. Mihm, H. P. Reisenauer, *Angew. Chem.* **1981**, *93*, 615–616; *Angew. Chem. Int. Ed. Engl.* **1981**, *20*, 597–598; b) G. Maier, G. Mihm, H. P. Reisenauer, *Chem. Ber.* **1984**, *117*, 2351–2368; c) G. Maier, G. Mihm, H. P. Reisenauer, D. Littmann, *Chem. Ber.* **1984**, *117*, 2369–2381; d) G. Maier, J. Glatthaar in *Organosilicon Chemistry—From Molecules to Materials* (Eds.: N. Auner, J. Weis), VCH, Weinheim, **1994**, pp. 131–138; e) G. Maier, H. P. Reisenauer, J. Glatthaar, *Chem. Eur. J.* **2002**, *8*, 4383–4391; f) G. Maier, J. Glatthaar, H. P. Reisenauer, *Chem. Ber.* **1989**, *122*, 2403–2405; g) G. Maier, J. Glatthaar, *Angew. Chem.* **1994**, *106*, 486–488; *Angew. Chem. Int. Ed. Engl.* **1994**, *33*, 473–475; h) M. Chen, L. Aihua, H. Lu, M. Zhou, *J. Phys. Chem. A* **2002**, *106*, 3077–3083; i) G. Maier, H. P. Reisenauer, H. Egenolf, J. Glatthaar in *Organosilicon Chemistry—From Molecules to Materials V* (Eds.: N. Auner, J. Weis), VCH, Weinheim, **2003**, pp. 5–10.

[2] a) M. R. Zachariah, C. F. Melius, *J. Phys. Chem. A* **1997**, *101*, 913–918; b) M. T. Nguyen, A. Van Keer, L. G. Vanquickenborne, *J. Org. Chem.* **1996**, *61*, 7077–7084; c) H. B. Schlegel, A. G. Baboul, *J. Am. Chem. Soc.* **1996**, *118*, 8444–8451; d) M. Driess, R. Janoschek, *J. Mol. Struct.* **1994**, *313*, 129–139; e) J. G. Lee, J. E. Boggs, A. H. Cowley, *J. Chem. Soc. Chem. Commun.* **1985**, *12*, 773–774; f) K. J. Dykema, T. N. Truong, M. S. Gordon, *J. Am. Chem. Soc.* **1985**, *107*, 4535–4541.

[3] Review: D. Bourisson, O. Guerett, F. P. Gabba¿, G. Bertrand, *Chem. Rev.* **2000**, *100*, 39–91.

[4] Y. van den Winkel, H. M. M. Bastiaans, F. Bickelhaupt, *Phosphorus Sulfur Silicon Relat. Elem.* **1990**, *49*/50, 333–336; G. Fritz, T. Vaahs, H. Fleischer, E. Matern, *Z. Anorg. Allg. Chem.* **1989**, *570*, 54–66.

[5] Reviews: a) F. Mathey in *Multiple Bonds and Low Coordination on Phosphorus Chemistry* (Eds.: M. Regitz, J. Scherer), Thieme, Stuttgart, **1990**; b) F. Mathey, N. H. Tran Huy, A. Marinetti, *Helv. Chim. Acta* **2001**, *84*, 2938–2957; c) K. Lammertsma, M. J. M. Vlaar, *Eur. J. Org. Chem.* **2002**, 1127–1138.

[6] Reviews describing the method: a) G. Maier, H. P. Reisenauer, H. Egenolf, J. Glatthaar in *Silicon Chemistry-From the Atom to Extended Systems* (Eds.: P. Jutzi, U. Schubert), Wiley-VCH, Weinheim, **2003**, pp. 4–19; b) G. Maier, H. P. Reisenauer, H. Egenolf, J. Glatthaar, L. Rösch in *Silicon for the Chemical Industry VI* (Eds.: H. A. Øye, H. M. Rong, L. Nygaard, G. Schüssler, J. Kr. Tuset), Trondheim, Norway, **2002**, pp. 285–297.

[7] P. E. Cade, *Can. J. Phys.* **1968**, *46*, 1989–1991.

[8] X. Li, S. I. Weissman, T.-S. Lin, P. P. Gaspar, *J. Am. Chem. Soc.* **1994**, *116*, 7899–7900.

 © 2004 Wiley-VCH Verlag GmbH & Co. KGaA, Weinheim

Chiral Solid-State Structures

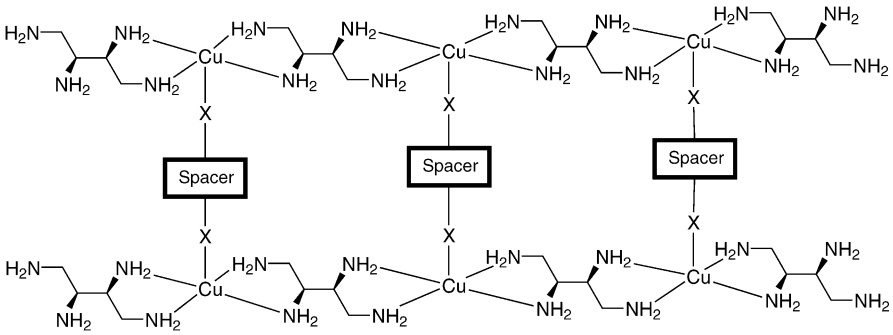
Rhenium–Chalcogenide–Cyano Clusters, Cu^{2+} Ions, and 1,2,3,4-Tetraaminobutane as Molecular Building Blocks for Chiral Coordination Polymers**

Yuri V. Mironov, Nikolai G. Naumov, Konstantin A. Brylev, Olga A. Efremova, Vladimir E. Fedorov, and Kaspar Hegetschweiler**

Dedicated to Professor Hans Rudolf Christen on the occasion of his 80th birthday

Metal–organic frameworks (MOFs) with an open structure have attracted considerable attention.[1,2] Such compounds are of interest as host matrices in supramolecular chemistry, and have potential as catalysts and as materials with special magnetic and optical properties. In this context, heterometallic and chiral MOFs are of particular interest.[3] A chiral network would allow selective binding of chiral guests, and the presence of different types of metal ions enables specific tuning of the electronic properties. A large number of papers have appeared within the last few years that have reported new, extended, metal-containing structures. However, most of these MOFs were obtained from achiral components, and consequently, only a limited number of chiral structures have been obtained. A straightforward strategy for the design of chiral, heterometallic MOFs would require 1) a readily accessible, chiral and enantiomericaly pure building block, 2) a rational method to control the structural parameters of the framework, and 3) a simple pathway to combine different metallic elements with each other.

In a preceding contribution, we presented the chiral 1,2*S*,3*S*,4-butanetetramine (*threo*-tab) as a promising building block for the construction of chiral coordination polymers.[4] This ligand coordinates preferably in a bis-bidentate mode with a metal–metal separation of about 7 Å (Scheme 1). The bis-bidentate coordination mode arises from steric constraints, which prevent binding of the four amino donor atoms to the same metal center. In aqueous solution, $[Cu(threo\text{-tab})]^{2+}$ formed oligomeric species with a linear chain structure and square-planar $\{CuN_4\}$ units. Additional binding of a bridging unit to the axial positions of the Cu^{II} centers would thus provide a promising route to new, two-dimensional and chiral MOFs with an open structure. The bridging unit would serve as a spacer, and its size and structure could be used to adjust the distance between individual $\{[Cu(threo\text{-tab})]^{2+}\}_\infty$ strands.



Scheme 1. Interconnection of individual $\{[Cu(threo\text{-tab})]^{2+}\}_\infty$ strands by anionic spacer ligands.

We have exploited this strategy, using a variety of well-known, anionic rhenium–chalcogenide–cyano clusters as bridging units and report here on the interlinking of linear $\{[Cu(threo\text{-tab})]^{2+}\}_\infty$ strands with $[Re_4Te_4(CN)_{12}]^{4-}$ and $[Re_6Q_8(CN)_6]^{4-}$ (Q = Te, Se, S).[5]

The crystalline solids **1**–**4** were prepared by direct combination of *threo*-tab, Cu^{2+}, and the rhenium–chalcogenide cluster anion in alkaline aqueous solution.

$[Cu(threo\text{-tab})]_2[Re_4Te_4(CN)_{12}] \cdot 6.5\,H_2O$ **1**

$[Cu(threo\text{-tab})]_2[Re_6Te_8(CN)_6] \cdot 13.5\,H_2O$ **2**

$[Cu_2(threo\text{-tab})_3(NH_3)][Re_6Se_8(CN)_6] \cdot 2\,H_2O$ **3**

$[Cu_2(threo\text{-tab})_3(NH_3)][Re_6S_8(CN)_6] \cdot 3\,H_2O$ **4**

The structures of **1**–**3** were elucidated by single-crystal X-ray diffraction.[6] The selenium compound **3** and the sulfur compound **4** are isotypic.[7] In all compounds, the $[Cu(threo\text{-tab})]^{2+}$ moieties adopted the above-mentioned chain structure, and the chains are interlinked by the cluster anions to form chiral, two-dimensional grids.

There is a clear influence of the individual steric properties of the four bridging units on the grid structure. In the heterocuboidal $[Re_4Te_4(CN)_{12}]^{4-}$ ion, the high number of cyano ligands enable different types of Cu···cluster···Cu

[*] Dr. Y. V. Mironov, Dr. N. G. Naumov, K. A. Brylev, Dr. O. A. Efremova, Prof. Dr. V. E. Fedorov
Institute of Inorganic Chemistry of the Russian Academy of Sciences
Pr. Lavrentieva 3, 630090, Novosibirsk (Russia)
Fax: (+7) 3832-344489
E-mail: fed@che.nsk.su.
Prof. Dr. K. Hegetschweiler
Universität des Saarlandes, Anorganische Chemie
Postfach 15 11 50, 66041 Saarbrücken (Germany)
Fax: (+49) 681-302-2663
E-mail: hegetschweiler@mx.uni-saarland.de

[**] Linear Primary Polyamines as Building Blocks for Coordination Polymers, Part 5. We thank Prof. W. S. Sheldrick (Bochum) and Dr. P. Osvath (Melbourne) for advice. This work was supported by the Russian Foundation for Basic Research (grant 02-03-32264), INTAS-00-00689, the Alexander von Humboldt Foundation (Y.V.M.), and the Fonds der Chemischen Industrie (K.H.). Part 4: A. Zimmer, T. Weyhermüller, K. Hegetschweiler in *Progress in Coordination and Bioinorganic Chemistry* (Eds.: M. Melnik, A. Sirota), Slovak Technical University Press, Bratislava, **2003**, pp. 201–206.

Supporting information for this article is available on the WWW under http://www.angewandte.org or from the author.

 DOI: 10.1002/anie.200351595 © 2004 Wiley-VCH Verlag GmbH & Co. KGaA, Weinheim

interactions (Figure 1a), and two of them are realized in **1** (Scheme 2). One chain is attached to the cluster by binding the two adjacent Cu atoms of a [Cu-(*threo*-tab)-Cu]$^{4+}$ moiety by two cyano groups of one single Re atom, whereas in the other chain the Cu atoms are connected to cyano groups of two different Re atoms. Owing to the lack of a center of inversion in the tetrahedral (local T_d) $[Re_4Te_4(CN)_{12}]^{4-}$ unit, all possible bridging modes will inherently result in a bent Cu···cluster···Cu arrangement.

The isostructural $[Re_6Q_8(CN)_6]^{4-}$ bridges in **2** and **3** (Q = Te, Se) comprise a Re_6 octahedron inscribed in a cube of eight μ_3-chalcogen atoms. Here, the Re atoms are only ligated by one single cyano ligand. Two different bridging modes must be considered with either a *cisoid* (local C_{2v}) or a *transoid* (local D_{4h}) structure (Scheme 2). Again, a bent Cu···cluster···Cu arrangement is expected for the *cisoid* C_{2v} mode due to the lack of a center of inversion, whereas the *transoid* D_{4h} mode is centrosymmetric and would provide a linear bridge. Interestingly, both modes are realized in **2** and **3**: In the tellurium derivative **2**, bent, *cisoid* bridges were formed, whereas in the selenium derivative **3** approximately linear, *transoid* bridges are observed (Figure 1b and 1c).

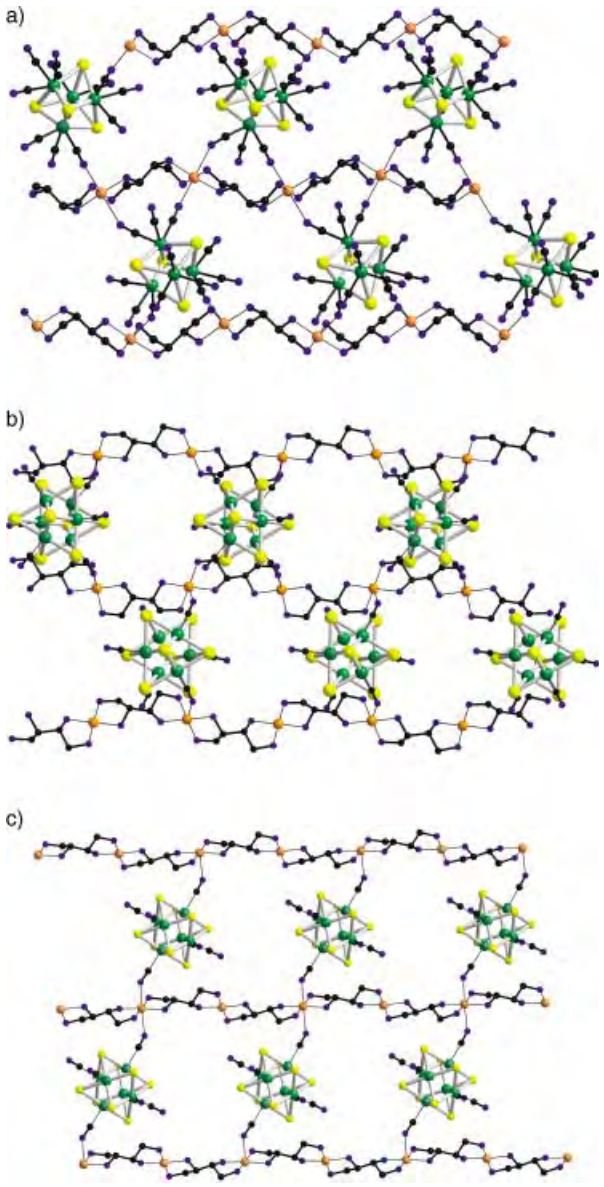
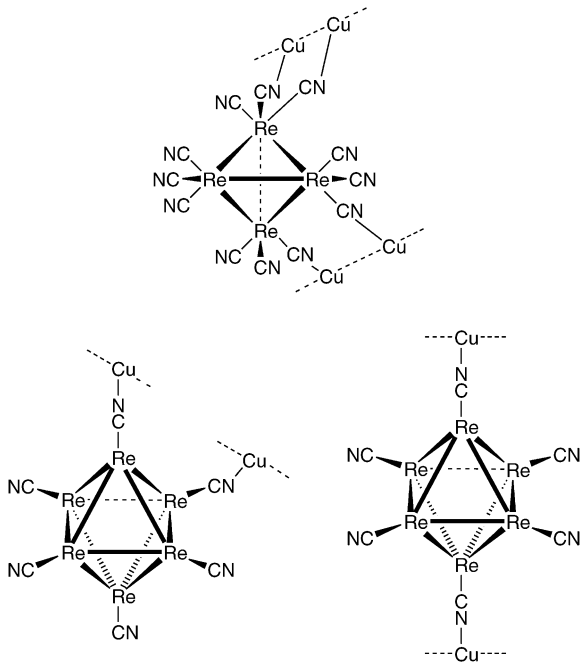


Figure 1. Ball-and-stick representations of the $\{Cu_{2n}(tab_{2n})(cluster)_n\}_\infty$ layer of a) **1**, b) **2**, and c) **3**. Hydrogen atoms and guest molecules (water, *threo*-tab) are omitted. Color code: Re: green; Te, Se: yellow; Cu: orange; N: blue; C: black.



Scheme 2. Schematic representation of the different types of bridging interactions in **1** (top), **2** (bottom left), and **3** (bottom right).

All three structures can be described as a stack of two-dimensional layers; however, the different bridging modes have a crucial influence on the packing characteristics. The bent bridging modes in **1** and **2** resulted in the formation of wavy layers, whereas the linear bridges of **3** generate approximately plane layers (see Figure S4 in the Supporting Information). In all three structures relatively large cavities are formed that are filled with H_2O or additional *threo*-tab molecules.[8] However, in **1** and **2**, the strongly undulating character of the $\{Cu_{2n}(tab_{2n})(cluster)_n\}_\infty$ layers prevent the formation of sufficiently large channels which would allow reversible incorporation of guest molecules.[9] This is different for **3**, in which a system of channels oriented parallel to the crystallographic *x* and *y* axis are formed (Figure 2).[10]

In this communication, we have introduced a new and straightforward synthetic pathway to chiral, heterometallic coordination polymers. The individual components, that is, the chiral *threo*-tab ligand, a labile, divalent transition-metal cation, and an oligonuclear, inert cyano complex, are readily available and the polymers can be prepared simply by combining these components in aqueous solution.

Cyano complexes of transition-metal cations are well established as bridging units in coordination polymers.[11] In recent times, Verdaguer and co-workers have used a variety of transition-metal cyano complexes for the construction of new magnetic materials.[12] The use of oligonuclear bridging units, as shown in our present contribution, proved to be of

 © 2004 Wiley-VCH Verlag GmbH & Co. KGaA, Weinheim

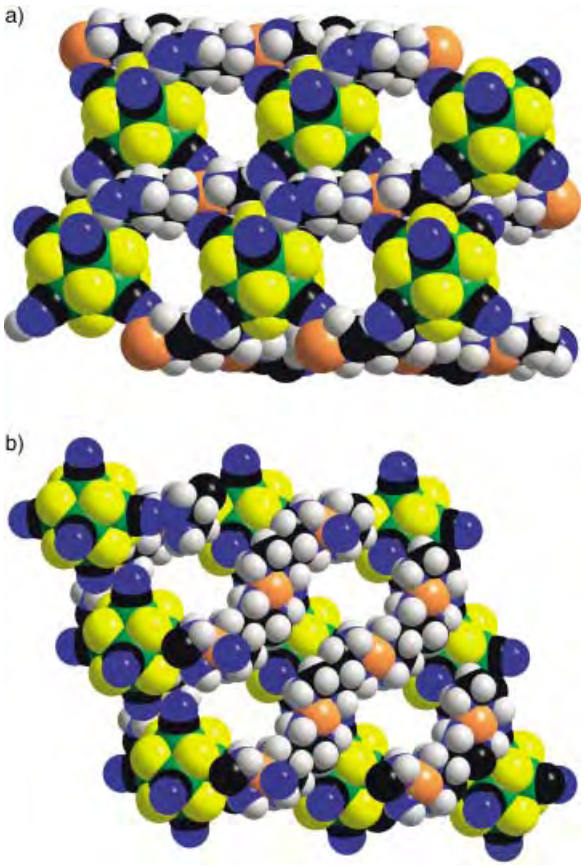


Figure 2. Space-filling models of the $\{Cu_{2n}(tab_{2n})(cluster)_n\}_\infty$ network of **3**.[10] Views along the crystallographic *x* (a) and *y* (b) axis, showing the channel structure of this compound. Views of the considerably smaller channels of **1** and **2** are provided as Supporting Information. Color code: Re: green; Te, Se: yellow; Cu: orange; N: blue; C: black; H: white.

particular interest, because it allows the design of open networks with sufficiently large voids for host–guest interactions. Most important, the use of the chiral, bis-bidentate *threo*-tab ligand guarantees the formation of a chiral crystal structure. It is also noteworthy that our strategy enables the design of two-dimensional networks with labile, coordinatively unsaturated transition-metal centers. Such 2D structures have the ideal prerequisites for the coating of suitable surfaces by a chiral monolayer.

Received: April 7, 2003
Revised: September 11, 2003 [Z51595]

Keywords: bridging ligands · chain structures · chirality · cluster compounds · polymers

[1] Comprehensive reviews: a) P. J. Hagrman, D. Hagrman, J. Zubieta, *Angew. Chem.* **1999**, *111*, 2798; *Angew. Chem. Int. Ed.* **1999**, *38*, 2638; b) B. Moulton, M. J. Zaworotko, *Chem. Rev.* **2001**, *101*, 1629; c) R. W. Saalfrank, E. Uller, B. Demleitner, I. Bernt, *Struct. Bonding (Berlin)* **2000**, *96*, 149; d) M. Eddaoudi, D. B. Moler, H. Li, B. Chen, T. M. Reineke, M. O'Keeffe, O. M. Yaghi, *Acc. Chem. Res.* **2001**, *34*, 319; e) U. S. Schubert, C. Eschbaumer, *Angew. Chem.* **2002**, *114*, 3016; *Angew. Chem. Int. Ed.* **2002**, *41*, 2892.

[2] Selection of recent research papers: a) R. Kitaura, K. Fujimoto, S.-i. Noro, M. Kondo, S. Kitagawa, *Angew. Chem.* **2002**, *114*, 141; *Angew. Chem. Int. Ed.* **2002**, *41*, 133; b) Y.-Q. Tian, C.-X. Cai, Y. Ji, X.-Z. You, S.-M. Peng, G.-H. Lee, *Angew. Chem.* **2002**, *114*, 1442; *Angew. Chem. Int. Ed.* **2002**, *41*, 1384; c) K.-M. Park, S.-Y. Kim, J. Heo, D. Whang, S. Sakamoto, K. Yamaguchi, K. Kim. *J. Am. Chem. Soc.* **2002**, *124*, 2140; d) R.-G. Xiong, X. Xue, H. Zhao, X.-Z. You, B. F. Abrahams, Z. Xue, *Angew. Chem.* **2002**, *114*, 3954; *Angew. Chem. Int. Ed.* **2002**, *41*, 3800; e) G. Seeber, A. L. Pickering, D.-L. Long, L. Cronin, *Chem. Commun.* **2003**, 2002.

[3] a) N. G. Pschirer, D. M. Ciurtin, M. D. Smith, U. H. F. Bunz, H.-C. zur Loye, *Angew. Chem.* **2002**, *114*, 603; *Angew. Chem. Int. Ed.* **2002**, *41*, 583; b) Y. Cui, O. R. Evans, H. L. Ngo, P. S. White, W. Lin, *Angew. Chem.* **2002**, *114*, 1207; *Angew. Chem. Int. Ed.* **2002**, *41*, 1159; c) J. Sun, L. Weng, Y. Zhou, J. Chen, Z. Chen, Z. Liu, D. Zhao, *Angew. Chem.* **2002**, *114*, 4651; *Angew. Chem. Int. Ed.* **2002**, *41*, 4471; d) O. Mamula, F. J. Monlien, A. Porquet, G. Hopfgartner, A. E. Merbach, A. von Zelewsky, *Chem. Eur. J.* **2001**, *7*, 533; e) L. Plasseraud, H. Maid, F. Hampel, R. W. Saalfrank, *Chem. Eur. J.* **2001**, *7*, 4007.

[4] A. Zimmer, D. Kuppert, T. Weyhermüller, I. Müller, K. Hegetschweiler, *Chem. Eur. J.* **2001**, *7*, 917.

[5] a) N. G. Naumov, A. V. Virovets, N. V. Podberezskaya, V. E. Fedorov, *J. Struct. Chem.* **1997**, *38*, 857; b) N. G. Naumov, A. V. Virovets, M. N. Sokolov, S. B. Artemkina, V. E. Fedorov, *Angew. Chem.* **1998**, *110*, 2043; *Angew. Chem. Int. Ed.* **1998**, *37*, 1943; c) Y. V. Mironov, A. V. Virovets, S. B. Artemkina, V. E. Fedorov, *Angew. Chem.* **1998**, *110*, 2656; *Angew. Chem. Int. Ed.* **1998**, *37*, 2507; d) N. G. Naumov, A. V. Virovets, Y. I. Mironov, S. B. Artemkina, V. E. Fedorov, *Ukr. Khim. Zhurn.* **1999**, *65*, 21; e) Y. V. Mironov, O. Oeckler, A. Simon, V. E. Fedorov, *Eur. J. Inorg. Chem.* **2001**, 2751; f) Y. V. Mironov, V. E. Fedorov, I. Ijjaali, J. A. Ibers, *Inorg. Chem.* **2001**, *40*, 6320.

[6] X-ray structural analyses: Siemens P4 diffractometer (for **1** and **2**) and Nonius Kappa CCD diffractometer (for **3**), graphite monochromator, $Mo_{K\alpha}$ radiation ($\lambda = 0.71073$ Å), ω-scans, SHELX-97 program set[13] for structure solution (direct methods) and refinement (full-matrix least-squares on F^2). Positions of hydrogen atoms were calculated (riding model). **1**: $C_{20}H_{41}Cu_2N_{20}O_{6.5}Re_4Te_4$ ($M_r = 2048.01$), $0.1 \times 0.1 \times 0.22$ mm, monoclinic, space group $P2_1$, $a = 9.782(2)$, $b = 12.487(7)$, $c = 20.017(6)$ Å, $\beta = 92.64(3)°$, $V = 2442.4(15)$ Å^3, $Z = 2$, $\rho_{calcd} = 2.785$ g cm^{-3}, $\mu = 13.123$ mm^{-1}, $2.04 < \theta < 25.0°$, $T = 293(2)$ K, empirical absorption correction (transmission coefficients: 0.998, 0.417). Reflections: 9261 collected, 8570 unique ($R_{int} = 0.0541$), 5890 observed [$I > 2\sigma(I)$]; 488 parameters refined with $R = 0.0668$ [$I > 2\sigma(I)$], w$R_2 = 0.1287$ (all data), GOF = 1.029. Abs. struct.: −0.029(14),[14] residual electron density: +1.465, −1.325 e Å^{-3}. **2**: $C_{14}H_{55}Cu_2N_{14}O_{13.5}Re_6Te_8$ ($M_r = 2900.80$), $0.08 \times 0.08 \times 0.08$ mm, orthorhombic, space group $P2_12_12_1$, $a = 13.767(3)$, $b = 19.692(4)$, $c = 21.780(4)$ Å, $V = 5905(2)$ Å^3, $Z = 4$, $\rho_{calcd} = 3.263$ g cm^{-3}, $\mu = 16.878$ mm^{-1}, $2.14 < \theta < 25.02°$, $T = 293(2)$ K, empirical absorption correction (transmission coefficient: 0.909, 0.573). Reflections: 11477 collected, 10406 unique ($R_{int} = 0.0578$), 5024 observed [$I > 2\sigma(I)$], 473 parameters refined with $R = 0.0725$ [$I > 2\sigma(I)$], w$R_2 = 0.1407$ (all data), GOF = 1.006. Abs. struct.: 0.03(2),[14] residual electron density: 1.216, −1.135 e Å^{-3}. **3**: $C_{18}H_{49}Cu_2N_{19}O_2Re_6Se_8$ ($M_r = 2439.72$), $0.1 \times 0.08 \times 0.05$ mm, triclinic, space group $P\bar{1}$ (no. 1), $a = 10.819(5)$, $b = 11.069(5)$, $c = 13.175(5)$ Å, $\alpha = 107.947(5)$, $\beta = 110.968(5)$, $\gamma = 92.593(5)°$, $V = 1380.0(10)$ Å^3, $Z = 1$, $\rho_{calcd} = 2.936$ g cm^{-3}, $\mu = 19.168$ mm^{-1}, $1.96 < \theta < 30.51°$, $T = 293(2)$ K, empirical absorption correction (transmission coefficient: 0.6079, 0.234). Reflections: 53986 collected, 16722 unique ($R_{int} = 0.0587$),

 © 2004 Wiley-VCH Verlag GmbH & Co. KGaA, Weinheim

11 852 observed [$I > 2\sigma(I)$]. The disordered (dangling) *threo*-tab ligand was refined by using two different sites with occupancies of 70 % and 30 % each (except N31 and N41 which received both full occupancy).[8] N31 and N41 were refined anisotropically, the remaining non-hydrogen atoms of the dangling *threo*-tab were refined isotropically. Some restraints were used to adjust the C–C and C–N bond lengths to meaningful values within the disordered moieties. The refinement of 445 parameters yielded $R = 0.0434$ [$I > 2\sigma(I)$], $wR_2 = 0.1344$ (all data), GOF = 1.03. Abs. struct.: −0.006(13),[14] residual electron density: +2.23, −1.49 e Å^{-3}. CCDC-207076 (**1**), CCDC-207077 (**2**), and CCDC-218525 (**3**) contain the supplementary crystallographic data for this paper. These data can be obtained free of charge via www.ccdc.cam.ac.uk/conts/retrieving.html (or from the Cambridge Crystallographic Data Centre, 12, Union Road, Cambridge CB2 1EZ, UK; fax: (+44) 1223-336-033; or deposit@ccdc.cam.ac.uk).

[7] Crystal data for **4**: $C_{18}H_{51}Cu_2N_{19}O_3Re_6S_8$ ($M_r = 2082.54$), triclinic, space group $P\bar{1}$ (no. 1), $a = 10.635(5)$, $b = 10.983(5)$, $c = 13.166(5)$ Å, $\alpha = 108.434(5)$, $\beta = 110.479(5)$, $\gamma = 92.856(5)^\circ$, $V = 1344.3(10)$ Å^3, $T = 293(2)$ K, $\rho_{calcd} = 2.573$ g cm^{-3}, $\mu = 14.575$ mm^{-1}.

[8] The size of the voids of **1** (308 Å^3), **2** (577 Å^3), and **3** (552 Å^3), which are accessible for guest molecules, have been calculated by using the program PLATON (A. L. Spek, PLATON, a Multipurpose Crystallographic Tool, Utrecht University, Utrecht, The Netherlands, **2001**; see also *Acta Crystallogr. Sect. A* **1990**, *46*, C34). In **1** and **2**, the voids are filled with mostly disordered H_2O molecules. In the Se derivative **3**, two H_2O molecules and an additional disordered *threo*-tab ligand which shows a very weak, monodentate interaction to Cu2 are found in the cavity. The N31 and N41 positions, which are in proximity to Cu2 show a significantly higher electron density than the other non-hydrogen atoms. We interpret this as an indication of an additional NH_3 (or H_2O) molecule which shares the position at random with the disordered *threo*-tab ligand.

[9] Thermogravimetric measurements of **2** show a rapid weight loss of about 8 % between 50 and 110 °C. This amount is in close agreement with the removal of the water of crystallization. IR spectroscopic measurements before and after heating confirmed this interpretation. The bands belonging to H_2O disappeared, whereas the vibrations of the cluster and the tab ligand in the range 500–2200 cm^{-1} remained virtually unchanged. However, the XRD powder diffraction patterns observed at 25 and 110 °C showed significant differences. Figures for the TG, IR and XRD measurements are provided as Supporting Information.

[10] In **3**, the Cu···*threo*-tab···Cu strands are oriented parallel to the *x*-*z* face diagonal, and the Cu···*cluster*···Cu linkages are parallel to the *y*-*z* face diagonal, resulting in infinite grids arranged parallel to the $(11\bar{1})$ plane. The channels have approximate dimensions of 4.0 × 5.2 Å (parallel to *x*) and 3.6 × 5.8 Å (parallel to *y*).

[11] a) V. P. Fedin, A. V. Virovets, I. V. Kalinina, V. N. Ikorskii, M. R. J. Elsegood, W. Clegg, *Eur. J. Inorg. Chem.* **2000**, 2341; b) J. S. Miller, J. L. Manson, *Acc. Chem. Res.* **2001**, *34*, 563; c) C. J. Shorrock, B.-Y. Xue, P. B. Kim, R. J. Batchelor, B. O. Patrick, D. B. Leznoff, *Inorg. Chem.* **2002**, *41*, 6743.

[12] a) M. Verdaguer, A. Bleuzen, V. Marvaud, J. Vaissermann, M. Seuleiman, C. Desplanches, A. Scuiller, C. Train, R. Garde, G. Gelly, C. Lomenech, I. Rosenman, P. Veillet, C. Cartier, F. Villain, *Coord. Chem. Rev.* **1999**, *190–192*, 1023; b) J. M. Herrera, D. Armentano, G. de Munno, F. Lloret, M. Julve, M. Verdaguer, *New J. Chem.* **2003**, *27*, 128.

[13] a) G. M. Sheldrick, SHELXS-97, Program for Crystal Structure Solution, University of Göttingen, Göttingen (Germany), **1997**; b) G. M. Sheldrick, SHELXL-97, Program for Crystal Structure Refinement, University of Göttingen, Göttingen (Germany), **1997**.

[14] H. D. Flack, *Acta Crystallogr. Sect. A* **1983**, *39*, 876.

 © 2004 Wiley-VCH Verlag GmbH & Co. KGaA, Weinheim

Metallocalixarenes

Pentanuclear Platinum(II) Macrocycles with Nucleobases**

*Michael J. Rauterkus and Bernt Krebs**

Macrocyclic metal complexes have attracted continuously growing attention in recent research activities owing to their outstanding chemical properties.[1] The immense potential of these self-assembling species is a result especially of their shape- and size-selective binding of small molecules.[2] Thus, a multitude of potential applications results, mainly in catalysis, sensing devices, and processes of molecular recognition and complexation.[3,4] Predominantly, the metal centers are found at the corners of these molecular cages, which are usually square or hexagonal in shape. Consequently, they can be categorized as the metal analogues of the corresponding calixarenes.[5] Bifunctional organic ligands such as 4,4′-bipyridine are widely used for connecting the metal atoms.

Nucleobases are capable of being incorporated in these nanoscaled macrocycles as well. Applying them with *cis*-configured platinum(II) and palladium(II) complexes as metal building blocks this approach leads to multinuclear complex compounds.[6,7] The metals' square-planar coordination spheres are completed by ligands, such as ethylenediamine or *cis*-arranged phosphanes. In the known platinum and palladium macrocycles, aromatic amine ligands are utilized very rarely.[2b,8] To date we have focused on the synthesis and characterization of cisplatin analogues with tertiary amines as chelating ligands.[9] These platinum(II) complexes exhibit significant cytostatic activities although they lack the ability to form stabilizing hydrogen bonds to the DNA's phosphate backbone.[10,11]

Herein we present the first complexes, which connect these two fields of research: three pentanuclear platinum(II) macrocycles, set up from a cisplatin analogue with aromatic nitrogen ligands and the nucleobases thymine (T) and uracil (U) (Figure 1).[12] The preparation of this novel type of metallocalixarenes succeeds in a highly selective way within a

[*] Prof. Dr. B. Krebs
Westfälische Wilhelms-Universität Münster
Institut für Anorganische und Analytische Chemie
Wilhelm-Klemm-Strasse 8, 48149 Münster (Germany)
Fax: (+49) 251-83-38366
E-mail: krebs@uni-muenster.de

Dr. M. J. Rauterkus
medac
Gesellschaft für klinische Spezialpräparate mbH
Fehlandtstrasse 3, 20354 Hamburg (Germany)

[**] The authors thank the W. C. Heraeus GmbH & Co. KG for the kind donation of the platinum salt used. Support by the Deutsche Forschungsgemeinschaft, the Fonds der Chemischen Industrie, the University of Münster and the medac GmbH is gratefully acknowledged. M.J.R thanks the Hanns Seidel Foundation, Munich, for financial support. All the experiments reported herein were carried out at the Institute of Inorganic and Analytical Chemistry, University of Münnster.

 © 2004 Wiley-VCH Verlag GmbH & Co. KGaA, Weinheim DOI: 10.1002/anie.200352950

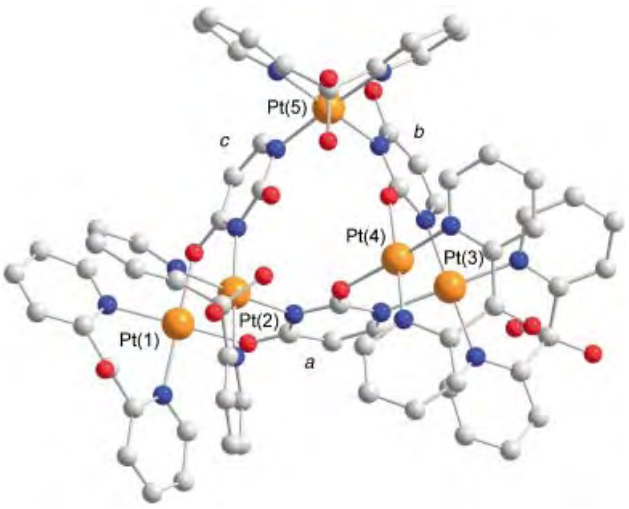


Figure 1. The pentanuclear complex cation of **1**: three uracilate ligands connect the two diplatinum centers and the monoplatinum center. Orange = Pt, blue = N, red = O, gray = C.

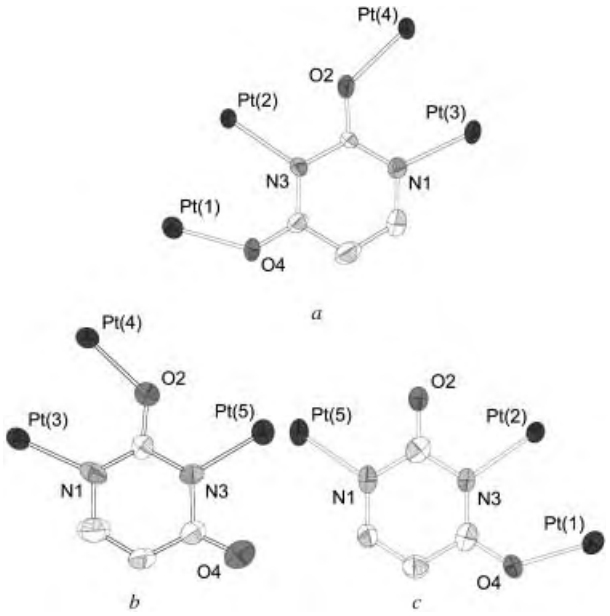


Figure 2. The uracil bases of **2** with coordinated platinum atoms (thermal ellipsoids set at 50% probability). The designations *a*–*c* are used correspondingly for the nucleobases of **1**–**3**.

few synthesis steps. 2,2′-Dipyridylketonedichloroplatinum(II) was used as a starting compound, the cytostatic activities of this compound have already been demonstrated by us in experiments with different tumor cell lines.[9a,13] In aqueous solution the bidentate ligand 2,2′-dipyridylketone (dpk) can react to give its corresponding hydrate form ($dpkOH_2$) by adding a water molecule to the ketone group bridging the two pyridine rings.

$[Pt_5(dpk)_2(dpkOH_2)_3(U)_3](BF_4)(NO_3)_3 \cdot 8H_2O$ **1**

$[Pt_5(dpk)_2(dpkOH_2)_3(U)_3](PF_6)(NO_3)_3 \cdot 9H_2O$ **2**

$[Pt_5(dpk)_2(dpkOH_2)_3(T)_3](ClO_4)_2(NO_3)_2 \cdot 15H_2O$ **3**

The ring-shaped cations in **1**, **2**, and **3** are built up by three different platinum subunits: two diplatinum and one monoplatinum center. Three dianionic nucleobases (uracilate in **1** and **2**, thyminate in **3**) link these structural units with each other. Simultaneously, they act as molecular bridges within the dinuclear substructures. Each platinum atom of the dinuclear substructures is coordinated by a dpk ligand, which is in the hydrated form in the chelates of Pt(2) and Pt(3). In **1**–**3** the coordination of 2,2′-dipyridylketone hydrate is also found within the mononuclear substructure of Pt(5). In this case the oxygen atoms of the nucleobases, the potential metal binding sites, are located above and below the Pt(5) coordination plane. Consequently, binding of a sixth platinum atom would cause disruptively strong steric interactions within the cyclic system. Thus, a dinuclear species is not formed in this subunit.

Two different ligands bound to the platinum atoms give two different platinum coordination environments. Within the dinuclear subunits Pt(2) and Pt(3), which are coordinated by the $dpkOH_2$ ligands, have square-planar coordination spheres consisting of four nitrogen atoms. The two other metal centers of the Pt_2 units have *cis*-N_2O_2 environments, each formed by a 2,2′-dipyridylketone ligand plus the exocyclic oxygen atoms of the uracil bases (in **1** and **2**) or the thymine bases (in **3**). Thus, the dinuclear substructures contain the bridging nucleobases in a head-to-head arrangement. The mononuclear platinum center is coordinated by two tertiary amine groups of a hydrated ligand. Accordingly, Pt(5) also has an N_4 environment. But in contrast to the dinuclear substructures, the Pt(5) coordination sphere is generated by the nitrogen atoms of two nucleobases, which are chemically not equivalent (N3 of nucleobase *b* and N1 of nucleobase *c*, Figure 2).

Thymine and uracil can coordinate to metal ions by their two endocyclic nitrogen atoms as well as by their two exocyclic oxygen atoms.[9a,14] However, often these potential donor atoms are only used partly. Within the macrocycles presented, the nucleobase *a* (uracil in **1** and **2**, thymine in **3**), which connects the dinuclear subunits to each other, coordinates to the four platinum centers of the subunits utilizing all N- and O-donor atoms. The two other U or T bases (*b* and *c*) each conjoin one of the Pt_2 units with the mononuclear platinum center. Accordingly, each of these bases forms three bonds to three platinum(II) ions. All the nucleobases point with their exocyclic oxygen atom O2, the potential binding site for a supramolecular *endo*-coordination, to the middle of the calixarene-like cation. Nucleobases *a* and *b* utilize this binding site for their bonds to Pt(4). Furthermore, nucleobase *b* provides an additional binding site for *exo*-coordination with its O(4)-donor atom, which is directed out of the macrocycle.

In contrast to the metallocalixarenes known to date these complex cations exhibit additional small-molecule coordination sites within their five-chelate ligands. The bridging keto (in dpk) and diol groups (in $dpkOH_2$) of the ligands can act as eight further potential reaction partners for the formation of supramolecular bonds, depending on the different orientations of the respective oxygen atoms. The dinuclear substructure Pt(1)···Pt(2) as well as the single platinum atom

 © 2004 Wiley-VCH Verlag GmbH & Co. KGaA, Weinheim

Pt(5) are bound to chelate ligands, of which the C–O groups point in the same direction as the O2 atoms of the nucleobases. In contrast, within the other structural part, Pt(3)···Pt(4), the keto and diol groups of the ligands point in opposite directions. This asymmetric arrangement of the C–O dipoles enables a binding of small molecules through hydrogen-bond formation at different sites of the voluminous cation (Figure 3).

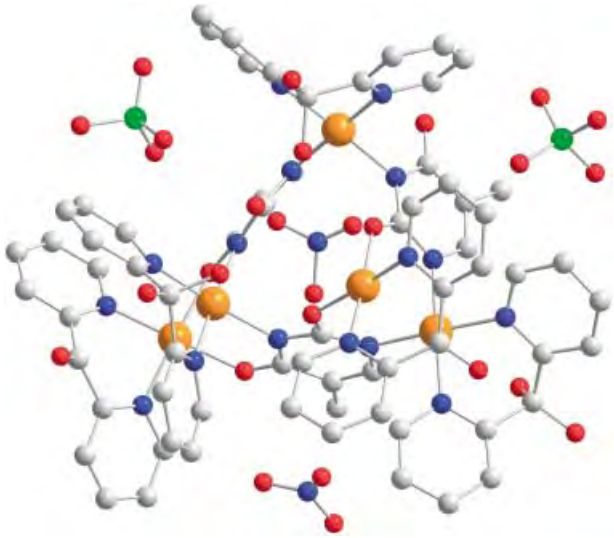


Figure 3. The calixarene-like, thyminato-bridged platinum(II) macrocycle of **3** with nitrate and perchlorate anions coordinated by supramolecular interactions. Green = Cl.

The isotypic Pt_5 complexes have the ability to coordinate different anions: nitrate, perchlorate, tetrafluoroborate, or hexafluorophosphate. Thus, the orientation of the anions into the direction of the cation dipoles does primarily not depend on their chemical nature, but on their small size compared to the pentanuclear cation. By this complexation of anions through hydrogen bonds the macrocycles exhibit a typical characteristic of calixarenes and their metal derivatives.

The three complex compounds presented are the first examples of a novel calixarene-like structure type, built up from a third-generation cisplatin analogue and bridging nucleobases. The synthesis of the pentanuclear cations succeeds reproducibly with the nucleobase uracil (in **1** and **2**) as well as with the nucleobase thymine (in **3**). This result underlines high stability of the compounds despite the high cationic charge density of five platinum(II) centers. The chelate ligands 2,2′-dipyridylketone and 2,2′-dipyridylketone hydrate provide further functional groups, supplementary to those of the DNA bases, for the formation of a dense hydrogen-bond network. Thus, different anions are bound at different sites of the Pt_5 complex by supramolecular interactions.

This crucial enlargement of possible coordination patterns opens new application potentials of anion recognition and complexation. The three self-assembling pentanuclear macrocycles provide new and important impulses to the ongoing field of metallocalixarene research owing to their so far unknown intrinsic asymmetry. Moreover, they build a bridge from cisplatin analogous complexes to supramolecular coordination chemistry.

Experimental Section

$[Pt(dpk)Cl_2]$ was prepared by treating the ligand 2,2′-dipyridylketone (1 mmol, 184 mg) with potassium tetrachloroplatinate(II) (1 mmol, 415 mg) in water. The mixture was stirred for 2 h while heating to 50 °C. The precipitated complex was collected by filtration and dried in a vacuum exsiccator over P_2O_5. For converting the dichloro complex into the diaqua complex $[Pt(dpk)Cl_2]$ (0.5 mmol, 450 mg) was suspended in water (10 mL). Then silver nitrate (1.95 equiv, 166 mg, 0.975 mmol) was added, the mixture was stirred overnight at room temperature. All light was excluded during the reaction by wrapping the reaction vessel with aluminum foil. The silver chloride formed was removed by centrifugation. An excess of uracil or thymine (0.35 mmol; 39 mg and 44 mg, respectively) was added to the freshly prepared solution. After stirring for 24 h at 40 °C the reaction mixture was allowed to cool. A few drops of an aqueous solution of sodium perchlorate, potassium hexafluorophosphate, or sodium tetrafluoroborate ($c = 0.2\ mol\,L^{-1}$) were added giving yellow to orange solutions. After a few days single crystals suitable for X-ray structure analyses formed. **1**: orange needles; yield 38 mg, 14 %; elemental analysis (%) calcd for $C_{67}H_{68}N_{19}O_{31}BF_4Pt_5$: C 29.83, H 2.50, N 9.87; found: C 29.48, H 2.32, N 9.62; IR (KBr pellet, 4000–400 cm^{-1}): $\tilde{\nu}$ = 3440m,br, 2927w, 1691m, 1621s, 1514m, 1483s, 1384s, 1317m, 1282m, 1145w, 1090m, 941w, 847w, 761w, 671w, 559w, 448w cm^{-1}. **2**: orange needles; yield 58 mg, 21 %; elemental analysis (%) calcd for $C_{67}H_{70}N_{19}O_{32}PF_6Pt_5$: C 29.01, H 2.54, N 9.59; found: C 28.94, H 2.49, N 9.47; IR (KBr pellet, 4000–400 cm^{-1}): $\tilde{\nu}$ = 3435 m,br, 3052w, 2927w, 1688m, 1597m, 1517m, 1480s, 1454m, 1384s, 1357s, 1315m, 1280m, 1092w, 1039w, 941w, 844m, 759 m, 691w, 671w, 579w, 557w, 442w cm^{-1}. **3**: yellow needles; yield 42 mg, 15 %; elemental analysis (%) calcd for $C_{70}H_{88}N_{18}O_{43}Cl_2Pt_5$: C 28.83, H 3.04, N 8.65; found: C 28.54, H 3.01, N 8.37; IR (KBr pellet, 4000–400 cm^{-1}): $\tilde{\nu}$ = 3433m,br, 1693w, 1629m, 1546w, 1483m, 1444m, 1384s, 1317m, 1298m, 1218w, 1149w, 1092m, 1042w, 939w, 864w, 800w, 762m, 671w, 625w, 579w, 490w, 441m cm^{-1}.

Received: September 25, 2003 [Z52950]
Published Online: February 2, 2004

Keywords: calixarenes · cisplatin · macrocycles · nucleobases · platinum

[1] a) S. Leininger, B. Olenyuk, P. J. Stang, *Chem. Rev.* **2000**, *100*, 853–908; b) B. J. Holliday, C. A. Mirkin, *Angew. Chem.* **2001**, *113*, 2076–2098; *Angew. Chem. Int. Ed.* **2001**, *40*, 2022–2043.
[2] a) J. A. R. Navarro, E. Freisinger, B. Lippert, *Inorg. Chem.* **2000**, *39*, 2301–2305; b) Z. Qin, M. C. Jennings, R. J. Puddephatt, *Inorg. Chem.* **2002**, *41*, 3967–3974.
[3] J. A. R. Navarro, B. Lippert, *Coord. Chem. Rev.* **1999**, *185–186*, 653–667.
[4] a) R.-D. Schnebeck, E. Freisinger, B. Lippert, *Angew. Chem.* **1999**, *111*, 235–238; *Angew. Chem. Int. Ed.* **1999**, *38*, 168–171; b) M. Fujita, K. Umemoto, M. Yoshizawa, N. Fujita, T. Kusukawa, K. Biradha, *Chem. Commun.* **2001**, 509–518.
[5] C. D. Gutsche, *Calixarenes*, *Monographs in Supramolecular Chemistry*, *Vol. 1*, The Royal Society of Chemistry, Cambridge, **1989**.
[6] a) H. Rauter, E. C. Hillgeris, A. Erxleben, B. Lippert, *J. Am. Chem. Soc.* **1994**, *116*, 616–624; b) H. Rauter, I. Mutikainen, M. Blomberg, C. J. L. Lock, P. Amo-Ochoa, E. Freisinger, L.

 © 2004 Wiley-VCH Verlag GmbH & Co. KGaA, Weinheim

Randaccio, E. Zangrando, E. Chiarparin, B. Lippert, *Angew. Chem.* **1997**, *109*, 1353 – 1357; *Angew. Chem. Int. Ed. Engl.* **1997**, *36*, 1296 – 1301; c) J. A. R. Navarro, E. Freisinger, B. Lippert, *Eur. J. Inorg. Chem.* **2000**, 147 – 151.

[7] a) L. Schenetti, G. Bandoli, A. Dolmella, G. Trovó, B. Longato, *Inorg. Chem.* **1994**, *33*, 3169 – 3176; b) B. Longato, G. Bandoli, G. Trovó, E. Marasciulo, G. Valle, *Inorg. Chem.* **1995**, *34*, 1745 – 1750.

[8] a) S.-W. Lai, M. C.-W. Chan, S.-M. Peng, C.-M. Che, *Angew. Chem.* **1999**, *111*, 708 – 710; *Angew. Chem. Int. Ed.* **1999**, *38*, 669 – 671; b) S.-Y. Yu, H. Huang, H.-B. Liu, Z.-N. Chen, R. Zhang, M. Fujita, *Angew. Chem.* **2003**, *115*, 710 – 714; *Angew. Chem. Int. Ed.* **2003**, *42*, 686 – 690.

[9] a) I. Puscasu, C. Mock, M. Rauterkus, A. Röndigs, G. Tallen, S. Gangopadhyay, J. E. A. Wolff, B. Krebs, *Z. Anorg. Allg. Chem.* **2001**, *627*, 1292 – 1298; b) M. J. Rauterkus, I. Puscasu, B. Krebs, *Inorg. Chim. Acta* **2002**, *339*, 438 – 444; c) M. J. Rauterkus, S. Fakih, C. Mock, I. Puscasu, B. Krebs, *Inorg. Chim. Acta* **2003**, *350*, 355 – 365.

[10] a) *Cisplatin—Chemistry and Biochemistry of a Leading Anticancer Drug* (Ed.: B. Lippert), Wiley-VCH, Weinheim, **1999**; b) M. J. Bloemink, H. Engelking, S. Karentzopoulos, B. Krebs, J. Reedijk, *Inorg. Chem.* **1996**, *35*, 619 – 627.

[11] a) G. Tallen, C. Mock, S. B. Gangopadhyay, B. Kangarloo, B. Krebs, J. E. A. Wolff, *Anticancer Res.* **2000**, *20*, 445 – 450; b) N. Möller, B. S. Kangarloo, I. Puscasu, C. Mock, B. Krebs, J. E. A. Wolff, *Anticancer Res.* **2000**, *20*, 4435 – 4440.

[12] Crystal structure analyses: Single crystal X-ray diffraction data were collected on a Bruker Nonius Smart diffractometer with a CCD detector ($\lambda(Cu_{K\alpha}) = 1.54184$ Å, $T = 100(2)$ K). The structure solutions were achieved by applying direct statistical methods of phase determination using the SHELXS program. A series of full-matrix least-squares refinements followed by Fourier syntheses (program SHELXL-97) gave all the remaining atom positions. The hydrogen atoms were refined on calculated positions adopting the riding model concept. **1**: crystal dimensions $0.13 \times 0.06 \times 0.04$ mm^3, triclinic, space group $P\bar{1}$, $a = 11.236(2)$, $b = 17.759(4)$, $c = 20.241(4)$ Å, $\alpha = 93.88(3)$, $\beta = 96.74(3)$, $\gamma = 94.25(3)°$, $V = 3988.0(1)$ Å^3, $\rho_{calcd} = 2.233$ g cm^{-3}, $2\theta_{max} = 142.82°$, 23542 reflections observed, 13368 independent reflections, $\mu = 16.941$ mm^{-1}, $R_1 = 0.0578$ and $wR_2 = 0.1618$ for $I > 2\sigma(I)$, $R_1 = 0.0701$ and $wR_2 = 0.1698$ for all reflections, 1020 parameters, GooF = 1.009 on $|F^2|$, max./min. residual electron density 3.764/−2.105 e Å^{-3}. **2**: crystal dimensions $0.20 \times 0.04 \times 0.02$ mm^3, triclinic, space group $P\bar{1}$, $a = 11.368(2)$, $b = 17.851(4)$, $c = 20.209(4)$ Å, $\alpha = 95.18(3)$, $\beta = 95.05(3)$, $\gamma = 95.02(3)°$, $V = 4049.5(1)$ Å^3, $\rho_{calcd} = 2.260$ g cm^{-3}, $2\theta_{max} = 142.66°$, 23388 reflections observed, 13455 independent reflections, $\mu = 16.937$ mm^{-1}, $R_1 = 0.0497$ and $wR_2 = 0.1336$ for $I > 2\sigma(I)$, $R_1 = 0.0636$ and $wR_2 = 0.1402$ for all reflections, 1160 parameters, GooF = 0.978 on $|F^2|$, max./min. residual electron density 3.858/−1.717 e Å^{-3}. **3**: crystal dimensions $0.12 \times 0.03 \times 0.02$ mm^3, triclinic, space group $P\bar{1}$, $a = 17.143(3)$, $b = 17.274(3)$, $c = 18.277(4)$ Å, $\alpha = 66.93(3)$, $\beta = 77.50(3)$, $\gamma = 64.11(3)°$, $V = 4473.0(2)$ Å^3, $\rho_{calcd} = 2.143$ g cm^{-3}, $2\theta_{max} = 143.80°$, 25458 reflections observed, 14824 independent reflections, $\mu = 15.739$ mm^{-1}, $R_1 = 0.0656$ and $wR_2 = 0.1648$ for $I > 2\sigma(I)$, $R_1 = 0.0943$ and $wR_2 = 0.1792$ for all reflections, 1233 parameters, GooF = 0.984 on $|F^2|$, max./min. residual electron density 3.146/−3.003 e Å^{-3}. CCDC-193927 (**1**), CCDC-193928 (**2**), and CCDC-193926 (**3**) contain the supplementary crystallographic data for this paper. These data can be obtained free of charge via www.ccdc.cam.ac.uk/conts/retrieving.html (or from the Cambridge Crystallographic Data Centre, 12 Union Road, Cambridge CB2 1EZ, UK; fax: (+44) 1223-336-033; or deposit@ccdc.cam.ac.uk).

[13] S. B. Gangopadhyay, A. Röndigs, S. B. Kangarloo, B. Krebs, J. E. A. Wolff, *Anticancer Res.* **2001**, *21*, 2039 – 2044.

[14] a) M. Grehl, B. Krebs, *Inorg. Chem.* **1994**, *33*, 3877 – 3885; b) E. Zangrando, F. Pichierri, L. Randaccio, B. Lippert, *Coord. Chem. Rev.* **1996**, *156*, 275 – 332.

 © 2004 Wiley-VCH Verlag GmbH & Co. KGaA, Weinheim

Cover Picture

Hiroaki Imai* and Yuya Oaki



The helical morphology shown in the cover picture, emerges from triclinic crystals through diffusion-limited growth. The backbone of the helical architecture comprises twisted twins of the tilted subunit crystal originating from the triclinic system. The results provide a fundamental basis for the formation of various helical morphologies that have already been reported. For more information see the Communication by H. Imai and Y. Oaki on page 1363 ff.

Contents

Angewandte EarlyView

The following articles are available online (in Wiley InterScience). You can find them at www.angewandte.org, under Full Text, Early View.

M. K. Runyon, B. L. Johnson-Kerner, R. F. Ismagilov:*
Minimal Functional Model of Hemostasis in a Biomimetic Microfluidic System
DOI: 10.1002/anie.200353428
Published online: February 24, 2004

S. Kraft, R. Beckhaus, D. Haase, W. Saak:*
Directed Reduction of Six-Membered Nitrogen Heterocycles—Selective Formation of Polynuclear Titanium Complexes
DOI: 10.1002/anie.200353021
Published online: February 23, 2004

S. S. Jain, F. A. L. Anet, C. J. Stahle, N. V. Hud:*
Enzymatic Behavior by Intercalating Molecules in a Template-Directed Ligation Reaction
DOI: 10.1002/anie.200353155
Published online: February 16, 2004

Articles judged by the referees or the editor as being either very important or very urgent are immediately edited, proof-read, and electronically published once the manuscript has arrived in the editorial office in final form. As long as there is no page number available these articles should be cited in the following manner:

Author(s) *Angew. Chem. Int. Ed.*, online publication date, DOI.

News

V. Percec Receives ACS Award in Polymer Chemistry ——— **1322**

G. K. S. Prakash Receives Award for Fluorine Chemistry ——— **1322**

N. Turro Receives ACS Award in Chemical Education ——— **1322**

Books

Persistence and Spatial Range of Environmental Chemicals ——— **1323** — Martin Scheringer — *reviewed by G. Schüürmann*

Catalysis from A to Z ——— **1324** — Boy Cornils, Wolfgang A.Herrmann, Robert Schlögl, Chi-Huey Wong — *reviewed by R. Stürmer*

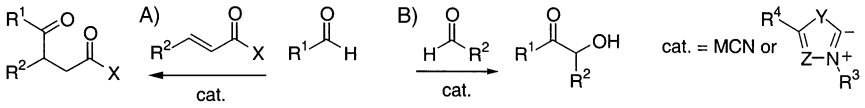
Pocket Guide to Biotechnology and Genetic Engineering ——— **1325** — Rolf D. Schmid — *reviewed by U. Bornscheuer*

Highlights

Umpolung Reactions

J. S. Johnson* ——— **1326 – 1328**

Catalyzed Reactions of Acyl Anion Equivalents

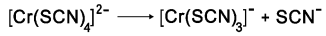


More than century after the description of the benzoin condensation, chemists are developing new approaches toward and new reactions involving aldehyde umpolung. This chemistry has been recently expressed in aldehyde/ketone benzoin condensations, aldehyde/imine couplings, and enantioselective benzoin (B) and Stetter (A) reactions (see scheme; M = K, Na, Bu_4N; Y = S, NR; Z = CH, N; X = alkoxy, alkyl).

Molecular Beams

D. Schröder* ——— **1329 – 1331**

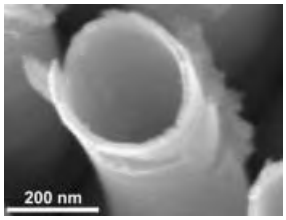
Coulomb Explosions and Stability of Multiply Charged Ions in the Gas Phase



Stopping ions from going to pieces: Multiply charged molecular ions have fascinating bonding schemes which must counterbalance the strong Coulomb repulsion of the charge centers. In molecular-beam experiments it has been possible to generate small multiply charged anions, such as $[Cr(SCN)_4]^{2-}$, and analyze their fragmentation behavior (see scheme).

© 2004 Wiley-VCH Verlag GmbH & Co. KGaA, Weinheim

Reviews



The spectrum of materials for nanotube walls can be broadened considerably by the simple and versatile technique of wetting porous templates. This opens up numerous possibilities for the functionalization of both porous membranes and individual nanotubes. These can be made from precious metals (see the scanning electron microscope image of a cross section of a Pd nanotube), high-performance polymers, or ferroelectric oxides, and exhibit nanotube walls with a specific fine structure.

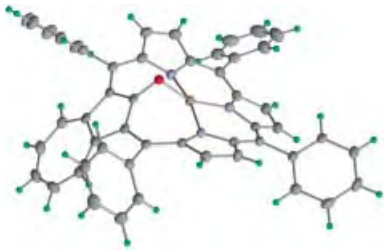
Nanostructures

M. Steinhart, R. B. Wehrspohn, U. Gösele, J. H. Wendorff* _____ **1334 – 1344**

Nanotubes by Template Wetting: A Modular Assembly System

Communications

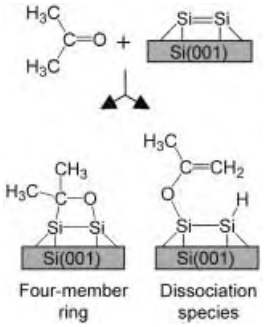
Abnormal upfield shifts for the external azulene protons are seen in the ^{1}H NMR spectra on oxidation of azuliporphyrins with copper(II) acetate to give highly distorted copper(II) complexes (see structure, brown Cu, blue N, red O, green H). These undergo demetalation with 10% trifluoroacetic acid/chloroform to give unique cross-conjugated ketones.



Porphyrin Oxidation

D. A. Colby, G. M. Ferrence, T. D. Lash* _____ **1346 – 1349**

Oxidative Metalation of Azuliporphyrins with Copper(II) Salts: Formation of a Porphyrin Analogue System with a Unique Fully Conjugated Nonaromatic Azulene Subunit

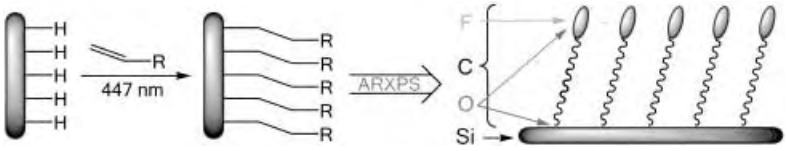


Changing the force: The driving force that determines the product distribution for acetone adsorbed on the Si(001) surface can be changed from kinetic (producing a four-member-ring species; see scheme) to thermodynamic (producing the dissociation species) upon raising the surface temperature. The results show that the binding of organic molecules to the Si(001) surface is in fact reversible.

Surface Chemistry

C. Hamai, A. Takagi, M. Taniguchi, T. Matsumoto,* T. Kawai ___ **1349 – 1352**

Kinetic and Thermodynamic Control by Chemical Bond Rearrangement on a Si(001) Surface



An extremely mild and practical method to attach organic monolayers on flat silicon surfaces by using visible light (447 nm; see scheme) was developed and the mechanism investigated. With high-resolution angle-resolved X-ray photoelectron spectroscopy (ARXPS) depth profiles of the elements in the monolayer (≈2 nm thickness) were obtained.

Monolayers

Q.-Y. Sun, L. C. P. M. de Smet, B. van Lagen, A. Wright, H. Zuilhof,* E. J. R. Sudhölter _____ **1352 – 1355**

Covalently Attached Monolayers on Hydrogen-Terminated Si(100): Extremely Mild Attachment by Visible Light

For the USA and Canada:
ANGEWANDTE CHEMIE International Edition (ISSN 1433-7851) is published weekly by Wiley-VCH PO Box 191161, D 69451 Weinheim, Germany. Air freight and mailing in the USA by Publications Expediting Inc. 200 Meacham Ave., Elmont, NY 11003. Periodicals postage paid at Jamaica NY 11431. US POSTMASTER: send address changes to *Angewandte Chemie*, Wiley-VCH, 111 River Street, Hoboken, NJ 07030. Annual subscription price for institutions: Europe € 3430.00/3118.00; outside Europe US$ 4499.00/4090.00 (valid for print and electronic/print or electronic delivery); for individuals who are personal members of a national chemical society, or whose institution already subscribes, or who are retired or self-employed consultants, print only: Europe € 248.00/outside Europe US$ 378.00. Postage and handling charges included. All Wiley-VCH prices are exclusive VAT.

 © 2004 Wiley-VCH Verlag GmbH & Co. KGaA, Weinheim

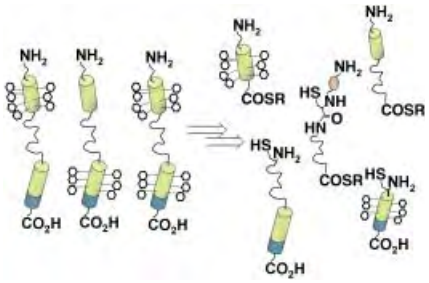
Contents

Glycoprotein Variants

D. Macmillan,*
C. R. Bertozzi ——— **1355 – 1359**

Modular Assembly of Glycoproteins: Towards the Synthesis of GlyCAM-1 by Using Expressed Protein Ligation

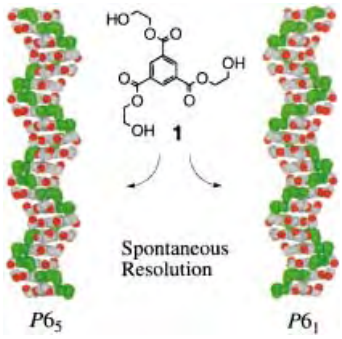
Put the two together: Physiologically relevant glycoproteins containing saccharides at predetermined sites, such as GlyCAM-1, can be generated from small synthetic and bacterially derived fragments by using the expressed protein ligation methodology. This technique was used for the synthesis of three semisynthetic GlyCAM-1 variants **1**–**3** (see scheme).



Crystal Engineering

I. Azumaya,* D. Uchida, T. Kato, A. Yokoyama, A. Tanatani, H. Takayanagi, T. Yokozawa* ——— **1360 – 1363**

Absolute Helical Arrangement of Stacked Benzene Rings: Heterogeneous Double-Helical Interaction Comprising a Hydrogen-Bonding Belt and an Offset Parallel Aromatic–Aromatic-Interaction Array



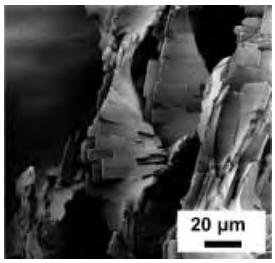
A resolution revolution? Self-assembled chiral structures resulting from the formation of two different helical interactions are found in the crystal structures of the achiral compound **1**. The interactions give rise to Ar–H···π and OH···O=C arrays. The chirality of the helices is spontaneously resolved within individual single crystals. Only one of the hydroxy groups contributes to the formation of a helical hydrogen-bonding array (shown in green).

Crystal Growth

H. Imai,* Y. Oaki ——— **1363 – 1368**

Emergence of Morphological Chirality from Twinned Crystals

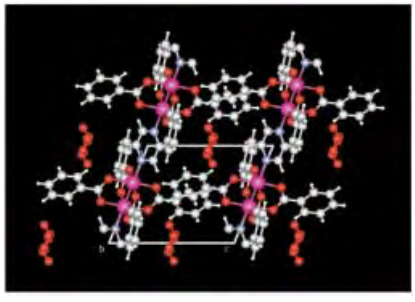
Twisted twins of subunit inorganic crystals make up the backbone of helical morphologies. Chirality emerges from crystals that are without molecular chirality through the assembly of tilted subunits under diffusion-limited conditions (see picture).



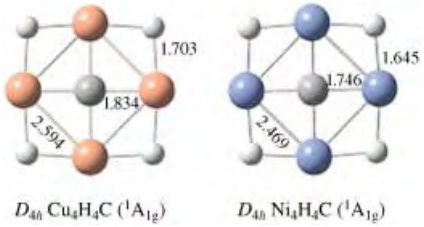
Single-Crystal Clathrates

S. Takamizawa,* E.-i. Nakata, T. Saito ——— **1368 – 1371**

Single-Crystal Adsorbents: A New Observation Field for Light Aggregates



A convenient method to generate single-crystal clathrates involves placing a single-crystal adsorbent into a gaseous guest atmosphere (see picture; Rh magenta, O red, C and H gray, N blue). The procedure has the potential for producing numerous low-dimensional aggregate crystals, and should be most effective for observing specific quantum effects in a variety of low-dimensional systems.



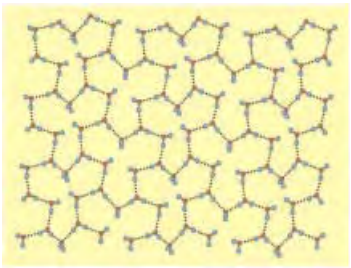
The first theoretical evidence for tetracoordinate planar nonmetals hosted at the centers of square hydrometal complexes M_4H_4X (M = Cu, Ni; X = B, C, N, O; see picture) has been obtained by ab initio calculations. These predictions may open a new branch of chemistry of nonmetal-centered hydrometals with potential applications as catalysts.

Tetracoordinate Planar Nonmetals

S.-D. Li,* G.-M. Ren, C.-Q. Miao, Z.-H. Jin ——— **1371 – 1373**

M_4H_4X: Hydrometals (M = Cu, Ni) Containing Tetracoordinate Planar Nonmetals (X = B, C, N, O)

Water rings: Two novel water chains and layers have been observed in supramolecular solid states. The structures can be interconverted by varying crystallization conditions. The water layer consisting of fused $(H_2O)_{12}$ rings (see structure, O red, H blue) resembles ice I_h.

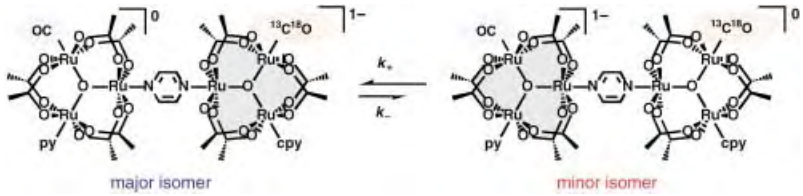


Supramolecular Chemistry

B.-Q. Ma,* H.-L. Sun, S. Gao* ——— **1374 – 1376**

Formation of Two-Dimensional Supramolecular Icelike Layer Containing $(H_2O)_{12}$ Rings

---



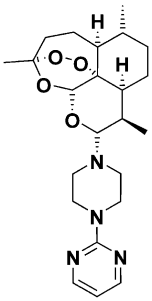
Upon electrochemical reduction, asymmetrically substituted dimers of Ru_3 clusters $[Ru_3O(OAc)_6(L)(CO)(\mu\text{-pz})Ru_3O(OAc)_6(L')(CO)]$ (pz = pyrazine, L and L′ are N ligands), exhibit IR spectral line coalescence in the ν_{CO} region. The IR spectra suggest the existence of two possible "charge-transfer isomers" for example, $[A^-–B]$ and $[A–B^-]$, in which A and B represent different Ru_3 moieties.

Charge Transfer

T. Ito,* N. Imai, T. Yamaguchi, T. Hamaguchi, C. H. Londergan, C. P. Kubiak* ——— **1376 – 1381**

Observation and Dynamics of "Charge-Transfer Isomers"

New leads for antimalarial drugs? 10-Alkylaminoartemisinin derivatives like that shown display in vivo antimalarial activities greater than those of the parent artemisinin. Previous conclusions regarding the chemical basis for the antimalarial activity of these compounds must be reconsidered.



Antimalarial Drugs

R. K. Haynes,* W.-Y. Ho, H.-W. Chan, B. Fugmann, J. Stetter, S. L. Croft, L. Vivas, W. Peters, B. L. Robinson ——— **1381 – 1385**

Highly Antimalaria-Active Artemisinin Derivatives: Biological Activity Does Not Correlate with Chemical Reactivity

 © 2004 Wiley-VCH Verlag GmbH & Co. KGaA, Weinheim

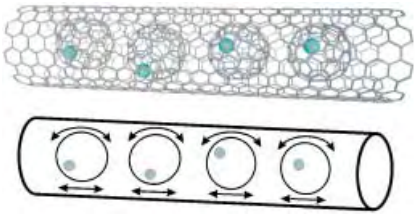
Contents

Fullerenes

A. N. Khlobystov,* K. Porfyrakis, M. Kanai, D. A. Britz, A. Ardavan, H. Shinohara, T. J. S. Dennis, G. A. D. Briggs* ——— **1386 – 1389**

Molecular Motion of Endohedral Fullerenes in Single-Walled Carbon Nanotubes

Rock and roll: Endohedral fullerenes Ce@C_{82} inserted in single-walled carbon nanotubes (SWNTs) interact by electrostatic interactions and exhibit unusual dynamic behavior. Translational oscillations and discontinuous molecular rotations are observed (by high-resolution transmission electron microscopy) for the first time for molecular arrays inside SWNTs (see picture; blue dot = endohedral Ce atom). The fullerene rotation rate

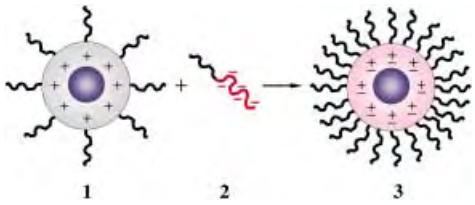


is different for isolated and aggregated nanotubes.

Block Copolymers

J. V. M. Weaver, Y. Tang, S. Liu, P. D. Iddon, R. Grigg, N. C. Billingham, S. P. Armes,* R. Hunter, S. P. Rannard — **1389 – 1392**

Preparation of Shell Cross-Linked Micelles by Polyelectrolyte Complexation

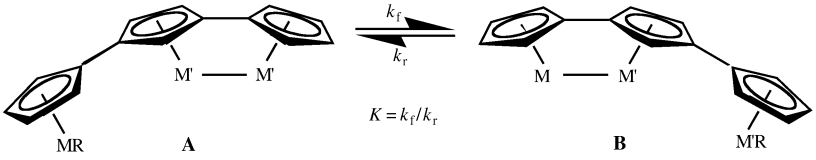


Shell shock: Shell cross-linked (SCL) micelles (**3**) are prepared by polyelectrolyte complexation by using a micelle-forming cationic ABC triblock copolymer (**1**) in conjunction with an anionic diblock copolymer cross-linker (**2**). This ionic cross-linking approach involves polymeric reagents that form physical complexes rapidly in aqueous solution at ambient temperature. Moreover, the product is surprisingly tolerant to added electrolyte.

Transition-Metal Complexes

J. K. Cammack, H. Amouri, P. W. Leonard, R. L. Myrabo, K. P. C. Vollhardt* ——— **1393 – 1397**

Electron Exchange Along the Tercyclopentadienyltrimetallic Scaffold: Kinetics, Equilibria, and Bond Strengths

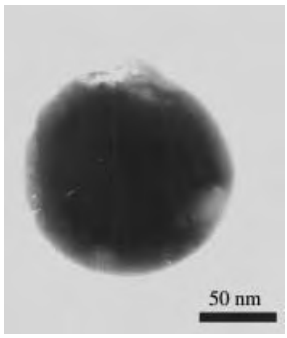


The metallomeric equilibrium between **A** and **B** can be quantified kinetically and thermodynamically by direct NMR techniques, which provide an insight into the mechanism of a fundamental organometallic displacement reaction and allows the estimation of relative metal–metal bond strengths in cyclopentadienyl–metal complexes (see scheme).

Heterogeneous Catalysis

J. Huang, T. Jiang, H. Gao, B. Han,* Z. Liu, W. Wu, Y. Chang, G. Zhao — **1397 – 1399**

Pd Nanoparticles Immobilized on Molecular Sieves by Ionic Liquids: Heterogeneous Catalysts for Solvent-Free Hydrogenation



A three-piece suite: The immobilization of a Pd-nanoparticle catalyst onto the surface of a molecular sieve by an ionic liquid (1,1,3,3-tetramethylguanidinium lactate) has been accomplished (see TEM image). The nanoparticle/ionic liquid/molecular sieve combination exhibits excellent synergistic effects that enhance the activity and durability of the catalyst for the hydrogenation of olefins.

 © 2004 Wiley-VCH Verlag GmbH & Co. KGaA, Weinheim

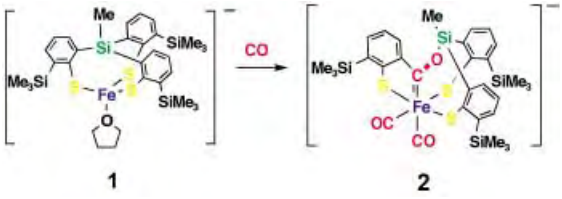


A new trump in the synthetic pack: The hidden potential of benzotriazoles to act as diazonium synthons has been witnessed in the reactions of 1-[(nonafluorobutyl)sulfonyl]-1*H*-1,2,3-benzotriazole with sodium phenoxide in which *ortho*-substituted azobenezenes were formed. The reaction can be steered towards *ortho* or *para* substitution simply by changing the solvent (this dichotomy is shown in an abstract fashion in the painting by Mathias Hansen).

Regioselectivity

X. Àlvarez Micó, T. Ziegler,*
L. R. Subramanian* ——— **1400 – 1403**

A Versatile Direct Approach to *ortho*-Substituted Azobenzenes from Benzotriazoles

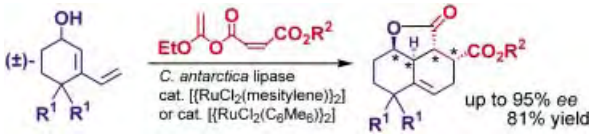


Fischer carbenes – a new angle: The insertion of carbon monoxide into an Si–C bond of the Fe^{II} complex **1**, which contains a tripodal thiolato ligand (see scheme), yields the Fischer carbene–thiolato complex **2**, whose molecular structure reveals the presence of a bonding interaction between the carbene carbon atom and the thiolato sulfur atoms.

Carbene Complexes

M. Yuki, T. Matsuo,
H. Kawaguchi* ——— **1404 – 1407**

Formation of an Iron(II) Carbene–Thiolato Complex by Insertion of Carbon Monoxide into an Si–C Bond



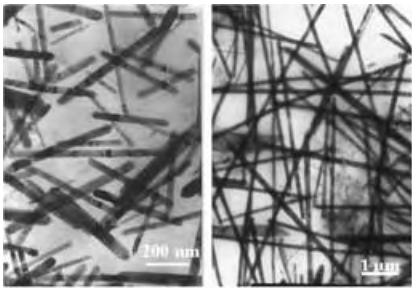
Combining chemistry: The use of a lipase and a ruthenium catalyst allows the direct preparation of polysubstituted decalines with high optical and chemical yields from racemic alcohols (see scheme). The lipase-catalyzed kinetic resolution of the racemic alcohols, the ruthenium-catalyzed racemization of the slow-reacting enantiomers, and an intramolecular Diels–Alder reaction of the resultant esters all occur under identical conditions.

Kinetic Resolutions

S. Akai, K. Tanimoto,
Y. Kita* ——— **1407 – 1410**

Lipase-Catalyzed Domino Dynamic Kinetic Resolution of Racemic 3-Vinylcyclohex-2-en-1-ols/Intramolecular Diels–Alder Reaction: One-Pot Synthesis of Optically Active Polysubstituted Decalins

HotMAIL! A microwave-assisted ionic-liquid (MAIL) method has been developed for controlled production of tellurium nanorods or nanowires (see pictures). The MAIL method is a fast, high-yield, and may be extended to synthesize a variety of other elemental and compound nanostructures.



Nanostructures

Y.-J. Zhu,* W.-W. Wang, R.-J. Qi,
X.-L. Hu ——— **1410 – 1414**

Microwave-Assisted Synthesis of Single-Crystalline Tellurium Nanorods and Nanowires in Ionic Liquids

 © 2004 Wiley-VCH Verlag GmbH & Co. KGaA, Weinheim

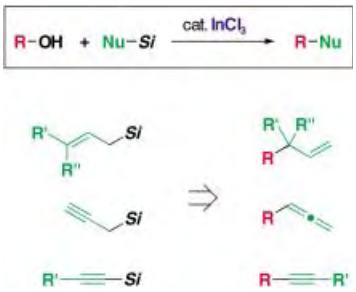
Contents

Direct Alkylation of Alcohols

M. Yasuda, T. Saito, M. Ueba, A. Baba* ——— **1414 – 1416**

Direct Substitution of the Hydroxy Group in Alcohols with Silyl Nucleophiles Catalyzed by Indium Trichloride

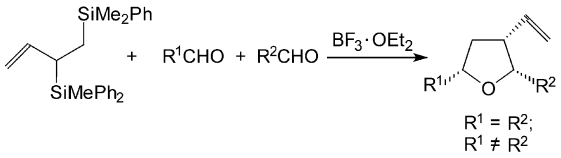
Straightforward substitution: An excellent combination of a silyl nucleophile and indium catalyst was used to accomplish the dehydroxylation/alkylation of alcohols under nearly neutral conditions (see scheme, *Si* = silyl group) even though this type of reaction usually requires at least an equimolar amount of acid.



Tetrahydrofuran Synthesis

T. K. Sarkar,* S. A. Haque, A. Basak ——— **1417 – 1419**

Bimetallic Reagents of Silicon: One-Pot Synthesis of 2,3,5-Trisubstituted Tetrahydrofurans by a Double Sakurai–Hosomi Reaction



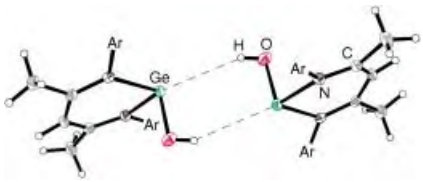
Good yields and high stereoselectivities are found in the cyclization of 1-silylmethyl allylic silanes with aldehydes. The silanes act as bimetallic coupling reagents and effect cyclization to yield a variety of 2,3,5-trisubstituted tetrahydrofurans in a one-pot procedure. A three-component cyclization with only one product can also be achieved with this methodology (see scheme).

A Germanium(II) Hydroxide

L. W. Pineda, V. Jancik, H. W. Roesky,* D. Neculai, A. M. Neculai ——— **1419 – 1421**

Preparation and Structure of the First Germanium(II) Hydroxide: The Congener of an Unknown Low-Valent Carbon Analogue

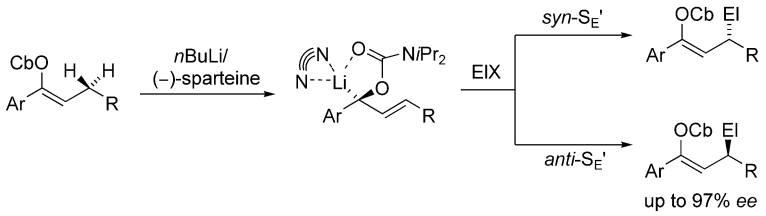
Trapping HCl with an Arduengo-type carbene was the key to preparing and isolating the first germanium(II) hydroxide [LGeOH] (L = HC{(CMe)(2,6-*i*Pr$_2$C$_6$H$_3$N)}$_2$) by hydrolysis of the corresponding chloride. In the solid state [LGeOH] forms dimers through an interaction of the OH group with the lone pair of another Ge atom (see picture; Ar = 2,6-*i*Pr$_2$C$_6$H$_3$).



Asymmetric Synthesis

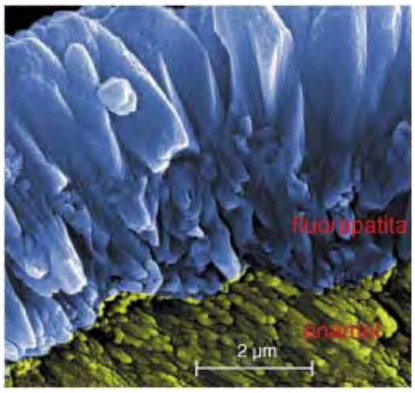
M. Seppi, R. Kalkofen, J. Reupohl, R. Fröhlich, D. Hoppe* ——— **1423 – 1427**

Highly Enantiomerically Enriched Ketone Homoenolate Reagents Prepared by (−)-Sparteine-Mediated γ-Deprotonation of Achiral 1-Alkenyl Carbamates



Homoenolate equivalents: Enantiotopos-differentiating deprotonation of achiral 1-alkenyl carbamates with the chiral base *n*-butyllithium/(−)-sparteine yields configurationally stable lithium homoenolate equivalents. In a subsequent *syn* or *anti* substitution (see scheme), γ-substituted *O*-(1-aryl-1-alkenyl) *N*,*N*-diisopropylcarbamates are formed with high enantio- and diastereoselectivity.

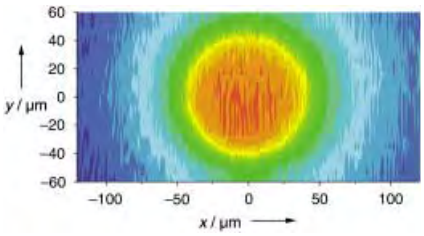
Something to get your teeth into: The continuous effect of acids in the mouth leads to dissolution of dental enamel. However, new technology could help to regenerate this unique biomineral. In vitro experiments show that the diffusion of suitable ions through a gelatin layer onto a tooth surface induces the mineralization of fluorapatite layers with a structure similar to tooth enamel (see picture).



Biomineralization

S. Busch* ____ **1428 – 1431**

Regeneration of Human Tooth Enamel



Nanoprobes for diffusion measurements: Nanometric-sized electrodes ($r = 80$ nm) have been constructed to map concentration profiles within the diffusion layer of a larger microelectrode ($r = 40$ µm) at high resolution (see picture). Comparisons with theoretical predictions demonstrate that, contrary to common wisdom, natural convection in the solution does, to some extent, affect diffusion at microelectrodes.

Microelectrochemistry

N. Baltes, L. Thouin, C. Amatore,*
J. Heinze* ____ **1431 – 1435**

Imaging Concentration Profiles of Redox-Active Species with Nanometric Amperometric Probes: Effect of Natural Convection on Transport at Microdisk Electrodes

VIP Communications labeled with this symbol have been judged by two referees as being "very important papers".

Looking for outstanding employees?

Do you need another expert for your excellent team?
... Chemists, PhD Students, Managers, Professors, Sales Representatives...

Place an advert in the printed version and have it made available online for 1 month, free of charge!

Angewandte Chemie International Edition
Advertising Sales Department: Marion Schulz
Phone: 0 62 01 - 60 65 65
Fax: 0 62 01 - 60 65 50
E-Mail: MSchulz@wiley-vch.de

Service

Keywords ____ *1438*

Authors ____ *1439*

Preview ____ *1441*

 © 2004 Wiley-VCH Verlag GmbH & Co. KGaA, Weinheim



V. Percec Receives ACS Award in Polymer Chemistry

Virgil Percec, born in 1946, completed his PhD in polymer chemistry at the Institute of Macromolecular Chemistry in Iasi (Romania) in 1976, then continued his research there on *cis* poly(phenylacetylene)s. He moved to the Institut für Makromolekulare Chemie at the Universität Freiburg in 1981, and the following year moved to the University of Akron (Ohio, USA). In 1982 he became assistant professor at the Case Western Reserve University in Cleveland (Ohio, USA), where he taught and carried out research until 1999, from 1986 as Professor of Macromolecular Science. Since 1999 he has been the Roy and Diana Vagelos Professor of Chemistry at the University of Pennsylvania in Philadelphia (USA).



V. Percec

Percec has been recognized by the American Chemical Society (ACS) for his work on the synthesis of covalent and supramolecular polymers, liquid-crystalline polymers, and dendrimers. Whereas his research was once concentrated on poly(aryl acetylene)s, metal-catalyzed ion-radical arylations, polymerizations under phase-transfer catalysis, and living radical polymerizations, its focus has increasingly shifted toward supramolecular chemistry. His latest Communication in *Angewandte Chemie* on the transformation of supramolecular dendrimers mediated by the fluorophobic effect was the cover-picture article in issue 36/2003.[1]

G. K. S. Prakash Receives Award for Fluorine Chemistry

Surya Prakash, professor at the University of Southern California, has been recognized by the ACS for his creative work in the field of fluorine chemistry. His work on trifluoromethyltrimethylsilane as a nucleophile for the introduction of CF_3 was ground-breaking. However, this is just one of many fluoroalkylation reagents developed in his laboratory. In his most recent Communication in *Angewandte Chemie* he describes difluoromethyl phenyl sulfone as a selective difluoromethylene dianion equivalent and the stereoselective one-pot synthesis of *anti*-2,2-difluoropropane-1,3-diols.[2] In addition to synthetic chemistry, he carries out mechanistic studies of reactive electrophilic intermediates in strongly acidic, nonnucleophilic media by broad-band NMR spectroscopy and other techniques. His research group also investigates the use of hydrocarbons in fuel cells.



G. K. Surya Prakash

Prakash was born in Bangalore (India) and studied chemistry at Bangalore University and at the Indian Institute of Technology in Madras. He completed his PhD in 1978 under the guidance of the later Nobel Laureate George Olah at the University of Southern California, where he now holds the George A. and Judith A. Olah Nobel Laureate Chair in Hydrocarbon Chemistry and is scientific co-director of the Loker Hydrocarbon Research Institute.

N. Turro Receives ACS Award in Chemical Education

The ACS has recognized Nicholas Turro with the George C. Pimentel Award in Chemical Education, for bringing together teams of faculty members and students to develop new computer tools for teaching. At the beginning of the 1990s, while the World Wide Web was still in its infancy, he and Leornard Fine developed an interactive program termed "IR Tutor" for the teaching or self-learning of IR spectroscopy. The program found application as a supplement to textbooks and as a tutorial for IR spectrometers. During the years 1995–98, in workshops with staff and students, he further developed the use of computers and networks in teaching, later with the involvement of faculty members from the humanities and social sciences.



N. Turro

Turro studied chemistry at Wesleyan University in Middletown, CT (USA) and completed his PhD in 1963 under the supervision of George Hammond at the California Institute of Technology in Pasadena (USA). After a postdoctoral year, Turro joined the faculty at Columbia University in New York, where he still teaches today, both as Professor of Chemical Engineering and Applied Chemistry and Professor of Earth and Environmental Engineering, and where he undertakes research in photochemistry and electron spin resonance spectroscopy.[3] He has also authored articles on the philosophy of science, including an Essay on the distinction between revolutionary and pathological science.[4]

[1] V. Percec, M. Glodde, G. Johansson, V. S. K. Balagurusamy, P. A. Heiney, *Angew. Chem.* **2003**, *115*, 4474; *Angew. Chem. Int. Ed.* **2003**, 42, 4338.

[2] G. K. S. Prakash, J. Hu, T. Mathew, G. A. Olah, *Angew. Chem.* **2003**, *115*, 5374; *Angew. Chem. Int. Ed.* **2003**, *42*, 5216.

[3] N. J. Turro, M. H. Kleinman, E. Karatekin, *Angew. Chem.* **2000**, *112*, 4608; *Angew. Chem. Int. Ed.* **2000**, *39*, 4436.

[4] N. J. Turro, *Angew. Chem.* **2000**, *112*, 2343; *Angew. Chem. Int. Ed.* **2000**, *39*, 2255

 © 2004 Wiley-VCH Verlag GmbH & Co. KGaA, Weinheim DOI: 10.1002/anie.200481029

Umpolung Reactions

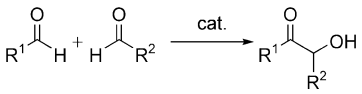
Catalyzed Reactions of Acyl Anion Equivalents

*Jeffrey S. Johnson**

Keywords:
aldehydes · benzoin condensation · homogeneous catalysis · ketones · umpolung

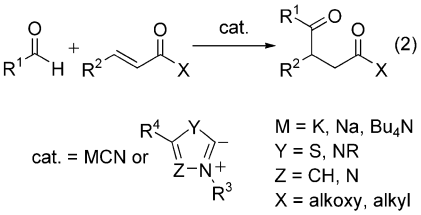
In comparison to catalytic reactions involving enolates, research addressing analogous catalytic chemistry of acyl anion equivalents has received considerably less attention.[1] This may be due in part to the attendant challenges in the latter class of reactions. Whereas the activation steps of a direct catalytic Michael or aldol reaction may, in the simplest analysis, be broken down into acid–base chemistry, the conversion of an aldehyde into a nucleophilic (d^1) center[2] is a less straightforward problem in reaction design. Organic chemists typically find recourse in the conversion of aldehydes into umpolung reagents such as dithianes and protected cyanohydrin derivatives, which may be converted into the derived carbanionic species with a strong base. Such approaches have proven extremely useful in a large number of contexts, but lack the step economy and aesthetic appeal of their enolate counterparts.

Increasingly, efforts are being directed at circumventing these shortcomings by accessing and augmenting classic reaction manifolds for effecting carbonyl-polarity reversal: the benzoin[3] and Stetter[4] reactions. Reactions of aldehydes with other aldehydes [Eq. (1)] or



(1)

α,β-unsaturated carbonyl compounds [Eq. (2)] mediated by cyanide or heteroazolium carbenes comprise the most

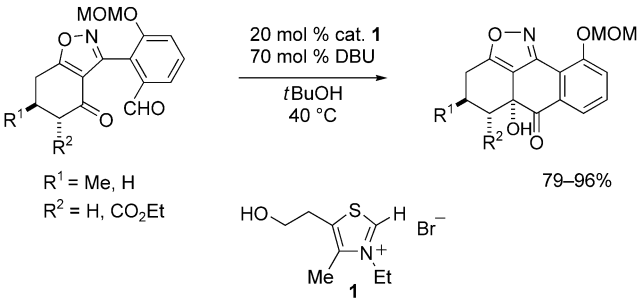


(2)

direct methods of acyl anion equivalence and have been developed accordingly.

Until recently, it was not known that ketones would engage in non-enzymatic benzoin-type behavior, although earlier studies from Hünig and Wehner had shown that silyloxy(nitrile) anions could add readily to ketone electrophiles under aprotic conditions.[5] Decarboxylative benzoin-type additions to ketones with pyruvate donors had previously been documented to proceed with a variety of thiamin diphosphate dependent (ThDP) enzymes.[6] The thermodynamics of an aldehyde/ketone coupling in the absence of CO_2 extrusion were uncertain until recent work by Suzuki and co-workers demonstrated that more traditional conditions (alcohol solvent, thiazolium carbene catalysis) could be used to effect intramolecular cross-benzoin reactions between an aldehyde and a ketone [Eq. (3); MOM = methoxymethyl, DBU = 1,8-diazabicyclo[5.4.0]undec-7-ene].[7] Notably, the reactions require no preactivation of either functional group. The products are significantly value-added: the reaction results in an annulation and a stereocontrolled introduction of a tertiary alcohol. The thiazolium carbene variant is significantly higher-yielding than its cyanide-catalyzed counterpart. Intermolecular aldehyde dimerization was notably suppressed. The absence of homo-benzoin product is likely due to a simple rate difference ($k_{intra} > k_{inter}$), but it is also conceivable that the dimeric benzoin is formed reversibly and that the intramolecular benzoin adduct acts as a thermodynamic sink. Unfortunately, significant amounts of the thiazolium salt precursor and base (DBU) are required; however, when higher concentrations are employed, the reactions are in some cases feasible at 5 mol% catalyst loading.

An interesting chemoselective benzoin condensation occurs in preference to intramolecular aldol addition: the six-membered ring α-hydroxycyclohexanone benzoin **2** is favored over the β-hydroxycycloheptanone aldol **3** (about 2.5:1) [Eq. (4)]. These results also beg the question: can the highly desirable intermolecular aldehyde/ketone cross-benzoin coupling be achieved under any circumstances?

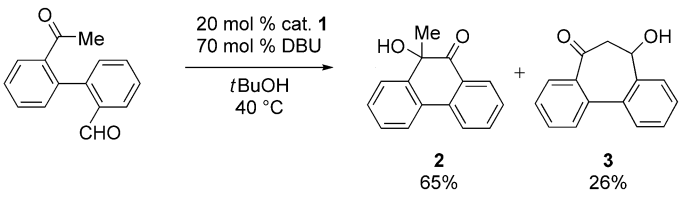


1

(3)

[*] Prof. J. S. Johnson
Department of Chemistry
University of North Carolina at Chapel Hill
Chapel Hill, NC 27599-3290
Fax: (+1) 919-962-2388
E-mail: jsj@unc.edu

 © 2004 Wiley-VCH Verlag GmbH & Co. KGaA, Weinheim DOI: 10.1002/anie.200301702

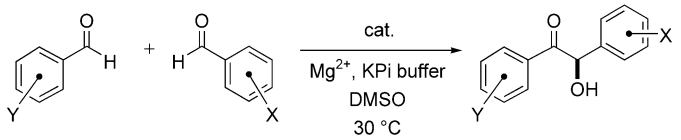


(4)

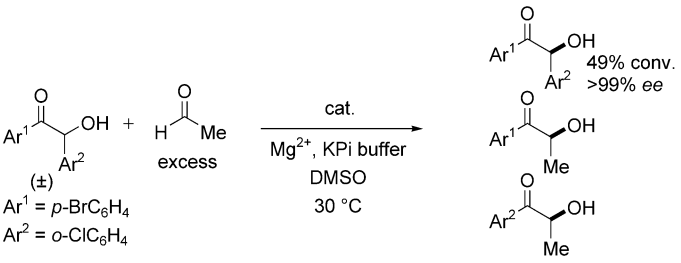
Such a reaction is a tall order indeed, given the absence of truly general aldehyde/aldehyde cross-benzoin reactions. Predicting the preferred product for a given pair of aldehydes can be challenging and, until the work of Müller and co-workers, an enantioselective mixed benzoin was not known.[8] Enzymatic catalysis was used advantageously to provide not only regioselectivity between a given pair of aldehydes, but enantiocontrol as well [Eq. (5); DMSO = dimethylsulfoxide]. The assigned donor–acceptor properties of a given aldehyde pair are often an outgrowth of the reversibility of the benzoin reaction; however, the results of Müller and co-workers indicate that kinetic control is possible. The enantioselective variants require a halogen in the *ortho* position of the acceptor aromatic aldehyde, but a range of substitution patterns is possible for the donor aldehyde. The thiamin diphosphate dependent benzaldehyde lyase was also capable of a highly selective kinetic resolution through retro-benzoin condensation: the liberated aldehydes from the reversal of the fast-reacting *R* enantiomer were trapped with acetaldehyde [Eq. (6)]. The unreacted *S* enantiomer was recovered in an enantiopure form. This procedure provides access to both mixed benzoin enantiomers, since formation of the *R* enantiomer is favored in the forward reaction.

Non-enzymatic methods were recently developed for catalyzed benzoin-type reactions that avoid the aforementioned substrate restrictions. Regiospecific cyanide-catalyzed mixed silyl benzoin reactions with broad substrate scope were achieved, albeit in racemic form and with the need to prepare acylsilanes as donors.[9]

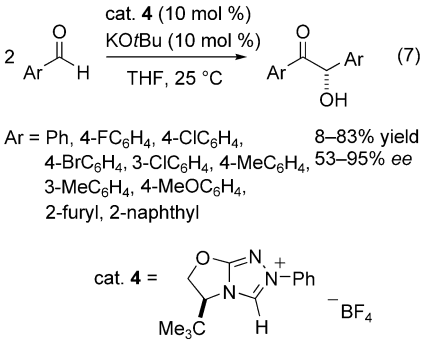
The use of scalemic heterazolium salts as catalyst precursors for enantioselective umpolung reactions was first introduced by Sheehan and Hara,[10] but was recently revitalized by remarkably selective new catalysts developed in the laboratories of Enders and of Rovis. The key advance with respect to both reactivity and selectivity has been the use of triazolium carbenes, rather than the traditional thiazolium carbene catalysts. Enantioselective dimerization of aromatic aldehydes was achieved through use of a *tert*-leucine-derived nucleophilic carbene catalyst [Eq. (7)].[11] Electron-rich aldehydes generally produced more highly enantioenriched α-hydroxyketones (up to 95% *ee*). Care was required with precise reaction conditions owing to the propensity of benzoins to racemize in the presence of the basic carbene.[12] The enolization problem always requires attention in asymmetric reactions catalyzed by heterazolium carbenes.



(5)



(6)

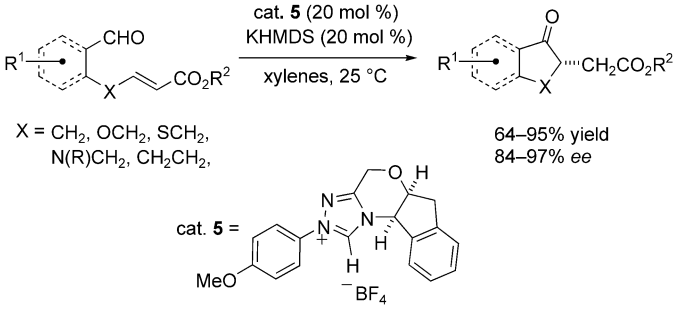


(7)

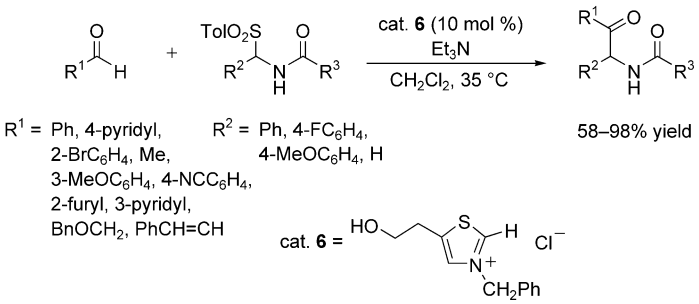
Enantioselective catalysis of intramolecular Stetter reactions was originally achieved by Enders et al.,[1] and recent efforts by Rovis and co-workers established the benchmark for enantiocontrol in this family of reactions.[13] Triazolium carbene catalysts derived from scalemic aminoindanol provided the annulated products with excellent enantioselectivity and chemical yield [Eq. (8); KHMDS = potassium hexamethyldisilazide]. An electron-donating group on the aromatic ring of the triazolium carbene provided the optimum combination of chemical yield and enantioselectivity. The catalyzed annulation reactions are notably tolerant of a range of linkers, although the benzofuranone product (X = O) is extremely susceptible to racemization. To date, the challenging intermolecular enantioselective Stetter reaction has met with limited success. Competitive formation of a stable conjugate adduct between the Michael acceptor and the carbene may be a culprit.[14]

Acylation of transient acylimines under thiazolium carbene catalysis was recently achieved by Murry, Frantz, and co-workers [Eq. (9)].[15] A key concern addressed by this work was the ability of the acylimine electrophile to compete with aldehyde; failure to do so would

 © 2004 Wiley-VCH Verlag GmbH & Co. KGaA, Weinheim



(8)



(9)

have led to simple benzoin condensation. The C=N π bond was generated in situ through the action of triethylamine on an arylsulfonyl amide, which then engaged the presumed thiazole enamine intermediate common to all benzoin-type catalysis. For a range of aldehydes and imines, yields were good to excellent. Interestingly, no homodimerization of either reactant was observed and the α-amido ketone products formed exhibit no proclivity toward reversion under the reaction conditions, as judged by crossover experiments. In contrast to many benzoin-type reactions, benzoin itself does not serve as a substrate for the reaction: the thiazolium carbene apparently does not catalyze the reverse reaction (PhC(O)-CH(OH)Ph → 2 PhCHO). The collective observations of kinetically-controlled product distribution bode well for the development of an asymmetric variant of this useful α-amido ketone synthesis.

The chemistry highlighted herein, all published within the last two years (and more than a century after the initial disclosure of the benzoin condensation), suggests a reemerging or more focused interest in developing new catalyzed methods involving d^1 nucleophiles. Efforts to produce more-active catalysts (lower catalyst loadings) and catalysts with expanded functional-group compatibility will undoubtedly continue. The inherent utility of the products derived from umpolung chemistry of aldehydes carries the attendant expectation of further creative chemistry in this field in the coming years.

[1] D. Enders, K. Breuer in *Comprehensive Asymmetric Catalysis*, *Vol. 3* (Eds.: E. N. Jacobsen, A. Pfaltz, H. Yamamoto, Eds.), Springer, New York, **1999**, pp. 1093 – 1102.

[2] D. Seebach, *Angew. Chem.* **1979**, *91*, 259 – 278; *Angew. Chem. Int. Ed. Engl.* **1979**, *18*, 239 – 258.

[3] W. S. Ide, J. S. Buck, *Org. React.* **1948**, *4*, 269 – 304.

[4] H. Stetter, H. Kuhlmann, *Org. React.* **1991**, *40*, 407 – 496.

[5] S. Hünig, G. Wehner, *Chem. Ber.* **1979**, *112*, 2062 – 2067.

[6] M. Pohl, B. Lingen, M. Müller, *Chem. Eur. J.* **2002**, *8*, 5288 – 5295.

[7] Y. Hachisu, J. W. Bode, K. Suzuki, *J. Am. Chem. Soc.* **2003**, *125*, 8432 – 8433.

[8] P. Dünkelmann, D. Kolter-Jung, A. Nitsche, A. S. Demir, P. Siegert, B. Lingen, M. Baumann, M. Pohl, M. Müller, *J. Am. Chem. Soc.* **2002**, *124*, 12084 – 12085.

[9] X. Linghu, J. S. Johnson, *Angew. Chem.* **2003**, *115*, 2638 – 2640; *Angew. Chem. Int. Ed.* **2003**, *42*, 2534 – 2536.

[10] J. C. Sheehan, T. Hara, *J. Org. Chem.* **1974**, *39*, 1196 – 1199.

[11] D. Enders, U. Kallfass, *Angew. Chem.* **2002**, *114*, 1822 – 1824; *Angew. Chem. Int. Ed.* **2002**, *41*, 1743 – 1745.

[12] Y.-K. Kim, A. Streitweiser, *J. Am. Chem. Soc.* **2002**, *124*, 5757 – 5761.

[13] M. S. Kerr, J. Read de Alaniz, T. Rovis, *J. Am. Chem. Soc.* **2002**, *124*, 10298 – 10299.

[14] D. Enders, K. Breuer, U. Kallfass, T. Balensiefer, *Synthesis* **2003**, 1292 – 1295.

[15] J. A. Murry, D. E. Frantz, A. Soheili, R. Tillyer, E. J. J. Grabowski, P. J. Reider, *J. Am. Chem. Soc.* **2001**, *123*, 9696 – 9697.

 © 2004 Wiley-VCH Verlag GmbH & Co. KGaA, Weinheim

Molecular Beams

Coulomb Explosions and Stability of Multiply Charged Ions in the Gas Phase**

*Detlef Schröder**

Keywords:
charge stripping · coulomb explosion · dianions · metal complexes · molecular beams

Since Pauling discussed the stability of the He_2^{2+} ion in 1933,[1] the existence of multiply charged molecular ions in the gas phase has attracted considerable attention because it challenges the fundamentals of chemical bonding.[2] Whereas an atom can get rid of all its electrons if enough energy is provided, molecules encounter an obvious problem in the absence of a stabilizing solvent environment because the electrons removed are essential for binding. Moreover, location of the charge on more than a single nucleus leads to strong electrostatic repulsion which may eventually result in charge separation, also referred to as Coulomb explosion. The latter term describes the situation quite adequately, because when the charges separate the electrostatic repulsion leads to a rapid release of kinetic energy, in the order of several electronvolts (eV). Consequently, almost all molecules can be ionized to monocations in the gas phase, whereas only a limited number of compounds form molecular dications, and only few small molecules exist as trications or in higher charge states.[3,4] In brief, the stability range of a molecular dication is determined by the crossing between the bonding potential-energy curve of AB^{2+} and the entirely repulsive interaction of the monocations A^+ and B^+ (Figure 1a).

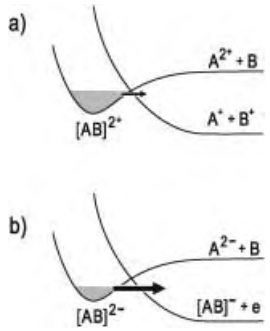


Figure 1. Schematic potential-energy surface of a) a dication $[AB]^{2+}$ and b) a dianion $[AB]^{2-}$ with the associated charge-separation asymptotes $A^+ + B^+$ and $[AB]^- + e^-$, respectively. The grey areas indicate the stability ranges of $[AB]^{2+}$ and $[AB]^{2-}$, and the horizontal arrows indicate the occurrence of tunneling through the potential-energy barrier.

The situation is even more extreme in small, multiply charged anions because electrons can easily tunnel through the potential-energy well formed by the crossing of the potential energy surfaces.As a result, the conditions required for the existence of long-lived dianions are more challenging (Figure 1b). About a decade ago, Cederbaum et al. pioneered research on dianions by means of extensive theoretical investigations, they suggested the existence of several small dianions[5] with $[BeF_4]^{2-}$ as the smallest member.[6,7]

Major progress in the research of multiply charged ions came from the invention of electrospray ionization (ESI)[8] because this method allows the generation of relatively small, multiply charged ions directly from solution. ESI is versatile in many respects and allows the generation of a manifold of multiply charged cations and anions. Other mass spectrometric methods also provide important information about multiply charged ions, particularly when it comes to small species.[9] Herein, some recent results about multiply charged cations and anions are addressed.

As far as cations are concerned, a number of interesting results have been reported in 2003. Thus, Duncan et al. have modified the conditions in a Smalley-type cluster-ion source to achieve surprisingly good yields of molecular dications, such as $[Mg(CO_2)_n]^{2+}$ ($n=1$–3), $[Si(Ar)_n]^{2+}$ ($n=1$–4), and $[Co(H_2O)]^{2+}$.[10] The $[Co(H_2O)]^{2+}$ ion is particularly suited to illustrate the fine balance that needs to be met in the optimization of the ionization conditions. Thus, the ionization energy (IE) of 17.08 eV of the Co^+ ion is more than 4 eV larger than $IE(H_2O) = 12.60$ eV. A strictly unimolecular collision of Co^{2+} ions formed upon laser ionization and neutral H_2O would therefore result in immediate electron transfer rather than association to the (metastable) bound $[Co(H_2O)]^{2+}$ state. In the other extreme, excessive cooling by an inert buffer gas would instead result in equilibration and thus lead to monocations only. The highest laser power on one hand and careful adjustment of gas pulses and gas pressures on the other led to success. While this new method has some limitations, it provides direct access to several molecular dications which are difficult to produce by other means.

A multiply charged ion which recently attracted much attention is the $[CO_2]^{2+}$ dication[11] because it has been

[*] Dr. D. Schröder
Institut für Chemie
Technische Universität Berlin
Strasse des 17. Juni 135, 10623 Berlin (Germany)
Fax: (+49) 30-314-21102
E-mail: df@www.chem.tu-berlin.de

[**] Financial support by the MCInet of the European Commission is acknowledged.

DOI: 10.1002/anie.200301728
© 2004 Wiley-VCH Verlag GmbH & Co. KGaA, Weinheim

proposed to play a role in nonthermal oxygen losses from the Martian atmosphere. In brief, the issue can be summarized as follows:[12] Unlike Earth, Mars lacks the atmospheric layers which protect from heavy radiation and thus energetic photons can penetrate. In higher layers of the Martian atmosphere, photons with energies above 37.4 eV can directly ionize the major component CO_2 to the corresponding dication. Even for the ground state of the $[CO_2]^{2+}$ dication, however, dissociation into the singly charged fragments $[CO]^+$ and O^+ is highly exothermic (ca. 5.1 eV).[13] Most of this energy is released as kinetic energy (Coulomb explosion) leading to fast-moving O^+ fragments which may eventually escape from the gravitational field of Mars.

As far as long-lived small molecules with even higher charge states are concerned, only a few trications are known and just a single tetracation has been detected.[4] In this respect, it is quite remarkable that the diatomic species $[UF]^{3+}$ even corresponds to a thermochemically stable diatomic trication;[14] here, the term "thermochemical stability" means that ground state of $[UF]^{3+}$ is lower in energy than all considerable fragments including the charge-separation asymptote $U^{2+} + F^+$. Recently, Harvey and Kaczorowska proposed the monocoordinate species $[Zr(CH_3CN)]^{4+}$ as a promising candidate for a small tetracation with a lifetime sufficient for detection, although the authors admit that the ion might be difficult to generate.[15] The achievable charge state is, of course, dependent on the size of the system. For metal complexes with slightly more extended solvation, multiply charged cations can easily be generated by ESI, for example, $[In(L)_4]^{3+}$ and $[Y(L)_5]^{3+}$ (with L = dimethylsulfoxide).[16,17]

As mentioned above, there exist more severe stability boundaries for multiply charged anions because charge reduction can proceed by electron tunneling. The oxalate dianion $[C_2O_4]^{2-}$ as well as the oxocarbon dianion $[C_5O_5]^{2-}$, for example, do not exist as free species in the gas phase. They can only be detected in the μs timeframe when solvated by several water molecules,[18,19] which is of interest for the analysis of these species. Likewise, in the series of 1,ω-diolatodiynes $^-O\text{-}(C{\equiv}C)_n\text{-}O^-$, the first species stable with respect to electron detachment is the dodecahexayne derivative $[C_{12}O_2]^{2-}$ $(n = 6)$.[20] In addition to electron detachment from multiply charged anions, Coulomb explosions can also occur without electron loss through the formation of two singly charged anions. Recent examples of such reactions deal with the dianions of iron–sulfur cubanes $[Fe_4S_4X_4]^{2-}$ (X = Cl, Br, SC_2H_5) which undergo symmetric cleavage to afford two $[Fe_2S_2X_2]^-$ units.[21,22] Quite remarkably, the corresponding monoanions $[Fe_4S_4X_4]^-$ have completely different dissociation patterns. Accordingly it was argued that Coulomb repulsion forces a symmetric cleavage of the cubane skeleton.[22]

A new methodological perspective has recently been added by Nielsen et al.[23] who generated reasonably small dianions by charge stripping (CS) of anions at a collision energy of 50 keV. Charge stripping was introduced in 1973 by Beynon et al.[24] and refers to electron removal from a mass-selected ion beam in high-energy collisions with a quasistationary target gas; usually monocations are converted into dications: $[AB]^+ \rightarrow [AB]^{2+} + e^-$. Nielsen et al. pursue the opposite approach by adding an electron to a mass-selected anion beam, so that the collision gas is also involved in the CS process. Three requirements were found to be essential for the success of this approach: 1) complexes of redox-active transition metals were chosen as precursor ions, so that the transition $[AB]^- + e^- \rightarrow [AB]^{2-}$ can occur without major changes in the bonding pattern. 2) An unusually large collision energy of 50 keV was applied to overcome the endothermicity of the CS process and to minimize interaction time between the fast-moving projectile ion and the target gas. 3) Sodium vapor, from which removal of an electron is relatively facile (IE = 5.14 eV), was chosen as a target. In marked contrast, no dianions were observed at all when dioxygen (IE = 12.07 eV) was used as a collision gas.

In their exploratory studies, Nielsen et al. demonstrate the occurrence of the CS processes $[Cr(SCN)_4]^- + e^- \rightarrow [Cr(SCN)_4]^{2-}$, $[Fe(CN)_4]^- + e^- \rightarrow [Fe(CN)_4]^{2-}$, and $[Pt(NO_2)_2]^- + e^- \rightarrow [Pt(NO_2)_2]^{2-}$, where the electrons are delivered by sodium in 50 keV collisions. In addition to the mere observation of CS occurring with anions, Nielsen et al. further investigated the dissociation behavior of the dianions formed by CS by means of energy-resolved experiments. The Coulomb explosion of the dianion $[Cr(SCN)_4]^{2-}$, for example, leads to the pair of the monoanions $[Cr(SCN)_3]^-$ and $[SCN]^-$ where both monoanion signals show characteristic peak broadenings owing to the large amount of kinetic energy released upon charge separation.

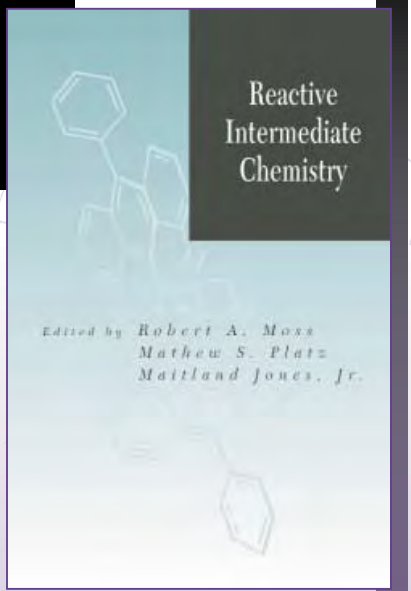
In conclusion, the chemistry and physics of multiply charged ions remains a formidable challenge to both experiment and theory, and recent progress in experimental techniques helps to address existing questions and to pose new ones. Upon first sight, small multiply charged ions might appear as a mere curiosity from mass spectrometric laboratories. More detailed consideration of the above examples demonstrates, however, that multiply charged ions may also play a role in practical applications or even atmospheric processes, not to speak about the enormous relevance of multiply charged ions in the analysis of biomolecules.

[1] L. Pauling, *J. Chem. Phys.* **1933**, *1*, 56.
[2] See for example the MCInet of the European Commission: http://www.chm.bris.ac.uk/pt/mcinet/welcome.htm.
[3] Large biomolecules can easily compensate many charges; for a recent example of a pentadecakisanion, see: J. Wu, S. A. McLuckey, *Int. J. Mass Spectrom.* **2003**, *228*, 577.
[4] D. Schröder, H. Schwarz, *J. Phys. Chem. A* **1999**, *103*, 7385.
[5] A. Dreuw, L. Cederbaum, *Chem. Rev.* **2002**, *102*, 181.
[6] H. G. Weickert, L. S. Cederbaum, *J. Chem. Phys.* **1993**, *99*, 8877.
[7] For experimental evidence, see: R. Middleton, J. Klein, *Phys. Rev. A* **1999**, *60*, 3515.
[8] J. B. Fenn, *Angew. Chem.* **2003**, *115*, 3999; *Angew. Chem. Int. Ed.* **2003**, *42*, 3871.
[9] For an example, see: D. Schröder, H. Schwarz, J. Wu, C. Wesdemiotis, *Chem. Phys. Lett.* **2001**, *343*, 258, and references therein.
[10] N. R. Walker, G. A. Grieves, J. B. Jaeger, R. S. Walters, M. A. Duncan, *Int. J. Mass Spectrom.* **2003**, *228*, 285.

 © 2004 Wiley-VCH Verlag GmbH & Co. KGaA, Weinheim

[11] P. Franceschi, R. Thissen, J. Zabka, J. Roithova, Z. Herman, O. Dutuit, *Int. J. Mass Spectrom.* **2003**, *228*, 507, and references therein.
[12] O. Witasse, O. Dutuit, J. Lilenstein, R. Thissen, J. Zabka, C. Alcaraz, P.-L. Blelly, S. W. Bougher, S. Engel, L. H. Andersen, K. Seiersen, *Geophys. Res. Lett.* **2002**, *29*, 104/1.
[13] H. Hogreve, *J. Phys. B* **1995**, *28*, L263.
[14] D. Schröder, M. Diefenbach, T. M. Klapötke, H. Schwarz, *Angew. Chem.* **1999**, *111*, 206; *Angew. Chem. Int. Ed.* **1999**, *38*, 137.
[15] J. N. Harvey, M. Kaczorowska, *Int. J. Mass Spectrom.* **2003**, *228*, 517.
[16] A. A. Shvartsburg, *J. Am. Chem. Soc.* **2002**, *124*, 12343.
[17] A. T. Blades, P. Jayaweera, M. G. Ikonomou, P. Kebarle, *Int. J. Mass Spectrom. Ion Processes* **1990**, *101*, 325.
[18] X.-B. Wang, X. Yang, J. B. Nicholas, L.-S. Wang, *J. Chem. Phys.* **2003**, *119*, 3631.
[19] T. B. Arthur, M. Peschke, P. Kebarle, *Int. J. Mass Spectrom.* **2003**, *228*, 1017.
[20] P. Schwerdtfeger, A. Hammerl, R. Wesendrup, *Int. J. Mass Spectrom.* **2003**, *228*, 341.
[21] X. Yang, X.-B. Wang, S. Q. Niu, C. J. Pickett, T. Ichiye, L.-S. Wang, *Phys. Rev. Lett.* **2002**, *89*, 163401.
[22] X. Yang, X.-B. Wang, L.-S. Wang, *Int. J. Mass Spectrom.* **2003**, *228*, 797.
[23] A. B. Nielsen, P. Hvelplund, B. Liu, S. B. Nielsen, S. Tomita, *J. Am. Chem. Soc.* **2003**, *125*, 9592.
[24] R. G. Cooks, T. Ast, J. H. Beynon, *Int. J. Mass Spectrom. Ion Phys.* **1973**, *11*, 490.

Reactive Intermediate Chemistry



Robert A. Moss, *Rutgers University*
Matthew S. Platz, *Ohio State University*
Maitland Jones, *Princeton University*

ISBN 0-471-23324-2 • 1,080 pages • Cloth
$99.95 / £64.50 / €90.90
December 2003

Reactive Intermediate Chemistry presents a detailed and timely examination of key intermediates central to the mechanisms of numerous organic chemical transformations. Spectroscopy, kinetics, and computational studies are integrated in chapters dealing with the chemistry of carbocations, carbanions, radicals, radical ions, carbenes, nitrenes, arynes, nitrenium ions, diradicals, etc. Nanosecond, picosecond, and femtosecond kinetic realms are explored, and applications of current dynamics and electronic structure calculations are examined.

WILEY

Reactive Intermediate Chemistry provides a deeper understanding of contemporary physical organic chemistry, and will assist chemists in the design of new reactions for the efficient synthesis of pharmaceuticals, fine chemicals, and agricultural products. Among its features, this authoritative volume is:

- Edited and authored by world-renowned leaders in physical organic chemistry.
- Ideal for use as a primary or supplemental graduate textbook for courses in mechanistic organic
- Enhanced by supplemental reading lists and summary overviews in each chapter.

CONTENTS

Preface

PART 1: REACTIVE INTERMEDIATES

1. Carbocations (R.A. McClelland)
2. Crossing the Borderline Between SN1 and SN2 Nucleophilic Substitution at Aliphatic Carbon(T.L. Amyes, et al.)
3. Carbanions (S. Gronert)
4. Radicals (M. Newcomb)
5. Non-Kekul Molecules as Reactive Intermediates (J.A. Berson)
6. Organic Radical Ions (H.D. Roth)
7. Singlet Carbenes (M. Jones Jr. and R.A. Moss)
8. Stable Singlet Carbenes (G. Bertrand)
9. Triplet Carbenes (H. Tomioka)
10. Atomic Carbon (P.B. Shevlin)
11. Nitrenes (M.S. Platz)
12. Synthetic Carbene and Nitrene Chemistry (M.P. Doyle)
13. Nitrenium Ions (D.E. Falvey)
14. Silylenes (W. Ando and N. Tokitoh)
15. Strained Hydrocarbons: Structures, Stability, and Reactivity (K.B. Wiberg)
16. Arynes (M. Winkler, et al.)

PART 2: METHODS AND TEMPORAL REGIMES

17. Matrix Isolation (T. Bally)
18. Nanosecond Laser Flash Photolysis: A Tool for Physical Organic Chemistry (J.C. Scaiano)
19. The Picosecond Realm (E. Hilinski)
20. Reactions on the Femtosecond Time Scale (J.E. Baldwin)
21. Potential Energy Surfaces and Reaction Dynamics (B.K. Carpenter)
22. The Partnership Between Electronic Structure Calculations and Experiments in the Study of Reactive Intermediates (W.T. Borden)

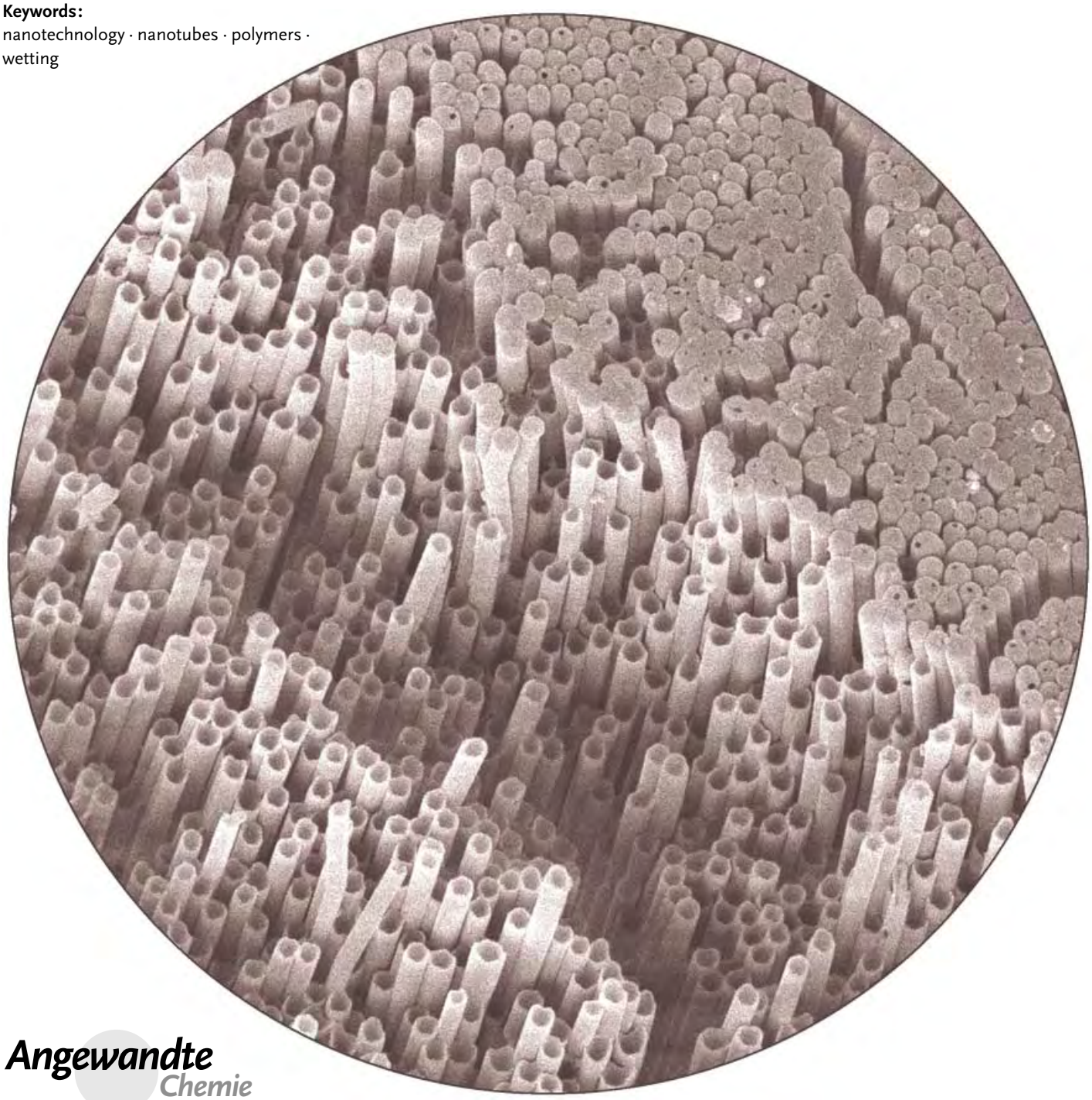
 © 2004 Wiley-VCH Verlag GmbH & Co. KGaA, Weinheim

Nanostructures

Nanotubes by Template Wetting: A Modular Assembly System

*Martin Steinhart, Ralf B. Wehrspohn, Ulrich Gösele, and Joachim H. Wendorff**

Keywords:
nanotechnology · nanotubes · polymers · wetting



Angewandte Chemie

 © 2004 Wiley-VCH Verlag GmbH & Co. KGaA, Weinheim DOI: 10.1002/anie.200300614

The wetting of porous templates with polymer melts and solutions or polymer-containing mixtures is a simple and versatile method for the preparation of tubular structures with diameters ranging from a few tens of nanometers to micrometers. The tube walls can be made of a multitude of materials, some of which have thus far been altogether impossible to use or very limited in their ability to be incorporated into nanostuctures. Template wetting also makes it possible to modify the nanotubes in a variety of ways, for example through the controlled generation of pores or the embedding of nanoparticles into the walls. This method offers a promising approach to functionalized nanotube–template hybrid systems and free-standing nanotubes.

From the Contents

1. Nanotubes—Beyond Carbon 1335
2. Nanotubes by Self-Assembly and Template Processes 1335
3. Nanotubes by Wetting 1336
4. Wetting of Porous Membranes 1337
5. The Modular Assembly System 1338
6. Potential Applications 1343

1. Nanotubes—Beyond Carbon

Since their discovery by Iijima over a decade ago,[1] nanotubes have often been equated with carbon nanotubes. Depending on their composition, they can have a variety of mechanical, electrical, and thermal properties;[2,3] can be conductors or semiconductors; and can have extremely high heat-conduction capabilities, or outstanding mechanical strength. Their application as components in composites, color flat-panel displays, and gas sensors, as well as in hydrogen and ion-storage units is under consideration or is about to be realized.[4] Carbon nanotubes with multiple graphite-like wall layers are produced by arcing between graphite electrodes,[1,5] or by the catalytic vapor deposition of carbohydrates in the presence of metal nanoparticles.[6] Single-walled carbon nanotubes (SWNTs) can be obtained by the combined use of catalysts and concentrated carbon-containing vapors, which are obtained by either arcing[7,8] or laser ablation. One modification of the production process is based on the implementation of conventional thin-layer techniques to prepare substrates for the growth of parallel carbon nanotubes through chemical vapor deposition. In this way we can obtain extensive nanotube arrays.[10,11]

In view of the understandable fascination with carbon nanotubes, their properties, and possible applications, the potential of nanotubes whose walls consist of other materials, such as polymers, metals, semiconductors, or ceramics, are often underrated. However, this is quite unjust, because carbon is in no way ideal as an all-purpose material for popular applications. In general, the tubular form offers considerable advantages, because nanotubes can be used as pipes, microcavities, or microcapsules, and can be arranged in parallel to functionalized membranes. When fixed in a porous membrane, nanotubes form easily handled nanostructured hybrid systems with extremely large surfaces, which have considerable advantages over systems involving nanoparticles formed by other means in such fields as catalysis and sensor technology. However, nanotubes can only be used in such applications if the chemical and physical properties of their walls can be tuned over a wide range. One prerequisite for this is naturally the ability to incorporate a broad spectrum of materials. The first applications for nanotubes not made of carbon were demonstrated by Martin and co-workers in such areas as the separation of racemic mixtures,[12] sensors,[13] substance separation,[14] or in membranes for selective ion transport.[15]

2. Nanotubes by Self-Assembly and Template Processes

The preparation of nanoscopic tubular objects is still an undertaking of material science, and can be extremely technically demanding. Frequently, special processes must be implemented or even developed to obtain materials with the required specifications. Correspondingly, methods have been described, which at least partially meet these demands. In general, two fundamental strategies have been pursued: 1) self-assembly and 2) the use of templates made of materials that can be easily nanostructured in a defined manner.

A process introduced by Schmidt and Eberl is based on rolling up a thin film, which is held under mechanical tension and attached to a sacrificial layer bound to a rigid substrate. When the sacrificial layer is removed, the film rolls itself into a nanotube.[16] Certain molecules, such as lipids,[17,18] peptides,[19] and block copolymers,[20] also exhibit the ability to self-assemble given the right conditions.[21] In this case, many individual, disorganized molecules come together to form highly ordered aggregates. Self-assembly is a very elegant

[*] Prof. Dr. J. H. Wendorff
Fachbereich Chemie und Wissenschaftliches Zentrum für Materialwissenschaften
Philipps-Universität
Hans-Meerwein-Strasse, 35032 Marburg (Germany)
Fax: (+49) 6421-282-8916
E-mail: wendorff@staff.uni-marburg.de
Dr. M. Steinhart, Prof. Dr. U. Gösele
Max-Planck-Institut für Mikrostrukturphysik
Weinberg 2, 06120 Halle (Germany)
Prof. Dr. R. B. Wehrspohn
Fachbereich Physik
Universität Paderborn
Warburger Strasse 100, 33098 Paderborn (Germany)

 DOI: 10.1002/anie.200300614 © 2004 Wiley-VCH Verlag GmbH & Co. KGaA, Weinheim

approach to nanostructured systems, because the tubes are made from building blocks that already have the required intrinsic structural information. Nature has perfected this principle for the synthesis of complex functional units; material science, on the other hand still has a long way to go. The limitations stem from two different problems: 1) only a small spectrum of materials is suited to self-organizational processes, and 2) while the precursor compounds can be tailored within certain limitations, it is difficult and expensive to then functionalize them as well. Self-assembly processes also offer limited flexibility with respect to the dimensions of the nanotubes.

These restrictions do not apply to template processes. Some materials can be nanostructured in a simple and controlled manner, and are therefore available for the preparation of templates, which can in turn be used for the synthesis of nanotubes from the actual target compound. Martin and co-workers first used nanoporous membranes.[22,23] For instance, when monomers are polymerized within the nanopores, it is possible to tune the wall thickness of the resulting polymers by choosing the right polymerization conditions, particularly the polymerization time.[24] Metallic nanotubes are attainable by electrochemical deposition in aluminum oxide templates with chemically modified pore walls,[25] as well as by electroless deposition.[26] Nanotubes made of inorganic semiconductors and metal oxides can be made by sol–gel processes.[27] Template methods initially yield template–nanotube hybrids. The detached nanotubes are then obtained by selective removal of the template.

Nanotubes with extremely large aspect ratios (the ratio of length to diameter) can be obtained in large quantities in woven or aligned forms by the coating and then selective removal of polymer nanofibers.[28–30] The nanofibers, whose diameters range from a few nanometers to a few micrometers, are formed by electrospinning, in which a strong electric field is used to pull a thin jet out of a drop of polymer solution or melt. The jet then is deposited in the form of a nanofiber.[31] The ability to obtain such high aspect ratios rests on the fact that electrospinning is, like extrusion processes, a continuous process. In addition, it is possible to use this method to obtain nanofibers, and thus nanotubes, with specific surface topologies.[32–34]

3. Nanotubes by Wetting

As versatile as the methods for the preparation of nanotubes described so far may be, two challenges remain: 1) important materials, including numerous high-performance polymers, copolymers, or mixtures of defined composition, cannot be made into nanotubes. 2) For many applications, it is essential to functionalize the nanotube walls by generating a specific fine structure. For example, one important question concerns the course of the crystallization processes within the walls, since the properties of crystalline or partially crystalline materials largely depend on the structure of the crystalline domains. One fascinating possibility for functionalization would be the generation of a



Martin Steinhart studied chemistry at the Universities of Hamburg and Marburg and received his doctorate under J. H. Wendorff in Marburg. In his research, he developed a process for the preparation of nanotubes by wetting of porous templates. Together with R. B. Wehrspohn he received the Wissenschaftsverbundpreis of the Buna Sow Leuna Olefinverbund GmbH in 2002. Since 2003 he has been a group manager in the U. Gösele division of the Max Planck Institute of Microstructure Physics in Halle. His research interests include complex one-dimensional nanostructures and hierarchical nanosystems.



Ralf B. Wehrspohn studied physics at the University of Oldenburg and received his PhD in 1997 at the École Polytechnique in Paris. Until 1999 he worked on thin-film transistors for new AMLCDs at Philips Research. From 1999 until 2003 he led the „Porous Materials/Photonic Crystals" group in the U. Gösele division of the Max Planck Institute of Microstructure Physics in Halle. Since April of 2003 he has held a chair in the Physics department at the University of Paderborn; his area of research is nanophotonic materials. He was awarded the Maier-Leibnitz Prize of the German Science Foundation in 2003.



Ulrich Gösele received his doctorate in physics in 1975 at the University of Stuttgart. In 1985 he was appointed as a full professor of materials science at Duke University and has been the director of the Max Planck Institute of Microstructure Physics in Halle since 1993. His research interests lie in the areas of defects and diffusion in semiconductors, ferroelectric thin films, waferbonding, porous materials, quantum dots, photonic crystals, silicon photonics, and silicon nanowires. He is a fellow of the American Physical Society and the Institute of Physics as well as a member of the German Academy of Natural Scientists Leopoldina and the board of directors of the Materials Research Society.



Joachim H. Wendorff obtained his PhD at the University of Marburg and subsequently transferred to a postdoctoral position at the University of Massachusetts, Amherst, working with Prof. F. P. Price. From 1976 until 1991 he was the director of the physics division at the German Plastics Institute in Darmstadt. He obtained his habilitation in 1982 with Prof. E. W. Fischer in Mainz and has held a chair for physical chemistry at the Philipps University in Marburg since 1991. In 2000–2001 he was the European Visiting Professor at the Key Centre for Polymer Colloids at the University of Sydney.

 © 2004 Wiley-VCH Verlag GmbH & Co. KGaA, Weinheim

fiberlike texture, which would bring to mind nanoactuators, piezoelectric actuators, or similar applications.

Composite systems with a highly defined phase morphology and thus a large internal phase interface could make it possible to direct transport processes within the nanotube walls. This is an important prerequisite for the implementation of nanotubes in the area of energy conversion in light-emitting diodes or solar cells, for example. The efficiency of such systems could be considerably increased if the domain structure could be tuned to the diffusion lengths of excitons or light-induced charges. This has already been shown in the case of uniform thin films on even substrates.[35–37] The selective removal of one component should lead to a specific surface roughness or nanoporosity of the tube walls. The surface area of the wall is thus increased further, which is advantageous for applications in catalysis, separation, or sensor technology. The pore size could also be used to modulate the transport of molecules through the wall of the tube.

It is thus necessary to develop a versatile but technically simple process for the preparation of nanotubes, which broadens the spectrum of available wall materials on the one hand, while allowing trouble-free modification for the tailoring of the nanotubes' structure and properties on the other. This could be possible by the controlled induction of phase transitions in the nanotube walls. The key to the solution of these problems is a familiar and thoroughly investigated phenomenon: wetting.[38,39] Complete wetting or spreading occurs when a thin film of liquid in equilibrium covers a substrate. While "soft" materials such as low-melting organic substances mostly have low surface energies (under 100 $mN\,m^{-1}$), "hard" inorganic materials with high melting points generally have high surface energies ranging from a few hundred to several thousand $mN\,m^{-1}$.[40,41] As a rule, solutions, mixtures, or melts with low surface energies spread over substances with higher surface energies.[42]

The nature of viscous liquids like polymer melts and solutions results in very slow spreading over uniform surfaces, with the frequent formation of precursor films.[43–45] These form around a spreading macroscopic drop of liquid, have thicknesses ranging from a few tens of nanometers down to a few hundred picometers, and cover areas of the substrate on the order of square centimeters (Figure 1). As it spreads,



Figure 1. Spreading drop with precursor film.

more and more material is drawn out of the macroscopic drop (whose height thus decreases) and into the precursor film. Ausserré et al. were the first to prove this experimentally for such cases, in which the nonvolatility of the liquid rules out matter transport via the gas phase.[46] The structure of the precursor film and the dynamics of its spreading cannot be described by macroscopic models. If the film thickness is in the mesoscopic range, then long-range intermolecular interactions, for example, must be taken into account.[43,44,47] It is clear that such wetting phenomena could be the key to a versatile method for the preparation of nanotubes.

4. Wetting of Porous Membranes

Organic polymers are among the materials with low surface energy.[40,42] Polymer melts are molten onto templates in excess, whereas wetting with polymer solutions occurs dropwise under ambient conditions (Figure 2a). It is to be

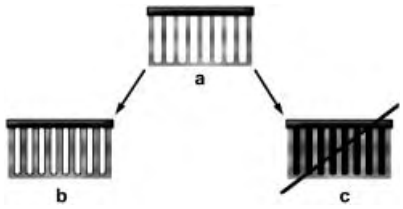


Figure 2. Wetting of porous templates with polymer melts or polymer-containing solutions: a) The fluid is brought in contact with the template. b) Within seconds, the pore walls are covered with a mesoscopic film of the liquid. c) Complete filling of the pore interior, if it occurs at all, happens on a completely different time scale.

expected that a mesoscopic film wets the walls of the pores in a manner analogous to the formation of precursor films on flat substrates (Figure 2b). As a prerequisite, the pore walls must have a high surface energy. The processes discussed here are microscopic in nature, in contrast to phenomena such as the Lotus effect,[48] which are associated with the macroscopic wettability of structured surfaces.

We can only speculate as to whether the equilibrium state corresponds to complete filling of the pore volume (Figure 2c and if it does, how this state is reached. On the one hand, the interface between the air and the inner shell surface would disappear, and cohesive energy might be gained. In that case, the state in which the pore walls are only wetted by a mesoscopic film would be kinetically stable (development toward equilibrium hindered or very slow)—because the adhesive forces between the polymer-containing liquid and the pore walls, which drive the spreading, would be neutralized—but not in equilibrium. On the other hand, as a result of the spatial limitations and the different interface energies of the outer shell surface (pore wall/nanotube wall) and the inner shell surface (nanotube wall/air), the molecules in the vicinity of pore walls may have a higher degree of order than those in the bulk. This would allow the formation of a phase boundary between those molecules in contact with the pore wall and those farther from the pore walls, that is, in the bulk. Phenomena such as autophobicity may also have to be taken into consideration. Autophobicity means that a droplet of a liquid shows nonwetting behavior on a thin surface layer of the same liquid. This would argue for the fact that equilibrium is already reached as soon as the pore walls are wetted by a mesoscopic film.

It remains unknown why low molecular weight fluids fill the entire pore space differently than polymers do. We presume that the polymer layer on the pore walls is particularly stable. Because of the unusually large dimensions of polymer molecules, the region near the pore wall, in which attractive interactions are in effect, is covered by a monolayer, so that most of the molecules are in direct contact with

 © 2004 Wiley-VCH Verlag GmbH & Co. KGaA, Weinheim

the pore wall. However, in the case of nonpolymeric materials, the influence of long-range intermolecular interactions could allow for a coating made of multiple layers of molecules. In those layers that are not in direct contact with the pore wall, the molecules could be relatively mobile; this could trigger the occurrence of instabilities, which could lead to the formation of a meniscus, and finally the complete filling of the pore.

With polymer melts as well as polymer solutions the pore walls are completely wetted, with complete reproduction of the pore structure and even to a pore depth (T_p) of 100 μm, within seconds.[49] The liquid film solidifies when cooling or evaporation of the solvent lead to crystallization or vitrification. Figure 3a depicts a pore opening from the top of a macroporous silicon membrane that has been wetted with polymethylmethacrylate (PMMA). It is clear that the interior of the pore has not been completely filled. The underside of a polyvinylidene fluoride (PVDF) wetted membrane of porous aluminum oxide (Al_2O_3) is shown in Figure 3b. The aluminum substrate that was bound to the membrane has been selectively etched away. The exposed tips of the PVDF nanotubes, which replicate the closed ends of the pores, are visible within the pores. As can be seen in Figure 3c, the thickness of the walls is typically about 10 nm. Pictured is a TEM image of an ultrathin section of an Al_2O_3 membrane wetted with a ten percent solution of polystyrene (PS). The dark region in the lower portion of the picture is the Al_2O_3 pore wall. In the upper portion of the picture, the cavity inside a PS nanotube appears light. In between the two is the roughly 10 nm nanotube wall, dyed with osmium tetroxide.

Polymers with ultrahigh molecular weights between 10^6 and 10^7 g mol^{-1}, such as polytetrafluoroethylene or polyethylene, which do not have the ability to flow viscously, owing to their extraordinarily high melt viscosity, will also spread on the pore walls if they are lightly pressed against the surface of the template. This indicates that the expansion of the polymer melt or solution over pore surfaces occurs by surface diffusion. The chain conformation would thus strongly deviate from the equilibrium conformation in the resting melts. The thicknesses measured for precursor films of polymers spreading on flat surfaces are in the subnanometer range, and are thus considerably smaller than the corresponding gyration radii (The gyration radius is a characteristic constant for polymers that take the form of statistical coils, and gives the average distance of the chain segments from the center of the molecule).[50] The polymer chains must thus lie flat on the substrate. If precursor films evolve on even substrates, it can be assumed that a limited amount of liquid spreads over an "infinite" substrate, whereas the surface of a single pore is finite and the reservoir of liquid with which it is in contact is "unlimited". In the wetting of pore walls, it is thus possible for a kinetically or thermodynamically stable state to form, which is distinguished by a wetting layer thickness of about 10–30 nm. When the diameters of the template pores become smaller than the wall thickness of the nanotubes, massive nanowires should form instead. Indeed, the pore volume of porous matrices with pore diameters in the subnanometer range can be completely filled by polymer melts.[51]

5. The Modular Assembly System

5.1. Ordered Porous Membranes as Templates

In order to be suitable as templates for the preparation of nanotubes, porous membranes must have pore walls with a high surface energy. Inorganic oxides meet this requirement. Since the mid 1990s, two materials that are particularly interesting for this purpose and have practically monodisperse pore diameter distributions in the nanometer and micrometer range have become the focus of much interest: porous aluminum oxide and macroporous silicon. These materials cover the pore diameter range from about 15 nm up to several micrometers (Figure 4). The pores can be arranged in a very regular fashion, and such templates are thus considered to be ordered.

Disordered porous aluminum oxide has been used for the eloxation of aluminum for over 100 years. In this process, the aluminum is potentiostatically anodized in diprotic acids (mostly sulfuric acid, oxalic acid, phosphoric acid, or chromic acid). Under certain conditions, a film of aluminum oxide with relatively even pores forms along the current lines. A detailed discussion of the pore formation process can be

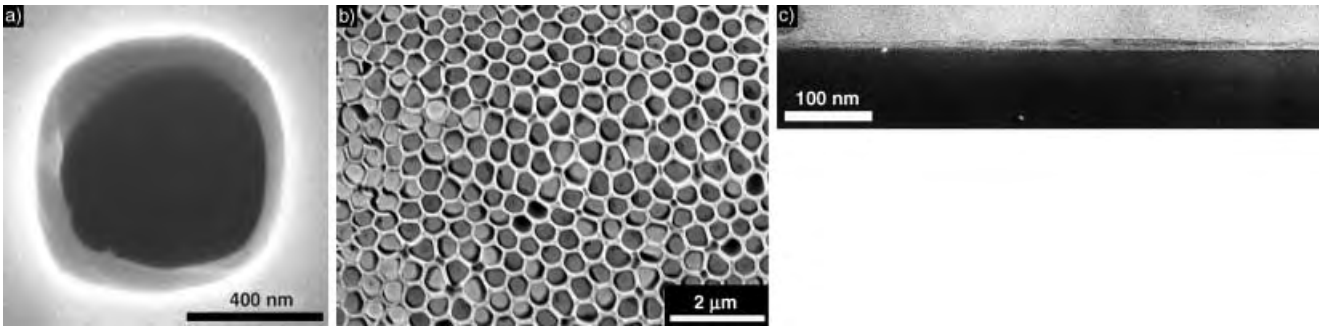


Figure 3. Wetted porous membranes: a) Scanning electron microscopy (SEM) image of a pore opening in macroporous PMMA-wetted Si. b) SEM image of the underside of a PVDF-wetted membrane of porous Al_2O_3 after selective etching of the aluminum substrate to which the membrane was bound. c) Transmission electron microscopy (TEM) image of an ultrathin section of a porous Al_2O_3 membrane wetted with a PS solution. The lower portion of the picture shows the Al_2O_3 pore wall, the middle portion depicts the wall of a PS nanotube, and the upper portion shows the cavity inside the nanotube.

 © 2004 Wiley-VCH Verlag GmbH & Co. KGaA, Weinheim

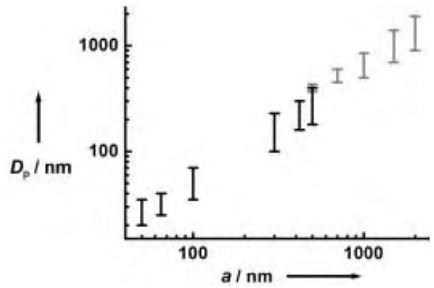


Figure 4. Overview of the pore diameters (D_p) and lattice constants (a) of the currently available highly ordered templates of aluminum oxide (black bars) and silicon (grey bars). Taken from reference [39].

found in the literature.[52,53] The pore diameters (D_p) typically lie between 15 and 400 nm, with a dispersity (calculated by dividing the standard deviation by the mean pore diameter) of at most 20% (Figure 5a). One hundred years after the first

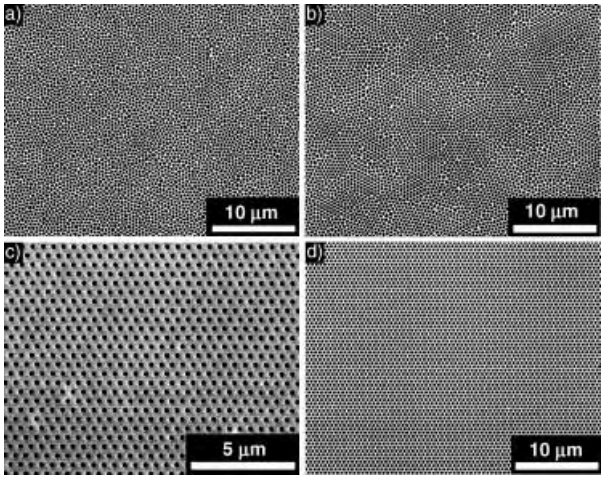


Figure 5. SEM images of porous membranes: a) disordered porous Al_2O_3, b) porous Al_2O_3 obtained by self-organized growth, c) Al_2O_3 prepared by a combination of nanoimprint lithography and self-organization, d) highly ordered macroporous Si. In all four systems $a = 500$ nm.

patent for disordered porous aluminum oxide,[54] Masuda and Fukuda were able to produce self-organized pore structures.[55] The self organization is induced during pore growth by lateral forces resulting from the expansion in volume on the conversion of aluminum to aluminum oxide.[56] In a two-step process,[55] self-organized pore structures can be produced, in which the pores form a hexagonal lattice with a porosity (fraction of the whole membrane surface taken up by pore openings) of 10% (10% porosity rule).[57] The distances between the centers of the pores a (the lattice constants) can be controlled by the conditions of the process. The domains typically stretch over 10–20 pore intervals and the dispersity of the pore sizes is 8%. The initial porosity of 10% can be increased by wet chemical processes after anodization. For example, the pore diameter for porous aluminum oxide with $a = 500$ nm after anodization can be increased from $D_p =$ 180 nm to 400 nm in a controlled manner by means of isotropic etching (Figure 5b). While self-organization allows access to pore structures with a polycrystalline degree of order, combination with lithographic methods makes it possible to produce extensive monodomains of pores with lateral dimensions ranging into the square centimeter range. Owing to its nanoroughness, direct electron beam lithography on aluminum gives unsatisfactory results, whereas nanoimprint processes are proving to be highly promising.[58] In this process it is necessary to match the lattice constants of the stamp to the correlation distances that result from the self-organized pore growth. Attainable pore diameter dispersities are below 2% (Figure 5c).

In parallel to this work, Lehmann developed an electrochemical method, also based on anodization, for the formation of ordered pore structures in silicon.[59] In this process, the silicon oxides or fluorides formed in the oxidation of silicon dissolve in an electrolyte containing hydrofluoric acid.[60] The processes involved are relatively complex and are extensively discussed in the literature.[59–61] Three growth processes can be distinguished, which lead to microporous ($D_p < 4$ nm), mesoporous ($4 < D_p < 100$ nm), and macroporous ($D_p > 100$ nm) silicon. The growth conditions for both n-silicon[59] and p-silicon[62] have been extensively investigated in recent years. The etch pits for the nucleation of the pores are as a rule generated lithographically. This process also results in extensive pore monodomains with lateral dimensions reaching the square centimeter range. The distance between pores can be set anywhere from $a = 500$ nm (Figure 5d) to $a = 20$ μm by variation of the process conditions. The pores are nearly perfectly vertically aligned, and can attain aspect ratios over 250.[63]

5.2. Wall Materials

Wetting of porous templates succeeds through contact with both polymer melts and polymer solutions under ambient conditions, which gives rise to the versatility of the method. The wetting step is preparatively simple and requires little effort. The fact that this process is based on a fundamental physical phenomenon, wetting, is the reason for the first major advantage of this method: practically all polymer-containing liquids with a low surface energy can be processed in this way. Aside from structural polymers like PS and PMMA, this particularly applies to high-performance polymers, which have been impossible or very difficult to nanostructure by conventional methods because of their unusual characteristics, such as insolubility in conventional solvents. High-performance polymers include technical plastics with outstanding mechanical, optical, or electronic properties; a high elasticity modulus; high impact strength; negligible cold flow; high continuous heat resistance, or particular biocompatibility.[64] Such materials are naturally also of considerable interest in nanotechnology, as minireactors, in the area of material separation, or for applications that require particular chemical or heat resistance. Polyether ether ketone (PEEK) and polytetrafluoroethylene (PTFE) are two such materials.

 © 2004 Wiley-VCH Verlag GmbH & Co. KGaA, Weinheim

PEEK[65] has a continuous service temperature of 250 °C, is insoluble in practically all common solvents, and demonstrates excellent chemical resistance. The melting point of the partially crystalline material is at about 340 °C. PEEK nanotubes have been produced by melting a film of the polymer on a template surface at 380 °C and subsequent removal of the Al_2O_3 template (Figures 6a, b).

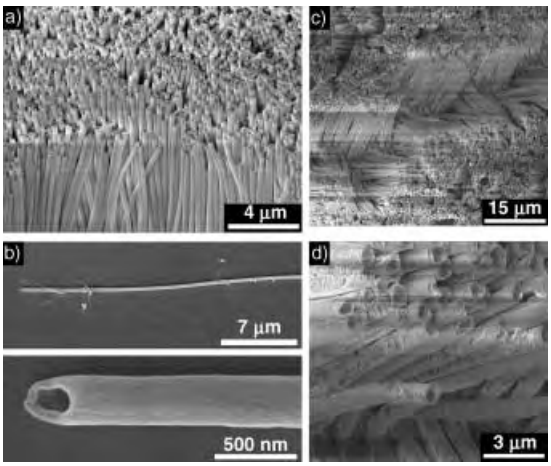


Figure 6. SEM images of nanotubes made from high-performance polymers: a) Array of PEEK nanotubes, b) individual PEEK nanotube, c, d) nanotubes made of ultra-high molecular weight PTFE.

An even larger challenge is the production of nanotubes from PTFE ("Teflon"). There has long been doubt about whether this would be possible at all, since commercially used PTFE has an extremely high molecular weight of 10^6 to 10^7 g mol^{-1}, is practically not flowable, and cannot be processed by the usual plastic molding techniques like extrusion or injection molding. The preparation of molded PTFE parts has thus fallen back on sintering. PTFE has highly interesting properties; it is insoluble, is stable toward nearly all chemicals, and has a very low surface energy as well as extreme toughness.

Experiments with Teflon CN (Dupont, Wilmington), a commercially available material, showed that wetting of pore walls occurs at a temperature of 400 °C when the polymer is gently pressed against the template surface. The walls of the resulting Teflon nanotubes (Figure 6c, d) are slightly ribbed. This could possibly be a result of the strongly divergent thermal expansion coefficients of the template and PTFE, as well as the large difference between the wetting and room temperatures, which leads to mechanical tension while cooling.

Multicomponent systems and composites with a defined composition can also be made into nanotubes. Thus polymers, which act as carriers in the wetting process, can be mixed with large proportions of inorganic components, which can then be chemically transformed within the walls of the composite nanotubes. One example of this is the formation of palladium nanotubes.[66] Palladium is of particular interest as a wall material, since nanoparticles or nanowires of this metal are used in catalysis,[67–70] sensors,[71] and hydrogen storage,[72] as well as other applications.

The preparation of Pd nanotubes occurs by wetting of porous templates with a mixture of palladium(II) acetate and a polymer in a solvent common to both. The polymer of choice was polylactide (PLA), first because, in the presence of polymers like PLA, which act as reducing agents, Pd^{II} is reduced to Pd^0 within seconds at only 160 °C; and second because PLA can be directly and easily removed by further tempering of the wetted templates at 350 °C, so that pure Pd nanotubes remain. Examples are shown in Figure 7, in which porous Al_2O_3 with pore diameters of 400 nm (a, b) and 55 nm (c) was used. The wall thickness of the Pd nanotubes is about 10 nm (Figure 7a). Their outer diameter corresponds to those of the template pores, either 400 nm (Figure 7b) or 55 nm (Figure 7c). It is also possible to fabricate nanotubes from ferroelectric and piezoelectric oxides such as lead zirconate titanate (PZT, $PbZr_{0.52}Ti_{0.48}O_3$) and barium titanate ($BaTiO_3$) in a similar manner.[73] In this case, precursor compounds that contain stoichiometric ratios of the metal cations are used for the wetting process.

5.3. Nanotube Powders and Organized Superstructures

Aside form their possible use as templates, materials with highly ordered pores are of interest in a wide spectrum of applications, including areas such as material separation, sensor technology, or photonics. The pores can either be open at both ends, or can have one end closed off. Wetting of the pore walls results in hybrid systems that contain nanotubes within the porous matrix. In this way, it is possible to tune the properties of the pore surface, such as the optical density, polarity, reactivity, and biocompatibility. Their use as functionalized photonic crystals, catalytic systems, or components in model systems for the investigation of the blood-brain barrier, have been discussed.

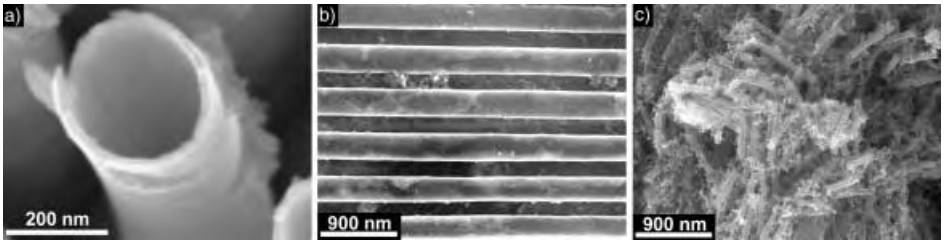


Figure 7. SEM images of Pd nanotubes: a) Cross-section of a Pd nanotube with a 400 nm diameter, b) parallel Pd nanotubes with a 400 nm diameter, c) powder of Pd nanotube segments with a 55 nm diameter.

 © 2004 Wiley-VCH Verlag GmbH & Co. KGaA, Weinheim

For the preparation of freestanding or powdered nanotubes, the templates are then dissolved. Since there are a large number of different formulations available for both acid and alkaline environments, the matrix can mostly be removed selectively and without damage to the nanotubes, even in the presence of sensitive polymeric components. With a 4 inch wafer, a single preparation can produce more than one hundred billion nanotubes.

By using stiff polymers or otherwise non-elastically deformable substances as wall materials and templates with thin pore walls, the degree of order of highly ordered template structures can be reproduced when these are wetted and selectively removed. For this, the highly ordered nanotubes must be attached to a substrate on at least one side. As a rule, some excess of the wetting fluid remains on the surface of the template after the wetting process. Mechanical removal of this excess fluid then frees up the openings of the coated pores. However, a film that has the same thickness as the nanotube walls and wets the upper surface of the pore walls will remain and bind the individual nanotubes together. These then form a highly ordered foil. An example of this with Pd as the wall material is depicted in Figure 8a. The excess wetting fluid that remains on the surface of the template can also act as the substrate to which the highly ordered nanotubes are fastened. In Figures 8b, and c, PMMA tubes bound by a 1 mm thick PMMA film are shown as an example.

5.4. Wall Morphologies

The functionality of nanotubes does not only stem from their dimensions and the type of wall material, but also from the inner structure of the nanotube walls. Specific wall morphologies can be generated by phase transitions or phase-separation processes in the nanotube walls.[66,74] The hollow cylinder geometry of the walls imposes a spatial confinement on the system: whereas the length of the nanotubes can be considered as infinite, the wall thickness and circumference are finite. In contrast to thin flat films, which have been intensively studied as model systems for spatially limiting geometries,[75–77] a curvature occurs, which is naturally highly significant for the evolution of the wall morphology.

An important phase transition in one-component systems is crystallization. The structure of crystalline domains to a large extent determines the mechanical, electrical, optical, and chemical properties of crystallizable substances. This is the case for actuators or sensors made of piezoelectric materials (coupling of mechanical deformation and electrical fields), pyrolectric materials (coupling of temperature changes and electrical fields), and ferroelectric materials (in which there can be spontaneous electrical polarization). As a rule, only certain crystal forms have the desired properties.

Particularly pronounced changes of corresponding material properties resulting from an interaction with an external electrical field will be attainable if the material is single-crystalline, or if is polycrystalline exhibiting a distinct crystalline texture. An investigation of crystallization in nanotube walls is thus of high interest. As a first step, it is necessary to determine if a crystalline texture is induced by the hollow-cylinder geometry. The partially crystalline polymer PVDF was chosen as a model system, because some of its crystal forms exhibit piezo-, pyro-, and ferroelectricity. In addition, it has extremely high chemical resistivity and biocompatibility, as well as a low surface energy, and is used in materials separation and in filter membranes.

Porous Al_2O_3 with $D_p = 400$ nm was wetted with a PVDF melt and thermally treated so that a well-formed and well characterizable crystalline phase, consisting only of α-PVDF, should be present in the nanotube walls. X-ray diffraction experiments were carried out on PVDF nanotubes that were perfectly aligned in the template. These experiments, in which the surface of the template was perpendicular to the plane formed by the incoming radiation beam and the detector, demonstrate the existence of a pronounced crystalline texture in the nanotube walls (Figure 9).[74] The diffractogram in Figure 9a is from an isotropic reference sample from melted PVDF pellets, which were otherwise prepared identically. It shows all of the reflections expected for α-PVDF,[78,79] with no

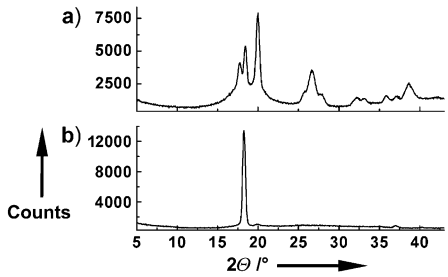


Figure 9. Diffractograms a) of an isotropic PVDF reference sample and b) of PVDF nanotubes ($D_p = 400$ nm) in a template, where the template surface is perpendicular to the plane formed by the primary beam and the refracted beam.

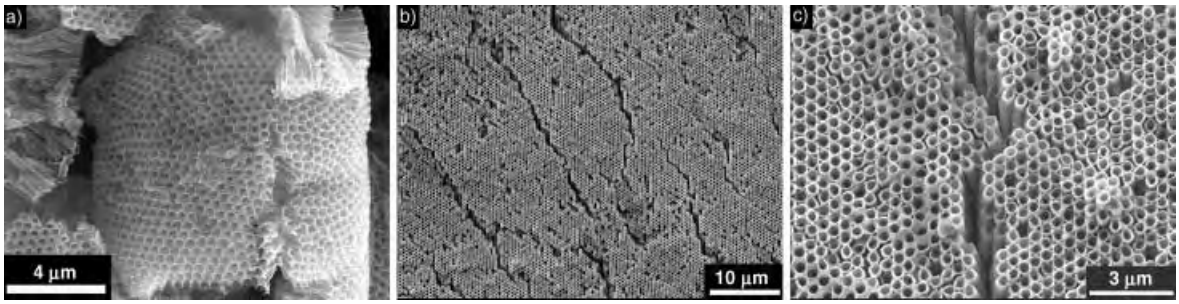


Figure 8. SEM images of highly ordered nanotube arrays made of Pd (a) and PMMA (b, c).

 © 2004 Wiley-VCH Verlag GmbH & Co. KGaA, Weinheim

indications of other modifications, as expected. In contrast, the oriented nanotubes with $D_p = 400$ nm generate only the (020) reflection of the α-form (Figure 9b). The PVDF crystallites in the nanotube walls must thus be oriented so that the crystallographic ⟨0*k*0⟩ direction, their main direction of growth,[80] is parallel to the long axis of the nanotube. This is thus the only direction in which the wall curvature equals zero, which is why this phenomenon can be described as curvature-directed crystallization.[74]

Although the nonpolar α-modification of PVDF does not yet demonstrate the desired piezoelectric properties, other systems have already shown that nanotubes that act as nanoactuators are attainable through template wetting. The nanotubes of ferroelectric and piezoelectric oxides, such as the PZT and $BaTiO_3$ discussed in Section 5.2, demonstrate piezoelectric hysteresis.[73]

An interesting expansion of the wetting concept is based on the use of multicomponent systems. Induction of decomposition processes by a leap in temperature, or the evaporation of a volatile solvent allows the generation of a specific phase morphology in the walls of the nanotubes. The ripening of the resulting phase morphology begins as soon as the phase separation starts. As well as the previously mentioned geometric limitations, wetting phenomena could also play a large role in this process. The ripening process occurs as long as the material forming the nanotube wall remains fluid, either because it is being annealed at correspondingly high temperatures or because it contains a sufficient quantity of a solvent. The driving force for ripening is the reduction of the originally large interface between the coexisting phases. This was examined in the case of Pd/PLA composite tubes, for example.[66] Figure 10 shows a TEM image of an ultrathin section of an Al_2O_3 template ($D_p = 400$ nm), whose pore walls (below, dark area) are covered with a 10 nm thick Pd/PLA composite layer (middle of picture). This contains Pd nanoparticles, visible as dark spots, with diameters of about 5–10 nm. Their morphology corresponds to an advanced state of ripening, as the palladium was originally finely dispersed.

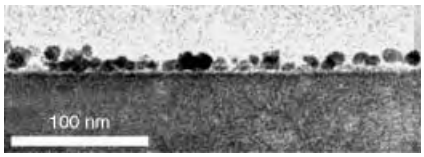


Figure 10. TEM image of an ultrathin section of an Al_2O_3 template (the pore wall is the dark area in the lower half of the picture) wetted with a PLA/Pd mixture. The wall of the PLA/Pd composite tube in the center of the picture contains Pd particles of about 10 nm.

Selective removal of PLA and the template leads to structured Pd nanotubes with walls consisting of sintered Pd nanoparticles. SEM and TEM images of Pd nanotubes with a 400 nm diameter and a morphology corresponding to a relatively early ripening stage are shown in Figures 11a and b. The rough, fine, and netlike structure of the walls can be discerned. In contrast, Figures 11c and d depict SEM and TEM images of Pd tubes with the same diameter but a wall morphology corresponding to a late ripening stage. The walls in this case are smoother and the Pd crystallites are larger. Figures 11e and f contain TEM images of Pd tubes with a 55 nm diameter after varying ripening times. These clearly show that the size of the Pd particles can be controlled by the duration of the ripening process. Larger Pd crystallites, such as those in Figures 11c, d, and f, correspond to a longer ripening time.[66]

5.5. Core-Shell Systems and Quantum-Dot-Containing Nanotubes

The highly variable principle of template wetting makes it possible to provide the nanotube walls with additional

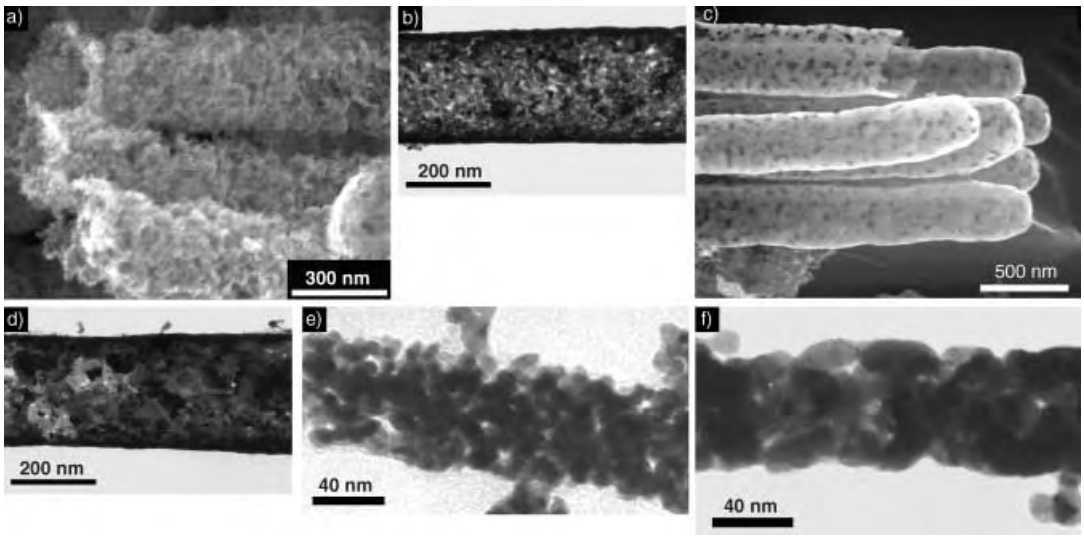


Figure 11. Pd nanotubes with structured walls: SEM (a) and TEM (b) images of nanotubes with a 400 nm diameter and a morphology corresponding to an early ripening state. SEM (c) and TEM (d) images of nanotubes with a 400 nm diameter and a morphology corresponding to a late ripening state. e,f) TEM images of Pd nanotubes with a 55 nm diameter and morphologies corresponding to early (e) and late (f) ripening state. Figure 11c was taken from reference [66].

 © 2004 Wiley-VCH Verlag GmbH & Co. KGaA, Weinheim

functionalities. If the wall material is transformed after template wetting, as described in Section 5.2, such that it has a high rather than a low surface energy, the nanotube walls can be coated through a second wetting step. It should thus be possible to increase the wall thickness in successive 10 nm steps, or to generate hybrid nanotubes with a core-shell morphology.[39] As an example, macroporous silicon was first coated with Pd, which was subsequently wetted with a PS melt in a second step. The resulting microtubes have a core-shell structure in which the PS core is surrounded with a Pd shell (Figure 12). In this way it is possible to produce polymer-metal hybrid nanotubes in which the metal layer's morphology is controllable.[39] This could result in hybrids that have higher mechanical stability than pure metal nanotubes, for example.



Figure 12. TEM image of a tube with a core-shell morphology, which was prepared by consecutive wetting steps. The outer shell is a network of Pd, the inner core consists of PS.

Another interesting possibility for functionalization is the embedding of semiconductor quantum dots in the nanotube walls. Such composite tubes should have interesting optical properties. Their preparation results from the dissolution of a carrier polymer in a colloid suspension of the quantum dots and subsequent template wetting. Light-emitting nanotubes are accessible in this way.[83] This process is particularly attractive because a regular arrangement of these tubes within a two-dimensional photonic crystal may result in hybrid systems, which could have specific emission properties.

6. Potential Applications

If it is possible to produce nanotubes with specific wall morphologies from a large spectrum of materials, very highly promising systems will be available for a plethora of very different applications. These lie in the areas of medicine and pharmaceuticals (tissue engineering, galenics, antifouling), packaging (high-thermal insulation), transport and separation, sensors (gas-, moisture-, and biosensors), chromatography, microreaction technology (nanotubes as microcavities, reaction chambers, and nanopipettes), storage of substances (fuel cells), microelectronics (interlayer dielectrics), electronics (nanocircuits, nanocables, nanocapacitors), and optics (light conduction, nanocapillaries for optical near-field microscopy). The nano- and mesoscale tubes could themselves be used as templates for the preparation of biomimetic nanostructures of a quality that would otherwise not be obtainable by artificial means. Examples of this would be hydroxyapatite, the basis for the formation of hard tissues in mammals (bones, teeth), protein storage, or artificial viruses. Nanotubes with dimensions into the 10 nm range open up undreamed of possibilities as functional units for steering physical and chemical phenomena. Quantum effects can occur, and transport processes and the speed of signal transmission could be controllable on a nanoscale. The concept of template wetting could be an important step toward tailored nanotubes for fundamental research as well as nanotechnology.

We thank the German Science Foundation for financial support (WE 2637/1 und WE 496/19), Böhringer Ingelheim for the supply of polylactide, Dr. P. Göring, J. Choi, K. Nielsch, K. Schwirn, S. L. Schweizer, J. Schilling and S. Matthias for the preparation of templates, M. Hellwig for SEM- and Dr. H. Hofmeister, Dr. A. K. Schaper, and Z. Jia for TEM investigations, and Dr. T. Frese for the use of Figures 1 and 2.

Received: June 3, 2003 [A614]

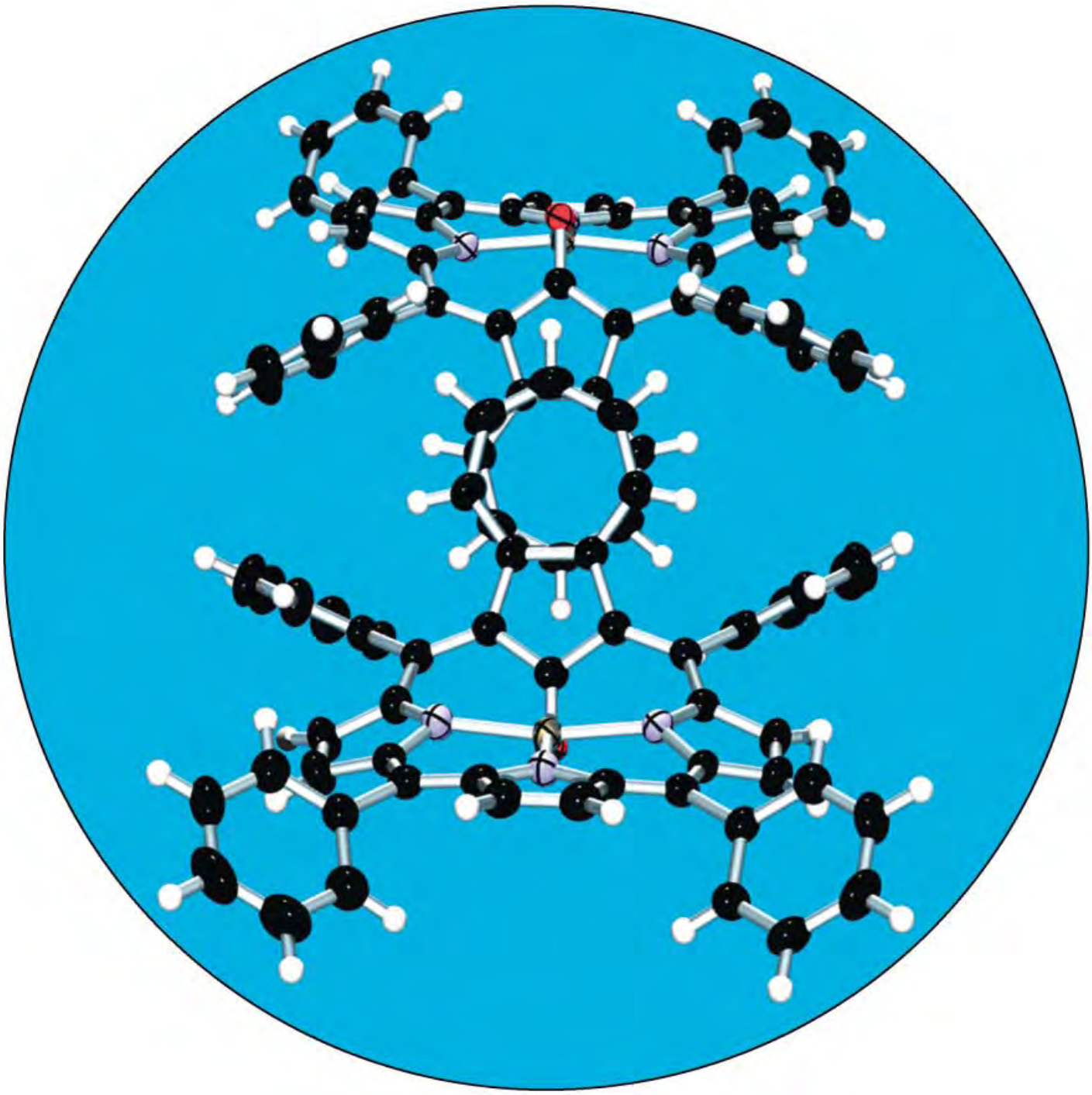
[1] S. Iijima, *Nature* **1991**, *354*, 56.
[2] C. Dekker, *Phys. Today* **1999**, *52*, 22.
[3] M. S. Dresselhaus, G. Dresselhaus, P. Avouris, *Carbon Nanotubes*, Springer, **2000.**
[4] See for example: C. P. Poole, Jr., F. J. Owens, *Introduction to Nanotechnology*, Wiley, New York, **2003**; "Nanotechnologie": *Spektrum der Wissenschaft Spezial*, **2002**, issue 2.
[5] T. W. Ebbesen, P. M. Ajayan, *Nature* **1992**, *358*, 220.
[6] S. Amelinckx, X. B. Zhang, D. Bernaerts, X. F. Zhang, V. Ivanov, J. B. Nagy, *Science* **1994**, *265*, 635.
[7] D. S. Bethune, C. H. Kiang, M. S. de Vries, G. Gorman, R. Savoy, J. Vazquez, R. Beyers, *Nature* **1993**, *363*, 605.
[8] C. Journet, W. K. Maser, P. Bernier, A. Loiseau, M. Lamy de - la Chappelle, S. Lefrant, P. Deniard, R. Lee, J. E. Fischer, *Nature* **1997**, *388*, 756.
[9] A. Thess, R. Lee, P. Nikolaev, H. Dai, P. Petit, J. Robert, C. Xu, Y. H. Lee, S. G. Kim, A. G. Rinzler, D. T. Colbert, G. E. Scuseria, D. Tomanek, J. E. Fischer, R. E. Smalley, *Science* **1996**, *273*, 483.
[10] M. Terrones, N. Grobert, J. Olivares, J. P. Zhang, H. Terrones, K. Kordatos, H. K. Hsu, J. P. Hare, P. D. Townsend, K. Prassides, A. K. Cheetham, H. W. Kroto, D. R. M. Walton, *Nature* **1997**, *388*, 52.
[11] Z. F. Ren, Z. P. Huang, J. W. Xu, J. H. Wang, P. Bush, M. P. Siegal, P. N. Provencio, *Science* **1998**, *282*, 1105.
[12] S. B. Lee, D. T. Mitchell, L. Trofin, T. K. Nevanen, H. Soderlund, C. R. Martin, *Science* **2002**, *296*, 2198.
[13] E. D. Steinle, D. T. Mitchell, M. Wirtz, S. B. Lee, V. Y. Young, C. R. Martin, *Anal. Chem.* **2002**, *74*, 2416.
[14] K. B. Jirage, J. C. Hulteen, C. R. Martin, *Science* **1997**, *278*, 655.
[15] M. Nishizawa, V. P. Menon, C. R. Martin, *Science* **1995**, *268*, 700.
[16] O. G. Schmidt, K. Eberl, *Nature* **2001**, *410*, 168.
[17] J. M. Schnur, *Science* **1993**, *262*, 1669.
[18] E. Evans, H. Brownman, A. Leung, D. Needham, D. Tirell, *Science* **1996**, *273*, 933.
[19] M. Ghadiri, J. R. Granja, R. A. Milligan, D. E. McRee, N. Khazanovich, *Nature* **1993**, *366*, 324.
[20] S. Steward, G. Liu, *Angew. Chem.* **2000**, *112*, 348; *Angew. Chem. Int. Ed.* **2000**, *39*, 340.
[21] G. M. Whitesides, J. P. Mathias, C. T. Seto, *Science* **1991**, *254*, 1312.
[22] C. R. Martin, *Science* **1994**, *266*, 1961.
[23] C. R. Martin, *Adv. Mater.* **1991**, *3*, 457.
[24] R. Parthasarathy, C. R. Martin, *Nature* **1994**, *369*, 298.
[25] C. J. Brumlik, C. R. Martin, *J. Am. Chem. Soc.* **1991**, *113*, 3174.
[26] V. P. Menon, C. R. Martin, *Anal. Chem.* **1995**, *67*, 1920.

 © 2004 Wiley-VCH Verlag GmbH & Co. KGaA, Weinheim

[27] B. Lakshmi, P. K. Dorhoeut, C. R. Martin, *Chem. Mater.* **1997**, *9*, 857.
[28] M. Bognitzki, H. Hou, M. Ishaque, T. Frese, M. Hellwig, C. Schwarte, A. Schaper, J. H. Wendorff, A. Greiner, *Adv. Mater.* **2000**, *12*, 637.
[29] H. Hou, Z. Jun, A. Reuning, A. Schaper, J. H. Wendorff, A. Greiner, *Macromolecules* **2002**, *35*, 2429.
[30] M. Bognitzki, T. Frese, J. H. Wendorff, A. Greiner, *Polym. Prepr. Am. Chem. Soc. Div. Polym. Chem.* **2000**, *82*, 45.
[31] D. H. Reneker, I. Chun, *Nanotechnology* **1996**, *7*, 216.
[32] M. Bognitzki, W. Czado, T. Frese, A. Schaper, M. Hellwig, M. Steinhart, A. Greiner, J. H. Wendorff, *Adv. Mater.* **2001**, *13*, 70.
[33] M. Bognitzki, W. Czado, T. Frese, A. Schaper, M. Hellwig, M. Steinhart, A. Greiner, J. H. Wendorff, *Polym. Eng. Sci.* **2001**, *41*, 982.
[34] R. Dersch, T. Liu, A. Schaper, A. Greiner, J. H. Wendorff, *J. Polym. Sci. Part. A* **2003**, *41*, 545.
[35] Y. Yang, A. J. Heeger, *Nature* **1994**, *372*, 344.
[36] M. Berggren, O. Inganäs, G. Gustafsson, J. Rasmusson, M. R. Andersson, T. Hjertberg, O. Wennerström, *Nature* **1994**, *372*, 444.
[37] J. J. M. Halls, C. A. Walsh, N. C. Greenham, E. A. Marseglia, R. H. Friend, S. C. Moratti, A. B. Holmes, *Nature* **1995**, *376*, 498.
[38] M. Steinhart, J. H. Wendorff, A. Greiner, R. B. Wehrspohn, K. Nielsch, J. Schilling, U. Gösele, *Science* **2002**, *296*, 1997.
[39] M. Steinhart, R. B. Wehrspohn, J. H. Wendorff, *ChemPhysChem*, **2003**, *4*, 1171.
[40] H. W. Fox, E. F. Hare, W. A. Zisman, *J. Phys. Chem.* **1955**, *59*, 1097.
[41] D. Myers, *Surfaces, Interfaces, and Colloids*, Wiley-VCH, New York, **1999**.
[42] S. Wu, *Polymer Interfaces and Adhesion*, Marcel Dekker, New York, **1982**.
[43] P. G. de Gennes, *Rev. Mod. Phys.* **1985**, *57*, 827.
[44] L. Léger, J. F. Joanny, *Rep. Prog. Phys.* **1992**, *55*, 431.
[45] J. C. Berg, *Wettability*, Marcel Dekker, New York, **1993**.
[46] D. Ausserré, A. M. Picard, C. Léger, *Phys. Rev. Lett.* **1986**, *57*, 2671.
[47] J. Israelachvili, *Intermolecular and Surface Forces*, Academic Press, London, **1991**.
[48] W. Barthlott, C. Neinhuis, *Planta* **1997**, *202*, 1.
[49] M. Steinhart, Dissertation, Philipps-Universität Marburg, **2003**.
[50] P. J. Flory, *Principles of Polymer Chemistry*, Cornell University Press, New York, **1953**.
[51] L. Naji, F. Kremer, R. Stannarius, *Liq. Cryst.* **1998**, *24*, 363.
[52] J. W. Diggle, T. C. Downie, C. W. Goulding, *Chem. Rev.* **1969**, *69*, 365.
[53] J. P. O'Sullivan, G. C. Wood, *Proc. R. Soc. London Ser. A* **1970**, *317*, 511.
[54] "Anodised Electrical Condensers und Current Directing Devices": C. Pollak, British Patent No. 933, **1898**.
[55] H. Masuda, K. Fukuda, *Science* **1995**, *268*, 1466.
[56] O. Jessensky, F. Müller, U. Gösele, *Appl. Phys. Lett.* **1998**, *72*, 1173.
[57] K. Nielsch, J. Choi, K. Schwirn, R. B. Wehrspohn, U. Gösele, *Nano Lett.* **2002**, *2*, 677.
[58] J. Choi, K. Nielsch, M. Reiche, R. B. Wehrspohn, U. Gösele, *J. Vac. Sci. Technol. B* **2003**, *21*, 763; H. Masuda, H. Yamada, M. Satoh, H. Asoh, M. Nakao, T. Tamamura, *Appl. Phys. Lett.* **1997**, *71*, 2770.
[59] V. Lehmann, *J. Electrochem. Soc.* **1993**, *140*, 2836.
[60] V. Lehmann, H. Föll, *J. Electrochem. Soc.* **1990**, *137*, 653.
[61] A. Birner, U. Grüning, S. Ottow, A. Schneider, F. Müller, V. Lehmann, H. Föll, U. Gösele, *Phys. Status Solidi A* **1998**, *165*, 111.
[62] J.-N. Chazalviel, F. Ozanam, R. B. Wehrspohn, *J. Electrochem. Soc.* **2002**, *149*, C511.
[63] R. B. Wehrspohn, J. Schilling, *Mater. Res. Bull.* **2001**, *8*, 623.
[64] *Römpp Lexikon Chemie*, Thieme, Stuttgart, **1997**, Elektronische Version of the 10th Edition.
[65] *Ullmann's Encyclopedia of Industrial Chemistry*, Wiley-VCH, 6th ed., Electronic Release, Weinheim, **2002**.
[66] M. Steinhart, Z. Jia, A. Schaper, R. B. Wehrspohn, U. Gösele, J. H. Wendorff, *Adv. Mater.* **2003**, *15*, 706.
[67] C. P. Mehnert, D. W. Weaver, J. Y. Ying, *J. Am. Chem. Soc.* **1998**, *120*, 12289.
[68] Y. Li, X. M. Hong, D. M. Collard, M. A. El-Sayed, *Org. Lett.* **2000**, *2*, 2385.
[69] S. Niwa, M. Eswaramoorthy, J. Nair, A. Raj, N. Itoh, H. Shoji, T. Namba, F. Mizukami, *Science* **2002**, *295*, 105.
[70] S. Kim, M. Kim, W. Y. Lee, T. Hyeon, *J. Am. Chem. Soc.* **2002**, *124*, 7642.
[71] F. Favier, E. C. Walter, M. P. Zach, T. Benter, R. M. Penner, *Science* **2001**, *293*, 2227.
[72] "Hydrogen in Metals III" (Ed.: H. Wipf): *Top. Appl. Phys.* **1997**, *73*.
[73] Y. Luo, I. Szafraniak, V. Nagarjan, R. Wehrspohn, M. Steinhart, J. H. Wendorff, N. D. Zakharov, R. Ramesh, A. Alexe, *Appl. Phys. Lett.* **2003**, *83*, 440.
[74] M. Steinhart, S. Senz, R. B. Wehrspohn, U. Gösele, J. H. Wendorff, *Macromolecules* **2003**, *36*, 3646.
[75] R. A. Jones, L. J. Norton, E. J. Kremer, F. S. Bates, P. Wiltius, *Phys. Rev. Lett.* **1991**, *66*, 1326.
[76] G. Krausch, C. Dai, E. J. Kramer, F. S. Bates, *Ber. Bunsen-Ges.* **1994**, *98*, 446.
[77] L. Sung, A. Karim, J. F. Douglas, C. C. Han, *Phys. Rev. Lett.* **1996**, *76*, 4368.
[78] R. Hasegawa, Y. Takahashi, Y. Chatani, H. Tadokoro, *Polym. J.* **1972**, *3*, 600.
[79] JCPDS-Datenbank, Eintrag 42-1650.
[80] A. J. Lovinger, *J. Polym. Sci. Part B* **1980**, *18*, 739.
[81] J. W. Cahn, *J. Chem. Phys.* **1977**, *66*, 3667.
[82] A. J. Liu, D. J. Durian, E. Herbolzheimer, S. A. Safran, *Phys. Rev. Lett.* **1990**, *65*, 1897.
[83] S. Richter, M. Steinhart, N. Gaponik, A. Eychmüller, H. Hofmeister, R. B. Wehrspohn, J. H. Wendorff, A. Rogach, M. Zacharias, *Chem. Mater.* submitted.

 © 2004 Wiley-VCH Verlag GmbH & Co. KGaA, Weinheim

Communications



Azuliporphyrins are an interesting family of porphyrin-like molecules with an azulene unit replacing one of the usual pyrrole rings. Lash and co-workers demonstrate on the following pages that azuliporphyrins undergo a unique oxidative metalation with copper(II) acetate that leads to 21-oxyazuliporphyrins, novel porphyrinoid ligands that possess an internal carbonyl moiety.

DOI: 10.1002/anie.200353189
© 2004 Wiley-VCH Verlag GmbH & Co. KGaA, Weinheim

Porphyrin Oxidation

Oxidative Metalation of Azuliporphyrins with Copper(II) Salts: Formation of a Porphyrin Analogue System with a Unique Fully Conjugated Nonaromatic Azulene Subunit**

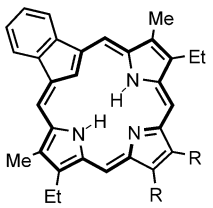
*Denise A. Colby, Gregory M. Ferrence, and Timothy D. Lash**

Carbaporphyrinoids are porphyrin analogues where one or more of the pyrrole subunits has been replaced by carbocyclic rings such as indene or azulene.[1,2] These systems often exhibit unusual spectroscopic and physical properties[3] and may show varying degrees of aromatic character.[4,5] A particularly promising aspect of carbaporphyrinoid chemistry has been the generation of organometallic derivatives using late-transition-block metals such as nickel, palladium, platinum,[6] and silver.[7] However, some attempts at metalation chemistry resulted in the formation of unexpected oxidation products instead.

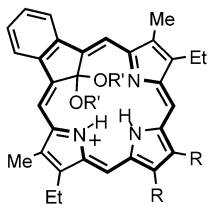
Benzocarbaporphyrins **1** were shown to react with ferric chloride in the presence of various alcohols to afford the benzo[18]annulene ketals **2** in excellent yields,[3] while more recently reaction of nonaromatic tetraphenylbenziporphyrin **3a** with silver(I) acetate was shown to afford the 22-acetoxy derivative **3b**.[8] Our recent studies have focused on the synthesis and chemistry of azuliporphyrins **4** and **5**—carbaporphyrinoids that show intermediary aromatic characteristics.[9–12] Azuliporphyrins react with nickel(II), palladium(II), or platinum(II) salts under mild conditions to afford the corresponding organometallic derivatives (for example, **6**–**8**).[6] We now report that azuliporphyrins **5** give an unusual oxidative metalation with copper(II) acetate to form a new porphyrinoid ligand system with highly modified spectroscopic properties.

Tetraphenylazuliporphyrin **5a**[11,12] reacted with copper(II) acetate in DMF or pyridine at room temperature over a period of 5–10 minutes to afford the green crystalline product **9a** in a 30% yield. Tetrakis(4-chlorophenyl)azuliporphyrin **5b** afforded a similar product **9b** under these conditions. The UV/Vis spectra for **9** were ill-defined with three medium absorptions between 350 and 520 nm. We had anticipated that these derivatives corresponded to the copper(II) complexes **10**. However, high-resolution mass spectrometric analysis demonstrated that an oxygen atom had been incorporated in addition to the copper ion. The electron paramagnetic resonance spectrum for **9a** showed that the metal was present in the copper(II) oxidation state and was coordinated to all three nitrogen atoms. Furuta et al. have shown that N-confused porphyrins react with copper(II) acetate under aerobic conditions to give copper(II) tripyrrinone derivatives where the "confused" ring has been degraded.[13,14] However, our data is consistent with the retention of the full carbaporphyrinoid ring skeleton and the product must therefore differ considerably from the products formed in the study of Furuta et al. The paramagnetic complex cannot be analyzed by NMR spectroscopy, so crystals of **9a** were used for X-ray diffraction analysis. The data obtained demonstrated that a regioselective oxidation of **5a** had occurred at the internal carbon atom to give the copper(II) chelate **9a**.[15]

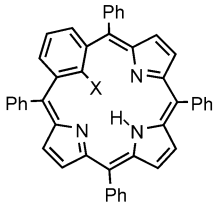
The most striking features of structure **9a** are the presence of an oxygen atom between C(21) and the copper center as well as the dramatic 52.96(3)° dihedral angle between azulene and the mean [18]annulene plane (Figure 1).[16] The latter can be clearly attributed to the steric requirements imposed by the oxygen atom bridging C21 and Cu. Although this is a



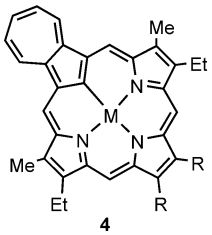
1 R = Et or Ph



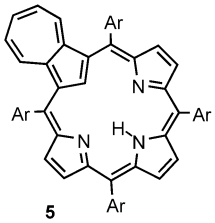
2 R' = Me, Et, *i*Pr, etc.



3 a. X = H; b. X = OAc

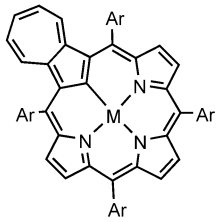


4

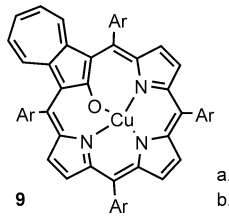


5

a. Ar = Ph
b. Ar = *p*-ClC$_6$H$_4$



6 M = Ni **7** M = Pd
8 M = Pt **10** M = Cu



9

a. Ar = Ph
b. Ar = *p*-ClC$_6$H$_4$

[*] D. A. Colby, Prof. Dr. G. M. Ferrence, Prof. Dr. T. D. Lash
Department of Chemistry
Illinois State University
Normal, IL 61790-4160 (USA)
Fax: (+1) 309-438-5538
E-mail: tdlash@ilstu.edu

[**] Part 32 in the series "Conjugated Macrocycles Related to the Porphyrins". This work was supported by the National Science Foundation under Grant No. CHE-0134472 (to T.D.L), the Petroleum Research Fund, administered by the American Chemical Society (to G.M.F. and T.D.L.), and Pfizer, Inc. (fellowship to D.A.C.). Low-temperature CCD X-ray data were collected by Dr. Robert McDonald at The University of Alberta Structure Determination Laboratory. Part 31: K. Miyake, T. D. Lash, *Chem. Commun.* **2004**, 178–179.

 © 2004 Wiley-VCH Verlag GmbH & Co. KGaA, Weinheim DOI: 10.1002/anie.200353189

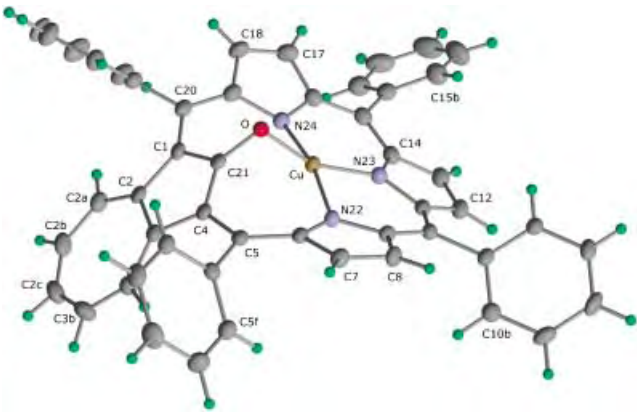
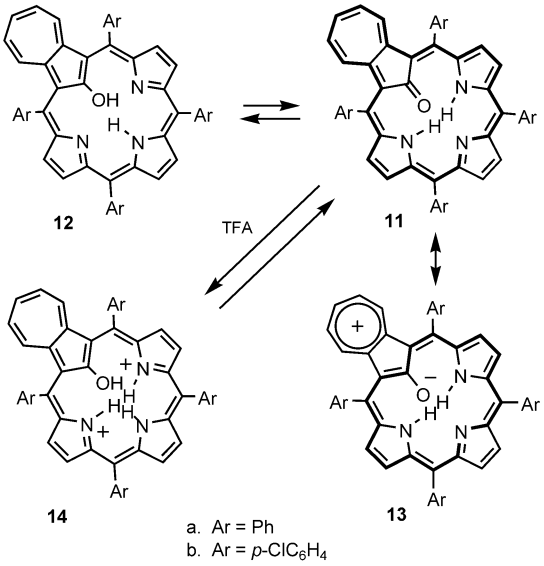


Figure 1. RASTEP drawing (50% probability level) of **9a**, with hydrogen atoms drawn arbitrarily small. Selected bond lengths [Å] and angles [°]: C21-O 1.302(3), C21-Cu 2.474(2), Cu-N23 1.911(2), Cu-O 1.938(2), Cu-N22 1.990(2), Cu-N24 2.003(2); C(21)-O-Cu 97.6(1), N23-Cu-O 157.22(8), N23-Cu-N22 93.56(8), O-Cu-N22 88.05(7), N23-Cu-N24 93.28(8), O-Cu-N24 89.02(8), N22-Cu-N24 168.90(8), N23-Cu-C21 171.33(8), O-Cu-C21 31.44(7), N22-Cu-C21 86.20(8), N24-Cu-C21 85.72(8), O-C21-C1 125(2), O-C21-C4 125.0(2), C1-C21-C4 109.7(2), O-C21-Cu 50.9(1), C1-C21-Cu 112.3(2), C4-C21-Cu 111.9(2), N23-Cu-O-C21 179.5(2).



Scheme 1. Tautomers, resonance contributors, and protonated forms of tetraaryloxyazuliporphyrins **11**.

unique structure, there is some resemblance to nickel(II) and copper(II) octaethylporphyrin *N*-oxides.[15,17] The remainder of the bonding parameters observed in **9a** appear to be routine. The C21–O and Cu–O separations of 1.302(3) and 1.938(2) Å, respectively, are typical for C-O-Cu^{2+} interactions, and the remainder of the macrocycle is distorted from planarity to a lesser extent, as demonstrated by the dihedral angles between the pyrrole rings and the mean [18]annulene plane of 15.8(1), 17.8(1), and 14.3(1)°.

Treatment of **9a** or **9b** with 10% trifluoroacetic acid (TFA)/chloroform afforded excellent yields of the corresponding demetalated 21-oxyazuliporphyrins **11**. The UV/Vis spectrum for free base **11a** showed a strong Soret-like band at 478 nm as well as three weaker absorptions at 554, 603, and 673 nm (Figure 2B). The protonated system formed in 1% TFA/$CHCl_3$ (Scheme 1) exhibited a Soret-like band at 480 nm and a broad far-red absorption centered at 837 nm. Despite the porphyrin-like features of the UV/Vis spectra, the ^{1}H NMR spectrum of **11a** in $CDCl_3$ showed no evidence of significant aromatic character (Figure 2A). Unlike the azuliporphyrin precursor, in which the cycloheptatrienyl protons resonate between $\delta = 6.9$ and 7.7 ppm, the external azulene protons in **11a** are shifted atypically upfield and resonate at $\delta = 5.16$ (2H, d), 5.38 (1H, t), and 5.69 ppm (2H, t). This observation strongly implies that the aromatic character of the azulene unit has been lost. On the other hand, the pyrrolic protons are only shifted upfield by approximately 0.1 ppm relative to the free base of **5a**. Demetalation of **9** could give rise to 21-hydroxyazuliporphyrins **12** or the corresponding keto tautomers **11**. The data is not consistent with **12**, and keto tautomers are generally favored when this type of situation arises in porphyrinoid systems.[3b,18] The ^{13}C NMR data show a carbonyl group at $\delta = 162.8$ ppm, while the IR spectrum of **11a** shows a strong carbonyl absorption at 1524 cm^{-1}. These data suggest that the carbonyl moiety is highly polarized, although strong hydrogen-bonding interactions undoubtedly contribute to the low frequency value observed for the carbonyl stretch. Several delocalization pathways are feasible

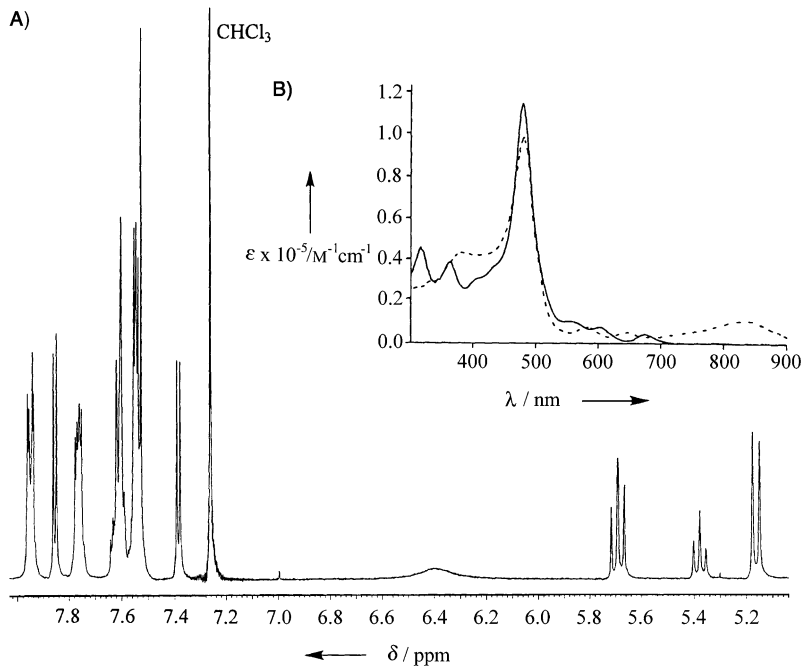


Figure 2. A) 400 MHz ^{1}H NMR spectrum of tetraphenyloxyazuliporphyrin **11a** showing the atypically upfield-shifted resonances for the external azulene protons between 5.1 and 5.7 ppm. B) UV/Vis spectra of ketone **11a** in 1% Et_3N/$CHCl_3$ (bold line, free base) and 1% TFA/$CHCl_3$ (dotted line, dication **14a**).

 © 2004 Wiley-VCH Verlag GmbH & Co. KGaA, Weinheim

for porphyrinoids **11**. The ketone structure has a 24π-electron pathway, and in principle could possess antiaromatic character; however, the upfield shifts seen in the ^{1}H NMR spectra of **11** fall considerably short of the values expected for a species with a paratropic ring current. Alternatively, dipolar resonance contributors such as **13** would provide a porphyrin-like 18π-electron delocalization pathway instead. The latter cannot be a dominant canonical form as the seven-membered ring does not have tropylium ion characteristics as evident from the observed ^{1}H NMR resonances. The unique spectroscopic characteristics of the oxyazuliporphyrin system must arise from a combination of factors and will require more detailed investigation. The ^{1}H NMR spectrum of the corresponding dication **14** in TFA/$CDCl_3$ shows significant diatropic character. The NH protons resonate upfield at $\delta = -0.2$ (1H) and 3.11 ppm (2H), compared to 6.40 ppm for **11**, while the pyrrolic protons show up at approximately 0.5 ppm further downfield than those of the free base. In addition, the azulene protons no longer gave abnormal upfield resonances. It would be expected that protonation would favor a species that resembles the aromatic resonance form **13**. Unfortunately, as with the azuliporphyrins **5**,[11,12] the ^{1}H NMR spectra for the dications are considerably broadened, most likely because of restricted conformational mobility in these crowded structures.

The origin of the oxygen atom in **9** remains to be determined. Mass spectrometric analysis of reactions carried out in the presence of ^{18}O labeled water showed that no ^{18}O was incorporated into the copper(II) complex. In addition, acetate was ruled out as the source of the oxygen because the same complex was formed using $CuCl_2$ instead of $Cu(OAc)_2$, albeit in lower yields.[19] However, our results demonstrate that the azuliporphyrin system holds new and surprising chemical properties and further work in this area is underway. In particular, we have found that oxyazuliporphyrins **11** show some promise as macrocyclic ligands and we have generated stable complexes of **11a** with nickel(II), palladium(II) and platinum(II), cations.

Experimental Section

9a: $Cu(OAc)_2 \cdot H_2O$ (230 mg, 1.16 mmol) (OAc = acetate) was added to a solution of **5a** (64.4 mg, 0.0954 mmol) in pyridine (65 mL) and the resulting mixture stirred under an atmosphere of nitrogen for 5 min. The mixture was diluted with chloroform (60 mL), washed with water (150 mL), and dried over sodium sulfate. The solvents were removed under reduced pressure and the residue purified by column chromatography on Grade 3 alumina eluting with 20% hexanes/dichloromethane. The product was collected as a red fraction. Recrystallization from chloroform-hexanes gave **9a** (21.3 mg, 0.0283 mmol, 30%) as shiny dark-green crystals, m.p. >350°C. UV/Vis ($CHCl_3$): λ_{max} (log ε) = 362 (4.57), 415 (4.62), 508 (4.77), 634 (3.90), 669 nm (3.69); HRMS (EI): calcd for $C_{50}H_{31}CuN_3O$: *m/z* 752.1763; found: 752.1760; elemental analysis (%) calcd for $C_{50}H_{31}CuN_3O \cdot 0.4\,CHCl_3$: C 75.56, H 3.95, N 5.24; found: C 75.46, H 4.14, N 5.26.

21-Oxyazuliporphyrin **11a**: Copper(II) complex **9a** (49.1 mg, 0.0652 mmol) was stirred with 10% TFA/chloroform (50 mL) for 15 min at room temperature. The mixture was washed with water and 5% sodium bicarbonate solution, dried over sodium sulfate, and evaporated to dryness. The residue was purified by column chromatography on Grade 3 alumina eluting with 50% CH_2Cl_2/$CHCl_3$. The demetalated product eluted as a purple band. Recrystallization from $CHCl_3$/hexanes afforded **11a** (40.9 mg, 0.0592 mmol, 91%) as shiny green crystals, m.p. 321–322°C (decomp). UV/Vis (1% Et_3N/$CHCl_3$): λ_{max} (log ε) = 318 (4.66), 363 (4.59), 478 (5.06), 554 (4.03), 603 (3.89), 673 nm (3.64); UV/Vis (1% TFA/$CHCl_3$): λ_{max} (log ε) = 312 (4.42), 337 (4.48), 380 (4.64), 480 (4.99), 579 (3.88), 643 (3.69), 837 nm (4.05); ^{1}H NMR (400 MHz, $CDCl_3$): $\delta = 5.16$ (2H, d, $J = 10.4$ Hz), 5.38 (1H, t, $J = 9.6$ Hz), 5.69 (2H, t, $J = 10.2$ Hz), 6.40 (2H, br s), 7.38 (2H, d, $J = 4.8$ Hz), 7.52 (2H, s), 7.53–7.56 (6H, m), 7.59–7.64 (6H, m), 7.75–7.78 (4H, m), 7.85 (2H, d, $J = 4.8$ Hz), 7.93–7.97 ppm (4H, m); ^{1}H NMR (400 MHz, TFA/$CHCl_3$, dication): $\delta = -0.23$ (1H, br s), 3.11 (2H, v br s), 7.26–7.36 (5H, m), 7.78–7.83 (8H, m), 7.90–7.96 (6H, m), 8.05–8.10 (4H, m), 8.25 (2H, s), 8.30 (2H, br d), 8.32–8.38 ppm (4H, m); ^{13}C NMR (100 MHz, $CDCl_3$): δ = 118.1, 125.8, 126.5, 127.4, 127.6, 128.4, 129.4, 131.0, 131.4, 131.7, 133.5, 134.5, 135.1, 139.5, 140.5, 141.3, 141.6, 144.8, 150.8, 162.8 ppm; HRMS (FAB): calcd for $C_{50}H_{33}N_3O$ + H: *m/z* 692.2702; found: 692.2701; elemental analysis (%) calcd for $C_{50}H_{33}N_3O \cdot CHCl_3$: C 75.51, H 4.22, N 5.18; found: C 75.01, H 4.29, N 5.20.

Received: October 29, 2003 [Z53189]
Published Online: January 27, 2004

Keywords: aromaticity · azulenes · copper · oxidation · porphyrinoids

[1] T. D. Lash in *The Porphyrin Handbook*, *Vol. 2* (Eds.: K. M. Kadish, K. M. Smith, R. Guilard), Academic Press, San Diego, **2000**, pp. 125–199.
[2] T. D. Lash, *Synlett* **2000**, 279–295.
[3] a) M. J. Hayes, J. D. Spence, T. D. Lash, *Chem. Commun.* **1998**, 2409–2410; b) T. D. Lash, M. A. Muckey, M. J. Hayes, D. Liu, J. D. Spence, G. M. Ferrence, *J. Org. Chem.* **2003**, *68*, 8558–8570.
[4] T. D. Lash, S. T. Chaney, D. T. Richter, *J. Org. Chem.* **1998**, *63*, 9076–9088.
[5] a) D. T. Richter, T. D. Lash, *Tetrahedron* **2001**, *57*, 3659–3673; b) J. T. Szymanski, T. D. Lash, *Tetrahedron Lett.* **2003**, *44*, 8613–8616.
[6] a) S. R. Graham, G. M. Ferrence, T. D. Lash, *Chem. Commun.* **2002**, 894–895; b) T. D. Lash, D. A. Colby, S. R. Graham, G. M. Ferrence, L. F. Szczepura, *Inorg. Chem.* **2003**, *42*, 7326–7338.
[7] M. A. Muckey, L. F. Szczepura, G. M. Ferrence, T. D. Lash, *Inorg. Chem.* **2002**, *41*, 4840–4842.
[8] a) M. Stepien, L. Latos-Grazynski, *Chem. Eur. J.* **2001**, *7*, 5113–5117; b) M. Stepien, L. Latos-Grazynski, *Org. Lett.* **2003**, *5*, 3379–3381.
[9] T. D. Lash, S. T. Chaney, *Angew. Chem.* **1997**, *109*, 867–868; *Angew. Chem. Int. Ed. Engl.* **1997**, *36*, 839–840.
[10] S. R. Graham, D. A. Colby, T. D. Lash, *Angew. Chem.* **2002**, *114*, 1429–1432; *Angew. Chem. Int. Ed.* **2002**, *41*, 1371–1374.
[11] D. A. Colby, T. D. Lash, *Chem. Eur. J.* **2002**, *8*, 5397–5402.
[12] T. D. Lash, D. A. Colby, G. M. Ferrence, *Eur. J. Org. Chem.* **2003**, 4533–4548.
[13] H. Furuta, H. Maeda, A. Osuka, *Org. Lett.* **2002**, *4*, 181–184.
[14] However, N-confused porphyrins can also form stable copper(II) organometallic derivatives; see a) P. J. Chmielewski, L. Latos-Grazynski, I. Schmidt, *Inorg. Chem.* **2000**, *39*, 5475–5482; b) H. Maeda, A. Osuka, Y. Ishikawa, I. Aritome, Y. Hisaeda, H. Furuta, *Org. Lett.* **2003**, *5*, 1293–1296; c) H. Maeda, Y. Ishikawa, T. Matsuda, A. Osuka, H. Furuta, *J. Am. Chem. Soc.* **2003**, *125*, 11822–11823.
[15] A μ-hydroxo iron dimer complex of a similar oxo N-confused porphyrin has been reported by Hung et al. The formation of this complex may be mechanistically related to the chemistry

 © 2004 Wiley-VCH Verlag GmbH & Co. KGaA, Weinheim

reported in this communication; see C.-H. Hung, W.-C. Chen, G.-H. Lee, S.-M. Peng, *Chem. Commun.* **2002**, 1516 – 1517.

[16] Crystal data for **9a** ($C_{50}H_{31}CuN_3O$): $M_r = 753.32$, $T = 193(2)$ K, green block, approximate dimensions $0.42 \times 0.12 \times 0.09$ mm^3, monoclinic, space group $P\bar{1}$ (No. 2), $a = 9.374(1)$, $b = 13.750(2)$, $c = 14.681(2)$ Å, $\alpha = 67.209(2)$, $\beta = 87.286(2)$, $\gamma = 86.332(2)°$, $V = 1740.4(3)$ Å^3, $Z = 2$, $\rho_{calcd} = 1.437$ Mg m^{-3}, $\mu = 0.674$ mm^{-1}, $\lambda_{(Mo-K\alpha)} = 0.71073$ Å, $2\Theta_{max} = 52.76°$, 9418 measured reflections, 6948 independent reflections, 496 refined parameters, GOF = 1.022, $R_1 = 0.042$ and $wR_2 = 0.104$ ($F_o^2 > 2\sigma(F_o^2)$), $R_1 = 0.057$ and $wR_2 = 0.110$ (for all data), max./min. residual electron density 0.679/−0.369 e Å^{-3}. Data collection and analysis were performed using standard techniques.[6b] CCDC-222542 contains the supplementary crystallographic data for this paper. These data can be obtained free of charge via www.ccdc.cam.ac.uk/conts/retrieving.html (or from the Cambridge Crystallographic Data Centre, 12, Union Road, Cambridge CB21EZ, UK; fax: (+44) 1223-336-033; or deposit@ccdc.cam.ac.uk).

[17] a) A. L. Balch, Y.-W. Chan, M. M. Olmstead, M. W. Renner, *J. Am. Chem. Soc.* **1985**, *107*, 2393 – 2398; b) A. L. Balch, Y.-W. Chan, M. M. Olmstead, *J. Am. Chem. Soc.* **1985**, *107*, 6510 – 6514.

[18] T. D. Lash, *J. Org. Chem.* **1992**, *57*, 4312 – 4315.

[19] Following the initial submission of this paper, we performed the oxidative metalation of **5a** with $Cu(OAc)_2$ in the presence of $^{18}O_2$. EI-MS shows substantial incorporation of the heavy isotope into the copper complex **9a**. This result demonstrates that the oxygen atom is derived from traces of molecular oxygen. The authors thank Professor C. D. Stevenson for her help in this isotope labeling study and Dr. S. L. Mullen, University of Illinois at Urbana-Champaign, for providing the mass spectrometry data.

 © 2004 Wiley-VCH Verlag GmbH & Co. KGaA, Weinheim

Surface Chemistry

Kinetic and Thermodynamic Control by Chemical Bond Rearrangement on a Si(001) Surface

Chiho Hamai, Akihiko Takagi, Masateru Taniguchi, Takuya Matsumoto, and Tomoji Kawai*

The (2×1)-reconstructed Si(001) surface, where the surface lattice structure undergoes a reconstruction in which adjacent silicon dimers pair together and form dimers through a σ bond and a π bond,[1] is intriguing in that the chemistry at the surface is frequently analogous to that in organic chemistry owing to its covalent nature. Alkenes, for example, are known to bind to silicon dimers on the Si(001) surface to produce four-member ring analogs in a similar way to [2+2] cycloaddition reactions in organic synthesis.[2] The mechanisms of cycloadditions on the surface have also been argued in terms of orbital symmetry in a similar fashion to organic chemistry.[3] However, it seems likely that adsorbate formation and organic synthesis are different in that it is usually difficult to control the product distributions of surface species on the Si(001) surface, that is, the relative efficiencies of specific reactions to side reactions, by changing reaction temperature. The selectivity of reactions has previously been discussed for the adsorption of 1,3-cyclohexadiene,[4] 2,3-dimethyl-1,3-butadiene,[5] and unsaturated ketones[6] on the Si(001) and Ge(001) surfaces. Those studies have investigated whether the degree of selectivity is determined by thermodynamic or by kinetic factors. However, the conversion from kinetically controlled reactions into thermodynamically controlled ones for the same organic compound by means of heating has not been observed on the Si(001) surface to date. This may be because the binding of organic molecules to the silicon surface is usually strong, which makes reactions irreversible.

Herein we report that the driving force that determines the product distribution for acetone adsorbed on the Si(001) surface can be changed from kinetic to thermodynamic by reversible binding upon raising the surface temperature. The results presented are of interest not only because controlling the degree of selectivity is of importance for future applications of organic-functionalized semiconductors, but also because it is found that the binding of organic molecules to the Si(001) surface is in fact reversible.

Figure 1 depicts two bonding configurations of a four-member-ring and a dissociation species which are produced when the acetone molecules are adsorbed on the Si(001) surface.[7] The relative efficiencies of the two reactions shown in Figure 1 were investigated using scanning tunneling microscopy (STM) in the surface temperature range from 340 K to 440 K (Figure 2a and b). Two separate features labeled A and B are visible in Figure 2, although their ratio differs between the images (see below). The A-type feature is a protrusion which appears to be centered above a silicon dimer. The B-type feature has a protrusion and a depression on a silicon dimer. It is suggested that these two features can be attributed to the four-member-ring and the dissociation species depicted

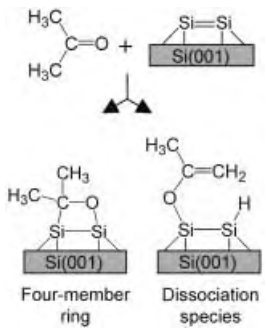


Figure 1. Reactions of acetone with the Si(001) surface. The molecules are bound to the surface to give a mixture of the four-member-ring and dissociation species.[7]

[*] Dr. C. Hamai, Dr. A. Takagi, Dr. M. Taniguchi, Dr. T. Matsumoto, Prof. Dr. T. Kawai
Institute of Scientific and Industrial Research
Osaka University
8-1 Mihogaoka, Ibaraki, Osaka 567-0047 (Japan)
Fax: (+81) 6-6875-2440
E-mail: matsumoto@sanken.osaka-u.ac.jp

Supporting information for this article is available on the WWW under http://www.angewandte.org or from the author.

 DOI: 10.1002/anie.200352074 © 2004 Wiley-VCH Verlag GmbH & Co. KGaA, Weinheim

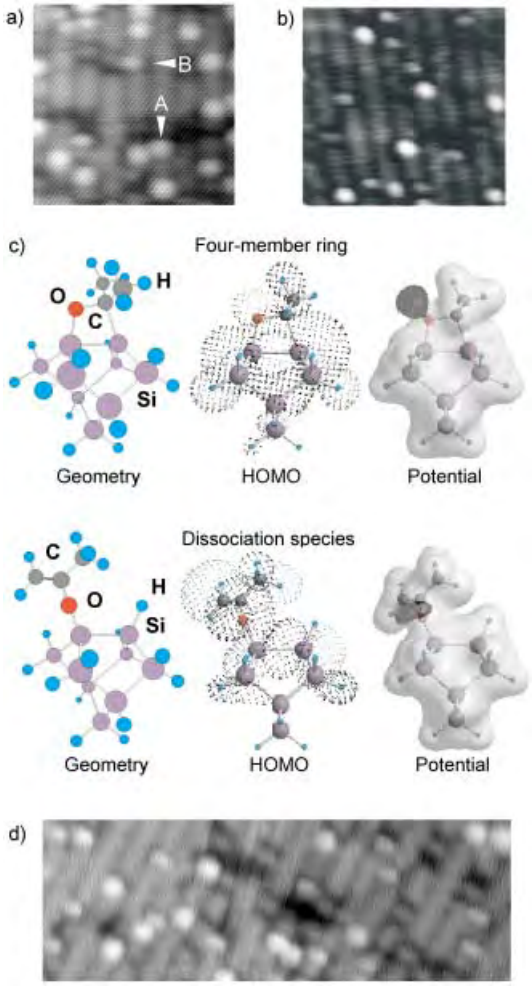


Figure 2. a), b) STM images obtained by exposing Si(001) samples at a) 365 K and b) 440 K to 0.3 L of acetone. The images were acquired with a tunneling current of 0.10 nA and a sample bias of −3.0 V. c) Optimized geometries, probability amplitudes of the HOMO, and electrostatic potentials. Gray and black surfaces for the electrostatic potentials show a difference in plus and minus signs for differential of the potentials. d) STM image obtained after annealing the sample at 420 K.

in Figure 1. Although the images in Figure 2a and b were taken with a sample bias of −3.0 V, it was found that the A-type and B-type features also had similar appearances at a sample bias of −2.0 V. With a sample bias of −2 V, the H–Si bond is imaged more darkly than intact silicon dimers on the Si(001) surfaces.[8] Therefore, it is expected that the dark image in the B-type features can be attributed to the Si–H group in the dissociation species. The A-type features can then be ascribed to the four-member ring.

STM images reflect the local density of states which exist near the Fermi level and tunneling barrier of a sample surface.[9] Therefore, the highest occupied molecular orbital (HOMO) and the electrostatic potentials were calculated using density functional theory (DFT) for the acetone molecules bound to the $[Si_9H_{12}]$ clusters shown in Figure 2c. This procedure was used to confirm the assignment of the A-type and B-type features which were observed in the filled-state images at negative sample biases. Figure 2c shows the optimized geometries, the probability amplitudes of the HOMO, and the electrostatic potentials calculated for the two surface species. The contour surfaces of the HOMO and the electrostatic potential for the four-member ring protrude over the adsorption site, which is in good agreement with the STM images of the A-type features where a protrusion is observed on a silicon dimer. On the other hand, the Si–H group in the dissociation species has a reduced HOMO density and an electrostatic potential which is lower than those for the entire four-member ring and for the vinyl ether group in the dissociation species (Figure 2c), which is in good agreement with the STM images of the B-type features where dark and bright halves are observed on a silicon dimer (Figure 2a, b). Comparison with previous STM studies on the hydrogen-atom-terminated Si(001) surface[8] and calculations of the HOMO and the electrostatic potential both support the idea that the A-type and B-type features are associated with the four-member-ring and the dissociation species, respectively.

In the images in Figure 2a and b, it can be seen that adsorption at 365 K produces predominantly in the four-member-ring species and adsorption at 440 K predominantly the dissociation species. To elucidate the connection between the product distribution and the reaction temperature, the product ratios were examined for Si(001) samples exposed to the compound at 340, 365, 380, 400, and 440 K. Figure 3a shows the distributions of the observed surface species, that is, the ratios of the four-member-ring: the dissociation species: the unidentified species. The relative efficiency of the dissociation reaction is enhanced when the reaction temperature is raised.

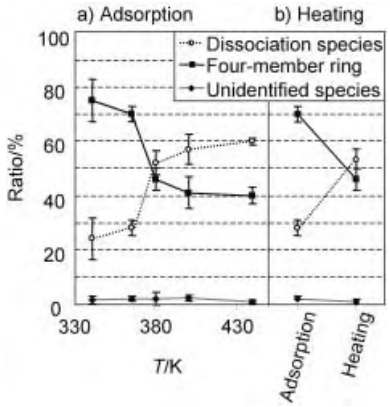


Figure 3. Product distributions of the four-member-ring, the dissociation species, and the unidentified species. The data were obtained by counting 440–1010 adsorbates in the STM images. a) The distributions for the Si(001) samples exposed to 0.3 L of acetone at various temperatures. b) The distributions for the Si(001) sample exposed to acetone at 365 K (left, adsorption) and subsequently annealed to 420 K (right, heating).

The surface species formed on the Si(001) surface were annealed to see whether the reactions were reversible. Figure 2d shows an image which was obtained by heating the Si(001) sample at 420 K for 90 s after it had been exposed to 0.3 L (1.0×10^{-8} Torr·30 s) of acetone at 365 K. Comparing

 © 2004 Wiley-VCH Verlag GmbH & Co. KGaA, Weinheim

the image in Figure 2d with that in Figure 2a, it can be seen that annealing to 420 K leads to an increase in the dissociation species. Figure 3b shows the product distribution before and after annealing to 420 K. The counting statistics show that successive heating at 420 K varies the ratio of dissociation species:four-member ring from 28:70 to 46:53, which reveals that the acetone molecules bound to the surface undergo changes upon subsequent heating. This result indicates that the reactions are reversible. Additionally, the STM images show that annealing at 420 K does not significantly alter the total coverage of the molecules. Exposing the Si(001) sample at 365 K to acetone resulted in coverages of 0.08 and 0.02 molecules per dimer for the four-member ring and the dissociation species, respectively, while subsequent heating at 420 K resulted in coverages of 0.04 and 0.06 molecules per dimer for the four-member ring and the dissociation species, respectively. The successive heating therefore appears not to decrease the sum of the coverages, which suggests that desorption of the molecules does not occur upon annealing.

To understand the energetics of the adsorption, the DFT calculations were carried out using the $[Si_9H_{12}]$ cluster models. The calculations predict that the adsorption energies of the four-member-ring and the dissociation species are 34.6 kcal mol^{-1} and 43.1 kcal mol^{-1}, respectively. The results of the calculations which show that the cycloaddition species is less stable than the dissociation species can be explained by the formation of a strained four-member ring in the cycloaddition reaction. Based on the experimental and computational data, it seems that the major surface species is changed from an energetically unfavorable species to an energetically favorable one when the reaction temperature is increased.

Since the experimental data suggest that the reactions are reversible, it is possible to consider that the adsorption is kinetically controlled at a low temperature and thermodynamically controlled at a high temperature. Kinetic control preferentially provides the less stable species, that is, the four-member ring at low temperature, if the activation energy for the cycloaddition is smaller than that for the dissociation. On the other hand, thermodynamic control gives rise to the dissociation species in preference to the four-member-ring species at high temperature, if the activation energy for the reverse reaction of dissociation is larger than that for the reverse reaction of cycloaddition. Because the STM images show that the desorption of the surface species does not explain the temperature dependence of the product distribution, it is expected that the conversion between the four-member ring and the dissociation species takes place via intermediates which are weakly bound to the surface (Figure 4). It seems that the rearrangement of chemical bonds via the intermediate on the surface enables competition between the kinetic and thermodynamic dominance. Using DFT calculations, it has recently been proposed that carbonyl compounds react with the Si(001) surface via a precursor in which the carbonyl oxygen center binds to the surface silicon atom through a dative bond.[10] Thus, the studies presented herein imply that the precursor, theoretically predicted in the recent reports, connects the cycloaddition reaction with the dissociation reaction on the potential energy surface.

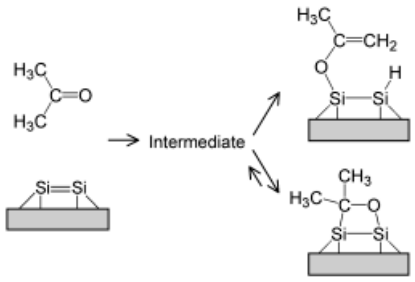


Figure 4. Adsorption mechanism. Conversion between the four-member rings and the dissociation species via intermediate formation accounts for the reversible binding.

In conclusion, we have found evidence that it is possible to control the product distribution on the Si(001) surface by changing the determinant factor from kinetic to thermodynamic control, which is a result of the reversible binding of the surface species. These results suggest approaches for future applications to increase the degree of selectivity in the attachment of organic molecules to the Si(001) surface.

Experimental Section

All experiments were performed in an ultrahigh vacuum (UHV) system with a base pressure of 5×10^{-11} Torr. Clean Si(001) surfaces (1–10 ohm cm resistivity, B-doped) were prepared by a published method.[11]. Acetone (Aldrich, 99.9+% purity) was subjected to several freeze–pump–thaw cycles prior to introduction into the UHV chamber. The temperatures of the samples were measured with an infrared optical pyrometer, followed by calibration using a thermocouple attached to an identical test sample. Exposures are expressed in Langmuir units ($1\ L = 1 \times 10^{-6}$ Torr s). The DFT calculations were performed for the acetone molecules bound to the $[Si_9H_{12}]$ clusters which have one exposed silicon dimer, using Gaussian 98 (B3LYP hybrid DFT method and 6-31+G(d) basis sets).[12]

Received: June 6, 2003
Revised: November 28, 2003 [Z52074]

Keywords: adsorption · kinetics · reaction mechanisms · silicon · thermodynamics

[1] a) H. N. Waltenburg, J. T. Yates, Jr., *Chem. Rev.* **1995**, *95*, 1589; b) J. D. Chadi, *Phys. Rev. Lett.* **1987**, *59*, 1961.
[2] a) U. Birkenheuer, U. Gutdeutsch, N. Rösch, A. Fink, S. Gokhale, D. Menzel, P. Trischberger, W. Widdra, *J. Chem. Phys.* **1998**, *108*, 9868; b) F. Matsui, H. W. Yeom, I. Matsuda, T. Ohta, *Phys. Rev. B* **2000**, *62*, 5036; c) G. P. Lopinski, D. J. Moffatt, D. D. M. Wayner, R. A. Wolkow, *J. Am. Chem. Soc.* **2000**, *122*, 3548; d) R. J. Hamers, J. S. Hovis, S. Lee, H. Liu, J. Shan, *J. Phys. Chem. B* **1997**, *101*, 1489; e) J. M. Buriak, *Chem. Rev.* **2002**, *102*, 1271.
[3] Q. Liu, R. Hoffmann, *J. Am. Chem. Soc.* **1995**, *117*, 4082.
[4] J. S. Hovis, H. Liu, R. J. Hamers, *J. Phys. Chem. B* **1998**, *102*, 6873.
[5] C. H. Choi, M. S. Gordon, *J. Am. Chem. Soc.* **1999**, *121*, 11311.
[6] G. T. Wang, C. Mui, C. B. Musgrave, S. F. Bent, *J. Am. Chem. Soc.* **2002**, *124*, 8990.
[7] See Supporting Information.
[8] a) D. Lin, R. Chen, *Phys. Rev. B* **1999**, *60*, R8461; b) M. Dürr, Z. Hu, A. Biedermann, U. Höfer, T. F. Heinz, *Phys. Rev. Lett.* **2002**, *88*, 46104.

 © 2004 Wiley-VCH Verlag GmbH & Co. KGaA, Weinheim

[9] R. J. Hamers, D. F. Padowitz in *Scanning Tunneling Microscopy and Spectroscopy* (Ed.: D. A. Bonnell), Wiley, New York, **2001**, pp. 59–110.
[10] a) J. A. Barriocanal, D. J. Doren, *J. Am. Chem. Soc.* **2001**, *123*, 7340; b) G. T. Wang, C. Mui, C. B. Musgrave, S. F. Bent, *J. Phys. Chem. B* **2001**, *105*, 12559; c) G. T. Wang, C. Mui, C. B. Musgrave, S. F. Bent, *J. Am. Chem. Soc.* **2002**, *124*, 8990.
[11] R. Akiyama, T. Matsumoto, T. Kawai, *Phys. Rev. B* **2000**, *62*, 2034.
[12] a) Gaussian 98 (Revision A.7), M. J. Frisch, G. W. Trucks, H. B. Schlegel, G. E. Scuseria, M. A. Robb, J. R. Cheeseman, V. G. Zakrzewski, J. A. Montgomery, R. E. Stratmann, J. C. Burant, S. Dapprich, J. M. Millam, A. D. Daniels, K. N. Kudin, M. C. Strain, O. Farkas, J. Tomasi, V. Barone, M. Cossi, R. Cammi, B. Mennucci, C. Pomelli, C. Adamo, S. Clifford, J. Ochterski, G. A. Petersson, P. Y. Ayala, Q. Cui, K. Morokuma, D. K. Malick, A. D. Rabuck, K. Raghavachari, J. B. Foresman, J. Cioslowski, J. V. Ortiz, A. G. Baboul, B. B. Stefanov, G. Liu, A. Liashenko, P. Piskorz, I. Komaromi, R. Gomperts, R. L. Martin, D. J. Fox, T. Keith, M. A. Al-Laham, C. Y. Peng, A. Nanayakkara, C. Gonzalez, M. Challacombe, P. M. W. Gill, B. G. Johnson, W. Chen, M. W. Wong, J. L. Andres, M. Head-Gordon, E. S. Replogle, J. A. Pople, Gaussian, Inc., Pittsburgh, PA, **1998**; b) A. D. Becke, *J. Chem. Phys.* **1993**, *98*, 1372; c) C. Lee, W. Yang, R. G. Parr, *Phys. Rev. B* **1988**, *37*, 785.

 © 2004 Wiley-VCH Verlag GmbH & Co. KGaA, Weinheim

Monolayers

Covalently Attached Monolayers on Hydrogen-Terminated Si(100): Extremely Mild Attachment by Visible Light**

Qiao-Yu Sun, Louis C. P. M. de Smet, Barend van Lagen, Andrew Wright, Han Zuilhof, and Ernst J. R. Sudhölter*

A "holy grail" in the attachment of monolayers on surfaces involves the use of ambient conditions that are compatible with a wide variety of functional groups. Such conditions would, for example, allow for the direct covalent attachment of many bioactive materials to a surface. In the field of covalently attached monolayers to well-defined Si surfaces presently reported attachment methods include thermal conditions and UV irradiation.[1–5] Although such reaction conditions yield stable[6,7] and densely packed monolayers,[8,9] they are too harsh to allow the use of labile bioactive materials. This situation has two ways out: In the first route, one attaches a precursor to the surface that can stand such harsh conditions, which is subsequently transformed into the bioactive monolayer. Such an approach has been taken by, for example, Hamers and co-workers,[10,11] and in the elegant DNA attachment studies of Horrocks, Houlton and co-workers.[11,13] The second route would make use of mild reaction conditions that are, in principle, compatible with such bioactive moieties. In the case of porous silicon, such an approach has been taken by Buriak and Stewart through either the use of a white-light-promoted reaction[14] or a hydride-abstracting agent.[15] Recently, Hamers reported the visible light (514 nm)-initiated modification of flat Si(111) and Si(001) surfaces by partial iodination.[16]

Herein, we further develop this second route by the formation of densely packed covalently attached monolayers by using a variety of unsaturated compounds on well-defined Si(100)–H (i.e., hydrogen-terminated) surfaces by visible light (447 nm) at room temperature. Angle-resolved X-ray photoelectron spectroscopy (ARXPS) and contact-angle measurements were used to evaluate the monolayers in detail.

Figure 1 shows the gradual formation of a hexadecyl monolayer upon irradiation of Si(100)–H wafers in the presence of 1-hexadecene. The water contact angle obtained after ≥ 10 h is 110°, which is comparable with the best literature values.[17]

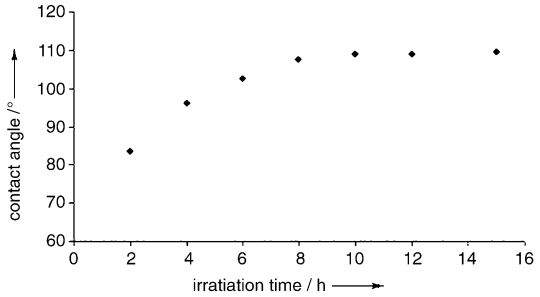


Figure 1. Static water contact angle of a hexadecyl monolayer on a hydrogen-terminated Si(100) surface as function of irradiation time (447 nm).

Table 1 lists the static water contact angle of the surfaces modified by a variety of 1-alkenes, 1-alkynes, and two ω-esterified-1-alkenes (compounds **I**, and **II**) by using this mild procedure, together with the corresponding results of the thermal radical reaction.[17] These results indicate that visible-light attachment yields monolayers with properties similar to those obtained from thermal radical reactions,[18] without the disadvantage of requiring a high temperature (165 °C). This has also been confirmed by using attenuated total reflection infra red (ATRIR) spectroscopy, which provided clear peaks for, for example, the antisymmetric and symmetric CH_2

[*] Dr. Q.-Y. Sun, L. C. P. M. de Smet, B. van Lagen, Dr. H. Zuilhof, Prof. Dr. E. J. R. Sudhölter
Laboratory of Organic Chemistry
Wageningen University
Dreijenplein 8, 6703 HB Wageningen (The Netherlands)
Fax: (+31) 317-484-914
E-mail: han.zuilhof@wur.nl
A. Wright
Thermo VG Scientific
The Birches Industrial Estate
Imberhorne Lane, East Grinstead RH19 1UB (UK)

[**] We thank the research school VLAG, the Netherlands Technology Foundation STW and the Human Frontier Science Program for financial support, and Cees Heijboer and Dr. Richard White (Thermo), and Dr. Klaus Simon (ASML) for stimulating discussions. Finally, we are thankful to a referee for constructive suggestions towards improvements of the manuscript.

 © 2004 Wiley-VCH Verlag GmbH & Co. KGaA, Weinheim DOI: 10.1002/anie.200352137

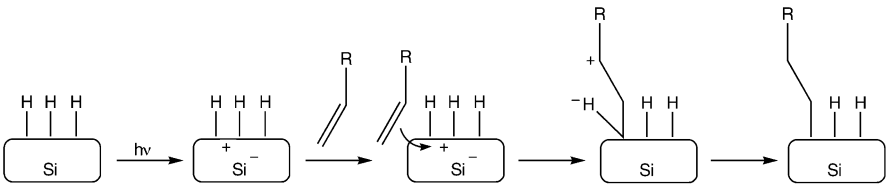
Table 1: Static water contact angles of monolayers on silicon surfaces prepared by the visible-light-initiated and thermal method.[a]

Reactants	Photochemical reaction	Thermal reaction
$CH{=}C\text{-}C_{10}H_{21}$	108	108[b]
$CH{=}C\text{-}C_{12}H_{25}$	110	110[b]
$CH{=}C\text{-}C_{14}H_{29}$	110	110[b]
$CH_2{=}CH\text{-}C_{10}H_{21}$	109	108[b]
$CH_2{=}CH\text{-}C_{12}H_{25}$	108	108[b]
$CH_2{=}CH\text{-}C_{14}H_{29}$	109	108[c]
$CH_2{=}CH\text{-}C_8H_{16}COOCH_3$ (**I**)	78	77[c]
$CH_2{=}CH\text{-}C_8H_{16}COOCH_2CF_3$ (**II**)	85	88[c]

[a] All experiments were performed at least twice; experimental error = ±1°. [b] Data taken from reference [17]. [c] Value obtained by using conditions as described in reference [17].

stretching vibrations. The precise position of the antisymmetric CH_2 stretching vibration ($2921.7 \pm 0.1\ cm^{-1}$ for monolayers derived from 1-hexadecene, and $2921.5 \pm 0.1\ cm^{-1}$ for those obtained photochemically from 1-hexadecyne), suggests a comparable quality as obtained for thermally prepared monolayers (≈ 2920–$2922\ cm^{-1}$).

Up to now, photoinduced hydrosilylation of unsaturated hydrocarbons onto H-terminated flat silicon surfaces had only been reported with UV light. The mechanism for UV-induced hydrosilylation involves photolytic homolysis of a surface Si–H bond, for example, a radical-induced reaction. Based on the Si–H bond dissociation energy on a silicon surface, a wavelength of shorter than 350[19–22]–380 nm[23] is necessary to obtain surface silicon radicals on H-terminated flat Si(111), which implies that a radical-based initiation is not in operation during the visible-light-promoted hydrosilylation reaction described here. Stewart, Buriak, and co-workers proposed an alternative mechanism to explain the white-light-promoted hydrosilylation of photoluminescent nanocrystalline silicon.[14,15] We hypothesize that this mechanism, perhaps rephrased in terms of surface plasmons,[24] depicted in Scheme 1, is also active here. If this mechanism is operative,



Scheme 1. Proposed mechanism for the hydrosylilation of Si(100)–H with 447 nm light.

it is expected—based on findings of Hamers and co-workers for the photo attachment of alkenes on partly iodine-terminated Si(111) and Si(001)[16]—that the required reaction time to obtain densely packed monolayers depends on the dopant concentration. This has indeed been found: after 5 h Si(100)–H with low dopant concentration (p- or n-type) yields contact angles $\approx 100°$. However, heavily doped p-type Si(100)–H is much harder to modify, and yields after 5 h a contact angle of $\approx 90°$, and after 10 h of only 104°, in line with the effects of the dopant on the band bending.

Fluorine-containing alkenyl esters were synthesized and photoattached to Si(100)–H wafers. Thus obtained monolayers of $CH_2{=}CHC_{13}H_{26}CO_2CH_2CF_3$ (**III**)[25] were analyzed by X-ray photoelectron spectroscopy (XPS), a very useful tool for the study of covalently attached monolayers on silicon.[10,11,16,19,22,26–34] Figure 2 shows the C_{1s}, F_{1s}, and Si_{2p}

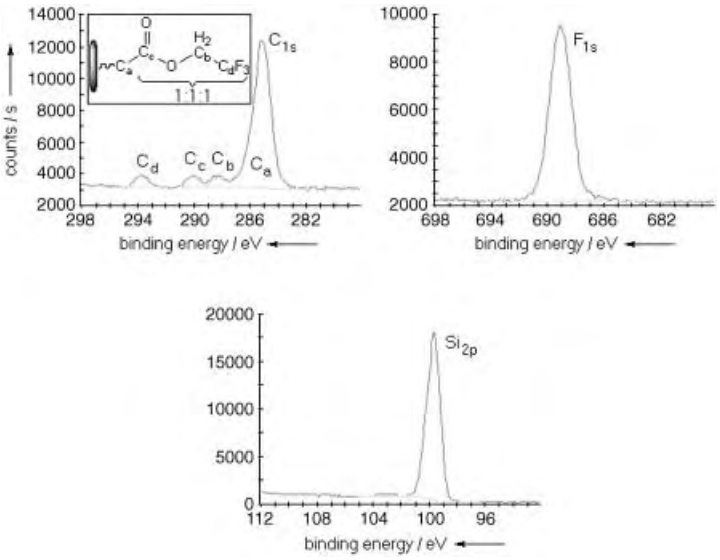


Figure 2. X-ray photoelectron region spectra of a monolayer of compound **III** on Si(100)–H prepared by the method of visible-light-induced hydrosilylation.

regions of the resulting XPS spectrum. The C_{1s} region spectrum shows peaks from 288 to 294 eV, which can be assigned to the different carbons in the trifluoroethyl ester moiety.[10] The presence of $C_{1s}D$ (294 eV) and F_{1s} (689 eV) signals indicates that a trifluoroethyl ester-terminated monolayer was formed on the Si(100)–H surface. Additionally, the silicon spectrum shows very little oxidation of the surface as evidenced by the small signal in the 101–103 eV region. The results are comparable to those obtained with UV light (254 nm) to attach the trifluoroethyl ester of undecylenic acid onto the Si(111)–H surface.[10]

An important issue in the preparation of surfaces for the application in sensor technology is the control over the amount and depth distribution of sensing functionalities in mixed monolayers. To study the relation between the ratio of two 1-alkenes in the solution and their relative amounts in the resulting mixed monolayer, mixed monolayers of compounds **I** and **II** were prepared. Figure 3 shows that the amount of F atoms (as measured by XPS) of the mixed monolayers increases linearly with an increasing molar fraction of compound **II** in the alkene solution from which the samples were prepared. This result implies that one can obtain a surface that can easily be defined by solution properties. Such a relation has previously been proposed based on indirect fluorescence labeling.[35]

 © 2004 Wiley-VCH Verlag GmbH & Co. KGaA, Weinheim

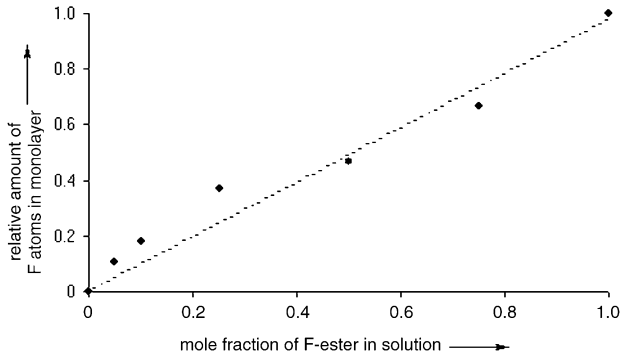


Figure 3. Linear correlation of the amount of F atoms in the photochemically prepared monolayers as function of the mole fraction of trifluoroethyl ester **II** in mixed solutions.

Since the diameter of the probe molecule—rhodamine—is larger than that of an alkyl spacer, it is unlikely that the observed linearity from a 0% to a 100% rhodamine-substituted monolayer can be attributed to a linearly changing composition of constant monolayer thickness/packing density of a densely packed monolayer. In addition, ATRIR has been used to study to the ratio of the ester carbonyl stretch to the total methylene asymmetric stretch as a function of the mole fraction of ethyl undec-1-enylate in 1-decene.[36] Although qualitatively in line with the present finding, quantification of monolayer IR data is harder than that of XPS data. The value of XPS was, for example, shown by detailed analysis of mixed monolayers of **III** with 1-hexadecene. The fluorine probe works well since quantitative XPS allows one to obtain the amount of F atoms of the surface directly for the total concentration range, while the constant packing density of the monolayer of both thermally and photochemically prepared monolayers could be ascertained from the $C_{1s}A$ signal.

Apart from with conventional XPS, the monolayers were also studied with parallel angle-resolved XPS (ARXPS) by using a 2D microchannel detector (MCD) that measures the intensity of the photoelectron emission as a function of emission angle. As a result the angle-resolved data are acquired simultaneously (Figure 4, top). This MCD permits ARXPS experiments without tilting the sample, and with a concomitantly constant analysis area for all detection angles. As a result, unparalleled resolution can be obtained with respect to the distribution of depths of the elements on the surface. Figure 4 (bottom) depicts a relative depth profile of such a mixed monolayer of compound **III**, for a monolayer of only 1.4 nm total thickness. To the best of our knowledge, this is the first report of an ARXPS-based relative depth profile on an ultrathin organic monolayer. The relative depth profile locates bulk Si at the bottom (Si_{2p}), subsequently the Si peak of Si atoms bound to O ($Si_{2p}Ox$), and the corresponding O atoms ($O_{1s}A$). Then the carbon-atom signals of the alkyl spacer and the oxygen-atom signals of the ester are found ($C_{1s}A$ and $O_{1s}B$), while on top the signals are found for $C_{1s}D$ and F_{1s} that belong to the CF_3 group (data for intermediate $C_{1s}B$ and $C_{1s}C$ are not shown). Signals for F_{1s} appear lower than $C_{1s}D$ owing to trace amounts of unresolved F atoms bound to the Si surface, which result from the etching step.

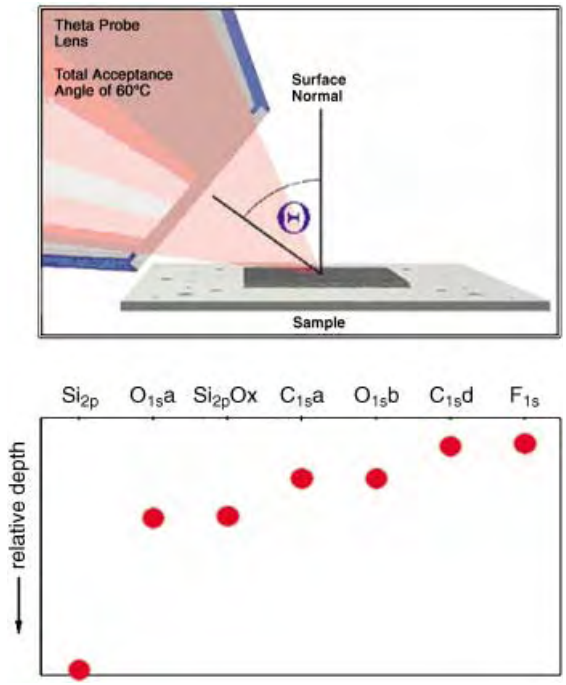


Figure 4. Schematic representation of the two-dimensional detection system (top), and relative depth profile of the elements of a Si sample modified by compound **III** (bottom).

We reported for the first time a visible-light induced reaction for attaching functional monolayers onto the Si(100)–H surface. According to the water contact angle the quality of monolayers derived in this way is as good as that of monolayers obtained by the thermal reaction. High-resolution ARXPS was used to provide detailed information about the depth distribution of the elements in the monolayer. Furthermore, it was shown by quantitative XPS that for appropriately sized functional groups, the surface composition can be easily defined by the solution composition. The combination of these techniques opens an attractive avenue for the attachment and characterization of (bio)active functionalization of monolayers on silicon,[37] including a variety of lithographic techniques.

Experimental Section

Materials: Single-polished Si(100): n-type, 500–550 μm thick, resistivity 1–2 Ωcm (Seltec Silicon, Mitsubishi Silicon America), p-type, 375 μm thick, resistivity 1–2 Ωcm (Bayer Solar Freiberg, Germany), p-type, 475 μm thick, resistivity 0.015–0.025 Ωcm (Okmetic Inc., USA). Other chemicals and purifications as in references.[7,17]

XPS and ARXPS measurements: XPS and ARXPS analyses were performed on a Theta Probe (Thermo VG Scientific, UK) by using a monochromatic $Al_{K\alpha}$ X-ray source with a 400 μm spot runs at 100 W under UHV conditions. The higher-resolution XPS data in Figure 2 were acquired in standard (non angle-resolving) mode by using scanned spectra at a pass energy of 100 eV. The snapshot mode of acquisition was used for the ARXPS data. This acquires spectral data across the full detector width at a fixed analyzer energy. The ARXPS snapshot spectra were acquired from 500×1 s frames at a pass energy of 150 eV. Sixteen angles were measured in the range of 23–83°. The relative surface sensitivity for a particular chemical species was determined by calculating the ratio of the sum of the

 © 2004 Wiley-VCH Verlag GmbH & Co. KGaA, Weinheim

relevant peak areas at three bulk-sensitive angles (23–35°) and the sum of the equivalent peak areas at three surface-sensitive angles (65–75°).

Monolayer preparation: Si(100) samples were cleaned in piranha solution (H_2SO_4:H_2O_2 = 2:1) at 90 °C for 2 h, and subsequently etched by using 2.5 % HF for 2 min. The alkene solution was flushed with N_2 for 30 min before and for 30 min after putting the fresh Si(100)–H wafer into the solution, before the light was turned on. The visible-light-initiated reaction was performed by irradiation of a wafer-containing 0.1 M solution of 1-alkene/1-alkyne in mesitylene with monochromatic 447 nm light (phosphor-coated pen lamp from Jelight Company, model 84-247-2, 32 nm bandwidth, $\approx 3\ mW\,cm^{-2}$ intensity at 2 cm) from 0.5 cm for 15 h under a N_2 atmosphere. Afterwards, the surface was excessively rinsed with PE40/60, EtOH and CH_2Cl_2.

Received: June 13, 2003
Revised: October 27, 2003 [Z52137]

Keywords: hydrosilylation · monolayers · photochemistry · silicon · X-ray photoelectron spectroscopy

[1] J. M. Buriak, *Chem. Rev.* **2002**, *102*, 1271.
[2] D. D. M. Wayner, R. A. Wolkow, *J. Chem. Soc. Perkin Trans. 1* **2002**, *2*, 23.
[3] A. B. Sieval, R. Linke, H. Zuilhof, E. J. R. Sudhölter, *Adv. Mater.* **2000**, *12*, 1457.
[4] M. Zarnikov, A. Küller, A. Shaporenko, E. Schmidt, W. Eck, Langmuir **2003**, *19*, 4682.
[5] A. Küller, W. Eck, V. Stadler, W. Geyer, A. Gölzhäuser, Appl. Phys. Lett. **2003**, *82*, 3776
[6] M. R. Linford, P. E. Fenter, P. M. Eisenberger, C. E. D. Chidsey, *J. Am. Chem. Soc.* **1995**, *117*, 3145.
[7] A. B. Sieval, A. L. Demirel, J. W. M. Nissink, M. R. Linford, J. H. van der Maas, W. H. de Jeu, H. Zuilhof, E. J. R. Sudhölter, *Langmuir* **1998**, *14*, 1759.
[8] A. B. Sieval, B. van den Hout, H. Zuilhof, E. J. R. Sudhölter, *Langmuir* **2000**, *16*, 2987.
[9] A. B. Sieval, B. van den Hout, H. Zuilhof, E. J. R. Sudhölter, *Langmuir* **2001**, *17*, 2172.
[10] T. Strother, W. Cai, X. S. Zhao, R. J. Hamers, L. M. Smith, *J. Am. Chem. Soc.* **2000**, *122*, 1205.
[11] Z. Lin, T. Strother, W. Cai, X. P. Cao, L. M. Smith, R. J. Hamers, *Langmuir* **2002**, *18*, 788.
[12] A. R. Pike, L. H. Lie, R. A. Eagling, L. C. Ryder, S. N. Patole, B. A. Connolly, B. R. Horrocks, A. Houlton, *Angew. Chem.* **2002**, *114*, 637; *Angew. Chem. Int. Ed.* **2002**, *41*, 615.
[13] A. R. Pike, S. N. Patole, N. C. Murray, T. Ilyas, B. A. Connolly, B. R. Horrocks, A. Houlton, *Adv. Mater.* **2003**, *15*, 254.
[14] M. P. Stewart, J. M. Buriak, *J. Am. Chem. Soc.* **2001**, *123*, 7821.
[15] J. M. Schmeltzer, L. A. Porter, M. P. Stewart, J. M. Buriak, *Langmuir* **2002**, *18*, 2971.
[16] W. Cai, Z. Lin, T. Strother, L. M. Smith, R. J. Hamers, *J. Phys. Chem. B* **2002**, *106*, 2656.
[17] A. B. Sieval, R. Opitz, H. P. A. Maas, M. G. Schoeman, G. Meijer, F. J. Vergeldt, H. Zuilhof, E. J. R. Sudhölter, *Langmuir* **2000**, *16*, 10359.
[18] A. B. Sieval, V. Vleeming, H. Zuilhof, E. J. R. Sudhölter, *Langmuir* **1999**, *15*, 8288.
[19] R. I. Cicero, M. R. Linford, C. E. D. Chidsey, *Langmuir* **2000**, *16*, 5688.
[20] J. Terry, M. R. Linford, C. Wigren, R. Y. Cao, P. Pianetta, C. E. D. Chidsey, *Appl. Phys. Lett.* **1997**, *71*, 1056.
[21] J. T. C. Wojtyk, M. Tomietto, R. Boukherroub, D. D. M. Wayner, *J. Am. Chem. Soc.* **2001**, *123*, 1535.
[22] R. Boukherroub, S. Morin, F. Bensebaa, D. D. M. Wayner, *Langmuir* **1999**, *15*, 3831.
[23] F. Effenberger, G. Gotz, B. Bidlingmaier, M. Wezstein, *Angew. Chem.* **1998**, *110*, 2651; *Angew. Chem. Int. Ed.* **1998**, *37*, 2462.
[24] W. L. Barnes, A. Dereux, T. W. Ebbesen, *Nature* **2003**, *424*, 824.
[25] The synthesis of compound **III** will be published elsewhere.
[26] A. Bansal, X. L. Li, S. I. Yi, W. H. Weinberg, N. S. Lewis, *J. Phys. Chem. B* **2001**, *105*, 10266.
[27] J. F. Zhang, C. Q. Cui, T. B. Lim, E. T. Kang, K. G. Neoh, S. L. Lim, K. L. Tan, *Chem. Mater.* **1999**, *11*, 1061.
[28] W. F. Bergerson, J. A. Mulder, R. P. Hsung, X. Y. Zhu, *J. Am. Chem. Soc.* **1999**, *121*, 454.
[29] N. Y. Kim, P. E. Laibinis, *J. Am. Chem. Soc.* **1998**, *120*, 4516.
[30] E. J. Lee, T. W. Bitner, J. S. Ha, M. J. Shane, M. J. Sailor, *J. Am. Chem. Soc.* **1996**, *118*, 5375.
[31] L. Hong, H. Sugimura, T. Furukawa, O. Takai, *Langmuir* **2003**, *19*, 1966.
[32] M. R. Linford, C. E. D. Chidsey, *Langmuir* **2002**, *18*, 6217.
[33] A. B. Sieval, R. Linke, G. Heij, G. Meijer, H. Zuilhof, E. J. R. Sudhölter, *Langmuir* **2001**, *17*, 7554.
[34] T. L. Niederhauser, G. L. Jiang, Y. Y. Lua, M. J. Dorff, A. T. Woolley, M. C. Asplund, D. A. Berges, M. R. Linford, *Langmuir* **2001**, *17*, 5889.
[35] F. Wei, X. S. Zhao, *Thin Solid Films* **2002**, *408*, 286.
[36] R. Boukherroub, D. D. M. Wayner, *J. Am. Chem. Soc.* **1999**, *121*, 11513.
[37] L. C. P. M. de Smet, G. A. Stork, G. H. F. Hurenkamp, Q.-Y. Sun, H. Topal, P. J. E. Vronen, A. B. Sieval, A. Wright, G. M. Visser, H. Zuilhof, E. J. R. Sudholter, *J. Am. Chem. Soc.* **2003**, *125*, 13916.

 © 2004 Wiley-VCH Verlag GmbH & Co. KGaA, Weinheim

Glycoprotein Variants

Modular Assembly of Glycoproteins: Towards the Synthesis of GlyCAM-1 by Using Expressed Protein Ligation**

Derek Macmillan and Carolyn R. Bertozzi*

Glycosylation is a vital protein modification for the normal growth and development of organisms.[1] However, establishing the biological significance of specific covalently bound

[*] Dr. D. Macmillan
School of Chemistry, University of Edinburgh
Kings Buildings, West Mains Road
Edinburgh, EH9 3JJ (GB)
Fax: (+44) 131 650 4743
E-mail: derek.macmillan@ed.ac.uk

Prof. C. R. Bertozzi
Center for New Directions in Organic Synthesis
Departments of Chemistry and Molecular and Cell Biology and
Howard Hughes Medical Institute, University of California
Berkeley, CA 94720 (USA)

[**] The center for New Directions in Organic Synthesis is supported by Bristol–Myers Squibb as Sponsoring Member and Novartis as Supporting Member. The authors acknowledge financial support from The National Science Foundation and the BBSRC.

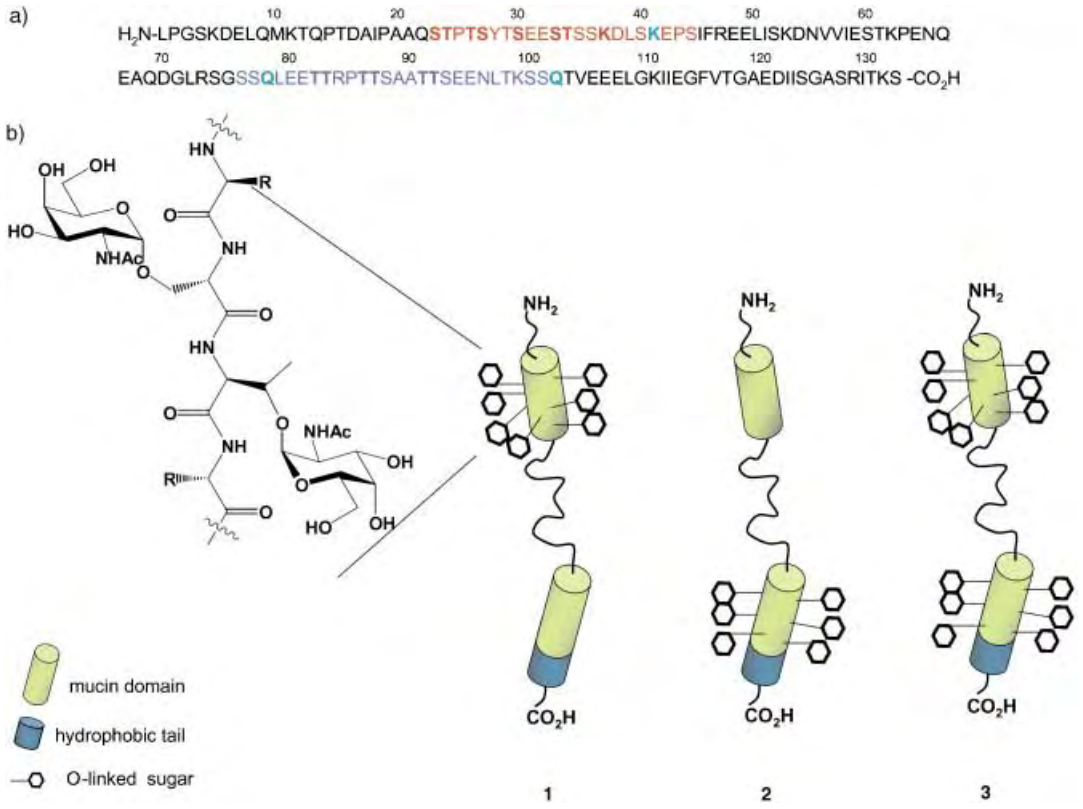
Supporting information for this article (synthetic procedures, HPLC traces, and ESI-MS data) is available on the WWW under http://www.angewandte.org or from the author.

 DOI: 10.1002/anie.200352673 © 2004 Wiley-VCH Verlag GmbH & Co. KGaA, Weinheim

oligosaccharides is difficult owing to glycoprotein microheterogeneity,[2] a phenomenon arising from the fact that protein glycosylation is not under direct genetic control. Consequently, a single glycoprotein can exist as a complex mixture of glycosylated forms termed "glycoforms" and analytical difficulties arising from this property have been a driving force for the development of new methods for the synthesis of glycoproteins with predefined oligosaccharides. Although bacteria lack the protein-glycosylation machinery of mammalian cells, they can be employed to express large quantities of recombinant proteins which allows subsequent chemical modifications to be monitored by using standard biophysical techniques.[3] More recently it has been shown that non-native N-linked glycans can be assembled in *Escherichia coli* after transformation with the N-linked glycosylation apparatus from *Campylobacter jejuni* and raises the possibility of glycan engineering in bacteria.[4] Furthermore, bacteria can produce useful protein fragments such as C-terminal thioesters which can be used in convergent protein-coupling techniques, such as native chemical ligation[5] and expressed protein ligation (EPL).[6] Glycoprotein assembly is particularly suited to EPL since synthetically derived glycopeptides[7] can be fused with bacterially derived protein fragments of large molecular weight to give glycoproteins.[8]

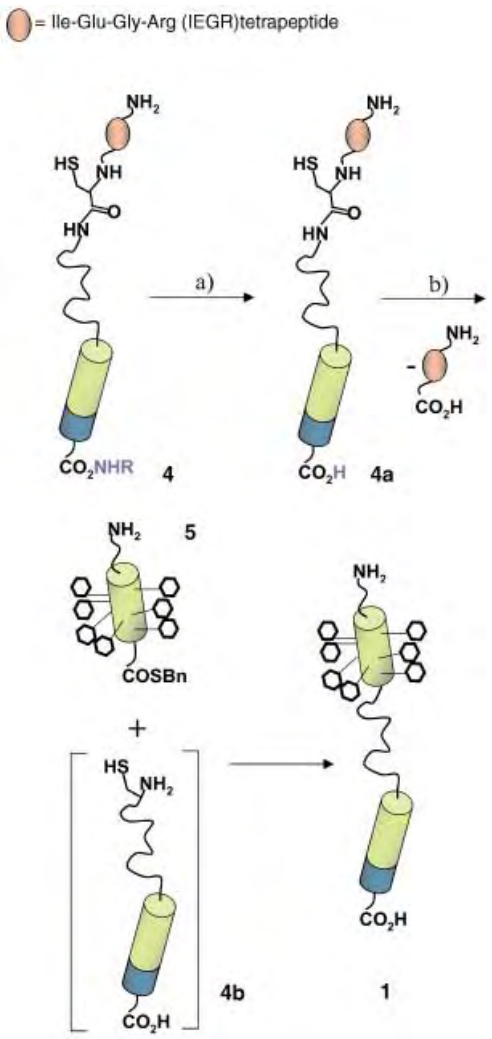
We have focused our efforts on GlyCAM-1, a mucin-like glycoprotein that functions as a ligand for the leukocyte adhesion molecule L-selectin. GlyCAM-1 comprises two mucin domains separated by a central, unglycosylated domain (Scheme 1). The mucin domains, which consist of clustered oligosaccharides characterized by α-*O*-glycosidic linkages between *N*-acetyl galactosamine (GalNAc) and the hydroxy groups of Ser/Thr residues of the protein backbone, are important for binding L-selectin through a 6-sulfo sialyl Lewis^X motif.[9] We aim to study the relevance of O-linked glycosylation to the structure and function of GlyCAM-1 through the synthesis of three separate semisynthetic variants: **1** contains the N-terminal mucin domain, **2** has a glycosylated C-terminal mucin domain, and **3** is glycosylated in both mucin domains (see Scheme 1). In this study we produced glycosylated forms of these targets with single GalNAc residues at the sites of glycosylation. It is possible to elaborate these GalNAc residues enzymatically[10] to generate fully functional GlyCAM-1.

First, we set out to prepare glycoform **1** from a synthetic glycopeptide thioester and a bacterially derived protein fragment. The unglycosylated GlyCAM-1 protein fragment **4** comprising GlyCAM-1 residues 41–132 (Scheme 2) was expressed from the commercially available IMPACT CN intein-fusion vector (pTYB-1).[8a] After cleavage from the intein-chitin binding domain (CBD) fusion protein with dithiothreitol (DTT, 50 mM), the target polypeptide **4a** was readily isolated in 5–10 mg quantities from one litre of bacterial cell culture and characterized by SDS-PAGE and LC-MS. A factor Xa protease recognition peptide, Ile-Glu-Gly-Arg (IEGR), was included as a protecting group for a



Scheme 1. a) Amino acid sequence of GlyCAM-1. The mucin domains are highlighted in red and blue and sites at which O-linked GalNAc was incorporated are shown in bold. Amino acid substitutions (to cysteine) were conducted at positions highlighted in green; b) target GlyCAM-1 glycoforms for semisynthesis by using expressed protein ligation.

 © 2004 Wiley-VCH Verlag GmbH & Co. KGaA, Weinheim



Scheme 2. Assembly of glycoform **1**. a) 50 mM DTT, 100 mM $NaHPO_3$; pH 8.0, 100 mM NaCl; b) Factor Xa protease, 5 mM $CaCl_2$, 100 mM $NaHPO_3$; pH 8.0, 100 mM NaCl, 2% MESNA. R = intein-CBD fusion protein, DTT = 1,4-dithiothreitol, MESNA = 2-mercaptoethanesulfonic acid.

latent N-terminal cysteine residue to prevent reaction with the intermediate peptide α-thioester formed during the cleavage of the intein-CBD fragment. The IEGR sequence was readily cleaved from precursor **4a** to form **4b** by using factor Xa protease, which liberated the N-terminal cysteine residue for subsequent ligation. In practice, the IEGR sequence was cleaved in situ and **4b** was not isolated. With recombinant peptide **4a** in hand, we embarked on the synthesis of glycopeptide **5** corresponding to the N-terminal mucin domain of GlyCAM-1.

The synthesis of glycopeptide α-thioester **5** was particularly challenging since seven glycoamino acids in close proximity had to be installed. The synthesis was conducted by using the 4-sulfamylbutyryl resin, as described by Shin et al.,[11] employing five equivalents of amino acid in each coupling step, and HBTU/HOBt (HBTU = *O*-benzotriazol-1-yl-*N*,*N*,*N*′,*N*′-tetramethyluronium-hexafluoro-phosphate, HOBt = 1-hydroxybenzotriazole) as the coupling reagents. The coupling time was seven hours for glycoamino acid building blocks Fmoc-Thr(α-*O*-GalNAc$(OAc)_3$-OH and Fmoc-Ser(α-*O*-GalNAc$(OAc)_3$-OH (Fmoc = 9-fluorenylmethyloxycarbonyl).[12] After synthesis, the resin was activated for cleavage by alkylation with iodoacetonitrile, and release of the fully protected glycopeptide α-thioester was effected with benzyl mercaptan and catalytic NaSPh.[13] After TFA-mediated (TFA = trifluoroacetic acid) removal of the remaining peptide backbone protecting groups, ether precipitation, and HPLC purification, the synthetic glycopeptide thioester **5** was obtained and characterized by electrospray mass spectrometry (Figure 1).

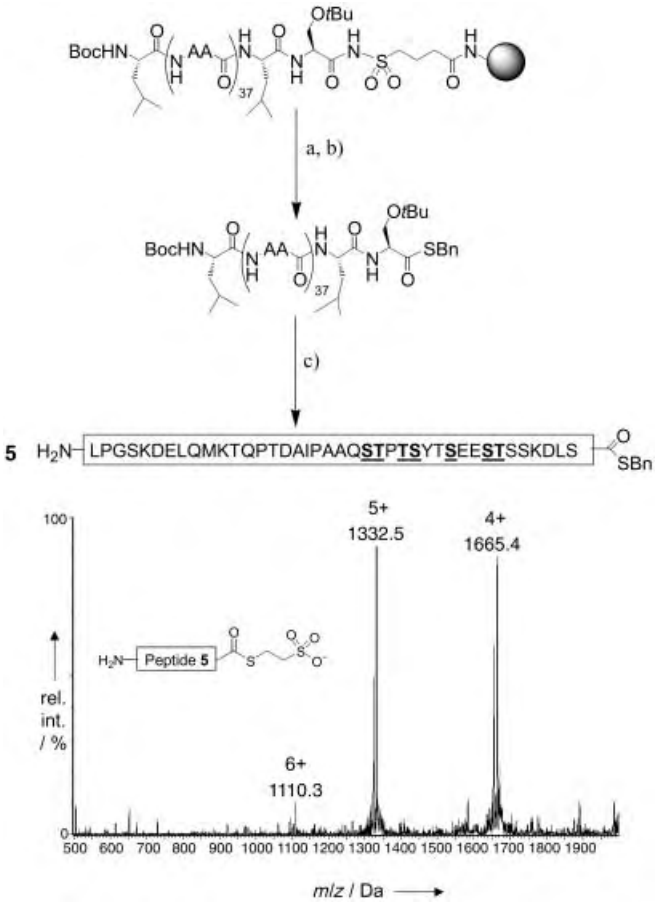


Figure 1. Synthesis and MS characterization of glycopeptide thioester **5**. Glycoamino acids were incorporated at positions indicated in bold, underlined type. a) ICH_2CN, DIPEA, DMF, 16 h; b) BnSH, NaSPh, THF, 16 h; c) 85% TFA, 5% EDT, 5% thioanisole, 5% H_2O, 4 h. 10% overall yield based on resin loading. Calculated mass (MESNA thioester) = 6654.8 Da, observed mass = 6656.9 Da. DIPEA, *N*,*N*-diisopropylethylamine; EDT = 1,2-ethanedithiol.

The ligation reaction between the fragments **4b** and **5** was carried out under nondenaturing conditions and was usually complete within 48 hours; the reaction was monitored by using LC-MS and was quantitative with respect to the limiting reagent (synthetic thioester). Excess reagents could also be recovered and nonspecific proteolysis was not observed. After ligation, the 21 acetyl esters originally present on the GalNAc residues of glycopeptide **5** were removed by using

 © 2004 Wiley-VCH Verlag GmbH & Co. KGaA, Weinheim

2% aqueous hydrazine to afford the target glycoprotein **1** (Figure 2) on a multimilligram scale. Note that the promiscuity of factor Xa for sequences similar to IEGR is well documented and this "one-pot" factor Xa cleavage and ligation procedure is likely to be protein dependant to some degree.

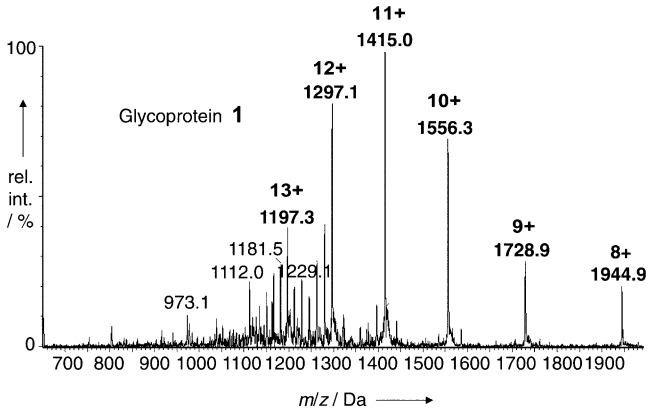
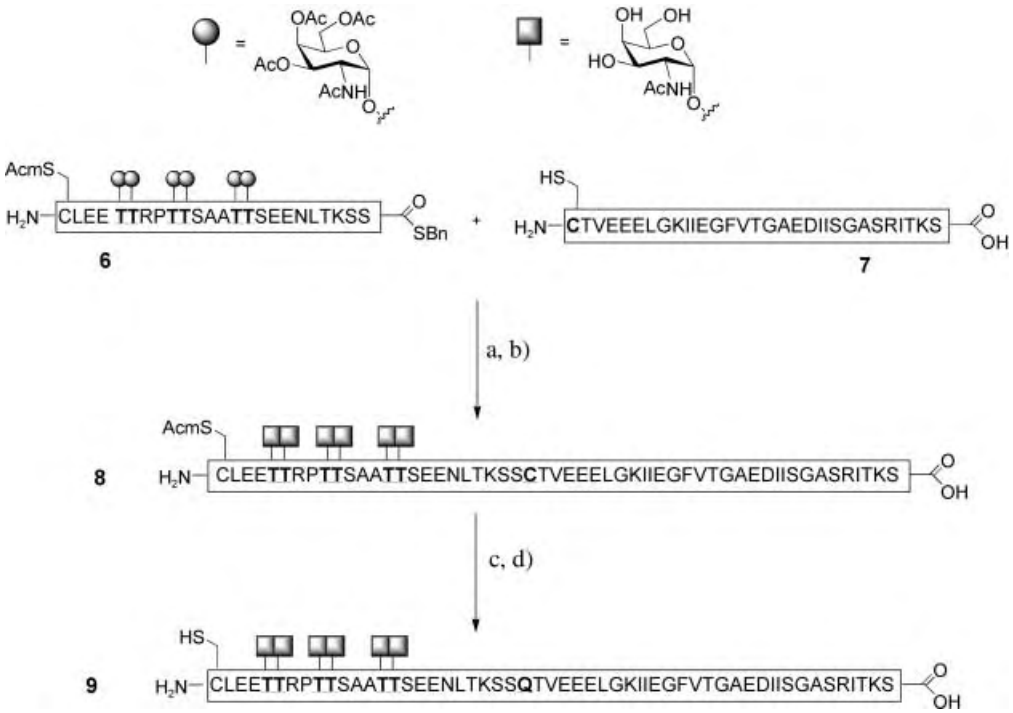


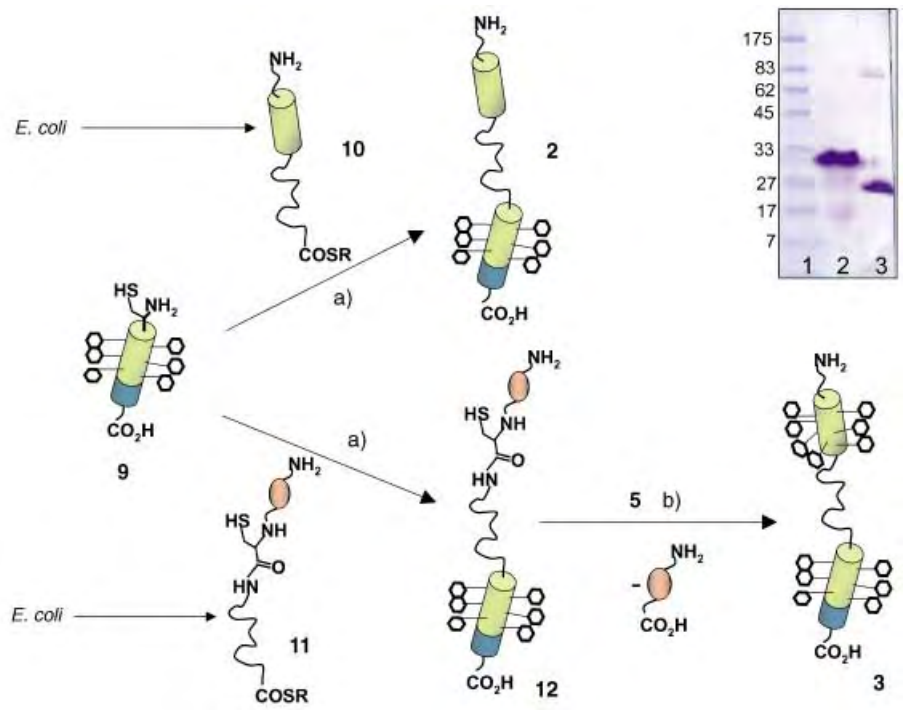
Figure 2. Electrospray MS analysis of HPLC purified glycoform **1**, calculated mass = 15550.3 Da, observed mass = 15550 Da.

The synthesis of glycoform **2** required a reversal of the above strategy, that is, a bacterially derived thioester and a synthetic glycopeptide bearing an N-terminal cysteine residue. Glycopeptide **9** (Scheme 3) was prepared in two sections that were joined by native chemical ligation. This approach was chosen since the C-terminal peptide was particularly hydrophobic, which hampered monitoring of the glycoamino acid coupling reactions by using the Kaiser ninhydrin test. Residues 78–101 (**6**) comprising the mucin domain were prepared as described above for thioester **5** except the N-terminal cysteine was temporarily protected with an *S*-acetamidomethyl group that was stable to the conditions required for cleavage from the resin. This thioester was then ligated to C-terminal residues 102–132 (**7**), prepared by standard Fmoc-based solid-phase peptide synthesis (SPPS) on NovaSyn-TGT resin, by native chemical ligation in sodium phosphate buffer (pH 8.0) and in the presence of 4% MESNA. The reaction was complete after 36 h, and following HPLC purification, the internal cysteine residue was capped by treatment with iodoacetamide added to a final concentration of 10 mM for 0.5 hours. The capping of this cysteine residue appeared essential for acceptable reaction rates and yields in subsequent ligations. Glycopeptide **8** was then purified by semipreparative HPLC and finally dissolved in 10% acetic acid. Upon overnight treatment with Hg^{II} acetate and excess 1,4-dithiothreitol (DTT) under argon, the desired C-terminal glycopeptide **9** was obtained (calculated molecular weight = 7067.4 Da, observed molecular weight = 7067.7 Da). This synthetic glycopeptide was then ligated to the bacterially derived thioester **10**[8a] (Scheme 4). The ligation was performed in sodium phosphate buffer (100 mM, pH 8.0) and yielded 25% (determined by HPLC) of the desired glycoform **2** with an observed molecular weight of 15510 Da (calculated molecular weight = 15509.7 Da). Though low yielding, the product and unreacted glycopeptide could be copurified by HPLC and resubjected to bacterially derived thioester **10** to drive the reaction to completion. In practice this ligation was conducted a total of three times to obtain reasonable yields (> 70%, determined by LC-MS) and



Scheme 3. Synthesis of the C-terminal mucin domain **9**. a) 200 mM $NaHPO_3$ buffer; pH 8.0, 4% MESNA, 24 h; b) 5% hydrazine hydrate, 10% DTT, 2 h; c) 2.5 mM iodoacetamide, 10 mM $NaHPO_3$ buffer; pH 8.0, 1 h; d) $Hg(OAc)_2$, 10% AcOH, 50 mM DTT, 16 h.

 © 2004 Wiley-VCH Verlag GmbH & Co. KGaA, Weinheim



Scheme 4. Schematic representation of the semisynthetic assembly of glycoforms **2** and **3**. a) 2% MESNA, 100 mM $NaHPO_3$; pH 8.0, 100 mM NaCl; b) Factor Xa protease, 5 mM $CaCl_2$, 100 mM $NaHPO_3$; pH 8.0, 100 mM NaCl, 2% MESNA. Analysis by coomassie blue stained gel electrophoresis (inset) 1) molecular weight markers; 2) glycoform **3**; 3) full-length unglycosylated GlyCAM-1.[16]

conducting this ligation under denaturing conditions may aid future attempts.

Glycoform **3** was then prepared by ligation of synthetic glycopeptide **9** to bacterially derived peptide thioester **11**[8a] resulting in intermediate **12** with an observed molecular weight of 11731.5 Da (calculated molecular weight = 11732.3 Da). As for the synthesis of glycoform **2**, this ligation reaction proceeded sluggishly and in low yield but could be driven to completion by copurification of **9** and **12** and resubjection of the mixture to bacterial thioester **11** as above. Intermediate **12** was then converted into glycoform **3** in the same manner as for the synthesis of glycoform **1** (Scheme 2). Finally, GlyCAM-1 has no native cysteine residues, therefore additional cysteine residues introduced for ligations (Cys41 for **1**, and Cys78 for **2**) were capped to resemble glutamine residues[14] in quantitative yield (determined by LC-MS) within 0.5 hours by the addition of iodoacetamide to glycoprotein samples.

In summary, we have applied protein semisynthesis to the preparation of three defined GlyCAM-1 glycoforms with as many as 13 *N*-acetylgalactosamine residues at predetermined positions. There have been a few recent reports of the application of native chemical ligation to the total synthesis of glycoproteins.[15] However, this is the first demonstration of the modular assembly of a physiologically relevant glycoprotein by using the expressed protein ligation technology and serves as a platform for the launch of biological investigations which will be reported in due course.

Received: August 18, 2003 [Z52673]

Keywords: expressed protein ligation · glycopeptides · glycoproteins · protein engineering · semisynthesis

[1] a) A. Varki, *Glycobiology* **1993**, *3*, 97; b) R. A. Dwek, *Chem. Rev.* **1996**, *96*, 683; c) A. Helenius, M. Aebi, *Science* **2001**, *291*, 2364; d) R. G. Spiro, *Glycobiology* **2002**, *12*, 43R.

[2] R. S. Rush, P. L. Derby, D. M. Smith, C. Merry, G. Rogers, M. F. Rohde, V. Katta, *Anal. Chem.* **1995**, *67*, 1442.

[3] B. G. Davis, *Chem. Rev.* **2002**, *102*, 579.

[4] M. Wacker, D. Linton, P. G. Hitchen, M. Nita-Lazar, S. M. Haslam, S. J. North, M. Panico, H. R. Morris, A. Dell, B. W. Wren, M. Aebi, *Science* **2002**, *298*, 1790.

[5] P. E. Dawson, S. B. H. Kent, *Annu. Rev. Biochem.* **2000**, *69*, 923.

[6] a) T. W. Muir, D. Sondhi, P. A. Cole, *Proc. Natl. Acad. Sci. USA* **1998**, *95*, 6705; b) R. M. Hofmann, T. W. Muir, *Curr. Opin. Biotechnol.* **2002**, *13*, 297; c) I. Giriat, T. W. Muir, *J. Am. Chem. Soc.* **2003**, *125*, 7180.

[7] H. Herzner, T. Reipen, M. Schultz, H. Kunz, *Chem. Rev.* **2000**, *100*, 4495.

[8] a) D. Macmillan, C. R. Bertozzi, *Tetrahedron* **2000**, *56*, 9515; b) T. J. W. Tolbert, C.-H. Wong, *J. Am. Chem. Soc.* **2000**, *122*, 5421.

[9] a) D. Crommie, S. D. Rosen, *J. Biol. Chem.* **1995**, *270*, 22614; b) S. Hemmerich, S. D. Rosen, *Biochemistry* **1994**, *33*, 4830; c) S. Hemmerich, C. R. Bertozzi, H. Leffler, S. D. Rosen, *Biochemistry* **1994**, *33*, 4820; d) S. Hemmerich, H. Leffler, S. D. Rosen, *J. Biol. Chem.* **1995**, *270*, 12035.

[10] a) E. C. Rodriguez, L. A. Marcaurelle, C. R. Bertozzi, *J. Org. Chem.* **1998**, *63*, 7134; b) A. Leppanen, S. P. White, J. Helin, R. P. McEver, R. D. Cummings, *J. Biol. Chem.* **2000**, *275*, 39569.

[11] Y. Shin, K. A. Winans, B. J. Backes, S. B. H. Kent, J. A. Ellman, C. R. Bertozzi, *J. Am. Chem. Soc.* **1999**, *121*, 11684.

[12] K. A. Winans, D. S. King, V. R. Rao, C. R. Bertozzi, *Biochemistry* **1999**, *38*, 11700.

[13] R. Ingenito, E. Bianchi, D. Fattori, A. Pessi, *J. Am. Chem. Soc.* **1999**, *121*, 11369.

[14] G. G. Kochendoerfer, S.-Y. Chen, F. Mao, S. Cressman, S. Traviglia, H. Shao, C. L. Hunter, D. W. Low, E. N. Cagle, M. Carnevali, V. Gueriguian, P. J. Keogh, H. Porter, S. M. Stratton, M. C. Wiedeke, J. Wilken, J. Tang, J. J. Levy, L. P. Miranda, M. M. Crnogorac, S. Kalbag, P. Botti, J. Schindler-Horvat, L. Savatski, J. W. Adamson, A. Kung, S. B. H. Kent, J. A. Bradburne, *Science* **2003**, *299*, 884.

[15] a) L. A. Marcaurelle, L. S. Mizoue, J. Wilken, L. Oldham, S. B. H. Kent, T. M. Handel, C. R. Bertozzi, *Chem. Eur. J.* **2001**, *7*, 1129; b) H. Hojo, E. Haginoya, Y. Matsumoto, Y. Nakahara, K. Nabeshima, B. P. Toole, Y. Watanabe, *Tetrahedron Lett.* **2003**, *44*, 2961c) J. S. Miller, V. Y. Dudkin, G. J. Lyon, T. W. Muir, S. J. Danishefsky, *Angew. Chem.* **2003**, *115*, 447; *Angew. Chem. Int. Ed.* **2003**, *42*, 431.

[16] Both proteins migrate with a higher apparent molecular mass than predicted, indeed almost twice that determined by mass spectrometry (full-length bacterially derived GlyCAM-1, observed mass (ESI-MS) = 14409 Da and 14451 Da for the acetylated species; semisynthetic GlyCAM-1 observed molecular mass (ESI-MS) = 16776 Da).

 © 2004 Wiley-VCH Verlag GmbH & Co. KGaA, Weinheim

Crystal Engineering

Absolute Helical Arrangement of Stacked Benzene Rings: Heterogeneous Double-Helical Interaction Comprising a Hydrogen-Bonding Belt and an Offset Parallel Aromatic–Aromatic-Interaction Array**

Isao Azumaya, Daisuke Uchida, Takako Kato, Akihiro Yokoyama, Aya Tanatani, Hiroaki Takayanagi, and Tsutomu Yokozawa**

Compounds that form helical structures in the crystalline state or in solution[1] have attracted much attention because living things utilize helical structures to store genetic information, and because compounds with a helical-ordered structure have provided new materials in solid- or liquid-crystal engineering.[2] There are several types of helical structure: a single strand that folds helically owing to solvophobic effect[3] or guest ligation,[4] a double or multiple helix of strands derived from cation or anion ligation,[5] or hydrogen bonding,[6] and a helical super-structure formed by conformationally helical or discotic small molecules through columnar stacking supported by hydrogen bonds,[7] for other examples see ref. [8]. In helical structures, a parallel aromatic–aromatic interaction[9] is often a very important driving force to stabilize the structure, and sometimes hydrogen bonding or other weak intermolecular interactions assist the formation of the highly ordered helical arrangement. Such a helical structure is intrinsically chiral, that is, it has a right-handed helix (*P*-helix) or a left-handed helix (*M*-helix), which are enantiomeric. Asymmetric synthesis to produce one enantiomeric helix is important, especially in self-assembling systems,[5–7] in foldamers,[1a] or in polymers with a helical structure induced by catalytic chiral initiation.[10] There are generally two kinds of driving forces to determine which helicity a compound will adopt, they are, an internal or an external chiral source. For example, the helicity of DNA is derived from the internal chirality of the chiral carbon atom in the deoxyribose chain. On the other hand, one of oligophenylacetylenes prepared by Moore and co-workers folded into a single helical form upon ligation of a chiral ligand.[4b,c] In this context, absolute asymmetric assembly of an achiral molecule is especially intriguing. In the course of our investigation[11] of spontaneous optical resolution,[12] we found a discotic compound, tris(2-hydroxyethyl)-1,3,5-benzenetricarboxylate (**1**), which crystallized as chiral crystals in which the nearly planar molecules were helically arranged within individual single crystals. The helicity of the triester **1** was derived from the helical arrangement of the molecules, supported by an array of hydrogen bonding through a single moiety and offset aromatic stacking of the adjacent molecules.

The triester **1**, which has an almost planar and highly symmetrical primary structure, was synthesized and crystallized from methanol/chloroform to give slender prismatic single crystals. A preliminary X-ray crystallographic analysis (Figure 1) revealed that the crystal belonged to the non-

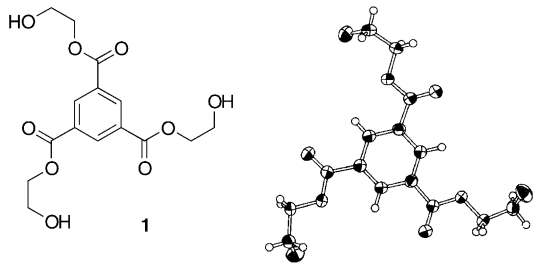


Figure 1. ORTEP drawing of the crystal structure of **1**. The thermal ellipsoids are set at 50% probability.

centrosymmetric space group $P6_1$ (or $P6_5$). This result was surprising, since the majority of achiral organic compounds tend to pack into centrosymmetric crystals. The most interesting feature is that the planar, discotic molecules were arranged in a columnar stack with a progressive helical twist between adjacent molecules to form helical superstructures in the crystal lattice. The chirality of the crystals was intrinsically derived from the helical arrangement of the molecules, assisted by the twist of the terminal hydroxy groups with respect to the plane of the central benzene ring, which leads to the generation of conformational chirality.

We measured the solid-state CD spectrum (in KBr) of several crystals of **1**.[13] The Cotton effect was characteristic of a helical structure of a chromophore.[14] As expected, we found two enantiomeric crystals which showed mirror-image curves in the region between 200–320 nm (Figure 2); one (red line in Figure 2) showed a negative Cotton effect at around 210 nm, a large positive one at 224 nm, a negative one at 248 nm, and two faint positive ones at 288 and 298 nm, and the other showed Cotton effects with the opposite sign at the corresponding wavelengths. Because one torsion angle of OC–aromatic ring unit was −2.7(4)° and the others were 0.1(4)° and 1.2(4)°, the Cotton effects of the crystal could be derived from the helical arrangement of the benzene rings of the molecule as well as torsion of one carbonyl group with respect to the central benzene ring.

The absolute structure could be determined[15] by comparison of the Flack parameter[16] for each space group ($P6_1$ or $P6_5$) using the least-squares method. For example, if the

[*] Dr. I. Azumaya, T. Kato, Prof. Dr. H. Takayanagi
Faculty of Pharmaceutical Sciences
Kitasato University
5-9-1 Shirokane, Minato-ku, Tokyo 108-8641 (Japan)
Fax: (+81) 334-42-5707
E-mail: azumayai@pharm.kitasato-u.ac.jp
D. Uchida, Dr. A. Yokoyama, Dr. A. Tanatani, Prof. Dr. T. Yokozawa
Department of Applied Chemistry
Kanagawa University
Kanagawa-ku, Yokohama 221-8686 (Japan)
Fax: (+81) 45-413-9770
E-mail: yokozt01@kanagawa-u.ac.jp

[**] I.A. acknowledges partial funding of this work by The Asahi Glass Foundation.

Supporting information (view of the left and right handed helixes) for this article is available on the WWW under http://www.angewandte.org or from the author.

 © 2004 Wiley-VCH Verlag GmbH & Co. KGaA, Weinheim DOI: 10.1002/anie.200352788

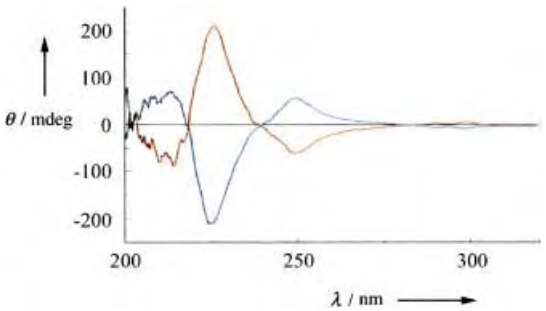


Figure 2. CD spectra of two enantiomeric crystals of **1** ($P6_1$: red line; $P6_5$: blue line) in KBr. A mixture of 250 μg of each crystal and 100 mg of KBr was well ground and formed into a transparent disk with a radius of 5 mm.

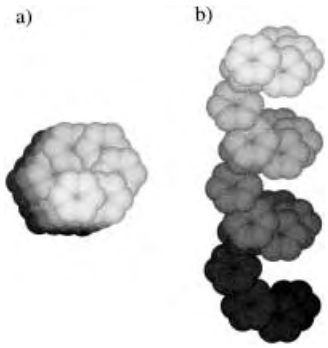


Figure 4. Top view (a) and tilted view (b) of the crystal packing of **1** showing the helical arrangement of the central benzene rings of the molecules. Neighboring benzene rings are stacked in an offset mode.

crystal that showed a positive Cotton effect at 224 nm was in the space group $P6_1$, the Flack parameter was 0.003 and in $P6_5$, it was 0.942, so the crystal was assigned to $P6_1$. On the other hand, if the crystal that showed a negative Cotton effect at 224 nm was in the space group $P6_1$, the Flack parameter was 1.036 and in $P6_5$, it was −0.041, so the crystal was assigned to $P6_5$. This correspondence between the Flack parameter and the sign of the Cotton effect was confirmed by examining at least three crystals for each enantiomer.

A further investigation of the crystal structure of **1** revealed that the arrangement of the molecule showed unique features. Only one of the three hydroxyethyloxycarbonyl groups formed a hydrogen bonding array between adjacent molecules, that is, the hydroxy group of a hydroxyethyloxycarbonyl group formed a hydrogen bond with the carbonyl group of a hydroxyethyloxycarbonyl group of the next molecule (Figure 3). This single-hydrogen-bond belt

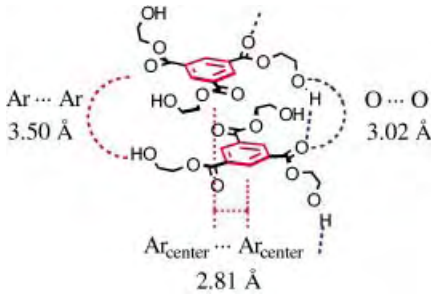


Figure 3. Schematic representation of the relative position of adjacent molecules in the crystal packing of **1**; red: benzene separations, blue: hydrogen-bonding distances.

forms a helical strand, which was right-handed for $P6_1$ and left-handed for $P6_5$.[17] Another remarkable feature is that the central benzene rings of the molecules exhibit circular offset stacking to form an enantiomeric single helix (Figure 4). These heterogeneous helical weak interactions have the same helicity. The attractive interaction between two aromatic rings in this structure would be strongest among various types of parallel stacking because an aromatic hydrogen center is located just above the center of the adjacent benzene ring.[9d,g–i] Because the unit cell has six molecules along the *c* axis, which gives rise to a complete turn in 21.0 Å, the distance between adjacent benzene rings is 3.50 Å. The exterior width of the array of molecules is about 12.5 Å, which is just over half of that of DNA (ca. 20 Å).

The stacked structure of **1** is reminiscent of the layered crystal structures of *N*,*N*′,*N*″-tris(2-methoxyethyl)benzene-1,3,5-tricarboxamide (**2**) which was reported to crystallize as chiral crystals belonging to space group $P2_1$.[7a] However, the triamide **2** showed straight stacking of the central benzene ring along the *b* axis, with complete overlap, and the distance between the central benzene rings is 3.60 Å. Further, the helical structure is derived from triple helices formed by hydrogen bonding between the secondary amide hydrogen and the carbonyl oxygen of the neighboring molecule. On the other hand, the helicity of the triester **1** was derived from a heterogeneous double-helical interaction, that is, a relatively weak, single hydrogen-bonding belt involving one of the hydroxyethyloxycarbonyl groups and an offset parallel aromatic–aromatic interaction between Ar–H and the center of the neighboring benzene ring to give the offset stacking. Our triester is the first example of an absolute helical arrangement of a single benzene ring in a parallel offset-stacking array that undergoes spontaneous resolution in the crystal, assisted by progressive hydrogen bonding; that is, the spontaneous resolution is driven by two different weak helical interactions which result in the formation of Ar–H···π and OH···O=C arrays. Such helical chirality induction of an achiral compound is of great interest, since such a system could be a simple model for spontaneous helical structure formation in nature.

Experimental Section

1: Preparation of 2-(*tert*-Butyldimethylsilyloxy)ethanol: dropwise, over 1 h, a solution of *tert*-butyldimethylsilyl chloride (15.1 g, 0.10 mol) in dry THF (500 mL) was added to a stirred solution of ethylene glycol (37.2 g, 0.60 mol) and imidazole (6.81 g, 0.10 mol) in dry THF (500 mL) at room temperature, and the mixture was stirred at room temperature for 6 h. After addition of water, THF was removed by evaporation under reduced pressure, and the residue was extracted with ethyl acetate. The organic layer was washed with water, dried over anhydrous $MgSO_4$, and concentrated under reduced pressure. The residue was purified by silica gel column chromatography (elution solvents: ethyl acetate/hexane = 1/4) to give 2-(*tert*-

 © 2004 Wiley-VCH Verlag GmbH & Co. KGaA, Weinheim

butyldimethylsilyloxy)ethanol as a colorless oil (14.1 g, 80%): ^{1}H NMR (200 MHz, $CDCl_3$): $\delta = 3.74$–3.40 (m, 4H), 2.47–2.33 (m, 1H), 0.85 (s, 9H), 0.03 ppm (s, 6H); ^{13}C NMR (50 MHz, $CDCl_3$): $\delta =$ 64.2, 63.7, 25.9, −5.4 ppm.

Tris[2-(*tert*-butyldimethylsilyloxy)ethyl]-1,3,5-benzenetricarboxylate: dropwise, over 3 h, a solution of 1,3,5-benzenetricarbonyl trichloride (5.88 g, 22 mmol) in dry CH_2Cl_2 (100 mL) was added to a stirred solution of 2-(*tert*-butyldimethylsilyloxy)ethanol (14.1 g, 80 mmol; see above) and triethylamine (8.06 g, 80 mmol) in dry CH_2Cl_2 (200 mL) at room temperature, and the mixture was stirred at room temperature for 3 days. After addition of water, the mixture was extracted with CH_2Cl_2, and the organic layer was washed with water, dried over anhydrous Na_2SO_4, and concentrated under reduced pressure. The residue was purified by silica gel column chromatography (elution solvents: ethyl acetate/hexane = 1/4) to give tris-[2-(*tert*-butyldimethylsilyloxy)ethyl]-1,3,5-benzenetricarboxylate as a yellow oil (13.6 g, 90%): ^{1}H NMR (200 MHz, $CDCl_3$): $\delta = 8.89$ (s, 3H), 4.45 (t, $J = 5.0$ Hz, 6H), 3.96 (t, $J = 5.0$ Hz, 6H), 0.90 (s, 27H), 0.09 ppm (s, 18H); ^{13}C NMR (125 MHz, $CDCl_3$): $\delta = 164.9$, 134.7, 131.3, 66.7, 61.1, 25.8, 18.3, −5.31 ppm; IR (neat) 2954, 2930, 2884, 2857, 1733, 1472 cm^{-1}.

Tris(2-hydroxyethyl)-1,3,5-benzenetricarboxylate (**1**): A mixture of tris[2-(*tert*-butyldimethylsilyloxy)ethyl]-1,3,5-benzenetricarboxylate (13.6 g, 20 mmol; see above), 6 M hydrochloric acid (1 mL), and THF (200 mL) was stirred at room temperature for 6 h, and concentrated under reduced pressure. The crude solid obtained was washed with hexane and dried in vacuo to give **1** as a colorless solid (6.11 g, 90%): ^{1}H NMR (600 MHz, [D$_6$]DMSO): $\delta = 8.74$ (s, 3H), 4.99 (t, $J = 5.4$ Hz, 3H), 4.39 (t, $J = 4.9$ Hz, 6H), 3.75 ppm (t, $J = 5.0$ Hz, 6H); ^{13}C NMR (151 MHz, [D$_6$]DMSO): $\delta = 164.5$, 133.8, 131.3, 67.5, 59.1 ppm; IR (KBr): $\tilde{\nu} = 3327$, 2955, 1722, 1441, 1242, 1078, 1025 cm^{-1}; Elemental analysis calcd (%) for $C_{15}H_{18}O_9$: C 52.63, H 5.30; found: C 52.60, H 5.34.

Received: September 4, 2003
Revised: October 27, 2003 [Z52788]

Keywords: chiral resolution · chirality · crystal engineering · helical structures · hydrogen bonds

[1] a) D. J. Hill, M. J. Mio, R. B. Prince, T. S. Hughes, J. S. Moore, *Chem. Rev.* **2001**, *101*, 3893–4011; b) J. J. L. M. Cornelissen, A. E. Rowan, R. J. M. Nolte, N. A. J. M. Sommerdijk, *Chem. Rev.* **2001**, *101*, 4039–4070; c) L. Brunsveld, B. J. B. Folmer, E. W. Meijer, R. P. Sijbesma, *Chem. Rev.* **2001**, *101*, 4071–4097; d) B. Gong, *Chem. Eur. J.* **2001**, *7*, 4336–4342; e) C. Schmuck, *Angew. Chem.* **2003**, *115*, 2552–2556; *Angew. Chem. Int. Ed.* **2003**, *42*, 2448–2452.

[2] G. R. Desiraju, *Angew. Chem.* **1995**, *107*, 2541–2558; *Angew. Chem. Int. Ed. Engl.* **1995**, *34*, 2311–2327.

[3] a) C. Nuckolls, T. J. Katz, G. Katz, P. J. Collings, L. Castellanos, *J. Am. Chem. Soc.* **1999**, *121*, 79–88; b) M. S. Gin, T. Yokozawa, R. B. Prince, J. S. Moore, *J. Am. Chem. Soc.* **1999**, *121*, 2643–2644; c) R. B. Prince, J. G. Saven, P. G. Wolynes, J. S. Moore, *J. Am. Chem. Soc.* **1999**, *121*, 3114–3121; d) W. Y. Yang, R. B. Prince, J. Sabelko, J. S. Moore, M. Gruebele, *J. Am. Chem. Soc.* **2000**, *122*, 3248–3249; e) C. Kübel, M. J. Mio, J. S. Moore, D. C. Martin, *J. Am. Chem. Soc.* **2002**, *124*, 8605–8610; f) D. Zhao, J. S. Moore, *J. Am. Chem. Soc.* **2002**, *124*, 9996–9997; g) D. J. Hill, J. S. Moore, *Proc. Natl. Acad. Sci. USA* **2002**, *99*, 5053–5057.

[4] a) T. Kawamoto, B. S. Hammes, B. Haggerty, G. P. A. Yap, A. L. Rheingold, A. S. Borovik, *J. Am. Chem. Soc.* **1996**, *118*, 285–286; b) R. B. Prince, S. A. Barnes, J. S. Moore, *J. Am. Chem. Soc.* **2000**, *122*, 2758–2762; c) A. Tanatani, M. J. Mio, J. S. Moore, *J. Am. Chem. Soc.* **2001**, *123*, 1792–1793; d) T. Nishinaga, A. Tanatani, K. Oh, J. S. Moore, *J. Am. Chem. Soc.* **2002**, *124*, 5934–5935.

[5] a) J.-M. Lehn, A. Rigault, J. Siegel, J. Harrowfield, B. Chevrier, D. Moras, *Proc. Natl. Acad. Sci. USA* **1987**, *84*, 2565–2569; b) U. Koert, M. M. Harding, J.-M. Lehn, *Nature* **1990**, *346*, 339–342; c) K. A. Hirsch, S. R. Wilson, J. S. Moore, *Chem. Commun.* **1998**, 13–14; d) S. J. Coles, J. G. Frey, P. A. Gale, M. B. Hursthouse, M. E. Light, K. Navakhun, G. L. Thomas, *Chem. Commun.* **2003**, 568–569; e) Y. Cui, H. L. Ngo, W. Lin, *Chem. Commun.* **2003**, 1388–1389.

[6] a) L. J. Prins, F. D. Jong, P. Timmerman, D. N. Reinhoudt, *Nature* **2000**, *408*, 181–184; b) L. J. Prins, E. E. Neuteboom, V. Paraschiv, M. Crego-Calama, P. Timmerman, D. N. Reinhoudt, *J. Org. Chem.* **2002**, *67*, 4808–4820.

[7] a) M. P. Lightfoot, F. S. Mair, R. G. Pritchard, J. E. Warren, *Chem. Commun.* **1999**, 1945–1946; b) S. J. Geib, C. Vicent, E. Fan, A. D. Hamilton, *Angew. Chem.* **1993**, *105*, 83–85; *Angew. Chem. Int. Ed. Engl.* **1993**, *32*, 119–121; c) T. B. Norsten, R. McDonald, N. R. Branda, *Chem. Commun.* **1999**, 719–720; d) P. Gangopadhyay, T. P. Radhakrishnan, *Angew. Chem.* **2001**, *113*, 2517–2521; *Angew. Chem. Int. Ed.* **2001**, *40*, 2451–2455; e) A. P. H. J. Schenning, P. Jonkheijm, E. Peeters, E. W. Meijer, *J. Am. Chem. Soc.* **2001**, *123*, 409–416; f) J. E. Field, D. Venkataraman, *Chem. Commun.* **2002**, 306–307; g) R. Shenhar, H. Wang, R. E. Hoffman, L. Frish, L. Avram, I. Willner, A. Rajca, M. Rabinovitz, *J. Am. Chem. Soc.* **2002**, *124*, 4685–4692; h) V. Král, F. P. Schmidtchen, K. Lang, M. Berger, *Org. Lett.* **2002**, *4*, 51–54.

[8] a) A. Tanatani, K. Yamaguchi, I. Azumaya, R. Fukutomi, K. Shudo, H. Kagechika, *J. Am. Chem. Soc.* **1998**, *120*, 6433–6442; b) V. Berl, I. Huc, R. G. Khoury, M. J. Krische, J.-M. Lehn, *Nature* **2000**, *407*, 720–723; c) C. Y. Li, S. Z. D. Cheng, X. Weng, J. J. Ge, F. Bai, J. Z. Zhang, B. H. Calhoun, F. W. Harris, L.-C. Chien, B. Lotz, *J. Am. Chem. Soc.* **2001**, *123*, 2462–2463.

[9] a) P. Hobza, H. L. Selzle, E. W. Schlag, *J. Am. Chem. Soc.* **1994**, *116*, 3500–3506; b) I. Dance, M. Scudder, *J. Chem. Soc. Chem. Commun.* **1995**, 1039–1040; c) V. E. Williams, R. P. Lemieux, G. R. J. Thatcher, *J. Org. Chem.* **1996**, *61*, 1927–1933; d) C. B. Martin, H. R. Mulla, P. G. Willis, A. Cammers-Goodwin, *J. Org. Chem.* **1999**, *64*, 7802–7806; e) P. Dapporto, P. Paoli, S. Roelens, *J. Org. Chem.* **2001**, *66*, 4930–4933; f) K. Biradha, M. Fujita, *Chem. Commun.* **2001**, 15–16; g) S. Tsuzuki, K. Honda, T. Uchimaru, M. Mikami, K. Tanabe, *J. Am. Chem. Soc.* **2002**, *124*, 104–112; h) M. J. Rashkin, M. L. Waters, *J. Am. Chem. Soc.* **2002**, *124*, 1860–1861; i) S. Tsuzuki, K. Honda, R. Azumi, *J. Am. Chem. Soc.* **2002**, *124*, 12200–12209; j) Y. Miyake, A. Hosoda, M. Takagaki, E. Nomura, H. Taniguchi, *Chem. Commun.* **2002**, 132–133.

[10] a) T. Nakano, Y. Okamoto, *Chem. Rev.* **2001**, *101*, 4013–4038; b) M. Ishikawa, K. Maeda, E. Yashima, *J. Am. Chem. Soc.* **2002**, *124*, 7448–7458; c) T. Aoki, T. Kaneko, N. Maruyama, A. Sumi, M. Takahasi, T. Sato, M. Teraguchi, *J. Am. Chem. Soc.* **2003**, *125*, 6346–6347.

[11] a) I. Azumaya, K. Yamaguchi, I. Okamoto, H. Kagechika, K. Shudo, *J. Am. Chem. Soc.* **1995**, *117*, 9083–9084; b) I. Azumaya, I. Okamoto, S. Nakayama, A. Tanatani, K. Yamaguchi, K. Shudo, H. Kagechika, *Tetrahedron* **1999**, *55*, 11237–11246; 1,2-bis(formylamino)benzene also gave chiral crystals: c) I. Azumaya, I. Okamoto, H. Takayanagi, *Anal. Sci.* **2003**, *19*, x3–x4; d) I. Azumaya, T. Kato, I Okamoto, R. Yamasaki, A. Tanatani, K. Yamaguchi, H. Kagechika, H. Takayanagi, *Org. Lett.* **2003**, *5*, 3939–3942.

[12] a) R. E. Pincock, K. R. Wilson, *J. Am. Chem. Soc.* **1971**, *93*, 1291–1292; b) R. E. Pincock, K. R. Wilson, *J. Chem. Educ.* **1973**, *50*, 455–457; c) F. Toda, M. Yagi, S. Soda, *J. Chem. Soc. Chem. Commun.* **1987**, 1413–1414; d) H. Koshima, T. Nakagawa, T. Matsuura, H. Miyamoto, F. Toda, *J. Org. Chem.* **1997**,

 © 2004 Wiley-VCH Verlag GmbH & Co. KGaA, Weinheim

62, 6322 – 6325; e) M. Sakamoto, *Chem. Eur. J.* **1997**, *3*, 684 – 689; f) B. Gong, C. Zheng, H. Zeng, J. Zhu, *J. Am. Chem. Soc.* **1999**, *121*, 9766 – 9767; g) R. Kuroda, Y. Imai, T. Sato, *Chirality* **2001**, *13*, 588 – 594; h) K. Asakura, T. Soga, T. Uchida, S. Osanai, D. K. Kondepudi, *Chirality* **2002**, *14*, 85 – 89; i) M. Sakamoto, T. Iwamoto, N. Nono, M. Ando, W. Arai, T. Mino, T. Fujita, *J. Org. Chem.* **2003**, *68*, 942 – 946.

[13] R. Kuroda, T. Honma, *Chirality* **2000**, *12*, 269 – 277.

[14] *Circular Dichroism: Principles and Applications*, 2nd ed. (Eds.: N. Berova, K. Nakanishi, R. W. Woody), Wiley-VCH, Weinheim, **2000**.

[15] Crystal data of **1a** ($P6_1$): $C_{15}H_{18}O_9$, $M_r = 342.30$, hexagonal, space group $P6_1$, $a = 11.304(1)$, $c = 20.997(4)$ Å, $V = 2323.5(6)$ Å^3, $Z = 6$, $\rho_{calcd} = 1.468\ g\,cm^{-3}$, $T = 296$ K, crystal size $0.20 \times 0.20 \times 0.20$ mm^3, $R = 0.043$, $R_w = 0.055$, GOF = 1.23 for 2817 reflections with $I > 0.0\sigma(I)$. The Flack absolute structure parameter has a value of 0.003(0.161), while the inverted stereochemistry requires a value of 0.942(0.154). Crystal data of **1b** ($P6_5$): $C_{15}H_{18}O_9$, $M_r = 342.30$, hexagonal, space group $P6_5$, $a = 11.3048(9)$, $c = 21.011(3)$ Å, $V = 2325.5(5)$ Å^3, $Z = 6$, $\rho_{calcd} = 1.466\ g\,cm^{-3}$, $T = 296$ K, crystal size $0.20 \times 0.20 \times 0.20$ mm^3, $R = 0.047$, $R_w = 0.067$, GOF = 1.29 for 2781 reflections with $I > 0.0\sigma(I)$. The Flack absolute structure parameter has a value of $-0.041(0.174)$, while the inverted stereochemistry requires a value of 1.036(0.164). CCDC-218393 (**1a**) and CCDC-218394 (**1b**) contain the supplementary crystallographic data for this paper. These data can be obtained free of charge via www.ccdc.cam.ac.uk/conts/retrieving.html (or from the Cambridge Crystallographic Data Centre, 12 Union Road, Cambridge CB21EZ, UK; fax: (+44) 1223-336-033; or deposit@ccdc.cam.ac.uk).

[16] H. D. Flack, *Acta Crystallogr. Sect. A* **1983**, *39*, 876 – 881.

[17] Only one of the hydroxy groups contributes to the formation of a single-helical hydrogen-bonding array of $-C{=}O\cdots HOCH_2$-$CH_2OC{=}O\cdots HO-$ (see Supporting Information). The two other hydroxy groups form weak hydrogen bonds with carbonyl groups on the next molecule, but do not form a hydrogen-bonding array.

 © 2004 Wiley-VCH Verlag GmbH & Co. KGaA, Weinheim

Crystal Growth

Emergence of Morphological Chirality from Twinned Crystals**

Hiroaki Imai and Yuya Oaki*

Helical and spiral architectures are fundamental shapes that have chirality and are observed in various environments and scales in nature. Their unique morphology is fascinating; the formation mechanisms for many kinds of helical forms are still a mystery. Biological polymers such as DNA, collagen, and agar produce helical chains from the nanometer to the submicron scale with a specific interaction through hydrogen bonding.[1] Artificially produced chiral organic molecules,[2] polymer chains,[3,4] and macromolecules[5] have been reported to induce twisted aggregates on various scales. In general, the formation of these helices was ascribed to the chirality of the components and hydrogen bonding originating from their asymmetric molecular structure. However, helical morphologies are not always attributable to only microscopic chirality at a molecular level. For example, macroscopic helical morphologies have also been observed with organic molecules,[6] polymers[7] and inorganic materials [8,9,13–18] without microscopic chirality. Helical whiskers, produced by vapor-phase deposition techniques, originate from the asymmetric behavior of a growing site at the top of each whisker[8] and dislocations in the crystal phase.[9] Well-known twisted ribbons in spherulites of polymer crystals without chirality have been characterized by X-ray diffraction and by modeling.[10,11] It was reported in 1929 that that several organic and inorganic crystal systems, except for cubic systems, induce twisted shapes.[12] However, the details of the shapes and growth conditions have not been previously described in the literature. In recent years, new families of helical shapes were discovered for barium sulfate,[13] calcium,[14] barium and strontium carbonates,[15] potassium dichromate,[16] manganese oxide,[17] and silica–surfactant composite.[18] Consequently, a novel concept is required to understand the emergence of these morphological chirality from achiral components.

We found that helical morphologies are generally grown with triclinic crystals in various kinds of gel matrices. The backbone of the unique architectures was observed to be

[*] Prof. H. Imai, Y. Oaki
Department of Applied Chemistry
Faculty of Science and Technology
Keio University
3-14-1 Hiyoshi, Kohoku-ku, Yokohama 223-8522 (Japan)
Fax: (+81) 45-566-1551
E-mail: hiroaki@applc.keio.ac.jp

[**] This work was supported by Grant-in-Aid for Scientific Research (No. 15560587) and 21 st Century COE program "KEIO Life Conjugate Chemistry" from the Ministry of Education, Culture, Sports, Science, and Technology, Japan. We thank Prof. D. K. Kondepdi at Wake Forest University for critically reading the manuscript.

Supporting information for this article is available on the WWW under http://www.angewandte.org or from the author.

 DOI: 10.1002/anie.200352891 © 2004 Wiley-VCH Verlag GmbH & Co. KGaA, Weinheim

composed of twin crystals twisted with a constant angle. The emergence of the macroscopic chiral morphology from achiral components is attributable to twisted assembly of tilted units in a diffusion field. Moreover, right-handed helices were predominantly obtained in a gel matrix consisting of biological macromolecules.

In total, four kinds of inorganic materials, including triclinic crystals ($K_2Cr_2O_7$ and H_3BO_3) and the cubic crystals ($Ba(NO_3)_2$ and NH_4Cl), were grown in various sorts of organic gel media (poly(vinyl alcohol) (PVA), poly(acrylic acid) (PAA), gelatin, agar, and pectin,). Crystals were grown from the precursor that contained a specified amount of the inorganic materials and gelling agents by lowering the temperature[19] (method 1) or by evaporation of water from the precursor (method 2). Detailed experimental procedure and conditions are described in the Experimental Section and in the figure legends.

As we have already reported,[19] the morphology of crystals grown in gel media by lowering the temperature (method 1) varied with the gel density. The fundamental variation of the morphologies was independent of the sorts of grown crystals and gelling agents. Polyhedral forms changed into skeletal and then dendritic shapes with increasing gel density. This evolution is ascribed to the change of growth behavior from a kinetic-limited mode into a diffusion-limited mode with suppression of the mobility of the solutes in the presence of gelling agents.[19] The main role of the gelling agents was the suppression of diffusion and the formation of a diffusion field. Consequently, gel media control the diffusion process and are otherwise inert for crystal growth. As shown in Figure 1 a–d, connected crystals consisting of platy subunits were produced through diffusion-limited growth with increasing gel density (method 1). Finally, twisted morphologies were observed in the branches of dendritic and spherulitic forms of the triclinic crystals ($K_2Cr_2O_7$ and H_3BO_3) grown in gel media at a relatively high density, regardless of the gelling agent. We could not detect the influence of the gelling agents on the crystallization process as a source of nucleation sites or scaffolds. Helical morphology also formed in the same growth condition by method 2 (Figure 1 e,f). On the other hand, twisted shapes were never found with cubic crystals (($Ba(NO_3)_2$, NH_4Cl)) under any conditions. These results suggest that the helical aggregates were produced through a diffusion-limited growth of triclinic crystals. However, detailed information of the structure of the unique aggregates was not obtained from the results shown in Figure 1.

We have successfully revealed the backbone for the foundation of helical aggregates, as shown in Figure 2 a–d. The twisted backbone was composed of platy subunits with a rotated connection both for $K_2Cr_2O_7$ and H_3BO_3, even though the shapes of the subunits are different. When the twisted platy subunits were not directly recognized on several helical forms as shown in Figure 1 f, the magnified SEM and TEM images clearly indicated the presence of the backbone inside the aggregates (Figure 3). Since the angles between the platy subunits at the connections were constant (Figure 2 c,d), the twisted backbone is deduced to be composed of twinned crystals. Tilted parallelogram subunits of $K_2Cr_2O_7$ surrounded by the $(2\bar{1}1)$, (010), and (001) planes were aligned along the

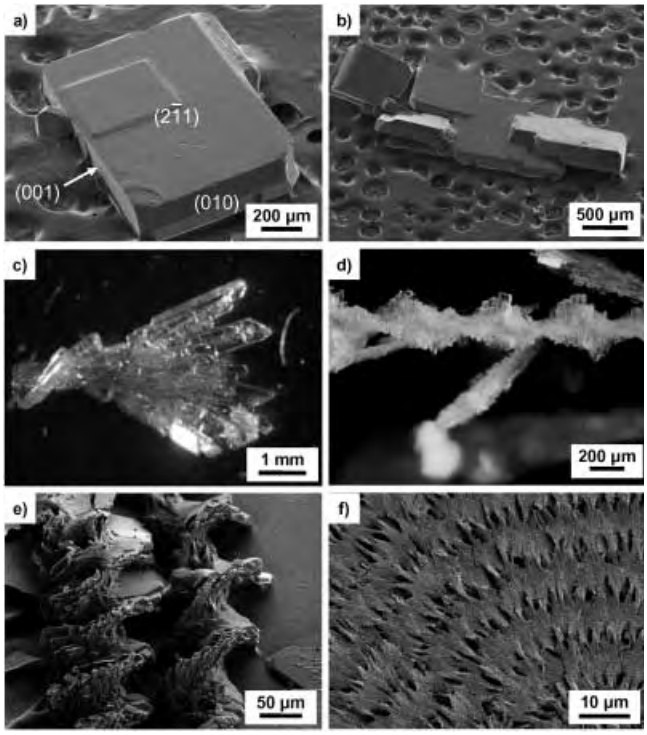


Figure 1. Typical optical microscopy and field-emission scanning electon microscope (FESEM) images of the twisted and helical architectures. a) Platy crystals at $C_{KC}=25.0$, $C_{ge}=0$, b) connection of the platy subunit crystals at $C_{KC}=25.0$, $C_{ge}=5.0$, c) twisted morphology consisting of the connections at $C_{KC}=25.0$, $C_{ge}=20.0$, d) helical forms at $C_{KC}=25.0$, $C_{ge}=25.0$. Twisted and helical morphology was formed through the connections of the platy subunits crystals with an increase of gel density (method 1; see Experimental Section). Various helical morphology grown by method 2 at $C_{KC}=3.0$, $C_{pe}=0.3$ (e), and $C_{KC}=2.0$, $C_{PAA}=0.02$ (f). These unique morphologies were found on triclinic crystals through diffusion-limited growth in gel matrices.

b axis with a rotation angle of about 12°. Hexagonal plates composed of the (100), (010), (001), and $(\bar{1}10)$ planes of H_3BO_3 were strung along the $\langle 100\rangle$, $\langle 010\rangle$, or $\langle \bar{1}10\rangle$ direction with a rotation angle of about 4.5°. The coincident lattice matching at the angles is estimated to be relatively good for these crystals because a suitable twin lattice with periodicity could be formed at the twin plane (see Supporting Information). Thus, the helical forms can be called "twisted twins." The rule of the connections was independent of the sorts of the gel matrices. The variation of the pitch of the helices depended on a change in the size of the subunits. A reduction in size increased the pitch of the twisting of the backbone. Figure 2 g,h shows a model of the twisted backbone with platy subunits (Figure 2 e,f) that were estimated from SEM images and unit-cell structures of $K_2Cr_2O_7$ and H_3BO_3 with specific angles for the connections. The backbones of the helical morphologies experimentally obtained are approximately reproduced by this simple simulation. These results support the idea that the twisted backbone consists of twins. The formation of twisted twins is ascribed to an increase in the influence of diffusion upon crystal growth in the gel media.

Figure 4 shows a nucleation point of helical (a) H_3BO_3 and (b) $K_2Cr_2O_7$ crystals grown in agar and PAA, respectively.

 © 2004 Wiley-VCH Verlag GmbH & Co. KGaA, Weinheim

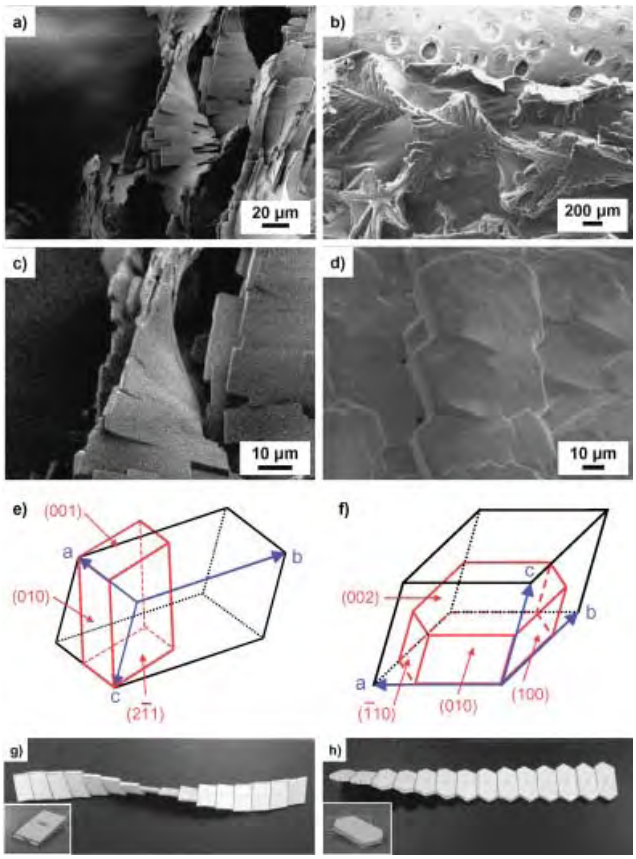


Figure 2. Backbone and detailed structure of unique helical forms. FESEM images of the backbone of (a) $K_2Cr_2O_7$ ($C_{KC}=3.0$, $C_{pe}=0.3$) and (b) H_3BO_3 ($C_{HB}=2.0$, $C_{ag}=0.2$) helices with twisted twins consisting of platy subunits. FESEM images of (c) $K_2Cr_2O_7$ and (d) H_3BO_3 twisted twins (magnification of (a) and (b), respectively). Schematic illustrations of (e) $K_2Cr_2O_7$ and (f) H_3BO_3 platy subunits estimated from FESEM images, XRD analysis, and unit cell structures. Simple models of the twisted backbones of (g) $K_2Cr_2O_7$ and (h) H_3BO_3 with platy subunits. We successfully obtained the backbone (a) and (b) of the helical morphologies consisting of the twisted twins (c) and (d). In addition, these morphologies were easily reproduced by a simple model (g) and (h) with platy subunits derived from those shown in (e) and (f).

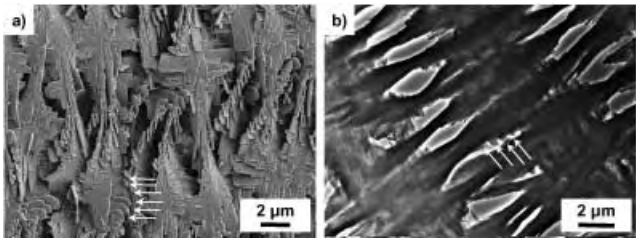


Figure 3. Magnified images of the backbone of the $K_2Cr_2O_7$ helical morphology. a) FESEM and b) TEM images clearly show the backbone structure of helical architecture consisting of the platy subunits.

Left- and right-handed twists are observed on the opposite side of the nucleation point. This observation suggests that the growth direction from the nucleation site determines the handedness of the helices. The specified direction of the twist did not change during the growth of the helical forms.

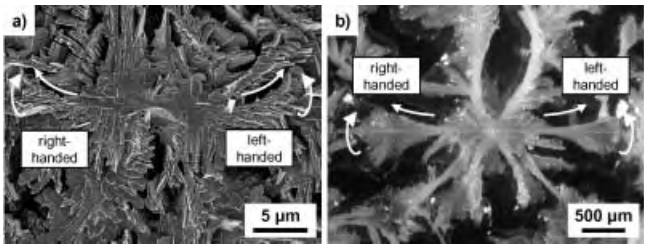


Figure 4. The nucleation point of (a) $K_2Cr_2O_7$ and (b) H_3BO_3 twisted forms grown in PAA and agar matrices, respectively. Left- and right-handed twists are observed on the opposite sides of the nucleation point, as indicated by the arrows.

Recently, Li, Cheng, and co-workers found the presence of twins in nanometer and micrometer scales in a helical polymer crystal consisting of chiral macromolecules.[20] Although their report also suggested the importance of twins for the construction of unique architectures, the correlation between the specific connections of twins and the helical morphology was not sufficiently clarified. The formation of helical architecture requires a pile of twisted twins with a constant angle and direction. Our results suggest that the architecture was achieved by the assembly of tilted subunits in a diffusion field. An increase in the gel density creates the condition for diffusion-limited growth by decreasing the mobility of solute molecules and ions. Consequently, the shapes of grown crystals change from polyhedral forms into regular dendrites and then into irregularly branching morphologies. The regular dendrites are usually composed of single crystals while the irregularly branching morphologies consisted of polycrystals. Thus, under highly diffusion-limited conditions, fast growth of the polycrystalline assembly is preferred over the formation of the more stable form of single crystals. In a diffusion field, the growth rate of a polycrystalline assembly is generally higher than that of single crystals because the growth along the direction of the highest gradient of the solute concentration is permitted in the former owing to an absence of a restriction of growth with specific crystal direction. Twin growth is inferred under moderately diffusion-limited conditions.[21,22] Therefore, the primary twisted unit is formed in a gel as twinned crystals (twins; Figure 1). Finally, the helical architecture is ascribed to assembly of the twinned crystals in a diffusion field. The connection is twisted owing to the tilt of the subunits originating from a lower symmetry of the triclinic crystal structure. The helical morphology with the triclinic crystals corresponds to the dendritic forms with cubic crystals.

When the diffusion process of solute molecules or ions determines the crystal growth, the gradient of the solute concentration around the growing surface is essential for the crystal morphology. The twisted assembly with a pile of tilted subunits in a diffusion field can be explained as follows: In a two-dimensional model, the higher driving force for crystal growth is obtained along direction A, which is the higher gradient of the concentration in a diffusion field (Figure 5a). The difference in the driving force is attributed to the asymmetry of a parallelogrammic subunit. In consequence, twins consisting of the same size of reverse subunits are

 © 2004 Wiley-VCH Verlag GmbH & Co. KGaA, Weinheim

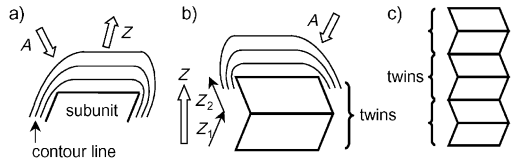


Figure 5. A two-dimensional growth model in a diffusion field. a) Growth of the asymmetric subunit along the higher concentration gradient (direction *A*) is preferable to the faster growth in a diffusion-limited condition. The gradient originated from the shape of the tilted subunit, b) thus, the reversed subunit forms the twins, and then the original growth direction (Z_1 and Z_2) is adjusted to *Z*. c) In this way, the faster growth was achieved to repeat formation of the twins.

produced to achieve faster growth as shown in Figure 5b, and the original growth direction (Z_1 and Z_2) is adjusted to direction *Z*. Since the more elongated reverse subunit would disturb the diffusion field and the faster growth, growth with the formation of the same size of the reverse twins is favorable even though excess interfacial energy is introduced. Therefore, a zigzag architecture would be created by the repetition of the twin formation (Figure 5c). Schultz also indicates that growth velocity is increased by spontaneous twin formation in twisted polymer crystals from the melt although experimental demonstration has not been carried out.[11] In three dimensions, the growth unit of triclinic crystals is tilted (Figure 6a). On the basis of the two-dimensional model, a pile of the same size of reverse subunits that rotate with an angle of 180° would be formed to achieve faster growth (Figure 6b). However, the nucleation probability of the completely reverse form is relatively small. Therefore, the growth direction *Z* is gradually adjusted by the accumulation of twins composed of slightly rotated subunits that have the same size as shown by Z_1, Z_2, Z_3... to Z_{15} (Figure 6). Since the angle of rotation is determined by the lattice matching on the twin plane, a series of twisted twins to reverse the growth direction is formed by a specified number of subunits with a constant angle. Then, the repetition of the twisted unit produces a continuous helical form (Figure 6g).

The direction of the rotation, which is associated with the handedness of the helices, depends on the tilt angle of the growth subunit. As shown in Figure 5b and Figure 6b, the growth direction *Z* of the tilted unit tends to be reversed in a diffusion field. In three dimensions, the daughter subunit is rotated to adjust *Z* toward the reversed position (Figure 6c). The rotated direction, clockwise or counterclockwise, could be explained as follows: Based on the assumption that the rotation of the daughter subunit around point O′ (the center of the top face of the mother subunit), movement of the furthest point P of the daughter subunit from point O (the center of the basal plane of the mother subunit) is essential to determine the rotation direction. Because the O–P distance provides the lowest concentration gradient for the growth of the tilted daughter subunit, the rotation with decrease in the O–P distance leads to advantageous growth conditions. The point P simply approaches the reverse position with counterclockwise rotation of the daughter subunit in the plan view of Figure 6c,d. In contrast, the O–P distance initially increases and then decreases with a clockwise rotation (Figure 6d). Since an increase in the O–P distance is disadvantageous for the reverse of the growth direction, counterclockwise rotation

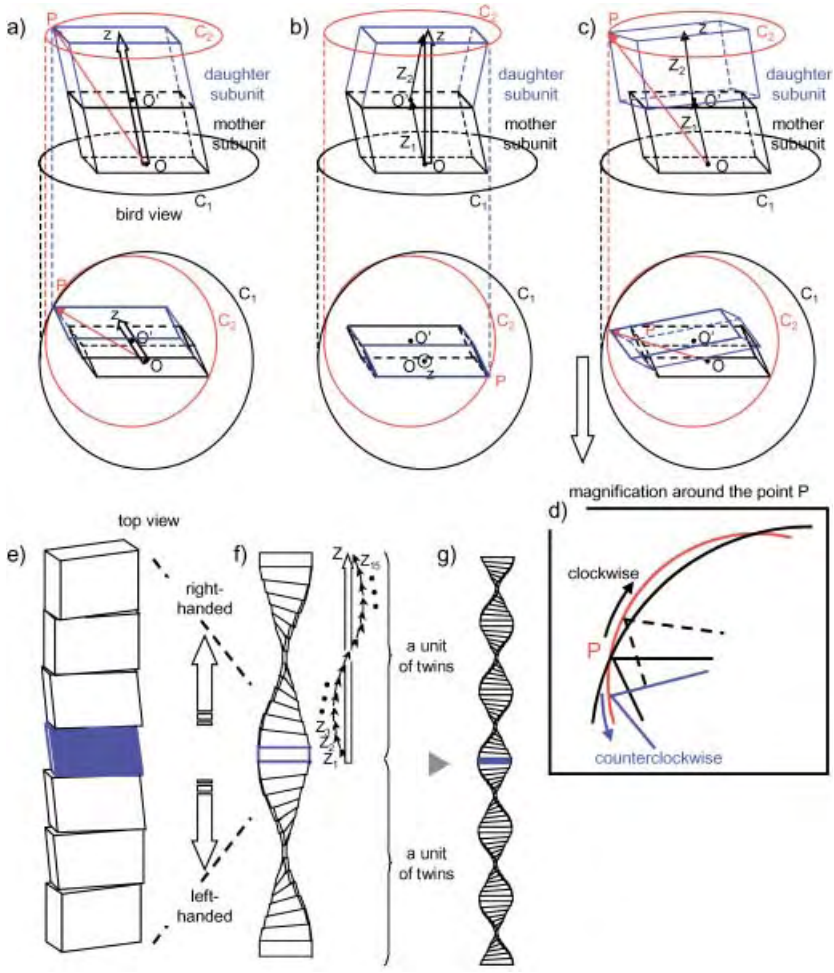


Figure 6. A three-dimensional growth model and formation mechanism of the helical morphology in a diffusion field. a) The growth subunit is tilted. b) The reverse twin could be formed to achieve the faster growth as seen in the two-dimensional model. c) In three dimensions, the formation of slightly rotated twin nuclei is more probable than that of reversed nuclei. d) Magnification of the region around point P, the twisted direction is determined by the variation of the O–P distance. In this case, counterclockwise rotation viewed from the upper sides is preferable to the clockwise rotation. e) According to this model, the upward and downward accumulations induce the right- and left-handed twists, respectively. f) Right- and left-handed units of twins are produced from the nucleation point. The growth direction (Z_1, Z_2, Z_3 to Z_{15}) is finally adjusted to *Z*. g) A pile of units forms helices; the specified direction of twist does not change during growth.

 © 2004 Wiley-VCH Verlag GmbH & Co. KGaA, Weinheim

is more favorable than clockwise rotation. Repetition of the rotation with a certain direction produces a series of twisted twins. Eventually, the formation of daughter subunits on the mother subunit occurs with the counterclockwise rotation, and a right-handed helix is then created with the upward accumulation of subunits, as shown in Figure 6e–g. The counterclockwise rotation is also favorable when the daughter subunits grow under the mother subunit in a manner similar to that described in the previous discussion. In this case, however, a left-handed helix is produced with the downward growth, as shown in Figure 5f. Therefore, right- and left-handed helices would be equally generated with the upward and downward growth, respectively. Actually, right-handed helices were observed on the opposite side of left-handed helices as shown in Figure 4. The pair formation of left- and right-handed helices from a nucleation site strongly supports our model for the formation of helical morphologies. Helical morphologies consisting of H_3BO_3 are also attributable to the same formation mechanism, although the shape of the subunits is different. Interestingly, right-handed helices dominante in the media consisting of biological macromolecules such as agar, gelatin, and pectin, whereas almost the same amounts of left- and right-handed helices were observed in PAA and PVA matrices. This fact indicates that the macroscopic chiral symmetry breaking was induced by the homochirality of the biological molecules. This unique phenomenon could be explained by the twisted-twin model and the stereospecific interaction between the chiral molecules and crystal planes. Details of the specific interaction on the surfaces of triclinic crystals are now under investigation. We identified the backbone of helical morphologies consisting of triclinic crystals. The essence of the formation of the chiral architecture from achiral components is the rotated accumulation of tilted subunits under conditions of diffusion-limited growth. The triclinic crystal structure is not always required for the formation of tilted-growth subunits. Thus, the formation model proposed here would be applicable to various helical architectures and complex morphologies, including twisted ribbons in polymer spherulites. The results described herein provide a novel guideline to the morphogenesis of various helical and twisted forms.

Experimental Section

Materials: We produced two kinds of triclinic crystals, potassium dichromate ($K_2Cr_2O_7$; Kanto chemical, 99.5%) and boric acid (H_3BO_3; Kanto chemical, 99.5%), in gel media to obtain conditions conducive to diffusion-limited growth. These products easily crystallized in aqueous solutions because their solubility varied steeply with temperature. Crystal growth occurred in supersaturated solutions in a gelling agent, such as PVA ($\bar{M}_w = 22000$; Junsei chemical), poly (acrylic acid) ($\bar{M}_w = 250000$, 35wt% aqueous solution; Aldrich chemical), gelatin (Kanto chemical), agar (Junsei chemical), and pectin (Kanto Chemical). Cubic crystals, barium nitrate ($Ba(NO_3)_2$; Koso chemical, 99.0%) and ammonium chloride (NH_4Cl; Kanto chemical, 99.0%), were also prepared by using the same conditions as a contrastive experiment.

Crystallization method 1**:** Inorganic crystals ($K_2Cr_2O_7$, H_3BO_3, $Ba(NO_3)_2$, NH_4Cl) were dissolved in 10 mL of purified hot water. After the crystals had completely dissolved, the solution was mixed with a gelling agent, and then the precursor solution was poured into a flat polystyrene vessel. Gelation of the mixture and subsequent crystal growth in the gel media were achieved by lowering the temperature from 60–100°C to 25°C (method 1).[19] The detailed concentration ranges to obtain the twisted and helical morphologies are described in our previous work[19] and in the figure legends.

Crystallization method 2: We also performed gelation and crystal growth simultaneously by evaporation of water from the mixture at 25°C (method 2). The 1–5 mL of the precursor solution were poured into a flat polystyrene vessel. Helical forms of $K_2Cr_2O_7$ were obtained from the follow concentration ranges; $C_{KC} = 1$–3, $C_{pv} = 0.2$, $C_{PAA} = 2.0$–4.0, $C_{ge} = 0.6$–1.0, $C_{ag} = 0.2$, and $C_{pe} = 0.2$–0.4. C_{KC}, C_{pv}, C_{PAA}, C_{ge}, C_{ag}, and C_{pe} indicate the initial concentration (g/100 g water) of $K_2Cr_2O_7$, PVA, PAA ($\bar{M}_W = 250000$; 35wt% aqueous solution), gelatin, agar, and pectin, respectively. Helical morphology of H_3BO_3 was produced from the precursor containing 1–2 g of H_3BO_3 and 0.2 g of agar per 100 g of water.

Characterization**:** Crystal morphologies were observed by using an optical microscope, a field-emission electron microscope (FESEM, Hitachi S-4700), and a field-emission transmission electron microscope (FETEM, Philips TECNAI F20). The morphologies obtained by method 2 were fundamentally the same as those by method 1. Subsequent observation of the products grown by method 2 was easily performed by using electron microscopes because the crystals were revealed with shrinkage of the matrix.

Received: September 16, 2003
Revised: November 11, 2003 [Z52891]
Published Online: January 27, 2004

Keywords: chirality · crystal growth · gels · helical structures

[1] a) D. S. Lawrence, T. Jiang, M. Levett, *Chem. Rev.* **1995**, *95*, 2229–2260; b) J.-M. Lehn, *Angew. Chem.* **1990**, *102*, 1347–1362; *Angew. Chem. Int. Ed. Engl.* **1990**, *29*, 1304–1319; c) A. H. Clark, S. B. R. Murphy, *Adv. Polym. Sci.* **1987**, *83*, 57–192.

[2] a) R. B. Prince, L. Brunsveld, E. W. Meijer, J. S. Moore, *Angew. Chem.* **2000**, *112*, 234–236; *Angew. Chem. Int. Ed.* **2000**, *39*, 228–230; b) D. A. Frankel, D. F. O'Brien, *J. Am. Chem. Soc.* **1994**, *116*, 10057–10069; c) S. Yamasaki, H. Tatumi, *Bull. Chem. Soc. Jpn.* **1994**, *67*, 906–911; d) K. Hanabusa, M. Yamada, M. Kimura, H. Shirai, *Angew. Chem.* **1996**, *108*, 2086–2088; *Angew. Chem. Int. Ed. Engl.* **1996**, *35*, 1949–1951; e) J. H. Jung, Y. Ono, K. Hanabusa, S. Shinkai, *J. Am. Chem. Soc.* **2000**, *122*, 5008–5009.

[3] a) A. L. McClellan, *J. Chem. Phys.* **1960**, *32*, 1271–1273; b) T. Tachibana, H. Kambara, *J. Am. Chem. Soc.* **1965**, *87*, 3015–3016.

[4] C. Y. Li, J. J. Ge, F. Bai, B. H. Calhoun, F. W. Harris, S. Z. D. Cheng, L. C. Chien, B. Lotz, H. D. Keith, *Macromolecules* **2001**, *34*, 3634–3641, and references therein.

[5] a) J. H. Gerorger, A. Singh, R. R. Price, J. M. Schnur, P. Yager, P. E. Schoen, *J. Am. Chem. Soc.* **1987**, *109*, 6169–6175; b) H. Ihara, M. Takafuji, C. Hirayama, D. F. O'Brien, *Langmuir* **1992**, *8*, 1548–1553; c) B. N. Thomas, C. M. Lindemann, R. C. Corcoran, C. L. Contant, J. E. Kirsch, J. P. Persichini, *J. Am. Chem. Soc.* **2002**, *124*, 1227–1233.

[6] a) W. E. Lindsell, P. N. Preston, J. M. Seddon, G. M. Rosair, A. J. Woodman, *Chem. Mater.* **2000**, *12*, 1572–1576; b) W. Yang, X. Chai, L. Chi, X. Liu, Y. Cao, R. Lu, Y. Jiang, X. Tang, H. Fuchs, T. Li, *Chem. Eur. J.* **1999**, *5*, 1144–1149.

[7] a) J. Liu, F. Zhang, T. He, *Macromol. Rapid Commun.* **2001**, *22*, 1340–1343; b) Z. Barteczak, A. S. Argon, R. E. Cohen, T. Kowalewski, *Polymer* **1999**, *40*, 2367–2380.

[8] a) R. T. K. Baer, P. S. Harris, S. Terry, *Nature* **1975**, *253*, 37–39; b) S. Yang, X. Chen, S. Motojima, *Appl. Phys. Lett.* **2002**, *81*, 3567–3569.

[9] G. W. Sears, *J. Chem. Phys.* **1959**, *31*, 53–54.

 © 2004 Wiley-VCH Verlag GmbH & Co. KGaA, Weinheim

[10] B. Lotz, J. C. Wittmann, *J. Polym. Sci. Part B* **1986**, *24*, 1541 – 1558.
[11] J. M. Schultz, *Polymer* **2003**, *44*, 433 – 441, and references therein.
[12] F. Bernauer, *Gedrillte Kristalle*, Gebrüder Borntraeger, Berlin, **1929**.
[13] a) M. Li, S. Mann, *Langmuir* **2000**, *16*, 7088 – 7094; b) J. D. Hopwood, S. Mann, *Chem. Mater.* **1997**, *9*, 1819 – 1828.
[14] L. A. Gower, D. A. Tirrell, *J. Cryst. Growth* **1998**, *191*, 153 – 160.
[15] a) J. M. Garcia-Ruiz, *J. Cryst. Growth* **1985**, *73*, 251 – 262; b) T. Terada, S. Yamabi, H. Imai, *J. Cryst. Growth* **2003**, *253*, 435 – 444.
[16] J. Suda, T. Nakayama, A. Nakahara, M. Matsushita, *J. Phys. Soc. Jpn.* **1996**, *95*, 771 – 777.
[17] O. Giraldo, S. L. Brock, M. Marquez, S. L. Suib, H. Hillhouse, M. Tsapatsis, *Nature* **2000**, *405*, 38.
[18] a) S. M. Yang, I. Sokolov, N. Coombs, C. T. Kresge, G. A. Ozin, *Adv. Mater.* **1999**, *11*, 1427 – 1431; b) W. J. Kim, S. M. Yang, *Adv. Mater.* **2001**, *13*, 1191 – 1194c) A. M. Seddon, H. M. Patel, S. L. Burkett, S. Mann, *Angew. Chem.* **2002**, *114*, 3114 – 3117; *Angew. Chem. Int. Ed.* **2002**, *41*, 2988 – 2991.
[19] Y. Oaki, H. Imai, *Cryst. Growth Des.* **2003**, *3*, 711 – 716.
[20] X. Weng, C. Y. Li, S. Jin, D. Zhang, J. Z. Zhang, F. Bai, F. W. Harris, S. Z. D. Cheng, *Macromolecules* **2002**, *35*, 9678 – 9686.
[21] M. J. Buerger, *Am. Mineral.* **1945**, *30*, 469 – 482.
[22] A. M. Cody, R. D. Cody, *J. Cryst. Growth* **1995**, *151*, 369 – 374.

 © 2004 Wiley-VCH Verlag GmbH & Co. KGaA, Weinheim

Single-Crystal Clathrates

Single-Crystal Adsorbents: A New Observation Field for Light Aggregates**

Satoshi Takamizawa, Ei-ichi Nakata, and Teruo Saito*

Determination of the properties of low-dimensional aggregates using gas clathrate compounds has interested researchers for the past 50 years.[1] The most ideal system for investigating the physicochemical properties of atomic/molecular aggregates would be single-crystal systems due to their extremely high degree of integrity and regularity. Such systems would contribute to a wide range of both pure and applied science; from basic objects to device applications. A single-crystal adsorbent is one of the goals that may be reached through the design of porous solids, and has been the subject of extensive study in recent years for its extended inorganic framework.[2] The ideal system should provide the long-awaited method for studying physicochemical properties of specific aggregate structures produced within the inner surface of the host solid. In fact, all previous observations were only characterized in powdered samples.[1,3] Here, we present a new convenient procedure for the inclusion of a light gas into a single-crystalline state by placing a crystal adsorbent in a gaseous guest atmosphere, which is efficient for ascertaining exact molecular/atomic structures with high resolution for included light aggregates such as oxygen.

We previously reported the empty crystal host of rhodium(II) benzoate pyrazine, $[Rh_2^{II}(bza)_4(pyz)]_n$ (**1**) (Figure 1),[4]

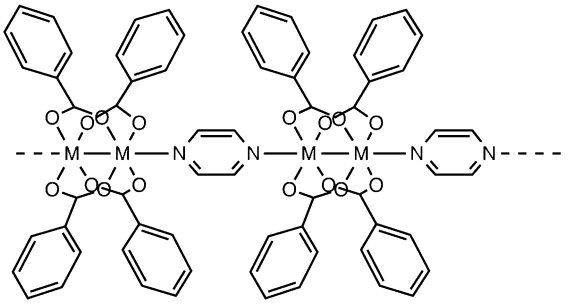


Figure 1. Infinite chain component of **1** ($M = Rh^{II}$).

which generated a CO_2 inclusion crystal by transition from a closed α phase to an open β phase through the process of smooth physisorption; the CO_2 guests are adsorbed into the generated narrow channels of the β lattice.[5] However, serious difficulties remain for other light-gas guests, such as oxygen, nitrogen, and especially hydrogen or helium due to their weak physisorbing capabilities. It was shown for crystal adsorbent **1** that the α–β phase transition obeys the Clausius–Clapeyron equation in terms of the temperature and pressure of the CO_2 gas. This correlation indicates the possibility that a phase transition could be induced by pressurizing the various gaseous guests (pressure swing), which produces inclusion crystals at low temperature, sufficient to crystallize the included guests (temperature swing). We attempted to construct low-dimensional aggregates inside a single crystal of **1** by the swinging method using oxygen gas; the specific cluster is likely to exhibit quantum effects through the magnetic interaction of unpaired electrons.[6]

X-ray diffraction measurements were conducted at temperatures of 298, 90, and 10 K under an oxygen atmosphere, which was prepared by sealing a glass capillary containing a single crystal of **1** and liquid oxygen (2 mm liquid in a 18 mm long capillary) in a liquid nitrogen bath. After the temperature was increased to room temperature, the pressure of the oxygen gas in the capillary was estimated to be ≈ 9 MPa. Surprisingly, the crystal remained intact and transparent under the conditions of high pressure and low temperature (Figure 2).

Single-crystal X-ray diffraction analysis demonstrated that the crystal of **1** had already undergone a phase transition from an α to a β lattice at room temperature,[7] which has one-dimensional channels (see Figure 3a and b), while X-ray crystallography could not locate the oxygen molecules in the channels, probably due to the thermal motion of the adsorbed oxygen. These results show that a bulk phase transition is

[*] Dr. S. Takamizawa, E.-i. Nakata, T. Saito
Graduate School of Integrated Science
Yokohama City University
Kanazawa-ku, Yokohama, Kanagawa 236-0027 (Japan)
Fax: (+81) 45-787-2187
E-mail: staka@yokohama-cu.ac.jp

[**] S.T. acknowledges the financial support of the Yokohama Academic Foundation.

Supporting information for this article is available on the WWW under http://www.angewandte.org or from the author.

 © 2004 Wiley-VCH Verlag GmbH & Co. KGaA, Weinheim DOI: 10.1002/anie.200352982

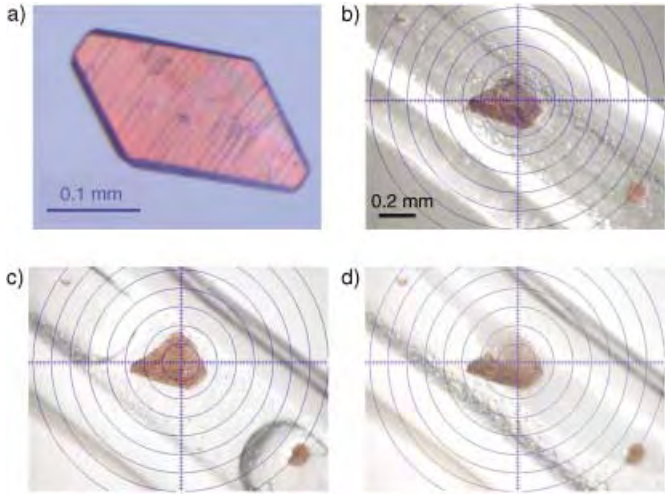


Figure 2. a) Photograph of a red single crystal of **1** under dry conditions; b–d) the same crystal placed in a thick-walled glass capillary and sealed under oxygen gas (≈9 MPa) at 298 K (b), 90 K (c), and 10 K (d). The crystal remained intact under high pressure and low temperature. Oxygen in the capillary was observed in different phases: in the gas phase at 298 K, in liquid–gas equilibrium at 90 K, and in the solid state at 10 K. Liquid oxygen and solid oxygen can be seen in (c) and (d), respectively.

enabled by the pressure swing in a considerably high temperature region for a light gaseous guest.[8] The crystal structure remains essentially unchanged, although the crystal cell parameters change slightly as the temperature decreases. On cooling, the oxygen inclusion crystal was determined to be **1**·3(O_2) at 90 K (see Figure 3c).[9] Oxygen gas, which diffuses in the generated channels of the β lattice, crystallizes between 298 K and 90 K and expands the cell volume by 2.4%, which is probably caused by an increase of the adsorbed oxygen in the channel. It should be noted that the observed temperature of crystallization is much higher than the freezing point of 54.4 K for bulk oxygen under atmospheric pressure, while the oxygen outside the crystal was in the liquid phase (Figure 2c). In comparison, for the case with carbon dioxide, the cell parameters of inclusion crystal **1**·3(O_2) are significantly different from those of **1**·3(CO_2) determined at 93 K (triclinic, $P\bar{1}$, $a = 9.556(3)$, $b = 10.318(4)$, $c = 11.079(5)$ Å, $\alpha = 70.18(3)$, $\beta = 66.12(3)$, $\gamma = 63.02(3)°$, $V = 873.7(6)$ Å^3),[5] in which the cell volume of **1**·3(O_2) is 3% less than that of **1**·3(CO_2). These observations of the flexibility of the crystal lattice clearly show the adjustable nature of **1** for variable guest structures. In addition, a 1.8% contraction of the inclusion crystal at 10 K[10,11] from that at 90 K is observed, which is primarily due to diminished thermal vibration (see Figure 3d).

At 90 K, the included oxygen molecules are coherently aligned in a linear fashion. The intermolecular distances between molecule centers among the contacted neighbors are 3.55 and 4.24 Å, forming molecular oxygen chains along the one-dimensional channels. The chain structure is most likely regulated by the channel structure (see Figure 3e and g). The parallel oxygen chains are effectively separated by a distance of ≈1 nm, which can be regarded as the first example of a single-molecular-chain oxygen crystal within a host lattice. The O–O atomic separations in the oxygen molecules were found to be too short (1.001(14) Å and 0.958(14) Å), which was determined without any constraints. However, a remarkable feature is that the included oxygen structure was easily located without disorder at the considerably high temperature of 90 K, where the thermal motion is effectively suppressed by the cooperative stabilization of the confined guest oxygen and the adjustable host lattice. In fact, even at 50 K, an extremely strongly disordered structure was observed for bulk oxygen in the γ phase.[12] In contrast, the O–O atomic separations in the oxygen molecules became reasonable at 10 K (1.147(17) Å and

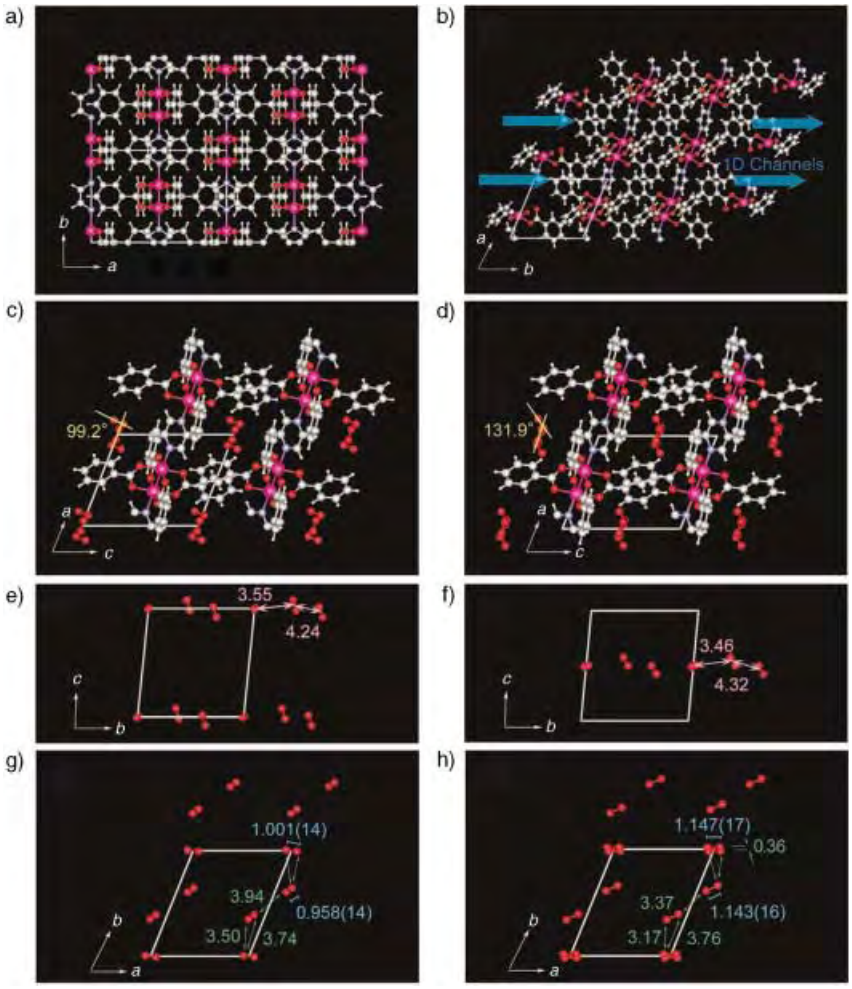


Figure 3. Crystal structure of **1** under various conditions: Pressure-swing transformation from a closed structure without gas (α lattice, *C*2/*m*, reported in ref. [5]) (a) to an open structure (β lattice, $P\bar{1}$) (b) under 9 MPa oxygen pressure at room temperature; views of an oxygen inclusion crystal viewed along the *b* axis at 90 K (c) and 10 K (d); molecular chains of oxygen molecules inside crystal **1** at 90 K (e, g) and 10 K (f, h) with selected distances [Å] and O-O···O-O torsion angles [°] (Rh magenta, O red, C and H gray, N blue).

 © 2004 Wiley-VCH Verlag GmbH & Co. KGaA, Weinheim

1.143(16) Å). These values represent the first exact bond lengths of molecular oxygen by single-crystal X-ray analysis, while the O–O bond length in α-phase solid oxygen was evaluated to be approximately between 1.15 and 1.22 Å by powder X-ray diffraction analysis at 23 K.[13] The periodic arrangement and configuration of the oxygen atoms in the chain became more crowded at 10 K. The intermolecular distances became short at (3.46 Å) and long (4.32 Å), respectively (see Figure 3 f). The longer separation is accompanied by a short contact between neighboring oxygen atoms at 3.37 Å; the shorter distance is realized by a separation of 0.36(9) Å of the separated oxygen molecules by disorder along the *c* edge (see Figure 3 f and h). The transformation in the oxygen chain indicates that a phase transition occurs in 1D systems of oxygen in regions of low temperature. Thus, a 1D oxygen system will be expected to show its unknown phases with properties of interest because many phases of 3D solid oxygen (bulk), and for 2D (on the surface) have been known to be correlated with specific magnetic properties and conductivity.[14]

The present construction procedure is considered quite effective for light guests, which are difficult to condense, because this method requires a certain gas pressure and can crystallize guests at considerably high temperatures. Furthermore, this procedure has the potential for producing various crystals within the structure of the single-crystal adsorbent, and preferred adsorbates under the control of thermodynamic factors. The derivatives of rhodium(II) benzoate pyrazine replaced with a different metal ion and substituted ligands would produce the first family of specifically designed single-crystal adsorbents. Our investigations[15] and the results for other gas-inclusion crystals will appear elsewhere. The homogeneity, anisotropy, integrity, and transparency of single-crystal adsorbents contributes to the establishment of new techniques for realizing simultaneous measurements for various specific aggregates inside a crystal lattice with new phases. This would be particularly effective for observing specific quantum effects in many low-dimensional systems.

Experimental Section

All single-crystal X-ray analyses were performed on a Bruker Smart APEX CCD area diffractometer with a helium-flow temperature controller (Japan Thermal Eng. TC-10 KCP) using graphite-monochromated $Mo_{K\alpha}$ radiation ($\lambda = 0.71073$ Å). Empirical absorption corrections were applied using the SADABS program. The structures were solved by direct methods (SHELXS 97) and refined by full-matrix least-squares calculations on F^2 (SHELXL-97) using the SHELX-TL program package. Non-hydrogen atoms were refined anisotropically; hydrogen atoms were fixed at calculated positions and refined using a riding model. CCDC-220620–220624 contain the supplementary crystallographic data for this paper. These data can be obtained free of charge via www.ccdc.cam.ac.uk/conts/retrieving.html (or from the Cambridge Crystallographic Data Centre, 12, Union Road, Cambridge CB21EZ, UK; fax: (+44) 1223-336-033; or deposit@ccdc.cam.ac.uk).

Received: October 1, 2003 [Z52982]

Keywords: clathrates · host–guest systems · nanostructures · solid-state structures · X-ray diffraction

[1] a) D. F. Evans, R. E. Richards, *Nature* **1952**, *170*, 246; b) A. H. Cooke, H. Meyer, W. P. Wolf, *Proc. R. Soc. London Ser. A* **1957**, *225*, 112–122.

[2] a) For example, O. M. Yaghi, M. O'Keefe, N. W. Ockwig, H. K. Chae, M. Eddaoudi, J. Kim, *Nature* **2003**, *423*, 705–714; b) W. Mori, S. Takamizawa in *Organometallic Conjugation* (Eds.: A. Nakamura, N. Ueyama, K. Yamaguchi), Kodansha Springer, Tokyo, **2002**, chap. 6, pp. 179–213; c) S. Inagaki, S. Guan, T. Ohsuma, O. Terasaki, *Nature* **2002**, *416*, 304–307.

[3] a) W. Mori, T. C. Kobayashi, J. Kurobe, K. Amaya, Y. Namuri, K. Kindo, H. A. Katori, T. Goto, N. Miura, S. Takamizawa, H. Nakamaya, K. Yamaguchi, *Mol. Cryst. Liq. Cryst.* **1997**, *306*, 1–7; b) R. Kitaura, S. Kitagawa, Y. Kubota, T. C. Kobayashi, K. Kindo, Y. Mita, A. Matsuo, M. Kobayashi, H. Chang, T. C. Ozawa, M. Suzuki, M. Sakata, M. Takata, *Science* **2002**, *298*, 2358–2361.

[4] S. Takamizawa, T. Hiroki, E. Nakata, K. Mochizuki, W. Mori, *Chem. Lett.* **2002**, 1208–1209.

[5] S. Takamizawa, E. Nakata, H. Yokoyama, K. Mochizuki, W. Mori, *Angew. Chem.* **2003**, *115*, 4467–4470; *Angew. Chem. Int. Ed.* **2003**, *42*, 4331–4334.

[6] a) F. D. M. Haldane, *Phys. Lett. A* **1983**, *93*, 464–468; b) M. Okumura, S. Yamanaka, W. Mori, K. Yamaguchi, *THEOCHEM* **1994**, *116*, 177–183; c) M. Otani, H. Miyagi, N. Suzuki, *Physica B* **1999**, *265*, 60–63.

[7] Crystal data for **1** at 298 K in ≈9 MPa of oxygen gas: 770.35 g mol^{-1}, triclinic, $P\bar{1}$, $a = 9.474(8)$, $b = 10.222(13)$, $c = 10.715(13)$ Å, $\alpha = 72.09(2)$, $\beta = 64.933(13)$, $\gamma = 62.737(14)°$, $V = 827.2(16)$ Å^3, $Z = 1$, $\rho_{calcd} = 1.546$ Mg m^{-3}, $R_1 = 0.0994$ (0.2202), $wR_2 = 0.2248$ (0.2726) for 770 reflections with $I > 2\sigma(I)$ (for 1721 reflections (2908 total measured)), GOF (F^2) = 0.957, largest diff. peak (hole) = 1.193(−2.763) e Å^{-3}.

[8] The α–β phase transition was not observed for **1** when wrapped up in silicon grease (under gas cut-off conditions) under an oxygen pressure of ≈10 MPa. This shows that gas adsorption causes the crystal-phase transition. Crystal data for **1** at 298 K (10 MPa): 770.35 g mol^{-1}, monoclinic, *C*2/*m*, $a = 18.12(3)$, $b = 9.552(13)$, $c = 12.352(18)$ Å, $\beta = 128.52(2)°$, $V = 1672(4)$ Å^3, $Z = 2$, $\rho_{calcd} = 1.530$ Mg m^{-3}, $R_1 = 0.0859$ (0.1377), $wR_2 = 0.2152$ (0.2404) for 569 reflections with $I > 2\sigma(I)$ (for 944 reflections (2707 total measured)), GOF (F^2) = 1.073, largest diff. peak (hole) = 1.152(−1.246) e Å^{-3}.

[9] Crystal data for **1**·3(O_2) at 90 K: 866.36 g mol^{-1}, triclinic, $P\bar{1}$, $a = 9.573(3)$, $b = 10.381(3)$, $c = 10.597(3)$ Å, $\alpha = 74.165(5)$, $\beta = 64.346(6)$, $\gamma = 63.723(6)°$, $V = 846.9(4)$ Å^3, $Z = 1$, $\rho_{calcd} = 1.699$ Mg m^{-3}, $R_1 = 0.0560$ (0.0982), $wR_2 = 0.1045$ (0.1182) for 2629 reflections with $I > 2\sigma(I)$ (for 4182 reflections (6175 total measured)), GOF (F^2) = 0.936, largest diff. peak (hole) = 2.160(−1.614) e Å^{-3}.

[10] Crystal data for **1**·3(O_2) at 10 K: 866.36 g mol^{-1}, triclinic, $P\bar{1}$, $a = 9.571(3)$, $b = 10.288(3)$, $c = 10.531(3)$ Å, $\alpha = 74.379(6)$, $\beta = 64.127(5)$, $\gamma = 63.558(5)°$, $V = 831.8(4)$ Å^3, $Z = 1$, $\rho_{calcd} = 1.730$ Mg m^{-3}, $R_1 = 0.0682$ (0.1114), $wR_2 = 0.1503$ (0.1775) for 2735 reflections with $I > 2\sigma(I)$ (for 4063 reflections (5802 total measured)), GOF (F^2) = 0.986, largest diff. peak (hole) = 3.451(−1.905) e Å^{-3}.

[11] The crystal structure of **1** at 10 K in an inert oil (under gas cut-off conditions) was regarded as the same structure as that of **1** at 93 K (γ phase) in an inert oil reported in ref [5]. Crystal data for **1** in an inert oil at 10 K: 770.35 g mol^{-1}, monoclinic, *C*2/*c*, $a = 17.384(4)$, $b = 9.5754(19)$, $c = 19.522(4)$ Å, $\beta = 98.561(8)°$, $V = 3213.4(12)$ Å^3, $Z = 4$, $\rho_{calcd} = 1.592$ Mg m^{-3}, $R_1 = 0.0625$ (0.1036), $wR_2 = 0.1210$ (0.1441) for 2852 reflections with $I > 2\sigma(I)$ (for 4049 reflections (11742 total measured)), GOF (F^2) = 1.093, largest diff. peak (hole) = 1.109(−1.542) e Å^{-3}.

 © 2004 Wiley-VCH Verlag GmbH & Co. KGaA, Weinheim

[12] T. H. Jordan, W. E. Streib, H. W. Smith, W. N. Lipscomb, *Acta Crystallogr.* **1964**, *17*, 777 – 778.
[13] C. S. Barrett, L. Meyer, J. Wasserman, *J. Chem. Phys.* **1967**, *47*, 592 – 597.
[14] a) K. Shimizu, K. Suhara, M. Ikumo, M. I. Eremets, K. Amaya, *Nature* **1998**, *393*, 767 – 769; b) T. Shibata, Y. Murakami, T. Watanuki, H. Suematsu, *Surf. Sci.* **1998**, *405*, 153 – 171.
[15] a) W. Mori, H. Hoshino, Y. Nishimoto, S. Takamizawa, *Chem. Lett.* **1999**, 331 – 332; b) W. Mori, H. Hoshino, K. Horikawa, Y. Nishimoto, S. Takamizawa, *Mol. Cryst. Liq. Cryst.* **2000**, *342*, 193 – 198; c) S. Takamizawa, E. Nakata, H. Yokoyama, *Inorg. Chem. Commun.* **2003**, *6*, 763 – 765; d) S. Takamizawa, E. Nakata, T. Saito, H. Yokoyama, *Inorg. Chem. Commun.* **2003**, *6*, 1326 – 1328; e) S. Takamizawa, E. Nakata, T. Saito, *Inorg. Chem. Commun.* **2004**, *7*, 1 – 3; f) S. Takamizawa, E. Nakata, T. Saito, *Inorg. Chem. Commun.* **2004**, *7*, 125 – 127.

 © 2004 Wiley-VCH Verlag GmbH & Co. KGaA, Weinheim

Tetracoordinate Planar Nonmetals

M_4H_4X: Hydrometals (M = Cu, Ni) Containing Tetracoordinate Planar Nonmetals (X = B, C, N, O)**

Si-Dian Li, Guang-Ming Ren, Chang-Qing Miao, and Zhi-Hao Jin*

Tetracoordinate planar carbon (that is, carbon atoms coordinated by four other atoms in a square-planar arrangement), first proposed by Hoffmann et al.[1] over thirty years ago, was recently observed in the vibrationally averaged D_{4h} $[Al_4C]^-$,[2] C_{2v} Al_3XC, $[Al_3XC]^-$ (X = Si,Ge),[3,4] and $[CAl_4]^{2-}$.[5] Tetracoordinate planar (TP) Si and Ge centers were also discovered in MAl_4 and $[MAl_4]^-$.[6] The TP bonding character of Group 14 elements, contrary to the conventional concept of tetrahedral C, Si, and Ge, is supported by excellent agreements between the measured photoelectron spectra and ab initio vertical detachment energies (VDE) of these molecules in the TP structures.

Here we extend the range of TP centers to include B, N, and O and the ligands from p-block elements to d-block transition metals (Cu and Ni). On the basis of ab initio optimization results, we present the first theoretical evidence that, in the form of the X-centered hydrometals M_4H_4X, these first-row nonmetals X (X = B, C, N, O) are tetracoordinated by four transition-metal ligands M (M = Cu, Ni) in perfect squares. Hydrocopper Cu_4H_4 and hydronickel Ni_4H_4 are found to be suitable for hosting these tetracoordinate planar nonmetals (TPNs) with the high symmetry of D_{4h}. To the best of our knowledge, neither experimental nor theoretical data on these unusual molecules are available to date. Our work was stimulated by the proposal of aromatic hydrocopper Cu_4H_4 at the DFT level.[7]

Various initial structures obtained at the B3LYP/Lanl2dz level were optimized at the B3LYP/6-311 + G(3df,p) level, and imaginary frequencies were checked at the same level. The DFT binding energies of 23.1 eV for D_{4h} Ni_4H_4C and 18.7 eV for C_{4v} Cu_4H_4C demonstrate the stability of these complexes with respect to dissociation. The B3LYP geometries were further refined with the second-order Møller–Plesset (MP2) procedure. We calculated the NMR shielding tensors using the gauge-independent atomic orbital (GIAO) procedure[8,9] at the B3LYP/6-311 + G(3df,p) level, and VDEs, ionization potentials (IPs), and electron affinities (EAs) utilizing the restricted outer valence Green function method (ROVGF)[10,11] with a smaller basis of 6-31 + G(d,p). The optimized MP2 bond parameters, normal vibrational frequencies, and electronic properties of these systems are provided in the Supporting Information. All the calculations were performed with the Gaussian 03 program.[12]

The optimized structures and corresponding HOMOs of the Cu_4H_4X series at the B3LYP level are depicted and compared with that of Cu_4H_4 in Figure 1a. The MP2 bond lengths were found to be about 5% shorter than the corresponding B3LYP values. Both $[Cu_4H_4N]^+$ and $[Cu_4H_4O]^{2+}$ have D_{4h} minima with TP N and TP O at the centers of the molecules. Their pyramidal (C_{4v}) and butterfly (D_{2d}) isomers are converted to the D_{4h} minima automatically during structural optimization, and other structures are either much higher in energy or high-order stationary points. Planar D_{4h} $[Cu_4H_4B]^-$ and Cu_4H_4C, on the other hand, were found to be transition states with imaginary frequencies of 266*i* and 135*i* cm^{-1}, respectively, and lie 0.962 and 0.124 eV higher in energy than the corresponding tetracoordinate pyramidal C_{4v} structures. These imaginary frequencies correspond to the A_{2u} vibrational mode, in which the central atom X moves up and down along the fourfold axis. Distortion of the D_{4h} structure in the A_{2u} mode leads to the C_{4v} global minimum, in which the X atom lies about 0.5 Å above the Cu_4 plane. Note that the HOMOs of both D_{4h} $[Cu_4H_4N]^+$ and $[Cu_4H_4O]^{2+}$ feature delocalized cyclic σ bonds along the -Cu-H-Cu- peripheries. This characteristic bond plays a critical role in stabilizing the D_{4h} structures of $[Cu_4H_4N]^+$ and $[Cu_4H_4O]^{2+}$, and it is clearly inherited in the pyramidal C_{4v} ground states of both $[Cu_4H_4B]^-$ and Cu_4H_4C, in which the nearly pure lone pair of $2p_z$ electrons of the central atom (discussed in detail below) overlaps partially with the cyclic σ bond. However, a cyclic σ HOMO does not exist in the D_{4h} transition states of Cu_4H_4C and $[Cu_4H_4B]^-$, which have Cu–H separations greater than 1.700 Å. Instead of forming delocalized cyclic σ bonds, both

[*] Prof. S.-D. Li, Dr. G.-M. Ren, C.-Q. Miao
Institute of Materials Sciences and
Department of Chemistry
Xinzhou Teachers' University
Xinzhou 034000, Shanxi (P. R. China)
Fax: (+86) 350-303-1845
E-mail: lisidian@yahoo.com
Prof. Z.-H. Jin
School of Materials Science and Engineering
Xian Jiaotong University
Xian 710049 (P. R. China)

[**] This work was financially supported by The Shanxi Natural Science Foundation. We are grateful to Dr. Hai-Jun Jiao and Hai-Shun Wu for inspiring discussions.

Supporting information for this article is available on the WWW under http://www.angewandte.org or from the author.

 DOI: 10.1002/anie.200353068 © 2004 Wiley-VCH Verlag GmbH & Co. KGaA, Weinheim

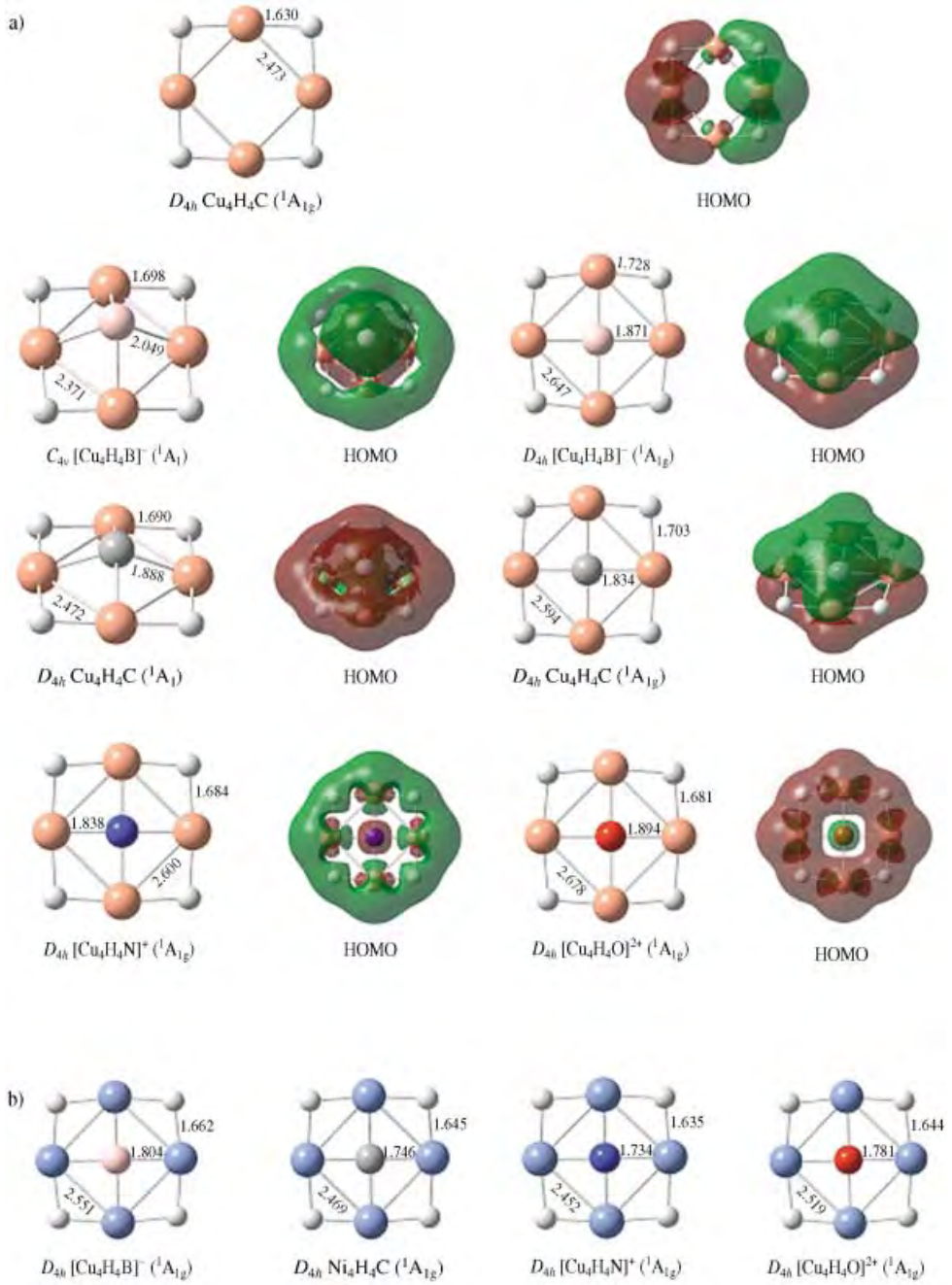


Figure 1. a) Optimized structures of the Cu_4H_4X series and their corresponding HOMOs, compared with those of hydrocopper Cu_4H_4; b) optimum structures of D_{4h} Ni_4H_4X (X = B, C, N, O) at the B3LYP/6-311+G(3df,p) level.

planar D_{4h} Cu_4H_4C and $[Cu_4H_4B]^-$ feature delocalized π HOMOs composed purely of contributions from the four Cu ligands and X center. This π interaction is not strong enough to prevent the D_{4h} planar structure from being distorted along the A_{2u} mode.

Natural bond orbital (NBO) analyses indicate that, in both D_{4h} and C_{4v} ground states, there is considerable electron transfer from the Cu ligands to the more electronegative center X, and the interactions between them exhibit clear ionic characteristics. For example, D_{4h} $[Cu_4H_4N]^+$ has atomic charges of Cu +1.00, N −1.62, and H −0.34 $|e|$ and the atomic charges of C_{4v} Cu_4H_4C are Cu +0.87, C −1.83, and H −0.41 $|e|$. In the transition states of D_{4h} $[Cu_4H_4B]^-$ and Cu_4H_4C, B and C carry even higher negative charges of −2.57 and −2.06 $|e|$ respectively. More detailed analysis shows that the central atoms X have three sp^2 hybrids and a nearly pure lone pair of $2p_z$ electrons perpendicular to the Cu_4 plane. For instance, the N atom in D_{4h} $[Cu_4H_4N]^+$ has the electron configuration $[He]2s^{1.95}2p_x^{1.32}2p_y^{1.32}2p_z^{1.96}$, and C in C_{4v} Cu_4H_4C has $[He]2s^{1.92}2p_x^{0.92}2p_y^{0.92}2p_z^{1.85}$, with both $2p_z$ atomic orbitals nearly fully filled. This observation is in line with Hoffmann's proposal[1] that the TP C in planar CH_4 has a pure lone pair of $2p_z$ electrons and there is considerable electron transfer from ligands H to central atom C.

 © 2004 Wiley-VCH Verlag GmbH & Co. KGaA, Weinheim

The coordination chemistry of X-centered hydronickel Ni_4H_4X is simpler. All the first-row nonmetals X = B, C, N, and O can be nicely fitted at the center of hydronickel Ni_4H_4 to form TPN centers (Figure 1b), and all these D_{4h} structures were confirmed to be true minima with no imaginary frequency. The NBO occupancy analyses indicate that, compared to Cu–X interactions, Ni–X bonds exhibit more covalent characteristics, except for Ni–O. This bonding feature is also supported by the observation that the nonmetal centers in D_{4h} Ni_4H_4X have much smaller negative charges than those in Cu_4H_4X. For example, the N center in D_{4h} $[Ni_4H_4N]^+$ carries a negative charge of $-0.79\,|e|$, about half the corresponding value of $-1.62\,|e|$ in D_{4h} $[Cu_4H_4N]^+$. In D_{4h} Ni_4H_4C, which represents the first TP carbon atom at the center of a perfect square of transition-metal atoms, Ni, C, and H atoms carry atomic charges of $+0.47$, -0.55, and $-0.33\,|e|$ and have electron configurations of $Ni[Ar]4s^{0.30}3d^{9.22}$, $C[He]2s^{1.49}2p^{3.01}$, and H $1s^{1.33}$, respectively. Here, the C center bears less than one-third of the negative charge of $-1.83\,|e|$ it carries in C_{4v} Cu_4H_4C. This charge distribution shows that the transfer of valence electrons from Ni to X is much less effective than that from Cu. The reduced charge transfer is partially reflected in the low occupancies of the $2p_z$ orbitals of the central atoms. For instance, B, C, N, and O centers in D_{4h} Ni_4H_4X systems have the electronic configurations of $B[He]2s^{1.20}2p_x^{0.84}2p_y^{0.84}2p_z^{0.39}$, $C[He]2s^{1.49}2p_x^{1.16}2p_y^{1.16}2p_z^{0.68}$, $N[He]2s^{1.69}2p_x^{1.48}2p_y^{1.48}2p_z^{1.09}$, and $O[He]2s^{1.84}2p_x^{1.73}2p_y^{1.73}2p_z^{1.55}$, respectively. The occupancies of the $2p_z$ orbitals increase quickly with increasing electronegativity of the central atoms. In addition, frequency analysis indicates that the H-bridged planar D_{4h} hydronickel Ni_4H_4 is a second-order transition state with two imaginary frequencies of $163i$ and $71i$ cm^{-1}. It is the introduction of an X atom at the center and the formation of four equivalent Ni–X interactions that stabilize the Ni_4H_4 square.

As nonmetal atoms X occupy the centers of heavy-atom squares in D_{4h} M_4H_4X, we checked the variation of relative NMR chemical shifts δ_H of the bridging H atoms in different systems to assess their aromaticity. Relative to the nuclear magnetic shielding tensor of H atoms (31.9 ppm) in T_d $Si(CH_3)_4$ (TMS), $\delta_H = -7.6$ ppm in benzene and -0.4 ppm in hydrocopper Cu_4H_4, with both demonstrating the ring-current effect of aromatic systems. The bridging H atoms in the M_4H_4X series, however, have positive δ_H values which show that these H atoms are located at higher field than $Si(CH_3)_4$ in NMR spectra. In the Cu_4H_4X series, $\delta_H = +1.4$, $+1.2$, $+0.8$, and $+3.7$ ppm for X = B, C, N, and O, respectively. In the Ni_4H_4X systems, the H atoms are shifted to even higher field. For instance, $\delta_H = +5.5$, $+4.3$, and $+3.2$ ppm for X = B, C, and N. These results are in line with $\delta_H = +0.6$ ppm for the two bridging H atoms in D_{2h} B_2H_6. The upfield NMR chemical shifts of bridging H atoms outside the M_4 squares show that, unlike aromatic benzene and hydrocopper,[7] M_4H_4X systems are nonaromatic. Introducing an X atom at the molecular center breaks the ring current in Cu_4H_4. These unusually high NMR chemical shifts could help to experimentally identify M_4H_4X molecules frozen in suitable matrices.

The lowest two VDEs of $[Cu_4H_4B]^-$, the first IP and EA of Cu_4H_4C, and first EAs of $[Cu_4H_4N]^+$ and $[Cu_4H_4O]^{2+}$ calculated at the B3LYP and MP2 levels generally agree well and lie within the energy ranges of conventional photoelectron measurements. For instance, C_{4v} $[Cu_4H_4B]^-$ has the two lowest VDEs of 2.51 and 4.86 eV, while the corresponding values of the D_{4h} transition state are 2.13 and 3.98 eV. For C_{4v} Cu_4H_4C, IP = 8.46 and EA = 0.97 eV. Its D_{4h} transition state has IP = 9.40 and EA = 0.38 eV. These values can be used in identifying corresponding species and distinguishing different isomers by gas-phase photoelectron spectroscopy.

In summary, we have presented the first theoretical evidence for TPN atoms hosted at the centers of perfect squares of transition-metal atoms, which parallels the result obtained for TP carbon[2] hosted at the center of an Al_4^{2-} square.[13] Latest optimization results indicate that heterocyclic hydrometal systems $Cu_xNi_yH_4$ ($x+y=4$) with lower symmetries exhibit similar behavior. These predictions await experimental confirmation, which would open a new branch of chemistry of hydrometals with TPN centers that may have important applications as catalysts.

Received: October 13, 2003 [Z53068]

Keywords: ab initio calculations · copper · density functional calculations · electronic structure · nickel

[1] R. Hoffmann, R. W. Alder, C. F. Wilcox, Jr., *J. Am. Chem. Soc.* **1970**, *92*, 4992.
[2] X. Li, L.-S. Wang, A. I. Boldyrev, J. Simons, *J. Am. Chem. Soc.* **1999**, *121*, 6033.
[3] L. S. Wang, A. I. Boldyrev, X. Li, J. Simons, *J. Am. Chem. Soc.* **2000**, *122*, 7681.
[4] X. Li, H.-J. Zhai, L.-S. Wang, *Chem. Phys. Lett.* **2002**, *357*, 415.
[5] X. Li, H.-F. Zhang, L.-S. Wang, G. D. Geske, A. I. Boldyrev, *Angew. Chem.* **2000**, *112*, 3776; *Angew. Chem. Int. Ed.* **2000**, *39*, 3630.
[6] A. I. Boldyrev, X. Li, L.-S. Wang, *Angew. Chem.* **2000**, *112*, 3445; *Angew. Chem. Int. Ed.* **2000**, *39*, 3307.
[7] A. C. Tsipis, C. A. Tsipis, *J. Am. Chem. Soc.* **2003**, *125*, 1136.
[8] R. Ditchfield, *Mol. Phys.* **1974**, *27*, 789 K. Wolinski, J. F. Hilton, P. Pulay, *J. Am. Chem. Soc.* **1990**, *112*, 8251.
[9] S.-D. Li, H.-L. Yu, H.-S. Wu, Z.-H. Jin, *J. Chem. Phys.* **2002**, *117*, 9543.
[10] W. von Niessen, J. Schirmer, L. S. Cederbaum, *Comput. Phys. Rep.* **1984**, *1*, 57.
[11] V. G. Zakrzewski, J. V. Ortiz, J. A. Nichols, D. Heryadi, D. L. Yeager, J. T. Golab, *Int. J. Quantum Chem.* **1996**, *60*, 29.
[12] Gaussian 03, Revision A.1, M. J. Frisch, G. W. Trucks, H. B. Schlegel, G. E. Scuseria, M. A. Robb, J. R. Cheeseman, V. G. Zakrzewski, J. A. Montgomery, R. E. Stratmann, J. C. Burant, S. Dapprich, J. M. Millam, A. D. Daniels, K. N. Kudin, M. C. Strain, O. Farkas, J. Tomasi, V. Barone, M. Cossi, R. Cammi, B. Mennucci, C. Pomelli, C. Adamo, S. Clifford, J. Ochterski, G. A. Petersson, P. Y. Ayala, Q. Cui, K. Morokuma, D. K. Malick, A. D. Rabuck, K. Raghavachari, J. B. Foresman, J. Cioslowski, J. V. Ortiz, B. B. Stefanov, G. Liu, A. Liashenko, P. Piskorz, I. Komaromi, R. Gomperts, R. L. Martin, D. J. Fox, T. Keith, M. A. Al-Laham, C. Y. Peng, A. Nanayakkara, C. Gonzalez, M. Challacombe, P. M. W. Gill, B. G. Johnson, W. Chen, M. W. Wong, J. L. Andres, M. Head-Gordon, E. S. Replogle, J. A. Pople, Gaussian, Inc., Pittsburgh, PA, **2003**.
[13] X. Li, A. E. Kuznetsov, H.-F. Zhang, A. I. Boldyrev, L.-S. Wang, *Science* **2001**, *291*, 859.

 © 2004 Wiley-VCH Verlag GmbH & Co. KGaA, Weinheim

Supramolecular Chemistry

Formation of Two-Dimensional Supramolecular Icelike Layer Containing $(H_2O)_{12}$ Rings**

Bao-Qing Ma, Hao-Ling Sun, and Song Gao**

Water is still not fully understood, though intensive investigations have been performed both experimentally and theoretically[1] because of its fundamental importance in biological and chemical processes.[2] Structural information of small water clusters is the first step towards understanding the behavior of bulk water. Thus, there has been an extensive investigation of water structures in recent years. A variety of water clusters including hexamers,[3,4] octamers,[5,6] and decamers,[7] found in a number of crystal hosts, have been structurally characterized and display very different configurations.

Structurally, the low-dimensional polymeric water/ice lies in between water clusters and bulk water and has physical properties closely associated with those of bulk water. However, understanding the growth of larger water clusters and how the clusters link to form a large network is still challenging, though some polymeric water phases consisting of basic water tetramer and hexamer subunits have been reported.[8–11] Very recently, two 2D water/ice layers containing large 12-[12] or 18-membered[13] water rings have been observed in solid states, which provide novel structural aspects of water and new insights into water with implications in biological environments. In this context, we describe two 1D and 2D water morphologies observed in the supramolecular solid-state complexes bpedo·2 H_2O (**1**) and bpedo·5 H_2O (**2**; bpedo = *trans*-bis(4-pyridyl)ethylene dioxide). The strong capability of O,O′-bifunctional 4-pyridyl spacers of forming hydrogen bonds with water molecules is known in supramolecular chemistry and crystal engineering.[14] Thus, employing such a compound is expected to facilitate the formation of various degrees of water aggregates.

Compounds **1** and **2** were obtained from methanol and aqueous solution, respectively. Single-crystal X-ray diffraction analysis[15] revealed that the hydrogen-bonding association of water molecules in compound **1** leads to the formation of 1D segregated water chain along the [001] direction (Figure 1). The chain consists of a sequence of O1w-O1w-O2w-O2w (Oxw = water oxygen center) with inversion centers lying in between two O1w and two O2w units. The inversion center leads to disorder of the water hydrogen atoms in the chain over two positions because of symmetry-imposed hydrogen-bonding interactions. The remaining hydrogen atom on each water is bonded to a bpedo moiety, which links the water chains in *trans*-mode (Scheme 1 a) into a 2D sheet (Figure 1). There are significant π–π interactions between adjacent bpedo molecules in the sheet which are separated by a distance of 3.22 Å.

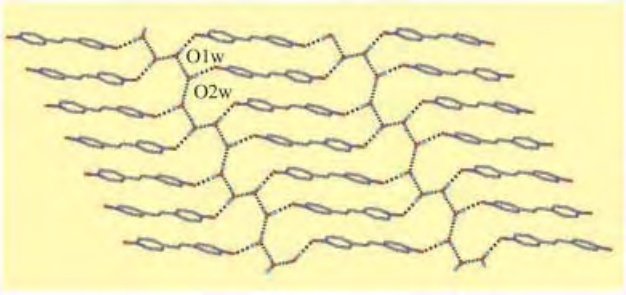
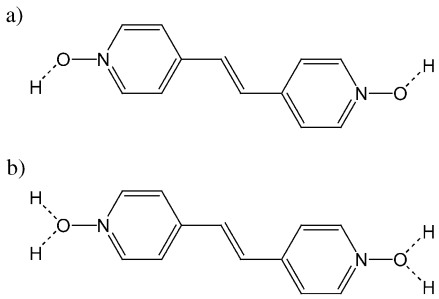


Figure 1. 2D sheet consisting of 1D segregated water chains and bpedo linker molecules in **1**.



Scheme 1. Hydrogen bonding of bpedo to water; a) *trans* mode, b) μ_4-hydrogen-bond mode.

Compound **2** contains an ordered 2D hydrogen-bonded water layer (Figure 2 a). Hydrogen-bonding association generates a 12-membered water ring consisting of six O3w, four O1w, and two O2w centers, which is symmetric over a crystallographic twofold axis passing through O1w. These 12-membered rings are fused together to form a 2D supramolecular $(H_2O)_{12}$ morphology with a corrugated sheet (Figure 2 b). The geometric parameters of the $(H_2O)_{12}$ ring are summarized in Table 1. The average O···O separation of 2.748 Å (90 K) or 2.776 Å (295 K) in the supramolecular $(H_2O)_{12}$ morphology is very close to the corresponding value of 2.759 Å in ice I_h.[16] Furthermore, the average O-O-O angle of 109.7° observed in $(H_2O)_{12}$ morphology is strikingly similar to the tetrahedral geometry, in agreement of the preferred tetrahedral hydrogen-bond arrangement for ice I_h, which further indicates the resemblance between $(H_2O)_{12}$ morphology and ice I_h.

In contrast to the recently observed ice layer, comprising $(H_2O)_{12}$ ring plus a dangling water molecule, which occurs only at very low temperature (20 K),[12] our $(H_2O)_{12}$ morphology can exist in a wide temperature range. The hydrogen-

[*] Dr. B.-Q. Ma, H.-L. Sun, Prof. S. Gao
State Key Laboratory of Rare Earth Materials Chemistry and Applications
PKU-HKU Joint Laboratory on Rare Earth Materials and Bioinorganic Chemistry, College of Chemistry and Molecular Engineering
Peking University, Beijing 100871 (P. R. China)
Fax: (+86) 10-6275-1708
E-mail: mabqing@yahoo.com
gaosong@pku.edu.cn

[**] This work was supported by the National Science Fund for Distinguished Young Scholars (20125104), NSFC No. 20221101, and the Research Fund for the Doctoral Program of Higher Education (20010001020).

 © 2004 Wiley-VCH Verlag GmbH & Co. KGaA, Weinheim DOI: 10.1002/anie.200353097

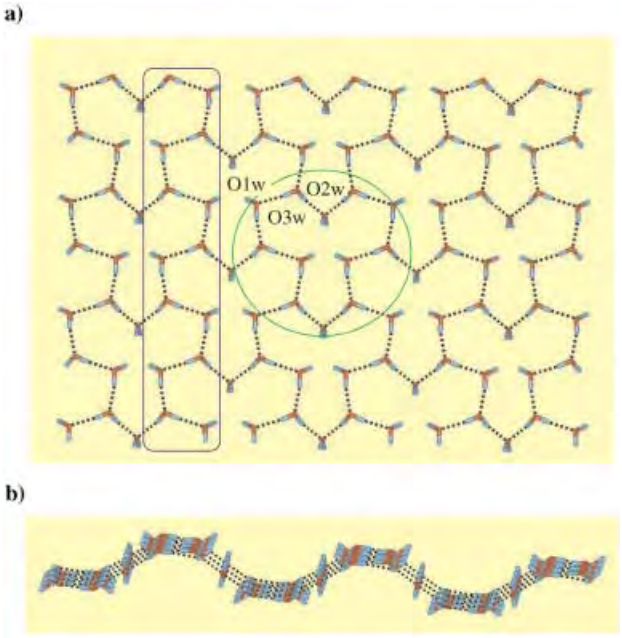


Figure 2. Supramolecular $(H_2O)_{12}$ water layer in **2**; a) Top view, the $(H_2O)_{12}$ ring is circled in green. The local structure boxed in blue shows a segregated chain similar to that in **1**. b) Side view.

Table 1: Hydrogen-bond parameters in compounds **1** and **2**.[a]

D–H···A	D–H [Å]	H···A [Å]	D···A [Å]	∢D-H···A [°]
		Compound **1**		
O1W-H···O1W	0.77(3)	1.98(4)	2.754(2)	176(4)
O1W-H···O2W	0.75(4)	2.04(4)	2.797(2)	175(4)
O2W-H···O2W	0.86(4)	1.91(4)	2.770(2)	174(5)
O2W-H···O1W	0.79(4)	2.01(4)	2.797(2)	172(3)
O1W-H···O1	0.88(2)	1.85(2)	2.722(2)	171(2)
O2W-H···O2	0.86(2)	1.89(2)	2.756(2)	174(2)
		Compound **2**		
O1W-H···O3W	0.85(2)	1.90(2)	2.7338(11)	168(2)
O3W-H···O2W	0.85(2)	1.94(4)	2.7759(9)	169(2)
O3W-H···O1W	0.85(2)	1.89(2)	2.7344(10)	172(2)
O1W-H···O1	0.87(2)	1.969(4)	2.7999(9)	159(2)
O2W-H···O1	0.86(2)	1.89(2)	2.7268(8)	166(2)

[a] Data are taken from the structures determined at 90 K.

bonded network of our $(H_2O)_{12}$ morphology does not show any significant changes on going from 90 to 295 K, which suggests structural uniformity. Moreover, the ice layer described here exhibits a novel topological motif with a pseudo C_{3v} symmetry, which differs from the reported irregular $(H_2O)_{12}$ ice phase.[12] Compared with 2D supramolecular $(H_2O)_{18}$ morphology which is structurally similar to liquid water,[13] the O···O separation in our $(H_2O)_{12}$ morphology is 0.1 Å shorter.

The remaining four hydrogen atoms per $(H_2O)_{12}$ water ring are bonded to two bpedo molecules, which act as bridges in a μ_4-hydrogen-bond fashion (Scheme 1b) to link these 2D water layers into a 3D network (Figure 3). The bpedo bridges are interweaved each other such that pyridine rings of one bpedo unit form π–π interactions with those of another. Notably, the water chain in **1** and layer in **2** can be viewed as

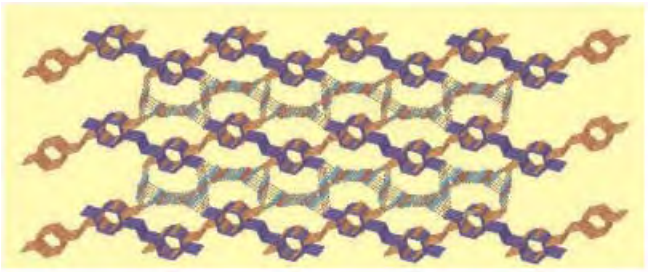


Figure 3. 2D supramolecular $(H_2O)_{12}$ water layers in **2** are connected by interweaved bpedo spacers into a 3D network.

building blocks, which are pillared by bpedo spacers to extend the dimensionality of the structure. In this sense, the water chain and layer are different from reported water clusters and other morphologies, which are situated within the host cavities or channels generated by organic or inorganic moieties.

The two compounds are interconvertible in the corresponding solvents. Recrystallization of **1** from water gave **2**, while dissolving **2** in methanol yielded **1**. The structural variation from 1D water chain in **1** to 2D water layer in **2** may be rationalized as follows: Within the methanol solution, the methanol presumably prevents the further growth of the water chain, while the water chain tends to grow in size without limitation in a water-enriched solution. A clear relationship between the two water phases exists. The water layer in **2** can be regarded as an evolution of water chain in **1** by adding water between the chains. The local structure of the $(H_2O)_{12}$ water layer (circled in blue in Figure 2a) displays a segregated chain motif, very similar to that observed in **1**. The extra water molecules are interspersed between water chains and bridge the neighboring chains to give the 2D layer. On the other hand, strong hydrogen-bonding ability of pyridine oxide linker employed here also plays a crucial role in promoting and stabilizing the aggregation of water molecules, thereby leading to the higher membered water rings. Compared with compound **1**, compound **2** easily loses its lattice water in air, which reflects the relatively weak interactions with the organic moiety in **2**. The hydrogen-bonding parameters give more evidence about the stability of the compounds. In **2** the average O···O separation of 2.763 Å between water layer and bpedo spacer is slightly longer than the average intrawater-layer O···O separation of 2.748 Å, while in **1** the average O···O separation of 2.739 Å between water chain and bpedo is significantly shorter than the average intrawater-chain hydrogen-bond length of 2.780 Å. These parameters imply that the water in **1** is more strongly affiliated to the organic spacers than in **2**.

In summary, structural variation from 1D water chain to 2D layer is realized by varying the crystallization conditions. The unique 2D ice layer has a great similarity with ice I_h and features a novel $(H_2O)_{12}$ ring. As water molecules play a crucial role in contributing to conformation, stability, function, and dynamics of biomacromolecules, the new water phases may provide insight into the hydrogen-bonding motif of the aqueous environment in living systems and enhance understanding of the 2D structural aspects of water.

 © 2004 Wiley-VCH Verlag GmbH & Co. KGaA, Weinheim

Experimental Section

trans-bis(4-pyridyl)ethylene dioxide (bpedo) was prepared by oxidizing *trans*-bis(4-pyridyl)ethylene.[17] Recrystallization from methanol and aqueous solution gave yellowish block crystals of **1** and yellow prismatic crystals of **2**, respectively. Dissolving **1** in aqueous solution generated crystal **2**, whereas dissolving **2** in methanol solution gave compound **1**. No precautions were taken to exclude adventitious water during the experiments.

Received: October 15, 2003 [Z53097]

Keywords: hydrogen bonds · N ligands · supramolecular chemistry · water

[1] a) K. Liu, M. G. Brown, C. Carter, R. J. Saykally, J. K. Gregory, D. C. Clary, *Nature* **1996**, *381*, 501; b) K. Nauta, R. E. Miller, *Science* **2000**, *287*, 293; c) F. Weinhold, *J. Chem. Phys.* **1998**, *109*, 367; d) J. M. Ugalde, I. Alkorta, J. Elguero, *Angew. Chem.* **2000**, *112*, 733; *Angew. Chem. Int. Ed.* **2000**, *39*, 717.

[2] R. Ludwig, *Angew. Chem.* **2001**, *113*, 1856; *Angew. Chem. Int. Ed.* **2001**, *40*, 1808.

[3] J. N. Moorthy, R. Natarajan, P. Venugopalan, *Angew. Chem.* **2002**, *114*, 3567; *Angew. Chem. Int. Ed.* **2002**, *41*, 3417.

[4] R. J. Doedens, E. Yphannes, M. I. Khan, *Chem. Commun.* **2002**, 62.

[5] J. L. Atwood, L. J. Barbour, T. J. Ness, C. L. Raston, P. L. Raston, *J. Am. Chem. Soc.* **2001**, *123*, 7192.

[6] W. B. Blanton, S. W. Gordon-Wylie, G. R. Clark, K. D. Jordan, J. T. Wood, U. Geiser, T. J. Collins, *J. Am. Chem. Soc.* **1999**, *121*, 3551.

[7] L. J. Barbour, G. W. Orr, J. L. Atwood, *Nature* **1998**, *393*, 671.

[8] R. Custelcean, C. Afloroaei, M. Vlassa, M. Polverejan, *Angew. Chem.* **2000**, *112*, 3224; *Angew. Chem. Int. Ed.* **2000**, *39*, 3094.

[9] K. M. Park, R. Kuroda, T. Iwamoto, *Angew. Chem.* **1993**, *105*, 939; *Angew. Chem. Int. Ed. Engl.* **1993**, *32*, 884.

[10] S. Pal, N. B. Sankaran, A. Samanta, *Angew. Chem.* **2003**, *115*, 1783; *Angew. Chem. Int. Ed.* **2003**, *42*, 1741.

[11] L. Infantes, S. Montherwell, *CrystEngComm* **2002**, *4*, 454.

[12] C. Janiak, T. G. Scharman, *J. Am. Chem. Soc.* **2002**, *124*, 14010.

[13] K. Raghuraman, K. K. Katti, L. J. Barbour, N. Pillarsetty, C. L. Barnes, K. V. Katti, *J. Am. Chem. Soc.* **2003**, *125*, 6955.

[14] a) B. Q. Ma, S. Gao, H. L. Sun, G. X. Xu, *J. Chem. Soc. Dalton Trans.* **2001**, 130; b) B. Q. Ma, H. L. Sun, S. Gao, G. X. Xu, *Inorg. Chem.* **2001**, *40*, 6247; c) A. J. Blake, M. T. Brett, N. R. Champness, A. N. Khlobystov, D. L. Long, C. Wilson, M. Schroder, *Chem. Commun.* **2001**, 2258.

[15] Crystal data: Compound **1**, $C_{12}H_{14}N_2O_4$, $M_r = 250.25$, triclinic, $P\bar{1}$, $a = 8.9776(9)$, $b = 9.0771(10)$, $c = 9.2190(10)$ Å, $\alpha = 64.532(3)$, $\beta = 87.186(3)$, $\gamma = 62.796(4)°$, $V = 592.97(11)$ Å^3, $Z = 2$, $\rho_{calcd} = 1.402$ Mg m^{-3}, $\mu = 0.107$ mm^{-1}, $F(000) = 264$, $GoF = 1.065$. A total of 4753 reflections were collected and 3063 are unique ($R_{int} = 0.0577$). $R1$ and $wR2$ are 0.0456 and 0.1303, respectively, for 228 parameters and 2615 reflections [$I > 2\sigma(I)$]. Compound **2**, $C_{12}H_{20}N_2O_7$, $M_r = 304.30$, orthorhombic, $Pbcn$, $a = 11.9300(8)$, $b = 7.2004(5)$, $c = 17.2426(12)$ Å, $V = 1481.15(18)$ Å^3, $Z = 4$, $\rho_{calcd} = 1.365$ Mg m^{-3}, $\mu = 0.113$ mm^{-1}, $F(000) = 648$, $GoF = 1.060$. A total of 18374 reflections were collected and 2211 are unique ($R_{int} = 0.1008$). $R1$ and $wR2$ are 0.0392 and 0.1061, respectively, for 137 parameters and 2008 reflections [$I > 2\sigma(I)$]. The data were collected on a SMART CCD 1000 with MoKα radiation ($\lambda = 0.71073$ Å) at 90 K. Room temperature data have also been collected for both compounds: Compound **1**, $C_{12}H_{14}N_2O_4$, $M_r = 250.25$, triclinic, $P\bar{1}$, $a = 9.015(2)$, $b = 9.175(3)$, $c = 9.325(2)$ Å, $\alpha = 64.586(11)$, $\beta = 86.382(11)$, $\gamma = 62.618(6)°$, $V = 609.9(3)$ Å^3, $Z = 2$, $\rho_{calcd} = 1.363$ Mg m^{-3}, $\mu = 0.104$ mm^{-1}, $F(000) = 264$, $GoF = 1.037$. A total of 2004 reflections were collected and 1811 are unique ($R_{int} = 0.0805$). $R1$ and $wR2$ are 0.0765 and 0.1952, respectively, for 217 parameters and 1446 reflections [$I > 2\sigma(I)$]. Compound **2**, $C_{12}H_{20}N_2O_7$, $M_r = 304.30$, orthorhombic, $Pbcn$, $a = 11.947(3)$, $b = 7.306(2)$, $c = 17.518(6)$ Å, $V = 1529.0(8)$ Å^3, $Z = 4$, $\rho_{calcd} = 1.322$ Mg m^{-3}, $\mu = 0.109$ mm^{-1}, $F(000) = 648$, $GoF = 1.001$. A total of 6121 reflections were collected and 2125 are unique ($R_{int} = 0.0729$). $R1$ and $wR2$ are 0.0506 and 0.1270, respectively, for 137 parameters and 1337 reflections [$I > 2\sigma(I)$]. The structures were solved by direction methods and refined by a full matrix least-squares technique based on F^2 using SHELXL 97 program. CCDC-219926–219929 (for compounds **1** and **2**) contain the supplementary crystallographic data for this paper. These data can be obtained free of charge via www.ccdc.cam.ac.uk/conts/retrieving.html (or from the Cambridge Crystallographic Data Centre, 12 Union Road, Cambridge CB2 1EZ, UK; fax: (+44) 1223-336-033; or deposit@ccdc.cam.ac.uk).

[16] The value is taken from the data at 200 K. D. Eisenberg, W. Kauzmann, *The Structure and Properties of Water*, Oxford University Press, Oxford, **1969**.

[17] a) W. J. Lu, L. P. Zhang, H. B. Song, Q. M. Wang, T. C. W. Mak, *New J. Chem.* **2002**, *26*, 775; b) B. Q. Ma, H. L. Sun, S. Gao, *Chem. Commun.* **2003**, 2164.

 © 2004 Wiley-VCH Verlag GmbH & Co. KGaA, Weinheim

Charge Transfer

Observation and Dynamics of "Charge-Transfer Isomers"**

Tasuku Ito, Naoyuki Imai, Tadashi Yamaguchi, Tomohiko Hamaguchi, Casey H. Londergan, and Clifford P. Kubiak**

We previously reported the measurement of rates of electron transfer (ET) by the coalescence of vibrational absorption bands in infrared (IR) spectra.[1,2] To observe the coalescence of vibrational bands in IR spectra, rates of chemical exchange

[*] Prof. T. Ito, N. Imai, Dr. T. Yamaguchi
Department of Chemistry, Graduate School of Science
Tohoku University. Sendai 980–8578(Japan)
Fax: (+81) 22-217-6548
E-mail: ito@agnus.chem.tohoku.ac.jp
Dr. C. H. Londergan, Prof. C. P. Kubiak
Department of Chemistry and Biochemistry
University of California
San Diego, La Jolla, CA 92093–0358 (USA)
Fax: (+1) 858-822-2665
E-mail: ckubiak@ucsd.edu
T. Hamaguchi
PRESTO, Japan Science and Technology Corporation
Sendai 980-8578 (Japan)

[**] This work was supported by Grant-in-Aid for Scientific Research (Priority Area "Metal Assembled Complexes" No. 10149102) from the Ministry of Education, Culture, Sports, Science, and Technology, and The U.S.—Japan Cooperative Science Program from JSPS and NSF. CPK and CHL gratefully acknowledge support from NSF (CHE-0079182) and an International Travel Award (INT-0087420) to support collaborative studies with the Ito research group.

 © 2004 Wiley-VCH Verlag GmbH & Co. KGaA, Weinheim DOI: 10.1002/anie.200353221

must be very fast, about 10^{11}–10^{12} s^{-1}.[1–3] The dynamic exchange observed in singly reduced symmetric intervalence charge-transfer complexes, $[A–A]^-$, occurs between the two equivalent charge distributions related by ET: $[A^––A]\rightleftarrows[A–A^–]$. Simulation of the extent of vibrational band coalescence in the IR spectrum can then be used to estimate the ET rate constants.[1,2] We now report the application of this method to study asymmetric charge-transfer complexes of the type $[A–B]^-$. We report several unprecedented findings, including the spectroscopic observation of both of the two possible charge-transfer isomers, for example, $[A^––B]$ and $[A–B^–]$, and dynamic exchange between them on the picosecond timescale.

In contrast to a symmetric charge-transfer complex $[A–A]^-$, intramolecular electron transfer in an asymmetric system $[A–B]^-$ is somewhat complicated. The question of whether an electron transfer will proceed within an asymmetric mixed valence state depends on two factors: (1) ΔG, the "driving force" or difference in free energy to attain $[A–B^–]$ starting from $[A^––B]$; (2) H_{AB}, the electronic coupling matrix element that quantum mechanically mixes the potential energy surfaces for $[A^––B]$ and $[A–B^–]$, stabilizes the resulting symmetric combination (lower surface), and destabilizes the antisymmetric combination (upper surface). This produces an energy separation of $2H_{AB}$ between the lower and upper surfaces at the crossing point (Figure 1). One

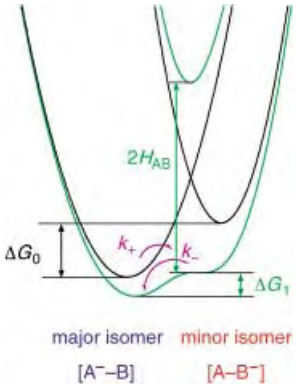


Figure 1. Marcus–Hush semiclassical model to describe ET in asymmetric charge transfer complexes, $[A–B]^-$.

complication of asymmetric mixed valency is that increased contributions of H_{AB} or ΔG work in opposite directions. Increases in H_{AB} tend to delocalize the electronic charge between A and B, whereas increases in ΔG tend to localize (trap) the charge. A more serious complication is that ΔG depends on H_{AB}. Note that electronic coupling (H_{AB}) has the effect of decreasing the free energy change for electron transfer from a value ΔG_0 in the diabatic case ($H_{AB}=0$) to a value of ΔG_1 in the adiabatic case. One special case that has escaped both experimental observation and theoretical discussion in the literature is that in which H_{AB} and ΔG are of appropriate magnitudes to permit the coexistence of similar populations of the two possible charge-transfer isomers: $[A^––B]$ and $[A–B^–]$. These could then exist as a major and a minor isomer, which exchange identity by intramolecular electron transfer. In particular, ET in the major isomer results in the formation of the minor isomer, and vice versa. In this letter, we present experimental evidence for the existence of such charge-transfer isomers. We describe how vibrational-band intensities and lineshapes in the IR are used to determine directly the difference in Gibbs free-energy, ΔG_1, and electron-transfer kinetics for strongly coupled asymmetric charge-transfer complexes.

The asymmetrical complexes $[Ru_3O(OAc)_6(L)(CO)(\mu\text{-}pz)Ru_3O(OAc)_6(L')(CO)]$ (pz = pyrazine, L = 4-dimethylaminopyridine (dmap), L′ = pyridine (py), **1**; L = py, L′ = 4-cyanopyridine (cpy), **2**; L = dmap, L′ = cpy, **3**) were prepared by modification of the procedures used to synthesize the symmetrical complexes. Each complex (**1**–**3**) displays two single-electron reduction waves in its cyclic voltammogram that correspond formally to $Ru_3^{III,III,II}$-pz-$Ru_3^{III,III,II}$/$Ru_3^{III,III,II}$-pz-$Ru_3^{III,II,II}$ (0/−1 overall charge) and then $Ru_3^{III,III,II}$-pz-$Ru_{33}^{III,II,II}$/$Ru_3^{III,II,II}$-pz-$Ru_3^{III,II,II}$ (−1/−2 overall charge; see Figure 2). This is completely analogous to the situation found in the symmetric complexes.[1,2] However, in contrast to the symmetric complexes, the magnitude of splitting between the two single-electron reduction waves, (0/−1) and (−1/−2), not only reflects the electronic interaction between the two Ru_3 clusters but also the difference in their intrinsic reduction potentials because of the different ligands present. The total splittings for the single-electron reductions of **1**–**3** are 410 mV

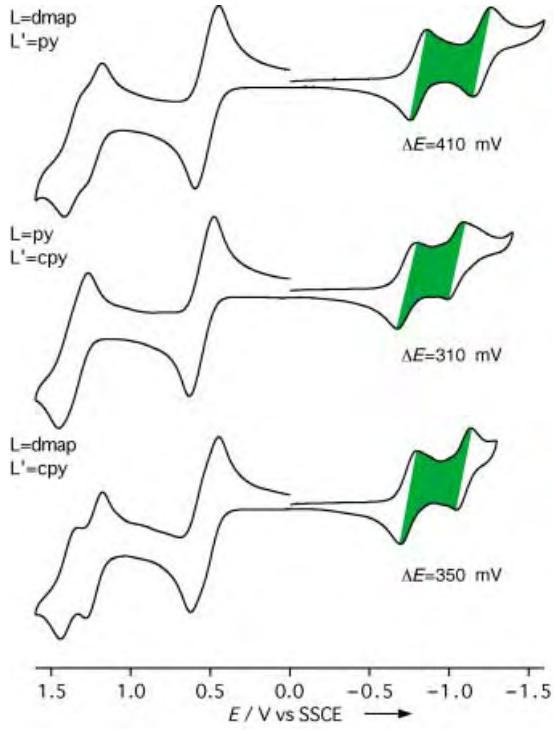


Figure 2. Cyclic voltammograms of the asymmetrically ligand substituted complexes: L = dmap, L′ = py (**1**); L = py, L′ = cpy (**2**); L = dmap, L′ = cpy (**3**). The two sequential single-electron reduction waves correspond to the (0/−1) and (−1/−2) redox processes. The measured splittings, ΔE, between the (0/−1) and (−1/−2) reduction waves reflect both the differences in intrinsic reduction potentials that depend on the ligands present and the degree of intercluster electronic coupling. SSCE = sodium-saturated calomel electrode.

 © 2004 Wiley-VCH Verlag GmbH & Co. KGaA, Weinheim

(**1**), 310 mV (**2**), and 350 mV (**3**). These compare with differences in intrinsic reduction potentials of the clusters, which depend only on the ligand set present,[4] 100 mV (**1**), 130 mV (**2**), and 230 mV (**3**). Thus, the differences in electrochemical splittings observed are significantly larger than the differences in intrinsic reduction potentials, which suggests that large intercluster electronic interactions exist in the mixed valence (−1) states of **1**–**3** (large H_{AB}). The differences in intrinsic reduction potentials also provide a reasonable estimate of ΔG_0, the Gibbs free energy for transferring an electron from a Ru_3 cluster with one type of ligand substitution to another in the absence of any perturbation from electronic coupling, H_{AB}.

The mixed valence (−1) states of **1**–**3** exhibit intense intervalence transfer (IT) absorptions in their electronic spectra.[5] This provides additional evidence of the high degree of electronic coupling that is present in the mixed valence states. Because these IT electronic-absorption bands are relatively broad and overlapped with other electronic transitions, it is not possible to resolve charge-transfer isomers. However, resolution can be achieved by vibrational spectroscopy. The vibrational spectra of the mixed-valence (−1) state were obtained using a custom low-temperature reflectance IR spectroelectrochemical (SE) cell under potentiostatic control.[6] The carbonyl stretching (ν(CO)) bands contain the most pertinent information. The ν(CO) spectra of the singly reduced states of **1**–**3** exhibit two broad and extensively overlapped bands, whereas the neutral (0) and doubly reduced (−2) states show single ν(CO) bands at higher and lower energy, respectively. The ν(CO) bands of **1** in the neutral (0), mixed valence (−1), and doubly reduced (−2) states are presented in Figure 3. In the case in which major and minor charge-transfer isomers exist in the spectrum of the mixed valence (−1) state, there will be four components to the overall ν(CO) spectral lineshape (Figure 4): (1) An intense high-frequency component from the unreduced cluster containing ligand L: major (L). (2) An intense low-frequency component from the reduced cluster containing ligand L′: major (L′). (3) A weak high-frequency component from the unreduced cluster containing ligand L′: minor (L′). (4) A weak low-frequency component from the reduced cluster containing ligand L: minor (L). Electron transfer within the major and minor isomers leads to two simultaneous two site chemical exchanges: major(L)/minor(L) and minor(L′)/major(L′). It is clear that the ν(CO) spectral lineshape of the intervalence charge transfer (−1) state of **1** (Figure 3 and 4) is too extensively overlapped to be interpreted meaningfully within the context of Figure 4. However, a remarkable simplification of the spectrum can be realized by selectively labeling one Ru_3 cluster with $^{13}C^{18}O$ while the other contains a CO ligand with natural abundances of isotopes (mostly $^{12}C^{16}O$). Such an isotopic substitution has the effect of shifting the $\nu(^{13}C^{18}O)$ frequencies some 85 cm^{-1} lower in energy than the $\nu(^{12}C^{16}O)$ bands. This has the additional effect of separating in frequency the major(L)/minor(L) exchange pair spectral components by 85 cm^{-1} from the minor(L′)/major(L′) pair in the mixed valence (−1) state. Figure 5 shows the ν(CO) spectra of $[Ru_3O(OAc)_6(L)(CO)(\mu\text{-pz})Ru_3O(OAc)_6(L')(^{13}C^{18}O)]$ (L = dmap, L′ = py (**1***); L = py, L′ = cpy (**2***); L = dmap, L′ = cpy (**3***)) in the neutral (0), mixed valence (−1), and doubly reduced (−2) states. The spectra of the neutral and −2 states each show two single ν(CO) bands, in which the lower-frequency band in each case corresponds to the $^{13}C^{18}O$ labeled Ru_3 cluster. The mixed valence (−1) states show two broad ν(CO) bands, each with a distinct shoulder on the inside. The overall spectra of the mixed valence (−1) states, Figure 5 (middle row), are precisely the results predicted for separating the nested major(L)/minor(L) and minor(L′)/major(L′) pairs of spectral

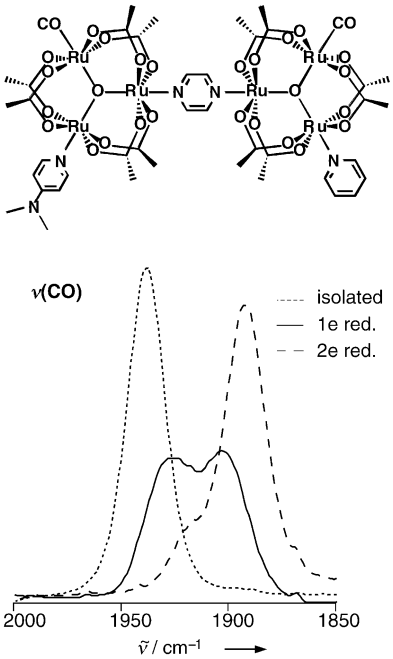


Figure 3. IRSE responses of **1** in the neutral (0) (....), mixed valence (−1) (——), and doubly reduced (−2) (-----) states. IRSE data were obtained at 233 K by using a low temperature thin layer cell[6] in CH_2Cl_2 solutions that contained 0.1 M tetrabutylammonium hexafluorophosphate as the supporting electrolyte.

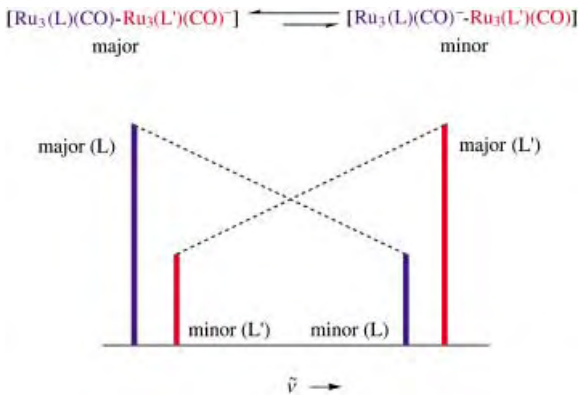


Figure 4. Schematic of exchange pairs in ν(CO) IR spectra of $\mathbf{1}^-$–$\mathbf{3}^-$. In the case where major and minor charge-transfer isomers exist, four peaks are expected. The resulting lineshapes are determined by both the relative populations (equilibrium constant) of major and minor isomers and the electron transfer rate constants that will tend to coalesce the spectral components that correspond to major(L)/minor(L) and minor(L′)/major(L′).

 © 2004 Wiley-VCH Verlag GmbH & Co. KGaA, Weinheim

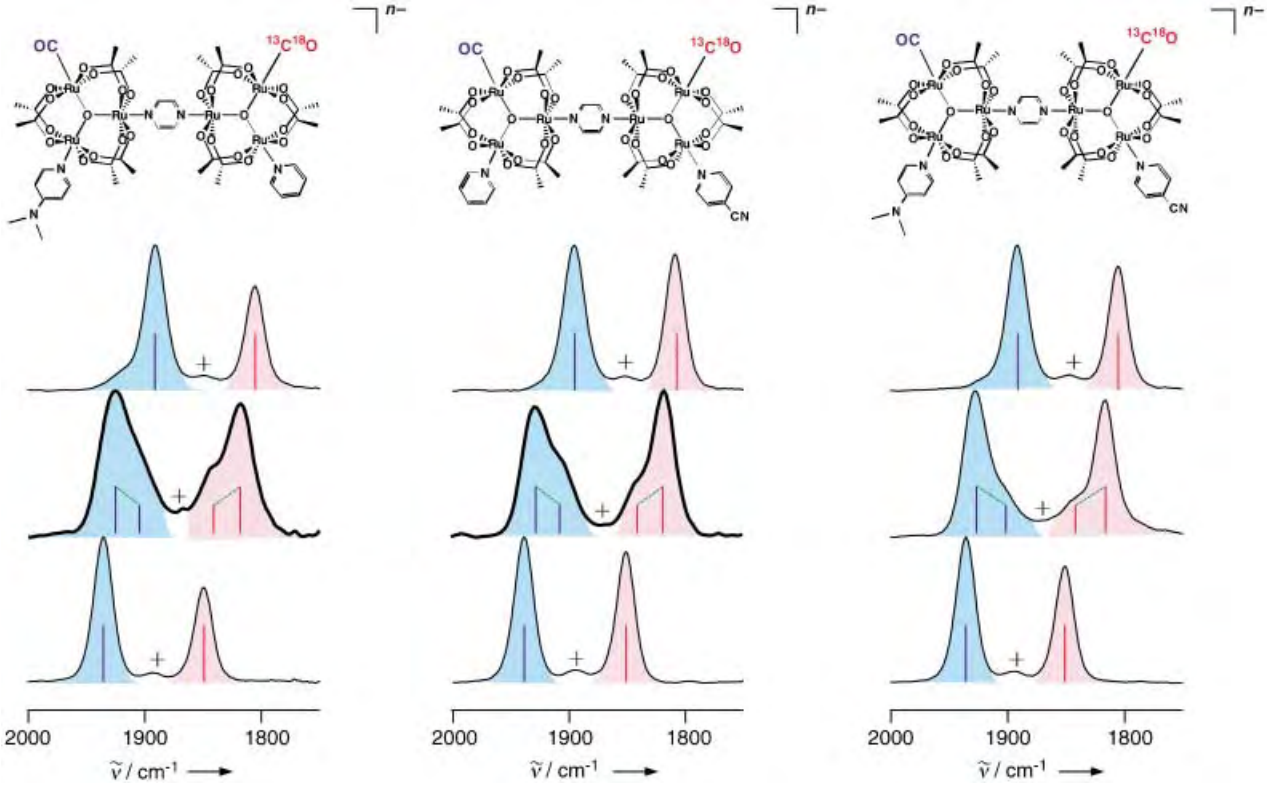


Figure 5. IRSE data for **1***, **2***, **3*** in the neutral (0; bottom row of spectra), mixed valence (−1; middle row of spectra), and doubly reduced (−2; top row of spectra) states. The small peaks identified by the "+" symbol correspond to $^{13}C^{16}O$ isotopic impurities.

components depicted in Figure 4 by isotope shifts. The peak assignments for the ν(CO) spectra of **1***, **2***, and **3*** in Figure 5 then in each case are (from high frequency to low frequency): major(L), minor(L), minor(L′), major(L′). These spectra provide compelling evidence for the presence of two charge transfer isomers. The fact that the bands are overlapped and broadened provides additional evidence that electron transfer is occurring to interconvert the charge transfer isomers on the IR timescale.

The IR spectra of **1***, **2***, and **3*** were analyzed by dynamic IR simulation with a modified version of VIBEXGL,[3,7] to obtain both the thermodynamics (major/minor equilibrium constant, K_{eq}, and derived free energy difference, ΔG_1) and kinetics (k_+, the rate constant for "uphill" (major→minor) ET) for charge-transfer isomers (see Table 1. It is clear that the populations of the minor isomers are far in excess of predictions based on differences in intrinsic reduction potentials. The values of K_{eq} predicted from ΔG_0 range from 150 (**1**) to 91 000 (**3**) (Table 1). The experimentally determined values of K_{eq} range from 1.6 (**1**) to 3.4 (**3**). The reason that charge transfer isomers can be observed in the present study then must be that the mixed valence (−1) states of **1**–**3** are so strongly electronically coupled that the diabatic free energies, ΔG_0, of 810–1850 cm^{-1} are reduced to (adiabatic) ΔG_1 values of only 75–200 cm^{-1}. The ν(CO) spectra in the mixed valence (−1) state (Figure 5) for each of **1***, **2***, and **3*** showed very small temperature dependence in favor of the major isomer at lower temperature in the range available experimentally (−40 to 7 °C). However, the spectral changes were so small

Table 1: Data for complexes **1**, **2**, and **3**.[a]

L-L′	ΔG_0 [cm^{-1}]	predicted (233 K)	actual (233 K)	ΔG_1 [cm^{-1}]	k_+ [$\times 10^{11}$ s^{-1}]
dmap-py (**1**)	810	150	1.6 ± 0.1	75	8.5 ± 0.5
py-cpy (**2**)	1050	650	2.4 ± 0.2	140	3.0 ± 0.5
dmap-cpy (**3**)	1850	91 000	3.4 ± 0.2	200	0.4 ± 0.2

[a] Diabatic and adiabatic free energies and equilibrium constants, experimentally determined total reorganization energies, and experimentally determined rate constants for forward electron transfer in the asymmetric charge transfer states.

(comparable to experimental error) that the effect of temperature on k_+ and K_{eq} could not be determined quantitatively.

Perhaps the most surprising result of the present study is that the large magnitudes of H_{AB} that evidently are sufficient to nearly equalize the populations of major and minor charge-transfer isomers are not sufficient to fully delocalize the systems to states with a single minimum. For example, Figure 6 presents the computed results of potential-energy surfaces developed by Sutin,[8] assuming an initial diabatic $\Delta G_0 = 810\ cm^{-1}$ and total reorganization energy $\lambda = 11\,500\ cm^{-1}$ ($\tilde{\nu}_{max}$ in ref. [6]), similar to values determined for **1**, as a function of increased electronic coupling, H_{AB}. At the point that the adiabatic free energy difference is diminished to $\Delta G_1 = 520\ cm^{-1}$ (for $H_{AB} = 4260\ cm^{-1}$), the double minimum required for two charge-transfer isomers is

 © 2004 Wiley-VCH Verlag GmbH & Co. KGaA, Weinheim

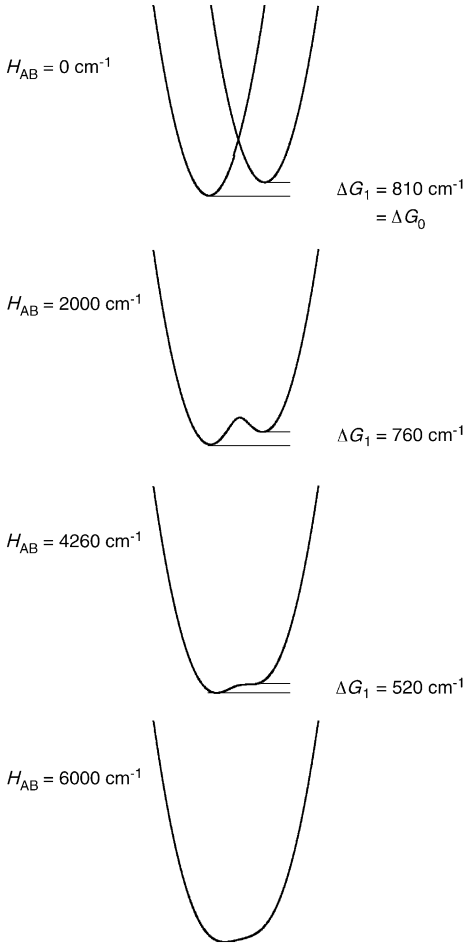


Figure 6. Diabatic (top) and adiabatic potential-energy surfaces showing how the Gibbs free-energy difference for electron transfer, ΔG_1, decreases as the electronic coupling, H_{AB}, increases. The potentials used[8] suggest that a single minimum (fully delocalized system) is attained at a value of $H_{AB} = 4260\ cm^{-1}$ if the initial diabatic driving force, ΔG_0, is 810 cm^{-1}.

no longer defined. Experimentally, we observe clear evidence of a double minimum: the presence of two charge-transfer isomers with relative populations 1.6:1, corresponding to $\Delta G_1 = 75\ cm^{-1}$. Why then, do these unusual complexes continue to exhibit dynamic exchange between alternate structures when they might otherwise achieve a single delocalized structure? It appears likely that these systems remain coupled to some other local dynamics (e.g., solvent, or molecular normal modes)[9,10] such that the equilibrated structure required for full electronic delocalization cannot be achieved. Experimental evidence of solvent control of the rates of ET in symmetrical systems related to **1–3** was reported recently.[11] Further studies should clarify the relative importance of local solvent and internal normal mode dynamics to the existence of charge transfer isomers.

Experimental Section

Preparation of **1–3**: The asymmetric dimers **1–3** were prepared in a way similar to the symmetric dimers by reacting equimolar quantities of $[Ru_3(\mu_3\text{-}O)(\mu\text{-}CH_3CO_2)_6(CO)(L)(H_2O)]$ and $[Ru_3(\mu_3\text{-}O)(\mu\text{-}CH_3CO_2)_6(CO)(L')(pz)]$. The dmap–py dimer,**1**, was prepared as follows. A mixture of $[Ru_3(\mu_3\text{-}O)(\mu\text{-}CH_3CO_2)_6(CO)(py)(H_2O)]$ (62 mg, 0.0775 mmol) and $[Ru_3(\mu_3\text{-}O)(\mu\text{-}CH_3CO_2)_6(CO)(dmap)(pz)]$ (70 mg, 0.0775 mmol) in CH_2Cl_2 (15 mL) was allowed to stand for 2 days at room temperature. The resulting solution was subjected to chromatography over silica gel with CH_2Cl_2/MeOH 99:1 (volume/volume) as the eluting agent. The compound was isolated from the main blue-green band. Yield 103 mg, 74%. Compounds **2** and **3** were prepared in a similar way with the use of appropriate Ru_3 cluster. For **1:** Elemental analysis (%) calcd for $Ru_6C_{42}H_{55}O_{28}N_5$: C 29.95, H 3.29, N 4.16; found: C 29.22, H 3.44, N 4.18. FABMS: *m*/*z* 1659, 1629 (calcd $[M-CO] = 1656$, $[M-2CO] = 1628$). ^{1}H NMR (270 MHz, $CDCl_3$): $\delta = 9.31$ (2H, pz), 9.21 (2H, py-*o*), 8.94 (2H + 2H, dmap-*o*, pz), 8.16 (1H, py-*p*), 8.07 (2H, py-*m*), 7.25 (2H, dmap-*m*), 3.34 (6H, dmap CH_3), 2.25 (6H, acetate CH_3), 2.21 (6H, acetate CH_3), 2.16 (6H, acetate CH_3), 2.11 (6H, acetate CH_3), 2.00 (6H, acetate CH_3), 1.95 ppm (6H, acetate CH_3). For **2:** Elemental analysis (%) calcd for $Ru_6C_{41}H_{49}O_{28}N_5{\cdot}3H_2O$: C 28.62, H 3.22, N 4.07%; found: C 28.47, H 3.11, N 4.10%. FABMS: *m*/*z* 1666, 1638, 1611 (calcd $[M] = 1667$, $[M-(CO)] = 1638$, $[M-2CO] = 1611$). ^{1}H NMR (270 MHz, $CDCl_3$): $\delta = 9.22$ (2H, pz), 9.09 (2H, py-*o*), 8.93 (2H, pz), 8.21 (2H, cpy-*m*), 8.15 (1H, py-*p*), 8.06 (2H, py-*m*), 2.26 (6H, acetate CH_3), 2.24 (6H, acetate CH_3), 2.18 (6H, acetate CH_3), 2.16 (6H, acetate CH_3), 2.03 (6H, acetate CH_3), 1.99 ppm (6H, acetate CH_3). For **3:** Elemental analysis (%) calcd for $Ru_6C_{43}H_{54}O_{28}N_5{\cdot}5H_2O$: C, 28.70, H, 3.59, N, 4.67%. Found: C 28.80, H 3.57, N 4.73%. FABMS: *m*/*z* 1653 (calcd $[M-2CO] = 1653$). ^{1}H NMR (270 MHz, $CDCl_3$): $\delta = 9.30$ (2H, pz), 9.08 (2H, pz), 8.92 (2H, dmap-*o*), 8.79 (2H, cpy-*o*), 8.22 (2H, cpy-*m*), 7.23 (2H, dmap-*m*), 3.34 (6H dmap CH_3), 2.26 (6H, acetate CH_3), 2.20 (6H, acetate CH_3), 2.18 (6H, acetate CH_3), 2.11 (6H, acetate CH_3), 2.03 (6H, acetate CH_3), 1.95 ppm (6H, acetate CH_3).

Preparation of **1***–**3***: Asymmetric dimers with $^{13}C^{18}O$ ligand were prepared similarly to the above mentioned method for **1–3** by using corresponding Ru_3 cluster with $^{13}C^{18}O$ ligand. $[Ru_3(\mu_3\text{-}O)(\mu\text{-}CH_3CO_2)_6(^{13}C^{18}O)(H_2O)(L)]$ was synthesized from $[Ru_3(\mu_3\text{-}O)(\mu\text{-}CH_3CO_2)_6(^{13}C^{18}O)(H_2O)_2]$. In all cases, isotopically labeled $^{13}C^{18}O$ was introduced onto the Ru_3 cluster fragment having the lower reduction potential. This produces the least complicated spectral overlaps of the ν(CO) spectra in the −1 states.

Received: November 3, 2003 [Z53221]

Keywords: charge transfer · electrochemistry · electron transfer · IR spectroscopy · mixed-valent compounds

[1] T. Ito, T. Hamaguchi, H. Nagino, T. Yamaguchi, H. Kido, I. S. Zavarine, T. Richmond, J. Washington, C. P. Kubiak, *J. Am. Chem. Soc.* **1999**, *121*, 4625–4632.

[2] T. Ito, T. Hamaguchi, H. Nagino, T. Yamaguchi, J. Washington, C. P. Kubiak, *Science* **1997**, *277*, 660–663.

[3] F.-W. Grevels, K. Kerpen, W. E. Klotzbücher, R. E. D. McClung, G. Russell, M. Viotte, K. Schaffner, *J. Am. Chem. Soc.* **1998**, *120*, 10423–11043.

[4] The intrinsic reduction potentials are taken as the mean value of (0/−1) and (−1/−2) reduction potentials in the symmetrically ligand substituted (dmap–dmap, py–py, and cpy–cpy) dimers.[1] In this case, the potentials for the (0/−1) and (−1/−2) redox couples are split only by electronic interactions. The mean value reflects the intrinsic reduction potential for one Ru3 cluster with a given ligand substitution in a dimer together with another similarly substituted Ru_3 cluster.

[5] Intervalence-transfer (IT) electronic-absorption spectroscopic data for the mixed valence (−1) states of **1–3**. $\tilde{\nu}_{max}$ (ε_{max}) = 11500 (16600) for **1**, 10500 (12200) for **2** and 10400 cm^{-1} (10100 $M^{-1}cm^{-1}$) for **3**.

 © 2004 Wiley-VCH Verlag GmbH & Co. KGaA, Weinheim

[6] I. S. Zavarine, C. P. Kubiak, *J. Electroanal. Chem.* **2001**, *495*, 106 – 109.
[7] R. E. D. McClung in *VibexGL: Program for the Simulation of IR Spectra of Exchanging Systems.*
[8] N. S. Sutin, *Prog. Inorg. Chem.* **1983**, *30*, 441 – 498.
[9] D. V. Matyushov, G. A. Voth, *J. Phys. Chem. A* **2000**, *104*, 6470 – 6484.
[10] K. D. Demadis, C. M. Hartshorn, T. J. Meyer, *Chem. Rev.* **2001**, *101*, 2655 – 2685.
[11] C. H. Londergan, J. C. Salsman, S. Ronco, L. M. Dolkas, C. P. Kubiak, *J. Am. Chem. Soc.* **2002**, *124*, 6236 – 6237.

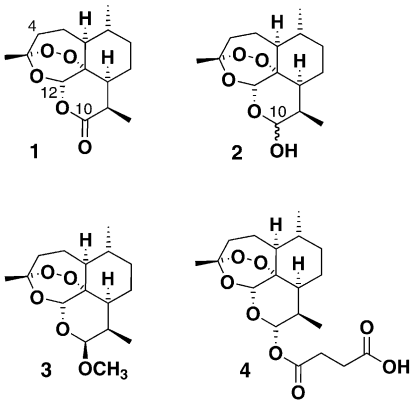
 © 2004 Wiley-VCH Verlag GmbH & Co. KGaA, Weinheim

Antimalarial Drugs

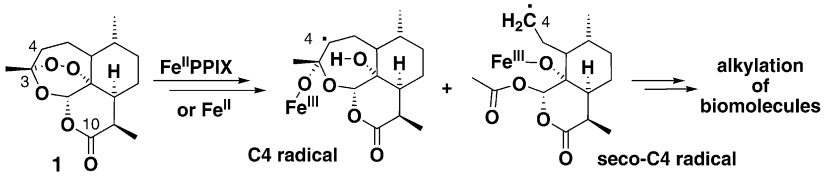
Highly Antimalaria-Active Artemisinin Derivatives: Biological Activity Does Not Correlate with Chemical Reactivity**

Richard K. Haynes, Wing-Yan Ho, Ho-Wai Chan, Burkhard Fugmann, Jörg Stetter, Simon L. Croft, Livia Vivas, Wallace Peters, and Brian L. Robinson*

Artemisinin (**1**, qinghaosu), and the derivatives dihydroartemisinin (DHA, **2**), artemether (**3**), and artesunate (**4**) are the most potent and rapidly acting antimalarial drugs.[1–3] Nevertheless, artemether (**3**) and artesunate (**4**) have short terminal half-lives, a consequence of facile metabolism to DHA,[4] a highly neurotoxic compound.[5–8] Therefore, there is an urgent need to develop practical routes to new derivatives that are more stable and do not undergo metabolism to DHA.[2,3,9]



The compounds act on all stages of the intraerythrocytic parasite, induce ultrastructural changes in parasite membranes,[10,11] and affect membrane and other proteins.[12] The bioactive agents are held to be C-centered radicals, generated by scission of the peroxide to give an alkoxyl radical, followed by abstraction of a hydrogen atom at C4 and cleavage of the C3–C4 bond (Scheme 1). Peroxide scission is induced either



Scheme 1. Proposed formation of C-centered radicals from artemisinin (**1**) by ferrous heme [Fe^{II}PPIX] or exogenous Fe^{II}. Fe^{III} ≡ ferric heme or Fe^{III}. Detailed discussions are given in refs.[25, 27].

by heme within the parasite food vacuole or by non-heme, "exogenous" iron. In both cases, iron must be in the +II state.[13,14] The C-centered radicals are held to alkylate undefined sensitive biomolecules in the parasite.[15–21] As artemisinin (**1**) reacts with heme to give covalent adducts,[22,23] a correlation has been drawn between this type of reaction and antimalarial activity for trioxanes in general.[24] For exogenous iron, trapping experiments with cysteine are also interpreted in terms of C-centered radicals.[25] On the basis of the hypothesis,[26] "rational design" in the synthesis of new analogues[15] and modular antimalarial drugs[27] has been claimed.

We are preparing new artemisinin derivatives in a program in which we address the problems of metabolism to DHA and of neurotoxicity, and seek to improve efficacy through the application of pharmacokinetic parameters

[*] Prof. Dr. R. K. Haynes, W.-Y. Ho, Dr. H.-W. Chan
Department of Chemistry
Hong Kong University of Science and Technology
Clear Water Bay, Kowloon, Hong Kong (P.R. China)
Fax: (+852) 2358-1594
E-mail: haynes@ust.hk
Dr. B. Fugmann[+]
Bayer AG Central Research
Head, Medicinal Chemistry
51368 Leverkusen (Germany)
Prof. Dr. J. Stetter[++]
Bayer AG Central Research
Chemistry for Life Sciences
51368 Leverkusen (Germany)
Dr. S. L. Croft, Dr. L. Vivas
Department of Infectious and Tropical Diseases
London School of Hygiene and Tropical Medicine
Keppel Street, London WC1E 7HT (UK)
Prof. Dr. W. Peters, B. L. Robinson
Centre for Tropical Antiprotozoal Chemotherapy
Northwick Park Institute for Medical Research
Block Y, Watford Road, Harrow, Middlesex HA1 3UJ (UK)
[+] Current affiliation:
Bayer AG, BBS, Science and Technology
51368 Leverkusen (Germany)
[++] Current affiliation:
Bayer AG, Corporate Development, Head of Innovation
51368 Leverkusen (Germany)
[**] This work was supported by grants from Bayer AG (Leverkusen, Germany) and by the Government of the HKSAR University Grants Council (grant no. HKUST 6091/02P).
Supporting information for this article is available on the WWW under http://www.angewandte.org or from the author.

 DOI: 10.1002/anie.200352343 © 2004 Wiley-VCH Verlag GmbH & Co. KGaA, Weinheim

designed to enhance solubility and adsorption of the neutral drug.[2] We now report that some of our compounds display very high activity in vivo against the malaria parasite, and they thereby provide an opportunity to test the current hypothesis for the mode of action.

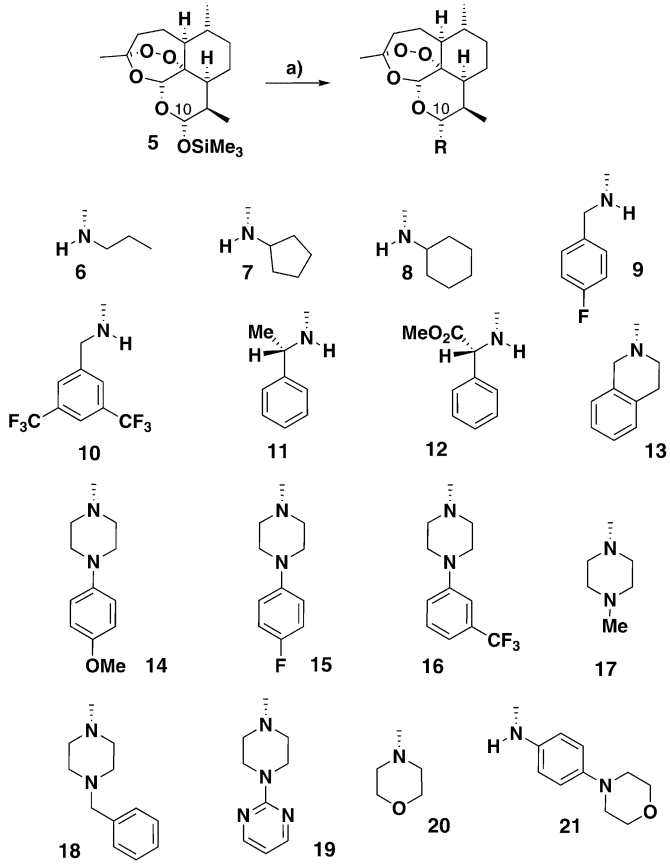
A solution of the DHA trimethylsilyl ether **5** in dichloromethane was treated with bromotrimethylsilane[28] and then with an excess of a primary or secondary alkylamine to give exclusively the 10α-alkylamino derivatives **6**–**20** (Scheme 2). Arylamino derivatives, for example, **21**, may also be prepared.[29] The reaction proceeds by means of nucleophilic displacement by the amine on the unstable 10β (axial) bromide intermediate, which is detectable in reaction mixtures by ^{1}H NMR spectroscopy.[28] Whilst yields are moderate (up to 60%), the method is straightforward and applicable to primary and secondary alkylamines, and primary aromatic amines.

Results of in vivo screens for compounds **17**–**20** conducted against chloroquine(CQ)-sensitive *P. berghei* and CQ-resistant *P. yoelii* in mice according to the Peters' four-day test are given in Table 1.[30] For comparative purposes, data acquired in the same screens for artesunate (**4**), the most active of the artemisinin derivatives currently in clinical use, and the aryl derivative **22** are also included.[28] For *P. berghei*, the amino derivatives are 3–26 times more active than artesunate when administered subcutaneously (*sc*), and 3–7 times more active when administered orally (*or*). For *P. yoelii*, the compounds are 2–81 times more active by the *sc* route (Table 1). The activities of compounds **18**–**20** in the murine malaria models appear to be superior to those of any other peroxide-containing antimalarial compound, either derived from artemisinin or of the synthetic trioxane-type, ever recorded. Thus, we have identified a new class of artemisinin derivatives with the potential for further development.

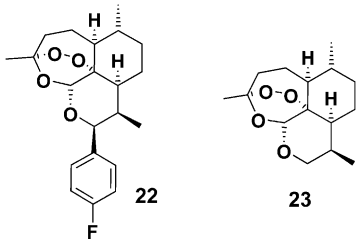
Table 1: In vivo screens against the chloroquine (CQ)-sensitive *P. berghei* N strain and the CQ-resistant *P. yoelii* NS strain according to the Peters four-day test; mice treated daily subcutaneously (*sc*) or orally (*po*) from day of infection (D0) through D+3; results (ED_{90} [mg kg^{-1}]) evaluated from parasite counts in peripheral blood on D+4.

Cmpd.	*P. berghei* ED_{90} [mg kg^{-1}: *sc*]	*P. berghei* ED_{90} [mg kg^{-1}: *po*]	*P. berghei* artesunate index[a] *sc*	*po*	*P. yoelii* ED_{90} [mg kg^{-1}: *sc*]	*P. yoelii* ED_{90} [mg kg^{-1}: *po*]	*P. yoelii* artesunate index[a] *sc*
4	4.6	9.3	1.0	1.0	42.0	–	1.0
17	1.45	3.5	3.2	2.66	22.0	–	1.9
18	0.78	2.4	5.9	3.88	0.85	3.0	49.4
19	0.46	1.5	10.0	6.2	0.52	2.0	81.0
20	0.18	1.3	25.6	7.15	1.25	1.84	33.6
22	1.16	5.0	4.0	1.86	1.08	–	39.6

[a] ED_{90}(**4**)/ED_{90}(derivative).



Scheme 2. Preparation of C10 aminoalkyl and aminoaryl derivatives **6**–**21** of DHA (**2**). a) 1. $SiMe_3Br$, CH_2Cl_2, 0°C, 45 min; 2. alkylamine (2.0 equiv), 0°C to room temperature, 12 h, then NH_4Cl/H_2O.



In order to evaluate the correlation between the antimalarial efficacy of these compounds with their reactivity towards ferrous heme or Fe^{III}, we also include the hydrolytically stable compounds **22** and **23**. The former possesses very good in vivo activities, especially against CQ-resistant *P. yoelii* (Table 1), and the latter, unlike artemisinin (**1**) and DHA (**2**), does not interact at all, for example, by complex formation, with ferric heme, and thereby does not interfere in formation of β-hematin or hemozoin, the heme dimer.[31] In comparison with artemisinin (**1**), compound **23** possesses superior in vitro activity against *P. falciparum* and is approximately equipotent in vivo against *P. berghei*.[32]

The heme experiments were carried out as previously described.[13] The artemisinin derivative, heme (ferriprotoporphyrin IX chloride), and L-cysteine (1 equiv of each) were stirred in buffered solution of deionized water/acetonitrile (1:1, pH 7.4) under nitrogen in the dark for 24 h.[33] After extraction with ether and dichloromethane, and then filtra-

 © 2004 Wiley-VCH Verlag GmbH & Co. KGaA, Weinheim

tion through Celite, the crude product mixture was examined by ^{1}H NMR spectroscopy with an internal standard (1,3,5-trimethoxybenzene) to determine the amounts of the unreacted derivative. The signal for H12 (for numbering, see **1**), a singlet which appears away from other signals in the spectra of these compounds, was used as the reference signal. The major products are presumed to be heme adducts of the artemisinin derivatives, which are insoluble in organic solvents;[13] no attempt was made to isolate them. The heme adduct from artemisinin has been thoroughly characterized.[23] For the amino derivatives **18** and **19**, the most significant by-product was DHA (**2**); very little of any other product was obtained for the other compounds (Table 2). The most striking observation is that compounds **22** and **23** do not undergo significant decomposition.

Table 2: Reaction of artemisinin derivatives with ferriprotoporphyrin IX chloride/L-cysteine (each 1 equiv) in buffered MeCN/H_2O (pH 7.4) during 24 h at 23 °C.

Cmpd.	Unreacted cmpd. [%]	Other products (%)
18	18	**2** (6), **24** (6), **25** (4)
19	62	**2** (18), **25** (2.5)
20	67	not determined
22	>99	not determined
23	>99	**27** + **30** (<1)

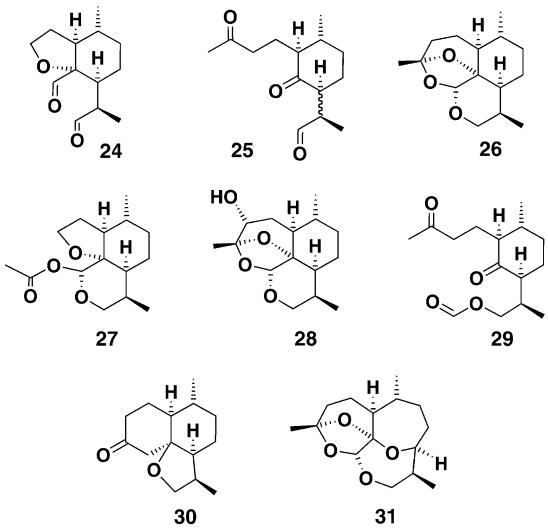
Next, the reactivity of the derivatives towards Fe^{II} was assessed (Table 3). Iron(II) sulfate in aqueous MeCN was used, in line with established practice in this type of

Table 3: Reaction of artemisinin derivatives with Fe^{II} sulfate in 1:1 MeCN/water during 24 h at 23 °C.

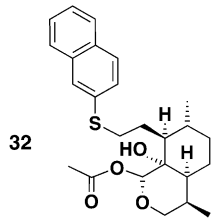
Artemisinin derivative	$FeSO_4 \cdot 7H_2O$ [equiv]	Unreacted derivative [%]	Other products (%)
18	0.3	96	**24** (3), **25** (1)
	1.0	63	**24** (25), **25** (12)
19	0.3	97	**24** (2), **25** (1)
	1.0	78	**24** (16), **25** (6)
23	0.3	0	**26** (1), **27** (41), **28** (51), **29** (5), **31** (1.5)
	1.0	0	**26** (<1), **27** (46), **28** (45), **29** (6), **31** (2.0)
19 + **23** (1 equiv)	0.3	**19:** 96, **23**: 4	**24** (3), **25** (1), **26** (6), **27** (43), **28** (41), **29** (6), **31** (0)
	1.0	**19**: 89, **23**: 0	**24** (7), **25** (4), **26** (13), **27** (41), **28** (41), **29** (5), **31** (0)

study.[20,21,25,34] The artemisinin derivative with iron(II) sulfate in 1:1 deionized water/MeCN was stirred at 23 °C for 24 h. The mixture was extracted with dichloromethane, and the products (**24**–**31**) were isolated by chromatography. Identity was secured by spectroscopic characterization and by comparison with literature data.[35,36]

Notably, the highly antimalarial-active compounds **18** and **19** displayed poor reactivity towards Fe^{II}. In contrast, compound **23** was completely decomposed. It may be argued that



the poor reactivity of the first two compounds towards Fe^{II} arises because the basic piperazinyl groups prevent the iron from entering into the redox chemistry associated with cleavage of the peroxide (cf. Scheme 1) through modulation of the pH of the aqueous reaction medium. However, that the Fe^{II} in fact remains catalytically active was established by treatment of equimolar mixtures of compounds **19** and **23** with iron(II) sulfate under the foregoing conditions. Each compound in the mixture behaved essentially as it did alone; that is, Fe^{II} remains catalytically active in inducing decomposition of **23**, whereas **19** was still unreactive (Table 3). Reactions with compound **23** were also run in the presence of 2-naphthalenethiol and iron(II) sulfate at different concentrations (0.005, 0.3, and 1.0 equiv). This did not greatly affect yields or ratios of products, although the unstable adduct **32** was obtained in variable, but low, yields.[37] Its formation belies the elaborate explanation[25] put forward for formation of cysteine adducts in related experiments.



In summary, we have developed a straightforward route to highly antimalaria-active artemisinin derivatives, which will be amenable for development of selected lead compounds. We also show that the hydrolytically stable compounds **22** and **23** are inert to ferrous heme, whereas under essentially the same conditions, compound **23** is completely decomposed by free Fe^{II}. In further contrast with the reactivity of **23**, the highly antimalaria-active alkylamino derivatives **18** and **19** are relatively unreactive towards free Fe^{II}. Their reactions in the presence of ferrous heme appears to depend partially on the nature of the amino group at C10. In any event, the formation of the hydrolysis product, DHA (**2**), in the heme reactions indicates activation of the piperazinyl substituent by complexation with heme-Fe^{II} or -Fe^{III} to displacement by water in the reaction medium takes place. In the reactions involving free Fe^{II}, it is possible that the piperazine forms a complex with Fe^{II}, and the amine–iron complex blocks access of further iron to the peroxide bridge.

 © 2004 Wiley-VCH Verlag GmbH & Co. KGaA, Weinheim

These results, coupled with those of earlier work,[13,31] and other arguments (see below), seem now to exclude the possibility that an activation pathway involving heme-Fe^{II} underpins antimalarial activity of artemisinin derivatives. In the case of free, that is, non-heme or "exogenous" Fe^{II}, others have sought to demonstrate a correlation between antimalarial activity and reactivity under the reaction conditions described herein.[20,21,25,34,38] However, as no such correlation exists for our compounds,[39] the use of such a probe to establish the chemical basis for antimalarial activity in general has to be treated with considerable caution, especially as so little is known of the biological environment in which the artemisinin derivative purportedly reacts with the iron. Given that the hypothesis involving "activation" of artemisinins by Fe^{II}, and the migration and reaction of the resulting C-centered radicals with sensitive biomolecules has its genesis in such studies,[15] the hypothesis itself must also be brought into question.

We have noted previously that several antimalaria-active trioxanes cannot obviously generate C-centered radicals according to the formalism of Scheme 1.[14,18,40] Whilst many peroxides are susceptible to reductive cleavage by ferrous iron,[41] a large number also display at best feeble antimalarial activity,[36,42] and further, the Fe^{III} formed by oxidation of Fe^{II} by the peroxide (cf. Scheme 1) is capable of oxidizing the C-centered radicals to carbocations.[40,43,44] Artemisinin derivatives do not inhibit but rather are potent inducers of Phase I-metabolizing P450 (CYP) enzymes, in which the heme hydroxylates the periphery of the molecule *syn* to the peroxide without interfering with it.[2] Further, the seco-C4 radical (Scheme 1) held to be produced in the reaction with ferrous heme clearly cannot be trapped by the L-cysteine (present work), or other thiols,[13] used to generate ferrous heme; clearly, if the C-centered seco-C4 is formed at all, it reacts exclusively with the proximate heme. In general, artemisinin and derivatives affect intraerythrocytic stages of the parasite in which catabolism of hemoglobin to produce heme does not take place, namely tiny rings and gametocytes, and further, locate to parasite membranes, not the food vacuole containing the heme.[10,45] Overall, the weight of evidence suggests that binding of the artemisinin to a specific target is involved, as we have pointed out previously.[2,18,31] The peroxide itself may be activated concomitantly with, or subsequent to, binding to generate either hydroperoxide, or derived electrophilic oxygenating agent, or oxygen-centered radical capable of inducing irreversible inhibition.[2,18,31,46]

Received: July 9, 2003 [Z52343]
Published Online: February 16, 2004

Keywords: heme proteins · iron · medicinal chemistry · peroxides · radicals

[1] Y. Li, Y.-L. Wu, *Med. Trop.* **1998**, *58*, Supplement 3, 9–12, and references therein; P. I. Trigg, *Econ. Med. Plant Res.* **1989**, *3*, 20–55; T. T. Hien, N. J. White, *Lancet* **1993**, *341*, 603–608; F. Nosten, T. T. Hien, N. J. White, *Med. Trop.* **1998**, *58*, 45–49; M. A. van Agtmael, T. A. Eggelte, C. J. van Boxtel, *Trends Pharmacol. Sci.* **1999**, *20*, 199–205; N. J. White, *Philos. Trans. R. Soc. London Ser. B* **1999**, *354*, 739–749; World Health Organization, *Trans. R. Soc. Trop. Med. Hyg.* **2000**, *94*, Supplement 1, 36–37.
[2] R. K. Haynes, *Curr. Opin. Infect. Dis.* **2001**, *14*, 719–726.
[3] Y. Li, Y.-L. Wu, *Curr. Med. Chem.* **2003**, *10*, 2197–2231.
[4] V. Navaratnam, S. M. Mansor, N. W. Sit, J. Grace, Q. G. Li, P. Olliaro, *Clin. Pharmacokinet.* **2000**, *39*, 255–270.
[5] R. F. Genovese, D. B. Newman, T. G. Brewer, *Pharmacol. Biochem. Behav.* **2000**, *67*, 37–44.
[6] A. Nontprasert, S. Pukrittayakamee, M. Nosten-Bertrand, S. Vanijanonta, N. J. White, *Am. J. Trop. Med. Hyg.* **2000**, *62*, 409–412.
[7] G. Schmuck, R. K. Haynes, *Neurotoxic. Res.* **2000**, *2*, 37–49.
[8] G. Schmuck, E. Roehrdanz, R. K. Haynes, R. Kahl, *Antimicrob. Agents Chemother.* **2002**, *46*, 821–827.
[9] F. Chorki, F. Grellepois, B. Crousse, V. D. Hoang, N. Van Hung, D. Bonnet-Delpon, J. P. Begue, *Org. Lett.* **2002**, *4*, 757–759.
[10] D. S. Ellis, Z. L. Li, H. M. Gu, W. Peters, B. L. Robinson, G. Tovey, D. C. Warhurst, *Ann. Trop. Med. Parasitol.* **1985**, *79*, 367–374.
[11] P.-Q. Chen, J. Yuan, Q.-Y. Du, *Zhongguo Yaoli Xuebao* **2000**, *21*, 234–238 [*Chem. Abstr.* **2000**, *132*, 317662, 2000:190391].
[12] W. Asawamahasadka, I. Ittarat, Y. M. Pu, H. Ziffer, S. R. Meshnick, *Antimicrob. Agents Chemother.* **1994**, *38*, 1854–1858; J. Bhisutthibhan, X.-Q. Pan, P. A. Hossler, D. J. Walker, C. A. Yowell, J. Carlton, J. B. Dame, S. R. Meshnick, *J. Biol. Chem.* **1998**, *273*, 16192–16198; T. Akompong, J. VanWye, N. Ghori, K. Haldar, *Mol. Biochem. Parasitol.* **1999**, *101*, 71–79.
[13] R. K. Haynes, S. C. Vonwiller, *Tetrahedron Lett.* **1996**, *37*, 253–256.
[14] R. K. Haynes, S. C. Vonwiller, *Tetrahedron Lett.* **1996**, *37*, 257–260.
[15] See inter alia G. H. Posner, C. H. Oh, *J. Am. Chem. Soc.*, **1992**, *114*, 8328–8329; G. H. Posner, C. H. Oh, D. Wang, L. Gerena, W. K. Milhous, S. R. Meshnick, W. Asawamahasadka, *J. Med. Chem.* **1994**, *37*, 1256–1258; G. H. Posner, J. N. Cumming, P. Ploypradith, C. H. Oh, *J. Am. Chem. Soc.* **1995**, *117*, 5885–5886; G. H. Posner, S. B. Park, L. Gonzalez, D. Wang, J. N. Cumming, D. Klinedinst, T. A. Shapiro, M. D. Bachi, *J. Am. Chem. Soc.* **1996**, *118*, 3537–3538; P. M. O'Neill, A. Miller, L. P. D. Bishop, S. Hindley, J. L. Maggs, S. A. Ward, S. M. Roberts, F. Scheinmann, A. V. Stachulski, G. H. Posner, B. K. Park, *J. Med. Chem.* **2001**, *44*, 58–68.
[16] S. R. Meshnick, T. E. Taylor, S. Kamchonwongpaisan, *Microbiol. Rev.* **1996**, *60*, 301–315.
[17] S. R. Meshnick, . C. W. Jefford, G. H. Posner, M. A. Avery, W. Peters, *Parasitol. Today* **1996**, *12*, 79–82; J. N. Cumming, P. Ploypradith, G. H. Posner, *Adv. Pharmacol.* **1997**, *37*, 253–297; G. H. Posner, J. N. Cumming, M. Krasavin, *Biomed. Chem.* **2000**, 289–309; G. H. Posner, M. Krasavin, M. McCutchen, P. Ploypradith, J. P. Maxwell, J. S. Elias, M. H. Parker in *Antimalarial Chemotherapy* (Ed.: P. J. Rosenthal), Humana Press, **2001**, pp. 255–263.
[18] P. Olliaro, R. K. Haynes, B. Meunier, Y. Yuthavong, *Trends Parasitol.* **2001**, *17*, 122–126.
[19] S. R. Meshnick, *Int. J. Parasitol.* **2002**, *32*, 1655–1660.
[20] W.-M. Wu, Y.-K. Wu, Y.-L. Wu, Z.-J. Yao, C.-M. Zhou, Y. Li, F. Shan, *J. Am. Chem. Soc.* **1998**, *120*, 3316–3325.
[21] D.-Y. Wang, Y.-K. Wu, Y.-L. Wu, Y. Li, F. Shan, *J. Chem. Soc. Perkin Trans. 1* **1999**, 1827–1831.
[22] Y. L. Hong, Y. Z. Yang, S. R. Meshnick, *Mol. Biochem. Parasitol.* **1994**, *63*, 121–128.
[23] A. Robert, J. Cazelles, B. Meunier, *Angew. Chem.* **2001**, *113*, 2008–2011; *Angew. Chem. Int. Ed.* **2001**, *40*, 1954–1957.
[24] A. Robert, B. Meunier, *Chem. Eur. J.* **1998**, *4*, 1287–1296; F. Zouhiri, D. Desmaële, J. D'Angelo, J. Mahuteau, C. Riche, F. Gay, L. Cicéron, *Tetrahedron Lett.* **1998**, *39*, 2897–2906; F. Zouhiri, D. Desma ële, J. D'Angelo, J. Mahuteau, C. Riche, F.

 © 2004 Wiley-VCH Verlag GmbH & Co. KGaA, Weinheim

Gay, L. Cicéron, *Eur. J. Org. Chem.* **1998**, 2897 – 2906; O. Provot, B. Camuzat-Dedenis, M. Hamzaoui, H. Moskowitz, J. Mayrargue, A. Robert, J. Cazelles, B. Meunier, F. Zouhiri, D. Desmaële, J. D'Angelo, J. Mahuteau, F. Gay, L. Cicéron, *Eur. J. Org. Chem.* **1999**, 1935 – 1938.

[25] Y.-K. Wu, Z.-Y. Wu, Y.-L. Wu, *Angew. Chem.* **1999**, *38*, 2730 – 2733; *Angew. Chem. Int. Ed.* **1999**, *38*, 2580 – 2582; Y.-K. Wu, Z.-Y. Yue, H.-H. Liu, *Helv. Chim. Acta* **2001**, *84*, 928 – 932; Y.-K. Wu, *Acc. Chem. Res.* **2002**, *35*, 255 – 259.

[26] In ref. [19], the statement is made to the effect that "19 other research groups in 11 countries have corroborated the importance of heme in the activation of artemisinin and its derivatives".

[27] O. Dechy-Cabaret, F. Benoit-Vical, A. Robert, B. Meunier, *ChemBioChem* **2000**, *1*, 281 – 283; A. Robert, O. Dechy-Cabaret, J. Cazelles, B. Meunier, *Acc. Chem. Res.* **2002**, *35*, 167 – 174.

[28] R. K. Haynes, H. W. Chan, M.-K. Cheung, S.-K. Chung, W.-L. Lam, H.-W. Tsang, A. Voerste, I. D. Williams, *Eur. J. Org. Chem.* **2003**, 2098 – 2114.

[29] Preparation of 10α-substituted alkylamino derivatives has not been previously reported. For preparation of the 10-arylamino derivatives, see Y.-H. Yang, Y. Li, Y.-L Shi, J.-D Yang, B.-A. Wu, *Bioorg. Med. Chem. Lett.* **1995**, *5*, 1791 – 1794; for an indirect preparation of the 10-arylamino derivatives bearing bromine at C9, see A. J. Lin, L.-Q. Li, D. L. Klayman, C. F. George, J. L. Flippen-Anderson, *J. Med. Chem.* **1990**, *33*, 2610 – 2614. Whilst these compounds display good efficacy in vitro, they have no significant activity in vivo.

[30] W. Peters, B. L. Robinson in *Handbook of Animal Models of Infection* (Eds.: O. Zak, M. Sande), Academic Press, London, **1999**, chap. 92, Section VI, pp. 756–771.

[31] R. K. Haynes, D. Monti, D. Taramelli, N. Basilico, S. Parapini, P. Olliaro, *Antimicrob. Agents Chemother.* **2003**, *47*, 1175; R. K. Haynes, D. Monti, D. Taramelli, N. Basilico, S. Parapini, P. Olliaro, *Antimicrob. Agents Chemother.* **2003**, *47*, 2712 – 2713.

[32] In vitro IC_{50} [ng mL^{-1}] values against W2 (chloroquine-resistant) and D6 strains of *P. falciparum*: **23**: 0.58, 0.15; artemisinin (**1**): 2.33, 1.21; in vivo against *P. berghei* in mice, **23** single dose D + 3, 640 mg kg^{-1} 5/5 cures: M. Jung, X. Li, D. A. Bustos, H. N. El Sohly, J. D. McChesney, W. K. Milhous, *J. Med. Chem.* **1990**, *33*, 1516 – 1518; in vivo against *P. berghei* in mice, **23** daily dose 60 mg kg^{-1}, 100% cure rate, artemisinin (**1**) 96% cure rate: B. Ye, G.-F. Wu, X.-Q. Jiao, *Acta Pharm. Sin.* **1991**, *26*, 228 – 230.

[33] The reactivity of artemisinin (**1**) under these conditions has been established; see ref. [13].

[34] W.-M. Wu, Z.-J. Yao, Y.-L. Wu, K. Jiang, Y.-F. Wang, H.-B. Chen, F. Shan, Y. Li, *Chem. Commun.* **1996**, 2213 – 2214; D.-Y. Wang, Y.-L. Wu, Y. Wu, J. Liang, Y. Li, *J. Chem. Soc. Perkin Trans. 1* **2001**, 605 – 609.

[35] For compounds **24**, **27**,and **28**, see ref. [20]; for compounds **25**, **29**, and **30**, see A. J. Lin, A. D. Theoharides, D. L. Klayman, *Tetrahedron* **1986**, *42*, 2181 – 2184; for compound **26**, see ref. [36] and M. Jung, X. Li, D. A. Bustos, H. N. ElSohly, J. D. McChesney, W. K. Milhous, *J. Med. Chem.* **1990**, *33*, 1516 – 1518; for compound **31**, see Y.-M. Pu, H. Yeh, H. Ziffer, *Heterocycles* **1993**, 36, 2099 – 2107. Detailed explanations have been presented previously for the formation of the products; see foregoing references, especially refs. [13,14,20,25,36].

[36] Treatment of compound **23** with anhydrous $FeBr_2$ in THF rapidly provides products **26** (8%) and **29** (79%): M. A. Avery, P.-C. Fan, J. M. Karle, J. D. Bonk, R. Miller, D. K. Goins, *J. Med. Chem.* **1996**, *39*, 1885 – 1897.

[37] Compound **32** is easily detected by thin-layer chromatography; however, it is admixed with approximately 15% of another adduct, possibly the C1-naphthyl-linked compound; oil, ^{1}H NMR spectrum (300 MHz, $CDCl_3$): δ = 8.16–7.36 (m, 7H), 5.97 (s, 1H), 3.68–3.60 (m, 1H), 3.48 (t, J = 11.7 Hz, 1H), 3.11–3.06 (m, 2H), 2.55–2.39 (m, 2H), 1.89 (s, 3H), 1.81–1.77 (m, 1H), 1.69–1.52 (m, 2H), 1.53–1.04 (m, 6H), 0.96–0.94 (d, J = 6.3 Hz, 3H), 0.78–0.76 ppm (d, J = 7.2 Hz, 3H).

[38] In ref. [21], it is reported that stereoisomeric naphthyl-10-deoxo-10-dihydroartemisinin derivatives differing in configuration at C9 and C10 react at markedly different rates with $FeSO_4$ in aqueous MeCN; the less reactive isomer in this case displays very low activity against *P. falciparum* in vitro.

[39] A referee contends that differences in reactivity may be due to different solubilities of the artemisinin derivatives in the reaction medium (1:1 MeCN/H_2O). In this respect, compound **20** is observed to be poorly soluble, but it is indeed decomposed by Fe^{II} (0.3 equiv) under the standard conditions (Table 3) to leave unreacted **20** (36%) and provide products **24** (13%) and **25** (6%), in addition to large amounts of as yet uncharacterized products bearing the morpholino substituent. Further, the contrasting reactivities of the benzylpiperazino compound **18** and 10-deoxo compound **23** towards each of heme-Fe^{II} and -Fe^{II} under essentially identical reaction conditions (Tables 2 and 3) are not in key with a solubility factor.

[40] R. K. Haynes, H.-O. Pai, A. Voerste, *Tetrahedron Lett.* **1999**, *40*, 4715 – 4718.

[41] For reviews and examples, see *Organic Peroxides* (Ed.: W. Ando), Wiley, Chichester, **1992**, chap. 3, pp. 174–178; *Organic Peroxides* (Ed.: W. Ando), Wiley, Chichester, **1992**, chap. 6, pp. 295–304.

[42] G. Rucker, E. Breitmaier, D. Manns, W. Maier, A. Marek, B. Heinzmann, K. Heiden, S. Seggeweis, *Arch. Pharm.* **1997**, *330*, 12 – 16.

[43] W. Herz, R. C. Ligroin, J. A. Turner, J. F. Blount, *J. Org. Chem.* **1977**, *42*, 1885.

[44] A. M. Szpilman, E. E. Korshin, R. Hoos, G. H. Posner, M. D. Bachi, *J. Org. Chem.* **2001**, *66*, 6531 – 6540.

[45] F. ter Kuile, N. J. White, P. H. Holloway, G. Pasvol, S. Krishna, *Exp. Parasitol.* **1993**, *76*, 85 – 95.

[46] After submission of the manuscript, it was reported that artemisinin (**1**) exerts its antimalarial activity through irreversible inhibition of the Ca^{2+}-dependent *Plasmodium falciparum* ATPase (PfATP6), as expressed in *Xenopus* oocytes: U. Eckstein-Ludwig, R. J. Webb, I. D. A. Van Goethem, J. M. East, A. G. Lee, M. Kimura, P. M. O'Neill, P. G. Bray, S. A. Ward, S. Krishna, *Nature* **2003**, *424*, 957 – 961. The enzyme is a transmembrane protein associated with the parasite endoplasmic reticulum. This beautiful work convincingly demonstrates the irrelevance of the heme-activation idea. Most importantly, the identification of the target will now allow for a rational examination of the mechanism of action of this remarkable class of antimalarial drug and the precise role, if any, played by iron in artemisinin activation at the binding site.

 © 2004 Wiley-VCH Verlag GmbH & Co. KGaA, Weinheim

Fullerenes

Molecular Motion of Endohedral Fullerenes in Single-Walled Carbon Nanotubes**

Andrei N. Khlobystov, Kyriakos Porfyrakis, Mito Kanai, David A. Britz, Arzhang Ardavan, Hisanori Shinohara, T. John S. Dennis, and G. Andrew D. Briggs**

Spherical carbon cages of fullerene molecules interact by van der Waals forces to form close-packed arrangements in the solid state, such as the face-centered cubic lattice formed by C_{60} at room temperature.[1] Owing to the low directionality and low energy of the interfullerene interactions neutral fullerene molecules (such as C_{60}) are freely rotating in the crystal at room temperature.[2] Contrasting to the empty fullerene cages, metal-containing endohedral fullerenes are known to have large electric dipole moments of 3–4 Debye.[3] Therefore, it should be expected that intermolecular interactions in the solid M@C_n, (M = metal center) are dominated by strong dipolar interactions. For example, fullerene Ce@C_{82} has a large dipole moment owing to the transfer of three valence electrons from the Ce atom to C_{82} cage.[4] This fullerene crystallizes in a hexagonal or a face-centered cubic close pack arrangement.[5] However, despite the dipole moment the fullerene Ce@C_{82} has been shown to retain its rotational freedom in the crystalline state with an energetic barrier of only 1.3 kJ mol^{-1}.[6]

In contrast to bulk-fullerene crystals, fullerene molecules inserted in single-walled carbon nanotubes (SWNTs) form linear chains in which each fullerene has only two nearest neighbors[7] as compared to 12 neighbors in the crystalline bulk fullerenes.[1,5] As a result the intermolecular interactions in these self-assembled carbon nanostructures, designated as C_n@SWNT, and the dynamic behavior of the encapsulated molecules are expected to be different to those in solid fullerenes. C_n@SWNTs exhibit unique electronic properties and are currently attracting attention as building blocks for functional nanodevices.[8,9] C_n@SWNTs structures containing magnetically active mono-metallofullerenes M@C_n are of interest as candidate materials for solid-state quantum computers.[10] We present herein for the first time a study on the molecular motion of mono-metallofullerene Ce@C_{82} chains inside SWNTs demonstrating different modes of translational and rotational motion.

Raw SWNTs (Aldrich) were purified by a combination of standard techniques.[11] Only nanotubes with diameters 13.5 Å and 15.0 Å (as shown by Raman spectroscopy; Supporting Information) were present in the samples used for the experiments. The purified SWNTs were effectively filled with C_{60}, C_{70}, and Ce@C_{82} (synthesized by DC arc-discharge method[12]) at 400–500 °C and 2×10^{-6} torr, which resulted in C_n@SWNT "peapod" structures in 60–90 % yields. The yield for inserting C_{82} in SWNTs was lower (≈ 30 %) even when an excess of C_{82} was used.

High-resolution transmission electron microscope (HRTEM, JEOL 4000EX, LaB_6, information limit 0.12 nm) imaging conditions have been carefully tuned by lowering the accelerating voltage of the microscope to 100 kV and reducing the beam current density to a minimum to enable a direct observation of the molecular motion for the mono-metallofullerene inside SWNTs. Under these conditions the amount of the energy transferable from the electrons to the specimen is significantly reduced[13] compared to the standard TEM imaging conditions. No beam damage was observed in sp^2-carbon structures under these conditions over a period of 20 min. Most of the micrographs were obtained by using 2 s exposures of a charge-coupled-device (CCD) detector. Translational motion can be observed for all types of C_n in SWNTs (Figure 1 a), which indicates that the molecules are mobile inside the nanotube at room temperature and move independently of one another. This effect is particularly noticeable in the peapod bundles where several nanotubes are aligned parallel to each other. Observation of the ends of the nanotubes and side-wall defects confirms that there is no relative motion of nanotubes within the bundle. It is remarkable that the molecules continue their translational motion even inside apparently completely filled nanotubes (Figure 1 b, c).

In contrast to the independent translations observed for sparsely filled nanotubes, the chains of fullerenes with regular van der Waals separations between the molecules undergo collective translations, so that the entire chain shifts in a short time without changing the intermolecular separations. The motion of an isolated molecule in sparsely filled nanotube (Figure 1 a) is not continuous: the molecule performs abrupt jumps with irregular intervals of approximately 10 s.

In contrast to isolated fullerenes the motion of the chains is significantly slower and appears to be more continuous than abrupt: the rectangular (Figure 1 b) and zigzag (Figure 1 c) arrangements do not transform immediately into each other. Instead the rearrangement occurs through a series of states

[*] Dr. A. N. Khlobystov, Dr. K. Porfyrakis, D. A. Britz, Prof. G. A. D. Briggs
Department of Materials
Oxford University
Parks Rd, Oxford, OX1 3PH (UK)
Fax: (+44) 1865-273789
E-mail: Andrei.Khlobystov@materials.ox.ac.uk
Andrew.Briggs@materials.ox.ac.uk
M. Kanai, Dr. T. J. S. Dennis
Centre for Materials Research, Queen Mary
University of London, Mile End Road, London, E1 4NS (UK)
Dr. A. Ardavan
Department of Physics, Oxford University
Parks Rd, Oxford, OX1 3PU (UK)
Prof. H. Shinohara
Department of Chemistry, Nagoya University
Nagoya 464-8602 (Japan)

[**] The work described here is supported through the Foresight LINK Award Nanoelectronics at the Quantum Edge (www.nanotech.org), funded by DTI, EPSRC (GR/R66029/01), and Hitachi Europe Ltd. T.J.S.D. thanks the Royal Society for a Joint Research Project (Japan), the EPSRC for grant GR/R55313/01. D.A.B. thanks the Overseas Research Student Scheme for funding. A.A. thanks the Royal Society.

Supporting information for this article is available on the WWW under http://www.angewandte.org or from the author.

 © 2004 Wiley-VCH Verlag GmbH & Co. KGaA, Weinheim DOI: 10.1002/anie.200352389

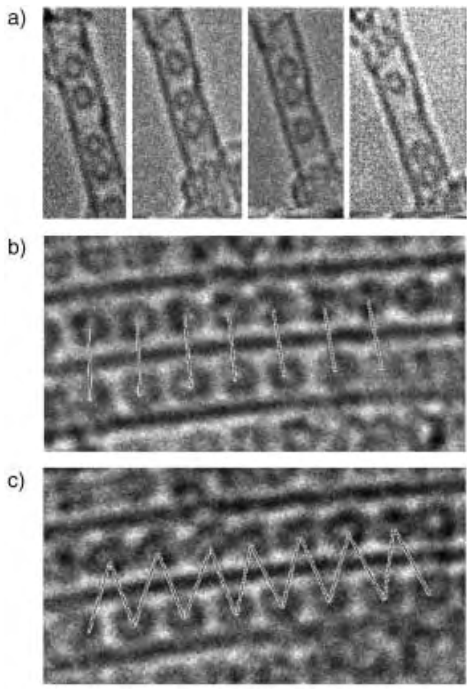


Figure 1. TEM micrographs showing translational motion of fullerenes in a) C_{82}@SWNT (time interval between photographs is 10 s) and b,c) in a bundle of (Ce@C_{82})@SWNT structures (time interval is $\approx$1 min).

intermediate between the two extreme cases shown in Figure 1 b and c. The chain translates in both directions, and its motion resembles irregular collective oscillations involving large numbers of fullerene molecules. The observation of the collective motions in SWNTs indicates a low energetic barrier for translation and provides explanation for the mechanism of molecular transport along the nanotube during the filling process. A chain of fullerenes does not create a blockage in SWNT and, therefore, the nanotube can be effectively filled along the entire its length from just one entrance point, provided that there is a constant supply of fullerenes from the gas phase. This notion is supported by the HRTEM analysis showing that nearly all nanotubes in the samples are either completely filled or completely empty, whereas partially filled nanotubes are very rare.

Another type of molecular motion, rotation, can, in principle, be observed by HRTEM for endohedral fullerene molecules, because an individual lanthanide atom can be clearly seen as a dark spot at the edge of the fullerene cage as a result of the high single atom contrast,[14] which is related to $Z^{2/3}$ where Z is the atomic number. Previous work reported the continuous spinning of fullerene Sm@C_{82} in SWNTs, so that the metal atom was not visible until the fullerene cages eventually became immobile as a result of beam damage.[15,16] A mixed dynamic behavior has been reported for Gd@C_{82} in the "peapod"-type structure where some cages are stationary and some are spinning.[17,18] Similar to the mono-metallofullerenes, bis(metallo)fullerenes can exhibit a tumbling motion (La_2@C_{80})[19] or total immobility (Sc_2@C_{84})[20] inside nanotubes. Although systematic experimental data on the dynamics of C_n@SWNT systems is very limited, it is possible to conclude that different rotational behavior of fullerenes is related to the energy of the intermolecular interactions inside SWNT. For example, the difference in charge distribution for Sm^{2+}@C_{82}^{2-} and Gd^{3+}@C_{82}^{3-} results in the relative rotational immobility observed for Gd@C_{82} as compared to Sm@C_{82}, which can be related to the stronger electrostatic intermolecular interactions for the latter, which restrict the free rotation.

Individual Ce atoms are visible as dark spots near the edges of the fullerene circles on the micrograph (Figure 2). Each Ce@C_{82} experiences the local electric field owing to the dipoles of neighboring molecules. As the positive end of the dipole moment of Ce@C_{82} coincides with the position of the Ce atom,[14] HRTEM reveals the orientation of Ce@C_{82} dipole moments inside SWNTs. The distribution of angle θ (Figure 3 a,b) indicates a preferential orientation for Ce@C_{82} with the dipole moment nearly parallel to the nanotube axis. Comparison of these angles (θ_1 and θ_2) for pairs of neighboring fullerenes shows a correlation between the orientations, thus, demonstrating that the dipole interactions influence the orientations of polar fullerene molecules in SWNTs (Figure 3 c). However, many fullerenes show significant deviations from the perfect order in SWNTs, as the impact of the electron beam and thermal motion at room temperature disrupt the order in the molecular chains.

A series of successive images with 2 s camera exposure time and with approximately 10 s interval between exposures revealed a discontinuous rotational motion of the fullerene molecules in isolated nanotubes (Figure 2 a–d): a particular Ce@C_{82} molecule stays stationary at a certain position for several seconds before it abruptly jumps to a new stable orientation. Similarly to the translational motion of isolated molecules, the process of switching between different orientations is fast and irregular so that only orientations of

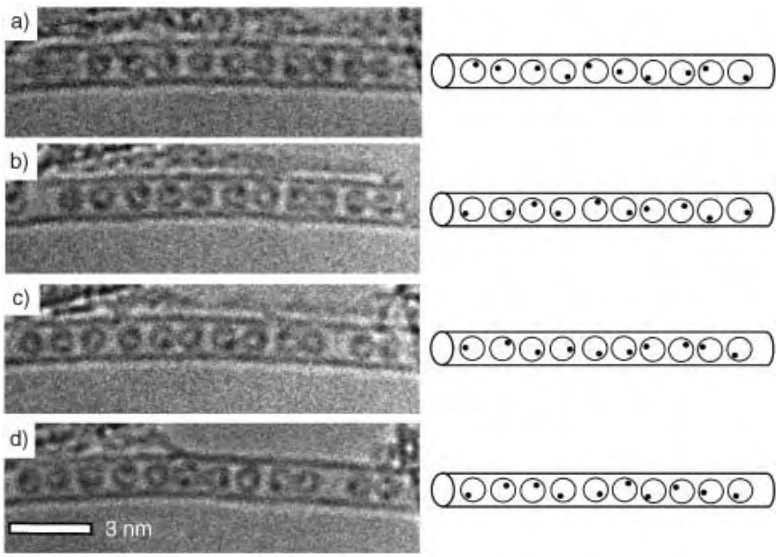


Figure 2. A series of successive HRTEM images of (Ce@C_{82})@SWNT and their schematic representation (a–d).

 © 2004 Wiley-VCH Verlag GmbH & Co. KGaA, Weinheim

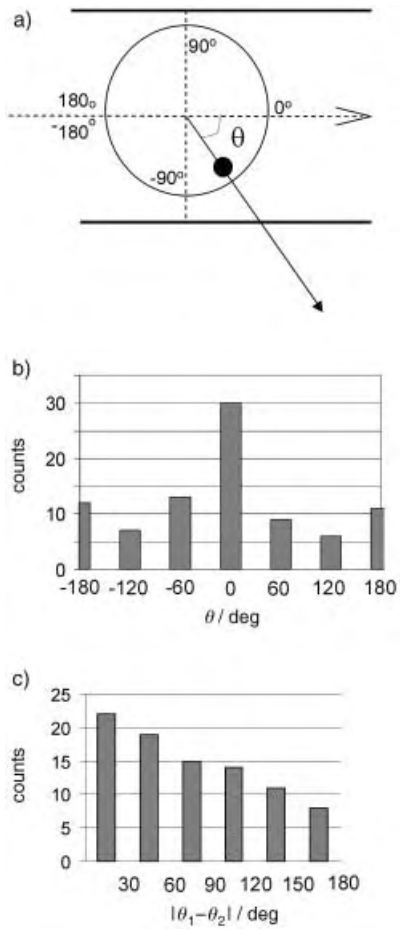


Figure 3. a) Schematic representation of Ce@C_n inside a nanotube: the nanotube direction is shown by a broken arrow, the dipole direction is shown by a solid arrow, θ is the angle between these directions. b) Experimental distribution of θ in (Ce@C_{82})@SWNTs. c) Distribution of $|\theta_1-\theta_2|$ for pairs of adjacent Ce@C_{82} molecules.

Ce@C_{82} corresponding to equilibrium positions can be captured on a CCD detector. The micrographs shown in Figure 2 represent a typical behavior of Ce@C_{82} observed for over 20 isolated nanotubes in different areas of the specimen dispersed on a 5 mm TEM grid. This motion is more likely to be associated with the molecular rotation than with a migration of the Ce atom within the fullerene, because a shift of the Ce atom with respect to the carbon cage requires the overcoming of a significant energetic barrier of 221 kJ mol^{-1}.[6] Thus, the relative energy required for metal rotation in a fixed cage is 170-times greater than that for the cage and metal rotating together in the crystal. The observed switching between equilibrium positions, as compared to a smooth continuous molecular rotation, indicates that the dipolar interfullerene interactions in the (Ce@C_{82})@SWNT system are significantly greater than in the crystal of Ce@C_{82} where molecules are freely rotating at temperatures above 80 K.[6] Each Ce@C_{82} in SWNT experiences the strong electrostatic field dominated by two nearest molecules (see Supporting Information), as compared to twelve nearest molecules in the close-packed crystalline Ce@C_{82}. Owing to the high symmetry of the electrostatic field in the crystal, each Ce@C_{82} molecule can exist in several energetically and geometrically equivalent orientations with a small barrier of 1.3 kJ mol^{-1} between them. However, the nearly free rotation in the crystal of Ce@C_{82} is substantially inhibited in the SWNT as a result of the lowering the symmetry of electrostatic potential for each fullerene.

We have also studied molecular rotation for peapods where each endohedral fullerene can interact with more than two neighboring molecules. (Ce@C_{82})@SWNTs structures spontaneously aggregate in small bundles with a distance of about 8 Å separating the molecules in adjacent nanotubes. Two or three spots appear on micrographs within each fullerene circle (Figure 4) that can be explained by fast

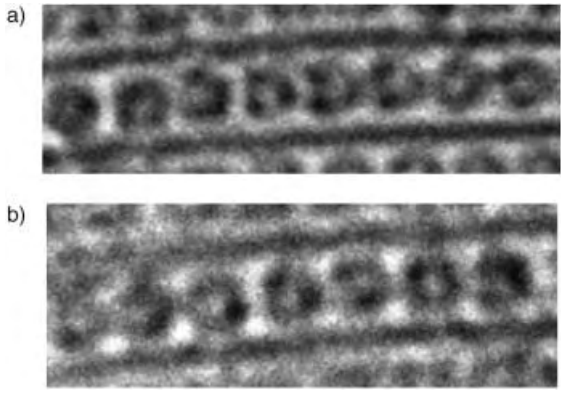


Figure 4. HRTEM micrographs of a bundle of (Ce@C_{82})@SWNT structures taken with a) 2 s and b) 1 s camera exposures.

switching orientations of Ce@C_{82} between two or three positions with a period shorter than the camera exposure time. At short camera exposures ($\approx$1 s) during the HRTEM imaging the Ce atom appears delocalized between two positions (Figure 4b), whereas at longer exposures (2 s) the Ce atom appears delocalized over three sites (Figure 4a). This effect has been observed for several areas of the specimen where two or more nanotubes are positioned in a close proximity. Attempts to use exposure times shorter than 1 s or longer than 2 s did not produce images with sufficient resolution because of a too low electron dose on the detector or excessive specimen drift, respectively.

The faster rate of discontinuous rotation for the endohedral fullerene in the bundle may be associated with dipolar interactions of each molecule with several molecules from adjacent nanotubes in addition to the interactions within the nanotube. This situation means the electrostatic potential around each fullerene has a complex symmetry, which causes orientational frustration for the Ce@C_{82} molecules. As a result, the molecular rotation in the bundle is less restricted than in the isolated nanotube. A bundle of (Ce@C_{82})@SWNTs can be viewed as an intermediate structure between a single "peapod" (Ce@C_{82})@SWNTs and the bulk crystal of the fullerene. Traditionally, bundles of C_n@SWNT are considered as "one dimensional" crystals[8] because of the molecular ordering within these structures, but our results indicate that they should in fact be considered to be "quasi-one-dimensional" or highly anisotropic three-dimensional structures.

 © 2004 Wiley-VCH Verlag GmbH & Co. KGaA, Weinheim

In summary, we have synthesized a carbon nanostructure ($Ce@C_{82}$)@SWNT containing isolated Ce atoms embedded in fullerenes. The molecules in nanotubes exhibit an unusual type of saltatory rotational motion visualized for the first time for mono-metallofullerenes. The alignment of the fullerene molecules and the rotational mode suggest the electrostatic dipole interaction influences the orientation of $Ce@C_{82}$ in the nanotube. The nature and rate of the molecular rotation is affected by the external electrostatic fields, such as the field of a neighboring ($Ce@C_{82}$)@SWNT structure within a bundle. In addition, cooperative translational oscillations have been observed for fullerene chains where the intermolecular separations are virtually unchanged as the entire molecular chain moves inside SWNT. It may be possible to exploit the dipolar interactions of this type to control the alignment of the molecular chains, thereby tuning the functional properties of the nanomaterials based on this type of carbon structures.

Received: July 16, 2003
Revised: September 24, 2003 [Z52389]

Keywords: carbon nanotubes · cerium · electron microscopy · fullerenes

[1] W. I. F. David, R. M. Ibberson, J. C. Matthewman, K. Prassides, T. J. S. Dennis, J. P. Hare, H. W. Kroto, R. Taylor, D. R. M. Walton, *Nature* **1991**, *353*, 147 – 149.
[2] P. Heiney, J. E. Fischer, A. R. McGhie, W. J. Romanow, A. M. Denenstein, J. P. McCauley, A. B. Smith, *Phys. Rev. Lett.* **1991**, *66*, 2911 – 2914.
[3] K. Laasonen, W. Andreoni, M. Parrinello, *Science* **1992**, *258*, 1916 – 1918.
[4] J. Q. Ding, L. T. Weng, S. H. Yang, *J. Phys. Chem.* **1996**, *100*, 11120 – 11121.
[5] C. J. Nuttall, Y. Inada, Y. Watanabe, K. Nagai, T. Muro, D. H. Chi, T. Takenobu, Y. Iwasa, K. Kikuchi, *Mol. Cryst. Liq. Cryst.* **2000**, *340*, 635 – 638.
[6] W. Sato, K. Sueki, K. Kikuchi, K. Kobayashi, K. Suzuki, Y. Achiba, H. Nakahara, Y. Ohkubo, F. Ambe, K. Asai, *Phys. Rev. Lett.* **1998**, *80*, 133 – 136.
[7] M. Monthioux, *Carbon* **2002**, *40*, 1809 – 1823, and references therein.
[8] T. Shimada, T. Okazaki, R. Taniguchi, T. Sugai, H. Shinohara, K. Suenaga, K. Ohno, S. Mizuno, S. Kishimoto, T. Mizutani, *Appl. Phys. Lett.* **2002**, *81*, 4067 – 4069.
[9] P. W. Chui, G. Gu, G. T. Kim, G. Philipp, S. Roth, S. F. Yang, S. Yang, *Appl. Phys. Lett.* **2001**, *79*, 3845 – 3847.
[10] A. Ardavan, M. Austwick, S. C. Benjamin, G. A. D. Briggs, T. J. S. Dennis, A. Ferguson, D. G. Hasko, M. Kanai, A. N. Khlobystov, B. W. Lovett, G. W. Morley, R. A. Oliver, D. G. Pettifer, K. Portyrakis, J. H. Reina, J. H. Rice, J. D. Smith, R. A. Taylor, D. A. Williams, C. Adelmann, H. Mariette, R. J. Hamers, *Philos. Trans. R. Soc. London Ser. A* **2003**, *361*, 1473 – 1485.
[11] J.-M. Moon, K. H. An, Y. H. Lee, Y. S. Park, D. J. Bae, G. S. Park, *J. Phys. Chem. B* **2001**, *105*, 5677 – 5681.
[12] H. Shinohara, *Rep. Prog. Phys.* **2000**, *63*, 843 – 892.
[13] B. W. Smith, D. E. Luzzi, *J. Appl. Phys.* **2001**, *90*, 3509 – 3515.
[14] K. Suenaga, T. Okazaki, K. Hirahara, S. Bandow, H. Kato, A. Taninaka, H. Shinohara, S. Iijima, *Appl. Phys. A* **2003**, *76*, 445 – 447.
[15] T. Okazaki, K. Suenaga, K. Hirahara, S. Bandow, S. Iijima , H. Shinohara, *Physica B + C* **2002**, *323*, 97 – 99.
[16] T. Okazaki, K. Suenaga, K. Hirahara, S. Bandow, S. Iijima, H. Shinohara, *J. Am. Chem. Soc.* **2001**, *123*, 9673 – 9674.
[17] K. Suenaga, T. Tence, C. Mory, C. Colliex, H. Kato, T. Okazaki, H. Shinohara, K. Hirahara, S. Bandow, S. Iijima, *Science* **2000**, *290*, 2280 – 2282.
[18] K. Hirahara, K. Suenaga, S. Bandow, H. Kato, T. Okazaki, H. Shinohara, S. Iijima, *Phys. Rev. Lett.* **2000**, *85*, 5384 – 5387.
[19] B. W. Smith, D. E. Luzzi, Y. Achiba, *Chem. Phys. Lett.* **2000**, *331*, 137 – 142.
[20] K. Suenaga, T. Okazaki, C. R. Wang, S. Bandow, H. Shinohara, S. Iijima, *Phys. Rev. Lett.* **2003**, *90*, 055506.

 © 2004 Wiley-VCH Verlag GmbH & Co. KGaA, Weinheim

Block Copolymers

Preparation of Shell Cross-Linked Micelles by Polyelectrolyte Complexation**

Jonathan V. M. Weaver, Yiqing Tang, Shiyong Liu, Peter D. Iddon, Rachel Grigg, Norman C. Billingham, Steven P. Armes, Robert Hunter, and Steven P. Rannard*

Covalent stabilization of micelles and vesicles has attracted increasing attention in recent years.[1–4] In particular, shell cross-linked (SCL) micelles are potentially useful nanosized vehicles for the delivery of various actives (e.g., drugs, fragrances, pesticides).[1–3] The first example of SCL micelles was described by Wooley and co-workers, who oligomerized pendent styrene groups by using radical chemistry.[1a] Our group has reported the use of 1,2-bis(2-iodoethoxy)ethane (BIEE) as a bifunctional cross-linker for the covalent stabilization of SCL micelles.[2] However, in view of its cost, toxicity, limited water solubility, and likely mutagenicity, BIEE is unlikely to be employed in commercial applications of SCL micelles, particularly in the biomedical field. The

[*] J. V. M. Weaver, Y. Tang, P. D. Iddon, R. Grigg, N. C. Billingham, Prof. Dr. S. P. Armes
Department of Chemistry, School of Life Sciences, University of Sussex
Falmer, Brighton, E. Sussex, BN1 9QJ (UK)
Fax: (+44) 1273-677196
E-mail: S.P.Armes@sussex.ac.uk
Dr. S. Liu
Department of Polymer Science and Engineering
University of Science and Technology of China
Hefei, Anhui, 230026 (P. R. China)
Dr. R. Hunter, Dr. S. P. Rannard
Unilever Research, Port Sunlight Laboratories
Quarry Road East, Bebington, Wirral, L63 3JW (UK)

[**] J.V.M.W. and P.D.I. thank EPSRC for a PhD studentship. J.V.M.W. thanks Cognis Performance Chemicals (Hythe (UK)) for CASE support and for the gift of the monohydroxy-capped PEO. P.D.I. thanks Avecia (Blackley (UK)) for CASE support. Y.T. and S.L. thank EPSRC for a post-doctoral fellowship (GR/S25845 and GR/N17409).

Supporting information for this article is available on the WWW under http://www.angewandte.org or from the author.

 DOI: 10.1002/anie.200352428 © 2004 Wiley-VCH Verlag GmbH & Co. KGaA, Weinheim

cross-linking strategies described by other workers are also rather unsatisfactory. For example, Wooley's group[1e] now favour the use of carbodiimide coupling chemistry to link carboxylic acid groups through diamines but this method suffers from expensive reagents and requires purification to remove small molecule by-products. Liu and co-workers[3a] prefer the UV-induced coupling of cinnamoyl groups; this is relatively "clean" chemistry but cinnamoyl groups are probably too hydrophobic to be suitable for use in aqueous media. It is clear that there is considerable scope for the development of new, improved cross-linking strategies.

Complexation of oppositely charged polyelectrolytes is a well-known phenomenon, which has been recently exploited in the context of layer-by-layer deposition[5] and also DNA condensation.[6] Moreover, Kabanov et al. have demonstrated that micellization can be induced by adding either a cationic homopolyelectrolyte (quaternized poly(4-vinylpyridine)) or a cationic surfactant (hexadecyltrimethylammonium bromide) to an aqueous solution of a molecularly dissolved neutral–anionic AB diblock copolymer, for example, poly(ethylene oxide-block-sodium methacrylate).[7] Both Harada and Kataoka and also Jerome's group have reported similar observations,[8] and very recently Schlaad and co-workers have exploited polyelectrolyte complexation in non-aqueous media to prepare vesicles.[9] In principle, polyelectrolyte complexation offers four advantages over conventional "small-molecule" cross-linking strategies: (1) polyelectrolytes are generally regarded as having low toxicity; (2) physical cross-linking means that there is no possibility of unwanted chemical modification of the active compound to be encapsulated; (3) there are no small-molecule by-products, hence purification is straightforward; (4) ionic cross-linking is, in principle, reversible in the presence of added salt. Furthermore, it might be reasonably expected that the glassy, rigid nature of the inter-polyelectrolyte complex layer would lead to efficient encapsulation (or at least retarded release) of the active hydrophobic compound within the micelle cores. Herein, we explore the feasibility of synthesizing SCL micelles by using either an anionic homopolymer or diblock copolymer as an ionic cross-linker for a cationic ABC triblock copolymer in which the cationic charge density resides in the central B block (see Figure 1).

The anionic cross-linkers, PEO_{113}–$NaStS_{34}$ diblock copolymer and $NaStS_{32}$ homopolymer (NaStS = sodium 4-styrenesulfonate), were each prepared by atom transfer radical polymerization (ATRP) in mixed aqueous media at 20 °C by using similar protocols to those described by Choi and Kim.[10] The $NaStS_{32}$ homopolymer had an $\bar{M}_n$ of 6900 and an $\bar{M}_w/\bar{M}_n$ of 1.26 as judged by aqueous gel-permeation chromatography (GPC) with near-monodisperse NaStS homopolymer calibration standards ($\bar{M}_n$ is the number-average molar mass, $\bar{M}_w$ is the weight-average molar mass). The PEO_{113}–$NaStS_{34}$ diblock copolymer was prepared by using a PEO-based macroinitiator[2d] ($DP_n = 113$, $\bar{M}_n = 5{,}100$, $\bar{M}_w/\bar{M}_n = 1.17$ with aqueous GPC and PEO standards; PEO = poly(ethylene oxide), DP_n is the degree of polymerization) and had an $\bar{M}_n$ of 12,000 as determined by ^{1}H NMR; aqueous GPC studies indicated an $\bar{M}_w/\bar{M}_n$ of 1.24 (with respect to NaStS homopolymer standards). The cationic ABC triblock copolymer was prepared by ATRP with the same PEO-based macroinitiator as that described above. This macroinitiator was used to polymerize 2-(dimethylamino)ethyl methacrylate (DMA) at ambient temperature in an 2:1 v/v isopropanol/water mixture. After 98% conversion, 2-(diethylamino)ethyl methacrylate (DEA) monomer was added to the reaction solution. The final $\bar{M}_n$ and polydispersity of the PEO_{113}–DMA_{38}–DEA_{54} triblock were determined to be 33100 g mol^{-1} and 1.20, respectively, as judged by THF GPC with poly(methyl methacrylate) standards. Assuming 100% macro-initiator efficiency and perfect blocking efficiency for the DEA polymerization, we esti-

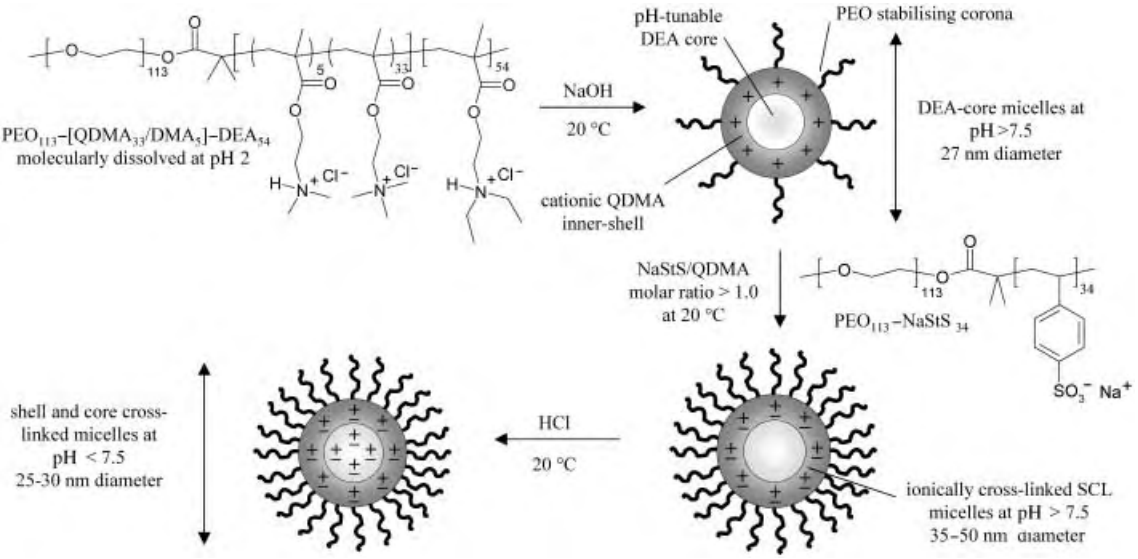


Figure 1. Schematic representation of the formation of shell cross-linked micelles by using an ionic cross-linking strategy. Conventional micelles formed by a PEO_{113}–[$QDMA_{33}$/DMA_5]–DEA_{50} triblock copolymer (see text for details) are stabilized by the addition of an anionic PEO_{113}–$NaStS_{34}$ diblock copolymer. At low pH the conventional micelles dissociate to form individual chains but the ionically cross-linked micelles remain intact, provided that an excess of the anionic diblock copolymer cross-linker is employed.

 © 2004 Wiley-VCH Verlag GmbH & Co. KGaA, Weinheim

mated the overall $\bar{M}_n$ of the triblock copolymer to be 21 000 g mol^{-1} by ^{1}H NMR by using the PEO as an end-group. The DMA residues were selectively quaternized in the presence of the more sterically congested DEA residues by using methyl iodide in THF at 20 °C[11] so as to create a permanently cationic central block (the degree of quaternization of the DMA block was determined to be approximately 88 % after 48 h by ^{1}H NMR). Thus the composition of the final quaternized triblock copolymer is given by PEO_{113}–[$QDMA_{33}$/DMA_5]–DEA_{54}, QDMA is methyl iodide-quaternized DMA residues. As expected, this quaternized triblock copolymer dissolved molecularly in acidic solution (the DEA block becomes protonated and hence hydrophilic at low pH)[11,12] but formed DEA-core micelles with an intensity-average diameter of around 26–28 nm above pH 7, as judged by both dynamic light scattering (DLS) studies (Figure 2a) and ^{1}H NMR spectroscopy (Figure 3). Static light scattering studies (multiangle Zimm plot analysis by using a DAWN DSP light scattering instrument) of the noncross-linked micelles at pH 9 indicated an $\bar{M}_w$ of 3.67×10^5 g mol^{-1}, which corresponds to a mean micelle aggregation number of approximately 10. In our initial experiments we attempted to ionically cross-link the QDMA residues of these DEA-core micelles by using the NaStS homopolymer. However, this shell cross-linking was not successful: on addition of the $NaStS_{32}$ homopolymer to the ABC triblock copolymer micelles at pH 10, a large increase in particle diameter from 26 nm to 56 nm was observed on increasing the NaStS/QDMA molar ratio from 0.4 to 0.8 (Figure 2a). This observation suggests that bridging flocculation of the micelles occurs, despite the relatively low molecular weight of the anionic cross-linker. On decreasing the solution pH at this NaStS/QDMA molar ratio, micellar dissociation occurred at around pH 6. This indicates that these ionically cross-linked micelles have insufficient stability to maintain their structural integrity once the core-forming DEA block becomes hydrophilic. Similar results were obtained with various other anionic homopolyelectrolytes, including poly(acrylic acid), poly(methacrylic acid) and poly(ammonium 2-sulfatoethyl methacrylate). However, ionic cross-linking was much more effective when the PEO_{113}–$NaStS_{34}$ diblock copolymer was used. Moreover, addition of this anionic diblock cross-linker led to a relatively small increase in the micelle diameter (Figure 2a); presumably the PEO chains of the anionic cross-linker reinforce the PEO corona of the PEO_{113}–[$QDMA_{33}$/DMA_5]–DEA_{54} micelles and hence suppress intermicelle bridging flocculation through enhanced steric stabilization. ^{1}H NMR spectroscopy studies confirmed that inter-polyelectrolyte complexation occurred as expected, since all the signals assigned to the QDMA residues and the NaStS

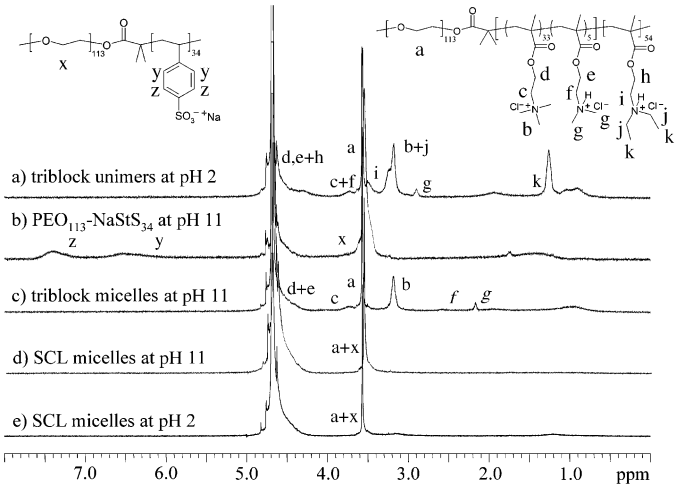


Figure 3. ^{1}H NMR spectra (D_2O) obtained for a) the PEO_{113}–[$QDMA_{33}$/DMA_5]–DEA_{54} triblock precursor at pH 2; b) the PEO_{113}–$NaStS_{34}$ diblock copolymer cross-linker; c) the PEO_{113}–[$QDMA_{33}$/DMA_5]–DEA_{54} micelles alone at pH 11; d) a binary mixture of these two block copolymers at pH 11 (NaStS/QDMA molar ratio = 2); e) the same binary mixture as that of (d) at pH 2 after addition of DCl. The italicized labels represent proton resonances due to deprotonated DMA residues not shown in the chemical structures.

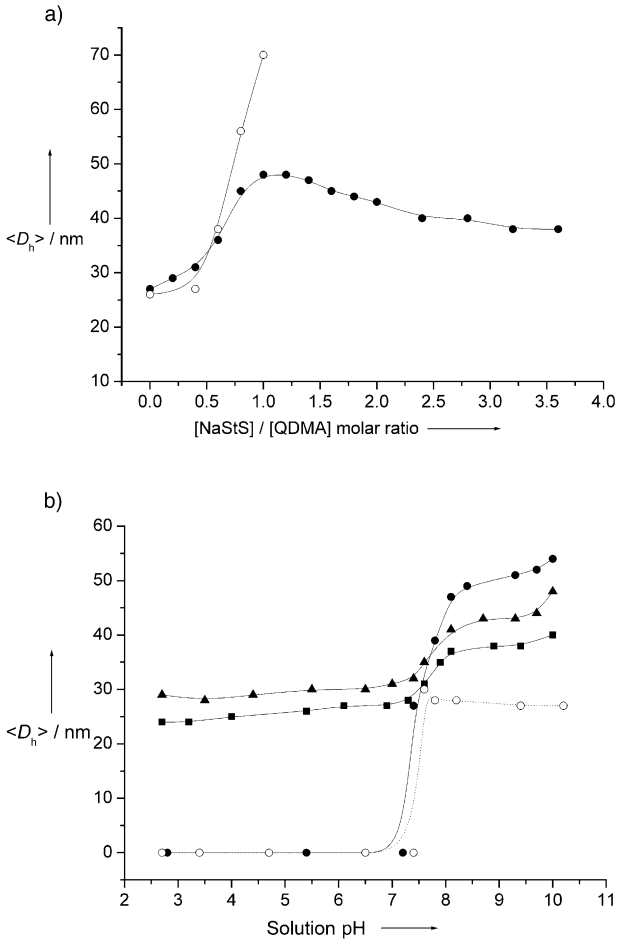


Figure 2. a) Variation of micelle diameter ($< D_h >$) as a function of NaStS/QDMA molar ratio at pH 10 and 20 °C for 5.0 g L^{-1} solutions containing the PEO_{113}–[$QDMA_{33}$/DMA_5]–DEA_{54} triblock copolymer and either the PEO_{113}–NaStS diblock copolymer (●) or a PNaStS homopolymer (○) as the ionic cross-linker. The lines serve as a guide to the eye. b) Variation of micelle diameter with solution pH for the conventional PEO_{113}–[$QDMA_{33}$/DMA_5]–DEA_{50} triblock copolymer micelles and the PEO_{113}–$NaStS_{34}$/PEO_{113}–[$QDMA_{33}$/DMA_5]-DEA_{54} shell cross-linked (SCL) micelles at NaStS/QDMA molar ratios of 2.0 (▲), 1.5 (■), 1.0 (●) and 0.0 (○).

 © 2004 Wiley-VCH Verlag GmbH & Co. KGaA, Weinheim

residues were suppressed on addition of the PEO_{113}–$NaStS_{34}$ cross-linker to the PEO_{113}–[$QDMA_{33}$/DMA_5]–DEA_{54} triblock copolymer micelles (see Figure 3). Again, the structural integrity of the SCL micelles was assessed by switching the solution pH from pH 10 to around pH 2, which leads to protonation of the DEA residues in the micelle cores. If ionic cross-linking had been unsuccessful, micellar dissociation would have occurred spontaneously below pH 7 as the protonated, cationic DEA chains are no longer hydrophobic. Instead, the micelles remain intact at pH 2. However, some micellar disintegration is observed if insufficient PEO_{113}–$NaStS_{34}$ cross-linker is present: the minimum NaStS/QDMA molar ratio required to preserve the micelles at low pH lies somewhere between 1.0 and 1.5 (see Figure 2b), which means that the PEO_{113}–$NaStS_{34}$ cross-linker must be present in reasonable excess. However, since the aromatic signals completely disappear in the ^{1}H NMR spectra recorded for the ionically cross-linked micelles at neutral pH (Figure 3), it seems that essentially all of the PEO_{113}-$NaStS_{34}$ diblock copolymer chains interact with the PEO_{113}–[$QDMA_{33}$/DMA_5]–DEA_{54} micelles. Previously, we observed that the ^{1}H NMR signals assigned to DEA residues in DEA-core SCL micelles were invisible at neutral pH but reappeared at low pH.[2d] However, in the present study, no signals due to protonated DEA residues were observed on addition of DCl. Presumably this is because the noncomplexed "excess" NaStS residues that are in the micelles at neutral pH are available to interact with the protonated DEA residues that are formed at low pH. Thus, we believe that the protonated micelle cores become ionically cross-linked in acidic solution, as well as the QDMA residues in the inner shell.[12]

Remarkably, DLS studies indicate that these ionically cross-linked SCL micelles (5.0 g L^{-1} triblock copolymer solution prepared by using a NaStS/QDMA molar ratio of either 1.5 or 2.0) retain their structural integrity at pH 3.3 in the presence of up to 1.0 M NaCl (see Supporting Information). Furthermore, the SCL micelles appear to be more stable when prepared with higher levels of the anionic diblock cross-linker. At higher levels of added electrolyte micellar dissociation occurs, as expected. Finally, DLS studies suggest that ionically cross-linked SCL micelles prepared at a NaStS/QDMA molar ratio of 2.0 in the absence of any electrolyte are stable to high dilution (< 0.08 g L^{-1}) at pH 3.3.

In summary, SCL micelles can be conveniently prepared simply by inter-polyelectrolyte complexation. The polymeric "reagent" forms physical complexes rapidly in aqueous solution at ambient temperature; ionic cross-linking is readily reversible as the SCL micelles dissociate in the presence of sufficient added electrolyte. However, a simple homopolyelectrolyte cross-linker only leads to flocculated micelles; it is necessary to use excess diblock copolymer for effective ionic cross-linking.

Received: July 21, 2003
Revised: November 6, 2003 [Z52428]

Keywords: block copolymers · drug delivery · micelles · polymerization

[1] a) K. B. Thurmond, T. Kowalewski, K. L. Wooley, *J. Am. Chem. Soc.* **1996**, *118*, 7239; b) H. Huang, T. Kowalewski, E. E. Remsen, R. Gertzmann, K. L. Wooley, *J. Am. Chem. Soc.* **1997**, *119*, 11653; c) H. Huang, E. E. Remsen, T. Kowalewski, K. L. Wooley, *J. Am. Chem. Soc.* **1999**, *121*, 3805; d) Q. Zhang, E. E. Remsen, K .L. Wooley, *J. Am. Chem. Soc.* **2000**, *122*, 3642; e) K. L. Wooley, *J. Polym. Sci. Part A* **2000**, *38*, 1397.

[2] a) V. Bütün, N. C. Billingham, S. P. Armes, *J. Am. Chem. Soc.* **1998**, *120*, 12135; b) V. Bütün, A. B. Lowe, N. C. Billingham, S. P. Armes, *J. Am. Chem. Soc.* **1999**, *121*, 4288; c) V. Bütün, X. S. Wang, M. V. de Paz Banez, K. L. Robinson, N. C. Billingham, S. P. Armes, Z. Tuzar, *Macromolecules* **2000**, *33*, 1; d) S. Liu, Y. Q. Tang, J. V. M. Weaver, N. C. Billingham, S. P. Armes, K. Tribe, *Macromolecules* **2002**, *35*, 6121.

[3] a) S. Stewart, G. J. Liu, *Chem. Mater.* **1999**, *11*, 4; b) X. H. Yan, F. T. Liu, Z. Li, G. J. Liu, *Macromolecules* **2001**, *34*, 9112; c) T. Sanji, Y. Nakatsuka, F. Kitayama, S. Sakurai, *Chem. Commun.* **1999**, 2201.

[4] a)S. I. Stupp, V. LeBonheur, K. Walker, L. S. Li, K. E. Huggins, M. Keser, A. Amstutz, *Science* **1997**, *276*, 384; b) M. Sauer, W. Meier, *Chem. Commun.* **2001**, 55.

[5] a) G. Decher, *Science* **1997**, *277*, 1232; b) F. Caruso, R. Caruso, H. Mohwald, *Science* **1998**, *282*, 1111.

[6] U. Rungsardthong, M. Deshpande, L. Bailey, M. Vamvakaki, S. P. Armes, M. C. Garnett, S. J. Stolnik, *J. Controlled Release* **2001**, *73*, 359.

[7] a) A. V. Kabanov, T. K. Bronich, V. A. Kabanov, K. Yu, A. Eisenberg, *Macromolecules* **1996**, *29*, 6797; b) S. V. Solomatin, T. K. Bronich, T. W. Bargar, A. Eisenberg, V. A. Kabanov, A. V. Kabanov, *Langmuir* **2003**, *19*, 8069.

[8] a) A. Harada, K. Kataoka, *Science* **1999**, *283*, 65; b) A. Harada, K. Kataoka, *Macromol. Symp.* **2001**, *172*, 1; c) A. Harada, K. Kataoka, *Macromolecules* **2003**, *36*, 4995; d) J. F. Gohy, S. K. Varshney, R. Jerome, *Macromolecules* **2001**, *34*, 2745; e) J. F. Gohy, S. K. Varshney, R. Jerome, *Macromolecules* **2001**, *34*, 3361.

[9] S. Schrage, R. Sigel, H. Schlaad, *Macromolecules* **2003**, *36*, 1417.

[10] C.-K. Choi, Y.-B. Kim, *Polym. Bull.* **2003**, *49*, 433.

[11] V. Bütün, S. P. Armes, N. C. Billingham, *Macromolecules* **2001**, *34*, 1148.

[12] Clearly there are two ways in which the protonated DEA residues could become charge-compensated. Either this core-forming block migrates to the inner shell to form a polyion complex or, alternatively, the "excess" anionic NaStS residues enter the cationic micelle cores. At this stage in our investigations we are not able to distinguish between these two possibilities.

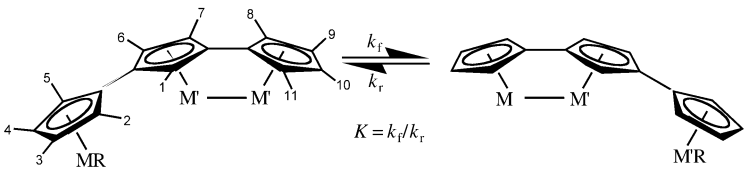
 © 2004 Wiley-VCH Verlag GmbH & Co. KGaA, Weinheim

Transition-Metal Complexes

Electron Exchange Along the Tercyclopentadienyltrimetallic Scaffold: Kinetics, Equilibria, and Bond Strengths**

*J. Kevin Cammack, Hani Amouri, Philip W. Leonard, Randy L. Myrabo, and K. Peter C. Vollhardt**

Electron transfer is fundamental to chemical reactivity.[1] A prototype example in organometallic chemistry is the attack of an anionic metal center on a metal–metal bond ($M^- + M'–M'$), which by nucleophilic substitution should lead to $M–M' + M'^-$. Such a result is not cleanly found, however, as the outcome of this mechanistically complex transformation is usually controlled by thermodynamic factors through electron redistribution to provide $M–M + M'^-$.[2] We report the first direct observation of such equilibria for cyclopentadienyl (Cp) metal complexes using NMR spectroscopy, mechanistic studies, and the use of the data for the estimation of CpM–M′Cp bond strengths. Key to these results is the employment of the tercyclopentadienyl (terCp) ligand as a frame on which to render the desired transformations intramolecular and regiospecific (Scheme 1).[3]



A **B**

1: M = M' = $Mo(CO)_3$, R = –
2: M = $W(CO)_3$, M' = $Mo(CO)_3$, R = –
3: M = $Mo(CO)_3$, M' = $W(CO)_3$, R = –
4: M = M' = $W(CO)_3$, R = –
5: M = $W(CO)_3$, M' = $Mo(CO)_3$, R = H
6: M = $Mo(CO)_3$, M' = $W(CO)_3$, R = H
7: M = $Cr(CO)_3$, M' = $Mo(CO)_3$, R = –
8: M = $Cr(CO)_3$, M' = $W(CO)_3$, R = –
9: M = $Mo(CO)_3$, M' = $Ru(CO)_2$, R = –
10: M = $Mo(CO)_3$, M' = $Ru(CO)_2$, R = H
11: M = $W(CO)_3$, M' = $Ru(CO)_2$, R = H
12: M = $Mo(CO)_3$, M' = $Ru(CO)_2$, R = CH_3

Scheme 1. Tercyclopentadienyl complexes investigated in this work.

[*] Dr. J. K. Cammack, Dr. H. Amouri, P. W. Leonard, Dr. R. L. Myrabo, Prof. K. P. C. Vollhardt
Center for New Directions in Organic Synthesis
Department of Chemistry, University of California at Berkeley
and
the Chemical Sciences Division, Lawrence Berkeley National Laboratory, Berkeley, California 94720-1460 (USA)
Fax: (+1) 510-643-5208
E-mail: kpcv@uclink.berkeley.edu

[**] This work was supported by the Director, Office of Energy Research, Office of Basic Energy Sciences, Chemical Sciences Division, of the U.S. Department of Energy, under Contract DE-AC03-76SF00098. A.H. and P.W.L. were aided by CNRS postdoctoral and NSF predoctoral stipends, respectively. We are grateful to Professors R. Bergman, M. Majda, A. Streitwieser, and M. Tilset for insightful comments. The Center for New Directions in Organic Synthesis is enabled by Bristol-Myers Squibb as a Sponsoring Member and Novartis as a Supporting Member.

The required materials were made according to described protocols (see Experimental Section),[3,4] with a minor modification for the preparation of the anions **1**–**4**, **7**, **8**, and **9**, which, to avoid (competing) reduction of the metal–metal bond, were generated using NaH or (for **9**) *t*BuOK. Structural proof of all new compounds rested on spectral data, conversion to stable methyl derivatives (in the case of the anions), and X-ray analyses of **3** and **4**. Particularly diagnostic were the ^{1}H NMR spectra, which could be assigned, as appropriate, by comparison with known systems or known substructures,[3] by exploiting the effect of the anisotropy of a metal–metal bond on the δ values of the attached fulvalene (Fv) nuclei,[5] via the characteristic three- ($\approx$3 Hz) and four-bond ($\approx$1.7 Hz) couplings in ligating cyclopentadienyls (Cps),[5b,c] by the occurrence of ^{183}W satellite signals, by way of the distinctive hydride absorptions, and through 2D-NOESY, TOCSY, COSY, and (in the case of rapid **A**/**B** exchange) EXSY experiments. Corroborating ^{13}C NMR data were particularly advantageous, especially in confirming the metal connectivity of the CO ligands.[6] The IR absorptions for the pendant CO groups revealed the composite patterns reflective of the individual $FvM–M^{(\prime)}$ and $CpM^{(\prime)}$ pieces, including ion association for the alkali salts of the anions,[7] the local symmetry of which could be restored by conversion to their ammonium analogues.[8]

While delocalized forms of anion **1** and its congeners are conceivable, the spectral data indicate largely localized arrays. Nevertheless, some of the negative charge on the isolated CpM^- segment appears to spread to the formally neutral neighbor, as evidenced by comparison with the properties of methylated relatives, for example, **1**–**4** (R = CH_3), and **12**. In particular, the hydrogen atoms 1 and 6–11 in the anions resonate at higher field than in their methylated relatives by an average of 0.15 ppm, and the corresponding dinuclear metal carbonyl stretching frequencies are attenuated by an average of $\approx$6 cm^{-1}. At the same time, charge depletion of the anionic center is indicated by more energetic CO bands ($\approx$11 cm^{-1}) than those measured for free $[CpM(CO)_3]^-$.[7b]

To define conclusively the relationship of the metals in the anions and to probe whether there are structural consequences of this charge delocalization, especially for the metal–metal bond, X-ray crystallographic analyses were performed on **3**- and **4**-$Na^+\cdot(THF)_5$. Their gross topologies were found to be almost identical to each other and to the known methylated **4** (R = CH_3),[3b] most notably marked by the anti configuration of the terCp sequence. Indeed, both compounds crystallize in the same space group ($P2_1$, no. 4) and are isomorphous. Because of problems with the data set for the structural solution of **4**, only **3** is described (Figure 1). The compound exists as a cocrystallisate in the thermodynamic ratio of the two isomers **A** and **B** and was successfully modeled as such.[9] The structural details for the $FvM–M^{(\prime)}$ fragment (e.g., the intermetallic distance) are, within experimental limits, very similar to those of the completely charge-localized methyl derivative,[3b] whereas the anionic CpM unit resembles (for example, with respect to

 DOI: 10.1002/anie.200352479 © 2004 Wiley-VCH Verlag GmbH & Co. KGaA, Weinheim

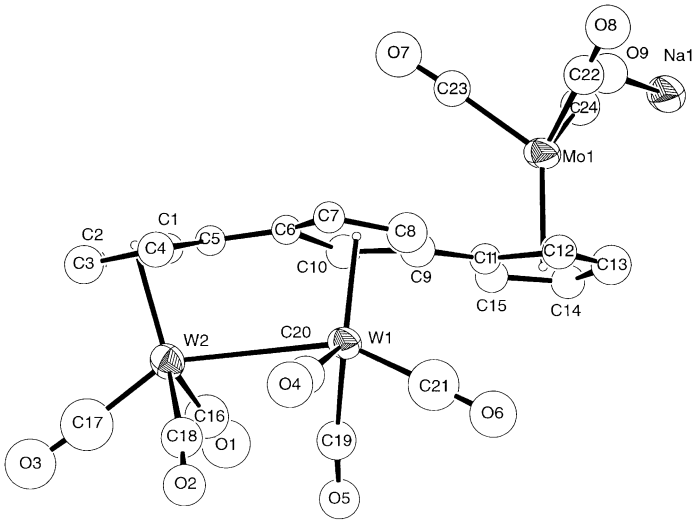
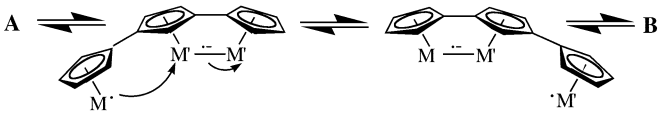


Figure 1. Averaged structure of **3**-Na^+·$(THF)_5$ in the crystal (from THF/pentane by diffusion), modeled as a 65:35 mixture of **A**:**B**. The metal labeling is arbitrarily that of the major form. The solvating THF molecules, of which four are ligating Na^+ ions, are omitted for clarity. Selected distances [Å] and angles [°] (compare with ref. [3b]): W1-W2 3.268(2), C5-C6 1.37(5), C9-C11 1.42(3), W1-Cp (centroid) 2.003, W2-Cp 2.165, Mo1-Cp 2.065; C4-C5-C6-C10 152(2), C1-C5-C6-C7 175(2).

average M–CO bond lengths) that of $[FvW_2(CO)_6]^{2-}$[10a] and other models.[10b] Thus, the effect of the charge on the remainder of the molecule seems minimal.

We find that the systems investigated are in equilibrium between the two forms **A** and **B**, directly observable as such for **1**–**6** and **11**, and/or approachable from one or both sides for **9**, **10**, and **12** (Table 1). Variable-temperature NMR experiments with the anions **1**–**4** revealed line broadening on warming, but because of the onset of decomposition at $>80\,°C$, the complexity of the spectra, and the required exacting kinetic modeling, only **2** was quantified in this manner (Table 1). In as much as it is representative of the structurally very similar anion series, the small $\Delta S^{\neq}$ value suggests little overall additional order in the transition state of the exchange. In conjunction with a clean first-order rate law and concentration-independent rate, these data point to a strictly intramolecular process. Kinetic data suitable for comparison within the series and with the rates reported for the intermolecular variants[2,11] were readily accessible for **1**–**4** by EXSY spectroscopy (Table 1), which show chemical exchange between six pairs of hydrogen atoms (e.g., H2/H11, H3/H10; Scheme 1).[12] The rates for **1** and **2** are independent of solvent polarity (CH_3CN, CH_2Cl_2, THF) and are unchanged (**1**) on adding up to a tenfold excess of $NaBF_4$ or using the pure Na^+ salt. The effective molarity k_{intra}/k_{inter}[11,13] for the exchanges in **1** and **4** is $\approx 10^5$ and $\approx 10^4$, respectively, consistent with their intramolecular nature. It also shows the absence of any unusual kinetic effects that might have been precipitated by the geometry of the systems.[14]

The two extreme mechanistic possibilities for these electron-transfer processes are nucleophilic substitution (either concerted or associative, perhaps with central Cp-ring slippage) and outer-sphere single-electron transfer (SET).[1,2] The latter would generate a dinuclear radical anion moiety,[15] which could equilibrate via an all-non-metal–metal-bonded diradical anion[15c] or by the direct S_{RN} displacement shown in Scheme 2. A distinction between these



Scheme 2. Electron-transfer mechanism of anions **1**–**4**.

options is often difficult.[1,2,16] Table 1 reveals a progressive rate decrease on going from **1** to **4**, incongruent with S_N2, considering the greater nucleophilicity of $[CpW(CO)_3^-]$ relative to $[CpMo(CO)_3^-]$ in methylations. The latter also show measurable effects of solvent polarity and the nature of the counterion, absent in our systems.[17] Particularly relevant are cases in which the leaving group is the same (i.e., $k_1/k_{2f} = 1.25$ and $k_{3f}/k_4 = 1.57$), data that speak against direct nucleophilic displacement. An associative mechanism with concurrent ring slippage[18] remains an option, however.[2a,c] SET appears most attractive, in particular because the trends in Table 1 follow those expected on the basis of redox potentials.[15b] Subsequent metal–metal bond homolysis to an intermediate diradical anion (equivalent to metal–metal bond homolysis in the starting anion) seems energetically unattractive, considering our activation parameters (Table 1), hence we suggest the mechanism depicted in Scheme 2.

The equilibrium data highlight the advantages of intramolecular exchange in

Table 1: Kinetic and/or equilibrium data for **1**–**12**, **A**→**B**, at 300 K in CH_3CN.

Compound	k [Hz]	K_{eq}	$\Delta H°$ [kcal mol^{-1}][a]	Compound	K_{eq}	$\Delta H°$ [kcal mol^{-1}][a]
1[b]	3.0	1.0		**6**[c]	30	1.0
2[b]	2.4 (k_f)	2.26[d]	−0.62	**7**	≤ 0.01[e]	≥ 9.7
	1.1 (k_r)			**8**	≤ 0.01[e]	≥ 9.8
3[b]	0.11 (k_f)[f]	0.32	0.81	**9**[g]	≤ 0.01	[h]
	0.36 (k_r)[f]			**10**[c,i]	≥ 100[e]	≤ -7.0
4[b]	0.07[f]	1.0		**11**[c,j]	2	−7.8
5[c]		0.03	−1.0	**12**[k]	≥ 100[e]	[h]

[a] Estimate of $\Delta BDE_{(M'-M')-(M-M')}$; see text. We use the (corrected) E_{ox} values (v) from Table I in ref.[19c]; Cr −0.688, Mo −0.385, W −0.379, Ru −0.941, and metal hydride BDEs (kcal mol^{-1}) from ref. [19a]; Mo-H 69.3, W-H 72.4, Ru-H 65.0. [b] Bu_4N^+ salts. NMR data and K values are unchanged from those of the Na^+ salts. [c] Equilibration is accelerated by added pyridine, retarded by added acetic acid. [d] In addition, complementary VT NMR analysis and theoretical fit of the coalescence of the signals for H1 ($\delta = 4.88$, **A**, and 4.97 ppm, **B**) furnishes $\Delta H^{\neq} = 16.2(\pm 2.4)$ kcal mol^{-1} and $\Delta S^{\neq} = -3.5(\pm 7)$ e.u. [e] $\Delta G° = +2.7$ kcal mol^{-1} (for $K_{eq} = 0.01$) or $= -2.7$ kcal mol^{-1} (for $K_{eq} = 100$). [f] Extrapolated from measurements at 313 (**3**) and 323 K (**4**). [g] Equilibrium established by deprotonation of either of the two hydrides **10A** and **B**. [h] Bracketing not meaningful. [i] Established by conversion of **10A** to **B** in THF. [j] Established by conversion of **11A** to **11B**. [k] Established by very slow (weeks), but clean, complete conversion of **12A** to **B** (see ref. [23d]).

 © 2004 Wiley-VCH Verlag GmbH & Co. KGaA, Weinheim

1–**4** in the estimation of (relative) bond strengths because structural, solvation, and entropy effects, and the imponderables of electrochemical measurements[19] should effectively cancel. For this purpose, we relate thermochemically the anions to their corresponding radicals. Specifically, the difference $\Delta H°$ in metal–metal bond dissociation energies (BDEs) in solution in going from **A** to **B** can be estimated from K (hence $\Delta G°$) of the anion equilibrium and the difference in the known oxidation potentials of the anionic fragments by Equation (1).[19]

$$\Delta H^o = -1.36 \log K - 23.1[E_{ox}(M^-) - E_{ox}(M'^-)]\ \text{kcal mol}^{-1} \quad \text{(all in } CH_3CN \text{ at 300 K)} \tag{1}$$

The results (Table 1) indicate a W–W bond that is only ≈ 2 kcal mol^{-1} stronger than a Mo–Mo bond, with the mixed-metal bond energy lying in between, as expected.[20] Turning to the literature on [{CpM(CO)$_3$}$_2$], the measured Mo–Mo BDE (32.5 kcal mol^{-1})[21a] appears reliable,[15a] however, that for W–W (56.0 kcal mol^{-1})[21b] has been queried repeatedly as being too high.[3c,19c,21c] Adopting the reasonable assumption that Fv intermetallic bonds are enthalpically equivalent to those in Cp dimers, certainly for lower triad metals,[22] we suggest 34.5 kcal mol^{-1}. Several control experiments support the validity of this approach. Thus, the $\Delta H°$ values for **5** and **6** [Eq. (2)] are exactly as expected, therefore negating the significance of any untoward anion effects.

$$\Delta H^o = -1.36 \log K - (\text{BDE}_{MH} - \text{BDE}_{M'H}) \tag{2}$$

For example, and to illustrate our procedure, for **5**: $\text{BDE}_{WH} = 72.4$ kcal mol^{-1},[19a,c] $\text{BDE}_{MoH} = 69.3$ kcal mol^{-1},[19a,c] $\text{BDE}_{MoMo} = 32.5$ kcal mol^{-1},[21a] $\text{BDE}_{WMo} = 33.5$ kcal mol^{-1}; hence, the isomerization **5a** to **5b** should be endothermic by $+2.1$ kcal mol^{-1}, providing a value of K of 0.03, as is observed. Similarly, the topological intermolecular equivalents of the equilibrations of **2** and **3**, namely $[FvMoW(CO)_6]^{2-} + [FvMo_2(CO)_6]$ ($K = 2.3$) or $[FvMoW(CO)_6]^{2-} + [FvW_2(CO)_6]$ ($K = 0.3$) conform with the values in Table 1 for **2** and **3**. They are also internally consistent ($[FvW_2(CO)_6]^{2-} + [FvMo_2(CO)_6]$, $K = 4$; expected: $2.3 \times (1/0.3) = 7.6$). The other entries in Table 1 serve to highlight the utility of the framework in confirming or questioning literature data. For example, for the equilibrium of **7**, the measured $K \leq 0.01$ provides $\Delta G° \geq +2.7$ kcal mol^{-1}. With $[E_{ox}(Cr^-) - E_{ox}(Mo^-)] = -0.688 - (-0.385)$ V $= -0.303$ V,[19a,c] one can derive a minimum estimate of 9.7 kcal mol^{-1} for how much weaker the Mo–Cr bond is relative to the Mo–Mo bond. This appears reasonable, since using BDE(Mo-Mo) = 32.5 kcal mol^{-1}[21a] and BDE(Cr-Cr) 14.7 kcal mol^{-1},[22] one would expect BDE(Cr-Mo) to be about 23.6 kcal mol^{-1} (the mean), that is, a value of $\Delta H°$ (Table 1) of 8.9 kcal mol^{-1}. A similar estimate for **8**, applying the new value for the W–W bond given above gives a value for $\Delta H°$ of 9.9 (found: ≥ 9.8) kcal mol^{-1}. Lesser agreement is evident in the Ru complexes. Because the equilibria of **9** and **12** lie in the direction dictated by the difference in E_{ox} values[19a,c] and metal–CH_3 energies,[23b,c] respectively, a meaningful estimation of their associated $\Delta H°$ values is not possible. However, those of **10** and, even better, **11** imply a Ru–Mo BDE of more than 7 kcal mol^{-1} less than that of Mo–Mo and, correspondingly, a Ru–W bond 7.8 kcal mol^{-1} weaker than that in W–W. These numbers would suggest Ru–Ru BDEs of < 20 kcal mol^{-1}, which are incompatibly low with other estimates and qualitative observations.[5b] The culprit may be a deficiently low Ru–H BDE (or, rather, a too negative value for $E_{ox}(Ru^-)$).[19] Such is indeed indicated by gas phase trends [BDE(Ru-H) > (Mo-H)],[23a] M–alkyl BDEs as they pertain to analog **12** (i.e. BDE[CpMo(CO)$_3$–CH$_3$] < BDE[CpRu(CO)$_3$–CH$_3$]),[23b,c] and the correspondence between hydride and alkylmetal bond strengths.[23a,e]

In summary, we have demonstrated the unique utility of the terCp ligand as a platform on which to carry out otherwise intractable kinetic and thermodynamic measurements of intramolecular electron (and ligand) exchange reactions along a trimetallic array. Future work is directed toward manipulation of the ligand (e.g., a central indenyl fragment, to further probe potential ring slippage) and the trimetallic array (e.g., rendition of an M-M′-M sequence for consonance with Marcus theory) for mechanistic purposes, and the juxtaposition of metal pairs judiciously chosen (e.g., $0 < K < 1$) to allow for the determination of their relative intermetallic bond strengths, a task of general importance in catalysis and mechanistic investigations.

Experimental Section

1-Na$^+$: red needles (from THF/hexanes); m.p. 107–110 °C (decomp); ^{1}H NMR (400 MHz, CD_3CN; numbering as in A in Scheme 1): $\delta =$ 5.71 (m, 2H, H5, H6), 5.41 (m, 1H, H10), 5.38 (m, 1H, H9), 5.30 (m, 1H, H2), 5.08 (m, 1H, H4), 5.02 (m, 1H, H3), 4.80 (t, $J = 1.8$ Hz, 1H, H1), 4.44 (m, 1H, H8), 4.39 (m, 1H, H7), 4.37 ppm (m, 1H, H11). ^{13}C{^{1}H} NMR (100 MHz, CD_3CN): $\delta = 235.7$ (Mo-*C*O), 110.2, 96.3, 95.6, 93.2, 87.7, 87.66, 87.60 (2C), 86.7, 86.6, 85.0 (2C), 84.6, 83.7, 80.2 ppm; IR (THF): $\tilde{\nu} = 2011$ (s), 1960 (s br), 1926 (s br), 1902 (s br), 1804 (m br), 1756 cm^{-1} (m br); MS (electrospray): m/z (%): 731 ([M^-], 100), 703 (50), 673 (48).

2-Na$^+$: ^{1}H NMR (300 MHz, CD_3CN): (isomer **A**) $\delta = 5.65$ (m, 1H, H6), 5.63 (m, 1H, H5), 5.38 (m, 2H, H9, H10), 5.26 (m, 1H, H2), 5.03 (m, 1H, H4), 4.98 (m, 1H, H3), 4.88 (t, $J = 1.6$ Hz, 1H, H1), 4.49 (m, 1H, H7), 4.46 ppm (m, 2H, H8, H11); (isomer **B**; numbering as in topology **A** of Scheme 1) $\delta = 5.63$ (m, 2H, H5, H6), 5.38 (m, 2H, H9, H10), 5.31 (m, 1H, H2), 5.03 (m, 1H, H4), 4.98 (m, 1H, H3), 4.97 (t, $J = 1.6$ Hz, 1H, H1), 4.68 (m, 1H, H8), 4.65 (m, 1H, H11), 4.55 ppm (dd, $J = 1.6, 1.1$ Hz, 1H, H7); IR (THF): $\tilde{\nu} = 2010$ (s), 1959 (s br), 1925 (s br), 1901 (s), 1802 (w), 1755 cm^{-1} (w).

3-Na$^+$·(THF)$_5$: dark red needles (from THF/pentane); m.p. 97–99 °C (decomp); ^{1}H NMR (300 MHz, CD_3CN): (isomer **A**) $\delta = 5.66$ (m, 1H, H6), 5.63 (m, 1H, H5), 5.40 (m, 1H, H10), 5.36 (m, 1H, H9), 5.33 (m, 1H, H2), 5.08 (m, 1H, H4), 5.07 (m, 1H, H1), 5.03 (m, 1H, H3), 4.74 (m, 1H, H8), 4.66 (m, 1H, H11), 4.65 ppm (m, 1H, H7); (isomer **B**) $\delta = 5.69$ (m, 1H, H6), 5.64 (m, 1H, H5), 5.40 (m, 1H, H10), 5.36 (m, 1H, H9), 5.28 (m, 1H, H2), 5.08 (m, 1H, H4), 5.03 (m, 1H, H3), 4.97 (t, $J = 1.9$ Hz, 1H, H1), 4.58 (m, 1H, H7), 4.53 (m, 1H, H8), 4.48 ppm (m, 1H, H11); IR (THF): $\tilde{\nu} = 2009$ (s), 2008(s), 1958 (vs), 1922 (s br), 1900 (m), 1799 (w), 1758 cm^{-1} (w); MS (electrospray): m/z (%): 907 ([M^-], 100).

4-Na$^+$: ^{1}H NMR (300 MHz, CD_3CN): $\delta = 5.66$ (m, 1H, H6), 5.61 (m, 1H, H5), 5.40 (m, 1H, 10), 5.38 (m, 1H, H9), 5.30 (m, 1H, H2), 5.09 (m, 2H, H1, H4), 5.05 (m, 1H, H3), 4.74 (m, 1H, H8), 4.68 (m, 1H, H11), 4.65 ppm (m, 1H, H7); IR (THF): $\tilde{\nu} = 2008$ (s), 1956 (s), 1921 (m), 1897 (m), 1799 (w), 1750 cm^{-1} (w).

 © 2004 Wiley-VCH Verlag GmbH & Co. KGaA, Weinheim

5A, B: ^{1}H NMR (300 MHz, CD_3CN, hydride signals): $\delta = -2.4$ (s, 0.03 H), -6.97 ppm (s, 1 H, $J(^{183}W\text{-}^1H) = 38$ Hz).

6A, B: ^{1}H NMR (300 MHz, CD_3CN, hydride signals): $\delta = -2.2$ (s, 0.03 H), -6.90 ppm (s, 1 H, $J(^{183}W\text{-}^1H) = 38$ Hz).

7: ^{1}H NMR (300 MHz, CD_3CN): $\delta = 5.63$ (dd, $J = 1.8$, 2.6 Hz, 1 H, H6), 5.38 (m, 2 H, H9, H10), 5.00 (m, 1 H, H5), 4.75 (t, $J = 1.6$ Hz, 1 H, H1), 4.60 (m, 1 H, H2), 4.43 (m, 4 H, H3, H4, H8, H11), 4.39 ppm (m, 1 H, H7); IR (THF): $\tilde{\nu} = 2010$ (s), 1962 (s), 1925 (s), 1899 (sh), 1794 (w), 1754 cm^{-1} (w).

8-Na^+ (isomer **A**): dark red needles (from THF/pentane); m.p. 103–105 °C (decomp); ^{1}H NMR (300 MHz, CD_3CN): $\delta = 5.62$ (dd, 1 H, $J = 3.0$, 1.8 Hz, H6), 5.40 (m, 1 H, H10), 5.36 (m, 1 H, H9), 5.03 (t, $J = 1.8$ Hz, 1 H, H1), 4.97 (m, 1 H, H5), 4.74 (m, 1 H, H8), 4.66 (m, 3 H, H2, H7, H11), 4.47 (m, 1 H, H4), 4.43 ppm (m, 1 H, H3); ^{13}C{^{1}H} NMR (100 MHz, CD_3CN, quaternary and W-*C*O carbon resonances not observed): $\delta = 245$ (Cr-*C*O), 89.8, 85.5, 85.5, 83.5, 83.5, 83.4, 82.7, 82.2, 82.0, 81.9, 78.9 ppm; IR (THF): $\tilde{\nu} = 2008$(s), 1955 (vs), 1920 (vs br), 1898 (m), 1803 (w), 1756 cm^{-1} (w); MS (electrospray): *m*/*z* (%): 859 ([M^-], 5), 727 (100).

9-Et_4N^+ (isomer **A**): yellow powder (from hexane/acetone); m.p. > 300 °C (decomp); ^{1}H NMR (500 MHz, CD_3CN): $\delta = 6.03$ (dd, $J =$ 2.8, 1.7 Hz, 1 H, H6), 5.79 (ddd, $J = 2.8$, 2.8, 1.6 Hz, 1 H, H9 or H10), 5.74 (ddd, $J = 2.8$, 2.8, 1.6 Hz, 1 H, H9 or H10), 5.70 (ddd, $J = 3.1$, 1.8, 1.8 Hz, 1 H, H5), 5.31 (ddd, $J = 3.0$, 1.9, 1.9 Hz, 1 H, H2), 5.06 (ddd, $J =$ 2.9, 2.9, 1.8 Hz, 1 H, H3 or H4), 5.03 (ddd, $J = 2.9$, 2.9, 1.8 Hz, 1 H, H3 or H4), 4.53 (dd, $J = 1.9$, 1.9 Hz, 1 H, H1), 4.21 (m, 1 H, H8), 4.00 (m, 2 H, H7, H11), 3.15 (q, $J = 7.2$ Hz, 8 H), 1.19 ppm (tt, $J = 7.2$, 1.8 Hz, 12 H); ^{13}C{^{1}H} NMR (125 MHz, CD_3CN): $\delta = 235.9$, 208.4, 207.4, 207.3, 206.8, 111.8, 97.3, 94.8, 92.5, 89.6, 89.5, 87.8, 87.4, 87.2, 87.0, 85.5, 79.9, 79.6, 78.2, 76.1, 53.0 (t, $J = 3.9$ Hz), 7.60 ppm; IR (CH_3CN): $\tilde{\nu} = 2008$, 1947, 1902, 1786, 1738 cm^{-1}; FAB-MS ([18]crown-6): *m*/*z*: 685 (M^-); (isomer **B**): ^{1}H NMR (300 MHz, CD_3CN, -70 °C): $\delta = 6.06$ (s, 1 H), 5.46 (s, 1 H), 5.38 (s, 1 H), 5.00 (m, 3 H), 4.76 (s, 2 H), 4.59 (s, 2 H), 4.22 ppm (s, 1 H).

10 (isomer **A**): ^{1}H NMR (400 MHz, [D_8]THF): $\delta = 6.22$ (m, 2 H), 5.84 (m, 1 H), 5.82 (m, 2 H), 5.59 (m, 1 H), 5.53 (m, 1 H), 4.74 (dd, $J =$ 1.8, 1.8 Hz, 1 H), 4.25 (m, 3 H), -5.25 ppm (s, 1 H); (isomer **B**): yellow-orange crystals (from hexane/acetone); m.p. 188–189 °C (decomp); ^{1}H NMR (400 MHz, [D_8]THF): $\delta = 6.22$ (dd, $J = 2.9$, 1.7 Hz, 1 H), 6.10 (ddd, $J = 2.9$, 1.7, 1.7 Hz, 1 H), 5.72 (ddd, $J = 2.9$, 1.7, 1.7 Hz, 1 H), 5.47 (ddd, $J = 2.8$, 2.8, 1.7 Hz, 1 H), 5.45 (m, 2 H), 5.42 (ddd, $J = 2.8$, 2.8, 1.7 Hz, 1 H), 4.77 (dd, $J = 1.8$, 1.8 Hz, 1 H), 4.65 (ddd, $J = 3.2$, 1.6, 1.6 Hz, 1 H), 4.64 (ddd, $J = 3.2$, 1.6, 1.6 Hz, 1 H), 4.25 (dd, $J = 2.9$, 1.9 Hz, 1 H), -10.89 ppm (s, 1 H); ^{13}C{^{1}H} NMR (100 MHz, [D_8]THF, -65 °C): $\delta = 236.2$, 224.0, 223.6, 206.2, 205.5, 202.03, 202.00, 103.1, 99.3, 98.3, 90.9, 88.1, 88.0, 86.9, 86.4, 86.3, 86.2 (2C), 85.3, 85.1, 76.6, 74.3 ppm; IR (THF): $\tilde{\nu} = 2025$, 1969, 1907, 1891 cm^{-1}; FAB-MS (sulfolane): *m*/*z*: 685 (M^+).

11 (isomer **A**): ^{1}H NMR (400 MHz, [D_8]THF): $\delta = 6.29$ (ddd, $J =$ 2.9, 1.8, 1.8 Hz, 1 H), 6.25 (dd, $J = 2.9$, 1.8 Hz, 1 H), 5.87 (m, 1 H), 5.84 (m, 1 H), 5.81 (m, 1 H), 5.67 (ddd, $J = 2.9$, 2.9, 1.8 Hz, 1 H), 5.61 (ddd, $J = 2.9$, 2.9, 1.8 Hz, 1 H), 4.75 (dd, $J = 1.8$, 1.8 Hz, 1 H), 4.29 (m, 3 H), -6.92 ppm (s, $J(^{183}W\text{-}H) = 37.4$ Hz, 1 H); (isomer **B**): $\delta = 6.24$ (dd, $J =$ 2.8, 1.7 Hz, 1 H), 6.09 (m, 1 H), 5.72 (m, 1 H), 5.47 (ddd, $J = 2.8$, 2.8, 1.7 Hz, 1 H), 5.43 (m, 3 H), 4.86 (dd, $J = 1.8$, 1.8 Hz, 1 H), 4.82 (m, 2 H), 4.34 (dd, $J = 2.9$, 2.0 Hz, 1 H), -10.88 ppm (s, 1 H).

12 (isomer **A**):[3b] ^{1}H NMR (300 MHz, [D_8]THF): $\delta = 6.21$ (dd, $J = 2.9$, 1.8 Hz, 1 H), 5.97 (ddd, $J = 2.8$, 1.8, 1.8 Hz, 1 H), 5.85 (m, 2 H), 5.55 (ddd, $J = 2.8$, 1.8, 1.8 Hz, 1 H), 5.48 (ddd, $J = 2.8$, 2.8, 1.8 Hz, 1 H), 5.39 (ddd, $J = 2.8$, 2.8, 1.8 Hz, 1 H), 4.71 (dd, $J = 1.8$, 1.8 Hz, 1 H), 4.31 (m, 3 H), 0.35 ppm (s, 3 H); (isomer **B**): ^{1}H NMR (400 MHz, [D_8]THF): $\delta = 6.16$ (dd, $J = 2.8$, 1.8 Hz, 1 H), 5.88 (m, 1 H), 5.51 (m, 1 H), 5.49 (m, 1 H), 5.45 (m, 3 H), 4.71 (dd, $J = 1.8$, 1.8 Hz, 1 H), 4.64 (m, 2 H), 4.28 (m, 1 H), 0.36 ppm (s, 3 H).

Received: July 25, 2003 [Z52479]
Published Online: February 9, 2004

Keywords: bond energy · cyclopentadienyl ligands · electron transfer · kinetics · metal–metal interactions · nucleophilic substitution

[1] *Electron Transfer in Chemistry*, *Vol. 1–5* (Ed.: V. Balzani), Wiley-VCH, Weinheim, **2001**.

[2] a) J. D. Atwood, M. S. Corraine-Pandolfino, Y. Zhen, W. S. Striejewske, C. K. Lai, P. Wang, *J. Coord. Chem.* **1994**, *32*, 65; b) Y. Zhen, J. D. Atwood, *Organometallics* **1991**, *10*, 2778; c) M. S. Corraine, J. D. Atwood, *Organometallics* **1991**, *10*, 2315; d) M. S. Corraine, J. D. Atwood, *Inorg. Chem.* **1989**, *28*, 3781; e) R. E. Dessy, P. M. Weissman, *J. Am. Chem. Soc.* **1966**, *88*, 5129; f) For the rare alternative, addition to generate clusters, see: A. T. T. Hsieh, M. J. Mays, *J. Organomet. Chem.* **1972**, *39*, 157.

[3] a) For a review, see: C. G. de Azevedo, K. P. C. Vollhardt, *Synlett* **2002**, 1019; b) R. Boese, R. L. Myrabo, D. A. Newman, K. P. C. Vollhardt, *Angew. Chem.* **1990**, *102*, 589; *Angew. Chem. Int. Ed. Engl.* **1990**, *29*, 549.

[4] All new isolated compounds gave satisfactory analytical and/or spectral data.

[5] a) D. J. Meyerhoff, R. Nunlist, M. Tilset, K. P. C. Vollhardt, *Magn. Reson. Chem.* **1986**, *24*, 709; b) R. Boese, J. K. Cammack, A. J. Matzger, K. Pflug, W. B. Tolman, K. P. C. Vollhardt, T. W. Weidman, *J. Am. Chem. Soc.* **1997**, *119*, 6757; c) C. G. de Azevedo, R. Boese, D. A. Newman, K. P. C. Vollhardt, *Organometallics* **1995**, *14*, 4980.

[6] B. E. Mann, B. F. Taylor, *^{13}C NMR Data for Organometallic Compounds*, Academic Press, London, **1981**.

[7] a) M. Y. Darensbourg, *Prog. Inorg. Chem.* **1985**, *33*, 221; b) M. Y. Darensbourg, P. Jimenez, J. R. Sackett, J. M. Hanckel, R. L. Kump, *J. Am. Chem. Soc.* **1982**, *104*, 1521.

[8] For example, the IR spectrum for **1**-Na^+ (Table 1) is a composite of that of [$FvMo_2(CO)_6$] ($\tilde{\nu} = 2010$, 1960, 1925, 1905 cm^{-1}) and ion-paired [$CpMo(CO)_3{}^-Na$]$^+$ ($\tilde{\nu} = 1899$, 1796, 1743 cm^{-1}), whereas for **1**-Bu_4N^+ the two low-energy bands merge to a single peak at 1792 cm^{-1}.

[9] Confirmed by dissolution of the crystals at -78 °C and NMR analysis. Crystal size $0.13 \times 0.11 \times 0.04$ mm^3, space group $P2_1$ (no. 4), scan range $3.00 < 2\theta < 46.2°$, $a = 10.7286(9)$, $b =$ 14.910(1), $c = 14.922(1)$ Å, $\beta = 102.659(2)°$, $V = 2328.9(3)$ Å^3, $Z = 2$, $\rho_{calcd} = 1.84$ g cm^{-3}, $\mu(Mo_{K\alpha}) = 52.70$ cm^{-1}, 6944 unique reflections at -97 °C, of which 3207 were taken as observed [$F_o > 3.00\sigma(F_o)$], $R = 0.064$, $R_w = 0.058$. CCDC-215769 contains the supplementary crystallographic data for this paper. These data can be obtained free of charge via www.ccdc.cam.ac.uk/conts/retrieving.html (or from the Cambridge Crystallographic Data Centre, 12, Union Road, Cambridge CB2 1EZ, UK; fax: (+44) 1223-336-033; or deposit@ccdc.cam.ac.uk).

[10] a) M. Tilset, K. P. C. Vollhardt, R. Boese, *Organometallics* **1994**, *13*, 3146; b) J. St. Denis, W. Butler, M. D. Glick, J. P. Oliver, *J. Am. Chem. Soc.* **1974**, *96*, 5427, and references therein.

[11] The second-order rate constants (at 300 K) of self-exchange of Cp-$d_5$$M^-Na^+$ with [{$CpM(CO)_3$}$_2$] (NMR) in THF are 3×10^{-5} and 2×10^{-5} M^{-1} s^{-1} for Mo and W, respectively.

[12] C. L. Perrin, T. J. Dwyer, *Chem. Rev.* **1990**, *90*, 935.

[13] G. Illuminati, L. Mandolini, *Acc. Chem. Res.* **1981**, *14*, 95.

[14] T. T. Chin, W. E. Geiger, A. L. Rheingold, *J. Am. Chem. Soc.* **1996**, *118*, 5002.

[15] See, amongst others: a) J. R. Pugh, T. J. Meyer, *J. Am. Chem. Soc.* **1992**, *114*, 3784; b) K. M. Kadish, D. A. Lacombe, J. E. Anderson, *Inorg. Chem.* **1986**, *25*, 2246; c) E. F. Dalton, S. Ching, R. W. Murray, *Inorg. Chem.* **1991**, *30*, 2642, and references therein.

[16] a) For a review, see: J.-M. Saveant, *Adv. Phys. Org. Chem.* **1990**, *26*, 1; b) for a recent pertinent attempt, see: T. V. Magdesieva,

I. V. Zhukov, K. P. Butin, *Vestn. Mosk. Univ. Ser. 2 Khim.* **1998**, *39*, 205.
[17] See: C.-K. Lai, W. G. Feighery, Y. Zhen, J. D. Atwood, *Inorg. Chem.* **1989**, *28*, 3929, and references therein.
[18] a) For a recent review, see: D. Zargarian, *Coord. Chem. Rev.* **2002**, *233–234*, 157, and references therein; b) ring slippage in CpMo may be faster than that in CpW systems: C. P. Casey, W. D. Jones, S. G. Harsy, *J. Organomet. Chem.* **1981**, *206*, C38.
[19] For pertinent reviews, see: a) M. Tilset in *Electron Transfer in Chemistry*, *Vol. 2* (Ed.: V. Balzani), Wiley-VCH, Weinheim, **2001**, p. 677; b) D. D. M. Wayner, V. D. Parker, *Acc. Chem. Res.* **1993**, *26*, 287; see also: c) M. Tilset, V. D. Parker, *J. Am. Chem. Soc.* **1989**, *111*, 6711 (Erratum: M. Tilset, V. D. Parker, *J. Am. Chem. Soc.* **1990**, *112*, 2843).
[20] T. Madach, H. Vahrenkamp, *Chem. Ber.* **1980**, *113*, 2675. This work indicates that the mixed-metal $\{CpM(CO)_3\}$ dimers of Cr with Mo or W have stronger intermetallic linkages than expected.
[21] a) S. Amer, G. Kramer, A. Poë, *J. Organomet. Chem.* **1981**, *209*, C28; b) J. R. Krause, D. R. Bidinosti, *Can. J. Chem.* **1975**, *53*, 628; c) J. T. Landrum, C. D. Hoff, *J. Organomet. Chem.* **1985**, *282*, 215.
[22] K. P. C. Vollhardt, J. K. Cammack, A. J. Matzger, A. Bauer, K. B. Capps, C. D. Hoff, *Inorg. Chem.* **1999**, *38*, 2624, and references therein.
[23] a) For a review, see: J. A. M. Simões, J. L. Beauchamp, *Chem. Rev.* **1990**, *90*, 629; b) $BDE[CpMo(CO)_3{-}CH_3] = 47.0$ kcal mol^{-1}: S. P. Nolan, R. L. de la Vega, C. D. Hoff, *J. Organomet. Chem.* **1986**, *315*, 187; c) $BDE[CpRu(CO)_3{-}CH_3] = 55.0$ kcal mol^{-1}, extrapolated from: C. Mancuso, J. Halpern, *J. Organomet. Chem.* **1992**, *428*, C8; d) The mechanism of this exchange reaction is likely to traverse through radicals: H. G. Alt, *Angew. Chem.* **1984**, *96*, 752; *Angew. Chem. Int. Ed. Engl.* **1984**, *23*, 766; e) J. A. Labinger, J. E. Bercaw, *Organometallics* **1988**, *7*, 926.

 © 2004 Wiley-VCH Verlag GmbH & Co. KGaA, Weinheim

Heterogeneous Catalysis

Pd Nanoparticles Immobilized on Molecular Sieves by Ionic Liquids: Heterogeneous Catalysts for Solvent-Free Hydrogenation**

Jun Huang, Tao Jiang, Haixiang Gao, Buxing Han, Zhimin Liu, Weize Wu, Yanhong Chang, and Guoying Zhao*

Ionic liquids (ILs) are attractive, environmentally acceptable solvents because they have a very low vapor pressure and can be used to replace volatile organic solvents.[1] ILs are good solvents for a wide range of inorganic, organic, and polymeric molecules and have been successfully used as solvents in many reactions.[2] Although the ability of biphasic catalysis in ILs has been successfully demonstrated, the chemical industry still prefers heterogeneous catalytic systems because of their ease of separation and the possibility of using a fixed-bed reactor. Furthermore, the use of a biphasic reaction system requires a large amount of IL, and on the basis of economic criteria and possible toxicological concerns, it is desirable to minimize the amount of utilized IL in reaction processes. Recently, Mehnert et al. reported a method for the immobilization of homogeneous Rh^+-based catalyst in an IL phase onto silica gel using a small amount of IL, which was used for hydrogenation and hydroformylation reactions. In their novel approach the IL layers on silica gel served as the reaction phase, in which the homogeneous Rh^+-based catalyst was dissolved.[3]

Nanoparticles have properties intermediate between those of bulk and single particles. The application of transition-metal nanoparticles in catalysis has attracted much attention.[4] They are expected to be suitable candidates for the design of highly active and selective catalysts. However, nanoparticles tend to aggregate to form larger particles because they have a very large surface area. Therefore, the stabilization of nanocatalysts by different methods has been studied extensively.[5] For example, many supported nanoparticles on molecular sieves have been used as catalysts; the incipient-wetness method is commonly used, which is convenient but leads to inhomogeneous particles and instable catalytic efficiency.[6] Ligand-protected nanoparticles supported on molecular sieves[7] and nanoclusters on SiO_2[8] were used as catalysts, with both achieving high activities, but with stabilities that were not satisfactory. Some nanoparticles stabilized by polyoxoanions and tetrabutylammonium ions were synthesized, characterized, and applied as catalysts for the hydrogenation of arenes or olefins in either organic solvents or water.[4d–i] Recently, metal nanoparticles formed in ILs were used directly as catalysts for the hydrogenation of olefins in biphasic liquid system.[9,10]

It is known that guanidine and guanidinium ions have the ability to form coordination complexes.[11] In this work, we conducted the first study of the immobilization of a nanoparticle catalyst onto a solid surface by an IL, and as an example, Pd nanoparticles were immobilized onto molecular sieves using the IL 1,1,3,3-tetramethylguanidinium lactate (TMGL). The catalytic system was used for solvent-free hydrogenation reactions, and unprecedented activity and stability was achieved. The combination of nanoparticles, the IL, and molecular sieves showed excellent synergistic effects to enhance the activity and durability of the catalyst, and this approach may find wide potential applications in transition-metal nanocatalysed reactions.

The solvent-free hydrogenation of cyclohexene, 1-hexene, and 1,3-cyclohexadiene was investigated (Table 1). The nanocatalyst showed unprecedented activity (entries 1–4) compared to the biphasic IL system or with a directly supported nanocatalyst (entries 5 and 6). The selectivity was very high for the hydrogenation of cyclohexadiene to cyclohexene (entry 3), which originates from the properties of Pd metal

[*] J. Huang, T. Jiang, H. Gao, Prof. B. Han, Z. Liu, W. Wu, Y. Chang, G. Zhao
Centre for Molecular Science
Institute of Chemistry, Chinese Academy of Sciences
Beijing 100080 (China)
Fax: (+86) 10-6256-2821
E-mail: Hanbx@iccas.ac.cn

[**] This work was financially supported by Ministry of Science and Technology of China (G2000048010) and National Natural Science Foundation of China (20133030, 20332030).

 DOI: 10.1002/anie.200352682 © 2004 Wiley-VCH Verlag GmbH & Co. KGaA, Weinheim

Table 1: Pd-catalyzed hydrogenation reactions, with nanoparticles actively supported on molecular sieves with a TMGL layer.

Entry	Olefins	Olefin/Pd molar ratio	T [°C]	t [h]	Conv. [%]	TOF [min^{-1}]
1[a]	cyclohexene	12000	20	10	100	20.0
2	cyclohexene	12000	40	7	100	28.3
3[b]	cyclohexadiene	12000	20	3	98	65.3
4	1-hexene	12000	20	3	100	66.7
5[c]	1-hexene	120	20	6	100	0.30
6[d]	cyclohexene	500	40	5	100	1.67
7[e]	cyclohexene	12000	20	10	100	20.0
8[f]	cyclohexene	12000	20	10	100	20.0
9[g]	cyclohexene	12000	20	10	100	20.0
10[h]	cyclohexene	12000	20	10	100	20.0

[a] The product was cyclohexane. [b] The product was cyclohexene; no cyclohexane was detected. [c] Based on data from Ref. [13] using phenanthroline-protected Pd nanoparticles. [d] The reaction was carried out using Pd nanoparticles in 1-*n*-butyl-3-methylimidazolium hexafluorophosphate (an IL) as the catalyst, see Ref. [10]. [e–h] The catalyst was used a second, third, fourth, and fifth time, respectively, after the experiment described in entry 1.

and the nanoscale size of the particle. Alkadienes are much more strongly adsorbed by the Pd nanoparticles than alkenes, which results in preferential hydrogenation of the alkadiene to the alkene.[12] Moreover, the small size of the Pd nanoparticles is also favorable in enhancing the selectivity.[12]

The catalyst used in entry 1 was reused for another four runs without any considerable loss of activity (entries 7–10). After reaction, the organic products were collected and analyzed by AAS (atomic absorption spectrum) method for Pd metal, and the Pd metal was not detected.

To our knowledge, it is very difficult to give the exact mechanism for the very high activity and stability of the catalytic system. However, we carried out some experiments that allowed us to obtain some useful information. The surface area and porous volume of the molecular sieves with the IL-stabilized Pd nanoparticles, as determined by nitrogen adsorption (desorption at 120 °C), were 383 $m^2 g^{-1}$ and 0.73 $cm^3 g^{-1}$, respectively, values which are smaller than those for unused molecular sieves (520 $m^2 g^{-1}$ and 0.87 $cm^3 g^{-1}$, respectively). The sieves were still hollow, however, and with a large surface area, which was favorable in offering a high activity. The size of the Pd particles in the THF/methanol solution (before immobilization) was determined by transmission electron microscopy (TEM), and the diameter of most of the Pd particles was in the range of 1–2 nm (Figure 1). A TEM experiment was also conducted to study the Pd agglomerations on the surface of the molecular sieves. No large Pd particles were observed on the surface of the support (Figure 2). Moreover, after five hydrogenation reactions, the nanocatalyst was washed with methanol and a black Pd metal suspension was obtained, in which the Pd particle size was also in the range of 1–2 nm, as characterized by TEM, which further confirmed that the Pd particles were not aggregated into larger particles on the molecular sieves. The catalyst contained 20 wt % IL, and the estimated average layer thickness of the IL on the surface of the molecular sieve was 0.4 nm. Since TMGL was alkaline, it could be adsorbed strongly onto the acidic surface of the molecular sieve. At the same time, the Pd nanoparticles were stabilized onto the surface of the molecular sieve, since guanidinium ions have a considerable ability for coordinate metal particles.[11] On the basis of these results, we can obtain a rough picture about the structure of the catalyst, as demonstrated in Figure 3. A thin layer of the IL is attached to the surface of the molecular sieve. The Pd particles do not come into direct contact with the molecular sieves but can still interact with their surface because the IL interacts strongly with both the Pd nanoparticles and the molecular sieves. The diameter of the Pd nanoparticles is larger than the thickness of the IL layer, and thus part of the Pd particles are not immersed in the IL layer. However, the Pd particles may be covered by the IL because the IL has ability to coordinate metal particles, as discussed above. All of these factors (e.g., large surface area, small size, and partial exposure of the Pd nanoparticles) are favorable towards enhancing the activity of the catalyst. Therefore, the IL, Pd

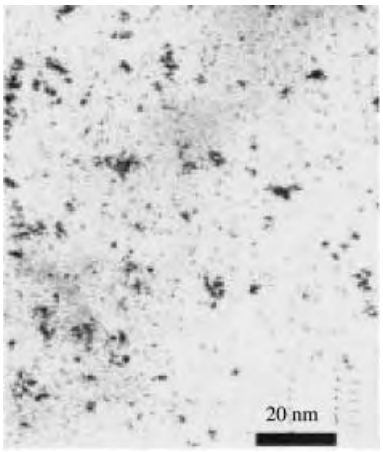


Figure 1. TEM micrograph of the Pd nanoparticles dispersed in methanol/THF.

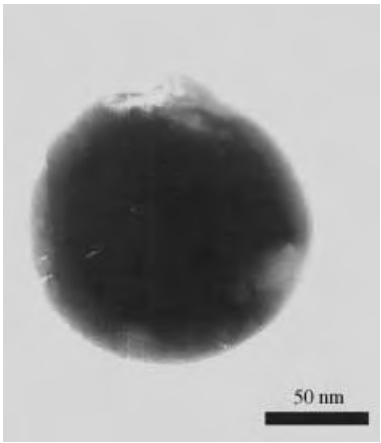


Figure 2. TEM micrograph of a molecular sieve with supported Pd nanoparticles.

 © 2004 Wiley-VCH Verlag GmbH & Co. KGaA, Weinheim

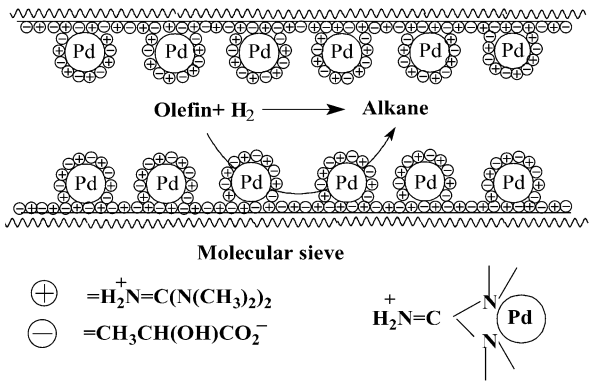


Figure 3. Illustration of the immobilization of Pd nanoparticles at the surface of a molecular sieve with an ionic liquid layer.

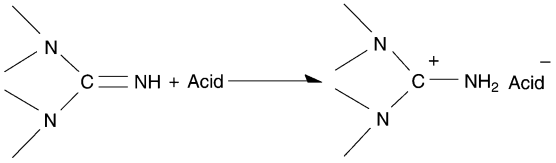
nanoparticles, and the molecular sieves exhibit an excellent synergistic effect.

In summary, the Pd nanoparticles immobilized onto molecular sieves by TMGL were very active and stable catalysts for the solvent-free hydrogenation of olefins. The excellent synergistic effects between the nanoparticles, the ionic liquid, and the molecular sieves enhance the activity, selectivity, and durability of the catalytic system.

Experimental Section

Molecular sieves (Si/Al = 1:1) with a porous diameter of 6.7 nm were employed, whose surface area and porous volume (determined by nitrogen adsorption) were 520 m^2g^{-1} and 0.87 cm^3g^{-1}, respectively. $Pd(OAc)_2$ was obtained from Acros Organics. All other reagents were obtained from the Beijing Chemical Reagent Company.

The IL was synthesized directly by neutralization of 1,1,3,3-tetramethylguanidine and lactic acid (Scheme 1), and the procedures were similar to those in literature.[14]



Scheme 1. Synthesis of the TMGL ionic liquid.

Received: August 20, 2003
Revised: December 29, 2003 [Z52682]

Keywords: heterogeneous catalysis · hydrogenation · ionic liquids · nanoparticles · palladium

[1] a) P. Wasserscheid, W. Keim, *Angew. Chem.* **2000**, *112*, 3926; *Angew. Chem. Int. Ed.* **2000**, *39*, 3772; b) H. Oliver-Bourbigou, L. Magna, *J. Mol. Catal. A* **2002**, *182*–183, 419; c) T. Welton, *Chem. Rev.* **1999**, *99*, 2071; d) A. Bösmann, G. Francio, E. Janssen, M. Solinas, W. Leitner, P. Wasserscheid, *Angew. Chem.* **2001**, *113*, 2769; *Angew. Chem. Int. Ed.* **2001**, *40*, 2697; e) J. Dupont, R. F. Souza, P. A. Z. Suarez, *Chem. Rev.* **2002**, *102*, 3667; f) L. A. Blanchard, D. Hancu, E. J. Beckman, J. F. Brennecke, *Nature* **1999**, *399*, 28.

[2] a) M. F. Sellin, P. B. Webb, D. J. Cole-Hamilton, *Chem. Commun.* **2001**, 781; b) A. L. Monteiro, F. K. Zinn, R. F. de Souza, J. Dupont, *Tetrahedron: Asymmetry* **1997**, *8*, 177; c) F. Liu, M. B. Abrams, R. T. Baker, W. Tumas, *Chem. Commun.* **2001**, 433; d) R. A. Brown, P. Pollet, E. McKoon, C. A. Eckert, C. L. Liotta, P. G. Jessop, *J. Am. Chem. Soc.* **2001**, *123*, 1254; e) C. J. Boxwell, P. J. Dyson, D. J. Ellis, T. Welton, *J. Am. Chem. Soc.* **2002**, *124*, 9334; f) T. Fischer, A. Sethi, T. Welton, J. Woolf, *Tetrahedron Lett.* **1999**, *40*, 793; g) B. Ellis, W. Keim, P. Wasserscheid, *Chem. Commun.* **1999**, 337; h) Z. S. Hou, B. X. Han, L. Gao, T. Jiang, Z. M. Liu, Y. H. Chang, X. G. Zhang, J. He, *New J. Chem.* **2002**, *26*, 1246.

[3] a) C. P. Mehnert, E. J. Mozeleski, R. A. Cook, *Chem. Commun.* **2002**, 3010; b) C. P. Mehnert, R. A. Cook, N. C. Dispenziere, M. Afework, *J. Am. Chem. Soc.* **2002**, *124*, 12932.

[4] a) A. M. Argo, J. F. Odzak, F. S. Lai, B. C. Gates, *Nature* **2002**, *415*, 623; b) A. T. Bell, *Science* **2003**, *299*, 1688; c) D. R. Rolison, *Science* **2003**, *299*, 1698; d) S. Ozkar, R. G. Finke, *J. Am. Chem. Soc.* **2002**, *124*, 5796; e) J. D. Aiken III, R. G. Finke, *J. Am. Chem. Soc.* **1999**, *121*, 8803; f) J. Schulz, A. Roucoux, H. Patin, *Chem. Eur. J.* **2000**, *6*, 618; g) J. Schulz, A. Roucoux, H. Patin, *Chem. Commun.* **1999**, 635; h) R. Raja, T. Khimyak, J. M. Thomas, S. Hermans, B. F. G. Johnson, *Angew. Chem.* **2001**, *113*, 4774; *Angew. Chem. Int. Ed.* **2001**, *40*, 4638; i) O. Vidoni, K. Philippot, C. Amiens, B. Chaudret, O. Balmes, J. Malm, J. Bovin, F. Senocq, M. Casanove, *Angew. Chem.* **1999**, *111*, 3950; *Angew. Chem. Int. Ed.* **1999**, *38*, 3736.

[5] a) A. Roucoux, J. Sehullz, H. Patin, *Chem. Rev.* **2002**, *102*, 3757; b) R. G. Finke in *Metal nanoparticles: synthesis, characterization and Application* (Eds.: D. L. Feldherim, C. A. Foss, Jr.), Marcel Dekker, New York, **2002**, chap. 2, pp. 17–54.

[6] a) P. Landon, P. J. Collier, A. J. Papworth, C. J. Kiely, G. J. Hutchings, *Chem. Commun.* **2002**, 2058; b) S. Hu, Y. Chen, *Ind. Eng. Chem. Res.* **2001**, *40*, 3127; c) M. A. Keane, P. M. Patterson, *J. Chem. Soc. Faraday Trans.* **1996**, *92*, 1413.

[7] N. Toshima, Y. Shiiraishi, T. Teranishi, M. Miyake, T. Tominaga, H. Watanable, W. Brijoux, H. Bönnemann, G. Schmid, *Appl. Organomet. Chem.* **2001**, *15*, 178.

[8] a) J. M. Thomas, B. F. G. Johnson, R. Raja, G. Sankar, P. A. Midgley, *Acc. Chem. Res.* **2003**, *36*, 20; b) R. Raja, G. Sankar, S. Herman, D. S. Shepherd, S. Bromley, J. M. Thomas, B. F. G. Johnson, *Chem. Commun.* **1999**, 1571; c) D. S. Shepherd, T. Maschmeyer, B. F. G. Johnson, J. M. Thomas, G. Sankar, D. Ozkaya, W. Z. Zhou, R. D. Oldroyd, *Angew. Chem.* **1997**, *109*, 2337; *Angew. Chem. Int. Ed. Engl.* **1997**, *36*, 2242; d) R. Raja, T. Khimyak, J. M. Thomas, S. Herman, B. F. G. Johnson, *Angew. Chem. Int. Ed.* **2001**, *113*, 4774; *Angew. Chem. Int. Ed.* **2001**, *40*, 4638.

[9] J. Dupont, G. S. Fonseca, A. P. Umpierre, P. F. P. Fichtner, S. R Teixeira, *J. Am. Chem. Soc.* **2002**, *124*, 4228.

[10] J. Huang, T. Jiang, B. Han, H. Gao, Y. Chang, G. Zhao, W. Wu, *Chem. Commun.* **2003**, 1654.

[11] a) S. Aoki, K. Iwaida, N. Hanamoto, M. Shiro, E. Kimura, *J. Am. Chem. Soc.* **2002**, *124*, 5256; b) P. J. Bailey, S. Pace, *Coord. Chem. Rev.* **2001**, 214, 91.

[12] *Handbook of Heterogeneous Catalysis*, *Vol. 5* (Eds.: G. Ertl, H. Knozinger, J. Weitkamp), Wiley-VCH, Weinheim, **1997**, p. 2184.

[13] a) G. Schmid, *Chem. Rev.* **1992**, *92*, 1709; b) G. Schmid, M. Harm, *J. Am. Chem. Soc.* **1993**, *115*, 2047.

[14] a) M. Hirao, H. Sugimoto, H. Ohno, *J. Electrochem. Soc.* **2000**, *147*, 4168; b) N. M. M. Mateus, L. C. Branco, N. M. T. Lourenço, C. A. M. Afonso, *Green Chem.* **2003**, *5*, 347.

 © 2004 Wiley-VCH Verlag GmbH & Co. KGaA, Weinheim

Regioselectivity

A Versatile Direct Approach to *ortho*-Substituted Azobenzenes from Benzotriazoles**

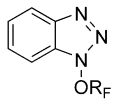
Xavier Àlvarez Micó, Thomas Ziegler, and Lakshiminarayanapuram R. Subramanian**

Benzotriazole (Bt) has been widely utilized by the research group of Katritzky as a synthetic auxiliary in a multitude of reactions.[1] Benzotriazole is an inexpensive, stable, and biologically innocuous compound[1a] which can be easily introduced into organic molecules. After conferring its multiple activating influences for carrying out precise transformation reactions, it can be easily removed and can generally be recycled. The early results in the chemistry of benzotriazole have been described by Katrizky and co-workers.[1e]

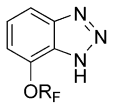
The benzotriazole ring is extremely stable and only rarely was ring cleavage encountered to give mostly products of nitrogen extrusion. For example, Grignard reagents open and modify the triazole ring and afford a variety of products.[2] Other methods for opening the benzotriazole ring are by photolysis and pyrolysis,[3] however, no actual ring opening of benzotriazole that has led to isolable azobenzenes has been reported.[1d]

We report here the pleasantly surprising chemistry of the hitherto unknown 1-[(nonafluorobutane)sulfonyl]-1*H*-benzotriazole (**3b**, BtNf) for the synthesis of *ortho*-azobenzenes in a direct and unprecedented approach.

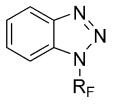
At the outset, our aim was to find out whether the perfluoroalkanesulfonates **1** and **3** derived from 1-hydroxybenzotriazole and benzotriazole, respectively, are suitable as perfluoroalknesulfonyl transfering agents for alcohols and phenols. Application of the known literature method[4] for the



1a: $R_F = SO_2CF_3$
1b: $R_F = SO_2C_4F_9$



2a: $R_F = SO_2CF_3$
2b: $R_F = SO_2C_4F_9$



3a: $R_F = SO_2CF_3$
3b: $R_F = SO_2C_4F_9$

preparation of aryl nonafluorobutanesulfonates (nonaflates) to synthesize the nonaflate **1b** surprisingly resulted in the isolation of the rearranged product **2b**.[5] Further investigations were then concentrated on the synthesis of sulfonyl compounds **3**.

The lower homologue of BtNf (**3b**), the 1-[(trifluoromethyl)sulfonyl]-1*H*-1,2,3-benzotriazole (**3a**), was prepared by Katritzky et al. and some of its reactions were studied.[6] However, the skeletal structure of benzotriazole remained intact in all of these reactions. We have now prepared 1-[(nonafluorobutyl)sulfonyl]-1*H*-1,2,3-benzotriazole (BtNf, **3b**) for the first time in 89% yield by treating 1-lithiobenzotriazole with nonafluorobutanesulfonyl fluoride in 1,2-dimethoxyethane at reflux temperature. BtNf (**3b**) decomposes in the presence of light and should be kept in the dark, preferably in a refrigerator. BtNf (**3b**) was fully characterized by its spectral properties and elemental analyses (see Experimental Section).

First we examined the reaction of phenol, which was chosen as the model compound, with the trifluoromethanesulfone (triflone) **3a**. The preliminary studies with **3a** were plagued by the formation of a mixture of two products, and hence all further explorations were conducted with the homologous nonafluorobutanesulfone (nonaflone) **3b**. The fact that the nonaflate group has been shown[7] to be a better leaving group than the triflate also prompted us to carry out the study with the nonaflone-substituted benzotriazole **3b**.

We attempted first the reaction of **3b** with phenol in the presence of several bases. After some experiments, sodium hydride was found to be the base of choice, and the reaction was conducted in toluene. The major product isolated after aqueous work-up was an orange product which was shown by spectral and analytical analyses to be the azo compound **4**. Although both *ortho*- and *para*-substituted azo compounds can be expected, the structure of the major product was unambiguously assigned as the *ortho*-substituted azo compound **4**, as supported by its X-ray crystallographic analysis.[8] Only a very small amount (ca. 5%) of the *para*-substituted derivative **5** was isolated by column chromatography. Evidently, the triazole ring underwent a ring-opening reaction by nucleophilic attack of the phenoxide anion. Although the presence of a strong electron-withdrawing substituent at N1 on benzotriazole has been shown to weaken the N1–N2 bond, thus leading to ring opening of the benzotriazole, they give products of nitrogen extrusion[1d] or undergo a Dimroth rearrangement when a 4-amino substituent is present.[9] The formation of the azo compound **4** from **3b** constitutes an entirely new reaction and is an efficient method for the formation of a wide variety of differently substituted aromatic azobenzenes.

This preliminary experiment of **3b** with the phenoxide ion enabled us to identify the products from the reaction of triflone **3a** as a mixture of the *ortho*-coupled azobenzene **4** ($R_F = SO_2CF_3$) with a free phenolic group and its corresponding trifluoromethanesulfonate ester (OTf instead OH).

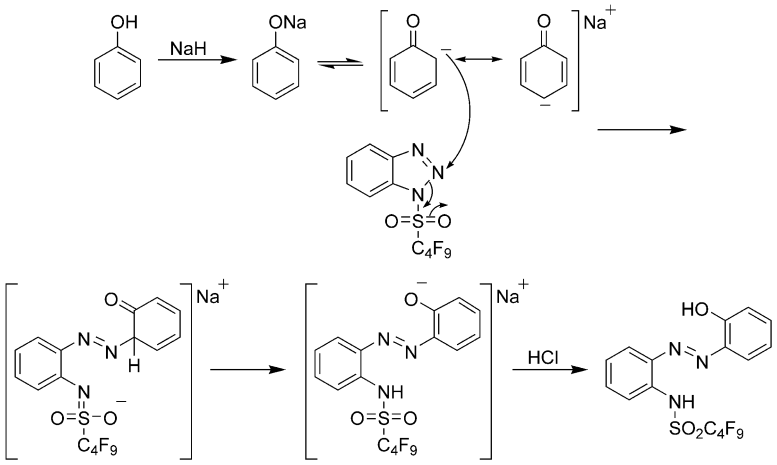
The mechanism for the formation of the azo compound is outlined in Scheme 1. The mesomeric anion formed by the reaction of sodium hydride with phenol attacks at the N2 position of the benzotriazole moiety. The highly electron-withdrawing nonafluorobutanesulfone group then results in the opening up of the ring which leads to **4** after proton shifts and acidic work-up. The formation of the *para*

[*] X. Àlvarez Micó, Prof. T. Ziegler, Dr. L. R. Subramanian
Institut für Organische Chemie
Universität Tübingen
Auf der Morgenstelle 18, 72076 Tübingen (Germany)
Fax: (+49) 7071-29-5244
E-mail: thomas.ziegler@uni-tuebingen.de
lrs@uni-tuebingen.de

[**] We thank Bayer AG for the generous gift of nonafluorobutanesulfonyl fluoride. The method for the formation of azobenzenes presented here has been submitted for a patent application.

Supporting information for this article is available on the WWW under http://www.angewandte.org or from the author.

 © 2004 Wiley-VCH Verlag GmbH & Co. KGaA, Weinheim DOI: 10.1002/anie.200352782

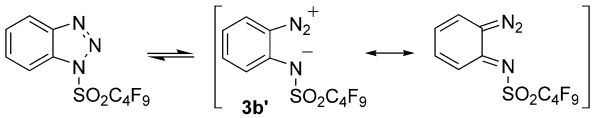


Scheme 1. Mechanism for the formation of the azo compound.

isomer can be considered to occur in a similar manner (not depicted).

Another possibility for the formation of **4** is a nucleophilic attack of the phenolate anion at the sulfur atom,[10] thus resulting in ring opening of the triazole moiety by a rearrangement reaction. However, this will lead only to the *ortho*-substituted product **4**.[11]

A mechanism involving a free diazonium intermediate existing in equilibrium with the benzotriazole **3b**′ (Scheme 2)



Scheme 2. Possible equilibrium involving **3b**′.

structure was also scrutinized.[12] The existence of a free diazonium species in equilibrium with the 1,2,3-triazole ring is known in the parent 1,2,3-triazole substituted with a sulfonyl group at N1. This equilibrium was confirmed by ^{1}H NMR spectroscopic studies.[13] In the benzotriazole series two compounds can be conceived to be in equilibrium with the diazo structure.

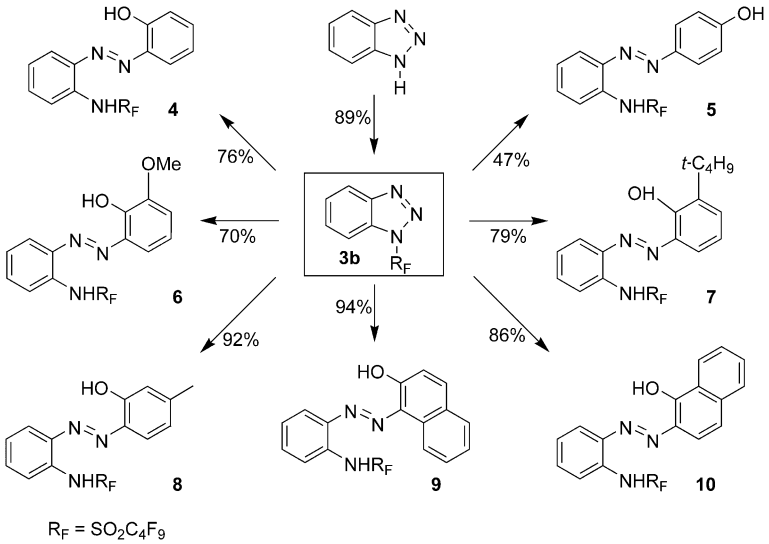
1-Nitrobenzotriazole,[14] was shown to react with amines; for example, piperidine gave an isolable piperidinium salt from the ring-opened benzotriazole. There was also a report[15] on the reversible thermochromic behavior of 1-cyanobenzotriazole, which is yellow in the melt and colorless in the crystalline state. No chemical evidence was obtained to indicate that the color might arise from ring opening to give the diazo-*N*-cyanoimine form, and no reactions of the cyano compound were reported. Experiments carried out on 1-nitrobenzotriazole by treating it with indolizine derivatives at room temperature were interpreted as an electron-transfer process, and the same process is attributed to the reaction of amines with 1-nitrobenzotriazole.[16]

Temperature-dependent NMR investigations were carried out to find out whether an equilibrium with a diazo structure does exist in the 1-nonafluorobutylsulfonylbenzotriazole **3b**. The signals in the aromatic region of the spectrum for molecule **3b** did not change when the sample was heated in [D_6]DMF up to a temperature of 100 °C. Spectra were recorded every 10 °C starting from ambient temperature. Above 100 °C, the compound starts to decompose to give a dark solution. No analysis of this sample could be carried out as the sample had completely decomposed.

Our coupling reactions were carried out at room temperature and on the basis of time-dependent NMR data it can be concluded that no free diazonium intermediate participates in the reaction. Also, no vibration corresponding to the N≡N group could be found in the IR spectrum of **3b**. We consider that, as far as the mechanism is concerned, the one shown in Scheme 1 is more probable, however, the other mechanism via the diazo structure cannot be completely ruled out at present.

The *para*-substituted aza compound **5**, the structure of which was proven by X-ray analysis,[17] could be obtained exclusively by conducting the reaction in *N*,*N*-dimethylformamide. This dipolar aprotic solvent probably blocks the *ortho* positions by coordination to the oxygen atom of the phenolate anion, thus directing the reaction to proceed exclusively to the *para* product **5** by the mechanism shown in Scheme 1. The lower yield of the *para* product relative to *ortho* products probably lies in the work-up from the reaction mixture containing DMF, as the yields have not yet been optimized.

A set of azobenzenes (Scheme 3) prepared by this method is listed in Table 1. The authentication of the *ortho* coupling in the reaction of benzotriazole **3b** with phenols in toluene is proved by the formation of products **6**–**8** from 2-methoxy-, 2-*tert*-butyl-, and 3-methylphenol, respectively. 2-Methoxyphenol and 2-*tert*-butylphenol gave more than 70% of the corresponding *ortho*-coupled products **6** and **7**, respectively,



Scheme 3. Azobenzenes prepared. Solvent: toluene for **4**–**10**, DMF for **5**.

 © 2004 Wiley-VCH Verlag GmbH & Co. KGaA, Weinheim

Table 1: Analytical data for azobenzenes **4**–**10**.

Product	Yield [%]	M.p. [°C]	Color	UV (MeCN) λ_{max} [nm] (ε mol^{-1} dm^3 cm^{-1})
4	76	134.2–135.1	orange	250 (11708), 321 (12021), 395 (8324)
5	47	129.5–130.0	red	250 (11334), 358 (19083)
6	70	134.0–135.0	yellowish brown	222 (23540), 333 (13380), 407 (8360)
7	79	88.7–91.3	orange	245 (11336), 326 (11559), 411 (8988)
8[a]	92	132.7–133.0	yellow	255 (22823), 325 (19315), 412 (18710)
9	94	174.0–174.7	red	212 (22617), 226 (21449), 235 (14598), 250 (8175), 277 (11095), 321 (3698), 518 (19036)
10	86	161.6–161.9	dark red	205 (40368), 245 (29965), 293 (20231), 524 (26772)

[a] The ring-opening reaction of benzotriazole **3b** proceeds quantitatively. Contains 8% of the other *ortho* isomer.

while 3-methylphenol quantitatively afforded the *ortho*-coupled azobenzenes **8** (92%) and the other *ortho* regioisomer (8%). β-Naphthol behaved in a typical way for a diazotization reaction and gave the *ortho* product, whereas α-naphthol showed opposite regioselectivity compared to that obtained in classical diazomethane reactions. The diazo compounds exhibit various colors depending upon the substituents (Table 1).

The *ortho* structure of the coupled products can be easily detected by the chemical shift of the phenolic OH group, which appears quite downfield at $\delta = 11$–16 ppm as a result of a hydrogen-bonding interaction with the neighboring nitrogen atom. In contrast, the phenolic OH group of the *para* product is found within the normal range of $\delta = 5$–6 ppm.

The aromatic azo compounds behave differently[18,19] in many of their reactions compared to the aliphatic diazo compounds.[20,21] Aromatic azo compounds are the largest and most important group of dyes used in the dye industry.[18,22–26] They have also found use in diazo-type photocopying processes and diazosulfonates are also beneficial as fungicides.[26] Although aromatic azo compounds are only represented to a marginal extent in pharmaceutical preparations,[27] azo groups have recently been included as substituents in some polycyclic compounds used as probes for chemical genetic studies.[28] Some other recent applications include their use for color marking of substrates in combinatorial chemistry[29] and in photosensitive nanocomposites.[30]

Aromatic azo compounds are still manufactured by the single most important synthetic route, that is, diazotization of aromatic amines followed by coupling with suitable acceptors.[18,22–26] In classical diazotization reactions, that is, treating a diazonium salt with an aromatic phenol or aniline derivative, the azo group usually does not enter at random, and for the phenol derivatives, the attack is always at the position *para* to the activating OH group. If this position is hindered, coupling will sometimes take place in the *ortho* position, albeit at a much slower rate.[24]

The Wallach rearrangement of azoxybenzenes[31] affords predominantly *p*-hydroxyazobenzenes. The thermolysis of 1:1 complexes of azoxybenzenes with $SbCl_5$ was reported[31] to give *o*-azobenzenes, but only in two instances were good yields obtained. The drawback of this reaction is that it necessitates the use of a harsh chemical ($SbCl_5$) and the prior preparation of azo compounds by a normal azo-coupling reaction and then oxidation to azoxybenzenes.

Of the two reported patent procedures, one describes the formation of the *ortho*-substituted azo-coupled product of α-naphthol in a heterogeneous water–organic solvent mixture (for example, water–dichloromethane) in 26% yield[32] and the other leads to *ortho* products only under strong alkaline conditions.[33] In the latter case, the intermediate formation of the mesomeric *o*-benzoquinone diazide is probably responsible for the *ortho* coupling.[33b] These variations in the reaction conditions have been done only in the case of α-naphthol to obtain various types of substituted azo dyes useful in the dye industry.

Bearing in mind the above mentioned literature data, to the best of our knowledge there exists no expedient direct method for the preparation of *ortho*-azobenzenes by a straight coupling reaction. Besides diazotization of aromatic amines, there are only a few methods, for example, diazotization of aryl hydrazines, transfer of an azo group by tosyl azides, known for the preparation of azobenzenes.[18,34,35]

In conclusion, the method presented here offers access to a wide palette of aromatic azo compounds by varying both the benzotriazole component as well as the nucleophile. Moreover, a total switch in the direction of attachment of the azo substituent can be envisaged. Although our investigations on this new reaction sequence continue, we believe that the above preliminary results provide ambitious guidelines for the preparation of keynote prototypes of *ortho*-substituted azobenzenes.

Experimental Section

3b: A 1.6 M solution of BuLi in hexanes (9.4 mL, 15 mmol) was added slowly to a stirred solution of **1** (1.8 g, 15 mmol) in anhydrous 1,2-dimethoxyethane (50 mL) at 0 °C under argon. After 1 h, nonafluorobutanesulfonyl fluoride (4.75 mL, 22.4 mmol) was added dropwise. The reaction mixture was stirred under reflux for about 3 h, with the progress of the reaction monitored by TLC. After completion of the reaction, the mixture was cooled to RT, and diluted with diethyl ether (100 mL). The organic layer was washed with aqueous saturated NH_4Cl solution (2×) and water (1×). After drying (Na_2SO_4), filtration, and removal of the solvent, the crude product was purified by chromatography on silica gel under protection from light (eluent: petroleum ether (b.p. 60–90 °C)/EtOAc, 4:1) to give **3b**; yield: 5.33 g (89%); m.p. 46.1–46.8 °C. IR (KBr): $\tilde{\nu} = 1356$, 1193 (SO_2), 1271, 1138, 1028 cm^{-1} (C-F); UV/Vis (MeCN): λ (ε mol^{-1} dm^3 cm^{-1}) = 211 (10650), 253 (5477), 293 (1477), 409 nm (352); ^{1}H NMR (250 MHz, $CDCl_3$): $\delta = 8.23$ (d, $J_{6,7} = 8.22$ Hz, 1H, H7), 7.98 (d, $J_{4,5} = 8.30$ Hz, 1H, H4), 7.75–7.85 (t, $J = 8.34$, 8.04 Hz, 1H, H6), 7.55–7.64 ppm (dd, $J = 8.84$, 7.53 Hz, 1H, H5); ^{13}C NMR (250 MHz, $CDCl_3$): $\delta = 145.3$ (C9), 132.1 (C8), 131.9 (C6), 127.2 (C5), 121.4 (C7), 111.8 ppm (C4); EI-MS: $m/z = 400.9$. Elemental analysis calcd for $C_{10}H_4F_9N_3O_2S$: C 29.94, H 1.00, N 10.47, S 7.99; found: C 30.06, H 0.93, N 10.36, S 8.16.

4: NaH (0.12 g, 60% suspension in oil) was added to a stirred solution of phenol (0.28 g, 3 mmol) and **3b** (1 g, 2.5 mmol) in anhydrous toluene (50 mL) at room temperature under argon. The

 © 2004 Wiley-VCH Verlag GmbH & Co. KGaA, Weinheim

mixture was allowed to stir for 7 h while controlling the progress of the reaction by TLC. At the end of this period, EtOAc (100 mL) and water (25 mL) were added, and the suspension was treated with conc. HCl until the color of the organic phase changed from red to orange-red. The aqueous phase must remain colorless during this time. The organic phase was separated, dried (Na_2SO_4), filtered, and the solvent was evaporated. The crude product was purified by chromatography over silica gel (eluent: petroleum ether (b.p. 60–90 °C)/EtOAc (30:1) containing 1% AcOH) to afford **4**; yield: 0.94 g (76%); m.p. 134.2–135.1 °C (petroleum ether (bp 60–90 °C)). IR (KBr): $\tilde{\nu} = 3441$ (NH, OH), 1349, 1184 (SO_2), 1285, 1252, 1135 cm^{-1} (CF); UV/Vis (MeCN): λ (ε $mol^{-1}dm^3cm^{-1}$) = 250 (11708), 321 (12021), 395 nm (8324); ^1H NMR (600 MHz, $CDCl_3$): $\delta = 12.00$ (s, 1H, OH), 11.86 (s, 1H, NH), 7.82–7.87 (m, 2H, H3, H6), 7.75 (d, $J = 7.92$ Hz, 1H, H3′), 7.44–7.50 (dd, $J = 7.32$, 8.52 Hz, 1H, H5), 7.37–7.44 (m, 2H, H4, H4′), 7.12–7.08 (t, $J = 7.32$, 7.92 Hz, 1H, H5′), 7.06 ppm (d, $J = 8.58$ Hz, 1H, H6′); ^{13}C NMR (600 MHz, $CDCl_3$): $\delta = 153.08$ (C2′), 137.34 (C2), 135.98 (C1′), 134.80 (C3′), 132.44 (C5), 131.43 (C4′), 130.27 (C6), 129.83 (C1), 126.12 (C4), 120.83 (C5′), 120.41 (C3), 118.72 ppm (C6′); EI-MS: $m/z = 494.9$ [M^+]. Elemental analysis calcd for $C_{16}H_{10}F_9N_3O_3S$: C 38.80, H 2.03, N 8.48, S 6.47; found: C 38.62, H 1.99, N 8.33, S 6.52.

Received: September 3, 2003 [Z52782]

Keywords: azo compounds · benzotriazoles · diastereoselectivity · *ortho*-coupling · solvent effects

[1] a) A. R. Katritzky, B. V. Rogovoy, *Chem. Eur. J.* **2003**, *9*, 4586; b) A. R. Katritzky, O. V. Denisko, *Pure Appl. Chem.* **2000**, *72*, 1597; c) A. R. Katritzky, *J. Heterocycl. Chem.* **1999**, *36*, 1501; d) A. R. Katritzky, X. Lan, J. Yang, O. V. Denisko, *Chem. Rev.* **1998**, *98*, 409; e) A. R. Katritzky, H. Wu, L. Xie, S. Rachwal, B. Rachwal, J. Jiang, G. Zhang, H. Lang, *Synthesis* **1995**, 1315; f) A. R. Katritzky, X. Lan, W.-Q. Fan, *Synthesis* **1994**, 445.

[2] A. R. Katritzky, S. Rachwal, R. J. Offerman, Z. Najzanek, A. K. Yagoub, Y. Zhang, *Chem. Ber.* **1990**, *123*, 1545.

[3] A. R. Katritzky, M. Soleiman, T. Davis, J. N. Lam, A. Maquestiau, D. Beugnies, R. Flammang, *J. Chem. Soc. Perkin Trans. 2* **1988**, 1071.

[4] L. R. Subramanian, A. G. Martinez, A. H. Fernandez, R. M. Alvarez, *Synthesis* **1984**, 481.

[5] This interesting rearrangement and the reactions of **2** will be reported later. The structure of **2** has been unambiguously proven by analytical, spectral, and X-ray data.

[6] a) A. R. Katritzky, J.-L. Moutou, Z. Yang, *Synlett* **1995**, 99; b) A. R. Katritzky, A. V. Ignatchenko, H. Lang, *Heterocycles* **1995**, *41*, 131.

[7] L. R. Subramanian, M. Hanack, *Chem. Ber.* **1972**, *105*, 1465.

[8] CCDC-219149 contains the supplementary crystallographic data for this paper. These data can be obtained free of charge via www.ccdc.cam.ac.uk/conts/retrieving.html (or from the Cambridge Crystallographic Data Centre, 12 Union Road, Cambridge CB21EZ, UK; fax: (+44) 1223-336-033; or deposit@ccdc.cam.ac.uk).

[9] A. R. Katritzky, F.-B. Ji, W.-Q. Fan, J. K. Gallos, J. V. Greenhill, R. W. King, P. J. Steel, *J. Org. Chem.* **1992**, *57*, 190.

[10] L. R. Subramanian, M. Hanack, L. W. K. Chang, M. A. Imhoff, P. von R. Schleyer, F. Effenberger, W. Kurtz, P. J. Stang, T. E. Dueber, *J. Org. Chem.* **1976**, *41*, 4099, and references therein.

[11] The mechanism is given in the Supporting Information.

[12] We thank one of the referees for the suggestion of considering this mechanism.

[13] a) G. Himbert, M. Regitz, *Chem. Ber.* **1972**, *105*, 2963; b) G. Himbert, M. Regitz, *Chem. Ber.* **1972**, *105*, 2975; c) G. Himbert, M. Regitz, *Justus Liebigs Ann. Chem.* **1973**, 1505.

[14] C. L. Habraken, C. Erkelens, J. R. Mellema, P. Cohen-Fernandes, *J. Org. Chem.* **1984**, *49*, 2197.

[15] M. E. Hermes, F. D. Marsh, *J. Am. Chem. Soc.* **1967**, *89*, 4760.

[16] M. Colonna, M. Poloni, *Gazz. Chim. Ital.* **1988**, *118*, 673.

[17] CCDC-219048 contains the supplementary crystallographic data for this paper. These data can be obtained free of charge via www.ccdc.cam.ac.uk/conts/retrieving.html (or from the Cambridge Crystallographic Data Centre, 12 Union Road, Cambridge CB21EZ, UK; fax: (+44) 1223-336-033; or deposit@ccdc.cam.ac.uk).

[18] H. Zollinger, *Diazo Chemistry*, *Vol. 1*, VCH, Weinheim, **1994**.

[19] K. H. Saunders, R. L. M. Allen, *Aromatic Diazo Compounds*, 3rd ed., Edward Arnold, Victoria, Australia, **1985**.

[20] M. Regitz, G. Maas, *Diazo Compounds*, Academic Press, New York, **1986**.

[21] H. Zollinger, *Diazo Chemistry*, *Vol. 2*, VCH, Weinheim, **1994**.

[22] H. Zollinger, *Color Chemistry*, 2nd ed., VCH, Weinheim, **1991**.

[23] *Riegel's Handbook of Industrial Chemistry*, 9th ed. (Ed.: J. A. Kent), Van Nostrand Reinhold, New York, **1992**, pp. 821–875.

[24] R. J. Chudgar in *Kirk-Othmer Encylopedia of Chemical Technology*, *Vol. 3* (Ed.: M. Howe-Grant), Wiley, New York, **1992**.

[25] K. Hunger, P. Mischke, W. Rieper in *Ullmann's Encyclopedia of Industrial Chemistry*, *Vol. A3* (Eds.: F. T. Campbell, R. Pfefferkorn, J. F. Rounsaville), VCH, Weinheim, **1985**, pp. 245–324.

[26] H. Hertel in *Ullmann's Encyclopedia of Industrial Chemistry*, *Vol. A8* (Eds.: L. Kaudy, R. Pfefferkorn, J. F. Rounsaville), VCH, Weinheim, **1987**, pp. 505–522.

[27] A. Kleeman, J. Engel, B. Kutscher, D. Reichert, *Pharmaceutical Substances*, Thieme, Stuttgart, **1999**.

[28] D. Barnes-Seeman, S. B. Park, A. N. Koehler, S. L. Schreiber, *Angew. Chem.* **2003**, *115*, 2478; *Angew. Chem. Int. Ed.* **2003**, *42*, 2376.

[29] P. Krattiger, C. McCarthy, A. Pfaltz, H. Wennemers, *Angew. Chem.* **2003**, *115*, 1763; *Angew. Chem. Int. Ed.* **2003**, *42*, 1722.

[30] N. Liu, Z. Chen, D. R. Dunphy, Y.-B. Jiang, R. A. Assiuk, C. J. Brinker, *Angew. Chem.* **2003**, *115*, 1773; *Angew. Chem. Int. Ed.* **2003**, *42*, 1731.

[31] a) J. Yamamoto, Y. Nishigaki, M. Imagawa, M. Umezu, T. Matsuura, *Chem. Lett.* **1976**, 261; b) J. yamamoto, Y. Nishigaki, M. Umezu, T. Matsuura, *Tetrahedron* **1980**, *36*, 3177.

[32] K. Bredereck, S. Ksraca, German Patent 2931807, **1981** [*Chem. Abstr.* **1981**, *94*, 210287].

[33] a) O. Knecht, O. Senn, DRP 741358, **1941** [*Chem. Zentralb.* **1942**, *113*(II), 2207]; b) K. H. Schündehütte in Houben-Weyl, *Vol. 10/3*, Thieme, Stuttgart, **1965**.

[34] *The Chemistry of the Hydrazo, Azo and Azoxy Groups* (Ed.: S. Patai), Wiley, London, **1975**.

[35] *The Chemistry of Diazonium and Diazo Groups*, *Vol. 2*, (Ed.: S. Patai), Wiley, London, **1997**.

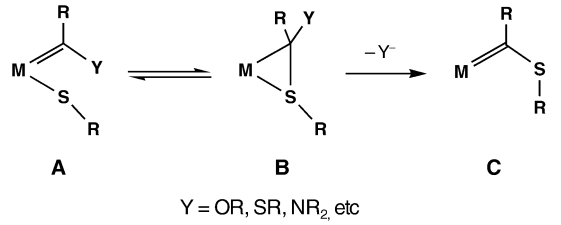
 © 2004 Wiley-VCH Verlag GmbH & Co. KGaA, Weinheim

Carbene Complexes

Formation of an Iron(II) Carbene–Thiolato Complex by Insertion of Carbon Monoxide into an Si–C Bond**

*Masahiro Yuki, Tsukasa Matsuo, and Hiroyuki Kawaguchi**

The carbene carbon atom in Fischer carbene complexes is well known to be susceptible to nucleophilic attack. Hence, complexes **A** bearing both Fischer carbene and thiolato ligands would be in equilibrium with the thiametalacyclopropane form **B**.[1] Although the existence of an equilibrium between **A** and **B** was supported by NMR spectroscopy and reactivity studies,[1a] such complexes are scarce.[2–4] A possible reason for this paucity lies in facile intramolecular nucleophilic substitution to form the RS-substituted carbene complex **C**.

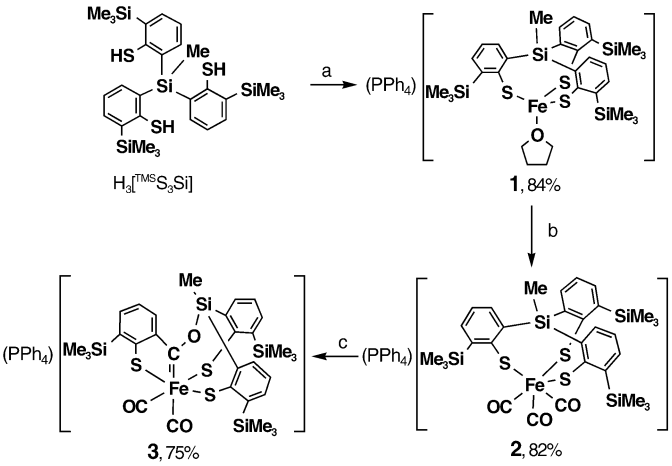


In our studies of transition-metal complexes of thiolato ligands,[5] we designed and synthesized the tridentate ligand $[^{TMS}S_3Si]^{3-}$ ($H_3[^{TMS}S_3Si]$ = tris(3-trimethylsilyl-2-mercaptophenyl)methylsilane).[6] On attempting to carbonylate an iron(II) complex of $[^{TMS}S_3Si]^{3-}$, namely **1**, we encountered an unexpected formation of a stable Fischer carbene–thiolato complex **3** (Scheme 1). Intriguingly, **3** exhibits a bonding interaction of the Fischer carbene carbon atom with the thiolato ligand.[7]

Treatment of $[Fe(CF_3SO_3)_2(CH_3CN)_2]$ with 1 equiv of $Li_3(^{TMS}S_3Si)$ followed by cation exchange with PPh_4Br afforded $PPh_4[Fe(^{TMS}S_3Si)(thf)]$ (**1**). The magnetic moment of **1** is typical of tetrahedral Fe^{II} centers ($\mu_{eff} = 4.77\,\mu_B$). Despite line-broadening and a paramagnetic shift of the resonances, the ^1H NMR spectrum exhibits five signals ascribed to the $[^{TMS}S_3Si]^{3-}$ ligand, and this suggests that the solution structure is consistent with C_3 symmetry.

[*] Dr. M. Yuki, Dr. T. Matsuo, Prof. Dr. H. Kawaguchi
Coordination Chemistry Laboratories
Institute for Molecular Science
Myodaiji, Okazaki, 444-8585 (Japan)
Fax: (+81) 564-55-5245
E-mail: hkawa@ims.ac.jp

[**] This work was supported by a Grant-in-Aid for Scientific Research (No. 14703008) and Priority Areas (No. 14078101 "Reaction Control of Dynamic Complexes") from Ministry of Education, Culture, Sports, Science, and Technology, Japan.



Scheme 1. Synthesis of **1**–**3**. a) 3 BuLi then $[Fe(CF_3SO_3)_2(CH_3CN)_2]$, THF; b) CO, THF, −48 °C; c) THF, RT.

An X-ray crystallographic study of **1** (Figure 1) showed that the iron atom is bound to the three sulfur donors and one THF molecule with an average Fe–S distance of 2.301 Å and an Fe–O distance of 2.130(2) Å.[8] The iron center has a tetrahedral environment with slight compression of the S-Fe-S angles (av 113.5°). The S-Fe-O angles average 104.7°. The bridging Si(1) atom assumes a tetrahedral geometry, and the atoms Fe and Si(1) are separated by 3.3701(9) Å. The strain in the eight-membered $\{FeS_2C_4Si\}$ ring of **1** is relieved by propeller twisting of the $[^{TMS}S_3Si]^{3-}$ ligand, which leads to average S-Fe-Si-C torsion angles of 41.9°.

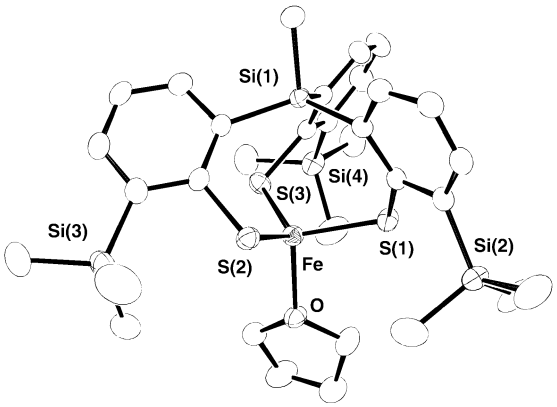


Figure 1. Structure of the anion of **1** with 50% ellipsoids. Selected bond lengths [Å] and angles [°]: Fe–S(1) 2.2798(9), Fe–S(2) 2.3097(9), Fe–S(3) 2.3129(9), Fe–O 2.130(2); S(1)-Fe-S(2) 106.02(3), S(1)-Fe-S(3) 112.00(3), S(2)-Fe-S(3) 122.62(3), S(1)-Fe-O 100.81(6), S(2)-Fe-O 110.13(7), S(3)-Fe-O 103.14(7).

Complex **1** smoothly reacted with 1 atm of CO in THF at −48 °C to give the diamagnetic carbonyl derivative $(PPh_4)[Fe(^{TMS}S_3Si)(CO)_3]$ (**2**). The ^1H NMR spectrum of **2** indicates that the symmetric coordination of the $[^{TMS}S_3Si]^{3-}$ ligand is retained. The $^{13}C\{^1H\}$ NMR resonance of the carbonyl ligands is found at $\delta = 209.6$ ppm. The IR spectrum of **2** displays two carbonyl stretching bands at 2052 and

 © 2004 Wiley-VCH Verlag GmbH & Co. KGaA, Weinheim DOI: 10.1002/anie.200352916

1990 cm^{-1}, indicative of a facial tricarbonyl geometry. Complex **2** is stable at low temperature, but is unstable in solution at ambient temperature. On warming to room temperature, the red solution gradually turned green, and complete conversion to complex **3** occurred.

The crystal structure of **3** revealed an unprecedented Fischer carbene–thiolato complex (Figure 2).[8] The coordination environment of the iron center is best described as distorted octahedral, with two mutually *cis* carbonyl ligands and a new [$^{TMS}S_3Si$]-derived tetradentate ligand in which the original trithiolato ligand has been transformed into a carbene–trithiolato moiety by insertion of CO into an Si–C bond. The Fe–C(29) bond length of 1.981(4) Å is at the long end of known Fe–C(carbene) bonds,[9] and the C(29) atom has trigonal-planar geometry, as evidenced by the sum of angles at C(29) of 352.7°. The Fe–S bond lengths, which range from 2.299(1) to 2.334(1) Å, are typical of low-spin Fe^{II} thiolato complexes.[10] It is noteworthy that the thiolato sulfur atom S(2) is in close proximity to the carbene carbon atom C(29), although the separation of 1.872(4) Å is longer than a normal C–S single bond ($C(sp^3)$–S 1.82 Å).[11] Longer C–S bonds (1.87–1.92 Å) have been observed for sulfur atoms bonded to spiro carbon atoms.[12] This structural feature suggests that substantial bonding interaction occurs between the vacant p orbital of the carbene carbon atom and the lone pair of the thiolato sulfur atom. This notion is also supported by the elongation of the C(29)–O(1) distance (1.409(5) Å) relative to those of Fischer carbene complexes.

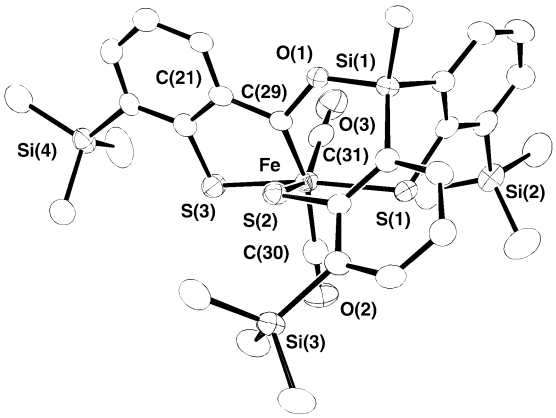
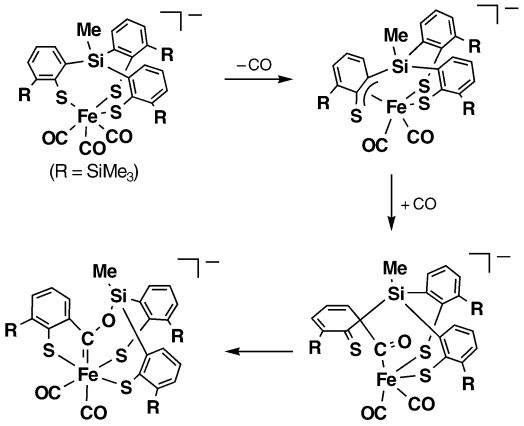


Figure 2. Structure of the anion of **3** with 50% ellipsoids. Selected bond lengths [Å] and angles [°]: Fe–S(1) 2.334(1), Fe–S(2) 2.299(1), Fe–S(3) 2.281(1), Fe–C(29) 1.981(4), Fe–C(30) 1.818(5), Fe–C(31) 1.745(5), S(2)–C(29) 1.872(4), Si(1)–O(1) 1.652(3), O(1)–C(29) 1.409(5), C(21)–C(29) 1.487(6); S(1)-Fe-S(2) 97.96(5), S(1)-Fe-S(3) 170.21(5), S(2)-Fe-S(3) 87.32(6), S(2)-Fe-C(29) 51.2(1), S(2)-Fe-C(30) 107.8(2), C(29)-Fe-C(31) 96.1(2), C(30)-Fe-C(31) 104.9(2), Fe-S(2)-C(29) 55.6(1), Fe-C(29)-S(2) 73.2(2), Fe-C(29)-O(1) 126.0(3), Fe-C(29)-C(21) 117.2(3), S(2)-C(29)-O(1) 114.8(3), S(2)-C(29)-C(21) 110.2(3), O(1)-C(29)-C(21) 109.5(3).

Spectroscopic data of **3** are consistent with the solid-state structure. The ^1H NMR spectrum reveals a total lack of symmetry in solution, as evidenced by three $SiMe_3$ singlets. In the $^{13}C\{^1H\}$ NMR spectrum of **3**-^{13}C, prepared with ^{13}CO, the carbene carbon atom resonates at $\delta = 128.6$ ppm as a doublet of doublets ($^2J_{C,C} = 11$, 7 Hz) and is accompanied by two doublets of doublets ascribed to two terminal carbonyl ligands at $\delta = 213.6$ ($J = 11$, 2 Hz) and 220.1 ppm ($J = 7$, 2 Hz). The chemical shift of the carbene carbon atom shows that this center is shielded relative to typical Fischer carbene complexes (220–350 ppm),[13] a difference that may arise from the interaction between the carbene carbon atom and the thiolato sulfur atom. In the IR spectrum, the carbonyl bands of **3** (1993, 1928 cm^{-1}) are at lower wavenumber than those of **2** because of the higher σ-donor/π-acceptor ratio of the carbene ligand relative to CO.

Scheme 2 shows the likely sequence of events in the formation of **3** from **2**. This transformation is presumed to involve loss of one CO ligand and η^1/η^3 rearrangement of one of the arylthiolate groups, followed by migratory insertion of the CO ligand into an Si–C bond and subsequent capture of the liberated CO. This would yield an acyl intermediate with a dearomatized ring, which could then undergo a net [1,3]-silyl migration to give a carbene species due to the high oxophilicity of the silicon atom. In arylthiolato complexes π coordination at the aryl substituent is uncommon. However, our recent finding that the arylthiolato ligand SC_6H_3-2,6-$(SiMe_3)_2$ can bind to the metal center though the aryl moiety could provide support for the η^1/η^3 rearrangement of this proposed mechanism.[5] Although carbonylation of early transition-metal and actinide complexes is well known to produce enolate complexes via insertion of CO into Si–C bonds,[14] this kind of intramolecular transformation is rare for late-transition-metal complexes. Recently, it was reported that a platinum complex with $Ph_2P{=}NSiMe_3$ ligands underwent insertion of CO into the N–Si bond and subsequent migration of the $SiMe_3$ group to generate an N,O-substituted carbene.[15]



Scheme 2. Proposed mechanism for the transformation of **2** into **3**.

To gain some insight into the kinetics of the formation of **3**, we monitored the disappearance of CO stretching absorptions in the IR spectrum of **2** from 277 to 296 K. The resulting data gave first-order plots with excellent correlation coefficients ($R^2 > 0.997$). An Arrhenius plot yielded values of $\Delta H^{\neq} = 125.3 \pm 3.3$ kJ mol^{-1} and $\Delta S^{\neq} = 122 \pm 11$ J mol^{-1} K^{-1}. Together with the observation that the rate of the reaction

 © 2004 Wiley-VCH Verlag GmbH & Co. KGaA, Weinheim

is slower in the presence of CO, the positive entropy of activation suggests a rate-limiting step involving CO loss from **2**. The formation of **3** might be driven by strain in the large chelate rings in **2**.

Finally, preliminary reactivity studies were carried out with **3**. Treatment of **3** with 1 equiv of methyl iodide gave a mixture of three products in which one of the three thiolato donors of the $[^{TMS}S_3Si]^{3-}$ ligand was methylated according to NMR spectroscopic data. The carbene moiety remains intact during the course of the reaction, in which a dithio(thioether)carbene ligand is formed. On the other hand, complex **3** was inert toward nucleophiles such as PEt_3.

In summary, we have synthesized the novel iron(II) trithiolato complex **1** containing the tripodal $[^{TMS}S_3Si]^{3-}$ ligand. Carbene–thiolato complex **3** was prepared by reaction of **1** with CO, in which insertion of CO into an Si–C bond took place. Since the coordinated THF molecule of **1** is labile, the trithiolato complex **1** could be a useful reagent for exploring the chemistry of iron–sulfur compounds relevant to the active sites in metalloenzymes. We are currently investigating the reactivity of **1** and **3**.

Experimental Section

1: A solution of $Li_3[^{TMS}S_3Si]$, prepared by reaction of $H_3[^{TMS}S_3Si]$ (428 mg, 0.729 mmol) with BuLi (1.58 M, 1.42 mL, 2.21 mmol) in THF (10 mL), was added to $[Fe(CF_3SO_3)_2(CH_3CN)_2]$ (317 mg, 0.728 mmol). The mixture was stirred for 15 min at room temperature, and a solution of PPh_4Br (305 mg, 0.727 mmol) in CH_3CN (3.5 mL) was added. After removal of the solvent in vacuo, recrystallization of the residue from THF/Et_2O afforded pale-yellow rods of **1** (643 mg, 84%); elemental analysis (%) calcd for $C_{56}H_{67}FeOPS_3Si_4$: C 63.97, H 6.42, S 9.15; found: C 63.83, H 6.53, S 8.67; ^{1}H NMR ([D$_8$]THF, 500 MHz, 23 °C): $\delta = 20.1$ (br, $w_{1/2} = 21$ Hz, 3H), 17.7 (br, $w_{1/2} = 40$ Hz, 3H), 8.35 (br, 8H, PPh_4^+), 8.09 (br, 12H, PPh_4^+), 6.99 (br, $w_{1/2} = 38$ Hz, 27H), −2.90 (br, $w_{1/2} = 27$ Hz, 3H), −25.3 ppm (br, $w_{1/2} = 24$ Hz, 3H); magnetic moment: $\mu_{eff} = 4.77\ \mu_B$.

2: A solution of **1** (368 mg, 0.35 mmol) in THF (3 mL) was treated with 1 atm of CO at −48 °C for 1 h. The red solution was concentrated and layered with Et_2O at −48 °C to give **2** (306 mg, 82%) as red plates; elemental analysis (%) calcd for $C_{55}H_{59}FeO_3PS_3Si_4$: C 62.12, H 5.59, S 9.05; found: C 61.95, H 5.93, S 8.30; IR (KBr): $\tilde{\nu}$(CO) = 2052 (s), 1990 cm^{-1} (s); ^{1}H NMR ([D$_8$]THF, 500 MHz, −30 °C): $\delta = 8.0$–7.6 (br, 20H, PPh_4^+), 7.19 (d, $J = 7.3$ Hz, 3H, ArH), 7.14 ($J = 6.8$ Hz, 3H, ArH), 6.75 (dd, $J = 6.8$, 7.3 Hz, 3H, ArH), 0.40 (s, 3H, SiMe), 0.27 ppm (s, 27H, $SiMe_3$). ^{13}C{^{1}H} NMR ([D$_8$]THF, 125 MHz, −30 °C): $\delta = 209.6$ (CO). ^{29}Si{^{1}H} NMR ([D$_8$]THF, 99 MHz, −30 °C) $\delta = -7.6$ ($SiMe_3$), −18.9 ppm (SiMe).

3: A solution of **2** (306 mg, 0.288 mmol) in THF (7 mL) was stirred for 2 h at room temperature. The resulting green solution was evaporated to dryness. The residue was washed with Et_2O and recrystallized from THF/Et_2O to give **3** as green plates (229 mg, 75%); elemental analysis (%) calcd for $C_{55}H_{59}FeO_3PS_3Si_4$: C 62.12, H 5.59, S 9.05; found: C 61.85, H 5.69, S 8.83; IR (KBr): $\tilde{\nu}$(CO) = 1993 (s), 1928 cm^{-1} (s); ^{1}H NMR ([D$_8$]THF, 500 MHz): $\delta = 8.0$–7.5 (m, 20H, PPh_4^+), 7.64 (d, $J = 7.3$ Hz, 1H), 7.34 (d, $J = 6.7$ Hz, 1H), 7.28 (d, $J = 6.7$ Hz, 1H), 7.19 (d, $J = 7.3$ Hz, 1H), 7.16 (d, $J = 7.3$ Hz, 1H), 6.89 (m, 2H), 6.83 (d, $J = 7.3$ Hz, 1H), 6.55 (m, 1H), 0.62 (s, 3H, SiMe), 0.331 (s, 9H, $SiMe_3$), 0.325 (s, 9H, $SiMe_3$), 0.28 ppm (s, 3H, $SiMe_3$); ^{13}C{^{1}H} NMR ([D$_8$]THF, **3**-^{13}C): $\delta = 219.8$ ($^2J_{C,C} = 11$, 2 Hz, CO), 213.3 ($J = 7$, 2 Hz, CO), 128.9 ppm ($J = 11$, 7 Hz, $C_{carbene}$); ^{29}Si NMR (DEPT, [D$_8$]THF, 99 MHz): $\delta = -5.0$, −6.3, −8.4 ($SiMe_3$), −15.1 ppm (SiMe).

Received: September 19, 2003 [Z52916]

Keywords: carbene ligands · insertions · iron · S ligands · tripodal ligands

[1] a) G. N. Glavee, R. J. Angelici, *J. Am. Chem. Soc.* **1989**, *111*, 3598–3603; b) D. Steinborn, *Angew. Chem.* **1992**, *104*, 392–412; *Angew. Chem. Int. Ed. Engl.* **1992**, *31*, 401–421.

[2] A variety of thiametallacyclopropane complexes has been reported: a) K. Miki, Y. Kai, N. Yasuoka, N. Kasai, *Bull. Chem. Soc. Jpn.* **1981**, *54*, 3639–3647; b) E. Rudulfo de Gil, L. F. Dahl, *J. Am. Chem. Soc.* **1969**, *91*, 3751–3756; c) R. A. Doyle, R. J. Angelici, *J. Organomet. Chem.* **1989**, *375*, 73–84; d) F. R. Kreißl, N. Ullrich, *J. Organomet. Chem.* **1992**, *440*, 335–339.

[3] N-Heterocyclic carbene complexes containing thiolato ligands are known: a) R. F. R. Jazzar, P. H. Bhatia, M. F. Mahon, M. K. Whittlesey, *Organometallics* **2003**, *22*, 670–683; b) D. Sellmann, W. Prechtel, F. Knoch, M. Moll, *Inorg. Chem.* **1993**, *32*, 538–546.

[4] A carbene complex with 1,1-ethylenedithiolato ligands was recently reported: J. Vincente, M. T. Chicote, S. Huertas, P. G. Jones, *Inorg. Chem.* **2003**, *42*, 4268–4274.

[5] T. Komuro, T. Matsuo, H. Kawaguchi, K. Tatsumi, *J. Am. Chem. Soc.* **2003**, *125*, 2070–2071.

[6] The synthesis of $H_3[^{TMS}S_3Si]$ is based on the well-known *ortho*-lithiation of lithium thiophenolate by *n*BuLi/*N*,*N*,*N*′,*N*′-tetramethylethylenediamine in hexane: a) G. D. Figuly, C. K. Loop, J. C. Martin, *J. Am. Chem. Soc.* **1989**, *111*, 654–668; b) E. Block, V. Eswarakrishnan, M. Gernon, G. Ofori-Okai, C. Saha, K. Tang, J. Zubieta, *J. Am. Chem. Soc.* **1989**, *111*, 658–665; c) M. Yuki, T. Komuro, T. Matsuo, H. Kawaguchi, K. Tatsumi, unpublished reasults.

[7] A bonding interaction between a carbene carbon atom and a neighboring chloro ligand was recently reported for the *N*-heterocyclic carbene complex of trichlorooxovanadium(v): C. D. Abernethy, G. M. Codd, M. D. Spicer, M. K. Taylor, *J. Am. Chem. Soc.* **2003**, *125*, 1128–1129.

[8] Crystal data for **1**: $C_{56}H_{67}FeOPS_3Si_4$, $M_r = 1051.49$, crystal dimensions $0.40 \times 0.25 \times 0.10$ mm, $a = 26.090(5)$, $b = 14.900(3)$, $c = 29.470(6)$ Å, $\beta = 100.560(3)°$, $V = 11262(4)$ Å^3, monoclinic, *C*2/*c* (no. 15), $Z = 8$, $\rho_{calcd} = 1.240$ g cm^{-3}, $F(000) = 4448$, $\mu = 5.29$ cm^{-1}, 42749 measured, 12534 independent, 9455 observed reflections ($F_o^2 > 2\sigma F_o^2$), R_1(observed data) = 0.054, wR_2(all data) = 0.137; Crystal data for **3**: $C_{55}H_{59}FeOPS_3Si_4$, $M_r = 1063.41$, crystal dimensions $0.45 \times 0.10 \times 0.03$ mm, $a = 18.717(7)$, $b = 15.436(6)$, $c = 20.571(8)$ Å, $\beta = 109.550(4)°$, $V = 5601(4)$ Å^3, monoclinic, $P2_1/n$ (no. 14), $Z = 4$, $\rho_{calcd} = 1.261$ g cm^{-3}, $F(000) = 2232$, $\mu = 5.35$ cm^{-1}, 44131 measured, 12801 independent, 7564 observed reflections ($F_o^2 > 2\sigma F_o^2$), R_1(observed data) = 0.075, wR_2(all data) = 0.189. Rigaku Saturn CCD system (**1**) or Murcury CCD system (**3**), $Mo_{K\alpha}$ radiation ($\lambda = 0.71070$ Å), graphite monochromator, $T = 173$ K; the structures were solved by direct methods and refined against F^2 for all independent reflections (heavy atoms with anisotropic temperature factors, H atoms located at calculated positions with isotropic temperature factors); CCDC-219529 (**1**) and -219530 (**3**) contain the supplementary crystallographic data for this paper. These data can be obtained free of charge via www.ccdc.cam.ac.uk/conts/retrieving.html (or from the Cambridge Crystallographic Data Centre, 12, Union Road, Cambridge CB21EZ, UK; fax: (+44) 1223-336-033; or deposit@ccdc.cam.ac.uk).

[9] a) V. Mahias, S. Vron, L. Toupet, C. Lapinte, *Organometallics* **1996**, *15*, 5399–5408; b) P. E. Riley, R. E. Davis, N. T. Allison, W. M. Jones, *Inorg. Chem.* **1982**, *21*, 1321–1328; c) J. Yin, J. Chen, W. Xu, Z. Zhang, Y. Tang, *Organometallics* **1988**, *7*, 21–25; d) A. G. M. Marrett, J. Mortier, M. Sabat, M. A. Sturgess, *Organometallics* **1988**, *7*, 2553–2561; e) D. V. Khasnis, H. Le Bozac, P. H. Dixneuf, *Organometallics* **1986**, *5*, 1772–1777;

 © 2004 Wiley-VCH Verlag GmbH & Co. KGaA, Weinheim

e) V. Esposito, E. Solari, C. Floriani, N. Re, C. Rizzoli, A. Chiesi-Villa, *Inorg. Chem.* **2000**, *39*, 2604 – 2613.
[10] a) D. G. McGuire, M. A. Khan, M. T. Ashby, *Inorg. Chem.* **2002**, *41*, 2202 – 2208; b) E. Delgado, B. Donnadieu, S. Garcia, F. Zamora, *J. Organomet. Chem.* **2002**, *649*, 21 – 24; c) D. Sellmann, J. Utz, F. W. Heinemann, *Inorg. Chem.* **1999**, *38*, 459 – 466; b) D. Sellmann, H. Kunstmann, F. Knoch, M. Moll, *Inorg. Chem.* **1988**, *27*, 4183 – 4149; c) R. B. English, L. R. Nassimbeni, R. J. Haines, *J. Chem. Soc. Dalton Trans.* **1978**, 1379 – 1385.
[11] F. A. Allen, O. Kennard, D. G. Watson, L. Brammer, A. G. Orpen, R. Taylor, *J. Chem. Soc. Perkin Trans. 2* **1987**, S1 – S19.
[12] W. K. Wong-Ng, S. C. Nyburg, *Acta Crystallogr. Sect. B* **1978**, *34*, 2910 – 2912.
[13] E. O. Fischer, *Adv. Organomet. Chem.* **1976**, *14*, 1 – 32; b) M. A. Gallop, W. R. Roper, *Adv. Organomet. Chem.* **1986**, *25*, 121 – 198; c) K. C. Brinkman, A. J. Blakeney, W. Krone-Schmidt, J. A. Gladysz, *Organometallics* **1984**, *3*, 1325 – 1332.
[14] a) P. Berno, R. Minhas, S. Hao, S. Gambarotta, *Organometallics* **1994**, *13*, 1052 – 1054; b) M. F. Lappert, C. L. Raston, L. M. Engelhardt, A. H. White, *J. Chem. Soc. Chem. Commun.* **1985**, 521 – 522; c) D. C. Sonnenberger, E. A. Mintz, T. J. Marks, *J. Am. Chem. Soc.* **1984**, *106*, 3484 – 3491; d) S. J. Shimpson, R. A. Andersen, *J. Am. Chem. Soc.* **1981**, *103*, 4063 – 4066.
[15] G. Lin, N. D. Jones, R. A. Gossage, R. McDonald, R. G. Cavell, *Angew. Chem.* **2003**, *115*, 4188 – 4191; *Angew. Chem. Int. Ed.* **2003**, *42*, 4054 – 4057.

 © 2004 Wiley-VCH Verlag GmbH & Co. KGaA, Weinheim

Kinetic Resolutions

Lipase-Catalyzed Domino Dynamic Kinetic Resolution of Racemic 3-Vinylcyclohex-2-en-1-ols/Intramolecular Diels–Alder Reaction: One-Pot Synthesis of Optically Active Polysubstituted Decalins**

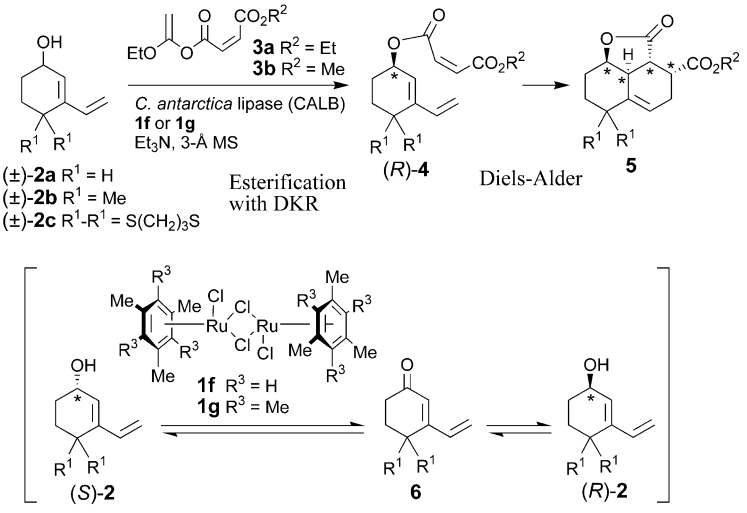
*Shuji Akai, Kouichi Tanimoto, and Yasuyuki Kita**

Over the past two decades the lipase-catalyzed kinetic resolution (KR) of racemic alcohols with acyl donors in organic solvents has gained increasing interest as an efficient method for the preparation of optically active compounds.[1] However, the inherent limitation of the yields to 50% at most has remained. Recently, lipase-catalyzed dynamic kinetic resolution (DKR) has been developed to overcome this problem.[2] In this reaction the KR was accompanied by the simultaneous racemization of the slow-reacting enantiomers of the alcohols with ruthenium catalysts such as [RuCl(indenyl)(PPh_3)$_2$] (**1a**),[3] [$Ru_2(CO)_4(\mu\text{-}H)(C_4Ph_4COHOCC_4Ph_4)$] (**1b**),[4] [$Ru(CO)_2Cl(C_4Ph_4CNHCHMe_2)$] (**1c**),[5] [{$RuCl_2$(*p*-cymene)}$_2$] (**1d**),[6] and [$Ru_2Cl_2(\mu\text{-}Cl)(\mu\text{-}H)$(*p*-cymene)$_2$] (**1e**)[6] to produce optically active esters in high yields. In both the DKR and the KR, however, the installed acyl groups have seldom been utilized as part of the constituent structure for subsequent intramolecular reactions,[7] and these groups are usually removed or replaced with other groups during subsequent transformations.[4b,c] A realization of the effective use of the acyl moiety by a domino procedure[8] has been highly desired because it could minimize the use of chemicals, reduce the waste, and shorten the transformation steps.

We have recently disclosed the first example of this concept, that is, the lipase-catalyzed KR of racemic furfuryl alcohols followed by the intramolecular Diels–Alder reaction to give tricyclic products with up to 99% *ee*; however, the yields were naturally less than 50%.[9] Herein we present the first lipase-catalyzed domino process that combines the DKR of racemic alcohols **2** by using functionalized ethoxyvinyl esters **3** and the Diels–Alder reaction of the intermediates (*R*)-**4**. The finding that the ruthenium catalysts (**1f** and **1g**) produced a fast racemization of the slow-reacting enantiomers (*S*)-**2** with reduced formation of the side products **6** was the key to the success of this process, and the products **5**, useful chiral intermediates for natural products such as compactin[10] and forskolin,[11] were directly obtained with up to 95% *ee* in 81% yield (Scheme 1).

Three separate reactions, that is, the enantioselective KR of (±)-**2**, the racemization of the slow-reacting enantiomer, and the Diels–Alder reaction of **4** have to proceed under identical conditions to achieve the domino reaction with DKR.

The lipases and organic solvents were first screened in the standard KR of (±)-**2a** with the ethoxyvinyl maleate **3a**,[12] and we found that the use of *Candida antarctica* lipase,



Scheme 1. Preparation of **5** by a lipase-catalyzed domino DKR/Diels–Alder reaction. MS = molecular sieves.

[*] Dr. S. Akai, K. Tanimoto, Prof. Dr. Y. Kita
Graduate School of Pharmaceutical Sciences
Osaka University, 1-6, Yamadaoka, Suita, Osaka 565-0871 (Japan)
Fax: (+81) 6-6879-8229
E-mail: kita@phs.osaka-u.ac.jp

[**] This work was supported by Grants-in-Aid for Scientific Research ((S) and (C)) and for Scientific Research on Priority Area (A) from the Ministry of Education, Culture, Sports, Science, and Technology, Japan. S.A. thanks the Takeda Science Foundation, Japan, for a research fellowship. Roche Diagnostics K.K., Japan, is thanked for the generous gift of the lipase.

Supporting information for this article is available on the WWW under http://www.angewandte.org or from the author.

 DOI: 10.1002/anie.200353044 © 2004 Wiley-VCH Verlag GmbH & Co. KGaA, Weinheim

fraction B (CALB, commercially available from Roche Diagnostics) in toluene caused the domino reaction to give **5a** ($R^1 = H$, $R^2 = Et$), although the enantioselectivity and the yield were poor (entry 1 in Table 1). On the other hand, the more polar solvents such as CH_2Cl_2, acetone, and MeCN were quite efficient for both the enzymatic resolution and the subsequent Diels–Alder reaction of **4a** ($R^1 = H$, $R^2 = Et$). After two days at 30 °C, **5a** (93–95 % *ee*, 35–43 % yield) was isolated, along with (*R*)-**4a** and (*S*)-**2a** (entries 2–4).[13,14] Prolonging the reaction time to five days completed the Diels–Alder reaction, and **5a** (90–93 % *ee*, 44–47 % yield) and (*S*)-**2a** (99 % *ee*, 46–50 % yield) were obtained (entries 5–7). Similar reactions at 40 °C, however, resulted in a slightly lower enantioselectivity (87–91 % *ee*), and therefore a reaction temperature lower than 40 °C was recommended.

The next and most critical subject in this study was the development of a highly effective catalyst for the racemization of (*S*)-**2a** at around 30 °C, because **1a–e** were not always effective for the lipase-catalyzed DKR at ambient temperature and often generated considerable amounts of ketones that caused a decrease in the yields of the desired products.[2–6]

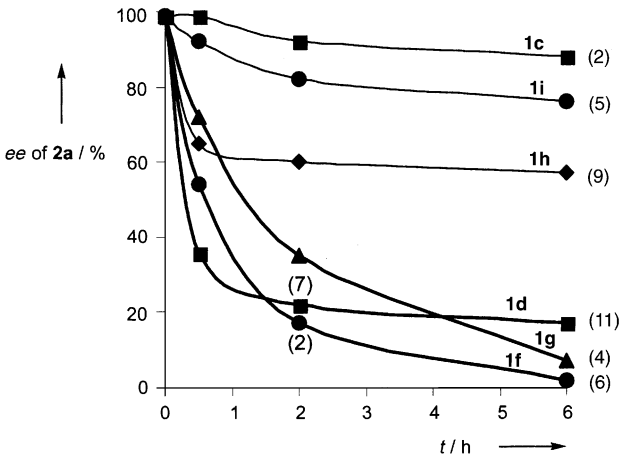


Figure 1. Time-course plot of the racemization of (*S*)-**2a** (99 % *ee*; 0.04 M) and the yield (%) of **6a** (shown in the parentheses) in CH_2Cl_2 with a ruthenium catalyst (**1c** (■), **1d** (■), **1f** (●), **1g** (▲), **1h** (◆), and **1i** (●)) at 25 °C. The combination of a ruthenium catalyst and a base (**1c** with *t*BuOK (8 and 10 mol %, respectively) or **1d**, **1f–i** and Et_3N (4 mol % and 1 equiv, respectively)) was used.

Table 1: Lipase-catalyzed KR of (±)-**2a** using **3a**.[a]

Entry	Solvent	*t* [days]	(*R*)-**4a**[a]		**5a**[b]		(*S*)-**2a**[b]	
			ee [%][b]	yield [%][c]	*ee* [%][b]	yield [%][c]	*ee* [%][b]	yield [%][c]
1	toluene	2	11	43	31	25	91	17
2	CH_2Cl_2	2	69	10	93	38	98	48
3	acetone	2	77	12	95	35	99	49
4	MeCN	2	91	7	93	43	99	44
5	CH_2Cl_2	5	trace	92	44	99	50	
6	acetone	5	trace	90	45	99	50	
7	MeCN	5	trace	93	47	99	46	

[a] A mixture of (±)-**2a** (0.12 mmol), **3a** (0.18 mmol), CALB (15 mg), and molecular sieves (3 Å; 60 mg) was stirred in a solvent (1.0 mL) at 30 °C. [b] For determination of the optical purity and the absolute stereochemistry, see ref. [14] and the Supporting Information, respectively. [c] Yields are based on ^{1}H NMR analysis.

Thus, the racemization of (*S*)-**2a** (99 % *ee*) with **1c** in CH_2Cl_2 at 25 °C was slow,[15] and that with **1d** provided an 11 % yield of the ketone **6a** after 6 h (Figure 1).

We found $[\{RuCl_2(mesitylene)\}_2]$ (**1f**) and $[\{RuCl_2(C_6Me_6)\}_2]$ (**1g**), which were readily available by the reported methods and stable at room temperature[16] but had not previously been used as catalysts for the racemization of optically active secondary alcohols, were more effective, and the reaction with these catalysts featured a higher reactivity and decreased formation of **6a**. On the other hand, the related catalysts $[\{RuCl_2(benzene)\}_2]$ (**1h**) and $[\{RuCl_2(anisole)\}_2]$ (**1i**) were not reactive (Figure 1). A further comparison of **1d**, **1f**, and **1g** for the racemization of (*S*)-**2a** in acetone disclosed that **1d** generated **6a** in 37 % yield with complete racemization, whereas **1f** and **1g** depressed the formation of **6a** to less than 10 % yield. A similar tendency was observed in MeCN (see the Supporting Information for further details).[17]

With these preliminary results in hand, we examined the domino DKR process with **1f** in CH_2Cl_2, acetone, or MeCN. Thus, a mixture of (±)-**2a**, **3a** (3 equiv), CALB, **1f** (4–10 mol %), Et_3N (3 equiv), and molecular sieves (3 Å) was stirred in the solvent at 35 °C. Although the reaction with 4 mol % of **1f** proceeded slowly because of the insufficient rate of racemization compared to the lipase-catalyzed KR, the use of 10 mol % of **1f** was found to be effective (Scheme 1). The reaction in acetone gave **5a** (95 % *ee*, 86 % yield as measured by ^{1}H NMR spectroscopy, 81 % yield after isolation) along with **6a** (9 % yield as measured by ^{1}H NMR spectroscopy; entry 2 in Table 2), and that in MeCN produced a similarly good result (**5a** with 97 % *ee* in 81 % yield as measured by ^{1}H NMR spectroscopy; entry 3). Compound **5a** was obtained with a lower optical purity in CH_2Cl_2 in an unsatisfactory yield as a result of the greater formation of **6a** (22 % yield; entry 1).

Under conditions similar to those listed in entry 2 in Table 2, the racemic alcohols **2a–c** and the acylating reagents (**3a**,**b**)[12] were subjected to the domino reaction, and the corresponding cycloadducts **5b–d** were isolated in good to high yields with more than 90 % *ee* (entries 4–6). This new procedure has the following advantages compared with the previous stepwise preparation of **5** from **2**: 1) the preparation of optically active **5a** and **5b** (entries 2 and 4) proceeds in higher yields than the previous preparation of the corresponding racemates (**5a**[10] and **5b**[13a] in 39 % and 67 % overall yields, respectively), and 2) the efficiency of our enzymatic resolution of (±)-**2c** (entry 6) is higher than that of the standard enzymatic KR of the same substrate.[18]

In addition, the one-pot synthesis was achieved from the preparation of **3b** from monomethyl maleate **7b** followed by the domino DKR process with (±)-**2a**. Catalyst **1d** was used for the first step because **1f** did not effectively accelerate the

 © 2004 Wiley-VCH Verlag GmbH & Co. KGaA, Weinheim

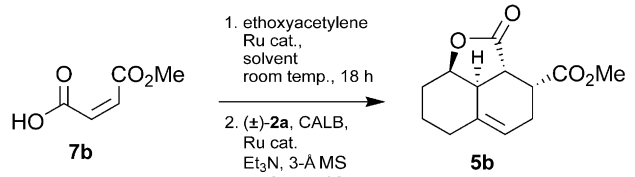
Table 2: Lipase-catalyzed domino DKR/Diels–Alder reaction of (±)-**2a–c** with **3a,b** to give **5**.[a]

Entry	(±)-**2**	**3**	Reaction conditions	**5**				**6** (Yield [%])[c]
				R^1	R^2	*ee* [%][b]	yield [%]	
1	(±)-**2a**	**3a**	CH_2Cl_2, 35 °C, 3 days	H	Et	**5a**: 82	73[c]	**6a** (22)
2	(±)-**2a**	**3a**	acetone, 35 °C, 3 days	H	Et	**5a**: 95	86[c] (81[d,e])	**6a** (9)
3	(±)-**2a**	**3a**	MeCN, 35 °C, 3 days	H	Et	**5a**: 97	81[c]	**6a** (13)
4	(±)-**2a**	**3b**	acetone, 35 °C, 3 days	H	Me	**5b**: 93	83[d,e]	**6a** (6)
5	(±)-**2b**	**3b**	acetone, 25 °C, 4 days	Me	Me	**5c**: 91	81[d,f]	**6b** (4)
6	(±)-**2c**	**3a**	acetone, 25 °C, 7.5 days	$S(CH_2)_3S$	Et	**5d**: 93	69[d,f,g]	**6c** (2)

[a] Typical procedure: A mixture of (±)-**2** (0.49 mmol), **3** (1.5 mmol), CALB (60 mg), **1f** (0.049 mmol), Et_3N (1.5 mmol), and molecular sieves (3 Å; 240 mg) was stirred in solvent (5 mL) in an argon atmosphere and the stated conditions. [b] For determination of the optical purity and the absolute stereochemistry, see ref. [14] and the Supporting Information, respectively. [c] Yield determined by ^{1}H NMR analysis. [d] Yield after isolation of the product. [e] A minor product (approximately 3–4% based on 500 MHz ^{1}H NMR analysis) that seemed to be a diastereomer was present as a contaminant after standard SiO_2 chromatography. [f] Obtained as a single diastereomer (500 MHz ^{1}H NMR analysis) after standard SiO_2 chromatography. [g] The diastereomer was obtained separately (approximately 8% yield) as well as **5d**.

addition of **7b** to ethoxyacetylene, and then (±)-**2a** and the reagents for the domino DKR reaction were added directly to give **5b** (94% *ee*, 81% yield; entry 1 in Table 3; see the Experimental Section for further details).[14] Another procedure involving **1g** for both steps also afforded **5b** (90% *ee*, 80% yield; entry 2 in Table 3). Although one disadvantage of these one-pot procedures is the long reaction time, we could obtain a potential strategy for a high-atom-economy process.

Table 3: One-pot synthesis of **5b** from **7b** and (±)-**2a**.



Entry	Ru cat./solvent for the first step	Ru cat./solvent for the second step	**5b**	
			ee value [%]	yield [%][a]
1	**1d** (0.5 mol%)/ acetone	**1f** (10 mol%)/ MeCN	94	81
2	**1g** (1 mol%)/ MeCN	**1g** (10 mol%)/ MeCN	90	80

[a] A minor product (≦3% based on 500 MHz ^{1}H NMR analysis) that seemed to be a diastereomer was present as a contaminant.

In conclusion, we have demonstrated here the first example of the combination of the domino reaction concept[8,9] and the DKR protocol,[2] a combination which is highly advantageous in terms of a simple and safe procedure, high chemical and optical yields at around room temperature, and the reduction of waste. From a mechanistic point of view, the successful use of acetone for the DKRs is extraordinary, because acetone acts as a hydrogen acceptor and thereby has been believed to accelerate the formation of the undesired ketones.[4a] Extensive study of other systems and the mechanistic elucidation are now in progress in our laboratory.

Experimental Section

3a: A mixture of ethoxyacetylene (1.88 mL, 23 mmol) and **1d** (92 mg, 0.15 mmol) in anhydrous acetone (50 mL) was stirred at 0 °C for 5 min under a nitrogen atmosphere, and a solution of monoethyl maleate **7a** (2.2 g, 15 mmol) in anhydrous acetone (20 mL) was added dropwise over 20 min. The reaction mixture was stirred at room temperature for 18 h and concentrated in vacuo to give **3a** (approximately 90% pure based on ^{1}H NMR analysis). Pure **3a** (1.59 g, 50% yield) was obtained by distillation as a colorless oil: b.p. 120–130 °C/0.4 Torr (bath temperature); ^{1}H NMR (300 MHz, $CDCl_3$): $\delta = 1.25$–1.41 (6H, m), 3.82 (1H, d, $J = 4.5$ Hz), 3.89 (2H, q, $J = 8$ Hz), 3.96 (1H, d, $J = 4.5$ Hz), 4.27 (2H, q, $J = 8$ Hz), 6.26 (1H, d, $J = 13$ Hz), 6.35 ppm (1H, d, $J = 13$ Hz); ^{13}C NMR (75 MHz, $CDCl_3$): $\delta = 14.0$, 14.1, 61.5, 65.0, 72.2, 127.7, 132.0, 156.6, 162.1, 164.9 ppm; IR (KBr): $\tilde{\nu} = 1759$, 1732, 1678 cm^{-1}; elemental analysis: calcd: C 56.07, H 6.59; found: C 55.79, H 6.54.

3b: b.p. 108–110 °C/1.5 Torr (bath temperature).

One-pot preparation of **5b** from **7b** and (±)-**2a** (entry 1 in Table 3): Similarly to the preparation of **3a**, a mixture of ethoxyacetylene (0.26 mL, 3.1 mmol), **7b** (0.27 g, 2.1 mmol), and **1d** (6.4 mg, 0.010 mmol) in anhydrous acetone (6 mL) was stirred at room temperature for 18 h and concentrated in vacuo. (±)-**2a** (60 mg, 0.49 mmol), **1f** (29 mg, 0.049 mmol), powdered molecular sieves (3 Å; predried at 140 °C, 1 Torr for 2 h, 120 mg), and CALB (60 mg) were successively added to this mixture. The flask was evacuated (approximately 20 Torr) at room temperature for 10 s and flushed with argon. Anhydrous MeCN (4 mL) and Et_3N (0.20 mL, 1.45 mmol) were added under an argon atmosphere, and the flask was sealed. The reaction mixture was stirred at 35 °C for 4.5 days and filtered through a celite pad. The filtrate was concentrated in vacuo, and the residue was purified by flash column chromatography on SiO_2 (hexanes/EtOAc, (5:1→2:1)) to give **5b** (92 mg, 81% yield) as white crystals. A minor product (≦3% based on 500 MHz ^{1}H NMR analysis) was also present that seemed to be a diastereomer. The optical purity of this product was determined to be 94% *ee* by HPLC with a Daicel Chiralcel OD chiral column (hexanes/*i*PrOH (90:10), flow rate = 1.0 mL min^{-1}). M.p. 73–74 °C; $[\alpha]_D^{27} = -32$ ($c = 1.0$ in $CHCl_3$); ^{1}H NMR, ^{13}C NMR, and IR spectroscopic data were in good agreement with the reported value of the racemate;[13a] elemental analysis: calcd: C 66.09, H 6.83; found: C 65.88, H 6.88.

Received: October 8, 2003 [Z53044]

Keywords: asymmetric synthesis · cycloaddition · domino reactions · kinetic resolution · lipases

[1] For recent reviews, see: a) U. T. Bornscheuer, R. J. Kazlauskas, *Hydrolases in Organic Synthesis: Regio- and Stereoselecive Biotransformations*, Wiley-VCH, Weinheim, **1999**; b) F. Theil, *Tetrahedron* **2000**, *56*, 2905–2919; c) K. Faber, *Biotransformations in Organic Chemistry*, 4th ed., Springer, Berlin, **2000**; d) S. M. Roberts, *J. Chem. Soc. Perkin Trans. 1* **2001**, 1475–1499; e) U. Hanefeld, *Org. Biomol. Chem.* **2003**, *1*, 2405–2415.

[2] For recent reviews, see: M.-J. Kim, Y. Ahn, J. Park, *Curr. Opin. Biotechnol.* **2002**, *13*, 578–587; O. Pàmies, J.-E. Bäckvall, *Chem. Rev.* **2003**, *103*, 3247–3261.

 © 2004 Wiley-VCH Verlag GmbH & Co. KGaA, Weinheim

[3] J. H. Koh, H. M. Jung, M.-J. Kim, J. Park, *Tetrahedron Lett.* **1999**, *40*, 6281 – 6284.
[4] a) B. A. Persson, A. L. E. Larsson, M. Le Ray, J.-E. Bäckvall, *J. Am. Chem. Soc.* **1999**, *121*, 1645 – 1650; b) O. Pàmies, J.-E. Bäckvall, *J. Org. Chem.* **2002**, *67*, 1261 – 1265; c) O. Pàmies, J.-E. Bäckvall, *J. Org. Chem.* **2002**, *67*, 9006 – 9010.
[5] J. H. Choi, Y. H. Kim, S. H. Nam, S. T. Shin, M.-J. Kim, J. Park, *Angew. Chem.* **2002**, *114*, 2479 – 2482; *Angew. Chem. Int. Ed.* **2002**, *41*, 2373 – 2376.
[6] D. Lee, E. A. Huh, M.-J. Kim, H. M. Jung, J. H. Koh, J. Park, *Org. Lett.* **2000**, *2*, 2377 – 2379.
[7] E. Brenna, C. Fuganti, P. Grasselli, S. Serra, *Eur. J. Org. Chem.* **2001**, 1349 – 1357.
[8] For related enzyme-initiated domino reactions, see: G. H. Müller, A. Lang, D. R. Seithel, H. Waldmann, *Chem. Eur. J.* **1998**, *4*, 2513 – 2522; S. F. Mayer, W. Kroutil, K. Faber, *Chem. Soc. Rev.* **2001**, *30*, 332 – 339.
[9] a) Y. Kita, T. Naka, M. Imanishi, S. Akai, Y. Takebe, M. Matsugi, *Chem. Commun.* **1998**, 1183 – 1184; b) S. Akai, T. Naka, S. Omura, K. Tanimoto, M. Imanishi, Y. Takebe, M. Matsugi, Y. Kita, *Chem. Eur. J.* **2002**, *8*, 4255 – 4264.
[10] K. Takatori, K. Hasegawa, S. Narai, M. Kajiwara, *Heterocycles* **1996**, *42*, 525 – 528.
[11] E. J. Corey, P. D. S. Jardine, T. Mohri, *Tetrahedron Lett.* **1988**, *29*, 6409 – 6412; S. Nagashima, K. Kanematsu, *Tetrahedron: Asymmetry* **1990**, *1*, 743 – 749; D. Calvo, M. Port, B. Delpech, R. Lett, *Tetrahedron Lett.* **1996**, *37*, 1023 – 1024.
[12] Novel acylating reagents (**3a**,**b**) were prepared by the addition of the monoalkyl maleate **7** to ethoxyacetylene in a similar way to the preparation of the related ethoxyvinyl esters.[9b] Although initial studies were carried out with purified **3** to examine diverse reaction conditions, a more practical one-pot method with crude **3** also gave a similar result, as shown in Table 3.
[13] The related intramolecular Diels–Alder reactions have been carried out at high temperatures, such as 120–150 °C, in aromatic solvents or with microwave irradiation; however, the yields of the products were moderate.[10,13a] We found that the reaction of **4a** in polar solvents gradually proceeded even at room temperature to give almost quantitative yields of **5a**. a) M. J. Batchelor, J. M. Mellor, *J. Chem. Soc. Perkin Trans. 1* **1989**, 985 – 995; for a similar example, see: b) P. Magnus, C. Walker, *Tetrahedron Lett.* **1986**, *27*, 651 – 654.
[14] Optically purity of the products was determined by HPLC analysis with a chiral column: Daicel Chiralcel OD for **2a**, **4a**, **5a**, and **5b**, Daicel Chiralpak AD-H for **5c** and **5d**. The absolute and relative stereochemistries of the products were determined as shown in the schemes (see the Supporting Information for further details).
[15] The reactivity of **1c** was confirmed by the complete racemization of 1-phenylethanol (99 % *ee*) within 1 h at room temperature according to the reported method.[5]
[16] a) M. A. Bennett, A. K. Smith, *J. Chem. Soc. Dalton Trans.* **1974**, 233 – 241; b) M. A. Bennett, T. W. Matheson, G. B. Robertson, A. K. Smith, P. A. Tucker, *Inorg. Chem.* **1980**, *19*, 1014 – 1021.
[17] The catalyst **1f** was also highly effective for the racemization of optically pure 3-hydroxy-1-phenylbut-1-ene, for which the use of **1d** or **1e** was reported to generate the corresponding ketones in 18–25 % combined yields[6] (see the Supporting Information for further details).
[18] S. Yamada, S. Nagashima, Y. Takaoka, S. Torihara, M. Tanaka, H. Suemune, M. Aso, *J. Chem. Soc. Perkin Trans. 1* **1998**, 1269 – 1274.

 © 2004 Wiley-VCH Verlag GmbH & Co. KGaA, Weinheim

Nanostructures

Microwave-Assisted Synthesis of Single-Crystalline Tellurium Nanorods and Nanowires in Ionic Liquids**

Ying-Jie Zhu, Wei-Wei Wang, Rui-Juan Qi, and Xian-Luo Hu*

Many chemical processes involve volatile organic solvents that evaporate into the atmosphere with detrimental effects on the environment and human health. As the introduction of cleaner technologies has become a major concern throughout both industry and academia, the search for alternatives to the damaging volatile solvents has become a high priority. Room-temperature ionic liquids (RTILs) have aroused increasing interest worldwide due to their high fluidity, low melting temperature and extended temperature range in the liquid state, air and water stability, low toxicity, nonflammability, high ionic conductivity, ability to dissolve a variety of materials, and importantly no measurable vapor pressure.[1–4] Therefore, negative environmental and safety problems arising from the use of volatile organic solvents can be avoided by using RTILs. Because of the above reasons, RTILs are actively being explored as possible "green" solvents[5] to substitute conventional volatile organic solvents in a variety of processes, including industrially important chemical processes.[6–10] They also offer fascinating possibilities for fundamental studies of their effects on chemical reactions and synthetic processes.[1–3,11]

In contrast to their application in organic chemistry, the use of RTILs in inorganic synthesis is still in its infancy. There have been only a few reports on the formation and stabilization, by using RTILs, of hollow TiO_2 microspheres,[12] and nanoparticles of palladium,[13] iridium[14] and platinum[15] that are recyclable catalysts for biphasic hydrogenation. Electrochemical deposition of nanocrystalline metals such as Al, Fe, and Al–Mn alloys has also been reported.[16] These metal nanoparticles prepared in ionic liquids were spherical in shape, and not nanorods nor nanowires. Nanorods and nanowires represent a class of 1D nanostructures, in which the carrier motion is restricted in two directions such that they usually show interesting properties that differ from those of the bulk or spherical nanoparticles of the same chemical composition.[17–18] These nanostructures have great potential

[*] Prof. Y.-J. Zhu, W.-W. Wang, R.-J. Qi, X.-L. Hu
State Key Laboratory of High Performance Ceramics and Superfine Microstructure
Shanghai Institute of Ceramics, Chinese Academy of Sciences
Shanghai 200050 (P. R. China)
Fax: (+86) 215-241-3122
E-mail: y.j.zhu@mail.sic.ac.cn

[**] Financial support from Chinese Academy of Sciences under the program for recruiting outstanding overseas Chinese (Hundred Talents Program) is gratefully acknowledged. We also thank the Innovation Research Fund from the Shanghai Institute of Ceramics, Chinese Academy of Sciences. We are grateful to Dr. Long Pan for helpful discussions.

 © 2004 Wiley-VCH Verlag GmbH & Co. KGaA, Weinheim DOI: 10.1002/anie.200353101

applications as important components and interconnects in nanodevices.[18–20]

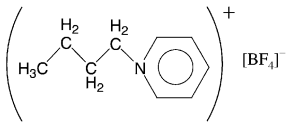
The application of microwave heating in synthetic chemistry is a fast-growing area of research.[21–22] Since the first reports of microwave-assisted synthesis in 1986,[23–24] microwave heating has been accepted as a promising method for rapid volumetric heating, which results in higher reaction rates and selectivities, reduction in reaction times often by orders of magnitude, and increasing yields of products compared to conventional heating methods. As a result, this has opened up the possibility of realizing new reactions in a very short time. From the perspective of microwave chemistry, one of the key important advantages of RTILs is the presence of large organic positive ions with a high polarizability. Therefore, RTILs are very good media for absorbing microwaves, thus leading to a very high heating rate. There has been a recent report[25] on the use of ionic liquids as aids for microwave heating of nonpolar solvents, thereby allowing them to be used as media for microwave-assisted chemistry. The addition of a small quantity of an ionic liquid to a nonpolar solvent can greatly increase the rate and yield of reactions. However, the application of microwave chemistry to materials synthesis in conjunction with ionic liquids has hardly been exploited despite these advantages.

By combining the advantages of both RTILs and microwave heating, we have developed a new microwave-assisted ionic liquid (MAIL) method for the fast controlled synthesis of tellurium (Te) nanorods and nanowires. Te is a p-type semiconductor with many useful and interesting properties, for example, photoconductivity, high piezoelectricity, thermoelectricity, and nonlinear optical responses. In addition, Te reacts readily with other elements to generate many functional materials. Recent progress has been made with the preparation of 1D nanostructures of Te.[26–30] Herein we demonstrate that the MAIL method is a fast, high-yield, seedless, template-free, and environmentally friendly green route for the production of Te nanorods and nanowires. This simple method does not need the subsequent complicated workup procedure required for the removal of the template or seed. This method may also be extended to the synthesis of a variety of other elemental and compound nanostructures. The conditions for preparing some typical samples by the MAIL method are listed in Table 1.

Table 1: Typical samples prepared by the MAIL method.[a]

Sample	Solution	Heating Method	T [°C]	t [min]	Morphology
1	TeO_2 (3 mg) + PVP (30 mg) + (BPy)[BF_4] (0.5 mL) + $NaBH_4$ (0.12 mL, 3.67 M)	microwave	180	10	nanorods
2	PVP (24 mg) + (BPy)[BF_4] (0.5 mL) + $NaBH_4$ (0.12 mL, 3.67 M) + TeO_2 (6 mg) + (BPy)[BF_4] (1 mL)	microwave	180	10	nanowires
3	same as sample 1	microwave	40–130	10	spherical
4	same as sample 1	microwave	130–150	10	nanorods + spherical
5	same as sample 1	oil bath	180	10	spherical
6	same as sample 1	oil bath	180	120	spherical + nanorods (minority)
7	TeO_2 (3 mg) + PVP (30 mg) + H_2O (0.5 mL) + $NaBH_4$ (0.12 mL, 3.67 M)	microwave	80–100	10	spherical
8	PVP (24 mg) + H_2O (0.5 mL) + $NaBH_4$ (0.12 mL, 3.67 M) + TeO_2 (6 mg) + H_2O (1 mL)	microwave	80–100	10	spherical
9	same ratios as sample 7 scaled up to a total volume of 30 mL	hydrothermal	180	10–90	spherical
10	same as sample 7 except no PVP, scaled up to a total volume of 30 mL by using (BPy)[BF_4] (2.3 mL)	hydrothermal	180	90	nanorods + spherical
11	same as sample 10	hydrothermal	180	600	nanowires (majority)

[a] See Experimental Section for details. PVP = polyvinylpyrrolidone, $BuPy^+[BF_4]^-$ = *N*-butylpyridinium tetrafluoroborate, the chemical structure of this ionic liquid is shown below:



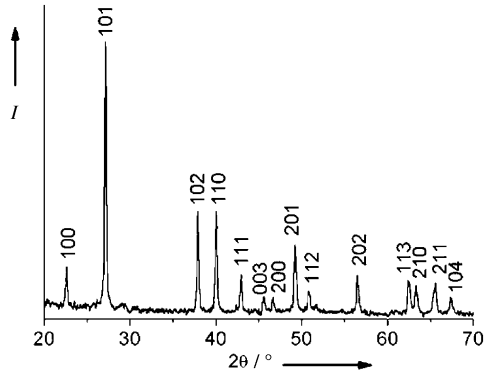


Figure 1. The XRD pattern of sample 1 prepared by the MAIL method at 180 °C for 10 min. The detailed preparation procedure is described in the Experimental Section. I = intensity, arbitrary units.

Figure 1 shows the XRD pattern of sample 1 prepared by the MAIL method at 180 °C for 10 min. From Figure 1 one can see that the product is a single phase of well-crystallized elemental Te with the hexagonal structure (space group: $P3_121$ (no. 152)). The measured lattice constants are a = 4.459 Å and c = 5.917 Å, which are consistent with the reported data (a = 4.457 Å, c = 5.927 Å, JCPDS file no. 36-1452). This result indicates that $NaBH_4$ has reduced TeO_2 to form Te in the ionic liquid $BuPy^+[BF_4]^-$ at 180 °C in 10 min. The yield of Te powder reached 94 % after the product was

 © 2004 Wiley-VCH Verlag GmbH & Co. KGaA, Weinheim

washed with absolute ethanol three times and distilled water two times, and dried at 60 °C in vacuum.

The morphologies, crystallization of samples prepared by the MAIL method were investigated with transmission electron microscopy (TEM). Figure 2 shows TEM micrographs of two typical samples consisting of Te nanorods and nanowires. The general reaction for the formation of Te may be simplified as follows:

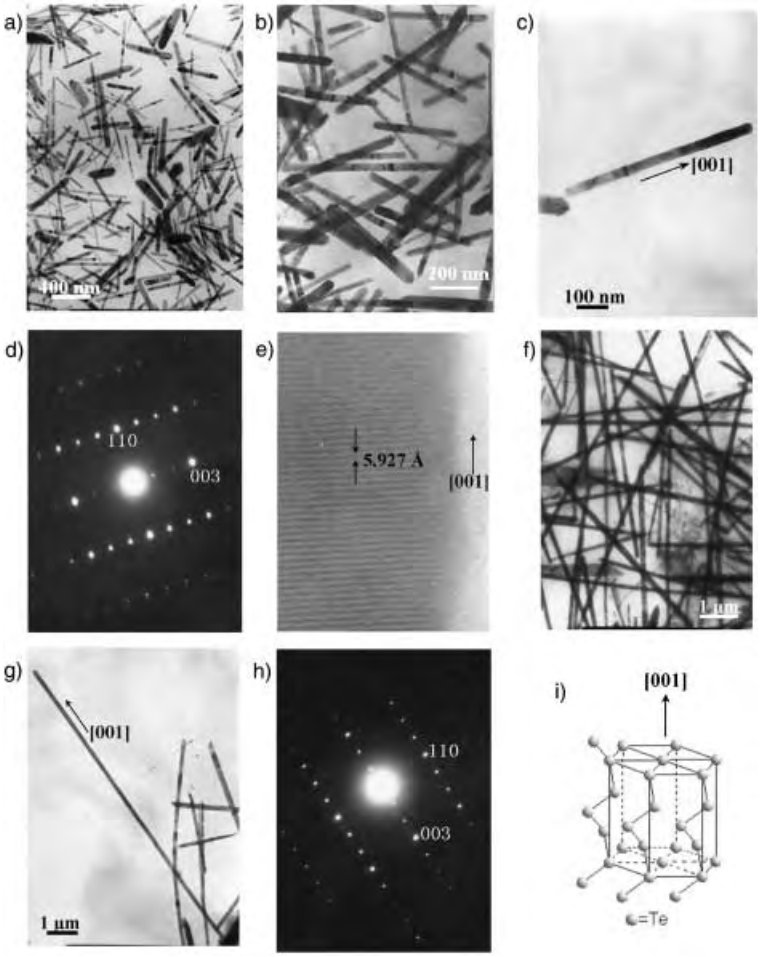


Figure 2. TEM micrographs of two typical samples prepared by the MAIL method. a) and b) sample 1; c) a single Te nanorod from sample 1 (Table 1); d) electron diffraction pattern of the same Te nanorod as shown in (c); e) high-resolution transmission electron microscopy (HRTEM) image of the same Te nanorod as shown in (c); f) and g) sample 2 (see Experimental Section); h) electron diffraction pattern of a single Te nanowire (the longest one in (g)); i) a schematic illustration showing the hexagonal crystal structure of Te and the [001] zone axis (*c* axis of the lattice).

$$TeO_2 + NaBH_4 \xrightarrow[\text{Microwave, } 180\,^{o}\text{C, } 10\,\text{min}]{BuPy^{+}[BF_4]^{-},\ PVP} \text{Te nanorods/nanowires} \qquad (1)$$

Figure 2a and b show TEM micrographs for the same sample as in Figure 1 (sample 1), from which one can see Te nanorods with diameters mostly ranging from ≈15 to ≈40 nm (a minority of them have diameters of 40 to 100 nm) and with lengths up to ≈700 nm. Each nanorod is straight and has a uniform diameter along its entire length. The aspect ratios of most nanorods are in the range from 10 to 20. The aspect ratio is defined as the length of the major axis divided by the width of the minor axis. Nanorods are defined as structures with widths of 1–100 nm and aspect ratios greater than 1 but less than 20; and nanowires are analogous structures with aspect ratios greater than 20.[31] Figure 2c shows a single Te nanorod with a diameter of 32 nm and a length of 610 nm (aspect ratio ≈19), its corresponding electron diffraction pattern is shown in Figure 2d which was obtained by focusing the electron beam along the $[1\bar{1}0]$ direction. Electron diffraction patterns on different nanorods or different positions of a given single nanorod were essentially the same as shown in Figure 2d, thus indicating that nanorods were single-crystalline. The electron diffraction pattern can be indexed to the hexagonal structure, which is consistent with the result obtained from XRD. Figure 2e shows the high-resolution transmission electron microscopy (HRTEM) micrograph of the same single nanorod as shown in Figure 2c, which provides more detailed structural information on these nanorods. The HRTEM shows that the nanorod is structurally single-crystalline with the periodic fringe spacing of 5.927 Å along the longitudinal axis of the nanorod, which corresponds to the interplanar spacing between the (001) planes of the hexagonal Te. This indicates that Te nanorods had the preferential growth direction along the [001] zone axis (*c* axis of the crystal lattice), which is consistent with the results obtained from Te nanorods prepared by other methods.[26,29]

By controlling the experimental parameters, exclusive nanowires or nanorods could be produced. Figure 2f shows the TEM micrograph of sample 2 prepared under a different procedure (see Experimental Section) from sample 1 by the MAIL method. One can see that nanowires instead of nanorods were produced. Most of these nanowires have diameters ranging from 20 to 100 nm, and a minority has diameters in the range of 100–500 nm. The lengths of these nanowires are tens of micrometers. Figure 2g shows several nanowires from sample 2. The corresponding electron diffraction pattern of the longest nanowire in Figure 2g is shown in Figure 2h. The electron diffraction pattern of the nanowire (Figure 2h) is essentially the same as that of the nanorod (Figure 2d), indicating that nanorods and nanowires have the same preferential growth direction along the [001] zone axis (*c* axis of the crystal lattice).

The temperature has a significant influence on the morphology of Te. $NaBH_4$ reacts with TeO_2 to form Te even at room temperature. However, no nanorods or nanowires were observed at temperatures between room temperature and 130 °C (Table 1, sample 3). Te nanorods as well as spherical nanoparticles were observed in the temperature range of 130 to 150 °C (sample 4). When the temperature was increased to 180 °C (sample 1) or higher, only nanorods were observed. However, diameters of nanorods increased significantly when the temperature was higher than 200 °C. A similar situation exists for the preparation of Te nanowires. Therefore, the optimum temperature for the production of Te nanorods or nanowires is around 180 °C.

 © 2004 Wiley-VCH Verlag GmbH & Co. KGaA, Weinheim

We investigated the influence of different heating methods on the morphology of Te. When the conventional heating method (oil bath) was used, no nanorods or nanowires were observed after heating at 180 °C for 10 min (Table 1, sample 5). Only a few nanorods could be observed if the heating time was increased to 2 h (sample 6). In contrast, exclusively nanorods or nanowires were produced by microwave-heating at 180 °C for only 10 min (samples 1 and 2). The heating time for synthesis of Te nanorods can be shortened by more than one order of magnitude by using microwave heating instead of conventional heating. The shorter microwave-heating time leads to enhanced efficiency and significant energy savings. This demonstrates the advantages of the MAIL method.

In a control experiment, we explored the possibility of using distilled water to replace ionic liquid $BuPy^+[BF_4]^-$ as the solvent. We used the same conditions and procedures as those used in samples 1 and 2 (Table 1), except with distilled water instead of $BuPy^+[BF_4]^-$ as the solvent. By microwave heating at temperatures between 80 and 100 °C (boiling point of water) for 10 min (samples 7 and 8), no nanorods or nanowires were observed. Similarly, only spherical Te nanoparticles were initially produced by reducing H_6TeO_6 by hydrazine (N_2H_4) in aqueous solution.[26] To increase the preparation temperature, each of reactant solutions was put into a 40 mL Teflon-lined stainless steel autoclave (75 % of total volume was filled). The autoclaves were sealed and hydrothermally treated at 180 °C for different times from 10 min to 1.5 h (sample 9). Nanorods or nanowires were still not observed. However, if small amount of $BuPy^+[BF_4]^-$ was added to replace PVP (sample 10), some nanorods were produced. If the hydrothermal heating time was increased to 10 h (sample 11), longer nanowires as a majority product with lengths up to tens of microns formed. These experiments show that ionic liquid $BuPy^+[BF_4]^-$ favors the formation of Te nanorods and nanowires.

The most cited classic model for shape-control is the Wulff facets theorem, which suggests that the shape of a crystal is determined by the relative specific surface energy of each facet of the crystal, giving a minimum total surface energy.[32] The shape of a single-crystalline nanostructure usually reflects the intrinsic crystal lattice symmetry. As shown in Figure 2i, Te has a highly anisotropic crystal structure consisting of helical chains of covalently bound atoms, thus having a strong tendency toward 1D growth.[26] However, the formation and growth of Te nanorods and nanowires can only be realized under appropriate conditions. Based on our experiments, we suggest that both the ionic liquid and microwave heating play an important role in the formation of Te nanorods and nanowires. The ionic liquid $BuPy^+[BF_4]^-$ consists of cation $BuPy^+$ and anion $[BF_4]^-$. The high ionic conductivity and polarizability of $BuPy^+$ make it an excellent microwave absorbing agent, thus leading to a high heating rate and a significantly shortened reaction time. The movement and polarization of ions under the rapidly changing electric field of the microwave reactor may result in transient, anisotropic micro-domains for the reaction system, facilitating the anisotropic growth of Te nanorods and nanowires. In addition to its acting as a solvent, it is likely that the ionic liquid acts as a capping reagent or a surfactant. We suggest that $BuPy^+$ ions act as a capping reagent and bind to the {001} facets less strongly than to other facets, leading to easier addition of Te atoms to the (001) facets and thus the preferential growth along *c* axis of the crystal lattice. The detailed formation mechanism of nanorods and nanowires in ionic liquids under the microwave heating needs to be further investigated.

In summary, we have developed a new MAIL method for the synthesis of Te nanorods and nanowires. This environment-friendly green method is a fast, high-yielding, seedless and template-free route, which avoids the subsequent complicated workup procedure normally needed to remove the template or seed. By controlling experimental parameters, exclusively Te nanorods or nanowires are synthesized. Our experiments show that both the ionic liquid and the microwave heating play an important role in the formation of Te nanorods and nanowires. As demonstrated by this successful example, the MAIL method may also be extended to synthesize other elemental and compound nanostructures. This will open up a new possibility for fast controlled production of a variety of 1D nanostructures in good yields by using desirable "green chemistry" methods. These related studies are in progress.

Experimental Section

All chemicals used were of analytical grade and purchased and used as received without further purification.

Sample 1 was prepared as follows: TeO_2 (3 mg) and PVP(30 mg) were mixed by a magnetic stirrer in a 10 mL tube that contained the ionic-liquid solvent $BuPy^+[BF_4]^-$ (0.5 mL) at room temperature. The suspension was microwave-heated to 180 °C (it took ≈40 s) at a power setting of 10 W, and two drops of 3.67 M $NaBH_4$ solution (≈0.12 mL) were added immediately at 180 °C. The solution was maintained at 180 °C for 10 min, then microwave heating was terminated and the solution was allowed to cool to room temperature.

Sample 2 was prepared as follows: PVP (24 mg) was dissolved in stirring $BuPy^+[BF_4]^-$ (0.5 mL) in a 10 mL tube at room temperature. Two drops of 3.67 M $NaBH_4$ aqueous solution (≈0.12 mL) were added at room temperature. The above solution was labeled solution A. TeO_2 (6 mg) was mixed into stirring $BuPy^+[BF_4]^-$ (1 mL) at room temperature, and this solution was labeled solution B. Solution A was microwave-heated to 180 °C at a power setting of 10 W (it took about 0.7 min), and solution B was immediately added dropwise at 180 °C. After the addition of solution B, the resulting solution was maintained at 180 °C for 10 min, then microwave heating was terminated and the solution was cooled to room temperature. The preparation conditions for other samples are listed in Table 1. Samples 3–6 (Table 1) were prepared under different conditions by using the same solution as that of sample 1. Samples 7 and 8 were prepared by the same means as that of sample 1 and sample 2, respectively, except using distilled water instead of $BuPy^+[BF_4]^-$. Samples 9–11 were prepared at 180 °C by the hydrothermal method. Black suspensions were obtained after microwave heating. The products were separated by centrifugation, washed with absolute ethanol three times and distilled water two times, and dried at 60 °C in vacuum.

The microwave oven (2.45 GHz, maximum power 300 W) used was a focused single-mode microwave synthesis system (Discover, CEM, USA). The unique, circular single-mode cavity ensured samples were in a homogenous highly dense microwave field. The system was equipped with an in situ magnetic stirring and a water-cooled condenser. Temperature was accurately controlled by auto-

 © 2004 Wiley-VCH Verlag GmbH & Co. KGaA, Weinheim

matic adjusting of microwave power. X-ray powder diffraction (XRD) patterns were recorded using a Rigaku D/max 2550 V X-ray diffractometer with high-intensity $Cu_{K\alpha}$ radiation ($\lambda = 1.54178$ Å) and a graphite monochromator. TEM images, selected area electron diffraction and HRTEM were taken with a JEOL JEM-2010 high-resolution transmission electron microscope.

Received: October 16, 2003 [Z53101]

Keywords: ionic liquids · microwave chemistry · nanostructures · tellurium

[1] T. Welton, *Chem. Rev.* **1999**, *99*, 2071.
[2] P. Wasserscheid, W. Keim, *Angew. Chem.* **2000**, *112*, 3926; *Angew. Chem. Int. Ed.* **2000**, *39*, 3772.
[3] J. Dupont, R. F. de Souza, P. A. Z. Suarez, *Chem. Rev.* **2002**, *102*, 3667.
[4] W. Xu, E. I. Cooper, C. A. Angell, *J. Phys. Chem. B* **2003**, *107*, 6170.
[5] L. A. Blanchard, D. Hancu, E. J. Beckman, J. F. Brennecke, *Nature* **1999**, *399*, 28.
[6] Y. Chauvin, H. Olivier-Bourbigou, *CHEMTECH* **1995**, *25*, 26.
[7] C. J. Adams, M. J. Earle, G. Roberts, K. R. Seddon, *Chem. Commun.* **1998**, 2097.
[8] M. J. Earle, P. B. McCormac, K. R. Seddon, *Chem. Commun.* **1998**, 2245.
[9] M. J. Earle, P. B. McCormac, K. R. Seddon, *Green Chem.* **1999**, *1*, 23.
[10] B. Ellis, W. Keim, P. J. Wasserscheid, *Chem. Commun.* **1999**, 337.
[11] K. Jin, X. Y. Huang, L. Pan, J. Li, A. Appel, S. Wherland, *Chem. Commun.* **2002**, 2872**.**
[12] T. Nakashima, N. Kimizuka, *J. Am. Chem. Soc.* **2003**, *125*, 6386.
[13] J. Huang, T. Jiang, B. X. Han, H. X. Gao, Y. H. Chang, G. Y. Zhao, W. Z. Wu, *Chem. Commun.* **2003**, 1654**.**
[14] J. Dupont, G. S. Fonseca, A. P. Umpierre, P. F. P. Fichtner, S. R. Teixeira, *J. Am. Chem. Soc.* **2002**, *124*, 4228.
[15] C. W. Scheeren, G. Machado, J. Dupont, P. F. P. Fichtner, S. R. Texeira, *Inorg. Chem.* **2003**, *42*, 4738.
[16] F. Endres, M. Bukowski, R. Hempelmann, H. Natter, *Angew. Chem.* **2003**, *115*, 3550; *Angew. Chem. Int. Ed.* **2003**, *42*, 3428.
[17] W. U. Huynh, J. J. Dittmer, A. P. Alivisatos, *Science* **2002**, *295*, 2425.
[18] X. Duan, Y. Huang, Y. Cui, J. Wang, C. M. Lieber, *Nature* **2001**, *409*, 66.
[19] S. Frank, P. Poncharal, Z. L. Wang, W. A. de Heer, *Science* **1998**, *280*, 1744.
[20] H. M. Huang, S. Mao, H. Feick, H. Yan, Y. Wu, H. Kind, E. Weber, R. Russo, P. Yang, *Science* **2001**, *292*, 1897.
[21] L. Perreux, A. Loupy, *Tetrahedron* **2001**, *57*, 9199.
[22] R. S. Varma, *Green Chem.* **2001**, *3*, 98.
[23] R. Gedye, F. Smith, K. Westaway, A. Humera, L. Baldisera, L. Laberge, L. Rousell, *Tetrahedron Lett.* **1986**, *27*, 279.
[24] R. Giguere, T. L. Bray, S. M. Duncan, G. Majetich, *Tetrahedron Lett.* **1986**, *27*, 4945.
[25] N. E. Leadbeater, H. M. Torenius, *J. Org. Chem.* **2002**, *67*, 3145.
[26] B. Mayers, Y. N. Xia, *J. Mater. Chem.* **2002**, *12*, 1875.
[27] B. Mayers, Y. N. Xia, *Adv. Mater.* **2002**, *14*, 279.
[28] M. S. Mo, J. H. Zeng, X. M. Liu, W. C. Yu, S. Y. Zhang, Y. T. Qian, *Adv. Mater.* **2002**, *14*, 1658.
[29] Z. P. Liu, Z. K. Hu, Q. Xie, B. J. Yang, J. Wu, Y. T. Qian, *J. Mater. Chem.* **2003**, *13*, 159.
[30] Y. J. Zhu, Y. T. Qian, H. Huang, M. W. Zhang, *J. Mater. Sci. Lett.* **1996**, *15*, 1700.
[31] J. Murphy and N. R. Jana, *Adv. Mater.* **2002**, *14*, 80.
[32] J. A. Venables, *Introduction to Surface and Thin Film Processes*, Cambridge University Press, Cambridge, **2000**, p. 4.

 © 2004 Wiley-VCH Verlag GmbH & Co. KGaA, Weinheim

Direct Alkylation of Alcohols

Direct Substitution of the Hydroxy Group in Alcohols with Silyl Nucleophiles Catalyzed by Indium Trichloride**

*Makoto Yasuda, Takahiro Saito, Masako Ueba, and Akio Baba**

Substitution of the hydroxy group in alcohols by nucleophiles intrinsically requires an equimolar (or greater) amount of acid because of the poor leaving ability of the OH group. To avoid the use of excessive amounts of acid, alcohols are usually transformed into the corresponding halides or related compounds that have good leaving groups before the treatment with the nucleophiles. In this context, direct substitution of alcohols in a catalytic manner under nearly neutral conditions would be a fascinating and ideal procedure for synthetic organic chemistry. We have previously reported the direct dehydroxylation of alcohols under catalytic conditions by using a chlorosilane/catalytic $InCl_3$ system.[1] We have now turned our attention to C–C bond formation by a direct substitution system with allylic nucleophiles.[2] In 1982, Cella reported allylation/dehydroxylation of alcohols by allylsilane in the presence of an excess amount of a Lewis acid.[3] This system, however, is only applicable to a narrow range of alcohols and gives a significant amount of side products. As a special case, hemiacetal is effectively alkylated by allylsilane to give the corresponding alkenes in high yields but this reaction requires more than an equimolar amount of BF_3.[4] Rubin and Gevorgyan recently reported allylation of certain alcohols in the presence of a boron catalyst although dehydration prevents the desired alkylating reaction in some cases.[5] Herein we report the direct substitution of the hydroxy group in alcohols by allyl-, propargyl-, and alkynylsilanes catalyzed by indium chloride. The system allows the desired alkylation of a wide range of applicable substrates under neutral conditions.

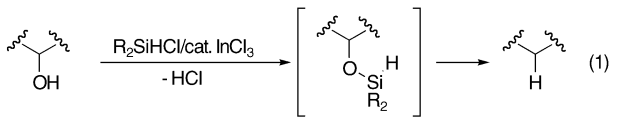
We have recently reported the direct reduction of alcohols[1,6] in a reaction with a silyl ether intermediate formed by removal of HCl, as shown in Equation (1). Therefore, we initially chose allylchlorodimethylsilane (**1**) as an allylic nucleophile in the reaction with benzhydrol (**2a**, Table 1). Although the uncatalyzed system resulted in no

[*] Dr. M. Yasuda, T. Saito, M. Ueba, Prof. Dr. A. Baba
Department of Molecular Chemistry and
Handai Frontier Research Center
Graduate School of Engineering, Osaka University
2-1 Yamadaoka, Suita, Osaka 565–0871 (Japan)
Fax: (+81) 6-6879-7387
E-mail: baba@chem.eng.osaka-u.ac.jp

[**] This work was supported by a Grant-in-Aid for Scientific Research from the Ministry of Education, Culture, Sports, Science, and Technology, Japan. Thanks are due to Mr. H. Moriguchi, Faculty of Engineering, Osaka University, for assistance in obtaining mass spectra.

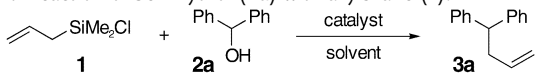
Supporting information for this article is available on the WWW under http://www.angewandte.org or from the author.

 © 2004 Wiley-VCH Verlag GmbH & Co. KGaA, Weinheim DOI: 10.1002/anie.200353121



(1)

Table 1: Reaction of benzhydrol (**2a**) with allylsilane (**1**).[a]



Entry	Catalyst	Solvent	Yield [%]
1	none	CH_2Cl_2	0
2	$InCl_3$	CH_2Cl_2	80
3	$AlCl_3$	CH_2Cl_2	0
4	$BF_3{\cdot}OEt_2$	CH_2Cl_2	0
5	$Sc(OTf)_3$[b]	CH_2Cl_2	13
6	$InCl_3$	THF[b]	0
7	$InCl_3$	DMF[b]	0
8	$InCl_3$	hexane	45

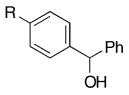
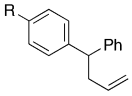
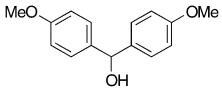
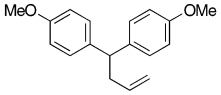
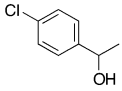
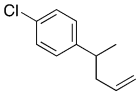
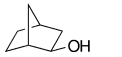
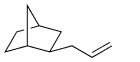
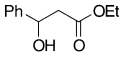
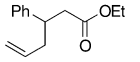
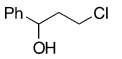
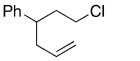
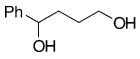
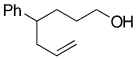
[a] All reactions were carried out in a solvent (1 mL) with allylsilane **1** (2.0 mmol), alcohol **2a** (1.0 mmol), and catalyst (0.05 mmol) at RT for 10 min. [b] Tf = trifluoromethanesulfonyl, THF = tetrahydrofuran, DMF = *N*,*N*-dimethylformamide.

reaction (entry 1), the loading of a catalytic amount of $InCl_3$ dramatically accelerated the reaction and led to the production of alkylated product **3a** in 80% yield (entry 2).[7] Strong Lewis acids such as $AlCl_3$ or $BF_3{\cdot}OEt_2$ were not effective for the alkylation (entries 3 and 4), probably because these catalysts are not stable under protic conditions. $Sc(OTf)_3$ only gave a low yield of **3a** (entry 5), even though it can generally be used in a protic solvent. Dichloromethane was the solvent of choice; THF, DMF, and hexane afforded unsatisfactory results (entries 6–8). The reaction was also attempted with the corresponding Grignard reagent (two equivalents of allylmagnesium chloride), which is a typical highly nucleophilic reagent, instead of **1**, but the starting alcohol was recovered after work-up under conditions with or without the $InCl_3$ catalyst. These results strongly suggest that the appropriate nucleophilicity of the allylic reagent and Lewis acidity of the catalyst, as well as tolerance of protic conditions, are important for the direct substitution pathway.

To investigate the scope and limitations of this reaction system with catalytic $InCl_3$, various alcohols **2** were examined and some of the results are shown in Table 2. Benzhydrol (**2a**) or its derivatives **2b–f** which have electron-donating or -withdrawing groups on the aryl rings were effectively allylated at room temperature in 10 min (entries 1–6). The reaction with 1-phenylethanol (**2g**) gave the corresponding alkene **3g** (entry 7) with side products that probably came from polymerization and/or a Friedel–Crafts reaction through the benzylic cationic species.[8] Use of three equivalents of silane **1** gave a higher yield of **3g** (entry 8). The simple benzyl alcohol gave intractable polymers rather than the desired product. The tertiary benzylic alcohol **2h** afforded the product **3h** (entries 9 and 10). Unfortunately, simple aliphatic alcohols, for example, 2-decanol, were not suitable substrates for the reaction system and gave none of the desired product. However, the norborneol **2j** gave allylated product **3j** in 52% yield as a single isomer (entry 13). The reaction with β-hydroxy ester **2k** gave the δ,ε-unsaturated ester **3k** without any side products modified at the ester moiety (entry 14).[9] Since there are few general methods to synthesize δ,ε-unsaturated esters by conjugate allylation of α,β-unsaturated esters, this type of reaction will provide an important way to access these compounds.[10] The chlorinated alcohols **2i** and **2l** were selectively transformed into **3i** and **3l**, respectively, with reaction at the hydroxy sites without affecting the chloride moieties (entries 11, 12, and 15). The diol **2m** was allylated selectively at the benzylic site to afford the primary alcohol **3m** after the workup with Bu_4NF (entry 16).

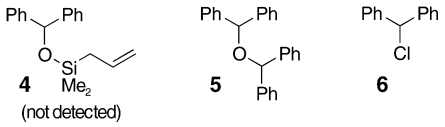
We performed an NMR spectroscopy study on a mixed solution of benzhydrol (**2a**), allylchlorodimethylsilane (**1**), and a catalytic amount of $InCl_3$ in CD_2Cl_2 at room temperature to investigate the reaction mechanism.[11] We had expected the silyl ether **4** to be formed by removal of HCl, as observed in the reduction system with $Ph_2SiClH/InCl_3$ reported by us [Eq. (1)].[1] However, species **4** was not

Table 2: Allylation of alcohols **2** with allylsilane **1** catalyzed by $InCl_3$.[a]

Entry	Alcohol		*t* [min]	Product		Yield [%]
1		**2a**: R = H	10		**3a**	80
2		**2b**: R = Me	10		**3b**	86
3		**2c**: R = Cl	10		**3c**	92
4		**2d**: R = NO_2	10		**3d**	80
5		**2e**: R = MeO	10		**3e**	82
6		**2f**	10		**3f**	67
7		**2g**	30		**3g**	46
8[b]			30			87
9		**2h**	30		**3h**	47
10[b]			30			59
11		**2i**	180		**3i**	62
12[b]			180			96
13[b]		**2j**	180		**3j**	52
14[c]		**2k**	60		**3k**	66
15		**2l**	180		**3l**	59
16[d,e]		**2m**	60		**3m**	56

[a] The reactions were carried out in dichloromethane (1 mL) with allylsilane **1** (2.0 mmol), alcohol **2** (1.0 mmol), and $InCl_3$ (0.05 mmol) at RT unless otherwise stated. [b] Allylsilane **1** (3.0 mmol), dichloromethane (2 mL). [c] Allylsilane **1** (3.0 mmol), dichloroethane (2 mL), 80°C. [d] Allylsilane **1** (4.0 mmol). [e] Bu_4NF was added during the workup.

 © 2004 Wiley-VCH Verlag GmbH & Co. KGaA, Weinheim

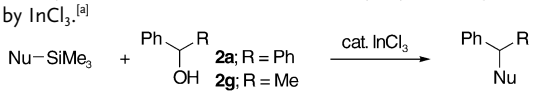


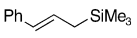
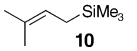
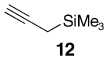
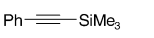
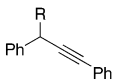
detected; signals for the dimeric ether **5** and a small amount of chloride **6** were observed instead (RT, 20 min), together with the allylated product **3a**.[12] In fact, no HCl was detected during the course of this reaction, whereas the reduction system with Ph_2SiHCl definitely generates HCl.[1] These results surprised us and showed that the mechanism of allylation is different from that of the reduction system,[1] although the exact reaction course is not yet clear.[13] The most important factor in this reaction is the unique character of the indium catalyst, which has 1) enough Lewis acidity to activate the C–O bond, 2) low oxophilicity to regenerate a catalysis from the substrate, and 3) stability under protic conditions. Those factors were realized in the direct substitution system with alcohols.

Since the removal of HCl was not observed during the course of the reaction, it might not be necessary to use the silane bearing the chlorine atom on its metal center. We examined some allylsilanes such as allyltrimethyl-, diallyldimethyl-, and trimethoxysilanes for the allylation of alcohols. Among these silanes, the desired alkylated product was only formed in satisfactory yield in the reaction with **2a** when allyltrimethylsilane (**7**) was used at 80 °C in dichloroethane (Table 3, entry 1). The reaction performed at room temperature gave no alkylated product. No **3a** was formed in the absence of the $InCl_3$ catalyst (entry 2). Gratifyingly, 1-phenylethanol (**2g**) gave **3g** without any side products (entry 3) while the reaction using allylchlorosilane (**1**) gave polymeric side products (see Table 2, entries 7 and 8). As those side products probably came from the benzylic chloride generated in situ, the Cl-free system with **7** was able to give a clean reaction with **2g**. The yield was increased to 87% by using three equivalents of **7** (entry 4). It is interesting that the reaction of γ-substituted allylsilanes **8** and **10** gave the products regioselectively in an exclusively γ-addition manner (entries 5–8). This system can be applied to other types of nucleophiles. In the case of the propargylsilane **12**, the regioselective formation of the allene **13** occurred exclusively through γ-addition (entries 9 and 10). The alkynylsilane **14** gave the desired products **15** in high yields (entries 11 and 12). As various types of trimethylsilyl compounds are available, the Cl-free system will expand the synthetic applications of this method.

In summary, we have demonstrated the direct substitution of the hydroxy group in alcohols by nucleophiles such as allylic-, propargyl-, and alkynylsilanes. The silyl nuclophile and $InCl_3$ make an indispensable combination to accelerate the unprecedented alkylative substitution with formation of a C–C bond. The details of the mechanism are now under investigation.

Table 3: Alkylation of alcohols **2** with trimethylsilyl nucleophiles catalyzed by $InCl_3$.[a]



Entry	Silane	Alcohol	*t* [h]	Product	Yield [%]
1	 **7**	**2a**	3	 **3a**	99
2[b]		**2a**	3		0
3		**2g**	3	**3g**	51
4[c]		**2g**	3		87
5	 **8**	**2a**	3	 **9a**	100
6	 **10**	**2a**	3	 **11a**	64
7		**2g**	3	**11g**	72
8[c]		**2g**	3		81
9	 **12**	**2a**	3	 **13a**	64
10		**2g**	6	**13g**	55
11	 **14**	**2a**	2	 **15a**	93
12[c]		**2g**	3		62

[a] The reactions were carried out in 1,2-dichloethane (2 mL) with silane (2.0 mmol), alcohol **2** (1.0 mmol), and $InCl_3$ (0.05 mmol) at 80 °C. [b] $InCl_3$ was not added. [c] Silane (3.0 mmol).

Received: October 21, 2003 [Z53121]

Keywords: alcohols · alkylation · homogeneous catalysis · indium · silanes

[1] M. Yasuda, Y. Onishi, M. Ueba, T. Miyai, A. Baba, *J. Org. Chem.* **2001**, *66*, 7741–7744.
[2] For recent reports of transition-metal-catalyzed C–C bond formation through direct substitution of allylic or propargylic alcohols with nucleophiles other than allylic ones, see: a) F. Ozawa, H. Okamoto, S. Kawagishi, S. Yamamoto, T. Minami, M. Yoshifuji, *J. Am. Chem. Soc.* **2002**, *124*, 10968–10969; b) Y. Nishibayashi, M. Yoshikawa, Y. Inada, M. Hidai, S. Uemura, *J. Am. Chem. Soc.* **2002**, *124*, 11846–11847.
[3] J. A. Cella, *J. Org. Chem.* **1982**, *47*, 2125–2130.
[4] A. Schmitt, H.-U. Reißig, *Eur. J. Org. Chem.* **2000**, 3893–3901.
[5] M. Rubin, V. Gevorgyan, *Org. Lett.* **2001**, *3*, 2705–2707.
[6] T. Miyai, M. Ueba, A. Baba, *Synlett* **1999**, 182–184.
[7] For $InCl_3$-catalyzed allylation of *gem*-diacetates by allylsilane, see: J. S. Yadav, B. V. Subba Reddy, C. Madhuri, G. Sabitha, *Chem. Lett.* **2001**, 18–19.
[8] The polymeric side products were observed in a similar type of reaction.[3,5]
[9] About 10% of a dehydrated product, ethyl 3-phenyl-2-propenoate, contaminated the reaction mixture and could be separated from the product by column chromatography.
[10] N. Kuhnert, J. Peverley, J. Robertson, *Tetrahedron Lett.* **1998**, *39*, 3215–3216.
[11] The NMR spectroscopy experiment was performed in dilute conditions (approximately 0.1M) to slow down the reaction.
[12] Our previous report[13b] suggests that the allylated silyl ether **4** could be formed by silanes, but **4** was not found in the reaction described in this paper.
[13] For the example including C–O bond cleavage with the silicon–indium system, see: a) Y. Onishi, D. Ogawa, M. Yasuda, A. Baba, *J. Am. Chem. Soc.* **2002**, *124*, 13690–13691; b) Y. Onishi, T. Ito, M. Yasuda, A. Baba, *Tetrahedron* **2002**, *58*, 8227–8235.

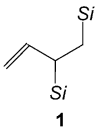
 © 2004 Wiley-VCH Verlag GmbH & Co. KGaA, Weinheim

Tetrahydrofuran Synthesis

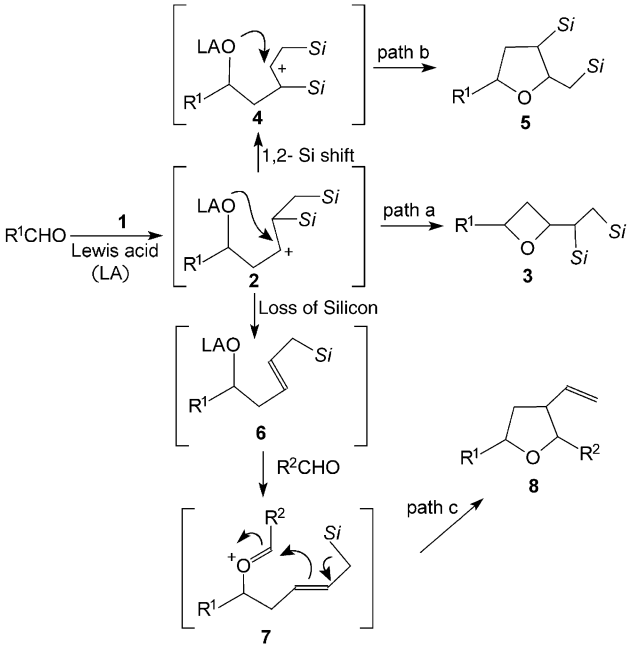
Bimetallic Reagents of Silicon: One-Pot Synthesis of 2,3,5-Trisubstituted Tetrahydrofurans by a Double Sakurai–Hosomi Reaction**

Tarun K. Sarkar, Sk. Anwarul Haque, and Arindrajit Basak*

Unsaturated bimetallic reagents containing Group 14 metals, such as silicon and tin, have recently emerged as versatile coupling reagents in organic synthesis.[1,2] These reagents are particularly appealing when both metals employ a "ferryman" service to yield metal-free cyclic products in a one-pot reaction. However, examples of such reactions are rare.[2] As part of our interest in allyl organometallic compounds of silicon,[3] we envisioned that 1-silylmethyl allylic silanes **1** could be useful synthetic building blocks. In the presence of a Lewis acid, a bis-silyl reagent such as **1** affords a β-silyl carbocation **2** (Scheme 1) when treated with an aldehyde. This carbocation may then collapse to give an oxetane **3** (path a)[4] or, more likely, undergo a 1,2-silyl migration to give the thermodynamically favored bis-β-silyl carbocation **4**,[5] which produces a trisubstituted tetrahydrofuran **5** (path b).[6] The latter was realized recently by Peng and Woerpel.[7] Additionally, a third pathway is also conceivable wherein **2** collapses to give a new allylic silane **6**. The allylic silane **6** should be less reactive than the starting allylic silane **1** because its π bond is more hindered. Introduction of a second aldehyde should yield a silicon-free tetrahydrofuran **8** by trapping of the oxocarbenium ion **7** (path c). While our studies were in progress Smitrovich and Woerpel[8] reported a single experiment on the synthesis of a tetrahydrofuran lacking silyl groups by reaction of a substituted silylmethyl allylic silane and an aldehyde; however, a pure product could not be obtained and a furan structure was only tentatively assigned. Herein, we provide the first report



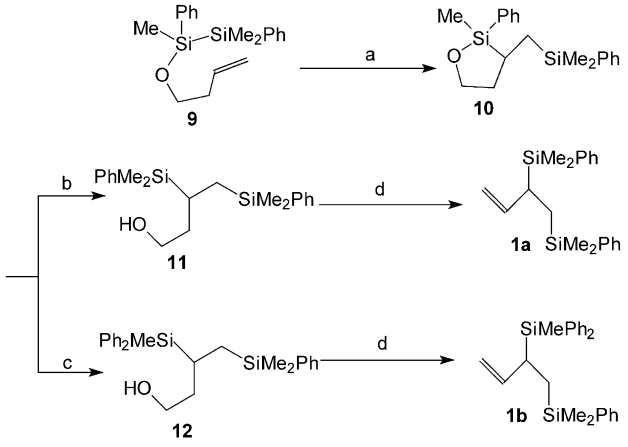
1



Scheme 1. Reaction of **1** with an aldehyde. *Si* = silyl group.

that silylmethyl allylic silanes of type **1** can be channeled through path c to yield only 2,3,5-trisubstituted tetrahydrofurans.

As the 1-silylmethyl allylic silanes **1a**,**b** (Scheme 2) selected for our study are novel, there were no reported procedures for their synthesis. Smitrovich and Woerpel



Scheme 2. Reagents and conditions: a) Me_3CCN (8 mol%), $Pd(OAc)_2$ (2 mol%), toluene, reflux, 80% yield; b) MeLi, Et_2O, 75% yield; c) PhLi, Et_2O, 80% yield; d) 1. *o*-$NO_2C_6H_4SeCN$, nBu_3P, THF; 2. H_2O_2 (30%), pyridine, CH_2Cl_2, 60–68% yield over two steps.

experienced great difficulties in preparing similar compounds but eventually succeeded by employing allylic displacement,[9] which unfortunately could not be applied in our case since only carbamates from secondary allyl alcohols are amenable to it. Thus, a convenient synthetic methodology to this family of allylic silanes was our initial task. Our successful route (Scheme 2) involved heating disilanyl ether **9** (prepared in

[*] Prof. T. K. Sarkar, S. A. Haque
Department of Chemistry
Indian Institute of Technology
Kharagpur-721302 (India)
Fax: (+91) 3222-282252-755303
E-mail: tksr@chem.iitkgp.ernet.in
Dr. A. Basak
Department of Chemistry
The University of Chicago
Chicago, IL 60637 (USA)

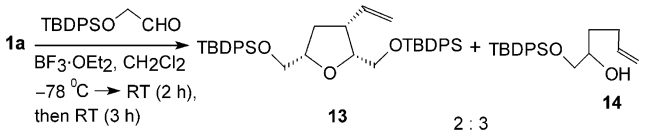
[**] This work has been financially supported by the DST, Govt. of India. We are grateful to Prof. H. Yamamoto (Chicago, IL, USA), Dr. C. Fehr, Dr. R. Brauchli, Dr. L. Wunsche (Firmenich, Geneva, Switzerland), and Prof. S. Uemura (Kyoto, Japan) for help with NMR spectroscopic and mass spectrometric analysis. Prof. M. Suginome (Kyoto, Japan) and Dr. S. Roy (IITKGP) are thanked for their helpful discussions. S.A.H. thanks the CSIR (India) for a research fellowship.

Supporting information for this article is available on the WWW under http://www.angewandte.org or from the author.

 DOI: 10.1002/anie.200353184 © 2004 Wiley-VCH Verlag GmbH & Co. KGaA, Weinheim

77% yield from 3-butene-1-ol and 1-chloro-1,2,2-trimethyl-1,2-diphenyldisilane) in the presence of $Pd(OAc)_2$ (2 mol%) and *tert*-butylisocyanide (8 mol%) under reflux in toluene. Intramolecular bis-silylation occurred readily to give the 1,2-oxasilolane **10** in good yield (80%).[10] Ring opening of **10** with either methyl- or phenyllithium in diethyl ether followed by Grieco dehydration[11] of the resulting alcohols **11** and **12** gave the desired allylic silanes **1a**,**b** in 45–55% overall yield from **10**.

Our initial idea for investigating the concept outlined in Scheme 1 was to treat the allylic silanes **1a**,**b** with an aldehyde containing a proximal heteroatom, such as oxygen, to allow the reaction to be performed under both chelation and nonchelation conditions. The choice of the aldehyde and reaction conditions were essential for the successful synthesis of tetrahydrofurans devoid of silicon appendages. Thus, in the presence of $BF_3{\cdot}OEt_2$,[12] **1a** was treated with (*tert*-butyldiphenylsilyloxy)ethanal to give tetrahydrofuran **13** (Scheme 3) admixed with the readily separable but undesired monoprotected glycol **14** (2:3, respectively). The latter was evidently

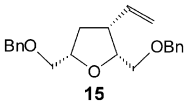
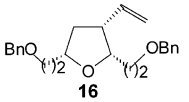
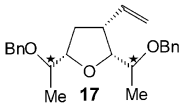
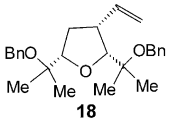


Scheme 3. The reaction of (*tert*-butyldiphenylsilyloxy)ethanal with allylic silane **1a**. TBDPSO = *tert*-butyldiphenylsilyloxy.

formed by protodesilylation of the in situ generated allylic silane (cf. **6**). Use of an additive, namely 2,6-di-*tert*-butyl-4-methylpyridine,[13] to remove traces of acid that would cause unwanted protodesilylation was ineffective. However, formation of **14** could be prevented by use of $BF_3{\cdot}OEt_2$ freshly distilled over calcium hydride to give only **13** in 50% yield. Additionally, **1b** was found to give **13** in a slightly higher yield (ca. 10%) under these conditions than did **1a**. Tetrahydrofuran **13** was formed as a single diastereomer, and the stereochemical outcome of the reaction is in accord with observations reported by Mohr.[14]

Encouraged by these findings, we investigated the scope and limitations of the one-pot tetrahydrofuran synthesis—the results of which are given in Table 1. $BF_3{\cdot}OEt_2$ was found to be the most effective Lewis acid (entry 1) and not $SnCl_4$ (entry 2), while $TiCl_4$ (entry 3) did not yield any traces of tetrahydrofuran **15**. The example in entry 4 shows the

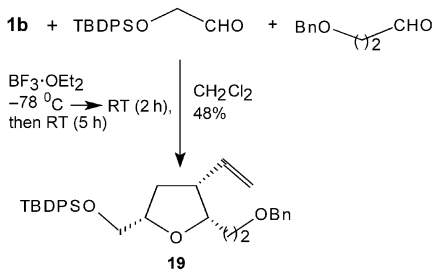
Table 1: Isolated yields for the reaction of allylic silane **1b** with aldehydes.

Entry	Aldehyde	Reaction conditions[a]	Products[b,c] (% yield)
1	BnO–CHO	$BF_3{\cdot}OEt_2$ −78 °C→RT (2 h), then RT (3 h)	 **15** (68%)
2		$SnCl_4$ −78 °C→RT (2 h), then RT (1 h)	(41%)
3		$TiCl_4$ −78 °C→RT (2 h), then RT (1 h)	(0%)
4	BnO–(CH2)2–CHO	$BF_3{\cdot}OEt_2$ −78 °C→RT (2 h), then RT (7 h)	 **16** (52%)
5	BnO–CH(Me)–CHO	$BF_3{\cdot}OEt_2$ −78 °C→RT (2 h), then RT (6 h)	 **17** (48%)
6	BnO–CMe2–CHO	$BF_3{\cdot}OEt_2$ −78 °C→RT (2 h), then RT (10 h)	 **18** (0%)

[a] All reactions were performed in CH_2Cl_2. [b] Yield of isolated pure material. [c] The product in entry 5 is a mixture of three diastereomers (3:1:1) with unknown configuration at the starred carbon atoms. LA = Lewis acid, RT = room temperature, Bn = benzyl.

compatibility of a β-alkoxy aldehyde to this reaction. Remarkably, **17** was obtained from 2-(benzyloxy)propanal as a mixture of three diastereomers (3:1:1, entry 5) from which the major one could be readily isolated by silica gel chromatography; however, the configuration at the extracyclic centers in this product remains undetermined at present. Incidentally, the reaction failed to give any tetrahydrofuran when the aldehyde is hindered (entry 6), although neither the aldehyde nor the starting allylic silane could be recovered.[15]

Finally, in our most dramatic result, three-component cyclizations were observed. For example, $BF_3{\cdot}OEt_2$ promoted the coupling of **1b** and two different aldehydes (Scheme 4) with the formation of a single product (**19**) in 48% yield uncontaminated by any regio- or stereoisomers. This synthesis was only possible because of the difference in reactivity between **1b** and the allylic silane formed in situ (cf. **6**) and between that of the two aldehydes.[16]



Scheme 4. Three-component reaction involving allylic silane **1b** with two different aldehydes. TBDPSO = *tert*-butyldiphenylsilyloxy, Bn = benzyl.

 © 2004 Wiley-VCH Verlag GmbH & Co. KGaA, Weinheim

In summary, 1-silylmethyl allylic silanes have been developed as new bimetallic reagents for rapid access to a variety of 2,3,5-trisubstituted tetrahydrofurans in good yields and with high stereoselectivities. The synthesis allows two different groups to be introduced at the 2 and 5 positions of the furan ring, which should enhance the utility of tetrahydrofuran synthesis and help promote its application in organic synthesis.

Received: October 29, 2003
Revised: December 8, 2003 [Z53184]

Keywords: cyclization · domino reactions · oxygen heterocycles · silanes · silicon

[1] For some recent work, see: a) G. E. Keck, J. A. Covel, T. Schiff, T. Yu, *Org. Lett.* **2002**, *4*, 1189; b) S. V. Mortlock, E. J. Thomas, *Tetrahedron* **1998**, *54*, 4663; c) M. Lautens, R. N. Ben, P. H. M. Delanghe, *Tetrahedron* **1996**, *52*, 7221, and references therein; d) M. Lautens, P. H. M. Delanghe, *Angew. Chem.* **1994**, *106*, 2557; *Angew. Chem. Int. Ed. Engl.* **1994**, *33*, 2448.
[2] a) M. M. Patel, J. R. Green, *Chem. Commun.* **1999**, 509; b) K. C. Nicolaou, T. K. Chakraborty, A. D. Piscopio, N. Minowa, P. Bertinato, *J. Am. Chem. Soc.* **1993**, *115*, 4419; c) A. Degl'Innocenti, P. Dembech, A. Mordini, A. Ricci, G. Seconi, *Synthesis* **1991**, 267.
[3] For a review of methods for the synthesis of allylsilanes, see: a) "Product subclass 40: allylsilanes": T. K. Sarkar, *Sci. Synth.* **2002**, *4*, 837; b) T. K. Sarkar, *Synthesis* **1990**, 1101; c) T. K. Sarkar, *Synthesis* **1990**, 969.
[4] T. Akiyama, M. Kirini, *Chem. Lett.* **1995**, 723.
[5] I. Fleming, S. K. Ghosh, *J. Chem. Soc. Perkin Trans. 1* **1998**, 2711.
[6] For pioneering work on the synthesis of tetrahydrofurans through a [3+2] cycloaddition of allylsilanes, see: a) J. S. Panek, M. Yang, *J. Am. Chem. Soc.* **1991**, *113*, 9868; b) J. S. Panek, R. Beresis, *J. Org. Chem.* **1993**, *58*, 809; c) for a review on cycloaddition reactions of allylsilanes, see: H.-J. Knölker, *J. Prakt. Chem.* **1997**, *339*, 304.
[7] Z.-H. Peng, K. A. Woerpel, *Org. Lett.* **2000**, *2*, 1379.
[8] J. H. Smitrovich, K. A. Woerpel, *Synthesis* **2002**, 2778.
[9] J. H. Smitrovich, K. A. Woerpel, *J. Org. Chem.* **2000**, *65*, 1601.
[10] a) M. Suginome, Y. Ito, *Chem. Rev.* **2000**, *100*, 3221; b) M. Murakami, M. Suginome, K. Fujimoto, H. Nakamura, P. G. Andersson, Y. Ito, *J. Am. Chem. Soc.* **1993**, *115*, 6487.
[11] I. Fleming, D. Waterson, *J. Chem. Soc. Perkin Trans. 1* **1984**, 1809.
[12] One or both oxygen atoms of the aldehyde may be complexed with $BF_3{\cdot}OEt_2$;[6b] another possibility is the formation of a chelated species, see: K. Maruyama, Y. Ishihara, Y. Yamamoto, *Tetrahedron Lett.* **1981**, *22*, 4235.
[13] S. R. Angle, N. A. El-Said, *J. Am. Chem. Soc.* **1999**, *121*, 10211.
[14] P. Mohr, *Tetrahedron Lett.* **1993**, *34*, 6251.
[15] Similarly, in our hands the use of isobutyraldehyde or benzaldehyde did not yield any characterizable products.
[16] The aldehyde group of (*tert*-butyldiphenylsilyloxy)ethanal is likely to be more electrophilic because of the inductive effect of the neighbouring silyloxy substituent and, therefore, more reactive than 3-(benzyloxy)propanal; see, also: J. S. Panek, M. Yang, *J. Am. Chem. Soc.* **1991**, *113*, 9868.

 © 2004 Wiley-VCH Verlag GmbH & Co. KGaA, Weinheim

A Germanium(II) Hydroxide

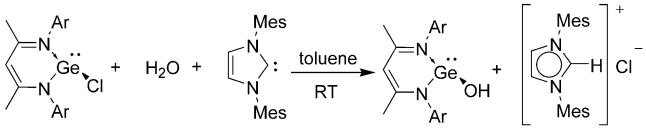
Preparation and Structure of the First Germanium(II) Hydroxide: The Congener of an Unknown Low-Valent Carbon Analogue**

Leslie W. Pineda, Vojtech Jancik, Herbert W. Roesky, Dante Neculai, and Ana M. Neculai*

Dedicated to Professor Pedro Aymonino on the occasion of his 75th birthday

In 1984 it was noted that the picture of the structural chemistry of hydroxides is far from complete,[1] and 20 years later this is still the case. In recent years, we have been interested in organometallic hydroxides. We reported on the preparation and structural characterization of unusual compounds such as $[LAl(OH)_2]$[2] ($L = HC\{(CMe)(2,6\text{-}iPr_2C_6H_3N)\}_2$), $[(Me_3Si)_3CSnO(OH)]_3$,[3] and $[(CpZr)_6(\mu_4\text{-}O)(\mu\text{-}O)_4(\mu\text{-}OH)_8]$,[4] and a series of experiments concerning the so-called water effect in organometallic chemistry.[5] Interestingly, only a few examples of well-characterized germanium(IV) hydroxides are known: Ph_3GeOH, $(C_{10}H_7)_3GeOH$, $(C_6H_{11})_3GeOH$,[6] $2\,tBu_2Ge(OH)_2\cdot(tBu_2GeO\text{-}H)_2O\cdot H_2O$,[7] and $[Fc(tBu)(OH)Ge]_2O$ [$Fc = CpFe(\eta^5\text{-}C_5H_4)$],[8] and no such compounds based on germanium(II) have been reported. The most common route to organogermanium hydroxides is through the hydrolysis of organohalogermanes, but they can be only isolated when the supporting ligand is bulky enough.[9]

Here we report on the hydrolysis of the stable germanium(II) chloride $[HC\{(CMe)(2,6\text{-}iPr_2C_6H_3N)\}_2GeCl]$ (**1**),[10] with a slight excess of water and one equivalent of 1,3-dimesitylimidazol-2-ylidene[11] (**2**; Mes = 2,4,6-$Me_3C_6H_2$) in toluene at room temperature, which led to the formation of $[HC\{(CMe)(2,6\text{-}iPr_2C_6H_3N)\}_2GeOH]$ (**3**) in good yield (Scheme 1). In contrast, conventional hydrolysis of **1** in the presence of an amine or in liquid ammonia was unsuccessful



1 **2** **3** **4**

Scheme 1. Ar = 2,6-$iPr_2C_6H_3$, Mes = 2,4,6-$Me_3C_6H_2$.

[*] Dipl.-Chem. L. W. Pineda, Dipl.-Chem. V. Jancik, Prof. Dr. H. W. Roesky, Dr. D. Neculai, Dr. A. M. Neculai
Institut für Anorganische Chemie
Universität Göttingen
Tammannstrasse 4, 37077 Göttingen (Germany)
Fax: (+49) 551-39-3373
E-mail: hroesky@gwdg.de

[**] This work was supported by the Deutsche Forschungsgemeinschaft and the Fonds der Chemischen Industrie. L.W.P thanks the Deutscher Akademischer Austauschdienst (DAAD) for a predoctoral fellowship.

 DOI: 10.1002/anie.200353205 © 2004 Wiley-VCH Verlag GmbH & Co. KGaA, Weinheim

due to the formation of several side products. Moreover, the separation of **3** from the amine·HCl adduct was not possible. Addition of HCl to the N-heterocyclic carbene **2** is clearly a key step in this reaction. The easy formation of **4** and its low solubility allow the separation of **3** from **4**.

Compound **3** is a yellow solid that is soluble in pentane, THF, dichloromethane, benzene, and diethyl ether, but insoluble in hexane. It was characterized by IR, ^{1}H, and ^{13}C NMR spectroscopy, EI mass spectrometry, elemental analysis, and X-ray single-crystal analysis. In the IR spectrum a sharp absorption around 3571 cm^{-1} can be attributed to the O–H stretching frequency. Theoretical calculations on $Ge(OH)_2$ showed that two vibrational frequencies could be expected at 3675 and 3735 cm^{-1}.[12] These values are in good agreement with that of **3** when it is taken into account that some symmetry constraints are involved. In addition, the monoanionic ligand in **3** might affect the vibrational frequency by means of its steric demand and bonding mode. The ^{1}H NMR spectrum shows the expected pattern for the β-diketiminato ligand[10] and a resonance for the hydroxide proton at high field ($\delta = 1.54$ ppm), which is in accordance with the chemical shift observed for the OH group in tBu$_2$Ge(OH)$_2$ ($\delta = 1.49$ ppm).[13] Surprisingly, the resonance for the corresponding group of $(FcN)_3GeOH$ (FcN = CpFe{η^5-$C_5H_3(CH_2NMe_2)$-2}) was found at $\delta = 8.98$ ppm.[14] The most intense peak in the EI mass spectrum appeared at $m/z = 403$ [M–Me–Ge–OH]$^+$, and the signal at $m/z = 508$ (25%) was assigned to the molecular ion [M]$^+$.

Single crystals of **3**[15] suitable for X-ray structural analysis were grown by maintaining the reaction mixture in toluene/hexane (2.5:1) at −20 °C for three weeks. Complex **3** crystallizes in the monoclinic space group $C12/c1$, with two half dimers in the asymmetric unit. In **3** a germanium atom is attached to two nitrogen atoms from the backbone of the chelating ligand and a hydroxyl group, and a lone pair presumably occupies the fourth coordination site, an assumption that is supported by the presence of an intermolecular interaction between the H atom of the OH group, which was located and refined, and another germanium atom (O–H···Ge 3.064(26) Å). The coordination geometry about germanium is derived from a distorted tetrahedron (Figure 1). The Ge–N bond lengths and N-Ge-N angle are 2.008(1) Å and 89.5(1)°, respectively. These data can be compared with the slightly shorter Ge–N bond lengths in **1** (1.988(2) and 1.997(3) Å) and [LGeF] (1.977(19) and 1.978(18) Å; L = HC{(CMe)(2,6-iPr$_2$C$_6$H$_3$N)}$_2$).[16] Conversely, the Ge–N bond lengths are slightly longer in [HB(3,5-Me$_2$pz)$_3$Ge]I,[17] (av 2.03(2) Å; pz = pyrazole ring) and [LGeMe] (2.008(2) and 2.038(2) Å).[16]

A noteworthy feature of compound **3** is the GeOH moiety (Ge–O 1.828(1), O–H 0.795(7) Å); the Ge–O bond length is in good agreement with those predicted for $Ge(OH)_2$ (av 1.804 Å).[12] Moreover, the O–H distance of **3** is somewhat shorter than that of water (0.96 Å). Interestingly, and as might be expected, shorter Ge–OH bond lengths are found in germanium(IV) compounds due to the smaller radius of Ge^{IV} relative to Ge^{II} (e.g., Ge–O 1.781(4) and 1.779(2) Å in tBu$_2$Ge(OH)$_2$,[13] and 1.779(5) Å in $(FcN)_3GeOH$).[14]

In summary, compound **3** is the first example of the hitherto unknown germanium(II) hydroxides. A low-coordinate carbon analogue of composition RC(OH) has so far not been reported. An RC(OH) species should be extremely unstable and rearrange to the corresponding aldehyde.

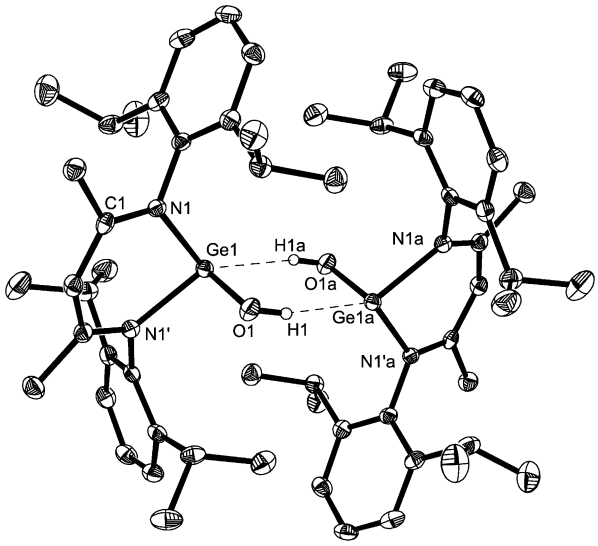


Figure 1. Thermal-ellipsoid plot of **3** at the 50% probability level. H atoms, except for the OH group, are omitted for clarity. Selected bond lengths [Å] and angles [°]: Ge1–O 1.828(1), Ge1–N1 2.008(1), Ge1–N1′ 2.008(1); O1-Ge1-N1 93.9(6), O1-Ge1-N1′ 94.8(6), N1-Ge1-N1′ 89.5(1).

Experimental Section

All manipulations were performed under a dry and oxygen-free atmosphere (N_2 or Ar) by using Schlenk-line and glove-box techniques.

3: **1** (1.28 g, 2.43 mmol) and **2** (0.74 g, 2.43 mmol) were dissolved in toluene (20 mL) at room temperature, then water (87.5 μL, 2.0 mmol) was slowly added, and the mixture was stirred. A white precipitate immediately formed. The reaction mixture was stirred for about 15 min, then the white precipitate was separated by filtration in vacuo. The remaining colorless solution was evaporated, and the resulting yellow solid of **3** was rinsed with hexane (2 × 10 mL) and dried in vacuo. Yield: 1.04 g (84%); m.p. 140 °C; IR (KBr): $\tilde{\nu} = 3571$, 2964, 2867, 1623, 1554, 1383, 1320, 1174, 1100, 1018, 918, 853, 795, 758, 588, 521, 366 cm^{-1}; ^{1}H NMR (200 MHz, C_6D_6): $\delta = 7.15$ (m, 6H, 2,6-iPr$_2$C$_6$H$_3$), 4.91 (s, 1H, γ-CH), 3.60–3.80 (sept, 2H, $(CH_3)_2$), 3.20–3.40 (sept, 2H, $(CH_3)_2$), 1.60 (s, 6H, CH_3), 1.54 (s, 1H, OH), 1.33 (d, 6H, $CH(CH_3)_2$), 1.29 (d, 6H, $CH(CH_3)_2$), 1.21 (d, 6H, $CH(CH_3)_2$), 1.12 ppm (d, 6H, $CH(CH_3)_2$); ^{13}C NMR (50.327 MHz, THF): $\delta =$ 163.31 (NC), 146.37 (NC), 143.62 (ArC), 141.00 (ArC), 124.87 (ArC), 124.06 (ArC), 96.98 (γ-C), 29.16 ($CH(CH_3)_2$), 28.02 ($CH(CH_3)_2$), 26.69 ($CH(CH_3)_2$), 24.73 ($CH(CH_3)_2$), 24.57 ($CH(CH_3)_2$), 24.08 ($CH(CH_3)_2$), 23.25 ppm ($NC(CH_3)$); MS (EI): m/z (%): 508 (25) [M]$^+$, 403 (100) [M–Me–Ge–OH]$^+$; elemental analysis (%) calcd for $C_{29}H_{42}GeN_2O$ (507.24): C 68.67, H 8.35, N 5.52; found: C 69.20, H 8.48, N 5.52.

Received: October 31, 2003 [Z53205]

Keywords: carbenes · germanium · hydrolysis · hydroxides

[1] a) A. F. Wells, *Structural Inorganic Chemistry*, Clarendon, Oxford, **1984**, p. 627; b) A. F. Holleman, E. Wiberg, *Lehrbuch*

der Anorganischen Chemie, Walter de Gruyter, Berlin, **1995**, p. 960; c) N. N. Greenwood, A. Earnshaw, *Chemistry of the Elements*, Butterworth-Heinemann, Oxford, **1997**, pp. 382–383.
[2] G. Bai, Y. Peng, H. W. Roesky, J. Li, H.-G. Schmidt, M. Noltemeyer, *Angew. Chem.* **2003**, *115*, 1164–1167; *Angew. Chem. Int. Ed.* **2003**, *42*, 1132–1135.
[3] J. Janssen, J. Magull, H. W. Roesky, *Angew. Chem.* **2002**, *114*, 1425–1427; *Angew. Chem. Int. Ed.* **2002**, *41*, 1365–1367.
[4] G. Bai, H. W. Roesky, J. Li, T. Labahn, F. Cimpoesu, J. Magull, *Organometallics* **2003**, *22*, 3034–3038.
[5] H. W. Roesky, M. G. Walawalkar, R. Murugavel, *Acc. Chem. Res.* **2001**, *34*, 201–211, and references therein.
[6] M. Lesbre, P. Mazerolles, J. Satgé, *The Organic Compounds of Germanium*, Wiley, London, **1971**, p. 403.
[7] J. Beckmann, K. Jurkschart, M. Schürmann, *Eur. J. Inorg. Chem.* **2000**, 939–941.
[8] Y. Zhang, F. Cervantes-Lee, K. H. Pannell, *Organometallics* **2003**, *22*, 510–515.
[9] P. Rivière, M. Rivière-Baudet, J. Satgé in *Comprehensive Organometallic Chemistry*, *Vol. 2* (Eds.: G. Wilkinson, F. G. A. Stone, E. W. Abel), Pergamon, Oxford, **1982**, pp. 405–503.
[10] Y. Ding, H. W. Roesky, M. Noltemeyer, H.-G. Schmidt, *Organometallics* **2001**, *20*, 1190–1194.
[11] a) A. J. Arduengo III, H. V. R. Dias, R. L. Harlow, M. Kline, *J. Am. Chem. Soc.* **1992**, *114*, 5530–5534; b) D. Bourissou, O. Guerrt, F. P. Gabbaï, G. Bertrand, *Chem. Rev.* **2000**, *100*, 39–91.
[12] J. R. T. Johnson, I. Panas, *Chem. Phys.* **1999**, *249*, 273–303.
[13] H. Puff, S. Franken, W. Schuh, W. Schwab, *J. Organomet. Chem.* **1983**, *254*, 33–41.
[14] A. Fischer, K. Jacob, F. T. Edelmann, *Z. Anorg. Allg. Chem.* **2003**, *629*, 963–967.
[15] Crystal data for **3**: $C_{29}H_{42}GeN_2O$, $M_r = 507.24$, monoclinic, space group $C12/c1$, $a = 24.765(3)$, $b = 15.155(2)$, $c = 14.700(2)$ Å, $\beta = 94.56(2)°$, $V = 5499.6(12)$ Å^3, $Z = 8$, $\rho_{calcd} = 2.251$ g cm^{-3}, $F(000) = 2160$, $\lambda = 1.54178$ Å, $T = 100(2)$ K, $\mu(Cu_{K\alpha}) = 1.66$ mm^{-1}. Data were collected on a Bruker three-circle diffractometer equipped with a SMART 6000 CCD detector. Intensity measurements were performed on a rapidly cooled crystal (dimensions $0.20 \times 0.10 \times 0.10$ mm) in the range $3.42 \leq 2\theta \leq 59.60°$. Of the 3752 measured reflections, 3635 were independent. The structure was solved by direct methods (SHELXS-97)[18] and refined for all data by full-matrix least-squares methods on F^2. The hydrogen atoms of C–H bonds were placed in idealized positions. The final refinements converged at $R1 = 0.0247$ for $I > 2\sigma(I)$ and $wR2 = 0.0650$ for all data. The final difference Fourier synthesis gave min./max. residual electron density of $-0.338/0.318$ e Å^{-3}. CCDC 222748 (**3**) contains the supplementary crystallographic data for this paper. These data can be obtained free of charge via www.ccdc.cam.ac.uk/conts/retrieving.html (or from the Cambridge Crystallographic Data Centre, 12, Union Road, Cambridge CB21EZ, UK; fax: (+44) 1223-336-033; or deposit@ccdc.cam.ac.uk).
[16] Y. Ding, H. Hao, H. W. Roesky, M. Noltemeyer, H.-G. Schmidt, *Organometallics* **2001**, *20*, 4806–4811. For comparison, see also a) Y. Ding, Q. Ma, H. W. Roesky, R. Herbst-Irmer, I. Usón, M. Noltemeyer, H.-G. Schmidt, *Organometallics* **2002**, *21*, 5216–5220; b) M. Stender, A. D. Phillips, P. P. Power, *Inorg. Chem.* **2001**, *40*, 5314–5315.
[17] D. L. Reger, P. S. Coan, *Inorg. Chem.* **1996**, *35*, 258–260.
[18] G. M. Sheldrick, SHELXS-97, Program for crystal structure refinement, University of Göttingen, Göttingen, Germany, **1997**.

 © 2004 Wiley-VCH Verlag GmbH & Co. KGaA, Weinheim

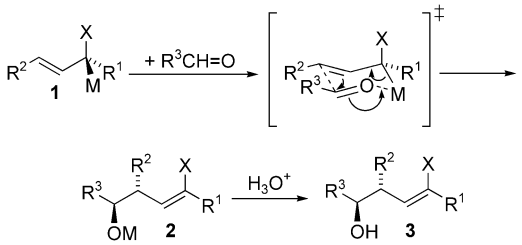
Asymmetric Synthesis

Highly Enantiomerically Enriched Ketone Homoenolate Reagents Prepared by (−)-Sparteine-Mediated γ-Deprotonation of Achiral 1-Alkenyl Carbamates**

*Michael Seppi, Rainer Kalkofen, Jens Reupohl, Roland Fröhlich, and Dieter Hoppe**

Dedicated to Professor Manfred T. Reetz on the occasion of his 60th birthday

Enantiomerically enriched, 1-hetero-substituted 2-alkenylmetal compounds **1** (e.g., M = Li, Ti(O*i*Pr)$_3$, Ti(NEt$_2$)$_3$) are powerful homoenolate reagents.[1] They react with aldehydes and ketones with virtually complete 1,3-transfer of chirality to form optically active homoaldol products **2**[2] (Scheme 1).[3] In



Scheme 1. Addition of homoenolate reagents to aldehydes.

the best homoenolate reagents **1** the substituent X is a complexing *N*,*N*-dialkylcarbamoyloxy group[2a–d] or a *tert*-butoxycarbonylamino group,[2e] both of which enhance the kinetic acidity in the deprotonation of the allylic precursor and are able to hold the counterion in compound **1** at the α-position.

The first known chiral allyllithium derivative configurationally stable below −70 °C was generated by deprotonation of an enantiomerically enriched, secondary allylic carbamate by *n*-butyllithium/*N*,*N*,*N*′,*N*′-tetramethylethylenediamine (TMEDA).[4] We also reported on the preparation of lithium compounds **1** obtained by kinetic resolution of racemic precursors by deprotonation with *n*-butyllithium/(−)-sparteine.[5,6] Lithium carbanions **1** (R^1 = H) derived from primary precursors could be generated by enantiotopos-differentiating deprotonation, but these only occasionally exhibit sufficient configurational stability.[2b,7] Alternatively, chiral auxiliaries were used for residue X.[8]

We now report on a surprising, simple, and efficient approach to 1-aryl ketone homoenolate reagents by enantiotopos-differentiating γ-deprotonation of 1-aryl-1-alkenyl *N*,*N*-diisopropylcarbamates by *n*-butyllithium/(−)-sparteine. When we attempted the asymmetric carbolithiation of enol carbamate **4a** (*Z*/*E* = 92:8)[10,11] and trapped the lithiated intermediate **6a** with acetone, we isolated the homoaldol product **8aa** in 69% yield and with 97% *ee* (Scheme 2). Subsequent experiments indicated that **8aa** has *R* configuration and is formed from the enantiomerically enriched homoenolate reagent (*S*)-**6a**. In turn, reagent (*S*)-**6a** arises from **4a** by deprotonation under the influence of the chiral base via the ternary complex **5a**. During the removal of the *pro*-*R* proton at C3 in the nine-membered cyclic transition state, the lithium cation migrates along the π system to position 1 to form the five-membered chelate (*S*)-**6a**. The prerequisites for intramolecular deprotonation are met only in the isomer (*Z*)-**4a**, since (*E*)-**4a** remains unchanged. Carbamates **4b–d** react analogously. The electrophiles **7** investigated—the dialkyl ketones **7a** and **7b**, triphenyltin chloride (**7c**), the acid chlorides **7d** and **7e**, the arene carboxaldehydes **7h** and **7i**, and alkanal **7l**—are added exclusively at the γ-position (Table 1).

The reactions of **4a** with triphenyltin chloride (**7c**) and *p*-bromobenzaldehyde (**7h**) (and subsequent oxidation of *ent*-**8ah**) afforded crystalline products *ent*-**8ac** and *ent*-**8af**, respectively, each with >90% *ee*. In X-ray crystal structure analyses with anomalous dispersion[12] both of them had the *S* configuration (Figure 1).

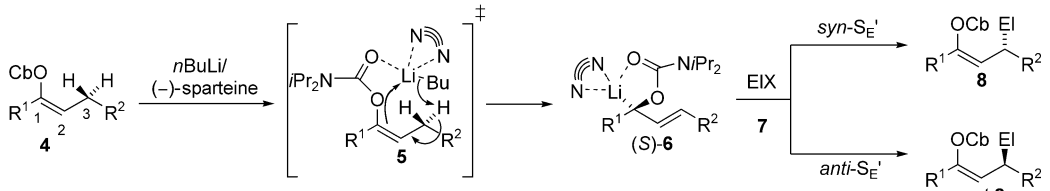
Since all of the investigated stannylations of allyllithium[13] and benzyllithium[14] derivatives proceed in an antarafacial manner by *anti*-S$_E$′ or stereoinvertive processes, the carbanionic intermediate **6a** has to be assigned the 1*S* configuration. Our experiments (Scheme 3) indicate that even *p*-bromobenzaldehyde (**7h**) undergoes an *anti*-S$_E$′ addition. Further evidence for this unusual result was provided by the following experiments: The lithium cation in **6a** was exchanged by reaction with chlorotris(diethylamino)titanium[15] (inversion of configuration), and the resulting *ent*-**9a** added onto aldehyde **7h** (*syn* addition).[2] Oxidation of the epimeric secondary alcohols *ent*-**8ah** yielded the ketone *ent*-**8af**, which was identical to a sample obtained from the lithium intermediate. This fact means that an antarafacial reaction step—the carbonyl addition—is involved in the lithium pathway B, as well.[16] In contrast, **6a** and acetone (**7a**) (Scheme 4) yield opposite enantiomers (*S*)-*ent*-**8aa** (pathway B) and (*R*)-**8aa** (pathway A), demonstrating that the lithium intermediate **6a** adds to dialkyl ketones in a *syn*-S$_E$′ process. The acylation by means of methyl chloroformate (**7e**) also proceeds predominantly in a *syn*-S$_E$′ process, as could be shown by transformation of the carboxylic ester (−)-**8ae** into alcohol (+)-**8aa** (Scheme 4).

The addition of the lithium compound **6a** to 2,2-dimethylpropanal (**7l**) and 2,2-dimethylpropanoyl chloride (**7d**) is also a *syn*-S$_E$′ process, as was concluded from an experiment similar to that depicted in Scheme 3. The aliphatic ketones, aldehydes, and acid chlorides are added to the lithium–

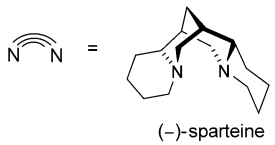
[*] Dr. M. Seppi, Dipl.-Chem. R. Kalkofen, J. Reupohl, Dr. R. Fröhlich, Prof. Dr. D. Hoppe
Organisch-Chemisches Institut
Westfälische Wilhelms-Universität Münster
Corrensstrasse 40, 48149 Münster (Germany)
Fax: (+49) 251-83-36531
E-mail: dhoppe@uni-muenster.de

[**] This work was supported by the Deutsche Forschungsgemeinschaft (SFB424) and the Fonds der Chemischen Industrie.

 DOI: 10.1002/anie.200352966 © 2004 Wiley-VCH Verlag GmbH & Co. KGaA, Weinheim

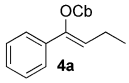
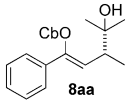
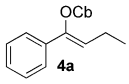
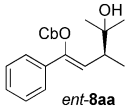
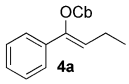
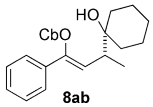
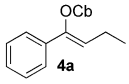
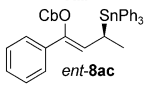
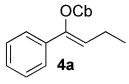
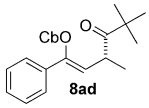
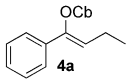
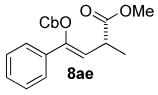
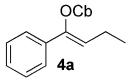
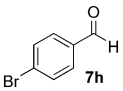
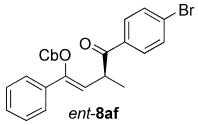
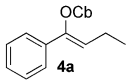
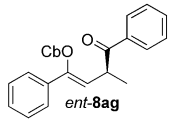
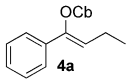
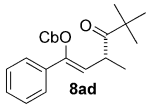
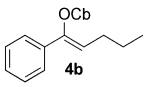
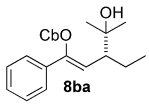
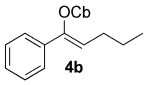
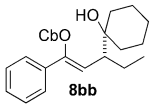


4	R^1	R^2
(*Z*)-**4a**	C_6H_5	CH_3
(*Z*)-**4b**	C_6H_5	C_2H_5
(*Z*)-**4c**	2-naphthyl	CH_3
(*Z*)-**4d**	4-ClC_6H_4	C_2H_5



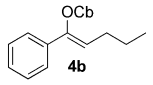
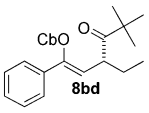
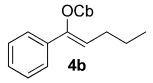
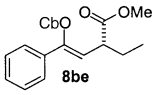
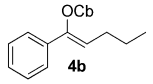
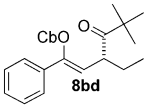
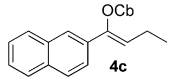
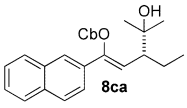
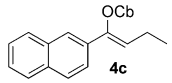
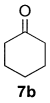
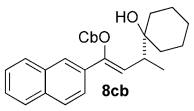
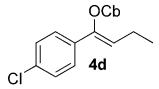
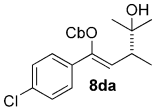
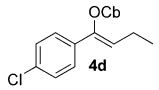
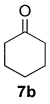
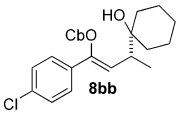
Scheme 2. Enantiotopos-differentiating γ-deprotonation of the *pro-R* protons by means of the chiral base *n*BuLi/(−)-sparteine. For ElX (**7**) see Table 1, Cb = carbamoyl.

Table 1: Reaction of lithium compounds **6** with different electrophiles.

Entry	Starting materials		Product	Yield [%]	*ee* [%][a]	$[\alpha]_D^{20}$[a]
1	 **4a**	 **7a**	 **8aa**	69	97	+87
2[b]	 **4a**	 **7a**	 *ent*-**8aa**	80	92	−83
3	 **4a**	 **7b**	 **8ab**	57	93	+49
4	 **4a**	Ph_3SnCl **7c**	 *ent*-**8ac**	78	94	+54
5	 **4a**	 **7d**	 **8ad**	81	77	−91
6	 **4a**	 **7e**	 **8ae**	78	78	−52
7[c,d]	 **4a**	 **7h**	 *ent*-**8af**	49	>90	+64
8[c,d]	 **4a**	 **7i**	 *ent*-**8ag**	70	86	+85
9[c,d]	 **4a**	 **7l**	 **8ad**	73	86	−105
10	 **4b**	 **7a**	 **8ba**	74	>95	+84
11	 **4b**	 **7b**	 **8bb**	75	>90	+51

 © 2004 Wiley-VCH Verlag GmbH & Co. KGaA, Weinheim

Table 1: (Continued)

Entry	Starting materials		Product	Yield [%]	*ee* [%][a]	$[\alpha]_D^{20}$[a]
12	 **4b**	 **7d**	 **8bd**	83	>95	−120
13	 **4b**	 **7e**	 **8be**	76	92	−64
14[c,d]	 **4b**	 **7l**	 **8bd**	72	>95	−129
15	 **4c**	 **7a**	 **8ca**	77	88	+84
16	 **4c**	 **7b**	 **8cb**	58	>95	+63
17	 **4d**	 **7a**	 **8da**	50	>95	+81
18	 **4d**	 **7b**	 **8bb**	58	>95	+57

[a] $c = 0.5$–1.28, $CHCl_3$. [b] Lithium species **6a** was treated with 3 equiv $[ClTi(NEt_2)_3]$ (Scheme 5). [c] Mixture of diastereomeric homoaldol adducts (ca. 1:1). [d] Oxidation of the crude product with pyridinium dichromate (PDC).

sparteine complexes in a suprafacial manner.[17] Apparently the lithium cation provides electrophilic assistance for the addition of carbonyl electrophiles. Aromatic aldehydes such as **7h** and **7i** undergo *anti* additions (Table 1, entries 7, 8);

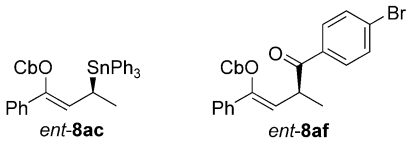
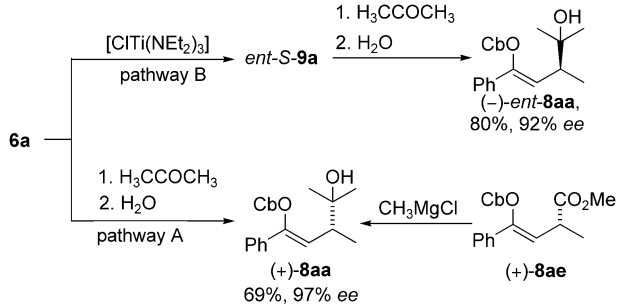
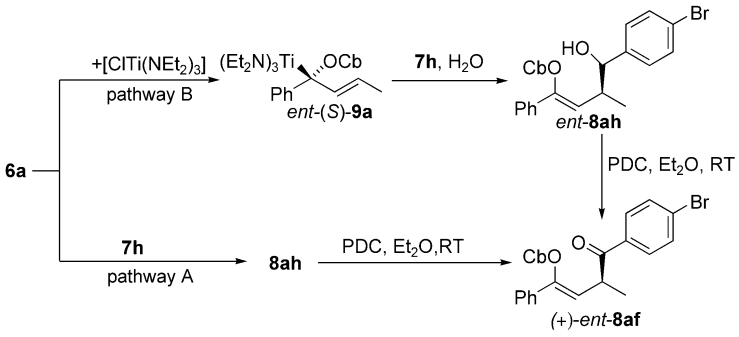


Figure 1. Formulas of the γ-products *ent*-**8ac** and *ent*-**8af**, which were analyzed by X-ray diffraction.



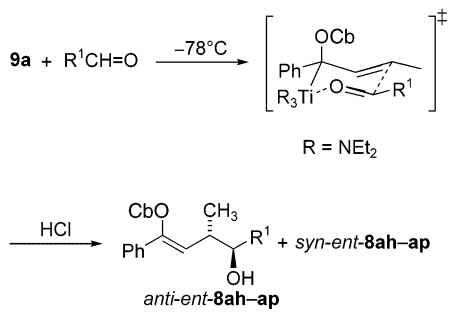
Scheme 4. Additions of (*S*)-**9a** and (*S*)-**6a** to acetone (**7a**) yield products of opposite configuration.



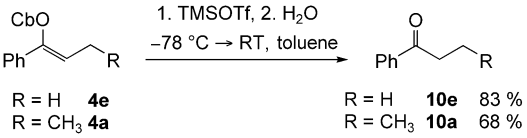
Scheme 3. Additions of (*S*)-**9a** and (*S*)-**6a** to *p*-bromobenzaldehyde (**7h**). Subsequent oxidation by pyridinium dichromate (PDC) leads to products of identical configuration.

presumably, an open-chain transition state is promoted by the formation of an intermediate π–π* complex.[18,14] Here, the approach from the face not covered by the solvated lithium cation is favored. The titanium compound (*S*)-**9a**, which generally is formed from **6a** with stereoinversion, adds to aldehydes reliably via a Zimmerman–Traxler transition state[19] and leads, combined with 1,3-chirality transfer, diastereoselectively to optically active homoaldol adducts *anti-ent*-**8** (Scheme 5, Table 2). Hydrolysis of 1-aryl-1-alkenyl carbamates to ketones is possible by treatment with trimethylsilyl triflate (TMSOTf) and subsequent addition of water (Scheme 6).

 © 2004 Wiley-VCH Verlag GmbH & Co. KGaA, Weinheim



Scheme 5. Reaction of titanium compound (*S*)-**9a** with different aldehydes to form highly enantioenriched homoaldol products. See Table 2 for R^1.



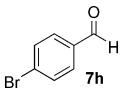
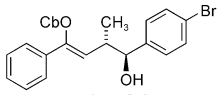
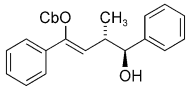
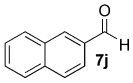
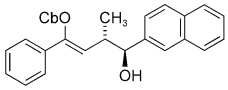
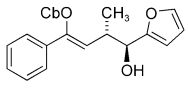
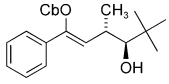
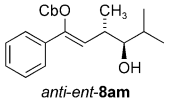
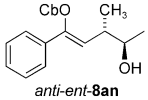
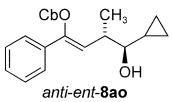
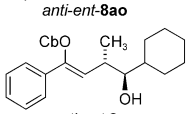
Scheme 6. Decarbamoylation of **4a** and **4e** by means of TMSOTf.

The (−)-sparteine-mediated γ-deprotonation of 1-alkenyl carbamates is an efficient and expandable approach to enantiomerically enriched homoenolate reagents starting from achiral precursors.[20] These react with the standard electrophiles investigated with high regio- and stereospecificity. From a mechanistic point of view, the highly stereoselective removal of a remote proton deserves particular attention.

Experimental Section

Synthesis of the homoaldol products *anti-ent*-**8ah**–**8ap**: To a solution of (−)-sparteine (0.353 g, 1.50 mmol) in dry toluene (2 mL) was added at −78 °C ca. 1.6 M butyllithium (1.4 mmol, 0.89 mL) in hexane. After the reaction mixture had been stirred for 10 min at −78 °C, a solution of carbamate **4a** (1.0 mmol) in toluene (1 mL) was added slowly. Stirring was continued for 1.5 h before a solution of $[ClTi(NEt_2)_3]$ (3.0 mmol) in toluene (2 mL) was added dropwise. After a transmetalation time of 2 h, the aldehyde **7** (3.0 mmol) was added at −78 °C, and stirring was continued for further 2 h. For workup, 2 N aq HCl (10 mL) was introduced to the flask. The aqueous phase was separated, and the aqueous solution was extracted with diethyl ether (3 × 25 mL, each). The combined organic extracts were

Table 2: Diastereo- and enantioselective homoaldol reaction, starting from **4a**.

Entry	Aldehyde	Product	Yield [%]	d.r.[a]	*ee* [%][a]	$[\alpha]_D^{20}$[b]
1	 **7h**	 *anti-ent*-**8ah**	66	95:5	97	−135
2	 **7i**	 *anti-ent*-**8ai**	71	98:2	95	−133
3	 **7j**	 *anti-ent*-**8aj**	49	97:3	93	−145
4	 **7k**	 *anti-ent*-**8ak**	82	97:3	95	−148
5	 **7l**	 *anti-ent*-**8al**	75	99:1	96	−73
6	 **7m**	 *anti-ent*-**8am**	78	99:1	94	−91
7	 **7n**	 *anti-ent*-**8an**	79	99:1	93	−95
8	 **7o**	 *anti-ent*-**8ao**	81	99:1	95	−100
9	 **7p**	 *anti-ent*-**8ap**	77	99:1	95	−85

[a] Determined by HPLC (column Chira Grom-2, solvent: hexane/2-propanol). [b] $c = 0.5$–1.25, $CHCl_3$.

 © 2004 Wiley-VCH Verlag GmbH & Co. KGaA, Weinheim

dried over $MgSO_4$, and the solvents evaporated in vacuo. The crude product *anti-ent*-**8** was purified by flash chromatography on silica gel (diethyl ether/petroleum ether 1:1). For the yields and stereochemical purity see Table 2.

Received: September 29, 2003 [Z52966]

Keywords: asymmetric synthesis · homoaldol reaction · lithium · sparteine · titanium

[1] Reviews: a) D. Hoppe, T. Hense, *Angew. Chem.* **1997**, *109*, 2376; *Angew. Chem. Int. Ed. Engl.* **1997**, *36*, 2282; b) D. Hoppe, F. Marr, M. Brüggemann, *Top. Organomet. Chem.* **2003**, *5*, 61; c) P. Beak, T. A. Johnson, D. D. Kim, S. H. Lim, *Top. Organomet. Chem.* **2003**, *5*, 134; d) H. Ahlbrecht, U. Beyer, *Synthesis* **1999**, 365.

[2] a) T. Krämer, J.-R. Schwark, D. Hoppe, *Tetrahedron Lett.* **1989**, *30*, 7037; b) D. Hoppe, O. Zschage, *Angew. Chem.* **1989**, *101*, 67; *Angew. Chem. Int. Ed. Engl.* **1989**, *28*, 69; c) D. Hoppe, O. Zschage, *Tetrahedron* **1992**, *48*, 5657; d) T. Krämer, D. Hoppe, *Tetrahedron Lett.* **1987**, *28*, 5149; e) M. C. Whisler, L. V. Vaillancourt, P. Beak, *Org. Lett.* **2000**, *2*, 2655.

[3] The direction of chirality transfer is reversed if **1** reacts from the 1-*exo*-conformation rather than the 1-*endo* configuration (as shown in Scheme 1).

[4] D. Hoppe, T. Krämer, *Angew. Chem.* **1986**, *98*, 171; *Angew. Chem. Int. Ed. Engl.* **1986**, *25*, 160.

[5] At least half of the racemic starting material is lost during this process.

[6] O. Zschage, J.-R. Schwark, D. Hoppe, *Angew. Chem.* **1990**, *102*, 336; *Angew. Chem. Int. Ed. Engl.* **1990**, *29*, 296.

[7] M. Özlügedik, J. Kristensen, B. Wibbeling, R. Fröhlich, D. Hoppe, *Eur. J. Org. Chem.* **2002**, 414.

[8] a) H. Roder, G. Helmchen, E.-M. Peters, K. Peters, H.-G. von Schnering, *Angew. Chem.* **1984**, *96*, 895; *Angew. Chem. Int. Ed. Engl.* **1984**, *23*, 898; b) D. Heimbach, D. Hoppe, *Synlett* **2000**, 950; c) M. Reggelin, C. Zurr, *Synthesis* **2000**, 1.

[9] For the asymmetric γ-deprotonation of enamines see the ref. [1d] and, in particular, the contributions of the author cited therein.

[10] J. G. Peters, M. Seppi, R. Fröhlich, D. Hoppe, *Synthesis* **2002**, 381.

[11] M. Seppi, Dissertation, Universität Münster, **2001**.

[12] X-ray crystal structure analysis of *ent*-**8ac**: $C_{35}H_{39}NO_2Sn$, $M_w = 624.36$, colorless crystal $0.35 \times 0.15 \times 0.10$ mm, $a = 10.625(1)$, $b = 14.474(1)$, $c = 11.047(1)$ Å, $\beta = 109.22(1)°$, $V = 1604.2(2)$ Å^3, $\rho_{calcd} = 1.293$ g cm^{-3}, $\mu = 65.52$ cm^{-1}, empirical absorption correction by ψ-scan data ($0.208 \le T \le 0.341$), $Z = 2$, monoclinic, space group $P2_1$ (no. 4), $\lambda = 1.54178$ Å, $T = 223$ K, $\omega/2\theta$ scans, 3591 reflections collected ($+h$, $+k$, $\pm l$), $(\sin\theta)/\lambda = 0.62$ Å^{-1}, 3407 independent ($R_{int} = 0.025$) and 3162 observed reflections [$I \ge 2\sigma(I)$], 3507 refined parameters, $R = 0.036$, $wR^2 = 0.097$, max. residual electron density 0.75 (-1.17) e Å^{-3}, Flack parameter $-0.003(9)$, hydrogen atoms calculated and refined as riding atoms. X-ray crystal structure analysis of *ent*-**8af**: $C_{24}H_{28}BrNO_3$, $M_w = 458.38$, colorless crystal $0.35 \times 0.20 \times 0.20$ mm, $a = 9.272(1)$, $b = 12.938(1)$, $c = 10.388(1)$ Å, $\beta = 112.00(1)°$, $V = 1155.4(2)$ Å^3, $\rho_{calcd} = 1.318$ g cm^{-3}, $\mu = 26.07$ cm^{-1}, empirical absorption correction via SORTAV ($0.462 \le T \le 0.624$), $Z = 2$, monoclinic, space group $P2_1$ (no. 4), $\lambda = 1.54178$ Å, $T = 223$ K, ω?and φ scans, 7530 reflections collected ($\pm h$, $\pm k$, $\pm l$), $[(\sin\theta)/\lambda] = 0.59$ Å^{-1}, 3077 independent ($R_{int} = 0.028$) and 2886 observed reflections [$I \ge 2\sigma(I)$], 268 refined parameters, $R = 0.029$, $wR^2 = 0.077$, max. residual electron density 0.22(-0.27) e Å^{-3}, Flack parameter $-0.030(18)$, hydrogens calculated and refined as riding atoms. Data sets were collected with an Enraf-Nonius CAD4 and Nonius KappaCCD diffractometers. Programs used: data collection EXPRESS (Nonius B.V., 1994) and COLLECT (Nonius B.V., 1998), data reduction MolEN (K. Fair, Enraf-Nonius B.V., 1990) and Denzo-SMN (Z. Otwinowski, W. Minor, *Methods Enzymol.* **1997**, *276*, 307), absorption corrections for CCD data SORTAV (R. H. Blessing, *Acta Crystallogr. Sect. A* **1995**, *51*, 33; R. H. Blessing, *J. Appl. Crystallogr.* **1997**, *30*, 421), structure solution SHELXS-97 (G. M. Sheldrick, *Acta Crystallogr. Sect. A* **1990**, *46*, 467), structure refinement SHELXL-97 (G. M. Sheldrick, Universität Göttingen, **1997**, E. Keller, Graphik SCHAKAL, Universität Freiburg, **1997**). CCDC-219962 and CCDC-219961 contains the supplementary crystallographic data for this paper. These data can be obtained free of charge via www.ccdc.cam.ac.uk/conts/retrieving.html (or from the Cambridge Crystallographic Data Centre, 12, Union Road, Cambridge CB21EZ, UK; fax: (+44) 1223-336-033; or deposit@ccdc.cam.ac.uk).

[13] H. Paulsen, C. Graeve, D. Hoppe, *Synthesis* **1996**, 141.

[14] a) A. Carstens, D. Hoppe, *Tetrahedron* **1994**, *50*, 6697; b) C. Derwing, D. Hoppe, *Synthesis* **1996**, 149; c) C. Derwing, H. Frank, D. Hoppe, *Eur. J. Org. Chem.* **1999**, 3511; d) F. Hammerschmidt, A. Hanninger, P. Perric, H. Völlenkle, H. Werner, *Eur. J. Org. Chem.* **1999**, 3511; e) N. C. Faibish, Y. S. Park, S. Lee, P. Beak, *J. Am. Chem. Soc.* **1997**, *119*, 11561.

[15] Reviews on titanation: a) M. T. Reetz, *Organotitanium Reagents in Organic Synthesis*, Springer, Berlin, **1986**; b) B. Weidmann, D. Seebach, *Angew. Chem.* **1983**, *95*, 12; *Angew. Chem. Int. Ed. Engl.* **1983**, *22*, 32; c) "Organotitanium Chemistry": M. T. Reetz in *Organometallics in Synthesis* (Ed.: M. Schlosser), Wiley, Chichester, **2002**, p. 817.

[16] Previously, only *syn*-S_E' additions of aldehydes have been reported.[1]

[17] The decreased enantioselectivity of 86% *ee* for the addition of the lithium compound **6a** to 2,2-dimethylpropanal (**7l**, Table 1, entry 9) indicates a tendency for *anti* addition. The tendency increases for branched alkanals and *n*-alkanals and causes the predominant formation of addition products *ent*-**8**.

[18] a) V. E. Williams, R. P. Lemieux, G. R. J. Thatcher, *J. Org. Chem.* **1996**, *61*, 1927; b) R. J. Wehmschulte, P. P. Power, *J. Am. Chem. Soc.* **1997**, *119*, 2847.

[19] H. E. Zimmerman, M. D. Traxler, *J. Am. Chem. Soc.* **1957**, *79*, 1920.

[20] J. Reubner, R. Fröhlich, D. Hoppe, *Org. Lett.* **2004**, *6*, in press.

 © 2004 Wiley-VCH Verlag GmbH & Co. KGaA, Weinheim

Biomineralization

Regeneration of Human Tooth Enamel**

*Susanne Busch**

Enamel, the exterior coating of vertebrate teeth, is a biomineral with remarkable hardness and resistance to physical and biochemical attack. The special features of enamel result from its composite nature,[1] as it is composed of substituted hydroxyapatite,[2] and organic macromolecules.[3] The tissue is assembled of needlelike crystals, bundled in parallel ordered prisms, but the exact microcrystalline alignment is specific to each individual.[4] As mature enamel is not living tissue, it is only scarcely remineralized after substantial mineral loss (e.g., caries). Currently, defects in enamel and the underlying dentine are usually refilled with unstructured substitutes like amalgam, ceramics, or polymer composites to prevent tooth death.

Various attempts to harden enamel surfaces[5] or remineralize tooth minerals have been undertaken, which include treatment with fluoride,[6] metastable calcium phosphate solution, or apatite particles.[7–11] Conditioning with apatite–protein composite nanoparticles leads to mineral depositions on dentine surfaces.[12] Until now the native structure of enamel has been thought too complex to be remodeled. Herein, an in vitro technique is introduced that induces the localized formation of an ordered enamel-like mineral on human teeth with tight contact to the substrate.[13] Parallel arrays of fluorapatite–protein composite particles up to a macroscopic length scale are formed. The results open up new possibilities for the remodeling of complex biological minerals in vitro, as well as the remineralization of superficial enamel defects in vivo with the advantage of lower acid solubility of fluorapatite compared to tooth enamel.

Basic investigations into the mineralization of fluorapatite in gelatin gels led to the formation of spherical composite particles that show remarkable similarities to tooth enamel in terms of morphology and chemical composition.[14–16] Like enamel, the resulting needlelike crystals have a large aspect ratio and contain about 2 wt % organic material (of composite character[17]). The main differences to enamel are the higher fluoride content of the particles, the composition of the organic component, and the shorter crystal length.

From these results a technique was developed to form dense fluorapatite layers on human enamel, which uses the diffusion of calcium ions from solution in a glycerine-enriched gelatin gel at 37 °C that contains phosphate and fluoride ions and covers the tooth surface. The ion gel is masked with another phosphate-free gel layer. To induce the mineralization of fluorapatite on the surface of the tooth, the prepared samples were immersed in a neutral calcium solution. The gel and calcium solution have to be exchanged periodically (see Experimental Section). A homogeneous enamel-like layer on top of the disk results with a thickness depending on the number of exchange cycles. Figure 1 a shows an SEM image of the side view of a layer grown for 10 days after five growth cycles. The tooth disk was cut so that the long axes of the enamel prisms are oriented perpendicular to the disk surface. Therefore, the crystals are visible from side-on as shown. The orientation of the enamel crystals and the newly crystallized fluorapatite is essentially parallel. The new layer, with a thickness of ≈ 5 μm, is not fully mature. The Knoop hardness number (KHN) was found to be 45 ± 30, similar to tooth dentine (50 ± 30).[18] After the 10th exchange cycle the fluorapatite layer looks more similar to enamel (Figure 1 b) and shows the same Knoop hardness (400 ± 100) as enamel within experimental error (400 ± 50).[19] A dense layer packing of uniform crystals is formed, but in contrast to human enamel the formed prisms are not flattened, but more like regular polygons, such as the fluorapatite crystals in the enameloid of sharks.[20]

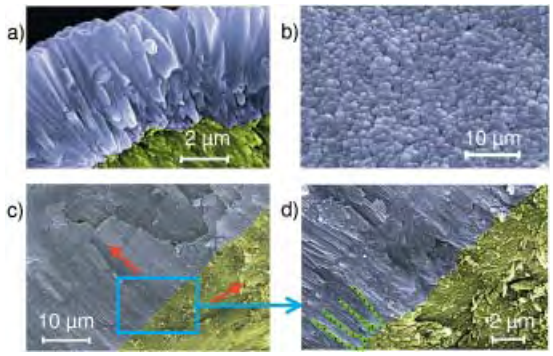


Figure 1. SEM images of fluorapatite layers on human enamel slices; for clarification the fluorapatite layer is colored blue and the enamel layer yellow. a) Side view of the enamel and fluorapatite layers after the 5th exchange cycle of the gel; b) the fluorapatite layer after 10 exchange cycles. A dense layer of homogeneous crystals can be seen. As the crystals on the surface mineralize last, they have not reached the mature state of the underlying area, and thus appear larger; c) side view of enamel and formed fluorapatite after the 36th exchange cycle of the gel. The dense, uniform layer is about 35-μm thick, which corresponds to a growth rate of $\approx 500\ \mathrm{nm\,day^{-1}}$ (red arrows indicate the main direction of crystal orientation); d) close-up of the borderline region between natural enamel and fluorapatite. Below left: the enamel prismlike bundles of fluorapatite are marked.

Figure 1 c shows an SEM image of a sample after the 36th exchange cycle with the enamel prisms running perpendicular to the long axis of the newly formed apatite needles. The SEM micrographs indicate that the new crystals are mostly oriented perpendicular to the surface of the substrate, and are unaffected by the prism orientation; the rate of growth is $\approx 500\ \mathrm{nm\,day^{-1}}$. Figure 1 d shows a close-up of the enamel–fluorapatite interface. The habit and size of both crystal types are similar and although the crystal orientation is not

[*] Dr. S. Busch
Max-Planck-Institut für Chemische Physik fester Stoffe
Nöthnitzer Strasse 40, 01187 Dresden (Germany)
Fax: (+49) 351-4646-3002
E-mail: busch@cpfs.mpg.de

[**] Prof. Rüdiger Kniep, Dr. Oliver Hochrein, Prof. Jürg Hulliger, and Jana Buder are thanked for their support, Dr. Jens Messerschmidt for providing fresh tooth samples, and Dr. Raul Cardoso for X-ray measurements.

 © 2004 Wiley-VCH Verlag GmbH & Co. KGaA, Weinheim DOI: 10.1002/anie.200352183

identical, the fit is nearly perfect. The fluorapatite crystals are partly bundled within these layers, as in natural enamel. The formation of mainly parallel-ordered fluorapatite crystals is verified by X-ray-diffraction (Figure 2a). Due to the perpendicular growth and preferred parallel orientation of the crystals, the 002, 004, 006, and 116 reflections are significantly enhanced. Such enhancement is also typical for enamel surfaces (Figure 2b), due to the far-reaching perpendicular arrangement of the enamel crystals, relative to the tooth surface.[21]

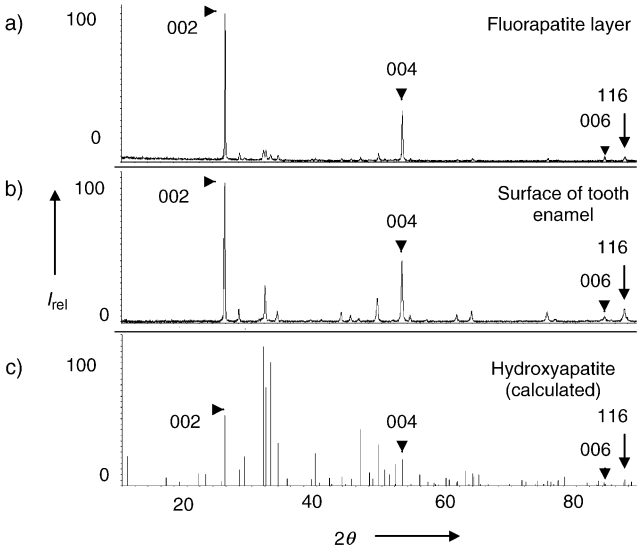


Figure 2. a) X-ray powder diffraction pattern of a fluorapatite layer after the 36th exchange cycle; b) X-ray powder diffraction pattern of the surface of a human incisor; c) a calculated X-ray powder diagram of hexagonal hydroxyapatite.[29] The intensity of certain reflections are enhanced because of strong preferential orientation of individual crystals of the fluorapatite layer and the enamel. Note that the positions of fluorapatite and hexagonal hydroxyapatite are essentially the same. In the case of fluorapatite the position of the reflections are slightly shifted to larger angles because of the smaller lattice parameters.[30]

To set up reaction conditions similar to those found in the human body, the gelatin gel was enriched with glycerine to increase the melting temperature to $\approx 40\,^{\circ}C$.[22] Direct diffusion of calcium ions into a phosphate-containing gel leads to significant precipitation of apatite at the liquid–gel border. Therefore, a shielding layer is introduced that is not enriched with phosphate and fluoride. The four-layer system (tooth, phosphate gel, shielding layer, and calcium solution) is maintained at 37 °C. At pH 5, the mobility of phosphate ions in the gel is reduced compared to that of calcium ions, while at $pH \geq 7$, or when phosphate/fluoride and calcium ions are exchanged, the shielding layer does not function.

To explain the observed crystal growth the following hypothesis is proposed: Positively charged amino groups of gelatinous polypeptides can form saltlike bonds to negatively charged phosphate groups on the apatite surface, and also to hydrogen phosphate ions in the gel. Interactions between acid side groups and calcium ions should be less intense because of the slightly acidic nature of the gel and the pK_s value of acid gelatin (≈ 9[23]). As a result the diffusion of calcium ions towards the tooth surface is faster than the movement of phosphate ions to the gel–liquid interface. Double-diffusion experiments show that the calcium ions have greater mobility in the gelatin gel; most of the mineralized fluorapatite is found on the side of the gel located near the phosphate solution.[24]

Heterogeneous nucleation on the surface of the tooth is induced; examinations of tooth disks with enamel prisms in different orientations relative to the disk surface always show a nearly perpendicular growth of fluorapatite needles relative to the substrate. This is also true for layers covering drilled holes in whole teeth, after the holes were filled with the gel and treated like the tooth disks. Figure 3 illustrates schematically a tooth with a drilled hole; the SEM image shown is of the side wall of such a hole, at which growth has been carried out. A correlation between the overall diffusion direction of the calcium ions and the growth direction can be ruled out. At around pH 5, the charged N-terminal groups of rodlike polypeptides attach to the phosphate groups on the enamel surface, with their long axes oriented perpendicular to the surface. Where nucleation of bone mineral occurs in the collagen-rich extracellulary matrix, there is some evidence that nucleation centers are most likely in regions of high polarity. This is the case in the gap and overlap zones of collagen, and likewise in all areas of the collagen fibrils with high concentrations of polar amino acids.[25] As the sequence of amino acids in collagen and acid-hydrolyzed gelatin is essentially identical, similar polar regions are expected to act as nucleation centers in gelatin. The gap and overlap zones present in native bone collagen that result from the typical quaternary structure of triple-helical collagen molecules are not expected to play a significant role in denatured gelatin, although the partial renaturation to a collagen-like structure is possible.[25] In the case of gelatin, nucleation sites may lie at the ends or between the parallel peptide rods, next to polar amino acid residues. In these regions a high concentration of immobilized hydrogen phosphate ions is expected due to the charged N-terminal amino acids and the side-groups from arginine, histidine, and lysine that make up about 0.8 % of the amino acids occurring in collagen type I.[26] The increase in pH during the diffusion of the neutral calcium solution decreases the solubility product of apatite. Mineralization is

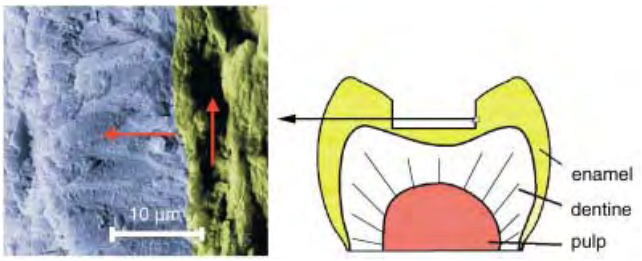


Figure 3. Schematic drawing of a tooth (without a root) with a drilled hole. The marked region corresponds to the SEM image of a side wall where growth has occurred (for clarification the fluorapatite layer is colored blue, the enamel layer yellow). The main direction of crystal orientation is indicated with red arrows.

 © 2004 Wiley-VCH Verlag GmbH & Co. KGaA, Weinheim

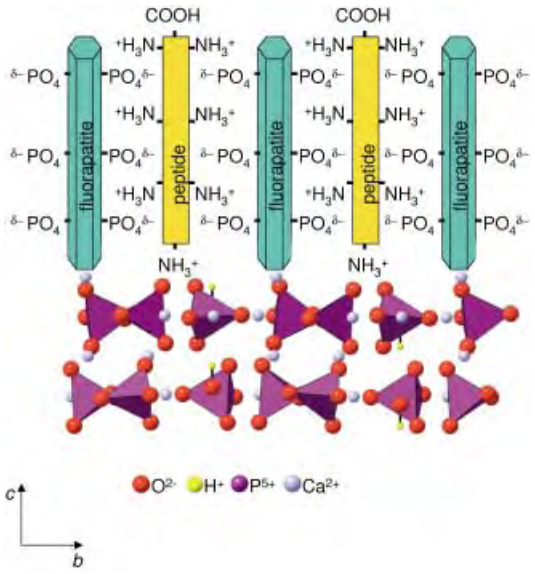


Figure 4. Hypothetical model for the orientation of gelatinous macromolecules on an apatitic surface and the early mineralization of fluorapatite. Phosphate ions are represented as tetrahedra. For simplification, all molecules are considered to be identical. As the exact size of the active organic molecules and the initial fluorapatite crystals are not yet known, the size correlation between organic and inorganic component is not exact. Moreover epitaxial interactions between apatite and gelatin are not discussed here as the superstructure of the active gelatin units is unknown. Phosphate ions on the apatitic enamel surface should be attracted to the positively charged N-terminal end of the peptides. Therefore the peptides should orientate perpendicular to the substrate and parallel to each other. Polar regions on the molecules attract ions which mineralize to apatite (templated by the ordered gelatin), which leads to the perpendicular growth of fluorapatite crystals (only the assumed mineralization between the organic molecules is shown). An interaction of calcium ions with carboxy groups is not taken into account, since the carboxy groups are neutral under the reaction conditions.

thus induced, and crystals arrange parallel to the organic molecules (Figure 4).

From fluorapatite composite aggregates grown in a double-diffusion cell, we conclude that the long axis of apatite and gelatin fibers are preferentially oriented parallel to each other.[17] A parallel orientation of apatite crystals and proteins is also observed for tooth enamel.[27] The induced perpendicular growth of fluorapatite crystals has certain advantages in medical applications: Just as enamel prisms are always oriented so that their long axes run perpendicular to the tooth surface,[21] the fluorapatite crystals also align in the same direction when grown on a natural tooth surface.

The similarity of the natural and the biomimetically grown mineral suggests that the experimental set-up is an attractive model for the mineralization of enamel in particular, but also for biomineralization in general, where a material mimics the morphology of a complex biomineral in some aspects. As in living systems, a composite of uniform particle size, morphology, and orientation is formed.[28] This technique has potential in dentistry as it offers a method of remineralizing teeth that are suffering from superficial mineral loss with a material closer to nature than any restorative material used to date. Moreover, a thin cover layer of the less soluble fluorapatite on tooth enamel should offer considerable protection against caries.

Experimental Section

Human molars were sliced with a diamond saw in disks with a thickness of $\approx 500\,\mu m$; different orientations of the enamel prisms relative to the slice surface were realized. The slices were degreased with absolute ethanol, and etched with 30 wt% phosphoric acid for 30 s to roughen the surface. The as-prepared disks were washed with deionized water and placed in a polyethylene tube. One gel was prepared by mixing gelatin (8.6 g; pig rind, 300 Bloom, acid hydrolyzed), glycerine (85%, 8.2 g), distilled water (7.3 mL), NaOH (2 M, 1.8 mL), AcOH (2 M, 2.7 mL; buffer system), NaF (13.8 mg), and Na_2HPO_4 (755.2 mg). A second gel was prepared by mixing gelatin (8.6 g), glycerine (8.2 g), and H_2O (11.8 g). The mixtures were allowed to swell for 30 min and then heated to 80 °C. Different tooth disks were first covered with a 2-mm-thick layer of the phosphate gel and then with a 2-mm-thick layer of ion-free gelatin. After gelification the polyethylene tube is filled with 10 mL of a neutral $CaCl_2$ solution (0.13 M) and the gel is immersed for 20–60 min. The tooth sections are maintained in a water bath at 37 °C. Immersion in the calcium solution is repeated every 24 h, and the gel has to be replaced every 48 h. To examine the growth behavior on complete teeth, a human molar with a hole 2 mm in diameter and 1 mm in depth was filled with the gels, and the calcium solution was added as described above. The fluorapatite layer was examined by X-ray powder diffraction (STOE STADI P) in the reflection mode ($Cu_{K\alpha 1}$ radiation, Ge monochromator).

Received: June 23, 2003
Revised: October 30, 2003 [Z52183]

Keywords: bioinorganic chemistry · biomineralization · composite structures · enamel · fluorapatite

[1] S. Mann, *Nature* **1988**, *332*, 119–124.
[2] E. D. Eanes, *J. Dent. Res.* **1979**, *58B*, 829–836.
[3] C. Robinson, S. J. Brookes, R. C. Shore, J. Kirkham, *Eur. J. Oral Sci.* **1998**, *106*, 282–291.
[4] G. Cevc, P. Cevc, M. Schara, U. Skaleric, *Nature* **1980**, *286*, 425–426.
[5] T. Koulourides, H. Cueto, W. Pigman, *Nature* **1961**, *189*, 226–227.
[6] T. Aoba, *Crit. Rev. Oral Biol. Med.* **1997**, *8*, 136–153.
[7] S. R. Brailsford, B. Shah, D. Simons, S. Gilbert, D. Clark, I. Ines, S. E. Adams, C. Allison, D. Beighton, *J. Dent. Res.* **2001**, *80*, 1828–1833.
[8] E. Lynch, A. Baysan, *Caries Res.* **2001**, *35*, 60–64.
[9] G. Dolchi, International Patent 00/03747, **2000.**
[10] K. Kropf, H. Dolhaine, M. Marcel, U. Brüninghaus, A. Weiss, U. Schrörken, L. Kintrup, A. Pastura, P. Wülknitz, R. Kniep, B. Eschen, M. Meinders, H. Laska, S. Müllner, International Patent 01/01930A2, **2001**.
[11] W. Wiedemann, International Patent 98/10736, **1998**.
[12] G. Schechner, **2002**, private communication.
[13] S. Busch, R. Kniep, WO 102 23 157.5, **2002**.
[14] S. Busch, H. Dolhaine, A. DuChesne, S. Heinz, O. Hochrein, F. Laeri, O. Podebrad, U. Fietze, T. Weiland, R. Kniep, *Eur. J. Inorg. Chem.* **1999**, 1643–1653.
[15] S. Busch, U. Schwarz, R. Kniep, *Chem. Mater.* **2001**, *13*, 3260–3271.
[16] R. Kniep, S. Busch, *Angew. Chem.* **1996**, *108*, 2788–2791; *Angew. Chem. Int. Ed. Engl.* **1996**, *35*, 2624–2626.
[17] S. Busch, U. Schwarz, R. Kniep, *Adv. Funct. Mater.* **2003**, *13*, 189–198.

 © 2004 Wiley-VCH Verlag GmbH & Co. KGaA, Weinheim

[18] Y. Hosoya, S. J. Marshall, L. G. Watanabe, G. W. Marshall, *Oper. Dent.* **2000**, *25*, 81 – 89.
[19] K. Collys, D. Slop, R. Cleymaet, D. Coomans, Y. Michotte, *Dent. Mater.* **1992**, *8*, 332 – 335.
[20] N. Kemp, J. H. Park, *Arch. Oral. Biol.* **1974**, *19*, 633 – 644.
[21] R. J. Radlanski, W. Seidl, G. Steding, A. Jäger, *Anat. Anz.* **1998**, *168*, 405 – 412.
[22] T. Leopold, *Z. Körperpflegemittel-*, *Parfümerie-*, *Riechstoff- und Aerosol-Industrie* **1990**, *16*, 639 – 645.
[23] I. Tomka, *Chimia* **1983**, *37*, 534 – 540.
[24] S. Busch, Ph.D. Thesis, University of Technology, Darmstadt, **1998.**
[25] M. E. Maitland, A. L. Arsenault, *Calcif. Tissue Int.* **1991**, *48*, 341 – 352.
[26] P. I. Rose in *Encyclopedia of Polymer Science and Engineering*, Wiley, London, **1987**.
[27] *Handbook of Microscopic Anatomy: Teeth* (Eds.: A. Oksche, L. Vollrath), Springer, Berlin, **1989**.
[28] A. L. Bianconi, J. Lin, A. R. Strzelecki, *Nature* **1991**, *349*, 315 – 317.
[29] K. Sudarsanan, R. A. Young, *Acta Crystallogr. Sect. B* **1982**, *24*, 1968 – 2038.
[30] K. Sudarsanan, P. E. Mackie, R. A. Young, *Mater. Res. Bull.* **1971**, *7*, 1331 – 1338.

 © 2004 Wiley-VCH Verlag GmbH & Co. KGaA, Weinheim

Microelectrochemistry

Imaging Concentration Profiles of Redox-Active Species with Nanometric Amperometric Probes: Effect of Natural Convection on Transport at Microdisk Electrodes**

Norman Baltes, Laurent Thouin, Christian Amatore, and Jürgen Heinze**

Microelectrochemistry opens new dimensions for the solution of many electroanalytical problems.[1,2] In this context, a fascinating new development is the electrochemical imaging of the topologies and reactivities of surfaces and layers. This can be performed by coupling scanning probe techniques with electrochemistry (scanning electrochemical microscopy; SECM).[3–6] The spatial resolution achieved in the measurements is directly related to the electrochemical techniques investigated and the properties of the probing electrodes used.[4] We recently demonstrated that potentiometric[7,8] and amperometric[8–11] detections could be performed with a microelectrode probe to map concentration profiles above an electrochemically active surface.

When the microelectrode tip is used as a potentiometric probe, it does not consume analyte. The concentration profile of electroactive species is thus not perturbed by the tip except for possible geometrical hindrance to the transport of molecules and ions. Furthermore, it is also possible to use ion-selective microtips[12–15] to investigate complex mechanisms.[7] However, despite its accuracy, potentiometric detection requires long detection times, since a redox equilibrium must be fully reached at the probe surface. Therefore, only steady-state concentration profiles can be probed, which prevents the study of transient processes. In addition, external assumptions are required to reconstruct absolute concentrations based on the electrochemical potential mapped. Finally, experimental conditions are sometimes restricted by the possible contamination of the electrochemical potential by other electrical potential sources such as ohmic drop potentials and diffusion potentials.[7]

By comparison, amperometric detection is more flexible and suitable because it avoids all the above difficulties,[8] provided that the electrochemical reaction occurring on the probe surface does not significantly disturb the diffusion layer under investigation. This, in turn, limits the applicability and the resolution of this method if averaging of concentration measured on the probe diffusion layer is significant and/or there are feedback effects between probe and substrate.[16,17] The method can be improved through the short time connection–polarization of the probe[9] or through the use of an additional chemical reaction known as a "chemical lens".[18] However, since the attainable resolution depends on both the probe radius and the distance between probe and substrate, another alternative is to use nanometer-sized probes (nanoprobes)[6,19–27] which allow one to increase the resolution and to de facto avoid such artefacts.

In this work, we demonstrate that in agreement with expectations the mapping of concentration profiles of redox-active species can be performed with excellent accuracy and resolution by using nanometric amperometric probes to investigate transport at micrometric level. Indeed, since the size of the zone in which significant concentration gradients develop at a spherical-type probe is at most similar to its radius, one expects that the current detected at a nanometric probe will be indicative of concentrations averaged over nanometric distances. This is a critical notion since this means that the nanometric probe is monitoring the true local concentration of a species and is almost immune to any side effects. In particular, we wish to take advantage of this increased spatial resolution to address the influence of natural convection[10] that necessarily affects the development of

[*] Dr. L. Thouin, Prof. Dr. C. Amatore
Ecole Normale Supérieure, Département de Chimie
UMR CNRS-ENS-UPMC 8640 "PASTEUR"
24 rue Lhomond, 75231 Paris Cedex 05 (France)
Fax: (+33) 1-4432-3863
E-mail: christian.amatore@ens.fr
Dipl.-Chem. N. Baltes, Prof. Dr. J. Heinze
Institut für Physikalische Chemie
Albert-Ludwigs-Universitäat Freiburg
Albertstrasse 21, 79104 Freiburg (Germany)
and
Freiburger Materialforschungszentrum (FMF)
Albert-Ludwigs-Universität Freiburg
Stefan-Meier-Strasse 21, 79104 Freiburg (Germany)
Fax: (+49) 761-203-6237
E-mail: juergen.heinze@physchem.uni-freiburg.de

[**] This work has been supported in part by the CNRS (UMR 8640), the French Ministry of Research, the Ecole Normale Supérieure in Paris, and by the Deutsche Forschungsgemeinschaft. Support from a specific bilateral cooperation program between France (Procope n°00237YE) and Germany (DAAD Akz.: 312-pro-ms) is also gratefully acknowledged.

 DOI: 10.1002/anie.200352662 © 2004 Wiley-VCH Verlag GmbH & Co. KGaA, Weinheim

hemispherical diffusion and thus of concentration distributions at microdiskelectrodes.[28]

The nanoelectrodes obtained by application of our fabrication procedure were characterized by cyclic voltammetry in a solution of 5 mM $[Ru(NH_3)_6]^{3+}$ containing 0.1 M KF.[23,27] Figure 1 shows several steady-state cyclic voltammograms monitored at several nanoelectrodes. Assuming that the electrode geometry is a perfect disk, the evaluation of the corresponding radius was performed by considering the diffusion-limited current. Radii were thus estimated as ranging approximately between 10 and 300 nm. These limits represent the variety of Pt nanoelectrodes that can be easily constructed by using our experimental procedure. Such discrepancies are due mainly to the polishing process, which has a significant impact on the final size of the electrode.

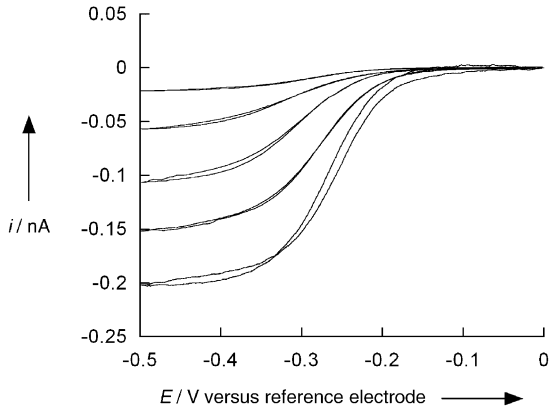


Figure 1. Steady-state voltammograms monitored at nanoelectrodes of various radii in 5 mM $[Ru(NH_3)_6]^{3+}$/0.1 M KF solution: radii (from top to bottom): 17, 45, 85, 125, and 165 nm based on their plateau currents. Scan rate 0.1 Vs^{-1}.

In scanning electrochemical microscopy these nanoelectrodes were used as amperometric probes to map concentration gradients above a larger electrode. Figure 2 shows a typical two-dimensional map. Qualitatively speaking, the resolution of the measurements is very satisfactory since the disk shape of the generator electrode is reproduced with a diameter comparable to its nominal size. Furthermore, the measurements are very stable over time so that such a two-dimensional map can be constructed from a series of measurements performed over at least 10 min without any alteration. Since the size of the probe is very small compared to the distance separating the two electrodes ($z = 5$ μm), no positive feedback is expected contrary to what should be observed in this case using micrometric probes.[29]

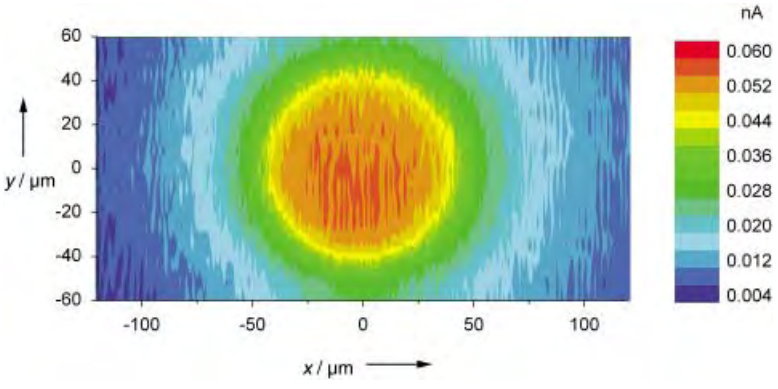


Figure 2. Two-dimensional map of currents (concentrations) measured by a nanoprobe (r = 80 nm, collector) in the vicinity of a microelectrode ($r = 40$ μm, generator). The nanoprobe was scanned parallel to the microelectrode plane at a constant vertical distance $z = 5$ μm with a speed of 8 μm s^{-1}. The generator potential of the microelectrode was placed on the plateau of the reduction wave of $[Ru(NH_3)_6]^{3+}$ ($E_{gen} = -0.45$ V versus reference electrode) and the nanoelectrode probe potential was set on the plateau of the $[Ru(NH_3)_6]^{2+}$ oxidation wave ($E_{probe} = 0$ V versus reference electrode). The bulk solution contained 5 mM $[Ru(NH_3)_6]Cl_3$ in an aqueous 0.1 M KF solution.

Figure 3 shows the steady-state currents monitored at a nanoelectrode ($r = 95$ nm) as a function of the distance to a microelectrode ($r = 250$ μm), where the nanoelectrode acts either as the collector (GC) or as the generator (CG), and the larger microelectrode plays the other role respectively. In this case, the nanoelectrode is displaced along the z axis perpendicular to the center of a micrometric (250 μm radius) electrode. In the CG mode the current remains almost constant up to the point at which the two electrodes have physical contact (i.e., $z = 0$). This constancy evidences the absence of feedback between the two electrodes.

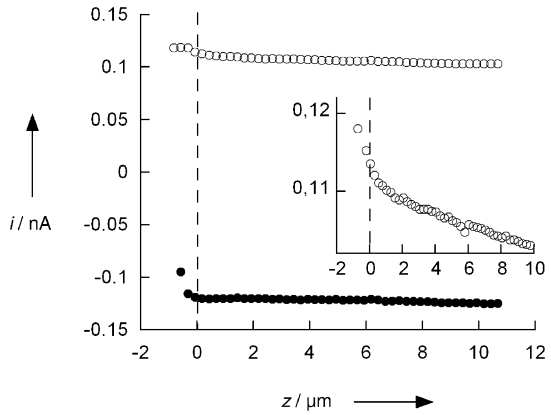


Figure 3. Approach curves monitored in GC (open circles) and CG (solid circles) modes using a nanometric tip ($r = 95$ nm) in the vicinity of a microelectrode ($r = 250$ μm). Inset: Expansion of the approach curve in GC mode. See Figure 2 for the other experimental conditions. See the text for the definitions of the GC and CG modes and for the meaning of data recorded at $z < 0$.

When the probe is pushed further (i.e., for data points $z < 0$ in Figure 3), the probe bends due to its high flexibility, and the related current drops dramatically, presumably owing to hindering effects, but no shortcut effect is noted. In the GC mode, the current varies linearly as a function of the distance separating the two electrodes since it monitors the almost linear variation of the Ru^{II} concentration gradient which is installed at close distances from the micrometric electrode. Indeed, a planar transport regime is expected over any micrometric

 © 2004 Wiley-VCH Verlag GmbH & Co. KGaA, Weinheim

electrode over distances that remain much smaller than its radius (250 μm in Figure 3).[29] When the two electrodes are touching (i.e., again $z<0$), the current increases up to a given limit. In both modes, the absolute values of the currents i that can be evaluated at $z=0$ are almost identical within the measured accuracy. This result demonstrates again that no feedback occurs between the electrodes and furthermore that Ru^{III} and Ru^{II} have approximately identical diffusion coefficients. Consequently, in each mode the current i measured locally by the probe electrode at any $z>0$ is proportional to the same extent to the local concentration C of either Ru^{III} (CG mode) or Ru^{II} (GC mode). Therefore, if i_0 denotes the absolute value of the average current measured by the probe upon reduction of Ru^{III} in a bulk solution of Ru^{III} with concentration C_0, the current ratio i/i_0 in the GC mode, is thus equivalent to the concentration ratio C/C_0 where C is the concentration of Ru^{II}.

Figure 4 shows the concentration profile (circles) of Ru^{II} monitored along the z axis perpendicular to the microelectrode (generator) and passing through its center. This

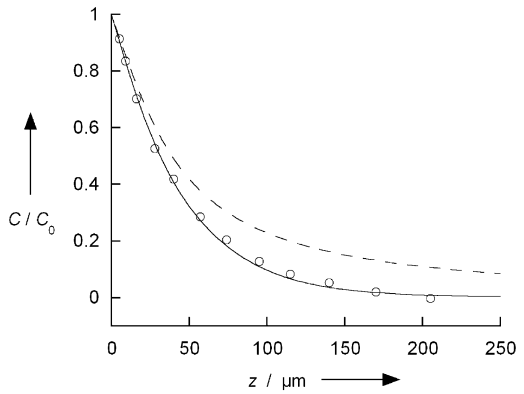


Figure 4. Concentration profile (circles) recorded near a generator microelectrode ($r=40$ μm) along its vertical z axis above its center ($x=y=0$ in Figure 2). The experimental profile (circles) is superimposed on those predicted by taking into account the effect of diffusion only (dashed line) or by including natural convection (solid line; $\delta=135$ μm, see text). See Figure 2 for the other experimental conditions.

experimental profile is compared to a series of two theoretical profiles predicted on the basis that transport occurs either exclusively by diffusion (dashed line) or is corrupted by natural convection (solid line), although the solution is motionless overall.[10] In the second case (i.e. mixed convective-diffusive transport), the theoretical model was adapted from that previously developed for planar diffusion, by extending it to include the case of transport at a microdisk electrode. Quantitative prediction by this model without any adjustment by fitting theoretical to experimental results is verified by independent experimental determination of the parameters r_0 and δ the microelectrode generator radius and the limiting thickness of the diffusion layer which is reached at a planar macroelectrode with infinite polarization times, respectively.[10] A value of $\delta=135$ μm was determined independently by monitoring steady-state concentration profiles under the same (i.e., identical hydrodynamic) experimental conditions in the vicinity of a macroelectrode (data not shown). After calculation, one observes that there is excellent agreement between the experimental and theoretical data at any relevant distance from the microelectrode surface. This result demonstrates the validity of the model and illustrates again that no positive feedback was observed under these experimental conditions.

The dashed line in Figure 4 represents the concentration profile obtained by resolving the diffusion equations without taking into account the effect of natural convection. One can see that even for a microelectrode with a radius of 40 μm, natural convection very significantly affects the concentration profile. Consequently this effect should contribute to some extent to its steady-state current. However, the gradient at the

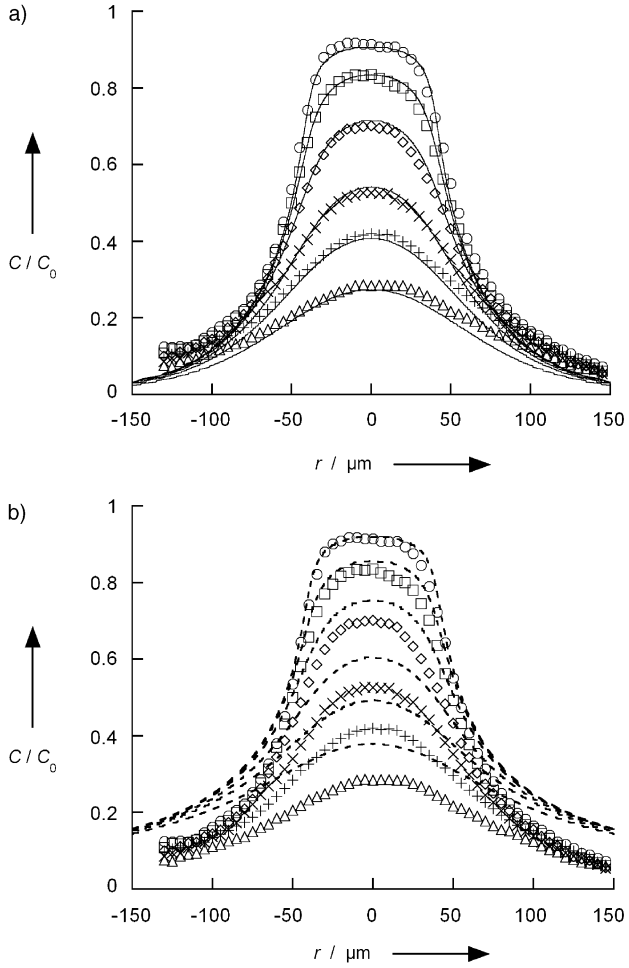


Figure 5. Experimental concentration profiles measured at various vertical distances z on top of the center of a generator microelectrode ($r=40$ μm) at various distances from its symmetry axis ($r=[x^2+y^2]^{1/2}$, see Figure 2) as a function of z: $z=5$ (circles), 9 (squares), 16 (diamonds), 28 (tilted crosses), 40 (crosses), and 57 μm (triangles). a) Comparison of the experimental concentrations with those predicted (solid lines) as a function of r for the same set of z values by taking into account mixed transport by diffusion and natural convection ($\delta=135$ μm, see text). b) Comparison of the experimental concentrations with those predicted (dashed lines) by taking into account transport by diffusion only. See Figure 2 for the other experimental conditions.

 © 2004 Wiley-VCH Verlag GmbH & Co. KGaA, Weinheim

electrode surface (i.e., the current) is only modestly affected, so that the two predicted curves are almost tangential near $z = 0$. This situation is characteristic of spherical type microelectrodes[30,31] and contrasts sharply with what occurs under planar diffusion, where the steady-state gradients are imposed by the natural convection,[10] as assumed by the classical Nernst layer approximation.

Figure 5a shows the concentration profiles obtained from several scans parallel to the microelectrode surface and performed at different constant distances z over the microelectrode plane. As in Figure 2, these concentration profiles demonstrate that the most important concentration gradients are located above the microelectrode surface and that they extend over distances which remain comparable to the microelectrode radius.[30,31]

Again, there is an excellent agreement between these data and those predicted when natural convection is taken into account. The influence of natural convection on transport and concentration patterns above the microelectrode, is only fully appreciated when the same experimental data are superimposed on the theoretical concentration profiles of exclusively diffusional transport (Figure 5b). One sees that the most significant deviations occur above about 10 μm, that is when the distance from the microelectrode surface is not much smaller than its radius.

The concentration profiles obtained experimentally illustrate the drastic role of natural convection even if the microelectrode generator currents remain almost unaffected. Further work is in progress and details about the influence of convection on planar–hemispherical diffusion will be discussed elsewhere.

Experimental Section

Solutions of $[Ru(NH_3)_6]Cl_3$ (5 mM, 98%, Aldrich) were prepared from Milli-Q reagent water (Millipore Corp.) with 0.1M KF (p.A., Merck) as supporting electrolyte. The solution was previously degassed by argon bubbling and maintained under a continuously renewed argon blanket during all the experiments.

The instrumentation for SECM measurements has been described in detail elsewhere.[27,32] The substrate, held at a 90° angle to the tip axis is carried by an x–y stage that is moved independently by two piezoelectric translators (P-731.20 and P-750.20, Physik Instrumente), controlled by a program controller (C-842 DC-Motor Controller, Physik Instrumente). They allow translations to be performed in the z direction with a 5 nm per step resolution. Additional stages (M-511.DG, Physik Instrumente) with a 300 nm increment are incorporated for larger translations up to 102 mm.

The whole setup was mounted on a vibration-insulating table (Mod 1-XL, Halcyonics) and shielded by using a home-built Faraday cage. A limiting speed of 8 $\mu m\,s^{-1}$ was applied to the probe to avoid locally any convection induced by its displacement.

A four-electrode configuration was used with a bipotentiostat (home-built). The reference electrode was a calomel electrode (KCl 0.1M) and the counter-electrode was a Pt sheet of 1 mm^2 diameter.

The Pt disk electrodes with radii of 250 μm and 40 μm used to generate the concentration profiles measured by the probes were cross-sections of Pt wires (500 μm and 80 μm nominal diameters respectively, Goodfellow) sealed in soft glass.

The nanometric electrodes were obtained by the following procedure.[23,27] A Pt wire of 25 μm diameter and 21 cm length sealed in a quartz capillary (250 μm outer diameter, Thomas recording) was positioned on a laser puller (P2000, Sutter Instruments) that the laser beam was focused on the center of the capillary. A hard pull was applied 10–100 ms before the end of the heating phase, leading to the formation of two Pt nanotips with Pt wires entirely sealed along the whole capillary. Rigidity of the electrode was assured, by inserting the capillary into a larger tube (1.5 mm outer diameter) except for the nanoelectrode tip, which protruded about 2–3 mm beyond the capillary-outer tube seal. This was important to avoid geometrical hindrance to diffusion by the probe. The tube and capillary were sealed together with a drop of epoxy and contact was made on the opposite side of the tip by inserting a Cu wire into the tube and using Hg to establish contact (puriss, Fluka).

A home-made polishing machine was specifically designed.[23,27,33] The distance between the tip and the polishing plate could be controlled by moving the holder with a micrometer screw; this was controlled optically by means of binoculars (Stemi 2000C, Zeiss). The self-adhesive polishing papers used were of 0.3 to 9 μm alumina grain size (Fibermet disks, Buehler).

Received: August 18, 2003 [Z52662]

Keywords: cyclic voltammetry · diffusion · electrochemistry · nanotechnology · scanning electrochemical microscopy

[1] J. Heinze, *Angew. Chem.* **1993**, *105*, 1327–1349; *Angew. Chem. Int. Ed. Engl.* **1993**, *32*, 1268–1288.
[2] J. W. Schultze, T. Osaka, *Electrochemical Microsystem Technologies*, Taylor & Francis, London, **2002**.
[3] K. Borgwarth, C. Ricken, D. G. Ebling, J. Heinze, *Fresenius J. Anal. Chem.* **1996**, *356*, 288–294.
[4] M. V. Mirkin, B. R. Horrocks, *Anal. Chim. Acta* **2000**, *406*, 119–146.
[5] A. J. Bard, M. V. Mirkin, *Scanning electrochemical microscopy*, Marcel Dekker, New York, **2001**.
[6] H. V. Macpherson, P. R. Unwin, *Anal. Chem.* **2001**, *73*, 550–557.
[7] C. Amatore, S. Szunerits, L. Thouin, *Electrochem. Commun.* **2000**, *2*, 248–253.
[8] C. Amatore, S. Szunerits, L. Thouin, J.-S. Warkocz, *Electroanalysis* **2001**, *13*, 646–652.
[9] C. Amatore, S. Szunerits, L. Thouin, J.-S. Warkocz, *Electrochem. Commun.* **2000**, *2*, 353–358.
[10] C. Amatore, S. Szunerits, L. Thouin, J.-S. Warkocz, *J. Electroanal. Chem.* **2001**, *500*, 62–70.
[11] C. Amatore, C. Pebay, O. Scialdone, S. Szunerits, L. Thouin, *Chem. Eur. J.* **2001**, *7*, 2933–2937.
[12] G. Denuault, M. H. Troise-Frank, L. M. Peter, *Faraday Discuss.* **1992**, *94*, 23–35.
[13] B. R. Horrocks, M. V. Mirkin, D. T. Pierce, A. J. Bard, *Anal. Chem.* **1993**, *65*, 1213–1224.
[14] C. Wei, A. J. Bard, G. Nagy, K. Toth, *Anal. Chem.* **1995**, *67*, 1346–1356.
[15] C. Wei, A. J. Bard, I. Kapui, G. Nagy, K. Toth, *Anal. Chem.* **1996**, *68*, 2651–2655.
[16] R. C. Engstrom, M. Weber, D. J. Wunder, R. Burgess, S. Winquist, *Anal. Chem.* **1986**, *58*, 844–848.
[17] R. C. Engstrom, T. Meaney, R. Tople, R. M. Wightman, *Anal. Chem.* **1987**, *59*, 2005–2010.
[18] K. Borgwarth, J. Heinze, *J. Electrochem. Soc.* **1996**, *146*, 3285–3289.
[19] R. M. Penner, M. J. Heben, T. L. Longin, N. S. Lewis, *Science* **1990**, *250*, 1118–1121.
[20] M. V. Mirkin, F. R. F. Fan, A. J. Bard, *J. Electroanal. Chem.* **1992**, *328*, 47–62.
[21] X. Zhang, W. Zhang, X. Zhou, B. Ogorevc, *Anal. Chem.* **1996**, *68*, 3338–3343.

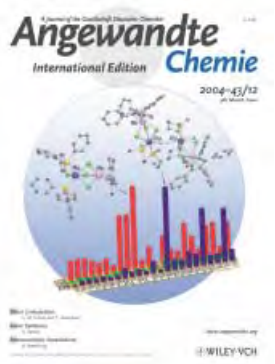
 © 2004 Wiley-VCH Verlag GmbH & Co. KGaA, Weinheim

[22] Y. H. Shao, M. V. Mirkin, G. Fish, S. Kokotov, D. Palanker, A. Lewis, *Anal. Chem.* **1997**, *69*, 1627 – 1634.
[23] J. Heinze, J. Ufheil, K. Borgwarth in *75th Bunsen-Meeting*, Leipzig, **1998**.
[24] C. J. Slevin, N. J. Gray, J. V. Macpherson, M. A. Webb, P. R. Unwin, *Electrochem. Commun.* **1999**, *1*, 282 – 288.
[25] J. L. Conyers, H. S. White, *Anal. Chem.* **2000**, *72*, 4441 – 4446.
[26] B. B. Katemann, W. Schuhmann, *Electroanalysis* **2002**, *14*, 22 – 28.
[27] J. Ufheil, C. Hess, K. Borgwarth, J. Heinze, *Phys. Chem. Phys.* submitted.
[28] In the following we use "natural convection" to denote the contribution to transport to and from an electrode surface which originates from convective modes that develop in locally still solution due to several sources (vibrations, thermal or density gradients, etc.) and result in the creation of eddies of micrometric dimensions which locally scramble the solution composition. For a detailed discussion of this phenomenon, see: C. Amatore, S. Szunerits, L. Thouin, J.-S. Warkocz, *J. Electroanal. Chem.* **2001**, 500, 62 – 70.
[29] J. Kwak, A. J. Bard, *Anal. Chem.* **1989**, *61*, 1221 – 1227.
[30] C. Amatore in *Physical Electrochemistry* (Ed.: I. Rubinstein), Marcel Dekker, New York, **1995**, pp. 131 – 208.
[31] C. Amatore, B. Fosset, *Anal. Chem.* **1996**, *68*, 4377 – 4388.
[32] K. Borgwarth, D. Ebling, J. Heinze, *Electrochim. Acta* **1995**, *40*, 1455 – 1460.
[33] J. Ufheil, K. Borgwarth, J. Heinze, *Anal. Chem.* **2002**, *74*, 1316 – 1321.

 © 2004 Wiley-VCH Verlag GmbH & Co. KGaA, Weinheim

Cover Picture

Laurent Quebatte, Rosario Scopelliti, and Kay Severin*



Highly efficient Rh–Ru catalysts for atom-transfer radical additions have been discovered in a fast screening assay. The catalyst library used in this assay was generated in situ by mixing chloro-bridged complexes of Ru^{II}, Ru^{III}, Ru^{IV}, Rh^{I}, Rh^{III}, Ir^{I}, Ir^{III}, Pd^{II}, and Pt^{II} with three different Ru^{II}–phosphane complexes. On page 1520 ff., K. Severin and co-workers describe the structures and reactivities of the new catalysts.

Contents

Angewandte EarlyView

The following articles are available online (in Wiley InterScience). You can find them at www.angewandte.org, under Full Text, Early View.

J. Rzayev, J. Penelle:*
HP-RAFT: A Free-Radical Polymerization Technique for Obtaining Living Polymers of Ultrahigh Molecular Weights
DOI: 10.1002/anie.200353025
Published online: March 1, 2004

T. Kawase, K. Tanaka, N. Shiono, Y. Seirai, M. Oda*:*
Onion-Type Complexation Based on Carbon Nanorings and a Buckminsterfullerene
DOI: 10.1002/anie.200353517
Published online: February 27, 2004

T. S. van Erp, E. J. Meijer:*
Proton-Assisted Ethylene Hydration in Aqueous Solution
DOI: 10.1002/anie.200353103
Published online: February 27, 2004

Articles judged by the referees or the editor as being either very important or very urgent are immediately edited, proof-read, and electronically published once the manuscript has arrived in the editorial office in final form. As long as there is no page number available these articles should be cited in the following manner:

Author(s) *Angew. Chem. Int. Ed.*, online publication date, DOI.

News

Süe Award to M. Verdaguer ——— **1456**

Prize for Coordination Chemistry to A. Bousseksou ——— **1456**

Reviews 2003: Competition Results ——— **1456**

Books

No Time to be Brief ——— **1457** C. P. Enz *reviewed by W. Kutzelnigg*

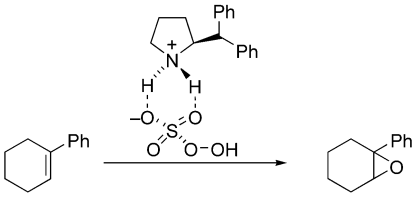
Magick, Mayhem, and Mavericks — **1458** Cathy Cobb *reviewed by P. Atkins*

Highlights

Catalytic Oxidation

A. Armstrong* ——— **1460 – 1462**

Amine-Catalyzed Epoxidation of Alkenes: A New Mechanism for the Activation of Oxone



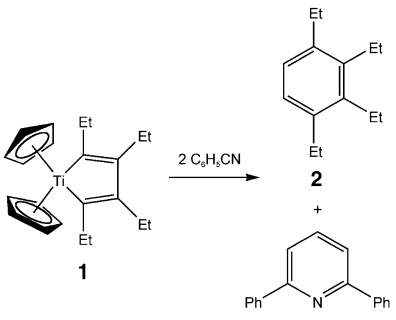
Some of the most promising systems emerging for the catalytic asymmetric epoxidation of alkenes involve the activation of oxone (active constituent $KHSO_5$). The discovery of catalysis by amines is an exciting development in this area of organocatalysis, and a new mechanism for the activation of oxone has been advanced with important consequences (see scheme).

Synthetic Methods

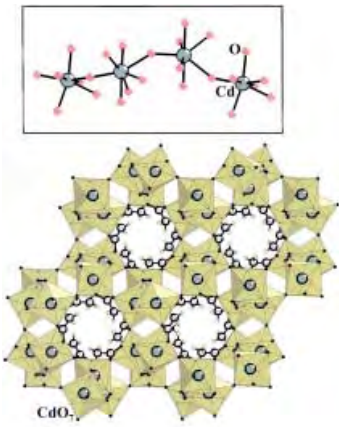
R. Kempe* ——— **1463 – 1464**

A New Arene Synthesis—Or: How Inert Is the Cyclopentadienyl Ligand?

A nice Cp recipe: The reaction of **1** with benzonitrile is a novel arene synthesis developed by Xi, Takahashi, and co-workers. Formally it is the breakdown of a cyclopentadienyl ligand into a C_2 fragment and a C_3 fragment which are then incorporated into a benzene and pyridine derivative, respectively. This synthetic variant has possible interesting applications in the preparation of oligoarenes.



Reviews



Metal carboxylates form a variety of fascinating open-framework structures (see picture). In this Review the synthesis, structure, and properties of various families of metal carboxylates, as well as organic–inorganic hybrid structures involving carboxylates, are presented. The use of carboxylate ligands as linking groups is of particularly interest.

Solid-State Structures

C. N. R. Rao,* S. Natarajan, R. Vaidhyanathan ——— **1466 – 1496**

Metal Carboxylates with Open Architectures

Communications



Completing RGB color space: The electrochemical and optical properties of the first electrochemically prepared conducting polymer that is green in its neutral form are reported. The extreme stability of this polymer after 10000 double potential steps makes it the best and only candidate for providing the missing third leg of RGB color space (red, blue, and green reflection; see picture) required for polymeric electrochromics.

Conducting Polymers

G. Sonmez, C. K. F. Shen, Y. Rubin, F. Wudl* ——— **1498 – 1502**

A Red, Green, and Blue (RGB) Polymeric Electrochromic Device (PECD): The Dawning of the PECD Era



Humidity-dependent electrical conductivity, which suggests possible applications in sensors, is exhibited by OCF-6GaSe, an open-framework gallium selenide assembled from T3 ($Ga_{10}Se_{20}^{10-}$) supertetrahedral clusters (picture, left). Furthermore, materials based on T4 ($Zn_4Ga_{16}Se_{35}^{14-}$, right), the largest supertetrahedral selenide cluster so far, were also obtained.

Supertetrahedral Clusters

X. Bu, N. Zheng, X. Wang, B. Wang, P. Feng* ——— **1502 – 1505**

Three-Dimensional Frameworks of Gallium Selenide Supertetrahedral Clusters

For the USA and Canada:
ANGEWANDTE CHEMIE International Edition (ISSN 1433-7851) is published weekly by Wiley-VCH PO Box 191161, D 69451 Weinheim, Germany. Air freight and mailing in the USA by Publications Expediting Inc. 200 Meacham Ave., Elmont, NY 11003. Periodicals postage paid at Jamaica NY 11431. US POSTMASTER: send address changes to *Angewandte Chemie*, Wiley-VCH, 111 River Street, Hoboken, NJ 07030. Annual subscription price for institutions: Europe € 3430.00/3118.00; outside Europe US$ 4499.00/4090.00 (valid for print and electronic/print or electronic delivery); for individuals who are personal members of a national chemical society, or whose institution already subscribes, or who are retired or self-employed consultants, print only: Europe € 248.00/outside Europe US$ 378.00. Postage and handling charges included. All Wiley-VCH prices are exclusive VAT.

 © 2004 Wiley-VCH Verlag GmbH & Co. KGaA, Weinheim

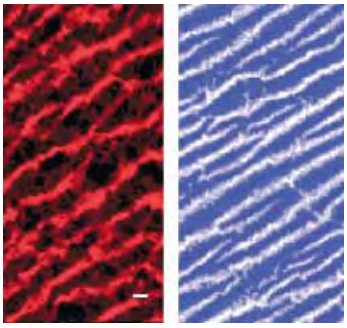
Contents

Mesoporous Materials

P. R. Giunta, R. P. Washington, T. D. Campbell, O. Steinbock,* A. E. Stiegman* ——— **1505 – 1507**

Preparation of Mesoporous Silica Monoliths with Ordered Arrays of Macrochannels Templated from Electric-Field-Oriented Hydrogels

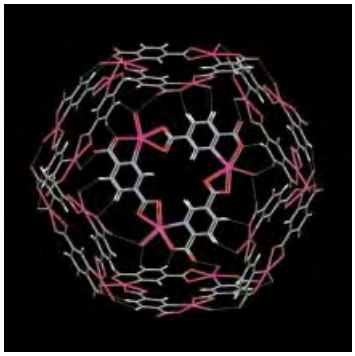
Silica monoliths with ordered arrays of micrometer-scale columns were fabricated from polyacrylamide gel templates. The preparation of the template involves the charged comonomer, N-acryloyl glycine, and is controlled by an externally applied electric field. This approach gives rise to the self-organization of columnar density patterns in the template (left; bar = 10 μm) that are recovered in the silica monoliths upon impregnation with tetramethylorthosilicate and subsequent calcination (right).



Microporous Materials

R. García-Zarracino, H. Höpfl* ——— **1507 – 1511**

A 3D Hybrid Network Containing Large Spherical Cavities Formed through a Combination of Metal Coordination and Hydrogen Bonding

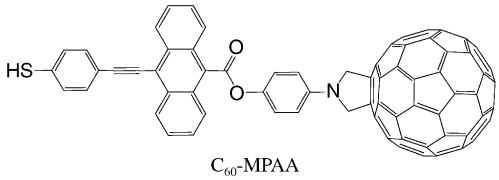


The hole story: A microporous material with cavities that have an internal volume of 1850 Å^3 has been formed from simple starting materials by combining them first through covalent coordination, and then through hydrogen-bonding interactions. The capsules in the 3D network can function as hosts for guest molecules such as triphenylmethane, sodium tetraphenylborate, and triptycene (see picture).

Fullerenes

S. H. Kang, H. Ma, M.-S. Kang, K.-S. Kim, A. K.-Y. Jen,* M. H. Zareie, M. Sarikaya* ——— **1512 – 1516**

Ordered Self-Assembly and Electronic Behavior of C_{60}–Anthrylphenylacetylene Hybrid



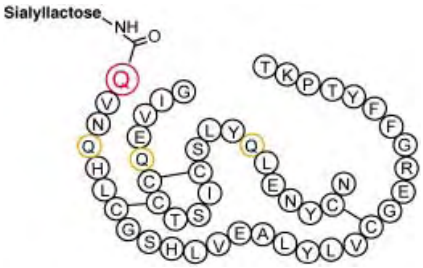
C_{60}-MPAA

A functional hybrid molecule, C_{60}–MPAA, has been designed and synthesized by taking advantage of the excellent physical and chemical properties of C_{60} and nanoscale ordering of anthryl-based self-assembled monolayers (SAMs). The SAM of C_{60}–MPAA exhibits stable and highly ordered 2D arrays that form an oblique lattice at room temperature and exhibit interesting electronic properties.

Drug Design

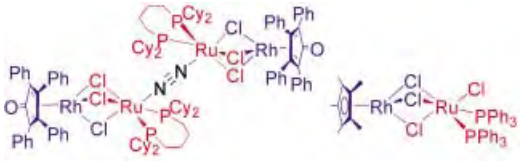
M. Sato, R. Sadamoto, K. Niikura, K. Monde, H. Kondo, S.-I. Nishimura* ——— **1516 – 1520**

Site-Specific Introduction of Sialic Acid into Insulin



More gain, less pain: A new long-acting insulin (see structure) was created by the enzymatic introduction of sialyllactose into mutant insulins. The glycosylation site was introduced into the insulin by point mutation without loss of biological activity. The experimental results with mice clearly demonstrated that the introduction of a sialic acid residue is crucial in prolonging glucose-lowering activity in the blood.

 © 2004 Wiley-VCH Verlag GmbH & Co. KGaA, Weinheim



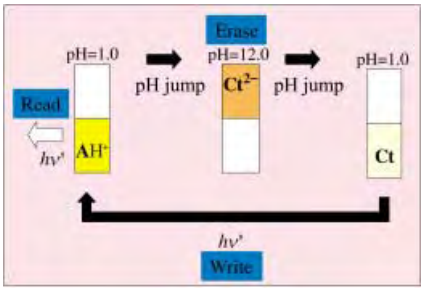
A radical alternative? Two highly efficient catalysts for atom-transfer radical additions were discovered in a parallel screening of bimetallic complexes. Both catalysts contain a rhodium-centered fragment (blue), which is connected through three chloro bridges to a ruthenium-centered fragment (red).

Bimetallic Catalysts

L. Quebatte, R. Scopelliti, K. Severin* ——— 1520 – 1524

Combinatorial Catalysis with Bimetallic Complexes: Robust and Efficient Catalysts for Atom-Transfer Radical Additions

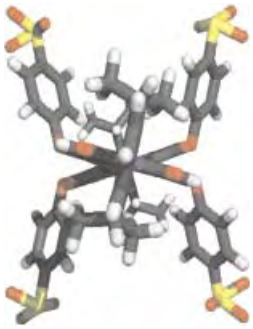
Switching colors: 4′,7-Dihydroxyflavylium (AH^+) in water–ionic liquid biphasic systems can be used as a write–read–erase system. In acid media, the chalcone (**Ct**) form is soluble in ionic liquids and is thermally metastable, but reacts photochemically (write) to give the yellow flavylium salt, which can be optically read without being erased. The system is prepared for a new cycle by two consecutive pH "jumps".



Molecular Switches

F. Pina,* J. C. Lima, A. J. Parola, C. A. M. Afonso ——— 1525 – 1527

Thermal and Photochemical Properties of 4′,7-Dihydroxyflavylium in Water–Ionic Liquid Biphasic Systems: A Write–Read–Erase Molecular Switch

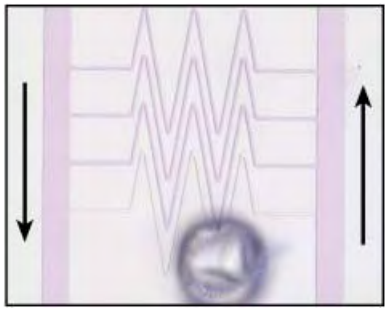


Dying to be seen: A series of water-soluble and highly fluorescent perylenetetracarboxdiimides (PDIs) have been synthesized in high yields by introducing charged groups into the bay region of PDI (see picture; C gray, H white, S yellow, O red). They can be used for staining living cells as they are nontoxic.

Water-Soluble Dyes

J. Qu, C. Kohl, M. Pottek, K. Müllen* ——— 1528 – 1531

Ionic Perylenetetracarboxdiimides: Highly Fluorescent and Water-Soluble Dyes for Biolabeling



The proof of the model is in the function: A minimal model of hemostasis (a complex biochemical network responsible for blood coagulation) may be implemented with only three chemical reactions, which creates a biomimetic functional microfluidic system that is capable of repairing itself (as modeled in the figure). This simple system shows threshold response and sensitivity to flow similar to that observed in hemostasis.

Biomimetics

M. K. Runyon, B. L. Johnson-Kerner, R. F. Ismagilov* ——— 1531 – 1536

Minimal Functional Model of Hemostasis in a Biomimetic Microfluidic System

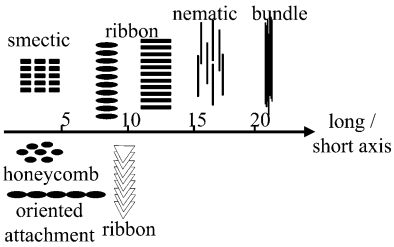
 © 2004 Wiley-VCH Verlag GmbH & Co. KGaA, Weinheim

Contents

Nanostructures

N. R. Jana* ——— 1536 – 1540

Shape Effect in Nanoparticle Self-Assembly

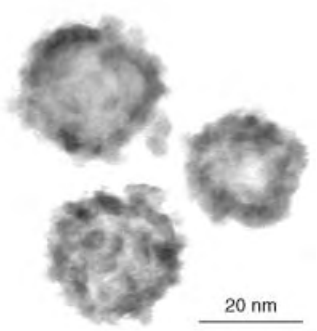


Particle anisotropy determines the way nanoparticles self-assemble, as shown in the picture. Gold and silver spheroids, rods, and plates with length-to-width ratios ranging from 1 to 25 show different liquid-crystalline order structures. These structures are analogous to the entropy-driven ordering that occurs at high volume fractions and is useful for large-scale ordering or shape separation.

Nanoparticles

H.-P. Liang, H.-M. Zhang, J.-S. Hu, Y.-G. Guo, L.-J. Wan,* C.-L. Bai* ——— 1540 – 1543

Pt Hollow Nanospheres: Facile Synthesis and Enhanced Electrocatalysts

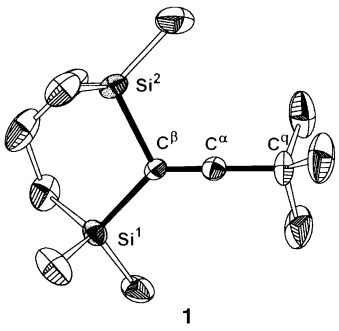


A facile large-scale preparation of Pt hollow nanospheres (see TEM image) makes use of Co nanoparticle as sacrificial templates. The nanospheres exhibit enhanced electrocatalytic activity. This method has been extended to the fabrication of industrially potentially useful Au, Pd, and other mono- and multimetallic hollow nanospheres.

Vinyl Cations

T. Müller,* M. Juhasz, C. A. Reed* ——— 1543 – 1546

The X-ray Structure of a Vinyl Cation



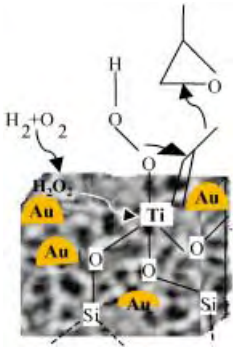
1

Thermodynamic stabilization by two β-silyl substituents and essentially nonnucleophilic reaction conditions are prerequisites for the preparation of the first structurally well-characterized vinyl cation **1** (see structure). The occurrence of β-Si–C hyperconjugation in **1** is indicated by unusually long Si–C^{β} bonds.

Epoxidation of Propene

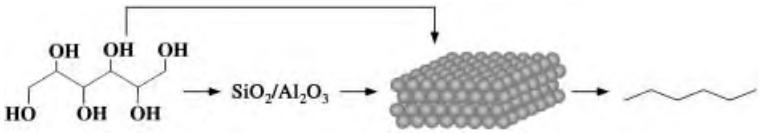
A. K. Sinha, S. Seelan, S. Tsubota, M. Haruta* ——— 1546 – 1548

A Three-Dimensional Mesoporous Titanosilicate Support for Gold Nanoparticles: Vapor-Phase Epoxidation of Propene with High Conversion



Direct selective gas-phase epoxidation of propene with commercially viable conversion has been achieved with catalysts consisting of gold nanoparticles (3–5 nm) supported on large-pore (> 7 nm) silylated mesoporous titanosilicates with $Ba(NO_3)_2$ as a promoter. The picture provides a plausible mechanism for the synergetic cooperation of the Au and Ti sites, which is superimposed onto a TEM image of the material.

© 2004 Wiley-VCH Verlag GmbH & Co. KGaA, Weinheim

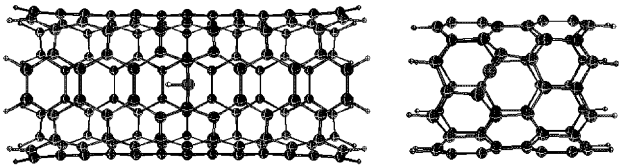


A clean stream of alkanes from renewable biomass resources is obtained through aqueous-phase reforming in a single reactor. Alkanes are produced from biomass-derived sorbitol through a bifunctional pathway (see scheme) that involves the dehydration of sorbitol on acid sites (SiO_2/Al_2O_3) and hydrogenation of intermediates on a metal catalyst under a H_2 atmosphere. Hydrogen is produced from sorbitol and water on the metal catalyst in the same reactor.

Alkane Production

G. W. Huber, R. D. Cortright, J. A. Dumesic* ——— **1549 – 1551**

Renewable Alkanes by Aqueous-Phase Reforming of Biomass-Derived Oxygenates



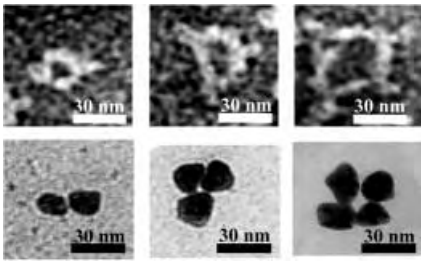
In contrast to earlier theoretical studies and experimental expectation, full high-level (B3LYP/6-31G*) computations on various nanotube models reveal that SWCNTs with O, NH, CH_2, and SiH_2 addends favor opened structures rather than three-membered rings. Furthermore, the diagonal C—C bonds in (8,0) zigzag nanotubes, rather than C—C bonds parallel to the axis, are the favorable sites for chemical modification.

Nanotubes

Z. Chen,* S. Nagase, A. Hirsch, R. C. Haddon, W. Thiel, P. von R. Schleyer* ——— **1552 – 1554**

Side-Wall Opening of Single-Walled Carbon Nanotubes (SWCNTs) by Chemical Modification: A Critical Theoretical Study

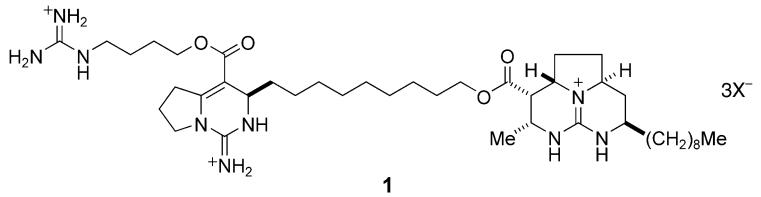
Immunoglobulin G templates: Clusters of gold nanoparticles are grown (see picture) from templates formed from the self-assembly of immunoglobulin Gs (IgGs) by using a synthetic divalent antigen. Carbohydrates inherent to IgGs create local nucleation centers for the electroless deposition of gold.



Nanostructures

J. Yang,* M. Mayer, J. K. Kriebel, P. Garstecki, G. M. Whitesides* ——— **1555 – 1558**

Self-Assembled Aggregates of IgGs as Templates for the Growth of Clusters of Gold Nanoparticles



1

One-step formation of an enone from a primary alcohol has been effectively applied in the total synthesis of batzelladine A (**1**). Successive 1,3-dipolar cycloadditions with a subsequent cyclization were used to form the tricyclic guanidine subunit of this natural product, which has the strongest inhibitory activity of HIV gp120-CD4 binding among the batzelladines.

Natural Product Synthesis

J. Shimokawa, K. Shirai, A. Tanatani, Y. Hashimoto, K. Nagasawa* ——— **1559 – 1562**

Enantioselective Total Synthesis of Batzelladine A

 © 2004 Wiley-VCH Verlag GmbH & Co. KGaA, Weinheim

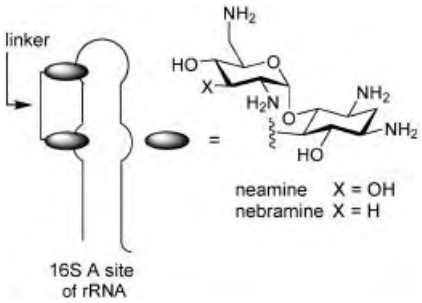
Contents

Drug Design

F. Agnelli, S. J. Sucheck,* K. A. Marby, D. Rabuka, S.-L. Yao, P. S. Sears, F.-S. Liang, C.-H. Wong* — **1562 – 1566**

Dimeric Aminoglycosides as Antibiotics

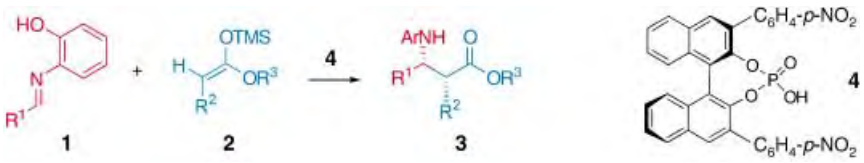
Double duty: Dimeric aminoglycoside antibiotics were designed by linking neamine or nebramine cores with various tethers differing in length and composition. The resulting dimeric aminoglycosides displayed high affinity for the 16S A site of ribosomal RNA (a representation of the complex is shown here) and were effective against various aminoglycoside-resistant bacterial strains.



Asymmetric Synthesis

T. Akiyama,* J. Itoh, K. Yokota, K. Fuchibe — **1566 – 1568**

Enantioselective Mannich-Type Reaction Catalyzed by a Chiral Brønsted Acid

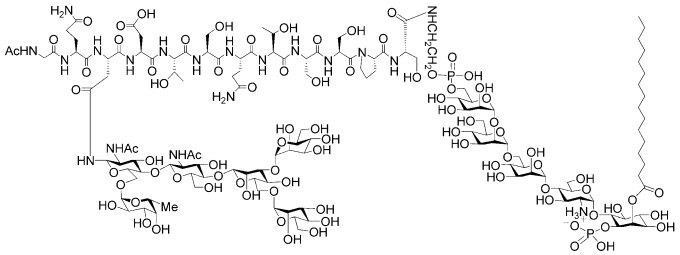


No metal required: The Mannich-type reaction of ketene silyl acetals **2** with aldimines **1** proceeded highly enantioselectively to afford the *syn* isomer of β-aminoesters **3** with up to 96% *ee* under the influence of a chiral Brønsted acid **4** derived from (*R*)-BINOL.

Glycopeptides

N. Shao, J. Xue, Z. Guo* — **1569 – 1573**

Chemical Synthesis of a Skeleton Structure of Sperm CD52—A GPI-Anchored Glycopeptide



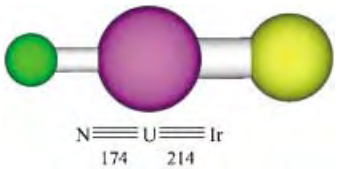
Going native: A highly convergent synthetic strategy was established to prepare a skeleton structure of sperm CD52 antigen (depicted), which represents the first chemical synthesis of a complex, all natively linked glycosylphosphatidylinositol (GPI)–glycopeptide conjugate.

Computer Chemistry

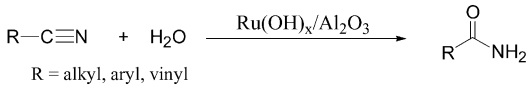
L. Gagliardi,* P. Pyykkö — **1573 – 1576**

Theoretical Search for Very Short Metal–Actinide Bonds: NUIr and Isoelectronic Systems

Cumulated triple bonds: A new class of molecules, the isoelectronic series of NUIr, (depicted) has been postulated and theoretically studied. The bond between the actinide and the 5d-metal atom is very short and is shown to correspond to triple bonding. The N–U bond is also a triple bond.



© 2004 Wiley-VCH Verlag GmbH & Co. KGaA, Weinheim

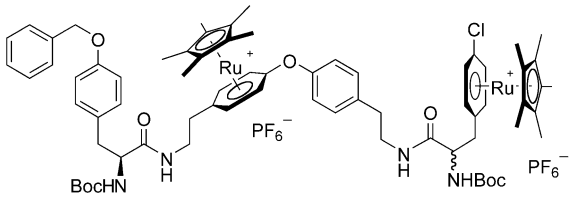


A broad range of amides is accessible in excellent yield (>99%) by hydration of the corresponding nitriles in water in the presence of the supported ruthenium catalyst $Ru(OH)_x/Al_2O_3$ (see scheme). For example, the industrially important conversion of acrylonitrile into acrylamide was achieved in quantitative yield and better than 99% selectivity. The catalyst can be reused without loss of catalytic activity and selectivity.

Catalytic Amide Synthesis

K. Yamaguchi, M. Matsushita, N. Mizuno* ——— 1576 – 1580

Efficient Hydration of Nitriles to Amides in Water, Catalyzed by Ruthenium Hydroxide Supported on Alumina



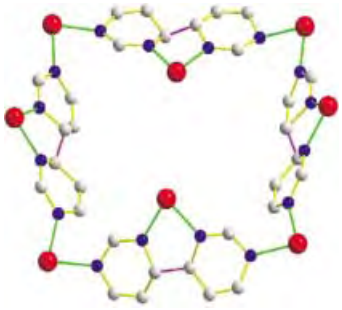
A packet of sandwiches: A new concept of modular assembly of novel, metal-labeled biooligomers starting from amino acid sandwich complexes is introduced. The first diaryl ether tetrapeptoid containing two ruthenium-sandwich labels is prepared (see picture; Boc = *tert*-butoxycarbonyl), it should now be possible to prepare longer peptoids by repetitive methods.

Bioinorganic Chemistry

A. Schmid, T. Lindel* ——— 1581 – 1583

Modular Synthesis of Ruthenium-Labeled Diaryl Ether Peptoids

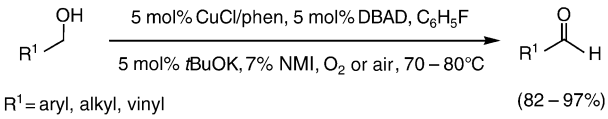
Two, three, four, or eight N-heterocycles react in the coordination sphere of titanium(II) compounds to give polynuclear titanium complexes (see picture, red = $TiCp_2$, blue = N, white = C). Simultaneously occurring C–C couplings mark a new strategy for the synthesis of self-assembled compounds of the early transition metals.



Self-Assembly

S. Kraft, R. Beckhaus,* D. Haase, W. Saak ——— 1583 – 1587

Directed Reduction of Six-Membered Nitrogen Heterocycles—Selective Formation of Polynuclear Titanium Complexes



An additive is the key to success: Catalytic amounts of *N*-methylimidazole are crucial for the aerobic oxidation of primary aliphatic alcohols in the presence of CuCl, 1,10-phenanthroline (phen), and di-*tert*-butyl azodicarboxylate (DBAD). This reaction, under neutral conditions, yields the aldehydes quantitatively and selectively without overoxidation to the carboxylic acids.

Oxidation with Air

I. E. Markó,* A. Gautier, R. Dumeunier, K. Doda, F. Philippart, S. M. Brown, C. J. Urch ——— 1588 – 1591

Efficient, Copper-Catalyzed, Aerobic Oxidation of Primary Alcohols

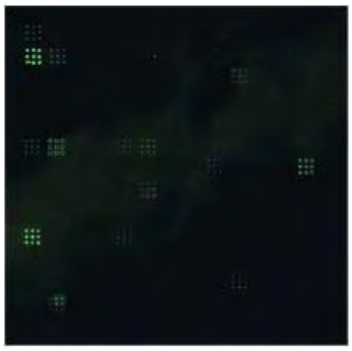
 © 2004 Wiley-VCH Verlag GmbH & Co. KGaA, Weinheim

Contents

Drug Design

M. D. Disney, S. Magnet, J. S. Blanchard, P. H. Seeberger* ——— **1591 – 1594**

Aminoglycoside Microarrays To Study Antibiotic Resistance

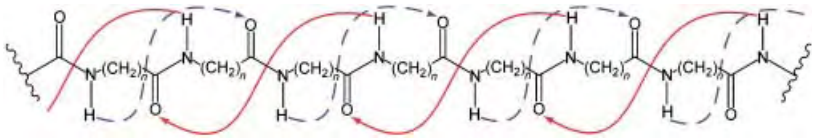


On to the next round! A sensitive microarray of immobilized aminoglycosides was used to study the binding of antibiotics to resistance-causing enzymes (see picture). This, in combination with other methods, will lead to the identification of new antibiotics that bind weakly to these enzymes and strongly to the therapeutic targets.

Peptide Structures

C. Baldauf, R. Günther, H.-J. Hofmann* ——— **1594 – 1597**

Mixed Helices—A General Folding Pattern in Homologous Peptides?



You may now exchange rings! "Mixed helices" along a peptide sequence, in which rings of different sizes are held together by hydrogen bonds in alternating directions (see picture), prove to be a general folding principle in homologous α-, β-, γ-, and δ-peptides.

VIP Communications labeled with this symbol have been judged by two referees as being "very important papers".

Looking for outstanding employees?

Do you need another expert for your excellent team?
... Chemists, PhD Students, Managers, Professors, Sales Representatives...

Place an advert in the printed version and have it made available online for 1 month, free of charge!

Angewandte Chemie International Edition
Advertising Sales Department: Marion Schulz
Phone: 0 62 01 - 60 65 65
Fax: 0 62 01 - 60 65 50
E-Mail: MSchulz@wiley-vch.de

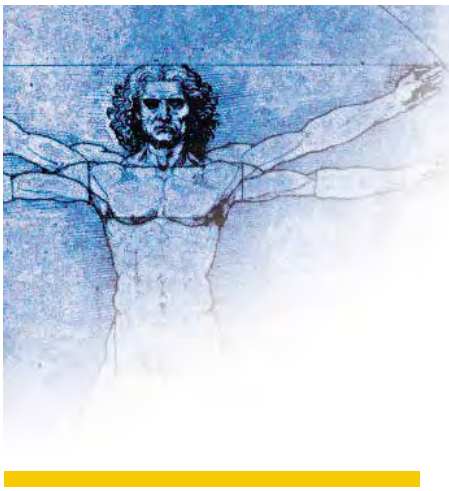
Service

Keywords ——— *1600*

Authors ——— *1601*

Angewandte's Sister Journals ——— *1598 – 1599*

Preview ——— *1603*



Süe Award to M. Verdaguer

Michel Verdaguer, emeritus professor at the Université Pierre et Marie Curie (Paris), has received the Grand Prix Süe of the French Chemical Society (Société Française de Chimie, SFC). The award is named after Pierre Süe, who worked in the field of artificial radioactive elements, and it has been awarded annually since 1997 for work of a high international standard.



M. Verdaguer

Verdaguer completed his PhD in 1984 on the synthesis and magnetic properties of bimetallic materials, under the supervision of Olivier Kahn in Orsay (near Paris), and in the same year received the Award of the Coordination Chemistry Division of the SFC for work on ferrimagnetic chains. In 1988 he became professor at the Université Pierre et Marie Curie in Paris. His research is focused on molecular magnets, such as Prussian Blue and other transition-metal–polycyanide complexes. Today he is particularly interested in multifunctional materials: molecular high-spin materials, photomagnetic materials, and optically active magnetic materials. He has contributed significantly to the development of the use of synchrotron irradiation in inorganic chemistry. He was one of the corresponding authors of a Communication on ferromagnetic cyanide-bridged iron(III)–cobalt(II) chains that appeared as the cover-picture article in issue 13/2003 of *Angewandte Chemie*.[1] Verdaguer shares the Süe Award with Jean-Louis Rivail (Université Nancy I, France), who has been recognized for his contributions to quantum chemistry.

Prize for Coordination Chemistry to A. Bousseksou

The Award of the Coordination Chemistry Division of the SFC for 2003 was presented to Azzedine Bousseksou. Bousseksou completed his PhD in 1992 under the guidance of F. Varret in Versailles (France) on thermal spin transitions in inorganic iron(III) compounds, which he investigated by Moessbauer spectroscopy. In 1993 he joined the Laboratory of Coordination Chemistry of the Centre National de la Recherche Scientifique (CNRS) in Toulouse (France). Since 2003 he has directed the research team "molecular physical properties". His research interests are concentrated on the mechanism of thermally induced spin transitions, which he investigates through high-field and pulsed experiments. Besides magnetically, optically, and electrically switchable bistable materials,[2] he is interested in size effects, as well as the exact calculation of the magnetic properties of clusters.



A. Bousseksou

Reviews 2003: Competition Results

The Gesellschaft Deutscher Chemiker (GDCh, German Chemical Society) has surveyed four chemistry departments in Germany, chosen at random, and 40 German corresponding authors in *Angewandte Chemie* to determine which Reviews in this journal in 2003 "were best able to offer a prospective chemist a competent, up-to-date, and comprehensive overview of a relevant area of chemistry". The top Reviews based on this survey were printed in a special issue for the Congress of Junior Lecturers, together with the 2002 Nobel Lectures by K. Wüthrich, K. Tanaka, and J. B. Fenn on the structural elucidation of large biomolecules by NMR and mass spectrometry. The approximately 350-page issue is to be made available to student members of the GDCh, but will also be used elsewhere for the advertisement of chemistry. The Reviews that received the most votes were those by Meyer, Castellano, and Diederich (interactions in molecular recognition processes, issue 11), Schrock and Hoveyda (Mo and W olefin-metathesis catalysts, issue 38), Hubbard and Walsh (vancomycin biosynthesis, issue 7), and—perhaps surprisingly—Evers, Staudigl, and co-workers on the preparation of single crystals of silicon and how the method that is still used today came about by chance (issue 46). Next came the Reviews by Copéret, Basset, and co-workers (organometallic chemistry on surfaces, issue 2), Connon and Blechert (olefin cross-metathesis, issue 17), Chen (mass spectrometry and the screening of homogeneous catalysts, issue 25), Fürstner (chemistry and biology of roseophilin and "bleeding hosts", issue 31), Hoffmann (*meso* compounds, issue 10), and Limberg (radicals in metal-assisted oxygenations, issue 48).

[1] R. Lescouëzec, J. Vaissermann, C. Ruiz-Pérez, F. Lloret, R. Carrasco, M. Julve, M. Verdaguer, Y. Dromzee, D. Gatteschi, W. Wernsdorfer, *Angew. Chem.* **2003**, *115*, 1521; *Angew. Chem. Int. Ed.* **2003**, *42*, 1483.

[2] G. Matouzenko, J. F. Létard, S. Lecocq, A. Bousseksou, L. Capes, L. Salmon, M. Perrin, O. Kahn, A. Collet, *Eur. J. Inorg. Chem.* **2001**, 2935.

 © 2004 Wiley-VCH Verlag GmbH & Co. KGaA, Weinheim DOI: 10.1002/anie.200481030

Catalytic Oxidation

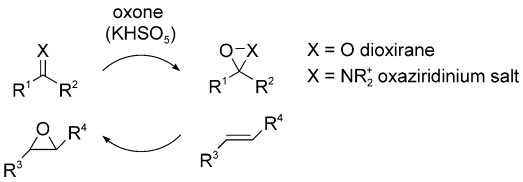
Amine-Catalyzed Epoxidation of Alkenes: A New Mechanism for the Activation of Oxone

*Alan Armstrong**

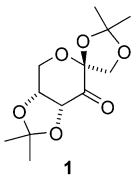
Keywords:
amines · catalysis · enantioselectivity · epoxidation · oxidation

Catalysis by small organic molecules—termed organocatalysis—is attracting intense current interest.[1] When compared to transition-metal-catalyzed processes, such reactions have advantages in terms of ease of product purification and their relative insensitivity to air and water, thus allowing easier experimental execution. The current renaissance in organocatalyzed C–C bond formation was preceded by extensive and ongoing efforts to develop methods for the asymmetric epoxidation of alkenes. Work in this area has been inspired not only by the practical advantages, but also by the need to extend the substrate scope of the main methods in the field to date: the Sharpless asymmetric epoxidation[2] and the use of Jacobsen–Katsuki (salen)Mn complexes.[3] Although both methods are widely applicable, the former is limited to allylic alcohol substrates, whereas the latter often gives poor results for *trans*-disubstituted and terminal alkenes.

The most productive organocatalytic alternatives so far have involved the activation of the triple salt oxone ($2\,KHSO_5 \cdot KHSO_4 \cdot K_2SO_4$).[4] Under appropriate conditions, the active constituent $KHSO_5$ of oxone converts ketones into reactive dioxirane species, which in turn effect efficient alkene epoxidation. This sequence is in principle catalytic in ketone (Scheme 1). In early work in this area a two-phase solvent system was employed in which the solubility properties of the alkene and ketone played a crucial role.[5] An important practical breakthrough was the development of an experimentally simple, self-buffering reaction system, which for the first time allowed a wide range of ketones to be screened as catalysts[6] and led to the development of several chiral ketones that gave rise to high enantioselectivity in the epoxidation of *trans*-disubstituted and trisubstituted alkenes.[7] The most notable of these chiral reagents is the ketone **1**, derived from D-fructose and introduced by Shi and co-workers.[8] Modified ketones reported more recently afford better results for *cis*- and monosubstituted alkenes,[9] as well as for α,β-unsaturated esters.[10]



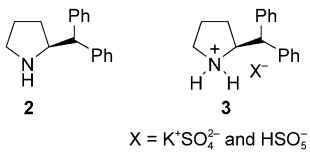
Scheme 1. Catalysis of oxone epoxidation by ketones (X = O) and iminium salts (X = NR_2^+).



1

An area closely related mechanistically to catalysis by ketones is the use of iminium salts as promoters, the reactions of which are presumed to proceed via the corresponding oxaziridinium salt (Scheme 1, X = NR_2^+).[11] The first asymmetric example,[12] which involved a dihydroisoquinolinium-based system, has been further developed by Page et al.[13] However, consistently high enantioselectivity across a range of alkene substitution patterns has yet to be achieved.[14] In principle, a diverse array of catalysts might be available if the iminium salt could be prepared from two separate components: an amine and a carbonyl compound. Along these lines, we reported the first examples of catalysis by exocyclic iminium salts derived from pyrrolidine and aromatic aldehydes, but attempts to extend this work to more hindered, chiral amines or carbonyl compounds were unsuccessful.[15] With the test alkene (*E*)-stilbene, control experiments revealed little epoxidation when the amine or carbonyl compound alone was employed, suggesting that the iminium salt was responsible for catalysis.

Yang and co-workers later found that in situ iminium formation was possible when appropriate carbonyl and amine partners were used.[16] Aggarwal and co-workers decided to examine in situ iminium formation with a different alkene—1-phenylcyclohexene—and found that epoxidation did indeed occur when the amine and carbonyl compound were mixed in the reaction system.[17] Remarkably, control experiments established that the epoxidation reaction was catalyzed by the amine alone, and asymmetric induction was observed when a chiral amine such as **2** was used! This finding led to extensive studies to elucidate the mechanistic role of the amine. In particular,



2 **3**

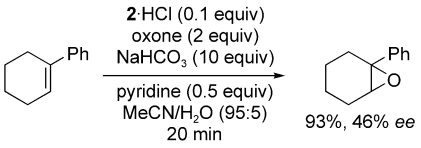
X = $K^+SO_4^{2-}$ and HSO_5^-

[*] Dr. A. Armstrong
Department of Chemistry
Imperial College London
South Kensington, London SW7 2AZ (UK)
Fax: (+44) 20-7594-5804
E-mail: a.armstrong@imperial.ac.uk

 © 2004 Wiley-VCH Verlag GmbH & Co. KGaA, Weinheim DOI: 10.1002/anie.200301716

the fact that enantioselectivity is observed suggests a close interaction between amine and alkene in the epoxidation transition state. Early results from the research group of Aggarwal[17] appeared to implicate the involvement of an amine radical cation, a species previously reported to be capable of alkene oxidation. However, subsequent irreproducibility of the key comparative control experiments[18] have now led Aggarwal and co-workers to look at the mechanism of the process further, and a recent publication implicates a novel and credible mechanism for the activation of oxone with important consequences.[19]

From a practical viewpoint, it was found that the use of the mono-HCl salt of the amine rather than the amine itself leads to far more reproducible results (Scheme 2). Pyridine is also added to the

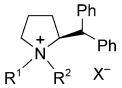


Scheme 2. Amine-catalyzed oxone epoxidation of 1-phenylcyclohexene

reaction mixture to minimize the formation of the diol through epoxide hydrolysis. In considering possible mechanisms, it is reasonable to wonder whether an oxidation product of the amine, such as the hydroxylamine or the nitrone, is responsible for catalysis. When the epoxidation process was performed at room temperature, the amine was indeed oxidized under the reaction conditions. However, its oxidation products were found not to promote the epoxidation reaction. Moreover, if the reaction was performed at −10 °C the alkene epoxidation still took place, but the amine salt could be recovered in good yield. It was discovered that the reaction of the amine **2** with oxone led to the formation of the complex **3**, which contained a mixture of the potassium sulfate and peroxymonosulfate anions. Crucially, the ammonium salt **3** promoted the epoxidation of 1-phenylcyclohexene with identical enantioselectivity to that observed for the catalytic system. This was good evidence that **3** is the active epoxidizing species. Hammett studies and trends in alkene reactivity further suggested that the active species in the amine-catalyzed epoxidation resembles a conventional electrophilic oxidant, such as *m*-chloroperbenzoic acid, more closely than an amine radical cation.

Why is the ammonium salt **3** more reactive than oxone itself? One reason is that the ammonium counterion acts as a phase-transfer catalyst, carrying the anion into the organic phase. However, systematic variations of the structure of the ammonium ion suggest that it plays a wider role. Aggarwal and co-workers found that the activity (and enantioselectivity) dropped in going from a secondary ammonium salt to its methylated tertiary counterpart, and that a quaternary ammonium salt was essentially unreactive (Table 1). This led them to

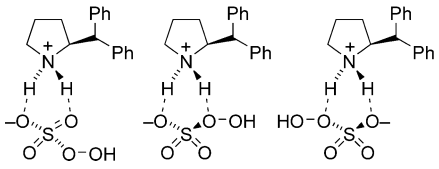
Table 1: Variation of yield and enantioselectivity with ammonium-salt structure in the oxone epoxidation of 1-phenylcyclohexene.



R^1	R^2	X	Yield [%]	*ee* of epoxide [%]
H	H	Cl	93	46
Me	H	Cl	58	5
Me	Me	BF_4	13	0

propose a novel mode of activation of oxone involving hydrogen bonding to the ammonium salt. The fact that this interaction can occur in several ways with differing orientations of the ammonium salt and HSO_5^- (Scheme 3) is likely to be deleterious to enantioselectivity.

The amine-catalyzed system has some way to go before it rivals ketone catalysis as a practical method for alkene epoxidation. Enantioselectivities



Scheme 3. Possible modes of interaction between a secondary ammonium salt and HSO_5^-.

are still modest even for the best combination of substrate and amine (66% *ee* for the epoxidation of 1-phenylcyclohexene with the naphthyl analogue of **2**·HCl). The scope is also limited to certain alkene substitution patterns: The reaction gives good conversion for trisubstituted alkenes, but not for terminal alkenes (apart from styrene), presumably as a result of their lower nucleophilicity. Inconsistent results are obtained for disubstituted alkenes; (*E*)-stilbene is unreactive because of its low solubility. Furthermore, a transition-state model to explain the observed sense of enantioselectivity has yet to be advanced. The stereoelectronic preferences in the dioxirane[20] and oxaziridinium[21] epoxidation systems are now well established, but a better understanding and better control of the mode of interaction of oxone with the ammonium salt will be necessary before similar levels of rationale can be attained in the amine-catalyzed case. Nevertheless, an understanding of the mechanism of the amine-catalyzed process is an important starting point towards fulfilling these academic and practical goals, and the fact that a wide variety of chiral amines is available suggests that progress can be made. The proposed mechanism also raises the exciting possibility of using other, non-ammonium, chiral hydrogen-bond donors as activators of oxone.

[1] P. I. Dalko, L. Moisan, *Angew. Chem.* **2001**, *113*, 3840–3864; *Angew. Chem. Int. Ed.* **2001**, *40*, 3726–3748.

[2] T. Katsuki, V. S. Martin, *Org. React.* **1996**, *48*, 1–300.

[3] E. N. Jacobsen, M. H. Wu, *Comprehensive Asymmetric Catalysis II* (Eds.: E. N. Jacobsen, A. Pfaltz, H. Yamamoto), Springer, Berlin, **1999**, pp. 649–677.

[4] For information and technical details about oxone, see: http://www.dupont.com/oxone/

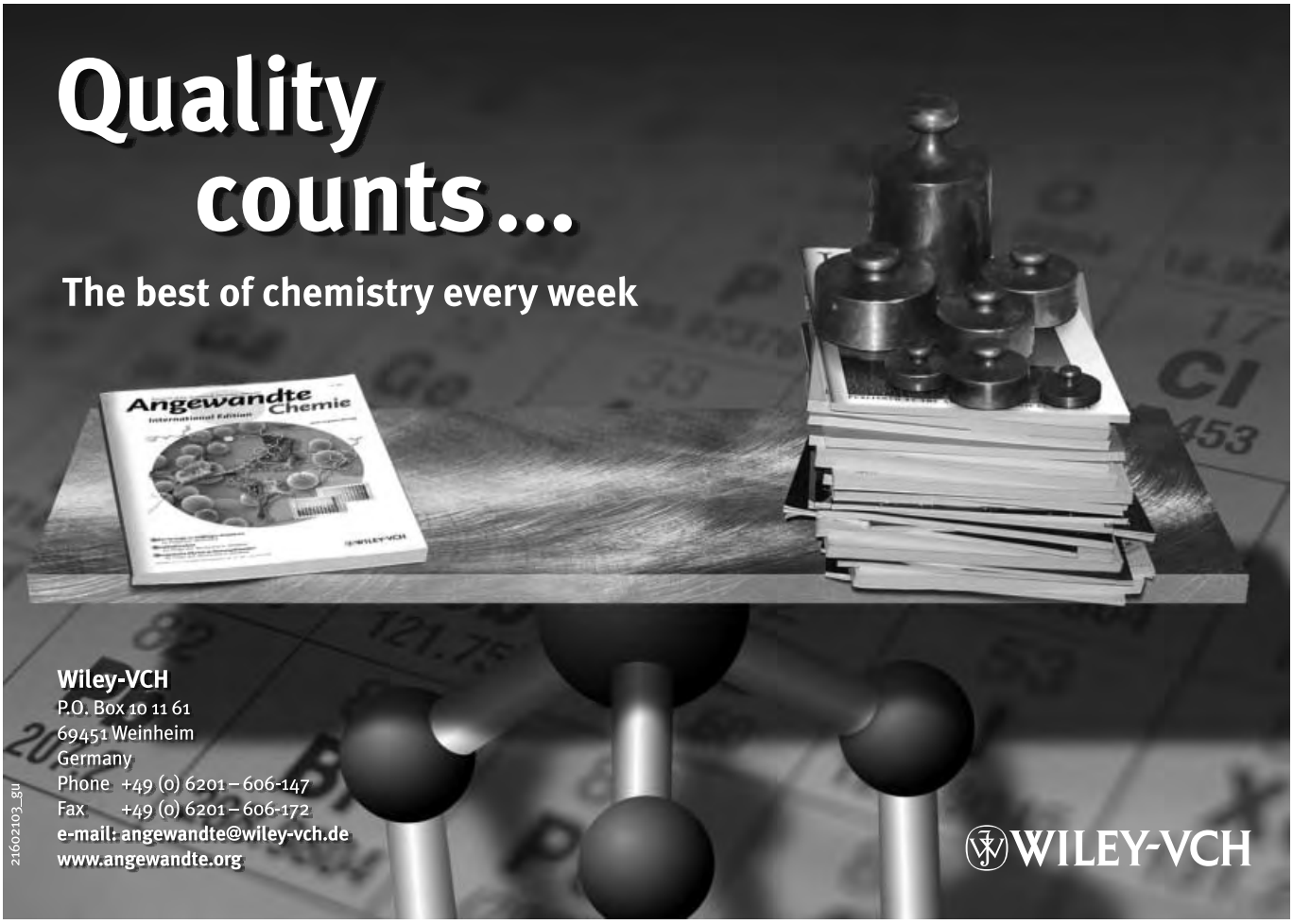
[5] S. E. Denmark, D. C. Forbes, D. S. Hays, J. S. Depue, R. G. Wilde, *J. Org. Chem.* **1995**, *60*, 1391–1407.

[6] D. Yang, M. K. Wong, Y. C. Yip, *J. Org. Chem.* **1995**, *60*, 3887–3889.

[7] For a review, see: M. Frohn, Y. Shi, *Synthesis* **2000**, 1979–2000; for recent examples, see: A. Armstrong, G. Ahmed, B. Dominguez-Fernandez, B. R. Hayter, J. S. Wailes, *J. Org. Chem.* **2002**, *67*, 8610–8617; T. K. M. Shing, Y. C. Leung, K. W. Yeung, *Tetrahedron*

 © 2004 Wiley-VCH Verlag GmbH & Co. KGaA, Weinheim

2003, *59*, 2159 – 2168; S. E. Denmark, H. Matsuhashi, *J. Org. Chem.* **2002**, *67*, 3479 – 3486.
[8] Z. X. Wang, Y. Tu, M. Frohn, J. R. Zhang, Y. Shi, *J. Am. Chem. Soc.* **1997**, *119*, 11224 – 11235.
[9] H. Q. Tian, X. G. She, H. W. Yu, L. H. Shu, Y. Shi, *J. Org. Chem.* **2002**, *67*, 2435 – 2446.
[10] X. Y. Wu, X. G. She, Y. A. Shi, *J. Am. Chem. Soc.* **2002**, *124*, 8792 – 8793.
[11] G. Hanquet, X. Lusinchi, P. Milliet, *C. R. Acad. Sci., Ser. II* **1991**, *313*, 625 – 628; G. Hanquet, X. Lusinchi, P. Milliet, *Tetrahedron Lett.* **1988**, *29*, 3941 – 3944; G. Hanquet, X. Lusinchi, P. Milliet, *Tetrahedron Lett.* **1987**, *28*, 6061 – 6064.
[12] L. Bohe, G. Hanquet, M. Lusinchi, X. Lusinchi, *Tetrahedron Lett.* **1993**, *34*, 7271 – 7274.
[13] P. C. B. Page, G. A. Rassias, D. Barros, A. Ardakani, B. Buckley, D. Bethell, T. A. D. Smith, A. M. Z. Slawin, *J. Org. Chem.* **2001**, *66*, 6926 – 6931.
[14] P. C. B. Page, G. A. Rassias, D. Barros, A. Ardakani, D. Bethell, E. Merifield, *Synlett* **2002**, 580 – 582; V. K. Aggarwal, M. F. Wang, *Chem. Commun.* **1996**, 191 – 192.
[15] A. Armstrong, G. Ahmed, I. Garnett, K. Goacolou, *Synlett* **1997**, 1075 – 1076; A. Armstrong, G. Ahmed, I. Garnett, K. Goacolou, J. S. Wailes, *Tetrahedron* **1999**, *55*, 2341 – 2352.
[16] M. K. Wong, L. M. Ho, Y. S. Zheng, C. Y. Ho, D. Yang, *Org. Lett.* **2001**, *3*, 2587 – 2590.
[17] M. F. A. Adamo, V. K. Aggarwal, M. A. Sage, *J. Am. Chem. Soc.* **2000**, *122*, 8317 – 8318.
[18] M. F. A. Adamo, V. K. Aggarwal, M. A. Sage, *J. Am. Chem. Soc.* **2002**, *124*, 11223 – 11223.
[19] V. K. Aggarwal, C. Lopin, F. Sandrinelli, *J. Am. Chem. Soc.* **2003**, *125*, 7596 – 7601.
[20] K. N. Houk, J. Liu, N. C. DeMello, K. R. Condroski, *J. Am. Chem. Soc.* **1997**, *119*, 10147 – 10152.
[21] I. Washington, K. N. Houk, *J. Am. Chem. Soc.* **2000**, *122*, 2948 – 2949; A. Armstrong, A. G. Draffan, *J. Chem. Soc. Perkin Trans. 1* **2001**, 2861 – 2873.



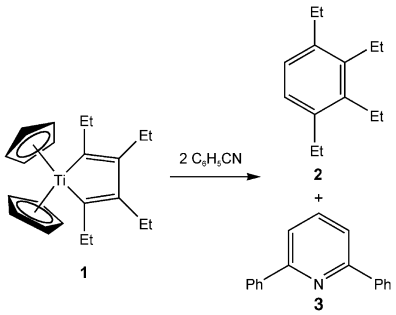
Synthetic Methods

A New Arene Synthesis—Or: How Inert Is the Cyclopentadienyl Ligand?**

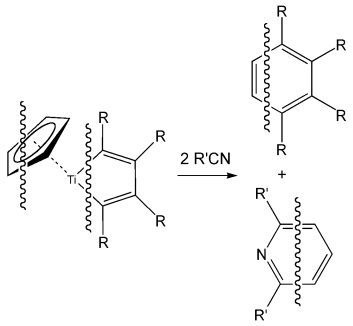
*Rhett Kempe**

Keywords:
arenes · C—C activation · cyclopentadienyl ligands · synthetic methods · titanium

For more than 50 years since their discovery[1–3] metal complexes containing η^5-cyclopentadienyl (C_5H_5; Cp) ligands have been investigated intensively, and since the middle of the 1970s group 4 metal complexes have attracted particular interest. This situation has arisen in part because of the discovery of the olefin-polymerization activity of these complexes when activated with MAO (methyl alumoxane),[4,5] because of their frontier orbitals that are capable of the activation of small molecules, and because of the stability of the metal–ligand bond. Recently Xi and Takahashi et al. achieved a breakthrough in the areas of activation and functionalization of cyclopentadienyl ligands bonded to titanium centers.[6] As expected, in the reaction of $[Cp_2TiBu_2]$ (Bu = *n*-butyl) with two equivalents of 3-hexyne the titanacyclopentadiene **1** is formed in the first step which then reacts with two equivalents of benzonitrile to form the benzene derivative **2** and the pyridine **3** (Scheme 1). The remaining nitrogen atom and the Cp–titanium moiety may be present as the nitrido complex $[(CpTiN)_4]$,[7] which is in agreement with the formation of NH_3 observed after aqueous workup. The outcome is a novel and interesting arene synthesis (Scheme 2). One of the two Cp rings of **1** is broken down into a C_2 fragment, which reacts with the titanacyclopentadiene unit to form the benzene derivative, and a C_3 fragment, which along with benzonitrile affords 2,6-diphenylpyridine.[6]



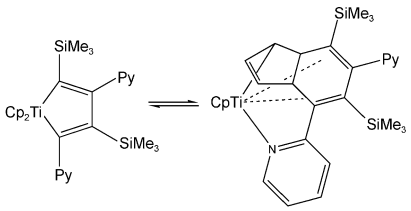
Scheme 1. Reaction of titanacyclopentadiene **1** with benzonitrile.



Scheme 2. Arene syntheses (R′ = phenyl).

The origin of the two- and three-atom fragments from one of the two Cp ligands was unambiguously confirmed by means of extensive experiments with isotopically labeled compounds. Thus the reaction with perdeuterated-Cp **1** or with the compound enriched with ^{13}C in the Cp ligand gives, respectively, the correspondingly deuterated and selectively ^{13}C-labeled benzene or pyridine derivatives. With ^{13}C-labeled benzonitrile the enriched isotopes are not incorporated into either the benzene or pyridine ring, but occur exclusively as phenyl substituents on the pyridine. If a mixture of half equivalent each of $[(C_5D_5)_2Ti(CPr)_4]$ (Pr = propyl) and $[(C_5H_5)_2Ti(CMe)_4]$ is used instead of **1** only deuterated tetrapropylbenzene and non-deuterated tetramethylbenzene are obtained, that is, bimolecular reaction pathways can be excluded.

The mechanism of this reaction is closely associated with the question of the stability of the Cp ligand. In the case of titanium in particular, substitution reactions have been observed in which the Cp ligand functions not only as an inert controlling ligand but also as a substrate. The most important reactions are the addition of coordinated S_5 to a Cp ligand,[8] fulvene formation,[9] and the intramolecular reactions of titanacyclopentadienyl units with Cp ligands observed by Rosenthal et al.[10] The latter reaction, which leads to dihydroindenyl complexes (Scheme 3), may be regarded as the first step in arene formation (Scheme 1). Next, dihydroindenyl cleavage probably occurs,[10] followed by benzene elimination, which is

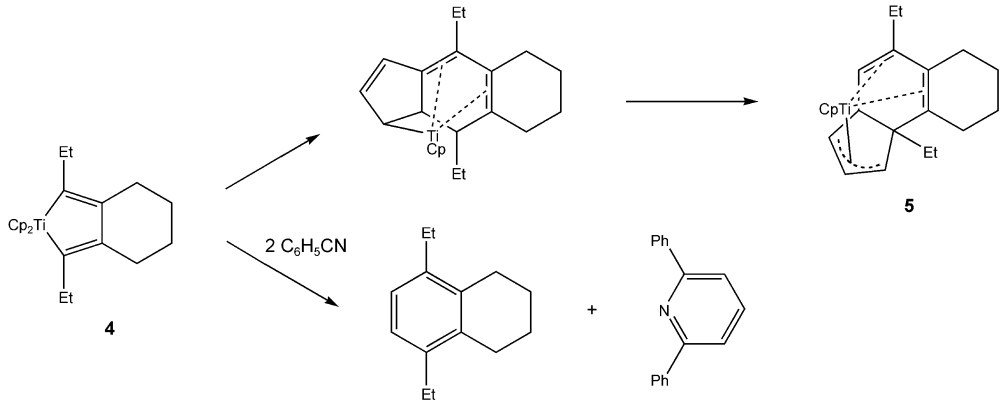


Scheme 3. Intramolecular coupling reaction of a titanacyclopentadiene moiety with a Cp ligand (Py = 2-pyridyl).

[*] Prof. Dr. R. Kempe
Universität Bayreuth
Lehrstuhl für Anorganische Chemie II
95440 Bayreuth (Germany)
Fax: (+49) 921-552-157
E-mail: kempe@uni-bayreuth.de

[**] I would like to thank U. Rosenthal and R. Schobert for helpful discussions.

DOI: 10.1002/anie.200301717
© 2004 Wiley-VCH Verlag GmbH & Co. KGaA, Weinheim

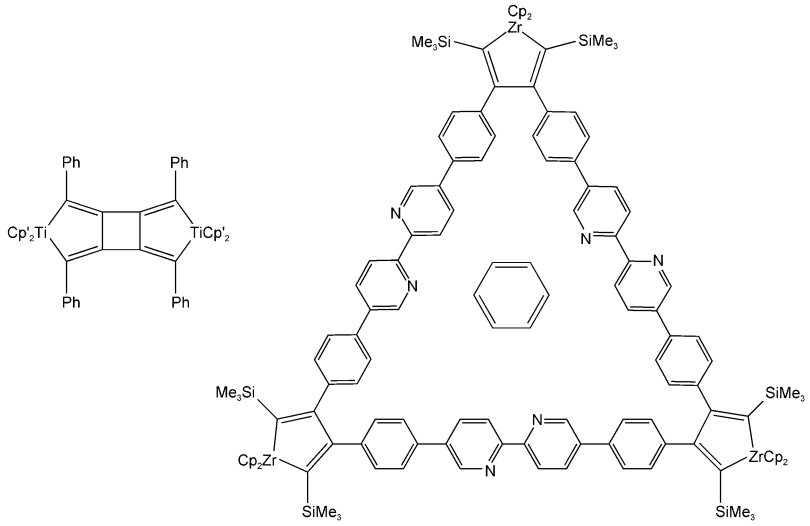


Scheme 4. Rearrangement of **4** to **5**[10] and the reaction of **4** to the benzene/pyridine derivate[6].

in agreement with the observation that first the benzene derivative is formed, then the pyridine derivate.[6]

Dihydroindenyl complexes of titanium are unstable; this results in bond cleavage which is necessary for benzene elimination (Scheme 4). Thus at room temperature **4** rearranges to **5** (75% yield).[10b] In the presence of benzonitrile, tetrahydronaphthalene is formed.[6]

The further course of the reaction could thus be investigated by the targeted reactions of the Rosenthal dihydroindenyl complexes with benzonitrile. This raises the question of which other functional groups apart from nitrile groups could participate in similar coupling reactions, as well as the question of the significance of such reactions. When the plethora of titanacyclopentadienes is considered the importance of these reactions lies in the area of arene synthesis. Can the dititanium tricyclic compounds (Scheme 5, right)[11] be used for arene synthesis, or even the titanium analogues of the oligozirconacyclopentadienes investigated in detail by Tilley et al. (Scheme 5, left)?[12] Moreover, such reactions are suitable for the preparation of selectively labeled isotopic benzene and pyridine derivatives. What bountiful, chemistry of the not-so-inert Cp ligand of the metallocenes of group 4 will be presented to us in the near future?



Scheme 5. Oligometallacyclopentadienes (Cp′ = methylcyclopentadienyl).

[1] T. J. Kealy, P. L. Pauson, *Nature* **1951**, *168*, 1039.

[2] G. Wilkinson, M. Rosenblum, M. C. Whiting, R. B. Woodward, *J. Am. Chem. Soc.* **1952**, *74*, 2125–2126.

[3] E. O. Fischer, W. Pfab, *Z. Naturforsch. B* **1952**, *7*, 377–379.

[4] A. Andersen, H.-G. Cordes, J. Herwig, W. Kaminsky, A. Merck, R. Mottweiler, J. Pein, H. Sinn, H.-J. Vollmer, *Angew. Chem.* **1976**, *88*, 689–690; *Angew. Chem. Int. Ed. Engl.* **1976**, *15*, 630–631.

[5] H. Sinn, W. Kaminsky, H.-J. Vollmer, R. Woldt, *Angew. Chem.* **1980**, *92*, 396–402; *Angew. Chem. Int. Ed. Engl.* **1980**, *19*, 390–396.

[6] Z. Xi, K. Sato, Y. Gao, J. Lu, T. Takahashi, *J. Am. Chem. Soc.* **2003**, *125*, 9568–9569.

[7] P. Gomez-Sal, A. Martin, M. Mena, C. Yelamos, *J. Chem. Soc. Chem. Commun.* **1995**, 2185–2186.

[8] D. M. Giolando, T. Rauchfuss, *J. Am. Chem. Soc.* **1984**, *106*, 6455–6456.

[9] a) R. Gleiter, W. Wittwer, *Chem. Ber.* **1994**, *127*, 1797–1798; b) W. E. Crowe, A. T. Vu, *J. Am. Chem. Soc.* **1996**, *118*, 5508–5509.

[10] a) U. Rosenthal, C. Lefeber, P. Arndt, A. Tillack, W. Baumann, R. Kempe, V. V. Burlakov, *J. Organomet. Chem.* **1995**, *503*, 221–223; b) A. Tillack, W. Baumann, A. Ohff, C. Lefeber, A. Spannenberg, R. Kempe, U. Rosenthal, *J. Organomet. Chem.* **1996**, *520*, 187–193; c) D. Thomas, N. Peulecke, V. V. Burlakov, W. Baumann, A. Spannenberg, R. Kempe, U. Rosenthal, *Z. Anorg. Allg. Chem.* **1998**, *624*, 919–924.

[11] P.-M. Pellny, V. V. Burlakov, N. Peulecke, W. Baumann, A. Spannenberg, R. Kempe, V. Francke, U. Rosenthal, *J. Organomet. Chem.* **1999**, *578*, 125–132.

[12] J. R. Nitschke, S. Zurcher, T. D. Tilley, *J. Am. Chem. Soc.* **2000**, *122*, 10345–10352.

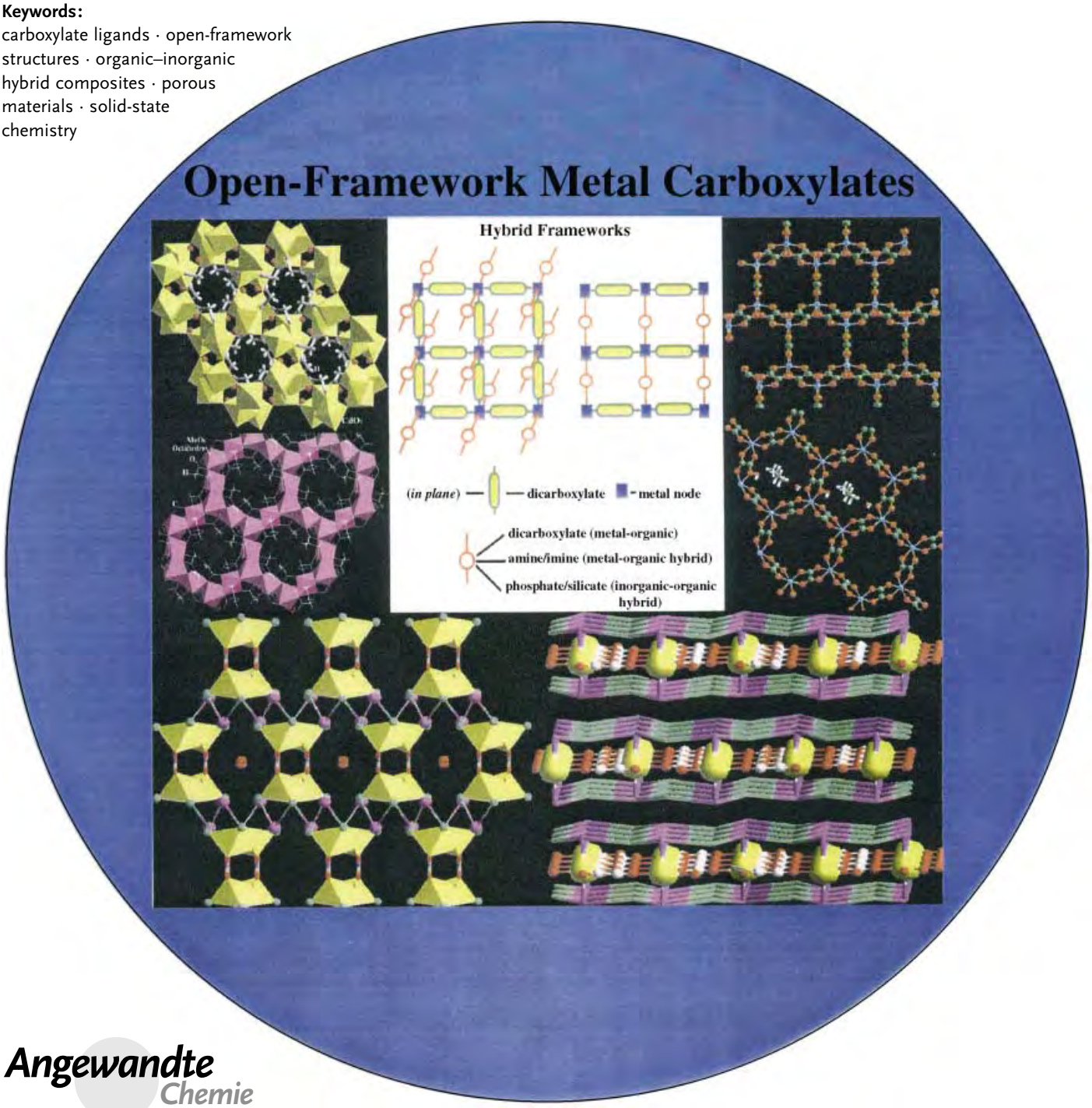
 © 2004 Wiley-VCH Verlag GmbH & Co. KGaA, Weinheim

Solid-State Structures

Metal Carboxylates with Open Architectures

C. N. R. Rao, Srinivasan Natarajan, and R. Vaidhyanathan*

Keywords:
carboxylate ligands · open-framework structures · organic–inorganic hybrid composites · porous materials · solid-state chemistry



© 2004 Wiley-VCH Verlag GmbH & Co. KGaA, Weinheim
DOI: 10.1002/anie.200300588

The field of inorganic open-framework materials is dominated by aluminosilicates and phosphates. The metal carboxylates have emerged as an important family in the last few years. This family includes not only mono- and dicarboxylates of transition, rare-earth, and main-group metals, but also a variety of hybrid structures. Some of the carboxylates possess novel adsorption and magnetic properties. Dicarboxylates and related species provide an effective means of designing novel hybrid structures with porous and other properties. In some of these structures, the dicarboxylate acts as a linker between two inorganic units. Hybrid nanocomposites are also of particular note, for example, cadmium oxalate host lattices that can accommodate extended alkali-metal halide structures. This Review discusses the synthesis, structure, and properties of various types of open-framework metal carboxylates.

From the Contents

1. Introduction	1467
2. Monocarboxylates	1467
3. Oxalates	1469
4. Higher Dicarboxylates	1477
5. Hybrid Compounds	1481
6. Cadmium Oxalates Incorporating Extended Alkali-Metal Halides	1489
7. Summary and Outlook	1490

1. Introduction

In recent years the area of inorganic open-framework materials has become one of intense research activity.[1–6] While one of the objectives of the research into open-framework solids is to find materials possessing channels and other features that make them porous, which can impart potential catalytic and sorption properties, the discovery of fascinating architectures of different dimensionalities has been equally exciting.

The aluminosilicates and metal phosphates, which constitute important prototype open-framework materials, have been discussed widely in the literature.[1,2] Several open-framework phosphates with dimensionalities varying between zero and three have been synthesized and characterized.[2a,h] A limitation with metal phosphates is that the structures comprise rigid polyhedra, such as tetrahedra and octahedra, which constitute the primary building units.[2a,d,5c] There has been much interest in designing hybrid materials containing inorganic and organic linkers, and several metal–organic frameworks possessing zeolitic structures have been reported.[6,7–9] One of the preoccupations today is to design novel structures involving both organic and inorganic components by employing novel synthetic tools as well as supramolecular chemistry. The design of hybrid structures takes advantage of metal coordination as well as the functionalities of the organic components, since the flexibility of the organic linkers renders such open architectures attractive.[5a,b,6–13]

The metal carboxylates are particularly interesting in that they not only form open-framework structures resulting from the presence of the carboxylate function itself, but also where the carboxylate group acts as a linker between inorganic moieties. Another interesting variety exists where the carboxylate unit coexists with a phosphate or arsenate group to give a hybrid structure. Some of the novel architectures of carboxylates are obtained by varying the nature of the reactants or the synthetic conditions, and by carrying out reactions in the presence of additives such as organic amines; the reactions are performed under hydro/solvothermal conditions. Accordingly, simple metal carboxylates such as formates and acetates crystallize in unusual structures under hydrothermal conditions.[6,14]

In this Review, we present a concise review of the structures and properties of the various of families of metal carboxylates. The Review is divided into six sections dealing with monocarboxylates, oxalates, aliphatic dicarboxylates, multifunctional dicarboxylates, hybrid compounds, and cadmium oxalates incorporating alkali halides. Strategies to design carboxylate networks are highlighted, and the comprehensive list of references provides linhs to the most up-to-date information. We particularly wish to recognize the review by Cheetham et al.,[2a] primarily dealing with open-framework metal phosphates, which appeared in this journal in 1999.

2. Monocarboxylates

Systematic investigations of open-framework structures constructed from monocarboxylate units are rather limited, but some of the metal monocarboxylates coexist with other ligands to form extended lattices of varying dimensionalities.[14] For example, copper formate tetrahydrate exhibits two-dimensional (2D) copper formate layers[15] that are separated by water molecules, while bismuth formate has a one-dimensional (1D) chain structure.[16] Monocarboxylates of alkali metals exhibit several polymorphic modifications.[17] Metal acetates tend to form dimers,[14a,c,d,18] the classic example being copper diacetate, which with further association forms an infinite array.[19] An interesting layered

[*] Prof. Dr. C. N. R. Rao, Prof. Dr. S. Natarajan, R. Vaidhyanathan
Chemistry and Physics of Materials Unit
Jawaharlal Nehru Centre for Advanced Scientific Research
Jakkur P. O., Bangalore 560 064 (India)
Fax: (+91) 80-846-2760
E-mail: cnrrao@jncasr.ac.in

 DOI: 10.1002/anie.200300588 © 2004 Wiley-VCH Verlag GmbH & Co. KGaA, Weinheim

compound based on copper acetate is $[\{Cu_2(O_2CMe)_4\}(tpt)_2]\cdot 2MeOH$, (tpt = 2,4,6-tris(4-pyridyl-1,3,5-triazine), which exhibits a large-pore structure; the metal acetate dimers are linked by *N*-donor ligands (Figure 1).[20] The

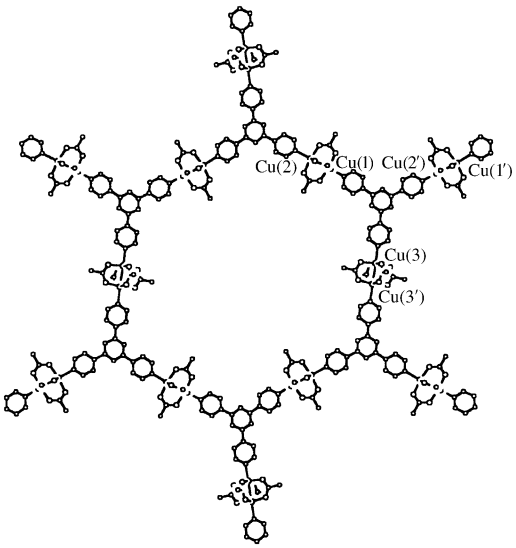


Figure 1. A hexagonal window (diameter ≈ 34–37 Å) in the (6,3) sheets of $[\{Cu_2(O_2CMe)_4\}_3(tpt)_2]\cdot 2MeOH$ (tpt = 2,4,6-tri(4-pyridyl-1,3,5-triazine).[20]

organic tpt groups link the acetate dimers, thus avoiding interpenetration through interlayer π–π interactions, which serves to stabilize the structure. Cotton and Kim[21] have employed cyanide ligands to connect metal acetate dimers to form molecular boxes and layered structures, thus providing a new avenue for the construction of neutral frameworks. For example, $[Rh_2(O_2CCF_3)_{42}(TCNE)]\cdot 2C_6H_6$ (TCNE = tetracyanoethylene) contains non-interpenetrating sheets formed by quasi-rectangular 30-membered rings. The sheets are again stabilized by significant π–π interactions between the $\{Rh_2(O_2CCF_3)_4\}$ and TCNE moieties.[21] The TCNE units themselves are linked via $\{Rh_2(O_2CCF_3)_4\}$ moieties, thus demonstrating the bridging role of the rhodium carboxylate complexes. Jacobson et al.[22] have prepared $K_3[Co(CN)_6]\cdot 2[Rh(O_2CMe)_4]$, in which the $\{Rh_2(O_2CMe)_4\}$ dimers are linked through the octahedral $\{Co(CN)_6\}$ unit to form a 2D structure with large windows.

High-nuclearity inorganic clusters formed by acetate ligands yield novel structures with interesting properties. Such clusters represent a bridge between molecular chemistry and solid-state chemistry, and provide a means of understanding their size-dependent physical properties.[23] Hydroxo, oxo, and carboxylate groups are used to prepare new nanoscopic compounds with such clusters, in which hydrophilic groups lie within the core and hydrophobic groups are located at the periphery.[24] High-nuclearity clusters can also be assembled into infinite coordination polymers.[25] $[Ba_9(MeCO_2)_{14}](ClO_4)_4$ (Figure 2), reported by

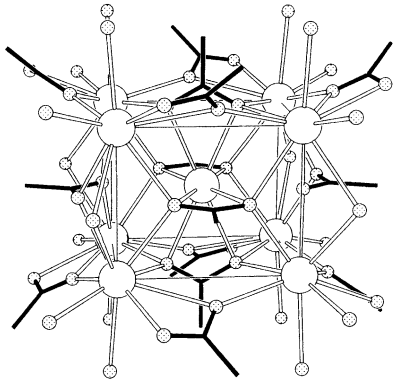


Figure 2. *I*-centered Ba_9 building block in $[Ba_9(O_2CMe)_{14}](ClO_4)_4$ held together by acetate bridges. Empty spheres: Ba, dotted spheres: O, thick bonds: H3C–C units of acetate ions.[26]

Dong et al.,[26] possesses a three-dimensional (3D) framework based on Ba_9 clusters. The structure consists of *I*-centered $[Ba_9(MeCO_2)_{14}]^{4+}$ tetragonal prisms that are connected by acetate and perchlorate bridges. The framework exhibits the μ^5-η^3:η^3 (a), μ^4-η^2:η^2 (b), and μ^3-η^2:η^2 bridging modes (Scheme 1); the μ^5 coordination mode is the highest possible coordination number that a metal center can display in such complexes.[27]

Meyer and co-workers have prepared and characterized heteronuclear rare-earth trichloroacetates that possess polymeric structures.[28] The structures have dimeric units that

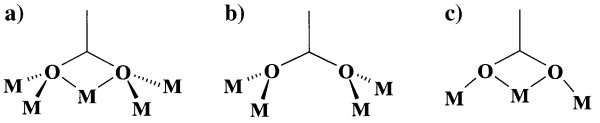


C. N. R. Rao gained his PhD from Purdue University and his DSc from the University of Mysore. He served as a faculty member at the Indian Institute of Technology (Kanpur) and the Indian Institute of Science (Bangalore) from 1959–1994 and has been associated with the Jawaharlal Nehru Center for Advanced Scientific Research (Bangalore) since 1989, where he is the Linus Pauling Research Professor. His research interests include solid-state and materials chemistry and nanomaterials. He is a Fellow of the Royal Society, a Foreign Associate of the US National Academy of Sciences and French Academy of Sciences, and a Foreign Member of several academies including those of Russia and Japan. He is also a member of the Pontifical Academy of Sciences.



S. Natarajan gained his PhD from the Indian Institute of Technology (Chennai) and carried out postdoctoral research at the Royal Institution of Great Britain and the University of California, Santa Barbara. He has been a member of the faculty of the Jawaharlal Nehru Center for Advanced Scientific Research since 1997, where he is an Associate Professor. His main research interests are in solid-state and materials chemistry, especially open-framework solids.

 © 2004 Wiley-VCH Verlag GmbH & Co. KGaA, Weinheim

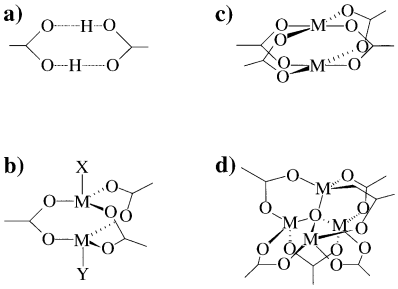


Scheme 1. Carboxylate ligands do not only coordinate in a mono- or bis-chelate fashion; here, three (c), four (b), and five (a) metal centers coordinate to one carboxylate group.

arise from the connectivity between two crystallographically distinct Nd atoms through four bridging bidentate carboxylate groups. The dimers are connected by square-planar copper–oxygen units to form a 1D chain. Exchange interactions between the f- and d-block ions gives rise to interesting optical and magnetic properties in these solids. In most of the metal monocarboxylates, extensive hydrogen-bond networks generally stabilize the structures.[14c,16,20,21,28,29]

Microporous metal hydroxyacetates exhibiting ion-exchange behavior have also been reported.[30] The 3D cobalt hydroxyacetate $[Co_5(OH)_2(O_2CMe)_8]\cdot 2H_2O$ has a structure that is built up entirely through edge-sharing cobalt–oxygen octahedra.[31] The acetate ligands, generated in situ by oxidative hydrolytic cleavage of an acetylacetonate ligand, exhibit both $\eta^1{:}\eta^2$ and the unusual $\eta^2{:}\eta^2$ coordination modes (Scheme 1). Recently, the 2D copper acetate [Cu(MeCO$_2$)(MeO)] was reported, in which acetate ligands containing tricoordinated oxygen atoms are found in addition to bridging methoxo groups.[32] In $(pipzH_2)(H_3O)$ $[Al_{15}(\mu^3\text{-}O)_4(\mu^3\text{-}OH)_6(\mu\text{-}OH)_{14}(hpdta)_4]\cdot pipz\cdot 41\,H_2O$ (pipz = piperazine, H_5hpdta = 2-hydroxypropane-1,3-diamine-*N*,*N*,*N*′,*N*′-tetraacetic acid),[33] Al_{15} aggregates with aluminium oxyhydroxide cores (of the brucite type) are assembled through hpdta linker groups.

Several structural motifs based on or related to carboxylates are profitably employed in the design of new solids with open structures (Scheme 2).[34] Among the many structural motifs commonly used in supramolecular chemistry,[34c] the simplest is the hydrogen-bonded dimer (a). The replacement of the proton in the dimer by various metal–acetate moieties (b–d) facilitates the assembly of 3D supramolecular networks through out-of-plane linkages. The use of the acetate dimer as a secondary building unit (SBU) in the design of rigid 3D metal–organic frameworks will be examined later in this Review. Paddle-wheel metal acetate clusters have been used to assemble encoded organic nodes (Figure 3).[35] This gives rise to an "inverted" metal–organic framework with compartmentalized cavities and walls that are accessible for further functionalization of the channels.



Scheme 2. a) An illustration of the doubly connected linear $R_2^2(8)$ carboxylate dimer; b–d) secondary building units (SBUs) in M^{II}-centered carboxylate compounds: square-planar (b), trigonal (c), and octahedral (d) nodes for the construction of coordination networks and assemblies. Note that the higher connectivity of the metal carboxylate SBUs is facilitated in part by the replacement of H^+ ions by more highly charged M^{2+} ions.[34a,b]

3. Oxalates

The oxalate ion acts as a rigid bidentate ligand that can facilitate the formation of extended structures by bridging metal centers. Many metal oxalate structures are reported in the literature including those occurring naturally as minerals.[36] A property of oxalate ions that has been of specific interest is their ability to mediate electronic effects between paramagnetic metal ions.[37] The oxalate moiety also acts as a linker between metal centers to yield open structures with dimensionalities ranging from zero and three.[38]

The 2D honeycomb structure is the most common for the oxalates.[39,40] This structure allows for large variations in molecule type and pore functionalization.[40] The ligating ability of the oxalate ion can be exploited for crystal engineering; formation through bis-chelation can give compounds with interesting physical properties, possibly due to the relatively short bonds between the metal centers.



R. Vaidhyanathan secured his BSc from St. Xavier's College (Tirunelveli) and an MSc and PhD from the Jawaharlal Nehru Center for Advanced Scientific Research (Bangalore). His work pertains to open-framework materials.

3.1. Transition-Metal Oxalates

3.1.1. Titanium and Zirconium Oxalates

Little is known about the oxalates of zirconium and titanium.[41] The titanyl oxalate $(NH_4)_2[TiO(ox)_2]\cdot H_2O$ (ox = C_2O_4), first described in 1974,[42] possesses cyclic $\{Ti_4O_4(ox)_8\}$ tetrameric units. The 1D coordination polymer $NH_4[Ti(ox)_2]\cdot 2H_2O$ is also known, in which the Ti center is found in a square-antiprismatic geometry.[43] Hydrothermal conditions have been employed to prepare titanium oxalates in the presence of organic amines.[44] These complexes contain the cyclic tetranuclear $[Ti_4O_4(ox)_8]^{8-}$ ion with organoammonium ions residing between the chains (Figure 4). To date, there have been no reports of 3D titanium oxalates.

 © 2004 Wiley-VCH Verlag GmbH & Co. KGaA, Weinheim

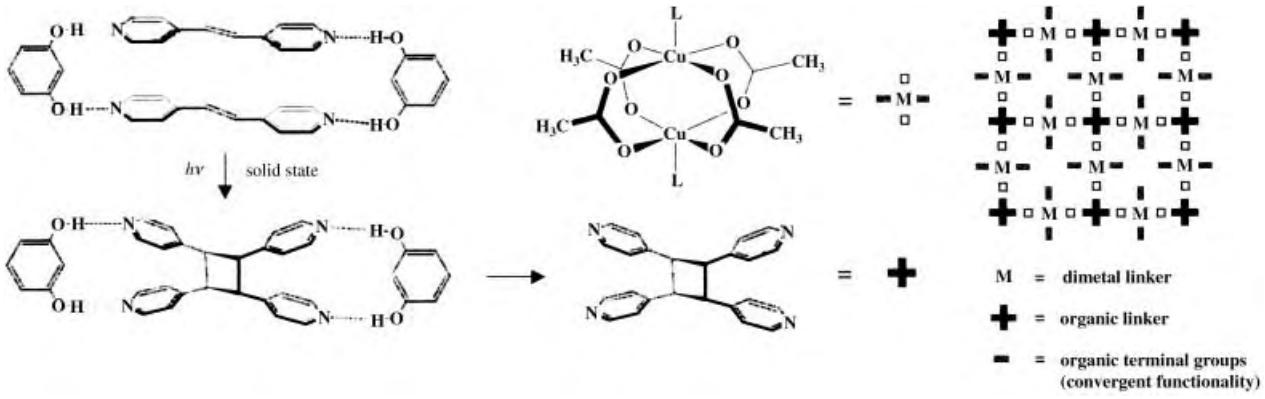


Figure 3. Construction of an open, inverted metal-organic framework (IMOF) using copper acetate dimers as linkers between tetrakis-(4-pyridyl)cyclobutane (4,4′-tpcb) units.[35]

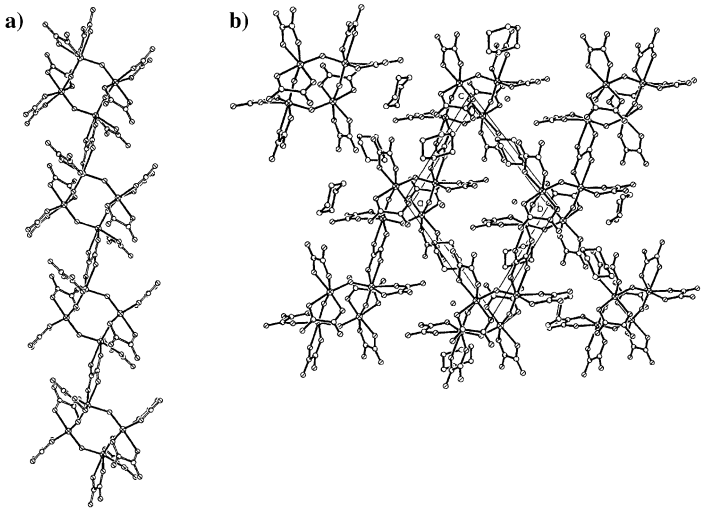


Figure 4. a) Section of the $\{[Ti_4O_4(ox)_7]^n_{6-}\}$ chain in $(C_4H_{12}N_2)_3[Ti_4O_4(ox)_7]\cdot 2H_2O$ ($ox = C_2O_4^{2-}$). Note the presence of both bridging and terminal oxalate groups. b) Structure of $(C_4H_{12}N_2)_3[Ti_4O_4(ox)_7]\cdot 2H_2O$ highlighting the apertures occupied by piperazine units.[44]

Zirconium oxalates are well known and are often isolated from aqueous solution.[45] The larger zirconium atoms can exhibit higher coordination than titanium,[46] and can form binuclear dimers as well as 1D polymeric chains. A series of open-framework oxalates containing zirconium and cadmium or lead along with alkali-metal or ammonium cations have been reported.[47] These compounds contain MO_8 (M = Zr, Cd) polyhedral units with dodecahedral or distorted square-antiprismatic geometry that are linked through oxalate oxygen atoms to give 3D open frameworks. In $[Pb_2Zr(ox)_4]\cdot n H_2O$, $\{PbO_8\}$ and $\{PbO_9\}$ units form two independent chains linked through the oxalate groups and the isolated $\{ZrO_8\}$ polyhedron to form a 3D structure.[47c] The zeolite-like storage of water molecules in the channels of some of these compounds has also been examined and the influence of water content on the lattice parameters has been studied. In $(NH_4)_2[CdZr(ox)_4]\cdot 3.9H_2O$ and $[H_3N(CH_2)_2NH_3][CdZr(ox)_4]\cdot 4.4H_2O$, right-handed metal–oxalate helical wires are formed through connectivity between the oxalate ions and the MO_8 polyhedra (M = Cd, Zr; Figure 5).[47a] The

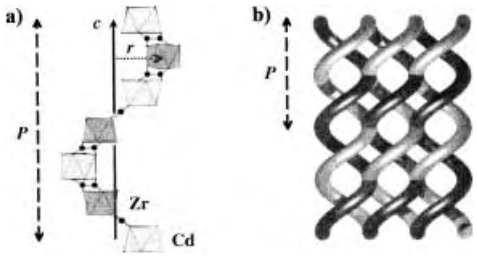


Figure 5. Helical representation of the anionic framework of $\{[CdZr(ox)_4]^{2-}_n\}$: a) structure of the metal–oxalate helical chain; b) a schematic representation of the helix interconnections. Helix parameters for $(NH_4)_2[CdZr(ox)_4]\cdot 3.9H_2O$: $P = 23.394(5)$ Å, $r = 4.5315(5)$ Å; for $(C_2H_{10}N_2)[CdZr(ox)_4]\cdot 4.4H_2O$: $P = 23.656(5)$ Å, $r = 4.553(5)$ Å.[47a]

oxalate unit serves to link the chains together to yield a 3D structure with channels (Figure 6). It is likely that the structure-directing property of the organoammonium ion plays a role in the formation of the helical structures.

3.1.2. *Transition-Metal Oxalates: Cr–Cu*

Transition-metal oxalates are of special interest since they can incorporate magnetic centers (with predetermined magnetic moments) by utilizing the various coordination modes of oxalate ligand. The structures of several transition-metal oxalates have been described.[36–39,48–51] Tamaki and co-workers have prepared 2D mixed-metal oxalates with Cr^{III} centers;[52] these η^3-complexes possess D_3 symmetry. The $[Cr(ox)_3]^{3-}$ ion acts as a building block by binding to three M^{II} centers (M = Fe, Co, Ni, Cu, Zn) ions through oxalate-ion bridges, thus forming an extended network. These compounds have three-dimensionally ordered ferromagnetic spins, and their channels are occupied by NBu_4^+ or alkali-metal cations. These complexes are an example of the design and tuning of

 © 2004 Wiley-VCH Verlag GmbH & Co. KGaA, Weinheim

the molecular components in extended structures to attain desirable properties.

Mixed-valent oxalates $A[M^{II}M^{III}(ox)_3]$ (A = monocation; M^{II} = Mn, Fe, Co, Ni, Cu, Zn; M^{III} = Cr, Fe, Co) have distinct magnetic properties, varying from paramagnetic to ferromagnetic or antiferromagnetic.[39c,48c,49b,49d,51a,51b] Chiral metal complexes have also been used to form layered magnets with oxalate networks, such as $[Cp_2^*Z^{III}][M^{II}M^{III}(ox)_3]$ (Z^{III} = Co, Fe, Mn; M^{II} = Mn, Fe, Co, Ni, Cu, Zn; M^{III} = Cr, Fe; Figure 7) and 3D anionic networks of the type $[Z^{II}(bpy)_3][M^{I}M^{III}(ox)_3]$ or $[[Z^{II}(bpy)_3][M^{II}M^{III}(ox)_3]$ (bpy = 2,2′-bipyridyl; Z^{II} = Fe, Co, Ni, Ru, Zn; M^{II} = Mn, Fe, Co, Cu; M^{III} = Cr, Fe; M^{I} = alkali metal, NH_4^+; Figure 8).[49c] An alternative way to describe these compounds would be to consider them as oxalate layers with 1D channels occupied by the bulky metal complex (Figure 7b). The interlayer separation in the 2D mixed-metal oxalates $[(C_nH_{2n+1})PPh_3][M^{II}Fe^{III}(ox)_3]$, with respect to varying cation chain lengths, follows the well known alternation effect.[53] The magnetic properties of these materials are well understood.

The design of chiral, porous metal oxalate structures using chiral starting materials has been explored.[39a] Thus, the 3D chiral magnetic lattice $[M^{z+}(ox)_3]^{(6-z)-}$ has been prepared from a preformed transition-metal complex and oxalate ions.[50a,54] Decurtins and co-workers[55]

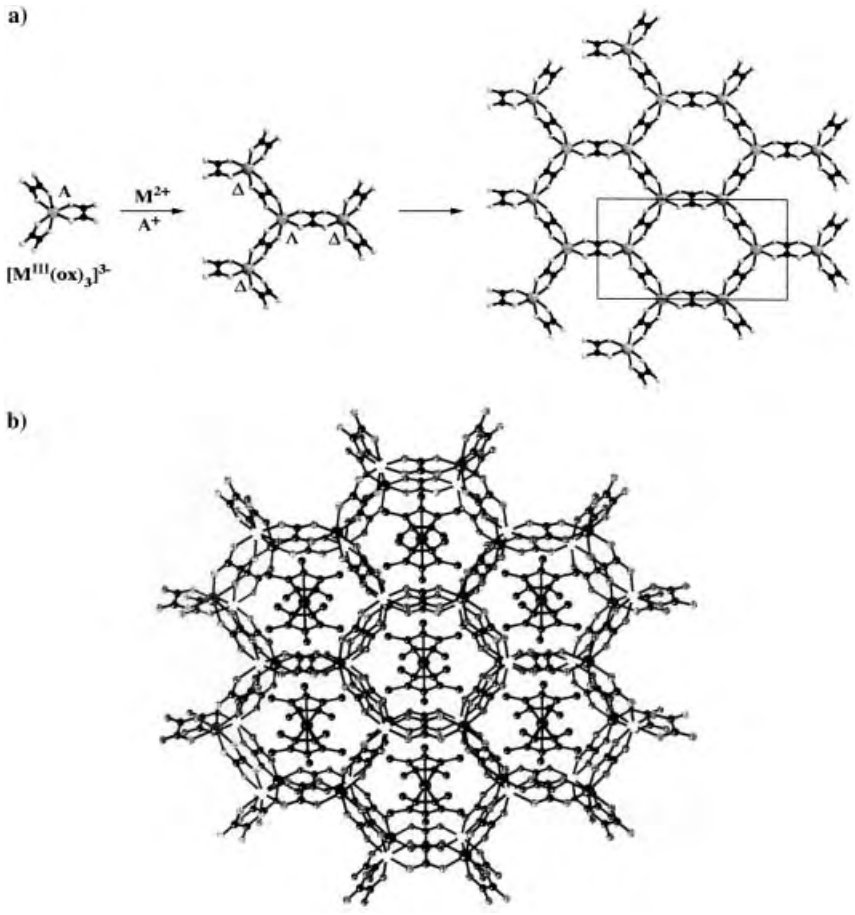


Figure 7. a) Alternating Λ and Δ isomers of tris(oxalato)metalate complexes in the presence of a bulky monocation; b) Perspective view of the eclipsed 2D layers in $[Cp_2^*Z][M^{II}M^{III}(ox)_3]$ (Z = Co, Fe, Mn; M^{III} = Fe, Cr; M^{II} = Mn, Fe, Co, Ni, Cu), which exhibits a magnetic moment.[49c]

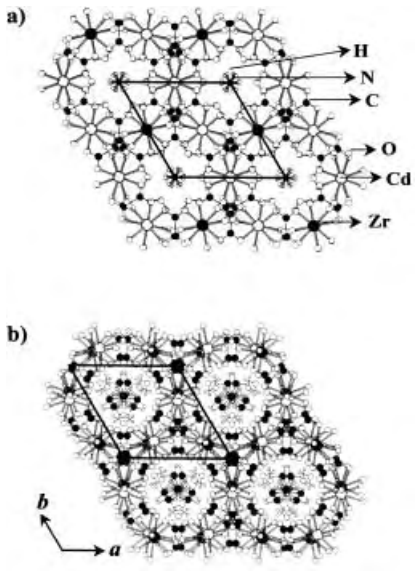


Figure 6. Projection (viewed along the *c* axis) of the structures of a) $(NH_4)_2[CdZr(ox)_4]\cdot 3.9\,H_2O$ and b) $(C_2N_2H_{10})[CdZr(ox)_4]\cdot 4.4\,H_2O$.[47a]

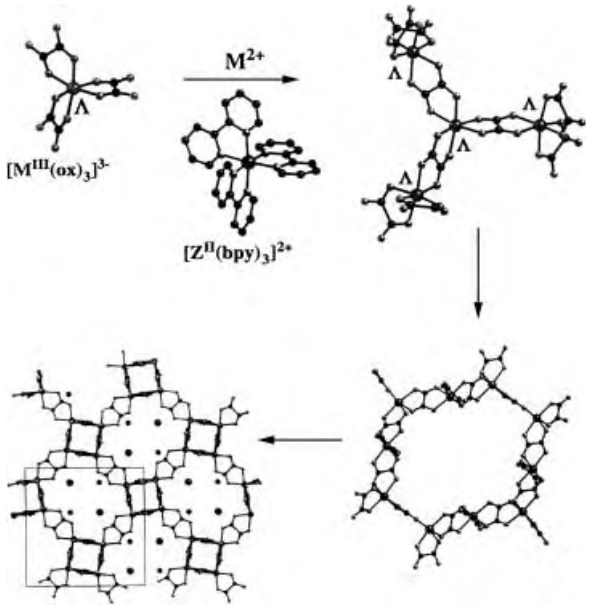


Figure 8. Construction of the 3D network of $\{[M^{II}M^{III}(ox)_3]_n^-\}$ by combination of Λ and Δ isomers of tris(oxalato)metalate complex monomers in the presence of a chiral metal complex Λ-$[Z(bpy)_3]^{2+}$ (Z = Co^{II}, Fe^{II}, Mn^{II}, Ni^{II}, Ru^{II}) that acts as a template.[49c]

 © 2004 Wiley-VCH Verlag GmbH & Co. KGaA, Weinheim

were able to tune the size of the cavity in the 3D metal–oxalate framework by varying the metal ions in framework. They also investigated the magnetic properties of these materials by changing using $[M(bpy)]^{2+}$ units of various metals within the zeolite-like cavities. The 3D supramolecular complex K[Cu(*trans*[14]dien)][Cr(ox)$_3$] has been described,[56] which has large helical tunnels ($\approx 21.2 \times 9.3$ Å) that are formed by the oxalate-bridged, octahedrally coordinated Cr and K centers. The Cu complex, which is coordinated to the framework via the oxalate ions and protrudes into the channel, can be chemically manipulated and exploited for potential applications.

Many other transition-metal oxalate frameworks with different templates, such as NH_4^+ ions, organoammonium ions, and metal complexes are also known.[38c,f,57] For example, the iron oxalate $(NH_4)_2[Fe_2O(ox)_2Cl_2]\cdot 2H_2O$ consists of a helical motif formed by the chiral linking of Fe atoms by the oxalate ions. These motifs are bridged by a μ-oxo group to form a 3D structure with helical tunnels that can be occupied by guest species.[58] The Fe–Fe separations of 3.384(2) (through the oxo ligand) and 5.496(2) Å (through the bisbidentate oxalate bridge) indicates the openness created by the presence of oxalate units in these structures. The templated iron oxalate framework also exhibits interesting ferromagnetic behavior with a Curie temperature (T_c) as high as 40 K (Figure 9). $Na_2[Co_2(ox)_3(H_2O)_2]$, a hydrothermally prepared 1D oxalate that possesses ladderlike topology, has been described and exhibits antiferromagnetic ordering.[59] On the other hand, $Ba_4[\{Fe(ox)(OH)\}_4(ox)Cl_2]$ possesses two distinct channels (concave and convex) that are formed by the linking of vertex-sharing FeO_6 octahedra through μ^2-OH bridges and oxalate ions in a monodentate fashion (Figure 10);[60] the concave channels (type 1) are occupied by Ba^{2+} and Cl^- ions, while the convex channels (type 2) are occupied by the oxalate ions.

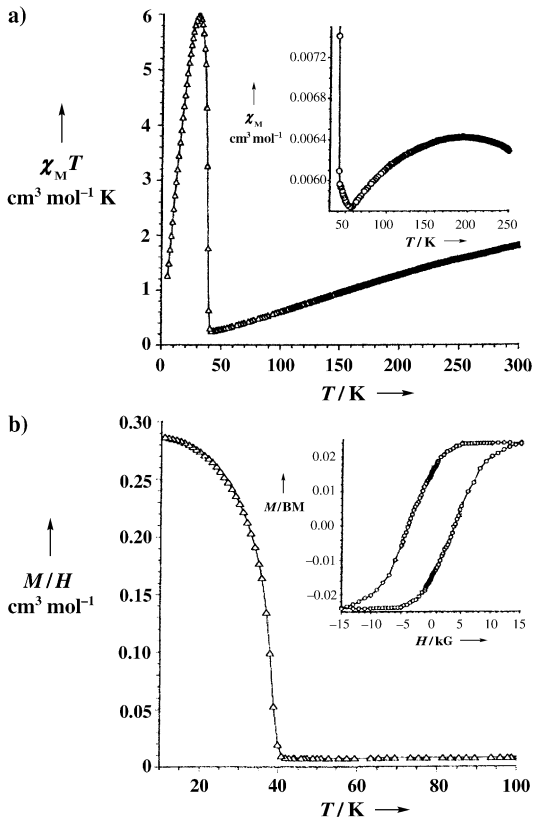


Figure 9. a) The variation of the $\chi_M T$ product for $(NH_4)_2[Fe_2O(ox)_2Cl_2]\cdot 2H_2O$ at $H = 100$ G. Inset: a plot of χ_M versus T; b) field-cooled magnetization for $(NH_4)_2[Fe_2O(ox)_2Cl_2]\cdot 2H_2O$ at $H = 100$ G. Inset: the hysterisis loop at 5 K.[58]

3.2. Zinc and Cadmium Oxalates

Zinc and cadmium oxalates of with various dimensionalities and open structures have been synthesized in the presence of alkali-metal ions and organic amines.[61–64] While the zero-dimensional (0D) oxalates are generally simple monomers or dimers with bridging oxalate ions,[61b] the 1D structures are formed by bridging of metal polyhedra through the oxalate units;[61b,62] these structures are stabilized by cooperative noncovalent interactions. The 2D layered oxalates adopt the common honeycomb structures with 12-membered apertures.[61,62] In some cases, the honeycomb layers are stacked one over the other to create psuedo-1D channels (Figure 11 a and b).[61c,62] The 3D oxalates generally possess honeycomb layers pillared or cross-linked by oxalate units (Figure 12 a).[61a,64] For example, a 3D zinc oxalate has been prepared that displays an interesting interrupted honeycomb structure, with channels that can allow water molecules to be reversibly adsorbed (Figure 12 b). Similar connectivities have been observed in tin(II) oxalates (Figure 13).[65,66] Scheme 3 shows the various connectivity patterns that can be found in oxalate structures; the wide variety of structures

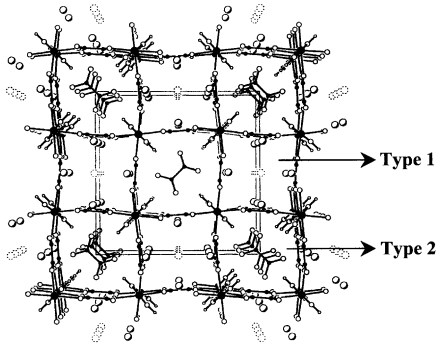


Figure 10. A perspective view of $Ba_4[\{Fe(ox)(OH)\}_4](ox)Cl_2$ showing {Fe(OH)} chains held together in a square lattice. Type 1 channels contain Ba^{2+} and Cl^- ions, while type 2 channels contain oxalate ions.[60]

that exist allow the design of complex 3D open-frameworks (thecolored illustration in the frontispiece of this Review shows a schematic representation of 3D metal–organic and inorganic–organic hybrid structures).

The reaction of Zn^{2+} ions with organoammonium oxalates has been shown to yield zinc oxalates of various dimensionalities (Figure 14).[61b] In view of the close relationship

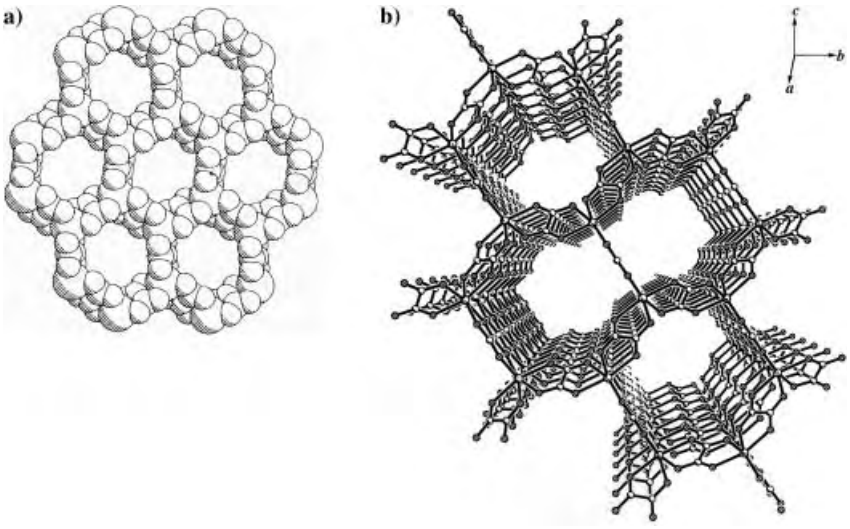


Figure 11. a) Space-filling diagram showing the open channels formed by the stacking of the 2D layers in $[Zn(ox)(C_6H_8N)_2]$;[62] b) 1D channels in the structure of $K(C_6N_2H_{13})[Zn_2(ox)_3]\cdot 4H_2O$ formed through molecular stacking.[61c]

between their structures, one can visualize a possible building-up process involved in the formation of higher dimensional structures from those of lower dimensionality (Scheme 4). The 0D monomer and dimer are reactive, which gives rise to 1D, 2D, and 3D extended structures.

A 3D cadmium oxalate that incorporates K^+ ions and imidazole moieties with in its channels has been prepared.[64] As in the 3D zinc oxalate structures, the structure bears both in-plane and out-of-plane linkages through oxalate units. Open-framework metal–organic cadmium chloride compounds, in which the cadmium chloride chains are assembled into three dimensions via the organic linkers (oxalate or piperazine) have been prepared under solvothermal conditions.[67a] The cadmium chloride chain in these compounds is similar to that in $CdCl_2$ and Cd(OH)Cl. In some of the oxalates the metal ions undertake ancillary coordination through bonding with, for example, water and amines.[62,67b] Coordination polymers of cadmium oxalates that possess such ancillary ligation from amine or imine-type ligands and infinite Cd-O-Cd linkages are known.[68] The bonded amine molecules interdigitate with the neighboring chains or layers to enhance π–π interactions or hydrogen-

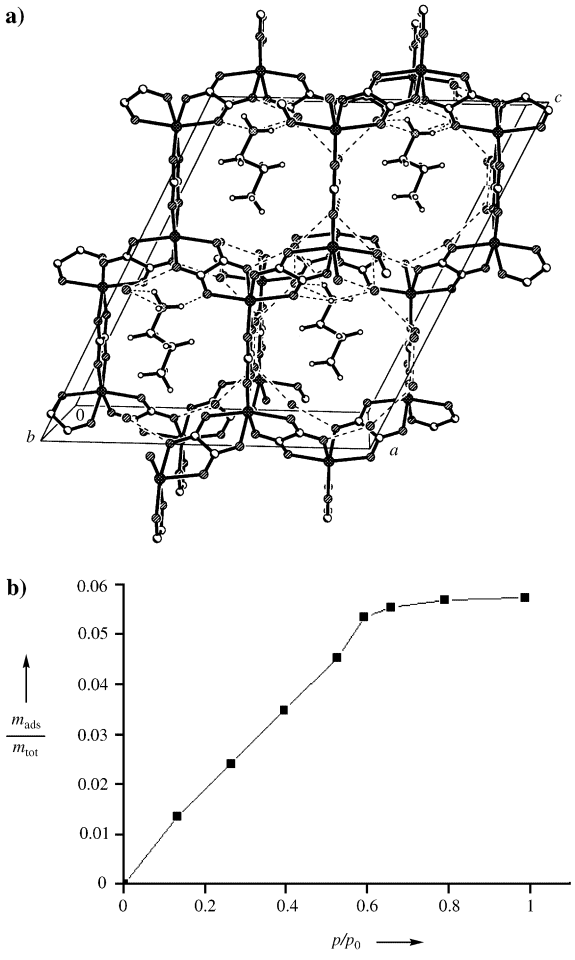


Figure 12. a) Structure of $(C_3H_7NH_3)_2[Zn_2(ox)_3]\cdot 3H_2O$ with 12-membered square channels. Propylammonium ions interact with the framework via hydrogen-bond interactions (dashed lines); b) room-temperature adsorption isotherm for H_2O in dehydrated $(C_3H_7NH_3)_2[Zn_2(ox)_3]$.[61a]

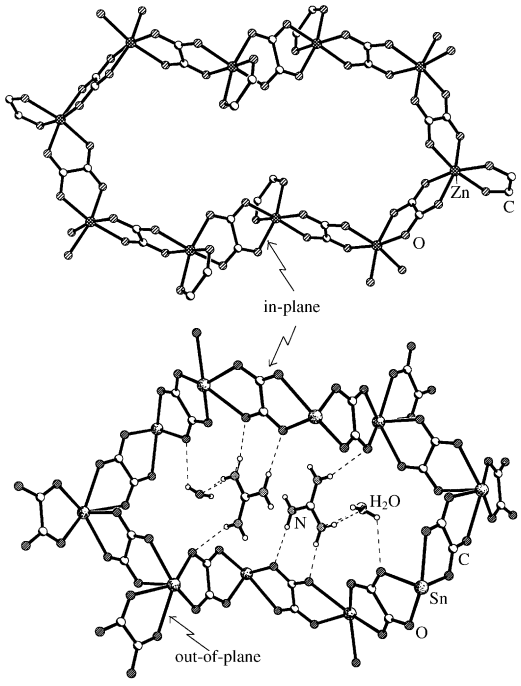
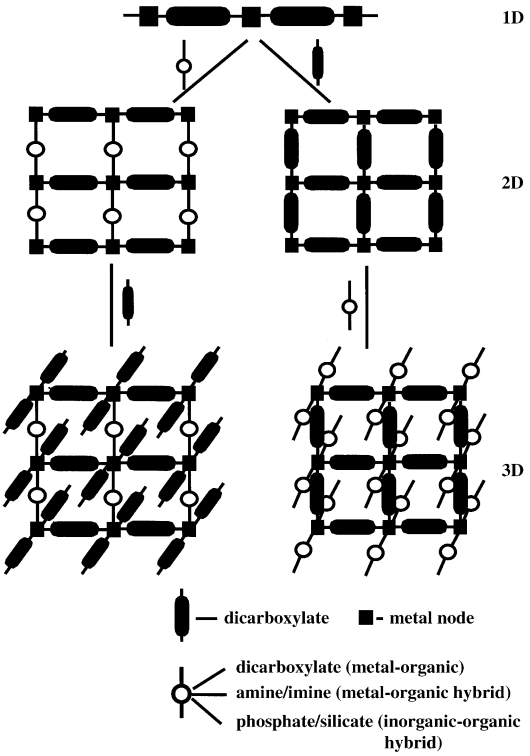


Figure 13. Structure of $(C_3H_7NH_3)_2[Zn_2(ox)_3]\cdot 3H_2O$ (above) exhibiting a 20-membered aperture, and a similar aperture in the the layered tin(II) oxalate $\{C(NH_2)_3\}_2[Sn_4(ox)_5]\cdot 2H_2O$. The replacement of a four-coordinate Sn^{II} center by a six-coordinate Zn center with two in-plane and two out-of-plane linkages can give the 3D zinc oxalate structure.[61a]

 © 2004 Wiley-VCH Verlag GmbH & Co. KGaA, Weinheim



Scheme 3. Hybrid 3D metal–organic systems formed from dicarboxylate ligands and inorganic linkers by transforming a reactive 1D chain through reaction with suitable reactants or precursors. The chain is just one example of a precursor; in principle, any other low-dimensional precursor could be utilized.

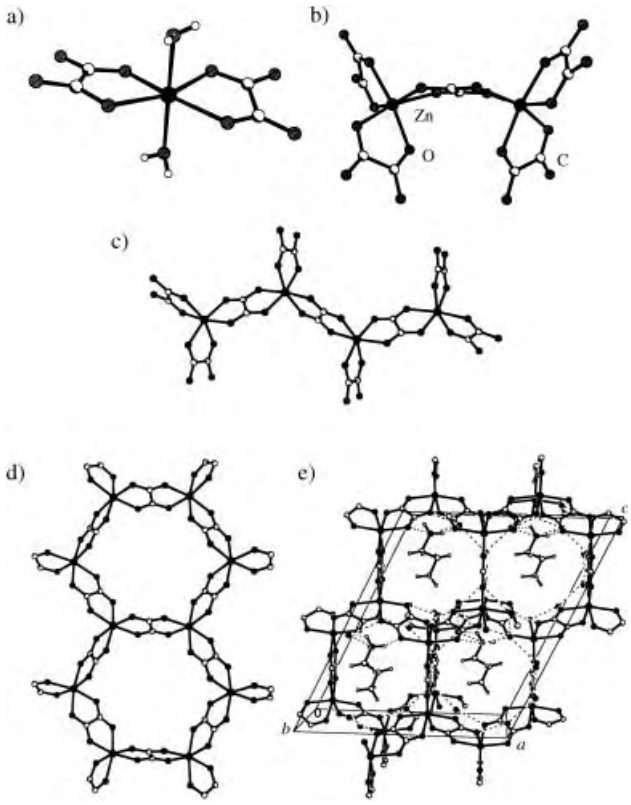


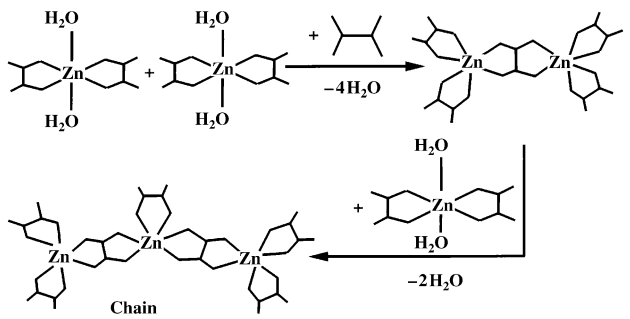
Figure 14. Various zinc oxalate structures obtained by the reaction of organoammonium oxalates and Zn^{2+} salts: a) monomer, b) dimer, c) 1D chain, d) 2D layer, and e) 3D structure. Note the close relationship between the structures.[61b]

bonding interactions, or to give more efficient packing (Figure 15). The transformation other dicarboxylates into oxalate species, and their further reaction with Zn^{2+} and Cd^{2+} ions to form extended metal–oxalate architectures has been observed.[69]

3.3. Rare-Earth-Metal Oxalates

Hydrated lanthanide oxalates have been prepared and characterized;[70] the loss of water molecules from such complexes invariably leads to the collapse of the structure.[71] Several rare-earth-metal oxalates have also been synthesized in the presence of alkali-metal cations.[72] Some of the rare-earth-metal oxalates possess cavities and channels.[73] Oxalato carbonates of the general formula $[\{Ln(H_2O)_2\}(ox)(CO_3)_2]$ (Ln = Eu–Ho) exhibit 2D and 3D structures.[74] Rare-earth-metal oxalate frameworks containing ammonium cations are known,[75,76a] and some mixed-metal rare-earth-metal oxalates with 2D and 3D structures possess zeolite-like properties (Figure 16).[76a–e] Thermal decomposition studies of $M[La(H_2O)_2(ox)_2]\cdot H_2O$ (M = K, NH_4) show the existence of crystalline anhydrous $K[La(ox)_2]$ and $(NH_4)[La(ox)_2]$, and in some cases ion-exchange properties have been observed.[76d,77]

A series of uranyl oxalates containing organoammonium ions or amine moieties were described, which exhibit variable coordination modes around the UO_2^{2+} ion.[78] Organoammonium ions have been utilized in the formation of rare-earth oxalates with open-framework structures.[79,80] For example, the yttrium oxalates $(C_6N_2H_{16})_{0.5}[Y(H_2O)(ox)_2]\cdot 2H_2O$ and $(C_5N_2H_{12})[Y(ox)_2]$ have 3D structures with Y in different coordination environments.[79] These oxalates possess layers with honeycomb-like apertures which are cross-linked by another oxalate unit to give 3D structures with channels that run in all three crystallographic directions (Figure 17a). The yttrium oxalates also show reversible adsorption behavior (Figure 17b). Recently, neodymium oxalates with dangling



Scheme 4. Formation of the zinc oxalate dimer from the 0D monomer and its transformation to 1D zinc oxalate chains via condensation reactions.[61b]

 © 2004 Wiley-VCH Verlag GmbH & Co. KGaA, Weinheim

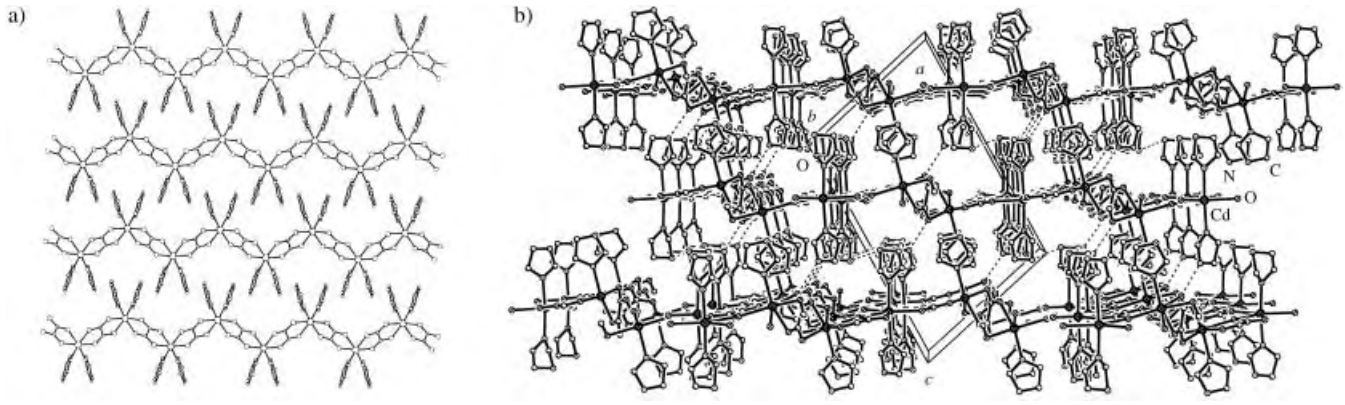


Figure 15. a) Interchain interdigitation of coordinated pyridine molecules in $[Zn(ox)(C_5H_5N)_2]$;[62] b) layered structure of $[Cd_2(ox)_2(C_3N_2H_4)_3(H_2O)]$ in which the bonded imidazole molecules point into the interlamellar regions and form stacks.[67b]

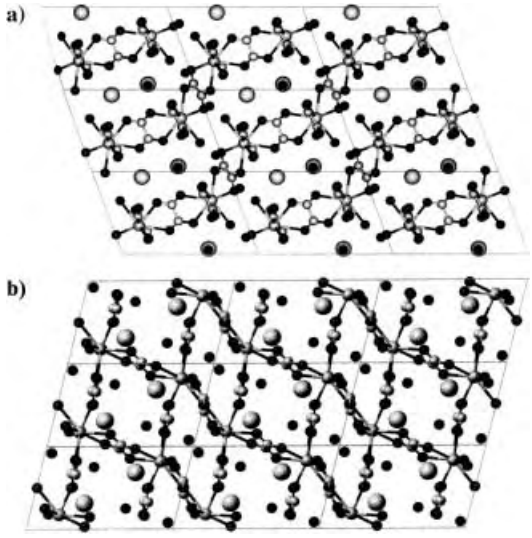


Figure 16. a) Projection of the structure of $K[La(ox)_2(H_2O)_2]\cdot H_2O$ that shows K^+ ions and water molecules present between the layers;[76a] b) Projection of the structure of $K[La(ox)_2(H_2O)_2]\cdot H_2O$ that highlights the four-membered rings formed by $\{[La(ox)]_4\}$ units.[76a]

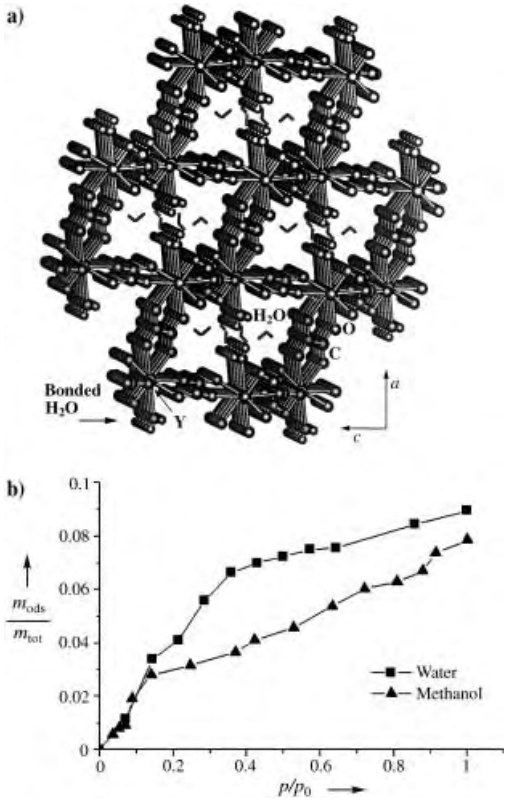


Figure 17. a) Structure of the 3D $(C_6N_2H_{16})_{0.5}[Y(ox)_2(H_2O)]\cdot 2H_2O$ showing rectangular zeolite-like channels. Note the proximity of the bonded water molecules that protrude into the channels; b) room-temperature adsorption isotherm for H_2O and CH_3OH in dehydrated $(C_6N_2H_{16})_{0.5}[Y(ox)_2(H_2O)]\cdot 2H_2O$.[79]

functional groups that protrude into accessible channels have been reported (Figure 18).[80] Other open-framework compounds based on carboxylate links that possess functionalized channels will be discussed later.

3.4. Oxalates of the Main-Group Elements

3.4.1. Oxalates of Al, Ga, In, Pb, and Bi

Oxalates of the main-group elements are scarce. Some of the hydrated oxalates of this category are listed in Table 1. In $[Ni(bpy)_3][NaAl(ox)_3]$ the octahedrally coordinated Al and Na atoms have D_3 symmetry and are linked through the oxalate units into a helical 3D network. The $[Ni(bpy)_3]^{2+}$ ions also have a D_3 symmetry and occupy the large voids within the anionic framework.[81] The mutual reflection of the symmetry of the templating cations and the framework is noteworthy. Other hydrated oxalates do not contain porous structures.[63,82–88]

3.4.2. Tin(II) Oxalates

Several tin oxalates with 0D, 1D, and 2D structures have recently been reported.[65,89–93] While the 0D structure has a

 © 2004 Wiley-VCH Verlag GmbH & Co. KGaA, Weinheim

Table 1: Main-group-metal oxalate hydrates and related compounds.[a]

Compound	Coordination geometry	Crystal data	Ref.
$(NH_4)_3[Al(ox)_3]\cdot 3H_2O$	$\{AlO_6\}$ octahedra	$P\bar{1}$; $a=7.888(4)$, $b=10.667(4)$, $c=10.643(2)$ Å $\alpha=83.33(2)$, $\beta=70.44(2)$, $\gamma=69.10(4)°$, $V=788.3$ Å^3	[82]
$[Ru(C_8N_2H_8)_3][NaAl(ox)_3]$	$\{AlO_6\}$ and $\{NaO_6\}$ octahedra	$P2_13$; $a=15.407(4)$ Å, $V=3657.2(16)$ Å^3	[83]
$[Ni(C_8N_2H_8)][NaAl(ox)_3]$	$\{AlO_6\}$ and $\{NaO_6\}$ octahedra	$P2_13$; a = 15.518(2) Å, $V=3736.9(8)$ Å^3	[81]
$(NH_4)_3[Ga(ox)_3]\cdot 3H_2O$	$\{GaO_6\}$ octahedra	$P\bar{1}$; $a=7.901(1)$, $b=10.674(2)$, $c=10.710(2)$ Å $\alpha=83.14(1)$, $\beta=70.18(1)$, $\gamma=69.88(1)°$, $V=798.0$ Å^3	[82]
$[In_2(ox)_3(H_2O)_4]\cdot 2H_2O$	$\{InO_7\}$ pentagonal bipyramid	$P2_1/c$; $a=10.189(1)$, $b=6.651(1)$, $c=11.162(1)$ Å, $\beta=95.64(1)°$, $V=752.7(1)$ Å^3	[84]
$NH_4[In(ox)_2]\cdot 2H_2O$	$\{InO_8\}$ archimedean antiprism	$P6_222$; $a=9.025(1)$, $c=11.343(1)$ Å, $V=800.0$ Å^3	[85]
$Na[In(ox)_2]\cdot 2H_2O$	$\{InO_8\}$ archimedean antiprism	$P6_222$; $a=8.739(1)$, $c=11.598(3)$ Å, $V=767.0$ Å^3	[85]
$[Pb(ox)]\cdot 2H_2O$	$\{PbO_8\}$ square antiprism	$Pnam$; $a=9.053(1)$, $b=8.036(1)$, $c=7.834(1)$ Å, $V=569.9(2)$ Å^3	[86]
$[Pb(ox)]\cdot 3H_2O$	$\{PbO_7\}$ pentagonal bipyramid	$P1$; $a=6.008(1)$, $b=6.671(1)$, $c=8.493(1)$ Å $\alpha=74.70(1)$, $\beta=74.33(1)$, $\gamma=80.98(1)°$	[63]
$[Pb_2(ox)(NO_3)_2]\cdot 2H_2O$	$\{PbO_7\}$ pentagonal bipyramid	$P2_1/c$; $a=10.623(2)$, $b=7.9559(9)$, $c=6.1932(5)$ Å $\beta=104.49(1)°$, $V=506.8(1)$ Å^3	[87]
$K[Bi(ox)_2]\cdot 5H_2O$	$\{BiO_8\}$ square antiprism	$Fd2d$; $a=8.7967(3)$, $b=16.1057(6)$, $c=17.1877(7)$ Å, $V=2435.1(2)$ Å^3	[88]

[a] ox = $[C_2O_4]^{2-}$.

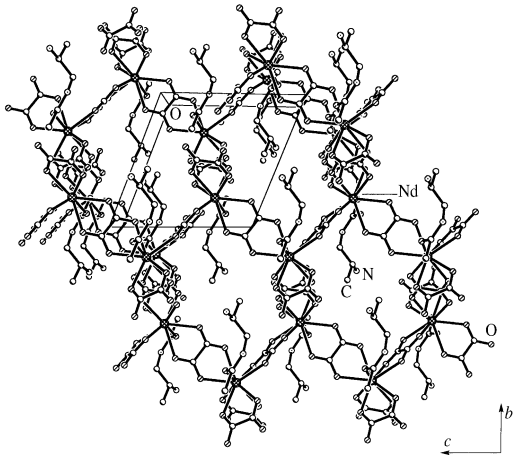


Figure 18. Structure of $\{OC(CH_3)NCH_2CH(CH_3)NH_3\}[Nd(ox)_2]\cdot H_2O$ with 12-membered channels and *N*-(2-aminopropylacetimide) groups protruding into the channels.[80]

typical monomeric structure that is stabilized through hydrogen bonding, the 1D tin oxalate is similar to the corresponding zinc oxalate $[Zn(ox)(py)_2]$,[62] and exhibits interchain interdigitation. The layered tin oxalates exhibit 8-, 12-, and 20-membered apertures within the layers, which are formed through the connectivity of the Sn atoms and the oxalate units (Figure 19). In $Na_4[Sn_4(ox)_3F_6]$, bonding between F^- ions bound to the Sn centers and Na^+ ions in the interlayer regions is observed.[91] The Sn atom is generally six-coordinated and the lone pair acts as the seventh coordinated species, which leads to a pseudo pentagonal-bipyramidal arrangement (Figure 20). The presence of lone pairs on tin centers not only influences the coordination geometry, but also directs the structure to some extent.

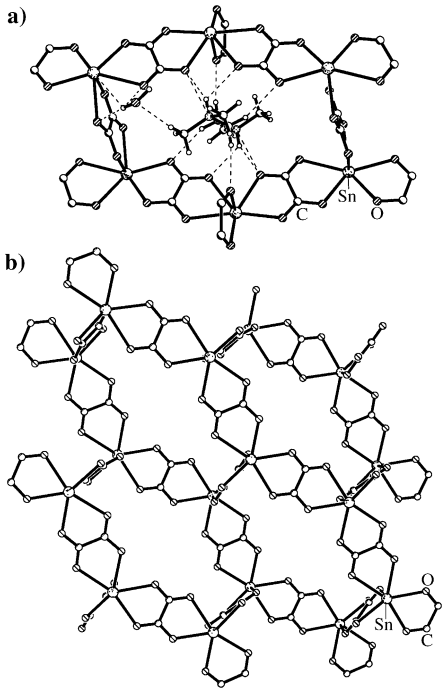


Figure 19. 12-membered windows in $\{(CH_3)_2NH(CH_2)_2NH(CH_3)_2\}[Sn_2(ox)_3]\cdot H_2O$. a) Hydrogen-bonding interactions between ammonium ions and water molecules with the framework within apertures; b) a view of one layer of the anionic framework.[65]

3.5. Oxalate Structure: A Perspective

The ability of the oxalate ligand to spawn a variety open-framework architectures both in the presence and absence of templating agents has already been shown. Nevertheless, the design of such architectures with predetermined structural

 © 2004 Wiley-VCH Verlag GmbH & Co. KGaA, Weinheim

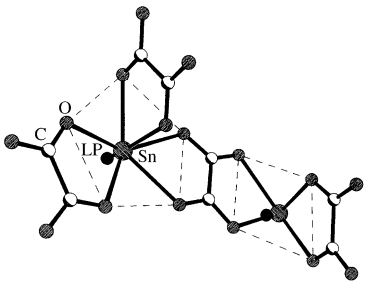
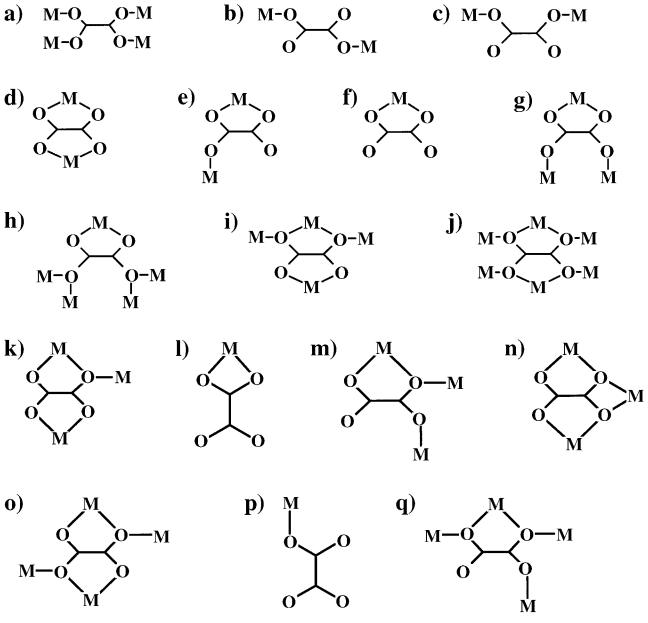


Figure 20. The structure of $\{C(NH_2)_3\}_2[Sn_4(ox)_5]\cdot 2H_2O$, in which the Sn centers are found in both pentagonal-bipyramidal and square-pyramidal geometries (LP = lone pair of electrons on Sn center).[65]

features and functionalities is far from being accomplished. It is therefore necessary to understand the behavior of the oxalate ligand in these open structures. Oxalate ligands can be monodentate,[68i] bidentate,[62–65] or show both coordination modes in the same compound;[38f] in addition, the oxygen atoms can be tricoordinate.[69a] A schematic representation of the various possible (and in some cases observed) modes of oxalate ligations are shown in Scheme 5.

A common feature of the low-dimensional oxalate structures is the presence of hydrogen-bond, π–π, or other weak interactions, which contribute to the cohesion of the structures. In the layered metal oxalates with templates, the stacking of the layers generally shows a shift of the layers along one or more crystallographic axis, either to achieve efficient packing or to promote hydrogen-bonding interactions.

The metal oxalate structures discussed hitherto suggest the possibility of generating complex supramolecular structures with multifarious properties and functionalities through utilizing the ability of the oxalate units to align metal centers in 2D or 3D assemblies. An alternative strategy for understanding oxalate structures involves net topology. In his recent review,[4c] Robson states "in the coordination polymer networks in which octahedral metal centers are chelated by three oxalates and each oxalate bridges two metal centers, both 2D hexagonal grid (6,3) nets[39a] and 3D (10,3)-a nets[4b] have been observed. Particularly interesting from the net point of view is $[Fe(2,2'\text{-bpy})_3][Fe_2(ox)_3]$ in which the anionic oxalate-bridged network adopts the (10,3)-a topology; within the cavities of the chiral anionic network are found chiral $[Fe(bpy)_3]^{2+}$ cations all with Δ configuration.[54a] In the 2D (6,3) nets, the absolute configurations of the metal centers are required to alternate, each Λ center being surrounded by three Δ centers and vice versa, whereas in the (10,3)-a nets the absolute configurations of all the metal centers in the network must be the same". Thus, it would be of interest to break down large open-framework structures into smaller fragments, and to understand such fragments in terms of nets. Another strategy would be to build 3D structures by connecting simpler predetermined building units, such as metal oxalate ladders, chains, or layers and linking these through bridging oxalates to reticulate channels with the desired magnetic characteristics. At the molecular level, it is also desirable to utilize basic building units that can carry precoded chemical information to generate larger framework structures.



Scheme 5. The possible coordination modes exhibited by oxalate ligands. Note the presence of monodentate (e.g., a–c), bidentate (e.g., d and f), and combinations of both mono- and bidentate (e.g., e and g) modes, and also the presence tricoordinate oxygen atoms (e.g., h–k): a) Ref. [60]; b) Ref. [206]; c) Ref. [68i]; d) Refs. [61a, 73a]; e) Ref. [38f]; f) Ref. [61b, 89]; g) Ref. [61e]; i) Ref. [67b]; k) Ref. [68f]; l) Ref. [78a]; n) Ref. [67b]; o) Ref. [67b]; p) Refs. [47c, 38f]; q) Ref. [90].

4. Higher Dicarboxylates

4.1. Flexible Aliphatic Dicarboxylates

Aliphatic dicarboxylates have good conformational freedom, which manifests itself in the various connecting modes that yield novel frameworks. In general, aliphatic carboxylates possess the following features: 1) bidentate and monodentate linking modes, 2) *cis–cis*, *trans–trans*, or *cis–trans* orientation, 3) tricoordinate oxygen-atom connectivity, 4) pillaring of the metal–oxygen layers or networks, and 5) the generation of secondary building units (SBUs) by acting as capping agents through their carboxylate moieties. Many compounds using $[OOC(CH_2)_nCOO]^{2-}$ ions have been prepared and characterized.[94–99] In some of these dicarboxylates, metal–oxide dimers (0D), chains (1D), or layers (2D) are linked or pillared by dicarboxylate ions to give higher dimensional frameworks (Figure 21 and Figure 22).[99d,e] The metal–oxygen layers have infinite M-O-M linkages formed through edge- or corner sharing of the $\{MO_x\}$ ($x = 4, 5, 6, 7$) polyhedra. Recently, cadmium succinates of various dimensionalities have been reported.[100] In these, a tetrahedral $\{Cd(suc)_4\}$ building unit ($suc = C_4H_4O_4$), yields 1D and 3D structures, the 3D structure possessing an interpentrated diamondoid toplogy (Figure 23).[100a] The cadmium succinate $[Cd_3(C_4H_4O_4)_2(OH)_2]$ has a SBU comparable to the SBU-4

 © 2004 Wiley-VCH Verlag GmbH & Co. KGaA, Weinheim

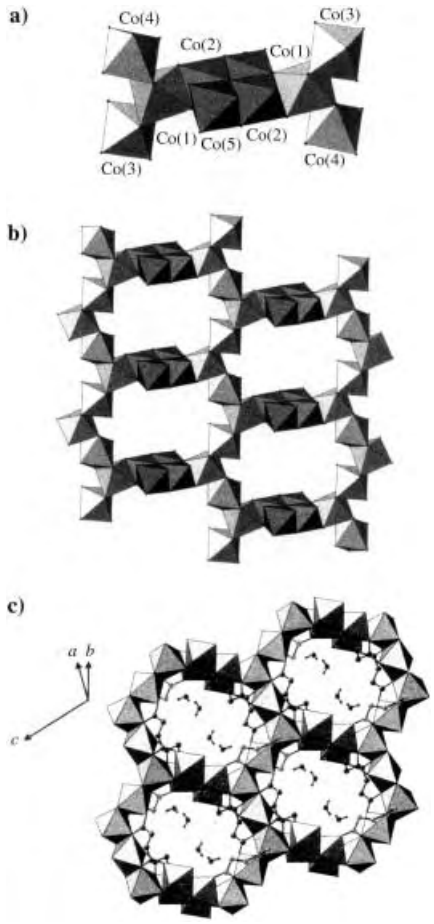


Figure 21. Secondary building units (SBUs) in $[Co_4(suc)_3(OH)_2(H_2O)_2]\cdot 2H_2O$: a) the tetrameric unit (dark) with 2 Co(2) and 2 Co(5) polyhedra. Co(1), Co(3), and Co(4) form a helical chain (b) that bind the tetramers; c) a view of one layer of the structure.[99c]

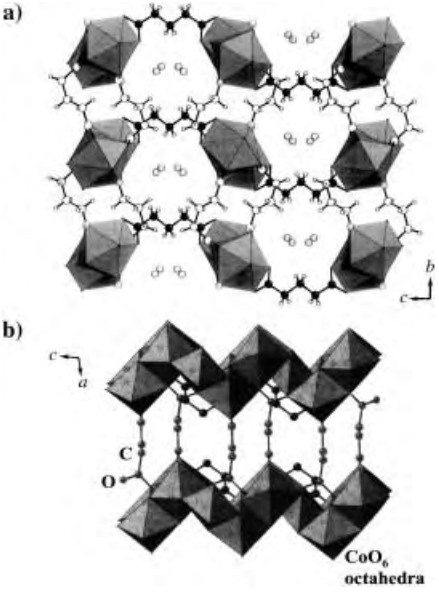


Figure 22. a) Projection of the structure of the glutarate $[\{Pr(H_2O)\}_2\{O_2C(CH_2)_3CO_2\}_3]\cdot 4H_2O$ with water molecules present in the channels;[99g] b) 3D structure of $[Co_5(suc)_4(OH)_2]$ (MIL-9) demonstrating the pillaring role of succinate anions.[99e]

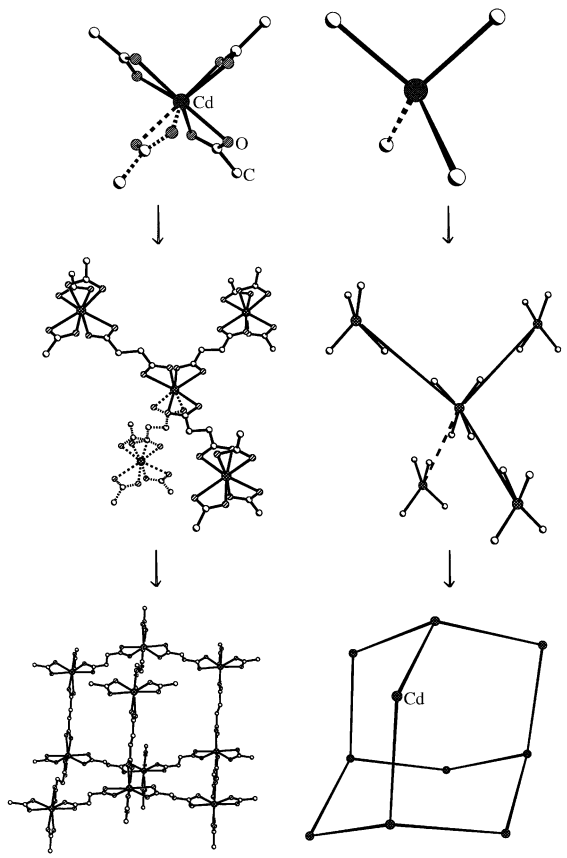


Figure 23. Structure of $(CN_3H_6)_2[Cd(suc)_2]$: The basic cadmium succinate tetrahedron, the supertetrahedron, and the adamantane unit are displayed to demonstrate the scale-up chemistry principle.[100a]

units found in many octahedral–tetrahedral metal–phosphate structures.[2d,5c] In addition, we have prepared the manganese adipate $[Mn\{O_2C(CH_2)_4CO_2\}(C_4H_8N_2)]$, which exhibits bound piperazine units located within channels.

Frameworks involving infinite M-O-M type linkages are also known.[31,101] Forster and Cheetham have described a nickel succinate $[Ni_7(suc)_6(OH)_2(H_2O)_2]\cdot 2H_2O$, which was prepared at the interface of a water/cyclohexanol mixture. (Figure 24).[101a] This compound exhibits an infinite Ni-O-Ni framework and has 1D hydrophobic channels. Similarly, cadmium malonate $[Cd(O_2CCH_2CO_2)(H_2O)]\cdot H_2O$, with

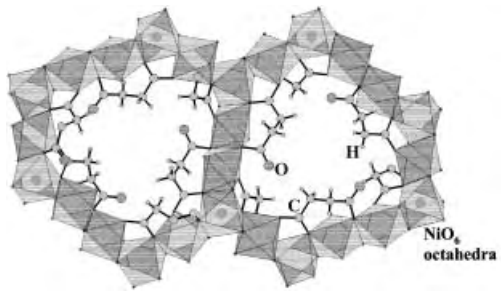


Figure 24. A view of the nickel succinate $[Ni_7(suc)_6(OH)_2(H_2O)_2]\cdot 2H_2O$ that highlights the hydrophobic channels, which are lined with methylene groups.[101a]

 © 2004 Wiley-VCH Verlag GmbH & Co. KGaA, Weinheim

infinite Cd-O-Cd connectivity, exhibits hydrophobic channels lined with methylene groups (Figure 25).[101b] Several open-framework transition-metal dicarboxylates with edge/corner

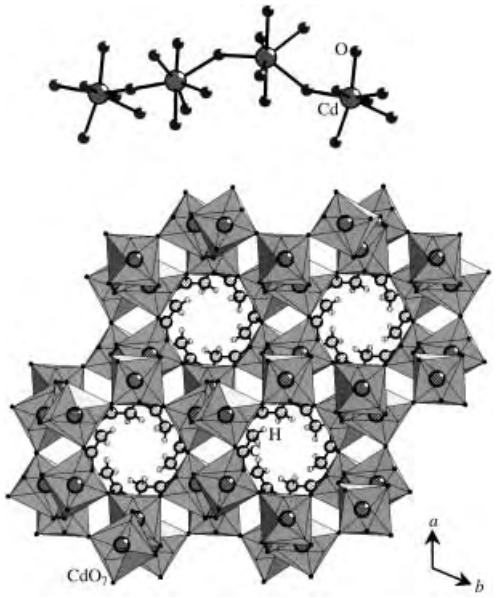


Figure 25. Structure of $[Cd(O_2CCH_2CO_2)(H_2O)]\cdot H_2O$ showing the 12-membered, methylene-lined hydrophobic channels. Above: the zigzag 1D Cd-O-Cd chains present in the strucuture.[101b]

sharing MO_6 (M = Co, Mn, Fe) octahedra are known.[102] The interlayer separations in these carboxylates is directly related to the length of the carbon backbone of the α,ω-dicarboxylic acid. The tetrahedral $\{XCd_4O_{24}\}$ (X = Cl, Br) cluster in $Na_3[Cd_5(C_4H_4O_4)_6X]$[100b] (Figure 26) is analogous to the $\{OZn_4\}$ clusters in $[Zn_4O(1,4\text{-bdc})_3]\cdot 8\,DMF\cdot C_6H_5Cl$ (H_2bdc = benzene dicarboxylic acid) described by Yaghi et al.[6c] Scheme 6 shows how complex structures can be broken down into more simple building blocks to assist the design of new inorganic–organic solids with open-framework structures.

The presence of infinite M-O-M connectivities in metal dicarboxylate structures facilitates electronic and magnetic exchange in one, two, or three dimensions. In the reported nickel fumarate,[99a] cobalt succinates,[99c,e] and cobalt adipate[98a] the possibility of braiding massive metal–organic structures with predetermined periodic M-O-M arrays has been demonstrated to give desired electronic, optical, and other useful properties, and to extend such interactions to larger dimensions via the mediating carboxylate linkages. For example, in the cobalt adipate compound the brucite-type $\{Co(OH)_3\}$ units are aligned by the adipate anions, and the compound exhibits interesting magnetic properties.[98a] These solids should be distinguished from the organodiammonium molybdenum oxides (MOXI-n family), based on bimetallic molybdenum oxides, described by Zubieta and co-workers.[4a] Metal dicarboxylate frameworks involving rare-earth-metal ions have been shown to possess interesting properties.[94d,98e,99d,99f,103] An essential feature in most of these structures is that the dicarboxylate ions participate in the

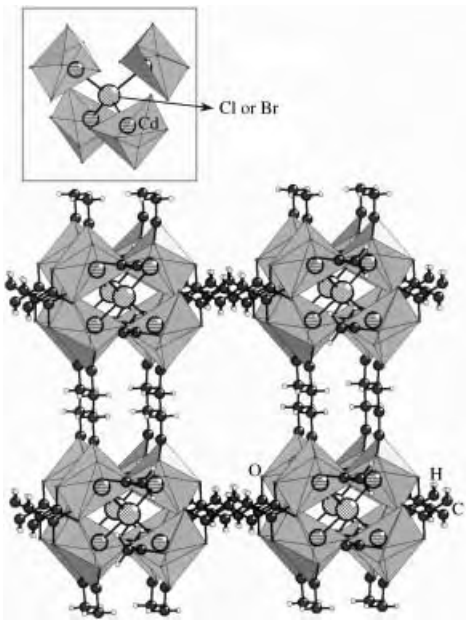
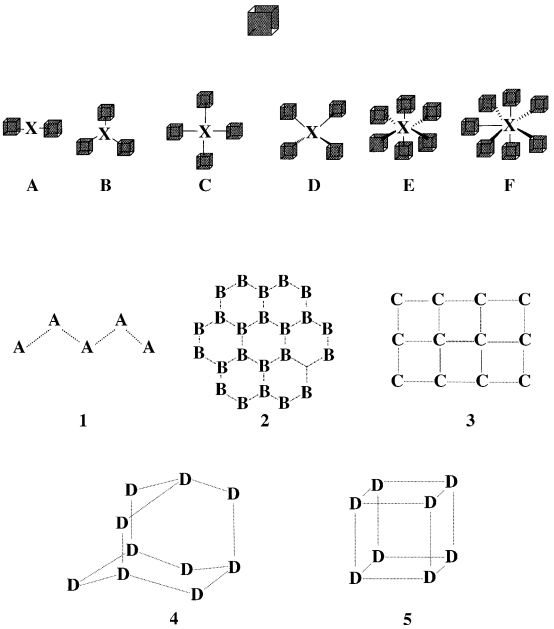


Figure 26. Cubelike architecture of $Na_3[Cd_5(suc)_6Cl]$: the $\{ClCd_4O_{24}\}$ clusters are connected through succinate linker groups (the centers of adjacent clusters are separated by 11.831 Å). Above: a $\{ClCd_4O_{24}\}$ cluster with a central Cl^- ion. In $Na_3[Cd_5(suc)_6Br]$, the Cl^- ion is replaced with Br^-.[100b]



Scheme 6. Complex 3D architectures built up from simpler primary and secondary building units. The cube on top is the primary building unit, which could be, for example, a tetrahedron, octahedron, or pentagonal bipyramid. **A**–**F** are secondary building units made from assembling the primary building units (SBUs with X = Cl, Br, O, S, Se etc.). **1**–**5** represent the tertiary building units (TBUs) from assembly of the SBUs.[100b]

skeleton along with the inorganic species, acting both as part of the extended oxide chains or sheets and as pillars between the latter, which is in contrast to the metal–organic framework (MOF) compounds of Yaghi et al., where isolated metal

 © 2004 Wiley-VCH Verlag GmbH & Co. KGaA, Weinheim

clusters are connected by organic linkers.[6] The wide variety of dicarboxylate-derived 3D metal–organic structures prompts an examination of the different roles performed by the dicarboxylate linkers in these solids. Scheme 7 illustrates several of the possible roles, some of which have already been observed.

The use of long-chain dicarboxylic acids in the construction of open-framework structures generally results in interpenetrated solids. Although interpenetrated structures contribute to metal–organic structures with lattices resembling inorganic networks, these catenated structures typically possess low porosities (<20%); this problem has been addressed by Yaghi and co-workers.[104] Robson and Batten[4b–d] refer to the inclusion of guest molecules into a framework so that they occupy positions where a second independent network is found within the parent structure. Porous architectures have been efficiently generated through "interweaving", a crystal-engineering tool that utilizes the minimal displacement between independent interpenetrating frameworks.[104]

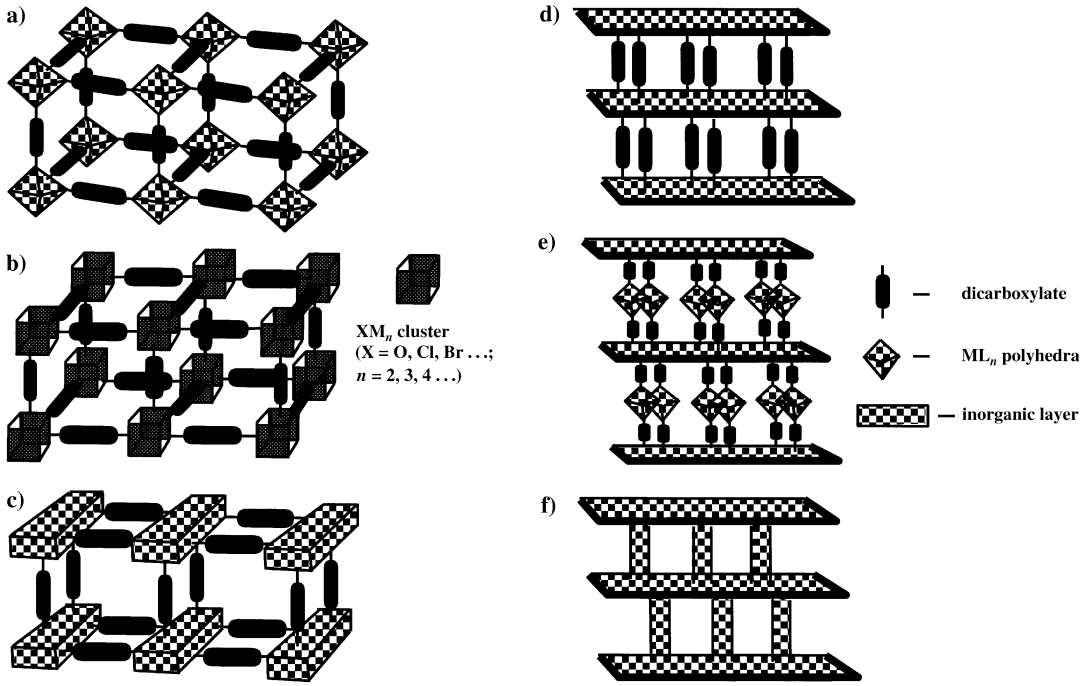
4.2. Multifunctional Carboxylates

A variety of open-framework solids prepared by using carboxylic acids with two or more carboxylate arms and a rigid cyclic backbone are known. The various features of many representative examples will be described below.

Several metal squarates and croconates have been reported.[105–107] In transition-metal-containing squarates, the metal is invariably in an octahedral coordination, with respect to the oxygen atoms. Molecular complexes involving squarate anions have been prepared and their magnetic properties investigated.[105] The observed structural diversity derives from differences in the binding modes and orientational preferences of the squarate anion. 1D squarates with chain structures are known;[106] in some metal squarates, the metal center exhibits ancillary coordination to water, DMF, or OH groups.[106] Vanadium, cobalt, and cadmium squarates with 2D layered structures have also been characterized.[108a,109a] In addition, a layered iron hydroxysquarate posessing $\{Fe(OH)_3O_3\}$ double chains has been prepared.[109b]

Many metal squarates with 3D structures have been reported.[108,110] In most of these the squarate anion is connected to the metal center through a fourfold monodentate linking mode. A neutral 3D vanadium squarate that contains dimers of edge-sharing $\{V^{III}O_6\}$ octahedra and where squarate anions exhibit μ^2 and μ^4 binding modes has been reported.[108a] The dense manganese squarate $[Mn_2(OH)_2(C_4O_4)]$, which exhibits antiferromagnetic behavior has also been described.[110a] Additionally, the 3D cobalt squarate $[Co_3(\mu^3\text{-}OH)_2(C_4O_4)_2]\cdot 3H_2O$, with brucite-type $\{Co(OH)_3\}$ double chains and squarate anions has been prepared.[110b] Similar brucite-type double chains have also been observed in cadmium chlorooxalate,[67a] cobalt adipate,[98a] and layered iron hydroxysquarate structures.[109b]

Some of the 3D squarates comprise cage networks that entrap solvent molecules in their cavities.[108b–d] The recently isolated metal squarates of the general formula $[M(H_2O)_2(C_4O_4)]$ (M = Co, Mn, Zn) possess structures



Scheme 7. 3D open-framework architectures generated through the linkage of various inorganic units by dicarboxylate units: a) Isolated polyhedra (either a dimer or trimer) connected in all directions by dicarboxylate linkers; b) metal clusters linked via dicarboxylate ligands; c) 1D inorganic metal–oxygen chains linked by dicarboxylate ligands; d) classical pillaring of inorganic metal–oxygen layers by dicarboxylate units; e) inorganic layers pillared by isolated polyhedra through coordinating dicarboxylate linkers; f) 3D structure arising from connectivity between polyhedra. Note that oxygen atoms from the dicarboxylate ligands are directly involved in the formation of the inorganic units.[101b]

 © 2004 Wiley-VCH Verlag GmbH & Co. KGaA, Weinheim

related to sodalite, thus demonstrating how square units can assemble to give a sodalite-like cage.[111] The structures of the squarates can be derived from the sodalite by replacing the $\{Al_2Si_2\}$ rings by the four-membered squarate C_4 rings and linking the squarate rings with octahedral $[M(H_2O)_2O_4]^{2-}$ ions (Figure 27). The 3D cobalt squarate $[(C_{12}H_8N_2)_4Co_2(\mu\text{-}C_4O_4)(H_2O)_2(C_4O_4)]\cdot 8H_2O$ exhibits reversible N_2 adsorption.[108e] The transformation of 1D Mn and Zn squarates into 3D cage networks of the form $[M(C_4O_4)(H_2O)_2]$ (M = Mn, Zn) has been achieved.[112]

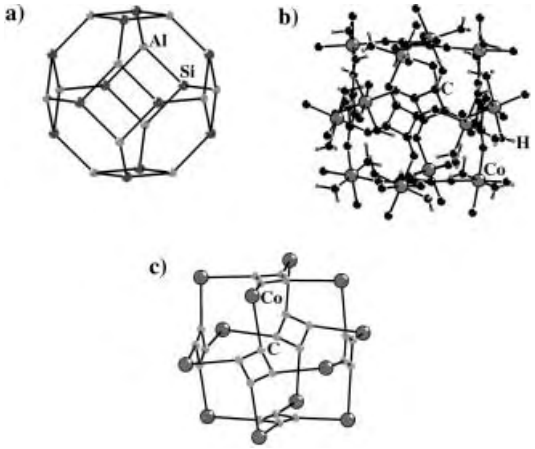


Figure 27. a) T-atom connectivity in an aluminosilicate sodalite cage; b) ball-and-stick view of the sodalite-like cage in $[Co(C_4O_4)(H_2O)_2]$; c) another view of $[Co(C_4O_4)(H_2O)_2]$, in which the O atoms have been omitted and the Co center is linked to the C atoms of the squarate ring to highlight the analogy with sodalite cages.[111]

A series of cerium squarates showing adsorption properties have been reported.[113a] They form as layer, tunnel, and 3D structures, with the common feature being the presence of infinite Ce-O-Ce chains linked by bis-chelating squarate units. The cerium atom in all of these structures is centered within a ninefold coordination sphere. Lanthanide oxalato squarates have also been described, in which oxalate-bridged pairs of $\{LnO_9\}$ (Ln = La, Ce, Eu) polyhedra are linked by squarate units to give 3D frameworks with tunnels that are occupied by water molecules.[88,113b] A layered oxalato squarate where the two anions are both part of the framework has been discovered recently.[113c]

Strontium and barium squarate trihydrates have been synthesized and characterized.[114] Whilst the eight-coordinate Sr complex forms a layered structure, the nine-coordinated Ba complex adopts a 3D structure. The layered $[Sr(C_4O_4)]\cdot 3H_2O$ forms $[Sr(C_4O_4)]\cdot H_2O$ on dehydration without losing its crystaline nature; both structures are stabilized by extensive hydrogen boding. The various structural relationships existing between the metal squarate networks have been discussed elaborately elsewhere.[115]

Unlike the squarates, open-framework structures based on croconates or rhodizonates are not currently known. Despite the early discovery of croconic acid and potassium croconate dihydrate in 1824,[116] it is only recently that metal croconates have recieved attention; various alkali-metal croconates stabilized by weak electrostatic interactions between the metal ion and the croconate mono- or dianion have been studied.[117] The structures possess significant π–π interactions, as well as hydrogen bonds. Transition-metal croconates of the general formula $[M(C_5O_5)(H_2O)_3]$ (M = Mn, Ni, Cu, Zn) with 1D polymeric chain structures have been synthesized.[118]

There are several reports of metal–organic frameworks constructed from multifunctional cyclic aliphatic and aromatic carboxylates;[10b,119–151] a list of such structures with brief structural descriptions is presented in Table 2. These structures clearly demonstrate the ability of rigid cyclic carboxylates to provide complex architectures from simple inorganic SBUs formed by metal–oxygen polyhedra (for example, Figure 28 shows the structure of chromium terephthalate.)[121]

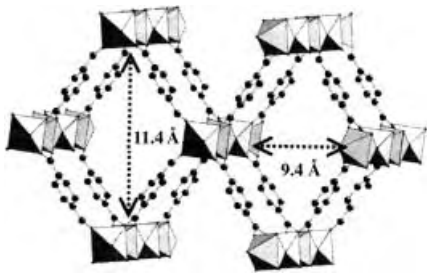


Figure 28. A view of [Cr(1,4-bdc)(OH)] (MIL-53ht) showing channels that are formed by four chains of corner-shared chromium octahedra and four 1,4-benzene dicarboxylate bridges.[121]

In addition to their adsorption and optical properties, some of these benzene multicarboxylate-based framework compounds exhibit interesting magnetic properties, as typified by a number of vanadium[10b] and cobalt[127] compounds that exhibit antiferromagnetic and ferrimagnetic characteristics, respectively.

5. Hybrid Compounds

5.1. Phosphato- and Arsenatooxalates

One family of hybrid structures is formed by incorporating two anionic building units, such as the phosphato- and arsanatooxalates, a large number of which have been synthesized (Table 3).[152–176] In the phosphatooxalates, the oxalate ion plays two roles; in some compounds, inorganic metal–phosphate layers are pillared with the oxalate ions, while in others the oxalate unit is an integral part of the layer, linking the metal–phosphate ladders to form hybrid layers. The manganese phosphatooxalate $[H_3N(CH_2)_3NH_3][Mn_2(HPO_4)_2(ox)(H_2O)_2]$ represents the hybrid layers (Figure 29a),[156] while the iron phosphatooxalate $[NH_3(CH_2)_2NH_3]_{1.5}[Fe_3PO_4(HPO_4)_3(ox)_{1.5}]\cdot x H_2O$ ($x = 1.5$–2.0)[162] represents the former (Figure 29b).[156]

 © 2004 Wiley-VCH Verlag GmbH & Co. KGaA, Weinheim

Table 2: Metal–organic hybrid materials with open-frameworks consisting of metal cations and multifunctional carboxylate ligands.

Compound	Dim.	Coordination geometry	Structure description	Ref.
$[M(Hbtc)(H_2O)_2]\cdot 0.5\,H_2O$ ($M = Sr$, Ba)[c]	2D	$\{MO_9\}$ polyhedra	The structure consists of alternating layers of doubly deprotonated 1,3,5-benzene tricarboxylate $(Hbtc)^{2-}$ ions and Sr^{2+} or Ba^{2+} cations. The layers stack to form channels in which water molecules reside; the water molecules can be reversibly adsorbed.	[119]
$[V^{III}(OH)(1,4\text{-bdc})\cdot x\,(1,4\text{-}H_2bdc)$ ($x \approx 0.75$; MIL-47as)[a,b]	3D	$\{VO_6\}$ octahedra	Four chains of corner-shared vanadium octahedra linked by $(1,4\text{-bdc})^{2-}$ units resulting in 1D tunnels (7.9×12.0 Å) along the [100] direction, with trapped $1,4\text{-}H_2bdc$ and water molecules. MIL-47 exhibits antiferromagnetic behavior.	[10b]
$[V^{IV}(O)(1,4\text{-bdc})]$ (MIL-47)[a,b]	3D	$\{VO_6\}$ octahedra	Same as MIL-47as but devoid of guest molecules. The structure has a flexible framework and shows interesting adsorption properties. The channels have dimensions of 10.5×11.0 Å.	[10b]
$[V^{III}(H_2O)]_3O(1,3\text{-bdc})_3]\cdot(Cl,\,9\,H_2O)$ (MIL-59)[a,b]	3D	$\{VO_6\}$ octahedra	3D frameworks built up from octahedral vanadium trimers that are joined through $(1,3\text{-bdc})^{2-}$ linkers to provide cages where water molecules and Cl^- ions are occluded. The material shows magnetic frustration.	[120]
$[Cr^{III}(OH)(1,4\text{-bdc})]\cdot 0.75\,(1,4\text{-}H_2bdc)$ (MIL-53as)[a,b]	3D	$\{CrO_6\}$ octahedra	3D structure built up by linking the chains of corner-sharing $\{Cr^{III}O_6\}$ octahedra with $(1,4\text{-bdc})^{2-}$ units, resulting in large pores occupied by guest $(1,4\text{-}H_2bdc)$ molecules. It is an antiferromagnet ($T_N = 65$ K).	[121, 122]
$[Cr^{III}(OH)(1,4\text{-bdc})]$ (MIL-53ht)[a,b]	3D	$\{CrO_6\}$ octahedra	Same topology as MIL-53as, but the channels are devoid of guest molecules. Upon removing guest molecules, the channels expand by up to 5 Å. The channels are hydrophilic due to OH groups protruding into them. Water adsorption forms $[Cr(OH)(1,4\text{-bdc})]\cdot H_2O$ (MIL-53lt), which exhibits canted antiferromagnetism, and has a Langmuir surface area of $> 1500\ m^2 g^{-1}$.	[121122]
$[Fe_2(1,2,4,5\text{-btec})]$ (MIL-62)[a,d]	3D	$\{FeO_6\}$ octahedra	The 3D structure is made up of edge-sharing $\{FeO_6\}$ octahedral chains linked by $(1,2,4,5\text{-btec})^{4-}$ units. Magnetic measurements indicate antiferromagnetic behavior, while Mössbauer measurements show the presence of competing quadrapolar and dipolar interactions.	[123]
$[Fe_3(H_2O)_5(1,3,5\text{-btc})_2]\cdot 3\,H_2O$ (MIL-65)[a,c]	3D	$\{FeO_6\}$ octahedra	The structure is built up from octahedral $\{Fe_2O_8(H_2O)_4\}$ dimers and isolated $\{FeO_4(H_2O)_2\}$ octahedra, interlinked through $(1,3,5\text{-btc})^{3-}$ ions. The resulting 3D architecture has channels occupied by water molecules. This compound shows paramagnetic behavior.	[124]
$K[M_3(1,3,5\text{-btc})_3]\cdot 5\,H_2O$ ($M = Fe$, Co) (MIL-45)[a,c]	3D	$\{MO_6\}$ octahedra	The Co (MIL-45a) and Fe/Co (MIL-45b) compounds are isostructural; they consist of undulating chains of MO_6 octahedra connected by distinct $(1,3,5\text{-btc})^{3-}$ and $(1,3,5\text{-Hbtc})^{2-}$ ions, which generates a 3D open-framework structure with channels occupied by K^+ ions and water molecules. Both the compounds are ferromagnetic.	[125]
$(C_4H_{11}N_2)_2[Co_4(OH)_2(H_2O)_2]\text{-}(1,2,4,5\text{-btec})_2\cdot 3\,H_2O$	3D	$\{CoO_5\}$ square pyramid and $\{CoO_5N\}$ octahedra	The structure consists of tetranuclear $\{Co_4(\mu_3\text{-}OH)_2(H_2O)_2\}$ clusters, which form 1D columns through hydrogen-bonding interactions. The columns are linked by the organic pyromellitate ligands into a 3D structure with 1D tunnels. The pendant piperazine molecules protrude into the channels, which are also occupied by guest water molecules. The compound is antiferromagnetic.	[126]
$[Co_2(OH)(1,2,3\text{-btc})(H_2O)]\cdot H_2O$[c]	3D	$\{CoO_6\}$ octahedra, $\{CoO_4\}$ tetrahedra and distorted $\{CoO_5\}$ trigonal bipyramid	The structure is based on a Δ-chain formed by $\{Co_3(\mu_3\text{-}OH)\}$ trimers. The chains are linked through $(1,2,3\text{-btc})^{3-}$ ions to give a 3D lattice reminiscent of the pyrochlore structure. The compound is paramagnetic.	[127]
$[Co_2(OH)(1,2,3\text{-btc})]$[c]	2D	$\{CoO_6\}$ octahedra and $\{CoO_4\}$ tetrahedra	The structure consists of layers of $\{Co_3(\mu_3\text{-}OH)\}$ units involving two independent CoO_6 octahedra, which are decorated on the surface by pendant $\{CoO_4$ tetrahedra$\}$. This material exhibits a ferrimagnetic behavior.	[127]
$[Co_3(H_2O)_6(1,3,5\text{-btc})(1,3,5\text{-Hbtc})(1,3,5\text{-}H_2btc)]\cdot 2\,H_2O$[c]	2D	$\{CoO_6\}$ octahedra	$(1,3,5\text{-btc})^{3-}$, $(1,3,5\text{-Hbtc})^{2-}$, and $(1,3,5\text{-}H_2btc)^-$ ions act as bridging elements for the Co centers. This leads to the formation of a nearly planar infinite net with triangular cavities partly occupied by water molecules.	[128]

 © 2004 Wiley-VCH Verlag GmbH & Co. KGaA, Weinheim

Table 2: (Continued)

Compound	Dim.	Coordination geometry	Structure description	Ref.
$K[Co_3(1,3,5\text{-btc})(1,3,5\text{-Hbtc})_2]\cdot 5\,H_2O$[c]	3D	$\{CoO_6\}$ octahedra	The 3D open-framework structure has sinusoidal chains of $\{CoO_6\}$ octahedra that are connected through via $(1,3,5\text{-btc})^{3-}$ and $(1,3,5\text{-Hbtc})^{2-}$ ions, such that the period of the sinusoidal wave is strongly correlated to the geometry of the $(1,3,5\text{-btc})^{3-}$ ion. Four such sinusoidal chains form rectangular tunnels, in which water molecules and K^+ ions reside. The material exhibits reversible dehydration properties.	[128]
$[Co_2(OH)_2(1,4\text{-bdc})]$[b]	3D	$\{CoO_6\}$ octahedra	Co hydroxide sheets are pillared by $(1,4\text{-bdc})^{2-}$ units, which results in a 3D structure. Intralayer interactions are ferromagnetic but the overall behavior is antiferromagnetic.	[129]
$[Co_2(1,2,4,5\text{-btec})(C_4N_2H_6)_4(H_2O)_4]\cdot H_2O$[d]	2D	$\{CoO_6\}$ octahedra	Each $(1,2,4,5\text{-btec})^{4-}$ ligand coordinates to four Co centers to produce 2D sheets that are corrugated such that the center of the ligand lies in the plane while the Co centers are bent above and below the plane. The spaces created by the corrugation between the sheets are occupied by *N*-methyl imidazole molecules bonded to the Co atoms.	[130]
$[Co_4(1,2,4,5\text{-btec})_2(bpy)_4(H_2O)_2]$[d]	2D	$\{CoO_6\}$ octahedra	The 2D structure consists of a chiral undulating (6,4) network that is formed through conncectivities between Co centers, $(1,2,4,5\text{-btec})^{4-}$ ions, and 2,2′-bipyridyl ligands. Though the layers are chiral the compound on the whole is racemic, with antiferromagnetic interactions between the Co centers.	[131]
$(H_4hpz)[Co_3(1,2,4,5\text{-btec})_2(H_2O)_{12}]\cdot 11\,H_2O$[d] ($H_4hpz$ = homopiperazonium)	1D, 2D	$\{CoO_6\}$ octahedra	The structure consists of neutral $\{[Co_2(1,2,4,5\text{-btec})(H_2O)_8]_n\}$ sheets. Anionic $[Co(1,2,4,5\text{-btec})(H_2O)_4]_n^{2-}$ chains are arranged in the interlamellar spaces along with the protonated homopiperazinium ions. Thus 1D and 2D structures co-exist.	[132]
$(H_4hpz)[Co(1,2,4,5\text{-btec})(H_2O)_3]\cdot 3\,H_2O$[d]	2D	$\{CoO_6\}$ octahedra	Between sheets of $[Co(btec)(H_2O)_3]_n^{2-}$ ions are located homopiperazinium ions and water molecules. The 1,2,4,5-btec units exhibit μ_4 and μ_2 bridging modes.	[132]
$[M_3(1,3,5\text{-btc})_2(\mu\text{-}H_2O)_2(H_2O)_2]\cdot 5\,H_2O$ (M = Co, Ni)[c]	3D	$\{MO_6\}$ octahedra	1D chains are formed by linking $\{Co_2O_{10}\}$ dimers with $\{CoO_6\}$ octahedra. The chains are connected by $(1,3,5\text{-btc})^{3-}$ ions to give a 3D structure. Both compounds are antiferromagnetic.	[133]
$(C_4H_{12}N_2)[M(1,2,4,5\text{-btec})(H_2O)_4]\cdot 4\,H_2O$[d] (M = Co^{II}, Ni^{II}, Zn^{II})	1D	$\{MO_6\}$ octahedra	$\{MO_6\}$ octahedral are linked by $(1,2,4,5\text{-btec})^{4-}$ ions to give 1D chains that are held together by the piperazinium ions via N—H···O hydrogen bonds.	[134]
$[Ni_3(1,3,5\text{-btc})_2(C_5H_5N)_6\{HOCH_2CH_2OH)_6]\cdot x\,HOCH_2CH_2OH\cdot y\,H_2O$ ($x\approx 3$, $y\approx 4$)	3D	$\{NiO_4N_2\}$ octahedra	The structure consists of four interpenetrating (10,3) nets that give rise to chiral channels that trap guest water and ethylene glycol molecules. The nature of the interpenetration is controlled by the auxiliary ligands.	[135]
$[Ni_3(1,3,5\text{-btc})_2(C_5H_5N)_6\{HOCH_2CH(OH)CH_3\}_3]\cdot 11\,HOCH_2CH(OH)CH_3\cdot 8\,H_2O$	3D	$\{NiO_4N_2\}$ octahedra	The structure consists of a distorted chiral framework having an interpenetrating (10,3) net topology. A 1,2-propanediol solvent molecule is bound to the metal center.	[136]
$[(NiL)_3(1,3,5\text{-btc})_2]\cdot 14\,H_2O$[c] (L = 3,10-bis(2-ethyl)-1,3,5,8,10,12-hexaazacyclotetradecane)	3D	$\{NiO_2N_4\}$ octahedra	Three Ni centers, each linked to four N atoms of the macrocycle are connected by a $(1,3,5\text{-btc})^{3-}$ ion to form a 2D layer in a brick-wall-like network. The layers are aligned to form a 1D channel accommodating water molecules, which selectively exchange with ethanol molecules.	[137]
$[Cu_3(1,3,5\text{-btc})_2(C_3H_4N_2)_6(H_2O)]\cdot 7\,H_2O$[c]	2D	$\{CuO_3N_2\}$ trigonal bipyramid and $\{CuO_3N_2\}$ square pyramid	The structure consists of dimeric and monomeric units formed through coordintaion of Cu^{2+} ions by the imidazole and the $(1,3,5\text{-btc})^{3-}$ ligands. The dimers are connected to the monomers via bridging carboxylate ligands resulting in infinite 2D sheets. Weak π–π interactions and hydrogen bonds create channels in which guest water molecules reside.	[138]
$[Cu_3(1,3,5\text{-btc})_2(C_4H_6N_2)_6(H_2O)]\cdot 16\,H_2O$[c]	2D	$\{CuO_3N_2\}$ trigonal bipyramid and $\{CuO_3N_2\}$ square pyramid	The structure exhibits 2D sheets similar to the those in $[Cu_3(1,3,5\text{-btc})_2(C_3H_3N_2)_6(H_2O)]\cdot 7\,H_2O$, with the ancillary coordination being provided by the *N*-methylimidazole ligands.	[138]

 © 2004 Wiley-VCH Verlag GmbH & Co. KGaA, Weinheim

Table 2: (Continued)

Compound	Dim.	Coordination geometry	Structure description	Ref.
$[\{Cu(C_{10}H_{26}N_6)\}_3(1,2,3\text{-btc})_2]\cdot 18\,H_2O$[c]	2D	$\{CuO_6\}$ octahedra	The Cu^{II} hexaazamacrocycle self assembles with two $(1,2,3\text{-btc})^{3-}$ ions to give a 2D architecture with honeycomb apertures. The layers stack to generate psuedo-1D channels containing water molecules, which can be partly exchanged with phenol.	[139]
$[Cu_2(1,2,4,5\text{-btec})(C_4N_2H_6)_4]$[d]	2D	$\{CuO_4\}$ square-planar coordination	The structure consists of 2D sheets formed by the btec ligands and the Cu^{II} ions. The two btec ligands *trans* to each other coordinate in a μ_4-bridging style to the Cu centers. The methylimidazole ligands bound to the Cu atoms interdigitate between the adjacent sheets.	[130]
$[Cd_3(1,3,5\text{-btc})_2]\cdot 13\,H_2O$[c]	2D	$\{CdO_5\}$ trigonal bipyramid and CdO_7 pentagonal bipyramid	The structure has a fundamental building unit composed of 5- and 7-coordintated Cd centers linked by $(1,3,5\text{-btc})^{3-}$ ions. The units are linked further through $(1,3,5\text{-btc})^{3-}$ ions to form a T-shaped molecular bilayer motif, interdigitated to form a 2D lattice.	[140]
$[Cd_3(1,3,5\text{-btc})_2]\cdot C_6N_2H_{12}\cdot 2\,H_2O$[c]	3D	$\{CdO_6\}$ and $\{CdO_5N\}$ octahedra	The structure has $\{Cd_3O\}$ trinuclear cores that are connected via $(1,3,5\text{-btc})^{3-}$ ions to yield "chicken-wire-like" 2D sheets that are stacked in a staggered fashion, and connected through out-of-plane $(1,3,5\text{-btc})^{3-}$ ions to form a 3D architecture.	[140]
$(Ph_3PCH_2Ph)[Cd(1,4\text{-bdc})Cl]\cdot 2\,H_2O$[b]	3D	$\{CdO_4Cl_2\}$ octahedra	$\{Cd_2Cl_2\}$ dimers with μ_2-Cl bridges are linked by two different out-of-plane $(1,4\text{-bdc})^{2-}$ ions to give an open architecture with rhombic channels that incorporate $(Ph_3PCH_2Ph)^+$ guests.	[141]
$[La(chdc)(Hchdc)]$ (H_2chdc = 1,4-cyclohexane dicarboxylic acid	2D	$\{LaO_9\}$ polyhedra	The structure consists of infinite edge-shared $\{LaO_9\}$ polyhedral chains, interleaved by the $(chdc)^{2-}$ ions and connected by $(Hchdc)^-$ ions.	[142]
$[La_2(chdc)_3(H_2O)_2]\cdot 2\,H_2O$	3D	$\{LaO_9\}$ polyhedra	The structure is similar to [La(chdc)(chdcH)] except that all of the anions are fully deprotonated and the interleaving chdc anions also connect between the Ln–O chains to give an interlocked 3D structure containing both bound and free water molecules; the guest water molecules can be reversibly adsorbed.	[142]
$[Ln_2(bhc)(H_2O)_6]$[e] (Ln = La to Er)	3D	$\{LnO_9\}$ polyhedra	Each $(bhc)^{6-}$ ion is connected to eight different Ln ions. Thus the Ln ions are bridged by the mellitate O atoms to form a corrugated 2D-sheet structure, which is pillared by the out-of-plane $(bhc)^{6-}$ ions into three-dimensions. This gives rise to 1D channels occupied by water molecules.	[143]
$[Ln_2(1,2\text{-bdc})_3(H_2O)]$ (Ln = La, Eu, Tb)[b]	2D	$\{LnO_8\}$ and $\{LnO_9\}$ polyhedra	The structure for Ln = La has layers of coplanar La atoms linked by 1,2-bdc units through two different bonding modes, while the isomorphous structures for Ln = Eu, Tb exhibit non-coplanar Ln atoms and the bdc anions show three different modes of connectivity.	[144]
$[Nd(1,2,4,5\text{-}H_2btec)_{0.5}(1,2,4,5\text{-btec})_{0.5}\cdot H_2O]$[d]	3D	$\{NdO_9\}$ polyhedra	Each $(1,2,4,5\text{-btec})^{4-}$ ligand links two Nd^{III} dimers to form a 1D chain structure. The chains are mutually linked by the carbonyl oxygen atom of the $(1,2,4,5\text{-}H_2btec)^{2-}$ ion into 2D layers, and through cross-linking of the layers by the bridging $(H_2btec)^{2-}$ and $(btec)^{4-}$ units to yield a 3D structure.	[145]
$[Eu^{III}_2(OH)_4(1,4\text{-bdc})]$ ($MIL\text{-}51_{HT}$)[a,b]	3D	$\{EuO_9\}$ monocapped antiprism	The structure consists of inorganic layers formed by the face-sharing europium polyhedra, which are pillared by $(1,4\text{-bdc})^{2-}$ units through a bidentate bridging mode to form the 3D structure.	[146]
$[Eu^{III}_2(H_2O)_2(OH)_4(1,4\text{-bdc})]$ ($MIL\text{-}51_{LT}$)[a,b]	3D	$\{EuO_9\}$ monocapped antiprism	Similar topology as $MIL\text{-}51_{HT}$ with the $(1,4\text{-bdc})^{2-}$ ions adopting a monodentate binding mode, hence the Eu atoms complete their coordination with a μ_2-O water molecule.	[146]
$[Eu^{II}(1,4\text{-bdc})]$ (MIL-52)[a,b]	3D	$\{EuO_8\}$ square antiprism	Inorganic layers made up of edge-sharing chains of europium polyhedra, which are linked by in-plane $(1,4\text{-bdc})^{2-}$ ions, are pillared by the out-of-plane ions to give a 3D structure.	[146]
$[Gd(1,2,4,5\text{-Hbtec})]$[d]	3D	$\{GdO_9\}$ polyhedra	Each Gd atom is linked by four $(Hbtec)^{3-}$ ions to form a 1D chain structure. Each adjacent layer is further linked through bridging carbonyl groups to produce a 3D structure.	[145]

 © 2004 Wiley-VCH Verlag GmbH & Co. KGaA, Weinheim

Table 2: (Continued)

Compound	Dim.	Coordination geometry	Structure description	Ref.
$[Gd(1,3,5\text{-btc})(H_2O)_3]\cdot 1.5\,H_2O$[c]	2D	$\{GdO_9\}$ tricapped trigonal prism	The structure consists of parallel double-sheet networks based on honeycomb-like molecular motifs where one corner is occupied by a Gd^{3+} ion and the other by a $(1,3,5\text{-btc})^{3-}$ ion. The adjacent layers are shifted and bridged by water molecules that reside in the interlayer spaces to give a hydrogen-bonded network.	[147]
$[Tb(1,2,4,5\text{-}H_2btec)_{0.5}(1,2,4,5\text{-btec})_{0.5}(H_2O)]\cdot 2\,H_2O$	3D	$\{TbO_9\}$ polyhedra	The $(btec)^{4-}$ ions act as a μ_6-bridge linking six different Tb centers; each Tb center is attached to three such ligands to form 2D layers that are interconnected via $(H_2btec)^{2-}$ ions to give a 3D structure.	[148]
$[Er_4(1,4\text{-bdc})_6]\cdot 6\,H_2O$[b]	3D	$\{ErO_8\}$ dodecahedron, ErO_7 capped trigonal prism, ErO_7 pentagonal bipyramid	The structure is formed through connectivities between the crystallographically independent Er atoms with 1,4-bdc units, which present two μ_4 and two μ_3 coordination modes.	[149]
$[Er_2(1,2,4,5\text{-btec})_{1.5}(H_2O)_4]\cdot 4\,H_2O$[d]	3D	$\{ErO_9\}$ and $\{ErO_8\}$ polyhedra	Two Er atoms are coordinated by six $(btec)^{4-}$ ions, which link in three different coordination modes to give the basic dinuclear building unit, which is further connected through btec units through different coordination modes to form a 3D structure with channels that are occupied by the guest water molecules.	[148]
$[Er(ctc)(H_2O)_2]\cdot 2.5\,H_2O$	3D	$\{ErO_9\}$ polyhedra	Each Er^{III} center is linked to four different $(ctc)^{3-}$ ligands, each of which is linked to five different Er atoms to generate the 3D structure with 1D channels along all the crystallographic axes, occupied by the water molecules. The material shows interesting hydration/dehydration properties.	[150]
$[Yb_4(1,2\text{-bdc})_6(H_2O)_2]$[b]	2D	$\{YbO_x\}$ polyhedra $x = 6$–9	The 2D structure is formed through the connectivity of Yb atoms, which exist in four different coordination environments, and the $(1,2\text{-bdc})^{2-}$ ions. The Yb centers are all non-coplanar, forming a wavelike arrangement that accommodates the steric requirements of the ligands.	[144]
$[\{Yb(1,2,4,5\text{-btec})_{0.75}(H_2O)_2\}_4]\cdot 6\,H_2O$[d]	3D	$\{YbO_8\}$ polyhedra	The macrocyclic $\{Yb_4(btec)_4(H_2O)_8\}$ unit constitutes the basic building block of the structure. Three Yb_4 units are linked together through Yb–O bonding to induce a new small cycle that generates a 2D layer structure with two kinds of pores; such layers are further linked by Yb^{III} ions and bridging $(btec)^{4-}$ ions to produce a novel 3D structure with channels.	[148]
$[Ln_2(bhc)(H_2O)_4]\cdot H_2O$ (Ln = Tm to Lu)	3D	$\{LnO_7\}$ polyhedra	As for the previous Ln compound, each $(bhc)^{6-}$ is coordinated to eight different Ln ions but the arrangement is entirely different. Two of the Ln ions are involved in the formation of 7-membered chelate rings and are bound to neighboring carboxylates to form a 3D network with a relatively open structure with large channels.	[143]
$[In_2(OH)_3(1,4\text{-bdc})_{1.5}]$[b]	3D	$\{InO_6\}$ octahedra	Corner-sharing In centers are connected via OH groups to give sheets of six-membered rings with the composition $\{[In_2(OH)_3]^{3+}_{inf}\}$; the sheets are pillared by $(1,4\text{-bdc})^{2-}$ ions to generate a 3D satructure.	[151]

[a] MIL: Material Institut Lavoisier. [b] H_2bdc = benzene dicarboxylic acid. [c] H_3btc = benzene tricarboxylic acid. [d] H_4btec = benzene tetracarboxylic acid. [e] H_6bhc = benzene hexacarboxylic acid.

The iron phosphatooxalate shows antiferromagnetic behavior ($T_N = 46$ K) and reversible adsorption behavior. A systematic phase study of the reactions of V_2O_5 in the $H_2C_2O_4$/H_3PO_4/NH_4OH system under hydrothermal syntheses has shown that oxalic acid plays the role of a reducing agent. Compounds isolated as single crystals occur in the H_3PO_4-rich regions, while the NH_4OH- and $H_2C_2O_4$-rich regions favor poorly crystalline phases that do not contain any oxalate ions.[154] The transformation of an 1D iron arsenatooxalate into 2D and 3D iron arsenates has also been reported.[175] It appears that the phosphato- and arsenatooxalates are intermediates between the oxalates and the phosphates (or arsenates).

Other open-framework structures involving mixed anions, such as the phosphatoacetate,[177] phosphonooxalate,[178,179] squaratooxalate,[113] carbonatooxalate,[74] isonicotinatooxalate,[69b] bipyridyl glutarate[95d] and bipyridyl squarate[180] structures are also known. These compounds exhibit various dimensionalities, with some of them exhibiting reversible dehydration and interesting optical properties.

 © 2004 Wiley-VCH Verlag GmbH & Co. KGaA, Weinheim

Table 3: Structural information of open-framework metal oxalatophosphates and -arsenates.[a]

Compound	Metal coordination	Dim.	Crystal parameters	Ref.
$(C_2H_{10}N_2)[\{VO(HPO_4)\}_2(ox)]$	$\{VO_6\}$ octahedra	2D	$P\bar{1}$; $a=6.3595(7)$, $b=6.6236(7)$, $c=9.224(1)$ Å $\alpha=98.216(2)$, $\beta=108.128(2)$, $\gamma=100.672(2)°$, $V=354.42(7)$ Å^3	[152]
$(CH_6N_3)_2[\{VO(HPO_4)\}_2(ox)]$	$\{VO_6\}$ octahedra	2D	$P\bar{1}$; $a=6.3825(8)$, $b=7.8877(9)$, $c=9.202(1)$ Å $\alpha=66.602(2)$, $\beta=71.757(2)$, $\gamma=79.821(2)°$, $V=403.07(8)$ Å^3	[152]
$(C_4N_2H_{12})[VO(HPO_4)(ox)]$	$\{VO_6\}$ octahedra	1D	$P2_12_12_1$; $a=6.4022(4)$, $b=12.4735(8)$, $c=14.653(1)$ Å $V=1170.2(1)$ Å^3	[153]
$(NH_4)_2[\{VO(HPO_4)\}_2(ox)]\cdot 5H_2O$	$\{VO_6\}$ octahedra	2D	$C2/m$; $a=17.735(2)$, $b=6.4180(6)$, $c=22.839(2)$ Å $\beta=102.017(2)°$, $V=2542.7(4)$ Å^3	[154]
$(C_6H_{16}N_2)[Mn_2(HPO_4)_2(ox)(H_2O)_2]$	$\{MnO_6\}$ octahedra	3D	$P2_1/n$; $a=5.9778(3)$, $b=16.6747(8)$, $c=8.4660(4)$ Å $\beta=90.384(1)°$, $V=843.85(6)$ Å^3	[155]
$(C_2H_{10}N_2)[Mn_2(HPO_4)_2(ox)(H_2O)_2]$	$\{MnO_6\}$ octahedra	3D	$P2_1/n$; $a=5.4573(4)$, $b=8.9650(7)$, $c=15.253(1)$ Å $\beta=98.924(1)°$, $V=737.22(8)$ Å^3	[155]
$(C_2H_{10}N_2)[Mn_4(HPO_4)_2(ox)_3(H_2O)_2]\cdot 2H_2O$	$\{MnO_6\}$ octahedra	3D	$P\bar{1}$; $a=7.830(4)$, $b=8.041(4)$, $c=9.652(7)$ Å $\alpha=76.29(5)$, $\beta=78.47(6)$, $\gamma=86.36(6)°$, $V=578.4(6)$ Å^3	[155]
$[Mn_4(PO_4)_2(ox)(H_2O)_2]$	$\{MnO_6\}$ octahedra and $\{MnO_5\}$ square pyramid	3D	$P2_1/c$; $a=10.263(3)$, $b=6.526(2)$, $c=10.082(3)$ Å $\beta=116.84(2)°$, $V=602.8(4)$ Å^3	[156]
$(C_3H_{12}N_2)[Mn_2(HPO_4)_2(ox)(H_2O)_2]$	$\{MnO_6\}$ octahedra	3D	$P2_1/n$; $a=5.474(2)$, $b=15.737(2)$, $c=9.056(2)$ Å $\beta=93.47(3)°$, $V=778.7(3)$ Å^3	[156]
$(s\text{-}C_5H_{14}N_2)[Fe_4(HPO_4)_2(ox)_3(H_2O)_2]$	$\{FeO_6\}$ octahedra	3D	$P1$; $a=7.6999(4)$, $b=7.9542(4)$, $c=9.8262(5)$ Å $\alpha=74.8444(7)$, $\beta=81.7716(8)$, $\gamma=85.4075(8)°$, $V=574.34(8)$ Å^3	[157]
$(s\text{-}C_5H_{14}N_2)[Fe_4(HPO_4)_2(ox)_3]$	$\{FeO_5\}$ square pyramid and $\{FeO_6\}$ octahedra	3D	$P2_1$; $a=7.5943(8)$, $b=7.8172(8)$, $c=18.318(2)$ Å $\beta=99.111(2)°$, $V=1073.8(3)$ Å^3	[157]
$(C_4H_{12}N_2)[Fe^{II}_4(HPO_4)_2(ox)_3]$	$\{FeO_4\}$ square pyramid and $\{FeO_6\}$ octahedra	3D	$P2_1/c$; $a=7.5573(4)$, $b=7.8188(4)$, $c=18.0421(9)$ Å $\beta=98.710(1)°$, $V=1053.8(1)$ Å^3	[158]
$(C_5H_{14}N_2)[Fe^{III}_2(HPO_4)_3(ox)]$	$\{FeO_6\}$ octahedra	3D	$P\bar{1}$; $a=6.3948(3)$, $b=9.1419(4)$, $c=16.1585(7)$ Å $\alpha=98.758(1)$, $\beta=93.443(1)$, $\gamma=108.488(1)°$, $V=879.50(7)$ Å^3	[158]
$[Fe_4(PO_4)_2(ox)(H_2O)_2]$	$\{FeO_5\}$ square pyramid and $\{FeO_6\}$ octahedra	3D	$P2_1/n$; $a=7.974(3)$, $b=4.817(3)$, $c=14.168(3)$ Å $\beta=94.70(3)°$, $V=542.4(4)$ Å^3	[159]
$(C_2H_{10}N_2)_{1.5}[Fe_3PO_4(HPO_4)_3(ox)_{1.5}]\cdot xH_2O$ ($x=1.5$–2.0)	$\{FeO_6\}$ octahedra	3D	$P3c1$; $a=13.630(3)$, $c=14.739(4)$ Å $V=2371.3(1)$ Å^3	[160]
$(C_{10}H_{28}N_4)[\{Fe_2(HPO_4)_3(ox)\}_2]$	$\{FeO_6\}$ octahedra	3D	$P2_1/n$; $a=10.829(1)$, $b=12.747(1)$, $c=12.397(1)$ Å $\beta=95.1(1)°$, $V=1704.4(3)$ Å^3	[161]
$[Fe_2(H_2O)_2(HPO_4)_2(ox)]\cdot H_2O$	$\{FeO_6\}$ octahedra	3D	$P2_1/c$; $a=4.840(2)$, $b=17.571(6)$, $c=7.342(4)$ Å $\beta=106.6(1)°$, $V=598.5(4)$ Å^3	[162]
$[Fe_2(H_2O)_2(HPO_4)_2(ox)]\cdot 2H_2O$	$\{FeO_6\}$ octahedra	3D	$P2_1/c$; $a=7.211(1)$, $b=9.294(1)$, $c=9.567(1)$ Å $\beta=103.4(1)°$, $V=623.8(1)$ Å^3	[162]
$(C_3H_{12}N_2)[\{Fe_2(HPO_4)_2(ox)_{1.5}\}_2]$	$\{FeO_6\}$ octahedra	3D	$P2_1/n$; $a=9.214(1)$, $b=15.201(2)$, $c=12.046(1)$ Å $\beta=101.9(1)°$, $V=1650.9(3)$ Å^3	[162]
$(C_3H_{12}N_2O)[\{Fe_2(HPO_4)_2(ox)_{1.5}\}_2]$	$\{FeO_6\}$ octahedra	3D	$P2_1/n$; $a=9.266(1)$, $b=15.204(1)$, $c=11.984(1)$ Å $\beta=102.2(1)°$, $V=1650.5(2)$ Å^3	[162]
$(C_4H_{12}N_2)_{0.5}[Fe_2(HPO_4)(ox)_{1.5}]$	$\{FeO_5\}$ trigonal pyramid and $\{FeO_6\}$ octahedra	3D	$P2_1/c$; $a=7.569(2)$, $b=7.821(2)$, $c=18.033(4)$ Å $\beta=98.8(1)°$, $V=1055.0(4)$ Å^3	[163]
$[Fe_2(H_2O)(PO_4)(ox)_{0.5}]$	$\{FeO_5\}$ trigonal pyramid and $\{FeO_6\}$ octahedra	3D	$P2_1/c$; $a=10.240(1)$, $b=6.375(3)$, $c=9.955(1)$ Å $\beta=117.3(1)°$, $V=577.4(1)$ Å^3	[163]
$(C_3H_{12}N_2)_{1.5}[Fe_3P_4O_{13}(OH)_3(ox)_{1.5}]$	$\{FeO_6\}$ octahedra	3D	$P3c1$; $a=13.656(1)$, $c=14.658(1)$ Å $V=2368.3(1)$ Å^3	[164]
$(C_4H_{12}N_2)_{0.5}[Co_2(HPO_4)(ox)_{1.5}]$	$\{CoO_5\}$ square pyramid and $\{CoO_6\}$ octahedra	3D	$P2_1/c$; $a=7.494(1)$, $b=7.726(1)$, $c=17.852(3)$ Å $\beta=97.7(1)°$, $V=1024.2(2)$ Å^3	[165]
$(C_3H_{12}N_2)[Zn_6(PO_4)_4(ox)]$	$\{ZnO_5\}$ square pyramid $\{ZnO_5\}$ trigonal bipyramid and $\{ZnO_4\}$ tetrahedra	3D	$P\bar{1}$; $a=5.0030(1)$, $b=8.5434(3)$, $c=12.4336(5)$ Å $\alpha=92.99$, $\beta=97.132(2)$, $\gamma=91.465(2)°$, $V=526.33(3)$ Å^3	[166]
$(C_2H_{10}N_2)_{2.5}[Al_4H(HPO_4)_4(H_2PO_4)_2(ox)_4]$	$\{AlO_6\}$ octahedra	2D	$C2/m$; $a=19.683(4)$, $b=12.360(3)$, $c=16.734(3)$ Å $\beta=110.51(3)°$, $V=3813(1)$ Å^3	[167]
$(C_4H_{12}N_2)[Al_2(PO_4)(HPO_4)(ox)]\cdot H_2O$	$\{AlO_6\}$ octahedra	3D	$Pccm$; $a=9.992(1)$, $b=11.644(1)$, $c=12.231(1)$ Å $V=1423.0(2)$ Å^3.	[168]
$K_2[Ga_4(PO_4)_4(ox)]\cdot 2H_2O$	$\{GaO_6\}$ octahedra and $\{GaO_4\}$ tetrahedra	3D	$P\bar{1}$; $a=7.9863(4)$, $b=8.2458(5)$, $c=8.7631(5)$ Å $\alpha=116.075(1)$, $\beta=100.825(1)$, $\gamma=104.033(1)°$, $V=473.3(1)$ Å^3	[169]

 © 2004 Wiley-VCH Verlag GmbH & Co. KGaA, Weinheim

Table 3: (Continued)

Compound	Metal coordination	Dim.	Crystal parameters	Ref.
$(C_{10}H_9N_2)[Ga_5(OH)_2(PO_4)_4(ox)]\cdot 2H_2O$	{GaO_4} tetrahedra and {GaO_6} octahedra	3D	$C2/c$; $a=18.3430(2)$, $b=15.9372(4)$, $c=9.1019(2)$ Å $\beta=90.867(1)°$, $V=2660.5(1)$ Å^3	[170]
$(C_{10}H_{28}N_4)[Ga_6(OH)_2(PO_4)_2(HPO_4)_4(ox)_3]\cdot 3.5H_2O$	{GaO_6} octahedra and {GaO_4} tetrahedra	3D	$P\bar{1}$; $a=9.0220(7)$, $b=9.1864(9)$, $c=13.4912(9)$ Å $\alpha=73.988(9)$, $\beta=79.199(7)$, $\gamma=78.775(7)°$, $V=1043.6(2)$ Å^3	[171]
$(C_4H_{12}N_2)[In_2(ox)(HPO_4)_3]\cdot H_2O$	{InO_6} octahedra	3D	$P2_1$; $a=6.5052(2)$, $b=17.5005(2)$, $c=8.1811(2)$ Å $\beta=107.656(1)°$, $V=887.50(5)$ Å^3	[172]
$[Sn_2(PO_4)(ox)_{0.5}]$	{SnO_3} pyramid and {SnO_4} square pyramid	2D	$P2_1/n$; $a=4.712(1)$, $b=5.862(1)$, $c=22.242(2)$ Å $\beta=95.77(1)°$, $V=611.3(1)$ Å^3	[173]
$(C_4H_{12}N_2)[VO(ox)HAsO_4]$	{VO_6} octahedra	1D	$P2_12_12_1$; $a=6.5595(1)$, $b=12.4689(1)$, $c=14.6363(1)$ Å $V=1197.10(3)$ Å^3	[153]
$(C_4H_{12}N_2)_2[Fe(HAsO_4)_6(ox)_2]$	{FeO_6} octahedra	3D	$P\bar{1}$; $a=11.1066(2)$, $b=12.9842(1)$, $c=13.4294(1)$ Å $\alpha=117.345(1)$, $\beta=93.668(1)$, $\gamma=93.879(1)°$, $V=1706.33(4)$ Å^3	[174]
$(C_4H_{12}N_2)[Fe(OH)(HAsO_4)(ox)]\cdot H_2O$	{FeO_6} octahedra	1D	$P\bar{1}$; $a=6.5668(3)$, $b=9.1040(3)$, $c=10.4715(4)$ Å $\alpha=86.35(1)$, $\beta=85.34(1)$, $\gamma=83.32(4)°$, $V=618.18(1)$ Å^3	[175]
$(C_6H_{20}N_3)[Zn_3(AsO_4)(HAsO_4)_2(ox)]$	{ZnO_4} tetrahedra and {ZnO_6} octahedra	3D	$P2_1/c$; $a=16.0857(2)$, $b=9.1973(2)$, $c=15.4216(3)$ Å $\beta=112.033(1)°$, $V=2114.92(7)$ Å^3	[176]

[a] ox = $[C_2O_4]^{2-}$.

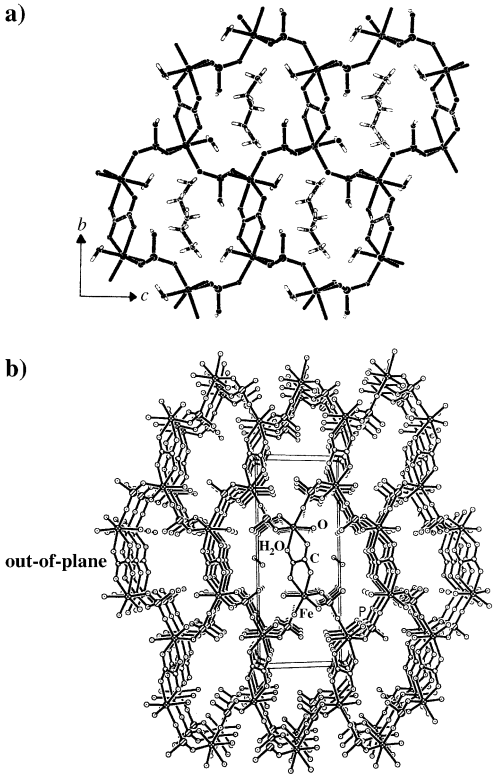


Figure 29. a) Structure of $\{H_3N(CH_2)_3NH_3\}[Mn_2(HPO_4)_2(ox)(H_2O)_2]$ showing the 12-membered apertures that form through conncectivities between the Mn centers and the in-plane oxalate and hydrogen phosphate moieties;[156] b) structure of $[Fe_2(HPO_4)_2(ox)(H_2O)_2]\cdot H_2O$ showing the channels formed by the linking of the iron hydrogen phosphate layers through the out-of-plane oxalate units; water molecules reside in the channels. Hydrogen bonds are omitted for clarity.[162]

5.2. Porous Hybrid Architectures

Engineering new microporous structures using metal–organic frameworks is a topic of current interest.[11e] To this end, different strategies have been employed with considerable success. Some of these materials not only show openness but also exhibit interesting physical and chemical properties, which makes them more interesting than their pure inorganic counterparts.[6–13] Special issues of journals dedicated to the design of hybrid nanoporous solids bear testimony to the rapid progress made in this area.[5b,6b] One of the strategies to prepare the hybrid solids is to use appropriate inorganic building units along with a rigid organic linker to bridge the building units. The carboxylate linkers can respond efficiently to chemical environments, thus enabling the tuning of the valency of the anion generated. They can also exhibit different modes of linking and generate SBUs.

The "top down" design principle (also referred as reticular synthesis) has been demonstrated recently by the arrangement of well defined molecular building blocks into periodic frameworks by copolymerizing them with organic linkers in a polar solvent under mild reaction conditions.[6b,181–184] This strategy yields stable porous structures, unlike the supramolecular assemblies. This strategy is exemplified by the preparation of metal–organic framework (MOF-n) structures, as illustrated in Figure 30.[181f]

Another strategy is to assemble the relevant inorganic/organic building units under suitable reaction conditions to give known inorganic frameworks (Figure 31).[6a,b] Large voids are created in these structures due to the use of long linkers. Interpenetration (maximal displacement of the catenated frameworks) and interweaving (minimal displacement of catenated frameworks) in the frameworks often

 © 2004 Wiley-VCH Verlag GmbH & Co. KGaA, Weinheim

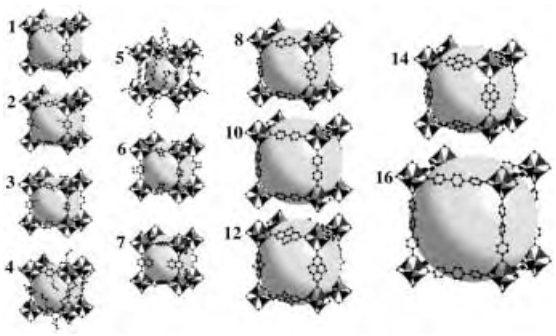


Figure 30. Structures of isoreticular metal–organic frameworks (IRMOF-*n*; *n* = 1–7, 8, 10, 12, 14, 16).[181f]

occurs where linkers with long organic backbones are employed. In some of the designed open-framework structures, manipulation of the steric factors and solvent molecules helps to prevent interpenetration.[104] Open-framework solids, prepared in this manner show remarkable thermal stabilities and adsorption behavior (Figure 32).[181a,f,183a,184a,184b] These hybrid compounds have been reviewed in detail.[6a,b,181f,183a,183c]

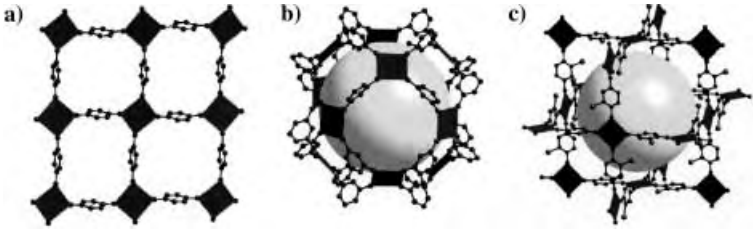


Figure 31. a) Linear 1,4-benzene dicarboxylate bridging ligands order the paddle-wheel units at 180° to each other to give a MOF-2 structure with a 4^4 square-grid arrangement; b) the bent 1,3-benzene dicarboxylate ligand results in the paddle-wheel units being arranged 120° to each other, which leads to the discrete truncated cuboctahedral MOP-1 structure (MOPM = metal–organic polyhedron); c) the 2-bromo-1,4-benzene dicarboxylate ligand places the paddle-wheel units at 90° angles to give an MOF-101 product with the NbO structure. The paddle-wheel unit is a SBU observed in most MOF-n structures.[181f]

The copper complex $[Cu_3(1,3,5\text{-btc})_2(H_2O)_3]$ (1,3,5-H_3btc = benzene 1,3,5-tricarboxylic acid), built up from dimeric copper(II) tetracarboxylate units exhibits an interesting structure and properties.[185] This compound has a neutral framework structure with square channels that are lined by aqua ligands (Figure 33), which can be replaced by organic functional groups.

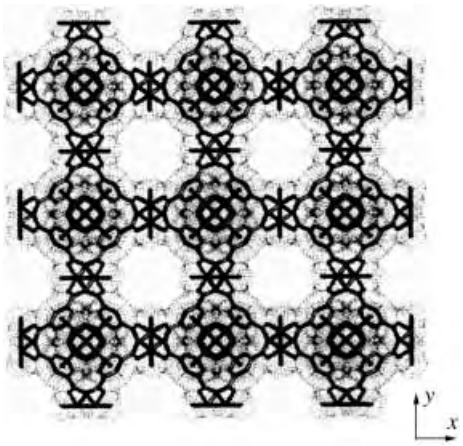
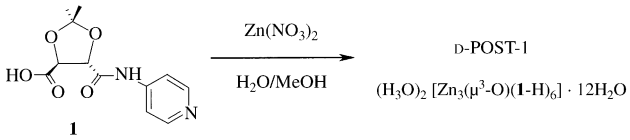


Figure 33. Structure of $[Cu_3(C_9H_3O_6)_2(H_2O)_3]$ (HKUST-1) showing nanochannels with fourfold symmetry.[185]

The homochiral metal–organic compound $(H_3O)_2[Zn_3(\mu^3\text{-O})(\mathbf{1}\text{-H})_6]\cdot 12H_2O$ (D-POST-**1**) has been prepared by using an oxo-bridged trinuclear enantiopure chiral metal carboxylate as a building block (Scheme 8).[186] The three zinc ions are connected to six carboxylate units through a bridging oxo group to form a trinuclear unit that acts as the SBU; the structure consists of 2D layers. The stacking of these layers leads to chiral 1D channels (≈13.4 Å). The three pyridyl groups that extrude into the interior of the channels impart ion-exchange properties.



Scheme 8. Synthesis of the zinc carboxylate D-POST-**1**, whose solid-state structure exhibits chiral channels.

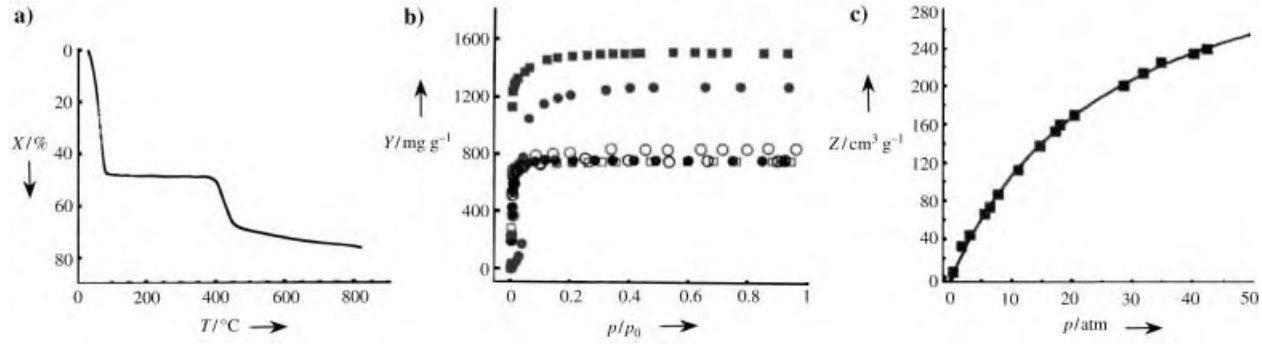


Figure 32. IRMOF-6: a) Thermogravimetric analysis; b) gas and organic vapor sorption isotherms (● N_2 adsorption, ○ N_2 desorption, □ C_6H_{12}, ■ CCl_4, ● CH_2Cl_2, ○ C_6H_6); c) uptake of methane gas, with a fit to the Langmuir equation (298 K).[181a]

 © 2004 Wiley-VCH Verlag GmbH & Co. KGaA, Weinheim

This compound also catalyzes transesterification reactions and shows remarkable enantioseparation due to the chiral environment of the channel (Figure 34).

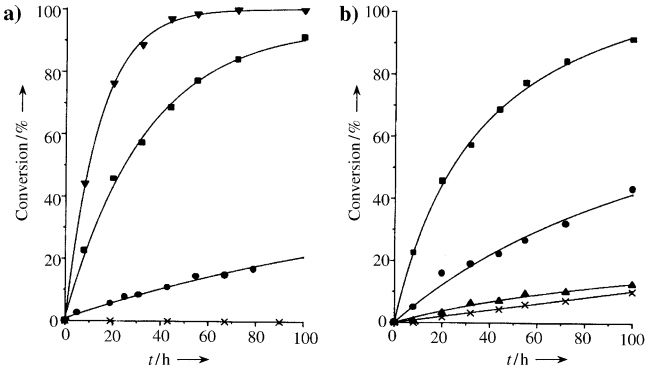


Figure 34. Catalytic activity of POST-**1** in transesterification reactions. a) Transesterification of 1-acetoxy-2,4-dinitrobenzene with ethanol in the presence of POST-**1**: ▼ methylester of **1**, ■ POST-**1**, ● methyl-POST-**1**; × no catalyst; b) transesterification of alchohols in the presence of POST-**1** (CCl_4, 27 °C): ■ ethanol, ● isobutanol, ▲ neopentanol, × 3,3,3-triphenyl-1-propanol.[186]

The thermally stable $[Zn_8(SiO_4)(1,4\text{-btc})_6]$ was recently prepared, which has a $\{Zn_8(SiO_4)\}$ core with SiO_4 tetrahedra occupying the center and bridging eight different Zn atoms, capped by terephthalate moieties.[187a] Porous hybrid compounds, in which metal dicarboxylate layers are pillared by other organic species, and which show high adsorption capabilities have been reported.[187b–d]

5.3. Carboxylates with Additional Binding Sites

A family of phosphonocarboxylates $(O_3PRCOO)^{3-}$ have been isolated where the end-groups can exhibit a variety of binding modes. Phosphonocarboxylates containing transition metals,[188] zinc,[189a] praseodymium,[189b] and main-group elements[190] are known. Longer-chain phosphonocarboxylic acids lead to open-framework structures with channels with irregular shapes and dimensions, owing to the greater flexiblity of the carbon backbone. Phosphonocarboxylates with an additional amino group give structures in which the channels are formed by the linking of metal centers through the PO_3 and CO_2 end groups, with the amino groups protruding into them,[191] which makes them amenable for chemical manipulation. The layers in the 3D hybrid compound $[\{K_2[CoO_3PCH_2N(CH_2CO_2)_2]\}_6]\cdot x\,H_2O$, which is prepared using (phosphonomethyl)iminodiacetic acid (PMIDA), are similar to those in the structure of gray arsenic.[192] Compounds of PMIDA with zinc and zirconium have also been synthesized.[193a,b] In addition, a lanthanoid–copper coordination polymer of the form $[Ln_2Cu_3\{HN(CH_2CO_2)_2\}_6]\cdot 8\,H_2O$ (Ln = La, Nd, Eu) has been reported recently.[194]

A family of nicotinates and isonicotinates with open architectures possessing properties arising from the unsymmetrical nature of the ligand, has been described.[195] The ligand was tailored to engender acentric diamandoid coordination networks by linking tetrahedral metal clusters and to tune the push–pull effects present in the ligand, thus imbuing second-order nonlinear optical activity in some of the compounds.[196] A thermally stable porous cobalt(II) nicotinate $[Co_2(H_2O)(C_6H_4O_2N)_4]\cdot G$ ($G = 0.5\,EtOH/0.5\,H_2O$ or $C_6H_5CH_2OH$) with channels containing ethanol, water, or benzyl alcohol molecules and showing reversible adsorption behavior has been isolated.[197] The 3D open-framework solid $[Cu(isonicotinate)_2]\cdot 2\,H_2O$ has spiral channels and exhibits solvent selectivity comparable to that of the zeolites.[198] $[Zn(C_6H_4O_2N)_2]\cdot MeOH\cdot 2\,H_2O$, with a $4^2\cdot 8^4$ net topology based solely on square planar nodes, occludes naphthalene and nitrobenzene guest molecules.[199] The use of pyrazine-carboxylate and Cu^{2+} ions gives rise to 1D chains and 2D layers, while Cd^{2+} ions lead to a unique 3D architecture.[200a] These compounds contain a 1D serpentine motif (resembling inosilicates) along with the 2D square grid to form the 3D architecture.[200b] The rational design of 3D strucutures by employing pyrazine-2,3-dicarboxylate in conjugation with pillaring ligands has been achieved; these compounds show interesting adsorption properties.[201a,b] A mixed-metal open-framework compound $[ZnCu(2,4\text{-pyridyldicarboxylate})_2(H_2O)_3(dmf)]\cdot DMF$, in which the Zn^{II} center is the node of the network, acting as a linker, and the Cu^{II} center is located in the channel wall has been characterized.[201c] The Cu^{II} ions are amenable for guest coordination. Other framework structures of different dimensionalities with pyridyldicarboxylate anions have also been reported.[202] 2,2′-bipyridyl-4,4′-carboxylic acid yields layered compounds with transition-metal ions[203a] and rigid 3D microporous frameworks with Cd^{2+} ions.[203b]

6. Cadmium Oxalates Incorporating Extended Alkali-Metal Halides

Recently, a new class of cadmium oxalates incorporating extended alkali-metal halides was described.[61e,204–206] These compounds may be considered as nanocomposites of unusual alkali-metal-halide structures within oxalate frameworks. Of particular interest is that simple metathetic reactions between cadmium halides and alkali-metal oxalates carried out under hydrothermal conditions yield these novel materials. An important feature in these solids is the close relationship between the host framework and the guest structure. The 3D cadmium oxalate host $[\{Cd(ox)\}_6]\cdot MCl\cdot 2\,H_2O$ (M = K, Rb), with a framework topology resembling that of the Chevrel-phase compounds,[207] can incorporate extended MCl structures (Figure 35 a). The unit-cell dimensions of the MCl–guest structure are twice that of the free MCl species (Figure 35 b). The stability of such an expanded lattice arises from the extra coordination to the framework and the water oxygen atoms. In the 2D cadmium oxalates $[Cd(ox)]\cdot 2\,MX\cdot H_2O$ (M = Rb, Cs; X = Cl, Br), alkali-metal halides possess layers comprising of six- and eight-membered apertures, resembling cyclohexane and cyclooctane molecules (See bottom right section of the frontispiece picture). Isolated cadmium oxalate units connected by the CsBr layers are also known.[205]

 © 2004 Wiley-VCH Verlag GmbH & Co. KGaA, Weinheim

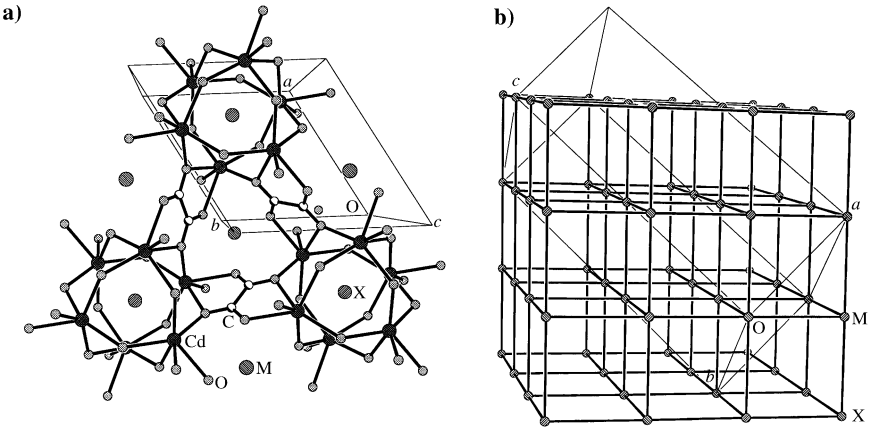
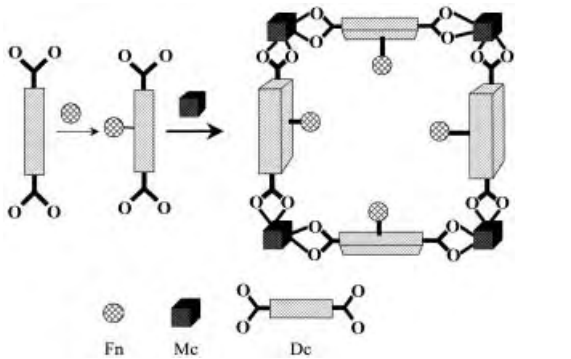


Figure 35. a) Structure of $[Cd_6(ox)_6]\cdot MX\cdot 2H_2O$ (M = K, Rb; X = Cl, Br) projected in the *ab* plane to show the intercluster oxalate connectivity. The M^+ ions are positioned outside the cluster; b) the expanded MX lattice in $[Cd_6(ox)_6]\cdot MX\cdot 2H_2O$.[205]

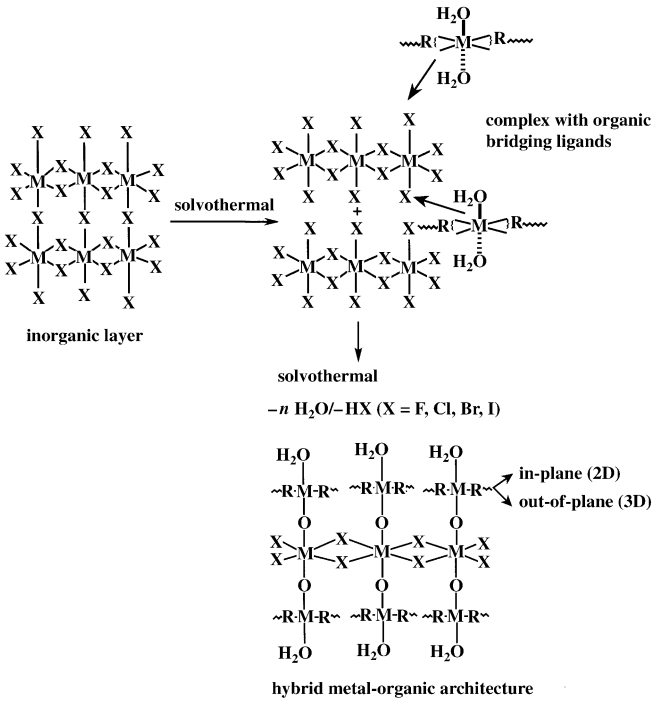
"Nanocomposite" hybrid compounds, such as the alkali-metal halide cadmium oxalates are examples of scale-up chemistry in which the host/guest controls the structure of the guest/host species. In $[Rb_2Cd(NO_3)(Cl)(ox)(H_2O)]$, the framework incorporates a rubidium excess (Rb_2NO_3) slab that is sandwiched between the cadmium chlorooxalate layers.[61e] 1D alkali-metal halide chains with zigzag and helical structures have also been embodied into cadmium oxalate and manganese oxalate frameworks.[205,206]

7. Summary and Outlook

The discussion of the various metal carboxylates with open architectures presented above should suffice to illustrate not only the variety of structures that exist, but also how the carboxylate unit provides an excellent means for designing novel materials by acting as a linker or by imparting unique structural features due to its functionalizability and flexibility. While metal carboxylates of different dimensionalities have been isolated to demonstrate the structural hierarchy in these systems, it has not yet been shown whether the lower dimensional structures can be transformed into higher dimensional ones. Thus there is much to be done in the design of carboxylate frameworks through suitable manipulation of the organic and the inorganic components by employing soft chemical procedures. It should be possible to obtain different environments in the channels of such 3D structures considering that even simple dicarboxylates crystallized under appropriate conditions give rise to channels with hydrophobic environments. Scheme 9 illustrates a possible strategy to synthesize frameworks with channels containing predetermined functionalities. In addition, a strategy for building up open-framework hybrid metal dicarboxylates by substituting an appropriate metal carboxylate unit into a desired structure is shown (Scheme 10). Recalling the recent report that extended alkali-metal halide structures of different dimensionalities can be incorporated into cadmium oxalate hosts by carrying out simple metathetic reactions between



Scheme 9. Designing functionalized channels by incorporating a predetermined functional moiety (Fn) into the dicarboxylate linker (Dc) and by binding the metal ions or metal clusters (Mc) via these functionally modified dicarboxylates.



Scheme 10. Synthesis of complex hybrid metal–organic architectures: Low-dimensional metal halide/hydroxide structures are aligned by replacing the Cl^- or OH^- ions with metal complexes that possess organic ligands capable of bridging the lower dimensional inorganic structures. Depending on the mode of linking provided by the organic linkers, the hybrid metal–organic structure can either be 2D or 3D. The generation of low-dimensional structures by the partial disintegration of the higher dimensional parent structure under suitable reaction conditions is also indicated. M = metal; X = F, Cl, Br, I, -OH, H_2O; R = dicarboxylate, 4,4′-bipyridyl, nicotinate, etc. Note that 1D inorganic chains can be introduced directly into the reaction medium.[67a]

 © 2004 Wiley-VCH Verlag GmbH & Co. KGaA, Weinheim

cadmium halides and alkali-metal oxalates under hydrothermal conditions,[61e] there is much to look forward to, with many more hybrid materials formed by carrying out reactions under different conditions imaginable. In this respect hydrothermal and solvothermal routes are likely to yield several more novel materials with interesting properties.

Received: February 18, 2003 [A588]

[1] a) R. M. Barrer, *Hydrothermal Chemistry of Zeolites*, Academic Press, London, **1982**; b) M. L. Occelli, H. C. Robson, *Zeolite Synthesis*, American Chemical Society, Washington, DC, **1989**; c) *Verified Syntheses of Zeolitic Materials* (Eds.: H. Robson, K. P. Lillerud, 2nd ed., Elsevier, Amsterdam, **2001**; d) M. T. Weller, S. E. Dann, *Curr. Opin. Solid State Mater. Sci.* **1998**, *3*, 137.

[2] a) A. K. Cheetham, G. Férey, T. Loiseau, *Angew. Chem.* **1999**, *111*, 3466; *Angew. Chem. Int. Ed.* **1999**, *38*, 3268; b) J. M. Thomas, *Angew. Chem.* **1999**, *111*, 3800; *Angew. Chem. Int. Ed.* **1999**, *38*, 3588; c) J. M. Thomas, *Chem. Eur. J.* **1997**, *3*, 1557; d) G. Férey, *C. R. Acad. Sci. Ser. IIc* **1998**, 1; e) F. Schüth, W. Schmidt, *Adv. Mater.* **2002**, *14*, 629; f) *Supramolecular Organization and Materials Design* (Eds.: W. Jones, C. N. R. Rao), Cambridge University Press, Cambridge, **2002**; g) C. N. R. Rao, *Proc. Indiana Acad. Sci.* **2002**, *113*, 363; h) S. Oliver, A. Kuperman, G. A. Ozin, *Angew. Chem.* **1998**, *110*, 48; *Angew. Chem. Int. Ed. Engl.* **1998**, *37*, 46.

[3] a) A. Müller, H. Reuter, S. Dillinger, *Angew. Chem.* **1995**, *107*, 2505; *Angew. Chem. Int. Ed. Engl.* **1995**, *34*, 2311; b) P. Y. Zavilij, M. S. Whittingham, *Acta Crystallogr. Sect. B* **1999**, *55*, 627.

[4] a) P. J. Hagrman, D. Hagrman, J. Zubieta, *Angew. Chem.* **1999**, *111*, 2798; *Angew. Chem. Int. Ed.* **1999**, *38*, 2638; b) S. R. Batten, R. Robson, *Angew. Chem.* **1998**, *110*, 1558; *Angew. Chem. Int. Ed.* **1998**, *37*, 1460, and references therein; c) R. Robson, *J. Chem. Soc. Dalton Trans.* **2000**, 3735; d) S. R. Batten, *CrystEngComm* **2001**, *18*, 1.

[5] a) G. Férey, *Chem. Mater.* **2001**, *13*, 3084; b) G. Férey, *J. Solid State Chem.* **2000**, *152*, 37, and related articles in the same issue; c) G. Férey, *J. Fluorine Chem.* **1995**, *72*, 187; d) A. Clearfield, *Curr. Opin. Solid State Mater. Sci.* **1996**, *1*, 268, and references therein; e) J. G. Mao, Z. Wang, A. Clearfield, *Inorg. Chem.* **2002**, *41*, 2334.

[6] a) M. Eddaoudi, D. B. Moler, H. Li, B. Chen, T. M. Reineke, M. O'Keeffe, O. M. Yaghi, *Acc. Chem. Res.* **2001**, *34*, 319, and references therein; b) M. Eddaoudi, J. Kim, D. Vodak, A. Sudik, J. Wachter, M. O'Keeffe, O. M. Yaghi, *Proc. Natl. Acad. Sci. USA* **2002**, *99*, 4900, and related articles in the same issue; c) H. Li, M. Eddaoudi, M. O'Keeffe, O. M. Yaghi, *Nature* **1999**, *402*, 276; d) O. M. Yaghi in *Metal Containing Polymeric Materials*, (Eds.: C. U. Pittman, C. E. Carraher, B. M. Culbertson, M. Zeldin, J. E. Sheets), Plenum, New York, **1996**, p. 219; e) O. M. Yaghi in *Modular Chemistry* (Ed.: J. Michl), Kluwer, Boston, **1997**, p. 663.

[7] a) J. M. Lehn, *Supramolecular Chemistry, Concepts and Perspectives*, VCH, Weinheim, **1995**; b) M. J. Zaworotko, *Nature* **1999**, *402*, 242; c) M. J. Zaworotko, *Nature* **1997**, *386*, 220; d) B. Moulton, M. J. Zaworotko, *Advances in Supramolecular Chemistry, Vol. 7*, JAI, Greenwich, CT, **2000**, p. 235, and references therein; e) P. J. Langley, J. Hulliger, *Chem. Soc. Rev.* **1999**, *28*, 279; f) P. H. Dinolfo, J. T. Hupp, *Chem. Mater.* **2001**, *13*, 3113.

[8] a) B. Moulton. M. J. Zaworotko, *Chem. Rev.* **2001**, *101*, 1629; b) M. J. Zaworotko, *Angew. Chem.* **2000**, *112*, 3180; *Angew. Chem. Int. Ed.* **2000**, *39*, 3052; c) S. I. Noro, S. Kitagawa, M. Kondo, K. Seki, *Angew. Chem.* **2000**, *112*, 2161; *Angew. Chem. Int. Ed.* **2000**, *39*, 2081; d) K. Biradha, Y. Hongo, M. Fujita, *Angew. Chem.* **2000**, *112*, 4001; *Angew. Chem. Int. Ed.* **2000**, *39*, 3843; e) K. Biradha, Y. Hongo, M. Fujita, *Angew. Chem.* **2002**, *114*, 3545; *Angew. Chem. Int. Ed.* **2002**, *41*, 3395; f) K. Biradha, M. Fujita, *Angew. Chem.* **2002**, *114*, 3542; *Angew. Chem. Int. Ed.* **2002**, *41*, 3392; g) M. Fujita, Y. J. Kwon, S. Washizu, O. Ogura, *J. Am. Chem. Soc.* **1994**, *116*, 1151.

[9] a) C. J. Kepert, M. J. Rosseinsky, *Chem. Commun.* **1999**, 375; b) E. J. Cussen, J. B. Claridge, M. J. Rosseinsky, C. J. Kepert, *J. Am. Chem. Soc.* **2002**, *124*, 9574, and references therein; c) Y. H. Kiang, G. B. Gardner, S. Lee, Z. Xu, E. B. Lobkovsky, *J. Am. Chem. Soc.* **1999**, *121*, 8204; d) L. C. Tabares, J. A. R. Navarro, J. M. Salas, *J. Am. Chem. Soc.* **2001**, *123*, 383; e) X. Xu, M. Nieuwenhuyzen, S. L. James, *Angew. Chem.* **2002**, *114*, 790; *Angew. Chem. Int. Ed.* **2002**, *41*, 764.

[10] a) J. Zhu, X. Bu, P. Feng, G. D. Stucky, *J. Am. Chem. Soc.* **2000**, *122*, 11563; b) K. Barthelet, J. Marrot, D. Riou, G. Férey, *Angew. Chem.* **2002**, *114*, 291; *Angew. Chem. Int. Ed.* **2002**, *41*, 281, and references therein; c) P. Losier, M. J. Zaworotko, *Angew. Chem.* **1996**, *108*, 2957; *Angew. Chem. Int. Ed. Engl.* **1996**, *35*, 2779.

[11] a) M. J. Zaworotko, *Chem. Soc. Rev.* **1994**, *23*, 283; b) C. M. Draznieks, S. Girard, G. Férey, J. C. Schon, Z. Cancarevic, M. Jansen, *Chem. Eur. J.* **2002**, *8*, 4103, and references therein; c) A. Hori, A. Akasaka, K. Biradha, S. Sakamoto, K. Yamaguchi, M. Fujita, *Angew. Chem.* **2002**, *114*, 3403; *Angew. Chem. Int. Ed.* **2002**, *41*, 3269, and references therein; d) B. Moulton, J. Lu, R. Hajndl, S. Hariharan, M. J. Zaworotko, *Angew. Chem.* **2002**, *114*, 2945; *Angew. Chem. Int. Ed.* **2002**, *41*, 2821; e) *Handbook of Porous Solids* (Eds.: F. Schüth, K. S. W. Sing, J. Weitkamp), Wiley-VCH, Weinheim, **2002**.

[12] a) D. Hagrman, P. J. Hagrman, J. Zubieta, *Angew. Chem.* **1999**, *111*, 3395; *Angew. Chem. Int. Ed.* **1999**, *38*, 3165; b) L. R. MacGillvray, R. H. Groeneman, J. L. Atwood, *J. Am. Chem. Soc.* **1998**, *120*, 2676; c) N. G. Pschirer, D. M. Ciurtin, M. D. Smith, U. H. F. Bunz, H. C. zur Loye, *Angew. Chem.* **2002**, *114*, 603; *Angew. Chem. Int. Ed.* **2002**, *41*, 583, and references therein.

[13] a) L. Carlucci, G. Ciani, D. M. Proserpio, A. Sironi, *J. Am. Chem. Soc.* **1995**, *117*, 4562; b) S. Subramanian, M. J. Zaworotko, *Angew. Chem.* **1995**, *107*, 2295; *Angew. Chem. Int. Ed. Engl.* **1995**, *34*, 2127.

[14] a) *Comprehensive Coordination Chemistry, Vol. 5*, (Ed.: G. Wilkinson), Pergamon, Toronto, Canada, **1987**; b) R. C. Mehrotra, R. Bohra, *Metal Carboxylates*, Academic Press, London, **1983**; c) Y. Liao, W. W. Schum, S. Miller, *J. Am. Chem. Soc.* **2002**, *124*, 9336; d) V. M. Rao, D. N. Sathyanarayana, H. Manohar, *J. Chem. Soc. Dalton Trans.* **1983**, 2167; e) G. Davey, F. S. Stephens, *J. Chem. Soc. A* **1971**, 103; f) I. Goldberg, F. H. Herbstein, *Acta Crystallogr. Sect. B* **1973**, *29*, 246.

[15] a) R. Kiriyama, *Acta Crystallogr.* **1954**, *7*, 482; b) R. Kiriyama, *Bull. Chem. Soc. Jpn.* **1962**, *35*, 1199.

[16] C. I. Stalhandske, *Acta Chem. Scand.* **1969**, *23*, 1525.

[17] J. Hatibarua, G. S. Parry, *Acta Crystallogr. Sect. B* **1972**, *28*, 3099, and references therein.

[18] a) B. Kozlevkar, N. Lah, S. Makuc, P. Segedin, F. Pohleven, *Acta Chim. Slov.* **2000**, *47*, 421; b) B. Morosin, R. C. Hughes, Z. G. Soos, *Acta Crystallogr. Sect. B* **1975**, *31*, 762; c) V. J. Pickardt, *Acta Crystallogr. Sect. B* **1981**, *37*, 1753.

[19] a) B. K. Koo, *Bull. Korean Chem. Soc.* **2001**, *22*, 113; b) J. E. Fiscus, S. Shotwell, R. C. Layland, M. D. Smith, H. C. zur Loye, U. H. F. Bunz, *Chem. Commun.* **2001**, 2674.

[20] S. R. Batten, B. F. Hoskins, B. Moubaraki, K. S. Murray, R. Robson, *Chem. Commun.* **2000**, 1095.

[21] F. A. Cotton, Y. Kim, *J. Am. Chem. Soc.* **1993**, *115*, 8511, and references therein.

 © 2004 Wiley-VCH Verlag GmbH & Co. KGaA, Weinheim

[22] J. Lu, W. T. A. Harrison, A. J. Jacobson, *Chem. Commun.* **1996**, 399.

[23] a) C. Cadiou, R. A. Coxell, A. Graham, A. Harrison, M. Helliwell, S. Parsons, R. E. P. Winpenny, *Chem. Commun.* **2002**, 1106, and references therein; b) D. J. Price, S. R. Batten, B. Moubaraki, K. S. Murray, *Chem. Commun.* **2002**, 762; c) M. Eshel, A. Bino, I. Felner, D. C. Johnston, M. Luban, L. L. Miller, *Inorg. Chem.* **2000**, *39*, 1376, and references therein; d) J. G. Mao, A. Clearfield, *Inorg. Chem.* **2002**, *41*, 2319.

[24] a) A. J. Blake, C. M. Grant, S. Parsons, J. M. Rawsons, R. E. P. Winpenny, *J. Chem. Soc. Chem. Commun.* **1994**, 2363; b) S. P. Watton, P. Fuhrmann, L. E. Pence, A. Caneschi, A. Cornia, G. L. Abbatti, S. J. Lippard, *Angew. Chem.* **1997**, *109*, 2917; *Angew. Chem. Int. Ed. Engl.* **1997**, *36*, 2774.

[25] a) H. L. Li, M. Eddaoudi, O. M. Yaghi, *Angew. Chem.* **1999**, *111*, 682; *Angew. Chem. Int. Ed.* **1999**, *38*, 653; b) Y. H. Liu, Y. L. Lu, H. C. Wu, J. C. Wang, K. L. Lu, *Inorg. Chem.* **2002**, *41*, 2592.

[26] G. Dong, Z. Bing-guang, D. C. Ying, P. Ke-liang, M. Qing-jin, *J. Chem. Soc. Dalton Trans.* **2002**, 3783.

[27] G. C. Guo, T. C. W. Mak, *Chem. Commun.* **1999**, 813.

[28] a) J. Legendziewicz, M. Borzechowska, G. Oczko, G. Meyer, *New J. Chem.* **2000**, *24*, 53; b) I. Kutlu, G. Meyer, G. Oczko, J. Legendziewicz, *Eur. J. Solid State Inorg. Chem.* **1997**, *34*, 231, and references therein; c) J. Legendziewicz, G. Oczko, G. Meyer, *Polyhedron* **1991**, *10*, 1921.

[29] R. G. Bryant, V. P. Chacko, M. C. Etter, *Inorg. Chem.* **1984**, *23*, 3580, and references therein.

[30] a) Y. Laget, C. Hornick, M. Drillon, *J. Mater. Chem.* **1999**, *9*, 169; b) S. Yamanaka, T. Sako, K. Seki, M. Hattori, *Solid State Ionics* **1992**, 53, 527; c) S. Yamanaka, T. Sako, M. Hattori, *Chem. Lett.* **1989**, 1869.

[31] R. Kuhlman, G. L. Schimek, J. W. Kolis, *Inorg. Chem.* **1999**, *38*, 194.

[32] I. A. Koval, P. Gamez, O. Roubeau, W. L. Driessen, M. Lutz, A. L. Spek, J. Reedijk, *Inorg. Chem.* **2003**, *42*, 868.

[33] W. Schmitt, E. Baissa, A. Mandel, C. E. Anson, A. K. Powell, *Angew. Chem.* **2001**, *113*, 3689; *Angew. Chem. Int. Ed.* **2001**, *40*, 3577.

[34] a) L. Brammer, M. D. Burgard, M. D. Eddleston, C. S. Rodger, N. P. Rath, H. Adams, *CrystEngComm* **2002**, *4*, 239; b) L. Brammer, M. D. Burgard, C. S. Rodger, J. K. Swearingen, N. P. Rath, *Chem. Commun.* **2001**, 2468; c) C. M. Rivas, L. Brammer, *Coord. Chem. Rev.*, **1999**, *183*, 43; d) G. R. Desiraju, *Crystal Engineering: The Design of Organic Solids*, Elsevier, New York, **1989**.

[35] G. S. Papaefstathiou, L. R. MacGillvray, *Angew. Chem.* **2002**, *114*, 2174; *Angew. Chem. Int. Ed.* **2002**, *41*, 2070.

[36] a) C. Sterling, *Nature* **1965**, *205*, 588, and references therein; b) C. Sterling, *Science* **1964**, *146*, 518; c) N. Gererd, G. W. Marion, A. T. Sorel, *Bull. Soc. Chim. Fr.* **1968**, *11*, 4367; d) O. C. Pluchery, J. C. Mutin, J. Bouillot, J. C. Niepce, *Acta Crystallogr. Sect. C* **1989**, *45*, 1699; e) I. L. Jenkins, F. H. Moore, M. J. Waterman, *J. Inorg. Nucl. Chem.* **1965**, *27*, 77.

[37] a) O. Kahn, *Molecular Magnetism*, VCH, Weinheim, Germany, **1993**, and references therein; b) P. Day, Science, **1993**, *261*, 431; c) O. Kahn, *Angew. Chem.* **1985**, *97*, 837; *Angew. Chem. Int. Ed. Engl.* **1985**, *24*, 834; d) M. Pilkington, S. Decurtins in *Magnetoscience from Molecules to Materials* (Eds.: J. S. Miller, M. Drillon), Wiley-VCH, Weinheim, **2001**, chap. 10; e) S. Decurtins, H. W. Schmalle, R. Pellaux, P. Fischer, A. Hauser, *Mol. Cryst. Liq. Cryst.* **1997**, *305*, 227; f) S. Decurtins, H. W. Schmalle, P. Schneuwly, R. Pellaux, J. Ensling, *Mol. Cryst. Liq. Cryst.* **1995**, *273*, 167; g) S. Decurtins, H. W. Schmalle, P. Schneuwly, L. M. Zheng, J. Ensling, A. Hauser, *Inorg. Chem.* **1995**, *34*, 5501.

[38] a) T. R. Felthouse, E. J. Laskowski, D. N. Hendrickson, *Inorg. Chem.* **1977**, *16*, 1077; b) H. K. Fun, S. S. Raj, X. Fang, L. M. Zheng, X. Q. Xin, *Acta Crystallogr. Sect. C* **1999**, *55*, 903; c) B. Modec, J. V. Brencic, D. Dolenc, J. Zubieta, *J. Chem. Soc. Dalton Trans.* **2002**, 4582; d) A. Escuer, R. Vicente, X. Solans, M. Font-Bardia, *Inorg. Chem.* **1994**, *33*, 6007; e) M. R. Sundberg, R. Kivekas, J. K. Koskimies, *J. Chem. Soc. Chem. Commun.* **1991**, 526; f) S. Kitagawa, T. Okubo, S. Kawata, M. Kondo, M. Katada, H. Kobayashi, *Inorg. Chem.*, **1995**, *34*, 4790, and references therein; g) G. D. Munno, R. Ruiz, F. Lloret, J. Faus, R. Sessoli, M. Julve, *Inorg. Chem.* **1995**, *34*, 408; h) S. Decurtins, H. W. Schmalle, R. Pellaux, A. Hauser, M. E. von Arx, P. Fischer, *Synth. Met.* **1997**, *85*, 1689.

[39] a) R. P. Farrell, T. W. Hambley, P. A. Lay, *Inorg. Chem.* **1995**, *34*, 757; b) L. Soto, J. Garcia, E. Escriva, J. P. Legros, J. P. Tuchagues, F. Dahan, A. Fuertes, *Inorg. Chem.* **1989**, *28*, 3378; c) R. Pellaux, H. W. Schmalle, S. Decurtins, P. Fischer, F. Fauth, B. Ouladdiaf, T. Hauss, *Physica B* **1997**, *234*, 783; d) R. Pellaux, H. W. Schmalle, S. Decurtins, R. Huber, P. Fischer, B. Ouladdiaf, T. Hauss, S. Decurtins, *Inorg. Chem.* **1997**, *36*, 2301.

[40] a) Y. H. Kiang, S. Lee, Z. Xu, W. Choe, G. B. Gardner, *Adv. Mater.* **2000**. *12*, 767; b) G. B. Gardner, D. Venkataraman, J. S. Moore, S. Lee, *Nature* **1995**, *374*, 792; c) D. D. MacNicol in *Inclusion Compounds*, *Vol. 2* (Eds: J. L. Atwood, J. E. Davies, D. D. MacNicol), Academic Press, London, **1984**, chap. 1; d) R. Bishop, I. G. Dance in *Inclusion Compounds*, *Vol. 4* (Eds: J. L. Atwood, J. E. Davies, D. D. MacNicol), Academic Press, London, **1991**, chap. 1.

[41] a) X. Li, Y. Lin, K. Zhou, *Chin. J. Struct. Chem.* **1984**, *3*, 45; b) M. G. B. Drew, D. J. Eve, *Inorg. Chim. Acta* **1977**, *25*, L111; c) G. L. Glen, J. V. Siverton, J. L. Hoard, *Inorg. Chem.* **1963**, *2*, 250; d) B. K. Prodic, Z. R. Toros, M. Sljukic, *Acta Crystallogr Sect. B* **1978**, *34*, 2001.

[42] G. M. H. van de Velde, S. Harkema, P. J. Gellings, *Inorg. Chim. Acta* **1974**, *11*, 243.

[43] R. B. English, D. J. Eve, *Inorg. Chim. Acta* **1993**, *203*, 219.

[44] Y. Fu, Y. Liu, Z. Shi, B. Li, W. Pang, *J. Solid State Chem.* **2002**, *163*, 427.

[45] R. C. Fay in *Comprehensive Coordination Chemistry*, *Vol. 3* (Eds: G. Wilkinson, R. D. Gillard, J. A. McCleverty), Pergamon, Oxford, England, **1987**, p. 411.

[46] a) R. Baggio, M. T. Garland, M. Perec, *Inorg. Chem.* **1997**, *36*, 737; b) R. Baggio, M. T. Garland, M. Perec, *Inorg. Chem.* **1997**, *36*, 3198; c) S. Morris, M. J. Almond, C. J. Cardin, M. G. B. Drew, D. A. Rice, Y. Zubavichus, *Polyhedron* **1998**, *17*, 2301, and references therein.

[47] a) E. Jeanneau, N. Audebrand, D. Louër, *Chem. Mater.* **2002**, *14*, 1187; b) E. Jeanneau, N. Audebrand, J. P. Auffrédic, D. Louër, *J. Mater. Chem.* **2001**, *11*, 2545; c) C. Boudaren, J. P. Auffrédic, M. Louër, D. Louër, *Chem. Mater.* **2000**, *12*, 2324; d) E. Jeanneau, N. Audebrand, D. Louër, *J. Mater. Chem.* **2002**, *12*, 2383.

[48] a) Z.-J. Zhong, N. Matsumoto, H. Okawa, S. Kida, *Chem. Lett.* **1990**, 87; b) L. O. Atovmyan, G. C. Shilov, R. N. Lyubovskaya, E. I. Zhilyaeva, N. S. Ovanesyan, S. I. Pirumova, I. G. Gusakovskaya, *JETP Lett.* **1993**, *58*, 766; c) M. Clemente-Leon, E. Coronado, J. R. Galan-Mascaros, C. J. Gomez-Garcia, *Chem. Commun.* **1997**, 1727; d) E. Coronado, J. R. Galan-Mascaros, C. J. Gomez-Garcia, J. Ensling, P. Gütlich, *Chem. Eur. J.* **2000**, *6*, 552; e) C. Mathoniere, S. G. Carling, D. Yusheng, P. Day, *J. Chem. Soc. Chem. Commun.* **1994**, 1551.

[49] a) G. D. Munno, M. Julve, F. Nicolo, F. Lloret, J. Faus, R. Ruiz, E. Sinn, *Angew. Chem.* **1993**, *105*, 588; *Angew. Chem. Int. Ed. Engl.* **1993**, *32*, 613; b) S. G. Carling, C. Mathoniere, P. Day, K. M. A. Malik, S. J. Coles, M. B. Hursthouse, *J. Chem. Soc. Dalton Trans.* **1996**, 1839; c) E. Coronado, M. Clemente-Leon, J. R. Galan-Mascaros, C. Gomenez-Saiz, C. J. Gomez-Garcia,

 © 2004 Wiley-VCH Verlag GmbH & Co. KGaA, Weinheim

E. Martinez-Ferrero, *J. Chem. Soc. Dalton Trans.* **2000**, 3955, and references therein; d) E. Coronado, J. R. Galan-Mascaros, C. J. Gomez-Garcia, J. M. Martinez-Agudo, *Adv. Mater.* **1999**, *11*, 558.

[50] a) S. Decurtins, H. W. Schmalle, R. Pellaux, R. Huber, P. Fischer, B. Ouladdiaf, *Adv. Mater.* **1996**, *8*, 647, and references therein; b) S. Decurtins, H. W. Schmalle, P. Schneuwly, J. Ensling, P. Gütlich, *J. Am. Chem. Soc.* **1994**, *116*, 9521.

[51] a) S. Decurtins, H. W. Schmalle, H. R. Oswald, A. Linden, J. Ensling, P. Gütlich, A. Hauser, *Inorg. Chim. Acta* **1994**, *216*, 65; b) C. J. Nuttall, P. Day, *Chem. Mater.* **1998**, *10*, 3050; c) H. W. Schmalle, R. Pellaux, S. Decurtins, *Z. Kristallogr.* **1996**, *211*, 533.

[52] H. Tamaki, Z. J. Zhong, N. Matsumoto, S. Kida, M. Koikawa, N. Achiwa, Y. Hashimoto, H. Okawa, *J. Am. Chem. Soc.* **1992**, *114*, 6974.

[53] I. D. Watts, S. G. Carling, P. Day, *J. Chem. Soc. Dalton Trans.* **2002**, 1429.

[54] a) S. Decurtins, H. W. Schmalle, P. Schneuwly, H. R. Oswald, *Inorg. Chem.* **1993**, *32*, 1888; b) S. Decurtins, H. W. Schmalle, R. Pellaux, P. Schneuwly, A. Hauser, *Inorg. Chem.* **1996**, *35*, 1451.

[55] R. Sieber, S. Decurtins, H. S. Evans, C. Wilson, D. Yufit, J. A. K. Howard, S. C. Capelli, A. Hauser, *Chem. Eur. J.* **2000**, *6*, 361.

[56] H. Y. Shen, W. M. Bu, D. Z. Liao, Z. H. Jiang, S. P. Yan, G. L. Wang, *Inorg. Chem.* **2000**, *39*, 2239.

[57] a) M. H. Molina, F. Lloret, C. R. Perez, M. Julve, *Inorg. Chem.* **1998**, *37*, 4131; b) M. Julve, M. Verdaguer, A. Gleizes, P. Levisalles, O. Kahn, *Inorg. Chem.* **1984**, *23*, 3808, and references therein; c) R. E. Oughtred, E. S. Raper, H. M. M. Shearer, *Acta Crystallogr. Sect. B* **1976**, *32*, 82.

[58] D. Armentano, G. De Munno, F. Lloret, A. V. Palii, M. Julve, *Inorg. Chem.* **2002**, *41*, 2007.

[59] D. J. Price, A. K. Powell, P. T. Wood, *J. Chem. Soc. Dalton Trans.* **2000**, 3566.

[60] D. J. Price, S. Tripp, A. K. Powell, P. T. Wood, *Chem. Eur. J.* **2001**, *7*, 200.

[61] a) R. Vaidhyanathan, S. Natarajan, A. K. Cheetham, C. N. R. Rao, *Chem. Mater.* **1999**, *11*, 3636; b) R. Vaidhyanathan, S. Natarajan, C. N. R. Rao, *J. Chem. Soc. Dalton Trans.* **2001**, 699; c) R. Vaidhyanathan, S. Natarajan, C. N. R. Rao, *Solid State Sci.* **2002**, *4*, 633; d) R. Vaidhyanathan, S. Natarajan, C. N. R. Rao, *J. Solid State Chem.* **2001**, *162*, 150; e) R. Vaidhyanathan, S. Natarajan, C. N. R. Rao, *J. Solid State Chem.* **2002**, *167*, 274; f) S. Natarajan, *Solid State Sci.* **2002**, *10*, 1331.

[62] O. R. Evans, W. Lin, *Cryst. Growth Des.* **2001**, *1*,9.

[63] S. Huang, R. Wang, T. C. W. Mak, *J. Crystallogr. Spectrosc. Res.* **1990**, *20*, 99.

[64] P. A. Prasad, S. Neeraj, S. Natarajan, C. N. R. Rao, *Chem. Commun.* **2000**, 1251.

[65] S. Natarajan, R. Vaidhyanathan, C. N. R. Rao, S. Ayyappan, A. K. Cheetham, *Chem. Mater.* **1999**, *11*, 1633.

[66] C. N. R. Rao, S. Natarajan, A. Choudhury, S. Neeraj, R. Vaidhyanathan, *Acta Crystallogr. Sect. B* **2001**, *57*, 1, and references therein.

[67] a) R. Vaidhyanathan, S. Natarajan, C. N. R. Rao, *Eur. J. Inorg. Chem.* **2003**, 1675; b) P. A. Prasad, S. Neeraj, R. Vaidhyanathan, S. Natarajan, *J. Solid State Chem.* **2002**, *166*, 128.

[68] a) J. C. Jansen, H. van Koningsveld, J. A. C. van Ooijen, *Cryst. Struct. Commun.* **1979**, *8*, 499; b) N. F. Curtis, I. R. N. McCormick, T. N. Waters, *J. Chem. Soc. Dalton*, **1963**, 1537; c) J. Y. Lu, M. A. Lawandy, J. Li, T. Yeun, C. L. Lin, *Inorg. Chem.* **1999**, *38*, 2695; d) M. A. Lawandy, L. Pan, X. Huang, J. Li, T. Yeun, C. L. Lin, *M. R. S. Symp. Proc.* **2001**, *658*, GG6.12.1; e) L. M. Zheng, X. Fang, K. H. Lii, H. H. Song, X. Q. Xin, H. K. Fun, K. Chinnakali, I. A. Razak, *J. Chem. Soc. Dalton Trans.* **1999**, 2311, and references therein; f) M. C. Munoz, M. Julve, F. Lloret, J. Faus, M. Andruh, *J. Chem. Soc. Dalton Trans.* **1998**, 3125; g) G. Marinescu, M. Andruh, R. Lescoueze, M. C. Munoz, J. Cano, F. Lloret, M. Julve, *New J. Chem.* **2000**, *24*, 527; h) O. Castillo, A. Luque, P. Romàn, F. Lloret, M. Julve, *Inorg. Chem.* **2001**, *40*, 5526; i) O. Castillo, A. Luque, J. Sertucha, P. Romàn, F. Lloret, *Inorg. Chem.* **2000**, *39*, 6142.

[69] a) P. Orioli, B. Bruni, M. D. Vaira, L. Messori, F. Piccioli, *Inorg. Chem.* **2002**, *41*, 4312; b) J. Y. Lu, J. Macias, J. Lu, J. E. Cmaidalka, *Cryst. Growth Des.* **2002**, *2*, 485.

[70] a) W. W. Wendlandt, T. D. George, G. R. Horton, *J. Inorg. Nucl. Chem.* **1961**, *273*, 273, and references therein; b) A. W. Wylie, *J. Chem. Soc.* **1947**, 1687; c) I. L. Jenkins, F. H. Moore, M. J. Waterman, *J. Inorg. Nucl. Chem.* **1965**, *27*, 77; d) R. M. Barrer, L. Ibbitson, *Trans. Faraday Soc.* **1944**, *40*, 195; e) R. M. Barrer, *Annu. Rep.* **1944**, *41*, 31.

[71] V. Gilpin, W. C. McCrone, *Anal. Chem.* **1952**, *24*, 225.

[72] a) I. A. Kahwa, F. R. Fronczek, J. Selbin, *Inorg. Chim. Acta* **1984**, *82*, 167; b) I. A. Kahwa, J. Selbin, *J. Therm. Anal.* **1983**, *28*, 359.

[73] a) E. Hansson, *Acta Chem. Scand.* **1970**, *24*, 2969; b) F. F. Cavillou, J. C. Trombe, *Solid State Sci.* **2002**, *4*, 1199; c) T. Bataille, D. Louër, *Acta Crystallogr. Sect. B* **2000**, *56*, 998; d) P. Klaus, J. P. Sutter, S. Golhen, L. Quahab, O. Khan, *Inorg. Chem.* **2000**, *39*, 1626, and references therein.

[74] a) S. Romero, A. Mosset, J. C. Trombe, *Eur. J. Solid State Inorg. Chem.* **1997**, *34*, 209, and refrences therein; b) S. Romero, A. Mosset, J. C. Trombe, *Eur. J. Solid State Inorg. Chem.* **1996**, *127*, 256.

[75] T. R. R. McDonald, J. M. Spink, *Acta Crystallogr.* **1967**, *23*, 944.

[76] a) T. Bataille, M. Louër, J. P. Auffrédic, D. Louër, *J. Solid State Chem.* **2000**, *150*, 81; b) T. Bataille, J. P. Auffrédic, D. Louër, *Chem. Mater.* **1999**, *11*, 1559; c) T. Bataille, J. P. Auffrédic, D. Louër, *J. Mater. Chem.* **2000**, *10*, 1707; d) T. Bataille, D. Louër, *Acta Crystallogr. Sect. C* **1999**, *55*, 1760; e) O. Genecova, J. Siftar, *J. Therm. Anal.* **1997**, *48*, 321.

[77] a) M. T. V. Ganzereli, L. Maggi, V. C. Caramella, *Appl. Radiat. Isot.* **1999**, *51*, 21; b) V. C. Caramella, L. Maggi, M. T. V. Ganzereli, *Appl. Radiat. Isot.* **1999**, *51*, 353.

[78] a) N. W. Alcock, *J. Chem. Soc. Dalton Trans.* **1973**, 1610; b) A. E. Bradley, J. E. Hatter, M. Nieuwenhuyzen, W. R. Pitner, K. R. Seddon, R. C. Thied, *Inorg. Chem.* **2002**, *41*, 1692.

[79] R. Vaidhyanathan, S. Natarajan, C. N. R. Rao, *Chem. Mater.* **2001**, *13*, 185.

[80] R. Vaidhyanathan, S. Natarajan, C. N. R. Rao, *Inorg. Chem.* **2002**, *41*, 4496.

[81] P. Romàn, C. G. Miralles, A. Luque, *J. Chem. Soc. Dalton Trans.* **1996**, 3985.

[82] N. Bulc, L. Golic, J. Siftar, *Acta Crystallogr. Sect. C* **1984**, *40*, 1829.

[83] R. Pellaux, S. Decurtins, H. W. Schmalle, *Acta Crystallogr. Sect. C* **1999**, *55*, 1075.

[84] N. Bulc, L. Golic, *Acta Crystallogr. Sect. C* **1983**, *39*, 174.

[85] N. Bulc, L. Golic, *Acta Crystallogr. Sect. C* **1983**, *39*, 176.

[86] A. V. Virovets, D. Y. Naumov, E. V. Boldyreva, N. V. Podberezskaya, *Acta Crystallogr. Sect. C* **1993**, *49*, 1882.

[87] C. Boudaren, J. P. Auffrédic, P. B. Rocherullé, D. Louër, P. Romàn, *Solid State Sci.* **2001**, *3*, 847.

[88] U. Heinl, P. Hinse, R. Mattes, *Z. Anorg. Allg. Chem.* **2001**, *627*, 2173.

[89] S. Ayyappan, A. K. Cheetham, S. Natarajan, C. N. R. Rao, *Chem. Mater.* **1998**, *10*, 3746.

[90] T. O. Salami, K. Marouchkin, P. Y. Zavilij, S. R. J. Oliver, *Chem. Mater.* **2002**, *14*, 4851.

[91] T. O. Salami, P. Y. Zavilij, S. R. J. Oliver, *Acta Crystallogr. Sect. E.* **2001**, *57*, m111.

[92] T. O. Salami, P. Y. Zavilij, S. R. J. Oliver, *Acta Crystallogr. Sect. E* **2001**, *57*, i49.

 © 2004 Wiley-VCH Verlag GmbH & Co. KGaA, Weinheim

[93] N. Audebrand, M. L. Vaillant, J. P. Auffrédic, D. Louër, *Solid State Sci.* **2001**, *3*, 483.
[94] a) Y. Q. Zheng, Z. P. Kong, *J. Solid State Chem.* **2002**, *166*, 279; b) F. Hohn, I. Pantenburg, U. Ruschewitz, *Chem. Eur. J.* **2002**, *8*, 4536; c) J. Sanchiz, Y. R. Martin, C. R. Perez, A. Mederos, F. Lloret, M. Julve, *New J. Chem.* **2002**, *26*, 1624; d) A. Michaelides, V. Kiritsis, S. Skoulika, A. Aubry, *Angew. Chem.* **1993**, *105*, 1525; *Angew. Chem. Int. Ed.* **1993**, *32*, 1495; e) B. Benmerad, A. G. Laidoudi, F. Balegroune, H. Birkedal, G. Chapuis, *Acta Crystallogr. Sect. C* **2000**, *56*, 789.
[95] a) B. Benmerad, A. G. Laidoudi, G. Bernardinelli, F. Balegroune, *Acta Crystallogr. Sect. C* **2000**, *56*, 321; b) E. V. Brusau, J. C. Pedregosa, G. E. Narda, G. Echeverria, G. Punte, *J. Solid State Chem.* **2000**, *153*, 1; c) E. V. Brusau, G. E. Narda, J. C. Pedregosa, G. Echeverria, G. Punte, *J. Solid State Chem.* **1999**, *143*, 174; d) B. Rather, M. J. Zaworotko, *Chem. Commun.* **2003**, 830; e) J. Perles, M. Iglesias, C. R. Valero, N. Snejko, *Chem. Commun.* **2003**, 346.
[96] a) M. Fleck, L. Bohaty, E. Tillmanns, *Z. Kristallogr.* **2001**, *216*, 633; b) P. S. Mukherjee, S. Dalai, G. Mostafa, E. Zangrando, T. H. Lu, G. Rogez, T. Mallah, N. R. Chaudhuri, *Chem. Commun.* **2001**, 1346; c) M. R. St.-J. Foreman, M. J. Plater, J. M. S. Skakle, *J. Chem. Soc. Dalton Trans.* **2001**, 1897; d) Y. Q. Zheng, J. L. Lin, Z. P. Kong, *Z. Anorg. Allg. Chem.* **2003**, *629*, 357; e) Y. Q. Zheng, J. L. Lin, *Z. Anorg. Allg. Chem.* **2003**, *629*, 578; f) J. Sun, Y. Q. Zheng, *Z. Anorg. Allg. Chem.* **2003**, *629*, 1001; g) T. A. Bowden, H. L. Milton, A. M. Z. Slawin, P. Lightfoot, *J. Chem. Soc. Dalton Trans.* **2003**, 936.
[97] a) P. M. Forster, A. K. Cheetham, *Chem. Mater.*, **2002**, *14*, 17; b) D. Chattopadhyay, S. K. Chattopadhyay, P. R. Lowe, C. H. Schwalbe, S. K. Mazumder, A. Rana, S. Ghosh, *J. Chem. Soc. Dalton Trans.* **1993**, 913; c) I. G. de Muro, M. Insausti, L. Lezama, M. K. Urtiaga, M. I. Arriortua, T. Rojo, *J. Chem. Soc. Dalton Trans.* **2000**, 3360; d) I. G. de Muro, F. A. Mautner, M. Insausti, L. Lezama, M. I. Arriortua, T. Rojo, *Inorg. Chem.* **1998**, *37*, 3243; e) M. Insausti, I. G. de Muro, L. Lorente, T. Rojo, E. H. Bocanegra, M. I. Arriortua, *Thermochim. Acta* **1996**, *287*, 81; f) J. Cernak, J. Chomic, C. Kappenstein, F. Robert, *J. Chem. Soc. Dalton Trans.* **1997**, 2981; g) A. D. Burrows, R. W. Harrington, M. F. Mahon, C. E. Price, *J. Chem. Soc. Dalton Trans.* **2000**, 3845; h) E. Suresh, M. M. Bhadbhade, K. Venkatasubramanian, *Polyhedron* **1999**, *18*, 657.
[98] a) M. Kurmoo, *J. Mater. Chem.* **1999**, *9*, 2595; b) E. Whelan, M. Devereux, M. McCann, V. McKee, *Chem. Commun.* **1997**, 427; c) E. A. H. Griffith, N. G. Charles, E. L. Amma, *Acta Crystallogr. Sect. B* **1982**, *38*, 262; d) K. H. Chung, E. Hong, Y. Do, C. H. Moon, *J. Chem. Soc. Chem. Commun.* **1995**, 2333; e) A. Michaelides, S. Skoulika, V. Kiritsis, A. Aubry, *J. Chem. Soc. Chem. Commun.* **1995**, 1415; f) S. M. Saadeh, K. L. Trojen, J. W. Kampf, W. E. Hatfield, V. L. Pecoraro, *Inorg. Chem.* **1993**, *32*, 3034; g) T. Glowiak, J. Legendziewicz, *Acta Crystallogr. Sect. C* **1986**, *42*, 1494; h) M. Post, J. Trotter, *J. Chem. Soc. Dalton Trans.* **1974**, 1922.
[99] a) N. Guillou, S. Pastre, C. Livage, G. Férey, *Chem. Commun.* **2002**, 2358; b) C. Livage, C. Egger, G. Férey, *Chem. Mater.* **2001**, *13*, 410; c) C. Livage, C. Egger, G. Férey, *Chem. Mater.* **1999**, *11*, 1546; d) F. Serpaggi, G. Férey, *J. Mater. Chem.* **1998**, *8*, 2737; e) C. Livage, C. Egger, M. Noguès, G. Férey, *J. Mater. Chem.* **1998**, *8*, 2743; f) F. Serpaggi, G. Férey, E. A. Fidancev, *J. Solid State Chem.* **1999**, *148*, 347; g) F. Serpaggi, T. Luxbacher, A. K. Cheetham, G. Férey, *J. Solid State Chem.* **1999**, *145*, 580; h) F. Serpaggi, G. Férey, *Microporous Mesoporous Mater.* **1999**, *32*, 311.
[100] a) R. Vaidhyanathan, S. Natarajan, C. N. R. Rao, *Inorg. Chem.* **2002**, *41*, 5226; b) R. Vaidhyanathan, S. Natarajan, C. N. R. Rao, *Cryst. Growth Des.* **2003**, *3*, 47.
[101] a) P. M. Forster, A. K. Cheetham, *Angew. Chem.* **2002**, *114*, 475; *Angew. Chem. Int. Ed.* **2002**, *41*, 457; b) R. Vaidhyanathan, S. Natarajan, C. N. R. Rao, *J. Chem. Soc. Dalton Trans.* **2003** 1459; c) N. Guillou, C. Livage, W. van Beek, M. Noguès, G. Férey, *Angew. Chem.* **2003**, *115*, 668; *Angew. Chem. Int. Ed.* **2003**, *42*, 644, and references therein.
[102] a) Y. Kim, E. W. Lee, D. Y. Jung, *Chem. Mater.* **2001**, *13*, 2684; b) Y. Kim, D. Y. Jung, *Bull. Korean Chem. Soc.* **2000**, *21*, 656; c) Y. Kim, D. Y. Jung, *Bull. Korean Chem. Soc.* **1999**, *20*, 827; d) E. W. Lee, Y. Kim, D. Y. Jung, *Inorg. Chem.* **2002**, *41*, 501; e) Y. Kim, D. Y. Jung, *Inorg. Chem.* **2000**, *39*, 1470.
[103] a) A. Dimos, D. Tsaousis, A. Michaelides, S. Skoulika, S. Golhen, L. Ouahab, C. Didierjean, A. Aubry, *Chem. Mater.* **2002**, *14*, 2616; b) B. Q. Ma, D. S. Zhang, S. Gao, T. Z. Jin, C. H. Yan, G. X. Xu, *Angew. Chem.* **2000**, *112*, 3790; *Angew. Chem. Int. Ed.* **2000**, *39*, 3644; c) R. Baggio, M. T. Garland, M. Perec, D. Vega, *Inorg. Chem.* **1996**, *35*, 2396; d) A. C. Rizzi, R. Calvo, R. Baggio, M. T. Garland, O. Pena, M. Perec, *Inorg. Chem.* **2002**, *41*, 5609.
[104] N. L. Rosi, M. Eddaoudi, J. Kim, M. O'Keeffe, O. M. Yaghi, *Angew. Chem.* **2002**, *114*, 294; *Angew. Chem. Int. Ed.* **2002**, *41*, 284, and references therein.
[105] a) M. I. Khan, Y. D. Chang, Q. Chen, J. Salta, Y. S. Lee, C. J. O'Connor, J. Zubieta, *Inorg. Chem.* **1994**, *33*, 6340; b) C. Castro, M. L. Calatyud, J. Sletten, F. Lloret, M. Julve, *J. Chem. Soc. Dalton Trans.* **1997**, 811, and references therein; c) G. J. Long, *Inorg. Chem.* **1978**, *17*, 2702; d) J. A. C. van Ooijen, J. Reedijk, A. L. Spek, *Inorg. Chem.* **1979**, *18*, 1184.
[106] a) A. Weiss, E. Riegler, I. A. H. Bohme, C. Robl, *Z. Naturforsch. B* **1986**, *41*, 18; b) C. Robl, W. F. Kuhs, *J. Solid State Chem.* **1988**, *75*, 15; c) G. M. Frankenbach, M. A. Beno, A. M. Kini, J. M. Williams, U. Welp, J. E. Thompson, M. H. Whangbo, *Inorg. Chim. Acta* **1992**, *192*, 195; d) M. Habenschuss, B. C. Gerstein, *J. Chem. Phys.* **1974**, *61*, 852; e) B. D. Alleyne, L. A. Hall, H. A. Hosein, H. Jaggernauth, A. J. P. White, D. J. Williams, *J. Chem. Soc. Dalton Trans.* **1998**, 3845.
[107] a) Q. Chen, S. Liu, J. Zubieta, *Inorg. Chim. Acta* **1990**, *175*, 241; b) N. C. Baenziger, D. G. Williams, *J. Am. Chem. Soc.* **1966**, *88*, 689; c) I. Castro, J. Sletten, L. K. Glaerum, F. Lloret, J. Faus, M. Julve, *J. Chem. Soc. Dalton Trans.* **1994**, 2777; d) C. C. Wang, C. H. Yang, G. H. Lee, *Inorg. Chem.* **2002**, *41*, 1015.
[108] a) K. J. Lin, K. H. Lii, *Angew. Chem.* **1997**, *109*, 2166; *Angew. Chem. Int. Ed. Engl.* **1997**, *36*, 2076; b) A. Weiss, E. Riegler, C. Robl, *Z. Naturoforsch. B* **1986**, *41*, 1329; c) A. Weiss, E. Riegler, C. Robl, *Z. Naturoforsch. B* **1986**, *41*, 1333; d) T. K. Maji, G. Mostafa, S. Sain, J. S. Prasad, N. R. Chaudhari, *CrystEngComm* **2001**, *37*, 1; e) S. F. Lai, C. Y. Cheng, K. J. Lin, *Chem. Commun.* **2001**, 1082.
[109] a) M. Dan, K. Shivshankar, A. K. Cheetham, C. N. R. Rao, *J. Solid State Chem.* **2003**, *174*, 60; b) J. C. Trombe, L. Sabadie, P. Millet, *Solid State Sci.* **2002**, *4*, 1209.
[110] a) C. S. Yufit, D. J. Price, J. A. K. Howard, S. O. H. Gutschke, A. K. Powell, P. T. Wood, *Chem. Commun.* **1999**, 1561; b) S. O. H. Gutschke, M. Molinier, A. K. Powell, P. T. Wood, *Angew. Chem.* **1997**, *109*, 1028; *Angew. Chem. Int. Ed. Engl.* **1997**, *36*, 991.
[111] S. Neeraj, M. L. Noy, C. N. R. Rao, A. K. Cheetham, *Solid State Sci.* **2002**, *10*, 1.
[112] O. M. Yaghi, G. Li, T. L. Groy, *J. Chem. Soc. Dalton Trans.* **1995**, 727.
[113] a) J. C. Trombe, J.-F. Petit, A. Gleizes, *Inorg. Chim. Acta* **1990**, *167*, 69; b) J. C. Trombe, J. F. Petit, A. Gleizes, *Eur. J. Solid State Inorg. Chem.* **1991**, *28*, 669; c) M. Dan, C. N. R. Rao, *Solid State Sci.* **2003**, *5*, 615.
[114] a) C. Robl, A. Weiss, *Z. Naturforsch. B* **1986**, *41*, 1490; b) C. Robl, A. Weiss, *Z. Naturforsch. B* **1986**, *41*, 1485.

 © 2004 Wiley-VCH Verlag GmbH & Co. KGaA, Weinheim

[115] C. R. Lee, C. C. Wang, Y. Wang, *Acta Crystallogr. Sect. B* **1996**, *52*, 966.
[116] L. Gmelin, *Ann. Phys. (Leipzig)* **1825**, *4*, 31.
[117] a) J. D. Dunitz, P. Seiler, W. Czechtizky, *Angew. Chem.* **2001**, *113*, 1829; *Angew. Chem. Int. Ed.* **2001**, *40*, 1779; b) D. Braga, L. Maini, F. Grepioni, *Chem. Eur. J.* **2002**, *8*, 1804.
[118] a) M. D. Glick, L. F. Dahl, *Inorg. Chem.* **1966**, *5*, 289; b) M. D. Glick, G. L. Downs, L. F. Dahl, *Inorg. Chem.* **1964**, *3*, 1712.
[119] M. J. Plater, A. J. Roberts, J. Marr, E. E. Lachowski, R. A. Howie, *J. Chem. Soc. Dalton Trans.* **1998**, 797.
[120] K. Barthelet, D. Riou, G. Férey, *Chem. Commun.* **2002**, 1492.
[121] F. Millange, C. Serre, G. Férey, *Chem. Commun.* **2002**, 822.
[122] C. Serre, F. Millange, C. Thouvenot, M. Noguès, G. Marsolier, D. Louër, G. Férey, *J. Am. Chem. Soc.* **2002**, *124*, 13519.
[123] M. Sanselme, J. M. Grenèche, M. R. Cavellec, G. Férey, *Chem. Commun.* **2002**, 2172.
[124] M. R. Cavellec, G. Férey, *Solid State Sci.* **2002**, *4*, 1221.
[125] M. R. Cavellec, C. Albinet, C. Livage, N. Guillou, M. Noguès, J. M. Grenèche, G. Férey, *Solid State Sci.* **2002**, *4*, 267.
[126] R. K. Chiang, N. T. Chuang, C. S. Wur, M. F. Chong, C. R. Lin, *J. Solid State Chem.* **2002**, *166*, 158.
[127] S. O. H. Gutschke, D. J. Price, A. K. Powell, P. T. Wood, *Angew. Chem.* **2001**, *113*, 1974; *Angew. Chem. Int. Ed.* **2001**, *40*, 1920.
[128] C. Livage, N. Guillou, J. Marrot, G. Férey, *Chem. Mater.* **2001**, *13*, 4387.
[129] Z. L. Huang, M. Drillon, N. Masciocchi, A. Sironi, J. T. Zhao, P. Rabu, P. Panissod, *Chem. Mater.* **2000**, *12*, 2805.
[130] D. Cheng, M. A. Khan, R. P. Houser, *J. Chem. Soc. Dalton Trans.* **2002**, 4555.
[131] Y. Li, H. Zhang, E. Wang, N. Hao, C. Hu, Y. Yan, D. Hall, *New J. Chem.* **2002**, *26*, 1619.
[132] D. Cheng, M. A. Khan, R. P. Houser, *Cryst. Growth Des.* **2002**, *2*, 415.
[133] H. Kumagai, M. A. Tanaka, K. Inoue, M. Kurmoo, *J. Mater. Chem.* **2001**, *11*, 2146.
[134] R. Murugavel, D. Krishnamurthy, M. Sathiyendiran, *J. Chem. Soc. Dalton Trans.* **2002**, 34.
[135] C. J. Kepert, T. J. Prior, M. J. Rosseinsky, *J. Am. Chem. Soc.* **2000**, *122*, 5158.
[136] C. J. Kepert, M. J. Rosseinsky, *Chem. Commun.* **1998**, 31.
[137] T. B. Lu, H. Xiang, R. L. Luck, L. Jiang, Z. W. Mao, L. N. Ji, *New J. Chem.* **2002**, *26*, 969.
[138] D. Cheng, M. A. Khan, R. P. Houser, *Inorg. Chem.* **2001**, *40*, 6858.
[139] J. W. Ko, K. S. Min, M. P. Suh, *Inorg. Chem.* **2002**, *41*, 2151.
[140] J. C. Dai, X. T. Wu, Z. Y. Fu, C. P. Cui, S. M. Hu, W. X. Du, L. M. Wu, H. H. Zhang, R. Q. Sun, *Inorg. Chem.* **2002**, *41*, 1391.
[141] J. C. Dai, X. T. Wu, Z. Y. Fu, S. H. Hu, W. X. Du, C. P. Cui, L. M. Wu, H. H. Zhang, R. Q. Sun, *Chem. Commun.* **2002**, 12.
[142] Y. Kim, D. Y. Jung, *Chem. Commun.* **2002**, 908.
[143] S. S. Y. Chui, A. Siu, X. Feng, Z. Y. Zhang, T. C. W. Mak, I. D. Williams, *Inorg. Chem. Commun.* **2001**, *4*, 467.
[144] Y. Wan, L. Jin, K. Wang, L. Zhang, X. Zheng, S. Lu, *New J. Chem.* **2002**, *26*, 1590.
[145] D. Sun, R. Cao, Y. Liang, Q. Shi, M. Hong, *J. Chem. Soc. Dalton Trans.* **2002**, 1847.
[146] C. Serre, F. Millange, J. Marrot, G. Férey, *Chem. Mater.* **2002**, *14*, 2409.
[147] C. Daiguebonne, Y. Gerault, O. Guillou, A. Lecerf, K. Boubekeur, P. Batail, M. Kahn, O. Kahn, *J. Alloys Compd.* **1998**, *275*, 50.
[148] R. Cao, D. Sun, Y. Liang, M. Hong, K. Tatsumi, Q. Shi, *Inorg. Chem.* **2002**, *41*, 2087.
[149] L. Pan, N. Zheng, Y. Wu, S. Han, R. Yang, X. Huang, J. Li, *Inorg. Chem.* **2001**, *40*, 828.
[150] L. Pan, E. B. Woodlock, X. Wang, *Inorg. Chem.* **2000**, *39*, 4174.
[151] B. G. Lor, E. G. Puebla, M. Iglesias, M. A. Monge, C. R. Valero, N. Snejko, *Inorg. Chem.* **2002**, *41*, 2429.
[152] J. Do, R. P. Bontchev, A. J. Jacobson, *Chem. Mater.* **2001**, *13*, 2601.
[153] Y. M. Tsai, S. L. Wang, C. H. Huang, K. H. Lii, *Inorg. Chem.* **1999**, *38*, 4183.
[154] J. Do, R. P. Bontchev, A. J. Jacobson, *Inorg. Chem.* **2000**, *39*, 3230.
[155] Z. A. D. Lethbridge, S. K. Tiwary, A. Harrison, P. Lightfoot, *J. Chem. Soc. Dalton Trans.* **2001**, 1904.
[156] Z. A. D. Lethbridge, A. D. Hillier, R. Cywinski, P. Lightfoot, *J. Chem. Soc. Dalton Trans.* **2000**, 1595.
[157] W. J. Chang, H. M. Lin, K. H. Lii, *J. Solid State Chem.* **2001**, *157*, 233.
[158] H. M. Lin, K. H. Lii, Y. C. Jiang, S. L. Wang, *Chem. Mater.* **1999**, *11*, 519.
[159] Z. A. D. Lethbridge, P. Lightfoot, *J. Solid State Chem.* **1999**, *143*, 58.
[160] A. Choudhury, S. Natarajan, C. N. R. Rao, *Chem. Mater.* **1999**, *11*, 2316.
[161] A. Choudhury, S. Natarajan, *J. Mater. Chem.* **1999**, *9*, 3113.
[162] A. Choudhury, S. Natarajan, C. N. R. Rao, *Chem. Eur. J.* **2000**, *6*, 1168.
[163] A. Choudhury, S. Natarajan, C. N. R. Rao, *J. Solid State Chem.* **1999**, *146*, 538.
[164] N. Rajic, D. Stojakovic, D. Hanzel, N. Z. Logar, V. Kaucic, *Microporous Mesoporous Mater.* **2002**, *55*, 313.
[165] A. Choudhury, S. Natarajan, *Solid State Sci.* **2000**, *2*, 365.
[166] S. Neeraj, S. Natarajan, C. N. R. Rao, *J. Chem. Soc. Dalton Trans.* **2001**, 289.
[167] P. Lightfoot, Z. A. D. Lethbridge, R. E. Morris, D. S. Wragg, P. A. Wright, A. Kvick, G. B. M. Vaughan, *J. Solid State Chem.* **1999**, *143*, 74.
[168] K. Kedarnath, A. Choudhury, S. Natarajan, *J. Solid State Chem.* **2000**, *150*, 324.
[169] L. C. Hung, H. M. Kao, K. H. Lii, *Chem. Mater.* **2000**, *12*, 2411.
[170] C. Y. Chen, P. P. Chu, K. H. Lii, *Chem. Commun.* **1999**, 1473.
[171] C. T. S. Choi, E. V. Anokhina, C. S. Day, Y. Zhao, F. Taulelle, C. Huguenard, Z. Gan, A. Lachgar, *Chem. Mater.* **2002**, *14*, 4096.
[172] Y. F. Huang, K. H. Lii, *J. Chem. Soc. Dalton Trans.* **1998**, 4085.
[173] S. Natarajan, *J. Solid State Chem.* **1998**, *139*, 200.
[174] S. Chakrabarti, M. A. Green, S. Natarajan, *Solid State Sci.* **2002**, *4*, 405.
[175] S. Chakrabarti, S. Natarajan, *Angew. Chem.* **2002**, *114*, 1272; *Angew. Chem. Int. Ed.* **2002**, *41*, 1224.
[176] S. Chakrabarti, S. Natarajan, *J. Chem. Soc. Dalton Trans.* **2002**, 4156.
[177] A. A. Ayi, A. Choudhury, S. Natarajan, C. N. R. Rao, *New J. Chem.* **2001**, *25*, 213.
[178] B. Adair, S. Natarajan, A. K. Cheetham, *J. Mater. Chem.* **1998**, *8*, 1477.
[179] N. Stock, G. D. Stucky, A. K. Cheetham, *Chem. Commun.* **2000**, 2277.
[180] C. Nather, J. Greve, I. Jess, *Chem. Mater.* **2002**, *14*, 4536.
[181] a) M. Eddaoudi, J. Kim, N. Rosi, D. Vodak, J. B. Wachter, M. O'Keeffe, O. M. Yaghi, *Science* **2002**, *295*, 469; b) M. Eddaoudi, J. Kim, M. O'Keeffe, O. M. Yaghi, *J. Am. Chem. Soc.* **2002**, *124*, 376; c) M. Eddaoudi, J. Kim, J. Wachter, H. K. Chae, M. O'Keeffe, O. M. Yaghi, *J. Am. Chem. Soc.* **2001**, *123*, 4368; d) B. Chen, M. Eddaoudi, T. M. Reineke, J. W. Kampf, M. O'Keeffe, O. M. Yaghi, *J. Am. Chem. Soc.* **2000**, *122*, 11559; e) M. Eddaoudi, H. Li, O. M. Yaghi, *J. Am. Chem. Soc.* **2000**, *122*, 1391; f) N. L. Rosi, M. Eddaoudi, J. Kim, M. O' Keeffe, O. M. Yaghi, *CrystEngComm* **2002**, *4*, 401.
[182] a) B. L. Chen, M. Eddaoudi, S. T. Hyde, M. O'Keeffe, O. M. Yaghi, *Science* **2001**, *291*, 1021; b) O. M. Yaghi, *Chem. Innovation* **2000**, *30*(10); c) T. Reineke, M. Eddoudi, D. Moler, M.

 © 2004 Wiley-VCH Verlag GmbH & Co. KGaA, Weinheim

O'Keeffe, O. M. Yaghi, *J. Am. Chem. Soc.* **2000**, *122*, 1391; d) T. J. Barton, L. M. Bull, W. G. Klemperer, D. A. Loy, B. McEnaney, M. Misono, P. A. Manson, G. Pez, G. W. Scherer, J. C. Vartuli, O. M. Yaghi, *Chem. Mater.* **1999**, *11*, 2633; e) T. M. Reineke, M. Eddaoudi, M. O'Keeffe, O. M. Yaghi, *Angew. Chem.* **1999**, *111*, 2712; *Angew. Chem. Int. Ed.* **1999**, *38*, 2590; f) T. Reineke, M. Eddaoudi, M. Fehr, D. Kelley, O. M. Yaghi, *J. Am. Chem. Soc.* **1999**, *121*, 1651.

[183] a) M. Eddaoudi, H. Li, T. Reineki, M. Fehr, D. Kelley, T. L. Groy, O. M. Yaghi, *Top. Catal.* **1999**, *9*, 105; b) H. Li, M. Eddaoudi, T. L. Groy, O. M. Yaghi, *J. Am. Chem. Soc.* **1998**, *120*, 8571; c) O. M. Yaghi, H. Li, C. Davis, D. Richardson, T. L. Groy, *Acc. Chem. Res.* **1998**, *31*, 474.

[184] a) O. M. Yaghi, C. E. Davis, G. Li, H. Li *J. Am. Chem. Soc.* **1997**, 119, 2861; b) O. M. Yaghi, G. Li, H. Li, *Nature*, **1995**, 378, 703.

[185] S. S. Y. Chui, S. M. F. Lo, J. P. H. Charmant, A. G. Orpen, I. D. Williams, *Science*, **1999**, *283*, 1148.

[186] J. S. Seo, D. Whang, H. Lee, S. I. Jun, J. Oh, Y. J. Jeon, K. Kim, *Nature* **2000**, *404*, 982.

[187] a) S. Y. Yang, L. S. Long, Y. B. Jiang, R. B. Huang, L. S. Zheng, *Chem. Mater.* **2002**, *14*, 3229; b) K. Seki, *Chem. Commun.* **2001**, 1496; c) K. Seki, *Langmuir* **2002**, *18*, 2441; d) T. J. Prior, D. Bradshaw, S. J. Teat, M. J. Rosseinsky, *Chem. Commun.* **2003**, 500.

[188] a) E. M. Sabbar, M. E. de Roy, J. P. Besse, *Mater. Res. Bull.* **1999**, *34*, 1023; b) E. M. Sabbar, M. E. de Roy, A. Ennaquadi, C. Gueho, J. P. Besse, *Chem. Mater.* **1998**, *10*, 3856; c) B. Bujoli, A. Corilleau, P. Palvadeau, J. Rouxel, *Eur. J. Solid State Inorg. Chem.* **1992**, *29*, 171; d) A. Distler, S. C. Sevov, *Chem. Commun.* **1998**, 959; e) S. Drumel, P. J. Janvier, M. B. Doeuff, B. Bujoli, *New J. Chem.* **1995**, *19*, 239; f) M. R. Cavellec, M. Sanselme, M. Noguès, J. M. Grenèche, G. Férey, *Solid State Sci.* **2002**, *4*, 619; g) D. A. Burwell, M. E. Thompson, *Chem. Mater.* **1991**, *3*, 14; h) D. A. Burwell, K. G. Valentine, J. H. Timmermans, M. E. Thompson, *J. Am. Chem. Soc.* **1992**, *114*, 4144.

[189] a) S. Drumel, P. Janvier, P. Barboux, M. B. Doeuff, B. Bujoli, *Inorg. Chem.* **1995**, *34*, 148; b) F. Serpaggi, G. Férey, *Inorg. Chem.* **1999**, *38*, 4741.

[190] a) G. B. Hix, D. S. Wragg, P. A. Wright, R. E. Morris, *J. Chem. Soc. Dalton Trans.* **1998**, 3359; b) F. Fredoueil, D. Massiot, D. M. Poojary, M. B. Doueff, A. Clearfield, B. Bujoli, *Chem. Commun.* **1998**, 175; c) S. Ayyappan, G. D. de Delgado, A. K. Cheetham, G. Férey, C. N. R. Rao, *J. Chem. Soc. Dalton Trans.* **1999**, 2905; d) N. Stock, S. A. Frey, G. D. Stucky, A. K. Cheetham, *J. Chem. Soc. Dalton Trans.* **2000**, 4292; e) N. Stock, *Solid State Sci.* **2002**, *4*, 1089; f) P. Janvier, S. Drumel, P. Piffard, B. Bujoli, *C. R. Acad. Sci. Ser. II* **1995**, *320*, 29.

[191] S. J. Hartman, E. Todorov, C. Cruz, S. C. Sevov, *Chem. Commun.* **2000**, 1213.

[192] S. O. H. Gutschke, D. J. Price, A. K. Powell, P. T. Wood, *Angew. Chem.* **1999**, *111*, 1158; *Angew. Chem. Int. Ed.* **1999**, *38*, 1088.

[193] a) J. G. Mao, A. Clearfield, *Inorg. Chem.* **2002**, *41*, 2319; b) B. Zhang, D. M. Poojary, A. Clearfield, G.-Z. Peng, *Chem. Mater.* **1996**, *8*, 1333.

[194] Y. P. Ren, L. S. Long, B. W. Mao, Y. Z. Yuan, R. B. Huang, L. S. Zheng, *Angew. Chem.* **2003**, *115*, 550; *Angew. Chem. Int. Ed.* **2003**, *42*, 532.

[195] a) R. G. Xiong, S. R. Wilson, W. Lin, *J. Chem. Soc. Dalton Trans.* **1998**, 4089; b) W. Lin, O. R. Evans, R. G. Xiong, Z. Wang, *J. Am. Chem. Soc.* **1998**, *120*, 13272; c) W. Lin, Z. Wang, L. Ma, *J. Am. Chem. Soc.* **1999**, *121*, 11249; d) O. R. Evans, W. Lin, *Inorg. Chem.* **2000**, *39*, 2189; e) O. R. Evans, R. G. Xiong, Z. Wang, G. K. Wong, W. Lin, *Angew. Chem.* **1999**, *111*, 557; *Angew. Chem. Int. Ed.* **1999**, *38*, 536; f) W. Chen, Q. Yue, C. Chen, H. M. Yuan, W. Xu, J. S. Chen, S. N. Wang, *J. Chem. Soc. Dalton Trans.* **2003**, 28.

[196] a) O. R. Evans, W. Lin, *Chem. Mater.* **2001**, *13*, 3009; b) O. R. Evans, W. Lin, *J. Chem. Soc. Dalton Trans.* **2000**, 3949; c) P. Ayyappan, O. R. Evans, W. Lin, *Inorg. Chem.* **2002**, *41*, 3328.

[197] Y. H. Liu, H. L. Tsai, Y. L. Lu, Y. S. Wen, J. C. Wang, K. L. Lu, *Inorg. Chem.* **2001**, *40*, 6426.

[198] J. Y. Lu, A. M. Babb, *Chem. Commun.* **2002**, 1340.

[199] B. Rather, B. Moulton, R. D. B. Walsh, M. J. Zaworotko, *Chem. Commun.* **2002**, 694.

[200] a) D. M. Ciurtin, M. D. Smith, H. C. zur Loye, *Inorg. Chim. Acta* **2001**, *324*, 46, and references therein; b) D. M. Ciurtin, M. D. Smith, H. C. zur Loye, *Chem. Commun.* **2002**, 74.

[201] a) R. Kitaura, K. Fujimoto, S.-i. Noro, M. Kondo, S. Kitagawa, *Angew. Chem.* **2002**, *114*, 141; *Angew. Chem. Int. Ed.* **2002**, *41*, 133; b) M. Kondo, T. Okubo, A. Asami, S. Noro, T. Yoshitomi, S. Kitagawa, T. Ishii, H. Matsuzaka, K. Seki, *Angew. Chem.* **1999**, *111*, 190; *Angew. Chem. Int. Ed.* **1999**, *38*, 140; c) S. I. Noro, S. Kitagawa, M. Yamashita, T. Wada, *Chem. Commun.* **2002**, 222.

[202] a) S. Takamizawa, W. Mori, M. Furihata, S. Takeda, K. Yamaguchi, *Inorg. Chim. Acta* **1998**, *283*, 268; b) Y. Liang, R. Cao, W. Su, M. Hong, W. Zhang, *Angew. Chem.* **2000**, *112*, 3442; *Angew. Chem. Int. Ed. Engl.* **2000**, *39*, 3304; c) Y. Liang, M. Hong, W. Su, R. Cao, W. Zhang, *Inorg. Chem.* **2001**, *40*, 4574; d) T. Whitfield, L. M. Zheng, X. Wang, A. J. Jacobson, *Solid State Sci.* **2001**, *3*, 829; e) X. Haitao, Z. Nengwu, X. Hanhui, W. Yonggang, Y. Ruyi, Y. Enyi, J. Xianglin, *J. Mol. Struct.* **2001**, *597*, 1, and references therein; f) L. A. Gerrard, P. T. Wood, *Chem. Commun.* **2000**, 2107.

[203] a) R. C. Finn, J. Zubieta, *Solid State Sci.* **2002**, *4*, 83, and references therein; b) Y. H. Liu, Y. L. Lu, H. C. Wu, J. C. Wang, K. L. Lu, *Inorg. Chem.* **2002**, *41*, 2592.

[204] R. Vaidhyanathan, S. Neeraj, P. A. Prasad, S. Natarajan, C. N. R. Rao, *Angew. Chem.* **2000**, *112*, 3612; *Angew. Chem. Int. Ed.* **2000**, *39*, 3470.

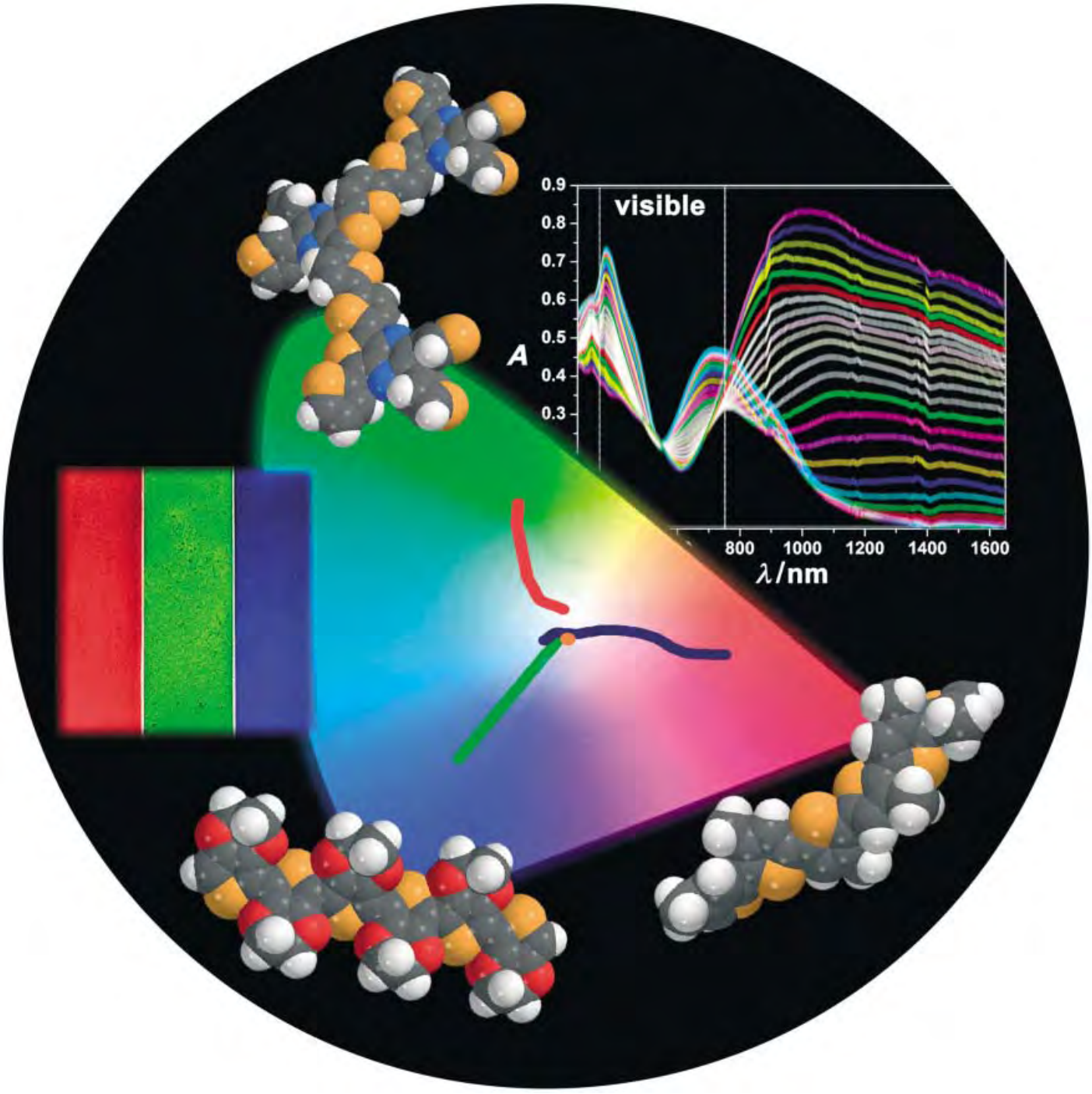
[205] R. Vaidhyanathan, S. Natarajan, C. N. R. Rao, *Chem. Mater.* **2001**, *13*, 3524.

[206] R. Vaidhyanathan, S. Natarajan, C. N. R. Rao, *Mater. Res. Bull.* **2003**, *38*, 477.

[207] a) G. V. Subba Rao, G. Balakrishnan, *Bull. Mater. Sci.* **1984**, *6*, 283; and references therein; b) G. V. Subba Rao, *Proc. Indian Natl. Sci. Acad. Part A* **1986**, *52*, 292.

 © 2004 Wiley-VCH Verlag GmbH & Co. KGaA, Weinheim

Communications



The first neutral, green conducting polymer has been synthesized. High green color saturation, fast switching, and extreme stability, make this material a promising candidate for the missing third leg of red, green, blue (RGB) color space and also brings polymer electrochromics closer to RGB realization. For more information see the Communication by Wudl et al. on the following pages.

DOI: 10.1002/anie.200352910
© 2004 Wiley-VCH Verlag GmbH & Co. KGaA, Weinheim

Conducting Polymers

A Red, Green, and Blue (RGB) Polymeric Electrochromic Device (PECD): The Dawning of the PECD Era**

*Gursel Sonmez, Clifton K. F. Shen, Yves Rubin, and Fred Wudl**

The ability to have three complementary colors, red, green, and blue (RGB) constitutes an important step forward to the use of conducting polymers in polymeric electrochromic devices (PECDs). Although many red and blue colored polymers in their neutral form have been reported, no green colored conducting polymer has been reported to date because of the difficulty to obtain the absorptions required in the visible region to reflect the color green. Herein we report the electrochemical and optical properties of the first electrochemically prepared, neutral, green-colored conjugated polymer. The extreme stability of this polymer after 10000 double potential steps makes it the best, and only, candidate for completing the third leg of color space for polymeric electrochromics.

In the last few decades, conducting polymers (CPs) have been very actively pursued.[1] Several discoveries brought the CPs to full commercialization with applications in electrochromic rearview mirrors,[2,3] windows,[4,5] thin-film transistors,[6] displays,[7,8] sensors,[9,10] polymer light-emitting diodes,[11,12] photovoltaics,[13] and electrochromic devices.[14–17] More recently, research on CPs has mostly focused on their optical properties in the visible[17–20] and near infra-red (NIR)[21–25] spectral regions. Poly(thiophene) derivatives have been the most studied materials because they exhibit fast switching times, outstanding stability and high contrast ratios in the visible and NIR regions.

The earliest electrochromic materials in the visible region were the inorganic tungsten trioxide (WO_3) and iridium dioxide (IrO_2).[26] Because of the increased versatility of organic materials (viologens, metallophtalocyanines, and conducting polymers),[27,28] these compounds have recently received the brunt of attention for potential electrochromic applications.[29] Among organic materials, conjugated polymers have several advantages over small molecules and inorganic solids; these are, outstanding coloration efficiency, fast switching times,[30,31] multiple colorations with the same material,[17,20] fine-tunability of the band gap (and the color),[32,33] high stability,[14,16] thin film flexibility and cost effectiveness.

The three primary colors, red, blue, and green, are required for commercial electrochromic application. When three legs of color space are completed, all other colors can be obtained according to color mixing theory[34] which states that if two color stimuli are mixed, the resulting color stimulus will lie somewhere along a straight line connecting two points on the chromaticity diagram. The position of the point depends on the ratio of the amounts of the two mixed colors. A "fine tuning" of color is possible by adjusting film thickness. Owing to its effect on the brightness of transmitted light, sample thickness has a large influence on the perceived color. Unfortunately, the polymers studied so far mainly absorb/reflect blue and red light in their neutral states. Since absorption at only one dominant wavelength is required to give blue or red, these can be obtained relatively easily by tuning the CP's band gap. At least two absorption bands (red and blue) are required to observe a green color. While these chromophores absorb red and blue in the neutral form of the polymer, they should also deplete together when the polymer is oxidized. However, control of both chromophores at the same time with the same applied potential is very difficult. This difficulty to create and deplete two absorption bands in the visible from the same polymer, make a green neutral polymer almost impossible to realize. It is important to note that green can be obtained by color mixing theory but in this case at least three polymers will be required to obtain another color, which would be green. Therefore, it is crucial to obtain a real green color from an individual polymer to complete the three main legs of color space.

Recently, our group has initiated a study to obtain a conjugated polymer which reflects green light in the neutral state and is transparent in the oxidized state. We believed that the goal could be achieved with the synthesis of a polymer backbone containing two well-defined, isolated, conjugated systems which absorb blue and red light. Thus, a 2,3-di(thien-3-yl)-5,7-di(thien-2-yl)thieno[3,4-*b*]pyrazine (DDTP) monomer that would afford two conjugated chains was designed and synthesized (Supporting Information; Figure S1). One chain has electron donor and acceptor groups to decrease the band gap, which results in absorption of the blue light at wavelengths longer than 600 nm, and the other chain absorbs in the red at wavelengths below 500 nm.

PolyDDTP (PDDTP) films[35] were synthesized on platinum or indium tin oxide (ITO) coated glass slides by oxidative electropolymerization from a mixture in dichloromethane and acetonitrile (20/80, v/v) solution containing 10^{-2} M monomer and 0.1 M tetrabutylammonium hexafluorophosphate (Bu_4NPF_6; Figure 1). The electrochemistry of polymerization and the polymer showed similar behavior to that of other CPs. An irreversible oxidation of the monomer appeared in the first cycle at +0.50 V versus Ag/Ag^+, followed by very fast deposition on subsequent cycles,

[*] Dr. G. Sonmez, Dr. C. K. F. Shen, Prof. Y. Rubin, Prof. F. Wudl
Department of Chemistry and Biochemistry and Exotic Materials Institute
University of California, Los Angeles, CA 90095-1569 (USA)
Fax: (+1) 310-8250767
E-mail: wudl@chem.ucla.edu

[**] We gratefully acknowledge financial support from the Air Force Office of Scientific Research through F49620-00-1-0103 and the Army Research Office through MURI DAAD19-99-1-0316. Instrumentation for this research was partially funded by NSF grand DGE-0114443. The authors would like to thank Prof. John R. Reynolds at University of Florida for helpful discussions. We thank Dr. Hieu Duong and Ryan Chiechi for recording the video display of color switching.

Supporting information (synthesis schemes, cyclic voltammograms) for this article is available on the WWW under http://www.angewandte.org or from the author.

 © 2004 Wiley-VCH Verlag GmbH & Co. KGaA, Weinheim DOI: 10.1002/anie.200352910

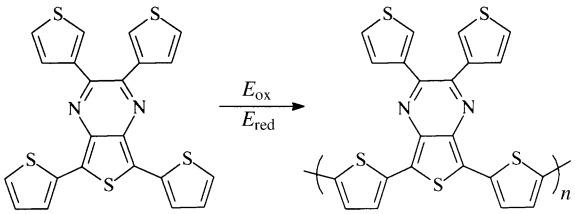


Figure 1. Electrochemical polymerization of DDTP.

owing to the redox system that grows rapidly at potentials lower than that of the monomer oxidation (Supporting Information; Figure S3). Note that the electrochemical oxidation of DDTP gives two oxidation peaks at 0.50 and 1.17 V (vs. Ag/Ag^+, Supporting Information; Figure S4). The first potential (0.50 V) corresponds to the oxidation of terthiophene and the second potential (1.17 V) may stem from the oxidation of 3-substituted thiophenes or follow-up reactions. As the monomer was polymerized at 0.50 V, the desired green material was obtained. A half-wave oxidation potential ($E^{ox}_{1/2}$) of the polymer, in monomer-free electrolyte solution, was observed at about 0.0 V (vs. Ag/Ag^+, Supporting Information; Figure S5). The linear dependence of the anodic and cathodic currents on the scan-rate demonstrates that the electrochemical processes are not diffusion limited. Since the main polymer backbone has both electron acceptor and donor groups, the polymer film can be both n- and p-doped. The half-wave reduction potential ($E^{red}_{1/2}$) of the polymer is at −1.42 V (vs. Ag/Ag^+, Supporting Information; Figure S6). From the difference between onset of oxidation and reduction potentials the band gap was determined to be approximately 1.15 eV.

The stability and the optical properties of the polymer for long-term switching between the oxidized and neutral states are the most important factors for the commercial application of CPs as PECDs. PDDTP films on a Pt button electrode were cycled 10000 times between their fully oxidized state at 0.58 V and the neutral state at −0.80 V in $LiClO_4$/propylene carbonate (PC; Figure 2). The charge involved during the electrochemical process was calculated for each voltammogram from the integration of the current during the redox process. The stability test of the polymer over a period of 10000 double potential cycles showed remarkable robustness without any significant charge or current loss. The cyclic voltammetry of the polymer was almost identical at the beginning and end of the stability test (Figure 2, insets). The small changes in the currents (ca. 4.5% increase in anodic and 1.5% decrease in cathodic peak current) and charge (ca. 10% increase) at the beginning of the stability test stem from the process of polymer electrochemical equilibrations. After reaching equilibrium at the 1500th cycle, the changes in anodic peak currents (i_{pa}), cathodic peak currents (i_{pc}) and the charge stored (Q_{stored}) are 0.26, 1.0, and 1.5%, respectively. This result indicates that PDDTP films can be cycled many times between oxidized and neutral states without any considerable change in electroactivity.

Figure 3 depicts the spectroelectrochemistry of PDDTP films. The π–π* transition of the neutral polymer (at −0.8 V vs. Ag/Ag^+) is split into two well-separated broad bands, as

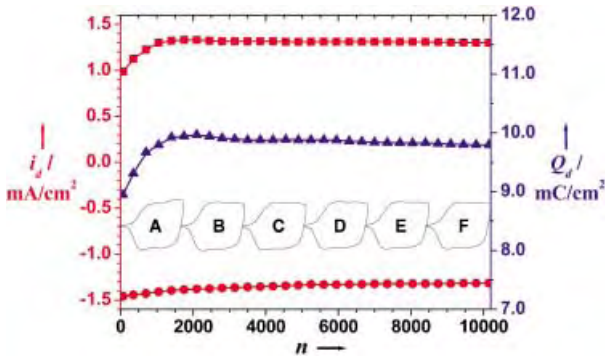


Figure 2. Stability test for long term switching: Variation of anodic (i_{pa}; ■) and cathodic (i_{pc}; ●) peak currents and the charge stored (Q_{stored}; ▲) by the polymer film as a function of number of cycles (n). The film was cycled more than 10000 times at a scan rate of 200 $mV s^{-1}$ between −0.80 and +0.58 V versus Ag/Ag^+ in 0.1 M $LiClO_4$/PC. The cyclic voltammograms inserted between the i_{pc} (●) and Q_{stored} (▲) curves show the essential invariability with cycle number; A = 500, B = 2000, C = 4000, D = 6000, E = 8000, F = 10000th cycle.

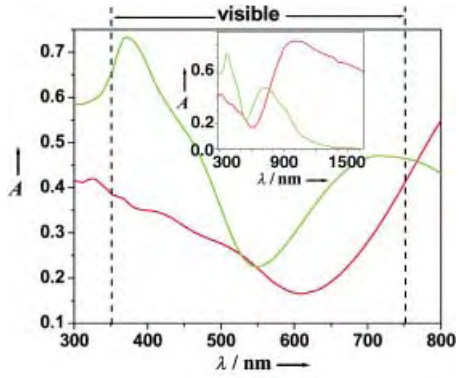


Figure 3. Spectroelectrochemistry of PDDTP film on an ITO-coated glass slide in 0.1 M Bu_4NPF_6/MeCN solution in two different oxidation states: neutral (——) and oxidized (——).

expected for green. One of these bands is located at wavelengths shorter than 500 nm with a maximum at 370 nm and covers the visible range, where red is absorbed. The other band is located at wavelengths longer than 600 nm, with a maximum at 725 nm; covering the visible range where blue is absorbed. The deep valley between these two absorption bands with a minimum at 550 nm controls the fine-tuning of the green color. The differences in transmittance (%ΔT) of the peaks at 370 and 725 nm and the lowest part of the valley at 550 nm are 42% and 27%, respectively. These values are sufficient to produce a highly saturated green color. Since the polymer has two absorption bands, the electronic band gaps are calculated from the onset of two π–π* transitions, which are 2.05 and 1.10 eV for the transitions at 377 and 725 nm, respectively. Noted that the band-gap value determined from electrochemistry is in agreement with the second value determined from spectroelectrochemistry. Upon electrochemical oxidation of the film, the π–π* transitions of both bands are depleted at the expense of an intense absorption band centered in the NIR, which corresponds to low-energy

 © 2004 Wiley-VCH Verlag GmbH & Co. KGaA, Weinheim

charge carriers. This depletion upon oxidation makes the polymer film more transparent but, unfortunately, residual absorptions remain in the visible region giving, a transmissive brown color. The detailed spectroelectrochemistry of PDDTP films as a function of applied potential is given in the Supporting Information (Figure S7).

The stability and response time upon electrochromic switching of the polymer film between its neutral and oxidized forms in the visible (370 and 725 nm) and NIR region (1600 nm) was monitored (Figure 4). The film was

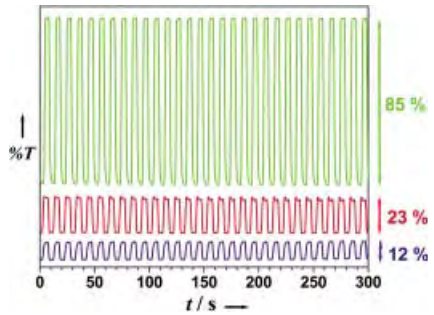


Figure 4. Double potential switching of PDDTP film on an ITO-coated glass slide at 370 (——), 725 (——), and 1600 (——) nm between its reduced state at −0.80 V and oxidized state at +0.58 V (vs. Ag/Ag^+) in 0.1 M Bu_4NPF_6/MeCN.

switched between its neutral (reduced) and oxidized form. The contrast ratios ($\Delta\%T$) of the polymer at 370, 725, and 1600 nm are 23, 12 and 85%, respectively. These transmittance changes in the visible are sufficient to change the color from green to transmissive yellowish-brown. The extreme stability of the $\Delta\%T$ in time and the fast switching property (about 0.5 s) at all three wavelengths makes this polymer a promising material for completion of the RGB colors.

After having demonstrated the electrochemistry, stability, and optical properties of our new polymer, we selected two well-known CPs, poly(3-methylthiophene) (P3MT) as the red and poly(3,4-ethylenedioxythiophene) (PEDOT) as the blue, to complete three legs of the color space. Representation of the hue and saturation for these two polymers with PDDTP is given in Figure 5. The colors of the polymers in their neutral states are located in the color space where the three main colors, RGB, are located. As the polymers are exposed to oxidation, they move towards the white point located at the center of the *x*–*y* color track and they become transparent. Lab and *Yxy* coordinates of P3MT, PEDOT, and PDDTP in their neutral and oxidized states are given in the Supporting Information (Table S1). Figure 6 shows the actual colors of these three polymers in a PECD. The polymer films present highly saturated RGB colors in their neutral state at the applied potential.[36]

In conclusion, the first neutral, green conducting polymer was synthesized. High green color saturation, fast switching, and extreme stability, make this material promising for completion of the deficient third leg of color space and also brings polymer electrochromics closer to RGB realization.

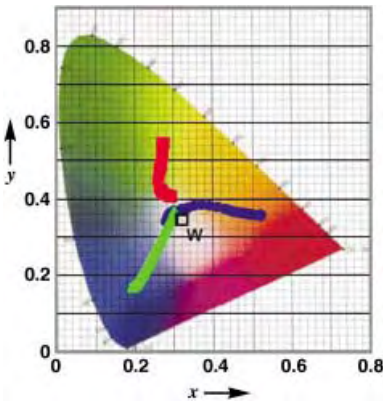


Figure 5. Representation of the hue and saturation *x*–*y* track for P3MT (●), PDDTP (■), and PEDOT (▲) film as the applied potential changes from −0.8 to +0.8 V (vs. Ag/Ag^+; W = white point).



Figure 6. RGB colors obtained from polymeric electrochromic device (PECD): P3MT, PDDTP, and PEDOT were used as red, green, and blue polymers, respectively. The polymer films were held at the same potential of −0.80 V (vs. Ag/Ag^+) to keep them in their neutral form.

Now that RGB is established, it will be only a matter of clever engineering to take full advantage of PECDs.

Experimental Section

All chemicals were purchased from Aldrich Chemical. Propylene carbonate (PC; 99.7%, anhydrous), dichloromethane (DCM) and acetonitrile (MeCN) were distilled over calcium hydride before use.

All reactions were performed under argon or glove box unless stated. The products were put under high vacuum overnight after flash chromatography. NMR spectroscopy studies were carried out on Bruker Avance-500 or Avance-600 spectrometers. Tetramethylsilane (TMS) was used as the internal standard for ^1H NMR and the deuterated solvent ($CDCl_3$) was used as a standard for ^{13}C NMR spectroscopy. FT-IR spectra were recorded on a Mattson Infinity IIa spectrometer with a DRIFT accessory from PIKE Technologies, on a diamond frit. High-resolution mass spectra (HRMS) were obtained with a VG ZAB-SE mass spectrometer with EI source. Column chromatography was performed on silica gel 230–400 mesh (flash) from E. Merck or from Scientific Absorbents; thin layer chromatography (TLC) was performed on glass plates coated with silica gel $^{60}F_{254}$ from E. Merck.

Electropolymerization was carried out with a BAS 100B/W potentiostat, employing a platinum button (diameter: 1.6 mm; area 0.02 cm^2) or ITO coated glass slides as working electrode, a platinum flag or wire as counter electrode, and a silver wire or 0.01M Ag/$AgNO_3$ (Ag/Ag^+) as reference. The electrolytes used were 0.1M of $LiClO_4$ or tetrabutylammonium hexafluorophosphate (Bu_4NPF_6) in PC, CH_2Cl_2, MeCN or mixture of MeCN and CH_2Cl_2. The electro-

 © 2004 Wiley-VCH Verlag GmbH & Co. KGaA, Weinheim

deposition was performed from a 0.01M solution of the monomer in the electrolyte potentiodynamically at a scan rate of 20 $mV s^{-1}$ or potentiostatically at 0.52 V vs. Ag/Ag^+. Cyclic voltammetry was carried out using the same electrode setup using monomer-free electrolyte solution.

Spectroelectrochemical data were recorded on a Shimadzu UV 3101PC UV/Vis-NIR spectrophotometer connected to a computer. A three-electrode cell assembly was used where the working electrode was an ITO-coated glass slides ($7 \times 50 \times 0.6$ mm, $R_s \leq 10\ \Omega/\square$, Delta Technologies Inc.), the counter electrode was a platinum wire, and a Ag wire was used as pseudo reference electrode. The pseudo reference was calibrated externally using a 5 mM solution of ferrocene (Fc/Fc^+) in the electrolyte ($E_{1/2}(Fc/Fc^+) = +0.140$ V vs. Ag wire and $+0.075$ V vs. Ag/Ag^+ in 0.1M $LiClO_4$/PC). The potentials are reported versus Ag/Ag^+. Polymer films for spectroelectrochemistry were prepared by potentiodynamic deposition on ITO-coated glass slides.

Colorimetry measurements were obtained using a Minolta Chroma Meter CS-100A and CIE recommended normal/normal (0/0) illuminating/viewing geometry for transmittance measurements.[37] As for spectroelectrochemistry, a three-electrode cell was employed. The potential was controlled by the same BAS 100B/W potentiostat. The sample was illuminated from behind by a D50 (5000 K) light source in a light booth (Minolta GTI ColorMatcher) specially designed to exclude external light and to illuminate from behind. The color coordinates are expressed in the CIE 1931 *Yxy* color space where the *Y* value is a measure of the luminance in Cd/m^2. The relative luminance, expressed in %, was calculated by dividing the *Y* value measured on the sample by the Y_0 value corresponding to the background. Note that the relative luminance is frequently reported instead of the luminance because it gives a more meaningful value.

A Fujifilm (FinePix 4500) digital camera was used to take photographs and movie of the polymer electrochromic device at high resolution.

DDTP: 1,2-di(thien-3-yl)ethane-1,2-dione (363 mg, 1.63 mmol)[39] and catalytic amount of *p*-toluene sulfonic acid (15 mg) were added to a solution of 3′,4′-diamino-2,2′:5′,2″-terthiophene (350 mg, 1.26 mmol)[38] in chloroform (50 mL), under argon atmosphere. The reaction mixture was heated under reflux for 12 h before cooling down. After removing all volatiles, the residue was redissolved in dichloromethane and absorbed onto silica gel. The crude product was purified by column chromatography on silica gel using a solvent mixture (hexanes:CH_2Cl_2 1:1) to give the pure product after removal of solvent as a dark purple powder in 94.2% yield (550 mg, 1.18 mmol). M.p. > 230 °C (dec.); ^{1}H NMR (500 MHz, $CDCl_3$): $\delta = 7.12$ (dd, $J = 5.0$ Hz, $J = 3.7$ Hz, 2H), 7.33 (dd, $J = 5.0$ Hz, $J = 3.0$ Hz, 2H), 7.39 (dd, $J = 5.0$ Hz, $J = 1.0$ Hz, 2H), 7.42 (dd, $J = 5.0$ Hz, $J = 1.2$ Hz, 2H), 7.60 (dd, $J = 3.0$ Hz, $J = 1.2$ Hz, 2H), 7.65 ppm (dd, $J = 3.7$ Hz, $J = 1.0$ Hz, 2H); ^{13}C NMR (125.7 MHz, $CDCl_3$): $\delta = 124.51$, 124.60, 125.21, 126.64, 127.26, 127.78, 129.00, 134.58, 137.12, 140.29, 148.09 ppm; HRMS calcd for $C_{22}H_{12}N_2S_5$ [M^+] 463.9604, found 463.9603.

Received: September 18, 2003 [Z52910]
Published Online: February 23, 2004

Keywords: conducting materials · electrochemistry · electrochromism · heterocycles · polymers

[1] *Handbook of Conducting Polymers* (Eds.: T. A. Skotheim, R. L. Elsenbaumer, J. R. Reynolds), 2nd ed., Marcel Dekker, New York, **1998**.
[2] H. J. Byker, (Gentex Corporation), **1990**, US Patent No. 4902108.
[3] R. G. Mortimer, *Chem. Soc. Rev.* **1997**, *26*, 147.
[4] C. G. Granqvist, A. Azens, A. Hjelm, L. Kullman, G. A. Niklasson, D. Ronnow, M. Stromme Mattsson, M. Veszelei, G. Vaivars, *Sol. Energy* **1998**, *63*, 199.
[5] R. D. Rauh, *Electrochim. Acta* **1999**, *44*, 3165.
[6] J. J. M. Halls, C. A. Walsh, N. C. Greenham, E. A. Marseglia, R. H. Friend, S. C. Moratti, A. B. Holmes, *Nature* **1995**, *376*, 498.
[7] P. M. S. Monk, *J. Electroanal. Chem.* **1997**, *432*, 175.
[8] K. Bange, *Sol. Energy Mater. Sol. Cells* **1999**, *58*, 1.
[9] K. J. Albert, N. S. Lewis, C. L. Schauer, G. A. Sotzing, S. E. Stitzel, T. P. Vaid, D. R. Walt, *Chem. Rev.* **2000**, *100*, 2595.
[10] D. T. McQuade, A. E. Pullen, T. M. Swager, *Chem. Rev.* **2000**, *100*, 2537.
[11] R. H. Friend, R. W. Gymer, A. B. Holmes, J. H. Burroughes, R. N. Marks, C. Taliani, D. D. C. Bradley, D. A. Dos Santos, J. L. Bredas, M. Logdlund, W. R. Salaneck, *Nature* **1999**, *397*, 121.
[12] A. Kraft, A. C. Grimsdale, A. B. Holmes, *Angew. Chem.* **1998**, *110*, 444; *Angew. Chem. Int. Ed.* **1998**, *37*, 402.
[13] C. J. Brabec, N. S. Sariciftci, J. C. Hummelen, *Adv. Funct. Mater.* **2001**, *11*, 15.
[14] P. K. H. Ho, D. S. Thomas, R. H. Friend, N. Tessler, *Science* **1999**, *285*, 233.
[15] I. Schwendeman, R. Hickman, G. Sonmez, P. Schottland, K. Zong, D. M. Welsh, J. R. Reynolds, *Chem. Mater.* **2002**, *14*, 3118.
[16] G. Sonmez, H. Meng, Q. Zhang, F. Wudl, *Adv. Funct. Mater.* **2003**, *13*, 726.
[17] G. Sonmez, H. Meng, F. Wudl, *Chem. Mater.*, in press.
[18] G. Sonmez, I. Schwendeman, P. Schottland, K. Zong, J. R. Reynolds, *Macromolecules* **2003**, *36*, 639.
[19] B. C. Thompson, P. Schottland, G. Sonmez, J. R. Reynolds, *Synth. Met.* **2001**, *119*, 333.
[20] B. C. Thompson, P. Schottland, K. Zong, J. R. Reynolds, *Chem. Mater.* **2000**, *12*, 1563.
[21] A. M. McDonagh, S. R. Bayly, D. J. Riley, M. D. Ward, J. A. McCleverty, M. A. Cowin, C. N. Morgan, R. Varrazza, R. V. Penty, I. H. White, *Chem. Mater.* **2000**, *12*, 2523.
[22] G. Sonmez, P. Schottland, K. Zong, J. R. Reynolds, *J. Mater. Chem.* **2001**, *11*, 289.
[23] P. Chandrasekhar, G. C. Birur, P. Stevens, S. Rawal, E. A. Pierson, K. L. Miller, *Synth. Met.* **2001**, *119*, 293.
[24] I. Schwendeman, J. Hwang, D. M. Welsh, D. B. Tanner, J. R. Reynolds, *Adv. Mater.* **2001**, *13*, 634.
[25] H. Meng, D. Tucker, S. Chaffins, Y. Chen, R. Helgeson, B. Dunn, F. Wudl, *Adv. Mater.* **2003**, *15*, 146.
[26] W. C. Dautremont-Smith, *Displays I*, **1982**, 3.
[27] P. M. S. Monk, R. J. Mortimer, D. R. Rosseinsky, *Electrochromism: Fundamentals and Applications*, VCH, Weinheim, **1995**.
[28] K. Bange, T. Bambke, *Adv. Mater.* **1990**, *2*, 10.
[29] R. J. Mortimer, *Electrochim. Acta* **1999**, *44*, 2971.
[30] S. A. Sapp, G. A. Sotzing, J. R. Reynolds, *Chem. Mater.* **1998**, *10*, 2101.
[31] A. Kumar, D. M. Welsh, M. C. Morvant, F. Piroux, K. A. Abboud, J. R. Reynolds, *Chem. Mater.* **1998**, *10*, 896.
[32] J. Roncali, *Chem. Rev.* **1997**, *97*, 173.
[33] H. S. Nalwa, *Handbook of Organic Conductive Molecules and Polymers*, Wiley, New York, **1997**.
[34] R. D. Overheim, D. L. Wagner, *Light and Color*, Wiley, New York, **1982**.
[35] Since PDDTP was insoluble in any solvent, an alkyl-substituted counterpart of the monomer (Supporting Information; Figure S2) was synthesized and electrochemically polymerized under the same conditions. Then polymer films were reduced electrochemically in monomer-free electrolyte solution and dissolved in [D_2]tetrachloroethane. ^{13}C NMR spectroscopy of the resulting polymer demonstrated that hydrogen atoms on the α and α′ positions of the thiophene rings labeled with the letters c and d (Supporting Information) remained after electrochemical polymerization confirming the proposed structure for PDDTP.

 © 2004 Wiley-VCH Verlag GmbH & Co. KGaA, Weinheim

The related work for alkyl-substituted PDDTP will be published separately.
[36] A device made by using initials of "Exotic Materials Institute" is also available, Figure S8 of Supporting Information.
[37] R. T. Markus in *Color for Science, Art and Technology* (Ed.: K. Nassau), Elsevier, Amsterdam, **1998**, pp. 31 – 96.
[38] C. Kitamura, S. Tanaka, Y. Yamashita, *Chem. Mater.* **1996**, *8*, 570.
[39] Using a reported procedure (F. Babudri, V. Fiandanese, G. Marchese, A. Punzi, *Tetrahedron Lett.* **1995**, *36*, 7305), 3-thienyl Grignard reagent was prepared from the corresponding 3-bromothiophene.

 © 2004 Wiley-VCH Verlag GmbH & Co. KGaA, Weinheim

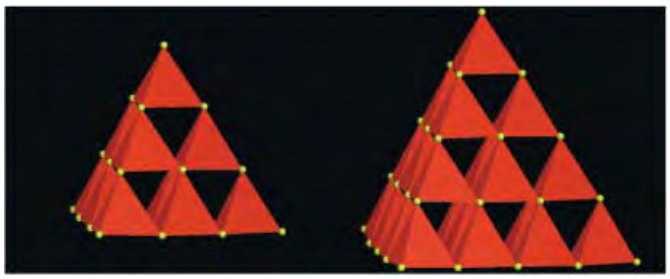


Figure 1. Polyhedral diagrams of T3 and T4 supertetrahedral clusters. The metal site is located at the center of each small red tetrahedron.

Supertetrahedral Clusters

Three-Dimensional Frameworks of Gallium Selenide Supertetrahedral Clusters**

*Xianhui Bu, Nanfeng Zheng, Xiqing Wang, Bing Wang, and Pingyun Feng**

Dense chalcogenides of Ga, In, and Tl have been extensively studied because of their intriguing stoichiometry and because many of them are semiconductors, photoconductors, or light emitters. On the other hand, while crystalline porous oxides have been known for a long time,[1] the development of crystalline porous chalcogenides, especially selenides and tellurides, is still in its early stages.[2–4] Compared to porous oxides, which are usually insulators, crystalline porous chalcogenides can have substantially higher electrical conductivity, which in combination with uniform porosity could lead to new applications in areas such as shape- and size-selective sensors and high-surface-area photocatalysts and photoelectrodes.[5]

One promising approach for the creation of crystalline porous chalcogenides is the directed assembly of chalcogenide clusters into three-dimensional (3D) frameworks.[3,4] Among the most common chalcogenide clusters are a series of supertetrahedral clusters denoted as T*n*. These clusters are regular tetrahedrally shaped fragments of the cubic ZnS-type lattice.[4] Here, *n* is the number of metal sites on each edge of the cluster (Figure 1). The large size of the supertetrahedral clusters usually leads to a highly open framework, particularly when the interpenetration of multiple sublattices is avoided.

[*] N. Zheng, X. Wang, B. Wang, Prof. P. Feng
Department of Chemistry
University of California
Riverside, CA 92521 (USA)
Fax: (+1) 909-787-4713
E-mail: pingyun.feng@ucr.edu
Prof. X. Bu
Department of Chemistry and Biochemistry
California State University
1250 Bellflower Blvd., Long Beach, CA 90840 (USA)

[**] We thank NSF and the donors of the Petroleum Research Fund (administered by the ACS).

Substantial success has recently been achieved with sulfides,[6–8] but the progress with selenides is much slower. Not only are there few 3D open-framework selenides, the types of supertetrahedral selenide clusters are also limited.[9–11] For example, although T5 sulfide clusters with as many as 35 metal atoms (e.g., $Cu_5In_{30}S_{56}^{17-}$) are known,[12] the largest supertetrahedral selenide cluster prior to this work has only ten metal atoms (T3, $In_{10}Se_{20}^{10-}$).[13] Larger clusters are desirable because they can be useful for studying the quantum size effect and can also serve as building blocks for constructing crystalline porous frameworks.[14] The gallium selenides are particularly challenging. Thus far, neither T3 (e.g., $Ga_{10}Se_{20}^{10-}$) nor T4 (e.g., $Zn_4Ga_{16}Se_{35}^{14-}$) clusters are known. To our knowledge, no 3D gallium selenide open frameworks were known prior to this work.

Here we report a series of 3D gallium selenide superlattices built up of supertetrahedral T3 and T4 clusters. Three 3D framework types (denoted as OCF-1ZnGaSe, OCF-6GaSe, and OCF-13GaSe, respectively; OCF = organically directed chalcogenide framework) were realized (Table 1). Similar to the synthesis of zeolites, the preparation of chalcogenide open frameworks is performed in an alkaline environment under hydrothermal conditions at 200 °C or below.[15] However, unlike the synthesis of zeolites, the self-assembly process in the chalcogenide system is usually preceded by redox reactions because one or more starting materials (e.g., S, Se, In) are in the elemental form.[16]

One of the most important advances reported here is the synthesis of the selenide T4 cluster $Zn_4Ga_{16}Se_{35}^{14-}$ in OCF-1ZnGaSe. This is the largest selenide supertetrahedral cluster made so far. Prior to this work, the largest selenide supertetrahedral clusters were the indium selenide T3 cluster $In_{10}Se_{20}^{10-}$ and ligand-terminated T3 clusters such as $[(CH_3)_4N]_4[Cd_{10}Se_4(SPh)_{16}]$.[13,17] The increase in the cluster size from T3 to T4 represents a significant advance towards the synthesis of large selenide supertetrahedral clusters such as T5 ($M_{35}X_{56}$) or T6 ($M_{56}X_{84}$).[7] Because of their uniform size and well-defined chemical composition, these supertetrahedral clusters could provide a unique opportunity for the study of quantum-confinement effects.[18]

Surprisingly, all three gallium selenide phases reported here are noncentrosymmetric, and none of them consists of two or more of the interpenetrating lattices that are common for these types of materials. This structural feature is also in contrast with the corresponding Ga–S system, in which all

 © 2004 Wiley-VCH Verlag GmbH & Co. KGaA, Weinheim DOI: 10.1002/anie.200352880

Table 1: A summary of crystallographic data[a] for selected structures synthesized in this study.

Name[b]	Composition	Space group	a [Å]	c [Å]	$R(F)$ [%]	$wR2$ [%] (all data)
OCF-1ZnGaSe-TMDP	$Zn_4Ga_{16}Se_{33}^{10-}$	$I\bar{4}2d$	41.311(7)	16.891(4)	8.33	28.9
OCF-6GaSe-TMDP	$Ga_{10}Se_{18}^{6-}$	$I\bar{4}2d$	17.064(3)	32.320(7)	5.66	20.5
OCF-13GaSe-DPM	$Ga_{10}Se_{18}^{6-}$	$I\bar{4}m2$	35.052(8)	17.402(6)	7.96	24.9
OCF-13GaSe-TMDP	$Ga_{10}Se_{18}^{6-}$	$I\bar{4}m2$	34.978(6)	17.212(4)	7.83	27.7
$(C_4H_{11}N_2)GaSe_2$	$GaSe_2^-$	$P2_1/c$	6.3025(9)	8.408(1)	2.55	6.25

[a] $R(F)=\Sigma||F_o|-|F_c||/\Sigma|F_o|$, where $F_o>4.0\sigma(F)$. For $GaSe_2$-PPZ, $b=16.660(2)$ Å, $\beta=105.144(3)°$. Crystal structures were solved from single-crystal data collected at 298 K on a SMART 1000 CCD diffractometer with $Mo_{K\alpha}$ radiation. The number of parameters and independent reflections were 241 and 4567 for OCF-1, 65 and 3070 for OCF-6, 132 and 3852 for OCF-13GaSe-DPM, 132 and 5151 for OCF-13GaSe-TMDP, and 95 and 1500 for $(C_4H_{11}N_2)GaSe_2$. CCDC 219205–219209 contain the supplementary crystallographic data for this paper. These data can be obtained free of charge via www.ccdc.cam.ac.uk/conts/retrieving.html (or from the Cambridge Crystallographic Data Centre, 12, Union Road, Cambridge CB2 1EZ, UK; fax: (+44) 1223-336-033; or deposit@ccdc.cam.ac.uk). [b] TMDP = 4,4′-trimethylenedipiperidine, $C_{13}H_{26}N_2$; DPM = dipiperidinomethane, $C_{11}H_{22}N_2$.

four known structure types are interpenetrating and centrosymmetric.[19]

Synthetically, there is a major difference between gallium selenides and gallium sulfides. While the presence of water promotes the crystal growth of the gallium selenides reported here, the synthesis of gallium sulfide superlattices is successful only in a nonaqueous system.[19] This difference between gallium selenides and gallium sulfides might be related to the relative hydrothermal stability of Ga–S and Ga–Se bonds.

The large cluster size and the absence of framework intergrowth help to generate a highly open architecture for these gallium selenides. The framework density, defined as the number of metal sites per 1000 Å^3, is 5.6, 4.3, and 3.7 for OCF-1ZnGaSe, OCF-6GaSe, and OCF-13GaSe, respectively. The percentage of the crystal volume occupied by extra-framework species is as high as 63, 70, and 73%, respectively.[20] These 3D selenides are by far the most open frameworks among known selenides.

All three phases also have large ring sizes, defined as the number of metal sites forming the window of the channel. OCF-1ZnGaSe contains windows of eight and four super-tetrahedral T4 clusters with a ring size of 32 (Figure 2C). To our knowledge, the topological type of OCF-1ZnGaSe is not known in dense inorganic compounds. OCF-6GaSe has a diamond-type structure in which T3 clusters occupy tetrahedral sites (Figure 2A). Only windows of six T3 clusters are present in OCF-6GaSe, giving rise to a ring size of 18. The framework topology of OCF-13GaSe is derived from the CrB_4-type network in which tetrahedral boron sites are replaced by T3 clusters (Figure 2B).[21] In OCF-13GaSe, windows with four, six, and eight T3 clusters are all present, giving rise to a maximum ring size of 24.

A notable synthetic feature here is that either Ga_2O_3 or Ga can be used as the source for Ga^{3+} cations. Prior to this work, elemental metals (In or Ga) were usually used as reagents in the synthesis of indium or gallium sulfides. Here, open-framework gallium selenides can be obtained from gallium oxide in the presence of Se and organic amines. This indicates that the reducing property of elemental metals is not essential for activating Se. It is likely that Se disproportionated into SeO_3^{2-} and Se^{2-} ions in aqueous solution.[22]

When attempts were made to synthesize centrosymmetric 3D framework selenides by employing nonaqueous conditions similar to those used for the preparation of gallium sulfides, an infinite chain structure (denoted as $GaSe_2$-PPZ, PPZ = piperazine) similar to that of fibrous SiS_2 is formed (Figure 2D). 1-(2-Aminoethyl)piperazine or piperazine can be used as the solvent. The chain consists of edge-sharing tetrahedral $GaSe_4^{5-}$ units. Despite its simple structure, the $GaSe_2^-$ chain has not been observed before. However, a fragment of this chain with six gallium atoms ($Ga_6Se_{14}^{10-}$) is known.[11]

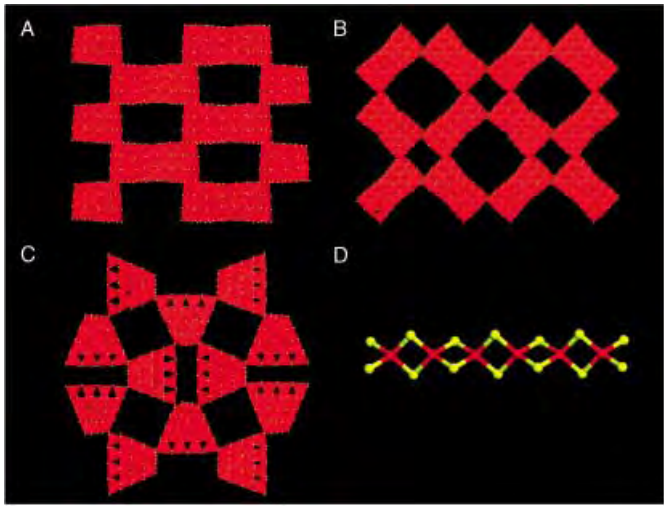


Figure 2. The 3D open frameworks of A) OCF-6GaSe, B) OCF-13GaSe, and C) OCF-1ZnGaSe, and D) the one-dimensional infinite chain in $GaSe_2$-PPZ.

Extra-framework species in the materials reported here are disordered, and their atomic positions could not be determined. Amines encapsulated in 3D chalcogenides are generally disordered, while those in lower-dimensional (i.e., 2D, 1D, and 0D) phases are ordered. In $GaSe_2$-PPZ, the negative charge of the $GaSe_2^-$ chain is balanced by monoprotonated piperazine molecules. The piperazine molecules are so well ordered that even the position of the additional proton can be located from single-crystal diffraction data, and this suggests that protonation occurs on a particular nitrogen atom, instead of being statistically distributed over two nitrogen atoms.

Alternating-current impedance measurements on a single crystal of OCF-6GaSe shows a humidity-dependent behavior of the electrical conductivity (Figure 3). With increasing relative humidity (RH), the specific conductivity σ increases by over two orders of magnitude and ranges from $1.32\times10^{-7}\,\Omega^{-1}\,cm^{-1}$ at 84.9% RH to $5.37\times10^{-5}\,\Omega^{-1}\,cm^{-1}$ at 100%

 © 2004 Wiley-VCH Verlag GmbH & Co. KGaA, Weinheim

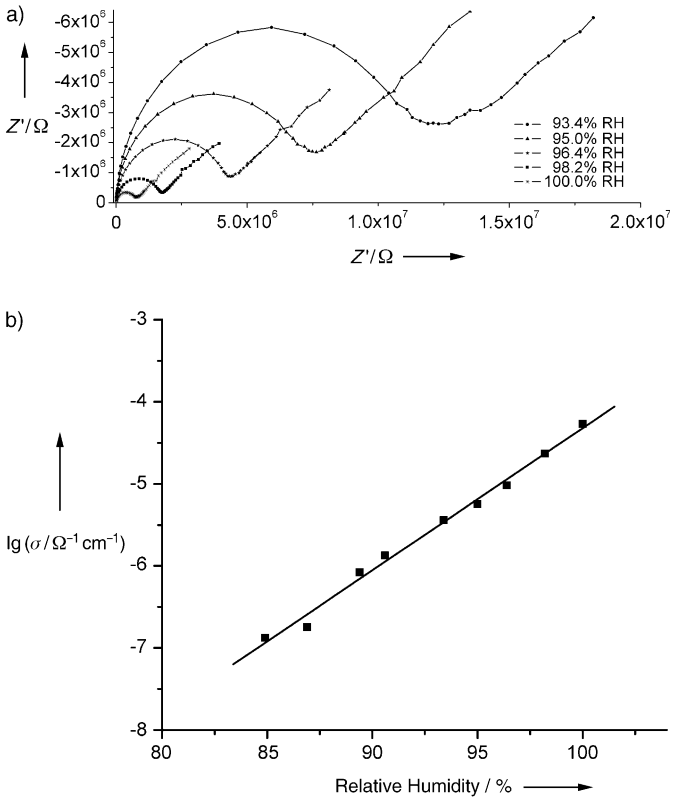


Figure 3. a) Alternating-current impedance plots at different humidities showing decreasing resistance with increasing RH for OCF-6GaSe-TMDP. b) Plot of electrical conductivity versus RH. The impedance plots were measured on a single-crystal sample by the ac impedance method using a Solartron 1260 frequency response analyzer.

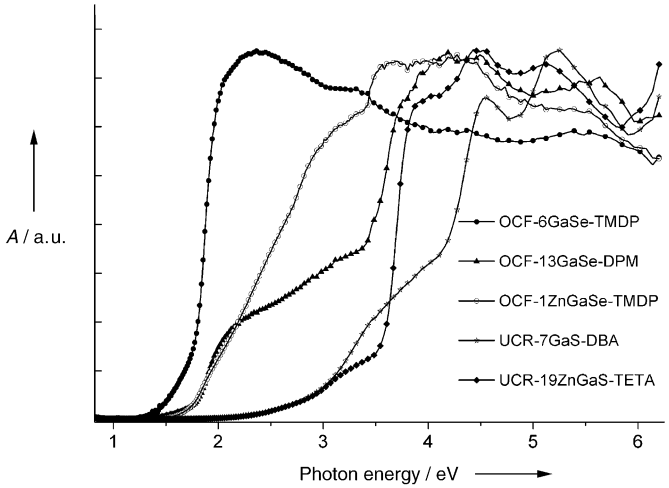


Figure 4. Optical absorption spectra of gallium sulfide and gallium selenide open-framework solids. Band gaps are 1.71 eV for OCF-1ZnGaSe-TMDP, 1.43 eV for OCF-6GaSe-TMDP, 1.76 eV for OCF-13GaSe-DPM, 2.60 eV for UCR-19ZnGaS-TETA (TETA = triethylenetetramine), and 2.84 eV for UCR-7GaS-DBA (DBA = di-*n*-butylamine). The absorption data were calculated from reflectance data by using the Kubelka–Munk function. $BaSO_4$ powder was used as reference (100% reflectance). UV/Vis/NIR diffuse reflectance spectra were measured on a Shimadzu UV 3101PC double-beam, double-monochromator spectrophotometer.

Keywords: cluster compounds · gallium · hydrothermal synthesis · microporous materials · selenium

RH. This property may have potential applications in electrochemical sensors.

The optical properties of the gallium selenides were studied by solid-state diffuse-reflectance UV/Vis/NIR spectroscopy. All phases show optical transitions with band gaps between 1.4 and 1.7 eV (Figure 4). The transition is likely to result from charge transfer from the Se^{2-}-dominated valence band to the Ga^{3+}-dominated conduction band. The similar values for the band gaps are consistent with the similar chemical compositions of the three phases. However, these band gaps are considerably smaller than those of corresponding gallium sulfides, which are about twice as large (2.6–2.8 eV).[19] Clearly, the framework anions have a much more dramatic impact on the band gap than framework cations.

In conclusion, the first 3D gallium selenide open frameworks have been synthesized, and their unique structural, optical, and electrical properties characterized. The T4 selenide cluster is the largest selenide supertetrahedral cluster synthesized so far. These gallium selenides are distinctly different from known gallium sulfide open frameworks in nearly every respect, including synthesis conditions and structural and optical properties. This work represents an important step in the synthetic development of heavy chalcogenide clusters and open-framework materials.

Received: September 16, 2003 [Z52880]

[1] P. Behrens, G. D. Stucky, *Comprehensive Supramolecular Chemistry*, *Vol. 7*, Pergamon, Oxford, **1996**, pp. 721 – 772.
[2] R. L. Bedard, S. T. Wilson, L. D. Vail, J. M. Bennett, E. M. Flanigen in *Zeolites: Facts, Figures, Future. Proceedings of the 8th International Zeolite Conference* (Eds.: P. A. Jacobs, R. A. van Santen), Elsevier, Amsterdam, **1989**, p. 375.
[3] N. Zheng, X. Bu, B. Wang, P. Feng, *Science* **2002**, *298*, 2366 – 2369.
[4] H. Li, A. Laine, M. O'Keeffe, O. M. Yaghi, *Science* **1999**, *283*, 1145 – 1147.
[5] S. Dhingra, M. G. Kanatzidis, *Science* **1992**, *258*, 1769 – 1772.
[6] R. W. J. Scott, M. J. MacLachlan, G. A. Ozin, *Curr. Opin. Solid State Mater. Sci.* **1999**, *4*, 113 – 121.
[7] H. Li, J. Kim, T. L. Groy, M. O'Keeffe, O. M. Yaghi, *J. Am. Chem. Soc.* **2001**, *123*, 4867 – 6868.
[8] C. Wang, Y. Li, X. Bu, N. Zheng, O. Zivkovic, C. Yang, P. Feng, *J. Am. Chem. Soc.* **2001**, *123*, 11506 – 11507.
[9] H. Ahari, A. Garcia, S. Kirby, G. A. Ozin, D. Young, A. J. Lough, *J. Chem. Soc. Dalton Trans.* **1998**, 2023.
[10] B. Krebs, D. Voelker, K.-O. Stiller, *Inorg. Chim. Acta* **1982**, *65*, L101-L102.
[11] B. Krebs, *Angew. Chem.* **1983**, *95*, 113 – 134; *Angew Chem. Int. Ed. Engl.* **1983**, *22*, 113 – 134.
[12] X. Bu, N. Zheng, Y. Li, P. Feng, *J. Am. Chem. Soc.* **2002**, *124*, 12646 – 12647.
[13] C. Wang, X. Bu, N. Zheng, P. Feng, *Chem. Commun.* **2002**, 1344 – 1345.
[14] T. Vossmeyer, G. Reck, L. Katsikas, E. T. K. Haupt, B. Schulz, H. Weller, *Science* **1995**, *267*, 1476 – 1479.
[15] OCF-1GaZnSe-TMDP, $(C_{13}H_{26}N_2H_2)_5(Zn_4Ga_{16}Se_{33})$: Ga (107.5 mg), Se (210.3 mg), $Zn(NO_3)_2{\cdot}6H_2O$ (157.1 mg), and TMDP (4,4′-trimethylenedipiperidine; 1.122 g) were mixed

 © 2004 Wiley-VCH Verlag GmbH & Co. KGaA, Weinheim

with H_2O (4.0212 g) in a 23-mL teflon-lined stainless steel autoclave and stirred for 30 min. The vessel was sealed and heated to 200 °C for 8 days. After cooling to room temperature, pale-yellow crystals were obtained in a yield of about 66 %. OCF-6GaSe-TMDP, $(C_{13}H_{26}N_2H_2)_3(Ga_{10}Se_{18})$: an autoclave containing Ga_2O_3 (101.1 mg), Se (213.4 mg), TMDP (1.1067 g), and H_2O (2.9683 g) was heated to 200 °C for 28 days, and pale-yellow octahedral crystals were obtained in a yield of about 77 %. UCR-13GaSe-DPM, $(C_{11}H_{22}N_2H_2)_3(Ga_{10}Se_{18})$: an autoclave containing Ga_2O_3 (101.1 mg), Se (211.3 mg), DPM (dipiperidinomethane; 1.0230 g), and H_2O (4.0288 g) was heated to 200 °C for 19 days, and pale-yellow crystals were obtained in a yield of about 84 %. $(C_4H_{11}N_2)GaSe_2$: an autoclave containing Ga (110.0 mg), Se (218.0 mg), piperazine (0.9508 g), and H_2O (3.1506 g) was heated to 200 °C for 8 days, and pale-yellow crystals were obtained in a yield of about 92 %.

[16] C. L. Cahill, J. B. Parise, *J. Chem. Soc. Dalton Trans.* **2000**, 1475 – 1482.

[17] I. Dance, A. Choy, M. L. Scudder, *J. Am. Chem. Soc.* **1984**, *106*, 6285 – 6295.

[18] A. Eichhofer, D. Fenske, *Dalton Trans.* **2000**, 941 – 944.

[19] N. Zheng, X. Bu, P. Feng, *J. Am. Chem. Soc.* **2003**, *125*, 1138 – 1139.

[20] A. L. Spek, *Acta Crystallogr. Sect. A* **1990**, *46*, C34.

[21] M. O'Keeffe, B. G. Hyde, *Crystal Structures I. Patterns and Symmetry*, Mineralogical Society of America, Washington, D.C., **1996**.

[22] W. S. Sheldrick, M. Wachhold, *Angew. Chem.* **1997**, *109*, 214 – 233; *Angew. Chem. Int. Ed. Engl.* **1997**, *36*, 206 – 224.

 © 2004 Wiley-VCH Verlag GmbH & Co. KGaA, Weinheim

Mesoporous Materials

Preparation of Mesoporous Silica Monoliths with Ordered Arrays of Macrochannels Templated from Electric-Field-Oriented Hydrogels**

Paul R. Giunta, Randy P. Washington, Tedric D. Campbell, Oliver Steinbock, and A. E. Stiegman**

The fabrication of ordered inorganic arrays of varying length scales and with multimodal porosities is of practical importance owing to their potential application in many areas of materials chemistry, including catalysis and separations science.[1,2] A common approach to the controlled synthesis of this class of materials, first exploited in the synthesis of the MCM-41 family of molecular sieves, is to polymerize the inorganic phase around an organic template by using a sol–gel process.[3] The organic phase is then removed by calcination leaving a void space that is a replica of the size, orientation, and arrangement in space of the template. By using multiple templates of different length scales, hierarchically porous inorganic structures containing various combinations of micro-, meso-, and macropores have been realized.[4–9] We report herein the creation of a mesoporous silica monolith that contains oriented macroporous channels, which is achieved by the application of an electric field to a hydrogel template during polymerization and cross-linking.[8,9] To the best of our knowledge, this is first time an external electric field has been used to create ordered, hierarchical meso-/macroporous silicate materials.

The template matrix is created through the electrical alignment of a polyacrylamide hydrogel, which is accomplished by copolymerizing a mixture of acrylamide functionalized with immobiline and bisacrylamide in the presence of an electric field (60 $V\,cm^{-1}$). The presence of this field creates interstitial voids of approximately 10 μm in diameter. The channel structure, which can be imaged through confocal microscopy, is present in the field-oriented hydrogel (Figure 1 a), but is replaced by a disordered structure (Figure 1 b) when no field is applied.

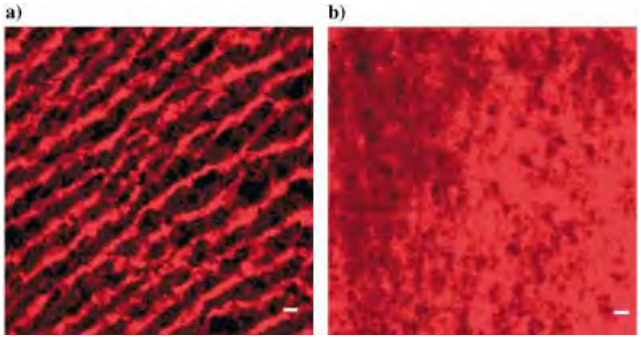


Figure 1. Fluorescence images of rhodamine-stained polyacrylamide hydrogels obtained by confocal laser scanning microscopy. The samples were polymerized in the presence (a) and the absence (b) of an externally applied electric field. Field of view: 210×210 μm^2; bar = 10 μm.

The silicate phase is introduced through the immersion of a freestanding hydrogel monolith in neat tetramethylorthosilicate (TMOS). Hydrolysis and condensation occurs as the TMOS infuses the hydrogel and reacts with water trapped in the voids. After a period of 24 h a hard solid white monolith, close in size to the hydrogel template, is formed. Calcination under O_2 at 500 °C removes the organic phase leaving a porous silica monolith.

Scanning electron micrographs of this material, imaged parallel to the electric field direction (Figure 2 a), show striations oriented in the field direction. No such features are observed when the disordered template is used, which suggests that the channel/hydrogel interface is replicated

[*] P. R. Giunta, Dr. R. P. Washington, T. D. Campbell, Prof. Dr. O. Steinbock, Prof. Dr. A. E. Stiegman
Department of Chemistry and Biochemistry
Florida State University
Tallahassee, FL 32306-4390 (USA)
Fax: (+1) 850-644-8281
E-mail: steinbck@chem.fsu.edu
stiegman@chem.fsu.edu

[**] This work was supported by the NSF (CHE-20023105) and the American Chemical Society Petroleum Research Fund (37278-G5). We thank Kim Riddle and John Ekman for technical assistance with microscopy.

 DOI: 10.1002/anie.200352813 © 2004 Wiley-VCH Verlag GmbH & Co. KGaA, Weinheim

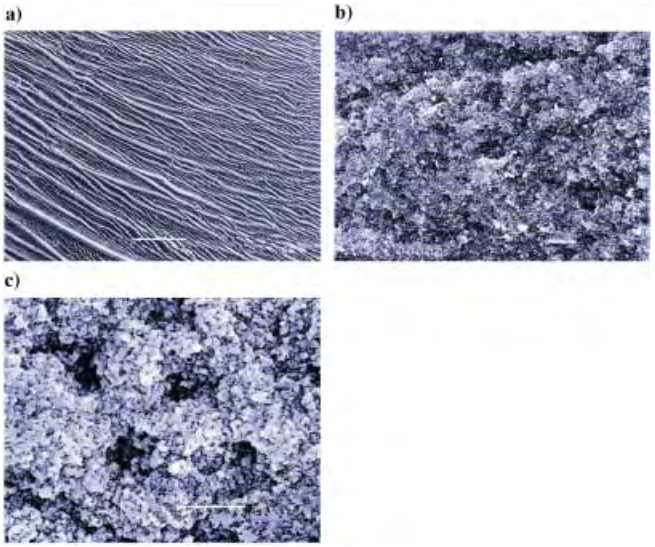


Figure 2. Scanning electron micrographs of calcinated silica monoliths created in electric-field-aligned polyacrylamide gels. The "striped" surfaces in (a) have a parallel orientation to the original electric field, whereas the "dotted" surface in (b,c) is perpendicular to the field vector. Field of view: a) $580\times435\ \mu m^2$; bar = 100 μm b) $110\times85\ \mu m^2$; bar = 10 μm, and c) $48\times37\ \mu m^2$; bar = 10 μm.

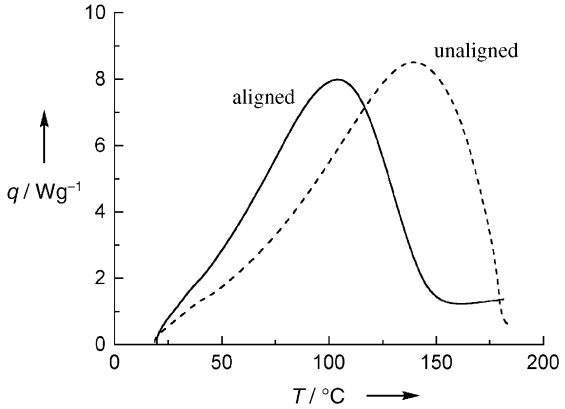


Figure 3. DSC measurements, collected at 20 K min^{-1}, of water desorption from templated silica. The solid and dashed lines correspond to material created in electric-field-aligned and unaligned hydrogels, respectively; q = heat flow.

during silicate formation. In general, hierarchical meso-/macroporous solids are made by using dual templates with the macropore region defined by a range of organized media at that scale length, including colloidal crystals of polymer spheres and even bacterial threads.[10–13] In the electric field oriented hydrogels the channels are empty and, potentially, can be filled with silica. However, prior to hydrolysis, TMOS has much greater solubility in the hydrogel itself and, as such, silicate formation preferentially occurs in this region during the initial stages of the reaction. This process defines an interface, as seen in the SEM image, and restricts the amount of silicate that reaches the channels, thus resulting in low-density silicate structures in the macrovoids. These structures are related to the difficult problem of achieving stable replicas of large voids (< 100 nm) in inorganic mineralization that was discussed by Mann and co-workers.[7] Evidence for these low-density regions can be seen in the bulk density, which is 0.806 g mL^{-1} for materials made from the field-oriented template and 0.960 g mL^{-1} for those made from a disordered hydrogels.

Figure 2b shows an SEM image of a field-oriented sample cut perpendicular to the field direction. In this orientation, the columns of low-density silica should appear as orifices of about 10 μm in diameter. The channel openings are vaguely discernible in the image but are occluded. However, after brief exposure to etching conditions (5 s immersion in 47% HF followed by neutralization in base), the openings of the channels (Figure 2c) are clearly evident, indicating that silica has been selectively removed from the low-density regions in the channels.

The effect of these channels on the physiochemical properties of the bulk materials can be demonstrated in a relatively straightforward fashion. Figure 3 shows differential scanning calorimetry (DSC) traces for water desorption from porous silica made from disordered and field-oriented templates. The field-oriented materials have an endotherm associated with desorption over a narrower temperature range with a maximum at 115 °C, close to the boiling point of pure water. Conversely, the disordered, purely mesoporous materials, have a broad desorption endotherm with a maximum at 150 °C. These differences are attributable to water acting as a pure liquid because of the large voids in which it is sequestered in the ordered material. Water trapped only in the mesoporous voids, which has a significant amount of interaction with the silica surface, desorbs over a wider temperature range and at a high average energy.

Information about the micro- and mesoporous regions of a hierarchically ordered material can be obtained through nitrogen-physisorption measurements. Isotherms collected on silica monoliths fabricated from both disordered and field-oriented hydrogels show a distinct hysteresis loop and are unambiguously of type IV which is characteristic of a mesoporous solid.[14] A BET (Brunauer, Emmett, and Teller) surface area of 314 and 337 m^2 g^{-1} for the disordered and oriented materials, respectively, is obtained from the isotherms.[15] The specific hysteresis loop displayed by the materials is one in which the desorption isotherm gradually diverges from the adsorption isotherm at high values of p/p^0 (p is the pressure of the gas, p^0 is the saturation pressure of the adsorbate) and then abruptly closes when the pores empty (type H3 in IUPAC notation). This is characteristic of slit-type pores found in adsorbents composed of plate-like particles in which the mechanisms of filling and emptying are completely different.[14] Such structures are directly evident in the SEM images of these materials (Figure 2b,c), which show that the walls between the channels, where the TMOS has penetrated the hydrogel network, consist of flat particles of ≈1 μm dimension. The single-point pore volumes were determined from the isotherms to be 0.52 and 0.73 cm^3 g^{-1}, with an average pore diameter 66.2 and 86.3 Å for the disordered and field-oriented matrices, respectively.

In summary, we have shown that ordered micrometer-scale arrays within organic templates are recovered in silica monoliths upon treatment with tetramethylorthosilicate and

 © 2004 Wiley-VCH Verlag GmbH & Co. KGaA, Weinheim

subsequent calcination. The underlying idea exploits the self-organization of periodic density patterns within the organic gel that we induce by using an externally applied electric field during polymerization. This approach allows the indirect, internal patterning of silica yielding hierarchical arrays of large aspect ratio in a highly efficient way. The anisotropic features of the silica monoliths fabricated could make them interesting materials for separation science and related applications.

Experimental Section

Preparation of polyacrylamide gels: Aligned and unaligned polyacrylamide gels were synthesized in a FisherBiotech vertical electrophoresis unit (FB-VE10-1) that was connected to a Bio-Rad power supply (Powerpac 3000). The electric-field-induced alignment was achieved by applying a constant voltage of 600 V to the polymerizing system. This procedure is similar to one reported by Charlionet et al. for the synthesis of oriented polyacrylamide gels for quick analysis of proteins and DNA.[16]

In a typical preparation, 0.70 g acrylamide (Fluka), 90 mg, *N*,*N*′-methylenebisacrylamide (Fluka), 0.25 mL of immobiline (0.20 M stock solution of *N*-acryloyl glycine; Pharmacia) and 0.25 g polyethylene glycol (Fluka) were added to 9.75 mL of distilled water. The freshly prepared solution was deoxygenated by purging with nitrogen. After the addition of 12.5 μL of ammonium persulfate (10% w/v; Fluka) and 20 μL of *N*,*N*,*N*′,*N*′-tetramethylethylenediamine (0.002 M; Aldrich), the stirred solution was transferred between two, previously silanized, glass plates spaced at 3 mm. A 1.5% agarose gel was used to prevent leakage within the vertical electrophoresis unit. The upper buffer solution of the electrophoresis unit contained 200 mM Tris (Pharmacia), 50 mM glycine (USB), and 2 mM ammonium persulfate, whereas the lower buffer contained 200 mM Tris and 50 mM glycine.

Preparation of silica gels: Tetramethylorthosilicate (98%; Aldrich) is vacuum distilled directly before use. A section of hydrogel is added to neat TMOS and is allowed to react overnight. The silica-loaded sample is removed and allowed to dry in air. The samples were then calcined at 500 °C under oxygen.

Received: September 8, 2003 [Z52813]

Keywords: gels · materials science · mesoporous materials · polymerization · silicon

[1] P. T. Tanev, M. Chibwe, T. J. Pinnavaia, *Nature* **1994**, *368*, 321.
[2] Y.-N. Jun, D. M. Dabbs, I. A. Aksay, S. Erramilli, *Langmuir* **1994**, *10*, 3377.
[3] N. K. Raman, M. T. Anderson, C. J. Brinker, *Chem. Mater.* **1996**, *8*, 1682.
[4] B. Lebeau, C. E. Fowler, S. Mann, C. Farcet, B. Charleux, C. Sanchez, *J. Mater. Chem.* **2000**, *10*, 2105.
[5] B. J. Zhang, S. A. Davis, S. Mann, *Chem. Mater.* **2002**, *14*, 1369.
[6] S. D. Sims, D. Walsh, S. Mann, *Adv. Mater.* **1998**, *10*, 151.
[7] M. Breulmann, S. A. Davis, S. Mann, H. P. Hentze, M. Antonietti, *Adv. Mater.* **2000**, *12*, 502.
[8] R. A. Caruso, J. H. Schattka, *Adv. Mater.* **2000**, *12*, 1921.
[9] R. A. Caruso, M. Antonietti, *Adv. Funct. Mater.* **2002**, *12*, 307.
[10] O. D. Velev, P. M. Tessier, A. M. Lenhoff, E. W. Kaler, *Nature* **1999**, *401*, 548.
[11] Y. J. Lee, J. S. Lee, Y. S. Park, K. B. Yoon, *Adv. Mater.* **2001**, *13*, 1259.
[12] S. A. Davis, S. L. Burkett, N. H. Mendelson, S. Mann, *Nature* **1997**, *385*, 420.
[13] D. Y. Zhao, P. D. Yang, B. F. Chmelka, G. D. Stucky, *Chem. Mater.* **1999**, *11*, 1174.
[14] S. J. Gregg, K. S. W. Sing, *Adsorption, Surface Area and Porosity*, 2nd ed., Academic Press, London, **1982**, p. 131.
[15] S. Brunauer, P. H. Emmett, E. Taller, *J. Am. Chem. Soc.* **1938**, *60*, 309.
[16] R. Charlionet, N. MachourMerlet, S. Leclerc, J. J. Malandain, *Electrophoresis* **1997**, *18*, 1133.

 © 2004 Wiley-VCH Verlag GmbH & Co. KGaA, Weinheim

Microporous Materials

A 3D Hybrid Network Containing Large Spherical Cavities Formed through a Combination of Metal Coordination and Hydrogen Bonding**

*Reyes García-Zarracino and Herbert Höpfl**

Dedicated to Professor Heinrich Nöth on the occasion of his 75th birthday

Assembling organic, organometallic, and/or inorganic building blocks to supramolecular structures through metal–ligand binding,[1] hydrogen bonds,[2] or π–π interactions[3] has become a powerful tool for the generation of large cagelike molecules or microporous substances with nanoscale cavities. Although important progress has been made in the construction of such assemblies by applying any one of these intermolecular interactions individually, a lot of research dealing with combinations of two or all three of them can still be carried out, thus allowing the construction of an almost infinite number of new supramolecular entities.[4]

Here, we report how a three-dimensional (3D) hybrid network containing large spherical cavities can be formed by the two-step self-assembly of 2,5-pyridinedicarboxylate and di-*n*-butyltin(IV) in a mixture of water and ethanol by using a combination of metal coordination and hydrogen-bonding interactions. We also describe the inclusion of hydrophobic molecules in this microporous material.

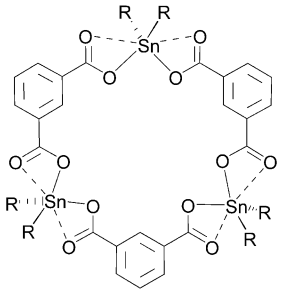
The preparation of the trinuclear macrocyclic complex $[\{(n\mathrm{Bu})_2\mathrm{Sn}(2,5\text{-pdc})(\mathrm{D})\}_3]$ (**2**; 2,5-pdc = 2,5-pyridinedicarboxylate; D = Lewis base, see below), which is similar to the synthesis of the recently reported, structurally related trimer $[\{(n\mathrm{Bu})_2\mathrm{Sn}(1,3\text{-bdc})\}_3]$ (**1**; 1,3-bdc = 1,3-benzenedicarboxylate), was carried out by the equimolar combination of di-*n*-

[*] R. García-Zarracino, Dr. H. Höpfl
Centro de Investigaciones Químicas
Universidad Autónoma del Estado de Morelos
Av. Universidad 1001, C.P. 62210 Cuernavaca (México)
Fax: (+52) 777-329-7997
E-mail: hhopfl@buzon.uaem.mx

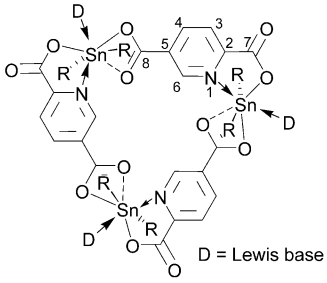
[**] This work was supported by CONACyT. The authors thank Dr. M. Sosa for the TGA data and Dr. F. Medrano for helpful discussions.

Supporting information for this article is available on the WWW under http://www.angewandte.org or from the author.

 DOI: 10.1002/anie.200352862 © 2004 Wiley-VCH Verlag GmbH & Co. KGaA, Weinheim



1 R = *n*Bu



2 R = *n*Bu

butyltin(IV) oxide and 2,5-pyridinedicarboxylic acid in a 5:1 solvent mixture of toluene and ethanol (72% yield).[5]

The formation of a 1:1 complex has been proved by integration of the ^{1}H NMR spectrum in CD_3OD. In contrast to **1**, complex **2** exhibits a five-membered NCCOSn chelate ring, with a N→Sn coordinative bond, whose presence in the complex can be shown by a downfield shift of the signal for the carbon atom in the *para* position relative to the pyridine nitrogen atom.[6] According to the ^{119}Sn NMR spectrum recorded in CD_3OD, the coordination number of the tin atom is seven ($\delta = -412$ ppm),[7] however, the signal is broadened, which indicates that the solvent molecules are interacting with the tin atom in a rapid-exchange equilibrium. That the structure is indeed cyclic in solution is evidenced by the FAB$^+$ mass spectrum, in which peaks of relatively high intensity at m/z 1194.22 and 1136.15 corresponding to the molecular ion of trinuclear $[\{(n\mathrm{Bu})_2\mathrm{Sn}(2,5\text{-pdc})\}_3]$ (**2**) and the corresponding ion formed through the loss of a *n*Bu group have been detected.

Crystallographic studies of crystals obtained from solutions in DMSO and MeOH showed that this structure is maintained in the solid state and that the heptacoordination of the tin atoms can be achieved either by coordination of solvent molecules like DMSO to the tin atoms, thus giving a crystal lattice with discrete molecules of the composition $[\{(n\mathrm{Bu})_2\mathrm{Sn}(2,5\text{-pdc})(\mathrm{DMSO})\}_3]$, or by intermolecular C=O→Sn coordination between neighboring molecules, giving a 2D polymeric coordination network of the composition $[\{[(n\mathrm{Bu})_2\mathrm{Sn}(2,5\text{-pdc})]_3\}_n]$.[8]

Interestingly, recrystallization of the latter compound in the presence of ethanol and water leads to a change in the molecular and/or supramolecular structure, since the solid-state IR spectrum changes significantly in the region corresponding to the vibrations of the carboxylate groups. While the spectrum of $[\{[(n\mathrm{Bu})_2\mathrm{Sn}(2,5\text{-pdc})]_3\}_n]$ reveals strong absorptions at $\tilde{\nu} = 1642$, 1604, 1404, and 1361 cm^{-1}, which correspond to the symmetric and antisymmetric carboxylate stretches,[5] the spectrum of the new compound shows bands at 1687, 1609, 1398, and 1333 cm^{-1}. New absorptions at $\tilde{\nu} =$ 2665 and 2552 cm^{-1} indicate the presence of hydrogen bonding within the structure, most probably involving water molecules coordinated to the tin atoms. In further experiments we discovered that a compound with the same characteristics can be prepared more readily from di-*n*-butyltin(IV) dichloride and the potassium salt of the ligand in a mixture of ethanol and water (see Experimental Section). Apparently, between zero and three ethanol molecules per trinuclear complex can be included in the solid state, as revealed by solution-state ^{1}H NMR spectra recorded on several occasions for different series of crystals. It seems that the number of ethanol molecules in the crystal lattice depends on the ethanol/water ratio used in the crystallization process, which indicates that the ethanol molecules are most probably located at interstitial sites in the crystal structure; these sites may be only partially filled and/or filled by additional water molecules instead of ethanol. The fact that all crystals obtained were cube-shaped and had the same unit cell (about 20 crystals have been examined), confirms this supposition. These observations and the detailed X-ray crystallographic study performed on one of the monocrystals showed their composition to be $[\{[(n\mathrm{Bu})_2\mathrm{Sn}(2,5\text{-pdc})(\mathrm{H_2O})]_3 \cdot 3\,\mathrm{H_2O} \cdot y\,\mathrm{EtOH}\}_n]$ (**3**, $0 < y < 3$); a crystal where $y = 3$ is discussed herein.

The crystal structure of $[\{[(n\mathrm{Bu})_2\mathrm{Sn}(2,5\text{-pdc})(\mathrm{H_2O})]_3 \cdot 3\,\mathrm{H_2O} \cdot 3\,\mathrm{EtOH}\}_n]$ consists of a chiral, highly symmetrical 3D hybrid network containing trinuclear complex molecules, in which each tin atom is strongly coordinated by one water molecule, $d(\mathrm{Sn\text{-}O}) = 2.287(4)$ Å.[5] The macrocycles are arranged in such a way that large spherical cavities are formed, whose centers are located at the 0,0,0 and $^1/_2,^1/_2,^1/_2$ positions in the cubic unit cell (space group $I23$).[9a] The unit cell of the title compound contains a capsule with nanometer dimensions (diameter ≈3.5 nm) being formed through hydrogen-bonding interactions between eight of the cyclotrimeric molecules (Figure 1).

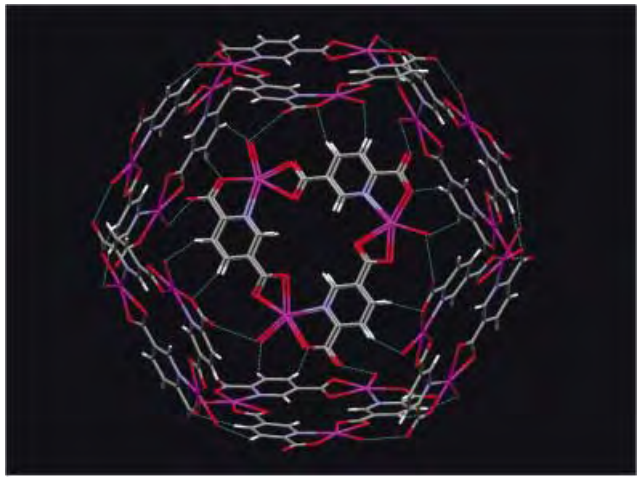


Figure 1. The unit cell of $[\{[(n\mathrm{Bu})_2\mathrm{Sn}(2,5\text{-pdc})(\mathrm{H_2O})]_3 \cdot 3\,\mathrm{H_2O} \cdot 3\,\mathrm{EtOH}\}_n]$ viewed along the [111] direction showing one of the capsules present in the crystal lattice (*n*Bu groups and uncoordinated solvent molecules have been omitted for clarity.

Each capsule consists of 24 $n\mathrm{Bu_2Sn}$ units and 24 ligand molecules giving a total of 48 starting components, which are held together by covalent coordination bonds to form $[\{(n\mathrm{Bu})_2\mathrm{Sn}(2,5\text{-pdc})(\mathrm{H_2O})\}_3]$ and a total of 36 hydrogen bonds of three different types to form the sphere: C–H···O interactions between one of the exocyclic aromatic CH groups and the oxygen atoms of the Sn–OH_2 water molecules

 © 2004 Wiley-VCH Verlag GmbH & Co. KGaA, Weinheim

(2.58 Å, 3.38 Å, 142°), C-H···O interactions between the second exocyclic aromatic CH group and the oxygen atoms of the chelate ring (2.45 Å, 3.33 Å, 154°), and O–H···O hydrogen bonds between the Sn–OH_2 water molecules and the uncoordinated carbonyl oxygen atoms (2.80 Å). Each trinuclear complex is involved in a total of 18 hydrogen bonds in the crystal lattice (Figure 2), which combine to form the 3D

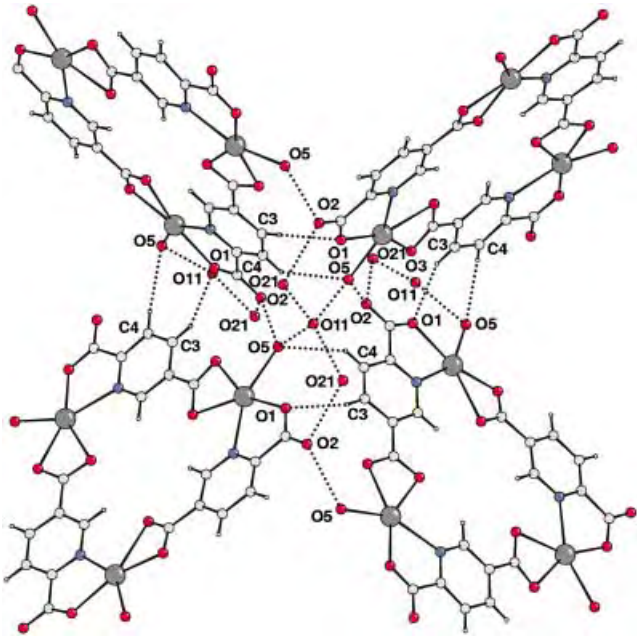


Figure 2. The intermolcular hydrogen-bonding interactions between $[\{(n\mathrm{Bu})_2\mathrm{Sn}(2,5\text{-pdc})(\mathrm{H_2O})\}_3]$ and uncoordinated solvent molecules present in the crystal lattice of $[\{[(n\mathrm{Bu})_2\mathrm{Sn}(2,5\text{-pdc})(\mathrm{H_2O})]_3\cdot 3\,\mathrm{H_2O}\cdot 3\,\mathrm{EtOH}\}_n]$. Oxygen atoms O11 correspond to uncoordinated water molecules and O21 to uncoordinated ethanol molecules. The hydrogen-bonding pattern shown is identical to the one found for the other two tin atoms in each complex molecule. The aliphatic groups of the tin complexes and ethanol molecules have been omitted for clarity.

network, and additionally in six further O–H···O hydrogen bonds to three ethanol and three water molecules (2.71–2.79 Å), which strengthen the union between the capsules in the 3D hybrid structure.

The capsules in the crystal lattice exhibit a body-centered-cubic packing motif in the solid state. However, the spherical supramolecular arrangements found in this crystal lattice can not be identified as isolated capsules, unlike for fullerenes. In this case, they are found as species that share faces with neighboring units, rather like the arrangement in a honeycomb. The eight trinuclear molecules of each capsule occupy the hexagonal faces of a truncated octahedron,[1f,10] in which the centers of two opposite faces are separated by a distance of 21.5 Å. Thus, the overall crystal structure can be described as a 3D network built up from the 3D union of truncated octahedra sharing all of their eight hexagonal faces with neighboring polyhedra.

Due to the 3D arrangement described above, half of the 48 butyl groups of one capsule are orientated into its interior, while the other half contributes to the filling of another eight neighboring capsules. Although in each capsule 24 butyl groups are oriented into the interior of the cavity, there still remain very large voids in the center, which have a volume of 1850 $Å^3$.[11] It should be mentioned that this is the only type of void present in the crystal structure and that their combined volume forms 24% of the crystal lattice volume; this space can be used to include guest molecules (see below). In the absence of guest molecules (other than solvents of crystallization), only smears of electron density could be detected within the cavities, which in this case therefore are most probably occupied by water molecules. Assuming a volume of 30 $Å^3$ for a single water molecule in the liquid phase, a maximum of 61 water molecules may be present per void.[12]

If the hydrogen-bonded, noncoordinated water and ethanol molecules present in the crystal lattice of $[\{[(n\mathrm{Bu})_2\mathrm{Sn}(2,5\text{-pdc})(\mathrm{H_2O})]_3\cdot 3\,\mathrm{H_2O}\cdot 3\,\mathrm{EtOH}\}_n]$ are omitted, channels of two different sizes can be identified along the [100], [010], [001], and [111] directions of the crystal lattice, whose bottlenecks correspond to the access windows into the interior of the capsules. Along the [100], [010], and [001] directions, the narrowest diameters of the channels are 6.3 Å, while along the [111] direction the diameter is 1.7 Å and corresponds to the diameter of the cavity localized in the center of the macrocyclic $[\{(n\mathrm{Bu})_2\mathrm{Sn}(2,5\text{-pdc})(\mathrm{H_2O})\}_3]$ (**2**) rings (Figure 3).

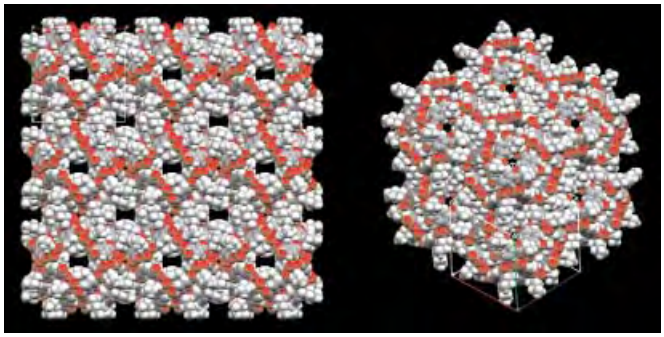


Figure 3. Channels along the [100], [010], [001], and [111] direction of the crystal lattice of $[\{[(n\mathrm{Bu})_2\mathrm{Sn}(2,5\text{-pdc})(\mathrm{H_2O})]_3\cdot 3\,\mathrm{H_2O}\cdot 3\,\mathrm{EtOH}\}_n]$ are observed when uncoordinated solvent molecules are omitted.

To evaluate the capacity of $[\{[(n\mathrm{Bu})_2\mathrm{Sn}(2,5\text{-pdc})(\mathrm{H_2O})]_3\cdot 3\,\mathrm{H_2O}\cdot y\,\mathrm{EtOH}\}_n]$ to act as a host for guest molecules, two different kinds of experiments have been carried out. First, a thermogravimetric analysis has been carried out to study the evacuation of the solvent molecules present at the intersitial sites. A continuous loss of weight starting at 30 °C is observed, which approaches 16.5% at 275 °C, after which decomposition occurs. However, during thermal treatment under vacuum the crystal lattice collapses at relatively low temperatures (< 100 °C). X-ray crystallography proves that the crystalline 3D hybrid network was transformed into an amorphous material. To evaluate the porosity of this material, crystals of the title compound were thermally treated for a period of 1.5 h (180 °C at 10 Torr) and then exposed to vapors of ethanol and THF. In both cases only a small quantity of guest molecules were included, however, in the presence of gaseous methylamine combined with THF (2 M solution in THF), a total of four molecules of

 © 2004 Wiley-VCH Verlag GmbH & Co. KGaA, Weinheim

$MeNH_2$ and one molecule of THF were included for every molecule of **2**, as shown by an integration of the ^1H NMR spectrum in CD_3OD. Therefore, assuming a volume of 48 Å^3 for $MeNH_2$ and of 135 Å^3 for THF, a total of 327 Å^3 of free space per complex molecule is available. For comparison, the analogous space in the title compound is 1850/4 = 460 Å^3. Studies in order to detail the function of the methylamine in the cavity formation are under way.

Cocrystallization experiments were also used to evaluate the host-binding capacity of $[\{[(n\mathrm{Bu})_2\mathrm{Sn}(2,5\text{-pdc})(H_2O)]_3 \cdot 3\,H_2O \cdot y\,\mathrm{EtOH}\}_n]$; diphenylmethane, triphenylmethane, sodium tetraphenylborate, and triptycene have been added to a solution of the starting materials in ethanol/water to form the tin complex. Since the 24 butyl groups oriented to the interior of the spherical cavities generate a hydrophobic environment, hydrophobic guests were initially studied. In all four cases a crystalline material was obtained, whose unit cell dimensions were identical to the ones found for $[\{[(n\mathrm{Bu})_2\mathrm{Sn}(2,5\text{-pdc})(H_2O)]_3 \cdot 3\,H_2O \cdot 3\,\mathrm{EtOH}\}_n]$. In all cases, electron density was located in the interior of the cavities, which indicates the presence of the guest molecules, however, due to disorder of the guests within the cavities, a well-refined solution of the structure could only be obtained in the case of the triphenylmethane inclusion complex.[9b] That in all four cases inclusion occurred was shown by integration of the ^1H NMR spectra of samples dissolved in CD_3OD. The guest molecules were included with different stoichiometries. In the case of diphenylmethane, an average of 2.5 molecules were included per capsule, such that 695 Å^3 of the available 1850 Å^3 were occupied; the remaining space is most probably filled by water molecules. In the other cases, 1.5 molecules of triphenylmethane (600 Å^3), one molecule of sodium tetraphenylborate (486 Å^3), and three molecules of triptycene (1260 Å^3) were found to be present in each void. Figures 4 and 5 give two views of the host–guest complex with triphenylmethane: Figure 4 shows one capsule occupied by two of the guest molecules, while Figure 5 provides a cross-sectional view of a capsule showing one guest molecule. In this case only water molecules (no ethanol molecules) have been found in the hydrogen-bonded network, which confirms the observation that the amount of ethanol molecules can indeed be zero. Although the void should be large enough for the inclusion of C_{60}, all attempts to prepare this inclusion complex have been unsuccessful so far, one of the problems being the insolubility of C_{60} in a mixture of ethanol and water.

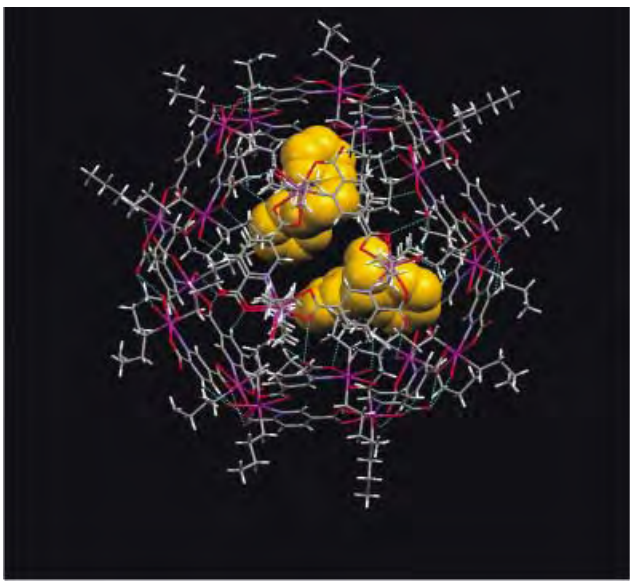


Figure 4. Inclusion of 2 equivalents of triphenylmethane in one of the capsules present in $[\{[(n\mathrm{Bu})_2\mathrm{Sn}(2,5\text{-pdc})(H_2O)]_3 \cdot 3\,H_2O \cdot 3\,\mathrm{EtOH}\}_n]$. Uncoordinated solvent molecules have been omitted for clarity.

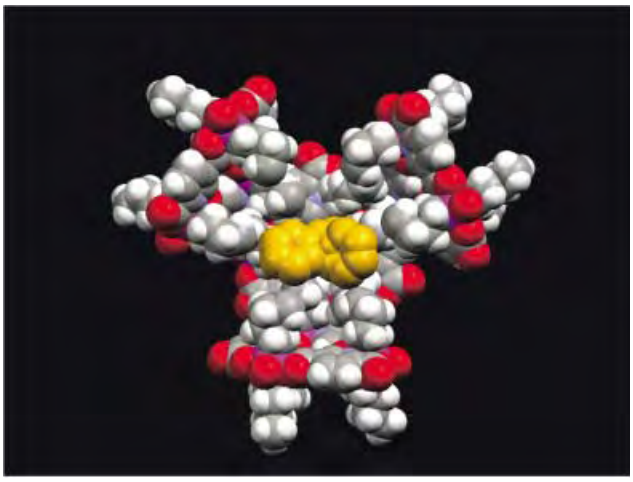


Figure 5. A cross-sectional view of the capsule shown in Figure 4 with one guest molecule.

In conclusion, we have shown that interesting supramolecular structures with large internal spherical cavities can be obtained from simple starting materials by assembling them in two steps; first by metal coordinative bonding, and then by combining these "intermediates" through hydrogen-bonding interactions. The spherical cavities in the supramolecular structure of $[\{[(n\mathrm{Bu})_2\mathrm{Sn}(2,5\text{-pdc})(H_2O)]_3 \cdot 3\,H_2O \cdot y\,\mathrm{EtOH}\}_n]$, whose size may be modulated varying the size of the organic substituents in the diorganotin groups, could be exploited further for the selective trapping of various guest molecules, the stabilization of labile reactive species, selective transport through channel systems, and for conducting chemical reactions by using the cavities as reaction vessels.

Experimental Section

2: A solution of 2,5-pyridinedicarboxylic acid (0.167 g, 1.00 mmol) and di-*n*-butyltin(IV) oxide (0.250 g, 1.00 mmol) was refluxed for 8 h using a Dean–Stark apparatus. After filtration of the light-yellow solid, the product was extracted with ethanol. The microcrystalline powder obtained after evaporation of the solvent is soluble in methanol, DMSO, and pyridine. Yield: 72%; m.p. 290°C (decomp).

3: A solution of di-*n*-butyltin(IV) dichloride (0.092 g, 0.30 mmol) in EtOH (2 mL) was added to a solution (6 mL) of 2,5-pyridinedicarboxylic acid (0.050 g, 0.30 mmol) and potassium hydroxide (0.034 g, 0.60 mmol) in EtOH/H_2O (3:1). After a few hours (though sometimes a few days) cubic, colorless crystals of **3** were formed. Crystals can be grown faster, if additional water is added to the reaction mixture after a few hours. According to the proportion of ethanol present in the reaction mixture, the quantity of ethanol

 © 2004 Wiley-VCH Verlag GmbH & Co. KGaA, Weinheim

present in the crystal lattice varies as shown by integration of ^{1}H NMR spectra of samples dissolved in CD_3OD. Yield: 77%; m.p. 290°C (dec.).

Cocrystallization reactions to form the inclusion compounds were carried out by adding an excess of the guest (triphenylmethane, diphenylmethane, triptycene, or sodium tetraphenylborate) dissolved in an EtOH solution.

X-ray diffraction studies were carried out on a BRUKER-AXS APEX diffractometer with a CCD area detector ($\lambda Mo_{K\alpha} = 0.71073$ Å, monochromator: graphite). Frames were collected at $T = 100$ K via ω-rotation ($\Delta/\omega = 0.3°$) at 10 s per frame.[13] The measured intensities were reduced to F^2 and corrected for absorption with SADABS.[14] Structure solution, refinement, and data output were carried out with the SHELXTL-NT program package.[15] Non-hydrogen atoms were refined anisotropically. Hydrogen atoms were placed in geometrically calculated positions using a riding model. Figures were created by the CRYSTALS[16] and MERCURY[17] software packages. Hydrogen-bonding interactions and voids in the crystal lattice were calculated by PLATON.[11]

CCDC-219315 and -219316 contains the supplementary crystallographic data for this paper. These data can be obtained free of charge via www.ccdc.cam.ac.uk/conts/retrieving.html (or from the Cambridge Crystallographic Data Centre, 12, Union Road, Cambridge CB2 1EZ, UK; fax: (+44) 1223-336-033; or deposit@ccdc.cam.ac.uk).

Received: September 15, 2003 [Z52862]

Keywords: carboxylate ligands · host–guest systems · self-assembly · supramolecular chemistry · tin

[1] For recent reviews see: a) R. W. Saalfrank, E. Uller, B. Demleitner, I. Bernt, *Struct. Bonding (Berlin)* **2000**, *96*, 149; b) G. F. Swiegers, T. J. Malefetse, *Chem. Rev.* **2000**, *100*, 3483; c) M. Fujita, K. Umemoto, M. Yoshizawa, N. Fujita, T. Kusukawa, K. Biradha, *Chem. Commun.* **2001**, 509; d) B. J. Holliday, C. A. Mirkin, *Angew. Chem.* **2001**, *113*, 2076; *Angew. Chem. Int. Ed.* **2001**, *40*, 2022; e) G. Férey, *Chem. Mater.* **2001**, *13*, 3084; f) B. Moulton, M. J. Zaworotko, *Chem. Rev.* **2001**, *101*, 1629; g) C. Janiak, *Dalton Trans.* **2003**, 2781.

[2] a) B. Hamelin, L. Jullien, C. Derouet, C. H. du Penhoat, P. Berthault, *J. Am. Chem. Soc.* **1998**, *120*, 8438; b) J. L. Atwood, L. J. Barbour, A. Jerga, *Chem. Commun.* **2001**, 2376; c) M. O. Vysotsky, I. Thondorf, V. Böhmer, *Chem. Commun.* **2001**, 1890; d) R. Zadmard, T. Schrader, T. Grawe, A. Kraft, *Org. Lett.* **2002**, *4*, 1687; e) F. Hof, S. L. Craig, C. Nuckolls, J. Rebek, Jr., *Angew. Chem.* **2002**, *114*, 1556; *Angew. Chem. Int. Ed.* **2002**, *41*, 1488; f) F. Corbellini, R. Fiammengo, P. Timmerman, M. Crego-Calama, K. Versluis, A. J. R. Heck, I. Luyten, D. N. Reinhoudt, *J. Am. Chem. Soc.* **2002**, *124*, 6569.

[3] D. Philp, J. F. Stoddart, *Angew. Chem.* **1996**, *108*, 1242; *Angew. Chem. Int. Ed. Engl.* **1996**, *35*, 1154.

[4] a) A. D. Burrows, C.-W. Chan, M. M. Chowdry, J. E. McGrady, D. M. P. Mingos, *Chem. Soc. Rev.* **1995**, *24*, 329; b) M. Munakata, L. P. Wu, M. Yamamoto, T. Kuroda-Sowa, M. Maekawa, *J. Am. Chem. Soc.* **1996**, *118*, 3117; c) D. Braga, F. Grepioni, G. R. Desiraju, *Chem. Rev.* **1998**, *98*, 1375; d) D. Braga, *Dalton Trans.* **2000**, 3705; e) C. B. Aakeröy, A. M. Beatty, *Aust. J. Chem.* **2001**, *54*, 409; f) A. M. Beatty, *CrystEngComm* **2001**, *51*, 1.

[5] R. García-Zarracino, J. Ramos-Quiñones, H. Höpfl, *Inorg. Chem.* **2003**, *42*, 3835.

[6] E. Gómez, R. Flores, G. Huerta, C. Alvarez-Toledano, R. A. Toscano, V. Santes, N. Nava, P. Sharma, *J. Organomet. Chem.* **2003**, *672*, 115.

[7] a) For [(nBu)$_2$Sn(pic)$_2$] (pic = 2-picolinate) a ^{119}Sn NMR shift of $\delta = -312$ ppm, typical for a hexacoordinate tin species, has been reported: J. Holecek, M. Nadvornik, K. Handlir, *J. Organomet. Chem.* **1986**, *315*, 299; b) in comparison, for the heptacoordinate complex [(Me)$_2$Sn(pic)$_2$(DMSO)] a chemical shift of $\delta = -451$ ppm was observed: T. P. Lockhart, F. Davidson, *Organometallics* **1987**, *6*, 2471.

[8] These results will be published in detail elsewhere.

[9] a) Crystal data for **3**: $C_{45}H_{69}N_3O_{15}Sn_3 \cdot 3H_2O \cdot 3EtOH$, $M_r = 1440.35$, $0.44 \times 0.46 \times 0.46$ mm^3, cubic, space group $I23$, $a = 24.8205(11)$ Å, $V = 15290.8(12)$ Å^3, $Z = 8$, $\rho_{calcd} = 1.251$, $2\theta_{max} = 25$, 4512 independent reflections, $R_1 = 0.041$ for 4502 reflections with $I > 2\sigma(I)$ and $wR_2 = 0.1243$ for all data, 243 parameters; b) Crystal data for the inclusion complex of **3** with triphenylmethane: $C_{45}H_{69}N_3O_{15}Sn_3 \cdot 5.5H_2O \cdot 0.375Ph_3CH$, $M_r = 1438.81$, crystal size $0.23 \times 0.22 \times 0.22$ mm^3, cubic, space group $I23$, $a = 24.8118(7)$ Å, $V = 15274.8(7)$ Å^3, $Z = 8$, $\rho_{calcd} = 1.278$, $2\theta_{max} = 25$, 4512 independent reflections, $R_1 = 0.056$ for 4476 for reflections with $I > 2\sigma(I)$, $wR_2 = 0.161$ for all data, 220 parameters.

[10] The truncated octahedron is an Archimedean solid: L. R. MacGillivray, J. L. Atwood, *Angew. Chem.* **1999**, *111*, 1080; *Angew. Chem. Int. Ed.* **1999**, *38*, 1018.

[11] PLATON, version 210103, A. L. Spek, *Acta Crystallogr. Sect. A* **1990**, *46*, C-34.

[12] If additional water molecules are considered to be present in these voids, the correct formula for the title compound should be [{[[(nBu)$_2$Sn(2,5-pdc)(H$_2$O)]$_3$·3H$_2$O·yEtOH·zH$_2$O}$_n$] with $0 < y < 3$ and $0 < z < 15$. It should be noted that according to the ^{1}H NMR spectra of crystals dissolved in CD_3OD, no more than one ethanol molecule was present per tin atom.

[13] Bruker Analytical X-ray Systems, SMART: Bruker Molecular Analysis Research Tool, Version 5.618, **2000**.

[14] Bruker Analytical X-ray Systems. SAINT + NT, Version 6.04, **2001**.

[15] Bruker Analytical X ray Systems, SHELXTL-NT, Version 6.10, **2000**.

[16] a) D. J. Watkin, C. K. Prout, J. R. Carruthers, P. W. Betteridge, T. I. Cooper, *CRYSTALS*, Issue 1, Chemical Crystallography Laboratory Oxford, Oxford, **2000**; b) D. J. Watkin, C. K. Prout, L. J. Pearce, *CAMERON*, Chemical Crystallography Laboratory Oxford, Oxford, **1996**.

[17] Cambridge Crystallographic Data Center, Mercury, Version 1.1.2, **2002**.

 © 2004 Wiley-VCH Verlag GmbH & Co. KGaA, Weinheim

Fullerenes

Ordered Self-Assembly and Electronic Behavior of C_{60}–Anthrylphenylacetylene Hybrid**

Seok Ho Kang, Hong Ma, Mun-Sik Kang, Kyoung-Soo Kim, Alex K.-Y. Jen, M. Hadi Zareie, and Mehmet Sarikaya**

The fullerene (C_{60}) molecule has very unique and attractive electronic, optical, and mechanical properties owing to its chemical properties and uniform, spherical, and nanoscale physical structure.[1] Recent studies revealed that thin films made of C_{60} exhibit a wide range of interesting characteristics such as charge transport, photoconductivity, superconductivity (upon doping with alkali metals), and biological activities.[2–3] The development of new C_{60}-based thin-film materials relies strongly on the development of novel synthetic and processing methodologies to modify C_{60}. Such methodologies include tailoring functional groups on C_{60} derivatives and covalently attaching fullerenes to solid-state supports to obtain a desirable optical or electronic response. Among many techniques explored, self-assembling C_{60}-based molecules on flat solid substrates has been found to be a good way to make thin films that also allow investigation of their physical properties, because self-assembled monolayers (SAMs) formed by chemisorption yield well-defined structures on substrates.[4] In the literature, there are many reports on attempts to construct SAMs of C_{60} to produce highly ordered and densely packed structures on substrates,[5–11] and there has been some success in this respect[12] especially the recently observed noncovalently bonded C_{60} at very low temperatures (5 K).[13] In a previous work related to the development of stable and ordered assemblies of conjugated molecular structures, we reported the self-assembly of (4-mercaptophenyl)anthrylacetylene (MPAA) on the surface of Au(111). These molecules tend to form highly ordered 2D stacked arrays through an interplay of strong π–π intermolecular stacking and chemisorptive gold–thiol interactions.[14] We also discovered that the electronic behavior of MPAA depends on its local ordering and the close stacking of the molecules in SAM films. Thus, on basis of the previous study, it may be possible to combine the excellent physical and chemical properties of C_{60} with the advantages offered by the controlled nanoscale ordering of MPAA-based SAMs. The hybridization of these two functional molecules and their stable assemblies may introduce new electrical or optical properties. To achieve this, a new synthetic methodology had to be developed to covalently connect these two molecules as a stable entity. Herein we report the design, synthesis, self-assembly, and functional characteristics of the new hybrid molecule.

In our molecular design, we took advantage of the MPAA moiety to form a rigid and stable footing on gold substrates for constructing well-ordered C_{60} films. Figure 1 shows the result of molecular modeling of C_{60}–MPAA (drawn by using the molecular mechanics 2, MM2, calculation method). The schematic suggests that the size of C_{60} (0.71 nm) is slightly smaller than that of MPAA moiety (0.92 nm). The small difference (0.21 nm) between the size of the two molecules is a critical parameter that could favor the close-packing of C_{60}–MPAA into 2D arrays on a Au(111) substrate.

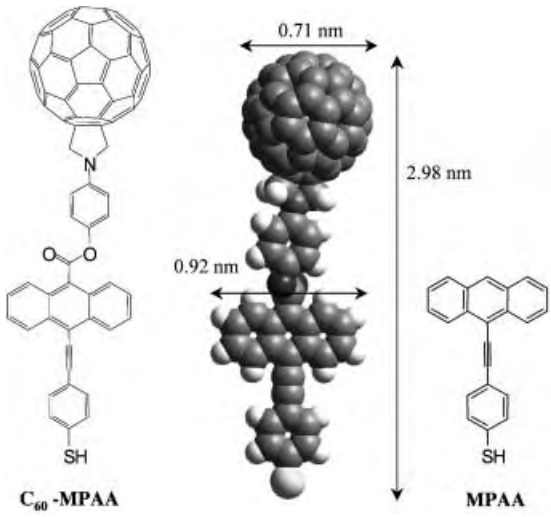


Figure 1. Schematic illustration of C_{60}–MPAA molecule based on MM2 calculation. The structure was optimized by force-field calculation by using Cerius 2 modeling program of Acelrys.

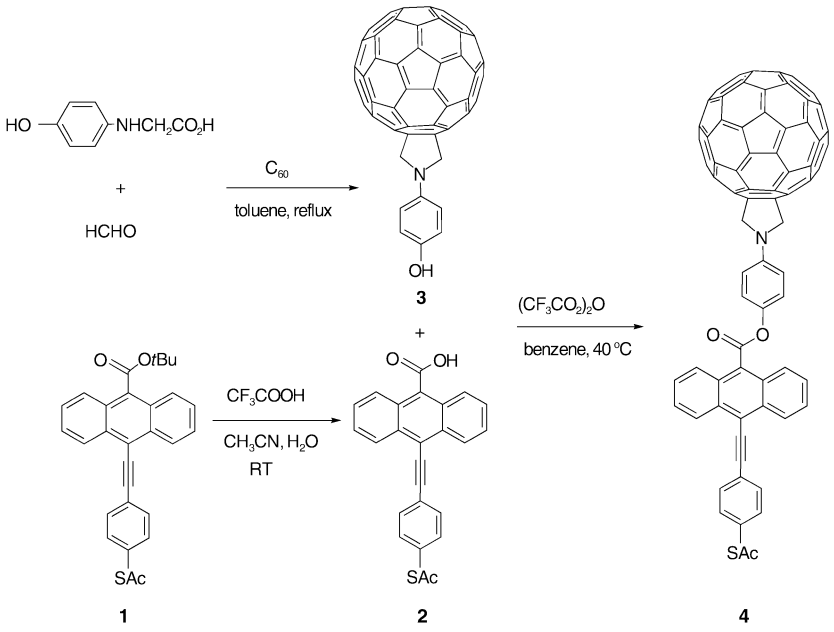
In our study, the C_{60}–MPAA hybrid molecule **4** was synthesized through the esterification of 9-(4-thioesterphenyl)-acetyleneanthracene-10-carboxylic acid **2** with *N*-(4-hydroxyphenyl)-3,4-fulleropyrrolidine **3** in the presence of a trace amount of trifluoroacetic anhydride as catalyst (Scheme 1). We employed the 1,3-dipolar cycloaddition methodology to functionalize C_{60} with azomethine ylides.[15] Paraformaldehyde, *N*-(4-hydroxyphenyl)glycine, and C_{60} were heated in refluxing toluene to afford *N*-(4-hydroxyphenyl)-3,4-fulleropyrrolidine **3** in 33% yield. 9-(4-Thioesterphenyl)-acetylene-anthracene-10-carboxylic acid **2** was synthesized by the acid-catalyzed deprotection of its *tert*-butyl ester precursor **1**, which was synthesized as shown in Scheme 2. The resulting coupled molecule **4** has an axis of twofold symmetry that runs through the length of the hybrid object. This symmetry has a profound effect on the control of the intermolecular forces that lead to the close packing of C_{60} on gold. All compounds were purified by column chromatog-

[*] Dr. S. H. Kang, Dr. H. Ma, Dr. M.-S. Kang, Dr. K.-S. Kim, Prof. A. K.-Y. Jen, Dr. M. H. Zareie, Prof. M. Sarikaya
Department of Materials Science and Engineering
University of Washington
Seattle, WA 98195-2120 (USA)
Fax: (+1) 206-543-3100
E-mail: ajen@u.washington.edu
sarikaya@u.washington.edu

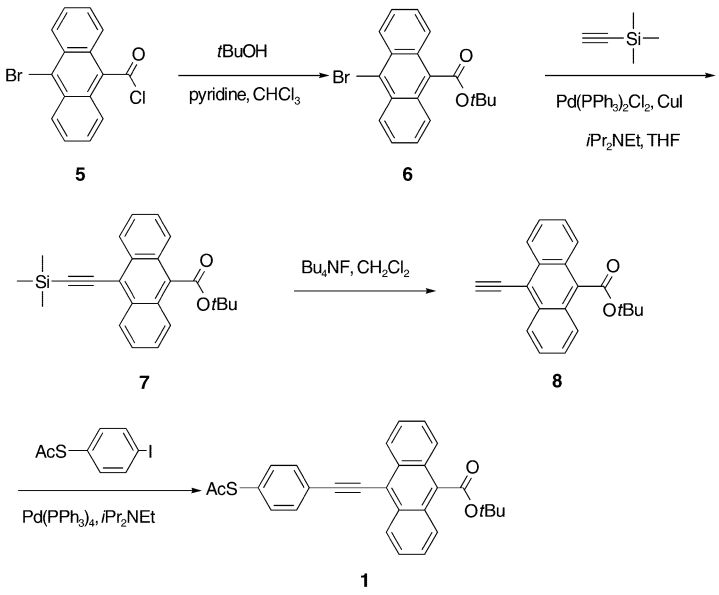
[**] This work was supported by ARO-DURINT (DAAD19-01-04999) and the Air Force Office of Scientific Research (AFOSR) under the Bioinspired Concept Program. Alex K.-Y. Jen thanks the Boeing–Johnson Foundation for its support.

Supporting information for this article is available on the WWW under http://www.angewandte.org or from the author.

 © 2004 Wiley-VCH Verlag GmbH & Co. KGaA, Weinheim DOI: 10.1002/anie.200353001



Scheme 1. Synthesis of C_{60}–MPAA with acetyl protection.



Scheme 2. Synthesis of 9-(4-thioesterphenyl)acetyleneanthracene-10-ester **1**.

raphy to give analytically pure materials, and their chemical structures were fully confirmed by ^1H, ^{13}C NMR spectroscopy and mass spectrometry.

SAM of C_{60}–MPAA hybrid was prepared by immersing Au(111)/mica substrate in a solution of **4** in THF/EtOH (1:10) at 25 °C for 24 h in the presence of a solution of ammonium hydroxide, thus hydrolyzing the acetyl protecting group. The thin film sample was then rinsed with THF and EtOH, and dried with a stream of nitrogen. The electrochemical properties of the C_{60}–MPAA hybrid as well as the SAM on Au were evaluated. This was carried out by using cyclic voltammetry (CV), with the molecules or assembly dissolved or immersed in a solvent mixture (toluene/acetonitrile = 4:1) that contained 0.1 M of Bu_4NPF_6 as electrolyte and swept at a rate of 100 $mV s^{-1}$ (Figure 2). Both the C_{60}–MPAA hybrid, and the assembly on Au showed two electrochemically accessible and stable reduction states of C_{60}. The CV profile for the hybrid exhibited two well-resolved reversible redox waves at $E_{1/2} = -0.56$ and -0.95 V versus Ag/AgCl. These values are typical for monofunctionalized C_{60}.[15] The first and the second peaks are attributed to successive one-electron reductions/oxidations of the C_{60} moiety. The CV results of C_{60}–MPAA/Au SAM also reveal well-defined redox waves and indicate that the hybrid molecules are strongly adsorbed on the gold surface. Although the first and second reduction potentials of the assembled films have shifted slightly to negative potentials ($E_{1/2} = -0.61$ and -0.99 V, respectively) compared to those of the hybrid molecule in solution (Figure 2), these results resemble those of previously reported C_{60} SAMs.[16]

Figure 3 shows a high-resolution scanning tunneling microscopy (STM) image of the C_{60}–MPAA SAM on Au(111)/mica recorded at room temperature. Each bright sphere indicates where a C_{60} core locates directly on top of an MPAA molecule. The image reveals a well-ordered 2D nanostructure that extends throughout a given textured Au grain. As shown in the power spectrum (Figure 3b) of the STM image (Figure 3a), the organization of the hybrid molecules in the self-assembled structure exhibits a pseudohexagonal arrangement. The oblique lattice formed by the hybrid molecule is characterized by a unit cell with $a = 1.00 \pm$

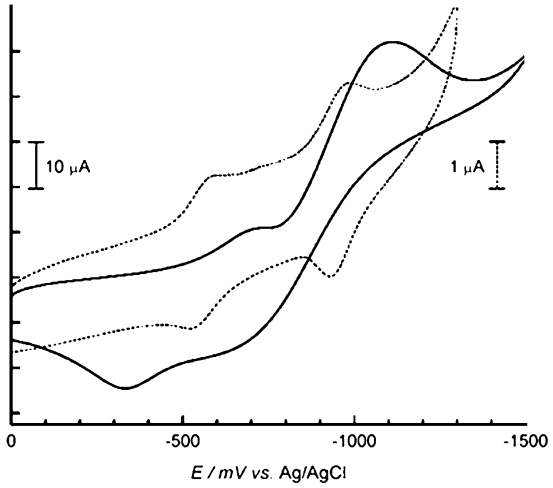


Figure 2. Cyclic voltammograms of C_{60}–MPAA (dotted line) and C_{60}–MPAA/Au (solid line) in toluene/acetonitrile = 4:1 with 0.1 M Bu_4NPF_6 at a sweep rate of 100 $mV s^{-1}$.

 © 2004 Wiley-VCH Verlag GmbH & Co. KGaA, Weinheim

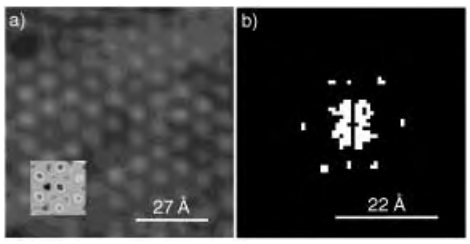


Figure 3. Room-temperature STM images of ordered assemblies of C_{60}–MPAA on Au(111) surface (constant current mode, U_t and average I are 200 mV and 100 pA, respectively). a) after 24 h self-assembly; inset: reconstructed image by using the transform in (b). b) Fourier transform of the periodic pattern shown in (a) reveals an oblique lattice.

0.25 nm, $b = 0.90 \pm 0.25$ nm; and the angle between them $\alpha = 62 \pm 0.5°$. It is well known that the self-assembly of C_{60} molecules on Au(111) results in the formation of perfectly hexagonal lattices with lattice parameters of about 0.9 nm.[15,17–19] The observation that the C_{60}–MPAA hybrid does not form perfectly hexagonal lattices requires further consideration.

The C_{60} molecule alone is spherical, and spherical particles on a flat surface organize into hexagonal lattice, the lowest energy state. In this supramolecular organization each particle has sixfold symmetry. However, as shown above, the hybrid molecule we synthesized forms an oblique structure with twofold symmetry (Figure 3b), probably because the C_{60}–MPAA hybrid molecule itself has twofold symmetry resulting from the asymmetric molecular architecture of the MPAA, that is, the planar MPAA part of the hybrid molecule is slightly larger than the C_{60} part. While C_{60} alone has a full 360° rotational freedom, this is not so true when it is tethered to the MPAA molecule and organized into a 2D ordered structure. Therefore, the twofold symmetry in the hybrid molecular architecture imposes a restriction on the rotation of the new molecule and forces it into an energetically more-favorable oblique-lattice conformation. This configuration is likely to correspond to a stable state at which centrally symmetric interactions among C_{60} molecules and planar interactions among MPAAs are compromised. It has also been demonstrated, in our earlier study,[14] that the MPAA ordered structure has an oblique lattice with lattice parameters significantly different ($a = 0.76$ nm and $b = 1.15$ nm) than in the lattice formed by the hybrid molecule studied here.

In addition to the structures, the dimensions of the lattices formed by C_{60} alone and that formed by hybridization with MPAA differ, providing clues to their relative stabilities. For example, a C_{60} film deposited directly on Au(111) surface shows a close-packed but unstable structure composed of mobile hexagonal arrays with an intercluster spacing of 1.1 nm.[15,17–19] Many other self-assembled structures based on alkylthiol-terminated fullerenes, fullerene-phenanthrolines, and disulfide-terminated fullerenes have also been reported. However, none of these earlier structures seem to have the same level of stable ordering as the hybrid molecule studied here. This stability is possibly due to the fact that alkyl chains in these SAMs are more dynamic, resulting in a loosely packed long-range organization of the molecular film.[5–11] Recently, it was reported that ordered C_{60} nanostructures can form on top of SAMs of alkylthiol films (on a Au(111) substrate) at 5 K.[12–13] In this case, the C_{60} molecules form closed packed hexagonal arrays with a nearest-neighbor distance of 1.0 nm. However, the resulting C_{60} arrays are not stable at room temperature. This instability is probably due to the detachment of C_{60} molecules from the alkylthiol along with their free rotation above the SAM film. In our work, the SAMs of the hybrid molecule, which is made up of C_{60} covalently bonded to MPAA, exhibit a high degree of ordering even at room temperature. The stable and robust nanoscale self-assembly and the resulting structure is a result of the interplay of intermolecular interactions among π–π stacked MPAA molecules in addition to interactions among the C_{60} molecules and the thiol–Au bonding.

We have also prepared composite samples of C_{60}–MPAA hybrid and MPAA molecules and observed their coassembly to assess their structure and corresponding electrical properties. Figure 4a is a room-temperature STM image that reveals

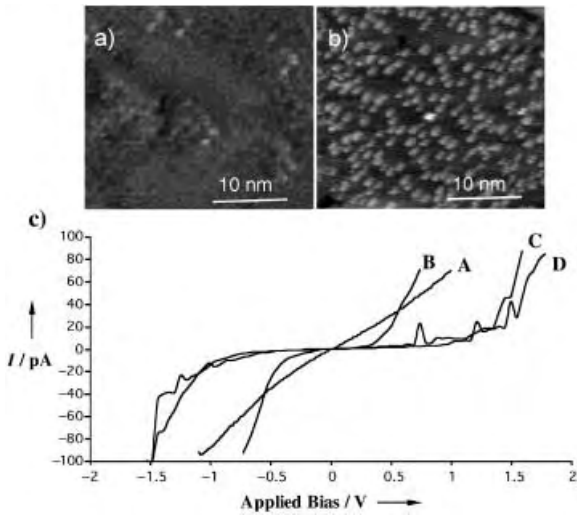


Figure 4. Room-temperature STM images of the molecular-ordered self-assemblies (both were recorded under constant current with U_t and average I being 200 mV and 100 pA, respectively). a) Assembly of C_{60}–MPAA observed after 24 h; b) Coassembly of C_{60}–MPAA and MPAA (ratio of compositions = 1:9) after 24 h. The bright spots in (b) corresponds to the aggregates of C_{60}–MPAA; c) Current-voltage characteristics of SAMs. A: Au(111); B: C_{60} only; C: C_{60}-MPAA in the homoassembly; D: C_{60}-MPAA co-assembled into MPAA (1:9).

a long-range molecularly ordered homoassembly of C_{60}–MPAA on a gold substrate. On the other hand, Figure 4b reveals coassembled structure of the C_{60}–MPAA hybrid (10%) with MPAA (90%) molecules. In latter case, the C_{60}–MPAA molecules form small, stable island-like aggregates that are fairly homogeneously distributed within the matrix of ordered MPAA molecules. The bright spots in Figure 4b represent the constant-current STM images of the hybrid molecules that are taller than those of the matrix molecules (2.98 nm versus 1.2 nm). The C_{60}–MPAA islands in Figure 4b contain a small number of molecules (1 to 3) and

 © 2004 Wiley-VCH Verlag GmbH & Co. KGaA, Weinheim

appear to be commensurate with the surrounding ordered molecular matrix, possibly a result of the twofold symmetry of the MPAA molecule in both regions.

We investigated electronic behavior of the C_{60}–MPAA SAMs by establishing their current/voltage (I/V) characteristics by scanning tunneling spectroscopy (STS; Figure 4c). The STS measurements were performed at a fixed tip–sample distance with the feedback loop being switched off. Each I/V curve was averaged over six successive voltage sweeps, with all six were typically within the measurement error. The time required for a complete spectroscopy measurement was below 1 second; therefore any influence of lateral drift was neglected.

Curves A, B, and C in Figure 4c show the I/V characteristics of bare Au(111), physically adsorbed C_{60} monolayer and homoassembled monolayer of C_{60}–MPAA on Au(111), respectively. Curve D in Figure 4c exhibits the I/V characteristics of the SAM of C_{60}–MPAA coassembled with MPAA. Both of the I/V curves of C_{60}–MPAA in homoassembly and coassembly show semiconducting behavior, evident when compared with the metallic characteristic of bare Au surface. The C_{60}–MPAA molecule, whether homoassembled or coassembled, has a much larger energy gap than that of pure C_{60} when it is directly physically adsorbed on Au. This difference is probably due to the fact that the introduction of anthrylphenyl acetylene moiety changes the electronic characteristics of the $C_{60,}$ which is verified by UV/Vis absorption spectra (reported elsewhere). Moreover, the STS spectra of the C_{60}–MPAA show multiple peaks in I/V curves (Figure 4c, curves C and D). These peaks resemble negative differential resistance (NDR) phenomenon reported earlier by Reed and co-workers.[20] The occurrence of the NDR effect is possibly due to the weak charge transfer between the MPAA and the electron-affinity of C_{60} at the molecular junction of C_{60}–MPAA. It should be noted that the I/V curves of the SAMs of neither C_{60} or MPAA[14] alone exhibit these peaks.

Another interesting point to note in the I/V curves corresponding to C_{60}–MPAA molecules in both homo and mixed states is that only weak (or no) apparent NDR-type peaks appear on the negative bias side. This finding may be an indication that charge transfer takes place more strongly in one direction, that is, from the electron-rich MPAA to the electron-deficient C_{60}. These peaks also exhibit very different bias voltage positions in the homo- and coassembled SAMs of C_{60}-MPAA (curves C and D in Figure 4c). The multiple peaks in I/V curves are especially clear in the coassembly state (Figure 4c, curve D) because of the measurements from isolated islands of C_{60}–MPAA. The differences in the characteristics of the peaks (number of peaks and their positions) may be due to a collective phenomena of different molecular surroundings of the C_{60}–MPAA molecules and their local ordering in these two SAMs; this would lead to different intermolecular interactions and changes in energy levels of molecular orbitals of the two assemblies. The more in-depth investigation of the electrical properties of these SAMs, especially verification of the possible NDR effect, could be carried out through STS measurements of the I/V characteristics by carefully isolating the hybrid molecules within the MPAA matrix, as planned in the near future.

In summary, we have designed and synthesized a novel functional hybrid molecule, C_{60}–MPAA, by taking advantage of the excellent physical and chemical properties of C_{60} and nanoscale ordering of anthryl-based SAMs. The self-assembled molecular films of C_{60}–MPAA exhibit stable and highly ordered 2D arrays that form an oblique lattice at room temperature. The self-assemblies of C_{60}–MPAA exhibit reversible electrochemical peaks and interesting electronic properties. The design strategy developed here should generally be applicable to other molecules for developing novel, well-ordered nanostructural assemblies and a wide range of thin film functional materials.

Received: October 2, 2003 [Z53001]

Keywords: fullerenes · molecular electronics · monolayers · nanostructures · self-assembly

[1] a) C. A. Mirkin, W. B. Caldwell, *Tetrahedron* **1996**, *52*, 5113–5130; b) M. Prato, *Top. Curr. Chem.* **1999**, *199*, 173–187; c) G. Yu, J. Gao, J. C. Hummelen, F. Wudl, A. J. Heeger, *Science* **1995**, *270*, 1789.
[2] M. Prato, *J. Mater. Chem.* **1997**, *7*, 10970–11109.
[3] F. Diederich, M. Gómez-López, *Chem. Soc. Rev.* **1999**, *28*, 263–277.
[4] a) *Self-assembled Monolayers of Thiols* (Eds.: A. Ulman), Academic, San Diego, **1998**; b) A. Ulman, *Chem. Rev.* **1996**, *96*, 1533; c) A. R. Bishop, R. G. Nuzzo, *Curr. Opin. Colloid Interface Sci.* **1996**, *1*, 127; d) F. Schreiber, *Prog. Surf. Sci.* **2000**, *65*, 151; e) M. Mrksich, G. M. Whitesides, *Annu. Rev. Biophys. Biomol. Struct.* **1996**, *25*, 55.
[5] W. B. Caldwell, K. Chen, C. A. Mirkin, S. J. Babinec, *Langmuir* **1993**, *9*, 1945–1947.
[6] V. V. Tsukruk, L. M. Lander, W. J. Brittain, *Langmuir* **1994**, *10*, 996–999.
[7] X. Shi, W. B. Caldwell, K. Chen, C. A. Mirkin, *J. Am. Chem. Soc.* **1994**, *116*, 11598–11599.
[8] F. Arias, L. A. Godínez, S. R. Wilson, A. E. Kaifer, L. Echegoyen, *J. Am. Chem. Soc.* **1996**, *118*, 6086–6087.
[9] O. Domínguez, L. Echegoyen, F. Cunha, N. Tao, *Langmuir* **1998**, *14*, 821–824.
[10] Y.-S. Shon, K. F. Kelly, N. J. Halas, T. R. Lee, *Langmuir* **1999**, *15*, 5329–5332.
[11] S. Zhang, D. Dong, L. Gan, Z. Liu, C. Huang, *New J. Chem.* **2001**, *25*, 606–610.
[12] a) T. Sakurai, X. D. Wang, K. Q. Xue, Y. Hasegawa, T. Hashizume, H. Shinohara, *Prog. Surf. Sci.* **1996**, *51*, 263; b) R. J. Wilson, G. Meijer, D. S. Bethune, R. D. Johnson, D. D. Chambliss, M. S. de Vries, H. E. Hunziker, H. R. Wendt, *Nature* **1990**, *348*, 621; c) A. Marchenko, J. Cousty, *Surf. Sci.* **2002**, *513*, 233.
[13] a) J. G. Hou, J. L. Yang, H. Q. Wang, Q. X. Li, C. G. Zeng, L. F. Yuan, B. Wang, D. M. Chen, Q. S. Zhu, *Nature* **2001**, *409*, 304–305; b) L. F. Yuan, J. L. Yang, H. Q. Wang, C. G. Zeng, Q. X. Li, B. Wang, J. G. Hou, Q. S. Zhu, D. M. Chen, *J. Am. Chem. Soc.* **2003**, *125*, 169–172.
[14] M. H. Zareie, H. Ma, B. W. Reed, A. K.-Y. Jen, M. Sarikaya, *Nano Lett.* **2003**, *3*, 139–142.
[15] L. Echegoyen, L. E. Echegoyen, *Acc. Chem. Res.* **1998**, *31*, 593–601.
[16] H. Imahori, T. Azuma, A. Ajavakom, H. Norieda, H. Yamada, Y. Sakata, *J. Phys. Chem. B* **1999**, *103*, 7233–7237.
[17] R. J. Willson, G. Meijer, D. S. Bethune, R. D. Johnson, D. D. Chambliss, M. S. de Vries, H. E. Hunziker, H. R. Wendt, *Nature* **1990**, *348*, 621–622.

 © 2004 Wiley-VCH Verlag GmbH & Co. KGaA, Weinheim

[18] L. D. Lamb, D. R. Huffman, R. K. Workman, S. Howells, T. Chen, D. Sarid, R. F. Ziolo, *Science* **1992**, *255*, 1413 – 1416.
[19] E. I. Altman, R. J. Colton, *Phys. Rev. B* **1993**, *48*, 18244 – 18249.
[20] a) J. Chen, M. A. Reed, A. M. Rawlett, J. M. Tour, *Science* **1999**, *286*, 1550; b) Y. Selzer, A. Salomon, J. Ghabboun, D. Cahen, *Angew. Chem.* **2002**, *114*, 855; *Angew. Chem. Int. Ed.* **2002**, *41*, 827; c) C. B. Gorman, R. L. Carroll, R. R. Fuierer, *Langmuir* **2001**, *17*, 6923; d) J. Cornil, Y. Karzazi, J. L. Brédas, *J. Am. Chem. Soc.* **2002**, *124*, 3516.

 © 2004 Wiley-VCH Verlag GmbH & Co. KGaA, Weinheim

Drug Design

Site-Specific Introduction of Sialic Acid into Insulin**

*Masaaki Sato, Reiko Sadamoto, Kenichi Niikura, Kenji Monde, Hirosato Kondo, and Shin-Ichiro Nishimura**

Insulin, a peptide hormone, is virtually the only effective drug for the treatment of diabetes.[1] The quantity of insulin required is increasing along with the number of patients, and the demand for insulin can be as much as 0.5–1.0 g per year per patient.[2] However, native insulin is broken down in the blood stream within a few hours of administration, mainly as a result of decomposition in the liver.[3] Several insulin derivatives have been investigated as possible long-acting insulins for decreasing the required frequency of administration.[3,4] Most of these insulin derivatives are less soluble than native insulin and are gradually released from the injection site into the blood stream.[4] The disadvantages of these long-acting insulins are in the complex administration procedure and the difficulty in controlling the circulating glucose levels.[5] It is expected that water-soluble long-acting insulin derivatives would overcome these problems.[5,6]

We focused on the increased solubility[7] and decreased degradation offered by the addition of a sugar chain, especially one containing a sialic acid moiety, for the development of new long-acting insulin derivatives. In the case of erythropoietin,[8] another widely used protein-based drug, it is known that the introduction of sugar chains containing sialic acid moieties through genetically controlled protein expression, for example, in mammalian cells, enhances the duration of the drug's effectiveness because the proteins with sialic acid on the surface are not easily decomposed in the liver. However, optimization of the glycosylation is difficult because of the inevitable variation, arising from the expression, in the number of sugar moieties per protein and in the site of introduction. Several chemical methods have been reported for making a uniformly glycosylated protein;[9] however, these chemical methods usually require relatively harsh conditions that may abolish protein functions.

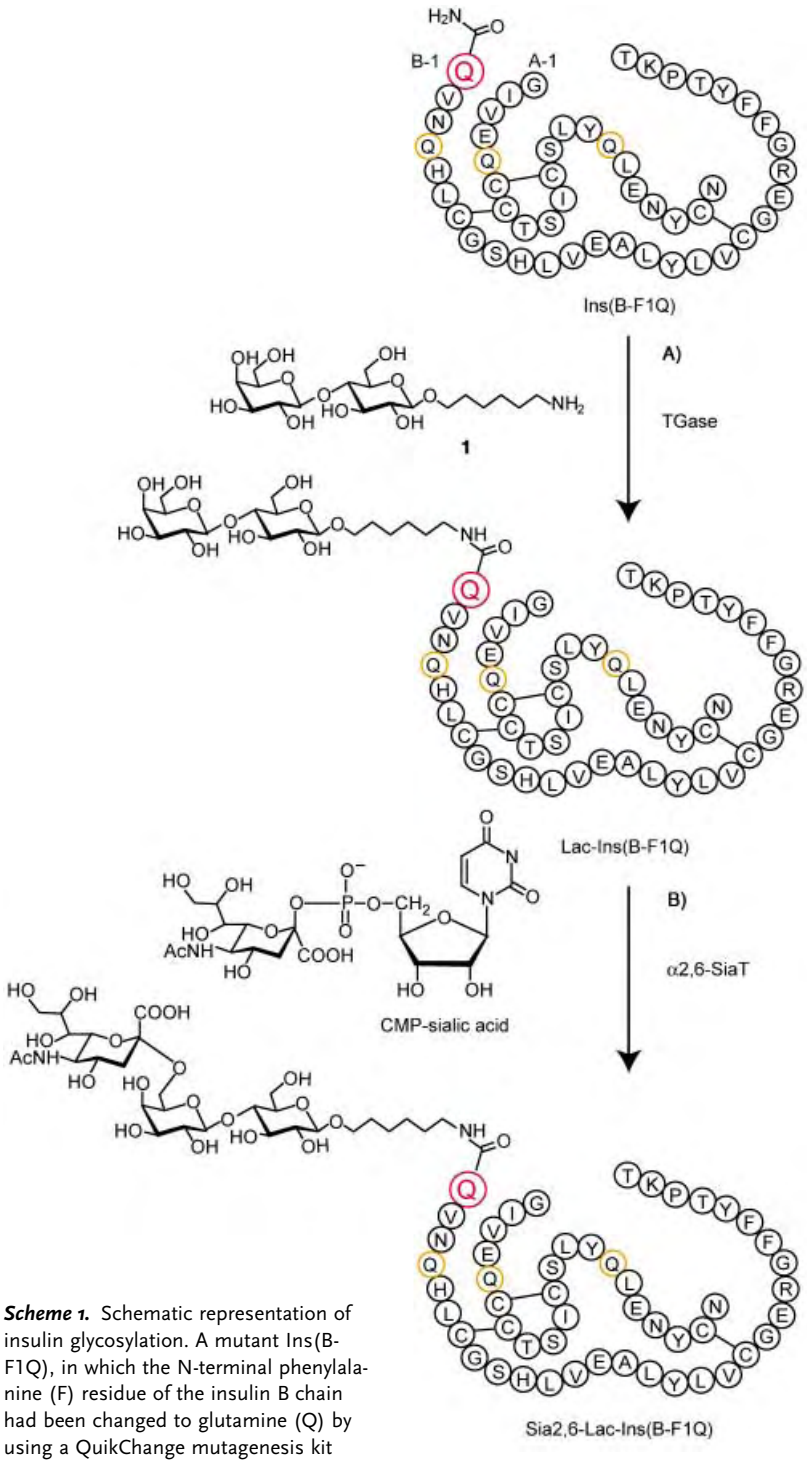
Herein, we describe a method for introducing a defined sugar moiety onto mutant insulins by enzymatic reactions (Scheme 1). After insertion of the lactose derivative through a transglutaminase reaction,[10] sialic acid can be introduced through a recombinant α2,6-sialyltransferase reaction.[11,12] These enzymatic reactions can proceed under physiological conditions. The insulin with the sialyl oligosaccharide is expected to demonstrate prolonged activity as a result of its resistance to decomposition in the liver.

Introduction of a sugar moiety to the glutamine residues by using TGase was reported to be a very effective method for obtaining sugar-modified peptides and proteins.[13] Recently, it was also demonstrated that an efficient synthesis of potent blockers of the influenza virus based on cyclic glycopeptides can be performed by using a TGase reaction.[12] Initially, we attempted to use the three glutamine residues in wild-type human insulin (Ins(WT)) as the reaction anchor to conjugate lactose derivative **1** through a TGase reaction. However, the sugar moiety was not effectively attached to the insulin (Figure 1 A), a result suggesting that all three glutamine residues are inaccessible to TGase. Therefore, we thought that some reactive glutamine residues should be added to the native insulin by point mutations. Human insulin consists of two separate chains, the A chain (21 amino acids) and the B chain (30 amino acids), joined together by a characteristic pattern of disulfide bridges[14] (Scheme 1). While the amino acid sequence of insulin is highly conserved in most animal species, species variations do exist, mainly in the amino acid sequence of the N-terminal region of the B chain. It has also been shown that modification of the N terminus of either the B or the A chain with a poly(ethylene glycol) chain or a simple monosaccharide residue has almost no negative effect on insulin bioactivity.[9b,15] Therefore, we created two mutagenetic insulins, Ins(B-F1Q) which has a glutamine residue instead of phenylalanine at the N terminus of the B chain and

[*] M. Sato, Dr. K. Niikura, Dr. K. Monde, Prof. S.-I. Nishimura
Division of Biological Sciences, Graduate School of Science
Frontier Research Center for Post-Genomic Science and Technology
Hokkaido University, Kita 21 Nishi 11, Sapporo 001-0021 (Japan)
Fax: (+81) 11-706-9042
E-mail: shin@glyco.sci.hokudai.ac.jp
Prof. S.-I. Nishimura
Japan Bioindustry Association
Sapporo 060-0810 (Japan)
Prof. S.-I. Nishimura
National Insutitute of Advanced Industrial Science and Technology (AIST)
Sapporo 062-8517 (Japan)
Dr. R. Sadamoto
Shionogi Laboratory of Biomolecular Chemistry
Division of Biological Science, Graduate School of Science
Frontier Research Center for Post-Genomic Science and Technology
Hokkaido University, Kita 21 Nishi 11, Sapporo 001-0021 (Japan)
Dr. H. Kondo
Discovery Research Laboratories
Shionogi & Co., Ltd., Osaka 553-0002 (Japan)

[**] This work was supported partly by a grant for "Research and Development on Glycocluster Controlling Biomolecules" from the New Energy and Industrial Technology Development Organization (NEDO). M.S. would like to thank Mr. A. Toda, Dr. K. Yamada, Dr. K. Iwata, Mr. T. Ohta, and Dr. H. Nakagawa for helpful discussions.

 © 2004 Wiley-VCH Verlag GmbH & Co. KGaA, Weinheim DOI: 10.1002/anie.200353058



Scheme 1. Schematic representation of insulin glycosylation. A mutant Ins(B-F1Q), in which the N-terminal phenylalanine (F) residue of the insulin B chain had been changed to glutamine (Q) by using a QuikChange mutagenesis kit (Stratagene), was overexpressed and purified from *Escherichia coli*. A) Chemoenzymatic glycosylation of Ins(B-F1Q) was carried out in 20 mM Tris buffer (pH 7.5) containing Ins(B-F1Q) (104 nmol), compound **1** (0.9 mmol), 5 mM $CaCl_2$, and TGase (4 U; Oriental Yeast Co.). The reaction mixture was incubated for 30 min at 37 °C. B) The sugar-elongation reaction of Lac-Ins(B-F1Q) was carried out in 50 mM sodium cacodylate buffer (pH 7.5, 1 mL) containing Lac-Ins(B-F1Q) (0.5 mg, 80.5 nmol), 0.6 mM CMP-sialic acid, 0.2% BSA, 1.6 mM $MnCl_2$, 0.2% Triton CF54, calf-intestine alkaline phosphatase (20 U), and recombinant α2,6-SiaT (150 mU, TOYOBO Co.). The reaction mixture was incubated for 2 h at 37 °C. TGase = transglutaminase, α2,6-SiaT = α2,6-sialyltransferase, Lac-Ins(B-F1Q) = lactose-displaying Ins(B-F1Q), Sia2,6-Lac-Ins(B-F1Q) = α2,6-sialylated Lac-Ins(B-F1Q), CMP = cytidine monophosphate, Tris = tris(hydroxymethyl)aminomethane, U = international unit, BSA = bovine serum albumin.

Ins(A-G1Q) which has a glutamine residue instead of glycine at the N terminus of the A chain.

First, we tested whether the mutagenetic insulins Ins(B-F1Q) and Ins(A-G1Q) retained their bioactivity by using streptozotocin-treated diabetic mice (STZ-treated mice). STZ-treated mice were separated into three groups at random, treated with a single subcutaneous dose of Ins(WT), Ins(B-F1Q), or Ins(A-G1Q), and then monitored for changes in blood-glucose level every hour for five hours (Figure 2). The dosage of all insulin preparations was adjusted to 1 U. The Ins(B-F1Q) action profile was very similar to that of wild-type insulin, a result showing that the biological potency of Ins(B-F1Q) was equal to that of Ins(WT). However, the glucose-lowering action of Ins(A-G1Q) was much weaker than that of the wild-type insulin. Therefore, we chose the active Ins(B-F1Q) for further modification with sugars.

The enzymatic reaction of Ins(B-F1Q) with a large excess of lactose derivative **1** was carried out in a Tris buffer (pH 7.5; Scheme 1). Mass spectrometric stidies showed that the modified insulin mostly had a single lactose moiety (Figure 1B). Purification of glycosylated insulin was performed by HPLC to afford the desired insulin Lac-Ins(B-F1Q) in around 50% yield. To determine the glycosylation site, Lac-Ins(B-F1Q) was treated with 2-thioethanol to cleave the disulfide bonds and divide it into two chains (the A and B chains); the molecular weights of the two peptide chains were then determined (Figure 1C). Mass spectrometry confirmed the glycosylation of the B chain occurred as expected. After purification of the B chain by HPLC, amino acid sequence analysis by using aminopeptidase M degradation was performed to determine the glycosylation site (Figure 1D). Treatment of the glycosylated B chain with aminopeptidase M, an exo-type protease that hydrolyzes peptides one by one from the N terminus, showed that not only the terminal glutamine residue (Q1) of the B chain but also the fourth glutamine residue (Q4) from the N terminus had been glycosylated by TGase. From the intensity of the fragment peaks corresponding to the peptides lacking only the N-terminal residues it seems that the glycosylation ratio between Q1 and Q4 is almost identical. Since the Q4 residue of the native insulin was not glycosylated by TGase, the phenylalanine → glutamine substitution at the N terminus is

 © 2004 Wiley-VCH Verlag GmbH & Co. KGaA, Weinheim

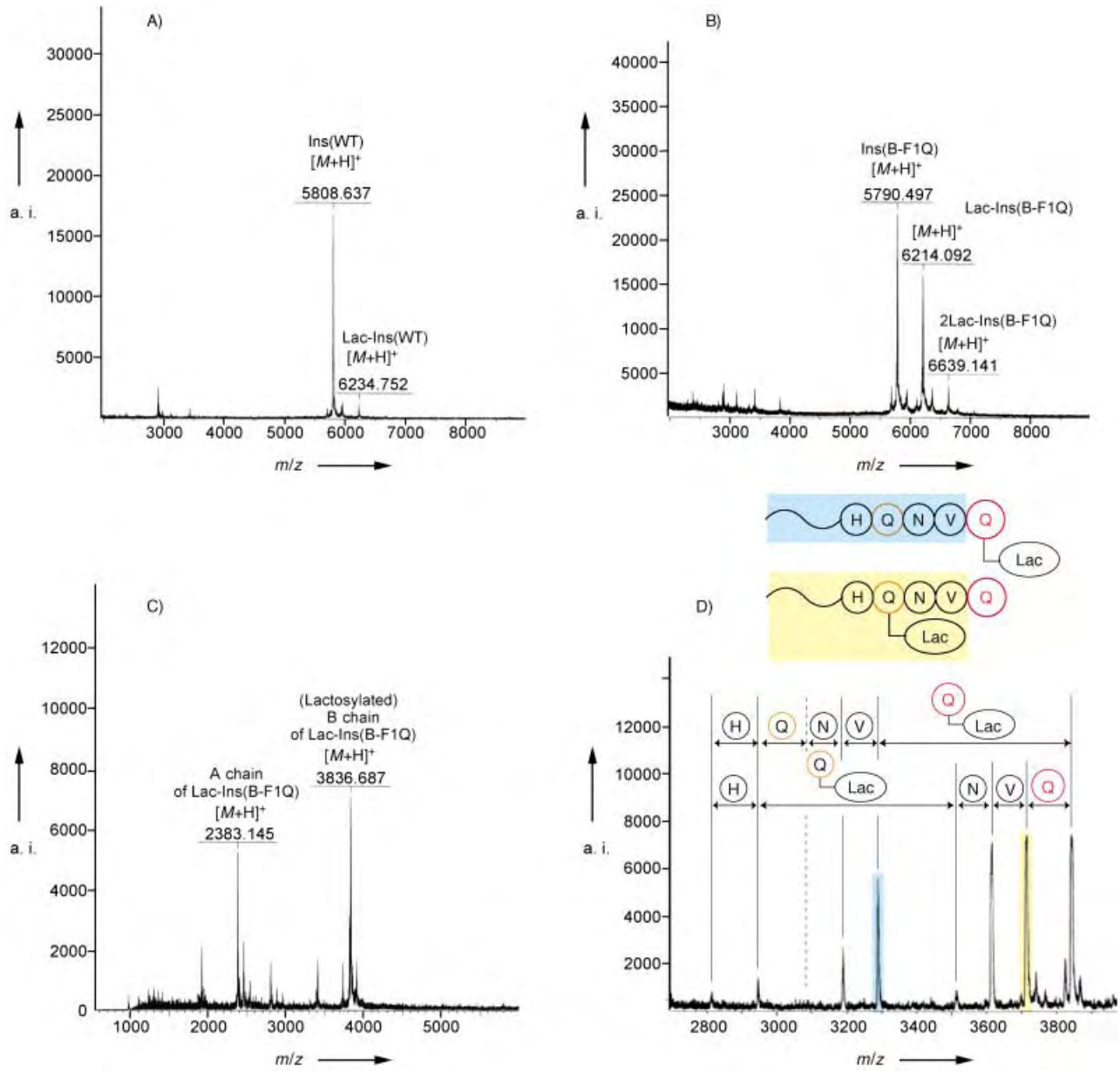


Figure 1. MALDI-TOF mass spectra of insulin and glycosylated insulin derivatives. A) Wild-type insulin after the TGase reaction. B) Ins(B-F1Q) after the TGase reaction. C) Lac-Ins(B-F1Q) after cleavage of the chains by 2-thioethanol (final concentration = 0.1 mmol mL^{-1}). D) Amino acid sequence analysis of the N terminus of the lactosylated B chain with aminopeptidase M. The lactosylated B chain was incubated with aminopeptidase M (final concentration = 1 U mL^{-1}; Roche) for 10 min at 37 °C. The reaction mixture was analyzed by MALDI-TOF (Bruker REFLEXIII) mass spectrometry. a.i. = arbitrary intensity.

thought to affect the microenvironment around Q4, thereby resulting in enhanced accessibility for TGase. The lactose-displaying insulin, which showed a single peak in the HPLC analysis, was found to be a mixture of two isomers, and we employed the mixture of Q1- and Q4-glycosylated insulin for further experiments.

The sialylation of Lac-Ins(B-F1Q) was performed by means of recombinant α2,6-SiaT, which transfers the sialic acid of CMP-sialic acid to position 6 of galactose (Scheme 1). The reaction mixtures were purified with reversed-phase HPLC to yield Sia2,6-Lac-Ins(B-F1Q).

To investigate if changes in the secondary/tertiary structure of the insulin molecule had occurred because of the mutation and glycosylation, far-UV/CD spectra of the insulin derivatives were compared to that of Ins(WT) (Figure 3). The spectrum of Ins(A-G1Q) was different from that of Ins(WT), a fact suggesting that the α-helix structure of the N terminus of the insulin A chain was changed by the point mutation. The spectra of Ins(B-F1Q) and Sia2,6-Lac-Ins(B-F1Q) were similar to that of Ins(WT). Therefore, the F1Q mutation and glycosylation at the N terminus of the insulin B chain had no effect on the overall structure, as evident from the CD spectra.

The biological activity of the two glycosylated insulin derivatives was also evaluated by using STZ-treated mice (Figure 2). The glycosylated insulins showed similar activity

 © 2004 Wiley-VCH Verlag GmbH & Co. KGaA, Weinheim

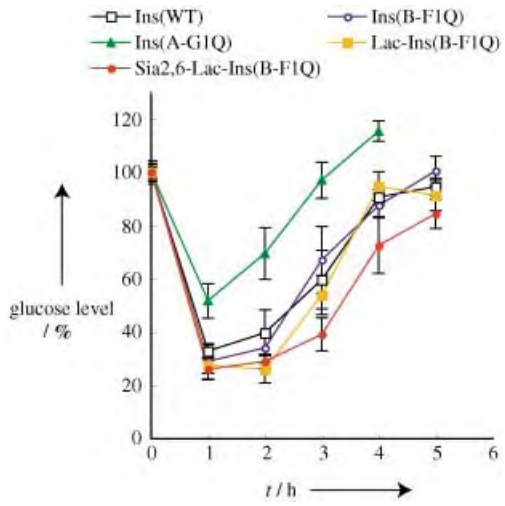


Figure 2. Changes in blood-glucose levels after the administration of insulin and glycosylated insulin derivatives. Mice (C57BL/6J, male, 7 weeks of age) were fasted for 18–20 h and then injected intraperitoneally with a single dose of streptozotocin (STZ; 200 mg kg^{-1} body weight; Wako). Mice with initial blood-glucose levels of above 400 mg dL^{-1} were selected for the monitoring of blood-glucose levels. Five mice were used for each insulin derivative. Blood samples were obtained from the tail vein at 0, 1, 2, 3, 4, and 5 h after subcutaneous administration of Ins(WT), Ins(B-F1Q), Ins(A-G1Q), Lac-Ins(B-F1Q), or Sia2,6-Lac-Ins(B-F1Q) (1 U of each). Blood-glucose levels were measured by using a Glucocard (Kyoto Daiichi Kagaku Co.). Data are presented as a percentage of the initial values ± standard error.

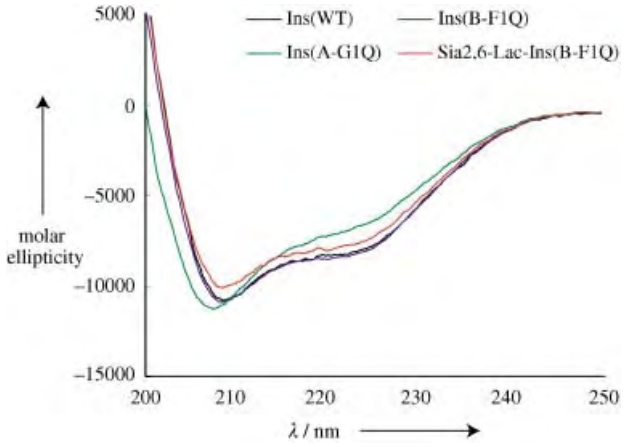


Figure 3. Circular dichroism spectra of insulin derivatives. All the insulin samples were dissolved in phosphate-buffered saline (pH 7.4). The protein concentrations were all adjusted to 40 μM by measurement of the UV absorption at 280 nm. CD measurements were performed on a Jasco-820 CD spectropolarimeter at 25 °C. For the far-UV/CD spectra, samples were scanned from 200–250 nm and accumulated 10 times at a resolution of 0.2 nm with a scanning speed of 100 nm min^{-1}. The cell length was 0.1 cm. All the CD data are expressed as the mean residue ellipticity.

shortly after subcutaneous injection, but the activity levels varied significantly with time. Lac-Ins(B-F1Q) had a slightly extended glucose-lowering effect compared to that of the wild type. However, Sia2,6-Lac-Ins(B-F1Q) displayed clearly prolonged glucose-lowering action, especially after three and four hours. We speculate that the long-acting effect of Sia2,6-Lac-Ins(B-F1Q) might be because the introduced sialic acid moiety increases the resistance against degradation of insulin in the liver.

In conclusion, we demonstrated that the point mutation of the N terminus of the insulin B chain enabled chemoenzymatic glycosylation to be achieved by combined use of a transglutaminase and a glycosyltransferase, thereby providing enzymatic access to link insulin and sugars. Sialyllactose-displaying insulin was found to show a prolonged duration of glucose-lowering action in the blood in vivo compared to the action of wild-type or lactose-displaying insulin, a result implying that the introduction of sialic acid to the protein is essential for prolonged activity in vivo. Our chemoenzymatic method generates artificial glycoproteins with a homogeneous glycoform and is suitable for large-scale production. This strategy is widely applicable for the synthesis of novel artificial glycopeptides and glycoproteins with improved and potent biological activity as protein-based drugs. Further study on the applications of this method is currently underway in our laboratory.

Experimental Section

Wild-type and mutant proinsulins were expressed and purified according to the procedure in ref. [16], except that arginine was used instead of methionine as a linker between the polyhistidine tag and the proinsulins for easy single cleavage.[17] The proinsulins were properly folded according to the protocol described in ref. [18]. The histidine tag and the C chain of the proinsulins were removed by trypsin cleavage.[17] Compound **1** was chemically synthesized according to the procedure described in ref. [12].

Received: October 10, 2003 [Z53058]

Keywords: drug design · glycoproteins · glycosylation · insulin · sialic acids

[1] a) O. Pillai, R. Panchagnula, *Drug Discovery Today* **2001**, *6*, 1056–1061; b) D. E. DeWitt, I. B. Hirsch, *JAMA J. Am. Med. Assoc.* **2003**, *289*, 2254–2264; c) D. E. DeWitt, D. C. Dugdale, *JAMA J. Am. Med. Assoc.* **2003**, *289*, 2265–2269.

[2] M. Schmidt, K. R. Babu, N. Khanna, S. Marten, U. Rinas, *J. Biotechnol.* **1999**, *68*, 71–83.

[3] E. Gershonov, Y. Shechter, M. Fridkin, *Diabetes* **1999**, *48*, 1437–1442.

[4] a) J. Markussen, P. Hougaard, U. Ribel, A. R. Sorensen, E. Sorensen, *Protein Eng.* **1987**, *1*, 205–213; b) J. Markussen, I. Diers, A. Engesgaard, M. T. Hansen, P. Hougaard, L. Langkjaer, K. Norris, U. Ribel, A. R. Sorensen, E. Sorensen, H. O. Voigt, *Protein Eng.* **1987**, *1*, 215–223; c) J. Markussen, I. Diers, P. Hougaard, L. Langkjaer, K. Norris, L. Snel, A. R. Sorensen, E. Sorensen, H. O. Voigt, *Protein Eng.* **1988**, *2*, 157–166.

[5] J. Markussen, S. Havelund, P. Kurtzhals, A. S. Andersen, J. Halstrom, E. Hasselager, U. D. Larsen, U. Ribel, L. Schaffer, K. Vad, I. Jonassen, *Diabetologia* **1996**, *39*, 281–288.

[6] a) E. Gershonov, I. Goldwaser, M. Fridkin, Y. Shechter, *J. Med. Chem.* **2000**, *43*, 2530–2537; b) P. Kurtzhals, B. Kiehr, A. R. Sorensen, *J. Pharm. Sci.* **1995**, *84*, 1164–1168.

[7] G. Walsh, *Protein Biochemistry and Biotechnology*, Wiley, Chichester, **2002**, p. 30.

 © 2004 Wiley-VCH Verlag GmbH & Co. KGaA, Weinheim

[8] a) J. C. Egrie, E. Dwyer, J. K. Browne, A. Hitz, M. A. Lykos, *Exp. Hematol.* **2003**, *31*, 290 – 299; b) J. C. Egrie, J. K. Browne, *Br. J. Cancer* **2001**, *84* (Suppl. 1), 3 – 10.
[9] a) M. Brownlee, A. Cerami, *Science* **1979**, *206*, 1190 – 1191; b) T. Uchio, M. Baudys, F. Liu, S. C. Song, S. W. Kim, *Adv. Drug Delivery Rev.* **1999**, *35*, 289 – 306; c) E. J. Bilsky, R. D. Egleton, S. A. Mitchell, M. M. Palian, P. Davis, J. D. Huber, H. Jones, H. I. Yamamura, J. Janders, T. P. Davis, F. Porreca, V. J. Hruby, R. Polt, *J. Med. Chem.* **2000**, *43*, 2586 – 2590; d) D. Macmillan, R. M. Bill, K. A. Sage, D. Fern, S. L. Flitsch, *Chem. Biol.* **2001**, *8*, 133 – 145.
[10] a) J. E. Folk, P. W. Cole, *Biochim. Biophys. Acta* **1966**, *122*, 244 – 264; b) T. Ohtsuka, M. Ota, N. Nio, M. Motoki, *Biosci. Biotechnol. Biochem.* **2000**, *64*, 2608 – 2613.
[11] a) H. J. Gross, R. Brossmer, *Glycoconjugate J.* **1995**, *12*, 739 – 746; b) A. Nagpurkar, D. Hunt, S. Mookerjea, *Int. J. Biochem. Cell Biol.* **1996**, *28*, 1337 – 1348c) E. R. Sjoberg, H. Kitagawa, J. Glushka, H. van Halbeek, J. C. Paulson, *J. Biol. Chem.* **1996**, *271*, 7450 – 7459.
[12] T. Ohta, N. Miura, N. Fujitani, F. Nakajima, K. Niikura, R. Sadamoto, C.-T. Guo, T. Suzuki, Y. Suzuki, K. Monde, S.-I. Nishimura, *Angew. Chem.* **2003**, *115*, 5344 – 5347; *Angew. Chem. Int. Ed.* **2003**, *42*, 5186 – 5189.
[13] D. Ramos, P. Rollin, W. Klaffke, *J. Org. Chem.* **2001**, *66*, 2948 – 2956.
[14] G. I. Bell, R. L. Pictet, W. J. Rutter, B. Cordell, E. Tischer, H. M. Goodman, *Nature* **1980**, *284*, 26 – 32.
[15] K. D. Hinds, S. W. Kim, *Adv. Drug Delivery Rev.* **2002**, *54*, 505 – 530.
[16] R. B. Mackin, *Protein Expression Purif.* **1999**, *15*, 308 – 313.
[17] P. Jonasson, J. Nilsson, E. Samuelsson, T. Moks, S. Stahl, M. Uhlen, *Eur. J. Biochem.* **1996**, *236*, 656 – 661.
[18] D. J. Cowley, R. B. Mackin, *FEBS Lett.* **1997**, *402*, 124 – 130.

 © 2004 Wiley-VCH Verlag GmbH & Co. KGaA, Weinheim

Bimetallic Catalysts

Combinatorial Catalysis with Bimetallic Complexes: Robust and Efficient Catalysts for Atom-Transfer Radical Additions

*Laurent Quebatte, Rosario Scopelliti, and Kay Severin**

Methods of combinatorial chemistry such as high-throughput screenings are increasingly being employed for the discovery and optimization of homogeneous transition-metal catalysts.[1] So far, most efforts have focused on mononuclear catalysts with ligands that are preferably built in a modular fashion. The screening of bi- or oligometallic catalysts represents a special challenge since the synthesis of a catalyst library is generally more difficult. Nevertheless, it would be interesting to include such compounds in screening assays because of the potentially superior performance of polynuclear catalysts as compared to their mononuclear counterparts.[2] In this context, complexes of the late transition metals in which two different metal fragments are connected by halo bridges appear to be of interest. The synthesis of such complexes is easy and can even be performed in situ.[3,4] Furthermore, due to the high intrinsic reactivity of halo-bridged complexes, they are well suited as catalyst precursors. In the following, we describe two chloro-bridged Rh–Ru complexes, which act as highly active catalyst precursors for atom-transfer radical additions (ATRAs) of polyhalogenated compounds to olefins (the "Kharasch reaction"). These catalysts were discovered in a parallel screening of bimetallic complexes.

Several transition-metal complexes are able to catalyze the anti-Markovnikov addition of polyhalogenated compounds to olefins.[5] Among these, Ru^{II}–phosphane complexes play a dominant role. For a long time, $[RuCl_2(PPh_3)_3]$ was considered to be the most active Ru-based ATRA catalyst,[5,6] and a variety of synthetically useful reactions were developed.[7] A drawback of this system, however, is the high catalyst loading (1–5%) and the harsh reaction conditions required ($T > 100\,^{\circ}C$). More recently, a number of new Ru^{II} catalysts with superior performance were developed.[8–10] So far, the pentamethylcyclopentadienyl (Cp*) complex $[Cp^*RuCl(PPh_3)_2]$[9] and its dicarbollide analogues $[(RR'S\text{-}C_2B_9RH_9)RuH(PPH_3)_2]$[10] show the highest activity, which allows the Kharasch addition of CCl_4 to styrene to be carried out at ambient temperature.[9]

The ruthenium-catalyzed Kharasch reaction is believed to proceed via a radical mechanism in the coordination sphere of the metal complex.[5] For reactions with $[RuCl_2(PPh_3)_3]$, the actual catalyst is presumably the fourteen-electron species $\{RuCl_2(PPh_3)_2\}$, which is generated by dissociation of PPh_3. This assumption is in agreement with the fact that the reaction is inhibited by an excess of PPh_3.[6] In a previous publication, we have reported that the $\{RuCl_2(PPh_3)_2\}$ fragment can be stabilized and solubilized using half-sandwich chloro complexes as labile ligands.[11] The resulting complexes $[L_nM(\mu\text{-}Cl)_3RuCl(PPh_3)_2]$ (L_nM = (arene)Ru, Cp*Ir, Cp*Rh) can be obtained in quantitative yield by reaction of the dimeric acetone adduct $[(PPh_3)_2(CH_3COCH_3)Ru(\mu\text{-}Cl)_3RuCl(PPh_3)_2]$ (**1**) with chloro-bridged half-sandwich complexes (Scheme 1). More recently, we have found that structurally related complexes with chelating 1,4-bis(diphenylphosphanyl)butane (dppb) or 1,4-bis(dicyclohexylphosphanyl)butane (dcypb) ligands instead of the two PPh_3 ligands can be synthesized (also in quantitative yield) using the aqua complex $[(dppb)ClRu(\mu\text{-}Cl)_2(\mu\text{-}OH_2)RuCl(dppb)]$ (**2**) or the dinitrogen complex $[(dcypb)(N_2)Ru(\mu\text{-}Cl)_3RuCl(dcypb)]$ (**3**) instead of **1**.[4]

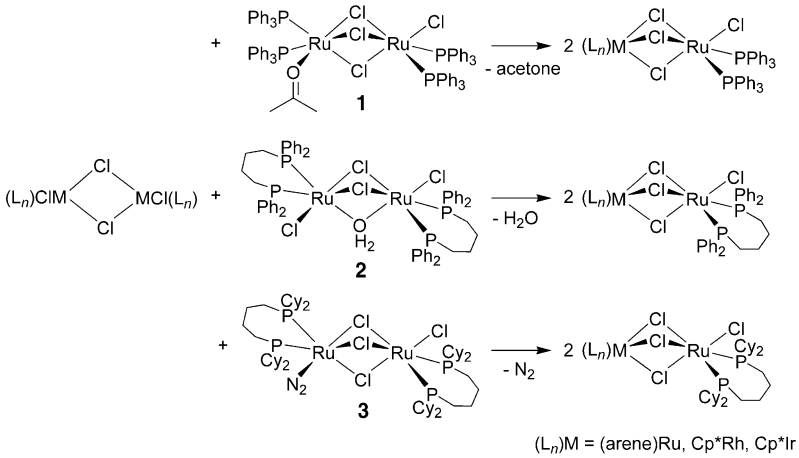
The reactions depicted in Scheme 1 are general, fast, and give rise to structurally defined products in quantitative yields. Therefore, they are ideally suited to generate a library of homo- and heterobimetallic complexes in a combinatorial fashion. To investigate whether compounds of this type are useful catalyst precursors for ATRA reactions, we have tested

[*] L. Quebatte, Dr. R. Scopelliti,[+] Prof. K. Severin
Institut des Sciences et Ingénierie Chimiques
École Polytechnique Fédérale de Lausanne
1015 Lausanne (Switzerland)
Fax: (+41) 21-693-9305
E-mail: kay.severin@epfl.ch

[+] X-ray structural analysis.

[**] X-ray structural analysis.

 © 2004 Wiley-VCH Verlag GmbH & Co. KGaA, Weinheim DOI: 10.1002/anie.200353084



Scheme 1. Synthesis of bimetallic complexes containing $\{RuCl_2(PR_3)_2\}$ fragments.

66 different complexes in a parallel fashion. Assuming that a reaction similar to that depicted in Scheme 1 would occur with other chloro-bridged complexes of the late transition metals, we have prepared mixtures of **1**, **2**, or **3** with various dimeric $[\{L_nM(\mu\text{-}Cl)\}_2]$ complexes of Ru^{II}, Ru^{III}, Ru^{IV}, Rh^{I}, Rh^{III}, Ir^{I}, Ir^{III}, Pd^{II}, and Pt^{II}.[12] These reactions were carried out simultaneously on a small scale and the resulting products were immediately tested in a parallel fashion for catalytic activity without purification.[13] As a benchmark reaction we have employed the addition of CCl_4 to styrene, which was analyzed by gas chromatography using an autosampler (Figure 1).

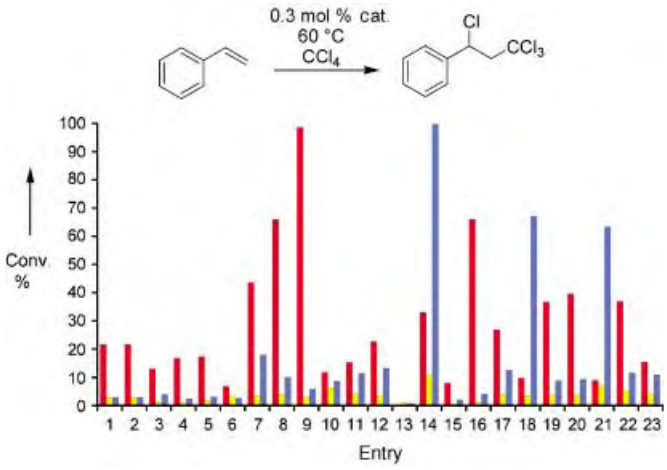


Figure 1. Parallel screening of catalyst activity using the addition of CCl_4 to styrene as a benchmark reaction. The catalysts were prepared in situ my mixing complex **1** (red), **2** (yellow), or **3** (blue) with: 1) $[\{(C_6H_6)RuCl(\mu\text{-}Cl)\}_2]$, 2) $[\{(C_6H_5CO_2Et)RuCl(\mu\text{-}Cl)\}_2]$, 3) $[\{(cymene)\text{-}RuCl(\mu\text{-}Cl)\}_2]$, 4) $[\{(C_6Me_6)RuCl(\mu\text{-}Cl)\}_2]$, 5) $[\{(1,3,5\text{-}C_6Et_3H_3)RuCl(\mu\text{-}Cl)\}_2]$, 6) $[\{(1,3,5\text{-}C_6H_3iPr_3)RuCl(\mu\text{-}Cl)\}_2]$, 7) $[\{(C_{10}H_{16})RuCl(\mu\text{-}Cl)\}_2]$, 8) $[\{Cp^*RuCl(\mu\text{-}Cl)\}_2]$, 9) $[\{Cp^*RhCl(\mu\text{-}Cl)\}_2]$, 10) $[\{(ppy)_2Rh(\mu\text{-}Cl)\}_2]$, 11) $[\{(allyl)_2Rh(\mu\text{-}Cl)\}_2]$, 12) $[\{(cod)Rh(\mu\text{-}Cl)\}_2]$, 13) $[\{(CO)_2Rh(\mu\text{-}Cl)\}_2]$, 14) $[\{(tpc)Rh(\mu\text{-}Cl)\}_2]$, 15) $[\{(cod)Ir(\mu\text{-}Cl)\}_2]$, 16) $[\{Cp^*IrCl(\mu\text{-}Cl)\}_2]$, 17) $[\{(PEt_3)PdCl(\mu\text{-}Cl)\}_2]$, 18) $[\{(PEt_3)_2Pd(\mu\text{-}Cl)\}_2](BF_4)_2$, 19) $[\{(C_9H_{12}N)Pd(\mu\text{-}Cl)\}_2]$, 20) $[\{(allyl)Pd(\mu\text{-}Cl)\}_2]$, 21) $[\{(PEt_3)_2Pt(\mu\text{-}Cl)\}_2](BF_4)_2$, 22) $[\{(C_{11}H_{14}NO_2)Pd(\mu\text{-}Cl)\}_2]$, 23) no additional complex. Reaction conditions: styrene (1.4 mmol), CCl_4 (2.0 mmol), first complex (**1**, **2**, or **3**) (2.3 μmol), second complex (4.6 μmol), $CHCl_3$ (600 μL), 60 °C. The conversion after 2 h is based on the consumption of styrene as determined by GC. For the reactions 1, 10, and 21, some precipitation could be observed during the reaction.

For reactions with the $\{RuCl_2(PPh_3)_2\}$ complex **1**, several of the in situ generated homo- and heterobimetallic complexes display a substantial catalytic activity (Figure 1, red bars). The highest activity is observed for reactions with a mixture of **1** and the Rh^{III} complex $[Cp^*RhCl(\mu\text{-}Cl)]_2$ (Figure 1, entry 9a; a = red, b = yellow, c = blue). The Rh^{I} complex $[\{(CO)_2Rh(\mu\text{-}Cl)\}_2]$, on the other hand, seems to inhibit the reaction completely (entry 13a). For mixtures containing the $\{RuCl_2(dppb)\}$ complex **2** (yellow bars), consistently low conversions were observed (1–11 %). This points to an intrinsic advantage of two monodentate PPh_3 ligands as compared to a chelating dppb co-ligand. Similarly, reactions with the $\{RuCl_2(dcypb)\}$ complex **3** gave low or moderate conversions with three notable exceptions: for mixtures with the cationic complexes $[\{(PEt_3)_2Pd(\mu\text{-}Cl)\}_2](BF_4)_2$ (entry 18c) and $[\{(PEt_3)_2Pt(\mu\text{-}Cl)\}_2](BF_4)_2$ (entry 21c) conversions of 67 % and 63 % were observed whereas a quantitative conversion was found for mixtures with the Rh^{I} complex $[\{(tpc)Rh(\mu\text{-}Cl)\}_2]$ (entry 14c; tpc = η^4-tetraphenylcyclopentadienone).

In a second set of experiments, we have tested the catalytic activity of all symmetrical complexes $[\{L_nM(\mu\text{-}Cl)\}_2]$ without the addition of the ruthenium complexes **1**–**3**. None of the complexes displayed any significant activity (conversion < 1 %). This indicates that the ruthenium–phosphane fragments are responsible for catalysis. The overall activity, however, is clearly modulated by the second metal fragment $\{L_nMCl\}$.

From the parallel screening, two promising catalyst precursors emerged. The first is formed by reaction of **1** with $[\{Cp^*RhCl(\mu\text{-}Cl)\}_2]$ and the second is formed by reaction of **3** with $[\{(tpc)Rh(\mu\text{-}Cl)\}_2]$. We have therefore repeated these reactions on a preparative scale from which we were able to isolate the heterometallic complexes $[Cp^*Rh(\mu\text{-}Cl)_3RuCl(PPh_3)_2]$ (**4**) and $[\{(tcp)Rh(\mu\text{-}Cl)_3Ru(dcypb)\}_2(\mu\text{-}N_2)]$ (**5**) in good yield. Both compounds were characterized by single-crystal X-ray analysis (Figures 2 and 3).[14]

The $\{Cp^*Rh\}$ fragment in **4** is coordinated through three chloro-bridges to the Ru–phosphane fragment. The Ru–Cl bond length of the terminal chloro ligand is smaller than the Ru–Cl bond lengths found for the bridging chloro ligands. As expected, the angle between the sterically demanding PPh_3 groups is enlarged resulting in a distorted octahedral geometry around the Ru atom. The plane defined by the Cp^* π ligand is almost parallel to that defined by the bridging chloro ligands.

Similar to what was found for complex **4**, the $\{(tcp)Rh\}$ fragment in **5** is coordinated through three chloro bridges to the Ru–phosphane fragment (Figure 3). Consequently, the Rh center exhibits a five-coordinate, electronically saturated configuration. This is in agreement with the known tendency of cyclopentadienone–rhodium complexes to form piano-stool-type complexes.[15] The ruthenium atom shows a dis-

 © 2004 Wiley-VCH Verlag GmbH & Co. KGaA, Weinheim

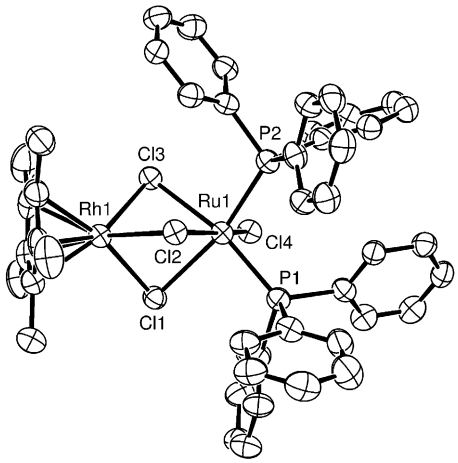


Figure 2. ORTEP drawing of the molecular structure of **4**. The hydrogen atoms are not shown for clarity. Selected bond lengths [Å] and angles [°]: Ru1-Cl4 = 2.375(2), Ru1-Cl2 = 2.436(2), Ru1-Cl3 = 2.399(2); P1-Ru1-P2 = 103.71(6), Cl4-Ru1-Cl2 = 169.42(6).

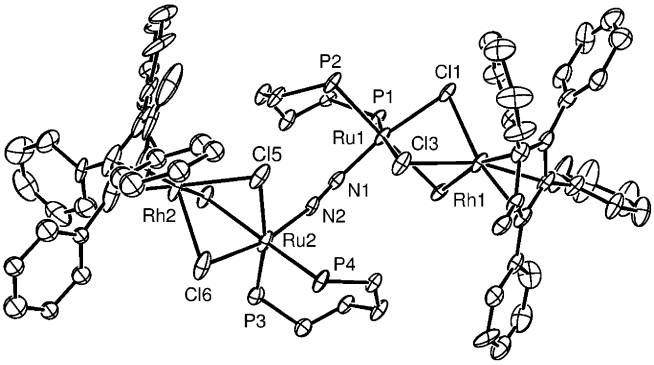


Figure 3. ORTEP drawing of the molecular structure of **5**. The hydrogen atoms, the cyclohexyl side chains, and the external solvent molecule are not shown for clarity. Selected bond lengths [Å] and angles [°]: Ru1-N1 = 1.963(10), Ru2-N2 = 1.985(9), N1-N2 = 1.118(12); P1-Ru1-P2 = 93.53(9), P3-Ru2-P4 = 94.14(11), N2-N1-Ru1 = 164.6(8), N1-N2-Ru2 = 164.2(8).

torted octahedral geometry with one coordination site being occupied by a dinitrogen ligand. The latter acts as an end-on bridging ligand that connects two heterobimetallic Rh^{I}–Ru^{II} complexes. The bond lengths and angles found for the $Ru(\mu^2\text{-}N_2)Ru$ moiety (Figure 3) are comparable to those observed for other ruthenium complexes with bridging N_2 ligands.[16]

With the isolated complexes **4** and **5**, we have performed a more detailed analysis of the catalytic performance using again the benchmark reaction between styrene and CCl_4. Apart from chloroform, toluene was employed as a solvent. The results are summarized in Table 1. The Rh^{I}–Ru^{II} complex **5** was found to display a very high activity surpassing not only that of the Rh^{III}–Ru^{II} complex **4** but also that of the previously described catalyst precursors $[RuCl_2(PPh_3)_3]$ and $[Cp^*RuCl(PPh_3)_2]$ (entries 1–6). A surprising discovery was that for catalysts **4** and **5**, reactions performed in "wet" chloroform and toluene gave better results than those performed in thoroughly dried solvents (entries 7–12). This is in sharp contrast to reactions catalyzed by $[RuCl_2(PPh_3)_3]$ or by the very sensitive[17] $[Cp^*RuCl(PPh_3)_2]$, for which traces of water were found to reduce the catalytic activity significantly (entries 11 and 12).

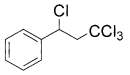
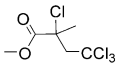
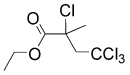
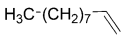
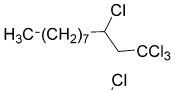
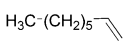
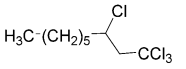
Table 1: Addition of CCl_4 to styrene, catalyzed by complex **4**, **5**, $[RuCl_2(PPh_3)_3]$, or $[Cp^*RuCl(PPh_3)_2]$.[a]

Entry	Catalyst	Solvent	Conv. [%]
1	**4**	toluene	23
2	**4**	chloroform	20
3	**5**	toluene	78
4	**5**	chloroform	94
5	$[RuCl_2(PPh_3)_3]$	chloroform	14
6	$[Cp^*RuCl(PPh_3)_2]$	chloroform	53
7	**4**	chloroform (saturated with H_2O)	37
8	**4**	toluene (saturated with H_2O)	36
9	**5**	toluene (saturated with H_2O)	76
10	**5**	chloroform (saturated with H_2O)	95
11	$[RuCl_2(PPh_3)_3]$	chloroform (saturated with H_2O)	7
12	$[Cp^*RuCl(PPh_3)_2]$	chloroform (saturated with H_2O)	29

[a] Reaction conditions: cat./styrene/CCl_4 = 1:300:432; [cat.] = 4.59 mM, 60 °C. The conversion is based on the consumption of styrene and was determined after 1 h by GC.

Next, we investigated the influence of the CCl_4 concentration on the activity of the new catalysts using "wet" chloroform as the solvent. Both complexes were found to display the highest activities for total CCl_4 concentrations of around 5.5 M (catalyst/substrate/CCl_4 = 1:300:1200). Using these optimized conditions, the scope of the new heterometallic catalyst precursors **4** and **5** was tested in reactions with various olefinic substrates (Table 2). For styrene and methylacrylates, near-total conversion of the substrate is observed

Table 2: Atom-transfer radical additions catalyzed by the heterobimetallic complexes **4** and **5**.[a]

Entry	Cat.	Substrate	Product	*t* [h]	Conv. [%]	Yield [%]
1	**4**			4	88	86
2	**5**			1	99	98
3	**4**			4	99	84
4	**5**			1	98	93
5	**4**			4	99	79
6	**5**			1	98	92
7	**4**			10	97	88
8	**5**			24	80	75
9	**4**			10	98	90
10	**5**			24	80	74

[a] Reaction conditions: cat./styrene/CCl_4 = 1:300:1200; [cat.] = 4.59 mM; solvent: $CHCl_3$ saturated with H_2O; 60 °C. The conversion is based on the consumption of the substrate and the yield is based on the formation of product as determined by GC or by ^1H NMR spectroscopy.

 © 2004 Wiley-VCH Verlag GmbH & Co. KGaA, Weinheim

after only 1 h for catalyst **5** and after 4 h for catalyst **4** (entries 1–6). The yields are slightly lower than the conversions due to the formation of oligomers, a problem generally encountered for these types of addition reactions.

Longer reaction times are required for 1-octene and 1-decene, two notoriously bad substrates for Kharasch reactions. It is interesting to note that for these substrates it is the Rh^{III}–Ru^{II} complex **4** that gives the better results: after 10 h, a yield of 88% and 90%, respectively, is found together with a nearly quantitative conversion (entry 7 and 9). These values are clearly superior to what is observed for other catalyst precursors. With $[Cp^*RuCl(PPh_3)_2]$, for example, a yield of 27% and a conversion of 46% was observed after 24 h under nearly identical conditions.[9]

The potential of the catalyst precursor **5** is further underlined by the high turnover frequencies (TOFs) and numbers (TONs) that can be achieved. For the addition of CCl_4 to styrene, for example, an initial TOF of 1200 h^{-1} and a total TON of 4500 has been determined (catalyst/substrate/CCl_4 = 1:6000:12000). These are among the highest values that have been reported for an ATRA catalyst.[18] The unique tetrameric structure of **5** points to a possible explanation for its exceptionally high catalytic activity: As for the starting material **3**, the dinitrogen ligand is expected to be labile. Upon liberation of this ligand, an unsaturated 16-electron ruthenium complex would be generated, which is then stabilized by the sterically demanding {(tcp)Rh} fragment and the large dcypb ligand. For complex **4**, the mode of activation is less evident. A plausible mechanism involves the cleavage of one or several halo bridges, as was suggested for a chloro-bridged Rh^{III}–Ru^{II} metathesis catalyst.[19] It is clear, however, that both the $\{Cp^*Rh^{III}\}$ and the $\{Ru^{II}(PPh_3)_2\}$ fragment are essential constituents of this new catalyst.

Aside from their high catalytic activity, complexes **4** and **5** offer some important advantages. Since they are obtained in reactions that are fast and quantitative, they can be generated in situ, prior to catalysis, without isolating the complexes. The corresponding starting materials are easily accessible, in particular for complex **4**. Of special interest is the fact that the catalysts display a good performance in organic solvents of moderate purity (saturated with water). Extensive purification of the solvents, as is required for other catalysts for the Kharasch reaction, is therefore not necessary. Current efforts in our laboratory are directed towards a deeper understanding of the mechanism of these new types of catalysts. Furthermore, we are investigating whether complexes **4** and **5** are useful catalysts for the closely related atom-transfer radical polymerization of olefins.[20]

Experimental Section

The complexes $[(dppb)ClRu(\mu\text{-}Cl)_2(\mu\text{-}OH_2)RuCl(dppb)]$,[21] $[(dcypb)(N_2)Ru(\mu\text{-}Cl)_3RuCl(dcypb)]$,[22] $[Cp^*Rh(\mu\text{-}Cl)_3RuCl(PPh_3)_2]$,[11] $[\{(C_6H_5CO_2Et)RuCl(\mu\text{-}Cl)\}_2]$,[23] $[\{(cymene)RuCl(\mu\text{-}Cl)\}_2]$,[24] $[\{(C_6H_6)RuCl(\mu\text{-}Cl)\}_2]$,[25] $[\{(C_6Me_6)RuCl(\mu\text{-}Cl)\}_2]$,[24] $[\{(1,3,5\text{-}C_6H_3Et_3)RuCl(\mu\text{-}Cl)\}_2]$,[26] $[\{(1,3,5\text{-}C_6H_3iPr_3)RuCl(\mu\text{-}Cl)\}_2]$,[26] $[\{(\eta^3\text{:}\eta^3\text{-}C_{10}H_{16})RuCl(\mu\text{-}Cl)\}_2]$,[27] $[\{Cp^*RuCl(\mu\text{-}Cl)\}_2]$,[28] $[\{Cp^*RhCl(\mu\text{-}Cl)\}_2]$,[29] $[\{Cp^*IrCl(\mu\text{-}Cl)\}_2]$, $[\{(ppy)_2Rh(\mu\text{-}Cl)\}_2]$ (ppy = pyridin-2-yl-2-phenyl),[30] $[\{(allyl)_2Rh(\mu\text{-}Cl)\}_2]$ (allyl = η^3-C_3H_5),[31] $[\{(cod)Rh(\mu\text{-}Cl)\}_2]$ (cod = η^4-cycloocta-1,5-diene),[32] $[\{(CO)_2Rh(\mu\text{-}Cl)\}_2]$,[33] $[\{(tpc)Rh(\mu\text{-}Cl)\}_2]$ (tpc = η^4-tetraphenylcyclopentadienone),[34] $[\{(cod)Ir(\mu\text{-}Cl)\}_2]$,[35] $[\{(PEt_3)PdCl(\mu\text{-}Cl)\}_2]$,[36] $[\{(C_9H_{12})Pd(\mu\text{-}Cl)\}_2]$ (C_9H_{12} = *ortho*-metalated *N*,*N*′-dimethylbenzylamine),[37] $[\{(PEt_3)_2Pt(\mu\text{-}Cl)\}_2](BF_4)_2$,[38] and $[\{(PEt_3)_2Pd(\mu\text{-}Cl)\}_2](BF_4)_2$[38] were prepared according to literature procedures. The complex $[\{(allyl)Pd(\mu\text{-}Cl)\}_2]$ was purchased from Fluka. Complex **4** was prepared as described in ref. [11]. Crystals were obtained by slow diffusion of pentane into a solution of **4** in THF.

5: A mixture of $[(dcypb)(N_2)Ru(\mu\text{-}Cl)_3RuCl(dcypb)]$ (110 mg, 86 μmol) and $[\{(tpc)Rh(\mu\text{-}Cl)\}_2]$ (90 mg, 86 μmol) in CH_2Cl_2 (10 mL) was stirred until a homogeneous solution was obtained. The solution was then poured into hexane (100 mL) to precipitate a red powder, which was filtered off and washed with pentane (2 × 20 mL) and dried under a flow of dinitrogen for at least 5 h (yield: 87%). Single crystals were obtained by slow diffusion of pentane into a solution of **5** in CH_2Cl_2. ^1H NMR (400 MHz, CD_2Cl_2): δ = 0.86–2.28 (m, 104H, dcypb), 7.11–7.82 ppm (m, 40H, $C_{29}H_{20}O$); ^{13}C NMR (101 MHz, CD_2Cl_2): δ = 14.24–40.21 (dcypb), 67.71 (d, $^1J_{C\text{-}Rh}$ = 11 Hz, tpc), 93.79 (d, $^1J_{C\text{-}Rh}$ = 13 Hz, tpc), 127.20–133.18 ppm (tpc); ^{31}P NMR (162 MHz, CD_2Cl_2): δ = 42.44 ppm; elemental analysis calcd (%) for $C_{114}H_{144}N_2O_2Cl_6P_4Rh_2Ru_2 \cdot 0.5\,C_6H_{14}$: C 59.49, H 6.44, N 1.19; found: C 59.76, H 6.50, N 1.09.

Received: October 14, 2003 [Z53084]
Published Online: February 16, 2004

Keywords: combinatorial chemistry · heterogeneous catalysis · Kharasch reaction · rhodium · ruthenium

[1] For recent reviews see: a) P. Chen, *Angew. Chem.* **2003**, *115*, 2938–2954; *Angew. Chem. Int. Ed.* **2003**, *42*, 2832–2847; b) C. Gennari, U. Piarulli, *Chem. Rev.* **2003**, *103*, 3071–3100; c) J. P. Stambuli, J. F. Hartwig, *Curr. Opin. Chem. Biol.* **2003**, *7*, 420–426; d) V. Murphy, A. F. Volpe, Jr., W. H. Weinberg, *Curr. Opin. Chem. Biol.* **2003**, *7*, 427–433; e) J. G. de Vries, A. H. M. de Vries, *Eur. J. Org. Chem.* **2003**, 799–811; f) A. Hagemeyer, B. Jandeleit, Y. Liu, D. M. Poojary, H. W. Turner, A. F. Volpe, Jr., W. H. Weinberg, *Appl. Catal. A* **2001**, *221*, 23–43; g) S. R. Gilbertson, *Prog. Inorg. Chem.* **2001**, *50*, 433–471; h) M. T. Reetz, *Angew. Chem.* **2001**, *113*, 292–320; *Angew. Chem. Int. Ed.* **2001**, *40*, 284–310; i) B. Jandeleit, D. J. Schaefer, T. S. Powers, H. W. Turner, W. H. Weinberg, *Angew. Chem.* **1999**, *111*, 2648–2689; *Angew. Chem. Int. Ed.* **1999**, *38*, 2494–2532; j) R. H. Crabtree, *Chem. Commun.* **1999**, 1611–1616; k) K. D. Shimizu, M. L. Snapper, A. H. Hoveyda, *Chem. Eur. J.* **1998**, *4*, 1885–1889.

[2] a) G. J. Rowlands, *Tetrahedron* **2001**, *57*, 1865–1882; b) B. Bosnich, *Inorg. Chem.* **1999**, *38*, 2554–2562; c) D. E. Fenton, *Chem. Soc. Rev.* **1999**, *28*, 159–168; d) E. K. van den Beuken, B. L. Feringa, *Tetrahedron* **1998**, *54*, 12985–13001; e) D. G. McCollum, B. Bosnich, *Inorg. Chim. Acta* **1998**, *270*, 13–19; f) H. Steinhagen, G. Helmchen, *Angew. Chem.* **1996**, *108*, 2489–2492; *Angew. Chem. Int. Ed. Engl.* **1996**, *35*, 2339–2342.

[3] K. Severin, *Chem. Eur. J.* **2002**, *8*, 1515–1518, and references therein.

[4] S. Gauthier, L. Quebatte, R. Scopelliti, K. Severin, *Chem. Eur. J.*, in press.

[5] J. Iqbal, B. Bhatia, N. K. Nayyar, *Chem. Rev.* **1994**, *94*, 519–564.

[6] W. J. Bland, R. Davis, J. L. A. Durrant, *J. Organomet. Chem.* **1985**, *280*, 397–406.

[7] a) H. Nagashima, H. Wakamatsu, N. Ozaki, T. Ishii, M. Watanabe, T. Tajima, K. Itoh, *J. Org. Chem.* **1992**, *57*, 1682–1689; b) G. M. Lee, S. M. Weinreb, *J. Org. Chem.* **1990**, *55*, 1281–1285; c) H. Nagashima, N. Ozaki, K. Seki, M. Ishii, K. Itoh, *J. Org. Chem.* **1989**, *54*, 4497–4499; d) T. K. Hayes, R. Villani, S. M. Weinreb, *J. Am. Chem. Soc.* **1988**, *110*, 5533–5543; e) T. K.

 © 2004 Wiley-VCH Verlag GmbH & Co. KGaA, Weinheim

Hayes, A. J. Freyer, M. Parvez, S. M. Weinreb, *J. Org. Chem.* **1986**, *51*, 5503 – 5505; f) H. Nagashima, K.-I. Ara, H. Wakamatsu, K. Itoh, *J. Chem. Soc. Chem. Commun.* **1985**, 518 – 519.

[8] a) A. Richel, S. Delfosse, C. Cremasco, L. Delaude, A. Demonceau, A. F. Noels, *Tetrahedron Lett.* **2003**, *44*, 6011 – 6015; b) B. De Clercq, F. Verpoort, *Tetrahedron Lett.* **2002**, *43*, 4687 – 4690; c) B. De Clercq, F. Verpoort, *Tetrahedron Lett.* **2001**, *42*, 8959 – 8963; d) F. Simal, S. Sebille, A. Demonceau, A. F. Noels, R. Nuñez, M. Abad, F. Teixidor, C. Viñas, *Tetrahedron Lett.* **2000**, *41*, 5347 – 5351; e) F. Simal, A. Demonceau, A. F. Noels, *Tetrahedron Lett.* **1999**, *40*, 5689 – 5693; f) J. A. Tallarico, L. M. Malnick, M. L. Snapper, *J. Org. Chem.* **1999**, *64*, 344 – 345.

[9] F. Simal, L. Wlodarczak, A. Demonceau, A. F. Noels, *Eur. J. Inorg. Chem.* **2001**, 2689 – 2695; b) F. Simal, L. Wlodarczak, A. Demonceau, A. F. Noels, *Tetrahedron Lett.* **2000**, *41*, 6071 – 6074.

[10] O. Tutusaus, C. Viñas, R. Núñez, F. Teixidor, A. Demonceau, S. Delfosse, A. F. Noels, I. Mata, E. Molins, *J. Am. Chem. Soc.* **2003**, *125*, 11 830 – 11 831.

[11] A. C. da Silva, H. Piotrowski, P. Mayer, K. Polborn, K. Severin, *Eur. J. Inorg. Chem.* **2001**, 685 – 691.

[12] For several combinations it is likely that doubly bridged (instead of triply bridged) complexes are formed.

[13] The chloro-bridged complexes $[\{L_nM(\mu\text{-}Cl)\}_2]$ were added in excess (Ru/M = 1:2) to enforce the formation of asymmetric $\{M(\mu\text{-}Cl)_xRu\}$ complexes.

[14] Crystal data for **4**: $C_{46}H_{45}Cl_4P_2RhRu$, $M_r = 1005.54$, triclinic, space group $P\bar{1}$ (No. 2), $a = 11.937(2)$, $b = 13.200(2)$, $c = 14.3916(14)$ Å, $\alpha = 81.696(12)$, $\beta = 77.383(14)$, $\gamma = 71.811(17)°$, $V = 2095.2(6)$ Å^3, $Z = 2$, $\rho_{calcd} = 1.594$ g cm^{-3}, $\mu = 1.119$ mm^{-1}, $F(000) = 1016$, crystal dimensions $0.30 \times 0.25 \times 0.21$ mm^3. Data collection: mar345 IPDS, $T = 140(2)$ K, $Mo_{K\alpha}$ radiation, $\lambda = 0.71070$ Å, $\theta = 3.54$–$25.02°$, $-14 \le h \le 14$, $-15 \le k \le 15$, $-17 \le l \le 16$, 12 667 reflections collected, 6930 independent reflections, $R_{int} = 0.0619$, 5600 observed reflections $[I > 2\sigma(I)]$, empirical absorption correction, max./min. transmission: 0.563/0.101. Refinement: $N_{ref} = 6930$, $N_{par} = 488$, R_1 $[I > 2\sigma(I)] = 0.0637$, wR_2 (all data) = 0.1948, $S = 1.135$, the weighting scheme is $w^{-1} = [\sigma^2(F_o^2) + (0.1112P)^2 + 3.8732P]$ with $P = (F_o^2 + 2F_c^2)/3$, max. and average shift/error = 0.000, 0.000, largest difference peak/minimum: 1.059/−1.173 e Å^{-3}. Structure solution and refinement by SHELX97 (G. M. Sheldrick, SHELX97, Programs for Crystal Structure Analysis, University of Göttingen, Göttingen (Germany), **1998**). H atoms were placed in calculated positions using the riding model. Crystal data for **5**: $C_{114}H_{144}Cl_6N_2O_2P_4Rh_2Ru_2 \cdot CH_2Cl_2$, $M_r = 2403.78$, monoclinic, space group $C2/c$ (No. 15), $a = 71.244(6)$, $b = 12.9605(11)$, $c = 24.9834(19)$ Å, $\beta = 94.136(11)$, $V = 23\,009(3)$ Å^3, $Z = 8$, $\rho_{calcd} = 1.388$ g cm^{-3}, $\mu = 0.829$ mm^{-1}, $F(000) = 9920$, crystal dimensions $0.36 \times 0.25 \times 0.13$ mm^3. Data collection: Oxford Diffraction KM4/Sapphire CCD, $T = 140(2)$ K, $Mo_{K\alpha}$ radiation, $\lambda = 0.71073$ Å, $\theta = 2.63$–$25.03°$, $-84 \le h \le 84$, $-13 \le k \le 13$, $-29 \le l \le 29$, 65 671 reflections collected, 19 222 independent reflections, $R_{int} = 0.1233$, 10 703 observed reflections $[I > 2\sigma(I)]$, no absorption correction. Refinement: $N_{ref} = 19\,222$, $N_{par} = 1183$, R_1 $[I > 2\sigma(I)] = 0.0933$, wR_2 (all data) = 0.2712, $S = 1.055$, the weighting scheme is $w^{-1} = [\sigma^2(F_o^2) + (0.1120P)^2 + 391.8266P]$ with $P = (F_o^2 + 2F_c^2)/3$, max. and average shift/error = 0.001, 0.000, largest difference peak/minimum: 1.821/−1.636 e Å^{-3}. Structure solution and refinement by SHELX97. H atoms were placed in calculated positions using the riding model. Disorder problems dealing with two phenyl rings and with the CH_2Cl_2 group have been handled using the split model for the aromatic rings and keeping the carbon atoms isotropically defined. DELU and DFIX cards have been employed to achieve reasonable displacement parameters for the whole structure and to obtain reasonable geometrical data for the solvent molecule, respectively. CCDC-221541 and -221542 contains the supplementary crystallographic data for this paper. These data can be obtained free of charge via www.ccdc.cam.ac.uk/conts/retrieving.html (or from the Cambridge Crystallographic Data Centre, 12 Union Road, Cambridge CB21EZ, UK; fax: (+44) 1223-336-033; or deposit@ccdc.cam.ac.uk).

[15] a) L. E. Harrington, J. F. Britten, D. W. Hughes, A. D. Bain, J.-Y. Thépot, M. J. McGlinchey, *J. Organomet. Chem.* **2002**, *656*, 243 – 257; b) H. K. Gupta, N. Rampersad, M. Stradiottto, M. J. McGlinchey, *Organometallics* **2000**, *19*, 184 – 191.

[16] a) L. Bonomo, C. Stern, E. Solari, R. Scopelliti, C. Floriani, *Angew. Chem.* **2001**, *113*, 1497 – 1500; *Angew. Chem. Int. Ed.* **2001**, *40*, 1449 – 1452; b) V. Rodriguez, I. Atheaux, B. Donnadieu, S. Sabo-Etienne, B. Chaudret, *Organometallics* **2000**, *19*, 2916 – 2926; c) D. G. Gusev, F. M. Dolgushin, M. Y. Antipin, *Organometallics* **2000**, *19*, 3429 – 3434; d) K. Abdur-Rashid, D. G. Gusev, A. J. Lough, R. H. Morris, *Organometallics* **2000**, *19*, 1652 – 1660; e) R. A. T. M. Abbenhuis, I. del Río, M. M. Bergshoef, J. Boersma, N. Veldman, A. L. Spek, G. van Koten, *Inorg. Chem.* **1998**, *37*, 1749 – 1758;

[17] J. R. Torres-Lubián, M. E. Sánchez-Castro, P. Juárez-Saavedra, J. Hernández-Martínez, B. Gordillo-Román, M. A. Paz-Sandoval, *J. Organomet. Chem.* **2002**, *663*, 127 – 133.

[18] To the best of our knowledge, there is only one catalyst for which slightly higher values have been reported (TOF = 1500 h^{-1} and TON = 9000 for the addition of CCl_4 to styrene; see ref. [10]).

[19] T. Weskamp, F. J. Kohl, W. Hieringer, D. Gleich, W. Herrmann, *Angew. Chem.* **1999**, *111*, 2573 – 2576; *Angew. Chem. Int. Ed.* **1999**, *38*, 2416 – 2419.

[20] Quite often, ATRA catalysts are also good catalysts for atom-transfer radical polymerizations (ATRPs). For some selected examples see refs. [8a, b, and d].

[21] K. S. MacFarlane, I. S. Thorburn, P. W. Cyr, D. E. K.-Y. Chau, S. J. Rettig, B. R. James, *Inorg. Chim. Acta* **1998**, *270*, 130 – 144.

[22] D. Amoroso, G. P. A. Yap, D. E. Fogg, *Can. J. Chem.* **2001**, *79*, 958 – 963.

[23] B. Therrien, T. R. Ward, M. Pilkington, C. Hoffmann, F. Gilardoni, J. Weber, *Organometallics* **1998**, *17*, 330 – 337.

[24] M. A. Bennett, T.-N. Huang, T. W. Matheson, A. K. Smith, *Inorg. Synth.* **1982**, *21*, 74 – 78.

[25] M. A. Bennett, A. K. Smith, *J. Chem. Soc. Dalton Trans.* **1974**, 233 – 241.

[26] J. W. Hull, W. L. Gladfelter, *Organometallics* **1984**, *3*, 605 – 613.

[27] D. N. Cox, R. Roulet, *Inorg. Chem.* **1990**, *29*, 1360 – 1365.

[28] U. Koelle, J. Kossakowski, *J. Organomet. Chem.* **1989**, *362*, 383 – 398.

[29] C. White, A. Yates, P. M. Maitlis, *Inorg. Synth.* **1992**, *29*, 1687 – 1692.

[30] J. H. van Diemen, J. G. Haasnoot, R. Hage, J. Reedijk, J. G. Vos, R. Wang, *Inorg. Chem.* **1991**, *30*, 4038 – 4043.

[31] J. Powell, B. L. Shaw, *J. Chem. Soc. A* **1968**, 583 – 596.

[32] G. Giordano, R. H. Crabtree, *Inorg. Synth.* **1990**, *28*, 88 – 90.

[33] R. Cramer, *Inorg. Synth.* **1974**, *15*, 14 – 18.

[34] N. A. Bailey, V. S. Jassal, R. Vefghi, C. White, *J. Chem. Soc. Dalton Trans.* **1987**, 2815 – 2822.

[35] J. L. Herde, J. C. Lambert, C. V. Senoff, *Inorg. Synth.* **1974**, *15*, 18 – 19.

[36] F. R. Hartley, *Organomet. Chem. Rev. Sect. A* **1970**, *6*, 119 – 137.

[37] A. C. Cope, E. C. Friedrich, *J. Am. Chem. Soc.* **1968**, *90*, 909 – 913.

[38] P. M. Treichel, K. P. Wagner, W. J. Knebel, *Inorg. Chim. Acta* **1972**, *6*, 674 – 676. The Pd complex was prepared in an analogous fashion.

 © 2004 Wiley-VCH Verlag GmbH & Co. KGaA, Weinheim

Molecular Switches

Thermal and Photochemical Properties of 4′,7-Dihydroxyflavylium in Water–Ionic Liquid Biphasic Systems: A Write–Read–Erase Molecular Switch**

Fernando Pina, João C. Lima, A. Jorge Parola, and Carlos A. M. Afonso*

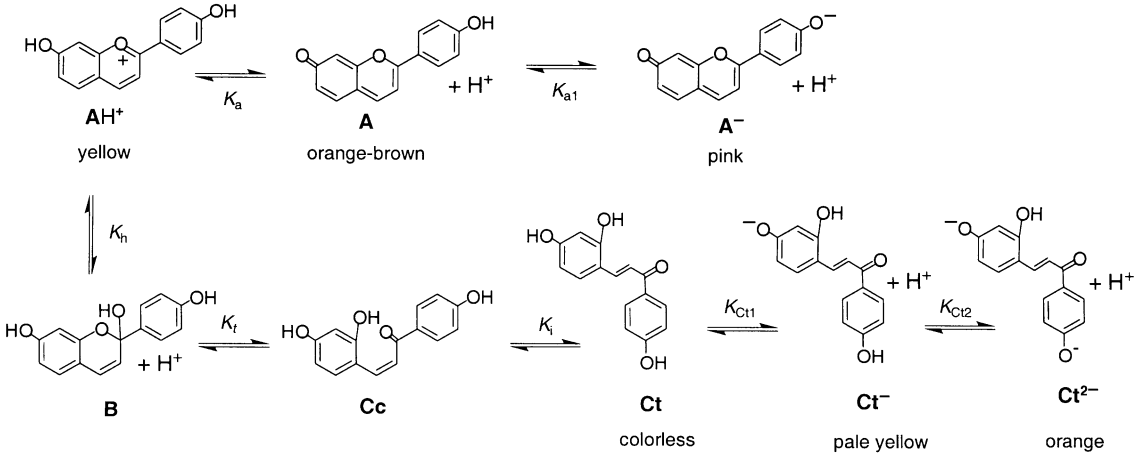
In the framework of supramolecular chemistry, synthetic flavylium salts can be envisaged as molecular systems that exist in different forms (multistate), which can be interconverted by different external stimuli (multifunctional).[1] Herein we explore a new dimension brought by ionic liquids to flavylium chemistry.

Room-temperature ionic liquids are thermally stable salts constituted by an organic cation and either an organic or inorganic anion. These liquids, unlike traditional inorganic molten salts, present a high degree of asymmetry that inhibits crystallization at room temperatures. They are air- and water-stable, exhibit a nonmeasurable vapor pressure, and solvate a variety of organic and inorganic compounds. For these reasons ionic liquids are emerging as alternative green solvents, that is, as reaction media in many transformations including catalysis,[2] biocatalysis,[3] and separation processes.[4]

In Scheme 1 the complex network of chemical reactions in which the compound 4′,7-dihydroxyflavylium is involved is represented.[5] We selected this particular flavylium salt, because: 1) it is stable over the whole pH range, 2) it exhibits a variety of colored species, which are easily identified and therefore a useful sensor to the "naked eye" in the ionic liquids, and 3) its thermal and photochemical behavior was previously characterized in water.[5–7]

In acidic water, five species of this compound can be distinguised: the flavylium cation ($\mathbf{A}H^+$); the quinoidal neutral base (**A**) formed upon deprotonation of $\mathbf{A}H^+$; the hemiketal (**B**) obtained by hydration of $\mathbf{A}H^+$; the *cis*-chalcone (**Cc**) resulting from tautomerization of **B**; and the *trans*-chalcone (**Ct**) owing to the isomerization of **Cc**. However, **B** and **Cc** are short-lived, transient species whose absorption spectra have not been observed experimentally.[5–7] In basic water, ionized quinoidal base ($\mathbf{A}^-$) and ionized *trans*-chalcones ($\mathbf{Ct}^-$ and $\mathbf{Ct}^{2-}$), obtained by deprotonation of the hydroxy groups, are found in equilibrium or as transient species.

The pH-dependent mole-fraction distribution of the species reported in Scheme 1 are represented in Figure 1, at equilibrium (red solid lines, bottom color bars), or as transient forms obtained immediately upon a pH stimulus (blue dotted lines, top color bars). From these data, it can be concluded that equilibrated solutions of 4′,7-dihydroxyflavylium are yellow at pH < 2, slightly orange-brown at pH 4–8, pale brown-pink at around pH 9, and orange at pH > 11. On the other hand, immediately upon a "direct" pH jump from pH 1 (yellow $\mathbf{A}H^+$) to pH 6 or pH 10, **A** (orange-brown) and $\mathbf{A}^-$ (pink), respectively, are formed (Figure 1a). In the case of "reverse" pH jumps, from ≈pH 12 (orange $\mathbf{Ct}^{2-}$), the transient species $\mathbf{Ct}^-$ (pale yellow) and **Ct** (colorless) can be detected (Figure 1b). In all pH jumps, the final equilibrium is



Scheme 1. Network of reactions involving 4′,7-dihydroxyflavylium in water.

reached after several minutes, depending on pH and temperature.

The photochemistry of 4′,7-dihydroxyflavylium in water is based on the efficient *trans–cis* photoisomerization of the chalcone.[6–7] In a typical photochemical experiment, a solution previously equilibrated in the pH range 3–6 and containing ≈90% **Ct** and ≈10% **A** is irradiated. Depending on the specific pH value, the formation of $\mathbf{A}H^+$ (yellow) or **A** (orange-brown) is observed. However, these species spontaneously revert back to the initial equilibrium concentrations;

[*] Prof. F. Pina, Dr. J. C. Lima, Dr. A. J. Parola, Dr. C. A. M. Afonso
REQUIMTE/CQFB
Departamento de Química, Faculdade de Ciências e Tecnologia
Universidade Nova de Lisboa
2829-516 Monte de Caparica (Portugal)
Fax: (+351) 21-294-8550
E-mail: fjp@dq.fct.unl.pt

[**] We thank the Fundação para a Ciência e Tecnologia and FEDER for projects POCTI/QUI/47357/2002 and POCTI/EQU/35437/1999.

Supporting information for this article is available on the WWW under http://www.angewandte.org or from the author.

 DOI: 10.1002/anie.200353131 © 2004 Wiley-VCH Verlag GmbH & Co. KGaA, Weinheim

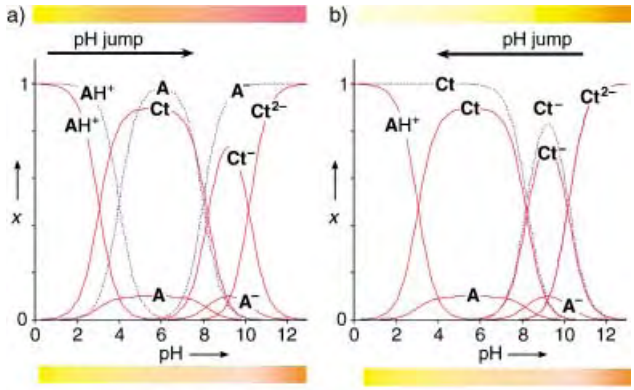


Figure 1. Mole-fraction distribution of the several species of 4′,7-dihydroxyflavylium in water, and color bars representing the corresponding color of the solution; a) pH jumps from pH 1 (yellow $\mathbf{AH}^+$) to less acidic or basic pH values lead to transient mole-fraction distributions immediately after the jump (blue dotted lines and top color bar) that evolve in time to reach a thermodynamic equilibrium (red solid lines and bottom color bar); b) "reverse" pH jumps from pH 12 (orange $\mathbf{Ct}^{2-}$) to less basic or acidic solutions lead to transient mole-fraction distributions immediately after the jump (blue dotted lines and top color bar) that evolve in time to reach a thermodynamic equilibrium (red solid lines and bottom color bar).

When aqueous solutions of 4′,7-dihydroxyflavylium are combined with the ionic liquid 1-*n*-butyl-3-methylimidazolium hexaflurophosphate ([bmim][PF_6]), the two solutions are not miscible, and several interesting phenomena take place. Figure 2 describes one sequence of steps that allows a description of a *write–read–erase* cycle and provides information on the ionic-liquid properties. In a typical experiment, an aqueous solution of 4′,7-dihydroxyflavylium perchlorate (2×10^{-5} M, 2 mL) at pH 1.0 was added to the ionic liquid (2 mL). Moderate shaking leads to the dissolution of all the flavylium cation in the ionic liquid in its orange-brown quinoidal base form, **A**. However, after shaking vigorously for approximately 1 minute, the bottom ionic-liquid solution becomes yellow, indicating that **A** was protonated to form the $\mathbf{AH}^+$ species.



Figure 2. a) 1-*n*-Butyl-3-methylimidazolium hexafluorophosphate, [bmim][PF6] (lower phase), 4′,7-dihydroxyflavylium perchlorate in 0.01 M HCl, $\mathbf{AH}^+$ species (upper phase); b) after moderate shaking, **A** species (lower phase); c) after vigorous shaking, $\mathbf{AH}^+$ species (lower phase); d) after making the aqueous phase alkaline (pH 12) with minimum shaking, $\mathbf{A}^-$ (lower phase), $\mathbf{Ct}^{2-}$ (upper phase); e) after moderate shaking; f) after vigorous shaking, $\mathbf{Ct}^{2-}$ species (upper phase); g) after reacidification of the aqueous phase and vigorous shaking, **Ct** species (lower phase); h) after irradiation of the ionic-liquid phase at 366 nm, $\mathbf{AH}^+$ species.

the process takes only several minutes. More information on the kinetics of the reaction network can be achieved by flash photolysis.[6,7] When the **Ct** species is submitted to a pulse of light, its absorption is bleached during the lifetime of the flash, but partial recovery of the absorbance occurs on a timescale of seconds. These results clearly indicate the lack of thermal barrier between the two chalcone species. On the other hand, the absorption of $\mathbf{AH}^+$ (or **A**) species increases, indicating that not all the photoproducts (**Cc**) revert back to **Ct**, but some go forward to form $\mathbf{AH}^+$ (or **A**) (Scheme 1). The process is complete when photochemically produced $\mathbf{AH}^+$ (or **A**) reverts spontaneously to **Ct** (timescale of minutes at room temperature at pH 3.5–5.5; see Figure 3S in the Supporting Information).

In a typical "optical memory", the write step consists of the use of light to irradiate the **Ct** species, which should give the $\mathbf{AH}^+$ (or **A**) form, whose color formation is the output of the system, its signal. To read this signal, a wavelength at which **Ct** does not absorb must be used, which can easily be selected as the flavylium species exhibits a red-shifted absorption band relative to the chalcones and is photochemically stable. The existence of a *cis–trans* thermal barrier that prevents the back reaction is required for the operation of such an "optical memory", otherwise the written information is erased before it can be read. The erasing of the "memory" and preparation for a new cycle can be achieved by a pH jump to basic medium, leading to $\mathbf{Ct}^{2-}$, followed by a "reverse" pH jump to regain the **Ct** species. Some synthetic flavylium salts, namely those with a single substituent such as an hydroxy or methoxy group in the 4′ position, exhibit these properties in water and have been used as models for "optical memories".[1] The lack of the *cis–trans* isomerization barrier of 4′,7-dihydroxyflavylium in aqueous solutions immediately excludes this compound for these purposes.

The flavylium cation, $\mathbf{AH}^+$, dissolved in the ionic liquid is the starting and finishing point of the proposed cycle. Figures 2d, e, and f show three stages obtained upon a jump from pH 1 to pH 12 in the aqueous phase. The final equilibrium in this step is obtained with the $\mathbf{Ct}^{2-}$ species completely dissolved in the aqueous phase (Figure 2f). The next step of the cycle consists of a pH jump in the aqueous phase back to pH 1, followed by vigorous mixing of the two phases. This procedure allows the **Ct** species formed in the aqueous phase to dissolve completely in the ionic liquid. The equilibrium species at this pH value ($\mathbf{AH}^+$) is formed at a slow rate, (after 1 hour at 40 °C, less than 2% of flavylium cation was formed) showing that, in contrast to the behavior in water, the **Ct** species in the ionic liquid exhibits a very large kinetic barrier that prevents rapid *cis–trans* isomerization, a requirement for a "memory" model.

It is known that ionic liquids based on the imidazolium cation (im) have an organized layer-by-layer structure and are not an ensemble of statistical aggregates of anions and cations.[8] In line with reported strong interactions between ionic liquids and solutes capable of π–π, n–π, or hydrogen bonding,[4c,9] a strong interaction of the **Ct** form with the ionic liquid is expected. The large kinetic barrier of *cis–trans* isomerization in the ionic liquid can be explained by this more rigid and stable distribution of **Ct** in the ionic liquid that needs

 © 2004 Wiley-VCH Verlag GmbH & Co. KGaA, Weinheim

to be disrupted during the thermal isomerization owing to the formation of less-planar intermediates, as well as by the large viscosity of the ionic liquid.

The spectral variations that occur upon steady-state irradiation at 365 nm of the **Ct** species dissolved in the ionic liquid are qualitatively similar to those previously reported for the 4′,7-dihydroxyflavylium in pure water (see Supporting Information).[6,7] Flash photolysis measurements are reported in Figure 3. Two processes that follow the light pulse were

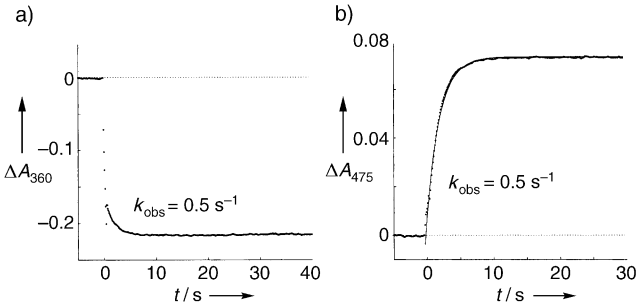
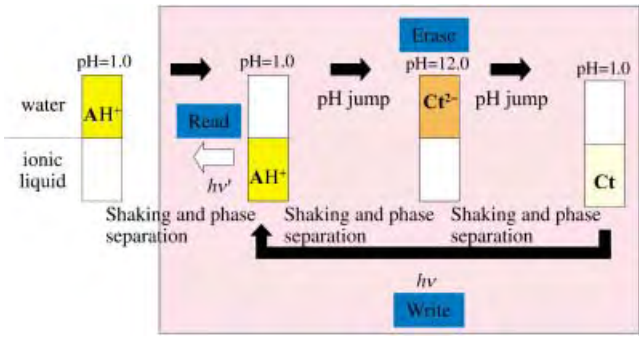


Figure 3. Flash photolysis of the **Ct** species in the ionic liquid, measured at: a) 360 nm (**Ct** absorption); b) 475 nm ($\mathbf{AH^+}$/**A** absorption).

identified. The first corresponds to the bleaching of the solution at 360 nm, which occurs during the lifetime of the flash. This process can be assigned to the *cis–trans* isomerization. The second process is the formation of $\mathbf{AH^+}$ from **Cc** ($k = 0.5\ s^{-1}$) clearly shown by the increasing absorption at 475 nm. According to the traces in Figure 3, neither recovery of the **Ct** absorption (Figure 3a) nor a decrease in $\mathbf{AH^+}$ absorption (Figure 3b) was observed, confirming the existence of the thermal barrier.[10]

In conclusion, the following write–read–erase cycle can be proposed:[11] 1) the *write* step consists of the irradiation of the **Ct** species dissolved in the ionic liquid, with formation of flavylium cation, $\mathbf{AH^+}$; 2) the information thus obtained can be *read* at a wavelength at which the $\mathbf{AH^+}$ (or **A**) absorbs but the **Ct** species does not, e.g. 475 nm; 3) to *erase* the system and prepare it for a new cycle, a sequence of operations need to be carried out: a jump to pH 12 and vigorous shaking to extract the compound from the ionic liquid into water in its $\mathbf{Ct^{2-}}$ form, followed by a second jump back to pH 1.0 and vigorous shaking to dissolve the **Ct** species in the ionic liquid (Scheme 2).



Scheme 2. Write–read–erase cycle of 4′,7-dihydroxyflavylium in a biphasic water/[bmim][PF6] system.

The advantage of the present cycle is that no significant mass variation occurs in the ionic liquid. Moreover, the top aqueous solutions or even the synthetic flavylium salt can be removed from the ionic liquid and substituted if necessary. Ionic liquids extend the possibility of using synthetic flavylium salts that lack a **Ct**→**Cc** thermal barrier, e.g. 4′,7-dihydroxyflavylium, as models for "optical memories".

Received: October 21, 2003 [Z53131]

Keywords: ionic liquids · molecular switches · optical memory · photochemistry

[1] a) F. Pina, M. Maestri, V. Balzani, *Handbook of Photochemistry and Photobiology*, *Vol. 3*, American Scientific Publication, Research Triangle Park, **2003**, chap. 9, pp. 411–449; b) F. Pina, M. J. Melo, M. Maestri, R. Ballardini, V. Balzani, *J. Am. Chem. Soc.* **1997**, *119*, 5556–5561; c) F. Pina, A. Roque, M. J. Melo, M. Maestri, L. Belladelli, V. Balzani, *Chem. Eur. J.* **1998**, *4*, 1184–1191; d) F. Pina, M. J. Melo, M. Maestri, P. Passaniti, V. Balzani, *J. Am. Chem. Soc.* **2000**, *122*, 4496–4498; e) A. Roque, C. Lodeiro, F. Pina, M. Maestri, S. Dumas, P. Passaniti, V. Balzani, *J. Am. Chem. Soc.* **2003**, *125*, 987–994.

[2] a) S. V. Dzyuba, R. A. Bartsch, *Angew. Chem.* **2003**, *115*, 158–160; *Angew. Chem. Int. Ed.* **2003**, *42*, 148–150; b) K. R. Seddon, *Nat. Mater.* **2003**, *2*, 1; c) J. H. Davis Jr. , P. A. Fox, *Chem. Commun.* **2003**, 1209–1212; d) H. Zhao, S. V. Malhotra, *Aldrichimica Acta* **2002**, *35*, 75–83; e) J. F. Brennecke, E. J. Maginn, *AIChE J.* **2001**, *47*, 2384–2389; f) J. Dupont, C. S. Consorti, J. Spencer, *J. Braz. Chem. Soc.* **2000**, *11*, 337–344; g) P. Wasserscheid, W. Keim, *Angew. Chem.* **2000**, *112*, 3926–3945; *Angew. Chem. Int. Ed.* **2000**, *39*, 3772–3789; h) T. Welton, *Chem. Rev.* **1999**, *99*, 2071–2083.

[3] a) J. Dupont, R. F. de Souza, P. A. Z. Suarez, *Chem. Rev.* **2002**, *102*, 3667–3692; b) R. Sheldon, *Chem. Commun.* **2001**, 2399–2407; c) C. M. Gordon, *Appl. Catal. A* **2001**, *222*, 101–117.

[4] a) J. D. Holbrey, A. E. Visser, S. K. Spear, W. M. Reichert, R. P. Swatloski, G. A. Broker, R. D. Rogers, *Green. Chem.* **2003**, *5*, 129–135; b) E. D. Bates, R. D. Mayton, I. Ntai, J. H. Davis, Jr., *J. Am. Chem. Soc.* **2002**, *124*, 926–927; c) L. C. Branco, J. G. Crespo, C. A. M. Afonso, *Angew. Chem.* **2002**, *41*, 2895–2897; *Angew. Chem. Int. Ed.* **2002**, *41*, 2771–2773; d) L. C. Branco, J. G. Crespo, C. A. M. Afonso, *Chem. Eur. J.* **2002**, *8*, 3865–3871; e) T. Schäfer, C. M. Rodrigues, C. A. M. Afonso, J. G. Crespo, *Chem. Commun.* **2001**, 1622–1623; f) A. G. Fadeev, M. M. Meagher, *Chem. Commun.* **2001**, 295–296.

[5] F. Pina, L. Benedito, M. J. Melo, A. J. Parola, J. C. Lima, A. L. Maçanita, *An. Quim. Int. Ed.* **1977**, *93*, 111–118.

[6] M. Maestri, R. Ballardini, F. Pina, M. J. Melo, *J. Chem. Educ.* **1997**, *74*, 1314–1316.

[7] F. Pina, M. J. Melo, R. Ballardini, L. Flamigni, M. Maestri, *New J. Chem.* **1997**, *21*, 969–976.

[8] a) J.-F. Huang, P.-Y. Chen, I.-W. Sun, S. P. Wang, *Inorg. Chim. Acta* **2001**, *320*, 7–11; b) J. Dupont, P. A. Z. Suarez, R. F. De Souza, R. A. Burrow, J.-P. Kintzinger, *Chem. Eur. J.* **2000**, *6*, 2377–2381; c) P. Bonhôte, A.-P. Dias, N. Papageorgiou, K. Kalyanasundaram, M. Grätzel, *Inorg. Chem.* **1996**, *35*, 1168–1178; d) J. Fuller, R. T. Carlin, H. C. De Long, D. Haworth, *J. Chem. Soc. Chem. Commun.* **1994**, 299–300.

[9] J. L. Anderson, J. Ding, T. Welton, D. W. Armstrong, *J. Am. Chem. Soc.* **2002**, *124*, 14247–14254.

[10] Compare with Figure 3S in the Supporting Information.

[11] An identical cycle was performed with [bmim][NTf_2] (Tf = trifluoromethanesulfonyl). In this case, the ionic-liquid phase is more turbid, thus making spectrophotometric measurements difficult.

 © 2004 Wiley-VCH Verlag GmbH & Co. KGaA, Weinheim

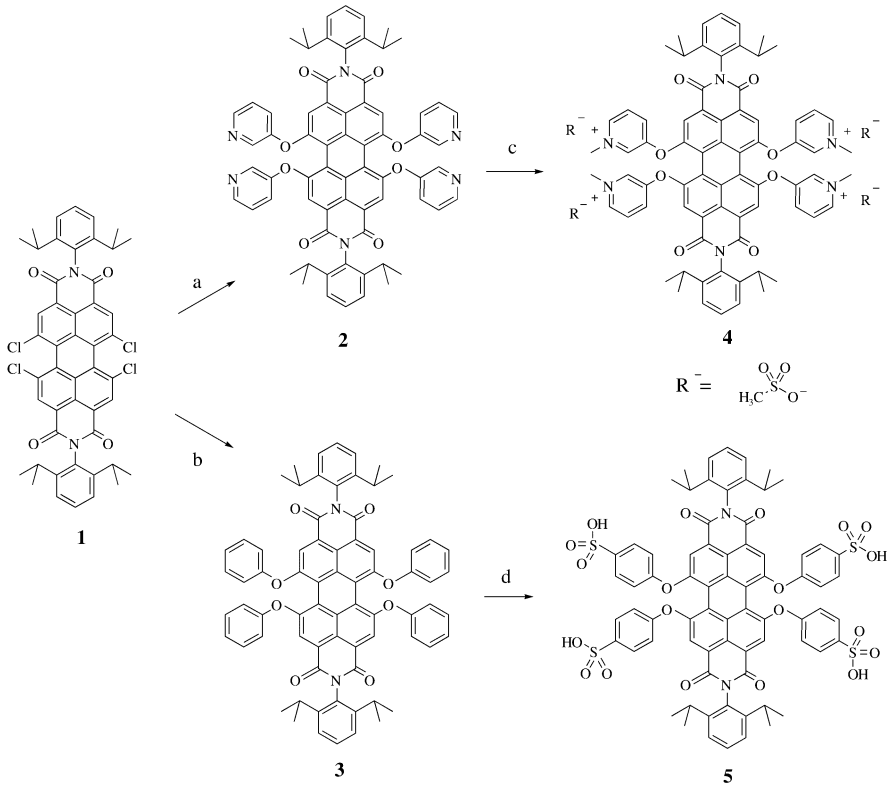
Water-Soluble Dyes

Ionic Perylenetetracarboxdiimides: Highly Fluorescent and Water-Soluble Dyes for Biolabeling**

*Jianqiang Qu, Christopher Kohl, Mark Pottek, and Klaus Müllen**

The use of water-soluble fluorescent labels for cells, antibodies, and DNA has rapidly expanded in recent years and has gained additional momentum owing to single-molecule spectroscopy.[1–3] Although there are a large variety of water-soluble chromophores commercially available today, most of them exhibit relatively low fluorescence quantum yields and/or photochemical stabilities. Cyanine dyes, for example, are highly instable towards oxygen and light, while xanthene dyes tend to aggregate in aqueous medium.[1,4] The ideal dye label should have the following characteristics: 1) good water solubility, 2) high fluorescence quantum yield, 3) high chemical and photostability, 4) nontoxicity, 5) good biocompatibility, 6) availability of monofunctional derivatives as an extrinsic covalently bound probe, as well as 7) possible commercial viability and scalable production. The highly fluorescent perylene-3,4,9,10-tetracarboxdiimide (PDI) chromophore is widely used as a commercial dye and pigment due to its outstanding chemical, thermal, and photochemical stability.[5] Furthermore, because of its brilliant color, strong absorption, and fluorescence, it has been extensively investigated as an active compound in reprographic processes,[6] photovoltaic cells,[7] light-emitting diodes,[8] other photonic devices,[9] and light-harvesting complexes.[10] Owing to the unique properties of PDIs, they should also be excellent biological probes; however, the retention of high fluorescence in aqueous medium is a critical issue. Up to now, only a few water-soluble PDI derivatives with functionalities in their imide moieties have been reported. They exhibit poor water solubility and/or very weak fluorescence in water with moderate fluorescence quantum yields of around 10% because of aggregation of the perylene chromophores.[11,12]

It is well-known that the solubility of PDI derivatives in organic solvents dramatically increases when substituents are attached in the bay region, resulting in a twist within the perylene core,[13] and that water solubility can be achieved by introducing charged groups on the hydrophobic dyes or pigments.[14] By successfully combining both structural features, we can produce highly fluorescent, water-soluble, and photostable PDIs for the first time. Furthermore, PDIs that contain multiple charged groups have been prepared as a monocarboxylic acid derivative for covalently attached labels in the field of biology. Initial cell-visualization experiments by using the novel labels are described below.



Scheme 1. a) 3-Pyridinol, *N*-methylpyrrolidone (NMP), K_2CO_3, 80 °C, 15 h, 85%; b) phenol, NMP, K_2CO_3, 80 °C, 15 h, 89%; c) 1) methyl iodide, methanol, reflux, 24 h, 95%; 2) silver methanesulfonate, methanol, room temperature, 5 h, 92%, d) conc. sulfuric acid, room temperature, 15 h, 93%.

The synthesis of the positively charged PDI **4** involves a phenoxylation with 3-pyridinol in 1-methyl-2-pyrrolidone followed by a quaternization, beginning with the tetrachloroperylenetetracarboxdiimide **1** (Scheme 1).[15] Because of the good solubility of PDI **2** in alcohols, the quaternization is performed with an excess of methyl iodide in methanol followed by a quantitative exchange of iodide with methanesulfonate counterions to give the desired water-soluble PDI **4**. A PDI with sulfonyl substituents **5** is obtained after phenox-

[*] J. Qu, C. Kohl, Dr. M. Pottek, Prof. Dr. K. Müllen
Max-Planck-Institut für Polymerforschung
Ackermannweg 10, 55128 Mainz (Germany)
Fax: (+49) 6131-379-350
E-mail: muellen@mpip-mainz.mpg.de

[**] Financial support from the Deutsche Forschungsgemeinschaft (Sonderforschungsbereich 625, Schwerpunktprogramm Organische Feldeffekt-Transistoren), the Bundesministerium für Bildung und Forschung (Zentrum für Multifunktionale Werkstoffe und Miniaturisierte Funktionseinheiten), and BASF AG is gratefully acknowledged.

 © 2004 Wiley-VCH Verlag GmbH & Co. KGaA, Weinheim DOI: 10.1002/anie.200353208

ylation of **1** with phenol (by using a similar procedure as for **2**), and the subsequent sulfonation with concentrated sulfuric acid at room temperature.

The asymmetric, chloro substituted PDI **7** is obtained by imidization by using two different arylamines with and without the carboxylic function. Isolation of the monoacids **7**, **8**, and **9** is easily performed by column chromatography, the eluent being a mixture of dichloromethane/acetone (10:1 v/v). The monofunctional water-soluble PDIs **10** and **11** are prepared in high yields by using the same reaction conditions as for **4** and **5** (Scheme 2). The structures of all compounds are confirmed by means of field desorption (FD) mass spectra, matrix-assisted laser desorption/ionization time-of-flight (MALDI-TOF) spectrometry and/or NMR spectroscopy.[16] These new chromophores have good thermal stability, with decomposition temperatures above 300 °C, and high water solubility. The saturation concentration of PDI **4** in water is above 1.0×10^{-2} M and 8.0×10^{-2} M for **5**. Monofunctional ionic PDIs **10** and **11** show similar water solubility in comparison to the symmetric ionic PDIs. Molecular-modeling studies[17] of PDIs **4** and **5** reveal a twist of the two naphthalene rings of about 28°[18] and a polar shell embedding the PDI fluorophore (not show here).

The UV/Vis absorption and emission spectra of **4**, **5**, **10**, and **11** are measured in water (Figure 1) and their fluorescence quantum yields are determined. An overview of the optical properties of all chromophores is given in Table 1. PDIs **4** and **5** have high extinction coefficients in water in comparison to tetraphenoxyperylenetetracarboxdiimide **3** in organic solvents ($\approx45000\,M^{-1}cm^{-1}$). Furthermore, the absorption spectra of all ionic PDIs in water in a concentration rage of $10\,mg\,mL^{-1}$–$1.0\times10^{-2}\,mg\,mL^{-1}$ exhibited the same vibrational fine structure of PDI, which suggest that ionic PDIs still present as monomers in high concentrations. A PDI that has positive charges, **4**, shows a blue shift

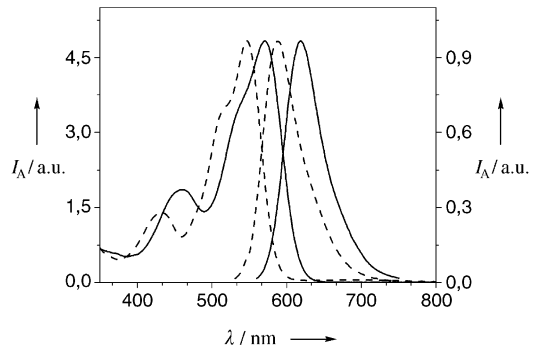
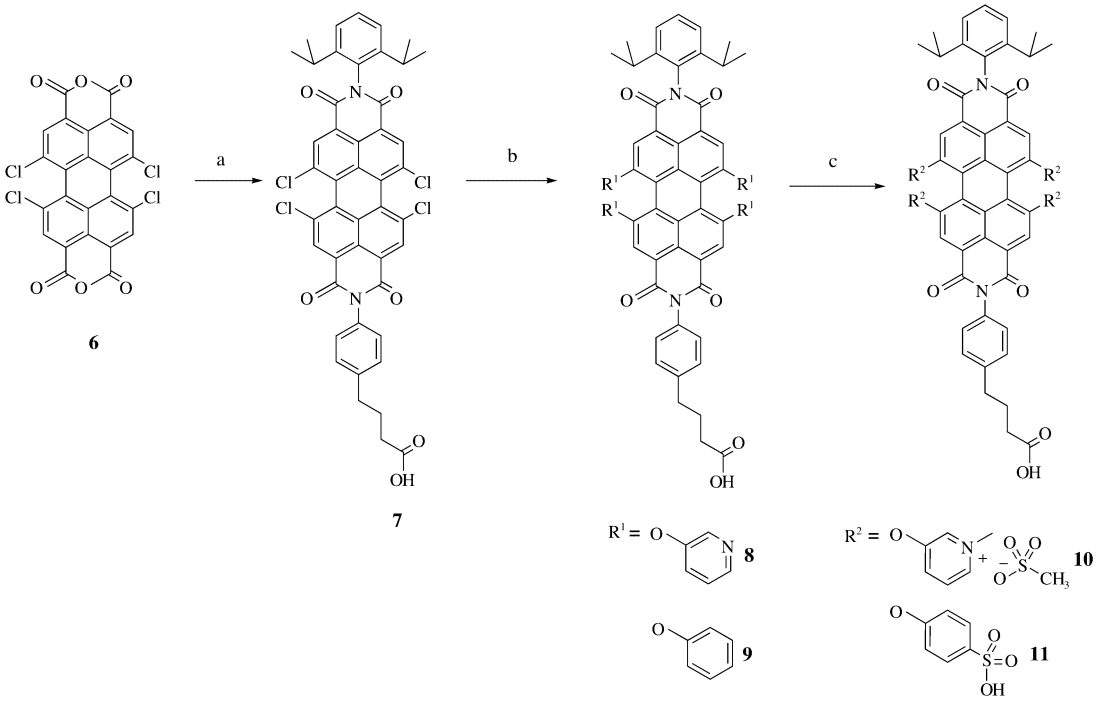


Figure 1. The normalized absorption spectra and fluorescence spectra of **4** (dash) and **5** (solid) in water.

Table 1: Absorption ($\lambda_{max,abs}$) and fluorescence maxima ($\lambda_{max,flu}$), and fluorescence quantum yields (Φ_f)[a] in water for **4**, **5**, **10**, **11**, and **12**.

Compound	$\lambda_{max,abs}$ [nm] (ε [$M^{-1}cm^{-1}$])	$\lambda_{max,flu}$ [nm]	Φ_f
4	434 (9766), 516 (24628), 547 (33751)	588	0.66
5	461 (10708), 541 (21026), 571 (27800)	619	0.58
10	432 (9456), 516 (21818), 547 (29974)	592	0.58
11	459 (9540), 541 (19261), 566 (23160)	618	0.49

[a] Φ_f was measured at room temperature using Cresyl Violet in methanol (the standard value is 0.54) as reference.[19]



Scheme 2. a) 2,6-Diisopropylaniline, 4-(4-aminophenyl)butyric acid, propionic acid, 140 °C, 5 h, 30%; b) **8**: 3-pyridinol, NMP, K_2CO_3, 80 °C, 15 h, 81%; **9**: phenol, NMP, K_2CO_3, 80 °C, 15 h, 80%; c) **10:** 1. methyl iodide, methanol, reflux, 24 h, 94%; 2. silver methanesulfonate, methanol, RT, 5 h, 90%; **11**: conc. sulfuric acid, RT 15 h, 92%.

 © 2004 Wiley-VCH Verlag GmbH & Co. KGaA, Weinheim

(≈20 nm) in comparison to the negatively charged PDI **5** due to the stronger electron withdrawing effect of pyridinium. All synthesized PDIs can be excited with 488 and 514 nm (Ar), 532 nm (Nd:YAG) laser lines, and with a 546 nm mercury arc line, owing to the presence of a broad and strong absorption band, to yield intense fluorescence. The dyes have high fluorescence quantum yields (Φ_f), which are measured by using Cresyl Violet in methanol as a reference.[19] PDIs with positive charges have similar Φ_f values to those that have negative charges (0.66 for **4**, 0.58 for **5**). The monofunctional dyes **10** and **11** show very similar optical properties to the analogous symmetric PDIs **4** and **5**. However, the fluorescence quantum yields of the monofunctional dyes are slightly lower (0.58 for **10**, 0.49 for **11**). Clearly the imide structure of the ionic PDIs influences the fluorescence in water.[20] These results validate our concept of introducing water solubility and high fluorescence quantum yield of PDIs in water by introducing substituents in the bay region and also explain the failure of approaches found in the early literature that were based upon functionalization of the imide units.[11,12] The ionic PDIs in water appear to retain photostability in comparison to PDIs in organic solvents or in the solid state.[21] The UV/Vis absorption and the fluorescence spectra of the water solution of PDIs **4** and **5** remain almost unchanged (their intensities decrease by about 6% for **4** and 1% for **5**) in sun light or after radiation with under UV light (365 nm) for one week.

The biological applicability of PDI **4** was demonstrated with a cardiac cell culture.[22] When they were subjected to a dye concentration of 3.0 mM, these cells became intensely fluorescent, which was most pronounced in the perinuclear region (Figure 2). This observation indicates an intracellular deposition of the dye, although the mechanism for entering the cells is not yet clear. After they were stained, the cells appeared healthy, as judged from their morphology, and were devoid of vacuoles and any other sign of structural degradation. In addition, the combination of the PDI treatment with nuclear staining by the blue fluorescent dye 4,6-diamidino-2-phenylindole (DAPI)[1] revealed the presence of double nuclei in some cells (indicated by arrows in Figure 2). Thus, the cells continued to proliferate in the presence of the PDI dye, which underlines the nontoxicity of the labels. Photostability and fluorescence intensity remained for a long period of time after contact with the cell culture, thus indicating that the dye is not metabolized by the cells. In addition, the fixation of the cells after staining does not degrade the fluorescence properties of the water-soluble PDI. These primary results are encouraging in terms of the applicability of commercially available dyes/pigments (PDIs) as biological fluorescent probes.

In summary, novel ionic PDI dyes and monofunctionalized ionic PDIs with positively or negatively charged substituents in the bay regions have been developed with simple procedures in high yields. This is the first time that water-soluble PDIs with high fluorescence quantum yields, high extinction coefficients, as well as significant photostability are reported. Due to their broad absorption bands, they can be excited with different excitation sources. The results with ionic PDI on living cells show that the water-soluble dyes are nontoxic and maintaining high fluorescence intensity and photostability. Our future research will concentrate on the mechanism of water-soluble PDIs entering the cells, the role of PDI dyes in specific cell organelles, and the study of DNA and proteins labeled with monofunctional PDIs through covalent bonds, thereby, also using methods of single molecule spectroscopy.[23,24]

Received: October 31, 2003 [Z53208]

Keywords: cell staining · chromophores · dyes/pigments · fluorescent dyes · water chemistry

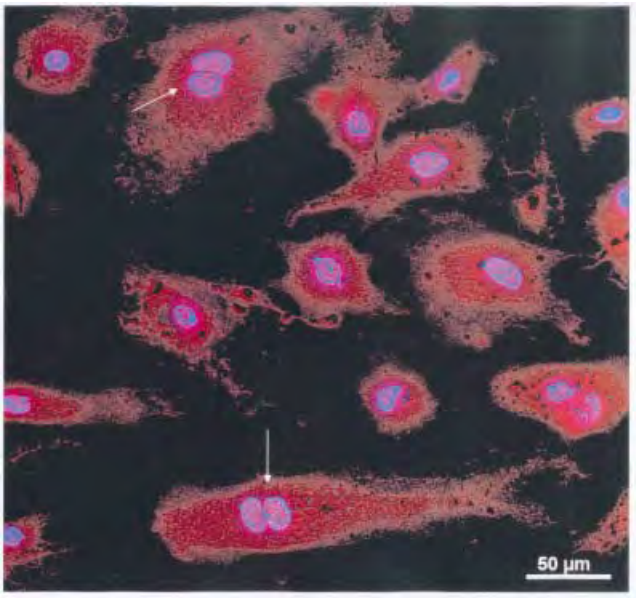


Figure 2. Staining of cardiac fibroblast and muscle cells by PDI **4** (red). The cells' nuclei (blue) were labeled by DAPI. Double nuclei (arrows) indicate ongoing cell division. Micrographs of both staining conditions were separately taken and subsequently overlaid (scale bar 50 µm).

[1] R. P. Haugland, *Handbook of Fluorescent Probes and Research Products*, 9th ed., Molecular Probes, Eugene, **2002**.
[2] G. Seisenberger, M. U. Ried, T. Endress, H. Buning, M. Hallek, C. Bräuchle, *Science* **2001**, *294*, 1929.
[3] M. Cotlet, J. Hofkens, M. Maus, T. Gensch, M. Van der Auweraer, J. Michiels, G. Dirix, M. Van Guyse, J. Vanderleyden, A. J. W. G. Visser, F. C. De Schryver, *J. Phys. Chem. B* **2001**, *105*, 4999.
[4] a) P. Chen, S. Sun, Y. Hu, Z. Qian, D. Zheng, *Dyes Pigm.* **1999**, *41*, 227; b) P. Gregory, *High-Technology Applications of Organic Colorants*, Plenum, New York, **1991**; c) G. W. Byers, S. Gross, P. M. Henrichs, *Photochem. Photobiol.* **1976**, *23*, 37; d) M. Fischer, J. Georges, *Chem. Phys. Lett.* **1996**, *260*, 115.
[5] a) Y. Nagao, T. Misono, *Dyes Pigm.* **1984**, *5*, 171; b) H. Zollinger, *Color Chemistry*, VCH, Weinheim, **1987**; c) R. M. Christie, *Polym. Int.* **1994**, *34*, 351.
[6] H. O. Loufty, A. M. Hor, P. Kazmaier, M. Tarn, *J. Imaging Sci.* **1989**, *33*, 151.
[7] a) L. Schmidt-Mende, A. Fechtenkötter, K. Müllen, E. Moons, R. H. Friend, J. D. MacKenzie, *Science* **2001**, *293*, 1119; b) A. J. Breeze, A. Salomon, D. S. Ginley, B. A. Gregg, *Appl. Phys. Lett.* **2002**, *81*, 3085.

 © 2004 Wiley-VCH Verlag GmbH & Co. KGaA, Weinheim

[8] J. Kalinowski, P. D. Marco, V. Fattori, L. Giuletti, M. Cocchi, *J. Appl. Phys.* **1998**, *83*, 4242.
[9] a) M. P. O'Neil, M. P. Niemczyk, W. A. Svec, D. Gosztola, G. L. Gaines, M. R. Wasielewski, *Science* **1992**, *257*, 63; b) R. Gvishi, R. Reisfeld, Z. Burshtein, *Chem. Phys. Lett.* **1993**, *213*, 338.
[10] a) F. Würthner, A. Sautter, *Org. Biomol. Chem.* **2003**, *1*, 240; b) T. Weil, E. Reuther, K. Müllen, *Angew. Chem.* **2002**, *114*, 1980; *Angew. Chem. Int. Ed.* **2002**, *41*, 1900; c) R. Gronheid, J. Hofkens, F. Kohn, T. Weil, E. Reuther, K. Müllen, F. C. De Schryver, *J. Am. Chem. Soc.* **2002**, *124*, 2418.
[11] G. Schnurpfeil, J. Stark, D. Wöhrle, *Dyes Pigm.* **1995**, *27*, 339.
[12] H. Langhals, German Patent DE-3703513, **1987**; H. Langhals, W. Jona, F. Einsiedl, S. Wohnlich, *Adv. Mater.* **1998**, *10*, 1022.
[13] a) F. Würthner, C. Thalacker, S. Diele, C. Tschierske, *Chem. Eur. J.* **2001**, *7*, 2245; b) J. Qu, N. G. Pschirer, D. Liu, A. Stefan, F. C. De Schryver, K. Müllen, *Chem. Eur. J.* **2004**, *10*, 528.
[14] R. Raue, *Rev. Prog. Color. Relat. Top.* **1984**, *14*, 187–203.
[15] H. Quante, PhD Thesis, Johannes Gutenberg University Mainz (Germany), **1995**.
[16] J. Qu, C. Kohl, T. Weil, K. Müllen, A detailed description of the synthesis and spectra of all compounds will be published separately together with other approaches toward water-soluble PDIs.
[17] The energy-minimized structures of ionic PDI have been obtained by applying the MM+ force field and the Conjugate Gradient algorithm implemented in the HyperChem 6.0 program from Hypercube Inc. The 3D structure of the PDI-core molecule was first calculated separately by using the semi-empirical PM3 method, and a global minimum was evaluated. Further, the four functional groups were attached to the core, and the geometry of the complete molecule was calculated with the MM+ force field and the Fletcher Reeves algorithm.
[18] F. Würthner, A. Sautter, C. Thalacker, *Angew. Chem.* **2000**, *112*, 1298; *Angew. Chem. Int. Ed.* **2000**, *39*, 1243.
[19] J. R. Lakowicz *Principles of Photoluminescence Spectroscopy*, 2nd ed., Kluwer Academic/Plenum Publishers, Dordrecht, **1999**.
[20] F. Würthner, S. Ahmed, C. Thalacker, T. debaerdemaeker, *Chem. Eur. J.* **2002**, *8*, 4742.
[21] G. Seybold, G. Wagenblast, *Dyes Pigm.* **1989**, *11*, 303.
[22] Cardiac cells were obtained from embryonic rat hearts (CD rats; Charles River) and cultivated on fibronectin (Roche Diagnostics, Mannheim, Germany) coated cover-slips for 4 days. Cultures were subjected to PDI dye **4** (0.3 mM in water) for 30 min at 37 °C, rinsed in nutrient mixture F-10 (Invitrogen Corp., Karlsruhe, Germany), and then fixed with 2% paraformaldehyde for 15 min at 4 °C. Subsequently, nuclear staining was achieved by incubation with 0.25 $\mu g\,mL^{-1}$ 4′,6-diamidino-2-phenylindole dihydrochloride (DAPI; Sigma, Taufkirchen, Germany) in PBS pH 7.4 for 4 min at room temperature. Cultures were mounted on microscopic slides and analyzed by using an Olympus IX70 microscope with a U-MNG (PDI dye) and U-MNU (DAPI) fluorescence filter set. Digital micrographs were taken by a cooled CCD device (Photometrics CoolSNAP fx; Roper Scientific, Germany) controlled by the imaging system MetaMorph (Universal Imaging Corp., Downingtown, PA, USA).
[23] C. Bräuchle, G. Seisenberger, T. Endress, M. U. Ried, H. Buning, M. Hallek, *ChemPhysChem* **2002**, *3*, 299.
[24] I. Scheblykin, G. Zoriniants, J. Hofkens, S. De Feyter, M. Van der Auweraer, F. C. De Schryver, *ChemPhysChem* **2003**, *4*, 260.

 © 2004 Wiley-VCH Verlag GmbH & Co. KGaA, Weinheim

Biomimetics

Minimal Functional Model of Hemostasis in a Biomimetic Microfluidic System**

*Matthew K. Runyon, Bethany L. Johnson-Kerner, and Rustem F. Ismagilov**

Biology is functional, and this function both inspires and puzzles. Inspiration from biology has led to the development of biomimetic systems—artificial systems that function by mimicking biology. Biomimetic systems have been successfully created in self-assembly,[1,2] materials,[3] chemical synthesis,[4] and surface chemistry.[5] They often provide insight into the puzzles of biology, because to develop a biomimetic system, models of biology must be created and tested. In this paper we show how this approach can be extended to a dynamic, nonequilibrium chemical system. We describe a minimal model of hemostasis, then show how this model may be implemented with chemical reactions and used to create a functional microfluidic system that is capable of repairing itself by mimicking hemostasis.

Hemostasis is a complex functional system that consists of approximately 80 coupled biochemical reactions that involve both soluble proteins and platelets. It is responsible for repairing damaged blood vessels and preventing excessive bleeding. It maintains blood in a fluid, clot-free state under normal conditions, but creates a localized solid clot in response to vascular damage.[6] The complexity of hemostasis is associated with a finely tuned self-regulation, essential for its function. This self-regulation is believed to be the basis of two essential features of healthy hemostasis: 1) Hemostasis shows a threshold response. There is no response to small regions of internal vascular damage present throughout the circulatory system, but full response to substantial damage of a blood vessel; 2) hemostasis acts locally. A clot formed in the region of substantial damage is confined to that region. These two features are responsible for preventing excessive clotting that obstructs the blood flow and is associated with life-threatening conditions such as deep-vein thrombosis.

Self-regulation in hemostasis is thought to be the direct result of a delicate balance between the initiation and inhibition modules; the flow of blood is essential to achieving this balance.[7–9] The network of interacting reactions in hemostasis is difficult to model;[10] this difficulty is inherent to complex reaction networks.[11,12] The interactions between reactions and the role of fluid flow are difficult to model by

[*] M. K. Runyon, B. L. Johnson-Kerner, Prof. R. F. Ismagilov
Department of Chemistry
The University of Chicago
5735 South Ellis Avenue, Chicago, IL 60637 (USA)
Fax: (+1) 773-702-0805
E-mail: r-ismagilov@uchicago.edu

[**] This work was supported by NSF CAREER Award, Office of Naval Research Young Investigator Award (N00014-03-10482), Searle Scholars Program, and by Dreyfus New Faculty Award. We thank Professors G. M. Whitesides, C. Chen, C. Hall, T. Van Ha, V. Turitto, and M. LaBarbera for invaluable suggestions.

 DOI: 10.1002/anie.200353428 © 2004 Wiley-VCH Verlag GmbH & Co. KGaA, Weinheim

considering isolated reactions of hemostasis. The system has to be modeled as a whole.[11,13,14] It is challenging to model hemostasis by explicitly treating fluid flow and each of approximately 80 reactions. Although such modeling gives valuable insights into the dynamics of hemostasis,[7] it would be difficult to use it as a basis of a biomimetic system. Therefore, simplifications are needed.

We simplified this complex system while still treating it as a whole using a modular approach.[15–18] We separated the system into three interacting modules (initiation, inhibition, and precipitation), and represented each module by a single reaction with appropriate kinetics (Figure 1). These modules

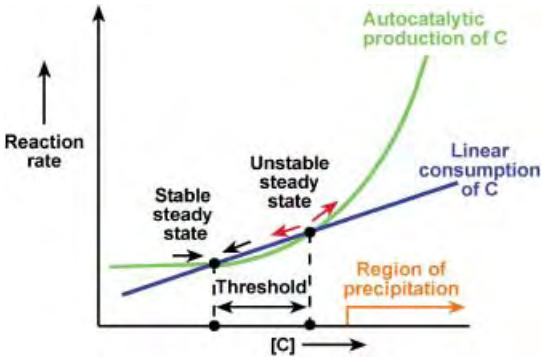


Figure 1. Graphical representation of the minimal kinetic model of self-regulation in hemostasis. The threshold response of hemostasis is modeled to arise from the existence of two steady states that correspond to the crossing points of the two reaction curves describing competing production and consumption of a control molecule C. The left steady state is stable. A small perturbation that decreases [C] from this steady state moves the system to the left, where the rate of production of C is higher than the rate of consumption, causing [C] to increase until the system returns to the steady state (black arrow). A small perturbation that increases [C] from this steady state moves the system to the right, where the rate of consumption exceeds the rate of production, causing [C] to decrease until the system returns to the steady state (black arrow). The right steady state is unstable by the same analysis (red arrows). An increase of [C] larger than the threshold (from the stable to the unstable steady state) triggers production of large amounts of C and causes precipitation.

are coupled—the initiation module is responsible for inducing the formation of the precipitate, and the inhibition module is responsible for preventing formation of precipitate and for dissolving precipitate that is already formed (in analogy to fibrinolysis). Threshold response is provided by the interactions of the inhibition and initiation modules, as was previously proposed.[19,20] The modules interact via a single control molecule C with concentration denoted [C]. We modeled the initiation module with an autocatalytic reaction that produces C with a rate proportional to $[C]^{\alpha}$ ($\alpha > 1$, green curve in Figure 1), modeled the inhibition module with a reaction that consumes C with a rate linearly proportional to [C] (blue line in Figure 1), and modeled the precipitation module with an equilibrium reaction that produces a precipitate at high concentrations of C (orange line in Figure 1). This model is minimal because removal of any of the three reactions should disrupt the function.

Hemostasis is a dynamic nonequilibrium system, therefore it was analyzed in terms of reaction rates and steady states, rather than equilibria (Figure 1). We modeled the threshold response observed in hemostasis[21] by a system with two steady states: one stable (left in Figure 1) and one unstable (right in Figure 1). Threshold response is common in systems with multiple stable and unstable steady states, and is the basis of excitability.[22] In our model, these steady states arise naturally from the kinetics of the initiation and inhibition modules; they correspond to the crossing points of the two curves (Figure 1), where the rate of production of C equals the rate of consumption of C. Multiple stable and unstable steady states have been proposed to exist in hemostasis and were used successfully to explain the effect of mass transfer on the rate of production of thrombin.[23] The stability of steady states is established using linear stability analysis[22] or graphically (Figure 1).

According to this minimal model, hemostasis is normally in the stable steady state. The threshold equals the difference between [C] at the unstable and stable steady states. Perturbations in [C] decay if they are smaller than the threshold. The system returns to the steady state after these perturbations. Perturbations in [C] grow if they are larger than the threshold. They increase [C] past the unstable (right) steady state, and lead to rapid production of C until the reagents are exhausted (this third steady state is not shown in Figure 1). The rapid production of [C] causes precipitation by the reaction of the precipitation module.

We created a biomimetic system by implementing this model using three chemical reactions that have hydronium (H_3O^+) ions as the control species C. The initiation and inhibition modules were constructed using the two competing chlorite-thiosulfate reactions well characterized by Epstein.[22,24–26]

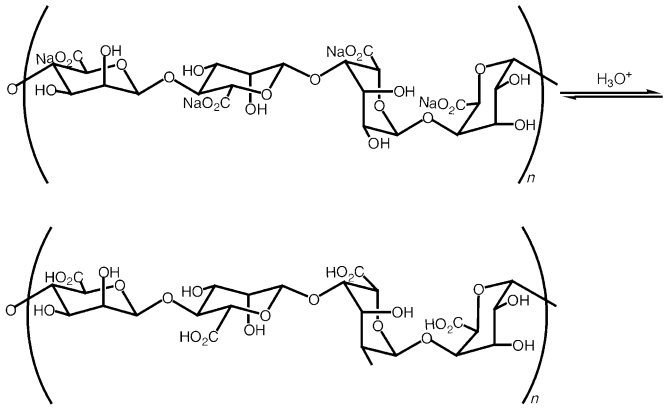
Reaction 1—autocatalytic production of H_3O^+ ions:

$$S_2O_3^{2-} + 2\,ClO_2^- + H_2O \rightarrow 2\,SO_4^{2-} + 2\,H_3O^+ + 2\,Cl^-$$
$$\text{Rate} \propto [H_3O^+]^2[Cl^-]$$

Reaction 2—linear consumption of H_3O^+ ions:

$$4\,S_2O_3^{2-} + ClO_2^- + 4\,H_3O^+ \rightarrow 2\,S_4O_6^{2-} + 2\,H_2O + Cl^-$$
$$\text{Rate} \propto [H_3O^+]$$

Reaction 3—gelling of sodium alginate in the excess of H_3O^+ ions:



 © 2004 Wiley-VCH Verlag GmbH & Co. KGaA, Weinheim

Reaction 1 produces H_3O^+ ions and is second-order autocatalytic with respect to $[H_3O^+]$. Reaction 2 consumes H_3O^+ ions and its rate is linearly proportional to $[H_3O^+]$. We used these reactions in the range of concentrations where they exhibit sensitivity to stirring and flow.[24] To allow for precipitation, we added a third reaction (Reaction 3) between H_3O^+ ions and a water-soluble sodium alginate. This reaction produces a gel of alginic acid at a high concentration of H_3O^+, when Reaction 1 becomes dominant.

The proof of the model is in the function. We used microfluidic systems to test if the model reactions could mimic hemostasis and to develop a functional microfluidic system with the ability to repair itself. The utility of this approach has been demonstrated by a self-repairing biomimetic system created to mimic the ability of vertebrae to reorganize after a deformation.[1] To create the biomimetic model of hemostasis, we designed networks of microfluidic channels to test whether the model reproduces two essential features of healthy hemostasis—both threshold and local response under conditions of flow.

Absence of blood flow is known to be detrimental for hemostasis, and it is a part of a classic Virchow's triad of factors that cause thrombosis, which can be described as excessive clotting that propagates into vessels that are not damaged.[6] Initiation of clotting through the extrinsic pathway is believed to occur when a patch of the subendothelial layer of a blood vessel is exposed by damage. In the absence of flow, autocatalysts produced by the damage activate soluble autocatalysts in the plasma.[27] Clotting initiated by the damaged patch propagates throughout the vessel,[28] leading to thrombosis.

We observed this phenomenon experimentally in our model system when the reaction mixture containing all of the components was placed into a microfluidic channel in the absence of flow. Initiation of the reaction in one region of the microfluidic channel led to propagation of the acidic chemical front[22] throughout the channel with a velocity (V_f) of 3.6 mm s^{-1} (Figure 2a). Formation of the gel of alginic acid in the acidic regions (yellow) is analogous to clot formation. The velocity V_f [m s^{-1}] of this planar chemical front (Figure 2a) can be estimated from the diffusion coefficient of the autocatalyst D_C [m^2 s^{-1}], and the normalized rate of the reaction V_r [s^{-1}]: $V_f \approx (V_r D_C)^{1/2}$. Once the reaction is initiated on a patch inside the microfluidic channel, the autocatalyst C is produced and diffuses out to increase [C] above the threshold concentration in the adjacent regions, which initiates the reaction and causes propagation of the front. If the patch is too small, the loss of the autocatalyst by diffusion from the patch is more rapid than the initiation of the reaction, and the front does not propagate because the concentration of the autocatalyst does not exceed the threshold. In the absence of flow the critical size of the patch p_c [m] can be estimated from the critical curvature in the eikonal equation, by comparing the rates of diffusion and reaction: $p_c \approx (D_C/V_r)^{1/2}$, or by expressing it as a function of the front velocity $p_c \approx D_C/V_f$.[29]

Fluid flow over the patch should increase p_c by removing the autocatalyst, and this effect has been predicted for

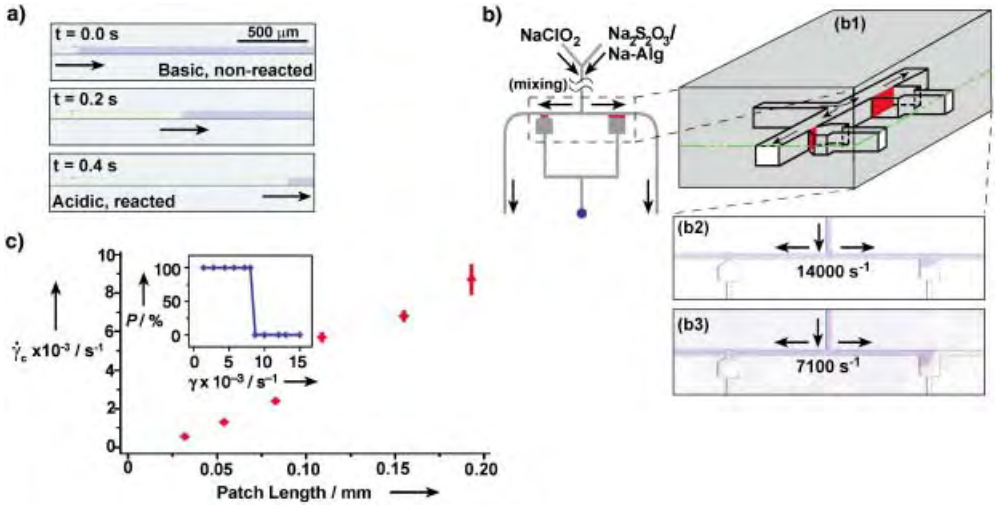


Figure 2. Chemical implementation of the minimal model. a) Behavior analogous to thrombosis in the absence of flow: Time-lapse images of propagation (3.6 mm s^{-1}) of the acidic chemical front, followed by gelling of alginic acid (clot), through a 50×50 μm^2 microfluidic channel; b) images showing the threshold response of the minimal model of hemostasis: (b1) is a schematic drawing of splitting region. The gray box represents PDMS, in which the channels were fabricated. Solutions were allowed to mix prior to reaching the region shown. In the absence of external stimuli the reaction mixture remained basic and clot-free (purple). (b2) is a microphotograph of the splitting region ($\dot{\gamma}$ = 14000 s^{-1}) after external initiation at the central outlet (blue dot). Clot propagation into the flowing regions was not seen at either the large (185-μm long) or small (60-μm long) acidic patches; the patches refer to the interfaces (red) between the acidic gel and the flowing basic solutions shown in the schematic drawings. (b3) is a microphotograph of the splitting region ($\dot{\gamma}$ = 7100 s^{-1}) after external initiation at the central outlet. Clot propagation into the flowing region was seen only at the large acidic patch; c) plot of critical shear rate ($\dot{\gamma}_c$) as a function of patch length. The inset shows a graph of probability of initiation (*P*) versus the shear rate, illustrating the typical threshold response observed. The 185 μm patch was used as an example. The purple solution was generated by mixing equal volumes of two aqueous solutions: 1) $Na_2S_2O_3$ (0.1 M, pH 9.3), the sodium salt of alginic acid (Na-Alg, 0.03 M), and bromophenol blue (0.001 M), and 2) $NaClO_2$ (0.03 M, pH 10.8). We used a pH indicator, bromophenol blue, to follow the propagation by a visible color change from purple (basic) to yellow (acidic). In all cases the depth of channels was 50 μm.

 © 2004 Wiley-VCH Verlag GmbH & Co. KGaA, Weinheim

hemostasis.[8] Initiation of clotting in hemostasis is predicted to show a threshold response with respect to both the size of the patch and shear rate of the flow.[8] It is believed that under normal physiological conditions there are multiple small patches of damaged surface on vessels,[7] but in the presence of flow these patches do not initiate clotting.

To test the threshold behavior of the model system in the presence of small acidic patches inside the channels, we designed a microfluidic device in which patches analogous to damaged surfaces can be easily introduced (Figure 2b). The reagents were allowed to continuously flow in through the two inlets and out though all three outlets. The solutions were allowed to mix completely before they reached the splitting region ((b1) in Figure 2b). Then the central outlet was blocked to stop the flow and initiate clotting in this channel. The clot propagated (similar to Figure 2a) into both dead volume regions, producing two patches ((b2) and (b3) in Figure 2b) of different sizes that presented H_3O^+-filled gel to the flowing solutions.

At shear rates ($\dot{\gamma}$) above 8000 s^{-1} neither of the patches induced clotting in the flowing reaction mixture ((b2) in Figure 2b), but below the critical shear rate ($\dot{\gamma}_c$) of 8000 s^{-1}, only the larger patch initiated clot formation in the flowing reaction mixture (b3; see inset in Figure 2c). We measured $\dot{\gamma}_c$ for patches ranging from 25–185 μm, and confirmed that the critical shear rate increases for larger patches. We confirmed that for sufficiently small patches the reaction did not initiate even in the absence of flow. We could not fabricate devices with sufficiently small patches for the reaction mixture with $V_f = 3.6$ mm s^{-1} studied in Figure 2c. We decreased the front velocity to $V_f = 0.96$ mm s^{-1} by increasing the initial pH value of the reaction mixture and slowing the reaction. For this mixture in the absence of flow the reaction did not initiate for patches below $p_c \approx 9$ μm, in surprisingly good agreement with the simple estimate of $p_c \approx D_H^+/V_f \approx 11$ μm, where $D_H^+ \approx 10^{-8}$ $m^2 s^{-1}$.

We tested whether our model could mimic the ultimate function of hemostasis: the ability to self-repair by localized clotting. To demonstrate this phenomenon we used a microfluidic device with a large (250 μm in width) inlet channel ("artery") and a large outlet channel ("vein") connected by a bed of 25 μm capillaries (Figure 3). This device was designed biomimetically so that the capillaries connected directly to a vessel with a much larger cross-sectional area, similar to the connections found in the human circulatory system (Figure 3a).[30] We introduced solutions into this device as in the experiment described in Figure 2b. In the absence of damage the flow was stable and no clotting occurred (Figure 3a). Puncturing the device with a syringe needle through the polydimethylsiloxane (PDMS) resulted in initial leakage, and formation of a small volume of the reaction mixture exposed to air with minimal fluid flow. In this region the reaction spontaneously initiated and a gel of alginic acid (yellow clot) formed, which blocked the damaged area and stopped the leakage of the solution. Spontaneous initiation of this reaction may be due to fluctuations of concentration,[24] but we have not excluded absorption of CO_2 from air, or evaporation of the solution as causes of initiation. The clot propagated throughout the damaged capillary, but remained localized within the capillary ((b1) in Figure 3b) and did not induce clotting in the larger channels, in analogy to the experiment described in (b2) in Figure 2b. As a control, we punctured such a microfluidic device when the solutions were lacking one of the reagents, sodium chlorite. In this case the damage to the device did not induce clot formation and resulted in continuous, severe leaking through the hole ((b2) in Figure 3b). We emphasize that this model is minimal and it will not explain all of the nuances of hemostasis. Self-repair in this biomimetic system is similar to the initial repair achieved by the formation of the hemostatic plug in biological systems. It is less sophisticated than complete biological repair, in which tissue eventually re-grows to replace the hemostatic plug.

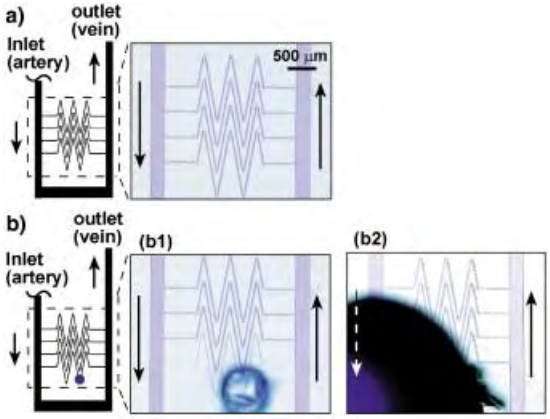


Figure 3. Biomimetically designed self-repairing microfluidic devices: a) Schematic drawing and a microphotograph of a solution prior to initiation in the biomimetic microfluidic device. The black arrows indicate the direction of flow; b) (b1) shows self-repair in the biomimetic device. Use of the complete reaction mixture ($Na_2S_2O_3$/Na-Alg and $NaClO_2$) resulted in formation of a localized clot and minimal leaking when the capillary bed was punctured (blue dot); (b2) shows when the $NaClO_2$ component of the reaction mixture was removed, puncturing the device in the same location as in (b1), led to severe leaking through the hole. All channels were 50-μm deep. Small channels (capillaries) were 25-μm wide and large channels were 250-μm wide.

This model may be also used for generating new hypotheses describing hemostasis. Traditionally, the evolution of vascular systems has been considered from the point of view of Murray's law, taking into account mass transport, gas exchange, and the hydrodynamic efficiency of pumping.[30] These criteria are clearly important for the overall structure and design of a vascular network, but they are more difficult to apply to the local features of the network, such as the geometry of junctions of blood vessels. For example, changes in the geometries of junctions of small vessels will not significantly affect the overall pressure drop for the flow of blood through the vascular system.

Here we propose a hypothesis that some local features may have evolved to accommodate the self-regulation of hemostasis. We designed a non-biomimetic network of channels, where small capillaries were connected to large veins and arteries through triangular expansions (Figure 4), rather than a direct connection,[30] as in the biomimetic device (Figure 3a). After the flow of reagents was established as in Figure 3a, the capillary was punctured with a syringe needle.

 © 2004 Wiley-VCH Verlag GmbH & Co. KGaA, Weinheim

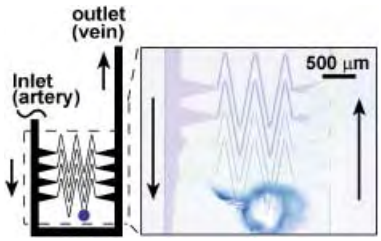


Figure 4. Use of a non-biomimetic capillary design to show the critical role of the ratio of cross-sectional surface areas of the capillaries and larger vessels. Here, the capillaries are joined to the larger vessels through an opening that is 300-μm wide. The device was able to self-repair when punctured, but the clot propagated into the larger vessels (yellow) due to the large acidic patch formed at the interface between the capillaries and the large vessels. All channels were 50-μm deep. Small channels (capillaries) were 25-μm wide and large channels were 250-μm wide. As in Figure 2, solutions of $Na_2S_2O_3$/Na-Alg and $NaClO_2$ mixed prior to reaching the region of interest.

The reaction initiated, and the clot stopped the leaking, just as it did in the biomimetic device. Unlike the biomimetic device, the response of this system was not local—when the clot propagated through the damaged capillary it did not stop at the capillary–vein junction, but propagated into both the vein and the artery (Figure 4).

There are two implications of experiments of this type. First, they may provide clues to the design of artificial vessels (e.g., those used for dialysis or bypass grafts) that do not induce clotting. Second, they may provide alternative perspectives on the evolution of vascular systems, traditionally considered from the points of view of mass transport, gas exchange, and the hydrodynamic efficiency of pumping, and not the ability of hemostasis to act locally.[30] This experiment suggests a hypothesis that properly functioning hemostasis may have presented an additional evolutionary constraint on the design of vascular systems in biology. We emphasize that this experiment in itself does not test the hypothesis, only suggests it. We are currently using the microfluidic devices we have designed for the model system (e.g., the device shown in Figure 2b) to test this hypothesis with blood, and to study the dynamics of hemostasis under controlled-flow conditions.

In this system only three chemical reactions have been sufficient to reproduce the function of the complex biochemical network of hemostasis. It is conceivable that one could add additional reactions to each module of the model system—while maintaining the overall kinetics of each module—to make it resemble hemostasis more closely. If such an incremental transformation is possible, one may speculate that hemostasis could have originated as a minimal system composed of a few reactions (at least three, with at least one reaction for each module). The spontaneous appearance of such a simple system early in evolution is not impossible. How to evolve hemostasis, from a minimal system with rather primitive function into a complex system with much more sophisticated function, is a fascinating question. The evolution of hemostasis is also interesting because it has been considered an "irreducibly complex" system; a system that does not function if any of the components are removed, and therefore a system that could not have evolved by incremental addition of components while maintaining its function.[31,32] One may speculate that such evolution could occur through redundant coexistence. For each of the three reactions in the original minimal system, a set of new reactions would have to evolve with the overall kinetics of the original reaction. The function of the system would not be disrupted during the evolution of the new set of reactions, as long as the original and the new reactions coexist. Once the new set of reactions evolves, the original reaction may be lost, also without the loss of function. Such a mechanism may be used in reverse to reduce the complexity of hemostasis without the loss of function (ultimately reducing it to as few as three reactions). These ideas are certainly speculative, but they may be used to generate testable hypotheses, and to stimulate and guide further investigation in hemostasis and other complex systems.

We conclude that we have succeeded in creating a minimal model of hemostasis that can be implemented with purely non-biochemical reactions in a microfluidic device. The system showed properties similar to those of hemostasis, and allowed us to create a biomimetic microfluidic device that repairs itself. This result complements the previous examples that use nonlinear interactions in chemical[33–35] or physical[36] systems for self-regulation and self-repair.[1] In general, the function of biochemical systems arises from interactions of multiple reactions away from thermodynamic equilibrium. We are especially excited by the opportunities and challenges that such functional biochemical systems present to synthetic chemists. Microfluidics may be used to "synthesize" systems of reactions by controlling interactions among the individual reactions, and maintaining them away from equilibrium. Such synthesis of functional systems of reactions (in addition to the synthesis of molecules and assemblies of molecules) could lead to practically useful developments, such as new types of functional microfluidic devices. Synthetic functional systems of chemical reactions may also help understand the biological systems by which they were inspired. As Richard Feynman put it, "what I cannot create, I do not understand."[37]

Received: November 28, 2003 [Z53428]
Published Online: February 24, 2004

Keywords: autocatalysis · biomimetic synthesis · hemostasis · microfluidic systems · self-repairing systems

[1] M. Boncheva, G. M. Whitesides, *Angew. Chem.* **2003**, *115*, 2748; *Angew. Chem. Int. Ed.* **2003**, *42*, 2644.
[2] G. M. Whitesides, B. Grzybowski, *Science* **2002**, *295*, 2418.
[3] S. Mann, D. D. Archibald, J. M. Didymus, T. Douglas, B. R. Heywood, F. C. Meldrum, N. J. Reeves, *Science* **1993**, *261*, 1286.
[4] H. E. Pelish, N. J. Westwood, Y. Feng, T. Kirchhausen, M. D. Shair, *J. Am. Chem. Soc.* **2001**, *123*, 6740.
[5] H. Y. Erbil, A. L. Demirel, Y. Avci, O. Mert, *Science* **2003**, *299*, 1377.
[6] R. S. Cotran, V. Kumar, T. Collins, *Robbins Pathological Basis of Disease*, 6th ed., W. B. Saunders Company, New York, **1999**.
[7] A. L. Kuharsky, A. L. Fogelson, *Biophys. J.* **2001**, *80*, 1050.
[8] E. Beltrami, J. Jesty, *Math. Biosci.* **2001**, *172*, 1.
[9] H. J. Weiss, V. T. Turitto, H. R. Baumgartner, *J. Lab. Clin. Med.* **1978**, *92*, 750.

 © 2004 Wiley-VCH Verlag GmbH & Co. KGaA, Weinheim

[10] S. L. Diamond, *Biophys. J.* **2001**, *80*, 1031.
[11] A. Arkin, P. D. Shen, J. Ross, *Science* **1997**, *277*, 1275.
[12] G. M. Whitesides, R. F. Ismagilov, *Science* **1999**, *284*, 89.
[13] W. Vance, A. Arkin, J. Ross, *Proc. Natl. Acad. Sci. USA* **2002**, *99*, 5816.
[14] T. Vicsek, *Nature* **2002**, *418*, 131.
[15] P. Nurse, *Nature* **2003**, *424*, 883.
[16] L. H. Hartwell, J. J. Hopfield, S. Leibler, A. W. Murray, *Nature* **1999**, *402*, C47.
[17] U. Alon, *Science* **2003**, *301*, 1866.
[18] W. Xiong, J. E. Ferrell, *Nature* **2003**, *426*, 460.
[19] A. L. Fogelson, A. L. Kuharsky, *J. Theor. Biol.* **1998**, *193*, 1.
[20] E. Beltrami, J. Jesty, *Proc. Natl. Acad. Sci. USA* **1995**, *92*, 8744.
[21] C. vantVeer, K. G. Mann, *J. Biol. Chem.* **1997**, *272*, 4367.
[22] I. R. Epstein, J. A. Pojman, *An Introduction to Nonlinear Chemical Dynamics Oscilllations, Waves, Patterns, and Chaos*, Oxford University Press, **1998**.
[23] D. Basmadjian, M. V. Sefton, S. A. Baldwin, *Biomaterials* **1997**, *18*, 1511.
[24] I. Nagypal, I. R. Epstein, *J. Phys. Chem.* **1986**, *90*, 6285.
[25] A. K. Horvath, I. Nagypal, I. R. Epstein, *J. Am. Chem. Soc.* **2002**, *124*, 10956.
[26] A. K. Horvath, I. Nagypal, I. R. Epstein, *J. Phys. Chem. A* **2003**, *107*, 10063.
[27] P. L. A. Giesen, U. Rauch, B. Bohrmann, D. Kling, M. Roque, J. T. Fallon, J. J. Badimon, J. Himber, M. A. Riederer, Y. Nemerson, *Proc. Natl. Acad. Sci. USA* **1999**, *96*, 2311.
[28] H. Partsch, *Curr. Opin. Pulm. Med.* **2002**, *8*, 389.
[29] A. Toth, V. Gaspar, K. Showalter, *J. Phys. Chem.* **1994**, *98*, 522.
[30] M. Labarbera, *Science* **1990**, *249*, 992.
[31] J. A. Coyne, *Nature* **1996**, *383*, 227.
[32] E. C. Scott, *Science* **2000**, *288*, 813.
[33] D. J. Beebe, J. S. Moore, J. M. Bauer, Q. Yu, R. H. Liu, C. Devadoss, B. H. Jo, *Nature* **2000**, *404*, 588.
[34] C. D. Mao, V. R. Thalladi, D. B. Wolfe, S. Whitesides, G. M. Whitesides, *J. Am. Chem. Soc.* **2002**, *124*, 14508.
[35] D. R. Reyes, M. M. Ghanem, G. M. Whitesides, A. Manz, *Lab Chip* **2002**, *2*, 113.
[36] A. Groisman, M. Enzelberger, S. R. Quake, *Science* **2003**, *300*, 955.
[37] A. Eschenmoser, M. V. Kisakurek, *Helv. Chim. Acta* **1996**, *79*, 1249.

 © 2004 Wiley-VCH Verlag GmbH & Co. KGaA, Weinheim

Nanostructures

Shape Effect in Nanoparticle Self-Assembly**

*Nikhil R. Jana**

The assembly of nanoparticles is a key step for their application as nanodevices. Self-assembly of nanomaterials strongly depends on interparticle interactions,[1,2] particle size distribution[1,2] and particle shape.[3–8] Current methods for assembling nanoparticles include capillary force,[9] template-directed patterning,[10] or surface derivatization of particles that modify interparticle interactions.[1,2] Spontaneous self-assembly of spherical nanoparticles occurs only with particles with a narrow size distribution, that is, those with a polydispersity $< 5\,\%$, and leads to a compact 2D or 3D structure.[1,2] In contrast, nonspherical nanoparticles show different types of self-assembly. Oriented attachment-based self-assembly and crystallization was observed for inorganic colloids and nanoparticles.[4,11,12] Various liquid-crystalline order structures such as nematic, columnar, and smectic phases are observed for rodlike and platelike particles at high volume fractions.[13–21] Similarly, bundle structures have been observed for nanowires and nanotubes.[22,23] However, the colloidal systems available for experimental study had a limited length scales and aspect-ratio ranges, namely, the tobacco mosaic virus (TMV) nanorods, β-FeOOH nanorods, gibbsite plates, boehmite rods, and higher-order smectic phases, which are often inhibited either because of shape polydispersity or the kinetic arrest into the gel phase because of the lack of suitable surface modification.[17,24] Recent synthetic advances that provide anisotropic nanoparticles of various size, shape, and dimension, provide an opportunity to examine theoretical predictions and to use them for the ordering of nanomaterials.[6–8,20,25,26] We have studied the self-assembly of gold–silver nanoparticles with various aspect ratios (length to width ratio for spheroids/rods and diameter to width ratio for plates) from 1–25, all having short axis diameter between 10–30 nm. We observed various types of self-assembly depending on shape and extent of particle anisotropy. (Figures 1–5) The observed self-assemblies are analogous to the entropy-driven ordering into liquid-crystalline phases, as originally proposed by Onsager[27] and latter verified by computer simulations,[28,29] and experimental work.[17,18]

[*] Dr. N. R. Jana
Department of Chemistry
Raja Rammohun Roy Mahavidyalaya
Radhanagar-712406, Hooghly WB (India)
and
Department of Chemistry and Biochemistry
University of Arkansas
Fayetteville, AR 72701 (USA)
Fax: (+1) 479-575-4049
E-mail: njana@uark.edu

[**] This research was supported by R. R. R. Mahavidyalaya, WB, India. The author thanks C. J. Murphy, University of South Carolina and T. Pal, Indian Institute of Technology-Kharagpur, for assistance.

 © 2004 Wiley-VCH Verlag GmbH & Co. KGaA, Weinheim DOI: 10.1002/anie.200352260

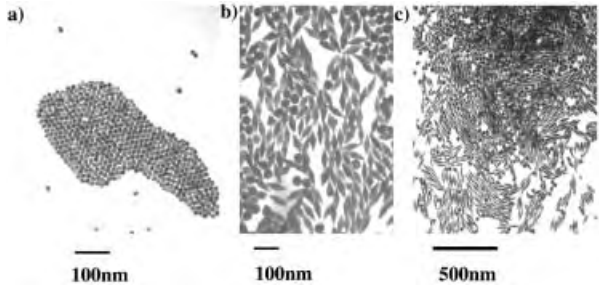


Figure 1. Honeycomb structures produced by gold spheroids of different anisotropy: a) aspect ratio 1.2, b) aspect ratio 3.5, and c) aspect ratio 6.5. Particle dispersion in water was ≈1% concentration by weight and 1–2 μL of this solution was deposited onto carbon-coated copper grid and solvent was slowly evaporated. The resulting dried film was investigated by transition electron microscopy (TEM).

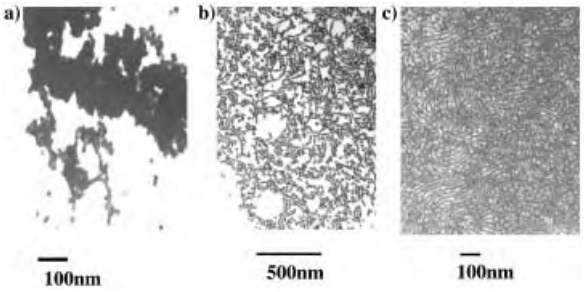


Figure 2. Oriented attachment observed by different anisotropic gold spheroids: a) aspect ratio 1.5 and b),c) aspect ratio 3.5. Particle dispersion in water was ≈0.1% concentration by weight. Concentration of free surfactants in solution was ≈0.0 as they were removed by successive centrifugation and redispersion cycles. TEM studies were carried out 48 h after preparing the dispersions by using 1–2 μL of the precipitated portion.

According to the Onsager's theory, hard rods interacting with repulsive forces could exhibit orientational ordering at densities far below the closest packing. The thermodynamic stability of these order structures arises from a gain in translational entropy that overrules the loss of orientational entropy associated with particle alignment.[27] These order structures strongly depend on the particle anisotropy.[28] Short rods (< 7 aspect ratio) exhibit direct isotropic–smectic phase transition but long rods show isotropic–nematic–smectic transitions.[28] We observed that spheroids with aspect ratios between 1 and 7 show orientational ordering that often leads to honeycomb structures (Figure 1); cylindrical nanorods and platelets with aspect ratios between 2 and 4 show higher order smectic 2D structures (Figure 3), but particles with aspect ratios 5–15 have lower-order 1D ribbon structures (Figure 4). As the aspect ratio was further increased, nematic ordering, bundle structures, or a weak tendency to from smectic 3D structures were observed depending on the experimental conditions.

A closer look into the smectic 2D structures show that small nanorods/plates form ribbon structures through side-by-side alignment and those ribbons further self-assemble, side-by-side, into a smectic array. (Figure 3) The aspect-ratio window is relatively small for this smectic array and needs a

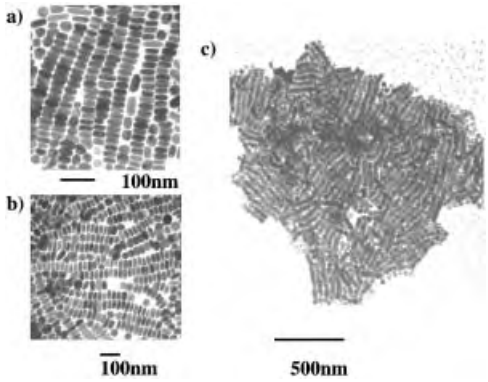


Figure 3. Smectic 2D ordering of silver nanorods/plates with aspect ratio 2–4: a) plates with aspect ratio of 2, b) rods with aspect ratio of 2, and c) rods with aspect ratio of 3.5 (some plates are also involved in this self-assembly). Particle dispersion in water was ≈2% concentration by weight. TEM studies were carried out 24 h after preparing the dispersions by using 1–2 μL of the precipitated portion.

narrow distribution (< 10%) of aspect ratio. However, we observed that the extent of anisotropy is more important than the nature of shape (i.e., rods or plates), thus both rods and plates can be involved in the same smectic array. In concentrated dispersions these rods slowly precipitate into these 2D structures. When this precipitate was observed under electron microscope, micrometer size 2D structures were observed without any isolated particles. No other type of ordering such as nematic or ribbon structure was observed, thus indicating that smectic ordering was only favorable as predicted earlier.[28] The precipitated nanorods can be redispersed in excess water and this diluted dispersion no longer produces a smectic array; mostly isolated particles are observed.

The honeycomb structures of spheroids do not show positional ordering, (Figure 1) however, 1D positional ordering occurs in the ribbon structures of particles with aspect ratios from 5 to 15. (Figure 4) The spheroids, plates, or

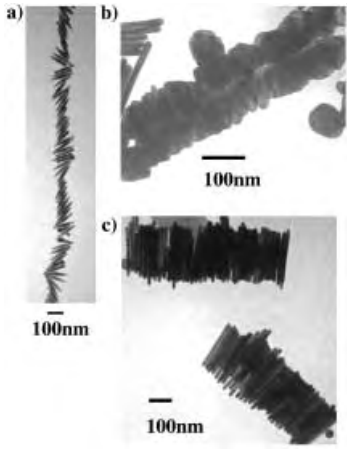


Figure 4. Ribbon structures of nanoparticles with higher aspect ratios: a) gold spheroids with aspect ratio of 7.5, b) gold plates with aspect ratio of 8 and two ribbons aligned size-by-size, and c) gold nanorods with aspect ratio 15. Particle dispersion in water was ≈5% concentrated. TEM study was carried out by using 1–2 μL of the dispersion.

 © 2004 Wiley-VCH Verlag GmbH & Co. KGaA, Weinheim

nanorods align almost parallel to each other and form linear arrays of small groups in which the nanoparticle long axis is perpendicular to the array axis. (Figure 4) A similar array was present throughout the microscopic grid. In some cases 2 or 3 ribbons stack with each other, thus showing a weak smectic ordering. The frequency of occurrence of ribbon structures (compared with isolated particles) and the length of the ribbons increase with an increase in the aspect ratio. For example the spheroids seldom form ribbon structures (rather than honeycomb structures), but plates and rods form ribbon structures very frequently. The average number of monomer spheroids and plates present in a ribbon structure is between 25 and 50, but this number increases to a few hundred as the aspect ratio increases to 15. With a further increase in anisotropy (aspect ratio 15–25), the 1D ribbon structure extends into 2D bundle structures with occasional side-by-size alignment of 2 or 3 bundles into 3D superstructures. (Figure 5) At lower surfactant concentrations these long

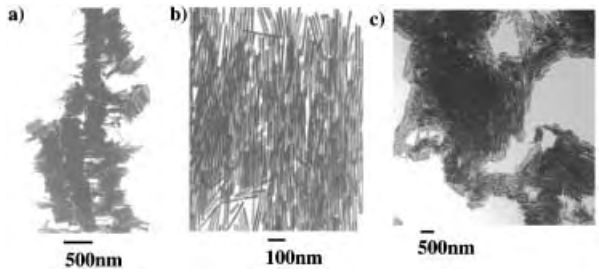


Figure 5. Self-assembly of gold nanorods with aspect of ratio 22: a) bundle structure at higher surfactant concentration with three bundles aligned size-by-size, and b,c) nematic order at lower surfactant concentration. Particle dispersion in water was ≈5% concentration by weight. TEM studies were carried out by using 1–2 μL of the dispersion.

rods exhibit nematic ordering. (Figure 5) Our observations are in general agreement with the theoretical prediction that higher structures are more favorable with increasing particle anisotropy.[28]

A very different type of self-assembly, previously known as oriented attachment,[11,12] was observed for spheroids at lower stabilizing surfactant condition. Spheroids undergo irreversible oriented attachment and form a linear array. (Figure 2) In this oriented attachment, particles appear fused almost end-to-end along their longitudinal axis and form linear chains. The long chains were often bent and sometimes formed coils and globules. This oriented attachment also occurs in polydispersed samples in which the spheres are mixed, thus leading to the selective precipitation of spheroids. This oriented attachment is irreversible and particles could not be redispersed. This type of particle assembly occurs at 0.01–0.1% volume fractions, which is much lower than the condition required for entropy-driven ordering.[24] The irreversible attachment leads to a lowering of the surface energy after the elimination of highly curved surfaces of individual spheroids, and is an enthalpy-favorable processes.[11,12] We presumed that a lower concentration of stabilizing surfactant would induce slow 1D aggregation (then fusing) of charged particles to minimize the repulsive interactions between particles.[30]

The self-assembly process was influenced by the presence of stabilizer surfactant, which was used in the particle synthesis. As the concentration of surfactant increased relative to a fixed particle concentration, the formation of order structures appeared to be more favorable than the formation of isolated particles. This was evident with the precipitation of smectic 2D short rods, an increase of ribbon structures for rods with aspect ratios 5–15, and an increase of bundle structures for rods with aspect ratios 15–25. The volume fractions we used were relatively low compared to the theoretical values determined by hard particle approximation.[17,24,28] Similar self-assembly at lower volume fraction was recently reported.[21] This is expected as the interaction of real colloids or nanoparticles with each other depends on the presence of an ionic and/or an organic stabilizing shell surrounding each particle, and Onsager's theory may be applicable to those particles that have an effective increased diameter.[27] In the case presented here, the particles are coated with a cationic surfactant and the presence of excess surfactant induce self-assembly. This surfactant shell causes the particles to have a net positive charge, and can induce interdigitation between particles.[5,19] When the surfactant was replaced by a dodecanethiol monolayer, no order structures were observed as surface charge was eliminated. These facts indicate that the role of the surfactant is to balance the repulsive and attractive interactions between particles. The excess surfactant may behave similarly to polymer that is often used to induce depletion attraction between colloids and to widen the regions over which phase transition can occur.[24]

The lateral capillary force that occurs during the drying processes of the particle dispersion may induce the self-assembly.[6] However, self-assembly was observed only at higher particle concentrations or with precipitates. When the solution was diluted and the precipitate was redispersed to make a dilute solution, no self-assembly was observed under a microscope. The separation of nanorods from a bulk solution of rod–sphere mixture indicates that capillary forces do not have major role in the self-assembly processes. Liquid-crystalline order structures were further confirmed when the sample solution or the precipitates were investigated under polarized-light microscopy and by small-angle X-ray scattering.[19] However, we are unable to make very concentrated particle dispersions for light-scattering studies as most of our sample dispersion immediately precipitates or becomes too turbid. Earlier reports show that concentrated particle dispersions often form gels unless the particle surfaces are properly modified with stabilizer.[17,24] In this respect surfactants may not be a good stabilizer, as they themselves can form liquid crystals or gels; currently, we are trying to modify the particle surface with polymers.

In real colloids, the polydispersity often inhibits crystallization.[1,2,16] For example, in a binary colloid mixture, dilute solutions are homogeneous as the mixing entropy dominates, but at higher concentration spontaneous phase separation often occurs. This phase separation increases the free volume and thus increases the translational entropy of colloids that

 © 2004 Wiley-VCH Verlag GmbH & Co. KGaA, Weinheim

compensates for the loss of mixing entropy. In this concentrated dispersion, particles of the same shape attract each other—a phenomenon that is known as "macromolecular crowding" in biology and "depletion attraction" in chemistry and physics.[16,24] To understand the role of polydispersity in the self-assembly process, we performed some control experiments. When the samples were studied before shape separation from spheres (10–50% spheres, the rest spheroids or nanorods), the self-assembly processes often led to spontaneous shape separation in micrometer length scale. The rods or spheroids self-assembled with each other, formed groups, and separated from the spheres. In other words, nanorods or spheroids recognize each other in a polydispersed sample and assemble into groups (Figure 6), which is very similar to what

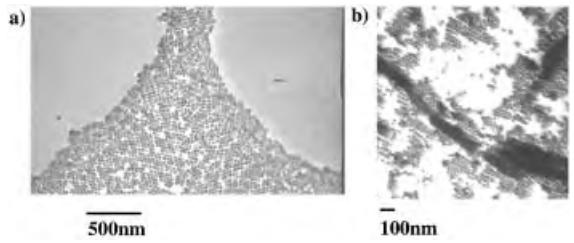


Figure 6. Self-assembly of gold nanorods in polydispersed sample: a) rods with aspect ratio of 2–4, and b) rods with aspect ratio of 5. In these samples rods are mixed with spheres (30–40% by number) of similar size and particles were 5% concentration by weight. TEM studies were carried out by using 1–2 μL of the dispersion.

occurs in the formation of bacteria colonies. Under similar conditions, spheres do not self-assemble. This is very similar to the recent observation by Lekkerkerker and co-workers in which the polydispersed (≈25%) plates show smectic transition during which spontaneous shape fractionation occurs.[18] Our results indicate that shape polydispersity may not inhibit crystallization under all experimental conditions, but may induce shape fractionation followed by the crystallization of each identical shapes—at least at the micrometer-length scale.

The above microscopic shape separation phenomenon can be used for bulk shape separation of nanorods and plates, if the experimental condition are properly designed.[26] When the polydispersed samples are prepared at high volume fractions (0.5–5%), nanorods or plates precipitate leaving only spheres in solution. The purified nanorods can be redispersed in suitable solvents as the self-assembly is a reversible processes. As the self-assembly process depends on the particle anisotropy, the separation conditions can be tuned for the step-by-step separation of different anisotropic particles.[26] For example, in a mixture of gold rods (aspect ratio 10–25), plates (aspect ratio 8) and spheres, as the concentration of particle dispersion increased, long rods precipitated first followed by short rods and finally plates, but spheres remained in solution. Similarly, for the mixture of silver rods (aspect ratio 2–4) and spheres, rods precipitated but spheres remained in solution. Separation efficiency can be increased by repeated precipitation–redispersion cycles.[26] This shape separation technique can be used to prepare high-purity nanorods and plates.

Our results indicate that self-assembly is strongly induced by shape. While under similar experimental conditions the spheres of similar size do not self-assemble unless they have a very tight size distribution, other shapes do self-assemble despite shape polydispersity. Both the nature of the self-assembly and the driving force for self-assembly depends on particle shape and particularly on the extent of shape anisotropy. These types of self-assemblies may be used for mesoscale self-assembly of nanomaterials to overcome problems by using nanosphere precursors.

Experimental Section

The nanoparticles of various shapes were prepared according to seeding-growth processes in aqueous surfactant (cetyl-trimethylammonium bromide, CTAB) media.[25] In the first step, 3–4 nm seeds of citrate-stabilized silver or gold nanoparticles are prepared by borohydride reduction. In the next step, the seeds are grown in a growth solution that contains additional metal salts and weak reducing agents as previously reported. [25] Nanorods or plates of different anisotropy are formed depending on the ratio of seed to metal salt, presence of shape inducing agents (namely, Ag^+ ions or cyclohexane) or by changing solution pH. The prepared nanoparticles are then separated from the spherical nanoparticles and excess surfactant by centrifugation at different speeds. Nanoparticles thus prepared have a surfactant coating that stabilizes their aqueous dispersion. Thermogravimetric analysis of separated nanoparticles shows the presence of 15–20% surfactant by mass, which is larger that the monolayer coverage (≈3%) surrounding the particles. After removal of the excess surfactant, nanoparticles are then subjected to purification cycles.[26] Typically, a dispersion of nanoparticles (0.5–5% concentration by weight of the respective metals) is prepared and then either preserved for few days or excess CTAB is added until a precipitate is observed. The precipitate is redispersed in water or in a fresh CTAB solution. The precipitation–redispersion cycles are repeated 4 or 5 times, after which the concentrated nanoparticle dispersions (up to 20% by weight) are obtained. For dodecanethiol capping, nanoparticle hydrosol is mixed with a toluene solution of the thiol and stirred vigorously for one hour. The thiol-coated nanoparticle aggregates form films at the water–toluene phase boundary, which can be used for microscopic study.

Received: June 30, 2003
Revised: November 24, 2003 [Z52260]

Keywords: gold · nanostructures · nanotechnology · self-assembly · silver

[1] C. P. Collier, T. Vossmeyer, J. R. Heath, *Annu. Rev. Phys. Chem.* **1998**, *49*, 371–404.
[2] M. P. Pileni, *J. Phys. Chem. B* **2001**, *105*, 3358–3371.
[3] Z. L. Wang, *J. Phys. Chem. B* **2000**, *104*, 1153–1175.
[4] B. A. Korgel, D. Fitzmaurice, *Adv. Mater.* **1998**, *10*, 661–665.
[5] M. Li, H. Schnablegger, S. Mann, *Nature* **1999**, *402*, 393–395.
[6] B. Nikoobakht, Z. L. Wang, M. A. El-Sayed, *J. Phys. Chem. B* **2000**, *104*, 8635–8640.
[7] K. Franklin, K. Serena, A. Jennifer, Y. Peidong, *J. Am. Chem. Soc.* **2001**, *123*, 4360–4361.
[8] V. F. Puntes, D. Zanchet, K. Can, C. K. Erdonmez, A. P. Alivisatos, *J. Am. Chem. Soc.* **2002**, *124*, 12874–12880.
[9] N. Bowden, F. Arias, T. Deng, G. M. Whitesides, *Langmuir* **2001**, *17*, 1757–1765.

 © 2004 Wiley-VCH Verlag GmbH & Co. KGaA, Weinheim

[10] A. P. Alivisatos, K. P. Johnsson, X. Peng, T. E. Wilson, C. J. Loweth, M. P. Bruchez Jr. , P. G. Schultz, *Nature* **1996**, *382*, 609 – 611.
[11] R. L. Penn, J. F. Banfield, *Science* **1998**, *281*, 969 – 971.
[12] C. Pacholski, A. Kornowski, H. Weller, *Angew. Chem.* **2002**, *114*, 1234 – 1237; *Angew. Chem. Int. Ed.* **2002**, *41*, 1188 – 1191.
[13] F. Livolant, A. M. Levelut, J. Douset, J. P. Benoit, *Nature* **1989**, *339*, 724 – 726.
[14] P. A. Buining, A. P. Philipse, H. N. W. Lekkerkerker, *Langmuir* **1994**, *10*, 2106 – 2114.
[15] Z. Dogic, S. Fraden, *Phys. Rev. Lett.* **1997**, *78*, 2417 – 2420.
[16] M. Adams, Z. Dogic, S. L. Keller, S. Fraden, *Nature* **1998**, *393*, 349 – 352.
[17] J-C P. Gabriel, P. Davidson, *Top. Curr. Chem.* **2003**, *226*, 119 – 172.
[18] K. van der, M. Felix, K. Kassapidou, H. N. W. Lekkerkerker, *Nature* **2000**, *406*, 868 – 871.
[19] N. R. Jana, L. A. Gearheart, S. O. Obare, C. J. Johnson, K. J. Edler, S. Mann, C. J. Murphy, *J. Mater. Chem.* **2002**, *12*, 2909 – 2912.
[20] L. Li, J. Walda, L. Manna, A. P. Alivisatos, *Nano Lett.* **2002**, *2*, 557 – 560.
[21] H. Maeda, Y. Maeda, *Phys. Rev. Lett.* **2003**, *90*, 18303.
[22] B. Vigolo, A. Pénicaud, C. Coulon, C. Sauder, R. Pailler, C. Journet, P. Bernier, P. Poulin, *Science* **2000**, *290*, 1331 – 1334.
[23] S.-H. Yu, M. Antonietti, H. Coelfen, J. Hartmann, *Nano Lett.* **2003**, *3*, 379 – 382.
[24] V. J. Anderson, H. N. W. Lekkerkerker, *Nature* **2002**, *416*, 810 – 814.
[25] a) N. R. Jana, L. Gearheart, C. J. Murphy, *Chem. Commun.* **2001**, 617 – 618; b) N. R. Jana, L. Gearheart, C. J. Murphy, *J. Phys Chem. B* **2001**, *105*, 4065 – 4067; c) N. R. Jana, L. Gearheart, C. J. Murphy, *Adv. Mater.* **2001**, *13*, 1389 – 1393; d) C. J. Murphy, N. R. Jana, *Adv. Mater.* **2002**, *14*, 80 – 82.
[26] N. R. Jana, *Chem. Commun.* **2003**, 1950 – 1951.
[27] L. Onsager, *Ann. N. Y. Acad. Sci.* **1949**, *51*, 627 – 659.
[28] M. A. Bates, D. Frenkel, *J. Chem. Phys.* **2000**, *112*, 10034 – 10041.
[29] M. A. Bates, D. Frenkel, *J. Chem. Phys.* **1998**, *109*, 6193 – 6199.
[30] B. V. Enustun, J. Turkevich, *J. Am. Chem. Soc.* **1963**, *85*, 3317 – 3328.

 © 2004 Wiley-VCH Verlag GmbH & Co. KGaA, Weinheim

Nanoparticles

Pt Hollow Nanospheres: Facile Synthesis and Enhanced Electrocatalysts**

Han-Pu Liang, Hui-Min Zhang, Jin-Song Hu, Yu-Guo Guo, Li-Jun Wan, and Chun-Li Bai**

Considerable attention has been paid to alternative energy sources such as hydrogen and fuel cells as energy sources in an attempt to relieve the pollution and energy crisis. Among various candidates, Pt has stimulated considerable research into its use as a catalyst in the production of hydrogen from methane, in automobile catalytic converters, and particularly in the direct methanol fuel cell (DMFC).[1] However, a critical problem with Pt-based catalysts is their prohibitive cost. Therefore, economical and effective alternative catalysts are required and cost-effective routes are being sought to make more-efficient Pt catalysts. To date, efforts have focused on the development of techniques to produce Pt catalysts with a high surface area to achieve high catalytic performance and utilization efficiency.[2]

Hollow metallic nanospheres exhibit catalytic activities different from their solid counterparts with the advantages of low density, saving of material, and reduction of costs. For example, Hyeon and co-workers reported that hollow Pd spheres show good catalytic activities in Suzuki cross-coupling reactions and can be reused many times without the loss of catalytic activity.[3] Traditional ways to fabricate hollow spheres have focused on various sacrificial templates, including polystyrene spheres,[4] silica spheres,[3,5] resin spheres,[6] vesicles,[7] liquid droplets,[8] and microemulsion droplets.[9] The common procedures of these methods relate to the removal of the core template or two immiscible liquid phases. The procedures are technically complicated, which limits their application to some extent. Recently, Xia and co-workers reported a one-step approach to produce metallic hollow nanospheres with average diameters of ≈ 50 nm by combining Ag nanoparticles with a solution of an appropriate salt precursor.[10] However, an AgCl precipitate was formed in the procedure, which made the procedure complicated and influenced the yield of hollow nanospheres. Herein we described a facile, efficient, and economical route to the

[*] H.-P. Liang,[+] H.-M. Zhang, J.-S. Hu,[+] Y.-G. Guo,[+] L.-J. Wan, C.-L. Bai
Center for Molecular Science, Institute of Chemistry
Chinese Academy of Sciences
Beijing 100080 (China)
Fax: (+86) 10-6255-8934
E-mail: wanlijun@iccas.ac.cn
clbai@iccas.ac.cn

[+] Also at the Graduate School of Chinese Academy of Sciences
Beijing 100064 (China)

[**] This work was supported by the National Natural Science Foundation of China (20025308 and 20177025), the National Key Project on Basic Research (Grant G2000077501), and the Chinese Academy of Sciences.

Supporting information for this article is available on the WWW under http://www.angewandte.org or from the author.

 © 2004 Wiley-VCH Verlag GmbH & Co. KGaA, Weinheim DOI: 10.1002/anie.200352956

large-scale synthesis of Pt hollow nanospheres with an average diameter of 24 nm. The synthesized Pt hollow nanospheres, composed of discrete Pt nanoparticles, show good electrocatalytic activity in the oxidation of methanol.

The key idea of our method for the synthesis of the Pt hollow nanospheres is to exploit the replacement reaction between Co nanoparticles and H_2PtCl_6. The fabrication of Co nanoparticles is an important step. The formation of Co particles is easily determined, as the solution undergoes a color change from transparent to dark. Citrate is present as a capping agent to prevent the growth of Co nanoparticles through repulsive forces between negatively charged cobalt nanoparticles. To avoid the oxidation of Co nanoparticles in the presence of atmospheric oxygen, nitrogen is bubbled through the solution during the whole procedure (see Experimental Section for details). As the standard reduction potential of the $PtCl_6^{2-}$/Pt redox pair (0.735 V vs. the standard hydrogen electrode (SHE)) is much higher than that of the Co^{2+}/Co redox pair (-0.277 vs. SHE), Co nanoparticles are immediately oxidized to cobalt ions when the solution of Co nanoparticles is added to the H_2PtCl_6 solution. The H_2PtCl_6 solution turns from pale yellow to black at the same time, which suggests the oxidation of Co nanoparticles and the formation of Pt hollow nanospheres. As this replacement reaction occurs rapidly, the Pt atoms nucleate and grow into very small particles, eventually evolving into a thin shell around the cobalt nanoparticles. The shell should have an incomplete porous structure because Co^{2+} and $PtCl_6^{2-}$ continuously diffuse across the shell until the Co nanoparticles have been completely consumed. Spherical Pt materials were fabricated on a large scale (see Figure S1 in the Supporting Information). If $NaBH_4$ reduces all the Co^{2+} to Co nanoparticles, the solutions of Co nanoparticles should react completely with H_2PtCl_6 on the basis of the stoichiometric relationship in Equation (1).

$$2\,Co + PtCl_6^{2-} = Pt + 2\,Co^{2+} + 6\,Cl^- \quad (1)$$

The structure and morphology of these Pt hollow nanospheres were investigated by transmission electron microscopy (TEM). Figure 1a is a typical large-scale TEM image. It was found that the centers of the spheres are brighter than the edges. The structural details are revealed in high-magnification TEM (Figure 1b). The individual Pt spheres are composed of an empty core with a shell, that is, a hollow structure. The thickness of the shell is ≈ 2 nm. The average diameter of the nanospheres was statistically calculated to be 24 ± 2 nm. From the high-magnification TEM image in Figure 1b, the shells of the Pt hollow nanospheres seem to be rough and consist of Pt nanoparticles with a size of ≈ 2 nm. Another feature is that the shell is incomplete and porous, not solid. This feature endows the Pt hollow nanospheres with a high surface area.

To evaluate the electrocatalytic activity of the Pt hollow nanospheres, solid Pt nanoclusters with roughly the same diameter as that of the Pt hollow nanospheres were fabricated by a seeding growth strategy. The morphology and structure of the solid Pt nanocluster was characterized by TEM. Figure 1c and d are the low- and high-magnification TEM images, respectively. In Figure 1c, well-dispersed Pt nanoclusters are observed. The average diameter of the clusters was statistically measured to be $\approx 29 \pm 3$ nm. From the high-magnification TEM image in Figure 1d, it can be seen that each cluster is composed of small nanoparticles with a size of ≈ 4 nm. The crystalline feature was confirmed by microelectronic diffraction pattern (see Figure S2). Both the Pt hollow nanospheres and nanoclusters adopt a typical face-centered-cubic polycrystalline structure.

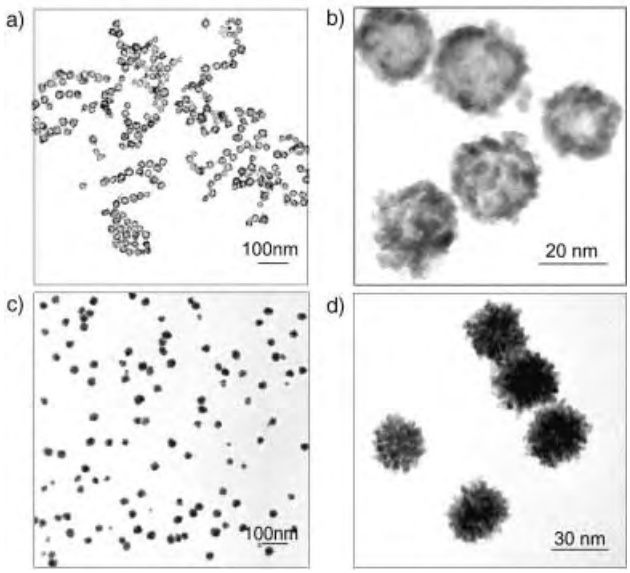


Figure 1. TEM images of Pt hollow nanospheres (a) and (b), and solid nanoclusters (c) and (d).

The electrocatalytic activity of the Pt hollow nanospheres for the oxidation of methanol was demonstrated and compared with that of solid Pt nanoclusters by using a well-used electrochemical reaction in a solution of H_2SO_4.[11] A glassy carbon disk electrode with a diameter of 3 mm was used. The loading of the hollow nanospheres and the solid nanoclusters on the electrode surface was the same (0.0175 mg cm^{-2}). From the voltammograms in Figure 2, both the Pt hollow nanospheres and nanoclusters show catalytic behavior for the electrooxidation of methanol by the appearance of an oxidation current in the positive potential region. The consistent appearance of the two voltammograms can be seen in the figure. The onset potentials are around 0.3 V (vs. SCE). The peak potentials for the oxidation of methanol are approximately 0.65 V (vs. SCE), in agreement with literature values.[11] The peak currents of the nanosphere and nanocluster catalysts are 54 μA and 19 μA, respectively. From the current measurements, it is clear that the catalytic activity of the Pt hollow nanospheres is twice that of the solid Pt nanoclusters. The remarkably high oxidation current for the hollow-sphere catalysts is directly related to the high surface area. Since Pt hollow nanospheres are coreless, a larger number of Pt nanospheres were obtained relative to that found with the same loading of solid Pt nanoclusters. Furthermore, the incomplete shell of hollow nanospheres may provide the interior surface for the catalytic reaction. If we assume that the inner and outer surfaces of a hollow

 © 2004 Wiley-VCH Verlag GmbH & Co. KGaA, Weinheim

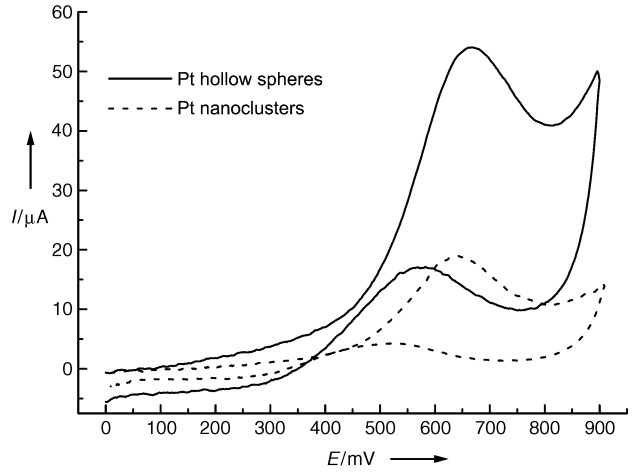


Figure 2. Cyclic voltammograms of Pt solid nanoclusters (dashed line) and hollow nanospheres (solid line) on a glass carbon disk electrode in H_2SO_4 (0.5 M) and methanol (0.6 M). The same loading of nanospheres and solid nanoclusters was applied to the electrodes (0.0175 mg cm^{-2}). Scan rate = 50 mV s^{-1}.

nanosphere can participate in the catalytic reaction, the surface area of the single hollow nanosphere is approximately 1.16 times as that of a single solid nanocluster. The higher surface area of Pt nanospheres results in a higher catalytic activity. Consequently, our results suggest a simple route to enhance the catalytic efficiency of Pt catalysts by a simple improvement of the morphology. Therefore, enhanced electrocatalysts can be obtained as hollow nanospheres without changing catalyst loadings.

In summary, a facile procedure for the large-scale synthesis of Pt hollow nanosphere catalysts was developed. The catalysts can be simply prepared at room temperature in a homogeneous solution with Co nanoparticles as sacrificial templates. The method presented herein is more cost-effective than previous methods. The incomplete and porous shells of the Pt hollow nanospheres have a higher surface area and therefore exhibit enhanced electrocatalytic performance. This approach was successfully extended to the fabrication of Au, Pd, and their bimetallic hollow nanospheres. These metallic hollow nanospheres could be useful in industrial applications including catalytic nanoreactors, plasmonic devices, and near-infrared absorbers.

Experimental Section

Cobalt chloride, $NaBH_4$, H_2PtCl_6, and citric acid were obtained from Beijing Chemical Reagent Ltd. and were used without further purification. The Co nanoparticles were fabricated by the addition of a solution of $CoCl_2$ (0.4 M; 0.1 mL) to a deaerated aqueous solution (100 mL) of $NaBH_4$ (4 mM) and citric acid (0.4 mM). For the preparation, a solution of citric acid and $NaBH_4$ was first prepared. $NaBH_4$ should be freshly dissolved. H_2 was evolved during the reaction and continued for several minutes. When gas evolution ceased, the resulting solution (100 mL) was immediately added to a stirred solution of H_2PtCl_6 (1 mM; 30 mL) at room temperature.

The obtained solution was centrifuged, and the precipitate was collected, washed, and dispersed by ultrasonic treatment, dropped onto a carbon-coated copper grid, and characterized by transmission electron microscopy (TEM, Philips TECNAI-20). A Hitachi S-4300F scanning electron microscope (SEM) equipped with an energy-dispersive X-ray analyzer (Phoenix) was used to determine the morphology and the composition of the hollow nanospheres.

Pt solid nanoclusters with roughly similar diameter were prepared by a seeding growth strategy. Pt seeds with diameters of ≈ 4 nm were fabricated according to Teranishi et al.[12] Briefly, a mixture of aqueous H_2PtCl_6 (6.0 mM; 5 mL; 30 μmol of Pt), water (4.5 mL), and poly(*N*-vinyl-2-pyrrolidone) (PVP; 30 μmol) in methanol (40.5 mL) was heated at reflux in a 100-mL flask for 3 h under air to synthesize the PVP-protected Pt nanoparticles. The above solution (1 mL) was added to the H_2PtCl_6 solution (1 mM; 10 mL). Excess ascorbic acid (100 mM; 1.2 mL) was added to the stirred solution. The reaction was continued until the solutions turned black in color, suggesting the formation of Pt nanoclusters.

Electrochemical measurements were conducted in an electrochemical cell with a three-electrode configuration at room temperature. The working electrode was a glassy carbon disk with a diameter of 3 mm, polished with Al_2O_3 paste and washed ultrasonically in Millipore water. The electrode was loaded with Pt nanospheres and nanoclusters. The same loading (0.0175 mg cm^{-2}) was used for the two catalysts. Electrocatalytic oxidation measurements were carried out in a solution of H_2SO_4 (0.5 M) and methanol (0.6 M) on a Basic Electrochemical System from EG&G instruments, Princeton Applied Research (PAR).

Received: September 25, 2003 [Z52956]

Keywords: cobalt · electrocatalysis · nanostructures · oxidation · platinum

[1] a) A. T. Bell, *Science* **2003**, *299*, 1688 – 1691; b) D. R. Rolison, *Science* **2003**, *299*, 1698 – 1701; c) L. Pino, V. Recupero, S. Beninati, A. K. Shukla, M. S. Hegde, P. Bera, *Appl. Catal. A* **2002**, *225*, 63 – 75.

[2] For example, see: a) T. S. Ahmadi, Z. L. Wang, T. C. Green, A. Henglein, M. A. El-sayed, *Science* **1996**, *272*, 1924 – 1925; b) Z. Zhou, S. Wang, W. Zhou, G. Wang, L. Jiang, W. Li, S. Song, J. Liu, G. Sun, Q. Xin, *Chem. Commun.* **2003**, 394 – 395; c) G. Vijayaraghavan, L. Gao, C. Korzeniewski, *Langmuir* **2003**, *19*, 2333 – 2337; d) X. Zhang, K.-Y. Chan, *Chem. Mater.* **2003**, *15*, 451 – 459; e) H. Uchida, Y. Mizuno, M. Watanabe, *J. Electrochem. Soc.* **2002**, *149*, A682-A687; f) H. Bönnemann, N. Waldöfner, *Chem. Mater.* **2002**, *14*, 1115 – 1120.

[3] S.-W. Kim, M. Kim, W. Y. Lee, T. Hyeon, *J. Am. Chem. Soc.* **2002**, *124*, 7642 – 7643.

[4] a) F. Caruso, R. A. Caruso, H. Möhwald, *Science* **1998**, *282*, 1111 – 1114; b) F. Caruso, X. Shi, R. A. Caruso, A. Susha, *Adv. Mater.* **2001**, *13*, 740 – 744; c) Z. Yang, Z. Niu, Y. Lu, Z. Hu, C. C. Han, *Angew. Chem.* **2003**, *115*, 1987 – 1989; *Angew. Chem. Int. Ed.* **2003**, *42*, 1943 – 1945; Corrigendum: Z. Yang, Z. Niu, Y. Lu, Z. Hu, C. C. Han, *Angew. Chem.* **2003**, *115*, 4867; *Angew. Chem. Int. Ed.* **2003**, *42*, 4719; d) M. L. Breen, A. D. Dinsmore, R. H. Pink, S. B. Qadri, B. R. Ratna, *Langmuir* **2001**, *17*, 903 – 907.

[5] a) Z. Dai, L. Dähne, H. Möhwald, B. Tiersch, *Angew. Chem.* **2002**, *114*, 4191 – 4194; *Angew. Chem. Int. Ed.* **2002**, *41*, 4019 – 4022; b) K. P. Velikov, A. van Blaaderen, *Langmuir* **2001**, *17*, 4779 – 4786.

[6] A. B. Bourlinos, M. A. Karakassides, D. Petridis, *Chem. Commun.* **2001**, 1518 – 1519.

[7] H. T. Schmidt, A. E. Ostafin, *Adv. Mater.* **2002**, *14*, 532 – 535.

[8] a) T. Nakashima, N. Kimizuka, *J. Am. Chem. Soc.* **2003**, *125*, 6386 – 6387; b) C. E. Fowler, D. Khushalani, S. Mann, *Chem. Commun.* **2001**, 2028 – 2029; c) X. Gao, J. Zhang, L. Zhang, *Adv. Mater.* **2002**, *14*, 290 – 293.

 © 2004 Wiley-VCH Verlag GmbH & Co. KGaA, Weinheim

[9] a) S. Schacht, Q. Huo, I. G. Voigt-Martin, G. D. Stucky, F. Schuth, *Science* **1996**, *273*, 768 – 771; b) D. Walsh, B. Lebeau, S. Mann, *Adv. Mater.* **1999**, *11*, 324 – 328; c) J. Jang, K. Lee, *Chem. Commun.* **2002**, 1098 – 1099; d) D. Zhang, L. Qi, J. Ma, H. Cheng, *Adv. Mater.* **2002**, *14*, 1499 – 1502; e) L. Qi, J. Li, J. Ma, *Adv. Mater.* **2002**, *14*, 300 – 303; f) M. S. Wong, J. N. Cha, K.-S. Choi, T. J. Deming, G. D. Stucky, *Nano Lett.* **2002**, *2*, 583 – 587; g) Q. Sun, P. J. Kooyman, J. G. Grossmann, P. H. H. Bomans, P. M. Frederik, P. C. M. M. Magusin, T. P. M. Beelen, R. A. van Santen, N. A. J. Sommerdijk, *Adv. Mater.* **2003**, *15*, 1097 – 1100.

[10] a) Y. Sun, Y. Xia, *Science* **2002**, *298*, 2176 – 2179; b) Y. Sun, B. T. Mayers, Y. Xia, *Adv. Mater.* **2003**, *15*, 641 – 646; c) Y. Sun, B. T. Mayers, Y. Xia, *Nano Lett.* **2002**, *2*, 481 – 485.

[11] a) T. Hyeon, S. Han, Y.-E. Sung, K.-W. Park, Y.-W. Kim, *Angew. Chem.* **2003**, *115*, 4488 – 4492; *Angew. Chem. Int. Ed.* **2003**, *42*, 4352 – 4356; b) W. X. Chen, J. Y. Lee, Z. Liu, *Chem. Commun.* **2002**, 2588 – 2589; c) K.-W. Park, J.-H. Choi, Y.-E. Sung, *J. Phys. Chem. B* **2003**, *107*, 5851 – 5856; d) S. M. Golabi, A. Nozad, *J. Electroanal. Chem.* **2002**, *521*, 161 – 167.

[12] T. Teranishi, M. Hosoe, T. Tanaka, M. Miyake, *J. Phys. Chem. B* **1999**, *103*, 3818 – 3827.

 © 2004 Wiley-VCH Verlag GmbH & Co. KGaA, Weinheim

Vinyl Cations

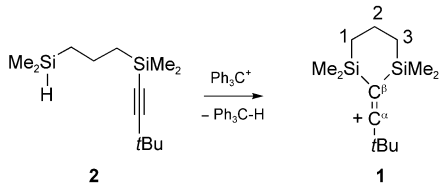
The X-ray Structure of a Vinyl Cation**

Thomas Müller, Mark Juhasz, and Christopher A. Reed**

Dedicated to Prof. Yitzhak Apeloig on the occasion of his 60th birthday.

Vinyl cations,[1] the dicoordinated unsaturated analogues of trivalent carbenium ions, were first detected by Grob and coworkers in the early 1960s in solvolysis reactions of α-aryl vinyl halides.[2] In the 1970s numerous investigations established vinyl cations as reaction intermediates in solvolysis reactions of activated alkenyl halides[3] and in reactions of electrophiles with alkynes.[4] The direct NMR detection of vinyl cations under superacidic reaction conditions at temperatures below −100 °C was achieved in the early 1990s and provided important information about their electronic structure.[5] We report herein the X-ray structure of the β-silyl substituted vinyl cation **1**, which provides the first direct experimental structural information about this important class of reaction intermediates.[6] In addition, the molecular structure of cation **1** gives direct structural evidence for the occurrence of β-silyl hyperconjugation in carbocations.[7]

Vinyl cation **1** was prepared by reaction of the alkynylsilane **2** with trityl ion as described previously for related cations (see Scheme 1).[8] The counterions were either tetrakis(pentafluorophenyl)borate, $[B(C_6F_5)_4]^-$, or the hexabromocarborane, $[CB_{11}H_6Br_6]^-$, chosen for their extreme inertness.[9] The former has advantages in NMR experiments because its salts form high concentrations of liquid clathrates while the latter is better for growing crystals. Cation **1** was characterized in a benzene solution by multinuclear NMR spectroscopy (see Table 1). The appearance of a single ^{29}Si NMR signal at $\delta^{29}Si = 29.1$ ppm indicates ring closure to a species that is symmetric on the NMR timescale. The C=C$^+$ unit of the vinyl cation is readily identified by the low-field resonance of the positively charged C^α atom at $\delta^{13}C =$ 202.4 ppm and that attributed to C^β at $\delta^{13}C = 75.3$ ppm. These NMR chemical shifts are very close to those found for similar β-silylsubstituted vinyl cations and are characteristic for the electronic situation found for a C=C double bond formed from a positively charged dicoordinated carbon atom and a second sp^2-hybridized trigonal carbon center.[5,8]



Scheme 1. Synthesis of vinyl cation **1**.

No solvent effect on the NMR chemical shift can be detected in aromatic hydrocarbons, that is, in toluene virtually the same NMR chemical shifts are observed ($\delta^{29}Si = 28.9$; $\delta^{13}C$ $(C^\alpha) = 202.7$; $\delta^{13}C$ $(C^\beta) = 75.5$ ppm, see Table 1). This indicates negligible cation solvent interactions at room temperature. In toluene solution the salts **1** $[B(C_6F_5)_4]$ and **1** $[CB_{11}H_6Br_6]$ are stable for weeks and this unusual stability is attributed to (1) the essentially nonnucleophilic reaction conditions and (2) the high thermodynamic stability due to the combined effect of two β-silyl substituents.

The influence of the β-silyl substituents on the electron distribution in cation **1** is indicated by the marked down-field shift of the ^{29}Si resonance at $\delta = 29.1$ ppm compared to the precursor alkinylsilane ($\delta = -16.9$ ppm). This is in agreement with significant delocalization of positive charge from the C^α atom to the β-positioned silyl groups. Furthermore, the ^1J(Si–C) coupling constant between the C^β atom and the silicon atoms is extremely small ($^1J(Si–C) = 15.7$ Hz, compared to regular $^1J(Si–C) \approx 60$ Hz in trialkylvinylsilanes).[10,11] This

[*] Dr. T. Müller
Institut für Anorganische und Analytische Chemie
der Johann Wolfgang Goethe–Universität Frankfurt/Main
Marie Curie Strasse 11, 60439 Frankfurt/Main (Germany)
Fax: (+49) 697-982-9188
E-mail: dr.thomas.mueller@chemie.uni-frankfurt.de
M. Juhasz, Prof. Dr. C. A. Reed
Department of Chemistry
University of California, Riverside 92521-0403 (USA)
Fax: (+1) 909-787-2027
E-mail: chris.reed@ucr.edu

[**] We thank Dr. Fook Tham for solution of the X-ray crystal structure. This work was supported by NSF grant CHE-0095206 and by the German Israeli Foundation (GIF).

Supporting information for this article is available on the WWW under http://www.angewandte.org or from the author.

 DOI: 10.1002/anie.200352986 © 2004 Wiley-VCH Verlag GmbH & Co. KGaA, Weinheim

Table 1: Experimental and theoretical ^{13}C and ^{29}Si NMR spectroscopic data of **1**. Coupling constants $^{n}J(XY)$ in Hz.

	$\delta^{13}C^{\alpha}$	$\delta^{13}C^{\beta}$	$\delta^{13}C^{1/3}$	$\delta^{13}C^{2}$	$\delta^{13}C^{q}$	$\delta^{13}C^{CH_3}$	$\delta^{13}C^{SiMe_2}$	$\delta^{29}Si$
1[a]	202.4	75.3	15.0	15.8	33.5	26.6	0.9	29.1
	$^{3}J(CH)=5.2$		$^{1}J(CH)=121.1$	$^{1}J(CH)=131.8$	$^{2}J(CH)=4.2$	$^{1}J(CH)=131.8$	$^{1}J(CH)=123.0$	$^{1}J(SiC)=55.3$
		$^{1}J(SiC)=15.7$	$^{1}J(SiC)=56.2$				$^{1}J(SiC)=55.7$	$^{1}J(SiC)=15.7$
1[b]	202.7	75.5	15.2	16.2	33.8	26.8	1.0	28.9
1[c,d]	215.7	82.6	20.3	20.7	39.4	29.6	3.7	31.8
	$^{3}J(CH)=5.1$		$^{1}J(CH)=120.3$	$^{1}J(CH)=127.7$	$^{2}J(CH)=3.0$	$^{1}J(CH)=128.4$	$^{1}J(CH)=121.7$	$^{1}J(SiC)=50.3, 49.1, 10.2$[e]
		$^{1}J(SiC)=10.2$	$^{1}J(SiC)=50.3$				$^{1}J(SiC)=49.1$	

[a] In $[D_6]$benzene at 300 K. [b] In $[D_8]$toluene at 300 K. [c] NMR chemical shifts δ calculated at the GIAO/B3LYP/6-311G(2d,p)//MP2/6-31G(d) level, $\sigma(^{13}C, TMS\ (T_d))=183.6$, $\sigma(^{29}Si, TMS\ (T_d))=329.1$). Nuclear chemical shift constants $^{n}J(XY)$ calculated at the GIAO/B3LYP/6-311G(d,p)//MP2/6-31G(d) level. [d] For the different silicon atoms (Si^1, Si^2) and the carbon atoms which are interrelated by the molecular motions ($C^{1/3}$, C^{SiMe_2}, C^{CH_3}), the mean values are given. [e] Coupling between Si and $C^{1/3}$, CH_3 and C^{β}, respectively.

suggests a rather unusual bonding situation between the C^{β} atom and the adjacent silicon atoms.

The vinyl cation **1** is further characterized by a very intense band in the IR spectra at $\tilde{\nu}=1987\ cm^{-1}$, which is assigned to the C=C$^+$ stretching vibration. This IR band is more intense than regular C=C stretch vibrations of C=C bonds and its position is strongly shifted to higher energy, which suggests a bond order of the C=C$^+$ bond in **1** significantly larger than 2.

Suitable crystals for X-ray analysis were obtained by recrystallization of **1** $[CB_{11}H_6Br_6]$ from 1,2-dichlorobenzene.[12] The solid-state structure of the salt reveals that the vinyl cation is clearly separated from the carborane anion (see Figure 1). No bromine atom of the anion approaches the positively charged C^{α} atom to a distance smaller than 720 pm. The disilacyclohexane ring of the vinyl cation **1** adopts a regular chair conformation with the two silicon atoms and the C^{β} and C^{α} atoms nearly coplanar ($\Theta(SiC^{\beta}C^{\alpha}Si=173.9°$). As previously predicted by calculations[13] and deduced from ^{13}C NMR chemical shift parameter,[5,8] the molecule is linear around the dicoordinated carbon atom C^{α} (bond angle $\alpha(C^{\beta}C^{\alpha}C)=178.8°$), which indicates an sp hybridization for C^{α} and, as a consequence, the C^{β}–C^{α} double bond is unusually short (122.1 pm) and approaches the length of a regular C–C triple bond. In addition, also the C^{α}–C single bond is short (144.9 pm). A quite remarkable feature of the molecular structure of **1** is the unusual length of the C^{β}–Si single bonds (198.4 and 194.6 pm), around 10 pm longer than regular single bonds between sp^2 hybridized carbon atoms and tetracoordinated silicon.[14] This bond elongation can be attributed to the interaction of the $\sigma(C^{\beta}Si)$ bond with the empty 2p orbital at C^{α} (i.e. β-silyl hyperconjugation). Although the NMR results indicate that **1** is symmetric in solution, in the solid state the two silicon atoms in **1** are clearly different. Not only are the C^{β}–Si single bonds markedly different from each other (by 3.8 pm) but also the $\alpha(Si\text{-}C^{\beta}\text{-}C^{\alpha})$ bond angles can be clearly distinguished (115.5° and 133.0°). The more acute bond angle is associated with the longer Si–C^{β} bond, which suggests more pronounced β silicon hyperconjugation for this group.

Density functional (B3LYP/6-31G(d)) as well as correlated ab initio calculations (MP2/6-31G(d))[15,16] predict very similar molecular structures for **1**, and these calculated gas-phase structures closely match the experimental solid-state geometry of **1** (see Figure 2). In particular, the unsymmetrical

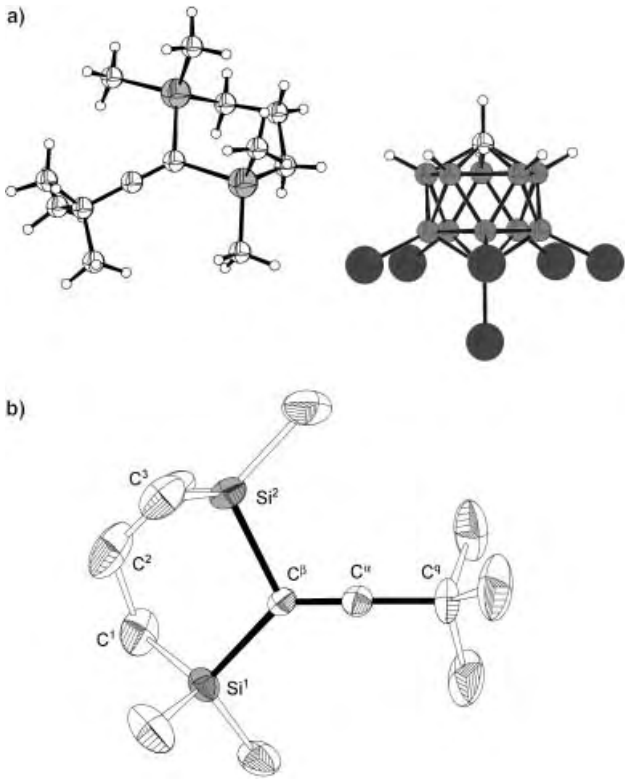


Figure 1. a) Perspective view of the asymmetric unit of the crystal structure of **1** $[CB_{11}H_6Br_5]$ (black Br; dark gray B; white C; gray Si). b) Molecular structure of vinyl cation **1** (hydrogen atoms omitted for clarity; thermal ellipsoids drawn at 30% probability level). Selected bond length [pm] and bond angles [°]: C^{β}-C^{α} = 122.1, C^{α}-C^{q} = 145.2, Si^2-C^{β} = 198.4, Si^1-C^{β} = 194.6, C^{β}-C^{α}-C^{q} = 178.8, Si^2C^{β}-C^{α} = 115.5, Si^1C^{β}-C^{α} = 133.0.

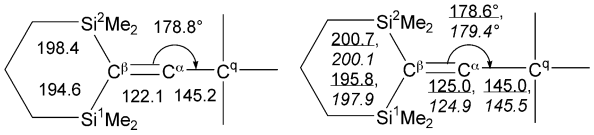
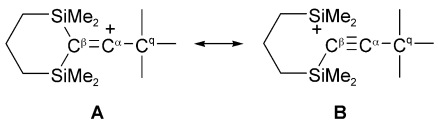


Figure 2. Comparison of experimental (left) and calculated (right; underlined, MP2/6-31G(d); italic, B3LYP6-31G(d)). Bond lengths [pm], bond angles [°], additional bond angles: Si^2C^{β}-C^{α} = 115.5, *112.3*, *118.0*, Si^1-C^{β}-C^{α} = 133.0, 133.5, *127.6*.

 © 2004 Wiley-VCH Verlag GmbH & Co. KGaA, Weinheim

arrangement of the silicon atoms at the central C=C$^+$ unit is found in the theoretical structures, which indicates that this arrangement is a result of an intrinsic bonding situation in cation **1** and not a consequence of crystal lattice or similar intermolecular interactions in the condensed phase. The C_s symmetrical structure of **1**, which has two identical Si–C$^\beta$ bonds, **1** (C_s), is the transition structure for the degenerate interconversion of two cations **1** (at B3LYP/6-31G(d)). Compound **1** (C_s), however, is merely 0.7 kcal mol^{-1} higher in energy than **1** (MP2/6-311G(d,p)//B3LYP/6-31G(d) + ΔZPVE), which suggests a time-averaged symmetry for cation **1** in solution and in the gas phase.

The unusual position of the C=C$^+$ stretch vibration in the IR spectra of **1** is in agreement with the results of density functional calculations. Thus, a frequency calculation at the B3LYP/6-31G(d) level of theory predicts for the C=C$^+$ bond stretch vibration a very strong IR absorption at 1956 cm^{-1}, close to the experimental observed IR band (1987 cm^{-1}).[18] Finally, calculations for NMR chemical shift[19] and nuclear spin–spin coupling constants[20] (see Table 1) agree well with the experiment, that is, δ^{29}Si = 31.8 ppm[21] compared to the measured value of 28.9 ppm. At the applied level of theory, δ^{13}C values for **1** are systematically predicted too far down field. The largest deviation is found for the ^{13}C NMR chemical shift of the positively charged C$^\alpha$ atom ($\Delta\delta^{13}$C = 13.3).[22] Theoretical and experimental ^{13}C NMR chemical shifts for **1** are however linearly correlated thereby confirming the validity of the computed structure.[23] An analysis[20] of the computed spin–spin coupling constants reveal that the unusually small ^1J(SiC$^\beta$) constant (calculated 10.2 Hz,[24] 15.7 Hz experimentally) is a consequence of the strongly reduced Fermi contact term.[25] This result suggests a very small s-orbital contribution for the Si–C$^\beta$ bonds, in agreement with a natural-bond-order (NBO) analysis[26] at the MP2/6-31G(d) level of theory, which indicate a contribution of the 3 s(Si) to the Si–C$^\beta$ σ bond of less than 15%. This analysis gives additional support for the occurrence of hyperconjugation in **1**. Strongly depleted Si–C$^\beta$ σ bonds (1.48 e and 1.77 e) and a formally empty C(2p) orbital at C$^\alpha$ with an occupation of 0.66 e are the result of electron delocalization from the bonding σ-Si-C$^\beta$ orbitals into the vacant C(2p). Thus, experimental (NMR, IR spectroscopic and structural) as well as theoretical data clearly indicate the occurrence of hyperconjugation between the occupied σ C$^\beta$–Si orbitals and the empty 2p(C$^\alpha$) orbital in vinyl cation **1**. This interaction can be straightforwardly described as resonance between the Lewis structures **A** and **B** (Scheme 2).[27]



A B

Scheme 2. Resonance structures for vinyl cation **1**.

Received: October 1, 2003 [Z52986]
Published Online: February 16, 2004

Keywords: carbocations · computer chemistry · hyperconjugation · silicon · X-ray diffraction

[1] For a recent monograph on vinyl cations: *Dicoordinated Carbocations* (Eds.: Z. Rappoport, P. J. Stang), Wiley, New York, **1997**.

[2] a) C. A. Grob, J. Csapilla, G. Cseh, *Helv. Chim. Acta* **1964**, *47*, 1590; b) C. A. Grob in *Dicoordinated Carbocations* (Eds.: Z. Rappoport, P. J. Stang), Wiley, **1997**, chap. 1, p. 1.

[3] a) M. Hanack, *Acc. Chem. Res.* **1976**, *9*, 364; b) T. Kitamura, H. Taniguchi, Y. Tsuno in *Dicoordinated Carbocations* (Eds.: Z. Rappoport, P. J. Stang), Wiley, New York, **1997**, chap. 7, p. 321; c) L. R. Subramanian, M. Hanack, *Chem. Rev.* **1972**, *72*, 1465.

[4] For reviews see: a) V. Lucchini, G. Modena, L. Pasquato in *Dicoordinated Carbocations* (Eds.: Z. Rappoport, P. J. Stang), Wiley, New York, **1997**, chap. 6, p. 237.

[5] H.-U. Siehl in *Dicoordinated Carbocations* (Eds.: Z. Rappoport, P. J. Stang), Wiley, **1997**, chap. 5, p. 189.

[6] For a previous report on the isolation of the neutral solid metallacarborane [CpFe^{II}HCB$_9$H$_9$C–C=CH$_2$] containing a -C=CH$_2$ group, see. L. I. Zakharkin, V. V. Kobak, *J. Organomet. Chem.* **1984**, *270*, 229.

[7] The isoelectronic neutral methylene boranes (R$_3$Si)$_2$C=B–R were previously synthesized and structurally characterized. a) R. Boese, P. Paetzold, A. Tapper, R. Ziembinski, *Chem. Ber.* **1989**, *122*, 1057; b) M. Pilz, M. Stadler, R. Hunold, J. Allwohn, W. Massa, A. Berndt, *Angew. Chem.* **1989**, *101*, 761; *Angew. Chem. Int. Ed. Engl.* **1989**, *28*, 784.

[8] T. Müller, R. Meyer, D. Lennartz, H.-U. Siehl, *Angew. Chem.* **2000**, *112*, 3203; *Angew. Chem. Int. Ed.* **2000**, *39*, 3074.

[9] C. A. Reed, *Acc. Chem. Res.* **1998**, *31*, 133.

[10] Y. Takeuchi, T. Takayama in *The chemistry of organosilicon compounds*, *Vol. 2* (Eds.: Z. Rappoport, Y. Apeloig), Wiley, New York, **1998** chap. 6, p. 267.

[11] A small ^1J(SnC) coupling constant was detected in a related distannylmethylene borane. M. Pilz, H. Michel, A. Berndt, *Angew. Chem.* **1990**, *102*, 438; *Angew. Chem. Int. Ed. Engl.* **1990**, *29*, 409.

[12] Crystal data for **1** [CB$_{11}$H$_6$Br$_6$], C$_{14}$H$_{33}$B$_{11}$Br$_6$Si$_2$, M_r = 860.69, crystal dimensions 0.19 × 0.18 × 0.04 mm^3, monoclinic, space group *P*2(1)/*c*, *a* = 12.250(3), *b* = 13.034(3), *c* = 20.639(5) Å, β = 104.293(6)°, *V* = 3193.3(13) Å^3, *Z* = 4, ρ_{calcd}* = 1.790 Mg m^{-3}, μ(Mo$_{K\alpha}$) = 7.701 mm^{-1}, *T* = 223(2) K, *F*(000) = 1648, $2\theta_{max}$ = 49.42°. 17628 reflections measured, of which 5441 were unique (R_{int} = 0.0551). Final R_1 = 0.0481 with wR_2 = 0.1165 for 5441 observed reflections with $I > 2\sigma(I)$. * Note: The bromo-carborane was over brominated by about 6%. The density was calculated by using the site occupancy factor ratio of 6%/94% for Br^7/H^6 attached to B^6 atom. The slight over bromination of the carborane is figured into the X-ray model and solution, thus improving the accuracy and R value. CCDC-220463 contains the supplementary crystallographic data for this paper. These data can be obtained free of charge via www.ccdc.cam.ac.uk/conts/retrieving.html (or from the Cambridge Crystallographic Data Centre, 12, Union Road, Cambridge CB21EZ, UK; fax: (+44) 1223-336-033; or deposit@ccdc.cam.ac.uk).

[13] a) R. Sustmann, J. E. Williams, M. J. S. Dewar, L. C. Allen, P. von R. Schleyer, *J. Am. Chem. Soc.* **1969**, *91*, 5350. b) For a review: Y. Apeloig, T. Müller in *Dicoordinated Carbocations* (Eds.: Z. Rappoport, P. J. Stang), Wiley, New York, **1997**, chap. 2, p. 9.

[14] M. Kaftory, M. Kapon, M. Botoshansky in *The chemistry of organosilicon compounds*, *Vol. 2* (Eds.: Z. Rappoport, Y. Apeloig), Wiley, New York, **1998**, chap. 5, p. 181.

[15] All calculations were performed with Gaussian 98 (Revision A.7), M. J. Frisch, G. W. Trucks, H. B. Schlegel, G. E. Scuseria, M. A. Robb, J. R. Cheeseman, V. G. Zakrzewski, J. A. Montgomery, R. E. Stratmann, J. C. Burant, S. Dapprich, J. M. Millam, A. D. Daniels, K. N. Kudin, M. C. Strain, O. Farkas,

 © 2004 Wiley-VCH Verlag GmbH & Co. KGaA, Weinheim

J. Tomasi, V. Barone, M. Cossi, R. Cammi, B. Mennucci, C. Pomelli, C. Adamo, S. Clifford, J. Ochterski, G. A. Petersson, P. Y. Ayala, Q. Cui, K. Morokuma, D. K. Malick, A. D. Rabuck, K. Raghavachari, J. B. Foresman, J. Cioslowski, J. V. Ortiz, B. B. Stefanov, G. Liu, A. Liashenko, P. Piskorz, I. Komaromi, R. Gomperts, R. L. Martin, D. J. Fox, T. Keith, M. A. Al-Laham, C. Y. Peng, A. Nanayakkara, C. Gonzalez, M. Challacombe, P. M. W. Gill, B. G. Johnson, W. Chen, M. W. Wong, J. L. Andres, M. Head-Gordon, E. S. Replogle, J. A. Pople, Gaussian, Inc., Pittsburgh, PA, **1998** and Gaussian 03 (Revision B.03), M. J. Frisch, G. W. Trucks, H. B. Schlegel, G. E. Scuseria, M. A. Robb, J. R. Cheeseman, V. G. Zakrzewski, J. A. Montgomery, R. E. Stratmann, J. C. Burant, S. Dapprich, J. M. Millam, A. D. Daniels, K. N. Kudin, M. C. Strain, O. Farkas, J. Tomasi, V. Barone, M. Cossi, R. Cammi, B. Mennucci, C. Pomelli, C. Adamo, S. Clifford, J. Ochterski, G. A. Petersson, P. Y. Ayala, Q. Cui, K. Morokuma, D. K. Malick, A. D. Rabuck, K. Raghavachari, J. B. Foresman, J. Cioslowski, J. V. Ortiz, B. B. Stefanov, G. Liu, A. Liashenko, P. Piskorz, I. Komaromi, R. Gomperts, R. L. Martin, D. J. Fox, T. Keith, M. A. Al-Laham, C. Y. Peng, A. Nanayakkara, C. Gonzalez, M. Challacombe, P. M. W. Gill, B. G. Johnson, W. Chen, M. W. Wong, J. L. Andres, M. Head-Gordon, E. S. Replogle, J. A. Pople, Gaussian, Inc. Pittsburgh, PA, **2003**.

[16] a) A. D. Becke, *Phys. Rev. A* **1988**, *38*, 3098; b) A. D. Becke, *J. Chem. Phys.* **1993**, *98*, 5648; c) B. G. Johnson, P. M. W. Gill, J. A. Pople, *J. Chem. Phys.* **1993**, *98*, 5612.

[17] According to density functional calculations at the B3LYP/6-31G(d) level of theory β-disilyl substituted vinyl cations having π-donating substituents at C^{α} do not show this unsymmetrical arrangement of the β-silylgroups. Thus, for the analogous phenyl substituted vinyl cation, equal $Si{-}C^{\beta}$ bond lengths of 197.3 pm have been calculated.[8]

[18] The calculated frequency of $\tilde{\nu} = 2031\ cm^{-1}$ is scaled with the global scaling factor of 0.963 suggested by Rauhut and Pulay. G. Rauhut, P. Pulay, *J. Phys. Chem.* **1995**, *99*, 3093.

[19] a) R. Ditchfield, *Mol. Phys.* **1974**, *27*, 789; b) K. Wolinski, J. F. Hilton, P. Pulay, *J. Am. Chem. Soc.* **1982**, *104*, 5667; c) J. Cheeseman, G. W. Trucks, T. A. Keith, M. Frisch, *J. Chem. Phys.* **1996**, *104*, 5497.

[20] a) T. Helgaker, M. Watson, N. C. Handy, *J. Chem. Phys.* **2000**, *113*, 9402; b) V. Sychrovsky, J. Gräfenstein, D. Cremer, *J. Chem. Phys.* **2000**, *113*, 3530.

[21] Mean value from $\delta^{29}(Si^1) = 23.7$ ppm and $\delta^{29}(Si^2) = 39.9$ ppm.

[22] DFT-based Gauge Independent Atomic Orbitals (GIAO) calculations fail to predict reliably $\delta^{13}C$ NMR chemical shift for the $C{=}C^{+}$ unit in vinyl cations. For reliable predictions of the $\delta^{13}C(C^{\alpha})$, the coupled-cluster method must be applied, which is, however, for **1** technically not feasible. a) J. F. Stanton, J. Gauss, H.-U. Siehl, *Chem. Phys. Lett.* **1996**, *262*, 183; b) H.-U. Siehl, T. Müller, H.-U. Siehl, *J. Phys. Org. Chem.* **2003**, *16*, 577.

[23] $\delta^{13}C^{theo} = (1.049 \pm 0.06)\ \delta^{13}C^{exp} + (3.50 \pm 0.53)$; $R = 0.99991$, 7 data points, for details see Supporting Information.

[24] Mean value from $^1J(Si^1C^{\beta}) = 17.2$ Hz and $^1J(Si^2C^{\beta}) = 3.2$ Hz.

[25] The Fermi contact contribution to $^1J(Si^1C^{\beta})$ is $+18.0$ Hz, compared to $+52.6$ Hz for $^1J(Si^1C^1)$.

[26] a) NBO 4.0. E. D. Glendening; J. K. Badenhoop, A. E. Reed, J. E. Carpenter, F. Weinhold, Theoretical Chemistry Institute, University of Wisconsin, Madison, WI, **1996**; b) A. E. Reed, L. A. Curtiss, F. Weinhold, *Chem. Rev.* **1988**, *88*, 899.

[27] Supporting Information (experimental details, analytical data, NMR spectra, absolute energies and structures of **1** at several theoretical levels, correlation between $\delta^{13}C^{theo}$ versus $\delta^{13}C^{exp}$) is available.

 © 2004 Wiley-VCH Verlag GmbH & Co. KGaA, Weinheim

Epoxidation of Propene

A Three-Dimensional Mesoporous Titanosilicate Support for Gold Nanoparticles: Vapor-Phase Epoxidation of Propene with High Conversion**

*Anil K. Sinha, Sindhu Seelan, Susumu Tsubota, and Masatake Haruta**

Gold nanoparticles deposited on TiO_2[1] provide a new route for the direct epoxidation of propene using molecular oxygen. Such an alternative direct gas-phase epoxidation process is of tremendous industrial significance and is more environmentally friendly than the multistep chlorohydrin and hydroperoxide processes that are currently employed.[2] We have established the viability of the vapor-phase epoxidation of propene over nanosize Au catalysts supported on Ti-containing supports such as TiO_2, TiO_2/SiO_2, TS-1, Ti-MCM-41, Ti-MCM-48, and Ti-containing hydrophobic silsequioxanes.[3–10] However, low conversion of propene, rapid catalyst deactivation, and regeneration problems have all been major hurdles in making the process commercially viable, even though propene oxide (PO) selectivity is greater than 90%. Based on a rough estimate for the commercialization of vapor-phase propylene epoxidation with H_2 and O_2, we set the following research targets: one-pass propylene conversion of 10%, PO selectivity of 90%, and hydrogen efficiency of 50%.

A new class of disordered mesoporous materials with channels of uniform width interconnected in a three-dimensional (3D) wormholelike fashion[11] have the advantage over their more ordered counterparts such as MCM-41 of better diffusion of reactants and products and thus overcome mass-transfer limitations. Furthermore, their higher thermal stability and cheap, easy, and reproducible preparation make these materials more suitable for industrial applications. The possibility to tailor their porosity (between 5 and 10 nm)[12] makes the mesopores easily accessible for a dispersion of 2–5 nm Au particles by the deposition–precipitation (DP) method,[1] in contrast to the narrower pores (3–4 nm) of MCM-type supports, for which access to the mesopores by Au nanoparticles is limited.

Here we demonstrate for the first time that it is possible to prepare a commercially viable Au catalyst for the direct

[*] Dr. S. Tsubota, Dr. M. Haruta
Research Institute for Green Technology
AIST, 16-1 Onogawa, Tsukuba 305-8569 (Japan)
Fax: (+81) 298-61-8240
E-mail: m.haruta@aist.go.jp
Dr. A. K. Sinha
Materials Department, Toyota Central R&D Laboratories Inc.
Nagakute, Aichi 480-1192 (Japan)
Dr. S. Seelan
Ceramic Research Institute, AIST, Shidami Science Park
Nagoya 463-8560, Aichi (Japan)

[**] A.K.S. thanks JSPS and AIST, Japan for a fellowship. S.S. acknowledges NEDO, Japan for a fellowship.

Supporting information for this article is available on the WWW under http://www.angewandte.org or from the author.

 © 2004 Wiley-VCH Verlag GmbH & Co. KGaA, Weinheim DOI: 10.1002/anie.200352900

epoxidation of propene. The catalyst is a high-Ti (3–6 mol%) 3D mesoporous silylated titanosilicate in which Au nanoparticles are dispersed on the surface and in the mesopores, and its activity is further promoted by an alkaline-earth-metal nitrate promoter. Our intention was to exploit the advantages of large-pore, 3D wormholelike mesoporous titanosilicates as supports for nanosized gold catalysts in the direct epoxidation of propene to PO with molecular oxygen. Moreover, it is possible to enhance the hydrophobicity of these titanosilicates by trimethylsilylation of the silanol sites, which is expected to enhance PO desorption and hence PO yield and also to slow down the deactivation of the catalyst. Furthermore, addition of certain metal salts as promoters can enhance the performance of the catalyst.

The X-ray powder diffraction patterns (Figure 1a) of calcined titanosilicate materials show a broad peak around

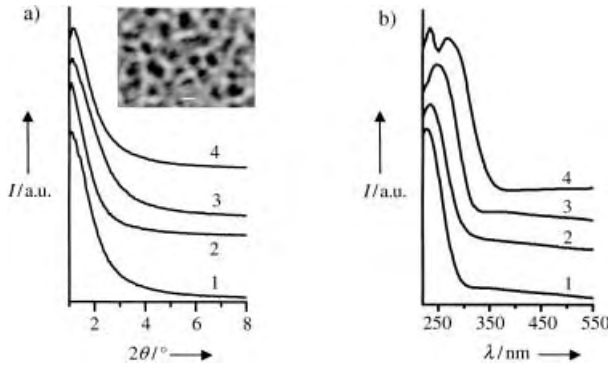


Figure 1. a) XRD spectra (inset: high-resolution TEM image; 3% Ti; scale bar = 6 nm), and b) diffuse-reflectance UV/Vis spectra of 3D mesoporous titanosilicates. Titanium concentrations: 1) 2.0 mol%, 2) 3.0 mol%, 3) 6.0 mol%, 4) 8.0 mol%. *I* = intensity.

$2\theta = 1.0$–$2.0°$, which is typical for disordered mesostructured materials. Such XRD patterns are similar to those of mesostructured MSU-1,[11] UTD-1,[12] HMS,[13] and KIT-1,[14] which have 3D networks of short, interconnected, wormhole-like mesopores. High-resolution TEM images (Figure 1a, inset) confirmed the presence of such uniform, 3D networks of short interconnected wormholelike channels. The diffuse-reflectance UV spectra (Figure 1b) show that samples with Ti concentrations of up to 6.0 mol% exhibit absorbance peaks at 220–245 nm, which result from tetrahedrally coordinated Ti centers, that is, most of the titanium is present as isolated tetrahedral species in the silica matrix. The samples yielded no peaks above 300 nm, which indicates the absence of any bulk titania. The sample with the highest titanium concentration (8 mol%) shows two clear peaks, one at 235 nm due to tetrahedrallly coordinated titanium, and another at 272 nm, attributable to higher (5-, 6-) coordinate Ti. The XPS analysis of titanosilicates with 2–6 mol% titanium content showed that the binding energy (BE) of the Ti $2p_{3/2}$ core level is about 460.0 eV, which indicates tetrahedral coordination of completely isolated Ti sites in the silica lattice.[15] However, the shift of the BE to 459.3 eV at higher Ti content (8 mol%) indicates incomplete isolation of Ti sites for high Ti content.[16] The BE is about 458.5 eV for aggregated Ti with octahedral coordination.[16] The BET surface area, Barrett–Joyner–Halenda (BJH) pore diameter, and mesopore volume were 838–896 $m^2 g^{-1}$, 7.1–9.2 nm, and 1.0–1.4 $cm^3 g^{-1}$, respectively.

Gold nanoparticles were deposited on all the supports by the DP method. The gold loading on the resultant materials was 0.3–0.4 wt%, and the average size of the well-dispersed Au nanoparticles was 3.0 ± 1.0 nm. An EXAFS/XANES analysis showed that the Au nanoparticles were completely metallic in nature.

Under similar reaction conditions, the Au catalysts supported on silylated mesoporous titanosilicates showed greatly enhanced catalytic activity for propene epoxidation (Figure 2, Table 1, catalysts 2–6). The propene conversion and PO selectivity increased conspicuously after silylation of the

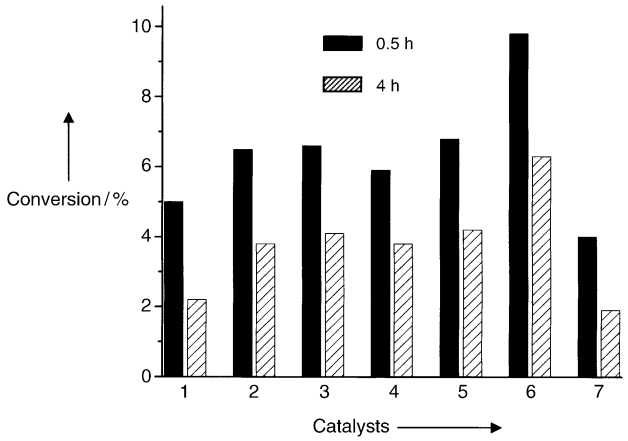


Figure 2. Propylene epoxidation over gold nanocatalysts deposited on 3D mesoporous titanosilicate: 1) 2 mol% Ti; 2) silylated catalyst 1; 3) silylated catalyst, 3 mol% Ti; 4) regenerated catalyst 3; 5) silylated catalyst, 6 mol% Ti; 6) $Ba(NO_3)_2$-promoted silylated catalyst 3. (7) Au/Ti-MCM-48.

Au/titanosilicate catalysts. The silylated catalysts with 3 and 6% Ti (catalysts 3 and 5), showed higher propene conversion than the silylated catalyst with 2% Ti (catalyst 2). Further enhancement of epoxidation activity was observed over a silylated catalyst (3 mol% Ti) impregnated with 1 wt% $Ba(NO_3)_2$, which had the highest propylene conversion of 9.8% and about 90% PO selectivity. This catalyst was much more active than Au/Ti-MCM-48 catalyst (Table 1). Enhanced propene conversion and PO selectivity can be attributed to the larger pore size and 3D mesoporosity of the support, which allow easy diffusion of reactants and products, while higher hydrophobicity due to silylation favors ready desorption of PO. It was also possible for the first time to regenerate the catalyst (catalyst 4) and regain about 90–95% of initial activity by treatment in 10 vol% H_2 and O_2 diluted in argon (for about 1–2 h) at 250°C. This is very important for making the process commercially viable.

Propene conversions decreased with on-stream time in all cases, but a relatively lower decrease was observed for silylated catalysts. This is attributable to the easy desorption of PO from the support surface and to passivation of surface acid sites, which prevents deactivation of the catalyst surface by oligomerized species formed from adsorbed PO at these sites.[7] Thus, silylation of Au catalysts supported on disordered titanosilicates has been found to have a very positive

 © 2004 Wiley-VCH Verlag GmbH & Co. KGaA, Weinheim

Table 1: Propylene epoxidation over gold nanoparticles deposited on mesoporous titanosilicates and reference materials.

Catalyst	Ti content (treatment)	TOS [h][a]	Conversion [%]		PO selectivity [%]	H_2 efficiency [%][b]
			C_3H_6	H_2		
1	2%	0.5	5.0	14.1	91.1	33.3
		4	2.2	7.7	95.5	41.0
2	2%	0.5	6.5	15.7	93.3	35.3
	(silylated)	4	3.8	9.7	96.4	34.0
3	3%	0.5	6.6	15.8	94.9	35.4
	(silylated)	4.0	4.1	10.2	95.8	31.8
4[c]	3%	0.5	5.9	15.2	94.1	29.4
	(silylated)	4.0	3.8	10.8	94.3	27.3
5	6%	0.5	6.8	17.5	90.1	23.6
	(silylated)	4.0	4.2	11.3	92.8	27.2
6[d]	3%	0.5	9.8	22.3	90.3	27.1
	(silylated)	4.0	6.3	16.7	92.3	34.6
Au/Ti-MCM-48	2%	0.5	4.1	35.2	91.2	8.9
		4	1.9	33.4	92.8	4.1
Au/Ti-MCM-48s	2%	0.5	2.7	21.3	94.2	10.1
	(silylated)	4	2.3	18.8	95.5	9.6

[a] TOS = time on stream. [b] Based on a stoichiometric reaction to produce PO and water. [c] Catalyst 3, regenerated with Ar-diluted H_2+O_2 for 1 h. [d] $Ba(NO_3)_2$-promoted catalyst.

influence on PO yield, in contrast to silylated Au/Ti-MCM-48 catalysts (Table 1). Furthermore, the addition of $Ba(NO_3)_2$ (as a promoter) to the Au/titanosilicate catalyst enhances propylene conversion, probably by promoting the formation of hydroperoxide-like species from H_2 and O_2, as well as by lowering the acidity of the catalyst. These titanosilicate-based catalysts also showed the best hydrogen efficiency. For example, the H_2 consumption was nearly 2–5 times lower than those observed for ordered MCM-type supports (Table 1), and this can be directly correlated to efficient utilization of hydroperoxide-like species generated in situ for epoxidation[3] due to better synergism between Au and Ti sites. The PO concentration in the exit gas for the Ti-MCM-48 based catalyst was about 0.1 vol%, while for catalyst 6 it contained about 1 vol% PO. The activity of the catalyst in terms of space–time yield is 130–150 $g\,L^{-1}\,h^{-1}$, which is in the desired range to make this process commercially viable. CO_2 was the major byproduct of the reaction, and traces of ethanal, propanal, and acetone were also observed.

In summary, we have demonstrated that highly dispersed gold nanoparticles supported on 3D mesoporous, silylated titanosilicates with large (>7 nm) pores in the presence of $Ba(NO_3)_2$ as a promoter are very efficient catalysts for the epoxidation of propene to PO with molecular O_2 and H_2. Further work on catalyst preparation, silylation optimization, metal salt promoters, and optimization of the balance between synergetic Au and Ti sites is underway and will result in the preparation of a commercially viable catalyst for propene epoxidation. Furthermore, these 3D mesoporous titanosilicates with a high titanium content (up to 8 mol%) can be expected to be highly active in other oxidation and epoxidation reactions.

Experimental Section

A modified sol–gel method was used to prepare mesoporous titanosilicates.[12] In a typical synthesis, titanium tetra-*n*-butoxide (2.1 g, for 6 mol% Ti) was added dropwise to tetraethyl orthosilicate (20.8 g) while stirring. Then triethanolamine (29.8 g) was added dropwise to the stirred mixture followed by the dropwise addition of deionized water (19.8 g). After stirring the solution for 1–2 h, tetraethylammonium hydroxide (14.7 g) was added dropwise. The final homogeneous mixture was aged at room temperature for 24 h, dried overnight at 100 °C, and then calcined at 700 °C for 10 h in air.

In a typical preparation of titanosilicate-supported Au catalysts by the DP method, an aqueous solution (100 mL) of $HAuCl_4{\cdot}4H_2O$ (2 mmol) was heated to 70 °C, and the pH value was adjusted to 7.0 by adding aqueous NaOH solution. The support (1.0 g) was suspended in the solution, and the pH value was readjusted to 7.0. The suspension was stirred for 1 h, after which the solid was collected by filtration, dried at 100 °C for 12 h, and then calcined at 300 °C for 8 h. The catalyst was placed in a vertical fixed-bed U-shaped quartz reactor (internal diameter = 10 mm) and pretreated in a flow of 10 vol% H_2 in Ar and 10 vol% O_2 in Ar for 30 min each at 250 °C. The catalysts were trimethylsilylated at 150 °C by passing methoxytrimethylsilane vapor (maintained at 25 °C) in an Ar stream over the catalyst bed for 15–30 min, followed by flushing with Ar at 200 °C (5 h) prior to catalytic measurements. Catalytic epoxidation was carried out at 160 °C with a feed containing 10 vol% each of C_3H_6, H_2, and O_2 in argon (space velocity 4000 $cm^3\,h^{-1}\,g^{-1}$ cat.). PO selectivity was calculated as: (moles of PO formed/moles of propene converted) × 100.

Received: September 17, 2003 [Z52900]

Keywords: epoxidation · gold · heterogeneous catalysis · mesoporous materials · titanosilicates

[1] T. Hayashi, K. Tanaka, M. Haruta, *J. Catal.* **1998**, *178*, 566.
[2] M. McCoy, *Chem. Eng. News* **2001**, *79*, 19.
[3] M. Haruta, *Catal. Today* **1997**, *36*, 153.
[4] B. S. Uphade, M. Okumura, S. Tsubota, M. Haruta, *Appl. Catal.* **2000**, *190*, 43.
[5] B. S. Uphade, Y. Yamada, M. Haruta, *Appl. Catal.* **2001**, *215*, 137.
[6] C. Qi, T. Akita, M. Okumura, M. Haruta, *Appl. Catal.* **2001**, *218*, 81.
[7] B. S. Uphade, T. Akita, T. Nakamura, M. Haruta, *J. Catal.* **2002**, *209*, 331.
[8] M. P. Kapoor, A. K. Sinha, S. Seelan, S. Inagaki, S. Tsubota, H. Yoshida, M. Haruta, *Chem. Commun.* **2002**, 2902.
[9] A. K. Sinha, S. Seelan, T. Akita, S. Tsubota, M. Haruta, *Appl. Catal.* **2003**, *240*, 243.
[10] A. K. Sinha, S. Seelan, T. Akita, S. Tsubota, M. Haruta, *Catal. Lett.* **2003**, *85*, 223.
[11] S. A. Bagshaw, E. Prouzet, T. J. Pinnavaia, *Science* **1995**, *269*, 1242.
[12] Z. Shan, E. Gianotti, J. C. Jansen, J. A. Peters, L. Marchese, T. Maschmeyer, *Chem. Eur. J.* **2001**, *7*, 1437.
[13] P. T. Tanev, T. J. Pinnavaia, *Science* **1995**, *267*, 865.
[14] R. Ryoo, J. M. Kim, C. H. Ko, C. H. Shin, *J. Phys. Chem.* **1996**, *100*, 17718.
[15] A. Y. Stakheev, E. S. Shpiro, J. Apijok, *J. Phys. Chem.* **1993**, *97*, 5668.
[16] M. Galan-Fereres, L. J. Alemany, R. Mariscal, M. A. Banares, J. A. Anderson, J. L. G. Fierro, *Chem. Mater.* **1995**, *7*, 1342.

 © 2004 Wiley-VCH Verlag GmbH & Co. KGaA, Weinheim

Alkane Production

Renewable Alkanes by Aqueous-Phase Reforming of Biomass-Derived Oxygenates**

*George W. Huber, Randy D. Cortright, and James A. Dumesic**

Research is being conducted world-wide to develop new technologies for the generation of energy from renewable resources. In this respect, it has recently been stated that "biomass is the only practical source of renewable liquid fuel".[1] Current technologies to produce liquid fuels from biomass are typically multistep and energy-intensive processes, including the production of ethanol by fermentation of biomass derived glucose,[2] bio-oils by pyrolysis or high pressure liquefaction of biomass,[3,4] polyols from hydrogenolysis of biomass derived sorbitol,[5] and biodiesel from vegetable oils.[6] Biomass can also be gasified to produce CO and H_2 (synthesis gas), which can be further processed to produce methanol or liquid alkanes by Fischer–Tropsch synthesis.[3] In addition, liquid hydrocarbons can be formed from biomass-derived carbohydrates over zeolite catalysts at temperatures from 570 to 920 K, accompanied by formation of carbonaceous residues on the catalyst.[7]

We have recently demonstrated that it is possible to produce hydrogen and light alkanes (primarily methane) by aqueous-phase reforming (APR) of biomass-derived oxygenates, including glucose, sorbitol, and glycerol.[8,9] The APR process offers a simple route for the production of renewable fuels from biomass, since this process takes place in a single reaction vessel. Herein, we show how aqueous-phase reforming of sorbitol (the sugar alcohol obtained by hydrogenation of glucose) can be tailored to selectively produce a clean stream of heavier alkanes consisting primarily of butane, pentane, and hexane. The conversion of sorbitol to alkanes plus CO_2 and water is an exothermic process that retains approximately 95% of the heating value and only 30% of the mass of the biomass-derived reactant.

Production of alkanes by aqueous-phase reforming of sorbitol takes place by a bifunctional reaction pathway that involves first the formation of hydrogen and CO_2 on the appropriate metal catalyst (such as Pt) and the dehydration of sorbitol on a solid acid catalyst (such as silica-alumina[10]). These initial steps are followed by hydrogenation of the dehydrated reaction intermediates on the metal catalyst. When these steps are balanced properly, the hydrogen produced in the first step is fully consumed by hydrogenation of the dehydrated reaction intermediates, which leads to the overall conversion of sorbitol to alkanes plus CO_2 and water.

Figure 1 shows the essential features of the bifunctional reaction pathway for the production of alkanes from sorbitol. Hydrogen is produced on the metal by cleavage of C–C bonds

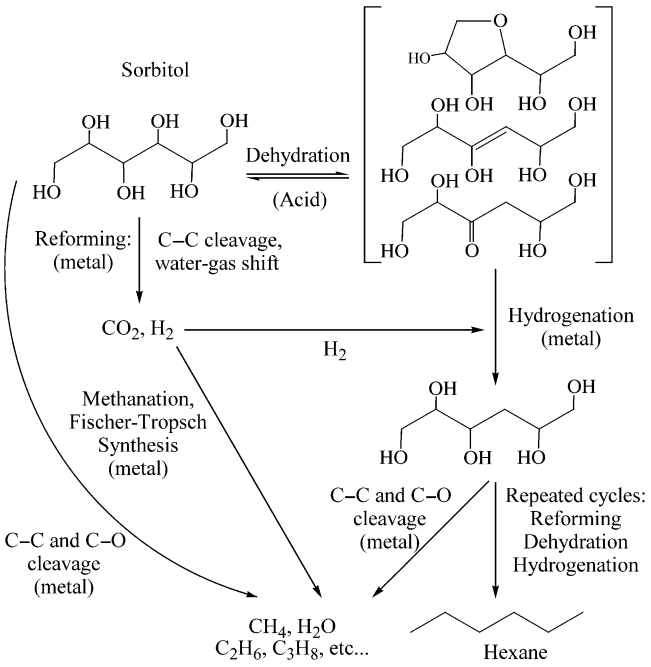


Figure 1. Reaction pathways for the production of alkanes from sorbitol over catalysts with metal and acidic components.

followed by the water–gas shift reaction. Dehydrated species such as ring compounds like isosorbide or enolic species are formed on acid sites,[11] which migrate to metal sites where they undergo hydrogenation reactions. Repeated cycling of dehydration and hydrogenation reactions in the presence of hydrogen leads to heavier alkanes (such as hexane) from sorbitol. Formation of lighter alkanes takes place by more rapid cleavage of C–C bonds compared to hydrogenation of dehydrated reaction intermediates. Lighter alkanes can also be formed by hydrogenation of CO and/or CO_2 on metals such as Ni and Ru.[12] Accordingly, the selectivities for production of various alkanes by aqueous-phase reforming depend on the relative rates of C–C bond cleavage, dehydration and hydrogenation reactions. The selectivities for the production of alkanes can be varied by changing the catalyst composition, the reaction conditions, and by modifying the reactor design. In addition, these selectivities can be modified by co-feeding hydrogen with the aqueous sorbitol feed, leading to a process in which sorbitol can be converted to alkanes and water without the formation of CO_2 (since hydrogen is supplied externally and need not be produced as an intermediate in the process). As another variation, the production of alkanes can be accomplished by replacing the

[*] G. W. Huber, R. D. Cortright, Prof. J. A. Dumesic
Chemical and Biological Engineering Department
University of Wisconsin
Madison, WI 53706 (USA)
Fax: (+1) 608-262-5434
E-mail: dumesic@engr.wisc.edu

[**] This work was supported by U.S. Department of Energy (DOE), Office of Basic Energy Sciences, Chemical Sciences Division, by the National Science Foundation (NSF) through a STTR grant, and by Conoco-Phillips. We thank John W. Shabaker, Marco Sanchez-Castillo, Bret Wagner, Juben Chheda and Rupali R. Davdi for technical assistance.

Supporting information for this article is available on the WWW under http://www.angewandte.org or from the author.

 DOI: 10.1002/anie.200353050 © 2004 Wiley-VCH Verlag GmbH & Co. KGaA, Weinheim

solid acid with a mineral acid (such as HCl) that is co-fed with the aqueous sorbitol reactant.

Table 1 summarizes the experimental results for aqueous-phase reforming of sorbitol at various reaction conditions. These data were collected over catalysts consisting of 4 wt% Pt/SiO_2–Al_2O_3 (Pt–SiAl), 3 wt% Pd/SiO_2–Al_2O_3 (Pd–SiAl), 3 wt% Pt/Al_2O_3 (Pt–Al) and physical mixtures of Pt–Al with SiO_2–Al_2O_3 (SiAl). The Al_2O_3 content of the SiO_2–Al_2O_3 support was 25 wt%. All data were collected after 20 h on-stream. Experimental details are given in the Supporting Information.

The Pt–SiAl catalyst showed no deactivation after 6 days on-stream at a conversion of 92% and 498 K. As shown in Table 1, the carbon selectivity for production of butane, pentane and hexane over Pt–SiAl varies from 58 to 89%, depending on the reaction conditions. The selectivity to hexane increases for the Pt–SiAl catalyst at 498 K as the pressure increases from 25.8 to 39.6 bar, and slightly decreases as the pressure is increased further to 52.7 bar. The alkanes are formed by a combination of metal and acidic components, since they are formed in only small amounts on the Pt–Al catalyst. The alkanes formed are straight-chain compounds with only minor amounts of branched isomers (less than 5%). Alkanes heavier than hexane were not formed under the reaction conditions of this study.

As shown in Figure 2, the selectivity for production of hexane increases when hydrogen is co-fed with the aqueous sorbitol stream. Thus, increasing the hydrogen partial pressure in the reactor increases the rate of hydrogenation compared to C–C bond cleavage on the metal catalyst surface. No major difference is observed in the alkane distribution as the temperature is increased from 498 to 538 K (Figure 2).

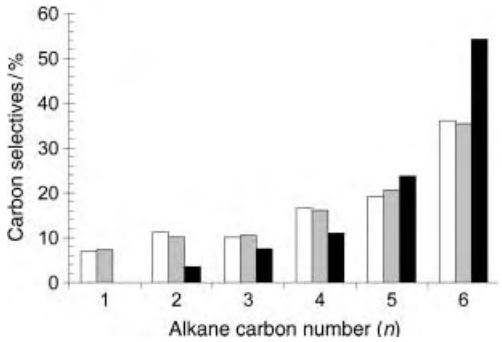


Figure 2. Carbon selectivities for aqueous-phase reforming of 5 wt% sorbitol over Pt–SiAl: white, 498 K and 34.8 bar; gray, 538 K and 60.7 bar, black; co-feeding H_2 at 498 K and 34.8 bar.

Figure 3a shows that the selectivities to heavier alkanes increase as more solid acid sites are added to a non-acidic Pt–Al catalyst by making physical mixtures of Pt–Al and SiAl. The alkane selectivities for an acidic Pt–SiAl catalyst and for a mixture of Pt–Al and SiAl components are similar, both having the same ratio of Pt to acid sites. The alkane distribution also shifts to heavier alkanes for the non-acidic Pt–Al catalyst when the pH of the aqueous sorbitol feed is lowered by the addition of HCl, as shown in Figure 3b.

By changing the nature of the metal component in the catalyst, one can vary the relative rates of C–C bond cleavage versus hydrogenation, thereby controlling the selectivities for the production of different alkanes. Reaction-kinetics studies

Table 1: Experimental data for aqueous phase reforming of 5 wt% sorbitol

Catalysts and additives to feed	Pt–SiAl							Pt–SiAl H_2[b]	Pt–SiAl H_2[b]	Pd–SiAl H_2[b]	Mix 1[c]	Mix 2[c]	Pt–Al	Pt-Al HCl pH 3	Pt–Al HCl pH 2	Pt–Al Void[d]
WHSV [h^{-1}][a]	1.3	1.3	1.3	1.3	1.3	1.3	1.3	1.3	1.3	0.29	1.4	0.46	0.75	0.75	0.75	2.4
Temperature [K]	498	498	498	498	498	538	538	498	498	538	538	538	538	538	538	538
Pressure [bar]	25.8	33.1	34.8	39.6	52.7	55.5	60.7	29.3	34.8	58.2	57.5	57.5	57.5	57.5	57.5	57.5
Carbon in liquid phase effluent [%]	16	13	10	10	27	8	8	12	11	28[e]	10	5	10	8	11	16
Carbon in gas phase effluent [%]	81	89	93	92	76	95	95	84	85	67	91	94	86	88	89	80
Carbon selectivity [%][f]																
CH_4	15	11	7	6	10	11	7	0	0	2	7	35	42	24	9	17
C_2H_6	13	9	11	8	10	9	10	3	4	2	9	20	25	19	7	9
C_3H_8	14	10	10	8	9	11	11	6	7	4	13	16	17	21	14	12
C_4H_{10}	20	18	17	17	15	17	16	11	11	8	18	12	8	15	22	17
C_5H_{12}	17	19	19	21	19	21	21	25	24	28	23	10	5	12	25	20
C_6H_{14}	21	33	36	40	37	31	35	55	54	56	30	7	3	9	23	25
Alkane to total gas phase carbon [%][g]	46	58	63	64	53	58	60	91	91	98	53	31	27	29	47	53
H_2 selectivity [%][h]	21	2	2	1	1	7	4	–	–	–	11	46	43	31	6	16

[a] WHSV = weight hourly space velocity; mass of sorbitol solution per mass of catalyst per hour. [b] H_2 co-fed at a gas-hourly space velocity of 120–900 h^{-1}. Densities of SiO_2-Al_2O_3 catalysts are 0.54 g cm^{-3}. [c] Mix 1 contains Pt-Al (1.45 g) and SiAl (1.11 g). Mix 2 contains Pt-Al (3.30 g) and SiAl (0.83 g). [d] Empty void space representing 70% of the total reactor volume located upstream from the catalyst bed. [e] Approximately 25% of the carbon was in a volatile organic liquid phase product and 3% of the carbon was in the aqueous phase product. The carbon selectivities are based on gas phase products. [f] Carbon selectivity = (moles alkane × number of carbon atoms in alkane)/(total moles of carbon atoms in alkane products) × 100. [g] The gas phase carbon consisted of alkanes and carbon dioxide. [h] % H_2 selectivity = (molecules H_2 produced/C atoms in gas phase) × (6/13) × 100.

 © 2004 Wiley-VCH Verlag GmbH & Co. KGaA, Weinheim

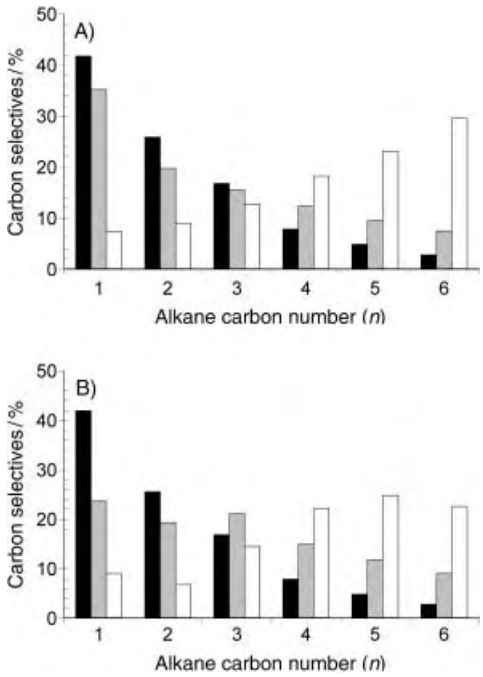


Figure 3. Carbon selectivities for aqueous-phase reforming of 5 wt% sorbitol at 538 K and 57.6 bar. A) Addition of solid acid to Pt–Al: black, Pt–Al; gray, mixture 2: Pt–Al (3.30 g) and SiAl (0.83 g); white, mixture 1: Pt–Al (1.45 g) and SiAl (1.11 g). B) Addition of mineral acid (HCl) in feed over Pt–Al: black, $pH_{feed} = 7$; gray, $pH_{feed} = 3$; white, $pH_{feed} = 2$.

for aqueous-phase reforming of ethylene glycol over silica-supported Pd and Pt catalysts indicate that the rate of C–C bond cleavage is approximately one order of magnitude lower for Pd than for Pt,[12] whereas Pd catalysts are used as hydrogenation catalysts for various reactions.[13] As shown in Table 1, a Pd–SiAl catalyst exhibits very high selectivity for the production of alkanes versus CO_2 when hydrogen is co-fed with aqueous sorbitol into the reactor, as the rate of C–C bond cleavage on Pd is slower than the rates of dehydration on acid sites and hydrogenation reactions on Pd sites. Furthermore, this catalyst system shows very high selectivity for the production of hexane. This example shows that effective bifunctional catalysts can be formulated by using metals that, by themselves on non-acidic supports, show low activities for hydrogen production by aqueous-phase reforming reactions. The hydrogen used for this process can be obtained by APR of sorbitol in a separate reactor over nonprecious metal catalysts.[8]

Another factor that affects the selectivities for the production of alkanes is the presence of void space in the reactor, in which sorbitol can undergo homogenous liquid-phase reactions. Products such as isosorbide and organic acids ($\approx$100–500 ppm) were observed in the liquid products from an empty reactor with a feed of 5 wt% sorbitol heated at 538 K and 57.5 bar, whereas negligible amounts of liquid products were observed at 498 K and 36.5 bar (both experiments conducted with similar liquid residence times as used for studies of supported Pt catalysts). As seen in Table 1, the presence of void space in the reactor at 538 K leads to higher selectivities for the production of alkanes over Pt–Al, since the intermediates formed by homogeneous reactions in the liquid phase are hydrogenated to alkanes over Pt.

The general conclusion from this work is that a clean stream of alkanes can be formed by aqueous-phase reforming of sorbitol over bifunctional catalyst systems in which sorbitol is repeatedly dehydrated by an acid catalyst (e.g., a solid acid or an aqueous mineral acid) and then hydrogenated on a metal catalyst (e.g., Pt or Pd). Hydrogen, which is needed for the hydrogenation reaction, can be produced in situ by aqueous-phase reforming of sorbitol over a catalyst (such as Pt) that facilitates C–C bond cleavage and water–gas shift reactions, or it can be co-fed to the reactor with the aqueous sorbitol reactant. The selectivities for production of heavier alkanes can be controlled by the choice of reaction conditions and by co-feeding hydrogen to the reactor. It is likely that advances in the understanding of new types of solid-acid catalysts[14] as well as new metal alloy catalysts[8] will lead to further process improvements.

Received: October 9, 2003 [Z53050]

Keywords: acidity · alkanes · basicity · heterogeneous catalysis · hydrogenation

[1] T. E. Bull, *Science* **1999**, *285*, 1209.
[2] R. Katzen, G. T. Tsao, *Adv. Biochem. Eng./Biotechnol.* **2000**, *70*, 77.
[3] D. L. Klass, *Biomass for Renewable Energy, Fuels, and Chemicals*, Academic Press, San Diego, **1998**.
[4] D. C. Elliott, D. Beckman, A. V. Bridgwater, J. P. Diebold, S. B. Gevert, Y. Solantausta, *Energy Fuels* **1991**, *5*, 399.
[5] T. A. Werpy, J. G. Frye, Jr., A. H. Zacher, D. J. Miller, US 2003/0119952A1, **2003**.
[6] F. Ma, M. A. Hanna, *Bioresour. Technol.* **1999**, *70*, 1.
[7] N. Y. Chen, L. R. Koenig, US 4503278, **1985**.
[8] G. W. Huber, J. W. Shabaker, J. A. Dumesic, *Science* **2003**, *300*, 2078.
[9] R. D. Cortright, R. R. Davda, J. A. Dumesic, *Nature* **2002**, *418*, 964.
[10] G. M. Kramer, G. B. McVicker, J. J. Ziemiak, *J. Catal.* **1985**, *92*, 355.
[11] P. Stoss, R. Hemmer, *Adv. Carbohydr. Chem. Biochem.* **1991**, *49*, 93.
[12] R. R. Davda, J. W. Shabaker, G. W. Huber, R. D. Cortright, J. A. Dumesic, *Appl. Catal. B* **2003**, *43*, 1.
[13] G. M. R. van Druten, V. Ponec, *Appl. Catal. A* **2000**, *191*, 163.
[14] D. G. Barton, S. L. Soled, G. D. Meitzner, G. A. Fuentes, E. Iglesia, *J. Catal.* **1999**, *181*, 57.

 © 2004 Wiley-VCH Verlag GmbH & Co. KGaA, Weinheim

Nanotubes

Side-Wall Opening of Single-Walled Carbon Nanotubes (SWCNTs) by Chemical Modification: A Critical Theoretical Study**

Zhongfang Chen, Shigeru Nagase, Andreas Hirsch, Robert C Haddon, Walter Thiel, and Paul von Ragué Schleyer**

Dedicated to Professor Henry F. Schaefer III on the occasion of his 60th birthday

Single-walled carbon nanotubes (SWCNTs) have unique electronic, mechanical, and structural characteristics; consequently, promising applications derived from these materials, such as chemical sensors or nanometer-scale electronic devices,[1] can be expected. Structurally altered nanotubes with appropriate addends should facilitate their use by improving solubility, processability, and ease of dispersion, as well as by providing sites for chemical attachment to surfaces and polymer matrices.[2]

A vexing problem is ascertaining the detailed structures of nanotube derivatives after their preparation. The characterization of functionalized SWCNTs is difficult; all experimental attempts to determine the precise location and mode of addition of newly attached groups have failed. SWCNT adducts with possible three-membered rings (3MRs) that result from oxygen, methylene, and NH additions are simple but very important side-wall functionalized derivatives. Oxidation reactions are used widely to purify nanotubes,[3] and the electrical properties of carbon nanotubes are extremely sensitive to oxygen exposure.[4] Methylene and NH adducts are the prototypes of the recently synthesized covalently bonded dichlorocarbene[5] and nitrene[6] adducts. The available theoretical studies on the structures of nanotube oxide[7] and dichlorocarbene adducts[8] that involve either armchair[7a,8] or zigzag tube[7b–f] models, employed rather unsatisfactory methodology (see below).

Owing to the large size of nanotubes, carefully chosen truncated models, appropriate for the problem being investigated, are required. One approach uses small nanotube fragments to simulate a full nanotube, but carries out computations at a relatively high level.[7b,9] The other approach uses the ONIOM technique,[10] which treats part of the system at a high theoretical level but the rest of the system at a lower level. This strategy allows larger systems to be simulated at a practical computational cost.[7a–c,11] Thus, a recent ONIOM(B3LYP/6-31G*:AM1) study employed a C_{16} fragment (Figure 1a) for the high-level computation to simulate the side-wall chemistry of the armchair SWCNTs.[7a,11a–11f] However, no systematic validation of the ONIOM approach for such applications is available.

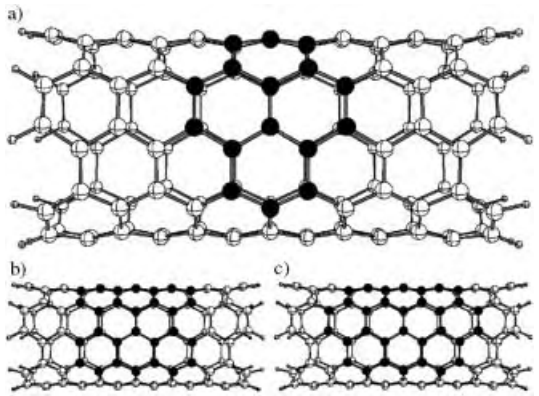


Figure 1. Thirteen-layered (5,5) tube model ($C_{130}H_{20}$), in which the highlighted a) 16, b) 28, and c) 32 atoms are used for the high-level treatment in the two-level ONIOM computations.

Herein we report B3LYP/6-31G* computations[12] on the O, CH_2, and NH nanotube derivatives, as well as the hypothetical SiH_2 adduct, for both (5,5) and (8,0) SWCNTs. In addition, several combinations of methods in the two-level ONIOM approach are evaluated.

(5,5) Armchair SWCNT Derivatives**:** The optimized structure of the NH adduct of the 13-layered tube model is shown in Figure 2 as an example (see the Supporting Information for others). The separations between the two C atoms at the site at which the O, CH_2, SiH_2, and NH addends are attached to the (5,5) armchair SWCNT models are all over 2 Å (Table 1). Regardless of the addend and of the length of the the (5,5) model, all the modified nanotubes have opened structures rather than 3MRs. We have obtained the

[*] Dr. Z. Chen, Prof. Dr. A. Hirsch, Prof. Dr. P. von R. Schleyer
Institut für Organische Chemie
Universität Erlangen-Nürnberg
Henkestrasse 42, 91054 Erlangen (Germany)
Fax: (+49) 9131-85-26864
E-mail: chen@organik.uni-erlangen.de
schleyer@chem.uga.edu

Prof. Dr. S. Nagase
Department of Theoretical Studies
Institute for Molecular Science
Okazaki 444-8585 (Japan)

Prof. Dr. R. C. Haddon
Departments of Chemical and Environmental Engineering and Chemistry and Center for Nanoscale Science & Engineering
University of California
Riverside, CA 92521 (USA)

Prof. Dr. W. Thiel
Max-Planck-Institut für Kohlenforschung
Kaiser-Wilhelm-Platz 1, 45470 Mülheim an der Ruhr (Germany)

Dr. Z. Chen, Prof. Dr. P. von R. Schleyer
Department of Chemistry and
Center for Computational Quantum Chemistry
University of Georgia
Athens, GA 30602 (USA)

[**] This work was supported by National Science Foundation Grant CHE-0209857, the University of Georgia, the Grant-in Aid for NAREGI Nanoscience Project, Scientific Research (B), and Scientific Research on Priority Area (A) from the Ministry of Education, Culture, Sports, Science and Technology of Japan, and FORCARBON.

Supporting information for this article is available on the WWW under http://www.angewandte.org or from the author.

 © 2004 Wiley-VCH Verlag GmbH & Co. KGaA, Weinheim DOI: 10.1002/anie.200353087

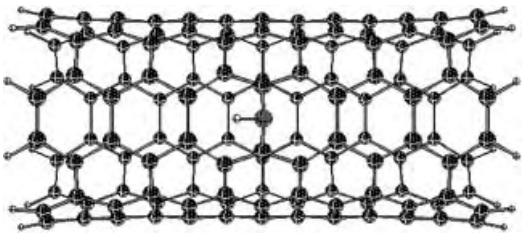


Figure 2. B3LYP/6-31G* optimized NH adduct of the 13-layered (5,5) SWCNT model.

Table 1: Distances (in Å) between two C atoms attached to the addend in *n*-layered (5,5) SWCNT derivatives (B3LYP/6-31G*).

n	O	CH_2	SiH_2	NH
5	2.141	2.250	2.542	2.179
7	2.049	2.142	2.379	2.086
9	2.139	2.231	2.478[a]	2.086
13	2.096	2.186	2.417	2.131

[a] Another minimum with a CC bond length of 1.723 Å is 16.8 kcal mol^{-1} higher in energy.

same result for the oxygen and methylene adducts of (10,10) SWCNTs that have typical nanotube diameters (see Supporting Information). The strain of the 3MR alternatives and their diminished aromaticity, as in the bridged 1,6-X-[10]annulenes,[13] is responsible for these open structures. These findings contradict earlier theoretical studies with the ONIOM method[7a,11f] and with GGA (general gradient approximation) exchange-correlation functionals by using a plane-wave basis set.[7g,14]

(8,0) zigzag SWCNTs: There are two sets of C–C bonds in zigzag SWCNTs (see Figure 3). Though no literature on the

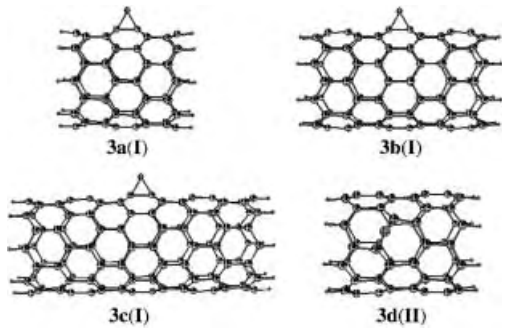


Figure 3. B3LYP/6-31G* optimized structures of (8,0) SWCNT oxide. (a)–(c) are 8-, 12- and 16-layered model with addition pattern **I**, and (d) is the 8-layered model with addition pattern **II**.

structures of CH_2, NH, and SiH_2 adducts with zigzag SWCNTs is available, oxygen adducts of such tubes have been well investigated. With the exception of the work reported in reference [7e], the C–C bond parallel to the tube axis was used as the site to model the reactions.[7b,d,f,g] We find that all the (8,0) tube oxides in this addition pattern (**I**) favor closed 3MRs (C–C bond lengths 1.464, 1.468, and 1.473 Å for Figure 3 a–c, respectively). However, the parallel C–C bonds in the zigzag SWCNTs have greater single-bond character, whereas the diagonal C–C bonds are more double-bond-like. Indeed, computations confirm our expectation that the oxide **3d** with addition-pattern **II** not only is 25.6 kcal mol^{-1} more stable than **3a**, but, as in the (5,5) adducts, also has an opened structure (2.126 Å) rather than a 3MR, in agreement with reference [7e]. This conclusion holds true for CH_2, NH, and SiH_2 adducts (see Supporting Information), whose addition-pattern **II** is more stable than **I** by 30.7, 29.5, and 20.4 kcal mol^{-1}, respectively.

ONIOM evaluation**:** Does the ONIOM model give reliable results for nanotubes? Table 2 summarizes a critical

Table 2: Distances (in Å) between the two C atoms where the addend in *n*-layered (5,5) SWCNT derivatives is attached.

13-layer	N_{high}[a]	O	CH_2	SiH_2	NH
B3LYP/6-31G*	full	2.096	2.186	2.417	2.131
HF/3-21G	full	2.133	2.140	2.314[b]	2.140
AM1[c]	full	2.216	2.224	2.366	2.174
ONIOM	16	1.586	1.694	1.719	1.636
(B3LYP/6-31G*	28	1.585	1.687	1.593	1.634
:AM1)	32	1.590	1.706	1.706	1.646
ONIOM	16	2.084	2.176	2.402	2.120
(B3LYP/6-31G*	28	2.090	2.182	2.411	2.126
:B3LYPSTO-3G)	32	2.083	2.176	2.398	2.118
ONIOM	16	1.559	1.651	1.669	1.599
(B3LYP/6-31G*	28	1.570	1.682	2.580	1.622
:HF/3–21G)	32	1.581	1.712	1.622	1.639

[a] Number of atoms at the high level in ONIOM approach. [b] Another minimum with a 1.789 Å bond length is 2.5 kcal mol^{-1} higher in energy. [c] Higher energy minima with closed 3MRs also were located (see Supporting Information).

evaluation that involves different combinations in the two-level ONIOM method for the 16-, 28-, and 32-atom high-level models (Figure 1). The B3LYP/6-31G* results on the adducts of the full $C_{130}H_{20}$ systems are used as reference; HF/3-21G and AM1 data on these full systems are included for comparison.

The full B3LYP/6-31G* results are reproduced at the full HF/3-21G and full AM1 levels: all the (5,5) tube adducts favor opened structures rather than 3MRs. However, higher-energy closed 3MR minima also were located for all the adducts at AM1 and for the SiH_2 adduct at HF/3-21G. But these closed 3MR forms did not survive further optimization at B3LYP/6-31G*.

In contrast, only the ONIOM(B3LYP/6-31G*:B3LYP-STO-3G) combination reproduces all the results from density functional theory. The combination of B3LYP/6-31G* with AM1 and with HF/3-21G fail since they predict closed 3MRs. This is surprising as both AM1 and HF/3-21G methods by themselves give opened structures (see Table 2). When the opened B3LYP geometry for the oxide was used as the starting structure for ONIOM optimization for the latter two combinations, only closed 3MRs resulted. The often-employed ONIOM(B3LYP:AM1) model as implemented in Gaussian 98[12] is thus not reliable, at least for the systems we studied. This underlines the need for careful validation of the ONIOM approach for any given application. The S-value

 © 2004 Wiley-VCH Verlag GmbH & Co. KGaA, Weinheim

test[15] (see Supporting Information) may be helpful in this regard.

In summary, the (5,5) armchair SWCNT derivatives investigated here have opened structures instead of 3MRs. Furthermore, the addends prefer attachment to the diagonal C–C bonds in (8,0) zigzag tubes, and also are prone to adopt opened rather than 3MR structures. Since armchair and zigzag tubes are two extremes for SWCNT structures, evidently the side-wall of SWCNTs can be opened by chemical modifications. As the often-used ONIOM(B3LYP:AM1) approach is not appropriate for the systems studied in this paper, serious limitations in the ONIOM approach to computational nanotube chemistry are apparent. Our computational results, that SWCNT derivatives favor opened rather than 3MR structures, may be verified experimentally with new advances in SWCNT solubilization and spectroscopic analysis. Experiments aimed at this purpose are under way.

Supporting Information available: AM1 results, optimized structures of (10,10) SWCNT adducts, S-value test, B3LYP/6-31G* structures for (5,5) and (8,0) SWCNT adducts.

Received: October 14, 2003 [Z53087]

Keywords: computer chemistry · density functional calculations · nanotubes · structure elucidation

[1] See recent reviews: a) R. H. Baughman, A. A. Zakhidov, W. A. de Heer, *Science* **2002**, *297*, 787–792; b) P. M. Ajayan, *Chem. Rev.* **1999**, *99*, 1787–1799; c) Guest editor R. C. Haddon, special issue on nanotubes in *Acc. Chem. Res.* **2002**, *35*, 997–1113.

[2] a) J. L. Bahr, J. M. Tour, *J. Mater. Chem.* **2002**, *12*, 1952–1958; b) S. B. Sinnott, *J. Nanosci. Nanotechnol.* **2002**, *2*, 113–123; c) A. Hirsch, *Angew. Chem.* **2002**, *114*, 1933–1939; *Angew. Chem. Int. Ed.* **2002**, *41*, 1853–1859; d) S. Banerjee, M. G. C. Kahn, S. S. Wong, *Chem. Eur. J.* **2003**, *9*, 1898–1908.

[3] For example, S. Banerjee, S. S. Wong, *J. Phys. Chem. B* **2002**, *106*, 12144–12151.

[4] P. G. Collins, K. Bradley, M. Ishigami, A. Zettl, *Science* **2000**, *287*, 1801–1804.

[5] a) J. Chen, M. A. Hamon, H. Hu, Y. Chen, A. M. Rao, P. C. Eklund, R. C. Haddon, *Science* **1998**, *282*, 95–98; b) K. Kamaras, M. E. Itkis, H. Hu, B. Zhao, R. C. Haddon, *Science* **2003**, *301*, 1501–1501; c) H. Hu, B. Zhao, M. A. Hamon, K. Kamaras, M. E. Itkis, R. C. Haddon, *J. Am. Chem. Soc.* **2003**, *125*, 14893–14900.

[6] M. Holzinger, J. Abraham, P. Whelan, R. Graupner, L. Ley, F. Hennrich, M. Kappes, A. Hirsch, *J. Am. Chem. Soc.* **2003**, *125*, 8566–8580.

[7] a) X. Lu, L. L. Zhang, X. Xu, N. Q. Wang, Q. Zhang, *J. Phys. Chem. B* **2002**, *106*, 2136–2139; b) S. Irle, A. Mews, K. Morokuma, *J. Phys. Chem. A* **2002**, *106*, 11973–11980; c) S. P. Walch, *Chem. Phys. Lett.* **2003**, *374*, 501–505; d) D. C. Sorescu, K. D. Jordan, P. Avouris, *J. Phys. Chem. B* **2001**, *105*, 11227–11232; e) S. Dag, O. Gülseren, T. Yildirim, S. Ciraci, *Phys. Rev. B* **2003**, *67*, 165424/1–10; f) D. J. Mann, M. D. Halls, *J. Chem. Phys.* **2002**, *116*, 9014–9020; g) S. P. Chan, G. Chen, X. G. Gong, Z. F. Liu, *Phys. Rev. Lett.* **2003**, *90*, 086403/1–4.

[8] R. F. Li, Z. F. Shang, G. C. Wang, Y. M. Pan, Z. S. Cai, X. Z. Zhao, *J. Mol. Struct. (Theochem)* **2002**, *583*, 241–247.

[9] For example, a) F. Nunzi, F. Mercuri, A. Sgamellotti, N. Re, *J. Phys. Chem. B* **2002**, *106*, 10622–10633; b) Z. Chen, A. Hirsch, W. Thiel, *ChemPhysChem* **2003**, *4*, 93–97.

[10] a) M. Svensson, S. Humbel, R. D. J. Froese, T. Matsubara, S. Sieber, K. Morokuma, *J. Phys. Chem.* **1996**, *100*, 19357–19363; b) S. Dapprich, I. Komáromi, K. S. Byun, K. Morokuma, M. J. Frisch, *J. Mol. Struct. (Theochem)* **1999**, *461*–462, 1–21.

[11] For example a) X. Lu, F. Tian, N. Q. Wang, Q. Zhang, *Org. Lett.* **2002**, *4*, 4313–4315; b) X. Lu, F. Tian, Y. B. Feng, X. Xu, N. Q. Wang, Q. Zhang, *Nano Lett.* **2002**, *2*, 1325–1327; c) X. Lu, F. Tian, X. Xu, N. Q. Wang, Q. Zhang, *J. Am. Chem. Soc.* **2003**, *125*, 10459–10464; d) X. Lu, Q. Yuan, Q. Zhang, *Org. Lett.* **2003**, *5*, 3527–3530; e) L. Long, X. Lu, F. Tian, Q. Zhang, *J. Org. Chem.* **2003**, *68*, 4495–4498; f) X. Lu, F. Tian, Q. Zhang, *J. Phys. Chem. B* **2003**, *107*, 8388–8391; g) C. W. Bauschlicher, *Chem. Phys. Lett.* **2000**, *322*, 237–241; h) C. W. Bauschlicher, *Nano Lett.* **2001**, *1*, 223–226; i) G. E. Froudakis, *Nano Lett.* **2001**, *1*, 531–533; j) V. A. Basiuk, E. V. Basiuk, J. M. Saniger-Blesa, *Nano Lett.* **2001**, *1*, 657–661; k) V. A. Basiuk, *Nano Lett.* **2002**, *2*, 835–839; l) C. W. Bauschlicher, C. R. So, *Nano Lett.* **2002**, *2*, 337–341; m) E. V. Basiuk, V. A. Basiuk, J. G. Banuelos, J. M. Saniger-Blesa, V. A. Pokrovskiy, T. Y. Gromovoy, A. V. Mischanchuk, B. G. Mischanchuk, *J. Phys. Chem. B* **2002**, *106*, 1588–1597; n) A. Ricca, J. A. Drocco, *Chem. Phys. Lett.* **2002**, *362*, 217–223; o) V. A. Basiuk, *J. Phys. Chem. B* **2003**, *107*, 8890–8897.

[12] Gaussian 98 (Revision A.11), M. J. Frisch, G. W. Trucks, H. B. Schlegel, G. E. Scuseria, M. A. Robb, J. R. Cheeseman, V. G. Zakrzewski, J. A. Montgomery, R. E. Stratmann, J. C. Burant, S. Dapprich, J. M. Millam, A. D. Daniels, K. N. Kudin, M. C. Strain, O. Farkas, J. Tomasi, V. Barone, M. Cossi, R. Cammi, B. Mennucci, C. Pomelli, C. Adamo, S. Clifford, J. Ochterski, G. A. Petersson, P. Y. Ayala, Q. Cui, K. Morokuma, D. K. Malick, A. D. Rabuck, K. Raghavachari, J. B. Foresman, J. Cioslowski, J. V. Ortiz, B. B. Stefanov, G. Liu, A. Liashenko, P. Piskorz, I. Komaromi, R. Gomperts, R. L. Martin, D. J. Fox, T. Keith, M. A. Al-Laham, C. Y. Peng, A. Nanayakkara, C. Gonzalez, M. Challacombe, P. M. W. Gill, B. G. Johnson, W. Chen, M. W. Wong, J. L. Andres, M. Head-Gordon, E. S. Replogle, J. A. Pople, Gaussian, Inc., Pittsburgh, PA, **1998**.

[13] H. Jiao, N. J. R. v. E. Hommes, P. v. R. Schleyer, *Org. Lett.* **2002**, *4*, 2393–2396.

[14] The open structure for six-layered (6,6) dioxide was obtained at B3LYP/6-31G* level. A minimum with a central closed 3MR can be located at HF/3-21G level, which, upon elongation of the distance between carbon atoms in this 3MR, is transformed into another minimum with two open 3MRs that is more stable by 14 kcal mol^{-1}. For the optimized structures see the Supporting Information.

[15] K. Morokuma, D. G. Musaev, T. Vreven, H. Basch, M. Torrent, D. V. Khoroshun, *IBM J. Res. Dev.* **2001**, *45*, 367–395.

 © 2004 Wiley-VCH Verlag GmbH & Co. KGaA, Weinheim

Nanostructures

Self-Assembled Aggregates of IgGs as Templates for the Growth of Clusters of Gold Nanoparticles**

Jerry Yang, Michael Mayer, Jennah K. Kriebel, Piotr Garstecki, and George M. Whitesides**

This paper describes a procedure for generating clusters of gold nanoparticles by using as templates oligomers (dimers, trimers, and tetramers) formed by self-assembly of immunoglobulin Gs (IgGs) with bivalent antigens, and by growing the nanoparticles from redox-active centers (aldehydes) derived from the integral carbohydrates located in the F_c portion of the IgGs. In this procedure, a significant fraction ($15 \pm 5\,\%$) of these gold nanoparticles occurs in multimeric clusters (mostly dimers), with a distance of about 30 nm between particles in a cluster. This distance is consistent with the spacing between carbohydrate groups in separate antibody molecules when the antibodies are preassembled into aggregates. This method combines molecular recognition (to assemble nucleating centers for growth of nanoparticles) with redox-active functional groups on the biomolecule (to generate the nucleating centers for electroless growth of gold) to form locally ordered sets of nanoparticles.

Nanoparticles of various shapes (e.g., wires, rectangles, stars, octahedra, truncated boxes, and spirals),[1] compositions (e.g., metals or minerals),[2] and arrangements of clusters (e.g., small multimeric aggregates or large superlattices)[3] are interesting for their potential uses for the miniaturization of optical and electronic devices (e.g., optical filters, optical detectors, conducting wires, molecular electronics, MEMS).[1b,c] New techniques for the fabrication of metallic and hybrid nanostructures with defined geometry may be useful for further realization of these types of devices.

The groups of Finn, Ben–Porat, Mann, Francis, and others have used biomolecular building blocks as the basis for bottom-up fabrication of metallic nanostructures and assemblies of nanoparticles.[1d,4] Viral particles and DNA modified with thiols on their exterior surface are useful in positioning gold nanoparticles; assemblies of nanoparticles based on organization by using DNA duplexes[3b,5] show characteristic shifts in plasmon absorption in aqueous solutions upon clustering of nanoparticles.[6] Feldheim and co-workers used synthetic thiol-based molecular templates to generate multimers (dimers, trimers, and tetramers) of preformed gold and silver nanoparticles for the study of the shifts in plasmon absorption that results from the formation of small aggregates of nanoparticles.[3a,7] Several groups have grown metallic nanostructures by processes that assume coordination of metal ions from solution to biomolecular or synthetic polymeric templates; reduction of the adhering metal ions afforded metallic nanostructures that reflect the structure of the templates from which they were derived.[1c,8]

Although several strategies successfully generate metallic structures from molecular templates, so far the variety of shapes of metallic nanostructures remains limited (mostly to large arrays and lines).[1,8] To demonstrate the combination of molecular self-assembly[9] with the generation of metallic nanostructures, we produced linear and cyclic aggregates of IgGs from a divalent interaction of a compound that contained two fluorescein groups with monoclonal IgGs derived from fluorescein isothiocyanate as antigens (anti-FITC; Figure 1).[10] We subsequently grew clusters of gold nanoparticles using these aggregates as templates. We show that pairs of redox-active functional groups (carbohydrates) present in biomolecular (IgG) aggregates can (after periodate oxidation) provide nucleation sites for the electroless deposition of gold, and that the resulting pairs of gold nanoparticles reflect the geometry of these aggregates. This approach provides a new, bottom-up route to metallic nanostructures.

We incubated a divalent derivative of fluorescein (**1**, Figure 1) in a solution of monoclonal anti-FITC IgG in various relative concentrations, and determined the size of the aggregates in the resulting mixture by size-exclusion HPLC.[18] We observed high conversion of IgGs into aggregated species ($\approx 73\,\%$ of the protein in solution aggregated into $\approx 91\,\%$ dimers, 8 % trimers, and $\approx 1\,\%$ tetramers) when we incubated a 2 μM solution of **1** with a 1 μM solution of IgG at 4 °C for 3 hrs.[19] Transmission electron microscope (TEM) imaging of the aggregates of antibodies deposited on a carbon-coated Formvar substrate revealed numerous cyclic structures (Figure 2a), consistent in size with oligomers (predominantly cyclic) of antibodies, but with indistinct shape (Figure 2b). The Supporting Information summarizes the experimental details of procedures used to form the aggregates of IgGs and to prepare the samples for imaging by TEM.

We formed individual gold nanoparticles on the IgG molecules by using the carbohydrate units present on IgGs to nucleate the growth of metal particles. All IgGs contain N-linked carbohydrate groups attached to the C_H2 domains in the F_c regions.[20] These carbohydrates are used routinely to link molecules to the F_c region by initial oxidation with $NaIO_4$ to produce aldehyde groups, followed by subsequent conjugation reactions.[21] Aldehydes derived from carbohydrates have also been used to reduce silver ions for silver-enhanced staining of biological tissues.[22] We used the aldehyde moieties derived from periodate oxidation of the carbohy-

[*] Prof. J. Yang, Dr. M. Mayer, J. K. Kriebel, Dr. P. Garstecki, Prof. G. M. Whitesides
Department of Chemistry and Chemical Biology
Harvard University
12 Oxford Street, Cambridge, MA 02138 (USA)
Fax (+1) 617-495-9857
E-mail: jyang@chem.ucsd.edu
gwhitesides@gmwgroup.harvard.edu

[**] This work was supported by the NIH (Grant GM30367). M.M. acknowledges the Swiss National Science Foundation for a postdoctoral fellowship. J.K. acknowledges support from the NDSEG for a predoctoral fellowship. P.G acknowledges the Foundation for Polish Science for a postdoctoral fellowship. We thank Dr. Declan Ryan for helpful discussions. IgGs = Immunoglobulin Gs.

Supporting information for this article is available on the WWW under http://www.angewandte.org or from the author.

 DOI: 10.1002/anie.200353161 © 2004 Wiley-VCH Verlag GmbH & Co. KGaA, Weinheim

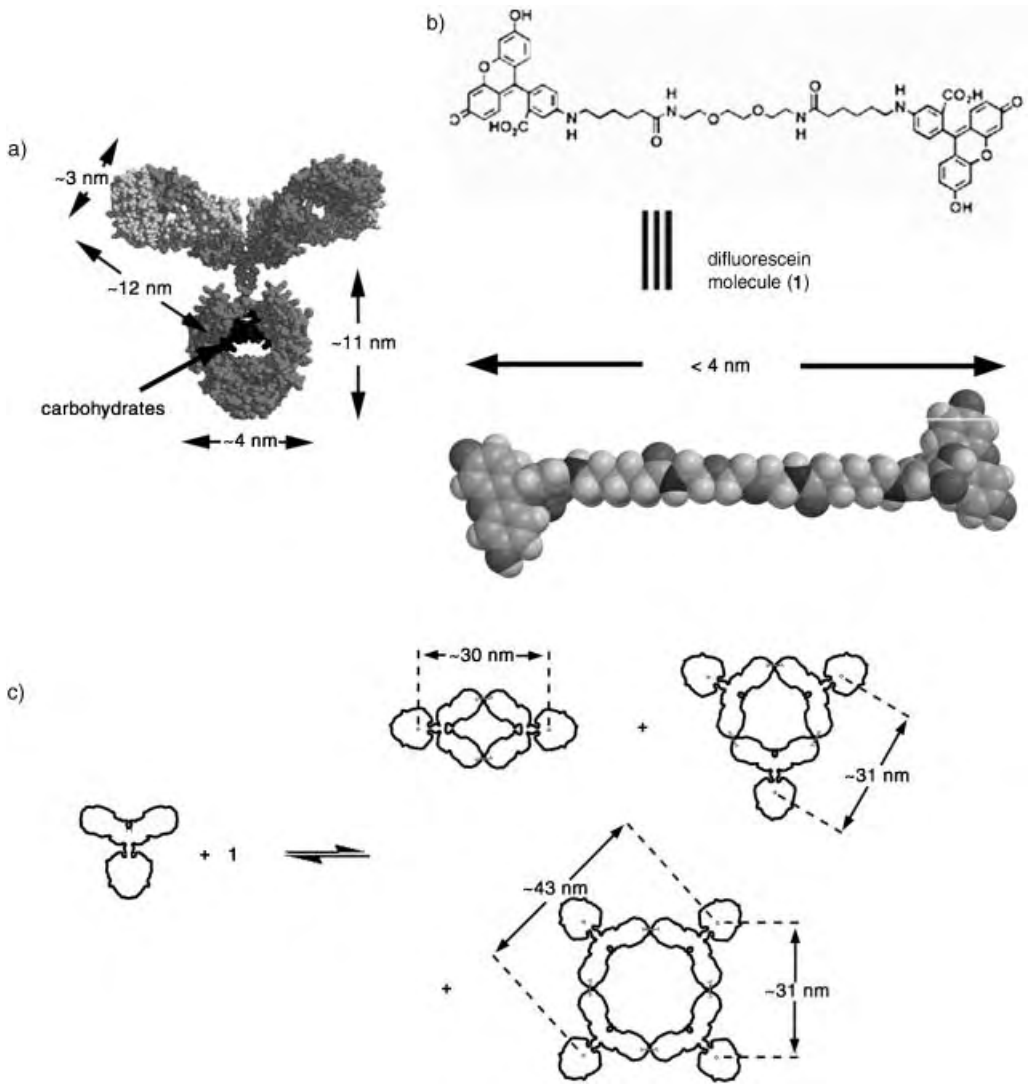


Figure 1. Schematic representation of complexes between anti-FITC IgGs and difluorescein antigen **1**: a) A reconstructed crystal structure of an IgG with the location of the carbohydrates shown in black;[25] b) schematic molecular representation of difluorescein molecule **1** (represented in an extended conformation); and c) schematic representation of cyclic oligomeric structures formed between anti-FITC IgGs and **1** (the IgGs and difluorescein antigens are drawn approximately to scale).

drates in the aggregates of IgGs to reduce a small group of silver atoms; the resulting cluster of silver atoms acted as the nucleus for electroless deposition of a gold nanoparticle.

We deposited a solution of aggregated IgG (2 μM **1** and 1 μM anti-FITC in 0.1 M phosphate buffer: pH 7.0, 0.3 M NaCl) on a Si_3N_4 membrane that had been cleaned with an air plasma. We treated the aggregates of IgGs on the surface with a solution of 10 mM $NaIO_4$ (in 0.02 M acetate buffer, pH 5.0, 0.15 M NaCl) for 60 min at 23 °C, followed by incubation of the surface with a 1 M solution of ethylene glycol for 20 min (to quench the excess periodate). We incubated the IgGs (for 90 min at 23 °C in the dark) with a 0.1 M solution of $AgNO_3$ (in 28–33 % aqueous NH_4OH, adjusted to pH 10.5) and subsequently treated the surface (for 0.5 to 2 min) with an electroless Au plating solution.[4d,23]

TEM examination revealed many clusters of nanoparticles (Figure 2e). We analyzed several large-area images (2320 × 1840 nm up to 3590 × 2843 nm) of substrates that contained these assemblies of nanoparticles by using software written to identify the distribution of nearest-neighbor distances for particles deposited on a surface (see Supporting Information for details). The image-analysis software identified a statistically significant excess in the number of particles (15 ± 5 %)[24] with the centers of the particles having a distance of nearest neighbors of 15 to 45 nm (with a maximum at ≈33 nm, Figure 3a). These distances are consistent with the expected distances (estimated from TEM examination of aggregates of IgGs, Figure 2a) between the carbohydrates in the F_c regions of adjacent antibodies in cyclic and linear aggregates (Figure 1). Similar analysis of substrates containing nanoparticles grown from deposited IgGs that were not preincubated with difluorescein **1** did not indicate a significant excess in the number of particles with a distance between nearest neighbors of 15 to 45 nm (Figure 3b). Instead, the analysis indicated a random distribution of distances between nearest neighbors.

 © 2004 Wiley-VCH Verlag GmbH & Co. KGaA, Weinheim

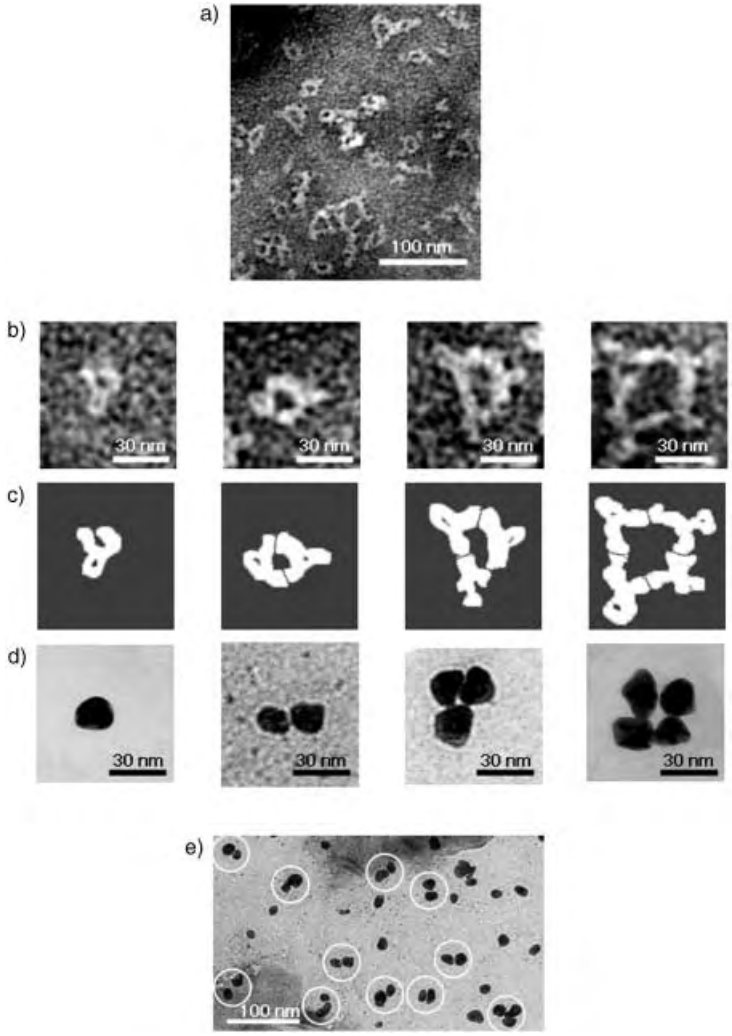


Figure 2. TEM images of aggregated antibodies. a) Image of anti-FITC IgG antibodies deposited from a solution of 1 μM protein after incubation with 2 μM solution of difluorescein antigen **1**; the substrate was negatively stained with a 2% uranyl acetate solution in water. Notice the numerous cyclic structures present. b) Magnified images of (from left to right) a single IgG molecule, cyclic dimer, cyclic trimer, and cyclic tetramer. c) Schematic representation of the corresponding IgG monomer, dimer, trimer, and tetramer in row (b) (obtained by hand-tracing threshold enhanced images of row b; the dotted lines were manually inserted to illustrate our interpretation of divisions between the individual antibody units in each aggregate structure). d) Magnified images of (from left to right) gold nanoparticles presumably grown from a single IgG molecule, a cyclic dimer, a cyclic trimer, and a cyclic tetramer after treatment with sodium periodate (60 min), ethylene glycol (20 min), silver nitrate (90 min), and electroless gold plating solution (2 min). These nanoparticles were grown to a diameter of 15–30 nm to clarify their geometric arrangement. e) Larger area of a sample of anti-FITC IgG deposited in the presence of difluorescein antigen **1** after they had been subjected to the metal-growth conditions (1 min exposure to gold electroless plating solution, clusters of nanoparticles are circled in white).

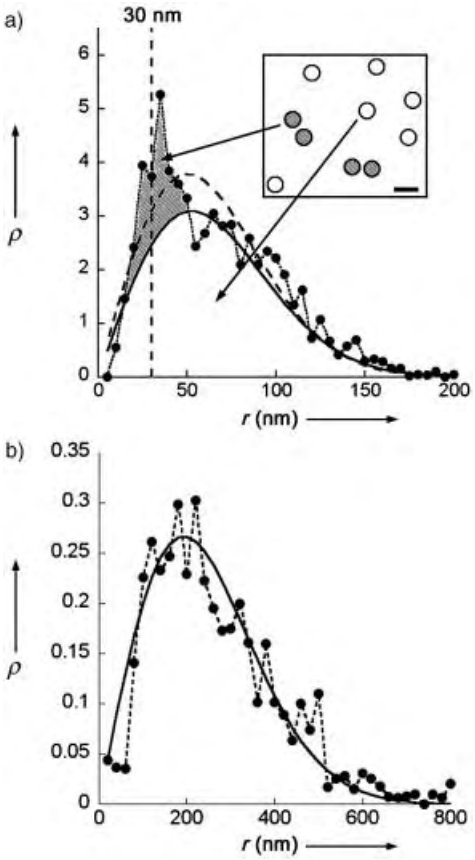


Figure 3. a) Comparison of the distribution of distances of nearest neighbors (DDNN) of particles grown from aggregated IgG templates (dotted line) with the theoretical DDNN for uniformly distributed, uncorrelated particles of the same number density (dashed line) and a density equal to 85% of the experimentally measured one (solid line). The shaded area corresponds to the excess in the density of particles incorporated into multimers compared to a random distribution of particles with a density approximated under the solid line. ρ (particles μm^{-2}) is the density of particles with nearest neighbors at a distance $r \pm \Delta r/2$. The scale bar of the inset corresponds to a distance of $\approx$30 nm. The bin size (Δr) is equal to 5 nm. b) Comparison of the DDNN of nanoparticles grown from IgGs (that were not previously incubated with difluorescein antigen **1**) (dotted line) with the reference DDNN for uniformly distributed, uncorrelated particles of the same number density (solid line). The bin size (Δr) is equal to 25 nm.

We did not observe nanoparticles when we omitted any of the steps in the metal growth procedure—that is, $NaIO_4$ oxidation of the carbohydrate, reduction of Ag^+, or electroless deposition of Au^+. We observed few nanoparticles on the surface under the metal-growth conditions in the absence of a deposited protein, or in the presence of bovine ubiquitin—a protein that does not contain a carbohydrate.

We have thus demonstrated that monoclonal anti-FITC IgGs spontaneously assemble into cyclic and linear oligomers in the presence of a divalent fluorescein antigen. These aggregated IgGs form nanostructures with linear, triangular, and square-planar geometries, and can serve as templates for the growth of clusters of nanoparticles. Further optimization is necessary to improve the disparity in shape, size, and distance between nanoparticles within an assembly.

The realization of growth of metal nanoparticles from a self-assembled molecular template, however, is a step towards generating a variety of tailored geometric metallic structures by using molecular precursors. Assemblies of nanoparticles show promise, for instance, for improved light-attenuating

 © 2004 Wiley-VCH Verlag GmbH & Co. KGaA, Weinheim

pigments (owing to more efficient scattering of UV light compared to conventional dye-based inks[2]) and for sensitive molecular diagnostic devices (owing to the colorimetric change upon binding of ligands[1e,3b]).

Received: October 27, 2003 [Z53161]

Keywords: antibodies · antigens · gold · nanostructures · self-assembly

[1] a) D. V. Goia, E. Matijevic, *New J. Chem.* **1998**, *22*, 1203; b) D. L. Feldheim, C. A. Foss, *Metal Nanoparticles: Synthesis, Characterization, and applications*, Marcel Dekker, New York, **2002**; c) A. Kiriy, S. Minko, G. Gorodyska, M. Stamm, *Nano Lett.* **2002**, *2*, 881; d) T. Scheibel, R. Parthasarathy, G. Sawicki, X. M. Lin, H. Jaeger, S. L. Lindquist, *Proc. Natl. Acad. Sci. USA* **2003**, *100*, 4527; e) A. J. Haes, R. P. Van Duyne, *J. Am. Chem. Soc.* **2002**, *124*, 10596.

[2] K. J. Klabunde, *Nanoscale materials in Chemistry*, Wiley, New York, **2001**.

[3] a) W. P. McConnell, J. P. Novak, L. C. Brousseau, R. R. Fuierer, R. C. Tenent, D. L. Feldheim, *J. Phys. Chem. B* **2000**, *104*, 8925; b) C. A. Mirkin, R. L. Letsinger, R. C. Mucic, J. J. Storhoff, *Nature* **1996**, *382*, 607; c) W. Shenton, S. A. Davis, S. Mann, *Adv. Mater.* **1999**, *11*, 449.

[4] a) Q. Wang, T. Lin, L. Tang, J. E. Johnson, M. G. Finn, *Angew. Chem.* **2002**, *114*, 477; *Angew. Chem. Int. Ed.* **2002**, *41*, 459; b) Q. Wang, T. Lin, J. E. Johnson, M. G. Finn, *Chem. Biol.* **2002**, *9*, 813; c) Q. Wang, E. Kaltgrad, T. Lin, J. E. Johnson, M. G. Finn, *Chem. Biol.* **2002**, *9*, 805; d) K. Keren, M. Krueger, R. Gilad, G. Ben-Yoseph, U. Sivan, E. Braun, *Science* **2002**, *297*, 72; e) C. Joachim, J. K. Gimzewski, A. Aviram, *Nature* **2000**, *408*, 541; f) W. Shenton, D. Pum, U. B. Sleytr, S. Mann, *Nature* **1997**, *389*, 585; g) C. Mao, C. E. Flynn, A. Hayhurst, R. Sweeney, J. Qi, G. Georgiou, B. Iverson, A. M. Belcher, *Proc. Natl. Acad. Sci. USA* **2003**, *100*, 6946; h) C. M. Niemeyer, W. Burger, J. Peplies, *Angew. Chem.* **1998**, *110*, 2391; *Angew. Chem. Int. Ed.* **1998**, *37*, 2265; i) S. Mann, W. Shenton, M. Li, S. Connolly, D. Fitzmaurice, *Adv. Mater.* **2000**, *12*, 147.

[5] A. P. Alivisatos, K. P. Johnsson, X. Peng, T. E. Wilson, C. J. Loweth, M. P. Bruchez, P. G. Schultz, *Nature* **1996**, *382*, 609; Professor Matthew B. Francis, personal communication.

[6] E. Dujardin, S. Mann, *Adv. Mater.* **2002**, *14*, 775.

[7] a) L. C. Brousseau, J. P. Novak, S. M. Marinakos, D. L. Feldheim, *Adv. Mater.* **1999**, *11*, 447; b) J. P. Novak, L. C. Brousseau, F. W. Vance, R. C. Johnson, B. I. Lemon, J. T. Hupp, D. L. Feldheim, *J. Am. Chem. Soc.* **2000**, *122*, 12029; c) J. P. Novak, D. L. Feldheim, *J. Am. Chem. Soc.* **2000**, *122*, 3979.

[8] a) M. Mertig, L. C. Ciacchi, R. Seidel, W. Pompe, A. De Vita, *Nano Lett.* **2002**, *2*, 841; b) S. Minko, A. Kiriy, G. Gorodyska, M. Stamm, *J. Am. Chem. Soc.* **2002**, *124*, 10192.

[9] E. E. Simanek, J. P. Mathias, C. T. Seto, D. Chin, M. Mammen, D. M. Gordon, G. M. Whitesides, *Acc. Chem. Res.* **1995**, *28*, 37.

[10] Green,[11] Valentine,[12] and others[13] described the spontaneous formation of linear and cyclic nanoscale complexes between polyclonal IgGs[14] (or IgEs) and divalent antigens.

[11] a) N. M. Green, *Adv. Immunol.* **1969**, *11*, 1; b) R. C. Valentine, N. M. Green, *J. Mol. Biol.* **1967**, *27*, 615.

[12] a) R. C. Valentine in *Nobel Symposium*, *Vol. 3*, Wiley-Interscience, New York, **1967**, p. 251; b) R. C. Valentine in *Proceedings of the European Regional Conference on Electron Microscopy*, *Vol. 2*, Rome, **1969**, p. 3.

[13] a) M. Mammen, S.-K. Choi, G. M. Whitesides, *Angew. Chem.* **1998**, *110*, 2909; *Angew. Chem. Int. Ed.* **1998**, *37*, 2755; b) B. Baird, B. Goldstein, R. Posner, K. Subramanian, B. Hashemi, D. Holowka, *J. Cell. Biochem.* **1994**, Suppl. 18C, 241; c) M. Dembo, B. Goldstein, A. K. Sobotka, L. M. Lichtenstein, *J. Immunol.* **1978**, *121*, 354; d) J. W. Erickson, R. G. Posner, B. Goldstein, D. Holowka, B. Baird, *Biochemistry* **1991**, *30*, 2357; e) R. G. Posner, J. W. Erickson, D. Holowka, B. Baird, B. Goldstein, *Biochemistry* **1991**, *30*, 2348; f) R. Schweitzerstenner, A. Licht, I. Pecht, *Biophys. J.* **1992**, *63*, 563.

[14] IgGs are proteins that comprise four polypeptide chains joined by disulfide bonds to give a Y-shaped glycoprotein.[15] There are two antigen-binding F_{ab} fragments and one crystallizable F_c fragment, which make up the three arms of the Y in the IgG molecules. The F_{ab} arms join the F_c region at a flexible hinge region; the angle between the two F_{ab} regions can vary from 40 to over 180 degrees;[16] the flexibility at the hinge allows for the generation of several different sizes and shapes of cyclic oligomers of IgGs. The length of the F_{ab} and F_c regions varies from organism to organism, but on average the F_{ab} fragment is about 12 nm long and the F_c fragment is about 11 nm long.[10a,17]

[15] C. A. Janeway, P. Travers, M. Walport, J. D. Capra, *Immunobiology*, 4th ed., Garland, New York, **1999**.

[16] M. Gerstein, A. M. Lesk, C. Chothia, *Biochemistry* **1994**, *33*, 6739.

[17] D. M. Crothers, H. Metzger, *Immunochemistry* **1972**, *9*, 341.

[18] We will report the details of these studies in solution elsewhere. The supporting information includes a representative size-exclusion HPLC chromatogram illustrating the conversion of IgGs to aggregated species.

[19] We separated these aggregates from the non-aggregated protein by FPLC (data not shown). Images of gold nanoparticles grown from a mixture of these purified aggregates appeared indistinguishable from images of particles grown from aggregates of IgGs that were not purified by FPLC.

[20] C. Branden, J. Tooze, *Introduction to Protein Structure*, 2nd ed., Garland, New York, **1999**.

[21] H. W. Morehead, K. W. Talmadge, D. J. O'Shannessy, C. J. Siebert, *J. Chromatogr.* **1991**, *587*, 171.

[22] a) A. Rambourg, C. P. Leblond, *J. Cell Biol.* **1967**, *32*, 27; b) J. J. Bozzola, L. D. Russell, *Electron Microscopy*, 2nd ed., Jones & Bartlett, Boston, **1999**.

[23] Staining and TEM-imaging experiments of IgGs on Si_3N_4 substrates indicate that washing the surfaces in aqueous solutions does not completely remove protein from the substrates.

[24] We believe the difference in the fraction of aggregated IgGs in solution (≈73% of the protein) and the fraction of clusters of nanoparticles grown from the carbohydrates on the IgGs (15 ± 5%) reflects the less than quantitative yield of the chemical reactions that generate the metal nanoparticles—that is, the oxidation of the carbohydrate units, the reduction of silver ions, and the electroless growth of gold.

[25] Adapted from J. Koolman, *Color Atlas of Biochemistry* Thieme, Stuttgart, 1996.

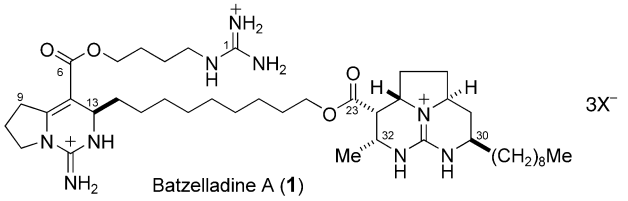
 © 2004 Wiley-VCH Verlag GmbH & Co. KGaA, Weinheim

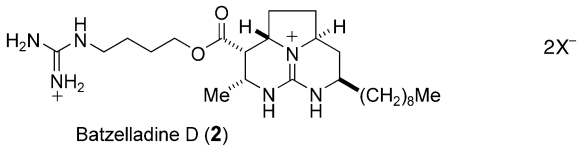
Natural Product Synthesis

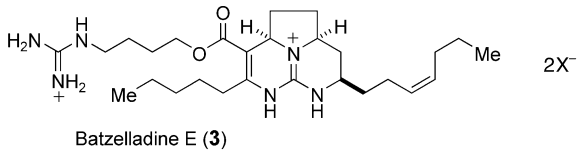
Enantioselective Total Synthesis of Batzelladine A**

*Jun Shimokawa, Koji Shirai, Aya Tanatani, Yuichi Hashimoto, and Kazuo Nagasawa**

Batzelladines A–I are members of a class of polycyclic guanidine alkaloids that were isolated from Bahamian and Jamaican sponges by scientists at SmithKline Beecham in 1995 and 1997.[1,2] The batzelladines are of much interest, as batzelladines A (**1**), B, and D (**2**) inhibit the binding of the

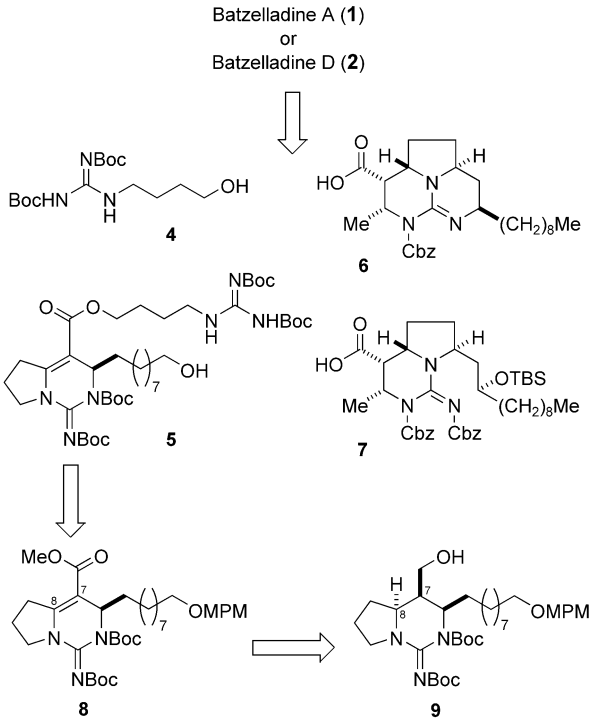






HIV glycoprotein gp120 to the human CD4 receptor,[1a] whereas batzelladines F–I were found to dissociate the protein tyrosine kinase $p56^{lck}$ from CD4.[1b] The unique structures of the batzelladines and their potential clinical importance in AIDS treatment have inspired considerable synthetic attention.[3–11] In 1998, Snider and Chen reported the total synthesis of batzelladine E (**3**) by a biomimetic synthetic route; this was the first synthetic success in this class of molecules.[5b] In 1999 and 2001, Overman and co-workers succeeded in the total synthesis of batzelladines D (**2**) and F, in which a tethered Biginelli reaction was applied effectively as a key step.[7] These syntheses led to structural revisions of batzelladines E (**3**) and F. In the case of batzelladine A (**1**), the absolute configuration was determined recently with the aid of synthetic efforts. The right-hand tricyclic guanidine subunit of **1** has the same structure as that in batzelladine D (**2**), the absolute configuration of which was established by the total synthesis of **2** by Overman and co-workers.[7a] The left-hand bicyclic guanidine subunit of **1** has one stereogenic center at C13. Duron and Gin recently synthesized the left-hand bicyclic guanidine moiety of **1**, which was also obtained by the methanolysis of natural **1**, and determined the absolute stereochemistry at C13 to be *R* by comparing the optical rotation values.[8] As we are interested in the unique structure of the batzelladines and the mechanism through which they modulate protein–protein interactions, we planned to synthesize the batzelladines and their derivatives for potential use as tools in biological studies. Herein, we report an enantioselective total synthesis of batzelladine A (**1**) based upon a strategy involving successive 1,3-dipolar cycloadditions.[11a]

As an approach to the synthesis of batzelladines A (**1**) and D (**2**)and their derivatives, it seemed reasonable to couple the side-chain alcohol **4** or **5** with the tricyclic guanidine carboxylic acid **6** by means of an esterification at the final stage of the synthesis (Scheme 1). However, the tricyclic guanidine carboxylic acid **6** did not undergo esterification or transesterification because of its axially oriented carboxylic acid group, as had already been noted by Snider and Chen, as well as Overman and co-workers, in the synthesis of **3**[5b] and **2**.[7a] In an effort to overcome this problem, we found that the



Scheme 1. Synthetic strategy toward batzelladines A and D. Boc = *tert*-butoxycarbonyl, Cbz = carbobenzyloxy, MPM = 4-methoxyphenylmethyl, TBS = *tert*-butyldimethylsilyl.

[*] J. Shimokawa, K. Shirai, Dr. A. Tanatani, Prof. Y. Hashimoto, Prof. K. Nagasawa
Institute of Molecular and Cellular Biosciences
University of Tokyo
Bunkyo-ku, Tokyo 113-0032 (Japan)
Fax: (+81) 3-5841-8495
E-mail: nagasawa@iam.u-tokyo.ac.jp

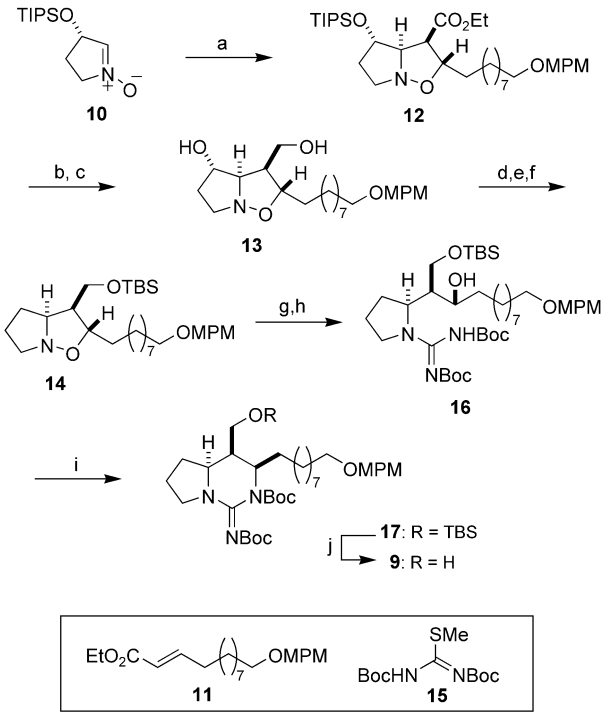
[**] We thank Prof. T. Nakata (Tokyo University of Science) and Dr. H. Koshino (RIKEN) for helpful discussions. This work has been supported by grants from the Pharmacy Research Encouragement Foundation, the Uehara Memorial Foundation, and the Mochida Memorial Foundation for Medical and Pharmaceutical Research.

Supporting information for this article is available on the WWW under http://www.angewandte.org or from the author.

 DOI: 10.1002/anie.200353200 © 2004 Wiley-VCH Verlag GmbH & Co. KGaA, Weinheim

esterification of the bicyclic guanidine carboxylic acid **7** (an analogue of **6**) with the side-chain alcohol **4** proceeded well, and this finding was applied to the synthesis of **2**.[11c] We planned to synthesize batzelladine A (**1**) based upon this strategy (Scheme 1). The left- and right-hand cyclic guanidine subunits **9** and **7** can be synthesized through a 1,3-dipolar cycloaddition strategy, and therefore the introduction of the required double bond at C7–C8 of **9** by means of oxidation was addressed at the outset of the synthesis of **1**.

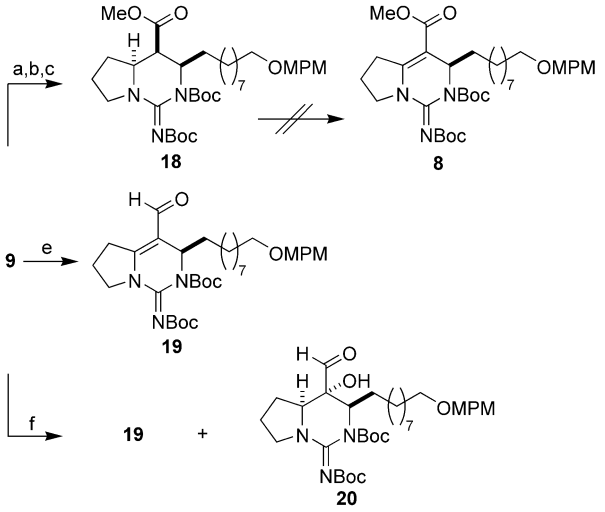
The synthesis of the bicyclic guanidine **9** began with a 1,3-dipolar cycloaddition reaction of the optically active nitrone **10** reported by Goti et al. (Scheme 2).[12] The 1,3-dipolar



Scheme 2. Synthesis of the bicyclic guanidine fragment: a) **11**, toluene, 90 °C; b) $LiAlH_4$, Et_2O, 0 °C; c) CsF, EtOH, 90 °C (59%, three steps); d) TBSCl, pyridine (81%); e) ClC(S)OPh, pyridine, DMAP (58%); f) $n$$Bu_3SnH$, AIBN (94%); g) $Pd(OH)_2$, H_2; h) **15**, $HgCl_2$, Et_3N, DMF (71%, two steps); i) PPh_3, DEAD, toluene (100%); j) TBAF, THF (81%). AIBN = azobisisobutyronitrile, DEAD = diethyl azodicarboxylate, DMAP = 4-dimethylaminopyridine, DMF = *N*,*N*-dimethylformamide, TIPS = triisopropylsilyl.

cycloaddition reaction between **10** and the ester **11** proceeded stereoselectively to give the isoxazolidine **12** as a single diastereomer. The ester group in **12** was reduced with $LiAlH_4$ to give the corresponding alcohol, and subsequent removal of the TIPS group with CsF gave the diol **13** in 59% yield from **10**. Selective protection of the primary alcohol as its TBS ether, followed by deoxygenation of the secondary alcohol at C9 by the Barton–McCombie method gave **14** in 44% yield from **13**. Reductive cleavage of the N–O bond of **14** with hydrogen in the presence of $Pd(OH)_2$, followed by guanidination of the resulting pyrrolidine with bis(Boc)-2-methyl-2-thiopseudourea (**15**) and mercury(II) chloride,[13] afforded the bis(Boc)-protected guanidine **16** in 71% yield from **14**. Cyclization of **16** under the Mitsunobu reaction conditions in the presence of DEAD and triphenylphosphane[14] provided the bicyclic guanidine **17** stereoselectively. Finally, removal of the TBS group with TBAF gave the primary alcohol **9** in 81% yield from **16**.

With the bicyclic guanidine alcohol **9** in hand, we next examined the conversion of **9** into the α,β-unsaturated carbonyl compound **5** through introduction of a double bond at C7–C8. Initially, we envisaged that oxidation of the primary alcohol **9** to the corresponding methyl ester and subsequent oxidation by the Sharpless method with an organoselenium reagent[15] or by the Saegusa–Tsuji method[16] would afford the α,β-unsaturated ester **8**. Thus, the alcohol **9** was oxidized to the corresponding carboxylic acid by means of a Swern oxidation followed by further oxidation with sodium chlorite[17] (Scheme 3). The carboxylic

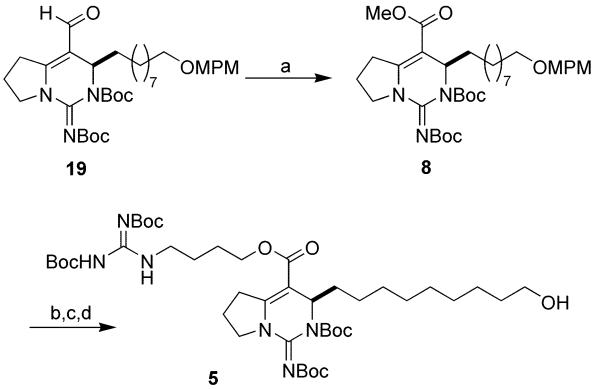


Scheme 3. Oxidation of **9** to **19**: a) $(COCl)_2$, DMSO, Et_3N, CH_2Cl_2; b) $NaClO_2$, NaH_2PO_4, 2-methyl-2-butene, tBuOH/H_2O; c) $TMSCHN_2$, benzene/MeOH (71%, three steps); e) TPAP, NMO, molecular sieves (4 Å), CH_2Cl_2 (47%); f) IBX, DMSO/toluene (**19**: 13%, **20**: 11%). DMSO = dimethyl sulfoxide, IBX = 2-iodoxybenzoic acid, NMO = 4-methylmorpholine *N*-oxide, TMS = trimethylsilyl, TPAP = tetrapropylammonium perruthenate.

acid obtained was treated with (trimethylsilyl)diazomethane[18] to give the methyl ester **18** in 71% overall yield. However, neither subsequent reaction with phenylselenenyl bromide in the presence of LDA nor attempted ketene silyl acetal formation afforded the desired product. We therefore examined direct formation of the α,β-unsaturated aldehyde **19** from the primary alcohol **9** with IBX, a reaction developed by Nicolaou et al.,[19] but only poor conversion into **19** was observed (13% yield), along with formation of the α-hydroxyaldehyde **20** (11% yield). Studies of various oxidation reagents for this conversion led to the interesting finding that TPAP–NMO oxidation of **9** gave **19** in 47% yield with complete regioselectivity. The mechanism and the basis of the selectivity of this reaction are not clear. We are attempting to elucidate the generality and mechanism of this oxidation reaction.[20]

 © 2004 Wiley-VCH Verlag GmbH & Co. KGaA, Weinheim

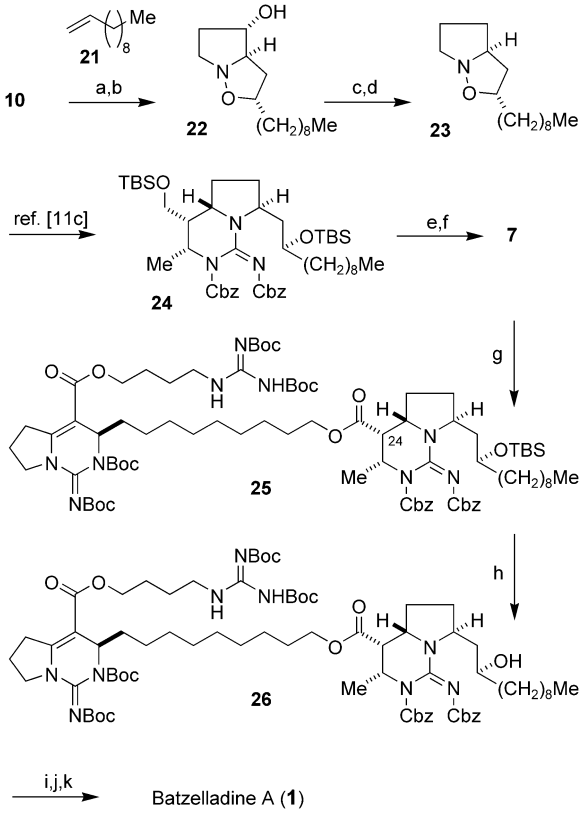
The aldehyde **19** was further oxidized with sodium chlorite to the corresponding carboxylic acid, and then treatment with (trimethylsilyl)diazomethane gave the methyl ester **8** in 86% yield (based on recovered aldehyde; Scheme 4). Hydrolysis of the methyl ester **8** with *n*PrSLi and subsequent condensation with the guanidine alcohol **4** provided the desired ester in 54% yield from **8**. Finally, the MPM group was removed with DDQ to give the alcohol **5** in 66% yield.



Scheme 4. Synthesis of **5**: a) $NaClO_2$, NaH_2PO_4, 2-methyl-2-butene, *t*BuOH/H_2O, $TMSCHN_2$ (53%; 86% based on recovered **19**); b) *n*PrSLi, HMPA; c) **4**, BOPCl, Et_3N, CH_2Cl_2 (54%, two steps); d) DDQ, CH_2Cl_2/H_2O (66%). BOP = bis(2-oxo-3-oxazolidinyl)phosphinic chloride, DDQ = 2,3-dichloro-5,6-dicyano-1,4-benzoquinone, HMPA = hexamethyl phosphoramide.

The synthesis of the optically active bicyclic guanidine carboxylic acid **7**, a precursor of the right-hand tricyclic guanidine, and the final stage of the synthesis of **1** were performed as illustrated in Scheme 5. Three components, the chiral nitrone **10**, 1-undecene (**21**), and methyl crotonate, were combined in successive 1,3-dipolar cycloadditions as reported previously to give the TBS ether **24**, which was then oxidized to give **7** in optically pure form.[11c] Treatment of the carboxylic acid **7** with the bicyclic guanidine alcohol **5** in the presence of EDCI and DMAP at room temperature gave the desired ester **25**, but epimerization at C24 occurred under these conditions to give an approximately 1:1 mixture of diastereomers. When the esterification reaction was performed at 0°C we found that the epimerization was suppressed and obtained **25** in 60% yield. The masked secondary alcohol functionality in **25** was deprotected with HF–pyridine to furnish **26** in 80% yield. The Cbz protecting groups were then cleaved with hydrogen in the presence of Pd/C, and cyclization of the resulting bicyclic guanidine to the desired tricyclic guanidine was carried out under the Mitsunobu reaction conditions. Finally, the four Boc groups were cleaved with TFA. The crude mixture obtained was purified by HPLC (PEGASIL-ODS, eluant: 50% MeCN/H_2O, 0.1% TFA) to give batzelladine A (**1**) as the trifluoroacetate salt in 24% yield from **26**. All of the data for synthetic **1** were in good agreement with reported values.[21]

In summary, the first enantioselective total synthesis of batzelladine A (**1**) has been described. A strategy of successive 1,3-dipolar cycloadditions was a key feature of the synthesis. During the course of these studies we discovered that the primary alcohol **9** could be converted into the α,β-unsaturated aldehyde **19** by reaction with TPAP/NMO, and this novel oxidation was applied effectively in the synthesis of the left-hand bicyclic guanidine fragment of **1**. The synthesis described should make it possible to prepare substantial amounts of batzelladines and their derivatives, and should thus aid efforts toward the elucidation of the mechanism through which these relatively small molecules modulate protein–protein interactions.



Scheme 5. Synthesis of the precursor **7** to the tricyclic guanidine subunit and conversion into **1**: a) 1-undecene (**21**), toluene, 90°C (75%); b) CsF, EtOH, 90°C (98%); c) ClC(S)OPh, pyridine, DMAP; d) nBu_3SnH, AIBN (51%, two steps); e) TBAF, THF (97%); f) Jones reagent, acetone; g) **5**, EDCI, DMAP, CH_2Cl_2 (60%, two steps); h) HF–pyridine, THF (80%); i) Pd/C, H_2; j) PPh_3, DEAD, toluene; k) TFA/CH_2Cl_2 (24%, three steps). EDCI = 3-(3-dimethylaminopropyl)-1-ethylcarbodiimide, TBAF = tetrabutylammonium fluoride.

Received: October 30, 2003 [Z53200]

Keywords: alkaloids · cycloaddition · natural products · oxidation · total synthesis

[1] a) A. D. Patil, N. V. Kumar, W. C. Kokke, M. F. Bean, A. J. Freyer, C. De Brosse, S. Mai, A. Truneh, D. J. Faulkner, B. Carté, A. L. Breen, R. P. Hertzberg, R. K. Johnson, J. W. Westley, B. C. M. Potts, *J. Org. Chem.* **1995**, *60*, 1182; b) A. D. Patil, A. J. Freyer, P. B. Taylor, B. Carté, G. Zuber, R. K. Johnson, D. J. Faulkner, *J. Org. Chem.* **1997**, *62*, 1814.

 © 2004 Wiley-VCH Verlag GmbH & Co. KGaA, Weinheim

[2] The identity of the source of these compounds was revised: a) J. C. Braekman, D. Daloze, R. Tavares, E. Hadju, R. W. M. Van Soest, *J. Nat. Prod.* **2000**, *63*, 193; b) R. W. M. Van Soest, J. C. Braekman, D. J. Faulkner, E. Hadju, M. K. Harper, J. Vacelet, *Bull. Inst. R. Sci. Nat. Belg.* **1996**, *66*, 89.
[3] A. V. Rama Rao, M. K. Gurjar, J. Vasudevan, *J. Chem. Soc. Chem. Commun.* **1995**, 1369.
[4] S. Louwrier, M. Ostendorf, A. Tuynman, H. Hiemstra, *Tetrahedron Lett.* **1996**, *37*, 905.
[5] a) B. B. Snider, J. Chen, A. D. Patil, A. J. Freyer, *Tetrahedron Lett.* **1996**, *37*, 6977; b) B. B. Snider, J. Chen, *Tetrahedron Lett.* **1998**, *39*, 5697; c) B. B. Snider, M. V. Busuyek, *J. Nat. Prod.* **1999**, *62*, 1707.
[6] a) G. P. Black, P. J. Murphy, N. D. A. Walshe, *Tetrahedron* **1998**, *54*, 9481; b) G. P. Black, P. J. Murphy, A. Thornhill, N. D. A. Walshe, C. Zanetti, *Tetrahedron* **1999**, *55*, 6547.
[7] a) F. Cohen, L. E. Overman, S. K. L. Sakata, *Org. Lett.* **1999**, *1*, 2169; b) F. Cohen, L. E. Overman, *J. Am. Chem. Soc.* **2001**, *123*, 10782; c) A. S. Franklin, S. K. Ly, G. H. Mackin, L. E. Overman, A. J. Shaka, *J. Org. Chem.* **1999**, *64*, 1512; d) A. I. McDonald, L. E. Overman, *J. Org. Chem.* **1999**, *64*, 1520; e) F. Cohen, S. K. Collins, L. E. Overman, *Org. Lett.* **2003**, *5*, 4485.
[8] S. G. Duron, D. Y. Gin, *Org. Lett.* **2001**, *3*, 1551.
[9] P. A. Evans, T. Manangan, *Tetrahedron Lett.* **2001**, *42*, 6637.
[10] M. C. Elliot, M. S. Long, *Tetrahedron Lett.* **2002**, *43*, 9191.
[11] a) K. Nagasawa, H. Koshino, T. Nakata, *Tetrahedron Lett.* **2001**, *42*, 4155; b) K. Nagasawa, T. Ishiwata, Y. Hashimoto, T. Nakata, *Tetrahedron Lett.* **2002**, *43*, 6383; c) T. Ishiwata, T. Hino, H. Koshino, Y. Hashimoto, T. Nakata, K. Nagasawa, *Org. Lett.* **2002**, *4*, 2921.
[12] A. Goti, M. Cacciarini, F. Cardona, A. Brandi, *Tetrahedron Lett.* **1999**, *40*, 2853.
[13] a) K. S. Kim, L. Qian, *Tetrahedron Lett.* **1993**, *34*, 7677; b) E. J. Iwanowicz, M. A. Poss, J. Lin, *Synth. Commun.* **1993**, *23*, 1443.
[14] D. S. Dodd, A. P. Kozikowski, *Tetrahedron Lett.* **1994**, *35*, 977.
[15] K. B. Sharpless, R. F. Lauer, A. Y. Teranishi, *J. Am. Chem. Soc.* **1973**, *95*, 6137.
[16] a) Y. Ito, T. Hirao, T. Saegusa, *J. Org. Chem.* **1978**, *43*, 1011; b) J. Tsuji, I. Minani, I. Shimizu, *Tetrahedron Lett.* **1983**, *24*, 5635; c) I. Minani, K. Takahashi, I. Shimizu, T. Kimura, J. Tsuji, *Tetrahedron* **1986**, *42*, 2971; d) J. Tsuji, K. Takahashi, I. Minani, I. Shimizu, *Tetrahedron Lett.* **1984**, *25*, 4783.
[17] a) G. A. Kraus, M. J. Taschner, *J. Org. Chem.* **1980**, *45*, 1175; b) G. A. Kraus, B. Roth, *J. Org. Chem.* **1980**, *45*, 4825; c) B. O. Lindgren, T. Nilsson, *Acta Chem. Scand.* **1973**, *27*, 888.
[18] N. Hashimoto, T. Aoyama, T. Shioiri, *Chem. Pharm. Bull.* **1981**, *29*, 1475.
[19] K. C. Nicolaou, Y.-L. Zhong, P. S. Baran, *J. Am. Chem. Soc.* **2000**, *122*, 7596.
[20] We currently believe the mechanism of this reaction to involve iminium formation by oxidation of the guanidine nitrogen atom at the ring junction, followed by isomerization to form the α,β-unsaturated aldehyde.
[21] Spectral data for synthetic **1**: $[\alpha]_D^{25} = +4.29$ ($c = 0.25$, MeOH) (lit:[1a] $[\alpha]_D^{25} = +8.9$ ($c = 2.3$, MeOH)); IR (neat): $\tilde{\nu} = 2925, 2854, 1732, 1697, 1683, 1648, 1637, 1558, 1347, 1092\ cm^{-1}$; ^1H NMR (500 MHz, CD_3OD): $\delta = 4.39$ (t, $J = 6.1$ Hz, 1H), 4.21 (t, $J = 6.4$ Hz, 2H), 4.13 (t, $J = 6.7$ Hz, 2H), 3.93 (m, 1H), 3.83 (m, 2H), 3.66 (m, 1H), 3.52 (m, 1H), 3.32 (m, 1H), 3.22 (t, $J = 7.3$ Hz, 2H), 3.12 (dd, $J = 4.6, 3.5$ Hz, 1H), 2.98 (m, 1H), 2.35 (m, 1H), 2.28–2.17 (m, 3H), 2.10 (m, 1H), 1.76 (m, 2H), 1.72–1.52 (m, 9H), 1.48–1.23 (m, 29H), 1.27 (t, $J = 6.7$ Hz, 3H), 0.89 ppm (t, $J = 6.7$ Hz, 3H); ^{13}C NMR (125 MHz, CD_3OD): $\delta = 170.7, 166.2, 158.7, 153.1, 152.7, 151.5, 103.3, 66.0, 65.1, 57.7, 57.3, 53.2, 51.2, 49.9, 48.8, 45.6, 42.0, 37.5, 36.9, 34.2, 33.0, 31.9, 31.4, 29.7, 29.3, 27.0, 26.6, 26.2, 25.2, 23.7, 22.9, 18.4, 14.4$ ppm; HRMS (FAB, MH^+): calcd for $C_{42}H_{74}N_9O_4$: 768.5864, found: 768.5866.

 © 2004 Wiley-VCH Verlag GmbH & Co. KGaA, Weinheim

Drug Design

Dimeric Aminoglycosides as Antibiotics**

Fabio Agnelli, Steven J. Sucheck, Kenneth A. Marby, David Rabuka, Su-Lan Yao, Pamela S. Sears, Fu-Sen Liang, and Chi-Huey Wong**

Aminoglycosides are an important class of natural products with antimicrobial activity against Gram-positive and Gram-negative bacteria.[1] They have important clinical applications in cases of opportunistic infections accompanying AIDS, cystic fibrosis, and cancer. They are primarily used against infections caused by Gram-negative bacteria, particularly *Pseudomonas aeruginosa*, which are the leading cause of morbidity and mortality in patients having cystic fibrosis (CF). However, the rapid emergence of aminoglycoside-resistant bacterial strains is limiting their efficacy and making the discovery of structurally novel and more potent classes of semisynthetic antibiotics a pressing necessity.[2]

Aminoglycosides exert their antibacterial action by selectively binding to the prokaryotic ribosome, and thereby impeding the synthesis of bacterial proteins.[3] In particular, 2-deoxystreptamine aminoglycosides (Figure 1) are known to selectively bind to the decoding A site on the 16S subunit of the ribosomal RNA, causing inhibition of translation and thus misreading of the genetic code.[4–10]

Structural studies modeling the interaction between neomycin-class aminoglycosides and the 16S A site of *E. coli* showed that multiple contacts occur between the major groove of the RNA and rings I and II of the antibiotic.[11–15] This conserved pseudodisaccharide motif is the essential pharmacophore responsible for most of the specificity of these interactions, while the rest of the molecule has a less well-defined role. Using surface plasmon resonance (SPR) and an immobilized 27-mer RNA construct (AS-wt), we discovered that neamine (the pseudodisaccharide corresponding to rings I and II of neomycin B, Figure 1) binds the oligonucleotide in a 2:1 stoichiometry, with a K_d of about 10 μM at each binding site. Relying on a favorable divalent interaction with the RNA target, we then constructed

[*] Dr. S. J. Sucheck, K. A. Marby, D. Rabuka, Dr. S.-L. Yao, Dr. P. S. Sears
Optimer Pharmaceuticals, Inc.
10110 Sorrento Valley Road, Suite C
San Diego, CA 92121 (USA)
Fax: (+1) 858-909-0737
E-mail: ssucheck@optimerpharma.com.
Dr. F. Agnelli, F.-S. Liang, Prof. C.-H. Wong
Department of Chemistry and Skaggs Institute for Chemical Biology
The Scripps Research Institute
10550 North Torrey Pines Road
La Jolla, CA 92037 (USA)
Fax: (+1) 858-784-2409
E-mail: wong@scripps.edu

[**] Supported by the NIH (grants GM 58439 to C.-H.W. and SBIR 1 R43 AI056617-01 to S.J.S.).

Supporting information for this article is available on the WWW under http://www.angewandte.org or from the author.

 © 2004 Wiley-VCH Verlag GmbH & Co. KGaA, Weinheim DOI: 10.1002/anie.200353225

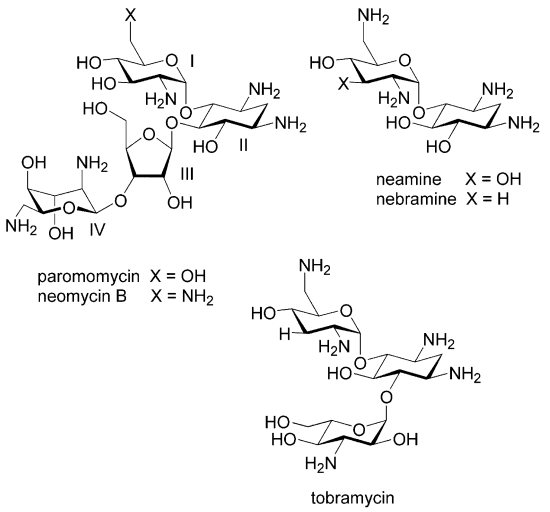


Figure 1. Structures of some representative aminoglycoside antibiotics of the 2-deoxystreptamine class.

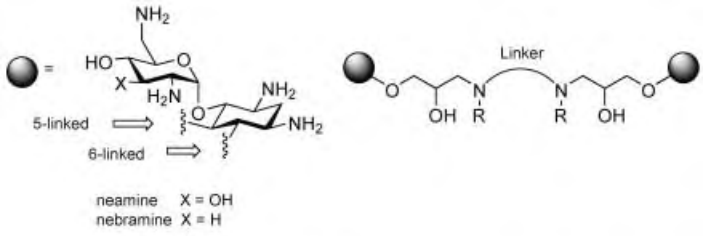
neamine dimers. It was determined that **1** (5-linked with a $(CH_2)_4$ tether) binds to AS-wt with a 1:1 stoichiometry, displaying a K_d of about 40 nM (Figure 2).[16]

Although this binding affinity is better than that of neomycin B, it is still about 250 times lower than the approximate theoretical value.[17] Since no direct structural information about the details of the divalent interaction is available, a rigorous rational-design approach was not possible. In order to improve the affinity of our dimers for RNA, we focused on three possible points of diversity: ring I of the pseudodisaccharide, the linker attachment points, and the linking domain. RNA affinity and antibiotic activity were monitored while structural modifications were introduced into compound **1** without modifying the tether length. At the same time the relative distance between the two neamine cores was systematically probed by using "unobtrusive" polyglycol tethers between 9 and 14 atoms in length, with the expectation that the activity would reach a maximum at the optimal distance between the two sites.

Compounds **5** and **9** were both prepared by an extension of the previously reported procedure,[16] starting from perazido perbenzyl derivatives of neamine and nebramine, respectively (see the Supporting Information for the experimental details). Compound **15** was derived from tobramycin (X = H, Figure 2) but displays a 4,5- (neomycin-type) linking pattern. In this case, after the diazo-transfer reaction, the α-D-glucopyranosyl bond of perazido tobramycin was cleaved by reaction with refluxing 1M H_2SO_4 in methanol (Scheme 1). The perazido nebramine so obtained was dissolved in 1:1 mixture of toluene and acetonitrile, placed on a rotary evaporator, and allowed to stir at 50 °C under reduced pressure with cyclohexanone dimethoxy ketal, in the presence of a catalytic amount of *p*-toluenesulfonic acid, to afford **10**. Subsequent benzylation of the free hydroxy group at C4′ and hydrolysis of the ketal afforded diol **11**. Treatment of the diol with tributyltin oxide followed by alkylation with BOMCl selectively freed the hydroxy group at C5′ for further manipulation. Compound **12** was then alkylated with (2*R*)-(−)-glycidyl tosylate, followed by treatment with 0.5 equivalents of *N*,*N*′-dibenzyl-1,4-diaminobutane. Staudinger reduction and catalytic hydrogenation finally gave deprotected dimer **15**.

The influence of the length and hydrophilicity of the linker was assessed by preparing two series of compounds: one with C_2-symmetric hydrophilic polyglycol tethers and the other with hydrophobic polymethylene tethers, as shown in Figure 3. The polyglycol linkers were obtained starting from the corresponding diallyl ethers, either by ozonolysis/borohydride reduction or hydroboration/oxidation reaction sequences, followed by standard tosylation conditions. The remaining linkers **17c** and **17f** were prepared by tosylation of commercially available tetra- and pentaethylene glycols, respectively. When a solution of the ditosylates **17** and two equivalents of perazido perbenzyl neamine **2** in DMF was treated with an excess of NaH, the reaction smoothly proceeded to afford protected dimers **18a–f** (Scheme 2). Surprisingly, when the corresponding bromides, iodides, and triflates were used, very sluggish reactions ensued. The order of addition of the reagents also proved to be crucial: preformation of the neamine alkoxide, followed by slow addition of the electrophile resulted in a complex mixture of products. A two-step catalytic hydrogenation finally afforded the deprotected dimers **19a–f** in 51–72% yields.[18] The more hydrophobic compounds **19g** and **19h** were obtained by similar routes, starting from commercial 1,10-decenediol and 1,12-dodecenediol, respectively.

When the series of polyglycol dimers **19a–f** was tested by means of SPR against immobilized AS-wt RNA, binding constants in the 1–8 μM range were



5-Linked Dimers

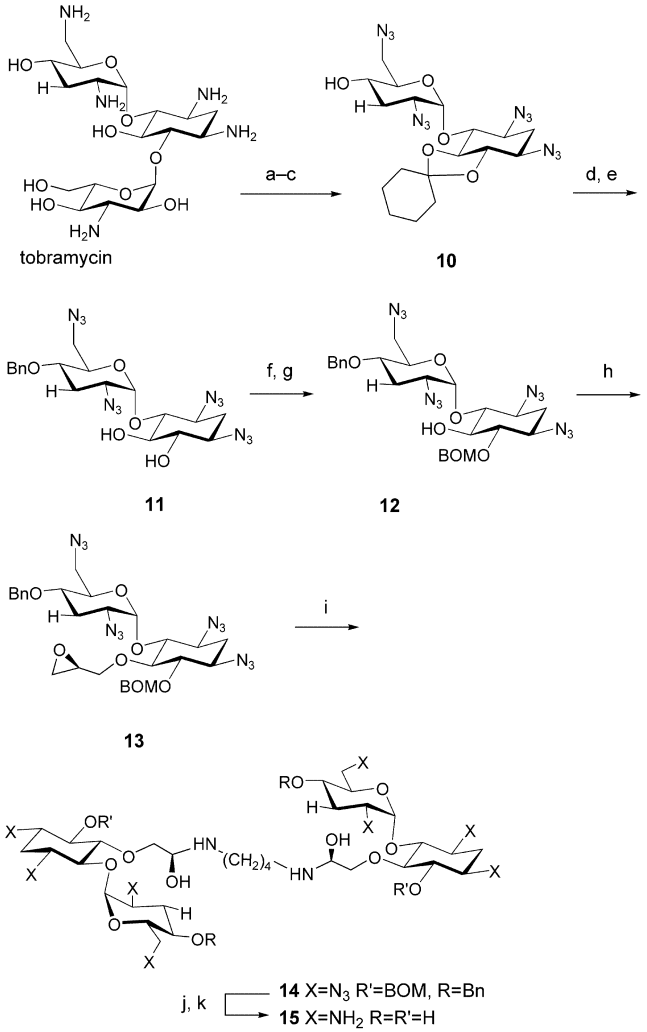
	Linker	X	R	K_d (nM)	MIC (μM) *S. aureus* ATCC 29213	MIC (μM) *E. coli* ATCC 25922	MIC (μM) *P. aeruginosa* ATCC 27853
1	$(CH_2)_4$	OH	CH_3	42	1.1	4.5	9
5	$(CH_2)_4$	OH	H	141	1.2	4.7	4.7
15	$(CH_2)_4$	H	H	166	2.5	20	5

6-Linked Dimers

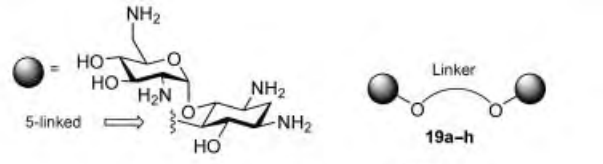
	Linker	X	R	K_d (nM)	MIC (μM) *S. aureus* ATCC 29213	MIC (μM) *E. coli* ATCC 25922	MIC (μM) *P. aeruginosa* ATCC 27853
9	$(CH_2)_4$	H	H	148	0.6	4.9	2.5

Figure 2. Structures, binding constants (K_d), and minimum inhibitory concentrations (MIC) for the neamine and nebramine dimers.

 © 2004 Wiley-VCH Verlag GmbH & Co. KGaA, Weinheim

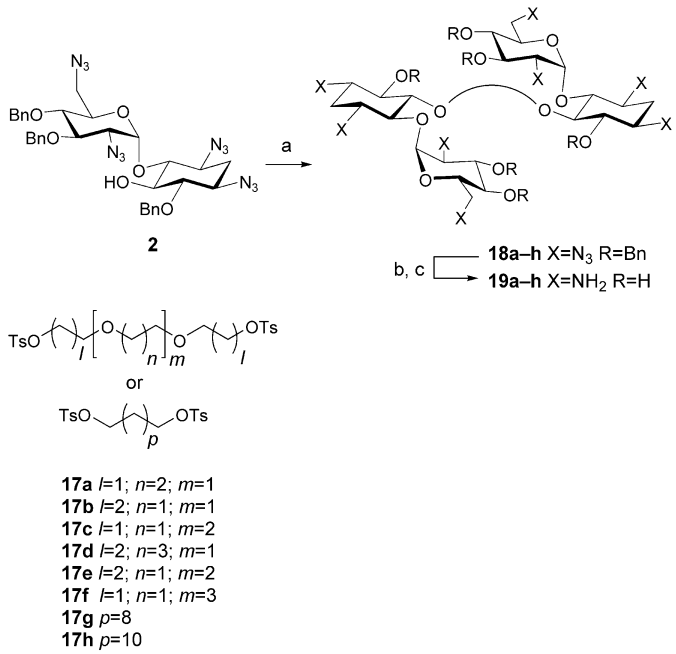


Scheme 1. Reagents and conditions: a) TfN_3, $CuSO_4$, TEA, MeOH, CH_2Cl_2, H_2O; b) H_2SO_4, MeOH, reflux; c) cyclohexanone dimethyl ketal, *p*TsOH, PhMe, MeCN, 50 °C, 20 mm Hg; d) BnBr, NaH, DMF; e) HCl, MeOH; f) SnO_2, PhMe, reflux; g) BOMCl, Bu_4NI; h) (*R*)-(−)-glycidyl tosylate, NaH, DMF; i) *N*,*N*′-dibenzyl-1,4-diaminobutane, EtOH, 70–85 °C; j) PMe_3, NH_4OH, H_2O, THF; k) H_2, $Pd(OH)_2/C$, H_2O/AcOH. BOMCl = benzyloxymethyl chloride, DMF = dimethylformamide, *p*TsOH = *p*-toluenesulfonic acid, TEA = triethylamine, Tf = trifluorosulfonyl.



	Linker	K_d (μM)	MIC (μM) *S. aureus* ATCC 27853	*E. coli* ATCC 25922	*P. aeruginosa* ATCC 27853
19a	$(CH_2)_2O(CH_2)_3O(CH_2)_2$	1.1	31	125	>250
19b	$(CH_2)_3O(CH_2)_2O(CH_2)_3$	3.6	125	>250	>250
19c	$(CH_2)_2[O(CH_2)_2]_2O(CH_2)_2$	1.8	62.5	>250	>250
19d	$(CH_2)_3O(CH_2)_4O(CH_2)_3$	3.3	>250	>250	>250
19e	$(CH_2)_3[O(CH_2)_2]_2O(CH_2)_3$	6.0	>250	>250	>250
19f	$(CH_2)_2[O(CH_2)_2]_3O(CH_2)_2$	1.4	62.5	>250	>250
19g	$(CH_2)_{10}$	5.3	>250	>250	>250
19h	$(CH_2)_{12}$	7.7	>250	>250	>250

Figure 3. Structures, binding constants (K_d), and minimum inhibitory concentrations (MIC) for neamine dimers with hydrophylic (**19a**–**f**) and hydrophobic (**19g**,**h**) tethers of increasing length. No obvious correlation is apparent between tether length and binding affinity.



Scheme 2. Reagents and conditions: a) **17a**–**h** (0.6 equiv), NaH, DMF; b) H_2, $Pd(OH)_2/C$, THF, MeOH; c) H_2, $Pd(OH)_2/C$, aq HCl (1 equiv), MeOH, H_2O.

found, with no obvious dependence of K_d on tether length (Figure 3). The antimicrobial activity was tested versus three standard, antibiotic-sensitive strains: *Staphylococcus aureus* (ATCC 29213), *Escherichia coli* (ATCC 25922), and *Pseudomonas aeruginosa* (ATCC 27853). The activity of the compounds was also weak, in some cases similar to that of neamine, but generally weakening with increasing tether length. A possible explanation for these results might reside in the high hydrophilicity of the linker. In order to test this hypothesis, two representative tether lengths (10 and 12 atoms) were chosen, and the more hydrophobic dimers **19g** and **19h** were synthesized. When tested against AS-wt RNA, they displayed K_d values and activities analogous to those of their polyether-linked counterparts.

The diaminobutane-linked dimers shown in Figure 2 possessed significant affinity and antimicrobial activity, and all displayed a binding stoichiometry of 1:1 for the RNA–antibiotic complex. Surprisingly, compound **5**, lacking the two *N*-methyl groups in the tether with respect to **1**, displayed slightly lower affinities and activities (about threefold) than its predecessor. These data might suggest that this additional hydrogen-bond-donating capability is not a fundamental

 © 2004 Wiley-VCH Verlag GmbH & Co. KGaA, Weinheim

feature for binding and that the basicity of the two nitrogen atoms might play a role in determining such properties.

The K_d values of the two nebramine-derived dimers **9** and **15** were comparable to those of the neamine-derived compounds (in the 150 nM range), showing very little contribution of the 3′-hydroxy group to binding. The position of the anchor points for the two dimers (4,6 tobramycin-like for **9** and 4,5 neomycin-like for **15**) seems to play no significant role in the RNA recognition. In spite of these similarities, the antimicrobial activity for the two compounds differed by a factor of four against *E. coli*. These findings, and in particular direct comparison of compounds **1**, **5**, **15**, **19d**, and **19h**, show that the contribution of the linker to binding cannot be neglected and that a more subtle balance of interactions governs the binding affinities of these small ligands.

The antimicrobial activity of the diaminobutane-linked dimers was further investigated against different panels of aminoglycoside-sensitive and -resistant *P. aeruginosa* strains obtained from CF clinical isolates. The neamine-derived compounds **1** and **5** and the nebramine-derived dimer **9** possess activity levels comparable to (and in some cases greater than) tobramycin, which is considered the current gold standard for treatment of CF infections (Table 1). A very common complication in CF-related *P. aeruginosa* infections is biofilm formation. Interestingly, when tested against a panel of biofilm-producing *P. aeruginosa* strains from CF isolates, the tobramycin-derived compound **15** was revealed to be uniquely effective and in many cases more potent than tobramycin itself (Table 2).

Table 1: MIC values [μg mL^{-1}] of tobramycin and compounds **1** and **5** against *S. aureus* ATCC 33591 (MRSA) and *P. aeruginosa* clinical isolates.

Organism	Resistance	Tobramycin	1	5
S. aureus ATCC 33591 (MRSA)	resistant	>64	16	16
P. aeruginosa (strain 034)[a]	sensitive	8	8	8
P. aeruginosa (strain 609)[a]	resistant	128	8	4
P. aeruginosa (strain 663)[a]	resistant	128	8	8
P. aeruginosa (PAE_NUH01)[b]	resistant	>200	12.5	6.3
P. aeruginosa (PAE_NUH02)[b]	resistant	50	6.3	6.3
P. aeruginosa (PAE_NUH03)[b]	resistant	50	6.3	6.3
P. aeruginosa (PAE_NUH04)[b]	resistant	100	6.3	3.1
P. aeruginosa (PAE_NUH05)[b]	resistant	100	6.3	3.1
P. aeruginosa (PAE_NUH06)[b]	resistant	100	12.5	6.3

[a] Strains obtained from the Foothills Medical Centre, Calgary, AB, Canada. [b] Strains obtained from National University Hospital, National University of Singapore.

Further SPR analysis of **1** and **5** interacting with other RNA targets of interest showed that both compounds are more active than neomycin B against the 16S A site (1.5- to 5-fold, Table 3). A possible explanation of this finding might reside in the increased positive charge density that these molecules bear with respect to neomycin B. However, a generally significant increase in selectivity for the 16S A site for compound **1** (and, to a lesser extent, compound **5**) reveals that more subtle factors govern the specificity of the aminoglycoside–RNA interaction. Indeed, design of more potent and selective binders remains the major challenge for future research in the field of aminoglycoside antibiotics.

Table 2: MIC [μg mL^{-1}] of compounds **9** and **15** against a panel of biofilm-producing *P. aeruginosa* from CF clinical isolates.

P. aeruginosa	Resistance	Tobramycin	9	15
27 EN	sensitive	4	2	1
64 EN	sensitive	8	32	4
24 EN	sensitive	4	64	2
25 EN	sensitive	8	>64	4
90 EM	resistant	64	>64	4
98 EM	resistant	16	4	0.5
89 EM	resistant	64	>64	4

Table 3: K_d [μM] and selectivity profile of neomycin B and compounds **1** and **5** for the 16S A site (expressed as the ratio of the binding constants, in parentheses) in RNAs of interest.

RNA[a]	Neomycin B	1	5
16S A site	0.2	0.04	0.14
Bcr-Abl	2 (10)	0.55 (14)	0.46 (3)
PAX3-FKHR	0.8 (4)	1.1 (27)	1.4 (10)
HIV-FSS	1.6 (8)	1.1 (27)	1.9 (13)
HIV-PAS mRNA	2 (10)	1.2 (30)	1.7 (12)
HCV-IIb IRES	2.9 (14)	0.58 (14)	0.83 (6)
HCV-IIId IRES	2.9 (14)	1.3 (32)	1.8 (13)
E. coli TG mRNA	2.8 (14)	1.6 (40)	2.7 (19)

[a] Arbitrary abbreviations used. HIV-FSS: HIV frameshift signal; HIV-PAS: HIV protease active site mRNA; HCV-IIb IRES: HCV IRES domain IIb; HCV-IIId IRES: HCV IRES domain IIId; *E. coli* TG: *E. coli* transglycosilase mRNA. See the Supporting Information for RNA sequences.

In conclusion, the neamine and nebramine dimers synthesized in this study represent a new class of aminoglycoside antibiotics that are active against several aminoglycoside-resistant bacterial strains and may show promise for the treatment of *P. aeruginosa* infections. In order to fully elucidate the structural details of the dimeric interaction and further improve the affinity, potency, and specificity of newly designed aminoglycoside antibiotics, additional studies are currently underway.

Received: November 3, 2003 [Z53225]

Keywords: aminoglycosides · antibiotics · carbohydrates · drug design · RNA recognition

[1] M. K. Kim, D. P. Nicolaou, *Infect. Dis. Ther.* **2002**, *28*, 125.
[2] For recent work on aminoglycosides see: B. Llano-Sotelo, E. F. Azucena, L. P. Kotra, S. Mobashery, C. S. Chow, *Chem. Biol.*

 © 2004 Wiley-VCH Verlag GmbH & Co. KGaA, Weinheim

2002, *9*, 455; J. Haddad, S. Vakulenko, S. Mobashery, *J. Am. Chem. Soc.* **1999**, *121*, 11922; J. Haddad, L. P. Kotra, B. Llano-Sotelo, C. Kim, E. F. Azucena, M. Liu, S. B. Vakulenko, C. S. Chow, S. Mobashery, *J. Am. Chem. Soc.* **2002**, *124*, 3229; S. Hanessian, M. Tremblay, A. Kornienko, N. Moitessier, *Tetrahedron* **2001**, *57*, 3255; S. Hanessian, M. Tremblay, E. E. Swayze, *Tetrahedron* **2003**, *59*, 983; S. Hanessian, A. Kornienko, E. E. Swayze, *Tetrahedron* **2003**, *59*, 995; N. W. Luedtke, Q. Liu, Y. Tor, *Biochemistry* **2003**, *42*, 1391; K. Michael, H. Wang, Y. Tor, *Bioorg. Med. Chem.* **1999**, *7*, 1951; S. R. Kirk, Y. Tor, *Bioorg. Med. Chem.* **1999**, *7*, 1979; S. R. Kirk, N. W. Luedtke, Y. Tor, *J. Am. Chem. Soc.* **2000**, *122*, 980; N. W. Luedtke, T. J. Baker, M. Goodman, Y. Tor, *J. Am. Chem. Soc.* **2000**, *122*, 12035; Y. Wang, R. R. Rando, *Chem. Biol.* **1995**, *2*, 281H. Wang, Y. Tor, *Angew. Chem.* **1998**, *110*, 117; *Angew. Chem. Int. Ed.* **1998**, *37*, 109.

[3] H. Umezawa, I. R. Hooper, *Aminoglycoside Antibiotics*, Springer, New York, **1982**.

[4] J. H. Cate, M. M. Yusupov, G. Z. Yusupova, T. N. Earnest, H. F. Noller, *Science* **1999**, *285*, 2095.

[5] W. M. Clemons, J. L. C. May, B. T. Wimberly, J. P. McCutcheon, M. S. Capel, V. Ramakrishnan, *Nature* **1999**, *400*, 833.

[6] D. Moazed, H. F. Noller, *Nature* **1987**, *327*, 389.

[7] P. Nissen, J. Hansen, N. Ban, P. B. Moore, T. A. Steitz, *Science* **2000**, *289*, 920.

[8] F. Schlunzen, R. Zarivach, J. Harms, A. Bashan, A. Tocilj, R. Albrecht, A. Yonath, F. Franceschi, *Nature* **2001**, *413*, 814.

[9] B. T. Wimberly, D. E. Brodersen, W. M. Clemons, R. J. Morgan-Warren, A. P. Carter, C. Vonrhein, T. Hartsch, V. Ramakrishnan, *Nature* **2000**, *407*, 327.

[10] M. M. Yusupov, G. Z. Yusupova, A. Baucom, K. Lieberman, T. N. Earnest, J. H. D. Cate, H. F. Noller, *Science* **2001**, *292*, 883.

[11] D. Fourmy, M. I. Recht, S. C. Blanchard, J. D. Puglisi, *Science* **1996**, *274*, 1367.

[12] D. Fourmy, M. I. Recht, J. Puglisi, *J. Mol. Biol.* **1998**, *277*, 347.

[13] S. R. Lynch, R. L. Gonzalez, J. D. Puglisi, *Structure* **2003**, *11*, 43.

[14] Q. Vicens, E. Westhof, *Chem. Biol.* **2002**, *9*, 747.

[15] Q. Vicens, E. Westhof, *Structure* **2002**, *10*, 647.

[16] Other dimers reported in the literature were based on a monomer with 1:1 stoichiometric binding, thus only slightly improving the affinity. See ref. [2] and S. J. Sucheck, A. L. Wong, K. M. Koeller, D. D. Boehr, K. A. Draker, P. Sears, G. D. Wright, C. H. Wong, *J. Am. Chem. Soc.* **2000**, *122*, 5230.

[17] Assuming independent binding events for each site, the total binding energy for a dimerically linked molecule ΔG_T should be the sum of the binding energies for each monomer, ΔG_1 and ΔG_2, plus the contribution of the linker ΔG_L. ΔG_L includes both the free energy of the linker interaction with the RNA and also a term that accounts for the reduced entropy change of binding due to the tethering of the monomers. If the effect of the linker is ignored in a first approximation, the resulting K_d should therefore be in the picomolar range.

[18] A single step deprotection using 20% $Pd(OH)_2/C$ (Degussa type) in 1:1 $AcOH/H_2O$ under H_2 could also be achieved when fresh catalyst was added after the reaction appeared to stop.

 © 2004 Wiley-VCH Verlag GmbH & Co. KGaA, Weinheim

Asymmetric Synthesis

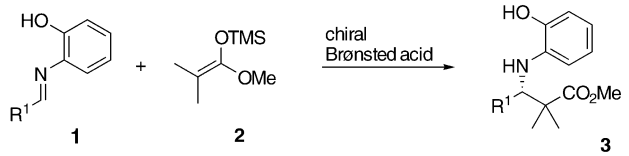
Enantioselective Mannich-Type Reaction Catalyzed by a Chiral Brønsted Acid**

Takahiko Akiyama, Junji Itoh, Koji Yokota, and Kohei Fuchibe*

The enantioselective Mannich-type reaction of an enolate or an enolate anion equivalent with aldimines constitutes a useful method for the preparation of chiral β-amino carbonyl compounds, which are the precursors of biologically important compounds such as β-lactams and β-amino acids. The development of chiral catalysts for the asymmetric Mannich-type reaction has attracted the attention of synthetic organic chemists.[1] Although stoichiometric amounts of chiral acid were employed initially,[2] a number of enantioselective catalysts such as chiral Lewis acid catalysts[3] and chiral base catalysts[4] have been developed lately.

In addition to metal-based chiral catalysts,[5] the use of small organic molecules as catalysts to promote asymmetric reactions has emerged as a new frontier in reaction methodology.[6] Accordingly, L-proline derivatives[7] and peptide derivatives[8] have been developed as catalysts for the Mannich-type reactions. We previously reported that Mannich-type reactions[9] and the aza-Diels–Alder reaction[10] proceed smoothly in the presence of a catalytic amount of a strong Brønsted acid. We thus postulated that the use of a chiral Brønsted acid, in which the proton is surrounded by bulky substituents, may lead to effective asymmetric induction. We report herein an enantioselective Mannich-type reaction of silyl enolates with aldimines catalyzed by a chiral metal-free Brønsted acid.[11,12]

First, treatment of aldimine **1a** (Scheme 1, $R^1 = Ph$) and ketene silyl acetal **2** (3.0 equiv) with 0.3 equivalents of the chiral phosphate **4a**[13,14,15] (which is readily prepared from (*R*)-BINOL; Scheme 2) in toluene at −78 °C led to a smooth Mannich-type reaction to give **3a** ($R^1 = Ph$). However, no enantioselectivity was observed (Table 1, entry 1), as deter-



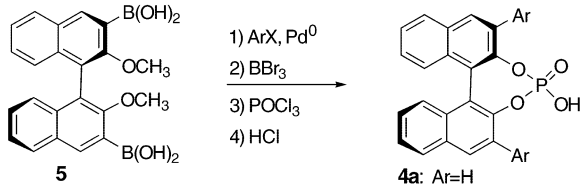
Scheme 1. Mannich-type reaction of aldimines **1** and ketene silyl acetals **2** to form β-aminoesters **3**.

[*] Prof. Dr. T. Akiyama, J. Itoh, K. Yokota, Dr. K. Fuchibe
Department of Chemistry, Faculty of Science
Gakushuin University
Mejiro, Toshima-ku, Tokyo 171-8588 (Japan)
Fax: (+81)-3-5992-1029
E-mail: takahiko.akiyama@gakushuin.ac.jp

[**] This work was supported by a Grant-in-Aid for Scientific Research (No. 15550042) from the Ministry of Education, Science, Sports, Culture, and Technology, Japan.

 © 2004 Wiley-VCH Verlag GmbH & Co. KGaA, Weinheim DOI: 10.1002/anie.200353240

mined by HPLC analysis with a chiral stationary phase column.[16] Next, we synthesized chiral phosphates **4b–e** by Suzuki coupling of bis(boronic acid) **5**[17] followed by demethylation and subsequent phosphorylation, as shown in Scheme 2. Introduction of aromatic groups at the 3,3′-



5

4a: Ar=H
4b: Ar=C_6H_5
4c: Ar=2,4,6-$Me_3C_6H_2$
4d: Ar=4-$MeOC_6H_4$
4e: Ar=4-$NO_2C_6H_4$

Scheme 2. Formation of chiral phosphates **4**, readily available from (*R*)-BINOL.

positions exerted a beneficial effect on the enantioselectivity. Use of **4b** as a chiral Brønsted acid in toluene increased the enantiofacial selectivity to 27% *ee* (Table 1, entry 2). The introduction of 4-nitrophenyl groups (i.e. **4e**) had a dual effect: 1) improvement of enantioselectivity to 87% *ee*, 2) acceleration of reaction rate, thereby allowing the reaction to go to completion in 4 h (Table 1, entry 5). The absolute stereochemistry of **3a** was determined by chiral HPLC analysis by comparison of the retention time with that found in the literature.[3c]

Table 1: Effect of the aromatic substituents of **4**.[a]

Entry	Ar	*t* [h]	Yield [%]	*ee* [%]
1	H	22	57	0
2	Ph	20	100	27
3	2,4,6-$Me_3C_6H_2$	27	100	60
4	4-$MeOC_6H_4$	46	99	52
5	4-$NO_2C_6H_4$	4	96	87

[a] Aldimine **1a** (R^1 = Ph) (1.0 equiv) and **2** (3.0 equiv) were treated with Brønsted acid **4** (30 mol%) in toluene at −78°C.

By further optimization of the reaction conditions, we found that the use of aromatic solvents led to high enantioselectivities, whereas protic solvents gave racemates.[18] Furthermore, a lower loading (10 mol%) of the Brønsted acid was sufficient to retain the high enantioselectivity. The results of the Mannich-type reaction of **2** with several aldimines catalyzed by chiral Brønsted acid **4e** are shown in Table 2.

Table 2: Catalytic enantioselective Mannich-type reactions.[a]

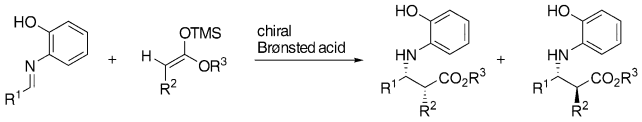
Entry	R^1	Product	Yield [%]	*ee* [%]
1	Ph	**3a**	98	89
2	*p*-MeC_6H_4	**3b**	100	89
3	*p*-FC_6H_4	**3c**	100	85
4	*p*-ClC_6H_4	**3d**	100	80

[a] Aldimine **1** (1.0 equiv) and **2** (1.5 equiv) were treated with **4e** (10 mol%) in toluene at −78°C for 24 h.

Aldimines derived from aromatic aldehydes afforded adducts with good to high enantioselectivities. The chemical yields were excellent in all cases.[19,20]

Next, other ketene silyl acetals were examined (Table 3). Monosubstituted ketene silyl acetals led to high *syn* selectivity as well as excellent enantioselectivity. The ketene silyl acetal derived from ethyl propionate furnished the corresponding ester in 96% *ee* (Table 3, entry 1). Substituted aromatic, heteroaromatic, and α,β-unsaturated aldimines also gave the corresponding adducts with high enantioselectivities (Table 3, entries 2–7). The reactions of ketene silyl acetals derived from ethyl 3-phenylpropionate (Table 3, entries 8–10) and methyl 2-triphenylsilyloxyacetate (Table 3, entry 11) also exhibited excellent *syn* selectivities[21] and high enantioselectivities.

Table 3: Diastereoselective Mannich-type reactions.[a]

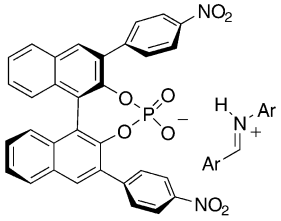


1 **6** **7**

Entry	R^1	R^2	R^3	Yield [%]	*syn*/*anti*	*ee* [%][b]
1	Ph	Me[c]	Et	100	87:13	96
2	*p*-$MeOC_6H_4$	Me[c]	Et	100	92:8	88
3	*p*-FC_6H_4	Me[c]	Et	100	91:9	84
4	*p*-ClC_6H_4	Me[c]	Et	100	86:14	83
5	*p*-MeC_6H_4	Me[c]	Et	100	94:6	81
6	2-Thienyl	Me[c]	Et	81	94:6	88
7	PhCH=CH	Me[c]	Et	91	95:5	90
8	Ph	$PhCH_2$[d]	Et	100	93:7	91
9	*p*-$MeOC_6H_4$	$PhCH_2$[d]	Et	92	93:7	87
10	PhCH=CH	$PhCH_2$[d]	Et	65	95:5	90
11	Ph	Ph_3SiO[e]	Me	79	100:0	91

[a] Aldimine **1** (1.0 equiv) and ketene silyl acetal **6** (1.5 equiv) were treated with **4e** (10 mol%) in toluene at −78°C for 24 h. [b] *ee* value of *syn* isomer. [c] *E*/*Z* = 87:13. [d] *E*/*Z* = 87:13. [e] *E*/*Z* = 91:9.

Because the use of *N*-benzylideneaniline in place of **1a** (R^1 = Ph) in the reaction with **2** lowered the enantioselectivity to 39% *ee*, we concluded that the presence of the hydroxy group in the *ortho* position of the aldimine is essential for the present enantioselective Mannich-type reaction. This reaction can be considered to proceed via an iminium salt, generated from the aldimine and the Brønsted acid. Although the precise mechanism has not been elucidated, it is supposed that 3,3′-diaryl groups, which are not coplanar with the naphthyl groups (see **8**), would effectively shield the phosphate moiety, leading to efficient asymmetric induction.[22] This is the first example of an enantioselective Mannich-type reaction in which the carbon–nitrogen double bond is



8

 © 2004 Wiley-VCH Verlag GmbH & Co. KGaA, Weinheim

activated by a strong, metal-free chiral Brønsted acid, even though chiral Brønsted acids were previously implicated in enantioselective Mannich-type reactions.[7,8]

In summary, we have developed a chiral Brønsted acid catalyzed enantioselective Mannich-type reaction of aldimines with silyl enolates, and β-aminoesters were obtained with high to excellent enantioselectivities under metal-free conditions. This method adds a new entry to the catalogue organo-catalyzed asymmetric reactions. This method can potentially be extended to a variety of enantioselective nucleophilic addition reactions to carbon–nitrogen double bonds. Further investigations to clarify the reaction mechanism and its application to other enantioselective reactions are in progress.

Experimental Section

General procedure (Table 3, Entry 1): A solution of **6** (R^2 = Me, R^3 = Et) (50 μL, 0.246 mmol) was added dropwise over 3 min to a solution of **1** (R^1 = Ph) (32.0 mg, 0.162 mmol) and **4e** (9.5 mg, 0.0161 mmol) in toluene (1 mL) at −78 °C. The reaction was stirred at this temperature for 17 h. The mixture was quenched by the addition of saturated solutions of $NaHCO_3$ and KF at −78 °C. After filtration over celite, the filtrate was extracted with ethyl acetate. The combined organic layers were washed successively washed with HCl (1N) and brine, dried over anhydrous Na_2SO_4, and concentrated to dryness. The remaining solid was purified by TLC (SiO_2, hexane/EtOAc 3:1) to give **7** (45.6 mg, 0.155 mmol) in 100% yield. The enantiomeric excess was determined on a Daicel Chiralpak AS-H column.

Received: November 3, 2003 [Z53240]

Keywords: asymmetric synthesis · Brønsted acids · enantioselectivity · organocatalysis · Schiff bases

[1] For reviews, see: S. Kobayashi, H. Ishitani, *Chem. Rev.* **1999**, *99*, 1069; E. F. Kleinman in *Comprehensive Organic Synthesis*, *Vol. 2* (Eds.: B. M. Trost, I. Fleming), Pergamon Press, Oxford, **1991**, p. 893; M. Arend, B. Westermann, N. Risch, *Angew. Chem.* **1998**, *110*, 1096; *Angew. Chem. Int. Ed.* **1998**, *37*, 1045; M. Arend, *Angew. Chem.* **1999**, *111*, 3047; *Angew. Chem. Int. Ed.* **1999**, *38*, 2873.

[2] a) K. Ishihara, M. Miyata, K. Hattori, T. Tada, H. Yamamoto, *J. Am. Chem. Soc.* **1994**, *116*, 10520; b) R. Müller, H. Goesmann, H. Waldmann, *Angew. Chem.* **1999**, *111*, 166; *Angew. Chem. Int. Ed.* **1999**, *38*, 184.

[3] a) H. Ishitani, M. Ueno, S. Kobayashi, *J. Am. Chem. Soc.* **1997**, *119*, 7153; b) S. Kobayashi, H. Ishitani, M. Ueno, *J. Am. Chem. Soc.* **1998**, *120*, 431; c) H. Ishitani, M. Ueno, S. Kobayashi, *J. Am. Chem. Soc.* **2000**, *122*, 8180; d) S. Kobayashi, T. Hamada, K. Manabe, *J. Am. Chem. Soc.* **2002**, *124*, 5640; e) E. Hagiwara, A. Fujii, M. Sodeoka, *J. Am. Chem. Soc.* **1998**, *120*, 2474; f) S. Xue, S. Yu, Y. Deng, W. D. Wulff, *Angew. Chem.* **2001**, *113*, 2331; *Angew. Chem. Int. Ed.* **2001**, *40*, 2271; g) B. M. Trost, L. R. Terrell, *J. Am. Chem. Soc.* **2003**, *125*, 338; h) K. Juhl, N. Gathergood, K. A. Jørgensen, *Angew. Chem.* **2001**, *113*, 3083; *Angew. Chem. Int. Ed.* **2001**, *40*, 2995; i) D. Ferraris, B. Young, T. Dudding, T. Lectka, *J. Am. Chem. Soc.* **1998**, *120*, 4548; j) A. E. Taggi, A. M. Hafez, T. Lectka, *Acc. Chem. Res.* **2003**, *36*, 10; k) S. Matsunaga, N. Kumagai, S. Harada, M. Shibasaki, *J. Am. Chem. Soc.* **2003**, *125*, 4712.

[4] For chiral-base-catalyzed reactions, see: H. Fujieda, M. Kanai, T. Kambara, A. Iida, K. Tomioka, *J. Am. Chem. Soc.* **1997**, *119*, 2060; K. Tomioka, H. Fujieda, S. Hayashi, M.-A. Hussein, T. Kambara, Y. Nomura, M. Kanai, K. Koga, *Chem. Commun.* **1999**, 715.

[5] E. N. Jacobsen, A. Pfaltz, H. Yamamoto in *Comprehensive Asymmetric Synthesis*, *Vol. I–III*, Springer, Berlin, **1999**; H. Tye, P. J. Comina, *J. Chem. Soc. Perkin Trans. 1* **2001**, 1729.

[6] P. I. Dalko, L. Moisan, *Angew. Chem.* **2001**, *113*, 3840; *Angew. Chem. Int. Ed.* **2001**, *40*, 3726; K. A. Ahrendt, C. J. Borths, D. W. C. MacMillan, *J. Am. Chem. Soc.* **2000**, *122*, 4243; S. Kobayashi, C. Ogawa, H. Konishi, M. Sugiura, *J. Am. Chem. Soc.* **2003**, *125*, 6610; K. Juhl, K. A. Jørgensen, *Angew. Chem.* **2003**, *115*, 1536; *Angew. Chem. Int. Ed.* **2003**, *42*, 1498; N. A. Paras, D. W. C. MacMillan, *J. Am. Chem. Soc.* **2002**, *124*, 7894.

[7] B. List, P. Pojarliev, W. T. Biller, H. J. Martin, *J. Am. Chem. Soc.* **2002**, *124*, 827; W. Notz, K. Sakthivel, T. Bui, G. Zhong, C. F. Barbas III, *Tetrahedron Lett.* **2001**, *42*, 199; A. Cordova, W. Notz, G. Zhong, J. M. Betancort, C. F. Barbas III, *J. Am. Chem. Soc.* **2002**, *124*, 1842; A. Cordova, S.-i. Watanabe, F. Tanaka, W. Notz, C. F. Barbas III, *J. Am. Chem. Soc.* **2002**, *124*, 1866; A. Cordova, C. F. Barbas III, *Tetrahedron Lett.* **2002**, *43*, 7749; Y. Hayashi, W. Tsuboi, I. Ashimine, T. Urushima, M. Shoji, K. Sakai, *Angew. Chem.* **2003**, *115*, 3805; *Angew. Chem. Int. Ed.* **2003**, *42*, 3677.

[8] P. Vachal, E. N. Jacobsen, *J. Am. Chem. Soc.* **2002**, *124*, 10012; A. G. Wenzel, E. N. Jacobsen, *J. Am. Chem. Soc.* **2002**, *124*, 12964.

[9] a) T. Akiyama, J. Takaya, H. Kagoshima, *Synlett* **1999**, 1045; b) T. Akiyama, J. Takaya, H. Kagoshima, *Synlett* **1999**, 1426; c) T. Akiyama, J. Takaya, H. Kagoshima, *Tetrahedron Lett.* **2001**, *42*, 4025; d) T. Akiyama, J. Takaya, H. Kagoshima, *Adv. Synth. Catal.* **2002**, *344*, 338; e) T. Akiyama, J. Itoh, K. Fuchibe, *Synlett* **2002**, 1269.

[10] T. Akiyama, J. Takaya, H. Kagoshima, *Tetrahedron Lett.* **1999**, *40*, 7831; T. Akiyama, K. Matsuda, K. Fuchibe, *Synlett* **2002**, 1898.

[11] For recent examples which claim the use of chiral Brønsted acids as activators, see: B. L. Hodous, G. C. Fu, *J. Am. Chem. Soc.* **2002**, *124*, 10006; C. Palomo, M. Oiarbide, J. M. Garcia, A. Gonzalez, A. Lecumberri, A. Linden, *J. Am. Chem. Soc.* **2002**, *124*, 10288; N. T. McDougal, S. E. Schaus, *J. Am. Chem. Soc.* **2003**, *125*, 12094; Y. Huang, A. K. Unni, A. N. Thadani, V. H. Rawal, *Nature* **2003**, *424*, 146.

[12] For a "Brønsted acid assisted chiral Lewis acid" promoted Mannich-type reaction, see reference [2a], in which a Lewis acid plays an important role.

[13] J. Jacques, C. Fouquey, *Org. Synth.* **1989**, *67*, 1.

[14] For use as a chiral resolving agent, see: S. H. Wilen, J. Z. Qi, *J. Org. Chem.* **1991**, *56*, 487.

[15] For an enantioselective asymmetric reaction in which a metal salt of a chiral BINOL phosphate is used, see: J. Inanaga, Y. Sugimoto, T. Hanamoto, *New J. Chem.* **1995**, *19*, 707; H. Furuno, T. Hanamoto, Y. Sugimoto, J. Inanaga, *Org. Lett.* **2000**, *2*, 49.

[16] Daicel Chiralpak AD-H was employed.

[17] P. Wipf, J.-K. Jung, *J. Org. Chem.* **2000**, *65*, 6319.

[18] The enantiomeric excesses in other solvents were as follows: 83% *ee* (EtC_6H_5), 30% *ee* (Et_2O), 13% *ee* (CH_2Cl_2), 0% *ee* (EtOH).

[19] The absolute stereochemistry of **3a** and **3d** were assigned to be *S* by comparison of the retention times of both enantiomers with literature data,[3c] and those of others were proposed to be *S* by analogy.

[20] The Mannich-type reaction with aldimines derived from aliphatic aldehydes was not successful.

[21] For the *syn*-selective Mannich-type reaction catalyzed by a Brønsted acid, see reference [9c].

[22] 4-$NO_2C_6H_4$ groups might enhance the activity by increasing the acidity of the phosphate group.

 © 2004 Wiley-VCH Verlag GmbH & Co. KGaA, Weinheim

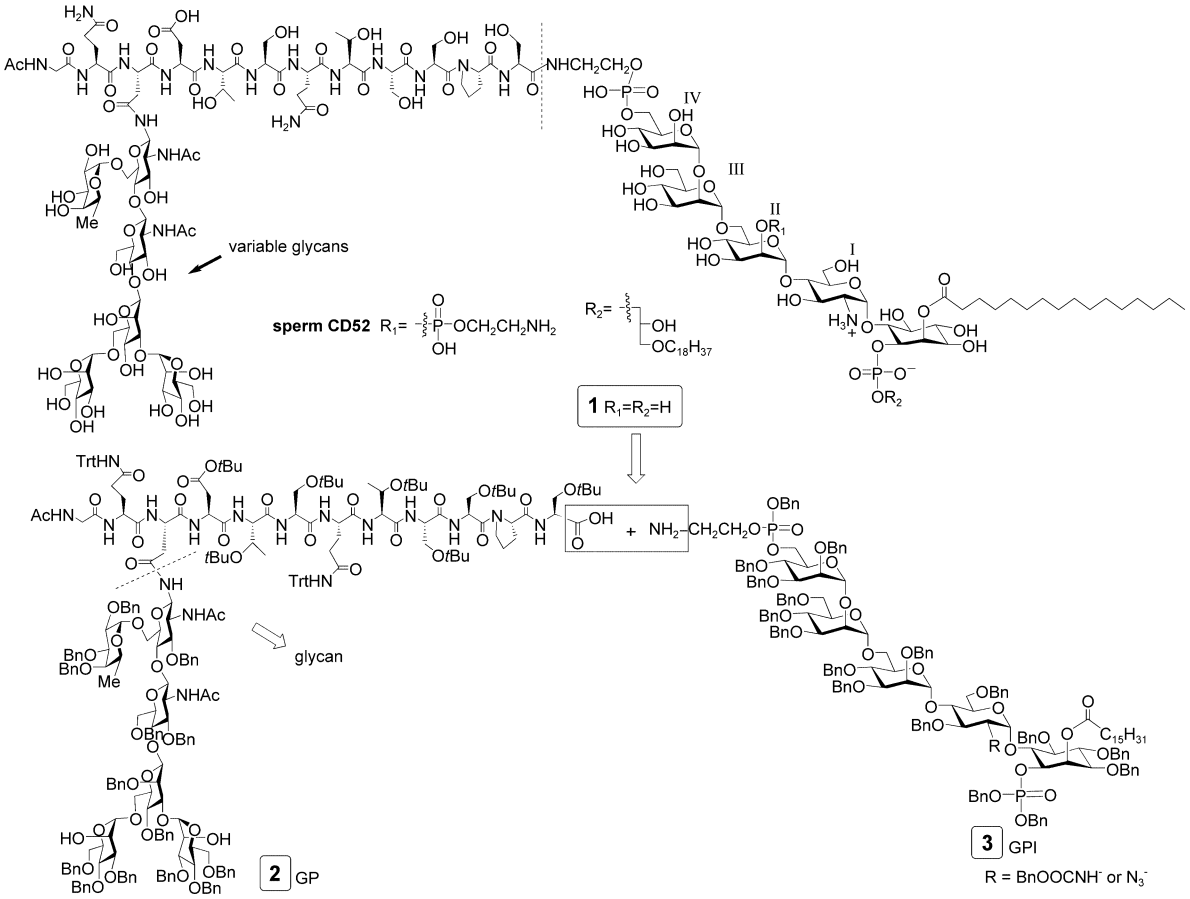
Glycopeptides

Chemical Synthesis of a Skeleton Structure of Sperm CD52—A GPI-Anchored Glycopeptide**

*Ning Shao, Jie Xue, and Zhongwu Guo**

Glycosylphosphatidylinositol (GPI)-anchored glycopeptides or glycoproteins are ubiquitously present on eukaryotic cells.[1] For example, CD52 antigen, which is expressed by virtually all human lymphocytes and sperms,[2,3] is a simple GPI-anchored glycopeptide, but it plays a critical role in the human immune and reproduction systems.[4–6] Sperm CD52 is involved in the human sperm–egg recognition and binding, while antibodies against lymphocyte CD52 have been used to treat several immune system-related diseases.

The structure of CD52 is rather typical as it has the phospholipid and the conserved GPI glycan linked to the inositol C1–*O* and C6–*O* positions and the glycopeptide to the GPI glycan nonreducing end C6–*O* position through a phosphoethanolamine bridge (Scheme 1).[2,3] Additional biomodifications of sperm CD52 GPI include a phosphoethanolamine group to the mannose II (Man^{II}) C2–*O* position and a large acyl group to the inositol C2–*O* position.[2] The peptide chain of CD52 is very short, consisting of 12 amino acids, and it has only one *N*-glycosylation site, to which complex and heterogeneous glycans are attached. The heterogeneity of CD52 glycoforms constitutes a major obstacle in accessing homogeneous antigens from biological sources.



Scheme 1. Retrosynthetic plan for **1**.

Due to its short peptide, simple glycosylation pattern, and intriguing biological activities, sperm CD52 is a useful model for structural and structure–activity relationship studies of GPI-anchored glycopeptides and glycoproteins. In this context, a practical synthetic method for it should be of great significance. However, there have been very few reports concerning the synthesis of GPI-anchored structures, even though a number of GPIs[7–16] and glycopeptides,[17,18] including CD52 GPI[19,20] and glycopeptides,[21,22] have been synthesized by chemical methods. The only synthetic studies towards GPI-anchored glycopeptides or proteins either used simple

[*] N. Shao, Dr. J. Xue, Prof. Z. Guo
Department of Chemistry, Case Western Reserve University
Cleveland, OH 44106-7078 (USA)
Fax: (+1) 216-368-3006
E-mail: zxg5@case.edu

[**] This work was supported in part by the Research Corporation (Research Innovation Award 0663), the American Chemical Society (PRF 37743-G), and the NIH/NCI (1R01 CA95142). We are also grateful to Dr. S. Chen and Mr. J. Faulk for the MS measurements.

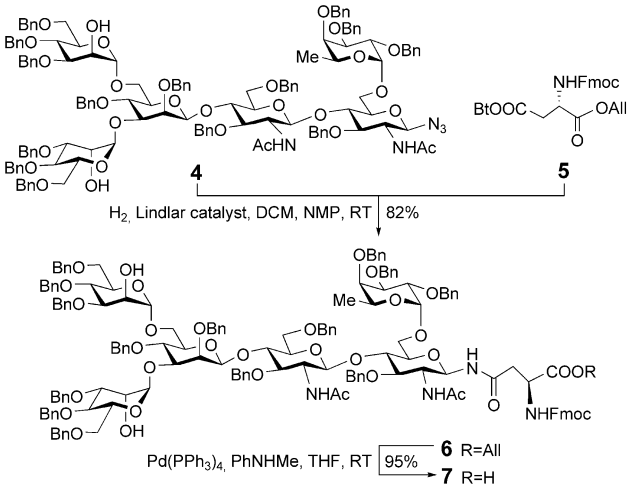
Supporting information for this article is available on the WWW under http://www.angewandte.org or from the author.

 DOI: 10.1002/anie.200353251 © 2004 Wiley-VCH Verlag GmbH & Co. KGaA, Weinheim

molecular models[19,23] or had an artificial linkage between the GPI and protein.[16] Chemical synthesis of complex, native GPI-anchored glycopeptides, which involves several areas of chemistry, remains a formidable challenge.

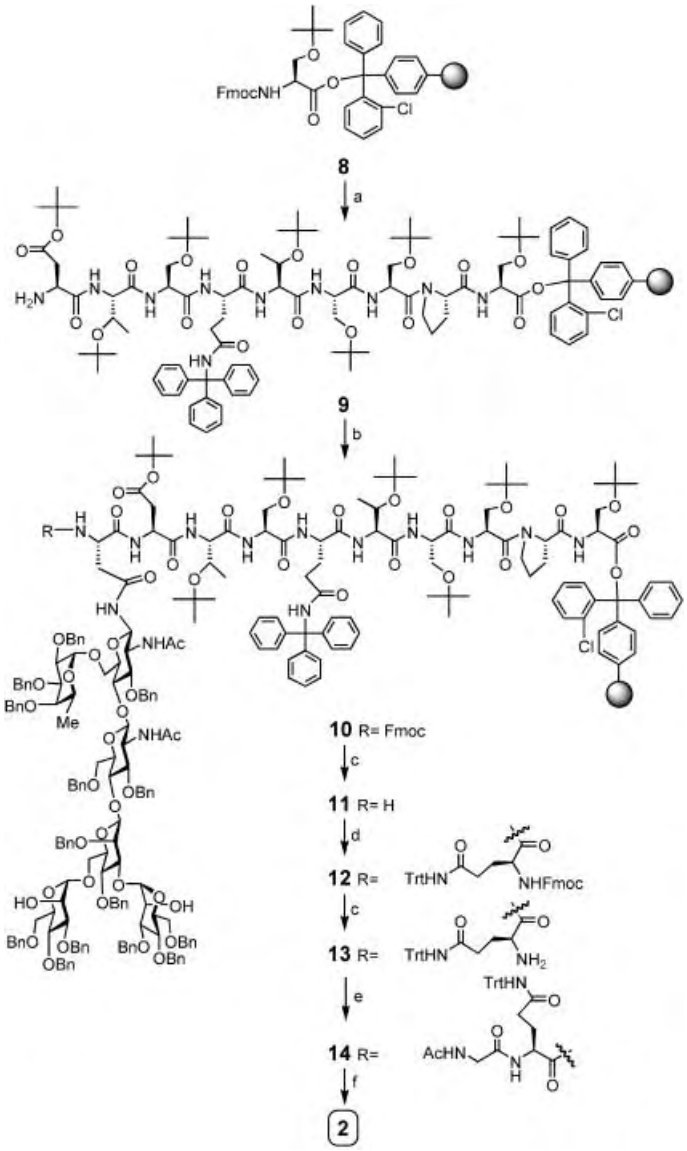
The work presented herein aims at the construction of natively linked GPI-glycopeptide conjugates, especially focusing on the strategic synthetic designs. For this purpose, a skeleton structure **1** (Scheme 1) of sperm CD52 without the glycerol lipid and the extra phosphoethanolamine of its GPI was established as the synthetic target. The omission of two functional groups can save us a few steps and problems in the GPI preparation.[20] For **1**, since an amide can be easily formed by the condensation reaction between a free amino group and a free carboxyl group, the amido bond between the GPI and the glycopeptide was cleaved first to offer two logical building blocks **2** and **3** (Scheme 1) that had very different properties. Moreover, because this linkage is shared by all GPI-anchored glycopeptides and glycoproteins, such a synthetic strategy may be of general significance. Thus, an important issue is the coupling between two complex segments, namely, the GPI and the glycopeptide. For **2** and **3**, we employed benzyl group as a permanent protection for the carbohydrate hydroxyl groups, as it can be easily removed under mild conditions later on. In the meantime, glycopeptide **2** was planned to have a fully protected peptide to prevent the potential interference of peptide side chains with the coupling reaction and the potential influence of a free peptide on the solubility and other properties of involved intermediates. Another important issue of this synthesis was thus preparing **2** and **3** in the properly protected form.

The *N*-glycan **4** with an azido group attached to the reducing end was prepared by a modified literature procedure,[24] which will be reported elsewhere. After the azido group of **4** was selectively reduced to a primary amine by Lindlar catalyst-catalyzed hydrogenation, it was coupled to the side chain of asparagine by the reaction with an active ester **5**. Because the glycan contained a benzylated fucosidic linkage that is extremely sensitive to acids,[25] the α-carboxyl group of **5** was protected by an allyl, instead of a *tert*-butyl (*t*Bu) group typically used in peptide synthesis, to circumvent acidic treatment during the deprotection.[26] Then, the allyl group was smoothly removed by $Pd(PPh_3)_4$ to afford **7** (Scheme 2), which was ready as a key building block for the glycopeptide assembly.



Scheme 2. Synthesis of the glycosyl asparagine **7**.

As mentioned earlier, except for the terminal carboxyl group, the peptide chain of glycopeptide **2** needed to be fully protected. In this case, the traditional solid-phase glycopeptide synthesis by using Wang resin[21] would not be useful, since the acidic conditions, such as 95% aqueous trifluoroacetic acid (TFA), used to retrieve glycopeptides from Wang resin would deprotect the amino acid side chains and affect the α-fucosidic linkage.[25] To deal with this problem, we employed the extremely acid-sensitive 2-chorotrityl resin[27] to synthesize **2** (Scheme 3). The ester bond between 2-

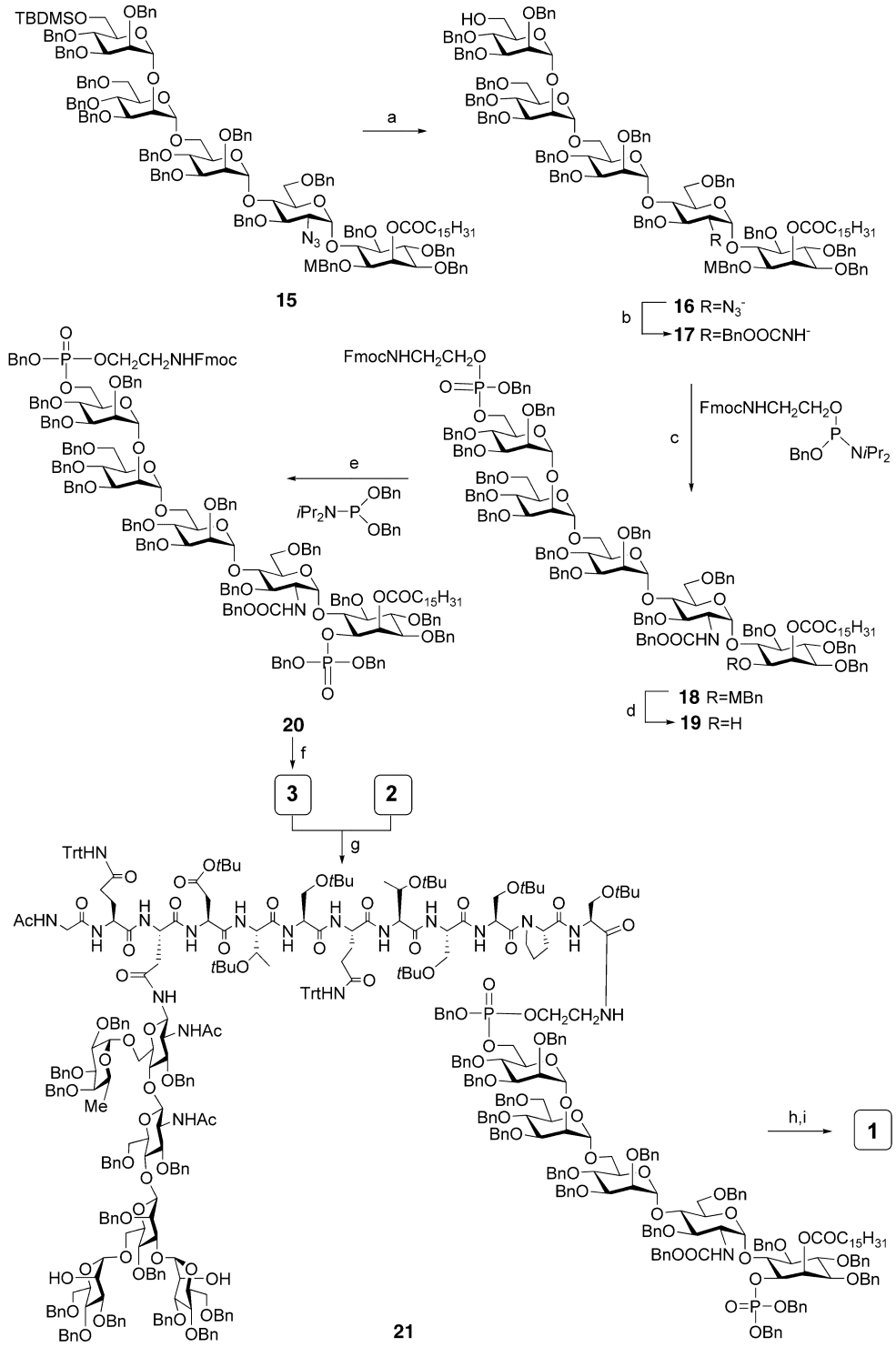


Scheme 3. Reagents and conditions: a) solid-phase peptide elongation by conventional Fmoc chemistry on an automatic peptide synthesizer;[30] b) **7**, HOBt, DCC, 0°C to RT, 24 h; c) 20% piperidine in NMP, RT, 2 h; d) Fmoc–Gln(Trt)–OH (Gln = glutamine), HOBt, DCC, NMP, RT, 2 h; e) Ac–Gly–OH (Gly = glycine), HOBt, DCC, NMP, RT, 2 h; f) HOAc, TFE, DCM (1:1:8), RT, 2 h, 70% (from **9**).

 © 2004 Wiley-VCH Verlag GmbH & Co. KGaA, Weinheim

chorotrityl resin and the peptide *C*-terminus could be cleaved by 1–20% acetic acid, the use of which did not affect the side-chain protecting groups of amino acids, including the trityl (Trt) group on glutamine.[28]

The glycopeptide assembly started from a commercially available resin, **8**, already loaded with a serine. The peptide was first elongated by the conventional Fmoc (9-fluorenylmethoxycarbonyl) chemistry on an automatic peptide synthesizer by using 2-*O*-(1*H*-7-azabenzotriazol-1-yl)-1,1,3,3-tetramethyluronium hexafluorophosphate (HATU) and *N*,*N*-diisopropylethylamine (DIEA) as the condensation reagents[29] to afford **9**. All amino acids employed were commercially



Scheme 4. Reagents and conditions: a) Tetrabutyl ammonium fluoride (TBAF), HOAc, DCM, 35–40°C, 3 days, 95%; b) PEt_3, CBz_2O, MeOH, DCM (1:2), RT, overnight, 70%; c) tetrazole, DCM, MeCN (3:1), RT, 6 h; then *t*BuOOH, 84%; d) TFA, DCM (1:9), RT, 0.5 h, >99%; e) tetrazole, DCM, MeCN (3:1), RT, 0.5 h; then *t*BuOOH; 57%. f) DBU, DCM, RT, 2 min, 90%; g) HOBt, EDC, DCM, NMP (2:1), RT, 1 day, 70%; h) 10% Pd/C, H_2, $CHCl_3$, MeOH, H_2O (10:10:3), 2 days; i) TFA in DCM (15%, containing 10% of $HSiEt_3$); then HPLC, 85% (two steps).

 © 2004 Wiley-VCH Verlag GmbH & Co. KGaA, Weinheim

available. Next, the glycosyl asparagine **7** was introduced manually to minimize the use of **7**. In this coupling, only 2 equivalents of **7** were used with *N*,*N*-dicyclohexylcarbodiimine (DCC) and *N*-hydroxybenzotriazole (HOBt) as the condensation reagents. Thereafter, manual *N*-deprotection of **10** with 20% piperidine in *N*-methylpyrrolidinone (NMP), followed by further peptide elongation by using Fmoc–amino acids and the standard protocols of solid-phase peptide synthesis,[30] resulted in the glycopeptide–resin conjugate **14.** It was finally treated with a mixture of acetic acid, trifluroethanol (TFE) and dichloromethane (DCM) (1:1:8) to offer a white solid, which was purified by preparative TLC. In addition to the expected glycopeptide **2** (13 mg), a non-glycosylated peptide (2 mg) was also obtained as a side product. According to this result, the coupling yield between **7** and **9** was about 70%. The NMR spectroscopy and MS data of **2** agreed well with the proposed structure. One possible concern about this synthesis was whether asparagine suffered from racemization during the coupling between **7** and **9**. Since no other product was obtained and the NMR spectra of **2** showed only one set of signals, we assumed that this side reaction, if any, was minimal.

Scheme 4 outlines the GPI synthesis as well as the final coupling and deprotection steps. First, the GPI core **15** was prepared according to a recently reported procedure.[19] Then, its nonreducing end C6-*O* position was deprotected to give **16**. The phosphorylation of **16** turned out to be problematic.[20] In contrast to all previous GPI syntheses,[7–16] the azido group was affected by the reaction to result in complex products. In fact, the acyl group at the inositol 2-*O* position caused a number of problems in the synthesis of sperm CD52 GPI, which was discussed separately.[20] To overcome this complication, the azido group was reduced with triethylphosphine and the resulted free amine was protected by a benzyloxycarbonyl (CBz) group to afford **17** that was phosphorylated smoothly. The Fmoc group was used to protect the amino group of phosphoethanolamine in **17** to facilitate the selective deprotection by a mild base later on. After the *p*-methoxylbenzyl (MBn) group of **18** was removed by TFA, the second phosphate was attached to the exposed inositol 1-hydroxyl group (57%). All intermediates were conveniently purified by column chromatography. Finally, treatment of **20** with diluted 1,8-diazabicyclo[5,4,0]undec-7-ene (DBU) in DCM for a brief period (2 min) gave the GPI building block **3**, which was practically pure and was thus directly used without further purification during the construction of the target molecule.

The coupling reaction between **2** and **3** was performed in a mixture of DCM and NMP (2:1) under a nitrogen atmosphere by using 1-[3-(dimethylamino)propyl]-3-ethylcarbodiimide hydrochloride (EDC) and HOBt (10 equivalents) as the condensation reagents,[31] which turned out to be very efficient. After one day of stirring at room temperature, the reaction mixture was worked up and the product was purified by column chromatography to give **21** in a 70% isolated yield. Compound **21** was well separated from both substrates by TLC and column chromatography. Its 1D, 2D NMR, and MS data were consistent with the expected structure. The NMR signals of its reporter groups, such as that of the carbohydrate anomeric protons, carbon atoms and some amino acid α-protons, were easily assigned. Moreover, from the NMR spectra, we could not identify the potential recemization product, which was consistent with our previous results with a simple molecular model.[19] Global deprotection of **21** was achieved in two steps, namely hydrogenolytic debenzylation in a hydrogen atmosphere with 10% Pd/C as the catalyst followed by removal of the peptide side-chain protecting groups by 15% TFA in DCM. It was important to observe this deprotection sequence, as the benzylated fucosidic linkage is much more labile to TFA than the free sugar. For example, 15% TFA could destroy the former within an hour but had little influence on the latter after several hours of treatment.[28] The final synthetic target **1**[32] was then thoroughly purified by reversed-phase HPLC by using a C_{18} column (250 mm × 10 mm). The presence of a long lipid chain resulted in its strong retention on the column. Therefore, with 40% *iso*-propanol/water (2 mL min^{-1}) as the eluent, **1** displayed a retention time of 37.5 min, while free CD52 glycopeptides were washed out from the same column by 2% *iso*-propanol/water in less than 25 min. The structure of **1** was supported by its high field NMR spectroscopy and MS.

In summary, this paper described the convergent synthesis of a skeleton structure of the sperm CD52 antigen, which represents the first chemical synthesis of a complex and all natively linked glycopeptide–GPI conjugate. Our general synthetic design was to separately prepare the protected glycopeptide and the GPI first. 2-Chlorotrityl resin that has an extremely acid-labile linker was used in the solid-phase synthesis of the glycopeptide to obtain its fully protected form. Next, the glycopeptide *C*-terminus and the GPI nonreducing end phosphoethanolamine group were selectively deprotected. Finally, the two segments were joined through an amido bond by using HOBt/EDC as the condensation reagents, to give the glycopeptide-GPI conjugate. The coupling reaction proved to be very efficient. Because this amido linkage is shared by various GPI-anchored glycopeptides or glycoproteins, we assume that the methods described herein may be useful for the synthesis of other similar structures.

Received: November 4, 2003 [Z53251]

Keywords: antigens · carbohydrates · glycopeptides · glycoproteins · solid-phase synthesis

[1] M. A. J. Ferguson, A. F. Williams, *Annu. Rev. Biochem.* **1988**, *57*, 285–320.
[2] S. Schroter, P. Derr, H. S. Conradt, M. Nimtz, G. Hale, C. Kirchhoff, *J. Biol. Chem.* **1999**, *274*, 29862–29873.
[3] A. Treumann, M. R. Lifely, P. Schneider, M. A. J. Ferguson, *J. Biol. Chem.* **1995**, *270*, 6088–6099.
[4] G. Hale, M.-Q. Xia, H. P. Tighe, J. S. Dyer, H. Waldmann, *Tissue Antigens* **1990**, *35*, 118–127.
[5] Y. Tsuji in *Immunology of Human Reproduction* (Eds.: M. Kurpisz, N. Fernandez), BIOS Sci. Pub., Oxford, **1995**, pp. 23–32.
[6] E. D. Eccleston, T. W. White, J. B. Howard, D. W. Hamilton, *Mol. Reprod. Dev.* **1994**, *37*, 110–119.
[7] A. Crossman, Jr., J. B. Brimacombe, M. A. J. Ferguson, T. K. Smith, *Carbohydr. Res.* **1999**, *321*, 42.

 © 2004 Wiley-VCH Verlag GmbH & Co. KGaA, Weinheim

[8] U. E. Udodong, R. Madsen, C. Roberts, B. Fraser-Reid, *J. Am. Chem. Soc.* **1993**, *115*, 7886 – 7887.
[9] A. S. Campbell, B. Fraser-Reid, *J. Am. Chem. Soc.* **1995**, *117*, 10387 – 10388.
[10] D. K. Baeschlin, A. R. Chaperon, V. Charbonneau, L. G. Green, S. V. Ley, U. Lücking, E. Walther, *Angew. Chem.* **1998**, *110*, 3609 – 3614; *Angew. Chem. Int. Ed.* **1998**, *37*, 3423 – 3428.
[11] N.-C. Reichardt, M. Martín-Lomas, *Angew. Chem.* **2003**, *115*, 4822 – 4825; *Angew. Chem. Int. Ed.* **2003**, *42*, 4674 – 4677.
[12] C. Murakata, T. Ogawa, *Carbohydr. Res.* **1992**, *235*, 95 – 114.
[13] T. G. Mayer, B. Kratzer, R. R. Schmidt, *Angew. Chem.* **1994**, *106*, 2289 – 2293; *Angew. Chem. Int. Ed. Engl.* **1994**, *33*, 2177 – 2181.
[14] K. Pekari, R. R. Schmidt, *J. Org. Chem.* **2003**, *68*, 129 – 1308.
[15] M. C. Hewitt, D. A. Snyder, P. H. Seeberger, *J. Am. Chem. Soc.* **2002**, *124*, 13434 – 13436.
[16] L. Schofield, M. C. Hewitt, K. Evans, M.-A. Siomos, P. H. Seeberger, *Nature* **2002**, *418*, 785 – 789.
[17] See review: O. Seitz, *ChemBioChem* **2000**, *1*, 214 – 246, and references therein.
[18] See review: H. Herzner, T. Reipen, M. Schultz, H. Kunz, *Chem. Rev.* **2000**, *100*, 4495 – 4537.
[19] J. Xue, N. Shao, Z. Guo, *J. Org. Chem.* **2003**, *68*, 4020 – 4029.
[20] J. Xue, Z. Guo, *J. Am. Chem. Soc.* **2003**, *125*, 16334 – 16339.
[21] Z. Guo, Y. Nakahara, Y. Nakahara, T. Ogawa, *Angew. Chem.* **1997**, *109*, 2442 – 2444; *Angew. Chem. Int. Ed.* **1997**, *36*, 1464 – 1467, and references therein.
[22] M. R. Pratt, C. R. Bertozzi, *J. Am. Chem. Soc.* **2003**, *125*, 6149 – 6159.
[23] Tanaka, Y. Nakahara, H. Hojo, Y. Nakahara, *Tetrahedron* **2003**, *59*, 4059 – 4067.
[24] Z. Guo, Y. Nakahara, Y. Nakahara, T. Ogawa, *Bioorg. Med. Chem.* **1997**, *5*, 1917 – 1924, and references therein.
[25] C. Unverzagt, H. Kunz, *Bioorg. Med. Chem.* **1994**, *2*, 1189 – 1201.
[26] M. Rosch, H. Herzner, W. Dippold, M. Wild, D. Vestweber, H. Kunz, *Angew. Chem.* **2001**, *113*, 3954 – 3957; *Angew. Chem. Int. Ed.* **2001**, *40*, 3836 – 3839.
[27] K. Barlos, D. Gatos, S. Kapolos, G. Papaphotiu, W. Schaefer, W. Yao, *Tetrahedron Lett.* **1989**, *30*, 3947 – 3950.
[28] N. Shao, J. Xue, Z. Guo, *J. Org. Chem.* **2003**, *68*, 9003 – 9011.
[29] L. A. Carpino, *J. Am. Chem. Soc.* **1993**, *115*, 4397 – 4398.
[30] M. Bodanszky, *Peptide chemistry: A practical textbook*, 2nd ed., Springer, Berlin, **1993**.
[31] L. A. Carpino, A. El-Faham, F. Albericio, *J. Org. Chem.* **1995**, *60*, 3561 – 3564.
[32] Selected data. **6**: $[\alpha]_D = -3.48$ ($c = 1.2$, $CHCl_3$). ^{1}H NMR (600 MHz, $CDCl_3$): $\delta = 7.73$–7.55 (m, 4H, Fmoc), 5.83 (m, 1H, All), 5.26 (m, 2H, N-H, All), 5.17 (dd, $J = 1.2$, 10.2 Hz, 1H, All), 5.13 (s, 1H, Man-1), 4.90 (s, 1H, Man 1(anomeric)), 4.82 (s, 1H, Fuc 1(Fuc = fucose), 4.72 (d, $J = 8.4$ Hz, 1H, GlcNAc 1), 4.70 (d, $J = 8.4$ Hz, 1H, GlcNAc 1 (GlcN = glucosamine), 4.51 (s, 1H, Man 1), 2.85 (dd, $J = 3.6$, 15.6 Hz, 1H, Asn β (Asn = asparagine), 2.62 (dd, J 3.0, 15.6 Hz, 1H, Asn β), 1.73 (s, 3H, Ac), 1.66 (s, 3H, Ac), 1.03 ppm (d, $J = 6.0$ Hz, 3H, Fuc 6). MALDI-TOF MS: Calcd for $C_{160}H_{173}O_{34}N_4Na$, 2717.183, found 2717.181 [M+H+Na$^+$]. **21**: TLC: $R_f = 0.41$ (DCM and MeOH 10:1). ^{1}H NMR ($CDCl_3$, 600 MHz): $\delta = 5.81$ (br, 1H, Ino 2 (Ino = inositol)), 5.31 (d, $J = 3$ Hz, 1H, GlcN 1), 5.25 (d, $J = 7$ Hz, 1H, GlcNAc 1), 5.11 (br, 2H, 2 Man 1), 4.85 (1H, Man 1), 4.76 (1H, Fuc 1), 4.71 (1H, Man 1), 4.69 (1H, GlcNAc 1), 4.67 (1H, Man 1), 4.45 (b, 1H, Man 1), 2.80–2.62 (m, 4H, Asp β(Asp = aspartic acid), Asn β), 1.76 (s, 3H, Ac), 1.72 (s, 3H, Ac), 1.01, 0.99 (2 d, $J = 6.0$ Hz, 6H, Fuc 6, Thr γ(Thr = threonine)), 0.87 ppm (t, $J = 7.2$ Hz, 3H, lipid–Me). ^{13}C (150 MHz, $CDCl_3$, from HMQC): $\delta = 101.4$ (2 Man 1), 101.2 (Man 1), 100.6 (GlcNAc 1), 100.0 (Man 1), 99.3 (GlcN 1, 2 Man 1), 98.0 (Fuc 1), 79.5 (GlcNAc 1), 68.0 ppm (Ino 2). ^{31}P NMR ($CDCl_3$): $\delta = -1.07$, -1.31 ppm. MALDI-TOF-MS: Calcd for $C_{426}H_{505}N_{19}O_{87}P_2$ 7346, found 7385 [M+K$^+$]. **1**: HPLC: Retention time = 37.5 min, C_{18} column (Discovery 250 mm × 10 mm), eluent: 40% *i*PrOH in H_2O (2.0 mL min^{-1}). ^{1}H NMR (D_2O, 600 MHz): $\delta = 5.24$ (br, 1H, Man 1), 5.14 (s, 1H, Man 1), 5.11 (br, 2H, 2 Man 1), 5.04 (br, 3H, Man 1, GlcNAc 1, Fuc 1), 4.93 (s, 1H, Man 1), 4.88 (br, 1H, Ser α(Ser = serine)), 4.83 (m, 1H, Asp α), 4.79 (bs, 1H, Ino 2), 4.75 (m, 1H, Asn α), 4.70 (d, 1H, GlcNAc 1), 4.26 (s, 1H, GlcN 1), 2.90–2.64 (m, 4H, Asn β, Asp β), 2.09, 2.07, 2.03 (3 s, 3 × 3H, 3 Ac), 1.30–1.15 (m, Fuc 6, Thr γ), 0.88 ppm (br, lipid-Me). MALDI-TOF MS: Calcd for $C_{135}H_{229}N_{19}O_{85}P_2$ 3538, found 3561 [M+Na$^+$].

 © 2004 Wiley-VCH Verlag GmbH & Co. KGaA, Weinheim

Computer Chemistry

Theoretical Search for Very Short Metal–Actinide Bonds: NUIr and Isoelectronic Systems**

Laura Gagliardi and Pekka Pyykkö*

It was recently discovered[1] that platinum can act, in discrete molecular groups, as a chemical analogue to oxygen. For instance the discrete molecular groups CPt, CPt_2, and CPt_3^{2-} were then found to have analogous bonding systems as CO, CO_2, and CO_3^{2-}, respectively. These analogues provide an example of the isolobal principle, now without any outside ligands on the Pt atom, a situation described as its "autogenic isolobality". These systems have multiple C–Pt bonds. The isolobal principle of Hoffmann refers to the similar chemical behavior of an sp hybrid and a metal atom with ligands, -ML_n. In "autogenic isolobality" a similar behavior occurs without the ligands, L.

Granted the extreme oxophilicity of the early actinides it is interesting to ask whether Pt or its neighbors could act as an oxygen analogue in uranyl, UO_2^{2+}. The isoelectronic neighbors, such as IrUIr as an analogue to the known NUN, immediately present themselves. It turned out that at least in the half-substituted case, the idea works. The suggestion is remotely favored by the existence of UPt_n ($n = 1$–3, 5) in the solid phase.[2] In general, the early-d–late-d metallic alloys, such as $CePt_2$ or $HfPt_3$, are astonishingly stable. This was described as Lewis acid–base interactions.[3] These suggested

[*] Dr. L. Gagliardi
Department of Physical Chemistry "F. Accascina"
University of Palermo
Viale delle Scienze
90128 Palermo (Italy)
Fax: (+39) 091-590-015
E-mail: laura.gagliardi@caspur.it
Prof. Dr. P. Pyykkö
Department of Chemistry
University of Helsinki
P.O.Box 55, 00014 Helsinki (Finland)

[**] This work was supported by Ministero dell'Università e della Ricerca Scientifica (MURST) and by The Academy of Finland, grants 173235 and 200903.

 DOI: 10.1002/anie.200353261 © 2004 Wiley-VCH Verlag GmbH & Co. KGaA, Weinheim

molecules would have multiple bonds. The molecule UAu_4 with a calculated single U^{IV}–Au bond of about 270 pm was recently predicted.[4] While Au is a pseudohalogen, Au^+ is for the present purpose a pseudochalcogen.

A further aspect is the conspicuous absence of strong actinide–actinide bonds in molecules. While a D_0 of 2.25(22) eV has been measured for diatomic U_2,[5] the only example on such a bond in singlet systems is the acetylene-like molecule predicted to be HTh≡ThH.[6] A theoretical treatment of U_2,[7,8] or even the possibly closed-shell and quintuply-bonded U_2^{2+} still presents daunting difficulties.[9] That would also make an An–M(5d) bond an interesting halfway achievement.

The only previous structurally characterized molecular actinide–M(*n*d) bonds that we are aware of, are the unbridged Th–Ru bond of 302.77(6) pm in $(Cp')_2Th^{I}Ru(Cp)(CO)_2$, ($Cp' = C_5Me_5$).[10,11] and the phosphido-bridged Th–Pt bond of 298.4(1) pm in the molecule $(C_5Me_5)_2Th(\mu\text{-}PPh_2)_2Pt(PMe_3)$, reported by Hay et al. [12] Theoretical calculations suggested a normal σ bond between Th and Pt.

Herein we report the results of a study of a series of new molecules with general formula EUM, E = C,N,O, or F. U is the uranium atom, and M = Re,Os,Ir, or Pt. These molecules turned out to be stable according to our quantum-chemical calculations and the bond between the uranium and the 5d metal is very short.

We have first carried out a quasirelativistic density functional theory (DFT) mapping of the trends of the E–U and U–M bond lengths and the singlet–triplet splittings in the EUM^q isoelectronic series. The results are shown in Table 1,

Table 1: Trends of the DFT-level singlet-state E–U and U–M bond lengths (in pm) for the EUM^q isoelectronic series.[a]

	Re	Os	Ir	Pt	Au
F	FURe 200, **207** +0.31				
O	$OURe^-$ 184, 209 +0.17	OUOs 179, 210 +0.38	$OUIr^+$ 175, 215 −0.27	$OUPt^{2+}$ 172, 226 −0.83	
N		$NUOs^-$ 176, 213 +1.16	NUIr 172, 218 +1.07	$NUPt^+$ **169**, 230 +0.17	$NUAu^{2+}$ 168, 256 −0.34
C				CUPt 175, 236 −0.21	

[a] Shortest bond lengths in boldface. $NUAu^{2+}$ is exceptionally a triplet state. The singlet-triplet splitting (in eV) is given below the bond lengths. Positive values indicate a singlet ground state.

where q is the charge chosen to obtain closed shells, isolelectronic with uranyl. Among the neutral species, a singlet ground state is most clearly favored at NUIr. The shortest N–U bond occurs at $NUPt^+$ and the shortest DFT singlet-state U–M bond of 207 pm occurs in FURe. Such a predicted bond length is extremely short. The four bonding orbitals are shown in Figure 1 for NUIr and also strongly suggest a N≡U≡Ir system with two well-developed triple bonds, as previously found for uranyl, NUN, and isoelectronic

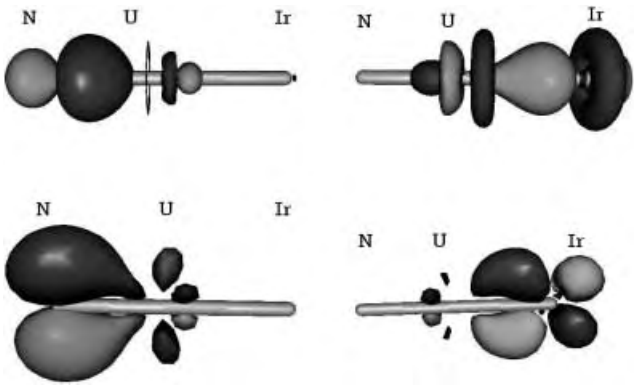


Figure 1. CASSCF molecular orbitals of NUIr.

systems.[13–17] The calculated dipole moment for NUIr is 0.24 Debye. with direction N(+) Ir(−). Both the smallness of the electric dipole moment of NUIr and the similarity of the CASSCF orbitals in Figure 1 suggest that the two bonds to the central uranium atom have a very similar character.

The DFT results can be compared with the CASPT2 results in Table 2, and are not found to change much. The CASPT2 electronic spectrum of NUIr up to 5 eV is reported

Table 2: Predicted species and bond distances (pm) in their ground state.

XUM	El. state	*R*(UX)	*R*(UM)	Δ*E*(Trip-Sing) [eV]
NUIr	$^1\Sigma^+$	172.2	218.4	+1.07
	$^3\Phi$	175.2	220.9	
NUIr[a]	$^1\Sigma^+$	174.9	216.7	+1.49[b]
NUIr[c]	$^1\Sigma^+$	174.1	214.5	
OUOs	$^1\Sigma^+$	179.2	210.2	+0.38
	$^3\Phi$	182.6	211.6	
FURe	$^1\Sigma^+$	200.1	206.7	+0.31
	$^3\Phi$	202.4	207.6	
CUPt	$^1\Sigma^+$	174.6	235.6	−0.21[b]
$NUOs^-$	$^1\Sigma^+$	213.2	176.2	+1.16
	$^3\Phi$	216.6	180.2	
$OURe^-$	$^1\Sigma^+$	184.1	209.1	+0.17
	$^3\Phi$	186.1	220.0	
$NUPt^+$	$^1\Sigma^+$	169.3	229.6	+0.17
	$^3\Phi$	173.0	236.7	
$NUAu^{2+}$	$^1\Sigma^+$	168.1	256.4	−0.34
	$^3\Phi$	173.2	279.1	
$OUIr^+$	$^1\Sigma^+$	174.6	215.0	−0.27
	$^3\Phi$	177.2	218.3	
$OUPt^{2+}$	$^1\Sigma^+$	171.6	226.3	−0.83
	$^3\Phi$	172.2	236.0	

[a] CASPT2 BS2. [b] Vertical. [c] CASPT2 BS3.

in Table 3. The ground state of NUIr is of $^1\Sigma^+$ type. The first excited state, $^1\prod$, lies 1.33 eV above the ground state. The first triplet excited state, $^3\Phi$, lies 1.49 eV above the ground state. The spectrum has been recalculated with the inclusion of spin–orbit coupling between all the spin–free singlet and triplet states reported in Table 3 and the first spin–orbit excited state is found to lie (vertically) 1.07 eV above the Ω_0 ground state. The inclusion of spin–orbit coupling does not have any effect on the structure of NUIr in its ground state.

 © 2004 Wiley-VCH Verlag GmbH & Co. KGaA, Weinheim

Table 3: CASPT2 vertical electronic spectrum for NUIr with BS2.

XUM	El. state	E [eV]	E [cm^{-1}]
	$^1\Sigma^+$	0.00	0.00
	$^1\Phi$	1.33	10727.7
	$^3\Phi$	1.49	12005.6
	$^1\Phi$	2.35	19015.0
	$^3\Phi$	2.61	21043.9
	$^3\Sigma^-$	3.11	25073.1
	$^3\Sigma^-$	3.14	25291.2
	$^1\Sigma^-$	3.41	27503.9
	$^1\Sigma^-$	3.54	28601.8
	$^3\Sigma^+$	4.51	36353.9
	$^3\Sigma^+$	5.08	40985.0

The bond along the molecule involves essentially σ- and π-bonding orbitals (see also below the discussion about the active space). The δ orbitals are strongly localized at Ir and only weakly bonding to U. As a simple test, a Mulliken population analysis for NUIr is shown in Table 4. The end atoms are only slightly negative. The U populations amount to $6d^{2.41}5f^{2.76}$. If the 7p is neglected, only a very slight 6p hole of −0.03 is assigned to U.

Table 4: CASPT2-BS2 Mulliken population analysis for NUIr.[a]

	N	U	Ir
δ	−0.24	+0.46	−0.22
s	3.65	12.28	11.37
p	3.49	29.97	24.15
d	0.20	32.41	27.58
f		16.76	14.10
g		0.12	

[a] δ is the partial charge on each atom, followed by the number of electrons in each type of orbitals.

The calculated vibrational frequencies are reported in Table 5. The U−M stretching vibrations are calculated to occur in the range from 300 to 400 cm^{-1}. All the systems are clearly linear.

In view of the potentially helpful $4d^{10}5s^0$ electron configuration of Pd, one attempt was made on $NUPd^+$. The U−Pd bond length was 231.5 pm and the triplet was clearly below the singlet. Other less promising tests were those on the symmetric, doubly substituted systems IrUIr and $PtUPt^{2+}$, analogous to the known NUN and OUO^{2+}. They both turned out to be linear. IrUIr has a triplet ground state, with a Ir−U bond length of 220.7 pm and harmonic frequencies in the range 56–367 cm^{-1}. $PtUPt^{2+}$ in its singlet state has a Pt−U bond length of 222.6 pm, and harmonic frequencies in the range 46–333 cm^{-1}. The triplet lies lower in energy than the singlet, but a full triplet optimization could not be carried out. The asymmetric OsUPt was also investigated and it has a triplet ground state with Os−U and U−Pt bond lengths of 211 and 239 pm, respectively, and harmonic frequencies in the range 53–385 cm^{-1}.

One possible way to create the present species might be by "brute force", which would involve the simultaneous evaporation of the three elements. Another possibility would be to start with the experimentally known diatomics IrN or UN.

Table 5: Harmonic B3LYP frequencies (cm^{-1}) and their IR intensities (km mol^{-1}) in parentheses with the BS1 basis set.

States	π		σ	σ
		NUIr		
$^1\Sigma^+$	100.63		320.35	1119.51
	(36.5)		(3.1)	(282.5)
$^3\Phi$	117.56		300.75	991.37
	(38.5)		(4.1)	(49.8)
		OUOs		
$^1\Sigma^+$	102.67		372.83	943.61
	(16.5)		(0.9)	(274.5)
$^3\Phi$	119.80		363.00	888.54
	(21.7)		(2.0)	(297.3)
		FURe		
$^1\Sigma^+$	39.30		390.96	628.81
	(3.8)		(1.1)	(96.7)
$^3\Phi$	62.80		368.86	594.64
	(6.2)		(0.0)	(113.5)
		$NUOs^-$		
$^1\Sigma^+$	105.11		344.48	1034.96
	(34.4)		(0.0)	(525.2)
$^3\Phi$	120.14		320.93	928.34
	(41.0)		(3.7)	(273.8)
		$OURe^-$		
$^1\Sigma^+$	89.76		377.50	857.09
	(9.2)		(0.2)	(325.2)
$^3\Phi$	87.76		309.61	828.46
	(15.4)		(0.4)	(333.1)

The exothermic reaction energies with a U or Ir atom are −460 and −510 kJ mol^{-1}, respectively.

IrN has a calculated bond length of 160.4 pm and a harmonic frequency of 1231 cm^{-1} in the $^1\Sigma^+$ ground state, compared to the experimental values of 160.68 pm and 1126 cm^{-1}.[18] UN has a calculated bond length of 174.4 and a harmonic frequency of 1052 cm^{-1} pm in the $^4\Sigma$ ground state, compared to the experimental value of 996 cm^{-1}.[19,20] In a previous study[17] the formation of NUN from U and N_2 was investigated, and NUN was found to lie about −230 kJ mol^{-1} lower in energy than U and N_2. The present results thus indicate that the energy balance would be even more favorable for NUIr. In conclusion, we are predicting the existence of a very short triple Ir≡U bond of about 215 pm in a closed-shell NUIr molecule.

Experimental Section

Computational methods: The calculations were performed at the B3LYP density functional level of theory. Some of the species were also studied by using the complete active space (CAS) SCF (SCF = self-consistent field) method[21] with dynamic correlation added by second-order perturbation theory (CASPT2).[22]

A 3s2p1d basis set of 6-31g* type was used for the light atoms, namely N and O. For the heavy atoms the core electrons were replaced with quasirelativistic pseudopotentials[23] resulting in 16, 17, 18, and 32 valence electrons for Os, Ir, Pt, and U, respectively. The corresponding valence basis sets were of 6s5p3d quality for Os, Ir, Pt, and 8s7p6d4f quality for U. We labeled such basis sets as BS1 basis sets. The CASSCF/CASPT2 calculations were performed with all electron basis sets of ANO type for all atoms. The exponents were optimized by using the Douglas–Kroll (DK) Hamiltonian. The contracted basis set was 4s3p2d for N, 8s7p5d3f for Ir, and 9s8p7d5f for U, indicated as BS2. The BS2 basis was further extended by one f

 © 2004 Wiley-VCH Verlag GmbH & Co. KGaA, Weinheim

function for N, one g function for Ir, and two g function for U, indicated as BS3.

In the CASPT2 calculations scalar relativistic effects were included with a DK Hamiltonian.[24,25] The effects of spin–orbit coupling were introduced by using a method based on the CASSCF state interaction approach (CASSI).[26,27] Here, the CASSCF wave function generated for a number of electronic states are allowed to mix under the influence of a spin–orbit Hamiltonian. The method has recently been described,[28] and we refer to this article for details.

In our recent study of the NUN system,[17] we found that it was important to include in the active space the nitrogen 2p orbitals and the corresponding UN antibonding orbitals of σ and π type. They are hybrid orbitals mixing 5f, 6d, and 7s. This gives an active space of 12 electrons in 12 orbitals (12/12). In the NUIr case, the 2p orbitals of one nitrogen atom have been replaced with the 4d orbitals of appropriate symmetry, namely 4d σ and π. Preliminary calculations, including also the unoccupied Ir 4d δ, indicated that the antibonding orbitals did not affect the results, so they have not been included in most of the calculations. The CASPT2 geometry optimization of NUIr was carried out numerically.

The DFT calculations have been performed with the Gaussian 98 package and the CASSCF/CASPT2 calculations with the MOLCAS 6.0 program.[29]

Received: November 5, 2003 [Z53261]

Keywords: computer chemistry · density functional calculations · iridium · multiple bonding · uranium

[1] P. Pyykkö, M. Patzschke, J. Suurpere, *Chem. Phys. Lett.* **2003**, *381*, 45 – 52.
[2] J. J. Katz, G. T. Seaborg, L. R. Morss, *The Chemistry of the Actinide Elements*, Part 1, 2nd ed., Chapman and Hall, London, **1986**, p. 234.
[3] L. Brewer, *J. Chem. Educ.* **1972**, *61*, 101 – 104.
[4] L. Gagliardi, *J. Am. Chem. Soc.* **2003**, *125*, 7504 – 7505.
[5] L. N. Gorokhov, A. M. Emel'yanov, Yu. S. Khodeev, *Teplofiz. Vys. Temp.* **1974**, *12*, 1307 – 1309.
[6] M. Straka, private communication.
[7] B. E. Bursten, G. A. Ozin, *Inorg. Chem.* **1984**, *23*, 2910 – 2911.
[8] M. Pepper, B. E. Bursten, *J. Am. Chem. Soc.* **1990**, *112*, 7803 – 7804.
[9] P. Pyykkö, N. Runeberg, B. A. Hess, unpublished results.
[10] R. S. Sternal, C. P. Brock, T. J. Marks, *J. Am. Chem. Soc.* **1985**, *107*, 8270 – 8272.
[11] B. E. Bursten, K. J. Novo-Gradac, *J. Am. Chem. Soc.* **1987**, *109*, 904 – 905.
[12] P. J. Hay, R. R. Ryan, K. V. Salazar, D. A. Wrobleski, A. P. Sattelberger, *J. Am. Chem. Soc.* **1986**, *108*, 313 – 315.
[13] R. G. Denning, *Struct. Bonding (Berlin)* **1992**, *79*, 215 – 276.
[14] P. Pyykkö, J. Li, N. Runeberg, *J. Phys. Chem.* **1994**, *98*, 4809 – 4813.
[15] M. Straka, K. G. Dyall, P. Pyykkö, *Theor. Chem. Acc.* **2001**, *106*, 393 – 403.
[16] L. Gagliardi, B. Roos, *Chem. Phys. Lett.* **2000**, *331*, 229 – 234.
[17] L. Gagliardi, G. La Manna, B. Roos, *Faraday Discuss.* **2003**, *124*, 63 – 68.
[18] R. Ram, J. Liévin, P. Bernath, *J. Mol. Spectrosc.* **1999**, *197*, 133 – 146.
[19] G. Kushto, P. Souter, L. Andrews, M. Neurock, *J. Chem. Phys.* **1997**, *106*, 5894 – 5903.
[20] K. Sankaran, K. Sundararajan, K. Viswanathan, *J. Phys. Chem. A* **2001**, *105*, 3995 – 4001.
[21] B. O. Roos in *Ab Initio Methods in Quantum Chemistry, Vol. II* (Ed.: K. P. Lawley), Wiley, Chichester, England, **1987**, p. 399.
[22] K. Andersson, P.-Å. Malmqvist, B. O. Roos, *J. Chem. Phys.* **1992**, *96*, 1218 – 1226.
[23] D. Andrae, U. Häussermann, M. Dolg, H. Stoll, H. Preuss, *Theor. Chim. Acta* **1990**, *77*, 123 – 141.
[24] N. Douglas, N. M. Kroll, *Ann. Phys.* **1974**, *82*, 89 – 155.
[25] B. Hess, *Phys. Rev. A* **1986**, *33*, 3742 – 3748.
[26] P.-Å. Malmqvist, *Int. J. Quantum Chem.* **1986**, *30*, 479 – 494.
[27] P.-Å. Malmqvist, B. O. Roos, *Chem. Phys. Lett.* **1989**, *155*, 189 – 194.
[28] P.-Å. Malmqvist, B. Roos, B. Schimmelpfenning, *Chem. Phys. Lett.* **2002**, *357*, 230 – 240.
[29] K. Andersson, M. Barysz, A. Bernhardsson, M. R. A. Blomberg, Y. Carissan, D. L. Cooper, M. P. Fülscher, L. Gagliardi, C. de Graaf, B. A. Hess, G. Karlström, R. Lindh, P.-Å. Malmqvist, T. Nakajima, P. Neogrády, J. Olsen, B. O. Roos, B. Schimmelpfennig, M. Schütz, L. Seijo, L. Serrano-Andrés, P. E. M. Siegbahn, J. Stålring, T. Thorsteinsson, V. Veryazov, P.-O. Widmark, MOLCAS *Version 6.0*, Dept. of Theor. Chem., Chem. Center, Univ. of Lund, P.O.B. 124, S-221 00 Lund, Sweden, Lund, **2003**.

 © 2004 Wiley-VCH Verlag GmbH & Co. KGaA, Weinheim

Catalytic Amide Synthesis

Efficient Hydration of Nitriles to Amides in Water, Catalyzed by Ruthenium Hydroxide Supported on Alumina**

*Kazuya Yamaguchi, Mitsunori Matsushita, and Noritaka Mizuno**

Hydration of nitriles to the corresponding amides is an important reaction in academia and industry because of their usefulness in a wide variety of applications such as intermediates in organic syntheses and as raw materials for engineering plastics, detergents, and lubricants.[1–4] For example, hydration of acrylonitrile produces annually more than 2×10^5 tons of acrylamide and is the most important technology for the production of this chemical.[4–6] Homogeneous hydration of nitriles is traditionally carried out with acids and bases such as H_2SO_4 and NaOH. However, carboxylic acids are formed as undesirable by-products by hydrolysis of the starting nitriles and amide products, especially under strongly basic conditions. In addition, many functional groups, for

[*] Dr. K. Yamaguchi, M. Matsushita, Prof. Dr. N. Mizuno
Department of Applied Chemistry, School of Engineering
The University of Tokyo
7-3-1 Hongo, Bunkyo-ku, Tokyo 113-8656 (Japan)
Fax: (+81) 3-5841-7220
E-mail: tmizuno@mail.ecc.u-tokyo.ac.jp

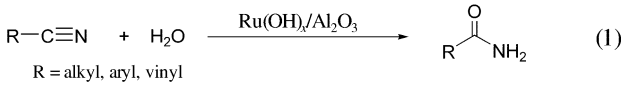
[**] This work was supported in part by the Core Research for Evolutional Science and Technology (CREST) program of Japan Science and Technology Agency (JST) and a Grant-in-Aid for Scientific Research from the Ministry of Education, Culture, Sports, Science, and Technology of Japan.

Supporting information for this article is available on the WWW under http://www.angewandte.org or from the author.

 © 2004 Wiley-VCH Verlag GmbH & Co. KGaA, Weinheim DOI: 10.1002/anie.200353461

example, carbon–carbon double bonds, do not tolerate such forcing conditions, which results in decreased selectivity for amides. Only under carefully controlled conditions with one of equivalent water with respect to the nitrile could hydration of a nitrile to an amide be selectively catalyzed by H_2SO_4 to give the corresponding amide sulfate salt. Since a stoichiometric amount of ammonia (two equivalents with respect to amide sulfate) is required to isolate the free amide, ammonium sulfate is produced as waste. Therefore, the development of an efficient, intrinsically non-waste-producing catalytic hydration system is of great importance.

Many efficient methods that use microorganisms for enzymatic hydration of nitriles[5,6] or homogeneous complexes of transition metals such as cobalt,[7] copper,[8] molybdenum,[9] ruthenium,[10] rhodium,[11] palladium,[12,13] and platinum[14,15] have been reported. However, these systems have disadvantages: difficulty in catalyst/product separation and necessity of special handling of microorganisms and metal complexes. Despite the advantages of heterogeneous hydration, for example, easy catalyst/product separation and recycling, only a few examples have been reported. Unactivated neutral alumina (stoichiometric hydration without water),[16] Raney copper,[4] KF/Al_2O_3,[17] KF/phosphate,[18] MnO_2/SiO_2,[19,20] Ru-substituted hydroxyapatite ($(RuCl)_2Ca_8(PO_4)_6(OH)_2$),[21] and $NaNO_3$ on fluoroapatite ($NaNO_3$/FAP)[22] are examples. However, turnover numbers are still very low (≤ 6) or stoichiometric, catalysts can not be reused, and/or the type of nitrile is limited. In this context, efficient, widely usable, reusable catalysts are so far unknown, although heterogeneous hydration systems are environmentally and technologically the most desirable.[23–25] Herein we report that the easily prepared, inexpensive supported ruthenium hydroxide catalyst $Ru(OH)_x/Al_2O_3$[26–28] is effective for the hydration of various nitriles to amides in water[29] under conditions that are entirely free of explosive, hazardous, or carcinogenic organic solvents, even in the workup steps [Eq. (1)].



(1)

First, the catalytic activity and selectivity for the hydration of benzonitrile to benzamide in water at 403 K were compared with those of a variety of ruthenium catalysts (Table 1). Hydration did not proceed in the absence of catalyst. γ-Al_2O_3 and γ-Al_2O_3 treated with NaOH did not show any catalytic activity under the present reaction conditions. Among the ruthenium catalysts tested, $Ru(OH)_x/Al_2O_3$ had the highest catalytic activity and selectivity for the hydration of benzonitrile to benzamide, and no benzoic acid could be detected. Under the same conditions, it was confirmed that $Ru(OH)_x/Al_2O_3$ did not catalyze the hydrolysis and dehydration of benzamide. The yield of benzamide was higher than those of heterogeneous catalysts such as anhydrous RuO_2, $Ru(OH)_3{\cdot}n\,H_2O$, and $(RuCl)_2Ca_8(PO_4)_6(OH)_2$, and of homogeneous ruthenium catalysts such as $RuCl_3{\cdot}n\,H_2O$ and $[RuCl_2(PPh_3)_3]$ 18-Electron ruthenium complexes such as $[RuCl_2(dmso)_4]$, $[RuCl_2(bpy)_2]$, and $[\{RuCl_2(p\text{-cymene})\}_2]$ were completely inactive.

Table 1: Hydration of benzonitrile to benzamide with various catalysts.[a]

Entry	Catalyst	Conversion of benzonitrile [%]	Selectivity to benzamide [%]	Rate × 10^3 [M min^{-1}]
1	$Ru(OH)_x/Al_2O_3$	47	>99	1.74
2[b]	$(RuCl)_2Ca_8(PO_4)_6(OH)_2$	7	>99	0.10
3	$Ru(OH)_3{\cdot}n\,H_2O$	7	>99	0.24
4	RuO_2	2	>99	0.06
5	$RuCl_3{\cdot}n\,H_2O$	28	>99	0.79
6	$[Ru(acac)_3]$	no reaction	–	0.00
7	$[RuCl_2(PPh_3)_3]$	no reaction	–	0.00
8	$[RuCl_2(DMSO)_4]$	no reaction	–	0.00
9	$[\{RuCl_2(p\text{-cymene})\}_2]$	no reaction	–	0.00
10	$[RuCl_2(bpy)_2]$	no reaction	–	0.00
11[c]	Al_2O_3	no reaction	–	0.00
12[c]	Al_2O_3 treated with NaOH	no reaction	–	0.00
13	NaOH	3	>99	0.05
14	H_2SO_4	no reaction	–	0.00
15	None	no reaction	–	0.00

[a] Reaction conditions: benzonitrile (1 mmol), catalyst (2 mol%), water (3 mL), 403 K, 3 h. Conversion and selectivity were determined by GC with an internal standard. [b] Prepared according to the procedure in ref. [20]. [c] 0.2 g. Wilgus et al.[16] reported that unactivated alumina could act as a stoichiometric reagent (two hydroxy functions for hydration of one nitrile molecule) for the hydration of nitriles in the absence of water. If the alumina used can act as a stoichiometric reagent in the same way, the maximum yield is estimated to be ca. 5%. However, alumina was completely inactive under these conditions, probably because of the presence of water in the present system.

When the hydration of benzonitrile was carried out at 413 K (see Experimental Section), a quantitative yield of benzamide was obtained after 6 h, as determined by GC analysis. The $Ru(OH)_x/Al_2O_3$ catalyst could be easily separated from the reaction mixture by filtration (Figure 1a and b). After separation of the catalyst, the filtrate was cooled to 273 K, and analytically pure white crystals of benzamide appeared (Figure 1c). The crystals were isolated from the water solvent by filtration or decantation in 90% yield. Recovered $Ru(OH)_x/Al_2O_3$ could be reused at least twice for the hydration of benzonitrile without appreciable loss of catalytic performance (entries 1–3 in Table 2). After the catalytic hydration of benzonitrile was completed under the conditions in Table 2, the reaction mixture was filtered to remove the $Ru(OH)_x/Al_2O_3$ and product amide. It was confirmed that no ruthenium was present in the filtrate by inductively coupled plasma atomic emission spectroscopy (ICP-AES; detection limit of 7 ppb). Then, benzonitrile (1 mmol) was again added to the filtrate and the solution was heated to 413 K. No conversion of benzonitrile was observed. These results show that any contribution to the observed catalysis from ruthenium species that leached into the reaction solution can be ruled out, and the observed catalysis is truly heterogeneous in nature.[30]

The scope of the present $Ru(OH)_x/Al_2O_3$ catalyst system with regard to various kinds of nitriles was examined. The results are summarized in Table 2. $Ru(OH)_x/Al_2O_3$ has high catalytic activity for hydrations of activated, unactivated, and

 © 2004 Wiley-VCH Verlag GmbH & Co. KGaA, Weinheim

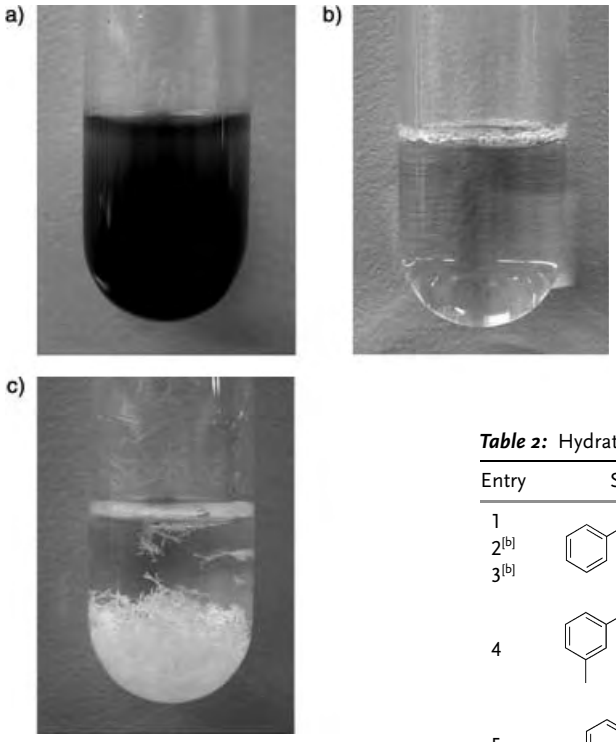
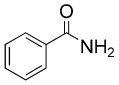
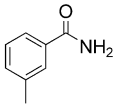
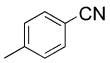
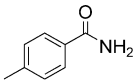
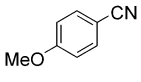
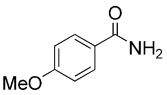
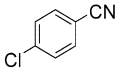
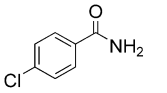
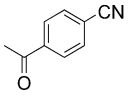
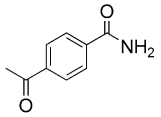
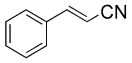
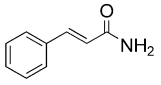
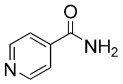
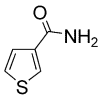
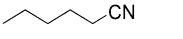
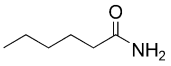
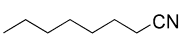
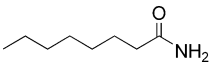


Figure 1. Hydration of benzonitrile to benzamide. a) Reaction mixture, b) filtrate after removal of $Ru(OH)_x/Al_2O_3$ by filtration at 363 K, and c) benzamide crystals obtained after cooling the filtrate.

heterocyclic nitriles in water. Benzonitriles were smoothly hydrated to give the corresponding benzamides in excellent yields (entries 1–8). The rates were not much influenced by the electronic effects of the substituents on the aromatic ring of benzonitriles. A larger scale experiment (tenfold scale-up, 0.4 mol% Ru) for benzonitrile at 423 K showed a turnover frequency (TOF) of 13 h^{-1}, and the turnover number (TON) reached 234. These values are the highest of those reported for the heterogeneous hydration of benzonitrile so far: KF/Al_2O_3 (TOF 0.2 h^{-1}, TON 0.5 based on KF),[17] KF/phosphate (0.2 h^{-1}, 0.9 based on KF),[18] MnO_2/SiO_2 (0.2 h^{-1}, 0.7 based on MnO_2),[19] $(RuCl)_2Ca_8(PO_4)_6(OH)_2$ (0.2 h^{-1}, 6 based on Ru),[21] and $NaNO_3$ on fluoroapatite ($NaNO_3$/FAP; 2 h^{-1}, 6 based on $NaNO_3$).[22] Hydration of the α,β-unsaturated nitrile cinnamonitrile proceeded only at the cyano group to afford the corresponding α,β-unsaturated amide (entry 9). Notably, the industrially important hydration of acrylonitrile proceeded with 2.3 mol% of $Ru(OH)_x/Al_2O_3$ at 393 K to afford a quantitative yield of acrylamide. Neither hydration of the carbon–carbon double bond nor polymerization of acrylonitrile and/or acrylamide occurred (entry 10). $Ru(OH)_x/Al_2O_3$ successfully catalyzed the hydration of various nitriles containing heteroatoms such as oxygen, nitrogen, and sulfur to the corresponding amides in high yields (entries 6, 8, 11, and 12). The less reactive aliphatic nitriles could also be hydrated to the corresponding aliphatic amides (entries 13 and 14).

In the hydration of toluonitriles, the lower reaction rate of *o*-tolunitrile (79% yield after 24 h) relative to *m*- and *p*-

Table 2: Hydration of various nitriles catalyzed by $Ru(OH)_x/Al_2O_3$.[a]

Entry	Substrate	Product	*t* [h]	Conversion [%]	Selectivity [%]
1			6	99	>99
2[b]			6	99	>99
3[b]			6	99	>99
4			6	96	>99
5			6	>99	99
6			6	>99	>99
7			6	>99	>99
8			6	>99	99
9			5	>99	99
10[c]			24	>99	>99
11			6	91	98
12			6	>99	>99
13[d]			10	92	99
14[d]			24	91	97

[a] Reaction conditions: nitrile (1 mmol), $Ru(OH)_x/Al_2O_3$ (4 mol% Ru), water (3 mL), 413 K. The conversion and selectivity were determined by GC with an internal standard. Traces of the corresponding carboxylic acids, formed by hydrolysis of starting nitriles or amide products, were found as by-products in some cases. Carbon balance for each reaction was greater than 95%. [b] These experiments used a recycled catalyst: 1st reuse (entry 2), 2nd reuse (entry 3). The reaction conditions were the same as in entry 1. The initial rates for the recycle runs were the same as that for the first run with fresh catalyst. [c] Reaction conditions: acrylonitrile (10 mmol), $Ru(OH)_x/Al_2O_3$ (2.3 mol% Ru), water (20 mL), 393 K. The conversion and selectivity were determined by ^1H NMR spectroscopic analysis with an internal standard. [d] The reaction was carried out at 403 K.

 © 2004 Wiley-VCH Verlag GmbH & Co. KGaA, Weinheim

toluonitrile indicates a steric effect. This observation strongly suggests that nitriles coordinate to the ruthenium center on the surface of $Ru(OH)_x/Al_2O_3$ and that hydration of nitriles proceeds by intramolecular attack of a ruthenium hydroxide species on the coordinated nitrile (steps 1 and 2). When the hydration of *o*-, *m*-, and *p*-toluonitriles was catalyzed by NaOH, the reactivity did not vary. In addition, the ρ value for NaOH-catalyzed hydration in water (external attack of water on the nitrile carbon atom catalyzed by free OH^-) should be positive, in contrast to the negative ρ value for the present $Ru(OH)_x/Al_2O_3$-catalyzed hydration (see below). The above observations show that free OH^- is not the active species. It was reported that cobalt(III) hydroxide undergoes coordination of a nitrile and that this favors nucleophilic attack of the metal hydroxide on the proximal nitrile carbon atom rather than on the distal carbon–carbon double bond, hydration of which is thus prevented. These results are in agreement with those for the present system and support coordination of a nitrile to Ru^{n+} (**II**). Competitive hydration of benzonitrile and *p*-substituted benzonitriles was carried out in water at 413 K. The order of reactivity was *p*-OCH_3 ($k_X/k_H = 1.28$) > *p*-CH_3 (1.01) > *p*-H (1.00) > *p*-Cl (0.79) > *p*-$COCH_3$ (0.70). The good linearity of Hammett plots ($\lg(k_X/k_H)$ versus Brown–Okamoto σ^+, see the Supporting Information) suggests that the present hydration proceeds with a single mechanism. The slope of the linear line gave a Hammett ρ value of -0.21. The negative Hammett ρ value might be due to the formation of a positively charged transition state at the carbon atom adjacent to the phenyl ring.

On the basis of these results, we propose the possible mechanism given in Figure 2 for the $Ru(OH)_x/Al_2O_3$-catalyzed hydration of nitriles. This catalytic hydration can be divided into steps 1–3: Initially, coordination of a nitrile to the ruthenium center proceeds to form **II** (step 1). Then, intramolecular nucleophilic attack of hydroxide species in **II** on the nitrile carbon atom takes place to afford the ruthenium iminolate species **III** or ruthenium η^2-amidate species **IV** (step 2). Step 2 may include the formation of a carbocation-type transition state. Regeneration of ruthenium hydroxide species **I** proceeds by the ligand exchange between water and **III** or **IV** together with the formation of the amide product (step 3).

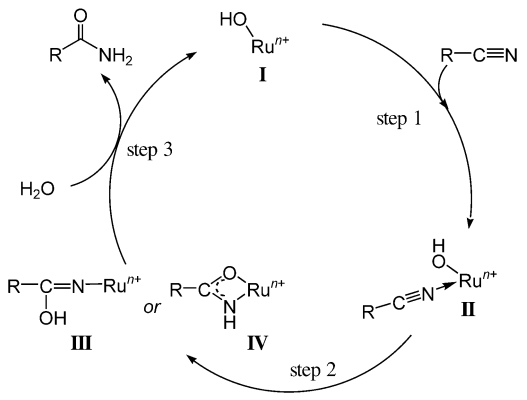


Figure 2. A proposed reaction mechanism for the $Ru(OH)_x/Al_2O_3$-catalyzed hydration of nitriles.

Kinetic studies revealed a zero-order dependence of the reaction rate on the concentration of water and a first-order dependence on both the amount of $Ru(OH)_x/Al_2O_3$ and the nitrile concentration (Supporting Information). The Arrhenius plots (observed rate constant k_{obs} versus T^{-1}) are also shown in the Supporting Information (383–423 K). Good linearity was observed for the Arrhenius plots, which gave the following activation parameters: $E_a = 71.5\ kJ\,mol^{-1}$, $\Delta H^{\ddagger}_{413\,K} = 68.1\ kJ\,mol^{-1}$, $\Delta S^{\ddagger}_{413\,K} = -155.3\ J\,mol^{-1}K^{-1}$, and $\Delta G^{\ddagger}_{413\,K} = 132.2\ kJ\,mol^{-1}$. The activation energy E_a is lower than that of hydration with H_2SO_4 ($E_a = 150.7\ kJ\,mol^{-1}$).[31] The hydration rate was independent of the content of D_2O (Supporting Information). These results show that O–H bond dissociation (step 3) is not included in the rate-limiting step under the present conditions.[32] The value of the activation entropy $\Delta S^{\ddagger}_{413\,K}$ suggests that a bimolecular transition state (step 2) is included in the rate-limiting step.[32]

In summary, $Ru(OH)_x/Al_2O_3$ can act as a heterogeneous catalyst for the hydration of nitriles in water. The hydration of both activated and unactivated nitriles can be performed with high conversion and selectivity to give the corresponding amides. Furthermore, catalyst/product separation is easy, and $Ru(OH)_x/Al_2O_3$ is recyclable.

Experimental Section

The $Ru(OH)_x/Al_2O_3$ catalyst was prepared by the procedure reported previously.[26–28] A typical $Ru(OH)_x/Al_2O_3$-catalyzed hydration was carried out as follows: Benzonitrile (5 mmol), $Ru(OH)_x/Al_2O_3$ (4 mol%), and water (15 mL) were placed in a Teflon vessel with a magnetic stir bar. Next, the Teflon vessel was quickly inserted into an autoclave, and then the autoclave was heated at 413 K (bath temperature). The reaction rates were not affected by stirring rates from 500 to 2000 rpm. After 6 h, benzamide was formed in >99% yield, as determined by GC analysis. $Ru(OH)_x/Al_2O_3$ was removed by filtration at 363 K. The filtrate was cooled to 273 K, and white crystals precipitated from the filtrate. The crystalline product was collected by simple filtration and dried in vacuo to give analytically pure benzamide in 90% yield. The recovered $Ru(OH)_x/Al_2O_3$ was further washed with hot water and an aqueous NaOH solution (pH 13) and then dried in vacuo before reuse.

Received: December 4, 2003 [Z53461]

Keywords: amides · cyanides · heterogeneous catalysis · hydration · ruthenium

[1] F. Matsuda, *Chemtech* **1977**, *7*, 306.
[2] C. E. Mabermann in *Encyclopedia of Chemical Technology*, *Vol. 1* (Ed.: J. I. Kroschwitz), Wiley, New York, **1991**, p. 251–266.
[3] D. Lipp in *Encyclopedia of Chemical Technology*, *Vol. 1* (Ed.: J. I. Kroschwitz), Wiley, New York, **1991**, p. 266–287.
[4] R. Opsahl in *Encyclopedia of Chemical Technology*, *Vol. 2* (Ed.: J. I. Kroschwitz), Wiley, New York, **1991**, p. 346–356.
[5] P. K. Mascharak, *Coord. Chem. Rev.* **2002**, *225*, 201, and references therein.

 © 2004 Wiley-VCH Verlag GmbH & Co. KGaA, Weinheim

[6] K. Ingvosersen, J. Kamphuis in *Enzyme Catalysis in Organic Synthesis*, *Vol. 1* (Eds.: K. Drauz, H. Waldmann), VCH, Weinheim, **1995**, p. 365 – 392.
[7] J. H. Kim, J. Britten, J. Chin, *J. Am. Chem. Soc.* **1993**, *115*, 3618.
[8] R. Breslow, R. Fairweather, J. Keana, *J. Am. Chem. Soc.* **1967**, *89*, 2135.
[9] K. L. Breno, M. D. Pluth, D. R. Tyler, *Organometallics* **2003**, *22*, 1203.
[10] S.-I. Murahashi, S. Sasao, E. Saito, T. Naota, *J. Org. Chem.* **1992**, *57*, 2521.
[11] M. C. K.-B. Dojoman, A. N. Ajjou, *Tetrahedron Lett.* **2000**, *41*, 4845.
[12] G. Villain, A. Gasket, P. H. Kalck, *J. Mol. Catal.* **1981**, *12*, 103.
[13] N. V. Kaminskaia, N. M. Kostic, *J. Chem. Soc. Dalton Trans.* **1996**, 3677.
[14] T. Ghaffar, A. W. Parkins, *Tetrahedron Lett.* **1995**, *36*, 8657.
[15] T. Ghaffar, A. W. Parkins, *J. Mol. Catal. A* **2000**, *160*, 249.
[16] C. P. Wilgus, S. Downing, E. Molitor, S. Bains, R. M. Pagni, G. W. Kabalka, *Tetrahedron Lett.* **1995**, *36*, 3469.
[17] C. G. Rao, *Synth. Commun.* **1982**, *12*, 177.
[18] S. Sebti, A. Rhiil, A. Saber, N. Hanafi, *Tetrahedron Lett.* **1996**, *37*, 6555.
[19] K.-T. Li, M.-H. Shih, H.-W. Huang, C.-J. Hu, *Synthesis* **1988**, 715.
[20] P. Breuilles, R. Leclerc, D. Uguen, *Tetrahedron Lett.* **1994**, *35*, 1401.
[21] K. Mori, K. Yamaguchi, T. Mizugaki, K. Ebitani, K. Kaneda, *Chem. Commun.* **2001**, 461.
[22] A. Solhy, A. Smahi, H. E. Badaoui, B. Elaabar, A. Amoukal, A. Tikad, S. Sebti, D. J. Macquarrie, *Tetrahedron Lett.* **2003**, *44*, 4031.
[23] P. T. Anastas, J. C. Warner, *Green Chemistry: Theory and Practice*, Oxford University Press, Oxford, **1998**.
[24] J. H. Clark, *Green Chem.* **1999**, *1*, 1.
[25] Thematic issue on "Green Chemistry", *Acc. Chem. Res.* **2002**, *35*, 685 – 816.
[26] K. Yamaguchi, N. Mizuno, *Angew. Chem.* **2002**, *114*, 4720; *Angew. Chem. Int. Ed.* **2002**, *41*, 4538.
[27] K. Yamaguchi, N. Mizuno, *Angew. Chem.* **2003**, *115*, 1517; *Angew. Chem. Int. Ed.* **2003**, *42*, 1479.
[28] K. Yamaguchi, N. Mizuno, *Chem. Eur. J.* **2003**, *9*, 4353.
[29] Thematic issue on "Organic Reaction in Water", *Adv. Synth. Catal.* **2002**, *3–4*, 219 – 451.
[30] R. A. Sheldon, M. Wallau, I. W. C. E. Arends, U. Schuchardt, *Acc. Chem. Res.* **1998**, *31*, 485.
[31] K. Sugiyama, H. Miura, Y. Nakano, H. Sekiwa, T. Matsuda, *Bull. Chem. Soc. Jpn.* **1986**, *59*, 2983.
[32] K. A. Connors, *Chemical Kinetics, The Study of Reaction Rates in Solution*, VCH, New York, **1990**.

 © 2004 Wiley-VCH Verlag GmbH & Co. KGaA, Weinheim

Bioinorganic Chemistry

Modular Synthesis of Ruthenium-Labeled Diaryl Ether Peptoids**

*Alexander Schmid and Thomas Lindel**

Dedicated to Professor Wolfgang Steglich on the occasion of his 70th birthday

Research on peptide-like ("peptoid"[1]) compounds is of basic relevance to bioorganic and bioinorganic chemistry. Important examples include the fascinating β- and γ-peptides.[2] Radioactive peptide metal complexes constitute a special case, promising the sensitive, selective detection or perhaps even the destruction of tumor cells; the biochemical selectivity is efficiently combined with high-energy radiation. The most prominent example used in nuclear medicine is ^{111}In radio-labeled octreotide which binds to receptors of the regulatory hormone somatostatin.[3] Beck et al. have reviewed the transition-metal complexes of amino acids and peptides as an emerging area of bioorganometallic chemistry.[4]

Peptides are normally labeled after their assembly, more recently this has also been possible at specially functionalized sites.[5] In general, however, the introduction of a large metal label into a small bioactive peptide may alter or even abolish its properties. Therefore, it would be desirable to be able to select from a pool of peptoids all of which are already metal labeled. Ruthenium isotopes appear to be suitable for labeling, because their half-lives range three days to one year[6] and because they can be incorporated into peptoids as chemically inert sandwich complexes. Ruthenium metallopharmaceuticals have recently been reviewed,[7,8] The potential of ruthenium isotpes[6] for applications in radiopharmacy had been recognized early on, but in the peptide area only small molecules, such as β-ruthenocenylalanine could be characterized.[20] Several research groups, in particular Pearson et al., used $[RuCp]^+$-($Cp = C_5H_5$) monolabeled peptoid diaryl ethers as intermediates for the synthesis of natural products.[9] Sheldrick et al. converted dipeptides and diketopiperazines into doubly $[RuCp^*]^+$-($Cp^* = C_5Me_5$) labeled peptoids.[10]

Ruthenium(III) chloride can directly be used as the source of radioactive, inert ruthenium sandwich complexes, because $[RuCp^*]^+$ sandwich complexes of benzenoid arenes can be synthesized in a single step.[13] Herein we report the synthesis and characterization of a complete initial sequence for the modular assembly of metal-labeled peptoids with a new architecture. This method, based on solid-supported processes, has the potential to be used in combinatorial chemistry. The approach relies on the two-fold use of $[RuCp^*]^+$ as both metal label and as activator of chloroaromates towards nucleophilic substitution by phenolates.[11] The resulting $[RuCp^*]^+$-complexed diaryl ether partial structures will enhance the protease stability of the peptoid.[12]

Figure 1 outlines the design of new oligopeptoids with alternating diaryl ether and amide bonds. Ruthenium labels

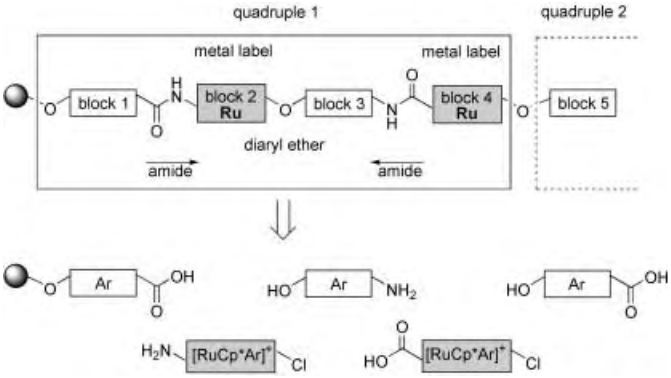


Figure 1. Modular architecture of ruthenium-labeled peptoids with alternating amide and diaryl ether bonds. After the first four building blocks, repetitive elongation steps are possible.

are incorporated with every second building block, which allows a high degree of metal-labeling. Unlike the assembly of regular peptides, four different elongation steps have to be performed to give a quadruple before repeating the synthetic cycle. Consequently, the synthesis of the initial tetrapeptoid is a key goal in developing an automated method for the modular synthesis of this new type of bioorganometallic oligomer.

Scheme 1 gives the synthesis of the doubly $[RuCp^*]^+$-labeled diaryl ether tetrapeptoid **7**. As η^5-ligand, Cp* was chosen instead of Cp because $[RuCp^*(\eta^6\text{-arene})]^+$ complexes can be assembled in a one-pot procedure starting from $RuCl_3 \cdot x\,H_2O$,[13] whereas the analogous Cp complexes require a four-step sequence.[14] As building blocks of the target tetrapeptoid **7** we used *N*-Boc-OBn-tyrosine (**1**), $[RuCp^*]^+$-complexed *p*-chlorophenylethylamine (**2**), tyramine (**4**), and the $[RuCp^*]^+$ complex of *N*-Boc-protected *p*-chlorophenyl alanine (**6**). The free carboxylic acid **6** is best synthesized via its ethyl ester[13b] which is then selectively hydrolyzed using LiOH in THF:H_2O (4:1) at 0 °C for 1 h.

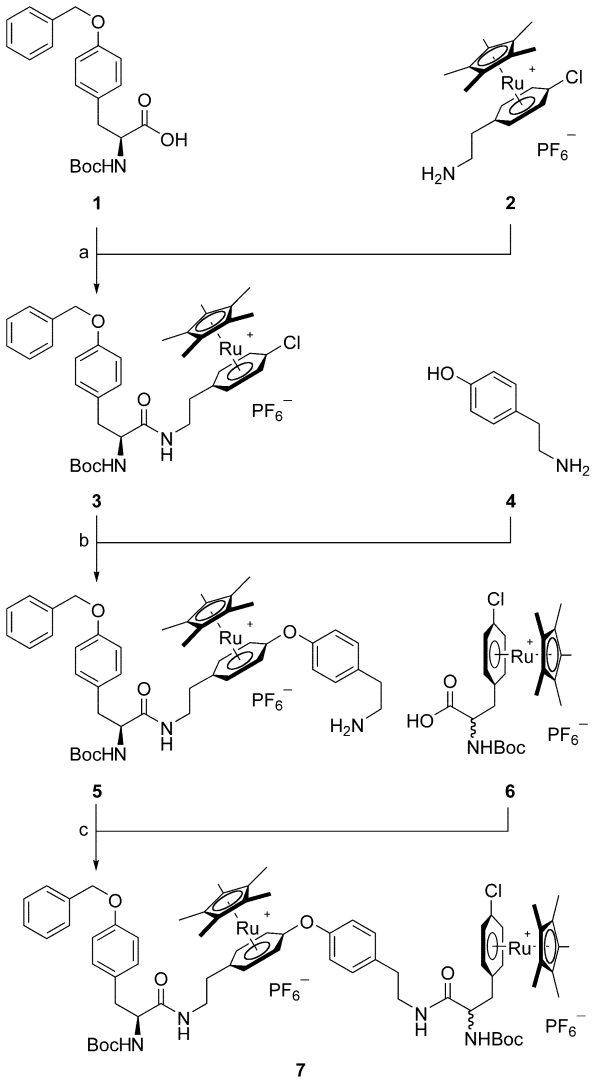
In the first amide coupling step, the acid **1** was converted into its pentafluorophenyl ester with in situ generated *tert*-butyl pentafluorophenyl carbonate.[15] Reaction with the free $[RuCp^*]^+$-complexed amine **2** provided the dipeptoid **3**. Treatment of **3** with tyramine (**4**) provided the $[RuCp^*]^+$ diaryl ether tripeptoid **5** in good yield. Reaction of **5** with **6** by the EDCI/HOBt method completed the synthetic cycle and gave the first tetrapeptoid **7** with two $[RuCp^*]^+$-sandwich labels. The benzyl group currently introduced with the first building block as a protecting group may later be replaced by a linker to solid phases.

[*] Dipl.-Chem. A. Schmid, Prof. Dr. T. Lindel
Ludwig-Maximilians-Universität
Department of Chemistry
Butenandtstrasse 5–13, 81377 Munich (Germany)
Fax: (+49) 89-218-077-734
E-mail: thomas.lindel@cup.uni-muenchen.de

[**] We thank the Degussa AG and Macherey-Nagel GmbH & Co KG for support.

Supporting information for this article is available on the WWW under http://www.angewandte.org or from the author.

 DOI: 10.1002/anie.200352927 © 2004 Wiley-VCH Verlag GmbH & Co. KGaA, Weinheim



Scheme 1. Synthesis of the doubly ruthenium-labeled tetrapeptoid **7** a) **1**, pentafluorophenol (1 equiv), Boc_2O (1 equiv), pyridine, 23 °C, 4 h; then **2**, 1 day, 23 °C, 1 day, 50 °C, 75 %. b) **4**, [18]crown-6, KO*t*Bu, THF:MeCN (1:1), 30 min, 0 °C; then transfer to precooled solution of **3**, −78 °C, 90 min, then 23 °C, 15 min, 64 %. c) **6**, HOBt, THF, EDCI, 0 °C, 15 min; then **5** in THF, iPr_2NEt, 0 °C to 23 °C, 24 h, 80 %; Boc = *tert*-butoxycarbonyl, HOBt = N-hydroxybenzotriazole, EDCI = *N*-ethyl-*N*′-(3-dimethylaminopropyl) carbodiimide.

Larger, permanently charged peptoids, such as the tripeptoid **5** and the tetrapeptoid **7**, require improved chromatography procedures for analysis and purification. The use of aminopropyl silica solid phases was already an important step towards the difficult purification of peptoid $[RuCp]^+$ complexes.[16] We now discovered that unsurpassed separation of the cationic $[RuCp^*]^+$ sandwich complexes can be achieved by using the silica-based Nucleosil SA stationary phase which has both adsorption and ion-exchange properties.[17] Anions and non-charged components of the reaction mixture eluted easily when using pure methanol as the mobile phase. The cationic products were then eluted employing a sodium acetate gradient in methanol.[18] The efficiency of this approach is shown by the separation of the three-component

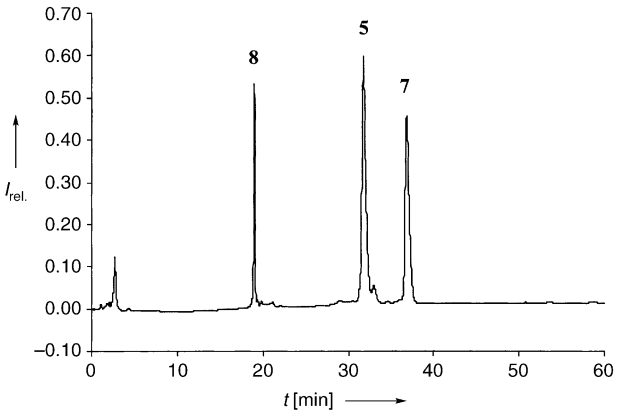
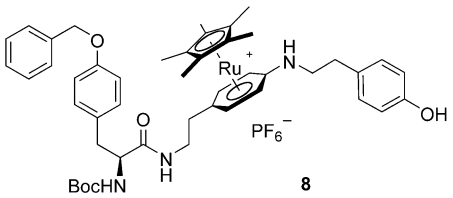


Figure 2. HPLC elution profile of a comparative mixture of the regioisomeric tripeptoids **5** and **8**, and of the tetrapeptoid **7**. For conditions see ref. [18].

mixture of the $[RuCp^*]^+$-labeled peptoids **5**, **7**, and **8** (see Figure 2).

The new chromatography method allowed us to investigate side products, specifically of the attack of the ambident nucleophile **4** on the dipeptoid **3**. We were able to isolate and fully characterize the tripeptoid **8** (a regioisomer of **5**) with an



$[RuCp^*]^+$ alkylarylamine partial structure. The pronounced NMR high-field shift of the protons of the benzenoid part of the sandwich structure of **8** (compared to the diaryl ether **5**), could indicate partial η^5 coordination and a double bond to a deprotonated nitrogen atom, as is observed for the corresponding sandwich complexes of free phenols.[19] However, the ^1H NMR spectrum clearly shows a signal at $\delta =$ 4.29 ppm,which was assigned to an NH proton by COSY, HSQC, and HMBC experiments, thus confirming η^6 coordination of the C_6 ring. The formation of **8** is best avoided by keeping the reaction mixture at −78 °C for at least 90 min and using 1.1 equivalents of **4**. The $[RuCp^*]^+$ sandwich complexes did not tend to decompose in aqueous solution or on exposure to air, the exception being the free amine **2** which should be prepared by deprotection of its Boc-protected precursor immediately prior to use.

Our approach offers the advantage of full control of the frequency and positions of $[RuCp^*]^+$ complexation. From the synthesis of the tetrapepoid **7**, repetitive steps are envisaged. The steric bulk of the Cp* unit restricts the number of possible conformations and we expect to find unusual secondary structures in the longer chain analogues.

Received: September 22, 2003 [Z52927]

 © 2004 Wiley-VCH Verlag GmbH & Co. KGaA, Weinheim

Keywords: bioinorganic chemistry · diaryl ethers · metal-labeling · peptoids · sandwich complexes

[1] The term "peptoid" ("-oid" from the ancient-Greek "ειδος"—"picture") was originally restricted to oligomers of *N*-substituted glycines: R. J. Simon, R. S. Kania, R. N. Zuckermann, V. D. Huebner, D. A. Jewell, S. Banville, S. Ng, L. Wang, S. Rosenberg, C. K. Marlowe, D. C. Spellmeyer, R. Tan, A. D. Frankel, D. V. Santi, F. E. Cohen, P. A. Bartlett, *Proc. Natl. Acad. Sci. USA* **1992**, *89*, 9367 – 9371.

[2] a) D. Seebach, T. Sifferlen, D. J. Bierbaum, M. Rueping, B. Jaun, B. Schweizer, J. Schaefer, A. K. Mehta, R. D. O'Connor, B. H. Meier, M. Ernst, A. Glättli, *Helv. Chim. Acta* **2002**, *85*, 2877 – 2917; b) D. Seebach, L. Schaeffer, M. Brenner, D. Hoyer, *Angew. Chem.* **2003**, *115*, 800 – 802; *Angew. Chem. Int. Ed.* **2003**, *42*, 776 – 777, and references therein.

[3] a) A. Janecka, M. Zubrzycka, T. Janecki, *J. Pept. Res.* **2001**, *53*, 91 – 107; b) A. J. van der Lely, W. W. de Herder, E. P. Krenning, D. J. Kwekkeboom, *Endocrine* **2003**, *20*, 307 – 311.

[4] K. Severin, R. Bergs, W. Beck, *Angew. Chem.* **1998**, *110*, 1722 – 1743; *Angew. Chem. Int. Ed.* **1998**, *37*, 1635 – 1654.

[5] W. E. P. Greenland, K. Howland, J. Hardy, I. Fogelman, P. J. Blower, *J. Med. Chem.* **2003**, *46*, 1751 – 1757, and references therein.

[6] ^{97}Ru (half-life 2.89 days, electron capture), ^{103}Ru (39.27 days, β^-), and ^{106}Ru (1.02 years, β^-); *Handbook of Chemistry and Physics*, 76th ed. (Ed.: D. R. Lide), CRC, Boca Raton, FL, **1995**, pp. 11 – 64.

[7] D. B. Grotjahn, *Coord. Chem. Rev.* **1999**, *190–192*, 1125 – 1141.

[8] M. J. Clarke, *Coord. Chem. Rev.* **2003**, *236*, 209 – 233.

[9] a) A. J. Pearson, J. G. Park, S. H. Yang, Y. H. Chuang, *J. Chem. Soc. Chem. Commun.* **1989**, 1363 – 1364; b) A. J. Pearson, S. Zigmantas, *Tetrahedron Lett.* **2001**, *42*, 8765 – 8768, and references therein; c) C. W. West, D. H. Rich, *Org. Lett.* **1999**, *1*, 1819 – 1822, and references therein; d) A. Marchetti, J. M. Ontoria, V. G. Matassa, *Synlett* **1999**, *1*, 1000 – 1002; e) S. Venkatraman, F. G. Njoroge, V. Girijavallabhan, A. T. McPhall, *J. Org. Chem.* **2002**, *67*, 3152 – 3155.

[10] a) W. S. Sheldrick, A. Gleichmann, *J. Organomet. Chem.* **1994**, *470*, 183 – 187; b) A. J. Gleichmann, J. M. Wolff, W. S. Sheldrick, *J. Chem. Soc. Dalton Trans.* **1995**, 1549 – 1554.

[11] a) A. N. Nesmeyanov, N. A. Vol'kenau, I. N. Bolesova, L. S. Shul'pina, *Dokl. Akad. Nauk SSSR* **1980**, *254*, 1408 – 1409; b) J. A. Segal, *J. Chem. Soc. Chem. Commun.* **1985**, 1338 – 1339.

[12] H. Eickhoff, G. Jung, A. Rieker, *Tetrahedron* **2001**, *57*, 353 – 364.

[13] a) A. R. Kudinov, M. I. Rybinskaya, Yu. T. Struchkov, A. I. Yanovskii, P. V. Petrovskii, *J. Organomet. Chem.* **1987**, *336*, 187 – 197; b) A. Schmid, H. Piotrowski, T. Lindel, *Eur. J. Inorg. Chem.* **2003**, 2255 – 2263.

[14] a) T. P. Gill, K. R. Mann, *Organometallics* **1982**, *1*, 485 – 488; b) B. M. Trost, C. M. Older, *Organometallics* **2002**, *21*, 2544 – 2546.

[15] M. Breslav, N. Doviborov, F. Naider, *J. Chem. Res. Synop.* **1994**, 362 – 363.

[16] a) D. Leone-Stumpf, T. Lindel, *Chem. Eur. J.* **2001**, *7*, 3961 – 3965; b) D. Leone-Stumpf, T. Lindel, *Eur. J. Org. Chem.* **2003**, 1853 – 1858.

[17] Nucleosil SA (Macherey-Nagel) is functionalized with *n*-propylbenzenesulfonic acid groups and has mostly been used for the separation of inorganic cations: M. M. Muenter, K. C. Stokes, R. T. Obie, J. R. Jezorek, *J. Chromatogr. A* **1999**, *844*, 39 – 51, and references therein.

[18] Stationary phase: Macherey-Nagel EC250/4 Nucleosil 100-5SA (length 25 cm, diameter 0.4 cm, particle size 5 μm). Mobile phase: MeOH (10 min), then gradient MeOH to MeOH/$NaOAc\cdot 3H_2O$ (0.74 M) within 40 min, then MeOH/$NaOAc\cdot 3H_2O$ (0.74 M) for 10 min. UV detection at 239 nm.

[19] L. Djakovitch, F. Moulines, D. Astruc, *New J. Chem.* **1996**, *20*, 1071 – 1080.

[20] W. H. Soine, C. E. Guyer, F. F. Knapp, Jr., *J. Med. Chem.* **1984**, *27*, 803 – 806.

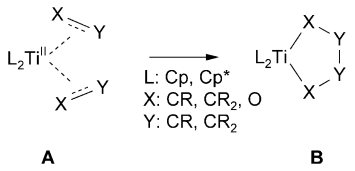
 © 2004 Wiley-VCH Verlag GmbH & Co. KGaA, Weinheim

Self-Assembly

Directed Reduction of Six-Membered Nitrogen Heterocycles—Selective Formation of Polynuclear Titanium Complexes**

Susanne Kraft, Rüdiger Beckhaus, Detlev Haase, and Wolfgang Saak*

Low-valent titanium compounds of the bent metallocene type have proven to be excellent templates for the linkage of π-bonding systems (**A**→**B**).[1] This is illustrated by the formation of titanacyclopentanes,[2] -pentenes,[3] -pentadienes,[4] -oxacyclopentenes[5] or -dioxacyclopentanes[6] in the early days of organometallic chemistry. The formation of homologous zirconium complexes by regioselective alkyne–alkyne coupling of spacer-separated dialkynes has reignited the interest in metallacyclopentadienes.[7] The use of the acetylene complexes synthesized by Rosenthal and co-workers was decisive for the latter developments.[7b,8]



Here we report on the reaction of titanocene precursors with six-membered N-heterocycles which leads, by way of selective C–C coupling, to the formation of polynuclear titanium compounds. Reaction of the titanocene complexes $[Cp_2Ti\{\eta^2\text{-}C_2(SiMe_3)_2\}]$ (**1**) and $[Cp^*_2Ti\{\eta^2\text{-}C_2(SiMe_3)_2\}]$ (**2**)[8] with triazine (**3**) at 25 (**1**) or 60 °C (**2**), respectively, led, after 48 h, to the dinuclear chelate complexes **4** or **5**,

[*] S. Kraft, Prof. Dr. R. Beckhaus, D. Haase, W. Saak
Institut für Reine und Angewandte Chemie
Fakultät für Mathematik und Naturwissenschaften
Carl von Ossietzky Universität Oldenburg
Postfach 2503, 26111 Oldenburg (Germany)
Fax: (+49) 441-798-3581
E-mail: ruediger.beckhaus@uni-oldenburg.de

[**] This work was supported by the Fonds der Chemischen Industrie and by the Karl-Ziegler-Stiftung of the Gesellschaft Deutscher Chemiker.

Supporting information for this article is available on the WWW under http://www.angewandte.org or from the author.

 DOI: 10.1002/anie.200353021 © 2004 Wiley-VCH Verlag GmbH & Co. KGaA, Weinheim

respectively, which can be isolated in 45% or 32%, respectively (Scheme 1).

Complexes **4** and **5** are sparingly soluble in aliphatic and aromatic hydrocarbons as well as in THF and decompose above 300°C, without melting. They display the expected molecular ion peak at *m*/*z* (%) 518 (90) (**4**) and 799 (40) (**5**) in the mass spectrum (EI, 70 eV). Owing to the low solubility, single crystals of **4** and **5** were grown in the reaction solutions. Figure 1 shows the molecular structure of **4** determined by X-ray crystallography.[9] Owing to a disorder at C2, **4** belongs to the highly symmetrical point group *mmm*.[10]

The reactions of alkyne complexes **1** or **2** with pyrazine (**6**) displayed varied behavior. As expected, in both cases the alkyne ligand is displaced: the tetranuclear, pyrazine-bridged titanium complex **7** is formed starting from **1**, whereas **2** reacts under spontaneous threefold C–C coupling to give the trinuclear chelate complex **8** (Scheme 1). The reaction of **1** with **6** occurs in THF at room temperature, as is evident from the color change from yellow-brown to deep purple; after 48 h crystalline **7** can be obtained in 43% yield from dilute reaction solutions. Complex **8** is formed at 60°C in THF or toluene in 60% yield. The molecular structures of **7** and **8** are shown in Figures 2 and 3, respectively.[9] Complex **7** is C_2-symmetrical. In addition, two THF molecules per four-membered ring **7** are contained in the crystal lattice. Like **7**, **8** is also C_2-symmetrical; Ti2 lies on the twofold axis. The three new C–C bonds generated lead to the formation of an ideal cyclohexane ring in the chair conformation.

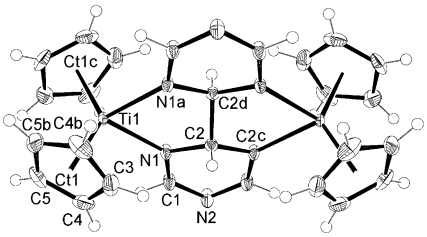
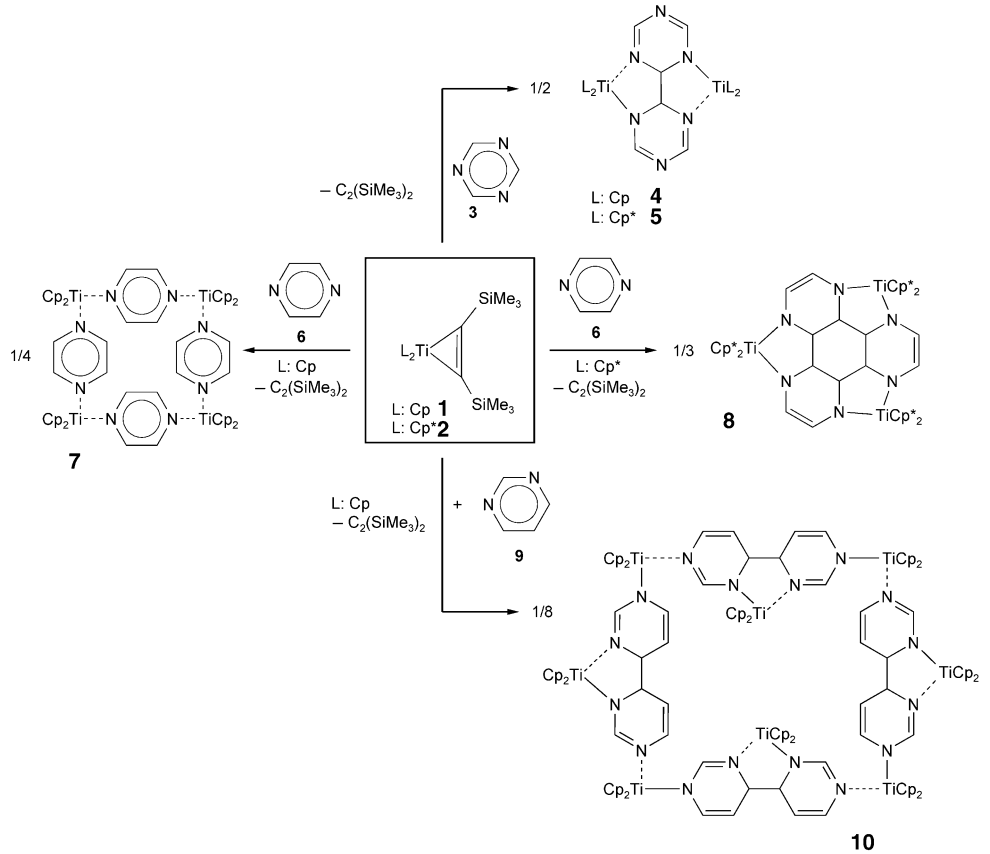


Figure 1. Structure of **4** in the crystal (50% probability, with H atoms). Selected bond lengths [Å] and angles [°]: Ti1-N1 2.2108(16), Ti1-Ct1 2.072, N1-C1 1.299(3), N1-C2 1.468(2), N2-C1 1.352(2), C2-C2c 1.501(6); N1-Ti1-N1a 76.13(9), Ct1-Ti1-Ct1c 133.09; Ct1 = ring centroid of C3–C4b, symmetry transformations for the generation of equivalent atoms: a) *y*, *x*, −*z*; b) *y*, *x*, *z*; c) *x*, *y*, −*z*, d) −*x*, −*y*, −*z*.

The reaction of **1** with pyrimidine (**9**) gives after 2 h at 64°C the octanuclear titanium complex **10** in the form of yellow, needlelike crystals in 80% yield (Scheme 1). Crystals suitable for the X-ray structure analysis were obtained by crystallization from toluene. The resulting molecular structure is shown in Figure 4.[9] Similar to **4**, **5**, **7**, and **8** no NMR spectra could be recorded for **10** because of its low solubility. In the crystal five equivalents of toluene were found per molecule of **10**. The octanuclear compound crystallizes in the polar space group *Pc*. The C(sp^3) centers formed by the C–C coupling show typical disorders.

The formation of **4**, **5**, and **10** is characterized in each case through the linkage of one C–C bond of the N-heterocycle (**3**,



Scheme 1. Reactions of the titanocene–alkyne complexes **1** and **2** with the N-heterocycles **3**, **6**, and **9**. Cp* = C_5Me_5.

 © 2004 Wiley-VCH Verlag GmbH & Co. KGaA, Weinheim

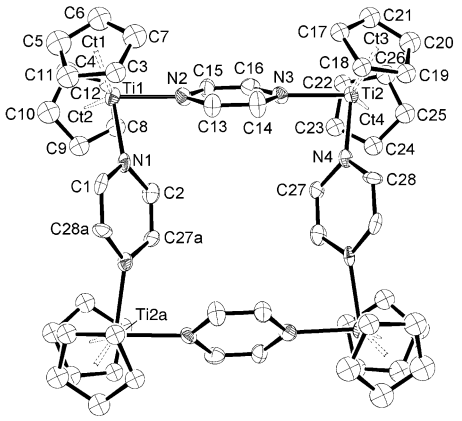


Figure 2. Structure of **7** in the crystal (50% proabability, without H atoms). Selected bond lengths [Å] and angles [°]: Ti1-N1 2.181(7), Ti1-N2 2.152(7), Ti1-Ct1 2.109, Ti1-Ct2 2.111, Ti2-N3 2.167(7), Ti2-N4 2.167(7), Ti2-Ct3 2.433, Ti2-Ct4 2.432, N1-C1 1.403(9), N1-C2 1.391(9), N2-C13 1.384(10), N2-C15 1.412(11), N3-C14 1.398(10), N3-C16 1.407(10), N4-C27 1.395(8), N4-C28 1.384(9), C1-C28a 1.359(10), C2-C27a 1.370(10), C13-C14 1.352(12), C15-C16 1.349(11); N1-Ti1-N2 84.4(2), Ct1-Ti1-Ct2 130.5, N3-Ti2-N4 84.2(2), Ct3-Ti2-Ct4 130.1; Ct1 = ring centroid of C3–C7, Ct2 = ring centroid of C8–C12, Ct3 = ring centroid of C17–C21, Ct4 = ring centroid of C22–C26, symmetry transformation for the generation of equivalent atoms: a) $-x, y, -z+0.5$.

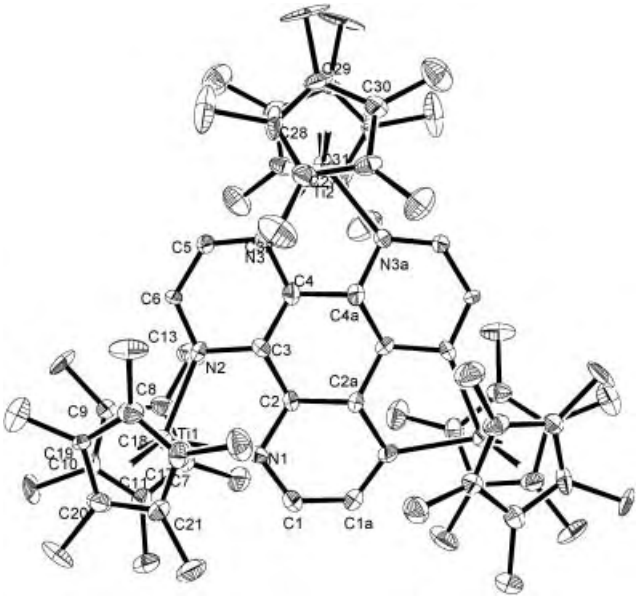


Figure 3. Structure of **8** in the crystal (50% probability, without H atoms). Selected bond lengths [Å] and angles [°]: Ti1-N1 2.212 (3), Ti1-N2 2.193 (2), Ti2-N3 2.184 (2), Ti1-Ct1 2.149, Ti1-Ct2 2.146, Ti2-Ct3 2.158, N1-C1 1.343(4), N1-C2 1.458 (4), N2-C3 1.446 (4), N2-C6 1.349 (4), N3-C4 1.460 (4), N3-C5 1.342 (4), C1-C1a 1.413 (6), C2-C2a 1.508 (7), C2-C3 1.496 (4), C3-C4 1.510 (4), C4-C4a 1.484 (7), C5-C6 1.413 (4); N1-Ti1-N2 76.97 (9), N3-Ti2-N3a 77.89 (12), Ct1-Ti1-Ct2 137.53, Ct3-Ti2-Ct3a 140,18. Ct1 = ring centroid of C7–C11, Ct2 = ring centroid of C17–C21, Ct3 = ring centroid of C27–C31, symmetry transformation for the generation of equivalent atoms: $a = -x+1, y, -z+0.5$.

9) used. Whereas in the reaction with **3**, only **4** or **5**, respectively, is formed even when **1** and **2** are used in excess, that is only the chelate positions are occupied, the

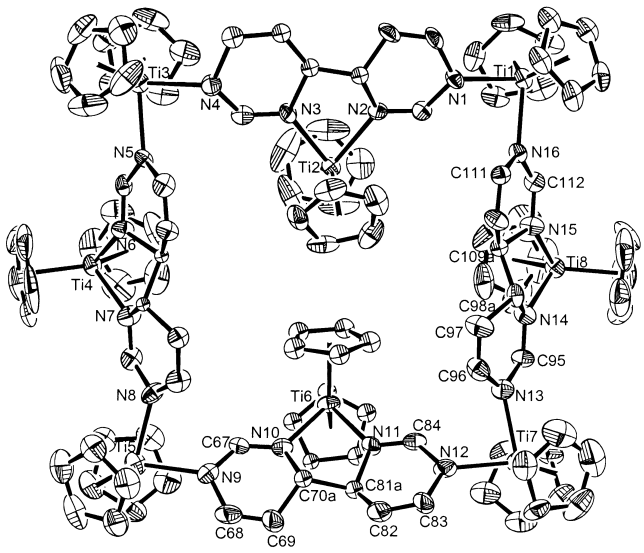


Figure 4. Structure of **10** in the crystal (50% probability, without H atoms). Selected bond lengths [Å] and angles [°] at the terminal Ti5 and Ti7 centers as well as at the chelate positions Ti6 and Ti8: Ti5-N9 2.193(6), Ti5-N8 2.205(6), Ti6-N10 2.155(6), Ti6-N11 2.157(5), Ti7-N12, 2.182(6), Ti7-N13 2.190(6), Ti8-N15 2.153(6), Ti8-N14 2.158(6), N9-C67 1.334(9), N9-C68 1.430(9), N10-C67 1.272(9), N10-C70a 1.569(15), N11-C84 1.301(9), N11-C81a 1.468(9), N12-C84 1.367(8), N12-C83 1.378(9), N13-C95 1.361(9), N13-C96 1.415(9), N14-C95 1.313(9), N14-C98a 1.552(10), N15-C112 1.317(9), N15-C109a 1.496(11), N16-C112 1.338(9), N16-C111 1.422(8), C68-C69 1.302(11), C69-C70a 1.529(18), C70a-C81a 1.602(19), C81a-C82 1.420(9), C82-C83 1.306(10), C96-C97 1.287(11), C97-C98a 1.502(12), C98a-C109a 1.500(14); N9-Ti5-N8 82.0(2), Ct-Ti5-Ct 131.72, N10-Ti6-N11 75.4(2), Ct-Ti6-Ct 133.48, N12-Ti7-N13 83.4(2), Ct-Ti7-Ct 131.88, N15-Ti8-N14 75.8(2), Ct-Ti8-Ct 135,16; Ct = ring centroid of the carbon atoms of the respective Cp ring.

reaction of **1** with **9** leads to the saturation of the terminal N atoms and thus to the octanuclear molecular aggregate **10**. In **10** the eight linked titanium centers form a puckered ring (see Figure 4), and the chelate centers are located above the plane of the terminal Cp_2Ti units. Two of the chelate positions (Ti2, Ti6) point towards the center of the ring, and Ti4 and Ti8 point outwards away from the ring. The formation of **4**, **5**, **8**, and **10** is accompanied by a loss of the aromaticity of the N-heterocycle employed. Along the new C–C bonds, the H atoms always adopt a *trans* position. Particularly notable is the formation of **8** from **2** in comparison to that of **7** from **1**. To the best of our knowledge, compound **7** is the first structurally characterized low-valent molecular square of titanium.[11] All the titanium atoms in **7** lie in one plane and form N-Ti-N angles of 84.4° or 84.2°. The bridging pyrazine molecules are rotated significantly with respect to each other; the titanium atoms are located outside the plane of the N-heterocycles (Ti1-Ti2a-N1 15.4°, Ti1-Ti2-N3 5.8°). Preliminary magnetic measurements reveal diamagnetic behavior for **7** in the temperature range between 25 and 325 K.[12,13]

The Ti–N distances in **4**, **5**, **7**, **8**, and **10** lie at the upper limit for pure Ti–N σ bonds without p_π–d_π interactions,[14] and correspond to the values expected for titanium-coordinated N-heterocycles.[15] The Ti–N distances within **4**, **5**, and **10** do not differ significantly, such that mesomeric forms can be

 © 2004 Wiley-VCH Verlag GmbH & Co. KGaA, Weinheim

assumed.[16] Bond lengths and angles of the titanocene units correspond to those for tetrahedral coordination geometry.

The formation of the C–C-coupled polynuclear complexes **4**, **5**, and **10** can be explained by the initial reduction of the heterocycles to radical anions, which has been described for several N-heterocycles in reactions with low-valent metal complexes[17] or by electrochemical reactions.[18] The C–C coupling in the reaction to give **10** occurs regioselectively at the C4 atom of the heterocycle, the same is true for the electrochemical coupling.[18a] The formation of **8** is particularly surprising, since pyrazine (**6**) is considered to be a typical bridging ligand and no defined C–C coupling at metal centers has been described to date for this heterocycle.[19]

For the investigations described herein, we employed a novel synthetic method, in which metal-linked complexes of polyvalent N-donor ligands are formed from readily accessible building blocks. The good solubility of the starting materials **1** and **2** allows a smooth separation of the (in most cases) sparingly soluble products. Further work on these systems should be able to show whether the record of the linkage of eight [Cp_2Ti] units can be beaten, and to what extent the observed self-assembly principles can be developed by using low-valent early transition metals and redox-active acceptor ligands.[20] The synthesis of **8** described herein could be the beginning of a new area of chemistry comparable to the chemistry of the HAT ligands which are difficult to access.[21]

Experimental Section

General: All titanium compounds were synthesized and handled in an inert gas atmosphere (Schlenk techniques). The solvents were thoroughly dried and saturated with nitrogen prior to use.

4: Compounds **1** (500 mg, 1.435 mmol)[22a] and **3** (116.3 mg, 1.435 mmol) were dissolved in THF (40 mL) at room temperature. In the course of 24 h the solution darkened in color and **4** precipitated in the form of black-green crystals, which were filtered, washed with *n*-hexane, and dried under vacuum (45%). M.p. >300°C; MS (70 eV): *m*/*z* (%): 518 (90) [M^+], 437 (20) [$M^+-C_3H_3N_3$], 398 (25), 316 (25), 259 (15), 178 (100) [Cp_2Ti], 113 (25); IR (KBr): $\tilde{\nu}=3079$ (w), 2998 (w), 2942 (w), 2855 (w), 799 (w), 1613 (s), 1478 (s), 1373 (s), 1348 (s), 1250 (s), 1109 (w), 1067 (w), 1009 (m), 899 (w), 843 (w), 799 (s), 721 (m), 642 (m), 590 (m), 378 cm^{-1} (m); C,H,N analysis calcd (%) for $C_{26}H_{26}N_6Ti_2$: C 60.26, H 5.06, N 16.22; found: C 60.01, H 5.28, N 15.89.

5: Compounds **2** (300 mg, 0.627 mmol)[22b] and **3** (51.5 mg, 0.627 mmol) were dissolved in THF (15 mL), and the solution was heated at 60°C without stirring for 48 h. This led to the precipitation of **5** in the form of orange-colored crystals. After decantation of the mother liquor, the crystals were washed with *n*-hexane and dried under vacuum (32%). M.p. >300°C; MS (70 eV): *m*/*z* (%): 799 (40) [M^+], 664 (40) [$M^+-C_{10}H_{15}$], 501 (25), 335 (65), 319 (80) [Cp_2^*Ti], 285 (25), 169 (100), 119 (30); exact mass determination *m*/*z* 798.4296, calcd 798.4308 ($C_{46}H_{66}N_6Ti_2$); IR (KBr): $\tilde{\nu}=2954$ (m), 2893 (m), 2855 (m), 1607 (s), 1479 (s), 1381 (m), 1346 (s), 1242 (s), 1113 (w), 1032 (m), 997 (s), 719 (s), 656 (s), 590 (s), 394 (s), 373 cm^{-1} (s); C,H,N analysis calcd (%) for $C_{46}H_{66}N_6Ti_2$: C 69.16, H 8.33, N 10.52; found: C 69.07, H 8.26, N 10.67.

7: Solutions of **1** (200 mg, 0.574 mmol) and **6** (46 mg, 0.574 mmol), each in THF (30 mL) THF, were combined, which led to a color change to deep purple. The solution was left for 48 h at room temperature, during which time **7** precipitated in the form of purple crystals. After decantation of the mother liquor, the crystals were washed with *n*-hexane and dried under vacuum (43%). M.p. >300°C; MS (70 eV): *m*/*z* (%): 178 (10) [Cp_2Ti^+], 80 (85) [$C_4H_4N_2^+$], 71 (95), 42 (100); IR (KBr): $\tilde{\nu}=3098$ (w), 2969 (w), 2863 (w), 1615 (w), 1441 (w), 1269 (w), 1065 (w), 1009 (m), 788 (s), 702 (s), 756 (m), 417 cm^{-1} (m); C,H,N analysis calcd (%) for $C_{56}H_{56}N_8Ti_4$: C 65.13, H 5.46, N 10.85; found: C 64.72, H 6.16, N 9.16.

8: Compounds **2** (500 mg, 1.045 mmol) and **6** (83.8 mg, 1.045 mmol) were dissolved in toluene (30 mL), and the solution was heated at 60°C without stirring for 24 h. This led to the precipitation of **8** in the form of dark brown crystals (60%). M.p. >300°C; IR (KBr): $\tilde{\nu}=3044$ (w), 2963 (w), 2895 (m), 2853 (w), 1651 (w), 1454 (m), 1375 (w), 1254 (s), 1211 (w), 1161 (w), 1090 (w), 1057 (w), 1017 (s), 791 cm^{-1} (w); C/H/N analysis calcd (%) for $C_{72}H_{102}N_6Ti_3$: C 72.35, H 8.60, N 6.03; found: C 72.55, H 8.47, N 6.10.

10: Compounds **1** (1000 mg, 2.87 mmol) and **9** (229.8 mg, (2.87 mmol) were dissolved in THF (15 mL) and heated to reflux for 2 h. This led to the precipitation of **10** in the form of yellow needles, and further product was obtained by the addition of *n*-hexane (15 mL) to the mixture. After cooling, filtration, and washing with *n*-hexane, the product was dried under vacuum (80%). M.p. >300°C (decomp); IR (KBr): $\tilde{\nu}=3094$ (w), 3044 (w), 2951 (w), 2851 (w), 2755 (w), 2554 (w), 1634 (s), 1532 (s), 1456 (w), 1393 (m), 1366 (m), 1317 (m), 1265 (s), 1181 (m), 1067 (w), 1013 (s), 988 (s), 909 (w), 891 (w), 793 (s), 735 (m), 667 (w), 627 (m), 596 (m), 374 cm^{-1} (m); C,H,N analysis calcd (%) for $C_{112}H_{112}N_{16}Ti_8$: C 65.14, H 5.47, N 10.85; found: C 64.96, H 5.57, N 10.73.

Received: October 6, 2003 [Z53021]
Published Online: February 23, 2004

Keywords: alkyne ligands · C–C coupling · nitrogen heterocycles · self-assembly · titanium

[1] I. Marek, *Titanium and Zirconium in Organic Synthesis*, Wiley-VCH, Weinheim, **2002**.
[2] a) R. H. Grubbs, A. Miyashita, *J. Am. Chem. Soc.* **1978**, *100*, 1300–1302; b) K. Mashima, N. Sakai, H. Takaya, *Bull. Chem. Soc. Jpn.* **1991**, *64*, 2475–2483; c) K. Mashima, H. Takaya, *Organometallics* **1985**, *4*, 1464–1466.
[3] a) G. Erker, U. Korek, R. Petrenz, A. L. Rheingold, *J. Organomet. Chem.* **1991**, *421*, 215–231; b) M. D. Rausch, L. P. Kleman, W. H. Boon, *Synth. React. Inorg. Met.-Org. Chem.* **1985**, *15*, 923–943.
[4] M. D. Rausch, *Pure Appl. Chem.* **1972**, *30*, 523–538.
[5] A. Ohff, S. Pulst, C. Lefeber, N. Peulecke, P. Arndt, V. V. Burlakov, U. Rosenthal, *Synlett* **1996**, 111–118.
[6] J. Scholz, M. Dlikan, K.-H. Thiele, *J. Prakt. Chem.* **1988**, *330*, 808–810.
[7] a) L. L. Schafer, J. R. Nitschke, S. S. H. Mao, F.-Q. Liu, G. Harder, M. Haufe, T. D. Tilley, *Chem. Eur. J.* **2002**, *8*, 74–83, and references therein; b) J. R. Nitschke, S. Zürcher, T. D. Tilley, *J. Am. Chem. Soc.* **2000**, *122*, 10345–10352.
[8] U. Rosenthal, V. V. Burlakov, P. Arndt, W. Baumann, A. Spannenberg, *Organometallics* **2003**, *22*, 884–900.
[9] Crystallographic data: STOE-IPDS diffractometer ($Mo_{K\alpha}$ radiation); **4**: 175 measurements, $\Delta\varphi$ per measurement 1.6°, $T=193$ K, crystal dimensions $0.40\times0.40\times0.17$ mm^3, $C_{26}H_{26}N_6Ti_2$, $M_r=518.33$, tetragonal, space group $P4_2/mnm$, $a=b=9.4328(4)$, $c=12.3908(7)$ Å, $V=1102.51(9)$ $Å^3$, $Z=2$, $\rho_{calcd}=1.561$ $g\,cm^{-3}$, $\mu(Mo_{K\alpha})=0.753$ mm^{-1}, $F(000)=536$, $\Theta_{max}=26.11°$, 11429 measured reflections, 618 independent reflections ($R_{int}=0.0570$), 546 observed reflections ($I>2\sigma I$)), 60 parameters, GOF (F^2) = 1.061, final *R* indices: $R_1=0.0258$, $wR_2=0.0643$, max./min. residual electron density 0.293/−0.202 e $Å^{-3}$. All atoms of the molecule were refined free. **5**: 245 measurements, $\Delta\varphi$ per measurement 1.1°, $T=193$ K, crystal dimensions $0.75\times0.28\times0.08$ mm^3, $C_{46}H_{66}N_6Ti_2$, $M_r=798.85$, triclinic, space group $P\bar{1}$, $a=10.8204(14)$, $b=12.2876(15)$, $c=17.634(2)$ Å, $\alpha=108.809(13)°$,

$\beta = 107.159(14)°$, $\gamma = 91.509(15)°$, $V = 2101.3(4)$ Å^3, $Z = 2$, $\rho_{calcd} = 1.263$ g cm^{-3}, $\mu(Mo_{K\alpha}) = 0.420$ mm^{-1}, $F(000) = 856$, $\Theta_{max} = 25.92°$, 22303 measured reflections, 7612 independent reflections ($R_{int} = 0.0694$), 4600 observed reflections ($I > 2\sigma(I)$), 485 parameters, GOF (F^2) = 1.011, final R indices: $R_1 = 0.0713$, $wR_2 = 0.1988$, max./min. residual electron density 0.936/−0.454 e Å^{-3}. All non-hydrogen atoms of the molecule were refined free. The H atom positions were calculated. **7**: 183 measurements, $\Delta\varphi$ per measurement 1.2°, $T = 193$ K, crystal dimensions $0.15 \times 0.07 \times 0.06$ mm^3, $C_{64}H_{72}N_8O_2Ti_4$, $M_r = 1176.90$, monoclinic, space group $C2/c$, $a = 21.0255(13)$, $b = 13.8828(13)$, $c = 19.2618(13)$ Å, $\beta = 92.115(8)°$, $V = 5618.6(7)$ Å^3, $Z = 4$, $\rho_{calcd} = 1.391$ g cm^{-3}, $\mu(Mo_{K\alpha}) = 0.601$ mm^{-1}, $F(000) = 2464$, $\Theta_{max} = 25.98°$, 20703 measured reflections, 5454 independent reflections ($R_{int} = 0.3236$), 1352 observed reflections ($I > 2\sigma(I)$), 203 parameters, GOF (F^2) = 0.714, final R indices: $R_1 = 0.0655$, $wR_2 = 0.0925$, max./min. residual electron density 0.944/−0.626 e Å^{-3}. The non-hydrogen atoms were anisotropically refined, the cyclopentadienyl rings were idealized and isotropically refined, the H atom positions were calculated, the solvent molecules are disordered and were refined with coupled U values at two positions with an occupancy ratio of 50:50. **8**: 200 measurements, $\Delta\varphi$ per measurement 1.0°, $T = 193(1)$ K, crystal dimensions $0.09 \times 0.08 \times 0.07$ mm^3, $C_{72}H_{102}N_6Ti_3$, $M_r = 1195.30$, monoclinic, space group $C2/c$, $a = 24.856(10)$, $b = 14.827(4)$, $c = 18.095(8)$ Å, $\beta = 108.45(5)°$, $V = 6326(4)$ Å^3, $Z = 4$, $\rho_{calcd} = 1.255$ g cm^{-3}, $\mu(Mo_{K\alpha}) = 0.417$ mm^{-1}, $F(000) = 2568$, $\Theta_{max} = 25.96°$, 24357 measured reflections, 6117 independent reflections ($R_{int} = 0.4457$), 1335 observed reflections ($I > 2\sigma(I)$), 339 parameters, GOF (F^2) = 0.678, final R indices: $R_1 = 0.0735$, $wR_2 = 0.1059$, max./min. residual electron density 0.415/−0.401 e Å^{-3}. All non-hydrogen atoms were anisotropically refined, the H atom positions were calculated. **10**: 215 measurements, $\Delta\varphi$ per measurement 1.0°, $T = 193$ K, crystal dimensions $0.37 \times 0.26 \times 0.06$ mm^3, $C_{147}H_{152}N_{16}Ti_8$, $M_r = 1263.02$, monoclinic, space group Pc, $a = 20.6583(7)$, $b = 21.7715(10)$, $c = 15.5313(5)$ Å, $\beta = 110.481(3)°$, $V = 6543.8(4)$ Å^3, $Z = 2$, $\rho_{calcd} = 1.282$ g cm^{-3}, $\mu(Mo_{K\alpha}) = 0.519$ mm^{-1}, $F(000) = 2644$, $\Theta_{max} = 25.85°$, 54156 measured reflections, 24879 independent reflections ($R_{int} = 0.1091$), 11557 observed reflections ($I > 2\sigma(I)$), 1103 parameters, GOF (F^2) = 0.835, final R indices: $R_1 = 0.0630$, $wR_2 = 0.1170$, max./min. residual electron density 0.527/−0.399 e Å^{-3}. All non-hydrogen atoms of the molecule were anisotropically refined, providing they were not disordered. The disordered atoms were refined at two positions with an occupancy ratio of 50:50 or 70:30, respectively. The H atom positions were calculated. The asymmetric unit contains five solvent molecules (toluene), which were isotropically refined. All structures were solved by using direct methods (SHELXS-86) and refined against F^2 (SHELXL-97).[23] CCDC-212226 (**4**), CCDC-212223 (**5**), CCDC-212225 (**7**), CCDC-212222 (**8**), and CCDC-212224 (**10**) contain the supplementary crystallographic data for this paper. These data can be obtained free of charge via www.ccdc.cam.ac.uk/conts/retrieving.html (or from the Cambridge Crystallographic Data Centre, 12, Union Road, Cambridge CB21EZ, UK; fax: (+44) 1223-336-033; or deposit@ccdc.cam.ac.uk).

[10] The molecular structure of **5** is given in the Supporting Information.

[11] A cationic Ti^{IV} compound was previously reported on the basis of NMR and MS data: P. J. Stang, J. A. Whiteford, *Res. Chem. Intermed.* **1996**, *22*, 659–665.

[12] We thank Prof. Dr. M. Jansen, Max-Planck-Institut für Festkörperforschung, Stuttgart, for the magnetic measurements.

[13] For comparison: A low-lying triplet state was found for the d^2 complex $[Cp_2Ti(2,2\text{-bpy})]$,[13a] whereas $[Cp^*_2Ti(2,2\text{-bpy})]$ is diamagnetic.[13b] a) A. M. McPherson, B. F. Fieselmann, D. L. Lichtenberger, G. L. McPherson, G. D. Stucky, *J. Am. Chem. Soc.* **1979**, *101*, 3425–3430; b) R. Gyepes, P. T. Witte, M. Horacek, I. Cisarova, K. Mach, *J. Organomet. Chem.* **1998**, *551*, 207–213.

[14] Example: $[Cp^*_2Ti{-}NPhMe]$ 2.054(2) Å: J. Feldman, J. C. Calabrese, *J. Chem. Soc. Chem. Commun.* **1991**, 1042–1044.

[15] Examples of Ti-coordinated N-heterocycles: $[Cp_2Ti(py)_2]^+$ 2.285(3), 2.258(3);[15a] $[Cp_2Ti(2,2\text{-bpy})]^{2+}$ 2.14(1) Å;[15b] $[Cp_2Ti(2,2\text{-bpy})]$ 2.159(6), 2.127(5) Å.[13b] a) A. Ohff, R. Kempe, W. Baumann, U. Rosenthal, *J. Organomet. Chem.* **1996**, *520*, 241–244; b) U. Thewalt, K. Berhalter, *J. Organomet. Chem.* **1986**, *302*, 193–200.

[16] See Supporting Information.

[17] Examples for the formation of dinuclear complexes by C–C coupling of N-heterocycles: phthalazine coupling to $[Cp_2Ti]$,[17a] $[Cp^*_2Yb]$,[17b] phenanthroline to $[Cp_2Ti]$,[17c] pyridazine to $[Cp^*_2Sm]$,[17d] pyridine to $Ti(OR)_2$.[17e] a) D. R. Corbin, G. D. Stucky, W. S. Willis, E. G. Sherry, *J. Am. Chem. Soc.* **1982**, *104*, 4298–4299; b) D. J. Berg, J. M. Boncella, R. A. Andersen, *Organometallics* **2002**, *21*, 4622–4631; c) D. R. Corbin, W. S. Willis, E. N. Duesler, G. D. Stucky, *J. Am. Chem. Soc.* **1980**, *102*, 5969–5971; d) W. J. Evans, D. K. Drummond, *J. Am. Chem. Soc.* **1989**, *111*, 3329–3335; e) L. D. Durfee, P. E. Fanwick, I. P. Rothwell, K. Folting, J. C. Huffman, *J. Am. Chem. Soc.* **1987**, *109*, 4720–4722.

[18] For comparison: electrochemical coupling of pyrimidine to 4,4-bipyrimidine,[18a] 1,3,5-triazine to 4,4-dihydrobitriazyl.[18b] a) G. Tapolsky, F. Robert, J. P. Launay, *New J. Chem.* **1988**, *12*, 761–764; b) H.-S. Chien, M. M. Labes, *J. Electrochem. Soc.* **1986**, *133*, 2509–2510.

[19] a) W. Kaim, *Angew. Chem.* **1983**, *95*, 201–221; *Angew. Chem. Int. Ed. Engl.* **1983**, *22*, 171–191; b) W. Kaim, *Acc. Chem. Res.* **1985**, *18*, 160–166.

[20] a) B. J. Holliday, C. A. Mirkin, *Angew. Chem.* **2001**, *113*, 2076–2097; *Angew. Chem. Int. Ed.* **2001**, *40*, 2022–2043; b) P. J. Stang, *Chem. Eur. J.* **1998**, *4*, 19–27.

[21] Multistep synthesis of 1,4,5,8,9,12-hexaazatriphenylene (HAT), in part through the use of explosive materials: ref. [21a–c], examples for HAT complexes: ref. [21d]. a) D. Z. Rogers, *J. Org. Chem.* **1986**, *51*, 3904–3905; b) M. S. P. Sarma, A. W. Czarnik, *Synthesis* **1988**, 72–73; c) J. T. Rademacher, K. Kanakarajan, A. W. Czarnik, *Synthesis* **1994**, 378–380; d) B. F. Abrahams, P. A. Jackson, R. Robson, *Angew. Chem.* **1998**, *110*, 2801–2804; *Angew. Chem. Int. Ed.* **1998**, *37*, 2656–2659.

[22] a) V. V. Burlakov, U. Rosenthal, P. V. Petrovsky, V. B. Shur, M. E. Volpin, *Metalloorg. Khim.* **1988**, *1*, 526–527; b) V. V. Burlakov, A. V. Polyakov, A. I. Yanovsky, Y. T. Struchkov, V. B. Shur, M. E. Vol′pin, U. Rosenthal, H. Görls, *J. Organomet. Chem.* **1994**, *476*, 197–206.

[23] G. M. Sheldrick, SHELXL-97, A Program for Refining Crystal Structures, Universität Göttingen, (Germany), **1997**.

 © 2004 Wiley-VCH Verlag GmbH & Co. KGaA, Weinheim

Oxidation with Air

Efficient, Copper-Catalyzed, Aerobic Oxidation of Primary Alcohols**

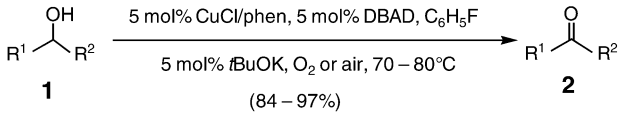
István E. Markó, Arnaud Gautier, Raphaël Dumeunier, Kanae Doda, Freddi Philippart, Stephen M. Brown, and Christopher J. Urch*

The oxidation of alcohols into aldehydes and ketones is of paramount importance in organic chemistry and numerous reagents have been reported to accomplish this transformation efficiently and selectively.[1] However, most of these oxidants are either toxic, hazardous, or required in large excess. From an economical and environmental viewpoint, catalytic oxidations are particularly interesting,[2] and major efforts have been devoted over the last few years to the discovery and development of efficient procedures employing O_2 (or air) or hydrogen peroxide as the ultimate stoichiometric oxidant.[3] These attractive catalytic systems utilize cheap and readily available reactants, display high atom economy[4] and release only innocuous by-products such as H_2O.[5] Whilst a large variety of ruthenium complexes have been shown to catalyze this reaction, either on their own[6] or with the assistance of various co-catalysts,[7] only a limited number of other metals, such as cobalt[8] and palladium,[9] have been successfully employed so far. In most cases, however, the range of substrates tolerated in these aerobic oxidations is limited to certain classes of alcohols.[10]

Sometime ago, we reported that the inexpensive and readily available CuCl/phen/DBAD complex (DBAD = di-*tert*-butyl azodicarboxylate, phen = 1,10-phenanthroline) was a competent catalyst for the aerobic oxidation of a wide range of alcohols **1** to give carbonyl compounds **2** (Scheme 1).[11] Subsequent optimization of our initial catalytic system led to an improved and highly efficient protocol for the oxidation of primary allylic and benzylic as well as secondary aliphatic, allylic, and benzylic alcohols under neutral conditions.[12] Unfortunately, and despite extensive efforts, primary aliphatic alcohols remained elusive recalcitrant substrates.

In this communication we report that the addition of a simple and inexpensive additive provides a modified catalyst that quantitatively oxidizes a large variety of primary alcohols to the corresponding aldehydes. To the best of our knowledge, the Yamaguchi–Mizuno heterogeneous ruthenium system[9h] and our CuCl/phen/DBAD complex are thus far the only systems for the aerobic oxidation of all classes of alcohols.

Closer examination of the oxidation of several primary aliphatic alcohols revealed intriguing features (Table 1). Whilst poor conversion of 1-decanol (**3**) to decanal (**4**) was achieved (Table 1, entry 1), dibenzyl leucinol (**5**) and *N*-Boc-prolinol (**7**) were quantitatively transformed into the corresponding aldehydes (entries 2 and 3). No racemization is observed with these enantiomerically pure substrates. The enhanced reactivity of **5** and **7** could be due either to an increased steric effect at the α-carbon center, to an electronic influence of the α-nitrogen substituent, or to a combination of both. To test the importance of steric hindrance, the aerobic oxidation of cyclohexanylmethanol (**9**) and adamantylmethanol (**11**) was carried out. Much to our surprise, oxidation of **9** afforded **10** in 70% conversion (entry 4) and transformation of **11** to **12** proceeded with 80% conversion (entry 5). Clearly, increased substitution at the α-position favors the oxidation of primary aliphatic alcohols, though the conversions are still not optimum.

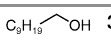
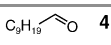
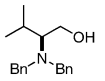
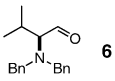
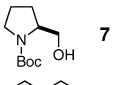
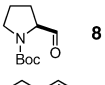
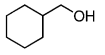
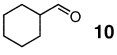
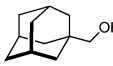
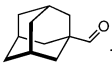


R^1, R^2 = aryl, alkyl, vinyl, H; DBAD = $tBuO_2C$-N=N-CO_2tBu

Scheme 1. Copper-catalyzed aerobic oxidation of alcohols.

In order to improve this transformation, selected additives were tested in the aerobic oxidation of 1-decanol (**3**). The high affinity of heterocyclic amines for copper salts, coupled with their ubiquitous presence as ligands in biologically active copper-containing proteins,[13] prompted us to investigate them initially. Some selected results are collected in Table 2. As can be seen, the conversion of 1-decanol (**3**) to the desired aldehyde **4** proceeded poorly in the absence of additive (Table 2, entry 1). In the presence of 5 mol% DMAP (4-*N*,*N*-dimethylaminopyridine), a significant increase in the transformation of **3** to **4** was observed (entry 2) and complete conversion was eventually reached using 10 mol% DMAP (entry 3). Interestingly, only 7 mol% NMI (*N*-methylimidazole) was required to transform **3** completely into **4** (entry 4).

Table 1: Copper-catalyzed aerobic oxidation of selected primary alcohols.

Entry	Substrate	Product	Conv. [%]	Yield [%][a]
1	 **3**	 **4**	60	51
2	 **5**	 **6**	100	84
3	 **7**	 **8**	100	97
4	 **9**	 **10**	70	64
5	 **11**	 **12**	80	77

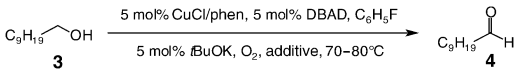
[a] Yield of isolated, pure product.

These conditions were next applied to the aerobic oxidation of a variety of primary alcohols. A selection of pertinent examples is displayed in Table 3. All the primary alcohols employed were quantitatively converted into the corresponding aldehydes with 100% selectivity. It is noteworthy that no trace of carboxylic acid was observed under these aerobic conditions.[14] The reaction tolerates both simple aliphatic primary alcohols (Table 3, entry 1) and more hindered derivatives (entries 2 and 3) as well as various protecting groups (entries 4 and 8). Simple alkenes are

 © 2004 Wiley-VCH Verlag GmbH & Co. KGaA, Weinheim DOI: 10.1002/anie.200353458

unaffected (entry 5), and base-sensitive substrates are smoothly oxidized (entry 6). It is interesting to note that under these neutral conditions, highly acid-sensitive substrates are also quantitatively converted into the correspond-

Table 2: Influence of additives on the aerobic oxidation of 1-decanol (**3**).



Entry	Additive	Amount [mol%]	Conv. [%][a]
1	–	–	60
2	DMAP 	5	80
3	DMAP 	10	100
4	NMI 	7	100

[a] The conversions were measured by capillary gas chromatography with an internal standard.

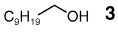
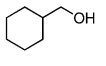
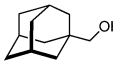
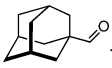
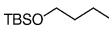
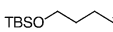
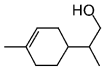
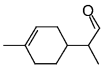
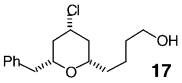
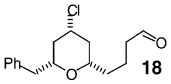
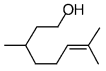
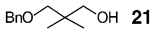
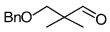
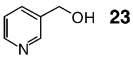
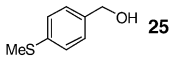
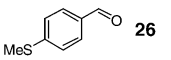
ing aldehydes (entry 7). Finally, a serious impediment in all the other reported aerobic oxidation protocols is their inability to oxidize alcohols possessing a chelating function, a nitrogen atom or a sulfur substituent. Such is not the case for the copper catalyst which transforms the strongly coordinating substrate **21** quantitatively into the aldehyde **22** (entry 8) and tolerates both heteroatoms (entries 9 and 10).

The remarkable effect of DMAP and NMI on the ability of the copper catalyst to oxidize efficiently a wide range of primary alcohols is surprising, and the origin of this effect was investigated, initially with the mechanistically simpler anaerobic system. In the absence of oxygen and NMI, 1-decanol was smoothly and quantitatively oxidized to decanal. Addition of 7 mol% NMI did not improve the conversion, nor the rate of the reaction; rather, NMI had a slightly retarding effect.[15]

In order to reconcile these observations with the previously established catalytic cycle for the aerobic oxidation of alcohols using the CuCl/phen/DBAD system, a new catalytic manifold has to be operative in the presence of NMI. The productive catalytic cycle begins with the ternary loaded complex **A** (Scheme 2). Intramolecular hydrogen transfer from the alkoxo ligand to the azo ligand generates copper(I) hydrazide **B**. Subsequent release of the aldehyde produces complex **C**, which is rapidly captured by oxygen, affording Cu^{II} hydrazide derivative **D**. Reorganization of **D** under the thermal conditions of the reaction leads to the hydroxocopper(I) species **E**. Finally, ligand exchange and elimination of water regenerates the active, loaded complex **A**, and a new catalytic cycle ensues.

Amongst the various active species in this system, complex **C**, bearing an empty coordination site, appears to be the most likely candidate to suffer a competitive deactivation by the primary alcohols.[16] Indeed, whilst **C** usually reacts rapidly with oxygen, it can occasionally undergo competitive coordination to an alcohol, producing the copper derivative **F** that might undergo hydrogen transfer and loss of the hydrazine substituent, resulting in the inactive complex **G**.[17,18]

Table 3: The copper-catalyzed aerobic oxidation of primary alcohols with NMI as an additive.[a]

Entry	Substrate	Product	Yield [%][a]
1	 **3**	 **4**	95
2	 **9**	 **10**	93
3	 **11**	 **12**	95
4	 **13**	 **14**	94
5	 **15**	 **16**	94
6	 **17**	 **18**	83
7	 **19**	 **20**	82
8	 **21**	 **22**	97
9	 **23**	 **24**	93
10	 **25**	 **26**	95

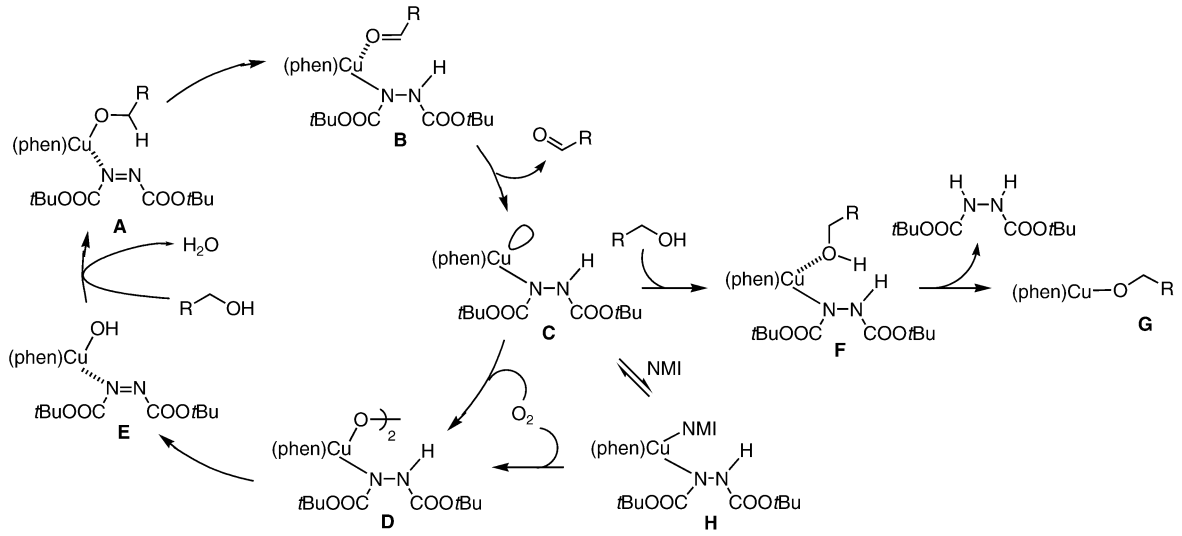
[a] Reaction conditions: entry 4, Table 2. [b] All yields are for pure, isolated products.

In the case of secondary alcohols, competitive coordination to **C** of the OH function or of dioxygen, largely favors the latter and the bis(copper) peroxide **D** is formed. However, when primary aliphatic alcohols are employed, coordination of the less hindered OH group now becomes competitive. The formation of inactive complex **G** gradually depletes the catalytic cycle in the active oxidizing species, and the reaction grinds to a halt. This mechanistic proposal also explains the observed increased conversions when more hindered aliphatic primary alcohols are employed.

The role of NMI and DMAP would thus be to bind rapidly and reversibly to copper complex **C**, generating intermediate **H**. Such coordination would preclude the competitive addition of the alcohol and suppress the undesired formation of the inert derivative **G**.[19,20]

In summary, we have shown that the use of the simple and inexpensive additive NMI strongly modified the course of the copper-catalyzed aerobic oxidation of primary aliphatic alcohols. Under these novel conditions, a wide range of primary substrates could be transformed efficiently into the corresponding aldehydes with no trace of overoxidized carboxylic acids. Moreover, the neutral conditions employed are compatible with base- and acid-sensitive substrates. Furthermore, these results have shed some light on an unsuspected decomposition pathway, the inhibition of which held the key to a highly successful aerobic oxidation

 © 2004 Wiley-VCH Verlag GmbH & Co. KGaA, Weinheim



Scheme 2. Proposed mechanism for the copper-catalyzed aerobic oxidation of alcohols.

procedure for primary alcohols. To the best of our knowledge, the Yamaguchi–Mizuno heterogeneous ruthenium system and our copper-catalyzed aerobic protocol are thus far the only catalytic procedures that are able to oxidize, with equal efficiency, substrates from all classes of alcohols.

Experimental Procedure

Aerobic oxidation of **3:** First 1,10-phenanthroline (180 mg, 1 mmol, 5 mol%) and then solid CuCl (100 mg, 1 mmol, 5 mol%) were added to 200 mL anhydrous FC_6H_5. After the suspension had been stirred for 5 min at room temperature, **3** (3.16 g, 20 mmol) was added followed by solid KO*t*Bu (112 mg, 1 mmol, 5 mol%). The resulting yellowish solution was stirred at room temperature for 10 min before NMI (120 mg, 1.4 mmol, 7 mol%) and DBAD (230 mg, 1 mmol, 5 mol%) were added. The reaction mixture was heated at reflux under a gentle stream of O_2 for 100 min. After the reaction mixture was cooled to 20 °C, celigel (4 g, 80/20 w/w mixture of celite and silica gel) was added and stirring was continued for 2 min. The solid residue was removed by filtration and washed with 200 mL ether. Evaporation of the solvents in vacuo afforded pure **4** as a colorless liquid (2.95 g, 95%).

Received: December 4, 2003 [Z53458]

Keywords: aerobic oxidation · alcohols · aldehydes · molecular oxygen · oxidation

[1] a) R. C. Larock in *Comprehensive Organic Transformations*, VCH, New York, **1989**, p. 604; b) G. Procter in *Comprehensive Organic Synthesis*, *Vol. 7* (Eds.: B. M. Trost, I. Flemming, S. V. Ley), Pergamon, Oxford, **1991**, p. 305; c) S. V. Ley, A. Madin in *Comprehensive Organic Synthesis*, *Vol. 7* (Eds.: B. M. Trost, I. Fleming, S. V. Ley), Pergamon, Oxford, **1991**, p. 251; d) T. V. Lee in *Comprehensive Organic*, *Synthesis*, *Vol. 7* (Eds.: B. M. Trost, I. Fleming, S. V. Ley), Pergamon, Oxford, **1991**, p. 291.

[2] a) R. A. Sheldon, J. K. Kochi in *Metal-Catalyzed Oxidations of Organic Compounds*, Academic Press, New York, **1981**; b) S. V. Ley, J. Norman, W. P. Griffith, S. P. Marsden, *Synthesis* **1994**, 639; c) S.-I. Murahashi, T. Naota, Y. Oda, N. Hirai, *Synlett* **1995**, 733.

[3] a) R. A. Sheldon in *Dioxygen Activation and Homogeneous Catalytic Oxidation* (Ed.: L. L. Simandi), Elsevier, Amsterdam, **1991**, p. 573; b) G. Strukul in *Catalytic Oxidations with Hydrogen Peroxide as Oxidant*, Kluwer Academic Publishers, London, **1992**; c) K. Sato, J. Takagi, M. Aoki, R. Noyori, *Tetrahedron Lett.* **1998**, *39*, 7549; d) K. Sato, M. Aoki, R. Noyori, *Science* **1998**, *281*, 1646; e) A. Berkessel, C. A. Sklorz, *Tetrahedron Lett.* **1999**, *40*, 7965.

[4] R. A. Sheldon, *Pure Appl. Chem.* **2000**, *72*, 1233, and references therein.

[5] For an excellent review, see: P. T. Anastas, M. M. Kirchhoff, *Acc. Chem. Res.* **2002**, *35*, 686, and references therein.

[6] a) K. Masutani, T. Uchida, R. Irie, T. Katsuki, *Tetrahedron Lett.* **2000**, *41*, 5119; b) M. Lee, S. Chang, *Tetrahedron Lett.* **2000**, *41*, 7507; c) R. A. Sheldon, I. W. C. E. Arends, A. Dijksman, *Catal. Today* **2000**, *57*, 157; d) M. Matsumoto, S. Ito, *J. Chem. Soc. Chem. Commun.* **1981**, 907; e) R. Lenz, S. V. Ley, *J. Chem. Soc. Perkin Trans. 1.* **1997**, 3291; f) B. Hinzen, R. Lenz, S. V. Ley, *Synthesis* **1998**, 977; g) A. Bleloch, B. F. G. Johnson, S. V. Ley, A. J. Price, D. S. Shephard, A. W. Thomas, *Chem. Commun.* **1999**, 1907.

[7] a) A. Dijksman, A. Marino-Gonzalez, A. Mairata i Payeras, I. W. C. E. Arends, R. A. Sheldon, *J. Am. Chem. Soc.* **2001**, *123*, 6826; b) S.-I. Murahashi, T. Naota, N. Hirai, *J. Org. Chem.* **1993**, *58*, 7318; c) T. Matsushita, K. Ebitani, K. Kaneda, *Chem. Commun.* **1999**, 265; d) for an excellent review, see: R. A. Sheldon, I. W. C. E. Arends, G.-J. ten Brink, A. Dijksman, *Acc. Chem. Res.* **2002**, *35*, 774.

[8] a) T. Iwahama, S. Sakaguchi, Y. Nishiyama, Y. Ishii, *Tetrahedron Lett.* **1995**, *36*, 6923; b) A. Hanyu, E. Takezawa, S. Sakaguchi, Y. Ishii, *Tetrahedron Lett.* **1998**, *39*, 5557; c) T. Iwahama, Y. Yoshino, T. Keitoku, S. Sakaguchi, Y. Ishii, *J. Org. Chem.* **2000**, *65*, 6502.

[9] a) T. F. Blackburn, J. Schwarts, *Chem. Commun.* **1997**, 157; b) K. Kaneda, Y. Fujie, K. Ebitani, *Tetrahedron Lett.* **1997**, *38*, 9023; c) G.-J. ten Brink, I. W. C. E. Arends, R. A. Sheldon, *Science* **2000**, *287*, 1636; d) K. Hallman, C. Moberg, *Adv. Synth. Catal.* **2001**, *343*, 260; e) T. Nishimura, T. Onoue, K. Ohe, S. Uemura, *J. Org. Chem.* **1999**, *64*, 6750; f) N. Kakiuchi, Y. Maeda, T. Nishimura, S. Uemura, *J. Org. Chem.* **2001**, *66*, 6620; g) M. J. Schultz, C. C. Park, M. S. Sigman, *Chem. Commun.* **2002**, 3034; h) K. Yamaguchi, N. Mizuno, *Angew. Chem.* **2002**, *114*, 4720; *Angew. Chem. Int. Ed.* **2002**, *41*, 4538.

 © 2004 Wiley-VCH Verlag GmbH & Co. KGaA, Weinheim

[10] See for example, refs. [7a, 7d, 9a, 9e, and 9f].
[11] a) I. E. Markó, P. R. Giles, M. Tsukazaki, S. M. Brown, C. J. Urch, *Science* **1996**, *274*, 2044; b) I. E. Markó, P. R. Giles, M. Tsukazaki, I. Chellé-Regnaut, C. J. Urch, S. M. Brown, *J. Am. Chem. Soc.* **1997**, *119*, 12661; c) I. E. Markó, P. R. Giles, M. Tsukazaki, S. M. Brown, C. J. Urch in *Transition Metals for Organic Synthesis*, *Vol. 2* (Eds.: M. Beller, C. Bolm), **1998**, chap. 2.12, p. 350.
[12] a) I. E. Markó, A. Gautier, I. Chellé-Regnaut, P. R. Giles, M. Tsukazaki, C. J. Urch, S. M. Brown, *J. Org. Chem.* **1998**, *63*, 7576; b) I. E. Markó, A. Gautier, J.-L. Mutonkole, R. Dumeunier, A. Ates, C. J. Urch, S. M. Brown, *J. Organomet. Chem.* **2001**, *624*, 344.
[13] a) K. D. Karlin, Y. Gultneh, *Prog. Inorg. Chem.* **1987**, *35*, 219; b) A. M. Sakharov, I. P. Skibida, *Kinet. Catal.* **1988**, *29*, 96; c) N. Kitajima, K. Fujisawa, C. Fujimoto, Y. Moro-oka, S. Hashimoto, T. Kitagawa, K. Toriumi, K. Tatsumi, A. Nakamura, *J. Am. Chem. Soc.* **1992**, *114*, 1277; d) E. I. Solomon, U. M. Sundaram, T. E. Machonkin, *Chem. Rev.* **1996**, *96*, 2563.
[14] The overoxidation of the aldehyde into the corresponding carboxylic acid has never been observed with this aerobic oxidation protocol. Whilst no proper explanation can be provided at this stage, it is possible that the copper catalyst protects the aldehyde towards further reaction with dioxygen. A similar observation has been reported by Sheldon et al.[7a]
[15] Whilst quantitative conversion of **3** into **4** occurred in the absence and presence of 7 mol% NMI, the oxidation of **3** proceeded more slowly in the presence of this additive (87% conversion after 30 min in the absence of NMI and 75% conversion after 30 min in the presence of NMI). The coordination of NMI to copper results in a slower exchange with the excess DBAD and hence, in a longer reaction time.
[16] Studies performed on the anaerobic version of this catalytic system revealed that aliphatic primary alcohols were oxidized with the same efficiency as all the other classes of alcohols, thus ruling out complexes **A**, **B**, and **E** as the culprit for the decomposition pathway. Whilst we could not experimentally rule out complex **D**, coordination of an alcohol to **D** should involve the participation of a pentacoordinated copper species. Whilst these are not uncommon, their formation requires a higher activation energy than the coordination to **C**.
[17] This hydrogen transfer is essentially an intramolecular acid–base reaction. The hydrogen on the coordinated alcohol function is acidified by coordination to the copper centre whilst the hydrazine ligand has basic properties. The elimination of the hydrazine substituent is irreversible under these neutral conditions. Indeed, in the absence of excess base, $DBADH_2$ is unable to displace the alkoxo ligand from the copper complex **G**.
[18] We have previously demonstrated[11a] that **G** was not a competent catalyst in the aerobic oxidation protocol when R = alkyl. Under anaerobic conditions, that is, in the presence of 1 equiv DBAD, **G** can efficiently regenerate the loaded ternary complex **A** and smooth oxidation ensues.
[19] I. E. Markó, M. Tsukazaki, P. R. Giles, S. M. Brown, C. J. Urch, *Angew. Chem.* **1997**, *109*, 2297; *Angew. Chem. Int. Ed. Engl.* **1997**, *36*, 2208.
[20] In full accord with this mechanistic rationale, the use of NMI and other heterocyclic nitrogen derivatives allows the preferential kinetic oxidation of primary aliphatic alcohols over secondary ones. Whilst the selectivities are not yet perfect, initial experiments have shown that the nature of the additive strongly affects the selectivity of this oxidation.

 © 2004 Wiley-VCH Verlag GmbH & Co. KGaA, Weinheim

Drug Design

Aminoglycoside Microarrays To Study Antibiotic Resistance**

*Matthew D. Disney, Sophie Magnet, John S. Blanchard, and Peter H. Seeberger**

Aminoglycosides are broad-spectrum antibiotics against a variety of clinically important bacteria. Their antibacterial effect is due to binding to bacterial 30S ribosomes and inhibiting protein synthesis. The therapeutic efficacy of aminoglycosides, however, has decreased recently because of increased antibiotic resistance.[1,2] Bacteria use several mechanisms to achieve resistance including decreased uptake of the drug into cells, mutation of the target, binding of the drug to proteins, and covalent modification of the drug by enzymes.[1,2] Enzymatic modification is the most common mechanism leading to aminoglycoside resistance. The result of aminoglycoside modification is a large decrease in binding

[*] Dr. M. D. Disney, Prof. P. H. Seeberger
Laboratory for Organic Chemistry
Swiss Federal Institute of Technology Zürich
ETH Hönggerberg HCI F315
Wolfgang-Pauli-Strasse 10, 8093 Zürich (Switzerland)
Fax: (+41) 163-31-235
E-mail: Seeberger@org.chem.ethz.ch

Dr. S. Magnet, Prof. J. S. Blanchard
Department of Biochemistry
Albert Einstein College of Medicine
Bronx, NY 10461 (USA)

[**] This research was supported by a Roche Foundation Postdoctoral Fellowship (to M.D.D.). P.H.S. thanks GlaxoSmithKline (Scholar Award), the Alfred P. Sloan Foundation (fellowship), and Merck for financial support. The work in the USA was supported by the NIH (grant AI33696).

Supporting information for this article is available on the WWW under http://www.angewandte.org or from the author.

 DOI: 10.1002/anie.200353236 © 2004 Wiley-VCH Verlag GmbH & Co. KGaA, Weinheim

affinity to the therapeutic target.[3] The development of high-throughput methods to identify compounds that weakly bind to resistance-causing proteins and strongly bind to therapeutic targets would facilitate the discovery of improved antibiotics. Such methods also allow for a better understanding of the interactions of antibiotics with therapeutic targets and resistance-causing proteins. Microarrays,[4–8] created by the immobilization of small molecules onto glass surfaces, provide a versatile platform for rapidly screening several thousand potential antibiotics in parallel for binding to therapeutic targets and resistance-causing proteins. These screens are particularly attractive since only miniscule amounts of potential antibiotics, therapeutic targets, and resistance-causing proteins are needed, and thus the limitations of current screening methods can be overcome.

Here we report the construction of aminoglycoside microarrays and their use in probing the binding of aminoglycosides to resistance-causing proteins. Two aminoglycoside acetyltransferases that cause antibiotic resistance, 2′-acetyltransferase (AAC(2′)) from *Mycobacterium tuberculosis*[9] and 6′-acetyltransferase (AAC(6′)) from *Salmonella enterica*[10] were used as examples. Hybridization of these enzymes to aminoglycoside arrays show that each immobilized aminoglycoside interacts with both AAC(2′) and AAC(6′). Furthermore, delivery of as little as picomoles of aminoglycoside to slides was sufficient for binding to be observed (Figure 1). The signal from mannose, a negative control, was much lower, indicating that specific interactions were detected.

Binding of aminoglycoside antibiotics to resistance enzymes can be grouped into two categories based on the fluorescence signal from the highest concentration spot (Figure 1). For AAC(6′), the strongest fluorescence arose from binding to amikacin, tobramycin, kanamycin B, lividomycin, neomycin, and ribostamycin. Kanamycin A, apramycin, paromomycin, gentamycin, and neamine resulted in lower signals. For AAC(2′), the strongest signals were observed for amikacin, paromomycin, tobramycin, and ribostamycin while kanamycin B, apramycin, kanamycin A, neamine, neomycin, lividomycin, and gentamycin displayed weaker signals.

To determine how hybridization of AAC(6′) to the aminoglycoside arrays correlates with protein–aminoglycoside binding measurements in solution, we made comparisons to a calorimetric study of aminoglycoside binding to AAC(6′).[11] This analysis shows a strong correlation between these different types of measurements. Calorimetry showed that ribostamycin, tobramycin, lividomycin, and neomycin have the strongest affinities, whereas kanamycin B, paromomycin, gentamycin C, kanamycin A, and amikacin had lower affinities to AAC(6′). Generally the array data and the calorimetry data correlate well when the affinities are classified as strong and stronger with the exception of amikacin, which had one of the strongest fluorescence signals with both enzymes. Amikacin, unlike most of the other aminoglycosides, contains two primary amino groups; the sterically least encumbered amino group is six carbon atoms removed from the 2,4-deoxystreptamine core. Thus, amikacin may be immobilized onto the surface differently than the other aminoglycosides, giving rise to the more intense signal.

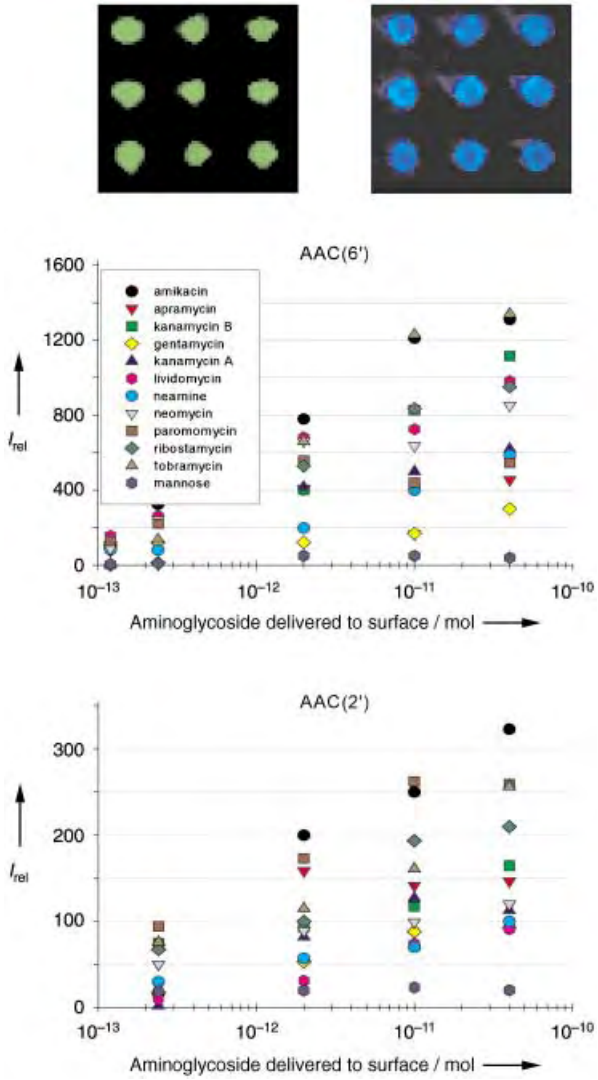
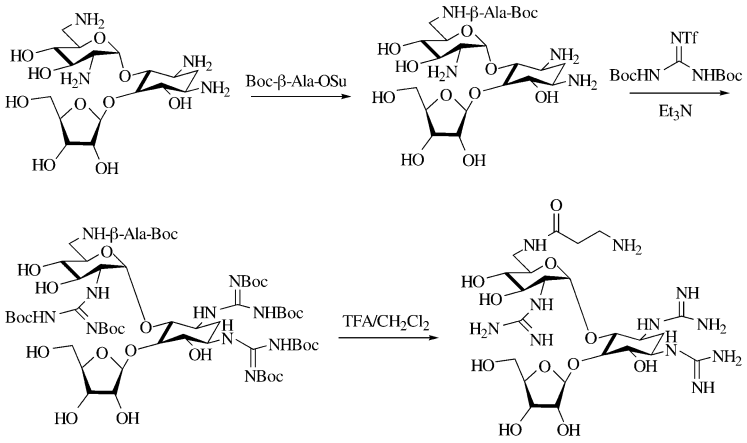


Figure 1. Top: Aminoglycoside microarray after hybridization with AAC(6′) (green) and AAC(2′) (blue). Bottom: Fluorescence intensities for the arrays of antibiotic hybrids after binding to the aminoglycosides.

In an effort to find inhibitors of antibiotic-resistance enzymes, a library of aminoglycoside mimetics was synthesized, arrayed, and screened for tight binding to by AAC(2′) and AAC(6′). Guanidinoglycosides[12,13] are an attractive set of aminoglycoside analogues for several reasons: 1) They are readily synthesized from aminoglycosides. 2) Their increased positive charge may allow them to bind more tightly to the aminoglycoside binding pocket present in resistance-causing enzymes that contain several negatively charged amino acids.[14] 3) The difference in the pK_a values of guanidino (pK_a ~ 12.5) and amino groups (pK_a ~ 8.8) suggests that guanidinoglycosides may not be substrates for AAC(2′) and AAC(6′).

A diverse set of guanidinoglycosides was synthesized (Scheme 1) by reacting each aminoglycoside with Boc-β-Ala-OSu to introduce a primary amino linker for immobilization, which was used to normalize surface loading for each library component. Guanidinylation using *N*,*N*′-di(Boc)-*N*″-triflyl-

 © 2004 Wiley-VCH Verlag GmbH & Co. KGaA, Weinheim



Scheme 1. The synthesis of an aminoglycoside mimetic library is illustrated by the synthesis of 6′-*N*-β-alanine-1,3,3′-*N*-guanidinoribostamycin; all other compounds were synthesized similarly. Boc = *t*-butoxycarbonyl, Tf = trifluoromethanesulfonyl, TFA = trifluoroacetic acid.



Figure 2. An array containing guanidinoglycosides and aminoglycosides that was incubated with fluorescein-labeled AAC(6′). Arrows point to 3×3 blocks of repetitive spots (spot diameter ≈150 μM) on the array that correspond to β-Ala-neomycin (1), β-Ala-guanidinoneomycin (2), β-Ala-ribosytamycin (3), and β-Ala-guanidinoribostamycin (4).

guanidine[12] typically required at least three days and reactions were stopped when mass spectrometry analysis indicated that no partially guanidinylated compounds were present. Treatment with a solution of trifluoroacetic acid (50 % CH_2Cl_2)[12] afforded the desired guanidinylated products in good overall yield (typical yields per step $>90\,\%$).

For a direct comparison of the effect of guanidinylation, both the guanidinoglycosides and the aminoglycosides equipped with a β-alanine linker were arrayed onto glass slides. In all cases after incubation of the arrays with fluorescently labeled AAC(2′) and AAC(6′), the arrayed guanidinoglycosides exhibited a stronger signal for binding to AAC(2′) and AAC(6′) than the corresponding aminoglycosides. The largest enhancement, sevenfold for AAC(2′) and eightfold for AAC(6′), was observed with β-Ala-guanidinoribostamycin (Table 1 and Figure 2). Based on these studies and calorimetry experiments that demonstrate that ribostamycin has the highest affinity to for AAC(6′), we chose β-Ala-guanidinoribostamycin for more detailed studies.

To determine if β-Ala-guanidinoribostamycin is a substrate for AAC(2′) or AAC(6′), kinetics experiments were performed at 37 °C and monitored spectrophotometically.[10] While ribostamycin is completely consumed after 10 min, β-Ala-guanidinoribostamycin did not react with either AAC(2′) or AAC(6′) (data not shown). In addition, β-Ala-guanidinoribostamycin inhibits both AAC(2′) and AAC(6′)(Table 2). In each case, 6′-β-Ala-guanidinoribostamycin was a noncompetitive inhibitor of the binding of ribostamycin to both AAC(2′) and AAC(6′). Data from the kinetics experiments was used to determine the effect on both K_{ii}, the intercept inhibition constant, and K_{is}, the slope inhibition constant. We found that 6′-β-Ala-guanidinoribostamycin inhibits AAC(6′) and AAC(2′) with K_{ii} and K_{is} values in the 10–200 micromolar range. The observation that 6′-β-Ala-guanidinoribostamycin is a noncompetitive inhibitor suggests that it binds to both the free enzyme and the acetyl-CoA enzyme complex, which is also suggested to be how lividomycin noncompetitively inhibits AAC(6′).[10]

In conclusion, we have developed a microarray method for screening antibiotics for binding to resistance-causing enzymes. When this method is used in combination with screening for tight binding of antibiotics to therapeutic

Table 1: Enhancement in binding to AAC(2′) and AAC(6′) by addition of guanidino groups to selected aminoglycosides.[a]

Aminoglycoside	AAC(6′)	AAC(2′)
kanamycin A	2.1	1.1
kanamycin B	1.6	5.5
neomycin	3.2	2.5
ribostamycin	7.5	6.7
paromomycin	1.4	1.1
lividomycin	1.1	1.8

[a] The enhancement is the increase in signal due to the presence of the guanidino groups and is calculated by dividing the signal from the guanidinoglycoside by the signal from the corresponding aminoglycoside.

Table 2: Inhibition of AAC(2′) and AAC(6′) by 6′-*N*-β-alanine-1,3,3′-*N*-guanidinoribostamycin.[a]

Aminoglycoside	K_M [μM]	V_{max} [10^{-2} min^{-1}][b]	K_{ii} [μM]	K_{is} [μM]
		AAC(6′)		
ribostamycin	4.4(±0.8)	18(±0.1)	92(±20)	17(±8)
kanamycin A	12(±3)	2.8(±0.2)	23(±7)	31(±15)
		AAC(2′)		
ribostamycin	4.4(±0.7)	4.4(±1.8)	134(±40)	39(±16)
kanamycin B	0.7(±0.2)	2.6(±0.2)	61(±20)	200(±50)

[a] Experiments to determine inhibition constants were performed with variable concentrations of aminoglycoside and inhibitor. For details see the Supplementary Information. [b] Rates are $\Delta A_{412}\,\text{min}^{-1}$.

 © 2004 Wiley-VCH Verlag GmbH & Co. KGaA, Weinheim

targets, new antibiotics that are weak binders to resistance-causing enzymes and tight binders to therapeutic targets can be identified. This new method was used to screen a series of aminoglycoside mimetics for high-affinity binding to the resistance-causing enzymes AAC(2′) and AAC(6′) in an effort to discover inhibitors of resistance. These screens identified 6′-β-Ala-guanidinoribostamycin as a high-affinity binder to both AAC(2′) and AAC(6′). Further experiments show that 6′-β-Ala-guanidinoribostamycin is not a substrate for either resistance enzymes and is an inhibitor of acylation of several clinically important antibiotics. This approach should prove valuable for screening libraries of compounds to discover improved antibiotics that evade current modes of bacterial resistance.

Received: November 3, 2003 [Z53236]

Keywords: antibiotics · bioorganic chemistry · carbohydrates · combinatorial chemistry · high-throughput screening

[1] C. Walsh, *Nature* **2000**, *406*, 775.
[2] G. D. Wright, *Curr. Opin. Chem. Biol.* **2003**, *7*, 563.
[3] B. Llano-Sotelo, E. F. Azucena, Jr., L. P. Kotra, S. Mobashery, C. S. Chow, *Chem. Biol.* **2002**, *9*, 455.
[4] D. Barnes-Seeman, S. B. Park, A. N. Koehler, S. L. Schreiber, *Angew. Chem.* **2003**, *115*, 2478; *Angew. Chem. Int. Ed.* **2003**, *42*, 2376.
[5] S. Fukui, T. Feizi, C. Galustian, A. M. Lawson, W. Chai, *Nat. Biotechnol.* **2002**, *20*, 1011.
[6] A. N. Koehler, A. F. Shamji, S. L. Schreiber, D. Barnes-Seeman, S. B. Park, *J. Am. Chem. Soc.* **2003**, *125*, 8420.
[7] G. MacBeath, A. N. Koehler, S. L. Schreiber, *J. Am. Chem. Soc.* **1999**, *121*, 7967.
[8] P. J. Hergenrother, K. M. Depew, S. L. Schreiber, *J. Am. Chem. Soc.* **2000**, *122*, 7849.
[9] S. S. Hegde, F. Javid-Majd, J. S. Blanchard, *J. Biol. Chem.* **2001**, *276*, 45876.
[10] S. Magnet, T. Lambert, P. Courvalin, J. S. Blanchard, *Biochemistry* **2001**, *40*, 3700.
[11] S. S. Hegde, T. K. Dam, C. F. Brewer, J. S. Blanchard, *Biochemistry* **2002**, *41*, 7519.
[12] T. J. Baker, N. W. Luedtke, Y. Tor, M. Goodman, *J. Org. Chem.* **2000**, *65*, 9054.
[13] N. W. Luedtke, T. J. Baker, M. Goodman, Y. Tor, *J. Am. Chem. Soc.* **2000**, *122*, 12035.
[14] M. W. Vetting, S. S. Hegde, F. Javid-Majd, J. S. Blanchard, S. L. Roderick, *Nat. Struct. Biol.* **2002**, *9*, 653.

 © 2004 Wiley-VCH Verlag GmbH & Co. KGaA, Weinheim

Peptide Structures

Mixed Helices—A General Folding Pattern in Homologous Peptides?**

*Carsten Baldauf, Robert Günther, and Hans-Jörg Hofmann**

Oligomers composed entirely of unnatural monomers that form characteristic secondary structures have attracted considerable attention in the last years.[1] The motivation for work in this area ranges from gaining a better understanding of the structure and function of biomolecules and imitating them to developing polymers with novel properties. Considerable stimulation of research on these foldamers[2] came from the investigation of β-peptides.[3] Numerous secondary structures were found in these β-peptides as well as in homologous γ- and δ-peptides.[1,4]

In their studies on β-peptides Seebach and co-workers found a unique type of secondary structure, which they referred to as a "mixed helix".[5] Other authors have also described such mixed helices in the meantime.[6] In the familiar periodic helices all corresponding backbone torsion angles of the monomer constituents have the same values, and all peptide bonds form hydrogen bonds of the same type. In contrast, the periodicity of the mixed helices emerges at the level of dimer units. Here, the monomer constituents have alternating values for the backbone torsion angles, and the peptide bonds form hydrogen bonds of different types in an alternating way as well. The CO and NH groups of adjacent peptide linkages are involved in hydrogen bonds that are formed alternatingly in the forward and backward directions. This leads to the formation of alternating hydrogen-bonded rings of different size along the sequence (Figure 1). In the mixed helices of the β-peptides 10-membered rings with an interaction between the amino acids i and $(i+1)$ in the forward direction are followed by 12-membered rings with an interaction between the amino acids i and $(i+3)$ in the backward direction of the sequence.

The existence of mixed helices in β-peptides raises the question whether this folding pattern might also exist in the homologous γ- and δ-peptides and even in the native α-peptides. The transfer of the folding principle to the homologous peptides leads to the hydrogen-bonding patterns with $i\rightarrow(i+1)/i\leftarrow(i+3)$ interactions of the amino acids (Figure 1). Moreover, it is feasible that this principle can be

[*] Dipl.-Biochem. C. Baldauf, Dr. R. Günther, Prof. H.-J. Hofmann
Institut für Biochemie, Universität Leipzig
Brüderstrasse 34, 04103 Leipzig (Germany)
Fax: (+49) 341-973-6998
E-mail: hofmann@uni-leipzig.de

[**] This work was supported by the Deutsche Forschungsgemeinschaft (Project HO2346/1 "Sekundärstrukturbildung in Peptiden mit nicht-proteinogenen Aminosäuren" and SFB 610 "Proteinzustände mit zellbiologischer und medizinischer Relevanz") and the Fonds der Chemischen Industrie.

Supporting information for this article is available on the WWW under http://www.angewandte.org or from the author.

 © 2004 Wiley-VCH Verlag GmbH & Co. KGaA, Weinheim DOI: 10.1002/anie.200353249

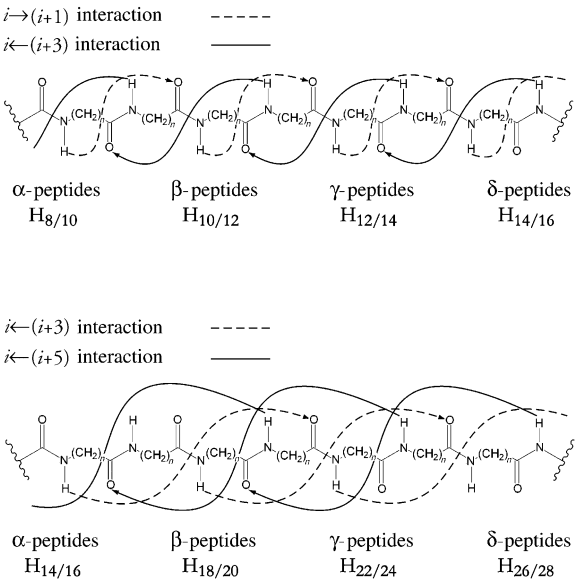


Figure 1. Alternative hydrogen-bonding patterns in mixed helices $H_{x/y}$ of homologous α- ($n=1$), β- ($n=2$), γ- ($n=3$), and δ-peptides ($n=4$). The index x/y denotes the number of atoms in the alternating hydrogen-bonded rings.

extended to mixed helices with still larger alternating ring systems, as for instance with an $i\rightarrow(i+3)/i\leftarrow(i+5)$ interaction of the amino acids (Figure 1). Finally, it would be interesting to find further structure alternatives for a given hydrogen-bonding pattern.

On the basis of theoretical methods it is possible to answer these questions. For this purpose the conformational space of hexamers of α-, β-, γ-, and δ-peptides was systematically searched for mixed helices having the hydrogen-bonding patterns shown in Figure 1. In this search the backbone torsion angles φ, θ, ζ, ρ, and ψ of the oligomers (cf. structures in Table 1) were systematically varied.[7] Thus, about 1.1×10^5, 1.7×10^6, 1.1×10^6, and 6.3×10^5 conformations were generated for the α-, β-, γ-, and δ-peptides, respectively. For the δ-peptides only mixed helices with the combination of the smaller rings according to Figure 1 were sought. Since boundary effects cannot be excluded in oligomers of six amino acids, the two possible orders of the alternating rings were considered in the hexamers. In the corresponding conformation pools the candidates for mixed helices were selected on the basis of general geometry criteria for the formation of hydrogen bonds. Dependent on the peptide and helix types, these were in between 5 and 30 conformations that fulfilled the hydrogen-bonding patterns in Figure 1. These structures were the starting points for geometry optimization[8a] at various levels of ab initio MO theory, which provide reliable results in the conformational analysis of peptides (HF/6-31G*, B3LYP/6-31G*).[9] The resulting stationary points on the potential energy surface were characterized by the eigenvalues of the matrix of force constants.

Both ab initio models show mixed helices as energy minima for all homologous peptides. For the β-, γ-, and δ-peptides there are even several representatives for the hydrogen-bonding patterns examined, which are denoted by superscripted Roman numbers on the helix symbol in Table 1. The mixed helix of the α-peptides shows a sequence of alternating 14- and 16-membered rings. Interestingly, the model structures of α-peptides with the smaller 8- and 10-membered rings could not be localized as energy minima. The basic patterns of the mixed helices in the various homologous peptides are characterized by the backbone torsion angles listed in Table 1. Figure 2 shows the most stable helices for

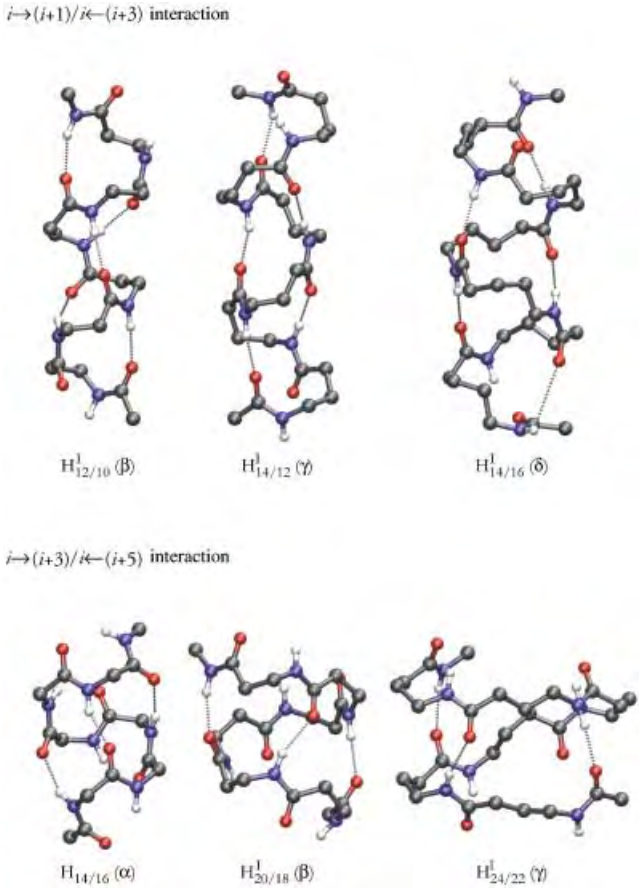


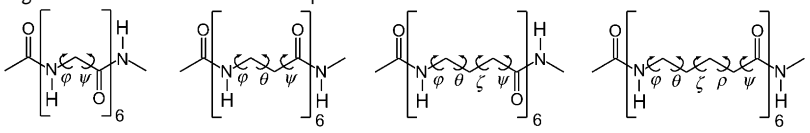
Figure 2. Most stable mixed helices in hexamers of homologous α-, β-, γ-, and δ-peptides for the investigated hydrogen-bonding patterns.

each peptide and hydrogen-bond type. Force field calculations (CHARMm23.1)[10] proved that the hexamer structures are maintained in sequences of up to 20 monomer constituents.

Even more impressive than the wide variety of mixed helices that are possible in the homologous peptides is the considerable stability of some of the structures in comparison to the periodic helices. This is most striking for the β-peptides (Table 1). In the case of the α-peptides, we selected the 3_{10}-helix characterized by 10-membered hydrogen-bonded rings for the energy comparison. For the β-peptides, the experimentally determined helices with 14- and 12-membered rings,[11] which are confirmed by our calculations as particularly stable, served as references to estimate the stability of the mixed-helix alternatives. The reference structure for the γ-peptides was an experimentally found and theoretically

 © 2004 Wiley-VCH Verlag GmbH & Co. KGaA, Weinheim

Table 1: Basic patterns of mixed helices in hexamers of α-, β-, γ-, and δ-peptides characterized by the corresponding backbone torsion angles[a] φ, θ, ζ, ρ, and ψ, and the relative energies[b] based on the most stable periodic helix.



α-peptides β-peptides γ-peptides δ-peptides

Type[c]	φ	θ	ζ	ρ	ψ	ΔE HF	ΔE B3LYP	ΔE PCM
α-Peptides								
$H_{14/16}$	81				−67	**−36.2**	**−65.3**	46.4
	−81				85			
H_{10}[d]	−63				−20	0.0	0.0	**0.0**
β-Peptides								
$H_{12/10}^{I}$	−102	61			89	**−82.6**	**−79.5**	**−10.7**
	90	66			−111			
$H_{12/10}^{II}$	87	61			−96	−44.1	−54.6	31.0
	−27	−50			160			
$H_{10/12}^{III}$	179	−62			−21	−45.9	−56.0	26.6
	−93	51			87			
$H_{20/18}^{I}$	91	66			171	−69.5	−57.4	12.8
	−79	−57			149			
$H_{20/18}^{II}$	99	67			173	−35.3	−28.1	36.7
	−150	57			47			
$H_{20/18}^{III}$	153	162			69	−27.9	−20.9	39.5
	73	52			−144			
$H_{18/20}^{IV}$	79	−171			100	−0.5	−1.4	67.7
	110	−48			−43			
H_{14}	−148	61			−138	13.4	26.0	0.0
H_{12}	−87	92			−109	0.0	0.0	22.6
γ-Peptides								
$H_{14/12}^{I}$	−91	79	−80		162	19.9	13.7	49.1
	94	84	−73		−29			
$H_{14/12}^{II}$	65	56	−126		−53	46.7	45.8	80.2
	−64	−37	−61		143			
$H_{24/22}^{I}$	74	−177	−80		−168	12.3	9.9	40.9
	−125	62	−77		154			
$H_{24/22}^{II}$	117	−68	−174		128	44.5	45.8	68.1
	−89	−72	83		58			
$H_{24/22}^{III}$	94	79	−66		−102	72.0	67.1	87.0
	123	64	66		16			
H_{14}	138	−60	−65		141	**0.0**	**0.0**	**0.0**
δ-Peptides								
$H_{14/16}^{I}$	−172	159	−77	−68	131	**−1.9**	−10.0	89.5
	76	69	−167	82	−126			
$H_{16/14}^{II}$	113	−54	−62	167	159	2.4	**−14.2**	90.0
	−126	82	−66	−67	164			
H_{10}	98	−62	−68	169	−85	0.0	0.0	40.2
H_8	180	66	−142	69	−173	19.1	28.2	**0.0**

[a] Angles in degrees. For reasons of space, only the angles of the two central amino acids are given. The angles of all amino acids at all levels of approximation are given in the Supporting Information. [b] Relative energies at the HF/6-31G*, DFT/B3LYP/6-31G*, and PCM//HF/6-31G* levels (solvent water) in kJ mol^{-1}. The most stable structures are indicated. The total energies of the periodic reference helices are given in the Supporting Information. [c] $H_{x/y}$ denotes a mixed helix with alternating hydrogen-bonded rings having *x* and *y* atoms, respectively. H_x denotes periodic helices with hydrogen-bonded rings of *x* atoms. [d] 3_{10}-helix.

confirmed periodic structure with 14-membered rings.[4a,12] Finally, structures with 8- and 10-membered rings, respectively, which proved to be the most stable periodic structures according to our calculations, were the reference structures for the δ-peptides. Both ab initio MO models agree fairly well in their stability predictions. Only for the δ-peptides are the two mixed helices and the periodic reference helix are energetically equivalent at the Hartree–Fock level, although the mixed helices are distinctly more stable according to the density functional theory.

It might be supposed that the influence of the medium could be the reason for the larger number of experimentally determined periodic helices in homologous peptides in comparison to the single representative of a mixed helix found until now. The hydrogen bonds in the mixed helix are formed alternately in forward and backward directions along the sequence. Thus, only a small helix dipole should result. This is confirmed by the dipole moments of $\mu = 3.8$ D for the hexamers of the most stable mixed helix of the β-peptides and $\mu = 31.5$ D for the periodic helix alternative with 14-membered rings. Since the formation of mixed helices is at a disadvantage in polar media, it is more likely to occur in less polar media. In order to estimate the influence of the environment, the solvation energies were calculated for the solvent water based on the polarizable continuum model (PCM//HF/6-31G*).[8b] The results indicate that the mixed helices, in particular those of the α-, γ-, and δ-peptides, indeed become more unstable than the periodic folding alternatives. Only the most stable mixed helices of the β-peptides remain competitive in strongly polar solvents (Table 1).

 © 2004 Wiley-VCH Verlag GmbH & Co. KGaA, Weinheim

The formation of mixed helices can also be influenced by the introduction of substituents into the monomer units.[13] Our calculations on models of mixed helices of β-peptides for all possible substitution patterns, which we will report on elsewhere, reveal that a mixed helix with alternate substituents at the α- and β-carbon atoms is especially stable. This substitution pattern is the same as that in the mixed helix found by Seebach and co-workers. Thus, mixed helices prove to be a novel and interesting alternative of general importance for determinining secondary structures in α-peptides and their homologues.

Received: November 4, 2003 [Z53249]

Keywords: ab initio calculations · conformational analysis · foldamers · peptides · secondary structure

[1] D. J. Hill, M. J. Mio, R. B. Prince, T. S. Hughes, J. S. Moore, *Chem. Rev.* **2001**, *101*, 3893.

[2] S. H. Gellman, *Acc. Chem. Res.* **1998**, *31*, 173.

[3] a) R. P. Cheng, S. H. Gellman, W. F. DeGrado, *Chem. Rev.* **2001**, *101*, 3219; b) D. Seebach, J. L. Matthews, *Chem. Commun.* **1997**, 2015; c) W. F. DeGrado, J. P. Schneider, Y. Hamuro, *J. Pept. Res.* **1999**, *54*, 206.

[4] a) T. Hintermann, K. Gademann, B. Jaun, D. Seebach, *Helv. Chim. Acta* **1998**, *81*, 983; b) S. Hanessian, X. Luo, R. Schaum, S. Michnick, *J. Am. Chem. Soc.* **1998**, *120*, 8569; c) D. D. Long, N. L. Hungerford, M. D. Smith, D. E. A. Brittain, D. G. Marquess, T. D. W. Claridge, G. W. J. Fleet, *Tetrahedron Lett.* **1999**, *40*, 2195.

[5] a) D. Seebach, K. Gademann, J. V. Schreiber, J. L. Matthews, T. Hintermann, B. Jaun, *Helv. Chim. Acta* **1997**, *80*, 2033; b) M. Rueping, J. V. Schreiber, G. Lelais, B. Jaun, D. Seebach, *Helv. Chim. Acta* **2002**, *85*, 2577.

[6] a) S. A. W. Gruner, B. Truffault, G. Voll, E. Locardi, M. Stöckle, H. Kessler, *Chem. Eur. J.* **2002**, *8*, 4366; b) G. V. M. Sharma, K. R. Reddy, P. R. Krishna, A. R. Sankar, K. Narsimulu, S. K. Kumar, P. Jayaprakash, B. Jagannadh, A. C. Kunwar, *J. Am. Chem. Soc.* **2003**, *125*, 13670.

[7] Variation of the backbone torsion angles based on the alternation conditions for mixed helices: α-peptides: φ, ψ in steps of 30°; β-peptides: φ, θ, ψ in steps of 30°; γ-peptides: φ, θ, ζ ,ψ in steps of 60°; δ-peptides: φ and ψ in steps of 60°, θ, ζ, and ρ in steps of 120°; changes of $\pm 15°$ were allowed for the torsion angle $\omega = 180°$ of the *trans*-peptide bonds.

[8] a) Gaussian 98 (Revision A.11.3), M. J. Frisch, G. W. Trucks, H. B. Schlegel, G. E. Scuseria, M. A. Robb, J. R. Cheeseman, V. G. Zakrzewski, J. A. Montgomery, R. E. Stratmann, J. C. Burant, S. Dapprich, J. M. Millam, A. D. Daniels, K. N. Kudin, M. C. Strain, O. Farkas, J. Tomasi, V. Barone, M. Cossi, R. Cammi, B. Mennucci, C. Pomelli, C. Adamo, S. Clifford, J. Ochterski, G. A. Petersson, P. Y. Ayala, Q. Cui, K. Morokuma, D. K. Malick, A. D. Rabuck, K. Raghavachari, J. B. Foresman, J. Cioslowski, J. V. Ortiz, B. B. Stefanov, G. Liu, A. Liashenko, P. Piskorz, I. Komaromi, R. Gomperts, R. L. Martin, D. J. Fox, T. Keith, M. A. Al-Laham, C. Y. Peng, A. Nanayakkara, C. Gonzalez, M. Challacombe, P. M. W. Gill, B. G. Johnson, W. Chen, M. W. Wong, J. L. Andres, M. Head-Gordon, E. S. Replogle, J. A. Pople, Gaussian, Inc., Pittsburgh, PA, **1998**; b) Gamess (Version: 20 JUN 2002 (R2)) M. W. Schmidt, K. K. Baldridge, J. A. Boatz, S. T. Elbert, M. S. Gordon, J. H. Jensen, S. Koseki, N. Matsunaga, K. A. Nguyen, S. J. Su, T. L. Windus, M. Dupuis, J. A. Montgomery, *J. Comput. Chem.* **1993**, *14*, 1347.

[9] a) T. Head-Gordon, M. Head-Gordon, M. J. Frisch, C. L. Brooks III, J. A. Pople, *J. Am. Chem. Soc.* **1991**, *113*, 5989; b) G. Endredi, A. Perczel, O. Farkas, M. A. McAllister, G. I. Csonka, J. Ladik, I. G. Csizmadia, *J. Mol. Struct.* **1997**, *391*, 15; c) K. Möhle, M. Gussmann, A. Rost, R. Cimiraglia, H.-J. Hofmann, *J. Phys. Chem. A* **1997**, *101*, 8571.

[10] a) F. A. Momany, R. Rone, *J. Comput. Chem.* **1992**, *13*, 888; b) F. A. Momany, R. Rone, H. Kunz, R. F. Frey, S. Q. Newton, L. Schäfer, *J. Mol. Struct.* **1993**, *286*, 1.

[11] a) D. Seebach, M. Overhand, F. N. M. Kühnle, B. Martinoni, L. Oberer, U. Hommel, H. Widmer, *Helv. Chim. Acta* **1996**, *79*, 913; b) D. H. Appella, L. A. Christianson, D. A. Klein, D. R. Powell, X. Huang, J. J. Barchi, Jr., S. H. Gellman, *Nature* **1997**, *387*, 381; c) K. Möhle, R. Günther, M. Thormann, N. Sewald, H.-J. Hofmann, *Biopolymers* **1999**, *50*, 167; d) Y.-D. Wu, D.-P. Wang, *J. Am. Chem. Soc.* **1998**, *120*, 13485; e) X. Daura, K. Gademann, B. Jaun, D. Seebach, W. F. van Gunsteren, A. E. Mark, *Angew. Chem.* **1999**, *111*, 249; *Angew. Chem. Int. Ed.* **1999**, *38*, 236; f) R. Günther, H.-J. Hofmann, K. Kuczera, *J. Phys. Chem. B* **2001**, *105*, 5559.

[12] C. Baldauf, R. Günther, H.-J. Hofmann, *Helv. Chim. Acta* **2003**, *86*, 2573.

[13] a) Y.-D. Wu, D. P. Wang, *J. Am. Chem. Soc.* **1999**, *121*, 9352; b) T. A. Martinek, F. Fülöp, *Eur. J. Biochem.* **2003**, *270*, 3657.

 © 2004 Wiley-VCH Verlag GmbH & Co. KGaA, Weinheim